OPENING SESSION

Room 6A-C 7:45 – 8:20 Chair: Chrit T. Moonen, President

7:45 **Welcome and Award Presentations**

2006 MANSFIELD LECTURE

Room 6A-C 8:20 – 9:00 Chair: Jeffrey L. Duerk

8:20 **Strategic Directions and the Role of Imaging in 21st Century Healthcare: The NIH Perspective**
Elias A. Zerhouni[1]
[1]National Institutes of Health, Bethesda, Maryland, USA

PLENARY LECTURES: Global Healthcare Challenges

Room 6A-C 9:00 - 10:15 Chairs: Qun Chen and Glyn Johnson

9:00 *1.* **Infectious Diseases: Is There a Role for MRI?**
Rakesh Kumar Gupta[1]
[1]Sanjay Ghandhi Institute for Medical Sciences, Lucknow, India

The impact of cutting edge MR technology in management of infectious diseases of the CNS is presented. MR has helped in the non-invasive specific diagnosis of brain infections such as tuberculosis, brain abscess and herpes simplex encephalitis. *In vivo* MR spectroscopy, perfusion and diffusion tensor imaging have been found to be useful in monitoring therapeutic response in these subjects and differential diagnosis of the intracranial lesions complicating AIDS.

9:25 *2.* **Opportunities and Challenges of MR in Developing Countries**
Jianping Dai[1]
[1]Beijing Tian Tan Hospital, Beijing, China

In recent years many developing countries are undergoing rapid, profound economic and social change and development. Being the largest developing country, China is taking advantage of this trend. With a population of about 1.3 billion, one-fifth of the world's total, China has a rapidly growing need and economic resources for advanced healthcare products, including MRI systems. With China as an example, we see unprecedented huge opportunities of MRI market in the developing world.

9:50 *3.* **Imaging COPD and Asthma - From Structure to Function**
Eduard E. de Lange[1]
[1]University of Virginia, Charlottesville, Virginia, USA

Chronic Obstructive Pulmonary Disease (COPD) and asthma are respiratory diseases of global importance. In this lecture we will discuss the appearances of the structural and functional findings of the lung as demonstrated in patients with these diseases using current clinical imaging modalities such as high resolution computed tomography, radionucleide scintigraphy and magnetic resonance (MR) imaging. Particular attention will be given to recent developments in hyperpolarized noble gas MR imaging as a method for high-resolution visualization of the lung airspaces and regional airflow, and for probing the lung microstructure using diffusion-weighted imaging.

CLINICAL CATEGORICAL COURSE
Hot Topics in Clinical Practice: Neuroimaging and Body Imaging

Room 6E 11:00 - 13:00 Chairs: Thomas M. Grist and John D. Port

Educational Objectives:
Upon completion of this session, participants should be able to:

- Describe five points that can be used to improve imaging strategies in important areas of clinical practice;
- Assess the applicability to clinical practice of three newer imaging techniques.

Neuroimaging:

The final five minutes of each presentation will be reserved for questions.

11:00 **Molecular Imaging with Cell Tracking in the CNS**
Letterio Politi

11:20 **Automated Changed Detection in Serial Imaging Studies of the Brain**
Bradley J. Erickson

11:40 **Cutting-Edge Imaging of the Spine**
Roland Bammer

Body Imaging:

12:00 **Hot Body MRI: Beyond Anatomy Towards Tissue Function**
Scott B. Reeder

12:20 **Hot Topics in Europe: Whole Body MRI**
Thomas C. Lauenstein

12:40 **Hot New MRA Techniques**
Martin R. Prince

CLINICAL MRI COURSE
Body MR Problem Solving

Room 6C 11:00 - 13:00 Chair: Caroline Reinhold

The Hepatitis C Patient:
Early Diagnosis of Cirrhosis and HCC

Educational Objectives:
Upon completion of this session, participants should be able to:

- Recognize early morphologic signs of cirrhosis, before nodular texture or contour abnormalities are evident;
- Describe the spectrum of findings of portal hypertension; and
- List the categories of nodular lesions, and be able to devise a differential diagnosis and appropriate follow-up.

Problem Solving with Breast MRI

Educational Objectives:
Upon completion of this session, participants should be able to:

- Identify useful clinical indications for breast MR imaging;
- Describe and apply diagnostic criteria for benign masses and non-mass-related enhancement; and
- Describe and apply diagnostic criteria for invasive and intraductal malignant lesions, as well as mass-related enhancement from DCIS.

11:00 **The Hepatitis C Patient: Early Diagnosis of Cirrhosis and HCC**
Donald G. Mitchell

12:00 **Problem Solving with Breast MR**
Christiane K. Kuhl

Non-Cartesian Parallel Reconstruction

Room 6D 11:00 - 13:00 Chairs: Walter F. Block and Stefan Kannengiesser

11:00 *4.* **The Combination of 2D SENSE and 2D Partial Fourier Homodyne Reconstruction: Achieving Acceleration Factors Greater Than the Number of Coils**

Houchun H. Hu[1], Ananth J. Madhuranthakam[2], Clifton R. Haider[1], David G. Kruger[1], James F. Glockner[1], John Huston III[1], Norbert G. Campeau[1], Stephen J. Riederer[1]

[1]Mayo Clinic College of Medicine, Rochester, Minnesota, USA; [2]GE Healthcare, Boston, Massachusetts, USA

Sensitivity encoding (SENSE) and 1D partial Fourier (PF) techniques accelerate MR acquisitions by collecting reduced k-space data. This work introduces a modified elliptical centric trajectory that combines 2D-SENSE and 2D-PF with homodyne reconstruction to improve resolution and speed performance in 3D contrast-enhanced MR angiography. Acceleration factor exceeding the number of coils are reliably achieved. Using four coils, seven-fold accelerated 19-second acquisitions with 2D SENSE-PF consistently yields diagnostic-quality angiograms with 1-mm resolution in the lower legs. Additional studies were performed using an eight-channel array in intracranial venography, where a whole-brain volume with 1-mm isotropic resolution is acquired in under 60 seconds.

11:12 *5.* **Artifact Reduction in Undersampled BLADE/PROPELLER MRI by K-Space Extrapolation Using Parallel Imaging**

Martin Blaimer[1], Kestutis Barkauskas[1], Stephan Kannengiesser[2], Felix Breuer[3], Peter M. Jakob[3], Jeffrey L. Duerk[1], Mark A. Griswold[1]

[1]University Hospitals of Cleveland and Case Western Reserve University, Cleveland, Ohio, USA; [2]Siemens Medical Solutions, Erlangen, Germany; [3]University of Würzburg, Würzburg, Germany

BLADE (a.k.a., PROPELLER) MRI is an efficient acquisition and reconstruction technique that allows motion correction. However, the scan time is increased compared to conventional imaging. Recently, k-space undersampled BLADE MRI was proposed for reducing the imaging time. However, this method introduces image artifacts. Here, we present a reconstruction approach that allows one to reduce these artifacts. It is based on a k-space extrapolation of acquired data using the parallel GRAPPA-Operator technique. Unlike other approaches incorporating parallel imaging, this method is totally self-calibrated and can still be combined with conventional parallel imaging to provide even further reductions in imaging time.

11:24 *6.* **A Self-Calibrated Parallel Imaging Method for Radial Trajectories**

Arjun Arunachalam[1], Alexei A. Samsonov[1], Walter F. Block[1]

[1]UW-Madison, Madison, Wisconsin, USA

A self-calibrated Parallel Imaging method with low reconstruction times is presented for two and three dimensional radial trajectories. The radially over sampled center of k-space is used to estimate individual receiver sensitivity profiles. Receiver sensitivities are then reintroduced in the image domain and the prohibitively large matrix inversion procedure is completed entirely in k-space by performing a small number of fast matrix inversions. The *in vivo* applicability of the method for 2D radial applications for acceleration factors of 2 and 4. In CE-MRA, scan times were reduced from 42 seconds to 14 seconds to achieve isotropic resolution along all three dimensions.

11:36 *7.* **3D Cylindrical GRAPPA**

Nicole Elizabeth Seiberlich[1], Felix A. Breuer[1], Martin Blaimer[1], Peter Speier[2], Mark A. Griswold[3], Peter M. Jakob[1]

[1]University of Würzburg, Würzburg, Bavaria, Germany; [2]Siemens AG Medical Solutions, Erlangen, Bavaria, Germany; [3]University Hospitals of Cleveland, Cleveland, Ohio, USA

The advantages of both 3D radial k-space sampling and parallel acquisition techniques for reducing motion artifacts, decreasing imaging time, and providing greater spatial resolution are well-known. This abstract proposes a novel method of applying the GRAPPA reconstruction method to undersampled 3D cylindrical k-space trajectories. Whereas previous authors have suggested using GRAPPA to reconstruct images with purely z-direction undersampling, we show that undersampling in both the z and angular directions provides better image quality and allows for higher acceleration factors. We also demonstrate that the application of a CAIPIRINHA-like rotation of the undersampled radial disks can further improve the reconstruction.

11:48 *8.* **Improving Rigid Head Motion Correction Using Parallel Imaging**

Roland Bammer[1], Chunlei Liu[1], Murat Aksoy[1]

[1]Stanford University, Stanford, California, USA

A novel method to determine and correct for rigid in-plane body motion is introduced. The method utilizes parallel imaging to correct for missing k-space data that result from the initial motion correction. The utility of the new method has been first verified in simulation studies and was then tested in healthy volunteers that were asked to move their head at three intensity levels (no, mild, and moderate motion) during data acquisition. A significant reduction of motion artifacts was observed. The new correction scheme is a promising tool for multi-shot DTI, PWI or fMRI studies to monitor and correct for motion.

12:00 ***9***. **Multi-Resolution Successive Iteration (MRSI) for Non-Cartesian SENSE Reconstruction**

Peng Qu[1], Bida Zhang[2, 3], Chunsheng Wang[1], Gary X. Shen[1]

[1]The University of Hong Kong, Hong Kong, People's Republic of China; [2]The Graduate School and Institute of Biophysics, The Chinese Academy of Sciences, Beijing, People's Republic of China; [3]Siemens Mindit Magnetic Resonance Ltd., Shenzhen, Guangdong, People's Republic of China

An improved reconstruction strategy ¡[a] the multi-resolution successive iteration (MRSI) method is proposed for non-Cartesian SENSE. The conjugate gradient (CG) reconstruction is performed in several successive phases with different level of resolution. In such a fashion, the iteration approaches the desired image with increasing resolution. *In vivo* results show that the total reconstruction time can be significantly reduced with this novel method.

12:12 ***10***. **BOSCO: Parallel Image Reconstruction Based on Successive Convolution Operations**

Peng Hu[1], Craig H. Meyer[1]

[1]University of Virginia, Charlottesville, Virginia, USA

We present a new approach for parallel imaging reconstruction for non-Cartesian trajectories: BOSCO (Based On Successive Convolution Operations). In our method, a normal gridding is performed for the data from each coil, followed by another convolution that suppresses the aliasing artifacts in one coil. The un-aliased sub-images from all the coils are combined using square-root of sum-of-squares to form the final image. *In vivo* spiral images show that BOSCO gives aliasing free images under acceleration factors of two and four, while maintaining sufficient SNR. As the two convolutions can be calculated relatively fast, BOSCO is a promising technique for real-time parallel imaging applications.

12:24 ***11***. **Noise Amplification in TPI-SENSE Parallel Imaging**

Yongxian Qian[1], Andy Stenger[2], Fernando Boada[1]

[1]University of Pittsburgh, Pittsburgh, Pennsylvania, USA; [2]University of Hawaii at Manoa, Honolulu, Hawaii, USA

Noise amplification in the TPI-SENSE imaging was investigated for a 4-element head coil array on a 3T scanner. Multiple noise trials and conjugate gradient SENSE reconstruction were used to calculate noise images for the reductions in polar (ring) and azimuthal (rotation) directions. The average standard derivation of the noise images showed that the noise amplification in the TPI-SENSE was significantly smaller than that expected for Cartesian sampling, and closely associated with the coil maps.

12:36 ***12***. **Efficient Parallel MRI with 3D Radials Using Accelerated PARS Reconstruction**

Jessica L. Klaers[1], Arjun Arunachalam[1], Walter F. Block[1], Alexey A. Samsonov[1]

[1]University of Wisconsin, Madison, Wisconsin, USA

The variable sampling density of radial trajectories has proven useful for robust imaging in the presence of motion, accelerated scanning through undersampling, and time-resolved imaging. Parallel MRI (pMRI) offers the opportunity to further accelerate 3D radial imaging. Recently, efficient modification of the Parallel MRI with Augmented Radius (PARS) technique was proposed and demonstrated with 2D radials. We extend the technique to 3D radial imaging for comprehensive imaging of the entire torso. An accelerated PARS pMRI technique has reduced computation to synthesize k-space data by a factor of 400 in a 3D non-Cartesian acquisition compared to original PARS.

12:48 ***13***. **Improved Iterative Non-Cartesian SENSE Reconstruction Using Inner-Regularization**

Peng Qu[1], Bida Zhang[2, 3], Jing Luo[2], Jianmin Wang[3], Gary X. Shen[1]

[1]The University of Hong Kong, Hong Kong, People's Republic of China; [2]The Graduate School and Institute of Biophysics, The Chinese Academy of Sciences, Beijing, People's Republic of China; [3]Siemens Mindit Magnetic Resonance Ltd., Shenzhen, Guangdong, People's Republic of China

The conjugate-gradient (CG)-based non-Cartesian SENSE reconstruction in many cases exhibits unstable convergence behavior. This is because the generalized encoding matrix (GEM) is usually seriously ill-conditioned due to the large dimension and the mixed encoding scheme. To overcome this difficulty, an improved iterative SENSE approach is presented. During a so-called Lanczos iteration process, inner-regularization can be incorporated into the reconstruction without touching the iteration process. With inner-regularization adaptively applied for every iteration loop, the convergence behavior of iterative SENSE can be significantly improved and noise booming can be avoided.

Experimental Cardiac MRI (Animal)

Room 4C - 3,4 11:00 - 13:00 Chairs: Paul A. Bottomley and Maria I. Altbach

11:00 ***14.*** **Tissue Characterization by Combining Delayed Hyperenhancement and Percent Edema Mapping – a R2-Map Based MRI Method in Canine Myocardial Infarction**

Pál Surányi[1, 2], Balázs Ruzsics[1], Pál Kiss[1, 2], Brigitta C. Brott[1], Tamás Simor[1, 2], Nada H. Saab-Ismail[2], Robert A. Baker[1], Gabriel A. Elgavish[1, 2]

[1]University of Alabama at Birmingham, Birmingham, Alabama, USA; [2]Elgavish Paramagnetics Inc., Hoover, Alabama, USA

A Tissue-Characterization-Mapping (TCM) MRI post-processing method is introduced. It differentiates myocardial edema, acute necrosis, hemorrhage and mature scar. The method combines the widely accepted delayed-contrast-enhancement(DE) method with our Percent Edema Mapping (PEM) method. PEM is a R2-based method for generating a map that reflects water-content in the infarcted heart. In dogs(n=6) four days after reperfused myocardial infarction, pixel-by-pixel R2-mapping was followed by DE imaging. Four dogs were sacrificed immediately and two were allowed to survive for eight weeks. Results of the TCM were compared to TTC-staining, validating the ability of TCM to accurately localize and quantify the various tissue types.

11:12 ***15.*** **Structural Basis for Regional Heterogeneity of Left Ventricular Function?**

Daniel B. Ennis[1], Lars Wigström[1, 2], Tom Nguyen[1], Stefan Skare[1], Roland Bammer[1], Neil B. Ingels[1], D C. Miller[1]

[1]Stanford University, Palo Alto, California, USA; [2]Linköping University, Linköping, Sweden

The complex, but highly ordered arrangement of myofibers in the ventricular wall is closely related to regional myocardial function. This work uses DTMRI measures in 5 sheep to demonstrate that midwall myofibers are not oriented in the circumferential direction in all regions of the left ventricle and furthermore that regional gradients in myofiber orientation are heterogeneous. In the lateral midwall fibers are oriented at an angle of ?=-13.9 ±8.0 . In comparison, septal midwall fibers average 9.6 ±11.8 . Regional differences of myofiber arrangement should impact regional function in addition to having implications for the interpretation of MRI tissue tagging strains.

11:24 ***16.*** **A High-Throughput MRI Method for Individualized Assessment of Left Ventricular Hypertrophy in Mice**

Luis Freay[1], Brent Sharp[1], Angela Tidwell[1], Zhi-Ming Ding[1], Alex Abuin[1], Zheng-Zheng Shi[1]

[1]Lexicon Genetics Incorporated, The Woodlands, Texas, USA

We report here a cardiac MRI protocol for rapid and repeated assessment of myocardial hypertrophy in mice. A modified fast gradient-echo cine sequence gated to both ECG and respiratory motion was used to measure mid-ventricular LV mass at days 0 and 7 of isoproterenol treatment in the same animal. Using this protocol, development of LV hypertrophy in all animals and an attenuation of the hypertrophy in animals receiving additional treatment of Enalapril was demonstrated. This non-invasive MRI method proved to be fast (18 min/animal), accurate, and more sensitive than autopsy due to its baseline-control capability.

11:36 ***17.*** **Self-Gated, Wireless Cine-MRI Allows Accurate and Time-Efficient Analysis of Mouse Heart Function When Conventional ECG-And Respiratory Gated Cine MRI Fails**

Cees J.A. Van Echteld[1], Marcel G.J. Nederhoff[1, 2], Bernard C.M. Te Boekhorst[1, 2], Cees W.A. Van de Kolk[1], Maurits A. Jansen[1, 2], Arno Nauerth[3]

[1]University Medical Center Utrecht, Utrecht, Netherlands; [2]InterUniversity Cardiology Institute of the Netherlands, Utrecht, Netherlands; [3]Bruker BioSpin MRI GmbH, Ettlingen, Germany

Conventional cardiac cine MR images are obtained with ECG and respiratory gating. In animal, and in particular in mouse, cardiac MRI, the quality of the ECG signal is variable and frequently deteriorates over time, especially for mice with myocardial infarction or cardiac hypertrophy. Sometimes ECG gated cardiac MRI is not possible at all due to severe cardiac conduction disturbances. Therefore, we have explored a newly developed navigator-based retrospective gating technique based on a gradient echo with very high temporal resolution on adult healthy control mice and mice with large myocardial infarctions. We conclude that self gated, wireless cine MRI 1)allows accurate analysis of mouse heart function when ECG and respiratory gated cine MRI fails, 2) allows a higher throughput, since the instrumentation with ECG electrodes is obviated and 3)shows less flow artifacts.

11:48 ***18.*** **High-Throughput µMRI Phenotyping of Right Ventricular Mouse Embryonic Abnormalities: Requirement for Intravascular Contrast Enhancement**

Youssef Zaim Wadghiri[1], Amanda Schneider[1], Emily N. Gray[1], Orlando Aristizabal[1], Daniel H. Turnbull[1], David E. Gutstein[1]

[1]New York University School of Medicine, New York, New York, USA

µMRI is becoming a well established screening tool to phenotype mouse mutants during development. The characterization of the mouse cardiac right ventricle (RV) is particularly challenging when conventional histology is used to evaluate the morphology of this asymmetric, crescent-shaped chamber. Based on a µMRI protocol initially proposed by Smith B.R. *et al.* (1994), we imaged a line of connexin43 (Cx43) mutant mouse embryos that are known to have heart malformations. Using a high throughput setup, highly detailed 3D image datasets (50µm isotropic resolution) can be obtained simultaneously from 4 fixed specimen previously infused with Gd-based contrast agents. Our results demonstrate that RV abnormalities in the Cx43 mouse line can be more reliably visualized with µMRI than with conventional histology. More importantly we show that the use of contrast agent can be critical to visualize the disruption of the architecture of the muscle wall in the embryonic heart, a phenotype that is variable.

12:00 ***19***. **Non-Invasive Myocardial and Hepatic R2* Assessment in a Juvenile Hematochromatosis Mouse Model at High Magnetic Field**

Peter R. Allegrini[1], Claudia Weidensteiner[1], Hanspeter Nick[1]
[1]Novartis Inst. for BioMedical Research, Basel, BS, Switzerland

Juvenile hemochromatosis leads to excess iron deposition in liver and heart. Cardiac failure is the most common cause of death of patients with iron overload. This study describes the development of non-invasive cardiac and hepatic iron determination by MRI based on R_2* assessment. A preliminary time course study with $HJV^{-/-}$ mice, a model of Juvenile hemochromatosis was performed. At the age of 6 months myocardial R_2* of $HJV^{-/-}$ was 136 s^{-1} (control 56 s^{-1}) whereas that of the liver amounted to 641 s^{-1} (control 82 s^{-1}). The feasibility of reproducible hepatic and myocardial R_2* assessment in mice was demonstrated.

12:12 ***20***. **Cardiac Cine MRI at 3.0T: Initial Experience with Gadomer-17 in a Swine Model**

Carissa Grace Fonseca[1], Kambiz Nael[1], Hanns-Joachim Weinmann[2], Glen Nyborg[1], Gerhard Laub[3], J Paul Finn[1]
[1]UCLA, Los Angeles, California, USA; [2]Schering AG, Berlin, Germany; [3]Siemens AG, Erlangen, Germany

At 3.0T, cardiac cine MRI using SSFP is limited by B0 inhomogeneity and magnetic susceptibility effects which heighten sensitivity to off-resonance artefacts. Spoiled gradient echo sequences, such as FLASH cine imaging, may have advantages over SSFP, at 3.0T, if the associated blood saturation effect can be overcome. The contrast agent – Gadomer-17, used with FLASH cine imaging in a swine model at 3.0T eliminated saturation effects, remarkably improving blood-pool signal intensity and spatial and temporal uniformity, thereby affording better delineation of the myocardium from blood-pool. This technique has the potential to outperform SSFP for cardiac cine imaging at 3.0T.

12:24 ***21***. **Non-Contrast Measurement of Myocardial Perfusion and Oxygenation by MRI: Comparison with PET in an Acute Coronary Stenotic Canine Model**

Kyle McCommis[1], Haosen Zhang[1], Shalonda W. Scott[1], Pilar Herrero[1], Robert J. Gropler[1], Jie Zheng[1]
[1]Washington University School of Medicine, St. Louis, Missouri, USA

Non-contrast quantification of myocardial blood flow (MBF) and oxygen OEF have been developed with arterial spin labeling and T2-BOLD methods. The aim of this study is to compare these novel MRI methods in the quantification of MBF and myocardial oxygen consumption (MVO2) with results obtained through PET. With an acute coronary artery stenosis in a canine model, ROI measurements of MBF and OEF by MRI were performed at rest and during dobutamine-induced stress. The MBF and MVO2 by MRI were correlated well with PET, while OEF during the stress was moderately correlated with PET result.

12:36 ***22***. **Characterizing Temporal B_0 Field Changes in the Rat Heart**

Richard D. Dortch[1], Mark D. Does[1]
[1]Vanderbilt University, Nashville, Tennessee, USA

Quantitative NMR measurements in the rat heart are made difficult by the presence of substantial background field gradients caused by the susceptibility difference that occurs at the lung-myocardium interface. In order to characterize these field gradients, field maps were measured at several points in the cardiac cycle. The highest off-resonance values found corresponded to areas near the lung-myocardium interface. Also, B_0 was found to change throughout the cardiac cycle. To assess the effect of time-varying field gradients on quantitative NMR measurements, transverse relaxation rates were measured. As expected, time-varying field gradients had a larger effect on R_2^* than R_2.

12:48 ***23***. **Mouse Cardiac MRI Using Open Birdcage Coil – Comparison with Single Loop and Body Coils**

Xiaobing Fan[1], Gregory S. Karczmar[1], Marta Zamora[1], Erica Markiewicz[1], Muhammad Haque[1], Brian B. Roman[1]
[1]University of Chicago, Chicago, Illinois, USA

An open birdcage coil was built to perform cardiac MR imaging of the mouse at 4.7T. Although the open design greatly benefits animal placement and physiological measurements, it was not clear how this design would compare with more widely implemented coil designs. Therefore, the quality of images acquired from an open birdcage coil were compared with those from a similar sized single loop surface coil and a 3.8 cm birdcage coil. The results demonstrate that the open birdcage coil provides greater sensitivity than the volume coil and higher signal/contrast to noise ratio and B1 homogeneity than the single loop surface coil.

MRI of Animal Models Other Than Stroke

Room 611 - 612 11:00 - 13:00 Chairs: Sheng-Kwei V. Song and Ed X. Wu

11:00 ***24***. Young Investigator Award Finalist: **Toward Accurate Diagnosis of White Matter Pathology Using Diffusion Tensor Imaging**

Matthew Dean Budde[1], Joong Hee Kim[1], Hsiao-Fang Liang[1], Robert E. Schmidt[1], John H. Russell[1], Anne H. Cross[1], Sheng-Kwei Song[1]

[1]Washington University, St Louis, Missouri, USA

The underlying pathological correlates of changes on diffusion tensor imaging (DTI) have not been adequately determined. We investigated injury to spinal cord white matter in two animal models to compare axial and radial diffusivities derived from DTI and histological markers of axon and myelin injury by registering the histological images to MRI and applying a receiver operating characteristic (ROC) analysis. Decreased axial and increased radial diffusivity are sensitive and specific markers of axonal damage and demyelination, respectively. Although relative anisotropy is sensitive to the two types of injury, it is not specific for either axon or myelin injury.

11:20 ***25***. **3D MRI and DTI of *Cnp1* Deficient Mice: A Model of Axonal Damage Without Affecting Myelin**

Susann Boretius[1], Sandra Goebbels[2], Takashi Watanabe[1], Klaus-Armin Nave[2], Jens Frahm[1], Thomas Michaelis[1]

[1]Max-Planck-Institut fuer biophysikalische Chemie, Goettingen, Germany; [2]Max-Planck-Institut fuer experimentelle Medizin, Goettingen, Germany

Genetically modified mice lacking the *Cnp1* gene develop axonal swelling and neurodegeneration throughout the brain without affecting myelin, that is its ultrastructure, periodicity, and physical stability. T1- and T2-weighted 3D MRI as well as diffusion tensor imaging (DTI) revealed reduced T2 contrast as well as an increased axial and radial diffusivity of white matter. T1 contrast and FA values remained unchanged. Complementary to other animal models of human multiple sclerosis such as EAE and cuprizone-induced demyelination, *Cnp1* deficient mice may allow for a better correlation of MRI contrast alteration and neurodegenerative pathology with special emphasis on axonal damage.

11:32 ***26***. **Diffusion Tensor Magnetic Resonance Imaging of Regeneration/degeneration After Rat Sciatic Nerve Injury**

MinSig Hwang[1, 2], George Q. Perrin[1], David Muir[1], Thomas H. Mareci[1, 2]

[1]University of Florida, Gainesville, Florida, USA; [2]National High Magnetic Field Laboratory, Gainesville, Florida, USA

Diffusion tensor imaging (DTI) was used to investigate spatiotemporally the structural changes in cut or crush excised rat sciatic nerves using a 17.6 T magnet. Fractional anisotropy (FA) of diffusion direction, and averaged rate of diffusion ([D]) were examined as DTI derived MR parameters for the quantification of the structural changes. Increasing FA and decreasing [D] may be used to follow the regenerating nerve after crush injury, and decreased FA and increased [D] may correlate with the irreversibly damaged to the nerve after cut injury. FA appears to be more sensitive indicator because it reflects these changes more significantly.

11:44 ***27***. **Axial Diffusivity Correlates with the Degree of Neurological Disability in a Mouse Model of Multiple Sclerosis**

Matthew Dean Budde[1], Hsiao-Fang Liang[1], Anne H. Cross[1], Sheng-Kwei Song[1]

[1]Washington University, St Louis, Missouri, USA

The pathology of Multiple Sclerosis (MS) exhibits varying degrees of inflammation, demyelination, and axonal damage. The directional diffusivities derived from diffusion tensor imaging (DTI), axial and radial diffusivity, have proven useful in detecting axonal and myelin damage, respectively. We applied DTI in addition to contrast enhancement imaging of the spinal cord white matter in mice with acute and chronic experimental autoimmune encephalomyelitis, an animal model of MS. The changes in contrast enhancement, radial diffusivity, and axial diffusivity reflected the pathological changes evident on histology. Axial diffusivity and the percentage of contrast enhancement significantly correlated with neurological disability.

11:56 ***28***. **Wallerian Degeneration in Visual Pathway Detected Using Diffusion Tensor Imaging**

Shu-Wei Sun[1], Hsiao-Fang Liang[1], Anne H. Cross[1], Sheng-Kwei Song[1]

[1]Washington University, St. Louis, Missouri, USA

The injury to retinal ganglion cells results in damages of optic nerve and tract as a consequence of Wallerian degeneration. After retinal ischemia, *in vivo* DTI has been applied to differentiate axonal and myelin damage in optic nerve. It is expected that the axonal damage would progress through chiasm reaching the contralateral optic tract. In this study, transient retinal ischemia was induced in the right eye of mice. At 14 days after the ischemia, this study demonstrated that the damage in optic nerve progresses to the contralateral optic tract resulting in both axonal and myelin damage.

12:08 ***29***. **Response to Therapy Measurement in a Mouse Model of Niemann-Pick Type C Disease Via Diffusion Tensor Imaging**

Silvia Lope-Piedrafita[1], Chad M. Hicks[1], Elizabeth S. Chaitkin[1], Iram Ahmad[1], Robert J. Gillies[1], Jean-Philippe Galons[1], Robert P. Erickson[1], Theodore P. Trouard[1]

[1]University of Arizona, Tucson, Arizona, USA

Niemann-Pick Type C (NPC) disease is a presently untreatable, homozygous recessive disorder affecting the intracellular trafficking of low density lipoprotein derived cholesterol. We have applied diffusion tensor imaging (DTI) to investigate the neurological abnormalities associated with NPC disease and its response to therapy. DTI was carried out in wildtype (WT) mice, NPC mice, and NPC mice treated with the neurosteroid Allopregnanolone at day 7. Fractional anisotropy (FA) analyses indicated that NPC mice have a preferential loss of brain volume with higher FA compared to WT mice. Treated NPC mice demonstrated a normalization of FA, although it was not complete.

12:20 ***30***. **Measurement of Cerebrospinal Fluid Flow in the Aqueduct of a Rat Model of Hydrocephalus**

Raphael D. Hazel[1], Erin J. McCormack[1], Janet Miller[2], Jie Li[2], Mei Yu[3], Helene Benveniste[1], Janes P. McAllister II[2], Michael Egnor[1], Mark E. Wagshul[1]

[1]Stony Brook University, Stony Brook, New York, USA; [2]Wayne State University School of Medicine, Detroit, Michigan, USA; [3]Brookhaven National Laboratory, Brookhaven, New York, USA

We demonstrate the use of a phase contrast balanced steady state free precession pulse sequence for the measurement of pulsatile flow of cerebrospinal fluid in the cerebral aqueduct of control rats, and new rat model of communicating hydrocephalus. Peak flow velocity is two times greater in the hydrocephalus rat compared to a control rat, and the stroke volume is five times greater compared to the control. The ability to make quantitative measures of CSF flow in the rat makes it possible to study CSF flow dynamics during the development of hydrocephalus and to test theoretical models of intracranial dynamics.

12:32 ***31***. **Measurement of Cerebral Blood Flow in Craniosynostotic Rabbits Using ASL-MRI**

Lesley M. Foley[1], Wendy Fellows-Mayle[2], T Kevin Hitchens[1], Joyce Horner[1], Joseph E. Losee[3], Michael I. Siegel[2], Mark P. Mooney[2], Chien Ho[1]

[1]Carnegie Mellon University, Pittsburgh, Pennsylvania, USA; [2]University of Pittsburgh, Pittsburgh, Pennsylvania, USA; [3]Children's Hospital of Pittsburgh, Pittsburgh, Pennsylvania, USA

Craniosynostosis occurs in 400 per 1,000,000 live births and is associated with elevated intracranial pressure (ICP). Elevated ICP in craniosynostosis is associated with changes in ventricle volume and cerebral blood flow (CBF). Rabbits with early onset coronal suture (EOCS) synostosis have significantly enlarged lateral ventricles. Measurement of CBF in these rabbits using ASL-MRI shows increased flow in the area of the lateral ventricles and the brain cortex. This may be associated with alterations in CSF.

12:44 ***32***. **Longitudinal Changes in Vascular Function in a Canine Aging Model Measured by Dynamic Contrast Enhanced MRI and the Correlation of Blood-Brain-Barrier Permeability with Beta-Amyloid Angiopathy Assessed by Immunohistochemical Staining**

Min-Ying Su[1], Viorela Pop[1], Long Vu[1], Yong Chu[1], Bruce A. Muggenburg[2], Orhan Nalcioglu[1], Elizabeth Head[1]

[1]University of California, Irvine, California, USA; [2]Lovelace Respiratory Research Institute, Albuquerque, New Mexico, USA

We investigated the changes in vascular volume and BBB permeability in a canine model of human aging during the critical aging decline period of 3 years. The interventions, anti-oxidant diet or environmental enrichment, improved the vascular function measured by dynamic contrast enhanced MRI. They increased the blood volume in the frontal lobe after one year, and delayed the BBB permeability worsening for 2 years compared to controls. MRI results demonstrated that BBB permeability was higher in occipital lobe than frontal lobe, which was higher than in parietal lobe, and the order was the same in A-beta angiopathy study using immunohistochemical staining.

Functional Lung MRI

Room 615 - 617 11:00 - 13:00 Chairs: Hiroto Hatabu and Shantanu Sinha

11:00 ***33***. **Wash-In Time of Molecular Oxygen from Dynamic Oxygen-Enhanced MRI: New Approach for Assessment of Smoking-Related Pulmonary Functional Loss**

Yoshiharu Ohno[1], Hisanobu Koyama[1], Munenobu Nogami[1], Makoto Obara[2], Hideaki Kawamitsu[3], Daisuke Takenaka[1], Marc van Cauteren[2], Hiroto Hatabu[4], Kazuro Sugimura[1]

[1]Kobe University Graduate School of Medicine, Kobe, Hyogo, Japan; [2]Philips Medical Systems, Tokyo, Japan; [3]Kobe University Hospital, Kobe, Hyogo, Japan; [4]Beth Israel Deaconess Medical Center, Boston, Massachusetts, USA

The purpose of the present study is to determine the capability of wash-in time of molecular oxygen from dynamic O2-enhanced MRI for assessment of smoking-related pulmonary functional loss. Overall O2-enhancement and mean wash-in time were correlated with Brinkmanfs index, FEV1% and DLCO/VA. Mean wash-in time had better correlation with Brinkmanfs index and FEV1%, and slightly wrong correlation with DLCO/VA, as compared with overall O2-enhancement. Wash-in time of molecular oxygen may have a potential for assessment of smoking-related pulmonary functional loss, and be more sensitive parameter to assess air-way dependent pulmonary functional loss.

11:12 ***34.*** **Correlation Between Oxygen Enhanced MR Imaging, Quantitative CT and Lung Function Tests: Before and After Endobronchial Valve Deployment**

Gregory Ernest Antonio[1], Alfred Brian Yu[1], David Yeung[1], Kwok K. Shing[2], Tak Wai Lee[1], Antony P. Yim[1], David S. Hui[1]

[1]The Chinese University of Hong Kong, Shatin, Hong Kong, People's Republic of China; [2]Prince of Wales Hospital, Shatin, Hong Kong, People's Republic of China

Oxygen enhanced MR imaging, quantitative CT and lung function tests were performed on nine patients before and after endobronchial valve deployment for non-surgical lung reduction to relieve dyspnoea. Our results showed a difference in all parameters before and after valve deployment, and that serial changes in MR oxygen-enhancement correlated well with changes in FVC and DLCO. On the other hand, serial changes in FEV1 correlated best with serial changes in coronal CT density (expiratory – inspiratory).

11:24 ***35.*** **Navigator Triggered Oxygen-Enhanced MRI in Patients with Interstitial Lung Disease**

Francesco Molinari[1], Monika Eichinger[2], Christian Fink[2, 3], Frank Risse[2], Lorenzo Bonomo[1], Hans-Ulrich Kauczor[2]

[1]Catholic University of Rome, Rome, Italy; [2]Deutsches Krebsforschungszentrum (DKFZ), Heidelberg, Germany; [3]Institute of Clinical Radiology, Munich, Germany

In this study we demonstrate the feasibility of simultaneous cardiac and respiratory synchronization in oxygen-enhanced MRI of the lung, using navigator and ECG trigger. A correlation between the results of navigator-triggered oxygen-enhanced MRI and the pulmonary function tests used to evaluate alveolar-capillary gas exchange was assessed in volunteers and in patients with interstitial lung disease.

11:36 ***36.*** **Single-Shot-Quantitative Perfusion Imaging of the Human Lung**

Eberhard Daniel Pracht[1], André Fischer[1], Johannes F. Arnold[1], Peter Michael Jakob[1]

[1]University of Würzburg, Würzburg, Bavaria, Germany

One drawback to quantitative perfusion imaging using arterial spin labelling techniques is the need for two images. The method presented yields quantitative perfusion information of the human lung by acquiring perfusion-weighted image in a single-shot. The described technique ensures the complete suppression of background tissue while almost completely preserving signal from the blood. The quantitative perfusion values varied over the lung parenchyma in end expiration over the range of 0.5 to 3 ml/s/ml. The ability to suppress not only lung tissue, but also different tissue types with varying T_1 values makes it a promising tool for diagnosis of several diseases.

11:48 ***37.*** **Assessment of Bolus Injection Protocol with Appropriate Concentration for Quantitative Assessment of Pulmonary Perfusion by Dynamic Contrast-Enhanced MR Imaging**

Yoshiharu Ohno[1], Kenya Murase[2], Munenobu Nogami[1], Hisanobu Koyama[1], Daisuke Takenaka[1], Hiroto Hatabu[3], Kazuro Sugimura[1]

[1]Kobe University Graduate School of Medicine, Kobe, Hyogo, Japan; [2]Osaka University Medical School, Suita, Osaka, Japan; [3]Beth Israel Deaconess Medical Center, Boston, Massachusetts, USA

The purpose of the present study was to determine the appropriate concentration for quantitative assessment of dynamic contrast-enhanced pulmonary MR imaging. Pulmonary blood flow were calculated from dynamic MR data (PBFMR) with three different concentration protocols (protocol A: 0.1mmol/mL, B: 0.3mmol/mL and C: 0.5mmol/mL), and compared with perfusion SPECT (PBF Perfusion SPECT). PBFMR using protocol B in <70 kg group and protocol C in >/= 70 kg group showed no significant difference, when compared with PBF Perfusion SPECT. In conclusion, appropriate concentration of bolus injection protocol for 3D dynamic MR imaging provides accurate and reproducible assessments of regional pulmonary perfusion parameters.

12:00 ***38.*** **Voxel-Wise Analysis of Lung Parenchymal Motion During Breathing Via a Non-Rigid Registration Algorithm in Human: Dynamic MRI in Different Postures**

Shigeto Kubo[1], Tessa A. Sundaram[2], Shigeru Kiryu[1], Yasutane Mori[1], James C. Gee[2], Hiroto Hatabu[1], Masaya Takahashi[1]

[1]Beth Israel Deaconess Medical Center, Boston, Massachusetts, USA; [2]University of Pennsylvania, Philadelphia, Pennsylvania, USA

We have recently established a novel method for quantifying lung parenchymal motion from a sequence of pulmonary MR images acquired over the respiratory cycle. By applying non-rigid registration algorithm, voxel-by-voxel deformation can be computed between successive MR images of the human lung. The purpose of this study was to explore the feasibility of this method to detect differences in regional pulmonary parenchymal motion during free breathing in both supine and prone postures.

12:12 ***39***. **Differentiation of Vasculopathy from Normal Pulmonary Vasculature Using Hyperpolarized Helium-3 MRI in Humans**

David Lipson[1], JiangSheng Yu[1], Sheeva Rajaei[1], Kiarash Emami[1], Stephen Kadlecek[1], Masaru Ishii[2], John MacDuffie Woodburn[1], Frank Hammond[1], Vahid Vahdat[1], Warren Gefter[1], Rahim R. Rizi[1]

[1]University of Pennsylvania, Philadelphia, Pennsylvania, USA; [2]Johns Hopkins University, Baltimore, Maryland, USA

Many lung diseases manifest with alterations in the pulmonary vasculature bed. We hypothesized that we could non-invasively differentiate pulmonary disease caused by vasculopathy, from normal subjects, based on differences in regional PAO2 and ventilation/perfusion using helium-3 MRI. Patients with vasculopathy have higher alveolar oxygen concentrations than normal subjects because of decreased uptake of oxygen from the alveolar space. Elevations in regional VA/Q represent an increased number of lung units with high ventilation/perfusion ratios due to vascular destruction. Hyperpolarized helium-3 MRI may non-invasively differentiate normal subjects from those with vasculopathy based on differences in regional PAO2 and regional ventilation/perfusion relationships.

12:24 ***40***. **Three-Dimensional Volumetric Analysis of the Lung During Respiration in Ventilated Mice**

Shigeto Kubo[1], Tessa A. Sundaram[2], James C. Gee[2], Hiroto Hatabu[1], Masaya Takahashi[1]

[1]Beth Israel Deaconess Medical Center, Boston, Massachusetts, USA; [2]University of Pennsylvania, Philadelphia, Pennsylvania, USA

Lung tissue compliance, which is derived from the slope of the pressure-volume curve, is an index of pulmonary function and is altered in several lung diseases. Positive end-expiratory pressure (PEEP) levels are varied to induce different respiratory mechanics in a controlled fashion to simulate pathological changes in an animal. In this study, we evaluated the volumetric changes in mechanically ventilated mice using 3D dynamic MRI over a respiratory cycle by controlling different PEEP and end-inspiratory pressure levels. The results were compared with the tissue mechanical properties measured by a small animal ventilator.

12:36 ***41***. **Compound 48/80 Induced Mast Cell Activation in the Lung**

Harry Karmouty Quintana[1, 2], Catherine Cannet[1], Stefan Zurbruegg[1], François-Xavier Blé[1], Lazzaro Mazzoni[1], John R. Fozard[1], Clive P. Page[3], Nicolau Beckmann[1]

[1]Novartis Institutes for BioMedical Research, Basel, Switzerland; [2]King's College London, London SE1 1UL, UK; [3]King's College London, London SE1 1UL, Switzerland

The effects of mast cell activation by compound 48/80 were investigated non-invasively in the lungs of naïve Brown Norway (BN) rats by proton magnetic resonance imaging (MRI). A peak edematous response was observed 24 h after 48/80 and was fully inhibited immediately following pre-treatment with a mast cell stabilizer (di-sodium cromoglycate, DSCG) and the steroid budesonide administered 1 h before or 3 h after 48/80. Histamine and 5-HT antagonists did not block the late phase (24h) edema induced by 48/80.

12:48 ***42***. **Assessment of Lung Function with Simultaneous Spirometric and Grid-Tagging MRI Measurements**

Abram Voorhees[1], Jing An[1], Kenneth I. Berger[1], Roberta M. Goldring[1], Qun Chen[1]

[1]New York University School of Medicine, New York, New York, USA

Simultaneous spirometry and MRI measurements were conducted for the validation of a regional, MRI-based, pulmonary function test. MRI spirometry uses grid-tagged images to dynamically track motion of the lungs during respiration. From displacement maps of the lung parenchyma, regional flow and volume change can be calculated. Results from conventional spirometry, in which the total volumetric air flow rate is measured through the mouth, and lung volume segmentation from MR images were compared with good agreement. This study demonstrates that lung segmentation in conjunction with MRI-based spirometry can be used to assess overall performance, i.e. global function, of the lung.

Multimodal Methods for Cancer Detection & Staging

Room 618 - 620 11:00 - 13:00 Chairs: Johannes T. Heverhagen and Sarah Nelson

11:00 ***43***. **Whole-Body MRI and 11C-Choline PET/CT in Patients with Prostate Cancer**

Heinz-Peter Wilhelm Schlemmer[1], Susanne-Martina Eschmann[1], Christina Pfannenberg[1], Philip Aschoff[1], Christian Mueller-Horvat[1], Matthias Lichy[1], Enno Rodegerts[1], Aristotelis Anastasiadis[1], Arnulf Stenzl[1], Roland Bares[1], Claus D. Claussen[1]

[1]University Hospital Tuebingen, Tuebingen, BW, Germany

The most favourable outcome achievable in patients with prostate cancer is associated with complete tumor resection. For optimizing therapeutic outcome and avoiding unnecessary complications it is a great need to obtain precise information about local tumor extension as well as distant tumor spread particularly to the most common sites, e.g. bone marrow and lymph nodes. Goal of this study is to compare the diagnostic potential of wb-MRI and Cho-PET/CT to detect distant tumor spread in patients with prostate cancer. Our initial data show, that wb-MRI is a very promising diagnostic tool to identify tumor spread in patients with prostate cancer. Particularly bone marrow involvement could better be detected by wb-MRI than by Cho-PET/CT. The synopsis of wb-MRI and Cho-PET results was most favorable with regard to both detection and interpretation of suspicious finding. Regarding the assessment of early lymph node involvement, however, both modalities detected only large metastases (>1cm) and may therefore be limited. So far, the combination of wb-MRI and endoMRI/MRS seems to be most useful to differentiate patients with localized disease and systemic progression during initial and repeated staging.

11:12 ***44.*** **Multimodality (MR/PET/CT) Monitoring Preoperative Systemic Therapy in Operable Breast Cancer**

Michael A. Jacobs[1], Vered Stearns[1], Antonio C. Wolff[1], Ronald Ouwerkerk[1], David Bluemke[1], Richard Wahl[1]

[1]Johns Hopkins School of Medicine, Baltimore, Maryland, USA

We have demonstrated the feasibility of monitoring preoperative systemic therapy in patients with operable breast cancer using multi-modality proton, sodium MR, and PET/CT imaging. Significant decrease in tumor volume, total sodium, and SUV were observed. These methods provide a basis for a comprehensive evaluation of the complex tumor environment by examining the changes in volume and sodium and glucose metabolism in response to therapy.

11:24 ***45.*** **STIR Turbo SE Imaging vs. Co-Registered FDG-PET/CT: Quantitative and Qualitative Assessment of N-Stage in Non-Small Cell Lung Cancer Patients**

Yoshiharu Ohno[1], Hisanobu Koyama[1], Munenobu Nogami[1], Daisuke Takenaka[1], Masahiko Fujii[1], Hiroto Hatabu[2], Kazuro Sugimura[1]

[1]Kobe University Graduate School of Medicine, Kobe, Hyogo, Japan; [2]Beth Israel Deaconess Medical Center, Boston, Massachusetts, USA

To compare diagnostic capabilities of N-stage in non-small cell lung cancer (NSCLC) patients between STIR turbo SE imaging (STIR MRI) and FDG-PET/CT, 115 consecutive patients were analyzed. Feasible threshold value of each method was determined on per node basis, and tested on per patient basis. When feasible threshold values were adapted, sensitivity and accuracy of quantitatively assessed STIR MRI were significantly higher than those of quantitatively and qualitatively assessed PET/CT. Sensitivity of qualitatively assessed STIR MRI was also significantly higher than that of qualitatively assessed PET/CT. In conclusion, STIR MRI is useful for diagnosis of N-stage in NSCLC patients.

11:36 ***46.*** **Whole-Body MRI Using a 32-Channel System Vs PET-CT for the Detection of Skeletal Metastases**

Gerwin Paul Schmidt[1], Stefan O. Schoenberg[1], Robert Stahl[1], Rupert Schmid[1], Peter Herzog[1], Maximilian F. Reiser[1], Andrea Baur-Melnyk[1]

[1]University Hospital Munich-Grosshadern, Munich, Bavaria, Germany

Accurate detection of bone metastases in staging and restaging of patients with a neoplastic disease is vital to assess therapeutic options and patient prognosis. However, established diagnostic algorithms e.g. using 99mTc-phosphonate-based skeletal scintigraphy may miss early stage disease in absence of an osteoblastic response. Alternatively, whole-body MRI and PET-CT, were tested for their performance as diagnostic tools for bone screening in this study. Our results indicate that both whole-body MRI and PET-CT are robust modalities for the detection of malignant bone disease. However, overall diagnostic performance of MRI was higher than of PET-CT. With the use of PAT on a multi-channel whole-body MR scanner bone marrow screening of the entire body with high resolution and precise diagnostic accuracy is feasible below 40 minutes.

11:48 ***47.*** **Multi-Contrast Whole-Body MRI Protocol Compared to Whole-Body PET/CT in Oncology**

Trevor La Folie[1], Bruno Triaire[1], Patrice Hervo[2], Charline Gabaudan[1], Patrick Richez[1], Jean Briant[1]

[1]Military Hospital Laveran, Marseille, France; [2]GE Healthcare Technology, Paris, France

The purpose of the study was to evaluate the efficacy of a multi-contrast whole-body MRI protocol for tumor staging. The MRI protocol used a three-dimensional diffusion-weighted Echo-Planar, STIR, and T1 weighted Fast Spoiled Gradient Echo with fat suppression following gadolinium administration. Results of 15 patients with various primary malignancies were compared with whole-body PET/CT. The use of a high b value diffusion-weighted sequence in the Whole-Body MRI protocol improved the detection of secondary lesions, particularly lymph nodes.

12:00 ***48.*** **Imaging of Illuminated Tissue During the Photodynamic Process by Photosensitized Bold MRI**

Catherine Brami[1], Iddo Pinkas[1], Avigdor Scherz[1], Yoram Salomon[1]

[1]The Weizmann Institute of Science, Rehovot, Israel

Vascular targeting photodynamic therapy (VTP) of tumors with circulating Pd-bacteriochlorophyll derivatives is presently in phase II clinical trials for prostate cancer. Its mechanism is based on intravascular light-dependent generation of cytotoxic ROS. Consequent accumulation of paramagnetic deoxyhemoglobin and blood stasis were reported by us as intrinsic markers for online monitoring of VTP by photosensitized fMRI. Here we newly demonstrate that upon application of short light flashes, coincidental BOLD contrast pulses trace the illuminated area, thereby signifying that BOLD MRI is capable of imaging the boundaries of the illuminated region in the tissue. Supported by STEBA BIOTECH and NEGMA LERADS, France.

12:12 ***49.*** **MR Colonography vs. Optical Colonoscopy: Comparison of Patient Acceptance in a Screening Population**

Sonja Kinner[1], Christiane A. Kuehle[1], Michael Nuefer[1], Susanne C. Goehde[1], Joerg Barkhausen[1], Thomas C. Lauenstein[1]

[1]University Hospital Essen, Essen, Germany

We compared MR colonography (MRC) in conjunction with fecal tagging to optical colonoscopy (OC) regarding patients` acceptance. 284 asymptomatic patients underwent both modalities within 4 weeks. Acceptance values were determined using a standardized questionnaire. Overall acceptance for MRC and OC failed to prove any statistically significant difference. As for dedicated aspects of the single examinations, bowel cleansing was the most displeasing part for OC. However, the placement of the rectal tube and the administration of an enema were rated most unpleasant for MRC.

12:24 ***50***. **Functional MRI of the Bowel: Detection of Perfusion Defects and Changes in the Water Diffusion**

Christian Hohl[1], Patrick Haage[1], Thorsten Schmidt[1], Heiner Brock[1], Felix Schoth[1], Georg Mühlenbruch[1], Gabriele Anja Krombach[1], Rolf W. Günther[1], Thoralf Niendorf[1]

[1]UK Aachen, Aachen, Germany

In mesenteric ischemia the interval between the onset of symptoms and irreversible damage of the bowel is app. 120-180 min. The early detection of bowel ischemia requires imaging methods which are (i) sensitive to changes in the blood supply or (ii) susceptible to the net water shift associated with the development of cytotoxic edema. For this reason this work studies (i) the detection of perfusion deficits in the mesenteric end-arteries using high spatial resolution contrast enhanced MRA and (ii) the detection of cytotoxic edema of the bowel wall by means of diffusion weighted (DWI) imaging.

12:36 ***51***. ***In Vivo* MRI and Intravital Optical Microscopy of Window Chambers in Mice**

Arthur F. Gmitro[1], Stephen Moore[1], Robert Gatenby[1]

[1]University of Arizona, Tucson, Arizona, USA

MRI is used routinely to study anatomic, physiologic, and functional aspects of tumor growth and tumor microenvironments. Intravital optical microscopic imaging of implanted window chambers is another approach that provides a method for direct high resolution imaging of tumors and the tumor-host interface. A key issue in both MRI and optical studies of biological properties is validation of methods. Cross validation of one technique (e.g. MRI) by another (e.g. intravital microscopy) could provide such an assessment. Here we report on the first *in vivo* experiments to demonstrate the dual imaging modalities of MRI and intravital optical microscopy.

12:48 ***52***. **Blood-Tumor Permeability (K) Measured with Dynamic Contrast Enhanced MRI and C14-AIB Autoradiography in a Rat Brain Tumor Model, a Validation Study**

Moira Catherine Ferrier[1], Hemant Sarin[1], Steve Huntz Fung[1], Bawarjan Schatlo[1], Sandeep Gupta[2], Ryszard Pluta[1], David Thomasson[1], John A. Butman[1]

[1]NIH, Bethesda, Maryland, USA; [2]General Electric, Baltimore, Maryland, USA

Dynamic contrast-enhanced MRI (DCE-MRI) data was analyzed using a direct convolution iteration method for solving equations of the general kinetic model to measure rat blood-tumor permeability. Ktrans from DCE-MRI was correlated to K1 from C14-AIB quantitative autoradiography (QAR) and found to be nearly identical. Our results validate use of this method to accurately measure permeability in rat brain tumors and suggest that it may accurately measure permeability values in human brain tumors as well.

Cartilage Imaging and Clinical Applications

Room 602 - 604 11:00 - 13:00 Chairs: Timothy J. Mosher and Miika T. Nieminen

11:00 ***53***. **Dosing Bias in DGEMRIC Due to BMI Differences**

Carl Johan Tiderius[1], Ashley Williams[1], Marisa Hori[1], Michelle Finnell[1], Leena Sharma[2], Pottumarthi Prasad[3], Deborah Burstein[1]

[1]Beth Israel Deaconess Medical Center, Boston, Massachusetts, USA; [2]Northwestern University, Chicago, Illinois, USA; [3]Evanston Northwestern Healthcare, Evanston, Illinois, USA

A correlation was found between BMI and plasma [Gd-DTPA2-], indicating a potential dosing bias in dGEMRIC. Dose bias will not be a factor in longitudinal studies where BMI doesn't change significantly, or when compartments within a knee are compared. However, in comparisons between individuals with a large range of BMI dosing by BMI, not weight, or post-process correction of the data must be considered. Correcting for dose bias did not change any previously reported conclusions regarding dGEMRIC versus radiographic metrics, and there was still a strong relationship between dGEMRIC and BMI in OA subjects.

11:12 ***54***. **Single-Slice DGEMRIC as a Predictor of Early Failure After a Periacetabular Osteotomy in Hip Dysplasia**

Rebecca Hope Jessel[1], Christoph Zilkens[1], Carl J. Tiderius[1], Young-Jo Kim[1]

[1]Children's Hospital Boston, Boston, Massachusetts, USA

The present study of 55 dysplastic hips that were treated with a periacetabular osteotomy confirms previous data showing that the dGEMRIC index correlates with clinically relevant parameters, such as pain and joint space width. Moreover, a low preoperative dGEMRIC index was shown to predicta a poor surgical outcome, i.e., total joint replacement within four years post-surgery. The study also shows that the analysis of one central slice over the hip joint provides similar information as a multislice protocol including most joint cartilage. We conclude that a single-slice dGEMRIC protocol can be used to identify dysplasia patients who could benefit from surgery.

11:24 ***55.*** **Relationship of T2 and DGEMRIC with Histologically Verified Degeneration of Human Cartilage at 1.5T**

Eveliina Lammentausta[1], Panu Kiviranta[1], Juha Töyräs[2], Ilkka Kiviranta[3], Miika Tapio Nieminen[4], Jukka Sakari Jurvelin[1, 2]

[1]University of Kuopio, Kuopio, Finland; [2]Kuopio University Hospital, Kuopio, Finland; [3]Jyväskylä Central Hospital, Jyväskylä, Finland; [4]Oulu University Hospital, Oulu, Finland

Samples from human cadaveric patellar cartilage were divided into three groups (Healthy, Early degeneration and Advanced degeneration) based on their Mankin score. Based on the present results, significant, degeneration dependent variation existed in superficial and bulk T2 values as well as in mechanical and compositional parameters of human patellar cartilage. These results indicate that elevated T2 relaxation time values effectively identify advanced degeneration of articular cartilage while dGEMRIC correlates relatively poorly with mechanical or compositional parameters in this setting.

11:36 ***56.*** **T2 Values of Patellar Cartilage in Subjects with Osteoarthritis**

Matthew F. Koff[1], Kimberly K. Amrami[1], Kenton R. Kaufman[1]

[1]Mayo Clinic, Rochester, Minnesota, USA

T2 values of articular cartilage have been proposed as a biomarker for osteoarthritis (OA). This study quantified differences of T2 values of patellar cartilage across different stages of OA as defined by radiological examination. 110 subjects were enrolled in the study. T2 values of patellar cartilage were calculated from a series of T2 weighted images. Patello-femoral OA stage was assigned based on weight bearing radiographs. No significant differences of T2 values were found across the stages of radiographic patello-femoral OA. Additional work is required to determine the benefits and sensitivity of T2 mapping in a clinical setting.

11:48 ***57.*** **Multiecho Ultrashort TE (UTE) Imaging and T2* Mapping of Knee Cartilage**

Jiang Du[1], Atsushi M. Takahashi[2], Ann Shimakawa[2], Jean H. Brittain[2], Mark Bydder[1], Graeme M. Bydder[1]

[1]University of California, San Diego, San Diego, California, USA; [2]Global Applied Science Laboratory, GE Healthcare, Menlo Park, California, USA

Magnetic resonance imaging has been used not only to detect changes in cartilage morphology, but also to quantify T1 and T2 which reflect changes in biochemical composition of cartilage with early osteoarthritis (OA). We present a multislice multiecho ultrashort TE (UTE) imaging pulse sequence which combines half pulse excitation and radial sampling. The initial echo time was 8 usec, followed by 11 echoes with an echo space of 5 msec. T2* maps were generated from the multiecho images using exponential fitting.

12:00 ***58.*** **T1rho Imaging of Mechanically Stressed Human Cartilage**

Daniel R. Thedens[1], Douglas R. Pedersen[1], James A. Martin[1], Thomas D. Brown[1]

[1]University of Iowa, Iowa City, Iowa, USA

T1rho relaxation is a promising marker for assessing cartilage proteoglycan content in vitro and *in vivo*. The purpose of this study was to investigate the feasibility of T1rho imaging to detect proteoglycan changes in human cartilage subjected to rigidly controlled and realistic mechanical stresses. A range of mechanical stresses were applied to fresh human cartilage samples in a 12-day regimen, followed by T1rho imaging in a 4.7 T small-bore magnet. The results showed considerable changes in T1rho at the greatest loading levels, suggesting T1rho imaging can detect proteoglycan changes directly resulting from controlled mechanical loading.

12:12 ***59.*** **The Effects of Mechanical and Osmotic Stress on Intact and PG-Depleted Cartilage**

Galit Saar[1], Hadassah Shinar[1], Gil Navon[1]

[1]Tel Aviv University, Tel Aviv, Israel

Intact and PG depleted bovine cartilage-bone plugs, equilibrated in deuterated saline were studied by 1D ^{2}H double quantum filtered spectroscopic MRI. At rest, we have found that the depletion had a minimal effect on the quadrupolar splitting indicating no change in the orientation of the fibers. Intact and depleted plugs exhibited different changes in their quadrupolar splittings when subjected to mechanical compression. Both intact and depleted cartilage lost the orientation dependence under osmotic stress indicating the loss of macroscopic order.

12:24 ***60.*** **Quantitative Assessment of Bone Marrow Edema and the Overlying Cartilage in OA and ACL Injuries Using MR Imaging and Spectroscopic Imaging at 3T**

Xiaojuan Li[1], Jesus Lozano[1], C. Benjamin Ma[1], Jan S. Bauer[1], Thomas M. Link[1], Sharmila Majumdar[1]

[1]University of California at San Francisco, San Francisco, California, USA

Bone marrow edema (BME) are presented commonly in knee osteoarthritis (OA) and anterior cruciate ligament (ACL) injuries, however, little is known about the natural history and significance of these lesions. This study aimed to assess BME using MR imaging and spectroscopic imaging and to evaluate the BME-overlying cartilage using T1rho quantification at 3T. Ten patients (4 OA and 6 ACL) were studied. T1rho values were significantly elevated in BME-overlying cartilage compared with surrounding cartilage (51.8±10.8ms vs. 43.0±8.3 ms, P=0.032). Quantitative MRI can allow us to critically evaluate the success of medical and surgical treatments of cartilage and bone injuries.

12:36 ***61***. **Doxycycline Slows MRI-Assessed Cartilage Volume Loss in the Guinea Pig Model of Osteoarthritis**

Jean Tessier[1], Jonathan Bowyer[1], Chris Heapy[1], Jacqueline Elliott[1], Rod Pickford[1], Jo Flannelly[1], Rose Maciewicz[1]
[1]Astrazeneca, Macclesfield, Cheshire, UK

In a previous placebo-controlled trial in obese women with unilateral radiographic knee OA, doxycycline reduced joint space width assessed by x-radiography by 40% compared to placebo. It is thought that this effect may be mediated by reducing levels of metalloproteinases. In this study we explored the effect of doxycycline on cartilage volume loss in the guinea pig model of OA using high resolution 3D gradient echo MRI and we correlate the findings with the activities of MMPs. We found that doxycycline treatment reduces cartilage loss significantly and completely suppress the activity levels of MMP13 and MMP8.

12:48 ***62***. **MR Derived Synovial Volume Reflects Disease Regression in Children with JRA**

Akila Rajagopal[1], T. Brent Graham[1], Bernard J. Dardzinski[1, 2]
[1]Cincinnati Children's Hospital Medical Center, Cincinnati, Ohio, USA; [2]University of Cincinnati College of Medicine, Cincinnati, Ohio, USA

Juvenile rheumatoid arthritis (JRA) is the most common form of arthritis in children. The inflamed synovium can be quantified with contrast enhanced MR imaging. Twenty children with JRA were enrolled in this study and were scanned during three visits (initial scan, 3 months and 1 year). Subjects had different JRA subtypes and duration of disease. Treatments during the course of the study included NSAID's, methotrexate, etanercept, and intra-articular corticosteroids. MR derived synovial volumes in the knees were significantly correlated with both clinical and laboratory outcome measures. The synovial volume declined following treatment while the clinical symptoms improved.

Spectroscopic Imaging Acquisition Techniques and Speed Optimization

Room 613 - 614 11:00 - 13:00 Chairs: Dikoma C. Shungu and Daniel M. Spielman

11:00 ***63***. **Field Map Based Automated Shimming for Organs Outside of the Human Brain**

Hoby Patrick Hetherington[1], Nikolai I. Avdievich[1], Jullie W. Pan[1]
[1]Albert Einstein College of Medicine, Bronx, New York, USA

For the brain a variety of automated non-iterative shimming methods using either columnar projections or images of phase evolution to generate B0 maps have been reported. Intrinsic to most of these methods is the assumption that there is only a single chemical species contributing to the image. While this view is valid in brain tissue, this is not necessarily true in tissues outside of the brain. We have developed a method based on B0 mapping using a modified Dixon acquisition to provide fully automated shimming of tissue where lipids dominate. We demonstrate this method in the human calf and liver.

11:12 ***64***. **Spectral Separation Analyses of Proton MRSI Data: Validation with Tumor Grade of Brain Glioma**

Sunitha B. Thakur[1], Yuzhuo Su[2], Sasan Karimi[1], Shuyan Du[3], Paul Sajda[3], Wei Huang[1], Lucas Parra[2]
[1]Memorial Sloan Kettering Cancer Center, New York, New York, USA; [2]City University of New York, New York, New York, USA; [3]Columbia University, New York, New York, USA

A constrained non-negative matrix factorization (NMF) algorithm was applied to analyze clinical proton MRSI data of brain gliomas (n = 14), extracting constituent spectra of tumor tissue, normal brain tissue, and residuals. The Cho-NAA patterns of the constituent tumor spectra were consistent with the pathologically proven tumor grades. This MRSI data analysis method resolves partial volume effect, reduces variability of *in vivo* spectra, and has potential in clinical applications, such as defining tumor margins, treatment planning of radiotherapy, and surgical decisions.

11:24 ***65***. **Spectroscopic Imaging of ^{1}H at 3T: Comparing SNR Between Traditional Phase Encoding and Echo-Planar Techniques in the Human Brain**

Matthew L. Zierhut[1, 2], Esin Ozturk[1, 2], Albert P. Chen[1, 2], Pieter Pels[2], Charles H. Cunningham[3], Daniel B. Vigneron[1, 2], Sarah J. Nelson[1, 2]
[1]UCSF/UCB Joint Graduate Group in Bioengineering, San Francisco, California, USA; [2]UCSF, San Francisco, California, USA; [3]Stanford University, Stanford, California, USA

The effects of various echo-planar spectroscopic imaging (EPSI) techniques on data quality were investigated for 1H spectroscopy in the human brain. Specifically, signal to noise ratio (SNR) was compared across imaging techniques for creatine, choline, and NAA. The results show a slight loss in relative SNR when compared to standard phase-encoded chemical shift imaging (CSI) throughout the various EPSI techniques. However, the spectroscopic data are still clinically acceptable, and there are less lipid aliasing artifacts.

11:36 ***66***. **Optimized Outer Volume Suppression for Slice Selective MRSI**

Anke Henning[1], Michael Schär[1, 2], Rolf F. Schulte[1], Klaas P. Pruessmann[1], Peter Boesiger[1]
[1]University and ETH Zurich, Zurich, Kanton Zurich, Switzerland; [2]John Hopkins University, Baltimore, Maryland, USA

In spite of highly-selective saturation pulses sufficient outer volume and especially fat suppression in MRSI could just be achieved in combination with PRESS localization, which causes immense chemical shift displacement at higher field strength. Slightly over-prescribed PRESS was only shown in combination with single suppression bands. In this work the flip angles of multitude, overlapping suppression bands were optimized considering the progressing T1 relaxation during the OVS scheme. T1 and B1 insensitive outer volume suppression in combination with largely over-prescribed PRESS MRSI and slice selective MRSI could be reached. The optimization was performed for highly-selective, broadband higher-order phase pulses (HOPP).

11:48 ***67.*** **3D SENSE Spectroscopic Imaging with Acceleration in Three Dimensions**

Ulrike Dydak[1], Cecilia Possanzini[2], Sebastian Kozerke[1], Marijn Kruiskamp[2], Dieter Meier[1], Roger Luechinger[1], Peter Boesiger[1]

[1]University and ETH Zurich, Zurich, Switzerland; [2]Philips Medical Systems, Best, Netherlands

Scan times in MR spectroscopic imaging (MRSI) can be reduced significantly by using SENSE. So far a maximal SENSE acceleration factor of two has been applied in one or two phase encoding dimensions of single or multi-slice MRSI. 3D MRSI is a sequence with three phase encoding dimensions, offering the possibility for SENSE acceleration in three dimensions. Using a 16-element coil with different coil sensitivities in all dimensions, we show initial results of 3D MRSI with a SENSE factor of 2x2x2. Furthermore, SENSE acceleration factors of 4, 6 and 9 are compared to conventional MRSI for a single slice measurement.

12:00 ***68.*** **Improvement in Multi-Slice 2D SENSE-MR Spectroscopic Imaging at 3T Using Frequency-Modulated Refocusing Pulses**

Richard Anthony Edward Edden[1], James Murdoch[2], Peter B. Barker[1]

[1]Johns Hopkins University, Baltimore, Maryland, USA; [2]Philips Medical Systems, Cleveland, Ohio, USA

Multi-slice MR Spectroscopic Imaging (MRSI) of the human brain at 3T offers reduced scan time and increased signal-to-noise ratios (SNR) compared to conventional MRSI techniques at 1.5T. However, the chemical shift artifact is exacerbated at the higher field strength, so that images of the different metabolites acquired with traditional sinc-gauss slice-selective refocusing pulses represent significantly different slices. In this abstract, a high bandwidth frequency-modulated slice selective pulse is compared to sinc-gauss refocusing pulses, demonstrating a significant improvement in the spatial localization of the images and a 15% improvement in SNR.

12:12 ***69.*** **High-Speed Volumetric Proton Echo Planar Spectroscopic Imaging (PEPSI) with RF Sensitivity Encoding Along Two Spatial Dimensions**

Ricardo Otazo[1, 2], Ramiro Jordon[2], Stefan Posse[1, 3]

[1]The MIND Institute, Albuquerque, New Mexico, USA; [2]University of New Mexico, Albuquerque, New Mexico, USA; [3]University of New Mexico School of Medicine, Albuquerque, New Mexico, USA

Proton Echo Planar Spectroscopic Imaging (PEPSI) offers fast spatial-spectral encoding, but 3D spatial encoding is still time consuming. We have previously demonstrated combination of PEPSI with SENSE acceleration along one spatial dimension. Here we present the combination of PEPSI with SENSE acceleration along two spatial dimensions to further accelerate 3D spectroscopic imaging. Up to 8-fold acceleration was feasible for a 32x32x16 spatial matrix using an 8-channel array coil.

12:24 ***70.*** **Single-Shot Interleaved Gradient Compensation of Susceptibility Induced Spectral Line Broadening in Proton Spectroscopic Echo-Planar Imaging (PEPSI)**

Arvind Caprihan[1, 2], Ting Li[2], Stefan Posse[2, 3]

[1]New Mexico Resonance, Albuquerque, New Mexico, USA; [2]The MIND Institute, Albuquerque, New Mexico, USA; [3]University of New Mexico, Albuquerque, New Mexico, USA

We present a novel, single-shot spectroscopic imaging method that compensates local gradients in regions that suffer from susceptibility related spectral line broadening. The method was integrated into a PEPSI sequence and uses a train of alternating gradient pulses of increasing strengths, interleaved into the spatial-spectral encoding scheme, to simultaneously collect an uncompensated and a compensated data set. Controlled spectral aliasing was used to overcome gradient slew rate and stimulation limitations. Metabolite maps show strongly reduced susceptibility effects in frontal lobe in human brain at 4 Tesla.

12:36 ***71.*** **Fast 3D ^{1}H Spectroscopic Imaging of the Human Brain at 3 Tesla Using "spectroscopic Missing Pulse – SSFP" with 3D Spatial Selection**

Christian Schuster[1, 2], Wolfgang Dreher[1, 2], Dieter Leibfritz[1, 2]

[1]University of Bremen, Bremen, Germany; [2]Center of Advanced Imaging (CAI), Bremen, Germany

In this study a novel SSFP based method for fast 3D ^{1}H spectroscopic imaging termed "spectroscopic Missing Pulse – SSFP" is presented which combines the high SNR_t and the short minimum measurement time of spectroscopic SSFP sequences with 3D spatial selection. The sequence was implemented on a 3T head scanner and applied to healthy volunteers. The technique provides 3D metabolic maps with good spatial and spectral resolution in about 6 minutes. As a separate water suppression is avoided and phase correction is not needed, "spectroscopic Missing Pulse – SSFP" is a very robust fast SI method with only minimal user interaction.

12:48 *72.* **Spectral-Spatial Excitation and Refocusing for Reduced Volume Mis-Registration at 7 Tesla**

Charles H. Cunningham[1], Daniel B. Vigneron[2], Albert P. Chen[2], Duan Xu[2], Michael Lustig[1], Douglas A. Kelley[3], John M. Pauly[1]

[1]Stanford University, Stanford, California, USA; [2]UC San Francisco, San Francisco, California, USA; [3]GE Healthcare Technologies, San Francisco, California, USA

For localized MR spectroscopy at high field (>= 3 T), chemical shift mis-registration of the excited/refocused volume is a major concern. In this abstract, the use of spectral-spatial pulses as a means to excite/refocus volumes without mis-registration is investigated for application at 7 T. Spectral-spatial pulses that completely eliminate chemical-shift mis-registration over the full bandwidth defined by the gradient oscillation frequency can be designed. In a tradeoff of spectral bandwidth for robustness, a partially adiabatic spectral-spatial pulse was designed. Experimental tests showed feasibility for long echo-time spectroscopy without chemical-shift mis-registration and insensitivity to RF inhomogeneity over a range of +/- 30%.

GOLD CORPORATE MEMBER LUNCHTIME SYMPOSIUM
Philips Medical Systems
Perspectives on High Field and Ultra-High Field Imaging

Room 6A-B 13:00 - 14:00

SPECIAL SYMPOSIUM
Grant Writing: Opportunities, Needs and Strategies

Room 6C 14:00 - 16:00 Chair: Michael V. Knopp

Educational Objectives:
Upon completion of this session, participants should be able to:

- Identify opportunities of grant funding in the MR domain;
- Recognize requirements for successful competition;
- Apply structured approaches to develop grant writing skills; and
- Learn from experiences of other investigators.

14:00 **Grants - A Strategic Perspective from a Funding Agency Point of View: Requirements and Expectations**
Roderic I. Pettigrew

14:30 **Grantsmanship: The Essentials**
Alan Jackson

15:00 **Grants - An Outcome Perspective: Looking Back from a Scientific Publication to Grant Funding - Lessons to Be Learned**
Val M. Runge

15:30 **Roundtable: Personal Experience and Strategies**
Michael V. Knopp, Moderator
T.J. Fitzgerald
Nina Mayr.
Anwar Padhani
Stefan Schoenberg
June S. Taylor

SMRT/ISMRM FORUM
Imaging of the Mother, Fetus and Newborn

Room 6D 14:00 - 16:00 Chairs: Jeffrey L. Duerk and Bobbi Lewis

Educational Objectives:
Upon completion of this session, participants should be able to:

- Recognize basic normal and abnormal fetal or neonatal anatomy;
- Explain issues related to patient preparation, anesthesia and patient handling in order to safely and efficiently expedite neonatal imaging studies;
- Optimize pulse sequence parameters and effectively utilize hardware peripherals in order to perform mother/fetus/neonate MRI; and
- Evaluate whether prenatal MRI can supplement or supplant another diagnostic examination.

The final five minutes of each presentation will be reserved for questions.

14:00 **Technical Aspects of Scanning the Pregnant Mother: A Technologist's Overview and Perspective**
Norman T. Farrar

14:30 **Fetal MR – Including the CNS (general techniques and uses with some specific discussion of CNS)**
Deborah Levine

15:00 **Imaging the Neonatal Brain: Specific Pathologies – Specific Imaging Protocols**
Mary Rutherford

15:30 **Imaging the Pediatric Patient: Specific Pathologies – Specific Imaging Protocols**
Pek-Lan Khong

CLINICAL SCIENCE FOCUS SESSION: Issues in Clinical Cardiac MRI

Room 4C - 3,4 14:00 - 16:00 Chairs: Michael Atalay and James C. Carr

14:00 *73.* **Regional Myocardial Perfusion Reserve Determined by Patlak Analysis of Myocardial Perfusion MRI Showed a Good Correlation with Coronary Flow Velocity Reserve Measured by Doppler Flow Wire**

Tairo Kurita[1], Kakuya Kitagawa[2], Katsuya Onishi[1], Kan Takeda[2], Takeshi Nakano[1], Hajime Sakuma[2]
[1]Mie University School of Medicine, Tsu, Mie, Japan; [2]Mie University, School of Medicine, Tsu, Mie, Japan

Regional myocardial perfusion reserve determined by quantitative analysis of myocardial perfusion MRI was compared with coronary flow velocity reserve measured by intra-coronary Doppler flow wire in 20 patients with coronary artery disease. MR myocardial perfusion reserve (average 1.74±0.46) analyzed by two-compartment, Patlak plot method showed a good linear correlation with Doppler coronary flow velocity reserve (average 1.95±0.70; R=0.73, p<0.001). Quantitative analysis of stress-rest myocardial perfusion MRI can provide accurate assessment of regional myocardial perfusion reserve in patients with coronary artery disease.

14:10 *74.* **Myocardial Triglyceride in Health and in Metabolic Disease**

Jonathan McGavock[1], Naomi Salas[1], Lidia S. Szczepaniak[1]
[1]UT Southwestern Medical Center, Dallas, Texas, USA

We tested hypothesis whether myocardial steatosis accompany the states of glucose intolerance and insulin resistance and if it correlates with cardiac function in 59 individuals. We have found a graded increase in myocardial triglyceride content with development of glucose intolerance and diabetes. Although it is unclear if myocardial steatosis is associated with decrements in left ventricular funciton in humans, these data provide intital support for the myocardial lipotoxicity theory in a clinical setting.

14:20 *75.* **High Field MR Imaging of Myocardial Viability: An Intraindividual Comparison of MRI at 3.0T vs. 1.5T**

Bernhard Klumpp[1], Ulrich Kramer[1], Tobias Hoevelborn[1], Andreas May[1], Michael Fenchel[1], Klaus Peter Lodemann[2], Norbert I. Stauder[1], Claus D. Claussen[1], Stephan Miller[1]
[1]Eberhard-Karls-University of Tuebingen, Tuebingen, Baden-Wuerttemberg, Germany; [2]Bracco Altana, Konstanz, Baden-Wuerttemberg, Germany

Determination of myocardial viability by delayed enhancement MR-imaging (DE MRI) is increasingly used prior to myocardial revascularization. Aim of our study was the evaluation of the potential benefit of DE MRI at 3.0T. In our ongoing study 20 patients with chronic myocardial infarction are examined at 3.0T and 1.5T. Myocardial viability is assessed using an IR turbo FLASH sequence (0.1 mmol Gadobenate Dimeglumine / kg BW). SNR, CNR and image quality were significantly higher at 3.0T (3.0T/1.5T: SNRinfarction=30.2/19.1, p<0.005, SNRmyocardium=4.3/3.9, p>0.1, CNR=26/15.2, p<0.005). These advantages may be exploited to achieve higher spatial resolution, decrease acquisition times or reduce contrast dose.

14:30 *76.* **Delayed Enhancement MRI Detects RF Ablation Pattern in the Left Atrium and Pulmonary Vein Ostia**

Dana Ceceilia Peters[1], John Wylie[1], Kraig V. Kissinger[2], Rene M. Botnar[3], Thomas Hauser[1], Vidal Essebag[1], Mark E. Josephson[1], Warren J. Manning[1]
[1]Beth Israel Deaconess Medical Center, and Harvard Medical School, Boston, Massachusetts, USA; [2]Beth Israel Deaconess Medical Center, Boston, Massachusetts, USA; [3]Technical University of Munich, Munich, Germany

The visualization of left atrium scar after RF ablation treatment of patients with atrial fibrillation would allow refinement of this treatment. We have developed a 3D high resolution delayed enhancement technique and applied it in 31 studies of patients before and/or after pulmonary vein isolation. Hyperenhancement of the left atrium and the pulmonary vein ostia was observed in 100% of good quality studies after ablation, and in 0% of good quality studies before ablation. Partial or complete circumferential ablation patterns could be detected, and a relationship between scar thickness and time since ablation was observed.

14:40 ***77.*** **Single Breath Hold Transient MR-Elastography of the Heart - Imaging Pulsed Shear Wave Propagation Induced by Aortic Valve Closure -**

Ralph Sinkus[1], Benjamin Robert[1], Jean-Luc Gennisson[1], Mickael Tanter[1], Mathias Fink[1]
[1]Laboratoire Ondes et Acoustique, Paris, France

Pulsed transient shear waves, generated by aortic valve closure, are visualized in the septum by a motion-sensitized balanced FFE sequence. Motion-sensitization is achieved by adding a sinusoidal gradient coding waves at 300Hz. Acquisition is performed in a single breath hold using a retrospectively gated ECG-triggered sequence, which is phase-locked to mechanical vibrations at 300Hz. 20 heart phases are acquired. Phase-profiles through the septum reveal the presence of shear waves present shortly after aortic valve closure. Identical experiments without a motion-sensitized gradient yield phase-profiles identical during the entire cardiac cycle. Obtained values for shear wave speed agree with findings from ultrasound.

14:50 ***78.*** **Delayed Enhancement Imaging with Increasing Flip Angles: Reducing Signal Changes During the Acquisition Window**

Dana Ceceilia Peters[1], Kraig V. Kissinger[1], Warren J. Manning[1]
[1]Beth Israel Deaconess Medical Center, and Harvard Medical School, Boston, Massachusetts, USA

Delayed hyperenhancement imaging of scar and inflammation is a powerful technique, which has recently been applied in high resolution applications such as vessel wall imaging. The typical signal evolution during the acquisition window for inversion recovery gradient echo acquisition is analyzed, demonstrating signal changes greater than 250% during the window. An alternative method using increasing flip angles is presented which provides constant signal during the acquisition, based on T1, TI, TR and heart-rate. The results of this method are compared to conventional methods in simulations, phantoms and patients.

15:00 ***79.*** **A Black Blood T2* Technique for Myocardial Iron Measurement in Thalassemia**

Taigang He[1, 2], Peter G. Gatehouse[1, 2], Paul Kirk[1, 2], Dudley J. Pennell[1, 2], David N. Firmin[1, 2]
[1]Royal Brompton Hospital, London, UK; [2]Imperial College of Science Technology and Medicine, London, UK

A black blood sequence was developed and compared with a conventional bright blood one to evaluate the effectiveness and reproducibility of T2* analysis for iron overload measurement in thalassemia. Fifteen human subjects were imaged and T2* analysis was performed by two independent observers. The black blood T2* technique yielded high SNR images, provided well defined borders and avoided blood signal contamination to the myocardium. It shows reduced inter-observer variability and likely improved accuracy, which will allow for better characterization of the myocardium and facilitates its clinical application. This technique may have potential to study other disease requiring T2* analysis.

15:10 ***80.*** **Ultrafast Viability Imaging in Less Than 10 Minutes**

Lincoln Diniz[1], Karin Dill[1], Al Zhang[2], Edwin Wu[1], James Carr[1]
[1]Northwestern University, Chicago, Illinois, USA; [2]Siemens Medical Systems, Chicago, Illinois, USA

Conventional viability imaging protocols can result in long table-top times thus limiting patient throughput in a busy practice. Parallel imaging and single-shot strategies can be employed to reduce overall acquisition times. In this study, we implemented real-time cine TrueFISP with TSENSE and delayed enhanced single-shot IR TrueFISP, in a group of 22 patients. This resulted in a significant reduction in overall imaging time and produced comparable results to conventional segmented techniques.

15:20 ***81.*** **Feasibility of Cardiac Magnetic Susceptibility Measurement in Patients with Iron Overload**

Zhiyue J. Wang[1, 2], Zili Chu[1, 2], Raja Muthupillai,[23], Rajesh Krishnamurthy[1, 2], Donald H. Mahoney[1, 2], Brigitta U. Mueller[1, 2], Kenneth L. McClain[1, 2], Roland Fischer[4], Taylor Chung[1, 2]
[1]Texas Children's Hospital, Houston, Texas, USA; [2]Baylor College of Medicine, Houston, Texas, USA; [3]Philips Medical Systems, Cleveland, Ohio, USA; [4]Children's Hospital & Reaserch Center Oakland, Oakland, California, USA

Iron overload in the heart is the leading cause of death for thalassemia patients receiving chronic transfusions. A method for measuring the cardiac iron concentration in patients has not been available in clinical practice. The purpose of this work is to demonstrate the feasibility of measuring the magnetic susceptibility of the left ventricle (LV) for patients with iron overload. We found that intercostal muscle was a reliable reference for epi-myocardial susceptibility. Furthermore, the blood inside LV can be used as reference for endo-myocardial susceptibility measurement. Results of the study suggest a strong correlation between 1/T2* and magnetic susceptibility of the LV.

15:30 ***82.*** **Bright-Blood Delayed Contrast-Enhanced Imaging for Improving the CNR Between Endocardial Scar and Blood**

Daniel Kim[1], Monvadi B. Srichai[1], Vivian S. Lee[1]
[1]New York University, New York, USA

Delayed contrast-enhanced (DCE) imaging is becoming a clinically acceptable diagnostic method for assessing the extent of myocardial scar. This inversion-recovery (IR) technique exhibits good contrast-to-noise ratio (CNR) between scar and normal myocardium. However, CNR between blood and endocardial scar is frequently poor, because the T1 values of blood and scar at the time of DCE imaging are similar. This limitation may lead to incorrect estimation of the infarct size and obscure the visualization of small endocardial scar. The purpose of this study was to develop a single acquisition bright-blood DSE pulse sequence for improving the CNR between blood and endocardial scar.

15:40 ***83.*** **Systolic-Phase Black-Blood Imaging for Fatty Tissue Detection in Arrhythmogenic Right Ventricular Dysplasia**

Glenn S. Slavin[1], Godtfred Holmvang[2], Ehud Schmidt[3]

[1]GE Healthcare, Bethesda, Maryland, USA; [2]Massachusetts General Hospital, Boston, Massachusetts, USA; [3]GE Healthcare, Boston, Massachusetts, USA

Arrhythmogenic right ventricular dysplasia (ARVD), one of the leading causes of sudden death, is a disease where RV muscle is replaced by fatty or fibrotic tissue. It is currently diagnosed with MRI utilizing a variety of imaging sequences to evaluate wall-motion abnormalities, the presence of scar tissue, and the presence of fatty regions in the right ventricular wall. A breath-held, black-blood fast spin echo (FSE) sequence, timed for the systolic cardiac phase, is presented. Data acquisition occurs at the cardiac phase where the RV is thickest, allowing for easier detection of small fat layers.

15:50 ***84.*** **Fat Suppressed Delayed Enhancement Imaging**

Sven Zuehlsdorff[1], Yiu-Cho Chung[1], Edwin Wu[2], James C. Carr[2], Orlando P. Simonetti[3]

[1]Siemens Medical Solutions USA, Inc., Chicago, Illinois, USA; [2]Northwestern University Feinberg School of Medicine, Chicago, Illinois, USA; [3]Ohio State University, Columbus, Ohio, USA

Inversion recovery techniques are widely used to image infarcted myocardium. Distinction between infarcts and epicardial fat may be difficult due to short longitudinal relaxation times in both species post contrast.In this work, two methods of fat suppression in infarct imaging were examined. We compared the performance of an IR segmented turboFLASH sequence with fat saturation preparation pulse, with an IR segmented turboFLASH sequence using spectral spatial excitation pulses. The two methods were first evaluated in healthy volunteers. The better method was then tested on patients with myocardial infarction. Reliable fat suppression was achieved by using spectral spatial excitation pulses.

CLINICAL SCIENCE FOCUS SESSION: Cutting Edge Body MRI

Room 615 - 617 14:00 - 16:00 Chairs: Brian A. Hargreaves and Donald G. Mitchell

14:00 ***85.*** **Image Functional Modeling (IFM) Using Hyperpolarized Helium MRI**

Jennifer Kenyon[1], Yang-Sheng Tzeng[1, 2], James Brian Zender[1], Lisa Marie Campana[1], George R. Washko[2], Elliot Israel[2], Mitchell S. Albert[2], Kenneth R. Lutchen[1]

[1]Boston University, Boston, Massachusetts, USA; [2]Brigham and Women's Hospital, Boston, Massachusetts, USA

Asthmatic lung structure can be assessed using Hyperpolarized (HP) 3He MRI. In this study we synthesized anatomically consistent airway tree models with HP 3He MRI imaging and oscillatory mechanics data to advance an approach called Image Functional Modeling (IFM). Specifically, ventilation information was extracted from the imaging data and imported into a 3D computational lung model. Matching the model-simulated ventilation and mechanics with measured data required heterogeneous constriction throughout the airway tree, primarily involving closures and constriction of small airways (<2mm). The IFM approach suggests the possibility of personalized assessment of airway dysfunction.

14:10 ***86.*** **Abnormalities of Lung Structure in Children with Bronchopulmonary Dysplasia as Assessed by Diffusion Hyperpolarized Helium-3 MRI**

Talissa A. Altes[1, 2], Jaime Mata[2], Deborah K. Froh[2], Alix Paget-Brown[2], Eduard E. de Lange[2], John P. Mugler[2]

[1]Children's Hospital of Philadelphia, Philadelphia, Pennsylvania, USA; [2]University of Virginia, Charlottesville, Virginia, USA

45 subjects, including 32 healthy subjects with a history of uncomplicated term birth and 13 with a history of preterm birth complicated by subsequent bronchopulmonary dysplasia (BPD), underwent diffusion hyperpolarized helium-3 MR. The subjects with BPD had a higher group average of the mean apparent diffusion coefficient (ADC) (0.198 cm2/s) than the healthy subjects (0.157 cm2/s), p=0.0001, and 38% of subjects with BPD had heterogeneous ADC maps while all of the healthy subjects had homogeneous ADC maps. Diffusion hyperpolarized helium-3 MR appears to be able to detect the expected lung structural abnormalities, including enlarged alveoli, in children with BPD.

14:20 ***87.*** **Diffusion Weighted Imaging of Prostate and Rectal Wall: Comparison of Biexponential and Monoexponential Modelled Diffusion Coefficients**

Sophie Florence Riches[1], Kate Hawtin[2], Nandita M. deSouza[1]

[1]Institute of Cancer Research & Royal Marsden NHS Trust, Sutton, Surrey, UK; [2]Hammersmith Hospitals NHS Trust, London, UK

Diffusion weighted (DW) MRI is increasingly being used to identify prostate cancer, particularly within the central gland (PCG) where T2-W imaging has poor contrast between benign and malignant nodules. In a study of 50 patients, endorectal single shot echo-planar DW-MRI with 11 b-values ranging from 0 – 800 s/mm2 was analysed with two different models. A biexponential model could not adequately describe the central gland, but identified a perfusion component in the peripheral zone and rectal tissues, allowing a true diffusion coefficient to be calculated which was statistically different from the monoexponentially derived values of the apparent diffusion coefficient.

14:30 ***88***. **Diffusion-Weighted MR Imaging for Pretreatment Prediction and Early Monitoring of Primary Rectal Cancer Response to Chemoradiation Therapy**

Ying Shi Sun[1], Xiao Peng Zhang[1], Lei Tang[1], Jie Li[1], Kun Cao[1]

[1]Beijing Cancer Hospital£ School of Oncology£Peking University, Beijing, People's Republic of China

The Purpose of this study is to evaluate the predictive and early monitoring value of DW-MRI on therapy outcome of combined chemoradiation in patients with primary carcinoma of the rectum. Materials and Methods Fifteen patients with primary rectal carcinoma (cT3) undergoing preoperative chemoradiation were recruited in the study. Diffusion weighted echo planar imaging was performed weekly on all 15 patients during the course of therapy using a GE 1.5T MR scanner with an 8-channel body phase-array coil. The imaging parameters are: TE/TR£ºminimum/6000 msec, FOV£º36cm, Matrix£º128x128 Slicethick£º5mm, Nex£º8. Two motion-probing gradients (b=0 and b=1000 sec/mm2) were employed to obtain the diffusion ¨Cweighted images. And SENSE (ASSET) technology was also used to reduce the distortion of EPI. The mean ADC values of the tumor region was calculated at before and 1st, 2nd , 4th week of therapy compared with the postsurgical histopathologic results. Results Patients were divided into two groups according to the postsurgical histopathologic results: with 9 patients in responder group and 6 patients in non-responder group. The mean ADC (10-3 mm2/s) value in non-responder group (1.36¡À0.13) was higher compared to that in responder group (1.11¡À0.14) before onset of chemoradiation therapy(t=3.158,p<0.05). The mean ADC values between the groups are significantly different. Responder group showed a significant increase of mean ADC value at the course of treatment. In the nonresponder group, no initial increase of ADC value was observed or a decrease was found. Discussion and Conclusion DW-MRI is able to detect difference and individual changes of tumor ADC values during the course of chemoradiation, reflect biological difference and changes within the tumor tissue, and has shown the potential for pretreatment Prediction and early monitoring of primary rectal cancer response to chemoradiation therapy.

14:40 ***89***. **Single Breathold Multi-Contrast 3D Abdominal Imaging**

Richard Winkelmann[1], Jan De Becker[2], Romhild Hoogeveen[2], Peter Börnert[3], Olaf Dössel[1]

[1]University of Karlsruhe, Karlsruhe, Germany; [2]Philips Medical Systems, Best, Netherlands; [3]Philips Research Laboratories, Hamburg, Germany

In abdominal MR-imaging, multiple contrasts are helpful for a clear and comprehensive diagnosis. To avoid image respiratory artifacts, breath-hold techniques are usually preferred which could be significantly speed up by the use of highly accelerated parallel imaging. This allows multiple acquisitions of large 3D abdominal volumes, choosing arbitrary contrast protocols, within a single breath-hold. Such multi-contrast, single breath-hold data show no spatial misregistration and could potentially improve and ease diagnosis. In-vivo studies on healthy volunteers have been carried out to demonstrate the technical feasibility of this approach.

14:50 ***90***. **MR Diffusion and ^{1}H MR Spectroscopy in Non-Alcoholic Fatty Liver Disease**

Susan Moyher Noworolski[1], Daniel B. Vigneron[1], Raphael Merriman[1], Aliya Qayyum[1]

[1]UCSF, San Francisco, California, USA

A single-shot fast spin-echo diffusion tensor imaging sequence and proton MR spectroscopy were applied to the liver in 10 healthy subjects and 12 patients with non-alcoholic fatty liver disease (NAFLD). Directionally-averaged apparent diffusion coefficient (Dav) and total lipids:water were compared to each other and to histopathological steatosis, inflammation, and fibrosis measures. In general, Dav decreased and lipids:water increased with increasing steatosis, inflammation, and fibrosis. When combined, Dav and lipids:water completely separated steatosis grades. Subjects with higher fibrosis stage(2-3) had low Dav and high lipids:water for given steatosis grades. MR diffusion and MRS have promise for the noninvasive evaluation of NAFLD.

15:00 ***91***. **Comparison of Proton Diffusion in Regenerative Nodules and Fibrosis in Explanted Human Liver**

Peter M. Malek[1], Richard Znamirowski[1], Diego A. Aguirre[1], Alyssa D. Chavez[1], Mark Bydder[1], Tanya Wolfson[1], Matthew D. Robson[2], Graeme M. Bydder[1], Claude B. Sirlin[1]

[1]University of California, San Diego, San Diego, California, USA; [2]Oxford University, Oxford, UK

The apparent diffusion coefficient (ADC) of liver is reduced in fibrotic liver disease. This reduction is generally assumed to be caused by the fibrosis itself. This assumption overlooks the potential contribution of non-fibrotic regenerative liver tissue, which constitutes the dominant fraction of total liver content. This study prospectively compared proton diffusion in fibrosis and regenerative nodules in explanted cirrhotic liver specimens, utilizing high-resolution DW images. Pathology was the reference for tissue classification. Proton diffusion was significantly more restricted in regenerative nodules than fibrosis. This suggests that regenerative tissue contributes significantly to the reduced liver ADC value observed in cirrhosis.

15:10 ***92***. **Liver Regeneration and Bioenergetic Changes Following Hepatic Irradiation and Hepatocyte Transplant *In Vivo* by ^{31}P MRSI**

Charles Landis[1], Laibin Liu[1], Biao Xi[1], Jayanta Roy-Chowdhury[1], Hoby Hetherington[1], Chandan Guha[1]

[1]Albert Einstein College of Medicine, Bronx, New York, USA

Radiation treatment has limited usage in the treatment of liver cancers due the development of radiation induced liver damage (RILD). Previous work has demonstrated that hepatocyte transplant (HT) could ameliorate RILD in rats. To study the metabolic changes that occur in RILD with and without HT, ^{31}P MRSI data was acquired in rats treated with partial hepatectomy (PH) alone, PH with hepatic irradiation (PHRT) or PHRT with HT. Persistently reduced [γ-ATP] and γ-ATP/Pi signal ratio were observed in rats after PHRT. Reduced γ-ATP/Pi but elevated [γ-ATP] were observed in rats receiving HT at 6 weeks, suggesting that transplanted hepatocytes can simultaneously restore metabolic function while replacing host hepatocytes damaged by RT.

15:20 ***93.*** **Texture Analysis of Combined Contrast Enhanced MR Imaging Permits Accurate Non-Invasive Staging of Liver Fibrosis**

Gautam Bahl[1], Alyssa D. Chavez[1], Julie Collins[1], Tanya D. Wolfson[1], Anthony C. Gamst[1], Giovanni C. Motta[1], Cynthia B. Behling[1], Tarek C. Hassanein[1], Graeme C. Bydder[1], Claude B. Sirlin[1]
[1]UCSD, San Diego, California, USA

Current staging of liver fibrosis requires biopsy, which is invasive and prone to sampling error. We assessed non-invasive grading of liver fibrosis using texture analysis of combined contrast enhanced MR imaging with histology as the reference in 122 patients. A blinded radiologist assessed MR images qualitatively. Additionally, 256 quantitative texture features were measured in each patient and a forward selection algorithm based on a Bayesian information criterion was used to build a model to predict histological fibrosis stage. Pairwise Spearman correlation showed excellent agreement between qualitative MR and pathology, quantitative MR and pathology, and qualitative MR and quantitative MR.

15:30 ***94.*** **Morphological Features of FNH in Gadoxetic Acid-Enhanced Liver MRI: Results of a Multicenter Trial**

Christoph J. Zech[1], Luigi Grazioli[2], Josy Breuer[3], Stefan O. Schoenberg[1], Maximilian F. Reiser[1], E. EOB-Study-Group[3]
[1]Munich University Hospitals - Grosshadern, Munich, Germany; [2]University of Brescia, Brescia, Italy; [3]Schering AG, Berlin, Germany

Focal nodular hyperplasia (FNH) is a common benign focal liver lesion. Since FNH is usually no indication for liver surgery, non-invasive characterization of this lesion is of high importance. This multicenter trial evaluates the diagnostic performance to characterize FNH and describes morphological and enhancement features of FNH in MRI with the hepato-cellular-specific contrast agent gadoxetic acid. The results show that gadoxetic acid – enhanced MRI provides a better characterization of FNH in comparison to pre-contrast MRI and spiral CT. In the early dynamic examination enhancement characteristics well known from extracellular contrast agents can be distinguished.

15:40 ***95.*** **Voxel-Based Analysis of Dynamic 3D Perfusion Images: Preliminary Results in Chronic Liver Disease**

Samson Wong[1], Artem Mikheev[1], Henry Rusinek[1], Vivian S. Lee[1], Bachir Taouli[1]
[1]NYU Medical Center, New York, New York, USA

We describe our early experience with a quick automated voxel-based analysis method to process 3D perfusion-weighted imaging of the liver, performed in 10 patients (5 cirrhotic, 5 non cirrhotic) using an interpolated 3D GE sequence after injection of 10 mL of Gd-DTPA. Post-processing was performed using an automated method that enabled misregistration correction. Color maps of time to peak (TTP) of contrast in liver parenchyma were obtained, and showed longer higher TTP in cirrhotic livers (47.7 vs. 20.0 sec., $p < 0.005$). Our study shows a potential usefulness of a quick automated method for post-processing of liver perfusion data.

15:50 ***96.*** **Time-Resolved Echo-Sharing Angiographic Technique Used in Conjunction with Volume-Interpolated Breath-Hold Examination MRI (Treat-Vibe): Feasibility of a 3-D Technique for Evaluation of the Liver with High Temporal Resolution Using a Triple- Arterial Phase Acquisition**

Stephen John Drew[1], Sarah Shock[1], Bachir Taouli[1], Elizabeth M. Hecht[1], Tejas Parikh[1], Ruth P. Lim[1], Randall Kroeker[2], Jian Xu[3], Vivian S. Lee[1]
[1]New York University Medical Center, New York, New York, USA; [2]Siemens Medical Solutions, Erlangen, Germany; [3]Siemens Medical Solutions, New York, New York, USA

Our objective was to assess the feasibility of a triple-phase arterial acquisition during a single breath-hold using a Time Resolved Echo-sharing Angiographic Technique-Volume Interpolated Breath-hold Examination technique with parallel imaging (GRAPPA) factor 2. For cirrhotics, the liver parenchymal enhancement varied in maximal enhancement during the three arterial phase acquisitions, and lesions had variable arterial enhancement. TREAT-VIBE acquisition is a feasible technique achieving high temporal resolution and incorporating optimal arterial phase enhancement of the liver parenchyma during contrast infusion. This may have important implications in detection of arterially enhancing lesions in the altered contrast kinetics of the cirrhotic liver.

ELECTRONIC POSTER DISCUSSION: Novel Contrast Agents & Methods

Room 618 - 620 14:00 - 16:00 Chairs: Ralph P. Mason and Samuel A. Wickline

14:00 ***97.*** **MEMRI of Glucose Activated Human Pancreatic Islets**

Lara Leoni[1], Suraj Serai[1], Muhammad Haque[1], Jose Oberholzer[1], Richard L. Magin[1], Brian B. Roman[1]
[1]University of Chicago, Chicago, Illinois, USA

The validity of MEMRI in assessing human pancreatic islet function was investigated. Glucose stimulated influx of calcium into ß-cells is necessary for insulin release. When present during glucose stimulation, extracellular Mn can enter ß-cells through voltage-gated calcium channels and its accumulation alters T1 and T2 relaxation times resulting in increased MR image contrast. High-resolution MR micro imaging of glucose activated isolated human islets showed a significant increase in MR contrast at 50 μM Mn and higher. Although concerns may exist about Mn toxicity, the doses employed did not exhibit any acute negative effects as glucose stimulation indices were normal.

14:10 ***98***. **Developing New Multicolor Protein MRI Contrast Agents**

Michael Thomas McMahon[1, 2], Assaf A. Gilad[1], Jeff W.M. Bulte[1], Peter C.M. van Zijl[1, 2]

[1]Johns Hopkins School of Medicine, Baltimore, Maryland, USA; [2]Kennedy Krieger Institute, Baltimore, Maryland, USA

We are interested in expanding the capabilities of cellular MR imaging by developing contrast agents which allow distinction between multiple cell populations. In this work, we present four prototype amino acid sequences, tested in-vitro, which can be discriminated from each other using MRI. These agents produce contrast through the Chemical Exchange Saturation Transfer (CEST) mechanism, with the colors coming from the frequency dependency of the contrast. The magnitude of the contrast is dependent on the rate of exchange, which we also show can be predicted. These new agents should allow improved visualization of, for example, tumor-host interactions through MRI.

14:20 ***99***. **Stimulation-Induced Changes in Temperature and PH Measured Simultaneously by ^{1}H CSI**

Daniel Coman[1], Hubert Trubel[1, 2], Basavaraju G. Sanganahalli[1], Fahmeed Hyder[1]

[1]Yale University, New Haven, CT 06510, USA; [2]University Witten/Herdecke, Wuppertal, Germany

In vivo measurements of brain temperature and pH in absolute units are greatly lacking in quantitative studies of function. Both temperature and pH are believed to be tightly regulated in the brain and small changes are thought to impact neurophysiology greatly. Here we demonstrate the application of a recently developed high speed ^{1}H CSI method using a lanthanide complex to measure accurate temperature (±0.05 C) and pH (±0.02) distributions in the brain. Preliminary results for baseline and stimulation conditions show great sensitivity of both parameters in the cortex. Studies are underway for delivering the MR biosensor into deeper brain regions.

14:30 ***100***. **Artificial Reporter Gene Providing MRI Contrast *In Vivo* Based on Chemical Exchange**

Assaf A. Gilad[1], Michael T. McMahon[1, 2], Piotr Walczak[1], Paul T. Winnard Jr[1], Venu Raman[1], Jeff W. M Bulte[1], Peter C.M. van Zijl[1, 2]

[1]Johns Hopkins University School of Medicine, Baltimore, Maryland, USA; [2]Kennedy Krieger Institute, Baltimore, Maryland, USA

LRP is an artificial gene that was designed and cloned in order to serve as a biomarker for *in vivo* tracking of cell biodistribution, and potentially for monitoring gene expression by MRI. This study demonstrates that LRP expression by genetically engineered 9L glioma cells, provides sufficient contrast to distinguish transplanted LRP-expressing tumors from control tumors and the surrounding mouse brain. Since LRP relies on saturation transfer after irradiation of specific protons, this work opens the possibility for making a family of reporter genes that can be use for imaging multiple targets simultaneously, in frequency selective manner.

14:40 ***101***. **A Novel Approach in the Development of 19F NMR Reporter to Assess LacZ Gene Expression**

Jian-Xin Yu[1], Ra Ren[1], Ralph P. Mason[1]

[1]The University of Texas Southwestern Medical Center at Dallas, Dallas, Texas, USA

A novel class of 19F NMR lacZ gene reporter molecule (LCD-1) was designed, synthesized and tested. The successful detection with lacZ stably transfected human breast tumor MCF-7 cells shows great promise for further exploration of these reporters for *in vivo* assessing lacZ gene expression.

14:50 ***102***. **Simultaneous ^{19}F and ^{1}H Imaging on a Clinical 3T MR Scanner**

Jochen Keupp[1], Peter Caesar Mazurkewitz[1], Ingmar Gräßlin[1], Tobias Schaeffter[1]

[1]Philips Research Laboratories, Hamburg, Germany

^{19}F MRI has been identified as ideal for detection and tracking of drugs, reporter molecules or nano-particles for molecular imaging. As there is no ^{19}F signal from biological tissue, only signal from exogenous contrast agents is displayed. For diagnostic localization, an anatomical proton image is required, which so far needs additional imaging time. An imaging system is presented, which allows simultaneous acquisition of ^{1}H and ^{19}F images. The associated imaging sequence employs concurrent dual-frequency RF pulses and acquisition windows. It is validated in a phantom study on a modified clinical 3T whole-body MR system using a double-tuned solenoid transmit/receive coil.

15:00 ***103***. **$H_2{}^{17}O$ as a "smart" T_2 Contrast Agent with Relaxivity Sensitive to Tissue Metabolic Status**

Peter Edward Thelwall[1], Xeve Silver[1], Stephen J. Blackband[1, 2]

[1]University of Florida, Gainesville, Florida, USA; [2]National High Magnetic Field Laboratory, Tallahassee, Florida, USA

$H_2{}^{17}O$ acts as a water proton T_2 relaxation agent due to scalar coupling interactions between ^{1}H and ^{17}O. This T_2 relaxivity effect is transmitted to bulk water by proton exchange, and thus T_2 relaxivity is proportional to exchange rate. As this rate is modulated by sample pH and phosphate content, $H_2{}^{17}O$ acts as a T_2 contrast agent sensitive to tissue metabolic status. We employed $H_2{}^{17}O$ to distinguish between normal and ischemic *in vivo* mouse brain in mice enriched with ~1.5% $H_2{}^{17}O$. Thus $H_2{}^{17}O$ acts as a minimally invasive “smart” contrast agent with relaxivity sensitive to tissue metabolic status.

15:10 ***104***. **Development of PARACEST MRI Contrast Agents to Assess Cartilage Glycosaminoglycan Concentrations**

Fei Dong[1], Megan Marsh[1], James Dennis[1], Marty D. Pagel[1]
[1]Case Western Reserve University, Cleveland, Ohio, USA

We have developed negatively-charged and charge-neutral PARACEST MRI agents to more accurately quantify the glycosaminoglycan content in cartilage. We can selectively detect a minimum CEST agent concentration of 2.8mM at a minimum 5% change in MR signal. The ratio of PARACEST agent concentrations that are simultaneously applied to healthy and GAG-depleted *ex vivo* rabbit cartilage samples correlated well with correlated with histopathological measurements. These results are being used to develop a single quantitative assessment of glycosaminoglycan content in cartilage during a single MRI scan session.

15:20 ***105***. **Power Optimization of *In-Vivo* Chemical Exchange Saturation Transfer (CEST) Contrast for PH Weighted Imaging**

Phillip Zhe Sun[1, 2], Jinyuan Zhou[1, 2], Judy Huang[1], Peter van Zijl[1, 2]
[1]Johns Hopkins University, Baltimore, Maryland, USA; [2]F.M.Kirby Center, Baltimore, Maryland, USA

CEST imaging provides a unique contrast, reflecting properties of sometimes unobservable labile protons of metabolites and mobile proteins. Using solution phantoms, the optimal irradiation power has been derived. However, CEST is complicated *in vivo* due to concomitant conventional MT. Here, we hypothesize that at weak and intermediate power, the endogenous CEST process can be modeled with an empirical equation developed for describing simultaneous proton transfer and spillover effects. The model fits well and could be applied to achieve great contrast improvement of pH-weighted imaging. Furthermore, this approach provides a strategy of reduction of energy deposit and duration for *in vivo* CEST imaging.

15:30 ***106***. **Spatio-Temporal Expression Control of a Heat Shock Promoter-Driven Transgene Delivered in the Kidney by Modified Mesenchymal Stem Cells: A Feasibility Study Using MR Guided Focused Ultrasound**

Beatrice Letavernier[1], Rares Salomir[2], Yahsoo Delmas[1], Claire Rome[3], Franck Couillaud[3], Alexis Desmouliere[1], Olivier Hauger[3], Nicolas Grenier[3], Christian Combe[1], Jean Ripoche[1], Chrit Moonen[3]
[1]University Bordeaux 2, Bordeaux, France; [2]University Bordeaux2, Bordeaux, France; [3]CNRS/University Bordeaux2, Bordeaux, France

Rat mesenchymal stem cells (MSC) line expressing a luciferase gene under the control of a Heat Shock Protein 70 minimal promoter were injected in the rat renal artery. The kidney was locally heated by MRI-guided focused ultrasound. Induction of expression of the luciferase gene was demonstrated in the heated region using histological examination.

15:40 ***107***. **Non-Invasive Assessment of Therapy-Induced Tumor Necrosis Using DTPA-Gd-Poly(L-Glutamic Acid)**

Edward F. Jackson[1], Emilio Esparza-Coss[1], Xiaoxia Wen[1], Chun Li[1]
[1]University of Texas M.D. Anderson Cancer Center, Houston, Texas, USA

A novel contrast agent, DTPA-Gd-poly(L-glutamic acid), was investigated as a marker for necrosis in tumors treated with poly(L-glutamic acid)-paclitaxel. PG-Gd results were compared to those obtained using degraded PG-Gd and MagnevistTM. Contrast agents were administered on Day 0 and images obtained at Days 0, 3, and 5. Treatment began on Day 1. Tumor enhancement was seen immediately following injection of degraded PG-Gd or Magnevist with no enhancement at Days 3 and 5. PG-Gd did not demonstrate acute enhancement, but caused pronounced enhancement on Days 3 and 5, with areas of enhancement corresponding to regions of necrosis seen on H&E sections.

15:50 ***108***. **Characterization and Potential of Gd-ACX, a New Contrast Agent for Magnetic Resonance Neuroimaging**

Hana Lahrech[1, 2], Adriana Teodora Perles-Barbacaru[1, 2], Soâd Aous[3], Régine Farion[1, 4], Jean-Claude Debouzy[3], Andrée Gadelle[5], Pascal Henri Fries[5]
[1]INSERM, U594, Grenoble, F-38043, France; [2]Univ Grenoble 1, Grenoble, F-38043, France; [3]Laboratoire de Biophysique Cellulaire et Moléculaire CRSSA, La Tronche, F-38702, France; [4]Univ Grenoble, Grenoble, F-38043, France; [5]Laboratoire de Reconnaissance Ionique/Service de Chimie Inorganique et Biologique (UMR-E 3 CEA-UJF), Grenoble, F-38054, France

The (3,6-per anhydro) α-cyclodextrin derivative (ACX) complexing Gd3+ has properties of a MRI contrast agent. The complex Gd-ACX is biocompatible, not nephrotoxic and little hemolytic up to 10 times the dose needed for *in vivo* MRI. The longitudinal and transversal relaxivities, 8.61 and 10.11 mM-1s-1 respectively, are superior to those of Gd-DOTA. Gd-ACX is characterized by a flat nuclear magnetic relaxation dispersion profile up to 100 MHz. It is shown to be a blood pool agent. No extravasation in a C6 glioma model in rats was observed, contrary to Gd-DOTA. Its potential for cerebral perfusion measurement is demonstrated.

CLINICAL SCIENCE FOCUS SESSION: Assessment of Prostate Cancer

Room 602 - 604 14:00 - 16:00 Chairs: N. R. Jagannathan and Daniel B. Vigneron

14:00 ***109***. **Dynamic Contrast Enhanced Imaging and Quantitative Analysis of Prostate Cancer at 3 Tesla**

Iclal Ocak[1], Marcelino Bernardo[2], Gregory Metzger[3, 4], Yolanda McKinney[5], Peter Choyke[1]

[1]National Cancer Institute, Bethesda, Maryland, USA; [2]SAIC-Frederick, Frederick, Maryland, USA; [3]Philips Medical Systems, Bethesda, Maryland, USA; [4]University of Minnesota, Bethesda, Maryland, USA; [5]National Institute of Health, Bethesda, Maryland, USA

Endorectal coil MRI of the prostate has been extensively studied at 1.5 T for detecting and staging prostate cancer. The potential advantage of 3.0 T MRI is higher signal to noise ratios leading to higher temporal and spatial resolution. In this study we evaluated T2-weighted, DCE-MRI images and pharmacokinetic parameters in 36 patients with biopsy proven prostate cancer with endorectal coil at 3.0 T. The combined sensitivity and specificity of T2-weighted and DCE-MRI images were 77% and 78%, respectively. Although all of the pharmacokinetic parameters were higher in biopsy proven cancer area than inflammatory and benign foci for an individual patient, there was considerable overlap in like regions across all patients. In spite of these results further investigations need to be performed on tumor pathophysiological parameters and the addition of MR spectroscopy to the T2W and DCE-MRI may further improve the results.

14:10 ***110***. **Analysis of Prostate DCE-MRI at 3T Using a Measured Arterial Input Function**

Martin Lowry[1], Lindsay W. Turnbull[1]

[1]University of Hull, Hull, UK

DCE-MRI of the prostate at 3T was implemented using multiple flip angles, for T1 determination, and a rapid dynamic 3D acquisition. Pharmacokinetic analysis using a 2-comparment model and the measured arterial input function revealed that mean T1, Max [Gd], Ktrans, and Ve in tumour were significantly greater than in peripheral zone but similar to those of BPH. In addition, for all tissues, Ktrans and Ve were positively correlated with Max [Gd]. Parameter maps of Ktrans proved superior to AUC maps in delineating the extent and heterogeneity of malignancy within the prostate.

14:20 ***111***. **MRI-Guided Prostate Biopsy for Individuals with Elevated or Increasing PSA Levels After Negative TRUS-Biopsy**

Matthias Philipp Lichy[1], Aristotelis Anastasiadis[1], Arnulf Stenzl[1], Claus D. Claussen[1], Heinz-Peter Schlemmer[1]

[1]University of Tuebingen, Tuebingen, BW, Germany

Purpose of this study was to establish MRI-guided biopsy for individuals with elevated or increasing PSA levels after negative TRUS- biopsy and suspicious (endo)MRI findings at 1.5 Tesla. A total of 26 patients were included so far. Prostate cancer was detected in 14 out of 26 cases (54%). MRI-guided biopsy of the prostate is a save and clinically feasible procedure. Based on our initial results it is a very promising method for tumor detection in individuals with elevated or increasing PSA-levels and negative former TRUS-biopsies.

14:30 ***112***. **Ferumoxtran-10 Enhanced MRI in Noninvasive Detection of Lymph Node Metastases; First Results in the Work-Up of Prostate Cancer in a Clinical Setting**

Alette Wilhelmina Daniels-Gooszen[1], Roel Heesakkers[2], Harrie Van den Bosch[1], John Wondergem[1], Evert Koldewijn[1], Ad Hendrikx[1], Jelle Barentsz[2]

[1]Catharina Hospital, Eindhoven, Netherlands; [2]UMC St Radboud, Nijmegen, Netherlands

With ferumoxtran-10 (lymphotrophic superparamagnetic nanoparticles) enhanced MRI lymph node metastases can be detected non-invasively. Sensitivity and specificity of this new technique performed in a clinical setting are evaluated. 120 consecutive patients were included. Ferumoxtran-10 enhanced MRI performed in a clinical setting of a general hospital showed a sensitivity of 89% and a specificity of 99% for the detection of lymph node metastases in prostate cancer. Additional positive lymph nodes outside the obturator fossa are found in 29%. In conclusion MRL seems a very promising and reliable technique for future workup in patients with prostate cancer.

14:40 ***113***. **3D 1H-MR Spectroscopic Imaging of the *In Vivo* Human Prostate at 3T with a Body Array Coil: A Step Towards MR Screening of Prostate Cancer?**

Tom WJ Scheenen[1], Stijn WTPJ Heijmink[1], Stefan A. Roell[2], Christina A. Hulsbergen-Van de Kaa[1], Jelle O. Barentsz[1], Arend Heerschap[1]

[1]Radboud University Nijmegen Medical Centre, Nijmegen, Netherlands; [2]Siemens Medical Solutions, Erlangen, Germany

3D 1H-MRSI was performed in 22 biopsy-proven prostate cancer patients without an endorectal coil at 3T. Spectroscopic signals from an elliptical weighted PRESS pulse sequence acquired with all elements of an 8-channel body array coil were combined into zero-order phased spectra for every individual voxel of the MRSI matrix. With whole-mount section histopathology as a standard of reference, the choline to citrate ratio of voxels in healthy and tumor tissue were calculated. Prostate cancer can now be detected throughout the whole prostate with a true voxel resolution of 1.0 cm3 in 8.5 minutes without using an endorectal coil.

14:50 ***114***. **Potential of 3D ^{1}H MRSI and DWI in Men with Increased PSA**

Virendra Kumar[1], N R. Jagannathan[1], Rajeev Kumar[1], S C. Das[1], Lokesh Jindal[1], Sanjay Thulkar[1], S Dutta Gupta[1], S N. Dwivedi[1], Stefan Roell[2], A K. Hemal[1], N P. Gupta[1]

[1]All India Institute of Medical Sciences, New Delhi, India; [2]Siemens, Erlangen, Germany

The potential of 3D ^{1}H MRSI and DWI was evaluated in men with increased prostate specific antigen (PSA). Both MRSI and DWI were carried out prior to sextant biopsy during the same scanning session. Metabolite ratio [Citrate/(Cho+Cr)] and ADC were calculated for identical voxels. It is observed that the region of the prostate that showed reduced metabolite ratios also showed low ADC. A positive correlation was observed between metabolite ratio and ADC (r = 0.6 to 0.9). MRSI and DWI may show early changes of malignancy especially in patients with PSA 4 – 20 ng/mL, thereby improving detection of malignancy.

15:00 ***115***. **Intermediate Results of IMAPS: An International Multi-Centre Assessment of Prostate MR Spectroscopy**

Tom Scheenen[1], Elisabeth Weiland S Roell[2], Paul van Hecke[3], Marc Lemort[4], Peter Bachert[5], Heinz-Peter Schlemmer[6], Jaoping Lu[7], Dale Broome[8], Geert Villeirs[9], Jurgen Futterer J Barentsz A Heerschap[1]

[1]Radboud University Nijmegen Medical Centre, Nijmegen, Netherlands; [2]Siemens Medical Solutions, Erlangen, Germany; [3]University Hospital, Katholieke Universiteit Leuven, Leuven, Belgium; [4]Jules Bordet Institute, Brussels, Belgium; [5]German Cancer Research Institute DKFZ, Heidelberg, Germany; [6]University of Tuebingen, Tuebingen, Germany; [7]Shanghai Changhai Hospital, Shanghai, People's Republic of China; [8]Loma Linda University Health Science Centre, Loma Linda, California, USA; [9]University Hospital Ghent, Ghent, Belgium

IMAPS is a multi-centre trial evaluating the use of 3D 1H-spectroscopic imaging of the prostate to detect and localize prostate cancer. Currently 67 patients contributed by 8 different institutions are included. The value of the (choline+creatine)/citrate integral ratio was evaluated for different healthy anatomical regions and for tumor tissue. Threshold values and corresponding numbers for sensitivity and specificity in detecting prostate cancer were calculated for these different tissues. Prostate cancer can better be detected in the peripheral zone than in the central gland, and the peri-urethral area needs to be evaluated with caution.

15:10 ***116***. **Combined Use of Endorectal MRS and Apparent Diffusion Coefficients to Increase Accuracy in Prostate Tumour Detection**

Stefan A. Reinsberg[1], [2], Geoffrey S. Payne[1], Sophie F. Riches[1], Sue Ashley[3], Nandita M. deSouza[1]

[1]Institute of Cancer Research, Sutton, Surrey, UK; [2]University of British Columbia, Vancouver, BC, Canada; [3]Royal Marsden NHS Trust, Sutton, Surrey, UK

Low sensitivity and specificity of conventional imaging for prostate cancer detection can be improved by the use of combined CSI and diffusion-weighted imaging. In a study with 42 patients at 1.5T we investigate the use of a combined metabolite ratio and ADC predictor for tumour detection. At a sensitivity of 93%, specificity of detecting lesions is significantly improved for the combined predictor 91% as compared to Cho/Cit alone (73%) or ADC alone (57%). An increase in CSI resolution will minimise partial volume effects and improve tumour detection further.

15:20 ***117***. **A Study of Differentiation Between Prostate Cancer and Prostatitis by 1H MR Spectroscopic Imaging (MRSI)**

Saying Li[1], Haodan Dang[1], Wenchao Wang[1], Chen Zhang[1], Cheng zhou[1], Min Chen[1]

[1]Beijing Hospital, Beijing, People's Republic of China

The purpose was to investigate the differential features of prostate cancer and prostatitis by 1H MR Spectroscopic Imaging (MRSI)Seventy-two voxels corresponding to the histopathologically confirmed regions of cancer or prostatitis in the peripheral zone were retrospectively evaluated using MRSI. Cancerous voxels were defined as CC/C¡Ý0.8. The changes in citrate and choline in each voxles were also evaluated. The CC/C for cancer voxels was significantly different from the ratios in the voxles with prostatitis ($p<0.05$). The overestimation for prostatitis was significantly reduced by adding the requirement that citrate was not or slightly decreased to normal level citrate (Cit/Norm.Cit ¡Ý 0.75).

15:30 ***118***. **Signal Loss in DCE-MRI Associated with Tumor Progression in Prostate Cancer Bone Metastasis Model**

Hagit Dafni[1], Sun Jin Kim[1], Kunal Panda[1], James A. Bankson[1], Sabrina M. Ronen[1]

[1]The University of Texas, MD Anderson Cancer Center, Houston, Texas, USA

Bone metastases are often resistant to conventional therapy, but response can be improved by combination with anti-vascular agents. A bone metastasis model was induced by intratibial injection of human prostate cancer cells (PC-3MM2). Dynamic contrast enhanced (DCE)-MRI using macromolecular contrast material (biotin-BSA-GdDTPA) showed progressive signal loss in the bone marrow, matching the progression of bone metastases. Loss of signal could be attributed to the increased interstitial fluid pressure in the tumor microenvironment. Extravasation of contrast material occurred only after osteolysis. These apparent vascular changes suggest that DCE-MRI could be used to monitor disease progression and drug-induced regression of bone metastases.

15:40 ***119***. **Correlation of Choline-Containing Metabolites with Gene Expression of Kennedy Cycle Enzymes**

John Kurhanewicz[1], Carissa Ferrer Santos[1], Thomas Nordling Butler[1], David Jae-hyeun Joun[1], Sarah J. Nelson[1], Daniel B. Vigneron[1], Mark Gunnard Swanson[1]

[1]UCSF, San Francisco, California, USA

Combined HR-MAS and gene expression studies of 16 human prostate biopsy samples (n=10 healthy, n=6 Gleason 3+3 cancers) demonstrated that the relatively higher levels of choline and lower levels of phosphocholine observed in the proton spectra of prostate cancer relative to breast cancer may be due to differences in the expression of several key Kennedy cycle enzymes that would lead to increased choline rather than phosphocholine. Specifically, choline kinase was not over-expressed while phospholipase D was over-expressed in prostate cancer, in contrast to breast cancer where choline kinase and phospholipase C were both over-expressed.

15:50 ***120***. **Characterizing the Physiological Environments of a Prostate Cancer Xenograft in Orthotopic and Subcutaneous Sites**

Zaver M. Bhujwalla[1], Arvind P. Pathak[1], Meiyappan Solaiyappan[1], Venu Raman[1], Paloma Ballesteros[2], Dmitri Artemov[1]

[1]The Johns Hopkins University School of Medicine, Baltimore, Maryland, USA; [2]UNED, Madrid, Spain

Invasive human cancer xenografts invade and metastasize more efficiently following orthotopic implantation compared to heterotopic subcutaneous implantation. We recently generated a stably transfected human prostate cancer cell line with green fluorescent protein (GFP) expression under the control of a hypoxia response element (HRE) and have characterized its response to hypoxia *in vivo*. Here we have used this cell line to characterize differences in the orthotopic and heterotopic environments of this xenograft model using MRSI (total choline, lactate/lipid, and extracellular pH), and optical detection of GFP expression (hypoxia).

Parallel RF Transmission Technology

Room 6E 16:30 - 18:30 Chairs: David I. Hoult and Ulrich Katscher

16:30 ***121***. **An 8 Channel Transmit Coil for Transmit Sense at 3T**

Vijayanand Alagappan[1], Graham C. Wiggins[1], Andreas Potthast[2], Kawin Setsompop[3], Elfar Adalsteinsson[3, 4], Lawrence L. Wald[1, 4]

[1]A. A. Martinos Center for Biomedical Imaging, Charlestown, Massachusetts, USA; [2]Siemens Medical Solutions, Charlestown, Massachusetts, USA; [3]MIT, Cambridge, Massachusetts, USA; [4]Harvard-MIT Division of Health Sciences and Technology, Cambridge, Massachusetts, USA

An 8 channel 3T transmit coil used for parallel excitation is presented to correct the B1 inhomogeneity at high field strengths, using spatially tailored RF pulses. The coil was tested in a prototype 8 transmit channel 3T Tim Trio system and validated using spatially tailored RF excitation pulses.

16:42 ***122***. **Transmit Coil Array for Accelerating 2D Excitation on an Eight-Channel Parallel Transmit System**

Yudong Zhu[1], Randy Giaquinto[1], Ronald Watkins[1], Adam Kerr[2], John Pauly[2], Mika Vogel[3], Joseph Piel[1], Thomas Foo[1], Ileana Hancu[1], Keith Park[1]

[1]GE Global Research Center, Niskayuna, New York, USA; [2]Stanford University, Stanford, California, USA; [3]GE Global Research Center, Munich, Germany

The multiple transmit coils at the front end of a parallel transmit architecture define the individual B1 profiles that, under the control of the parallel RF pulses, are weighted and superimposed to form the composite RF field. The coils thus play a central role in the induction of appropriate B1 spatiotemporal variations that affect excitation acceleration and the concomitant E field that dictates SAR. In this study some of the important aspects of a transmit array's construction/application were examined. An effort to design and build an improved version of a previously reported array is described as a specific example.

16:54 ***123***. **An Eight Channel Transmit/Receive Body Coil for 3T**

Peter Vernickel[1], Peter Röschmann[2], Christian Findeklee[2], Kai Michael Luedeke[2], Christoph Leussler[2], Johan Overweg[2], Ulrich Katscher[2], Ingmar Graesslin[2], Klaus Schuenemann[3]

[1]TuTech Innovation, Hamburg, Germany; [2]Philips Research Laboratories, Hamburg, Germany; [3]Technical University Hamburg-Harburg, Hamburg, Germany

Multi-channel transmit MR systems bear the potential of compensating signal intensity variations occurring at higher field strengths due to dielectric resonances. Methods like RF shimming and local excitation in combination with Transmit Sense can be applied to compensate for these effects. Moreover, methods like Transmit Sense can be applied to excite arbitrarily shaped pattern efficiently. The implementation of these methods adds new requirements to the MRI hardware, especially with respect to the number of RF transmit channels. This work describes the implementation and testing of a decoupled eight-element transmit/receive body coil for 3T and its integration into a standard clinical MRI scanner.

17:06 ***124***. **Six Channel Transmit-Receive Coil Array for Whole Body Imaging at 4T**

Sven Junge[1], Peter Ullmann[2], Frank Seifert[3], Thorsten Thiel[1]

[1]Bruker BioSpin MRI GmbH, Ettlingen, Germany; [2]University Hospital Freiburg, Freiburg, Germany; [3]Physikalisch-Technische Bundesanstalt, Berlin, Germany

Whole body imaging at high magnetic field strength above 3T is limited by the increase in RF-power requirements and SAR. In order to overcome these restrictions we designed a novel multi-transmit and multi-receive body coil by combining current-sheet-antenna (CSA) and loop coil elements. It allows high-field cardiac and abdominal imaging at 4 Tesla with low RF-power levels and therefore significantly reduced energy deposition compared to large transmit volume body-coils. The CSA coil-setup provides excellent parallel imaging capabilities (e.g. GRAPPA) and can be used in combination with multiple transmit channels for Transmit SENSE applications.

17:18 ***125***. **Implementation of Mode-Scanning Excitation Method with a 16-Ch Transmit/Receive Volume Strip Array at 7T**

Ray F. Lee[1], Ryan Brown[2], Gabor Mizsei[3], Rong Xue[1], Tamer Ibrahim[4], Hugo Chang[5], Yi Wang[2], Cornel Stephanescu[1]

[1]New York University, New York, USA; [2]Cornell University, New York, New York, USA; [3]Mount Sinai School of Medicine, New York, New York, USA; [4]University of Oklahoma, Norman, Oklahoma, USA; [5]Siemens Medical Solution, Inc., New York, New York, USA

At high fields, especially 7T or above, the interaction between coil and sample is so pronounced that not only the sample loading has to be included in tuning (as in lower fields), but also the sample dielectric resonance has to be considered to determine the magnetic field pattern of the coil. The Mode-Scanning Excitation (MSE) method was previously proposed and simulated to obtain the desired transmit field pattern of any arbitrary sample inside a volume strip array (VSA) by inverse design of the voltage amplitudes and phases at transmit ports based on a set of pre-scan measurements. In this study, a 7T 16-ch transmit/receive coil and its 16-way transmit/receive RF interface was built to prove the feasibility of the MSE method. Our experimental results show that desired regional excitation patterns at specified locations can be achieved by MSE in presence of sample dielectric resonance.

17:30 ***126***. **A 32 Channel Lattice Transmission Line Array for Parallel MRI**

Gregor Adriany[1], Ark Gozubuyuk[1], Johannes Ritter[1], Carl Snyder[1], Pierre-Francois Van de Moortele[1], Steen Moeller[1], J Thomas Vaughan[1], Kamil Ugurbil[1]

[1]University of Minnesota, Minneapolis, Minnesota, USA

We present a 32 channel lattice head array based on transmission lines for very high field. For this, a combination of concentric transmission line elements was pursued to demonstrate that they can be used both in parallel and perpendicular orientation to the magnetic field and to investigate whether an array consisting of a combination of both type of elements improves SNR and parallel imaging performance. Our results demonstrate that concentric arrangements of transmission line arrays are feasible at 7 Tesla and improve the achievable reduction factors significantly.

17:42 ***127***. **A Flexible 8-Channel RF Transmit Array System for Parallel Excitation**

Ulrich Fontius[1], Rudi Baumgartl[1], Uwe Boettcher[1], Gerald Doerfler[1], Franz Hebrank[2], Daniel Fischer[1], Hendrik Jeschke[1], Stephan Kannengießer[1], Gernot Kwapil[1], Ulrich Nerreter[1], Jürgen Nistler[1], Georg Pirkl[1], Andreas Potthast[2], Stefan Roell[1], Stefan Schor[1], Bernd Stoeckel[3], Elfar Adelsteinson[4], Gregor Adriany[5], Vijayanand Alagappan[6], Borjan Gagoski[4], Kawin Setsompop[4], Lawrence L. Wald[6], Franz Schmitt[1]

[1]Siemens Medical Solutions, Erlangen, Germany; [2]Siemens Medical Solutions, Charlestown, Massachusetts, USA; [3]Siemens Medical Solutions, New York, New York, USA; [4]MIT, Cambridge, Massachusetts, USA; [5]Center for MR Research, Minneapolis, Minnesota, USA; [6]MGH Martinos Center, Charlestown, Massachusetts, USA

Imaging of human sized subjects at ultra high fields, such as 7T, suffers intrinsically from the interaction of the B1 field with the dielectric human tissue. B1 shimming and TX-Sense have been proposed to improve the homogeneity of the B1 field. With the exception of the 3 channel system of Ullman *et al*., previous parallel excitation work has been limited to modelling with a single TX channel system. We demonstrate a modular approach to adding TX channels to a clinical scanner. The system is also well suited to multinuclear spectroscopy and ASL experiments utilizing multiple labelling coils, as well as dynamic shimming with up to 21 shim channels.

17:54 ***128***. **A Vector Modulation Transmit Array System**

Greig Cameron Scott[1], Pascal Stang[1], William Overall[1], Adam Kerr[1], John Pauly[1]

[1]Stanford University, Stanford, California, USA

Transmit coil arrays have gained interest as a means of shortening selective excitation. However, a more urgent need exists in interventional MRI, where RF safety with guidewire coupling remains a major concern. We propose a transmit array system with the goal of creating safe RF excitations in the presence of guidewires. We are prototyping vector modulator electronics, low cost RF power amplifiers, and a 3 coil array to test feasibility of our approach.

18:06 ***129***. **Whole Body 3T MRI System with Eight Parallel RF Transmission Channels**

Ingmar Graesslin[1], Peter Vernickel[2], Joachim Schmidt[1], Christian Findeklee[1], Peter Röschmann[1], Christoph Leussler[1], Paul Haaker[1], Horst Laudan[1], Kai Michael Luedeke[1], Josef Scholz[1], Steffen Buller[1], Jochen Keupp[1], Peter Börnert[1], Henk Dingemans[3], Giel Mens[3], Gerrit Vissers[3], Krelis Blom[3], Nico Swennen[3], Jan vd Heijden[3], Leo Mollevanger[3], Paul Harvey[3], Ulrich Katscher[1]

[1]Philips Research Laboratories, Hamburg, Germany; [2]TuTech Innovation, Hamburg, Germany; [3]Philips Medical Systems, Best, Netherlands

Dielectric resonance effects diminish the quality of body MR images at main fields at 3T or above. Parallel RF transmission techniques bear the potential of compensating for these effects through RF shimming or local excitation. This paper describes the first MRI prototype system based on a modified clinical MR scanner, which features whole body imaging at 3T using genuine eight-channel transmitter/receiver (Tx/Rx) technology. The system offers a multi-channel transmit and a standard single channel-imaging mode. Examples for the imaging results of the MRI experiments in both modes are shown.

18:18 ***130***. **A Parallel Transceiver for Human Imaging at 9.4T**

Lance DelaBarre[1], Carl J. Snyder[1], Kamil Ugurbil[1], J Thomas Vaughan[1]

[1]University of Minnesota, Minneapolis, Minnesota, USA

At 9.4T, the short Larmor wavelength of RF in the human head produces an inhomogenous distribution of B_1. To correct some of these variations, a parallel transceiver was designed and tested. Each element in a multichannel coil has a separate RF path, which includes a dedicated broadband amplifier and digital receiver. Each coil is independently computer-controlled with digital phase shifters and programmable attenuators modifying the waveform prior to amplification. This additional control will facilitate feedback driven B_1 shimming and other applications.

MR PHYSICS AND TECHNIQUES FOR CLINICIANS

Room 6C 16:30 - 18:30 Chairs: Frank R. Korosec and Joseph C. McGowan

Educational Objectives:
Upon completion of this session, participants should be able to:

- Define and describe the fundamental principles of MR imaging, including the definition of spin magnetization, the Larmor relationship, relaxation phenomena, and the process of using the spin magnetization to produce an image;
- Explain imaging pulse sequences based upon spin and gradient echoes, including fast spin echo and echo planar techniques;
- Design MR imaging protocols for diagnostic applications considering image contrast, spatial resolution, acquisition time, signal-to-noise ratio, and artifacts; and
- Describe the principles and capabilities of various advanced MR techniques including, diffusion, vascular and cardiac MRI.

16:30 **Spin Gymnastics I**
Donald B. Plewes

17:10 **Spin Gymnastics II**
Walter Kucharczyk

17:50 **Hardware**
Steven M. Conolly

Diffusion Imaging: Clinical Applications

Room 6D 16:30 - 18:30 Chairs: Jeffrey J. Neil and Carlo Pierpaoli

16:30 ***131***. **Normal Appearing White Matter Damage is Associated with Neuropsychiatric Symptoms in Systemic Lupus Erythematosus**

Pamela L. Peterson[1], T Barrick[1], P Rich[2], A Clifton, F Howe[1], C Clark[1], J Axford[1]

[1]St. George's University London, London, England UK; [2]St.George's Hospital NHS Trust, London, England UK

The attribution of neuropsychiatric events to systemic lupus erythematosus (SLE) remains challenging, as there is no single diagnostic test and the symptoms of neuropsychiatric SLE are diverse and non-specific. We have used diffusion tensor imaging to investigate structural changes in patients with normal conventional MRI scans and found that damage to normal appearing white matter is associated with neuropsychiatric events in SLE.

16:42 ***132***. **Diffusion Tensor Fractional Anisotropy is a Potential Surrogate Marker for Neuroinflammatory Molecules in Brain Abscess**

Asht Mangal Mishra[1], Rakesh Kumar Gupta[1], Kavindra Nath[1], Amit Prasad[1], Khader M. Hasan[2], Kashi Nath Prasad[1], Mazhar Husain[3], Nuzhat Husain[3], Shalini Kumar[4], Ponnada A. Narayana[2]

[1]Sanjay Gandhi Post Graduate Institute of Medical Sciences, Lucknow, Uttar Pradesh, India; [2]University of Texas Medical School at Houston, Houston, Texas, USA; [3]King George's Medical University, Lucknow, Uttar Pradesh, India; [4]University of California at Los Angeles, Los Angeles, California, USA

DTI data were acquired from five patients with brain abscess (BA) with an aim to look for the reasons for high fractional anisotropy (FA) value in the cavity and the wall of BA. Neuroinflammatory molecules (NMs) (intercellular cell adhesion molecule-1, lymphocyte function associated antigen-1, tumor necrosis factor-á and interleukin-1â) from the pus were quantified using reverse transcription-polymerase chain reaction to observe relationship of NMs with FA. Positive correlation between FA and NMs and between NMs and immunodetection of NMs in the wall of BA suggests that FA is a surrogate marker of active neuroinflammation in BA.

16:54 ***133***. **Long-Term Diffusion Changes in the Corpus Callosum of Patients with Severe Traumatic Brain Injury**

Annette S. Nielsen[1], Karam Sidaros[1], Matthew G. Liptrot[1], Henrik Kahr Mathiesen[1], Egill Rostrup[1]

[1]Copenhagen University Hospital Hvidovre, Copenhagen, Denmark

Diffuse axonal injury is the dominating type of primary neuronal injury in patients with severe blunt head trauma. To investigate the long-term changes of diffusion parameters following trauma, we performed a DTI study with approximately one-year follow-up on patients with severe traumatic brain injury. In the corpus callosum, fractional anisotropy decreased ($p<0.001$), ADC increased ($p=0.012$) and mean of the eigenvalues $\lambda 2$ and $\lambda 3$ increased ($p<0.001$). These findings are consistent with an ongoing degeneration following diffuse axonal injury.

17:06 ***134***. **Arcuate Fasciculus Maturation is Impaired Bilaterally in Pediatric Traumatic Brain Injury: A DTI Study at 3.0 T**

Khader M. Hasan[1], Ambika Sankar[1], Larry Kramer[1], Mary R. Prasad[1], Linda Ewing-Cobbs[1]

[1]University of Texas Medical Scool, Houston, Texas, USA

Closed head traumatic brain injury (TBI) is a major cause of disability and morbidity amongst school-age children. Diffuse axonal injury (DAI) caused by shear-strain deformation disrupting the cytoskeletal network and axonal membranes is the primary pathophysiological consequence of TBI. In this preliminary report entire brain DTI was used on 19 healthy pediatric controls and 14 TBI children to assess the effect of trauma on the arcuate fasciculus, which is an important white matter structure involved in language. We demonstrate using the FA and transverse diffusivity that TBI arrests bilaterally the matuarion trend of this lateralized structure.We demonstarte that using the transverse diffusivity and FA that this is attributed to impairement of myelin repair and remyelination mechansisms.

17:18 ***135***. **Brain Morphometry Using Diffusion-Weighted Magnetic Resonance Imaging: Application to Studying Subjects at High Genetic Risk for Schizophrenia**

Kamila Urszula Szulc[1], Babak A. Ardekani[2], Matthew J. Hoptman, [12], Craig A. Branch[2], Arthika Bappal[2], Hilary Bertisch, [12], Kyle Brown[2], Magda Majcher[2], Lynn E. DeLisi, [12]

[1]NYU School of Medicine, New York, New York, USA; [2]Nathan S. Kline Institute for Psychiatric Research, Orangeburg, New York, USA

In this abstract a recently proposed apparent diffusion coefficient (ADC) based method of assessing cortical atrophy is applied to studying subjects at high genetic risk for schizophrenia. The innovation of this method is the assertion that ADC may be used as a marker of cortical volume deficits. Four regions were identified in which subjects at high genetic risk with schizophrenia and patients had increased ADC. These data indicate that subtle cortical atrophy may already be occurring in people at high-risk for developing schizophrenia prior to actually showing clinical signs of the illness.

17:30 ***136***. **Assessment of White Matter Damage in Subacute Sclerosing Panencephalitis Using Quantitative Diffusion Tensor MRI**

Richa Trivedi[1], Rakesh Kumar Gupta[1], Atul Agarwal[2], Khader M. Hasan[3], Arun Gupta[1], Kashi Nath Prasad[1], Ponnada A. Narayana[3]

[1]Sanjay Gandhi Post Graduate Institute of Medical Sciences, Lucknow, Uttar Pradesh, India; [2]King George Medical University, Lucknow, Uttar Pradesh, India; [3]University of Texas Medical School at Houston, Houston, Texas, USA

Diffusion tensor imaging data were acquired from twelve patients of stage II subacute sclerosing panencephalitis (SSPE) and ten age and sex-matched healthy controls. Fractional anisotropy (FA) and mean diffusivity (MD) values were calculated in the periventricular white matter, corpus callosum and posterior limb of the internal capsule in patients as well as healthy controls. Statistically significant decreased FA in white matter and increased MD in the parieto-occipital region were found in patients with normal as well as abnormal conventional imaging compared to healthy controls. We conclude that FA and MD changes are widespread in the white matter in SSPE that may help in the early diagnosis and management of these patients.

17:42 ***137***. **ADC Measurement in the Middle Cerebellar Peduncle Allows the Differentiation of MSA from PD and PSP**

Caterina Tonon[1], Raffaele Lodi[1], Giuseppe Nicoletti[2], Francesco Fera[2], Emil Malucelli[1], David Neil Manners[1], Francesca Condino[2], Pierfrancesco Pugliese[2], Gennarina Arabia[2], Mario Zappia[2], Aldo Quattrone[2], Bruno Barbiroli[1]

[1]Università di Bologna, Bologna, Italy, [2]Institute of Neurological Sciences, Mangone (Cosenza), Italy

Clinical differentiation of Parkinson's disease (PD) from parkinsonian syndromes such as multiple system atrophy (MSA) and progressive supranuclear palsy (PSP) is difficult in the early stage of the disease, with a high rate of misdiagnosis. We used DWI to extensively assess ADC values in the middle cerebellar peduncles (MCP), brainstem, basal ganglia and cerebral white matter regions in patients with PD, MSA, and PSP. ADC in the MCP differentiated MSA patients both from PSP, PD patients and healthy volunteers with 100% sensitivity and 100% specificity. ADC measurement of MCP should be included in the clinical work-up of parkinsonian syndromes.

17:54 ***138***. **A Study on Patients with Temporal Lobe Epilepsy Showed a Relationship of a Circle in a Plane Defined by FA and Trace Jointly**

Jiun-Jie Wang[1], Chia-Lung Yang[1], You-Zen Lu[2], Yau-Yau Wai[2], Tzuu-Kang Chy[2]

[1]Chang Gung University, TaoYuan, Taiwan; [2]Chang Gung Memorial Hospital, TaoYuan, Taiwan

Increased diffusivity was detected in the epileptic hippocampus and the ipsilateral temporal structures associated with a decreased anisotropy along the temporal lobe. However, from such observations it is difficult to determine the microstructural changes because the change in mean diffusivity and anisotropy is not directly related and therefore segmented. This study showed a simple relationship existed, which defined a circle in a coordinate system of FA and normalized trace. The combined information described the change in the microenvironment in water diffusion in epileptic patients.

18:06 ***139***. **Postmortem Interval Alters the Water Relaxation and Diffusion Properties of Nervous Tissue – Implications for High Resolution MRI of Human Autopsy Samples**

Timothy Michael Shepherd[1], Jeremy Flint[1], Peter Edward Thelwall[1], Greg J. Stanisz[2], Stephen John Blackband[1]

[1]University of Florida, Gainesville, Florida, USA; [2]Sunnybrook & Women's CHSC/University of Toronto, Toronto, Ontario, Canada

Stunning high-resolution MRI images of human brain autopsy samples have been presented at the ISMRM, yet the origins of these samples should be more suspect. This study investigated the impact of postmortem interval to 4formaldehdye fixation on the relaxation and diffusion MRI properties of nervous tissue.

18:18 ***140***. **Advantages of Fast Spin-Echo Diffusion Weighted Imaging in Detecting Small Stroke Lesions**

Josef P. Debbins[1], John Karis[1], James G. Pipe[1]

[1]St. Joseph's Hospital, Phoenix, Arizona, USA

Stroke lesion detection is improved using diffusion-weighted Propeller imaging when compared with standard single-shot EPI DWI methods, particularly for very small lesions. We investigate the mechanisms of this small lesion improvement, particularly local susceptibility from T2* effects due to increased deoxyhemoglobin concentrations. Results show that Propeller diffusion imaging improves lesion conspicuity when compared to standard single shot EPI diffusion methods and thus provides a better estimate of total stroke.

Myocardial Function

Room 4C - 3,4 16:30 - 18:30 Chairs: Nael F. Osman and Bernd Wintersperger

16:30 ***141***. Young Investigator Award Finalist: **Detailed Analysis of Myocardial Motion in Volunteers and Patients Using High Temporal Resolution MR Tissue Phase Mapping**

Bernd André Jung[1], Daniela Föll[1], Petra Böttler[1], Steffen Petersen[2], Jürgen Hennig[1], Michael Markl[1]

[1]University Hospital, Freiburg, Germany; [2]John Radcliffe Hospital, Oxford, UK

Since diastolic dysfunction accounts for up to one half of the cases of heart failure, abnormal regional left ventricular wall motion is an important clinical marker in multiple cardiac pathologies. Tissue Doppler imaging (TDI) is an established method allowing for the detection and investigation in regional myocardial motion with high temporal resolution. Drawbacks of TDI are related to limitations of the acoustic window and the dependance of myocardial velocities on the angle of insonation. In order to overcome limitations of TDI, respiratory gated MR phase contrast measurements with high temporal resolution were performed in 12 volunteers and 2 patients with LV hypertrophy and characteristical findings in myocardial motion were discussed.

16:50 ***142***. **Highly Accelerated K-T SENSE Using Large Coil Arrays**

Viton Vitanis[1], Christof Baltes[1], Jeffrey Tsao[2], Michael Schacht Hansen[3], Peter Boesiger[1], Sebastian Kozerke[1]

[1]Institute for Biomedical Engineering, University and Swiss Federal Institute of Technology Zurich, Zurich, Switzerland; [2]Novartis Institutes for BioMedical Research, Cambridge, Massachussets, USA; [3]Centre for Medical Image Computing, University College of London, London, UK

k-t SENSE enables significant scan accelerations in dynamic imaging. However, dynamic image features may become blurred with increasing acceleration factors. When using large receiver arrays the spatial encoding capability of multiple independent coils may be exploited to partially replace the role of training information. At large acceleration factors, however, this approach is limited by noise amplification from coil encoding. In this work, modified sampling is proposed which favors the temporal dimension by skipping spatial phase-encodes entirely. The approach is shown to provide improved temporal fidelity in 2D cine imaging of the heart with up to 16-fold acceleration.

17:02 ***143***. **Gated and Real-Time Wideband SSFP Cardiac Imaging at 3T**

Hsu-Lei Lee[1], Gerald M. Pohost[1], Krishna S. Nayak[1]

[1]University of Southern California, Los Angeles, California, USA

SSFP cardiac imaging at 3T suffers from off-resonance artifacts and has limited readout duration. Wideband SSFP can solve these problem by providing an efficient scheme for acquiring SSFP images with long readouts, which will allow the high SNR of 3T SSFP to be translated into higher spatial and temporal resolution. In this work we implemented wbSSFP for 3T cardiac imaging in both PG-gated 2DFT imaging and real-time imaging with a 3.2ms long three-echo EPI readout. A significant improvement over conventional SSFP was observed in both cases.

17:14 ***144***. **Cine-Navigator Imaging: Self-Navigating Respiratory Motion Correction for Free-Breathing Cardiac Cine-MRI**

Angela Leung[1], Richard Thompson[1]

[1]University of Alberta, Edmonton, AB, Canada

Respiratory motion artifacts in cine-imaging of the heart are avoided by breath-holding, which limits the information that can be acquired in a given study and excludes patients that are unable to perform breath-holds, particularly children. We use an interleaved segmented radial k-space approach to acquire real-time images throughout a free-breathing conventional gated-segmented experiment, using the same k-space data for both purposes. Real-time images are used for self-navigating image registration and motion correction of k-space data prior to the ultimate gated-segmented reconstruction. Significant improvement over uncorrected images (up to 67% increase in edge sharpness) is shown in volunteer studies.

17:26 ***145***. **Highly Accelerated Real-Time Imaging of Cardiac Function Using a 32 Channel Phased Array at 3 T**

Tobias Wichmann[1, 2], Titus Lanz[1], Mark A. Griswold[3], Andreas Greiser[4], Mathias Nittka[4], Peter M. Jakob[2]

[1]Rapid Biomedical GmbH, Rimpar, Germany; [2]University of Würzburg, Würzburg, Germany; [3]Case Western Reserve University, Cleveland, Ohio, USA; [4]Siemens Medical Solutions, Erlangen, Germany

The purpose of this study was to gauge the performance of a 32 channel array in cardiac imaging at 3T using high parallel imaging accelerations. This combination is shown to provide significant improvement in imaging speed while maintaining good image quality. In particular, real-time acquisitions are shown at acceleration factors of 7 using TSENSE. In addition, high-resolution free-breathing real-time images were obtained with an in-plane spatial resolution of 2.8x1.2mm, which is similar to the typical breathhold protocol used today in the clinical routine. We believe this technology could allow clinical use of ungated, free-breathing real time imaging of cardiac function.

17:38 ***146***. **Simultaneous Imaging of Myocardial Function and Viability in Patients**

ElSayed H. Ibrahim[1], Matthias Stuber[1], Robert G. Weiss[1], Amy E. Spooner[1], Nael F. Osman[1]

[1]Johns Hopkins University, Baltimore, Maryland, USA

The assessment of myocardial viability is important for therapeutic decision-making in patients with myocardial infarction. In addition, cardiac functional images provide complementary information about myocardium. Composite strain encoding (C-SENC) imaging provides simultaneous functional and viability images of myocardium. In this work, the method was tested on seven patients, and the resulting viability images were validated against conventional delayed-enhancement (DE) images. The two images showed good agreement in determining myocardial infarction. C-SENC imaging took almost the same time as DE imaging, but resulted in additional functional images. This allowed for constructing one composite image that showed both functional and viability information.

17:50 ***147***. **Respiratory Self-Gating with PROPELLER Encoding: Application to Free-Breathing Cardiac Imaging**

Teng-Yi Huang[1], Yi-Jui Liu[2], Chun-Jung Juan[3], Cheng-Yu Chen[3], Brigitte P. Poncelet[4], Kenneth K. Kwong[4]

[1]National Taiwan University of Science and Technology, Taipei, Taiwan, Taiwan; [2]Feng Chia University, Taichung, Taiwan; [3]Tri-Service General Hospital and National Defense Medical Center, Taipei, Taiwan; [4]MGH/MIT/HMS Athinoula A. Martinos Center for Biomedical Imaging, Charlestown, Massachusetts, USA

For the clinical cardiac MR imaging application, patients are generally required to hold their breath during the scan to minimize the motion-related artifacts. The PROPELLER encoding method can reconstruct a low-resolution image, which can be used to extract respiratory trace, from every single blade due to k-space center oversampling. In this study, we investigated the possibility of extracting respiratory motion trace with the low-resolution images acquired by PROPELLER encoding for the application of free-breathing high resolution cardiac imaging.

18:02 ***148***. **Measuring LV-RV Interventricular Dyssynchrony Using Cine DENSE MRI**

Bruce Shawn Spottiswoode[1], Xiaodong Zhong[2], Rajan A. Patel[2], Patrick A. Helm[2], Bongani M. Mayosi[3], Christopher M. Kramer[2], Ernesta M. Meintjes[1], Frederick H. Epstein[2]

[1]University of Cape Town, Cape Town, Western Cape, South Africa; [2]University of Virginia, Charlottesville, Virginia, USA; [3]Groote Schuur Hospital and University of Cape Town, Cape Town, Western Cape, South Africa

Cine DENSE MRI has been shown to provide a detailed mapping of mechanical activation of left ventricular (LV) myocardium. Echocardiography results show that measures of combined left and right ventricular dyssynchrony are better predictors for response to cardiac resynchronisation therapy (CRT) than LV dyssynchrony alone. In this study we adapt the cine DENSE methods to measure strain in both the LV and the right ventricle (RV). Results from normal volunteers and patients with heart failure are presented, clearly demonstrating delays to onset of strain. Cine DENSE measurements of interventricular RV-LV dyssynchrony may improve our ability to prospectively identify CRT responders.

18:14 ***149***. ***In Vivo* MR Elastography of the Human Heart: Initial Results**

Jens Rump[1], Sebastian Papazoglou[1], Dieter Klatt[1], Uwe Hamhaber[2], Jürgen Braun[2], Ingolf Sack[1]

[1]Institute of Radiology, Berlin, Germany; [2]Institute of Medical Informatics, Berlin, Germany

The assessment of myocardial stiffness could be important for detecting early states of heart diseases and predicting the development of heart insufficiency. Here, first successful *in vivo* MR Elastography (MRE) experiments on the human heart are presented. A new sequence design in steady-state free precession – MRE enabled us to combine a low-frequency shear-wave excitation of the interventricular septum with fast motion sensitization and short MR-repetition times. Initial results on three healthy volunteers indicate the presence of two independent shear moduli (16 ± 8 kPa and 2.25 ± 1.8 kPa) similarly to the anisotropy of the elasticity observed in skeletal muscle.

High Resolution/High Field Spectroscopy in Human and Animal Models

Room 611 - 612 16:30 - 18:30 Chairs: Sebastián Cerdán and Tracy R. McKnight

16:30 ***150***. **Functional ^{1}H NMR Spectroscopy in Cat Visual Cortex**

Ivan Tkac[1], Kamil Ugurbil[1], Noam Harel[1]

[1]University of Minnesota, Minneapolis, Minnesota, USA

Neuronal activity in primary visual cortex of cats has been extensively investigated using different fMRI techniques. The primary goal of this study was to investigate the feasibility of determining the detection threshold for multiple brain metabolites with highly resolved *in vivo* ^{1}H NMR spectroscopy in the cat visual cortex at 9.4 T. Exceptional spectral quality was achieved which allowed reliable quantification of 16 brain metabolites (CRLB < 15%). Preliminary data showed that during visual stimulation the concentration of all metabolites varied within the detection threshold range of the spectroscopic method (±0.2 µmol/g).

16:42 ***151***. **Dynamics of Human Brain Metabolites During Prolonged Visual Stimulation as Revealed by 1H-MRS at 7 T**

Silvia Mangia[1], Ivan Tkac[1], Rolf Gruetter[2], Pierre-Francois Van De Moortele[1], Bruno Maraviglia[3], Kamil Ugurbil[1]

[1]University of Minnesota, Minneapolis, Minnesota, USA; [2]Centre d'Imagerie Biomedicale, EPFL and Univ. of Lausanne and Geneva, Lausanne, Switzerland; [3]University of Rome "La Sapienza", Rome, Italy

By means of ultra-short echo-time STEAM (TE = 6 ms), we determined on twelve subjects the time-course of lactate and other metabolites during prolonged visual stimulation at 7 T. The group analysis revealed significant concentration changes for lactate (+20%), glutamate (+2%), aspartate (-20%) and glucose (-15%). In general, changes in metabolite concentrations were within ±0.2 µmol/g. Lactate increased within 1-2 min by about 0.2 µmol/g and returned to baseline after the stimulus ended. The reported changes of opposite sign in aspartate and glutamate implicated that amino-acid homeostasis is affected by physiological stimulations.

16:54 ***152***. **Localized ^{1}H MR Spectroscopy in the Primary Visual Cortex (V1) of the Macaque Monkey**

Christoph Juchem[1], Nikos K. Logothetis[1], Josef Pfeuffer[1, 2]

[1]Max-Planck-Institute for Biological Cybernetics, Tuebingen, BW, Germany; [2]Siemens Medical Solutions, Erlangen, B, Germany

The primary visual cortex (V1) is one of the elementary targets, when visual function and cortical reorganization are investigated. Neurotransmitters and substances involved in the energy metabolism of the brain are thought to be key compounds for a deeper understanding of the underlying processes. Here, 1H MR spectroscopy from small volumes positioned exclusively within the macaque V1 in direct vicinity to the cranial bone is reported. Optimizations in combined passive and active shimming, outer volume suppression and RF pulse design allowed the full quantification of 10 metabolites including creatine and phosphocreatine from a very localized voxel of monkey cortex V1 (5x1.6x5 mm3, 40 iL).

17:06 ***153***. **^{1}H MRSI Revealed Influence of Genetic Background on Neuronal Behavior in Murine Model of HIV-1 Encephalitis**

Jay A. Nelson[1], Santhi Gorantla[1], Huanyu Dou[1], Melissa Mellon[1], Jennifer M. Bradley[1], Danette Kibuule[1], Howard E. Gendelman[1], Michael D. Boska[1], Larisa Poluektova[1]

[1]University of Nebraska Medical Center, Omaha, Nebraska, USA

Murine models of human immunodeficient virus type-1 encephalitis (HIVE), C.B.-17/SCID and Rag-2$^{-/-}\gamma c^{-/-}$, were compared for their ability to mimic human pathology. Mice were injected in the subcortex with infected human monocyte derived macrophages (MDM) and data were collected 7-days post-infection. Compared to Rag-2$^{-/-}\gamma c^{-/-}$, C.B.-17/SCID mice showed increased microglia activation, astrocytosis, neuronal damage, TNF-α and IL-1β, enhanced chemoattraction of peripheral MDM and reduced MDM numbers in brain tissue. C.B.-17/SCID also had reduced concentrations of NAA/Cre globally. The increased and widely distributed inflammatory responses with increased neuronal damage in the C.B.-17/SCID model better mimics HIVE pathology than the Rag-2$^{-/-}\gamma c^{-/-}$ murine model.

17:18 ***154***. ***In Vivo* Detection of Dynamic ^{13}C Isotopomer Turnover from [U-^{13}C]-Glucose**

Su Xu[1], Wenjun Zhu[1], Jun Shen[1]

[1]National Institute of Mental Health, Bethesda, Maryland, USA

An INEPT-based ^{13}C MRS method was used to detect dynamic isotopomer turnover in the rat brain at 11.7 T. The isotopomer patterns of both glutamate and glutamine C4 consist predominantly of a quartet (from consecutive labeling at C3, C4 and C5) and a doublet (from consecutive labeling at C4 and C5 but not at C3). A lag in the transition of glutamine C4 pattern from doublet-dominance to quartet dominance as compared to glutamate C4 was observed, which is consistent with the concept of the precursor-product relationship between glutamate and glutamine and a significant cerebral glutamate-glutamine cycle.

17:30 ***155***. **Spectroscopic Monitoring of an Experimental Brain Lesion Treated by Cell Transplantation**

Vít Herynek[1, 2], Katerina Glogarová[2, 3], Pavla Jendelová[2, 3], Eva Syková[2, 4], Milan Hájek[1, 2]

[1]Institute for Clinical and Experimental Medicine, Prague, Czech Republic; [2]2nd Faculty of Medicine, Charles University, Prague, Czech Republic; [3]Institute of Experimental Medicine ASCR, Prague, Czech Republic; [4]Institute of Experimental Medicine, ASCR, Prague, Czech Republic

An experimental cortical lesion in the rat brain was monitored after treatment by cell transplantation. Higher concentrations of NAA and glutamate and lower concentrations of glutamine, as assessed by 1H MRS, in treated animals compared to untreated ones indicated faster recovery of the affected tissue after cell therapy. Although complete recovery or replacement of damaged neurons cannot be expected within a short time period, transplanted cells might rescue partially damaged cells, resulting in a decrease in the penumbra area and enabling faster regeneration of the tissue.

17:42 ***156***. **CSI of Mouse Brain Tumors at 7 Tesla with 0.8µl Voxel Resolution**

Rui Simoes[1, 2], Claudia Diekmann[3], Sebastián Cerdán[4], Carles Arús[1]

[1]Universitat Autònoma de Barcelona, Barcelona, Spain; [2]Universidade de Coimbra, Coimbra, Portugal; [3]Bruker BioSpin MRI GmbH, Ettlingen, Germany; [4]Instituto de Investigaciones Biomédicas Alberto Sols UAM-CSIC, Madrid, Spain

Routine CSI acquisition on mouse models of human disease is now possible with a new generation of commercially available equipment. In this preliminary study, brain tumors were induced in mice by intracranial injection of C6 glioma cells. Animals harboring a brain tumor, identified by CE-T1 MRI, underwent CSI studies at 7T either in a PharmaScan 70/16 or in a BioSpec 70/30 (Bruker, Germany). The highly resolved CSI data obtained (0.8 µl voxels) opens exciting avenues for new spectroscopic applications in mouse models, suggesting that in the future CSI information can be correlated with molecular phenotype in heterogeneous tumors.

17:54 ***157***. **Lack of Brain Edema in Acute on Chronic Liver Failure Results from Compensatory Mechanisms in Skletetal Muscle and Brain**

Claudia Zwingmann[1, 2], Chris Rose[1], Dieter Leibfritz[2], Roger Butterworth[1]

[1]Hospital Saint-Luc, Montreal, Quebec, Canada; [2]University of Bremen, Bremen, Germany

In acute Hepatic Encephalopathy (HE), the major cause of death is brain edema. Brain edema is rarely encountered in acute-on-chronic liver failure (ACLF). We investigated whether ALF and ACLF result in differences in relation to the onset of brain edema, blood ammonia and cerebral metabolism using *ex vivo* NMR. ALF caused significant changes compared to ACLF: a) increased brain water, 2. increased arterial ammonia concentrations, 3. decreased brain glutamine synthesis through pyruvate carboxylase, 4. increased brain lactate synthesis, and 5. decreased brain aspartate synthesis. Our observations suggest that impaired brain energy metabolism and ammonia play a key role in ALF.

18:06 ***158***. **NAA is Reduced During the Latent Period Preceding Pilocarpine-Induced Epilepsy**

William A. Gomes[1, 2], Kan Takahashi[2], Cynthia Pan[2], Fred Alexander Lado[2], Hoby Patrick Hetherington[2]

[1]Montefiore Medical Center, Bronx, New York, USA; [2]Albert Einstein College of Medicine, Bronx, New York, USA

Reductions in NAA enable localization of seizure foci in temporal lobe epilepsy (TLE). To determine whether deficits in NAA precede the onset of overt seizures or are solely a consequence of chronic seizures, we measured hippocampal NAA in the pilocarpine rat model of TLE. In this model of human TLE, NAA is reduced prior to the development of spontaneous seizures, suggesting that spectroscopic studies of NAA may provide an early marker of epileptogenesis. If validated in patients, this may allow identification of patients at risk for epilepsy following a first seizure.

18:18 ***159***. **Increased Cortical TCA Cycle Rate During Functional Stimulation Determined at 11.7 Tesla**

Jehoon Yang[1], Dawen Li[1], Jun Shen[1]
[1]NIMH, Bethesda, Maryland, USA

Glutamate C4 turnover from [1,6-$^{13}C_2$]glucose with and without forepaw stimulation was measured at 11.7 Tesla using POCE spectroscopy from a 35 µL voxel located at the primary somatosensory cortex of alpha-chloralose anesthetized rat brain. The TCA cycle rate was found to increase by ~39% due to functional stimulation (from 0.49±0.10, n = 5, to 0.68±0.11 µmol/g/min, n = 6, mean±SD, $p < 0.05$, unpaired t test). No significant change in the glutamate-glutamine cycling flux was found from the *in vivo* turnover time courses (0.19±0.07 vs. 0.15±0.07 µmol/g/min).

fMRI of the Normal Human Brain: Cognition, Language, Vision

Room 615 - 617 16:30 - 18:30 Chairs: Frederik Barkhof and John C. Gore

16:30 ***160***. **The Neural Network of Mental Calculation in Child Abacus Experts and Nonexperts**

Feiyan Chen[1], Zhenghui Hu[2], Xiaowei Tang[1], Pengcheng Shi[2]
[1]Zhejiang University, Hangzhou, Zhejiang, People's Republic of China; [2]Hong Kong University of Science and Technology, Hang Kong, People's Republic of China

Abacus mental calculation (AMC) experts refer to those who have been trained and also demonstrated extraordinary capability of mental calculation. In this study, child AMC experts and nonexperts were required to perform mental calculations through visual stimuli during MRI scanning sessions. We found a substantially different functional connectivity networks for child AMC experts and non-experts during mental calculation experiments. It demonstrates that the different neural networks and functional connectivity degree of mental calculation between two groups may be related to the cognitive strategies implied in the processing of mental calculation.

16:42 ***161***. **Differences Between Boys and Girls in the Correlation of Functional Brain Connectivity and Intelligence**

Vincent J. Schmithorst[1], Scott K. Holland[1]
[1]Children's Hospital Medical Center, Cincinnati, Ohio, USA

The neuroanatomical correlates of intelligence and their developmental trajectories in boys and girls were investigated using functional MRI (fMRI). A large cohort of over three hundred children performed the task of silent verb generation. Regions were found in the left hemisphere exhibiting positive correlations of functional activation with IQ, including the medial temporal gyrus, prefrontal cortex (Broca's area), medial frontal gyrus, precuneus, and cingulate gyrus. Using a data-driven analysis procedure, a sex-X-IQ-X-age interaction was demonstrated in the functional connectivity between regions in the left hemisphere. Our results provide evidence for disparate neuroanatomical bases underlying intelligence in boys and girls.

16:54 ***162***. **Steady State Functional Connectivity Modulated by Demand in Working Memory**

Allen T. Newton[1], Victoria L. Morgan[1], John C. Gore[1]
[1]Vanderbilt University, Nashville, Tennessee, USA

Steady state correlations in low frequency BOLD signals have been interpreted as revealing functional connectivity between regions within the human brain. It is still not well understood how they may change as a function of cognitive demand. Our goal is to investigate whether inter-regional correlations in low frequency BOLD signals are functions of demand using the N-back task. Significant differences were found between resting state data and data during task performance. These data confirm that the demand introduced by a higher order cognitive task increase the low frequency correlations between regions known to be involved in the task.

17:06 ***163***. **Functional MRI Activation Patterns Based on Subject's Reaction Times in a Verb Generation Task**

Mayuresh S. Korgaonkar[1], Susan Fiore[1], Candice J. Perkins[1], Nancy K. Squires[1], Mark E. Wagshul[1]
[1]Stony Brook University, Stony Brook, New York, USA

Verb generation tasks have been exclusively used in the past to study neural activity associated with language processing and has also shown to be a reliable predictor of laterality in contrast to simple picture naming or word reading tasks. The goal of this study was to develop a task which could be used to understand differences in brain areas recruited in identifying differential difficulty stimuli based on reaction times which could be used in assessment of aphasia therapy. Differential level of activation was seen in the inferior frontal gyrus (BA45) with a longer hemodynamic response associated with the difficult stimuli.

17:18 ***164***. **Spectral Differences in Language Processing Areas in Good and Dyslexic Readers**

Larissa I. Stanberry[1], Todd Richards[2], Virginia W. Berninger[2], Rajesh Nandy[3], Elizabeth Aylward[2], Kenneth Maravilla[2], Dietmar Cordes[2]
[1]University of Washington, Everett, Washington, USA; [2]University of Washington, Seattle, Washington, USA; [3]University of California Los Angeles, Los Angeles, California, USA

The purpose of this abstract is to compare the spectral properties of the fMRI signal changes in areas associated with phonological processing (inferior frontal gyrus (IFG) and angular gyrus (AG)) in good and dyslexic readers. Our preliminary results indicate lack of temporal coherence between the right IFG and other regions studied here across the entire task. They also suggests possible functional discontinuity of the left IFG and right IFG in dyslexic readers and a possibly compensatory role of the left IFG in the reading strategies employed by dyslexics.

17:30 ***165***. **Measuring Language Laterality Using Functional Connectivity**

Anthony B. Waites[1, 2], Peter Mannfolk[1], Johan Olsrud[1], Marnie E. Shaw[3], David F. Abbott[2], Graeme D. Jackson[2]
[1]Lund University Hospital, Lund, Sweden; [2]Brain Research Institute, Melbourne, Australia; [3]Flinders University, Adelaide, Australia

Determination of language laterality index (LI) helps preserve function following neurosurgery. However, some subjects show little activation, or have difficulty performing the task. The purpose of the present study was to measure LI with functional connectivity, without using a language task. Twelve healthy subjects performed a verbal fluency task, together with a period of continuous rest. LI based only on resting data correlated with the conventional activation LI, and it was possible to threshold to distinguish typical from atypical LI with 100% concordance. This approach enables LI measurement in subjects of any age, and with decreased cognitive ability.

17:42 ***166***. **Why Does Language Laterality Index Vary?**

Anthony B. Waites[1], Peter Mannfolk[1], Johan Olsrud[1], David F. Abbott[2], Graeme D. Jackson[2]
[1]Lund University Hospital, Lund, Sweden; [2]Brain Research Institute, Melbourne, Australia

Measurement of language lateralisation is of great benefit for surgical planning. fMRI measures of laterality index (LI) are not totally concordant with Wada test, and show variability with analysis method. This study investigates the extent to which this variability depends on methodological issues, versus variability in the underlying cognitive networks. Twelve subjects performed a language fMRI study, and LI was calculated in a number of ways. Further, simulated data was investigated. LI was found to vary as a function of threshold in individual subjects, and this variation was subject-specific, making a single threshold inappropriate.

17:54 ***167***. **Using CASL Perfusion fMRI to Image Natural Vision**

Hengyi Rao[1, 2], Jiongjiong Wang[1], Kathy Tang[1], Wei Pan[2], John A. Detre[1]
[1]University of Pennsylvania, Philadelphia, Pennsylvania, USA; [2]Sun Yat-Sen University, Guangzhou, People's Republic of China

Due to its noninvasive CBF quantification and long-term temporal stability, ASL perfusion fMRI provides an appealing approach for imaging brain activity during natural conditions. The present study used ASL perfusion fMRI to image brain activity when subjects were freely viewing a cartoon movie. The results revealed significant CBF increases in multiple visual pathway and frontal areas. The concurrent CBF and BOLD activities in MT showed significant associations with subjects' motion perception. These results suggest the feasibility of ASL perfusion fMRI for imaging brain activity during natural vision and support the maintained functional segregation and specialization during complex natural vision.

18:06 ***168***. **Multiple Spotlights of Visual Attention?**

Carmen Morawetz[1], Petra Holz[1], Jürgen Baudewig[1], Stefan Treue[2], Peter Dechent[1]
[1]MR-Research in Neurology and Psychiatry, Medical Faculty, Georg-August University, Goettingen, Germany; [2]Cognitive Neuroscience Laboratory, German Primate Center, Goettingen, Germany

Different models have been proposed to account for the distribution of attentional resources in visual space: "zoom lens", "single spotlight", and "multiple spotlights" theory. The present study aimed at the verification of previous reported findings that the attentional spotlight can be split among multiple, spatially separated locations. Subjects had to deploy their attention either to a single peripheral location or two non-contiguous regions performing a match/mismatch judgement. Contrasting the two attentional tasks in all subjects increased activation was observed in the defined ROIs, intervening (fovea) and task-irrelevant regions. Our findings support the classical view of a single spotlight of attention.

18:18 ***169***. **Utilization of Binocular Inhibitory Interaction for Reliable fMRI Mapping of Human Ocular Dominance Columns**

Nanyin Zhang[1], Xiao-Hong Zhu[1], Essa Yacoub[1], Kamil Ugurbil[1], Wei Chen[1]
[1]University of Minnesota, Minneapolis, Minnesota, USA

A fMRI approach based on the binocular inhibition between the left-eye and right-eye ocular dominance columns (ODCs) is introduced for spatially differentiating and mapping ODCs in human brain. This approach does not require the image subtraction so that is insensitive the degree of symmetry of the BOLD activities from the neighboring ODCs. The reliability of maps generated with the proposed approach can be examined from multiple aspects: human ODC morphology, difference between high-resolution and low-resolution maps, mapping reproducibility and mapping reversibility. The results validated the proposed approach which should provide reliability and accuracy for spatially mapping the functional column structures in human brain.

Prostate Cancer

Room 618 - 620 16:30 - 18:30 Chairs: Jelle O. Barentsz and Robert V. Mulkern

16:30 ***170***. **A Comparison of Image Quality and Prostate Cancer Localization and Staging Performance Between Body Array Coil and Endorectal Coil MR Imaging at 3T**

Stijn W. Heijmink[1], Jurgen J. Fütterer[1], Satoru Takahashi[1], Tom W. Scheenen[1], Christina A. Hulsbergen-v.d. Kaa[1], J. Alfred Witjes[1], Jelle O. Barentsz[1]

[1]Radboud University Nijmegen Medical Center, Nijmegen, Gelderland, Netherlands

When going from 1.5T to 3T it is unclear whether the endorectal coil (ERC) is still necessary for localizing and staging prostate cancer. Therefore, this study compared the image quality, localization and staging accuracies of prostate cancer at 3T between body array coil (BAC) and ERC MR imaging. Significantly more motion artifacts were present at ERC imaging compared with BAC imaging. All other image quality characteristics improved significantly with ERC imaging. Although image quality improved, localization performance was equal for BAC and ERC imaging. For staging, however, the ERC was necessary to achieve high sensitivity in detecting locally advanced disease.

16:42 ***171***. **Dynamic Contrast-Enhanced Analysis of the Prostate at 3T with a Body Array Coil is Feasible and Increases Prostate Cancer Localization Performance**

Stijn W. Heijmink[1], Jurgen J. Fütterer[1], Pieter C, Vos[1], Tom W. Scheenen[1], Henkjan J. Huisman[1], Christina A. Hulsbergen-v.d. Kaa[1], J. Alfred Witjes[1], Jelle O. Barentsz[1]

[1]Radboud University Nijmegen Medical Center, Nijmegen, Gelderland, Netherlands

T2-weighted and dynamic-contrast enhanced (DCE) MR imaging with a body array coil at 3T was performed in 17 consecutive patients with biopsy-proven prostate cancer. Two radiologists scored the presence of cancer in a 16-segment model on a five-point probability scale. Whole-mount section histopathology was the standard of reference. Dynamic contrast-enhanced MR imaging with a body array coil was feasible and by combining the DCE parameters the localization performance increased significantly compared with T2-weighted imaging.

16:54 ***172***. **3T MR of the Prostate: Reducing Susceptibility Gradients by Inflating the Endo-Rectal Coil with a Barium Suspension**

Yael Rosen[1], B Nicolas Bloch[1], Robert E. Lenkinski[1], Robert L. Greenman[1], Robert P. Marquis[1], Neil M. Rofsky[1]

[1]Beth Israel Deaconess Medical Center, Boston, Massachusetts, USA

Most prostate MRS/MRI studies are performed with an endo-rectal coil inflated with air, which induces susceptibility gradients within the gland. Using perfluorocarbon instead of air has been previously shown to improve spectral resolution. We assessed the suitability of a barium suspension by determining field maps in normal volunteers when the endo-rectal coil was inflated with air, perfluorocarbon and barium successively. The barium suspension, as well as the perfluorocarbon, provided a significantly better field homogeneity than air. Further studies are underway to compare the benefits of using barium suspensions or perfluorocarbon on *in vivo* 3D-CSI spectra of the prostate at 3T.

17:06 ***173***. **MR Spectroscopic Imaging as a Tool for Guiding Prostatic Biopsy in Patients with Prior Negative Biopsy**

Claudia Testa[1], Riccardo Schiavina[1], Raffaele Lodi[1], Eugenio Salizzoni[1], Barbara Corti[1], Caterina Tonon[1], Manuela Coe[1], Walter F. Grigioni[1], Antonia D'Errico[1], Giuseppe Martorana[1], Romeo Canini[1], Bruno Barbiroli[1]

[1]Università di Bologna, Bologna, Italy

The benefit of a “voxel”-guided biopsy on the basis of 3D-MRSI results was evaluated in patients with high risk of prostate cancer. MRSI-biopsy detection rate was 40% and 45% on a patients by patiens and a core by core analysis in the peripheral zone respectively. The good diagnostic accuracy (72%) and negative predictive value (100%) show that prostate cancer detection can be improved by TRUS-biopsy and hopefully cores number at successive biopsies can be reduced. A stringent criterion to classify transitional zone voxels as malignant suggest that "voxel-guided" TRUS-biopsy can be extended to the transitional zone with good accuracy.

17:18 ***174***. **Exclusion of False Positive Identification of Prostate Cancer Using Diffusion Anisotropy**

Junqian G. Xu[1], Peter A. Humphrey[1], Adam S. Kibel[1], Vamsidhar R. Narra[1], Sheng-Kwei Song[1]

[1]Washington University in St. Louis, St. Louis, Missouri, USA

To examine the potential utility of diffusion anisotropy in prostate cancer patient management, thirteen patients scheduled for radical prostatectomy surgery were examined by diffusion tensor imaging (DTI) *in vivo*. After surgery, prostate specimens were examined *via ex vivo* DTI, and by histology after formalin fixation. Corresponding MRI and histology findings confirm that elevated diffusion anisotropy in the central gland can facilitate differentiating benign prostatic hyperplasia from prostate cancer.

17:30 ***175***. **Specific MRI Detection of PSMA-Expressing Prostate Cancer Uisng 3C6 MAb-Conjugated SPIONs**

Laurel O. Sillerud[1], Natalie L. Adolphi[2], Rita Serda[1], Marco Bisoffi[1], Ming Ji[1]
[1]University of New Mexico, Albuquerque, New Mexico, USA; [2]New Mexico Resonance, Albuquerque, New Mexico, USA

We demonstrate a new contrast agent, synthesized from commercial streptavidin superparamagnetic iron oxide nanoparticles (SPIONs) conjugated to 3C6 antibodies, which selectively enhances the T1 contrast of human prostate cancer cells that overexpress prostate specific membrane antigen (PSMA).

17:42 ***176***. **A Clinical Comparison of Rigid and Inflatable Endorectal Coil Probes for MRI and 3D MRSI of the Prostate**

Susan Moyher Noworolski[1], Jason C. Crane[1], Daniel B. Vigneron[1], John Kurhanewicz[1]
[1]UCSF, San Francisco, California, USA

Endorectal probes can provide improved signal to noise (S/N) over a pelvic phased array, but may produce image artifacts. Four probe setups were evaluated for image motion artifacts and spectral quality: two rigid coils and an inflatable probe filled with either air or fluid. The probes have different tradeoffs. The rigid probes provided higher S/N (260% and 240% increase), but suffered more motion artifacts versus the inflatable probes. The fluid-inflated probes produced excellent quality images and spectra and had the shortest time to manually shim, but do distort the prostate. Rigid probes may be preferred for particular applications.

17:54 ***177***. **Assessment of Pharmacokinetic Parameters by Different Models in Dynamic Contrast-Enhanced MRI of Prostate**

Guang Jia[1], Johannes T. Heverhagen[1], Jiachao Liang[1], Klaus T. Baudendistel[1], Andrea L. Levine[1], Thomas J. Rosol[1], Michael V. Knopp[1]
[1]The Ohio State University, Columbus, Ohio, USA

Quantitative analysis of DCE-MRI data needs pharmacokinetic models with well mixture compartments. Different pharmacokinetic models were used for analyzing DCE-MRI data and the generated pharmacokinetic parameters were used to characterize the microcirculation in the prostate. In order to select the most appropriate pharmacokinetic model to characterize the time-signal intensity curves in prostate, this study systematically compared four available pharmacokinetic models on fitting different regions in beagle prostate by investigating the goodness-of-fit and reproducibility of the models.

18:06 ***178***. **Quantitative Analysis of Benign Prostate Hyperplasia with Apparent Diffusion Coefficient**

Feiyu Li[1], Xiaoying Wang[1], Yufeng Xu[1], Jiangxi Xiao[1], Xuexiang Jiang[1]
[1]Peking University First Hospital, Beijing, People's Republic of China

BPH was probably the most frequent lesion in senior and it may be misdiagnosed as prostate cancer on T2W image and MRS. It remained unclear about the impact of BPH on the ADC value. The purpose of our study is to quantitatively analyze the ADC values of different types of BPH, and to compare them with ADC values of Pca. Seventeen BPH patients and fifteen Pca patients were divided into three groups: glandular BPH, stromal BPH and Pca. The ADC values of gBPH, sBPH and Pca were measured. Statistically significant difference could be detected among them.

18:18 ***179***. **Dynamic Contrast-Enhanced Magnetic Resonance Imaging as a Biologic Marker to Non-Invasively Assess the Effect of Finasteride on Prostatic Suburethral Microcirculation**

Guang Jia[1], Johannes T. Heverhagen[1], Hans Polzer[1], Richard V. Jacko[1], Jiachao Liang[1], Jun Zhang[1], Andrea L. Levine[1], Thomas J. Rosol[1], Michael V. Knopp[1]
[1]The Ohio State University, Columbus, Ohio, USA

The important questions to be addressed about finasteride treatment include, what is the optimum dose and how long should the patients be treated. An effective non-invasive tool may be helpful to solve these questions by monitoring the changes in prostatic microcirculation. In this study we investigated dynamic contrast-enhanced magnetic resonance imaging (DCE-MRI) of the prostate and assessed the potential of the pharmacokinetic parameters as biomarkers to evaluate microvascular changes in the prostatic suburethral tissue in an experimental dog prostate model.

Novel Nanoparticle Contrast Agents

Room 602 - 604 16:30 - 18:30 Chairs: Jeff W. M. Bulte and Klaas Nicolay

16:30 ***180***. **Novel MRI Reporter Gene for Determination of Cell Viability**

Phillip C. Yang[1], Manickam Krishnan[1], Sally Zhang[1], Takayasu Arai[1], Thomas Quertermous[1], Irving Weissman[1], Joe Wu[1], Micha Drukker[1], Robert Robbins[1]
[1]Stanford University, Stanford, California, USA

A novel MRI reporter gene driven by constitutively expressed CMV/ubiquitin promoter has been targeted to specific recombinant fusion gene designed to express antigenic epitopes on the surface of mouse embryonic stem cells (mESC). Employing commercially available SPIO-tagged monoclonal antibodies (SPIO-MAb) specific to these surface epitopes, viable mESC transfected with a reporter gene will generate MRI signal from SPIO-Mab linked to the epitopes. In vitro proof-of-concept was performed to demonstrate generation of MR signal from the molecular marker of mESC viability.

16:42 ***181***. **Microarray Analysis of the Effect of Feridex-Labeling on Gene Expression in Neural Stem Cells**

Piotr Walczak[1], Assaf A. Gilad[1], Dorota A. Kedziorek[1], Jesus Ruiz-Cabello[1], Bradley Barnett[1], Jeff W. Bulte[1]
[1]Johns Hopkins University, Baltimore, Maryland, USA

MRI cell tracking using Feridex has found many biological applications and has recently entered the clinic. However, little is known about potential down- or upregulation of gene expression following labeling. As iron catalyzes many biological reactions, robust safety data will be required by regulatory agencies before widespread clinical implementation. We have performed microarray analysis of over 40,000 genes in Feridex-labeled neural stem cells. Surprisingly, we detected a significant change in gene expression for more than 400 genes, with maximal changes at 1-2 days following labeling. These results may have implications for FDA-approval of SPIO-based cell tracking.

16:54 ***182***. **Imaging of Islet Transplantation in a Pre-Clinical Animal Model Using an FDA-Approved Contrast Agent: *In Vivo* Studies**

Natalia Evgenov[1], Zdravka Medarova[1], Pamela Pantazopoulos[1], Simone Leyting[1], Guangping Dai[1], Anna Moore[1]
[1]Massachusetts General Hospital, Charlestown, Massachusetts, USA

Islet transplantation is an effective therapy for patients with Type 1 diabetes mellitus. It is critical to develop reliable non-invasive imaging techniques that can determine graft location and survival after transplantation. We used the FDA-approved commercially available contrast agent FERIDEX, to label human pancreatic islets for *in vivo* detection by MR imaging in a clinically relevant animal model of islet transplantation. The results of our study demonstrated a direct correlation between the apparent decrease in the number of intrahepatically transplanted islets on MR images and the rate of apoptosis observed by histological methods.

17:06 ***183***. **Multimodality Molecular Imaging of Tumor Angiogenesis Using Quantum Dots**

Willem J.M. Mulder[1], Gustav J. Strijkers[1], Celso de Mello Donegá[2], Ricardo J. Brandwijk[3], Patrick T.K. Chin[1], Rolf Koole[2], Karolien Castermans[3], Gert Storm[2], Arjan W. Griffioen[3], Klaas Nicolay[1]
[1]Eindhoven University of Technology, Eindhoven, Netherlands; [2]Utrecht University, Utrecht, Netherlands; [3]Maastricht University, Maastricht, Netherlands

We developed quantum dots with a pegylated and paramagnetic coating (pQDs) to make them detectable by both MR and optical imaging. The pQDs were made specific for angiogenic blood vessels by conjugating them with multiple RGD-peptides. The specificity of this novel contrast agent was verified in vitro. Upon intravenous administration of RGD-pQDs in tumor bearing mice intravital microscopy and MRI was performed, which allowed the multimodality visualization of activated tumor endothelium.

17:18 ***184***. **Differentiation of Glioma from Radiation Necrosis by MRI Using Magnetically Labeled Cells**

Ali Syed Arbab[1], Ali M. Rad[1], ASM Iskander[1], Steve L. Brwon[1], Swayamprava Panda[1], Karyn A. Ledbetter[1], Guangliang Ding[1], James R. Ewing[1], Hamid Soltanian-Zadeh[1], Donald J. Peck[1]
[1]Henry Ford Health System, Detroit, Michigan, USA

Angiogenesis in glioma are typically permeable to contrast agents, and can thus be detected by contrast-enhanced MRI or CT. However, areas of radiation necrosis can also show enhancement due to active inflammatory reactions and increasing vascular permeability. One distinguishing characteristic, however, is that there is little active angiogenesis at the site of radiation necrosis. Moreover, there is no proof that radiation necrosis can initiate immunogenic reaction. Based on the vascularity and immunogenic reaction, glioma could be differentiated from radiation necrosis by MRI using magnetically labeled endothelial progenitor cells and sensitized T-cell.

17:30 ***185***. **Fluorine MR Angiography with Intravenously Delivered Nanoparticle Emulsions at 1.5 T**

Anne Morawski Neubauer[1], Shelton D. Caruthers[1, 2], Todd D. Williams[1], Frank D. Hockett[1], Tillman Cyrus[1], John S. Allen[1], Gregory M. Lanza[1], Samuel A. Wickline[1]
[1]Washington University, St. Louis, Missouri, USA; [2]Philips Medical Systems, Best, Netherlands

Fluorine magnetic resonance imaging, with its lack of competing background signal, has been used for a variety of applications including mapping oxygen tension, studying tumor metabolism, and imaging of vasculature and organ perfusion (1,2,3). In this work, we sought to characterize the use of a systemically-injected perfluoro-15-crown-5-ether fluorinated nanoparticle contrast agent for MR angiography at the clinical field strength 1.5 T.

17:42 ***186***. **Assessing Early Effects of Angiogenesis Inhibitors Using MR Molecular Imaging**

Willem J.M. Mulder[1], Gustav J. Strijkers[1], Daisy W.J. van der Schaft[2], Gert Storm[3], Kevin H. Mayo[4], Arjan W. Griffioen[2], Klaas Nicolay[1]
[1]Eindhoven University of Technology, Eindhoven, Netherlands; [2]Maastricht University, Maastricht, Netherlands; [3]Utrecht University, Utrecht, Netherlands; [4]University of Minnesota, Minneapolis, Minnesota, USA

In this study we assessed the early effects of anti-angiogenesis therapies with MR molecular imaging, using paramagnetic and fluorescent RGD-conjugated liposomes. Tumor bearing mice were treated with either Endostatin or Anginex. Mice that were not treated served as a control group. After 3 days of treatment mice were imaged using T1-weighted MRI before and after injecting the contrast agent. The percentages of voxels within the tumors that showed contrast enhancement were compared between the 3 groups and revealed a significant decrease for the Endostatin treatment group as compared to the control group.

17:54 ***187***. **Labeling and Imaging Stem/Progenitor Cells with Multiple Unique Nanoparticulate Fluorine Markers: the Potential for Multispectral Stem Cell Detection with 19F MRI**

Junjie Chen[1], Kathy Crowder[1], Jason Brant[1], Anne M. Neubauer[1], Shelton D. Caruthers[2], Gregory M. Lanza[1], Samuel A. Wickline[1]

[1]Washington University, St. Louis, Missouri, USA; [2]Philips Medical System, St. Louis, Missouri, USA

We and others have shown previously that 19F MRI of liquid perfluorocarbon (PFC) nanoparticles may present a unique and sensitive cell label (fluorine) that cannot be obscured by traditional tissue background proton signal. In the present study, we aimed to explore the possibility of creating multiple unique and differentiable PFC labels for stem cells. Our results showed that perfluoro-15-crown-5 ether and perfluorooctylbromide nanoparticles could serve as simultaneous intracellular markers with the use of 19F MRS/MRI at 11.7T.

18:06 ***188***. **Gd@(Carbon Nanostructures) as High Relaxivity Nanoprobes Magnetic Resonance Imaging**

Balaji Sitaraman[1], Raja Muthupillai[2], LA Tran[1], RA Bolskar[1], Scott D. Flamm[3], AG Mikos[1], LJ Wilson[1]

[1]Rice University, Houston, Texas, USA; [2]Philips Medical Systems, and Baylor College of Medicine, Houston, Texas, USA; [3]St. Luke's Episcopal Hospital, Houston, Texas, USA

Carbon nanostructures containing paramagnetic gadolinium (Gd) exhibit unusually large proton relaxivities compared to commercially available Gd-based MR contrast agents used today. We report the results from our first MRI phantom studies on two such nano-probes, Gd@C60 metallofullerenes, and Gd@ultrashort tubes (nanotubes). Our results show that, even at modest concentrations of Gd, these nanoprobes show extremely large signal enhancements. The high proton relaxivity of these probes, coupled with their ability to translocate across cell membranes with minimal cytotoxicity may render them attractive candidates for cellular MRI.

18:18 ***189***. **Ultra-Short Echo Time Difference (USTED) Data Acquisition for T2* Contrast Reversal**

Fernando Emilio Boada[1], Erik Wiener[1]

[1]University of Pittsburgh, Pittsburgh, Pennsylvania, USA

MR cell tracking studies capitalize on the strong B0 inhomogeneity defect produced by small paramagnetic particles (SPA). Recent studies have demonstrated the sensitivity of such approaches for detecting cell migration during organ transplant and stem cell implantation (1). Although the contrast mechanism that SPA-based approaches rely on is very effective, the signal loss due to the large field inhomogeneity could sometimes limit the usefulness of the technique. In this work we present a theoretical and experimental demonstration of the use of dual-echo, ultra-short echo time difference (USTED) data acquisitions for improving the usefulness of T2*-weighted scans in cell tracking studies.

Interventional MRI: Thermal Therapy

Room 613 - 614 16:30 - 18:30 Chairs: Nathan J. McDannold and Sherif G. Nour

16:30 ***190***. ***In Vivo*** **Targeted Drug Delivery to the Brain Using MRI Guidance of Focused Ultrasound**

Lisa Hsu Treat[1, 2], Nathan McDannold[1], Natalia Vykhodtseva[1], Yongzhi Zhang[1], Karen Tam[1], Kullervo Hynynen[1]

[1]Harvard Medical School and Brigham & Women's Hospital, Boston, Massachusetts, USA; [2]Harvard-MIT Division of Health Sciences and Technology, Cambridge, Massachusetts, USA

We investigated the effect of focused ultrasound on the absorption of liposome-encapsulated doxorubicin in the rodent brain and the use of MRI as an indicator of blood-brain barrier permeability. By applying focused ultrasound in the presence of microbubbles, we achieved targeted drug delivery to the brain *in vivo*. Tissue drug concentrations in sonicated brain were significantly different from unexposed control samples ($p = 0.01$) and corresponded with cytotoxic levels measured in various human tumors. Increased MR signal enhancement at the focal location on contrast-enhanced T1w FSE images correlated with increased penetration of doxorubicin into brain tissue ($r = 0.85$).

16:42 ***191***. **Simultaneous MR Temperature Imaging and Radiofrequency Ablation of Human Liver Tumor: A Preliminary Study**

Matthieu Lepetit-Coiffe[1], Olivier Seror[1], Bruno Quesson[1], Hervé Laumonier[2], Sébastien d'Attoma[3], Chrit Moonen[1], Hervé Trillaud[1, 2]

[1]CNRS/University Bordeaux 2, Bordeaux, France; [2]Service de Radiologie, Bordeaux, France; [3]Tyco Healthcare, Plaisir, France

Radiofrequency (RF) thermo ablation is a mini invasive technique used for tumor ablation, but combination with quantitative MR thermometry is challenging due to artifacts induced by RF generators. In this preliminar study, a MR compatible RF device was used to perform local monopolar RF ablation on 6 human hepatic tumors *in vivo*. Temperature uncertainty remained under 2 Cand thermal dose maps calculated from real-time quantitative temperature images were found to be in good agreement with local contrasts changes observed on T1-(post gadolinium injection)and T2-weighted images obtained just after ablation. No local or distant recurrence was observed after 12months of follow up.

16:54 ***192***. **Is the Thermal Dose a Reliable and Precise Indicator of Tissue Ablation? a Pig Liver Radiofrequency Thermo-Ablation Under Quantitative MR-Temperature Mapping**

Olivier Seror[1], Matthieu Lepetit-Coiffé[1], Hervé Trillaud[2], Brigitte LeBail[3], Chrit Moonen[1], Bruno Quesson[1]

[1]Laboratire d'Imagerie Moléculaire et Fonctionnelle, Bordeaux, France; [2]CHU Saint André, Bordeaux, France; [3]Laboratoire d'Anatomie Pathologique - C.H.U Pellegrin, Bordeaux, France

Quantitative temperature mapping, associated with continous cumulative thermal dose (TD) assessment, has been suggested for guidance of RF ablation. This study on large animals demonstrates that high quality temperature maps can be obtained on pig liver *in vivo* on a clinical scanner simultaneously with RF ablation, using appropriate filtering. Apparent lesion dimensions measured on TD maps correlated with histologically determined lesions.

17:06 ***193***. **Magnetic Resonance Guided Focused Ultrasound Surgery (MRgFUS) with Interleaved Technique: Initial Experience for a More Rapid Treatment of Uterine Fibroids**

George Alan Holland[1], Arik Hananel, MD[2], Mary H. Briggs[1], Alison B. Dick[1], Raffaele Bruno[1]

[1]Lahey Clinic, Burlington, Massachusetts, USA; [2]InSightec, Tirat Carmel, Israel

The purpose of this study was to evaluate a more rapid MRgFUS technique using a manual interleaved MRgFUS (iMRgFUS) treatment of uterine fibroids. Methods: 33 iMRgFUS treatments were performed in 23/28 women. Treatments were manually divided into non-overlapping regions. The cooling time was decreased from 90 to 45 secondsResults: iMRgFUS permitted up to 127 versus 60 sonications in a 3-hour treatment resulting in treatments in 60% of the time. There were no serious adverse events with the iMRgFUS. 13/15 had marked relief and none of the patients have had alternative treatments.Discussion: iMRgFUS is a safe method for rapid treatment of fibroids.

17:18 ***194***. **Correlation of T1-Weighted and Diffusion-Weighted Imaging After MR-Guided High Intensity Focused Ultrasound Treatment**

Michael A. Jacobs[1],David H. Gultekin[1], Hyun S. Kim[1]

[1]Johns Hopkins School of Medicine, Baltimore, Maryland, USA

We have demonstrated that the area defined by DWI and cT1WI are highly correlated after treatment of uterine fibroids by MRg-FUS. The experimental data indicate that the combination of DWI and cT1WI can effectively be used in the assessment of the treatment of uterine fibroids by MRg-FUS ablation and the areas are highly matched.

17:30 ***195***. **Transurethral Multi-Sectored Ultrasound Applicators for Conformal Thermal Therapy of the Prostate with MR Temperature Monitoring**

Adam M. Kinsey[1, 2], Chris J. Diederich[1, 2], William H. Nau[1], Kim Butts Pauly[3], Viola Rieke[3], Graham Sommer[3]

[1]University of California, San Francisco, San Francisco, California, USA; [2]University of California, Berkeley and San Francisco, San Francisco, California, USA; [3]Stanford University, Stanford, California, USA

Transurethral ultrasound applicators with multiple sectors on a tubular transducer were developed for BPH and prostate cancer treatment. The devices conformed a thermal dose to a target area in the angular, axial, and radial dimensions. Evaluations of device heating patterns and characteristics were conducted in a 0.5T interventional scanner in three canine prostates. The multi-sectored ultrasound applicators developed in this study created large thermal lesions (>15mm in diameter) in relatively short treatment times (~10min). With real-time MR temperature imaging feedback, the devices were able deliver a targeted without requiring any applicator movement or manipulation during treatment.

17:42 ***196***. **Investigation of DWI to Evaluate Prostate Thermal and Cryo Lesions**

Jing Chen[1], Bruce L. Daniel[1], Donna M. Bouley[1], Graham Sommer[1], Kim Butts Pauly[1]

[1]Stanford University, Stanford, California, USA

Fast, accurate and repeatable lesion evaluation is desirable for MRI-guided prostate therapies. In this work we investigate the use of diffusion weighted imaging (DWI) to estimate the cell viability immediately after the treatments. Line scan diffusion imaging is performed on six canine prostates with MRI-guided high intensity ultrasound thermal therapy or cryoablation. Significant ADC value reduction is observed in the thermal/cryo lesions. The necrotic tissue has an ADC trace value of approximately 0.001 mm^2/second. Evident correlation between DWI and histology result is presented.

17:54 ***197***. **Acute Histopathological Changes in Canine Prostates Treated with High Intensity Ultrasound or Cryosurgery: Correlation with Contrast Enhanced MR Images**

Donna Michelle Bouley[1], Bruce Daniel[1], Kim Butts Pauly[1], Erin Liu[1], Chris Diederich[2], Will Nau[2], Graham Sommer[1]

[1]Stanford University, Stanford, California, USA; [2]UCSF, San Francisco, California, USA

The clinician's ability to monitor and accurately predict the extent of targeted tissue damage that results from minimally invasive cancer therapies is paramount for the successful outcome of the therapy and the safety of the patient. In this study, the histopathological lesions created by high intensity ultrasound and cryosurgery are evaluated in a canine prostate model. Gross and microscopic lesions are compared with contrast enhanced MR images in order to provide the clinician with valuable information that should aid in real time monitoring of lesion induction and extent of tissue damage with MRI.

18:06 ***198***. **Optimization of the Self-Reference Thermometry Using Isolated Regions for Complex Signal Estimation**

Daisuke Kokuryo[1], Kagayaki Kuroda[2, 3], Etsuko Kumamoto[4, 5], Bilgin Keserci[6], Atsuya Okada[7], Toshiya Kaihara[5], Susumu Fujii[5]

[1]Graduate School of Science and Technology, Kobe University, Kobe, Hyogo, Japan; [2]Graduate School of Information Science and Technology, Tokai University, Hiratsuka, Kanagawa, Japan; [3]Institute of Biomedical Research and Innovation, Kobe, Hyogo, Japan; [4]Information Science and Technology Center, Kobe University, Kobe, Hyogo, Japan; [5]Faculty of Engineering, Kobe University, Kobe, Hyogo, Japan; [6]MR Imaging Application Tech Center, GE Yokogawa Medical Systems Ltd, Hino, Tokyo, Japan; [7]Iseikai Hospital, Osaka, Japan

In the "referenceless", or self-reference thermometry technique, temperature estimation errors could be increased when thermal changes, or spatial irregularities, in the complex signals were included in the region for estimation (RFE), which was placed to surround the region of interest (ROI) covering the spot of heating. To solve this problem, size, shape and placement of RFE('s) were devised to serve better temperature monitoring capability for focused ultrasound surgery of uterine fibroids. Errors in temperature estimation with a single, "doughnut-like" RFE located on the tissue boundary were significantly reduced by using multiple, spatially-isolated RFE's allocated to avoid the tissue boundary.

18:18 ***199***. **Referenceless PRF Thermometry with Multi-Echo Processing**

Viola Rieke[1], Adam M. Kinsey[2], William H. Nau[2], Chris J. Diederich[2], Graham Sommer[1], Kim Butts Pauly[1]

[1]Stanford University, Stanford, California, USA; [2]University of California, San Francisco, San Francisco, California, USA

Referenceless proton resonance frequency (PRF) shift thermometry is a motion insensitive method to monitor thermal ablation. A new three echo pulse sequence is proposed with varying k-space coverage for each echo in order to allow reconstruction of both a low resolution temperature image and a high resolution anatomical image, without a decrease in temporal resolution. The method is demonstrated in phantoms and during *in vivo* canine prostate ablation.

STUDY GROUP
Diffusion & Perfusion

Room 6D 18:30 - 20:30

18:30 **Business Meeting**
19:00 **Scientific Meeting: "Can Diffusion MR Measure Anything?"**
- 19:00 **Yes, but Caveat Emptor**
  Joseph J. H. Ackerman, William Greenleaf Eliot Professor and Chair, Department of Chemistry, Washington University, St. Louis, Missouri, USA
- 19:30 **Confusion with Diffusion; an Illusion?**
  Stephen J. Blackband, Associate Professor, Evelyn F. & William L. McKnight Brain Institute, University of Florida, Gainesville, Florida, USA

20:00 **Panel Discussion**

STUDY GROUP
Cardiac MR

Room 4C-3,4 18:30 - 20:30

18:30 **Business Meeting**
18:45 **Scientific Meeting: "Emerging Applications and Technology in Cardiovascular MR"**
- 19:05 **Interventional Cardiovascular MRI**
  Jeffrey L. Duerk, Case Western Reserve University, Cleveland, Ohio, USA
- 18:45 **Transmit SENSE for High-Field Cardiovascular MR**
  Peter Boernert, Philips Research, Hamburg, Germany
- 19:25 **Ultimate Limits of Parallel Cardiovascular MRI**
  Florian Wiesinger, GE Global Research, Munich, Germany
- 19:45 **High Resolution MRI Cardiac Strain Mapping**
  Nael Osman, Johns Hopkins University, Baltimore, Maryland, USA
- 20:00 **Panel Discussion**

STUDY GROUP
MR Safety

Room 611-612 18:30 - 20:30

18:30 **Business Meeting**
- 18:30 **Welcome Statement and Announcement of Group Formation: Opening session, with brief presentation on major areas of MR safety that needs focus for more research**
  Alayar Kangarlu, Columbia University, New York, New York, USA
- 18:40 **History of Study Group: Brief history of formation of the group and statistics of its membership population**
  J. Daniel Schaefer, GE Healthcare, Milwaukee, Wisconsin, USA

18:50 **Scientific Meeting**
- 18:50 **MR Safety Issues: Considerations at High Fields**
  Alayar Kangarlu, Columbia University, New York, New York, USA
- 19:10 **RF Power Deposition, General Considerations and Implications of Implants/Devices**
  Tamer S. Ibrahim, University of Pittsburgh, Pittsburgh, Pennsylvania, USA
- 19:30 **Gradient Safety at High Field**
  John A. Nyenhuis, Purdue University, West Lafayette, Indiana, USA
- 19:50 **MRI Safety for Implants and Devices: Update 2006**
  Frank G. Shellock, University of Southern California and Institute for Magnetic Resonance Safety, Education and Research, Los Angeles, California, USA
- 20:10 **Round Table Discussion by Presenters, with further discussion of the role of the MR of Safety Study Group and invitation and instruction for membership, inviting suggestion for mid-year meeting**

STUDY GROUP
Current Issues in Brain Function

Room 615-617 18:30 - 20:30

18:30 **Business Meeting**

18:50 **Scientific Meeting: "Other Measures of Brain Function: Metabolic Markers and Contrast Mechanisms"**
- 18:50 ***In Vivo* Multinuclear MRS for Studying Brain Bioenergetics and Function**
  Wei Chen, University of Minnesota, Minneapolis, Minnesota, USA
- 19:10 **Temperature Mapping in fMRI**
  Robert E. Lenkinski, Harvard Medical School, Boston, Massachusetts, USA
- 19:30 **17O T1p Imaging**
  Ravinder Reddy, University of Pennsylvania, Philadelphia, Pennsylvania, USA
- 19:50 **Intermolecular Double Quantum Coherence**
  Jianhui Zhong, University of Rochester, Rochester, New York, USA
- 20:10 **Discussion**

STUDY GROUP
Dynamic NMR Spectroscopy

Room 618-620 18:30 - 20:30

18:30 **Business Meeting**

18:45 **Scientific Meeting**
- 18:45 ***In Vivo* 13C NMR Spectroscopy at 9.4 Tesla: From Animal to Human**
  Pierre-Gilles Henry, Center for Magnetic Resonance Research, Department of Radiology, Minneapolis, Minnesota, USA
- 19:25 **Dynamic 13C MRS in Human Brain Disease**
  Stefan Blüml, Childrens Hospital Los Angeles, Department of Radiology, Los Angeles, California, USA
- 20:05 **Panel Discussion**

STUDY GROUP
Musculoskeletal MR

Room 602-604 18:30 - 20:30

18:30 **Scientific Meeting**
- 18:30 **The Development of Specialized Coils for Musculoskeletal Imaging**
  Edmund Kwok,University of Rochester, Rochester, New York, USA
- 19:00 **Ultrashort TE Imaging of the Musculoskeletal System**
  Graeme Bydder, University of California, San Diego, La Jolla, California, USA
- 19:30 **Fat Suppression Techniques for Musculoskeletal Imaging**
  Scott Reeder, University of Wisconsin, Madison, Wisconsin, USA

20:00 **Business Meeting**

STUDY GROUP
Hyperpolarized Media MR

Room 613-614 18:30 - 20:30

18:30 **Business Meeting**
18:45 **Scientific Meeting: "Methods and Applications of Hyperpolarized Spins"**
- 18:45 **Recent Advances in Noble Gas Spin-Exchange Optical Pumping**
  Stephen Kadlecek, Department of Radiology, University of Pennsylvania, Philadelphia, Pennsylvania, USA
- 19:15 **Pharmaceutical Perspective on Development and Value of MR Imaging of Hyperpolarized Gases**
  Barry T. Peterson, Director of Global Clinical Technology, Pfizer, Global Research and Development, Groton, Connecticut, USA
- 19:45 **Hyperpolarized Spins Beyond the Noble Gases**
  Joachim Bargon, Institute of Theoretical and Physical Chemistry, University of Bonn, Bonn, Germany
- 20:15 **Panel Discussion**

MORNING CATEGORICAL COURSE
Technical Advances in Body MR

Room 618-620 7:00 – 8:00 Chairs: Neil M. Rofsky, Daniel K. Sodickson, and Bachir Taouli

Educational Objectives:
Upon completion of this session, participants should be able to:

- Evaluate important developments in MRI technology, including high field imaging and parallel imaging;
- Identify the technical challenges associated with effective application of this technology for body imaging; and
- Describe the potential applications of new technologies in body imaging, including areas such as diffusion and perfusion MRI, and MR spectroscopy.

Advances in High Field Imaging

07:00 **High Field Imaging: A Technical Perspective**
Douglas A. C. Kelley

07:30 **High Field Body Imaging: A Clinical Perspective**
Robert R. Edelman

MORNING CATEGORICAL COURSE
Cardiovascular Imaging

Room 6D 7:00 – 8:00 Chairs: Qun Chen and James F.M. Meaney

Educational Objectives:
Upon completion of this session, participants should be able to:

- Implement a robust protocol for clinical evaluation of arteries with both non-contrast and contrast-enhanced techniques;

- Identify the strengths and weaknesses of 3T MRI vs. 1.5T MRI for cardiovascular assessment;
- Recognize the value of parallel imaging for cardiovascular assessment at higher magnetic field (>1.5T);
- Select a comprehensive time-efficient protocol incorporating anatomical and functional cardiac evaluation;
- Explain the value of MRI for the assessment of non-coronary artery disease; and
- Recognize the strengths and also the limitations of current techniques.

MR Angiography

07:00 **Body and Peripheral MRA**
Thomas M. Grist

07:20 **Non-Contrast MRA**
Mitsue Miyazaki

07:40 **Coronary MRA**
René M. Botnar

MORNING CATEGORICAL COURSE
Clinical DTI/PWI/fMRI

Room 4C-3,4 7:00 – 8:00 Chairs: Alberto Bizzi and Soonmee Cha

Educational Objectives:
Upon completion of this session, participants should be able to:

- Describe the main applications and contributions of fMRI, DTI, and tractography and bolus tracking and arterial labeling perfusion MR imaging in clinical neuroscience;

- Describe the technical requirements necessary to implement robust, accurate, and repeatable clinical advanced MR studies in patients with neurological diseases;
- List the potential contribution of PWI, DTI and fMRI to formulate diagnosis, prognosis, and evaluate different therapeutic strategies in the neurological diseases focus of this course;
- Discuss the basic MR principles involved in the quantification of angiogenesis and permeability using perfusion MR imaging;
- Implement new quantitative MR methods that may quantify cumulative brain damage that better correlate with the disability score;
- Recognize challenges, limitations and pitfalls of performing advanced MR studies to answer clinical questions in neurological patients; and
- Implement Quality Assurance (QA) procedures necessary to run a reliable and successful advanced MRI clinic.

Angiogenesis and Permeability: Perfusion MRI

07:00 **What Can Quantitative DCE T1-Weighted MR Imaging Tell Us?**
Paul S. Tofts

07:30 **Grading, Therapy Monitoring, and Predicting Outcome of Glioma**
Soonmee Cha

MORNING CATEGORICAL COURSE
MR Hardware/Engineering

Room 611-612 7:00 – 8:00 Chairs: Steven M. Conolly and Steven M. Wright

Educational Objectives:
Upon completion of this session, participants should be able to:

- List and compare implementations of static field magnet designs for clinical MRI;

- Recognize that there are fundamental limits on our ability to shim out steep field variations (such as those in the sinuses);
- Describe advances in shim system design;
- Explain the differences between arrays designed to optimize SNR vs. those designed for partial parallel imaging;
- Compare and contrast arrays designed for transmit and receive applications;
- Describe algorithms for designing RF pulses for parallel imaging;
- Compare and contrast ESR and NMR; and
- Describe several applications of hyper-polarized 13C and explain methodological differences between conventional MRI and hyperpolarized MRI.

B_0/Shims

07:00 **B_0**
Johan A. Overweg

07:30 **Shims**
Peter Jezzard

MORNING CATEGORICAL COURSE
Human MRI and MRS at High Static Magnetic Fields: The Promise, the Challenges, the Solutions

Room 615-617 7:00 – 8:00 Chairs: Joseph A. Helpern and Dikoma C. Shungu

Educational Objectives:
Upon completion of this session, participants should be able to:

- Describe the general behavior of B_0 and B_1 fields in the human body when the Larmor frequency is of the order of or greater than 100 MHz;

- List the problems faced in trying to obtain a homogeneous B_0 field and a B_1 field;
- Recognize the challenges of developing RF coils for high field applications;

- Recognize the challenges of whole-body imaging at high fields and list potential solutions;
- List recent methodological advances for detecting neurotransmitters by MRS at high fields;
- Recognize the challenges of implementing heteronuclear spin-spin decoupling at high static fields;
- Describe the benefits of high field for BOLD contrast;
- Describe the interaction between high magnetic fields and biological systems; and
- List organizations responsible for regulating exposure to magnetic fields.

07:00 **Impediments to High Field MR – A Look at B_0 and B1 Field Behavior**
David I. Hoult

07:30 **How to do RF at High Fields**
J. Thomas Vaughan

MORNING CATEGORICAL COURSE
New Horizons in Musculoskeletal MRI

Room 613-614 7:00 – 8:00 Chairs: Joshua M. Farber and Timothy J. Mosher

Educational Objectives:
Upon completion of this session, participants should be able to:

- Recognize patterns of abnormal hip biomechanics and associated MRI findings in femoral acetabular impingement syndrome;
- Apply knowledge of normal articular cartilage maturation and joint development in interpretation of pediatric musculoskeletal MRI;
- Recognize the role of normal and abnormal biomechanics and the associated MRI findings in normal joint physiology and development of overuse injuries;
- Identify emerging translational research applications in the field of musculoskeletal MRI:
- Describe new MRI techniques for tracking mesenchymal stem cells;
- Recognize new applications of molecular imaging in the study of musculoskeletal diseases.

Femoral Acetabular Impingement: Concepts and Clinical Applications

The final five minutes of each presentation will be reserved for questions.

07:00 **Biomechanics of Femoral Acetabular Impingement**
Thaddeus Laird

07:30 **MR Imaging of Femoral Acetabular Impingement**
William E. Palmer

MORNING CATEGORICAL COURSE
Quantitative Neuro MRI

Room 602-604 7:00 – 8:00 Chairs: Fernando Calamante and Annemie Van der Linden

Educational Objectives:
Upon completion of this session, participants should be able to:

- Discuss the latest advances in the field of arterial spin labeling, their current limitations, and identify their potential role in basic and clinical science;
- Demonstrate the role of MR methods to assess oxygen consumption non-invasively, and illustrate potential applications;
- Describe the various approaches to measure the arterial input function using dynamic-susceptibility contrast MRI, and describe their limitations and implications to measure absolute cerebral blood flow,explain the latest advances of dynamic contrast-enhanced MRI to measure non-perfusion parameters, and assure proper formation of echoes.
- Recognize the limitations of the diffusion tensor model and identify more advanced methodologies to characterize areas with multiple fiber directions more accurately, as well as to describe the latest advances on fiber-tracking, including the concept of probabilistic tractography;

- Apply statistical approaches to perform voxel-based analysis for group comparison, and
- Describe image analysis techniques to characterize brain deformation.

Latest Advances in Arterial Spin Labeling and Oxygen Consumption Measurements

07:00 **Latest Advances in Arterial Spin Labeling**
Eric C. Wong

07:30 **Measuring Oxygen Consumption Using MRI: What Can and Cannot be Done**
Peter C. M. van Zijl

MORNING CATEGORICAL COURSE
Unsolved Problems and Unmet Needs in Magnetic Resonance

Room 6E 7:00 – 8:00 Chairs: Stuart Crozier and Michael B. Smith

Educational Objectives:
Upon completion of this session, participants should be able to:

- Identify and assess a sampling of key unsolved problems and unmet needs in the field of magnetic resonance;
- Establish criteria for successful solutions to such problems;
- Consider any large-scale coordination across our field or with other fields that may be called for to address some classes of research or clinical needs;
- Identify and share additional unsolved problems or unmet needs in your areas of interest.

What are we missing? Seeing through metal and devining with RF coils

07:00 **Introduction**
Daniel K. Sodickson

07:15 **Techniques for MR Imaging Near Metallic Implants**
Garry E. Gold

07:30 **Prospects of Absolute B1 Calibration**
Florian Wiesinger

07:45 **Open Discussion**

PLENARY LECTURES: Technologies to Accelerate Applications

Room 6A-C 8:15 - 9:30 Chairs: Steven M. Conolly, Hiroyuki Fujita, and Steven M. Wright

8:15 ***200***. **1.5T Vs 3.0T: A Technical and Application Update**
Axel Haase[1]
[1]University of Würzburg, Würzburg, Germany

Higher magnetic field strengths result in a higher signal to noise ratio (SNR), altered relaxation time constants (T1 and T2), increased spectral and spatial resolution. There are also adverse effects, which can be avoided when MRI pulse programs and hardware, especially MRI coils are optimized. It becomes more and more evident that the field of 3,0 T MRI is also of advantage for all versions of parallel imaging techniques. Advantages for clinical applications of 3,0 T have been shown for practically all organs and for many diseases. The present state of technology and clinical applications will be summarized in this presentation.

8:40 ***201***. **Prospects for Acceleration and Dose Reduction in Selected MR and X-Ray CT Cardiovascular Applications**

Charles A. Mistretta[1]

[1]University of Wisconsin, Madison, Wisconsin, USA

There are likely to be significant advances in the acceleration of data acquisition in cardiovascular MR and X-ray CT in the near future. This presentation will emphasize an acquisition and reconstruction algorithm that has produced, with *in vivo* imaging and multiple simulations, acceleration factors between ten and several hundred for MR acquisitions that represent a motion free time series of images or images involving a series of variations in MR parameters. For the case of X-ray CT, simulations involving the decimation of *in vivo* data suggest that dose in CT contrast-enhanced time series can be significantly reduced.

9:05 ***202***. **Parallel Imaging Update: How Many Elements Do We Need?**

Lawrence L. Wald[1]

[1]Massachusetts General Hospital, Charlestown, Massachusetts, USA

Virtually all clinical coils utilize receive-only arrays with 4 to, more recently, 32 elements. Both sensitivity and accelerated encoding motivates even higher numbers of array elements. In the logical extension of this approach, the number of elements is increased ad infinitum and the size of the elements is reduced (to cover a fixed anatomical territory). With unlimited access to receive channels, a different paradigm emerges for RF coil design. We are just beginning to explore at what point the utility of this approach exhausts itself and what factors limit the gains in array coil SNR and acceleration capability.

Pulse Sequences: I

Room 6E 10:30 - 12:30 Chairs: Charles A. Mistretta and Dwight G. Nishimura

10:30 ***203***. **Ultra-Fast MR Velocity Measurement Using Spin-Tagging and Single-Echo Acquisition (SEA) Imaging**

Steven M. Wright[1], *Mary Preston McDougall*[1], *Naresh Yallapragada*[1]

[1]Texas A&M University, College Station, Texas, USA

As MRI evolves into a functional imaging tool, the potential for using MRI to image extremely rapid, non-periodic or one-time events is of growing interest. This abstract demonstrates the combination of spin-tagging RF pulses with single-echo acquisition (SEA) imaging to achieve real-time velocity visualization with frame rates of 200 images per second. The method is tested on a gelatin phantom rotating at 600 revolutions per minute. Although the array coil elements are 2-mm wide in the narrow dimension, 1-mm wide spin-tags are visualized through the use of a phase compensation gradient pulse optimized for detecting high-frequencies rather than signal-to-noise.

10:42 ***204***. **Ultra Fast Dynamic Contrast Enhanced Time Resolved UNFOLD Imaging**

Umesh Rudrapatna[1], *Manojkumar Saranathan*[1]

[1]Indian Institute of Science, Bangalore, Karnataka, India

Dynamic Contrast Enhanced (DCE) MRI has become an indispensable tool for tumor diagnostics. Any improvement in the achievable temporal resolution can be very useful, due to the trade-off between spatial and temporal resolution that exists in the current imaging schemes. This work reports a novel strategy of combining UNFOLD with time resolved imaging to effect acceleration factors of 6 and higher, thereby pushing the capabilities of DCE-MRI further. A new, computationally efficient, sinc-interpolation based reconstruction strategy has also been proposed. Tests conducted on real and simulated data validate the accuracy and increase in temporal resolution obtained using this new acquisition-reconstruction technique.

10:54 ***205***. **Adaptive Dynamic Imaging in Cardiac MR Fluoroscopy: First *In-Vivo* Results**

Nitin Aggarwal[1], *Brad Sutton*[1], *Yoram Bresler*[1]

[1]University of Illinois, Urbana-Champaign, Urbana, Illinois, USA

We present the Adaptive Dynamic Imaging (ADI) method for cardiac fluoroscopy that adapts both the MR data acquisition and the reconstruction to the subject being imaged. We demonstrate that with such an approach a high spatial and temporal resolution cardiac cine can be reconstructed with acquiring data at a sub-Nyquist rate and without cardiac gating.

11:06 ***206***. **Comparison of Three Accelerated Pulse Sequences for Quantitative Myocardial Perfusion Imaging Using TSENSE**

Stefan Weber[1, 2], *Andrea Kronfeld*[1], *R. Peter Kunz*[1], *Martin Fiebich*[2], *Karl Friedrich Kreitner*[1], *Wolfgang Günther Schreiber*[1]

[1]Mainz University Medical School, Mainz, Germany; [2]University of Applied Sciences Giessen-Friedberg, Giessen, Germany

Three established pulse sequences for first-pass myocardial perfusion imaging (SR-TurboFLASH, SR-TrueFISP and SR-Interleaved Gradient EPI) were compared with regard to image quality obtained while using TSENSE with an acceleration factor of two. Phantom studies showed that the linearity of the signal intensity with contrast agent concentration is increased when using TSENSE and therefore quantification may be improved. In a volunteer study TrueFISP yielded the best SNR, CNR and quality scores. It is therefore considered most suitable for quantitative analysis of myocardial perfusion.

11:18 ***207***. **High-Resolution Cartilage Imaging with Wideband SSFP**

Hsu-Lei Lee[1], Garry Gold[2], Krishna S. Nayak[1]
[1]University of Southern California, Los Angeles, California, USA; [2]Stanford University, Palo Alto, California, USA

SSFP cartilage imaging benefits from high SNR efficiency and excellent contrast between cartilage and synovial fluid, but has limited TR because of the off-resonance banding artifact. It's difficult to achieve high spatial resolution given the restricted readout time. In this work we applied wideband SSFP to knee imaging to extend the readout duration while maintaing a sufficient passband bandwidth. Patellar cartilage images of high in-plane resolution (0.15mm x 0.3mm) and T2/T1 contrast were obtained with reduced off-resonance artifacts compared to conventional SSFP.

11 :30 ***208***. **A Fast Method to Measure Trabecular Bone Thickness Anisotropy**

Branimir Vasilic[1], Felix W. Wehrli[1]
[1]University of Pennsylvania Medical Center, Philadelphia, Pennsylvania, USA

The autocorrelation function (ACF) can be used to estimate the thickness anisotropy tensor of trabecular bone. The ACF is calculated from MR acquired k-space data. We show that aniosotropic acquisitions can be utilized to greatly decrease scan times while increasing the signal to noise ratio and preserving the accuracy of high resolution scans in determining the principal values of the thickness anisotropy tensor. The proposed fast anisotropic autocorrelation readout (FAAR) technique is demonstrated with measurements of a phantom consisting of periodicly spaced soybean oil inclusions.

11:42 ***209***. **3D Magnetization Prepared Elliptical Centric Fast Gradient Echo Imaging**

Chen Lin[1], Mathew A. Bernstein[1]
[1]Mayo Clinic College of Medicine, Rochester, Minnesota, USA

3D magnetization prepared fast gradient echo MR sequence, such as MP-RAGE, has many useful applications because it provides good spatial resolution and T1 contrast. This technique can be further improved with a segmented and recessed elliptical centric view order and by substituting the acquisition of views in k-space corners with zeros. This study shows that this novel acquisiton strategy can provide images with better signal-to-noise ratio (SNR), contrast-to-noise ratio (CNR) and less artifacts than MP-RAGE while reducing scan time.

11:54 ***210***. **Sliding Phase Encoding in Table-Motion Direction for Fast Continuously Moving Table Imaging**

Shinji Kurokawa[1], Yo Taniguchi[1], Tetsuhiko Takahashi[2], Hisaaki Ochi[1]
[1]Hitachi, Ltd., Kokubunji, Tokyo, Japan; [2]Hitachi Medical Corporation, Kashiwa, Chiba, Japan

Continuously moving table imaging improves extended FOV imaging speed. However, it is limited in that the directions of the phase-encoding and table-motion should not be parallel. Therefore, when homogeneous space is narrow in the table-motion direction or higher resolution is needed in the orthogonal direction of the table-motion, the read-out direction is forcibly set in an inefficient direction and the imaging time increases. To prevent this, we propose a new encoding and reconstruction that is applicable in the table-motion direction. Phantom experiments show that the proposed methods successfully reconstruct images.

12:06 ***211***. **Contrast Manipulation in 3D Whole-Body Continuously Moving Table MRI Using Magnetization Preparation and K-Space Segmentation**

Jochen Keupp[1], Peter Börnert[1], Bernd Aldefeld[1]
[1]Philips Research Laboratories, Hamburg, Germany

The ability to create clinically relevant image contrasts in continuously moving table (CMT) imaging is a pre-requisite to enable applications such as metastases screening in cancer patients. In this paper, feasibility of contrast manipulations for 3D CMT imaging is studied, which requires special attention with respect to the timing of the preparation pulses and the type of segmentation to avoid table-motion induced image artifacts. Different magnetization preparations and k-space segmentations were studied in experiments on healthy volunteers showing a robust image quality.

12:18 ***212***. **Respiratory-Gated Continuously Moving Table 3D MRI**

Bernd Aldefeld[1], Peter Börnert[1], Jochen Keupp[1], Kay Nehrke[1]
[1]Philips Research Laboratories, Hamburg, Germany

Continuously moving table whole-body MR imaging is improved using respiratory motion detection and gating. A dual-velocity scan is applied, using lower velocity in combination with gating only when data are acquired from the abdominal and chest regions, whereas higher velocity is used during most part of the scan. Improved image quality is obtained in head-to-toe volunteer scans.

CLINICAL CATEGORICAL COURSE
Body/Cardiovascular Imaging at 3T: Is it Ready for Clinical Prime Time?

Room 6C 10:30 - 12:30 Chairs: Elizabeth M. Hecht and Stefan G. Ruehm

Educational Objectives
Upon completion of this session, participants should be able to:

- Describe the basic physics of imaging at 3T and its effects on signal to noise, relaxation rates, susceptibility, chemical shift, power deposition, and patient safety;

- List advantages and disadvantages of body and cardiovascular imaging at 1.5 and 3T;
- Explain why protocols optimized for 1.5T may not be optimal for 3.0T; and
- Recognize the sequence parameters that may need adjusting to optimize protocols at 3T, and discuss specifically which sequences may or may not improve at 3T.

10:30 **Introduction to Body Imaging at 3T: Theoretical Advantages and Practical Challenges**
Neil M. Rofsky

10:45 **Musculoskeletal Imaging at 3T**
Garry E. Gold

11:05 **Abdominal and Pelvic Imaging at 3T**
Elizabeth M. Hecht

11:30 **Cardiovascular Imaging at 3T**
Stefan O. Schoenberg

11:55 **Body and Breast at 3T: Where is the Added Value Compared to 1.5T**
Christiane K. Kuhl

12:15 **Questions and Answers**

CLINICAL MRI COURSE
Neuro MR Problem Solving

Room 6D 10:30 – 12:30 Chair: Elias R. Melhem

Educational Objectives
Upon completion of this session, participants should be able to:

- Implement DTI, perfusion, and MR spectroscopy in brain neoplasms;

- Recognize the role of DTI, perfusion, and MR spectroscopy in evaluation of brain neoplasms;
- Identify limitations of DTI, perfusion, and MR spectroscopy in evaluation of brain neoplasms; and
- Apply an algorithmic approach to the evaluation of brain neoplasms-based advanced MR imaging.

10:30 **How to Use Parallel Imaging Techniques to Improve the Efficiency of Clinical CNS Imaging Protocols**
Meng Law

11:30 **MR Angiography of the Carotids and Circle-of-Willis: Technical and Clinical Dilemmas**
Ronald L. Wolf

Emerging RF Coil Technology

Room 4C - 3,4 10:30 - 12:30 Chairs: Hiroyuki Fujita and Christoph Leussler

10:30 ***213***. **7T Body Imaging: First Results**
J. Thomas Vaughan[1], Carl Snyder[1], Lance DelaBarre[1], Lizann Bolinger[2], Jinfeng Tian[1], Peter Andersen[1], John Strupp[1], Gregor Adriany[1], Kamil Ugurbil[1]
[1]University of Minnesota, Minneapolis, Minnesota, USA; [2]National Research Council-Canada, Winnipeg, MB, Canada

The objective of this study was to investigate the feasibility of whole body human imaging at 7T. To accomplish this study new 300 MHz body coils and receivers had to be modeled, designed, built and applied. Human body images were acquired in three dimensions. The first 7T images show promise for safe and successful whole body imaging at 7T.

10:42 ***214***. **A 7 Tesla Gradient Mode Birdcage Coil for Improved Temporal and Occipital Lobe SNR**

Graham Charles Wiggins[1], Oliver Kraff[2], Elizabeth Zakszewski[1], Vijay Alagappan[1], Christopher John Wiggins[1], Lawrence L. Wald[1]

[1]Massachusetts General Hospital, Charlestown, Massachusetts, USA; [2]University Hospital Essen, Essen, Germany

We compare the use of two of modes of a birdcage coil - homogeneous and gradient - for human brain imaging at 7T. These give complementary field distributions, with the gradient coil being particularly suited to imaging the temporal and occipital lobes.

10:54 ***215***. **An Inductive Resonator for 7T with Transmission Line Segments for Strong Coupling**

Joseph Murphy-Boesch[1], Yun-Jeong Yang[1], Shumin Wang[2]

[1]USA Instruments, Inc., Aurora, Ohio, USA; [2]NINDS of the NIH, Bethesda, Maryland, USA

An Inductive Resonator for the Head is described using Transmission Line Segments for strong inductive coupling of the mesh elements. A circuit analysis is presented that provides a means for tuning the resonator at high field (7T). The resonator exhibits a strongly coupled high-pass mode distribution with capacitors located only in the legs or cross-members of the coil. The virtual grounds of these segments and the distributed capacitance of cross-members minimize Electric fields.

11:06 ***216***. **Development of Micro-Strip Coils for Breast Imaging**

Jian-xiong Wang[1], Han Wang, Yangmei Li[1], Donald B. Plewes[1]

[1]Sunnybrook & Women's College Health Science Centre, Toronto, ON, Canada

A micro-strip coil developed to overcome strongly coupled surface coils in parallel imaging setting is presented. Due to its natural shielding structure, the micro-strip coil has both decoupling and isolation properties. It opens the possibility for different coil geometries with improved SNR for breast MRI.

11:18 ***217***. **Concentrically Shielded Surface Coils - A New Method for Decoupling Phased Array Elements**

Titus Lanz[1], Mark Griswold[2]

[1]Rapid Biomedical GmbH, Rimpar, Germany; [2]Case Western University, Cleveland, Ohio, USA

In this abstract we present a new method of decoupling neighboring elements based on the use of concentric shields which is compatible with a gapped coil arrangement and yields good SNR and good isolation between the elements even at 1.5T. Nevertheless, the Q drop shows that the shielded coil can be made sample noise dominant and with sufficient SNR for use in an array arrangement. We believe this general concept will be useful for the construction of arrays with a large number of elements.

11:30 ***218***. **Observation of Radiation Damping Effects in a Birdcage Resonator with Hyperpolarized 3He at 1.5T**

Kevin Teh[1], Nicola de Zanche[2], Jim M. Wild[1]

[1]University of Sheffield, Sheffield, Yorkshire, UK; [2]ETH, Zurich, Switzerland

In this work, radiation-damping effects were investigated with a birdcage resonator with samples of hyperpolarized 3He at 1.5T. To our knowledge this is the first report of radiation damping in a birdcage resonator with samples hyperpolarized or otherwise. This experimental observation of radiation damping could help shed light on the meaning and definition of the filling factor for a birdcage resonator, and its relationship with the quality factor. The presence and diagnosis of radiation damping in HP gas MR also has major implications in RF calibration experiments in HP gas MRI, where accurate knowledge of the flip angle is imperative.

11:42 ***219***. **Cantilever Heterodyne Mixing and Filtering for MRI**

Modhurin Banerjee[1], Charles A. Paulson[1], Daniel van der Weide[1], Thomas M. Grist[1]

[1]University of Wisconsin, Madison, Madison, Wisconsin, USA

This project is to realize NMR antennas for wideband frequency detection using magnetic force microscopy (MFM).Micron-scale current loops on micro-fabricated cantilevers produce magnetic dipole forces to make the cantilever oscillate at its mechanical resonance frequency. Theoretical calculations and experimental demonstration has shown that frequency tunable, micro-mechanical detector suggested here can be used to exceed the performance of a standard NMR detector if Johnson noise can be eliminated via cryogenic cooling.

11:54 ***220***. **Single Cable Transmission for Multi-Channel MRI Using Frequency Division Multiplexing**

Juan Wei[1], Jing Yuan[1], Gary X. Shen[1]

[1]The University of Hong Kong, Hong Kong, People's Republic of China

Parallel imaging and RF array coils require a great quantity of MRI channels, which can produce ghosting and interference to decrease imaging SNR. In this work, we make use of a frequency division multiplexing (FDM) technique to combine several channel signals and transmit them in single cable. At present the PCB board is prototyped and tested with the signal generator. We propose to build the completed circuit with coil array on board to recover the multi-channel FID signals.

12:06 ***221***. **A High-Temperature Superconducting Volume Coil for Magnetic Resonance Microscopy at 9.4T**

John Nouls[1], Mike Izenson[2], Hal Greeley[2], Mark Bagley[2], Jay Rozzi[2], G A. Johnson[1]
[1]Duke University, Durham, North Carolina, USA; [2]Creare Inc., Hanover, New Hampshire, USA

We present a novel superconducting volume coil consisting of spiral coils in Helmholtz pair configuration for magnetic resonance microscopy of the mouse brain at 9.4T. Spiral coils can be tuned easily by hand. The probe resonance frequency is adjusted by changing the spacing between the coils, cooled by tightly temperature-controlled recirculating helium. The spiral was modeled by a radiofrequency simulation software. Agreement between modeled and experimental coil resonance frequency was excellent. Experimental magnetic field homogeneity was good. The quality factor improved by a factor of eight, as compared to a similar copper coil. Signal-to-noise ratio improvement is currently being investigated.

12:18 ***222***. **Method to Extract the Non-Linear Characteristics of High Temperature Superconducting (HTS) RF Coils**

Olivier Girard[1], Jean-Christophe Ginefri[1], Luc Darrasse[1]
[1]CNRS - Universite Paris Sud, Orsay, France

High-temperature superconducting (HTS) surface coils can strongly improve the SNR in MR microscopy. However the implementation of such RF coils remains difficult since power levels involved during transmission lead to a non-linear response. This results in flip-angle misadjustements and severe shape distortion of slice-selective soft pulses. We describe here a method for complete RF coils characterization accounting for non-linear conduction. The non-linear characteristics is required to compensate for the undesirable effects and to help designing more convenient matching circuits or RF coils based on improved materials or geometries.

Manganese Enhanced MRI: Multiple Applications

Room 611 - 612 10:30 - 12:30 Chairs: Robia G. Pautler and Anne-Marie Van der Linden

10:30 ***223***. ***In Vivo* Visualization of Cytoarchitecture to Define Boundaries in Cortex, Thalamic Nuclei and Superior Colliculus Using Manganese Enhanced MRI**

Carolyn W-H Wu[1], Stephen J. Dodd[1], Alan P. Koretsky[1]
[1]National Institutes of Health, Bethesda, Maryland, USA

The cerebral cortex is divided into areas based on cytoarchitectonics, according to the thickness of cortical layers and neuronal density. A shortcoming of present cytoarchitectonic techniques is they require histology on fixed and sectioned tissue. Manganese-enhanced MRI (MEMRI) has proven useful for visualizing anatomical structures, neuronal connections and activity in the brain *in vivo*. In the present study, we demonstrate that MEMRI can also be used to delineate cortical areas and visualize subcortical structures. The implication of the study enables noninvasive imaging to study the organization and functions of normal and pathological brains.

10:42 ***224***. **Manganese SynapticTransfer Index (MSTI): A Novel Approach to Assess Neuronal Physiology in Mouse Models of Neurodegeneration**

Karen Smith[1], Hui Zheng[1], Robia Pautler[1]
[1]Baylor College of Medicine, Houston, Texas, USA

It would be extremely useful to have a sensitive, *in vivo* assay that could detect changes in neurological function. Here we develop an extension of MEMRI tract tracing to measure changes in the efficiency of trans-synaptic manganese transfer. We demonstrate that this is a sensitive biomarker of alterations in brain physiology by analyzing two mouse models with established changes in brain function.

10:54 ***225***. **Quantitative Manganese Tract Tracing: Concentration Dependence**

Andrew Lowe[1], Ian D. Thompson[1, 2], Nicola R. Sibson[1]
[1]University of Oxford, Oxford, Oxfordshire, UK; [2]Kings College London, London, UK

Varying manganese concentration load within the vitreous humor of adult mice has confirmed differential degrees of resultant tectal terminal labelling using magnetic resonance imaging. Quantitative evaluation of T1 relaxation times within the superior colliculus has enabled the robust assessment of the within and between subject effects of intra-ocular manganese loading. The differential decreases in T1 relaxation times within the superior colliculi suggest varying concentrations of manganese may effect optimal, unfavourable and undesirable consequences.

11:06 ***226***. **Variations in Relaxivity of Manganese Between Regions in Rat Brain**

Na Zhang[1, 2], Vanessa Ann Fitsanakis[3], Michael Aschner, [1,3], Malcolm J. Avison[1], John C. Gore[1, 2]
[1]Vanderbilt University Medical Center, Nashville, Tennessee, USA; [2]Vanderbilt University, Nashville, Tennessee, USA; [3]Vanderbilt University School of Medicine, Nashville, Tennessee, USA

Manganese (Mn) is an essential metal that is neurotoxic at high levels but which has been used with MRI *in vivo* to track neuronal architecture. As part of a toxicological study that aims to determine the pattern of Mn distribution in rat brain following weekly injections of Mn, we measured the effective relaxivity of Mn *in vivo* in different regions of the brain. The variations found suggest Mn takes different chemical or physical forms in different parts of the brain, which may be relevant for studies that assume the relaxivity is constant.

11:18 ***227***. **_In Vivo_ Manganese-Enhanced MRI (MEMRI) of the Appetite Regulations, Correlation with C-Fos Expression**

Yu-Ting Kuo[1, 2], James RC Parkinson[1], Owais B. Chaudhri[1], Amy H. Herlihy[1], Po-Wah So[1], Caroline J. Small[1], Steve R. Bloom[1], Jimmy D. Bell[1]

[1]Hammersmith Hospital, Imperial College London, London, UK; [2]Faculty of Medicine, School of Medicine, Kaohsiung Medical University, Kaohsiung, Taiwan

Obesity is a major problem across the world. The discovery of appetite-regulating neuropeptides is providing new insights into the mechanisms associated with appetite and may lead to new pharmacological targets for treatment. MEMRI has been proposed to delineate neuronal connectivity in animals. In this study we have used MEMRI to determine the neuronal activations associated with appetite regulations and have also determined the effect of manganese on neuronal activation by c-fos expression. The results from this study suggest that MEMRI can be used to establish the site, degree and timing of neuronal activity associated appetite regulations without affecting c-fos expression.

11:30 ***228***. **Using Manganese Enhanced MRI to Reveal Active Olfactory Circuitry in Response to Odorant Stimuli**

Kai-Hsiang Chuang[1], Jung Hee Lee[1], Afonso C. Silva[1], Leonardo Belluscio[1], Alan P. Koretsky[1]

[1]National Institutes of Health, Bethesda, Maryland, USA

To investigate the circuitry activated by odorants in the mammalian olfactory bulb (OB) we adapted a functional imaging technique known as manganese-enhanced MRI (MEMRI). A functional map of the odorant in the OB can be detected by quantifying regional signal enhancement as manganese traces from active olfactory neurons in the nose and enters the OB. Odor maps of the glomerular layer for three different odorants were obtained. Furthermore, activation of a single glomerulus could be observed by comparing MEMRI maps to specific glomeruli that were visualized with green fluorescent protein. The ability of manganese to trace trans-synaptically should enable depicting the organizational pattern of the signal transduced to deeper parts of the OB and into the brain.

11:42 ***229***. **Statistical Mapping of Auditory Activity by Manganese-Enhanced MRI**

Xin Yu[1], Dan Sanes[2], Jing Zou[3], Youssef Zaim Wadghiri[1], Daniel Turnbull[1]

[1]New York University School of Medicine, New York, USA; [2]New York University, New York, USA; [3]University of Maryland, College Park, Maryland, USA

Mn-enhanced MRI (MEMRI) can be used to produce 3D representations of sound-evoked activity in the awake mouse, consistent with previous electrophysiological activity maps. Significantly, our studies revealed a clear coding of sound frequency and amplitude in the mouse midbrain. The 3D spatial distribution of the frequency- and amplitude- sensitive neurons has been demonstrated in the midbrain by an unbiased statistical analysis of MEMRI data. These results further our understanding of the signal processing in the auditory system and broaden the application of MEMRI to studies of sensory perception in the brain.

11:54 ***230***. **MRI Assessment of Status Epilepticus Induced Hippocampal Plasticity After Systemic Mn Administration**

Riikka Johanna Immonen[1], Asla Pitkänen[1], Olli Gröhn[1]

[1]A.I.Virtanen Institute for Molecular Sciences, University of Kuopio, Kuopio, Finland

Mn2+-enhanced magnetic resonance imaging (MEMRI) has potential to reveal functional, structural and connectional alterations in high spatial resolution. This work was designed to test if systemic Mn-injection provides a robust MEMRI approach for detection of mossy fiber sprouting, and to assess the possible accumulation of systemically injected Mn into hippocampus during status epilepticus. Mn-enhancement was not increased by status epilepticus 15-37 hours after kainic acid (KA) injection. However, 2 months after KA-injection marked changes in shape and thickness of the CA3 and dentate gyrus as well as in intensity of CA1 subregions of hippocampus were detected, attributed to axonal sprouting.

12:06 ***231***. **The Use of MEMRI to Measure _In Vivo_ Axonal Transport Rates in a Murine Model of Alzheimer's Disease**

Karen Brown Smith[1], Mitchell E. Deshazer[1], Hui Zheng[1], Robia G. Pautler[1]

[1]Baylor College of Medicine, Houston, Texas, USA

Methods to detect Alzheimer's Disease prior to plaque formation are desperately needed for diagnosis and screening of potential treatments. We have extended the use of manganese enhanced MRI (MEMRI) to a transgenic mouse model of Alzheimer's Disease (tg2576) for the detection of changes in manganese transport prior to recorded amyloid plaque accumulation. Our findings demonstrate that this method may be developed for the *in vivo* detection of axonal transport deficits in mouse models of Alzheimer's Disease.

12:18 ***232***. ***In Vivo* Staining of Apoptosis by Manganase-Enhanced Magnetic Resonance Imaging (MEMRI) in the Hypoxic-Ischemic Newborn Rat**

Jin Taek Kim[1], Keun Ho Lim[2], Hee Jin Cho[2], Jung Hee Lee[3], Ki Soo Kim[1]

[1]University of Ulsan College of Medicine, seoul, Republic of Korea; [2]Asan Institute for Life Sciences, seoul, Republic of Korea; [3]Sungkyunkwan University School of Medicine, seoul, Republic of Korea

This study was designed to investigate the usefulness of MEMRI for *in vivo* detection of apoptosis for hypoxic-ischemic newborn rat brain. MEMRI showed high signal intensity regions at 72 hours after injury and Mn2+ administration. The signal intensity of the enhanced regions increased in time upto 1 week. Those enhanced regions in MRI were matched with TUNEL staining for apoptosis. The result of this study suggests that MEMRI can be an tool for *in vivo* staining of apoptosis.

fMRI Analysis and Correction Methods

Room 615 - 617 10:30 - 12:30 Chairs: Lizann Bolinger and Stephen M. Smith

10:30 ***233***. **A Data-Driven Method for Analysis of Associated Time Courses Found from Group Independent Component Analysis**

Vincent J. Schmithorst[1], Scott K. Holland[1]

[1]Children's Hospital Medical Center, Cincinnati, Ohio, USA

A data-driven method for analyzing the associated time courses obtained from group Independent Component Analysis (ICA) of functional MRI (fMRI) data is proposed. The method can be used for between-groups analyses or correlations with covariates of interest in a General Linear Model (GLM) framework. Changes in the shape of the hemodynamic response function (HRF) yield different information than changes in the activation intensities. The effectiveness of the method, with greater sensitivity than a hypothesis-driven approach, is demonstrated via the investigation of age-related and performance-related effects in a cohort of normal children ages 5-18 performing a word-picture matching task.

10:42 ***234***. **Estimation of the Intrinsic Dimensionality of fMRI Data**

Dietmar Cordes[1], Rajesh Nandy[2]

[1]University of Washington, Seattle, Washington, USA; [2]UCLA, Los Angeles, California, USA

A new method based on an autoregressive noise model of order 1 is introduced to the problem of detecting the number of components in fMRI data. Unlike current information-theoretic criteria like AIC, MDL and related PPCA, which do not incorporate autocorrelations in the noise, the new method leads to more consistent estimates of the model order, as illustrated in simulated and real fMRI resting-state data.

10:54 ***235***. **Component Based Noise Correction for Perfusion fMRI**

Yashar Behzadi[1], Khaled Restom[1], Joanna Perthen[1], Thomas T. Liu[1]

[1]UCSD, San Diego, California, USA

Perfusion based functional magnetic resonance (fMRI) utilizing arterial spin labeling (ASL) techniques has several potential advantages over traditional blood oxygenation level dependent (BOLD) based imaging, such as 1) better localization of neural activity and 2) potentially less inter-subject variability. However, the ASL signal exhibits low signal-to-noise and is often confounded by physiological noise sources. Here we develop and characterize a component based algorithm (CompCor) for the identification and removal of structured noise elements in perfusion based fMRI. We show that CompCor removes respiration induced noise and significantly increases ASL sensitivity.

11:06 ***236***. **Unsupervised Modelling of Physiological Noise Artifacts in fMRI DataΦ**

Kristoffer Hougaard Madsen[1, 2], Torben Ellegaard Lund[2]

[1]Technical University of Denmark, Kgs. Lyngby, Denmark; [2]Copenhagen University Hospital, Hvidovre, Copenhagen, Denmark

This study suggests a way to obtain nuisance regressors to correct for artefacts such as cardiac and respiratory noise in fMRI time series without measures of cardiac and respiratory cycles. We show that including these regressors in the design matrix reduces correlation and non-normality in the residual errors. In addition, the obtained regressors are in fact similar to the ones obtained using measures of cardiac and respiratory cycles. Furthermore, we show that these regresssors surpass other methods in terms of reducing non-normality and correlations in the residual errors.

11:18 ***237***. **A Multi-Channel Recursive Least Squares Filter for Motion and Ballistocardiogram Artefacts in EEG Recorded in the MR Scanner**

Richard Andrew J. Masterton[1, 2], David F. Abbott[1], Steve Fleming[1], Graeme D. Jackson[1, 2]

[1]Brain Research Institute, Melbourne, Victoria, Australia; [2]University of Melbourne, Melbourne, Victoria, Australia

Recording EEG during fMRI scanning permits the identification of hemodynamic changes associated with EEG events. However, subject motion within the MR scanner can cause unpredictable and frustrating artefacts on the EEG. Here we present a new method for recording motion in the MR scanner that is particularly suited for filtering motion artefacts from the EEG. We apply this filter to simulated and real EEG recordings and demonstrate that it can achieve a marked reduction in motion artefacts whilst preserving the underlying EEG signal.

11:30 ***238***. **Gradient Noise Cancelling for Simultaneous EEG-fMRI Recording**

Michiro Negishi[1], Robert Todd Constable[1]
[1]Yale University, School of Medicine, New Haven, Connecticut, USA

Artifacts induced in the EEG during simultaneous EEG-fMRI acquisition are commonly removed by average waveform subtraction methods. However, these methods require EEG sampling timing correction, which is not suited for online artifact removal. We implemented a noise cancellation method utilizing dummy leads placed close to EEG electrodes. Since signals from the electrodes and the dummy leads are sampled at the same time, timing correction is unnecessary. With bipolar wiring and RF artifact-free recording, the artifact recorded from a phantom in a 3T scanner was 290 and 3.3 microvolts RMS before and after noise removal, demonstrating the effectiveness of the method.

11:42 ***239***. **A Noise Cancellation Scheme for fMRI Involving Participant Speech**

Ian Atkinson[1], Theodore Claiborne[1], Michael P. Flannery[1], Keith R. Thulborn[1]
[1]University of Illinois at Chicago, Chicago, Illinois, USA

The substantial acoustic noise produced by EPI sequences often used for fMRI make functional studies involving analysis of participant speech challenging. We proposed an adaptive technique for suppressing gradient noise from human speech. Experimental results indicate that proposed method is able to effectively cancel the noise induced by the switching gradients while preserving frequencies in typical human voice. When applied to human speech, the proposed scheme increased the ability of a naïve listener to correctly identify individual English words spoken during fMRI by an average of 21.6% and decreased the time required to make this identification by an average of 17.5%.

11:54 ***240***. **Evaluating the Effect of Task-Correlated Subject Motion in fMRI Experiments Upon the Inferred BOLD Activation Maps**

Bas Gobets[1], Jan-Henry Seppenwoolde[1], Suzanne Koudijs[1], Josien Pluim[1], Matthias J. P. van Osch[2]
[1]Image Sciences Institute, Utrecht, Netherlands; [2]Leiden University Medical Center, Leiden, Netherlands

A new approach is proposed to investigate the effects of motion upon the accuracy of fMRI studies. In this approach an fMRI experiment is conducted during which the entire planned stack of slices is moved between scans, according to precisely defined motion parameters. By comparing the activation map obtained this way to that obtained in a standard fMRI experiment, effect of (task-correlated) motion can be studied. The method is applied to investigate the effects of task-correlated motion such as observed in an fMRI study of hemiparetic children, upon the accuracy of the inferred BOLD activation maps in that study.

12:06 ***241***. **Real-Time Prospective Slice-By-Slice Motion Correction for fMRI in Freely Moving Subjects**

Oliver Speck[1], Maxim Zaitsev[1]
[1]University Hospital Freiburg, Freiburg, Germany

Subject motion is still the major source of data quality degradation in functional MRI studies. Most of the established methods correct motion between successive repetitions based on the acquired imaging volumes either retrospectively or prospectively. We introduce a prospective method using external optical tracking that corrects motion on a slice-by-slice basis to continuously follow the motion of the head with the imaging volume. This method enables to acquire fMRI data even in the presence of significant motion during the acquisition of a single volume. The results show that this method is superior to image based correction methods.

12:18 ***242***. **Expanded Design of Web-Distributed Software fMRI Phantoms**

David Pickens[1], Yong Li[1], Victoria Morgan[1], Benoit Dawant[1], Ning Xu[1], J Michael Fitzpatrick[1]
[1]Vanderbilt University, Nashville, Tennessee, USA

We have previously described a set of software phantoms designed to simulate real fMRI studies, but with known amounts of motion, noise, and activation. These phantoms can be used to evaluate fMRI image processing software and are precomputed for download from our web site. In this abstract we describe an expanded design for our phantoms to simulate slice timing artifacts, varied hemodynamic response functions, baseline drift, spin history effects, and motion-induced susceptibility artifacts. These phantoms will be distributed by an extended, interactive web site so that users can select the characteristics of phantoms to meet their needs.

Human Brain MRS in Neuropsychiatric Disease and Dementia

Room 618 - 620 10:30 - 12:30 Chairs: Kim M. Cecil and Clifford R. Jack

10:30 ***243***. **^{1}H MRSI Comparison of Chronic Fatigue Syndrome and Generalized Anxiety Disorder**

Xiangling Mao[1], Kathryn A. Keegan[2], Victor Otcheretko[2], Eric L. Smith[3], Jeremy D. Coplan[3], Susan Levine[4], Jack M. Gorman[2], Sanjay Mathew[2], Dikoma C. Shungu[1]

[1]Weill Medical College of Cornell University, New York, USA; [2]Mount Sinai School of Medcine, New York, New York, USA; [3]SUNY Downstate Medical Center, New York, New York, USA; [4]Infectious Disease Specialist, New York, New York, USA

This study used 1H MRSI to explore regional differences in the neurometabolic profiles of chronic fatigue syndrome (CFS), generalized anxiety disorder (GAD), and healthy volunteers. Sixteen GAD patients, sixteen CFS patients, and fifteen medically healthy controls underwent clinical assessment and 1H MR spectroscopy. CFS patients had markedly higher ventricular lactate than did GAD patients or healthy volunteers. Lactate was highly correlated with fatigue severity across groups, suggesting a specific relationship between subjective fatigue and brain lactate concentrations. Validation of ventricular lactate as a reliable diagnostic marker of CFS must await further study.

10:42 ***244***. **Global and Regional Brain Metabolic Deficits in Autism**

Tim J. DeVito[1, 2], Dick Drost[1, 2], Peter C. Williamson[2], Nagalingham Rajakumar[2], Richard W. Neufeld[2], William Pavlosky[2], Rob Nicolson[2]

[1]Lawson Health Research Institute, London, Ontario, Canada; [2]University of Western Ontario, London, Ontario, Canada

Twenty-seven boys with autism and a control group of 30 healthy boys underwent a combined MRI/MRSI experimental protocol at 3.0 tesla. Proton metabolite amplitudes were quantified in numerous localized regions of interest, and mean global gray and white matter metabolite levels were estimated using voxel-wise partial-volume regression analysis. Patients exhibited distributed regional deficits in NAA, Glx and Myo. Global tissue-specific analysis revealed significant reduction in global gray matter NAA, Glx and Myo. Global white matter metabolite levels did not differ between groups.

10:54 ***245***. **Age-Dependence and Clinical Correlates of Brain Metabolism in Rett Syndrome**

Luciano Farage[1], Izlem Izbudak[1], Genila Bibat[2], Lidia M. Nagae-Poetscher[1], Walter Kaufmann[2], Peter B. Barker[1], SakkuBai Naidu[2], Alena Horska[1]

[1]Jonhs Hopkins Medical Institutions, Baltimore, Maryland, USA; [2]Kennedy Krieger Institute, Baltimore, Maryland, USA

Thirty-five girls with a neurodevelopmental disorder of Rett Syndrome (RTT) and eight healthy girls were examined with single voxel proton MR spectroscopy at short TE. Spectra were acquired from the left frontal white matter. Compared to controls, a 10% lower NAA/Cr and a 174% higher mI/Cr was detected in RTT. NAA/Cr decreased and mI/Cr increased with age in RTT while both ratios were stable in controls. Age-related changes of NAA/Cr and mI/Cr in RTT are suggestive of progressive axonal damage with accompanying gliosis.

11:06 ***246***. **^{1}H MRSI in the Putamen and Thalamus of Homosexual Pedophiles Does Not Show Similarities to OCD**

Gabriele Ende[1], Christine Kief[1], Alexander Sartorius[1], Sigi Walter[1], Matthias Ruf[1], Fritz A. Henn[1], Josef Bailer[1], Harald Dressing[1]

[1]Central Institute of Mental Health, Mannheim, Germany

As pedophilia is characterized by socially deviant, repetitive, highly arousing sexual fantasies, urges and activities, it shares some phenomenological similarities with obsessive compulsive disorder (OCD), which is also characterized by inadequate urges and poorly inhibited, repetitive behaviors. Providing that pedophilia does indeed share neurobiological similarities with OCD we hypothesized differences in striatal N-Acetylaspartate (NAA) as previously reported for OCD patients. We conducted a 2D ^{1}H MRSI study in 10 homosexual pedophiles compared to 10 healthy controls matched for age and education and did not find the hypothesized differences.

11:18 ***247***. ***In-Vivo* 3T ^{1}H Magnetic Resonance Spectroscopy of the Brain Reveals Elevated *scyllo*-Inositol in Patients with Mild Alzheimer's Disease**

Henry Randall Griffith[1], Chris C. Stewart[1], Jan A. den Hollander[1], William T. Evanochko[1], Lindy E. Harrell[1], Edward Y. Zamrini[1], John C. Brockington[1], Daniel C. Marson[1]

[1]University of Alabama at Birmingham, Birmingham, Alabama, USA

In-vivo ^{1}H magnetic resonance spectroscopy (^{1}H MRS) reveals brain metabolism abnormalities, including reduced *N*-acetylaspartate and elevated *myo*-inositol, in patients with mild Alzheimer's disease (AD) and mild cognitive impairment (MCI). We are aware of no studies that have documented abnormal *scyllo*-inositol (sI) levels in AD and MCI. This study compared 3T ^{1}H MRS of sI in the posterior cingulate gyrus across mild AD, MCI and healthy older adults. sI/ creatine (Cr) ratio was significantly higher in mild AD patients compared to controls, a finding not reported in past MRS studies. Further research with sI in AD appears warranted.

11:30 ***248***. **Longitudinal Change in ^{1}H MRS Metabolites in Mild Cognitive Impairment and Alzheimer's Disease**

Kejal Kantarci[1], Stephen Weigand[1], Ronald Petersen[1], Bradley Boeve[1], David Knopman[1], Jeffrey Gunter[1], Denise Reyes[1], Maria Shiung[1], Peter O'Brien[1], Glenn Smith[1], Robert Ivnik[1], Eric Tangalos[1], Clifford Jack, Jr.[1]

[1]Mayo Clinic, Rochester, Minnesota, USA

We measured the longitudinal ^{1}H MRS metabolite changes in normal elderly, patients with Alzheimer's disease (AD), and amnestic mild cognitive impairment (MCI), many of whom have prodromal AD, and compared ^{1}H MRS metabolite ratios and ventricular MRI volumes in tracking clinical disease progression in AD. The neuronal integrity marker NAA/Cr declines steadily starting from the prodromal stages of AD. The change in ^{1}H MRS metabolite ratios correlate with clinical progression as strongly as the rate of ventricular expansion, suggesting that both ^{1}H MRS and MR volumetric markers may be equally useful in monitoring drug effects in patients with AD.

11:42 ***249***. **Elevated Creatine and Myo-Inositol Levels Correlate with Verbal and Visual Memory Tasks in Mild Cognitive Impairment**

Sarah Andrea Dunham[1], Kathleen L. Fuchs[1], Scott A. Wylie[1], Carol A. Manning[1], Jack Knight-Scott[1]

[1]University of Virginia, Charlottesville, Virginia, USA

In this study, we examined the validity of the assumption that total creatine (tCr = creatine + phosphocreatine) is a stable metabolite reference for the calculation of metabolite concentrations in mild cognitive impairment (MCI). 10 ms TE ^{1}H MRS data were collected from 9 participants with MCI and 8 healthy elderly adults in the posterior cingulate gyrus at 1.5T. Creatine (tCr, p=0.002) and myo-inositol (mI, p=0.012) concentrations were elevated in the MCI participants relative to the healthy controls. Post hoc comparisons between psychometric indices of visual and verbal recall and the tCr and mI concentrations revealed significant negative correlations ($p < 0.001$). That is, increased tCr and mI concentrations were associated with reduced performance on memory measures. Multiple linear regression of mI and tCr on the scores for visual and verbal memory yielded correlation coefficients of 0.797 and 0.814, respectively, with a minimum power of 98% for each regression. There was no significant correlation with a general measure of cognitive integrity (Stroop color-word), indicating that the change in tCr and mI may be specific to the site (posterior cingulate) and/or to the cognitive process (memory).

11:54 ***250***. **Cerebral Metabolic Changes in Rheumatoid Arthritis**

Bart Jeroen Emmer[1], A. E. van der Bijl[1], F. C. Breedveld[1], T.W.J. Huizinga[1], M.A. van Buchem[1], J. van der Grond[1]

[1]Leiden University Medical Center, Leiden, Zuid-Holland, Netherlands

Although patients with rheumatoid arthritis (RA) generally suffer from non-specific subjective neuropsychiatric complaints, the effects of RA on the brain are currently unknown. In this study we aimed to detect cerebral metabolic abnormalities in RA patients using 1H-MRS. 35 RA patients with varying disease activity and 28 healthy control subjects underwent single voxel 1H-MRS in the left centrum semi-ovale. Active RA patients had decreased NAA/choline and increased choline/creatine ratios compared to inactive RA patients. Moreover, both ratios correlated significantly with the erythrocyte sedimentation rate. Our data show that increased choline levels are associated with disease activity, indicating impaired membrane metabolism.

12:06 ***251***. **Monitoring Effects of Dietary Glycine Loading on Brain Glycine Levels with TE-Averaged ^{1}H MRS**

Andrew Paul Prescot[1], Perry F. Renshaw[1], Dost Ongur[1], Eden A. Evins[2], Tanya Barros[1], Julie Covell[1], John Brown[3], Liqun Wang[3], Maurizio Fava[2], Marc J. Kaufman[1]

[1]McLean Hospital, Belmont, Massachusetts, USA; [2]Massachusetts General Hospital, Boston, Massachusetts, USA; [3]GlaxoSmithKline, Greenford, England UK

Glycine (Gly) serves as an essential coagonist for the glutamatergic N-methyl D-aspartate (NMDA) receptor subtype. NMDA receptor hypofunction is implicated in the pathophysiology of schizophrenia. Several clinical trials have reported that dietary Gly administration has promise for reducing negative symptoms in schizophrenia. High-dose dietary Gly therapy increases serum levels in schizophrenics, although clinical responses to Gly loading are highly variable. This report describes the acquisition of TE-averaged ^{1}H-MR spectra from two groups of healthy subjects, one participating in a test-retest variability study, and a second group who participated in a high-dose Gly-loading study, to determine whether TE-averaged ^{1}H-MRS can detect brain Gly increases.

12:18 ***252***. **Age-Related Changes in Long and Short Echo Time Proton Magnetic Resonance Spectroscopy of the Brain**

Dominick John McIntyre[1], Rebecca Ann Charlton[1], Hugh S. Markus[1], Franklyn Arron Howe[1]

[1]St George's, University of London, London, England UK

Long and short echo proton spectroscopic imaging were used to investigate white matter metabolite ratios and R_2 relaxation rates in 90 volunteers aged 50-90. Midline lipid was detected in some subjects, the incidence increasing significantly with age. The R_2 of NAA and the NAA/creatine ratio at both echo times significantly correlated with age. The choline/creatine ratio fell just short of significance. The results are consistent with creatine increasing with age. Correlations were similar at both echo times, with lower p values at short echo. As short echo also detects more metabolites, we recommend its use for future ageing studies.

On the Go: Muscles on the Move

Room 602 - 604 10:30 - 12:30 Chairs: Cornelius J. Faber and William B. Morrison

10:30 ***253***. **Correlation Between T2 and Diffusion Coefficient in Exercised Muscle**

Zaid Q. Ababneh[1], Riad Ababneh[2], Stephan E. Maier[2], Carl Winalski[2], Koichi Oshio[2], Robert V. Mulkern[3]
[1]BIDMC, Boston, Massachusetts, USA; [2]Brigham and Women's Hospital, Boston, Massachusetts, USA; [3]Children's Hospital, Boston, Massachusetts, USA

The increase in T2 relaxation times of skeletal muscle after exercise has been correlated with the increase of the diffusion coefficient D in the tibialis anterior of six subjects. The T2 and D measurements were acquired in approximately 90 s intervals before and for approximately 10 minutes after flexion exercise and were highly correlated, indicating that any model used to explain T2 increases with exercise must also account for increased diffusion coefficients

10:42 ***254***. **T2 Recovery Unable to Distinguish Anaerobic Exercise from Aerobic**

Anders T. Nygren[1], Barbara Norman[1], Eva Jansson[1]
[1]Karolinska Institutet, Stockholm, Sweden

T2 of skeletal muscle has been shown to be affected by ischemic conditions, thereby raising the question if anaerobic exercise may induce a different T2 recovery as to the response of a predominantly aerobic exercise. To induce a marked anaerobic metabolism in skeletal muscles, a wingate exercise test was performed. The exercise resulted in increased muscle volume and plasma venous lactate with delayed blood flow recovery. However, maximal T2 value post-exercise or the recovery rate were not different than after a high intensity endurance exercise. Therefore, T2 seems unable to distinguish the anaerobically driven exercise from a predominantly aerobic exercise.

10:54 ***255***. **Measured Decrease in T1 Relaxation Time in Skeletal Muscle on Oxygen Inhalation**

Deirdre McGrath[1], Josephine Naish[1], Paul Beatty[1], Alan Jackson[1], John Waterton[2], Chris Taylor[1], Geoff Parker[1]
[1]University of Manchester, Manchester, Lancashire, UK; [2]AstraZeneca, Alderley Park, Macclesfield, Cheshire, UK

Dissolved oxygen can be used as a contrast agent in MRI due to the paramagnetic properties of the oxygen molecule. A modest increase in the longitudinal relaxation rate R1 of water protons is induced by O2, and the increase is proportional to the dissolved oxygen concentration. Measurements of oxygenation using these effects can provide an indication of tissue perfusion and metabolism.We discovered that contrary to previous findings, the T1 of skeletal muscle is reduced significantly in hyperoxic conditions. We also obtained measures of the time course of regional signal intensity change for healthy skeletal muscle during oxygen wash-in and wash-out.

11:06 ***256***. **Application of Cine DENSE MRI to Studying Skeletal Muscle Mechanics During Joint Motion**

Xiaodong Zhong[1], Silvia S. Blemker[2], Bruce S. Spottiswoode[3], Patrick A. Helm[1], Aaron T. Hess[3], Frederick H. Epstein[1]
[1]University of Virginia, Charlottesville, Virginia, USA; [2]Stanford University, Stanford, California, USA; [3]University of Cape Town, Cape Town, Western Cape, South Africa

The feasibility of using cine DENSE to quantify skeletal muscle displacement and strain was investigated. An EPI cine DENSE sequence was used to acquire displacement encoded dynamic images of biceps and triceps brachii muscles during elbow flexion. The direction of muscle tissue motion was consistent with the muscles' mechanical actions, and the peak displacements occurred along the centerline of the muscles. Strain results demonstrate nonuniform shortening along the centerline region and uniform shortening along the anterior region. Cine DENSE provides a reliable means to measure muscle displacement and strain during joint motion.

11:18 ***257***. **Age Dependence of Water Diffusivity in Human Skeletal Muscle**

Craig J. Galban[1], Stefan Maderwald[2], Frank Stock[2], Katja Brauck[2], Mark E. Ladd[2]
[1]National Institutes of Health, Bethesda, Maryland, USA; [2]University Hospital of Essen, Essen, North Rhein Westphalia, Germany

Diffusion tensor imaging was used to determine if water diffusivity within human calf muscles is sensitive to the physical characteristics (height, weight, or body mass index) or age of healthy male subjects. The eigenvalues, trace of the diffusion tensor, and two anisotropic parameters were calculated and compared in four muscles: soleus, lateral and medial gastrocnemius, and anterior tibialis. This study concluded that the physiological and morphological changes that occur with age significantly contribute to the diffusion measurements in skeletal muscle.

11:30 ***258***. **Effects of Gd Bolus on DTI Measurements in Skeletal Muscle**

Sonya Bells[1], Michael D. Noseworthy[1]
[1]McMaster University, Hamilton, ON, Canada

Diffusion tensor imaging is now a commonly used MR procedure. However, it is done either before or after Gd contrast enhanced scans without sound knowledge of the agent's effect on tensor measurements. In this study we show that Gd contrast affects calculated diffusion tensor parameters, thus suggesting DTI should be performed prior to contrast enhanced scans.

11:42 ***259***. **Mechanisms Associated with Deep Pressure Ulcers; A Multi-Parametric MRI Study**

Anke Stekelenburg[1], Gustav J. Strijkers[1], Cees W.J Oomens[1], Dan L. Bader[2], Klaas Nicolay[1]
[1]Eindhoven University of Technology, Eindhoven, Netherlands; [2]Queen Mary, University of London, London, UK

Pressure ulcers represent a serious health and financial problem. Deep pressure ulcers often initiate in the muscle layer near bony prominences. A rat model was developed in which the tibialis anterior muscle was loaded with an indenter. In this study three MRI techniques and a finite element model were applied to this model in order to distinguish between the different factors that contribute to muscle damage during and after compressive loading. The importance of deformation was demonstrated by differences in response to compressive versus ischemic loading, and by a close correlation between location of damage and high shear strain.

11:54 ***260***. **Local Inflammatory Response Due to Burn Coincides with Intramyocellular Lipid Accumulation**

Haihui Cao[1, 2], Qunhao Zhang[2], Loukas G. Astrakas[1, 2], Hongyue Yu[1], Christian Farrar[2], Michael N. Mindrinos[3], Ronald G. Tompkins[2], Laurence G. Rahme[2], A. Aria Tzika[1, 2]
[1]Massachusetts General Hospital and Shriners Institute, Harvard Medical School, Boston, Massachusetts, USA; [2]Massachusetts General Hospital, Harvard Medical School, Boston, Massachusetts, USA; [3]Stanford University, Palo Alto, California, USA

We report that High Resolution Magic Angle Spinning (HRMAS) 1H MR Spectroscopy has detected intramyocellular lipid (IMCL) accumulation in burned versus normal mice. These IMCLs of the former were paralleled by increased expression of mitochondrial uncoupling protein 3 (UCP3) and increased levels of circulating fatty acids. Our findings are consistent with the hypothesis that IMCLs and UCP3 increase after burn in order to protect the myoskeletal mitochondria from the deleterious effect of increased mitochondrial matrix free fatty acids.

12:06 ***261***. **MRI of Denervated Skeletal Muscle for the Diagnosis of Peripheral Nerve Injury**

Eiko Yamabe[1], Toshiyasu Nakamura[1], Koichi Oshio[1], Yoshito Kikuchi[2], Hiroyasu Ikegami[1], Yoshiaki Toyama[1]
[1]School of Medicine, Keio University, Tokyo, Japan; [2]Saitama Municipal Hospital, Saitama, Japan

T2-weighted MR image of denervated skeletal muscle shows high signal intensity. However the relationship between the degree of peripheral nerve injury and the signal intensity is unknown. We investigated the signal changes in T2 weighed images and measured T2 value using various degrees of nerve injury models of rats. Differences in signal intensity can be quantified by measuring T2 value of the target muscle of injured nerve. We can evaluate the degree of nerve injury by the changes in T2 weighed images and the time course of T2 value.

12:18 ***262***. **Preliminary Study for Systemic Sclerosis Staging with MRI**

Jinnan Wang[1], Vasily Yarnykh[1], Chun Yuan[1], Jo Fleming[1], Stephen Schwartz[1]
[1]University of Washington, Seattle, Washington, USA

Systemic sclerosis (SSc) is a rare disease that causes systemic proliferation of connective tissue. High resolution MRI technique was firstly used to study sub-skin layer soft tissue condition, blood supply and vessel wall thickness in human forearms and fingers. By *in vivo* venous flow and vessel morphology quantification, MRI has been shown to be potentially a powerful tool for future SSc study.

MR Tracking and Intervention

Room 613 - 614 10:30 - 12:30 Chairs: Ergin Atalar and Albert C. Lardo

10:30 ***263***. **A Reflection Mode Fiber-Optic Faraday Sensor for Device Localization in Interventional MRI**

Eissa Nadi Aguor[1], Sebastian Brenner[1], Reiner Umathum[1], Wolfhard Semmler[1], Michael Bock[1]
[1]German Cancer Research Center, Heidelberg, Germany

A position-sensor based on the Faraday Effect could be a safe alternative to active tracking coils that use electrically conducting structures in MR-guided interventions with the risk of device heating. The fiber-coupled sensor attenuates traversing light as a function of both the strength of a surrounding magnetic field and the sensor-orientation towards the field-direction. To integrate a Faraday sensor into an interventional device the use of only one fiber for both sensor illumination and signal readout would be advantageous. In this work we present a single fiber sensor-design and prove its operability in the MR environment.

10:42 ***264***. **A Novel Catheter Tracking Method Using Reversed Polarization**

Haydar Çelik[1], Aslý Ulutürk[2], Yiðitcan Eryaman[1], Turgut Tali[2], Ergin Atalar[1, 3]
[1]Bilkent University, Ankara, Turkey; [2]Gazi University, Ankara, Turkey; [3]The Johns Hopkins University, Baltimore, Maryland, USA

Recently, the use of an inductively coupled RF (ICRF) coil in catheter tracking has been introduced. As it was described, visualization of ICRF coil in all sequences and flip angles may be difficult. Here, we proposed a novel ICRF coil tracking method which enables separate visualization of the catheter and the body in one color-coded image by utilization of reverse and forward polarization modes of a receive-only birdcage coil.

10:54 ***265***. **Novel Optically Tunable Capacitor for RF Safe Tuning and Decoupling of Intravascular MR Coils**

Steffen Weiss[1], Thorsten Uelzen[2], Guido Pantel[3], Joerg Mueller[2]

[1]Philips Research Laboratories, Hamburg, Germany; [2]Hamburg University of Technology, Hamburg, Germany; [3]MRI Devices Daum GmbH, Schwerin, Germany

A very compact optically tunable capacitor based on a dedicated metal-oxide-semiconductor interface is proposed, that allows remote optical tuning and decoupling of miniature receive coils for intravascular imaging and catheter tracking. The capacitor is illuminated by laser light guided in an optical fiber and is therefore inherently RF safe, whereas PIN diode based active decoupling would require leads that are prone to RF heating. The capacitance of the device are measured as a function of the incident light power. The device is applied to tune a prototype intravascular receive coil to resonance that can be expanded and therefore changes its inductance.

11:06 ***266***. **Resistively Coupled Interventional Device Visualization**

Greig Cameron Scott[1], William Overall[1], Juan Santos[1], John Pauly[1]

[1]Stanford University, Stanford, California, USA

We present feasibility tests demonstrating that RF ablation electrodes and nitinol guide wires can be resistively coupled to an MRI receiver port to provide sensitive reception. The tissue forms part of the circuit with an external pad acting as signal ground. Placement of the ground pad will also modulate sensitivity. Phantom tests at 1.5T and 0.5T provide high SNR amplitude and phase images. *In vivo* imaging at 0.5T on a rabbit verified the concept for guidewire imaging.

11:18 ***267***. **Cellular Encapsulation and MRI Tracking with Self-Assembled RF Shielded Devices**

Barjor Gimi[1], Dmitri Artemov[1], Timothy Leong[2], Zaver M. Bhujwalla[1], David Gracias[2]

[1]The Johns Hopkins University School of Medicine, Baltimore, Maryland, USA; [2]Johns Hopkins University, Baltimore, Maryland, USA

This paper describes a strategy for the microencapulation of cells and biotherapeutic products using a novel approach to self-assemble 3D metallic containers from 2D photolithographically micropatterned precursors. These containers can be easily detected and tracked with MRI through the RF shielding effect, providing characteristic hypointensity within the container. This demonstration is the first step toward the design of micropatterned, encapsulation devices that can serve as biosensors and can be used in a myriad of interventional applications. Since the strategy is compatible with MEMS, we envision the mounting of electromechanical modules, such as RF microcoils, on the surfaces of these devices.

11:30 ***268***. **Real-Time Virtual Endoscopy for MR-Guided Aortic Interventions**

Klaus J. Kirchberg[1, 2], Andreas Wimmer[1, 2], Christine H. Lorenz[3]

[1]Siemens Corporate Research, Princeton, New Jersey, USA; [2]University of Erlangen, Erlangen, Germany; [3]Siemens Corporate Research, Baltimore, Maryland, USA

Moving from traditional diagnostic MR imaging to MR-guided interventions requires not only specialized pulse sequences, but also novel means of visualization and navigation. We propose an interactive, segmentation-based approach to render a virtual endoscopic view of the aorta in real-time. A 3D/4D model is generated and then continuously updated based on the subsequently acquired MR images. The model construction, updating and rendering is integrated in a graphical scanner control and automation framework.

11:42 ***269***. **Real-Time MR-Guided Endovascular Stent-Graft Placement in an Animal Model of Aortic Dissection**

Harald H. Quick[1], Holger Eggebrecht[1], Hilmar Kuehl[1], Gernot M. Kaiser[1], Stephanie Aker[1], Michael O. Zenge[1], Frank Breukmann[1], Frank Stock[1], Mark E. Ladd[1]

[1]University Hospital Essen, Essen, Germany

Real-time MRI guided endovascular stent-graft placement for therapy of experimental aortic dissection in a pig model has been evaluated. Dissections of the descending thoracic aorta were successfully created under x-ray in 8 domestic pigs. Subsequent stent-graft implantation was performed under rtMRI guidance. In 7/8 pigs, rtMRI permitted: 1) safe navigation from the iliac arteries to the thoracic aorta, 2) precise positioning, and 3) successful deployment of the stent-grafts. Post-interventional MRI demonstrated correct stent-graft positioning and complete false lumen obliteration as confirmed by necropsy. Besides pre-interventional evaluation and procedure guidance, MRI permits immediate post-interventional anatomic and functional evaluation of procedure success.

11:54 ***270***. **MR-Guided Trans Apical Delivery of a Self Expanding Heart Valve Prosthesis Equipped with a Resonant Circuit: Initial Experiences in a Porcine Model**

Andreas Melzer[1], Keith Horvath[2], Michael Guttman[2], Ming Li[2], Erwin Immel[1, 3], Robert Lederman[2], Jan Spilner[4], Christine Lorenz[5], Elliot McVeigh[2]

[1]INSITE med. University Gelsenkrichen, Gelsenkirchen, Germany; [2]NIH, Bethesda, Maryland, USA; [3]Biophan, Castrop Rauxel, Germany; [4]RWTH Aachen, Aachen, Germany; [5]Siemens, Erlangen, Germany

MRI guided implantation of inductively coupled self expanding stents based heart valve prosthesis

12:06 ***271***. **Fusion of Delayed Hyperenhancement MRI with Live X-Ray Imaging for Guidance of Targeted Endomyocardial Injections of Therapeutic Cells**

Luis F. Gutiérrez[1, 2], Ranil de Silva[2], Amish N. Raval[2], Naheed Banu, Elliot R. McVeigh, [12], Cengizhan Ozturk[2], Robert J. Lederman[2]

[1]Johns Hopkins University School of Medicine, Baltimore, Maryland, USA; [2]NHLBI, NIH, Bethesda, Maryland, USA

MRI and X-ray fluoroscopy provide complementary information for diagnosis and treatment of myocardial infarction. We fused pre-procedural delayed-hyperenhancement MRI with live X-ray to guide endomyocardial injection of iron-labeled mesenchymal stromal cells to the infarcts of 12 swine. Injections were identified on post-injection T2*-weighted MRI for *in vivo* quantitative measurement of registration error. Injections were also spiked with tissue dye for visualization on *ex vivo* TTC-stained heart slices. Fusion-predicted injection locations mapped onto DHE images compared favorably with dye staining on necropsy, and *in vivo* error was 3.2±2.6 mm (n=64). Fusion of DHE-MRI and live X-ray enables accurate, targeted endomyocardial injections.

12:18 ***272***. **MR-Guided Electrophysiology Interventions**

Richard Philip Mallozzi[1], Renee A. Guhde[1], Eric Fiveland[1], Robert D. Darrow[1], Charles L. Dumoulin[1], Ehud J. Schmidt[2], Jeremy D. Dando[3], Dale E. Just[3], Godtfred Holmvang[4], Zachary J. Malchano[4], Srinivas R. Dukkipati[4], Vivek Y. Reddy[4]

[1]GE Global Research, Niskayuna, New York, USA; [2]GE Healthcare, Waukesha, Wisconsin, USA; [3]St. Jude Medical, Minnetonka, Minnesota, USA; [4]Massachusetts General Hospital, Boston, Massachusetts, USA

A system for performing electrophysiology interventions under real-time MRI guidance has been developed, with the target of treating atrial fibrillation and ventricular tachycardia. Voltage maps have been acquired on five infarcted pigs under both MRI guidance and the clinical gold standard, CARTO (Biosense-Webster)and compared. Simultaneous RF ablation and MR Imaging has been performed with no degradation of image quality.

GOLD CORPORATE MEMBER LUNCHTIME SYMPOSIUM
Siemens Medical Solutions
syngo MR Applications. Powered by Tim.

Room 6A-B 12:30 - 13:30

CLINICAL MRI COURSE
MR Neurography for Musculoskeletal Radiologists

Room 6C 13:30 – 15:30 Chair: Kimberly K. Amrami

MR Neurography – Imaging Peripheral Nerves

Educational Objectives:
Upon completion of this session, participants should be able to:

- Describe the appropriate techniques for MR neurography of peripheral nerves;
- Identify specific patterns of disease using MR neurography;
- Apply these techniques for specific indications; and
- Explain the role of image reformatting and post-processing for MR neurography.

Diagnosis and Treatment of Peripheral Nerve Problems

Educational Objectives:
Upon completion of this session, participants should be able to:

- Describe the application of MR neurography for directing fascicular biopsy;
- Explain the role of MR of peripheral nerves in clinical decision making; and
- Describe MR findings in specific disease affecting peripheral nerves.

13:30 **MR Neurography – Imaging Peripheral Nerves**
Kenneth R. Maravilla

14:30 **The Role of MRI in the Diagnosis and Treatment of Peripheral Nerve Problems**
Robert J. Spinner

CLINICAL SCIENCE FOCUS SESSION: Diffusion Tensor Tractography: Clinical Applications

Room 6D 13:30 - 15:30 Chairs: Yukio Miki and A. Gregory Sorensen

13:30 *273.* **Focal Wallerian Degeneration of Corpus Callosum in Large Middle Cerebral Artery Stroke: Serial Diffusion Tensor Imaging**

Sona Saksena[1], Rakesh Kumar Gupta[1], Khader M. Hasan[2], Atul Agarwal[3], Mohammad Haris[1], Chandra M. Pandey[1], Ponnada A. Narayana[2]

[1]Sanjay Gandhi Post-Graduate Institute of Medical Sciences, Lucknow, Uttar Pradesh, India; [2]University of Texas Medical School at Houston, Houston, USA, USA; [3]King George's Medical University, Lucknow, Uttar Pradesh, India

Diffusion tensor imaging data were acquired from eight patients with symptoms of large middle cerebral arterial territory stroke and eight healthy age matched controls at different time points. Region-of-interest analysis was performed on seven segments of the corpus callosum for determining the fractional anisotropy (FA), mean diffusivity, and the corresponding callosal cross-sectional areas. A significant temporal decline in FA values was observed suggesting cortico-callosal wallerian degeneration in these patients.

13:40 ***274***. **Diffusion Tensor Imaging Demonstrates the Evolution of Axonal Degeneration After Corpus Callosotomy**

Luis Concha[1], Donald W. Gross[1], Christian Beaulieu[1]
[1]University of Alberta, Edmonton, Alberta, Canada

Axonal degeneration of white matter is a key consequence of neuronalor axonal injury. Diffusion parameters were followed using diffusiontensor imaging (DTI) in three patients who underwent surgicalbisection of the corpus callosum. Diffusion anisotropy was reduced ina spatially dependent manner at one week and remained low 2-4 monthsafter the surgery. The lower FA was due to a reduction in paralleldiffusivity (consistent with axonal fragmentation) at 1 week, whereas an increase in perpendicular diffusivity (consistent with myelin degradation) was responsible at 2-4 months. DTI is capable of non-invasively following and staging Wallerian Degeneration in white matter.

13:50 ***275***. **Bootstrap-Based Longitudinal Analysis of DTI Estimates (BLADE): Applications in Clinically Isolated Syndrome Patients**

SungWon Chung[1], Daniel Pelletier[1], Jeffrey I. Berman[1], Meredith A. Metcalf[1], Roland G. Henry[1]
[1]University of California, San Francisco, San Francisco, California, USA

A novel approach of longitudinal DTI analysis, incorporating uncertainty information acquired by bootstrap on voxel-by-voxel basis, is illustrated and applied to patients with clinically isolated syndromes suggestive of multiple sclerosis. Using this approach, we were able to detect localized changes of fractional anisotropy over time, which would be difficult with histogram or ROI analyses. This method's capability to follow individual patients on voxel level may be useful in monitoring the changes in specific axonal pathways and provide new information relevant to disease progression and treatment effects in the study of axonal degeneration in normal controls and neurological disorders.

14:00 ***276***. **Quantitative Entire Brain Diffusion Tensor Imaging of Spina Bifida Meningomyelocele Children at 3.0T: Preliminary Evidence of Neurodevelopmental Brain Plasticity**

Khader M. Hasan[1], Ambika Sankar[1], Larry Kramer[1], Linda Ewing-Cobbs[2], Michael Brandt[2], Julia Hannay[3], Susan Blaser[4], Maureen Dennis[5], Jack M. Fletcher[2]
[1]University of Texas Medical School, Houston, Texas, USA; [2]UofT, Houston, Texas, USA; [3]UofH, Houston, Texas, USA; [4]HSC, Toronto, ON, Canada; [5]Hospital for Sick Children, Toronto, Ontario, Canada

Spina Bifida Meningomyelocele (SBM) is a common congenital neurodevelopmental disorder with a rate of 0.5-1 per 1000 live births. SBM is caused by incomplete neural tube closure during the first 5-6 weeks of gestation and results in abnormal function and maturation of the spinal cord and brain. Quantitative MRI of SBM is generally scant. In this report, we present the first diffusion tensor imaging study on SBM children to demonstaret evidence of brain plasticity in SBM, including regions that are not directly affected. In this preliminary report, we have used an optimally designed entire brain DT-MRI protocol at 3.0 T in combination with conventional MRI sequences to document regional differences between 19 healthy pediatric controls and 10 children with SBM.

14:10 ***277***. **Assessing White Matter Integrity with DTI in a Large Group of ALS Patients**

Caroline Sage[1], Ronald Peeters[1], Wim Robberecht[1], Stefan Sunaert[1]
[1]University Hospital of the Catholic University of Leuven, Leuven, Belgium

Amyotrophic lateral sclerosis (ALS) is a neurodegenerative condition of complex pathology in humans, primarily involving motor neurons in the cerebral cortex (upper motor neurons), the brainstem and the spinal cord (lower motor neurons). In this 3T study, using DTI (16 directions of diffusion, b=800 s/mm^2) with voxel based statistics and fiber tractography, significant changes in fractional anisotropy (FA), diffusivity (MD), and DTI fiber count in a group of 33 patients compared to 21 healthy controls were observed in corticospinal tract, but also frontal and parietal white matter tracts projecting from/to the motor system.

14:20 ***278***. **Non-Invasive Mapping of Corticofugal Fibers from Multiple Motor Areas: Useful Tool for Assessing Disconnection After Sub-Cortical Stroke?**

Jennifer Michelle Newton[1], [2], Nick S. Ward[1], Geoffrey J. Parker[3], Ralf Deichmann[1], Daniel C. Alexander[1], Karl J. Friston[1], Richard SJ Frackowiak[1]
[1]University College London, London, UK; [2]UCLA, Los Angeles, California, USA; [3]University of Manchester, Manchester, UK

Here we describe the trajectories of the corticofugal connections from each major component of the motor system using probabilistic tractography in normal subjects. We then infer damage to corticofugal pathways in patients with sub-cortical stroke by comparing the overlap between significant regions of reduced anisotropy with the trajectories of corticofugal fibers to each motor area in the normal subjects. We found that these inferred disconnections could explain enhanced handgrip related responses, as assessed with functional MRI, in the ipsilesional motor system. These results confirm that selective disruption of motor corticofugal fibers influences functional reorganization in individual patients.

14:30 ***279***. **Semi-Automated Fiber-Based Analysis of Group Differences in DTI**

Lori R. Arlinghaus[1], Rui Li[1], Benoit M. Dawant[1], Zhaohua Ding[1], Junghee Lee[1], Sohee Park[1], Adam W. Anderson[1]
[1]Vanderbilt University, Nashville, Tennessee, USA

The definition of point-correspondence between subjects is a major challenge in the implementation of fiber-based (FB) analysis methods of DTI data. We have developed a FB analysis scheme which provides semi-automated seed point selection and point-correspondence definition based upon the co-registration of the diffusion tensor image spaces. This method was applied to a study of FA differences between control and schizophrenic subjects in the cingulum, uncinate, and arcuate fasciculi. We found our method to be consistent with the results of ROI and VB analysis.

14:40 ***280***. **Probabilistic Diffusion Tractography: A Potential Tool to Assess the Rate of Disease Progression in ALS**

Olga Ciccarelli[1], Tim E. Behrens[2], Dan R. Altmann, [13], R W. Orrell[4], [5], R S. Howard[4], Heidi Johansen-Berg[2], David H. Miller[1], Paul M. Matthews[2], Alan J. Thompson[1]
[1]Institute of Neurology, London, UK; [2]FMRIB, Oxford, UK; [3]Medical Statistics Unit, London, UK; [4]NHNN, London, UK; [5]Royal Free and Univ. College Medical School, London, UK

We developed two voxel-based measures of connectivity along the tractography-derived cortico-spinal tract and studied 13 patients with Amyotrophic Lateral Sclerosis (ALS) and 19 controls. Patients with a rapid disease progression rate had significantly lower connectivity measures than controls in the left CST. Strong associations between these connectivity measures and the rate of disease progression were found. These findings suggest that the newly developed summary connectivity measures are sensitive markers of structural damage in the CST that is associated with the rate of disease progression

14:50 ***281***. **Corticocortical Connectivity of Probst Bundle Fibers in Callosal Dysgenesis Revealed by Diffusion Tensor Imaging Fiber Tractography**

SungWon Chung[1], Pratik Mukherjee[1], Roland G. Henry[1], Jeffrey I. Berman[1], Steven W. Hetts[1], Anthony James Barkovich[1], Elliott H. Sherr[1]
[1]University of California, San Francisco, San Francisco, California, USA

DTI fiber tractography was used to noninvasively map the connectivity patterns of Probst bundle fibers in one adolescent and two adults with callosal dysgenesis. In a normal adult volunteer, fiber tracking of the corpus callosum showed the expected homotopic organization. In callosal dysgenesis, the dominant corticocortical connectivity of the Probst bundles was between medial frontal lobe and the ipsilateral superior parietal area. In the only subject without left hemispheric cortical malformations, connectivity was also identified between left medial prefrontal cortex and left anterior temporal lobe, but not in the right hemisphere of any of the 3 experimental subjects.

15:00 ***282***. **DSI Tractography Demonstrates Connectivity Remodelling After Stroke**

Cristina Granziera[1], Van Wedeen[1], Thomas Benner[1], Ruopeng Wang[1], Gregory A. Sorensen[1]
[1]NMR-MGH Center, Charlestown, Massachusetts, USA

We studied a patient with a clinical picture of Wernicke's aphasia (fluent aphasia: impaired comprehension, naming and repetition) due to a lesion in the posterior region of the left superior temporal gyrus and involving the inferior part of the parietal lobe.Using DSI tractography, we could map the post-stroke remodelling of fibers located the stroke region and directly involved in the pathophysiology of the clinical picture (arcuate fasciculum). This work demonstrates that DSI could be used to study the connectivity involved in stroke recovery giving an anatomical insight into the complex mechanisms leading to functional improvement after an ischemic lesion.

15:10 ***283***. **Quantitative Tract-Of-Interest Metrics for White Matter Integrity Based on Diffusion Tensor MRI Data**

Stephanie Y. Lee[1], Stephen Correia[2], David F. Tate[2], Robert H. Paul[2], Song Zhang[2], Stephen P. Salloway[2], Paul F. Malloy[2], David H. Laidlaw[1]
[1]Brown University, Providence, Rhode Island, USA; [2]Brown Medical School, Providence, Rhode Island, USA

Problem: To provide initial validity data on new quantitative DTI tractography metrics for assessing cerebral white matter integrity.Method: From whole-brain streamtube models of white matter pathways we calculated the number of streamtubes and their summed total length (TL). Additional metrics included TL weighted for average linear anisotropy and normalized for intracranial volume. Results: Patients with vascular cognitive impairment had significantly lower values ($p<.05$) than the controls on all length metrics but not the number of streamtubes. Conclusions: These results provide preliminary evidence that these new quantitative DTI tractography metrics hold promise for examining group differences in white matter health.

15:20 ***284***. **Diffusion Tensor Tractography in Schizophrenia**

Vincent Alfonso Magnotta[1], Adix Michael[1], Kelvin Lim[2], Arvind Caprihan[3], Randy Lyanne Gollub[4], Nancy Andreasen[1,3]
[1]The University of Iowa, Iowa City, Iowa, USA; [2]The University of Minnesota, Minneapolis, Minnesota, USA; [3]The MIND Institute, Albuquerque, New Mexico, USA; [4]Massachusetts General Hospital, Boston, Massachusetts, USA

A novel tract tracing algorithm was applied to study connectivity of the cerebellum and thalamus in patients with schizophrenia compared to a control sample. The patients had overall lower fractional anisotropy values along the identified tracts. Discrete areas of deficits were seen in both fiber tracts (left and right) in similar locations.

ELECTRONIC POSTER DISCUSSION: Parallel Imaging Reconstruction

Room 4C - 3,4 13:30 - 15:30 Chairs: Mark A. Griswold and David J. Larkman

13:30 ***285***. **Spatially Variant GRAPPA**

Eugene G. Kholmovski[1], Dennis L. Parker[1]
[1]University of Utah, Salt Lake City, Utah, USA

GRAPPA, widely used technique for parallel MRI, has serious limitations for high reduction factors. Recently, new algorithms have been proposed to resolve this GRAPPA limitation. These algorithms exploit all available data dimensions to find reconstruction coefficients allowing more reliable reconstruction for high reduction factors. However, inclusion of additional data dimensions in the reconstruction substantially increases the number of reconstruction coefficients resulting in low computational efficiency of these new algorithms. A novel algorithm has been developed that achieves equivalent image quality for high reduction factors as the multi-dimensional auto-calibrating techniques but has computational efficiency comparable with the computational efficiency of GRAPPA.

13:40 ***286***. **A 3D GRAPPA Algorithm for Volumetric Parallel Imaging**

Felix Breuer[1], Martin Blaimer[2], Nicole Seiberlich[1], Mark Griswold[2], Peter Jakob[1]
[1]University of Würzburg, Würzburg, Germany; [2]University Hospitals of Cleveland, Cleveland, Ohio, USA

It has been shown that the GRAPPA method is the method of choice in applications where sensitivity maps, as required for SENSE reconstruction, are hard to obtain. This is for example the case in regions with low SNR, such as the lung. In this work, a 3D GRAPPA reconstruction algorithm for volumetric parallel imaging is presented, which is more efficient than previous proposed k-space based strategies. The method is described for conventional rectangular scan-time reductions in two spatial dimensions and 2D CAIPIRINHA-type reductions where sampling positions are shifted with respect to each other.

13:50 ***287***. **Potential Pitfalls of Including Reference Data in Parallel Imaging Reconstructions at High Acceleration**

Donglai Huo[1], Mark Griswold[1], Martin Blaimer[1], David Wilson[1]
[1]Case Western Reserve University, Cleveland, Ohio, USA

In GRAPPA, the ACS (Auto Calibration Signal) lines are used to determine coil-weighting factors and can be included directly in the. Park *et al*. proposed shifting the calibration region to higher frequency in the PE direction. This modification can improve overall image quality, but at high acceleration factors, it can create shading and blurring of the image. Adding center reference data can reduce these artifacts, but the residual artifact is still a big issue in clinical applications requiring fine details. One should be careful when incorporating reference data in a GRAPPA reconstruction, in particular at high acceleration factors.

14:00 ***288***. **Regularized Channel-Dependent Kernel Deconvolution for Resolution Enhancement in SEA Imaging**

Jim X. Ji[1], Jong Bum Son[1], Mary P. McDougall[1], Steven M. Wright[1]
[1]Texas A&M University, College Station, Texas, USA

Single Echo Acquisition (SEA) is a completely parallel imaging method that can obtain a 2-D image using only a single echo. In doing so, it utilizes a bank of 64 or more mm-size linear phased-array elements with highly localized sensitivity. Nevertheless, the spatial resolution of the SEA images is still limited by the coil sensitivity profiles, which are not completely localized to the desirable voxel size. In this work, we developed a deconvolution method for resolution enhancement in SEA imaging. To address the highly ill-conditioning problem, Tikhonov's regularization is adopted to constrain the deconvolution process. Preliminary computer simulation results using data collected from a 4.7 Tesla scanner show that the new method can achieve super resolution when appropriate channel sensitivity is available.

14:10 ***289***. **Improving KtSENSE by Adaptively Selecting the Regularization Image**

Dan Xu[1], Kevin Franklin King[2], Zhi-Pei Liang[1]
[1]University of Illinois at Urbana-Champaign, Urbana, Illinois, USA; [2]General Electric Healthcare, Milwaukee, Wisconsin, USA

The recently-proposed ktSENSE has shown very encouraging results with a factor of 5-8 improvement in imaging speed for several dynamic imaging applications. This paper presents an improvement on the method by providing adaptively-selected the regularization image for image reconstruction. Specifically, a variable-density, sequentially interleaved sampling pattern with references is proposed for data acquisition. This scheme provides sufficient ¡ auxiliary¡± data to reconstruct high-resolution time-varying images using a generalized series model, which are then used as regularization images (adaptive to each time frame) to remove aliasing effects due to undersampling along both the time and k axes. Cardiac imaging experiments were carried out using the proposed method and compared with ktSENSE and other methods, which showed a substantially improved temporal resolution and less image artifacts.

14:20 ***290***. **Noise Characteristics of Arterial Spin Labeling fMRI Using Spiral SENSE at 3T**

Joanna E. Perthen[1], Mark Bydder[1], Khaled Restom[1], Thomas T. Liu[1]
[1]UCSD, San Diego, California, USA

In this study, the effect of parallel imaging on the noise characteristics of ASL fMRI data was investigated. Whilst thermal noise increased as the length of the acquisition window shortens, the contribution of respiratory noise was found to decrease, possibly reflecting the fact that there is less time for accrual of global phase errors induced by expansion of the thoracic cavity. Functional data show that in areas of the brain contaminated by respiratory noise, the use of physiological noise correction schemes gives the largest improvement in SNR when using long readout windows.

14:30 ***291***. **fMRI at Ultra High Field (7T) with GRAPPA and SENSE**

Steen Moeller[1], Ute Goerke[1], Kâmil Ugurbil[1]
[1]University of Minnesota, Minneapolis, Minnesota, USA

Parallel imaging is a reconstruction technique which has enabled the trading of spatial SNR for either higher spatial or faster temporal resolution. The impact on the CNR for optimal fMRI studies is compared between SENSE and GRAPPA with a 1-dimensional reduction factor of 4. The noise, t-scores, p-values, and number of activated pixels are used to measure the differences.

14:40 ***292***. **Applying Parallel Imaging in Hyperpolarized ^{3}He *In Vivo* MRI to Achieve High Acceleration Factor Without the Conventional SNR Penalty**

Ray F. Lee[1], Glyn Johnson[1], Bernd Stockel[2], Rorbert Trampel[1], Igor Kamenetskiy[1], Georgeann McGuinness[1]
[1]New York University, New York, USA; [2]Siemens Medical Solutions, Inc., New York, USA

The continual depletion of the signal level over the course of excitations in hyperpolarized 3He MRI results in a SNR that can be independent of the number of excitations. This suggests that one can use parallel MRI to gain both temporal and spatial resolution without conventional loss in the SNR. Using a 24ch phased array and parallel 3He MRI with a reduction factor of 16 (4x4), an entire lung can be imaged in 13ms and one breath-hold.

14:50 ***293***. **Simultaneous Slice Excitation and Reconstruction for Single Shot EPI**

Rita G. Nunes[1], Joseph V. Hajnal[1], Xavier Golay[2], David J. Larkman[1]
[1]Hammersmith Hospital, Imperial College London, London, UK; [2]Singapore Bioimaging Consortium, Singapore, Singapore

For single shot EPI, reduction in the number of phase encodes associated with parallel imaging has a small impact on scan time Typically 20-30% with a speedup factor of 2. Where time is critical, a better strategy for single shot imaging is to excite multiple slices simultaneously. However, this method suffers from high g-factor when transverse slice geometries are used because of unfavourable coil geometry We propose a new method to introduce an arbitrary shift between two simultaneously excited single shot EPI slices, allowing them to be separated by PPI with acceptable g-factors. We have demonstrated the method *in vivo*.

15:00 ***294***. **Automatic Coil Element Selection for Parallel Imaging of Localized Regions**

Martin Buehrer[1], Peter Boesiger[1], Sebastian Kozerke[1]
[1]ETH Zuerich, Zuerich, Switzerland

Large coil arrays with multiple independent coil elements are advantageous in parallel imaging. At this stage, however, data handling and increased computational effort lead to long reconstruction times. If an imaging region smaller than area covered by the array is targeted, it may be beneficial to select a subset of coil elements without significant SNR loss. In this work an efficient algorithm is presented which automatically determines an optimal element selection for a given imaging region. Given a cardiac 32-element array a considerable number of elements can be deactivated for parallel imaging of the coronary arteries without significant SNR loss.

15:10 ***295***. **Physiological Noise Correction with Increasing Acceleration in SENSE-EPI**

R. Allen Waggoner[1], Mauro Costagli[1], Ken'ichi Ueno[1], Keiji Tanaka[1], Kang Cheng[1]
[1]RIKEN - Brain Science Institute, Wako-shi, Saitama, Japan

Retrospective correction of physiological fluctuations, has been a useful tool for minimizing the variance in EPI time series, for BOLD-fMRI studies. However in accelerated parallel imaging the intrinsic noise increases with acceleration factor, while the physiological noise does not. This study explores the effectiveness of retrospective correction of physiological noise as a function of acceleration factor.

15:20 ***296***. **GRAPPA Reconstruction of Sensitivity Encoded 2D and 3D Proton Echo Planar Spectroscopic Imaging (PEPSI) with SNR Adaptive Recalibrating**

Martin Rueckert[1, 2], Ricardo Otazo[1, 2], Stefan Posse[1, 3]
[1]MIND Institute, Albuquerque, New Mexico, USA; [2]University of New Mexico, Albuquerque, New Mexico, USA; [3]University of New Mexico School of Medicine, Albuquerque, New Mexico, USA

It is demonstrated that high-speed spectroscopic imaging using the PEPSI method, sensitivity encoded by an 8-channel surface RF coil array, can be 4-fold accelerated without significant loss in spectral quality by using GRAPPA parallel imaging. This approach enables PEPSI acquisitions to be performed in less than 3 minutes for 3D spatial encoding and in just a few seconds for 2D spatial encoding. It is shown that the quality of the reconstruction can be improved by adjusting the SNR of the GRAPPA calibration reference to the SNR of the PEPSI-data.

CLINICAL SCIENCE FOCUS SESSION: Women's Imaging

Room 611 - 612 13:30 - 15:30 Chairs: Nola Hylton and Evis Sala

13:30 ***297***. **Screening Women at Genetic Risk of Breast Cancer Using DCE-MRI: The Effect of Gene Mutation Status on Detection Sensitivity, Specificity and Cancer Characteristics**

Martin Osmund Leach[1], T Maribs Study Group[1]

[1]Institute of Cancer Research, Sutton, Surrey, UK

MRI is a sensitive method of detecting cancer in younger women at genetic risk of breast cancer. Combination of MRI with XRM provides a test with a sensitivity of 86%-94%, compared with about 40% for XRM alone. Decisions on how to provide screening for such high risk groups depends on a knowledge of sensitivity in particular risk groups. In this study we present sensitivity and specificity for MRI and XRM alone and in combination in women with BRCA1 or BRCA2 breast cancer predisposition mutations, or women at high familial risk who tested negative for both of these mutations.

13:40 ***298***. **MR Imaging of Ductal Carcinoma In Situ: Morphological Appearances, Kinetic Features, and Choline Quantification with Pathological Correlation**

Jeon-Hor Chen[1, 2], H. J. Yu[1], H-M Baik[1], M-Y Su[1], O. Nalcioglu[1]

[1]University of California, Irvine, Irvine, CA 92697, USA; [2]China Medical University Hospital, Taichung, Taiwan

This study showed a high percentage of DCIS (13/31) was presented with multiple foci of enhancement scattering in a region and presented as clumped pattern in MIPs. Kinetic assessment showed no correlation between the tumor grades and types of enhancement. Intermediate grade DCIS showed higher frequency of rapid initial and washout than high grade DCIS. This finding supported studies that intermediate grade DCIS has even higher microvascular density than that of low and high grade DCIS. Our study also demonstrated that choline level is detectable in DCIS, a finding different from previous reports showing no detectable choline in DCIS patients

13:50 ***299***. **MRI Monitoring of Neoadjuvant Chemotherapy Response in Breast Cancer of Different Phenotypes to Doxorubicin-Cyclophosphamide Followed by Taxane + Carboplatin ± Trastuzumab Regimen**

Min-Ying Su[1], Hon J. Yu[1], Jeon-Hor Chen[1], Rita S. Mehta[1], Toni Schubbert[1], David J-B Hsiang[1], Philip M. Carpenter[1], Orhan Nalcioglu[1]

[1]University of California, Irvine, California, USA

The response of breast cancer to AC, and AC followed by Carboplatin-Taxel ± Herceptin was studied in 53 patients. The lesions were classified into 4 types: mass, multi-nodule, diffuse, and septal pattern. With the more aggressive Taxane protocol, 25/36 achieved a complete response on MRI, with 18/21 cases proven to have a pathological complete response. The responses to three treatment regimens were significantly different, CR was found in 0/13 in AC groups, 13/23 in Her2/neu negative patients receiving AC+TCa, and 12/12 in Her2/neu positive patients receiving AC+TCaH. The MRI phenotype was not associated with response, thus not a good predictor.

14:00 ***300***. **Predicting the Response of Neo-Adjuvant Chemotherapy in Locally Advanced Breast Cancer Patients by Diffusion Weighted Imaging**

K A. Danishad[1], V Seenu[1], N R. Jagannathan[1]

[1]All India Institute of Medical Sciences, New Delhi, Delhi, India

Diffusion weighted MR imaging was carried out in breast cancer patients prior to neo-adjuvant chemotherapy and after chemotherapy along with twelve normal subjects. The ADC value obtained in tumors was significantly lower compared to the normal breast indicating high cellularity and restricted water diffusion. Significant increase in ADC from pre-therapy value was observed after therapy in responders while non responders showed only a marginal increase. Chemotherapy induced reduction in tumor volume was correlated with the change in ADC. The study proved the significance of DW-MRI in the evaluation of the response of the tumor to therapy in a clinical setting.

14:10 ***301***. **Comparison of T1 Fat Saturation vs. High Spectral and Spatial Resolution MRI of Breast Lesions**

Xiaobing Fan[1], Gillian Newstead[1], Milica Medved[1], Sean Foxley[1], Marta Zamora[1], Sunnaz Arkani-Hammad[1], Funmi Olopade[1], Hiroyuki Abe[1], Gregory S. Karczmar[1]

[1]University of Chicago, Chicago, Illinois, USA

High resolution echo-planar spectroscopic images (EPSI) of breast were compared with conventional T1-weighted fat saturated images acquired with the same resolution, slice thickness, and slice location. Women with suspicious breast lesions were imaged on 1.5 Tesla scanners. Images with intensity proportional to the water signal peak height in each voxel were synthesized from the EPSI datasets. The results demonstrated that fat suppression, tumor edge delineation, lesion conspicuity, and image texture were improved in the water peak height images. The water peak height images can be an additional clinical tool to improve detection and diagnosis of breast cancer.

14:20 ***302***. **Highly Accelerated IDEAL-SPGR Breast Imaging**

Charles Alexander McKenzie[1, 2], Randy O. Giaquinto[3], Aaron Grant[4, 5], Ajit Shankaranarayanan[6], David Gurr[7], Ananth Madhuranthakam[8], Huanzhou Yu[6], Anja Brau[6], Ann Shimakawa[6], Sanjay Joshi[7], Vinod V. Menon[7], Andres Carrillo[7], Theodore Steger[7], Susan M. LaRuche[4], Norman Farrar[4], Charles L. Dumoulin[3], Jean H. Brittain[6], Scott B. Reeder[9], Neil M. Rofsky[4, 5], Daniel K. Sodickson[4, 5]

[1]Beth Israel Deaconess Medical Center, Boston, Massachusetts, USA; [2]Harvard Medical School, Boston, Massachusetts, USA; [3]GE Global Research, Niskayuna, New York, USA; [4]Radiology, Beth Israel Deaconess Medical Center, Boston, Massachusetts, USA; [5]Radiology, Harvard Medical School, Boston, Massachusetts, USA; [6]Global Applied Science Laboratory, GE Healthcare, Menlo Park, California, USA; [7]GE Healthcare, Waukesha, Wisconsin, USA; [8]Global Applied Science Laboratory, GE Healthcare, Boston, Massachusetts, USA; [9]University of Wisconsin Medical School, Madison, Wisconsin, USA

This work evaluates the feasibility of using large acceleration factors (>6x) in combination with the Iterative Decomposition of water and fat with Echo Asymmetry and Least-squares estimation (IDEAL) for dynamic contrast enhanced breast MRI. The major drawback of IDEAL is the additional time needed to acquire three images to produce separate water and fat images. Combining large parallel imaging accelerations with IDEAL techniques eliminates this time penalty. IDEAL with parallel imaging acceleration factors as high as 9.6x was applied to T1w SPGR dynamic contrast enhanced imaging. The advantages of IDEAL over standard fat-suppressed imaging are demonstrated in protocols for breast cancer screening or evaluation.

14:30 ***303***. **Cervical Cancer: Value of an Endovaginal Coil Magnetic Resonance Imaging Technique in Detecting Small Volume Disease and Assessing Parametrial Extension**

Nandita deSouza[1, 2], Roberto Dina[2], Angus McIndoe[2], William Patrick Soutter[2]

[1]Institute of Cancer Research, Sutton, Surrey, UK; [2]Hammersmith Hospital, London, UK

Endovaginal magnetic resonance imaging has high sensitivity in the preoperative staging of uterine cervical cancer even for tumors ≤1cm^3. It is an invaluable technique in planning fertility-conserving or radical surgical treatment of early stage cervical cancer.

14:40 ***304***. **Hypointense Malignant Ovarian Tumors on T2-Weighted Images: MR-Pathologic Correlation**

Mayumi Takeuchi[1], Kenji Matsuzaki[1], Hiromu Nishitani[1], Hisanori Uehara[1]

[1]Univ. of Tokushima, Tokushima, Japan

Very rare hypointense malignant tumors of the ovary on T2-weighted images are evaluated with pathologic correlation. T2 shortening of the pathologies were caused by primary and secondary ovarian stromal proliferation in Krukenberg's tumor, malignant carcinoid tumor, and malignant Brenner tumor, and by mucinous, viscid proteinous material and/or coagulated necrosis in mucinous cystadenocarcinoma, clear cell carcinoma (solid variant), and choriocarcinoma. Preoperative diagnosis of these tumors from benign sex-cord stromal tumors, which may often show hypointensity on T2-weighted images, is important and should be made by their characteristic clinical and imaging findings.

14:50 ***305***. **Value of Diffusion-Weighted Images in Ovarian Tumors**

Takashi Koyama[1], Ken Tamai[1], Shigeaki Umeoka[1], Tsuneo Saga[1], Shingo Fujii[1], Kaori Togashi[1]

[1]Kyoto University, School of Medicine, Kyoto, Japan

The purpose of this study was to investigate value of DWI for detecting ovarian tumors, peritoneal implants, and metastatic lymphadenopathy and for differentiating benignancy and malignancy. In our series of 33 patients with surgically confirmed ovarian tumors, T2WI and fusion images with DWI were evaluated regarding the presence of abnormal intensity, peritoneal implants and lymphadenopathy. Abnormal signal was observed in all ovarian cancers. However, benign endometrial cysts and dermoid cyst also showed high intensity on DWI. Fusion image with DWI was superior to T2WI in demonstrating peritoneal implants and metastatic lymphadenopathy.

15:00 ***306***. **Comparison of Dynamic TrueFisp Versus HASTE Imaging for the Evaluation of Pelvic Floor Dysfunction**

Elizabeth M. Hecht[1], Bachir Taouli[1], Samson Wong[1], James S. Babb[1], Genevieve L. Bennett[1]

[1]New York University, New York, USA

The purpose of this study is to compare dynamic True Fisp and HASTE sequences to determine if one demonstrates a greater degree of pelvic floor dysfunction. Greater degrees of organ prolapse in all three pelvic compartments were diagnosed using the dynamic True Fisp when compared to the static HASTE sequence. The ability to image in real time with the True Fisp sequence may allow for more physiologic evaluation of the pelvic floor.

15:10 ***307***. **Role of MR Imaging in Diagnosis of Urethra Hypermobility and Intrinsic Sphincter Deficiency in Women with Stress Urinary Incontinence**

Katarzyna J. Macura[1], Rene R. Genadry[1], David A. Bluemke[1]

[1]Johns Hopkins Medical Institutions, Baltimore, Maryland, USA

This work reports on age-matched urethral sphincter size comparison between continent and incontinent women based on intraurethral MR imaging. We also report on correlations between MRI findings and urodynamics which have not been previously documented. This work shows that although, the decrease in urethral sphincter volume has been associated with stress incontinence in women it is also associated with normal aging. There is high correlation between several urodynamics variables and MRI findings which promises that MRI may become an important adjunct tool in the evaluation of women with stress urinary incontinence.

15:20 ***308***. **Evaluations of the Female Pelvis: Comparison of 3D T2-Weighted FSE Images Using ASSET and 2D T2-Weighted FSE Images in Three Planes**

Takayuki Masui[1], Motoyuki Katayama[1], Kimihiko Sato[1], Masahiro Sugiyama[1], Hidekazu Seo[1], Atsushi Nozaki[2], Masaya Hirano[2]

[1]Seirei Hamamatsu General Hospital, Hamamatsu, Shizuoka, Japan; [2]GE Yokogawa Medical Systems, Hino, Tokyo, Japan

For evaluation of the female pelvis, 2D T2-weighted FSE imaging in the axial and sagittal planes is important. With parallel imaging technique, 3D T2-weighted imaging can be one of the options for the replacement of all 2D T2-weighted images. In the current study, comparison of the abilities of one set of 2D T2-weighted images in axial, sagittal and perpendicular to the axis of the uterus planes with that of 3D T2-weighted images for the evaluation of the female pelvis was made. 3D T2-weighted FSE images give useful information and can be substitute for 2D T2-weighted FSE images in three planes.

CLINICAL SCIENCE FOCUS SESSION: Characterization of CNS Disorders using fMRI

Room 615 - 617 13:30 - 15:30 Chairs: Thomas Ernst and Stefan Sunaert

13:30 ***309***. **Analyzing Differences of Static BOLD-Sensitive Whole Brain MR Images: Application in Dementia**

Serge A. Rombouts[1], Philip Scheltens[1], Joost Kuijer[1], Frederik Barkhof[1]

[1]VU University Medical Center, Amsterdam, Netherlands

Eighteen patients with Alzheimer's disease, 28 patients with mild cognitive impairment and 41 healthy elderly controls participated. Static (no time series) BOLD-sensitive reference state EPI images (visual fixation) showed decreased signal in patients in the hippocampus, posterior cingulate cortex / precuneus, insula / putamen, and parietal cortex. This shows that not only brain (de)activation is altered in dementia with fMRI, but also the static signal during the reference condition in certain regions. Most of these differences are likely caused by grey matter atrophy, although decreased metabolism, or perhaps iron deposition may also contribute.

13:40 ***310***. **Model-Free Group Analysis Shows Altered BOLD Networks in Dementia**

Serge A. Rombouts[1], Jeske S. Damoiseaux[1], Frederik Barkhof[1], Philip Scheltens[1], Stephen M. Smith[2], Christian F. Beckmann[2]

[1]VU University Medical Center, Amsterdam, Netherlands; [2]John Radcliffe Hospital, Oxford, UK

Tensorial probabilistic independent component analysis (T-PICA) is a newly developed, exploratory, model free technique that can be used to analyze group fMRI data. T-PICA was applied to analyze on/off fMRI data (face encoding versus fixation) in 18 patients with Alzheimer's disease, 28 with mild cognitive impairment, and 41 healthy elderly controls. This showed decreased reactivity in patients in activated networks of cognitive, motor, and visual processing. Reactivity was also decreased in the deactivated default mode network. Furthermore, T-PICA appeared more sensitive to detect group differences than the commonly applied model-based technique.

13:50 ***311***. **Vascular Versus Neuronal Defects in Amyotrophic Lateral Sclerosis: An fMRI Study**

Caroline Sage[1], Ronald Peeters[1], Wim Robberecht[1], Stefan Sunaert[1]

[1]University Hospital of the Catholic University of Leuven, Leuven, Belgium

Amyotrophic lateral sclerosis (ALS) is a neurodegenerative condition of complex pathology, primarily involving motor neurons in the cerebral cortex, the brainstem and the spinal cord. Patients lose the ability to generate and execute voluntary movements. Apart from neuronal loss, vascular deficits could play a role in the physiopathology of ALS. We performed an fMRI study, assessing the activation pattern in the brain during the performance of a motor task, an imaginary motor task and an alternating hyperventilation/breath-hold task. The obtained activation patterns were compared to controls, to evaluate whether vascular and/or neuronal defects contribute to the physiopathology of ALS.

14:00 ***312***. **fMRI Reveals Declined Activation of Prefrontal Cortex in Epilepsy Patients on Topiramate Therapy**

Jacobus F.A. Jansen[1, 2], Albert P. Aldenkamp[1, 3], H. J.Marian Majoie[1, 3], Rianne P. Reijs[1, 3], Marc C.T.F.M de Krom[1], Paul A.M. Hofman[1], M. Eline Kooi[1, 2], Klaas Nicolay, [12], Walter H. Backes[1, 2]

[1]University Hospital Maastricht, Maastricht, Netherlands; [2]Eindhoven University of Technology, Eindhoven, Netherlands; [3]Epilepsy Centre Kempenhaeghe, Heeze, Netherlands

The antiepileptic drug topiramate is often associated with cognitive side effects. We used fMRI of covert word generation to examine brain activation abnormalities associated with topiramate-induced cognitive impairment in patients with epilepsy. Compared with a control epilepsy group, the topiramate group showed significantly less activation in the language-mediating cortical regions (left inferior prefrontal cortex (IPC) and the medial prefrontal cortex (MPC)) together with significant lower neuropsychological language scores. Furthermore, the IPC and MPC display a higher relative sensitivity to TPM treatment than other brain regions.These findings suggest that topiramate has a critical effect on the cerebral neural systems that mediate expressive language.

14:10 ***313***. **Amygdala Activity in Major Depression: Modulation by Serotonergic Genes**

Harald Kugel[1], Udo Dannlowski[1], Patricia Ohrmann[1], Jochen Bauer[1], Bernhard T. Baune[1], Christa Hohoff[1], Anette Kersting[1], Volker Arolt[1], Walter Heindel[1], Jürgen Deckert[1], Thomas Suslow[1]

[1]University of Muenster, Muenster, NRW, Germany

Polymorphisms of genes involved in serotonergic neurotransmission, e.g., the serotonin transporter gene (5-HTT) and the serotonin receptor 1A (5-HT_{1A}) gene, have been implicated in the pathogenesis of depression. From studies in healthy controls it was suggested that the gene's effect might be mediated via dysfunctional amygdala activity, a brain structure critical for emotion processing. The data of this study suggest that in patients with major depression, amygdala excitability in response to emotionally relevant stimuli is influenced by the 5HT_{1A}-1019C/G and the 5-HTTLPR polymorphism.

14:20 ***314***. **Anxiety Disease: Decreased of Functional Connectivity in Left Superior Temporal Gyrus (GTs) and Right GTs**

Zhao Xiaohu[1], Hu Zhenghui[2], Wang Peijun[1], Shi Pengcheng[2]

[1]Tong Ji Hospital of Tong Ji University, Shanghai, People's Republic of China; [2]Hong Kong University of Science and Technology, Hong Kong, People's Republic of China

In this study, we attempt to characterize the joint interactions between left superior temporal gyrus (GTs) and right GTs during processing of differential emotional words in anxiety patients and control subjects. Our result suggests decreased information flow among two brain region during processing of anxiety word to neutral word in anxiety patients.

14:30 ***315***. **Neurocognitive Mapping of Visuospatial Judgment in Healthy Subjects and Chronic Alcoholics – an fMRI Study**

Manisha Bhattacharya[1], Senthil S. Kumaran[1], Shilpi Modi[1], Subash Khushu[1]

[1]Institute of Nuclear Medicine and Allied Sciences, DELHI, India

Neurocognitive mapping for visuospatial tasks has been carried out in healthy volunteers and chronic alcoholics, using BOLD technique. Significant activations observed in the parietal, occipital lobes and frontal cortex in healthy subjects are attributed to spatial representation and the processing of spatial information and attention shifting. In alcoholics, activations were quite less in the above regions as compared to controls, indicating impairment.

14:40 ***316***. **Effect of Prenatal Alcohol Exposure on Brain Activation During Arithmetic Task**

Priya Santhanam[1], Xiaoping Hu[1], Scott J. Peltier[1], Zhihao Li[1], Claire D. Coles[2], Mary Ellen Lynch[2]

[1]Emory University, Atlanta, Georgia, USA; [2]Emory University School of Medicine, Atlanta, Georgia, USA

Prenatal alcohol exposure (PAE) is known to be associated with structural abnormalities, including diminished growth and microcephaly. The present study examines the effects of PAE on brain activation during an arithmetic task. Seven characterized PAE subjects and 7 control subjects were asked to perform a basic arithmetic task using a block-design paradigm. Significant activation was present in temporal, prefrontal, posterior cingulate, angular gyrus, and parietal regions in PAE subjects, while control subjects demonstrated activation in the temporal and prefrontal regions only ($p<0.05$). Results suggest a PAE subject must utilize more neurons in the parietal and prefrontal regions for arithmetic tasks.

14:50 ***317***. **Age-Related Increase in Brain Reserve in HIV Subject During Attention Tasks**

Linda Chang[1], Renat Yakupov[1], Laura Girton[2], Tara Nash[1], Helenna Nakama[1], Thomas Ernst[1]

[1]University of Hawaii, John A. Burns School of Medicine, Honolulu, Hawaii, USA; [2]Queens Medical Center, Honolulu, Hawaii, USA

Aging and HIV-infection both may lead to decreased ability to attend. Functional MRI was performed in 39 HIV-subjects [17 with cognitive deficits (HIV-CD) and 22 neuroasymptomatic (HIV-NA)] and 19 seronegative controls (SN) during visual attention tasks to evaluate possible interactive effects of aging and HIV. Age-dependent increases in activation were greater in the parietal regions of HIV-NA, but in the prefrontal regions of HIV-CD. These findings suggest, with aging, HIV may cause even less efficient usage of the normal network, but greater usage of the reserve regions. Cognitive deficits ensued in HIV-CD when the reserve capacity was exhausted on more difficult tasks.

15:00 ***318***. **fMRI and Carotid Artery Intima-Media Thickness in Patients with Cardiovascular Disease**

Andreana Petrova Haley[1], Lawrence H. Sweet[1], Daniel E. Forman[2], Athena Poppas[1], Robert H. Paul[1], John Gunstad[3], Rohald A. Cohen[1]

[1]Brown University, Providence, Rhode Island, USA; [2]Harvard Medical School, Boston, Massachusetts, USA; [3]Kent State University, Kent, Ohio, USA

The purpose of this study was to examine the relationship between a non-invasive marker of cardiovascular health, common carotid artery intima-media thickness (CCA IMT), and fMRI activation during a verbal working memory task in patients with cardiovascular disease. IMT was measured by B-mode ultrasound. Increased CCA IMT was associated with significant decreases in both task related signal intensity and number of recruited voxels in the left dorsolateral prefrontal cortex. These results confirm the vulnerability of attention-executive networks to damage due to cerebrovascular disease, and reaffirm the need for elucidating the relationships between vascular health, cerebral perfusion, and brain function.

15:10 ***319***. **Cortical Activation in Tinnitus Patients Studied with fMRI**

Arthur Peter Wunderlich[1], Carlos Schönfeldt-Lecuona[2], Kristina Liener[2], Edgar Bachor[3], Wolfgang Freund[1]

[1]Univ.-Clinic Ulm, Ulm, Baden-Wuerttemberg, Germany; [2]Univ.-Clinic Ulm, Ulm, Germany; [3]SRH Zentralklinikum, Suhl, Germany

To investigate anomalities in brain activation as underlying cause for tinnitus, we scanned 17 tinnitus patients and 9 normal hearing controls with fMRI. Five beeps per second, each 50 ms in duration, at three frequencies (3 kHz ± 2%) and silence were presented blockwise pseudorandomly distributed by calibrated headphones above MR acoustic noise level. Subject's attention was focused to the tones with a tone decision task. Data were analysed using SPM99. The tinnitus group showed prefrontal activation which was not detectable in controls. Random effect analysis between both groups revealed subcortical areas to be activated in patients superior to controls.

15:20 ***320***. **Investigations of LGN Activation During Recovery from Acute Optic Neuritis**

Kirsten Nielsen[1], Kristoffer Hougaard Madsen[1, 2], Jette Lautrup Frederiksen[3], Anna Tsakiri[3], Arnold Skimminge[1], Torben Ellegaard Lund[1]

[1]Copenhagen University Hospital, Hvidovre, Denmark; [2]Informatics and Mathematical Modelling, Technical University of Denmark, Denmark; [3]Copenhagen University Hospital, Glostrup, Denmark

To further elucidate the mechanisms of recovery of vision in acute optic neuritis (ON), we conducted a longitudinal fMRI-study at 3T of activation of the lateral geniculate nucleus (LGN) during visual stimulation of patients with ON. Sixteen patients were examined acutely, and two weeks, three and six months later.At each time-point we calculated the average BOLD signal change in LGN during stimulation of affected and unaffected eyes. We found a clear tendency towards smaller differences in LGN activation between affected and unaffected eyes over time, indicating that the amount of signals reaching LGN from affected eyes increases during recovery.

ELECTRONIC POSTER DISCUSSION: Novel Methods to Generate Contrast

Room 602 - 604 13:30 - 15:30 Chairs: Steven M. Conolly and Stacie I. Ringleb

13:30 ***321***. **Passive Array Mechanical Driver for Magnetic Resonance Elastography of the Breast**

Vyacheslav Khozikov[1], Phillip J. Rossman[1], Richard L. Ehman[1]

[1]Mayo Clinic and Foundation, Rochester, Minnesota, USA

The purpose of this research was to develop a novel mechanical wave driver device for Magnetic Resonance Elastography of the Breast. The design goal was to develop a driver can be used with any breast RF coil, including multichannel designs. The driver is entirely passiv, non-metallic, and consists of an array of elastic tubes Experimental testing with a breast phantom demonstrates that the driver provides uniform shear wave illumination, and other favorable characteristics, making it an attractive alternative to a special combined driver/RF coil for breast MRE.

13:40 ***322***. **Monitoring Adipogenesis in Tissue-Engineered Fat *In Vitro* Using Microscopic Magnetic Resonance Elastography**

Shadi F. Othman[1], Michael S. Stosich[1], Huihui Xu[1], Nicholas W. Marion[1], Jeremy Mao[1], Richard L. Magin[1]

[1]University of Illinois at Chicago, Chicago, Illinois, USA

Repair of extensive soft tissue damage is difficult. Tissue engineering can reduce patients suffering and speed recovery if allogeneic implants can be designed to mimic normal adipogenesis. In this study, we use μMRE to monitor the mechanical properties of tissue engineered fat by visualizing low frequency (550 Hz) shear waves with high spatial resolution (109 μm x 109 μm x 500 μm). Excellent contrast was observed in vitro over a 3 weeks growth period corresponding to the normal adipogenic development of tissue engineered fat. A 400% (5.8 kPa to 1.4 kPa) reduction in the shear stiffness of the fat was observed.

13:50 ***323***. ***In Vivo* Quantification of Induced Liver Fibrosis in an Animal Study Using MR-Elastography**

Najat Salameh[1], Frank Peeters[1], Ralph Sinkus[2], Jorge Abarca-Quinones[1], Laurence Annet[1], Leon ter Beek[3], Bernard E. Van Beers[1]

[1]Université Catholique de Louvain, Brussels, 1200, Belgium; [2]ESPCI, Paris, 75231, France; [3]Philips Medical Systems, 3511, Best, Netherlands

The aim of the study was to assess if MR-elastography (MRE) can be used to quantify the degree of liver fibrosis *in vivo*. Ten rats with liver fibrosis and five normal rats were examined with MRE. The visco-elastic parameters obtained the Maxwell models were correlated to the percentage of liver fibrosis determined by histopathology. Significant correlations were observed between the visco-elastic properties and the percentage of liver fibrosis. These results suggest that MRE is a reliable method to quantify liver fibrosis.

14:00 ***324***. **Real Time Prospective Voxel Position Correction with Interleaved Reference Scan Using an Optical Motion Tracking System**

Martin Büchert[1], Oliver Speck[1], Jürgen Hennig[1], Maxim Zaitsev[1]
[1]University Hospital Freiburg, Freiburg, Germany

Subject motion during MRS investigations is a factor limiting the quality and the diagnostic value of the results. In this abstract a possibility of interfacing the MR scanner with an external optical motion tracking system, capable of determining object's position with sub-millimetre accuracy at a high update rate is demonstrated. Thereafter the information on the object motion is used in real time to update the position of the voxel during the acquisition on every sequence repetition. The degenerative effects of the frequency shifts, induced by the sample motion are effectively suppressed by the interleaved reference scan method.

14:10 ***325***. **Validation of a Dynamic MR Elastography Technique Customized for In Vitro Biomechanical Assessment of Articular Cartilage Under High Frequency Cyclical Shear**

Orlando Lopez[1], Armando Manduca[1], Richard L. Ehman[1]
[1]Mayo Clinic, Rochester, Minnesota, USA

Assessment of internal mechanical properties in articular cartilage by dynamic MR Elastography (MRE) requires customized methods for adequate generation and visualization of high-frequency (> 1 kHz) propagating shear waves. Sensitivity and repeatability of the technique were validated using sets of homogeneous, cartilage-mimicking, small and stiff dual-layered phantoms (2.5 mm thick per layer) made of wirosil silicone. Results demonstrated the sensitivity of customized dynamic MRE to detect differences in mechanical properties within small-stiff, multilayered, cartilage mimicking materials. Dynamic MRE of bovine articular cartilage also assessed differences in mechanical properties between superficial- and deep-layers.

14:20 ***326***. **MR Microscopy of Rat Hippocampal Slice Cultures: A Novel Model for Studying Cellular Processes and Chronic Perturbations to Tissue Microstructure**

Timothy Michael Shepherd[1], Bjorn Scheffler[1], Michael A. King[1], Greg J. Stanisz[2], Dennis A. Steindler[1], Stephen John Blackband[1]
[1]University of Florida, Gainesville, Florida, USA; [2]Sunnybrook & Women's CHSC/University of Toronto, Toronto, Ontario, Canada

We report MRI microscopy of hippocampal slice cultures, which can be sustained viably for several weeks. This novel method should aid investigations of chronic tissue pathology, such as beta-amyloid plaque formation, and facilitate investigations that employ stem cell or molecular imaging techniques.

14:30 ***327***. **Towards Rapid Planar MR Elastography of the Human Brain: A 3D Analysis of *In Vivo* Shear Wave Propagation**

Uwe Hamhaber[1], Jens Rump[2], Sebastian Papazoglou[2], Dieter Klatt[2], Ingolf Sack[2], Jürgen Braun[1]
[1]Institute of Medical Informatics, Berlin, Germany; [2]Institute of Radiology, Berlin, Germany

MR elastography (MRE) allows the monitoring of strain wave fields for determining elastic constants of soft tissue.However, a correct reconstruction of elastograms requires the acquisition of full 3D wave fields which tremendously extends the time consumption of elastographic studies.Here, a method is proposed to reduce the dimensionality of the reconstruction of brain MRE wave images. A 3D analysis of the shear wave propagation through the brain yielded specific slice positions which enable to deduce shear elasticities with geometrically related error margins of 25%. Using planar MRE, the elasticity of the human brain can be estimated within seconds.

14:40 ***328***. **Desynchronized Motion Encoding in Rapid Steady-State Free Precession MR Elastography**

Jens Rump[1], Dieter Klatt[1], Sebastian Papazoglou[1], Uwe Hamhaber[2], Jürgen Braun[2], Ingolf Sack[1]
[1]Institute of Radiology, Berlin, Germany; [2]Institute of Medical Informatics, Berlin, Germany

To accelerate *in vivo* MR elastography studies of highly viscous tissue we propose the use of low-frequency shear vibrations matched to the repetition time of fast SSFP sequences which include oscillating gradients for motion sensitization. In SSFP-MRE the frequency of the motion encoding gradient is desynchronized with the vibration frequency, which allows decreasing the vibration frequency without compromising the image quality due to enhanced T2*-dephasing. Despite desynchronized vibration-encoding the sensitivity of SSFP-MRE to harmonic motions is only slightly reduced compared to classical MRE. This tradeoff is overcompensated by the benefit of using low-vibration frequencies which result in high deflection amplitudes.

14:50 ***329***. **Observation of Shear Wave Dispersion Using Anharmonic MR Elastography**

Dieter Klatt[1], Jens Rump[1], Sebastian Papazoglou[1], Uwe Hamhaber[2], Jürgen Braun[2], Ingolf Sack[1]
[1]Institute of Radiology, Berlin, Germany; [2]Institute of Medical Informatics, Berlin, Germany

MR Elastography (MRE) is capable to test mechanical properties of soft tissue using harmonic shear vibrations. Here, the use of anharmonic vibrations is proposed for analyzing the wave propagation in dispersive media at multiple frequencies. The bandwidth of the motion sensitive gradient in our MRE sequence was adjusted to encode multiple frequencies simultaneously. Experiments on tissue specimens were conducted using ramp-shaped actuator vibrations. Comparison to sinusoidal wave excitation revealed non-linear elastic material properties. Initial *in vivo* studies clearly showed 50Hz- and 100Hz-vibrations in the human liver, which could be used to estimate the viscosity according to Voigt's dispersion relation.

15:00 ***330***. **Directional Filtering for Multiple-Driver Magnetic Resonance Elastography Data**

David S. Lake[1], Armando Manduca[1], Yogesh Kannan Mariappan[1], Richard L. Ehman[1]
[1]Mayo Clinic College of Medicine, Rochester, Minnesota, USA

Magnetic resonance elastography (MRE) requires the application of harmonic mechanical excitation to an object. In some cases, adequate displacement may not be present in certain regions due to attenuation and shadowing effects. Excitation with multiple, phased array drivers can provide more uniform illumination of an object, but the wave field from such driving can be very complex, with interference patterns yielding areas of low amplitude and hence low SNR that can negatively impact inversion algorithms. Spatio-temporal directional filtering can separate interfering waves traveling in different directions so they can be processed separately, and dramatically improve inversion results.

15:10 ***331***. **Reconstruction of Irregular Conductivity Distributions Using MREIT at Low Current Levels**

Ozlem Birgul[1], Lutfi Tugan Muftuler[1], Mark J. Hamamura[1], Orhan Nalcioglu[1]
[1]University of California, Irvine, California, USA

Magnetic resonance-electrical impedance tomography (MREIT) is an imaging modality that reconstructs conductivity from magnetic field measurements generated by a current distribution. Since the conductivity values of malignant, benign, and normal tissues are significantly different, this information can be used in classification to improve specificity in breast cancer. There are several studies to determine the capabilities of MREIT using simple cases but none investigates performance in detecting irregular and more complex conductivity distributions, which models the real life cases more accurately. In this study, we showed that it is possible to resolve a 6mm inhomogeneity within an irregular region using MREIT.

15:20 ***332***. ***In Vivo* MRI Based Electrical Impedance Tomography of Malignant Tumors**

L Tugan Muftuler[1], Mark Hamamura[1], Ozlem Birgul[1], Orhan Nalcioglu[1]
[1]University of California, Irvine, California, USA

Previously, we reported preliminary results with MR based Electrical Impedance Tomography (MREIT) on several phantoms and a few animals. In the presented study, we applied the technique on ten tumor-bearing rats and collected MREIT images to investigate the potential of MREIT for characterizing malignant tumors. Results show that the tumors had significantly higher mean conductivity compared to the mean of conductivity in the rest of the body. Although heterogeneity of conductivity was observed in the tumor, the mean was still higher than the background.

Pulse Sequences: II

Room 6E 16:00 - 18:00 Chairs: Sean B. Fain and Craig H. Meyer

16:00 ***333***. Young Investigator Award Finalist: **Dynamic Magnetic Resonance Inverse Imaging of Human Brain Function**

Fa-Hsuan Lin[1], Lawrence L. Wald[1], Kenneth K. Kwong[1], Seppo P. Ahlfors[1], Matti S. Hamaleinen[1], John W. Belliveau[1]
[1]Massachusetts General Hospital, Charlestown, Massachusetts, USA

Inspired by electroencephalography (EEG) and magnetoencephalography (MEG) source localization, we develop MR Inverse Imaging (InI) to achieve an order-of-magnitude speed-up in dynamic MR measurements. Spatially resolved dynamic changes and associated statistical inference maps can be obtained with millisecond temporal resolution using spatial information encoded with the detector geometry of a 90-channel head array. We introduce the InI theoretical framework and demonstrate the InI in classical BOLD PRESTO fMRI with 20-ms temporal resolution. The InI approach can be combined with other MR contrast preparation mechanism for the ultra-fast characterization of functional contrast sources associated with neuronal activation.

16:20 ***334***. **Ultrashort TE Imaging of the Short T2 Components in White Matter Using Half Pulse Excitation and Spiral Sampling**

Jiang Du[1], Mark Bydder[1], Atsushi M. Takahashi[2], Ann Shimakawa[2], Jean H. Brittain[2], Graeme M. Bydder[1]
[1]University of California, San Diego, San Diego, California, USA; [2]Global Applied Science Laboratory, GE Healthcare, Menlo Park, California, USA

There are short T2 components in the white matter which can not be detected with conventional magnetic resonance imaging sequences. We present an ultrashort TE imaging pulse sequence which combines half pulse excitation and spiral sampling. The ultrashort T2 components in the white matter were selective depicted with an ultrashort echo time of 8 usec, while the long T2 components were suppressed using a long slice selective inversion pulse and dual-echo echo subtraction.

16:32 ***335***. **HYPR PR-TRICKS: Highly Undersampled Hybrid Radial/Cartesian Acquisition with HighlY Constrained BackPRojection Reconstruction for Time Resolved MRI**

Yijing Wu[1], Yan Wu[1], Frank R. Korosec[1], Oliver Wieben[1], Jiang Du[2], Charies A. Mistretta[1]
[1]University of Wisconsin, Madison, Wisconsin, USA; [2]University of California, San Diego, San Diego, California, USA

A time-resolved hybrid radial/Cartesian acqusition, PR-TRICKS, is combined with a newly developed method, HighlY constrained back PRojection (HYPR) reconstruction, provides artifact-free images with overall Nyquist undersampling factors of 200 or more. This greatly improves both the temporal and spatial resolution.

16:44 ***336***. **Three Dimensional SPI PC-MRA at 3 Tesla**

Kishor V. Koladia[1], James Grant Pipe[1]
[1]St. Joseph's Hospital, Phoenix, Arizona, USA

This work investigates the application of Spiral Projection Imaging for 3D multi-venc Phase Contrast MRA at 3 Tesla, using an 8-channel head coil, with retrospective ECG gating. The higher field strength and phased array coils greatly enhance the SNR of the resulting PC-MRA images.

16:56 ***337***. **Formation of Primary Spin Echoes During Global Coherent Free Precession Improves Longevity of "Memory" Effect**

Wolfgang Gerhard Rehwald[1], Enn-Ling Chen, Burkhard Sievers, Raymond J. Kim, Robert M. Judd
[1]Siemens Medical Solutions/ Duke University, Durham, North Carolina, USA

We describe a new global coherent free precession technique based on spin echoes (SE-GCFP) rather than gradient echoes (GRE-GCFP). The limitation of GRE-GCFP that signal "memory" is only about 200 ms due to T2* decay is overcome by repeated spin rephasing. Greater filling distances are achieved. We establish that spin echoes can be formed during GCFP despite the complexity of maintaining global phase coherence in the setting of multi-dimensional blood flow. Phantom data demonstrate that SE-GCFP dramatically increases signal "memory", implying that *in vivo* images will allow visualization of blood flow much further than previously demonstrated for GRE-GCFP.

17:08 ***338***. **Improved 3D Spin-Echo Imaging Using Frequency-Swept Pulses**

Jang-Yeon Park[1], Olli H J Gröhn[2], Michael Garwood[1]
[1]Center for Magnetic Resonance Research and Department of Radiology, University of Minnesota, Minneapolis, Minnesota, USA; [2]A.I.Virtanen Institute for Molecular Sciences, University of Kuopio, Kuopio, Finland

Adiabatic full-passage (AFP) pulses have desirable properties that are commonly exploited in NMR (eg, insensitivity to B1-inhomogeneity and ability to invert broad bandwidths). Although AFP pulses can produce refocusing in spin-echo MRI sequences, even numbers of AFP pulses are required to compensate the non-linear magnetization phase. Recently, it was shown that phase compensating using an even number of slab-selective AFP pulses is unnecessary when spatial-encoding is performed in the slab-selection direction. Here, phase profiles produced by AFP pulses in spin-echo sequences are analytically described and shown to produce a "pseudo-echo". Image reconstruction using a sliding window function is also described.

17:20 ***339***. **Fully Balanced Steady State 3D-Spin-Echo (BSSSE) Imaging at 3 Tesla**

Roland Krug[1], Eric T. Han[2], Suchandrima Banerjee[1], Sharmila Majumdar[1]
[1]UCSF, San Francisco, California, USA; [2]GE Healthcare, Global Applied Science Laboratory, Menlo Park, California, USA

In this work a rapid fully balanced steady state spin-echo sequence (bSSSE) has been designed and implemented on a 3 Tesla whole-body MR scanner. Its performance was compared to previously used gradient-echo and spin-echo based sequences. SE sequences are less prone to off-resonance frequencies arising from magnetic field inhomogeneities. SNR and SNR efficiency of bSSSE outperforms that of previous introduced non-balanced SSSE sequences. We applied the new sequence to *in vivo* high-resolution MRI of trabecular bone. The resulting trabecular microstructure was more clearly depicted compared to previously used spin-echo and gradient-echo based sequences in a clinically reasonable imaging time.

17:32 ***340***. **Arbitrary Fields of View in Radial Imaging**

Peder E Z Larson[1], Paul T. Gurney[1], Dwight G. Nishimura[1]
[1]Stanford University, Stanford, California, USA

We have developed a method to support arbitrary fields of view (FOVs) in radial imaging techniques, such as 2D and 3D projection reconstruction (PR) as well as 3D cones. Non-circular FOVs, such as ellipses and rectangles, allow for scan time reductions without inducing artifacts. When applied to undersampled dynamic imaging, the unaliased region of support for motion need not be circular. The method is based on non-uniform angular sampling density, and also supports anisotropic resolutions.

17:44 ***341***. **MRI Using a Concentric Rings Trajectory with Built-In Off-Resonance Correction**

Hochong H. Wu[1], Jin Hyung Lee[1], Dwight G. Nishimura[1]
[1]Stanford University, Stanford, California, USA

In this work, we design a pulse sequence that samples k-space with a set of concentric rings. Advantages associated with such a readout trajectory include flexible polar sampling in k-space, and flexible trade-off between image resolution and scan time. This sequence can be readily extended to variable-density k-space coverage and can be used for efficient dynamic MRI. As with non-Cartesian trajectories, off-resonance blurring degrades image quality. We correct for off-resonance blur by retracing rings near the center of k-space to obtain a field map with no extra scan time, and then employ multi-frequency reconstruction.

MR PHYSICS AND TECHNIQUES FOR CLINICIANS

Room 6C 16:00 - 18:00 Chairs: Frank R. Korosec and Joseph C. McGowan

Educational Objectives:
Upon completion of this session, participants should be able to:

- Define and describe the fundamental principles of MR imaging, including the definition of spin magnetization, the Larmor relationship, relaxation phenomena, and the process of using the spin magnetization to produce an image;
- Explain imaging pulse sequences based upon spin and gradient echoes, including fast spin echo and echo planar techniques;
- Design MR imaging protocols for diagnostic applications considering image contrast, spatial resolution, acquisition time, signal-to-noise ratio, and artifacts; and
- Describe the principles and capabilities of various advanced MR techniques including, diffusion, vascular and cardiac MRI.

16:00 **Spin Echo**
R. Scott Hinks

16:40 **Gradient Echo**
Michael Markl

17:20 **Fast Spin Echo**
Joseph C. McGowan

Improvements in Diffusion Analysis

Room 6D 16:00 - 18:00 Chairs: Andrew L. Alexander and Adam W. Anderson

16:00 ***342***. **Utilization of Proton Density Gradients in the Estimation of Diffusion Tensors**
Steven J. Haker[1], Stephan E. Maier[1], Robert V. Mulkern[1]
[1]Brigham and Women's Hospital, Boston, Massachusetts, USA

We present a principled method for the incorporation of proton densityinformation within the standard diffusion tensor estimation technique.

16:12 ***343***. **Evaluation of Anisotropic Filtering for DTI as a Function of SNR**
Jee Eun Lee[1, 2], Moo K. Chung[1, 2], Andew L. Alexander[1, 2]
[1]University of Wisconsin, Madison, Wisconsin, USA; [2]Waisman Laboratory for Functional Brain Imaging and Behavior, Madison, Wisconsin, USA

The sensitivity to noise in DTI measures increases as the higher spatial resolution of DTI is gained. An anisotropic Gaussian filter based on the diffusion tensor was recently proposed for preferential image blurring along the white matter tracts directions, which minimizes partial volume averaging artifacts. In this study, we evaluated the performance of powered anisotropic Gaussian kernel smoothing using higher resolution human brain DTI data with different SNR levels. The study demonstrates that for SNR levels between 10 and 20, filtering does improve the overall accuracy of DTI brain measurements and both the optimal type and amount of filtering depends upon the SNR of the data. However, for moderately high SNR, filtering will likely introduce more error than is removed.

16:24 ***344***. **Evaluation of SNR Performance and Utility of High Spatial and Angular Resolution Denoised 1mm3 Isotropic DTI of Entire Human Brain at 3.0 T**
Khader M. Hasan[1], K Rodenacker[2], Klaus R. Hahn[2]
[1]University of Texas Medical Scool, Houston, Texas, USA; [2]GSF-National Research Center for Environment and Health, Neuherberg, Bavaria, Germany

In vivo application of quantitative DTI methods to study the contributors to the healthy developing and diseased tissue anisotropy is limiteddue to the selection of large voxels that excerbate the partial volume artifacts of gray matter and CSF even on large compact structures such as the corpus callosum. *In vivo* studies of healthy and diseased structures such as the prostate, cortex, cerebellum, optic nerve and spinal cord generally demand high spatial resolution. In this work we demonstarte and validate the SNR performance and time efficiency of human brain data acquired at 3.0 T using 1mmx1mmx1mm true isotropic resolution without replicated averaging or interpolation. The acquisition uses a multi faceted high angular resolution alternating polarity icosahedral scheme and the data are denoised using a recently described procedure. The results in both whie and gray matter demonstarte the advanatge of this acquisition-processing strategy over the time consuming replicated averaging choice.

16:36 ***345***. **Noise Correction on Rician Distributed Data for Fiber Orientation Estimators**

Rafael Alonso Clarke[1, 2], Paola Scifo[2], Flavio Dell'Acqua[2], Giovanna Rizzo,[23], Giuseppe Scotti[1, 2], Ferruccio Fazio[2, 3]
[1]Università Vita-Salute San Raffaele, Milan, Italy; [2]Scientific Institute H San Raffaele, Milan, Italy; [3]CNR, Milan, Italy

New complex tissue microstructure estimators have been presented in order to resolve the white matter fiber orientations through Diffusion Weighted Imaging (DWI). These algorithms are based on signal profile and, since the Rician statistics behaviour has not been taken into account, the estimations are affected by noise artifacts. We present a signal profile correction based on the Maximum-Likelihood as a preprocessing for fiber orientation estimators.

16:48 ***346***. **A New Rician Noise Bias Correction**

Marzieh Nezamzadeh[1], Ian Cameron,[12]
[1]Carleton University, Ottawa, ON, Canada; [2]The Ottawa Hospital, Ottawa, ON, Canada

It is well known that pixel intensities of magnitude MR images are biased by Rician noise. This is particularly noticeable for SNR < 2. Rician noise bias corrections from the literature work well for SNR > 2 but not for SNR < 2. Furthermore, the distribution of these "corrected" data points is far from Gaussian. This can have significant implications if the data is further processed using least squares procedures, which assume a Gaussian distribution of data points. In this work a new and improved procedure for Rician noise bias correction for small SNR is presented which gives a better estimate of the true signal value and produces a Gaussian-like distribution function for the corrected data.

17:00 ***347***. **Estimation of the Cross-Terms for All B-Matrix Elements with an Isotropic Phantom**

Kamil A. Il'yasov[1]
[1]University Hospital Freiburg, Freiburg, Germany

Accurate DTI calculations require exactly b-matrix calculations, taking into account all diffusion weighting (DW) and imaging gradients. However a routine user mostly has no exact information on pulse sequence details. In such a case cross terms between imaging and DW gradients are ignored and the b-matrix is approximated from the diffusion encoding direction and the "nominal" b-factor. This work presents a new method to estimate the unknown cross terms between imaging and DW gradients. The method based on calibration measurements on a phantom with isotropic diffusion and improves the accuracy of DTI calculations in tissues with diffusion anisotropy.

17:12 ***348***. **Mutual Information Estimation Using K-Space Data: An Application for Eddy-Current Distortion Correction in Diffusion Tensor Imaging**

Udomchai Techavipoo[1], John Lackey[1], Jianrong Shi[1], Xin Guan[1], Song Lai[1]
[1]Thomas Jefferson University, Philadelphia, Pennsylvania, USA

Mutual information between diffusion-weighted and T2-weighted images, used for eddy-current distortion correction in diffusion tensor imaging, is generally estimated using linear interpolation and partial volume methods. These methods create artifacts on MI and reduce the accuracy of the distortion-correction parameters. We developed a method based on the shifting theorem to discover pixel values in any specific coordinates without interpolation. Upsampling was applied to reduce the computational time. The joint probability between two images was smoothed using 2D-Gaussian kernel. The results indicate major improvement in terms of principal-components variances and visual qualities of fractional anisotropy images and brain-fiber-orientation color maps.

17:24 ***349***. **Efficient, Robust, Nonlinear, and Guaranteed Positive Definite Diffusion Tensor Estimation**

Robert W. Cox[1], Daniel Glen[1]
[1]Department of Health and Human Services, Bethesda, Maryland, USA

We describe a method to estimate the diffusion tensor D directly from the nonlinear relationship between diffusion-weighted images and D. A modified gradient descent algorithm is used, one which ensures that D remains positive definite. Iterative reweighting is applied to remove outliers.

17:36 ***350***. **Robust Interpolation of DT-MRI Data Using Tensor Splines**

Angelos Barmpoutis[1], Baba C. Vemuri[1], Timothy M. Shepherd[1], John Forder[1]
[1]University of Florida, Gainesville, Florida, USA

Interpolation is a fundamental problem in the field of medical imaging. To correctly perform interpolation of diffusion tensors one needs to first identify the space in which these diffusion tensors live and then define an appropriate metric in this space for interpolation and computation of lengths of paths, averages etc. The space of diffusion tensors is known to be a curved space of negative curvature. We make use of this to define an appropriate metric to perform interpolation and other tasks. Interpolation is essential in many applications such as image registration, atlas construction etc.

17:48 ***351***. **Fiber-Oriented Regularization of Diffusion Tensor Images**

Yonggang Lu[1], Jing Qi[2], Adam Anderson[1], John C. Gore[1], Zhaohua Ding[1]
[1]Vanderbilt University, Nashville, Tennessee, USA; [2]The First Affiliated Hospital of Nanjing Medical University, Nanjing, People's Republic of China

A fiber-oriented Bayesian regularization method was proposed to suppress the confounding effects of noise and partial volume averaging in diffusion tensor fiber tractography. Compared to conventional Gaussian and anisotropic tensor regularization methods, this new method has not only the functions of noise reduction and boundary preservation but also robustness to partial volume averaging, as demonstrated by experiments with synthetic data.

Cell Labelling Methods and Imaging

Room 4C - 3,4 16:00 - 18:00 Chairs: Mathias Hoehn and Michal Neeman

16:00 ***352***. **Bioenergetics Measured by *In Vivo* ^{31}P MRSI in Hind Limb Muscles Correlates with Functional Performance Before and After Stem Cell Treatment in a Mouse Model of Peripheral Vascular Disease**

Xiao-Hong Zhu[1], Aernout Luttun[2], Jonathan McCue[2], Betsy Schroeder[2], Meredith Seaborn[2], Catherine Verfaillie[2], Fei Du[1], Yi Zhang[1], Xiaoliang Zhang[1], Wei Chen[1]

[1]CMRR, Minneapolis, Minnesota, USA; [2]Stem Cell Institute, University, Minneapolis, Minnesota, USA

Continuous and objective monitoring of the effect of (stem cell) therapy in trials with patients suffering from peripheral vascular disease (PVD) is a challenge. A limb ischemia mouse model was used to test *in vivo* ^{31}P MRS combined with MRI as a non-invasive technique to evaluate functional benefits of stem cell transplantation. Functional assessment of muscles was scored by a swim test. The bioenergetic changes measured by MRS in ischemic hind limb muscles spatially correlated with the ischemic energy status of the muscle, temporally correlated with functional muscle performance and successful stem cell engraftment reflecting functional improvement upon stem cell transplantation. Therefore, MRS/MRI could be useful to monitor the effect of (stem cell) treatments in patients.

16:12 ***353***. ***In-Vivo* MR Monitoring of Magnetically Labeled Mesenchymal Stem Cells in Kidneys After Selective Intrarenal Injection in a Glomerulonephritis Model in Rats at 3T**

Harald Ittrich[1], Friedrich Thaiss[1], Claudia Lange[1], Hannes Dahnke[2], Christoph Leussler[2], Tobias Schaeffter[2], Gerhard Adam[1], Claus Nolte-Ernsting[1]

[1]University Hospital Hamburg Eppendorf, Hamburg, Germany; [2]Philips Research Laboratories Hamburg, Hamburg, Germany

We evaluated MRI for *in vivo* tracking of selective intraarterial injected superparamagnetic iron oxide particle-labeled mesenchymal stem cells (MSC) in a rat model of an Anti-Thy1 glomerulonephritis. 10^6 labeled rMSC were injected in one renal artery. In-vivo T2*weighted MR Imaging and T2* Relaxometry were performed repetitively up to day 22 in a clinical 3T scanner and correlated with histology. Significant SNR and T2* decrease was observed in kidney of injection side up to 3 weeks after administration in MSC group with glomerular predominance. Delayed MSC migration to liver and spleen was observed. The study demonstrates the potential of MRI for *in vivo* cell-tracking of therapeutically administered, magnetically labeled MSC.

16:24 ***354***. **Unique and Rapid 19F Imaging of Stem Cells Labeled with Perfluorocarbon Nanoparticles at 11.7T and 1.5T**

Anne Morawski Neubauer[1], Kathy Crowder[1], Shelton D. Caruthers[1], Jason Brandt[1], Frank D. Hockett[1], Jan Nolta[1], Gregory M. Lanza[1], Samuel A. Wickline[1], Junjie Chen[1]

[1]Washington University, St. Louis, Missouri, USA

Stem cell tracking is rapidly developing as a new application of magnetic resonance imaging because it allows for precise anatomical localization of the cells as they migrate in living tissue. While most current labeling methods have centered on the use of iron oxide particles to produce “negative” contrast, we have developed a liquid perfluorocarbon nanoparticle that is readily endocytosed by stem/progenitor cells and allows for 19F imaging for tracking. In this work, we demonstrate the use of these particles for imaging of labeled cells in vitro at both 11.7 T and 1.5T, and in mouse skeletal muscle at 11.7 T.

16:36 ***355***. **MRI of Neural Progenitor Migration in the Developing Mouse Brain**

Abby E. Deans[1], Youssef Zaim Wadghiri[1], Daniel H. Turnbull[1]

[1]New York University School of Medicine, New York, USA

Micron-sized particles of iron oxide (MPIO) have recently been shown to label stem cells in culture and *in vivo*. We used MPIO to label neural progenitor cells in situ in the medial and lateral ganglionic eminences of the embryonic mouse forebrain. Five days after labeling, T2*-MRI at 7T and histology of *ex vivo* samples demonstrated that neuronal progenitors had taken up particles and migrated to the expected locations in the cortex and striatum. These results show promise for this approach in future *in vivo* cell migration studies in the embryonic mouse brain.

16:48 ***356***. **Validation of Magnetoliposomes as MR Contrast Agents for In Situ Labeling of Endogenous Neuronal Progenitor Cells in the Mouse Brain**

Ruth Vreys[1], Christa Peleman[2], Martine Geraerts[3], Marcel De Cuyper[2], Zeger Debyser[3], Veerle Baekelandt[3], Annemie Van der Linden[1]

[1]University of Antwerp, Antwerp, Belgium; [2]KULAK, Kortrijk, Belgium; [3]KULeuven, Leuven, Belgium

MRI has recently become a powerful tool for *in vivo* non-invasive monitoring of the migration of superparamagnetic iron oxide labeled stem cells. In our study we stereotactically injected four different types of Magnetoliposomes (MLs) in the Rostral Migration Stream (RMS) of healthy adult mice to evaluate their potentials for labeling endogenous neuronal progenitor cells. The observed migration of the contrast agents along the RMS appeared to be relocation of the ML’s along the white matter tract that runs in parallel with the RMS and no stem cell migration. This was confirmed by ML’s migrating along other white matter tracts.

17:00 ***357***. **Measures of Bone Marrow-Derived Monocyte Migration Into Brain During HIV-1 Encephalitis: Implications for the Pathogenesis and Treatment of HIV-1 Infection of the Nervous System**

Michael D. Boska[1], Huanyu Dou[1], Jay A. Nelson[1], Jeffrey Kingsley[1], Mariano Uberti[1], R. Lee Mosley[1], Howard E. Gendelman[1]

[1]University of Nebraska Medical Center, Omaha, Nebraska, USA

Superparamagnetic iron oxide (SPIO) labeling of mouse bone marrow derived macrophages (BMM) has been used to track body and brain trafficking of i.v. injected BMM. Detection by T2* weighted MRI has been used to track cell distribution over time and endpoints were validated by Prussian blue stained histological analyses of BMM density. Results demonstrate, for the first time, that non-invasive tracking of BMM into HIV-1 encephalitic brain tissue can be detected by T2* weighted MRI of SPIO labeled BMM with cells primarily found in the region of HIV-1 infected cells in a mouse model of HIV-1 encephalitis.

17:12 ***358***. **MR Tracking of Lineage-Restricted Neural Precursors Following Transplantation Into the Adult Spinal Cord**

Angelo C. Lepore[1], Piotr Walczak[2], Itzhak Fischer[1], Mahendra S. Rao[3], Jeff W. Bulte[2]

[1]Drexel University College of Medicine, Philadelphia, Pennsylvania, USA; [2]Johns Hopkins University School of Medicine, Baltimore, Maryland, USA; [3]National Institute of Aging, Baltimore, Maryland, USA

Mixtures of neuronal-restricted precursor cells (NRPs) and glial-restricted precursor cells (GRPs) display robust survival and extensive migration following transplantation into both the intact and injured spinal cord. Following magnetic labeling of NRPs/GRPs from a transgene rat, allowing proper histological analysis of live cell distribution, cells migrated over 5 mm distances and differentiated into all three neural lineages *in vivo*. An hereto unreported specific infiltration of macrophages was observed only for labeled cells; however the majority of iron particles remained in grafted cells. Thus, iron oxide labeling does not impede cell differentiation and can accurately depict transplanted cells by MRI

17:24 ***359***. **Fluorine Diffusion Measurements Confirm Intracellular Labeling of Perflurocarbon Nanoparticles in Therapeutic Stem/Progenitor Cells as Tracking Agents**

Junjie Chen[1], Kathy Crowder[1], Jason Brant[1], Gregory M. Lanza[1], Samuel A. Wickline[1]

[1]Washington University, St. Louis, Missouri, USA

The ability to track transplanted therapeutic cells *in vivo* is critical for elucidating mechanisms of cell migration and differentiation. 19F MRI of liquid perfluorocarbon nanoparticles (PFC NP: 200 nm) may offer a unique and sensitive cell marker (fluorine) that cannot be obscured by traditional tissue background proton signal. We proposed that 19F diffusion weighted MRS/MRI could provide a non-invasive method to confirm intracellular labeling of stem/progenitor cells by specifically detecting intracellular PFC NP as its diffusivity decreases dramatically upon successful cell labeling.

17:36 ***360***. **Selective MRI of Magnetically Labeled Cells – a Comparative Evaluation of Positive Contrast Techniques**

Jan-Henry Seppenwoolde[1], Raoul Oude Engberink[1], Annette van der Toorn[1], Erwin L.A. Blezer[1], Chris J.G. Bakker[1]

[1]University Medical Center Utrecht, Utrecht, Netherlands

This work describes a comparative evaluation of three types of selective MR imaging of magnetically labeled cells: the white marker method (WM), the spectrally selective RF method (SSRF), and the off-resonance balanced gradient-echo method (OBM). Comparison was done by simulations, in vitro experiments, and *in vivo* rat experiments with photothrombotic brain lesions. The results show that the described methods have their own specific issues: OBM has the least flexibility with a very narrow optimum, SSRF has more flexibility but yields relatively small markers, and WM has the most flexibility and yields larger markers with a very robust contrast.

17:48 ***361***. **Optimal Positive Contrast of Labeled Cells Via Conventional 3D Imaging**

Hannes Dahnke[1], Wei Liu[2], Joseph Frank[3], Tobias Schaeffter[1]

[1]Philips Research Laboratories, Hamburg, Germany; [2]Philips Research Laboratories, Briarcliff, New York, USA; [3]National Institutes of Health, Bethesda, Maryland, USA

Contrast agents based on super paramagnetic iron oxides SPIOs are widely used for cell labeling. The cell detection is hampered by the negative contrast the SPIOs introduce in conventional imaging. We propose a method to calculate an optimal positive contrast image by determining a map of the susceptibility gradients from a regular 3D image dataset. This avoids the use of dedicated positive contrast sequences and does not require prior knowledge about the local SPIO concentration; in addition to that, the map of the susceptibility gradients contains quantitative information that could be used for SPIO quantification.

Advances in Coronary MRA

Room 611 - 612 16:00 - 18:00 Chairs: Hajime Sakuma and Matthias Stuber

16:00 ***362***. **Evaluation of Coronary Atherosclerotic Plaque Using Navigator Coronary MR Angiography with Reference to 64-MDCT Coronary Angiography**

Xin Liu[1], Wei Sun[2]
[1]PLA General Hospital, Beijing, People's Republic of China; [2]GE Healthcare,China, Beijing, People's Republic of China

Using coronary MR angiography with SSFP (1.5T) to scan 15 non-calcified plaques with significant stenosis and 4 severe calcified plaques detected by 64-slice CT in 15 patients. Nine non-calcified plaques were detected as low signal and the stenosis were correctly evaluated compared to CT. Six non-calcified plaques were not detected might be caused by smaller size in 4 and rich fibrous component in 2. Four calcified plaques showed no significant stenosis on MR. High-spatial resolution and black blood MR technique should be developed to increase the ability of detection for the small size plaque (<2.3 mm) and fibrous-rich plaque.

16:12 ***363***. **Real-Time Cardiac Fat Navigator Gated SSFP 3D Coronary MRA Using a Fast Kaiser Magnetization Preparation**

Thanh D. Nguyen[1], Pascal Spincemaille[1], Martin R. Prince[1], Yi Wang[1]
[1]Weill Medical College of Cornell University, New York, New York, USA

The objective of this study is to demonstrate the feasibility of employing the recently developed cardiac fat navigator in free-breathing SSFP 3D coronary MRA. The time delay between the navigator echo and the imaging echoes is reduced to approximately 24 ms by eliminating the need for a separate fat saturation pulse and by using a fast Kaiser ramp preparation with 6 RF pulses. Our preliminary human study (n = 11) shows that this approach provides better image quality than both the $\alpha/2$ preparation ($p<0.0025$) and the linear ramp preparation with 20 RF pulses ($p<0.025$).

16:24 ***364***. **Respiratory Self-Gated 4D Coronary MRA**

Peng Lai[1], Andrew C. Larson[1], Jaeseok Park[2], James C. Carr[1], Debiao Li[1]
[1]Northwestern University, Chicago, Illinois, USA; [2]Siemens Medical Solutions, Erlangen, Germany

The purpose of this work was to investigate the feasibility of a respiratory self-gating (RSG) technique for free-breathing 3D cine (4D) coronary MRA, which aimed to resolve the respiratory and cardiac motion artefact problem. In our method, real-time RSG signal was derived from direct measurement of heart motion. Volunteer studies and statistical analysis showed the effectiveness of this technique for suppression of respiratory motion. With the capability of achieving phase images over an entire cardiac cycle, the image with best visualization the coronary can be retrospectively selected.

16:36 ***365***. **Simultaneous Projection of Multi-Branched Vessels with Their Surroundings on a Single Image from Coronary MRA**

Shmuel Aharon[1], Ozcan Oksuz[1, 2], Christine H. Lorenz[1]
[1]Siemens Corporate Research, Princeton, New Jersey, USA; [2]Bilkent University, Bilkent Ankara, Turkey

This study's goal was to develop a method for visualizing coronary MRA datasets, with simultaneous projection of multi-branched vessels and their surroundings on a single image without distortion and artifacts. The algorithm uses the vessels centerlines specified by a semi-automatic tracking algorithm and/or manual user specification. We successfully visualized data from eight patients, with processing time for an inexperienced user of less than 5 minutes per data set. The presented method provides simultaneous projection of multi-branched vessels with their surrounding without distortion, and allows rapid delineation of both the left and right coronary arteries on a single image.

16:48 ***366***. **Navigator-Gated Whole Heart Coronary MRI: Comparison of 3D TrueFisp Cartesian and Radial Acquisitions**

Sonia Nielles-Vallespin[1], Peter Speier[1], Xiaoming Bi[2], Debiao Li[2], Edgar Mueller[1]
[1]Siemens AG Medical Solutions, Erlangen, Germany; [2]Northwestern University, Chicago, Illinois, USA

3D TrueFISP navigator-gated whole heart coronary images acquired using Cartesian and radial sampling were compared in terms of SNR, CNR and vessel sharpness in four healthy volunteers. With an average total acquisition time of 10-13 min, the Cartesian data have lower and anisotropic resolution (voxel size $1.1\times1.1\times2.2$ mm^3), thus higher SNR and CNR, while the radial data have higher and true isotropic resolution (voxel size $1.1\times1.1\times1.1$ mm^3) and improved vessel sharpness.

17:00 ***367***. **Non-Model Based Correction of Respiratory Motion Using Beat-To-Beat 3D Spiral Fat-Selective Imaging**

Jennifer Keegan[1], Peter D. Gatehouse[1], Guang-Zhong Yang[2], David N. Firmin[1]
[1]Royal Brompton Hospital, London, UK; [2]Imperial College, London, UK

Current methods of correcting coronary artery scans for respiratory motion rely on navigator-based motion models developed from a calibrating pre-scan. As an alternative, we propose a non-model based post-processing approach to respiratory correction using the cross-correlation of low resolution 3D spiral fat-selective images which are acquired on every cardiac cycle immediately prior to the data segment contrbuting to the high resolution image. We have demonstrated the feasibility of this approach with 3d spiral coronary artery vessel wall scanning where high quality images have been obtained with 100% respiratory efficiency.

17:12 ***368***. **Cardiac Phase Resolved 3D Coronary MRA Using Balanced SSFP and a Spiral Trajectory**

Bryan Kressler[1, 2], Pascal Spincemaille[2], Thanh D. Nguyen[2], Martin R. Prince[2], Yi Wang, [12]
[1]Cornell University, Ithaca, New York, USA; [2]Weill Medical College of Cornell University, New York, New York, USA

A cardiac phase resolved 3D coronary MR angiography sequence is developed using balanced SSFP and a 3D stack of spirals trajectory. A shifting fat saturation scheme is employed to distribute the dead time associated with fat saturation evenly throughout the cardiac cycle. A sliding window reconstruction is performed to generate 16 cardiac phases. The motion of the coronary arteries can be visualized throughout the cardiac cycle, allowing selection of the cardiac phase with the sharpest visualization of the coronary arteries.

17:24 ***369***. **Evaluation of Whole-Heart Coronary MRA Completed in 5 Minutes Using "Paddle-Wheel" Balanced SSFP**

Shigeo Okuda[1], Koichi Oshio[1], Akihiro Tanimoto[1], Hiroshi Shinmoto[1], Minoru Yamada[1], Sachio Kuribayashi[1]
[1]Keio University School of Medicine, Tokyo, Japan

We implemented "paddle-wheel" balanced SSFP on a 1.5T clinical scanner and obtained whole-heart coronary MRA of 10 patients. The imaging parameters were: 224 readout points, 300 projections, 64 slices, TR/TE = 4.0/2.0 msec, FOV = 30-35 cm, acquisition matrices = 256x256. Respiratory navigator was not used during image acquisition and respiratory motion was corrected on a workstation by using image data itself for navigation. The image acquisition time was completed in 5 minutes. The average image quality was assessed on 4-point-scale (4 = excellent) as 3.36, 2.58 and 2.22 for RCA, LAD and LCX, respectively.

17:36 ***370***. **Tailoring Transient Balanced Gradient Echo Coronary MRA at 3.0T**

Michael Schär[1, 2], Reza Nezafat[3], Matthias Stuber[1], Peter Boesiger[4], Sebastian Kozerke[4]
[1]Johns Hopkins University, Baltimore, Maryland, USA; [2]Philips Medical Systems, Cleveland, Ohio, USA; [3]National Institutes of Health, Bethesda, Maryland, USA; [4]University and ETH Zurich, Zurich, Switzerland

Balanced SSFP sequences have shown high potential for coronary MRA at 1.5T. At 3.0T, however, increased inhomogeneities of the magnetic field and the radio frequency field together with power deposition limitations cause increased off-resonance and flow related artifacts in the transient phase. This was addressed with a number of sequence changes including binomial pre-saturation followed by a Kaiser-Bessel shaped flip angle sweep to reduce transient oscillations, variable-rate selective excitation pulses to reduce repetition time, and adiabatic refocusing pulses for T2-preparation. Combined with localized shimming and resonance frequency determination excellent image quality was achieved in angiograms of the right coronary artery.

17:48 ***371***. **Spiral PILS Coronary Artery Imaging**

Peng Hu[1], Craig H. Meyer[1]
[1]University of Virginia, Charlottesville, Virginia, USA

The goal of this study is to apply the partially parallel imaging with localized sensitivities (PILS) technique to spiral coronary artery imaging. We use spiral trajectories that are under-sampled between interleaves and a Fermi mask is applied to each coil image generated by gridding to suppress aliasing artifacts. The resulting coil images are combined using square-root of sum-of-squares to reconstruct the final image. Spiral coronary images are acquired and aliasing-free bright blood and black blood images are successfully reconstructed using spiral PILS. As a high SNR parallel imaging method, PILS is a valuable tool in breath-held coronary artery imaging.

BOLD: Origins and Interactions

Room 615 - 617 16:00 - 18:00 Chairs: Richard B. Buxton and Oliver Speck

16:00 ***372***. **Metabolic Origin of BOLD Signal Fluctuations During Extended Rest and Light Sleep**

Masaki Fukunaga[1], Silvina G. Horovitz[1], Jacco A. de Zwart[1], Peter van Gelderen[1], Susan C. Fulton[1], Thomas J. Balkin[2], Jeff H. Duyn[1]

[1]National Institutes of Health, Bethesda, Maryland, USA; [2]Walter Reed Army Institute of Research, Silver Spring, Maryland, USA

Recent BOLD fMRI studies have demonstrated the existence of ongoing activity in the absence of stimuli. However, the origin of this activity remains unknown, and might be purely vascular. In order to investigate this, we performed concurrent BOLD and perfusion-based fMRI and used the ratio of their fluctuation levels to establish metabolic involvement. We found that this ratio was similar between rest, sleep, and a visual task and significantly lower compared to a breatholding task. These results suggest that the phenomenon of resting state BOLD activity represents a metabolic process and continues during sleep

16:12 ***373***. **Reducing Inter-Voxel Variability of the BOLD Response with Measurement of Resting Blood Flow**

Yashar Behzadi[1], Khaled Restom[1], Joanna Perthen[1], Thomas T. Liu[1]

[1]UCSD, San Diego, California, USA

The BOLD signal used in fMRI is dependent on regional differences on the cerebral blood flow (CBF), cerebral blood volume (CBV), and oxidative metabolism. Previous studies have attempted to account for the regional differences in the intensity of the BOLD response by hypercapnic normalization. In particular, studies showed that normalized BOLD signal induced by a motor task was consistent across different magnetic fields and pulse sequences. However, hypercapnic normalization involves the delivery of C02 and may be difficult to implement for select clinical subject populations. Here we investigate the use of resting CBF as a possible alternative normalization technique by first examining the dependence of the functional BOLD response on resting CBF.

16:24 ***374***. **Relationship Between Changes in Cerebral Arterial Blood Volume and Flow as Measured by MOTIVE with ASL During Neural Activation**

Tae Kim[1], Kristy Hendrich[1], Kazuto Masamoto[1], Seong-Gi Kim[1]

[1]University of Pittsburgh, Pittsburgh, Pennsylvania, USA

Changes in cerebral arterial blood volume (δCBVa) and flow (δCBF)were simultaneously measured during stimulation by modulation of tissue and vessel (MOTIVE) signals with arterial spin labeling. Activation maps of CBVa and CBF were successfully obtained for all animals with the high-sensitivity technique.δCBVa increases were correlated with δCBF increases; δCBVa (ml/100g) = 0.0054 (min^{-1}) ×δCBF (ml/100g/min)+ 0.13 (R=0.87). This indicates that stimulation-induced increases in CBF are not due to velocity changes, but are mostly due to arterial vessel dilation.

16:36 ***375***. **Simultaneous MRI Acquisition of Activation-Induced Change in Blood Flow, Blood Volume and Blood Exygenation: A Human Brain Study**

Wen-Chau Wu[1], Eric C. Wong[1]

[1]University of California, San Diego, La Jolla, California, USA

Inter-scan variations such as subject motion and physiological status can complicate the interpretation of fMRI data. Yang *et al* recently proposed a method that combined FAIR and VASO to simultaneously acquire images with contrasts of CBV, CBF and BOLD. The optimal inversion slab thickness, however, could vary with individuals, slice orientation and flow velocity. Besides, low SNR is an inherent disadvantage of current VASO technique. Here we describe a modified sequence for the same purpose by implementing an alternative VASO technique with higher SNR and less sensitivity to inversion efficiency, at the expanse of half temporal resolution.

16:48 ***376***. **Quantification of Arterial and Total Cerebral Blood Volume: Arterial Changes Dominate During Neural Activation**

Tae Kim[1], Kristy Hendrich[1], Seong-Gi Kim[1]

[1]University of Pittsburgh, Pittsburgh, Pennsylvania, USA

Changes in arterial cerebral blood volume (δCBVa) during stimulation were quantified by modulation of tissue and vessel (MOTIVE) signals with arterial spin labeling, and then compared with changes in total cerebral blood volume (δCBVt) determined by injection of contrast agent. There are no significant differences between δCBVa and δCBVt. These results demonstrate that total blood volume changes occurring during neural activation are mainly due to arterial volume changes rather than venous volume changes. This implies that BOLD signal changes are due mostly to the mismatch between cerebral blood flow and oxygen consumption.

17:00 ***377***. **Quantitative Hippocampal Perfusion Response to a Memory Encoding Task: A Comparison Between Healthy Young and Elderly Adults**

Khaled Restom[1], Katherine J. Bangen[1, 2], Joanna E. Perthen[1], Mark W. Bondi, [13], Thomas T. Liu[1]

[1]University of California, San Diego, La Jolla, California, USA; [2]UCSD/SDSU Joint Doctoral Program, San Diego, California, USA; [3]Veteren Affairs Healthcare System, San Diego, California, USA

Quantitative perfusion based fMRI utilizing ASL techniques has the potential to be a useful tool for studying the progression of cognitive diseases, such as Alzheimer's. However, due to the low inherent sensitivity of ASL, the application of this technique to the investigation of cognitive function has been limited. Here we show that ASL can be used in both young and elderly adults to obtain robust and reliable measures of functional perfusion activation in the hippocampus with a memory encoding task. This study supports the feasibility of using ASL to measure perfusion changes associated with cognitive function in older populations.

17:12 ***378***. **3T Pseudo-Continuous ASL Perfusion fMRI with Background-Suppressed Single Shot 3D GRASE During Memory Encoding**

Maria Asuncion Fernandez-Seara[1], Ze Wang[1], Jiongjiong Wang[1], Marc Korczykowski[1], Matthias Guenther[2], David Feinberg[2], John A. Detre[1]

[1]University of Pennsylvania Medical Center, Philadelphia, Pennsylvania, USA; [2]Advanced MRI Technologies, Sebastopol, California, USA

ASL perfusion-based fMRI was used to detect activation of the hippocampus during a memory encoding task. Perfusion data were acquired using a pseudo-continuous ASL approach combined with a background suppressed single shot 3D GRASE read-out and compared with BOLD results. Perfusion fMRI yielded stronger group activation, consistent with prior observations for sensorimotor tasks.

17:24 ***379***. **Evidence for a Slow Water Diffusion Pool Swelling During Activation of Human Visual Cortex**

Denis Le Bihan[1, 2], Shinichi Urayama[1], Toshihiko Aso[1], Takahashi Hanakawa[1], Hideano Fukuyama[1]

[1]Kyoto University Graduate School of Medicine, Kyoto, Japan; [2]CEA, Orsay, France

A transient decrease of water diffusion has been reported during activation of visual cortex. We have investigated signal changes at different degrees of diffusion sensitization using a 2-compartment diffusion model. At 3T activation of visual cortex was detected in our 6 subjects though a diffusion-weighted signal increase, but the signal change increased with b value. This increase was well modeled by a swelling of the slow diffusion pool (+0.56%) and a shrinking of the fast diffusion pool (-0.44%), suggesting a shift of water from the fast to the slow diffusion pools. Although the nature of the pools is still unclear diffusion-sensitized MRI might provide direct and quantitative access to a physiological surrogate of cortical activation.

17:36 ***380***. **Comparing BOLD Resonses of TMS, Median Nerve Stimulation and Voluntary Finger Movements**

Vera Kessler[1], Peter Dechent[1], Jürgen Baudewig[1]

[1]MR-Research in Neurology and Psychiatry, Medical Faculty, Georg-August-University, Göttingen, Germany

The combination of transcranial magnetic stimulation (TMS) with functional magnetic resonance imaging (fMRI) provides the possibility to directly visualize the TMS induced changes in brain activity at a high spatial and temporal resolution. Using interleaved TMS/fMRI we compared the activations shown after stimulation with TMS with the ones seen after voluntary finger movement and peripheral median nerve stimulation. Both supra- and subthreshold TMS of the primary motor cortex and median nerve stimulation resulted in the activation of cortical and subcortical structures involved in the motor network that are similar to the ones seen during voluntary thumb movement.

17:48 ***381***. **Visualizing Virtual Brain Lesions: Simultaneously Combining fMRI and TMS**

Jürgen Baudewig[1], A. Kohler[2], Sven Bestmann[3], D. E. J. Linden[4], Peter Dechent[1], R. Goebel[5], A. T. Sack[5]

[1]MR-Research in Neurology and Psychiatry, Medical Faculty, Georg-August-University, Göttingen, Germany; [2]Dept. of Neurophysiology, MPI for Brain Research, Frankfurt, Germany; [3]Institute of Cognitive Neuroscience & Wellcome Dept. of Imaging Neuroscience, University College, London, UK; [4]School of Psychology, University of Wales, Bangor, UK; [5]5Department of Cognitive Neuroscience, Faculty of Psychology, Maastricht University, Maastricht, Netherlands

Applying transcranial magnetic stimulation (TMS) can temporary and specifically impair behavioural performance. This non-invasive virtual lesion technique thus allows investigating the causal relationship between stimulated brain regions and a specific behavioural or cognitive function. Here we simultaneously combine fMRI and TMS during the execution of behaviourally controlled visuospatial tasks in order to visualize the physiological consequences of a virtual brain lesion as measured by TMS-induced changes of BOLD responses. We found a task-specific behavioural impairment of the TMS that was mirrored by task-specific fMRI signal reductions at the site of stimulation as well as within connected brain structures.

Measuring Vascular Function in Cancer

Room 618 - 620 16:00 - 18:00 Chairs: David L. Buckley and Jeffrey L. Evelhoch

16:00 ***382***. **Use of a High Temporal Resolution Population-Averaged Arterial Input Function to Improve DCE-MRI Reproducibility in Phase I Clinical Trial Settings**

Geoff James Martin Parker[1], Caleb Roberts[1], Andrew Macdonald[1], Sue Cheung[1], Giovanni A, Buonaccorsi[1], David L. Buckley[1], Alan Jackson[1], Yvonne Watson[1], Karen Davies[1], Gordon C. Jayson[2]

[1]University of Manchester, Manchester, UK; [2]Christie Hospital, Manchester, UK

T1-weighted 3D time series data were acquired in the abdomen of cancer patients during a phase I clinical drug trial to allow dynamic contrast-enhanced MRI (DCE-MRI) analysis of tumour microvasculature. The arterial input function (AIF) was measured in each patient at two pre-dose visits following a standardised bolus administration of gadodiamide. Tracer kinetic modeling output using measured AIFs was compared with the results of modeling using a high temporal resolution population AIF. Large improvements in the reproducibility of DCE-MRI model parameters are demonstrated when using the population AIF indicating the potential for increased sensitivity to therapy-induced change.

16:12 ***383***. **Blood Plasma Gd-DTPA Concentration Derived from Skeletal Muscle is Comparable with a Direct Measurement from the Aorta**

Simon Walker-Samuel[1], Benjamin R. Knowles[1], James A. d'Arcy[1], Neil J. Smith[2], Chris Parker[3], Gina Brown[3], Martin O. Leach[1], David J. Collins[1]

[1]Institute of Cancer Research, Sutton, Surrey, UK; [2]Mayday University Hospital, Thornton Heath, Surrey, UK; [3]Royal Marsden and NHS Foundation Trust, Sutton, Surrey, UK

Recent methodological advances have enabled the use of a reference tissue such as skeletal muscle to quantify DCE-MRI pharmacokinetics. This study aimed to compare blood plasma concentration curves derived from muscle with that measured directly in the aorta, in order to validate the reference tissue approach. It was found that, within the uncertainties of the methodology, both measurements are equivalent using published values of Ktrans and ve in skeletal muscle.

16:24 ***384***. **Tumor Arterial Input Function (AIF) Estimation in DCE-MRI Studies Using a Multiple Reference Tissue Method**

Cheng Yang[1], Walter M. Stadler[1], Milica Medved[1], Gregory S. Karczmar[1]

[1]University of Chicago, Chicago, Illinois, USA

We have developed a multiple reference tissue method (MRTM) to estimate the contrast agent arterial input function (AIF) in DCE-MRI. Its central assumption is that the AIFs of the multiple (2 or more) reference tissues have the same shape. Due to the heterogeneity of tumors, multiple reference tissues can be obtained from a single tumor ROI using a cluster analysis. The applications to clinical DCE-MRI data of renal cell cancer suggest that the MRTM can be generally applied. The estimated AIFs provide excellent fit to the data and closely resemble the AIFs measured by blood sampling reported in the literature.

16:36 ***385***. **T_1 Measurement of Flowing Blood and Arterial Input Function Determination for Quantitative 3D T_1 –weighted DCE-MRI**

Hai-Ling Margaret Cheng[1, 2]

[1]The University of Toronto, Toronto, Ontario, Canada; [2]The Hospital for Sick Children, Toronto, Ontario, Canada

Accurate measurement of the arterial input function (AIF) is challenging but necessary for reliable quantitative DCE-MRI. A method is proposed for accurate T_1 measurement in flowing blood and simultaneous monitoring of AIF and tissue uptake of Gadomer. Results in rabbits (N=10) showed that measured pre-injection blood T_1s were accurate and that individually derived AIFs followed expected biexponential decay characteristics. DCE-MRI analysis of blood volume in muscle based on individual AIFs was reliable and reproducible. The proposed method for accurate blood T_1 measurement combined with reproducible AIF extraction, can greatly improve the accuracy and reproducibility of DCE-MRI analysis.

16:48 ***386***. **Towards the Absolute Quantitation of DCE-MRI Pharmacokinetic Parameters: Addressing the Assumption of Constant Contrast Reagent Relaxivity and Its Effect on K^{trans}**

Greg Metzger[1, 2], David Thomasson[3], Marcelino Bernardo[4, 5], Peter Choyke[5]

[1]Philips Medical Systems, Bethesda, Maryland, USA; [2]University of Minnesota, Minneapolis, Minnesota, USA; [3]Clinical Center, Bethesda, Maryland, USA; [4]SAIC, Frederick, Maryland, USA; [5]National Cancer Institute, Bethesda, Maryland, USA

The assumption of constant relaxivity in the analysis of dynamic contrast enhanced MRI data is demonstrated to lead to an overestimation of Ktrans, the endothelial transfer constant, which characterizes the wash-in of contrast from the blood plasma to the extrvascular-extracellular space. By generating relaxivity correction maps derived from patient dependent magnetization transfer studies, the need for assuming constant relaxivity can be avoided. Average Gd-DTPA concentrations decreased by 22.9% using previous phantom calibration results relating magnetization transfer ratios to changes in relaxivity. This resulted in a decrease in the estimated Ktrans values.

17:00 ***387***. **Quantification of Proton Exchange by Histological Verification of Fractional Blood Volume Determined by an Intravascular T1 Contrast Agent at Prostate Tissue and Prostate Tumor**

Lutz Lüdemann[1], Ole Gemeinhardt[1], Guido Correia Carreira[1], Hagen Rehbein[1], Carsten Warmuth[1], Matthias Taupitz[1], Dirk Beyersdorff[1]

[1]Charité, Berlin, Germany

Quantification of blood volume by using blood pool contrast agents becomes available. A verification study is presented. Blood volume was determined in the same subject by MRI and histology. The differences of both methods were used to determine the impact of proton exchange on the MRI blood volume.

17:12 ***388***. **Simultaneous Determination of Perfusion and Microvascular Permeability: Measurement Precision with T_1-Weighted DCE-MRI**

Lucy Elizabeth Kershaw[1], David L. Buckley[1]

[1]University of Manchester, Manchester, UK

Two methods for estimating the bolus arrival time in T_1-weighted dynamic contrast enhanced MRI data were compared, and a bootstrap error analysis was used to estimate precision in simultaneous measurements of microvascular perfusion and permeability using the adiabatic approximation to the tissue homogeneity model. An independent method for estimating bolus arrival time was found to be more accurate and precise than a model-fitting approach. Both perfusion and permeability could be measured with acceptable accuracy.

17:24 ***389***. **Effect of Transcytolemmal Water Exchange in DCE-MRI Data Analysis of Human Head and Neck Cancer**

Sungheon Kim[1], Harry Quon[1], Laurie A. Loevner[1], Mark Rosen[1], Alex M. Kilger[1], Jerry D. Glickson[1], Harish Poptani[1]

[1]University of Pennsylvania, Philadelphia, Pennsylvania, USA

The dynamics of contrast reagent uptake has often been analyzed using the Kety-Schmidt two-compartment model assuming the trancytolemmal water exchange rate does not affect the DCE-MRI data. Recently, it has been demonstrated in animal tumor models that deviations from this assumption need to be taken into account. In the present study, we compared the goodness of fitting for Kety-Schmidt model with or without taking into account the trancytolemmal water exchange rate and conclude that the effect of water exchange needs to be considered in the quantitative analysis of contrast reagent uptake in human head and neck cancer.

17:36 ***390***. **Incorporating the Effects of Transcytolemmal Water Exchange in the Reference Region Model for DCE-MRI Analysis**

Thomas Yankeelov[1], Laura M. DeBusk[1], P. Charles Lin[1], John C. Gore[1]

[1]Vanderbilt University, Nashville, Tennessee, USA

The effects of transcytolemmal water exchange are incorporated into a reference region model for the analysis of dynamic contrast enhanced MRI data.

17:48 ***391***. **Error Propagation in Vessel Size Index Imaging**

Emmanuel L. Barbier[1, 2], Samuel Valable[1, 2], Cédric Lucatelli[1, 2], Irène Troprès,[23], Christoph Segebarth[1, 2] Chantal Rémy[1, 2]

[1]U594, Grenoble, F-38043, France; [2]Univ Grenoble 1, Grenoble, F-38043, France; [3]IFR1, Grenoble, F-38043, France

The vessel size index (VSI) provides information on the distribution of vessel radii in a voxel. It can be obtained by measuring the changes in R_2 and in R_2* induced by the injection of an intravascular contrast agent, the apparent diffusion coefficient, and the variation of susceptibility difference between blood and tissue before and after contrast injection. Since VSI depends on numerous factors, this study aims to characterize each contribution to the error on VSI so as to estimate the smallest change in VSI that can be detected and to identify directions for acquisition scheme optimization.

Hepatobiliary MRI

Room 602 - 604 16:00 - 18:00 Chairs: Shahid M. Hussain and Richard C. Semelka

16:00 ***392***. **Improved Background Suppression for 3D-MRCP Using T2-Prep**

Reed F. Busse[1], Jean H. Brittain[1], Scott B. Reeder[2], Frederick Kelcz[2]

[1]GE Healthcare, Madison, Wisconsin, USA; [2]University of Wisconsin, Madison, Wisconsin, USA

High contrast, high resolution MRCP is demonstrated using a 3D-FRFSE sequence with T2-Prep. MRCP requires strong suppression of background signal in order to visualize small bile and pancreatic ducts. T2-Prep improves background suppression by allowing magnetization in short and moderate T2 materials to decay before beginning acquisition. In particular, this reduces the undesirable high spatial frequency contribution from blood vessels. Incompletely saturated fat decays more rapidly during the prep phase with widely spaced refocusing pulses, overcoming the "bright fat" effect that is notable in FSE. PSF analysis and *in vivo* experiments are presented.

16:12 ***393***. **Detecting Cancer of the Bile Duct: Multivariate Analysis of ^{1}H MRS of Bile**

Tedros Bezabeh[1], Nils Albiin[2], Ulrika Broomé[2], Brian Dolenko[1], Bo Lindberg[2], Urban Arnelo[2], Ian CP Smith[1]

[1]NRC Institute for Biodiagnostics, Winnipeg, Manitoba, Canada; [2]Karolinska Institute, Karolinska University Hospital Huddinge, Stockholm, Sweden

Strictures in the bile duct resulting from malignant changes (cholangiocarcinoma) are difficult to distinguish from their benign counterparts, particularly in patients with primary sclerosing cholangitis (PSC), a benign chronic condition. The ability to detect early malignant changes in patients with PSC is critical in the appropriate treatment and management of these patients. 1-H MRS of bile was utilized in this study to assess the diagnostic potential of the technique. Using multivariate methods of analysis, 3 spectral regions were identified as being discriminatory and with the help of these regions; a classification accuracy of 100% was obtained in differentiating normal and PSC patients from those harboring cancer.

16:24 ***394***. **MR-Guided Delivery of Magnetoencapsulated Pancreatic Islets in a Swine Model**

Brad P. Barnett[1], Perry Karmarkar[1], Wesley Gilson[1], Piotr Walczak[1], Di Qian[1], Dara L. Kraitchman[1], Matthias Stuber[1], Jeff WM Bulte[1], Aravind Arepally[1]

[1]Johns Hopkins University School of Medicine, Baltimore, Maryland, USA

Recent advances in pancreatic islet cell transplantation for type I diabetes mellitus have provided insulin-independence in patients through successful engraftment. Nevertheless, the current percutaneous hepatic approach to transplantation carries a significant risk of bleeding and portal vein thrombosis. With these considerations in mind, we developed a novel approach to deliver and image islets following intraportal infusion in swine. Human islets were magnetoencapsulated (microencapsulation in an alginate based Feridex containing formulation) thereby providing both a means of immuno-isolation and MR-trackability. Utilizing MR guidance to access the portal vein via a transvenous approach magnetoencapsulated islets were delivered and subsequently imaged.

16:36 ***395***. **Quantitative MRI/MRS of Nonalcoholic Fatty Liver Disease (NAFLD)**

William H. Perman[1], Brent Neuschwander-Tetri[2], Elizabeth Brunt[3], Eldad Bialecki[3], Dean Palmer[3], Isin Akduman[3], John Olynyk[4], Gen Balci[3]

[1]St. Louis University School of Medicine, St. Louis, Missouri, USA; [2]St. Louis University, St. Louis, Missouri, USA; [3]St. Louis University School of Medicine, St. Louis, Missouri, USA; [4]University of Western Austrailia, Fremantle, Australia

We performed quantitative MRI and MRS on 25 patients diagnosed with NAFLD in order to correlate the histologic measures of the disease (steatosis, inflammation and fibrosis) with the MRI and MRS parameters of calculated T1 and T2, percent fat, percent magnetization transfer (MT%), and diffusion coefficient (D). Significant changes in liver T1 were highly correlated with inflammation alone, significant percent fat correlated with decreased T1 and T2, significant changes in MT and D do not appear to correlate with histology. Summary: quantitative liver MRI/MRS is sensitive to changes due to disease, but the changes do not always correlate with histology.

16:48 ***396***. **SPIOs and Low Molecular Weight Gd Chelates Are Synergistic for Direct Visualization of Advanced Liver Fibrosis**

Fiona Mary Hughes[1], Mark Bydder[1], Alyssa Chavez[1], Collins Julie[1], Richard Znamirowski[1], Wolfson Tanya[1], Cynthia Behling[1], Graeme Bydder[1], Claude Sirlin[1]

[1]UCSD, San Diego, California, USA

Super-paramagnetic iron oxides (SPIO) and gadolinium (Gd) chelates increase visibility of liver fibrosis on MR imaging by different mechanisms. This study compared the visibility of advanced liver fibrosis on unenhanced, Gd-enhanced, SPIO-enhanced, and combined (SPIO + Gd) contrast-enhanced MR images. In 58 consecutive cirrhotic patients imaged with four different spoiled gradient recalled echo sequences, fibrosis-liver contrast to noise ratio was significantly higher with combined contrast enhancement than with SPIO or Gd alone, and was higher with SPIO or Gd than without any contrast enhancement. The results indicate that SPIO and Gd are synergistic for detecting advanced liver fibrosis.

17:00 ***397***. **Robust Measurement of Hepatic Perfusion Using an Interleaved Saturation Prepared Double Echo Sequence: Comparison of Dual-Input and Gradient Models**

Kieren G. Hollingsworth[1], Martin J. Graves[1], Daniel J. Emmens, David John Lomas[1]

[1]University of Cambridge & Addenbrooke's Hospital, Cambridge, UK

Measuring hepatic perfusion robustly with MRI is a complex problem that requires accurate estimations of the aortic and portal venous gadolinium concentrations with sufficient temporal resolution following transient bolus injection. This work presents a solution using an interleaved saturation prepared sequence that collects a short saturation time, low spatial resolution, image of the aorta and a longer saturation time, higher spatial resolution, image of the hepatic parenchyma. Parallel reconstruction methods allow both images to be acquired within a single heartbeat. Dual-input model and heuristic estimates of liver perfusion are performed and compared in 6 healthy volunteers.

17:12 ***398***. **MR Elastography of the Liver in an Animal Model of Hepatic Fibrosis**

Meng Yin[1], Armando Manduca[1], Peter C. Harris[1], Vicente E. Torres[1], Richard L. Ehman[1]
[1]Mayo Clinic College of Medicine, Rochester, Minnesota, USA

At present, the gold standard for diagnosing hepatic fibrosis is liver biopsy, which is an invasive procedure, with risks of complications, potential sampling errors, and subjective histology grading problems. MR Elastography (MRE) is a modified phase-contrast MRI technique for quantitatively assessing the mechanical properties of soft tissues by visualizing propagating shear waves in soft tissues. It could be a promising non-invasive quantitative diagnostic method to assess hepatic fibrosis. Therefore, the underlying relationship between hepatic fibrosis extent and the corresponding MRE measurements of the liver tissues was quantitatively evaluated in an *in vivo* animal model of ARPKD mice.

17:24 ***399***. **Fast Planar Steady-State Free Precession MR Elastography on Human Liver**

Dieter Klatt[1], Patrick Asbach[1], Jens Rump[1], Sebastian Papazoglou[1], Uwe Hamhaber[2], Jürgen Braun[2], Ingolf Sack[1]
[1]Institute of Radiology, Berlin, Germany; [2]Institute of Medical Informatics, Berlin, Germany

Classical MR elastography (MRE) experiments applied to human liver suffer from extended time consumption due to slow vibration frequencies and the acquisition of 3D-strain wave fields for calculating elastograms. We propose the application of fast balanced SSFP-MRE for acquiring phase-difference wave images within 3 seconds. The combination of SSFP-MRE with alternating slice subtraction allows the use of low mechanical excitation frequencies below 50 Hz. Transversal wave excitation allows reducing the dimensionality of the wave inversion problem. Using the new planar SSFP-MRE method 8 healthy volunteers and 3 patients were investigated within an individual study time of 2 minutes.

17:36 ***400***. **Feasibility of a Respiratory-Triggered SSEPI Diffusion-Weighted Sequence for Liver Imaging Using Navigator Echo Technique: Comparison with Breath-Hold Diffusion-Weighted Sequence**

Alison Sandberg[1], Tejas Parikh[1], Glyn Johnson[1], Alto Stemmer[2], Jian Xu[3], Bachir Taouli[1]
[1]NYU Medical Center, New York, New York, USA; [2]Siemens Medical Solutions, Erlangen, Germany; [3]Siemens Medical Solutions, Malvern, Pennsylvania, USA

Our objective was to implement a new non breath-hold (NBH) SSEPI diffusion-weighted imaging (DWI) sequence combined with a navigator echo technique for liver imaging and to compare it with a breath-hold (BH) DWI sequence at b=0, 50 and 500 sec/mm2. NBH DWI showed significantly better image quality and better normalized liver signal ratio. In addition, lesion to liver contrast ratio was significantly higher with NBH DWI. ADCs of liver and focal lesions with both sequences were significantly correlated. The use of a navigator echo to trigger a SSEPI DWI sequence improves image quality and liver lesion conspicuity.

17:48 ***401***. **Detection of Colorectal Liver Metastases by Diffusion-Weighted Imaging**

Erica Scurr[1], Angela Riddell[1], Gina Brown[1], David Collins[1], Baris Kanber[2], Nandita deSouza[2], Dow-Mu Koh[2]
[1]Royal Marsden NHS Foundation Trust, Sutton, Surrey, UK; [2]Institute of Cancer Research, Sutton, Surrey, UK

The use of diffusion weighted imaging (DWI) has a good sensitivity and specificity for detection of colorectal cancer liver metastases. However, artefacts due to cardiac motion make DWI an inadequate diagnostic test for the left lobe of the liver. Quantitation of ADCs has utility in differentiating between benign cysts and metastases, but not between hemangiomas and metastases at b values 0-500 s/mm^2.

Multinuclear Spectroscopy of the Brain

Room 613 - 614 16:00 - 18:00 Chairs: Arend Heerschap and Brian D. Ross

16:00 ***402***. **Localized ^{13}C NMR Measurement of NAA and GSH Turnover in the Human Brain Over Multiple Days**

Pierre-Gilles Henry[1], Gulin Oz[1], Elizabeth R. Seaquist[1], Kamil Ugurbil[1], Rolf Gruetter[1]
[1]University of Minnesota, Minneapolis, Minnesota, USA

[1-^{13}C]glucose was infused i.v. in four healthy human volunteers for up to 50 hours in order to measure ^{13}C label incorporation into metabolites with a low metabolic rate such as N-acetyl-aspartate (NAA) and glutathione (GSH). Our results indicate that the entire pool of NAA is metabolically active, and that the time constant for NAA turnover is about 30 hours in the human brain. Our results also demonstrate the feasibility of measuring glutathione turnover from glutamate in the human brain.

16:12 ***403***. **13C MRS to Study Human Brain Metabolism During HYPOglycemia is Feasible**

Marinette van der Graaf[1], Bastiaan E. de Galan[1], Dennis W.J. Klomp[1], Cees J.J. Tack[1], Arend Heerschap[1]
[1]Radboud University Nijmegen Medical Center, Nijmegen, Netherlands

13C-MRS studies on human brain metabolism are generally performed using 13C-1-glucose infusion under HYPERglycemic conditions to obtain sufficient signal-to-noise ratio of the 13C-labeled metabolite signals. However, this study shows the feasibility to obtain time curves of the 13C-MR metabolite signals under HYPOglycemic conditions by the application of an optimized hyperinsulinemic hypoglycemic clamp method, a 13C/1H volume head coil, and an ISIS-DEPT pulse sequence at 3T. This method not only allows studies on normal brain metabolism during hypoglycemia, but it also opens possibilities to study differences in hypoglycemic brain metabolism of diabetic patients with and without hypoglycemia unawareness.

16:24 ***404***. **Quantification of Undecoupled ^{13}C NMR Spectra in the Brain**

Dinesh K. Deelchand[1], Kamil Ugurbil[1], Pierre-Gilles Henry[1]
[1]University of Minnesota, Minneapolis, Minnesota, USA

Proton-decoupling has restricted the implementation of ^{13}C NMR spectroscopy for human studies at ultra-high fields, mainly due to power deposition. We show that incorporation of ^{13}C label into brain amino acids can be monitored accurately using localized ^{13}C spectroscopy without ^{1}H-decoupling in rat brain at 9.4T. Quantification was performed using LCModel with prior knowledge of J-coupling constants. Although the Cramer-Rao Bounds observed in undecoupled spectra were higher than decoupled spectra, the degradation was less than the peak S/N loss while both metabolites time courses were in excellent agreement. The study suggests the possibility of performing ^{13}C human studies at fields>4T.

16:36 ***405***. **Does Brain Glycogen Supply Fuel for Neuronal Activation?**

Gulin Oz[1], Pierre-Gilles Henry[1], Pierre-Francois van de Moortele[1], Elizabeth R. Seaquist[1], Rolf Gruetter[1]
[1]University of Minnesota, Minneapolis, Minnesota, USA

Utilization of brain glycogen during brain activation was investigated after pre-labeling glycogen with i.v. infusions of [1-^{13}C]glucose over extended periods (13-50 h) in five healthy volunteers. No difference in [1-^{13}C]glycogen signal localized to the visual cortex was observed after 20 minutes of visual stimulation with a checkerboard pattern. This observation supports the hypothesis that bulk brain glycogen is mobilized when glucose supply becomes rate-limiting for metabolism. A small fraction of glycogen may still be highly active under normal physiology.

16:48 ***406***. **Sensitivity Enhanced and Localized 13C MRS to Study Glucose Uptake and Metabolism in Mouse Brain**

Christine Nabuurs[1], Dennis Klomp[1], Hermien Kan[1], Arend Heerschap[1]
[1]Radboud University Medical Center, Nijmegen, Netherlands

In vivo 13C MRS measurements with 13C labeled compounds in mice would provide a valuable technique for a better understanding of neurometabolism, especially when feasible in transgenic mice models. Here we present an experimental setup that enables the first 3D localized 13C MRS detection at physiological conditions in mice brain. With polarization transfer techniques and efficient RF coils, a substantial signal enhancement was obtained. The achieved high temporal en spectral resolution of localized 13C MRS opens new opportunities to study neurometabolic fluxes in mouse models.

17:00 ***407***. **Detection of Lactate Dehydrogenase Reaction *In Vivo* Using Carbon-13 Magnetization Transfer**

Su Xu[1], Jun Shen[1]
[1]National Institute of Mental Health, Bethesda, Maryland, USA

The carbon-13 magnetization transfer effect due to the rapid exchange between pyruvate and lactate catalyzed by lactate dehydrogenase is reported. The carbonyl carbon of pyruvate at 207.9 ppm was saturated after intravenous infusion of [2-^{13}C]glucose and bicuculline. The results demonstrate that the magnetization transfer effect of lactate dehydrogenase could be used as a novel marker accessible to the noninvasive MRS techniques for studying many physiological and pathological conditions such as cancer.

17:12 ***408***. **Glial Glutamate Dysfunction in Schizophrenia: 13C Acetate MRS**

Kent Christopher Harris[1]
[1]Huntington Medical Research Institute, Pasadena, California, USA

With our earlier 1-13C glucose MRS data, we demonstrated direct support for the role of glutamate in schizophrenia.In this study, the known glial fuel sodium acetate, enriched in carbon 1 position (2mg/kg/min over 1 hour = approximately 10g total) administered intravenously, is traced in the brain into its glial and neuronal compartments to directly determine the *in vivo* rates of the Krebs Cycle, glutamate-glutamine cycle and oxidative pathways. We describe reduced bicarbonate production from 1-13C acetate. We conclude glial elements of the glutamate glutamine cycle are abnormal in schizophrenic subjects.

17:24 ***409***. **High-Field ^{17}O Study of 3D $CMRO_2$ Imaging in Human Visual Cortex**

Xiao-Hong Zhu[1], Xiaoliang Zhang[1], Nanyin Zhang[1], Yi Zhang[1], John Strupp[1], Kamil Ugurbil[1], Wei Chen[1]
[1]CMRR, Radiology Department, University of Minneasota Medical School, Minneapolis, Minnesota, USA

It is important to develop an MR approach for noninvasively imaging the cerebral metabolic rate of oxygen ($CMRO_2$) which plays an essential role in brain function at both physiological and pathological states. We have conducted a preliminary study to examine the feasibility of using *in vivo* ^{17}O MR spectroscopic imaging (MRSI) for directly obtaining 3D $CMRO_2$ images in the human visual cortex (V1) at 7T during a 2-3 minute inhalation of $^{17}O_2$. Our preliminary results indicate an excellent ^{17}O SNR for detecting the accumulation rate of the $H_2{}^{17}O$ in brain tissue being metabolized from the inhalated $^{17}O_2$. A significant increase of $CMRO_2$ upon stimulation was observed in our initial study.

17:36 ***410***. **T_2-Labelling of Phosphate by ^{17}O – a Method with Potential for *In Vivo* Studies of Phosphorus Metabolism**

Peter Edward Thelwall[1]
[1]University of Florida, Gainesville, Florida, USA

As ^{31}P has 100% natural abundance and is the only MR-visible stable isotope of phosphorus, tracer studies analogous to those employed with ^{13}C are not appicable to MR studies of the metabolism of phosphorus-containing compounds. Previous studies have labelled phosphate with ^{17}O or ^{18}O, detecting the presence of these isotopes by mass spectrometry or by the isotope effect of ^{18}O on the ^{31}P chemical shift. However, neither of these methods is applicable to *in vivo* studies. We present a method to detect ^{17}O-labelled phosphate via the scalar coupling interaction between ^{31}P and ^{17}O, which is applicable to *in vivo* studies.

17:48 ***411***. **Rapid Interleaved Proton and Phosphorous MRS at 4T: Metabolic Effects of Hyperventilation**

Seth D. Friedman[1], *Eric J. Jensen*[2], *Blaise D. Frederick*[2], *Stephen R. Dager*[3], *Perry F. Renshaw*[2]
[1]University of Washington, Seattle, Washington, USA; [2]Harvard, McLean, Massachusetts, USA; [3]University of Washington, Seattle, Washington, USA

Hyperventilation (HV), a common feature of many diseases, results in a constellation of metabolic compensatory changes. Though a number of animal and human studies have suggested metabolic changes are mild in degree, an alternative conclusion from several animal studies is that hyperventilation results in major metabolic compromise. Since anesthesia effects may be a potential confound, we wanted to clearly characterize the degree ofmetabolic effects in the awake human, using dual interleaved 1H and 31P at 4T as a methodological probe.

BRONZE CORPORATE MEMBER SYMPOSIUM
Berlex Imaging / Schering AG
Breast MRI Hot Topics

Room 6C 18:15 - 19:45

Faculty:
Constance D. Lehman
Christiane K. Kuhl
Nola M. Hylton

BRONZE CORPORATE MEMBER SYMPOSIUM
Varian, Inc.
Pushing the Envelope with High Fields

Room 6D 18:15 - 19:45

18:15 Reception

18:30 **Ultra High Field MR *In Vivo*: Adventures on a Varian/Magnex 12 Tesla Scanner**
Joseph J. H. Ackerman

18:50 **The Indispensable Role of High Fields in Studies of Brain Function and Neurochemistry**
Kamil Ugurbil

19:10 **Spectroscopic Imaging at High Field: From Mouse to Man**
Hoby Hetherington

19:30 **Moore's Law for Magnets**
Rory Warner

BRONZE CORPORATE MEMBER SYMPOSIUM
Bracco
The Quest for Signal: Developments in MR Sequences and Contrast Agents

Room 4C-3,4 18:15 - 19:45

MORNING CATEGORICAL COURSE
Technical Advances in Body MR

Room 618-620 7:00 – 8:00 Chairs: Neil M. Rofsky, Daniel K. Sodickson, and Bachir Taouli

Educational Objectives:
Upon completion of this session, participants should be able to:

- Evaluate important developments in MRI technology, including high field imaging and parallel imaging;
- Identify the technical challenges associated with effective application of this technology for body imaging; and
- Describe the potential applications of new technologies in body imaging, including areas such as diffusion and perfusion MRI, and MR spectroscopy.

Advances in Coil Design and Multichannel Imaging for Body MRI

07:00 **Coils, Receivers, and Parallel Imaging: A Technical Perspective**
Charles A. McKenzie

07:30 **Parallel Imaging: A Clinical Perspective**
Neil M. Rofsky

MORNING CATEGORICAL COURSE
Cardiovascular Imaging

Room 6D 7:00 – 8:00 Chairs: Qun Chen and James F.M. Meaney

Educational Objectives:
Upon completion of this session, participants should be able to:

- Implement a robust protocol for clinical evaluation of arteries with both non-contrast and contrast-enhanced techniques;

- Identify the strengths and weaknesses of 3T MRI vs. 1.5T MRI for cardiovascular assessment;
- Recognize the value of parallel imaging for cardiovascular assessment at higher magnetic field (>1.5T);
- Select a comprehensive time-efficient protocol incorporating anatomical and functional cardiac evaluation;
- Explain the value of MRI for the assessment of non-coronary artery disease; and
- Recognize the strengths and also the limitations of current techniques.

Cardiovascular MRI at High Field – Is 3T better than 1.5T?

07:00 **MRA at 3.0T**
Neil M. Rofsky

07:20 **Cardiac MRI at 3.0T**
J. Paul Finn

07:40 **Cardiovascular Parallel Imaging at 3.0T**
Thoralf Niendorf

MORNING CATEGORICAL COURSE
Clinical DTI/PWI/fMRI

Room 4C-3,4 7:00 – 8:00 Chairs: Alberto Bizzi and Soonmee Cha

Educational Objectives:
Upon completion of this session, participants should be able to:

- Describe the main applications and contributions of fMRI, DTI, and tractography and bolus tracking and arterial labeling perfusion MR imaging in clinical neuroscience;
- Describe the technical requirements necessary to implement robust, accurate, and repeatable clinical advanced MR studies in patients with neurological diseases;
- List the potential contribution of PWI, DTI and fMRI to formulate diagnosis, prognosis, and evaluate different therapeutic strategies in the neurological diseases focus of this course;
- Discuss the basic MR principles involved in the quantification of angiogenesis and permeability using perfusion MR imaging;
- Implement new quantitative MR methods that may quantify cumulative brain damage that better correlate with the disability score;
- Recognize challenges, limitations and pitfalls of performing advanced MR studies to answer clinical questions in neurological patients; and
- Implement Quality Assurance (QA) procedures necessary to run a reliable and successful advanced MRI clinic.

Measuring Extent of White Matter Disease: Diffusion MRI

07:00 **Diffusion Tensor Imaging of Traumatic Brain Injury**
Pratik Mukherjee

07:30 **Clinical Output of DTI Measurements in Multiple Sclerosis**
Olga Ciccarelli

MORNING CATEGORICAL COURSE
MR Hardware/Engineering

Room 611-612 7:00 – 8:00 Chairs: Steven M. Conolly and Steven M. Wright

Educational Objectives:
Upon completion of this session, participants should be able to:

- List and compare implementations of static field magnet designs for clinical MRI;
- Recognize that there are fundamental limits on our ability to shim out steep field variations (such as those in the sinuses);
- Describe advances in shim system design;
- Explain the differences between arrays designed to optimize SNR vs. those designed for partial parallel imaging;
- Compare and contrast arrays designed for transmit and receive applications;
- Describe algorithms for designing RF pulses for parallel imaging;
- Compare and contrast ESR and NMR; and
- Describe several applications of hyper-polarized 13C and explain methodological differences between conventional MRI and hyperpolarized MRI.

Receivers and RF Arrays

07:00 **Array Systems**
Nicola de Zanche

07:20 **Receivers System**
Arne Reykowski

MORNING CATEGORICAL COURSE
Human MRI and MRS at High Static Magnetic Fields: The Promise, the Challenges, the Solutions

Room 615-617 7:00 – 8:00 Chairs: Joseph A. Helpern and Dikoma C. Shungu

Educational Objectives:
Upon completion of this session, participants should be able to:

- Describe the general behavior of B_0 and B_1 fields in the human body when the Larmor frequency is of the order of or greater than 100 MHz;
- List the problems faced in trying to obtain a homogeneous B_0 field and a B_1 field;
- Recognize the challenges of developing RF coils for high field applications;
- Recognize the challenges of whole-body imaging at high fields and list potential solutions;
- List recent methodological advances for detecting neurotransmitters by MRS at high fields;
- Recognize the challenges of implementing heteronuclear spin-spin decoupling at high static fields;
- Describe the benefits of high field for BOLD contrast;
- Describe the interaction between high magnetic fields and biological systems; and
- List organizations responsible for regulating exposure to magnetic fields.

07:00 **High Resolution Imaging: Why is it Important for T_1 Weighted Imaging, MRA and SWI?**
E. Mark Haacke

07:20 **Parallel Excitation: Making SENSE of High-Field Body MRI**
Yudong Zhu

MORNING CATEGORICAL COURSE
New Horizons in Musculoskeletal MRI

Room 613-614 7:00 – 8:00 Chairs: Joshua M. Farber and Timothy J. Mosher

Educational Objectives:
Upon completion of this session, participants should be able to:

- Recognize patterns of abnormal hip biomechanics and associated MRI findings in femoral acetabular impingement syndrome;
- Apply knowledge of normal articular cartilage maturation and joint development in interpretation of pediatric musculoskeletal MRI;
- Recognize the role of normal and abnormal biomechanics and the associated MRI findings in normal joint physiology and development of overuse injuries;
- Identify emerging translational research applications in the field of musculoskeletal MRI:
- Describe new MRI techniques for tracking mesenchymal stem cells;
- Recognize new applications of molecular imaging in the study of musculoskeletal diseases.

Pediatric Cartilage Imaging

The final five minutes of each talk will be reserved for questions.

07:00 **MRI Evaluation of Cartilage Maturation**
Miika T. Nieminen

07:30 **MR Imaging of Cartilage in the Pediatric Patient**
Tal Laor

MORNING CATEGORICAL COURSE
Quantitative Neuro MRI

Room 602-604 7:00 – 8:00 Chairs: Fernando Calamante and Annemie Van der Linden

Educational Objectives:
Upon completion of this session, participants should be able to:

- Discuss the latest advances in the field of arterial spin labeling, their current limitations, and identify their potential role in basic and clinical science;
- Demonstrate the role of MR methods to assess oxygen consumption non-invasively, and illustrate potential applications;
- Describe the various approaches to measure the arterial input function using dynamic-susceptibility contrast MRI and describe their limitations and implications to measure absolute cerebral blood flow, explain the latest advances of dynamic contrast-enhanced MRI to measure non-perfusion parameters, and assure formation of proper echoes;
- Recognize the limitations of the diffusion tensor model and identify more advanced methodologies to characterize areas with multiple fiber directions more accurately, as well as to describe the latest advances on fiber-tracking, including the concept of probabilistic tractography;
- Apply statistical approaches to perform voxel-based analysis for group comparison, and
- Describe image analysis techniques to characterize brain deformation.

Dynamic Susceptibility-Contrast MRI

07:00 **Quantification Issues in Bolus-Tracking Perfusion MRI**
Matthias J. P. van Osch

07:30 **Steady-State and First-Pass Contrast Agent Methods to Evaluate CBV, Vascular Morphology and Permeability**
Kathleen M. Schmainda

MORNING CATEGORICAL COURSE
Unsolved Problems and Unmet Needs in Magnetic Resonance

Room 6E 7:00 – 8:00 Chairs: John A. Detre and Michael E. Moseley

Educational Objectives:
Upon completion of this session, participants should be able to:

- Identify and assess a sampling of key unsolved problems and unmet needs in the field of magnetic resonance;
- Establish criteria for successful solutions to such problems;
- Consider any large-scale coordination across our field or with other fields that may be called for to address some classes of research or clinical needs;
- Identify and share additional unsolved problems or unmet needs in your areas of interest.

Can MRI provide a noninvasive biopsy?

07:00 **Cytoarchitectonic MRI: Can MRI Be Used to Quantify Neural Tissue?**
Itamar Ronen

07:15 **Tissue Structure through Diffusion and Transverse Relaxation Measurements**
Valerij G. Kiselev

07:30 **Unresolved Issues in Diffusion and Perfusion MRI: A Consensus from the Study Group**
Derek K. Jones

07:45 **Open Discussion**

PLENARY LECTURES: The Role of Imaging in Understanding Obesity and its Complications

Room 6A-C 8:15 - 9:30 Chairs: Dikoma C. Shungu and Joshua Farber

8:15 ***412***. **MR Spectroscopy in Obesity and Its Complications: Diabetes and Insulin Resistance**
Gerald I. Shulman[1]
[1]Yale University School of Medicine, New Haven, Connecticut, USA

Type 2 diabetes is the most common metabolic disease in the world and it is the leading cause of blindness, endstage renal disease and non-traumatic loss of limb in most industrialized countries. While the primary cause of this disease is unknown, insulin resistance plays a major role in its development. This presentation will focus on recent studies using 13C, 31P and 1H magnetic resonance spectroscopy techniques in humans to examine the mechanism of fat induced hepatic and muscle insulin resistance and more recent 13C and 31P magnetic resonance studies that have implicated functional defects in mitochondrial activity in the pathogenesis of insulin resistance.

8:40 ***413***. **Functional Imaging in Obesity and Its Complications: Understanding Food Craving and Satiety**
J. Daniel Ragland[1]
[1]University of Pennsylvania, Philadelphia, Pennsylvania, USA

Food craving is an intense desire to eat a specific food. This presentation shows how diet manipulation and cue-induction techniques can be used to trigger food cravings while individuals are undergoing functional magnetic resonance imaging (fMRI). Subjects received either normal or monotonous diets prior to scanning and were presented with liked versus monotonous food cues during imaging. As predicted, monotonous diet was accompanied by increased craving during fMRI and by differential activation in limbic, paralimbic, and basal ganglia regions. Results suggest a common neural substrate for food and drug craving, and are discussed in relationship to the obesity literature.

9:05 ***414***. **When Fat is Good: The Biomechanical Role of Fat in the Musculoskeletal System**
Mark Schweitzer[1]
[1]Hospital for Joint Diseases, New York, USA

Conceptually fat almost always has primary purposes and secondary affects. For example: Systemically the primary purpose of fat is an energy store, the secondary affects leads to bone hypertrophy protecting against fracture but causing osteoarthritis. In the musculoskeletal system, one of the primary affects of fat is an articular cushion. . Another primary affect is as a space holder. In some ways the primary and secondary affects interact with each other. For example: following articular disease synovial fat can hypertrophy when injured but can increasing articular cushioning.Lastly some systemic processes such as diabetes and neurologic disorders cause alterations in skeletal fat leading to MSK infections.

SOUNDS & VISIONS - Reloaded

Room 6A-C 9:30 - 10:30 Chairs: Mark E. Ladd and Harald H. Quick

CLINICAL CATEGORICAL COURSE
Cardiovascular Imaging

Room 6E 11:00 – 13:00 Chairs: David A. Bluemke and J. Paul Finn

Educational Objectives:
Upon completion of this session, participants should be able to:

- Describe advances in coronary MRA using whole heart techniques;
- List applications of high field MRI for cardiovascular imaging;
- Explain the use of contrast enhanced myocardial MRI for the evaluation of myocardial fibrosis/scar;
- Describe advanced MRI methods for evaluation of peripheral arterial disease.

11:00 **Coronary Whole Heart MRA**
Debiao Li

11:30 **MRA at 3T**
J. Paul Finn

12:00 **Advances in Delayed Gadolinium MRI of Heart and Vessels**
Joao A. C. Lima

12:30 **Peripheral MRA: Competing in the MDCT Era**
Jörg Barkhausen

New Developments in Parallel Imaging RF Array Coil Design

Room 6C 11:00 - 13:00 Chairs: Mary McDougall and Larence L. Wald

11:00 ***415***. **A 32 Channel Receive-Only Head Coil and Detunable Transmit Birdcage Coil for 7 Tesla Brain Imaging**
Graham Charles Wiggins[1], Christopher John Wiggins[1], Andreas Potthast[2], Vijay Alagappan[1], Oliver Kraff[3], Arne Reykowski[4], Lawrence L. Wald[1]
[1]Massachusetts General Hospital, Charlestown, Massachusetts, USA; [2]Siemens Medical Solutions, Inc, Malvern, Pennsylvania, USA; [3]University Hospital Essen, Essen, Germany; [4]Invivo Corporation, Gainesville, Florida, USA

We demonstrate a 32 channel phased array head coil for use at 7T. The receive coil and dedicated transmit birdcage fit within a 36cm head gradient coil. The 32 overlapping circular receive coils are arranged with a soccer ball geometry over a close fitting helmet. The array provided SNR gains of 2-fold in the center of the head and 5-fold or more in the cortex. The g-factor performance was also examined and found to be slightly better than a 3T 32 channel coil with identical element geometry, and much better than an 7T 8 channel close-fitting array.

11:12 ***416***. **An Adjustable 8-Channel Coil Array for MRI of the Human Wrist**
Jurek Antonin Massner[1], Nicola De Zanche[1], Klaas Paul Pruessmann[1]
[1]University and ETH Zurich, Zurich, Switzerland

Wrist imaging demands very high resolution due to a large number of subtle structures in a small volume, thus calling for receiver ar-rays that fit the anatomy closely for highest SNR yield. To address issues like variable wrist size, handling and patient comfort we have developed a coil array that optimizes its SNR performance by adjusting to each individual wrist. Variable coil interaction was addressed mainly by preamplifier decoupling. However, the best SNR was obtained with moderate coupling in favor of preamplifier noise matching. Consistently excellent SNR efficiency is demonstrated by selected *in vivo* results from wrists of varying size.

11:24 ***417***. **Experimental and Numerical Investigations of SENSE Array Performances from High to Ultra-High Field Strengths**
Shumin Wang[1], Patrick J. Ledden[2], Jacco A. de Zwart[1], Peter van Gelderen[1], Alan Koretsky[1], Jeff H. Duyn[1]
[1]LFMI, NINDS, National Institutes of Health, Bethesda, Maryland, USA; [2]Nova Medical, Inc., Wilmington, Massachusetts, USA

To verify earlier theoretical predictions of increased parallel imaging performance at high field, closely gapped arrays were compared at various field strengths, both experimentally and numerically. Experiments were conducted at 1.5, 3.0 and 7.0 Tesla respectively to verify the simulation results. The simulation was then extended to 11.7, 14.0 and 21.0 Tesla. Consistent with earlier studies, the simulations showed an improvement of SENSE performance at high field strengths, in particular for higher acceleration rates. Furthermore, experimental results obtained at 1.5 T, 3.0 T and 7.0 T closely matched the simulations.

11:36 ***418***. **36 Channel Peripheral Angio Matrix Coil for 3 Tesla**
Volker Matschl[1], Helmut Kess[1], Karsten Jahns[1], Heinz Hahn[1], Helmut Greim[1], Harald Kramer[2], Stefan Schoenberg[2], Hubertus Fischer[1]
[1]Siemens Medical Solutions, Erlangen, Germany; [2]University of Munich - Grosshadern Campus, Munich, Germany

A new peripheral angio coil with 36 integrated coil elements is presented for 3 Tesla. It will be shown why an overlap antenna design is preferable for these applications. The SNR and the iPAT performance from the overlap in comparison to the gap design were evaluated. Based on these results examinations on volunteers were performed.

11:48 ***419***. **An 8 Channel Shoulder Coil for High Resolusion Imaging**
Yoshinori Hamamura[1], Brian Brown[1], Kyle Johnson[1], Jeff Hathaway[1], Ken Meurer[1], Murray Wheeler[1]
[1]Invivo, Pewaukee, Wisconsin, USA

An 8 channel shoulder coil with high surface SNR and deep tissue SNR is presented by optimizing the loop layout and introducing dual hinging mechanism to fit various patients body tightly. 1.5T and 3T coils were built and evaluated by both phantom and volunteer images. Phantom SNR showed 1.2 times higher than conventional four-channel coil at the labrum position and 2.0 times at the surface. Volunteer images showed SNR improvement at both medial and surface regions.

12:00 ***420***. **An Optimised 16-Element Head Coil for 7T with Integrated Preamplifiers**

Yun-Jeong Yang[1], Nicholas Castrilla[1], Cliff Mills[1], Verna Fitzsimmons[2], Joseph Murphy-Boesch[1]
[1]USA Instruments, Inc., Aurora, Ohio, USA; [2]Kent State University, Kent, Ohio, USA

An 16- Element close-fitting head coil insert is described for acquiring high-sensitivity images of the brain at 7 Tesla. The insert was designed to fit within the cylindrical volume of a transmit volume coil, and its former has been optimized for a wide range of head sizes. Twelve coil elements were distributed around the dome of the head and four placed over the cerebellum for whole brain coverage. Staggering of two layers of elements azimuthally provided greater overlap in the S-I direction. Low-impedance preamps integrated into the assembly provide high sensitivity and good isolation among the elements.

12:12 ***421***. **High-Field Transmission Line Arrays for Transmit and Receive**

Carl J. Snyder[1], Lance DelaBarre[1], Can Akgun[1], Steen Moeller[1], Gregor Adriany[1], Kamil Ugurbil[1], John Thomas Vaughan[1]
[1]University of Minnesota, Minneapolis, Minnesota, USA

At high-fields, transmission line arrays and multi-channel TEM coils have show to be useful transceivers, but the extension to using these transmission line resonator arrays in a receive-only array has not been strongly pursued. Here we have developed a 16-element, receive-only transmission line resonator array to be used in conjunction with a 16-element transmission line vloume array for high-field imaging. The receiver array had improved SNR and spatial sensitivity then the larger volume array. The receiver array also shows improved cortical homogeneity over more traditional loop arrays

12:24 ***422***. **Twenty-Four Channel Receive-Only Array for Brain Imaging at 7T**

Patrick J. Ledden[1], Azma Mareyam[1], Shumin Wang[2], Peter van Gelderen[2], Jeff H. Duyn[2]
[1]Nova Medical, Inc., Wilmington, Massachusetts, USA; [2]National Institutes of Health, Bethesda, Maryland, USA

The availability of increasing numbers of receivers on 7T MRI scanners leads to the question of how to optimally make use of these additional channels. For this work, we describe a 24 channel receive-only array using radially gapped columns of overlapping elements parallel to B0 for brain imaging at 7T. This element geometry provided dramatically improved sensitivity improvements over a quadrature channel volume coil and more modest yet significant sensitivity improvements eight channel radially gapped coil of similar size. Axial plane G factors were low and this coil geometry allows for SENSE acquisition in other planes

12:36 ***423***. **A 28 Channel Bi-Lateral Breast Array for Accelerated MR Imaging**

Randy O. Giaquinto[1], Charles McKenzie[2], Daniel K. Sodickson[2], Aaron K. Grant[2], Gordon E. Murtagh[1], Robert L. Furman[1], Leo J. Swider[1], Christopher J. Hardy[1], Charles L. Dumoulin[1]
[1]GE Global Research, Niskayuna, New York, USA; [2]Beth Israel Deaconess Medical Center, Boston, Massachusetts, USA

A breast imaging table with a built-in 28-channel breast coil array was constructed. The performance of the coil array was evaluated in phantoms and human volunteers. The excellent sensitivity of the rf coils in the breast imaging table and the large number of independent elements permit MR imaging with substantial acceleration factors. This in turn affords greater flexibility in reducing scan times, increasing resolution and choice of protocol.

12:48 ***424***. **Measuring Practical Coil Array Performance with Respect to Ultimate Intrinsic SNR: A Tool for Array Design and Assessment**

Riccardo Lattanzi[1, 2], Aaron K. Grant[2], Michael A. Ohliger[1, 2], Daniel K. Sodickson, [12]
[1]Harvard-MIT, Cambridge, Massachusetts, USA; [2]Beth Israel Deaconess Medical Center, Boston, Massachusetts, USA

A method for evaluating the absolute SNR performance of radiofrequency detector coils for traditional or parallel imaging is described. Measured SNR is expressed pixel by pixel as a fraction of the ultimate achievable SNR (computed using electrodynamic considerations for a given object and image plane geometry, and scaled to account for pulse-sequence-specific factors). In this work, coil performance maps were generated as a function of parallel imaging acceleration factor for a linear 8-element array atop a cylindrical phantom. For this array, a maximum of nearly 45% of optimal performance for unaccelerated imaging and nearly 60% for accelerated imaging was observed.

Enhanced Contrast Using Non-Traditional Methods

Room 6D 11:00 - 13:00 Chairs: Klaus Scheffler and Dmitriy A. Yablonskiy

11:00 ***425***. Young Investigator Award Finalist: **Improving MRI Differentiation of Gray and White Matter in Epileptogenic Lesions Based on Nonlinear Feedback**

Susie Yi Huang[1], Stephanie M. Wolahan[1], Gary W. Mathern[1], Dennis J. Chute[1], Massoud Akhtari[1], Snow T. Nguyen[1], My Huynh[1], Noriko Salamon[1], Yung-Ya Lin[1]
[1]University of California, Los Angeles, Los Angeles, California, USA

A new method for enhancing MRI contrast between gray and white matter in epileptogenic lesions is demonstrated. This method uses the radiation damping feedback interaction in high-field MRI to amplify contrast due to small differences in resonance frequency in gray and white matter corresponding to variations in tissue susceptibility. High-resolution radiation damping-enhanced images of in vitro brain tissue from five patients were acquired at 14T and compared against conventional T1-weighted, T2-weighted, and proton density images and simulated radiation damping-enhanced images. The radiation damping-enhanced images yielded 5x better contrast-to-noise ratios on average than the best T1-weighted, T2-weighted, or proton density images.

11:20 ***426***. **Z-Spectral Asymmetry Caused by Radiation Damping**

Johanna Narvainen[1], David C. Williamson[1, 2], Risto A. Kauppinen[3], Gareth A. Morris[1]

[1]University of Manchester, Manchester, England, UK; [2]University of York, York, England UK; [3]University of Birmingham, Birmingham, England UK

It is shown that radiation damping interacts with small probe tuning errors to cause significant asymmetry in Z-spectra of water and 0.4 M aqueous urea at 400 MHz. This may obscure the Z-spectrum asymmetry caused by chemical exchange and complicate the *in vivo* determination of pH via Z-spectroscopy when high Q coils and high fields are used.

11:32 ***427***. **MR Imaging with T_1 Dispersion Contrast**

Sharon E. Ungersma[1], Nathaniel I. Matter[1], Jonathan W. Hardy[1], Ross D. Venook[1], Albert Macovski[1], Steven M. Conolly[2], Greig C. Scott[1]

[1]Stanford University, Stanford, California, USA; [2]University of California, Berkeley, Berkeley, California, USA

Prepolarized MRI can polarize a sample at high field, then allow the magnetization to decay at an "evolutionary" field strength before imaging at low field. The difference between images collected with two different evolutionary field strengths yields an image with contrast reflecting the slope of the T_1 vs. field dispersion curve over a small field range. We present *in vivo* images of the wrist and foot with protein-content contrast using our method for creating T_1 dispersion contrast between fat (no protein), which has roughly constant T_1, and muscle tissue (high protein), which has rapidly varying T_1 near the quadrupole dips.

11:44 ***428***. **Amide Proton Transfer Imaging of Human Brain Tumors Distinguishes Tumor from Brain Tissue at the Periphery**

Craig K. Jones[1, 2], Michael J. Schlosser[2], Peter C.M. van Zijl[1, 2], Martin G. Pomper[2], Jinyuan Zhou[1, 2]

[1]Kennedy Krieger Institute, Baltimore, Maryland, USA; [2]Johns Hopkins University, Baltimore, Maryland, USA

In the amide proton transfer (APT) effect, endogenous mobile protein or peptide amide protons are saturated and exchange with free water protons, thereby reducing the measurable water signal. Ten brain tumor patients were scanned with APT, T2w, T1w, FLAIR and DWI imaging. The quantitative analysis showed that the APT contrast was able to distinguish active tumor from normal appearing white matter or peritumoral edema better than the standard clinical measures

11:56 ***429***. **Gradient Echo Plural Contrast Imaging (GEPCI)**

Adil Bashir[1], Dmitriy A. Yablonskiy[1]

[1]Washington University, St. Louis, Missouri, USA

In MRI spin echo (SE) pulse sequences are used to eliminate magnetic field inhomogeneity effects and create T2 contrast. However, SE techniques suffer from a number of artifacts including restrictions on RF power deposition limiting their clinical applications especially at high field MRI. In this study we demonstrate *in vivo* application of FID-based technique - Gradient Echo Plural Contrast Imaging (GEPCI) – that also allows elimination of magnetic inhomogeneity effects and does not suffer from restrictions on RF power. The technique allows generation of T2, T2*, T1 and spin density images in a single scan, hence the title – Plural Contrast Imaging.

12:08 ***430***. **Off-Resonance Separation for Positive Contrast Imaging of Iron-Oxide Labeled Cells**

Scott Brian Reeder[1], Anthony Z. Faranesh[2], Ian Y. Chen[2], Catherine D. Gard[1], Sam S. Gambhir[2], Oliver Wieben[1], Garry E. Gold[2]

[1]University of Wisconsin, Madison, Wisconsin, USA; [2]Stanford University, Stanford, California, USA

Detection of SPIO labeled cells with MR has traditionally relied on T2* weighted imaging to attenuate image signal, creating dark regions in the image, or "negative contrast". In this work, we describe a novel "positive contrast" method that acquires a small number of complex images at slightly different echo shifts facilitating the separation of off-resonance spins near SPIO labeled cells from on-resonance spins. Labeled cells appear as focal bright areas that can be color coded and recombined with the on-resonance image that provides anatomical reference. Examples with SPIO labeled myoblasts are shown.

12:20 ***431***. **Positive Contrast MR Imaging of Iron Oxide Nanoparticles with Simultaneous Suppression of Fat and Water Signals**

Ioannis Koktzoglou[1], Rohan Dharmakumar[1], Debiao Li[1]

[1]Northwestern University, Chicago, Illinois, USA

Positive contrast imaging (PCI) has been proposed for MR imaging of spatially-dependent magnetic field differences due to the presence of iron oxide particulates. However, a major limitation with PCI *in vivo* is imaging in the presence of off-resonant fat. This work sought to describe the strategy of simultaneous suppression of on-resonant water and fat signals through a single pre-saturation pulse for positive contrast imaging of iron oxide particulates in the presence of fat. Imaging results in phantoms supported theoretical predictions.

12:32 ***432***. **Microscopic Susceptibility-Induced Steady-State Perturbation: Theory and Experiment**

Oliver Bieri[1], Klaus Scheffler[1]
[1]University of Basel, University Hospital, Basel, Switzerland

Development of models that describe susceptibility effects in a microvascular network in a Hahn spin-echo and gradient-echo type of experiment have a long history and are profoundly investigated. Although other type of measurement protocols such as steady state sequences may have a better sensitivity to mesoscopic paramagnetic structures, such protocols have not yet been investigated. A model, based on Monte Carlo simulations and experiments with microspheres is derived that describes microscopic susceptibility-based contrast in a balanced SSFP type of sequence – prototypic for all steady state protocols. Susceptibility effects show up as an overall reduction in steady state amplitude that depends on the repetition time and susceptibility difference, as well as on relaxation times and on flip angle and finally, a scaling law will be given.

12:44 ***433***. **Dephased MRI – Separating Magnetic Susceptibility Effects from Partial Volume Effects**

Jan-Henry Seppenwoolde[1], Koen L. Vincken[1], Chris J.G. Bakker[1]
[1]University Medical Center Utrecht, Utrecht, Netherlands

By applying dephasing gradients, called 'dephased MRI', local magnetic field inhomogeneities (e.g. created by magnetically labeled cells) can be selectively visualized with positive contrast. Next to that, dephased MRI improves visualization of sub-voxel structures by partial-volume effects. What remained unclear so far was the actual contribution of partial volume (PV) and magnetic susceptibility (X) effects in creating the dephased MRI signal. In this work, we present the theory and supportive phantom experiments of two strategies to separate PV and X-effects during application of dephased MRI. The results show that both strategies are successful in eliminating PV effects.

Tracts, Maps & Atlases

Room 4C - 3,4 11:00 - 13:00 Chairs: Timothy E. J. Behrens and Derek K. Jones

11:00 ***434***. **Definition of Connection Significance Using Probabilistic Tractography**

David Mark Morris[1], Karl V. Embleton[1], Geoff J. Parker[1]
[1]University of Manchester, Manchester, UK

Probabilistic diffusion tractography methods conventionally define probability in terms of the frequency with which a particular connection is observed during a Monte Carlo process. This is not an ideal representation of connection probability as it does not explicitly take into account the possibility that the observed frequency of connection could have been observed by chance. This leads to distance-related artefacts in the probability of connection maps. We demonstrate that the use of a null distribution of connection, together with appropriate statistical analysis, allows for the definition of connection significance from a seed voxel and also corrects for distance-related artefacts.

11:12 ***435***. **Tractography Gone Wild: Probabilistic Tracking Using the Wild Bootstrap**

Derek K. Jones[1]
[1]Institute of Psychiatry, London, UK

The bootstrap is a powerful tool in DT-MRI tractography, allowing assignment of confidence to reconstructed pathways without any prior assumptions about the data. It is unlikely to find widespread acceptance, however, due to the long acquisition times that are needed for robust bootstrapping. We discuss the application of an alternative to conventional bootstrapping – Wild Bootstrapping, to fiber tracking. This allows extraction of probability distributions from data collected in a fraction of the time that conventional bootstrapping requires. We show good agreement between the two methods, indicating that previously published bootstrap-dependent methods may be brought within the clinical domain.

11:24 ***436***. **Imaging the Brain Neuronal Network with Diffusion MRI: A Way to Understand Its Global Architecture**

Patric Hagmann[1, 2], Maciej Kurant[2], Xavier Gigandet[2], Patrick Thiran[2], Van Wedeen[3], Reto Meuli[1], Jean-Philippe Thiran[2]
[1]University Hospital, Lausanne, Switzerland; [2]Ecole Polytechnique Fédérale, Lausanne, Switzerland; [3]Harvard Medical School, Charlestown, Massachusetts, USA

In order to better understand the high complexity of the brain, the detailed study of its individual components clearly seems insufficient. The backbone of complexity in the nervous system is composed of the large scale architectural characteristics of the neuronal network. Newly, by the advent of MR tractography, its investigation is accessible. We report on two important network characteristics that were already guessed from functional investigations and animal *ex vivo* studies, but never directly addressed in the human subject, ie the small world and hierarchical architecture of the human long-range brain axonal network.

11:36 ***437***. **Multiscale White Matter Fiber Tract Coregistration: A New Feature-Based Approach to Align Diffusion Tensor Data**

Alexander Leemans[1], Jan Sijbers[1], Steve De Backer[1], Everhard Vandervliet[2], Paul Parizel[2]
[1]University of Antwerp, Antwerp, Belgium; [2]University Hospital Antwerp, Antwerp, Belgium

In this work, we developed an automatic multiscale three-dimensional (3D) feature-based DTI coregistration technique based on the local curvature ς and torsion τ of the White Matter (WM) fiber pathways. This fully automatic and analytic (no iterations) technique inherently allows region of interest (ROI) coregistration, is adequate to perform both global and local transformations, and makes the calculation of the diffusion tensor reorientation superfluous. Simulations with synthetic diffusion tensor data have been elaborated to evaluate the performance and an *in vivo* example has been worked out, demonstrating feasibility of the proposed technique to align experimental data.

11:48 ***438***. **Creating Large Scale Population Atlases Using Diffusion Tensor Images**

Ragini Verma[1], Christos Davatzikos[1]
[1]University of Pennsylvania, Philadelphia, Pennsylvania, USA

We propose a novel framework for the statistical analysis of diffusion tensor images applicable to large population studies, which addresses the challenging problems of tensor statistics, unaddressable by commonly used linear statistical methods, due to the inherent non-linearity of tensors. We perform multivariate statistical analysis on tensors by identifying the underlying manifold of the set of tensors under consideration using the Isomap manifold learning technique and defining geodesic distances between tensors along the manifold. Application on human brains with simulated pathology and average population atlasing, show that the proposed statistical analysis method properly captures statistical relationships among tensor image data, while identifying group differences.

12:00 ***439***. **A High-Dimensional Fiber Tract Atlas**

Lauren O'Donnell[1], Carl-Fredrik Westin, [1,2]
[1]MIT, Cambridge, Massachusetts, USA; [2]Harvard Medical School, Boston, Massachusetts, USA

We present a method for creation of an atlas of major white matter fiber tracts. The method employs population clustering to generate fiber bundles, and can be applied in a straightforward way to label new subjects. We perform tractography in 5 DTI datasets then apply spectral clustering to the paths, producing population clusters in the high-dimensional spectral embedding space. These clusters are labeled with anatomical information and grouped into desired bundles, creating an atlas. We label the tracts of a new subject by embedding them into the atlas space using the Nystrom method, and assigning paths to the nearest cluster.

12:12 ***440***. **3D DT-MRI Atlas of Macaque Brain**

Hao Huang[1], Mark Walker[1], Sarah Ying[1], David Zee[1], Peter van Zijl[1, 2], Susumu Mori[1, 2]
[1]Johns Hopkins University School of Medicine, Baltimore, Maryland, USA; [2]Kennedy Krieger Institute, Baltimore, Maryland, USA

Macaque brains have been widely used in neuroscience research. Although there are several 2D atlases, they are not always suitable for studies that require 3D registration such as electrode reading and functional mapping. The purpose of this project is to establish a 3D DT-MRI atlas of the macaque brain in stereotaxic coordinates. High resolution T2 weighted and DTI images were acquired and various neural structures were assigned and segmented. Software was developed to explore the images and segmentation results. This atlas is being developed for the purposes of education, anatomical reference, and data registration.

12:24 ***441***. **Relative Contribution of Motor and Association Fibres to the White Matter Underlying Motor Cortex in Human and Macaque**

Timothy E.J. Behrens[1], Mark William Woolrich[1], Heidi Johansen-Berg[1], Mark Pinsk[2], Wolfgang Richter[2], Marlene Richter[2], Charles Gross[2], Sabine Kastner[2], Matthew D. Robson[1], Jim K. Rilling[3]
[1]University of Oxford, Oxford, Oxon, UK; [2]Princeton University, Princeton, New Jersey, USA; [3]Emory University, Atlanta, Georgia, USA

By explicit modelling of local complexity in the diffusion signal, we are able to make quantitative estimates of the relative contributions of different fibre populations. In the well known region of fibre complexity under motor cortex, we find a notable evolution from macaque to human. In the macaque brain, motor pathways dominate this region; in the human brain language fibres dominate.

12:36 ***442***. **Correlating DTI Fiber Clusters with White Matter Anatomy**

Song Zhang[1], Steve Correia[2], David F. Tate[2], David H. Laidlaw[1]
[1]Brown University, Providence, Rhode Island, USA; [2]Brown Medical School, Providence, Rhode Island, USA

We evaluated the accuracy of automated DTI fiber clustering results for representing known white matter features in four normal subjects. Two expert raters provided confidence ratings for identifying 11 white matter fiber tracts bilaterally in the clustered models. Large coherent fiber tracts were identified with high confidence, whereas some smaller tracts were missing. Some of the missing tracts were identifiable in an unclustered model with prior anatomical knowledge. The results demonstrate that the clustering algorithm can produce anatomically-relevant results, but dropout of smaller fiber pathways indicate the need for improvements in DTI imaging and modeling.

12:48 ***443***. **Tract-Based Spatial Statistics: Voxelwise Analysis of Multi-Subject Diffusion Data**

Stephen Mark Smith[1], Mark Jenkinson[1], Heidi Johansen-Berg[1], Daniel Rueckert[2], Thomas E. Nichols[3], Clare Mackay[1], Kate E. Watkins[1], Olga Ciccarelli[4], M Zaheer Cader[1], Andreas J. Bartsch[5], Paul M. Matthews[1], Timothy E J Behrens[1]

[1]fMRIB, Oxford University, UK; [2]Dept Computing, Imperial College London, UK; [3]University of Michigan, Ann Arbor, Michigan, USA; [4]Institute of Neurology, University College London, UK; [5]Dept of Neuroradiology, University of Würzburg, Germany

Many imaging studies are using DTI data in voxelwise ("VBM-style") analyses in order to localise brain change related to development, degeneration and disease. However, there has not been a satisfactory solution to the question of how to align FA images from multiple subjects in a way that allows valid conclusions to be drawn from the subsequent voxelwise analysis. Furthermore, the arbitrariness of the spatial smoothing extent has not yet been resolved. We present a method, Tract-Based Spatial Statistics (TBSS), that aims to solve these issues via nonlinear registration followed by projection onto an alignment-invariant tract representation (the "mean FA skeleton").

Human White Matter Disease

Room 611 - 612 11:00 - 13:00 Chairs: Micheal D. Phillips and Gioacchino Tedeschi

11:00 ***444***. **T_1 Tissue Specific Imaging in Multiple Sclerosis: Sensitivity and Specificity Issues**

Vasiliki N. Ikonomidou[1], Francesca Bagnato[1], Peter van Gelderen[1], Marco Riva[1], Fernanda Tovar-Moll[1], Jacco A. de Zwart[1], Silvina G. Horovitz[1], Joan Ohayon[1], Henry F. McFarland[1], Jeff H. Duyn[1]

[1]National Institutes of Health, Bethesda, Maryland, USA

Brain tissue degeneration in multiple sclerosis (MS) is associated with changes in T_1 and T_2. Conventional T_1 weighted imaging fails to visualize early changes in white matter, and doesn't characterize different degrees of damage. We applied a recently introduced Tissue Selective Imaging (TSI) technique to generate images of white matter, gray matter and cerebrospinal fluid of MS patients based on T_1. Preliminary evaluation (n=6) suggests that the new technique has superior sensitivity over conventional ones, depicts early T_1 changes in white matter, and allows characterization of lesions with large T_1 values and damage sustained in later stages of MS.

11:12 ***445***. **Voxelwise MT Analysis Shows Less Pronounced Brain Tissue Damage in Benign MS Than in Early Relapsing MS**

Marco Battaglini[1], Maria Laura Stromillo[1], Maria Laura Bartolozzi[2], Valentina Zipoli[3], Benedetta Goretti[3], Leonello Guidi[2], Emilio Portaccio[3], Antonio Giorgio[1], Antonio Federico[1], Maria Pia Amato[3], Nicola De Stefano[1]

[1]University of Siena, Siena, Italy; [2]Empoli Hospital, Empoli, Italy; [3]University of Florence, Florence, Italy

Results of the present study demonstrate that, despite the presence of significantly more WM lesions and much longer disease duration, focal and diffuse structural brain damage as measured by MTr is significantly less pronounced in B-MS than in a cohort of RR-MS at their earliest disease stages. This might be possibly due to more effective repair mechanisms to demyelination in patients with B-MS than in RR-MS. On this basis, the use of MTr might be helpful in differentiating patients with benign form of MS from those with a typical disabling course of the disease.

11:24 ***446***. **Long-T_2 Imaging: Evidence of a New Water Reservoir in Multiple Sclerosis**

Cornelia Laule[1], Irene M. Vavasour[1], Anthony L. Traboulsee[1], David K.B. Li[1], Alex L. MacKay[1]

[1]University of British Columbia, Vancouver, BC, Canada

The purpose of this study was to better define the T_2 distribution in MS lesions and NAWM with particular emphasis on identifying potential long T_2 components. Forty-eight echo T_2-relaxation data was acquired in 20 MS patients. Decreased myelin water, increased geometric mean T_2 (GMT_2) and increased peak width of the intra/extracellular (IE) peak were observed in MS lesions relative to NAWM. A new water reservoir with a markedly prolonged T_2 peak (200-800ms) was identified in 30% of lesions and several NAWM regions. Those lesions with a Long-T_2 peak also exhibited longer IE GMT2 than those lesions without a Long-T_2 signal.

11:36 ***447***. **MRI of Post Mortem Multiple Sclerosis Brain: Quantifying the Effects of Formalin Fixation**

Klaus DG Schmierer[1], Daniel J. Tozer[1], Claudia AM Wheeler-Kingshott[1], Phil A. Boulby[1], Harold G. Parkes[1], Tarek A. Yousry[1], Paul S. Tofts[1], David H. Miller[1]

[1]Institute of Neurology, UCL, London, England, UK

Quantitative magnetic resonance imaging (qMRI) of post mortem (PM) multiple sclerosis (MS) brain is being used to probe MS. There is limited information about changes of qMRI indices in PM MS brain following fixation. We studied T_1 relaxation time (T_1), magnetisation transfer ratio (MTR), fraction of macromolecular protons (f_B), mean diffusivity and fractional anisotropy as well as the association of qMR with pathological indices. Changes due to fixation were dependent on MR sequence used and tissue compartment (lesions, normal-appearing white matter) studied. MTR was the strongest predictor of myelin in fresh tissue whereas after fixation T_1 and f_B were more reliable.

11:48 ***448***. **De- Or Hypomyelination in Myelinopathia Centralis Diffusa/Leukoencephalopathy with Vanishing White Matter? Insights from Localized Proton MRS**

Steffi F. Dreha-Kulaczewski[1], Peter Dechent[1], Jürgen Finsterbusch[2], Knut Brockmann[1], Bernd Wilken[3], Jutta Gärtner[1], Jens Frahm[2], Folker Hanefeld[1]

[1]Georg-August-University, Goettingen, Lower Saxony, Germany; [2]Biomedizinische Forschungs GmbH am MPI für biophysikalische Chemie, Goettingen, Lower Saxony, Germany; [3]Clinic of Pediatric Neurology, Kassel, Lower Saxony, Germany

De- and hypomyelination are discussed in the pathogenesis of white matter (WM) disorders. Both produce distinct metabolite patterns detectable by proton MRS as demyelination is characterized by elevated Cho, whereas hypomyelination causes decreased concentrations of Cho. The newly discovered Myelinopathia Centralis Diffusa/Leukoencephalopathy with Vanishing White Matter (MCD/VWM) is neuropathologically characterized by loss of WM tissue. However the pathophysiology leading to the profound MRI-detectable WM changes already at onset of symptoms is still not fully understood. Ten patients with MCD/VWM were studied longitudinally using localized proton MRS. At early stages, a relatively high Cho was detected, indicating an initial demyelinating process.

12:00 ***449***. **Diffusion Tensor Imaging Study of Pelizaeus-Merzbacher Disease**

Jeremy Laukka[1], Malek Makki[2], James Garbern[1]

[1]Wayne State University, Detroit, Michigan, USA; [2]Children's Hospital of Michigan, Detroit, Michigan, USA

Pelizaeus-Merzbacher disease (PMD) is an X-linked leukodystrophy caused by any of a wide variety of mutations affecting proteolipid protein1 (PLP1), the most abundant protein in central nervous system myelin. Severe missense mutations cause oligodendrocyte apoptosis through activation of the unfolded protein response (UPR), which secondary severe hypomyelination. Less severe mutations cause little or no oligodendrocyte apoptosis or hypomyelination, but result in relatively late-onset axonal degeneration. To infer neuropathological changes in PMD, DT-MRI was performed on seven PMD patients with diverse PLP1 mutations and we compared diffusivity and anisotropy of their internal capsules to that of age matched normal control subjects.

12:12 ***450***. **Microembolization is a Likely Contributing Factor to Leukoaraiosis in Patients with Symptomatic Carotid Artery Disease**

Nishath Altaf[1, 2], Paul S. Morgan[1], Lucy Daniels[1], John R. Gladman[1], Shane T. MacSweeney[2], Tim Jaspan[1], Alan R. Moody[3], Dorothee P. Auer[1]

[1]University of Nottingham, Nottingham, Nottinghamshire, UK; [2]Queen's Medical Centre, Nottingham, Nottinghamshire, UK; [3]Sunnybrook and Women's College Health Sciences Centre, Ontario, Canada

The evidence for an association of leukoaraiosis or white matter hyperintense lesions (WMHL) with large vessel atherosclerosis is highly controversial. The aim of this study was to determine if the extent of WMHL was associated with the unstable carotid plaque as characterized by Magnetic resonance direct thrombus imaging (MRDTI). MRDTI and brain FLAIR imaging was performed in a cohort of 178 patients with symptomatic carotid disease. The extent of WMHL in the affected cerebral hemisphere is associated with the unstable MRDTI +ve carotid plaque and in contrast, symptoms were only associated with the number of lacunar lesions.

12:24 ***451***. **Detection of Change in CNS Involvement in NPSLE with Magnetization Transfer Imaging**

Bart Jeroen Emmer[1], S C. Steens[1], G M. Steup-Beekman[1], J van der Grond[1], F Admiraal-Behloul[1], H Olofsen[1], G P. Bosma[1], W J. Ouwendijk[1], T W. Huizinga[1], M A. van Buchem[1]

[1]Leiden University Medical Center, Leiden, Zuid-Holland, Netherlands

In neuro-psychiatric systemic lupus erythematosus (NPSLE) magnetization transfer imaging (MTI) has been associated with disease activity. However, it is unknown whether MTI is also sensitive to changes in individual neurological or psychiatric symptoms, which typically occur in NPSLE patients. 19 NPSLE patients underwent MTI on two separate occasions. In patients who clinically improved the MTR peak height increased significantly. In patients who were clinically stable, MTI did not change. In patients who clinically deteriorated, the MTR peak height decreased significantly. These findings suggest that MTI could be a valuable additional tool to objectify neurological or psychiatric complaints in NPSLE patients.

12:36 ***452***. **Validation of a White-Matter Specific Dual MR/optical Contrast Agent for High-Resolution Imaging**

Megan L. Blackwell[1, 2], Christian T. Farrar[1], Bruce R. Rosen[1, 2]

[1]Martinos Center for Biomedical Imaging, Charlestown, Massachusetts, USA; [2]Massachusetts Institute of Technology, Cambridge, Massachusetts, USA

In this work, we address three remaining questions about Luxol Fast Blue, a dual MR/optical white-matter specific contrast agent: 1) the relaxivity of LFB at 14T, 2) the duration LFB-stained samples should be immersed in lithium carbonate differentiating solution, and 3) the histological validation of LFB distribution within tissue samples. In addition, high-resolution MR images of samples treated with LFB display enhanced vertical bands, which may be radial organizations of neocortical axons. LFB and other specific, exogenous contrast agents hold much promise for enhancing the cytoarchitecture in high-resolution, high-field MR imaging.

12:48 ***453***. **Diffusion Measurement of Human Optic Nerve Using Fat Suppressed Diffusion Turbo FLASH Sequence**

Junqian G. Xu[1], Sheng-Kwei Song[1]
[1]Washington University in St. Louis, St. Louis, Missouri, USA

To avoid susceptibility induced distortion with a conventional echo planar imaging based diffusion sequence, a phase cycled centric-order diffusion turbo FLASH sequence was developed with fat suppression. Accurate diffusion tensor measurement of human optic nerve is demonstrated with fat saturation in two healthy volunteers.

fMRI: Metabolic and Vascular Responses

Room 615 - 617 11:00 - 13:00 Chairs: R. Todd Constable and Kamil Uludag

11:00 ***454***. **CBF/CMRO2 Coupling Measurements with Calibrated BOLD-fMRI: Bias Due to Voxel Selection**

Oleg Leontiev[1], Richard Buxton[1]
[1]University of California, San Diego, La Jolla, California, USA

The coupling ratio n of the fractional changes in CBF and CMRO2 during neural activation can be measured reproducibly with a calibrated BOLD technique. However, the estimated value of n varies from approximately 2-5 depending on the method of choosing a region of interest (ROI) for averaging, suggesting the presence of a strong bias due to voxel selection. A possible explanation of the source of the bias is the inclusion of venous structures when either a BOLD-localizer or a V1 retinotopic map is used for constructing the ROI. Given these biases, a functional flow localizer is recommended.

11:12 ***455***. **Differences in Cerebrovascular Reactivity in Males Versus Females Obtained Using BOLD MRI and Alternating States of End-Tidal CO2**

Andrea Kassner[1], Julien Poublanc[2], George Tomlinson[1], David Mikulis[2], Adrian Crawley[2]
[1]University of Toronto, Toronto, Ontario, Canada; [2]The Toronto Western Hospital, Toronto, Ontario, Canada

Combining CO2 manipulation with BOLD MRI is a promising for assessing regional differences in cerebrovascular reactivity (CVR) which is a measurement of the brains autoregulatory capacity and important for the assessment of vascular disorders in which autoregulation is compromised or exhausted. The characterization of these pathophysiological conditions in the cerebral circulation, however, requires the knowledge of potential physiological gender-dependent differences in CVR. The objective of this study was to evaluate gender differences in CVR in normal subjects using quantitative CVR measurements by correlating BOLD MR signal intensity with square wave changes in end-tidal pressure of CO2 (pET CO2).

11:24 ***456***. **Enhancement of BOLD Response Using Carbogen Modulation**

Chou-Ming Cheng[1], Tzu-Chen Yeh[1, 2], Jen-Chuen Hsieh[1, 2], Low-Tone Ho[1, 2]
[1]Taipei Veterans General Hospital, Taipei, Taiwan, Taiwan; [2]National Yang-Ming University, Taipei, Taiwan, Taiwan

fMRI is used to investigate cortical activity based on BOLD response. In this study, carbogen modulation is introduced to enhance BOLD response because of vascular autoregulation. The visual tasks with and without carbogen inhalation were proposed to show the dynamic coupling between carbogen inhalation and BOLD response. The results demonstrated significant BOLD increase by carbogen modulation.

11:36 ***457***. **Direct Imaging of $CMRO_2$ in Cat Visual Cortex at Rest and Visual Stimulation**

Xiao-Hong Zhu[1], Yi Zhang[1], Nanying Zhang[1], Xiaoliang Zhang[1], Kamil Ugurbil[1], Wei Chen[1]
[1]CMRR, Department of Radiology, University of Minnesota Medical School, Minneapolis, Minnesota, USA

Whether and how much $CMRO_2$ increases during brain activation and how it influences BOLD-based fMRI have been debated for a long time. A major difficulty for resolving this controversy is the lack of reliable techniques for directly imaging $CMRO_2$. Recent developments in the high-field ^{17}O NMR methodology provide a promising tool for noninvasively imaging $CMRO_2$ in animals. We have applied this methodology for obtaining 3D $CMRO_2$ imaging in the cat visual cortex at both resting state and visual stimulation with short inhalation of $^{17}O_2$ gas. The results indicate (i) a substantial $CMRO_2$ increase in the activated regions and (ii) an essential role of oxidative metabolism in brain function.

11:48 ***458***. **Quantitative BOLD: Separation of Effects from Blood Volume and Oxygen Extraction Fraction**

Xiang He[1], Dmitriy A. Yablonskiy[1]
[1]Washington University School of Medicine, St. Louis, Missouri, USA

Measurement of oxygen extraction fraction (OEF) is essential for understanding the baseline state of the human brain both in health and decease. Separation of contributions from OEF and cerebral deoxygenated blood volume (DBV) is also important for better understanding of BOLD signal. Herein we propose a theoretic BOLD model that incorporates MR signals from white and gray matters, intravascular blood and cerebrospinal fluid. Data are acquired using multi-gradient echo sequence (GESSE). Results show a relatively uniform OEF distribution (43.5±11.5%) in a good agreement with PET data as well as a contrast of DBV between gray (1.37±0.25%) and white (0.67±0.11%) matters.

12:00 ***459***. **Concurrent Nulling of Blood and CSF Signal (VASO-FLAIR) Allows for Simultaneous Measurement of CBV and CSF Volume Fractions**

Manus J. Donahue[1], Richard A. Edden[1], Jason M. Zhao[1], Peter C M van Zijl[1]
[1]Johns Hopkins University, Baltimore, Maryland, USA

Quantification of hemodynamic parameters is often imprecise due to imperfect knowledge of CSF volume fractions. We developed a novel VASO-FLAIR technique, which nulls blood and CSF signals simultaneously through the application of two appropriately-spaced, non-spatially-selective inversion pulses. We show that CSF and blood volume fractions can be rapidly quantified by sequentially acquiring VASO data (blood-nulling with a single non-selective inversion), VASO-FLAIR data, and a CSF reference signal in the ventricles, and processing these data with knowledge of tissue T1 and T2 relaxation times.

12:12 ***460***. **Sensitivity of the Vascular Occupancy (VASO) Method Estimated Using a Multicompartmental Blood-Tissue Model**

Stefan K. Piechnik[1], Peter Jezzard[1]
[1]University of Oxford, Oxford, Oxfordshire, UK

Inclusion of the measurement of cerebral blood volume (CBV) changes may enhance our understanding of functional imaging contrasts. We analyse the properties of the vascular occupancy (VASO) method to estimate relative changes in CBV through complementary changes in signal arising from the tissue. VASO depends on CBV but in a complex way, which makes it difficult to use as a marker of relative CBV changes without a-priori calibration for the resting CBV and the partial volume of tissues.

12:24 ***461***. **HASTE Sequences for Functional MRI: BOLD and VASO**

Benedikt A. Poser[1], David G. Norris[1]
[1]FC Donders Centre for Cognitive Neuroimaging, Nijmegen, Netherlands

The benefits of the HASTE sequence applied to fMRI at 3T are investigated. Multiply-refocused sequences combine the advantage of being artifact free with the improved spatial BOLD signal localization of SE techniques. First *in vivo* results with visual and emotional stimulation paradigms indicate that (a) T2 weighted partial Fourier, parallel accelerated HASTE has at least equal BOLD sensitivity than SE-EPI, and (b) that VASO HASTE is markedly more sensitive to CBV changes than EPI based VASO.

12:36 ***462***. **Comparison of Conventional BOLD and CBV-Weighted fMRI Iso-Orientation Column Maps in Cat Visual Cortex**

Chan hong Moon[1], Hiro Fukuda[1], Ping Wang[1], Seong-gi Kim[1]
[1]Dept. of Neurobiology, Pittsburgh, Pennsylvania, USA

Assignment of higher conventional BOLD signal change is not clear, because the high BOLD signal change could indicate the active or inactive neuronal sites, depending on the inter-distance between orientation columns and spatial point spread functions of metablic and hemo-dynamic responses. So, here we obtained the orientation column map using conventional BOLD technique and continuous stimulation to increase the sensitivity of orientation. And we compared this BOLD map with the well confirmed CBV-weighed fMRI columnar map to confirm the activation sites of BOLD.

12:48 ***463***. **Baseline and Functional Vessel Size Index Imaging in Cat Visual Cortex: Insights Into Hemodynamic Regulation**

Fuqiang Zhao[1], Ping Wang[1], Kristy Hendrich[1], Seong-Gi Kim[1]
[1]Pittsburgh University, Pittsburgh, Pennsylvania, USA

Comparative sizes of vessels which dilate in response to neural activation were determined by calculation of relative baseline and functional vessel-size-indices (VSI). Baseline signal changes induced by MION (monocrystalline iron oxide nanoparticles) injection and functional signal changes before and after MION injection were simultaneously measured in the same cat by echo planar imaging with vessel-size-independent gradient-echo and vessel-size-dependent spin-echo techniques. In most of the cortex, functional VSI is larger than baseline VSI, suggesting that functional vasodilation occurs in vessels larger than capillaries.

Pre-Clinical Assessment of Vascular Function

Room 618 - 620 11:00 - 13:00 Chairs: Natarajan Raghunand and Simon P. Robinson

11:00 ***464***. **Vascular Tortuosity is Culprit to Abnormal Perfusion in 9L Gliosarcoma Tumor**

Moses Morakortoi Darpolor[1], Robert C. Molthen[2], Francisca C. Wu[3], Kathleen M. Schmainda[3]
[1]Marquette University, Milwaukee, Wisconsin, USA; [2]Dept. of Veterans Affair, Zablocki VAMC, Milwaukee, Wisconsin, USA; [3]Medical College of Wisconsin, Milwaukee, Wisconsin, USA

Cerebral perfusion in brain tumor is quite inefficient as demonstrated by dynamic susceptibility contrast magnetic resonance imaging (DSC-MRI). This inefficient perfusion is attributed to the density of irregularly shaped vessels in rat brain tumors as elucidate by micro-computed tomography of intact vessel tree. It is shown that the density of tortuous vessels is the prime suspect of abnormal perfusion. Validation of DSC-MRI parameters could ensure its use to assess vessel attributes in brain tumors.

11:12 ***465***. **Assessment of Mouse Glioma Vasculature Using SPIO and Small Molecule Contrast Agents: Sequential Implementation of Alternate Perfusion MRI Methodologies**

Martin Mugar Pike[1], Catherine P. Langford[1], Cristine D. Neumann[1], L Burt Nabors[1], G Yancey Gillespie[1]
[1]University of Alabama at Birmingham, Birmingham, Alabama, USA

A macromolecular superparamagnetic iron oxide (SPIO) contrast agent, Ferridex, was successfully employed to address first pass extravasation problems in the application of dynamic susceptibility contrast MRI (DSC-MRI) cerebral blood flow (CBF) measurements in models of mouse glioma. Furthermore, in the same imaging session, the approach was combined with dynamic contrast enhanced MRI assessments of vascular permeability using a small molecule contrast agent, in order to obtain a comprehensive assessment of mouse glioma vascularization. The approach lays the groundwork for noninvasive and highly diagnostic investigations of anti-angiogenesis strategies in mouse models of malignant glioma.

11:24 ***466***. **The Role of VEGF in Growth of Brain Metastases from Single Cells as Visualized by Contrast Enhanced MRI**

Kirsten Tracy[1], Juan Juan Yin[1], Jeeva Munasinghe[1], Erik Shaprio[1], Alan Koretsky[1], Kathleen Kelly[1]
[1]National Institutes of Health, Bethesda, Maryland, USA

Brain metastasis occurs in 20-40% of cancer patients; however, the contributing factors are poorly understood. Over-expression of VEGF may contribute to metastatic growth by increasing angiogenesis. This study determines if VEGF inhibition affects the growth of established metastases utilizing various parameters of tumor progression as visualized by MRI. A xenograft model of brain metastasis was initiated from hematogenously delivered single cells labeled with iron-oxide particles. Using 3-D gradient echo MRI, we tracked the growth of the labeled tumor cells in mice being treated with a VEGF receptor antagonist and found that treatment did result in fewer and smaller brain metastases.

11:36 ***467***. **The Role of Platelet-Derived Growth Factor on Tumour Vascular Function and Morphology *In Vivo* Assessed by Susceptibility Magnetic Resonance Imaging**

Simon P. Robinson[1], Christian Ludwig[2], Janna Paulsson[3], John R. Griffiths[1], Arne Ostman[3]
[1]St. George's, University of London, London, UK; [2]University of Birmingham, Birmingham, UK; [3]Karolinska Institute, Stockholm, Sweden

Platelet-derived growth factor (PDGF) contributes to numerous processes in tumour progression, including recruitment of pericytes and angiogenesis. Intrinsic-susceptibility MRI, sensitive to changes in endogenous deoxyhaemoglobin, was used to investigate the effects of PDGF on tumour vascular maturation and function *in vivo*. The transverse relaxation rate R_2* of PDGF expressing B16 and control B16 melanomas was quantified during air, hypercapnia and hyperoxia challenge. Hypercapnia induced a negligible reduction in tumour R_2*, whereas hyperoxia significantly reduced R_2* of both tumour types, this reduction being significantly greater in the PDGF expressing tumours, consistent with increased pericyte coverage increasing blood vessel function *in vivo.*

11:48 ***468***. **Vascular Targeting Photodynamic Therapy (VTP): Correlations Between Hemodynamic and Photosensitized fMRI Response Parameters in the Mouse Ear Tumor Model**

Noa Madar[1], Catherine Brami[1], Vyacheslav Kalchenko[1], Avigdor Scherz[1], Michal Neeman[1], Yoram Salomon[1]
[1]The Weizmann Institute of Sciences, Rehovot, Israel

Vascular Targeting Photodynamic therapy (VTP) relies on local photogeneration of a circulating photosensitizer and generation of cytotoxic reactive oxygen species leading to tumor eradication. To further understand the mechanistic basis of photosensitized MRI, the vascular response during VTP was examined online on the mouse ear model by IntraVital microscopy and fMRI. Increased tumor BOLD contrast during VTP was correlated with decrease in blood flow velocity, and contained two phases, one early (tVTP<5min) light-dependent and reversible, followed by a light-independent late phase (5min>tVTP>10min); characterized by irreversible high BOLD contrast. Supported by STEBA BIOTECH & NEGMA LERADS, France

12:00 ***469***. **Assessment of Spin Echo BOLD FMR Imaging as a Prognostic Tool for Determining Chemotherapeutic Efficacy**

Arup Bhattacharya[1], Richard Mazurchuk[1], Joseph A. Spernyak[1], Shousong Cao[1], Farukh A. Durrani[1], Youcef M. Rustum[1]
[1]Roswell Park Cancer Institute, Buffalo, New York, USA

Spin echo BOLD fMR imaging using T_2weighted spin echo based RARE phase encoding and carbogen breathing was used to serially scan head and neck squamous cell carcinoma xenografts growing in nude mice during chemotherapy for predicting chemotherapeutic response. Linear regression analysis between responders *vs.* non-responders indicated a significantly (P_{slope} = 0.088, $P_{Elevation}$ = 0.001) different trend between the tumors that respond vs. those that did not. The earliest time point that was found to be predictive using this method was day 5 of chemotherapy when tumor regression was minimal (< 20%). BOLD fMR change reflects the changing intratumoral microenvironmental milieu, including neoangiogenic microvessel density, in response to chemotherapy.

12:12 ***470***. **Characterizing Hypoxia-Induced Alterations in ECM Integrity of Solid Tumors *In Vivo* Using MRI and Fluorescent Microscopy**

Arvind P. Pathak[1], Venu Raman[1], Dmitri Artemov[1], Zaver M. Bhujwalla[1]
[1]Johns Hopkins University School of Medicine, Baltimore, Maryland, USA

Tumor microenvironmental factors are critical determinants in the phenotypic traits of cancer. Of these, hypoxia is known to induce drug/radiation resistance, and select for a more aggressive phenotype. However, the relationship between hypoxia, the resultant ECM remodeling and macromolecular transport *in vivo* remains largely unexplored. Hypoxia is known to induce collagen deposition, and induce upregulation of various matrix metalloproteinases (MMPs) that remodel the ECM and affect the movement of macromolecules. Here for the first time we have related the macromolecular movement through the ECM to tumor hypoxia, using optical molecular imaging of tumor hypoxia in conjunction with novel MRI analyses.

12:24 ***471***. **Molecular Imaging and Targeted Anti-Angiogenic Therapy in Cancer with $Alpha_{nu}beta_3$-Targeted Nanoparticles**

Patrick M. Winter[1], Shelton D. Caruthers[1, 2], Todd A. Williams[1], John S. Allen[1], Thomas D. Harris[3], Samuel A. Wickline[1], Gregory M. Lanza[1]
[1]Washington University, St. Louis, Missouri, USA; [2]2Philips Medical Systems, Cleveland, Ohio, USA; [3]Bristol-Myers Squibb Medical Imaging, Billerica, Massachusetts, USA

This study presents preliminary results using integrin targeted perfluorocarbon nanoparticles for targeted delivery of fumagillin (an anti-angiogenic drug) in tumor bearing rabbits with follow-on molecular imaging of angiogenesis to assess therapeutic effect. Rabbits were treated 6, 9, and 12 days after tumor implantation. Sixteen days post-implantation, fumagillin treated tumors were significantly smaller than controls. Molecular imaging of angiogenesis showed both the area and amount of MRI signal enhancement tended to be lower in treated vs. control tumors, suggesting reduced neovascular proliferation. The results of this pilot study imply that targeted fumagillin nanoparticles may suppress angiogenesis and inhibit tumor development.

12:36 ***472***. **Multi Parameter High-Resolution Magnetic Resonance Imaging and Spectroscopy of Tumors**

Philipp Moerchel[1], Gerd Melkus[1], Volker Christian Behr[1], Markus Kotas[1], Peter Jakob[1], Michael Flentje[1]
[1]University of Würzburg, Würzburg, Germany

An MRI and MRS protocol to measure oxygenation, perfusion, and lactate distribution *in vivo* and with a high spatial resolution on different tumor models was implemented on a 17.6 Tesla wide-bore spectrometer. In order to compare the MR-results with data from bioluminescence, these tumors were histologicaly processed.The results consistently show a good correlation between the MR and histology data. Differences in MR-Parameters (particularly the lactate concentration) between the tumor models could be detected in MR, possibly allowing an identification of the tumor *in vivo*. With such *in vivo* data, radiological therapies and treatment could be accomplished more efficiently.

12:48 ***473***. **HRMAS 1H Spectroscopy of the Novel VEGF-RTK Inhibitor AG013736 in a Breast Cancer Model**

Lisa J. Wilmes[1], Samson Jarso[1], Maria G. Pallavicini[2], David R. Shalinsky[3], John Kurhanewicz[1], Nola M. Hylton[1]
[1]University of California San Francisco, San Francisco, California, USA; [2]University of California Merced, Merced, California, USA; [3]Pfizer Global Research and Development, La Jolla, California, USA

High-resolution magic angle spinning (HRMAS) 1H spectroscopy was utilized to investigate the treatment effects of the novel vascular endothelial growth factor receptor (VEGFR) tyrosine kinase inhibitor (TKI), AG-013736, in a human breast cancer xenograft model. Tumor samples evaluated after 7 days of AG013736 treatment showed a 3.5-fold increase in total lipid and a 2-fold decrease in total choline compared to untreated controls. 2D TOCSY showed that phosphocholine, glycerophosphocholine and choline decreased in treated tumors. These metabolic changes may reflect treatment-induced necrosis or apoptosis. Previous studies have shown that AG013736 treatment inhibited tumor growth and decreased tumor endothelial transfer constant.

Diet and Exercise: The Physiology of Obesity

Room 602 - 604 11:00 - 13:00 Chairs: Chris Boesch and Peter G. Morris

11:00 ***474***. **Measurement of Ectopic Fat Deposition in Genetically Modified Mice Fed a High Fat Diet**

Didier Laurent[1], Brittany Yerby[1], Farid Sari-Sarraf[1], Erica Hirsch[1], John Gounarides[1], Thomas Daniels[1], Xiaomei Wang[1], Stacey Wade[1], Shamina Rangwala[1]
[1]Novartis Institutes for Biomedical Research Inc, Cambridge, Massachusetts, USA

In-vivo MRI and localized ^{1}H-MRS were used to monitor ectopic fat storage induced by high-fat feeding in estrogen-related receptor α (ERRα) deficient mice. After 2 months on the diet, intramyocellular lipids (IMCL) in the *tibialis anterior* muscle of wild-type mice increased by ~3-fold while virtually no change was detected in ERRα knockout mice. In contrast to the expected phenotype, ERRα knockout mice also displayed a ~5-fold increase in intrahepatic lipid contents and levels of visceral adiposity similar to wild-type mice, suggesting normal lipid absorption.

11:12 ***475.*** **Anti-Adipogenic Effects of a Diet High in Resistant Starch**

Po-Wah So[1], Wei-Sheng Yu[1], Jimmy David Bell[1], Gary Frost
[1]Hammersmith Hospital, Imperial College London, London, UK

Approaches to ameliorating obesity include ingestion of low glycaemic index (GI) foods. High GI foods induce high blood glucose levels leading to hyperinsulinaemia, linked to the 'metabolic syndrome'. In this study, the effect of diets high in resistant starch (and of low GI) on adiposity and intrahepatocellular lipid (IHCL) levels was investigated by 1H MRS in a murine model. Maintenance on a diet high in resistant starch leads to similar weight gain to that on a low resistant starch diet but the former diet led to both comparatively lower adipose tissue deposition and accumulation of IHCL levels than the latter.

11:24 ***476.*** **^{13}C MRS Study of Postprandial Glycogen Storage to Investigate the Second Meal Effect**

Emily Leverton[1], Bhavana Solanky[1], Ana Jovanovich[2], Johanna Snaar[1], Roy Taylor[2], Peter Morris[1]
[1]University of Nottingham, Nottingham, UK; [2]University of Newcastle upon Tyne, Newcastle upon Tyne, UK

^{13}C spectroscopy was used to investigate the second meal effect. The rise in blood glucose after breakfast is much greater than the rise after a lunch. This is possibly due to suppressed hepatic glycogen output after lunch. Our study was designed to investigate this by observing the differences in glycogen levels for subjects given breakfast plus lunch and lunch only in the liver and thigh.We found that the increase in hepatic glycogen levels after lunch were 61% higher in subjects that had breakfast. A similar trend was observed in the thigh glycogen concentrations with the increment being 50% higher.

11:36 ***477.*** **Regional and Intracellular Lipid Stores: Impact of a 12 Week Randomized Cross Over Study of Isonitrogenous Low Fat vs. Low Carbohydrate Weight Loss Diets**

Min-Hui Cui[1], V. Tomuta[1], G. Goswami[1], H. Jayatillake[1], G. Cruikshank[1], C-J Segal-Isaacson[1], B. Cowell[1], J.-H. Hwang[1], D.T. Stein[1]
[1]Albert Einstein College of Medicine, Bronx, New York, USA

The effect of low fat vs. low carbohydrate diet weight loss on regional and intracellular lipid stores and insulin sensitivity is reported. 8 subjects underwent 6 weeks one diet and crossed-over to the other diet for another 6 weeks. IHL, SAT and VAT decreased with weight loss, not different on LC vs. LF diet. On the other hand, IMCL increased significantly after LC diet and declined after LF diet. The peripheral insulin sensitivity was significantly improved from basal after LC diet accompanied by a decrease in plasma triglyceride.

11:48 ***478.*** **Relationship of Soleus Muscle Intramyocellular Lipid (IMCL) and C-Reactive Protein (CRP) Levels in Healthy Asian Indian Males**

Virendra Kumar[1], Manish Rathi[1], Sanjeev Sinha[1], Mahesh Kumar[1], Anoop Misra[1], Ravindra Mohan Pandey[1], Manjari Dwivedi[1], Kalpana Luthra[1], N R. Jagannathan[1]
[1]All India Institute of Medical Sciences, New Delhi, Delhi, India

In the present study we estimated the IMCL content in soleus muscle in 30 healthy Asian Indian males using ^{1}H MR spectroscopy and correlated it with body mass index, measures of abdominal obesity, percentage of body fat, serum lipoproteins, fasting and post-oral glucose load serum insulin levels and other surrogate markers of insulin resistance. Soleus muscle IMCL content correlated significantly with measure of generalized and abdominal obesity but not with insulin sensitivity or CRP levels in healthy Asian Indian males

12:00 ***479.*** **Relevance of Visceral Adipose Tissue and Intrahepatic Lipids in the Pathogenesis of Insulin Resistance – a Cross-Sectional Study**

Jürgen Machann[1], Claus Thamer[2], Birgit Schnödt[1], Norbert Stefan[2], Hans-Ulrich Häring[2], Claus D. Claussen[3], Andreas Fritsche[2], Fritz Schick[1]
[1]Section on Experimental Radiology, Tübingen, Germany; [2]Department of Endocrinology, Metabolism and Pathobiochemistry, Tübingen, Germany; [3]Department of Diagnostic Radiology, Tübingen, Germany

Quantification of different lipid compartments is essential for identification of risk-factors for development of type 2 diabetes as not only the total lipid content but also its distribution is important. Aim of the study was determination of visceral adipose tissue (VAT) and intrahepatic lipids (IHL) in a cohort at increased risk for type 2 diabetes and correlation with insulin sensitivity. 180 volunteers were examined by MRI and MRS and linear correlation coefficients amounted to r=-0.61 and –0.40 for females/males for VAT and r=-0.61 and –0.51 for IHL. Both lipid compartments seem to be involved in the pathogenesis of insulin resistance.

12:12 ***480.*** **"Real-Time" Detection of Intramyocellular Lipids (IMCL) During Exercise by Means of 1H-MRS**

Michael Ith[1], Thomas Benz[1, 2], Roland Kreis[1], Chris Boesch[1]
[1]University & Inselspital Berne, Berne, Switzerland; [2]ETH Zurich, Zurich, Switzerland

A method is proposed that uses 1H-MRS to directly assess IMCL levels during exercise in eight male volunteers. Comparing IMCL usage of the tibialis anterior muscle during 3 hours of continuous or 3h of intermittent running revealed no significant difference, indicating that the 12 minutes breaks for MRS-measurements every half hour do not influence the IMCL metabolism. During both exercise sessions about 50% of the initial amount of IMCL was used. Measurements every 30 minutes revealed that only 5% of the total IMCL consumption was used during the initial 30 minutes, whereas 19% was used during each of the remaining bouts.

12:24 ***481***. **MRI and MRS for Detection of Changes in Adipose Tissue Distribution After Lifestyle Intervention**

Jürgen Machann[1], Claus Thamer[2], Birgit Schnödt[1], Norbert Stefan[2], Hans-Ulrich Häring[2], Claus D. Claussen[3], Andreas Fritsche[2], Fritz Schick[1]

[1]Section on Experimental Radiology, Tübingen, Germany; [2]Department of Endocrinology, Metabolism and Pathobiochemistry, Tübingen, Germany; [3]Department of Diagnostic Radiology, Tübingen, Germany

Quantification of changes in adipose tissue after lifestyle intervention in a group of 130 volunteers at increased risk for type 2 diabetes. MR examinations before and after participation in a dietary intervention and increased activity (at least 4 h sports/week). Separation of different lipid compartments by MRI, additionally determination of intrahepatic lipids (IHL) by MRS. Volunteers with weight loss (n=90) are characterized by massive reduction of visceral adipose tissue (VAT) and IHL. In volunteers with increased body weight, these compartments were nearly unchanged. VAT and IHL seem to be very important lipid compartments and are metabolically highly active.

12:36 ***482***. **^{13}C MRS of Muscle and Hepatic Glycogen Metabolism in Type I Diabetes to Investigate Muscle Exhaustion**

Bhavana Shantilal Solanky[1], Emily Leverton[1], Johanna Snaar[1], kamalakkannan Chokkalingam[2], Luke Norton[2], Ian Macdonald[2], Peter G. Morris[1]

[1]University of Nottingham, Nottingham, UK; [2]Queen's Medical Centre, Nottingham, UK

By using ^{13}C MRS, the postprandial hepatic and muscle glycogen storage after intense exercise in subjects with type I diabetes was compared to normal healthy subjects. It was expected that the exhaustion suffered by type I diabetics during exercise may be due to low glycogen stores. The study found hepatic glycogen homeostasis behaves similarly to controls when blood insulin levels are controlled. Thigh muscle glycogen storage differed from controls, with the levels remaining higher after exercise. This suggests that a failure for the muscle to utilise glycogen may be the reason behind exhaustion in type I diabetics.

12:48 ***483***. **A Comparison of Different Methodologies to Study Skeletal Muscle Mitochondrial Function in Type 2 Diabetes Patients**

Henk M.M.L. De Feyter[1], Stephan S.F. Praet[2], Luc J. van Loon[2], Jeanine J. Prompers[1], Klaas Nicolay[1]

[1]Eindhoven University of Technology, Eindhoven, Netherlands; [2]Maastricht University, Maastricht, Netherlands

Recent studies suggest that mitochondrial dysfunction plays a key role in the pathogenesis of skeletal muscle insulin resistance and Type 2 diabetes (T2D). Various experimental methods can be used to evaluate mitochondrial function. The interrelationship between *in vivo* ^{31}P magnetic resonance spectroscopy (MRS) parameters of skeletal muscle mitochondrial function, whole-body spiro-ergometry and *in vitro* tissue markers of oxidative capacity was evaluated in T2D patients. The results of the different methods correlated well, which suggest that they all represent proper estimates of mitochondrial function in T2D patients.

MRS of GABA, Glutamate and Glutathione: Detection Methods, Sensitivity Enhancement and Brain Mapping

Room 613 - 614 11:00 - 13:00 Chairs: Ralph E. Hurd and Melissa J. Terpstra

11:00 ***484***. **Rapid Brain Glutamate Mapping in Central and Peripheral Gray Matter at 3 and 4 Tesla Using Short TE Proton-Echo-Planar-Spectroscopic-Imaging (PEPSI)**

Stefan Posse[1, 2], Ricardo Otazo[1, 3], Arvind Caprihan[1, 4], Juan Bustillo[2], Hongji Chen[2], Chun Zuo[5], Perry Renshaw[5], Vincent Magnotta[6], Bryon Mueller[7], Kelvin O. Lim[7], Kamil Ugurbil[7], Paul Mullins[1], Charles Gasparovic[1], Jeffry R. Alger[8]

[1]The MIND Institute, Albuquerque, New Mexico, USA; [2]University of New Mexico School of Medicine, Albuquerque, New Mexico, USA; [3]University of New Mexico, Albuquerque, New Mexico, USA; [4]New Mexico Resonance, Albuquerque, New Mexico, USA; [5]Harvard University, Boston, Massachusetts, USA; [6]University of Iowa, Iowa City, Iowa, USA; [7]University of Minnesota, Minneapolis, Minnesota, USA; [8]University of California in Los Angeles, Los Angeles, California, USA

In this study we assess the reliability of mapping glutamate and other multiplet resonances at 3 and 4 Tesla across a whole brain slice that includes peripheral gray matter using the Proton-Echo-Planar-Spectroscopic-Imaging (PEPSI) method. Glutamate maps displayed approximately two-fold concentration differences between white matter and central and peripheral gray matter areas, and mean Cramer-Rao lower bounds of 8 % across the entire slice. Smaller, but consistent gray /white matter differences were also seen in Cr maps. Mean CRLBs at 4 T in supra-ventricular slices were significantly smaller than at 3 T ($p < 0.05$, except Ala and Gln).

11:12 ***485***. **Glutamate Levels in Normal Appearing White and Gray Matter in Multiple Sclerosis Using TE-Averaged MRSI at 3T**

Radhika Srinivasan[1], Sarah Nelson[1], Stephen Hauser[1], Daniel Pelletier[1]
[1]University of California, San Francisco, California, USA

Histopathological and animal models in Multiple Sclerosis have provided compelling evidence of a glutamate mediated disease process in Multiple Sclerosis (MS). Using a two-dimensional spectroscopic imaging technique that results in an unobstructed detection of glutamate at 3T we evaluate glutamate levels in the normal appearing white matter (NAWM) and normal appearing gray matter (NAGM) in a large cohort of Multiple Sclerosis patients and compare these levels to control white matter (WM) and gray matter (GM). A significant ($p<0.001$) increase in glutamate in the NAWM relative to control WM was found. The glutamate levels in the NAGM in patients was comparable to control GM.

11:24 ***486***. **Gender, Age and Regional Differences of Brain Glutamate Concentration in Healthy Subjects**

Napapon Sailasuta[1], Thomas Ernst[1], Linda Chang[1]
[1]John A, Burns School of Medicine, University of Hawaii, Honolulu, Hawaii, USA

Single voxel TE-averaged PRESS was performed in four brain regions (frontal white, frontal gray and parietal gray matter, and basal ganglia) of healthy subjects to determine if the brain glutamate (GLU) concentration varies with age, gender or region. As expected, regional differences in glutamate concentration were observed, with the frontal gray matter showing the highest GLU concentrations. The GLU concentration decreased significantly with age in the frontal white matter ($p=0.036$), parietal gray matter ($p=0.001$) and basal ganglia ($p=0.019$) regions. However, the glutamate concentration did not vary significantly between males ($n=16$) and females ($n=8$) in any of the four brain regions.

11:36 ***487***. **Measurement of Heterogeneous Distribution of GABA in Gray and White Matters in the Human Brain Using Selective Multiple Quantum Chemical Shift Imaging of GABA**

In-Young Choi[1, 2], Sang-Pil Lee[1, 2], Hellmut Merkle[3], Jun Shen[3]
[1]University of Kansas Medical Center, Kansas City, Kansas, USA; [2]The Nathan Kline Institute, Orangeburg, New York, USA; [3]NIH, Bethesda, Maryland, USA

In vivo assessment of heterogeneous distribution of GABA in the human brain is fraught with technical challenges. We developed a selective multiple quantum GABA CSI technique based on a two-echo acquisition scheme for simultaneous measurement of GABA and creatine. The simultaneously measured creatine served as concentration and phase references, providing more robust GABA measurements. Throughout the entire GABA CSI slice, contamination from overlapping signals was minimized. It was found that GABA is about three-fold more concentrated in gray matter than white matter in the human brain *in vivo*.

11:48 ***488***. **Evaluation of GABA Detection Sensitivity Gains Achieved with an 8-Channel Phased-Array Head Coil at 3.0 T in the Human Dorsolateral Prefrontal Cortex Using the J-Editing Technique**

Dikoma C. Shungu[1], Xiangling Mao[1], Lawrence S. Kegeles[2]
[1]Weill Medical College of Cornell University, New York, New York, USA; [2]College of Physicians and Surgeons of Columbia University, New York, New York, USA

Low brain GABA concentrations make its *in vivo* detection challenging. It was recently demonstrated that use of the J-editing difference technique with a phased-array head coil at 3.0 T can significantly enhance GABA detection sensitivity for a voxel in the human dorsolateral prefrontal cortex. In this study, we evaluated the tradeoffs for these GABA detection sensitivity gains achieved with an 8-channel phased-array coil at 3.0 T between voxel size and scan time that can be made without sacrificing spectral quality.

12:00 ***489***. **Test-Retest Reliability of Dorsolateral Prefrontal Cortical GABA Measurement Using an 8-Channel Phased-Array Head Coil with the J-Editing Technique at 3T**

Lawrence S. Kegeles[1], Xiangling Mao[2], Jonathan Dyke[2], Robyn Gonzales[1], Tacara N. Soones[1], Dikoma C. Shungu, [12]
[1]Columbia University, New York, New York, USA; [2]Weill Medical College of Cornell University, New York, New York, USA

Measurement of brain GABA and glutamate/glutamine in the dorsolateral prefrontal cortex (DLPFC) is of central interest in many neuropsychiatric disorders. Previous work has shown the feasibility of reliable measurements at 3T with MRS and the J editing technique using a single-channel quadrature volume head coil, with fairly large (19.5 cc) voxel of interest (VOI). Significant SNR gains have been found to be attainable in this region with a multichannel phased-array coil. This study shows the feasibility of utilizing the SNR gains of a multichannel phased-array coil to reduce the DLPFC VOI volume to 9 cc without degradation of test-retest reliability.

12:12 ***490***. **Residual Water as a Navigator in GABA Editing Spectroscopy**

Jan Willem W.C. van der Veen[1], Jun Shen[1]
[1]NIH, NIMH, Bethesda, Maryland, USA

GABA is the primary inhibitory neurotransmitter involved in a variety of psychiatric and neurological disorders. Due to the intense creatine methyl signal at 3.0 ppm, small movements of the subject and carrier frequency drift can lead to severe subtraction errors using the conventional two-step subtraction editing methods. Accurate and objective phase correction requires a phase marker with high SNR and an automatic routine with minimal user intervention. Here we report a robust phase correction routine using residual water as the internal navigator signal, which significantly minimized subtraction errors in GABA editing.

12:24 ***491***. ***In Vivo* Evaluation of the Concentration of Macromolecule Species Involved in GABA Editing**

Changho Choi[1], Nicholas J. Coupland[1], Paramjit P. Bhardwaj[1], Nikolai Malykhin[1], Dan Gheorghiu[1], Peter S. Allen[1]
[1]University of Alberta, Edmonton, Alberta, Canada

An *in vivo* study for evaluation of the concentration of macromolecule (MM) species involved as a primary contaminant in GABA C4 proton editing is reported. Two types of double-quantum filtering sequences, designed for selective detection of GABA and MM, gave a filtered signal ratio of 1.0±0.2 (mean±SD, n=2), at TE = 82 ms, for the human prefrontal cortex. With the signal retention ratios from the density-matrix simulation, the MM-to-GABA concentration ratio was evaluated to be 6±1, for GABA-to-MM T_1 and T_2 ratios both at 5.

12:36 ***492***. **Simultaneous Detection of Unobstructed Glutamate and Glutamine Using Standard STEAM with Optimized Sequence Parameters at 3, 4, 4.7, 7, and 9.4 Tesla - A Simulation Study**

Shaolin Yang[1], Jiani Hu[2], Elliot A. Stein[1], Yihong Yang[1]
[1]National Institute on Drug Abuse, NIH, Baltimore, Maryland, USA; [2]Wayne State University, Detroit, Michigan, USA

The Glutamate (Glu) and Glutamine (Gln) signals in one-dimensional 1H MR spectra usually overlap around 2.3-2.5 ppm, particularly at low field strengths. Various techniques have been developed for reliable detection and quantification of these compounds. A recent report proposed simultaneous detection of Glu and Gln (and GABA) using standard STEAM spectroscopy at 4T. The basic idea was to find optimal sequence parameters, at which the individual Glu and Gln signals around 2.3-2.5 ppm appeared as pseudo-singlets, thus minimizing the signal overlap. In this study we examine the feasibility of the idea at various field strengths.

12:48 ***493***. **Double Edited NMR Spectroscoy for Detection of an Antioxidant Profile in the Human Brain *In Vivo***

Melissa Terpstra[1], Rolf Gruetter[1]
[1]University of MN, Minneapolis, Minnesota, USA

Edited NMR spectroscopy typically exploits J-coupling to uncover a single target resonance. In this study, a second target resonance (GSH), was deliberately added to vitamin C (ascorbate) edited spectoscopy. Double Editing With (DEW) PRESS localization was developed for simultaneous detection of the two most concentrated non-enzymatic antixidants in the human brain. Each double edited spectrum contained separable ascorbate and GSH resonances, and used the same measurement time as single editing. The DEW spectra measured in four normal volunteers at 4T were highly reproducible. DEW can be adapted for editing of Multiple coupling systems (MEW) and implemented with other editing techniques.

CLINICAL MRI HANDS-ON WORKSHOP 1
Neuro and Musculoskeletal Protocol Optimization
GE Healthcare

Room 4F(1) 11:00 – 13:00 Chairs: Kimberly K. Amrami and Alberto Bizzi

CLINICAL MRI HANDS-ON WORKSHOP 1
Neuro and Musculoskeletal Protocol Optimization
Philips Medical Systems

Room 4F(2) 11:00 – 13:00 Chairs: Kimberly K. Amrami and Alberto Bizzi

CLINICAL MRI HANDS-ON WORKSHOP 1
Neuro and Musculoskeletal Protocol Optimization
Siemens Medical Solutions

Room 4F(3) 11:00 – 13:00 Chairs: Kimberly K. Amrami and Alberto Bizzi

GOLD CORPORATE MEMBER LUNCHTIME SYMPOSIUM
GE Healthcare

Room 6A-B 13:00 – 14:00

CLINICAL SCIENCE FOCUS SESSION: Human Stroke: From Disease Markers to Patient Management

Room 6D 14:00 - 16:00 Chair: A. Gregory Sorensen

14:00 ***494***. **Clinical Diagnosis and Treatment of Stroke and Trauma in a Neurovascular XMR Suite**
Andrew Jeremy M. Kiruluta[1, 2], Pamela W. Schaefer[1], Jim Rabinov[1], Johnny Pryor[1], Joshua A. Hirsch[1], Julian He[1], Ehud J. Schmidt, [13], R. Gilberto Gonzalez[1]
[1]MGH, Boston, Massachusetts, USA; [2]Harvard University, Cambridge, Massachusetts, USA; [3]GE, Milwaukee, Wisconsin, USA

Combining the high quality 3D anatomical information obtained from MR with the high spatial and temporal resolution of x-ray imaging is of potentially great benefit in acute stroke monitoring and treatment as well as other neurological diseases whose treatment requires a short interventional window. The presence of an MR scanner in the emergency department (ED) greatly enhances the utility of the XMR suite since acute stroke patients appear first in the ED. Clinical treatment of stroke in the XMR suite is currently underway combining catheter placement under x-ray guidance for thrombolysis treatment of acute stroke following MR based imaging diagnosis.

14:10 ***495***. **Intracranial Phase Contrast MRA with Vastly Under-Sampled Isotropic Projection Reconstruction (PC-VIPR): Initial Experience at 3.0 Tesla**
Darren Lum[1], Kevin Johnson[1], Oliver Wieben[1], Aquilla Turk[1], Beverly Aagaard-Kienitz[1], Frank Korosec[1], Charles Mistretta[1], Patrick Turski[1]
[1]University of Wisconsin - Madison, Madison, Wisconsin, USA

Phase-contrast MRA with vastly under-sampled isotropic projection reconstruction (PC-VIPR) is a promising technique, capable of producing high resolution angiographic images as well as quantitative flow information over a large imaging volume in a single exam. In this study, we present our initial experience on the imaging characteristics and performance of PC-VIPR of the intracranial vasculature at 3.0T. Specifically, we compare the contrast to noise ratios (CNR) of various intracranial vessel beds obtained from PC-VIPR exams acquired at 1.5T and 3.0T. In addition, we assess the image quality of PC-VIPR versus 3D Time-of-Flight MRA at 3.0T.

14:20 ***496***. **Perfusion Weighted MRI is Valuable in Identifying Persisting Vessel Occlusion in Acute Posterior Inferior Cerebellar Artery (PICA) Ischemia**
Simone Claudia Bukow[1], Kristina Szabo[1], Rolf Kern[1], Martin Griebe[1], C-H Lie[2], Michael G. Hennerici[1], Achim Gass[1, 3]
[1]Universitätsklinikum Mannheim, University of Heidelberg, Mannheim, Baden-Württemberg, Germany; [2]Institute of Medicine,, Juelich, Nordrhein-Westfalen, Germany; [3]Universitätsspital Basel, Basel, Switzerland

For various reasons most acute MRI studies have focused on anterior circulation stroke. This study analyzes in 16 patients with acute PICA stroke the value of combined diffusion-weighted MRI (DWI), PWI and MRA in acute stroke in the territory of the posterior inferior cerebellar artery (PICA) in comparison with vascular ultrasound ECD/TCCD findings. PWI showed hypoperfusion in the PICA territory in 9/16 patients, demonstrating persistent vessel pathology. Matching results for PWI and MRA and/or ECD/TCCD were found in only 11/16 patients (pattern 1 and 4). In 5/16 patients the results were not matching and PWI was valuable as it either demonstrated lack of hypoperfusion despite indications of arterial obstruction (pattern 2) or demonstrated hypoperfusion indicating persistent vessel pathology, which could not be detected by means of MRA or ECD/TCD (pattern 3). In PICA territory ischemia the high contrast visualization with a combination of DWI and PWI helps to achieve the diagnosis of persistent vessel pathology and identifies the extent of the abnormalities and tissue at risk for infarction.

14:30 ***497***. **3D GRASE ASL is Highly Sensitive to Detect Hyperperfusion States in Patients with Acute Stroke**
Rolf Kern[1], Matthias Guenther[1], Kristina Szabo[1], Martin Griebe[1], Fabrizio Sallustio[1], Michael Hennerici[1], Achim Gass[1]
[1]Universitätsklinikum Mannheim, University of Heidelberg, Mannheim, Germany

Hyperperfusion states usually reflect increase of CBV and/or CBF after recanalization and vasoparesis or in pathological states of high energy demand. In stroke, assessment of hyperperfusion may have therapeutic implications for stroke patients since thrombolysis may be needless or even harmful if vessel recanalization has already occurred. Arterial spin labeling (ASL) techniques provide non-invasive information on cerebral perfusion. Hyperperfusion states demonstrating areas with recanalization with earlier contrast arrival on TTP were detected in 7/36. Areas of hyperperfusion were clearly visualised on 3D-GRASE ASL perfusion maps, more easily discernible than on DSC derived perfusion maps.

14:40 ***498***. **Methods for In-Line Calculation of Perfusion Parameter Images**

Rudolf Stollberger[1], Franz Payer[1], Christian Enzinger[1], Franz Ebner[1], Franz Fazekas[2]
[1]Medical University of Graz, Graz, Austria; [2]Medical Uiversity of Graz, Graz, Austria

For in-line calculation of cerebral haemodynamic parameter images the maximum slope method was assessed by a simulation study and in comparison with deconvolution techniques for clinical data. Additionally the lag-time of a correlation analysis between a local voxel and the global bolus was considers as analogue to the mean transit time. With advanced methods for data preprocessing the maximum slope method performed equally well as deconvolution techniques. The lag times was found to be even more robust than the MTT calculated from the normalized residue function.

14:50 ***499***. **The Physiological Significance of the Tmax Parameter in Bolus Tracking MRI**

Soren Christensen[1], Ona Wu[2], Henrik Karstoft[3], Niels Hjort[1], Ken Butcher[4, 5], Stephen Davis[5], Leif Østergaard[1]
[1]Aarhus Sygehus, Aarhus, Denmark; [2]Massachusetts General Hospital, Boston, Massachusetts, USA; [3]University College of Aarhus, Aarhus, Denmark; [4]University of Sydney, Sydney, New South Wales, Australia; [5]Royal Melbourne Hospital, Melbourne, Victoria, Australia

The Tmax parameter calculated in bolus tracking studies has proved a promising penumbra marker, yet an interpretation of the pathophysiology it reflects is lacking. We investigate which physical parameters affect Tmax by using simulations and then subsequently use the results to examine 2 acute stroke patients. We conclude that Tmax reflects primarily the time to travel of blood from the site of AIF selection to the tissue and to a lesser extent MTT. Tmax has several attractive features as a metric in acute stroke but sources of confounders do exist and must be taken into account when interpreting data.

15:00 ***500***. **Predicting Tissue Outcome in Acute Human Stroke Using Temporally Adaptive MRI-Based Algorithms**

Ona Wu[1], Lee H. Schwamm[2], Walter J. Koroshetz[2], Thomas Benner[1], William A. Copen[2], R. Gilberto Gonzalez[2], A. Gregory Sorensen[1]
[1]Massachusetts General Hospital, Charlestown, Massachusetts, USA; [2]Massachusetts General Hospital, Boston, Massachusetts, USA

Tissue viability after stroke depends on depth and duration of the ischemic insult. Infarction risk was estimated on a voxel-wise basis by combining serial DWI and PWI and ischemia duration (i.e., time from symptom onset to MR acquisition) from stroke patients imaged <12h from onset. Models incorporating temporal information performed significantly better (p<02) in predicting final infarction at chronic timepoints (Youden's J=.46±.2) compared to models that did not (J=.40±.2) and performed equivalently acutely. Ischemia duration is an important factor that modulates interpretation of DWI and PWI in relation to tissue salvageability; therefore, its incorporation into MR-based algorithms improves infarction prediction.

15:10 ***501***. **Fully Automated Prediction of Irreversible Cerebral Infarction Using Diffusion and Perfusion MRI in the Multi-Center MR RESCUE Clinical Trial**

Timothy J. Schaewe[1], Jeffry R. Alger[1], Jennifer Shin[1], Brittany Copenhaver[1], Chelsea S. Kidwell[2, 3]
[1]David Geffen School of Medicine at UCLA, Los Angeles, California, USA; [2]Georgetown University, Washington, District of Columbia, USA; [3]Washington Hospital Center, Washington, District of Columbia, USA

MR and Recanalization of Stroke Clots Using Embolectomy (MR RESCUE) is an NIH-sponsored, multi-center clinical trial of mechanical embolectomy versus medical management using acute MRI for patient stratification and randomization. For this trial we have developed an automated computer system that generates a predictive map of irreversible infarct versus salvageable (penumbral) tissue from perfusion- and diffusion-weighted MRI. The computed predictive map is used to categorize patients according to the presence or absence of salvageable tissue to prove or disprove the hypothesis that acute MRI may be used to identify patients most likely to respond to mechanical embolectomy for treatment of acute ischemic stroke. The system is presently deployed at 10 (of 20 planned) clinical sites in the United States and Canada.

15:20 ***502***. **Determination of the Ischemic Threshold for Cell Death in Acute Stroke**

Wanyong Shin[1], Matthew T. Walker[2], Ali Shaibani[2], Rahul N. Sawlani[1], Medhi Rohany[2], Ty Allen Cashen[1], Timothy J. Carroll[1, 2]
[1]Northwestern University, Chicago, Illinois, USA; [2]Northwestern University Feinberg School of Medicine, Chicago, Illinois, USA

The Bookend method has been presented with water exchange effects correctionfor quantitative cerebral blood flow (qCBF) measurement. Acute strokepatients were scanned with the Bookend protocol, and qCBF maps wereobtained. The diagnostic accuracy for ischemic threshold was determinedusing an ROC analysis, and the ischemic threshold values were estimated in white matter and gray matter, respectively.

15:30 ***503***. **Effects of MR Perfusion Parameters Selection on the Prediction of Tissue Infarction in Acute Human Stroke**

Ona Wu[1], Walter J. Koroshetz[2], R. Gilberto Gonzalez[2], Thomas Benner[1], Chloe J. Lopez[1], Mingwang Zhu[1], Joanie Cacciola[2], Chris Melinosky[1], Hakan Ay[1], Aneesh B. Singhal[2], A. Gregory Sorensen[1]

[1]Massachusetts General Hospital, Charlestown, Massachusetts, USA; [2]Massachusetts General Hospital, Boston, Massachusetts, USA

Acute stroke patients not receiving thrombolysis (n=80) were retrospectively analyzed to determine whether multiparametric algorithms could be used to objectively select perfusion parameters for predicting tissue infarction. Models were generated with PWI parameters calculated by deconvolving with AIFs from ipsilateral or contralateral hemisphere, using standard or delay-insensitive methods. Separate models incorporating tracer-arrival time (DELAY) as a covariate were developed. The inclusion of DELAY as a parameter significantly ($p<.01$) increased performance accuracy ($\Delta AUC=.01\pm.02$) for all models, suggesting that the transit time for tracer arrival is an important indicator of tissue at risk of infarction in patients not receiving aggressive therapeutic intervention.

15:40 ***504***. **Heterogeneity of Brain Inflammation Following Human Ischemic Stroke: Evidence from USPIO - Enhanced MRI**

Michael Schroeter[1], Andreas Saleh[1], Adrian Ringelstein[1], Sebastian Jander[1]

[1]Heinrich Heine-University, Duesseldorf, NRW, Germany

Heterogeneity of stroke is regarded one of the main obstacles for establishing new therapeutic approaches. New methods are demanded to get additional *in vivo* pathophysiological information to tailor stroke therapy more individually. USPIO-enhanced MRI gives valuable new information after stroke. In an ongoing study. we found USPIO-enhancement in three out of nine patients in early post stroke MRI. USPIO enhancement is suggested to reflect divergent dynamics and spatial patterns of macrophage infiltration after stroke and may help to select patients suitable for studying anti-inflammatory therapeutic strategies after stroke.

15:50 ***505***. **Assessment of Image Quality in a Prospective Clinical Trial of Conventional vs. SENSE DWI at 1.5T**

Scott K. Nagle[1], David B. Clayton[1], Maarten G. Lansberg[1], Gregory W. Albers[1], Roland Bammer[1]

[1]Stanford University, Stanford, California, USA

Diffusion-weighted imaging (DWI) has proven indispensable in the diagnosis of acute stroke. Most DWI sequences use single-shot EPI methods; however, the long read-out time of these sequences leaves them sensitive to off-resonance and T2*-blurring effects. Applying parallel imaging techniques to DWI (SENSE DWI) may reduce these effects and improving the overall quality of clinical DWI scans. The authors present the results of a prospective clinical trial comparing conventional DWI with SENSE DWI sequences on a 1.5T scanner. The SENSE DWI scans demonstrated a significant reduction in susceptibility artifact and blurring and improved overall image quality in the majority of scans.

CLINICAL SCIENCE FOCUS SESSION: MR Angiography: Why Use Gadolinium

Room 4C - 3,4 14:00 - 16:00 Chairs: Mitsue Miyazaki and Freddy Ståhlberg

14:00 ***506***. **ECG-Gated High Resolution Contrast-Enhanced MR Angiography of Thoracic Aorta**

Elliott Groves[1], Timothy Carroll[1], Karin Dill[1], Carina Yang[1], Lincoln Diniz[1], James Carr[1]

[1]Northwestern University, Chicago, Illinois, USA

Contrast-enhanced magnetic resonance angiography (CE-MRA) is routinely used as a first-line tool for assessing the thoracic aorta.The proximal aorta is not infrequently obscured by motion artifact due to cardiac pulsation. With acceleration techniques such as parallel imaging it is now possible to implement CE-MRA with ECG-gating. This study shows a significant improvement in sharpness of the aortic root for ECG-gated MRA compared to ungated MRA in a group of 50 patients. This may result in improved detection of pathology particularly in the region of the aortic sinuses.

14:10 ***507***. **Impact of ECG-Gating in Contrast-Enhanced MR Angiography for the Assessment of the Left Atrium and the Pulmonary Veins**

Marcus Katoh[1], Arno Buecker[1], Georg Muehlenbruch[1], Patrick Schauerte[1], Rolf W. Guenther[1], Elmar Spuentrup[1]

[1]RWTH Aachen University Hospital, Aachen, Germany

A contrast-enhanced MR angiography (ceMRA) sequence was combined with ECG-gating for improved visualization of the left atrium, pulmonary veins and the great thoracic vessels. In twelve patients ceMRA was performed with and without ECG-gating on a 1.5 Tesla MR-system (Gyroscan Intera, Philips Medical Systems, Best, NL). Contour sharpness, SNR, CNR, and the subjective artifact level were analyzed. Using an ECG-gated ceMRA sequence, cardiac motion and vessel pulsation artifacts were significantly reduced leading to significantly increased contour sharpness of the left atrium and the thoracic vessels. In addition, higher SNR and CNR were found using ECG-gated ceMRA compared to standard ceMRA.

14:20 ***508***. **Free-Breathing Steady-State Free-Precession (SSFP) MR Angiography of the Renal Arteries Without Contrast Agent: A Prospective Intraindividual Comparison with High-Spatial-Resolution Contrast-Enhanced MR Angiography**

Michael Wyss[1, 2], Antonio Braghetti[3], Mario Alerci[3], Paolo Santini[3], Marcello Di Valentino[3], Romhild Hoogeveen[4], Marcus Katoh[5], Augusto Gallino[3], Rolf Wyttenbach[3]

[1]ETH and University, Zuerich, CH, Switzerland; [2]Philips Medical Systems, Zuerich, CH, Switzerland; [3]Ospedale San Giovanni, Bellinzona, CH, Switzerland; [4]Philips Medical Systems, Best, DA, Netherlands; [5]University Hospital, University of Technology, Aachen, D, Germany

The current state-of-the-art magnetic resonance angiographic technique for screening of renal artery stenosis is contrast-enhanced (CE) magnetic resonance angiography (MRA). Our study compares a free-breathing navigator-gated 3D SSFP MRA technique without the use of T1 contrast agent with high-resolution 3D CE-MRA. Free-breathing 3D SSFP MRA showed a high diagnostic accuracy for detection of renal artery stenosis and therefore can potentially be used for screening of renovascular disease in hypertensive patients without the need for contrast media. However severity of renal artery stenosis may be overestimated by SSFP MR angiography due to signal loss distal to the stenotic lesion.

14:30 ***509***. **Navigator Steady State Free Precession for Renal Artery Screening - Has the Time Come?**

Jeffrey Harold Maki[1, 2], William B. Eubank[1, 2], Romhild Maki Hoogeveen[3], David J. Glickerman[1, 2], Juan A. Millan[2], Sudhakaer Pipavath[2], Gregory J. Wilson[4]

[1]Puget Sound VAHCS, Seattle, Washington, USA; [2]University of Washington, Seattle, Washington, USA; [3]Philips Medical, Best, Netherlands; [4]Philips Medical, Cleveland, Ohio, USA

Forty patients underwent navigator Steady State Free Precession (Nav SSFP) and contrast-enhanced (CE) renal artery MR angiography to evaluate Nav SSFP as a screening test to rule out renal artery stenosis (RAS). The incidence of RAS (>50%) by CE-MRA was 25%. Nav SSFP had a sensitivity of 100%, specificity of 80%, and negative predictive value of 100% for the detection of RAS. The perfect sensitivity in combination with high specificity makes Nav SSFP an ideal candidate for a fast, less-expensive, non-contrast screening test for renal artery stenosis.

14:40 ***510***. **Non-Gadolinium Enhanced MRA of the Distal Lower Extremities**

Ruth P. Lim[1], Elizabeth M. Hecht[1], Jian Xu[2], Samson Wong[1], James S. Babb[1], Bachir Taouli[1], Stephen J. Drew[1], Tejas Parikh[1], Vivian S. Lee[1]

[1]NYU Medical Center, New York, New York, USA; [2]Siemens Medical Solutions USA, New York, New York, USA

A novel non-contrast enhanced MRA technique called ECG-gated HASTE is compared with two contrast-enhanced techniques, time-resolved and conventional bolus chase MRA for the evaluation of the infragenual arteries. 16 patients were examined, with 10 below-knee segments per leg, for technical quality and clinical findings. The study showed significant differences ($p<0.05$) in accuracy of the non-contrast technique, with mildly decreased visualization of vessel length and overestimation of stenosis. However, with continued development, non-contrast MRA has potential as a rapid, entirely non-invasive examination.

14:50 ***511***. **Time Resolved MRA for the Classification of Endoleaks After Endovascular Aneurysm Repair**

Robert H. Siegelbaum[1], Emil Cohen[1], Shaun M. Honig[1], Robert Lookstein[1], Michael Marin[1]

[1]Mount Sinai Medical Center, New York, New York, USA

Utilization of time resolved MRA for the classification of endoleaks post endovascular stent graft repair of abdominal aortic aneurysms.

15:00 ***512***. **Effect of Dose Bisection at 3.0T on Contrast-Enhanced Magnetic Resonance Angiography of the Renal Arteries**

Christoph U. Herborn[1], David M. Watkins[2], Val M. Runge[2], L Gill Naul[2], Gerhard Adam[1]

[1]University Medical Center, Hamburg, Germany; [2]Scott and White Hospital, Temple, Texas, USA

Aim of the study was to intraindividually compare two doses of gadolinium for contrast-enhanced enhanced three-dimensional Magnetic Resonance Angiography (CE-MRA) in patients suspected of renal artery stenosis. 22 patients underwent MR imaging of the renal arteries at 1.5T (0.2 mmol/kg) and 3.0T (0.1 mmol/kg). Random consensus readout was performed. While mean image quality did not show any statistically significant differences between the two doses and field strength SNR and CNR values were statistically significant different with the greater dose at 1.5T as compared to the lower dose at 3.0T. Further dose studies for optimized renal CE-MRA are warranted.

15:10 ***513***. **Magnetic Resonance Angiography (MRA) of the Lower Extremities with Parallel Imaging and a Dedicated 36 Element Matrix-Coil at 3 Tesla**

Harald Kramer[1], Bernd J. Wintersperger[1], Volker Matschl[2], Peter Schmitt[2], Michele Picciolo[1], Maximilian F. Reiser[1], Stefan O. Schoenberg[1]

[1]University Hospital of Munich - Grosshadern Campus, Munich, Germany, Germany; [2]Siemens Medical Solutions, Erlangen, Germany, Germany

One of the last drawbacks of MRA was the reduced spatial resolution compared to DSA and CTA. The implementation of dedicated angiography matrix-coils in combination with parallel imaging and high field strength offer the possibility of high spatial resolution without ionizing radiation or nephrotoxic contrast agents. A prototype of a dedicated peripheral angiography matrix-coil helped to compensate the loss of SNR when using parallel acquisition techniques.

15:20 ***514***. **Prevalence and Distribution of Atherosclerotic Abnormalities in Subjects Aged 70 Examined with Whole-Body MRA**

Tomas Hansen[1], Johan Wikström[1], Lars Lind[2], Lars Johansson[1], Håkan Ahlström[1]
[1]Dept of Radiology, Uppsala University, Uppsala, Sweden; [2]Dept of Medical Sciences, Uppsala University, Uppsala, Sweden

303 subjects were examined. The vessels were divided into 26 segments and evaluated according to stenosis, occlusion or aneurysms. 99% of the 7878 segments were possible to evaluate. 94 subjects (31%) had stenoses with more than 50% diameter reduction or occlusions, including 7 aneurysms. 112 subjects (37%) had only stenoses less then 50%, though 5 of them had aneurysms. 95 subjects (31%) had no abnormalities. 2 subjects had aneurysms without other vascular abnormalities. This study gives the prevalence and severity of atherosclerotic abnormalities in a random sample of 70 year old subjects examined with whole-body MRA at 1,5 T scanner.

15:30 ***515***. **Detection of Intravascular Hematocrit in Equilibrium Phase Imaging Using a Blood Pool Agent**

Maisie S. Wang[1], David Robert Haynor[1, 2], Gregory J. Wilson[3], Jeffrey Harold Maki[1, 2]
[1]University of Washington, Seattle, Washington, USA; [2]Puget Sound VAHCS, Seattle, Washington, USA; [3]Philips Medical, Bothell, Washington, USA

Intravascular hematocrit can occur during the time period of equilibrium phase imaging, particularly in slow flowing or stagnant veins. It consists of a layering between contrast-enhanced and less-enhanced layers that can appear similar to the type of filling defect seen with deep vein thrombosis (DVT). This layering effect has not been reported in MR venography, likely because equilibrium imaging is not typically performed. Blood pool agents allow intravascular HCT to be observed during equilibrium phase imaging. Flow characteristics and the enhancement patterns of the HCT layering effect were examined in *ex vivo* and *in vivo* studies.

15:40 ***516***. **High-Resolution Magnetic Resonance Lymphangiography in Patients with Primary and Secondary Lymphedema**

Christian Lohrmann[1], Etelka Foeldi[2], Oliver Speck[1], Mathias Langer[1]
[1]University Hospital of Freiburg, Freiburg, Germany; [2]Foeldi Clinic for Lymphology, Hinterzarten, Germany

Up to now lymphoscintigraphy has been the primary imaging modality in diagnosing patients with suspected extremity lymphedema. However, this method has the disadvantages of ionizing radiation exposure and poor spatial and temporal resolution, limiting its value for accurate assessment of the lymphatic anatomy and function. We present a new technique for visualizing non-invasively the lymphatic vessels and accompanying complications in patients with primary and secondary lymphedema. The method is not aimed at the depiction of lymph node morphology but can provide complementary information about the lymphatic vessels when lymph nodes are examined with super-paramagnetic iron oxide particles in cancer patients.

15:50 ***517***. **MR Evaluation of Deep Venous Thrombosis (DVT) of the Lower Extremities Using Ferumoxytol,**

Wei Li[1, 2], John Salanitri[1, 2], Eugene Dunkle[1], Sean Tutton[1, 2], Linda Pierchala[1], Paula Jacobs[3], Pottumarthi V. Prasad[1, 2], Robert R. Edelman[1, 2]
[1]Evanston Northwestern Healthcare, Evanston, Illinois, USA; [2]Northwestern University Feinberg School of Medicine, Chicago, Illinois, USA; [3]Advanced Magnetics, Inc, Cambridge, Massachusetts, USA

MR venography has been previously reported using 2D TOF and gadolinium-enhanced MRA. The former is inefficient and suffers from sensitivity to flow patterns, whereas the latter suffers from rapid leakage of contrast agent. Nine patients with known DVT of lower extremities were evaluated with MR venography using an iron oxide blood pool agent, ferumoxytol. Pre-contrast TOF, post-contrast TRICKS, 3D SPGR bright blood, and T2 FSE dark blood sequences were acquired. Dual contrast, artifact-free images of DVT were obtained in all subjects. The results suggest that ferumoxytol MR venography offers great potential for detection of DVT.

ELECTRONIC POSTER DISCUSSION: MR Engineering Forum

Room 611 - 612 14:00 - 16:00 Chairs: Arne Reykowski and Steven M. Wright

14:00 ***518***. ***In-Vivo*** **Human Brain Inhomogeneity Estimation Using Susceptibility Registration and Rapid Field Simulation**

Kevin Matthew Koch[1], Douglas L. Rothman[1], Robin A. de Graaf[1]
[1]Yale University, New Haven, Connecticut, USA

Rapid *in vivo* inhomogeneity simulations have recently been presented which exploit the small susceptibilities (<10-4) of materials compatible with magnetic resonance studies. These simulations present an alternative to time consuming image based field mapping. Such field maps are useful for large-volume shim optimization and post-acquisition geometric distortion correction of echo-planar images. Utilizing field simulations for these purposes requires estimation of the susceptibility distribution within a sample. This can be accomplished by nonlinearly registering a fixed susceptibility model to standard MRI acquisitions. Here, we present the methods of this inhomogeneity estimation procedure and its agreement with experimentally measured field maps.

14:10 ***519***. **Adjustable Subject-Specific Passive Shims Using Optimized Distributions of Bismuth and Zirconium**

Kevin Matthew Koch[1], Peter M. Brown[1], Douglas L. Rothman[1], Robin A. de Graaf[1]
[1]Yale University, New Haven, Connecticut, USA

Low order spherical harmonic shims cannot globally compensate *in vivo* field inhomogeneity near significant magnetic susceptibility boundaries. Subject-specific passive shims offer a means to globally compensate these higher-order effects. Through linear response theory, we have developed a method to optimize the placement of diamagnetic Bismuth and paramagnetic Zirconium elements. Here, we demonstrate the utility and accuracy of this method through the optimization, construction, and use of a global passive shim for the mouse brain.

14:20 ***520***. **Shielding and Energy Advantages of Capped Elliptical Coil Structures**

Tanvir Noor Baig[1], Timothy P. Eagan[1], Labros S. Petropoulos[1, 2], William A. Edelstein[1, 3], Matthew Finnerty[1], Xin Chen[1], Robert W. Brown[1]
[1]Case Western Reerve University, Cleveland, Ohio, USA; [2]Hitachi Medical Systems America, Twinsburg, Ohio, USA; [3]MRScience LLC, Schenectady, New York, USA

We have designed a capped actively shielded gradient coil on an elliptical coil form. Compared to conventional uncapped elliptical and cylindrical gradients, our design substantially reduces the fringe fields, the associated eddy currents in the inner bore and consequent acoustic noise power. In addition, there is a good reduction in magnetic energy. The fringe fields are reduced 70%, largely because of the end caps, and the magnetic energy is lessened because of the reduced cross sectional area. The magnetic energy is reduced, relative to cylindrical designs, by 35% for the z-gradient and 19% for the transverse gradients.

14:30 ***521***. **Gradient Arrays for High Performance Multiple Region MRI**

Dennis L. Parker[1], J. Rock Hadley[1]
[1]University of Utah, Salt Lake City, Utah, USA

This paper demonstrates that multiple region gradient arrays have the potential to improve gradient performance, with increased total imaging field of view and reduced total magnetic field excursions to reduce the potential for nerve stimulation. Simulated annealing is used to generate optimal coil designs for single and dual region gradient systems. Performance factors are substantially improved.

14:40 ***522***. **A New Look at RF Power Requirements in MRI**

Tamer S. Ibrahim[1], Lin Tang[1], Doney Abraham[1]
[1]University of Oklahoma, Norman, Oklahoma, USA

In this work, we closely study the RF power/frequency dependence up to frequencies nearing 12 Tesla on a variety of electrical load sizes, configurations, and RF coils. Using full wave modeling, we provide power relations by using RF optimization in the excitation chain to achieve highly homogenous flip angles with a fixed uniformity criteria at B0 field strengths ranging from 4T up to 9.4 T for human head imaging.

14:50 ***523***. **Miniature Form-Fitting Transmission Line Resonator for In-Vivo Small-Animal Imaging at 2.35 T**

Jean-Christophe Ginefri[1], Marion Woytasik[1], Olivier Girard[1], Jean-Sebastien Raynaud[2], Elisabeth Dufour-Gergam[1], Philippe Robert[2], Luc Darrasse[1]
[1]Université Paris Sud, Orsay, France; [2]Guerbet Research, Aulnay-Sous-Bois, France

Performances of 11 mm diameter form-fitting Multiturn Transmission Line Resonator (MTLR) fabricated on a flexible polyimide film using microtechnological processes are presented. As compared to a similar but flattened MTLR and to a standard 10 cm volume coil, the form-fitted MTLR achieved SNR gains up to 2 and 8 respectively on images acquired at 2.35 T with a cylindrical doped-water phantom of 10mm diameter.An *in vivo* subcutaneous model tumor image with a 156x78x1000 μm^3 voxels and a SNR of about 35 was performed in the mouse with the form-fitting MTLR.

15:00 ***524***. **Clinical Integration of a Phosphorus-31 Coil Insert Into a System Head Coil at 3T**

David Michael Peterson[1, 2], Hee-Won Kim[1]
[1]University of Florida, Gainesville, Florida, USA; [2]Midwest RF, LLC, Hartland, Wisconsin, USA

In order to make MNS a reality in the clinical environment, steps must be taken to integrate MNS into the proton imaging. The first step for this is through coil designs that minimally impact proton imaging while preserving the integrity of the MNS coil.

15:10 ***525***. **A Dual-Tuned Half Volume Coil for $^{13}C\{^1H\}$ MRS: Two Open Coils in One**

Atiyah Yahya[1], Peter S. Allen[1]
[1]University of Alberta, Edmonton, Alberta, Canada

In $^{13}C\{^1H\}$ studies a coil system that resonates at both the frequencies of ^{13}C and ^1H is required. We present here a single-unit, dual-tuned, half-volume coil that is based upon the open coil design (half birdcage). To make it dual-tuned, each alternate leg was tuned to one of the two frequencies alternately and a trap circuit was placed in each leg to block current at the unwanted frequency. The efficacy of the coil was verified on the human calf at 3 T.

15:20 ***526***. **An Integrated Signal-To-Noise Ratio Approach for Phased-Array Coil Health Check**

Ceylan Celil Guclu[1], Steven J. Huff[1]

[1]GE Healthcare, Waukesha, Wisconsin, USA

As the number of channels increases on commercial MRI scanners, it is getting more difficult to identify individual coil element failures, and collecting reliable SNR data. The purpose of this study was (i) to design an automated software tool with appropriate protocols to identify element failures in a multi-coil array (a.k.a Phased-Array Coil), (ii) to make the method immune to other internal and external disturbances, i.e. improving the gage repeatability and reproducibility.

15:30 ***527***. **Four-Element 300 MHz Superconducting Array for Parallel Imaging**

Jaroslaw Wosik[1], Krzysztof Nesteruk[2], Maged Kamel[1], Lian Xue[1], Lei-Ming Xie[1], Kurt H. Bockhorst[3], Ponnada A. Narayana[3]

[1]University of Houston and Texas Center for Superconductivity, Houston, Texas, USA; [2]Institute of Physics Polish Academy of Sciences, Warsaw, Poland; [3]The University of Texas, Health Science Center, Houston, Texas, USA

We report on the recent development of a 300-MHz superconducting array for parallel MRI of small animals. Two four-elements arrays were designed with one made of copper and the other with HTS thin films. Each array comprises of four 18mm-diameter coils with built-in capacitors for capacitive coupling/matching/tuning and decoupling. The closed cycle pulsed tube refrigerator was used to cool the array and the associated electronics to 55 K. Both arrays were fully tested at 7.0T Bruker scanner and the obtained SNR gain of the cooled Cu and HTS arrays over room temperature Cu were 100 % and 160%, respectively.

15:40 ***528***. **Inductively Decoupled Microstrip Array at 9.4T**

Bing Wu[1], Xiaoliang Zhang[2], Gary X. Shen[1]

[1]The University of Hong Kong, Hong Kong, People's Republic of China; [2]University of Minnesota, Minneapolis, Minnesota, USA

In this study, an inductive decoupling technique of microstrip array for ultra high fields has been discussed. The decoupling inductance is nearly independent of resonant frequency. Thus microstrip arrays can be tuned and work well at the magnetic fields higher than 7T. For the prototype of volume array, the introduced inductors can reduce the mutual coupling not only between adjacent elements, but also between non-adjacent elements.

15:50 ***529***. **9.4T Human Imaging: Preliminary Results**

J. Thomas Vaughan[1], Lance DelaBarre[1], Carl Snyder[1], Jinfeng Tian[1], Peter Andersen[1], John Strupp[1], Gregor Adriany[1], Pierre-Francois van de Moortele[1], Kamil Ugurbil[1]

[1]University of Minnesota, Minneapolis, Minnesota, USA

Preliminary results of human head imaging at 9.4T are reported. To achieve safe and successful brain images at this new high-field bench mark, new RF technology and methods were required. Fortuitously the short Larmor wavelengths responsible for RF related artifacts also facilitate the B1 field phase and gain control required to compensate these artifacts. The multi-channel transceiver equipment, RF coils and interactive methods required to optimize image homogeneity and other criteria at 9.4T are presented. First of a kind 9.4T images so acquired are shown.

ELECTRONIC POSTER DISCUSSION: The Future of BOLD? Resting State Signals and Multiple Modalities

Room 615 - 617 14:00 - 16:00 Chairs: Xavier G. Golay and Mark Jenkinson

14:00 ***530***. **Impaired Default-Mode Network Activity in Schizophrenia: A Resting-State fMRI Study**

Tuomo Starck[1], Harri Littow[1], Jani Anttola[1], Michael Greicius[2], Osmo Tervonen[1], Matti Isohanni[1], Vesa J. Kiviniemi[1]

[1]Oulu University Hospital, Oulu, Finland; [2]Stanford University School of Medicine, Stanford, California, Finland

Functional MRI can be used in detecting impaired connectivity of brain networks. The resting-state activity of the default-mode network was compared between schizophrenics fulfilling DSM-III-R criteria and controls in a cohort study. Normal default mode network and new inversely correlated activity was identified in the healthy controls. Schizophrenics had reduced default mode network activity in the posterior cingulate cortex and in hippocampi, and the new inverse activity showed significant deficit in the ventral temporal areas. In addition, the resting-state activity of the primary sensory regions and the default-mode network were also more mixed in the schizophrenics.

14:10 ***531***. **BOLD fMRI Resting State Activity and the Network of Default Mode Brain Function**

Silvina G. Horovitz[1], Masaki Fukunaga[1], Jacco A. de Zwart[1], Peter van Gelderen[1], Susan C. Fulton[1], Thomas J. Balkin[2], Jeff H. Duyn[1]

[1]National Institutes of Health, Bethesda, Maryland, USA; [2]Walter Reed Army Institute of Research, Silver Spring, Maryland, USA

Recent BOLD fMRI studies suggest that, during rest, some brain regions increase their activity in a spatially correlated fashion. These regions have been hypothesized to constitute a network involved with so-called "default mode" activity, which possibly supports non goal-directed behavior and monitoring of the environment. In this study, we investigated the role of default mode activity by performing simultaneous EEG-fMRI while subjects rested and slept. The BOLD fluctuation level was maintained during sleep (stages 1-2) in most brain regions, including the default-mode network. This suggests that default mode activity does not represent conscious mentation.

14:20 ***532***. **Resting-State Functional Connectivity in Rat Brain**

Hanbing Lu[1], Leah Gitajn[1], William Rea[1], Elliot A. Stein[1], Yihong Yang[1]
[1]National Institute on Drug Abuse, Baltimore, Maryland, USA

Resting-state fMRI can be used to reveal functional connectivity in the brain. While the technique has been successfully used in humans, fewer studies have been reported on animals, particularly rats. There are several challenges in the use of resting-state fMRI in animal studies, including uncertainty of anesthesia effects on the synchronized low-frequency fluctuations and potential confounds of faster cardiac pulsations, particularly in small animals like rats. In this study, we attempted to measure resting-state functional signals in rats anesthetized with alpha-chloralose and with injection of superparamagnetic contrast agent (ferumoxtran-10) for reducing signals contributed from blood.

14:30 ***533***. **Tissue Specificity of Nonlinear Dynamics in Baseline fMRI**

Gopikrishna Deshpande[1], Stephen LaConte[1], Scott Peltier[1], Xiaoping Hu[1]
[1]Georgia Institute of Technology and Emory University, Atlanta, Georgia, USA

In this work, we investigated the nonlinear dynamical properties of BOLDresting state fluctuations. EPI data were acquired at 3T in 5 restingsubjects. Patterns of singularity in the complex plane and Lempel-Zivcomplexity were used to study the deterministic nonlinearity in fMRI. Weobserved greater nonlinearity and determinism in gray matter compared to whitematter and CSF. The removal of respiratory and cardiac pulsations decreasedthe nonlinearity and determinism but did not alter the relative differencebetween gray matter and white matter. Therefore, tissue-specific deterministicnonlinearity may reflect native physiological and metabolic fluctuationsrather than physiological artifacts due to respiration and cardiac pulsation.

14:40 ***534***. **Mapping Resting-State Functional Connectivity by Perfusion MRI**

Kai-Hsiang Chuang[1], Peter van Gelderen[1], Jerzy Bodurka[1], Vasiliki Ikonomidou[1], Alan Koretsky[1], Jeff Duyn[1], S. Lalith Talagala[1]
[1]National Institutes of Health, Bethesda, Maryland, USA

Resting-state low frequency (< 0.08 Hz) fluctuation of BOLD signal has been shown to exhibit high correlation among functionally connected regions. However, it is challenging to detect functional connectivity based on perfusion MRI. This work shows that combination of continuous arterial spin labeling (CASL) using a neck labeling coil and 16-channel receiver coil provides adequate sensitivity to reliably identify functionally connected brain regions based on resting-state CBF fluctuations. Furthermore, we also demonstrate that a proper labeling strategy can frequency shift the ASL signal so that perfusion time-courses can be obtained without BOLD contamination.

14:50 ***535***. **An Index of Low Frequency (0.1 Hz) Spectral Power Predicts Changes in the Amplitude and Shape of the BOLD Response**

Thomas Liu[1], Yashar Behzadi[1], Khaled Restom[1], Gretchen Smith[2], Jeanne Townsend[2]
[1]UCSD Center for fMRI, La Jolla, California, USA; [2]UCSD, La Jolla, California, USA

The amplitude and shape of the BOLD signal used in most fMRI studies can be altered by shifts in the baseline vascular state due to factors such as medication, age, and disease. We show that a normalized measure of the power in low frequency (0.1 Hz) components of the BOLD response to a randomized stimulus can be used to probe the baseline vascular state. In preliminary experiments, the normalized measure accounted for 40 to 80% of the variability in BOLD parameters due to both differences in age and the administration of vasoactive agents.

15:00 ***536***. **Multiple Networks for Interhemispheric Integration in the Visual Brain: fMRI BOLD Response Increases with EEG Synchronization**

Eleonora Fornari[1], Maria G. Knyazeva[1], Philippe Maeder[1], Reto Meuli[1]
[1]Centre Hospitalier Universitaire Vaudois (CHUV), Lausanne, Switzerland

Natural images contain a wide spectrum of spatial information, ranging from low to high spatial frequencies (SF). Our study, combining fMRI and EEG techniques, was aimed at mapping neural assemblies involved in the Gestalt-based interhemispheric integration of bilateral stimuli systematically varying in spatial frequencies. Visual stimuli of various spatial frequencies induce SF-specific pattern of activation and of interhemispheric EEG synchronization in the beta-gamma band. fMRI and EEG data suggest involvement of occipital and parietal neuronal networks in the processing of different spatial frequencies. Linear relation between BOLD and EEG coherence suggests that local activation can be boosted by synchronization.

15:10 ***537***. **Simultaneous Recordings of BOLD fMRI and Electrophysiological Responses to Whisker Stimulation in Conscious Rabbits**

Limin Li[1, 2], Andrew C. Talk[1, 2], G Iordanescu[1, 2], Craig Weiss[2], John F. Disterhoft[2], Alice M. Wyrwicz[1, 2]
[1]ENH Research Institute, Evanston, Illinois, USA; [2]Feinberg School of Medicine, Northwestern University, Chicago, Illinois, USA

We report preliminary results of simultaneous recordings of BOLD fMRI and electrophysiological responses from conscious rabbits during whisker stimulation at frequencies of 10 – 75Hz. Our data demonstrate strong correlations of BOLD fMRI responses with neuronal activity. This work suggests a useful model system to study the neurophysiological base of fMRI responses.

15:20 ***538***. **Inferring Blood Volume, Blood Flow and Blood Oxygenation Changes from Functional ASL Data**

Mark William Woolrich[1], Peter Chiarelli[1], Danial Gallichan[1], Thomas T. Liu[2]

[1]University of Oxford, Oxford, Oxon, UK; [2]UCSD, San Diego, California, USA

Functional MRI techniques such as Arterial Spin Labelling (ASL), Vascular Space Occupancy (VASO) and Blood Oxyenation Level Dependent (BOLD) have been developed to investigate the different haemodynamic changes of cerebral blood flow (CBF), cerebral blood volume (CBV), and blood oxygenation respectively. We propose an approach which infers these three haemodynamic changes simultaneously via a physiological model of ASL data acquired at multiple echo times. The physiological model describes the contributions of the changes in CBF, CBV and BOLD to the measured data. This can be achieved with a fairly simple model of the physiology. The method infers physiologically plausible haemodynamic changes in response to a visual task. We also demonstrate increased sensitivity in inferring CBF when compared to standard approaches of extracting it from tag-control differencing of ASL data. This approach means that a range of complementary information can be efficiently and simultaneously gathered in functional brain studies, offering enhanced detection power and improved data interpretation, particularly in studies where it is difficult to reliably reproduce conditions between sessions.

15:30 ***539***. **fMRI Measurement of $CMRO_2$ Using a Comprehensive Biophysical Model: Compared with PET**

Ai-Ling Lin[1], Peter T. Fox[1], Jia-Hong Gao[1]

[1]University of Texas Health Science Center at San Antonio, San Antonio, Texas, USA

Mapping changes in the cerebral metabolic rate of oxygen ($CMRO_2$)in human brain during neuronal activation has been performed using both PET and fMRI. It has been noted that the $\delta CMRO_2/CMRO_2$measured by fMRI (based on a simplified biophysical model) in previous studies was significantly different both in its values and pattern of the frequency dependence when compared with those measured by PET. By using a recently developed and more comprehensive biophysical model and improved data acquisition strategy, the fMRI-determined $CMRO_2$were re-evaluated and the new fMRI data shows substantial improvement in its agreement with previous PET results.

15:40 ***540***. **Modeling of BOLD Components in the Statistical Analysis of Perfusion-Based fMRI Experiments**

Eric Edward Roller[1, 2], Khaled Restom[1, 2], Thomas T. Liu[2]

[1]UCSD, La Jolla, California, USA; [2]UCSD Center for fMRI, La Jolla, California, USA

Perfusion based fMRI with arterial spin labeling (ASL) suffers from inherently low sensitivity. As a result, optimal analysis methods are required to make ASL a robust and widely applicable tool. Here we present an extension of a general linear model for the analysis of ASL data. We show that the incorporation of a BOLD-weighted static tissue term is critical for achieving optimal statistical power for acquisitions with long echo times (TE= 30 ms) but can be neglected for acquisitions with short echo times (TE = 9 ms).

15:50 ***541***. **Investigating the Relation Between Steady-State HBOLD and FBOLD Signals in fMRI Studies**

Chun-Jung Juan[1, 2], Yi-Jui Liu[3], Hsiao-Wen Chung[2], Cheng-Yu Chen[1], Tsu-Chen Chao[2], Yi-Yo Shih[2], Hwa-San Liu[2], Chou-Yin Wang, [24], Cheng-Wen Ko[5]

[1]Tri-Service General Hospital and National Defense Medical Center, Taipei, Taiwan; [2]National Taiwan University, Taipei, Taiwan; [3]Feng-Chia University, Taichung, Taiwan; [4]Tri-Service General Hospital, Taipei, Taiwan; [5]National Sun Yat-sen University, Kaohsiung, Taiwan

The neuron-activity related BOLD signals (fBOLD) could be interfered by the BOLD signals coming from the inhaled CO2 (hBOLD). Prior studies have focused on the relation between the fBOLD and hBOLD, however, leading to discrepant results. We hypothesize that the cerebrovascular reserve might be limited by original global vasodilatation at high inspired CO2 fractions, restrict further neuroactivity-related vasodilatation, and then attenuate the BOLD signal change. In this study, we broaden the range of CO2 concentration from room air to 7% and extend the experiment duration to cover the transient and steady states BOLD responses.

CLINICAL SCIENCE FOCUS SESSION: Novel MR Clinical Applications in the Musculoskeletal System

Room 602 - 604 14:00 - 16:00 Chairs: Kimberly K. Amrami and Sharmila Majumdar

14:00 ***542***. **Changes in Achilles Tendon Compliance from 30 Days of Chronic Unloading and Subsequent 3 Weeks of Rehabilitation – an MR Phase Contrast Study at 3T**

Dongsuk Shin[1], Sinyeob Ahn[1], Haedong Lee[1], John Hodgson[1], Taija Finni[1], Reggie Edgerton[1], Shantanu Sinha[1]

[1]University of California, Los Angeles, California, USA

We used phase contrast cine magnetic resonance imaging to quantify tendon compliance. This study aims to (i) show the feasibility of using PC MRI technique for noninvasive measurement of the Achilles tendon compliance with significant precision and accuracy and (ii) quantify changes in the tendon compliance from 30 days of chronic unloading and consequent atrophy followed by 6 weeks of physical rehabilitation. The stiffness decreased as a result of muscle atrophy and gradually recovered to near normal level by the end of 3 weeks. These changes of compliance seem to indicate that muscle atrophy elicits changes not only in muscle activity but also in material properties of passive tissues.

14:10 ***543***. **Diffusion Tensor Imaging of the Human Calf - Comparison Between 1.5T and 3.0T - Preliminary Experience**

Nadja Saupe[1], Lawrence M. White[1], Marshall S. Sussman[1], Mike D. Noseworthy[2]

[1]Mount Sinai Hospital and University Health Network, Toronto, Ontario, Canada; [2]St. Joseph's Healthcare, Hamilton, Ontario, Canada

DT-MRI, offers the opportunity to study the microstructure of skeletal muscle. The theory is that cell membranes and other structures restrict the diffusion of molecules and that for elongated cells and other media with anisotropic tortuosity, this restriction is greater in some directions than in others.The aim of this study was to evaluate the imaging parameters necessary to perform DT-MRI at 1.5T and 3T in normal humal skeletal muscle using different b-values and to calculate and to determine a number of quantitative parameters to characterize diffusion anisotropy in organized tissue.The study demonstrates useful parameters to perform DT-MRI at 1.5T and 3T.DT-MRI at 1.5 and 3T provides *in vivo* validation of quantitative structural analysis of human skeletal muscle.

14:20 ***544***. **Effects of Muscle Atrophy on the Heterogeneity of Strain Distribution and Other Characteristics of the Human Triceps Surae Muscle-Tendon Complex**

Dongsuk Shin[1], Haedong Lee[1], Sinyeob Ahn[1], John Hodgson[1], Taija Finni[1], Reggie Edgerton[1], Shantanu Sinha[1]

[1]University of California, Los Angeles, California, USA

We observed changes in the strain dynamics of the posterior soleus aponeurosis-tendon complex, the volume and strength of the triceps surae muscles before/after muscle atrophy and during the subsequent rehabilitation period (0, 1, 3, 6 weeks). These changes were investigated using the velocity encoded phcase contrast cine magnetic resonance imaging. Spatial strain ditribution changed after ULLS for 60% of the subjects . MVC anke plantarflexion torque decreased by 60% and gradually recovered to pre ULLS level by the end of 6-week rehabilitation. The solues, medial gastrocnemius volume changed 5.14%, and 8.01%, respectively. The lateral gastrocnemius volume remained unchaged.

14:30 ***545***. **Quantitative Diffusion and Fat Imaging of Vertebral Compression Fractures**

Blake Allen Cannon[1], Ashok J. Kumar[1], Colleen Costelloe[1], Patrick LeRoux[2], Jingfei Ma[1]

[1]University of Texas M. D. Anderson Cancer Center, Houston, Texas, USA; [2]GE Healthcare Technologies, Buc Cedex, France

Several published studies indicate that diffusion weighted imaging (DWI) and fat/water in-phase and opposed-phase imaging are useful in characterizing the nature of a vertebral compression fracture (VCF). In this work, we used a non-CPMG fast spin echo based diffusion technique and a spin echo based two-point Dixon technique to measure, in the same sessions, the apparent diffusion coefficient (ADC) and relative fat content in 14 cancer patients with VCFs. Our results show that between benign and malignant VCFs, the mean ADC value is statistically different. In contrast, no significant difference is found for the fat content.

14:40 ***546***. **Quantitative Micro-MRI Demonstrates Significant Effects on Trabecular Bone Architecture in Response to Antiresorptive Therapy**

Felix W. Wehrli[1], Glenn A. Ladinsky[1], Branimir Vasilic[1], Babette S. Zemel[1], Alexander C. Wright[1], Hee Kwon Song[1], Punam K. Saha[1], Helen Peachy[1], Peter J. Snyder[1]

[1]University of Pennsylvania, Philadelphia, Pennsylvania, USA

Advances in MR image acquisition and processing techniques now have made possible direct imaging of trabecular microarchitecture and assessment of the topological changes that occur during the pathogenesis and treatment of patients with osteoporosis. Comparing a group of women ages 45-55 years in early menopause treated with estrogen against a control group without hormonal therapy, we provide evidence for the postulated architectural changes in response to antiresorptive treatment and show that these effects can be visualized *in vivo* in individual patients.

14:50 ***547***. **MR Imaging Study of Relationships Between Lumbar Bone Density, Paravertebral Muscle Bulk and Perfusion Indices in Postmenopausal Osteoporosis**

Steven Yang[1], James Francis Griffith[1], David Yeung[1]

[1]The Chinese University of Hong Kong, Shatin, Hong Kong, People's Republic of China

Loss of skeletal muscle mass or sarcopenia and osteoporosis are both features of aging commonly observed among postmenopausal women. However, it is unclear whether these changes are related or do they occur independently of each other. In addition, little is known whether there is any relationship between lumbar muscle mass and muscle perfusion variables. Our goal in this study was to address these questions through study of the interrelationships among sarcopenia, osteoporosis, and perfusion indices of the lumbar spine in female elderly patients of similar age.

15:00 ***548***. **The Diagnostic Ability of Diffusion Weighted Imaging with Background Body Signal Suppression (DWIBS) in Bone Metastasis**

Behnaz Goudarzi[1], Riwa Kishimoto[1], Kyosan Yoshikawa[1], Susumu Kandatsu[1], Shuhei Komatsu[1], Hiroyuki Ishikawa[1], Makhtum Shahnazi[2], Hirohiko Tsujii[1]

[1]National Institute of Radiological Science, Chiba, Japan; [2]Loghman University Hospital, Tehran, Iran

Recently High resolution diffusion-weighted imaging with background body signal suppression (DWIBS) and 3D images offers significant improvement for whole body screening strategies for detecting malignancy. The authors present a report of performing DWIBS in 10 patients with different kinds of tumors and bone metastasis in order to assess its ability in detecting bone metastasis. DWIBS data were compared with 11C- methionine positron emission tomography (MET-PET) and whole body bone scan. We believe DWIBS is a very sensitive method for detecting bone metastasis especially in pelvic cavity which is superior to MET-PET and bone scan; although for providing specifity side-by-side comparison with conventional MRI is necessary.

15:10 ***549***. **Potential of SPIO in the Diagnosis of Bone Metastasis - Preliminary Examination for Clinical Application**

Yuko Fukuda[1], Kumiko Ando[1], Reiichi Ishikura[1], Natsuko Tsuda[2], Naoki Kato[2], Norio Nakao[1]

[1]Hyogo College of Medicine, Nishinomiya, Hyogo, Japan; [2]Nihon Schering K.K., Osaka, Japan

In preliminary experiment using the model rabbits, we have reported that a superparamagnetic iron oxide (SPIO) enhanced magnetic resonance imaging (MRI) has a potential in the differential diagnosis of bone metastasis and inflammation. In this study, we clinically investigated optimal imaging parameters and scan timing of bone marrow with healthy volunteers as well as a potential of SPIO for the differential diagnosis with patients. Optimal imaging parameters and scan timing were short TI inversion recovery and at 3 hours after a ferucarbotran injection. SPIO enhanced MRI could detect bone metastasis in patients at a clinically approved liver imaging dose.

15:20 ***550***. **Examiner Variability of T2 of Cartilage in Subjects with Osteoarthritis**

Matthew F. Koff[1], Fazel A. Khan[1], Kimberly K. Amrami[1], Kenton R. Kaufman[1]

[1]Mayo Clinic, Rochester, Minnesota, USA

T2 values of articular cartilage have been proposed as a biomarker for osteoarthritis (OA). This study evaluated the repeatability of T2 calculations of cartilage in patients with osteoarthritis. 20 subjects with patello-femoral OA were enrolled. A series of T2 weighted images were acquired to calculate T2 values of patellar cartilage. Images were digitized twice by two examiners. Inter-examiner and intra-examiner repeatability was high, both with mean T2 differences of less than 1 ms. This study will aid in determining the clinical applicability of T2 mapping in a clinical setting.

15:30 ***551***. **Dynamic Contrast Enhanced MRI of Synovium in Rheumatoid Arthritis Patients: Response to Intra-Articular Therapy and Relationship to Magnetization Transfer Contrast**

Lawrence Yao[1], Melanie Kotys[1], Mildred Wilson[1], Sandeep N. Gupta[2], David M. Thomasson[1], Raphaela Goldbach-Mansky[1]

[1]NIH, Bethesda, Maryland, USA; [2]General Electric Heathcare, Hanover, Maryland, USA

In patients with rheumatoid arthritis (RA) dynamic contrast enhanced magnetic resonance imaging (DCE-MRI) may yield information about disease activity not reflected by changes in synovial volume. We examined changes in synovium occurring after intra-articular steroid therapy as reflected by standardized kinetic parameters derived from DCE-MRI. We examined the relationship of these parameters and magnetization transfer contrast (MTC) in synovium, hypothesizing that MTC might serve as a marker for more chronic synovial pannus. Our preliminary results, however, did not support this hypothesis. Intra-articular therapy led to consistently reduced synovial volume and spatially variable decreases in Ktrans.

15:40 ***552***. **Using MR Elastography to Evaluate Plantar Soft Tissue Damage in Diabetics**

John B. Weaver[1], Yvonne Y. Cheung[1], Timothy B. Miller[2], Marvin M. Doyley[1], Phillip R. Perrinez[2], Huifang Wang[2], James S. Wrobel[3], Richard J. Comi[1], Francis E. Kennedy[2], Keith D. Paulsen[2]

[1]Dartmouth-Hitchcock Medical Center, Lebanon, New Hampshire, USA; [2]Dartmouth College, Hanover, New Hampshire, USA; [3]Rosalind Franklin University of Medicine and Science, Chicago, Illinois, USA

Damage done by the impact of walking on the heel fat pad was evaluated by comparing the shear modulus in the regions where the impacts of walking is highest to the shear modulus where there is little impact. Four diabetic subjects and 7 normal subjects were evaluated. In the diabetic subjects, the region under the calcaneus was significantly softer than peripheral regions indicating that the fat pads were damaged from walking. There was no indication of damage in the normals. The damage observed in the diabetic subjects increased monotonically with the number of years the subject has had diabetes.

15:50 ***553***. **Does 3.0 T MRI Improve Diagnosis of Internal Derangement of the Knee?**

Ritu Rajwar[1], Timothy John Mosher[1], Eric A. Walker[1], Jason Robert Stuck[1], Scott A. Lynch[1], Kevin P. Black[1]

[1]Penn State University, Hershey, Pennsylvania, USA

A retrospective evaluation of 134 knee MRI cases with surgical correlation were used to compare the sensitivity and specificity of 1.5 T with 3.0 T MRI in diagnosis of full thickness ACL tear, medial and lateral meniscal tear, and chondrosis of patellar, femoral, and tibial cartilage. There was no significant difference in sensitivity or specificity in diagnosis of ACL or meniscal tears between the two field strengths. There was a trend for greater specificity in diagnosis of chondral lesions using 3.0 T. We conclude 3.0 T MRI of the knee has diagnostic efficacy equivalent to that of 1.5 T.

CLINICAL MRI HANDS-ON WORKSHOP 2
Body and Cardiovascular Protocol Optimization
GE Healthcare

Room 4F(1) 14:00 – 16:00 Chairs: David A. Bluemke and Caroline Reinhold

CLINICAL MRI HANDS-ON WORKSHOP 2
Body and Cardiovascular Protocol Optimization
Philips Medical Systems

Room 4F(2) 14:00 – 16:00 Chairs: David A. Bluemke and Caroline Reinhold

CLINICAL MRI HANDS-ON WORKSHOP 2
Body and Cardiovascular Protocol Optimization
Siemens Medical Solutions

Room 4F(3) 14:00 – 16:00 Chairs: David A. Bluemke and Caroline Reinhold

Molecular Imaging in Atherosclerosis

Room 6E 16:30 - 18:30 Chairs: Zahi A. Fayad and Patrick M. Winter

16:30 ***554.*** **Multimodality Validation and Mechanistic Explanation of Functional Restoration of Murine Model of Myocardial Infarction by Mouse Embryonic Stem Cells**

Phillip C. Yang[1], Shoko Ikeda[1], Brett Fenster[1], Stephen Hendry[1], Sally Zhang[1], Micha Drukker[1], Irv Weissman[1], Philip Tsao[1], Robert C. Robbins[1]

[1]Stanford University, Stanford, California, USA

In this study, multi-modality validation of MR evaluation of myocardial restoration following transplantation of mouse embryonic stem cells (mESC) has been performed. Furthermore, the mechanisms underlying functional restoration of the injured myocardium in murine model of myocardial infarction have been investigated.

16:42 ***555.*** **MRI Tracking of the Regional Persistence of Feridex-Labeled Mesenchymal Stem Cells in a Canine Myocardial Infarction Model**

Ana Victoria Soto[1], Wesley D. Gilson[1], Dorota Kedziorek[1], Adit Tal[1], Danielle Crawford[1], Parag Karmarker[1], Randell G. Young[2], Mark F. Pittenger[3], Jeff W. M. Bulte[1], Dara L. Kraitchman[1]

[1]Johns Hopkins University, Baltimore, Maryland, USA; [2]Osiris Therapeutics, Inc, Baltimore, Maryland, USA; [3]Johns Hopkins University School of Medicine, Baltimore, Maryland, USA

The purpose was to determine the regional persistence and migration of targeted SPIO-labeled mesenchymal stem cells (MSCs) in a canine model of myocardial infarction over 2 months. Dogs were subjected to a coronary artery occlusion followed by reperfusion to create an AMI. Autologous MSCs were then delivered to each dog. Images were obtained to localize injection sites for 2 months to assess persistence in comparison to infarct transmurality. MSCs have a higher tendency to remain in the infarct which indicates this area may be the preferred for targeting. Reduction in injection sites represents cell death and migration within the heart.

16:54 ***556.*** **Tracking of Intra-Coronary Delivered Mesenchymal Stem Cells Using MRI in a Porcine Model of Myocardial Infarction**

John J. Graham[1], Warren D. Foltz[2], Yeusong Yang[1], Jay S. Detsky[3], Graham A. Wright[1, 3], Alexander J. Dick[1]

[1]Sunnybrook and Women's College Health Sciences Centre, Toronto, ON, Canada; [2]St Michael's Hospital, Toronto, ON, Canada; [3]University of Toronto, Toronto, ON, Canada

Stem cells are increasingly being used to regenerate infarcted myocardium. MR imaging has demonstrated capabilities for delineating magnetically-labeled cells *in vivo* as focal hypointensities. We have developed a model enabling MRI tracking of intra-coronary delivered, magnetically and fluorescently labeled, mesenchymal stem cells in a porcine model of reperfused AMI. Immediately following cell delivery, using an FSPGR sequence, the cells' magnetic label was observed predominantly in the infarct border rather than within the infarct itself. Post-mortem fluorescent imaging showed concordance of the cells' fluorescent labels with the regions of hypointensity seen on MRI.

17:06 ***557***. **Relationship Between Macrophage Content and MRI Signal Intensity of Atherosclerosis Using Gadolinium-Containing Immunomicelles Targeted to Macrophage Scavenger Receptor**

Smbat Amirbekian[1], Vardan Amirbekian[2], Juan Gilberto S. Aguinaldo, Juan Carlos Frias, Venkatesh Mani, Karen C. Briley-Saebo, Esad Vucic, Marc Sirol, Zahi Adel Fayad

[1]Emory University School of Medicine - Mount Sinai School of Medicine, New York, USA; [2]Johns Hopkins University School of Medicine - Mount Sinai School of Medicine, New York, USA

Macrophages play a vital role in the pathogenesis of atherosclerosis. They are major sources of inflammation. Furthermore, the necrotic core of ruptured/thrombosed plaques often contains a high content of macrophages. Gadolinium-containing immunomicelles have demonstrated *in vivo* efficacy in imaging of atherosclerosis using ApoE-knockout mice. The aim of the current study is to evaluate the relationship between macrophage content of atherosclerotic plaques and *in vivo* MRI signal-intensity in the atherosclerotic aorta using immunomicelles as a contrast-agent targeted to macrophages. There appears to be a significant connection between atherosclerosis macrophage content and MRI signal-intensity using immunomicelles. The investigation is ongoing to determine significance level.

17:18 ***558***. **Method for Specific Detection of Plaque Angiogenesis in the Cholesterol-Fed Apolipoprotein-E Deficient Mouse with MR Fluorine Spectroscopy of Integrin-Targeted Perfluorocarbon Nanoparticles at 11.7T**

Emily A. Waters[1, 2], John Stacy Allen[2], Huiying Zhang[2], Gregory M. Lanza[2], Samuel A. Wickline, [12], Junjie Chen[2]

[1]Washington University in St. Louis, St. Louis, Missouri, USA; [2]Washington University School of Medicine, St. Louis, Missouri, USA

We developed a novel method using high-field MR spectroscopy to detect angiogenesis in aortic atherosclerotic plaques of Apolipoprotein-E deficient mice. We used a targeted perfluorocarbon-based nanoparticle contrast agent, which binds specifically to $\alpha_v\beta_3$ integrin (expressed on neovasculature endothelium). Fluorine MRS was performed at 11.7T on excised aortas of mice treated with nanoparticles and then euthanized, and signal was readily apparent. Localized spectroscopy showed stronger fluorine signal from the aortic arch than the descending aorta, consistent with pathological observation of disease distribution. This method enables definitive detection of angiogenesis in atherosclerotic plaques, and is sensitive to spatial variations in disease extent.

17:30 ***559***. **Imaging of Atherosclerosis *In Vivo* Using a Magnetic Resonance Contrast Probe Molecularly Targeted to Matrix Metalloproteinases (MMPs)**

Smbat Amirbekian[1], Juan Gilberto S. Aguinaldo, Vardan Amirbekian[2], Marc Sirol, Fabien Hyafil, Esad Vucic, Venkatesh Mani, Eric Lancelot[3], Claire Corot[3], Zahi Adel Fayad

[1]Emory University School of Medicine - Mount Sinai School of Medicine, New York, USA; [2]Johns Hopkins University School of Medicine - Mount Sinai School of Medicine, New York, USA; [3]Guerbet, Paris, France

We tested the *in vivo* ability of P947 to detect and assess atherosclerosis using molecular MRI. P947 contains a ligand to matrix-metalloproteinases (MMPs) that is attached to a gadolinium-chelate making it into a molecular MRI contrast-agent. MMPs play a very important role in atherosclerosis plaque progression and rupture leading to thrombosis. Our results show that compared to several controls, including a scrambled version of P947(P1135), P947 facilitated excellent enhancement of atherosclerosis in ApoE-knockout mice. P947 provided a 125% normalized increase in signal-intensity of atherosclerotic vessels compared to controls. The results were corroborated using pathology, MMP immunohistochemistry techniques and MMP zymography methods.

17:42 ***560***. **Visualizing the Uptake of Combidex® (Ferumoxtran-10) in a Rat Model of AAA Using Positive and Negative Contrast Methods**

Joan M. Greve[1], Eiketsu Sho[2], Maureen Tedesco[1], Masahiro Terashima[1], Michael V. McConnell[1], Ronald L. Dalman[1], Maj Hedehus[3], Charles H. Cunningham[1], Steven M. Conolly[4], Charles A. Taylor[1]

[1]Stanford University, Stanford, California, USA; [2]KAI Pharmaceuticals, Inc., South San Francisco, California, USA; [3]Varian, Inc., Palo Alto, California, USA; [4]University of California Berkeley, Berkeley, California, USA

Inflammation may play a role in abdominal aortic aneurysm (AAA) disease. Visualizing inflammation using MRI is possible by administering certain USPIOs. We assessed the potential of using ferumoxtran-10 to visualize vessel wall inflammation in a rat model of AAA using gradient echo (GE) techniques and off-resonance (OR) techniques that exploit field inhomogeneity near iron particles. There was good correspondence between the methods. The majority of signal was derived from spleen and lymph nodes. This is one of the first studies to extend OR methods beyond proof-of-concept. The technique is reproducible, provides high-throughput, and is specific to the USPIO induced inhomogeneities.

17:54 ***561***. ***In Vivo* MR Imaging of Bone Marrow Cell Trafficking to Atherosclerotic Plaques**

Bensheng Qiu[1], Fabao Gao[1], Piotr Walczak[1], Jiangyang Zhang[1], Sourav Kar[1], Jeff WM Bulte[1], Xiaoming Yang[1]

[1]Johns Hopkins Univ School of Medicine, Baltimore, Maryland, USA

This study evaluated the potential use of MRI to monitor, *in vivo*, trafficking of magnetically labeled bone marrow (BM) cells to atherosclerotic lesions. Feridex-labeled or unlabeled LacZ-BM cells were transplanted into ApoE-/- mice with atherosclerotic lesions. *In vivo* MR imaging showed large MR signal voids in the ascending aorta of mice with Feridex-BM transplantation, which were not visualized in the control mice with unlabeled BM transplantation or without BM transplantation. Results of this study demonstrate the potential of monitoring BM cell trafficking to atherosclerotic plaques using *in vivo* MR imaging.

18:06 ***562***. **Molecular Imaging of Angiogenic Therapy in Peripheral Vascular Disease with $Alpha_{nu}beta_3$-Targeted Nanoparticles**

Patrick M. Winter[1], Shelton D. Caruthers[1, 2], John S. Allen[1], Todd A. Williams[1], Thomas D. Harris[3], Samuel A. Wickline[1], Gregory M. Lanza[1]

[1]Washington University, St. Louis, Missouri, USA; [2]Philips Medical Systems, Cleveland, Ohio, USA; [3]Bristol-Myers Squibb Medical Imaging, Billerica, Massachusetts, USA

Molecular imaging of angiogenesis using a targeted paramagnetic nanoparticle contrast agent was studied for detecting angiogenesis in an animal model of peripheral vascular disease. Ten days post surgical ligation of one femoral artery, MRI molecular imaging showed increased angiogenesis in the ischemic vs. control hindlimbs. Similarly, X-ray angiography performed 40 days post-surgery showed a greater number of mature vessels in the ischemic vs. control limbs. This data demonstrates that targeted paramagnetic nanoparticles can be utilized to specifically detect the molecular signatures of angiogenesis in skeletal muscle far earlier than traditional X-ray angiography techniques.

18:18 ***563***. **Positive Contrast MR Imaging of *In Vivo* Atherosclerosis in a Rabbit Model Using Ultrasmall Iron Oxide Particles**

Karen C. Briley-Saebo[1], Venkatesh Mani[1], Fabien Hyafil[1], Zahi A. Fayad[1]

[1]Mount Sinai School of Medicine, New York, New York, USA

Recent in-vitro studies using GRe Acquisition for Superparmagnmetic Particles (GRASP) sequence show that GRE sequences with manually controlled dephasing gradients resulted in positive signal enhancement in gels containing iron particles. The purpose of our study was to verify the *in vivo* efficacy of GRASP to produce positive signal in plaques of atherosclerotic rabbits after administration of 4.7 mg Fe/kg USPIO (fractionated-Feridex). All imaging was performed at 1.5T using T2* GRE and GRASP sequences both pre and 24-hours post USPIO injection. The results of the study strongly suggest that GRASP sequence may be used to verify uptake of USPIO in plaque macrophages.

MR PHYSICS AND TECHNIQUES FOR CLINICIANS

Room 6C 16:30 - 18:30 Chairs: Frank R. Korosec and Joseph C. McGowan

Educational Objectives:
Upon completion of this session, participants should be able to:

- Define and describe the fundamental principles of MR imaging, including the definition of spin magnetization, the Larmor relationship, relaxation phenomena, and the process of using the spin magnetization to produce an image;
- Explain imaging pulse sequences based upon spin and gradient echoes, including fast spin echo and echo planar techniques;
- Design MR imaging protocols for diagnostic applications considering image contrast, spatial resolution, acquisition time, signal-to-noise ratio, and artifacts; and
- Describe the principles and capabilities of various advanced MR techniques including, diffusion, vascular and cardiac MRI.

16:30 **Imaging Options and Their Effects on SNR**
Frank R. Korosec

17:10 **Ultrafast Imaging**
Marcus Alley

17:50 **Field Strength Dependence in MRI-Advantages and Artifacts at 3T**
Matt A. Bernstein

MR Angiography: Pushing the Limits

Room 6D 16:30 - 18:30 Chairs: Elizabeth Hecht and Susanne C. Ladd

16:30 ***564***. **Cardiovascular Whole-Body MRI with Parallel Acquisition Techniques (PAT) and Matrix-Coils at 3 Tesla: Comparison to 1.5 Tesla**

Harald Kramer[1], Sabine Weckbach[1], Henrik J. Michaely[1], Konstantin Nikolaou[1], Maximilian F. Reiser[1], Stefan O. Schoenberg[1]

[1]University Hospital of Munich - Grosshadern Campus, Munich, Germany, Germany

Recent developments in MR hard- and software made it possible to perform whole body MRI at the same high image quality as it is known from organ based MR exams. The next step to perform state of the art cardiovascular whole body imaging is to implement it to high field strength like 3 Tesla. The combination of matrix-coil systems, parallel imaging and 3 Tesla offer the possibility to image the entire cardiovascular system within reasonable time at high image quality.

16:42 ***565***. **Scout-Less Stepping Table Whole-Body Contrast-Enhanced MR Angiography**

Wei Li[1, 2], Anthony T. Vu[3], Eugene Dunkle[1], Robert R. Edelman[1, 2]

[1]Evanston Northwestern Healthcare, Evanston, Illinois, USA; [2]Northwestern University Feinberg School of Medicine, Chicago, Illinois, USA; [3]GE Healthcare, Waukesha, Wisconsin, USA

A scout-less imaging method for step-table whole-body contrast-enhanced magnetic resonance angiography is described. This method uses non-selective RF excitation for rapid data acquisition using predetermined settings for the 3D volumes and table-shifts. Because the data are acquired through the total thickness of the body, there is no need for acquisition of multiple scout images and manual positioning of the multiple imaging volumes. The entire four-station study, including mask and angiogram images, can be completed in seven minutes or less.

16:54 ***566***. **Whole Body MR Angiography at 3.0T on a 32 Channel System: Initial Results**

Kambiz Nael[1], Roya Saleh[1], Michael Fenchel[1], Mayil Krishnam[1], Gerhard Laub[2], Stefan G. Ruehm[1], John Paul Finn[1]

[1]David Geffen School of Medicine at UCLA, Los Angeles, California, USA; [2]Siemens, Los Angeles, California, USA

Sixteen subjects underwent multi-station whole body MR angiography using a 32-channel 3.0T system with multi-coil technology. Implementation of high acceleration parallel acquisition, and flexible table movement capabilities, result in acquisition of isotopic submillimeter voxels throughout the body, sufficient for diagnosis in most vascular territories.

17:06 ***567***. **Contrast-Enhanced Supraaortic MRA at 3.0T Using 8-Channel and 16-Channel Neurovascular Coils and Parallel Acquisition with Acceleration Factors Ranging from 1 to 9**

Winfried A. Willinek[1], Jürgen Gieseke[1], Dariusch R. Hadizadeh[1], Marcus von Falkenhausen[1], Marco Nijenhuis[2], Romhild Hoogeveen[2], Horst Urbach[1], Hans H. Schild[1]

[1]University of Bonn, Bonn, NRW, Germany; [2]Philips Medical Systems, Best, NL, Netherlands

Contrast-enhanced MRA of the supraaortic arteries was performed on a clinical whole body 3.0T MRI using parallel imaging with high SENSE acceleration factors (SF) ranging from 1 to 9 and using 8- and 16-channel neurovascular coils. In 23 subjects, MRA with SENSE (i.e. SF 2, 4, 9) allowed for higher spatial resolution, shorter acquisition time and improved anatomic coverage (365 slices instead of 150 with SF 1) that included vascular structures of the head and neck arteries that were not covered by the standard MRA protocol with SF 1.

17:18 ***568***. **A Parallel Acquisition Optimized Peripheral Vascular Coil for Combination Time Resolved and High Resolution Peripheral CE-MRA**

Jeffrey Harold Maki[1, 2], Gregory J. Wilson[3], Romhild Maki Hoogeveen[4], William B. Eubank[1, 2], David J. Glickerman[1, 2], Joseph Whitnah[2], Mark B. Mathis[2], Cecil E. Hayes[2]

[1]Puget Sound VAHCS, Seattle, Washington, USA; [2]University of Washington, Seattle, Washington, USA; [3]Philips Medical, Cleveland, Ohio, USA; [4]Philips Medical, Best, Netherlands

An 18 channel three-station peripheral MRA prototype coil optimized for parallel imaging (SENSE) was built and tested. SENSE factors of up to five are possible at all stations. Using this coil, time-resolved (keyhole technique, 3-4 s per timeframe) 3D intermediate resolution calf-station MRA can be performed and used a.) to aid in diagnosis, and b.) to optimally choose imaging and parallel imaging factors such that high-resolution single-injection moving table peripheral CE-MRA can be performed without confounding venous enhancement.

17:30 ***569***. **Carotid Artery Disease: Effects of Doubling and Tripling Spatial Resolution in 3D Contrast-Enhanced Elliptical Centric Magnetic Resonance Angiography**

Brad Hnatiuk[1], Derek Emery[1], Alan Wilman[1]

[1]University of Alberta, Edmonton, Alberta, Canada

In contrast-enhanced 3D MRA, higher resolution is always desirable, but this requires increased acquisition times. The limitation on acquisition times for carotid artery contrast-enhanced MRA has recently shifted from venous contamination and arterial signal prolongation, to patient motion and signal-to-noise issues. This work addresses the effects of doubling and tripling image resolution in 110 consecutive patients presenting with suspected carotid artery disease. The work assesses the associated losses in SNR and potential increased patient motion. The higher resolution was found to be warranted for maximizing diagnostic value in patients with severe carotid stenosis, but not in normal arteries.

17:42 ***570***. **3D Time-Resolved Contrast-Enhanced MRA with Sliding Subtraction**

Ty Allen Cashen[1], James C. Carr[2], Matthew T. Walker[2], John K. Hopkins[2], Wanyong Shin[1], Timothy J. Carroll[1, 2]
[1]Northwestern University, Chicago, Illinois, USA; [2]Northwestern University Feinberg School of Medicine, Chicago, Illinois, USA

We have developed a novel 3D MR angiographic technique with high frame rate to serve as a noninvasive alternative or adjunct to X-ray DSA. 3D images were acquired of a single hemisphere of the intracranial vasculature with 1.1 x 1.1 x 2.5 mm spatial resolution and 0.3 s/frame temporal resolution after sliding window reconstruction. The sliding subtraction method yielded images with strong artery-vein separation in time, background suppression, and immunity to motion artifacts. The radial trajectory was used to provide uniform vessel enhancement without the high-pass filter effect found with Cartesian sliding window techniques.

17:54 ***571***. **"Shoot and Scoot" MR Angiography: Clinical Experience in a Symptomatic Population with Peripheral Vascular Disease**

Jean Michel M. Serfaty[1], Jean Pierre P. Laissy[1], Pelin Aksit[2], Elisabeth Schouman-Claeys[1], Patrice Hervo[3]
[1]University Hospital of Bichat, Paris, France; [2]GE Healthcare Technology, Baltimore, Maryland, USA; [3]GE Healthcare Technology, Buc, France

We assessed an improved version of the single injection multi-station bolus chase MRA technique known as "Shoot and Scoot" (SNS) in a symptomatic population of patients with peripheral arterial occlusive disease of the lower limbs. By enabling a faster bolus chase, SNS permitted to reduce venous contamination at infrapopliteal arterial vasculature while preserving spatial resolution compared to standard multi-station peripheral MRA methods, and preserving SNR compared to multiple injection approaches to imaging the peripheral vascular tree.

18:06 ***572***. **A Curved Thigh Cuff for Suppressing Venous Enhancement on Peripheral MRA**

Martin R. Prince[1], Hale Ersoy[2], Honglei Zhang[1], Hui Xu[3], Minh Chao[1], Kiyarash Mohajer[1], Bernard Ho[1]
[1]Weill Medical College of Cornell University, New York, New York, USA; [2]Brigham and Womens Hospital, Harvard Medical School, Boston, Massachusetts, USA; [3]Cornell University, Ithaca, New York, USA

A curved cuff was developed for thigh compression to eliminate venous contamination at the calf station of bolus chase peripheral MRA. It uses a Urethane laminate with a Velcro surface and a curved shape optimized for a snug fit on the conical shape of the leg. Inflation is uniform and controlled with 59 spot welds. The cuff has o-ring sealed connectors to a coiled conduit for inflation via an MRI compatible hand inflator or a high precision autoinflator connected to a pressure source. Consistent effective venous compression is achieved with this dedicated cuff system compared to MRA without venous compression.

18:18 ***573***. **Intraindividual Comparison of High-Spatial Resolution Abdominal MRA at 1.5T and 3.0T**

Henrik Jakob Michaely[1], Harald Kramer[1], Kambiz Nael[2], Sabine Weckbach[1], Maximilian F. Reiser[1], Stefan O. Schoenberg[1]
[1]University of Munich, Munich, Bavaria, Germany; [2]UCLA, Los Angeles, California, USA

An intraindividual comparison study of abdominal MRA at 1.5T and 3.0T is presented. 15 volunteers were imaged at both field strength. The MRA sequences featured high spatial resolution (1x0.8x1mm³ at 1.5T / 0.9x0.8x0.9mm³ at 3T), a fast image acquisition enabled by parallel imaging factor 3. Image quality was rated by two radiologists, CNR was measured.MRA at 3T proved to have significantly higher CNR and fewer artifacts. Vessel visibility was equal with better vessel conspicuity at 3T.Even with broader anatomic coverage, a 20% reduced voxel size and scan time MRA at 3.0T was superior to 1.5T MRA.

Functional Breast Imaging

Room 4C - 3,4 16:30 - 18:30 Chairs: Donald B. Plewes and Hans H. Schild

16:30 ***574***. **Evaluation of Choline Concentrations in Malignant Breast Lesions in Predicting Response to Neoadjuvant Chemotherapy**

Peuen Clara Tan[1], Martin Lowry[1], David J. Manton[1], Lindsay W. Turnbull[1]
[1]University of Hull, Hull, Yorkshire, UK

A measurement of the *in vivo* T1 and T2 relaxation times of water and choline in malignant breast lesions, as well as a study using these values to obtain lesion choline concentrations and follow their changes throughout neoadjuvant chemotherapy, is reported here. We found no apparent difference in behaviour of [choline] between responsive and non-responsive lesions. This could be because [choline] is indicative of the tumour cells' biological status rather than clinical response to drugs. Monitoring [choline] of malignant breast lesions therefore does not appear to be a robust way of predicting their response to chemotherapy.

16:42 ***575.*** **Changes in Lesion T2 and Volume Predict Response of Malignant Breast Lesions to Neoadjuvant Chemotherapy**

Peuen Clara Tan[1], Martin Lowry[1], David J. Manton[1], Lindsay W. Turnbull[1]
[1]University of Hull, Hull, Yorkshire, UK

We report here an investigation into both imaging and spectroscopic methods of measuring the water T2 of malignant breast lesions, and their utility in predicting response to neoadjuvant chemotherapy, both alone and in combination with lesion volumes. We found that imaging and spectroscopy produced similar T2 values, and the ratio of the product of the lesion T2 and volume after the 2nd cycle to those pre-treatment is a good predictor of ultimate lesion response, with PPV and NPV of 95.5% and 84.6% respectively.

16:54 ***576.*** **Blood Oxygenation Level Dependent (BOLD) and Gd-DTPA Contrast MRI for Early Evaluation of Breast Cancer Chemotherapy**

Lan Jiang[1], Roderick McColl[1], Paul Weatherall[1], Debu Tripathy[1], Ralph P. Mason[1]
[1]UT Southwestern Medical Center, Dallas, Texas, USA

Tumor microcirculation and oxygenation play very important roles in tumor growth and responsiveness to cytotoxic treatment. In order to explore using BOLD technique to evaluate cancer chemotherapy in clinic, we used the BOLD and DCE technique to assess breast cancer chemotherapy. Ten female patients with locally advanced breast cancer were treated with preoperative chemotherapy. MRI was performed on a Philips 1.5 T clinical scanner. Our result showed a strong correlation between high relative signal intensity of BOLD response and better therapeutic efficacy. BOLD may provide an indication of tumor physiology that responded to certain therapies.

17:06 ***577.*** **MRI Measurements of Tumor Size and Pharmacokinetic Parameters as Early Predictor Variables in Breast Cancer Patients Undergoing Neoadjuvant AC-Chemotherapy**

Hon J. Yu[1], Min-Ying Su[1], Rita Mehta[1], Orhan Nalcioglu[1]
[1]University of California, Irvine, California, USA

Neoadjuvant chemotherapy, which plays an important role in breast-cancer therapy, requires a reliable means to predict the response of tumor at early times once the chemotherapy is initiated so that the patient could be spared from ineffective treatment. MRI measurements of tumor-size and pharmacokinetic parameters (Ktran and kep) were investigated in 27 breast cancer patients undergoing neoadjuvant AC-chemotherapy to ascertain their values as predictors of response. Statistically significant reductions in both parameters were observed after 1-2 cycles of AC only for the responders predicting their response after 4 cycles of AC, complementing the size-reduction observed after 1-2 cycles of AC.

17:18 ***578.*** **Discrimination of Choline-Positive Invasive Breast Carcinomas Using Water-To-Fat Ratio: A Proton MRS Study**

Sunitha B. Thakur[1], Lia Bartella[1], Nicole M. Ishill[1], Elizabeth A. Morris[1], Laura Liberman[1], David D. Dershaw[1], Hedvig Hricak[1], Jason A. Koutcher[1], Wei Huang[1]
[1]Memorial Sloan Kettering Cancer Center, New York, New York, USA

Choline concentrations [Cho] and water-to-fat (W/F) ratios were calculated from proton MRS data of 42 patients with pathologically proven breast cancer (invasive ductal carcinoma (IDC) or invasive lobular carcinoma (ILC)), who exhibited Cho-positive MRS findings. W/F ratio was obtained from the reference MRS scan without water suppression, while [Cho] was calculated using the water signal as internal reference. There is no significant difference in [Cho] between the IDC and ILC groups. However, W/F ratio is significantly higher in IDCs than ILCs, and performs significantly better compared to [Cho] in differentiating the two breast malignancies with high sensitivity and specificity.

17:30 ***579.*** **A Quantitative Study of Various Metabolites in Breast Tumors by *In-Vitro* Proton MR Spectroscopy and Its Statistical Evaluation**

Ankita Pandey[1], Puja Ramakant[2], Sandeep Kumar[2], A.N. Srivastava[2], Mukesh Srivastava[1], Raja Roy
[1]Central Drug Research Institute, Lucknow, Uttar Pradesh, India; [2]King George's Medical University, Lucknow, Uttar Pradesh, India

PROTON MR quantitative analysis in breast tumors, fibroadenomas (n=10) and ductal carcinomas (n=13) along with their respective controls (n=23) were carried out on twelve metabolites viz. formate, myo-inositol, glycine, a-GPC, choline, Cr/PCr, glutamine, succinate, glutamate, acetate, alanine and lactate. Multivariate discriminant function analysis (DFA) was performed to find out important descriptors for the discrimination of fibroadenomas and ductal carcinomas (CA), along with their control tissues. The best discrimination between fibroadenomas and ductal carcinomas was obtained with the combined effect of Glycine and Choline as marker metabolites ($p < 0.01$). The proposed model could classify 95.65% cases correctly between the fibroadenoma and ductal carcinoma, with the sensitivity of 92.3% and the specificity of 100%.

17:42 ***580***. **Preliminary Experience with Breast ^{1}H MRS at 7 Tesla**

Patrick John Bolan[1], Carl J. Snyder[1], Lance J. DelaBarre[1], Lizann Bolinger[2], Michael Garwood[1], J Thomas Vaughan[1]
[1]University of Minnesota, Minneapolis, Minnesota, USA; [2]National Research Council Canada, Winnipeg, Manitoba, Canada

This work describes our initial experience in performing *in vivo* MRS of the human breast at very high field. Using a unilateral transmit/receive coil design and single-voxel localized spectroscopy, a total choline resonance was detected and quantified in 4/5 normal subjects, and a taurine resonance was observed in 2/5 same subjects. Additionally, we report measurements of respiration-induced frequency variations and relaxation rates for water and lipid resonances. These preliminary data show that 7 Tesla breast MRS is feasible and may lead to improved spectroscopic characterization of breast lesions.

17:54 ***581***. **Proton Chemical Shift Imaging for Characterization of Heterogeneous Human Breast Tumors**

Hyun-Man Baik[1], Min-Ying Su[1], Hon J Yu[1], Jeon-Hor Chen[1], O. Nalcioglu[1]
[1]University of California-Irvine, Irvine, California, USA

The chemical-shift imaging (CSI) is a useful technique for analyzing the regional heterogeneity of tumor metabolites. We applied high-resolution 2D-CSI technique to measure the spatial heterogeneity of choline-containing compounds (Cho) in malignant and benign breast lesions and demonstrated the feasibility of this technique for characterizing breast tumors within an acceptable scan time. Therefore, we conclude that the use of CSI technique for a clinical 1.5T study might be of value for further characterization of DCE-MRI enhanced lesions to improve specificity.

18:06 ***582***. **Quantification of Choline-Containing Compounds in Malignant Breast Cancer by ^{1}H Single-Voxel MR Spectroscopy at 1.5T**

Hyun-Man Baik[1], Min-Ying Su[1], Hon J Yu[1], O. Nalcioglu[1]
[1]University of California-Irvine, Irvine, California, USA

To investigate the feasibility of internal reference method for quantifying the Cho concentrations in patients with malignant breast tumors using a clinical 1.5T scanner, and to compare the Cho concentration range measured with the current method with previously published results. We have performed single-voxel MR spectroscopy and demonstrated the potential of the method for the absolute quantification of Cho metabolite in malignant breast lesions. The Cho levels from 28 spectra (82 %) were in a range of 0.76 ?10.22 mmol/kg, which seems to be consistent with previously published value (i.e., 0 ?10 mmol/kg).

18:18 ***583***. **Optimal K-Space Acquisition Reordering for Intermittent Fat Saturation in Breast MRI**

Kimberly L. Desmond[1], Elizabeth Ramsay[2], Don B. Plewes[1, 2]
[1]University of Toronto, Toronto, Ontario, Canada; [2]Sunnybrook and Women's College Health Sciences Centre, Toronto, Ontario, Canada

We demonstrate a method of partial-k-space fat suppression for 3D scans which significantly reduces the extension in imaging time while producing images which are visually equivalent to those produced with the conventional full-k-space saturation technique. Fat saturation pulses are performed intermittently while the k-space acquisition is reordered to optimize the distribution of the fat suppression, accounting for the regrowth of the fat signal via the Bloch equations. Using the reordered method we could achieve excellent fat suppression even when only 1% of k-space received a fat saturation pulse, allowing for the temporal resolution of 3D image sets to be doubled.

MRS Sensitivity Enhancement Techniques for 13C and Other Nuclei through Hyperpolarization

Room 611 - 612 16:30 - 18:30 Chairs: Rolf Gruetter and Brian D. Ross

16:30 ***584***. **Metabolic Imaging with Hyperpolarized ^{13}C and Multi-Echo, Single-Shot RARE**

Sven Månsson[1], Jochen Leupold[2], Oliver Wieben[3], René In't Zandt[4], Peter Magnusson[4], Edvin Johansson[4], John Stefan Petersson[4]
[1]Malmö University Hospital, Malmö, Sweden; [2]University Hospital Freiburg, Freiburg, Germany; [3]University of Wisconsin, Madison, Wisconsin, USA; [4]Amersham Health R&D, Malmö, Sweden

Chemical shift imaging (CSI) is traditionally used to create images with both spectral and spatial information. Long scan time and a large number of RF excitations make CSI less suited for metabolic imaging of hyperpolarized substances. In this work, a fast multi-echo RARE sequence was implemented and used for acquisition of metabolic maps after injection of hyperpolarized 13C in a pig. For comparison, a CSI dataset was acquired as well. The scan times of the sequences were 0.6 s and 24 s, respectively. Despite the big difference in acquisition strategy, the distribution of metabolites were found similar with both sequences.

16:42 ***585***. **Fast Chemical Shift Imaging of Hyperpolarized ^{13}C Substrates**

Alexander Peter Lin[1, 2], Thao T. Tran[1], Pratip Bhattacharya, [23], Kent Harris[3], Brian David Ross[3]
[1]Rudi Schulte Research Institute, Pasadena, California, USA; [2]California Institute of Technology, Pasadena, California, USA; [3]Huntington Medical Research Institutes, Pasadena, California, USA

Fast chemical shift imaging allows for *in vitro* and *in vivo* visualization of chemical shift as well as spatial localization of ^{13}C substrates within the fast relaxation time frame of hyperpolarization. Multiple CSI acquisitions allows for dynamic time course of signal intensities that is sensitive to multiple hyperpolarized reagents for periods of up to 5 minutes post hyperpolarization. *In vivo* experiments in rats demonstrate that this technique has great potential to observe metabolism using hyperpolarized reagents that were previously beyond detection.

16:54 ***586***. **Carbon-13 Metabolic Imaging at 3T Using Hyperpolarized 13C-1-Pyruvate**

Susan J. Kohler[1], YiFen Yen[1], Jan Wolber[2], Rene in't Zandt[2], Andreas Gram[2], Fredrik Ellner[2], Mikkel Thaning[2], Albert Chen[3], Mark Albers[3], Robert Bok[3], James Tropp[4], Sarah Nelson[3], Daniel Vigneron[3], John Kurhanewicz[3], Ralph Hurd[1]

[1]GE Healthcare, Menlo Park, California, USA; [2]GE Healthcare, Malmo, Sweden; [3]University of California San Francisco, San Francisco, California, USA; [4]GE Healthcare, Fremont, California, USA

This study explores metabolic imaging on a clinical 3T scanner using hyperpolarized pyruvate labeled with 99% 13C in the C1 position.

17:06 ***587***. **High-Resolution Hyperpolarized C-13 Spectroscopic Imaging of the TRAMP Mouse at 3T**

Albert P. Chen[1, 2], Mark Albers[1, 2], Susan J. Kohler[3], Yi-fen Yen[3], Ralph E. Hurd[3], James Tropp[3], Pieter Pels[1], Matthew L. Zierhut[1, 2], Robert Bok[1], Sarah J. Nelson[1, 2], John Kurhanewicz[1, 2], Daniel B. Vigneron[1, 2]

[1]UCSF, San Francisco, California, USA; [2]UCSF/UCB, San Francisco, California, USA; [3]GE Healthcare, Menlo Park, California, USA

High resolution MR imaging and dynamic hyperpolarized C-13 spectroscopic imaging was applied to the study of normal mice and transgenic mouse models of prostate cancer. The goal of this study was to assess the feasibility of detecting hyperpolarized pyruvate and its metabolic products localized to the prostate and cancer nodules in transgenic models of prostate cancer.

17:18 ***588***. **Limits of Detection of Hyperpolarized ^{13}C *In Vitro* and *In Vivo***

Brian David Ross[1], Alexander Peter Lin[2, 3], Pratip Bhattacharya[1, 3], Kent Harris[1], Keiko Kanamori[1], Anna Freundlich[2], Thao Tran[2]

[1]Huntington Medical Research Institutes, Pasadena, California, USA; [2]Rudi Schulte Research Institute, Pasadena, California, USA; [3]California Institute of Technology, Pasadena, California, USA

Hyperpolarization of ^{13}C exceeding 10,000 fold allows sub-second *in vivo* imaging and spectroscopy. Contrast agents are administered at concentrations of 0.3 – 0.5M, creating toxic, hyperosmolar and redox-metabolic stress which may mask the biological interpretation. This Abstracts establishes the lower limit of *in vivo* detection of hyperpolarized ^{13}C with the aim of creating physiologically acceptable experimental conditions for this novel technology. Hyperpolarized ^{13}C MRI is demonstrated in the 1 – 10 mM range.

17:30 ***589***. **Polarization Transfer for Sensitivity-Enhanced Spectroscopy Using a Single RF Transmit-Channel on (Clinical) MR Systems**

Dennis W.J. Klomp[1], Arno P.M. Kentgens[2], Arend Heerschap[1]

[1]Radboud University Nijmegen Medical Center, Nijmegen, Netherlands; [2]Radboud University Nijmegen, Nijmegen, Netherlands

Polarization transfer techniques are commonly used to enhance sensitivity and improve localization in multi-nuclear MR spectroscopy. Clinical MR scanners are in general not equipped with a second transmit RF channel making conventional polarization transfer techniques like Distortionless Enhanced Polarization Transfer (DEPT) impossible. Here we present that DEPT with sequential pulses (DEPT-SP) can be used on a single transmit channel with the same sensitivity and bandwidth performance. Validated by simulations, phantom and *in vivo* measurements at 3T, we show that polarization transfer methods can be implemented for *in vivo* MRS without the need for an additional RF transmit channel.

17:42 ***590***. **^{13}C Spectroscopic Imaging of Glycogen in Rat Brain**

Hongxia Lei[1, 2], Rolf Gruetter[1, 2]

[1]EPFL, Lausanne, Switzerland; [2]University of Minnesota, Minneapolis, Minnesota, USA

To date, *in vivo* localized ^{13}C MRS is the only non-invasive method to assess brain glycogen under physiological condition. The present study implemented and demonstrated feasibility to assess brain glycogen distribution using 1D CSI in rat with ^{13}C glucose label administration and visually confirmed the performance of 3D OVS localization.

17:54 ***591***. **Hunting for Cerebral [2-^{13}C]GABA Signal Derived *In Vivo* from Glia-Specific Substrate [2-^{13}C]acetate**

Jehoon Yang[1], Shizhe Steve Li[1], Stephen Fox[2], John Bacher[3], Robert B. Innis[1], Jun Shen[1]

[1]NIMH, Bethesda, Maryland, USA; [2]NCI, Frederick, Maryland, USA; [3]ORS, Bethesda, Maryland, USA

Acetate has been demonstrated to be a glia-specific substrate. Brain [2-^{13}C]GABA signal derived from [2-^{13}C]acetate is a measure of the glutamine-GABA cycle. In this study, spectrally resolved cerebral [2-^{13}C]GABA signal derived from intravenously infused [2-^{13}C]acetate was detected *in vivo* in the POCE spectra in vigabatrin-treated rats at 11.7 Tesla. However, in the intact brain, the [2-^{13}C]GABA signal derived *in vivo* from [2-^{13}C]acetate is not significantly above the noise level after extensive signal averaging using either ^{1}H{^{13}C} POCE spectroscopy of rat brain at 11.7 Tesla or ^{13}C{^{1}H} polarization transfer spectroscopy of the monkey brain at 4.7 Tesla.

18:06 ***592***. **Non-Linear Effects of Strong Coupling in ^{13}C Edited ^{1}H NMR Spectra Obtained Without Decoupling**

Julien Valette[1], Fawzi Boumezbeur[1], Malgorzata Marjanska[2], Kâmil Ugurbil[2], Vincent Lebon[1], Pierre-Gilles Henry[2]
[1]CEA-SHFJ, Orsay, France; [2]CMRR, University of Minnesota, Minneapolis, Minnesota, USA

Analysis of *in vivo* ^{13}C edited ^{1}H NMR spectra is hampered by spectral overlap, and linear combination modeling is being increasingly used to overcome this problem. Up to now, it was implicitly assumed that isotopomer spectra are linear, i.e. the spectrum of any isotopomer (labeled at several carbon positions) can be linearly decomposed to a basis-set consisting of spectra of isotopomers labeled at only one carbon position. In this work this assumption of linearity is investigated. It is demonstrated that, when ^{13}C decoupling is not performed, the linearity assumption is intrinsically incorrect for strongly coupled systems such as glutamate.

18:18 ***593***. **Simultaneous Observation of Lungs and Brain to Enhance Versatility of 129Xe Washout Curve Analysis in Mouse Brain**

Hideaki Fujiwara[1], Takashi Masutani[2], Michiko Narazaki[2], Hirohiko Imai[2], Tetsuya Wakayama[2], Atsuomi Kimura[2]
[1]Osaka University, Suita, Osaka, Japan; [2]Osaka University, 1-7 Yamadaoka, Suita, Osaka, Japan

129Xe washout curve analysis in brain is improved methodologically by simultaneously observing lungs and brain to remove the effect of lung parameters and by simplifying the formulation of the effect of rf pulses which is destructive to the residual HP magnetization. Thus, 129Xe apparent relaxation time in mouse brain has become determined in each mouse without citation of standard values for lung parameters. This method will be useful for the detection of changes in the net (not apparent) relaxation time and cerebral blood flow when any stimulus, which is known to affect only one of these two, is given.

RF Pulse Design

Room 615 - 617 16:30 - 18:30 Chairs: Peter Börnert and V. Andrew Stenger

16:30 ***594***. **Design of T_2 Selective Excitation Pulse Trains for Knee Imaging**

Logi Vidarsson[1], Charles Cunningham[1], Peder Eric Zufael Larson[1], Garry Gold[1], John Pauly[1]
[1]Stanford University, Stanford, California, USA

Linear combination filtering is a new post-processing method that canbe used to generate T_2 selective images, showing onlytissues with T_2 of interest. However a multi-echo datasetis required which calls for long scan-times. In this work we presentan equivalent T_2 selective RF pulse, this leads tosignificant scan-time reductions as only a single acquisition isrequired. In addition, multiple slices can be acquired in seriesfollowing a single preparation pulse.

16:42 ***595***. **Broadband RF Pulses with Polynomial-Phase Response**

Rolf F. Schulte[1], Jeffrey Tsao[2], Peter Boesiger[1], Klaas P. Pruessmann[1]
[1]University and ETH Zurich, Zurich, Switzerland; [2]Novartis Institutes for Biomedical Research, Inc., Cambridge, Massachusetts, USA

The bandwidth of common linear-phase RF pulses is tightly limited by the maximal feasible B_1 amplitude. For reducing B_1 requirements and hence increasing the achievable bandwidth, targeting a quadratic-phase response can be argued to be nearly optimal. Nevertheless, as shown in this work significant further B_1 reduction can be accomplished with higher-order polynomial corrections to the quadratic phase. A non-linear optimisation scheme is introduced, using a direct search algorithm for approximating the optimal polynomial phase adjustment. For fixed pulse duration and B_1 limit, this approach enables increases in bandwidth and selectivity by factors of two and more.

16:54 ***596***. **Spectrally Selective B1 Insensitive T2 Preparation Sequence for 3T Imaging**

Reza Nezafat[1], [2], John Andrew Derbyshire[1], Ronald Ouwerkerk[2], Matthias Stuber[2], Elliot R. McVeigh[1]
[1]Lab of Cardiac Energetics, Division of Intramural Research, NHLBI, NIH, DHHS, Bethesda, Maryland, USA; [2]Johns Hopkins University, Baltimore, Maryland, USA

T2 magnetization preparation and spectrally selective fat suppression sequences are commonly used to enhance the imaging contrast. Increased B1 inhomogeneity at 3 T necessitates a preparation sequence that is more robust with respect to B1 inhomogeneity. We propose a spectrally selective B1 insensitive T2 Prep sequence for imaging at 3T. Numerical simulations, phantom and *in vivo* images acquired using this technique are presented.

17:06 ***597***. **Validation of B1+ Non-Uniformity Correction in the Chest at 3T Using TIP-COMP**

Kyunghyun Sung[1], Charles H. Cunningham[2], Krishna S. Nayak[1]
[1]University of Southern California, Los Angeles, California, USA; [2]Stanford University, Stanford, California, USA

For *in vivo* magnetic resonance imaging at high field it is essential to consider the homogeneity of the active B1 field (B1+), particularly if surface coils are used for RF transmission. In this work, Transmit In-Plane Compensation (TIP-COMP) RF pulse, which can be dynamically adapted to different ROIs and B1+ variations, *in vivo* validation in the chest, and real-time B1+ measurement and compensation at 3T are presented. In-vivo abdominal and cardiac imaging results are presented. Compared to conventional excitation, TIP-COMP reduced flip-angle variations from 30.1% to 7.9% over the heart at 3T.

17:18 ***598***. **Flexible Feature Specific Inner-Volume Selection with Transmit SENSE: Methods and Applications in Humans, Animals and Biological Samples**

Peter Ullmann[1], Ralf Haueisen[2], Sven Junge[2], Frank Seifert[3], Florian Schubert[3], Markus Wick[2], Wolfgang Ruhm[2], Jürgen Hennig[1]

[1]University Hospital Freiburg, Freiburg, Germany; [2]Bruker BioSpin MRI GmbH, Ettlingen, Germany; [3]Physikalisch-Technische Bundesanstalt, Berlin, Germany

The theoretical concept of Parallel Excitation or Transmit SENSE has been known for a few years now and recently experimental implementations have been achieved that have confirmed the predictions of the Transmit SENSE theory. The present study focuses on the evaluation of Transmit SENSE for biological and medical applications. First *in vivo* images of inner-volume selection using Transmit SENSE have been acquired in humans and animals. Furthermore, experiments of reduced-FOV imaging and double parallel TX/RX imaging have been carried out in a biological sample.

17:30 ***599***. **RF Power Deposition and "g-Factor" in Parallel Transmit**

Yudong Zhu[1]

[1]GE Global Research Center, Niskayuna, New York, USA

The departure from the standard practice of striving for B1 homogeneity provides parallel excitation with a unique leverage to ameliorate some of the issues that are especially prominent at high B0 strength, including excitation profile-uniformity degradation and high specific absorption rate (SAR). To further advance the new excitation technology, we developed a fast method for calculating SAR-minimized RF pulses given a target excitation profile, introduced parallel excitation "g-factor", and established an analysis framework that can be potentially useful guiding transmit array designs and establishing the ultimate intrinsic SAR in parallel transmit.

17:42 ***600***. **Experimental Verification of Over- And Underdetermined Transmit SENSE**

Ulrich Katscher[1], Ingmar Graesslin[1], Henk Dingemans[2], Giel Mens[2]

[1]Philips Research Laboratories, Hamburg, Germany; [2]Philips Medical Systems, Best, Netherlands

A major goal of parallel transmission is to reduce the length of spatially selective RF pulses, which might be applied, e.g., for RF shimming or localized excitation. The reduction of the pulse duration, however, is accompanied with a decreasing accuracy of the excited spatial pattern. In this study, the trade-off between RF pulse duration and excitation accuracy is investigated with an experimental MR system equipped with an 8-channel whole body RF coil capable for parallel transmission.

17:54 ***601***. **SAR-Analysis for Transmit SENSE with a 4-Channel Head Array at 3 T**

Peter Ullmann[1], Gerd Wuebbeler[2], Sven Junge[3], Frank Seifert[2], Wolfgang Ruhm[3], Jürgen Hennig[1]

[1]University Hospital Freiburg, Freiburg, Germany; [2]Physikalisch-Technische Bundesanstalt, Berlin, Germany; [3]Bruker BioSpin MRI GmbH, Ettlingen, Germany

The concept of Transmit SENSE has gained considerable interest in the past few years and is now on the cusp of being evaluated for practical applications. One very important safety issue in this context is the behavior of the specific absorption rate when performing Transmit SENSE experiments. In this study a detailed SAR-analysis of Transmit SENSE with an existing 4-element head array, based on numerical simulations of the electromagnetic fields, has been performed and has revealed a rather complex dependence of RF power and SAR from various parameters such as excitation pattern, k-space trajectory and reduction factor.

18:06 ***602***. **Reduction of B1 Inhomogeneity Using Transmit SENSE Slice-Select Pulses**

Zhenghui Zhang[1], Chun Yu Yip[2], William A. Grissom[2], Fernando E. Boada[1], Douglas C. Noll[3], Victor Andrew Stenger[4]

[1]University of Pittsburgh, Pittsburgh, Pennsylvania, USA; [2]University of Michigan, Ann Arbor, Michigan, USA; [3]University of Michigan, Ann Arbor, Michigan, USA; [4]University of Hawaii, Honolulu, Hawaii, USA

A major limitation of high field MRI is B1 inhomogeneity. Transmit SENSE (XSENSE) methods have been suggested as a means to address this limitation due to the inclusion of the transmit spatial sensitivity in the RF design. We developed a novel small-tip-angle fast-k_z XSENSE 3D tailored RF pulse that is 4.3ms in length with a 5mm slice thickness. XSENSE accleration factors were used to increase the excitation resolution without increasing pulse length. The pulse was demonstrated *in vivo* at 3T using a body coil and 8-channel receiver array. Brain images acquired with the XSENSE pulse showed reduced B1 inhomogeneity.

18:18 ***603***. **Parallel Excitation Pulse Design Using Bayesian Inference Theory**

Florian Wiesinger[1], Mika W. Vogel[1], Yudong Zhu[2], Joseph E. Piel[2], Randy O. Giaquinto[2], Wolfgang Loew[1], Hartmut Koenig[1], Patrick Gross[1]

[1]GE Global Research, Munich, Germany; [2]GE Global Research, Niskayuna, New York, USA

One of the most promising technological developments of recent years was the extension of parallel imaging from the receive case towards signal excitation with transmit arrays. Most importantly parallel transmission holds great promise for achieving improved excitation homogenization, reduced pulse length for extended multi-dimensional selective excitations, reduction of the SAR and mitigation of B0 induced blurring. In this work a novel parallel transmit pulse design framework based on Bayesian inference theory is presented, which enables the incorporation of prior knowledge in a comprehensive fashion. In addition to numerical Biot-Savart simulations, experimental results of parallel transmission at 3T are presented.

Brain Tumors: fMRI and DTI

Room 618 - 620 16:30 - 18:30 Chairs: Alberto Bizzi and Andrei I. Holodny

16:30 ***604***. **The Reliability of Presurgical fMRI Language Lateralization in Patients with Primary Brain Tumors and Prior Surgery**

Kyung Peck[1], Nicole Petrovich[1], Bob Hou[1], Dmitry Bogomolny[1], Vivian Tabar[1], Philip Gutin[1], Andrei Holodny[1]
[1]Memorial Sloan-Kettering Cancer Center, New York, USA

The Intracarotid Amobarbital Procedure (known as the WADA test) is currently the gold standard for establishing hemispheric dominance for language. However, due to its invasive nature, it is hoped that functional MRI, a non-invasive, imaging method, will replace the WADA test. We investigated data obtained from glioma patients with and without prior surgery and characterize the effects of such on the laterality index using fMRI. Despite the presence of tumor and artifact from previous surgery, the effects of tumor and surgical MR artifact were not be sufficient to affect the overall hemispheric measurement of LI and fMRI revealed the expected left hemispheric dominance from both groups.

16:42 ***605***. **MRI-Derived RCBV Can Guide Intraoperative Diagnosis of Brain Tumors**

Kathleen Marie Schmainda[1], John L. Ulmer[1], M Davian[1], B D. Ward[1], Scott D. Rand[1], Hendrikus GJ Krouwer[1]
[1]Medical College of Wisconsin, Milwaukee, Wisconsin, USA

When removing brain tumor tissue, an intraoperative (IOP) diagnosis based on tissue frozen sections are fundamental to the strategy of neurosurgeons. However, in practice, the intraoperative and final diagnoses are discordant. In this study we demonstrate the potential for MRI-derived rCBV information to guide the IOP diagnosis. Specifically, in the 41 brain tumor patients studied there was agreement between IOP and final diagnosis in only 49% of the cases. In contrast by choosing a normalized GE rCBV = 2.0, the probability of correctly predicting high-grade tumor was 90% and incorrectly classifying high-grade as low grade, only 10%.

16:54 ***606***. **Effect of Abnormal Neovasculature and Metabolites on the BOLD fMRI Activation Volume for Brain Tumor Patients**

Bob L. Hou[1], Sunitha B. Thakur[1], Kyung K. Peck[1], Nicole M. Petrovich[1], Wei Huang[1], Philip H. Gutin[1], Andrei I. Holodny[1]
[1]Memorial Sloan-Kettering Cancer Center, New York, USA

Our results for the cases of GBM in PMC suggest that the presence of abnormal neovasculature (indicated by the high rCBV ratios) and the resultant decoupling of neuronal activity and blood flow lead to a muted BOLD response. Lactate peaks in tumor side PMCs suggest hypoxia which implies a) that the vessels may be nearly maximally dilated which further limits the BOLD response b) a corresponding decrease in oxygen consumption for resulting in even small BOLD response. If a tumor was not allocated in the PMC, the BOLD signal (i.e., the ratio) was much closer to the normal value.

17:06 ***607***. **The Use of Diffusion Tensor Metrics and Tractography in Differentiating Between Infiltrating and Well-Circumscribed Tumors of the Posterior Fossa**

Yvonne W. Lui[1], Meng Law[1], James S. Babb[1], Effie George[1], Maxine Ames[1], Glyn Johnson[1]
[1]NYU Medical Center, New York, New York, USA

Are DTI metrics and tractography useful in distinguishing between infiltrating and well-circumscribed posterior fossa tumors? DTI was performed in subjects and controls. Of 36 patients, 16 had infiltrating tumors and 20 had well-circumscribed lesions. Subjects had elevated MD, decreased FA, elevated Elong, and elevated Etrans compared to controls in areas of T2 prolongation. Corticospinal tracts with T2 prolongation demonstrated higher MD, lower FA, and higher Etrans in infiltrating tumors compared with circumscribed tumors. Differences between patient groups were also seen in NAWM. Circumscribed lesions displaced fiber tracts, whereas gliomas disrupted them. DTI can help to characterize posterior fossa tumors.

17:18 ***608***. **DTI and Tractography Metrics Discriminate Between Brain Tumour Types *In Vivo***

Tiernan James Dermot Byrnes[1], Thomas R. Barrick[1], Christophe Ladroue[1], B A. Bell[1], Christopher A. Clark[1]
[1]St. George's University of London, London, UK

Brain tumour diagnosis is necessary to determine patient management; however surgical biopsy has a significant risk of morbidity and mortality. We studied 36 patients with three brain tumour types using diffusion tensor imaging and tractography. Mean FA, MD, tensor shape metrics and streamline density for both the tumour and its surrounding oedema were computed. Using a principal component analysis and linear discriminant analysis we demonstrate the ability of DTI metrics when combined with tractography to discriminate between the 3 most prevalent brain tumour types, namely glioblastoma, meningioma, and metastasis. This technique could potentially reduce the requirement for invasive biopsy.

17:30 ***609***. **An Evaluation of Clinical Usefulness of DTI Derived Image Information in Infra- And Supratentorial Brain Tumors**

Kristina Szabo[1], Claudius Thome[1], Gerrit Schubert[1], Jochen G. Hirsch[2], Christina Rossmanith[1], Michael G. Hennerici[1], Achim Gass[1]

[1]University Hospital Mannheim, Mannheim, Germany; [2]University Hospital Basel, Basel, Switzerland

We used a "subjective" expert educated approach to evaluate the potential value of DTI derived information. We considered a systematic neurosurgical expert review as usually performed on conventional MRI and in addition DTI derived imaging in patients with different etiologies of mass lesions. Both lesion characteristics and anatomical information on the main white mattter pathways were felt to be useful adjunct information not changing the principal decision to perform surgery but frequently altering considerations concerning surgical approach or extent of tumor resection or preoperative surgical risk assessments.

17:42 ***610***. **The Predictive Value of Diffuse Tensor Imaging and Tractography in Determining Neurological Status and Outcome in Patients with Brainstem and Posterior Fossa Tumors**

Yvonne W. Lui[1], Meng Law[1], James S. Babb[1], Keren Tuvia[1], Glyn Johnson[1]

[1]NYU Medical Center, New York, New York, USA

Do DTI findings correlate with clinical findings in patients with posterior fossa tumors? Of 29 patients with posterior fossa tumors who had MRI with DTI, 3 had bilateral weakness, 6 had unilateral weakness, 17 had no weakness, 4 had no exam. Patients with diminished/disrupted left-sided motor tractography were more likely to have right-sided weakness than subjects with normal left-sided tractography. MD and Elong in the pyramidal tracts and FA in the medial lemniscus/central tegmental tracts were predictive of progression. There is an association between diminution/disruption of left-sided motor tractography and right-sided weakness. Several DTI metrics are predictive of progression.

17:54 ***611***. **Combining Functional MRI and Diffusion Tensor Imaging in the Pre-Operative Assessment of the Hand and Foot Fibers Within the Corticospinal Tract**

Meike Vernooij[1], Marion Smits[1], Piotr Wielopolski[1], Henri Vrooman[1], Gavin Houston[2], Arnaud Vincent[1], Gabriel Krestin[1], Aad van der Lugt[1]

[1]Erasmus MC, Rotterdam, ZH, Netherlands; [2]ASL Europe, GE Healthcare, Den Bosch, Brabant, Netherlands

Functional MRI (fMRI) has an important role in identifying the location of the primary motor area pre-operatively. Less attention has been given to the course of the corticospinal tract (CST) which can be depicted with Diffusion tensor imaging (DTI). We found that combining fMRI and DTI in the pre-operative assessment of brain tumor patients can provide essential information not only on the location of functional cortical areas, but also on the course of important white matter tracts, and their relationship to the tumor, specifically of the hand and foot fibers within the CST.

18:06 ***612***. ***In Vivo* DTI-Based Tractography of Intra-Cranial Rat Brain Tumors**

Sungheon Kim[1], Stephen Pickup[1], Oliver Hsu[1], Harish Poptani[1]

[1]University of Pennsylvania, Philadelphia, Pennsylvania, USA

There have been only a limited number of *in vivo* and *ex vivo* reports on tractography of the rat brain without providing a systematic approach to reconstruct individual white matter fiber bundles. The availability of DTI-based tractography of rat brain *in vivo* might be useful for studying changes in the white matter tracts due to a pathology. These studies could then be validated with invasive measurements that are not feasible in the clinic. We developed a DTI data acquisition and tractography method for *in vivo* rat brain and demonstrated its application in monitoring the growth of intra-cranial rat tumor.

18:18 ***613***. **Development and Evolution of Glioma After ENU Exposure: A Model of Malignant Transformation of Low Grade Gliomas**

Binulal Nelson Sathy[1], Yi-Hua Hsu[1], Taichang Jang[2], Lawrence Recht[2], Chen Chang[1]

[1]Functional and Micro-MRI Center, Institute of Biomedical Sciences, Academia Sinica, Taipei, Taiwan; [2]Departments of Neurology and Clinical Neurosciences, Stanford University, Stanford, California, USA

MRI was used to detect the evolution of chemically induced experimental brain tumors in rats after in utero exposure to ethyl-nitrosourea (ENU). Both T2WI and DWI were used to acquire brain images every 15 days from postnatal day 30 to day 210. T2WI images of early and advanced gliomas were correlated with histology. Tumor growth rate and CNR were serially assessed during tumor development.

MRI of Animal Models on Stroke and Traumatic Brain Injury

Room 602 - 604 16:30 - 18:30 Chairs: Rick M. Dijkhuizen and Risto A. Kauppinen

16:30 ***614***. **Correlation Between Brain-Water T2 Relaxometry and 1H MRSI Following Perinatal Transient Cerebral Hypoxia-Ischemia**

Enrico De Vita[1, 2], Alan Bainbridge[1], Osuke Iwata[2], Sachi Iwata[2], Daniel West[2], John S. Thornton[3], Roger J. Ordidge[2], John Wyatt[2], Nicola J. Robertson[2], Ernest B. Cady[1]

[1]University College London Hospitals NHS Foundation Trust, London, UK; [2]University College London, London, UK; [3]National Hospital for Neurology and Neurosurgery, London, UK

Proton MRS localised to deep grey matter provides useful prognostic information in neonatal encephalopathy (NE) before conventional MRI becomes reliable. T2 relaxometry within 3 days of birth may also provide prognostic information in infants with NE. We investigated the change in brain-water T2 after transient hypoxia-ischaemia (HI) and the relationship between T2 and metabolite ratios obtained with 1H MRS imaging in a piglet model of transient HI. As in NE infants, T2 increased following transient HI. Significant correlations were observed between T2 and most 1H metabolite ratios. T2 relaxometry may provide a useful early prognostic alternative to1H MRS.

16:42 ***615***. **Delineating the Boundary Between the Ischemic Penumbra and Regions of Oligaemia Using PH-Weighted MRI (PHWI)**

Phillip Zhe Sun[1, 2], Jinyuan Zhou[1, 2], Weiyun Sun[1], Judy Huang[1], Peter van Zijl[1, 2]

[1]Johns Hopkins University, Baltimore, Maryland, USA; [2]Kennedy Krieger Institute, Baltimore, Maryland, USA

Permanent middle cerebral artery occlusion was studied to test whether pH-weighted imaging (pHWI) can subdivide PWI-DWI mismatch into regions of benign oligaemia and a true penumbra (viable area with impaired metabolism). Regions of pH-deficit were always larger than or equal to regions of cellular depolarization (DWI-deficit) and smaller than or equal to PWI-deficits. Group analysis showed that pHWI-deficits at 3.5 hr predicted well resulting infarct at 24 hr endpoint. Final infarcts were smaller than PWI-deficits (65-90%, depending on occlusion severity) and, in most cases, much larger than initial DWI-deficits. These data support that pHWI can separate penumbra and benign oligaemia.

16:54 ***616***. **Early Disturbance and Subsequent Reorganization of Neuronal Connectivity as Studied with Manganese-Enhanced MRI After Stroke in Rats**

Jet van der Zijden[1], Ona Wu[1, 2], Annette van der Toorn[1], Rick Martin Dijkhuizen[1]

[1]University Medical Center Utrecht, Utrecht, Netherlands; [2]Massachussetts General Hospital/Harvard Medical School, Charlestown, Massachusetts, USA

Loss of function and subsequent spontaneous recovery after stroke have been associated with structural alterations of neuronal circuitry in the brain. In this study, restoration of function is correlated with temporal changes in neuronal connections after stroke in rats as studies with manganese-enhanced MRI. Loss of manganese enhancement, suggestive of disturbed connectivity in the sensorimotor network at 2 weeks after stroke was paralleled by severe loss of function. Subsequent recovery of function may be associated with restored ipsilateral connectivity and increased transhemispheric connectivity as indicated by increased manganese distribution at chronic stages after stroke.

17:06 ***617***. **Serial Triple Quantum Sodium MRI During Non-Human Primate Focal Brain Ischemia**

George C. LaVerde[1], Charles A. Jungreis[2], E. Nemoto[1], Costin Tanase[1], Fernando E. Boada[1]

[1]University of Pittsburgh, Pittsburgh, Pennsylvania, USA; [2]Temple University, Philadelphia, Pennsylvania, USA

Triple quantum sodium MRI techniques have been demonstrated *in vivo* in a non-human primate model of focal brain ischemia. TQ sodium MRI hyperintensity was demonstrated in the ischemic hemisphere relative to the contralateral hemisphere as early as 34 minutes after the onset of ischemia. The TQ sodium MRI hyperintensity corresponded to the anatomical location of the ischemic cortex as indicated by the registration of the TQ image data with anatomical proton MR image data. We believe that the TQ sodium MRI hyperintensity in the ischemic hemisphere is a result of the increase in the intracellular sodium concentration that occurs in ischemia.

17:18 ***618***. **Endogenous and Exogenous Inflammatory Cell Responses Following Transient Ischaemia in Mice**

Adam Denes[1, 2], Rishma Vidyasagar[2], Jianghua Feng[2], Johanna Närväinen[2], Barry McColl[2], Risto A. Kauppinen[2], Stuart Allan[2]

[1]MTA KOKI, Budapest, Hungary; [2]University of Manchester, Manchester, UK

Macrophages are detected *in vivo* by MRI using AMI-227. Macrophage invasion and microglial activation are known to happen in acute stroke, yet contribution of these cells to infaction process is not clear. Here, mice were subjected to 30 minutes middle cerebral artery occlusion, injected daily with AMI-227/Magnevist and monitored daily for infarct evolution. Histology showed that resident microglia become rapidly activated, proliferated and phagocytosed neutrophils, while only a small infiltrating exogenous macrophage population was observed by 72 hours. Thus, blood-borne macrophages are not profoundly involved in the development of ischaemic infarction in this experimental model.

17:30 ***619***. **Visualisation of Phagocytic Cells in a Mouse Brain After Traumatic Brain Injury with Micron-Sized Iron-Oxide Particles: A Preliminary Report**

Lesley M. Foley[1], T Kevin Hitchens[1], Patrick M. Kochanek[2], John A. Melick[2], Chien Ho[1]
[1]Carnegie Mellon University, Pittsburgh, Pennsylvania, USA; [2]University of Pittsburgh School of Medicine, Pittsburgh, Pennsylvania, USA

Micron-sized iron-oxide particles (MPIO) were used to label mononuclear phagocytes *in vivo*. MRI was able to detect the presence of these labeled macrophages and their response after controlled cortical impact injury. MPIO's were seen in the injured brain as hypointense spots, but were not present in an intact brain which questions their ability to cross the blood-brain-barrier. With this technique, MRI has great potential to understand the cellular mechanisms behind secondary injury after TBI and the role CBF plays.

17:42 ***620***. **Prediction of Ischemic Tissue Fate----Comparison Among 30-Min, 60-Min and Permanent Occlusion Groups**

Qiang Shen[1], Hongxia Ren[1], Jürgen Bardutzky[2], Marc Fisher[3], Timothy Q. Duong[1]
[1]Emory Unviersity, Atlanta, Georgia, USA; [2]University of Heidelberg, Heidelberg, Germany; [3]The University of Massachusetts Medical School, Worcester, Massachusetts, USA

An algorithm was extended to statistically predict ischemic tissue fate in stroke rats subjected to 30-min and 60-min MCA occlusion. Perfusion and diffusion imaging was performed and an automated clustering (ISODATA) technique was used to classify tissue types. Probability profiles were derived and probability maps of risk of subsequent infarction were computed for a separate experimental group as ischemia progressed. The accuracy of these predictions was compared with that of the permanent stroke data reported previously. These predictions give probability maps of infarction based on valuable data obtained soon after stroke and thus have significant clinical value.

17:54 ***621***. **Early Detection of Brain Function Recovery Following Stroke. A Longitudinal fMRI Study of the Rat**

Pedro Ramos-Cabrer[1], Ralph Weber[1], Carlos Justicia[1], Dirk Wiedermann[1], Mathias Hoehn[1]
[1]Max-Planck-Institute for Neurological Research, Cologne, Germany

We present a method to predict functional outcome of rats after stroke. Combined BOLD-fMRI and electrophysiological longitudinal studies were performed on rats during 7 weeks after MCAO, acquiring EPI images during electrical stimulation of the forepaws. Following stroke we observed: 1) Animals with unaltered BOLD and SSEPs. 2) Animals with transient (2-3 weeks) loss of BOLD signal and distortion of SSEPs in the affected hemisphere. 3) Animals with permanent loss of BOLD and SSEPs in the affected hemisphere. The observation of abnormal electrical activity and lack of BOLD, provides early indication of late functional recovery following stroke.

18:06 ***622***. **Quantitative MRI Correlates with Long-Term Functional Outcome After Traumatic Brain Injury in Rat**

Riikka Johanna Immonen[1], Irina Kharatishvili[1], Heidi Gröhn[2], Asla Pitkänen[1], Olli Gröhn[1]
[1]A.I.Virtanen Institute for Molecular Sciences, University of Kuopio, Kuopio, Finland; [2]Kuopio University Hospital, Kuopio, Finland

Progressive tissue damage after head trauma was studied using volumetric and quantitative MRI. MRI results obtained in the acute and subacute phase 3 hours - 23 days after induction of TBI correlated with the functional outcome as assessed using Morris water maze test 7 months later. This provides evidence that MRI may facilitate the prediction of the functional outcome after TBI.

18:18 ***623***. **MRI Detection of White Matter Remodeling After Neural Progenitor Cell Treatment of Stroke**

Quan Jiang[1], Zhenggang Zhang[1], Guangliang Ding[1], Brian Silver[1], He Meng[1], Siamak Pourabdollah Nejad D.[1], Lei Wang[1], Lian Li[1], Hassan Bagher-Ebadian[1], Jiani Hu[2], Ali S. Arbab[1], James R. Ewing[1], Michael Chopp[1]
[1]Henry Ford Health System, Detroit, Michigan, USA; [2]Wayne State University, Detroit, Michigan, USA

We investigated the effects of neural progenitor cell (NPC) treatment of stroke in rat. We found that MRI can detect white matter reorganization after NPC treatment of stroke. White matter reorganization after NPC treatment of stroke is dominantly located in the extended area of corpus callosum in striatum. FA differentiated white matter reorganized brain tissue from other ischemic damaged tissues. T1, T2, and T1sat provide complementary information to characterize status of ischemic tissue with and without brain remodeling. Of these MRI methods, DTI related parameters appear to be the most useful to identify the location of white matter reorganization.

Fat-Water Imaging

Room 613 - 614 16:30 - 18:30 Chairs: Arthur F. Gmitro and Scott B. Reeder

16:30 ***624***. **IDEAL Water-Fat Separation with Simultaneous T2* Estimation**

Huanzhou Yu[1], Charles A. McKenzie[2], Ann Shimakawa[1], Norbert J. Pelc[3], Jean H. Brittain[4], Scott B. Reeder[5]

[1]GE Healthcare, Menlo Park, California, USA; [2]Beth Israel-Deaconess Medical Center and Harvard Medical School, Boston, Massachusetts, USA; [3]Stanford University, Stanford, California, USA; [4]GE Healthcare, Madison, Wisconsin, USA; [5]University of Wisconsin, Madison, Wisconsin, USA

For three-point water-fat decomposition methods, T2* decay has been assumed to be negligible. However, T2* may be shortened in situations such as in patients with hemochromatosis. It can be difficult to separate water and fat in the presence of shortened T2* or to estimate T2* in the presence of multiple chemical species due to their interference with one another. We propose an algorithm to achieve water-fat separation and T2* estimation simultaneously. Promising results were obtained from phantom studies. This T2*-IDEAL technique has potential applications in quantitative assessment of patients with conditions such as hemochromatosis and fatty infiltration of the liver.

16:42 ***625***. **Fast Water and Fat Imaging Using a Radial GRASE Technique with the IDEAL Algorithm**

Zhiqiang LI[1], Scott W. Squire[1], Arthur F. Gmitro[1], Maria I. Altbach[1]

[1]University of Arizona, Tucson, Arizona, USA

The performance of water and fat separation with conventional 3-point Dixon methods is limited by the phase unwrapping algorithm and tissue connectivity. Recently an IDEAL algorithm was proposed to generate robust water and fat separation. In this work we propose an asymmetrical radial GRASE technique combined with the IDEAL algorithm to achieve better time efficiency, robust water and fat separation, and high noise performance. With this technique, one complete data set can be acquired in a breath hold which makes it attractive for abdominal or cardiac imaging.

16:54 ***626***. **On the Application of the DIXON Method in Balanced SSFP Imaging**

Hyeonjin Kim[1], Alexander B. Pinus[1], Philip S. Murphy[2], R Todd Constable[1]

[1]Yale University School of Medicine, New Haven, Connecticut, USA; [2]Global Clinical Sciences, Pfizer, Sandwich, UK

The principle of the DIXON method for water-fat decomposition is preferentially used in balanced SSFP sequences (bSSFPs) by exploiting the spin-echo like signal behavior. Nonetheless, due to temporal shift of the echo which is commonly neglected, the integrity of the resultant water-only and fat-only images can be degraded. The consequence of neglecting such echo-shift in bSSFP on water-fat decomposition was examined by using the iterative least-squares estimation method in combination with trueFISP. The results demonstrate that the performance of any DIXON+bSSFP combinations can differ from pixel to pixel depending on an ROI due to the temporally variable echo formation.

17:06 ***627***. **Gradient Reversal Technique Revisited for Simultaneous Water and Fat Imaging at High Field**

Haiying Tang[1], Ed X. Wu[2], Richard Kennan[1], Haiying Liu[1]

[1]Merck Research Laboratories, Rahway, New Jersey, USA; [2]The University of Hong Kong, Hong Kong SAR, People's Republic of China

Qualitative and quantitative MR imaging of water and fat is of great importance in obesity and diabetic research, osteoarthritis cartilage visualization, body composition measurement, and drug evaluation studies. In this study, we revisited the gradient reversal technique, along with a chemical-shift-specific slice-selection (C4S) method. Simultaneous water and fat imaging approach was implemented at 11.7T. Using this technique, high quality water and fat images at the identical slice locations with in-plane chemical-shift correction were acquired in a single acquisition without increase in acquisition time. Applications in *in vivo* quantitative tissue lipid imaging were demonstrated.

17:18 ***628***. **A Single Scan Two-Point Dixon Technique Using Bunched Phase Encoding**

Hisamoto Moriguchi[1], Mark A. Griswold[1], Jeffrey L. Sunshine[1], Jeffrey L. Duerk[1]

[1]University Hospitals of Cleveland / Case Western Reserve University, Cleveland, Ohio, USA

The two-point Dixon (2PD) technique is capable of achieving unambiguous water-fat separation even in the presence of magnetic field inhomogeneities. However, the need to acquire two sets of images prolongs scan time, giving rise to the primary drawback of the 2PD technique. Bunched Phase Encoding (BPE) has recently been proposed as a new fast data acquisition method in MRI. In BPE, the total number of TR cycles can be reduced. In this study, it is shown that the total acquisition time of the 2PD technique can be reduced to that of a single acquisition by capitalizing on the BPE technique.

17:30 ***629***. **Water-Fat Separation at 3T with IDEAL and 3DPR**

Ethan K. Brodsky[1], Scott B. Reeder[1], Huanzhou Yu[2], Walter F. Block[1]

[1]University of Wisconsin, Madison, Wisconsin, USA; [2]GE Healthcare, Menlo Park, California, USA

SPGR-VIPR is a 3DPR acquisition with high isotropic resolution over a large FOV. While multiple echo VIPR provides inherent partial fat suppression, this suppression and other frequency-selective methods fail in areas of high B_0 inhomogeneity. We extend VIPR to acquire eight half-echos per TR, generating complex images at varying echo times. Separate fat and water images are calculated using the IDEAL algorithm which compensates for B_0 inhomogeneities. Whereas scan time increases are often required to use IDEAL with Cartesian acquisitions, this technique requires no increase in scan time and will actually increase data acquisition efficiency.

17:42 ***630***. **Regional Iterative Phasor Extraction (RIPE): Effective Phase Correction for Water-Fat Imaging**

Qing-San Xiang[1]

[1]University of British Columbia, Vancouver, BC, Canada

Phase error is a key issue for water-fat imaging, which can be corrected with Regional Iterative Phasor Extraction (RIPE). Two error phasor candidates are calculated. An initial error phasor map is estimated either by simple averaging or other algorithms along with a confidence map. The two error phasor candidates are compared with the initial error phasor after smoothing, and the one closer is selected as a new error phasor estimate. This "smooth and compare" iteration is repeated till a stabilized error phasor is found, and subsequently removed from the acquired complex images leading to unambiguous water and fat solutions.

17:54 ***631***. **Comparison of In and Out of Phase Imaging and IDEAL Fat-Water Separation for Liver Imaging at 3.0 T**

Charles Alexander McKenzie[1, 2], *Daniel Sacchetti*[3], *Scott Fredericks*[3], *Michael Schuster*[3], *Martin Smith*[3], *Huanzhou Yu*[4], *Anja Brau*[4], *Ann Shimakawa*[4], *Jean H. Brittain*[4], *Scott B. Reeder*[5], *Ivan Pedrosa,* [23], *Neil M. Rofsky,* [23]

[1]Beth Israel Deaconess Medical Center, Boston, Massachusetts, USA; [2]Radiology, Harvard Medical School, Boston, Massachusetts, USA; [3]Radiology, Beth Israel Deaconess Medical Center, Boston, Massachusetts, USA; [4]Global Applied Science Laboratory, GE Healthcare, Menlo Park, California, USA; [5]University of Wisconsin Medical School, Madison, Wisconsin, USA

This work evaluates the feasibility of using T1-weighted Iterative Decomposition of water and fat with Echo Asymmetry and Least-squares estimation (IDEAL) imaging to replace In and Out of Phase (IOP) imaging at 3.0T. Because IDEAL produces separate fat-only and water-only images it has potential advantages over IOP for the detection of hepatic fat and iron. IDEAL and IOP images were acquired in 41 patients referred for liver imaging. Three radiologists compared the resulting images in a random and blinded fashion. T1 weighted IDEAL imaging was found to provide increased confidence in the diagnosis of hepatic fat and iron compared to IOP.

18:06 ***632***. **Multi-Echo IDEAL Water-Fat Separation for Rapid Imaging of Cartilage**

Garry E. Gold[1], *Scott B. Reeder*[2], *Huanzhou Yu*[3], *Jean H. Brittain*[4], *Brian A. Hargreaves*[1]

[1]Stanford University, Stanford, California, USA; [2]University of Wisconsin, Madison, Wisconsin, USA; [3]GE Healthcare, Menlo Park, California, USA; [4]GE Healthcare, Madison, Wisconsin, USA

Three-dimensional imaging of articular cartilage with fat suppression is useful in both the clinical and research settings. Wide use of these technqiues, however, is limited by long scan times. We have developed a fat-water separation method based on IDEAL (Iterative Decomposition of water and fat with Echo Asymmetry and Least-squares estimation) that acquires multiple echoes per TR. We compared multi-echo IDEAL gradient echo imaging (IDEAL-GRE) to fat-suppressed spoiled gradient echo imaging (FS-SPGR) in the knees of healthy volunteers at 1.5T. Multi-echo IDEAL-GRE provides robust water-fat separation, shorter imaging times, and higher cartilage SNR efficiency than FS-SPGR.

18:18 ***633***. **T2-TIDE-BSSFP Imaging with Simple and Robust Fat Suppression**

Yin-Cheng Kasuga Huang[1], *Teng-Yi Huang*[2], *Hsiao-Wen Chung*[1, 3]

[1]National Taiwan University, Taipei City, Taiwan; [2]National Taiwan University of Science And Technology, Taipei City, Taiwan; [3]Tri-Service General Hospital and National Defense Medical Center, Taipei City, Taiwan

A robust fat-suppression approach is proposed as an adjunct to the T_2-TIDE-bSSFP (balanced SSFP imaging with transition into driven equilibrium with T_2-weighting) imaging technique. The scheme employs a simple addition of half Fourier option, which places the fat frequency within the null-signal bands which span for a wide range of off-resonance frequencies. During signal evolution, a substantial signal void in the central *k*-space thus leads to effective fat suppression. Imaging experiments in the abdomen agree well with theoretical calculations. The proposed method has potential for routine clinical applications in abdominal and cardiac imaging.

STUDY GROUP
MR Engineering

Room 4C-3,4 19:30 - 21:30

STUDY GROUP
MR in Drug Research

Room 611-612 19:30 - 21:30

19:30 **Business Meeting**
19:45 **Scientific Meeting: "Current Status of MRI in Drug Discovery"**

- 19:45 **Potential Uses of Magnetic Resonance Imaging in Development of Therapies for Atheroma**
  Zahi A. Fayad, The Eva and Morris Feld Cardiovascular MRI Research Laboratory, Mount Sinai School of Medicine, New York, New York, USA
- 20:10 **Applications of MRI in the Development of Drugs for Musculoskeletal Disorders**
  John Waterton, Discovery Enabling Capabilities & Sciences, AstraZeneca, Alderly Edge, United Kingdom
- 20:35 **MRI in the Development of Drugs for Neurological Disorders: An Industry View**
  Paul Matthews, GlaxoSmithKline, London, England, UK
- 21:00 **Biomarker Consortium Update**
  Jeffrey L. Evelhoch, Medical Sciences – Imaging, Amgen, Inc., Thousand Oaks, California, USA
- 21:15 **Panel Discussion**

STUDY GROUP
MR Flow & Motion Quantitation

Room 615-617 19:30 - 21:30

19:30 **Business Meeting**
19:45 **Scientific Meeting**

- 19:45 **Tagging Analysis**
  Nael Osman, Johns Hopkins University, Baltimore, Maryland, USA
- 20:05 **Real-Time Color Flow**
  Krishna Nayak, University of Southern California, Los Angeles, California, USA
- 20:25 **7D Flow**
  Oliver Wieben, University of Wisconsin, Madison, Wisconsin, USA
- 21:45 **Clinical Application of Flow & Motion Imaging**
  Susan Yeon, Beth Israel Deaconess Medical Center, Boston, Massachusetts, USA
- 21:00 **Panel Discussion**

STUDY GROUP
Molecular & Cellular Imaging

Room 618-620 19:30 - 21:30

19:30 **Business Meeting**
19:45 **Scientific Meeting: "Reporter Genes for MRI"**

- 19:45 **The Transgene Reporter Approach for the Induction of Selective MRI Contrast**
  Eric Ahrens, Carnegie Mellon University, Pittsburgh, Pennsylvania, USA
- 20:15 **Ferritin as a Tissue Specific MRI Reporter of Inducible Gene Expression in Transgenic Mice**
  Michal Neeman, Weizmann Institute of Science, Rehovot, Israel
- 20:45 **Cellular MRI Contrast Via Co-Expression of Transferrin Receptor and Ferritin**
  Abby Deans, New York University School of Medicine, New York, New York, USA
- 21:00 **Frequency Selective MR Reporter Gene Based on Chemical Exchange**
  Assaf Gilad, Johns Hopkins University School of Medicine, Baltimore, Maryland, USA
- 21:15 **Spatio-Temporal Expression Control of a Heat Shock Promoter-Driven Transgene Delivered in the Kidney by Modified Mesenchymal Stem Cells: A Feasibility Study**
  Olivier Hauger, INSERM, Bordeaux, France

STUDY GROUP

White Matter Diseases

Room 602-604 19:30 - 21:30

STUDY GROUP
Interventional MRI

Room 613-614 19:30 - 21:30

MORNING CATEGORICAL COURSE
Technical Advances in Body MR

Room 618-620 7:00 – 8:00 Chairs: Neil M. Rofsky, Daniel K. Sodickson, and Bachir Taouli

Educational Objectives:
Upon completion of this session, participants should be able to:

- Evaluate important developments in MRI technology, including high field imaging and parallel imaging;
- Identify the technical challenges associated with effective application of this technology for body imaging; and
- Describe the potential applications of new technologies in body imaging, including areas such as diffusion and perfusion MRI, and MR spectroscopy.

Applications: Functional Imaging

07:00 **DWI in Body Imaging**
Elizabeth Hecht

07:30 **PWI in Body Imaging**
Anwar R. Padhani

MORNING CATEGORICAL COURSE
Cardiovascular Imaging

Room 6D 7:00 – 8:00 Chairs: Qun Chen and James F.M. Meaney

Educational Objectives:
Upon completion of this session, participants should be able to:

- Implement a robust protocol for clinical evaluation of arteries with both non-contrast and contrast-enhanced techniques;
- Identify the strengths and weaknesses of 3T MRI vs. 1.5T MRI for cardiovascular assessment;
- Recognize the value of parallel imaging for cardiovascular assessment at higher magnetic field (>1.5T);
- Select a comprehensive time-efficient protocol incorporating anatomical and functional cardiac evaluation;
- Explain the value of MRI for the assessment of non-coronary artery disease; and
- Recognize the strengths and also the limitations of current techniques.

MRI of Myocardial Function, Perfusion and Viability

07:00 **MRI of Global and Regional Myocardial Function**
Leon Axel

07:20 **MRI of Myocardial Perfusion**
Steve D. Wolff

07:40 **MRI of Myocardial Viability**
Raymond J. Kim

MORNING CATEGORICAL COURSE
Clinical DTI/PWI/fMRI

Room 4C-3,4 7:00 – 8:00 Chairs: Alberto Bizzi and Soonmee Cha

Educational Objectives:
Upon completion of this session, participants should be able to:

- Describe the main applications and contributions of fMRI, DTI, and tractography and bolus tracking and arterial labeling perfusion MR imaging in clinical neuroscience;

- Describe the technical requirements necessary to implement robust, accurate, and repeatable clinical advanced MR studies in patients with neurological diseases;
- List the potential contribution of PWI, DTI and fMRI to formulate diagnosis, prognosis, and evaluate different therapeutic strategies in the neurological diseases focus of this course;
- Discuss the basic MR principles involved in the quantification of angiogenesis and permeability using perfusion MR imaging;
- Implement new quantitative MR methods that may quantify cumulative brain damage that better correlate with the disability score;
- Recognize challenges, limitations and pitfalls of performing advanced MR studies to answer clinical questions in neurological patients; and
- Implement Quality Assurance (QA) procedures necessary to run a reliable and successful advanced MRI clinic.

Brain Function and Cortical Reorganization: Functional MRI

07:00 **Functional Connectivity**
Mark J. Lowe

07:30 **Combining fMRI and DTI Applications**
Andrei I. Holodny

MORNING CATEGORICAL COURSE
MR Hardware/Engineering

Room 611-612 7:00 – 8:00 Chairs: Steven M. Conolly and Steven M. Wright

Educational Objectives:
Upon completion of this session, participants should be able to:

- List and compare implementations of static field magnet designs for clinical MRI;

- Recognize that there are fundamental limits on our ability to shim out steep field variations (such as those in the sinuses);
- Describe advances in shim system design;
- Explain the differences between arrays designed to optimize SNR vs. those designed for partial parallel imaging;
- Compare and contrast arrays designed for transmit and receive applications;
- Describe algorithms for designing RF pulses for parallel imaging;
- Compare and contrast ESR and NMR; and
- Describe several applications of hyper-polarized 13C and explain methodological differences between conventional MRI and hyperpolarized MRI.

Transmit SENSE for RF Homogeneity, SAR Reduction, and Fast RF Pulses

07:00 **Transmit Arrays Design**
Christopher J. Hardy

07:20 **RF Pulse Design for Transmit SENSE**
Douglas C. Noll

MORNING CATEGORICAL COURSE
Human MRI and MRS at High Static Magnetic Fields: The Promise, the Challenges, the Solutions

Room 615-617 7:00 – 8:00 Chairs: Joseph A. Helpern and Dikoma C. Shungu

Educational Objectives:
Upon completion of this session, participants should be able to:

- Describe the general behavior of B_0 and B_1 fields in the human body when the Larmor frequency is of the order of or greater than 100 MHz;

- List the problems faced in trying to obtain a homogeneous B_0 field and a B_1 field;
- Recognize the challenges of developing RF coils for high field applications;

- Recognize the challenges of whole-body imaging at high fields and list potential solutions;
- List recent methodological advances for detecting neurotransmitters by MRS at high fields;
- Recognize the challenges of implementing heteronuclear spin-spin decoupling at high static fields;
- Describe the benefits of high field for BOLD contrast;
- Describe the interaction between high magnetic fields and biological systems; and
- List organizations responsible for regulating exposure to magnetic fields.

07:00 **Advances in Spectral Editing: MRS of Neurotransmitters**
Peter S. Allen

07:20 **Broadband Decoupling at High Field: Challenges and Solutions**
Robin A. de Graaf

MORNING CATEGORICAL COURSE
New Horizons in Musculoskeletal MRI

Room 613-614 7:00 – 8:00 Chairs: Joshua M. Farber and Timothy J. Mosher

Educational Objectives:
Upon completion of this session, participants should be able to:

- Recognize patterns of abnormal hip biomechanics and associated MRI findings in femoral acetabular impingement syndrome;
- Apply knowledge of normal articular cartilage maturation and joint development in interpretation of pediatric musculoskeletal MRI;
- Recognize the role of normal and abnormal biomechanics and the associated MRI findings in normal joint physiology and development of overuse injuries;
- Identify emerging translational research applications in the field of musculoskeletal MRI:
- Describe new MRI techniques for tracking mesenchymal stem cells;
- Recognize new applications of molecular imaging in the study of musculoskeletal diseases.

MRI and Exercise: Translational Research: From Biomechanics to the Athlete

The final five minutes of each talk will be reserved for questions.

07:00 **Functional Cartilage MRI**
Peter A. Hardy

07:30 **Overuse Injuries in Elite Athletes**
William B. Morrison

MORNING CATEGORICAL COURSE
Quantitative Neuro MRI

Room 602-604 7:00 – 8:00 Chairs: Fernando Calamante and Annemie Van der Linden

Educational Objectives:
Upon completion of this session, participants should be able to:

- Discuss the latest advances in the field of arterial spin labeling, their current limitations, and identify their potential role in basic and clinical science;
- Demonstrate the role of MR methods to assess oxygen consumption non-invasively, and illustrate potential applications;
- Describe the various approaches to measure the arterial input function using dynamic-susceptibility contrast MRI and describe their limitations and implications to measure absolute cerebral blood flow, explain the latest advances of dynamic contrast-enhanced MRI to measure non-perfusion parameters, and assure formation of proper echoes;

- Recognize the limitations of the diffusion tensor model and identify more advanced methodologies to characterize areas with multiple fiber directions more accurately, as well as to describe the latest advances on fiber-tracking, including the concept of probabilistic tractography;
- Apply statistical approaches to perform voxel-based analysis for group comparison, and
- Describe image analysis techniques to characterize brain deformation.

Diffusion MRI

07:00 **Recent Advances to Resolve Multiple Fibers Using Diffusion MRI**
Jacques-Donald Tournier

07:30 **Recent Advances in Fiber Tracking**
Geoff J. M. Parker

MORNING CATEGORICAL COURSE
Unsolved Problems and Unmet Needs in Magnetic Resonance

Room 6E 7:00 – 8:00 Chairs: Thomas M. Grist and Martin R. Prince

Educational Objectives:
Upon completion of this session, participants should be able to:

- Identify and assess a sampling of key unsolved problems and unmet needs in the field of magnetic resonance;
- Establish criteria for successful solutions to such problems;
- Consider any large-scale coordination across our field or with other fields that may be called for to address some classes of research or clinical needs;
- Identify and share additional unsolved problems or unmet needs in your areas of interest.

Will new contrast agents revolutionize MRI?

07:00 **Exclusively MRI – Based Molecular Imaging: Can Magnetic Labeling of Physiologically Important Compounds via DNP or Parahydrogen-Induced Hyperpolarization Provide a Potential Supplement or Replacement of PET?**
Joachim Bargon

07:15 **Direct Detection of Neuromodulation**
Rachel Katz-Brull

07:30 **Development of Static Tracers for Myocardial Perfusion Imaging by MRI**
Timothy F. Christian

07:45 **Open Discussion**

2006 LAUTERBUR LECTURE

Room 6A-C 8:05 – 8:45 Chair: J. Paul Finn, President

8:05 **Functional Brain Imaging: An Evolving Perspective**
Marcus E. Raichle[1]
[1]Washington University School of Medicine, St. Louis, Missouri, USA

8:45 **YIA and Poster Award Presentations**
J. Paul Finn, President

PLENARY LECTURES: The Making of the Brain: Development Plasticity

Room 6A-C 8:50 - 10:00 Chairs: Petra Hüppi and Weili Lin

8:50 ***634***. **Developmental and Genetic Factors Underlying the Complexity and Variability of Cortical Convolutions**
David van Essen[1]
[1]Washington University School of Medicine, St. Louis, Missouri, USA

This presentation describes a surface-based approach to analyzing human cortical convolutions. It involves quantitative analyses of folding patterns in several different groups. Comparison between the left and right hemispheres of normal subjects revealed eight localized asymmetries. Comparison between men and women revealed no significant difference in average shape, but greater shape diversity in male right hemispheres. Analysis of specific disease conditions revealed 35 folding abnormalities in Williams Syndrome and several folding abnormalities in autism. These results provide useful insights regarding variability of cortical folding patterns in health and disease and suggest hypotheses regarding developmental mechanisms underlying normal and abnormal folding.

9:15 ***635***. **Prematurity and Developmental Plasticity in the Brain**
David G. Gadian[1]
[1]Institute of Child Health, London, England, UK

Developmental plasticity may be defined as the ability of cells or tissue to develop in response to their environment. The transition from fetal to postnatal life constitutes a major change in environment, and if this occurs prematurely, then in response it can be expected that there may be a different developmental trajectory from that associated with term birth. It is becoming more widely appreciated that such differences may have a strong influence on long-term health. This presentation focuses on the role that MRI can play in understanding how prematurity impacts on brain structure and function.

9:40 ***636***. **Digital Dynamic Brain Atlases**
Arthur W. Toga[1]
[1]University of California, Los Angeles, California, USA

Dynamic brain maps offer key biological markers for understanding development and a wide range of nervous system processes and disorders including development, aging, neurodegenerative diseases and mental illness. When fully implemented at a clinical level, such tools can serve an important diagnostic role by quantifying the range and confidence limits of normality from brain structure and function. When fully implemented at a clinical level, such tools can serve an important diagnostic role by quantifying the range and confidence limits of normality from brain structure and function. When applied to individual patients and patient populations, they can also quantify disease burden and provide objective, quantifiable tools for use in experimental therapies and therapeutic trials.

Diffusion: A Window in Fiber Architecture

Room 6E 10:30 - 12:30 Chairs: Yoram Cohen and Felix W. Wehrli

10:30 ***637***. **AxCaliber – a Method to Measure the Axon Diameter Distribution and Density in Neuronal Tissues**

Yaniv Assaf[1, 2], Tamar Blumenfeld[1], Gome Levin[1], Yossi Yovel[1], Peter J. Basser[3]

[1]Tel Aviv University, Tel Aviv, Israel; [2]Tel Aviv Sourasky Medical Center, Tel Aviv, Israel; [3]National Institutes of Health, Bethesda, Maryland, USA

The morphology of white matter is determined histologically using myeloarchitectural staining. Parameters that help distinguish different white matter fascicles are the axon diameter distribution and the axonal density. Here we use the composite hindered and restricted model of diffusion (CHARMED) framework to measure these two features in porcine spinal cord. Combined with cluster analysis, CHARMED-MRI distinguished six areas in the spinal cord resembling regions in the corresponding histological images. This MRI methodology may advance morphological studies to assess changes in axon diameter distribution or axon content associated with development, disease, degeneration, regeneration, or trauma in the CNS or PNS.

10:42 ***638***. **Structural Information of Different Nerve Types from High B-Value Q-Space Diffusion MRS**

Amnon Bar-Shir[1], Yoram Cohen[1]

[1]Tel-Aviv University, Tel-Aviv, Israel

High b-value q-space diffusion MR were claimed to provide structural information under certain experimental conditions. Here, we use this methodology to examine the mean displacement in optic and sciatic nerves as a function of the diffusion time. The mean displacements of the sciatic nerves (both components) were found to be significantly larger than in the optic nerves. The slow diffusing component of the optic nerves was found to be the most restricted one. The extracted sizes were found to be comparable with those observed by microscope images suggesting that high-b value q-space diffusion MR can be regarded as "virtual histology".

10:54 ***639***. **Comparison of MR Diffusion Anisotropy with Axon Density**

Fatemeh Noushin Golabchi[1], Dana H. Brooks[1], William Scott Hoge[2], Hatsuho Mamata[2], Stephan E. Maier[2]

[1]Northeastern University, Boston, Massachusetts, USA; [2]Brigham and Women's Hospital, Harvard Medical School, Boston, Massachusetts, USA

In nerve fibers, water diffusion is strongly influenced by the presence of axon membranes and myelin sheaths. With diffusion tensor magnetic resonance imaging, rotationally invariant measures of diffusion restriction such as fractional anisotropy (FA) can be obtained. Here we compare FA measured in axial spinal cord specimen sections with the density of axons determined from corresponding histological images. Results show there is a high positive linear correlation between the FA maps, and their corresponding computed axon density maps.

11:06 ***640***. **Q-Space Propagator Maps of Mouse Spinal Cord Provide Insight Into Regional Axonal Architecture**

Henry H. Ong[1], Alex C. Wright[1], Suzanne L. Wehrli[2], Andre Souza[1], Eric D. Schwartz[1], Punam K. Saha[1], Felix W. Wehrli[1]

[1]Department of Radiology, University of Pennsylvania, Philadelphia, Pennsylvania, USA; [2]Children's Hospital of Philadelphia, Philadelphia, Pennsylvania, USA

Q-space imaging offers potential for indirect tissue architecture quantification by exploiting regularity in porous systems. Using a custom-built 50T/m z-gradient/RF coil set, we have created high-resolution propagator maps at 0.65 micron resolution of cervical and thoracic spinal cord regions for three healthy adult mice. The calculated propagator FWHM, which is proportional to axon diameter, was assigned to each pixel location. Focusing on three WM tracts that showed characteristically different mean axon diameters (cuneatus, gracilis, and rubrospinal tract), the propagator maps showed significant differences in FWHM between each region that correlated with mean diameters as computed from histologic images.

11:18 ***641***. **How Accurately Can the Diffusion Profiles Predict Multiple Fiber Orientations? - A Study on General Fiber Crossings in Diffusion MRI**

Wang Zhan[1], Yihong Yang[1]

[1]National Institute on Drug Abuse, NIH, Baltimore, Maryland, USA

High angular resolution diffusion (HARD) imaging and q-space imaging techniques have been developed to identify intravoxel multi-fiber components, based on the measured profiles of apparent diffusion coefficient (ADC) and orientation distribution function (ODF), respectively. The exact relationship between local maxima of the diffusion profiles and the actual orientations of fibers is crucial for accurate determination of the fiber orientation, but has not yet been systematically investigated. The present study aims to examine the accuracy of these profile-based methods by directly comparing the angular deviations between the estimated local maxima of the profiles and the real fiber orientations under various conditions.

11:30 ***642***. **Accuracy Assessment of Q-Ball Imaging with Phantom Models**

Kuan-Hung Cho[1], Chun-Hung Yeh[2], Yi-Ping Chao[1], Jyh-Horng Chen[1], Ching-Po Lin[2]

[1]Dept. of Electrical Engineering, National Taiwan University, Taipei, Taiwan; [2]National Yang-Ming University, Taipei, Taiwan

Q-ball imaging can be used to estimate intravoxel complex fiber coherence by measuring ODF. However, criteria of QBI parameter selection have not been studied. In this study, we evaluated QBI accuracy in mapping complex fiber coherence by phantom models with different b-value, SNR and diffusion time. The results showed that QBI can map coherent and crossing fiber accurately with angular error of 4.67 ±0.36 and 1.07 ±5.13 , respectively. This study implied that QBI with 92 encoding points, along with adequate diffusion time and SNR, could map complex fiber coherence accurately in clinical system.

11:42 ***643***. **Optimal Encoding Points for Diffusion Spectrum Imaging: Using Bi-Gaussian Extrapolation**

Chun-Hung Yeh[1], Kuan-Hung Cho[2], Yi-Chia Li[1], Hsuan-Cheng Lin[1], Ching-Po Lin[3]

[1]Institute of Radiological Sciences, National Yang-Ming University, Taipei, Taiwan; [2]Interdisciplinary MRI/MRS Lab, Department of Electrical Engineering, National Taiwan University, Taipei, Taiwan; [3]Institute of Neuroscience, National Yang-Ming University, Taipei, Taiwan

Diffusion spectrum imaging (DSI) is capable of defining complex orientational coherence within MR voxel. To establish the adequately sampling points over q-space, however, usually results in a long scan time. Additionally, diffusion q-value is generally limited by the available gradient strength in clinical machine and therefore produces the truncation error in 3D probability density function (PDF) reconstruction. To acquire the complex fiber orientations while avoiding these drawbacks, this study reduced DSI encoding points as well as maximum q-value by applying a bi-Gaussian curve fitting over the q-space. Both Monte-Carlo simulation and MR experiments showed that this method can decrease DSI acquisition time while preserving the PDF patterns and primary orientations.

11:54 ***644***. **Optimal Imaging Parameters for Minimum Angular Discrimination in Diffusion Spectrum Imaging**

Yi-Chia Li[1], Kuan-Hung Cho[2], Kun-Hsien Chou[3], Ching-Po Lin[4]

[1]Institute of Radiological Sciences, National Yang Ming University, Taipei, Taiwan; [2]Institute of Electrical Engineering, National Taiwan University, Taipei, Taiwan; [3]Institute of Biomedical Engineering, National Yang Ming University, Taipei, Taiwan; [4]Institute of Neuroscience, National Yang Ming University, Taipei, Taiwan

In this study, Monte-Carlo simulation was used to optimize the DSI imaging parameters for intersecting crossing fiber mapping. We synthesized diffusion MRI measurements of two crossing fibers. The results showed that DSI could differentiate smaller crossing fibers (≤ 30 °) under clinical gradient limitations with higher b-value encoding. The criteria for DSI parameter selection were also optimized.

12:06 ***645***. **Improved Characterisation of Crossing Fibres: Spherical Deconvolution Combined with Tikhonov Regularization**

J-Donald Tournier[1], Fernando Calamante[1], Alan Connelly[1]

[1]Brain Research Institute, Melbourne, Australia

The diffusion tensor is commonly used to estimate fibre orientations from diffusion-weighted data, but cannot describe crossing fibre regions. We have recently proposed the spherical deconvolution technique for estimating the fibre orientation distribution (FOD) that effectively removes this limitation. Here we present a method for significantly improving the angular resolution of the reconstructed FOD, based on the unphysical nature of negative lobes in the FOD. This information was incorporated as a constraint in a Tikhonov regularisation formulation of spherical deconvolution. The improved angular resolution allows fibres crossing at smaller angles to be resolved, which is essential for reliable fibre-tracking.

12:18 ***646***. **Quantitative Comparison Between Hybrid Diffusion Imaging and Diffusion Spectrum Imaging**

Yu-Chien Wu[1], Andrew L. Alexander[1]

[1]University of Wisconsin-Madison, Madison, Wisconsin, USA

Many approaches have been proposed to study the complex diffusion behavior in brain tissues with crossing white matter (WM) fibers. Hybrid diffusion imaging (HYDI) combines the advantages of diffusion spectrum imaging (DSI) and high angular resolution diffusion imaging for complex diffusion characterization. In this study, Monte Carlo noise simulations were used to compare the measurements accuracy of DSI and HYDI for estimating the properties of the diffusion displacement spectra in complex WM. HYDI and DSI performed similarly for estimating scalar measures of the diffusion spectrum, whereas the outer HYDI shell was generally superior for resolving and characterizing crossing WM orientations.

CLINICAL CATEGORICAL COURSE
Stroke Imaging

Room 6C 10:30 - 12:30 Chairs: Weili Lin and A. Gregory Sorensen

Educational Objectives
Upon completion of this session, participants should be able to:

- Describe the underlying biological factors associated with neuroprotection and its potential implications for MRI;

- Recognize the status of currently ongoing clinical trials where MR plays a critical role;
- Determine how MR can potentially be further utilized for imaging acute stroke patients;
- Evaluate whether or not a higher field strength is beneficial for the management of acute stroke patients; and
- Identify the needed new MR technologies to further improve the management of acute stroke patients.

10:30 **Neuroprotection: Biological Background and MR Implications**
Michael Chopp

10:55 **The Current Status of Ongoing Clinical Trials: Beyond 3 Hours**
Howard A. Rowley

11:20 **The Perspective of Pathophysiology – Guided Stroke Therapy**
Arno Villringer

11:45 **MR Wish List for Stroke Neurologists: What are we Missing?**
Jeffrey Saver

12:10 **Questions and Answers**

CLINICAL MRI COURSE
Cardiac Problem Solving: Imaging the Coronary Arteries in 2006 - CT vs. MRCA

Room 6D 10:30 – 12:30 Chairs: Victor A. Ferrari and Matthias Stuber

Educational Objectives
Upon completion of this session, participants should be able to:

- Identify the clinical indications for coronary artery imaging with MR and CT;

- Describe the advantages and disadvantages of current MR and CT techniques for use in coronary angiography;
- Discuss the risks and benefits regarding safety considerations for CTA vs. MRCA; and
- Explain the uses and limitations of CT and MRI for plaque characterization and vessel wall imaging.

10:30 **Can CT be Reliably Used for Plaque Characterization and Vessel Wall Imaging?**
Zahi A. Fayad

10:50 **Advanced MR Coronary Imaging at 3T: Promise or Perils?**
Debiao Li

11:10 **CTA vs. MRCA: Technical and Clinical Perspective**
Konstantin Nikolaou

11:30 **Head-to-Head Comparison of CT and MRCA**
Bernhard Gerber

11:50 **Assessing the Myocardium: Ischemia, Prognosis and Viability**
Daniel Berman

Plaque Imaging: Techniques and Clinical Relevance

Room 4C - 3,4 10:30 - 12:30 Chairs: Philippe Douek and Chun Yuan

10:30 *647.* **High Resolution *In Vivo* Magnetic Resonance Imaging and Image Quantitation of the Progression of the Murine Aortic Atherosclerotic Plaque**

Haiying Tang[1], Haiying Liu[1], Sandra E. Rex_Rabe[1], Ray Rosa[1], Corey Miller[1], Donald S. Williams[1], Larry Peterson[1], Richard Hargreaves[1]
[1]Merck Research Laboratories, Rahway, New Jersey, USA

MRI is becoming an important imaging modality for detecting and characterizing atherosclerosis because of its non-invasive and high-resolution capability. Atherosclerotic plaque detection requires imaging protocols with high spatial resolution and high contrast-to-noise ratio. Our purpose was to establish a high resolution *in vivo* MRI technique for the evaluation and quantitation of the progression of atherosclerosis in a transgenic mouse model based on Ldlr null. High resolution 3D MR imaging and quantitation of aortic atherosclerotic plaque were demonstrated.

10:42 ***648***. **Contrast-Enhanced MRI at 3T of Experimental Atherosclerotic Lesions Using QIR-FSE and DTPA(Gd)**

John A. Ronald[1, 2], Josh Zhang[1], Amanda Marie Hamilton[2], Kem A. Rogers[2], Robert A. Hegele[1], Brian K. Rutt[1, 2]
[1]Robarts Research Institute, London, Ontario, Canada; [2]University of Western Ontario, London, Ontario, Canada

Contrast-enhanced MRI of atherosclerotic lesions using DTPA(Gd) is useful for improved detection of diseased vessel wall in humans. However, similar results in a non-balloon injured animal model with a pulse sequence optimized for accurate quantitative analysis of enhancement has not been achieved. Here we report on work focused on using a quadruple inversion recovery fast-spin-echo sequence (QIR-FSE) at 3T for creating a robust system capable of assessing vessel wall enhancement and agent wash-in and wash-out kinetics in a cholesterol-fed, non-balloon injured rabbit model following conventional DTPA(Gd) and novel Gd-based agent administration.

10:54 ***649***. **Qualitative and Quantitative Estimation of High Risk Atherosclerotic Plaques in WHHL Animals with Gadofluorine M – Enhanced MRI at 3T**

Harald Ittrich[1], Andrew N. Priest[1], Tim Nielsen[2], Tobias Schaeffter[2], Christoph Weber[1], Bernd Misselwitz[3], Hanns-Joachim Weinmann[3], Gerhard Adam[1]
[1]University Hospital Hamburg Eppendorf, Hamburg, Germany; [2]Philips Research Laboratories Hamburg, Hamburg, Germany; [3]Schering AG, Berlin, Germany

Atherosclerotic plaque imaging in MRI at 3T with low dose Gadofluorine M (Schering AG, previous studies:100µmol/kg) using 3D InversionRecovery-TurboFLASH sequences and quantitative assessment of the contrast agent uptake using T1 relaxation measurements was performed in hyperlipidemic rabbits (WHHL) compared to normal controls (NZW). Gadofluorine-enhanced MRI improves detection of early atherosclerotic plaques down to 25µmol/kg injection dose ($p<0.05$). Look-Locker sequence allows a quantitative determination of R1 of the aortic wall, which showed a linear correlation to injection dose ($R^2=0.9924$). This techniques hold promise for detection of initial stages, longitudinal evaluation of plaque progression and monitoring of pharmaceutical therapy in clinical practise.

11:06 ***650***. **MR Histology of Advanced Atherosclerotic Lesions of ApoE-Knockout Mice**

Anna V. Naumova[1], Vasily Yarnykh[1], Marina Ferguson[1], Michael Rosenfeld[1], Chun Yuan[1]
[1]University of Washington, Seattle, Washington, USA

Transgenic mice are widely used as animal models for the study of atherosclerosis. The major challenges for histological MR imaging of atherosclerotic lesions in mice are the very high-resolution requirement, the need to image long vessel segments, and prohibitively long scan time. This study has shown an ability of non-invasively determination of advanced atherosclerotic lesions composition and precise quantification of the major plaque components in the different vascular beds. A time-efficient microimaging protocol for MR histological imaging on mice was developed. Advanced atherosclerotic lesions in ApoE-knockout mice are characterized by high calcification and presence of the large fibrofatty nodules.

11:18 ***651***. **Diffusion Weighted 3D Dark Blood SSFP Imaging of the Thoracic Aorta: Initial Clinical Evaluation**

Anish Kirpalani[1], Ioannis Koktzoglou[1], Karin Dill[1], Timothy Carroll[1], Debiao Li[1], James Carr[1]
[1]Northwestern University, Chicago, Illinois, USA

Diffusion weighted 3D SSFP dark blood imaging can be a powerful tool in both vessel wall imaging and in 3D MR angiography.

11:30 ***652***. **Three-Dimensional Black-Blood Vessel Wall Imaging with Diffusion-Prepared Segmented Steady-State Free Precession**

Ioannis Koktzoglou[1], Debiao Li[1]
[1]Northwestern University, Chicago, Illinois, USA

A 3D diffusion-prepared segmented steady-state free precession (SSFP) MR imaging sequence (3D DIFF-SSFP) was developed and applied for thick-slab black-blood vessel wall imaging of the thoracic aorta and the carotid arteries. The developed segmented 3D DIFF-SSFP sequence was found to robustly suppress blood signal and yield higher wall-lumen CNR efficiency than 2D double inversion-recovery fast spin-echo imaging ($p < 0.05$). Segmented 3D DIFF-SSFP appears to be a promising sequence for efficient black-blood imaging of large vascular territories.

11:42 ***653***. **3D Dark Blood TSE for Carotid Vessel Wall Imaging**

Yiu-Cho Chung[1, 2], Marion Menzel[3], Subha V. Raman[4], Orlando P. Simonetti[4]
[1]Siemens Medical Solutions USA, Inc, Chicago, Illinois, USA; [2]Northwestern Universtiy, Chicago, Illinois, USA; [3]Siemens AG, Med, Erlangen, Germany; [4]Ohio State University, Columbus, Ohio, USA

In the carotids, plaque identification is typically performed using 2D TSE since scan time for 3D TSE is long. For instance, high resolution T1 weighted 3D TSE for a 24mm slab requires 6 minutes. 3D dark blood TrueFISP is encouraging but optimal blood suppression limits slab thickness. We propose here a new approach to 3D, T2 weighted high-resolution dark blood TSE technique capable of imaging a 180mm slab along the length of the carotids in about 6 minutes. We shall show here the technique's potential in vessel wall imaging, dark blood MRA, localization, and plaque characterization at the carotids.

11:54 ***654***. ***In Vivo* High-Resolution Volumetric Imaging of Carotid Complicated Plaque: 3-Dimensional High-Resolution Magnetic Resonance Direct Thrombus Imaging (HiresMRDTI)**

Richard Bitar[1, 2], Alan R. Moody, [12], General Leung[2], Sean Symons[1, 2], Susan Crisp[2], Corwyn Rowsell[1], Jagdish Butany[1, 3], Alexander Kiss[4], D James Sahlas[2], David Gladstone[2], Robert Maggisano[2]

[1]University of Toronto, Toronto, Ontario, Canada; [2]Sunnybrook and Women's College HSC, Toronto, Ontario, Canada; [3]University Health Network, Toronto, Ontario, Canada; [4]Institutes for Clinical Evaluative Sciences, Toronto, Ontario, Canada

hiresMRDTI allows very good delineation of the exact location of intraplaque hemorrhage/ thrombosis in the plaque, resulting in good-to-very good agreement between imaging and histology. Being a 3D technique, hiresMRDTI allows multiplanar reformations, as well as providing a large number of images for analysis.

12:06 ***655***. **Incidence of AHA Type 4/5 Atherosclerotic Plaque and Outcome in Patients with Suspected Acute TIA/Stroke: A Prospective, Observational MRI Study Using Novel 3D Turbo Spin Echo, Continuously Variable Flip Angle, Double Inversion Recovery Technique**

Jaywant Philip Parmar[1], Erol Baskurt[1], John P. Mugler[2]

[1]University of Virginia Health System, Charlottesville, Virginia, USA; [2]University of Virginia, Charlottesville, Virginia, USA

Introduction:The AHA type 4 atherosclerotic plaque is considered to be presymptomatic but vulnerable. We sought to identify the incidence of this plaque type in clinically suspected stroke patients being imaged by hospital MRI.Methods:Prospective, observational design study using 3D fast spin echo, double inversion recovery, variable flip angle MR imaging, clinical imaging and clinical chart review.Results: Infrequent association of type 4 plaques to cerebral ischemia and a frequent association with stenosis were observed. Fair interobserver agreement found.Conclusion: AHA model of disease is supported by MRI and chart review.

12:18 ***656***. **Vulnerable Lesion Correlates to Accelerated Recurrence of Cerebral Infarction: Carotid Magnetic Resonance Imaging Study**

Kai Lin[1], Zhao-Qi Zhang[2], Biao Lu[2]

[1]Beijing Institute of Heart Lung and Blood vessel diseases, Beijing, People's Republic of China; [2]Beijing Anzhen Hospital, Beijing, People's Republic of China

Carotid atherosclerosis may correlate ischemic cerebral disease. In this experiment,we enrolled 50patients haing two times of cerebral infarction and exmined their carotid bifurcation. We classified the lesion in carotid wall according to its signal and shape using criteria of AHA as an template. It demonstrated that patients with a MRI defined vulnerable plaque prone to had a shorter interval between the two cerebral infarctions.

Neuronal Activation: Novel (Unconventional) Detection Methods

Room 611 - 612 10:30 - 12:30 Chairs: Peter A. Bandettini and Karla L. Miller

10:30 ***657***. **Is the Neuromagnetic Field in the Human Brain Detectable by MRI in Practice?**

Hendrik Mandelkow[1], Pascal Halder[2], Nicola de Zanche[1], Daniel Brandeis[2], Peter Boesiger[1]

[1]University and ETH Zurich, Zurich, ZH, Switzerland; [2]University of Zurich, Zurich, ZH, Switzerland

We explore the possibility for direct detection of neuronal currents by fast dynamic MRI in conjunction with fully simultaneous recordings of the EEG. Specifically, our experiment is designed to localize the current source of alpha waves by analyzing the spectral coherence of EEG channel and MRI voxel time series recorded simultaneously in human subjects. A phantom containing a dipolar current source was constructed to determine the sensitivity of the measurement and to validate the analytical approach. The analysis of our *in vivo* and in-vitro data indicates that a moderate improvement in SNR may render alpha waves detectable by this kind of correlation analysis, but the specificity of any such approach may be limited due to physiological confounds like cardiac pulsation.

10:42 ***658***. **Detection of MR Signal Modulation Due to Magnetic Fields from Axonal Currents in the Human Visual System Using LED Stimulation**

Li Sze Chow[1], Greg Cook[1], Elspeth H. Whitby[1], Martyn Paley[1]

[1]University of Sheffield, Sheffield, South Yorkshire, UK

The aim of this study is to directly detect axonal currents in the human optic nerve, visual cortex and corpus callosum with LED stimulation using a GE-EPI sequence at 1.5T and 3.0T. It assumes modulation of the MR signal by the magnetic fields of weak axonal currents, which can be detected as image perturbations with the appropriate processing. MR signal fluctuations measured *in vivo* are consistent with a Lorentzian model for a symmetrical axonal field distribution within a voxel, from which axonal field strengths have been estimated.

10:54 ***659***. **Finding NAMO (Neuroelectric Activity Under Magnetic-Field Oscillations) with MRI *In Vivo***

Trong-Kha Truong[1], Allen W. Song[1]
[1]Duke University, Durham, North Carolina, USA

The direct, real-time, and non-invasive imaging of neural activity *in vivo* using MRI could have a significant impact in neurosciences. Previous attempts at detecting the magnetic field changes induced by neuronal currents *in vivo* have been challenging, because of the extremely small signal changes as well as confounding factors such as the BOLD effect. Here, we describe a novel technique that uses oscillating magnetic field gradients to detect the Lorentz effect induced by neuroelectric activity, and demonstrate its effectiveness in imaging sensory nerve activation *in vivo* in the human median nerve during electrical stimulation of the wrist.

11:06 ***660***. **MR-Encephalography: 'Imaging' Without Gradients Using Multichannel Receiver Coils: Applications to Physiological Measurements**

Jürgen Klaus Hennig[1], Kai Zhong[1], Oliver Speck[1]
[1]University Hospital, Freiburg, Germany

First results of MR-Encephalography based on data acquisition with multiple coils are presented. Spatial information is provided by the sensitive volume of the coils (OVOC= one-voxel-one-coil imaging) without any gradients. A conventional image acquired with identical parameters is used as a template for constrained reconstruction using the continuously sampled coil signals as weighting factors. The ultimate imaging speed of this approach is limited only by the receiver bandwidth. Applications on resting state brain using a standard 8-channel head coil illustrate the very high temporal resolution and signal-to-noise to observe the spatiotemporal pattern of breathing and ECG-related signal variations.

11:18 ***661***. **Rapid Time-Series Mapping of the Longitudinal Relaxation Time of the Brain During Neuronal Activity**

Jung-Jiin Hsu[1], Gary H. Glover[1]
[1]Lucas Center for Imaging, Stanford University School of Medicine, Stanford, California, USA

There have been reports on the change of the longitudinal relaxation time T1 related to the neuronal activity but these results are inferred from T1-weighted scans rather than direct T1 measurement. Recently, a rapid method of T1 mapping has been developed which is capable of obtaining T1 values at a time resolution feasible for brain fMRI. With this novel method, we have detected neuronal activation by direct mapping of the longitudinal relaxation time.

11:30 ***662***. **Towards T2 Weighted fMRI of the Whole Brain at Ultra-High Fields**

Johannes Ritter[1], Pierre-Francois van de Moortele[1], U. Goerke[1], Kamil Ugurbil[1]
[1]University of Minnesota, Minneapolis, Minnesota, USA

Spin Echo (SE) BOLD based Functional Magnetic Resonance Imaging (fMRI) is less sensitive to the extra vascular response from larger vessels and, at ultra-high magnetic fields, is less sensitive to blood contributions to functional mapping signals. Hence, SE fMRI is less contaminated by contributions which may originate far from the actual site of neuronal activation than Gradient-recalled Echo (GE) fMRI. A major disadvantage of SE fMRI signals is that the mapping signals are inherently weak. However, they increase supralinearly with magnetic field and attain usable magnitudes at ~7 Tesla or above. Thus, SE fMRI at ultra-high magnetic fields provide a high contrast-to-noise ratio (CNR) and high spatial accuracy method for functional mapping (see for instance [1], [2]). Specific absorption rate (SAR) considerations, however, have been a limiting factor in pursuing multi slice SE Echo-Planar Imaging (EPI) at ultra high field strengths. In this study, a slab wise T2 magnetization preparation followed by a multislice series of GE EPI readouts is presented. This method reduces SAR significantly. Robust BOLD responses are observed.

11:42 ***663***. **Increased T2-Sensitivity in BOLD fMRI Using Stimulated Echoes: A Monte-Carlo Simulation**

Ute Goerke[1], Kamil Ugurbil[1]
[1]CMRR/University of Minnesota, Minneapolis, Minnesota, USA

Monte-Carlo simulations were applied to calculate the relative BOLD signal changes in a stimulated echo sequence. The model was based on the diffusion of water molecules in the presence of local magnetic field variations in the vicinity of capillaries and venules. Neighboring vessels were included to account for long diffusion times. The predicted increase of the relative signal change with longer echo and mixing time is consistent with experimental results. It is concluded that more efficient dynamic averaging is the main mechanism for the enhanced T_2-sensitivity of the STE.

11:54 ***664***. **Characterization of SSFP fMRI Signal and Noise: A Comparison with GRE at Multiple Field Strengths**

Karla L. Miller[1], Peter Jezzard[1], Stephen M. Smith[1], Graham C. Wiggins[2], Christopher J. Wiggins[2]
[1]Oxford University, Oxford, UK; [2]Massachusetts General Hospital, Charlestown, Massachusetts, USA

Balanced steady-state free precession (SSFP) has recently been demonstrated to detect brain activity, with the potential to decouple functional contrast from sources of image artifacts. However, the dynamics of this functional contrast have yet to be explored, as have the noise properties of SSFP fMRI. This work experimentally characterizes SSFP fMRI signal via comparison with GRE over two TR and three field strengths. Our results indicate that SSFP has both higher contrast and higher noise than matched GRE sequences, indicating a fundamentally different source of contrast than conventional BOLD

12:06 ***665***. **High Field Balanced-SSFP fMRI: Examining a Diffusion Contrast Mechanism Using Varied Flip-Angles**

Chris Van Bowen[1], Jeff Mason[2], Ravi S. Menon[2], Joseph Sandor Gati[2]
[1]National Research Council, Halifax, Nova Scotia, Canada; [2]Robarts Research Institute, London, Ontario, Canada

Although T2* weighted, gradient echo based fMRI has become a standard acquisition tool for neuroscientific investigation, many questions still exist as to the spatial specificity of the functional patterns observed relative to neuronal activity. Two main problems persist with T2* weighted fMRI: (i) an oversensitivity to oxygenation changes in large draining veins located distal to the site of activation; and (ii) an inability to perform robust T2* fMRI analysis in regions of strong field inhomogeneity. This paper proposes the use of b-SSFP at high field (4T) using on-resonance acquisitions. We show b-SSFP fMRI acquisitions have comparable sensitivity to the BOLD mechanism as traditional T2*-EPI acquisitions. Additionally, we demonstrate increased sensitivity with flip angle in tissue, consistent with a diffusion contrast mechanism, and negative signal changes within obvious draining veins, aiding large vessel suppression.

12:18 ***666***. **Feasibility of Velocity Selective Arterial Spin Labeling in Functional MRI**

Wen-Chau Wu[1], Julie Bykowski[1], Eric C. Wong[1]
[1]University of California, San Diego, La Jolla, California, USA

The feasibility of velocity selective arterial spin labeling (VS-ASL) has been validated in baseline CBF measurement but not in fMRI study yet. This abstract reports the discrepancy and compatibility between VS and conventional ASL fMRI in human visual cortex. Experiment results show that two techniques detect compatible spatial distribution of neuronal activation. VS-ASL further provides information of vasculature that contributes to neuronal activity from different flow direction. Meanwhile, caution has to be taken when averaging signal time curves over multiple directions of VS encoding. Flow variation during activation has negligible effect on localization (voxel size = 3.4x3.4x7 mm^3).

Cerebral Perfusion: Methodology

Room 615 - 617 10:30 - 12:30 Chairs: Matthias Guenther and Leif Østergaard

10:30 ***667***. **Rapid Imaging of Multiple Vascular Territories Using Cycled Arterial Spin Labeling with Independent Component Analysis**

Matthias Guenther[1], [2]
[1]Universitätsklinikum, Mannheim, Germany; [2]Advanced MRI Technologies, Sebastopol, California, USA

A method for regional ASL imaging is presented in which selected vascular territories were visualized at 1.5T in 2 minutes using a new labeling cycled scheme (cycled ASL) which varies the selective labeling of different inflow arteries before image acquisition with a single shot 3D GRASE read-out. When subject motion caused improper slab positioning of arterial labeling, the separation of vascular territories could be markedly improved using independent component analysis.

10:42 ***668***. **Vessel Encoded Arterial Spin Labeling Using Pseudo-Continuous Tagging**

Eric C. Wong[1]
[1]University of California, San Diego, La Jolla, California, USA

We introduce here an arterial spin labeling method in which groups of vessels can be simultaneously encoded to provide maps of vascular territories with high SNR efficiency. Based on pseudo-continuous tagging, this method uses additional transverse gradient pulses and an RF phase cycling scheme to provide optimal Hadamard encoding of the vessels. In principle, any number of vessels can be encoded and reconstructed to provide vascular territory maps in the same scan time and with the same SNR as a single conventional ASL scan. Examples in the human brain are shown.

10:54 ***669***. **Dual Vessel Arterial Spin Labeling Scheme for Regional Perfusion Imaging**

Ivan Zimine[1], Esben Thade Petersen[1], Xavier Golay, [1,2]
[1]National Neuroscience Institute, Singapore, Singapore; [2]ASTAR, Singapore, Singapore

Recently introduced Regional Perfusions Imaging (RPI) techniques have great clinical potential for evaluation of patients with cerebro-vascular disorders. In the original approach, three ASL acquisitions with selective labeling of left and right ICAs and posterior arteries was necessary to obtain regional flow information. Here, we propose a new labeling scheme allowing obtaining identical RPI maps using only two ASL acquisitions. The new method is based on simultaneous labeling of lateral and posterior circulation, and a simple combination of the data allows extraction of individual flow territories. Demonstration of the approach on 7 individuals provided matching flow territories and perfusion values.

11:06 ***670***. ***In Vivo* Measurement of the Longitudinal Relaxation Time of Arterial Blood (T_{1a}) in the Mouse Using a Pulsed Arterial Spin Labeling Approach**

David L. Thomas[1], Mark F. Lythgoe[1], David G. Gadian[1], Roger J. Ordidge[1]
[1]University College London, London, UK

A novel method for the measurement of the longitudinal relaxation time of arterial blood (T_{1a}) is presented. The standard FAIR acquisition scheme was modified by incorporating a global saturation pulse before the recovery period. By doing this, the FAIR tissue signal has a monoexponential dependence on recovery time, with T_{1a} as the time constant. Therefore, T_{1a} can be calculated from FAIR measurements performed over a range of recovery times. This eliminates many of the difficulties associated with the measurement of T_{1a}. Experiments performed in the mouse at 2.35T produced a mean value of 1.51s for T_{1a}, consistent with published values.

11:18 ***671***. **Effect of Tag Dispersion on Fast ASL Methods**

Gregory R. Lee[1], Luis Hernandez-Garcia[1], Douglas Noll[1]
[1]University of Michigan, Ann Arbor, Michigan, USA

A model for the turbo-CASL perfusion signal in the presence of dispersion of the tag bolus is presented. Simulations demonstrate an attenuation of the turbo CASL signal peak that becomes more pronounced with increasing tag dispersion. This signal attenuation is less severe for traditional CASL acquisitions with long TR values. Fits to two-coil turbo-CASL data from a human subject were improved significantly when tag dispersion was allowed. The average FWHM of the fitted Rayleigh PDF dispersion kernel was 0.89 seconds. Flow estimates for gray matter voxels increased by 15.6% on average when dispersion was taken into account.

11:30 ***672***. **Imaging Microvascular Flow Distributions Using Residue Function Shape Characteristics**

Kim Mouridsen[1], Stefan Kiebel[2], Niels Hjort[1], Leif Østergaard[1]
[1]Aarhus University Hospital, Aarhus, Denmark; [2]Institute of Neurology, London, UK

DSC-MRI is widely used for determination of perfusion parameters such as CBF, CBV and MTT which are used for assessing tissue viability in acute stroke. However, important information about the capillary flow patterns contained in the residue function is not quantified. We use a previously published vascular model to estimate perfusion parameters as well as residue function shape characteristics. Simulations demonstrate that the algorithm can identify a large class of residue functions from exponential to box-car. In a case of acute MCA occlusion we show that different microvascular flow profiles may underlie perfusion lesions observed on CBF and MTT maps.

11:42 ***673***. **PERMEATE: High Temporal Resolution Multi-Echo/Multi-Slice Dynamic Susceptibility Contrast Perfusion Imaging Using GRAPPA EPI**

Rexford Newbould[1], Stefan Skare[1], David B. Clayton[1], Marcus T. Alley[1], Gregory Albers[1], Maarten Lansberg[1], Roland Bammer[1]
[1]Stanford University, Stanford, California, USA

A high temporal resolution dynamic susceptibility contrast (DSC) perfusion sequence is presented, which collects multi-slice and multi-echo volumes with a high temporal resolution, about 1s in clinical practice. A multi-shot interleaved EPI sequence is used, allowing self-calibrating parallel imaging within a volume. Data acquisition is ordered to allow each shot to be reconstructed into a full dataset, or combined for increased SNR. Several echoes are collected in each volume, allowing Δ R2* calculation unbiased by T1 effects or the need for baseline acquisitions. CBF and CBV maps have been calculated from both stroke patients and volunteers.

11:54 ***674***. **Robust Semi-Automated Arterial Input Function Identification Using Self Organizing Maps**

Jinesh J. Jain[1], Wilburn E. Reddick[1]
[1]St. Jude Children's Research Hospital, Memphis, Tennessee, USA

Absolute quantification of cerebral blood flow and volume using dynamic-susceptibility contrast MRI relies on deconvolution of the arterial input function - commonly estimated from signal changes in a major artery. We present an automated technique to determine the local AIF by the selection of best-candidate arterial pixels using a Kohonen Self-Organizing Map. The technique, validated across five patients over three exams each, identified not just the blood vessels but also yielded unique classes for artery and vein. The technique leads to accurate calculation of the perfusion maps and may aid in normalizing results over various exams and patients.

12:06 ***675***. **Absolute Quantification of Cerebral Blood Flow in Normal Volunteers: Dynamic Susceptibility Contrast MRI Compared with Xe-133-SPECT**

Linda Knutsson[1], Siv Börjesson[2], Elna-Marie Larsson[3], Jarl Risberg[2], Lars Gustafsson[4], Ulla Passant[4], Freddy Ståhlberg[1, 3], Ronnie Wirestam[1]
[1]Department of Medical Radiation Physics, Lund, Sweden; [2]Department of Psychology, Lund, Sweden; [3]Department of Diagnostic Radiology, Lund, Sweden; [4]Department of Psychogeriatrics, Lund, Sweden

Reproducible absolute quantification of cerebral blood flow (CBF) is desirable, for example, in therapy monitoring, in the assessment of ischemic threshold levels in acute ischemic stroke and when a global reduction of CBF can be expected as, for example, in patients with dementia. In this study, a comparison between CBF estimates from dynamic susceptibility contrast (DSC) MRI and Xe-133-SPECT was performed in 20 healthy volunteers. The correlation between CBF estimates obtained by DSC-MRI and Xe-133-SPECT was quite reasonable (r=0.76) and if proportionality between the DSC-MRI-based and SPECT-based CBF results is assumed, i.e. CBF(MRI)=k·CBF(SPECT), the present data indicates that k=2.16.

12:18 ***676***. **Basal CBF and CBF fMRI of Rhesus Monkeys on a Siemens Trio 3T Using a Three-Coil Continuous Arterial-Spin-Labeling Technique**

Xiaodong Zhang[1], Edward Auerbach[2], Tsukasa Nagaoka[1], Robbie Champion[1], Lei Zhou[3], Xiaoping Hu[3], Christopher Edmonds[1], Xiangyang Ma[1], Timothy Q. Duong[1]

[1]Emory University, Atlanta, Georgia, USA; [2]University of Minnesota Medical School, Minneapolis, Minnesota, USA; [3]Emory University/Georgia Tech, Atlanta, Georgia, USA

This study reported the implementation of a three-coil continuous arterial-spin-labeling technique on a Siemens 3T Trio for non-human primate research. High quality basal cerebral-blood-flow (CBF) images were obtained in 4 mins with 1.5 mm isotropic resolution. CBF fMRI were obtained with a 7-second resolution. Combined CBF and BOLD fMRI associated with hypercapnic challenge showed robust and heterogeneous signal changes across the entire brain as expected. fMRI were studied under graded isoflurane concentrations. This technology is expected to provide a non-invasive means to study physiology, function, neurovascular coupling, and metabolism (i.e., CMRO2) for non-human primate research.

Cell Tracking and Targeted Contrast Agents in Cancer

Room 618 - 620 10:30 - 12:30 Chairs: Alexei A. Bogdanov and Joseph A. Frank

10:30 ***677***. ***In Vivo* Tracking of Growth and Dormancy of Solitary Cells in a Mouse Model of Breast Cancer Metastasis to Brain Using MRI**

Chris Heyn[1, 2], John A. Ronald[1, 3], Soha S. Ramadan[1, 3], Jonatan A. Snir[1], Andrea M. Barry[1], Lisa T. MacKenzie[3, 4], David J. Mikulis[2, 5], Diane Palmieri[6], Julie L. Bronder[6], Patricia S. Steeg[6], Toshiyuki Yoneda[7], Ian C. MacDonald[3], Ann F. Chambers[3, 4], Brian K. Rutt[1, 3], Paula J. Foster[1, 3]

[1]Robarts Research Institute, London, ON, Canada; [2]University of Toronto, Toronto, ON, Canada; [3]University of Western Ontario, London, ON, Canada; [4]London Regional Cancer Program, London, ON, Canada; [5]Toronto Western Hospital of The University Health Network, Toronto, ON, Canada; [6]Center for Cancer Research, NCI, Bethesda, Maryland, USA; [7]The University of Texas Health Science Center at San Antonio, San Antonio, Texas, USA

For breast cancer patients, metastasis to the brain is a complication associated with a poor prognosis. In this abstract, the fate of iron-oxide-labeled breast cancer cells is tracked non-invasively with MRI in a mouse model of brain metastasis. Using this technique, the distribution of single cancer cells was visualized in the entire mouse brain and the proportion of cells that were cleared, remained dormant, or grew into tumours was quantified. This work reports a substantial new capability of MRI for imaging metastasis development in a relevant model, with clear application for studying the biology and drug response of brain metastases.

10:42 ***678***. **Expression of Transferrin Receptor and Ferritin Following Ferumoxides - Protamine Sulfate Labeling of Cells: Implications for Cellular Magnetic Resonance Imaging**

Edyta Pawelczyk[1], Ali S. Arbab[2], Sunil Pandit[3], Elbert Hu[1], Joseph A. Frank[1]

[1]National Institutes of Health, Bethesda, Maryland, USA; [2]Henry Ford Health System, Detroit, Michigan, USA; [3]Clinical Center, Bethesda, Maryland, USA

Ferumoxides-protamine sulfate (FE-Pro) complexes are used for labeling of cells to monitor cell trafficking by *in vivo* MRI. The objective was to evaluate the effects of FE-Pro labeling on the expression of transferrin receptor and ferritin, proteins involved in iron transport and storage in mesenchymal stem cells, HeLa and primary macrophages. FE-Pro labeled cells were cultured from 1 to 4 weeks and evaluated for transferrin receptor and ferritin mRNA by RT-PCR, and protein levels by Western blot. FE-Pro labeling elicited physiological changes in iron metabolism/storage and showed that cells can process the increase in intracellular iron load.

10:54 ***679***. **Sentinel Node Imaging of the Breast in Mice Using a Dual-Labeled Nano-Sized MRI/near Infrared (NIR) Optical Hybrid Contrast Agent, G6-Cy5.5**

Hisataka Kobayashi[1], Vladimir S. Talanov[1], Marcelino Bernardo[2], Celeste A. Regino[1], Yoshinori Koyama[1], Yukihiro Hama[1], Martin W. Brechbiel[1], Peter L. Choyke[1]

[1]NCI/NIH, Bethesda, Maryland, USA; [2]SAIC-Frederick, NCI/NIH, Bethesda, Maryland, USA

The presence of lymph node metastases greatly affects prognosis of breast cancer patients. Current methods do not allow for real time surgical guidance. We have synthesized a single hybrid probe, which could be used for MRI and near infrared (NIR) optical imaging of the sentinel node for preoperative and intraoperative localization. The SLNs of the breast tissue could be easily identified using the G6-Cy5.5 agent with MRI and during surgery with NIR optical imaging. The signal arising from SLNs on MR were sufficient for identifying the SLN.

11:06 ***680***. **Noninvasive MR Quantification of Magnetically Labeled Tumor Cells in Rats**

Wei Liu[1], Daniel Herzka[1], Hannes Dahnke[2], Bobbi K. Lewis[3], E. Kay Jordan[3], Naheed Banu[3], Tobias Schaeffter[2], Joseph A. Frank[3]

[1]Philips Research North America, Briarcliff Manor, New York, USA; [2]Philips Research Germany, Hamburg, Germany; [3]National Insititue of Health, Bethesda, Maryland, USA

Quantifying the number of labeled stem cells in target tissues in experimental models is of great importance to optimize dose and timing of cellular therapy in clinical trials. In this study, we investigated the quantitative relationship between iron labeled cells and tissue R2* relaxation rate in a tumor rat model. The *in vivo* experiments demonstrated an excellent linear correlation between the number of iron labeled cells and tissue R2*. Our data further illustrates that R2* measurement is a reliable and sensitive approach for the *in vivo* quantification of iron labeled cells.

11:18 ***681***. **High-Resolution Fluorescence Microscopy and MRI Reveals Mechanism of Lymphatic Metastasis**

Maya Dadiani[1], Dalia Seger[1], Vyacheslav Kalchenko[1], Ady Yosepovich[2], Yaron Hassid[1], Raanan Margalit[1], Hadassa Degani[1]

[1]Weizmann Institute of Science, Rehovot, Israel; [2]Sheba Medical Center and Sackler Faculty of Medicine, Tel Aviv, Israel

Metastatic spread to regional lymph nodes is one of the earliest events of tumor cell dissemination. We aimed to characterize metastatic spread into the lymphatic system using combined high-resolution MRI and fluorescent microscopy. We captured spontaneous metastasizing cells moving along the lymphatic flow by fluorescent videomicroscopy. Micrometastases in lymph nodes were clearly observed, facilitating examination by MRI. A designed Gd-DTPA infusion protocol enhanced the drainage pathways in lymph nodes. Invaded tumor cells in metastatic lymph node appeared to block the normal lymphatic drainage, seen as enhancement of the outer rim only that correlated to a metastatic rim observed in histopathology.

11:30 ***682***. **Tracking Recruitment of Fibroblasts to Ovarian Carcinoma Tumors by MRI**

Dorit Granot[1], Michal Neeman[1]

[1]Weizmann Institute of Science, Rehovot, Israel

Fibroblasts, as critical components of tumor microenvironment, are vital contributors to tumor progression. With the motivation of studying their biology in tumor angiogenesis, we labeled fibroblasts in-vitro with biotin-BSA-GdDTPA contrast material (CM) to monitor their *in vivo* recruitment to ovarian carcinoma tumors. R1 measurements confirmed visibility of pre-labeled fibroblasts and demonstrated their recruitment to tumors after subcutaneous as well as intraperitoneal administration. Increased CM visibility with cell proliferation was detected in-vitro and *in vivo*. These studies demonstrate the feasibility for tracking fibroblast recruitment into the tumor stroma by MRI, and would enable determination of the biological contribution of these cells.

11:42 ***683***. **Internalization of Annexin A5-USPIOs by Apoptotic Cells**

Geralda A.F. van Tilborg[1], Gustav J. Strijkers[1], H. Duimel[2], Paul Bomans[2], Peter M. Frederik[2], Chris P.M. Reutelingsperger[3], Klaas Nicolay[1]

[1]Eindhoven University of Technology, Eindhoven, Netherlands; [2]University of Maastricht, Maastricht, Netherlands; [3]Maastricht University, Maastricht, Netherlands

AnnexinA5-USPIOs enable the detection of apoptosis with MRI. The protein annexinA5 was recently shown to be internalized by cells that are co-exposed to apoptotic stimuli. In this study we show that annexinA5-USPIOs are also internalized by cells that are coexposed to an apoptotic stimulus. The particles were localized to distinct intracellular vesicles. This finding has importantconsequences for the optimal detection of apoptosis since homogeneously distributed particles induce shorter T2 and T2* relaxation times compared to clustered particles.

11:54 ***684***. **New Vanadium-Based MRI Probes for Early Detection of Cancer**

Devkumar Mustafi[1], Sean Foxley[1], Marta Zamora[1], Marvin W. Makinen[1], Gregory S. Karczmar[1]

[1]The University of Chicago, Chicago, Illinois, USA

A novel class of MRI contrast agents, containing VO2+-chelated organic ligands, namely VO(acetylacetonato)2, has been developed. These contrast agents target specifically receptor proteins in glycolysis and are taken up by highly glycolytic cells. We have demonstrated that these compounds have very little toxicity in rats. The relaxivity of VO(acac)2 is comparable to that of low molecular weight Gd3+-complexes; and it provided excellent T1 and T2* contrasts compared to Gd-DTPA in high-resolution MR images of rodent tumors. The preliminary biochemical, biophysical, and cell-biological data showed a great potential to develop the first MRI contrast agents that are sensitive to cancer metabolism.

12:06 ***685***. **Tumor-Targeted Enzyme Mediated MR Signal Amplification Using Paramagnetic Substrates**

Alexei A. Bogdanov[1], Hye-Won Kang[1], David Gordon Bennett[2], Manuel Querol[1], Anna Y. Yudina[1], Iris Verel[3], Christopher H. Sotak, [12]

[1]UMASS Medical School, Worcester, Massachusetts, USA; [2]Worcester Polytechnic Institute, Worcester, Massachusetts, USA; [3]Phillips Research, Eindhoven, Netherlands

A novel combination of a pre-targeting system of cancer-specific antibody-enzyme conjugates and a paramagnetic substrate has been designed for tumor-specific receptor MR imaging. Monoclonal antibody conjugates linked to horseradish peroxidase (HRP) or glucose oxidase (GO) were synthesized by using bisaromatic hydrazone bonds. Purified conjugates were tested in vitro and *in vivo* using human squamous carcinoma model in the presence of bis-(5-hydroxytrypatmide)-DTPA(Gd) paramagnetic HRP substrate (5HT-DTPAGd). L6 (anti-L6 protein family, a pan-carcinoma specific monoclonal antibody, mAb) was tested for tumor cell pre-targeting and showed strong and specific regional tumor T1 signal enhancement on MRI after the injection of 0.2-0.25 mmol dose of 5HT-DTPAGd/kg.

12:18 ***686***. **Polyamine-Substituted Gd-DTPA: Intracellular, Tumor-Selective, High-Retention MRI Contrast Agents**

William E. Hull[1], Markus Wolf[1], Sabine Heiland[2], Ulrike Bauder-Wuest[1], Michael Eisenhut[1]
[1]German Cancer Research Center (DKFZ), Heidelberg, Germany; [2]University of Heidelberg, Heidelberg, Germany

Intracellular Gd(III) contrast agents with polyamine-substituted DTPA ligands have been synthesized. They exhibit relaxivities r1 of 2-8 s–1 mM–1, high uptake (10-100 µM) via polyamine transporters into cultured B16 melanoma and MH3924A Morris hepatoma cells, and are retained within tumor cells for at least 24 h. *In vivo* MRI studies with subcutaneous MH3924A in the rat at 2.35 T demonstrate that the expected T1-wt. contrast enhancement in tumor is achieved with these novel agents, even at 24 h post Gd injection.

Reconstruction Methods

Room 602 - 604 10:30 - 12:30 Chairs: John Pauly and Jeffrey Tsao

10:30 ***687***. **Reconstruction of Under-Sampled Dynamic Images by Modeling the Motion of Object Elements**

Claudia Prieto[1], Roberto Mir[1], Philip Batchelor[2], Derek L. G. Hill[2], Marcelo Guarini[1], Pablo Irarrazaval[1]
[1]Pontificia Universidad Catolica de Chile, Santiago, Chile; [2]University College London, London, UK

We propose a new method to reconstruct under-sampled *in vivo* dynamic images. This technique recovers the lost data from the motion estimation of each object element (obel, think of a piece of tissue) in a continuous space. The results show that the method can effectively reconstruct sequences of 2D cardiac images with an under-sampling factor of 4. Furthermore, the method obtains the vectors of movement of each obel and does not require the motion to be confined to a part of the field of view or to a portion of the temporal frequency.

10:42 ***688***. **Highly Constrained Back Projection (HYPR): Theory and Potential MRI Applications**

Oliver Wieben[1], Julia Velikina[1], Walter F. Block[1], John Perry[1], Yijing Wu[1], Kevin M. Johnson[1], Yan Wu[1], Frank K. Korosec[1], Charles A. Mistretta[1]
[1]University of Wisconsin, Madison, Wisconsin, USA

This study investigates a novel, non-iterative, unfiltered backprojection algorithm that effectively allows for the acquisition and reconstruction of a time series with higher temporal resolution while maintaining high SNR and a low artifact level. The technique was evaluated in simulations by synthesizing numerical phantoms for fMRI and MR spectroscopy and by generating undersampled 2D images obtained from contrast-enhanced MRA, breast perfusion, diffusion, and CT perfusion imaging to investigate artifacts and waveform fidelity. Subsequently, HYPR data were acquired in phantom studies and in CE-MRA using PR TRICKS. Significant acquisition acceleration factors were possible in a wide range of applications.

10:54 ***689***. **X-F Choice Reconstruction of Dynamic Undersampled MR Data Applied to DCE-MRA**

Shaihan Malik[1], Stephan Schmitz[1], Declan O'Regan[1], Jo Hajnal[1]
[1]Hammersmith Hospital, Imperial College London, London, England, UK

Dynamic undersampling in the 'k-t' domain causes aliasing in the conjugate x-f domain, which must be resolved. Based on the observation that signal distribution in x-f space is sparse, x-f choice reconstruction proceeds by reducing the size of problem to solve for each aliased voxel group to locally reflect the true amount of signal overlap. Overlaps are resolved using coil sensitivity data. The problem size is inferred from a model x-f space constructed directly from undersampled data using a k-means clustering approach, meaning no training scan is required. Presented are images from *in vivo* application and a validation study.

11:06 ***690***. ***k-T* Denoising – Exploiting Spatiotemporal Correlations for Signal-To-Noise Improvement in Dynamic Imaging**

Jeffrey Tsao[1], Oleg Tarnavski[1], Melissa Privetera[1], Suraj Shetty[1]
[1]Novartis Institutes for BioMedical Research, Inc., Cambridge, Massachusetts, USA

k-t denoising is a means of improving the signal-to-noise ratio in dynamic imaging by exploiting the spatiotemporal correlations within natural image series. In *k-t* denoising, the raw data are split into two copies. One undergoes spatial filtering, and is then used to estimate the signal covariance for denoising the second copy in *x-f* space (*x* = spatial position, *f* = conjugate axis of time). *k-t* denoising is similar to *k-t* BLAST and *k-t* SENSE, but without acceleration. This opens up new possibilities of alternative and more effective transforms. Cine cardiac images of ob/ob mice show significant noise reduction.

11:18 ***691***. **Accelerating Dynamic Spiral MRI by Algebraic Reconstruction from Undersampled *k-t* Space**

Taehoon Shin[1], Jon Fredrik Nielsen[1], Krishna S. Nayak[1]
[1]University of Southern California, Los Angeles, California, USA

The temporal resolution of dynamic MRI can be increased by sampling a fraction of *k*-space in an interleaved fashion, which causes spatial and temporal aliasing. We describe algebraically and graphically the aliasing process in dynamic spiral imaging to formulate unaliasing as a set of inverse problems. Since each linear system is numerically rank deficient, zero assumption in the solution and regularization are proposed. To reduce required memory and computation time, conjugate gradient method is employed as an iterative linear solver. In-vivo experiments using real-time spiral cardiac imaging demonstrate improved temporal resolution of the proposed method.

11:30 ***692***. **An Application of Highly Constrained Backprojection (HYPR) to Time-Resolved VIPR Acquisition**

Julia V. Velikina[1], Charles A. Mistretta[1], Kevin M. Johnson[1], Oliver Wieben[1]
[1]University of Wisconsin - Madison, Madison, Wisconsin, USA

We present an application of the new Highly Constrained Backprojection (HYPR) method to 3D time-resolved VIPR acquisition. HYPR is a simple non-iterative backprojection algorithm that uses a composite image obtained from all of the acquired data to constrain the backprojection process. This significantly reduces streak artifacts and increases the SNR. The application of HYPR to time-resolved VIPR acquisition allows increasing the undersampling factor from the present value of 50 up to 600. This improvement can be used to increase the number of time frames, decrease the number of projections per time frame and overall scan time while maintaining the SNR.

11:42 ***693***. **Anti-Alias Imaging by Fresnel Scalable Image Reconstruction**

Satoshi Ito[1], Shun Nakamura[1], Yoshifumi Yamada[1], Kunio Tanaka[2]
[1]Utsunomiya University, Utsunomiya, Tochigi, Japan; [2]Asahikawa Medical College, Asahikawa, Hokkaido, Japan

A novel image reconstruction technique, which avoids aliasing artifacts by scalable image reconstruction in Magnetic Resonance Imaging, is proposed. The signal obtained in the phase-scrambling Fourier imaging technique can be transformed to the signal described in the Fresnel transform equation of the objects. Therefore, image reconstruction can be performed not only by inverse Fourier transform but also by inverse Fresnel transform. Image reconstruction by inverse Fresnel transform allows optional scaling of images Thus, alias-free images can be reconstructed even from signals that produce serious aliasing artifacts by standard inverse Fourier transform reconstruction.

11:54 ***694***. **Bunched Phase Encoding in Projection Reconstruction**

Hisamoto Moriguchi[1], Mark A. Griswold[1], Jeffrey L. Sunshine[1], Jeffrey L. Duerk[1]
[1]University Hospitals of Cleveland / Case Western Reserve University, Cleveland, Ohio, USA

Projection reconstruction (PR) acquisitions have several advantages over rectilinear acquisitions. However, streaking artifacts remain and thus degrade image quality when the number of projections is significantly reduced. Bunched Phase Encoding (BPE) has recently been proposed as a new fast data acquisition method in rectilinear sampling in MRI. In BPE, the total number of TR cycles and hence the scan time can be reduced. In this study, rectilinear BPE have been extended to PR to reduce the number of projections. The newly proposed PR-BPE acquisition represents a very useful method to reduce acquisition time in PR MRI while maintaining image quality.

12:06 ***695***. **Rapid MR Imaging with "Compressed Sensing" and Randomly Under-Sampled 3DFT Trajectories**

Michael Lustig[1], David L. Donoho[1], John Mark Pauly[1]
[1]Stanford University, Stanford, California, USA

A rapid imaging method that exploits sparsity or compressibility of MR images using randomly under-sampled 3DFT trajectories and "Compressed Sensing" reconstruction is proposed. Indeed, pure 2D random sampling is impractical for MR hardware, however, randomly under-sampling the phase encodes in a 3D Cartesian scan is practical, involves no overhead, is robust, simple to implement and is purely random in two dimensions. Moreover, scan-time reduction in 3D Cartesian scans is always an issue. A 5-fold scan time reduction in Magnetic Resonance Angiography is demonstrated. Finally, a method to evaluate the effective randomness of a randomly under-sampled trajectory is presented.

12:18 ***696***. **MR Image Reconstruction from Sparse Radial Samples Using Bregman Iteration**

Ti-chiun Chang[1], Lin He[2], Tong Fang[1]
[1]Siemens Corporate Research, Inc., Princeton, New Jersey, USA; [2]UCLA, Los Angeles, California, USA

MR image reconstruction from undersampled MR measurement data usually results in image artifacts and poor SNR. To improve reconstructed image quality, we develop an iterative reconstruction algorithm that is based on the sparse representations of the images, which is realized by both the gradient operation and wavelet transform. We formulate a cost functional that includes the L1 norm of the sparse representations and a constraint term that is imposed by the raw measurement data in k-space. The functional is then minimized by the conjugate gradient (CG) algorithm and further refined by Bregman iteration. Our experimental results achieve high image quality with significantly less image artifacts as compared with the conventional gridding algorithm. Our approach is suitable for the MRI applications where real-time reconstruction is not critical

EM Fields: Computation and Validation

Room 613 - 614 10:30 - 12:30 Chairs: Stuart Crozier and Tamer S. Ibrahim

10:30 ***697***. **Accurate Absolute Thermal Monitoring with RF Radiometry**

AbdElMonem El-Sharkawy[1], Paul Sotiriadis[1], Paul Bottomley[1], Ergin Atalar[1]
[1]Johns Hopkins University, Baltimore, Maryland, USA

The MRI scanner can be used as a radiometer to passively measure noise power emitted by the human body and obtain absolute thermal measurement. The accuracy of thermal measurements depends critically on the precision with which the receiver coils can be matched and tuned to eliminate variations in the receiver chain characteristics. Here we present a new impedance sensing system for RF radiometry that has an accuracy of 0.1Ω. The system allows for continuous impedance sensing, matching and calibration that achieve, in phantom studies, temperature detection with accuracy of 0.2°C. This offers the potential for real-time SAR monitoring

10:42 ***698***. **Real Time Measurement of Heating Near Metallic Implants Throughout a Phantom Using Phase-Shift MR Thermometry**

Howard Bassen[1], Anthony Kam[2], Wolfgang Kainz[1], Gonzalo Mendoza[1], Honghui Wang[2]
[1]Food and Drug Administration, Rockville, Maryland, USA; [2]National Institutes of Health, Bethesda, Maryland, USA

We demonstrated real time acquisition of MRI-induced heating near a simulated medical device lead (an insulated wire with exposed tip). This preliminary thermometry provided a resolution of better than 0.5 ºC, spatial resolution of 1.2 x 1.2 x 3 mm, and a sample rate of 3.1 sec. This is adequate for local temperature measurements near small implants per ASTM F2182 MRI safety test standard. This method has the potential to be a valuable tool for in vitro and *in vivo* viewing and measuring MRI-induced heating near implants in real time.

10:54 ***699***. **High Frequency Electromagnetic Analysis Using Hybrid MOM/FEM Method**

Bing Keong Li[1], Bin Xu[1], Feng Liu[1], Hon Tat Hui[1], Stuart Crozier[1]
[1]University of Queensland, Brisbane, Queensland, Australia

As the magnetic field strength of current human MRI system increases, the size of the human body becomes comparable to the operating wavelength and coil-sample interactions become significant. Numerical techniques based on solving Maxwell's full-wave equations are essential for the prediction of fields in loads and can provide vital information in designing RF coils and in understanding the behavior of the coils when they are loaded with biological structures. Several, full-wave numerical methods; for example, the popular FDTD, hybrid MOM/FDTD and hybrid DGF/MOM have been suggested. In this work, a new full-wave electromagnetic modeling using hybrid MoM/FEM is presented.

11:06 ***700***. **7 Tesla Whole-Slice and Localized Excitation Everywhere in the Human Head**

Tamer S. Ibrahim[1]
[1]The University of Oklahoma, Norman, Oklahoma, USA

In this work, a multi-port excitation technique is numerically implemented at 7 Tesla MRI to provide 1) homogenous whole-slice (axial, sagittal, or coronal) head excitation and 2) highly localized excitation within the same slices, all with the same the RF coil. The method is tested using a full wave model of a coil loaded with an anatomically detailed human head mesh. The proposed approach is solely based on RF shimming. The results demonstrate that both whole-slice homogeneity as well as localized excitation can be achieved within any slice of the human head at 7 Tesla (298 MHz).

11:18 ***701***. **Achieving Uniform In-Plane B1 Amplitude in a 3D Volume for High Field MRI: A Computer Simulation Study**

Zhiyue J. Wang[1, 2], Zili Chu[1, 2]
[1]Texas Children's Hospital, Houston, Texas, USA; [2]Baylor College of Medicine, Houston, Texas, USA

In high field MRI, the RF field patterns demonstrate wavelength effects that depend on the geometry of the sample. We consider the use of an excitation array coil employing "composite excitation elements" consisting of three small current loops with axes along the x, y and z directions, respectively. The excitation elements are distributed to surround the volume of excitation. In each current loop, the current amplitude and phase are independently adjustable. Computer simulations on a human head using the finite-difference time-domain numerical method demonstrated that B1 amplitude with a high degree of in-plane homogeneity can be achieved in a 3D volume.

11:30 ***702***. **Multi-Coil Composite Pulses for Whole-Brain Homogeneity Improved Over RF Shimming Alone**

Christopher M. Collins[1], Zhangwei Wang[1], Weihua Mao[1], Jieming Fang[1], Wanzhan Liu[2], Gregor Adriany[2], J. Thomas Vaughan[2], Kamil Ugurbil[2], Michael B. Smith[1]
[1]Penn State College of Medicine, Hershey, Pennsylvania, USA; [2]University of Minnesota, Minneapolis, Minnesota, USA

In recent years a number of methods for improving image homogeneity in high field MRI have been proposed, some of them relying on separate control of RF coils in a transmit array. Here we combine accurate RF field calculations with accurate representations of the Bloch equation to demonstrate that by using multiple individually-optimized pulses, more homogeneous distributions in available signal intensity over the entire brain volume can be achieved at 300 MHz than when using a single optimized (or RF shimmed) pulse with the same transmit array.

11:42 ***703***. **Simulating the SNR of High-Field RF Coils by the Surface Integral-Equation Method**

Shumin Wang[1], Patrick J. Ledden[2], Jeff H. Duyn[1]
[1]LFMI, NINDS, National Institutes of Health, Bethesda, Maryland, USA; [2]Nova Medical, Inc., Wilmington, Massachusetts, USA

A surface integral-equation-based approach is developed for simulating the SNR of high-field RF coils. This method formulates the equations on the surfaces of RF coils and the phantom. As a result, very high modeling accuracy and computational efficiency can be achieved. Numerical results of an eight-channel coil array for brain imaging at 7.0 Tesla further demonstrate the validity, accuracy and efficiency of this approach.

11:54 ***704***. **Discrete Design Method of a Transverse Gradient Coil for Magnetic Resonance Imaging**

Shmaryu Shvartsman[1], Gordon DeMeester[1], Michael Morich[1]
[1]Philips Medical Systems, Cleveland, Ohio, USA

In this work we describe a discrete gradient coil design method that does not include some of the essential steps of continuous current based minimum energy design methods. The key concept is that all characteristics of a transverse gradient, such as coil inductance, spatial distribution of the magnetic field, coil resistance, and slew rate of the coil, are expressed through the set of z-intercepts where the coil current pattern intersects the cardinal axes, for example Zi along f=0 and f=p for an X-gradient. We illustrate the advantages of the discrete design method with the example of a whole body gradient.

12:06 ***705***. **A Simple Relationship for High Efficiency-Gradient Uniformity Trade-Offs in Multi-Layer Asymmetric Gradient Coils**

Hector Sanchez Lopez[1], Feng Liu[1], Adnan Trakic[1], Stuart Crozier[1]
[1]University of Queensland, Brisbane, Queensland, Australia

In this work, we have studied the influence of DSV size, coil length and radius, relative axial offset position of DSV and target gradient field uniformity over the figure of merit in multi-layer asymmetric transverse gradient coils. A simple linear function that defines the optimal coil length to produce a maximum figure of merit given a DSV size, coil radius, axial offset position and introduced uniformity error is obtained. Applying the method and the linear functions derived, high quality solutions are obtained.

12:18 ***706***. **Comparison of Peak Simulated Electric Fields with PNS Locations**

Rebecca Emily Feldman[1], Christopher M. Collins[2], Blaine Alexander Chronik[1]
[1]University of Western Ontario, London, Ontario, Canada; [2]The Pennsylvania State University College of Medicine, Hershey, Pennsylvania, Canada

Gradient coil induced electric fields are simulated in a Visible Man model of a human male head, neck, and torso. The simulation indicates that tissue geometry plays a large role in the magnitude of the field experienced. In addition to large fields accumulating at locations on the surface of the body, such as the tip of the nose, internal air cavities also demonstrate enhanced electric fields. The locations of large simulated electric field include the sinus cavities as well as an air cavity in the chest. These locations of high simulated field are compared to the locations of actual stimulation.

CLINICAL MRI HANDS-ON WORKSHOP 1 (REPEAT)
Neuro and Musculoskeletal Protocol Optimization
GE Healthcare

Room 4F(1) 10:30 – 12:30 Chairs: Kimberly Amrami and Alberto Bizzi

CLINICAL MRI HANDS-ON WORKSHOP 1 (REPEAT)
Neuro and Musculoskeletal Protocol Optimization
Philips Medical Systems

Room 4F(2) 10:30 – 12:30 Chairs: Kimberly Amrami and Alberto Bizzi

CLINICAL MRI HANDS-ON WORKSHOP 1 (REPEAT)
Neuro and Musculoskeletal Protocol Optimization
Siemens Medical Solutions

Room 4F(3) 10:30 – 12:30 Chairs: Kimberly Amrami and Alberto Bizzi

GOLD CORPORATE MEMBER LUNCHTIME SYMPOSIUM
GE Healthcare

Room 6E 12:30 – 13:30

GOLD CORPORATE MEMBER LUNCHTIME SYMPOSIUM
Philips Medical Systems
SmartExam: The First MR with IQ

Room 6C 12:30 – 13:30

GOLD CORPORATE MEMBER LUNCHTIME SYMPOSIUM
Siemens Medical Solutions
Developments in Molecular MRI

Room 6D 12:30 – 13:30

ELECTRONIC POSTER DISCUSSION: Diffusion: Simulation, Attenuation, Computation, and Application

Room 6E 13:30 - 15:30 Chairs: Peter J. Basser and David G. Norris

13:30 ***707***. **A Theoretical Model of Water Diffusion in Brain Tissue**
Sune Nørhøj Jespersen[1], Christopher D. Kroenke[2], G. Larry Bretthorst[2], Joseph J. H. Ackerman[2], Dmitriy A. Yablonskiy[2]
[1]University of Aarhus, Aarhus, Denmark; [2]Washington University, St. Louis, Missouri, USA

We present a new theoretical model that reflects basic diffusion properties of brain tissue at the cellular level. Neuronal tissue (gray and white matter) is modeled as a distribution of long cylinders, and water associated with these cylinders exhibits anisotropic diffusion. Diffusion outside the neurons, in glia cells and extracellular space, is assumed isotropic on the time scale of the diffusion measurement. To test the model, 153 diffusion weighted images with varying amplitude and direction of diffusion gradients were collected from a fixed baboon brain. Considerable agreement is found between the theoretical model and experimental data.

13:40 ***708***. **Simulating Water Diffusion in Tissues with an Improved Finite Difference Method**
Junzhong Xu[1], Mark D. Does[1], John C. Gore[1]
[1]Vanderbilt University, Nashville, Tennessee, USA

To conquer the two main limitations to the use of the finite difference (FD) method to the numerical study of diffusion in biological tissues; the edge effect and the long computing time, we have developed a novel hybrid discretization scheme algorithm and a tightly-coupled FD model that uses parallel computing technique. The simulated results show that our modified FD approach constrains the computing errors to a level of less than 5% for diffusion time as long as 100ms, and reduces 97.5% of the computing time. Those improvements make the FD method suitable for even long diffusion times and large-scale complex tissues.

13:50 ***709***. **A Fractal Model of Diffusion Weighted MRI in Brain Tissue**
Brian Hansen[1], Peter Vestergaard-Poulsen[1, 2]
[1]Aarhus University, Aarhus, Denmark; [2]Aarhus University Hospital, Aarhus, Denmark

We present a new model of Diffusion Weighted MRI in brain tissue using a computer generated DLA cluster to mimic grey matter cells. Neuronal growth is related to the growth-mechanism named Diffusion Limited Aggregation (DLA). This causes similarity between neurons and DLA clusters. A population of random walkers is allowed to diffuse on the DLA cluster to simulate an intra-cellular spin pool. We also include a population of diffusing extra-cellular spins. The spin populations have independent properties of diffusion and relaxation and we allow exchange between compartments. Our model also includes a random distribution of static traps to model macro-molecular signal sinks.

14:00 ***710***. **Rician Noise Corrected and Multi-Component Analyzed Diffusion Signal Decays for Human Brain Tissue In-Vivo at High B-Values**

Marzieh Nezamzadeh[1], Ian Cameron[2]

[1]Ottawa General Hospital, Carleton University, ottawa, ON, Canada; [2]Ottawa general Hospital, Ottawa, ON, Canada

Restricted diffusion of water molecules in human brain was examined at high b-values over a range of diffusion times to evaluate the apparent diffusion coefficients from the signal decays. Reliable diffusion information requires the removal of Rician noise bias from the decay particularly at high b-values with low SNR and a multi-component analysis. Using this approach, we observed the three major components in the spectrum of diffusion coefficients from the voxel signal decay and small diffusion time dependence for the smallest diffusion coefficient, which has not previously been reported. This observation was compared with the exchange theory for a human model.

14:10 ***711***. **Comparison of Stretched Exponential and Non-Negative Least Squares Fitting Methods for Multi-Exponential Diffusion Decay Curves**

Lanette J. Friesen Waldner[1], Brian K. Rutt[1]

[1]Robarts Research Institute, London, Ontario, Canada

Fitting of multi-exponential decay curves is not trivial. Diffusion decay curves were fit using two different fitting methods: non-negative least squares (NNLS) and a form of the stretched exponential fit. Diffusion decay curves were obtained from twelve tumours in an animal model pre- and post-sacrifice of the animal. Both fitting methods showed significant differences ($p<0.05$) between the pre- and post-sacrifice decay curves. The sum of the squares of the residuals was higher for the stretched exponential method than the NNLS method both pre- and post-sacrifice suggesting that NNLS provides a better fit to the decay curves in this study.

14:20 ***712***. **q-Space Analysis of Diffusion Measurements in Myelinated and Non-Myelinated Nerves: Restriction vs. Exchange**

Itamar Ronen[1], James Hamilton[1], Dae-Shik Kim[1]

[1]Boston University School of Medicine, Boston, Massachusetts, USA

In this work, diffusion weighted spectra were collected from three radically different mammalian nerves: optic, vagus and sciatic nerves freshly obtained from rhesus monkeys. q-space analysis performed on these data shows that displacement RMS is unbounded and reaches beyond the average axonal diameter of all three nerves even at relatively short diffusion times. These results are then interpreted according to the well-characterized cytoarchitectonics of these nerves. One possible conclusion is that interplay between axonal diameter, axonal packing and transmembrane permeability plays a major role in defining water diffusion characteristics in neural tissue, both in myelinated and non-myelinated nerves.

14:30 ***713***. **Extension of the Diffusion Orientation Transform (DOT) to Multiexponential Signal Attenuation**

Evren Ozarslan[1], [2], Baba C. Vemuri[2], Stephen J. Blackband[2]

[1]National Institutes of Health, Bethesda, Maryland, USA; [2]University of Florida, Gainesville, Florida, USA

The diffusion orientation transform (DOT) enables the estimation of water displacement probability profiles from high angular resolution diffusion-weighted MRI data. The method assumes independent monoexponential signal attenuations along different directions if a single spherical shell is sampled. When several concentric shells in q-space are sampled, the transform can trivially be extended to multiexponential signal attenuations. Although estimated fiber orientations seem unaffected, the proposed extension of the DOT improves the resolution of individual fiber populations. The method has the potential to yield a significant reduction in the required number of acquisitions for 3-dimensional q-space imaging.

14:40 ***714***. ***In Vivo* Comparison of Q-Ball, Spherical Deconvolution and Diffusion Orientation Transform HARDI for Fiber Orientation Estimation Using the Bootstrap Method**

Christopher P. Hess[1], Pratik Mukherjee[1], Jeffrey I. Berman[1], Eric T. Han[2], Duan Xu[1], Roland G. Henry[1], Daniel B. Vigneron[1]

[1]University of California San Francisco (UCSF), San Francisco, California, USA; [2]GE Healthcare Global Applied Science Laboratory, Menlo Park, California, USA

Prior research comparing high angular resolution diffusion imaging (HARDI) reconstruction methods has relied on numerical simulations to assess accuracy in resolving multiple fiber orientations. In this study, we apply the bootstrap concept to determine the *in vivo* precision of fiber orientation estimates derived from q-ball, spherical deconvolution, and diffusion orientation transform reconstructions. We compare the estimation uncertainty of each technique and assess the degree to which mean estimates of orientation differ across techniques. The results suggest that, for typical sparsely sampled HARDI data that might be acquired in the clinical setting, the three methods yield nearly equivalent directional information.

14:50 ***715***. **White Matter Tractography Analysis of the Connectivity Patterns of the Visual Cortical Areas**

Mariana Lazar[1], Paul Thottakara[2], Bryan Baxter[1], Andrew L. Alexander[1]

[1]University of Wisconsin, Madison, Wisconsin, USA; [2]University of Michigan, Ann Arbor, Michigan, USA

White matter tractography with DTI was used to examine the anatomical connectivity patterns of several cortical areas involved in visual processing situated in the occipital (Brodmann's areas 17, 18, 19), parietal (Brodmann's area 39), and temporal (Brodmann's area 37) lobes. Brodmann's areas templates were used to define regions of interest and select the corresponding white matter connectivity patterns. Probabilistic connectivity maps of each Brodmann's area were constructed by averaging the connectivity patterns for 16 subjects in a normalized coordinate space. Patterns of connectivity characteristic to each region were found. These patterns appear to be consistent across subjects.

15:00 *716*. **Quantitative Imaging of White Matter Microstructure in Canine Brain Using High Angular DTI Microscopy**

Ping Wang[1], Jian-Ming Zhu[1]
[1]Wake Forest University School of Medicine, Winston-Salem, North Carolina, USA

The current proposed method provided an accurate and yet quantitative imaging method to map white matter microstructure in fixed canine brain. Using this procedure, extremely high resolution microstructural images can be obtained. This will lead the most accurate method currently available to study functional microanantomy in brains, in particular, of animal models.

15:10 *717*. **DTI-Driven Segmentation of Human Cortex - Methods, Validation and Reproducibility**

Johannes C. Klein[1], Tim Edward John Behrens[1], Matthew D. Robson[1], Clare E. Mackay[1], Des J. Higham[2], Heidi Johansen-Berg[1]
[1]University of Oxford, Oxford, Oxfordshire, UK; [2]University of Strathclyde, Glasgow, Scotland, UK

We describe and validate an automated method to separate functional areas of the human cortex based on their connectivity profiles using probabilistic diffusion tractography. Inter-session reproducibility is established. Ongoing research suggests that the method is also extendable to deep gray structures.

15:20 *718*. **A Multimodal Imaging Study Using Anatomical and DTI Data**

Dongrong Xu[1], Xuejun Hao[1], Ravi Bansal[1], Kerstin J. Plessen, [12], Weidong Geng[3], Bradley S. Peterson[1]
[1]Columbia University & New York State Psychiatric Institute, New York, New York, USA; [2]University of Bergen, Bergen, Norway; [3]Zhejiang University, Hangzhou, Zhejiang, People's Republic of China

Diffusion tensor imaging provides information on the connectivity of white matter fibers in the brain, which is undetectable using other imaging modalities. In most applications, DTI data are analyzed independently from other imaging modalities, with regions of interest (ROIs) for fiber tracking identified manually by experts. However, the accuracy of manual segmentation can be unreliable because of morphometric and functional variations between individual brains. Moreover, the procedure is time consuming and subjective. Based on our previous work on image co-registration across modalities and neural fiber tracking, we propose an automated framework that uses data from multiple imaging modalities to identify ROIs for fiber tracking. We demonstrate the effectiveness of our procedure through application to a population of Tourette's syndrome (TS) patients and a group of age-matched normal controls. Our procedure requires minimal human intervention and is therefore relatively objective and accurate.

CLINICAL MRI COURSE
Vascular Problem Solving and Case Presentation

Room 6C 13:30 - 15:30 Chair: Georg Bongartz

Educational Objectives:
Upon completion of this session, participants should be able to:

- Identify frequently encountered vascular lesions and recognize common artifacts when imaging the vessels of the neck;
- Correctly detect and grade renal artery stenosis, assess renoparenchymal disease and differentiate various vascular and nonvascular renal diseases;
- Describe the critical role of MRA in non-invasive imaging of the extremity arteries and recognize how limitations and artifacts can be overcome.

The last 10 minutes of each talk will be reserved for questions.

13:30 **Vessels of the Neck**
John Huston III

14:10 **Evaluation of Renal Vascular Disease**
Stefan O. Schoenberg

14:50 **MRA of the Run-Off's: Hands and Feet**
James F. M. Meaney

CLINICAL SCIENCE FOCUS SESSION: Alzheimer's and Other Degenerative Diseases

Room 4C - 3,4 13:30 - 15:30 Chairs: John D. Port and Nicola De Stefano

13:30 ***719***. **Greater Blood Flow Reduction in Mild Diffuse Lewy Body Disease Than in Mild Alzheimer's Disease**

Tamara Fong[1], Daniel Press[1], David Charles Alsop[1]
[1]Beth Israel Deaconess Medical Center, Boston, Massachusetts, USA

Arterial Spin Labeling(ASL) blood flow abnormalities in subjects diagnosed with mild Diffuse Lewy Body Disease(DLBD) were compared to normal controls and subjects with mild Alzheimer's Disease. Blood flow abnormalities were similar in spatial distribution for the two dementias but the magnitude of the abnormality was more pronounced in the DLBD patients despite lower impairment. These results suggest ASL blood flow MRI may have low specificity for differentiating these two common dementias and that cholinergic dysfunction, which is greater in DLBD than AD, may be related to cortical flow abnormalities.

13:40 ***720***. **Combining CASL with Uni- And Multi-Variate Methods for Early Detection of Alzheimer's Disease**

Iris Asllani[1], Christian Habeck[1], Ajna Borogovac[1], Yaakov Stern[1], Truman Brown[1]
[1]Columbia University, New York, New York, USA

We present preliminary data showing the feasibility of combining CASL with multivariate statistical analysis for discrimination between AD subjects and healthy controls.

13:50 ***721***. **Regional Degradation of White Matter Ultrastructure in Mild Cognitive Impairment and Alzheimer's Disease by Diffusion Tensor Imaging**

Yu Zhang[1], Norbert Schuff[1], G-H Jahng[1], Whitney Bayne[1], Susumu Mori[2], L Schad[3], Susanne Mueller[1], Joel Kramer, Kristine Yaffe, Hellen Chang Chui[4], William J. Jagust[5], Bruce L. Miller, Michael W. Weiner[1]
[1]VA Medical Center and UC San Francisco, San Francisco, California, USA; [2]Johns Hopkins University, Baltimore, Maryland, USA; [3]German Cancer Research Institute, Heidelberg, Germany; [4]University of Southern California, Los Angeles, California, USA; [5]Lawrence Berkeley National, Laboratory and UC Berkeley, Berkeley, California, USA

Diffusion tension imaging (DTI) was used to determine the usefulness of degradation of cingulum fibers in diagnosis of mild cognitive impairment (MCI) and Alzheimer's disease (AD). The result showed that degradation of the cingulum fibers measured by fractional anisotropy (FA) was already detectable in MCI and becomes more regionally widespread in AD. Furthermore, adding DTI to hippocampal volume significantly improved the classification of MCI and AD from normal aging. In conclusion, assessment of cingulum fibers using DTI is more powerful than assessment of hippocampal atrophy for early changes in MCI and therefore may be a sensitive marker for AD pathology.

14:00 ***722***. **Thin Slice Magnetic Resonance Histological Imaging and Co-Regisitration of Beta-Amyloid Plaques**

Mark David Meadowcroft[1], Shutong Zhang[2], James R. Connor[1], Michael B. Smith[1], Qing X. Yang[1]
[1]Pennsylvania State University - College of Medicine, Hershey, Pennsylvania, USA; [2]The University of Pennsylvania, Philadelphia, Pennsylvania, USA

There continue to be difficulties within the literature regarding the co-registration of the through plane MRI data with histological preparations of dissected tissue samples. This problem has been addressed with the fabrication of the histological coil at a field strength of 3.0 T. Using this coil, imaging human brain tissue samples to obtain a one to one relationship between image parameter maps and the histological chemical stains is possible. This coil has been used to specifically address the problem of co-registering the hypo-intensities found in the MR images with focal iron deposition and Aâ plaque distribution. These data show novel results supporting such a correlation when using the same tissue sample for both MR imaging and histological staining.

14:10 ***723***. **Alterations in Cerebral Microstructual Integrity in Normal Aging and in Alzheimer's Disease: A Multi-Contrast Diffusion MRI Study**

Hanzhang Lu[1], Jens H. Jensen[1], Cathy Hu[1], Maria F. Falangola[1], Anita Ramani[1], Steven Ferris[1], Joseph A. Helpern[1]
[1]New York University, New York, USA

Recently we developed a diffusion kurtosis imaging (DKI) technique that can measure conventional diffusion tensor as well as the non-Gaussian behavior of water diffusion in the tissue. Here DKI is applied to four patient groups: Alzheimer's Disease patients, Mild cognitive impairment patients, age-matched controls, and young adult controls. Mean diffusivity (MD), fractional anisotropy (FA) and mean kurtosis (MK) parametric maps were computed. ROI analysis shows that the FA and MK increase while MD decreases among the four groups. Histograms reveal that MK have multiple peaks corresponding to different tissue types and is capable of differentiating volume atrophy from microstructual alterations.

14:20 *724*. **DTI Measures Predict the Performance on Cognitive Tests in Elderly and Patients with Early Alzheimer's Disease**

Hongyan Ni[1], Jianhui Zhong[1], Voyko Kavcic[2]

[1]University of Rochester, Rochester, New York, USA; [2]University of rochester, Rochester, New York, USA

Alzheimer's disease (AD), a neurodegenerative disorder associated with progressive functional decline, affects somal, dendritic, and axonal structures in the brain. We hypothesized that alteration in the white matter (WM) correlates with cognitive status. We tested this assumption on15 AD patients and 18 age-matched controls by neuropsychological testing and by DTI measurements of major WM structures. The results showed that the DTI measures can predict 13 % to 55 % of variance in the performance on 5 of 7 neuropsychological tests. These findings demonstrate that cognitive performance does not depend only on the intact cortex but also on intact WM structures.

14:30 *725*. **Towards an Early Prognosis of Alzheimer's Disease: Probing the Diffusion Characteristics of the Entorhinal Cortex and Perforant Pathway with Turboprop-DTI**

Minzhi Gui[1], Ana Solodkin[2], James A. Mastrianni[2], Konstantinos Arfanakis[1]

[1]Illinois Institute of Technology, Chicago, Illinois, USA; [2]University of Chicago, Chicago, Illinois, USA

The earliest neuropathological changes of AD appear in the entorhinal cortex (EC) and perforant pathway (PP). In this study, Turboprop-DTI was used to detect changes in the diffusion characteristics of EC/PP in patients with AD. It is demonstrated that FA/trace of EC/PP are more sensitive in separating AD patients from normal controls than conventional hippocampus and EC/PP volume measurements. Furthermore, the EC/PP diffusion characteristics for some MCI subjects were similar to those of AD patients. This may indicate that the particular MCI subjects are more probable to develop AD than MCI subjects with normal appearing EC/PP diffusion properties.

14:40 *726*. **Asymptomatic Members with SOD1 Mutation in a Large Kindred with Familial Amyotrophic Lateral Sclerosis Have Abnormal Water Diffusion Characterisitcs**

Man Cheuk Ng[1], Jenny T. Ho[2], S. L. Ho[1], Raymond Lee[2], Geng Li[3], Y. Q. Song[1], K. H. Chan[1], T. S. Cheng[1], Edward S. Yang[1], L. Y. Leong[2]

[1]The University of Hong Kong, Pokfulam, N/A, Hong Kong, People's Republic of China; [2]Queen Mary Hospital, N/A, Hong Kong, People's Republic of China; [3]The Jockey Club MRI Centre, The University of Hong Kong, Pokfulam, N/A, Hong Kong, People's Republic of China

DTI was carried out in FALS/SALS patients and familial members with SOD1 mutation (AFALS) who may be in a pre-symptomatic phase of ALS. The changes in FA and TT were investigated in CBT/CST and in whole brain. In FALS/SALS, diffusion pattern changes were found in cerebral peduncle, internal capsule, sub-cortical white matter, cerebellum and frontal lobe while in AFALS, abnormal pattern could also be detected in the cerebral peduncle, cerebellum and frontal lobe but with a smaller extent. Our study indicates that DTI can show early diffusion changes in members with SOD1 mutation in FALS prior to symptom-onset.

14:50 *727*. **Robust Assessment of Cortical Thinning in Brain MRI by Generalized Complexity Measures**

Karl Young[1, 2], Norbert Schuff[1, 2]

[1]University of California San Francisco, San Francisco, California, USA; [2]Veterans Affairs Medical Center, San Francisco, California, USA

Recent brain MRI studies of aging and dementia have suggested methods for measuring cortical thinning. Though promising, these methods depend on a number of parameters. A robust method for detecting cortical thinning via complexity measures, requiring a single choice, the distance scale for the analysis, is presented in this study. The methods are demonstrated using a data set of 50 segmented T1 MRI images, 25 of which had the cortical surface in the right superior temporal gyrus artificially thinned. The method proved robust to normal population variations, and sensitive to even slight focal changes in cortical thinning.

15:00 *728*. **Gray Matter Thinning Demonstrated in ALS Using Novel Thickness Maps**

Don C. Bigler[1], Kevin R. Scott[1], Mark D. Meadowcroft[1], Jianli X. Wang[1], Helen E. Stephens[1], Zachary Simmons[1], Qing X. Yang[1], Michael B. Smith[1]

[1]Penn State College of Medicine, Hershey, Pennsylvania, USA

Amyotrophic lateral sclerosis (ALS) is one of the most common neuromuscular diseases worldwide with no known cure and is invariably fatal. Presently the progression of the disease within the brain is not well understood. In this study, novel gray matter thickness maps of age and sex matched controls and ALS subjects are visually inspected to determine if thinning in the primary motor cortex may be used for diagnosis and monitoring of disease progression in ALS. Results suggest that this technique may be useful for this purpose.

15:10 ***729***. **Thalamic Involvement Following Mild Brain Injury: *In Vivo* Occult Pathology Demonstrated by Diffusion Kurtosis Imaging**

Yulin Ge[1], Hanzhang Lu[1], Jens H. Jensen[1], Joseph A. Helpern[1], Joseph Reaume[1], Robert I. Grossman[1]
[1]New York University School of Medicine, New York City, New York, USA

Diffusional kurtosis (DK) is defined as reflecting the non-Gaussian water diffusion properties in the biologic tissues. DK imaging is an extension of conventional diffusion imaging and provides a specific measure for the deviation of water diffusion from the Gaussian behavior in tissues with heterogeneous solution, thus, is a sensitive method for the degree of tissue structural complexity. In this study, we have compared the DK imaging and diffusion tensor (DT) imaging in different brain regions including thalamus in patients with mild traumatic brain injury (MTBI) and in age-matched normal controls to investigate the thalamic involvement in MTBI.

15:20 ***730***. **Brain Morphometry in Methamphetamine Users in Relation to Cumulative Drug Exposure**

Renat Yakupov[1], Linda Chang[1], Dan Alicata[1], Darlene Ramones[1], Christine Cloak[1], Thomas Ernst[1]
[1]University of Hawaii, John A. Burns School of Medicine, Honolulu, Hawaii, USA

22 current or recently abstinent methamphetamine (METH) users and 27 controls were evaluated with voxel-based morphometry (VBM, SPM2), using 3T MRI. METH-associated differences in gray matter (GM), white matter (WM) and CSF, as well as their relationships with lifetime METH usage, were evaluated. METH subjects had increased frontal WM volumes but decreased CSF volumes in temporo-parietal regions. Increased brain volumes might be due to increased inflammation in these brain regions. METH exposure correlated negatively with frontal and occipital GM volumes and positively with posterior cingulate CSF, suggesting additional brain alterations with heavy METH use.

CLINICAL SCIENCE FOCUS SESSION: Pediatric Brain: Advanced MR Modalities

Room 611 - 612 13:30 - 15:30 Chairs: Joseph V. Hajnal and Daniel B. Vigneron

13:30 ***731***. **A Novel Approach to Accurate 3D High Resolution and High SNR Fetal Brain Imaging**

Shuzhou Jiang[1], Hui Xue[1], Alan Glover[2], Mary A. Rutherford[1], Joseph V. Hajnal[1]
[1]Hammersmith Hospital, Imperial College London, London, UK; [2]Department of Radiology Hammermsith Hospital, London, UK

We present a novel method to reconstruct isotropic high resolution 3D images of fetal brains in-utero. After continuous scanning to acquire a repeated series of parallel slices using single-shot FSE, image registration is used to correct for fetal motion. Compounding of multiple images increases SNR, so imaging parameters can be chosen to provide high resolution at the expense of SNR in individual images. The method has been tested on adult and neonatal brain images, and on two normal fetuses imaged at 1.5T. In all cases self-consistent 3D brain images with anatomical details clearly visible in all planes were successfully reconstructed.

13:40 ***732***. **Advances in T1-Based Fluid Oxymetry**

Greg Zaharchuk[1], Reed F. Busse[2], Guy Rosenthal[1], Geoffery T. Manley[1], Orit A. Glenn[1], Eric Han[2], William P. Dillon[1]
[1]UC San Francisco, San Francisco, California, USA; [2]GE Healthcare, Menlo Park, California, USA

Recent studies have shown that it is possible to measure absolute oxygen partial pressure (pO_2) non-invasively in human body fluids with a dualshot nonequilibrium saturation recovery single-shot fast spin echo technique. Such a method promises insight into normal physiology as well as into changes during disease or treatment. This abstract reports mean CSF, vitreous, and bladder urine oxygenation in normal young adults. Also, potential errors due to fluid protein content and partial volume error are analyzed. Finally, the first images and measurements of pO_2 in fetal CSF and vitreous *in utero* are presented.

13:50 ***733***. **3D MRSI of the Premature Brain: Defining Normal and Abnormal Maturational Changes**

Natalie Noonan Charlton[1], Duan Xu[1], Steve P. Miller[1], Srivathsa C. Veeraraghavan[1], Dong Hyun Kim[1], Pratik Mukherjee[1], A J. Barkovich[1], Daniel B. Vigneron[1]
[1]University of California, San Francisco, California, USA

In this study, lactate-edited 3D MRSI was applied in a large (N=97exams) population of premature infants to define the anatomic and maturational changes in infants with normal 1-year neurodevelopmental outcome and to investigate metabolic abnormalities in those with poor neurodevelopmental outcome. NAA/CHO levels were found to increase significantly with age in all anatomic regions with varying rates. The infants with very poor outcome demonstrated abnormal LAC/NAA and LAC/CHO ratios at least 2.5 standard deviations above the means defined in the age-matched normative data.

14:00 *734*. **Regional Variation in Human Thalamic Maturation Revealed by Diffusion Tensor Imaging of Premature Newborns**

Amy Robin deIpolyi[1], Pratik Mukherjee[1], Srivathsa Veeraraghavan[1], Jeffrey I. Berman[1], Roland G. Henry[1], Daniel B. Vigneron[1], A. James Barkovich[1]

[1]University of California, San Francisco, San Francisco, California, USA

Diffusion tensor imaging (DTI) has revealed regional heterogeneity in preterm neocortical maturation. We examined whether this is also true of thalamic nuclei that are reciprocally interconnected with different cortical areas. We found that, throughout the thalamus, mean diffusivity and all three eigenvalues correlated negatively with age, whereas in most regions, anisotropy correlated positively with age. First-order thalamic relay nuclei projecting to primary sensorimotor cortex have lower diffusivity and eigenvalues, but higher anisotropy, than higher-order thalamic nuclei projecting to neocortical association areas. Our data support the hypothesis that the thalamus exhibits a hierarchical pattern of maturation analogous to the preterm neocortex.

14:10 *735*. **Accelerated Development in the Visual Areas of Preterm Infants? A Voxel-Based Morphometry Study on Diffusion Tensor MR Imaging**

Monica Gimenez[1, 2], Maria J. Miranda[3], Peter A. Born[3], Zoltan Nagy[4], Terry Jernigan[3, 5], Egill Rostrup[3]

[1]University of Barcelona, Barcelona, Spain; [2]Institut d'Investigacions Biomèdiques August Pi i Sunyer (IDIBAPS), Hospital Clínic, Barcelona, Spain; [3]Danish Research Centre for Magnetic Resonance, Copenhagen University Hospital, Copenhagen, Denmark; [4]Karolinska Institute, Stockholm, Sweden; [5]Laboratory of Cognitive Imaging (LOCI), La Jolla, California, USA

Premature birth has been related to delayed brain maturation, but the possibility of a more rapid maturation of certain brain areas has not been directly demonstrated. We compared brain maturation by a voxel-based morphometry approach in diffusion images in a sample of preterm newborns compared to a control group. Both groups were MR scanned at similar postmenstrual ages. When compared with the full-term group, the preterm infants at full-term age showed an increase in FA in areas related to visual function. Our findings may lead to new investigations evaluating the adaptive mechanisms of the immature developing brain at early stages.

14:20 *736*. **Non-Invasive Assessment of Connectivity in Two Year Old Infants Who Were Born Preterm: A Probabilistic Tractography Approach**

Serena J. Counsell[1], Leigh E. Dyet[2], David J. Larkman[1], Rita G. Nunes[1], James P. Boardman[1], Joanna M. Allsop[1], Julie Fitzpatrick[1], Latha Srinivasan[1], Frances M. Cowan[1], Joseph V. Hajnal[1], A David Edwards[1], Mary A. Rutherford[1]

[1]Imperial College London, London, UK; [2]Imperial College London, London, UK

The aim of this study was to visualise connectivity in the brain of infants who were born preterm. We studied twelve infants who were born at a median of 31 weeks gestational age and imaged at a median corrected age of 24.6 months. Thalamo-cortical projections and connectivity distributions from seed points positioned in numerous white matter tracts were visualised. Abnormalities were identified in an infant with white matter lesions. This study suggests that a probablilistic tractography approach will be useful in assessing connectivity in brain development and in infants who have focal lesions.

14:30 *737*. **Apparent Diffusion Coefficient in Children and Adolescents: Effect of Age and Correlation with Neuropsychological Measures of Frontal Brain Function**

David Bonekamp[1], Carolyn T. Wells[1], Melissa Matson[1], E. Mark Mahone[1], Rena J. Geckle[1], Amanda Barnes[1], Susumu Mori[1, 2], Alena Horska[1]

[1]Johns Hopkins University School of Medicine, Baltimore, Maryland, USA; [2]Kennedy Krieger Institute, Baltimore, Maryland, USA

To determine structural correlates of neurobehavioral functioning, and to examine white matter maturation in children between 5 and 18 years, we obtained measurements of ADC bilaterally in 15 white matter tracts with a region of interest based data analysis approach. ADC decreased with age in 5 of 15 regions in the left hemisphere and in 3 regions in the right hemisphere. Right anterior white matter ADC significantly predicted scores of Bead Memory, a test of visual working memory considered to be related to functioning in the dorsolateral prefrontal cortex (right greater than left). Regional ADC in locations considered to be less or not related to Bead Memory showed no significant association.

14:40 *738*. **Late Development of the Superior Longitudinal Fasciculus Revealed by Diffusion Tensor Imaging (DTI)**

Jiangyang Zhang[1], Alan C. Evans[2], Laurent Hermoye[3], Pamela Donohue[4], Setsu Wakana[1], Weihong Zhang[1], Michael I. Miller[5], Peter C.M. van Zijl[1, 6], Susumu Mori[1]

[1]Johns Hopkins University School of Medicine, Baltimore, Maryland, USA; [2]Montreal Neurological Institute, Montreal, QC, Canada; [3]Univerisity Catholique de Louvain, Saint-Luc Univerisity Hospital, Brussels, Belgium; [4]Johns Hopkins School of Medicine, Baltimore, Maryland, USA; [5]Johns Hopkins University, Baltimore, Maryland, USA; [6]Kennedy Krieger Institute, Baltimore, Maryland, USA

Development of association pathways in human brain from newborn to adult was studied using DTI. Images from 82 subjects were normalized to the widely used Montreal Neurological Institute (MNI) template using 12-parameter affine transformations. Subjects were organized into 7 age groups and average diffusion tensor images were generated for each group. After normalization, morphological changes of association pathways were studied in the common coordinates. We applied a voxel-based method to quantify these changes. The results identified the superior longitudinal fasciculus (SLF) as the major tract maturing slowest in the postnatal stages.

14:50 ***739***. **Reading Ability Correlates with White Matter Anisotropy in Elementary School Children**

Christian Beaulieu[1], Christopher Plewes[1], Lindsay Snook[1], Dawne Roy[1], Luis Concha[1], Linda Phillips[1]
[1]University of Alberta, Edmonton, Alberta, Canada

Previous diffusion tensor imaging (DTI) studies have demonstrated correlations between reading ability and fractional anisotropy (FA) in the left temporo-parietal white matter in adults and older children (~11 years old). The purpose of this study was to determine whether similar correlations between FA in the brain and reading ability exist in two even younger cohorts of children (Kindergarten - Grade 1, ages 5-7; Grades 2 – 4, ages 7-10) with varying levels of skill. It is demonstrated that localized white matter connectivity in the brain is related to reading performance in elementary school children whom are emerging readers.

15:00 ***740***. **The Development of Functional and Effective Connectivity for Narrative Processing in Children Investigated Via Functional MRI and Multivariate Autoregressive Modeling**

Vincent J. Schmithorst[1], Scott K. Holland[1]
[1]Children's Hospital Medical Center, Cincinnati, Ohio, USA

A functional MRI (fMRI) study involving narrative comprehension was conducted on a cohort of normal children ages 5-18. Activation was seen in Wernicke's area and the middle frontal gyrus bilaterally, and Broca's area in the left hemisphere. The functional connectivity between Wernicke's areas in both hemispheres, and between Wernicke's and Broca's area, increased with age. In addition, using Multivariate Autoregressive Modeling (MAR), feedback networks were found involving effective connectivity from Broca's area and the middle frontal gyrus to Wernicke's area, and the effective connectivity from Broca's area to Wernicke's area in the left hemisphere increased with age.

15:10 ***741***. **Age-Related Changes in Cerebral White and Grey Matter Structures from Infancy to Adulthood: A Voxel-Based Morphometry Study**

Samiuel Groeschel[1], Brigitte Vollmer[1], Alan Connelly[1]
[1]UCL Institute of Child Health, London, UK

In order to quantify and localise morphometric changes during brain development structural high resolution MRI data of 159 subjects from birth to 30 years of age were analysed using voxel-based morphometry. The total volumes of both grey and white matter increase non-linearly over this age range. Relative to brain size, overall grey matter volume decreases non-linearly over this age range, whereas overall relative white matter volume increases. Regression analyses with age as a covariate have been performed during childhood, adolescence, and young adulthood, revealing regional changes in tissue concentration and volume both in grey and white matter structures.

15:20 ***742***. **CASL Perfusion fMRI Revealed Altered Resting Brain Function in Prenatally Cocaine Exposed Teenagers**

Hengyi Rao[1], Hallam Hurt[2], Marc Korczykowski[1], Joan Giannetta[2], David Shera, Brian B. Avants[1], James Gee[1], John A. Detre[1], Jiongjiong Wang[1]
[1]University of Pennsylvania, Philadelphia, Pennsylvania, USA; [2]The Children's Hospital of Philadelphia, Philadelphia, Pennsylvania, USA

The present study used CASL perfusion fMRI and optimized VBM to explore the effect of prenatal cocaine exposure (PCE) on the neurocognitive development of adolescents' brain. Compared to socioeconomically matched controls, perfusion fMRI observed globally reduced CBF particularly in the posterior brain, while regional CBF was relatively increased in anterior brain areas involved in emotional and arousal processing in cocaine-exposed teenagers. Optimized VBM revealed that PCE may increase the gray matter volume in the insula-amygdala areas. These results supported that PCE affects emotional processing and suggested that PCE may alter the spatial distribution of resting brain function in adolescents.

ELECTRONIC POSTER DISCUSSION: Correction Strategies

Room 615 - 617 13:30 - 15:30 Chairs: Frank R. Korosec and Ravi S. Menon

13:30 ***743***. **Field Map Constrained Nonrigid Registration Method for Correction of Distortions in EP Images**

Yong Li[1], Ning Xu[1], John Michael Fitzpatrick[1], Victoria L. Morgan[1], David R. Pickens[1], Benoit M. Dawant[1]
[1]Vanderbilt University, Nashville, Tennessee, USA

Image post-processing techniques have been widely used in distortion correction for Echo Planar (EP) images. Two main strategies among them are field map and nonrigid registration methods. The combination of these two methods has not yet been investigated. Here, we use a measured field map as a constraint for the registration process and we utilize nonrigid registration to compensate inaccuracies in field map measurements. The proposed methodology is demonstrated on simulated images and on a real EP image of a phantom.

13:40 ***744***. **Correction of EPI Nyquist Ghosting Caused by the Non-Uniform Frequency Response of the MRI Receiver Chain**

Oliver Josephs[1], Nikolaus Weiskopf[1], Ralf Deichmann[1]
[1]University College London, London, UK

The acquisition time in rectilinear echo-planar imaging (EPI) is usually minimized by bi-directional scanning in the readout (RO) direction. Differences between the two acquisition directions lead to systematic signal variations between alternate phase-encoding lines and so to Nyquist ghosting. Recently, the MRI receiver frequency response has been shown to contribute a spatially variable ghost, because it leads to different amplitude modulations for the two acquisition directions. Here, we report a method for reducing this type of ghosting and show its effectiveness experimentally.

13:50 ***745***. **An X,y Phase Correction Method to Eliminate Image Ghosts in Single and Multi Shot EPI**

Yuval Zur[1]
[1]GE Healthcare Technologies, Tirat Carmel, Israel

Single and multi shot EPI recon is very sensitive to inconsistencies, i.e. a phase difference F(x, y) between k space lines acquired during alternate read gradient polarity or during different shots. F(x, y) is caused by position dependent eddy currents, anisotropy of the gradient system and field inhomogeneity, and is a function of the readout (x) and phase encoding (y) directions. In this abstract, we propose a simple pre scan and a close form algorithm to calculate F(x, y) and correct the image for any arbitrary number of shots. Experimental data show that this technique robustly eliminates EPI artifacts below detection levels in all imaging directions, even in systems with suboptimal calibrations.

14:00 ***746***. **Real-Time Motion Correction in 3D EPI Using Cloverleaf Navigators**

Laurence Marie Wastiaux[1], Anders M. Dale[2], Andre J. van der Kouwe[1]
[1]Athinoula A. Martinos Center for Biomedical Imaging, Massachusetts General Hospital, Charlestown, Massachusetts, USA; [2]University of California, San Diego, La Jolla, California, USA

Echo Planar Imaging is the method of choice for functional MR Imaging studies where rapid scanning is required to follow brain activations. While multi-slice EPI is commonly used to acquire 3D datasets, 3D EPI offers the advantages of better contiguous slices and higher signal to noise ratio but is more sensitive to subject's motion. To increase the image quality of 3D EPI scans and reduce the effects of motion, we have developed a 3D EPI sequence with embedded cloverleaf navigators, which estimate rigid body motion in real-time and adjust the acquisition parameters accordingly between the acquisition of each partition.

14:10 ***747***. **Full and Hybrid 2-Dimensional Navigator Echo Correction: New Techniques to Suppress Respiratory-Induced Physiological Noise in Echo-Planar Functional MRI**

Robert L. Barry[1, 2], Ravi S. Menon[1, 2]
[1]Robarts Research Institute, London, Ontario, Canada; [2]University of Western Ontario, London, Ontario, Canada

Functional MRI acquired using multi-shot EPI is particularly sensitive to spatially and temporally varying frequency offsets induced by respiration. As global and 1D navigator echo correction techniques have been shown to both amplify and suppress respiratory-induced physiological noise in different regions of an image, the use of full 2D navigator echo correction is investigated. Using a priori information of the slow spatial variations of this induced frequency offset map, the full 2D correction approach is modified to design a computationally efficient hybrid 2D navigator echo correction technique for 2-shot EPI with noise suppression performance comparable to its full 2D counterpart.

14:20 ***748***. **Real-Time B0 and First Order Shim Correction During Motion Correction with Cloverleaf Navigators**

Andre Jan Willem van der Kouwe[1], Thomas Benner[1], Anders Martin Dale[2]
[1]Massachusetts General Hospital, Charlestown, Massachusetts, USA; [2]University of California at San Diego, La Jolla, California, USA

Various types of navigators have been used for rigid body motion correction and shim correction during imaging. We demonstrate that cloverleaf navigators can be used to achieve real-time rigid body motion correction as well as real-time tracking of zero and first order B0 changes (frequency and linear shim changes) due to effects such as subject motion, breathing and scanner frequency drift. We show that B0 tracking improves the accuracy of the motion estimates and therefore also improves image quality indirectly.

14:30 ***749***. **Eddy Current-Induced Artifact Reduction in Spiral Trajectory Balanced-SSFP for Transition-Band SSFP fMRI**

Jongho Lee[1], John M. Pauly[1]
[1]Stanford University, Stanford, California, USA

Eddy currents in balanced SSFP can cause serious artifacts. In nonphase-cycled balanced SSFP, the direction of the undesired spin dephasing induced from eddy currents is not alternated by the RF phase cycle; therefore conventional sequential phase encodes ordering or rotational interleaves ordering causes phase accumulation. 'Alternating interleaves ordering (or phase encodes ordering)' is suggested to remove the piling of the eddy current-induced spin dephasing. Significant reduction in imaging artifacts and phase changes in FID is observed with this new ordering method.

14:40 *750*. **Real-Time RF Pulse Adjustment for B0 Drift Correction**

Thomas Benner[1], André J.W. van der Kouwe[1], Graham C. Wiggins[1], A. Gregory Sorensen[1]
[1]Athinoula A. Martinos Center, Charlestown, Massachusetts, USA

High duty cycle scans can cause MR scanner frequency drift due to shim heating. This leads to image shift and decreased effectiveness of fat saturation pulses and can result in image artifacts. Methods to correct image shift have been proposed, however, these do not correct the saturation effectiveness. We propose a real-time RF pulse adjustment to synchronize the RF pulses of the sequence with the scanner frequency drift based on the estimation of the frequency drift from the phase correction lines. Real-time RF pulse adjustment is found effective to correct for image drift as well as decreasing fat saturation effectiveness.

14:50 *751*. **Real-Time B0 Field Drift Compensation in Balanced SSFP: Stabilization of the Activation Band in Transition-Band SSFP fMRI**

Jongho Lee[1], Juan M. Santos[1], John M. Pauly[1]
[1]Stanford University, Stanford, California, USA

B0 field drift shifts the activation band in transition-band SSFP fMRI. This results in the degradation of functional contrast and the reduction of spatial coverage. We utilized a real-time feed-back system to measure and compensate for this drift. About 0.23 ~ 0.26 ppm/hr of drift was measured and successfully compensated for.

15:00 *752*. **Real Time Shimming for Compensation of Respiration Induced Field Changes**

Peter van Gelderen[1], Jacco Adrianus de Zwart[1], Piotr Starewicz[2], Robert Scott Hinks[3], Jeff Hendricus Duyn[1]
[1]National Institues of Health, Bethesda, Maryland, USA; [2]Resonance Research, Inc., Billerica, Massachusetts, USA; [3]GE Healthcare, Milwaukee, Wisconsin, USA

A system was designed for real time shimming to compensate respiration induced field changes. The feasbility of real time shimming is demonstrated for brain imaging at 7T, showing a marked increase in phase stability and image quality compared to scans without this compensation. The system can be used with all types scans, as it does not require any sequence modification.

15:10 *753*. **An *In-Vivo* Image Intensity Correction Method for High Field Systems**

Ceylan Celil Guclu[1], Hiroyuki Kabasawa[2], Zhu Li[1]
[1]GE Healthcare, Waukesha, Wisconsin, USA; [2]GE Yokogawa Medical Systems, Hino-shi, Tokyo, Japan

In this work we developed a technique to reduce the dielectric effect related image non-uniformity at high field. The method is practical for all routine clinical high field imaging. Phantom and volunteer scans performed to test the efficiency and robustness of the technique. Some of the results were presented in the text.

15:20 *754*. **Automated Lipid Artefact Removal for DTI Using Multiple Coils**

David J. Larkman[1], Philip G. Batchelor[2], Serena Counsell[1], Joseph V. Hajnal[1]
[1]Hammersmith Hospital, Imperial College London, London, UK; [2]University College London, London, UK

DTI is extremely sensitive to imperfect fat suppression as the immobile lipid protons signal is largely unaffected by the diffusion gradients whilst signal in the rest of the brain is suppressed. In our experience imperfect fat suppression at 3T is not uncommon. In this study we develop a practical, automated and robust method of identifying problem pixels and correcting them. We apply the method to Diffusion Weighted Imaging (DWI) and demonstrate that errors introduced by lipid contamination can be eliminated entirely from apparent diffusion coefficient (ADC) maps and fractional anisotropy (FA) maps, both of which are extremely sensitive to it.

CLINICAL SCIENCE FOCUS SESSION: MR as a Predictive of Response Biomarkers to Cancer Treatment

Room 618 - 620 13:30 - 15:30 Chairs: Peter L. Choyke and Frederik L. Giesel

13:30 *755*. **Prognostic Power of DCE-MRI Heterogeneity Analysis in Patients with Advanced Solid Tumours**

Yvonne Watson[1], Sue Cheung[1], Caleb Roberts[1], Gio A. Buonaccorsi[1], Karen E. Davies[1], Alan Jackson[1], Chan Ton[2], Lynn Broughton[2], Fiona Power[2], Gordon C. Jayson[2], Zhihui Lang[3], Saifee Mullamitha[2], Robert Beckman[3], Geoff J M Parker[1]
[1]University of Manchester, Manchester, UK; [2]Christie Hospital, Manchester, UK; [3]Centocor, Malvern, Pennsylvania, USA

22 patients were enrolled for a dynamic contrast-enhanced (DCE)-MRI study of the effects of a novel antivascular agent. Although no clear drug effect was discernable, we observed that small differences in average tumour microvascular characteristics were present that distinguished patients with progressive disease from those with stable or better disease. Widespread differences of large magnitude between these groups were apparent on histogram analysis, indicating the importance of accounting for intra-tumour heterogeneity when interpreting the findings of DCE-MRI studies. We conclude that heterogeneity in DCE-MRI parameters is of potential prognostic value.

13:40 ***756***. **Predicting Recurrence Patterns of Gliomas Using Diffusion Tensor Imaging**

Stephen John Price[1], Rajesh Jena[1], Neil Gunn Burnet[1], T. Adrian Carpenter[1], John D. Pickard[1], Jonathan H. Gillard[1]
[1]University of Cambridge, Cambridge, UK

Gliomas are one of the most heterogeneous tumours yet we treat them all the same. If we could identify different phenotypes it might allow us to individualise treatment. By splitting the diffusion tensor into its isotropic and anisotropic components we have identified three groups of abnormality that can predict recurrence patterns in 92% of cases. Diffuse abnormalities usually predict a general increase in tumour size. Localised abnormalities usually predict recurrence in the direction of this abnormality. For the few patients with minimal abnormality this appears to predict slow progression and may be a marker of long-term survival.

13:50 ***757***. **Predicting Grade of Cerebral Glioma Using Vascular-Space-Occupancy (VASO) MRI**

Hanzhang Lu[1], Erica Pollack[1], Robert Young[1], James S. Babb[1], Glyn Johnson[1], Jens H. Jensen[1], Joseph A. Helpern[1], Meng Law[1]
[1]New York University, New York, USA

Cerebral glioma is an aggressive form of brain tumor characterized by angiogenesis and breakdown of blood-brain-barrier. The extent of these hemodynamic changes is known to be correlated with the grade of the tumor. Using a recently developed Vascular-Space-Occupancy (VASO) MRI technique that is sensitive to changes in both CBV and vascular permeability, we examined the relationship between VASO parameters and the tumor grade in 39 patients with primary glial neoplasms. The results show different VASO parameters in grade 1, 2 and 3 gliomas, and both VASOTumor (p=0.0006) and VASORatio (p=0.0004) can be used as a significant predictor of tumor grades.

14:00 ***758***. **Pre-Surgery Lactate, Lipid, and ADC Predict Survival for Patients with Glioblastoma Multiforme**

Forrest W. Crawford[1], Inas S. Khayal[1], Kathleen R. Lamborn[1], Rebeca Choy[1], Suja Saraswathy[1], Ilwoo Park[1], Joonmi Oh[1], Soonmee Cha[1], Susan Chang[1], Sarah J. Nelson[1]
[1]University of California, San Francisco, California, USA

Accurate prediction of survival for newly diagnosed Glioblastoma Multiforme (GBM) patients could assist oncologists in evaluation of the effectiveness of new therapies in clinical trials by providing an improved baseline estimate of survival. We studied 54 patients with GBM who had undergone no prior resection or treatment to determine whether MR spectroscopic imaging or diffusion-weighted MRI markers would predict survival immediately prior to surgery. The results of our study suggest that the average normalized values of lactate and lipid measured within the T2 hyperintense region, and ADC measured within the contrast-enhancing and necrotic regions may be predictive of survival.

14:10 ***759***. **Dynamic Tumor Regression During Radiation Therapy Predicts Treatment Outcome in Cervical Cancer**

Jian Zhong Wang[1], Nina A. Mayr[1], William TC Yuh[1], Joseph F. Montebello[1], John C. Grecula[1], Dee H. Wu[2], Kenneth F. Wegner[2], Susan M. Edwards[2], Nilendu Gupta[1], Michael V. Knopp[1]
[1]The Ohio State University, Columbus, Ohio, USA; [2]University of Oklahoma Health Science Center, Oklahoma City, Oklahoma, USA

MRI-based volumetric tumor regression parameters (regression rate or area under regression curve) predicts long-term local tumor control and survival in cervical cancer. If tumor shows >10% residual volume at the conclusion of treatment, the risk for local failure and death are so high (> 80%) that aggressive intervention is warranted.

14:20 ***760***. **Use of Dynamic Contrast-Enhanced MRI to Predict Drug Uptake in Patients**

Alain Oregioni[1], Simon Walker-Samuel[1], James Darcy[1], David J. Collins[1], Chooi P. Lee[1], Michael Tracey[2], Maeli J. Campbell[3], Ian R. Judson[1], Paul Workman[1], Martin O. Leach[1], Geoffrey S. Payne[1]
[1]Institute of Cancer Research and Royal Marsden NHS Trust, Sutton, Surrey, UK; [2]SRI International, Menlo Park, California, USA; [3]Cancer Research UK, London, UK

Detection and prediction of drug delivery to target tissues is of crucial importance in treating disease. We have investigated whether the vascular parameters derived from dynamic contrast-enhanced MRI predict uptake of an agent currently in phase 1 clinical trial (SR4554), as measured with 19F MR spectroscopy. Good correlations are observed between drug delivery and dynamic contrast enhanced derived vascular parameters Ve (r=0.828, p=0.022), KTrans (r=0.741, p=0.057), rBV (r=0.812, p=0.026) and rBF (r=0.910, p=0.044).

14:30 ***761***. **The Effect of Heterogeneous Tumour Enhancement on the Assessment of Response to Treatment**

Simon Walker-Samuel[1], N. Jane Taylor[2], Anwar R. Padhani[2], Martin O. Leach[1], David J. Collins[1]
[1]Institute of Cancer Research, Sutton, Surrey, UK; [2]Mount Vernon Hospital, Northwood, Middlesex, UK

Response to treatment of cancer is usually assessed using DCE-MRI by either evaluating the change in the fit to a whole-tumour averaged uptake curve or by the change in summary statistics such as mean, median, etc. following pixel-by-pixel analysis. This study aimed to assess the relative sensitivity of each approach using simulations of heterogeneous tumour enhancement and spatially heterogeneous response. It is shown that median and mean measurements are more sensitive to change than whole-tumour fitting but that neither approach reflects the known, localised therapeutic response.

14:40 ***762***. **MRI Measures of Tumor Perfusion and T_2 Relaxation in Response to Radiotherapy for Prostate Cancer**

David L. Buckley[1], Lucy E. Kershaw[1], John P. Logue[2], Charles E. Hutchinson[1]
[1]University of Manchester, Manchester, Greater Manchester, UK; [2]Christie Hospital, Manchester, Greater Manchester, UK

The purpose of this study was to assess the vascular and MR relaxation characteristics of the prostate gland in response to radiotherapy. Twenty-two patients were studied before and one year after radiotherapy using T_1 and T_2 mapping, dynamic contrast-enhanced MRI and a distributed parameter tracer kinetic model. Following treatment tumor perfusion was significantly reduced and the permeability of microvessels in nearby muscle increased. Pre-treatment measures of tumor T_2 and relative perfusion were found to differ between responders and non-responders.

14:50 ***763***. **Parametric DCE-MRI HPI Maps - A Qualitative and Quantitative Analysis in Phase I Clinical Trial Patients with Liver Metastases**

Keiko Miyazaki[1], Simon Walker-Samuel[1], Benjamin Richard Knowles[1], N J. Taylor[2], A R. Padhani[2], Tony Wallace[1], Adrian Tang[1], Mark White[3], David Hawkes[3], David Atkinson[3], David J. Collins[1], Martin O. Leach[1], D M. Koh[1]
[1]The Institute of Cancer Research and The Royal Marsden NHS Trust, Sutton, Surrey, UK; [2]Mount Vernon Hospital, Northwood, Middlesex, UK; [3]University College of London, London, UK

The aim of this study was to qualitatively and quantitatively assess parametric HPI maps obtained using DCE-MRI in a group of Phase I clinical trial patients with metastatic liver disease. MR signal intensities were converted to gadolinium concentrations and the HPI values were calculated from the DCE-MRI concentration-time curves. Qualitative analysis of HPI maps in patients with metastatic liver disease showed striking increase in relative arterial perfusion around hepatic metastases. Quantitative measurements of whole liver and tumoral HPIs showed good reproducibility. Quantitative HPI therefore, may be investigated as a potential marker for treatment response in clinical drug trials.

15:00 ***764***. **Evaluation of the Effects of the Triple Angiokinase Inhibitor BIBF 1120 on Tumor Vasculature in a Phase I Clinical Trial Using Dynamic Contrast-Enhanced MRI (DCE-MRI)**

Ralph Strecker[1], Klaus Mross[2], Martin Stefanic[3], Lothar de Rossi[3], Jürgen Hennig[1]
[1]University Hospital, Freiburg, Germany; [2]Tumorbiology Center, Freiburg, Germany; [3]Boehringer-Ingelheim Pharma GmbH & CO KG, Biberach, Germany

DCE-MRI using an IR trueFISP protocol was applied in a clinical phase I trial of the novel triple angiokinase inhibitor BIBF 1120. A reduction of >40% in iAUC/ Ktrans was observed in a considerable number of patients with a maximum (11/35) after 2 cycles (56 days) of treatment. Most of the responders were treated with doses in the range of 250-300mg once daily and 250mg twice daily BIBF 1120. DCE-MRI results suggest an antiangiogenic effect of BIBF 1120.

15:10 ***765***. **Dynamic MRI Evaluation of the Triple Receptor Tyrosine Kinase Inhibitor BIBF 1120 in Patients with Advanced Solid Tumours**

Anwar R. Padhani[1], N Jane Taylor[1], James A. d'Arcy[2], Simon Walker-Samuel[2], David J. Collins[2], Benjamin Knowles[2], J. James Stirling[1], Toni Wallace[2], Dow-Mu Koh[2], Adrian Tang[2], Chooi Lee[2], Graham Temple[3], Gordon J S Rustin[1], Martin O. Leach[2]
[1]Mount Vernon Hospital, Northwood, Middlesex HA6 2RN, UK; [2]Royal Marsden Hospital, Sutton, Surrey SM2 5PT, UK; [3]Boehringer Ingelheim, Bracknell, Berkshire RG12 8YS, UK

Antivascular effects of a triple receptor tyrosine kinase inhibitor (BIBF-1120 acting against VEGF, FGF and PDGF) are explored by dynamic MRI (DCE-MRI) in a multicentre phase I clinical study. Antiangiogenesis effects are seen in isolated patients and in cohort analyses. There was no clear evidence for drug dose dependence but patients with metastatic liver disease appeared to have the largest antivascular effects.

15:20 ***766***. **Single and Multi-Centre DCE-MRI Reproducibility in Phase I Clinical Trials**

N. Jane Taylor[1], James A. d'Arcy[2], Simon Walker-Samuel[2], Katharine J. Lankester[3], David J. Collins[2], Benjamin Knowles[2], David L. White[4], Yves Miaux[4], Joyce Suhy[4], Ali Guermazi[4], J James Stirling[1], Toni Wallace[2], Dow-Mu Koh[2], Adrian Tang[2], Chooi Lee[2], Gordon J S Rustin[1], Martin O. Leach[2], Anwar R. Padhani[1]
[1]Mount Vernon Hospital, Northwood, Middlesex HA6 2RN, UK; [2]Royal Marsden Hospital, Sutton, Surrey SM2 5PT, UK; [3]Royal Marsden Hospital, London, SW3 6JJ, UK; [4]Synarc, Inc., San Francisco, CA 94105, USA

The measurement of test-retest variability is integral to trial design of phase I antiangiogenesis and angiolytic drugs where dynamic MRI (DCE-MRI) is used to evaluate the effect of drug on tumour vasculature. Knowing kinetic parameter reproducibility enables the identification genuine pharmoacodynamic effects and this information can then be used to identify a biologically active dose. In this study we compare single and multiple centres DCE-MRI studies with the aim of identifying the change in K^{trans} that would be significant for a single patient and for typical Phase I dosing cohort sizes of 3 and 6 patients.

CLINICAL MRI HANDS-ON WORKSHOP 2 (REPEAT)
Body and Cardiovascular Protocol Optimization
GE Healthcare

Room 4F(1) 13:30 – 15:30 Chairs: David A. Bluemke and Caroline Reinhold

CLINICAL MRI HANDS-ON WORKSHOP 2 (REPEAT)
Body and Cardiovascular Protocol Optimization
Philips Medical Systems

Room 4F(2) 13:30 – 15:30 Chairs: David A. Bluemke and Caroline Reinhold

CLINICAL MRI HANDS-ON WORKSHOP 2 (REPEAT)
Body and Cardiovascular Protocol Optimization
Siemens Medical Solutions

Room 4F(3) 13:30 – 15:30 Chairs: David A. Bluemke and Caroline Reinhold

Brain Architecture, Function and Development: Analysis By Diffusion Tensor Imaging

Room 6E 16:00 - 18:00 Chairs: Susumu M. Mori and Kei Yamada

16:00 ***767***. **Sex Differences in White Matter Diffusion Anisotropy in the Normal Pediatric Population**
Vincent J. Schmithorst[1], Mark DiFrancesco[1], Bernard J. Dardzinski[1], Scott K. Holland[1]
[1]Children's Hospital Medical Center, Cincinnati, Ohio, USA

Possible sex differences in diffusion fractional anisotropy (FA) of brain white matter were investigated in a cohort of normal children ages 5-18. A modified voxelwise analysis technique was utilized which reduces the risk of spurious results due to imperfect spatial normalization. Boys displayed greater FA in inferior fronto-temporal white matter, the genu of the corpus callosum, the corticospinal tract, and left inferior parietal white matter; no regions were found with greater FA in girls. Post-hoc analyses revealed no sex-by-age interaction effects. The results indicate different developmental trajectories in white matter maturation between boys and girls.

16:12 ***768***. **Between Session and Between Subject Reproducibility of Diffusion MR and Tractography Measures**
Einar Heiervang[1], Timothy EJ Behrens[2], Clare M. Mackay[2], Matthew D Robson[2], Heidi Johansen-Berg[2]
[1]Haukeland University Hospital, Bergen, Norway; [2]University of Oxford, Oxford, UK

Diffusion MR and tractography are increasingly used to generate quantitative measures for clinical studies. Interpretation of such results depends on a good understanding of the variability of these measures but evidence on this variability is limited. We scanned 8 subjects on 3 occasions to characterise within and between subject variability of quantitative diffusion measures including histogram measures of fractional anisotropy (FA), ROI analyses of FA, and measures generated from tractography. The variability measures that we present can be used to estimate required sample sizes to detect differences between populations.

16:24 ***769***. **Auditory-Language Networks Involving the Superior Temporal Gyrus: Patterns of Connection and Lateralization**
Hamied Ahmad Haroon[1], Matthew A. Lambon Ralph[1], Yvonne Watson[1], Olga Ciccarelli[2], Claudia A M Wheeler-Kingshott[2], Daniel C. Alexander[3], Simona Luzzi[4], Geoffrey J M Parker[1]
[1]The University of Manchester, Manchester, England, UK; [2]Institute of Neurology, UCL, London, England, UK; [3]University College London, London, England, UK; [4]University of Ancona, Ancona, Italy

To date, neuroanatomy of the human brain has only been inferred from either studies in non-human primates or from the results of functional neuroimaging studies. We have used probabilistic tractography, incorporating crossing fibre information, to assess anatomical connection of human superior temporal gyrus (STG) *in vivo*. We provide evidence for parcellation of the human STG according to auditory/language connections that show close compatibility with invasive non-human primate studies. We also present evidence for clear lateralization of intra- and extra-STG anatomical connection involved with some aspects of higher auditory/language processing, whilst demonstrating no structural lateralization of connections serving primary auditory processing.

16:36 ***770***. **White Matter Development During Late Adolescence in Healthy Males: A Cross-Sectional Diffusion Tensor Imaging Study**

Manzar Ashtari[1], Khader M. Hasan[2], Hana Kester[3], Babak Ardekani[4], Kelly Cervellione[3], Jinghow Wu[3], Carolyn McIlree[3], Philip R. Szeszko[3], Sanjiv Kumra[3]

[1]North Shore Long Island Jewish Health System, New Hyde Park, New York, USA; [2]University of Texas Medical School, Houston, Texas, USA; [3]North Shore Long Island Jewish Health System, Glen Oaks, New York, USA; [4]Nathan Klein Institute, Rockland, New York, USA

The authors investigated white matter maturation as reflected by changes in anisotropy with age in a cohort of healthy adolescent males. Twenty-four healthy volunteers were divided into two groups based on a median age split and were studied using DTI and voxelwise analysis. Increased FA and parallel anisotropy were observed in older adolescents in the left arcuate fasciculus. Verbal fluency and verbal comprehension were correlated with higher FA in this area. The increased FA and parallel anisotropy may reflect a tendency in reduced tortuousity and/or increased axonal fiber organization to a more parallel orientation during brain maturation in late adolescent.

16:48 ***771***. **Application of DTI in Human Fetal Brain Development Study**

Hao Huang[1], Linda Richards[2], Rong Xue[3], Peter van Zijl[1, 4], Susumu Mori[1, 4]

[1]Johns Hopkins University School of Medicine, Baltimore, Maryland, USA; [2]The University of Queensland, St Lucia, Queensland, Australia; [3]New York University, New York, New York, USA; [4]Kennedy Krieger Institute, Baltimore, Maryland, USA

DT-MRI has been proved to be an effective technique for the study of normal and injured developing human brain. High resolution DTI data was acquired for fixed fetal brains from 13 to 21 gestational weeks. High contrasts from diffusion tensor can delineate most neural structures of developing fetal brains. To quantify the correlation of the primary eigenvector orientation and cortical surface morphology, the angles between the normal vectors of cortical surface and primary eigenvector of diffusion tensor were measured to reveal the growth pattern of cortical surface. DTI not only provides the high contrast for structure identification and 3D reconstruction, but also helps understanding of cortical surface folding.

17:00 ***772***. **Voxel-Based Investigation of White Matter Changes in Normal Ageing Using Diffusion Tensor Imaging**

Thomas Richard Barrick[1], Rebecca Anne Charlton[1], Michael O'Sullivan[1], Hugh S. Markus[1], Chris A. Clark[1]

[1]Saint George's, University of London, London, UK

Voxel-based statistical analyses of diffusion parameters allow us to investigate anatomical distribution of white matter damage across the ageing brain. Here we present data from a large sample of normal older adults in which we analyse 3D mean diffusivity (MD) and fractional anisotropy (FA) maps, and investigate MD and FA perpendicular to the mid-sagittal plane (2D column maps) and through coronal slices (1D coronal slice profiles) in standard space. Our results indicate a decline of white matter integrity across the whole brain, but with the anterior frontal lobes being particularly affected.

17:12 ***773***. **The Somatotopic Organization of Thalamocortical Projection Fibers Through the Centrum Semiovale**

Kei Yamada[1], Osamu Kizu[1], Hirotoshi Ito[1], Takao Kubota[1], Kentaro Akazawa[1], Hiroyuki Oouchi[1], Shigenori Matsushima[1], Tsunehiko Nishimura[1]

[1]Kyoto Prefectural University of Medicine, Kyoto, Japan

The sensory tract trajectory towards the cerebral cortex has not been previously thoroughly investigated. By using diffusion tensor imaging (DTI) based tractography, we elucidated the course of the sensory tract through the supratentorial brain. Seven healthy normal volunteers underwent MR scanning using a 1.5 Tesla imager. All the sensory tracts had a posterior rotation as they traveled through the centrum semiovale towards the cortex. When the pair of tracts was viewed as a unit, the sensorimotor tracts of the lower extremity formed the axis of rotation around which the other parts of the pyramidal and sensory homunculus turned.

17:24 ***774***. **The Minimum Detectable Change in Water Diffusion Across DTI Sessions**

Raymond Wei-Meng Lau[1], Bradley Gordon Goodyear[1]

[1]University of Calgary, Calgary, AB, Canada

As myelin is destroyed during the progression of Multiple Sclerosis, the local fractional anisotropy (FA) of water diffusion as measured by diffusion tensor imaging (DTI) decreases. To track disease progression and assess treatment, there is a need to measure FA during the progression of MS in individual patients. In this study, we determine the minimum detectable change in FA, mean diffusion (MD), and transverse diffusion (TD) across imaging sessions. As a result, this will determine if the precision of FA, MD, and TD is sufficient for clinical use to monitor the progression of white matter disease.

17:36 *775.* **Diffusion Tensor Axial Diffusivities Are Different in the Body of the Corpus Callosum of Age-Matched Male and Female Adults**

Khader M. Hasan[1], Chul W. Ahn[2], Rakesh K. Gupta[3], Larry Kramer[1], Linda Ewing-Cobbs[2], Jack M. Fletcher[2], Ponnada A. Narayana[1]

[1]University of Texas Medical School, Houston, Texas, USA; [2]UofT, Houston, Texas, USA; [3]SGPGIMS, Lucknow, UP, India

The contributors to human *in vivo* tissue diffusion anisotropy remain to be unresolved even for the simplest white matter structure such as the corpus callousm (CC) which is known to have heterogeneous axonal density and myelination levels. DTI literature on gender based differences in ansiotropy are llargely inconsistent. In this report, we use the transverse and longitudinal eigenvalues on the seven segments of the corpora callosa of 16 males and 16 age-matched females and show that subtle microstructural differences in the water molecular diffusion in large myelinated fibers can be detected using optimized entire brain DTI at high SNR and using the principal eigenvalues as a more specific morphological index.

17:48 *776.* **Temporo-Parietal White Matter Pathway Asymmetry Underlies Functional Laterality**

Thomas Richard Barrick[1], Nigel Lawes[1], Clare E. Mackay[2], Chris A. Clark[1]

[1]Saint George's, University of London, London, UK; [2]University of Oxford, Oxford, UK

White matter pathway asymmetry was investigated using diffusion tensor tractography in a normalised image dataset of 30 right handed young healthy individuals for pathways passing between the temporal and parietal lobes. We identified, for the first time, a rightwardly asymmetric pathway connecting the posterior part of the temporal lobe to the superior parietal lobule. This pathway may be related to auditory-spatial function for which there is evidence for a rightward laterality from functional imaging studies and may also be implicated in verbal and auditory spatial working memory function.

MR PHYSICS AND TECHNIQUES FOR CLINICIANS

Room 6C 16:00 - 18:00 Chairs: Frank R. Korosec and Joseph C. McGowan

Educational Objectives:
Upon completion of this session, participants should be able to:

- Define and describe the fundamental principles of MR imaging, including the definition of spin magnetization, the Larmor relationship, relaxation phenomena, and the process of using the spin magnetization to produce an image;
- Explain imaging pulse sequences based upon spin and gradient echoes, including fast spin echo and echo planar techniques;
- Design MR imaging protocols for diagnostic applications considering image contrast, spatial resolution, acquisition time, signal-to-noise ratio, and artifacts; and
- Describe the principles and capabilities of various advanced MR techniques including, diffusion, vascular and cardiac MRI.

16:00 **Diffusion MRI**
Konstantinos Arfanakis

16:40 **MR Angiography**
Jean H. Brittain

17:20 **Cardiac MRI**
Oliver Wieben

Emerging MR Systems Concepts

Room 6D 16:00 - 18:00 Chairs: Blaine A. Chronik and Jacob D. Willig

16:00 *777.* **Continuous-Wave MRI of Short-T_2 Solid Materials**

David J. Lurie[1], Andrew J. Fagan[2], Gareth R. Davies[1], James M. Hutchison[1]

[1]University of Aberdeen, Aberdeen, Scotland, UK; [2]Trinity College, Dublin, Ireland

Many solid materials exhibit extremely short T_2 relaxation times, which may be as short as 10-20μs in rigid solids. This makes them impossible to image by standard pulsed MRI. We have developed a solid imaging technique based on continuous-wave (CW) detection, which has in practice no lower limit on the T_2 of the solid being imaged. CW-MRI was implemented at 7T (300 MHz). One-dimensional projections are obtained by sweeping B_0 through resonance in the presence of a continuously-applied gradient. Stepwise rotation of the gradient through 180° allows image reconstruction from the projections. 2D and 3D images of rigid solids have been produced.

16:12 ***778***. **Torque-Figure of Merit Trade-Off in Multi-Layer Asymmetric Gradient Coils**

Hector Sanchez Lopez[1], Feng Liu[1], Adnan Trakic[1], Stuart Crozier[1]
[1]University of Queensland, Brisbane, Queensland, Australia

In the present research we describe the relationship between the figure of merit and target torque minimization value for multi-layer asymmetric transverse gradient coils taking into account the real field profile of long and short bore symmetric and asymmetric magnets. Two torque/force minimization strategies are introduced in order to obtain asymmetric transverse gradient coils with a high minimum torque-maximum figure of merit trade-off. Simple current pattern, minimum torque, high performance head asymmetric gradient coils are obtained combining the real external magnetic field effects over the gradient coil with a specific axial position of the gradient coil's DSV.

16:24 ***779***. **Insert Dome Gradient Coils for Brain Imaging**

James Leggett[1], Dan Green[1], Richard Bowtell[1]
[1]University of Nottingham, Nottingham, UK

Insert gradient coils offer significant advantages for brain imaging. Head-sized hemispherical gradient coils offer further improvements in performance compared with cylindrical coils. This enhanced performance is compromised when torque-balancing is incorporated into the design of transverse hemispherical coils. We show how the addition of a short, cylindrical coil section to the open end of the hemisphere, overcomes this problem, allowing the design of torque-balanced gradient coils which have significantly higher efficiency at fixed inductance than conventional cylindrical insert coils. A full three-axis, dome gradient coil set has been designed, built and subsequently used in brain imaging experiments at 3 T.

16:36 ***780***. **Local Planar Gradients with Order-Of-Magnitude Strength and Speed Advantage**

Bulent Aksel[1], Bruce D. Collick[2], Luca Marinelli[1], William D. Barber[1], Paul A. Bottomley[3], Christopher J. Hardy[1]
[1]General Electric, Niskayuna, New York, USA; [2]General Electric, Waukesha, Wisconsin, USA; [3]Johns Hopkins University, Baltimore, Maryland, USA

We have designed, built, and tested a planar gradient set producing gradient fields of 250 mT/m in X and Y, and 500 mT/m in Z at 320 A current. This is an order-of-magnitude increase in performance over present clinical systems, but in a limited field-of-view (FOV). Because FOV is limited, dB/dt levels remain within safe levels so the gradient system can be used for rapid, high-resolution, and efficient diffusion-weighted MRI. Initial imaging experiments on normal volunteers show excellent image quality after correcting for gradient nonlinearity, without excessive coil heating or movement.

16:48 ***781***. **Advances in NMR Probe Technology for Magnetic Field Monitoring**

Nicola De Zanche[1], Christoph Barmet[1], Jurek A. Massner[1], Klaas Paul Pruessmann[1]
[1]University and ETH Zurich, Zurich, Switzerland

We report recent advances in the design and integration of NMR probes for monitoring the spatiotemporal magnetic field evolution during MR experiments. New choices of sample and matching materials have been essential for improving signal lifetimes and in miniaturizing the NMR samples to prevent dephasing in high-resolution scans. Solid-state matching has critically improved the probe handling and durability. Arbitrary probe configurations are enabled by a modular mounting system. For reliable operation at high field, RF crosstalk has been addressed by refined cabling. The potential of large probe arrays and flexible mounting is illustrated by an example of second-order field monitoring.

17:00 ***782***. **3D Prepolarized MRI with RARE**

Nathaniel I. Matter[1], Greig C. Scott[1], Ross D. Venook[1], Sharon E. Ungersma[1], Thomas Grafendorfer[2], Albert Macovski[1], Steven M. Conolly, [12]
[1]Stanford University, Stanford, California, USA; [2]University of California at Berkeley, Berkeley, California, USA

Prepolarized MRI (PMRI) with pulsed electromagnets has the potential to produce diagnostic quality 0.5-1.0 T images with significantly reduced cost, susceptibility artifacts, specific absorption rate, and gradient noise. We describe the use of three techniques to achieve efficient, artifact-free RARE in PMRI: electro-motive force (EMF) cancellation during field ramping, phase compensation of CPMG echo trains, and quadratic nulling of concomitant gradient fields. We demonstrate the use of prepolarized RARE to acquire *in vivo* wrist images with T_1 and fat-suppressed T_2 weighting using clinical resolution and scan times.

17:12 ***783***. **A Broadband Tunable Surface Coil and Magnetic Force Detector for MRI**

Charles Andrew Paulson[1], Modhurin Banerjee[1], Krishna Kurpad[1], Thomas M. Grist[1], Daniel Warren van der Weide[1]
[1]The University of Wisconsin, Madison, Wisconsin, USA

We demonstrate detection of high frequency magnetic fields using a cantilever with an integrated magnetic loop. The detection works be frequency mixing with the magnetic fields of a sample. A broadband loop antenna gathers fields to be detected and step-up transforms them at the location of the cantilever. We demonstrate broadband performance of the system by detecting a range of frequencies between 10 and 1000 MHz. The Q of our detection system is extremely high (10,000+), and it increases linearly with frequency. Also, our detection system requires no capacitor, thus minimizing dielectric coupling.

17:24 ***784***. **Comparison of Optical Modulation Methods for RF Coil Interlinks**

Jing Yuan[1], Juan Wei[1], Gary X. Shen[1]
[1]The University of Hong Kong, Hong Kong, People's Republic of China

Optical modulation method is one of the key factors in the optical link design for MRI RF coil interlinks. In this work, link performances of direct modulation by laser diode and external modulation by Mach Zehnder Interferometer are compared in the aspects of power gain, modulation bandwidth, noise figure and dynamic range. An external optical link can achieve better performance by the use of a low noise and high power laser. However, a direct optical link shows advantages in link structure, compact size and low cost. It is more feasible in engineering for large coil array interlinks.

17:36 ***785***. **Combining PET and MRI - Challenges in Developing an MR Compatible PET Insert**

Ciprian Catana[1], Yibao Wu[1], Martin S. Judenhofer[2], Jeffrey H. Walton[1], Bo Joseph Peng[1], Jacob Willig-Onwuachi[1, 3], Bernd J. Pichler[2], Simon R. Cherry[1]
[1]University of California, Davis, Davis, California, USA; [2]University of Tuebingen, Tuebingen, Germany; [3]UCDMC, Sacramento, California, USA

PET and MRI are two widely utilized imaging techniques that are largely complementary in the information they provide. Integrating PET and MRI into a single system may benefit a range of existing studies where data from both modalities is required, and may also lead to new applications in molecular imaging. We are building a PET scanner insert for preclinical MRI systems by using field-insensitive position sensitive avalanche photodiodes coupled, via short lengths of optical fibers, to arrays of LSO scintillator crystals. The fibers are used to minimize radiofrequency interference between the RF and gradient coils, and the PET detector system.

17:48 ***786***. **Resolution Improvement of PET in PET/MRI Combined System**

Hao Peng[1], William H. Handler[1], James W. Odegaard[1], Peter J. Simpson[1], Blaine A. Chronik[1]
[1]University of Western Ontario, London, Ontario, Canada

The integration of anatomical and functional imaging modality such as PET/CT and PET/MRI has caused intensive interests in the recent years, which provide more accurate diagnosis information and effective patient management. PET resolution is mainly determined by the point spread function (PSF) of isotopes, detector size ands system diameter. MRI can improve the PET system resolution by reducing the PSF. This effect is most significant in small animal PET system and for high energy isotopes such as 68Ga and 82Rb. A Monte-Carlo simulation was used to study the PET system resolution improvement as a function of different magnetic field strengths, for a small animal PET system.

Cardiac: From Acquisition to Quantitative Data

Room 4C - 3,4 16:00 - 18:00 Chairs: Dara L. Kraitchman and Orlando P. Simonetti

16:00 ***787***. **Transcapillary Transport of Gd-DTPA in the Human Heart Increases in Proportion to Myocardial Blood Flow**

Michael Jerosch-Herold[1], Xin Li[1], Charles S. Springer[1]
[1]Oregon Health & Science University, Portland, Oregon, USA

The degree of transcapillary transport of extracellular Gd-contrast during the first pass can be confounded by transcapillary water exchange. A linear 3-site exchange model is combined with the Kety-Schmidt tracer kinetic model to determine the dependence of the capillary transfer rate constant for Gd-DTPA on myocardial blood flow. The capillary transfer rate constant was found to increase with flow, in agreement with the concept of capillary recruitment during vasodilation.

16:12 ***788***. **Multimodality Visualization of MR Functional Information Fused with CT Coronary Vasculature**

Rakesh Mullick[1], Vivek Vaidya[1], Kokku Raghu[1], Stuart Clarkson[2], Cindy Comeau[3]
[1]GE Research, Bangalore, India; [2]GE Healthcare, Milwaukee, Wisconsin, USA; [3]ACI, CRF, New York, New York, USA

Mutual Information based multi-modality registration methods are engaged in combination with automated vascular segmentation and image acquisition information for unified visualization of cardiac function and anatomy. Cardiac physiology is imaged using rapid MR methods (short-axis) to assess viability, perfusion, and myocardial wall-motion, while the coronary vasculature is derived from high-resolution CT Angiography (axial) data. An interactive environment to visualize Phased MR data and 3D MIP has been developed. An early embodiment of this integrated paradigm is prepared for clinical evaluation.

16:24 ***789***. **Multi-Stage Clustering of Different Heart Tissues in Patients Using Composite Strain Encoding (C-SENC) MRI Images**

ElSayed H. Ibrahim[1], Robert G. Weiss[1], Amy E. Spooner[1], Nael F. Osman[1]
[1]Johns Hopkins University, Baltimore, Maryland, USA

The combination of myocardial functional and viability images is important for therapeutic decision making in patients with myocardial infarction. Composite strain encoding (C-SENC) imaging provides both functional and viability images at the same cardiac phase. This allows for applying automatic clustering techniques without suffering from misregistration problems. In this work, a multi-stage unsupervised clustering technique was applied to the resulting C-SENC images of seven patients. The technique used both fuzzy c-means (FCM) and ISODATA clustering methods. Normal myocardium, infarction, and blood were successfully identified using the proposed technique. In addition, different degrees of contractility were assigned to the non-infarcted myocardium.

16:36 ***790***. **Contribution of Endocardial Trabeculae and Papillary Muscles to Left Ventricular Volumes**

Amol S. Pednekar[1, 2], Raja Muthupillai, [23], Benjamin Cheong[2], Scott D. Flamm[2]
[1]Philips Medical Systems, Bothell, Washington, USA; [2]St.Luke's Episcopal Hospital and Texas Heart Institute, Houston, Texas, USA; [3]Philips Medical Systems, Cleveland, Ohio, USA

Presently, estimation of left ventricular (LV) ejection fraction (EF) from cine-MRI requires manual tracings of the LV cavity, which introduces considerable variability in amounts of endocardial trabeculae (T) and papillary muscles (P) included in end-diastolic (ED) and end-systole (ES) volumes. Two experienced observers delineated the endocardium circumscribing P and T, and one observer drew an additional contours circumscribing P separately at ED and ES. An automatic algorithm estimated the LV blood volume. From these measures, we quantitatively evaluated the relative contributions of tissues T and P to LV volumes at ED and ES, and to EF, using Bland Altman analyses.

16:48 ***791***. **32-Channel Non-Angulated Cine Cardiac Volumes - Automatic Reformatting**

Nicholas Michael Ian Noble[1, 2], Vivek Muthurangu[2], Redha Boubertakh, [12], Richard Winkelmann[3], Robert A. Johnson[2], Sanjeet Hedge[2], Peter Boernert[4], Reza S. Razavi[2], Derek Lionel Glendon Hill[1]
[1]University College London, London, UK; [2]King's College London, London, UK; [3]University of Karlsruhe, Hamburg, Germany; [4]Philips Medical Systems, Hamburg, Germany

Traditional evaluations of cardiac function typically require: scan-planning, two-chamber, four-chamber and short axis acquisitions. This work used a 32-channel coil array in conjunction with SENSE to acquire cine non-angulated volumes of the heart in a single breath-hold. These volumes are isotropic and can thus be reformatted in any orientation - removing the need for multiple acquisitions. We removed the need for manual planning by automatically identifying the short axis and two- and four-chamber orientations via registration to a cadaver atlas. Our technique is quick and all of the view planes identified were deemed clinically acceptable

17:00 ***792***. **Self-Gated Cine MRI for Clinical Wall Motion Abnormality Studies**

Pavani Chalasani[1], Dave N. Sandman[2], Mark Crowe[2], Orlando P. Simonetti[3], Edwin Wu[2], James Carr[2], Andrew Larson[2]
[1]Advocate Illinois Masonic Medical Center, Chicago, Illinois, USA; [2]Northwestern University, Chicago, Illinois, USA; [3]Ohio State University, Columbus, Ohio, USA

Electrocardiogram (ECG)-gating uses an R-wave trigger to synchronize segmented cine data acquisition to the cardiac cycle. ECG gating has been known to have some disadvantages. Self-gating (SG) techniques have been described which potentially eliminate the need for external physiological signal monitoring. SG cine has recently shown to provide equivalent image quality to ECG gated cine in a limited sample of healthy volunteers and patients. However, the SG synchronization signal is largely dependent upon cardiac tissue motion and blood flow and therefore further clinical validation of the SG technique in wall motion abnormality was necessary. The purpose of this study was to assess such clinical effectiveness.

17:12 ***793***. **Automatic Assessment of Left Ventricular Contraction Synchronicity in Cine MRI Studies**

Sebastian Ordas[1], Catalina Tobon-Gomez[1], Critina Moure[2], Marina Huguet[2], Alejandro Federico Frangi[1]
[1]Computational Imaging Laboratory, Pompeu Fabra University, Barcelona, Spain; [2]CETIR-Sant Jordi Cardiovascular Centre, Barcelona, Spain

In this work we present a processing pipeline for automatic global and regional cardiac function analysis employing all available images of a routinely acquired cine CMRI study. The study was tailored to seek for new parameters that could enhance current recommendations for the Cardiac Resynchronization Therapy (CRT), an emerging technique that attempts to restore contractile coordination in dyssynchronous hearts, to those patients most likely to benefit from it. Cine CMRI studies combined with automatic 3D functional analysis, allows to calculate currently assessed dyssynchrony indexes, in an accurate and reproducible way, within the time of a routine examination. Moreover, together with the haemodynamic evaluation of the whole cardiac cycle and contraction patterns, all within the same automatic analysis, the presented methodology provides a compact framework for fast and accurate information providing, aiming to improve CRT planning and candidate recruiting.

17:24 ***794***. **Motion-Guided Segmentation of the Left Ventricle for Cine DENSE MRI**

Bruce Shawn Spottiswoode[1], Xiaodong Zhong[2], Christine H. Lorenz[3], Bongani M. Mayosi[4], Ernesta M. Meintjes[1], Frederick H. Epstein[2]

[1]University of Cape Town, Cape Town, Western Cape, South Africa; [2]University of Virginia, Charlottesville, Virginia, USA; [3]Siemens, Baltimore, Maryland, USA; [4]Groote Schuur Hospital and University of Cape Town, Cape Town, Western Cape, South Africa

Cine DENSE MRI allows myocardial motion to be tracked through the cardiac cycle at a high spatial resolution. We introduce a novel segmentation method that uses the encoded motion in the myocardium to guide a set of contours through time. The method is successfully validated in 320 out of 336 images (95.2%). This algorithm reduces the total user interaction in cine DENSE analysis to the manual demarcation of the myocardium for a single frame. The method is fast and independent of the cardiac imaging plane and the shape of the predefined contour.

17:36 ***795***. **A Synthetic Data Set for Validation of Tracer Kinetic Modelling and Model-Driven Registration in DCE-MRI**

Giovanni Alessandro Buonaccorsi[1], Geoff J.M. Parker[1]

[1]University of Manchester, Manchester, UK

Analytical techniques for DCE-MRI would benefit from validation against ground truth, but patient data is generally unsuitable for this purpose. We have therefore developed a framework for generating synthetic DCE-MRI data sets that includes the incorporation of an appropriate kinetic model and the addition of motion and noise. We have applied tracer kinetic model fitting and kinetic model-driven registration to a simple synthetic data set generated using this framework, with positive results. We propose that synthetic data of this type will prove invaluable for validating DCE-MRI techniques, particularly when these are to be used in clinical trials.

17:48 ***796***. **MR Elastography of the Heart: Initial Feasibility**

Arunark Kolipaka[1], Kiaran P. McGee[1], Philip A. Araoz[1], Phillip J. Rossman[1], Richard L. Ehman[1]

[1]Mayo Clinic, College of Medicine, Rochester, Minnesota, USA

Changes in the mechanical properties of myocardium are associated with a variety of cardiac disease processes. MR elastography (MRE) has been used to quantitate shear stiffness in the absence of organ motion. We hypothesize that gated acquisition sequences employed in cardiac MR can be adapted to current MRE sequences to provide shear stiffness measures of organs undergoing periodic motion. This work describes the development and initial evaluation of a gated MRE sequence in a spherical phantom undergoing period volumetric and pressure changes. The results indicate the initial feasibility of quantitating the shear stiffness of an organ undergoing these cyclic variations.

fMRI: Drug Modulated Effects in Animals

Room 611 - 612 16:00 - 18:00 Chairs: Markus Rudin and Afonso C. Silva

16:00 ***797***. **Negative BOLD Signals Correlate with Synchronized Delta Oscillations Induced by Heroin in the Nucleus Accumbens of the Rat Brain**

Shi-Jiang Li[1], Feng Luo[1], Marie Schulte[1], Anthony Hudetz[1]

[1]Medical College of Wisconsin, Milwaukee, Wisconsin, USA

It is not clear how negative BOLD signals are linked to changes in field potentials. In the present study, a rat model was employed and the measurements of local EEG changes in the nucleus accumbens were performed before, during and after systemic administration of heroin. Under the same experimental conditions, a negative BOLD signal in the nucleus accumbens was robustly measured. The analysis of EEG oscillations revealed that heroin shifted the mean power frequency from 8Hz to 3Hz and that this frequency shift was correlated with the negative BOLD signal that could be resulted from the GABAergic inhibitory activity.

16:12 ***798***. **BOLD Response to the Agonist THC and to the Selective Antagonist, Rimonabant: an fMRI Study in the Rat Brain**

Jennifer Ann Stark[1], Steve R. Williams[1], Simon M. Luckman[1]

[1]University of Manchester, Manchester, UK

Delta-9-tetrahydrocannabinol (THC), an agonist at cannabinoid 1 receptors in the brain, increases food intake in sated animals. We are investigating appetite regulation by cannabinoids in rats using high field BOLD fMRI. Animals were administered either THC or the cannabinoid receptor 1 antagonist rimonabant, and their brains scanned. Drug groups were analysed separately using SPM2 due to drug vehicles being different. Results show that rimonabant had consistent opposite effects in areas modulated by THC.

16:24 ***799***. **Confounding Effects of Volatile Anesthesia on CBV Assessment in Rodent Forebrain Following Acute Alcohol Challenge: A Study of Isoflurane and Halothane Anesthesia**

Feng Luo[1], Zhixin Li[1], Young R. Kim[2], Steven Treistman[1], Craig F. Ferris[1]
[1]UMass, Worcester, Massachusetts, USA; [2]MGH, Boston, Massachusetts, USA

The present study is the first to use phMRI to evaluate ethanol-induced changes in brain activity in animals. As a first step in this line of investigation, it was critical to characterize the responsiveness of the anesthetized and conscious animal to an acute dose of EtOH. CBV response to EtOH under isoflurane, halothane anesthesia and awake condition were examined. Both isoflurane and halothane produced a heterogeneous perfusion background with region specific suppression in cortex. This confounds faithful representation of brain responses to acute EtOH challenge. Animal in fully conscious preparation is warranted for further EtOH imaging studies.

16:36 ***800***. **Baseline Dependence of the fMRI Response: Elucidating the Variable Effects of Induction Agents**

Basavaraju Ganganna Sanganahalli[1], Peter Herman[1, 2], Fahmeed Hyder[1]
[1]Yale University, New Haven, Connecticut, USA; [2]Semmelweis University, Budapest, Hungary

Functional brain imaging in animals provides an essential platform for investigating mechanisms of neurometabolic-neurovascular coupling and to understand the BOLD response. While α-chloralose has become the popular anesthetic of choice for functional studies in rodents, prior to the treatment of this drug a variety of volatile agents are used during the surgical preparation phase of the experiment. Here we demonstrated the time dependent (i.e., baseline) effects on BOLD response and neuronal firing using rat forepaw model under α-chloralose by using three volatile induction agents (halothane, isoflurane, enflurane). Graded increase in BOLD and neuronal firing was observed with time.

16:48 ***801***. **The Effects of Clonidine and Idazoxan on Cerebral Blood Flow in Rats Studied by Arterial Spin Labeling Magnetic Resonance Perfusion Imaging**

Xiaoxia Du[1], Hao Lei[1]
[1]Wuhan Institute of Physics & Mathematics, Chinese Academy of Sciences, Wuhan, Hubei, People's Republic of China

Clonidine is a widely used anti-hypertension drug. In this study, we investigated the effects of clonidine and its antagonist idazoxan on CBF in rat using MR perfusion imaging. It is shown that clonidine induces global CBF reduction in the idazoxan-naive rats, which can be reversed, in a region-dependent manner however, by the subsequent idazoxan administration. Pretreatment with idazoxan diminishes the effects of clonidine on CBF in the cortex and hypothalamus/septal region, but not in the striatum. Such observation might be related to the fact that clonidine can affect local CBF through its direct effect on central α_2-adrenergic and imidazoline receptors.

17:00 ***802***. **PhMRI of Brain Deactivation: Effects of the Antiepileptic Agent Tiagabine on Cerebral Haemodynamics**

Alessandro Gozzi[1], Laura Ceolin[1], Adam Schwarz[1], Torsten Reese[1], Valerio Crestan[1], Angelo Bifone[1]
[1]Centre of Excellence for Drug Discovery, Psychiatry, GlaxoSmithKline, Verona, Italy

The interpretation of negative responses in pharmacological MRI has been a contentious matter in recent literature. We have used MRI, Laser Doppler Flowmetry, and fluorescence quenching methods to measure the individual components of the response to a pharmacological challenge with Tiagabine, a GABAergic drug that lowers neuronal activity in the cortex. Tiagabine produced a marked cortical reduction in both rCBV and LDF, consistent with reduced local metabolism. However, a sustained increase in pO2 was observed, suggesting that during cortical GABAergic deactivation, tissue oxygen consumption decreases more than oxygen supply.

17:12 ***803***. **The Cerebrovascular Coupling Under COX-2 Blockade**

Bojana Stefanovic[1], Francesca Bosetti[2], Afonso C. Silva[1]
[1]NINDS, NIH, Bethesda, Maryland, USA; [2]NIA, NIH, Bethesda, Maryland, USA

The inhibition of COX-2 was found to produce a pronounced disturbance in the cerebrovascular coupling in anesthetized rats. The administration of Meloxicam attenuated the CBF response to forepaw stimulation by ~70% and the BOLD response by ~50% of their respective predrug magnitudes, while SEP responses remained unaffected. The administration of PGE2 produced a parial recovery of the hemodynamic responses, suggesting a modulatory role of COX-2 in the cerebrovascular coupling. The persistence of the neuronal response despite much attenuated hemodynamics is indicative of a metabolic buffer in the tissue.

17:24 ***804***. **The Coupling Between BOLD, CBF, CBV, and SEP Responses Under NO Blockade**

Bojana Stefanovic[1], Wolfram Schwindt[2], Mathias Hoehn[3], Afonso C. Silva[1]
[1]NINDS, NIH, Bethesda, Maryland, USA; [2]Universitätsklinikum Münster, Muenster, Germany; [3]Max-Planck-Institute for Neurological Research, Cologne, Germany

The inhibition of neuronally derived nitric oxide synthase was found to produce a pronounced and sustained disturbance in the coupling between hemodynamic and neuronal responses to functional stimulation in anesthetized rats. The administration of an ip bolus of 7-NI (50 mg/kg) attenuated the CBF response to forepaw stimulation by ~90%. In turn, BOLD response decreased by 60% and CBV by 50%, while the SEP amplitude declined by only ~25%. The disproportionately large hemodynamic, relative to neuronal response attenuation, testifies to an existence of a metabolic buffer in the tissue.

17:36 ***805***. **Functional Magnetic Resonance Imaging (fMRI) of Neurotrophin-3 (NT3) Treated Spinal Cord Injured Rats**

Jaivijay Ramu[1], Kurt H. Bockhorst[2], Kishore V. Mogatadakala[2], Ray J. Grill[2], Ponnada A. Narayana[2]
[1]University of Houston, Houston, Texas, USA; [2]University of Texas, Houston, Texas, USA

We have investigated cortical activation, using functional magnetic resonance imaging (fMRI), in spinal cord injured rodents treated with the neurotrophin, NT3. The NT3 treated animals have shown extensive activation in both cortical and subcortical structures in response to electrical stimulation of the forepaw. The extent of shift in the center of mass and volume of activation in each structure was calculated using automatic cluster analysis. These results indicate extensive cortical reorganization in NT3 treated spinal cord injury.

17:48 ***806***. **Lamina-Specific Anatomical and Functional Imaging of Normal and Diabetic Rat Retina**

Haiying Cheng[1], Darin E. Olson[1], Yongjun Liu[1], Perter M. Thule[1], Machelle T. Pardue,[1,2], Timothy Q. Duong[1]
[1]Emory University, Atlanta, Georgia, USA; [2]Atlanta VA Medical Center, Atlanta, Georgia, USA

High-resolution MRI and BOLD-fMRI were used to compare laminar dimensions and vascular responsiveness in retina of diabetic (DM) and non-diabetic control (Con) rats. The widths of inner and middle retinal layers were similar in DM and Con. By contrast, outer layer width of DM retinas was significantly greater than Con, suggesting vascular complication. The numbers of activated pixels associated with hyperoxia- and hypercapnia-induced BOLD fMRI in different layers were reduced relative to Con, suggesting damages to neurovascular coupling integrity. MRI could provide powerful insights into how diabetic retinopathy affects the vasculatures in the retina and the neural tissues they subserve.

Cerebral Vessels: Morphology and Territories

Room 615 - 617 16:00 - 18:00 Chairs: Mark C. DeLano and Stephen J. Riederer

16:00 ***807***. **4D Time-Resolved Angiography with CENTRA Keyhole (4D-TRAK) and SENSE Using a Total Acceleration Factor of 60 as Compared with Catheter Angiography in Patients with Cerebral Arteriovenous Malformations at 3.0T**

Dariusch Reza Hadizadeh[1], Jürgen Gieseke[1], Romhild Hoogeveen[2], Markus von Falkenhausen[1], Bernhard Meyer[1], Horst Urbach[1], Hans H. Schild[1], Winfried A. Willinek[1]
[1]University of Bonn, Bonn, Germany; [2]Philips Medical Systems, Best, Netherlands

Contrast enhanced 4D time-resolved MR angiography with CENTRA Keyhole (4D TRAK) and parallel imaging (SENSE) was performed at 3.0 Tesla in 10 patients with cerebral arteriovenous malformations (cAVM) and compared with DSA. A total acceleration of 6 (Keyhole) x 8 (SENSE) x 1.25 (half Fourier) = 60 was achieved yielding a temporal resolution of 608 msec./dynamic. In 10/10 patients, 4D TRAK allowed for reliable classification of cAVM according to Spetzler and Martin matched with DSA.

16:12 ***808***. **Whole-Brain 3D Contrast-Enhanced MR Venography with Robust 4 to 8-Fold 2D-SENSE and Sub-Mm Spatial Resolution in Approximately 60 Seconds**

Houchun H. Hu[1], Clifton R. Haider[1], David G. Kruger[1], John Huston III[1], Norbert G. Campeau[1], Stephen J. Riederer[1]
[1]Mayo Clinic College of Medicine, Rochester, Minnesota, USA

3D contrast-enhanced MR venography (CE-MRV) requires an imaging volume that encompasses the full anterior/posterior and right/left extent of the brain. 3D CE-MRV also requires sub-millimeter resolution for accurate visualization of the intracranial venous system. The long acquisition time of CE-MRV is an ideal candidate for 2D-Sensitivity Encoding (SENSE). In this work, we hypothesize that with an eight-element head coil, 4-8x 2D-SENSE can be reliably achieved with robust reconstructions at the 1.5T field. In 14 volunteers, 2D-SENSE-acquired images (0.8x0.8x1.0 mm^3) show no reconstruction artifacts, exhibit excellent visualization of the large dural sinuses and cerebral veins, and maintain adequate SNR for diagnosis.

16:24 ***809***. **Integration of Scan Time Reduction Techniques with Rearranged Elliptical Centric K-Space Acquisition for 3DTOF MRA at 3.0T**

Chen Lin[1], Mathew A. Bernstein[1], John Huston III[1]
[1]Mayo Clinic College of Medicine, Rochester, Minnesota, USA

3DTOF MRA is a useful, but slow technique, especially when multiple slabs are needed to provide adequate coverage. To achieve reduction of scan time, a combination of variable TR, not acquiring views in k-space corners, and parallel imaging is shown to be effective. These techniques are integrated with rearranged elliptical centric view order which allows simultaneous low SAR MT background suppression and flow artifact suppression. A 40% reduction in scan time with no obvious impact on image quality is obtained without parallel imaging, and a 70% reduction with minor impact is achieved with an acceleration factor of 2.

16:36 ***810***. **High Resolution Magnetic Resonance Venography at 3 Tesla: Optimized Acquisition, Reconstruction, and Post-Processing**

Eugene G. Kholmovski[1], Dennis L. Parker[1]
[1]University of Utah, Salt Lake City, Utah, USA

Magnetic resonance venography (MRV) based on susceptibility weighted imaging can be used for detailed study of intracranial venous vasculature. The main problems with the existing MRV techniques are long scan time (20 minutes and longer) and poor visibility of small veins due to relatively large voxel volume (0.25 mm3 or larger). The composite method for intracranial MRV including optimized data acquisition, image reconstruction, and post-processing has been developed and successfully applied to more than 20 studies. The method allows acquisition of high quality venograms with improved small vessel visibility in acceptable scan time (less than 10 minutes).

16:48 ***811***. **High Resolution Thoracic and Neurovascular 3T MRI for the Comprehensive Assessment of Inflammatory Disease**

Michael Markl[1], Markus Uhl[1], Oliver Wieben[2], Mathias Langer[1], Jürgen Hennig[1], Thorsten Bley[1]
[1]University Hospital Freiburg, Freiburg, Germany; [2]University of Wisconsin, Madison, Wisconsin, USA

A new MR protocol for the combined assessment of thoracic and neurovascular arterial anatomy and subsequent evaluation of inflammatory disease in cranial vessels walls at 3T has been investigated. Contrast-enhanced MR Angiography and additional pre- and post contrast T1 weighted turbo spin echo imaging permits the depiction of large parts of the thoracic and neurovascular geometry with large coverage in combination with the assessment of morphology and potential inflammatory changes in cranial artery walls with high, sub-millimeter detail. The feasibility for the diagnosis of rheumatologic diseases and potential for the identification of simultaneous arteriosclerotic involvement was demonstrated in seven patients.

17:00 ***812***. **Time-Resolved 3D Contrast-Enhanced MRA with 2D Homodyne and View Sharing for Contrast Bolus Dynamics of the Brain**

Clifton R. Haider[1], Houchun Harry Hu[1], Annanth J. Madhuranthakam[2], David G. Kruger[1], Norbert G. Campeau[1], John Huston 3rd[1], Stephen J. Riederer[1]
[1]Mayo Clinic College of Medicine, Rochester, Minnesota, USA; [2]GE ASL East, Boston, Massachusetts, USA

Time-resolved (TR) imaging can effectively capture bolus dynamics in 3D contrast-enhanced (CE) MRA. Recently, an elliptical centric (EC) technique that encompasses projection-like sampling with 2D-homodyne (HD) reconstruction was demonstrated in non-TR CE-MRA. The sampling consists of a central ellipse and an outer annulus with alternating asymmetric vanes across the conjugate ky-kz axes. In this work, we hypothesize that this technique can be extended to TR imaging by updating the ellipse, selectively acquiring portions of the annulus, and performing HD for appropriate views during each reconstruction cycle. The method is demonstrated in intracranial vasculature with a 2.3 second frame rate.

17:12 ***813***. **Tracking Vascular Supply Using Bolus Tracking MRI**

Soren Christensen[1], Fernando Calamante[2], Christoph Manka[3], Leif Østergaard[1]
[1]Aarhus Sygehus, Aarhus, Denmark; [2]Brain Research Institute, Melbourne, Victoria, Australia; [3]University of Bonn, Bonn, Germany

Bolus tracking studies are widely used in settings of acute stroke. We propose a new application of Bolus Tracking that will estimate the likely supply routes of blood for a given voxel. We outline the theoretical background and illustrate the method in 2 acute stroke cases. Results show promise that information on collateral supply, vascular territories and density of supplying vessels can be derived from this method.

17:24 ***814***. **Ultrahigh Field (>7T) Time-Of-Flight and Phase Contrast Magnetic Resonance Angiography of the Intracerebral Arteries**

Johannes T. Heverhagen[1], John Duraj[2], Petra Schmalbrock[1], Michael R. Thompson[2], Donald Chakeres[1], Michael V. Knopp[1]
[1]The Ohio State University, Columbus, Ohio, USA; [2]Philips Medical Systems, Cleveland, Ohio, USA

The purpose of this study was to evaluate the feasibility of TOF and PC MR Angiography of the intracerebral arteries in a whole body 7T MR scanner and to compare the results with clinical MR systems at 1.5T and 3T. PC and TOF MRAs were acquired in a 7T MR scanner and in clinical 3T and 1.5T scanners. Ultrahigh field MRAs demonstrate higher order branches with smaller calibers than conventional MRAs. This study demonstrates the feasibility of both TOF and PCMRA of the brain in a whole body 7T MR scanner with improved arterial contrast and vessel conspicuity compared to lower clinical field strengths.

17:36 ***815***. **Effect of Normal Aging in the Flows of the Cerebral Blood and the Cerebro-Spinal Fluid**

Olivier Baledent[1], Souraya Stoquart el Sankari[1], Catherine Gondry-jouet[1], Malek Makki[2], Marc-etienne Meyer[1]
[1]Hospital, amiens, picardie, France; [2]Children's Hospital of Michigan, detroit, michigan, USA

We investigated the age effect on the dynamic of normal brain by quantifying flows and volumes of cerebral blood (CB), and cerebro-spinal fluid (CSF). We studied 31 healthy adults, 19 young persons (27±4 years) and 12 elderly persons (71±9 years) using Phase-Contrast MRI. Within the elderly population we found a significant decrease of the CSF stroke volume at the level of the aqueduct and cervical spaces and a significant decrease of CB flow compared that of the young group. These findings are useful to study neurologic pathologies related to aging such as hydrocephalus, Parkinson and Alzheimer diseases.

17:48 ***816***. **Wall Shear Stress of Swine Model with Induced Carotid Artery Stenosis**

Sinyeob Ahn[1], Akira Ishii[1], Dongsuk Shin[1], Fernando Vinuela[1], Shantanu Sinha[1]
[1]University of California, Los Angeles, California, USA

Swine model was introduced by creating stenosis at a common carotid artery after surgical partial ligation. High resolution MR-PC imaging was performed to estimate wall shear stress concurrently with temporally-resolved histo-pathological investigation during the development of atherosclerotic plaques. Low and/or oscillating wall shear stress was observed at the proximal region to the stenosis where advanced atherosclerotic plaques were developed. The distal region to the stenosis showed relatively high wall shear stress with little oscillation, depending upon the vessel geometry. Calculated wall shear stress based on PC-MRI datasets was consistent with Doppler velocimetry measurement.

Brain Tumors: The New Frontier

Room 618 - 620 16:00 - 18:00 Chairs: Aaron S. Field and Elias R. Melhem

16:00 ***817***. **Magnetic Resonance Spectroscopic Imaging of Choline Diffusion in Experimental Gliomas During the Programmed Cell Death**

Kimmo Lehtimäki[1], Timo Liimatainen[1], Juhana Hakumäki[1, 2]
[1]University of Kuopio, Kuopio, FI, Finland; [2]Kuopio University Hospital, Kuopio, FI, Finland

In this study, we quantified apparent diffusion coefficient (ADC) maps for the choline moiety (CHO) from BT4C/HSV-tk gliomas undergoing programmed cell death by using diffusion MRSI. CHO diffusion maps revealed that the ADC values in the border sections of the tumors were systematically 10-30% lower than in the center section in single animals. Most importantly, the ADC values of CHO in tumor center sections became significantly reduced by day 4 from the start of ganciclovir treatment. During treatment the ADC of CHO was reduced by more than 50% demonstrating the potential of this index for imaging of apoptotic cell shrinkage.

16:12 ***818***. **MRI Follow-Up of Monocyte/macrophages Colonisation of a Rat Brain Tumour**

Samuel Valable[1, 2], Emmanuel L. Barbier[1, 2], Myriam Bernaudin[3, 4], Simon Roussel[3, 4], Edwige Petit[3, 4], Chantal Remy[1, 2]
[1]U594, Grenoble, F-38043, France; [2]Univ grenoble 1, Grenoble, F-38043, France; [3]UMR 6185, Caen, F-14074, France; [4]Université de Caen, Caen, F-14074, France

As brain tumors are highly attractive for macrophages, these cells could be used as vectors for anti-tumoral therapy. We aimed to visualize by MRI if intravenously injected monocytes present the capacity of colonizing brain tumors. Monocytes were labeled with fluorescent and magnetic particles. FACS revealed that the labeling is near one hundred percent and that cells are not altered by the labeling. When intravenously injected, monocytes were attracted by the tumor itself. A cellular strategy using monocytes as vectors might be used to target the tumour. MRI could help following the fate of the cells and the efficacy of the treatment.

16:24 ***819***. **Correlation of Choline and Apparent Diffusion Coefficient in Glioma Patients**

Inas S. Khayal[1], Kathleen R. Lamborn[1], Forrest W. Crawford[1], Suja Saraswathy[1], Joonmi Oh[1], Susan M. Chang[1], Soonmee Cha[1], Tracy R. McKnight[1], Sarah J. Nelson[1]
[1]University of California, San Francisco, California, USA

Gliomas are spatially heterogeneous brain tumors; non-invasive methods for evaluating this heterogeneity are important in directing patient treatment. Previous studies have shown an inverse correlation of ADC to choline for heterogeneous grades and regions; this study suggests there is an inverse correlation specifically in Grade IV patients, but not in Grade II. This implies that there is independent information to be acquired from both diffusion and spectroscopic imaging. Furthermore, the range of values for ADC and choline within a Grade IV tumor are large and require image-guided biopsy to accurately correlate these values to cell density.

16:36 ***820***. **First Clinical Evaluation of Vessel Size Imaging in Human Glial Brain Tumors**

Tobias Breyer[1], Peter Galt[2], Valerij G. Kiselev[2], Oliver Speck[2], Irina K. Mader[1]
[1]Dept. of Neuroradiology, Freiburg, Germany; [2]MR Physics, Freiburg, Germany

Intracranial tumors vary greatly in the extent of microvascularization, which cannot be imaged directly by current MR-techniques. The purpose of this study was to measure the vessel-size-index (VSI) in patients with glial tumors of different WHO tumor grades (II through IV), and to evaluate whether a higher tumor grade shows also an increased microvascularization. ROI analysis of normal gray matter, thalamus, normal white matter, cerebrospinal fluid and solid tumor was performed. The VSI of glial brain tumors was increased compared to normal appearing white matter, which showed smallest standard deviation.

16:48 ***821***. **Improved Identification of *true* Hot-Spots in Intra-Axial Neoplasms by Coregistration of Blood Volume Maps and Morphological Data**

Kyrre E. Emblem[1], Paulina Due-Tonnessen[1], Baard Nedregaard[1], J. K. Hald[1], E A. Jacobsen[1], Atle Bjornerud[1]
[1]Rikshospitalet University Hospital, Oslo, Norway

One challenge with tumor grading based on relative cerebral blood volume (rCBV) maps is to identify the true tumor volume avoiding large vessels and edema. This study used rCBV maps derived from first-pass gradient echo perfusion MR as coregistered overlays on both morphological T1-w SE and T2-w FSE images in patients with intra-axial tumors. The preliminary results of this ongoing study shows that this method has the potential to be an important aid in differentiating vessels from true high rCBV regions.

17:00 ***822***. **Dynamic Susceptibility Contrast Perfusion MRI of Angiogenesis and Microscopic Tumoral Infiltration in the Corpus Callosum of Patients with Gliomas**

Jean Yves Gauvrit[1, 2], Meng Law[1], S Papadaki[1], E St. Clair[1], M Inglese[1], G Johnson[1]
[1]New York University Medical Center, New York, New York, USA; [2]Hopital R Salengro, Lille, France

The purpose of this study is to determine if there are microvascular changes within the normal appearing CC and contralateral white matter of patients with gliomas and if there are differences between glioma grades

17:12 ***823***. **Characterization of Intra-Axial Neoplasms by Histogram Analysis of Total Tumor Volume from MR-Derived Cerebral Blood Volume Maps**

Kyrre E. Emblem[1], Baard Nedregaard[1], Paulina Due-Tonnessen[1], Eva Astrid Jacobsen[1], John K. Hald[1], Atle Bjornerud[1]
[1]Rikshospitalet University Hospital, Oslo, Norway

One limitation with tumor grading based on relative cerebral blood volume (rCBV) is the user dependent selection of tumor 'hot-spots' which is critical for correct tumor grading. We propose an alternative method based on histogram analysis of the entire tumor volume, using the histogram shape and frequency distribution to differentiate high-grade from low-grade tumors in rCBV maps derived from first-pass GRE-EPI perfusion MR. The initial results of this ongoing study suggest that this may be an improved alternative to grading brain tumors from rCBV maps with less user bias.

17:24 ***824***. **Use of Cerebral Blood Volume as a Potential Surrogate Marker of Vascular Normalization in 9L Gliosarcoma Tumor**

Moses Morakortoi Darpolor[1], Francisca C. Wu[2], Kathleen M. Schmainda[2]
[1]Marquette University, Milwaukee, Wisconsin, USA; [2]Medical College of Wisconsin, Milwaukee, Wisconsin, USA

Antiangiogenic treatment provides a transitory period of vascular normalization that is suitable for drug delivery to tumor microenvironment, which may improve the efficiency of chemotherapy or radiotherapy. Immunohistochemistry, anti-CD31, showed some regression in vessel size after dexamethasone therapy as possible indication of vascular "normalization". However, non-invasive imaging techniques are in great need to delineate vascular "normalization" in brain tumors. Cerebral blood volume measure from dynamic susceptibility contrast magnetic resonance imaging (DSC-MRI) is a potential surrogate marker to characterize the "normalization" of tumor vasculatures during antiangiogenic therapy.

17:36 ***825***. **Quantitative Cerebral Blood Volume Measurement Using the Bookend Method : Water Exchange Effect Correction and Diagnosis on Tumor in Gradient-Echo and Spin-Echo EPI**

Wanyong Shin[1], Sandra W. Horowitz[2], Ty Allen Cashen[1], Timothy J. Carroll[1, 2]
[1]Northwestern University, Chicago, Illinois, USA; [2]Northwestern University Feinberg School of Medicine, Chicago, Illinois, USA

However qunatitative cerebral blood volume (qCBV) measurement can diagnose the abnormalties of the brain, accurate qCBV measurement with a whole brain coverage has remained challenaging in clinical use. Quantification of relative CBV maps from dinamic susceptibility contrast analysis was performed by the Bookend method with correction of water exchange effects. Based on qCBV maps, pre-confirmed tumor was diagnosed and compared with normal tissue in gradient-echo and spin-echo EPI.

17:48 ***826***. **Relative Cerebral Blood Volume is a Measure of Angiogenesis in Brain Tuberculoma and Its Therapeutic Implications**

Rakesh Kumar Gupta[1], Mohammad Haris[1], Nuzhat Husain[2], Mazhar Husain[2], Kashi Nath Prasad[1], Mohan Pauliah[1], Chhitij Srivastava[2], Mukesh Tripathi[1], Manu Rastogi[2], Sanjay Bihari[1], Divya Rathore[3], Ram Kishore S. Rathore[3]
[1]Sanjay Gandhi Post Graduate Institute of Medical Sciences, Lucknow, Uttar Pradesh, India; [2]King George's Medical University, Lucknow, Uttar Pradesh, India; [3]Indian Institute of Technology, Kanpur, Uttar Pradesh, India

Dynamic contrast enhanced (DCE) MRI has been performed in 15 patients with (9 excised and 6 follow-up) brain tuberculomas. The relative cerebral blood volume in case of excised tuberculoma correlated significantly with cellular component and histopathologically derived microvascular density (MVD) and vascular endothelial growth factor (VEGF). In case of follow-up patients, there was significant decrease in cellular component at three time points with significant decrease in relative cerebral blood volume (rCBV) in response to anti-tuberculous therapy. We conclude that rCBV is a surrogate marker of angiogenesis in brain tuberculoma.

Tissue Segmentation and Co-registration

Room 602 - 604 16:00 - 18:00 Chairs: R. Mark Henkelman and Henry Rusinek

16:00 ***827***. **_Shape-Contexts_: Automatic Computation of 3D Landmarks Applied to the Generation of an Atlas of the Knee**

Julio Carballido-Gamio[1], Sharmila Majumdar[1]
[1]University of California, San Francisco, San Francisco, California, USA

Robust 3D scale-rotational-translational invariant *shape-contexts* are presented to compute plausible landmarks and applied to the generation of an atlas of the knee. A mean femoral shape as well as a mean cartilage thickness map were succesfully generated. Results suggest that the technique could be easily applicable to the creation of other mean shapes as well as mean maps of different tissue properties.

16:12 ***828***. **Segmentation of Prostate MRI Volumes Using 3D Shape Model Constrained Tissue Classification**

Philip Daniel Allen[1], James Graham[1], David Williamson[2], Charles Hutchinson[1]
[1]University of Manchester, Manchester, UK; [2]University of York, York, UK

Benign Prostatic Hyperplasia is a non-cancerous enlargement of the prostate that can cause constriction of the urethra. Evaluation of potential drug treatments designed to shrink the prostate requires a means of quantifying their effect. In an MR image the prostate has two distinct zones and the relative volumes of these has been shown to be sensitive to the progress of BPH and the degree of urinary flow obstruction. Here we present a method of semi-automatic prostate segmentation in MR images using grey level voxel classification, coupled with a 3D point distribution model to provide a smooth, anatomically credible spatial constraint.

16:24 ***829***. **Markov Shape Models: Object Boundary Identification in Serial Magnetic Resonance Images**

Hunter Reeve Underhill[1], William S. Kerwin[1]
[1]University of Washington, Seattle, Washington, USA

A method to perform object boundary identification in sequential images is presented. Building on the structure of the Active Shape Model, the proposed technique utilizes object descriptors from the previous image to refine the search in the current image. The underlying idea is similar to Markov random processes and is therefore referred to as a "Markov Shape Model." The method is successfully applied to outer-wall boundary detection of the common carotid artery and its highly variable bifurcation in a sequence of magnetic resonance images (MRIs). The technique may be an effective tool for automated object boundary detection in MRI.

16:36 ***830***. **Simultaneous Segmentation and Registration of MR Images**

Cristian A. Tejos[1], Marcelo Guarini[1], Pablo Irarrazaval[1]
[1]Pontificia Universidad Catolica de Chile, Santiago, Chile

In medical imaging studies that analyse the evolution of structures through time, objects of interest need to be not only segmented, but also registered to correct pose changes resulting from the re-positioning of patients in the scanner. A few researchers have successfully integrated both processes, however, the existing joint segmentation and registration techniques provide geometrically distorted results due to their pixel-based characteristics, or correspond to 2D schemes without 3D extensions. The Simplex Mesh Diffusion Snake technique, a recently developed prior knowledge-based deformable model segmentation algorithm, is here employed to perform simultaneously segmentation and registration of synthetic and real MR images, with sub-pixel accuracy.

16:48 ***831***. **An Iterative Framework for Registration and Segmentation of Dynamic Three-Dimensional MR Renography**

Ting Song[1], Vivian Lee[2], Henry Rusinek[2], Samson Wong[2], Andew Laine[1]
[1]Columbia University, New York, New York, USA; [2]New York University Medical Center, New York, New York, USA

Our purpose was to develop a computer aided iterative registration and segmentation algorithms and to evaluate them four 4-D MR renography datasets. Without decoupling registration and segmentation problem, we achieved satisfied results in that refined average translation error was almost within half a voxel and rotation error was less than one degree. Compared with two manual segmented ROIs, computer calculated ROIs showed consistent and accurate results in overlaps and volumes.

17:00 ***832***. **A Feature-Based Approach to Combine Multimodal Brain Imaging Data**

Vince Calhoun[1]
[1]Institute of Living/Yale University, Hartford, Connecticut, USA

Approaches for combining or fusing data in brain imaging can be put on aspectrum with meta-analysis (highly distilled data) to examine convergentevidence at one end and large-scale computational modeling (highly detailedtheoretical modeling) at the other end. In between are methods that attemptto do direct data fusion. In this study, we present a general ICA fusionframework and introduce a method to assess the value of combining differenttypes of data by using a discrimination metric based on the Kullback-Leibler(KL) divergence to evaluate the joint distributions. The data types we focuson in this paper are fMRI, structural MRI (sMRI), and EEG. We show that bycombining modalities in certain ways, performance (ability to distinguishschizophrenia patients from controls) is improved.

17:12 ***833***. **Registration of MALDI Mass Spectrometry Images and MR Parametric Maps for Relaxomic Analysis**

Tuhin Kumar Sinha[1], Jeffrey James Luci[1], Sheerin Khatib Shahidi[1], Dale Shannon Cornett[1], John Christopher Gore[1], Benoit M. Dawant[1]

[1]Vanderbilt University, Nashville, Tennessee, USA

The work presented here explores the accurate alignment of tissue proteomic imaging via MALDI mass spectrometry (MS) and MR imaging. The goal is to provide a cohesive imaging study where each voxel in the image volume is a multivariate signal of various MR parameters (R1, R2, qMT, etc.) and tissue protein composition as determined by MS imaging. We demonstrate a comprehensive registration protocol to align MALDI MS images to corresponding locations in MR parametric spaces.

17:24 ***834***. **Automatic Prospective Registration of High Resolution Trabecular Bone Images of the Tibia**

Janet H. Blumenfeld[1, 2], Julio Carballido-Gamio[1], Radhika Srinivasan[1], Ileana Hancu[3], Daniel J. Blezek[3], Sharmila Majumdar[1]

[1]University of California, San Francisco, San Francisco, California, USA; [2]UCSF-UCB Joint Graduate Group in Bioengineering, Berkeley, California, USA; [3]GE Global Research Center, Niskayuna, New York, USA

The purpose of this work was to demonstrate the feasibility of prospective MR image registration of high-resolution trabecular bone images of the tibia. The registration technique, which is based on mutual information, utilizes a baseline and a follow-up scan to compute registration parameters that are subsequently used to prescribe an aligned follow-up acquisition. Results suggest that there is a possibility that this algorithm is robust enough to be used in several different musculoskeletal imaging applications.

17:36 ***835***. **Blind Source Separation of Signals from Dynamic Contrast Enhanced Breast Magnetic Resonance Images**

Bao Zhang[1], Yi Wang[2], Steven Roys[1], Rao P. Gullapalli[1]

[1]University of Maryland School of Medicine, Baltimore, Maryland, USA; [2]University of Maryland Baltimore County, Catonsville, Maryland, USA

Dynamic contrast enhanced breast magnetic resonance imaging is known to differentiating benign from malignant breast lesions with high sensitivity and specificity. However the large amount of images generated makes the clinical diagnosis labor intensive. We explore here the use of blind source separation (BSS), a statistical technique to analyze the data automatically. BSS identified successfully all the lesions that were clinically diagnosed. The first two independent components from any given data satisfied the clinical diagnosis. No lesions that were clinically diagnosed were missed by BSS. The successful application of BSS to dynamic contrast-enhanced breast MRI demonstrates that BSS is capable of extracting lesion's dynamic response automatically.

17:48 ***836***. **Four-Step Approach for Flattenning Brain Surface Onto Sphere and Plane**

Min Jeong Kwon[1], HyunWook Park[1]

[1]Korea Advanced Institute of Science and Technology, Daejeon, Republic of Korea

Flattening of the brain surface onto sphere and plane is widely used to view the buried sulci of cerebral cortex. Conventional parametric deformable models usually result in self-intersection and the resultant triangles may overlap at thin and deep concave region because vertices are deformed by combination of the external forces. Although some algorithms solve the overlap problem, they require heavy computation and do not guarantee no-overlap between triangles. This paper proposes a method that flattens the brain surface onto sphere and plane without overlap between triangles, with small computational time, and with minimized metric distortion. The proposed method organized by four steps each of which takes charge of specific purpose. In each step, deformation is performed just by one force and the effect of force is maximized. Flattening to sphere and plane need three and four steps, respectively. Vertices are deformed in 2D Spherical coordinates for flattening to sphere in order for vertices to exist exactly on sphere and 2D Cartesian coordinates for flattening to plane.

Gastrointestinal MR Imaging and Techniques

Room 613 - 614 16:00 - 18:00 Chairs: David J. Lomas and Neil M. Rofsky

16:00 ***837***. **Redistribution of Abdominal Blood Flow Following Meal Ingestion**

John J. Totman[1], Luca Marciani[1], Steve Foley[1], Eugene Campbell[1], Robin C. Spiller[1], Penny A. Gowland[1]

[1]University of Nottingham, Nottingham, UK

Blood flow in the superior mesenteric artery increases upon a meal challenge. The aim of this study was to use phase contrast MRI to monitor serially the separate haemodynamic responses to a food challenge of the SMA and descending aorta in healthy volunteers. At time t=30 min after feeding we observed a four-fold increase in blood flow in the SMA ($p<0.05$) and a concomitant 44% decrease in the Aorta ($p<0.05$). Such non-invasive serial monitoring techniques could have clinical potential in impaired gut blood supply conditions such as Irritable Bowel Syndrome, mesenteric ischemia and postprandial hypotension in the aged /diabetic population.

16:12 ***838***. **Functional Evaluation of the Postoperative Gastrointestinal Tract Using Kinematic MR Imaging: Quantitative Assessment of Peristaltic Activity**

Mizuki Nishino[1, 2], Shingo Iwata[2], Katsumi Hayakawa[2], Shotarou Kanao[2], Taisuke Morimoto[2], Sumio Mukaihara[2], Hiroto Hatabu[1]

[1]Beth Israel Deaconess Medical Center, Boston, Massachusetts, USA; [2]Kyoto City Hospital, Kyoto, Japan

Assessment of peristaltic activity in reconstructed gastrointestinal tract is difficult without an established quantitative method. We aim to demonstrate the feasibility of kinematic MRI in visualization and evaluation of peristaltic activity of reconstructed gastrointestinal tract. We studied 16 patients with gastrointestinal reconstruction. In all patients, kinematic MRI demonstrated peristaltic activities of the reconstructed gastrointestinal tracts, and the frequency and velocity were measured. Kinematic MR imaging is feasible for visualization and evaluation of peristaltic activity in the reconstructed gastrointestinal tract with quantitative measurement of frequency and velocity, providing a novel and simple technique for evaluating surgical effects of gastrointestinal peristaltic function.

16:24 ***839***. **Gastric Emptying, Transit Times and Visualisation of Alginate Beads in the Gastro-Intestinal Tract**

Caroline L. Hoad[1], Eleanor F. Cox[1], Phillipa Rayment[2], Robin C. Spiller[3], Peter J. Wright[1], Michael Butler[2], Luca Marciani[3], Penelope A. Gowland[1]

[1]University of Nottingham, Nottingham, UK; [2]Corporate Research, Unilever R & D, Colworth, Beds., UK; [3]University Hospital, Nottingham, UK

Gastric emptying and intestinal transit times were measured in 7 healthy volunteers who consumed 2 different types of alginate beads (weakly and strongly gelled). The beads were visualised in the small intestine using RARE images and different areas of the small intestine were compared by dividing the region into 4 quadrants. Gastric emptying times for the strongly gelling beads were longer compared to the weakly gelling beads. The intestinal transit time was 120 minutes for both bead types. Quadrant analysis of the beads found that they were more visible in the lower compared to the upper quadrants of the bowel.

16:36 ***840***. **Gastrointestinal Effects of Bran: A MRI Study**

Luca Marciani[1], John J. Totman[1], Caroline L. Hoad[1], Steve Evans[1], Amisha Mistry[1], Robin C. Spiller[1], Penny A. Gowland[1]

[1]University of Nottingham, Nottingham, England, UK

The symptoms of IBS can be aggravated by bran but the underlying mechanisms are currently unknown. This study aimed to exploit the potential of MRI to test the hypothesis that bran acts via mechanical stimulation of secretions. We measured gastric emptying, small bowel water content and size of colon segments following a standard rice pudding test meal with or without bran in twelve healthy volunteers. We could confirm the substantial effect of coarse bran on the small intestine. The technique is non-invasive and allows serial studies. It is ideally suited to study mechanisms of secretion using serotonin agonists and antagonists.

16:48 ***841***. **MR Colonography with Fecal Tagging: Do Individual Patient Characteristics Influence Image Quality?**

Sonja Kinner[1], Christiane A. Kuehle[1], Michael Nuefer[1], Susanne C. Goehde[1], Joerg Barkhausen[1], Thomas C. Lauenstein[1]

[1]University Hospital Essen, Essen, Germany

We evaluated the effect of different patient characteristics such as age and body mass index on the image quality of MR colonography (MRC) in conjunction with fecal tagging. 397 asymptomatic patients were included, who ingested a barium-based tagging agent prior to the MRC. The degree of stool tagging was assessed visually on a segmental basis. In 95% of the segments fecal material was sufficiently tagged while in 5% visible stool strongly impeded image analysis. However, no correlation was found between the success rate of tagging and patients` characteristics.

17:00 ***842***. **Preoperative Detection and Staging of Esophageal Cancer by Diffusion-Weighted MR Imaging and FDG-PET**

Yuji Nakamoto[1], Takashi Koyama[1], Shigeaki Umeoka[1], Ken Tamai[1], Tatsuya Higashi[1], Tsuneo Saga[1], Kaori Togashi[1]

[1]Kyoto University, Kyoto, Japan

In preoperative evaluation of esophageal cancer, DWI yielded a slightly higher diagnostic accuracy than FDG-PET.

17:12 ***843***. **Preliminary Evaluation of MR Diffusion-Weighted Imaging in Diagnosing Pancreatic Carcinoma**

Ying Li[1], Xiao-peng Zhang[1], Lei Tang[1], Ying-shi Sun[1]

[1]Beijing Cancer Hospital & Peking University School of Oncology, Beijing, People's Republic of China

The purpose is to evaluate the efficacy and limitation of DWI in diagnosing pancreatic carcinoma. Twelve pancreatic carcinoma patients and 12 healthy volunteers underwent MR DWI scan with 1.5T MR system, b=0, 800s/mm2. The SIR and CNR of tumors in DWI image were higher than that in T1WI and T2WI. The ADC of tumor was higher than peri-tumor pancreas. When ADC of 1.30¡Á10-3mm2/s was chosen, the sensitivity and specificity of diagnosis were 75% and 62.5%, respectively. DWI and ADC are useful to diagnose pancreatic carcinoma .The main limitations are the relatively small volume of pancreas and the signal heterogeneity.

17:24 ***844***. **Reduced Acquisition Time in Fat Saturated Abdominal Imaging Using HoPE: A Clinical Evaluation**

Dominik Paul[1], Jens Walcher[1], Hans-Peter Fautz[1], Jürgen Hennig[1], Oliver Schäfer[1]
[1]University Hospital, Freiburg, Germany

Frequency selective fat saturation is an established method to increase diagnostic value in abdominal imaging, but on the cost of reduced scan efficiency. A method to increase scan efficiency while maintaining fat saturation and image quality is HoPE. A clinical study was performed on 32 patients to evaluate HoPE in clinical abdominal gradient echo imaging. Qualitative and quantitative analysis showed no significant difference in image quality, contrast, SNR, and intra abdominal fat suppression, but improved artifact behavior. Using HoPE an acquisition time reduction of up to 40% was achieved.

17:36 ***845***. **Isotropic Diffusion Weighted MR Imaging with Tetrahedral Gradients in the Upper Abdomen**

Masatoshi Hori[1], Takamichi Murakami[1], Tonsok Kim[1], Hiromitsu Onishi[1], Masatomo Kuwabara[1], Kaname Tomoda[1], Hironobu Nakamura[1], Masaya Hirano[2], Atsushi Nozaki[2]
[1]Osaka University Graduate School of Medicine, Suita, Osaka, Japan; [2]GE Yokogawa Medical, Hino, Tokyo, Japan

The purpose of this study was to determine efficacy of the isotropic diffusion weighted MR sequence using tetrahedral technique in the upper abdomen by comparison with conventional sequence using orthogonal gradients. Twenty patients were included in this study. Images obtained with each technique were subjectively graded based on the signal homogeneity in the liver, image distortion, and overall image quality. Apparent diffusion coefficient values of the liver and the spleen were also calculated. The results were compared between the techniques. The tetrahedral gradient diffusion technique showed significantly better image quality than the conventional orthogonal technique.

17:48 ***846***. **The Utility of TrueFISP in Abdominal Imaging: Analysis of Vascular Assessment and Liver Lesion Detection**

Dejana Radulovic[1], Iain Donald Craik Kirkpatrick[1], Mervyn A. Kroeker[1], Neal Pawlyshyn[1]
[1]University of Manitoba, Winnipeg, Manitoba, Canada

To study TrueFISP in assessing vasculature of the abdomen and detecting liver lesions, imaging of 143 patients was performed with post-contrast 3DVIBE and TrueFISP and HASTE acquisitions with either 7-10mm or 5mm slice thickness. Two blinded radiologists scored visualization of the aorta, IVC, splenic, hepatic, and portal veins. TrueFISP scored significantly higher at 5mm than at 7-10mm, and at 5mm were superior to 3DVIBE for all vessels ($p<0.001$) except the aorta. All 6 thrombi were seen with TrueFISP. Sensitivity for liver lesion detection was inferior to HASTE. TrueFISP offers a valuable alternative for vascular imaging in patients without intravenous access.

MORNING CATEGORICAL COURSE
Technical Advances in Body MR

Room 618-620 7:00 – 8:00 Chairs: Neil M. Rofsky, Daniel K. Sodickson, and Bachir Taouli

Educational Objectives:
Upon completion of this session, participants should be able to:

- Evaluate important developments in MRI technology, including high field imaging and parallel imaging;
- Identify the technical challenges associated with effective application of this technology for body imaging; and
- Describe the potential applications of new technologies in body imaging, including areas such as diffusion and perfusion MRI, and MR spectroscopy.

Applications: Metabolic Imaging

07:00 **Body MR Spectroscopy**
John Kurhanewicz

07:30 **Fat-Water Imaging**
Scott B. Reeder

MORNING CATEGORICAL COURSE
Cardiovascular Imaging

Room 6D 7:00 – 8:00 Chairs: Qun Chen and James F.M. Meaney

Educational Objectives:
Upon completion of this session, participants should be able to:

- Implement a robust protocol for clinical evaluation of arteries with both non-contrast and contrast-enhanced techniques;

- Identify the strengths and weaknesses of 3T MRI vs. 1.5T MRI for cardiovascular assessment;
- Recognize the value of parallel imaging for cardiovascular assessment at higher magnetic field (>1.5T);
- Select a comprehensive time-efficient protocol incorporating anatomical and functional cardiac evaluation;
- Explain the value of MRI for the assessment of non-coronary artery disease; and
- Recognize the strengths and also the limitations of current techniques.

MRI of Non-Coronary Artery Disease

07:00 **Arrthymogenic Conditions**
David A. Bluemke

07:30 **Other Cardiomyopathies**
Jeanette Schulz-Menger

MORNING CATEGORICAL COURSE
Clinical DTI/PWI/fMRI

Room 4C-3,4 7:00 – 8:00 Chairs: Alberto Bizzi and Soonmee Cha

Educational Objectives:
Upon completion of this session, participants should be able to:

- Describe the main applications and contributions of fMRI, DTI, and tractography and bolus tracking and arterial labeling perfusion MR imaging in clinical neuroscience;

- Describe the technical requirements necessary to implement robust, accurate, and repeatable clinical advanced MR studies in patients with neurological diseases;

- List the potential contribution of PWI, DTI and fMRI to formulate diagnosis, prognosis, and evaluate different therapeutic strategies in the neurological diseases focus of this course;
- Discuss the basic MR principles involved in the quantification of angiogenesis and permeability using perfusion MR imaging;
- Implement new quantitative MR methods that may quantify cumulative brain damage that better correlate with the disability score;
- Recognize challenges, limitations and pitfalls of performing advanced MR studies to answer clinical questions in neurological patients; and
- Implement Quality Assurance (QA) procedures necessary to run a reliable and successful advanced MRI clinic.

Advanced Imaging of the Pediatric Brain

07:00 **Diffusion MRI in the Fetus and Newborn**
Andrea Righini

07:30 **Measuring Brain Perfusion in the Pediatric Brain**
Michela Tosetti

MORNING CATEGORICAL COURSE
MR Hardware/Engineering

Room 611-612 7:00 – 8:00 Chairs: Steven M. Conolly and Steven M. Wright

Educational Objectives:
Upon completion of this session, participants should be able to:

- List and compare implementations of static field magnet designs for clinical MRI;

- Recognize that there are fundamental limits on our ability to shim out steep field variations (such as those in the sinuses);
- Describe advances in shim system design;
- Explain the differences between arrays designed to optimize SNR vs. those designed for partial parallel imaging;
- Compare and contrast arrays designed for transmit and receive applications;
- Describe algorithms for designing RF pulses for parallel imaging;
- Compare and contrast ESR and NMR; and
- Describe several applications of hyper-polarized C_{13} and explain methodological differences between conventional MRI and hyperpolarized MRI.

Emerging Methods

07:00 **ESR**
David J. Lurie

07:20 **Hyperpolarized C13**
J. Stefan Petersson

MORNING CATEGORICAL COURSE
Human MRI and MRS at High Static Magnetic Fields: The Promise, the Challenges, the Solutions

Room 615-617 7:00 – 8:00 Chairs: Joseph A. Helpern and Dikoma C. Shungu

Educational Objectives:
Upon completion of this session, participants should be able to:

- Describe the general behavior of B_0 and B_1 fields in the human body when the Larmor frequency is of the order of or greater than 100 MHz;

- List the problems faced in trying to obtain a homogeneous B_0 field and a B_1 field;
- Recognize the challenges of developing RF coils for high field applications;
- Recognize the challenges of whole-body imaging at high fields and list potential solutions;
- List recent methodological advances for detecting neurotransmitters by MRS at high fields;

- Recognize the challenges of implementing heteronuclear spin-spin decoupling at high static fields;
- Describe the benefits of high field for BOLD contrast;
- Describe the interaction between high magnetic fields and biological systems; and
- List organizations responsible for regulating exposure to magnetic fields.

07:00 **Getting BOLDer with High Field fMRI**
Xiaoping P. Hu

07:30 **Static Magnetic Fields: Bioeffects, Regulation and Management**
Penny Anne Gowland

MORNING CATEGORICAL COURSE
New Horizons in Musculoskeletal MRI

Room 613-614 7:00 – 8:00 Chairs: Joshua M. Farber and Timothy J. Mosher

Educational Objectives:
Upon completion of this session, participants should be able to:

- Recognize patterns of abnormal hip biomechanics and associated MRI findings in femoral acetabular impingement syndrome;
- Apply knowledge of normal articular cartilage maturation and joint development in interpretation of pediatric musculoskeletal MRI;
- Recognize the role of normal and abnormal biomechanics and the associated MRI findings in normal joint physiology and development of overuse injuries;
- Identify emerging translational research applications in the field of musculoskeletal MRI:
- Describe new MRI techniques for tracking mesenchymal stem cells;
- Recognize new applications of molecular imaging in the study of musculoskeletal diseases.

MRI Applications for Stem Cell Research in the Musculoskeletal System

The final five minutes of each talk will be reserved for questions.

07:00 **MRI Techniques for Stem Cell Trafficking**
Erik M. Shapiro

07:30 **Stem Cell Research Opportunities in the Musculoskeletal System**
Jeff W. M. Bulte

MORNING CATEGORICAL COURSE
Quantitative Neuro MRI

Room 602-604 7:00 – 8:00 Chairs: Fernando Calamante and Annemie Van der Linden

Educational Objectives:
Upon completion of this session, participants should be able to:

- Discuss the latest advances in the field of arterial spin labeling, their current limitations, and identify their potential role in basic and clinical science;
- Demonstrate the role of MR methods to assess oxygen consumption non-invasively, and illustrate potential applications;
- Describe the various approaches to measure the arterial input function using dynamic-susceptibility contrast MRI and describe their limitations and implications to measure absolute cerebral blood flow, explain the latest advances of dynamic contrast-enhanced MRI to measure non-perfusion parameters, and assure formation of proper echoes;
- Recognize the limitations of the diffusion tensor model and identify more advanced methodologies to characterize areas with multiple fiber directions more accurately, as well as to describe the latest advances on fiber-tracking, including the concept of probabilistic tractography;
- Apply statistical approaches to perform voxel-based analysis for group comparison, and

- Describe image analysis techniques to characterize brain deformation.

Group Comparison and Longitudinal Studies

07:00 **Voxel-Based Analyses**
Gareth J. Barker

07:30 **Techniques for Measuring Brain Deformation**
Derek L. G. Hill

MORNING CATEGORICAL COURSE
Unsolved Problems and Unmet Needs in Magnetic Resonance

Room 6E 7:00 – 8:00 Chairs: Richard W. Bowtell and David I. Hoult

Educational Objectives:
Upon completion of this session, participants should be able to:

- Identify and assess a sampling of key unsolved problems and unmet needs in the field of magnetic resonance;
- Establish criteria for successful solutions to such problems;
- Consider any large-scale coordination across our field or with other fields that may be called for to address some classes of research or clinical needs;
- Identify and share additional unsolved problems or unmet needs in your areas of interest.

Do we need a virtual scanner, or do we understand real ones?

07:00 **Need for a Non-Commercial Open-Source MR Simulator**
Ralf B. Loeffler

07:15 **Does the Principle of Reciprocity Hold at High Field MR?**
Jinghua Wang

07:30 **Open Discussion**

07:45 **Conclusion**
Daniel K. Sodickson

PLENARY LECTURES: Clinical Trials

Room 6A-C 8:15 - 9:30 Chairs: David A. Bluemke and Michael V. Knopp

8:15 ***847.*** **MRI in Multicenter Trials: Challenges and Limitations**
Mitchell D. Schnall[1]
[1]University of Pennsylvania, Philadelphia, Pennsylvania, USA

Multicenter clinical trials in MRI will continue to be more important to validate applications and innovations. There are many challenges in performing these trials including design, standardization, quantitation and quality control. Better training in multicenter clinical trials within the MRI community is necessary for it to provide leadership clinical trials involving MRI.

8:40 ***848.*** **MR as a Biomarker in Clinical Trials**
Jeffrey L. Evelhoch[1]
[1]Amgen, Inc., Thousand Oaks, California, USA

Imaging is a powerful biomarker that can provide information about many biological/pathobiological processes. MR can serve as a biomarker in many diseases including multiple sclerosis, cancer, arthritis, atherosclerosis and others. Examples of how MR is used in clinical trials developing human therapeutics will be presented. However, prior to use as a biomarker, it must be demonstrated that the MR method is qualified for its intended use. Public-private partnerships among industry, government bodies, academia and not-for-profit organizations could both reduce the cost and speed the process of developing and qualifying MR biomarkers. Ongoing consortia involving MR biomarkers will be considered.

9:05 ***849***. **Challenges in the Use and Approval of Novel Diagnostic Agents**

Jelle O. Barentsz[1]

[1]University Hospital Nijmegen, Nijmegen, Netherlands

This course will specifically discuss the challenges in performing clinical trials with novel diagnostic agents with high clinical potential. General guidelines will be given, and skills of the primary investigator required for good outcome will be discussed. More in detail, problems which may arise will be illustrated, using examples of new diagnostic MR agents. In this respect endorectal coil dynamic MRI & MRSI in prostate cancer, USPIO for detection of very small lymph node metastases, and a new oral MN-based liver contrast agent for improved detection of small metastases will be shown.

CLINICAL CATEGORICAL COURSE
Therapy Assessment

Room 6E 10:30 – 12:30 Chair: Michael V. Knopp

Educational Objectives:
Upon completion of this session, participants should be able to:

- Identify opportunities to use MR for non-invasive assessment of therapy;
- Recognize requirements for standardization of acquisition and analysis;
- Apply standardized approaches to use the potential of MR within clinical use; and
- Explain current concepts in image based assessment.

The final five minutes of each talk will be reserved for questions.

10:30 **The Needs and Opportunities of Imaging as Bio- or Surrogate Markers – A Strategic Perspective**
Daniel C. Sullivan

11:00 **Goals for Assessment of Response – A Clinical and Cooperative Trial Structure**
Lawrence H. Schwartz

11:30 **Integrating MR Response Information within Trials: A Quality Assurance Perspective**
T. J. Fitzgerald

12:00 **Using MR to Assess Therapeutic Response – An Investigator's Perspective**
Johannes T. Heverhagen

Advances in Diffusion Acquisition and Sequence Design

Room 6C 10:30 - 12:30 Chairs: Roland Bammer and James G. Pipe

10:30 ***850***. **Multislice Inner Volume MRI for Spinal Cord Diffusion Imaging**

Bertram Jakob Wilm[1, 2]*, Jonas Sevensson*[1, 3]*, Urs Gamper*[2]*, Anke Henning*[2]*, Peter Boesiger*[2]*, Spyros Kollias*[1]

[1]Institute of Neuroradiology, Zurich, Switzerland; [2]Institute of Biomedical Engineering, Zurich, Switzerland; [3]Department of Radiation Physics, Malmö, Sweden

Diffusion weighted imaging (DWI) of the spinal cord is complicated by strong susceptibility gradients as well as physiological motion. To reduce susceptibility effects and motion artifacts at the same time we present a single-shot spin echo EPI technique with a reduced field of view in the phase encoding direction. To avoid fold over a spatially selective signal profile and outer volume suppression are incorporated. The combination of these techniques enables high resolution DWI within all regions of the spinal cord.

10:42 ***851***. **Diffusion Encoding with 2D Gradient Trajectories Yields Natural Contrast for 3D Fiber Orientation**

Van J. Wedeen[1]*, Guangping Dai*[1]*, Wen-Yih Isaac Tseng*[2]*, Roupeng Wang*[1]*, Thomas Benner*[1]

[1]Athinoula A. Martinos Center, Charlestown, Massachusetts, USA; [2]National Taiwan University College of Medicine, Taipei, Taiwan

A novel diffusion contrast mechanism is presented. Gradient pulse trains following appropriate trajectories within a prescribed 2D plane in q-space create diffusion contrast specific for fibers oriented perpendicular to the specified plane. Theory and experimental data, tractography in fixed marmoset brain and in human subjects, are presented, showing that high-resolution diffusion MRI with such gradients yield accurate fiber orientation density functions directly from the signal, without need of reconstruction by integral transform. Opportunities are discussed for quantitation of fiber geometry including fiber diameter.

10:54 ***852***. **Whole-Brain High Angular Resolution Diffusion Imaging Within a Clinically Feasible Acquisition Time**

Pratik Mukherjee[1], Christopher P. Hess[1], Eric T. Han[2], Duan Xu[1], Daniel B. Vigneron[1]
[1]University of California, San Francisco, California, USA; [2]GE Healthcare Global Applied Science Laboratory, Menlo Park, California, USA

Whole-brain 3T HARDI with 55 diffusion-encoding directions and b=3000 s/mm-sq was performed at 2.2 mm isotropic voxel resolution within a 15 minute acquisition time on five adult normal volunteers, two traumatic brain injury patients, and two patients with agenesis of the corpus callosum. Multimodal intravoxel fiber orientations were derived from the HARDI data using three different techniques: spherical harmonic q-ball, spherical deconvolution, and the diffusion orientation transform. All 3 methods provided effective visualization of normal complex white matter architecture in the volunteers and aberrant or injured white matter in the patients. Whole-brain HARDI is feasible for routine clinical application.

11:06 ***853***. **Turbo Segmented Spiral Diffusion Tensor Imaging: Acquiring Whole K-Data Using Multi-Segments Within Single-Shot Time Window**

Tiejun Zhao[1], Danli Wang[1], Xiaoping Hu[1]
[1]Emory University/Georgia Tech, Atlanta, Georgia, USA

A new diffusion weighted sequence is developed based on segmented spiral and experimentally demonstrated. With this method, all the segments for covering the desired k-space are acquired after a single diffusion weighting. Compared to the previous multi-shot methods, the new method is less sensitive to motion and does not require navigators.

11:18 ***854***. **A New Propeller EPI Design Using Short Axis Readouts**

Stefan Skare[1], Rexford Newbould[1], David B. Clayton[1], Roland Bammer[1]
[1]Stanford University, Palo Alto, California, USA

A new propeller EPI design is presented. Difference to earlier propeller EPI method is that the readout is played out along the short-axis rather than the long-axis of the blades. This results in reduction of Nyquist ghosts and distortions per blade, which means less blurring in the reconstructed image. Also, since the number of phase encoding points of the blads determines k_max, higher image resolutions does not increase the distortions and blurring.

11:30 ***855***. **Improved High-Resolution SNAILS DTI with a Spiral-In Navigator**

Chunlei Liu[1], Roland Bammer[1], Michael Moseley[1]
[1]Stanford University, Stanford, California, USA

Variable density (VD) spiral has been applied in SNAILS for the acquisition of high-resolution diffusion weighted images. By oversampling the center of k-space, SNAILS provides the capability to navigate the motion-induced phase errors. However oversampling increases off-resonance blurring. A method is proposed to improve SNAILS by applying a spiral-in phase navigator. This extra navigator reduces the oversampling factor of the VD spiral, while maintaining a reasonable high SNR to compensate residual artifacts. *In vivo* high-resolution DTI is demonstrated using two VD spiral pitch factors. The navigator enables a smaller pitch factor and improves the image SNR and contrast.

11:42 ***856***. **Multi-Shot Diffusion-Weighted PROPELLER MRI of the Abdomen**

Jie Deng[1], Alto Stemmer[2], Frank H. Miller[1], Thomas K. Rhee[1], Riad Salem[1], Debiao Li[1], Reed A. Omary[1], Andrew C. Larson[1]
[1]Northwestern University, Chicago, Illinois, USA; [2]Siemens Medical Solutions, Erlangen, Germany

Single-shot diffusion-weighted EPI (DW-EPI) techniques are routinely used for neuroimaging applications due to relative insensitivity to bulk motion artifacts. However, these single-shot techniques can suffer significant image distortion, chemical shift artifacts, and reduced spatial resolution. The recently introduced DW-PROPELLER strategy offers the potential to overcome these limitations. The PROPELLER sequence uses a multi-shot acquisition strategy while permitting segmental phase correction to reduce bulk motion artifacts. Our study evaluated the feasibility of using the multi-shot DW-PROPELLER sequence for diffusion-weighted imaging of the abdomen. We tested the hypothesis that DW-PROPELLER provides accurate quantitative diffusion measurements while improving qualitative image quality compared to single-shot DW-EPI.

11:54 ***857***. **Diffusion Imaging Using MinD SAP-EPI**

Stefan Skare[1], Rexford Newbould[1], David B. Clayton[1], Roland Bammer[1]
[1]Stanford University, Palo Alto, California, USA

MinD SAP-EPI stands for Minimum Distortion Short-Axis readout Propeller EPI. It is based on a new propeller EPI design with readout along the short-axis of the blade to reduce distortions. To reduce distortions further, GRAPPA with R=4 was used on a 4-shot DW SAP-EPI. Combining SAP-EPI with R=4, gives about 12 times less distortions. Finally, by identifying propeller blades pairs, oriented 180 degrees apart, distortion & motion correction was performed on the magnitude blade pair images using RGPM. After correction, the two blade pairs are averaged and Fourier transformed back to k-space for simultaneous regridding.

12:06 ***858***. **Diffusion Tensor Imaging with HighlY Constrained BackPRojection (HYPR)**

Andrew L. Alexander[1], Jee Eun Lee[1], Charles A. Mistretta[1]
[1]University of Wisconsin, Madison, Wisconsin, USA

This study examines the feasibility of a highly constrained reconstruction method for undersampled diffusion-weighted projection imaging with diffusion measurements obtained with high angular resolution. Simulations of a DTI experiment with projection imaging were performed. The highly constrained filter backprojection (HYPR) method demonstrated considerably reduced artifacts and increased SNR in the reconstructed images relative to standard filtered backprojection using an undersampling acceleration factor of 20.

12:18 ***859***. **Q-Ball Imaging with PROPELLER Acceleration**

Ming-Chung Chou[1, 2], Hsiao-Wen Chung[1, 2], Teng-Yi Huang[3], Hua-Shan Liu[1, 2], Chao-Ying Wang[1, 2], Ming-Long Wu[1], Cheng-Yu Chen[2]
[1]National Taiwan University, Taipei, Taiwan, Taiwan; [2]Tri-Service General Hospital, Taipei, Taiwan, Taiwan; [3]National Taiwan University of Science and Technology, Taipei, Taiwan, Taiwan

We proposed PROPELLER QBI technique using PROPELLER EPI acquisition for acceleration to reduce scan time. Herein we used PROPELLER keyhole reconstruction to form 252 high-resolution DWIs from 252 low-resolution blade DWIs. In our preliminary results, this approach can reduce whole brain QBI images to 18 minutes.

Hyperpolarized Gas Imaging

Room 6D 10:30 - 12:30 Chairs: Bastiaan Driehuys and Jim Wild

10:30 ***860***. **Hyperpolarzied 129Xe Human Gas Exchange at 0.2T with XTC**

Samuel Patz[1], Iga Muradian[2], Mirko I. Hrovat[3], James P. Butler[4], George P. Topulos[1], Steven Ketel[2], Iulian C. Ruset[2], Silviu Covrig[2], F. William Hersman[2], Massimo Ferrigno[1]
[1]Brigham and Women's Hospital, Boston, Massachusetts, USA; [2]University of New Hampshire, Durham, New Hampshire, USA; [3]Mirtech, Inc., Brockton, Massachusetts, USA; [4]Harvard School of Public Health, Boston, Massachusetts, USA

Xenon Transfer Contrast (XTC), developed by Ruppert *et al* (MRM 51:676-687,2004), has been used to measure gas exchange, i.e. 129Xe diffusion from alveolar gas to lung parenchymal tissue, in animal lungs. This method provides an indirect measure of gas exchange from alveoli to tissue by looking at the modulation on the gas phase signal after applying multiple 180's to the dissolved phase. Here we modify this method to allow all data to be acquired in a single breath-hold and also report the first human pulmonary gas exchange results with this method.

10:42 ***861***. **Real-Time Production and *In Vivo* Imaging of Hyperpolarized ^{129}Xe**

Bastiaan Driehuys[1], Gary Price Cofer[1], Jim Pollaro[1]
[1]Duke University, Durham, North Carolina, USA

MRI using hyperpolarized ^{3}He and ^{129}Xe is challenging due to the non-renewable magnetization and single gas batches generally available for imaging. However, the polarization physics of ^{129}Xe, lends itself to real-time and continuous production as has been demonstrated for in vitro NMR spectroscopy applications. However, *in vivo* imaging requires gas pressures to be stepped down to physiologic levels, and ^{129}Xe to be polarized faster. Here, we demonstrate the capability to perform *in vivo* imaging using hyperpolarized ^{129}Xe flowing directly and continuously from the polarizer to the subject.

10:54 ***862***. **Imaging Pulmonary Gas Exchange Using Hyperpolarized ^{129}Xe**

Bastiaan Driehuys[1], Gary Price Cofer[1], Jim Pollaro[1], Julie Boslego[1], Lawrence Hedlund[1], G A. Johnson[1]
[1]Duke University, Durham, North Carolina, USA

We present a method for imaging pulmonary gas exchange enabled by differentially imaging ^{129}Xe that is taken up in lung tissue versus capillary blood. The ^{129}Xe-blood image is sensitive to micron scale changes in the thickness of the blood gas barrier which will delay the appearance of the characteristic 211ppm blood resonance. We both validate and demonstrate the utility of the method by showing that ^{129}Xe uptake in blood is impaired in rats with unilateral fibrosis. Blood/tissue separation was achieved by using a 1-point variant of the Dixon technique in combination with projection encoding.

11:06 ***863***. **Characterizing Surface-To-Volume Ratio Using Hyperpolarized Xenon-129 Exchange Dynamics in a Rabbit Model**

Jing Cai[1], Jaime F. Mata[1], Kai Ruppert[2], Talissa Anne Altes, [13], W A. Tobias[1], H-T J. Wang[1], G D. Cates Jr[1], John P. Mugler III[1], James R. Brookeman[1]
[1]University of Virginia, Charlottesville, Virginia, USA; [2]AMRIT, Sebastopol, California, USA; [3]Children's Hospital of Philadelphia, Philadelphia, Pennsylvania, USA

In this study we investigated whether MR measurements of hyperpolarized Xe-129 inter-phase exchange can characterize the surface-to-volume ratio (S/V) of the lung. Lung emphysema was induced in 5 rabbits to produce S/V changes; 3 rabbits were used as control. Depolarization of the gas-phase signal was measured after ventilation with 50cc hyperpolarized Xe-129. Slopes of the depolarization curves were calculated and compared with S/V from morphology. The emphysema group demonstrated a lower slope (0.732¡À0.106) than the control group (0.907¡À0.0448). Slopes correlated well (r=0.9551) with S/V. The results suggest this technique may be useful to detect changes in S/V of the lung.

11:18 ***864***. **MR Grid-Tagging Using Hyperpolarized Helium-3 for Quantitative Assessment of Regional Pulmonary Biomechanics**

Jing Cai[1], Talissa Anne Altes,[12], Wilson Miller[1], Jaime F. Mata[1], Xiaodong Zhong[1], Eduard E. de Lange[1], John P. Mugler III[1], James R. Brookeman[1]

[1]University of Virginia, Charlottesville, Virginia, USA; [2]Children's Hospital of Philadelphia, Philadelphia, Pennsylvania, USA

The purpose of this study was to develop a MR grid-tagging sequence for hyperpolarized He-3 (hp He-3) and to evaluate its ability to quantify human lung biomechanics. Six healthy subjects underwent MR imaging at inspiration and expiration after inhalation of 150-400cc hp He-3. Displacement, first and second principal strains (E1 and E2), and regional ventilation were determined. MR images show clearly defined grid tag lines at both inspiration and expiration. Lung displacement, E1, E2, and ventilation are generally homogenous throughout the lungs. These preliminary results demonstrate the feasibility of quantitative assessment of regional pulmonary mechanics using this technique.

11:30 ***865***. **Helium-3 Phase-Contrast Velocimetry on a Human Airway Model for Validation of Computational Fluid Dynamic Simulation**

Ludovic de Rochefort[1], Xavier Maître[1], Laurence Vial[2, 3], Redouane Fodil[4], Bruno Louis[4], Daniel Isabey[4], Marc Thiriet[2], Georges Caillibotte[3], Gabriela Sbirlea-Apiou[3], Jacques Bittoun[1], Emmanuel Durand[1]

[1]U2R2M, UMR 8081, CNRS, Université Paris-Sud, Le Kremlin-Bicêtre, France; [2]Laboratoire Jacques Louis Lions, UMR 7598, CNRS, Université Paris VI, Paris, France; [3]Centre de Recherche Claude Delorme (CRCD Air Liquide), Les Loges-en-Josas, France; [4]Biomécanique Cellulaire et Respiratoire, UMR651, INSERM, Université Paris XII, Créteil, France

A dedicated MR sequence combining phase contrast and radial imaging was applied on hyperpolarized helium-3 to map velocity on gas. The three velocity components could be measured with good temporal and spatial resolutions (1 s, 1.5 mm for in-plane resolution in a 1 cm thick slice) on physiologically relevant phantoms: a curved pipe and an airway tree reconstructed from CT-scans thoracic images. The technique was first evaluated quantitatively and computational fluid dynamic simulations on a patient-specific geometry could then be validated by the MR experiments.

11:42 ***866***. **High Temporal Resolution Hyperpolarized Helium Imaging**

Vinay Manjunath Pai[1], Igor E. Kamenetskiy[1], Ray F. Lee[1], Glyn Johnson[1]

[1]New York University, New York, New York, USA

High temporal resolution dynamical imaging of the lungs using hyperpolarized helium can be used for diagnosis of many pulmonary diseases. We present a SSFP based multi-echo approach which permits us to acquire relatively high temporal resolution cine data of the lungs when imaged with hyperpolarized helium.

11:54 ***867***. **3D He-3 Ventilation Imaging Using Multi-Echo VIPR**

James H. Holmes[1], Youngkyoo Jung[1], Rafael L. O'Halloran[1], Walter F. Block[1], Eric T. Peterson[1], Sean B. Fain[1]

[1]University of Madison-Wisconsin, Madison, Wisconsin, USA

Hyperpolarized (HP) gas MRI with 3D isotropic resolution will likely improve depiction and analysis of lung structures by reducing partial voluming and providing true cubic voxels for segmentation and measurement. The hypothesis of this work is that multi-echo 3D under-sampled Projection acquisition can provide the desired isotropic resolution in HP gas MRI of the lungs with sufficient SNR efficiency and k-space coverage relative to conventional acquisition techniques. Moreover, the use of multiple echoes per TR will mitigate loss due to RF-decay and reduce under-sampling artifact to improve the attainable resolution within a breath-hold.

12:06 ***868***. **Simultaneous Measurements of Regional Alveolar Oxygen Pressure, Oxygen Depletion Rate and Apparent Diffusion Coefficient by Hyperpolarized 3He MRI**

JiangSheng Yu[1], Masaru Ishii[2], Stephen Kadlecek[1], John MacDuffie Woodburn[1], Kiarash Emami[1], Sheeva Rajaei[1], Frank Hammond[1], Vahid Vahdat[1], Warren Gefter[1], David Lipson[1], Timothy W.I. Clark[3], Benjamin M. Brainard[1], Letitia R. Cheatham[1], Rahim R. Rizi[1]

[1]University of Pennsylvania, Philadelphia, Pennsylvania, USA; [2]Johns Hopkins University, Baltimore, Maryland, USA; [3]New York University, New York, New York, USA

Regional alveolar partial pressures of oxygen and regional oxygen depletion rates are important parameters describing lung function, while the apparent diffusion coefficient gives valuable insight into the lung's microstructure. Here we present a new nonlinear fitting technique for simultaneously measuring all of these parameters. This represents to the best of our knowledge the first example of the direct and simultaneous correlation of regional oxygen measurements to lung structure.

12:18 ***869***. **Single Scan 3D PO2 Mapping with Hyperpolarized 3He MRI**

Jim M. Wild[1], Kevin Teh[1], Neil Woodhouse[1], Rob Ireland[1], Stan Fichele[1], Edwin van Beek, [12], Martyn Paley[1]
[1]University of Sheffield, Sheffield, Yorkshire, UK; [2]University of Iowa, Iowa, USA

A single scan method of 3D mapping of lung pO2 with 3He has been developed to increase scan speed and reduce errors associated with breath-hold repeatability and mis-registration in multiple breath-hold 3D p02 mapping. The accuracy of the sequence is demonstrated with gas phantoms and *in vivo* experiments on a healthy normal. The *in vivo* values for the initial pO2 (p0) are in agreement with those published previously with a 2 scan 3D method and whole lung projection methods. The initial 3D B1 mapping reference scan could be used for subsequent images acquired with reduced phase encoded parallel imaging.

Phase Contrast: Go With The Flow

Room 4C - 3,4 10:30 - 12:30 Chairs: Krishna S. Nayak and Vinay Pai

10:30 ***870***. **Quantification of Turbulence Intensity by Generalizing Phase-Contrast MRI**

Petter Dyverfeldt[1], Andreas Sigfridsson[1], John-Peder E. Kvitting[1, 2], Tino Ebbers[1]
[1]Linköping University, Linköping, Sweden; [2]Linköping University Hospital, Linköping, Sweden

Turbulent flow is believed to be implicated in the pathogenesis of several cardiovascular diseases. Generalizing phase-contrast MRI and exploiting the phenomenon of signal loss, we propose a method for direct measurement of the standard deviation of the velocity distribution within a voxel. Standard deviation, in one direction, is obtained from the magnitude of two PC-MRI measurements with different first gradient moments. An in-vitro comparison with published LDA results shows good agreement. This method allows for quantitative studies of turbulence and may be useful in the assessment of heart valves and detection and analysis of turbulence in predilection areas of atherosclerosis.

10:42 ***871***. **Segmentation and Characterization of Vortical Flow Patterns in MRI Phase-Contrast Velocity Data**

Lars Wigström[1, 2], Thomas Hope[1], Mary T. Draney[1], Einar Heiberg[2], Ann F. Bolger, [23], Marcus T. Alley[1], Norbert J. Pelc[1], D Craig Miller[1], Robert J. Herfkens[1]
[1]Stanford University, Stanford, California, USA; [2]Linköping University, Linköping, Sweden; [3]University of California, San Francisco, California, USA

Phase-contrast magnetic resonance imaging provides a unique method to accurately estimate velocities within a 3D region during the complete cardiac cycle. This enables studies of flow patterns in the heart and great vessels to provide new physiological insights. An automatic and objective characterization of flow patterns would be of great importance for the definition of normal and abnormal flow. In this study, new image processing and visualization tools have been developed to automatically locate and quantify flow patterns of interest, based on the acquired velocity vector data.

10:54 ***872***. **Application of UNFOLD to Real-Time Fourier Velocity Encoding**

Christopher K. Macgowan[1], Bruno Madore[2]
[1]University of Toronto & Hospital for Sick Children, Toronto, ON, Canada; [2]Harvard Medical School & Brigham and Women's Hospital, Boston, Massachusetts, USA

A method is presented and experimentally validated to remove aliasing artifacts from real-time Fourier velocity encoding (FVE) using UNFOLD. UNFOLD cannot be applied directly to real-time FVE data because the measured flow patterns already possess large temporal bandwidths that would interfere with UNFOLD encoding. We show that it is possible to suppress the signal modulation related to flow by pre-processing the FVE data, which then allows artifact removal using UNFOLD. This approach will enable more aggressive undersampling of k-space without compromising flow measurement.

11:06 ***873***. **Fast PC Flow Measurements Using Undersampled Projection Reconstruction: Preliminary Results in a Swine Model**

Andrew L. Wentland[1], Frank R. Korosec[1], Oliver Wieben[1], Karl K. Vigen[1], Thomas M. Grist[1]
[1]University of Wisconsin, Madison, Wisconsin, USA

Accurate flow measurements are difficult to obtain within the time of a patient's breathhold. Previous studies using a cine PC undersampled projection reconstruction (PRPC) technique have shown that accurate flow measurements can be obtained in the time of a breathhold. In this study we used a swine model to evaluate the PRPC technique in comparison with a Fourier-based PC acquisition. Flow measurements in the aorta and renal arteries correlated well between the two methods. Undersampled PRPC offers benefits over the Fourier-based method, which may provide increased ability to evaluate the hemodynamic significance of stenoses for improved treatment planning.

11:18 ***874***. **Highly Accelerated Quantitative Flow Measurements Using *k-T* SENSE with Large Coil Arrays**

Christof Baltes[1], Michael Schacht Hansen[2], Kay Nehrke[3], Jeffrey Tsao[4], Peter Boesiger[1], Sebastian Kozerke[1]

[1]University & ETH, Zurich, Switzerland; [2]Guy's Hospital, King's College, London, UK; [3]Philips Research Laboratories, Hamburg, Germany; [4]Novartis Institutes for BioMedical Research, Inc., Cambridge, Massachusetts, USA

The feasibility of accelerating data collection in phase-contrast (PC) velocity mapping using *k-t* SENSE has been demonstrated recently. However, the accuracy of flow quantification was compromised at high acceleration factors due to slight temporal low-pass filtering. In this work, the impact of large coil arrays on the accuracy of *k-t* SENSE accelerated flow measurements was investigated. A fully sampled reference dataset was acquired and a subset of these data was used to simulate 16-fold accelerated PC flow measurements. It is demonstrated that the accuracy of quantitative flow measurements improves when using a larger number of coil elements.

11:30 ***875***. **Influence of Aerobic Fitness and Hypertension on Aortic Stiffness Throughout the Adult Age Span**

Kenneth A. Kraft[1], Ding-Yu Fei[1], Yung-Yeh Chang[1], Ross Arena[1]

[1]Virginia Commonwealth Univ., Richmond, Virginia, USA

We tested the hypothesis that MR-derived central arterial stiffness, as determined by aortic wave velocity (AWV) measurements, would differ across the adult age span in the following 3 groups: healthy sedentary, healthy athletic and persons with systolic hypertension. A total of 275 men and women (ages 21 – 84 years) underwent cardiopulmonary exercise testing and AWV measurements using rapid-acquisition MR sequences. Consistent with our hypothesis, the mean AWV was significantly different for each group, with athletes exhibiting the lowest, and hypertensives the highest average aortic wave velocities.

11:42 ***876***. **Time-Resolved 3D MR Flow Analysis at 3T: Insights Into Major Hemodynamic Changes Associated with Aortic Pathologies**

Michael Markl[1], Alex Frydrychowicz[1], Andreas Harloff[1], Ernst Weigang[1], Benrd Jung[1], Mathias Langer[1], Jürgen Hennig[1]

[1]University Hospital Freiburg, Freiburg, Germany

The intrinsic sensitivity of MRI to flow offers the unique possibility to acquire spatially registered information about vascular hemodynamics simultaneously with the morphological data within a single experiment. In this study, blood flow characteristics associated with common aortic pathologies were analyzed and compared to healthy controls using time resolved and respiration controlled 3D velocity MR mapping. 3D blood flow visualization revealed considerable alterations in local blood flow characteristics compared to normal volunteers. Specifically, relatively small geometric changes such as prosthesis implantation or mild ascending aortic aneurysm resulted in major disturbances of local vascular hemodynamics.

11:54 ***877***. **Time-Resolved 3D MR Velocity Mapping in a Realistic Vascular Rapid-Prototyping Model of the Thoracic Aorta**

Christian Canstein[1], [2], Pavel Dagarov[3], Bernd Jung[1], Ralf Schumacher[3], Jürg Küffer[3], Jürgen Hennig[1], Michael Markl[1]

[1]Universitätsklinikum Freiburg, Freiburg, Germany; [2]Universität Konstanz, Konstanz, Germany; [3]Fachhochschule beider Basel (FHBB), Muttenz, Switzerland

Using rapid prototyping technology a vascular geometry as measured by contrast enhanced MR-Angiography was transformed into a realistic solid flow phantom with large anatomical coverage and high spatial resolution. Integration into a flow circuit with patient-specific pulsatile inflow and application of time-resolved 3D MR velocity mapping permitted detail analysis of local and global flow dynamics in a realistic patient-specific environment. Different visualisation tools were applied to identify the 3D flow patterns inside the vessels which were found to be in good agreement with previously reported aortic blood flow patterns.

12:06 ***878***. **Tri-Directional Velocity-Encoding Phase Contrast MRI in Patients Undergoing Aortic Valve-Sparing Root Replacement**

Karin Dill[1], Timothy Carroll[1], Andrew Larson[1], Thomas Gleason[1], Al Zhang[2], Gert Reiter[3], James Carr[4]

[1]Northwestern University, Chicago, Illinois, USA; [2]Siemens Medical Systems, Chicago, Illinois, USA; [3]Siemens Medical Systems, Austria, Austria; [4]Northwestern University, Chicago, Illinois, USA

We have evaluate aortic flow characteristics in patients undergoing a unique valve sparing aortic root replacement surgery. A three directional flow quantification pulse sequence a analysis software elucidate the hemodynamic advantages of this proceedure.

12:18 ***879***. **Pulse Sequences for Phase-Contrast SSFP Imaging from a Single Steady-State**

Jon-Fredrik Nielsen[1], Krishna S. Nayak[1]

[1]University of Southern California, Los Angeles, California, USA

Steady-state phase contrast (SSPC) imaging achieves rapid flow measurements with high phase-signal-to-noise-ratio . However, due to the sensitivity of SSFP to eddy-current-induced phase variations from one TR to the next, two separate steady states are typically established (one for each value of the gradient first moment). This produces phase-contrast measurement errors in regions where the two images are not in perfect spatial alignment, and requires careful switching between the two steady states. We introduce two approaches to SSPC imaging from a single steady-state: (1) gradient inversion within a single TR, and (2) interleaved SSPC imaging using "VENC pairing".

Spinal Cord Imaging

Room 611 - 612 10:30 - 12:30 Chairs: Hanzhang Lu and Edward D. Wirth

10:30 ***880***. **Fast Contour Extraction in High Resolution *In Vivo* Rat Spinal Cord MR Images**

Xiang Deng[1], Ponnada A. Narayana[1]
[1]University of Texas Medical School at Houston, Houston, Texas, USA

A fast unsupervised method for contour extraction in high resolution *in vivo* rat spinal cord MR images is developed and implemented. This technique is based on a B-spline snake defined in polar coordinate system. It deforms toward the spinal cord contour by minimization of a weighted sum of the external and internal energy of the snake. Our experimental results on 24 images from 3 normal rats demonstrate that this method can detect the spinal cord contours in 1.6 seconds. This method is highly reproducible and the computed contours correlate well with manually defined contours.

10:42 ***881***. **Spinal Cord MT Imaging Correlates with Somatosensory Evoked Potentials in Adrenomyeloneuropathy**

Asif Mahmood[1, 2], Seth A. Smith[1, 2], Ronnie Abi-Raad[2], William A. Trescher[2, 3], Gerald V. Raymond, [12], Peter C.M. Van Zijl, [12], Hugo W. Moser, [12]
[1]Johns Hopkins University, Baltimore, Maryland, USA; [2]Kennedy Krieger Institution, Baltimore, Maryland, USA; [3]M.S. Hershey Medical Center, Pennsylvania State University, Hershey, Pennsylvania, USA

CSF normalized MTw imaging (MTCSF) showed sensitivity to neurological disability and quantitative sensory-motor tests in Adrenomyeloneuropathy, the adult form of X-ALD. Our purpose was to determine the association between central abnormalities detected by Somatosensory evoked potential (reflective of myelin integrity) of upper and lower limbs and dorsal column MTCSF. A significant positive correlation between each subject's mean dorsal column MTCSFint value and SSEP of central latency and interpeak latency was seen. We conclude that abnormalities seen by conventional SSEP of care are corroborated by imaging findings and thus corroborate each other in the *in vivo* detection of non-inflammatory demyelinating pathology.

10:54 ***882***. ***In Vivo* Longitudinal Diffusion Tensor Imaging of Spinal Cord Injury in Rats**

Aparna A. Deo[1], Raymond J. Grill[2], Khader M. Hasan[2], Ponnada A. Narayana[2]
[1]University of Houston, Houston, Texas, USA; [2]University of Texas, Houston, Texas, USA

In vivo longitudinal DTI of rat spinal cord injury (SCI) was performed over a period of eight weeks post-injury. The fractional anisotropy (FA) and individual eigenvalues were estimated for the ventral, dorsal, and lateral white matter. In all the three regions, the DTI metrics were observed to be significantly different in injured cords relative to the uninjured controls close to the epicenter of the injury. The spatio-temporal changes in the DTI metrics revealed a region specific recovery pattern. Analysis of the longitudinal and transverse diffusivities suggests the presence of remyelination and demyelination, but not axonal recovery, in injured cord tissue.

11:06 ***883***. **Logitudinal *In Vivo* DTI Assessment of Contusion Injury and Secondary Degeneration in Mouse Spinal Cord**

Joong H. Kim[1], Sheng-Kwei Song[1]
[1]Washington University, St. Louis, Missouri, USA

Longitudinal DTI was performed to assess injury progression of the residual ventrolateral white matter in contusion injured mouse spinal cord. The temporal and spatial evolution of secondary injury in white matter was clearly observed via the RA time course. The time courses of axial and radial diffusivity further suggest that axonal injury preceded demyelination in the white matter of this contusion spinal cord injury model. Longitudinal measurements *in vivo* reduce derived parameter uncertainty caused inter-animal differences when measurements are made *ex vivo* at single time points.

11:18 ***884***. **Quantitative Measurement of Spinal Cord Blood Volume (SCBV) in Humans Using Vascular-Space-Occupancy (VASO) MRI**

Hanzhang Lu[1], Meng Law[1], Stephen M. Hesseltine[1], Otto Rapalino[1], Jens H. Jensen[1], Joseph A. Helpern[1]
[1]New York University, New York, USA

While MRI techniques for brain perfusion measurement are well established, the perfusion quantification in spinal cord is more difficult because the dynamically acquired EPI images often show significant distortions and, more importantly, the arterial input function required for quantification is not readily measurable in the spinal cord. In this study, a steady state approach is used that acquires two VASO images before and after the contrast agent (Gd-DTPA) injection. This technique allows the calculation of spinal cord blood volume (SCBV) in physiological units. The results show an averaged SCBV of 4.12±0.65ml blood/100ml tissue in six subjects.

11:30 ***885***. **Differentiation of Spinal Cord Arteries and Veins Based on Temporal Separation with Dynamic Contrast-Enhanced MR Angiography**

Karolien Jaspers[1], Robbert J. Nijenhuis[2], Walter H. Backes[2]
[1]Eindhoven University of Technology, Eindhoven, Netherlands; [2]Maastricht University Hospital, Maastricht, Netherlands

Very small spinal cord arteries and veins were dynamically resolved using keyhole dynamic contrast-enhanced MR angiography in healthy volunteers and thoraco-abdominal aortic aneurysm patients. Venous enhancement appeared at least one dynamic phase (6 - 8 s) later than arterial enhancement. According to computer simulations the keyhole fraction should be taken as large as possible to account for the peripheral k-space information of the small vessels, and to avoid signal intensity loss and vessel blurring as much as possible.

11:42 ***886***. **Comparison of Phased Array Versus Implantable Coil for Rat Spinal Cord MRI**

Andrew C. Yung[1], Katie Carr[2], Piotr Kozlowski[1, 2]
[1]University of British Columbia High Field MRI Centre, Vancouver, BC, Canada; [2]Prostate Centre Vancouver General Hospital, Vancouver, BC, Canada

A 4-element phased array was compared with an inductively coupled implantable coil system for imaging of rat spinal cord at 7T. Ex vivo gradient echo FLASH images on the same rat were acquired using both coil systems, achieving adequate SNR in the spinal cord at 100 micron spatial resolution at reasonable imaging times. The implantable coil generated 2.4 times more SNR than the phased array. The phased array is a good choice if noninvasiveness and long-term reliability are desired, whereas the implantable coil can be used if maximal SNR is critical.

11:54 ***887***. **Integrated Brain and Biplanar Spinal Cord MRI Using Parallel Imaging and Multi-Array Coil Technology**

Katrin Weier MD[1], Yvonne Naegelin MD[1], Alain Thoeni[1], Jochen G. Hirsch[1], Ludwig Kappos MD[1], David Leppert MD[1, 2], Ernst-Wilhem Radue MD[1], Achim Gass MD[1]
[1]University Hospital Basel, Basel, BS, Switzerland; [2]GlaxoSmithKline R&D, Harlow, UK

We investigated the sensitivity and potential gain of combined brain and fast spinal cord imaging schemes. Brain and entire cord MRI with high resolution sagittal and transverse MRI was performed in a cohort of 256 MS patients. A SIEMENS 1.5T Avanto unit with TIM and parallel imaging techniques, both essential for the fast and complete assessment of the whole neuro-axis was used. Additional transverse MRI adds further information as some focal lesions can be detected, that are difficult to visualise on sagittal slices and that diffuse signal change can be ascertained or detected.

12:06 ***888***. **Diffusion Tensor Imaging Evaluation of the Cervical Spinal Cord in Spondylosis: Evaluation of Changes in Major and Minor Eigenvalues**

Stephen M. Hesseltine[1], Meng Law[1], Scott Lopez[1], James Babb[1], Glyn Johnson[1]
[1]New York University, New York, New York, USA

Diffusion tensor imaging (DTI) has shown promise in the evaluation of spinal cord white matter tracts in spondylosis. The purpose of this study is to compare spinal cord DTI metrics in patients with severe multilevel spondylosis with normal volunteers, evaluating changes in FA and MD as well as in the major and minor eigenvalues. Increased minor eigenvalues seen in the setting of chronic spondylosis suggests possible microscopic demyelination and axonal compromise.

12:18 ***889***. **Spinal Cord MRS in and Beyond the Cervical Spine**

Anke Henning[1], Michael Schär[1, 2], Spyridon Kollias[3], Dieter Meier[1], Peter Boesiger[1], Ulrike Dydak[1]
[1]University and ETH Zurich, Zurich, Kanton Zurich, Switzerland; [2]John Hopkins University, Baltimore, Maryland, USA; [3]Universital Hospital Zurich, Zurich, Kanton Zurich, Switzerland

Spinal cord MRS has been mainly restricted to the brain-stem and the upper part of the cervical spine. In this work first MRS patient data from the thoracic spinal cord are shown. Furthermore the spectral quality as well as its consistency over different volunteers and patients in the cervical spine was improved. Both was possible due to a combination of outer-volume suppression bands with a very sharp excitation profile, based on quadratic-phase (QPP) and higher-order-phase (HOPP) saturation pulses, and localized higher-order shimming, based on high-resolution cardiac-triggered B0-mapping.

fMRI: Spatial & Temporal Signal Characteristics

Room 615 - 617 10:30 - 12:30 Chairs: Stuart Clare and Seong-Gi Kim

10:30 ***890***. **Spatial Specificity of Post-Stimulus BOLD Undershoot Signal**

Fuqiang Zhao[1], Ping Wang[1], Tao Jin[1], Seong-Gi Kim[1]
[1]Pittsburgh University, Pittsburgh, Pennsylvania, USA

Spatial specificity of the post-stimulus BOLD undershoot signal has been tested by high-resolution fMRI in response to visual stimulus of isoflurane-anesthetized cats at 9.4T using GE techniques. BOLD and CBV-weighted data were acquired without and with injection of MION, respectively. The positive BOLD signal was spread across the cortical layers, while both post-stimulus BOLD undershoot and CBV-weighted fMRI signals peaked at the middle cortical layer. Additional BOLD study was performed to investigate TE dependence of post-stimulus BOLD signal. The post-stimulus BOLD undershoot is TE-dependent and is ikely caused by the elevated oxygen consumption.

10:42 ***891***. **Retinotopic Mapping of Human Visual Cortex Using Arterial Spin Labeling**

Zhaohui M. Liu[1, 2], Xiaoping Hu[1]

[1]Emory University, Atlanta, Georgia, USA; [2]WPI & UMass Medical School, Worcester, Massachusetts, USA

Retinotopic mapping using BOLD fMRI has been well established. BOLD offers high sensitivity but low spatial specificity due to its susceptibility to large draining vessel contamination. Perfusion fMRI might provide complementary data and potentially may even result in more accurate retinotopic map. We acquired human retinotopic mapping using both pulsed ASL (PASL) fMRI and BOLD fMRI and compared them. Different visual areas were detected successfully using both fMRI methods. General overlap of activated voxels in two methods is about 65% and in V1, overlap is up to 96%. Reliability study of PASL shows comparable true detection rate relative to BOLD.

10:54 ***892***. **Detection of Orientation Specific Activation Zones in Human V1 Using fMRI**

Essa Yacoub[1], Kamil Ugurbil[1], Noam Harel[1]

[1]University of Minnesota, Minneapolis, Minnesota, USA

The development of high field systems have allowed for improved capabilities of BOLD fMRI. Higher signal to noise ratios as well as increased spatial specificity have made robust mapping of cortical columns in humans attainable. Several groups have previously demonstrated ocular dominance columns (ODC) maps in humans using fMRI; however, to date there haven't been any studies that have successfully mapped orientation specific activation in humans directly. In this work, we show for the first time, direct mapping of orientation specific domains in humans with respect to established ODC maps.

11:06 ***893***. **High Resolution 3D fMRI of Human Visual Cortex with Elimination of Large Venous Vessels**

Markus Barth[1, 2], David G. Norris[1]

[1]Radboud University, Nijmegen, Netherlands; [2]MUW, Vienna, Austria

We propose a very high-resolution, 3D gradient echo technique with a two-fold partial parallel imaging acceleration to perform fMRI using a block design at isotropic sub-millimeter resolution ($0.75x0.75x0.75mm^3$). Visual stimulation leads to very robust activation in primary visual areas. Using this technique it is also possible to directly identify and remove large vein effects from activation maps. Results show that this procedure clearly improves the quality of activation maps and that the remaining portion is highly localized to grey matter. Despite the relatively long measurement time this technique holds promise for the identification of small functional units.

11:18 ***894***. **Temporal Encoded Orientation Maps with CBV-Weighted fMRI in Primary Visual Cortex**

Chan Hong Moon[1], Hiro Fukuda[1], Seong-gi Kim[1]

[1]Dept. of Neurobiology, Pittsburgh, Pennsylvania, USA

In order to increase the sensitivity of orientation-selective fMRI signals, temporally-encoded continuous stimulation was used with an ultrahigh magnetic field. Iso-orientation maps of fMRI were compared with those of optical imaging of intrinsic signal with 570nm wavelength in the same anesthetized cats. Location of active columns in the fMRI maps well matched with that of the optical imaging maps. This implies that an increase in blood volume (plasma and red blood cells) should occur in microvessels confined to the iso-orientation column. With the confirmed fMRI, functional architecture can be mapped in the brain where optical imaging can not be used.

11:30 ***895***. **The Dependence of BOLD fMRI and Somatosensory Evoked Potentials on Stimulation of the Rat Forepaw with Various Pulse Waveforms**

Artem G. Goloshevsky[1], Afonso C. Silva[1], Stephen J. Dodd[1], Alan P. Koretsky[1]

[1]National Institute of Neurological Disorders and Stroke, National Institutes of Health, Bethesda, Maryland, USA

The frequency and amplitude of stimulation pulses, as well as the duration of trains of pulses, were varied in the previous studies of the coupling between neuronal activity and hemodynamics in the rat model. Increases in neuronal activity and cerebral blood flow (CBF) were reported as linearly coupled. Hemodynamics underlie the contrast in functional MRI of the brain. In this study, we investigated the effects of the stimulation pulse waveforms on neuronal activity, as measured by recordings of somatosensory evoked potentials (SEPs), and BOLD fMRI in rats. Each pulse waveform was characterized by its frequency content. The results indicated that stimulation pulses with power at lower frequencies elicited stronger SEPs but decreased fMRI responses, compared to pulses with power at higher frequencies, which elicited weaker SEPs but larger fMRI responses.

11:42 ***896***. **Understanding the Intra- And Extravascular Contributions to the BOLD Effect Through Simulations**

Jose P. Marques[1], Richard W. Bowtell[2]

[1]Universidade de Coimbra, Coimbra, Portugal; [2]University of Nottingham, Nottingham, UK

By using a 3D finite element method to simulate BOLD signal changes produced by infinite cylinders and a more realistic model of the human cortical vasculature and comparing the results obtained, this abstract assesses the reliability of the infinite cylinder model used previously in the literature. A simple parametrisation of R2* changes as a function of blood volume and susceptibility has also been carried out, allowing a discussion of the variable form of the haemodynamic response at different fields. Using the realistic model it is also possible to explore the coupling between intra and extravascular contrast.

11:54 ***897***. **Temporal Analysis of the BOLD Response Using High Temporal Resolution Echo Volumar Imaging**

Cécile Rabrait[1], Philippe Ciuciu[1], Cyril Poupon[1], Denis Le Bihan[1], Franck Lethimmonier[1]
[1]Commissariat à l'Energie Atomique, Orsay, France, France

We describe the first fMRI results obtained with a new acquisition method : zoomed 2D parallel Echo Volumar Imaging. It allows high scanning rates (200ms/volume) and gives a higher SNR than EPI. Robust activation detection is demonstrated both in block and event-related paradigms, with high statistical thresholds. Then, an unsupervised statistical analysis with no predetermined hrf analytic model is performed and the estimated single-trial hemodynamic response function shows a good shape and a putative early dip. With the high temporal resolution reached, this method is a well adapted device to investigate the temporal features of the BOLD signal.

12:06 ***898***. **Swelling of Slow Water Diffusion Pool Precedes Hemodynamic Response During Activation of Human Visual Cortex**

Denis Le Bihan[1], Toshihiko Aso[1], Shinichi Urayama[1], Takahashi Hanakawa[1], Hideano Fukuyama[1]
[1]Kyoto University Graduate School of Medicine, Kyoto, Japan

A transient decrease of water diffusion has been reported during activation of visual cortex. We have investigated its temporal relationship with activation. At 3T activation of visual cortex was detected in our 6 subjects through a diffusion-weighted signal increase. Using a diffusion biexponential model the diffusion signal time course was converted into a slow diffusion pool swelling time course. The diffusion-derived time courses showed no initial dip, but a post-stimulus undershoot was present. Although the diffusion-derived and the BOLD time courses were similar in shape, the BOLD time course always lagged behind the diffusion-derived time course during the activation period with an average of 2.4 +/- 0.7s. Diffusion-sensitized MRI might provide a quantitative access to an early and direct physiological surrogate of cortical activation.

12:18 ***899***. **CBF, BOLD, CBV and $CMRO_2$ fMRI at 500-Ms Temporal Resolution**

Qiang Shen[1], Hongxia Ren[1], Timothy Q. Duong[1]
[1]Emory Unviersity, Atlanta, Georgia, USA

Gradient-echo BOLD, CBF, CBV and CMRO2 fMRI signals were measured with 500-ms resolution associated with rat forepaw stimulation. Percent changes and onset times were analyzed for three cortical layers. BOLD change was largest in Layer I-III whereas CBF, CBV and CMRO2 changes were largest in Layer IV-V. Only BOLD time course from Layer I-III showed a post-stimulus undershoot. CBV increased first but was overtaken by CBF. BOLD significantly lagged both CBF and CBV. These results suggest that CBF change arises largely from arterioles, CBV change has some venous contribution during steady state, and BOLD signal is weighted by draining veins.

Proton MRS of Human Brain Disease

Room 618 - 620 10:30 - 12:30 Chairs: Peter B. Barker and Michela Tosetti

10:30 ***900***. **NAA/Cr Tightly Correlates with Extracellular GABA in Surgically Treated Hippocampal Epilepsy**

Jullie W. Pan[1], Idil Cavus[2], Dennis Spencer[2], Hoby Hetherington[1]
[1]Albert Einstein College of Medicine, Bronx, New York, USA; [2]Yale University School of Medicine, New Haven, Connecticut, USA

While it is known that extracellular GABA can be elevated in the seizure focus, the etiology of its increase is unknown. Animal and human studies of extracellular GABA in epilepsy have shown several abnormalities in GABA physiology, and that relatively mild mitochondrial injury results in increased GABA release. We correlated 1H MR spectroscopic imaging data from n=14 epilepsy patients undergoing microdialysis studies of extracellular GABA, finding an unusually strong correlation between GABA concentrations with NAA/Cr (R=-0.96, p<1xe-4). This argues that GABA release, enhanced under conditions of mitochondrial injury is heavily controlling extracellular GABA levels.

10:42 ***901***. **Brain 1H MRSI and Formal Thought Disorder in Pediatric Complex Partial Epilepsy**

Joseph O'Neill[1], Jennifer Levitt[1], Erin Lanphier[1], Caroline Bailey[2], S Gurbani[3], James Alger[4], Rachel Caplan[1]
[1]UCLA NPI Child Psychiatry, Los Angeles, California, USA; [2]UCLA MRRC, Los Angeles, California, USA; [3]UC Irvine Pediatrics, Irvine, California, USA; [4]UCLA Neurology, Los Angeles, California, USA

MRS abnormalities are known in childhood epilepsy, but are understudied in relation to use of language to organize and formulate thoughts, formal thought disorder (FTD). We acquired 1H MRSI (TR/TE = 2300/272 ms) from widespread extrafocal brain regions in children with Complex Partial Seizures (CPS) and age-matched controls. In CPS, below-normal NAA/Cr and NAA/Cho and above-normal Cr and Cho were registered in bilateral parietal lobes and right striatum. In CPS in left parietal lobe, cortical NAA/Cr and white-matter Cr correlated with FTD. Extrafocal neuron damage (NAA) and gliosis (Cr, Cho) in pediatric CPS may contribute to thought disorder.

10:54 ***902***. **Thalamic and Hippocampal Dysfunction in TLE Measured by MRS**

Hoby Patrick Hetherington[1], Ruben I. Kuzniecky[2], Kenneth Vives[3], Dennis D. Spencer[3], Jullie W. Pan[1]
[1]Albert Einstein College of Medicine, Bronx, New York, USA; [2]New York University, New York, New York, USA; [3]Yale University, New Haven, Connecticut, USA

Recent work by Pan has demonstrated that there are significant declines in energetics (PCr/ATP) in the contralateral hippocampus, thalami and basal ganglia of patients with temporal lobe epilepsy. This finding supports the role of an anatomical network of involved structures in the pathophysiology of temporal lobe epilepsy. Previously, Kuzniecky reported that decrements in NAA in the contralateral hippocampus were associated with seizure recurrence following temporal lobectomy. In this work we demonstrate that decreases NAA in the network are: 1) anatomically correlated and 2) can they be used to lateralize the focus and predict surgical outcome.

11:06 ***903***. **Quantitation of Cellular and Biochemical Alterations in Hereditary Ataxias by 1H MRS at 4 Tesla**

Gulin Oz[1], Isabelle Iltis[1], Diane Hutter[1], Christopher M. Gomez[1]
[1]University of Minnesota, Minneapolis, Minnesota, USA

Neurochemical profiles of the vermis, cerebellar white matter and pons of healthy volunteers (N=10) and patients with spinocerebellar ataxias (SCA2 and SCA6, N=4 in each group) were obtained by ultrashort-echo STEAM spectroscopy and LCModel. Concentrations of 9-12 metabolites were measured reliably and corrected for atrophy. Major alterations in the profile indicating processes such as neuron loss, gliosis and reduced glucose utilization were observed in all three volumes-of-interest. The pattern of involvement of the three regions agreed well with the known pathology of these two ataxia types.

11:18 ***904***. **Cerebral Metabolic Abnormalities and Correlations with Cognition in Children with Pervasive Developmental Disorder: A Preliminary Proton MRS Study**

Luminita Alina Tudorica[1], Lidia Gabis[2], Allen Azizian[1], Susan Sclafani[1], John Bilski[1], Patricia Roche[1], Carla DeVincent[1], John Pomeroy[1], Wei Huang[3]
[1]State University of New York, Stony Brook, New York, USA; [2]Safra Children's Hospital, Tel Hashomer, Israel; [3]Memorial Sloan-Kettering Cancer Center, New York, New York, USA

Single-voxel proton MR spectra were acquired from left and right hippocampus-amygdala (LHA and RHA) regions and cerebellum of children with Pervasive Developmental Disorder (PDD) and healthy controls. In all or some of the brain regions examined, NAA/Cr was significantly decreased, while Cho/Cr and mI/Cr were significantly increased in the PDD group. LHA Cho/Cr was inversely associated with visual discrimination ability, while RHA NAA/Cr and mI/Cr were positively related to performance IQ. Combined approach of proton MRS and neuropsychological measurements may provide insight in understanding the underlying neuropathology of PDD.

11:30 ***905***. **Correlation Between Choline Containing Metabolites and Choline Kinase in Untreated Pediatric Brain Tumors**

Deborah E. Schofield[1], Ashok Panigrahy[2], Mark D. Krieger[2], Marvin D. Nelson[2], Floyd H. Gilles[2], Ignacio Gonzalez-Gomez[2], Stefan Bluml[2], [3]
[1]Childresn Hospital Los Angeles, Los Angeles, California, USA; [2]Childrens Hospital Los Angeles, Los Angeles, California, USA; [3]Rudi Schulte Reserach Institute, Santa Barbara, California, USA

Synopsis not available.

11:42 ***906***. **Brain Metabolite Changes Detected by MRS in Early Onset Type-1 Diabetes**

Robert Mark Wellard[1], Debbie Rankin[2], Debra Boyce[2], Graeme David Jackson[1], George Werther[2], Elisabeth Northam[2]
[1]Brain Research Institute, Melbourne, Victoria, Australia; [2]Royal Children's Hospital, Melbourne, Victoria, Australia

The biological correlates of subtle neuropsychological deficits observed in early-onset diabetes are not understood. This study aimed to use MRS to examine differences in brain metabolite profile on frontal lobe, temporal lobe and basal ganglia of a cohort of type-1 diabetics 13-15 years after diagnosis, compared to a matched control group. Short echo single voxel MRS, recorded at 3T, showed increased myoinositol in all regions, reduced NAA in frontal lobe and basal ganglia and increased total choline in frontal lobes. The observed metabolite differences suggest that region-specific long-term cellular changes accompany the neuropsychological deficits recorded in the patient group.

11:54 ***907***. **Magnetic Resonance Spectroscopic Imaging is Sensitive to Severity in Traumatic Brain Injury**

William M. Brooks[1], Sandra B. Hall[1], JoAnn Lierman[1], Allan L. Schmitt[1], Linda R. Ladesich[1], Thomas M. Malone[1], Robin L. Aupperle[1], Cary R. Savage[1]
[1]University of Kansas Medical Center, Kansas City, Kansas, USA

Traumatic brain injury (TBI) is a complex clinical entity with few effective methods for assessing severity of injury and for predicting outcome. Magnetic resonance spectroscopy provides a powerful means to assess brain metabolism following TBI. The overall aim was to determine whether sampling a large volume of brain issue using spectroscopic imaging approaches was sensitive to severity of brain injury. We found that averaged metabolites were significantly altered in patients following TBI. We also found that metabolite markers of membrane injury and of glial activation could discriminate mild injury from severe. These results might be helpful to elucidate cellular and molecular mechanisms.

12:06 ***908***. **Biochemical and Anatomical Characterization of Minimal HE**

Albert Michael Thomas[1], Nader Binesh[2], Rajesh Kumar[2], Sherry Liu[2], Bhagyashree Sawale[2], Amir Huda[3], Steven Han[2]
[1]University of California Los Angeles (UCLA) School of Medicine, Los Angeles, California, USA; [2]UCLA School of Medicine, Los Angeles, California, USA; [3]California State University, Fresno, California, USA

Sixteen patients with minimal hepatic encephalopathy (HE) and eighteen healthy controls were investigated using T1-weighted MRI, T2-weighted MRI and single-voxel-based 2D L-COSY. 2D spectra were recorded in the frontal and occipital regions, and neuropsychological tests. MRI of HE patients showed 23% increase in the globus pallidus signal intensities and increase of T2 in the frontal and occipital white matter. 2D MRS of HE showed significantly elevated combined glutamate and glutamine to creatine ratios, as well as reduced ratios of choline, taurine and myo-inositol compared to controls. Our preliminary data report both biochemical and anatomical changes in minimal HE patients compared to controls.

12:18 ***909***. **Proton MRS at 3 Tesla Reveals Altered Neurochemistry in Smokers**

Florian Schubert[1], Frank Seifert[1], Malek Bajbouj[2], Jürgen Gallinat[2]
[1]Physikalisch-Technische Bundesanstalt, Berlin, Germany; [2]Charite University Medicine, Berlin, Germany

We compared neurochemical parameters in smokers and healthy nonsmokers. MRS at 3T was performed in 13 subjects of each group, acquiring PRESS spectra from the left hippocampus and the anterior cingulate, and quantifying concentrations of choline-containing compounds (tCho), creatine+phosphocreatine, NAA, and glutamate. The NAA level in hippocampus was lower in smokers than in nonsmokers ($p=0.023$), and the concentration of tCho in the cingulate was positively correlated with the amount of smoking ($p=0.002$). These results are in line with growing evidence that hippocampal neurons are susceptible to neurotoxic nicotine effects, and may indicate membrane alterations in cortical regions of heavy smokers.

Microscopy, ESR, and Other Nuclei

Room 602 - 604 10:30 - 12:30 Chairs: Cornelius J. Faber and Jay L. Zweier

10:30 ***910***. **Improved Temporal and Spatial Resolution *In Vivo* Oxymetry Using Time-Domain EPR Imaging**

Sankaran Subramanian[1], Ken-ichiro Matsumoto[1], Fuminori Hyodo[1], Nallathamby Devasahayam[1], Calvin A. Johnson[1], James B. Mitchell[1], Cherukuri M. Krishna[1]
[1]National Institutes of Health, Bethesda, Maryland, USA

Electron Paramagnetic Resonance (EPR) is a spectroscopic technique that detects and characterizes free radicals. EPR is capable of providing direct measurements of tissue oxygen concentration in a manner that is not dependent on complex biological processes. We describe the use of single-point imaging (SPI) in radiofrequency, Fourier-transform EPR. We present the techniques for performing oxygen imaging using EPR with phantoms and *in vivo*. Results from mouse tumor models demonstrate that the SPI EPR imaging technique readily distinguishes between normal and tumor legs and can track the changes in tissue oxygen concentration in response to percentage of oxygen in breathing gas.

10:42 ***911***. **Noninvasive *In Vivo* Redox Status Study by Fast Acquisition Proton Electron Double Resonance Imaging**

Haihong Li[1], Arturo Cardounel[1], Xiaoqing Xi[1], Ziqi Sun[1], Yuanmu Deng[1], Sergy Petryakov[1], Periannan Kuppusamy[1], Jay L. Zweier[1]
[1]Davis Heart & Lung Research Institute, Ohio State University, Columbus, Ohio, USA

In order to map and monitor fast metabolism state of free radicals *in vivo*, temporal and spatial resolution are very critical. A suitable fast acquisition proton electron double resonance imaging sequence based on fast spin echo pulse sequence was developed and first time applied for noninvasive *in vivo* redox status study of mice. Temporal resolution (~ 3.4 s) and spatial resolution (~ 1.2 mm) were achieved. Both control and treated mice were studied by using TEMPONE nitroxide as probe. It was demonstrated that Cardax treatment significantly altered the tissue redox status of the mice heart and reduced the oxidant levels.

10:54 ***912***. **Shear-Wave Scatter Contrast Enhancement in Steady-State MR Elastography**

Ingolf Sack[1], Jens Rump[1], Sebastian Papazoglou[1], Dieter Klatt[1], Uwe Hamhaber[2], Eckbert Gedat[2], Jürgen Braun[2]
[1]Institute of Radiology, Berlin, Germany; [2]Institute of Medical Informatics, Berlin, Germany

In MR elastography (MRE) shear wave images are acquired to test non-invasively the mechanics of soft tissue. Here, a method is proposed for analyzing minor amplitude changes of shear waves in steady-state MRE wave images. As result, a new image contrast is obtained that displays anatomical structures due to externally applied motion. We ascribe the new contrast to differences in the mechanical impedance in heterogeneous tissue causing a scattering of shear waves. The new shear-wave scatter contrast enhancement (SCE) is applied to *in vivo* MRE of the human brain and the liver.

11:06 ***913***. **Efficient ^{19}F Imaging of Multi-Spectral-Line Contrast Agents: Aliasing Serves to Minimize Time Encoding**

Jochen Keupp[1], Tobias Schaeffter[1]
[1]Philips Research Laboratories, Hamburg, Germany

^{19}F MR imaging allows direct quantification of nano-particles or fluorinated (anti-cancer) drugs for molecular imaging. However, ^{19}F MR imaging is generally complicated by chemical shift artifacts induced by multi-line spectra with a shift range of around 100 ppm. Many counter measures have been described which typically lead to reduced SNR (line selection/saturation) or long imaging time (chemical shift encoding). A time encoding scheme with minimum number of equidistant encoding steps is proposed and demonstrated in a phantom study, which combines all spectral lines in a single image with optimized SNR and scan efficiency.

11:18 ***914***. **Comparison of Genetic and Environmental Murine Models of Amyotrophic Lateral Sclerosis in Fixed Spinal Cords Using MR Microscopy**

Michael S. Petrik[1], Jason M.B. Wilson[1], Samuel Colles Grant[2, 3], Stephen John Blackband,[34], Xiaoyang Shan[5], J. D. Schulz[1], S. Singh[1], Charles Krieger[5], Chistopher A. Shaw[1]
[1]University of British Columbia, Vancouver, BC, Canada; [2]Florida State University, Tallahassee, Florida, USA; [3]National High Magnetic Field Laboratory, Tallahassee, Florida, USA; [4]University of Florida, Gainesville, Florida, USA; [5]Simon Fraser University, Burnaby, BC, Canada

Murine models of familial Amyotrophic Lateral Sclerosis (ALS) employ mice over-expressing human mutant SOD1 (mSOD) genes while sporadic ALS may be better represented in mice fed a cycad neurotoxin. In this study, spinal cord tissue from mSOD mice were compared to previous studies of cycad-fed mice using MR microscopy performed at 17.6 T. Volumetric analysis of 3D images acquired at ~40-micron isotropic resolutions showed significantly decreased volumes in total grey (-16%) and white matter (-20%) of mSOD lumbar cords. Previously, cycad-fed lumbar cords showed similarly decreased volumes in lumbar spinal cord grey matter but no involvement of the white matter.

11:30 ***915***. **Imaging of Embryonic Cardiovascular Development with High-Field MR Microscopy**

Bianca Hogers[1, 2], Robert E Poelmann[1]
[1]Leiden University Medical Center, Leiden, The Netherlands, Netherlands; [2]Leiden Institute of Chemistry, Leiden, The Netherlands, Netherlands

(Ultra) high field MR microscopy has been used to follow up embryonic development *in vivo* with emphasis on heart development and to study possible side effects of the MRI procedure. Quail embryos were longitudinally studied with MRI to cover all stages of heart development. The obtained resolution was sufficient to detect all important cardiac structures and enough to detect congenital malformations in the future. There were no harmfull effects of MRI on embryonic development.

11:42 ***916***. **SSFP-Based Spectral Editing for Imaging of ^{19}F Contrast Agents**

Jochen Keupp[1], Tobias Schaeffter[1]
[1]Philips Research Laboratories, Hamburg, Germany

Typical shortcomings of non-proton MRI can be addressed by steady-state free precession (SSFP) methods, which offer a high signal level, short imaging time and spectral selective properties. Imaging of ^{19}F contrast agents can benefit particularly from SSFP because of the complex multi-line spectra with large chemical shift (CS) range. The CS artifact of perfluoro-octyl-bromide can be reduced to two main components using the SSFP frequency response. Weak components, which cause image blurring, are eliminated. The remaining components can be combined in a single image after Dixon-type CS compensation. ^{19}F phantom experiments were performed on a clinical 3T MR scanner.

11:54 ***917***. **Monitoring Chick Development in Ovo Using a 7T MRI System**

Maureen Bain[1], Andrew J. Fagen[2], James Mullin[1], Iain McNaught[1], Barrie Condon[1]
[1]Glasgow University, Glasgow, Scotland, UK; [2]Trinity College Institute of Neuroscience, Dublin 2, Republic of Ireland., Ireland

This study was undertaken using a state-of-the-art ultra high field (7 Tesla) MRI system to assess the feasibility of monitoring chick development and growth in ovo throughout the incubation period (21 days). Chick movement was problematic from day 8 but this was minimized by cooling the eggs in a fridge (4oC) for 1 hour prior to imaging. Image quality was excellent allowing the growth of individual organs including the brain, liver and heart to be continuously monitored from day 12 of incubation through to hatching. MRI has many benefits over more traditional invasive methods of monitoring chick development and growth.

12:06 ***918***. ***In Vivo* Sodium Imaging at 4T Using Conical-SPRITE and 3DGRE: A First Comparison**

Sandro Romanzetti[1], Joachim Kaffanke[1], Meghan Halse[2], Bruce Balcom[2], Nadim Jon Shah[1, 3]

[1]Research Centre Juelich, Juelich, Germany; [2]University of New Brunswick, Fredericton, New Brunswick, Canada; [3]University of Dortmund, Dortmund, Germany

Physiological processes taking place in the cell rely upon highly regulated intra- (10 mM) and extracellular (150 mM) sodium ion concentrations. Variations of sodium concentration from these values are indicative of diseases. The measurement of Tissue Sodium Concentration (TSC) is therefore important to understand disease grade and tissue viability. However, difficulties such as low sensitivity and complex relaxation behaviour are associated with ^{23}Na imaging. In this study performed at 4T, *in vivo* ^{23}Na images acquired using Conical-SPRITE are compared to images acquired using an optimised 3D Gradient Echo on a normal healthy volunteer brain. Conical SPRITE images show very good signal-to-noise ratios but are characterised by blurring which hinders exact anatomical determination. On the other hand, 3DGRE delivers images with good anatomical details but almost completely loses the fast component of the ^{23}Na signal.

12:18 ***919***. **Optimized Sodium Imaging of the Human Brain at 4.7 Tesla**

Robert W. Stobbe[1], Christian Beaulieu[1]

[1]University of Alberta, Edmonton, Alberta, Canada

Sodium images of the human brain are acquired using pulse-length and flip-angle optimization for SNR (considering a given scan duration) based on constant specific absorption rate. This optimization is performed using simulation with relaxation parameters measured in the human brain. Twisted projection acquisition is employed producing images with an acquisition voxel size of 3.2 mm isotropic at 4.7 Tesla in 10 minutes.

Relaxometry

Room 613 - 614 10:30 - 12:30 Chairs: Penny A. Gowland and Klaus Scheffler

10:30 ***920***. **T_1 Measurements at 7T with Application to Tissue Specific Imaging**

Vasiliki N. Ikonomidou[1], Peter van Gelderen[1], Jacco A. de Zwart[1], Jeff H. Duyn[1]

[1]National Institutes of Health, Bethesda, Maryland, USA

Tissue T_1 properties are important for contrast and sensitivity in many MRI applications as well as MRI sequence design and optimization. T_1 determination through exponential fitting of the inversion recovery curve is often hampered by ill-conditioning of the mathematical problem. In this work we present T_1 measurements at 7 T obtained using logarithmic sampling, which improves the robustness of the fitting process. The resulting values were used for application of a tissue specific imaging sequence that allows selective tissue imaging based on differences in T_1.

10:42 ***921***. **T_1 Measurements for Cortical Grey Matter, White Matter and Sub-Cortical Grey Matter at 7T**

P J. Wright[1], A Peters[1], M Brookes[1], R Coxon[1], P Morris[1], S Francis[1], R Bowtell[1], P Gowland[1]

[1]University of Nottingham, Nottingham, UK

T1 has been measured in human brain at 7T using an IR-TSE sequence. T1 maps and high resolution T1-weighted images have been acquired from 6 subjects. The T1 in cortical white matter was 1017 ± 86ms and the T1 in cortical grey matter was 1654 ± 21ms averaged over all subjects. The T1 in the caudate nucleus was measured to be 1480 ± 63ms, while the T1 in the putamen was 1327 ± 45ms. T1 maps and high resolution T1-weighted images have been obtained.

10:54 ***922***. **EKG-Triggered, Navigator-Gated SSFP Saturation Recovery for Quantitative T1 Mapping with High Resolution During Free Breathing**

Christian Stehning[1], Kay Nehrke[1], René Michael Botnar[2], Stefanie Winkelmann[1], Tobias Schaeffter[1]

[1]Philips Research Laboratories, Hamburg, Germany; [2]Technical University Munich, Muenchen, Germany

To allow for T1 quantification in the presence of cardiac- and respiratory motion, an enhanced saturation recovery sequence is presented. EKG-triggering is employed to exclude cardiac motion, and respiratory navigator gating allows for data acquisition during free breathing. Thus, breath holding is not required, and T1 maps, e.g. of the myocardium, can be acquired with high spatial resolution, while patient comfort is improved substantially. First results were obtained in phantoms and *in vivo*.

11:06 ***923***. **The Effects of Magnetic Field Inhomogeneity on FLASH-Based T_1 Measurements**

Dionyssios Mintzopoulos[1], Souheil Inati[2]

[1]Harvard Medical School, Boston, Massachusetts, USA; [2]New York University, New York, New York, USA

Multiple FLASH experiments with different flip angles and/or repetition times have been proposed as an efficient, fast, low SAR method for measuring T1 *in vivo*. Using analytical arguments and numerical experiments we show that the simultaneous estimation of the physical parameters T1, spindensity and B1 from finite-TR FLASH data is ill-posed, irrespective of the number of flip angles and TRs, short or long.

11:18 ***924***. **Single-Shot R1-Mapping Strategies for Dynamic Contrast Agent Quantification**

Stefanie Winkelmann[1], Tobias Schaeffter[2], Christian Stehning[2], Rene M. Botnar[3], Olaf Doessel[1]

[1]University of Karlsruhe, Karlsruhe, Germany; [2]Philips Research Laboratories, Hamburg, Germany; [3]Technical University Munich, Munich, Germany

We investigated the use of radial imaging and k-space preparation filters in single-shot R1-mapping for dynamic contrast agent quantification in carotid imaging. Two optimized sampling schemes for multiple image generation from a single shot data set were compared. Both techniques yielded accurate R1-maps in about 2s for a sub-millimeter in-plane resolution in phantoms and healthy volunteers. The results for short R1 values, as in the presence of contrast agents, was superior for the golden cut based profile order due to the high flexibility in time-point resolution.

11:30 ***925***. **Iterative T2 Estimation from Highly Undersampled Radial Fast Spin-Echo Data**

Christian Graff[1], Zhiqiang Li[1], Ali Bilgin[1], Maria Altbach[1], Arthur F. Gmitro[1], Eric W. Clarkson[1]

[1]University of Arizona, Tucson, Arizona, USA

T2-weighted imaging is a valuable method for the diagnosis of many pathological disorders, though T2 measurements are lengthy and impractical for routine clinical use. Recently a radial fast-spin echo method was developed which greatly reduces acquisition time. Data acquired in this way is very undersampled in spatial high frequencies, which results in errors in the T2 estimation of small objects. We present an iterative reconstruction technique based on projection onto convex sets (POCS), which can extract accurate T2 estimates from this undersampled data set.

11:42 ***926***. **Comparison of T2* Measurements in Human Brain at 1.5, 3 and 7 T**

Andrew Michael Peters[1], Matthew J. Brookes[1], Frank G C Hoogenraad[2], Penny Anne Gowland[1], Susan Tracey Francis[1], Peter G. Morris[1], Richard William Bowtell[1]

[1]University of Nottingham, Nottingham, UK; [2]Philips Medical Systems, Best, Netherlands

The characterisation of T2* in brain tissue is important for optimisation of MRI protocols. It may also be relevant in the identification of diseased tissue, since T2* values are affected by iron content. Here, we employ a modified EPI sequence in order to measure T2* in cortical grey matter, white matter, and deep grey matter nuclei, for three field strengths. We show that, R2* scales approximately linearly with field strength. Further, in agreement with previous studies we find that the average T2* in cortical grey matter is longer than that in grey matter nuclei.

11:54 ***927***. **Ultrashort T2* Relaxometry in Iron Labeled Tumors**

Wei Liu[1], Hannes Dahnke[2], Bobbi K. Lewis[3], E. Kay Jordan[3], Naheed Banu[3], Tobias Schaeffter[2], Joseph A. Frank[3]

[1]Philips Research North America, Briarcliff Manor, New York, USA; [2]Philips Research Germany, Hamburg, Germany; [3]National Insititue of Health, Bethesda, Maryland, USA

A new method was proposed to measure fast decaying T2* relaxation in tissues containing highly concentrated iron labeled cells, where T2* decay is too rapid for regular multiple gradient echo T2* mapping. *In vivo* MR experiments in rats with iron labeled tumors demonstrate that this method can quantify ultrashort T2* down to 1 millisecond or less. Combined with the regular T2* mapping, the new technique is expected to improve the *in vivo* quantification and monitoring of tissues containing heavily iron labeled cells.

12:06 ***928***. **Proton Imaging of Silanes to Map Tissue Oxygenation Levels (PISTOL): A New Tool for Quantitative Tissue Oximetry**

Vikram D. Kodibagkar[1], Ralph P. Mason[1]

[1]UT Southwestern Medical Center at Dallas, Dallas, Texas, USA

The linear dependence of the spin lattice relaxation rate, R_1, of the ^{19}F NMR resonances of fluorocarbons on pO_2 is well known and has been studied extensively. Recently, hexamethyldisiloxane (HMDSO) was presented as a potential analogous ^1H NMR pO_2 reporter molecule and bulk pO_2 measurements were obtained by ^1H spectroscopy. We have now extended application to present an imaging based method, PISTOL (Proton Imaging of Silanes to map Tissue Oxygenation Levels), and use HMDSO to map tissue oxygenation in rat thigh muscle in response to oxygen challenge. Dynamic changes in pO_2 were assessed with respect to respiratory challenge. Given the lack of toxicity and ready availability of HMDSO, we believe it has great potential as a pO_2 reporter molecule in the clinic.

12:18 ***929***. **Anomalous Iron-Induced CPMG Relaxation: Importance of Particle Size**

Nilesh Ghugre[1], Cathleen M. Enriquez[1], John C. Wood[1]

[1]Childrens Hospital Los Angeles, Keck School of Medicine, University of Southern California, Los Angeles, California, USA

MRI based non-invasive detection of tissue iron overload is becoming a clinically important tool. Compared to single-echo, CPMG techniques are faster and may offer greater insight into the effective size of iron clusters as well as residence/exchange times of proton pools. However, they exhibit complicated non-monoexponential signal decay and anomalous T2 behavior with echo-spacing(τ) in human liver. In order to investigate, we studied T2-τ behavior for three paramagnetic particles of different radii: ferritin (~7 nm), Feridex (~30 nm) and synthetic liposomes (400 nm). Our relaxometry observations suggest that iron particles must have a critical physical size to produce *in vivo* behavior.

TRADITIONAL POSTERS

MRI in Animal Models Other Than Stroke

Room 4E Monday 14:00 - 16:00

930. MRI Microscopy of Alzheimer Plaques in APP751 Transgenic Mice: Effect of TE and Spatial Resolution on Plaque Detectability

Amnon Bar-Shir[1], Yoram Cohen[1]
[1]Tel-Aviv University, Tel-Aviv, Israel

Amyloid plaques are the hallmark of Alzheimer disease (AD) but their identifications by non-invasive methods is difficult. Here we demonstrate for the first time, that Aβ plaques can be detected in APP751 transgenic (tg) mice without the need for contrast agents. In addition, we demonstrate that an in-plane resolution of 50µm and slice thickness of 100µm are optimal for the detection of Aβ plaques in this tg strain. As expected, longer TE in the gradient echo sequence also increases the detectability of the Aβ plaques, however, these images can be problematic due to their relatively low SNR.

931. Screening Mutagenic Mice with Ventricular Mutation: A Longitudinal Study

Yu-Ying Tung[1], Ching-Po Lin[2], Chen Chang[1]
[1]Functional and Micro-MRI Center, Institute of Biomedical Sciences, Academia Sinica, Taipei, Taiwan; [2]Institute of Neuroscience, National Yang-Ming University, Taipei, Taiwan

To screen mice with ventricular mutation, longitudinal mice ventricular volumes of each compartment were established using high resolution 3D T2 weighted MR images.

932. Evaluation of Neurodegeneration in a Mouse Model of INCL by MRI and Spectroscopic Analyses

Alison Heffer[1], Jeeva P. Munasinghe[1], Zhongjian Zhang[1], Sandra L. Hofmann[2], Alan P. Koretsky[1], Anil Mukherjee[1]
[1]National Institutes of Health, Bethesda, Maryland, USA; [2]University of Texas, Dallas, Texas, USA

Infantile Neuronal Ceroid Lipofuscinosis (INCL) is a childhood neurodegenerative storage disorder. Although children with INCL are normal birth, they are blind by two years of age and brain-dead by four. Rapid brain atrophy and altered chemical composition are characteristic of INCL. Using a mouse model of INCL that mimics the human disease, we analyzed the brains of these mice at 3, 4, 5 and 6 months of age using quantitative MRI, T2, ADC, relative cerebral blood flow, cerebral blood volume, Gd2+ infusion and MRS. The results suggest that these methods are useful in evaluating novel therapeutic interventions in this disease.

933. Longitudinal Study of the Development of Beta-Amyloid Plaque Burden in a Transgenic Mouse Model of Alzheimer's Disease, Using *In Vivo* Magnetic Resonance Imaging

Niels Braakman[1], Jörg Matysik[1], Sjoerd G. van Duinen[2], Fons Verbeek[1], Reinhard Schliebs[3], Huub J. M. de Groot[1], Alia Alia[1]
[1]Leiden University, Leiden, Netherlands; [2]Leiden University Medical Center, Leiden, Netherlands; [3]University of Leipzig, Leipzig, Germany

The development of non-invasive *in vivo* methods for imaging Alzheimer's pathology, such as Aβ plaques, has been a major challenge in recent years, with several groups developing magnetic resonance imaging methods for the visualization of Aβ. In this study we focus on developing magnetic resonance micro-imaging (µMRI) as a diagnostic tool for longitudinal studies to evaluate the progression of AD. So far longitudinal studies were only possible by studying different animals from different age groups. µMRI presents the unique possibility of studying the development within the same animals, over time.

934. *In Vivo* Quantification of Neuronal Degeneration in the G93A-SOD1 Transgenic Mouse Model of ALS by T_2 Mapping

Heiko G. Niessen[1], Frank Angenstein, [12], Kerstin Sander[2], Hans-Jochen Heinze[1], Henning Scheich[2], Stefan Vielhaber[1]
[1]University of Magdeburg, Magdeburg, LSA, Germany; [2]Leibniz Institute for Neurobiology, Magdeburg, LSA, Germany

G93A-SOD1 transgenic mice are used as an animal model to study the pathogenesis and the efficacy of drugs in amyotrophic lateral sclerosis (ALS). Here, we used T_2 mapping in the brain to monitor motor neuron degeneration at early stages of ALS. Depending on the disease progression, ALS mice showed significantly increased T_2 values in brain stem motor nuclei Nc. V, VII, XII, and spinal cord, whereas no change was observed in motor cortex and thalamus. Consequently, the parameter T_2 can be applied as a magnetic resonance progression marker that may allow for the screening of putative treatments of ALS.

935. Development of a VBM Protocol for Assessing Regional Gray and White Matter Brain Changes in a Canine Model of Aging

P D. Tapp[1], Kevin Head[1], Elizabeth Head[1], Nortan W. Milgram[2], Bruce A. Muggenburg[3], Orhan Nalcioglu[1], Min-Ying Su[1]

[1]University of California, Irvine, California, USA; [2]University of Toronto, Toronto, Ontario, Canada; [3]Lovelace Respiratory Research Institute, Albuquerque, New Mexico, USA

VBM was performed on 62 scans to assess regional brain changes in a canine model of human aging. Standard dog brain templates and probability maps were created from 192 scans. In males and females, GM atrophy was greatest in the frontal and temporal lobes, respectively. In WM, atrophy was largest in the optic nerve bundle and alveus of the hippocampus for males and females, respectively. Consistent with earlier manual planimetry, frontal lobe atrophy was observed in aging dogs. Moreover, age-related atrophy was more widespread than initially reported and varied among males and females using VBM procedures.

936. Comparison of MRI with Histopathology in T-Cell Clone Mediated Mouse EAE

Susann Boretius[1], Steffan Nessler[2], Christine Stadelmann[3], Takashi Watanabe[1], Jens Frahm[1], Thomas Michaelis[1]

[1]Max-Planck-Institut fuer biophysikalische Chemie, Goettingen, Germany; [2]Heinrich-Heine-University, Duesseldorf, Germany; [3]Gerog-August-University, Goettingen, Germany

In a clonal EAE mouse model two dominant lesion patterns with distinct histopathological findings were identified. Type A lesions were characterized by a reduction of signal intensity on both T1- and T2-weighted images, whereas type B lesions appeared as hyperintensities on T2- and slightly reduced or isointense signals on T1-weighted images. Histopathologically, type A lesions showed a significantly higher inflammatory cell density and more myelin loss than type B. Thus, high resolution 3D MRI not only proved useful for the assessment of lesion pathology, but also offers a promising tool to monitor lesion development and novel therapeutic strategies.

937. Axonal Injury is Detected by Postmortem DTI Before Fixation (But Not After)

Shu-Wei Sun[1], Hsiao-Fang Liang[1], Sheng-Kwei Song[1]

[1]Washington University, St. Louis, Missouri, USA

Reduced sensitivity of *ex vivo* DTI in detecting axonal damage has been reported. It is hypothesized that the structural changes caused by formalin fixation reduces the sensitivity of axial diffusivity to detect the injury. In this study, the DTI of injured optic nerve from mice *in vivo* live and in situ after death was conducted. The diffusion coefficients decreased 60% in both control and injured optic nerves after death, but the lesion contrast was preserved. The present data suggests that without the effect of formalin fixation the axial diffusivity is able to detect the axonal damage in the dead tissue.

938. Temporal Evaluations of the EAE-Induced Pathologies in the Grey Matter of Chronic Relapsing EAE

Anil Zechariah[1], Yi-Hua Hsu[1], Chen Chang[1]

[1]Functional and Micro-MRI Center, Institute of Biomedical Sciences, Academia Sinica, Taipei, Taiwan

The present study aims in providing new insights into the mechanism of pathogenesis occurring during multiple sclerosis (MS) by utilizing experimental autoimmune encephalomyelitis (EAE), a well-accepted MS animal model. Complex pathology of MS is associated with the formation of plaques in the white matter and abnormalities in the grey matter during the disease attack. Temporal evaluation of the clinical and pathological disease progression was carried out using the conventional MR techniques along with localized proton MR spectroscopy (MRS) and contrast enhanced MRI. Our results demonstrated the temporal changes in brain structure and metabolites concentration before, during and after the EAE attack.

939. Sequential Cerebral MRI of Listeria Brain Stem Encephalitis in Mice - Visualization of Sub-Clinical Lesions

Christian Brekken[1], Ellen-Ann Antal[2], Pål Erik Goa[1], Tina Bugge Pedersen[1], Else Løberg[2], Kjetil Klaveness Melby[2], Jan Mæhlen[2], Olav Haraldseth[1]

[1]Norwegian University of Science and Technology, FUGE MIC, Trondheim, Norway; [2]University of Oslo, Ullevaal University Hospital, Oslo, Norway

Brain stem encephalitis may arise during infection with the bacterium Listeria monocytogenes. Early diagnosis is of vital importance. The aim of this study was to test the ability of sequential cerebral MRI (7T) to visualize early brain stem encephalitis in mice. The MRI protocol consisted of tri-axial and sagittal scout scans, axial T2-w, and axial or 3D T1-w started ~10 min after i.p. injection of Gadodiamide. Our study shows that cerebral MRI examination can identify listeria brain stem encephalitis at a sub-clinical stage in mice. The MDEFT images demonstrate the applicability of this sequence in post-contrast T1-weighted MRI at 7T.

940. Increased Dietary Lysine and Associated Age Dependent Bilateral Striatal Damage in Glutaryl-CoA Dehydrogenase Deficient Mice

William Zinnanti[1], Jelena Lazovic[2], Keith Cheng[1], Michael B. Smith[1]
[1]Penn State College of Medicine, Hershey, Pennsylvania, USA; [2]California Institute of Technology, Pasadena, California, USA

Deficiency in glutaryl-CoA dehydrogenease (GCDH), leads to accumulation of glutaryl-CoA and glutaric acid. Affected individuals may suffer striatal degeneration within the first few years of life. Pathophysiology of the selective striatal vulnerability remains unclear, and an animal model of striatal specific injury is still missing. We exposed Gcdh -/- mice to high lysine diet. High lysine diet resulted in vasogenic edema within the striatum and death in 75% of 4-week-old Gcdh -/- mice. In 8-week-old Gcdh -/- mice after 6 weeks on high lysine diet increased vacuolation of the striatal patches and neuronal loss within cortex were observed.

941. MRI Changes in CBF, Diffusion and T2 After Seizures Induced by GluR5 Agonist Infusion in Rat Before 180 Mins

Jeeva P. Munasinghe[1], Madhumitha Banerjee[1], Maria Acosta[1], Alison Heffer[1], S-I Yamaguchi[1], Michael A. Rogawski[1], Afonso C. Silva[1], Alan P. Koretsky[1], William H. Theodore[1]
[1]National Institutes of Health, Bethesda, Maryland, USA

Glutamate receptor activation may evoke epileptogenesis and structural derangements. ATPA, KA and AMPA, activating varied receptor subtypes, were infused intra amygdalar (i.a) and i.v. in rats; seizures lasted 60 minutes. Arterial spin labeling, a 7T, 72/ 25 mm volume/surface rf coil ensemble generated axial slice CBF, T2 and ADC maps. Amygdalar infusion produced widespread brain activation. Saline had no effect. i.v. animals showed rapid global increases, particularly neocortical. Drug T2 and ADC effects possibly were limited to limbic regions due to relatively short seizure duration. MRI evidence of potential cytotoxic injury can occur after one hour of seizure activity.

942. High-Resolution MRI of NPC Mice Shows Neurological Changes Prior to Onset of Disease Symptoms

Chad Hicks[1], Silvia Lope-Piedrafita[1], Elizabeth Chaitkin[1], Emelia Allee-Jumbo[1], Lan Lin[2], Robert Erickson[1], Kewei Chen[3], Gene Alexander[2], Theodore Trouard[1]
[1]University of Arizona, Tucson, Arizona, USA; [2]Arizona State University, Tempe, Arizona, USA; [3]PET Center, Phoenix, Arizona, USA

High-resolution (100um isotropic) 3D MRI was used to longitudinally track brain volume changes in NPC mice versus controls. NPC mice were found to exhibit retarded growth and eventual atrophy compared to controls. Also, NPC mice showed hyperintensity in white-matter tract indicating a lack of myelin.

943. The Impact of Hydrocephalus in Experimental Meningitis

Christian Brandt[1], Helle J. Simonsen[2], Lise Vejby Søgaard[2], Olaf B. Paulson[2], Ian J. Rowland[2]
[1]Statens Serum Institut, Copenhagen, Denmark; [2]Copenhagen University Hospital, Hvidovre, Denmark

The aims of this study were to follow the evolution of experimental meningitis in a rat model and to identify critical events in the disease process using MR imaging methods. Clinical and motor scores were obtained and compared with the size of the ventricles. Over time the ventricles gradually increased in size and this expansion was closely associated with deterioration in clinical and motor scores. The results suggest that expansion of the ventricles leads to compression, reduced perfusion and damage to cortical tissue and is a critical component of the disease process.

944. Intranasal Insulin Delivery is Protective Against Diabetes Mellitus-Related Brain Atrophy and White Matter Abnormalities in Experimental Diabetes Mellitus

Cory Toth[1], Ursula I. Tuor[1], Douglas Zochodne[1]
[1]University of Calgary, Calgary, Alberta, Canada

Diabetes mellitus (DM) is associated with cognitive decline, brain atrophy, white matter changes, and even dementia. We studied experimental DM in mice receiving intranasal delivery of insulin or placebo. Compared to control mice, DM mice showed cognitive decline after 6-7 months which was prevented by intranasal insulin, which also prevented brain atrophy. Intranasal insulin prevents brain atrophy in experimental DM.

945. *In Vivo* Study of the Development of Hippocampal Subregions by High-Resolution Diffusion Weighted Imaging

Hsiao-Wen Chen[1], [2], Yi-Hua Hsu[2], Wei-C. Chu[1], Chen Chang[2]
[1]Institute of Biomedical Engineering, National Yang-Ming University, Taipei, Taiwan; [2]Functional and Micro-MRI Center, Institute of Biomedical Sciences, Academia Sinica, Taipei, Taiwan

The presented study was aimed to non-invasively and *in vivo* image the hippocampal subregions by using high-resolution diffusion weighted imaging (DWI). Further, the ADC measurements belong to three different diffusion directions were applied to quantitatively evaluate the morphogenesis of neuronal cell bodies and dendrites in hippocampus during early postnatal stages. The development of an *in vivo* detection tool to monitor detailed structural changes in hippocampus can provide a new insight into the pathogenesis in hippocampal subregions.

946. MRI Assessment of Aß-Iron Complex in PS/APP Mouse Brain

Maria F. Falangola[1, 2], Sang-Pil Lee[3], Jens H. Jensen[1], Hanzhang Lu[1], Ralph A. Nixon[2], Karen Duff[2], Joseph A. Helpern[1, 2]

[1]New York University School of Medicine, New York, New York, USA; [2]Nathan Kline Institute, Orangeburg, New York, USA; [3]University of Kansas Medical Center, Kansas City, Kansas, USA

The presence of iron in Aß plaques in PS/APP transgenic mouse model of Alzheimer pathology has been suggested to be a significant factor responsible for reducing T2 and the source of the intrinsic MRI contrast of Aß plaques seen in these animals. In this study, we investigated the relationship between areas of MR signal hypo-intensities, Magnetic Field Correlation and the presence Aß-iron complex (Perls' stain and anti-ferritin immunochemistry). We showed that ferritin-iron contained in the Aß plaque is the source of MRI contrast responsible for reduction of T2 and increase of MFC values in the brain of this mouse model.

Animal Brain MRS 13C, 17OZ, 7Li, 15N

Room 4E Monday 14:00 - 16:00

947. The Anaplerotic Metabolic Flux Through Pyruvate Carboxylase is a Prerequisite for Ammonia Detoxification in Acute and Chronic Liver Failure

Claudia Zwingmann[1, 2], Roger Butterworth[1], Dieter Leibfritz[2]

[1]Hospital Saint-Luc, Montreal, Quebec, Canada; [2]University of Bremen, Bremen, Germany

Liver failure results in acute or chronic Hepatic Encephalopthay (HE) - due to ammonia neurotoxicity. It is suggested that the osmotic effect of astrocytic glutamine is responsible for developmentof HE. We suggest that, rather than glutamine accumulation, limited glutamine synthesis account for HE development. In order to evaluate the association of anaplerosis with glutamine synthesis in HE, high resolution NMR was used to measure carbon flux in brain, liver and muscle of rats with different forms of liver failure. The data show that the muscle is the major organ for ammonia detoxification, and that glutamine formation is dependent on anaplerotic flux through pyruvate carboxylase.

948. Glucose Metabolism in Animals with a Traumatic Brain Injury: A 13C NMR Study

Brenda L. Bartnik[1, 2], David A. Hovda[2], Richard L. Sutton[2]

[1]Loma Linda University, Loma Linda, California, USA; [2]University of California Los Angeles, Los Angeles, California, USA

Traumatic brain injury is associated with metabolic alterations that may contribute to energy crisis. The present study was designed to explore the metabolic fate of [1, 2 13C2] glucose in the rat cortex 3.5h and 24h after a fluid percussion injury, where we have previously established a period of immediate hyperglycolysis followed by a decrease in ATP synthesis and a period of metabolic depression. Our results show an injury induced decrease in glucose utilization and subsequent glutamate and glutamine isotopomer labeling. Increased metabolism through the pentose phosphate and pyruvate recycling pathways suggest an increased need for reducing equivalents after injury.

949. Neuronal-Glial Glucose Oxidation and Glutamatergic-GABAergic Function Revealed by ^{13}C MRS Studies

Fahmeed Hyder[1], Anant Bahadur Patel[1], Albert Gjedde[2], Douglas L. Rothman[1], Kevin L. Behar[1], Robert G. Shulman[1]

[1]Magnetic Resonance Research Center, Yale University, New Haven, Connecticut, USA; [2]Aarhus University, Aarhus, Denmark

Recent ^{13}C MRS results, of total cycling ($V_{cyc(tot)}$), neuronal and glial glucose oxidation ($CMR_{glc(ox),N}$), are used to revise a model of neurotransmitter cycling and energy metabolism which excluded energetics of glia and GABA neurons. The revised model shows that neurons produce ~3.7× more ATP oxidatively than glia, and glutamatergic neurons generate ~4.6× more ATP than GABAergic neurons. Although neurons produce ~79% of total oxidative ATP, neuronal glucose uptake is only ~30% of the total glucose oxidized. Glial lactate still makes the major contribution to neuronal oxidation. The relationship observed between $\Delta CMR_{glc(ox),N}$ and $\Delta V_{cyc(tot)}$ is maintained by glial glycolysis as before.

950. Investigation of the Role of GABA Reuptake in GABAergic Neurotransmission

Anant Bahadur Patel[1], Robin A. de Graaf[1], Douglas L. Rothman[1], Kevin L. Behar[1]

[1]Magnetic Resonance Research Center, Yale University, New Haven, Connecticut, USA

The purpose of the present study was to assess the potential contribution of the GABA reuptake pathway to total GABA release. Cerebral metabolic rates were measured in halothane anesthetized rats using *in vivo* ^{1}H-[^{13}C]-NMR in conjunction with intravenous [1,6-$^{13}C_2$]glucose infusion under conditions in which the primary neuronal GABA transporter (GAT-1) was blocked by tiagabine. Glutamatergic and GABAergic neurotransmission is decreased slightly following tiagabine treatment suggesting a high degree of coupling, possibly due to reduced glutamatergic activity of the elevated extracellular GABA expected with tiagabine treatment. We conclude that the contribution of neuronal reuptake to synaptically released GABA is less than previously expected.

951. Comparison of Amino Acid Turnover Rates in Cortex and Isolated Nerve Terminals of the Anesthetized Rat

Anant Bahadur Patel[1], James CK Lai[2], Golam MI Chowdhury[1], Douglas L. Rothman[1], Kevin L. Behar[1]
[1]Magnetic Resonance Research Center, Yale University, New Haven, Connecticut, USA; [2]Idaho State University, Pocatello, Idaho, USA

In the present study we investigated neurotransmitter metabolism in nerve terminals and compared them with the values in cortical tissue. Halothane anesthetized rats were infused with either [1,6-$^{13}C_2$]glucose or [2-^{13}C]acetate for different times. ^{13}C Enrichments of metabolites were measured in isolated nerve terminals and cortical extracts using ^{1}H-[^{13}C]-NMR spectroscopy. Nerve terminal ^{13}C enrichments from [1,6-$^{13}C_2$]glucose were lower than for cortex but higher during infusion of [2-^{13}C]acetate indicating substantial dilution from glial glutamine. The turnover rate of the nerve terminal pool of neurotransmitters glutamate and GABA appears to be similar to tissue rates assessed *in vivo* by NMR.

952. Evaluation of the Simplified Method for Mapping Cerebral Metabolic Rate of Oxygen Based on ^{17}O NMR Approach

Nanyin Zhang[1], Xiao-Hong Zhu[1], Wei Chen[1]
[1]University of Minnesota, Minneapolis, Minnesota, USA

Various factors that may have impacts on the simplified $^{17}O_2$ approach for $CMRO_2$ measurement are extensively studied. The simulation results validate the simplified method in measuring $CMRO_2$ in relative large ranges of physiologic/pathologic conditions as well as different experimental environments. Comparisons between the linear and quadratic fitting models confirm the notion that quadratic fitting gives more accurate but less reliable results whereas linear fitting gives less accurate but more reliable results. However, there is no statistic significance to distinguish the linear fitting model from the quadratic model in the variation range of the parameters examined.

953. Estimating Intracellular Lithium in Brain *In Vivo* by Lithium-7 MRS

Richard A. Komoroski[1], John M. Pearce[2]
[1]University of Cincinnati, Cincinnati, Ohio, USA; [2]University of Arkansas for Medical Sciences, Little Rock, Arkansas, USA

The fraction of intracellular lithium (Li) in the brain for subjects under treatment for bipolar disorder is not known. Localized 7Li MRS can measure the total Li concentration in brain *in vivo*. Biexponential 7Li T2s in rat brain *in vivo* were measured so as to estimate the Li compartmental distribution. These biexponential T2 results were also used for estimating Li compartmental distribution from previously determined monoexponential T2 decays by a simple linear approximation. Unlike for Na, a substantial fraction of Li enters the cell. Depending on estimation method, an average % intracellular Li of 49-63% was found.

954. Glial Glutamine Release and Neuronal Reuptake by SAT1 Studied *In Vivo* by N-15 NMR and Microdialysis

Keiko Kanamori[1], Brian D. Ross[1]
[1]Huntington Medical Research Institutes, Pasadena, California, USA

Kinetics and mechanism of transport of glutamine from glia to the neuron *in vivo* - a key step in the glutamine/glutamate cycle - are unknown. The time-course of extracellular glutamine (GLN) and its N-15 enrichment was determined, in the presence and absence of transport inhibitors, by a combination of N-15 NMR and microdialysis/gradient heteronuclear single-quantum correlation NMR. The rate of glial glutamine release to the extracellular fluid (ECF) was 2.8 micromol/g/h in mildly hyperammonemic rat brain at steady-state brain glutamine concentration of 8.5 micromol/g. Transporter SAT1 mediates at least 85% of neuronal uptake of extracellular GLN.

Brain: Different Types of Relaxation and Angiography

Room 4E Monday 14:00 - 16:00

955. Chromium-Enhanced MRI of Myelinated Structures in Mouse Brain *In Vivo*

Takashi Watanabe[1], Roland Tammer[1], Susann Boretius[1], Jens Frahm[1], Thomas Michaelis[1]
[1]Max-Planck-Institut für biophysikalische Chemie, Göttingen, Germany

Intracerebroventricular microinjection of potassium dichromate resulted in an enhancement of white matter tracts in T1-weighted MRI of mouse brain *in vivo* (2.35 T, 150 µm isotropic resolution). Pronounced signal increases were observed in corpus callosum, anterior commissure, and fornix as well as in the mammillothalamic tract and fasciculus retroflexus. The results suggest the diffusion of diamagnetic chromium(VI) to be followed by a reduction to paramagnetic chromium(III) due to the oxidation of myelin lipids and subsequent chromium retention. Without an enhancement of gray matter structures such as the hippocampal formation, chromium-induced contrast reveals novel information different from that obtainable using manganese.

956. Regional T1 Relaxation Time and Tissue Content Changes of Hippocampus in Bipolar Disorder

Wen-Jang Chu[1], Stephen M. Strakowski[1], Hoby P. Hetherington[2], Mellissa P. DelBello[1], Cal M. Adler[1], Jing-Huei Lee[1]
[1]Univ. of Cincinnati, Cincinnati, Ohio, USA; [2]Albert Einstein College of Medicine, Bronx, New York, USA

The mood dysfunction that is present in bipolar disorder (BD; manic depressive illness) patients could be related to the abnormalities in specific brain regions that modulate emotion. The changes of gray matter content in amygdale have been reported in several BD studies. The reported studies of hippocampus, which also is an important region involved in mood disorders, are few. The present work investigated the tissue content changes (gray and white matters, and cerebral spinal fluid) in hippocampus in BD patients, and healthy volunteers using T1-relaxation-time-based tissue segmentation methods.

957. Establishment of an *In Vivo* Iron and R_2* Calibration Curve

Mark David Meadowcroft[1], James R. Connor[1], Jian-li Wang[1], Xiaoyu Sun[1], Michael B. Smith[1], Qing X. Yang[1]
[1]Pennsylvania State University - College of Medicine, Hershey, Pennsylvania, USA

The inability to regulate iron leading to abnormally elevated levels in brain tissue has been associated with several neurodegenerative disorders including Parkinson's, Huntington (HD) and Alzheimer's disease. Iron distribution in tissue acts as a natural contrast agent for magnetic resonance imaging because the transverse relaxation rate R2* (=1/T2*) is a sensitive MRI parameter for evaluation of tissue iron concentration. With the iron loading animal model used here, we show that elevated iron levels in various brain regions do positively correlate to higher R2* relaxation values. This data supports the initiative to create and validate a model of R2* relaxation and the corresponding iron concentration within brain tissue.

958. 3D-Relaxometry - Quantitative T1 and T2 Brain Mapping at 3T

Burkhard Mädler[1, 2], Trudy Harris[3], Alex L. MacKay[2]
[1]UBC Hospital, Vancouver, BC, Canada; [2]University of British Columbia, Vancouver, BC, Canada; [3]Vancouver Coastal Health, Vancouver, BC, Canada

We demonstrated the feasibility of two novel 3D imaging techniques for the purpose of quantitative T1 as well as multi-component T2-relaxation measurements under clinical relevant time constrains (<25min) at high magnetic field strength (3T). T1 measurements were performed by means of a 3D inversion prepared ultra-fast gradient echo sequence with radial encoding and elliptical k-space shutter. A 3D 32-echo CPMG sequence with slab selective refocusing pulses were used for multi-component T2 measurements.

959. Normal Regional T_1 and T_2 Relaxation Times of the Brain at 3T

Christabel E.C. Lee[1], Eva H. Baker[1], David M. Thomasson[1]
[1]NIH, Bethesda, Maryland, USA

The recent trend is to apply quantitative measurements to a variety of brain diseases, since quantifiable abnormalities are detectable in areas of the brain that have normal visual appearance on T_1- and T_2-weighted images. Quantitative measurements have the potential to be used for establishing objective diagnostic criteria. They also can detect subtle changes over time, useful for monitoring progression of disease or response to treatment. As a reference for future studies of disease, it is helpful to have a thorough description of what is normal. The purpose of this study is to establish reference values and estimate normal variance. We have produced an extensive table of normal values for different regions of the brain, covering more regions with more subjects than previous reports.

960. Long T_2 Imaging: Evidence of a New Water Reservoir in Phenylketonuria

Cornelia Laule[1], Sumia A. Tahir[1], Sandra M. Sirrs[1], Elana E. Brief[2], Carole Bishop[1], David KB Li[1], Alex L. MacKay[1]
[1]University of British Columbia, Vancouver, BC, Canada; [2]Simon Fraser University, Burnaby, BC, Canada

Our goal was to fully characterize the T2 distribution in phenylketonuria (PKU) white matter. 48-echo T_2 relaxation data was acquired in 15 PKU subjects and 15 controls. A new water reservoir with a markedly prolonged T_2 peak (200-800ms) was identified in PKU NAWM and lesions. Decreased myelin water and increased water content was observed in both PKU NAWM and lesions relative to controls. NAWM is not normal in PKU but exists in two forms: (1)Areas which appear normal on proton density (PD), T_2 and Long-T_2 map images (2)Areas which appear normal on PD/T_2 images but are hyperintense on Long-T_2 maps.

961. Multicomponent T2 Analysis of Rat Brain and Spinal Cord at 9.4 T

Cheryl Rae McCreary[1], Debbie Anne Kelly[1], Boguslaw Tomanek[2], Tadeusz Foniok[2], Dave Kirk[1], Jeff Frank Dunn[1]
[1]University of Calgary, Calgary, AB, Canada; [2]National Research Council, Calgary, AB, Canada

Rat spinal cord and brain T2 values at 9.4T were quantified. Although historically single exponential analysis has been used to quantify T2, there is increasing evidence that *in vivo* T2 is better determined through multi-exponential analysis. We used multiple processing methods to determine the impact of single or multi-exponential analysis for T2 quantification. These results show that for most brain regions at 9.4T, two decay functions account for the shape of the decay curve. The average T2 of rat cortex was 48.8±1.8 ms with single exponential and was a combination of 26±15 and 52±15 ms for a double exponential fitting.

962. Positive Contrast Susceptibility Weighted Imaging of Physiologic Calcification in Humans

John A. Butman[1], Wei Liu[2], Tobias Schaeffter[3]
[1]National Institutes of Health, Bethesda, Maryland, USA; [2]Philips Research North America, Briarcliff Manor, New York, USA; [3]Philips Research Germany, Hamburg, Germany

Positive contrast mechanisms have been proposed to improve contrast and specificity in susceptibility weighted imaging. In this *in vivo* study, we investigated the use of gradient rephasing positive contrast technique for the detection of susceptibility induced signal loss arising from calcium deposition in the normal human brain. We have demonstrated that the gradient rephasing technique could provide adequate positive contrast for the detection of calcium deposition. To improve the conspicuity of calcifications, hemorrhage, or other susceptibility inducing lesions, methods of vascular and CSF suppression need to be incorporated into the positive contrast sequence.

963. A Novel Technique to Study Mouse Cerebrovasculature Using MR Guided Micro-CT

Brige Paul Chugh[1, 2], Lisa X. Yu[1], R. Mark Henkelman[1], John G. Sled[1]
[1]Mouse Imaging Centre (MICe), Toronto, Ontario, Canada; [2]University of Toronto, Toronto, Ontario, Canada

A new method for high resolution mapping of vascular density in the mouse brain is described that uses micro-CT and high resolution MRI. In this method an intravascular contrast agent that is visible in both CT and MRI is employed so that images of the same specimen can be registered on the basis of neurovascular landmarks. This accurate registration permitted a flat map reconstructed from the MRI of the cerebral cortex to be combined with the corresponding CT data to yield blood density maps over the cortex. These blood density maps reveal quantitative differences in vasculature between the cerebral cortex and the whole brain.

964. USPIO Enhanced Susceptibility Weighted Magnetic Resonance Imaging of the Mouse Brain Vascular Architecture

Bob Hamans[1], Markus Barth[2], William Leenders[1], Arend Heerschap[1]
[1]Radboud University Medical Centre, Nijmegen, Netherlands; [2]Radboud University, Nijmegen, Netherlands

Due to the small size of the mouse brain, visualizing its vascular structure is a challenge. The novel MR method of susceptibility weighted imaging (SWI) allows for small brain vessels (mostly veins) to be visualized. Nevertheless the method is not sufficient for detailed imaging of mouse brain vasculature. For this purpose we introduced SWI after loading with USPIO as blood pool contrast to increase local susceptibility. Substantially enhanced visibility of the presence of both large and small vessels was realized in this way, which opens the way to study brain vasculature in mouse models in a new way.

965. Cerebral MR Angiography in Mice with a New Blood Pool Agent (P792)

Nadine El Tannir El Tayara[1], Christine Walczak[1], Andreas Volk[1], Marc Dhenain[1, 2]
[1]Institut Curie, Orsay, France; [2]CEA-CNRS URA 2210, Orsay, France

In this study, we evaluated a new blood pool agent, the P792 (Vistarem®, Guerbet France), to perform cerebral angiography in mice. Angiograms acquired at 4.7T after injection of P792 were compared to Time of Flight (TOF) images and to those acquired after injection of Gd-Dota (Dotarem®, Guerbet, France). P792 allowed visualization of the venous vasculature in addition to the arterial vasculature already identified on TOF images. Angiograms reconstructed after head tissue removal were very similar with Gd-Dota and P792, as the number of displayed vessels was not increased.

966. Cerebral Magnetic Resonance Angiography of the Mouse Lemur Primate

Nadine El Tannir El Tayara[1], Fabienne Aujard[2], Jean Luc Picq[3], Andreas Volk[1], Marc Dhenain[1, 4]
[1]Institut Curie, Orsay, France; [2]CNRS UMR 5176, Brunoy, France; [3]Paris 8 University, EA 2027, Saint-Denis, France; [4]CEA-CNRS URA 2210, Orsay, France

Time of flight (TOF) methods were used to describe the cerebrovasculature of the mouse lemur Primate. Its angiogram was compared to that of rodents (mice and rats). 2D TOF techniques were applied to mouse lemurs because 3D techniques (that could be used for rodents) displayed only few arteries, probably because of the relatively low cerebral flow velocity in these animals. Angiograms from lemurs and rodents displayed several similarities with respect to the disposition and extend of most vessels however some differences, such as a smaller circle of Willis in lemurs could be highlighted.

967. T1 Relaxation in Mouse Brain at 9.4 and 17.6 Tesla

Rob C.G. van de Ven[1], Bianca Hogers[1], Arn Ma Ja Ms van den Maagdenberg[1], Rune R. Frants[1], Huub J. de Groot[2], Rob E. Poelmann[1], Suzanne R. Kiihne[2], Louise van der Weerd[1]
[1]Leiden University Medical Centre, Leiden, Netherlands; [2]Leiden University, Leiden, Netherlands

The application of higher field strengths requires knowledge of the relaxation rates at these fields for proper adjustment of image acquisition parameters. We provide the first *in vivo* T1 relaxation maps of mouse brain at 17.6 T and compare those with measurements at 9.4 T. The implications on SNR and CNR are discussed, as is the overall effect of T1, T2 and proton density on gray/white matter contrast at ultra-high field.

968. Enhanced T_2 Contrast for MR Histology of the Mouse Brain

Anjum Ali Sharief[1], [2], G Allan Johnson[2]
[1]Duke University, Durham, North Carolina, USA; [2]Duke University Medical Center, Durham, North Carolina, USA

T2-weighted contrast in the mouse brain at high fields has been a challenge due to the degrading effects of diffusion- and susceptibility- induced losses. This work illustrates a robust 3D CPMG sequence capable of producing isotropic 43-micron resolution T2-weighted images of the actively stained mouse brain at 9.4T. The signal and contrast is further enhanced with the application of a Fourier transform along the temporal dimension. The results show a detailed visualization of mouse brain structures like multiple cortical layers and thalamic nuclei not reported before in T2-weighted acquisitions.

969. Age Dependence of Transverse Relaxation at 3.0 T in Normal Human Brain

Jianli Wang[1], Xiaoyu Sun[1], Erin Zimmermann[1], Robert Grunfeld[1], Mark D. Meadowcroft[1], James R. Connor[1], Michael B. Smith[1], Qing X. Yang[1]
[1]Penn State College of Medicine, Hershey, Pennsylvania, USA

The age dependence of transverse relaxation rate R2 (1/T2) in the human brain was systemically studied on 37 9-50 year old normal volunteers at 3 T using a high resolution multi-echo spin-echo sequence. Voxel-based analysis showed an evident age dependence of R2 in most deep brain gray matter structures within the studied age range. Regression analyses revealed that an increase of R2 follows a similar logarithmic trend in most of these structures. No significant difference was observed between the two gender groups. The normalized data provide an important baseline for clinical applications of quantitative R2 mapping of brain.

970. High Field MRI Demonstrates Global Brain Iron Overload in Aceruloplasminemia

John F. Schenck[1], Earl A. Zimmerman[2], David L. Henderson[1]
[1]GE Global Research, Schenectady, New York, USA; [2]Albany Medical College, Albany, New York, USA

For the first time 3T MRI is reported along with quantitative T2 values for the rare genetic iron-storage disease aceruloplasminemia. A striking decrease in T2 is found throughout the brain including the thalamus, white matter and hippocampus. This suggests that in other neurodegenerative diseases it may be useful to investigate the possibility of iron-dependent T2 changes in regions not normally associated with iron accumulation.

971. T2* Relaxometry for Quantitative MR Imaging of Iron Deposits in Substantia Nigra of Parkinson's Disease Brain

Eunhee Kim[1], Jung Hee Lee[1], Sung Tae Kim[1], Won Yong Lee[1], Hong Sik Byun[1]
[1]Samsung Medical Center Sungkyunkwan University School of Medicine, Seoul, Republic of Korea

There has been great interest to quantitatively measure the brain iron content using MRI. The iron deposit in the brain is known to be associated with physiology and functions of many diseases. In this study, we employed ¥ÄB0 corrected T2* mapping to patients with Parkinson's disease to see whether the T2* can effectively reflect the iron content accumulated in the brain due to pathologic condition. The T2* values in the substantia nigra are shorter for idiopathic Parkinson's disease patients than for controls. The result of this study suggests us a potential of the T2* relaxometry as a diagnostic imaging method.

972. Impact of Spatial Distribution of T2 and T1 Lesion Volume on Disability and Brain Atrophy

Michael G. Dwyer[1], Sara Hussein[1], Nadir Abdelrahman[1], Viritha Yella[1], Niels P. Bergsland[1], Robert Zivadinov[1]
[1]Buffalo Neuroimaging Analyis Center, Buffalo, New York, USA

While lesion volume is a useful metric for describing inflammatory disease burden in patients with multiple sclerosis (MS), it fails to capture information about the spatial distribution of acute inflammatory activity. Metrics including spatial information may therefore be more relevant in terms of clinical disability. To investigate this possibility, we examined MRI scans from 301 patients with MS. We calculated measures of spatial standard deviation, moment of inertia, Frobenius norm, and centroid size. Except for spatial standard deviation, we found slightly better correlations between each of these measures and disability than that found for volume alone.

973. Fluid-Attenuated $T_{1\rho}$ of the Human Brain *In Vivo*

Ari Borthakur[1], Gul Moonis[1], Laura Spece[1], Elias R. Melhem[1], Christopher M. Clark[1], John Q. Trojanowski[1], Virginia M.-Y. Lee[1], Ravinder Reddy[1]
[1]University of Pennsylvania, Philadelphia, Pennsylvania, USA

A fluid-attenuated $T_{1\rho}$ MRI pulse sequence was developed and utilized to measure $T_{1\rho}$ in the brain of an Alzheimer's disease (AD) patient and two age-matched healthy volunteers. $T_{1\rho}$ maps were generated from fluid-attenuated and non-attenuated $T_{1\rho}$ sequences and compared on the same individuals. Average $T_{1\rho}$ from the fluid-attenuated map (91±8ms) were significantly ($p<0.01$) lower from the non-attenuated $T_{1\rho}$ maps (84±7ms) in regions containing CSF in the AD patient but insignificantly different in the healthy volunteers' brains. The new pulse sequence will be employed to obtain $T_{1\rho}$ maps from more AD patients and age-matched controls.

974. Changes in Brain Tissue Distribution and T2 Relaxation Time in Early Onset Type-1 Diabetes

Robert Mark Wellard[1], Gaby Pell[1], Debbie Rankin[2], Debra Boyce[2], Graeme David Jackson[1], George Werther[2], Elisabeth Northam[2]

[1]Brain Research Isntitute, Melbourne, Victoria, Australia; [2]Royal Children's Hospital, Melbourne, Victoria, Australia

The biological correlates of subtle neuropsychological deficits observed in early-onset diabetes are not well understood. MR techniques allow examination of disease related morphological changes. We aimed to use volume based analysis of structural images and T2 relaxation time measurements to compare brains from a cohort of type-1 diabetics 13-15 years after diagnosis with a matched control group. Diabetes and years of disease were associated with region-specific grey (medial frontal gyrus, thalamus), white matter (inferior temporal gyrus) and T2 relaxation changes (superior temporal gyrus and lentiform nucleus). The results indicate structures associated with the neuropsychological deficits observed in diabetes.

975. Mouse Brain Iron Distribution: Histochemical and Quantitative MRI (7T) Assessment

Sang-Pil Lee[1], Maria F. Falangola[2, 3], Jens H. Jensen[2], Hanzhang Lu[2], Ralph A. Nixon[3], Karen Duff[3], Joseph A. Helpern[2, 3]

[1]University of Kansas Medical Center, Kansas City, Kansas, USA; [2]New York University School of Medicine, New York, New York, USA; [3]Nathan Kline Institute, Orangeburg, New York, USA

Recently, we have developed a new MR technique called Magnetic Field Correlation (MFC) Imaging for measuring microscopic magnetic field inhomogeneities, such as those generated by iron-rich cells. MFC it is not influenced by molecular relaxation mechanisms. In this study, we investigated the relationship between quantitative MFC, R2, R2* and R2' values and iron distribution in normal mouse brain at 7Tesla. Our data suggest that MFC imaging provides a distinct MR measure and can be a potentially useful tool for assessing brain iron and the role of brain iron disruption in the pathogenesis of many neurodegenerative diseases.

976. Use of Double Inversion Recovery for Characterizing Diffusion of Myelin Water

Trevor Andrews[1], Michael Osborne[1], Mark D. Does[1]

[1]Vanderbilt University, Nashville, Tennessee, USA

To develop more complete and accurate mathematical models of white matter it is necessary to obtain a more detailed charaterization of the intracompartmental NMR properties of white matter. In this study a novel method was used to determine apparent diffusion coefficients (ADC) for the myelin water compartment in toad sciatic nerve. ADC values were found for both parallel and perpendicular to the long axis of the nerve.

977. Comparison of Magnetization Transfer Ratios in White Matter and Gray Matter of Neonatal, Juvenile, and Adult Rats

Rae Anne Kokotailo[1], Tadeusz Foniok[2], Min Qiao[2], Boguslaw Tomanek, [12], Ursula I. Tuor, [12]

[1]University of Calgary, Calgary, Alberta, Canada; [2]Institute for Biodiagnostics (West), Calgary, Alberta, Canada

Magnetization transfer (MT) imaging is potentially useful for detecting cerebral white matter injury. MT imaging was performed on neonatal, juvenile, and adult rats. The MT ratio (MTR) increased during development, particularly for white matter and its variation with an increasing number of saturation pulses or RF power were similar irrespective of age (i.e., 60-80 pulses and 60 μT in single slice experiments). When subjected to hypoxia-ischemia, white and gray matter MTR was substantially reduced. Thus, MT was sensitive to developmental cerebral changes and hypoxic-ischemic injury. Optimization of the technique was similar for all ages and injured tissue.

978. Does Repeated Injections of an Iron-Based Contrast Agent Lead to an Accumulation of Iron in the Brain Parenchyma?

Samuel Valable[1, 2], Christoph Segebarth[1, 2], Chantal Remy[1, 2], Emmanuel Barbier[1, 2]

[1]U594, Grenoble, F-38043, France; [2]Univ grenoble 1, Grenoble, F-38043, France

Vessel Size Index (VSI) MRI technique aims at providing data on the microvasculature. To date, is has been applied only at a unique time point. We aimed to verify if VSI imaging could be done at different time points. Rat bearing tumors received multiple injections of Sinerem and the evolution of the VSI was assessed. In the contralateral side, no variations of VSI were observed. Histological analysis revealed no accumulation of iron in the brain. In the tumor, we observed an increase of the VSI as a function of time. In conclusion, VSI imaging could be used to follow the evolution of the vasculature.

979. A 3T MRI Study of Brain Iron Deposition in Parkinson's Disease and MSA Patients Using PRIME

Lauren Wallis[1], Richard Grunewald[1], Harriet Joy[2], Paul Griffiths[1], Martyn Paley[1]

[1]University of Sheffield, Sheffield, Yorkshire, UK; [2]University of Southampton, Southampton, Hampshire, UK

Brain iron deposition was measured in relation to the pathology of Parkinsonfs Disease (PD) and multiple systems atrophy (MSA). Seventy scans were obtained on a 3T system using a partially refocused interleaved multiple echo (PRIME) sequence to yield R2 and R2* (and hence R2Œ) values for regions of interest within the basal ganglia. Patientsf movement severity was assessed off medication. R2Œ values showed significant relationships to symptom severity and disease duration in differential locations between the two patient groups. R2f measures may therefore aid understanding of the disease processes and help to assist diagnosis of the more rare condition MSA

980. High Resolution MR Imaging Reveals the Angioarchitecture of Human Cerebral Cavernous Malformations

Palamadai Nilakantan Venkatasubramanian[1, 2], Robert Shenkar[1], Jin Chen Zhao[1], Issam Awad[1], Alice Wyrwicz[1]
[1]ENH Research Institute, Evanston, Illinois, USA; [2]Nothwestern University School of Medicine, Chicago, Illinois, USA

Cerebral cavernus malformations (CCM)grow by a process of vascular cavern proliferation and consist mainly of blood-filled caverns lined by a single layer of endothelial cells. Biologic activity in CCMs include angiogenesis and inflammation demonstrated by hemosiderin laden macrophages. Although MR imaging is helpful in detecting the presence of CCMs in patients, clinical images do not reveal the angioarchitecture of CCMs. High resolution MR imaging of excised human CCMs at high field strength exquisitely captures caverns at various stages of proliferation without the use of any external contrast agent. An improved understanding of lesion genesis and proliferation in CCMs may lead to more specifically tailored treatments for patients.

981. MP-RAGE Compared to 3D IR SPGR for Optimal T1 Contrast and Image Quality in the Brain at 3T

Chen Lin[1], Robert E. Watson[1], Heidi A. Ward[1], Charlotte H. Rydberg[1], Robert J. Witte[1], Matt A. Bernstein[1]
[1]Mayo Clinic College of Medicine, Rochester, Minnesota, USA

We compare two commonly-used T1-weighted volumetric pulse sequences (MP-RAGE and IR-SPGR) at 3T on a series of ten healthy volunteers. The acquisition protocols are adjusted so that the scan times are both 7:23. SNR measurements in both grey and white matter are reported, as is the grey-white contrast to noise ratio. Results of a blinded review by radiologists on qualitative features including image sharpness and artifact level is also provided. Both pulse sequence techniques performed well, but a systematic preference for MP-RAGE was observed.

982. Secular-T2 MRI: Quantitative MRI of the Cerebrum and Cerebellum in 24 Subjects

Suzuko Suzuki[1], Osamu Sakai[1], Hernán Jara[1]
[1]Boston University School of Medicine, Boston, Massachusetts, USA

Purpose: To study comparatively the whole-brain distributions of T1, T2, and secular-T2 (T2(sec)) in adult human subjects over a wide age range, and to investigate potential spectral differences between the four main brain compartments: left and right cerebral and cerebellar hemispheres. Methods: Images obtained with the mixed-TSE pulse sequence were postprocessed for generating T1 and T2 distributions, which were spatially self-coregistered. These were used for computing the distribution of the T2(sec) on a pixel-by-pixel basis. Segmentation was done with a modified dual-space clustering algorithm Conclusion: Strong age effect was noted in the T1 spectra in the cerebrum. By removing the T1 contribution, an age independent parameter, namely T2(sec) was found in the adult brain. Described technique could be useful in the study of normal and pathologic brain aging.

983. T2 Relaxation Times of the Limbic System: Comparison of 1.5 T and 3.0 T

Eung Y. Kim[1], Xavier Golay[2, 3], Seung-Koo Lee[1], Sei Y. Kim[1], Dong J. Kim[1], Jinna Kim[1], Sam S. Kim[4], Dong I. Kim[1]
[1]Research Institute of Radiologic Science, Yonsei University College of Medicine, Seoul, Republic of Korea; [2]Singapore Bioimaging Consortium, ASTAR, Singapore, Singapore; [3]National Neuroscience Institute, Singapore, Singapore; [4]Kangwon National University College of Medicine, Chunchon, Republic of Korea

The hippocampus shows higher signal intensity than that of the cingulate gyrus on FLAIR imaging at 1.5 T. T2 relaxation time decreases at 3.0 T with respect to 1.5 T. The purpose of this study was to compare T2 relaxation times in the hippocampus, cingulate gyrus, amygdaloid body, and insular cortex between 1.5 T and 3.0 T MR imagers. In conclusion, T2 relaxation time decrease in the cingulate gyrus was less than the insular cortex, amygdaloid body, and hippocampus at 3.0 T, resulting in relatively higher signal intensity compared with that of the hippocampus on FLAIR at 3.0 T.

984. Examination of White Matter Abnormalities in Cocaine Dependence Using Multi-Slice T2 Relaxography

Bryon A. Mueller[1, 2], Sheila M. Specker[1], Logi Vidarsson[3], Jeff R. Wozniak[1], John M. Pauly[3], Kelvin O. Lim[1, 2]
[1]University of Minnesota, Minneapolis, Minnesota, USA; [2]Center for Magnetic Resonance Research, Minneapolis, Minnesota, USA; [3]Stanford University, Stanford, California, USA

Neuroimaging studies have found white matter abnormalities in cocaine dependent subjects. Other magnetic resonance techniques for examining white matter have recently become available, and have the potential to provide complimentary information about the underlying pathophysiology of cocaine use. T2 relaxography provides a quantitative method for measuring the signal from water trapped in the myelin sheath. We report preliminary results from T2 relaxography data from ten cocaine dependent subjects and eight healthy controls. These preliminary suggest differences in white matter between CD subjects and controls.

Spinal Cord MRI

Room 4E Monday 14:00 - 16:00

985. Preliminary Application Study of MR Perfusion Imaging and Diffusion Tensor Imaging in Tumor Like Lesions in the Cervical Spinal Cord

Xiang Liu[1], Wei Tian[1], Yoshimitsu Ohgiya[2], Sven Ekholm[1], Per-Lennart Westesson[1]

[1]University of Rochester School of Medicine & Dentistry, Rochester, New York, USA; [2]University of Rochester School of Medicine & Dentistry, Rochestrer, New York, USA

There is little clinical cervical functional MR study, especially about cervical MR perfusion weighted imaging(PWI) and diffusion tensor imaging(DTI) in cervical tumor-like lesions, although there were advanced development in MR hardware and sequence. Our study is to evaluate the application of MR PWI and DTI in tumor like lesions of the cervical spinal cord. 8 patients were enrolled in this study. The relative cerebral blood volume (rCBV) and Fractional anisotropy (FA) of lesions and normal tissues were analyzed. There are 4 patients with increased perfusion and 4 patients with decreased perfusion including one patient of cervical radiation injury, the lesion was enhanced after contrast and MR PWI revealed progressive decreased perfusion. All lesions were with decreased FA values. Our study proves that MR PWI and DTI are available for the cervical spinal cord tumor like lesions; combining cervical PWI and DTI could supply perfusion information and decreased anisotropy of these lesions, which are important for clinical diagnosis.

986. Diffusion Tensor MRI of the Spinal Cord in Amyotrophic Lateral Sclerosis

Paola Valsasina[1, 2], Beatrice Benedetti[1, 2], Domenico Caputo[1], Michele Perini[3], Massimo Filippi[1, 2]

[1]Fondazione Don Gnocchi, Milan, Italy, Italy; [2]Hospital San Raffaele, Milan, Italy, Italy; [3]Ospedale di Gallarate, Gallarate, Italy, Italy

In this study, we performed histogram analysis of cervical cord MD and FA in 14 patients with amyotrophic lateral sclerosis (ALS) and in 13 healthy subjects, to find the extent of cord damage in these patients. Compared to controls, ALS patients had significantly reduced average FA and cervical cord cross-sectional area. This study shows that DTI-MRI of spinal cord is feasible in patients with ALS and allows to grade the extent of cord damage. The most likely pathological substrates of the diffusion and atrophy changes found are axonal loss (due to cortico-spinal tract degeneration) and reactive gliosis.

987. Diffusion Tensor MR Imaging of the Spinal Cord in Patients with Multiple Sclerosis

Yoshimitsu Ohgiya[1, 2], Masaki Oka[3], Akio Hiwatashi[2], Xiang Liu[2], Naoya Kakimoto[2], Tadashi Kitahara[4], Takehiko Gokan[1], Sven Ekholm[2], Per-Lennart Westesson[2]

[1]Showa University School of Medicine, Tokyo, Japan; [2]University of Rochester Medical Center, Rochester, New York, USA; [3]Kikunakinen Hospital, Yokohama, Japan; [4]Showa University Fujigaoka Hospital, Yokohama-shi, Japan

we found a gradient of white matter abnormality in spinal cord extending from the plaques visible on T2-weighted imaging to the outside of the plaques in FA values. Diffusion tensor MR imaging may be more sensitive than T2-weighted imaging for assessing disease burden and monitoring effects for therapy.

988. Diffusion Anisotropy in WM Depends on Myelin Content in a Diffusion Time-Dependent Manner: Evidence from High B Value Q-Space Diffusion MR of Myelin Deficient Rat Spinal Cord

Inbal Eti Biton[1], Ian D. Duncan[2], Yoram Cohen[1]

[1]Tel-Aviv University, Tel-Aviv, Israel; [2]University of Wisconsin-Madison, Madison, Wisconsin, USA

The relative importance of myelin in the determining diffusion anisotropy of water in white matter (WM) remains elusive. To address this problem, high b value q-space diffusion MRS and MRI were performed on myelin deficient (md) and age-matched control spinal cords at different diffusion times and gradient pulse durations. Although differences in the diffusion characteristics between the two groups was observed at all diffusion times, diffusion anisotropy was apparent only at relatively long diffusion times. The possible implications of these results on the use of diffusion anisotropy for detecting WM abnormalities is briefly discussed.

989. DWI Assessment of a Transgenic Mouse Model for ALS

Haitham Abdelmoaty[1], Melinda West[1], Yasvir Tesiram[1], Andrew Abbott[1], Rebecca Blindauer[1], Kenneth Hensley[1], Rheal A. Towner[1]

[1]Oklahoma Medical Research Foundation, Oklahoma City, Oklahoma, USA

Amyotrophic lateral sclerosis (ALS) is a fatal neurodegenerative disease affecting the upper and lower motor neurons. ALS affects 60,000 to 100,000 individual at any given time. The disease is inexorable with no effective cure with 1-5 years life expectancy following onset. This study examined the spinal cords of G93A-SOD1 mice, a transgenic mouse model for ALS, with diffusion weighted imaging (DWI). Measuring translational diffusion of water with DWI allows the detection of biophysical changes in the spinal cord. A measure of this increase with time can shed light on where and when damage occurs in the spinal cord. This study demonstrates that DWI can provide non-invasive evaluation of ALS pathology without having to obtain invasive histology.

990. *In Vivo* Regional Diffustion Tensor Metrics of Rodent Spinal Cord

Aparna A. Deo[1], Khader M. Hasan[2], Ponnada A. Narayana[2]
[1]University of Houston, Houston, Texas, USA; [2]University of Texas, Houston, Texas, USA

Values of the mean diffusivity, fractional anisotropy, transverse and longitudinal diffusivites (or eigenvalues) from different white matter regions of the thoracic spinal cord are determined. The values of the majority of the DTI metrics show regional dependence. In particular, the regional differences in the longitudinal and transverse diffusivities appear to reflect the differences in the axonal morphology and degree of myelination. The values of these DTI metrics should be useful in improving the pathologic specificity of the injured spinal cord tissue.

991. Contrast-Enhanced High Resolution MR Angiography of the Rat Spinal Region

Ketan B. Ghaghada[1, 2], Kurt H. Bockhorst[3], Srinivasan Mukundan[4, 5], Ponnada A. Narayana[3], Ananth V. Annapragada, [12]
[1]University of Houston, Houston, Texas, USA; [2]University of Texas Health Science Center, Houston, Texas, USA; [3]University of Texas-Houston Medical School, Houston, Texas, USA; [4]Duke University Medical Center, Durham, North Carolina, USA; [5]Duke University, Durham, North Carolina, USA

The current study demonstrates the ability to perform contrast-enhanced high resolution imaging of the rat spinal region using a liposomal blood pool contrast agent.

992. MRI of Blood-Spinal Cord Barrier Disruption in Mice with Experimental Autoimmune Encephalomyelitis

Angela Eileen Schellenberg[1], Richard Buist[1], V Wee Yong[2], Marc R. Del Bigio[1], James Peeling[1]
[1]University of Manitoba, Winnipeg, Manitoba, Canada; [2]University of Calgary, Calgary, Alberta, Canada

Experimental autoimmune encephalomyelitis (EAE) is an animal model of demyelinating disease that exhibits cellular infiltration and a breakdown in the blood-spinal cord barrier (BSB) in mice. Contrast-enhanced MR images were acquired to detect BSB disruption in the spinal cord of C57BL/6 mice at the onset of EAE disease signs, peak disease, and remission. Mice were sacrificed following imaging and the spinal cords were assessed in situ for general features of inflammation (Hematoxylin and Eosin), BSB leak (IgG), and activated macrophages/microglia (GS lectin). Spinal cord enhancement was greatest at the onset of disease signs which corresponded to foci of dense infiltrates at the periphery of the spinal cord.

993. Double-Subtraction MIP MR Angiography to Detect the Artery of Adamkiewicz -Differentiating It from Drainage Vein-

Hideki Hyodoh[1], Hidenari Akiba[1], Mitsuharu Tamakawa[1], Kazusa Hyodoh[1], Naoya Yama[1], Taishi Sato[1], Yuriko Kawaai[1], Masato Hareyama[1]
[1]Sapporo Medical University, Sapporo, Japan

The artery of Adamkiewicz was detected in 81.3% of patients. Double subtraction MRA is useful to detect the artery of Adamkiewicz when it is necessary to differentiate from drainage vein.

994. Labeling Transected Axons with Intracellular Gd-DTPA for Micro-MRI of Lamprey Spinal Cord Injury

Alexander C. Wright[1], Li-Qing Jin[1], Guixin Zhang[1], Suzanne L. Wehrli[2], Michael E. Selzer[1], David B. Hackney[1], Felix W. Wehrli[1]
[1]University of Pennsylvania Medical Center, Philadelphia, Pennsylvania, USA; [2]Children's Hospital of Philadelphia, Philadelphia, Pennsylvania, USA

A novel method for MR microimaging of large axons in the lamprey spinal cord has been developed in which transected axons are labeled *in vivo* with Gd-DTPA. Excised spinal cords then can be imaged using μ-MRI. The results demonstrate contrast agent uptake among a subset of axons, yielding highly enhanced intra-axonal signal on heavily T1-weighted images. The method will facilitate tracking axonal degeneration and regeneration in this well-characterized animal model.

995. Dynamic *In Vivo* T1 Relaxation Measurements of Mouse Spinal Cord for Manganese-Enhanced MRI at 9.4 T

Xiping Liu[1], Guofan Xu[1], Gaohong Wu[1], Qian Yin[1], Shi-Jiang Li[1]
[1]Medical College of Wisconsin, Milwaukee, Wisconsin, USA

T1 relaxation time of mouse spinal cord after systemic adminstration of manganese chloride was first time mwasured dynamically. T1 and R1 values for both white matter and gray matter were determined for various post-MnCl2 injection time point. Fastest manganese uptake interval was calculated to get the best timing for neural stimulation.

996. Detection of Ipsilateral and Contralateral Activation Components in Unilateral Fingers-Tapping Using Spinal BOLD fMRI

M. C. Ng[1, 2], Edward X. Wu, H. F. Lau, Yong Hu, Edward S. Yang[1], D. K. Luk
[1]The Jockey Club MRI Centre, The University of Hong Kong, Pokfulam, Hong Kong, People's Republic of China; [2]Department of Orthopaedics and Traumatology, The University of Hong Kong, Pokfulam, Hong Kong, People's Republic of China

Ipsilateral activation component has been reported in brain fMRI studies using unilateral finger motion. However, the ipsilateral component is usually task-dependent and sparsely distributed. In this study, spinal BOLD fMRI has been performed on 4 healthy right-handed volunteers performing unilateral fingers-tapping to investigate the ipsilateral and contralateral activation inside the cervical spinal cord. Our results showed that more activation were found at the spinal level C5-C6/C7. Bilateral activation was observed in all subjects both in left/right hand fingers-tapping. Spinal fMRI was sensitive to detect bilateral firing in fingers-tapping using dominant or non-dominant hands.

997. Characterization of Spinal Cord Motion: a Source of Errors in Spinal fMRI?

Chase R. Figley[1], Patrick W. Stroman[1]
[1]Queen's University, Kingston, Ontario, Canada

It is hypothesized that spinal cord motion is the dominant source of systematic error in current spinal fMRI methods. However, there is little information in existing literature regarding the magnitude, direction, timing, or cause of this motion. The current study investigates spinal cord motion as a function of the cardiac cycle, as CSF and blood flow are believed to cause the motion of the cord. It was determined that cord motion occurs in the anterior/posterior direction, with peak displacement of 1 to 1.5 millimeters, depending on the rostral/caudal location. Motion in the right/left direction was determined to be negligible.

Perfusion Imaging in Animal Models

Room 4E Monday 14:00 - 16:00

998. Real Time Monitoring of Hyperosmolar Blood Brain Barrier Disruption Using MRI

Marie Blanchette[1], Martin Pellerin[1], Luc Tremblay[1], David Fortin[1], Martin Lepage[1]
[1]Université de Sherbrooke, Sherbrooke, QC, Canada

Different approaches have been advocated to improve delivery across the blood brain barrier (BBB). One such strategy is the osmotic opening of the BBB. This study was initiated with the goal of characterizing spatially and temporally the BBBD procedure with MRI. We report on the amplitude, rate of accumulation and localization of a contrast agent injected shortly after BBBD.

999. Implementation and Evaluation of an MRI Protocol for Assessment of Cerebrovascular Reserve in the Rhesus Monkey – Characterizing the Aging Brain

Alexandre Coimbra[1], Marie A. Holahan[1], Yevgen Tymofyeyev[1], Richard Hargreaves[1], Jacquelynn J. Cook[1], Donald S. Williams[1]
[1]Merck Research Laboratories, West Point, Pennsylvania, USA

Cerebrovascular autoregulation ensures adequate blood perfusion to match demands for oxygen and nutrients. Cerebrovascular reserve (CVR) is defined as the maximal capacity under a vasodilatory challenge. The present work used MRI to measure CVR in rhesus brains, in order to evaluate its responsiveness and test-retest repeatability in readiness for possible use in clinical trials.

1000. Steady-State Quantification of δR_2 (SSTAR2) with Combidex for Measuring Cerebral Blood Volume

Jeff Frank Dunn[1], Debbie Anne Kelly[1], Cheryl Rae McCreary[1], Randy Tyson[2], Dave Kirk[1], Tad Foniok[2]
[1]University of Calgary, Calgary, AB, Canada; [2]National Research Council, Calgary, AB, Canada

Angiogenesis research requires non-invasive methods for studying the growth and regression of vessels. This study quantifies the relaxation rate R2 before and after infusion of the super-paramagnetic susceptibility agent, Combidex and relates the changes to serum Combidex to quantify CBV. We use T2 imaging with short echo times to ensure selective sensitivity to the microvasculature. Practical issues are studied such as the effect of changing echo time and the differences observed when analyzing the data with single or multi-exponential models. The greatest precision was obtained with a single-exponential model, 3ms interecho spacing and 128 echoes. CBV was measured at 2.1%v/v.

1001. Rapid Steady State T1 Method for Cerebral Blood Volume Fraction Mapping: Sensitivity Determination Under Hypercapnia

Adriana Teodora Perles-Barbacaru[1, 2], Hana Lahrech[1, 2]
[1]INSERM, U594, Grenoble, F-38043, France; [2]Univ Grenoble 1, Grenoble, F-38043, France

The sensitivity of the rapid steady state T1 method for measuring physiologic cerebral blood volume fraction (CBV) changes is demonstrated by means of hypercapnia experiments in healthy rats. The normocapnic CBV measured with this method is in the order of 3.3 % and the CBV reactivity to hypercapnia is about 1% of the normocapnic CBV value per mmHg PaCO2. For this study, P760 (an experimental Gd-contrast agent from Guerbet Laboratories) was used for its high r1-relaxivity, and it has been shown that the method works equally well with Gd-DOTA at 0.2 to 0.3 mmol/kg, doses well tolerated by human.

1002. Quantitative Analysis of Distribution and Clearance Rate of Charged and Uncharged Gd-Chelates in Rat Brain

Paul A. Schornack[1], Ping Wang[1], Seong-Gi Kim[1]
[1]University of Pittsburgh, Pittsburgh, Pennsylvania, USA

In the goal of this study is to quantitatively analyze the distribution characteristics of the Gd-chelates, GdDTPA-BMA, GdDTPA2-, or GdDOTP5-, in rat brain. The blood brain barrier precludes delivery by vascular routes so agents were infused directly into ventricular cerebrospinal fluid yielding useful quantities of agent throughout the brain parenchyma for many hours after infusion. Identical quantities of each respective agent were delivered by direct infusion at a constant rate over 5 hours into the left lateral ventricle. Qualitative preliminary results were presented previously and we now present quantitative results obtained from fitting the contrast agent clearance curves from regions of interest throughout the entire brain volume.

1003. Developing an Arterial Spin Labeling Technique for Measuring Cerebral Blood Flow in Pediatrics: Comparison with Computed Tomography Perfusion

Adrian Matthew Yuri Koziak[1, 2], Jeff Winter[1, 2], Ting-Yim Lee[1, 2], Robert Terry Thompson[1, 2], Keith St. Lawrence[1, 2]
[1]Lawson Health Research Institute, London, Ontario, Canada; [2]University of Western Ontario, London, Ontario, Canada

As part of a longterm strategy of developing an arterial spin labeling (ASL) technique for imaging cerebral blood flow (CBF) in neonates, the purpose of this study was to validate the ASL CBF measurements by comparison with perfusion computed tomography (pCT). Images of CBF were collected with ASL and pCT in a neonatal animal model (piglets). The two techniques showed similar flow patterns and there was reasonable agreement in the global CBF measurements. However, vascular artifacts were evident with both techniques, which needs to be addressed in future work.

1004. Arterial Spin Labeling Measurement of Arterial Perfusion Territories Using a Localized Labeling RF Coil

Fernando Fernandes Paiva[1, 2], George Carlos Nascimento[1], Alberto Tannus[2], Afonso Costa Silva[1]
[1]National Institutes of Health, Bethesda, Maryland, USA; [2]Universidade de Sao Paulo, Sao Carlos, SP, Brazil

Arterial perfusion territories of major cerebral feeding arteries were acquired with high SNR using a three coil system comprised of a homogeneous volume excitation coil, a receive-only quadrature surface coil and a localized labeling coil. Vessel selectivity was achieved by utilizing oblique labeling planes while exploring the limited spatial coverage of the labeling coil. Perfusion territory maps of both left and right common carotid arteries, as well as of the vertebral arteries, were acquired. The method described allows use of different angles of labeling to evaluate perfusion territories including those from arteries that are not uniquely accessible.

1005. Limits on Quantification of Perfusion and Capillary Permeability Surface Area Product Using FAIR ASL

John Carr[1], David Buckley[1], Jean Tessier[2], Geoff Parker[1]
[1]University of Manchester, Manchester, Greater Manchester, UK; [2]AstraZeneca, Macclesfield, Cheshire, UK

In this study we look specifically at the use of ASL in normal brain of rats and humans to measure F and PS. We investigate the experimental limits on F and PS quantification using simulations and experimental verification in rat brain at 9.4 T. We ascertain the expected error on FAIR-based F and PS measurements and quantify the % changes in these parameters that can be resolved experimentally. Our results allow us to judge the feasibility of PS measurements the precision of F using FAIR ASL.

Tissue Segmentation and Coregistration

Room 4E Monday 14:00 - 16:00

1006. Identifying Tissue Types in MR Imaging of Benign Prostatic Hyperplasia

Seok Ping Ang[1], Philip Daniel Allen[1], James Graham[1], Charles Edward Hutchinson[1]
[1]The University of Manchester, Manchester, UK

This study investiagated the use of image texture analysis in classification of Benign Prostatic Hyperplasia as stromal or non-stromal. The distinction has important implication for drug treatment and can only be reliably made by histology. Texture measurements based on grey-level co-occurrence matrices were taken from the central gland regions of T2-weighted fat-suppressed images from 19 patients with BPH. Several image features produced classification into the two groups that agreed significantly (values in the range 0.14 to 0.41) with a semi-quantitative visual assessment based on published criteria that has been shown to accurately correspond to histological type.

1007. Can Texture Analysis of MR Images Discriminate the Severity of Hepatic Fibrosis? a Patient Study with Histological Correlation

Kieren Grant Hollingsworth[1], Susan Davies[2], David J. Lomas[1]
[1]University of Cambridge, Cambridge, Cambridgeshire, UK; [2]Addenbrookes Hospital, Cambridge, Cambridgeshire, UK

Hepatic fibrosis is not usually directly observable in MR images until the onset of end-stage cirrhosis. A training set of healthy volunteers and end-stage cirrhotic patients had previously been used to identify discriminating texture parameters. In this work these parameters are applied to an evaluation set of healthy subjects and patients with hepatic fibrosis of varying severity, confirmed on liver biopsy: the effect of changing the discretization step of the texture analysis is evaluated. The evaluation set confirms that the parameters can discriminate grades 0-2 fibrosis from fibrosis grades 3-6 but low numbers in the intermediate grades prevent further discrimination.

1008. Validation and Implementation of an Automated Boundary Finding Algorithm for Muscle Anatomy Studies

Bruce M. Damon[1], Drew A. Lansdown[1], Zhaohua Ding[1]
[1]Vanderbilt University, Nashville, Tennessee, USA

Measurements of muscle volume are important in many biomechanical, applied physiology, and pathophysiology studies. While anatomical MRI provides a precise and accurate means for making these measurements, the need to hand-define regions of interest in multiple imaging slices is subjective and time-consuming. Here, we validate a boundary finding algorithm that uses a combined model of prior shape and smoothness with computer-generated phantoms. The algorithm significantly reduced user input, and ROI quality indices were outstanding. The algorithm was then implemented in anatomical MR images of the leg.

1009. Improving Automatic Tibial Medial Cartilage Segmentation by Incorporating Femoral Cartilage Compartment

Jenny Folkesson[1], Ole Fogh Olsen[1], Erik Dam[1, 2], Paola Pettersen[2], Claus Christiansen[2]
[1]IT University of Copenhagen, Copenhagen, DK, Denmark; [2]Center for Clinical and Basic Research, Ballerup, DK, Denmark

In treatment development intended for osteoarthritis, quantitative evaluation of the articular cartilage is important. We have developed a tibial medial cartilage segmentation method for knees scans acquried by a low-field scanner. A classifier trained to recognize tibial medial cartilage classifies each voxel in the knee scans as cartilage or not cartilage. The method is significantly improved by incorporating estimates of femoral medial cartilage locations. The method is fully automatic and is performed directly in 3D.

1010. Automatic 3D Registration of Trabecular Bone Images Using a Collection of Regional 2D Registrations

Jeremy Magland[1], Branamir Vasilic[1], Wei Lin[1], Felix W. Wehrli[1]
[1]University of Pennsylvania Medical Center, Philadelphia, Pennsylvania, USA

An efficient algorithm is presented for automatically registering serial high-resolution 3D MR images of trabecular bone (TB). Such a 3D registration is important in longitudinal studies which seek to identify small changes in trabecular architecture over time. One difficulty is that the soft tissue adjacent to bone is not rigidly connected to the TB region of interest (ROI). Thus, a successful technique must isolate and register only the ROI. An automatic segmentation algorithm is first used to roughly locate the region of interest within the baseline and follow-up scans. A collection of random 2D regions within the baseline ROI are then matched to the follow-up scan using the local trabecular pattern, and these local registrations are fit to a global 3D rigid transformation. The algorithm was tested on nine subjects who were scanned at two time points as a part of a clinical study. In each case, the fully automatic algorithm succeeded in less than 30 seconds with sub-pixel accuracy.

1011. Fuzzy Logic Analysis and Reconstruction of Bone Structure from High-Resolution MRI

Florent Chandelier[1], David Dupuis[1], Luc Tremblay[1], Akbar Darabi[1], Gamal Baroud[1], Martin Lepage[1]
[1]Université de Sherbrooke, Sherbrooke, QC, Canada

The broad objective of this work is to have a better understanding of geometrical changes associated with osteoporotic bones and emerging techniques to repair the fractured bone by the use of medical cements. This methodological study focuses on combining high-resolution MRI together with advanced methods of image analysis, which is a 3D Fuzzy Distance Transform, for the assessment of the key geometrical features of bone. We report on the thickness distribution of a complete vertebra.

1012. Fuzzy C-Means Based Tissue Classification in the Presence of Noise and Field Inhomogeneity

Binjian Sun[1, 2], Don P. Giddens[1], Marijn E . Brummer[1, 2], John N. Oshinski[1, 2]
[1]Georgia Institute of Technology, Atlanta, Georgia, USA; [2]Emory University, Atlanta, Georgia, USA

We have developed a novel MAGIC-FCM algorithm that mitigates tissue misclassification due to intensity variations in traditional FCM algorithm. This model takes into consideration of both spatial constraint and inhomogeneity field characteristics when performing the classification. The proposed method can be used implicitly or explicitly to achieved the improved classification comparing to traditional FCM technique. It effectively suppresses the intensity variations in medical images and can be easily implemented. Improved segmentation results were achieved using the proposed algorithm with fixed parameters compared to uncorrected classification or correction by existing methods.

1013. Multi-Criteria Seeded Region Growing for Multi-Contrast MRI

Arnaud Garcia[1, 2], Corinne Vachier[1], Antoine Rosset[2], Jean-Paul Vallee[2]
[1]ENS Cachan, CACHAN, France; [2]Geneva University Hospital, Geneva, Switzerland

In many application fields and especially in medical imaging, the segmentation of an object or organ requires to take into account a great number of criteria of several types: morphological, statistical, geometrical... Considering the attributes extraction step solved, the underlying question is that of the adaptation of standard segmentation algorithms acting on gray-scale images to multi-valued images or vectorial images. In this paper, we propose to solve this question with the seeded region-growing algorithm (SRG) available in OsiriX. The procedure we proposed is called multi-criteria seeded region growing (MSRG); it is illustrated and discussed on several MRI examples.

1014. A Semi-Automatic Ventricular Border Segmentation Package Based on Multi-Phase Levelset Segmentation

Qi Duan[1], Daniel Moses[2], Monvadi B. Srichai[2], Vinay M. Pai[2], Andrew F. Laine[1]
[1]Columbia University, New York, New York, USA; [2]New York University Medical Center, New York, New York, USA

A semi-automatic package for segmenting along endocardial and epicardial boarders of the myocardium has been developed based on multi-phase level set method. The software package was tested on several different cardiac MRI image sets and evaluated by human experts. Faster segmentation times, relative to manual segmentation, make it potentially useful for analyzing volumetric cardiac cine datasets obtained clinically.

1015. Three Dimensional Tracking of Tag Intersections in Tagged MRI

Yu Shimizu[1], XiuYi Jin[2], Akira Amano[1], Tetsuya Matsuda[1]
[1]Kyoto University, Kyoto, Japan; [2]Advanced Software Technology & Mechatronics Research Institute of Kyoto, Kyoto, Japan

Tagged magnetic resonance imaging allows for non-invasive *in vivo* measurement of tissue deformation by creating planes of magnetic saturation, which exhibit themselves as black lines in the images. For reliable spatio temporal tracking of the tags sophisticated image analysis methods are of necessity. A time consuming step, when using the common two-dimensional approaches, is the matching of the tag lines to tag surfaces through the slices. Here, an algorithm is presented, which is based on tracing the tag-intersections in a three-dimensional and in this way the tedious process of reassigning the slices becomes superfluous.

1016. Dynamic Monitoring of the Rat Uterus Using 3D Automatic Segmentation

Erez Eyal[1], Ayelet Akselrod-Ballin[1], Meirav Galun[1], Edna Furman-Haran[1], Chidambaram Gunanathan[1], Ronen Basri[1], Achi Brandt[1], David Milstein[1], Hadassa Degani[1]
[1]Weizmann Institute of Science, Rehovot, Israel

The uterus is a classical target organ of estrogen and its endocrine activity is mediated by the estrogen receptor. We demonstrate MR protocols to monitor the uterus *in vivo* coupled to a novel 3D multi-channel multiscale automatic segmentation algorithm, inspired by algebraic multigrid methods (AMG), and a latter refinement by morphological operator. The segmentation was applied to rapidly delineate the uterus structure and separate uterine endometrial and myometrial tissues. It was further employed to analyze dynamic MRI experiments of a novel contrast agent that binds specifically to the estrogen receptor and enhances the endometrial tissue in a specific manner.

1017. A Knowledge-Guided Active Model Method of Cortical Structure Segmentation on Pediatric MR Images

Zuyao Y. Shan[1], Carlos Parra[2], Qing Ji[1], Jinesh Jain[1], Wilburn E. Reddick[1, 2]
[1]St. Jude Children's Research Hospital, Memphis, Tennessee, USA; [2]University of Memphis, Memphis, Tennessee, USA

A knowledge-guided active model (KAM) method was developed with a novel object function similar to the Gibbs free energy. Ten cortical structures were segmented by KAM. The average volumetric agreement between KAM and manually defined structures (0.97) was higher than the volumetric agreement for SPM2 (0.90). The similarity measurements (kappa) between KAM and manually defined structures (0.95) were significantly higher (P ¡Ü 0.001) than those for SPM2 (0.86). KAM can potentially be used to segment cortical structures for conformal radiation therapy planning and for quantitative evaluation of changes in disease or abnormality.

1018. Investigation of Sources of Variance in the Analysis of Structural Data with Voxel Based Morphometry

Gaby S. Pell[1], Heath Pardoe[1], Regula S. Briellmann[1], David F. Abbott[1], Graeme D. Jackson[1]
[1]Brain Research Institute, Melbourne, Victoria, Australia

Voxel-based morphometry (VBM) is a popular technique for the analysis of volume differences between groups of structural images. It is believed to be limited to comparisons of the images acquired with the acquisition scheme and on the same scanner. This study was undertaken to investigate the potential of multi-centre VBM (i.e., analysis of images obtained with different acquisition methods or at different sites) by investigating the sources of confounding variance that would be introduced. The effects of differing voxel sizes and orientations and that of different RF coils are shown to be especially significant, but pooling the data appears to diminish the likelihood of artefactual results.

1019. Clustering of Brain Tumors by Segmentation of Magnetic Resonance Data

Patrick W. T. Krooshof[1], Geert J. Postma[1], Willem J. Melssen[1], Lutgarde M. C. Buydens[1]
[1]Radboud University Nijmegen, Nijmegen, Gld, Netherlands

Previous research has shown that clustering of Magnetic Resonance data facilitates the diagnosis of brain tumors. However, the study did not include spatial information in the clustering of Magnetic Resonance Imaging (MRI) data. Additionally, the clustering results were not stable.The aim of this study is to investigate the added value of the inclusion of spatial information in the clustering of multivariate MRI images to facilitate the interpretation of MR data.A recently developed methodology uses spatial information to obtain initial parameters for the clustering of a stack of MRI images. With the clustering procedure, unique segmentations are obtained.

1020. MediCAD: An Integrated Visualization System for DTI and fMRI Fusion with Anatomical MRI for Presurgical Planning

Xin Guan[1, 2], Song Lai[1], John Lackey[1], Jianrong Shi[1], Udomachai Techavipoo[1], Klaus Mueller[2], Adam Flanders[1], David Andrews[1]
[1]Thomas Jefferson University, Philadelphia, Pennsylvania, USA; [2]Stony Brook University, Stony Brook, New York, USA

To obtain insight to the massive data that modern MRI technology provides, neurosurgeons and research scientists require an integrated system that reads multiple modalities of data, visualizes the information in an intuitive fashion, and offers instant user feedback. Similar systems have been designed and used in practice but require large-scale workstations. To relieve budget concerned hospitals and research labs from this requirement, we designed MediCAD, a software package that runs on personal computers with interactive frame rate. This software not only adds to user convenience, but offers information that is otherwise not intuitive.

1021. MR Image Content-Adaptive Finite Element Mesh Generation

Won Hee Lee[1], Tae-Seong Kim[1, 2], Min Hyung Cho[1], Soo Yeol Lee[1]
[1]Functional and Metabolic Imaging Center, Kyung Hee University, Yongin, Kyungki, Republic of Korea; [2]Functional and Metabolic Imaging Center, Kyung Hee University, Yongin, Kyungki, Republic of Korea

In various fields such as biomechanics and bioelectromagnetics, information in MR images is effectively utilized via finite element analysis (FEA) as an analytical tool. Although mesh generation is a critical step in FEA, most conventional mesh generators have limitations of handling complex biological geometries. In this work, we present an efficient and automatic mesh generation method that produces meshes adaptive to the content of MR images. The presented content-adaptive mesh (cMESH) generator could be a valuable tool toward the fields where MRI-based FEA is critical.

Diffusion: Analysis and Processing

Room 4E Monday 14:00 - 16:00

1022. Reproducibility of Tractography Results: Turboprop-DTI vs. Spin-Echo Echo-Planar DTI

Minzhi Gui[1], Mariana Lazar[2], Konstantinos Arfanakis[1]
[1]Illinois Institute of Technology, Chicago, Illinois, USA; [2]University of Wisconsin-Madison, Madison, Wisconsin, USA

The purpose of this study was to compare the intra-session and inter-session reproducibility of fiber-tracking results obtained from spin-echo echo-planar DTI (SE-EPI-DTI) and Turboprop-DTI datasets. It was demonstrated that the intra-session reproducibility of tractography results was similar for both Turboprop-DTI and SE-EPI-DTI data. However, the inter-session reproducibility was higher for Turboprop-DTI than SE-EPI-DTI data. This was due to the fact that the susceptibility-related distortions and artifacts, which affect tractography results in SE-EPI-DTI, depend on head positioning.

1023. Anomalous Diffusion and Non-Monoexponential B-Decay

Matt G. Hall[1], Clare Mackay[2], Matthew D. Robson[2], Thomas R. Barrick[3]
[1]University College London, London, UK; [2]University of Oxford, Oxford, UK; [3]St Georges, University of London, London, UK

We present an alternative interpretation of the non-monoexponential signal attenuation with b-value observed in diffusion imaging of the brain in terms of the theory of anomalous diffusion. We derive a scaling relation and analyse the results of an experiment that reproduces non-monoexponential decay in terms of this relation. We show that the assumption of anomalous diffusion leads to a simpler fitting problem than is the case for the biexponential model typically assumed. Results indicate that diffusion in cortical grey and white matter is consistant with a sub-diffusion hypothesis.

1024. Automated Correction of EPI Geometric Distortions Applied to Diffusion Tensor Imaging

Maxim Zaitsev[1], Jürgen Hennig[1], Kamil A. Il'yasov[1]
[1]University Hospital Freiburg, Freiburg, Germany

Single shot diffusion weighted EPI is commonly used for DTI. EPI is prone to geometric distortions, which scale with the main magnetic field, causing difficulties in DTI interpretation at 3T and above. Several distortion correction techniques have been proposed; nevertheless none is used routinely, probably because of their limited stability and the need for operator input. Yet, a method of point spread function mapping has proven to perform extremely well for functional MRI. The purpose of this study was to adapt this distortion correction method to DTI and evaluate the effect of the corrections on fibre tracking results.

1025. Image Noise Considerations for PROPELLER K-Space Sampling

Ashish Anil Tamhane[1], Mark A. Anastasio[1], Konstantinos Arfanakis[1]
[1]Illinois Institute of Technology, Chicago, Illinois, USA

PROPELLER-MRI is a data acquisition and reconstruction technique with greatly reduced sensitivity to motion and magnetic field inhomogeneities. The purpose of this work was to study the characteristics of image noise for PROPELLER k-space sampling. First, the properties of noise in PROPELLER were compared to those in Cartesian sampling. Also, the noise characteristics of PROPELLER were studied as a function of different acquisition and reconstruction parameters. The findings of this study will facilitate the design of optimal acquisition and reconstruction strategies.

1026. Adaptive Combination of Phased Array Signals for Diffusion Imaging

Thomas Benner[1], Vladimir Jellus[2], Ruopeng Wang[1], Van J. Wedeen[1], André J.W. van der Kouwe[1], Graham C. Wiggins[1], A. Gregory Sorensen[1]
[1]Athinoula A. Martinos Center, Charlestown, Massachusetts, USA; [2]Siemens Medical Solutions, Erlangen, Germany

Diffusion-weighted MR images exhibit low SNR, especially at high spatial resolutions. Signals from phased array coils are usually combined as sum-of-squares (SoS) which is sub-optimal in low SNR conditions. We present the advantages of a reconstruction method based on matched filtering (adaptive combination, AC) for tractography. 1 mm isotropic DTI scans were done on a phantom and two subjects using both reconstruction methods. Whole brain fiber tracking was performed and the number of fibers registered for several length ranges. AC reconstruction reduces background signal intensity and leads to larger number of fibers in all but one length range.

1027. Indices for Probabilistic Tractography Through Regions of Fibre Crossing

Guy B. Williams[1], Tim P. Hosey[1], Sally G. Harding[1], Thomas Adrian Carpenter[1]
[1]University of Cambridge, Cambridge, Cambridgeshire, UK

In recent years many algorithms for probabilistic fibre tracking have been proposed. Conventionally, partial volume problems due to crossing fibres have been considered a source of noise in the data. Where information about fibre heterogeneity is available, the path of least deflection has been chosen and tracks are assumed not to bifurcate. Using a two fibre model we present an algorithm for calculating the probability of connection using tractography and simultaneously estimating the proportion of fibres within a seed voxel that connect to target voxels.

1028. From ADC to Probability Profiles: The Diffusion Orientation Transform

Evren Ozarslan[1, 2], Timothy M. Shepherd[2], Baba C. Vemuri[2], Stephen J. Blackband[2], Thomas H. Mareci[2]
[1]National Institutes of Health, Bethesda, Maryland, USA; [2]University of Florida, Gainesville, Florida, USA

The diffusion orientation transform establishes a direct link between the probabilities for water displacements and the apparent diffusion coefficients (ADCs) that can be obtained from high angular resolution diffusion imaging. ADCs can be transformed into a spherical tensor enabling the computation of the probabilities via a Laplace series. Alternatively, the probability profile can be reconstructed directly. A matrix formulation of the method enables a simple implementation of the transform. Smoother probability profiles can be obtained by a simple modification of the signal values. Both simulation and experimental results demonstrate the ability of the DOT to accurately resolve fiber orientation heterogeneity.

1029. Landmark Guided Spatial Normalization of Diffusion Tensor Images in the Presence of Large Deformations

Nominated for an ISMRM Poster Award

Ragini Verma[1], Christos Davatzikos[1]
[1]University of Pennsylvania, Philadelphia, Pennsylvania, USA

We propose a method of correspondence detection in diffusion tensor images by using a unique morphological signature of each voxel which oncorporates the anisotropy, diffusivity and orientation information provided by tensors. This proves to be a key step in enhancing existing spatial normalization routines for diffusion tensor images (DTI), by adding the white matter context to the information provided by other scalar measures computed from DTI or other MR modalities. This is especially useful in the case of registering brain tumor images to a healthy template brain, as is required in large population studies.

1030. Comparison of Diffusion Tensor Imaging Between Temporal Lobe Epilepsy and Normal Controls Using Statistical Parametric Mapping

Nominated for an ISMRM Poster Award

Rahyeong Juh[1, 2], Min Ying Su[1], Chang Uk Lee[2], Tae Suk Suh[2], Orhan Nalcioglu[1]
[1]University of California, Irvine, California, USA; [2]Catholic University of Korea, Seoul, Republic of Korea

Voxel-based statistical analysis can be performed to compare changes in a group of patients or each individual patient to a control group; however, spatial normalization is required to minimize the anatomical variability between studied subjects. In this study we investigated whether the seizure focus in patients with temporal lobe epilepsy (TLE) can be identified compared to controls. The templates for ADC and FA were generated from the control subjects. Each individual TLE patient was compared to the normal group data to investigate whether the seizure focus can be identified. Also the group comparison was performed using statistical parametric mapping analysis.

1031. Quantitative Correlation-Time Diffusion MRI of the Brain: *In Vivo* Measurements and Comparison to Conventional Echoplanar Diffusion MRI

Benjamin Pan Liu[1], Osamu Sakai[1], Hernan Jara[2]
[1]Boston Medical Center, Boston, Massachusetts, USA; [2]Boston University Medical Center, Boston, Massachusetts, USA

Diffusion imaging using a mixed turbo spin echo sequence and correlation-time diffusion mapping technique was compared to conventional single shot spin echo echoplanar diffusion imaging. Based on Bloembergen-Purcell-Pound relaxation theory, diffusion maps were calculated as a function of coregistered proton density and T1 maps to reduce effects of non-diffusional motion and artifacts. Diffusion imaging was performed in phantoms and 12 human subjects, showing a strong global correlation between both techniques of diffusion coefficient mapping. However, compared to conventional PFG-encoded SS-SE-EPI diffusion maps, correlation-time diffusion mapping demonstrated better image quality and a higher gray-white matter contrast.

Diffusion Acquisition Methods

Room 4E Monday 14:00 - 16:00

1032. Simulations of Motion-Insensitive Diffusion Imaging Based on the Distant Dipolar Field

Tao Lin[1], Huijun Sun[1], Congbo Cai[1], Zhong Chen[1, 2], Shuhui Cai[1], Jianhui Zhong[2]
[1]Xiamen University, Xiamen, Fujian, People's Republic of China; [2]University of Rochester, Rochester, New York, USA

Diffusion-weighted (DW) MRI is commonly achieved with the use of pulsed-gradient spin-echo (PGSE) method. However, images acquired by this method often exhibit ghosts because of sample's macroscopic motion. These motion artifacts can be mostly eliminated by using the distant dipolar field (DDF) method, which relies on the refocusing of spatially modulated transverse magnetization by the DDF within the sample itself. In this report, DW images using both DDF and PGSE method were simulated. The results demonstrate that with the equivalent diffusion weighting, DW-DDF images are much less sensitive to the macroscopic sample motion, thus having fewer motion artifacts than traditional DW-PGSE images.

1033. Diffusion Weighted EPI vs. MinD SAP-EPI at 7T

Stefan Skare[1], Tie-Qiang Li[2], Rexford Newbould[1], David B. Clayton[1], Roland Bammer[1]
[1]Stanford University, Palo Alto, California, USA; [2]National Institute of Health, Bethesda, Maryland, USA

The performance of our newly developed MinD DW-SAP-EPI is here evaluated at 7T with respect to distortion and effective resolution. Comparisons are being made to conventional DW-EPI and also FSE, where the latter is used as a geometric reference without diffusion weighting.

1034. Benefits of Higher Magnetic Fields for Diffusion Tensor Imaging (DTI) Based on Single-Shot STEAM MRI Sequences: *In Vivo* Mouse Brain Studies at 2.35 T and 7 T

Susann Boretius[1], Jens Wuerfel[2], Frauke Zipp[2], Takashi Watanabe[1], Jens Frahm[1], Thomas Michaelis[1]
[1]Max-Planck-Institut fuer biophysikalische Chemie, Goettingen, Germany; [2]Research Center, Charite University Hospital, Berlin, Germany

Diffusion-weighted single-shot STEAM MRI takes full advantage of the increased longitudinal magnetization and prolonged T1 relaxation time at higher magnetic field strengths without suffering from geometric distortions and signal losses due to susceptibility artifacts. The signal gain can be successfully invested either in a corresponding reduction of measurement time or an increase of spatial resolution. Mouse brain studies at 7 T resulted in a pronounced improvement of fractional anisotropy and main diffusion direction maps in comparison to data obtained at 2.35 T.

1035. Ordering Diffusion-Weighted MRI Measurements Improves Results from Partially Completed Scans

Philip A. Cook[1], Mark R. Symms[1], Philip A. Boulby[1], Daniel C. Alexander[1]
[1]University College London, London, UK

Diffusion-MRI often uses a spherical sampling scheme, which acquires images sequentially with diffusion weighting gradients in unique directions distributed isotropically on the hemisphere. If not all of the measurements can be completed, the quality of results from the partial scan is sensitive to the order of the gradient directions in the scanner protocol. A partial scan may cover parts of the hemisphere densely but other parts sparsely and thus provide poor spherical coverage. We present a method to optimise maximise the spherical coverage of partial scans without affecting the spherical sampling of the complete acquisition.

1036. Phantom Optimization for Diffusion Tensor Magnetic Resonance Imaging

Els Fieremans[1], Steven Delputte[1], Yves De Deene[2], Yves D'Asseler[1], Rik Achten[2], Ignace Lemahieu[1], Rik Van de Walle[1]
[1]Ghent University, Ghent, Belgium; [2]Ghent University Hospital, Ghent, Belgium

The main application of diffusion tensor imaging (DTI) is to study the white matter geometry *in vivo*. To validate this technique, we have proposed a flexible hardware phantom by using parallel fibers of woven strands tightly held together by a shrinking tube. In this abstract, the short- and long- time diffusion behaviour of extra cellular diffusion between fibers is modelled by Monte Carlo simulations and experimentally evaluated. The results show that the packing density and the fiber diamter are the most effecting parameters in the phantom design for DTI.

1037. PROPELLER and Turboprop Acquisition Parameters for Optimal Motion Correction

Ashish Anil Tamhane[1], James G. Pipe[2], Konstantinos Arfanakis[1]
[1]Illinois Institute of Technology, Chicago, Illinois, USA; [2]Barrow Neurological Institute, Phoenix, Arizona, USA

PROPELLER-MRI and Turboprop-MRI are considerably less sensitive to motion than their precursors, multi-shot fast spin echo (FSE) and gradient & spin-echo (GRASE) respectively. In the PROPELLER family of sequences, data are collected along blades centered at the origin of k-space. The amount of translation and rotation of the object is estimated for each blade through comparison of the common low spatial frequency information between blades, and subsequently corrected. In this study, the effects of PROPELLER and Turboprop acquisition parameters on motion correction were investigated. Acquisition parameters that ensure optimal motion correction were proposed.

1038. Navigated Multi-Shot EPI Diffusion Imaging of the Spine

David Atkinson[1], Serena J. Counsell[2], David J. Larkman[2], Jo V. Hajnal[2], Philip G. Batchelor[1], Derek LG Hill[1]
[1]University College London, London, UK; [2]Hammersmith Hospital, Imperial College London, London, UK

Multi-shot EPI diffusion weighted imaging is used to present transverse images of the spine with improved resolution and reduced distortion compared to single-shot images. The image reconstruction uses: two dimensional image-domain phase corrections determined from a navigator following every shot, data from multiple averages, multiple coils and coil sensitivity information. The acquisition physics is expressed as matrix multiplications or equivalently as image operations. Consideration of these approaches permits the use of conjugate gradient based reconstructions to yield diffusion weighted images of the spine and nerve root.

1039. Optimization of K-Space Undersampled DW PROPELLER Using Fast RIGR Algorithm

Yutaka Natsuaki[1, 2], Michael H. Buonocore, [23], Thomas E. Nordahl, [23], Ruth E. Salo, [23]
[1]UC Davis, Davis, California, USA; [2]UC Davis Imaging Research Center, Sacramento, California, USA; [3]UCDMC, Sacramento, California, USA

Diffusion-Weighted (DW) PROPELLER is a DW MRI acquisition method that is free from the EPI-related artifacts (e.g. image distortion) and has integrated motion correction scheme. However, the practicality of DW PROPELLER MRI is hindered from its markedly long scan time. In the present work, a novel DW PROPELLER MRI scan time reduction method using k-space undersampling with Fast RIGR (Reduced-encoding Imaging by Generalized-series Reconstruction) algorithm is presented.

1040. Rapid Diffusion-Weighted Thermometry (DWT) Using 3D Singleshot Stimulated EPI

Nick Todd[1], S.E. Kim[1], E.K. Jeong[1], D.L. Parker[1]
[1]University of Utah, Salt Lake City, Utah, USA

Molecular diffusivity in MRI is usually measured using conventional 2D singleshot diffusion weighted-EPI. This method is limited because of strong distortions that occur at tissue/air or tissue/bone interfaces. A new pulse sequence, 3D singleshot DW stimulated echo planar imaging (3D ss-DWSTEPI) has been developed to overcome this problem. We present a preliminary study in which 3D ss-DWSTEPI is applied to the diffusion method of temperature measurement. Initial results are promising, as 3D ss-DWSTEPI is a rapid imaging technique, it is almost free from motion and susceptibility artifacts, and measured diffusion coefficients at different temperatures correlate well to previously measured values.

1041. Diffusion Spectrum Imaging Using Body-Center-Cubic Sampling Scheme

Wen-Yang Chiang[1], Van J. Wedeen[2], Li-Wei Kuo[3], Ming-Hwei Perng[1], Wen-Yih Isaac Tseng[4]
[1]National Tsing Hua University, Hsinchu, Taiwan; [2]Harvard Medical School, Charlestown, Massachusetts, USA; [3]National Taiwan University, Taipei, Taiwan; [4]National Taiwan University College of Medicine, Taipei, Taiwan

In order to shorten the data acquisition time of diffusion spectrum imaging (DSI) [1], a new homogeneous sampling scheme in q-space is proposed that the body-center cubic (BCC) sampling lattice, which was previously experimented in CT or MRI [2], is used instead of the Cartesian one. For spherical band-limited 3D signal, BCC sampling lattice is one of the most efficient sampling schemes, and the sampling efficiency of BCC is 30% higher than the conventional Cartesian one [2]. Because there are similar features in the diffusion spectrum of DSI, using BCC sampling scheme may reduce sampling number up to 30% theoretically, which means 30% reduction of data acquisition time. Once the q-space data of BCC lattice is acquired, probability density function (PDF) is reconstructed directly by BCC inverse discrete Fourier transform (IDFT) without interpolation. In addition, BCC sampling method saves data storage volume for 30% as well.

1042. High-Resolution Whole Brain Cardiac Gated Diffusion Tensor Imaging

Joelle Elita Sarlls[1], Rexford D. Newbould[2], Maria I. Altbach[1], Arthur F. Gmitro[1], Theodore P. Trouard[1]
[1]University of Arizona, Tucson, Arizona, USA; [2]Stanford, Stanford, California, USA

Radial-FSE methods enable high-resolution diffusion-weighted imaging, in two dimensions, without sensitivity to bulk rigid body motion and/or magnetic field inhomogeneity. In the present work, these methods are extended to three dimensions allowing high spatial resolution to be obtained equally in all dimensions while maintaining a high SNR. This technique also allows all regions of the brain to be measured with diffusion tensor imaging, including areas of susceptibility like the inferior temporal and anterior frontal lobes. In addition, the sequence has been cardiac gated to reduce residual non-rigid body motion due to cardiac pulsation.

1043. Reduce Encoding of Diffusion Spectrum Imaging with Cross-Term Correction

Kuan-Hung Cho[1], Chun-Hung Yeh[2], Yi-Ping Chao[1], Jyh-Horng Chen[1], Ching-Po Lin[2]
[1]Dept. of Electrical Engineering, National Taiwan University, Taipei, Taiwan; [2]National Yang-Ming University, Taipei, Taiwan

Diffusion spectrum imaging can define complex fiber structures accurately. However, the scanning procedure is time-consuming under current 515 data sampling scheme. Based on the property that diffusion echo signal is spherical symmetry, a reduced encoding scheme was proposed in this study. 515 encoding points were reconstructed from 298 hemi-spherical points in q-space posterior to cross-term correction calculated from pulse sequence. The results of coherent fiber, 45 , and 90 crossing fibers phantom models showed angular error of 0o, 42.05 ±1.97 , and 91.38 ±4.78 , respectively. Applying cross-term correction, we demonstrated that DSI with half-spherical encoding points is feasible while preserving fiber orientations.

1044. Halving Imaging Time of Whole Brain Diffusion Spectrum Imaging (DSI) Using Simultaneous Echo Refocusing (SER) EPI

Timothy G. Reese[1], Thomas Benner[1], Ruopeng Wang[1], David A. Feinberg[2], Van J. Wedeen[1]
[1]Massachusetts General Hospital, Boston, Massachusetts, USA; [2]Advanced MRI Technologies, Sebastapol, California, USA

We present a method for reducing the total scan time of DSI by nearly one half to 11 minutes using SER-EPI. This step to reduce the scan time of DSI enables the incorporation of DSI imaging into routine use and clinical protocols.

1045. Multi-Shot DWI with Iterative Phase and Field Inhomogeneity Corrections

Bryan Mackenzie Donald[1], Robert C. Welsh[1], Jeffrey A. Fessler[1], Douglas C. Noll[1]
[1]University of Michigan, Ann Arbor, Michigan, USA

Diffusion Tensor Imaging (DTI) is an emerging tool for analyzing the health of brain white matter. It also offers the potential to track connectivity between brain regions. There are often problems with field inhomogeneity distortions and shot-to-shot phase variations owing to bulk patient motion during the large DTI gradients. In this study we examine an image reconstruction approach that iteratively corrects for both of these issues. Results show improved feature resolution and functional anisotropy maps in the frontal lobes and corpus callosum over an equivalent sequence without field inhomogeneity correction.

1046. Multi-Shot, Diffusion-Weighted Imaging at 3T Using Readout-Segmented EPI and GRAPPA

David Andrew Porter[1], Robin M. Heidemann[1]
[1]Siemens Medical Solutions, Erlangen, Germany

The increased signal-to-noise at 3T is a particular benefit in diffusion-weighted imaging due to the inherently low signal levels. However, routine diffusion-weighted image quality is degraded by the sensitivity of single-shot EPI to the increased susceptibility and T2* decay effects at 3T. A number of options exist for improvement using multi-shot methods. This study investigated the readout-segmented EPI technique, using a GRAPPA reconstruction to give a reduction in EPI echo-train length. The method was found to give a substantial reduction in susceptibility artefact, allowing high-resolution T2- and trace-weighted images to be acquired with typical scan times of around 3 minutes.

1047. 2D-Navigator-Based Re-Acquisition for Motion Artefact Suppression in Multi-Shot, Diffusion-Weighted Imaging

David Andrew Porter[1]
[1]Siemens Medical Solutions, Erlangen, Germany

Non-linear 2D navigator-based phase correction is usually effective at removing artefacts in multi-shot diffusion-weighted imaging. However, it can fail sporadically due to high-spatial-frequency phase variation, for which the spatial resolution in the 2D navigator data is insufficient. This paper proposes a method for identifying data affected in this way based upon the measurement of the k-space signal distribution in a 2D navigator. It is also demonstrated how the information can be used during the measurement to reduce artefact by re-acquiring the unusable data. Sample data, acquired by combining the 2D-navigator-based re-acquisition scheme with the readout-segmented EPI sequence, are presented.

1048. Correlation Time Diffusion Coefficient Mapping of the Abdomen with Respiratory Triggered Mixed-TSE: A Non-Pulsed Field Gradient Technique

Hernan Jara[1], Rodrigo Diaz Garbizu[2], Jorge Andres Soto[1]
[1]Boston University Medical Center, Boston, Massachusetts, USA; [2]Boston University, Boston, Massachusetts, USA

Purpose: To develop a diffusion coefficient mapping technique for abdominal imaging with much reduced sensitivity to non-diffusional motions. Methods: Scans were performed with the mixed-TSE pulse sequence using respiratory triggering. PD, T1, and T2 maps were generated and used as input to a Bloembergen-Purcell-Pound model for computing the diffusion coefficient on a pixel-by-pixel basis. Conclusion: A diffusion coefficient mapping technique with much reduced motion artifact vulnerability has been developed. Image quality approaches that of the directly acquired images.

1049. Diffusion Tensor Encoding Schemes Optimized for White Matter Fibers with Selected Orientations

Huiling Peng[1], *Konstantinos Arfanakis*[1]
[1]Illinois Institute of Technology, Chicago, Illinois, USA

The accuracy of diffusion tensor imaging (DTI) measurements depends on the encoding scheme used. Most current acquisition schemes contain diffusion directions uniformly distributed in 3D space, in order to provide equal noise levels for fibers in any orientation. However, when considering specific fiber-bundles, the range of fiber orientations is limited. Based on this observation, we have developed a method to produce encoding schemes that minimize the noise of various tensor-derived scalar quantities for tensors with primary eigenvector orientations within a cone with a specified opening angle.

1050. Use of Gradient Crushers on Multiple Axes for Diffusion Imaging of Thin Slices with Reduced TE

Theodore R. Steger[1], *Zhu Li*[1], *R. Scott Hinks*[1], *Bryan J. Mock*[1]
[1]GE Healthcare, Waukesha, Wisconsin, USA

By applying gradient crushers simultaneously on all three axes during diffusion imaging, adequate crushing may be obtained for thin slices with a reduced TE compared with slice select crushers alone.

1051. Isotropic Steady State Diffusion Weighted Imaging

Taek Soo Kim[1], *Garry Evan Gold*[1], *John Mark Pauly*[1]
[1]Stanford University, Stanford, California, USA

Steady-state diffusion weighted imaging (SS-DWI) is potentially efficacious in the diagnosis of stroke location. However, white matter anisotropic tissues produce hyper- and hypo-intense signal and can make the stroke locate indiscernible. In this work we introduce isotropic steady-state diffusion weighted imaging (isotropic SS-DWI), which creates quasi-isotropic diffusion weighting and reduces the effect of diffusion anisotropy notably.

1052. Ghost-Free Spin-Echo Echo Planar Imaging Method for Diffusion Weighted Images Using Adaptive RF Pulses

Yeji Han[1], *Jinyoung Hwang*[1], *Jun-Young Chung*[1], *HyunWook Park*[1]
[1]Korea Advanced Institute of Science and Technology, Daejeon, Republic of Korea

Single-shot spin-echo echo planar imaging (SE-EPI) has become the dominant method for performing diffusion-weighted imaging (DWI) because it is fast and less sensitive to motion compared to other methods. Although the SE-DW-EPI provides images with less motion-related artifacts, it has its innate problems such as low spatial resolution, shape distortions, and N/2 ghosts. We used adaptive RF selection pulses that are applied in the phase encoding direction to excite alternate halves of the FOV. Each half of the field of view (FOV) is acquired separately and concatenated in the image domain. Thus, we can acquire ghost-free DW-EPI images.

1053. Diffusion Anisotropy Measurement at the Crossing Fiber by Using Ga Priorh Fiber Information

Hiroyuki Kabasawa[1], *Yoshitaka Masutani*[1], *Osamu Abe*[1], *Shigeki Aoki*[1], *Kuni Ohtomo*[1]
[1]University of Tokyo, Bunkyou-ku, Tokyo, Japan

Typical diffusion anisotropy index, such as Fractional Anisotropy are accurate at single fiber but this index has its intrinsic limitation at crossing fiber. To overcome this limitation high angular resolution diffusion measurement or q-space measurement were used. However these methods requires long scan time and applying those methods to clinical is virtually impossible. In this study, diffusion properties were estimated from sparse DTI data to reduce scan time. Fiber directions were estimated by novel image processing method. Multi-directional diffusion-weighted images were analyzed with the estimated fiber directions as ga priorh information to measure diffusion properties at the crossing fiber voxel.

1054. Accurate Quantification of Diffusion in Heterogeneous Systems Using the New Magic Asymmetric Gradient (MAG) Technique

Phillip Zhe Sun[1, 2]
[1]Johns Hopkins University, Baltimore, Maryland, USA; [2]Kennedy Krieger Institute, Baltimore, Maryland, USA

Pulsed field gradient (PFG) measurements have been used to characterize complex structures such as porous media and biological tissue. However, it is comprised of areas with strongly magnetic susceptibilities difference, leading to severe background gradients. Recently, magic asymmetric gradient (MAG) technique was proposed to suppress the cross term between applied and background gradients and can correct for contributions from varying background gradients. In this study, we showed that the MAG technique can quantify diffusion and structure accurately in heterogeneous systems. The combination of MAG and bipolar PFG techniques provides a unique contrast of quantifying varying background gradients.

1055. High Resolution DTI of Localized Volume, Using 3D Singleshot STimulated EPI

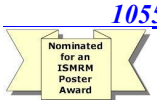

Eun-Kee Jeong[1], *Seong-Eun Kim*[1], *Eugene G. Kholmovski*[1], *Dennis L. Parker*[1]
[1]University of Utah, Salt Lake City, Utah, USA

This work reports on a novel 3D singleshot diffusion MRI technique, which completes the acquisition of the total k-space of a limited 3D volume after a single diffusion-preparation. As a stimulated echo technique, the DW longitudinal magnetization undergoes T1 rather than T2 decay. Reduced volume excitation techniques are used to limit the imaging volume, reduce the time required to acquire each complete plane of k-space and thereby reduce both T2* decay during the k-space plane and T1 decay along the slice-encoding direction. Images obtained with 3D ss-IMIV-STEPI have been free of severe susceptibility and motion artifacts. The technique should be useful for high-resolution 3D DTI of limited volumes of interest.

1056. PROPELLER EPI with Reversed Gradient Method for High Resolution DTI at 3.0T Without Field-Map Correction

Hing-Chiu Chang[1], Tzu-Chao Chuang[1], Teng-Yi Huang[2], Hsiao-Wen Chung[1, 3], Cheng-Yu Chen[3], Fu-Nien Wang[1], Kenneth K. Kwong[4]

[1]National Taiwan University, Taipei, Taiwan; [2]National Taiwan University of Science and Technology, Taipei, Taiwan; [3]Tri-Service General Hospital, Taipei, Taiwan; [4]Massachusetts General Hospital, Charlestown, Massachusetts, USA

We propose a modified reversed gradient method (RG) to reduce image blurring for PROPELLER EPI acquisition, which is compatible with parallel imaging, to generate high-resolution DTI without the need for field map correction. Our RG-corrected PROPELLER EPI images acquired near the skull base exhibited much less blurring than those without RG correction. The RG is computationally economic, therefore does not increase image reconstruction time substantially, and it also corrects EPI distortions arising from eddy current effects. The RG is an effective approach for high-resolution diffusion tensor imaging with PROPELLER EPI acquisition using large matrix size at high fields.

1057. *In Vivo* Diffusion Tensor Imaging of Rat Brain Acquired with a 3T Clinical MRI System and a High Strength Insert Gradient Coil

Dirk Mayer[1], Elfar Adalsteinsson[2, 3], Brian K. Rutt[4], Natalie Zahr[1], Edith V. Sullivan[1], Adolf Pfefferbaum, [15]

[1]Stanford University, Stanford, California, USA; [2]Harvard-MIT Division of Health Sciences and Technology, Cambridge, Massachusetts, USA; [3]MIT, Cambridge, Massachusetts, USA; [4]Robarts Research Institute, London, Ontario, Canada; [5]SRI International, Menlo Park, California, USA

We developed *in vivo* echo-planar diffusion tensor imaging with isotropic resolution (0.5mm) to examine white matter microstructure of the rat brain on a human 3T scanner equipped with a high-strength insert gradient coil. Diffusion-weighting in 6 noncollinear directions with the same 6 directions in opposite polarity compensated for diffusion effects of imaging gradients. Fractional anisotropy (FA) images acquired in 46-92min revealed white matter structures and primary fiber orientations. Mean FA in the corpus callosum genu was 52.2%±8.8SD and 34.0±5.0SD in the anterior commissure. Clinical scanners with insert gradients enable application of similar pulse sequences and field strength in translational research.

1058. A Novel Method of Partitioning Diffusion Weighting Schemes for Efficient Comparisons of DTI Protocols

Bennett Allan Landman[1], Jonathan A. D. Farrell, [12], Susumu Mori, [12], Jerry L. Prince[1, 3]

[1]Johns Hopkins School of Medicine, Baltimore, Maryland, USA; [2]Kennedy Krieger Institute, Baltimore, Maryland, USA; [3]Johns Hopkins University, Baltimore, Maryland, USA

We present a methodology that enables reuse of diffusion weighted data from a single acquisition in subsets. These results closely approximate those independently achievable with optimized schemes of fewer DWDs. First, we show how to derive optimal subsets from an existing master set of DWDs. Second, we perform de novo joint optimization of both master and subsets of particular sizes simultaneously. Our methodology is applicable to any DTI study which computes diffusion tensors from subsets of available data. We demonstrate an efficient means to assess DTI derived contrasts as a function of diffusion encoding scheme and to augment existing schemes.

Diffusion: Precision, Accuracy, and Effects of Experimental Design

Room 4E Monday 14:00 - 16:00

1059. Reproducibility Study of Quantitative Diffusion Characteristics

Christine Ojango[1], Dorothee Auer[1], Steven Jackson[1], Paul S. Morgan[1]

[1]University of Nottingham, Nottingham, UK

The variability of the parameters measured with diffusion tensor imaging (DTI) is a main concern for the longitudinal studies monitoring disease. We investigated the reproducibility of DTI parameters during one imaging session of one volunteer. The results are highly reproducible showing the stability of scanner performance. The study was repeated on another scanner with different field strength and reproducible diffusion parameters in white matter were seen between scanners.

1060. Reliability of FA and ADC Measures in the Healthy Brain: Implications for Longitudinal DTI Studies

Rachel Scheidegger[1, 2], Ying Wu[1, 2], Renee Ochs[1], Pippa Storey[1, 2], Robert Edelman[1, 2], Ann Ragin[1, 2]

[1]Feinberg School of Medicine, Northwestern University, Chicago, Illinois, USA; [2]Evanston Northwestern Healthcare, Evanston, Illinois, USA

Diffusion tensor imaging (DTI) may have considerable potential in the diagnosis and monitoring of neurological diseases. The inter-session reliability of whole brain, white matter, and gray matter DTI measurements was analyzed across a one year period along with intra-rater, inter-rater, and inter-tool reproducibility. Results show that apparent diffusion coefficient (ADC) measures tended to be more reproducible than fractional anisotropy (FA) measures and agreement for whole-brain measures was higher than for ROI measures. This study supports the feasibility of longitudinal DTI studies of central nervous system disorders, while underscoring the necessity of pre-study standardization of MR sequences and procedures, and inclusion of control subjects.

1061. Multivariate Statistical Comparison of Diffusion Tensor Maps in Normal Aging

Brandon Whitcher[1], David S. Tuch[2]
[1]GlaxoSmithKline, Greenford, Middlesex, UK; [2]Massachusetts General Hospital, Charlestown, Massachusetts, USA

Recently there have been efforts to develop multivariate hypothesis tests suitable for group comparison of tensors; yet it is not clear whether such tests actually provide greater statistical sensitivity or additional anatomical information over standard univariate tests on fractional anisotropy. Here, we provide results from numerical simulations and DTI data from a normal aging study.

1062. Sensitivity of Voxel-Based Analysis of DTI Images to the Warping Strategy

Gaby S. Pell[1], Heath Pardoe[1], Regula S. Briellmann[1], David F. Abbott[1], Graeme D. Jackson[1]
[1]Brain Research Institute, Melbourne, Victoria, Australia

Voxel-based analysis has become a popular method for the quantitative analysis of changes in DTI parameters between subject groups. It relies on the warping of the images from different subjects to a common space. However, there is no consensus as to how to best perform this warping step. In a study of subjects with epilepsy, the data was analysed using eight alternative warping strategies. The areas of fractional anisotropy change are shown to vary greatly with the warping step, while the Trace changes were relatively consistent. Results reported with this technique should be interpreted in this light and appropriate regard taken of the chosen warping procedure.

1063. Voxelwise Analysis of FA Data: Session and Subject Variability, Gaussianity and Dependence on Acquisition

Stephen Mark Smith[1], Heidi Johansen-Berg[1], Clare Mackay[1], Timothy E J Behrens[1], Andreas J. Bartsch[2]
[1]fMRIB, Oxford University, UK; [2]Dept Neuroradiology, University of Würzburg, Germany

We have recently proposed a new approach to voxelwise analysis of FA data: Tract-Based Spatial Statistics (TBSS). TBSS pre-aligns all subjects' FA data, creates a mean-FA-based white-matter skeleton image, and then projects each subject's FA image onto this skeleton, before carrying out cross-subject voxelwise analysis. Here we investigate: a) the cross-subject Gaussianity of FA data; b) the cross-session and cross-subject variability in FA when pre-processed by pure nonlinear registration, TBSS and by hand; and c) the dependence of cross-subject FA variability on different DTI acquisitions (6 vs. 60 directions and single-channel vs. parallel imaging).

1064. Anatomic Versus Fractional Anisotropy Images for Registration of Group DTI Morphometry Data

Kendra Klang[1], Marcel Jackowski[1], Robert Fulbright[1], Xenios Papademetris[1], Cheryl Lacadie[1], Hemant Tagare[1], Sally Shaywitz[1], Bennett Shaywitz[1], Robert Todd Constable[1]
[1]Yale University, New Haven, Connecticut, USA

Diffusion tensor imaging shows promise for investigating differences in white matter structure across study groups. Most analyses to date register the individual subject anatomic T2 weighted data to a reference brain volume and then apply the same transformation matrix to the DTI data. This work demonstrates that if the fractional anisotropy maps, primarily representing white matter structures, are instead registered to a reference FA map using a nonlinear registration algorithm, then the inter-subject variance for specific white matter structures decreases, increasing the sensitivity to small differences between groups.

1065. Analytical Expressions for Noise Propagation in Diffusion Tensor Imaging

Yuji Shen[1], Ida Pu[2], Chris Clark[1]
[1]St. George's, University of London, London, UK; [2]Goldsmiths College, University of London, London, UK

Parameters derived from diffusion tensor imaging (DTI) are sensitive to errors arising from noise in diffusion-weighted imaging (DWI) data. We present an analytical determination of errors arising due to noise in the eigenvalues and eigenvectors and a range of tensor metrics calculated from these parameters. In particular, an appraisal of errors in the principal eigenvector has implications for tractography, which utilises this information to map the white matter pathways of the brain. The derived expressions for the errors in the tensor metrics can be used to calculate the errors encountered for any tensor and signal to noise ratio (SNR) conditions.

1066. The Asymptotic Distribution of Diffusion Tensor and Fractional Anisotropy Estimates

John David Carew[1], Cheng Guan Koay[2], Grace Wahba[1], Andrew L. Alexander[1], Peter J. Basser[2], Mary Elizabeth Meyerand[1]
[1]University of Wisconsin, Madison, Wisconsin, USA; [2]National Institutes of Health, Bethesda, Maryland, USA

Error propagation in diffusion tensor imaging (DTI) has general interest since it tells us how noise in diffusion-weighted images propagates to estimates of the tensor and functions of the tensor estimate (e.g., fractional anisotropy (FA)). In this paper we derive asymptotic properties of the nonlinear least squares estimator (NLSE) of the diffusion tensor. We show that the NLSE of the diffusion tensor is a maximum likelihood estimator under normal noise assumptions. This connection allows us to directly apply the theory of maximum likelihood estimation to obtain asymptotic properties. In particular, we show that the NLSE is consistent and asymptotically normal. Furthermore, any continuously differentiable function of the tensor estimate is also consistent and asymptotically normal. To illustrate and validate the theory we derive the asymptotic distribution of FA and show, with simulations, that for as little as 6 directions, the asymptotic distribution of FA is very close to the empirical distribution.

1067. Error Propagation Framework for Diffusion Tensor Imaging

Cheng Guan Koay[1], Lin-Ching Chang[1], Carlo Pierpaoli[1], Peter J. Basser[1]
[1]NICHD, National Institutes of Health, Bethesda, Maryland, USA

In general, only one estimate of a tensor is obtained in each voxel in a DTI experiment. Since the tensor estimate itself is derived from the noisy diffusion-weighted signals, here we derive the SD of the tensor and tensor-derived quantities by error propagation from the DW signals. The proposed technique is shown to produce precise estimate of the SD of FA. The simulation results show that the variability in tensor-derived quantities is largely due to the variability in the reference signal if the DTI model includes the reference signal as a parameter to be estimated. A simple procedure is provided to ameliorate this problem.

1068. Motion Correction in Diffusion Magnetic Resonance Imaging

Yu Bai[1], Philip A. Cook[1], Hui Zhang[2], Daniel C. Alexander[1]
[1]University College London, London, UK; [2]University of Pennsylvania, Philadelphia, Pennsylvania, USA

This abstract reveals an artifact in diffusion images introduced by standard motion and distortion correction methods for high angular-resolution acquisition and introduces a new correction scheme that avoids the artifact. The artifact is the misalignment of the tissues boundaries between T2 and FA maps. As our new methods choose different reference images for different diffusion gradients, they avoid the mismatching caused by the intensity differences between component images.

1069. Magnitude-Based Spike Noise Correction for Diffusion Tensor Imaging

sofia Chavez[1], Matt Sodomsky[1], Pippa Storey[2], Simon Graham[1, 3]
[1]Sunnybrook and Women's College Health Sciences Centre, Toronto, Canada; [2]Evanston Northwestern Healthcare, Evanston, Illinois, USA; [3]University of Toronto, Toronto, ON, Canada

Spike noise is a common source of image artefact on MRI systems and is particularly problematic for diffusion tensor imaging (DTI). It is a problem that is difficult to trouble-shoot and often results in loss of data. Currently, there is no magnitude-based spike noise correction algorithm that can be directly applied to DTI. This paper presents a methodology for spike noise detection and correction based on a magnitude-derived pseudo-k-space. The methodology makes use of spike-free images to identify and correct the spike signature. It has been shown to work successfully on a wide range of spike noise occurrences.

1070. A Combined Distortion Corrected Protocol for Diffusion Weighted Tractography and fMRI

Karl Vincent Embleton[1], Matthew A. Lambon Ralph[1], Geoff J. M. Parker[1]
[1]University of Manchester, Manchester, UK

We present a protocol for combined distortion corrected diffusion-weighted (DW) echo planar imaging (EPI) and spin-echo (SE)-EPI fMRI based on the dual k-space traversal technique that relies on obtaining two images with opposite direction distortion. Novel features include a registration algorithm to ensure image pairs are aligned in the frequency-encode direction, an algorithm for reducing correction artefacts due to large signal voids in DW images and a distortion corrected fMRI protocol optimized for minimum repetition time. Results indicate that SE-EPI fMRI at 3T is sensitive enough to detect activation in the temporal and frontal lobes from a word categorisation task.

1071. Impact of Partial Volume Effect on Fiber Coherence Index (FCI) Calculation: A Simulation Study

Girish Srinivasan[1, 2], Aziz H. Poonawalla, [23], Xiaohong Joe Zhou[2]
[1]University of Illinois at Chicago, Chicago, Illinois, USA; [2]University of Illinois Medical Center, Chicago, Illinois, USA; [3]M. D. Anderson Cancer Center, Houston, Texas, USA

Fiber coherence index (FCI) was recently introduced as a vector-based diffusion tensor parameter for characterizing tissue structural integrity. This parameter is sensitive to partial volume effect because of a spatial vector correlation calculation. In this simulation study, we have analyzed the impact of partial volume effect on FCI for three types of fibers (straight, bent, and branching/crossing fibers) with varying sizes between 0.5 and 6 mm. The results provide a number of useful guidelines to properly use FCI on specific fibers for clinical applications, when the partial volume effect is a concern.

1072. Effects of the Gradient Number to Resolve Two Crossing Fiber Tracts in HARDI

Dae-Jin Kim[1], Hae-Jeong Park[2, 3], In Young Kim[1], Sun I. Kim[1]
[1]Hanyang University, Seoul, Republic of Korea; [2]Yonsei University, College of Medicine, Seoul, Republic of Korea; [3]Division of Nuclear Medicine, Severance Hospital, Seoul, Republic of Korea

Conventional DTI is unable to estimate the multiple fiber orientations within a voxel. HARDI is one of the novel methods for estimating the distributions of intravoxel multiple fiber orientations. Spherical harmonic decomposition (SHD) is used to quantitatively characterize the apparent diffusion profile in the HARDI approach. The performance of the SHD in HARDI in terms of gradient resolution, crossing angle and noise has not fully understood yet. The aim of this study is to analyze the ability to separate crossing fibers in simulations and human brain data in terms of the number of diffusion gradients, fiber crossing angle and noise.

1073. Effect of Diffusion Time and Diffusion Gradient Strength on the Mean Diffusivity of DTI in Healthy Human Brain

Song Gao[1], Shanglian Bao[1], Hongrun Ren[2]
[1]Beijing Key Laboratory of Medical Physics and Engineering, Peking University, Beijing, People's Republic of China; [2]Cangzhou medical college, Cangzhou, People's Republic of China

The effects of diffusion time on ADC and MD were controversial in previous studies. Moreover, the effect of the diffusion gradient strength has received little attention. In this study, a new experimental protocol is designed to evaluate the effect of the two parameters. The results show that the varying diffusion time or diffusion gradient strength produces a significant effect on MD, which could not be explained by previous theory.

1074. Diffusion Time Dependence of DTI Measurements

Shu-Wei Sun[1], Sheng-Kwei Song[1]
[1]Washington University, St. Louis, Missouri, USA

The effects of restrictions on diffusion measurements are investigated by performing diffusion tensor imaging (DTI) with short and long diffusion time on fixed mouse brain. Both constant b and constant q value approaches were employed. Each line of k-space data was acquired in an interleaved fashion for collecting short and long diffusion time DTI data to eliminate the inter-measurement variation. The results suggest that ADC decreased with increasing diffusion time whether constant q or constant b value was maintained. A more significant ADC reduction was observed in constant q value approach.

1075. Effects of Diffusion Weighting Scheme and SNR on DTI-Derived Fractional Anisotropy at 1.5T

Jonathan Andrew David Farrell[1, 2], Bennett Allen Landman[2], Craig K. Jones, [12], Seth A. Smith[1, 2], Jerry L. Prince[2, 3], Peter C.M. van Zijl, [12], Susumu Mori, [12]
[1]Kennedy Krieger Institute, Baltimore, Maryland, USA; [2]Johns Hopkins University School of Medicine, Baltimore, Maryland, USA; [3]Johns Hopkins University, Baltimore, Maryland, USA

The quantity and composition of DTI data can differ within or between imaging sites, and this impacts the compatibility of DTI-derived results. We investigated how scan repetition and increased directional resolution (number of unique diffusion weighted images in a dataset) impact fractional anisotropy (FA) in a clinical DTI study. By grouping data from 15 DTI datasets in each of three scan sessions, we show that 1) scan repetition alleviates the upward bias in low FA regions observed at low SNR and 2) in an equal scan time comparison FA was not sensitive to diffusion weighting schemes with similar condition numbers.

1076. Finite Pulse Widths Improve Fibre Orientation Estimates in Diffusion Tensor MRI

Matt G. Hall[1], Daniel C. Alexander[1]
[1]University College London, London, UK

We consider the effect of finite pulse widths on the directional concentration of principle eigenvectors of diffusion tensors acquired from simulations of random walkers on an isotropic substrate. We find that wider pulse widths lead to more reliable estimations of principle eigenvector orientation in the presence of noise.

1077. Analysis of Systematic Errors on Estimated Parameters in Q-Space MRI

Frank Peeters[1], Thierry Duprez[1], Guy Cosnard[1]
[1]St-Luc University Hospital, UCL, Brussels, Belgium

We have investigated the effects of finite duration gradients on the estimated parameters in q-space MRI on the basis of a simple model: one dimensional restricted diffusion between planar boundaries. In this case the MR-signal could be calculated exactly. Different reconstruction schemes of the probability density function were considered: direct Fourier reconstruction together with a scaling and dilation correction and a Gram-Charlier expansion. Three characterizing parameters were analyzed: return-to-origin probability, standard deviation and kurtosis. It turns out that large systematic errors will result depending on the gradient timings. Moreover, the concept of an effective diffusion time seems not to work.

The Normal Brain: Analysis by Tractography

Room 4E Monday 14:00 - 16:00

1078. Combined DTI Fiber Tracking and Histological 3D Atlas Mapping of Sensorimotor, Associative and Limbic Cortico – Striatal Circuits

Nominated for an ISMRM Poster Award

Saâd Jbabdi[1], Eric Bardinet[2], Habib Benali[1], Didier Dormont[2], Kamil Ugurbil[3], Jérôme Yelnik[4], Stéphane Lehéricy[1, 3]
[1]Inserm/UPMC, Paris, France; [2]CNRS, Paris, France; [3]University of Minnesota, Minneapolis, Minnesota, USA; [4]Inserm, Paris, France

The purpose of this study was to combine diffusion tensor fiber tracking and 3D deformable histological atlas of the human basal ganglia to build a probabilistic map of cortico – striatal connections. Results provide a 3D atlas and connectivity-based segmentation of the striatum. Visualization of cortico-striatal connections allows delineating the sensorimotor, associative and limbic territories of the basal ganglia.

1079. Cortico-Cortical Connectivity Revealed by DTI-Based Tractography

Hao Huang[1], Jerry L. Prince[2], Aaron Carass[2], Bennett Landman[1], Peter C.M. van Zijl[1, 3], Susumu Mori[1, 3]
[1]Johns Hopkins University School of Medicine, Baltimore, Maryland, USA; [2]Johns Hopkins University, Baltimore, Maryland, USA; [3]Kennedy Krieger Institute, Baltimore, Maryland, USA

Diffusion tensor imaging has been shown to be an effective way to delineate trajectories of the white matter tracts. Anatomy of large white matter tracts in deep white matter has been well documented in histology in the past and many of these tracts can be faithfully reconstructed by DTI-based fiber tracking. But little is known about the anatomy of subcortical white matter. The purpose of this study is to use tractography to identify reproducible short-range cortico-cortical fibers. To perform this study, the cortex in each subject was parcellated as regions of interest (ROIs) for fiber tracking, and the tractography was performed with brute force and multi-ROI line tracing method based on FACT. Ipsilateral and contralateral cortico-cortical connectivity were studied.

1080. Automatic Segmentation of the Pyramidal Tract Basing on Whole-Brain DTI Imaging

Felix Schoth[1], Uli Buergel[1], Paul Stracke[1]
[1]UK Aachen, Aachen, NRW, Germany

A segmentation of the pyramidal tract is expected to improve neuro-navigation. We investigated 10 healthy subjects with DTI. One segmentation method used line propagation and selected paths who connected the peduncel cerebri to Brodmann area 4. The second method was voxel based and chose the voxels according to direction of the main diffusion component, the anisotropy and T1-intensity in a fuzzy logic approach. The segmentations reflect histological findings. The voxel based method showed less mean errors. Line propagation methods are expected to be more efficient in a disturbed anatomy. Both methods can also be applied for other large fiber tracts.

1081. Cortical Mapping Inside Out: Mapping of Cortical Areas Associated with Specific White Matter Tracts Using Diffusion Tensor Imaging and Tractography

Kegang Hua[1], Jiangyang Zhang[1], Setsu Wakana[1], Huang Hao[1], Hangyi Jiang[1], Peter van Zijl[1, 2], Susumu Mori[1, 2]
[1]Johns Hopkins University, Baltimore, Maryland, USA; [2]F. M. Kirby Research Center for Functional Brain Imaging, Baltimore, Maryland, USA

Three-dimensional tractography based on DTI can identify connected cortical regions. However, tractography is known to have errors and unknown validity. In this study, we tackled these issues by creating population-averaged connectivity maps. The probabilistic maps were created for 7 major tracts using data from 28 normal subjects. Almost entire cortical regions were connected by 4 major association fibers. High degree of symmetry was observed, but three well-clustered regions are apparent for the superior longitudinal fasciculus only in the dominant hemisphere. These regions were identified as Wernicke's area, Broca's area, and supermarginal gyrus, which are known major language areas.

1082. Voxel Based Versus Region of Interest Analysis in Diffusion Tensor Imaging of Neurodevelopment

Lindsay Snook[1], Chris Plewes[1], Christian Beaulieu[1]
[1]University of Alberta, Edmonton, Alberta, Canada

Diffusion tensor imaging (DTI) studies of neurodevelopment demonstrate more widespread changes in the white matter than standard T1-weighted MRI. However, the degree of reported changes depends also on the analysis method. The purpose of this study is to determine whether voxel based analysis and region of interest methods lead to different conclusions of neurodevelopment on the same DTI data set, consisting of 32 children aged 8 – 12 years and 28 young adults aged 21 – 27 years.

1083. Regional Variability of Aging and Gender Difference in Human Corpus Callosum: A Diffusion Tensor MRI Study at 4 Tesla

Yu Zhang[1], Geon-Ho Jahng[1], An-Tao Du[1], Michael W. Weiner[1], Norbert Schuff[1]
[1]UC San Francisco and Center for Imaging of Neurodegenerative Diseases (CIND), VA Medical Center, San Francisco, California, USA

4 Tesla MRI and Diffusion Tensor Tractography were used to study age and gender related fractional anisotropy (FA) and mean diffusivity (MD) changes in the corpus callosum (CC). FA decreased with age in anterior CC and MD increased with age in anterior and body CC, while age effect on posterior CC wasn't detected. In addition, a trend of higher FA values in women than in men was found in anterior CC. The results indicate that healthy aging is associated with diminished fiber integrity in anterior CC, which may help to better understand the topology of age-associated brain alterations.

1084. Tract Probability Map in Stereotaxic Spaces and Analysis of Asymmetry

Kegang Hua[1], Jiangyang Zhang[1], Setsu Wakana[1], Hangyi Jiang[1], Peter van Zijl[1, 2], Susumu Mori[1, 2]
[1]Johns Hopkins University, Baltimore, Maryland, USA; [2]F. M. Kirby Research Center for Functional Brain Imaging, Baltimore, Maryland, USA

Three-dimensional tractography is known to be sensitive to noise, partial volume effects, and complex axonal structures. In this paper, we used a probabilistic approach to tackle these issues. Tracking results of 10 prominent white matter tracts from 28 normal subjects were normalized into common templates and probabilistic maps were generated. The quantification results indicated that 4 tracts related to the temporal lobe are larger in the left hemisphere. The probabilistic maps can be used as an atlas of these tracts and to test effects of diseases on sizes of specific white matter tracts.

1085. Evaluation of Somatotopic Organization of Corticospinal Tracts in the Cerebral Peduncle: Results of Diffusion-Tensor MR Tractography

Ji Kang Park[1], Bong Soo Kim[1], Guk Myung Choi[1], Hyung Soo Khang[2]
[1]Cheju National University Hospital, Jeju, Republic of Korea; [2]Eulji University Hospital, Daejeon, Republic of Korea

We examined the 9 healthy right-handed subjects by diffusion tensor MRI (DTI) and fiber tractography (FT). We evaluated the location and somatotopic organization of the corticospinal tract (CSTs) in the cerebral peduncle (CP). Unlike the posterior limb of internal capsule, hand fiber located slightly anteriorly and medially to the foot fiber in the CP.

1086. The Analysis of the Water Diffusivity Within White Matter Tract in Cuprizone-Induced Mouse Model Using Various Indices by the Diffusion Tensor Ellipsoid

Chien-Yuan Lin[1, 2], Pei-ching Chang[2], Chung-Yi Hong[2], Jyh-Hong Chen[1], Chen Chang[2]
[1]Interdisciplinary MRI/MRS Lab, Department of Electrical Engineering, National Taiwan University, Taipei, Taiwan; [2]Functional and Micro-MRI Center, Institute of Biomedical Sciences, Academia Sinica, Taipei, Taiwan

The goal of this study is to explore the ability of various diffusion tensor indices in detecting the abnormality of white matter tract (WMT) in cuprizone-induced mouse model. The results demonstrate that the analysis of size, shape and similarity of diffusion tensor ellipsoid are able to provide the different insight in tissue architecture which is promising for monitoring the changes of white matter structure in the development, aging and disease

Resting State BOLD and Connectivity

Room 4E Monday 14:00 - 16:00

1087. The Frequency Profile of TE-Dependent BOLD Physiological Fluctuations

Kevin Murphy[1], Rasmus M. Birn[1], Peter A. Bandettini[1]
[1]National Institute of Mental Health, Bethesda, Maryland, USA

By examining multi-echo time series data, TE-dependent physiological noise can be separated from non-TE dependent noise sources creating a potential method to cleanly separate BOLD from non-BOLD (and therefore non-neuronal) fluctuations. We investigate this technique further by characterizing the frequency components of the TE dependent and independent signal changes. We found that the TE-dependent BOLD-related physiological fluctuations are primarily at low frequencies, suggesting perhaps spontaneous neuronal activity. However, the results indicate that several non-neuronally related fluctuations also show a TE dependence making it difficult to cleanly separate neuronal from non-neuronal physiological noise.

1088. Capacity Scores of Functional Synchrony in MCI Subjects Are Significantly Lower Than in Age-Matched Controls Determined by ICA Analysis

Zhilin Wu[1], Yin Xu[1], Guofan Xu[1], Shi-Jiang Li[1]
[1]Medical College of Wisconsin, Milwaukee, Wisconsin, USA

Studies have shown that the hippocampus is an important region involved in early Alzheimer's disease (AD) onset. To test our hypothesis that the functional synchrony between the hippocampus regions and other brain regions is deteriorated in MCI subjects, we examined the resting state fMRI voxel time courses for mildly cognitive impaired (MCI) and age-matched control subjects. Independent component analysis (ICA) on spontaneous low frequency fluctuations revealed a significant decrease in functional synchrony among MCI subjects when compared to the controls. The capacity score was obtained as an indicator of functional synchrony and it could be served as a preclinical risk marker for AD.

1089. Functional Connectivity in the Resting Brain Revealed by Group-Level Independent Component Analysis

Sharon Chen[1, 2], Thomas J. Ross[1], Keh-Shih Chuang[2], Elliot A. Stein[1], Yihong Yang[1]
[1]National Institute on Drug Abuse, NIH, Baltimore, Maryland, USA; [2]National Tsing-Hua University, Hsin Chu, Taiwan, Taiwan

Coherent low-frequency fluctuations in the resting-state fMRI signal have been used to study functional connectivity. The majority of these studies have utilized hypothesis-driven methods, such as cross-correlation analysis with presumed seed points, to obtain brain connectivity maps. Independent component analysis (ICA) is a data-driven method and has been recently used to reveal resting-state functional networks without a priori seed points. In this study, we used group ICA (gICA) to analyze resting-state fMRI data to improve sensitivity and reduce bias from individual differences. Our results show that patterns of connectivity, including the "default mode" of brain networks, can be consistently obtained by gICA.

1090. Resting State Connectivity of Anterior and Posterior Cingulate Corteces Using Potts Spin Model

Larissa I. Stanberry[1], Alejandro Murua[2], Dietmar Cordes[3]
[1]University of Washington, Everett, Washington, USA; [2]University of Montreal, Montreal, QC, Canada; [3]University of Washington, Seattle, Washington, USA

In this paper we use a clustering method based on the Potts spin model to determine functional networks specific to the anterior cingulate cortex (ACC) and posterior cingulate cortex (PCC) in a group of nine healthy adult males. The Potts spin model provides a powerful tool to automatically identify functional networks under various conditions and requires no assumption of the number of clusters or their underlying distribution. Resulting networks reflect functional connections to the brain regions implicated in the default mode hypothesis including parahippocampal, fusiform, precentral and frontal gyri. We also compared spectral properties of the ACC and PCC.

1091. The Use of Multiple Physiologic Parameter Regression Increases Gray Matter Temporal Signal to Noise by Up to 50%

Rasmus Matthias Birn[1], Kevin Murphy[1], Jerzy Bodurka[1], Peter Anthony Bandettini[1]
[1]National Institute of Mental Health, Bethesda, Maryland, USA

The temporal signal-to-noise ratio achievable in T2*-weighted MR imaging time series is limited by physiologic noise. The goal of the present study is to compare and evaluate the effectiveness of five additive physiologic noise corrections: 1) RETROICOR to reduce fluctuations at cardiac and respiration frequencies, followed by regressing out 2) respiration volume changes, 3) motion parameters, 4) global signal average, and 5) the average signal over white matter. We found that in addition to more conventional physiologic correction routines, regressing out estimated motion parameters and slower changes in respiration volume lead to TSNR improvements of up to 45% gray matter.

1092. The Effect of Cardiac Pulsation on fMRI Data Analysis

Wen-Chau Wu[1], Eric C. Wong[1]
[1]University of California, San Diego, La Jolla, California, USA

BOLD signal can be modulated by baseline perfusion that can change with physiological condition and cardiac pulsation. We acquired functional data in synchrony with different cardiac phases and made a comparison with current method that analyzes data over multiple perfusion status. Compatible spatial specificity was found in ASL and BOLD data as images were acquired at different or mixed cardiac phases. Smaller BOLD signal change and larger post stimulus undershoot were found at high baseline perfusion. Gated fMRI has higher effective temporal resolution and can be used for detecting finer hemodynamics.

1093. Examination of Non-Physiological Sources of 1/f-Like Noise in EPI Power Spectra

David A. Soltysik[1], Vinai Roopchansingh[1], James S. Hyde[1]
[1]Medical College of Wisconsin, Milwaukee, Wisconsin, USA

Understanding the noise structure of EPI time-series is important for fMRI data analysis. Previous studies have found a 1/f-like noise structure in data collected from human brains and phantoms. In this study, the 1/f-like shape has been quantized on a voxelwise basis by fitting EPI power spectra to $1/f^{\alpha}$ curves. α values are seen to vary across tissue type, phantom type, TR, and voxel size. Based on the results revealed here, it is believed small voxel acquisition is desired to avoid 1/f-like noise from non-physiological sources when performing fMRI.

1094. Simple Model to Describe Weisskoff EPI Temporal Stability Test - Analogy with Physiological Noise Model in Oxygenation-Sensitive fMRI

Jerzy Bodurka[1], Peter Bandettini[1]
[1]NIMH, NIH, Bethesda, Maryland, USA

Weisskoff introduced a simple EPI temporal stability test for fMRI. In this method, the EPI time series fluctuations are measured on the phantom and plot as a function of the square ROI length. As ROI length increases the deviation of this plot from the theoretical value (1/(n*SNR), where SNR is an image signal to noise ratio) characterized MRI scanner related instabilities. Here we have proposed a simple model and derive an analytical formula to describe the Weisskoff EPI temporal stability test. We have also shown an analogy with physiological noise model in oxygenation-sensitive fMRI. Simplicity of this analytical approach can be used to characterize and quantify MRI scanner performance for given hardware settings/imperfections and gained insight in scanner related noise contribution to human fMRI data.

1095. Vasomotor Independence of BOLD-Based fMRI Resting Rhythms

Tzu-Chen Yeh[1, 2], Chou-Ming Cheng[1, 2], Wen-Jui Kuo[2], Jen-Chuen Hsieh[1, 2], Low-Tone Ho[1, 2]
[1]Taipei Veternas General Hospital, Taipei, Taiwan, Taiwan; [2]National Yang-Ming University, Taipei, Taiwan, Taiwan

The characteristic tripod resting rhythm has been identified with very low frequency signal fluctuation (VLF, 0.01~0.03 Hz) using 3T fMRI studies. Physiological cardio-respiratory aliasing signals and spontaneous vasomotor reactivity have been proposed for the origins of resting rhythms. In this blood-oxygen-level-dependence (BOLD)-based fMRI study of normal subjects, verification of cerebral resting tripod signal was obtained when cerebral blood flow (CBF) was independently modulated by the inhaling graded carbogens (0.003~5% CO2, 20% O2 and 80~75% N2). Tripod resting rhythm was concluded to represent the true neural activities during awake resting state.

1096. Fingerprints of Resting BOLD-Based fMRI

Tzu-Chen Yeh[1, 2], Chou-Ming Cheng[1], Wen-Jui Kuo[3], Jen-Chuen Hsieh[1], Low-Tone Ho[1]
[1]Taipei Veternas General Hospital, Taipei, Taiwan, Taiwan; [2]National Health Research Institutes, Taipei, Miaoli, Taiwan; [3]National Yang-Ming University, Taipei, Taiwan, Taiwan

A consistent and characteristic tripod pattern of resting rhythm has been detected by BOLD-based 3T fMRI studies of awaked human brains. Correlates of the tripod component involved posterior medial cortices (interpretation of environment), posterior lateral cortices, ventral medial prefrontal cortex (integration of information from internal/external environments) and dorsal medial prefrontal cortex (monitoring and reporting one¡¦s mental states). With spatiotemporal results of resting fMRI using independent component analyses, tripod signal components of different subjects were characterized by individual specificity and longitudinal reproducibility using correlation analyses and evaluation of Bhattacharyya distance. Furthermore, the existence of ¡§cerebro-prints (the fingerprints of brain)¡¨ was proposed.

1097. Temporal Autocorrelation of Noise for BOLD and IRON fMRI

Francisca Pais Leite[1], Doug Greve[2], Wim Vanduffel[2], Joseph B. Mandeville[2]
[1]MIT, Cambridge, Massachusetts, USA; [2]A A Martinos Center for Biomedical Imaging, Charlestown, Massachusetts, USA

IRON contrast has much better functional sensitivity than BOLD contrast, both in block designs and in ER designs using randomization of ISIs and/or event types. This work examines temporal noise using BOLD and IRON contrasts. We observe temporal correlations within a first order autocorrelation model, whose dominant source is likely to be signal dependent physiological noise. The BOLD noise correlation is twice that of IRON, but the AR noise scaling has relatively little effect on differences between BOLD and IRON sensitivities. The spatial distribution differs between the methods, probably reflecting different underlying physiology.

1098. Time-Dependent Analysis of Functional Connectivity Using Low Frequency BOLD Fluctuations (LFBF) in Visual Areas

Jochen G. Hirsch[1], Mark J. Lowe[2], Christina Rossmanith[3], Achim Gass[1, 3]
[1]University Hospital Basel, Basel, Switzerland; [2]The Cleveland Clinic Foundation, Cleveland, Ohio, USA; [3]University Hospital Mannheim, Mannheim, Germany

Functionally related regions of the brain show synchronized low frequency BOLD fluctuations, as shown with BOLD MRI as well as with other techniques. Experimental studies suggest that these fluctuations reflect oscillations of neuronal activity. Current evaluation strategies in LFBF analysis focus on primary functional networks and calculate cross-correlation figures based on the condition of synchrony (functional connectivity MRI). We extended the fcMRI analysis into the time domain by estimating the time-dependent cross-correlation function. Preliminary studies in 6 normal controls reveal the impact of synchrony as well as the additional information when considering the time dependence of the cross-correlation function.

1099. Spatio-Temporal Characteristics of Correlated Brain Activity During Awake Rest and Early Sleep

Masaki Fukunaga[1], Silvina G. Horovitz[1], Jacco A. de Zwart[1], Peter van Gelderen[1], Susan C. Fulton[1], Thomas J. Balkin[2], Jeff H. Duyn[1]
[1]National Institutes of Health, Bethesda, Maryland, USA; [2]Walter Reed Army Institute of Research, Silver Spring, Maryland, USA

During rest, a number of physiologic processes remain active in the human brain, some of which cause spatio-temporal patterns of correlated activity observable with BOLD fMRI. However, it is unclear whether this activity represents active cognitive processes. To investigate this, we performed fMRI during various levels of alertness including awake rest and early sleep. We found that spatially correlated activity continues during early sleep, indicating that it does not require a high level of alertness or consciousness, and suggesting that it does not represent conscious mentation.

1100. Local Coherence as a Measure of Localized Co-Ordination in the Brain: An Application to Anesthesia

Gopikrishna Deshpande[1], Stephen LaConte[1], Scott Peltier[1], Chantal Kerssens[2], Stephan B. Hamann, Peter S. Sebel[2], Michael Byas-Smith[2], Xiaoping Hu[1]
[1]Georgia Institute of Technology and Emory University, Atlanta, Georgia, USA; [2]Emory University School of Medicine, Atlanta, Georgia, USA

In this work, we introduce the concept of local coherence (LC) and demonstrate the utility of the concept with application to changes in the brain due to anesthesia. LC represents the average correlation a pixel has with its neighbors and is generated as a map over the entire brain. This is in contrast to functional connectivity which assesses the low-frequency correlation between anatomically distributed regions of the brain. Our results show that the LC in the brain decreases in the deep anesthetic state and partially recovers in the light anesthetic state except in the frontal areas.

1101. Mapping Functional Connectivity Using Potts Spin Model

Larissa I. Stanberry[1], Alejandro Murua[2], Dietmar Cordes[3]
[1]University of Washington, Everett, Washington, USA; [2]University of Montreal, Montreal, QC, Canada; [3]University of Washington, Seattle, Washington, USA

In this paper we introduce a clustering method based on the Potts spin model that provides a powerful tool to determine functionally connected regions of the brain. The Potts spin model is a thermodynamic model used in statistical physics and provides an intuitively simple approach to clustering since it requires no assumption of the number of clusters or their underlying distribution. The method is demonstrated on fMRI data using a conventional finger-tapping task to obtain functional connectivity maps of motor activity.

fMRI: Cognition and Language

Room 4E Monday 14:00 - 16:00

1102. Event Related Negative BOLD Response Observed in an Attention Switching Task

Zhihao Li[1], Scott Peltier[1], Xiaoping Hu[1]
[1]Emory University/Georgia Tech, Atlanta, Georgia, USA

Widespread negative impulse response was observed in an attention shift fMRI study. Our data suggested that it has a similar physiological basis as the initial dip. This negative response can be used to investigate brain functions.

1103. 7 Tesla fMRI of Mental Maze Solving in the Human Superior Parietal Lobule Using Parallel Imaging

Trenton Jerde[1], Scott Lewis[1], Ute Goerke[1], Pierre-Francois Van De Moortele[1], Gregor Adriany[1], Steen Moeller[1], Kamil Ugurbil[1], Apostolos Georgopoulos[1]
[1]University of Minnesota, Minneapolis, Minnesota, USA

We used a 7 T magnet and parallel imaging to show that single voxels in the human superior parietal lobule (SPL) are “tuned” for the direction of attention. Subjects mentally traversed four directions of a maze. Single voxels were directionally tuned, with approximately the same number of tuned voxels in each hemisphere. Preferred directions in the two hemispheres were distributed evenly across the 360-degree continuum. These results lay the groundwork for analyses of the functional representation of visuospatial information in the SPL, and they demonstrate the efficacy of imaging highly specific cognitive functions at high magnetic fields.

1104. Sensory Perception and Spatial Judgement Imagery Patterns in Healthy and Visually Handicapped Subjects - An fMRI Study

Senthil S. Kumaran[1], Subash Khushu[1], Shilpi Modi[1], Manisha Bhattacharya[1], Rajendra Prasad Tripathi[1]
[1]Institute of Nuclear Medicine and Allied Sciences, Delhi, India

Functional MRI experiments were carried out in 6 healthy and 2 blind subjects for sensory perceptive condition and spatial judgement at 1.5T. It was observed that blind subjects recruit neural areas responsible for visuospatial judgement for parametric identification. Visuospatial judgement recruit similar areas of the brain in visually handicapped subjects as in controls, even though they did not have any visual experience and accessed their environment using nonvisual modalities.

1105. Imagine Yourself Flying in MRI: Disagreement Between Visual Scene and Supine Position During fMRI

Kayako Matsuo[1], Chikako Kato[2], Haruo Isoda[3], Yasuo Takehara[3], Hiroyasu Takeda[3], Epifanio Tila Bagarinao[4], Toshiharu Nakai[1]
[1]National Center for Geriatrics and Gerontology, Obu, Aichi, Japan; [2]Toyohashi Sozo University, Toyohashi, Aichi, Japan; [3]Hamamatsu University School of Medicine, Hamamatsu, Shizuoka, Japan; [4]National Institute of Advanced Industrial Science and Technology (AIST), Tsukuba, Ibaraki, Japan

Functional MRI was conducted during subjects, lying on their back, seeing a bird's-eye view of a plane going and returning horizontally over the earth (Prone condition). Thus, the orientation of the visual scene contradicted the body position. As compared with a condition of looking up a plane crossing in the sky (Supine condition), the Prone condition augmented bilateral activation around the visual cortex and parahippocampal gyrus. These increases of activation during the disagreement between the visual and somatosensory information might be related to the object-based visual processing of displayed scenes in disregard of the subjects’ own proprioceptive/vestibular information.

1106. Gender Differences in the Topological Map Within the Parietal Lobes

Peter Brotchie[1], Shaun Seixas[2], Shoane Ip[3], Graeme Jackson[4]
[1]Geelong Hospital, Geelong, Victoria, Australia; [2]Swinburne University, Melbourne, Victoria, Azerbaijan; [3]University of Melbourne, Melbourne, Victoria, Australia; [4]Brain Research Institute, Melbourne, Victoria, Australia

Subjects were trained in a simple navigation task. During data acquisition, the subjects’ location within the environment was unexpectedly perturbed. BOLD signal changes related to the perturbation of the subject’s location in the environment were detected within the parietal cortex bilaterally. The activity was stronger on the left for males and stronger on the right for females. By controlling for all other aspects of the task, we believe we have demonstrated that this functional activity is related to the maintenance of a spatial topological map of the environment.

1107. Gender and Hormone Levels Influence Cortical Activation During Synonym Generation. an fMRI Study Across Menstrual Cycle and Sex at 3 T

Harald Kugel[1], Carsten Konrad[1], Sonja Schoening[1], Sebastian Schaefer[1], Pirus Beizai[1], Eva Pletziger[1], Patricia Ohrmann[1], Anette Kersting[1], Walter Heindel[1], Volker Arolt[1], Almut Engelien[1]
[1]University of Muenster, Muenster, NRW, Germany

As known from data from animal experiments, steroid hormones have an effect on brain function. Previous investigations in humans have shown that the level of sexual hormones and the menstrual cycle can influence activation of cortical networks. The results of this study demonstrate that the activation of cortical networks by generation of synonyms depends significantly on sex and menstrual cycle.

1108. Decrease in CMRO2 for Memory-Encoding Tasks in the Hippocampus of Mild Cognitive Impairment Subjects

Guofan Xu[1], Gaohong Wu[1], Yin Xu[1], Shi-Jiang Li[1]
[1]Medical College of WI, Milwaukee, Wisconsin, USA

It has been shown that the cerebral metabolism rate of oxygenation (CMRO2) changes could be derived by combined measurements of BOLD and CBF changes. Because the CMRO2 change could directly indicate localized neuronal activities, it is hypothesized that the CMRO2 changes would be a better biomarker to distinguish normal elderly individuals and mild cognitive impaired subjects. In the present study, regional CMRO2 changes induced by the memory-encoding task in hippocampus were obtained. The CMRO2 changes not only were significantly different between the normal elderly group and MCI group, but also significantly correlated with RAVL memory scores.

1109. Localisation of Regions of Hedonia in the Normal Brain Using an Original, Event-Related, Group Specific, Sporting Paradigm

John McLean[1], David Brennan[1], Barrie Condon[1], Jonathan Cavanagh[1], David Wyper[1], Jennifer Chisholm[1]
[1]Institute of Neurological Sciences, Glasgow, UK

This study aimed to localise regions of hedonia in the normal brain. This was achived by using an event-related, group specific, sporting paradigm. The stimuli were digital video clips from football (soccer) matches. Eight healthy male subjects were imaged. Reward (Goals being scored) and non-reward (Missed goal scoring opportunities) elements were presented in order to resolve pleasurable emotions from those of anticipation. This was achieved without the requirement for any subject decision making process.

1110. Brain Activation Induced by Acupoint Stimulation in the Yin Meridian: fMRI Study

Geng Li[1], Annie M. Y Tang[1], Gina G. Jing[1], Edward S. Yang[1]
[1]The University of Hong Kong, HK, HKSAR, People's Republic of China

In Chinese medical thinking, Yin meridians do not pass through the brain leading to the belief that their stimulation would not yield brain activation. Yet, pericardium meridian, a Yin meridian, and brain functions constitute a functional unit. We postulate that stimulation of PE 6 in the pericardium meridian would induce brain activation. 14 normal right-handed male subjects were studied using fMRI with manual acupuncture and electrical acupuncture, respectively. We observed brain activation following stimulation of PE 6 in the superior temporal gyrus and superior longitudinal fasciculus bilaterally as well as in the medial area of the frontal gyrus.

1111. Investigating the Emotional Responses to Commercials Using fMRI

Nelson J. Klahr[1], Feng Shen[1], Paul Wright[1], Goujun He[1], Jorge Villegas[1], Jon Morris[1], Yijun Liu[1]
[1]University of Florida, Gainesville, Florida, USA

After watching five separate commercials, twelve participants were asked to convey their feelings in terms of pleasure, arousal, and dominance by selecting the most appropriate Self-Assessment Manikin (SAM) out of five possible choices. The results of the behavioral and imaging data suggest that the field of neuromarketing can account for correlations between the emotions elicited by stimuli that act on apriori neural substrates. These findings may lead to predicting changes in consumer attitudes towards purchasing various products and with corresponding patterns of BOLD signal and neural activation.

1112. Does the Task Make a Difference? Comparison of Active and Passive Processing of Emotional Words with Functional Neuroimaging

Traute Demirakca[1], Matthias Ruf[2], Tim Wokrina[2], Gabriele Ende[2]
[1]Heidelberg Academy of Sciences, Heidelberg, Germany; [2]Central Institute of Mental Health, Mannheim, Germany

The influence of the task on neuronal activation concerning emotional processing is not known so far. We compared an active processing task with a passive reading task. Passive processing of negative adjectives yielded stronger activation in left inferior frontal gyrus, left superior frontal gyrus and the left inferior parietal lobe. Active processing leads to an elevated BOLD response in the anterior cingulate cortex and the medial frontal gyrus. However, no significant differences between the two tasks in terms of emotional processing could be found. Activation differences for lexical processing in the precuneus and parietal regions may be a consequence of the elevated attention in the active task.

1113. Processing Lexical Semantic Information in Seond Language Shaped Native Langauge by Event-Related fMRI

Jeong-Seok Kim[1], Bom-Soo Kim[1], Sin-Soo Jeun[1], Bo-Young Choe[1]
[1]College of Medicine, The catholic University of Korea, Seoul, Republic of Korea

The purpose of the present functional magnetic resonance imaging (fMRI) investigation was to examine the modulation of neural activity with respect to language translation. It is a complex task that entails an interaction between a second language (L2) and the native language(L1). To study the underlying mechanisms, we used fMRI to show bilingual's brain activity in phonological processing of reading English words (L2) shaped Korean words (L1). In our fMRI study, nine Korean-English bilingual subjects performed the experiment while they covertly read four type words such as Korean words, Korean words of foreign origin, English words shaped Korean words, English words. fMRI results reveal that the right occipital-temporal and the left inferior frontal areas have a greater response to the presentation of English words shaped Korean words than for other type words. These results may indicate a change in brain circuitry underlying relational processes of language translation, with transition from a similarity-based process system in the occipital-temporal lobes to a language-related processing system in the left prefrontal cortex.

1114. Detection of Short Term Effect of Violent Video Game: An fMRI Study Using Emotional Face Matching Task

Yang Wang[1], Vincent Mathews[1], Andrew Kalnin[1], Kristine Mosier[1], David Dunn[1], William Kronenberger[1]
[1]Indiana University School of Medicine, Indianapolis, Indiana, USA

To determine the short term effect of video game playing on brain function, the BOLD responses to an emotional face matching task were measured immediately after playing a violent or nonviolent video game. fMRI group map showed significantly more activation in prefrontal cortex by subjects playing nonviolent video game than that of playing nonviolent video game. Preliminary results may reflect decreased capacity for active emotion regulation as a result of violent game playing.

1115. Verbal Working Memory in Digital Calculations: A Functional MRI Study

Quan Zhang[1], Yunting Zhang[1], Wei Li[1], Jing Zhang[1]
[1]General Hospital, Tianjin medical University, Tianjin, People's Republic of China

Digital calculation was one of the important cognitive actions in daily life. Recent neuropsychological and behavioral studies showed that calculation may be done based on the language process. This study aimed to observe activation of functional areas related to verbal working memory in digital calculations with block-designed fMRI experiments. Subvocal number reading, simple and complex calculation experiments were preformed on healthy volunteers. Our results showed that verbal working memory was not necessary for subvocal number reading, but was even necessary in dealing with simple arithmetic problem, and verbal working memory had the loading effect during calculations.

1116. fMRI During Overt Production of Alternating Elemental English Sounds

James S. Hyde[1], David A. Soltysik[1], Vinai Roopchansingh[1]
[1]Medical College of Wisconsin, Milwaukee, Wisconsin, USA

An 8-cycle block trial, where each cycle consists of rapid alternation between two sounds spoken overtly for 14 s followed by 14 s rest, gives rise to intense fMRI signals at 3T using 2 × 2 × 2 mm voxels. Motion-induced susceptibility artifacts tend to be at the repetition frequency of the two sounds, which is much higher than the repetition frequency of the task cycle, resulting in a minimal number of false positives. It is concluded that this new paradigm will be useful in fMRI studies of the neurophysiology of sound production.

1117. Reliability of Language Paradigms in fMRI for Pre-Operative Mapping

Koushik Govindarajan[1], Shashwath Ashok Meda[1], Zahid Latif[1], Ewart Mark Haacke[1, 2], Randall Reed Benson[3]
[1]Wayne State University, Detroit, Michigan, USA; [2]MRI Institute for Biomedical Research, Detroit, Michigan, USA;
[3]Wayne State University School of Medicine, Detroit, Michigan, USA

BOLD functional MRI (fMRI) has usefulness in presurgical planning of lesions. The goal here is to map important functional cortex (e.g. motor, language and memory) in the area of the resection to minimize postoperative deficits. The clinical standards are invasive and have limitations. We try to evaluate the reliability of some of the essentially used fMRI paradigms. We use data from 4 patients on blocked design paradigms designed to look into language activation. A ROI based approach is taken to separate activated clusters from group averaged t-maps and we use a count of suprathreshold voxels to assess activation on individual t-maps for these clusters. Plots showing a percentage ratio of this activation depict the reliability of language paradigms used in fMRI. Further evaluation would yield substantial evidence to make progress in proving the clinical utility of fMRI.

1118. fMRI of Voice Production

Jürgen Baudewig[1], A. Olthoff[2], E. Kruse[2], Peter Dechent[1]
[1]MR-Research in Neurology and Psychiatry, University of Göttingen, Göttingen, Germany; [2]Dept of Phoniatrics and Pedaudiology, Medical Faculty, Georg-August-, Göttingen, Germany

A crucial part in voice production is the motor function of the larynx. In this study we examined the BOLD response during active, non-verbal phonation (singing quints) and performed several control experiments in order to differentiate pure motor control of the voice box from voice production. A main finding is the laryngeal representation in the sensorimotor cortex below the hand area but clearly above the lower end of the central sulcus. This is in contrast to former interpretations of the human humunculus but in good accordance with TMS experiments finding laryngeal motor cortex 8 cm lateral from midline.

1119. Lateralization of Brain Function in Cognitive Music Processing of Chord Versus Rhythm

Yi-Yu Shih[1], Yen-Hsiang Wang[1], Cheng-Wen Ko[2], Hsiao-Wen Chung[1]
[1]National Taiwan University, Taipei, Taiwan; [2]National Sun Yat-sen University, Kaohsiung, Taiwan

The difference of brain function between chord distinguishing and rhythm recognition was investigated on 7 subjects using fMRI. The left lateralization phenomenon was found in both tasks, with Brodmann's area (BA) 6 and 40 being the common activation regions. BA9, 22, and 38 showed slight activations with similar left-side lateralization. BA44 and 45 were individually activated exclusively in chord distinguishing and rhythm recognition, respectively, differentiating the unique properties of chord and rhythm and providing a linkage between music cognition and speech expression.

1120. Developmental fMRI Changes Associated with Relational Reasoning

Paul J. Eslinger[1], Jianli Wang[1], Clancy Blair[2], Bryn Lipovsky[1], David Baker[2], Steve Thorne[2], David Gamson[2], Qing X. Yang[1], Lisa Rohrer[2]
[1]Penn State College of Medicine, Hershey, Pennsylvania, USA; [2]Penn State University, University Park, Pennsylvania, USA

fMRI study of relational reasoning in typical children and adolescents 8-19 years of age revealed significant activations in occipital-parietal cortices (functionally associated with visuospatial perception/knowledge), occipital-temporal cortices bilaterally (functionally associated with visual pattern perception), and prefrontal and anterior cingulate regions (functionally associated with working memory, relational reasoning, conflict resolution, and decision-making). Age regression analyses indicated that bilateral parietal cortex activations increased with developmental age while prefrontal, anterior cingulate, and subcortical brain regions decreased in activity with age. Results suggest that younger children engage more widespread neural networks in relational reasoning tasks, but develop more focal parietal lobe activation with age.

1121. Designing a Language Task for Clinical Routine - An Application of Incremental Analysis of T-Statistics for Task Design

Toshiharu Nakai[1], Epifanio Bagarinao[2], Kayako Matsuo[1], Yuko Ohgami[3], Chikako Kato[4]
[1]National Center for Geriatrics and Gerontology, Ohbu, Aichi, Japan; [2]AIST, Tsukuba, Ibaragi, Japan; [3]Ochanomizu University Graduate School of Humanitics and Science, Bunkyo-ku, Tokyo, Japan; [4]Toyohashi Sozo College, Toyohashi, Aichi, Japan

In order to establish a task design to detect language areas for clinical usage, the effect of task block ordering to combine multiple tasks in one session was investigated. Three kinds of language tasks were included. An alternative performance of each condition gave better detection of the activity in Broca?fs area and Wernicke?fs area than a sequential performance did, although both designs included the same number of the task blocks. It was suggest that a combined task design with alternative performance of each condition in one session (9.5 min) may be a routine method for clinical fMRI.

1122. Hand Movement and Overt Speech Assessed by fMRI: Does a Combined Task Facilitate the Motor Execution?

Laura Mancini[1], Serge Pinto[2], Robert Brehmer[3], John S. Thornton[1], Marjan Jahanshahi[2], Tarek Yousry[1], Patricia Limousin-Dowsey[2]
[1]National Hospital for Neurology and Neurosurgery, London, UK; [2]Institute of Neurology, University College London, London, UK; [3]Queen Square Imaging Centre, London, UK

Concurrent verbal and manual task performance has been less studied than single tasks. Nevertheless, they are of great interest as they are implicated in complex human behaviour. In this study, cerebral activation profiles during speech-production (SP), hand-movement (HM) and combined SP/HM tasks have been compared. Our results suggest that the simultaneous motor execution of the same motor program with the hand and the orofacial areas, combined the cortical motor and cerebellar activations in addition to other regions such as the SMA. The added complexity of the combined task requires an additional motor coordination probably mediated by the SMA.

1123. Functional Imaging of Brainstem Structures Involved in Voiding Control

Jürgen Baudewig[1], Sandra Rebmann[2], Petra Holz[1], R.-H. Ringert[2], Peter Dechent[1]
[1]MR-Research in Neurology and Psychiatry, Medical Faculty, Georg-August-University, Göttingen, Germany; [2]Department of Urology, Medical Faculty, Georg-August-University, Göttingen, Germany

The pontine micturition center and the periaqueductal grey were known to be involved in voiding. Nevertheless no fMRI studies demonstrating activations in this brainstem structures during voiding were published yet. We present a study focused on the involvement of these brain regions in pelvic floor muscle control. fMRI was performed at 3T in healthy women, who were instructed to imitate micturition. The most striking results were well-localized activations in the region of periaqueductal grey and the pontine micturition centre. To our knowledge, this is the first study using fMRI to demonstrate micturition-related activity in these brainstem structures.

1124. fMRI of Taste and Aroma Associations

Sally Fathy Eldeghaidy[1], Luca Marciani[1], Johann Pfeiffer[1], Kay Head[1], Joanne Hort[1], Andy J. Taylor[1], Robin C. Spiller[1], Penny A. Gowland[1], Susan Francis[1]
[1]University of Nottingham, Nottingham, England, UK

We have previously developed improved methods to study the cortical representation of taste and retro-nasal aroma stimuli. This study on 6 subjects aimed to assess the cortical representation of taste and retro-nasal aroma associations using fMRI and an improved paradigm. We delivered randomly taste, aroma, taste plus aroma, and control stimuli. We have been able to detect the cortical representation of associations of taste and aroma (versus unimodal taste or unimodal aroma) in a protocol that is closer to the typical experience of consuming liquid foods.

1125. A Comparative Study of Functional Magnetic Resonance Imaging on Two Clinical MRI Systems Using an Auditory Paradigm

Shelley A. Waugh[1], Stephen James Gandy[1], Richard Stephen Nicholas[1], John Graeme Houston[1]
[1]Ninewells Hospital and Medical School, Dundee, Angus, UK

A fMRI study using an auditory paradigm was conducted on eight volunteers in order to compare functional imaging capabilities of two scanners: a Siemens Magnetom Avanto and a Magnetom Symphony. Sequence parameters and stimulus volumes were matched between the two scanners. The results demonstrated different patterns of activation that changed with increasing stimulus volume. This was attributed to the differences in gradient acoustic noise between the two scanners, and its interaction with the subject's perception of the stimulus.

1126. Functional Properties of the Posterior Cingulate Cortex and the Posterior Insula: Characterization Using Basic Types of Coherent and Incoherent Motion Stimuli

Peter Dechent[1], Andrea Antal[2], Petra Holz[1], Walter Paulus[2], Jürgen Baudewig[1]
[1]MR-Research in Neurology and Psychiatry, Medical Faculty, Georg-August-University, Göttingen, Germany;
[2]Department of Clinical Neurophysiology, Medical Faculty, Georg-August-University, Göttingen, Germany

Many neuroimaging studies have investigated visual motion processing in the human brain. However, some of the areas involved are only poorly characterized. Therefore, we used fMRI and simple visual motion patterns to describe the properties of the posterior cingulate gyrus and the posterior insula. All motion stimuli resulted in bilateral activation of the target areas. However, coherent motion induced stronger activation in those regions compared to incoherent motion. Considering the literature, the present findings suggest that the posterior cingulate gyrus and the posterior insula serve multiple functions, one of which is the processing of basic visual motion information.

fMRI: Primary Sensory/Motor Applications

Room 4E Monday 14:00 - 16:00

1127. Daily Priming Stimulation of the Motor Cortex Reduces Hemodynamics

Christopher B. Glielmi[1], Andrew J. Butler[2], Dmitriy M. Niyazov[1], Warren G. Darling[3], Charles M. Epstein[2], Jay L. Alberts[4], Xiaoping P. Hu[1]
[1]Emory University/GA Tech, Atlanta, Georgia, USA; [2]Emory University School of Medicine, Atlanta, Georgia, USA; [3]University of Iowa, Iowa City, Iowa, USA; [4]Cleveland Clinic Foundation Lerner Research Institute, Cleveland, Ohio, USA

Repetitive transcranial magnetic stimulation (rTMS) at low-frequency (1 Hz) can lead to inhibition of local cortical excitability. While past work demonstrates that priming stimulation before low frequency stimulation can enhance cortical inhibition, there is little evidence regarding the long-lasting effects of low frequency rTMS. This study examines the effect of 1 Hz rTMS, both with and without 6 Hz priming, on 5 consecutive days and long-term follow-up to elucidate the effect of rTMS on underlying neural activity using BOLD fMRI. Results exhibit significant voxel reduction as low frequency rTMS is continued over 5 days.

1128. Auditory-Visual Multisensory Interactions Within Primary Cortices Revealed by BOLD Peak Facilitation

Roberto Martuzzi[1], [2], Micah Murray[1], Christoph Michel[3], Philippe Maeder[1], Jean-Philippe Thiran[2], Stephanie Clarke[1], Reto Meuli[1]
[1]Lausanne University Hospital, Lausanne, Switzerland; [2]EPFL, Lausanne, Switzerland; [3]Geneva University Hospital, Lausanne, Switzerland

Studies in animals have shown multisensory interactions within primary cortices. Here, we provide corresponding, non-invasive evidence in humans, by analyzing the BOLD signal dynamics in response to rudimentary visual, auditory, or simultaneous auditory-visual stimuli during a simple reaction time task. Activation maps show that primary cortices of each sensory modality responded to both visual and auditory stimulation, indicative of multisensory convergence. Peak latencies within primary visual and auditory areas were also statistically compared, and exhibited earlier BOLD responses to multisensory auditory-visual stimuli than either unisensory condition. The implication is that brain areas traditionally considered unisensory contribute to multisensory interactions.

1129. Reduced Spurious Activation by Continued Controlled Attention in fMRI Measurements of Primary Sensory Areas

Lei Zhang[1], Jürgen Hennig[1], Kai Zhong[1], Oliver Speck[1]
[1]University Hospital Freiburg, Freiburg, Germany

The goal of this study was to control the subjects' attention during the fMRI experiment, especially for studies of primary sensory areas, and to measure and compare the influence of controlled attention on the activation. The subjects' attention is directed towards random transient color changes of the fixation point. With this controlled attention, the amount of false positive activation outside the primary visual areas is significantly reduced. Visual response is also reduced due to the absence of attentional modulation between baseline and activation state. Therefore, only the intended effect of sensory input is detected.

1130. Reproducibility of Trial-Based Functional MRI on Motor Imagery

Seung-Schik Yoo[1], Heather M. O'Leary[1], Jong-Hwan Lee[1], Nan-Kuei Chen[1], Lawrence P. Panych[1], Hyunwook Park[2], Ferenc A. Jolesz[1]
[1]Brigham and Women's Hospital, Harvard Medical School, Boston, Massachusetts, USA; [2]KAIST, Daejon, ChoongNam, Republic of Korea

We report on reproducibility of cortical activation characterized by repeated fMRI runs (ten times) during the performance of a motor imagery task and a passive auditory stimulation as a control task. Two parameters, the size of activation and BOLD signal contrast, were measured from the regions-of-interest for 10 subjects across different threshold conditions. The results suggest that a measurement of BOLD signal itself is a more reliable indicator of paradigm-related brain activation during repeated fMRI scans.

1131. Effective Connectivity of the Human Motor System: Differences in Subcortical Influences During Automatic and Effortful Movements

Suzanne T. Witt[1], Matthew W. Schmidt[1], Jo-Anne C. Lazarus[1], M Elizabeth Meyerand[1]
[1]University of Wisconsin, Madison, Wisconsin, USA

We present for the first time evidence for differences in the activity of subcortical motor structures involved in automatic and effortful movements. In line with functional activation maps generated for the two motor conditions, effective connectivity results from structural equation modeling suggest that the putamen preferentially influences the cortical motor structures during automatic movements, while the cerebellum preferentially influences the cortical motor structures during effortful movements. The estimated path coefficients also indicate a general increase in drive of the motor cortices during effortful movements.

1132. Plasticity of the Primary Motor Cortex in Bilateral Upper-Extremities Amputees with Different Foot Movement Skill

Xiao Jing Yu[1], Shi Zheng Zhang[1]
[1]Sir Run Run Shaw Hospital, Medical College of Zhejiang University, Hangzhou City, Zhejiang Province, People's Republic of China

The study aimed at investigating the primary motor cortex (PM) plasticity of five both upper extremities amputees with different foot movement skill. fMRI data showed that tope tapping of the amputees possessing more excellent foot movement skill activated the bilateral hand area, and top movement of the amputees possessing less skill activated the contralateral hand area. The amputees without foot movement skill only activate the foot area while toe tapping. We consider that plasticity of PM is responsible for obtaining foot movement skill and reorganization of PM in the amputee is related with higher and more complex brain functions.

1133. Two Types of Sensory and Motor Cortical Reorganization in Hemiplegia Following Early Cerebral Damage: Correlation of Clinical Outcome with Neurophysiological and fMRI Findings

Paolo Bonanni[1], Laura Biagi[1], Michela Tosetti[1], Domenico Montanaro[2], Giovanni Cioni[1]
[1]Stella Maris Scientific Institute, Pisa, PI, Italy; [2]National Research Council, Pisa, PI, Italy

Only one study has investigated the afferent projections to sensory cortex and has shown that the predominant afferent projection of the affected hand is directed to the contralateral hemisphere. These findings indicate that there could be an interhemispheric dissociation between afferent inputs and efferent corticomotor output. Moreover, it is not clear if there exists any correlation between type of reorganization and outcome of sensorimotor function, probably since this function was not evaluated with standardized criteria. Using clinical, somatosensory evoked potentials, transcranial magnetic stimulation and fMRI methods, we investigated cortical sensorimotor reorganization of affected hand in patients with hemiplegic cerebral palsy.

1134. Differences in fMRI Brain Activation Between Left and Right Handed Subjects Executing Diverse Tasks

Ronald Peeters[1], Kirsten Vandewalle[1], Stefan Sunaert[1], Paul Van Hecke[1]
[1]University Hospital of the Catholic University of Leuven, Leuven, Belgium

Differences between left and right handed persons have been studied in several fMRI experiments, but there is still no consensus about a possible difference between right and left handed subjects. In this experiment we explored the differences between groups of left and right handed subjects. The tasks performed by the subjects are a bimanual easy and difficult self paced finger tapping task and a toe movement task. Differences have been observed between the groups of left handed and right handed volunteers in several regions of the brain performing these different tasks.

1135. Cortical Activation Associated with Tactile Movement in Attentive Subjects

M K. Syed[1], Abdelmalek Benattayallah[2], J Fulford[3], I R. Summers[1]
[1]School of Physics, Exeter, UK; [2]School of Physics, Exeter, N/A, UK; [3]Children's Health and Exercise Research Centre, Exeter, UK

In this study, moving tactile stimuli were generated by an array-stimulator (100-elements) placed under the index finger to produce virtual-touch sensations during fMRI. The present study compares activation from moving and stationary tactile-stimuli. Subjects were required to attend to the stimuli.Both the moving and stationary tactile-stimuli produce significant activation of SI, SII and the posterior parietal-cortex, in agreement with previous studies. For 320Hz stimuli, activation is significantly enhanced for moving-stimuli, compared to stationary-stimuli. A similar result was obtained from analysis of data pooled over 40Hz and 320Hz stimuli. For 40Hz stimuli an equivalent result was obtained at a lower significance level.

1136. Where in Human Brain is the Representation of Grasping Movements?

Noriaki Hattori[1], Hiroshi Shibasaki[1], Lewis Wheaton[1], Tao Wu[1], Masao Matsuhashi[1], Mark Hallett[1]
[1]NINDS/NIH, Bethesda, Maryland, USA

Although numerous studies have been conducted to clarify the mechanisms of grasping movements, those studies have not directly demonstrated the location where the representation of ggraspingh is stored. In this study, we conducted an event-related fMRI study in which subjects were required to make a judgment as to whether various objects visually presented were graspable by one hand (G-judgment) or not (N-judgment). The results showed that only the left inferior parietal lobule (IPL) was more activated in the G-judgment condition compared with the N-judgment condition. This finding indicates that representations of grasping movements may be stored in the left IPL.

1137. Age-Related Motor and Nociceptive Cortical Processing Changes Revealed with fMRI

Raimi L. Quiton[1, 2], Gauri Bedekar, [23], Steven R. Roys[2], Jiachen Zhuo[2], Michael L. Keaser[1], Joel D. Greenspan[1, 2] Rao P. Gullapalli[2]
[1]University of Maryland Dental School, Baltimore, Maryland, USA; [2]University of Maryland School of Medicine, Baltimore, Maryland, USA; [3]University of Maryland Baltimore County, Catonsville, Maryland, USA

The decline in cognitive, motor, and sensory function with healthy aging is attributable to neuroanatomical and neurophysiological changes in the brain with age. In this study we used fMRI to compare motor and nociceptive cortical processing changes between two age groups. No difference in spatial activation was found for both the nociceptive and motor paradigms. However, significantly lower fMRI amplitude responses were found among the elderly for the pain paradigm bilaterally in the anterior insula and for the right-hand finger tapping task. These activated regions also showed a significant decrease in gray matter volumes which may explain the reduced activity.

1138. Differences Observed in Subcortical Motor Structures Active During Automatic and Effortful Movements

Suzanne T. Witt[1], Kathryn M. McMillan[2], M Elizabeth Meyerand[1]
[1]University of Wisconsin, Madison, Wisconsin, USA; [2]University of Nashville, Nashville, Tennessee, USA

Functional activation maps indicate that a dichotomy exists between the subcortical motor structures involved in automatic and effortful movements. The basal ganglia, in particular, the putamen is preferentially active during automatic movements; the cerebellum, in the region of the dentate nuclei, is preferentially active during effortful movements. This observed dichotomy is similar to results from previous studies examining internally generated and externally guided movements.

1139. Undershoot-Like Signal Associated with Effort-Induced Mirror Movements

Chihiro Kuroki[1], Koichi Oshio[2], Seiji Ogawa[1], Isao Yokoi[3]
[1]Hamano life science research foundation, Tokyo, Japan; [2]Keio University School of Medicine, Tokyo, Japan; [3]Oita University School of Medicine, Oita, Japan

Twenty six healty volunteers participated in this study. Subjects performed sequential high-speed unimanual finger/thumb tapping. BOLD and VASO fMRI were performed. Before and during scanning, EMG recording were made from bilateral flexor pollicis brevis muscle (data not shown). Mirror movements were seen in all subjects. In the ipsilateral brain region, the BOLD signal increase was much smaller than in cotralateral region, but a clear undershoot signal was seen. This might suggest a possibility of a separate mechanism behind the undershoot BOLD signal.

1140. Impact of Feeding on Olfactory Bulb Response Detected by fMRI

Fuqiang Xu[1], James Shafer[1], Godon M. Shepherd[1], Fahmeed Hyder[1], Douglus L. Rothman[1]
[1]Yale Medical School, New Haven, Connecticut, USA

Olfactory sensitivity and perceptual odor-quality are affected by feeding. The spatial activity pattern in the olfactory bulb codes the peripheral olfactory information and serves as the basis for various olfactory functions. We applied fMRI (9.4T) at glomerular resolution to reveal the activity patterns in the bulb as a function of blood glucose levels, which is associated with feeding. The pattern intensity, not topography, of the same stimuli was modified by feeding conditions. The results provide novel information about how odor patterns and perception are related to feeding conditions thus to assess the role of olfaction in the obesity epidemic.

1141. A Parametrized Approach to BOLD Calibration for the Olfactory Bulb

James Schafer[1], Fuqiang Xu[1], Douglas L. Rothman[1], Fahmeed Hyder[1]
[1]Yale Medical School, New Haven, Connecticut, USA

BOLD calibration in the olfactory bulb is complex due to its highly laminar structure/function and inability to use prior methods (e.g., 13C MRS or hypercapnia) to provide additional measurements. Stimulation-induced change in the BOLD signal (δs) depends on activity dependent change in oxidative metabolism (δm) which is coupled with changes in blood flow (δf) and volume (δv). If δs, δf, and δv can be measured in a reproducible manner for the same voxels with different stimuli, then the BOLD signal can be calibrated by parametrization. Preliminary results of this new process for BOLD calibration are shown and discussed.

1142. fMRI Study of Auditory- Somatosensory Multisensory Interaction

Hiroaki Mano[1], Masahiro Umeda[1], Masaki Fukunaga[1], Yu Ito[2], Toshihiro Higuchi[1], Chuzo Tanaka[1]
[1]Meiji University of Oriental Medicine, Nantan-shi, Kyoto, Japan; [2]Kyoto University, Kyoto, Japan

In this study, we investigated the correlation between the hemodynamic response to auditory, somatosensory stimuli and simultaneously given stimuli, by means of functional magnetic resonance. We presented all subjects to unimodal auditory (A) or tactile (T) stimuli, respectively, or both of them simultaneously(AT), using the right ear and palm. The differences of the responses across the A , T and AT were compared. We found significant signal decrease in the region of right temporal gyrus during AT than A,T ,which indicates the existence of an audio-tactile interaction suppressing the response to AT stimuli in the right superior temporal gyrus.

1143. Pain fMRI Studies Are Improved by Slice-Wise Removal of Cardiac Noise

Keith M. Vogt[1], James William Ibinson[1], Robert Harold Small[1], Petra Schmalbrock[1]
[1]The Ohio State University, Columbus, Ohio, USA

This study directly measured subject's pulse plethysmograph during functional MRI experiments with painful stimulation, during which cardiovascular changes are significant. This measured cardiac data was used to remove the cardiac noise in the time-ordered image data from each image slice by linear regression. Subsequent statistical analysis of activation coinciding with the pain stimulus paradigm showed 23% better fit of the general linear model, as measured by the average change in the adjusted coefficient of determination across all voxels. Areas exhibiting strong correlation to cardiac noise were those associated with large cerebral vessels, consistent with previously published maps.

1144. Functional Magnetic Resonance Imaging of the Human Spinal Cord and Brainstem During Heat Stimulation

Patrick W. Stroman[1], Catherine M. Cahill[1]
[1]Queen's University, Kingston, Ontario, Canada

A novel method for mapping function in gray matter along the entire spinothalamic tract has been developed for the purposes of studying pain in humans. fMRI data span 20 cm and include the entire cervical spinal cord, brainstem, and thalamus. The method used is an adaptation of spinal fMRI methods. Results demonstrate consistent activity in the spinal cord gray matter, the medulla, and in the thalamus. Comparisons of active regions observed with warm and hot stimuli, and with repeated stimuli, demonstrate variations consistent with noxious or innocuous stimulation. This method provides an objective means of studying pain in humans.

1145. Functional MRI of the Responses of the Human Hypothalamus to Sweet Taste and Calories

Paul Smeets[1, 2], Matthias van Osch, [13], Cees de Graaf, [24], Annette Stafleu[2], Jeroen van der Grond, [13]
[1]University Medical Center Utrecht, Utrecht, Netherlands; [2]TNO Quality of Life, Zeist, Utrecht, Netherlands; [3]Leiden University Medical Center, Leiden, Netherlands; [4]Wageningen University, Wageningen, Netherlands

Evidence exists that caloric beverages do not elicit appropriate anticipatory physiologic responses. This leads to excessive energy intake. We investigated the effects of sweet taste and calories on the fMRI signal in the hypothalamus and on blood glucose and insulin concentrations. Five men were scanned four times for 37 min. After 7 min they ingested one of four stimuli: water, a glucose, an aspartame (sweet taste) or a maltodextrin solution (nonsweet carbohydrate). We found that only glucose triggered a prolonged signal decrease. Our findings suggest that both sweet taste and energy content are required for a hypothalamic response.

1146. Intense Aerobic Training Has No Effect on BOLD-Based Brain Functional Imaging

Jill M. Slade[1], Theodore F. Towse[1], Mark C. DeLano[1], Ronald A. Meyer[1]
[1]Michigan State University, East Lansing, Michigan, USA

Systemic factors such as age or caffeine ingestion have been shown to alter the BOLD response during fmri studies. This study examined if intense aerobic exercise training, which has widespread systemic effects, alters the BOLD fmri response.

fMRI: CNS Disorders and Pharmacological Modulation

Room 4E Monday 14:00 - 16:00

1147. Neural Correlates to the Episodic Memory Continuum from Health to Alzheimer's Disease

Arthur Peter Wunderlich[1], Matthias Riepe[2], Georg Grön[3]

[1]Univ.-Clinic Ulm, Ulm, Baden-Wuerttemberg, Germany; [2]Charite - University Medicine, Berlin, Germany; [3]Univ.-Clinic Ulm, Ulm, Germany

Behaviorally, episodic memory in health and Alzheimer's Disease (AD) is thought to reflect a continuum. If so, neural correlates should exist which reflect this. This study was undertaken to look for neural correlates of episodic memory continuum in appropriate subjects. Twelve patients with mild AD and 24 healthy subjects, divided into two subgroups reflecting memory task performance were investigated with fMRI while performing an episodic memory task. Analysis was designed to reveal areas with increasing activation from high-performing healthy subjects to AD patients. We identified four areas: parahippocampal gyrus, hippocampus proper, lingual and fusiform gyri and inferior temporal gyrus.

1148. BOLD Deactivation Response to Hand Tapping in Multiple Sclerosis Patients

Stephanie C. Manson[1, 2], Christiane Wegner[1], Frederica Agosta[3], Frederick Barkhof[4], Christian Beckmann[1], Olga Ciccarelli[5], Nicola De Stefano[6], Franz Fazekas[7], Massimo Filippi[3], Joe A. Frank[2], Achim Gass[8], Jochen Hirsch[8], Heidi Johansen-Berg[1], Ludwig Kappos[8], Tijmen Korteweg[4], Laura Mancini[5], Francesco Manfredonia[5], Silvia Marino[6], David H. Miller[5], Xavier Montalban[9], Jacqueline Palace[1], Chris Polman[4], Maria Rocca[3], Stefan Ropele[7], Alex Rovira[9], Steve Smith[1], Alan Thompson[5], John Thornton[5], Tarek Yousry[5], Paul M. Matthews[1]

[1]Oxford University, Oxford, UK; [2]National Institutes of Health, Bethesda, Maryland, USA; [3]University Ospedale San Raffaele Milan, Milan, Italy; [4]VU University Medical Centre, Amsterdam, Netherlands; [5]University College London, London, UK; [6]University of Siena, Siena, Italy; [7]Medical University Graz, Graz, Austria; [8]University of Basel, Basel, Switzerland; [9]Hospital Vall d'Hebron, Barcelona, Spain

Many conclusions about cortical reorganization within the multiple sclerosis brain have been previously drawn from BOLD activation data. Here we use the deactivation contrast (rest minus task) to draw clinically relevant conclusions about reorganization in multiple sclerosis. Additionally, our multi-centre study exhibits that it is possible to get consistent data amongst multiple sites.

1149. Cortical Activation Volume During a Bilateral Motor Task in Multiple Sclerosis Patient: a Study of the Effect of Subject Motion and Task Performance

Mark J. Lowe[1], Craig Israel Horenstein[1], Devyani Bedekar[1], Ruth Ann Marie[1], Lael Stone[1], Pallab K. Bhattacharyya[1], Mario Dzemidzic[1], Michael D. Phillips[1]

[1]The Cleveland Clinic Foundation, Cleveland, Ohio, USA

During performance of a bilateral complex finger tapping paradigm, the number of significantly activated voxels occurring in the sensory and motor regions were calculated for multiple sclerosis patients (MS) and controls. When all subjects were analyzed, there was no difference in the volume of cortical activation between subject groups. However, when subjects displaying significant motion-related artifact were excluded from the analysis, the control subjects had significantly more activation than MS patients. Furthermore, when both groups were stratified according to task performance, the poor performing controls had a similar activation volume in comparison to MS patients.

1150. Strength and Onset of Basal Ganglia Activation in Parkinson's Disease Patients and Healthy Subjects During Different Movement Conditions

Christian Windischberger[1], Ross Cunnington[2], Birgit Hoheisel[1], Lüder Deecke[1], Ewald Moser[1]

[1]Medical University of Vienna, Vienna, Austria; [2]University of Melbourne, Melbourne, Australia

PD patients on standard medication and age-matched healthy controls were examined while performing finger movements according to (1) a predictable cue, (2) an unpredictable cue and (3) self-initiated. Increased activation during unpredictable and self-initiated finger movements compared to movements performed according to a predictable cue was found in the Putamen of PD patients, but not in the control group. During self-initiated movements activation in the left Caudate occurred significantly later in PD patients than in controls. Differences in activation onsets and strengths between conditions indicate altered movement strategies in PD patients compared to the healthy control group.

1151. Altered Cortical Activation in ALS Differs in Motor and Extra-Motor Regions

Biba Rhiannon Stanton[1], Andy Simmons[1], Victoria Williams[1], Camilla Blain[1], Peter Nigel Leigh[1]

[1]Institute of Psychiatry, King's College London, London, UK

There is evidence of altered cortical activation during motor tasks in patients with Amyotrophic Lateral Sclerosis (ALS), but previous studies have failed to adequately control for weakness. 16 ALS patients, 9 patients with lower motor neurone syndromes (matched for upper limb weakness) and 17 controls performed a block design paradigm contrasting freely selected right hand movements against rest. ALS patients showed increased activation around the sensorimotor cortex, but reduced activation in pre-frontal regions compared to controls and LMN patients. We conclude that these changes are not simply an artefact of weakness, but relate specifically to upper motor neurone pathology in ALS.

1152. Neuropathological Correlates of Movement Disorders in Normal Pressure Hydrocephalus (NPH)

Ekkehard H.G.K. Kuestermann[1], Markus Ebke[2], Anne Heinermann[2], Günther Schwendemann[2], Manfred Herrmann[1], Dieter Leibfritz[1]

[1]University of Bremen, Bremen, Germany; [2]Klinikum Bremen-Ost, Bremen, Germany

This functional MR study investigates neuronal correlates of movement disorders in normal pressure hydrocephalus (NPH) patients before and after lumbar puncture for NPH treatment. Imaginary movement tasks elicited in individuals activations in hippocampal regions which were not predicted by current hypotheses.

1153. Serotonergic Modulation of the Anterior Cingluate and STS During Emotion Processing

Gordon D. Waiter[1], Justin H.G. Williams[2], Alison D. Murray[1], Andrew Whiten[3], David Perrett[3]

[1]University of Aberdeen, Aberdeen, Grampian, UK; [2]University of Aberdeen, Aberdeen, UK; [3]University of St Andrews, St Andrews, Fife, UK

Effective processing of emotional signals is essential for human survival. However, the identification of facial emotion may be impaired in a number of psychopathological conditions associated with disruption to serotonergic function. The anterior cingulated is the region where attentional and emotional functions are integrated and it plays a major role in modulating emotional responses. During the reading of emotional expression, serotonergic manipulation reduces activity in brain structures that serve emotional processing activities. Empathic function is likely to be affected by serotonergic function, which may have implications for our understanding of autism, depression and other conditions where serotonergic function could be compromised.

1154. Spatial Non-Uniformity of the CBF Response to Sevoflurane: Implications for fMRI

Maolin Qiu[1], Ramachandran Ramani[2], R Todd Constable[1]

[1]Yale University School of Medicine, Hew Haven, Connecticut, USA; [2]Yale University School of Medicine, New Haven, Connecticut, USA

Quantitative measures of the change in CMRO2, can be obtained through models relating regional cerebral blood flow (rCBF) and blood oxygen level dependent (BOLD) contrast. This abstract presents results from a study showing the complicated effects of an anesthetic agent on basal neuronal activity. Most important for fMRI studies, the spatial-specificity of the drug-induced incremental changes in rCBF and the confounding vascular effect of the agent, are investigated.

1155. Effects of 0.25MAC Sevoflurane on Functional Magnetic Resonance Imaging - In-Vivo Study of Normal Human Subjects and Implications to Data Interpretation

Maolin Qiu[1], Ramachandran Ramani[2], R. Todd Constable[1]

[1]Yale University School of Medicine, Hew Haven, Connecticut, USA; [2]Yale University School of Medicine, New Haven, Connecticut, USA

Quantification fMRI uses BOLD and CBF mapping to obtain relative changes in oxidative metabolism (cerebral metabolic rate for O2, CMRO2). This approach is needed to investigate the functionally related activity in the presence of different levels of baseline activity induced by anesthetic agents. However, it is not clear in these models how this empirical relationship between flow and function is affected by anesthetics. This work presents results demonstrating altered coupling of rCBF, BOLD and CMRO2 in the presence of visual and auditory stimuli during anesthesia with 0.25 MAC sevoflurane using simultaneous BOLD and CBF fMRI techniques.

1156. Time-Related Neural Activity During Cue-Induced Heroin Craving: A Preliminary Study

Yan Fang[1], Chunming Xie[1], Haiyan Meng[1], Zheng Yang[1]

[1]Institute of Basic Medical Sciences, Haidian, Beijing, People's Republic of China

To study the cue-induced heroin craving, we used a method which could investigate the time-related neural activity by non-linear regression with a beta model. We found that during different time, the activated brain regions such as nucleus accumbens, anterior nucleus and the medial frontal gyrus were very different by comparing the heroin subjects and the healthy volunteers watching the heroin movie. This might show us a time relationship between these regions related to craving.

1157. Extraction of Pharmacokinetic Parameters from Human Brain Cocaine BOLD Responses

Peter R. Kufahl[1], Robert Risinger[1], Alan Bloom[1], Shi-Jiang Li[1]

[1]Medical College of Wisconsin, Milwaukee, Wisconsin, USA

Cocaine activation of the orbitofrontal cortex, ventral striatum and dorsal caudate in cocaine-dependent human subjects was observed with the BOLD signal. The transient deflections from baseline (pre-cocaine infusion) levels were modeled with a single-compartment pharmacokinetic model. Parameters from this model were numerically determined and used to estimate cocaine absorption and clearance in brain tissue. Variability of these parameters associated with experimental conditions and consistency with the pharmacology literature were assessed.

1158. Imaging RCBF Changes in Response to Insulin-Induced Hypoglycemia at 3T Using Three-Coil CASL

Edward J. Auerbach[1], Jyothi P. Rao[1], Kamil Ugurbil[1], Elizabeth R. Seaquist[1]
[1]University of Minnesota, Minneapolis, Minnesota, USA

Previous studies have used PET to map changes in regional cerebral blood flow (rCBF) in response to hypoglycemia, but the spatial resolution of PET is typically low (8-10 mm). Higher resolution would be advantageous for localizing smaller structures involved in hypoglycemia detection and counterregulation. In this study, three-coil CASL was implemented and utilized on a 3 Tesla clinical scanner to determine if changes in rCBF detected at a resolution of 2 × 2 × 3 mm could be used to identify those regions that are activated in response to hypoglycemia.

1159. Pharmacological fMRI: Measuring Opioid Effects Upon the BOLD Response to Hypercapnia

Kyle TS Pattinson[1], Stephen D. Mayhew[1], Richard Rogers[1], Irene Tracey[1], Richard G. Wise[1]
[1]Oxford University, Oxford, Oxfordshire, UK

This study investigated the effect of a mu-opioid agonist remifentanil, upon cerebrovascular CO2 reactivity, using BOLD fMRI. We delivered hypercapnic challenges to human volunteers, while controlling potential opioid-induced respiratory depression. We compared the BOLD signal increase to elevated CO2 before and during remifentanil administration. We have determined that remifentanil does not have a generalised effect on CO2 responsiveness in the cerebral vasculature. This allows us to interpret drug induced changes in BOLD signal with more confidence and we suggest that similar methodology to assess pharmacological influences on vascular reactivity should be used when investigating new compounds with fMRI.

1160. Bayesian Source Separation of Drug-Induced BOLD Responses with Correlated Reference Functions

Peter R. Kufahl[1], Daniel Rowe[1], Shi-Jiang Li[1]
[1]Medical College of Wisconsin, Milwaukee, Wisconsin, USA

The multivariate technique Bayesian Source Separation (BSS) was employed to investigate the drug-induced BOLD response of paralimbic human cortex, using the simultaneously measured BOLD signals of subcortical afferents as reference waveforms. BSS yielded improved activation statistics, and revealed significant interaction between the reference waveforms. BSS was shown to be a potentially useful probe of complex BOLD data relating drug-induced brain activity of different regions of interest.

1161. Comparison of Analysis Techniques for Direct Pharmacological Challenge-fMRI

Shane McKie[1], Paul Richardson[1], Jane Lees[1], John William Francis Deakin[1], Steve Ross Williams[1]
[1]University of Manchester, Manchester, UK

Direct pharmacological challenge-fMRI is a method to study the dynamic effects of drugs on brain haemodynamics. We have developed an alternative analysis method using SPM to detect drug-induced BOLD signal changes without prior knowledge of pharmacokinetics or subjective effects. Two psychiatric drugs (mCPP and ketamine) were used and the subjective effects measured. Our results show that this method of analysis is more robust than using the subjective ratings as it allows for individual differences and latency effects between brain regions.

1162. Working Memory and Go/NoGo Task in Gilles-De-La-Tourette Patients

Irene Neuner[1, 2], Hans P. Wegener[1], Tony Stoecker[1], Thilo Kellermann[2], Corinna Ehlen[2], Tilo Kircher[2], Jon N. Shah[1, 3], Frank Schneider[2]
[1]Research Centre Juelich, Juelich, NRW, Germany; [2]RWTH Aachen University, Aachen, NRW, Germany; [3]University of Dortmund, Dortmund, NRW, Germany

Tourette-Syndrome is a neuropsychiatric disorder with motor and vocal tics as prominent symptoms. The origin of the tics is attributed to a dysfunction of the cortico-striato-thalamo-cortical circuitry. Using fMRI at 1.5T, we studied 13 Tourette patients (mean 32.0 SD 10.2 years) and 13 matched healthy volunteers. In a blocked design they performed a working memory task and a Go/No-Go task. Subjects were videotaped with a custom-made, MR-compatible camera system. The results indicate complex frontal dysfunction in Tourette-Syndrome. The task dependent and varying patterns of deactivation or activation of frontal areas distinguishes Tourette patients from controls.

1163. Imaging Cerebral Blood Flow Changes Due to Pain with Arterial Spin Labeling

Daron G. Owen[1, 2], Yves Bureau[1, 2], Alex W. Thomas[1, 2], Frank S. Prato[1, 2], Keith S. St. Lawrence[1, 2]
[1]Lawson Health Research Institute, London, Ontario, Canada; [2]University of Western Ontario, London, Ontario, Canada

A limitation with BOLD fMRI for pain imaging is the inability to measure chronic pain. An alternative way to image pain is arterial spin labeling (ASL), although the reduced sensitivity of ASL could be a problem here. To overcome this limitation, we collected ASL data on a 3T magnet equipped with an 8-channel phased array coil. Using an experimental acute pain model, we demonstrated that ASL could detect activations in most of the areas typically associated with pain. This study suggests that with improved sensitivity, ASL offers the real possibility of imaging chronic pain with fMRI.

1164. The Cerebral Neural System Responsible for Salivation: A Functional MRI Study

Bob L. Hou[1], Kyung K. Peck[1], Christopher Kim[2], Nicole M. Petrovich[1], Dmitry Bogomolny[1], Dennis Kraus[1], Andrei I. Holodny[1]

[1]Memorial Sloan-Kettering Cancer Center, New York, USA; [2]University of Cincinnati, Cincinnati, Ihio, USA

We contributed evidence toward the determination of the neural network involved in salivation. Functional MRI results demonstrated that the salivation activated three cortical areas: the left orbital gyrus - a crucial part of the olfactory system, the left and right insula related to the gustatory system, and the postcentral (sensory) gyrus. These areas were activated even by the "Imagination" paradigm – when the subjects did not actually taste, smell or touch the lemon on the screen. This appears to represent the well-know Pavlovian response seen in animals and humans.

Cardiac Perfusion

Room 4E Monday 14:00 - 16:00

1165. Parametric Aspects of First Pass DCE MRI Myocardial Studies

Xin Li[1], Charles Springer[1], Michael Jerosch-Herold[1]

[1]Oregon Health & Science University, Portland, Oregon, USA

Values for parameters measuring a pseudo first-order rate constant for contrast reagent (CR) extravasation, Ktrans, and the blood volume fraction, vb, can be determined from the pharmacokinetic analysis of first-pass Dynamic-Contrast-Enhanced (DCE) MRI myocardial data. These vary between the resting and hyperemic conditions.

1166. Myocardial Stress Perfusion Dynamic Signal Evaluation Algorithm Comparison

Yi Wang[1, 2], Bin Luo[1], Sunil T. Mathew[1], Nora Ngai, PhD[1], Marguerite Roth[1], Jing Han[1], Nathaniel Reichek[1, 2]

[1]St. Francis Hospital, Roslyn, New York, USA; [2]State University of New York, Stony Brook, New York, USA

We studied six different perfusion quantification methods that are commonly used in stress perfusion imaging to evaluate their coefficient of variation in seven normal subjects. Three slope-based, semi-quantitative algorithms and three model-based quantitative algorithms were used in each subject. The results showed a smaller variation using a constrained algorithm compared to any other method. Furthermore, the flow reserves from the model-based methods were more consistent with each other and had higher values than the slope-based methods.

1167. Correction of Myocardial Perfusion Reserve Data from First-Pass MR Imaging at 3.0 Tesla with Parallel Imaging

Chun Ruan[1], Scott Yang[1], Kenneth Cusi[1], Feng Gao[1], Geoffrey D. Clarke[1]

[1]University of Texas Health Science Center at San Antonio, San Antonio, Texas, USA

In this study, the image nonuniformities were evaluated for 3T MRI first-pass contrast-enhanced myocardial perfusion imaging and a method was developed to compensate for these artifacts and evaluate their influence on the myocardial perfusion reserve index (MPRI) in normal subjects. The results demonstrated that the assessment of myocardial perfusion reserve at 3T is clinically feasible and desirable due to superior SNR, spatial and temporal resolution. The established normative MPRI can serve as a reference value for perfusion studies at 3T and could be used to screen patients with suspected CAD and follow-up treatment.

1168. Optimization of Contrast Medium Administration for First-Pass Myocardial Perfusion at 3T MR System

Mao-Yuan Marine Su[1], Woeichyn Chu[1], Hsi-Yu Yu[2], Wen-Yih Isaac Tseng[3]

[1]Institute of Biomedical Engerening, National Yang-Ming University, Taipei, Taiwan; [2]Department of Surgery, National Taiwan University Hospital, Taipei, Taiwan; [3]Center for Optoelectronic Biomedicine, National Taiwan University College of Medicine, Taipei, Taiwan

Although administration of Gd-DTPA for first-pass myocardial perfusion study has been optimized at 1.5T, it may be different at 3T MR system due to inherent differences in T1/T2 relaxation times. In this study, we evaluated different protocols of contrast medium (CM) administration for myocardial perfusion at 3T MR system. We found that not only CM dosage but also injection duration were crucial to achieve linearity of CM dose with respect to SI and to maintain adequate bolus contrast. Our study suggests that Gd-DTPA of less than 0.05 mmole/kg and injection duration of less than 2 sec are optimum for quantitative analysis of myocardial perfusion study at 3T MR system.

1169. Kinetic Models and Blood Signal Modeling for Dynamic Cardiac MRI Perfusion Studies

Edward DiBella[1], Nate Pack[1], Chris J. McGann[1]

[1]University of Utah, Salt Lake City, Utah, USA

A large number of analysis methods have been used for quantitative or semi-quantitative analysis of cardiac dynamic contrast MRI data. These models are most often used without regard to signal from the blood in the tissue or from spillover of blood signal in the left ventricular blood pool. A systematic comparison of five different models, some with and some without blood signal modeling is performed. The model with the lowest error in the fit and the lowest coefficient of variation had the most parameters (5) including two for modeling signal from the blood.

1170. Comparison of the Reproducibility of Myocardial Perfusion Measurements Using TrueFISP and TurboFLASH

Andrea Kronfeld[1], Agnes Zelinka[1], Georg Horstick[1], Karl Friedrich Kreitner[1], Wolfgang Günther Schreiber[1]
[1]Mainz University Medical School, Mainz, Germany

To compare intra- and interobserver variability of semi quantitative myocardial perfusion MRI with TrueFISP and TurboFLASH pulse sequences at low dose contrast agent dosage (0.04 mmol/kg BW) with each pulse sequence 20 patients were examined and myocardial perfusion reserve (MPR) was determined by 2 observers. Inter- and intraobserver variability were calculated for the TurboFLASH pulse sequence ((24±22)%, (26±23)% respectively) and for the TrueFISP pulse sequence ((21±20)%, (23±22)% respectively). In both cases the TrueFISP pulse sequence shows a significant better signal noise ratio and reproducibility and should be used for determination of MPR.

1171. Perfusion of an Empty-Beating Heart, a New Good Technique to Protect Hypertrophied Hearts for Valve Surgery

Jian Wang[1, 2], Gang Li[1], Bo Xiang[1], Marco Gruwel[1], Mike Jackson[1], Hongyu Liu[2], Tomas A Salerno[3], Roxanne Deslauriers[1], Ganghong Tian[1]
[1]Institute for Biodiagnostics, National Research Council, Winnipeg, Manitoba, Canada; [2]the Fourth Affiliated Hospital, Harbin Medical University, Harbin, People's Republic of China; [3]University of Miami, Jackson Memorial Hospital, Miami, Florida, USA

Conventional heart protection techniques may cause postoperative heart dysfunction or heart failure, particularly in the patients with hypertrophied hearts. The present study was to develop a new heart protection method for protection of hypertrophied hearts. We found that our new technique completely prevented the detrimental effects of the conventional techniques and was able to maintain normal myocardial fluid homeostasis and energy metabolism even in presence of a moderate coronary stenosis.

1172. Rate of Myocardial Contrast Enhancement with Extracellular Contrast Agent and Relationship to Perfusion Reserve

Michael Jerosch-Herold[1, 2], Naveen S. Murthy[2], Carsten Rickers[2, 3], Arthur E. Stillman, [2 4]
[1]Oregon Health & Science University, Portland, Oregon, USA; [2]University of Minnesota, Minneapolis, Minnesota, USA; [3]University of Kiel, Kiel, Schleswig-Holstein, Germany; [4]Cleveland Clinic Foundation, Cleveland, Ohio, USA

The rate of myocardial contrast enhancement is sensitive to changes in myocardial blood flow, but this relationship has not been systematically investigated. Starting with the central volume principle we derive an approximation between blood flow and rate of contrast enhancement, which is used to estimate the myocardial perfusion reserve, a clinically important parameter for assessing the hemodynamic signifcant of coronary lesions.

1173. A Novel BOLD-Sensitive SSFP Technique with Applications for Cardiac Imaging

Jordin D. Green[1], Andreas Kumar[2], Matthias G. Friedrich[2]
[1]Siemens Medical Solutions, Calgary, AB, Canada; [2]University of Calgary, Calgary, AB, Canada

Steady-state Free Precession (SSFP) is used for many cardiac applications, and under certain conditions is sensitive to the BOLD (Blood Oxygen-Level Dependent) effect. The purpose of this study is to demonstrate a new BOLD-sensitive SSFP sequence which is designed for use in the heart. We used an arm cuff model of ischemia in 11 volunteers and detected a signal change of 2.4% (baseline to ischemia) and 2.1% (baseline to hyperemia). These results are statistically significant ($p<0.05$) and comparable to other cardiac BOLD imaging techniques.

1174. Improvement of T_1 Accuracy with the Correction of Imperfect Excitation Flip Angle: Toward the Application of Arterial Spin Labeling

Haosen Zhang[1], Jinghua Wang[2], Pamela K. Woodard[1], Jie Zheng[1]
[1]Washington University School of Medicine, St. Louis, Missouri, USA; [2]Yale University School Medical Center, New Haven, Connecticut, USA

The aim of this study was to investigate B1 inhomogeneity effect on the accuracy of T1 calculated with a T1 regression algorithm adapted for inversion (IR) prepared single shot gradient echo (GRE) based arterial spin labeling sequence. In the simulation, we found that 90% efficiency of the nominal excitation flip angle (α) resulted in 1.5% overestimation of the actual T1 (900 ms). To improve the accuracy of the measured T1 in a phantom, we corrected the measured excitation flip angle in the T1 fitting, which might increase the final accuracy of the calculated T1 (approximately 3~4% error of the true T1).

1175. The Local Effective Flip Angle in the Presence of Highly Inhomogeneous B1-Fields and Flow

Florian Fidler[1], Peter Michael Jakob[1]
[1]University of Würzburg, Würzburg, Frankonia, Germany

The proposed method can easily access the local effective flip angle in highly inhomogeneous B1-fields that covers through-plane flow effects as well as slice profile.

1176. $^{1}H_2O$ MR Relaxography of the Perfused Rat Heart

Marie Poirier-Quinot[1, 2], Huamei He[1, 2], Charles S. Springer[3], James A. Balschi[1, 2]
[1]Brigham and Women's Hospital, Boston, Massachusetts, USA; [2]Harvard Medical School, Boston, Massachusetts, USA; [3]OHSU, Portland, Oregon, USA

This study measured $^{1}H_2O$ T_1 relaxation times of isolated rat hearts perfused with steady-state GdDTPA concentrations. Relaxographic analysis of the $^{1}H_2O$ T_1 decays and analysis with two site exchange modified Bloch equations (2SX) revealed intracellular (p_i) and extracellular (p_e) water populations (tissue water volume fractions) and the average lifetime of intracellular water molecules (τ_i). In the perfused heart we found: $\tau_i = 0.18$ sec and $p_i = 0.24$. Zero flow ischemia caused vascular collapse and a decrease in p_e; τ_i increased to 0.28 sec. $^{1}H_2O$ relaxography can measure myocardial intra- and extracellular volumes and τ_i during normal and disease states.

1177. Development of a Rapid, Automated Shim Approach for Cardiac MR in Mice *In Vivo*

Jurgen E. Schneider[1], Peter Jezzard[1]
[1]University of Oxford, Oxford, Oxon, UK

A novel, automated shim method, optimised for application to cardiac MR in mice, is reported. It is able to homogenize the B0-field in an arbitrarily shaped, but connected region of interest, using available linear, 2nd and 3rd order shim terms. Initial experiments in phantoms and mouse hearts *in vivo* show the superiority of this approach over manual shimming.

1178. Manganese-Enhanced Magnetic Resonance *In Vivo* Imaging of Rat Myocardium Using FLASH: Comparative Study of Contrast at 2.35T and 7T

Morten Bruvold[1], Tina Pavlin[1], Heidi Brurok[1], Per Jynge[1], John Georg Seland[1]
[1]Norwegian University of Science and Technology, Trondheim, Norway

In recent years, Manganese Enhanced MRI (MEMRI) has been studied in myocardial and brain tissue. To increase specificity of MR, it is essential to optimize both contrast and SNR. While the contrast in MEMRI is generated by increased T1-relaxivity, little is known about the effect of T1 dispersion on the contrast in MEMRI. Our study compares the contrast generated in rat myocardium using MEMRI at two different field strengths. Results show that an increased contrast is expected when MEMRI is performed at higher field strengths.

Myocardial Viability

Room 4E Monday 14:00 - 16:00

1179. A Multi-Parameter Analysis for the Optimization of Delayed Enhancement Imaging Using Known Myocardial T1 Values

Puneet Sharma[1], John N. Oshinski[1, 2]
[1]Emory University, Atlanta, Georgia, USA; [2]Georgia Tech, Atlanta, Georgia, USA

This study deals with a computational analysis of the delayed enhancement technique. We present a mathematical model that allows the investigation of not just the inversion time, but a wide variety of paramters such as flip angle, TR, lines/segment, segment interval time, etc. To this end, the viability sequence can be analyzed completely. We show that with the use of known T1 values of infarct and normal myocardium, one can optimize the sequence over many variables. We found that the optimal flip angle is independent of time post-contrast, and that the optimal inversion time is larger than the null-point TI, in terms of producing higher signal contrast between infarct and normal myocardium.

1180. Comparison of Delayed Contrast-Enhanced Viability Imaging at 1.5T and 3T: Initial Experience

Puneet Sharma[1], Mushabbar Syed[1], John N. Oshinski[1]
[1]Emory University, Atlanta, Georgia, USA

This invesitigation focuses on comparing delayed enhancement imaging at 3T with traditional methods performed at 1.5T. We intended to study the feasibility and image quality of the technique, and outline the potential benefits garnered by the application of higher field strengths. We found that, in general, higher infarct tissue SNR is achieved at 3T, improving infarct-to-remote myocardium image contrast. There was also a marginal benefit in blood-to-infarct contrast. Albeit one case with significant T2* dephasing in the infarct region, we conclude that 3T delayed enhancement imaging may provide increased infarct delineation afforded by improved SNR and CNR.

1181. Myocardial Infarction: Optimization of Delay Time at Delayed Contrast-Enhanced MR Imaging at 3T

Xiao Ying Wang[1], Wei Sun[2], Xue Xiang Jiang[3]
[1]Peking University First Hospital, BeiJing, People's Republic of China; [2]GE healthcare, Beijing, People's Republic of China; [3]
Peking University First Hospital, Beijing, People's Republic of China

Contrast-enhanced magnetic resonance imaging allows detection of nonviable myocardium. Hardware and acquisition sequences have improved image quality while simplifying cardiac examinations. 3T MR examination may be better than 1.5T theoretically due to the higher SNR, but there still a long way for the improvement of the technique. The aim of this paper is to find the optimum time for delay enhancement examination at 3T.

1182. Phasesensitive Inversion Recovery (PSIR) Single Shot TrueFISP for Assessment of Myocardial Infarction at 3 Tesla

Armin Michael Huber[1], Kerstin Bauner[1], Bernd Wintersperger[1], Michaela Schmidt[2], Edgar Mueller[2], Scott Reeder[3], Maximilian Reiser[1], Stefan Schoenberg[1]

[1]Klinikum Großhadern, München, Bayern, Germany; [2]Siemens Medical Solutions, Erlangen, Bayern, Germany; [3]University of Wisconsin, Madison, Wisconsin, USA

Imaging myocardial infarction at 3 Tesla compared to 1.5 Tesla allows for a gain of CNR when a PSIR Single Shot TrueFISP sequence is used. The volume and transmural extent of myocardial infarction can be determined with high diagnostic accuary compared to a reference technique at 1.5 Tesla.

1183. Differences in Null Points Between the Left and Right Ventricles in Contrast-Enhanced Inversion-Recovery MRI in Patients with Cardiac Diseases

Yasuo Amano[1], Tatsuo Kumazaki[1]

[1]Nippon Medical School, Tokyo, Japan

The purpose of this study was to assess the differences in the null points and signals of myocardia between right and left ventricles (RV and LV) in contrast-enhanced inversion-recovery MRI. Using Look-Locker imaging, null points of the RV myocardium were found to be shorter than those of the LV myocardium in nine of 26 patients. In these patients, the signal difference between the myocardia of the RV and LV was large in delayed contrast-enhanced MRI. Delayed contrast-enhanced MRI with a shorter inversion time should be performed to evaluate late enhancement of the RV myocardium.

1184. A Single Shot Myocardial Delayed Enhancement Technique Compared to Conventional 2D MDE

David W. Stanley[1], James F. Glockner[2], Thomas K. Foo[3]

[1]GE Healthcare, Proctor, Minnesota, USA; [2]Mayo Clinic, Rochester, Minnesota, USA; [3]GE Global Research, Niskayuna, New York, USA

Patients were referred for myocardial viability evaluation using 2D MDE and sshmde. Both sequences were evaluated and rated for perceived SNR, perceived CNR, myocardial suppression, infarct visualization, image artifacts, and overall image quality by a radiologist experienced in cardiac MRI. Preliminary results are promising using sshmde to decrease over all exam times while maintaining image quality to that of the conventional 2D MDE technique

1185. Initial Clinical Evaluation of a Substraction Delayed Enhancement Technique in Myocardial Infarction

Alban B. Redheuil[1], [2], Patrice Hervo[3], Séverine Peyrard, Thomas Foo[4], Elie Mousseaux

[1]HEGP - European Hospital Georges Pompidou - University of Paris-Descartes, PARIS, France; [2]INSERM, PARIS, France; [3]General Electric, Buc, Ile de France, France; [4]General Electric, Niskayuna, New York, USA

Initial application of a substraction technique using 2 delayed enhancement fast inversion recovery images at short and long TI times to improve contrast in the delineation of infart-blood and infarct normal myocardium borders on a myocardial infarction population.

1186. Evaluation of High-Resolution 3D Myocardial MR Delayed Contrast Enhancement Acquired During Free Breathing Using Realtime Motion Correction

Kenichi Yokoyama[1], Toshiaki Nitatori[1], Nahoko Kanke[1], Shinju Suzuki[1], Shuji Takahashi[1], Shuhei Takemoto[2], Shinichi Kitase[2], Shigehide Kuhara[2]

[1]Kyorin University school of medicine, Mitaka-shi, Tokyo, Japan; [2]Toshiba medical systems corporation, Bunkyo-ku, Tokyo, Japan

We evaluated a method that permits acquisition of high-resolution images during free breathing using real-time motion correction.This method can be performed with a high success rate in patients who have difficulty holding their breath and with accuratrly assessing the extent and stage of infarcted regions.

1187. *In Vivo* Risk Zone Assessment in the Rat at 1.5T Using Manganese Enhanced Magnetic Resonance Imaging (MEMRI)

Jean-Luc Daire[1], Jean-Noel Hyacinthe[1], Idil Gunes Tatar[1], Karin Montet-Abou[1], Marko Ivancevic[1], Manu Costa-Jorge M[1], Denis Morel[1], Jean-Paul Vallée[1]

[1]University Hospital of Geneva, Geneva, Switzerland

We examined the feasibility in manganese-enhanced MRI (MEMRI) of the risk zone assessment in the rat, based on a MnCl2 injection during and 6 hours after a coronary artery occlusion model at 1.5T. A clear deficit of enhancement was observed in all cases with a high correlation with the risk zone depict by methylene blue technique for group who received MnCl2 during occlusion and the infarct size measured by TTC for animals injected after occlusion. This work demonstrates the potential of MEMRI to assess the risk zone and not only the infarct area in rat at 1.5T.

1188. Delineation of Ischemically Injured Myocardium on T1 Weighted MRI After Intravenous Injection of SHU555A

Gabriele Anja Krombach[1], Yavuz Temur[1], Miriam Dehles[1], Rolf W. Günther[1], Arno Bücker[1]
[1]University Hospital Aachen, Aachen, NRW, Germany

The SPIO SHU555A was intravenously injected in 7 pigs with acute reperfused myocardial infarction. T1 values of left ventricular blood, ischemically injured and remote myocardium were repeatedly measured over an observation period of 3 hours. The T1 value of ischemically injured myocardium gradually decreases from 875 ± 61 ms to 588 ± 54 ms (remote myocardium 787 ± 31 ms prior injection and 759 ± 22 ms, 3 hours after injection of SHU 555A). ANOVA showed a significant difference of regional T1 for remote myocardium and infarcted myocardium, starting 60 min after injection of SHU555A. SHU555A has the potential for delineating the spatial extent of ischemically injured myocardium stably over a time period of at least two hours.

1189. Dynamic Distribution of Extracellular and Blood-Pool Contrast Agents in Acutely Infarcted Myocardium

Jian Wang[1, 2], Gang Li[1], Bo Xiang[1], Macro Gruwel[1], Jixian Deng[1], Hongyu Liu[2], Mike Jackson[1], Roxanne Deslauriers[1], Ganghong Tian[1]
[1]Institute for Biodiagnostics, National Research Council, Winnipeg, Manitoba, Canada; [2]the Fourth Affiliated Hospital, Harbin Medical University, Harbin, People's Republic of China

The present study was to assess distribution characteristics of extracellular and blood-pool contrast agents in acutely-infarcted myocardium. Gd-DTPA and Vistarem were chosen as a representative for the extracellular and blood-pool contrast agent, respectively. It was found that Gd-DTPA rapidly entered infarct and normal myocardium and reached its maximum distribution coefficient in the two regions in a short period. In contrast, Vistarem entered infarct and normal myocardium with much slower rates. It took more than 10 minutes for Vistarem to show different distribution coefficients between the two regions. The results suggest that both types of contrast agents could differentiate viable from nonviable myocardium. However, it requires a longer period for a blood-pool contrast agent to reach its maximum distribution co-efficient.

1190. Cardiac Function and Infarct Size Assessment in the Rat at 1.5T

Jean-Luc Daire[1], Karin Montet-Abou[1], Jean-Noel Hyacinthe[1], Idil Gunes Tatar[1], Marko Ivancevic[1], Manu Costa-Jorge M[1], Michèle Brunet[1], Denis Morel[1], Jean-Paul Vallee[1]
[1]University Hospital of Geneva, Geneva, Switzerland

The aim of this work is to demonstrate in a coronary artery occlusion model the feasibility of cardiac function imaging and infarct size assessment in rat on a 1.5T clinical MR system. Based on MR cine imaging and delayed enhancement, 7 rats were imaged at days 0, 2 and 9 after occlusion. MR imaging allowed to well describe infarct area and cardiac function in all cases with a good correlation with histological experiments. We also observed a natural partial recovery of heart function by an increase of global and local contraction.

1191. Positive Enhancement of Microvascular Obstruction in Reperfused Acute Myocardial Infarction Using T1 Prep Look-Locker Sequence: A Short Time-Course Study

Yuesong Yang[1], Warren D. Foltz[1, 2], John J. Graham[1], Jay Detsky[1], Alexander J. Dick[1], Graham A. Wright[1]
[1]Sunnybrook and Women's College Health Sciences Centre, Toronto, Ontario, Canada; [2]St.Michael Hospital, Toronto, Ontario, Canada

DE-MRI has been used for the determination of myocardial viability and can delineate the extent of myocardial infarction as a positive contrast. However, negative contrast can result from microvascular obstruction (MO) that is a strong unfavorable predictor for clinical outcome in these patients. A noninvasive MRI technique with positive enhancement of MO will improve the identification of MO, and thus would have value in MRI evaluation in patients with AMI. This study investigates a T1 prep acquisition during a Gd-DTPA infusion for the positive enhancement of MO in a porcine model of reperfused AMI and demonstrates its early time course.

1192. Assessment of Myocardial Infarction in Mice by Contrast-Enhanced MR Imaging Using an Inversion Recovery Pulse Sequence at 9.4T

Catherine Chapon[1], Amy Herlihy[1], Kishore Bhakoo[1]
[1]Hammersmith Hospital, Imperial College, London, London, UK

In order to accurately assess myocardial infarction in mice, delayed-enhancement imaging using an inversion recovery (IR) pulse sequence was used at 9.4T. Two days post-infarction, magnetization-prepared FLASH was performed prior to and following Gd-DOTA administration to determine the optimal inversion time (TI) for myocardial infarction IR imaging. At the optimal TI, the contrast-to-noise ratio between infarcted and normal myocardium was maximal leading to an accurate definition of infarct area. Therefore, an IR delayed enhancement can be performed to assess myocardial infarction in small animals despite of the rapid heart rate and increased longitudinal relaxation times at 9.4T.

1193. In-Vivo Cardiac IRON Imaging of MR Fluoroscopically Delivered Mesenchymal Stem Cells

Matthias Stuber[1], Wesley D. Gilson[1], Saurabh Shah[1], Dorota Kedziorek[1], Jeff W.M. Bulte[1], Dara L. Kraitchman[1]
[1]Johns Hopkins University, Baltimore, Maryland, USA

The use of superparamagnetic particles has shown great promise for cardiac stem cell research. However, competing sources of negative contrast and constant intrinsic and extrinsic myocardial motion adversely affect the interrogation of iron-labeled stem cells that are injected into the myocardium. For these reasons, we have developed a motion-suppressed 1.5T and 3T imaging sequence that enables hyperintense *in vivo* visualization of iron labeled stem cells.

Cardiomyopathy and Heart Structure

Room 4E Monday 14:00 - 16:00

1194. Quantification of Myocardial Lipid Using a Breath Hold Multiecho Technique at 3.0 Tesla

Declan Patrick O'Regan[1], Martina F. Callaghan[1], Stephan A. Schmitz[1], Rossi P. Naoumova[1], Julie Fitzpatrick[1], Joanna Allsop[1], Joseph V. Hajnal[1]
[1]Hammersmith Hospital, Imperial College, London, UK

The accumulation of lipid within the myocardium is associated with impairment of both systolic and diastolic function in animal models. A black blood cardiac-triggered gradient echo sequence was designed to acquire five echoes during a single breath-hold on a 3.0 tesla MRI system. The echo times were chosen such that fat and water resonances were either in-phase or out-of-phase with respect to each other. Images were acquired of lipid emulsion phantoms and in both volunteers and patients. A curve fitting model was used to derive the relative fat and water content of myocardium.

1195. Quantification of Cardiac Fat Volume in Humans Using 3D SSFP Imaging

Thanh D. Nguyen[1], Pascal Spincemaille[1], Martin R. Prince[1], Yi Wang[1]
[1]Weill Medical College of Cornell University, New York, New York, USA

Cardiac fat signal has been used successfully for measuring bulk cardiac motion. The accuracy of this novel approach depends upon the amount of fat within and around the heart. Currently, quantitative description of the human cardiac fat is lacking. The objective of this study is to estimate the cardiac fat volume using a fast 3D fat-selective pulse sequence. Our preliminary data show that the cardiac fat volume is substantial (115 ± 52 ml, or 11 ± 3% of the heart volume, n = 5).

1196. Early Murine Embryonic Cardiac Hypertrophy Associated with Increased Ganglioside Storage

Lingyun Hu[1], Yingying Sun[1], Dibya Sen[1], Sarah H. Shahmoradian[1], Robia G. Pautler[1]
[1]Baylor College of Medicine, Houston, Texas, USA

In this study, MRI was utilized to evaluate the role of ganglioside, GM2, in the embryonic cardiac development in a mouse model of Sandhoff's disease.

1197. MRI Assessment of a Novel Mouse Model of Hypertrophic Cardiomyopathy

Sarah Heloko Shahmoradian[1], Lingyun Hu[1], Yingying Sun[1], Doug Mann[1], Robia G. Pautler[1]
[1]Baylor College of Medicine, Houston, Texas, USA

In this study, MRI was used to characterize for the very first time the cardiac physiology and anatomy of the hexosamidase B knockout mouse (hexB-/-), a mouse model of Sandhoff's disease, The stroke volume and total heart muscle thickness of hexB-/- and control mice were compared at 6-8 weeks of age as well as at 15 – 19 weeks, just prior to the age when the hexB-/- mice typically perish.

1198. No Evidence for Iron Overload in the Heart of Multitransfused Elderly Patients with Sideroblastic Anemia (RARS): A Quantitative T2* Weighted MRI Study

Eli Konen[1], Tammar Kushnir[1], Asher Winder[2], Yael Eshet[1], Merav Leiba[1], Eliezer Rachmilewitz[2]
[1]The Chaim Sheba Medical Center, Tel Hashomer, Israel; [2]Wolfson Medical Center, Holon, Israel

Iron overload is a known complication in multitransfused patients with MDS, contributing to morbidity and mortality. Studies in thalassemia demonstrated no correlation between iron levels in liver and heart. The purpose of this study was to use quantitative, noninvasive, T2* weighted MRI to evaluate the degree of iron overload in the heart and liver of transfused patients with the sideroblastic form of MDS. Our results suggest that iron accumulation in these patients is primarily in the liver and not in the heart. Thus, the mechanism of iron deposition in the heart seems to be different in different anemias.

1199. A Mutual Information Approach to Automatic Detection of Heart Rejection in MRI

Hsun-Hsien Chang[1], José M-F Moura[1], Yijen L. Wu[1], Chien Ho[1]
[1]Carnegie Mellon University, Pittsburgh, Pennsylvania, USA

This paper develops an automatic algorithm to detect early rejection of transplanted hearts imaged by tagged MRI. We consider a mutual information based approach that compares the similarities of the regional motions between a test heart and a healthy one. Low mutual information means that the test regional motions are quite different from the healthy template and are classified as abnormal. The experiment shows good results of our algorithm.

1200. A Time-Based Study of Changes in T1 and T2 Components in Excised Rat Myocardium

Morten Bruvold[1], John Georg Seland[1], Sissel Skarra[1], Heidi Brurok[1], Per Jynge[1]
[1]Norwegian University of Science and Technology, Trondheim, Norway

Myocardial water is affected by different processes during ischemia. Cell swelling and contracture, alter distribution of myocardial water between the intracellular and extracellular compartments. This study aims to follow the progress of water redistribution by relaxographic measurements of multiple T1 and T2 components in excised rat myocardium. The use of T2-relaxography is promising in describing the status of ischemic progress and other processes altering the water distribution in biological tissue. Tissue-T1, influenced by the presence of ic Mn, could be used in combination with T2-relaxography to obtain information about equilibrium water exchange between ic and ec compartments during ischemic progress.

1201. MR Estimation of Myocardial Ferritin Iron and Hemosiderin Iron in Thalassemia Major

Christina Louise Tosti[1], Haiying Tang[2], Jens H. Jensen[3], Sujit Sheth[1], Srirama V. Swaminathan[1, 4], Kristi Hultman[1], Andjela Azabagic[1], Karen Altmann[1], Ashwin Prakash[1], Beth F. Printz[1], Anthony L. Brown[1], Allan J. Hordof[1], Nancy F. Olivieri[5], Gary M. Brittenham[1], Truman R. Brown[1]
[1]Columbia University, New York, New York, USA; [2]Merk Research Laboratories, Rahway, New Jersey, USA; [3]New York University School of Medicine, New York, New York, USA; [4]Philips Medical Systems, Cleveland, Ohio, USA; [5]University of Toronto, Toronto, Ontario, Canada

In this study we have used a multi-echo spin echo CPMG-like technique and a T2 quantification model to estimate the amount of hemosiderin iron and ferritin iron in the myocardial tissue of 13 patients with thalassemia major. We have found a strong correlation between our parameter related to the ferritin concentration and reduced echo shortening fraction. Our parameter related to the hemosiderin concentration is less correlated with the changes in heart function. These results suggest that ferritin is more closely related to cardiac dysfunction in thalassemia major.

1202. 4D Mouse Cardiac Isotropic Black-Blood Imaging for Phenotyping

Akiva Feintuch[1], Jonathan Bishop[1], Lorinda Davidson[1], Stuart S. Berr[2], Frederick H. Epstein[2], Brent A. French[2], Benoit G. Bruneau[1], R Mark Henkelman[1, 3]
[1]Hospital for Sick Children, Toronto, Ontario, Canada; [2]University of Virginia, Charlottesville, Virginia, USA; [3]University of Toronto, Toronto, Ontario, Canada

The mouse cardiac imaging environment differs from the human one in several factors. These include a much shorter cardiac cycle longer scan time possibilities and consequently less sensitivity to respiration. In that context, this study demonstrates how to perform 4D whole heart imaging which is optimized for segmentation and phenotyping analysis. A black-blood protocol is used for enhanced tissue-blood contrast combined with a MOTSA technique for full heart coverage. The effectiveness of this method is demonstrated on a mutant mouse.

1203. 3D MR Microscopy Rendering with Non-Uniformity Correction and a Non-Linear Adaptive Noise Filter for Studies of a Transgenic Mouse Heart Model of Myxomatous Valvular Disease

Jeff Frank Dunn[1], Nicholas W. Shworak[2], Siu C. Chan[1], Brian O'Brien[1], Jaret Hargreaves[1], Robert T. Palac[2], Jean Belding Fay[3], Dave Kirk[1], Tadeusz Foniok[4], J Ross Mitchell[1]
[1]University of Calgary, Calgary, AB, Canada; [2]Dartmouth Medical School, Hanover, New Hampshire, USA; [3]Dartmouth-Hitchcock Medical Center, Lebanon, New Hampshire, USA; [4]National Research Council, Calgary, AB, Canada

3D MR microscopy was used to image isolated hearts to study myxomatous valvular disease (MVD) in a unique transgenic mouse. Valve damage was confirmed *in vivo* with echocardiography. 3D gradient echo MRI was undertaken at 9.4T in gadolinium enhancement to obtain pixel resolution of 50x50x78µm. Significant post-processing was undertaken with novel 3D rendering software that has such efficiency improvements to allow it to operate interactively on a desktop computer. Processing included non-uniformity correction and a non-linear adaptive noise filter. Images are shown of surface rendering and of mitral valves of mouse hearts.

1204. 3T Ex-Vivo High Angular Diffusion Tensor Imaging of the Heart

Steven Dymarkowski[1], Caroline Sage[1], Ronald Peeters[1], Jan D'hooge[1], Piet Claus[1], Frank Rademakers[1], Jan Bogaert[1], Stefan Sunaert[1]
[1]University Hospital of the Catholic University of Leuven, Leuven, Belgium

The ventricular myocardium has a complex spatial organization, with muscle fiber orientation varying as a function of transmural location. Diffusion tensor imaging (DTI) may be used to measure this fiber orientation. High angular DTI in an acquisition time of less than 50 minutes and analysis with fiber tractography shows that the mid-wall fibers are mostly oriented concentrically, while epi- and endocardial muscle fiber orientation is mostly diagonal, consistent with known histology. A high angular configuration map reveals that the muscle fibers of the mid-wall cardiac tissue have predominantly a single orientation, while endo- and epicardial fibers have crossing diagonal fibers.

1205. Self-Gated, Reduced Field-Of-View Diffusion Tensor Imaging of the Human Heart at 3.0T

Urs Gamper[1], Sebastian Kozerke[1], Peter Boesiger[1]
[1]University and ETH Zurich, Zurich, Switzerland

Cardiac diffusion imaging in the *in vivo* heart is hampered by cardiac bulk motion, respiratory motion, chemical shift and susceptibility gradients around the heart. In this work a combined approach to diffusion imaging of the heart is presented employing motion-compensated diffusion encoding gradients with single-shot echo-planar imaging at 3T. Computer simulations were used to study phase dispersion from realistic cardiac bulk motion in the presence of bipolar diffusion encoding gradients to derive optimal sequence timing parameters. In-vivo data in short-axis view orientation were obtained during free-breathing. Results reveal known myocardial muscle fiber structure.

1206. Examination of the Effects of Myocardial Hypertrophy on Myocardial Microvascular Volume and Blood Oxygenation

Jeffrey M. Dendy[1, 2], Cynthia B. Paschal, [12], John C. Gore, [12]
[1]Vanderbilt University Hospital, Nashville, Tennessee, USA; [2]Vanderbilt University, Nashville, Tennessee, USA

We examine the effects of myocardial hypertrophy on myocardial microvascular volume and blood oxygenation level changes using iron oxide nanoparticles and adenosine. By measuring the changes in R2* at baseline and with the administration of adenosine, and repeating the measurements in the presence of the intravascular iron oxide contrast agent, blood volume maps and blood oxygenation maps were developed. R2* maps with and without adenosine, before and after the administration of monocrystalline iron oxide nanoparticle were calculated in healthy rats and rats with drug-induced myocardial hypertrophy. The method demonstrated a decrease in response of hypertrophic myocardium to adenosine.

Cardiac Post Processing

Room 4E Monday 14:00 - 16:00

1207. Automated Registration of Multiple Single Breath-Hold Cardiac MRI Images

Piotr J. Slomka[1], David Fieno[1], Vaibhav Goyal[1], Hidetaka Nishina[1], Tejas Mehta[1], Louise Thomson[1], Amit Ramesh[1], James Gerlach[1], Daniel S. Berman[1], Guido Germano[1]
[1]Cedars-Sinai Medical Center, Los Angeles, California, USA

Cine cardiac MRI (cMRI) images are typically acquired as multiple slices with one slice position and/or orientation per breath-hold. These multiple images are often misaligned due to patient motion. We developed a novel image processing technique, which allows registering multi breath-hold short-axis (SA), 2-chamber (2CH), and 4-chamber (4CH) cMRI views into common 3D spatial coordinates. Studies from 20 consecutive patients (10 males, 10 females) undergoing cMRI exams, with 2CH, 4CH, and SA cine (20 phases), each acquired in separate breath-holds, with pixel size 1.3-1.8 mm were analyzed retrospectively. 2CH, 4CH and SA image planes were brought into common 3D coordinates by dynamic profile registration technique. The overall accuracy of the automatic algorithm was 1.0±0.9 mm for the 2CH to 4CH registration, and 1.1±1.0 mm, 1.1±1.2 mm, and 2.0±1.8 mm for SA registration in midventricular, basal and apical regions respectively. The alignment algorithm can be used as a completely automated and accurate pre-processing step in the analysis of cMRI data reducing the spatial misregistration between planes acquired at different breath-holds and allowing integrated 3D spatial visualization of multiple planes.

1208. Registration of Short and Long-Axis Images in Cine Cardiac MRI

Tao Li[1], Thomas Stewart Denney[1]
[1]Auburn University, Auburn University, Alabama, USA

Cardiac MR images acquired over multiple breath-holds are often misregistered due to patient motion or inconsistent respiration. This misregistration must be corrected before performing three-dimensional analysis of wall geometry or other parameters. Existing registration methods address the issue of short-axis image registration, but long-axis images are needed to analyze the apex of the heart and can help register short-axis images. A new registration method is presented that uses myocardial contours identified in long-axis images to register short-axis images and short-axis contours to register long-axis images. The method is validated on simulated data and imaging studies from 15 human subjects.

1209. Retrospective CINE MRI of the Mouse Heart

Edwin Heijman[1], Wolter de Graaf[1], Claudia Diekmann[2], Arno Nauerth[2], Gustav J. Strijkers[1], Klaas Nicolay[3]
[1]Eindhoven University of Technology, Eindhoven, Netherlands; [2]Bruker BioSpin MRI GmbH, Ettlingen, Germany; [3], Eindhoven University of Technology, Eindhoven, Netherlands

We present a retrospective CINE FLASH sequence for mouse cardiac MRI, which uses a slice refocusing signal to derive heart as well as respiratory cycles retrospectively. The method was compared to traditional triggered and gated CINE FLASH. The retrospective CINE MRI sequence showed an excellent steady state signal behavior in the myocardial wall compared to the traditional methods but had a lower SNR. The measured heart and respiration rates showed an excellent match with the values extracted from the retrospective reconstruction program. The CINE FLASH images generated by the retrospective method were essentially free of motion artifacts.

1210. Cardiac Function by SSFP MRI: Accuracy of Measurement of Left Ventricular Ejection Fraction Per Slice Number and Location

Roya Saleh[1], Carissa G. Fonseca[2], Vibhas Deshpande[3], Kambiz Nael[4], Gerhard Laub[5], John Paul Finn[1]

[1]David Geffen School of Medicine at UCLA, Los Angeles, California, USA; [2]David Geffen School of Medicine, los angeles, California, USA; [3]Siemens Medical Solutions, los Angeles, California, USA; [4]David Geffen School of medicine at UCLA, Los Angeles, California, USA; [5]Siemens Medical Solutions, Los Angeles, California, USA

Contouring of the left ventricular myocardium, on cardiac MR images, in order to measure ejection fraction can be a time-consuming and tedious process as there are often 6 or more short-axis image planes per data-set. We have found that contouring of as few as 2 representative short-axis slices generates a value for ejection fraction that is comparable to the value obtained by contouring 6 slices equally spaced from base to apex. This approach greatly reduced the analysis time, and may prove highly practical and time-saving in patients without marked regional variations in ejection fraction.

1211. Automatic Computation of Ejection Fraction Using Spatio-Temporal Information

Amol S. Pednekar[1, 2], Raja Muthupillai, [23], Benjamin Cheong[2], Scott D. Flamm[2]

[1]Philips Medical Systems, Bothell, Washington, USA; [2]St. Luke's Episcopal Hospital and Texas Heart Institute, Houston, Texas, USA; [3]Philips Medical Systems, Cleveland, Ohio, USA

The current clinical practice of manually tracing the endocardium to compute the left ventricular (LV) ejection fraction (EF) from cine-magnetic resonance images (cine-MRI) is labor intensive, time consuming, and operator dependent. We used spatio-temporal information in the cine-MRI to automatically estimate the EF in 64 subjects (21 volunteers, and 43 patients). This entirely data-driven, multi-step approach incorporates apriori geometric information from the acquisition and spatial-temporal information intrinsic to cardiac cine-MRI. The results show that the mean bias values determined by Bland-Altman analysis for end-diastolic and end-systolic volumes and hence for EF are in close agreement with inter- and intra-observer variability.

1212. Assessment of Cardiac Function with a Three-Dimensional Shape Model Based on Surface Harmonics

Julien Sénégas[1], Paul Martin Bansmann[2], Alexander Stork[2], Gerhard Adam[2], Henrik Thoms[3]

[1]Philips Research, Hamburg, Germany; [2]University Hospital Eppendorf, Hamburg, Germany; [3]Bauhaus University, Weimar, Germany

A new, three-dimensional model of the cardiac ventricles is proposed. It relies on a description with surface harmonics in a prolate spheroidal coordinate system. We show how the standard method, which applies only to closed, star-shaped surfaces, can be extended to model open surfaces as well as the non star-shaped right-ventricle. This shape model allows to perform a functional analysis on the basis of both short-axis and long-axis cine acquisitions. Different volume computation methods obtained with the proposed model are presented and compared to the traditional Simpson's rule. The advantages of combining slices with different orientations are discussed.

1213. Optimization of Contour Detection in Cardiac MRI Using Active Appearance Models: Definition of the Training Set

emmanuelle Angelié[1], Sophia F.I. Matzken[1], Boudewijn P.F. Lelieveldt[1], Rob J. van der Geest[1], J H.C. Reiber[1]

[1]LUMC, Leiden, Netherlands

Active appearance models (AAMs) have been successfully used for image segmentation in cardiac MR (1). But its availability in clinical routine remains still low. This work aims at defining the optimal training set used in the AAM to bring it closer to the clinical routine: The minimal number of images to be included and the characteristics of the images were our focuses. We concluded that a minimal number of 150 images (mixture of 80% normal and 20% pathological) should define the training set.

1214. Comparison of Echocardiography and MRI for Measuring Left Ventricular Mass in the Rat

Chris McCabe[1], Willy Gsell[1], Lindsay Gallagher[1], Jim Mullin[1], Kirsten Gilday[1], Delyth Graham[1], Elisabeth Beattie[1], Anna Dominiczak[1], Iseabail Mhairi Macrae[1], Barrie Condon[1]

[1]Glasgow University, Glasgow, Lanarkshire, UK

The aim of the present study was to evaluate the use of MRI for measuring left ventricular (LV) mass and to compare this with the most commonly used technique in animals: echocardiography. We found multi slice MRI analysis of LV mass correlated well with post mortem LV mass values while both single slice MRI and echocardiography resulted in a significant overestimation of LV mass. Single slice MRI gave significantly higher ejection fraction (EF) values compared to multi slice MRI analysis of EF. Further studies are required to establish whether such overestimations impact on echocardiography's sensitivity to detect changes with disease.

1215. MR-Guided Evaluation of Post-Infarction Ventricular Tachycardia

Hiroshi Ashikaga[1], Bruce Hopenfeld[1], Elliot R. McVeigh[1]

[1]National Heart, Lung and Blood Institute, Bethesda, Maryland, USA

Fatal ventricular tachycardia (VT) can be prevented by catheter-based radiofrequency ablation of myocardial scar, but the procedure can be technically challenging, because it is guided only by electrophysiological parameters within the ventricles. We have developed a technique to merge MR-derived geometrical data of the myocardial scar with the electrophysiological information so detailed scar geometry help predict the foci of reentry circuits. This MR-guided visualization technique can help localize the reentry VT circuit with reference to the 3-D scar geometry.

1216. PTAGs: Partial K-Space Tagging Combined with SSFP

Vinay Manjunath Pai[1]
[1]New York University, New York, New York, USA

While myocardial tagging is an established approach for evaluating cardiac wall function, its practical application has been hindered by various issues. Some of the difficulties have included segmenting of epicardial and endocardial contours, and loss of information from early systolic phases when SSFP-based sequences are used. We present a partial tagging approach which may be useful in alleviating these problems. In this approach, a multi-echo SSFP tagging sequence is acquired in such a way that the central k-space region is untagged. This provides untagged and tagged cine datasets simultaneously, and eliminates transition artifacts typically observed in early systolic phases.

1217. Automated Adaptive Analysis of Tagged Magnetic Resonance Images of the Mouse Heart

Evren U. Azeloglu[1]*, Haiying Tang*[2,3]*, Richard K. Chen*[3]*, Hina W. Chaudhry*[3]*, Ed X. Wu*[4]*, Glenn R. Gaudette*[5]*, Kevin D. Costa*[1]
[1]Columbia University, New York, New York, USA; [2]Merck Rearch Laboratories, Rahway, New Jersey, USA; [3]Columbia University College of Physicians & Surgeons, New York, New York, USA; [4]The University of Hong Kong, Hong Kong SAR, People's Republic of China; [5]UMass Medical School, Worcester, Massachusetts, USA

The full potential of tagged MRI of the mouse heart for non-invasive evaluation of cardiac mechanics in transgenic animals has not been realized due to excessive user involvement with available image processing algorithms. Therefore, we developed an automated, rapid, high-resolution analysis technique, called High Density Mapping (HDM), that uses spectral correlation to efficiently quantify regional wall deformation, does not entail tracking of individual tags, and involves minimal user interaction. HDM analysis distinguishes regional mechanics in healthy and infarcted mice within 2 minutes. This new method may help promote the practical use of tagged MRI in mice and other species.

1218. Noise Suppression in Displacement Imaging Using an Adaptive Spatial Filter

Jean C. Honorio[1]*, Eric Bennett*[2]*, James Hahn*[1]*, Han Wen*[2]
[1]George Washington University, Washington, D.C., D.C., USA; [2]National Institutes of Health, Bethesda, Maryland, USA

In the recent development of rapid imaging techniques of myocardial wall motion such as cine-DENSE, noise in the displacement data needs to be reduced with spatial or temporal filtering. Spatial filtering is the choice in cases where the temporal resolution needs to be preserved, for example for characterizing contractile dyssynchrony. Standard low-pass filters blur anatomical boundaries and reduce transmural resolution. We designed a filter that adapts to the local wall contour and achieves the smoothing effect without loss of transmural resolution or blurring at the boundaries.

1219. Improving HARP Cardiac Strain Mapping Using Nonlinear Diffusion

Khaled Z. Abd-Elmoniem[1]*, Vijay Parthasarathy*[1]*, Jerry L. Prince*[1]
[1]Johns Hopkins University, Baltimore, Maryland, USA

In this work, we propose a smoothing method based on anisotropic diffusion that filters the HARP derivatives strictly within the myocardium without the need for prior segmentation. The information about tissue geometry and the strain distribution is used to restrict the smoothing to within the myocardium, thereby ensuring minimum distortion of the final strain map. Preliminary results demonstrate the ability of anisotropic diffusion to reduce artifacts and improve strain accuracy over existing methods.

1220. A Quantitative Comparison Between 2-Dimensional and 3-Dimensional Circumferential Strain in the Human Heart

Sandra R R Tecelão[1]*, Jaco J M Zwanenburg*[2]*, Joost P A Kuijer*[2]*, J T. Marcus*[2]
[1]University of Lisbon, Lisbon, Portugal; [2]VU University Medical Center, Amsterdam, Netherlands

The purpose of this study is to compare the 2D and 3D circumferential strain assessed with MR tagging. 6 healthy volunteers and 5 asymptomatic patients with left bundle-branch block were evaluated. The 2D and 3D timing and peaks of circumferential shortening were compared and the cross correlation was computed. No significant differences between these parameters were observed and high positive correlation coefficients were obtained. This study shows that there is no significant difference between 2D and 3D circumferential strain. Because the 2D strain computation is less time consuming, circumferential shortening should be measured using this approach.

1221. Myocardial Fiber Tracking Based on High Temporal Resolution Tissue Phase Mapping Data: Principles and Implications for Cardiac Fiber Structures

Bernd André Jung[1]*, Michael Markl*[1]*, Jürgen Hennig*[1]
[1]University Hospital, Freiburg, Germany

Information on the structure and dynamics of the muscle fibers in the human heart might provide significant insight into principles of the mechanics of ventricular contraction. Fiber orientation is inherently linked to cardiac wall motion, which can be measured with phase contrast MRI. This technique might be used to derive surrogate parameters describing the fiber structure of the left ventricle. High temporal resolution phase contrast measurements were performed during free-breathing. Based on the assumption that accelerations are related to the forces generated by the muscle fibers, a postprocessing evaluation with a tracking algorithm for acceleration fields derived from the velocity data was applied to different cardiac frames.

1222. Study of Myocardial Fiber Length Distribution with Diffusion Tensor MRI

Yin Wu[1], Haiying Tang[2], M. C. Ng[1], Jian Yang[1], H. F. Tse[1], C. P. Lau[1], E. S. Yang[1], E. X. Wu[1]
[1]The University of Hong Kong, Hong Kong, People's Republic of China; [2]Merck Research Laboratories, Rahway, New Jersey, USA

Diffusion tensor MRI (DTI) is a nondestructive method to map myocardial fiber organization. Many studies have been done on myocardial fiber orientation. However, cardiac contraction is also related with myocardial fiber length, but its study is limited so far. The current study aims to provide information of myocardial fiber length distribution in formalin-fixed porcine heart samples. DTI with medium diffusion resolution (15 directions) was performed. Fiber length distribution as a function of fiber helix angle was investigated in multiple short-axis slices located from base to apex of the left ventricles. Results show that longer fibers likely run circumferentially, and fibers located at middle and upper ventricle are generally longer than those near apex. The results provide supplementary structural information on myocardial fiber architecture and cardiac mechanics.

1223. Segmentation Based Registration of Myocardium in Cardiac Perfusion Images

Ganesh Adluru[1], Edward VR DiBella[1]
[1]University of Utah, Salt Lake City, Utah, USA

Registration and segmentation of myocardial perfusion images are important steps to extract qualitative and quantitative information. The two steps can be used to improve each other. We propose a method to achieve accurate registration of myocardium which uses a level set segmentation method to improve registration. A coarse registration is first performed to aid the automatic segmentation of the left ventricular blood pool and the segmentation is then used to improve the registration of the left ventricular myocardium. The method is tested on cardiac data and compares well with manual registration.

Diffusion Weighted Imaging of the Abdomen

Room 4E Monday 14:00 - 16:00

1224. Low B-Value Diffusion Weighted Imaging in the Evaluation of Hepatic Metastases from Neuroendocrine Tumor

David W. Stanley[1], James F. Glockner[2], Naoki Takahashi[2], Steven L. Williams[2]
[1]GE Healthcare, Proctor, Minnesota, USA; [2]Mayo Clinic, Rochester, Minnesota, USA

Patients with liver metastases from neuroendocrine tumors were evaluated with MRI using DWI, FSE, and dynamic contrast enhanced LAVA. DWI had superior lesion conspicuity compared with FSE and CE-LAVA, although it also had lower scores for perceived SNR, and degree of image artifacts. The preferred sequence was CE-LAVA in 13/28 cases, DWI in 10/28 cases and FSE in 5/28 cases.

1225. Evaluation of Cirrhosis and Chronic Hepatitis with Diffusion Weighted Imaging and ADC Measurements

Xinhao Cynthia Fan[1], Hero K. Hussain[1], Vikas Gulani[1], Saroja Adusumilli[1], Jorge A. Marrero[1], Thomas L. Chenevert[1]
[1]University of Michigan, Ann Arbor, Michigan, USA

Diffusion-weighted imaging and ADC values were obtained for 19 cases of cirrhotic livers, 4 cases of chronic hepatitis and 11 cases of normal livers (b=0 and 500 sec/mm2). In comparison with that of normal livers, ADC value is significantly decreased for cirrhosis and mildly decreased for chronic hepatitis.

1226. Diffusion-Weighted MR Imaging of Hepatocellular Carcinoma with Single-Shot Echo-Planar Imaging : Assessment of Early Response to Transcather Arterial Chemotherapy Embolism(TACE)

Wu Bin[1], Peng Weijun[1]
[1]Cancer Hospital, Shanghai, People's Republic of China

Diffusion-weighted magnetic resonance imaging (DWMRI) enables noninvasive characterization of tissue biology on the basis of their water diffusion properties. DWMRI should be sensitive to reveal several physiologic and morphologic characteristics of tissue associated with the slow or fast diffusion of water molecules. These characteristics include cell density and tissue viability, as well as changes in tissue in response to various treatments. In this work, we explore to study the feasibility of using DWMRI with breath-hold for upper abdominal organ like liver and to evaluate the use of DWIMRI for early assessment of hepatocelluar carcinoma(HCC) response to transcather arterial chemoembolism (TACE)

1227. Diffusion-Weighted MRI for Determination of Hepatocellular Carcinoma Response to Yttrium-90 Radioembolization

Jie Deng[1], Frank H. Miller[1], Thomas K. Rhee[1], Kent T. Sato[1], Mary F. Mulcahy[1], Riad Salem[1], Reed A. Omary[1], Andrew C. Larson[1]

[1]Northwestern University, Chicago, Illinois, USA

Hepatocellular carcinoma (HCC) is the fourth leading cause of cancer death in the United States. Yttrium-90 radioembolization is an emerging HCC treatment that delivers internal radiation to lesions via catheter-directed intra-arterial administration of 90Y microspheres. Early, non-invasive, biomarkers for predicting response to 90Y therapy could greatly benefit HCC patients. Tumor size changes are the traditional criteria used to non-invasively assess HCC response, but may not correlate with therapeutic efficacy. Recent studies have demonstrated that quantitative diffusion-weighted MRI (DW-MRI) may provide sensitive clinical biomarkers for the early stratification of therapy response in brain tumors and breast metastases. However, no studies have validated DW-MRI detection of water mobility changes in HCC tissue after 90Y radioembolization. The purpose of this study was to test the hypothesis that DW-MRI can detect increased water diffusion secondary to HCC tissue alteration following 90Y therapy.

1228. Utility of Diffusion Weighted MRI in Patients Undergoing Locoregional Treatment of Malignant Liver Tumours

Sudhakar Kundapur Venkatesh[1], Shih Chang Wang[1], Gabriel Lau[1], Fiona Leung[1]

[1]National University Hospital, Singapore, Singapore

Hepatic tumors treated with either chemoembolisation or RFA were studied with DWI. ADC maps may depict tumor necrosis better than T1 and T2W imaging

1229. Study of a Diffusion-Weighted Single-Shot Spin Echo Echo Planar Imaging Sequence Using Parallel Imaging of Focal Liver Lesions: Comparison with a T2-Weighted Turbo Spin Echo Technique

Kenneth Coenegrachts[1], Joost Delanote[1], Leon ter Beek[2], Marc Haspeslagh[1], Shandra Bipat[3], Jaap Stoker[3], Luc Steyaert[1], Hans Rigauts[1], Jan Walther Casselman[1]

[1]AZ St.-Jan AV, Bruges, West-Flandres, Belgium; [2]Philips Medical Systems, Best, Netherlands; [3]Academic Medical Center, Amsterdam, Netherlands

To compare diffusion-weighted Single-Shot Spin Echo Echo Planar Imaging (SS SE-EPI DWI) with T2-weighted Turbo Spin Echo (T2w TSE) in detecting focal liver lesions (focus on small (< 10mm) lesions). Twenty-four patients suspected for malignant liver lesions underwent the above mentioned sequences. The T2w TSE and SS SE-EPI DWI with b-values 0, 20, 300 and 800 s/mm2 were compared. Biliary cysts were best ($p < 0.05$) detected with T2w TSE and hemangiomas and metastases were best ($p < 0.05$) detected with SS SE-EPI DWI with b=20 s/mm2. SS SE-EPI DWI using low b-values seems useful in detecting focal liver lesions.

1230. Free-Breathing and High B-Value Diffusion-Weighted MR Images of Hepatic Cavernous Hemangiomas

Mayumi Takeuchi[1], Kenji Matsuzaki[1], Hitoshi Kubo[1], Masafumi Harada[1], Hiromu Nishitani[1]

[1]Univ. of Tokushima, Tokushima, Japan

We evaluated hepatic hemangiomas by free-breathing and high b-value DWI, and corresponding isotropic ADC maps to differentiate hemangiomas from cysts. Forty-five hemangiomas and forty-five cysts were evaluated. Forty-one hemangiomas (91%) showed high signal intensity, whereas all forty-five cysts showed iso to low signal intensity on DWI. The ADCs were 1.94 +/- 0.45 in hemangiomas, and 3.32 +/- 0.44 in cysts ($0.0001 > p$). DWI may be useful for the diagnosis of hemangiomas in differentiation from cysts without the administration of contrast medium. The ADC values may be helpful for the diagnosis of hemangiomas which do not show high signal intensity on DWI.

1231. Physiological Changes of Liver ADC Values During Cardiac Cycle Using DW-EPI

Masahiro Umeda[1], Chuzo Tanaka[1], Toshihiro Higuchi[1], Yasuharu Watanabe[2], Makoto Kitamura[1], Ichio Aoki[1], Shoji Naruse[3]

[1]Meiji University of Oriental Medicine, Nantan-shi, Kyoto, Japan; [2]Meiji School of Oriental Medicine, Suita-shi, Osaka, Japan; [3]Kyoto Prefectural University of Medicine, Kyoto-shi, Kyoto, Japan

DWI with low b in X direction using single shot EPI was performed for the liver. The signal change of the left lobe was found to be dependent on the cardiac phase. The signal of the left lobe in DWI was decreased during the diastole. Cine mode gradient echo MRI showed that in this period the cardiac muscle exerts pressure on the left liver lobe and deforms it. This signal decrease might be driven from that tissue water, which was moved incoherently during the application of the MPG. This effect is important for the correct ADC measurement of the liver.

1232. Detailed Diffusion Measurements of the Liver and Spleen Over Extended B-Factor Ranges

Hiroshi Shinmoto[1], Koichi Oshio[1], Akihiro Tanimoto[1], Nobuya Higuchi[1], Shigeo Okuda[1], Sachio Kuribayashi[1], Robert V. Mulkern[2]

[1]Keio University School of Medicine, Tokyo, Japan; [2]Children's Hospital, Harvard Medical School, Boston, Massachusetts, USA

We have made detailed diffusion measurements of the liver and spleen using multiple b-factors ranging up to 4000 s/mm^2. The signal decay versus b-factor over the extended range demonstrates a biexponential in both organs. The fast diffusion coefficients for the liver and spleen were 1.76}0.41 and 1.50}0.36 x 10^{-3}mm^2/s, respectively. The slow diffusion coefficients for the liver and spleen were 0.39}0.14 and 0.31}0.11 x 10^{-3}mm^2/s, respectively. The clinical utility of the biexponential parameterization is unclear, though clearly offers new and unique information for tissue characterization in the liver and spleen.

1233. Evaluation of Lymph Nodes in the Abdomen and Pelvis of the Children Using Diffusion-Weighted MR Imaging

Hidekazu Seo[1], Takayuki Masui[1], Motoyuki Katayama[1], Kimihiko Sato[1], Masahiro Sugiyama[1], Atsushi Nozaki[2], Masaya Hirano[2]

[1]Seirei Hamamatsu General Hospital, Hamamatsu, Shizuoka, Japan; [2]General Electtric Yokogawa Medical Systems, Hino, Tokyo, Japan

We evaluated the usefulness of DWI with high b-value during free-breathing for recognizing lymph nodes and residual tumor in the abdomen and pelvis of the children. As a result, DWI is a sensitive technique for recognizing lymph nodes in children. It might be usefulness to obtain DWI taking a few minutes in addition to the conventional MR sequences without radiation exposure and contrast material for the purpose of the detection of lymph nodes.

1234. Diffusion Weighted Imaging in Native and Transplanted Human Kidneys at 3T. Initial Experience

Peter Vermathen[1], Ute Eisenberger[1], Chris Boesch[1], Harriet C. Thoeny[1]

[1]University & Inselspital, Berne, Switzerland

In this feasibility study diffusion-weighted imaging (DWI) was performed in native kidneys of nine healthy subjects and in two patients with transplanted kidneys using a 3T MR-scanner. One multiple breath-hold and one untriggered DWI measurement was performed in each subject. The study clearly demonstrates that DWI is feasible at 3T and provides reliable results. No substantial improvements for breath-hold scans versus untriggered acquisitions were detected. Currently, DWI at 3T of human kidneys does not provide better results than at 1.5T. Geometric distortions play a minor role, if parallel imaging is employed allowing for short TE times.

1235. Diffusion-Tensor MR Imaging of the Kidney at 3.0 and 1.5 Tesla

Aki Kido[1], Masako Kataoka[1], Akira Yamamoto[1], Yuji Nakamoto[1], Takashi Koyama[1], Yoji Maetani[1], Hiroyoshi Isoda[1], Shigeaki Umeoka[1], Ken Tamai[1], Nobuko Morisawa[1], Tsuneo Saga[1], Susumu Mori[2], Kaori Togashi[1]

[1]Kyoto University, Kyoto, Japan; [2]Johns Hopkins University, Baltimore, Maryland, USA

This study aimed to assess the feasibility of respiration-triggered diffusion tensor imaging (DTI) of the normal kidney and to compare the results obtained with 3.0T and 1.5T imagers. FA and ADC values in cortex and medulla of the kidney were evaluated. DTI of the kidney at 3T showed better contrast between cortex and medulla and smaller standard deviation than those obtained at 1.5T in both FA and ADC values. The FA and ADC values were almost equal between DTIs obtained by 3T and 1.5T and agree with those values reported previously.

Cartilage Techniques and Applications

Room 4E Monday 14:00 - 16:00

1236. Males Have Thicker Load-Bearing Patellofemoral Joint Cartilage Than Females

Christine Elizabeth Draper[1], Thor F. Besier[1], Gary S. Beaupre,[12], Scott L. Delp[1], Garry E. Gold[1]

[1]Stanford University, Stanford, California, USA; [2]VA Palo Alto Health Care System, Palo Alto, California, USA

Articular cartilage thickness affects cartilage stress during joint loading. *In vivo* measurements of cartilage thickness at the patellofemoral joint may help to understand normal and pathological joint mechanics. Since cartilage stress is higher in regions of joint contact, estimates of the cartilage thickness in these regions may be more relevant than previous thickness estimates. We defined regions of joint contact during knee flexion and used MR images to estimate the cartilage thickness of young, healthy males and females in these regions. We found that males had thicker load-bearing cartilage on the patella and anterior femur than females.

1237. Magnetic Resonance Imaging of the Transverse Ligament of the Atlas and the Alar Ligaments Using Ultrashort TE (UTE) Pulse Sequences

Michael Benjamin[1], Richard M. Znamirowski[2], Rhonda L. Turner[2], Mark Bydder[2], Tudor H. Hughes[2], Graeme M. Bydder[2]

[1]Cardiff University, Cardiff, Wales, UK; [2]University of California, San Diego, San Diego, California, USA

Ultrashort TE imaging was used to study the transverse ligament of the Atlas and the alar ligaments in 6 normal adult volunteers. High signal regions were identified in the transverse ligament posterior to the odontoid process and extending laterally. They were also seen at the attachments of the alar ligaments. The features are consistent with the presence of fibrocartilage in the ligaments as described in anatomical studies. The distribution of fibrocartilage reflects its function in resisting compression and shear force. Fibrocartilage is also an important antigenic target in rheumatoid arthritis and seronegative disease.

1238. Collagen Signal Enhancement Using a Fast Magic Echo

Kevin F. King[1]

[1]GE Healthcare, Waukesha, Wisconsin, USA

Collagen exhibits orientation-dependent signal amplitude and T2 due to residual dipolar coupling. A magic echo can be used to refocus dipolar coupling and increase signal amplitude and T2. Although its effectiveness has been demonstrated in 2D spin echo pulse sequences, the magic echo uses hard RF pulses and, for multislice imaging, is more suited for 3D pulse sequences. A magic echo was implemented in a 3D Fast Spin Echo sequence. T2-weighted images of phantoms and volunteers show the expected increase in collagen signal. Some increase in ghosting and blurring relative to a conventional 3D Fast Spin Echo is also observed.

1239. Relationship of Joint Space Width and Cartilage T2 Values in Subjects with Osteoarthritis

Matthew F. Koff[1], Kimberly K. Amrami[1], Kenton R. Kaufman[1]

[1]Mayo Clinic, Rochester, Minnesota, USA

Joint space width (JSW) is routinely measured to assess stage of osteoarthritis within diarthrodial joints. This study examined the relationship between patellar cartilage T2 values and patello-femoral JSW measurements. 113 subjects were enrolled in the study. T2 values of patellar cartilage were calculated from a series of T2 weighted images. A series of sagittal spiral fast SPGR images were acquired for patello-femoral JSW measurements. No correlation was found between T2 and JSW for combined and individual stages of patello-femoral OA. Measurement of patello-femoral JSW may not be used as a surrogate for patellar cartilage T2 values.

1240. An MR Microscopy Study Comparing Distal Interphalangeal Joint Arthropathy in Patients with Psoriatic Arthritis and Osteoarthritis

Steven Frederick Tanner[1], Ai-Lyn Tan[1], Andrew J. Grainger[2], Paul Emery[1], Dennis McGonagle[1]

[1]University of Leeds, Leeds, UK; [2]Leeds General Infirmary, Leeds, UK

MR microscopy techniques have been used to compare the distal interphalangeal joints in healthy volunteers and patients with psoriatic arthritis and osteoarthritis. The study has revealed more prominent inflammatory changes in psoriatic disease relative to those in osteoarthritis. Whilst these results are in accordance with the generally held views that psoriatic arthritis is primarily an inflammatory condition and osteoarthritis is associated with joint degeneration, there are some interesting parallels between these conditions. Our results show abnormalities in tendons and ligaments at clinical presentation in both conditions suggesting that biomechanical factors may affect the phenotypic expression of both diseases.

1241. High Resolution 3D T2-Weighted Imaging for Evaluation of Cartilage Lesions of the Knee

H. Glenn Reynolds[1], Hiroshi Yoshioka[2], Gesa Neumann[2], Philipp Lang[2]

[1]GE Healthcare, Milwuakee, Wisconsin, USA; [2]Brigham and Women's Hospital, Boston, Massachusetts, USA

Magnetic resonance imaging (MRI) is an excellent modality for non-invasive evaluation of cartilage lesions in knees. T2-weighted contrast with low to intermediate cartilage signal and high fluid signal is one of the primary methods to establish contrast in cartilage. Although several types of pulse sequences have been proposed for evaluating cartilage (1,2), the optimum sequence(s) has yet to be determined. The purpose of this study is to generate diagnostic-quality T2-weighted images with high spatial resolution at 3.0 Tesla, all within 10 minutes. We propose the use of the refocused SSFP echo to generate T2-weighted images for better delineation of cartilage and fluid in muscular-skeletal joints.

1242. Should Hip DGEMRIC Be Performed Early or Late After the Contrast Injection?

Carl Johan Tiderius[1], Rebecca Jessel[2], Young-Jo Kim[2], Deborah Burstein[1]

[1]Beth Israel Medical Center, Boston, Massachusetts, USA; [2]Children's Hospital, Boston, Massachusetts, USA

Eight asymptomatic volunteers and 4 patients with early OA were imaged with hip dGEMRIC at 30, 65, 100 and 135 minutes after IV Gd-DTPA2-injection. In asymptomatics, T1Gd continued to decline after 65 minutes, whereas T1Gd in patients was low already at 30 min and did not change over time. At all time-points, T1Gd was lower in the patients ($p<0.001$) with the greatest difference at 30 min due to the wash-in differential. dGEMRIC imaging of the hip at 30 min has the advantages of higher sensitivity and logistical ease, but potentially less specificity to GAG and a higher variability.

1243. 3D Surface Map Analysis of DGEMRIC Changes in the Knee

Jose Gerardo Tamez-Pena[1], Saara Totterman[1], A Williams[2], N Krishnan[2], C McKenzie[2], D Burstein[2]
[1]VirtualScopics, Rochester, New York, USA; [2]Beth Israel Deaconess Medical Center, Boston, Massachusetts, USA

3D rendering of cartilage was applied to 3D dGEMRIC images of the knee, and used to analyze data from five female marathon runners. Significant areas of the central medial condyle showed change in the dGEMRIC Index one day after running. After 1 week the affected area was reduced and six week after running the cartilage tissue returned to its pre-marathon stage. The 3D rendering techniques provide an analytical tool that can be exploited to measure changes in dGEMRIC over the full area of the joint cartilage, which may supplement the currently utilized 2D approaches to evaluate dGEMRIC changes.

1244. Mapping MR Parameters of Human Articular Cartilage Degeneration Using Magnetic Resonance Microscopy

Shadi F. Othman[1], Jessy Moinness[1], Jun Li[2], Huihui Xu[1], Carol Muehleman[2], Richard L. Magin[1]
[1]University of Illinois at Chicago, Chicago, Illinois, USA; [2]Rush University Medical Center, Chicago, Illinois, USA

Assessment of articular cartilage degeneration is an important step in the staging of joint disease. MRI could play a bigger role in diagnosis if we can better understand the relationship between cartilage structure, MR relaxation (T2) and water diffusion (ADC). In this study, we correlated the tissue structure in human cartilage at different stages of deterioration with the MR properties of each layer. The ADC and T2 relaxation time of normal cartilage are not constant within the cartilage, reflecting its colligative properties and water content. The ADC values increased in the cartilage with disease progression.

1245. Localized Cartilage Assessment with Three-Dimensional DGEMRIC and Quantitative MRI in Patients with Femoroacetabular Impingement

Derek C. Wilson[1], Burkhard Maedler[2], Donald S. Garbuz[1], Clive P. Duncan[1], Felix Eckstein[3], David R. Wilson[1]
[1]University of British Columbia and Vancouver Coastal Health Research Institute, Vancouver, BC, Canada; [2]Philips Medical Systems, Vancouver, BC, Canada; [3]Paracelsus Private Medical University, Salzburg, Austria

Femoroacetabular impingement (FAI), in which femoral deformities lead to localized damage of the labrum and/or cartilage, has been proposed as a mechanism explaining idiopathic osteoarthritis. To assess localized cartilage degeneration we performed qMRI and 3D-dGEMRIC scans on patients diagnosed with FAI and matched controls. Femoral and acetabular cartilage was segmented to determine cartilage volume and mean/maximum thickness. T1-maps were generated to show the localized glycosaminoglycan distribution within the hip cartilage. Lower cartilage volume was seen in symptomatic patients and regional variation was seen in the dGEMRIC index for all subjects. Our results show the feasibility of comprehensive morphological assessments for hip cartilage and justify making localized dGEMRIC measurements in pathologies such as FAI.

1246. $T_{1\rho}$ in Articular Cartilage and the Loss of Proteoglycans

Vladimir Mlynarik[1], [2], Pavol Szomolanyi[1], [3], Irene Sulzbacher[1], Siegfried Trattnig[1]
[1]Medical University of Vienna, Vienna, Austria; [2]Ecole Polytechnique Federale de Lausanne, Lausanne, Switzerland; [3]Slovak Academy of Sciences, Bratislava, Slovakia

T_2 and $T_{1\rho}$ relaxation maps of articular cartilage were obtained from patients undergoing total joint replacement and were compared with the corresponding histological slices stained with Safranin. Visual appearance of the T_2 and $T_{1\rho}$ maps was similar. No clear correlation between the $T_{1\rho}$ and concentration of proteoglycans was observed.

1247. Complications in the Quantification of GAG in Cartilage with $T_{1\rho}$ Imaging

Jeffrey James Luci[1], Bobby Gibbons[1], John C. Gore[1]
[1]Vanderbilt University, Nashville, Tennessee, USA

Data are presented that describe some complications of using $T_{1\rho}$ relaxometry for the quantification of GAG in cartilage. In vitro studies suggest that collagen has similar contributions to $R_{1\rho}$, and may confound the ability to infer GAG content in cartilage.

1248. Rigid Matching of Two 3D Patellae Data Sets for Voxel Based Comparison

José G. Raya[1], Robert Stahl[1], Thomas Mendlik[1], Olaf Dietrich[1], Maximilian F. Reiser[1], Christian Glaser[1]
[1]Ludwig Maximilian University of Munich, Munich, Germany

We demonstrate that a simple rigid matching is able to position corresponding MRI data sets in space so that short time comparisons of measurements can be made on a voxel basis with good accuracy. Reliability of the method was assessed both comparing repeated measurements on healthy volunteers and performing numerical simulations. A comparison of T2 relaxation times and cartilage thickness after matching showed a mean relative error of 11.9%. Simulations on mathematical patella models showed a good correlation of the calculated and exact positions.

1249. High Resolution 3D $T_{1\rho}$ MRI of Knee Joint at 3.0T with Parallel Imaging

Sait Kubilay Pakin[1], Conrado Cavalcanti[1], Renata La Rocca[1], Mark E. Schweitzer[1], Ravinder Reddy Regatte[1]
[1]New York University, School of Medicine, New York, New York, USA

We implemented and demonstrated high resolution 3D-$T_{1\rho}$ -mapping at 3.0T employing an 8-channel phased-array coil and parallel imaging (GRAPPA with acceleration factor 2). High resolution $T_{1\rho}$ images are acquired and high resolution 3D-$T_{1\rho}$ -maps are computed for both healthy subjects and OA patients by combining spin-lock imaging with GRAPPA. The capability of generating high resolution $T_{1\rho}$ maps shows promise for accurate localization of areas with elevated $T_{1\rho}$ values in early OA subjects and potential detailed follow-up.

1250. Rapid 3D-$T_{1\rho}$ Mapping of Knee Joint at 3.0T with Parallel Imaging

Sait Kubilay Pakin[1], Jian Xu[2], Mark E. Schweitzer[1], Ravinder Regatte[1]

[1]New York University, School of Medicine, New York, New York, USA; [2]Siemens Medical solutions Inc, New York, New York, USA

$T_{1\rho}$ -weighted MRI has been shown to be sensitive to early biochemical changes in cartilage. Total imaging time and RF energy deposition are two major concerns for implementing spin-lock techniques at high field strengths (3.0T). In this work, parallel imaging is utilized to provide solutions to these problems. The feasibility of 3D-$T_{1\rho}$ -weighted MRI of knee joint with parallel imaging (GRAPPA) is shown. The reproducibility of 3D-$T_{1\rho}$ maps as a function of acceleration factor (AF) in order to reduce the total imaging time and deposited RF energy is also demonstrated in phantom and *in vivo* studies.

1251. High Resolution 3D Cartilage Imaging of the Knee at 3T in Five Minutes Using IDEAL-SPGR and Parallel Imaging

David B. Siepmann[1], Jeffrey M. McGovern[2], Garry E. Gold[3], Jean H. Brittain[4], Scott B. Reeder[1]

[1]University of Wisconsin, Madison, Wisconsin, USA; [2]GE Healthcare, Waukesha, Wisconsin, USA; [3]Stanford University, Palo Alto, California, USA; [4]GE Healthcare, Madison, Wisconsin, USA

Traditionally, the gold standard for knee cartilage evaluation has been 3D SPGR with fat saturation. The IDEAL method (Iterative Decomposition of water and fat with Echo Asymmetry and Least-squares estimation) provides robust fat/water separation with greater SNR efficiency than fat saturation. This work combines IDEAL with parallel imaging at 3.0T to provide high resolution, high SNR cartilage imaging within five minutes. IDEAL demonstrated 31% higher patellar cartilage SNR ($p<0.05$) when compared to FS-SPGR with the same resolution and imaging time. Cartilage/Fluid contrast-to-noise resolution was 168% higher ($p<0.05$) for IDEAL-SPGR than for FS-SPGR.

1252. High Field MRI of Musculoskeletal System at 7.0T: SNR, Contrast and Relaxation Times

Sait Kubilay Pakin[1], Conrado Cavalcanti[1], Renata La Rocca[1], Charles Saylor[2], Bernd Stoeckel[3], Mark E. Schweitzer[1], Ravinder Reddy Regatte[1]

[1]New York University, School of Medicine, New York, New York, USA; [2]*In vivo* Corp., Gainesville, Florida, USA; [3]Siemens Medical solutions Inc, New York, New York, USA

SNR, contrast and relaxation times of the knee joint were measured at 7.0T using a whole body scanner. High resolution 3D-FLASH provides excellent contrast among various musculoskeletal tissues *in vivo*. This study demonstrated that there is ~35-45% increase in T1 when compared to 3T but no significant changes in T2 are observed. The T2 advantage can be exploited for improving spatial and temporal resolution especially for musculoskeletal system at 7T.

1253. Optimum Methods for the Preservation of Cartilage Samples in MR Microimaging Studies

Holly Corianda Canuto[1], Kenneth W. Fishbein[1], Preeti Bajaj[2], Nancy P. Camacho[3], Richard G. Spencer[1]

[1]National Institutes of Health, Baltimore, Maryland, USA; [2]Johns Hopkins University, Baltimore, Maryland, USA; [3]The Hospital for Special Surgery, New York, New York, USA

Multi-modality cartilage studies often require sample transportation between facilities and significant periods of storage in addition to lengthy MRI experimental times. We investigated four storage solutions and combinations of freezing and cold unfrozen storage to determine an optimal protocol to maintain cartilage homeostasis, reflected by biochemical and MRI-based matrix analyses over a 4 month period. Composition and parameters such as T2 and magnetization transfer rate were best maintained by storage of cartilage samples at 4 C with the addition of protease inhibitors, while freezing led to more rapid loss of matrix components and changes in MRI parameters.

1254. The Effects of Formalin Fixation and Crosslinking on MRI Contrast in Bovine Nasal Cartilage Explants

Kenneth W. Fishbein[1], Yehezkiel A. Gluzband[1], Masaru Kaku[2], Hasina Togore[3], Sue A. Shapses[3], Mitsuo Yamauchi[2], Richard G. Spencer[1]

[1]National Institutes of Health, Baltimore, Maryland, USA; [2]University of North Carolina, Chapel Hill, North Carolina, USA; [3]Rutgers University, New Brunswick, New Jersey, USA

MR microscopy studies are often performed on formalin-fixed tissue samples, since fixation improves stability and compatibility with histology. However, little is known about MR contrast changes upon fixation, particularly in non-neural tissue. Accordingly, we investigated the effect of formalin fixation on T2 and magnetization transfer (MT) in bovine nasal cartilage, a spatially-homogeneous model for articular cartilage. We found significant decreases in T2 and increases in MT effects. These changes persist upon washout of residual formalin. Based on biochemical analyses, we attribute these latter effects to formaldehyde-induced crosslinking, which may immobilize GAG sidechains, thereby enhancing their contribution to MT in cartilage.

1255. Effectiveness of a Biomaterial Adhesive in Integrating a Hydrogel with Surrounding Tissue in Rabbit Cartilage Defects

Sharan Ramaswamy[1], Ilksen Gurkan[2], Blanka Sharma[3], Kenneth W. Fishbein[1], Brett Cascio[2], Jennifer Elisseeff[3], Richard G. Spencer[1]

[1]National Institutes of Health, Baltimore, Maryland, USA; [2]Johns Hopkins University School of Medicine, Baltimore, Maryland, USA; [3]Johns Hopkins University, Baltimore, Maryland, USA

Hydrogel-based cartilage repair is of potential significant therapeutic interest. In situ gel photopolymerization represents one such approach. An important consideration in this repair procedure is the stability of the hydrogel within the cartilage defect. We monitored this stability using MRI, evaluating repair in rabbit joints after a 4-week period of residence in the living animal, and further investigated CS-MA-ald as a bonding material. Our results indicate that cartilage integration can be evaluated with MRI, and that this bonding agent permits improved integration of the implant with surrounding tissue and augments early cartilage repair.

1256. A Non -Invasive Assay of Matrix Metalloproteinase Induced Musculoskeletal Syndrome in Rats Using High Resolution Magnetic Resonance Imaging

Richard P. Kennan[1], Carol Ann Keohane[1], Jesse Jackson[1], Richard Hajdu[1], Donald S. Williams[2], Suzanne Miller Mandala[1], Haiying Liu[1]

[1]Merck & Co. Inc, Rahway, New Jersey, USA; [2]Merck & Co. Inc, West Point, Pennsylvania, USA

Matrix metalloproteinases (MMPs) are considered excellent targets for drug development for arthritis and cancer. The clinical utility of MMP inhibitors has been restricted by a musculoskeletal side effect observed in humans and animal models. The objective of this study was to use MRI to characterize pathologic changes in a rat model of MMP–induced musculoskeletal syndrome (MSS). MRI detected growth plate and synovial fluid increases well before clinical signs. Over time, the growth plate increased by 5-fold, in agreement with previous histologic studies. Synovial fluid accumulated supra-linearly by 12 fold and was closely correlated with onset of behavioral symptoms.

1257. MRI and Image Quantitation for Assessment of the Growth Effects of Anabolic Steroid Precursors in a Guinea Pig Model

Haiying Tang[1], [2], Ed X. Wu[3], Joseph R. Vasselli[4]

[1]Merck Research Laboratories, Rahway, New Jersey, USA; [2]Columbia University College of Physicians & Surgeons, New York, New York, USA; [3]The University of Hong Kong, Hong Kong SAR, People's Republic of China; [4]St. Luke's Roosevelt Hospital, Columbia University, New York, New York, USA

MRI and image quantitation play an expanding role in modern drug research. With effective image segmentation and analysis methods, *in vivo* and longitudinal tissue growth can be assessed. The effects of the nandrolone and testosterone steroids on muscle growth have been investigated previously, in which MRI acquisition and analysis protocol were established, and excellent correlations were found between MRI measurement and dissection analyzes. In this study, the MRI protocol was used to evaluate the anabolic potential of 4 steroid precursors. The effects on muscle growth in castrated guinea pigs, in comparison with that of respective positive control steroids were determined.

Pre-Clinical Cancer Metabolism and Microenvironments

Room 4E Monday 14:00 - 16:00

1258. Effects of Hypoxia on Invasion, Metabolism, Proliferation, Proteinase Activities and Gene Expression of a Human Prostate Cancer Cell Line

Ellen Ackerstaff[1], Dmitri Artemov[1], Zaver M. Bhujwalla[1]

[1]Johns Hopkins University School of Medicine, Baltimore, Maryland, USA

Oxygen tensions below 10 mmHg in human tumors have been linked to decreased patient survival. Using our MR-compatible invasion assay, we demonstrated that despite increased endogenous activities of selected proteinases hypoxia can reduce cancer cell invasion. The presence of endothelial cells can ameliorate this reduction in invasion, which might be partly explained by their higher endogenous proteinase activities. In the cancer cells, hypoxia decreased cell proliferation and up- and down-regulated multiple genes related to invasion, angiogenesis, cell cycle and energy and lipid metabolism. Our MR results could not be explained solely by proteinase activity and gene expression changes, demonstrating the importance of combining gene and protein expression analysis with functional assays.

1259. Complex Relationship Between Changes in Oxygenation Status and Changes in R2* : The Case of Insulin and NS-398, Two Inhibitors of Oxygen Consumption

Bénédicte F. Jordan[1], Nathalie Crokart[1], Christine Baudelet[1], Gregory O. Cron[1], Reginald Ansiaux[1], Bernard Gallez[1]

[1]Université Catholique de Louvain, Brussels, B, Belgium

Insulin and NS-398 inhibit oxygen consumption in experimental tumor models, thereby increasing oxygenation and radiosensitization. The aim of this work was to use MRI to study changes in hemodynamics after administration of those oxygen consumption inhibitors. We compared BOLD parameters with DCE-MRI data as well as with pO2 results obtained by EPR oximetry. Variations in BOLD SI and R2* did not reflect the change in pO2. To explain the discrepancy between changes in pO2 and the lack of change in R2*, it may be noted that EPR provides extracellular measurements whereas ÄR2* results from the intravascular compartment only.

1260. *In Vivo* ^{19}F MRS and ^{19}F 2D-CSI Investigation of a Fluorine Labeled 2-Nitroimidazole (TF-MISO). A Potential Functional Reporter of Hypoxia in Solid Tumors

Daniel Procissi[1, 2], Filip Claus[1], Jacek Koziorowski[1], Paul Burgman[1], Cornelia Matei[1], Sunitha Thakur[1], Clifton Ling[1], Jason A. Koutcher[1]

[1]Memorial Sloan Kettering Cancer Center, New York, New York, USA; [2]California Institute of Technology, Pasadena, California, USA

We report a ^{19}F magnetic resoance spectroscopy (MRS) and ^{19}F chemical shift imaging (CSI) *in vivo* investigation of a 2-Nitroimidazole agent labeled with three fluorine atoms (TF-MISO) . *In vitro* cellular uptake results have shown how this compound is hypoxia selective. Here we demonstrate how it is possible to use it (1) as a *in vivo* ^{19}F MRS reporter of hypoxia in solid tumors, (2) how it is possible to functionally image the tumor distribution of the compound by ^{19}F CSI and, using the same radio frequency setup, 3) obtain high resolution anatomical ^{1}H reference images which provide context in terms of tissue hetereogeneity.

1261. Hypoxia Regulates Phosphocholine and Total Choline Concentrations in Human Prostate Cancer Cells

Kristine Glunde[1], Venu Raman[1], Zaver M. Bhujwalla[1]

[1]The Johns Hopkins University School of Medicine, Baltimore, Maryland, USA

Hypoxic regions are frequently found in the tumor microenvironment. Hypoxic conditions cause cells to stabilize hypoxia inducible factor (HIF-1α), a transcriptional activator binding to hypoxia response elements (HRE) in hypoxia-inducible genes. Using combined MRS and optical imaging, we previously demonstrated a strong spatial association between regions of hypoxia and elevated total choline (tCho) levels in human prostate cancer xenografts stably expressing green fluorescent protein (GFP) under the control of an HRE. Here we have extended our study to demonstrate that hypoxia drives up phosphocholine (PC) and tCho levels in wild-type PC-3 cells, mediated by an increased expression of choline kinase.

1262. A Metabolomic Study of HIF-2a Over-Expressed and Empty Vector 7860 Renal Tumours Using *In Vivo* and In Vitro 1H MRS

Helen Troy[1], Yuen Li Chung[1], Basetti Madhu[2], Adrian L. Harris[2], Simon Wigfield[2], Shet Biswas[2], Marion Stubbs[1], J R. Griffiths[2]

[1]St. George's University of London, London, UK; [2]John Radcliffe Hospital, Oxford, UK

We used 1H MRS both *in vivo* and in vitro (of the tissue extracts) to study the role of HIF-2a in tumour metabolism by measuring metabolites in xenografts grown up from HIF-2a over-expressing renal tumour and empty vector (EV) cells. The HIF-2a over-expressers grew faster than the EV tumours. They had significantly more choline *in vivo* and more free choline, phosphocholine (PC), taurine, creatine and glucose in vitro and surprisingly had less lactate when compared with EV tumours. We conclude that the faster growing HIF2a over-expressing tumours use a more oxidative metabolism than the slower growing EV tumours.

1263. Effects of Targeted Nanoparticle-Based Antiangiogenic Therapy on Brain Tumor Metabolism and Progression - MicroPET and MRI Study on a Rat Glioblastoma Model

Yi-Shan Yang[1], Leroy Sims[1], Steven Choi[1], Yingyun Wang[1], Samira Guccione[1]

[1]Stanford University, Stanford, California, USA

Anti-angiogenic therapy is an important tool for brain tumor.

1264. Improved Mapping of Extracellular PH in C6 Gliomas by ^{1}H MRSI Shows Low Correlation Between Lactate Concentration and PHe Changes Induced by Infusion of Glucose

Peggy Provent[1, 2], Régine Farion[1, 2], Pilar López Larrubia[3], Marina Benito[3], Bassem Hiba[1, 2], Paloma Ballesteros[3], Chantal Rémy[1, 2], Christoph Segebarth[1, 2], Sebastián Cerdán[3], Jonathan A. Coles[1, 2], María-Luisa García-Martín[3]

[1]U594, Grenoble, F-38043, France; [2]Univ Grenoble 1, Grenoble, F-38043, France; [3]Instituto de Investigaciones Biomédicas, Madrid, 28029, Spain

Extracellular pH (pHe) is more acid in tumors than in normal tissue and shows a very heterogeneous distribution within the tumor. Because most tumors exhibit a characteristic high glycolytic metabolism, it became widely accepted that this is the main cause of tumor acidity. In a previous work, using one of these new methodologies, we reported that no correlation between pH and lactate concentration could be found *in vivo* in C6 gliomas. In the current communication we further investigated the correlation between glycolytic metabolism and tumor acidity by looking at the changes in lactate concentration and pHe produced by glucose infusion.

1265. C6 Glioma Cells Depict an Active Pyruvate Recycling System That is Redox Sensitive

Tiago B. Rodrigues[1, 2], Gemma Ruiz[1], Genoveva Mateos[1], Sebastián Cerdán[1]

[1]Instituto de Investigaciones Biomédicas "Alberto Sols", Madrid, Spain; [2]University of Coimbra, Coimbra, Portugal

The pyruvate recycling pathway has been demonstrated in intact brain and astrocyte cultures as well as in the intact liver. Pyruvate recycling has been proposed to be involved in intracellular protection against redox and free-radical stress, but no direct evidences have been presented on its redox sensitivity. Here, we report the presence of pyruvate recycling in C6 glioma cells and demonstrate its dependence on the intracellular redox state. Our results show that C6 glioma cells, depict a considerable activity of the pyruvate recycling system, which increases remarkably under oxidized redox conditions. These findings support a detoxifying function for this pathway.

1266. Choline Kinase Suppression Increases Tumor Lipid Content and Vascular Volume in a Human Breast Cancer Model

Kristine Glunde[1], Dmitri Artemov[1], Venu Raman[1], Zaver M. Bhujwalla[1]
[1]The Johns Hopkins University School of Medicine, Baltimore, Maryland, USA

Increased choline kinase (Chk) expression is a primary cause of elevated phosphocholine (PC) and total choline (tCho) levels in breast cancers. Chk suppression in breast tumors is currently being explored as potential therapeutic strategy. We have characterized, for the first time, the effect of suppressing Chk on tumor lipid/lactate content and vascularization in tumor xenografts from human MDA-MB-231 breast cancer cells stably expressing small interfering RNA against Chk (siRNA-chk). Multiparametric co-localized maps of vascular volume, permeability, and total choline and lipid were obtained with ^{1}H MRI/MRSI. Both the lipid signal and vascular volume were significantly higher in Chk-suppressed breast tumors compared to controls.

1267. Concurrent Use of *In Vivo* 19F and 31P MRS at 9.4T to Monitor the Pathway for 5FC Conversion to Fluorinated Nucleotides and FUDP-Sugars in a Human Glioma Xenograft Treated with Ad5.CMV.CDUPRT/5FC Therapy

Huadong Zeng[1], Vera Simonenko[1], Yun Jiang[1], Thian C. Ng[1]
[1]University of Alabama at Birmingham, Birmingham, Alabama, USA

Concurrent 31P-MRS and 19F studies at high field 9.4T enabled us to determine the fluorinated intermediates and their cytotoxic mechanisms in tumors treated with Ad5.CMV.CD.UPRT/5FC gene therapy. We have shown for the first time the observation of FUDP-sugars *in vivo* via 31P-MRS. The elevated FUDP-sugars peaks are in consistent with the increasingly accumulated FNuct in glioma tumors observed by *in vivo* 19F MRS.

1268. Metabolic Response of Human Prostate Cancer Post 17 AAG Treatment in a Mouse Model

H Carl Le[1], Mihaela Lupu[2], Cornelia Matei[2], David Solit[2], Neal Rosen[2], Jason A. Koutcher[2]
[1]MSKCC, New York, USA; [2]MSKCC, New York, New York, USA

Hsp90 inhibitor 17AAG is being studies as a chemotherapy agent against prostate cancers. It has been shown to cause tumor growth arrest and partial shrinkage. Using total choline as a tumor proliferation surrogate maker, we compare the metabolic response of the hormone sensitive and resistant human prostate cancer CWR22 after 17AAG treatment. Differential responses of the two cancer lines shows that 17AAG can be a promising agent for the resistant line and that 1H MRS is a sensitive technique for tumor monitoring.

1269. Choline Kinase Downregulation by SiRNA Reduces Phosphocholine and Total Choline, and Enhances Treatment of Breast Cancer Cells with 5-Fluorouracil

Noriko Mori[1], Kristine Glunde[1], Tomoyo Takagi[1], Raman Venu[1], Zaver M. Bhujwalla[1]
[1]The Johns Hopkins University School of Medicine, Baltimore, Maryland, USA

The elevation of phosphocholine (PC) and total choline-containing compounds (tCho) is one of the common features in cancer. Increased choline kinase (ChK) expression and activity may cause this elevation. Here we used small interfering RNA against ChK (siRNA-chk) to knock down ChK expression, and determine its effect on cell viability and proliferation alone and in combination with 5-Fluorouracil (5-FU). Transient siRNA-chk transfection significantly reduced PC and tCho levels detected by ^{1}H NMR spectroscopy in malignant breast cancer cells and significantly decreased cell viability/proliferation to levels comparable with 5-FU alone. Treatment with 5-FU in combination with siRNA-chk transfection enhanced this reduction.

1270. A Metabolically Accurate Prostate Tissue Culture Model for ^{13}C Labeling Studies

Mark J. Albers[1], Robert G. Sellers[2], Daniel B. Vigneron, Sarah J. Nelson, [1], Donna M. Peehl[2], John Kurhanewicz
[1]UC Berkeley / UC San Francisco, San Francisco, California, USA; [2]Stanford Medical Center, Sanford, California, USA

A new human prostate tissue culture system was investigated to determine if the metabolic profiles mimic those observed *in vivo* and to determine if the tissue would incorporate ^{13}C labeled substrates added to the medium. The tissue samples were incubated with ^{13}C-3 Pyruvate and metabolic information was measured using HR-MAS spectroscopy. For each sample, a carbon-decoupled proton spectrum and an HSQC were acquired and the amount of ^{13}C enrichment was calculated. The spectra from these samples contained all the metabolites present in *in vivo* spectra and exhibited the expected changes with cancer. Finally, ^{13}C enrichment was found in glutamate, lactate, and alanine.

1271. Effects of Gd-DTPA on *In Vivo* ^{1}H MRS Choline Signals Observed in HT-29 Xenografts

Basetti Madhu[1], Simon P. Robinson[2], John R. Griffiths[1]
[1]St. George's, University of London, London, England, UK; [2]St. George's, University of London,, London, England, UK

The impact of contrast agent GD-DTPA on choline signals in HT-29 xenografts grown subcutaneously on nude mice was studied by *in vivo* ^{1}H MRS. Short echo time spectra by PRESS localization did not show any significant changes in choline peak area. However long echo time spectra revealed significant reduction of choline peak area after the administration of Gd-DTPA. The significant correlation between the choline and water signal intra voxel enhancements indicates a direct contact of choline with the contrast agent, implying that the choline observed in these tumours mostly resides in the interstial and extracellular space.

1272. Transmembrane PH Gradients in Tumor Cells: Observations Using 19F NMR of Promising New Reporter Molecules

Weina Cui[1], Li Liu[1], Peter Peschke[2], Uwe Haberkorn[2], Ralph P. Mason[1]
[1]UT Southwestern Medical Center at Dallas, Dallas, Texas, USA; [2]DKFZ, Heidelberg, Germany

We have been developing novel pH indicators and report progress in the development of useful 19F NMR reporter molecules. We had shown that 6-fluoropyridoxol (FPOL) could be used to measure transmembrane pH gradients in whole blood and perfused hearts. 6-fluoropyridoxamine (FPAM) is a close analog of FPOL and has a large chemical shift response to pH and a pKa = 7.05. Like FPOL, FPAM shows two signals in whole blood and perfused hearts. Unlike FPOL, FPAM shows two signals in cultures of several types of mammalian cells, suggesting it can be useful for investigating transmembrane pH gradients.

Vascular Postprocessing

Room 4E Monday 14:00 - 16:00

1273. Robust Vessel Path Tracking in Imperfect Volumetric Data

Noel Christopher Codella[1], Yi Wang[1], Ramin Zabih[2]
[1]Cornell Weill Medical College, New York, New York, USA; [2]Cornell University, Ithaca, New York, USA

In this work we present a fast and efficient algorithm that can determine the path of an artery of any length, visualized in 3D angiography data with low SNR and loss of contrast along one side of the artery from neighboring structures, while relying on minimal user input. Arterial dimensions can be simultaneously recorded during program execution. The required user input consists of two points that define the initial arterial axial vector, and a tracking length limit. A fixed number of other inputs controlling edge detection and scan resolution also exist, but are optional.

1274. Fast, Reliable Carotid Plaque Burden Measurements with Interactive Snakes

William Sean Kerwin[1], Dongxiang Xu[1], Fei Liu[1], Norihide Takaya[1], Baocheng Chu[1], Howard Klein[2], William Ross[2]
[1]University of Washington, Seattle, Washington, USA; [2]Pathway MRI, Inc., Seattle, Washington, USA

MRI measurements of carotid artery wall volume, thickness, and maximal area, have become important parameters of atherosclerotic disease severity and surrogate markers for therapeutic response. To assist in these measurements, we developed interactive Snakes (I-Snakes), which offer a highly automated and flexible interface for measuring plaque burden. Tests of I-Snakes show that plaque boundaries can be extracted in 1-2 minutes per artery and yield significant improvements in scan-to-scan reproducibility compared to manual outlining

1275. Neovascularization in the Carotid Atherosclerotic Plaque Can Be Identified by Dynamic Contrast-Enhanced High Resolution 3TMRI

Jing Han[1], Jian Cai[1], Lin Ma[1], Xin Liu[1]
[1]PLA general Hospital, Beijing, People's Republic of China

The gadolinium-based dynamic contrast-enhanced MRI can detect the major carotid atherosclerotic plaque components *in vivo* due to their characteristic enhancement patterns, especially to identify neovascularization-rich area (NRA).The NRA showed highest peak intensity enhancement and shorter time to peak (TTP) than other plague components. The TTP can provide useful information to detect NRA. Accurately identifying the presence of neovasculature based on DCE MRI may provide valuable information on predicting plaque stability.

1276. Robust Image Segmentation Through Outlier Handling Application to Automatic Plaque Burden Assessment

Karim Lekadir[1], Robert Merrifield[1], Niall Keenan[2], Dudley Pennell[2], Guang-Zhong Yang[1]
[1]Imperial College, London, UK; [2]Royal Brompton and Harefield Trust, London, UK

This abstract presents a robust automatic segmentation method that can be used for automated plaque burden assessment using CMR. Manual delineation can be problematic as it is time consuming and subject to significant operator bias. On the other hand, existing automatic techniques suffer from lack of accuracy when some landmarks lie on incorrect boundary positions due to noise and artefacts. The proposed method is able to detect and correct these outliers using an invariant shape representation. The validation on real data demonstrates high accuracy and robustness. The result shows a potential clinical value for longitudinal studies of plaque burden.

1277. Reproducibility Assessment of Morphology-Enhanced Probabilistic Plaque Segmentation (MEPPS) on Two Baseline Magnetic Resonance Scans

Fei Liu[1], Dongxiang Xu[1], Baocheng Chu[1], Tobias Saam[1], Norihide Takaya[1], Hunter Underhill[1], Thomas S. Hatsukami[1, 2], Chun Yuan[1], William S. Kerwin[1]

[1]University of Washington, Seattle, Washington, USA; [2]VA Puget Sound Health Care System, Seattle, Washington, USA

MRI is a promising noninvasive technique for characterizing atherosclerotic plaque composition *in vivo*, with an end-goal of assessing plaque vulnerability. In a previous study, MEPPS was introduced as a promising algorithm for automatic *in vivo* plaque component analysis. This study evaluates the *in vivo* reproducibility of plaque segmentation by MEPPS. Both the visual and quantitative comparison between manual drawing and MEPPS segmentation demonstrates that MEPPS and manual drawing achieve comparable reproducibility. Thus, MEPPS can be used in therapeutic clinical trials and in prospective longitudinal studies to examine carotid atherosclerotic plaque progression and regression to reduce radiologists' work in large studies.

1278. Aorta Segmentation Using Elliptical Deformable Templates

Ersin Bayram[1, 2], William Gregory Hundley[3], Craig Alan Hamilton[1]

[1]Virginia Tech-Wake Forest University, Winston-Salem, North Carolina, USA; [2]GE Healthcare, Waukesha, Wisconsin, USA; [3]
Wake Forest University School of Medicine, Winston Salem, North Carolina, USA

Vessel segmentation is important for many diagnostic tasks such as blood flow quantification and shear stress calculations; yet it is challenging as vessel's shape and position vary throughout the cardiac cycle. Manual delineation is considered the gold standard; however it is time consuming and observer-dependent. The proposed deformable template assumes an elliptical equilibrium shape, but deforms to the underlying vessel thru simulated annealing, which is governed by the shape constraints and local image features. The method is applied to the quantification of flow in ascending aorta phase contrast images. Comparison with manual analysis reveals that the proposed technique is fast and reliable.

1279. Reproducibility Study of Wall Segmentation Approach in Evaluating PAD Patient with MRI

Dongxiang Xu[1], Timothy J. Carroll[2], Lu Tian[2], James Carr[2], Kiang Liu[2], Debiao Li[2], Mary M. McDermott[2], Chun Yuan[1]

[1]University of Washington, Seattle, Washington, USA; [2]Northwestern University, Chicago, Illinois, USA

Peripheral arterial disease (PAD) is a common condition that is highly correlated with increased rates of functional impairment and decline and is associated with an increased risk of cardiovascular events. In recent years, high resolution MR imaging has been considered as the most promising imaging modality for assessing atherosclerotic plaque burden in many vascular beds [1]. However, there has been little research that uses MRI's ability to analyze atherosclerotic plaque burden in the lower extremity arteries. In this study, we use MRI cross sectional images to quantitatively analyze vessel wall morphology, in particular the following plaque characteristics: normalized total plaque volume, maximum arterial wall thickness, and mean arterial wall thickness – the three independent measures of plaque burden in PAD evaluation.

1280. Complex Subtraction – a Flow-Independent Method for Vessel Wall Imaging Shortly After Gadofluorine Injection

Ioannis Koktzoglou[1], Bernd Misselwitz[2], Hanns-Joachim Weinmann[2], Debiao Li[1]

[1]Northwestern University, Chicago, Illinois, USA; [2]Schering AG, Berlin, Germany

While flow-dependent methods such as double inversion-recovery and saturation work well to eliminate blood signal in non-contrast enhanced vessel wall imaging studies, these methods can fail after injection of T1-shortening contrast agents. Gadofluorine, a T1-shortening blood-pool contrast agent, has recently been shown to selectively enhance atherosclerotic arterial wall after injection. This work sought to investigate whether complex subtraction can be used as a flow-independent method for eliminating blood signal shortly after gadofluorine injection. Results indicate that complex subtraction appears to be a promising, flow-independent technique for eliminating blood signal during gadofluorine-enhanced vessel wall imaging.

ESR

Room 4E Monday 14:00 - 16:00

1281. Potentiation of Cyclophosphamide Chemotherapy Using the Antiangiogenic Drug Thalidomide: Importance of Optimal Scheduling to Exploit the Normalization Window of the Tumor Vasculature

Jerome Segers[1], Vincent Difazio[2], Reginald Ansiaux[1], Philippe Martinive[1], Olivier Feron[1], Pierre Wallemacq[2], Bernard Gallez[1]

[1]UCL, Woluwe, Bruxelles, Belgium; [2]Saint-Luc Hospital, Woluwe, Bruxelles, Belgium

At the early phase of anti-angiogenic treatments, a transient "normalization" of the tumor vasculature occurs, with a transient increase in tumor perfusion. EPR oximetry can been used to determine the timing of this normalization after thalidomide treatment. The technique allowed us to predict the optimal timing during thalidomide treatment for the administration of the cytotoxic agent cyclophosphamide. Indeed, a good correlation was observed between the reoxygenation of the tumor and improved delivery of drug into the tumor.

1282. New Formulation of EPR Oxygen Sensors Dispersed in Thermo-Reversible Hydrogels

Mustapha Dinguizli[1], *Nelson Beghein*[1], *Bernard Gallez*[1]
[1]Université catholique de Louvain, Brussels, B, Belgium

In vivo EPR oximetry is a powerful method to measure oxygenation of tissues. In order to minimize diffusion and migration of paramagnetic particles *in vivo*, we developed a new type of thermo-reversible hydrogel (poloxamer) containing charcoal particles. This system has an interesting property: it is fluid at 5 C but becomes a gel at 37 C (*in vivo*). The purpose of this study was to examine the performance of this system in muscle and tumors

1283. Modulated Radiation Force of US as Shear Wave Source in Microscopic MRE

Thomas J. Royston[1], *Shadi F. Othman*[1], *Faik Can Meral*[1], *Bulent B. Ozer*[1], *Richard L. Magin*[1]
[1]University of Illinois at Chicago, Chicago, Illinois, USA

Microscopic magnetic resonance elastography (μ MRE) is a high resolution imaging technique for measuring the viscoelastic properties of small synthetic and biological samples. Taking MRE to the microscopic scale requires stronger static fields, stronger magnetic field gradients, higher performance RF coils, and more compact, higher frequency shear wave actuators. Modulated radiation force of ultrasound (MRFU) is used to create a localized shear wave source within the test sample enabling μ MRE probing up to 5 kHz. Use of confocal and amplitude-modulated ultrasound transducers to create such a source within the working constraints of the μ MRE system is investigated.

1284. Performance Comparison of the Spatial Autocorrelation Function and the Mean Intercept-Length in the Determination of Trabecular Bone Anisotropy in the *In Vivo* Environment

Michael Jeffrey Wald[1], *Branimir Vasilic*[1], *Punam K. Saha*[1], *Felix W. Wehrli*[1]
[1]Department of Radiology, University of Pennsylvania Medical Center, Philadelphia, Pennsylvania, USA

Recent research suggests that structure contributes to bone strength in a manner complementary to bone mineral density. Besides parameters of scale such as trabecular bone thickness and volume fraction, the trabeculae are oriented preferentially along the major stress lines, leading to an angular dependence of such parameters as trabecular separation. The structural anisotropy is of pivotal importance to the bone's mechanical competence and is most commonly characterized by the mean-intercept-length (MIL) method. Here, we investigate the performance of the spatial autocorrelation function, a threshold-independent approach, as an alternative method that we hypothesized had significant advantages over the MIL technique with respect to *in vivo* imaging.

1285. An Automated On-The-Fly Detection and Correction Procedure for EPR Imaging Data Acquisition

Rizwan Ahmad[1], *Bradley Clymer*[1], *Yuanmmu Deng*[1], *Deepti Vikram*[1], *Sergey Petryakov*[1], *Periannan Kuppusamy*[1], *Jay L. Zweier*[1]
[1]The Ohio State University, Columbus, Ohio, USA

In this work, a fully automated procedure to monitor the performance and stability of an EPR system for projection data acquisition is demonstrated. The purpose of this scheme is to ensure that the quality of acquired data is optimum for a given hardware/software configuration. For this purpose, noise contents of each acquired projection are quantified and measured against those of zero-gradient projection which is set as a quality benchmark. The projections containing substantial amount of extra noise as compared to zero-gradient projection are identified. Hence, the proposed technique not only monitors the quality of acquisition effectively but also saves a substantial amount of acquisition time as we are not required to repeat the whole experiment in which only a small fraction of data is damaged.

1286. Application of Over Magnetic Field Modulation in EPR Oximetry

Yuanmu Deng[1], *Ramasamy P. Pandian*[1], *Rizwan Ahmad*[1], *Periannan Kuppusamy*[1], *Jay L. Zweier*[1]
[1]The Ohio State University School of Medicine, Columbus, Ohio, USA

The over-modulation technique was applied to EPR oximetry experiments. Modulation amplitudes in the range of 2-18 times the intrinsic linewidth of the oxygen probe were applied to increase the signal-to-noise ratio of spectra. The intrinsic linewidth of the probe at different oxygen concentrations was accurately extracted through curve fitting from the modulation-broadened spectra.

Human Lung Imaging Techniques

Room 4E Monday 14:00 - 16:00

1287. Quantitative Contrast-Enhanced Perfusion Measurements of the Human Lung

Markus Oechsner[1], *Matti Mühlhäusler*[1], *Peter M. Jakob*[1], *Meinrad Beer*[1], *Dietbert Hahn*[1], *Matthias Beissert*[1], *Matthias Spindler*[1], *Herbert Köstler*[1]
[1]University of Würzburg, Würzburg, Bavaria, Germany

In the present work, first-pass contrast-enhanced pulmonary perfusion was measured with injection of a 1ml bolus. Using the prebolus approach, perfusion was also quantified after administration of 3ml contrast agent. Additionally, the lung volume and the heart-time-volume were measured to calculate the value for the global lung perfusion (GLP). All perfusion values show good agreement with the literature and the 1ml and 3ml values correlate well with the global lung perfusion.

1288. Comparison of Hyperpolarized 3-He Administration Methods in Healthy and Diseased Subjects

Neil Woodhouse[1], Jim M. Wild[1], Gary H. Mills[2], Sally Fleming[2], Stan Fichele[1], Edwin JR van Beek[3]
[1]University of Sheffield, Sheffield, South Yorkshire, UK; [2]Sheffield Teaching Hospitals NHS Trust, Sheffield, South Yorkshire, UK; [3]University of Iowa, Iowa City, Iowa, USA

To determine the physiological effects and responses to hypoxic and anoxic breath holds containing 3-He in 2 patient groups (Healthy and Emphysema) using two separate methods of administration; the first a bag and tube containing 3-He and N2, the second a computer controlled applicator device driven by a ventilator. Oxygen saturation (SpO2) was measured for the first minute following each breathing maneuver. The healthy group showed the largest mean drop of 4%. While the group with emphysema showed only a 1% drop in SpO2. None of the participants reported any ill effects for either method.

1289. Short-Breath-Hold PO2 Imaging with 3He: Initial Experience in Lung Disease

G Wilson Miller[1], Eduard E. de Lange[1], Jaime F. Mata[1], Jing Cai[1], Gordon D. Cates[1], W A. Tobias[1], John P. Mugler III[1]
[1]University of Virginia, Charlottesville, Virginia, USA

We report on intial experience using a short-breath-hold hyperpolarized 3He technique to obtain maps of intrapulmonary oxygen partial pressures (pO2) in patients with lung disease. Two single-lung-transplant COPD patients were imaged. Features of the pO2 maps are interpreted within the context of chronic obstructive pulmonary disease, and potential pitfalls of the underlying pO2 measurement strategy are discussed.

1290. Regional Ventilation Differences at Large Lung Volumes Assessed Using Hyperpolarized ^{3}He MRI

Jessica Dickey Gereige[1], Yanping Sun[1], Joey Karim Mansour[1], Francine L. Jacobson[1, 2], Peter Lindholm[3], James P. Butler[2], Stephen H. Loring[4], Massimo Ferrigno[1], Mitchell S. Albert[1]
[1]Brigham and Women's Hospital, Boston, Massachusetts, USA; [2]Harvard Medical School, Boston, Massachusetts, USA; [3]Karolinska Institutet, Stockholm, Sweden; [4]Beth Israel Deaconess Medical Center, Boston, Massachusetts, USA

Pulmonary expansion at high lung volumes is believed to be homogeneous. However, there are no direct measurements *in vivo* of regional variations at high lung volumes. We studied regional lung ventilation differences using hyperpolarized ^{3}He MRI. Images were obtained upon breath-hold after inhaling 1 liter of ^{3}He at two different lung volumes: functional residual capacity (FRC) and total lung capacity (TLC). Our results show a sharp increase in ventilatory volume at TLC near the pericardial region of the lung. We believe this is caused by high regional compliance ratios, which may be due to this region's concave nature.

1291. Real-Time MR Imaging and Tracking of Regional Lung Motion During Forced Breathing Maneuvers

Abram Voorhees[1], Jing An[1], Kenneth I. Berger[1], Roberta M. Goldring[1], Leon Axel[1], Qun Chen[1]
[1]New York University School of Medicine, New York, New York, USA

Real-time imaging and tracking of lung motion was performed for forced breathing maneuvers using a turboFLASH sequence. The goal of this study was to acquire images with both high temporal resolution and a sufficient level of visible lung structure for parenchyma motion-tracking. Forced expirations were successfully imaged at 10 frames per second. Results show good contrast in the lungs allowing use of established motion-tracking algorithms for regional analysis of lung mechanics. This study demonstrates the potential for regional assessment of lung function while performing a full battery of pulmonary function tests.

1292. Towards a Normative Lung Atlas: Validation of Physiologically Appropriate Temporal Reparameterization of Dynamic Lung MR Sequences

Tessa Sundaram[1], Shigeto Kubo[2], Masaya Takahashi[2], James Gee[1], Hiroto Hatabu[2]
[1]University of Pennsylvania, Philadelphia, Pennsylvania, USA; [2]Beth Israel Deaconess Medical Center, Harvard University, Boston, Massachusetts, USA

Lung MR can be used to noninvasively visualize and assess pulmonary anatomy and dynamics. We have previously demonstrated and validated non-rigid registration algorithms for computing the motion between successive images. However, the problem of spatiotemporally matching individuals with unique respiratory rates and lung capacities is challenging. Using a specialized algorithm, we can interpolate anatomies at specified positions along the geodesic path between two images. We reconstruct these intermediate images using total lung deformation as our parametric basis, and thereby interpolate at the same physiologic point in the respiratory cycles of multiple individuals to construct a normative atlas.

1293. Optimal Breathing Protocol for Dynamic Contrast Enhanced MRI of Solitary Pulmonary Nodule at 3T

Aya Kino[1], Masaya Takahashi[1], Takeshi Kubo[1], Danielle Coute[1], Simon K. Ashiku[1], J. Anthony Parker[1], Malcolm M. DeCamp[1], Robert E. Lenkinski[1], Hiroto Hatabu[1]
[1]Beth Israel Deaconess Medical Center, Boston, Massachusetts, USA

The purpose of this study was to evaluate optimal breath instructions that provide less lung parenchyma movement, which can target small lung lesions during dynamic contrast-enhanced MRI scans. Our preliminary results indicate that dynamic contrasted-enhanced MRI of pulmonary nodule is feasible when a shallow breathing protocol is adopted. MR perfusion study of solitary pulmonary nodule using 3T MR system with high spatial and temporal resolution may provide a secondary characterizing method to distinguish benign from malignant nodules with minimal associated risks, thereby avoiding unnecessary intervention for benign lung nodules and associated mortality /morbidity.

1294. T_1 and D of Perfluorocarbon-O_2 Mixtures for Lung Imaging

Yulin V. Chang[1], Mark S. Conradi[1]
[1]Washington University, St. Louis, Missouri, USA

Experimental measurements of the relaxation time T_1 and diffusion D of perfluorocarbon (PFC) gas mixtures with oxygen are reported. The data will allow determination of local free diffusivity of the PFC gas in lung *in vivo* by localized T_1 measurements. Knowledge of the free diffusivity is crucial for calculating the local surface-to-volume ratio in lung, which would be an important parameter in understanding and diagnosing emphysema.

1295. Rapid Production of Hyperpolarized 3He Gas for MRI

Brian Saam[1], Richard E. Jacob[2], Benjamin C. Anger[1], Kevin R. Minard[2]
[1]University of Utah, Salt Lake City, Utah, USA; [2]Pacific Northwest National Laboratory, Richland, Washington, USA

Hyperpolarized ^{3}He has widespread interest as a signal source for MRI in the lung. Two recent advances in the physics of spin-exchange optical pumping (SEOP) have led to dramatic enhancements in the efficiency of generating hyperpolarized ^{3}He: the use of spectrally narrowed diode-laser arrays and "hybrid" SEOP, which employs both potassium and rubidium as alkali-metal intermediaries. We have combined these techniques in constructing two polarizers, both a prototype and more fully engineered system. We report up to 50% ^{3}He polarization in 0.5 bar L of gas in valved and refillable glass cells, achieved in 4 h.

1296. Using Laser Frequency Narrowing Techniques to Improve Production of Hyperpolarized Xe for Imaging and Surface Analysis

Cavin Lee Talbot[1], Marlies Elly Joy Friese[1], Halina Rubinsztein-Dunlop[1], Katie M. Baldwin[1], Andrew K. Whittaker[1], Ian Brereton[1], Norman R. heckenberg[1], David M. Doddrell[1], Deming Wang[1]
[1]The University of Queensland, Brisbane, Queensland, Australia

We produce hyperpolarized xenon for NMR/MRI by spin exchange optical pumping (SEOP), using a 30W LDA. SEOP efficiency is improved by frequency narrowing the LDA, doubling the spin polarization and thus doubling the NMR signal strength.

1297. Hyperpolarized 129Xe Human Pulmonary Gas Exchange with 3-Point Dixon Technique

Iga Muradian[1, 2], Samuel Patz[2], J. P. Butler[3], G. P. Topulos[2], M. I. Hrovat[4], S. Covrig[1], S. Ketel[1], I. Russet[1], F. W. Hersman[1]
[1]University of New Hampshire, Durham, New Hampshire, USA; [2]Brigham and Women's Hospital, Boston, Massachusetts, USA; [3]Harvard School of Public Health, Boston, Massachusetts, USA; [4]Mirtech Inc., Brockton, Massachusetts, USA

Magnetic Resonance images of human pulmonary gas exchange, i.e. diffusion of gaseous hyperpolarized 129Xe from the alveolar gas space into the parenchymal tissue, were obtained. Here we report a direct measurement of both the gas and tissue signals and their ratio, which gives the fraction of gas exchanged into tissue during a specified exchange time. This ratio is also proportional to a functional parameter of the lung, local surface area per unit volume S/V.

1298. Quantification of Pulmonary Perfusion Using SEEPAGE

André Fischer[1], Eberhard Daniel Pracht[1], Peter Michael Jakob[1]
[1]University of Würzburg, Würzburg, Bavaria, Germany

The standard method for assessing pulmonary perfusion images is contrast-enhanced MRI, which involves the injection of a contrast-agent. In this abstract, we present a non-invasive functional imaging sequence which requires no injections and provides a quantification of pulmonary perfusion on a voxel-by-voxel basis. Due to the initial saturation of the desired slice, an excellent suppression of stationary tissue is achievable. Our perfusion values obtained during breathhold at end expiration in the lung parenchyma varied from 1.0 to 2.5 ml/min/ml, a physiologically reasonable range. Since a perfusion-weighted image can be acquired in seconds this method shows promise for future clinical application

1299. Structural Lung Parenchyma: Breath-Hold Isotropic Imaging Using 3D SSFP

Piotr Wielopolski[1], Maarten Lequin[1]
[1]Erasmus MC, Rotterdam, ZH, Netherlands

In this study, we have focused on studying the possibilities of 3D SSFP scanning for volumetric imaging of the lung using the inherent high signal-to-noise (SNR) of the SSFP signal and the short TR/TE combinations that can be currently achieved in state-of-the-art MRI hardware. This expands the role of MRI in the diagnosis of lung parenchyma for many diseases that were previously the domain of CT. Therapy can be followed more effectively with this setup.

1300. Radial MRI of the Human Lung

Falko Lohberger[1], Michael Amann[1], Lothar R. Schad[1]
[1]German Cancer Research Center, Heidelberg, Germany

Lung MRI is very challenging because of low proton density, cardiac and respiratory motion and susceptibility effects (T2*≈1ms). Radial k-space sampling techniques provide very short echo and readout times. Additionally, they are motion insensitive due to central k-space averaging effects and thus being well suited for lung imaging. The implemented radial technique provides improved visibility of lung parenchyma and small vessels compared to conventional Cartesian gradient echo sampling. Furthermore it provides significantly reduced motion artifacts. Fast on-line reconstruction allows for immediate clinical diagnosis.

1301. MR Imaging of the Thorax During Whole-Body MRI: Evaluation of Different MR Sequences and Comparison to Thoracic CT

Bernd B. Frericks[1], Bernhard Meyer[1], Tanja Nentwig[2], Karl J. Wolf[1], Frank K. Wacker[1]
[1]Charité, Campus Benjamin Franklin, Berlin, Germany; [2]Imaging Science Institute, Siemens, Berlin, Germany

The diagnostic accuracy of four MR sequences (axial and coronal T2w-STIR, axial T2w-TSE, contrast-enhanced 3D-VIBE) for lung imaging in a whole-body MRI protocol for cancer patients was evaluated. MDCT detected 63 pulmonary lesions in 24 tumor patients. Sensitivities of the MR-sequences were: axial STIR 89%, coronal STIR 91%, axial T2w-TSE 87%, axial CE-3D-VIBE 81%. A maximum of 2 false positive findings were detected with each sequence. All missed lesions were either calcified or smaller than 5mm. Our results indicate that pulmonary MR imaging as part of a whole-body MRI is feasible and yields a diagnostic accuracy comparable to chest CT.

1302. A Self-Navigated Feedback Method for Fast Gradient-Echo Imaging of Hyperpolarized 3He Using Variable Flip Angles

G Wilson Miller[1], John P. Mugler III[1], Jing Cai[1], Jaime Mata[1], Eduard E. de Lange[1], Gordon D. Cates[1], W A. Tobias[1], James R. Brookeman[1]
[1]University of Virginia, Charlottesville, Virginia, USA

A feedback algorithm was incorporated as part of a 3D fast-gradient-echo sequence for hyperpolarized 3He lung imaging using variable flip angles. Signal measurements are acquired periodically during sequence execution, and the observed signal evolution is analyzed to calibrate the transmitter voltage and T1. Based on these measurements, the variable flip angle sequence is adjusted to ensure optimum usage of the available hyperpolarized magnetization.

1303. Parallel Phase-Encoded Images with Hyperpolarized Gas

Xavier Maître[1], Olivier Girard[1], Ludovic De Rochefort[1], Clarisse Halawani[1], Emmanuel Durand[1], Luc Darrasse[1]
[1]CNRS - Universite Paris Sud, Orsay, France

A four-channel RF-coil array was designed to perform accelerated hyperpolarized helium-3 MRI in the human lung with a 0.1 T whole-body MRI unit. Initial evaluation was based on a phantom replica of a human-lung cross-section, allowing comparison between numerical simulations and actually-acquired experimental data that address specific issues with hyperpolarized substances. First accelerated imaging acquisitions were achieved. They exhibited fairly good SNR both in vitro and *in vivo*. Phantom images with scan time reduction have been reconstructed while keeping same SNR by imposing constant the Fourier-domain filtering effect inherent to prepared magnetization. Centrically-reordered scans led to negligible reconstruction artifacts.

1304. Human Pulmonary Gas State Imaging at 0.2T with Hyperpolarized 129Xe

Samuel Patz[1], Iga Muradian, [12], Mirko I. Hrovat[3], James P. Butler[4], George P. Topulos[1], Steven Ketel[2], Iulian C. Ruset[2], Silviu Covrig[2], F. William Hersman[2]
[1]Brigham and Women's Hospital, Boston, Massachusetts, USA; [2]University of New Hampshire, Durham, New Hampshire, USA; [3]Mirtech, Inc., Brockton, Massachusetts, USA; [4]Harvard School of Public Health, Boston, Massachusetts, USA

This abstract presents an overview of human pulmonary gas-state imaging results with hyperpolarized 129Xe from over 120 breath-hold experiments on 10 different human subjects at 0.2T. Results include 2D multi-slice ventilation and ADC images as well as dynamic (movies) of inhalation and exhalation.

1305. Human Pulmonary PO2 at 0.2T with Hyperpolarized 129Xe

Mirko I. Hrovat[1], Iga Muradian[2], Steven Ketel[2], F. William Hersman[2], Samuel Patz[3], James P. Butler[4], George P. Topulos[3], Iulian C. Ruset[2], Silviu Covrig[2]
[1]Mirtech, Inc., Brockton, Massachusetts, USA; [2]University of New Hampshire, Durham, New Hampshire, USA; [3]Brigham and Women's Hospital, Boston, Massachusetts, USA; [4]Harvard School of Public Health, Boston, Massachusetts, USA

Variable flip angle techniques may be used to enhance measurements of intrapulmonary pO2 and temporal pO2 depletion utilizing hyperpolarized gasses. The Bloch equations have been modified to take into account the effects of magnetization depletion due to rf excitation. Thus new sequences are devisable to potentially provide a more sensitive indicator of lung pO2 and in particular temporal pO2 depletion due to Oxygen uptake. Regional pO2 measurements with hyperpolarized 3He have been reported [1,2]. Initial results are reported using hyperpolarized Xe in humans indicating that interpretation of hyperpolarized Xe measurements as a measure of intrapulmonary pO2 is potentially more difficult.

1306. Optimised FLASH Sequences for Examinations of the Human Lung at 0.2 Tesla

Markus Oechsner[1], Meinrad Beer[1], Eberhard D. Pracht[1], Herbert Köstler[1], Dietbert Hahn[1], Markus Weininger[1], Matthias Beissert[1], Peter M. Jakob[1]
[1]University of Würzburg, Würzburg, Bavaria, Germany

The object of this work is the optimisation of 2D- and 3D FLASH sequences for examinations of the human lung at 0.2 Tesla The relaxation times T1 and T2* were measured and appropriate sequence parameters were calculated. The optimised FLASH sequences provide a high SNR in lung parenchyma and simultaneously allows for the aquisition of an adequate number of images in one breath-hold. First examinations of cystic fibrosis showed a clear contrast between healthy and diseased tissue. Examinations of the human lung with FLASH sequences seem to be promising at low magnetic fields.

1307. Oxygen-Enhanced MRI of the Lung at 3 Tesla: Feasibility and T1 Relaxation Times

Olaf Dietrich[1], José G. Raya[1], Ulrike Fasol[1], Michael Peller[1], Maximilian F. Reiser[1], Stefan O. Schoenberg[1]
[1]Ludwig Maximilian University of Munich, Munich, Germany

The purpose of this study was to demonstrate the feasibility of oxygen-enhanced MRI (O_2-MRI) of the lung at a field strength of 3 Tesla and to determine the T1 relaxation time of lung tissue at 3 Tesla during inhalation of room air and oxygen. 3 volunteers were examined with a non-selective saturation recovery HASTE sequence. The mean T1 values of lung tissue found were (1281±124)ms during inhalation of room air and (1102±135 ms during inhalation of oxygen, i.e. oxygen breathing reduced T1 by 14%. Our results demonstrate that O_2-MRI of the lung using a saturation-prepared HASTE sequence is feasible.

1308. Half-Fourier Single-Shot Turbo Spin-Echo (HASTE) of the Lung at 3T: Feasibility Study Using Parallel Imaging with 32-Receiver Channel Technology

Christian Fink[1], Olaf Dietrich[1], Roger Eibel[1], Peter Herzog[1], Daniel Theisen[1], Titus Lanz[2], Maximilian F. Reiser[1], Stefan O. Schoenberg[1]
[1]University of Munich, Munich, NA, Germany; [2]Rapid Biomedical, Rimpar, NA, Germany

In this study the feasibility of HASTE of the lung at 3T using parallel imaging with a dedicated 32-receiver channel technology was assessed. Our results indicate that acceleration factors up to 4 can be achieved without degradation of the image quality (e.g. due to artefacts and poor signal to noise ratio). Expiratory scanning may be favourable to compensate for susceptibility associated signal loss of the lung at 3T.

1309. Comparing Gd Contrast and Non-Contrast Lung Perfusion Imaging at 1.5T and 3T

Sergei I. Obruchkov[1], Michael D. Noseworthy[1]
[1]McMaster University, Hamilton, Ontario, Canada

Two different approaches to lung perfusion were examined, a non contrast free breathing technique with respiratory and cardiac gating was compared to a breath held Gd-enhanced lung perfusion MR imaging. Two techniques were evaluated at two field strengths: 3T and 1.5T. Despite worsening susceptibility at higher field, a 3T MR scanner can be used for evaluation of lung perfusion. We suggest increased SNR at higher field allows non-contrast based MR perfusion imaging comparable to Gd-based bolus methods. Making it possible performing perfusion imaging in clinical populations, where the use of breath holds is often intolerable by patients.

1310. Influence of Inspiration Level on Hyperpolarized ^{3}He ADC in Healthy Lungs

Lise Vejby Søgaard[1], Trine Stavngaard[1], Jörg Schmiedeskamp[2], Wolfgang G. Schreiber[3]
[1]Copenhagen University Hospital, Hvidovre, Denmark; [2]Johannes Gutenberg-University, Mainz, Germany; [3]Johannes Gutenberg-University Medical School, Mainz, Germany

Hyperpolarized ^{3}He ADC is a sensitive probe of the micro-structure in the lung and may have the potential to detect early changes in emphysema and to monitor treatment response in patients. However, the ADC dependence on inspiration level has not been studied in much detail previously. In this work the ADC was measured for four different inspiration levels in three healthy subjects. The ADC values were found to increase with increasing respiratory level. Careful control of the inspiration status is nescessary in order to detect small changes in longitudinal studies and in the diagnosis of early emphysema.

1311. Nonlinear Fitting Method for High Resolution Mapping of Apparent Diffusion Coefficient (ADC) by Hyperpolarized 3He

JiangSheng Yu[1], Stephen Kadlecek[1], Masaru Ishii[2], John MacDuffie Woodburn[1], Kiarash Emami[1], Vahid Vahdat[1], Sheeva Rajaei[1], Frank Hammond[1], Letitia R. Cheatham[1], Benjamin M. Brainard[1], Timothy W.I. Clark[3], David A. Lipson[1], Warren B. Gefter[1], Rahim R. Rizi[1]
[1]University of Pennsylvania, Philadelphia, Pennsylvania, USA; [2]Johns Hopkins University, Baltimore, Maryland, USA; [3]New York University, New York, New York, USA

Hyperpolarized 3He diffusion MRI imaging shows the promise of measuring the lung structure at the microscopic level non-invasively, characterized by the Apparent Diffusion Coefficient (ADC)[1]. The conventional linear fitting method is prone to noise perturbation when image resolution is high. We present here a nonlinear fitting technique for accurate high resolution ADC mapping.

1312. Time Dependence of ^{3}He Diffusion in the Human Lung: Measurement in the Long-Time Regime Using Stimulated Echoes

Nominated for an ISMRM Poster Award

Chengbo Wang[1], Grady W. Miller[1], Talissa A. Altes, [1,2], Eduard E. de Lange[1], John P. Mugler, III[1]
[1]University of Virginia, Charlottesville, Virginia, USA; [2]Children's Hospital of Philadephia, Philadelphia, Pennsylvania, USA

A stimulated-echo-based technique was developed for measuring the long-time-scale apparent diffusion coefficient (ADC) of hyperpolarized ^{3}He in the lung. Computer simulations and phantom studies were used to validate our method. In ten healthy subjects, we found that the long-time-scale global ADC decreased substantially with increasing diffusion time. ADC maps in healthy subjects were uniform. In two COPD subjects, global ADC values at all diffusion times and the means of ADC maps were both significantly elevated compared to healthy subjects. In addition, regional elevation of ADC values was far more conspicuous on long-time-scale ADC maps than on short-time-scale ADC maps.

1313. Evidence of Background-Gradient Effects in GRE-Based ^{3}He Diffusion MRI

John P. Mugler III[1], Jaime F. Mata[1], Talissa A. Altes[1, 2], G. Wilson Miller[1], Eduard E. de Lange[1], William A. Tobias[1], Gordon D. Cates Jr. [1], James R. Brookeman[1]

[1]University of Virginia, Charlottesville, Virginia, USA; [2]Children's Hospital of Philadelphia, Philadelphia, Pennsylvania, USA

Since ^{3}He diffusion MRI commonly uses GRE-based methods, and because the lung by nature contains countless air-tissue interfaces, which lead to a very inhomogeneous magnetic environment, it is reasonable to expect that susceptibility-induced background gradients may influence ^{3}He ADC measurements. For GRE-based diffusion acquisitions that use a pair of bipolar gradient waveforms with an intervening time delay for diffusion sensitization, we observed an increase in the measured ADC with an increase in the time delay and, in a subject with COPD that exhibited a wide range of ADC values, we observed that this increase is inversely correlated with ADC value.

1314. The Relationship Between ^{3}He ADC and Lung Volume

Jason C. Woods[1], David S. Gierada[1], Yulin V. Chang[1], Barbara A. Lutey[1], Andrew J. Bierhals[1], Dmitriy A. Yablonskiy[1], Mark S. Conradi[1]

[1]Washington University, St Louis, Missouri, USA

^{3}He diffusion MRI has the likely application of characterizing alveolar spaces in health and disease. Recent comparisons to morphometry in healthy and diseased lungs has more rigidly validated the ^{3}He ADC as indicating alveolar size. The relationship between ^{3}He diffusivity and lung volume, however, is largely unknown. We imaged three volunteers and four normal donor lungs (rejected for transplantation) at multiple inflation volumes and determined that ADC is a weak, linear function of lung volume in the range of normal inspiration. For a volume of 0.5 times the lung's TLC, ADC is reduced to 78% of its value at TLC.

1315. Single Scan Acquisition of Hyperpolarized 3He Ventilation Images and ADC Images Using a Hybrid 2D Sequence

Jim M. Wild[1], Neil Woodhouse[1], Kevin Teh[1]

[1]University of Sheffield, Sheffield, Yorkshire, UK

A hybrid 2D ADC-ventilation sequence is presented which uses low flip angles to acquire both exams in the same breath-hold. The performance of the sequence was investigated *in vivo* in comparison with a conventional 2D ventilation imaging sequence. Acquisition of the ADC and ventilation images in one breath-hold provides ventilation images with comparable SNR and accurate high-resolution ADC images. The hybrid sequence used 2/3 of the gas needed for separate ADC and ventilation exams and saved the subject performing and extra breath-hold. The data is inherently registered allowing quantitative cross correlation between high spatial resolution ADC and ventilation data.

1316. How to Optimize *b*-Values for *In Vivo* Lung Morphometry with ^{3}He Diffusion MR

Alexander L. Sukstanskii[1], Yulin V. Chang[1], G. Larry Bretthorst[1], Mark S. Conradi[1], Dmitriy A. Yablonskiy[1]

[1]Washington University, St. Louis, Missouri, USA

In vivo lung morphometry can be evaluated based on measurement of anisotropic diffusion of 3He gas in acinar lung airways. However, for this method to become a robust tool for clinical and research applications, the accuracy of this method has to be analyzed. Herein we present a theoretical analysis of estimated experimental errors inherent to this approach. We derive expressions representing a dependence of the errors on experimental conditions and diffusion pulse sequence b-values. We demonstrate that accurate results can be achieved for a rather broad range of b-values, well compatible with the capabilities of clinical MRI scanners.

1317. Diffusion Corrected Reconstructions of Partial Pressure of Oxygen Using Polarized Gas MRI

Masaru Ishii[1, 2], JiangSheng Yu[2], Vahid Vahdat[2], John MacDuffie Woodburn[2], Sheeva Rajaei[2], Kiarash Emami[2], Frank Hammond[2], Stephen Kadlecek[2], Rahim R. Rizi[2]

[1]Johns Hopkins University, Baltimore, Maryland, USA; [2]University of Pennsylvania, Philadelphia, Pennsylvania, USA

Hyperpolarized (HP) 3He MRI measures of regional oxygen tensions provide important insight into lung function under physiologic and pathophysiologic conditions. This stems from the unique correlation between the lung's steady state oxygen tensions and its ventilation perfusion ratios; a similar relationship exists between the lung's the oxygen degradation rate and local alveolar perfusion. Thus these measures are of great interest to pulmonologists and physiologists. Current HP oxygen measurement techniques assume that diffusion of the HP gas during the measurement cycle affects the measured signal intensity negligibly. We show that under many conditions this assumption is false and severely degrades measurement accuracy; we present the first direct oxygen reconstruction algorithm for measuring regional oxygen tensions in the presence of a diffusing HP contrast agent. Numerical simulations and experimental results are presented as well.

1318. Quantification of Lung Tumor Volume and Rotation During Respiration Using 3D Dynamic Parallel MRI with View Sharing – Preliminary Results

Christian Plathow[1], Max Schoebinger[2], Christian Fink[3], Holger Hof[2], Claus Claussen[4], Heinz-Peter Meinzer[2], Hans-Ulrich Kauczor[2]

[1]Eberhard-Karls-University Tuebingen, Tuebingen, Baden-Württemberg, Germany; [2]German Cancer Research Center, Heidelberg, Baden-Wuerttemberg, Germany; [3]University of Munich, Munich, Bavaria, Germany; [4]Eberhard-Karls University, Tuebingen, Baden-Wuerttemberg, Germany

3D dMRI techniques using parallel imaging in combination with view-sharing and dedicated postprocessing techniques make it possible to non-invasively quantify volume and rotation of pulmonary nodules during respiration.

1319. Oxygen-Enhanced MRI of the Lung: Optimized Calculation of Difference Images

Olaf Dietrich[1], Michael Peller[1], Ulrike Fasol[1], Christoph Losert[1], Konstantin Nikolaou[1], Maximilian F. Reiser[1], Stefan O. Schoenberg[1]

[1]Ludwig Maximilian University of Munich, Munich, Germany

The purpose of this study was to analyze how the calculated relative signal increase (δS_{rel}) in oxygen-enhanced lung MRI depends on the intermediary signal observed immediately after switching the gas supply. 4×20 repetitions (1:air, 2:O_2, 3:air, 4:O_2) were continuously acquired in 10 healthy volunteers. Data was post-processed discarding between 0 and 19 repetitions after each change of gas supply before calculating δS_{rel}. The averaged δS_{rel} increases from 9.4% to 17.4% with increasing number of discarded acquisitions; the ratio of δS_{rel} and spatial standard deviation of δS_{rel} has a maximum at 5 to 8 discarded acquisitions.

1320. A Diffusion Coefficient Distribution Model to Describe the B-Value Dependence of ADC in Diffusion-Weighted Hyperpolarized Gas MRI

Rafael Luis O'Halloran[1], James H. Holmes[1], Andrew L. Alexander[1], Sean B. Fain[1]

[1]University of Wisconsin, Madison, Wisconsin, USA

A quantitative model for understanding the dependence of apparent diffusion coefficient on b-value is presented. In this model it is possible to obtain information about the degree of restricted diffusion in the medium of interest. The model is applied to hyperpolarized (HP) gas MRI data from two porous phantoms and rat lungs and appears to agree well with expected levels of restriction.

1321. Computer Simulations and Experimental Tests of Surface-To-Volume Measurements Using 3He NMR

Michael Carl[1], G Wilson Miller[1], John P. Mugler III[1], Gordon D. Cates[1]

[1]University of Virginia, Charlottesville, Virginia, USA

The feasibility of surface-to-volume measurements using gas diffusion NMR is explored. Computer simulations were performed and compared with the results of experimental tests conducted on a one-inch sphere containing hyperpolarized 3He.

1322. Long-Range Diffusion of ^{3}He in Lungs: Evidence for Collateral Ventilation Pathways from Comparison of Computer Simulations and Measurements

Seth-Emil Thomas Bartel[1], Susan E. Haywood[1], Mark S. Conradi[1], Jason C. Woods[1], David S. Gierada[1]

[1]Washington University, St. Louis, Missouri, USA

A computer simulation of diffusion within a regular symmetric dichotomous branching model of human lungs has shown the long-range effective diffusivity to be roughly 20 times smaller than what has previously been measured in healthy lungs. Collateral ventilation pathways, which were not implemented in the simulation, may help explain this discrepancy. The simulations and measurements on a healthy volunteer at two different lung volumes preliminarily suggest the role of collateral pathways in long-range diffusion.

1323. Experimental Study of Gas Diffusion in a Pulmonary Acinus Model

Dayane Habib[1], Denis Grebenkov[1], Xavier Maître[1], Ludovic De Rochefort[1], Emmanuel Durand[1], Geneviève Guillot[1]

[1]Université Paris-Sud Bât.220, Orsay, France

The 3D architecture of the pulmonary acinus is a dichotomic branching structure. This could play a role in the non-Gaussian behavior of the signal attenuation as a function of gradient intensity, for measurements of 3He diffusion in human lungs, previously attributed to anisotropic diffusion. A 3D phantom (channels of 3 mm size, total size 28 mm) with a branching structure topologically equivalent to that of the acinus was built, in which diffusion-weighted measurements were performed and compared to different models and to numerical simulations. The numerical approach was in better agreement with the experiments than the existing models.

1324. Quantitative MR Imaging of 3He Gas Transport in Model Airways

Kevin R. Minard[1], Richard E. Jacob[1]
[1]Pacific Northwest National Laboratory, Richland, Washington, USA

The feasibility of quantifying gas transport in the major airways of adult rats is examined by employing two-dimensional (2D) constant-time imaging (CTI) for measuring the dynamics of hyperpolarized (HP) 3He in a straight pipe with a diameter comparable to the rat trachea. At physiological flow rates, measured maps of axial flow and diffusion are shown to be accurately predicted using a simple transport model that describes 3He's diffusion across flow lamina. Since the diffusion-mediated model is generally applicable to any flow conduit, results provide a quantitative basis for studying gas transport with noninvasive 3He MRI.

1325. Velocimetry of Hyperpolarized Rare Gases: Phantom Studies and First *In Vivo* Results

Wolfgang Kilian[1], Max Strowig[1], Frank Seifert[1]
[1]Physikalisch-Technische Bundesanstalt, 10587 Berlin, Germany

For characterizing lung diseases or optimizing artificial respiration there is great interest in the dynamics of gas flow to the lungs. We have implied and tested a MR sequence for measuring gas-flow velocities using phase encoding techniques in combination with hyperpolarized ^{129}Xe gas. To reduce artifacts, the k-space lines of the flow compensated and the flow weighted images were sampled in an interleaved scheme. In tests with phantoms we found excellent agreement between theoretically calculated velocities and those derived from the MR measurements. In the *in vivo* measurements we got good velocity maps within the trachea.

1326. Quantitation of Pulmonary Structure Via Registration and Normalization of Serial ^{3}He MR Images

James Gee[1], Tessa Sundaram[1], Brian Avants[1], Pablo Burstein[1], Paul Yushkevich[1], Hui Zhang[1], Ingrid Casselbrant[2], Per Akeson[2], Goran Pettersson[3], Brad Wyman[4], Barry Peterson[4]
[1]University of Pennsylvania, Philadelphia, Pennsylvania, USA; [2]Malmo University Hospital, Malmo, Sweden; [3]General Electric, Malmo, Sweden; [4]Pfizer, Groton, Connecticut, USA

MR imaging of inhaled hyperpolarized helium has been shown to provide reproducible measures of lung structure. This work demonstrates that registration can be performed both to align individual longitudinal 3He MR images and to normalize this data from different individuals to a lung atlas. The former capability enables maps of longitudinal changes in ADC value to be automatically obtained, and the latter normalization makes possible regional or voxelwise comparisons of ADC behavior in different subject groups. These results indicate the feasibility of anatomically detailed detection and monitoring of lung structural changes in health and disease with hyperpolarized gas imaging.

Lung Imaging: Animal Model & Hyperpolarized Gases

Room 4E Monday 14:00 - 16:00

1327. Improved Determination of Hyperpolarized ^{129}Xe T_1 in the Rat Brain

Xin Zhou[1], Mary Lynn Mazzanti[1], Jianbing James Chen[1], Joey Karim Mansour[1], Jessica Dickey Gereige[1], Arvind K. Venkatesh[1], Yanping Sun[1], Robert V. Mulkern[1], Mitchell S. Albert[1]
[1]Brigham and Women's Hospital, Harvard Medical School, Boston, Massachusetts, USA

Signal dynamics properties of hyperpolarized (HP) ^{129}Xe are important for magnetic resonance imaging of the brain. However, the published T_1 values of HP ^{129}Xe in rat brain vary widely, ranging from 3.6 to 26 seconds. In our study, by applying an SNR threshold to minimize the effect of noise, 2 approaches to measuring the T_1 of HP ^{129}Xe in the rat brain yielded values of 14.9±1.4 and 16.4±2.2 seconds, respectively, which are highly consistent.

1328. Hyperpolarized 13C MRI Cineangiography of Pulmonary Perfusion

Masaru Ishii[1], Kiarash Emami[2], Stephen Kadlecek[2], Sheeva Rajaei[2], JiangSheng Yu[2], John MacDuffie Woodburn[2], Frank Hammond[2], Vahid Vahdat[2], J Stefan Petersson[3], Klaes Golman[3], Rahim R. Rizi[2]
[1]Johns Hopkins University, Baltimore, Maryland, USA; [2]University of Pennsylvania, Philadelphia, Pennsylvania, USA; [3]GE Healthcare, Malmo, Sweden

Noninvasive measures of pulmonary perfusion may prove useful for the understanding of many physiologic and pathophysiologic conditions. In this work, we present a study of MRI cineangiogrpahy of pulmonary perfusion using a water-soluble hyperpolarized (HP) 13C MRI contrast agent- 2-hydroxyethy acrylate. We show that HP 13C MRI is well suited to these types of studies due to its high temporal resolution, absence of background signal, and large signal to noise ratios.

1329. Parametric Mapping of Ex-Vivo Mouse Lung at 9.4 Tesla with Air-Inflation Fixation Method

Hidemasa Uematsu[1], Suzanne L. Wehrli[2], Masaya Takahashi[3], Hiroto Hatabu[3], Toshio Asakura[2]
[1]University of Fukui, Fukui, Japan; [2]Children's Hospital of Philadelphia, Philadelphia, Pennsylvania, USA; [3]Beth Israel Deaconess Medical Center, Harvard Medical School, Boston, Massachusetts, USA

We hypothesized that MRI of isolated lungs would produce a considerable signal enabling characterization of the relaxation times of various lung disorders. Wild-type mice and transgenic sickle mice were included in the study. Diffuse signal increase was demonstrated in transgenic mice lungs. The mean T1 and T2 of transgenic mice were significantly lower than those of wild-type mice. Histological analysis of transgenic mice lungs revealed numerous deformed red blood cells occupying the capillaries and small vessels, causing significant reduction in relaxation time due to deoxy-Hb. T1 and T2 characterization may provide additional information regarding lung disorders.

1330. A Delivery System for Hyperpolarized 129Xe MRI of Small Animal Lungs

Shing-Jong Huang[1], Chao-Hsien Hsieh[2], Jyh-Horng Chen[2], Shang-Bin Liu[1], Yeun-Chung Chang[3]
[1]Academia Sinica, Taipei, Taiwan; [2]National Taiwan University, Taipei, Taiwan; [3]National Taiwan University Hospital and College of Medicine, Taipei, Taiwan

Hyperpolarized (HP) 129Xe MRI has been demonstrated as a promising tool for diagnosis of pulmonary diseases. In this preliminary study, we designed and tested a storage/delivery system for HP 129Xe MRI to facilitate freezing and thawing cyclic operations while preserving majority of the spin depolarization with sustainable relaxation. The spin-lattice relaxation times (T1) of HP 129Xe gas in the storage and the delivery chamber were found to be 155.0 and 71.4 minutes, respectively, and hence practical for applications of HP 129Xe MRI in small animal lung and related disease diagnosis studies, which have been undertaken.

1331. Respiratory-Gated 3D Fast Spin-Echo for Oxygen-Enhanced MR Imaging of Mice Lungs

Kristina Nancy Watt[1, 2], Brian J. Nieman[1, 2], Jonathan Bishop[1], Ryan Mark Henkelman[1, 2], Josette Chen[1, 2]
[1]Mouse Imaging Centre (MICe), Hospital for Sick Children, Toronto, ON, Canada; [2]University of Toronto, Toronto, ON, Canada

Oxygen-enhanced MR imaging enables evaluation of regional lung ventilation by using inhaled molecular oxygen as a paramagnetic contrast agent. Oxygen-induced increases in signal intensity of lung parenchyma are often obscured by motion artifacts arising from cardiopulmonary physiology. Addressing this limitation, this study presents a cardiac-triggered respiratory-gated 3D fast spin-echo sequence suitable for small animal oxygen-enhanced imaging. Ghosting artifacts due to variations in cardiac and respiratory rates were reduced with a gating scheme that maintained steady-state magnetization. It is demonstrated in oxygen-enhanced imaging of a normal free-breathing mouse and shows potential for future application to studies of experimental mouse models.

1332. Experimental Validation of a Model for the Field Dependence of the SNR of Hyperpolarized Noble Gas MR Imaging of Rodent Lungs *In Vivo*

Juan Parra-Robles[1], William Dominguez Viqueira[1], Alexei Ouriadov[1], Wilfred Lam[1], Nishard Abdeen[2], Giles E. Santyr[1]
[1]Robarts Research Institute, London, Ontario, Canada; [2]Carleton University, Ottawa, Ontario, Canada

In this work the magnetic field strength dependence of the SNR for imaging of small animal lungs *in vivo* is experimentally verified for rat lung images and spectra obtained at 17 mT and 1.89 T using xenon gas and at 3T using helium. In order to estimate the field strength giving optimal SNR, the ratio of noise contributions between the coil and the sample is theoretically predicted and experimentally measured for a range of resonant frequencies and coil and sample sizes. This study validates the theoretical model *in vivo* for the field dependence of the SNR and indicates that high field strengths (frequencies) may be optimal for HNG lung imaging of small animals such as rats (80-100 MHz) and mice (100-130 MHz).

1333. Registered ^{3}He Ventilation and ^{1}H Perfusion Dynamic Contrast Enhanced MRI in the Rodent Lung

Nilesh N. Mistry[1], Jim R. Pollaro[1], Laurence W. Hedlund[1], Glenn Allan Johnson[1]
[1]Duke University, Durham, North Carolina, USA

Pulmonary function estimates for disease models such as pulmonary emboli, airway obstruction, pneumonitis provide useful information to the pulmonary physiologists. Dynamic contrast enhanced (DCE) MRI is difficult to perform in the rodent lungs due to its low proton density, large number of air/tissue interfaces, and higher spatio-temporal resolution requirements compared to humans. This work explores the feasibility of performing combined ^{3}He (ventilation) and DCE ^{1}H (perfusion) imaging in the rat. Successful dynamic first pass data acquisition is possible using multiple controlled bolus injections. Qualitative and quantitative analysis can be performed providing useful functional ventilation/perfusion information.

1334. Comparison of Hyperpolarized Helium MR Imaging of Regional Ventilation with Xenon-Enhanced CT in Rodents

Giles Santyr[1], Wilfred Lam[1], Alexei Ouriadov[1], Maria Drangova[1], David McCormack[2], David Holdsworth[1]
[1]Robarts Research Institute, London, Ontario, Canada; [2]London Health Sciences Centre, London, Ontario, Canada

Hyperpolarized helium gas can be used to measure regional ventilation in the rodent lung, however, this approach requires knowledge and or assumptions involving spin-lattice relaxation, T1, of the gas in the ventilator system and in the lung; the latter requiring knowledge of the alveolar oxygen partial pressure. An established method for regional ventilation mapping is xenon-enhanced CT, which is independent of relaxation effects. In this work, helium MR imaging and xenon-enhanced CT imaging of ventilation are compared in rats. The results indicate that ventilation measurements obtained by helium MR are comparable to xenon-enhanced CT without the associated x-ray dose.

1335. Measurement of Nonlinear Decay of Alveolar Partial Pressure of Oxygen in Mice Using 3He-MRI

Katarzyna Cieslar[1], Hasan Alsaid[2], Vasile Stupar[2], Sophie Gaillard[2], Rachida Fissoune[2], Emmanuelle Canet-Soulas[2], Yannick Cremillieux[2]

[1]Jagiellonian University, Institute of Physics, Krakow, Poland; [2]Univeriste Claude Bernard Lyon1, Lyon, France

The objective of the study was to measure the time course of oxygen partial pressure (pO2) in the mouse lung. During breath-hold oxygen removal from the lungs in exponential with time. However, all previous studies assumed linear decrease of pO2 during short periods of apnea. High metabolic rate of mice results in pO2 decay time being in the range of attainable imaging time posing a demand to use a nonlinear model of pO2 decrease. We show in this study that it is possible to perform pO2 measurements in mice using this novel approach.

1336. *In Vivo* Measurement of T2 Relaxation of Mouse Lungs During Inspiration and Expiration

Lars E. Olsson[1], Paul D. Hockings[1]

[1]AstraZeneca, Mölndal, Sweden

T2 relaxation of mouse lungs at end-expiration and end-inspiration was measured *in vivo* at 4.7 T (CPMG, interecho time 3.5 ms). T2 was longer ($p<0.01$) at end-expiration (9.7±0.7 ms) than at end-inspiration (9.0±0.8 ms). Relative proton density (lung/muscle tissue) was higher ($p<0.001$) during expiration (0.61±0.06), than inspiration (0.48±0.05). T2 increased linearly ($p< 0.001$, $r2=0.49$) with increasing proton density. To our knowledge, this is the first time the phenomenon is observed *in vivo* and for a normal breathing cycle.

1337. Alveolar Oxygen Partial Pressure and Oxygen Depletion Rate Mapping in Rats Using 3He-MRI

Katarzyna Cieslar[1], Vasile Stupar[2], Sophie Gaillard[2], Emmanuelle Canet-Soulas[2], Yannick Cremillieux[2]

[1]Jagiellonian University, Institute of Physics, Krakow, Poland; [2]Univeriste Claude Bernard Lyon1, Lyon, France

Alveolar partial pressure of oxygen (pO2) and its depletion rate (R) are important parameters for lung function assessment. Since there is variety of well established rodent animal models of lung diseases regional information on these parameters in small animals is desirable. For this purpose a novel single acquisition pO2 sensitive method has been developed with sliding window technique used for RF flip angle correction. The first maps of initial pO2 and R in rats are demonstrated using this protocol.

1338. Retrospective Cine ^{3}He Ventilation Imaging Under Spontaneous Breathing Conditions: A Non Invasive Imaging Protocol for Small Animal Lung Function Imaging

Vasile Stupar[1], Emmanuelle Canet Soulas[1], Hasan Alsaid[1], Sophie Gaillard[1], Nicolau Beckmann[2], Yannick Crémillieux[1]

[1]Laboratoire de RMN, UMR CNRS5012, Université Lyon1, ESCPE, Villeurbanne, France; [2]Discovery Technologies, Novartis Institutes for BioMedical Research, Basel, Switzerland

Up to date, small animal hyperpolarized 3He ventilation studies have been performed using animal tracheotomy or intubation procedures combined with assisted ventilation. These approaches are traumatic for the animal and are not suited for longitudinal studies. In this work we propose and demonstrate a non-invasive ventilation imaging protocol based on spontaneous animal breathing combined with retrospective radial CINE imaging and sliding window techniques. The complete breathing cycle was imaged by shifting the 100ms acquisition window by 5ms. This imaging protocol makes possible the performance of longitudinal studies for the investigation of pulmonary physiological or physio-pathological processes in small animals.

1339. Detection of Pulmonary Emboli by Hyperpolarized Carbon-13 in Pig Model

Masaru Ishii[1], Stephen Kadlecek[2], JiangSheng Yu[2], Sheeva Rajaei[2], Kiarash Emami[2], Vahid Vahdat[2], John MacDuffie Woodburn[2], Frank Hammond[2], J Stefan Petersson[3], Klaes Golman[3], Rahim R. Rizi[2]

[1]Johns Hopkins University, Baltimore, Maryland, USA; [2]University of Pennsylvania, Philadelphia, Pennsylvania, USA; [3]GE Healthcare, Malmo, Sweden

Water-soluble hyperpolarized (HP) 13C compounds represent a new class of MRI contrast agents which may revolutionize metabolic and functional imaging. We present a novel technique for the detection of pulmonary emboli created in a porcine model using the HP MRI contrast agent 2-hydroxyethyl acrylate. Our results indicate that HP 13C MRI angiography is a viable method for detecting pulmonary emboli.

1340. Nonlinear Fitting Method for the Measurements of Regional Alveolar Oxygen Pressure and Oxygen Depletion Rate by Hyperpolarized 3He MRI

JiangSheng Yu[1], Kiarash Emami[1], Masaru Ishii[2], John MacDuffie Woodburn[1], Sheeva Rajaei[1], David Lipson[1], Vahid Vahdat[1], Stephen Kadlecek[1], Frank Hammond[1], Timothy W.I. Clark[3], Benjamin M. Brainard[1], Letitia R. Cheatham[1], Warren B. Gefter[1], Rahim R. Rizi[1]

[1]University of Pennsylvania, Philadelphia, Pennsylvania, USA; [2]Johns Hopkins University, Baltimore, Maryland, USA; [3]New York University School of Medicine, New York, New York, USA

The regional alveolar oxygen partial pressure and regional oxygen depletion rate are important functional lung parameters. We present here a new nonlinear fitting technique for measuring these parameters, with a new timing scheme suitable for managing multiple-slice measurements.

1341. Diffusion Imaging with Hyperpolarized Helium MR in Surfactant Protien C Deficient Mice

Casey B. Orellana[1], Yulin V. Chang[1], Jason C. Woods[1], Richard E. Jacob[1], John A. Engelbach[1], Jeffrey A. Whitsett[2], Mark S. Conradi[1], Jeff J. Neil[1]

[1]Washington University, St. Louis, Missouri, USA; [2]Cincinnati Children's Hospital Medical Center, Cincinnati, Ohio, USA

Hyperpolarized 3He diffusion imaging was employed to evaluate normal and surfactant protein C deficient mice. Mice were imaged at age 8-10 months of age, a time at which pulmonary fibrosis would be expected to reduce alveolar size in affected mice. The apparent diffusion coefficients in two control animals were 0.144 and 0.181 cm2/s, as compared with 0.127 ± 0.020 cm2/s (n = 4) in surfactant-deficient animals. This study demonstrates the feasibility of making 3He diffusion measurements in transgenic mice. Further, the trend towards lower apparent diffusion coefficient values in affected animals is consistent with known pulmonary pathology in this model.

1342. Three-Dimensional Magnetic Resonance Microscopy of Pulmonary Solitary Tumors in Transgenic Mice

Masaya Takahashi[1], Shigeto Kubo[1], Elena Levantini[1], Susumu Kobayashi[1], Olivier Kocher[1], Daniel G. Tenen[1]

[1]Beth Israel Deaconess Medical Center, Boston, Massachusetts, USA

The field of cancer modeling in mice is progressing at an accelerated pace to create mouse models that accurately reproduce the genetic and histopathological alterations present in human tumors. This has highlighted the need to follow the temporal and spatial patterns of pulmonary solitary tumor progression in small rodents. Using synergistic strategies to increase MR microscopic sensitivity, we attempted to detect, characterize and volumetrically analyze the pulmonary solitary tumors *in vivo*. The results showed that the correlation with histological findings was over 95%, which offers the promise of *in vivo* MR microscopic assessment of pulmonary solitary tumors in transgenic mice.

1343. Evaluation of Emphysema Severity and Progression in a Rabbit Model: A Comparison of Hyperpolarized He-3 and Xe-129 ADC with Morphometry

Jaime Mata[1], Talissa Altes[1, 2], Jing Cai[1], Kai Ruppert[3], Wayne Mitzner[4], James Brookeman[1], William Tobias[1], James Wang[1], Gordon Cates[1], John Mugler III[1]

[1]University of Virginia, Charlottesville, Virginia, USA; [2]Children's Hospital of Philadelphia, Philadelphia, Pennsylvania, USA; [3]AMRIT, Sebastopol, California, USA; [4]Johns Hopkins University, Baltimore, Maryland, USA

In this study, hyperpolarized helium-3 and xenon-129 Apparent Diffusion Coefficient values were measured multiple times in the lungs of rabbits with induced emphysema during 8 weeks following elastase administration. Histology and morphometry of the lungs were performed at the end of the 8-week period and correlated with the *in vivo* ADC values.

1344. SPI Measurement of MR Signal and T2* in Order to Characterize Emphysema Type Changes in a Tight Skin Mouse Model

Lars E. Olsson[1], Maria Lindahl[2], Malin Palmér[1], Martina Kvist Reimer[2], Leif Hultin[1], Per-Ola Önnervik[2], Paul D. Hockings[1]

[1]AstraZeneca, Mölndal, Sweden; [2]AstraZeneca, Lund, Sweden

MR signal intensity at short detection times (0.2 ms and 0.4 ms) and T2* of *in vivo* mouse lungs was measured at 4.7 T using Single Point Imaging. The Tight Skin mouse was used as a model for emphysema. *In vivo* microCT scanning and histology were used as reference methods. MR signal and T2* was significantly lower in lungs with emphysema than in controls. MR signal in lung parenchyma correlated linearly with CT mass density, and T2* correlated linearly with the alveoli size (MLI).

1345. Quantitative Assessment of Lung Volume Reduction Surgery Effectiveness in Improving Functional Pulmonary Performance of Emphysematous Subjects - A Small Animal Model

Kiarash Emami[1], Masaru Ishii[2], Jianliang Zhu[1], John MacDuffie Woodburn[1], Jiangsheng Yu[1], Stephen J. Kadlecek[1], Vahid Vahdat[1], Benjamin M. Brainard[1], Michael E. Friscia[1], Joseph B. Shrager[1], Rahim R. Rizi[1]

[1]University of Pennsylvania, Philadelphia, Pennsylvania, USA; [2]Johns Hopkins University, Baltimore, Maryland, USA

Emphysema is an obstructive lung disorder characterized by the progressive destruction of the lung parenchyma, leading to a loss of surface area for gas exchange, reduction in lung elastic recoil, and irreversible airflow obstruction. Lung volume reduction surgery (LVRS), which involves the surgical resection of the lung to improve the mechanics of respiration and thus gas exchange, has recently become recognized as an effective treatment for emphysema. In this work, we study the improvements in lung compliance, fractional ventilation, and lung architecture, measured by hyperpolarized (HP) 3He MRI, brought about by LVRS. Preliminary data suggests that LVRS improves regional compliance and fractional ventilation when regions of the lung with severely aberrant compliance are resected suggesting that HP 3He MRI measures of lung function may play an important role in patient selection of LRVS candidates.

1346. Elastase Induced Emphysematous Development Assessed by Proton MRI in Spontaneously Breathing Rats

Harry Karmouty Quintana[1, 2], Catherine Cannet[1], Stefan Zurbruegg[1], Lazzaro Mazzoni[1], John R. Fozard[1], Clive P. Page[2], Nicolau Beckmann[1]

[1]Novartis Institutes for BioMedical Research, Basel, Switzerland; [2]King's College London, London SE1 1UL, UK

Proton MRI was used to follow, in the rat lung, the effects of porcine pancreatic elastase challenge in a model of emphysema. Edematous signals seen 24h after intra-tracheal elastase administration completely resolved two weeks later. From this time point onwards, parenchymal signals were significantly reduced in several regions of the lung and an increase in lung volume observed, consistent with air trapping due to airspace enlargement and reduction in alveoli number revealed by histology. These data suggest that, in rats, emphysema is induced early following elastase. Treatment with all-trans-retinoic acid did not show a reversal of elastase induced effects.

1347. ^{3}He Imaging of Methacholine Challenge in Mouse Models of Asthma

Bastiaan Driehuys[1], Gary P. Cofer[1], Jim Pollaro[1], Julia K.L. Walker[1], David A. Schwartz[2], G A. Johnson[1]

[1]Duke University, Durham, North Carolina, USA; [2]National Institute for Environmental Health Sciences, Research Triangle Park, North Carolina, USA

The study of asthma increasingly relies on transgenic and knock-out mouse models to elucidate the fundamental underpinnings of this disease. Currently, only global measurements of airway pressure before and after methacholine challenge are the primary tool available, leaving fundamental questions unanswered, such as the degree of small versus large airway involvement, whether the site of broncho-constriction is reproducible, and the degree to which mouse models reproduce human disease. Here, we present the first observation of methacholine challenge in mice using a 5 minute scan consuming 100ml of hyperpolarized ^{3}He.

1348. Characterisation of Lipopolysaccharide Induced Pulmonary Oedema in Rats by MRI

Sarah Hotee[1, 2], Kumar Changani[2], Alan White[2], Kishore Bhakoo[1], Jimmy Bell[1]

[1]Imaging Sciences Department, Hammersmith, London, UK; [2]GSK, The Frythe, Welwyn, UK

Lipopolysaccharide (LPS) is an ubiquitous endotoxin which produces many of the pathophysiological features of acute respiratory distress syndrome (ARDS) including; rapid pulmonary oedema development, and pulmonary neutrophil influx. An understanding of the processes and mechanisms in early phase ARDS is essential for the development of therapeutic intervention. This study characterises the regional development of oedema and quantifies its volume over time (<4 hours post LPS challenge).

1349. MR Imaging of *Ex-Vivo* Rat Lung with Acute Respiratory Distress Syndrome: Air-Inflation Fixation Method

Nobuyuki Kosaka[1], Hidemasa Uematsu[1], Hirohiko Kimura[1], Akinobu Kita[2], Harumi Itoh[1]

[1]University of Fukui, Fukui, Japan; [2]University of Fukui Hospital, Fukui, Japan

We hypothesized that MRI could provide new information on an acute respiratory distress syndrome (ARDS) lung model using air-inflation fixation method. Seven ARDS rats were analyzed using a 1.5 T MR scanner with dual 3-inch surface coils. Lung injuries were visualized as the reticular signal increase of lung parenchyma in all subjects. The T1 and T2 values of ARDS lungs were 883.1±176.5 ms and 54.6±8.3 ms, respectively. The combination of MR imaging and the air-inflation fixation method could provide parametric information such as T1 and T2 values simultaneously with anatomical information in diffuse lung disease.

1350. Non-Invasive Monitoring of Lung Transplant Viability in a Small Animal Model Using MRI and PET

James H. Holmes[1], Rudolf K. Braun[1], Rafael L. O'Halloran[1], Zhuzai Xiang[1], Ronald L. Sorkness[1], Robert W. Pyzalski[1], Eric T. Peterson[1], Robert B. Love[1], Sean B. Fain[1]

[1]University of Madison-Wisconsin, Madison, Wisconsin, USA

Imaging holds promise for longitudinal assessment of lung transplant to assess individual organ viability regionally. The hypothesis of this study is that non-invasive MR imaging techniques can be used for early assessment of organ viability in lung transplant. Four rats received left lung transplants and were imaged at 1 and 2 weeks post-transplant using hyperpolarized He-3 MRI, T1-weighted proton MRI, and FDG PET. Changes detected in imaging were correlated to pathology of the lungs after 2 weeks. This work demonstrates the ability to assess transplant viability qualitatively using MRI techniques during longitudinal small animal studies.

Consoles and Interfaces

Room 4E Monday 14:00 - 16:00

1351. An Integrated MR Console / MR Physics Simulation System

Jonathan Sharp[1], Donghui Yin[2], Randy Tyson[1], Kan Lo[1], Boguslaw Tomanek[1]
[1]National Research Council of Canada, Calgary, Alberta, Canada; [2]National Research Council of Canada, Winnipeg, Manitoba, Canada

We describe the design and application of an integrated MR console / MR physics simulation system. The system consists of a research MR console, a full-function hardware-independent pulse programming environment (over 40 sequences implemented); and a 44 CPU parallel Linux cluster for full Bloch equation simulations with stochastic spin modeling. The system allows precise side-by-side comparisons of experimental vs. simulated data for any real (not simplified) pulse sequence, and has numerous applications in MR research and development. The console has been installed on a 9.4T MRI. Real and simulated data are shown for a SSFP sequence.

1352. A Scalable Prototype MR Console Using USB

Pascal Stang[1], Nathaniel Matter[1], Steve Conolly[2], John Pauly[1], Greig Scott[1]
[1]Stanford University, Stanford, California, USA; [2]UC Berkeley, Berkeley, California, USA

Modern MR systems are trending towards large parallel receiver and transmitter arrays. We are building a modular MR console as a set of Universal Serial Bus peripherals on a USB 2.0 High-Speed backbone to target parallel transmit and receive applications. Each USB node includes an embedded 32-bit controller, USB interface, and digital RF blocks or gradient coil outputs. We have demonstrated imaging using our prototype console with pulse sequencing, console control, and image reconstruction all from within Matlab. Our approach harnesses the scalability of USB, and modularity of digital RF technology and embedded systems, to enable parallel imaging in MRI.

1353. Electrically Isolated Power Delivery for MRI Applications

Jan Gustav Werthen[1], Mort J. Cohen[1], Ta-Chung Wu[1], Seni Widjaja[1]
[1]JDS Uniphase, San Jose, California, USA

Photonic power, a means of converting laser light over fiber into electric power, offers several advantages compared to copper in powering electronics in high magnetic fields. Photonic power is a fully-isolated, non-conductive means of powering imaging coils, control electronics, and video monitors in MR systems. Advantages include improved noise immunity, enhanced imaging, reduced risk of patient RF burns, and more reliable patient surveillance techniques. This paper will describe the implementation of this technology for use in a broad array of applications in the MRI environment.

1354. Surface MRI Using a Rastered Backprojection

Joseph P. Hornak[1], Christina L. Bray[1], Tyler Lucero[1], Allison Bright[1]
[1]RIT, Rochester, New York, USA

Magnetic resonance imaging (MRI) is typically performed by placing the imaged object within a spatially homogeneous magnetic and radio frequency (RF) fields. This convention restricts MRI to system geometries which surround the imaged object with a magnet and RF coil. Many applications could benefit from a surface MRI device where magnet and RF coil are adjacent to the imaged object. We have developed a proof-of-concept surface MRI system which uses an inhomogeneous magnetic field, RF surface coil, and unique reconstruction method to produce tomographic images. Details of our unique system and reconstruction technique, along with phantom images, are presented.

1355. Integration of an External Motion Tracking System with the MR Scanner for Highly Accurate Real-Time Prospective Motion Correction

Maxim Zaitsev[1], Christian Dold[2], Jürgen Hennig[1], Oliver Speck[1]
[1]University Hospital Freiburg, Freiburg, Germany; [2]Fraunhofer Institute for Computer Graphics, Darmstadt, Germany

Motion artefacts in MRI are a significant problem. Remedial approaches proposed typically require severe modifications of imaging techniques. The use of an external motion tracking hardware in combination with prospective real-time update of the imaging coordinates allows MR imaging of moving objects with the vast majority of standard techniques. High resolution imaging places stringent requirements on both spatial and temporal accuracy of the motion data. In this work a high precision stereoscopic motion tracking system is integrated with a scanner, a novel method for coordinate calibration is proposed and the total latency of the system is measured experimentally.

Multimodality and Novel Systems

Room 4E Monday 14:00 - 16:00

1356. Signal Optimization of Magnetic Field Pulses in Field-Cycled MRI

Jamu Krishna Alford[1], William Bradfield Handler[1], Timothy James Scholl[1], Blaine Alexander Chronik[1]
[1]University of Western Ontario, London, Ontario, Canada

Fielded-cycled MRI uses resistive magnets instead of superconducting magnets to produce tissue magnetization. Due to the T1 dispersion curve, modification of the magnetic waveforms will produce different amounts of magnetization. This design study discuses the benefits of various pulse sequences from the point of view of power-supply choice. It was found that that simple constant-voltage supplies produce magnetization equivalent to more complicated power-supplies for a given amount of magnet heating.

1357. Magnet Design and Construction for a Field-Cycled MRI/PET System

Kyle Michael Gilbert[1], William Bradfield Handler[1], Timothy James Scholl[1], Blaine Alexander Chronik[1]
[1]The University of Western Ontario, London, Ontario, Canada

Field-cycled MRI employs two actively controlled resistive magnets to polarize and subsequently image an object, the benefits of which include an increase in T1 dispersion contrast and a reduction in susceptibility artifacts. Due to the versatility in design of the main resistive magnets, an allotment of space can be made for the integration of a PET ring or SPECT camera. The construction of the main magnets for a dual-modality, field-cycled MRI/PET system is presented.

1358. Placing a PET Insert in the Bore of a 7T Magnet: Initial Study of the Interactions of the MRI System with the PET Shielding

Bo Joseph Peng[1], Ciprian Catana[1], Jeff Walton[1], Simon R. Cherry[1], Jacob Willig-Onwuachi[1, 2]
[1]University of California, Davis, California, USA; [2]UCDMC, Sacramento, California, USA

A new PET insert is being built for simultaneous PET and MR imaging at 7T with the PET electronics placed inside the magnet bore. Results are presented for preliminary investigation of interactions between the PET shielding and the MR system. Initial concerns regarding gradient eddy currents, RF coupling, and B0 field uniformity are explored.

1359. Evaluation of Mesh Photomultiplier Tube Operation for Dual Modality PET/MRI Systems

Hao Peng[1], William H. Handler[1], Kyle M. Gilbert[1], Tim J. Scholl[1], Peter J. Simpson[1], Blaine A. Chronik[1]
[1]University of Western Ontario, London, Ontario, Canada

Beside the benefits achieved in combined PET/CT, several additional advantages can be achieved in PET/MRI such as better spatial and temporal correlation, flexible imaging region location and dynamic studies with fMRI. Field cycled MRI (FC-MRI) is an alternative method for performing an MRI that uses two resistive magnets in place of the single superconducting magnet. Two major characteristics of this system, open bore configuration and low fringe field distribution facilitate the design of a PET/FC-MRI system and reduce the magnetic field immunity requirement of PET detectors. A mesh photomultiplier tube (PMT), is expected to be more immune to the magnetic field than conventional PMTs and potentially be used to improve the PET system resolution. The feasibility of implementing the simultaneous PET/FC-MRI based on mesh PMTs was studied.

1360. Magnetic Field Inhomogeneities Induced by PET Detector Scintillators in Dual Modality MRI/PET Systems

Parisa Jamali[1], Blaine Alexander Chronik[1]
[1]The University of Western Ontario, London, Ontario, Canada

There is currently a great interest in combining magnetic resonance imaging (MRI) systems with Positron Emission Tomografy (PET). one the most potential advantages of this combination is the ability to obtain high resolution MR images of anatomoy while simultaeously collecting the functional imaging attainable with PET. One of the magor challange to this combination is the electro magnetic interference between PET detector and main magnet of MR system . by understanding the field inhomogeneity created by Pet we can design electromagnet correction coils to minimize magnetic interference

1361. Constraints Imposed on MRI in a Mixed Modality PET/MRI System

William Bradfield Handler[1], Blaine Alexander Chronik[1]
[1]University of Western Ontario, London, Ontario, Canada

Mixing PET with MRI requires an understanding of the effect of the MRI system on PET. Loss of signal and image artifacting in PET has been investigated for the various MRI configurations.

1362. Development of Endoscopic Radiation Probe for Fusion Imaging with MRI

Takao Goto[1], Yuji Iwadate[1], Edgar Carlos[1], Hiroshi Sato[2], Koji Watabe[2], Hiroshi Motomura[3], Akira Maekawa[3], Toru Kanoi[4], Kazuhiro Saito[5], Hidehiro Iida[2], Tetsuji Tsukamoto[1]

[1]GE Yokogawa Medical Systems Ltd., Hino-shi, Tokyo, Japan; [2]National Cardiovascular Center Research Institute, Osaka, Japan; [3]Nihon Medi-Physics Co. Ltd., Tokyo, Japan; [4]Universal Giken Co. Ltd., Odawara, Japan; [5]SD Giken Co. Ltd., Sakado, Japan

Endoscopy and X-ray have been used broadly in diagnostic tests for digestive organs. However these tests are not functional and detectability of early stage cancers depends on the experience of the radiologist. We propose a new fusion imaging of MRI and an endoscopic radiation probe (ERP) detecting 18F-FDG. A MRI marker was prepared to register both images. The ERP sensitivity was 18.4 cps/kBq and signals from point sources (3.8 KBq, 16.1 KBq) were separated in spite of the existence of a gamma ray background. MIP images of the MRI marker allowed us to identify the angular direction of the marker.

Gradient Subsystems

Room 4E Monday 14:00 - 16:00

1363. Measuring the Gradient Subsystem Bandwidth at 7T

Douglas A C Kelley[1]

[1]GE Healthcare, San Francisco, California, USA

Interaction between the gradient coil and the static field can reduce the effective bandwidth of the gradient subsystem at 7T. This study demonstrates the use of gradient trajectory mapping to characterize the available gradient waveform bandwidth.

1364. Phantom-Based Evaluation of Gradient Nonlinearity for Quantitative Neurological MRI Studies

Richard Philip Mallozzi[1], Daniel J. Blezek[1], Jeffrey L. Gunter[2], Clifford R. Jack, Jr.[2], Joshua R. Levy[3]

[1]GE Global Research, Niskayuna, New York, USA; [2]Mayo Clinic, Rochester, New York, USA; [3]The Phantom Laboratory, Inc., Greenwich, New York, USA

Structural MRI is a promising technique to diagnose and track the progression of Alzheimer's Disease. Quantitative structural studies require precise control of geometric distortion, both longitudinally and between scanners. We have developed a phantom-based method for evaluating and correcting distortion due to gradient nonlinearity for use in quantitative MRI studies.

1365. Practical Implementation of the Stream Function Method for Design of Arbitrary-Geometry Gradient Coils

Nominated for an ISMRM Poster Award

Rostislav A. Lemdiasov[1], Reinhold Ludwig[2]

[1]Insight Neuroimaging Systems, Worcester, Massachusetts, USA; [2]Worcester Polytechnic Institute, Worcester, Massachusetts, USA

A novel method for the design of short and ultra-short gradient coils for MRI is used to generate layouts for three gradient coils. It is shown how the theoretical stream function formulation translates into practical design. The coils are wound on Plexiglas formers and assembled into a prototype gradient coil set. The gradient coil set is tested in a 4.7T animal scanner under low-current conditions and with the goal of testing the numerical predictions of gradient strength and field linearity. It will be demonstrated that these tests underscore the practicality and efficiency of this novel design method.

1366. Novel Design Method for Gradient Coil Structures with Reduced Acoustic Noise Characteristics

Victor Taracila[1], Labros S. Petropoulos[1, 2], Robert W. Brown[1]

[1]Case Western Reserve University, Cleveland, Ohio, USA; [2]Hitachi Medical Systems, Twinsburg, Ohio, USA

A new approach to the design of actively shielded 3D gradient coils is presented. We consider the minimization of the vibrational total power as part of a target field method algorithm. Taking into account the full profile effects of the 1.5 T main magnetic field in the vicinity of primary and shielding gradient coil, it is possible to find new current patterns that reduce the acoustic noise signature of the gradient coil by more than 5 dB per gradient with no significant change in the vital gradient coil performance and characteristics.

1367. Z-Intercept Method for Improved SUSHI Gradient Solutions

Shmaryu Shvartsman[1, 2], Robert Brown[2], Victor Taracila[2], Timothy Eagan[2]

[1]Philips Medical Systems, Cleveland, Ohio, USA; [2]Case Western Reserve University, Cleveland, Ohio, USA

Good solutions to the SUSHI shielding equation, motivated by the desire for ultra-short gradients, often have current reversals and have been investigated previously using continuous current density solutions. In this work we show that a discrete coil design method can be applied to solve the SUSHI problem, with a priori use of current reversals on the primary coil. A key is that all characteristics of a transverse gradient are expressed through the set of z-intercepts where the current patterns intersect the cardinal axis ö=0. We illustrate the method with an X-gradient design having reduced turns density and improved magnetic performance.

1368. Design and Fabrication of a Three-Axis Hybrid-Quadrupole Gradient Coil for MR of the Breast

Karen Lynn VanderWerf[1], Josh Thomas de Bever[1], Kim Butts Pauly[2], Blaine Alexander Chronik[1]
[1]University of Western Ontario, London, Ontario, Canada; [2]Stanford University, Stanford, California, USA

In order to obtain the high gradient slew rates and strengths necessary for real-time SSFP and diffusion-weighted imaging of breast lesions, we have proposed the design of a three-axis hybrid-quadrupole gradient coil. This coil has a transverse orientation and is composed of two hybrid-quadrupole coils for the Gx and Gz axes and a fingerprint coil for the Gy coil. In this abstract, we report the proposed design for all axes of the coil.

1369. Design of Localized Surface Gradient Coil for DWI of the Carotid Artery

Rebecca Emily Feldman[1], Brian K. Rutt[1], Blaine Alexander Chronik[1]
[1]University of Western Ontario, London, Ontario, Canada

Diffusion weighted imaging can be difficult to implement *in vivo*. It is especially difficult to use in imaging of the carotid artery as the T2 values in the neck are quite small. A surface coil, in the shape of a butterfly coil, is proposed. This coil would be used as a fourth gradient channel. The efficiency of the surface coil is calculated and compared to a general whole body gradient coil and a custom head gradient coil.

1370. A High-Performance Head Gradient Coil for 7T Systems

Axel vom Endt[1], Ralph Kimmlingen[1], Jörg Riegler[1], Eva Eberlein[1], Franz Schmitt[1]
[1]Siemens Medical Solutions, Erlangen, Germany

Head gradient coils allow for higher gradient performance compared to whole-body gradients without running into peripheral nerve stimulation limits. A new WIP head gradient coil with 400 (670) mm inner (outer) diameter, passive and active shim is presented. Key features are: gradient strength 80 mT/m, slew rate 400 T/m/s, asymmetric design to accommodate shoulder cut-outs for improved patient access, asymmetric shim coils with minimized inductive coupling between shims and gradients, force and torque compensation on all axes. The increased inner diameter compared to existing head gradient coils is used for a noise encapsulation, which can support a RF transmit coil.

1371. Discrete Design of an Insert Gradient Coil for Head Imaging in High Field MRI

Shmaryu Shvartsman[1], Gordon DeMeester[1], Michael Morich[1]
[1]Philips Medical Systems, Cleveland, Ohio, USA

We present designs for a transverse head insert gradient coil using a discrete coil design method. The targets for the gradient are: 60mT/m gradient strength, 600mT/m/ms slew rate, and 24cm FoV. The gradient is sized to fit within a whole body gradient. In designing such a gradient we use the method of z-intercepts. The concept of this approach is that all characteristics of a transverse gradient can be expressed through the set of z-intercepts where the coil current patterns intersect the cardinal axis ö=0, for an X-gradient. Unshielded symmetric design with shoulder cutouts and shielded asymmetric design are investigated.

1372. FDTD Analysis of Transient Eddy Currents Induced by Gradient Coil Switching in MRI

Adnan Trakic[1], Hua Wang[1], Feng Liu[1], Hector Sanchez Lopez[1], Stuart Crozier[1]
[1]The University of Queensland, Brisbane, QLD, Australia

In Magnetic Resonance Imaging (MRI), pulsing of magnetic field gradients induces time-varying eddy currents in nearby conductors. These secondary fields are a major cause of concern, since they degrade the image quality by causing misregistration and intensity/phase variations in both images and spectra.A robust analysis scheme allows more complete design and optimisation of gradient coil/magnet combinations and provides indicative predictions of the pre-emphasis and B0-shift compensation waveforms required. A recently proposed three-dimensional (3D), low-frequency Finite-Difference Time-Domain (FDTD) method in cylindrical coordinates is employed to analyse temporal eddy currents and manifest effects (e.g. B0-shift) induced by pulsed actively shielded symmetric/asymmetric transverse x-gradient head and whole body z-coils.

1373. Cylindrical 3D FDTD Algorithm for the Computation of Low Frequency Transient Eddy Currents in MRI

Adnan Trakic[1], Hua Wang[1], Feng Liu[1], Hector Sanchez Lopez[1], Stuart Crozier[1]
[1]The University of Queensland, Brisbane, QLD, Australia

Most Magnetic Resonance Imaging (MRI) spatial encoding techniques employ low-frequency pulsed magnetic field gradients that undesirably induce multi-exponentially decaying eddy currents in nearby conducting structures of the MRI system. A numerical description of eddy current associated temporal characteristics encountered during gradient switching is undeniably of great importance to the MRI field. A robust analysis scheme would allow more complete design and optimization of gradient coil/magnet combinations and gives indicative predictions of the pre-emphasis and B0-shift compensation waveforms required. This work outlines a three-dimensional (3D) finite-difference time-domain (FDTD) method in cylindrical coordinates for the modelling of low-frequency transient eddy currents in MRI.

1374. Measurement of Cross-Axis Gradient Eddy Currents

Atsushi Mark Takahashi[1], R Scott Hinks[2]
[1]GE Healthcare, Menlo Park, California, USA; [2]GE Healthcare, Waukesha, Wisconsin, USA

Cross axis gradient eddy currents have been observed and characterization and compensation is necessary for optimal image quality. This work expands the self-encoding method to measure both on-axis and cross-axis eddy current effects.

1375. Spherical Harmonic Inductive Detection (SHID) Coils for Negative Feedback Control of Eddy Current Fields

Karl Edler[1], Glen Kolansky[1], David Ian Hoult[1]
[1]National Research Council Canada, Winnipeg, Manitoba, Canada

The theoretical groundwork for a novel class of coils that may enable a new strategy for the design of gradient coils is presented. The novel coils facilitate monitoring, by means of Faraday induction, the rates of change of the individual spherical harmonic components of a transient magnetic field. A set of these coils could then incorporated, in conjunction with an electrical shim set, in a negative feedback system that actively corrects those components as they arise.

Bo: Magnets and Inhomogeneity Considerations

Room 4E Monday 14:00 - 16:00

1376. Development of a New MgB_2 Superconducting Open MRI Magnet

Roberto Marabotto[1], Leonardo Bertora[1], Marco Modica[1], Davide Nardelli[1], Daniele Damiani[1], Giovanni Grasso[2], Alessandro Carrozzi[3]
[1]Ansaldo Superconduttori, Genova, Italy; [2]Columbus Superconductors, Genova, Italy; [3]Paramed, Genova, Italy

After the recent discovery of the superconductivity in MgB_2, a lot of work has been done to introduce MgB_2 conductors in MRI magnets. The main advantages would be relative low costs and working temperatures between LTC and HTC typical values. Ansaldo Superconduttori is developing a cryogen-free open MRI magnet based on a new developed MgB_2 superconductor. We will report on the main features of the magnet design and the most significant results obtained during MgB_2 tape and demo coil tests. All collected data confirm our preliminary design assumptions, and we are currently completing the prototype magnet.

1377. The Theoretical Basis of Rectangular Magnet and Coil Design

David Ian Hoult[1]
[1]National Research Council Canada, Winnipeg, Manitoba, Canada

A solution is given in Cartesian coordinates to the expansion of the field produced by a current element in a basis set comprising solutions of Laplace's equation. With this apparently new solution to a vexing problem, it is shown that there is a weighted Fourier relationship between a target magnetic field and a current distribution in parallel xy planes; and a Laplace transform relationship between current and field z variation. An example is given of the current distribution needed to produce a field homogeneous over a cuboid, and the relationship between target field roll-off and field z variation highlighted.

1378. A Pyrolytic Graphite Foam for Magnetic Susceptibility Matching to Human Tissue

Steven Michael Conolly[1, 2], Brian Andrew Hargreaves[2], Alex Chih-Ming Chen[1], Lizabeth Yue Li[2]
[1]UC Berkeley, Berkeley, California, USA; [2]Stanford University, Stanford, California, USA

Field gradients near air-tissue susceptibility interfaces can lead to artifacts including poor fat suppression, image shifts, blurring, ordropouts. External water bags can remove the susceptibility gradient from the imaging volume, but these are heavy and are incompatible withembedded RF coils. Here we introduce a pyrolytic graphite foam that matches human tissue susceptibility, is ten times less dense thanwater, and is compatible with embedded RF coil arrays, includingphased array and SENSE arrays. PG foams could significantly improve the robustness of MRI near the skin, especially for high field MRI, b-SSFP, and spectroscopy.

1379. Development of a Compact MRI for Early Diagnosis and Follow Up of Rheumatoid Arthritis

Shinya Handa[1], Hiroshi Yoshioka[2], Sadanori Tomiha[1], Tomoyuki Haishi[3], Katsumi Kose[1]
[1]University of Tsukuba, Tsukuba, Ibaraki, Japan; [2]Bringham Women's Hospital, Boston, Massachusetts, USA; [3]MRTechnology, Tsukuba, Ibraki, Japan

A compact MRI, whose magnet, gradient coil set, and pulse sequences were optimized for a hand, was developed. The total weight was 600kg, the installation space about $2m^2$, and the examination time was 16 minutes. As a result, this system could be used even in a small clinic for early diagnosis and follow-up of rheumatoid arthritis.

1380. Design and Construction of an Optimized Open-Access Human-Scale MRI Magnet for Posture Dependent Lung Studies

Leo L. Tsai[1, 2], Matthew S. Rosen[1], Ross W. Mair[1], Ronald L. Walsworth[1, 3]
[1]Harvard-Smithsonian Center for Astrophysics, Cambridge, Massachusetts, USA; [2]Harvard Medical School & MIT, Cambridge, Massachusetts, USA; [3]Harvard University, Cambridge, Massachusetts, USA

We have built an optimized low-field open-access MRI system specifically designed for orientation-dependent pulmonary ^{3}He human imaging. A B_0 homogeneity under 40 Hz across a 35 cm DSV at 5 mT, combined with effective noise filtering, allowed high sensitivity ^{1}H and ^{3}He NMR and MRI at 5 mT. The MRI system has more than one order-of-magnitude improvement in B_0 and noise suppression over a previous engineering prototype system, and optimized planar gradient coils have shortened imaging times. These improvements allow us to achieve a target of 2 x 2 x 20 mm resolution for rapid ^{3}He imaging.

1381. Design and Implementation of a Standalone Magnet Field Drift Correction Unit

Terence William Nixon[1], *Scott McIntyre*[1], *Douglas Lyle Rothman*[1], *Robin Alexander de Graaf*[1]
[1]Yale University, New Haven, Connecticut, USA

A custom Field Drift Correction Unit (FDCU) was designed and built to compensate for temporal magnetic field drifts. The multi nuclei unit was designed to be interfaced to any spectrometer that has access to the real and imaginary outputs of a receiver as well as access to the Z0 shim drive. The results shown demonstrate that the unit is able to keep the magnet to within +/- 0.2 Hz of a reference scan even in the presence of a heat induced 28 Hz drift over a 30 minute period

1382. A Priori Imposed Discrete Topology Considerations in Designing Transverse Resistive Shim Coils

Victor Taracila[1], *Shmaryu Shvartsman*[1, 2], *Robert W. Brown*[1]
[1]Case Western Reserve University, Cleveland, Ohio, USA; [2]Philips Medical Systems, Cleveland, Ohio, USA

Transverse gradients and shims have always represented a challenge to design and build. The target field method has revolutionized the design of such coils. Still, many approximations had to be considered, such as truncating the secondary windings, choosing the constraint points for the target field (for high-order tesseral shims this is especially difficult), and discretizing continuous current density distributions. The field qualities found for the continuous case may become altered when real wires are used. A new approach is applied to the design of resistive transverse shims in order to address these difficulties.

Computational Electromagnetics

Room 4E Monday 14:00 - 16:00

1383. Exploring the Limits of RF Shimming: Single Slice and Whole Brain Field Optimizations at Up to 600 MHz with Transmit Arrays of Up to 80 Elements

Weihua Mao[1], *Christopher M. Collins*[1], *Michael B. Smith*[1]
[1]Penn State University College of Medicine, Hershey, Pennsylvania, USA

Simulation and experiment have shown that separate control of magnitude and phase of individual coil drives in a transmit array can be used to provide significant improvement in homogeneity of RF fields, flip angles, and available signal intensity in high field MRI. Due to Maxwell's equations and wavelength effects, however, there are fundamental limits of what homogeneity can be achieved by RF shimming alone with any number of coils. Here we investigate the possibilities of reducing inhomogeneities at very high frequencies with a large number of coils. With a large number of coils, results are impressive (though some limitations can be seen) even for whole-brain RF shimming at 600 MHz.

1384. 3D Simulation Technique to Obtain Input Impedance and Frequency Response of Empty/Biologically Loaded RF Coils with Experimental Verifications

Tamer S. Ibrahim[1], *Doney Abraham*[1], *Roney Abraham*[1], *Ryan Gilbert*[2]
[1]University of Oklahoma, Norman, Oklahoma, USA; [2]Ohio State University, Columbus, Ohio, USA

In this abstract, discussion of a new method to obtain the frequency response and input impedance of MRI coils using 3D computational electromagnetics methods is provided. Studies of a TEM resonator empty and loaded (with a spherical phantom as well as an anatomically detailed human head) are provided, in addition to experimental verification of the results obtained using the new simulation technique. Comparison of the frequency response of all 16 drive ports of a head-loaded TEM coil is provided showing the variations in the coil's input impedances.

1385. A High Performance FDTD Scheme for MRI Applications

Hua Wang[1], *Adnan Trakic*[1], *Feng Liu*[1], *Marek E. Bialkowski*[1], *Stuart Crozier*[1]
[1]School of Information Technology and Electrical Engineering, University of Queensland, Brisbane, Queensland, Australia

With the current trend in Magnetic Resonance Technology towards high field strengths, the demand on single processing structures in large-scale and high-resolution applications is ever increasing. Therefore exploration of alternative computational architectures becomes necessary. This work presents a robust and optimised parallel computational scheme based on the Finite-Difference Time-Domain (FDTD) method that employs the pervasive Message-Passing Interface (MPI) library for efficient computation and communication. The potential of the algorithm is demonstrated on two different applications regarding the analysis of low-frequency transient eddy currents during switching of magnetic field gradients and the interaction of radio frequency (RF) fields with whole human body inside a birdcage resonator.

1386. An Analysis of an Extended Cavity TEM Coil

Graeme McKinnon[1], *Eddy Boskamp*[1]
[1]GE Healthcare, Waukesha, Wisconsin, USA

Integrating an RF body coil into a gradient structure is one approach for increasing the patient bore diameter. In one practical embodiment the RF coil is necessarily very short. However, an extended RF cavity in the space between the primary and shield gradient windings can improve the RF performance substantially. Here a TEM coil with an extended cavity is analyzed both numerically, using the finite-difference time-domain, and with a physically model; and performance as a function of cavity length is characterized.

1387. Excitation of a TEM Mode in a Birdcage Resonator

Shahed Reza[1], Charles A. Saylor[1]
[1]Invivo Corp., Gainesville, Florida, USA

This presentation demonstrates the use of FEM-based electromagnetic simulations in the design of high frequency volume coils. A prototype 7T coil was observed to undergo a significant change in its current distribution when loaded with a saline phantom. Using FEM simulations permitted us to quickly analyze the modes of the resonant structure, including additional modes caused by stray capacitance, and to determine the effects of sample loading on these modes. This information enabled us to redesign the coil by changing the capacitance distribution, thereby dramatically reducing the effect of sample loading on the current distribution.

1388. Obtaining Patient Specific RF Field Maps: Comparison of B1+ Measurements and Simulations for a Human Pelvis

C. A.T. van den Berg[1], L. W. Bartels[1], B. van den Bergen[1], H. Kroeze[1], J. J.W. Lagendijk[1]
[1]University Medical Centre, Utrecht, Netherlands

Parallel imaging and excitation techniques require the acquisition of excitation and sensitivity field maps of patients. In this study we compared an experimental B1+ field mapping technique with FDTD simulations of the same patient pelvis anatomy. We obtained a very well agreement between measurements and simulations. The B1+ distribution is built up of a global pattern caused by the elliptical human pelvis plus a local anatomy dependent part. While the measured B1+ maps show more details, the electromagnetic simulations also provide information about the receive and electric fields. These methods can be applied to parallel excitation and imaging with transceive coils.

1389. B1-Mapping for 3T Body Imaging

Zhiyong Zhai[1], David Foxall[1], Gordon DeMeester[1], Michael Morich[1], John Duraj[1]
[1]Philips Medical Systems, Cleveland, Ohio, USA

Increased image intensity non-uniformity is a main concern for clinical 3T body imaging when compared with conventional 1.5T results. The cause is poor B1-field uniformity due to electro-dynamic effects. Knowledge of the B1-field spatial distribution inside a patient provides useful data to correct the problem and can lead to improved image quality. Here we present the results of B1-field calculation made using the FDTD method for a loaded 3T quadrature body coil, and compare these with B1-mapping in a volunteer.

1390. Toward Understanding SAR Patterns in the Human Head at High Field (200 to 400 MHz) MRI with Volume Coils

Zhangwei Wang[1], Christopher M. Collins[1], Michael B. Smith[1]
[1]Penn State College of Medicine, Hershey, Pennsylvania, USA

Some recent numerical calculations have indicated a region of relatively high SAR near the center of the brain (1, 2). This can seem counter-intuitive from analytical theory, which predicts a low-SAR region near the center of a symmetric sample in a symmetric magnetic field (3). Here we compare SAR distributions in a homogeneous, symmetric sample (sphere) placed in the center of a volume coil with those for a heterogeneous human head with the majority of brain above the coil center. It is seen that in this case the overall pattern in the brain has some similarities to that in the upper half of the sphere, helping to explain the region of high SAR near the center of the brain.

1391. Improving the Signal Uniformity at 400 MHz: Sequential Multi-Channel Excitation with Intermediate Active Shims

Victor Taracila[1], Labros S. Petropoulos[1, 2], Timothy P. Eagan[1], Robert W. Brown[1]
[1]Case Western Reserve University, Cleveland, Ohio, USA; [2]Hitachi Medical Systems, Twinsburg, Ohio, USA

We present an alternative way to improve signal uniformity of a birdcage by using multi-channel excitations in one combined RF pulse to decrease the scanning time. To build up a uniform transverse magnetization constructively for the entire sample cross-section and at any flip angle, it is necessary to utilize additional small fields, referred to here as “active” shims (such shims are not driven at the Larmor frequency), interspersed with the RF pulses. Due to topological spin singularities associated with the channels n=2,3,… , the uniformity of the signal can only be achieved locally and not over the entire sample cross-section.

1392. Capping Off the Actively Shielded Cylindrical Gradient Story

Tanvir Noor Baig[1], Timothy P. Eagan[1], Labros S. Petropoulos[1, 2], William A. Edelstein[1, 3], Robert W. Brown[1]
[1]Case Western Reerve University, Cleveland, Ohio, USA; [2]Hitachi Medical Systems America, Twinsburg, Ohio, USA; [3]MRScience LLC, Schenectady, New York, USA

Eddy currents produced by the residual field from actively shielded gradients cause the inner bore of the cryostat to vibrate. These vibrations produce acoustic noise and the eddy currents affect image acquisition and processing. We propose a new design for an actively shielded, cylindrical transverse gradient coil with endcaps. The active windings of the shielding coil are extended over the ends of the gradient coil form and inward to its inner radius. The design was accomplishied using a ‘target-field-like” approach. The peak fringe field reduction with this approach is observed to be approximately 70%.

1393. FMag - Fast Computation of Static Magnetic Field Perturbation Due to Inhomogeneous Media

Amir Boag[1], Vadim Timchenko[1], Arnon Neufeld[2], Christine Letrou[3]
[1]Tel Aviv University, Tel Aviv, Israel; [2]Tel Aviv Sourasky Medical Center, Tel Aviv, Israel; [3]CNRS UMR 5157, Evry, France

A novel computational scheme (FMag) is proposed for fast evaluation of the magnetic field, Bo, perturbation due to varying magnetic permeabilities of the biological tissues. The computational task is formulated as an integral equation for the perturbation of the magnetic field relative to the externally impressed field, where the magnetic permeability variation serves as a source term. Solution of the integral equation is evaluated in just one iteration comprising FFT-accelerated convolution of the source term with the Green's function. The proposed technique is compared with analytic solution and commercial software.

1394. A Simple Approach of Combined Passive and Active Shimming for *In Vivo* MR Spectroscopy at High Magnetic Field

Christoph Juchem[1], Bernd Muller-Bierl[2], Fritz Schick[2], Nikos K. Logothetis[1], Josef Pfeuffer[1, 3]
[1]Max-Planck-Institute for Biological Cybernetics, Tuebingen, BW, Germany; [2]University of Tuebingen, Tuebingen, BW, Germany; [3]Siemens Medical Solutions, Erlangen, B, Germany

High magnetic fields increase are advantageous for MRS, since sensitivity and spectral dispersion are increased, however, spectral peaks are also broadened *in vivo* due to stronger susceptibility-induced effects. The shim requirements on our 7T monkey system exceeded the capabilities for active shimming tenfold, which were overcome by the optimized combination of passive and active shimming. Simple ferro-shim geometries of only two pieces per shim term were numerically optimized to generate the second order spherical harmonic shim fields. The removal of large scale field inhomogeneities was achieved by mounting the ferro-shims on a cylinder surface that surrounded the monkey head and the RF coils. Subsequently, high accuracy adjustment of the active shims was done with FASTMAP. The experimental effort for the passive shimming was acceptable, the shimming was reproducible between sessions; no eddy current or spike artifacts were introduced. The presented methods are of high practical relevance for shimming on high field systems and/or shimming of anatomical regions which inherently require high shim fields.

1395. Sampling Area-Based Mixed Model for T1-MRI Brain Tissues

Zeng Dong[1, 2], Yao De Zhong[1], Gong Qi Yong[3]
[1]School of Life Science and Technology, Chengdu, Sicuan, People's Republic of China; [2]HMMRC, Chengdu, sicuan, People's Republic of China; [3]HMRRC, Chengdu, Sicuan, People's Republic of China

We mainly focused on the classifiction of GM,WM and CSF, and try to solve separating PVE model int discrete one and assigning low intensity cortex voxels into CSF using the MRF-MAP framework

Interventional MR

Room 4E Monday 14:00 - 16:00

1396. An Actively Segmented Transmission Line for Improved MR Safety of Interventional Devices

Reiner Umathum[1], Sven Müller[1], Wolfhard Semmler[1], Michael Bock[1]
[1]German Cancer Research Center, Heidelberg, Germany

Active tracking catheters using transmission lines over the full length of the devices represent a serious hazard for intravascular applications due to excessive tissue heating. In this work we propose an approach, where the transmission line is electronically divided into several short sections by RF switches. These sections are well isolated from each other during transmit phase so that resonant coupling and thus excessive tissue heating is avoided. In receive phase the integrated switches reconnect all segments to a full length low loss transmission line.

1397. Three-Dimensional Catheter Tracking Using Real-Time Volumetric Imaging

Redha Boubertakh[1, 2], Nicholas MI Noble, [12], Vivek Muthurangu[1], Richard Winkelmann[3], Peter Börnert[4], Derek L. G. Hill[2], Reza S. Razavi[1]
[1]King's College London, London, UK; [2]University College London, London, UK; [3]University of Karlsruhe, Karlsruhe, Germany; [4]Philips Research Laboratories, Hamburg, Germany

Passive catheter visualization in MR guided cardiac catheterization is limited by ambiguity in catheter identification as well as the need for manual tracking. In this study we present an adaptive subtraction technique that allows safe and automated 3D passive catheter tracking in real-time interventional volumes. Results on a volunteer and a vessel phantom showed that the tip of a balloon angiographic catheter could be successfully localized and tracked in 3D, in the presence of both cardiac and respiratory motion. The three-dimensional nature of this technique can thus greatly improve catheter navigation and reduce the need of a skilled operator.

1398. Multi-Mode Probes for MR-Guided Therapeutic Endovascular Interventions

Orhan Unal[1], Krishna Kurpad[1], Thomas M. Grist[1]
[1]University of Wisconsin, Madison, Wisconsin, USA

Multi-mode or all-in-one intravascular MR probes that combine the functionalities of a tracking coil, an imaging coil, and an inductively coupled self-resonator (wireless marker) into one will be presented. Such probes may significantly reduce the risk of injury to the vasculature by obviating device switch during an endovascular intervention.

1399. Towards MRI-Guided Vascular Intervention with an Electromagnetic Tracking System and 3D Navigation Software

Daniel F. Kacher[1], Simon P. DiMaio[1], Eigil Samset[1], Barry Fetics[2], Erez Nevo[2], Ferenc A. Jolesz[1]
[1]Brigham and Women's Hospital, Boston, Massachusetts, USA; [2]Robin Medical, Baltimore, Maryland, USA

MRI-guidance has increasing potential to augment or replace conventional X-ray fluoroscopy in cardiac, peripheral-, and neuro- vascular interventions. Recently, an FDA approved electromagnetic tracking system that utilizes the scanner's gradients has emerged. Coupling such tracking systems with near real-time imaging and 3D visualization of previously acquired data sets yields a powerful tool for the interventionalist. The position and orientation of a sensor is determined by comparing the gradient coil current to the induced current in the coils of the sensor. Feasibility of navigation was shown with fusion of rendered roadmap images to real-time images acquired based on sensor position.

1400. ECG Triggered MRI-Guided Navigation for Cardiac Interventions

Eigil Samset[1, 2], Dan Kacher[1], Pelin Aksit[3], Glenn Hammond Reynolds[4], Laurance M. Epstein[1], Ferenc A. Jolesz[1]
[1]Brigham and Women's Hospital, Boston, Massachusetts, USA; [2]University of Oslo, Oslo, Norway; [3]Global Applied Science Laboratory, GE Healthcare, Baltimore, Maryland, USA; [4]Global Applied Science Laboratory, GE Healthcare, Boston, Massachusetts, USA

The purpose of this study was to enable concomitant navigation on 3D cardiac cine loops as well as real-time imaging using ECG triggering for accurate temporal registration and synchronization. A navigation system was developed to be able to visualize ECG-gated MRI volume cine loops in three orthogonal cross sections as well as using a volume rendering engine. At the same time real-time images can be displayed in the 3D view and annotated with tracked devices such as catheters. The real-time 2D images are spatially and temporarily registered with the 3D roadmap.

1401. Micro-Transmit Active Point Source Tracking for Eliminating RF Tissue Heating

Richard Philip Mallozzi[1], Eric Fiveland[1], Renee A. Guhde[1], Charles L. Dumoulin[1]
[1]GE Global Research, Niskayuna, New York, USA

Conducting structures such as catheters, guidewires, and pacemaker leads placed in an MR scanner present a danger of RF tissue heating due to induced current and voltage standing waves on the device. Such danger limits many promising interventional procedures. A method for tracking catheters and other devices in an MR scanner has been developed that produces no measurable heating. The method uses small tracking coils to transmit the RF field in addition to receive, eliminating the large volume RF excitation that leads to heating.

1402. Dynamic Coil Selection for Interactive Catheter Tracking with Parallel Imaging

Sven Müller[1], Reiner Umathum[1], Sebastian Ley[1], Wolfhard Semmler[1], Michael Bock[1]
[1]German Cancer Research Center, Heidelberg, 69120, Germany

A dynamic coil selection algorithm is presented to reduce the reconstruction time during real time parallel MRI. Coil data are dynamically selected for reconstruction based on their relative distance to the current imaging slice. In an animal experiment this technique was combined with parallel image acquisition and active catheter tracking. An active catheter was imaged during insertion into the abdominal aorta and the heart at a frame rate of 4 images/s.

1403. Automatic Device Tracking: A Multi Slice Approach

Sven Zuehlsdorff[1], Ingmar Viohl[2], Peng Hu[3], Peter Speier[4]
[1]Siemens Medical Solutions USA, Inc., Chicago, Illinois, USA; [2]Interventional Imaging, Inc., Cleveland, Ohio, USA; [3]University of Virginia, Charlottesville, Virginia, USA; [4]Siemens AG Medical Solutions, Erlangen, Germany

Interactive real time MRI has been successfully demonstrated in MR-guided interventions using active devices either for visualization or tracking. In this work, a generalized interactive multi slice sequence with tip tracking capability is presented. The sequence allows the real time selection of multiple slices in oblique orientations with a user selectable update frequency: a central slice containing the device is updated more frequently to enhance device tracking and an outer slice is used to visualize a relatively static anatomy. This work demonstrates these features in a vessel phantom study using a commercial grade catheter (Interventional Imaging, Inc. Cleveland, Ohio).

1404. Evaluation of a Novel Catheter-Vessel Model for MRI to Access Infused Drug Distribution in Target Artery and Catheter Design

Takeshi Yoshikawa[1], Koji Uchida[2], Yoshiharu Ohno[1], Shozo Hirota[3], Masahiko Fujii[1], Hajime Kitagaki[2], Kazuro Sugimura[1]
[1]Kobe University Graduate School of Medicine, Kobe, Hyogo, Japan; [2]Shimane University School of Medicine, Izumo, Shimane, Japan; [3]Hyogo Medical College, Nishinomiya, Hyogo, Japan

The purpose of this study was to investigate the efficacy of a new catheter-vessel model for MRI to evaluate of drug distribution and to optimize of catheter design for intra-arterial infusion therapy. The model consisted of a hepatic artery simulant tube through which water flowed continuously and a water cistern. Catheters were inserted into the tube and a gadolinium contrast medium was injected. Axial images of the tube were obtained. 5- and 2.7-Fr catheter were tested. Drug distribution near the catheter tips was clearly visualized and mixing points could be determined. This model appeared to be effective.

1405. Development of RF Coil for Integration System of Endoscope with MRI for Esophageal Examination

Yuichiro Matsuoka[1], Takashi Ozaki[2], Yasuhiro Mori[3], Kenichi Murakami[3], Makiya Matsumoto[4], Etsuko Kumamoto[3], Kyo Imagawa[2], Masakazu Gotanda[2], Kagayaki Kuroda[1, 4]

[1]Institute of Biomedical Research and Innovation, Kobe, Hyogo, Japan; [2]Olympus Medical Systems Corporation, Hachioji, Tokyo, Japan; [3]Kobe University, Kobe, Hyogo, Japan; [4]Tokai University, Hiratsuka, Kanagawa, Japan

Final purpose of this study is integration of endoscopy and MRI, which could provide precise diagnosis of tumor invasion. For this system, specific RF coil for the endoscope on 3T MRI was developed, which could facilitate to determine and identify location of MR image on optical image. The availability of the developed coil was exhibited by the MR image of gelatin phantom including fruit. And also the influence of the endoscope equipments on MRI was considered as not so serious matter. Basic function of the developed MR-endoscope system could be useful for the examination of tumor invasion.

1406. Evaluation of a Transformer Based Transmission Line for Improved RF Safety of Devices at 3T

Steffen Weiss[1], Peter Vernickel[2], Tobias Schaeffter[1], Bernhard Gleich[1]

[1]Philips Research Laboratories, Hamburg, Germany; [2]TuTech Innovation GmbH, Hamburg, Germany

A transmission line that had been proposed previously to improve RF safety of interventional devices at 1.5T was modified and evaluated for the use at 3T. Improved transformers achieving a higher common mode suppression were built and their signal transmission was measured. A transmission line with six such transformers was characterized and implemented in an active tracking catheter. In this catheter, RF heating during high SAR imaging was limited to 0.4 C whereas RF heating by 13.6 C occurred for a standard catheter under identical conditions. Active catheter tracking with the transformer catheter in a phantom performed robustly, and tracking projections with high SNR were acquired.

1407. MRI Assessment of Renal Function During Percutaneous Transluminal Angioplasty of Renal Artery Stenosis in Swine

Ty Allen Cashen[1], Jonathan K. Park[2], Wanyong Shin[1], Thomas K. Rhee[2], Brian E. Schirf[2], Andrew C. Larson[2], Pottumarthi Prasad[2], Debiao Li[1, 2], Timothy J. Carroll[1, 2], Reed A. Omary[2]

[1]Northwestern University, Chicago, Illinois, USA; [2]Northwestern University Feinberg School of Medicine, Chicago, Illinois, USA

We tested the hypothesis that MRI can successfully detect changes in renal function at the time of renal percutaneous transluminal angioplasty (PTA) in a swine model of renal artery stenosis (RAS). Before and after X-ray-guided PTA, pigs were imaged on a 3.0 T MR scanner to obtain functional kidney measurements. Glomerular filtration rate (GFR), extraction fraction (EF), and the renal blood flow (RBF) were measured pre- and post-procedure. Increases in GFR and EF following PTA were statistically significant, but changes in RBF were not. This combined X-ray/MR approach is now possible in a clinical setting with new hybrid X-ray/MR scanners.

1408. CE-MRA and PC-MRI in the Evaluation of Hemodynamics in Intracranial Aneurysms

Gabriel Acevedo-Bolton[1], Alastair Martin[2], Vitaliy Rayz[1], Michael Lawton[2], Randall Higashida[2], Brad Dispensa[2], William Young[2], Liang-Der Jou[3], David Saloner, [12]

[1]VA San Francisco, San Francisco, California, USA; [2]UCSF, San Francisco, California, USA; [3]University of Pittsburgh, Pittsburgh, Pennsylvania, USA

CE-MRA and PC-MRI were used to acquire lumen geometry and input and outflow flow as input to computational fluid dynamics models of patients with giant intracranial aneurysms. *In vivo* and *in vitro* phantom validation studies were performed to confirm the computational fluid dynamics predictions. This methodology was used to evaluate the relative merits of potential interventional treatments.

1409. Validation of an ECG Restoration Method Using a Linear Time-Invariant Model of Eddy Currents in Tissue

Landon William Locke[1], Weitian Chen[1], Craig Meyer[1], Walter J. Rogers[1]

[1]University of Virginia, Charlottesville, Virginia, USA

Time-varying magnetic gradients produce dramatic noise on ECG waveforms due to their inducement of eddy currents in tissue. This presents a challenge for patient monitoring and cardiac gating during interventional MR procedures. It has been proposed that this noise can be effectively removed by modeling the effect of the gradients on the ECG signal as a linear time-invariant (LTI) system. We verified this fundamental assumption by testing the system for the following properties: scalability, homogeneity, and superposition. Our results indicate that these properties are reasonably verified and that it is appropriate to model the system as LTI.

1410. Fusion of 3D MRI and X-Ray Fluoroscopy

Volker Rasche[1], Christof Burgstahler, [12], Markus Kunze[1], Nico Merkle[1], Jochen Woehrle[1], Vinzenz Hombach[1]

[1]University of Ulm, Ulm, Germany; [2]University Hospital of Tuebingen, Tuebingen, Germany

The accuracy of the registration between three-dimensional MRI and X-ray fluoroscopy was evaluated for a flat-panel X-Ray detector system. It could be shown that without any complex calibration of the X-ray system a sub-mm accuracy of the registration can be achieved.

1411. Rapid Prototyping of Stent Design by Means of Efficient Simulation of Intra-Voxel Dephasing

Thies Halvor Jochimsen[1], Torsten Scheuermann[2]
[1]Stanford University, Palo Alto, California, USA; [2]Boston Scientific, Munich, Bavaria, Germany

To allow rapid prototyping of stents, a simulation strategy has been implemented which allows evaluation of MR compatability of different stent designs. It includes a calculation of electromagnetic fields around the stent material used as input to the simulation of MRI by means of a novel approach which efficiently calculates intra-voxel dephasing.

1412. Meningioma Embolization Assessment with Interventional Magnetic Resonance Imaging

Alastair Martin[1], Soonmee Cha[1], Randall Higashida[1], Van Halbach[1], Chris Dowd[1], Michael McDermott[1], David Saloner[1]
[1]University of California - San Francisco, San Francisco, California, USA

Selective intra-arterial injection of dilute MR contrast media is used to assess the vascular bed of meningeal tumors prior to and following embolization therapy. MR is an excellent means of assessing the vascular bed of feeding arteries and clearly demonstrated the treated and untreated portion of the neoplasm following therapy. Very low contrast dose is necessary, making repeated assessment during therapy practical. MR appears to be more sensitive than conventional x-ray angiographic techniques for depicting tissue fed by a selected vessel, and has the additional advantage of providing a volumetric assessment.

1413. Design and Development of a Prototype Endocavitary Probe for High Intensity Focused Ultrasound Delivery with Magnetic Resonance Imaging Thermometry and Guidance

Iain Wharton[1], Ian Rivens[1], Gail ter Haar[1], David Gilderdale, David Collins, Jeff Hand[2], Paul Abel[2], Nandita deSouza
[1]Joint Department of Physics, Institute of Cancer Research, Sutton, Surrey, UK; [2]Imperial College, London, W12 0NN, UK

This study describes development of an endocavitary probe comprising an MR compatible HIFU transducer integrated with an MR receiver coil for MR guided thermal ablation. The ability to produce phase images capable of detecting small (<5 deg C temperature rises) was demonstrated. Implementation of local shimming optimizes this.

1414. MRI-Comptaible Ultrasound for Image Guided Therapy

Annie MeiYee Tang[1], Daniel F. Kacher[2, 3], Kelvin K. Wong, [23], Geng Li[1, 4], Ferenc A. Jolesz[2, 3], Edward S. Yang[1]
[1]The University of Hong Kong, Pokfulam, Hong Kong, People's Republic of China; [2]Brigham and Women's Hospital, Boston, Massachusetts, USA; [3]Harvard Medical School, Boston, Massachusetts, USA; [4]The University of Hong Kong, Pokfulam, Hong Kong, People's Republic of China

The purpose of this study is to test the feasibility of simultaneous MR and Ultrasound (US) imaging for image guided therapies (IGT). Simultaneous capturing of multi-modal images potentially provides more information for real time IGT. We present a method for acquiring MR images in a known orientation with respect to US image and demonstrate concurrent real-time imaging in a phantom with both modalities. Preliminary results suggested that US and MRI can operate concurrently. Future directions include real time non-linear registration of US and MRI, active tracking and remote manipulation of US probe and biopsy needle.

1415. An Electromagnetic Model for Cool-Tip RF Needle Artifacts in Magnetic Resonance Imaging

Bilgin Keserci[1], Etsuko Kumamoto[2], Kagayaki Kuroda[3, 4]
[1]GE Healthcare, Tokyo, Japan; [2]Kobe University, Kobe, Japan; [3]Institute of Biomedical Research and Innovation, Kobe, Japan; [4]Tokai University, Hiratsuka, Kanagawa, Japan

One problem that can occur in MRI with materials having susceptibility artifacts, which can cause severe degradation, or more subtle effects that can lead to misinterpretation of the MR image. Another problem that occurs with such material is deflection in the magnetic field. The aim of this study was to develop an electromagnetic model to derive the susceptibility artifacts of the cool-tip RF needle in magnetic resonance imaging.

1416. Targeted Delivery of Antibodies Through the Blood-Brain Barrier by MRI-Guided Focused Ultrasound

Manabu Kinoshita[1], Nathan McDannold[1], Ferenc A. Jolesz[1], Kullervo Hynynen[1]
[1]Brigham and Women's Hospital and Harvard Medical School, Boston, Massachusetts, USA

The blood-brain-barrier (BBB) is a persistent obstacle for the local delivery of macromolecular therapeutic agents to the central nervous system (CNS). Many drugs that show potential for treating CNS diseases cannot cross the BBB and there is a need for a non-invasive targeted drug delivery method that allows local therapy of the CNS using larger molecules. To overcome this problem, we developed a non-invasive technique that allows the image-guided local disruption of the BBB. Our major aims in this study were to 1) demonstrate that intravenously administered dopamine D4 receptor-targeting antibody crossed the BBB and recognized its antigens by using our MRI-guided focused ultrasound BBB disruption technique and 2) investigate whether or not we can monitor the extent of BBB disruption by the obtained MR images.

1417. Thermosensitive Mn^{2+}-Liposomes for MR-Guided Hyperthermia

Herbert M. Reinl[1], Martin Hossan[1], Michael Peller[1], Lars Lindner[1], Maximilian Reiser[1]
[1]Universitätsklinikum München - Grosshadern, Munich, Germany

Newly designed long circulating liposomes are shown to be a temperature sensitive contrast agent for MRI when $MnSO_4$ is trapped inside. At the therapeutic temperature of hyperthermia of 42-43 C the Mn^{2+} is set free, and can be detected by T_1 changes in a MRI-Hyperthermia hybrid-system. Our results indicate that our new liposomal system has the potentiality to improve monitoring of hyperthermia and thus the therapeutic outcome. Moreover, the liposomes may also be used for specific release of chemotherapeutics by moderate hyperthermia.

1418. Real Time Quantitative Temperature Imaging Allows Accurate Prediction of the Size of Radiofrequency Ablation in Rabbit Liver

Matthieu Lepetit-Coiffe[1], Olivier Seror[1], Brigitte Le Bail[2], Chrit Moonen[1], Hervé Trillaud[1], Bruno Quesson[1]
[1]CNRS/University Bordeaux 2, Bordeaux, France; [2]C.H.U Pellegrin, Bordeaux, France

High quality, quantitative, temperature mapping of the rabbit liver is feasible during RF ablation allowing real time assessment of the cumulative thermal dose (TD). T1, T2 weighted, dynamic contrast enhanced imaging at day 0, 4 and 8 after MRI guided RF ablation were compared to thermal dose images using histological evaluation as the gold standard, and shown to give a systematic underestimation whereas TD maps showed high prediction accuracy. Therefore, TD maps show promise in guidance and end-point determination of RF ablation procedures.

1419. Ultrafast 1D Approach for Phase or Frequency Mapping for MRI-Based Temperature Measurement

Nathan McDannold[1], Nankuei Chen[1], Koichi Oshio[1], Kullervo Hynynen[1], Robert V. Mulkern[2]
[1]Harvard Medical School/Brigham and Women's Hospital, Boston, Massachusetts, USA; [2]Harvard Medical School/Children's Hospital, Boston, Massachusetts, USA

Rapid 1D temperature measurements were achieved by sampling single columns. The columns were excited with a slice selective 90-180 pair and up to 32 echoes were sampled in order to rapidly measure frequency or phase shifts. By using each echo as an individual measurement, 4066 1D temperature measurements were acquired in 40 sec during ultrasound heating in a phantom. It was possible to acquire frequency measurements in the heart of a volunteer. Temperature monitoring of short sonications in moving organs such as the heart may be feasible with this method.

1420. Correction of Proton Resonance Frequency Shift Temperature Maps for Magnetic Field Disturbances Using Fat Signal

Andriy V. Shmatukha[1], Paul R. Harvey[2], Chris J.G. Bakker[1]
[1]University Medical Center Utrecht, Utrecht, Netherlands; [2]Philips Medical Systems, Best, Netherlands

The Proton Resonance Frequency Shift (PRFS) method of MRI temperature mapping is sensitive to magnetic field disturbances. Such disturbances are misinterpreted as artifact temperature changes. Our technique uses the fat signal, which does not exhibit a temperature-dependent frequency shift, for recovering correct PRFS temperature maps. It is based on the utilization of two gradient echoes acquired around an RF echo within one repetition interval using water- and fat-selective scans as well as a specially designed post-processing algorithm. Accurate and reliable temperature estimations were obtained in phantom experiments in spite of inter-scan motion and field disturbances up to 1.4 ppm.

1421. Respiratory Induced Resonance Offset Correction for PRFS Temperature Maps

Andriy V. Shmatukha[1], Chris J.G. Bakker[1]
[1]University Medical Center Utrecht, Utrecht, Netherlands

Respiratory Induced Resonance Offset (RIRO) handicaps the accuracy of the Proton Resonance Frequency Shift (PRFS) method of temperature mapping. We propose a compensation technique. Baseline images characterizing RIRO at a variety of respiratory cycle instants are acquired before a thermal treatment. During the treatment, the temperature evolution is found from two successive images and corrected for the additional contribution caused by RIRO using the pre-treatment baseline images acquired at the identical instances of the respiratory cycle. Our method is shown to improve the accuracy and stability of PRFS temperature maps in the presence of RIRO and motion in phantom experiments.

1422. Echo Combination to Reduce Temperature Measurement Errors in the Presence of Fat

Viola Rieke[1], Kim Butts Pauly[1]
[1]Stanford University, Stanford, California, USA

Lipids create errors in temperature estimation with the proton resonant frequency (PRF) shift method. Fat suppression is commonly used in tissues with lipid content, but increases imaging time and is difficult at low field strengths. In this study, we investigate a method to substantially reduce these errors by refocusing several gradient echoes and combining the corresponding temperature maps. This echo combination technique eliminates the need for fat suppression in tissues such as the liver.

1423. Consistency of Signal Intensity and R2* in Frozen Porcine Kidney and Liver

Elena Kaye[1], Sonal Josan[1], Kim Butts Pauly[1]
[1]Stanford University, Palo Alto, California, USA

MR-guided cryoablation is a promising method for the minimally invasive therapy of prostate, liver, and kidney tumors. It is known that the relaxation rate R2* increases in frozen tissue, it is not known how consistent these MR parameters are between tissue types. We report Signal Intensity and R2* values for freshly excised *ex vivo* frozen tissue of two different types, porcine kidney and liver. Our results showed that the slope of the line fit of R2*(T) and decay of SI in frozen tissue did not depend on tissue type, however the intersect values varied considerably between liver and kidney.

1424. Improvements in R2* Mapping During *In Vivo* Cryoablation

Aiming Lu[1], Bruce L. Daniel[1], Kim B. Pauly[1]
[1]Stanford University, Stanford, California, USA

Tissue R2* has been shown to be a promising MR parameter for temperature mapping during cryoablation of prostate cancer. However, mapping of R2* *in vivo* requires ultra-short echo times (TEs) and has been sensitive to eddy currents. In this work a multiple-echo PR readout was used following a half-RF excitation to reduce TE to 100 ms, and eddy currents are carefully measured and compensated. *In vivo* R2* maps with improved quality have been obtained in the canine prostate throughout the cryoablation. The proposed technique has been shown to be a very promising approach for temperature monitoring during cryosurgery.

1425. Image Processing for On-Line Reduction of Thermometry Artifacts

Baudouin Denis de Senneville[1], Bruno Quesson[1], Pascal Desbarats[2], Charles Mougenot[1], Chrit Moonen[1]
[1]Laboratoire Imagerie Moléculaire et fonctionnelle, Bordeaux, France; [2]LaBRI, Bordeaux, France

The Proton Resonance Frequency (PRF) technique gives an estimate of the temperature changes by comparing phase contrast between dynamically acquired images and reference data sets. However, organ displacements due to physiological activity (heart and respiration) may induce important artefacts on apparent temperature maps. When motion effects have been reduced in the MR pulse sequences (e.g. saturation slabs, respiratory and/or cardiac synchronisation, navigators), additional image post-processing may be applied to reduce inter-scan motion related errors in PRF. The implemented approach demonstrates that temperature correction can be performed on line even without synchronisation techniques.

1426. Magnetization Transfer for Early Assessment of Hepatic Tumors Treated with Thermal Ablation

Ahmed M. Gharib[1], Melanie S. Kotys[1], David M. Thomasson[1], Julia K. Locklin[1], Brad J. Wood[1]
[1]National Institutes of Health, Bethesda, Maryland, USA

Validated imaging techniques for thermal ablation of hepatic tumors may serve as early detection of untreated tumor, potentially impacting survival in specific clinical scenarios. Magnetization transfer (MT) liver imaging was performed in two patients three days before and one day after radiofrequency ablation of liver neoplasms. MT ratio maps showed that burned normal liver tended to have lower values than normal liver. Pre- and post-treatment ratios of the lesion were considerably different, and post-treatment values tended to normalize to values of normal remote liver. Analysis suggests that MT could provide useful information about the relationship of tumor to treatment zone.

1427. Respiratory and Cardiac Motion Induced B0 Fluctuations in the Breast: Implications for PRFS-Based Temperature Monitoring

Nicky H.G.M. Peters[1], Lambertus W. Bartels[1], Ferry Lalezari[1], Koen L. Vincken[1], Jan L. Verwoerd[2], Willem P.Th.M. Mali[1], Chris J.G. Bakker[1]
[1]University Medical Center Utrecht, Utrecht, Netherlands; [2]Philips Nederland BV, Medical Systems, Eindhoven, Netherlands

Proton resonance frequency shift based temperature mapping in the breast is hindered by local magnetic field inhomogeneities. We postulate a method for measuring field disturbances in the breast due to respiration and cardiac motion and describe the implications for PRFS-based thermometry. Field disturbances due to regular respiration were approximately 0.15 ppm (+/- 15¢ªC), due to maximum capacity respiration 0.25 ppm (+/- 25¢ªC), and less than 0.03 ppm (+/- 3¢ªC) due to cardiac motion. We concluded that respiration-induced field disturbances cause significant phase shifts in the breasts that need correction for accurate thermometry during MR-guided focused ultrasound.

1428. Feasibility of Diffusion-Weighted MR Imaging and ADC Map to Predict Necrosis of Uterine Fibroids During MR Imaging-Guided Focused Ultrasound Surgery

Atsuya Okada[1], Takamichi Murakami[2], Hironobu Nakamura[2], Bilgin Keserci[3]
[1]Iseikai Hospital, Osaka, Japan; [2]Osaka University, Suita, Japan; [3]GE Healthcare, Hino, Japan

The purpose of this study is to evaluate the feasibility of Diffusion-weighted MR Imaging in the prediction of necrosis of MR Imaging-guided FUS for Uterine Fibroids.

1429. A New MRI Method for Monitoring Thermal Coagulation

Dina Carasso[1], *Gil Navon*[1]
[1]Tel Aviv University, Tel Aviv, Israel

A new MRI method, based upon magnetization exchange between macromolecules and water in tissues (MEXI) is presented. Coagulated tissue has much faster magnetization exchange rate leading to the new contrast. The method was tested for porcine liver and porcine muscle. A good contrast was obtained between fresh and coagulated tissues.

1430. MR Temperature Imaging Using an Aliased Fat-Water Fast Chemical Shift Acquisition

R. Jason Stafford[1], *Ken Pin Hwang*[1, 2], *Andrew M. Elliott*[1], *Anil M. Shetty*[1], *John D. Hazle*[1]
[1]The University of Texas M. D. Anderson Cancer Center, Houston, Texas, USA; [2]GE Healthcare Technologies, Waukesha, Wisconsin, USA

A fast chemical shift imaging technique for magnetic resonance temperature imaging is explored in which the echo-spacing constraints are purposely relaxed to alias the fat-water spectrum in order to gain efficiency in both resolution and acquisition time. When incorporated with a partially parallel acquisition, the resulting technique maintains the advantages of a CSI based techniques, such as the ability to use the lipid signal as an internal reference, but has a spatio temporal resolution acceptable for monitoring most thermal therapies. Initial calibration results and measurements using the sequence are discussed.

1431. Simultaneous Monitoring of MRgFUS Temperature and Tissue Stiffness in Real Time

Nominated for an ISMRM Poster Award

Yuan Le[1], *Svetlana V. Primak*[1], *Kevin J. Glaser*[1], *Armando Manduca*[1], *Richard L. Ehman*[1], *Joel P. Felmlee*[1]
[1]Mayo Clinic College of Medicine, Rochester, Minnesota, USA

This work is to study the feasibility of simultaneous monitoring of the temperature and tissue stiffness change during focused ultrasound treatment using 1D MR elastography. The results shows that the phase shift in the MRE data due to temperature can be detected and correlate well with the temperature measured by thermometer. In the tissue and animal test it is shown that the trend of temperature change and stiffness change in treated tissue can be calculated from the 1D MRE data in real time. This result shows promising of using 1D MRE as a means of focused ultrasound therapy monitoring.

1432. Pilot Study Correlating Tissue Stiffness and Gross Pathology of MRgFUS Thermal Lesions in Human Liver Cancer Xenoplant Tissue

Svetlana Primak[1], *Yuan Le*[1], *Jinping Lai*[1], *Lewis Roberts*[1], *Carol Reynolds*[1], *Phil Rossman*[1], *Joel Felmlee*[1]
[1]Mayo Foundation, Rochester, Minnesota, USA

The purpose of these experiments was to evaluate stiffness change after MRgFUS in a nude mouse model with human liver cancer xenoplant (Hep3B cells). Our data confirm that tissue stiffness determined using MRE elastography correlates with cellular level thermal damage or necrosis in liver cancer tissue. Further *in vivo* experiments are suggested on finding correlation of stifness change on FUS power level and determining stiffness of baseline necrosis in future work

1433. Use of PROPELLOR for MR Thermometry

James R. MacFall[1], *Thomas Raidy*[1], *Omar Arabe*[1], *Thad Samulski*[1]
[1]Duke University Medical Center, Durham, North Carolina, USA

It is possible to use the temperature sensitivity of the tissue water proton resonant frequency shift (PRFS) or the apparent diffusion coefficient (ADC) to measure temperature change. While the PRFS method has good temporal and spatial resolution, it suffers from sensitivity to motion and drift. The ADC method is less sensitive to motion and drift but suffers from low resolution and image distortion due to the use of diffusion-weighted (DW) single shot echo-planar imaging (EPI) methods. In this study we evaluate the extent to which multi-shot DW PROPELLOR imaging can improve the ADC temperature change measurement method.

1434. MR Guided Microwave Surgery for Liver Tumor with MR Gradient-Based Tracking System

Shigeyuki Naka[1], *Yoshimasa Kurumi*[1], *Shigehiro Morikawa*[2], *Hisanori Shiomi*[1], *Tohru Tani*[1], *Hasnine A. Haque*[3]
[1]Shiga University of Medical Science, Otsu, Shiga, Japan; [2]Shiga University of Medical Science, Otsu, shiga, Japan; [3]GE Yokogawa Medical Systems, Hino, Tokyo, Japan

Using a new real-time MRI navigation system with MR gradient-based tracking system, eight patients were treated by microwave surgery. The new locator system is the MR gradient-based tracking system, which can provide the real time 6-degree of freedom tracking during MR imaging and eliminate the line-of sight problem of the optical tracking system. In the all case, microwave surgery was performed successfully without significant complication. The microwave surgery using the newly developed navigation system with the MR gradient-based tracking system is a feasible and effective procedure in treatment of the liver tumor.

1435. Contrast Enhanced MRI Guided Photodynamic Therapy for Non-Invasive Treatment of Cancer

Anagha Vaidya[1], Tianye Ke[2], YongEn Sun[2], Eun-Kee Jeong[2], ZhengRong Lu[2]
[1]Unviersity of Utah, Salt Lake City, Utah, USA; [2]University of Utah, Salt lake city, Utah, USA

MRI-guided photodynamic therapy is advantageous over current interventional therapies due to its non-invasive nature. Efficient detection of tumors and dynamic tracking of drugs by MRI would facilitate site-directed irradiation, avoiding non-specific exposure. For this dual purpose, we have developed polymer conjugates where both mesochlorin e6 (photosensitizer) and Gd-DOTA (contrast agent) were attached to the poly-(L-glutamic acid). Polymer conjugates without drug served as controls. MRI contrast enhancement and efficiency of PDT were evaluated in mice tumor models.The conjugates showed increased contrast enhancement on MR images in tumor tissue at 18 hours post injection. Compared to controls, animals receiving drug showed tumor regression and 100% survival.

1436. Quantitative Real-Time Imaging for MR-Guided Internal Radiation Therapy

Stefanie Winkelmann[1], Jan-Henry Seppenwoolde[2], Peter R. Seevinck[2], Evert-jan P.A. Vonken[2], Tobias Schaeffter[3], Chris J. G. Bakker[2], Olaf Doessel[1]
[1]University of Karlsruhe, Karlsruhe, Germany; [2]University Medical Center, Utrecht, Netherlands; [3]Philips Research Laboratories, Hamburg, Germany

For accurate MR-guidance of the local delivery of drugs or agents, online and fast quantitative feedback about the dynamic biodistribution is strongly required. In this work, a simultaneous imaging and R2*-mapping technique was successfully applied to quantitative monitoring of the distribution of microspheres that were loaded with the paramagnetic radionuclide Holmium. These microspheres are currently under investigation for MR-guided internal radiation therapy of liver tumors. The technique profits from time-efficient sampling of a radial multi-gradient-echo sequence and yielded adequate morphologic images and R2*-maps during the selective administration of Holmium-loaded microspheres to parts of the livers of two living pigs.

1437. Adult Stem Cells from Adipose Tissue for Cardiac Repair

Jixian Deng[1], Jian Wang[1], Gang Li[2], Bo Xiang[1], Marcu Gruwel[1], Yan Li[3], Terak Kashour[1], Mike Jackson[1], Roxanne Deslauriers[1], Ganghong Tian[1]
[1]Institute for Biodiagnostics,National Research Council, Winnipeg, Manitoba, Canada; [2]Harbin Medical University, Harbin, Helongjiang, People's Republic of China; [3]National Microbiology Laboratory, Winnipeg, Manitoba, Canada

Stem cell therapy, especially with adult stem cells, has a great promise for ischemic heart disease. Because of its potential to trans-differentiation into cardiomyocytes and high number, we believe that the stem cells in adipose tissue may be a good cell source for cardiac repair. The present study was to develop methods for isolation, culture, labeling of the adipose-derived stem cells chemically and genetically. We have successfully obtained adipose-derived stem cells from the mouse, rat, and pig. The stem cells labeled with ferumoxide could be monitored with MRI for approximately two weeks. Transfection of the stem cells with adenovirus-GFP did not significantly affect their proliferation ability and viability.

1438. Simultaneous Quantitative Flow-Measurement Using MRI and Optical Coherence Doppler Tomography

Hon J. Yu[1], Gultekin Gulsen[1], Zhongping Chen[1], Orhan Nalcioglu[1]
[1]University of California, Irvine, California, USA

This abstract presents a development of MR-compatible Optical Coherence Doppler Tomography (OCDT) system via a fiber-optic based Michelson interferometer and a MR-compatible optical probe. OCDT system is capable of simultaneously imaging static structure and spatially resolved flow dynamics of sample in very high resolution (order of 10 *f*Ým), which could be used to complement MRI in such application as capillary-level blood flow measurement or to validate MRI measurement when used simultaneously. The system¡¦s MR-compatibility and performance was tested with 4T MRI scanner using a laminar-flow phantom. The results show a good quantitative correlation of velocity profile (R2=0.96) between these two imaging modalities.

1439. Three-Dimensional MR Tracking of Convective Therapy Distribution in Prostate

Anil Shetty[1], Roger J. Stafford[1], Andrew M. Elliott[1], Wes Kassouf[1], Gordon A. Brown[1], Louis L. Pisters[1], L Clifton Stephens[1], Peggy T. Tinkey[1], Luc Bidaut[1], John D. Hazle[1]
[1]The University of Texas M.D.Anderson Cancer Center, Houston, Texas, USA

Convective delivery of therapy is a minimally invasive alternative for systemic delivery of chemotherapy and other cancer treatments, such as gene therapy, for localized tumor sites. Convective delivery of gene therapy in prostate cancer may help maximize gene transfection. This research investigates the feasibility of using MRI to non-invasively assess the distribution of a convectively delivered solution in an *in vivo* canine prostate model. Differing injection schema were investigated using a surrogate solution of Gadolinium-DTPA and methylene blue (to mimic vector distribution), injected intraprostatically. Methylene blue distributions on pathology photographs correlated well with the Gadolinium-DTPA distributions observed from MRI.

1440. Needle Placement Accuracy in MRI-Guided Prostate Biopsy of Prostate Cancer

Nobuhiko Hata[1], Philip Blumenfeld[1], Simon DiMaio[1], Kelly Zou[1], Steven Haker[1], Clare MC Tempany[1]
[1]Brigham and Women's Hospital and Harvard Medical School, Boston, Massachusetts, USA

This work aims to quantify needle placement accuracy in MRI-guided core biopsy of the prostate. Needle placement error was assessed in 10 clinical prostate biopsy cases, retrospectively. The source of placement errors was evaluated by in controlled phantom studies. The mean and standard deviation of the errors in targeted biopsies was 6.5±3.5mm. Relatively small correlation was found among different tissue types in trials with the symmetric needle ($p=0.23$), compared to trials with the asymmetric needle ($p<0.0001$). The analysis of needle susceptibility artifact yielded a mean artifact shift of 1.6±0.4mm along the direction of the frequency encoding. The results suggested that current accuracy of MRI-guided core biopsy of prostate has room for improvement and use of symmetric needle may be useful.

1441. Image-Guided Interventional Device for 3D Access and Localization of Breast Lesions

Xu Zhai[1], Ray Harter[2], Catherine Moran[1], Orhan Unal[1], Frederick Kelcz[1], Sean B. Fain[1]
[1]University of Wisconsin-Madison, Madison, Wisconsin, USA; [2]Marvel Medtech, LLC., Madison, Wisconsin, USA

A practical and easy system for localization and trajectory planning for MRI image guided biopsy and intervention in three dimensions has been designed and implemented. The system is designed to allow more direct access to the suspect lesion and integration of 3D images with different contrasts into the planning process. The planning and localization procedure is designed to make remote controlled intervention more robust, safe, and practical in the MR setting.

1442. Implementation of Real-Time Safety Control for Image-Guided Procedures Inside Cylindrical Scanners with MR-Compatible Manipulators

Eftychios Christoforou[1], Angel Lee[1], Nikolaos V. Tsekos[1]
[1]Washington University in St. Louis, St. Louis, Missouri, USA

The aim of this work is to develop a versatile MR image-based control scheme for safe and collision-free operation of MR-compatible manipulators inside high-field MR cylindrical scanners for performing interventions with real-time image guidance. For this purpose MR images are used to construct a solid model of the volume occupied by a subject inside the scanner and define the allowable space of maneuvering. The current position of the manipulator relevant to the patient is updated in real-time and is ensured that the prohibited operation volume is not violated. This implement was successfully tested experimentally using free-hand control of the manipulator.

1443. Freehand Performance of Interventions with Manipulator-Driven Real-Time Update of the Imaging Plane

Erbil Akbudak[1], Sven Zuehlsdorff[2], Eftychios Christoforou[1], Alpay Ozcan[1], Menelaos Karanikolas[1], Nikolaos V. Tsekos[1]
[1]Washington University, St. Louis, Missouri, USA; [2]Siemens Medical Solutions, Chicago, Illinois, USA

The purpose of this work is to develop and evaluate freehand manual control of an MR-compatible manipulator, combined with on-the-fly adjustment of the imaging plane position and orientation, for performing interventions with real-time MR guidance. Manipulator-driven update of the imaging plane allowed scouting the subject for the target and identifying the path of insertion, aiming the interventional tool and monitoring target acquisition.

1444. Real Time Imaging with Automatic Slice Positioning Controlled by an Interventional Assistance System

Michael Bock[1], Stefanie Guthmann[2], Bernd Gutmann[2], Jaane Rauschenberg[1], Sven Zuehlsdorff[3], Wolfhard Semmler[1]
[1]German Cancer Research Center, Heidelberg, 69120, Germany; [2]InnoMedic GmbH, Herxheim, Germany; [3]Siemens Medical Solutions, Chicago, Illinois, USA

In robot-assisted interventions in closed-bore MR magnets a continuous alignment of slice position and orientation with the interventional device is required. In this work a network interface was developed that transfers measured device coordinates to the MRI host computer. The interface was combined with a dedicated real-time pulse sequence where slice position and orientation are updated. Compared to slice tracking with MR marker coils this direct control system is simpler to realize and does not require any additional rf hardware.

1445. 3.0T MRI-Guided Breast Interventions: First Clinical Experience

Maurice A.A.J. van den Bosch[1], Carla Meeuwis[1], K. A.F. Houwert[1], M. A. Fernandez-Gallardo[1], R. van Hillegersberg[1], M. E.I. Schipper[1], W. P.Th.M. Mali[1]
[1]University Medical Center Utrecht, Utrecht, Netherlands

In this feasibility study we report our first clinical experience with MRI-guided breast interventions in a 3.0T closed bore magnet. We developed a high-resolution T1-FFE protocol (voxel 0.66x0.66x0.80) for optimal assessment of lesion morphology and monitoring of the needle during the biopsy procedures. Three MRI-guided needle localizations were performed by using a freehand technique and four MRI-guided large core needle biopsies were performed with a commercial available stereotactic biopsy device. All procedures were technically successful resulting in 3 benign lesions and 4 malignant lesions. Needle artifacts were reduced to a maximum of 5mm in diameter for the 13-gauge guiding needles.

1446. MRI-Guided Prostate Biopsy in Two Different Standard 1.5 T Scanners Using an Endorectal Biopsy Device

Karl Engelhard[1], Hans-Peter Hollenbach[2], Berthold Kiefer[2], Axel Winkel[3], Dirk Engehausen[4]
[1]Martha-Maria Hospital, Nuremberg, Germany; [2]Siemens Medical Solution, Erlangen, Germany; [3]Invivo Germany GmbH, Schwerin, Germany; [4]University of Erlangen-Nuremberg, Erlangen, Germany

Testing the valence of a MRI-guided prostate biopsy device. 50 patients with elevated PSA, negative tumor prostate biopsies underwent a MRI guided prostate biopsy in two 1.5T units.Tumor suspectetd areas were punctered using a biopsy device with a MR-visible needle guide controlled with a real time TrueFISP and a T2-weighted TSE sequence. Core biopsies were taken in the magnet with the patient in supine position. In cases of prostate cancer an excellent correlation was found between the site of biopsy and the histological results. The method can be effective in increasing primary tumor positive biopsies.

1447. A Voice Command Interface for Real-Time Interventional MR Imaging

Jochen von Spiczak[1, 2], Eigil Samset[1, 3], Daniel F. Kacher[1], Catherina R. Burghart[2], Ferenc A. Jolesz[1, 4] Simon P. DiMaio[1]
[1]Brigham & Women's Hospital, Boston, Massachusetts, USA; [2]University of Karlsruhe, Karlsruhe, Germany; [3]University of Oslo, Oslo, Norway; [4]Harvard Medical School, Boston, Massachusetts, USA

A voice command interface for real-time interventional MR imaging was developed for interactively controlling scan plane position and orientation from within the scanner room. The new interface gives complete control of MRI scanning back to the responsible user and allows for faster, direct adjustments of the scan plane. The feasibility of a voice command approach to scanner control and its inherent advantages over common practice for a number of applications were shown. The investigation of several workflow parameters illustrates the potential of the system to save time and improve efficacy when performing repeated imaging tasks.

1448. Biopsy Needle with Markers – Design of an MR Compatible Needle for High-Precision Needle Tip Positioning

Bernd Michael Müller-Bierl[1], Hansjörg Graf[1], Claudius König[1], Philippe Laurent Pereira[1], Fritz Schick[1]
[1]University Clinic Tübingen, Tübingen, Baden-Württemberg, Germany

Needle tip visualization is of high importance when performing biopsies under magnetic resonance (MR) imaging control. The exact position of the needle tip is, however, often obscured by the artifact of the needle. We investigated a newly developed biopsy needle design using a diamagnetic coating for several fast MR sequences (FLASH, FISP and TSE).

1449. Motorized Remote-Center-Of-Motion Constraint Robot to Assist MR-Guided Microwave Thermocoagulation of Liver Tumors

Shigehiro Morikawa[1], Nobuhiko Hata[2], Toshiro Inubusi[1], Koich Demura[1], Koichiro Murakami[1], Masahito Morita[1], Shigeyuki Naka[1], Yoshimasa Kurumi[1], Hasnine Akter Haque[3]
[1]Shiga University of Medical Science, Ohtsu, Shiga, Japan; [2]Brigham and Women's Hospital, Boston, Massachusetts, USA; [3]GE Yokogawa Medical Systems, Hino, Tokyo, Japan

In order to assist MR image guided microwave thermocoagulation therapy of liver tumors, we have developed a motorized robot, which consists of a passive end effecter with two-degree-of-freedom rotation and active XYZ-base stages with three-degree-of-freedom. The remote-center-of-motion constraint of this robot worked properly in the magnet to catch the target from various positions and it is helpful for surgeons to choose optimal puncture route. The design of this robot is also competent for the clinical use in the near future.

1450. MR Guided Percutaneous Intramyocardial Injection of Contrast Medium Solution to Infarct Borders After Delineation of the Infarct with High Molecular Contrast Media: Measurement of T1 Values

Gabriele Anja Krombach[1], Yavuz Temur[1], Joachim Georg Pfeffer[1], Christian Hohl[1], Sylvia Kinzel[1], Rolf W. Günther[1], Arno Bücker[1]
[1]University Hospital Aachen, Aachen, NRW, Germany

In 12 pigs reperfused myocardial infarction was induced. SHU 555A or MS325 were intravenously injected in order to delineate the infarct. After sufficient contrast between infracted and remote myocardium was obtained, intramyocardial injection was stared. The borders of the infarct were selected as target areas. Real-time MR imaging allowed for advancing a needle catheter from a carotid artery sheath into the left ventricle, inserting it into the myocardium, and injecting a Gd-DTPA-BMA solution. The described technique is a promising tool for minimally invasive percutaneous delivery of substances and visualization of their distribution.

MRI in Animal Models for Stroke and Traumatic Brain Injury

Room 4E Tuesday 13:30 - 15:30

1451. Early MRI Characterization of Cerebral Edema Following Diffuse Traumatic Brain Injury in Rat

Yohan van de Looij[1, 2], Hana Lahrech[1, 2], Gilles Francony[1, 2], Olivier Carle[1, 2], Régine Farion[1, 2], Christoph Segebarth[1, 2], Jean-François Payen[1, 2]

[1]INSERM U594, Grenoble, France; [2]Univ Joseph Fourier, Grenoble, France

The objective of this work was to characterize brain edema early after diffuse brain traumatic injury in rats. Evaluation of brain edema was achieved using diffusion, quantitative T1 and T2 MR Imaging. The Blood-Brain-Barrier (BBB) permeability was examined after administration of Gd-Dota and manganese Contrast Agents (CA). Histology and microgravimetry were performed to confirm MRI results. The diffusion results revealed that ADC is a promising parameter for the early detection of post-traumatic cerebral edema. The early ADC decrease provides evidence that cellular edema is predominant, confirmed by the CA MRI and histological results where the BBB is found intact.

1452. The Effect of Interleukin-1 on Local Brain Temperature During Focal Cerebral Ischemia in the Rat: A ^{1}H Magnetic Resonance Spectroscopic Imaging Study

Adrian Robert Parry-Jones[1], Timo Liimatainen[2], Nancy Jane Rothwell[1], Risto Antero Kauppinen[3], Olli H J Grohn[2]

[1]University of Manchester, Manchester, UK; [2]University of Kuopio, Kuopio, Finland; [3]University of Birmingham, Birmingham, UK

The pyrogen and pro-inflammatory cytokine interleukin-1 (IL-1) may exacerbate experimental stroke in part by increasing ischemic brain temperature. Rats undergoing middle cerebral artery occlusion received IL-1 or vehicle and brain temperature maps were generated by ^{1}H-magnetic resonance spectroscopic imaging. IL-1 increased infarct volumes but rectal temperature (T_r) did not vary significantly between groups. At occlusion, ischemic brain temperature relative to T_r was -0.6±0.6 C for vehicle and -1.2±0.9 C for IL-1. During reperfusion these differences were +0.6±0.9 C for vehicle and -0.6±1.0 C for IL-1. Thus, IL-1 reduces ischemic brain temperature which may be a consequence of increased depth of ischemia.

1453. Direct Evidence That Activating the Interleukin 1 Type I Receptor Enhances Ischemic Brain Damage

Jelena Lazovic[1], Anirban Basu[2], Raymond P. Rothstein[3], Michael B. Smith[4], Steven W. Levison[3]

[1]California Institute of Technology, Pasadena, California, USA; [2]National Brain Research Center, Gurgaon, India; [3]University of Medicine and Dentistry, East Orange, New Jersey, USA; [4]The Pennsylvania State University, Hershey, Pennsylvania, USA

Recovery from ischemic brain damage is affected by many variables including neuroinflammation. We used a model of hypoxia-ischemia (H/I) to establish whether the IL-1 type 1 Receptor (IL-1R1) is necessary for IL-1 to exacerbate brain damage. MRI was used to examine the extent of injury prior to and after addition of IL-1 following H/I. WT animals injected with IL-1 two days following H/I had an 8% increased volume of the hyperintense T2-signal at 7 days compared to 24 h. In contrast, the volume of the hyperintense T2-signal was 5% reduced in IL-1R1 null animals at 7 days following H/I.

1454. *In Vivo* Measurement of Blood Flow After Traumatic Brain Injury in Rats Using Susceptibility Weighted Imaging

Yimin Shen[1], Jiani Hu[1], Christian W. Kreipke[1], Theodor Petrov[1], E Mark Haacke[1, 2]

[1]Wayne State University School of Medicine, Detroit, Michigan, USA; [2]MRI Institute of Biomedical Research, Detroit, Michigan, USA

Magnetic resonance imaging and, in particular, susceptibility weighted imaging (SWI) is proving to be a sensitive means to monitor changes in function after traumatic brain injury (TBI). In this study, we have focused on an *in vivo* rat model post TBI after a weight drop has induced brain damage. The rats are then scanned over a number of time points from several hours to several weeks. The blood phase analyses in SWI imaging suggests local and global reductions in blood flow in agreement with arterial spin labeling methods and previous results published in the field.

1455. Delayed Thalamic Damage After Stroke: Discriminator for Recovery Success from Functional Loss in the Cortex of the Rat

Carlos Justicia[1], Pedro Ramos-Cabrer[1], Ralph Weber[1], Dirk Wiedermann[1], Cordula Strecker[1], Christiane Sprenger[1], Mathias Hoehn[1]

[1]Max-Planck-Institute for Neurological Research, Cologne, Germany

Following MCAO in the rat, damages affecting thalamocortical projections can cause secondary neuronal degeneration in the thalamus, which may explain lack of activity in the S1 cortical areas. Repetitive fMRI, SSEPs and behavioural experiments were performed for 7 weeks after MCAO, finishing with histology. Only animals with permanent loss of BOLD response in the S1 showed gliosis and neuronal death in both the ventral-posteromedial (VPM) and the ventral-posterolateral (VPL) thalamic nuclei. In animals with transient BOLD loss (<3 weeks) only the VPM was affected. Secondary damages to thalamic regions can aggravate the functional outcome after stroke. Recurrence of BOLD will depend on the extension of this delayed damage.

1456. The Response of the Fetal Brain to Antenatal Hypoxia-Ischemia Detected by Diffusion-Weighted Imaging

Alexander Drobyshevsky[1], Matthew Derrick[1], Alice M. Wyrwicz[1], Pottumarthi Prasad[1], Xinhai Ji[1], Ila Englof[2], Sidhartha Tan[1]

[1]Evanston Northwestern Healthcare, Evanston, Illinois, USA; [2]Evanston Northwestern Healthcare, Evanston,, Illinois, USA

We utilized a clinically relevant fetal animal model which exhibits a CP phenotype in newborn rabbit pups following fetal H-I, to examine the feasibility of developing prognostic biomarkers of later brain injury. Time course of ADC of individual fetus brains was examined serially during hypoxia period, and after 4, 24, 72 hours on GE 3T magnet. To investigate regional differences during hypoxia with higher spatial resolution, diffusion weighted imaging were performed on fetuses at E25 and E29 with a surface coil on 4.7 T Bruker scanner.

1457. Unilateral Common Carotid Artery Occlusion: A Transient Ischemia Model Well Suited to MR Studies

Jeremy Joseph Flint[1], Stephen J. Blackband[1, 2], Peter E. Thelwall[1]

[1]University of Florida, Gainesville, Florida, USA; [2]National High Magnetic Field Laboratory, Tallahassee, Florida, USA

We have employed a modified version of the Rice-Vannucci model of cerebral hypoxia to produce focal hypoxic lesions in adult rats. The model requires ligation of one carotid artery followed by exposure to a low-oxygen environment, resulting in a hypoxic lesion ipsilateral to artery ligation. This model is well suited to MR studies of hypoxia as initiation of and recovery from hypoxic insult is effected by changing the anesthetic carrier gas, requiring no physical manipulation of the animal. We acquired diffusion weighted images from rats under normoxic, hypoxic and post mortem conditions, and observed focal lesions during hypoxia.

1458. MRI Investigation of Combination Treatment of Embolic Stroke in Rat with Rt-PA and Atorvastatin

Guangliang Ding[1], Quan Jiang[1], Lian Li[1], Li Zhang[1], Zheng Gang Zhang[1], Swayamprava Panda[1], James R. Ewing[1], Michael Chopp[1]

[1]Henry Ford Health Sciences Center, Detroit, Michigan, USA

The combined rt-PA and atorvastatin treatment at 4h after the embolic MCAo significantly reduced microvascular perfusion deficits compared with the control animals. In the combination treated rats, MRA and CBF images show MCA recanalization and recovery of CBF, respectively, which match the cerebral microvascular patency data obtained from fluorescence microscopy. This may be attributed to atorvastatin, which increases the efficacy of fibrinolytic therapy with rt-PA and protects microvessels downstream of the occluded MCA from secondary occlusion. The MRI maps reflect the enhanced tissue perfusion or the reduction of ischemic lesion after the combination treatment with rt-PA and atorvastatin.

1459. Spatiotemporal Pattern of USPIO Enhancement in Experimental Stroke Lesions Depends on the Type of Ischemic Injury: A 9,4 T MRI Study

Michael Schroeter[1], Ana M. Oros-Peusquens[2], Marko Irkens[2], Avdo Celik[2], Andreas Saleh[1], Nadim J. Shah[2], Sebastian Jander[1]

[1]Heinrich Heine-University, Duesseldorf, Germany; [2]Research Centre Juelich, Juelich, Germany

Focal cerebral ischemia elicits a profound inflammatory response which essentially contributes to the functional and morphological sequelae of stroke. USPIO enable the visualization of cellular inflammation. We investigated two stroke models that distinguish divergent stroke pathogenesis and pathophysiology. At the early stage of 2 days after ischemia iron deposition could be only detected in the transient MCAO model whereas in permanent ischemia induced via PT iron-positive cells did not appear before 7 days after the insult. USPIO-enhanced MRI is therefore capable to noninvasively detect pathophysiological heterogeneity and might be a promising tool for targeting anti-inflammatory therapy in stroke.

1460. MR Imaging of Rat Monocytes Homing Towards an Area of Cerebral Infarction

Raoul David Oude Engberink[1], Erik I. Hoff[2], Susanne M. van der Pol[3], Erwin L. Blezer[1], Helga E. de Vries[3]

[1]University Medical Center Utrecht, Utrecht, Netherlands; [2]Department of Neurology, Maastricht, Netherlands; [3]VU Medical Center, Amsterdam, Netherlands

This work describes MR tracking of rat monocytes migrating towards an area of tissue damage in an animal model for cerebral infarctions (photothrombosis). A frequently used method, intravenous administration of ultra small superparamagnetic particles of iron oxides (USPIO), is compared to a more specific method of transplantation of pre-labeled monocytes containing SPIOs. 5 days after induction of the infarct animals are transplanted iv either with USPIOs or SPIO-labeled monocytes. T2*W imaging is performed before, 24h and 72h after transplantation. Results indicate that monitoring pre-labeled monocytes may be a better tool to study macrophage activity in brain inflammation.

1461. fMRI of Delayed Albumin Treatment During Stroke Recovery in Rats: Implication for Fast Neuronal Habituation in Recovering Brains

Young Ro Kim[1], Mauritz P.A. van Meer[1], Joseph B. Mandeville[1], Emiri Tejima[2], George Dai[1], Kamil Topalkara[3], Jianhua Qui[3], Rick M. Dijkhuizen[4], Mike A. Moskowitz[3], Eng H. Lo[2], Bruce R. Rosen[1]

[1]Athinoula Martinos Center for Biomedical Imaging/ Massachusetts General Hospital, Charlestown, Massachusetts, USA; [2]Neuroprotection Research laboratory/ Massachusetts General Hospital, Charlestown, Massachusetts, USA; [3]Stroke and Neurovascular Regulation Laboratory/ Massachusetts General Hospital, Charlestown, Massachusetts, USA; [4]Image Sciences Institute, University Medical Center Utrecht, The Netherlands, Charlestown, Massachusetts, USA

Accumulating experimental and clinical data suggest that albumin may be neuroprotective for stroke. Here, we use fMRI to evaluate the therapeutic efficacy of albumin and its effects on the recovery of stimuli-induced cerebral hemodynamics. Temporal characteristics of the ipsilesional somatosensory BOLD responses in the albumin-treated rats appeared considerably altered compared to those of contralesional responses while such temporal alterations were not pronounced for the CBV responses. These characteristic fMRI temporal profiles of the albumin-treated brains may be due to altered neuronal responses rather than altered neurovascular coupling, which implies an unusually fast habituation of neuronal responses in the lesional cortex.

1462. Dynamic Tissue Fates Tracking in Acute and Sub-Acute Phase of a Transient Occlusion Rat Model

Qiang Shen[1], Hongxia Ren[1], Jürgen Bardutzky[2], Marc Fisher[3], Timothy Q. Duong[1]

[1]Emory Unviersity, Atlanta, Georgia, USA; [2]University of Heidelberg, Heidelberg, Germany; [3]The University of Massachusetts Medical School, Worcester, Massachusetts, USA

The acute and sub-acute phase spatiotemporal dynamics of 30 minutes transient focal ischemic brain injury in rats were evaluated on a pixel-by-pixel basis using quantitative CBF and ADC measurements. The core and mismatch tissues before reperfusion were categorized to six groups according to their fates. The ADC and CBF values of different groups were dynamically tracked and tissue volume percentages were also summarized. About one third core tissues were permanently recovered. More than 70% mismatch pixels were salvaged by reperfusion. Hyper-perfusion was observed at 24-hr post-occlusion and could imply the presence of secondary injury.

1463. Time Course of Water Diffusivity in the Rat Brain After Global Ischemia

Ivan Vorisek[1, 2], Helena Neprasova[1], Miroslava Anderova[1], Daniel Jirak[3], Milan Hajek[3], Alexandr Chvatal[1], Eva Sykova[1, 2]

[1]Institute of Experimental Medicine ASCR, Prague, Czech Republic, Czech Republic; [2]Charles University, 2nd Medical Faculty, Prague, Prague, Czech Republic, Czech Republic; [3]Institute for Clinical and Experimental Medicine, Prague, Czech Republic, Czech Republic

We investigated the apparent diffusion coefficient of water (ADC_W) in the CA1 region of the hippocampus after global cerebral ischemia in the rat. The results were correlated with immunohistochemical analysis. An elevated ADC_W three days after reperfusion coincided with neuronal death. A subsequent increase in ADCw five weeks after reperfusion correlated with the activation of a caspase-3 dependent pathway of astrocytic death. We conclude that ADC_W can reflect changes in a number of cell elements, cell morphology or other cell properties connected with apoptosis.

1464. Brain Tissue Regeneration Following Activation of Endogenous Stem Cells in Animal Model of Stroke

Nancy J. Lobaugh[1], Anna Erlandsson[2], Hai-Ling Margaret Cheng[3], Voytek Gretka[1], Cindi Morshead[2], Greg J. Stanisz[1]

[1]Sunnybrook & Womens' CHSC, Toronto, ON, Canada; [2]University of Toronto, Toronto, ON, Canada; [3]Hospital for Sick Children, Toronto, ON, Canada

In this study, we used a rat model of stroke to demonstrate the feasibility of using MR to distinguish between regenerating and pathological tissues when using stem cell based therapies. Focal ischemia was induced in Wistar rats and endogenous neural precursor cells were activated with growth factors. Three weeks post-stroke MR imaging demonstrated formation of heterogenous tissue plug. Quantitative measurements of T1 and T2 relaxation times correlated very well with immunohistochemical analysis. The effects were more pronounced by 42 days post-stroke, where the extend of tissue recovery was significantly larger.

1465. Application of a Rat Stroke Model for Preclinical Evaluation of Anti-Stroke Drugs: Noninvasive Monitoring with Comprehensive Magnetic Resonance Imaging

Feng Chen[1], Yicheng Ni[1], Nobuo Nagai[2], Yasuhiro Suzuki[2], Desire Collen[2], Guy Marchal[2]

[1]Catholic University of Leuven, Leuven, Flamms Brabant, Belgium; [2]Catholic University of Leuven, Leuven, Flaams Brabant, Belgium

Utilizing the rodent stroke model and available MRI facilities, the present experimental system proved to be beneficial for anti-stroke drug evaluation. Comprehensive MRI approach allows noninvasive assessment of the therapeutic effects of μPli and tPA and their hemorrhagic transformation in rats. μPli may be a potential alternative to tPA with higher safety for ischemic stroke treatment.

1466. Correlation of Proton Transfer Ratio and Intracellular PH in Acute Ischaemia

Kimmo T. Jokivarsi[1], Heidi I. Gröhn[1], Olli H. Gröhn[1], Risto A. Kauppinen[2]

[1]A.I. Virtanen Institute for Molecular Sciences, University of Kuopio, Kuopio, Finland; [2]School of Sport and Exercise Sciences, University of Birmingham, Birmingham, UK

Acidification has been shown to enhance tissue damage caused by ischaemia. Proton transfer ratio (PTR) has been recently introduced as a means to determine intracellular pH (pHi). PTR was measured in transient middle cerebral artery occlusion model of rat, compared with pHi status of the brain and progression of ischaemic tissue alterations as assessed by T1rho and diffusion MRI. A strong correlation was seen between change in PTR and pHi derived from lactate concentration, as measured by 1H MRS. These results show that cellular acidification is a key factor affecting change in PTR due to ischaemia.

1467. Comparison of Cerebral Blood Flow Estimates in the Ischemic Area of Rat Brain Obtained with Dynamic Susceptibility Contrast and Continuous Arterial Spin Labeling

Ryo Kagaya[1, 2], Kazuhiro Nakamura[2, 3], Yasushi Kondoh[2], Masanobu Ibaraki[2], Jeff Kershaw[2, 3], Guoyue Chen[1], Iwao Kanno[2]

[1]Akita Pref Univ, Ugo-Honjoh, Japan; [2]Akita Res Inst of Brain and Vessels, Akita, Japan; [3]Akita Industry Promotion Found, Akita, Japan

The maximum value of the logarithmic signal ratio (max$\delta R2^*$) in DSC is occasionally used as an indicator of the CBF in the rat brain. A comparison of the CBF indicated by continuous arterial spin labeling (CASL) and max$\delta R2^*$ was performed in the ischemic rat brain. When the estimated CBF values were lower than 50% of the normal level, the ischemic brain area estimated from the max$\delta R2^*$ method was significantly smaller than that obtained with the CASL method ($p<0.05$). This study indicates that the CBF estimated with DSC may be overestimated in ischemic brain areas.

1468. Quantitative T2* Measurements of Fetal Brain Oxygenation During Hypoxia with MRI at 3T: Correlation with Blood Gas Analyses

Ulrike Wedegärtner[1], Hendrik Kooijman[2], Andrew N. Priest[1], Mikhail Tchirikov[1], Hobe J. Schröder[1], Gerhard Adam[1]

[1]University Hospital Hamburg-Eppendorf, Hamburg, Germany; [2]Philips Medical Systems, Hamburg, Germany

OLD might be an important tool to detect and monitor the fetus at risk, which is still a major problem in obstetrics. But MRI delivers only arbitrary units of the signal intensities. Quantitative multiecho-sequences allow the determination of absolute MRI values (T2 and T2* relaxation times). The purpose of this study is the determination of oxygen saturation in the fetal brain during hypoxia by T2* measurements and comparison with fetal blood gas analysis. There is a reasonable correlation between SO2 measured from MRI and determined by fetal blood samples. MRI thus has potential to assess fetal cerebral oxygen saturation non-invasively.

1469. Timecourse of Early CBF Changes After Controlled Cortical Impact in Mice

Lesley M. Foley[1], T Kevin Hitchens[1], Patrick M. Kochanek[2], John A. Melick[2], Chien Ho[1]

[1]Carnegie Mellon University, Pittsburgh, Pennsylvania, USA; [2]University of Pittsburgh School of Medicine, Pittsburgh, Pennsylvania, USA

Trauma can produce alterations of physiological processes such as cerebral autoregulation due to hypoperfusion, therefore it is important to study how targeting cerebral hemodynamics may improve neurological outcome. Approximately one hour after injury cerebral blood flow (CBF) was lowered over the entire ipsilateral hemisphere and it remained that way over the course of the experiment. Animals that had a craniotomy only, had lowered CBF in a pattern similar to the injured animals, but CBF recovered in all regions except the cortex under the contusion by experiment end.

1470. Post-Ischaemic Gene Therapy for Stroke: An MRI Study

Romina Aron Badin[1], Mark F. Lythgoe[1], Martin D. King[1], David S. Latchman[1], David G. Gadian[1]

[1]Institute of Child Health, University College London, London, UK

In spite of the many experimental studies on stroke, the development of effective therapies has been disappointing. Moreover, the increasing number of therapies attempting repair and regeneration has enhanced the need for investigation of functional outcome. This study addresses both these issues by evaluating the effects of heat shock protein treatment on stroke via longitudinal non-invasive MRI measurements of lesion size and via long term sensorimotor testing. Viral gene therapy with two proteins was attempted early after stroke induction. Results indicate that post-ischaemic overexpression of one of the proteins significantly reduces lesion size and affects behavioural recovery in a rat model of transient ischaemia.

1471. Temporal and Spatial Evolution of MR Derived Cerebral Metabolic Rate of Oxygen Utilization Index in Acute Middle Cerebral Artery Occlusion Stroke Rats

Hongyu An[1], Yasheng Chen[1], Liansheng Chang[1], Weili Lin[1]

[1]University of North Carolina at Chapel Hill, Chapel Hill, North Carolina, USA

In this study, the temporal and spatial evolution of MR measured cerebral metabolic rate of oxygen utilization index (MR-COMI) was studied during acute stage and its correlation with the final tissue outcome defined by 24 hours T2 images after MCAO was examined in a middle cerebral artery occlusion rat model. Lesions recruited to final infarction usually have a substantial reduction in MR_COMI, while the reversible lesions with compromised acute CBF but without final T2 lesions only show modest reduction in MR_COMI and comparable MR_COMI were obtained in the ipsi- and contra-lateral hemisphere in rats without CBF/T2 lesion.

1472. Cerebral Edema Induced by Synchrotron Microbeam Radiation Therapy in the Healthy Mouse Brain. Characterization by Means of Diffusion Tensor Imaging

Yohan van de Looij[1], Raphaël Serduc[1], Gilles Francony[1], Olivier Verdonck[1], Elke Brauer[2], Boudewijn van der Sanden[1], Christoph Segebarth[1], Chantal Remy[1], Hana Lahrech[1]
[1]UJF/INSERM U594, Grenoble, France; [2]European Synchrotron Radiation Facility, Grenoble, France

Conventional radiotherapy of brain tumors may induce significant necrosis and edema in the surrounding healthy brain, which can be characterized by modification of the Apparent Diffusion Coefficient (ADC). Microbeam Radiation Therapy (MRT) may significantly reduce radiation damage in the healthy brain tissue by spatial microfractionation of the absorbed radiation dose. The aim of this work was to verify this hypothesis by DTI and micogravimetric methods. Minor and transient cellular edema has only been detected 1 day after a 312 Gy exposure which makes MRT a promising tool in the treatment of malignant brain tumors while preserving healthy tissue.

1473. High Resolution Sodium Imaging of Rat and Mouse Models of Stroke at 17.6 T

Thomas Neuberger[1, 2], Andrew Webb[1, 2]
[1]Penn State University, University Park, Pennsylvania, USA; [2]University of Würzburg, Würzburg, Germany

This work presents the first *in vivo* high resolution sodium images acquired from two different mouse model of stroke, as well as one for rat. Submillimeter voxel sizes were achieved using density weighted chemical shift imaging techniques at high field. Localization of the infarct from the sodium images agreed well with those from T_2- and diffusion-weighted proton imaging. Measurement of the sodium T_1 relaxation times showed slightly higher values in the infarcted region of the mouse brain than for normal tissue, with excellent reproducibility during the study.

Animal Brain MRS: 1H MRS

Room 4E Tuesday 13:30 - 15:30

1474. Effect of Iron Deficiency on Developing Rat Striatum

Ivan Tkac[1], Kay L. Ward[1], Barbara Felt[2], Betsy Lozoff[2], Michael K. Georgieff[1], Raghavendra Rao[1]
[1]University of Minnesota, Minneapolis, Minnesota, USA; [2]University of Michigan, Ann Arbor, Michigan, USA

Gestational and postnatal iron deficiency (ID) impairs hippocampus-dependent recognition memory and is accompanied by changes in the neurochemical profile. In this study *in vivo* ^{1}H NMR spectroscopy at 9.4 T was used to investigate effects of ID on developing rat striatum. Developmental trajectories of the ID group (n=10) and the control group (n=10) were similar. However, small but significant changes in concentrations of multiple metabolites (Gln, Glu, Glc, Lac, myo-Ins, NAA, tCho, Tau) and metabolite ratio (PCr/Cr) between the groups were observed. Neurochemical changes correlated with delayed performance in striatum-dependent behavioral tests in the ID group.

1475. Water and Metabolite Proton T1 and T2 Relaxation in Rat Brain *In Vivo*

Robin A. de Graaf[1], Peter B. Brown[1], Scott McIntyre[1], Terence W. Nixon[1], Kevin L. Behar[1], Douglas L. Rothman[1]
[1]Yale University, New Haven, Connecticut, USA

A comprehensive and quantitative measurement of T1 and T2 relaxation times of water and metabolites in rat brain under identical experimental conditions at three high magnetic field strengths (4.0 T, 9.4 T and 11.7 T) is presented. Water relaxation show a highly significant increase (T1) and decrease (T2) with increasing field strength for all nine analyzed brain structures. Similar, but less pronounced, effects were observed for all metabolites. Among other features, this data shows that while spectral resolution continues to increase with field strength, SNR in T1/T2 based anatomical MRI may actually decrease at higher magnetic fields.

1476. Monitoring De- And Re- Myelination MR Spectroscopy Surrogate Markers in the Mouse Brain at 9.4 T

Wafaa Zaaraoui[1, 2], Mathilde Deloire[3], Michel Merle[2], Gerard Raffard[2], Marc Biran[2], Maria Inglese[1], Klaus G. Petry[3], Jean-Michel Franconi[2], Oded Gonen[1], Vincent Dousset[3]
[1]New York University, New York, New York, USA; [2]RMSB UMR 5536, Bordeaux, France; [3]EA2966 Universite Victor Segalen Bordeaux, Bordeaux, France

Proton MR spectroscopy (1H-MRS) is frequently used to augment the sensitivity of MRI with metabolic specificity. The main surrogate markers monitored by 1H-MRS are the N-acetylaspartate (NAA) which is exclusive to neuronal cells, the mixture of free and phosphor-creatine (Cr) reflecting cell energetics, and the composite of free and phospho-choline (Cho) which reflects membrane turnover. Unfortunately, increases or declines in their levels are rarely definitive of the underlying process. For example, a decline in NAA may reflect neuronal dysfunction (which may be recoverable) or loss, which is permanent. Likewise, elevated Cho may indicate membrane destruction or recovery or even an admixture of the two processes. There has been precious little direct validation, i.e., direct quantitative pathological verification, of the underlying molecular processes steering the MR observed behavior of these surrogates. The goal of this study was to validate the nature of the MRS surrogate markers in a known model of de- and re- myelination in a mouse brain and verify these observations with pathological validation.

1477. MR Studies of Aging in the Hippocampus of the FBNF1 Rat Show Correlations with Behavioral and Structural Degeneration

Ira Driscoll[1, 2], Robert S. Sutherland[2], Boguslaw Tomanek[3], Jeff F. Dunn[3], William M. Brooks[4]
[1]National Institute on Aging, Baltimore, Maryland, USA; [2]University of Lethbridge, Lethbridge, Alberta, Canada; [3]University of Calgary, Calgary, Alberta, Canada; [4]University of Kansas Medical Center, Kansas City, Kansas, USA

We conducted a multi-modality analysis of age-related characteristics in the hippocampus of young, middle-aged, and old FBNF1 rats, examining the relationships between aging, hippocampus, and memory, using a combination of behavioral, non-invasive MR imaging and spectroscopy, and post-mortem neuroanatomical measures. Aging was associated with functional deficits on hippocampus-dependent memory tasks, which were accompanied by structural alterations observed both *in vivo* (MRI-hippocampal volume) and post-mortem (neuronal density). Neuronal metabolic integrity (MRS-NAA levels) seemed preserved. This pattern of age-related alterations closely resembles previously reported pattern in humans and suggests FBNF1 rats to be a useful model of normal human aging.

1478. *In Vivo* Observation of Hypernatremia During Sodium Lactate Infusion

Su Xu[1], Wenjun Zhu[1], Jun Shen[1]
[1]National Institute of Mental Health, Bethesda, Maryland, USA

Hypernatremia was observed *in vivo* during sodium lactate infusion. The effect of hypernatremia on brain metabolites was quantitatively analyzed using ^{1}H MRS of α-chloralose anesthetized rat brain performed at 11.7 T. The levels of aspartate ($F(8,72)=2.258$, $P<0.03$), glutamate ($F(8,72)=10.545$, $P<0.0005$) and taurine ($F(8,72)=3.689$, $P<0.001$) were found to be altered significantly due to prolonged sodium lactate infusion, consistent with the known effect of hypernatremia observed in previous *in vivo* studies. During sodium lactate infusion, the lactate levels in both artery ($F(8,56)=6.681$, $P<0.0005$) and brain ($F(8,72)=11.198$, $P<0.0005$) were significantly increased which are consistent with previous findings in rats using *in vivo* ^{1}H MRS.

1479. Acute Administration of Nicotine Reduced Myo-Inositol and GABA Levels in Nucleus Accumbens in Rats

Serguei Liachenko[1], Robert Durham[1], Lori Badura[2], Peter Snyder[2]
[1]Pfizer, Inc., Ann Arbor, Michigan, USA; [2]Pfizer, Inc., Groton, Connecticut, USA

The potential reinforcing properties of compounds are an important consideration in the development of CNS-active drugs. Myo-inositol is a marker of glial-neuronal interactions, which are one mechanism of modulation of rewarding properties of addictive compounds. We found that acute administration of nicotine decreased the concentration of myo-inositol and GABA measured with MRS at 7 Tesla in nucleus accumbens in rats. Further investigation of addiction mechanisms and development of biomarkers for drug research is warranted.

1480. Effects of Chronic Morphine Treatment on Metabolism of Glutamate and GABA in Rat Prefrontal Cortex Studied by *Ex Vivo* High Resolution ^{1}H NMR Spectroscopy

Hongchang Gao[1], Yun Xiang[1, 2], Hang Zhu[1], Ninglei Sun[3], Yuanye Ma[3], Maili Liu[1], Hao Lei[1]
[1]Wuhan Institute of Physics & Mathematics, Chinese Academy of Sciences, Wuhan, Hubei, People's Republic of China; [2]Jianghan University, Wuhan, Hubei, People's Republic of China; [3]Kunming Institute of Zoology, Chinese Academy of Sciences, Kunming, Yunnan, People's Republic of China

The effects of chronic morphine treatment and subsequent withdrawal on the metabolism of glutamate (Glu)-GABA neurotransmitter systems in the prefrontal cortex (PFC) of rats were studied by *ex vivo* high resolution ^{1}H nuclear magnetic resonance spectroscopy. It is shown that chronic morphine treatment induces a progressive increase in GABA, and concurrent decreases in Glu and Glu/GABA ratio. Such changes are reversible during subsequent withdrawal, and might be manifestations of adaptive alterations of the neurotransmitter systems in response to repeated morphine exposures. The results are also consistent with the previous results showing that the PFC activities are reduced in drug addicts.

1481. Morphological and Metabolic Changes in the Brain of 6-Hydroxydopamine Treated Rats Observed by MRI and *In Vivo* ^{1}H MRS

Fang Fang[1], Yuanyi Ma[2], Shuzhen Kong[2], Min He[2], Hao Lei[1]
[1]Wuhan Institute of Physics & Mathematics, Chinese Academy of Sciences, Wuhan, Hubei, People's Republic of China; [2]Kunming Medical College, Kunming, Yunnan, People's Republic of China

MRI and *in vivo* ^{1}H MRS were used to investigate in rats the morphological and metabolic changes of the brain induced by unilateral stereotaxic injection of 6-hydroxydopamine (6-OHDA) into the substantia nigra (SN), a commonly used procedure known to cause Parkinsonism. Compared to their contralateral counterparts, the ipsilateral SN showed significantly lower T_2 and T_2*, likely due to iron deposition in this region, and the ipsilateral striatum showed significantly decreased NAA/Cr and NAA/Cho ratios, presumably as a result of 6-OHDA induced dopaminergic neuron loss in the SN and its effects on striatal dopaminergic neurons via nigrostriatal pathway.

1482. Methylphenidate Administration During Adolescence Produces Long-Term Effects in Adult Rat Brain: A 1H MRS *In Vivo* Study

Rossella Canese[1], Walter Adriani[1], Franca Podo[1], Giovanni Laviola[1]
[1]Istituto Superiore di Sanità, Rome, Italy

Long-term effects of methylphenidate (a drug currently used for treatment of children affected by attention deficit hyperactivity disorder) were investigated in selected brain regions of adult rats, following exposure to this drug during adolescence. Our data indicate that adolescent MPH exposure produces long-term metabolic changes in reward-related circuits. These enduring MRS-detectable biochemical modifications may perhaps account for the finding of reduced basal behavioral impulsivity in the adult rat.

1483. Metabolic Responses in Kanic Acid Induced Lesion in Rat

Hui Mao[1], Donna Toufexis[2], Xiaoxia Wang[1], Shaoxiong Wu[2], Agnes Lacreuse[2]
[1]Emory University School of Medicine, Atlanta, Georgia, USA; [2]Emory University, Atlanta, Georgia, USA

We demonstrated the meatbolite profiling can be obatined using MAS NMR in the classic animal model of brain injury/epilepic lesion in kainic acid induced lesion in rat.

1484. Creatine Uptake Kinetics in Brain and Skeletal Muscle of GAMT Deficient Knockout Mice

Hermien Elise Kan[1], Esther Meeuwissen[1], Andor Veltien[1], Dirk Isbrandt[2], Arend Heerschap[1]
[1]Radboud University Nijmegen Medical Center, Nijmegen, Netherlands; [2]University of Hamburg, Hamburg, Germany

In guanidinoacetate methyltransferase deficiency (GAMT-/-) creatine (Cr) concentrations in skeletal muscle and brain are severely reduced. We performed a detailed study of the Cr increase during Cr supplementation in a knockout mouse model of this disorder using 1H-MRS. Our results show that in GAMT-/- mice, Cr concentrations in skeletal muscle and brain increase in the course of days. Cr concentrations increase faster in skeletal muscle compared to brain, however, this is only apparent in the first week of supplementation. Regulation and expression of the Cr transporter in skeletal muscle and the blood-brain-barrier likely play a role in the observed differences.

1485. MRI and MRS Study of a Transgenic Mouse Model of D1 Dopamine Receptor Positive Striatal Cell Depletion

Ke Fang[1], Ilsa Gantois[1], Hong Xin Wang[1], Qi Zhu Wu[1], Qing Yang[1], John Drago[1], Gary Francis Egan[1]
[1]Howard Flory Institute, Melbourne, Vic, Australia

We have created a transgenic mouse model with post-natal striatal D1 receptor positive (D1R+) cell loss [1] to mimic the human Parkinson-plus syndromes and Huntington's disease (HD). Transgenic mice survive for an extended period of time allowing us a significant experimental time window to elucidate the mechanisms of brain disorders characterized by striatal cell loss. Several MRS studies have shown the striatal impaired energy metabolism and neuronal dysfunction in HD mouse model and human. The purpose of this study was to investigate brain changes using MRI and MRS in a transgenic model of D1R+ cell depletion. T2-weighted RARE MRI and 1H PRESS MRS were used to reveal anatomical changes and to monitor brain metabolism respectively.

1486. Metabolic Interactions Between Glutamatergic and Dopaminergic Neurotransmiter Systems Are Mediated Through D1, But Not D2, Dopamine Receptors

Tiago B. Rodrigues[1], [2], Ana B. Martin[3], Patricia Sanchéz[1], Sebastián Cerdán[1], Rosario Moratalla[3]
[1]Inst. Inv. Biomedicas "Alberto Sols", Madrid, Spain; [2]University of Coimbra, Coimbra, Portugal; [3]Inst. Cajal, Madrid, Spain

Dopaminergic neurotransmission is modulated by dopamine D1 and D2 receptors, which appear to play a fundamental role in a variety of physiopathological states, including Parkinson's disease and cocaine addiction. These disturbances involve also alterations in glutamatergic neurotransmission, suggesting that cross modulation may exist between both neurotransmitter systems. However, the mechanisms of the interaction between dopaminergic and glutamatergic neurotransmissions remain unknown. We explore here these interactions using transgenic knock-out mice deficient in the dopamine D1 and D2 receptors, evaluating by ^{13}C-NMR the glutamine cycle and associated glutamatergic neurotransmission. Removal of D1 receptors, but not D2 receptors, stimulate glutamatergic neurotransmission.

1487. Aggregation-Induced Reduction in T_2 Relaxation Time of MR Visible Lipids Observed in Ischemic Rat Brain

Li Wei[1], Hao Lei[1]
[1]Wuhan Institute of Physics & Mathematics, Chinese Academy of Sciences, Wuhan, Hubei, People's Republic of China

1MR visible lipids (MRVL) have been associated with inflammatory responses and apoptosis. Quantification of MRVL, however, can be complicated by the facts that different MRVL species could have different T2 and T2 of MRVL could change with disease evolution. *In vivo* 1H MRS was used to monitor temporal changes of MRVL and their apparent T2 in a rat model of transient focal ischemia. The results show that apparent T2 of the MRVL in the ischemic lesion decreases as the lesion matures, having a time course that coincides with that of the increases in amount and size of the lipid droplets.

1488. Identification of Neural Stem Cells in Rat Brain Using Their Specific Magnetic Resonance Spectroscopy Signature

Raphael D. Hazel[1], Louis N. Manganas[2], Xueying Zhang[3], Mei Yu[4], Petar M. Djuric[3], Helene Benveniste[3], Mark E. Wagshul[3], Mirjana Maletic-Savatic, [23]

[1]Stony Brook University, Stony Brook, New Yory, USA; [2]Cold Spring Harbor Laboratory, Cold Spring Harbor, New York, USA; [3]Stony Brook University, Stony Brook, New York, USA; [4]Brookhaven National Laboratory, Brookhaven, New York, USA

We present a novel technique for identifying neural stemcells (NSC) in rodent brain which uses a NSC specific signaturedetectable by high resolution microMRI spectroscopy. We havesuccessfully demonstrated the usefulness of this method for detecting and quantifying both endogenous and exogenous NSC *in vivo*. This raises thepossibility of tracking survival and distribution of implanted NSC inhuman brain.

1489. The Effect of Paramagnetic Manganese Cations on ^{1}H MR Spectroscopy of the Brain

Kathrine Skak Madsen[1, 2], David Alberg Holm[1, 3], Lise Vejby Søgaard[1], Gert Rene Christoffersen[2], Ian John Rowland[1]

[1]Copenhagen University Hospital, Hvidovre, Denmark; [2]University of Copenhagen, Copenhagen, Denmark; [3]Technical University of Denmark, Copenhagen, Denmark

The influence of paramagnetic manganese (Mn) cations on proton brain spectra was investigated *in vivo* and in phantom studies. Using a Mn-enhanced neural tracing model, spectra acquired from the two adjacent regions of the superior colliculi show minimal effects from the manganese within the spectroscopic voxel. The large relaxivity measured for NAA suggests that if the metabolite and paramagnetic Mn^{2+} cations are within the same cellular compartment, significant relaxation effects could influence the apparent ^{1}H MRS metabolic profile obtained from brain tissue. This effect should be taken into account when performing spectroscopic investigations on brain regions with increased Mn concentrations.

1490. Measurement of T_1 Relaxation Times of Major Metabolites in the Mouse Brain at 11.7 and 17.6 Tesla Using Voxel-Localized Proton Magnetic Resonance Spectroscopy

Thomas Neuberger[1, 2], Andrew Webb[1, 2], Cornelius Faber[2], Volker Christian Behr[2], Stefan Neubauer[3], Jürgen E. Schneider[3]

[1]Huck Institute Magnetic Resonance Centre, University Park, Pennsylvania, USA; [2]University of Würzburg, Würzburg, Germany; [3]University of Oxford, Oxford, UK

Characterization of the relaxation times of brain metabolites at different field strengths is important both for optimizing data acquisition parameters and for establishing control conditions in order to measure changes induced by pathology. In this work, water-suppressed localized ^{1}H-MR spectroscopy has been performed on volumes less than 20 μL in the mouse brain *in vivo* at 11.7 and at 17.6 tesla. Our results show a slight increase of the T_1 values from 11.7 to 17.6 tesla.

1491. Quantitative MR Spectroscopic Evaluation of Radiation-Induced Brain Injury in a Rat Model

Todd Atwood[1], Mike Robbins[1], Jian-Ming Zhu[1]

[1]Wake Forest University School of Medicine, Winston Salem, North Carolina, USA

In vivo localized MRS offers a tool to non-invasively study the metabolic and neuro-chemical changes throughout radiation treatment, which could help determine bio-markers that are relevant to normal tissue injury. This could also lead to the development of an accurate noninvasive imaging procedure to detect the neuro-functional changes at early stages. The specific aim of the current study was to detect and determine, using MRS, the long term neuro-chemical changes in rat brain associated with exposure to a clinically relevant dose of irradiation.

1492. Quantitative 1H MRS in the Rat Hippocampus After Global Ischemia

Daniel Jirak[1, 2], Ivan Vorisek[3], Eva Sykova[4], Milan Hajek[1, 2]

[1]IKEM, Prague 4, Czech Republic; [2]Charles University, 2nd Faculty of Medicine, Prague, Czech Republic; [3]Institute of Experimental Medicine,, Prague, Czech Republic; [4]Institute of Experimental Medicine, Prague, Czech Republic

The aim of our study was to determine, using proton MR spectroscopy, metabolic changes in the rat hippocampus after ischemia during one month. The concentrations of Cho, Cr, Ins and Tau did not change significantly during whole experiment. Gln changed significantly from controls 1 week after occlusion of carotides, we observed its decrease. Concentration of Glu significantly increased only 1 day after ischemia, and then returned to normal. NAA+NAAG decreased significantly 3 days and 1 week after ischemia. Our results support published data which referred to a decline in NAA concentration and increase in Glu concentration after ischemia.

1493. *In Vivo* Brain NMR Spectroscopy of Alpha-Mannosidosis in a Feline Model

Sergey Magnitsky[1], Charles H. Vite[2], Stephen Pickup[1], David Aleman[2], John H. Wolfe[2], Harish Poptani[3]

[1]The University of Pennsylvania, Philadelphia, Pennsylvania, USA; [2]University of Pennsylvania School of Veterinary Medicine, Philadelphia, Pennsylvania, USA; [3]The University of Pennsylvania,, Philadelphia, Pennsylvania, USA

A mutation in the MANB gene causes the lysosomal storage disease alpha-mannosidosis (AMD). In the brain, it leads to accumulation of mannose-rich oligosaccharides, swelling of neurons and glia, neuronal loss, gliosis and demyelination. *In vivo* NMR spectroscopy was performed in normal and AMD affected cat brains. A significant increase of signal intensity at 2.02 and 3.6 ppm was detected in the cortex and cerebellum of affected animals. The increased intensity of these signals may be due to the high concentration of mannose-rich oligosaccharides in these animals. We conclude that 1H-MRS studies may assist in diagnosis of AMD disease.

1494. [1]HMRS in a Monkey Model of AIDS and Opiates

Christine Carol Cloak[1], Linda Chang[1], Shawn O'Neil[2], Thomas M. Ernst[1], Dan Anderson[3], Robert M. Donahoe[4]
[1]University of Hawaii, JABSOM, Honolulu, Hawaii, USA; [2]Harvard Medical School, Southborough, Massachusetts, USA; [3]Emory University, Atlanta, Georgia, USA; [4]University of Utah, School of Medicine, Salt Lake City, Utah, USA

We evaluated possible interactive effects of opiates and immunodeficiency virus infections on the brain in a rhesus macaque primate model. Frontal gray matter, frontal white matter, putamen, and caudate brain extracts from morphine-dependent and saline-control monkeys, infected with simian immunodeficiency virus (SIVsmm9), were studied with *ex vivo* [1]HMRS. Morphine-exposed monkeys had significantly higher frontal white matter N-acetyl compounds than saline-controls, suggesting a protective effect of morphine. Several other interesting trends were observed. This study improves our understanding of how opiates affect AIDS progression and shows the feasibility of using the SIV model and [1]HMRS to study HIV1-opioid interactions.

1495. Genotype Specific Alterations Detected in the Neurochemical Profiles of Aged Transgenic Mouse Models of Alzheimer's Disease

Malgorzata Marjanska[1], Geoffrey L. Curran[2], Thomas M. Wengenack[2], Pierre-Gilles Henry[1], Robin L. Bliss[1], Joseph F. Poduslo[2], Clifford R. Jack, Jr.[2], Kamil Ugurbil[1], Michael Garwood[1]
[1]University of Minnesota, Minneapolis, Minnesota, USA; [2]Mayo Clinic College of Medicine, Rochester, Minnesota, USA

Proton magnetic resonance spectroscopy offers a non-invasive way to quantify many metabolites *in vivo*. Metabolite levels are sensitive to different *in vivo* pathologic processes at the molecular or cellular level; e.g. *myo*-inositol (mIns) and taurine are thought to be markers for osmotic stress or astrogliosis. Murine models of Alzheimer's disease (AD) have been created by inserting human mutations associated with abnormal processing of amyloid β protein. These mutations of amyloid precursor protein (APP) and presenilin (PS) 1 or 2 produce hereditary AD in humans. Recently spectroscopic analysis of single transgenic APP, and double transgenic PS2APP and APP-PS1 mice brains showed neurochemical profiles which deviate from that seen in wild-type mice as the transgenic mice age. The purpose of this study was to compare the levels of the metabolites in question, mIns and taurine, in different mouse models of Alzheimer's disease: APP, PS1, APP-PS1 and wild-type. We hypothesized that the neurochemical profiles of these transgenic mice at old age would be genotype specific and vary as a function of age and amyloid burden.

1496. The Pathophysiogical Basis of Brain Swelling of Grey vs. White Matter in Acute Liver Failure Are Different: Lessons from a Study Using MARS

Claudia Zwingmann[1], [2], Chris Rose[1], Surajit Sen[3], Nathan Davies[4], Roger Frank Butterworth[1], Dieter Leibfritz[2], Lars Marius Ytrebo[5], Arthur Revhaug[5], Rajiv Jalan[6]
[1]Hospital Saint-Luc, Montreal, Quebec, Canada; [2]University of Bremen, Bremen, Germany; [3]State University of New York, Buffalo, New York, USA; [4]University College London, London, UK; [5]University Hospital of Northern Norway, Tromso, Norway; [6]Royal Free & University College Medical School, London, UK

Encephalopathy in acute liver failure (ALF) is characterised by increased brain water in grey and white matter (GM and WM). Our aim was to perform *ex vivo* 1H-NMR to explore previous observations that albumin dialysis (MARS) reduces cerebral swelling only in the WM. In ALF, brain water increases in GM and WM. However only 6/11 metabolite changes are similar. The MARS-induced normalisation of brain water in the WM was paralleled by a normalization of 7/11 metabolites. Since MARS only normalised WM tissue water, this suggests that increases in brain water in WM vs GM are associated with different pathophysiological mechanisms.

1497. Effect of Blood Flow on Brain Temperature Distribution

Mingming Zhu[1], [2], Joseph J. H. Ackerman[1], [2], Alexander L. Sukstanskii[2], Dmitriy A. Yablonskiy, [12]
[1]Washington University, St. Louis, Missouri, USA; [2]Washington University School of Medicine, St. Louis, Missouri, USA

Temperature measurements in the rat brain reveal a gradient with the center of the brain being warmer than the brain surface. Detail theoretical analysis predicts that the temperature distribution near the brain surface is exponential with a characteristic "screening" length D dependent upon the CBF. This study provides direct experimental evidence confirming the theoretical relationship between D and CBF. Consequently, measurement of brain temperature profiles provides quantitative assessment of blood flow. Temperature profiles were evaluated by means of non-invasive MR spectroscopy and validated by direct thermocouple measurements. CBF was measured using the microsphere tracer technique.

Brain: Miscellaneous MRI

Room 4E Tuesday 13:30 - 15:30

1498. The Association of Low-Dosage Sex Hormone Replacement Therapy and the Aging Brain Using 3.0T MR Scanner

Hu Ling[1], Jin Zheng Yu[1], Feng Feng[1], Ge Qinsheng[1], Li Mingli[1]
[1]Peking Union Medical College Hospital, Beijing, People's Republic of China

Dementia and memory loss are society problem in aging persons. The incidence of dementia in postmenopausal women is much higher than the same years men. Alzheimer's disease closely related to E2 levels. But a lot of data show normal-dose HRT can do noting about preventing dementia to PMW. In our research work, Using 3.0T MR scanner, we can evaluate whether small-dose(1/4 less) long-term hormone replacement therapy is useful to prolonged degeneration of aging brain. Hippocampus atrophy and small cerebral vascular disease are two main character of dementia. According this research we draw the conclusion that small-dose long-term HRT can postpone PMW from brain early degeneration.

1499. Early Experience from the Application of a Noninvasive MRI-Based Measurement of Intracranial Pressure in Hydrocephalus

Noam Alperin[1], Josh Niebruegge[1], Terry Lichtor[2], Roberta Glick[2]
[1]University of Illinois at Chicago, Chicago, Illinois, USA; [2]Cook County Hospital, Chicago, Illinois, USA

Diversion of CSF in hydrocephalus by shunting is often necessary. However, shunting is associated with high failure rate (40% in the first year). The decision to place or revised a shunt is based on symptoms and radiographic imaging of ventricular size. Because symptoms often may not be specific and ventricular size may not correlate with abnormal ICP there is a need for a diagnostic test to assist in the treatment decision. We reports early experience from the first application of an MRI-based measurement of ICP in hydrocephalus. Patients with symptoms suggestive of elevated ICP or shunt malfunction underwent MR-ICP and were retrospectively evaluated with respect to the short-term outcome to assess its predictive values.

1500. Neuroprotective Effect of Long-Term Low Dose Hormone Replacement Therapy on Postmenopausal Women Brain Hippocampus

Hu Ling[1], Yue Yun[2], Zuo Pingping[2], Jin Zheng Yu[1], Feng Feng[1], Ge Qinsheng[1]
[1]Peking Union Medical College Hospital, Beijing, People's Republic of China; [2]Institute of Basic Medical Sciences, Chinese Academy of Medical Sciences & Peking Union Medical Coll, Beijing, People's Republic of China

Dementia and memory loss are society problem in aging persons. Alzheimer's disease closely related to E2 levels. But a lot of data show normal-dose HRT can do nothing about preventing dementia to postmenopausal women. In our research work, we select PMW (HRT group 14 cases, control group 11 cases)with susceptible genes of AD (ApoE¦Å3/¦Å4) , using 3.0T MR scanner we measured the hippocampus volumes, showed that the left and right hippocampus volumes in the HRT group were larger than the control group, and there were obvious differences ($P<0.05$). which indicate that long-term low dose HRT can avoid hippocampus atrophy, which is beneficial to maintaining function of brain and prevention of AD.

1501. Will Piecewise Continuous Echo Spacing Adversely Affect the T_2 Distribution?

Thorarin Albert Bjarnason[1]
[1]University of Calgary, Calgary, AB, Canada

Effects of diffusion weighting when using a piecewise-continuous echo spacing to measure T_2 relaxation were explored. Traditional multi-echo acquisitions acquire 32-echoes equally spaced collecting out to 320ms. Potentially prolonged T_2 components of the order 500ms are undersampled. A piecewise-continuous echo spacing allows one to collect out to 1120ms, thus better sampling relaxation data that could potentially contain a prolonged component. Three cases were studied: crusher gradients, read gradients, and both together. The following simulation work confirms that prolong components measured reflect microstructure and are not an artifact of the acquisition scheme.

1502. Magic Echo Imaging of the Brain at 1.5 T

Walter R.T. Witschey II[1], Brian K. Bronzo[1], Arijitt Borthakur[1], Ravinder Reddy[1]
[1]University of Pennsylvania, Philadelphia, Pennsylvania, USA

Magic echo imaging has been previously shown to generate a new kind of dipolar image contrast. In this study, we consider practical implementation, restrictions and advantages to magic echo imaging in the brain. We show the first magic echo brain images among a series of healthy volunteers and demonstrate T2 enhancement over conventional spin echo imaging. Methods for generating magic echo T2 maps are outlined and methods for eliminating the zero-peak artifact are shown. The effect of this T2 enhancement on image contrast is also taken into consideration.

1503. PET Restoration by Maximization of MRI-PET Mutual Information

Yong Chu[1], Min-Ying Su[1], Mark Mandelkern[1], Orhan Nalcioglu[1]
[1]University of California, Irvine, California, USA

The criterion of maximization of mutual information (MMI) is proposed to apply a priori information from high-resolution MR images on restoration of low-resolution PET images. The results, including improved resolution, sharper edges, better contrast, higher SNR, small structure and lesion detectability, and more accurate radioactivity concentration, were demonstrated using a realistic digital brain phantom. The proposed method was also applied in a clinical epilepsy study, and proven to improve the quality of restored PET images. This method can be easily implemented to improve the resolution and quantitative accuracy of functional PET or SPECT images when the MRI is available.

1504. Variability of Automated Shape Analyses of Fixed Brain Mouse MRI

Jason Lerch[1], Shoshana Tsatskis[1], John Sled[1], Natasa Kovacevic[1], R. Mark Henkelman[1]
[1]Mouse Imaging Centre, Toronto, Ontario, Canada

The study of phenotype/genotype relationships can be performed rapidly and accurately using high-resolution MRI on inbred mouse models. This abstract investigated the variability of an automated non-linear registration based shape analysis framework in 32µm fixed brain MRI, where the mouse brains remained inside the skull in order to reduce shape changes due to specimen handling. We found lower variance and higher statistical power using this improved protocol when compared to previous results.

1505. Pre-Processing Strategies to Improve Longitudinal MRI Repeatability

Kelvin Wong[1, 2], Xiaoyin Xu[2], Geoffrey Young[2], Stephen Wong[1, 2]
[1]Harvard Medical School, Boston, Massachusetts, USA; [2]Brigham and Women's Hospital, Boston, Massachusetts, USA

Image registration has been commonly used in MRI in putting different images together at the same spatial coordinates for normalization and comparison purposes. 2D acquisitions are known to produce inaccurate registration due to the highly anisotropic voxels. In mouse brain MRI, 2D techniques are frequently used to achieve high spatial resolution and to avoid physiological motion artifacts of in 3D sequence. In this paper we presented some strategies to characterize registration accuracy and how to accurately image the same location every time on the same mouse. It would be useful in monitoring disease progression as well as improving detection accuracy.

1506. Biocompatibility of Sapphire and Borosilicate Glass for Neural Prosthesis Using MRI and Histopathology

Kaushik Saranath Parthasarathy[1], Yimin Shen[1], Kelley Brabant[1], Jie Li[1], Yu Cheng[1], Gregory William Auner[1], James Pat McAllister II[1], Ewart Mark Haacke[1]
[1]Wayne State University, Detroit, Michigan, USA

The research has an emphasis on *in vivo* testing of biocompatibility of novel materials namely for development of neural prosthesis for treating blindness, Parkinson's disease and movement disorders. We analyzed the compatibility of sapphire and borosilicon glass by assessing the inflammation, edema and hemorrhage around the implant. Hemorrhage, inflammation and tissue interference were observed in the sapphire implanted animals on 10th and 28th day. Thus MRI techniques may provide a non-invasive tool to monitor the resolution of inflammation and hemorrhages after implantation, and for the better design of neuro - prosthetic devices.

1507. Using MRI Images for Determination of Near-Infrared Regions of Sensitivity in Rodent Brain

Hamid Dehghani[1], Jeff Frank Dunn[2]
[1]University of Exeter, Exeter, UK; [2]University of Calgary, Calgary, AB, Canada

Near-infrared imaging and spectroscopy is being used increasingly to study brain physiology and biochemistry in animals and humans. Interpretation of these studies requires information on light penetration. This project combines MRI and NIR data. It uses MR images to obtain 3D structural information in rodent heads. This information was used as a-priori knowledge to predict light paths in rodent brain. Predictions were modeled as a function of wavelength and distance between the source and detector. Reconstructions show a small dependence on wavelength and that the optimum fiber separation for obtaining cortical information from a mouse brain is approximately 5mm.

1508. SWI Filtered Phase Images Demonstrate That Tissue Iron in the Midbrain Correlates with Local Capillary Density

Ewart Mark Haacke, Ph.D. [1, 2], Elena Svilenova Manova[1], Muhammed Ayaz[2], Asadullah Khan[2], Daniel K. Kido[3], Wolff Kirsch[3]
[1]Wayne State University, Detroit, Michigan, USA; [2]The MRI Institute for Biomedical Research, Detroit, Michigan, USA; [3]Loma Linda University, Loma Linda, California, USA

Iron plays a key role in many neurological processes in the brain and in neuro-degenerative diseases. We observed that the filtered phase images in susceptibility weighted imaging (SWI) correlate with the vascular content of a number of structures in the midbrain. The goal is to demonstrate that the SWI phase corresponds to the local non-heme iron content and not the local venous blood supply. The ability to map this type of iron may prove to be a new means to map brain iron associated with vessels and may prove useful in the identification and longitudinal follow-up of neuro-degenerative diseases.

1509. Voxel-Based Morphometry Analysis of Structural Gray Matter Volume Variations Across Idiopathic and Cryptogenic Epilepsy Syndromes

Heath Pardoe[1], Gaby S. Pell[1], Anne T. Berg[2], David F. Abbott[1], Graeme D. Jackson[1]
[1]Brain Research Institute, Melbourne, Victoria, Australia; [2]Northern Illinois University, DeKalb, Illinois, USA

Voxel-based morphometry was used to investigate structural variations in a unique cohort of idiopathic and cryptogenic epilepsy syndromes. Childhood absence epilepsy, Cryptogenic Localization Related Epilepsy and Benign Rolandic Epilepsy syndromes were investigated for gray matter volume decreases. The regions of gray matter volume decrease correlated well with regions of BOLD signal change in idiopathic epilepsies observed in an independent fMRI study.

1510. Cerebrospinal Fluid Pulsatility Model and Its Validation

Jieun Kim[1], Neil A. Thacker[1], Paul A. Bromiley[1], Stephen J. Payne[2], Alan Jackson[1]
[1]University of Manchester, Manchester, UK; [2]University of Oxford, Oxford, UK

Observation of equilibrium among the arterial flow, CSF flows and venous flowwithin cranium is crucial in clinical conditions such as hydrocephalus,vascular dementia which could occur when the equilibrium is disturbed.Flow-sensitive MR images show that intracranial CSF flow is pulsatile and is driven bythe arterial flow into the brain. We have developed an electrical circuitequivalent model of intracranial pulsatility and verified the model usingflow date obtained from MR images of 24 normal subjects. We have obtaineda set of parameter from a subsetof the normal subject which can explain intracranial pulsatile flows.

1511. Perfusion Weighted MR in NPSLE

Bart Jeroen Emmer[1], M J. van Osch[1], D van As[1], O Wu[2], G M. Steup-Beekman[1], S C. Steens[1], T W. Huizinga[1], M A. van Buchem[1], J van der Grond[1]

[1]Leiden University Medical Center, Leiden, Zuid-Holland, Netherlands; [2]Massachusetts General Hospital, Charlestown, Massachusetts, USA

Systemic lupus erythematosus (SLE) is an autoimmune disease mediated by antibodies. Up to 70 percent of SLE patients develop neuropsychiatric (NP) symptoms. It is still unknown whether NP symptoms in SLE are related to ischemia or to anti-neuronal antibodies. We determined brain perfusion parameters in NPSLE patients and compared them to values in control subjects. We applied bolus-tracking perfusion MR in 16 active and 26 inactive NPSLE patients and 11 controls. No significant differences in CBF or CBV were found. Our results do not suggest that widespread ischemia is involved in the etiology of NP symptoms of SLE patients.

1512. Contrast-Enhanced First Pass Perfusion MR Imaging in Patients with Subclinical Hepatic Encephalopathy

Li Tao[1], Ma Lin[1], Li Tao[1]

[1]PLA General Hospital, Beijing, People's Republic of China China

Subclinical hepatic encephalopathy (SHE) means the patients with hepatic disease have no obvious clinical symptoms, but characteristic neuropsychologic tests are abnormal. This study investigated 12 patients with SHE and 10 volunteers perfusion pattern in basal ganglion using GRE-EPI sequence. The CBF, CBV and MTT ratios of basal ganglion, thalamus versus ipsilateral white matter were calculated and compared with control group. The results showed the MTT values statistically reduced and CBF values statistically increased in pallidus and putamen. In conclusion, MRI is higher in temporal, spatial resolution and anatomy location than SPECT. MTT is the most sensitive perfusion parameter.

1513. Central Pontine Myelinolysis After Liver Transplantation: MR Diffusion, Spectroscopy, and Perfusion Findings

Yong Guo[1], Jinhua Hu[2], Wei Lin[1], Kuihong Zheng[1]

[1]General navy Hospital, Beijing, People's Republic of China; [2]302 Hospital of PLA, Beijing, People's Republic of China

MR perfusion of CPM was not reported. One case of CPM after liver transplantation was performed with DWI, MRS, MR perfusion. On acute phase, pontine lesion showed obviously high signal intensity on DWI with a decreased ADC value, decreased NAA / Cr ratio and increased Cho/Cr ratio, increased perfusion on CBV map. On later phase, lesion showed iso-signal intensity on DWI, further decreased NAA / Cr ratio and increased Cho/Cr ratio, decreased perfusion. The increase in lesion perfusion in acute phase may reflect higher metabolic activity due to an increase in cell number and activity.

Eyes, Glands, and Neck

Room 4E Tuesday 13:30 - 15:30

1514. Characteristic MRI Findings of Metastatic Neuroblastomas and Chloromas in the Orbit in Children

Junfang Xian[1], Zhenchang Wang[1], Liyan He[1]

[1]Beijing Tongren Hospital, Beijing, People's Republic of China

Accurate diagnosis of metastases is of the utmost importance for treatment planning, for children with metastatic neuroblastomas and chloromas in the orbit often present initially with orbital manifestations. All fourteen patients appeared a soft tissue mass with lytic bone destruction. Postcontrast T1W images with fat suppression demonstrated extensive high signal intensity within the bone marrow of bilateral lateral orbital walls and greater wings of the sphenoid bone as well as bilateral petrous apices, which were the specific findings different from those of other lesions including the Langerhans' cell histiocytosis and the rhabdomyosarcoma.

1515. Assessment of Orbital Masses Using Dynamic Contrast-Enhanced MR Imaging

Liyan He[1], Jun Fang Xian[1], Zhen Chang Wang[1], Zhong Lin Liu[1], Fei Yan[1], Yan Tao Niu[1], Bo Zhao[1]

[1]Beijing tongren Hospital, Beijing, People's Republic of China

The purpose of our study is to assess the orbital masses using dynamic contrast-enhanced MR imaging.Eighty-three patients with the orbital masses including twenty malignant masses and sixty-three benign masses were studied.The results showed that there was significant difference in Teak, WR, slope and MCI between benign and malignant tumors of the orbit.Dynamic contrast-enhanced MR imaging is useful in differentiating benign from malignant tumors of the orbit.

1516. Study of Ocular Drug Delivery Using Contrast-Enhanced Magnetic Resonance Imaging

Stephanie Kim[1, 2], Craig J. Galban[1], Michael R. Robinson[1], Karl G. Csaky[1], Martin J. Lizak[1], Ginger Tansey[1], Nam Sun Wang[2], Robert J. Lutz[1]

[1]NIH, Bethesda, Maryland, USA; [2]University of Maryland, College Park, Maryland, USA

Contrast enhanced (CE)-MRI was utilized to determine the effects of various barriers and clearances in ocular drug delivery. Gd-DTPA was administered *in vivo* by continuous infusion into rabbit eyes and spatial and temporal distributions of Gd-DTPA in various ocular tissues were obtained. Resulting scans show that effective ocular drug delivery requires high infusion rates of drug to achieve delivery to the posterior regions of the eye and sustained infusion to minimize loss through rapid retinal clearance.

1517. *In Vivo* Echo Planar Diffusion Tensor Imaging of the Optic Nerve in Rats

Marte Thuen[1], Anders Kristoffersen[2], Torgil Riise Vandberg[2], Trond Erling Singstad[2], Olav Haraldseth[1], Christian Brekken[1]

[1]Norwegian University for Science and Technology, Trondheim, Norway; [2]St. Olavs Hospital HF, Trondheim, Norway

A protocol for *in vivo* echo planar diffusion tensor imaging was developed. Diffusion sensitizing gradients were applied along 12 non-collinear directions with 8 b-values in the range of 0-3000 s/mm^2. The sequence was repeated 4 times, giving an acquisition time of 40 minutes. The results were high quality DTI-EPI images with few geometrical distortions, which were confirmed by manganese-enhanced MRI. Within the optic nerve, the mean diffusivity and fractional anisotropy were 1.088±0.224 μm^2/ms and 0.780±0.056, and the axial and radial diffusivities were 2.368±0.447μm^2/ms and 0.449±0.148 μm^2/ms. There was a statistical significant difference between the axial and radial diffusivity ($p<0.001$).

1518. First Report of Diffusion Tensor Imaging of the Murine Eye

Saurav Chandra[1], Kyle Padgett[1], John R. Forder[2]

[1]University of Florida, Gainesville, Florida, USA; [2]McKnight Brain Institute, University of Florida, Gainesville, Florida, USA

The main objective of our study was to determine the feasibility of DTI methods in the murine eye for neuronal fiber orientation, an uncharted area so far. We have acquired extremely high resolution datasets in excised mouse eyes of up to 20 microns isotropic so as to image 6 individual retinal layers. Some of the major observations of this study were that diffusion in the retina is anisotropic and the direction of diffusion is along the retinal layers rather than across layers. This study will aid future ocular studies involving macular degeneration, diabetes and glaucoma.

1519. Does the Use of Passive Occlusion Combined with a Sialogogue Improve MR Sialography ?

Jo Ann Hugill[1], Kieren Grant Hollingsworth[2], Evis Sala[2], David J. Lomas[2]

[1]Addenbrookes Hospital, Cambridge, Cambridgeshire, UK; [2]University of Cambridge, Cambridge, Cambridgeshire, UK

When compared with conventional X-ray techniques, that use cannulation and injection of contrast medium to distend the salivary ducts, MR sialography is limited by the saliva volume and low intrinsic signal to noise ratio of the technique. This work, in 12 healthy volunteers, compares a 3D MIP MR sialography technique with no preparation with the same technique using both a passive occlusal device and a sialogogue to enhance saliva production immediately prior to the study. The results indicate that the enhancement approach significantly improved the visualisation of the main and secondary ducts with no increase in artefacts.

1520. Differentiating Squamous Cell Carcinoma from Other Types of Tumors in the Head and Neck Region by ^{1}H MRS

Tedros Bezabeh[1], Olva Odlum[1, 2], Richard Nason[1, 3], Paul Kerr[3], Donna Sutherland[3], Rakesh Patel[1], Ian C.P. Smith[1]

[1]National Research Council, Institute for Biodiagnostics, Winnipeg, Manitoba, Canada; [2]University of Manitoba, Winnipeg, Manitoba, Canada; [3]CancerCare Manitoba, Winnipeg, Manitoba, Canada

The majority of head and neck tumors are squamous cell carcinoma (SCC). However, other types of tumors are also found in this region. Initial clinical presentation and standard histopathologic assessment may not help in differentiating the different types of tumors. It is essential to know if a given tumor is non-SCC since that will require special staining techniques for reliable identification and appropriate treatment strategy. 1H MRS data were acquired on tissue specimens obtained from ninety-six head and neck cancer patients (89 SCC, 7 non-SCC) and analyzed using pattern recognition methods. The non-SCC samples were found to have spectral profiles that are not characteristic of SCC.

1521. Dynamic Magnetic Resonance Imaging of Swallowing Using a Synchronized Sampling Method

Yasutoshi Honda[1], Yoshinobu Yanagi[1], Noriko Kawai[1], Kanji Kishi[1], Dang Jianwu[2]

[1]Graduate school of Medicine, Dentistry and Pharmaceutical Sciences, Okayama University, Okayama-shi, Okayama, Japan; [2]Japan Advanced Institute of Science and Technology, Nomi, Ishikawa, Japan

This investigation was planed to observe the dynamic motion of swallowing. The motion of swalowing is too first to depict the images using a general method. We performed the synchronized sampling method. This method is used the auditory stimuli from the external trigger. It made the observation of swallowing prossece possible. I hope you like it!

1522. Apparent Diffusion Coefficient in Malignant Lymphoma and Carcinoma Involving Cavernous Sinus Evaluated by Line Scan Diffusion-Weighted Imaging

Masayuki Maeda[1], *Hajime Sakuma*[1], *Kan Takeda*[1]
[1]Mie University School of Medicine, Tsu, Mie, Japan

To evaluate the apparent diffusion coefficient (ADC) of malignant lymphomas and carcinomas involving cavernous sinus by line scan diffusion-weighted imaging (LSDWI) and to determine the usefulness of this method for differentiating between the two tumors. Four patients with malignant lymphomas and six patients with carcinomas were prospectively studied. Malignant lymphomas showed significantly lower ADC value than carcinomas. ADC provides additional useful information about differentiation between these tumors.

1523. Dynamic MRI of Vocal Cords Using Carotid Phased Array Coils

Marc Uwe Schlamann[1], *Stefan Maderwald*[1], *Goetz Lehnerdt*[1], *Isabel Wanke*[1], *Roya Jeyrani*[1], *Susanne Ladd*[1]
[1]University of Essen Medical School, Essen, Germany

The aim of this study was the evaluation of a noninvasive method to assess the motility of the vocal cords in patients with hoarseness of unknown etiology. We included 12 patients. All exams were performed using a 1.5 Tesla scanner with a phased array carotid coil. A repetitive coronal real-time SSPS image with a temporal resolution of 4 images per second was acquired. MRI findings were compared to the results of the endoscopic examination. Dynamic MRI was able to detect all cases of paresis of the vocal cords (7 of 12 patients).

1524. Characterization of a MRI Compatible Head / Neck Immobilization and Repositioning Device for Longitudinal Studies of the Carotid Artery

Emilee S. Minalga[1], *J. Rock Hadley*[1], *Dennis L. Parker*[1]
[1]University of Utah, Salt Lake City, Utah, USA

To improve repeatability of longitudinal studies of patients with carotid artery disease, we have developed an MRI compatible device that allows immobilization of the head and neck with accurate repositioning. Performance of this device was assessed in repeated positioning of normal volunteers and in a preliminary longitudinal study of patients with mild carotid artery disease.

1525. Technique for Acquiring MR Images of CSF Flow During a Valsalva Maneuver

Andrew L. Wentland[1], *Oliver Wieben*[1], *Charles A. Mistretta*[1], *Frank R. Korosec*[1], *Victor M. Haughton*[1]
[1]University of Wisconsin, Madison, Wisconsin, USA

Some Chiari I patients exhibit Valsalva-induced headaches. Hypothetically, the Valsalva maneuver creates CSF flow abnormalities. We have used an undersampled phase contrast projection reconstruction (PR PC) technique for evaluating CSF flow within the time span of a Valsalva maneuver in volunteers and Chiari I patients. Data have shown a significant increase in CSF flow in patients during a Valsalva maneuver but not in volunteers.

1526. Evaluation of Aneurysm Hemodynamics Using Phase Contrast Vastly Undersampled Isotropic Projection Imaging

Kevin Michael Johnson[1], *Roham Moftakhar*[1], *Beverly Aagaard*[1], *Chuck Mistretta*[1]
[1]University of Wisconsin-Madison, Madison, Wisconsin, USA

Currently, the size, morphology, and location of aneurysms are evaluated as possible predictors of rupture in the diagnosis of vascular disease. However, more reliable predictors for which aneurysms are at risk of rupture are needed. Using a novel MR imaging sequence, PC VIPR, we have obtained correlative intra-aneurismal pressure measurements in the canine bifurcation and side wall aneurysm model; and demonstrated methods for both qualitative and quantitative fluid velocimetry. Initial canine studies show quantitative correlation of pressure gradients calculated using PC VIPR and those obtained using invasive catheterization.

1527. Anatomic Imaging of the Soft Palate During Phonation as an Aid in Cleft Palate Presurgical Planning

James S. Hyde[1], *David A. Soltysik*[1], *Andrzej Jesmanowicz*[1], *Arun K. Gosain*[2]
[1]Medical College of Wisconsin, Milwaukee, Wisconsin, USA; [2]Children's Hospital of Wisconsin, Milwaukee, Wisconsin, USA

Improved SNR in imaging of the soft palate in seven normal adults is reported at 3T using an 8-channel head coil. The purpose of the study was to develop a protocol that can be used with children of age 5 to 10. Both 7 and 14 s scan times during phonation of vowels and nasoconsonants were evaluated. In addition, high resolution images of the soft palate could routinely be obtained in one minute scans without motional artifacts by instructing the subject to rest and nose breathe. The soft palate rests statically against the tongue during sustained nose breathing.

1528. Dynamic MRI of the Orbit

Marco Piccirelli[1, 2], Roger Luechinger[1], Oliver Bergamin[2], Michaela Soellinger[1], Andrea Rutz[1], Christof Baltes[1], Peter Boesiger[1]

[1]Swiss Federal Institute of Technology & University of Zürich, Zürich, ZH, Switzerland; [2]University Hospital of Zürich, Zürich, ZH, Switzerland

In clinical routine, static MRI serves for detecting mechanical disorders of the orbit. In complex cases there is a need for understanding the dynamics of eye movements and therefore for valuable MRI recording techniques. Using k-t BLAST for dynamic and high-resolution 3D-TFE sequence, the scan time was shortened to be acceptable for subjects without reducing the sharpness of the extraocular muscles. CSPAMM and CDENSE motion encoded images provided information of the movement of homogeneous orbital regions like the vitreous humor and the extraocular muscles. CDENSE showed higher motion sensitivity compared to CSPAMM, but at the cost of greater noise sensitivity.

Cerebral Blood Flow and Dynamic Contrast Perfusion

Room 4E Tuesday 13:30 - 15:30

1529. Relaxivity of Blood Pool Contrast Agent Depends on the Host Tissue as Suggested by Semianalytical Simulations

Birgitte Fuglsang Jensen[1], Leif Østergaard[1], Valerij G. Kiselev[2]

[1]Aarhus University Hospital, Aarhus, Denmark, Denmark; [2]University Hospital Freiburg, Freiburg, Germany, Germany

Concentration of MRI contrast agents (CA) is commonly determined indirectly using their relaxation effect. In quantitative perfusion studies, the change in the relaxation following a bolus passage is converted into concentrations assuming identical relaxivities for tissue and blood. Simulations presented in this study demonstrate that the relaxivity of blood pool CA depends significantly on both the host tissue and the pulse sequence, in agreement with previous experiments. In particular, the relaxation effect of Gd-based CA in brain tissues is several-fold larger than in bulk blood. The results can be applied to quantitation of perfusion, functional MRI and vessel size imaging.

1530. Intercompartmental Water Exchange Effects in DCE MRI

Xin Li[1], William Rooney[1], Charles Springer[1]

[1]Oregon Health & Science University, Portland, Oregon, USA

In Dynamic Contrast Enhanced (DCE) MRI results, the relative importance of the major equilibrium water exchange systems [transendothelial (te), and transcytolemmal (tc)] depends principally on the magnitude of the pseudo first-order rate constant for contrast reagent (CR) extravasation, Ktrans. Here, simulations are used to clearly show this.

1531. Investigations on the Non-Mono Exponential Signal Decay in Presence of a Single Vessel: Simulations, Phantom and *In Vivo* Measurements

Jan Sedlacik[1], Alexander Rauscher[1], Jürgen Rainer Reichenbach[1]

[1]Friedrich Schiller Universität, Jena, Thüringen, Germany

In this work the single vessel model was employed to estimate the blood oxygenation level of veins. The theoretical signal decay was investigated and verified by numerical and analytical simulations as well as in phantom measurements. The signal decay was found to be dependent on the voxel shape for vessels, which were oriented perpendicular to the main magnetic field due to the extravascular field inhomogeneities. The *in vivo* values of the blood oxygenation level extracted from the signal curves of a multi-echo gradient-echo sequence were in good agreement with values from physiology.

1532. A Re-Examination of the Impact of Dispersion on Quantitative Cerebral Blood Flow Measurements

Linda Ko[1], Marina Salluzzi[1], Richard Frayne[1], Michael Smith[1]

[1]University of Calgary, Calgary, Alberta, Canada

We re-examine the impact of dispersion upon the accuracy of quantitative cerebral blood flow (CBF) measurements by using a tracer-delay-insensitive singular value decomposition deconvolution algorithm. We demonstrate that under most circumstances dispersion will lead to the anticipated under-estimation of the perfusion level; with the level of under-estimation dependent on the dispersion model chosen. However we explain why dispersion can give rise to enhanced, rather than depressed, CBF estimates under conditions that can arise in the infarcted brain (arterial-tissue-delay < 0 s).

1533. The Effects of Background Micro-Circulation in the AIF Measured from DSC MRI of the Brain

Zhiyue J. Wang[1, 2], Robert J. Thornton[1, 2], Jeremy Y. Jones[1, 2]

[1]Baylor College of Medicine, Houston, Texas, USA; [2]Texas Children's Hospital, Houston, Texas, USA

In dynamic susceptibility contrast MRI, the shape of the arterial input function (AIF) is commonly obtained in the near vicinity of the middle cerebral artery (MCA). However, the tissue regions where the AIF is sampled also have significant perfusion, which causes T2* changes. We investigate whether correction of this effect will introduce significant changes in the measurement of the AIF. In the correction procedure, subtracted from the δR2* sampled in the immediate vicinity of the MCA was the δR2* sampled in a nearby region of gray matter away from the MCA. We demonstrate that in the brain, this correction of δR2* due to tissue perfusion leads to a narrower width of the AIF curve, and the peak of the AIF also moved to a slightly earlier time relative to the time of arrival. Using the corrected AIF, longer mean transit times were obtained from both gray and white matter areas.

1534. Automated Selection of Arterial Input Function (AIF) Pixels in DCE-MRI

Andreas Pohlmann[1], Katja Oberholzer[1], Wolfgang G. Schreiber[1]
[1]Johannes Gutenberg University Medical School, Mainz, Germany

When estimating the AIF from a dynamic images series a high reproducibility in identifying the most adequate arterial pixels is crucial for reliably detecting changes in perfusion. Generally used manual outlining of ROIs is prone to introducing large variations. However, recently developed automated AIF detection methods are either very specific (score/threshold based methods) and thus difficult to apply to other imaging locations or employ complicated mathematical techniques (e.g. fuzzy clustering) that are not easily implemented. We have developed a simple adaptive and flexible method that automatically selects AIF pixels, while using available prior information and requiring only minimal user interaction.

1535. Automated Computation of the Vascular Input Function for Dynamic Contrast-Enhanced MRI of the Brain

Sandeep Narendra Gupta[1], John A. Butman[2]
[1]GE Healthcare, Hanover, Maryland, USA; [2]Clinical Center, NIH, Bethesda, Maryland, USA

Dynamic contrast-enhanced MRI analysis using the 2-compartment General Kinetic Model can be used to characterize contrast medium kinetics based on 3 parameters (Ktrans, kep, and fPV). Solving this model requires an explicit vascular input function. Manual identification of the input function is subjective and more prone to errors. We present here a fast, fully automatic method for estimating the VIF from 3D brain DCEMRI data. The method first computes a mask from the data to emphasize vasculature, and then reliably selects pixels which exhibit enhancement characteristics of vessels. Results comparing the two methods on 15 clinical cases are presented.

1536. Visualization of Distinct Collateral Flow Territories in Patients with Symptomatic Carotid Artery Occlusion

Peter Jan van Laar[1], Jeroen Hendrikse[1], Willem Mali[1], Karin Klijn[1], Jaap Kappelle[1], Matthias van Osch[2], Jeroen van der Grond[2]
[1]University Medical Center, Utrecht, Netherlands; [2]Leiden University Medical Center, Leiden, Netherlands

Patients with occlusion of the internal carotid artery (ICA) strongly rely on collateral pathways to maintain adequate cerebral perfusion pressure. However, the actual contribution of these collateral pathways is still difficult to assess or to quantify. With non-invasive selective arterial spin labeling we studied the extent of the collateral flow territories in 23 symptomatic patients with ICA occlusion and 68 control subjects. Our results show that in patients the middle cerebral artery flow territory ipsilateral to the occluded ICA is dependent on the posterior circulation, whereas the ipsilateral anterior cerebral artery flow territory is supplied by the contralateral ICA.

1537. Improved Contrast in Dynamic Contrast Enhanced MRI by Combining Complex In-Phase and Opposed-Phase Data: Simulations and Phantom Experiment

Karl-Heinz Herrmann[1], Alexander Rauscher[1], Werner A. Kaiser[1], Jürgen R. Reichenbach[1]
[1]IDIR, Friedrich-Schiller University, Jena, Germany

MR signal formation of voxels with partially volumed fat and water tissue was simulated to demonstrate the possibility of contrast amplifications by combining complex in-phase and opposed-phase data. A contrast gain up to a factor of 2 was observed in simulations and confirmed in phantom measurements. A dual echo sequence, which imposes no time penalty for dynamic MRI studies, can be used to calculate fat/water separations.

1538. Voxel-Wise Exact T1 Estimation for Accurate Quantitation of Perfusion Indices Using Fast 3D-SPGR in Intracranial Mass Lesion

RKS Rathore[1], Anup Singh[1], RK Gupta[2], P Mohan[2], Md Haris[2], Getaneh Bayu[1], Divya KS Rathore[1], Ankur Purwar[1], Manoj K. Sarma[1]
[1]Indian Institute of Technology, Kanpur, UP, India; [2]Sanjay Gandhi Postgraduate Institute of Medical Sciences, Lucknow, UP, India

The conversion of signal (S) to absolute Gadolinium-DTPA concentration [Gd] for quantitative perfusion studies continues to be problematic. The conversion of the signal from a spoiled gradient echo sequence to concentration requires pre contrast T1 for which multipoint inversion recovery has been one of the most precise mean of measuring T1 in tissues; determination of T1 using this, however, requires a long scan time. Here we propose and demonstrate a very promising new method requiring less scan time for voxel-wise exact T1 estimation followed by a quantitative analysis of dynamic concentration curve for the measurement of various perfusion indices.

1539. Extraction of the Contribution of the First Bolus Passage to the Signal in Dynamic Perfusion Measurements

Peter Gall[1], Oliver Speck[1], Ralph Strecker[1], Valerij G. Kiselev[1]
[1]University Hospital Freiburg, Freiburg, Germany

Dynamic perfusion measurements are based on the tracer dilution theory, that uses the signal of the first bolus passage of an injected tracer. In a circular flow, the injected bolus will appear repeatedly at the observation point. In order to use the tracer dilution theory, the first bolus passage has to be isolated from the recirculatory contributions. In this work, a new method for the first bolus passage extraction is presented and compared to the commonly used gamma variate fit approach.

1540. Accurate Dynamic Susceptibility Contrast MR Perfusion Quantification Using Spatiotemporal Noise Filtering Algorithms

Jayme C. Kosior[1, 2], Richard Frayne, [12]
[1]University of Calgary, Calgary, Alberta, Canada; [2]Foothills Medical Centre, Calgary Health Region, Calgary, Alberta, Canada

Quantitative cerebral blood flow (CBF) values obtained from dynamic susceptibility contrast MR perfusion data are subject to variation due to non-stationary noise artifacts, which cause deconvolution algorithms to become unstable. The purpose of this study was to investigate 4D noise filtering algorithms (space and time) to improve the accuracy of CBF estimates. We compared 4D-Gaussian, 4D-anisotropic diffusion and 4D-bilateral filtering algorithms using a novel digital brain perfusion phantom and a stroke patient. The bilateral filter provided the most accurate CBF estimates in heterogeneous tissue regions and performed comparably well to Gaussian filtering in homogenous tissue regions.

1541. Adaptive SVD Thresholding is Shown to Be More Appropriate for Partial Brain Scans (*TR* = 1 S) Rather Than Full Brain Scans (*TR* = 2 S)

Michael Smith[1], Marina Salluzzi[1], Richard Frayne[1]
[1]University of Calgary, Calgary, Alberta, Canada

Application of SVD eigen-value thresholds ensure deconvolution stability but remove high frequency signal and noise components; compromising the accuracy of the CBF estimates. Adaptive SVD thresholds have been suggested for minimizing this error. Severe aliasing related distortions should be expected given that the low temporal resolution available with DSC image sequences does not meet the Nyquist sampling criteria for the residue functions. However, the individual aliasing of the sampled values in the arterial and tissue signals showed as more important. Adaptive thresholding proved appropriate for partial (TR = 1 s) but not full (TR = 2 s) brain scans.

1542. Thresholding Artefacts in SSVD and OSVD Deconvolution

Louise Gyldensted[1], Kim Mouridsen[1], Leif Østergaard[1]
[1]Aarhus University Hospital, Aarhus, Denmark

Deconvolution methods are widely used in perfusion-weighted MRI for obtaining CBF, CBV and MTT, but are sensitive to thresholding. Typically a single threshold depending on SNR is determined for the whole brain. We have found optimized thresholds for different SNRs for sSVD and oSVD and compared the two methods. We found that over-regularization in sSVD increases the delay-sensitivity, causing MTT overestimation in the posterior vascular territory. oSVD we have found to be less sensitive to over-regularization. However we report a general overestimation of MTT values in oSVD compared to sSVD.

1543. Estimation of Red Blood Cell Flow Using Microbubbles as a Contrast Agent for DSC-MRI

Christopher Chad Quarles[1], Ronald R. Price[1], John Christopher Gore[1]
[1]Vanderbilt University, Nashville, Tennessee, USA

In this study we evaluate the utility of gas-filled, encapsulated microbubbles as an intravascular first pass susceptibility contrast agent for DSC-MRI in normal rat brain tissue. Microbubbles have a diameter and vascular distribution similar to that of red blood cells. On average, the maximum measured δR2* following microbubble injection was 1/3 of that produced by 3 mg/kg of the iron oxide agent, ferumoxytol, at 9.4T. Unlike the rapid passage of ferumoxytol through cerebral tissue the duration of the microbubble signal enhancement was greatly prolonged, which prevented the calculation of microbubble flow using standard first pass tracer kinetic methods.

1544. Quantitative Cerebral Blood Flow Measurement at 3.0T : The Comparison of GE-EPI and SE-EPI

Wanyong Shin[1], Ty Allen Cashen[1], Jeffrey Miller[2], Matthew T. Walker[2], Medhi Rohany[2], Timothy J. Carroll[1, 2]
[1]Northwestern University, Chicago, Illinois, USA; [2]Northwestern University Feinberg School of Medicine, Chicago, Illinois, USA

Gradient echo (GE)- and spin ehco (SE)- echo planar imaging (EPI) have been used for dynamic susceptibility analysis with each advantage and limitation. SE-EPI with parallel imaging technique at high magnetic field has been presented to compensate low signal-to-noise and long TR for a whole brain coverage. Using the Bookend method with water exchange correction, consequencially acquired relative cerebral blood flow (CBF) images from GE- and SE-EPI have been quantified. quantitative CBF measurement from GE-and SE-EPI has been compared and validated with the published values

1545. High Resolution Dynamic-Susceptibility Contrast Perfusion Imaging Using Multi-Echo Parallel EPI

Thies Halvor Jochimsen[1], Rexford Newbould[1], Stefan Skare[1], David B. Clayton[1], Michael E. Moseley[1], Roland Bammer[1]
[1]Stanford University, Palo Alto, California, USA

The combination of parallel imaging with multi-echo EPI allows dynamic-contrast enhancement-based high-resolution perfusion imaging. The multi-echo technique provides accurate estimation of the arterial input function. Furthermore, cerebral blood volume and flow can be assessed undisturbed from changes in longitudinal relaxation. Together with parallel imaging, artifact-reduced high-resolution maps are obtained.

1546. T2* Perfusion Imaging at 7.0 Tesla Using 3D PRESTO: Initial Results

Christoph A. Manka[1], Christiane K. Kuhl[1], Lukas Scheef[1], Carsten Meyer[1], Michael R. Thompson[2], John Duraj[2], Frank Gerardus Hoogenraad[3], Jürgen Gieseke[4], Hans H. Schild[1]

[1]University of Bonn, Bonn, Germany; [2]Philips Medical Systems, Cleveland, Ohio, USA; [3]Philips Medical Systems, Best, Netherlands; [4]Philips Medical Systems, Bonn, NRW, Germany

7.0 Tesla ultra high field systems are currently being introduced for clinical imaging, focusing on high resolution structural imaging and fMRI applications due to the inherent gain of SNR. However, no perfusion results have yet been shown. Single-shot EPI at 7.0 Tesla will suffer from severe distortions, while multi-shot techniques can often not establish the required temporal resolution. In this abstract we investigated the use of a multi-shot technique with echo-shifting to overcome some of the distortions and to prevent low temporal resolution. Good perfusion results were obtained, showing the first perfusion maps at 7.0Tesla.

1547. The Age Dependence of QCBF Measure with the Bookend Technique

Timothy J. Carroll[1], Wanyong Shin[2], Hyun Jeong[1], Matthew Walker[1], Ali Shaibani[1], Medhi Rohany[1], James Carr[1], Ty Cashen[1]

[1]Northwestern University, Chicago, Illinois, USA; [2]Northwestern, Chicago, Illinois, USA

We have performed a validation study of an MRI pulse sequence which quantifies cerebral perfusion.

1548. Variability in QCBF Obtained from Deconvolution-Based Perfusion-Weighted MR Techniques

Daniel James Niven[1], Jayme C. Kosior[1, 2], Peter J. Dickhoff[3], Imanuel Dzialowski[4, 5], Suresh Subramaniam[4, 5] Andrew M. Demchuk[4, 5], Richard Frayne[1, 6]

[1]Seaman Family MR Centre, Foothills Medical Centre, Calgary Health Region, Calgary, Alberta, Canada; [2]Electrical and Computer Engineering, University of Calgary, Calgary, Alberta, Canada; [3]Diagnostic Imaging, Rockyview General Hospital, Calgary Health Region, Calgary, Alberta, Canada; [4]Clinical Neurosciences, University of Calgary, Calgary, Alberta, Canada; [5]Calgary Stroke Program, Foothills Medical Centre, Calgary Health Region, Calgary, Alberta, Canada; [6]Radiology, University of Calgary, Calgary, Alberta, Canada

We sought to evaluate the inter- and intra-observer variability, as well as the effect of AIF and ROI selection on qCBF variability. This study was a retrospective cohort study in which twelve patients with acute ischemic stroke (AIS) were imaged on a 3T MR scanner (DWI and PWI imaging). ROI selection ($p < 0.001$), embolic AIS etiology ($p < 0.001$), and observer ($p = 0.034$) significantly impact overall qCBF variability. AIF selection, i.e., manual versus semi-automated, does not contribute significantly to overall variability. There is significant intra- and inter-observer variability in qCBF based on the results of simple regression analyses.

1549. Assessment of the Computational Efficiency of Perfusion Deconvolution Algorithms for Application to Acute Stroke

Sylvia Drabycz[1], J Ross Mitchell[1]

[1]University of Calgary, Calgary, Alberta, Canada

The computational efficiency of three perfusion deconvolution algorithms was analyzed: circular SVD (oSVD), reformulated SVD (rSVD) and Fourier division (FD). Simulations were performed with varying number of timepoints, N. Perfusion-weighted images from 9 acute stroke patients were also analyzed. rSVD, oSVD and FD produced similar results but had significant differences in terms of execution speed. Simulations showed that the computation times for oSVD and rSVD increased rapidly with N while FD remained approximately constant. FD appears to be the most efficient approach when N>=48, suggesting it should be used for clinical applications over the algebraic SVD algorithms.

1550. Digital Anthropomorphic Perfusion Phantom for the Evaluation of DSC-MR Perfusion Algorithms

Jayme C. Kosior[1, 2], Richard Frayne, [1,2]

[1]University of Calgary, Calgary, Alberta, Canada; [2]Foothills Medical Centre, Calgary Health Region, Calgary, Alberta, Canada

Our purpose is to develop a digital anthropomorphic perfusion phantom that can be used to evaluate the accuracy and robustness of bolus-tracking perfusion-imaging algorithms in the presence of simulated acquisition artifacts (i.e., noise). This phantom represents a significant advancement compared to previous perfusion-imaging approaches that have relied on simulated 1D-signals for evaluation, since the phantom can also be used to evaluate spatiotemporal algorithms (i.e., noise filters). In this work, we use the phantom to demonstrate the effects of patient motion on cerebral blood flow estimates compared with the results obtained using a registration algorithm to correct for the motion.

1551. Improving the Sensitivity of Total Cerebral Blood Flow Measurement by Cine Phase Contrast MRI

Noam Alperin[1], Sang H. Lee[1]

[1]University of Illinois at Chicago, Chicago, Illinois, USA

Quantitation of cerebral blood flow (CBF) is potentially important for understanding normal brain function and for characterization of the disease sate in many neurological problems. Xenon enhanced CT, and dynamic contrast enhanced CT and MRI, measure regional CBF normalized for brain's weight. Phase contrast MRI techniques measure total CBF (tCBF) and therefore are potentially useful in detecting global changes in the brain such as diffuse head trauma or dementia. However, currently these measurements suffer from large inter-individual variability, which has limited their usefulness. This study aims to determine whether tCBF, normalized for brain volume, has a smaller inter-individual variability and thereby greater sensitivity.

1552. Demonstration of Direct and Complete Collateral Compensation During Carotid Artery Compression by MR Flow Monitoring

Jan-Henry Seppenwoolde[1], Jeroen Hendrikse[1], Henk Johan Nanang Streefkerk[2], Berend Hillen[2], Chris J.G. Bakker[1]
[1]University Medical Center Utrecht, Utrecht, Netherlands; [2]University Medical Center St Radboud, Nijmegen, Netherlands

Using 2D phase contrast flow monitoring, this study demonstrates the ability of cerebral vasculature to compensate with direct, and –on average- complete collateral compensation for a drop in perfusion pressure caused by a temporary occlusion of the one of the internal carotid arteries. In 15 healthy subjects, the average volume flow in the compressed ICA decreased with 4.88 ml/s to 0.15 ml/s. The average volume flow in the contralateral ICA increased with 3.27 ml/s to 8.96 ml/s and in the basilar artery with 1.92 ml/s to 4.46 ml/s.

Pediatric Brain

Room 4E Tuesday 13:30 - 15:30

1553. Association Between MR Changes Early in Therapy and Later Neurocognitive Performance in Children Treated for Acute Lymphoblastic Leukemia

Wilburn E. Reddick[1], Courtney L. Dirksen[1], John O. Glass[1], Cheng Cheng[1], Ching-Hon Pui[1]
[1]St. Jude Children's Research Hospital, Memphis, Tennessee, USA

This project focuses on detecting leukoencephalopathy early during therapy for ALL in 70 subjects and its association with neurocognitive performance 2.5 years later. Conventional MR imaging was performed (T1, T2, PD, and FLAIR) and analyzed with an automated computer-aided detection algorithm for leukoencephalopathy. Neurocognitive assessments were acquired, stratified by MR examination, and then assessed between groups using a two-way ANOVA. All intelligence and some verbal learning measures were significantly lower in patients with leukoencephalopathy. None of the academic achievement measures were significantly different between patient groups or normative test averages. This study establishes a significant relationship between MR changes seen early in therapy and later neurocognitive impact in children treated for ALL.

1554. Relationship of Temporal Lobe Volume to Neuropsychological Test Performance in Healthy Children and Adolescents

Carolyn Theresa Wells[1], Ernest Mark Mahone[1], Melissa Matson[1], Wendy R. Kates[1, 2], Trisha Hay[2], Alena Horska[3]
[1]Johns Hopkins University School of Medicine, Baltimore, Maryland, USA; [2]SUNY Upstate Medical University, Syracuse, New York, USA; [3]Johns Hopkins University, Baltimore, Maryland, USA

The present study examined the relationship between temporal lobe volumes and performance on neuropsychological tests hypothesized to measure either left (Peabody Picture Vocabulary Test-III/PPVT-III) or right (Beery Visual Perception) temporal lobe functioning in a sample of 37 healthy children. After controlling for total cranial gray matter volume, left temporal (but not left frontal) gray matter volume significantly predicted PPVT-III scores. Right temporal (but not right frontal) gray matter volume significantly predicted Visual Perception scores. This convergent and discriminant evidence supports the use of volumetric MRI in healthy children for establishing the ecological validity of neuropsychological tests.

1555. Non-Invasive Imaging of Endogenous Magnetic Particle Deposits in Biological Tissue Using Magnetic Resonance Imaging

Heath Pardoe[1], Gaby S. Pell[1], Graeme D. Jackson[1]
[1]Brain Research Institute, Melbourne, Victoria, Australia

Homing pigeons are able to navigate using the Earth's magnetic field. This magnetic sensing ability is linked to the presence of trace quantities of naturally occurring iron-based magnetic particles in the tissue of the bird. This study investigated the use of MRI to obtain high resolution in vitro images of a pigeon head and located regions of discrete hypointensity areas along the upper beak tissue that may correspond to these iron-based magnetic particle deposits.

1556. Cerebral Gray and White Matter T2 in Autism Spectrum Disorder

Helen Petropoulos[1], Seth D. Friedman[1], Dennis W. Shaw[1], Alan A. Artru[1], Geraldine Dawson[1], Stephen R. Dager[1]
[1]University of Washington, Seattle, Washington, USA

Autism Spectrum Disorder (ASD) is a clinically defined syndrome with reported enlarged brain volumes. We used quantitative T2 to assess whether accelerated development could account for these volumetric findings. FSE images acquired from children with ASD, developmental delay (DD), and typical development (TD) were segmented into gray matter (GM) and white matter (WM) to produce masks used to calculate T2 for either tissue type. ASD children had prolonged GM T2 compared to TD children. DD children had prolonged GM and WM T2 compared to ASD and TD children. Prolonged GM T2 in ASD may signify abnormalities that are specific to autism.

1557. Diffusion Tensor Imaging Findings in Rett Syndrome Patients

Izlem Izbudak[1], Luciano Farage[1], David Bonekamp[1], Weihong Zhang[1], Genila Bibat[2], Sussumu Mori[1], SakkuBai Naidu[2], Alena Horska[1]
[1]Jonhs Hopkins Medical Institutions, Baltimore, Maryland, USA; [2]Kennedy Krieger Institute, Baltimore, Maryland, USA

Twenty Rett Syndrome(RTT) girls and ten normal controls were evaluated by diffusion tensor imaging by measures of fractional anisotropy (FA) and apparent diffusion coefficent (ADC). Significant age related evolution of DTI values were found in our study in both patients and controls. No overall difference in ADC and FA between the hemispheres was detected. FA in the Rett patients was lower in the forceps minor, in the genu of corpus callosum and in the posterior thalamic radiation. Involvement of specific white matter tracts in RTT might indicate regions of vulnerability that could be target to treatment strategies in the future.

1558. Faster Quantitative Brain Imaging in Pediatric Patients by Using IR-TrueFISP

Claudia Maria Hillenbrand[1], Ralf Berthold Loeffler[1], John O. Glass[1], Wilburn Eugene Reddick[1]
[1]St. Jude Children's Research Hospital, Memphis, Tennessee, USA

IR-TrueFISP was recently introduced for quantification of tissue relaxation times. With IR-TrueFISP only a single acquisition is needed to calculate T_1-, T_2-, PD- maps and synthetic images with various contrasts such as FLAIR. In this study, we compared IR-TrueFISP with conventional methods to measure brain relaxation times in 5 pediatric patients. Data acquisition was 6 times faster with IR-TrueFISP, and there was excellent correlation between respective T_1 and T_2 maps ($p<0.001$).

1559. *In Vivo* Detection of Age-Related Brain Iron Differences with MFC

Anita Ramani[1], Jens H. Jensen[1], Amy L. Krain[1], Jing Yang[1], Caixia Hu[1], Hanzhang Lu[1], Joseph A. Helpern[1]
[1]New York University School of Medicine, New York, New York, USA

The purpose of this study was to investigate age-related differences in brain iron in adolescents and adults by using magnetic field correlation (MFC) imaging, a novel quantitative MRI method for estimating brain iron. The MFC is a sensitive measure of the regional distribution of iron in the brain, and can be measured using an asymmetric spin echo sequence. We have previously provided feasibility of this method *in vivo*. In this abstract, we have measured regional brain MFC values in both normal adolescents and adults, and have correlated the MFC with putative iron concentrations.

1560. Comparison of BOLD Signal Changes in the Fetal Brain at 3T with Local PO2 Measurements

Ulrike Wedegärtner[1], Andrew N. Priest[1], Hendrik Kooijman[2], Mikhail Tchirikov[1], Hobe J. Schröder[1], Gerhard Adam[1]
[1]University Hospital Hamburg-Eppendorf, Hamburg, Germany; [2]Philips Medical Systems, Hamburg, Germany

To consider fetal BOLD-MRI as a test modality to detect the fetus at risk, it is necessary to compare BOLD signal (SI) changes with defined changes of fetal tissue oxygenation. Recently, a non-O2-consuming fluorescent-fibre-optic probe has been developed. The purpose of this study was to compare BOLD-SI changes with local intracerebral oxygen tension measurements in the fetal brain during hypoxia in a sheep model. We conclude that BOLD-SI changes reflect changes of local brain pO2-values. R2*-changes in the brain correlate with local brain pO2-values. Therefore R2* provides information about fetal brain tissue oxygenation, which is important for fetal surveillance.

1561. Quantitative MR Imaging and Spectroscopy in Childhood White Matter Disorders

Patrick van der Voorn[1], Petra J.W. Pouwels[1], Augustinus A.M. Hart[2], Frederik Barkhof[1], Marjo S. van der Knaap[1]
[1]VU University Medical Center, Amsterdam, Netherlands; [2]Academic Medical Center, Amsterdam, Netherlands

MR imaging is highly sensitive in the detection of white matter lesions. In contrast, it has a limited specificity with regard to the pathology underlying the white matter signal abnormalities. Our aim was to investigate whether quantitative MR parameters, including MTR, ADC, FA and MRS metabolite concentrations, allow discrimination of different types of pathology underlying white matter signal abnormalities. MRS, DTI and MTI was performed in 41 leukodystrophy patients and 41 controls.Linear discriminant analysis showed that 95% of all patients were classified correctly using total creatine, choline-containing compounds, myo-inositol, MTR and ADC. Adding other parameters did not improve this.

1562. Fast 3D Pediatric Brain MRSI

Dong-Hyun Kim[1], Meng Gu[2], Charles Cunningham[2], Albert Chen[1], Fiona Baumer[1], Orit Glenn[1], Daniel Vigneron[1], Daniel Spielman[2], Anthony James Barkovich[1]
[1]University of California, San Francisco, California, USA; [2]Stanford University, Stanford, California, USA

We have developed a robust fast 3D MRSI protocol targeted for pediatric neuro imaging. In this abstract, we show the feasibility of the technique to acquire spectroscopic imaging data from infants/children in 6:24 minutes. Preliminary quantitative spectral analysis was performed in the corticospinal tract to correlate metabolic variations in those with motor delay.

Neuro-Oncology

Room 4E Tuesday 13:30 - 15:30

1563. Evaluating the Impact of Cancer Therapy on the Developing Brain

Wilburn E. Reddick[1], John O. Glass[1], Jinesh J. Jain[1], Nicholas S. Phillips[1], Qing Ji[1], Robert J. Ogg[1], Thomas E. Merchant[1], Amar Gajjar[1]

[1]St. Jude Children's Research Hospital, Memphis, Tennessee, USA

This study presents a comprehensive MR evaluation of the impact of cancer therapy on the developing brains of children treated for cancer. Conventional imaging for tissue segmentation, dynamic-susceptibility contrast imaging, and diffusion tensor imaging were acquired, processed and fused with composite radiation dosimetry to assess WM. Evaluations were conducted at baseline, post cranial irradiation, and at 12 month follow-up for five subjects. White matter volumes significantly increased immediately post irradiation but returned to baseline values. Diffusion measures of ADC in the posterior quadrants decreased significantly immediately post irradiation and were still depressed at follow-up. CBV/CBF values were not significantly changed but MTT was significantly shorter at follow-up.

1564. Longitudinal Evaluation of HSV Brain Tumor Therapy Using Diffusion Tensor MR Imaging

Wei Bian[1], Narasimha Shastry Akella[1], Steven T. Moore[1], William T. Evanochko[1], Matthias Karrasch[2], Axel Mescheder[2], James M. Markert[1], Louis B. Nabors[1]

[1]University of Alabama at Birmingham, Birmingham, Alabama, USA; [2]Medigene AG, Munich, Germany

G207 is a modified type-1 herpes simplex virus that is used to kill cancer cells. Diffusion tensor MR imaging can measure pathological changes at the cellular level and was used to assess G207-therapy response. We report a study investigating mean diffusivity and fractional anisotropy values as surrogate markers for quantitative efficacy evaluation of G207-therapy. Three patients with malignant brain tumors were imaged longitudinally using conventional anatomic and diffusion tensor MRI. Changes in mean diffusivity and fractional anisotropy in the tumor margins were calculated. Results suggest that these parameters complement traditional volumetric approaches while evaluating therapy response.

1565. Computer-Aided Detection of Brain Tumor Invasion Using Morphological and Diffusion-Weighted MR

Todd Robert Jensen[1], [2], Xin Feng[1], John L. Ulmer[2], Kathleen M. Schmainda[2]

[1]Marquette University, Milwaukee, Wisconsin, USA; [2]Medical College of Wisconsin, Milwaukee, Wisconsin, USA

Computer-aided detection (CAD) of tumors using information obtained from medical imaging has been applied successfully for cases of breast and lung cancers. This study used CAD to detect brain tumor invasion using morphological and diffusion-weighted MRI.

1566. The Added Value of MRS in Brain Tumor Diagnosis

Margarida Julià-Sapé[1], Indira E. Coronel[1], Marta Serrallonga[2], Carles Majós[2], Ana Paula Candiota[1], Mònica Cos[2], Oscar Godino[3], Juan-José Acebes[3], Carles Aguilera[2], Carles Arús[1]

[1]Universitat Autònoma de Barcelona, Cerdanyola del Vallès, Barcelona, Spain; [2]IDI-Bellvitge, Institut de Diagnòstic per la Imatge, L'Hospitalet del Llobregat, Barcelona, Spain; [3]Hospital Universitari de Bellvitge, L'Hospitalet del Llobregat, Barcelona, Spain

To-date, no prospective studies have tested whether SV MRS at 1.5T significantly helps MRI in typing and grading brain tumors. A one-year prospective study at a single institution was conducted for this purpose. MRI and MRS information was analyzed independently. Then, radiologists and spectroscopists respectively exchanged their predicted tumor types and confidence ratings and reevaluated MRI and MRS. MRS was analyzed integrating several pre-existing decision-support systems for classifying brain tumors. Statistically significant differences were found for several tumor types and grades. With current decision-support systems, MRS significantly helps MRI in discriminating high-grade from low-grade tumors.

1567. Supervised Pattern Recognition for Predicting the Appearance of Contrast-Enhancement in High-Grade Gliomas Using Multimodality MRI and MRSI

Michael C. Lee[1], Susan M. Chang[1], Sarah J. Nelson[1]

[1]University of California, San Francisco, California, USA

The appearance of contrast-enhancement in high-grade gliomas indicates a significant breakdown of the blood-brain barrier. We are interested in determining which spectroscopic, diffusion, and perfusion parameters are most predictive of the appearance of contrast enhancement at a later date. We hypothesize that data obtained prior to radiotherapy provide information that can be useful in predicting the location of the contrast-enhancing lesion after radiotherapy. A genetic algorithm is used to select and scale features for an optimized *k*-nearest-neighbor classification algorithm. By comparing the receiver-operating characteristic curves, we demonstrate that the optimized classifier significantly outperforms thresholding on any single-variable in the study.

1568. Lessons from Functional Brain Mapping in Pre- And Intra- Operation for Low-Grade Glioma: Insights Into Associations Between Tumour and Brain Plasticity

Zi Xiao Li[1], Jian Ping Dai[1], Tao Jiang[2], Shao Wu Li[1], Zhong Zhang[2], Cai Jie Duan[3], Yi Lin Sun[4], Pei Yi Gao[1], Jun Ma[1]

[1]The Capital University of Medical Science Affiliated Beijing Tian Tan Hospital, Beijing, People's Republic of China; [2]The Capital University of Medical Science Affiliated Beijing Tian Tan Hospital, Beijing, Chile; [3]Beijing University, Beijing, People's Republic of China; [4]Beijing Neurosurgery Institute, Beijing, People's Republic of China

To explore brain language function reorganization in response to progressive growth of low-grade gliomas (LGGs) using preoperative functional MRI (BOLD-fMRI and diffusion tensor imaging (DTI)) and intraoperative functional brain mapping (direct electrical stimulation). For patients with LGGs affecting the left language regions, two ways were recruited into language processing networks during progressive growth. One is intra-hemisphere, and the other is inter-hemisphere. Our data provide evidence of effective plasticity in the progressive growth of the LGGs, which should assist presurgical planning, define surgical indications, predict the risk of postoperative deficit and aspects of operative surgical neuro-ocology.

1569. Comparison of MRI Contrast Enhancement by Motexafin Gadolinium and Omniscan in Glioblastoma Multiforme

Genevieve Ning Wu[1], Judith M. Ford[1], Robert B. Lufkin[1], Jeffry R. Alger[1]

[1]Univ. of California at Los Angeles, Los Angeles, California, USA

Motexafin Gadolinium (MGd) is an investigational radiation enhancer, which can be detected with MRI. We studied glioblastoma multiforme patients who received MGd to compare the MGd enhancement pattern with that produced by Omniscan. The volume of Omniscan enhancement was significantly larger than the volume of MGd enhancement. On average Omniscan produced a 20% higher signal enhancement in comparison to MGd. The weaker MGd enhancement may result from the tendency of GBMs to be relatively necrotic tumors combined with the fact that MGd binds to tumor cells. MGd appeared to label both active and necrotic tumor areas.

1570. Imaging Blood Vessel Volume in High Grade Gliomas at 3T Using Susceptibility-Weighted Imaging and Dynamic Susceptibility Contrast Perfusion MRI

Janine M. Lupo[1], Michael C. Lee[1], Soonmee Cha[1], Susan M. Chang[1], Sarah J. Nelson[1]

[1]University of California, San Francisco, California, USA

As MRI scanners move to higher field strengths, traditional techniques to measure relative cerebral blood volume in brain tumors such as dynamic susceptibility-contrast perfusion MRI become a challenge due to increased B0 inhomogeneity and magnetic susceptibility differences that cause signal drop out and geometric distortions in echo-planar imaging. New methods are needed to assess vessel density from susceptibility-weighted imaging and to evaluate the potential of this technique at higher field strengths compared to DSC MRI. This study demonstrates how SWI and DSC MRI are different but complementary techniques that can be combined to more accurately assess tumor vascularity.

1571. Multi-Parametric Composite Maps in Recurrent Brain Tumor Patients

Kathryn M. McMillan[1], Baxter P. Rogers[1], Cheng Guan Koay[2], M Elizabeth Meyerand[3]

[1]Vanderbilt University, Nashville, Tennessee, USA; [2]NIH, Bethesda, Maryland, USA; [3]University of Wisconsin, Madison, Wisconsin, USA

Recurrent glioblastoma multiforme patients were studied using CSI, diffusion, perfusion, and BOLD-based hypoxia mapping. Relevant techniques were chosen for each patient and composite maps were formed via a novel overlap technique and ISODATA clustering methods. The maps appear to be similar in the size and location of the final clusters. We are encouraged that these maps could be incorporated into treatment planning.

1572. Quantitative Characterization of Functional and Morphological Properties of Tumor Vasculature in High-Grade Gliomas

Vijaya Nagesh[1], Thomas L. Chenevert[1], Larry Junck[1], Christina I. Tsien[1], Brian D. Ross[1], Theodore S. Lawrence[1], Yue Cao[1]

[1]University of Michigan, Ann Arbor, Michigan, USA

Understanding the structural and functional characteristics of the vascular microenvironment in gliomas is essential in design of therapeutic strategies. Alterations in the vascular properties in intratumor and peritumor may not be distinguishable by cerebral blood flow (CBF) or cerebral blood volume (CBV) alone. The objective was to examine the empirical and physiological relationships between CBF and CBV to estimate vasculature-specific hemodynamic characteristics in intratumor, peritumoral and normal brain tissue. Progressive abnormalities in functional and morphological characteristics of vascular bed were noted, with significant chaos and disorder in tumor, but mild abnormality in peritumoral tissue.

1573. Accuracy Evaluation of a First-Pass Pharmacokinetic Model (FPPM) for Simultaneous Mapping of Blood Volume and Microvascular Permeability in Brain Tumors

Hua-Shan Liu[1, 2], Hsiao-Wen Chung[1, 2], Ming-Chung Chou[1, 2], Chun-Jung Juan[1, 2], Cheng-Yu Chen[2]
[1]National Taiwan University, Taipei, Taiwan, Taiwan; [2]Tri-Service General Hospital, Taipei, Taiwan, Taiwan

For the purpose of simultaneously evaluating the cerebral blood volume and microvascular permeability, we implemented a currently developed first-pass pharmacokinetic model to investigate the accuracy of estimates from this model. A contrast concentration curve added with white Gaussian noise was simulated to assess the accuracy of this method. Our simulation shows that accurate measures of vascular plasma volume is produced which is free from the problem of overestimation from slow wash-out due to vessel tortuosity or second-pass transit, while Ktrans shows low tolerance of noise and kep seems inaccurate even at high SNR.

1574. Permeability Fitting of DSC Perfusion Data Through Constrained Optimization

Talin Tasciyan[1]
[1]Medical Numerics Inc, Sterling, Virginia, USA

A fitting method is described to simultaneously determine the CBV and permeability transfer and rate constants with a total of 5 parameters using the Marquardt Levenberg algorithm with additional constraints. The results demonstrate the robustness of the fitting process and the reliability of the constraints in ensuring that the primary contribution to the overall fit is from the bolus term and not from the leakage.

1575. Comparison of T1 to T2* Derived Parametric Maps in Brain Tumor Patients

Matthew L. Zierhut[1, 2], Soonmee Cha[2], Michael C. Lee[2], Mary Katherine Mayo[2], Sarah J. Nelson[1, 2]
[1]UCSF/UCB Joint Graduate Group in Bioengineering, San Francisco, California, USA; [2]UCSF, San Francisco, California, USA

This study compares two DCE-MRI methods to investigate which is more useful for brain tumor characterization, as measured by histologic tumor grade. T2* derived parameters for cerebral blood volume (CBV) and MR signal recovery were compared to T1 derived parameters of fractional blood volume (fBV) and vascular permeability (KPS). Both methods' blood volume parameters correlate well with literature. KPS was found to have a significant correlation with tumor grade ($p<0.02$). No other parameters showed a significant correlation with tumor grade. These results suggest that T1 derived parameters may be more useful than T2* derived parameters for characterizing brain tumor grade.

1576. rCBV Estimates in Tumor vs. Normal Brain Depend on Acquisition and Analysis Methods

Eric Scott Paulson[1], Douglas Edward Prah[1], Kathleen M. Schmainda[1]
[1]Medical College of Wisconsin, Milwaukee, Wisconsin, USA

The goal of this study was to investigate how different acquisition and analysis methods influence rCBV estimate variations in tumor versus normal brain. Two methods were used to acquire dynamic T2*-weighted images and rCBV was determined by numerical integration over the entire concentration-time curve and by fitting a gamma-variate function to the first pass of the concentration-time curve. Gamma-variate and numerical integration derived rCBV values were found to be similar in normal brain, but this agreement diminished in regions of tumor. These results signify the dependence of rCBV estimates on acquisition and analysis methods.

Metabolic and White Matter MRS

Room 4E Tuesday 13:30 - 15:30

1577. Reproducibility of ^{1}H-MR Spectroscopic Imaging in the Centrum Semi-Ovale in Patients with Multiple Sclerosis

Jop Mostert[1], Jeroen van der Grond[2], Jacques De Keyser[1], Hans Hoogduin[1]
[1]University Medical Center Groningen, University of Groningen, Groningen, Netherlands; [2]University Medical Center Leiden, Leiden, Netherlands

The reproducibility of ^{1}H-MR spectroscopic imaging at the centrum semi-ovale over a time span of 4 weeks was investigated in clinically stable MS patients. NAA/Cr ratios were reproducible with a coefficient of variation of 5.3 and 3.9% in gray and white matter, respectively. This indicates that ^{1}H MR spectroscopic imaging can potentially be used as a surrogate marker in MS.

1578. Whole Brain N-Acetylaspartate Concentration as a Surrogate Marker for Benign Multiple Sclerosis

Daniel Rigotti[1], Tyson Oberndorfer[1], James Babb[1], Clyde Markowitz[2], Joseph Herbert[1], Oded Gonen[1]
[1]NYU School of Medicine, New York, New York, USA; [2]UPenn Medical Center, Philadelphia, Pennsylvania, USA

Multiple sclerosis (MS) is a progressive autoimmune disorder characterized be demyelination and neurodegeneration that affects millions of people per year worldwide. Approximately twenty percent of MS patients experience a benign disease course that is generally diagnosed only after many years of relatively no clinical symptoms. To address this issue we show that the whole-brain concentration of the neuronal marker N-acetylaspartate (WBNAA) is significantly higher in patients with benign MS than not only patients with more malignant forms of MS, but also normal healthy controls. We assert that WBNAA may serve as a surrogate marker for a more timely diagnosis distinction between benign MS versus other types of MS.

1579. Brain Metabolism in Primary Progressive Multiple Sclerosis:A Three-Dimensional Proton MR Spectroscopy Study at 3T

Meredith Spindler[1], Sarah Brown[1], Joseph Herbert[1], Hina Jaggi[1], Matilde Inglese[1], Oded Gonen[1]
[1]New York University, New York, New York, USA

The primary-progressive type of multiple sclerosis (PPMS) affects a minority of patients diagnosed with this disease, and due to differing pathologies, the markers used for the more common types of MS cannot be used for therapeutic monitoring or prediction of the disease course in PPMS. In this study, 3D proton magnetic resonance spectroscopy (1H-MRS) was used to quantify the concentrations of 4 potential disease markers in eight PPMS patients and eight age and gender-matched controls. N-acetylaspartate (NAA) levels were found to be 16.9% lower in PPMS patients than in controls, whereas no significant difference was found in choline (Cho), creatine (Cr), or myo-inositol (mI) concentrations, and no significant correlations with EDSS or disease duration were found.

1580. Temporal Lobe Biochemistry and Non-Verbal Neurocognitive Function in Myotonic Dystrophy Type I

Deidre J. Devier[1], Charles Gasparovic, [12], Rex E. Jung[1], [2], Richard Campbell[1], Alejandro Tobon[1], Leslie Morrison[1]
[1]University of New Mexico, Albuquerque, New Mexico, USA; [2]MIND Institute, Albuquerque, New Mexico, USA

A tendency towards non-verbal learning disability is characteristic of Myotonic Dystrophy type I (DM1). This study explores the relationship between neurocognitive performance and brain metabolites measured across the temporal lobe with (1H-MRSI) in 7 patients with DM1and 9 healthy controls. In patients, we found significant correlations between Right Temporal NAA/Cr and delayed recall of the Rey Complex Figure and Facial Recognition subtests, both non-verbal memory tasks thought to measure right temporal lobe function. These findings support the notion of a non-verbal learning disability in patients with DM1 and provide insight into a possible biochemical mechanism.

1581. Metabolic Changes in Juvenile Myoclonic and Frontal Lobe Epilepsy by ^{1}H MR Spectroscopy

Hyun-Man Baik[1], Barbara Swartz[2], Long Vu[1], Hui Liu[1], O. Nalcioglu[1], Min-Ying Su[1]
[1]University of California-Irvine, Irvine, California, USA; [2]Haog Hospital, Newport Beach, California, USA

To evaluate the metabolic changes from the anterior cingulate in JME patients and patients with frontal lobe epilepsy (FLE) compared to normal age-matched controls, and to investigate whether metabolic abnormalities are associated with thalamo-cortical loop dysfunction. Single-voxel MR spectroscopy was performed using a STEAM sequence. JME patients showed significantly lower NAA/Cr and $(NAA/H_2O)x10^3$ compared to controls ($p = 0.04$; $p = 0.01$). The FLE patients also had significantly lower NAA compared to controls ($p = 0.04$; $p = 0.04$). We demonstrated that ^{1}H-MRS can be used to detect the metabolic changes not visible with structural MR imaging in JME and FLE patients.

1582. Quantitative MR Spectroscopy for Monitoring Treatment of Cerebrotendinous Xanthomatosis

Eva H. Baker[1], Jennifer L. McKeon[1], Robert D. Shamburek[1]
[1]NIH, Bethesda, Maryland, USA

Cerebrotendinous xanthomatosis (CTX) is a rare inborn error of metabolism, 27-sterol hydroxylase deficiency. Dysfunction of this enzyme results in abnormal metabolism of cholesterol; instead of normal production of the bile acids chenodeoxycholate and cholate, an alternative pathway produces cholestanol and bile alcohol. Cholestanol accumulates in most body tissues, including the brain, producing a variety of neurological symptoms. The disease progresses unless treated.Two siblings with CTX were studied with quantitative MRS prior to and following one year of treatment. Changes in symptoms and serum metabolites correlated with changes in brain metabolites measured by quantitative MRS. Our findings suggest that the treatment not only halts progression of the disease, but it probably also reverses of some of the damage to the brain.

1583. Blind Recovery of 1H MRSI Spectral Signatures of Batten Disease and Melas

Shuyan Du[1], Xiangling Mao[2], Paul Sajda[1], Dikoma C. Shungu[2]
[1]Columbia University, New York, New York, USA; [2]Weill Medical College of Cornell University, New York, New York, USA

Advanced MR hardware and spectroscopic imaging techniques have enabled dramatic improvements in the spatio-temporal resolution of MRSI data acquisition. However such gains bring in an undesired side effect: high dimensional spectroscopic imaging datasets which challenge available analysis methods. Recently, we introduced cNMF, a new data analysis method for recovering physically meaningful spectral signatures by decomposing the observed spectral data into two matrices. In this study we demonstrate that by applying cNMF to multislice 1H MRSI data of two neurodegenerative diseases affecting children : Batten disease and MELAS, whose phenotypic and radiologic similarities make it difficult to differentiate between them without extensive and costly genetic analyses, we can both extract their respective spectral patterns as well as the spatial distributions of lesion patterns critical for differentiation.

1584. Serial Proton MRS of Neurometabolic Alterations in Hereditary Spastic Paraplegia with Thin Corpus Callosum (HSP-TCC)

Steffi F. Dreha-Kulaczeski[1], Knut Brockmann[1], Gunther Helms[1], Jens Frahm[2], Jutta Gärtner[1], Peter Dechent[1]
[1]Georg-August-University, Goettingen, Lower Saxony, Germany; [2]Biomedizinische Forschungs GmbH am MPI für biophysikalische Chemie, Goettingen, Lower Saxony, Germany

HSP-TCC is a complicated form within the group of hereditary spastic paraplegias characterized by a marked thinning of the corpus callosum. We report a follow-up proton MRS study of a patient at age 20 and 25 yrs., in the latter case combined with DWI. Over that period the clinical course progressed. While MRI did not change significantly, MRS disclosed a progressive reduction of tNAA and a significant increase of Ins. The pattern is consistent with progressive neuroaxonal loss accompanied by astrogliosis which is in good agreement with histopathological findings. The ongoing neurometabolic alterations leading to clinical deterioration were best appreciated by MRS.

1585. Assessment of the Metabolic Changes in Type 2 Diabetes Mellitus Using Magnetic Resonance Spectroscopy

Shilpi Modi[1], Manisha Bhattacharya[1], S S. Kumaran[1], T Sekhri[1], S Khushu[1]
[1]INMAS, Delhi, India

Proton MRS (3.4cc single voxel) was used to assess the metabolic changes in right/left frontal white matter, left parietal white matter and left occipital gray matter and 31P spectrum from right skeletal muscle of subjects with a history of type 2 diabetes mellitus (DM2) and subjects affected with both DM2 and hypothyroidism. In DM2 a reduction in NAA/Cr in the frontal white matter and occipital gray matter, increased Cho/Cr value in occipital gray matter and reduction in PCr/Pi and an elevation in PDE/ATP values (in muscle) were observed. The changes are attributed to impaired energy metabolism and neuronal loss in these patients.

1586. Use of Opioids in Asphyxiated Term Neonates: Effect on Brain Metabolites and Outcomes

Barbara Holshouser[1], Danilyn M. Angeles[2], Nathaniel D. Wycliffe[1], Douglas Deming[1], Carrie Carr[2], Lawrence C. Sowers[2], Stephen Ashwal[1]
[1]Loma Linda University Medical Center, Loma Linda, California, USA; [2]Loma Linda University, Loma Linda, California, USA

To examine the hypothesis that opioids administered during the first week of life can decrease the severity of neurological injury in term-asphyxiated newborns, we compared metabolite data from proton magnetic resonance spectroscopy (MRS) in control, opioid-treated and non-treated neonates. Glutamate/glutamine (Glx) and choline (Cho) ratios correlated with tissue-damaging procedures (TDPs) in the first 4 days of life. NAA ratios were significantly decreased and lactate was present in 39% of non-opioid treated neonates ($p < 0.05$). MRS metabolite data measured in the first 3 weeks after injury correlate with neurological outcome. Our results suggest that opioids may be neuroprotective after neonatal asphyxia.

1587. Anti-TNF-Alpha Does Not Cause Acute Demyelination

Bart Jeroen Emmer[1], A E. van der Bijl[1], F C. Breedveld[1], T W. Huizinga[1], M A. van Buchem[1], J van der Grond[1]
[1]Leiden University Medical Center, Leiden, Zuid-Holland, Netherlands

Neurological symptoms have been reported in arthritis patients treated with anti-TNF-á. It has been suggested that symptoms could be the result of demyelination. To find such changes, we performed Magnetization Transfer Imaging, DWI and MRS of the brain in patients before and after anti-TNF-á administration. MTI histogram peak heights of white and gray matter decreased significantly after the use of anti-TNF-á. No changes were observed in ADC or metabolite ratios. Our results suggest that although MTI parameters point at a decreased parenchymal integrity after the use of anti-TNF-á, it is not likely that demeylination is one of the major effects.

Brain Registration and Normalization Techniques

Room 4E Tuesday 13:30 - 15:30

1588. Robust Anatomy Recognition for Automated MR Neuro Scan Planning

Stewart Young[1], Daniel Bystrov[1], Thomas Netsch[1], Rene Bergmans[2], Arianne van Muiswinkel[2], Fredy Visser[2], Rudolf Springorum[2], Frank Hoogenraad[2], Jürgen Gieseke[3]
[1]Philips Research, Hamburg, Germany; [2]Philips Medical Systems, Best, Netherlands; [3]University of Bonn, Bonn, Germany

A novel method for automated planning of scan geometries for MR scans of the brain is presented. The approach is based on the robust identification of a set of anatomical landmarks in a 3D survey image. A clinical trial was carried out over a six-month period, in which the reliability of the system was tested. Results are presented to demonstrate the accuracy of estimation of the mid-sagittal plane and landmark estimation. The approach was shown to be very robust, successfully planning geometries for all patients, including in the presence of large tumors, significant metal-induced artefacts and in patients with extensive brain resections. Over 230 clinical patients were scanned in the trial, and in each case the system provided a suitable initialization of the planning. There were no outliers observed.

1589. Iterative Tensor-Based Registration

Ravichandran Rajaram[1], Carlo Ciulla[1], E Mark Haacke[1]
[1]The MRI Institute for Biomedical Research, Detroit, Michigan, USA

This work presents an algorithm for registering 3D-MRI brain images. Processing steps consist of the application of: (i) a low pass Hanning filter to the k-space data, (ii) the Fourier Transform Theorem to correct for misplacement, and (iii) iterative enforcement of tensor-based registration. Results show improvement of registration both qualitatively as substantiated by a clear reduction of Gibbs ringing artifacts, and quantitatively by the reduction of the shift error to less than 0.001 of the voxel size for translation and 0.01 for rotation.

1590. Comparison of Two Spatial Normalization Methods in the Elderly Brain

Weiying Dai[1], Owen T. Carmichael, [12], Oscar L. Lopez[1], H. Michael Gach, [13]
[1]University of Pittsburgh, Pittsburgh, Pennsylvania, USA; [2]Carnegie Mellon University, Pittsburgh, Pennsylvania, USA; [3]Nevada Cancer Institute, Las Vegas, Nevada, USA

Spatial normalization involves transforming all of the subjects' data to the same stereotactic space to facilitate the comparison of different subjects. Two normalization methods were compared in the elderly brain for registration accuracy of two local structures and statistical comparisons of subject groups for the entire cerebrum: 1) statistical parametric mapping (SPM), and 2) Chen's fully deformable method. Chen's method provided excellent registration of the left hippocampus and left thalamus, while SPM misplaced the regions. Chen's method revealed markedly larger regions of statistical significance (on average by 230%) than SPM for 13 of 14 brain regions of interest.

1591. Evaluation of a Symmetric Diffeomorphic Registration Algorithm for Analyzing Neurodegenerative Disease

Brian Avants[1], James Gee[1], Murray Grossman[1]
[1]University of Pennsylvania, Philadelphia, Pennsylvania, USA

Our recently developed algorithm, symmetric diffeomorphic image registration, allows rigorous quantification of neurodegenerative disease. We show the benefits of our method in comparison to a standard elastic deformation model (Demons) for discovering statistically significant differences in populations through normalization. A comparison to gold standard results confirms that the new method outperforms Demons in terms of reproducing manual labelings and in terms of giving significant results.

1592. Non-Rigid Registration of Functional to Anatomical Brain MR Images Using Constrained Optimization

Ali Gholipour[1], Nasser Kehtarnavaz[1], Kaundinya Gopinath[2], Richard Briggs[2], Michael Devous[2], Robert Haley[2]
[1]University of Texas at Dallas, Richardson, Texas, USA; [2]University of Texas Southwestern Medical Center, Dallas, Texas, USA

Accurate registration of functional to anatomical brain MR images is needed for brain functional localization. Due to the effect of nonlinear distortions in fast functional echo planar imaging, even after rigid registration and resampling, mismatches of a few millimeters may occur in overlaying the activation maps from the functional image space to the anatomical image space. A non-rigid registration algorithm based on a bound constrained optimization technique, a Bspline free-form deformation model, and the mutual information similarity measure has been developed in this study. The experiments show that this algorithm provides practically significant enhancement in the registration of functional to anatomical brain MR images.

1593. Automated Versus Manual Scan Positioning: A Quantitative Analysis

Rudolf Springorum[1], Frank Hoogenraad[1], Rene Bergmans[1], Stewart Young[2], Daniel Bystrov[2], Clemens Bos[1]
[1]Philips Medical Systems, Best, Netherlands; [2]Philips Research, Hamburg, Germany

Automated scan prescription holds the promise of improving workflow and planning consistency. This study focuses on axial geometry planning in the brain. Accuracy and variation are compared between an automated planning system and scan prescription by experienced technologists. Prescribed off-center and angulation parameters were analyzed. The automated planning routine was accurate to within 1.5 degrees on all angulations. Particularly, the alignment to the corpus callosum shows less variation with the automated planning routine, viz. 1.3 degrees, versus an interoperator variability of 2.2 degrees. In conclusion, at sites where several technologists perform scan prescription, automatic planning can significantly improve consistency.

1594. Measurement of Subpixel Motion of the Lateral Ventricular Walls

Mark E. Wagshul[1], Michael R. Egnor[1], James Manzione[1], Erin J. McCormack[1], Abram Voorhees[2], Timothy Wei[3]
[1]Stony Brook University, Stony Brook, New York, USA; [2]New York University, New York, New York, USA; [3]Rutgers University, New Brunswick, New Jersey, USA

While pulsations of CSF in the brain are presumed to be driven by the arterial pulse entering the cranium, the means of transfer of these pulsations from the arteries to the ventricles remains a mystery. Using 3D cardiac gated, cine balanced SSFP images of the ventricles and motion tracking techniques, subpixel wall motion over the cardiac cycle was observed. Peak motion was approximately 0.1 pixels, primarily of the superior wall of the lateral ventricle. Further development of this technique will allow accurate measurement of net ventricular wall motion, which may help explain CSF flow patterns in diseases such as hydrocephalus.

1595. Realignment Strategies in ASL Timeseries

Karam Sidaros[1], Anders Jespersen[2], Torben E. Lund[1]
[1]Copenhagen University Hospital Hvidovre, Hvidovre, Denmark; [2]Copenhagen University Hospital Frederiksberg, Copenhagen, Denmark

Realignment parameter curves for ASL timeseries sometimes exhibit high-frequency modulations that could arise from the small perfusion-related difference between tag and control images. We compare three realignment strategies and test the detection of respiration and pulsation induced motion as well systematic tag-control differences. We find that the high frequency modulations in the realignment parameters are in fact due to respiration-induced motion and that systematic tag-control differences in the realignment parameters only arise in one of the compared methods. Furthermore, we find that not modelling the respiration effects in ASL timeseries leads to non-white noise in the residuals.

1596. Measurement of Pulsatile Brain Motion in a Patient with a Meningioma

Michaela Soellinger[1], Andrea Kaspar Rutz[1], Sebastian Kozerke[1], Miroslava Bjeljac[2], Peter Boesiger[1]
[1]University and ETH Zurich, Zurich, Switzerland; [2]University Hospital Zurich, Zurich, Switzerland

The intracranial blood flow, which initiates pulsatile expansion of brain tissue can be interpreted as an internal force. Alterations of the elastic properties of brain tissue are reflected in changes of brain displacement maps. Such displacement maps were acquired from a patient with a meningioma. A 2D cine DENSE imaging method was used. Strain maps were derived from the displacement maps. The displacement maps showed reduced tissue displacement within the tumor. The strain maps derived from anterior-posterior displacements indicated a stiffer mass compared to surrounding tissue at the location of the tumor.

Brain Segmentation Techniques

Room 4E Tuesday 13:30 - 15:30

1597. Improved Segmentation of Intracranial Volumes Using a Combination of T1- And T2-Weighted 3D MRI

Gunther Helms[1], Kai Kallenberg[1, 2], Peter Dechent[1]
[1]Göttingen University, Faculty of Medicine, Göttingen, Germany; [2]Göttingen University, Göttingen, Germany

Major problems of brain extraction and segmentation when using the fMRIB software library (FSL) can be overcome by T2-contrast features. T1w (MDEFT) and T2w (SPACE) structural 3D-MRI (1 mm resolution) were acquired at 3 Tesla. Postprocessing comprised rigid-body coregistration, brain extraction, segmentation, and volumetry. T1-contrast provided reliable segmentation of gray and white matter; T2-contrast delineation of the intracranial space and identification of a hypointense class of “non-brain”, representing vessels and connective tissue. Mismatches in sub-volumes determined from one single contrast could be largely explained by the 4-class results. This approach may improve assessment of cortical atrophy in ageing and dementia.

1598. Reproducibility of Automated Brain Morphometric Estimates Derived from Multi-Site Structural MRI Studies

Jorge Jovicich[1], Silvester Czanner[1], Xiao Han[1], Douglas Greve[1], Jenni Pacheco[1], Evelina Busa[1], Andre van der Kouwe[1], Bruce Fischl[1, 2], Anders Dale[3]
[1]1MGH/MIT/HMS Athinoula Martinos Center for Biomedical Imaging, Charlestown, Massachusetts, USA; [2]Massachusetts Institute of Technology, Cambridge, Massachusetts, USA; [3]University of California San Diego, San Diego, California, USA

Neuroimaging longitudinal and multi-site studies of change over time are becoming increasingly a standard element of clinical neuropsychiatric research. These studies create the imperative to characterize and correct technological sources of variance that limit image reproducibility in high-resolution structural MRI studies. Here we extend previous work to study the variability of morphometry results, cortical thickness and subcortical volume estimates, using data from a group of 5 healthy volunteers that were scanned twice at each of five different sites having clinical 1.5T systems (GE, Siemens, Picker). The measured cross-site variability was under 10%. Gradient non-linearity correction did not significantly reduce it.

1599. Segmentation of Gray- And White Matter on MR Brain Images in Multiple Sclerosis

Sushmita Datta[1], Balasrinivasa Rao Sajja[1], Renjie He[1], Jerry S. Wolinsky[1], Ponnada A. Narayana[1]
[1]Medical School, The University of Texas at Houston, Houston, Texas, USA

Atrophy of gray- and white matter (GM and WM, respectively) provides important information about pathology in multiple sclerosis. However, the partial volume averaging between different tissues, even when the slice thickness is small, results in false classification of GM and WM, making accurate estimation of these tissue volumes difficult. An iterative procedure based on the combination of partial volume averaging and bias field correction is proposed for accurate classification of GM and WM. This method was applied to 14 MS patients with excellent results.

1600. Histogram-Based Acceleration on EM Algorithm for Segmentation of Multi-Spectral MRI with Contextual Constrains

Renjie He[1], Sushmita Datta[1], Balasrinivasa Rao Sajja[1], Ponnada A. Narayana[1]
[1]University of Texas Medical School at Houston, houston, texas, USA

An extension of the histogram-based fast FCM to EM algorithm is presented in this paper for the segmentation of multi-spectral MRI, with the basic idea of contextual constrains applied. The combination provided a faster and more liable method compare to conventional MRI segmentation using EM to find maximum likelihood mixture densities parameters.

1601. Virtual Definition of Tissue by Cluster Analysis of Multi-Parametric MR Imaging (Virtual-Dot-Com Imaging)

Yossi Yovel[1], Yaniv Assaf[1, 2]
[1]Tel Aviv University, Tel Aviv, Israel; [2]Tel Aviv Sourasky Medical Cener, Tel Aviv, Israel

Resolution and contrast limits of MRI restrict our current ability to segment and characterize certain tissues. In this study we devised an algorithm (virtual-dot-com imaging) that segments brain tissue based on contrast differences from a multi-parametric MRI protocol. The algorithm uses contrast dynamic range stretching and cluster analysis to segment the tissue to statistically distinct clusters. Using this approach we were able to segment the thalamus to 7 clusters similar to histological atlas. Each cluster could be characterized with a unique contrast finger print. This methodology has the potential for indirect detection of the myelo- and cyto-architecture properties of tissues.

1602. Optimum Template Selection for Atlas-Based Segmentation

Minjie Wu[1], Jessica LoSurdo[1], Pilar Lopez-Garcia[2], Cameron Stuart Carter[2], Howard Jay Aizenstein[1]
[1]University of Pittsburgh, Pittsburgh, Pennsylvania, USA; [2]University of California at Davis, Sacramento, California, USA

Atlas-based segmentation typically uses a single atlas (e.g., MNI Colin27) for region identification. However, a single template is limited for structures, such as the anterior cingulate cortex (ACC), which have significant individual structural variations. An automated template selection method (with normalized mutual information metric) was developed to select the template (from multiple templates) optimized for ACC segmentation for each subject. The ACC segmentation overlap-ratio (9 subjects) using the optimum template selection approach outperformed the segmentation from individual templates ($p=0.0024$). These results highlight the importance of template selection for atlas-based segmentation and demonstrate an automated approach using a family of templates.

1603. Significant Local Shape Differences of the Brain Ventricles in Alzheimer's Patients Compared to Healthy Elderly

Luca Ferrarini[1], Walter Miguel Palm[1], Hans Olofsen[1], Mark A. van Buchem[1], Johan H C Reiber[1], Faiza Amiraal-Behloul[1]
[1]Leiden University Medical Center, Leiden, Netherlands

The goal of this work was to identify global and local shape differences of the brain ventricles of patients with Alzheimer's disease (AD) compared to age-matched healthy elderly. Using a fully automatic shape modeling technique, we captured the ventricles shape and shape variations of 29 AD subjects and 25 controls matched for age. By applying permutation tests on every single node of a mesh representation of the shapes, we identified the local areas with most significant differences.

1604. Segmentation of Age-Related White-Matter Changes in a Large-Scale, Multi-Centre Study

Tim Dyrby[1], Egill Rostrup[1], Elisabeth Catherine Wilhelmina van Straaten[2], Frederik Barkhof[2], Stefan Ropele[3], Lars Kai Hansen[4], Gunhild Waldemar[5]
[1]Copenhagen University Hospital, Hvidovre, Copenhagen, Denmark; [2]VU Medical Center, Amsterdam, Netherlands; [3]Karl Franzens University, Graz, Austria; [4]Danish Technical University, Copenhagen, Denmark; [5]Copenhagen Univ. Hospital, Rigshospitalet, Copenhagen, Denmark

Since age-related white matter changes are being recognised as a marker of vascular pathology, and are associated with motor and cognitive deficits, their automated quantification may be of great importance in multicentre studies. The robustness of an artificial neural network (ANN) segmentation is investigated and compared to manual delineation in a large dataset. When scan quality was optimal high correlation coefficients were found (avg. of 0.89), demonstrating the cross-centre generalisability of ANN methods. Anatomical and pathophysiological expert knowledge was a minor source of discrepancy, and suboptimal data quality a major cause of discrepancy. Centre-specific training sets may give further improvement.

1605. Automatic Cortex Extraction and Gray/White Matter Segmentation from T1-Weighted MRI with Geodesic Active Contours

Albert Huang[1], Rafeef Abugharbieh[1], Roger Tam[1], Anthony Traboulsee[1]
[1]The University of British Columbia, Vancouver, BC, Canada

We present a novel automatic 3D segmentation method for extracting brain cortex from T1-weighted MRI scans and segmenting gray and white matter by incorporating a statistical as well as a geometric model in a unified segmentation scheme. Combined with the expectation maximization algorithm, and both voxel probability and image gradient and curvature information, geodesic active contours are evolved to segment the cortex and brain tissues. The robustness and accuracy of our proposed method are validated with both synthetic and real data. Both quantitative and qualitative results indicate superior and consistent performance when compared with standard techniques including SPM and FSL.

1606. The Size of Corpus Callosum Normalized by the Intracranial or Brain Parenchymal Volume Exhibits a Significant Difference Between Male and Female Brains

Nobuhiro Takaya[1], Hidehiro Watanabe[1], Fumiyuki Mitsumori[1]
[1]National Institute for Environmental Studies, Tsukuba, Ibaraki, Japan

Sex-difference of corpus callosum is a long standing controversy. We extracted the cross-sectional area of corpus callosum in the mid-sagittal plane as well as volumes of total grey, white matters and CSF in 33 male and 36 female subjects. The absolute area of corpus callosum did not show significant sex-difference However, the normalized area by the intracranial or parenchymal volume exhibited a significant difference. Considering that individual differences in the brain size and age-dependent change are compensated in the normalized area, it is concluded that there is a significant sex-difference in the size of corpus callosum.

1607. De-Scalping of the Brain in Echo Planar DT-MRI

Ankur Purwar[1], RK Gupta[2], Manoj Kumar Sarma[1], Getaneh Bayu[1], Anup Singh[1], Divya KS Rathore[1], Sona Saksena[2], Richa Trivedi[2], Ashtmangal Mishra[2], Mohammad Haris[2], P Mohan[2], RKS Rathore[1]
[1]Indian Institute of Technology, Kanpur, UP, India; [2]Sanjay Gandhi Post Graduate Institute of Medical Sciences, Lucknow, UP, India

De-scalping a brain stack has applications in visualization, surface rendering, decreasing algorithmic complexity, etc. Many applications of brain imaging improve through it, e.g., (a) in DT-MRI registration of b0-images to DW stacks containing a considerable portion of eyeballs, skin etc., (b) tissue-type segmentation via DT-MRI, which helps in isolating brain tissue from other parts such as CSF, (c) in the removal of strong ghosting effects in EPI, (d) dynamic range in visualization of DT-MR metrics improves. This work describes an effective automatic procedure for de-scalping brain for EPI-MR axial images, which has favorable performance as compared with BET in MRI-Cro.

1608. A Simple Method for the Automatic Measurement of Cortical Thickness

Don C. Bigler[1], Qing X. Yang[1], Michael B. Smith[1]
[1]Penn State College of Medicine, Hershey, Pennsylvania, USA

A simple and effective voxel-based method for measuring cortical thickness is presented that uses Euclidian distance and the gray matter output of any brain segmentation tool. The method is less calculation-intensive than surface-based techniques and is independent of the segmentation tool used. Validation was performed with images of fundamental geometric shapes and an example image of cortical thickness is demonstrated.

1609. Semi-Automated Segmentation of Brain Tumor Lesions in MR Images

Suja Saraswathy[1], Forrest Crawford[1], Sarah J. Nelson[1]
[1]University of California, San Francisco, California, USA

Objective, rapid and reproducible methods of measuring tumor volume are of utmost importance to clinicians in assessing the response to treatment and in guiding appropriate therapy for serial studies. We implemented and validated a region growing method based on simple statistics that could be applied to images with different types of contrast and has the potential for not only reducing the variability in measurements, but also the time required to analyze serial changes in lesion volume. The algorithm was used to successfully segment hyperintense lesions in FLAIR and T2 images and both hyper-and hypointense lesions separately in T1 contrast enhanced images. The results show that volume measurements obtained using this method are in good agreement with manually segmented data.

1610. Brain Tumor Image Segmentation Using Neural Networks

Miguel Martín-Landrove[1], Raúl Villalta[1]
[1]Centro de Resonancia Magnética, Facultad de Ciencias, Universidad Central de Venezuela, Caracas, District of Columbia, Venezuela

A new method that combines MRS with multiecho T2-weighted images is proposed to obtain nosologic maps with appropriate spatial resolution for treatment considerations. Neural networks are used to classify relaxation data according to spectroscopic information and combine it in the generation of nosologic maps. Results are compared with other segmentation methods based in the analysis of relaxation rate distributions by inverse Laplace transform algorithms showing a high degree of correspondence and an improvement in processing time, what makes this methodology suitable for the analysis of a high number of images, typically acquired fro 3D treatment planning in radiotherapy or radiosurgery.

Diffusion Modeling and its Application to Microstructure

Room 4E Tuesday 13:30 - 15:30

1611. A Model of Diffusion Weighted MRI in Grey Matter - A Multiparametric Approach Using Global Solutions

Peter Vestergaard-Poulsen[1], [2], Brian Hansen[1]
[1]Aarhus University, Aarhus, Denmark; [2]Aarhus University Hospital, Aarhus, Denmark

The underlying cellular mechanisms responsible for the ADC change seen in stroke are still uncertain. In a brain tissue model including T2 relaxation and exchange effects model output from all combinations of a wide range of values of all model parameters were compared with experimental data obtained from grey matter in normal volunteers to ensure global solutions. The results support the hypothesis that T2 relaxation cannot be neglected in modelling water diffusion of brain tissue due to indications of slow exchange and T2 heterogeneity between compartments hence predicting a dependence of the ADC on the echo time

1612. A Finite Difference Model of Diffusion Applied to Ischemia

Kevin D. Harkins[1], Jean-Philippe Galons[1], Timothy W. Secomb[1], Joe L. Divijak[1], Theodore P. Trouard[1]
[1]University of Arizona, Tucson, Arizona, USA

A finite difference (FD) model of water diffusion within a two-dimensional (2D) array of semi-permeable cells separated by extracellular space has been developed. The FD model enables the evaluation of the effect of several biophysical parameters on water diffusion including cell size, cell volume fraction and membrane permeability as well as the intrinsic T2-relaxation and diffusion coefficients in the intra- and extracellular spaces. In this report, the effect of cellular swelling is modeled and compared to experimental results obtained from clinical stroke and ischemia experiments performed in cell cultures.

1613. Diffusion Weighted Signal at Short Times in the Presence of Impermeable Interfaces

Astrid From Frøhlich[1], [2], Leif Østergaard[1], Valerij G. Kiselev[2]
[1]Aarhus University Hospital, Aarhus, Denmark; [2]University Hospital Freiburg, Freiburg, Germany

The nonlinear dependence between the logarithm of the diffusion weighted signal, lnS, and the b-value is studied. The cumulant expansion of the signal is advocated instead of using the common biexponential fit. This implies that lnS is a power series in b, which is shown to converge in a large parametric range using the basic model of a flat, impermeable boundary. To a realistic accuracy, the signal is determined by the first two coefficients, which are related to the geometry of the restrictive boundaries. In this case, the fitting parameters of the biexponential function are not defined uniquely.

1614. Analysis of Water Diffusion and Magnetization Transfer Ratio in Optic Nerves After Crush Injury

Masaya Takahashi[1], Timothy K. Vartanian[1], David B. Hackney[1]
[1]Beth Israel Deaconess Medical Center, Boston, Massachusetts, USA

MRI determination of the apparent diffusion coefficient (ADC) in nervous tissue has demonstrated sensitivity to axonal diameter and density. The magnetization transfer ratio (MTR) has been shown to be an indicator of tissue injury. In the present study, we performed the MRI measurements of ADCs and MTR in the rat optic nerve crush injury model at one week and one month after the surgery. The results demonstrated that MR determination of ADC and MTR correlated with time after injury and severity of axonal damage and both parameters would be evaluated together as a stronger indicator than any one parameter alone.

1615. Decreased Diffusion Coefficients in Suspected Prostate Cancer Regions in Peripheral Zone: A Comparison with Increased (Cho + Cr)/Cit Ratios from Magnetic Resonance Spectroscopy

Agnieszka Szot Barnes[1], Steven J. Haker[1], Stephan E. Maier[1], Clare m. Tempany[1], Robert V. Mulkern[1]
[1]Brigham and Women's Hospital, Boston, Massachusetts, USA

In this study, diffusion coefficients from prostate peripheral zone (PZ) regions suspicious for cancer are compared with suspect healthy PZ regions in biopsy-confirmed cancer patients. MRS studies of the same patients allow for a comparison of D values in these PZ regions with the corresponding (Cho + Cr)/Cit ratios. We conclude that D maps with reasonably high spatial resolution demonstrate reduced D values in suspected PZ regions of cancer and may be acquired in reasonable scan times. As such, D maps may prove useful for helping target these regions for localized therapies or biopsies.

1616. Q-Space Analysis of Intracellular Water Diffusion in Cultured Cells

Jean-Philippe Galons[1], Joseph L. Divijak[1], Silvia Lope-Piedrafita[1], Kevin Harkins[1], Robert J. Gillies[1], Theodore Trouard[1]
[1]University of Arizona, Tucson, Arizona, USA

The complexity of biological tissues, with multiple compartments each with its own diffusion and relaxation properties require complex formalisms to model water signal in most MRI or MRS experiments. In this communication we take advantage of a Gd-DTPA induced magnetic susceptibility shift of the resonance frequency of extracellular water to perform a q-space analysis of the intracellular water diffusion using the signal originating exclusively from the intracellular space.

1617. Separating Intra- And Extracellular Water Signals in Rat Brain Using Gd-DPTA-Enhanced Diffusion-Weighted MRI

Timothy Michael Shepherd[1], Peter Edward Thelwall[1], Christopher M. Sotak[2], Stephen John Blackband[1]
[1]University of Florida, Gainesville, Florida, USA; [2]Worcester Polytechnic Institute, Worcester, Massachusetts, USA

This study investigated trasmembrane water exchange in viable rat cortical brain slices with previously described methods that employ Gd-DPTA to alter the T_1 properties of extracellular water and thus resolve the intra- and extracellular water signals using diffusion-weighted inversion recovery pulse sequences. Data obtained suggest that Gd-DTPA concentrations exceeding 8 mM are needed for transmembrane water exchange to be in an intermediate or slow regime relative to the T_1 relaxation rate.

1618. Multi-Component Apparent Diffusion Coefficients in the Rabbit VX2 Tumor Model

Jie Deng[1], Thomas K. Rhee[1], Gayle E. Woloschak[1], Tatjana Paunesku[1], Reed A. Omary[1], Andrew C. Larson[1]
[1]Northwestern University, Chicago, Illinois, USA

Diffusion-weighted magnetic resonance imaging (DW-MRI) techniques permit quantitative *in vivo* measurement of local water diffusion characteristics within tissues. Multiple studies have demonstrated using DW-MRI to detect early changes in tumor tissue diffusion properties predictive of therapy response. However, most of these studies assumed mono-exponential decay characteristics primarily sensitive to high-mobility extracellular water populations. Recent studies in murine breast cancer models and clinical brain metastases demonstrated bi-exponential diffusion decay properties within tumors. DW-MRI over a wider range of b-values permits derivation of two-compartment diffusion components and interrogation of both low-mobility (intra-cellular or bound water molecules) and high-mobility (extra-cellular) water populations. In this study we performed conventional and high b-value diffusion weighted imaging in the VX2 rabbit tumor model commonly used to evaluate liver tumor therapies. The purpose of this study was to determine the feasibility of deriving bi-exponential diffusion characteristics in the VX2 tumor model.

1619. The Intracellular Water Diffusion Coefficient of Cultured Microbead-Adherent HeLa Cells is ≥ 1 $\mu m^2/ms$

Lin Zhao[1], Christopher D. Kroenke[1], Joseph J. H. Ackerman[1], Jeffrey J. Neil[1]
[1]Washington University in St. Louis, St. Louis, Missouri, USA

A flow-related MR method was used to select the intracellular water signal from perfused microbead-adherent mammalian cells. By this means, the diffusion properties of intracellular water of HeLa cells were studied at various diffusion times. A statistical model of intracellular water diffusion fit the data well and was validated with optical microscopy. The intracellular water "free" diffusion coefficient is ≥ 1 $\mu m^2/ms$.

1620. Subcompartmental Cesium Diffusion in Healthy and Globally Ischemic Rat Brain

James A. Goodman[1], Joseph J.H. Ackerman[1], Jeffrey J. Neil[1]
[1]Washington University in St. Louis, St. Louis, Missouri, USA

Cesium-133 can be used as a compartment specific analog of water motion *in vivo*. One extracellular and two intracellular resonances have been observed in brains of live ^{133}Cs loaded rats. In healthy brain tissue the two intracellular resonances have similar ADCs, 1.0 ± 0.2 and 0.9 ± 0.4 $\mu m^2/ms$. Following global ischemia the first ADC remains unchanged while the second drops to 0.24 ± 0.04 $\mu m^2/ms$. Findings suggest that the decrease in intracellular water ADC associated with cell injury is not uniform across different subcellular compartments and is due mainly to a decrease in the ADC of water in organelles.

1621. Diffusion Exchange Weighted (DEW) Imaging

Saadallah Ramadan[1], Carolyn Mountford[1]
[1]Institute for Magnetic Resonance Research, Sydney, NSW, Australia

Correlation of diffusion coefficient with other molecular properties has been used to gain insight into molecular structures and dynamics. A diffusion-exchange weighted (DEW) sequence has been developed to measure ADC with exchange in a 3T whole body MR scanner. The exchange of protons from one compartment to another, with different ADCs, provides insight into physical properties of tissue. The ADC in the brain was found to be dependent on exchange time, with ADC decreasing with increased exchange time. The DEW imaging technique can also increase contrast to the image based on the exchange property, a function of various cell properties.

1622. Accuracy of Q-Space Derived Parameters in MRI - A Phantom Study of System-Induced Limitations

Jimmy Lätt[1], Daniel Topgaard[1], Ronnie Wirestam[1], Carin Malmborg[1], Olle Söderman[1], Freddy Ståhlberg[1], Sara Brockstedt[1]
[1]Lund University, Lund, Sweden

The aim of this study was to compare the system performance regarding q-space measurements between a 3.0T clinical MRI scanner and a 4.7T NMR spectrometer. Phantom measurements were performed on n-decane, at the two systems. The measurements give similar D and the measured FWHM values differ between the two systems, due to different resolution limits. In MRI, Gmax is a limiting factor for achieving high q-values and hence, it will also affect the minimum obtainable resolution. In the same way the resolution affects the kurtosis measure since the signal attenuation curve will no longer represent a full Gaussian distribution.

1623. Diffusion Weighted µMRI of Isolated Human Pancreatic Islets

Muhammad E. Haque[1], Suraj D. Serai[2], Lara Leoni[1], Robert V. Honeychuck[3], Jose Oberholzer[4], Brian B. Roman[1]
[1]University of Chicago, Chicago, Illinois, USA; [2]University of Illinois at Chicago, Chicago, Illinois, USA; [3]George Mason University, Fairfax, Virginia, USA; [4]University of Illinois, Chicago, Illinois, USA

Lack of an accurate assessment of functional pancreatic ß-cells mass is an obstacle for islet transplantation as a treatment for diabetes. A pancreatic islet is an island of cells, sizing from 100 µm to 500 µm containing approximately one to two million insulin producing ß-cells. Non-invasive diffusion weighted contrast was used to assess islet functionality and viability. Islet viability was confirmed by Trypan blue staining before and after imaging. We used in-vitro MR- microscopy to measure the diffusion coefficients of human islets under various conditions and optimized the diffusion weighted contrast. Diffusion coefficients demonstrated sensitivity to islet function and viability.

1624. Localization Regime of Restricted Diffusion in a Model Pulmonary Acinus

Denis S. Grebenkov[1], Geneviève Guillot[1]
[1]C.N.R.S. UMR8081 Université Paris-Sud, Orsay, France

The Monte Carlo simulations of restricted diffusion in 3D branching labyrinths of a model pulmonary acinus has revealed the appearance of the localization regime at high gradient intensity. This non-Gaussian regime is well known for porous materials and characterized by a stretch-exponential decay of the NMR signal as a function of the gradient strength. It gave the best fit for numerical data, as compared to the classical isotropic and anisotropic Gaussian models. These findings should be taken into account for future analysis of *in vivo* data.

1625. Dependence of Apparent Diffusion Coefficient on Cellular Structure

Dmitry S. Novikov[1], Valerij G. Kiselev[2]
[1]Princeton University, Princeton, New Jersey, USA; [2]University Hospital Freiburg, Freiburg, Germany

Water diffusion in tissues is hindered by complex cellular structure. This justifies using diffusion measurements as a structural probe. But just how sensitive such a probe can be? Addressing this question is important since acquiring the signal over a voxel is equivalent to performing statistical averaging of the tissue properties over a macroscopic scale. This may strongly reduce the information content of the ADC. By characterizing the local tissue diffusivity in terms of its correlation functions, here we present generic arguments why in fact the ADC remains sensitive to the microscopic details of the structural organization of the medium.

1626. Microscopic MRI Assessment of Human Articular Cartilage Degeneration Using Q-Space Analysis

Shadi F. Othman[1], Osama Abdullah[1], Richard L. Magin[1], Xiaohong Joe Zhou[1]
[1]University of Illinois at Chicago, Chicago, Illinois, USA

q-Space analysis of the diffusion experiment provides tissue structural information not easily obtained by other methods. Articular cartilage is a heterogeneous tissue with anisotropic structure and water content. In this study, we applied *q*--Space analysis to characterize the different layers of cartilage (superficial, middle, and deep zone) using diffusion data from seven diffusion gradient directions. The mean displacement of water molecules and the probability for zero displacement varied in different zones for both normal and diseased cartilage. Increasing isotropy appears to be correlated with the progression of disease.

1627. Diffusive Diffraction Measured with MRI at 7T

Egbert Gedat[1], Susanne Müller[2], Thomas Tolxdorff[1], Jürgen Braun[1]
[1]Institut für Medizinische Informatik, Berlin, Germany; [2]Klinik für Neurologie, Berlin, Germany

Observability of diffusive diffraction with volume selective MRI was demonstrated. A bundle of 55 water-filled glass capillaries with 100 µm inner diameter was placed in a 7T Bruker BioSpec. The stimulated echo amplitude in a volume selective STEAM sequence was evaluated with respect to the diffusion weighting gradients. Diffusion weighting was applied parallel and perpendicular to the capillaries' axes. In perpendicular direction two diffraction minima are clearly visible, while in parallel direction ordinary echo attenuation was observed. Thus, we conclude that diffusive diffraction is observable with MRI and may be applied to biological systems.

1628. The Variance of DTI-Derived Parameters Via First-Order Perturbation Methods

Lin-Ching Chang[1], Carlo Pierpaoli[1], Peter J. Basser[1]
[1]NIH, Bethesda, Maryland, USA

Monte Carlo and Bootstrap methods provide powerful statistical tools for determining the effects of background noise in diffusion weighted imaging (DWI) data on diffusion tensor MR imaging (DTI) -derived parameters, and for optimizing the design of DTI experiments. These empirical methods do not provide analytical relationships between the variance of the distribution of noise in the DWI data and the variance of DTI-derived parameters. Here we use the 1st-order matrix perturbation method to determine how noise in DWI data affects the uncertainty in the estimated tensors. Monte Carlo simulations of DTI experiments are performed to validate these formulae, and to determine their applicability over a broad range of experimental design parameters.

1629. Modelling Uncertainty in Two Fibre-Orientation Estimates Within a Voxel

Philip A. Cook[1], Daniel C. Alexander[1]
[1]University College London, London, UK

The Probabilistic Index of Connectivity tractography method uses Monte-Carlo streamline generation to create maps of connection probability. A probability density function (PDF) is associated with the fibre orientation in each voxel. We present a new model of the fibre-orientation PDF that models the uncertainty of two distinct fibre orientations within a voxel. Unlike previous work, the new model does not assume circular contours of the PDF on the sphere. We show an example of the model where a Gaussian mixture model is used to estimate the two fibre orientations in a simulated fibre crossing.

1630. Sensitivity of Diffusion-Weighted-Steady State Free Precession to Diffusion Anisotropy

Jennifer Andrea McNab[1], Karla L. Miller[1]
[1]University of Oxford, Oxford, UK

DW-SSFP signal attenuation is characterized in the context of 2D anisotropic diffusion. The DW-SSFP attenuated signal profile is shaped differently than that of DW-SE, with less narrowing at the principle diffusion axis. This difference in shape is explained by looking at the weighted summation of 'single echo' attenuation profiles. The anisotropy contrast is contributed by the long STE components and thus it may be of interest to find ways to isolate these longer STEs. Diffusion tensor analysis from DW-SSFP should be possible, however, a new formalism will be required to extract information about the diffusion tensor from DW-SSFP data.

1631. Numerical Simulation of Double Wave Vector Diffusion Experiments

Martin A. Koch[1], Jürgen Finsterbusch[1]
[1]University Medical Center Hamburg-Eppendorf, Hamburg, Germany

Double wave vector (DWV) diffusion weighting might provide a means to acquire information on cell size and shape. In numerical simulations we test a theoretical description of the DWV signal in a situation where the approximating assumptions are not strictly met. We show how the dependence of the signal on the angle between the diffusion gradient directions changes upon variation of the waiting period between 2nd and 3rd gradient pulse. This is done to consolidate seemingly contradicting experimental results concerning the angle at which the largest signal attenuation occurs.

1632. Isoflurane Strongly Affects the Diffusion of Intracellular Metabolites in the Brain, Revealing the Contribution of Subcellular Restriction to Metabolite ADC

Julien Valette[1], Martine Guillermier[2], Philippe Hantraye, [12], Gilles Bloch[1], Vincent Lebon[1]
[1]CEA-SHFJ, Orsay, France; [2]URA CEA-CNRS 2210, Orsay, France

Isoflurane is commonly used for diffusion NMR spectroscopy experiments in animals. However, isoflurane is known to impact membrane fluidity, possibly increasing permeability to metabolites. In this work the effect of isoflurane on metabolite ADCs is evaluated using diffusion tensor spectroscopy in the monkey brain. Metabolite ADCs exhibit strong increases when isoflurane dose varies from 1% to 2%. This is interpreted as a consequence of the facilitated exchange between subcellular structures at high isoflurane dose, while metabolites remain confined in these structures under normal conditions. This work provides new insights for interpreting ADC values as measured by diffusion NMR spectroscopy.

1633. Effects of Cellular Mitosis on the Apparent Diffusion Coefficient of Synchronized HeLa Cells

Daniel C. Colvin[1], Natasha Deane[1], Coe Foutch[1], Mark D. Does[1], John C. Gore[1]
[1]Vanderbilt University, Nashville, Tennessee, USA

The presence of restrictive barriers in biological tissues serves to reduce the apparent diffusion coefficient (ADC) of self-diffusing water molecules, compared to that of unrestricted water. At long diffusion times, a single diffusing molecule may experience a variety of local environments and barriers, and thus a reduced ADC reflects structure over the size of a cell or larger. However, at shorter diffusion times, the ADC is affected by boundaries of a much smaller spatial dimension and thus reveals changes on a subcellular scale. We have therefore used ADC as a measure of the effects of internal reorganization during cellular mitosis.

Myocardial Function and Strain Analysis

Room 4E Tuesday 13:30 - 15:30

1634. Single Breath-Hold Whole-Heart 3D CINE Imaging Using Kt-BLAST and Kt-SENSE

Marcus Katoh[1], Elmar Spuentrup[1], Arno Buecker[1], Marc Kouwenhoven[2], Jürgen Bunke[2], Rolf W. Guenther[1], Thoralf Niendorf[1], Thoralf Niendorf[1]
[1]RWTH Aachen University Hospital, Aachen, Germany; [2]Philips Medical Systems, Best, Netherlands

kt-BLAST and kt-SENSE were combined with a whole-heart 3D steady-state free-precession (SSFP) CINE sequence to allow data acquisition during a single breath-hold. Global cardiac function of seven volunteers was assessed using a 5- and 8-fold accelerated 3D CINE approach. Image quality was compared to conventional 2D CINE imaging. In addition, physiological parameters of the left ventricle (EDV, ESV, SV, EF, and LVM) were analyzed. Whole-heart 3D imaging demonstrated good image quality allowing for image reformation in arbitrary orientation. The value of measured EDV, SV, EF, and LVM, however, were significantly smaller compared to 2D imaging.

1635. Fast 3D Cine Steady-State Free Precession Imaging with Sensitivity Encoding for Assessment of Left Ventricular Function in a Single Breath-Hold

Neil B. Mascarenhas[1], Raja Muthupillai[2, 3], Benjamin Cheong[2], Mercedes Pereyra[2], Scott D. Flamm,[12]

[1]Baylor College of Medicine, Houston, Texas, USA; [2]St. Luke's Episcopal Hospital/Texas Heart Institute, Houston, Texas, USA; [3]Philips Medical Systems, Cleveland, Ohio, USA

Steady-state free precession (SSFP) is the sequence of choice for evaluating left ventricular (LV) function, but conventional 2-dimensional (2D) techniques require multiple breath-holds. We combined 3-dimensional (3D) SSFP with sensitivity encoding (SENSE) to achieve a single breath-hold acquisition. We imaged 23 individuals with both the 2D and 3D sequences and compared these two methods for quantifying LV function. 3D SSFP imaging with SENSE reduced the acquisition time to a single breath-hold and provided LV function assessment comparable to that obtained with conventional 2D SSFP imaging.

1636. Single Breath-Hold 3D Cine Imaging of the Heart: A Non-Angulated Isotropic Acquisition Using SENSE on a 32 Channel System

Vivek Muthurangu[1], Nicholas MI Noble[2], Redha Boubertakh[1], Richard Winkelmann[3], Peter Börnert[4], Derek L. G. Hill[2], Reza S. Razavi[1]

[1]King's College London, London, UK; [2]University College London, London, UK; [3]University of Karlsruhe, Karlsruhe, Germany; [4]Philips Research Laboratories, Hamburg, Germany

Single breath-hold cardiac 3D cine imaging requires minimal planning and subsequent 2D reformatting allows analysis of cardiac function. In 8 volunteers 3D cine data was acquired on a 32 channel system using 2D sensitivity encoding. Image sharpness, contrast and motion fidelity of reformatted 2D cine images were diagnostic. However, they were not equivalent to conventionally acquired 2D cine images. Volumetry results were comparable. However end diastolic volume was underestimated and end systolic volume was overestimated when using reformatted short axis data. We believe that once optimized this technique will allow more widespread use of cardiovascular magnetic resonance.

1637. Minimized Off-Resonance Effects with Centric Radial SSFP for Imaging Cardiac Function

Matthew D. Robson[1], Stefan Neubauer[1]

[1]Oxford University, Oxford, Oxfordshire, UK

Steady-State Free Precession offers excellent contrast to noise ratio when imaging the human heart, and when used as a single slice cine acquisition is the preferred approach for imaging cardiac function clinically. Single slice centric-radial steady-state free precession (cr-SSFP) provides the shortest TR for the 2D SSFP sequence, which will minimize the off-resonance artefact sometimes seen with these sequences, especially at 3Tesla. This approach has been implemented as a cine acquisition on clinical scanner at 1.5T and 3T and is demonstrated to provide high quality images across a larger frequency range than the standard clinical Cartesian SSFP methods.

1638. A Reproducibility Comparison of Quantitative Left Ventricular Assessments in Healthy Volunteers Using Different MRI Scanners - Implications for Multicentre Cardiac MRI Studies

Stephen J. Gandy[1], Shelley A. Waugh[1], R Stephen Nicholas[1], Helen Simpson[2], Wendy Milne[1], Tracy Rylott[3], J Graeme Houston[1]

[1]NHS Tayside, Ninewells Hospital, Dundee, Angus, UK; [2]School of Medicine, University of Dundee, Dundee, Angus, UK; [3]NHS Tayside, Perth Royal Infirmary, Perth, Perthshire, UK

In this study multicentre reproducibility of left ventricular cardiac MRI parameters was investigated. Volunteers were imaged twice on a Siemens scanner and once on a GE scanner over two months, and short-axis myocardial borders were segmented by two observers. Scan-to-scan parameter variations (e.g. ejection fraction, left ventricular mass) were similar whether derived from the same or different scanners. However, scan-to-scan variations were larger than single timepoint test-retest variations, and interobserver variability was larger than intraobserver variability. It is possible to simulate longitudinal multicentre conditions and obtain reproducible left ventricular measurements, but single or multiple segmenter use should be carefully considered.

1639. Range of Biventricular Dimensions and Function Evaluated by Steady State Free Precession Cine Magnetic Resonance in Patients with Repaired Tetralogy of Fallot

Margaret Mary Samyn[1], Andrew J. Powell[1], Ruchira Garg[1], Laureen Sena[1], Tal Geva[1]

[1]Children's Hospital Boston, Boston, Massachusetts, USA

Cardiac magnetic resonance (CMR)imaging studies have shown that ventricular volumes, measured by steady state free precession (SSFP)cine CMR imaging, are larger and mass is lower when compared with fast gradient echo (GRE) cine CMR data. CMR can be used for serial assessment of patients with tetraology of Fallot (TOF), who experience many clinical problems related to residual right ventricular outflow tract obstruction, pulmonary regurgitation, and right ventricular dysfunction. This study uses SSFP cine CMR to characterize the range of biventricular dimensions and function in a large cohort of patients (n = 300)with repaired TOF, allowing comparisons between repair with a RVOT patch and RV-to-pulmonary artery conduit.

1640. Longitudinal, Radial, and Circumferential Myocardial Velocities in Patients with Ventricular Dyssynchrony

Jana Delfino[1], Mobit Bhasin, Angel Leon, Robert Eisner, John Oshinski[1]
[1]Georgia Institute of Technology/ Emory University, Atlanta, Georgia, USA

The purpose of this study was to quantify three-dimensional (radial, circumferential and longitudinal) myocardial velocities in normal volunteers and patients with dyssynchrony using navigator-echo gated MR phase velocity mapping. Longitudinal, radial and circumferential velocities were compared between normal volunteers and patients. Significant differences were found in both the radial and longitudinal, but not the circumferential, peak systolic velocities between normal volunteers and dyssynchrony patients. The timing of peak systolic contraction was also found to be significantly delayed in the lateral wall of dyssynchrony patients compared to normal volunteers.

1641. Pre- And Postcontrast Three-Dimensional Cardiac Cine MRI Using SENSE and K-T BLAST

Yasuo Amano[1], Tatsuo Kumazaki[1], Yuriko Suzuki[2]
[1]Nippon Medical School, Tokyo, Japan; [2]Philips Medical System, Tokyo, Japan

The purpose of this study was to evaluate the usefulness of 3D cardiac cine MRI compared with 2D cine MRI. SENSE and k-t BLAST were employed to speed up the 3D cine MRI, and consequently permitted the breath-hold 3D cardiac cine MRI with the functional data comparable to the 2D cine MRI. The use of gadolinium injection increased the contrast between myocardium and ventricular cavity in the 3D cine MRI, whereas precontrast 3D cine MRI provided the acceptable contrast. Three-dimensional cardiac cine MRI using SENSE or k-t BLAST was useful for rapid acquisition of cardiac functions.

1642. Acquisition of Black-Blood Cine Cardiac Images in a Single Heartbeat at 3.0T

Ahmed S. Fahmy[1], Li Pan[1], Nael F. Osman[1]
[1]Johns Hopkins University, Baltimore, Maryland, USA

Cine black-blood images of the heart were successfully produced using stimulated echo mode (STEAM) after correction of deformation-induced artifacts. Because of the splitting of the image acquisition over several cardiac cycles, the method required at least one breath-hold in order to acquire the entire cine sequence. In this work, we present implementation of the STEAM sequence on 3.0T scanners that produces black-blood cine sequences of the heart acquired in a period of a single cardiac cycle. The method depends on efficient fat suppression technique combined with interleaved spiral acquisition of the k-space.

1643. A Double Navigator Approach to Double Inversion Recovery Fast Spin Echo Imaging in Black Blood Cardiac MRI

Pascal Spincemaille[1], Thanh D. Nguyen[1], Martin Prince[1], Yi Wang[1]
[1]Weill Medical College of Cornell University, New York, USA

A method using double navigators, real time slice tracking and registration, and a real time PAWS gating algorithm was developed for a double inversion black blood 2D fast spin echo sequence. Compared to the previous single navigator method, the double navigator method reduced image artifacts due to the respiration induced misregistration between selective inversion location and image location, allowing high quality free-breathing black blood cardiac imaging.

1644. MR Compatible Heart Phantom for Medical Research

Holger Timinger[1], Sascha Krueger[1], Joern Borgert[1]
[1]Philips Research, Hamburg, Germany

We present a pneumatically driven dynamic heart phantom for development and evaluation in medical research. The phantom contains an elastic ventricle phantom including vasculature which is reproducibly deformed by simulated heartbeat and respiration. Motion patterns and vasculature can be customized depending on the application to be simulated. The phantom can be imaged using MRT, CT, or X-ray. The phantoms control unit provides simulated ECG and respiratory signals. Possible applications include imaging tests, interventional and flow experiments. During evaluation, no B0 inhomogeneity was detected and gated 3D MR images of the moving phantom showed no motion artefacts at all.

1645. An MRI-Based Beating Heart Model

Qing Wei[1], Stuart Crozier[1], Ben Appleton[1], Ling Xia[2], Feng Liu[1], Stephen Wilson[1], Wendy Strugnell[3], Richard Slaughter[3], Robyn Riley[3]
[1]The University of Queensland, Brisbane, Queensland, Australia; [2]ZheJiang University, HangZhou, ZheJiang, People's Republic of China; [3]The Prince Charles Hospital, Brisbane, Queensland, Australia

In this report, we use cardiac MRI to generate a personalised electrical heart model so as to investigate the cardiac electrical activities and its resulting body surface Electrocardiographic potentials (BSPM). The BSPM and endocardial potentials can then be used for the detection of life threatening arrhythmias and other diseases. In our study, we construct a beating heart model based on our segmented myocardial contours from multiple-slice MRI time sequences. The moving heart model is then situated inside a MRI-based electromagnetic human torso model. The ECG simulations demonstrate that the inclusion of heart motion is essential to accurately model surface potentials.

1646. Balanced 2D Radial Acquisition SSFP of the Mouse Heart at 7 Tesla

Elizabeth Kathleen Bucholz[1], G. Allan Johnson[1]
[1]Duke University, Durham, North Carolina, USA

A 2D Radial Acquisition(RA) SSFP sequence was developed at 7T for the purpose ofcine mouse heart imaging. RA was chosen due to its immunity to motion artifactsand signal fluctuations, shorter repetition time, and reduced gradient demands.In the phantom, RA-SSFP resulted in 4X increase in SNR. In the live mouse,RA-SSFP increased SNR in the myocardium and blood by a factor of 2 and 1.5respectively. The sequence was designed to allow encoding on the outward andinward trajectory resulting in the formation of two images with ability toincrease SNR, temporal resolution and create BO maps.

1647. Direct Measurement of Intra Ventricular and Atrial Pressures Concurrent with MR Image Acquisiton

S. David Smith[1], [2], Helene Benveniste[2], [3], G. Ron Morris[4], Svante Hojer[5], Igor Izrailtyan[3], Mei Yu[2], Congwu Du[2], Zhongchi Luo[6], Yu Ma[2], Hai-Dee Lee[2], Igor Feinstein[7]
[1]INNOVISION Diagnostic Imaging Corp., Bellport, New York, USA; [2]Brookhaven National Laboratories, Upton, New York, USA; [3]Stony Brook Hospital, Stony Brook, New York, USA; [4]SA Instruments, Inc., Stony Brook, New York, USA; [5]Samba Instruments, Inc., Gotenburg, Sweden; [6]Stony Brook University, Stony Brook, New York, USA; [7]New York University, New York, New York, USA

Synopsis not available.

1648. Slice Refocusing Signal for Retrospective Reconstruction of CINE Cardiac MR Images

Arno Nauerth[1], Edwin Heijman[2], Claudia Diekmann[1]
[1]Bruker BioSpin MRI GmbH, Ettlingen, Germany; [2]Eindhoven University of Technology, Eindhoven, Netherlands

A prerequisite for cardiac MRI is the alignment of the data acquisition with the respiration and the cardiac cycles. Several techniques have been developed in order to overcome the major problems of conventional ECG triggering and respiratory gating. The proposed self-gating sequence widens the scope of cardiac MRI significantly. Once a dataset is acquired, one has a free choice of reconstructing cardiac movies and respiration movies with an arbitrarily number of movie frames. Furthermore, there are several possibilities to deal with diseased animals where other techniques simply fail

1649. Optimal Combination of Phase Cycling and Gradient Spoiling in DENSE Displacement Mapping

Eric Bennett[1], Bruce Spottiswoode[2], Christine H. Lorenz[2], Han Wen[1]
[1]National Institutes of Health, Bethesda, Maryland, USA; [2]Siemens, Bethesda, Maryland, USA

In DENSE and HARP displacement imaging the signal is a mixture of several k-space echoes and it is desirable to separate them or suppress the unwanted ones. These echoes acquire different phase factors from displacement encoding gradient and from phase shifts of the RF pulses in the encoding step, so they can be separated with phase-cycling of the RF pulses, and can be selectively suppressed with encoding gradient. The former costs more scan time and the latter causes signal reduction in the presence of strain. The optimal combination of the two is identified in the heart in this abstract.

1650. Combining 2D DENSE and SENC to Calculate the 3D Strain Tensor

Aaron Timothy Hess[1], Xiaodong Zhong[2], Bruce Shawn Spottiswoode[1], Frederick H. Epstein[2], Ernesta M. Meintjes[1]
[1]University of Cape Town, Cape Town, Western Cape, South Africa; [2]University of Virginia, Charlottesville, Virginia, USA

This study presents the methodology for combining cine DENSE and cine SENC acquisitions to form an intramyocardial 3D strain tensor. The outcome is a single slice of strain data produced by combining two adjacent image planes of two dimensional cine DENSE with a single cine SENC acquisition. The technique was evaluated in four volunteers.

1651. DENSE and HARP: Two Views on the Same Technique of Phase-Based Strain Imaging

Joost Kuijer[1], Mark B. Hofman[1], Jaco J. Zwanenburg[1], J. Tim Marcus[1], Albert C. Van Rossum[1], Rob M. Heethaar[1]
[1]VU University Medical Centre, Amsterdam, NL, Netherlands

Recent publications in the field of myocardial strain analysis show an increasing interest in phase-based strain quantification, using either the DENSE or the HARP technique. Historically, both techniques arose from a different framework. Both techniques have evolved since their introduction, thereby becoming more similar over time and losing their distinct features. However, in literature, both techniques are still regarded as distinctly different techniques, where a more general treatment of phase-based strain imaging is justified. This abstract discusses differences and similarities between HARP and DENSE in imaging and reconstruction, concluding that DENSE and HARP are actually one and the same technique.

1652. More Comprehensive Cardiac DENSE MR Imaging by Combination of Short Axis and Long Axis Data

Abbas Nasiraei Moghaddam[1], Han Wen[2], Morteza Gharib[1]
[1]California Institute of Technology, Pasadena, California, USA; [2]NIH/NHLBI, Bethesda, Maryland, USA

In this study we have shown the feasibility of the combination of cardiac Short Axis (S.A) and Long Axis (L.A) images that provides a more comprehensive data from DENSE MRI in 20 to 40% shorter time. Estimating the magnitude of the displacement field for a region on one of the S.A layers by its adjacent S.A and L.A neighbors resulted in 29% relative root mean squared (rms) error. It is almost equal to the 24% relative rms difference of the same parameter calculated based on S.A and L.A acquisitions for the points on the intersection of those layers.

1653. Fast 3D Dense Tracking of Cardiac Material Points Using ZHARP: In-Vivo Validation and Comparison with 3D SF-HARP

Khaled Z. Abd-Elmoniem[1], Matthias Stuber[1], Jerry L. Prince[1]
[1]Johns Hopkins University, Baltimore, Maryland, USA

In this study, we extend zHARP to multi-slice SA acquisition and tracking with the objectives of 3D dense displacement mapping throughout the heart without the need of extra LA acquisitions. We also compare the performance of zHARP to 3D SF-HARP. Phantom experiments show strong accordance between the two methods while *in vivo* results show the zHARP 3D tracking is less sensitive to heart rate variations.

1654. Real-Time Single-Shot CINE Imaging of Through-Slice Strain in the Human Heart

Han Wen[1], Eric Bennett[1]
[1]National Institutes of Health, Bethesda, Maryland, USA

Clinical applications of cardiac MRI increasingly require realtime assessment of regional function. This abstract presents cine imaging of through-slice strain over multiple cardiac phases in a single shot. It is based on the DENSE displacement mapping technique and is useful for monitoring cardiac function under changes of physiological condition, such as stress tests.

1655. Navigator Gated High Temporal Resolution Tissue Phase Mapping of Myocardial Motion

Bernd André Jung[1], Maxim Zaitsev[1], Jürgen Hennig[1], Michael Markl[1]
[1]University Hospital, Freiburg, Germany

Data acquisition for Tissue Phase Mapping (TPM) in the myocardium is typically based on multiple breath-held 2D measurements. In order to overcome limitations of breath-hold acquisitions, an improved navigator-guided technique was implemented. TPM measurements with 3D velocity encoding were performed in 12 volunteers during breath-hold periods with a temporal resolution of 69 ms and compared to free breathing acquisitions with a temporal resolution of 13.8 ms. Measurements with high temporal resolution reveal details in the motion pattern of velocity time courses. Results are highly promising such that high resolution TPM may offer the possibility to assess previously undetectable motion abnormality details associated with pathological left ventricular performance.

1656. Toward True Myocardial Plannar Strain Using ZHARP: Experimental In-Vivo Validation

Khaled Z. Abd-Elmoniem[1], Matthias Stuber[1], Jerry L. Prince[1]
[1]Johns Hopkins University, Baltimore, Maryland, USA

The purpose of this research is to develop and test a method that provides a true planar strain map for a given imaged slice. The method takes the through-plane motion into consideration and corrects for the false strain component caused by through-plane rotation. Phantom and *in vivo* results demonstrating the ability to remove the through-plane rotation effect from the strain maps are presented.

1657. Comparison of Myocardial Velocities Obtained with Magnetic Resonance Phase Velocity Mapping and Tissue Doppler Imaging in Normal Subjects and Patients with Left Ventricular Dyssynchrony

Jana Delfino[1], Mobit Bhasin[1], Robert Cole[1], Angel Leon[1], Robert Eisner[1], John Merlino[1], John Oshinski[1]
[1]Georgia Institute of Technology/ Emory University, Atlanta, Georgia, USA

Measurements and reproducibility of longitudinal myocardial velocity and time to peak longitudinal velocity made with MR PVM and Tissue Doppler Imaging (TDI) were compared in 10 normal volunteers and 10 patients with dyssynchrony. MR and TDI measurements correlated well (r=0.86) in both normal subjects and patients with dyssynchrony. However, MR PVM velocities consistently exceeded TDI velocities. MR and TDI agreed strongly in measuring the time to peak velocity (r=0.97). The reproducibility of TDI and MR PVM appeared similar in measuring peak velocities (13.1% vs. 11.0 %, respectively, p=NS) and time to peak velocity (9.1% vs. 5.7 %, respectively, p=NS).

1658. The Effect of Noise on the Accuracy of Strain Measurment When Using Strain Encoded (SENC) MRI

Tamer Yousef[1], Nael F. Osman[1]
[1]Johns Hopkins University, Baltimore, Maryland, USA

In this abstract, a thorough analysis of noise effect on the measurements of strain from SENC and how this guides the selection of the SENC pulse sequence parameters.

1659. VaFA: Replacing CSPAMM

Vinay Manjunath Pai[1], Daniel Kim[1]
[1]New York University, New York, New York, USA

Complementary SPAMM (or CSPAMM) is a popular approach to acquire tagged datasets due to its ability to provide dark blood contrast, and permit faster segmentation of the cardiac cine data. However, since CSPAMM requires two separate acquisitions, misregistration between the two acquisitions can frequently arise, affecting the accuracy of any wall function quantification performed subsequent to the segmentation. We present an alternative approach, VaFA, for obtaining SPAMM data with dark blood contrast in a single acquisition. This approach eliminates the issue of misregistration, and due to the dark blood contrast, can provide similar segmentation benefits as CSPAMM.

Lung Imaging: Applications

Room 4E Tuesday 13:30 - 15:30

1660. Quantitative Regional Lung Ventilation- Results in 15 Single Lung Transplanted Patients

Hans-Georg Topf[1], P Biondetti[2], Maren Zapke[1], Rainer Kuth[3], M Deimling[3], C Chefd´hotel[4], B Geiger[5], Thomas Rupprecht[6]
[1]Childrens Hospital, Erlangen, Germany; [2]Clinico, Milano, Italy; [3]Siemens, Erlangen, Germany; [4]Siemens, Princeton, U, USA; [5]Siemens, U, Germany; [6]Childrens Hospital, Bayreuth, Germany

Presented are measurements in 15 lung transplanted patients. The measured values and the regional color coded ventilation maps were in concordance to the clinical expectations. The fact that only on side of the lung was transplanted and the other side was kept allows to compare healthy and pathological lung tissue at the same time. We demonstrate a clinical application of a novel technique for quantitative calculation of regional pulmonary ventilation. The measured values were in concordance to the previous experiments, the clinical expectations and the lung function studies.

1661. Is There a Diagnostic Potential of Magnetization Transfer MRI in Patients with Lung Cancer?

Johannes F. T. Arnold[1], Markus Kotas[1], Eberhard D. Pracht[1], Michael Flentje[1], Peter Michael Jakob[1]
[1]University of Würzburg, Würzburg, Bavaria, Germany

To date, the only modalities routinely used for lung cancer radiation therapy planning are CT or CT in combination with FDG-PET. While MRI cannot match CT in terms of resolution, magnetization transfer prepared MRI (MT-MRI) could provide auxiliary functional information in non-small cell lung cancer patients. Our preliminary study shows the potential of MT-MRI in creating various contrasts in lung tumor masses, which otherwise appear homogenous in images from standard MRI sequences.

1662. The Role of Hyperpolarized 3-Helium MRI in NSCLC

Rob H. Ireland[1], Mark McJury[2], Matthew Q. Hatton[3], Neil Woodhouse[1], Edwin JR van Beek[4], Jim M. Wild[1]
[1]University of Sheffield, Sheffield, UK; [2]Belvoir Park Hospital, Belfast, UK; [3]Weston Park Hospital, Sheffield, UK; [4]University of Iowa, Iowa City, Iowa, USA

The feasibility of image registration of hyperpolarized 3-helium (^{3}He) MRI and radiotherapy treatment planning CT is demonstrated for six patients with non-small cell lung cancer (NSCLC). Knowledge of lung function derived from ^{3}He images may enable radiation fields to be targeted to limit the treatment dose to healthy regions of lung and therefore reduce the risk of radiation pneumonitis.

1663. Ventilation Heterogeneity Indices Computed from Hyperpolarized ^{3}He MRI Captures Differences Between Asthmatic and Non-Asthmatic Lungs

Yang-Sheng Tzeng[1, 2], Niral Shah, [12], Joey Mansour[1], Jessica Gereige[1], George Washko[1], Elliot Israel[1], Kenneth Lutchen[2], Mitchell Albert[1]
[1]Brigham & Women's Hospital, Boston, Massachusetts, USA; [2]Boston University, Boston, Massachusetts, USA

In an attempt to characterize ventilation heterogeneity, average local coefficient-of-variation and standard deviation of pixel intensity have been computed for hyperpolarized ^{3}He MR images obtained during static ventilation. The images were acquired from asthmatics and non-asthmatics, before methacholine challenge, after methacholine challenge, and after deep inspirations. Statistically significant changes in these indices from one phase to another, as well as differences between the two subject populations, corroborate current understanding of asthmatic hyper-reactivity, and the inability of deep inspirations to reverse asthmatic bronchoconstriction.

1664. Assessing the Temporal Changes of the Regional Ventilation in the Lungs of Asthmatics with Hyperpolarized Helium-3 MR Imaging

Talissa A. Altes[1], [2], John J. Battiston[2], Adam P. Juersivich[2], John P. Mugler[2], Thomas AE Platts-Mills[2], Eduard E. de Lange[2]

[1]Children's Hospital of Philadelphia, Philadelphia, Pennsylvania, USA; [2]University of Virginia, Charlottesville, Virginia, USA

37 asthmatics underwent hyperpolarized helium-3 MR twice: 20 on the same day and 17 on two different days, mean time between scans 4.3 min and 78 days respectively. The percent of the ventilation defects present on the first scan that were present in the same location on the second scan was 86%(23%) for the subjects scanned on the same day and 67%(25%) for subjects scanned on two different days. The surprisingly large number of ventilation defects that persisted or recurred in the same location on scans widely separated in time suggests that asthma is a regional disease.

1665. Comparison of Diffusion Weighted Helium-3 MRI in Patients with Asthma Versus Those with COPD

Sean B. Fain[1], Tallissa A. Altes[2], Rafael O'Halloran[1], Ronald L. Sorkness[1], Michael D. Evans[1], Frank R. Korosec[1], Thomas M. Grist[1]

[1]University of Wisconsin, Madison, Wisconsin, USA; [2]University of Pennsylvania, Philadelphia, Pennsylvania, USA

Helium-3 diffusion weighted MRI was applied to subjects with asthma with no smoking history. The apparent diffusion coefficient (ADC) for the subjects with asthma (N = 21, Age 35 ± 13 yrs) was compared to identical measures in healthy never-smokers (N = 24, Age = 50 ± 15 yrs), and patients with COPD grouped with active smokers (N = 16, Age = 53 ± 17 yrs). Results of a group-wise comparison show that mean ADC is significantly reduced in subjects with asthma compared to healthy never-smokers and active smokers with and without COPD even after age correction.

1666. Helium-3 Apparent Diffusion Coefficient MRI Compared to CT in Emphysema Patients

Per Åkeson[1], Sandra Diaz[1], Ingrid Casselbrant[1], Eeva Piitulainen[1], Per Wollmer[1], Göran Pettersson[2], Peter Magnusson[2], Barry Peterson[3]

[1]Malmö University Hospital, Malmö, Sweden; [2]GE Healthcare, Malmö, Sweden; [3]Pfizer Inc., Groton, Connecticut, USA

The goal of this study is to compare the Apparent Diffusion Coefficient of hyperpolarized 3He -Inhalation MRI with Emphysema Index of multislice CT in patients with early emphysema. 22 patients were examined with hyperpolarized 3He inhalation at 1.5T. The mean ADC calculated from 3HeMRI correlated well with EI calculated from CT imaging, but the MRI method does not involve the use of ionizing radiation. Furthermore, compared to EI, the mean ADC had a stronger correlation with DLCO, the physiological measure of emphysema. These results help establish the validity of 3HeMRI for assessing lung structure in patients with emphysema.

1667. Velocity Encoding MRI with SENSE: Utility for Assessment of Disease Severity in Pulmonary Emphysema Patients

Munenobu Nogami[1], Yoshiharu Ohno[1], Hisanobu Koyama[1], Daisuke Takenaka[1], Masahiko Fujii[1], Kazuro Sugimura[1]

[1]Kobe University Graduate School of Medicine, Kobe, Hyogo, Japan

Diagnosis of right ventricular failure due to secondary pulmonary hypertension in patients with pulmonary emphysema (cor pulmonale) is considered essential to estimate their prognosis. Recently, velocity encoding MR (velocity-MRI) imaging has been proposed as a substitute for cardiac echocardiography or catheterization for assessment of hemodynamic information in cardio-pulmonary disease. We hypothesize that parameters from velocity-MRI can assess severity of pulmonary emphysema according to functional and morphological information, and may play an important role for management of pulmonary emphysema. The purpose of present study was to determine the utility of velocity-MRI for quantitative assessment of severity of pulmonary emphysema.

1668. Early Detection of Emphysema by Hyperpolarized Helium-3 MRI Through Measuring Regional Fractional Ventilation

Kiarash Emami[1], Martin Fischer[1], Jianliang Zhu[1], Masaru Ishii[2], Vahid Vahdat[1], Stephen Kadlecek[1], John MacDuffie Woodburn[1], Michael E. Friscia[1], JiangSheng Yu[1], Rahim R. Rizi[1], Joseph Shrager[1]

[1]University of Pennsylvania, Philadelphia, Pennsylvania, USA; [2]Johns Hopkins University, Baltimore, Maryland, USA

Emphysema is a devastating disease associated with significant morbidities and mortalities. The early detection of emphysema is of fundamental importance to the diagnosis and treatment of this disease. In this work, we show that regional measures of fractional ventilation using hyperpolarized helium-3 MRI can detect early forms of emphysema and that it is a sensitive marker of disease progression. A comparison between functional MRI parameters and histology is presented as well.

Muscle Spectroscopy

Room 4E Tuesday 13:30 - 15:30

1669. Measurement of Intramyocellular Lipids in Obese Subjects Using Spectroscopic Imaging with High Spatial Resolution

Jan Weis[1], Lars Johansson[2], Frederic Courivaud[3], Anders Karlsson[1], Håkan Ahlström[1]
[1]Uppsala University Hospital, Uppsala, Sweden, Sweden; [2]Astra Zeneca R&D, Uppsala, Sweden, Sweden; [3]Philips Medical Systems, Oslo, Norway, Norway

IMCL quantification in obese subjects by single voxel spectroscopy and conventional spectroscopic imaging fails often due to overlap of IMCL by strong extramyocellular lipids (EMCL), and by strong signal contamination from subcutaneous fat and bone marrow. We demonstrate, that solution of those obstacles can be high-resolution spectroscopic imaging with 128 phase encoding steps and read gradient during acquisition. Small voxels that can be achieved facilitate differentiation between EMCL and IMCL. The method offers the possibility to study different muscle groups and the variation of lipids within one muscle.

1670. Separation of the Intra- And Extracellular Apparent Diffusion Coefficients (ADC) of Water in Rat Skeletal Muscle Using Spectroscopic MEMRI

Karl G. Helmer[1], John G. Seland[2], Nils Henninger[3], Christopher H. Sotak[1, 3]
[1]Worcester Polytechnic Institute, Worcester, Massachusetts, USA; [2]Norwegian University of Science and Technology, Trondheim, Norway; [3]UMass/Memorial Healthcare, Worcester, Massachusetts, USA

MEMRI was used to separate intracellular (IC) and extracellular (EC) water signals in rat skeletal muscle. Infusion of MnCl2 was through a stairstep schedule using concentrations from 20-70 mM. Diffusion-weighted (DW) inversion-recovery data was fit using a bi-exponential form and the resulting DW compartmental M0 values were then fit for the compartmental ADC values. The separation of water compartment signals was verified using an inverse-Laplace transform method. Results show that the increased relaxivity of Mn2+ over that of GdDTPA2- allows for the separation of the IC and EC signals and the measurement of their ADCs.

1671. *In Vivo* Quantification of Intramyocellular Lipid in Mouse Hindleg Muscle

Rachida Fissoune[1], Bassem Hiba[2], Marc Janier[2], André Briguet[1]
[1]Laboratoire de RMN CNRS UMR 5012, Lyon, France; [2]Animage Plateforme of Small Animal Imaging, Lyon, France

In vivo 1H-MRS has been applied successfully in human and animal to investigate the muscle lipids metabolism. However, no *in vivo* studies of IMCL pools from mice have been published because of the small size of muscle and the strong EMCL signal contamination. This study shows that a good selection of the VOI, the position of muscle in order to B0 and high shim quality are necessary to obtain a good discrimination between lipids resonances.we demonstrate that non-invasive *in vivo* 1H-MRS can be used for lipids quantification in mouse muscles. That could be interesting for metabolic and physiologic investigations of obesity, diabetes and insulin resistance mouse models.

1672. IMCL Changes During Moderate Endurance Exercise as Measured by Three Different Methods

Tom Dresselaers[1], Katrien De Bock[1], Paul Van Hecke[1], Peter Hespel[1]
[1]K.U.Leuven, Leuven, Belgium, Belgium

We report the first study to compare the effect of moderate intensity endurance exercise on intramyocellular lipids (IMCL) utilization as measured with three methods: non-invasively using 1H MRS and two invasive techniques: Oil-Red-O (ORO) staining and a biochemical assay. Both 1H MRS and ORO staining revealed equal IMCL breakdown during exercise whereas no decrease could be detected whenever IMCL content was analyzed biochemically.

1673. MRI Measurement of Advanced Glycation End Products: The MRI Hyperglycemic Damage Index

Andres Rahal[1], Gary D. Fullerton[1]
[1]The University of Texas Health Science Center at San Antonio, San Antonio, Texas, USA

Hypothesis: MRI can detect and measure glycation of tendon collagen in-vitro. MRI of samples incubated in glucose vs. controls shows increased signal intensity (SI) over time (to a maximum of 7.3 times over controls), greater on sequences with short TE, small flip angles, and with samples parallel to the main magnetic field (P). MRI of samples oriented at the magic angle (MA, 55º to Bo) showed increased SI of glycated tendons up to 1.5 times over controls. A glycation index was calculated and plotted versus incubation time (up to 30 weeks) extrapolated to years at 180 mg/dl of glucose.

1674. ^{1}H-MRSI in Human Calf Muscles at 3T: Ordering Effects and Intra-Myocellular Lipids

Peter Vermathen[1], Roland Kreis[1], Chris Boesch[1]
[1]University & Inselspital, Berne, Switzerland

Eighteen MRSI measurements in different calf muscles of nine subjects were performed at 3T. The separation between resonances from intramyocellular lipids (IMCL) and from bulk lipids was clearly improved at 3T with complete separation in some spectra. Cr and Tau showed the expected dipolar splitting depending on the muscle fiber orientation, however, better resolved than at 1.5T. While 24x24 MRSI (acquisition time 10 min) is sufficient to determine metabolite concentrations and fiber orientations in numerous muscles, higher spatial resolution measurements (80x80) with longer acquisition times are feasible and may be helpful in studies of obese subjects.

1675. Response of Insulin-Dependent Type 2 Diabetic Subjects to a 5-Month Exercise Training Program

Henk M.M.L. De Feyter[1], Stephan S.F. Praet[2], Luc J. van Loon[2], Jeanine J. Prompers[1], Klaas Nicolay[1]
[1]Eindhoven University of Technology, Eindhoven, Netherlands; [2]Maastricht University, Maastricht, Netherlands

Insulin-dependent Type 2 diabetes patients were studied before and after 5 months of combined strength and endurance exercise training. Intramyocellular lipids (IMCL) and mitochondrial function were measured using ^{1}H and ^{31}P MRS, respectively, whereas blood glucose homeostasis was evaluated by plasma HbA_1c and fasting plasma glucose measurements. Although IMCL levels did not change and oxidative capacity did not improve, the exercise training did result in an increased maximal workload per kg body mass and a modest, though significant improvement of blood glucose homeostasis.

1676. Assesment of the Fat Content of Proximal Femur and Adjacent Muscle in Patients with Osteoarthritis

Trevor S. Ahearn[1], Thomas W. Redpath[1], Richard M. Aspden[1], James D. Hutchison[1], Scott I.K. Semple[1], David J. Knight[1]
[1]University of Aberdeen, Aberdeen, UK

Osteoarthritis has traditionally been thought of as a disease that erodes cartilage, however it has been proposed that osteoarthritis may be a systemic disorder with numerous precursors. One such precursor may be an altered lipid metabolism. In this abstract we have used the Dixon 2 point technique to measure lipid content in the proximal femur and adjacent muscle in 16 patients and 11 healthy volunteers. A significant difference in muscle lipid content was found. The bone lipid differences were insignificant. Further work is required to clarify these results using an age matched group.

1677. PPARδ Agonist Treatment Increases Skeletal Muscle Lipid Metabolism Without Altering Mitochondrial Coupling: An *In Vivo* Magnetic Resonance Spectroscopy Study

Dewen Yang[1], Warren M. Casey[1], Alan R. Olzinski[1], Carolyn Williams[1], Stephen C. Lenhard[1], Jeffrey J. Legos[1], Terrance C. Hawk[1], Susanta K. Sarkar[1], Steve J. Newsholme[1], Beat M. Jucker[1]
[1]GlaxoSmithKline, King of Prussia, Pennsylvania, USA

PPARδ nuclear receptor activation results in activation of genes involved in skeletal muscle fatty acid oxidation and mitochondrial uncoupling. In present study, we examined the temporal and dose dependent response of a selective PPARδ agonist (GW610742X) treatment on intramyocellular lipid (IMCL) content and mitochondrial energy coupling efficiency rat hindlimb by *in vivo* MRS. There was a dose dependent decrease in soleus muscle IMCL/tCr ratio that was consistent with an increase in relative fat oxidation rate. However there was no alteration in hindlimb mitochondrial coupling efficiency measured as the ratio of unidirectional ATP synthesis to TCA cycle flux.

1678. The Typical IMCL Distribution Pattern in Rat Tibialis Anterior Muscle Remains Unchanged After High-Fat Diet or Fasting

Henk M.M.L. De Feyter[1], Klaas Nicolay[1], Jeanine J. Prompers[1]
[1]Eindhoven University of Technology, Eindhoven, Netherlands

Recently, we showed a pronounced inhomogeneous distribution of intramyocellular lipids (IMCL) within rat tibialis anterior muscle (TA), which correlated with the typical fiber type regionalization. The present study reports on high-fat diet and fasting as dietary interventions to manipulate IMCL levels and the typical pattern of IMCL distribution in the rat TA muscle.Fasting did not induce any changes in the TA IMCL levels, in contrast to the high-fat diet, which increased the IMCL levels in the TA by ~100%. The typical IMCL distribution pattern, however, did not change, despite the dietary interventions.

1679. Magnetic Resonance Findings and Serum Creatine Kinase Measurements in Acute Human Skeletal Muscle Injury

Tatiana Zaraiskaya[1], Dinesh Kumbhare[2], Michael D. Noseworthy[1]
[1]McMaster University, Hamilton, Ontario, Canada; [2]St.Joseph's Healthcare, Hamilton, Ontario, Canada

Measurement of blood serum creatine kinase (CK) is a widely used biochemical test to grade/stage musculoskeletal pathology. This test suffers from lack of anatomical specificity and a brief diagnostic window as the CK level returns to normal well before healing is complete. Magnetic resonance imaging (MRI), in particular, diffusion tensor magnetic resonance imaging (DT-MRI) has been successfully used to detect changes in pathological muscle tissue due to injury. The eigenvalues and eigenvectors of the diffusion tensor provide information about local tissue anisotropy. In addition tissue fractional anisotropy (FA) and apparent diffusion coefficient (ADC) may be calculated, which are provide reliable estimation of altered cellular geometry. In this study, we applied DT-MRI to temporally characterize structural changes associated with thigh muscle biopsy. These measurements were correlated with standard clinical measurement of serum CK.

1680. Reproducibility of Muscle Metabolism Parameters in Children Determined by ^{31}P Spectroscopy

Jonathan Fulford[1], Neil Armstrong[1], Alan Barker[1], Deborah Welford[1], Joanne Welsman[1]
[1]University of Exeter, Exeter, Devon, UK

The study examined the reproducibility of ^{31}P-MRS muscle energetic measurements during incremental exhaustive exercise tests in children. Three progressive tests to volitional exhaustion (end exercise) were undertaken and dynamic changes in muscle phosphocreatine (PCr), inorganic phosphate (Pi) and intracellular pH determined. From plots of Pi/PCr and pH against work rate, intracellular thresholds (ITs) were determined. Coefficients of variation (CV) for Pi/PCr and pH ITs were 9.2 % and 9.9 %. End exercise CVs for pH and Pi/PCr were 1.0 % and 50.9 %, respectively. Thus, when examining exercise characteristics from children, IT values provide greater reliability than those obtained from end exercise.

1681. *In Vivo* Assessment by 31P-MRS of Skeletal Muscle Mitochondrial Function in Patients on Long-Term Home Parenteral Nutrition

Loris Pironi[1], Emil Malucelli[2], Cristina Guidetti[1], Caterina Tonon[2], Claudia Testa[2], Raffaele Lodi[2], Bruno Barbiroli[2], Stefano Iotti[2]

[1]Università di Bologna, Bologna, Italy; [2]University of Bologna, Bologna, Italy

We assessed the mitochondrial functionality in a group of patients affected by Chronic Intestinal Failure receiving long-term home parenteral nutrition (HPN) to understand to what extent the nutritional status affects the bioenergetics of skeletal muscle. Results show that patients may present an impairment in the skeletal muscle energy metabolism which, however is not related to the HPN infusion frequency, duration and energy content. We hypothesise that the mitochondrial dysfunction may be a consequence of the peroxidative stress due to intravenous lipid infusion leading to an increased concentration of reactive oxygen species.

1682. OPA1 Mutations Result in a Deficit of *In Vivo* Mitochondrial ATP Production in Patients with Autosomal Dominant Optic Atrophy

R Lodi[1], C Tonon[1], D Manners[1], E Malucelli[1], C Testa[1], M L. Valentino[1], P Barboni[2], S Schaich[3], S Schimpf[3], B Wissinger[3], V Carelli[1], B Barbiroli[1]

[1]Università di Bologna, Bologna, Italy, Italy; [2]Centro Salus, Bologna, Italy, Italy; [3]Molekulargenetisches Labor der Universitats-Augenklinik, Tubingen, Germany, Germany

Autosomal dominant optic atrophy (ADOA), the most common form of hereditary optic neuropathy, in most patients is due to a mutation within the OPA1 gene. OPA1 encodes a ubiquitously expressed GTPase related to dynamins, implicated in the formation and maintenance of mitochondrial network and morphology. Calf muscle oxidative metabolism was assessed by 31P-MRS in 15 patients with ADOA: 10 with mutations in the OPA1 gene and 5 without. Post-exercise PCr re-synthesis rate was significantly reduced in ADOA patients with OPA1 mutations but not in those without. Our *in vivo* results support the central role of mitochondrial dysfunction in the pathophysiology of OPA1-related ADOA

1683. Bioenergetic Defects in Muscles of Polymyositis Patients: Quantitative MRI and P-31 MRS Investigation

Jing Qi[1, 2], Nancy Josephine Olsen[1, 3], Kenneth John Niermann[1], Jane Harting Park[1]

[1]Vanderbilt University Medical School, Nashville, Tennessee, USA; [2]Nanjing Medical University, Nanjing, Jiangsu, People's Republic of China; [3]UT Southwestern Medical School, Dallas, Texas, USA

Polymyositis (PM) is an inflammatory disease characterized by severe proximal weakness, inflammation and/or fat infiltration in the muscles, and elevated serum levels of muscle enzymes. ATP and PCr levels in quadriceps muscles showed 43% and 38% decreases during rest, exercise and recovery as compared to normal controls. Moreover, PM muscles showed increased Pi/PCr ratios and ADP levels, as well as decreased phosphorylation potentials. These data indicated defects in mitochondrial oxidative phosphorylation and are consistent with clinical fatigue and reduced work capacity. MRI and P-31MRS were instrumental in the elucidation of the pathophysiological mechanisms for PM disease progression.

1684. Intersubject Differences in the Effect of Acidosis on Phosphocreatine Recovery Kinetics After Exercise

Jeanine J. Prompers[1], Henk M.M.L. De Feyter[1], Nicole M.A. van den Broek[1], Larry A.H.J. de Graaf[1], Klaas Nicolay[1]

[1]Eindhoven University of Technology, Eindhoven, Netherlands

^{31}P magnetic resonance spectroscopy can be used to measure oxidative capacity of skeletal muscle by determining the rate of phosphocreatine (PCr) recovery after exercise. However, cytosolic pH has a strong influence on the kinetics of PCr recovery and therefore at a low end-exercise pH PCr recovery might not be a good measure of oxidative capacity. We investigated the intersubject differences in the effect of acidosis on PCr recovery kinetics in healthy subjects. The pH dependence of the rate of PCr recovery differed among subjects and therefore no general formula can be applied to correct for differences in end-exercise pH.

1685. Mitochondrial Capacity and Oxygenation Measured by ^{31}P MRS and Near Infrared Spectroscopy in Healthy and Diabetic Subjects

Jonathan Fulford[1], Rajagopalan Sriraman[2], Claire Ball[2], John Tooke[2], Neil Armstrong[1], Angela Shore[2]

[1]University of Exeter, Exeter, Devon, UK; [2]Peninsula Medical School, Exeter, Devon, UK

^{31}P MRS and near infrared spectroscopy (NIRS) were undertaken during an exercise protocol to measure mitochondrial capacity and oxygenation status in healthy and diabetic subjects. Significant differences were obtained for the PCr recovery rate constant, tau and the NIRS rate constant, t_{NIR} following exercise cessation. Values of 38.9 ± 16.7 sec and 75.8 ± 42.5 sec ($p=0.014$) for tau and 0.48 ± 0.31 mins^{-1} and 0.21 ± 0.05 mins^{-1} ($p=0.033$) for t_{NIR}, were obtained for healthy and diabetic subjects respectively. This supports the hypothesis that diabetic subjects have impaired mitochondrial capacity (larger tau) and oxygenation (smaller t_{NIR}).

1686. A Quantitative Study of Bioenergetics in Skeletal Muscle Lacking Carbonic Anhydrase III by 31P Magnetic Resonance Spectroscopy

Min Liu[1], Glenn Walter[1], Neeti Pathare[1], Un-jin Zimmerman[2], Robert E. Forster[2], Krista Vandenborne[1]
[1]University of Florida, Gainesville, Florida, USA; [2]University of Pennsylvania, Philadelphia, Pennsylvania, USA

The purpose of this study was to provide *in vivo* experimental evidence for the biological importance of carbonic anhydrase (CA) III in energy metabolism of skeletal muscle by 31P magnetic resonance spectroscopy. Compared to wild type mice, no significant differences were observed in the resting phosphate concentration, PCr depletion and pH kinetics during electrical stimulation. However, CA III knock out mice showed a slower rate of PCr recovery. These data suggested that CA III may play an important role in maintaining the bioenergetics' capacity of skeletal muscle following high intensive stimulation.

1687. Direct Quantification of Lactate and High Energy Phosphates in Exercising Human Skeletal Muscle by Interleaved Localised ^{1}H DQF, ^{1}H- And ^{31}P STEAM

Martin Meyerspeer[1], Graham J. Kemp[2], Vladimir Mlynárik[1], Martin Kršňák[3], Julia Szendroedi[1], Michael Roden[4], Ewald Moser[1, 3]
[1]Vienna Medical University, Wien, Austria; [2]University of Liverpool, Faculty of Medicine,, Liverpool, UK; [3]Medical University of Vienna, Wien, Austria; [4]Hanusch Hospital Vienna, Wien, Austria

An interleaved ^{31}P- and ^{1}H MRS method is presented bywhich lactate accumulation and the accompanying changes in phosphorusmetabolites, pH and total creatine concentration can be monitored in calfmuscle during plantar flexion exercise and recovery. A localiseddouble quantum filter for suppression of lipids at 1.3 ppm is implementedwith short TE to account for orientation dependent dipolar coupling oflactate in anisotropic muscle tissue, enabling backcalculation of lactateabsolute quantification. We show good agreement between directly measuredlactate and that measured biochemically and inferred indirectly from^{31}P MRS data.

1688. Energy Metabolism in the Extensor Muscles of the Hand and Wrist of Musicians with Overuse Syndrome Studied by 31P-MRS

Angel Moreno-Torres[1], Jaume Rosset[2], Jesus Pujol[3], Silvia Fàbregas[2]
[1]Centre Diagnostic Pedralbes - Cetir Grup Mèdic, Esplugues de Llobregat, Spain; [2]Institut de Fisiologia i Medicina de l'Art, Terrassa, Spain; [3]Institut d'Alta Tecnologia, Barcelona, Spain

We sought to study the energy metabolism of the pathological hand and wrist extrinsic extensor muscles in musicians with overuse syndrome during a low-intensity exercise protocol by 31P-MRS. The results showed a Pi peak splitting into a high-pH and a low-pH component associated with the overuse condition, an incapacity to reach the Pi/PCr steady-state observed in control subjects and twofold higher values of such ratio in subjects showing Pi peak splitting compared with subjects who did not. Such results suggest that the extensor muscles in overuse patients have a greater reliance on glycolitic sources of energy and diminish oxidative performance.

1689. Skeletal Muscle Hydrogen Ion Concentration Stimulates Ventilatory Drive Through Direct Neural Pathways as Shown by ^{31}P MRS

Christian Thomas Farrar[1], Mirko I. Hrovat[1], Anne V. LaRaia[2], Gregory D. Lewis[2], Paul P. Pappagianopoulos[2], David M. Systrom[2]
[1]Massachusetts General Hospital, Charlestown, Massachusetts, USA; [2]Massachusetts General Hospital, Boston, Massachusetts, USA

^{31}P magnetic resonance spectroscopy (MRS) is used to measure intracellular pH (pHi) during exercise. The decreased pHi observed during exercise is correlated with measures of increased ventilatory drive even under conditions that restrict possible vascular mediated chemical signaling of central neural circuits. This suggests that skeletal muscle hydrogen ion concentration stimulates ventilatory drive in the normal human through direct neural pathways during exercise. This is in contrast to previous models of ventilatory control where arterial chemoreceptors were argued to be stimulated by increased blood concentrations of metabolites such as lactic acid.

MSK/Body: Spine, Bone, Muscle, Tendon, Misc.

Room 4E Tuesday 13:30 - 15:30

1690. Prediction of Bone Mechanical Properties Using Quantitative MRI

Eveliina Lammentausta[1], Mikko Antero Hakulinen[1], Ilkka Kiviranta[2], Jukka Sakari Jurvelin[1, 3], Miika Tapio Nieminen[4]
[1]University of Kuopio, Kuopio, Finland; [2]Jyväskylä Central Hospital, Jyväskylä, Finland; [3]Kuopio University Hospital, Kuopio, Finland; [4]Oulu University Hospital, Oulu, Finland

Human cadaveric patellae (N=14) were investigated. T2* relaxation time and MRI-derived apparent bone volume fraction were correlated with bone mineral density and apparent bone area fraction obtained from pQCT measurements. Moderate statistically significant linear correlations were found between MRI and pQCT parameters. The present results demonstrate the feasibility of MRI methods in evaluating trabecular bone density and structure. The prediction of bone composition and the mechanical properties can be further improved by combining two MRI methodologies developed for the assessment of trabecular bone.

1691. *In-Vivo* Micro-MRI of Trabecular Bone in the Ovariectomized Rhesus at 3T

Paul J. McCracken[1], Marie A. Holahan[1], Parker D. Mathers[1], Jacquelynn J. Cook[1], Donald B. Kimmel[1], Richard Hargreaves[1], Le T. Duong[1], Donald S. Williams[1]
[1]Merck Research Laboratories, West Point, Pennsylvania, USA

Osteoporosis is currently assessed using BMD measurements, which does not characterize the microarchitecture of trabecular bone, a better predictor of fracture risk. Trabecular bone ì-MRI was used to examine bone architecture (BVF, TrN, TrTh, TrSp) in sham operated and ovariectomized rhesus monkeys as a model for osteoporosis and compared to traditional BMD measurements. These ì-MRI studies on bone morphology in the OVX model suggest this technique may have value in assessing bone disease and in drug discovery and development. The data suggest ì-MRI can evaluate key parameters of bone structure extending our ability to assess bone pathology beyond BMD measurement.

1692. *In-Vivo* MR Microscopy of Trabecular Structure of a Human Finger Using a Small Permanent Magnet

Nachiko Iita[1], Katsumi Kose[1]
[1]University of Tsukuba, Tsukuba, Ibaraki, Japan

MR microscopy of a human finger was performed using a portable MR microscope equipped with a small (27cm x 18cm x 24cm) permanent magnet (1.0 T). 3D MR microscopic images of 192 micron cube voxels were acquired with a 3D spin-echo sequence. As a result, trabecular architecture of a middle finger was clearly visualized. It is concluded that the MR microscope developed in this study has a great promise as a bone examination tool.

1693. Trabecular Bone Structure and Anisotropy Studies Via Diffusion-Based MR

Eric Edward Sigmund[1], Hyungjoon Cho[1], Yi-Qiao Song[1], Steve Byrnes, [12], Peiqiu Chen, [12], Edward X. Guo[3], Truman Brown[3]
[1]Schlumberger-Doll Research, Ridgefield, Connecticut, USA; [2]Harvard University, Cambridge, Massachusetts, USA; [3]Columbia University, New York, New York, USA

We present MR diffusion characterizations of trabecular bone providing geometrical information (projected surface-to-volume ratio S/V) without high resolution imaging. The first technique employs magnetization decay due to diffusion in internal fields (DDIF), while the second measures time-dependent diffusion coefficients via applied field gradients. We found that both methods probe the projected S/V ratio for the full range of the samples. Two regimes of strength-geometry relationship were found: a weak regime with constant anisotropy, and a strong regime with increasing anisotropy. These geometrical parameters from the diffusion techniques are likely to be useful for clinical bone evaluation.

1694. Measurements of Bone Marrow Proton Relaxation Times and Trabecular Bone Volume Fraction (TBVF) of the Calcaneus for 100 Subjects Using a Compact MRI

Sadanori Tomiha[1], Nachiko Iita[1], Fumi Okada[1], Shinya Handa[1], Katsumi Kose[1]
[1]University of Tsukuba, Tsukuba, Ibaraki, Japan

Relaxation times (T1 and T2) of bone marrow protons and trabecular bone volume fraction (TBVF) of the calcaneus were measured for 100 female subjects. It was found and suggested that relaxation times of bone marrow protons have no correlation with TBVF and T1 has a definite correlation with elastic or mechanical property of the bone marrow. Distribution of T2 of bone marrow protons was relatively small compared with that of T1. As a result it was concluded that T2 correction scan could be skipped for adult healthy subjects, which could reduce the examination time to 50%.

1695. Pathophysiology of Bone Marrow Edema: Insights from Dynamic Contrast Enhanced MR Imaging

Edward W. Jung[1], Glenn A. Tung[1], Jonathan P. Dyke[2], Jonathan H. Lee[3], D McK Ciombor[1], Roy K. Aaron[1]
[1]Brown Medical School, Providence, Rhode Island, USA; [2]Weill Cornell Medical College, New York, New York, USA; [3]Columbia University Medical School, New York, New York, USA

Bone marrow edema (BME) has been associated with such diseases as osteoarthritis, traumatic injury, and osteonecrosis. In many cases, BME is associated with pain; however, the pathophysiology of BME is not known. Studies have demonstrated increased intraosseous pressure in BME that could lead to diminished blood flow and hypoxia, altered osteoblastic cytokine expression, and osteocyte necrosis. The pharmacokinetic modeling of bone perfusion using dynamic contrast enhanced-MR imaging (DCE-MRI) has been used to assess various bone pathology. In this study, we investigate perfusion kinetics of BME using DCE-MRI in a Dunkin-Hartley guinea pig model of osteoarthritis and in human subjects with BME.

1696. Contrast-Enhanced MRI with Fat Suppression Using T_1 Dispersion

Sharon E. Ungersma[1], Nathaniel I. Matter[1], Ross D. Venook[1], Albert Macovski[1], Greig C. Scott[1], Garry E. Gold[1], Steven M. Conolly[2]
[1]Stanford University, Stanford, California, USA; [2]University of California, Berkeley, Berkeley, California, USA

Prepolarized MRI can polarize a sample at one field, then allow the magnetization to evolve at an "evolutionary" field strength before imaging. Subtracting images collected with two different evolutionary field strengths yields contrast reflecting the slope of the T_1 vs. field dispersion curve. Gadolinium-based contrast agents have a significant slope to their T_1 dispersion curves. Because fat has a flat T_1 dispersion curve, subtracting images with different evolution field strengths will remove the fat signal. This technique can therefore be used to suppress fat signal while retaining contrast-enhanced signal, which is important for diagnosing bone marrow diseases such as osteomyelitis.

1697. Water and Fat Suppressed Proton Projection MRI (WASPI) of Rat Femur Bone with Sub-Millimeter Resolution

Yaotang Wu[1], Jerome L. Ackerman[2], David A. Chesler[2], Guangping Dai[2], Mirko I. Hrovat[3], Brian D. Snyder[4], Ara Nazarian[4], Melvin J. Glimcher[1]

[1]Children's Hospital, Boston, Massachusetts, USA; [2]Massachusetts General Hospital, Boston, Massachusetts, USA; [3]Mirtech Inc, Brockton, Massachusetts, USA; [4]Beth Israel Deaconess Medical Center, Boston, Massachusetts, USA

Rat bone specimens are widely studied by micro-CT, which only reflects the mineral content of bone, but not the solid matrix content (mostly collagen) of bone. The feasibility of water and fat suppressed proton projection MRI (WASPI) to image the solid matrix content of rat whole bone specimens has been explored, meeting the challenges of small sample size and the demanding sub millimeter resolution. Proton solid-bone-matrix-only MR images with 0.4 mm resolution of rat femur were obtained for the first time to the best of our knowledge. This method provides a non-invasive means to study bone matrix in small animals.

1698. Trabecular Bone Volume Fraction (TBVF) Measurements of 108 Young Children Using a Compact MRI

Sadanori Tomiha[1], Katsumi Kose[1], Naomi Omi[1], Kayoko Kamemoto[1]

[1]University of Tsukuba, Tsukuba, Ibaraki, Japan

Trabecular bone volume fraction (TBVF) of 108 young children (age:2-12) was measured using a compact MRI operated at 0.21 T. The children were measured while sitting on a chair with their heels in the small magnet. Although not a few subjects gave motion artifacts on the MR images, TBVF of 69 subjects was successfully calculated and clear positive correlations of TBVF with age, height, and weight were observed. As a result it is concluded that the compact MRI is a very useful and may be exclusive tool for bone density measurements of young children.

1699. MRI Characterization of Trabecular Bone Structure by Exploring Bone Microscopic Susceptibility Effect

Shing Chung Cheung[1], Jian Yang[1], Sai Kam Hui[1], Ed Xuekui Wu[1]

[1]The University of Hong Kong, Pokfulam, Hong Kong, People's Republic of China

Bone strength depends on bone mineral density (BMD) as well as properties related to bone quality, such as the microarchitecture of trabecular bone. Structural parameters, such as trabecular thickness, can also critically influence the mechanical competence and thus resistance to fracture of bone. Complex bone structure can induce microscopic susceptibility effect and alter the bone transverse relaxation properties, which are expected to become more prominent at high field. This study aims to examine such susceptibility effect at 3T and explore the possibility of using bone as an endogenous contrast agent to derive the structural information in human trabecular bone.

1700. Basic Clinical Imaging Techniques in Prepolarized MRI

Nathaniel I. Matter[1], Greig C. Scott[1], Ross D. Venook[1], Sharon E. Ungersma[1], Thomas Grafendorfer, [1,2], John M. Pauly[1], Albert Macovski[1], Steven M. Conolly, [1,2]

[1]Stanford University, Stanford, California, USA; [2]University of California at Berkeley, Berkeley, California, USA

Prepolarized MRI has the potential to produce diagnostic quality images of human extremities using an inexpensive pulsed magnet system consisting of water-cooled copper electromagnets. We adapted GRE, spin echo, RARE and STIR techniques to produce T_1- and fat suppressed T_2-weighted wrist images with clinical resolution and scan time on our 0.4T/0.13T prepolarized MRI system. We also demonstrated the ability of PMRI to image near metal objects *in vivo*.

1701. Prepolarized MRI: Reducing Susceptibility Artifacts Around Metal Orthopedic Implants Without Sacrificing Image Quality

Ross Venook[1], Nathaniel Matter[1], Meena Ramachandran[1], Sharon Ungersma[1], Garry Gold[1], Nicholas Giori[2], Albert Macovski[1], Greig Scott[1], Steven Conolly[3]

[1]Stanford University, Stanford, California, USA; [2]VA Palo Alto Healthcare System, Palo Alto, California, USA; [3]U.C. Berkeley, Berkeley, California, USA

Conventional MRI near implants suffers from severe artifacts that scale with scanner magnetic field. Prepolarized MRI (PMRI) is a new system that reduces artifacts near metal without sacrificing image quality. Here we present the first *in vivo* images that demonstrate PMRI images near metal orthopedic hardware and compare artifact and diagnostic image quality to images from a 1.5 T scanner.

1702. Combined Rotational/Translational Motion Correction Using Autofocusing for High-Resolution Trabecular Bone Images

Wei Lin[1], Glenn Ladinsky[1], Felix W. Wehrli[1], Hee Kwon Song[1]

[1]University of Pennsylvania Medical Center, Philadelphia, Pennsylvania, USA

In high-resolution trabecular bone imaging, motion correction is particularly relevant due to the small voxel size and the long scan time. It is also more challenging due to low image SNR (~9). In this work, combined rotational/translational motion correction using autofocusing was demonstrated in a large clinical data set. Results show consistent improvements in image quality as visually observed and as evidenced by the changes in the architectural parameters, when compared with translational motion correction only using a 2-D navigator echo technique.

1703. Using the Phase for MR Image Segmentation: Application to the Bone of the Knee

Pierrick Bourgeat[1], Peter Stanwell[2], Saad Ramadan[2], Sebastien Ourselin[1]

[1]BioMedia Lab, Autonomous Systems Laboratory, ICT Centre, CSIRO, Sydney, NSW, Australia; [2]University of Sydney, Sydney, NSW, Australia

This abstract considers the problem of tissue classification in 3D MRI by the mean of texture analysis. The main contribution is the use of the phase of the complex MR image, to derive texture features. Phase can give information about tissue interfaces and provide a good discrimination between the bone and the surrounding tissues but is usually not used because of the phase unwrapping problem. We present a method to extract textural information from the phase, without the need of phase unwrapping. The textural information extracted from the magnitude and the phase can be combined to improve tissue classification.

1704. Observation of Anisotropic Properties of Skeletal Muscle in MR Elastography Via a Needle Device

Queenie C. C. Chan[1], Geng Li[1], Richard L. Ehman[2], Edward S. Yang[1]

[1]The University of Hong Kong, Pokfulam, Hong Kong, People's Republic of China; [2]Mayo Clinic and Foundation, Rochester, Minnesota, USA

Magnetic Resonance Elastography (MRE) is a technique for measuring the mechanical properties of tissue. This *in vivo* human study was aimed to evaluate the anisotropic properties of skeletal muscle with an acoustic wave produced by an inserted moving needle, using MRE. The experiments showed that the elasticity of muscle is different when measured parallel and perpendicular to the fibers, confirming that skeletal muscle is mechanically anisotropic, and indicating the feasibility of measuring this independent tissue characterization parameter.

1705. MR-Elastography Reveals Skeletal Muscle Elasticity Changes in Patients with Hypogonadism Prior to Testosterone Substitution and After 6 Months

Katja Brauck[1], Stefan Maderwald[1], Craig Galban[1], Burkhard Herrmann[1], Frank Stock[1], Mark Ladd[1]

[1]University Hospital Essen, Essen, NRW, Germany

Men afflicted with hypogonadism have reduced fat-free mass and in some cases a loss in muscle strength. We hypothesize that muscle elasticity of the lower extremities changes in patients with hypogonadism after initiation of testosterone substitution. The shear modulus of the soleus muscle was measured non-invasively using MR elastography (MRE) at 0%, 5%, 10%, 15%, and 20% of the subject's maximum applied force. The results showed statistical differences in patients prior to testosterone substitution and after 6 months of treatment.

1706. The Effects of Deoxyhemoglobin and Flow Rate on R2' in Hindlimb Perfused Skeletal Muscle

Otto Alexander Sanchez[1], Bruce M. Damon[1]

[1]Vanderbilt University, Nashville, Tennessee, USA

Hindlimb perfusion of mice with bovine erythrocytes and Krebs-Henseleit buffer was use to study the effects of changing flow rate and blood oxygenation on relaxation parameters. Despite increasing flow rate, blood volume measured using VASO in the skeletal muscle did not increase. Arterio-venous oxygen difference was observed at higher flow rates, as well as a decrease in venous deoxyhemoglobin. This was significantly associated with lower R2'. This study confirms that in skeletal muscle tissue oxygenation is the most important parameter affecting relaxation parameters.

1707. Dual Gradient-Echo Imaging of Ischemia/Reperfusion in Skeletal Muscle

Bruce M. Damon[1], Jennifer L. Hornberger[1], Jane A. Kent-Braun[2]

[1]Vanderbilt University, Nashville, Tennessee, USA; [2]University of Massachusetts, Amherst, Massachusetts, USA

Brief MRI signal intensity transients have been reported following short isometric contractions and may be useful indices of vascular function in applied physiology and pathophysiology studies. While generally reflecting a muscle BOLD response, their exact physiological mechanism remains unclear. Using dual gradient-echo EPI acquisitions (TE/TE=1000/6, 46 ms) and near-infrared spectroscopy measurements of total hemoglobin and oxyhemoglobin saturation obtained during 5 min of suprasystolic blood pressure cuff inflation, we show here that short-echo signals reflect changes in blood volume and long-echo signals reflect changes in blood oxygenation.

1708. Idiopathic Inflammatory Myositis: Analysis of Magnetic Resonance Imaging Using IDL to Enhance Diagnosis

Charles Edward Hutchinson[1], Harriet Chaney[1], Robert C. Cooper[2], Judith E. Kilgallon[3]

[1]University of Manchester, Manchester, UK; [2]Salford Royal Hospital NHS Trust, Salford, UK; [3]Christie Hospital NHS Trust, Manchester, UK

MR of Myositis is less reliable than we expected. However by using image analysis based on the T1 weighted and STIR axial images it is possible to greatly improve the ability to use MR images to make the diagnosis of Myositis. The IDL based program has shown itself to be more reliable than any other technique for establishing the diagnosis of myositis.

1709. Fast Spatially Resolved Measurement of R2' and R2 of Each Component of Cancellous Bone Marrow and Correlation of R2' with Trabecular Bone Volume Fraction (BVF)

Catherine E. Jones[1], Jeremy F. Magland[1], Aranee Techawiboonwong[1], Felix W. Wehrli[1]
[1]University of Pennsylvania Medical Center, Philadelphia, Pennsylvania, USA

Bone - bone marrow susceptibility differences cause local perturbations of the magnetic field in the marrow spaces of cancellous bone and thus enhanced R2' (line broadening). A rapid and accurate method for measuring R2' would be useful for assessing cancellous bone density and architecture. Here, we show that by mapping the evolution of the signal before and after a phase-reversal RF pulse with the GESFIDE sequence, spectra can be generated as Fourier transforms of the descending and ascending portion of the signal. From the resulting linewidths R2' can be computed. Cancellous bone volume fraction was measured from high-resolution anatomic images was highly correlated with R2' obtained in this manner.

1710. Potential Metabolic Markers for Intervertebral Disc Pain

Kayvan Keshari[1], John Kurhanewicz[1], Serena Hu[1], Thomas Link[1], Jeffrey Lotz[1], Sharmila Majumdar[1]
[1]University of California, San Francisco, San Francisco, California, USA

Conventional imaging methods of assessing the painful, degenerated intervertebral disc focus solely on morphologic criteria. However, it is well-known that there is a poor correlation between morphologic findings and patient symptoms. The goal of this in vitro study is to utilize quantitative high-resolution magic angle spinning (HR-MAS) NMR spectroscopy as a tool to characterize potential metabolic markers. Relative to deformity patients, those with discogenic back pain demonstrate significantly lower Proteoglycan/Lactate and Proteoglycan/collagen breakdown ratios ($p<0.05$). Our results suggest that spectroscopic biochemical markers may characterize processes that correlate with discogenic pain.

1711. Dynamic Contrast Enhanced MR Imaging and ^{1}H MR Spectroscopy Study of Post Menopausal Osteoporosis

James Francis Griffith[1], David Yeung[1], Gregory E. Antonio[1]
[1]The Chinese University of Hong Kong, Shatin, Hong Kong, People's Republic of China

Osteoporosis is a disease characterized by reduced bone strength predisposing to fracture. MRI/MRS enables investigation of various aspects of bone physiology, namely marrow fat content and perfusion that may provide insight as to the pathogenesis of osteoporosis. The vertebral bodies and the erector spinae muscles are both supplied by the paired segmental lumbar arteries. If a reduction in bone marrow perfusion indices are related to general circulatory impairment or atherosclerosis in the aorta or main lumbar arteries, a similar reduction in perfusion indices is to be expected to occur in the erector spinae muscle. The aims of this study were: (a) to determine if comparable changes in vertebral marrow fat content and perfusion indices, reported in male subjects of differing bone density, are also seen in female subjects; (b) to examine the relationship between vertebral marrow and erector spinae muscle perfusion indices and bone density.

1712. Magic Angle MR Microscopy and T2 Quantification of Intervertebral Discs Highlights the 3-Dimensional Collagen Structure

Jeff Frank Dunn[1], Tad Foniok[2], John Robert Matyas[1]
[1]University of Calgary, Calgary, AB, Canada; [2]National Research Council, Calgary, AB, Canada

MRI with T2 quantification and MR microscopy was used to image bovine caudal discs at 9.4T. Imaging was done at two orientations with respect to Bo to maximize the magic angle effect. This was combined with water analysis, polarized light microscopy and photographs of cryosections. Annular striations were visualized that extended between the endplates. Cryosections showed similar structures. These changed T2 and signal with orientation, indicating organized collagen. Water was lower in the annulus. The nucleus showed texture suggestive of some degree of collagen organization. This MRI imaging showed novel information about the macroscopic structure of disc cartilage.

1713. Apparent Diffusion Coefficient Measurement for Evaluation of Vertebral Normal Variations in the Lumbar Spine

Youichi Sato[1], Eito Kozawa[1], Naoko Nishi[1], Takayuki Hoshino[1], Atsuko Heshiki[1]
[1]Saitama Medical School, Moroyama-chou, Saitama, Japan

The purpose of this study is to measure ADC value based on diffusion weighted MRI in the vertebrae of lumbar spine and evaluate location dependent. Forty-two patients were entered the study. DWIs were obtained with spine echo sequences and three b factors=0,300 and 800. Mean and SDs were calculated. The mean values of ADC were compared the Tucky-Kramer test using commercially available software. Significance was defined at p less than 0.01. The mean ADC for vertebrae were L1:L2:L3:L4:L5=34.8+/-22.3:26.3+/-18.1:32.1+/-16.3:37.3+/-15.7: 45.3+/-23.1 x 10-5 mm2/sec, respectively. The mean ADC for L5 was significantly higher than that of L1, L2, L3 and L4 ($p<0.01$).

1714. Normal Variations in the Vertebral Appearrence on Opposed-Phase MRI: We Need to Know Normal Bone Marrow Appearrence

Eito Kozawa[1], Waka Mizukoshi[1], Takayuki Hoshino[1], Atsuko Heshiki[1]
[1]Saitama Medical School, Moroyama-chou, Saitama, Japan

To demonstrate normal vertebral bone marrow in normal individually and analyze the distribution of red and yellow marrow. Twohundred fouty-five subjects were entered the study. All subjects were studied with 1.5 T MRI units. Bone marrow pattern of opposed-phase image was analyzed visually in the spine. Mean and SDs of age were calculated for each bone marrow pattern. The mean values were compared the Tukey-Kramer test using at p less than 0.01. Bone marrow signal patterns were classified into five types. Statistically significant differences ($p<0.01$) were seen on type 5 and other types by the Tukey-Kramer test ($p<0.01$).

1715. *In Vivo* MR T1rho Mapping in Lumbar Vertebral Discs at 3T: A Preliminary Study

Xiaojuan Li[1], Eric T. Han[2], Thomas M. Link[1], Sharmila Majumdar[1]
[1]University of California at San Francisco, San Francisco, California, USA; [2]GE Healthcare Global, Menlo Park, California, USA

Degenerative disc disease is one of the causes of lower back pain. It has been suggested that T1rho relaxation time may probe changes of proteoglycan in the early stages of disc degeneration. In this study we aimed to develop a sagittal T1rho mapping technique and to evaluate its *in vivo* imaging feasibility. Six volunteers were studied at 3T. The T1rho values range from 61.5 ms to 135.1 ms. The average coefficient of variation was 5.64% for median T1rho values in all 16 discs. A volunteer who complained of lower back pain showed lower T1rho in S1-L5 and L4-L5 discs.

1716. Characterization of Intervertebral Disc Degeneration with T1ñ Imaging

Chenyang Wang[1], Walter Witschey[1], Wade Johannessen[1], Sampreet Niyogi[1], Ari Borthakur[1], Dawn M. Elliott[1], Ravinder Reddy[1]
[1]University of Pennsylvania, Philadelphia, Pennsylvania, USA

We obtained T1ñ maps for nine cadaver spine specimens (mean age: 45, range: 22-66) at 1.5 T. The average T1r relaxation time and the range of observed T1r throughout the L2/L3 intervertebral disk nucleus pulposus are shown to decrease with specimen age. We show here the average T1r relaxation time and T1r range has strong linear correlation with age, with correlation coefficient R= 0.82 and R=0.87, respectively.

1717. Improved Assessment of Degenerative Intervertebral Discs with a Novel Magic Echo Mapping Technique

Walter R.T. Witschey II[1], C Wang[1], Brian K. Bronzo[1], Wade Johannessen[1], Dawn M. Elliott[1], Ravinder Reddy[1]
[1]University of Pennsylvania, Philadelphia, Pennsylvania, USA

The primary objective of this research was to develop a novel, quantitative relaxation mapping technique for monitoring the biochemical and structural changes that occur in human IVDs during DDD. We show that the magic echo pulse sequence is more sensitive to the hypointense region of the IVD than standard spin echo imaging techniques. 35% increase in T2 is shown among regions of the nucleus pulposus and may provide a quantitative measure of disc degeneration with improved dynamic range relative to T2 mapping.

1718. Quantitative 3D- $T1_\rho$ Weighted MRI of Lumbar Spine at 3.0T

Famory -. Niang[1], Sait Kubilay Pakin[1], Mark E. Schweitzer[1], Ravinder R. Regatte[1]
[1]New York University School of Medicine, New York, New York, USA

The purpose of the work was to demonstrate the feasibility of measuring 3D-T1rho MRI for *in vivo* quantitation of lumbar spine at a 3T clinical scanner. Spatial heterogeneity of T1*f*â among S1-L5, L5-L4 and L4-L3 locations were observed on all five volunteers and this may be due to the variations in biochemical content (mainly GAG), load distribution and water content. The preliminary results demonstrate that it is possible to quantify 3D-T1rho MRI of lumbar spine *in vivo* without exceeding the RF power deposition at 3T clinical scanner.

1719. *In Vivo* Assessment of Human Lumbar Disc Degeneration

Ari Borthakur[1], Joshua D. Auerbach[1], Wade Johannessen[1], Carol A. Dolinskas[2], Richard A. Balderston[2], Dawn M. Elliott[1], Ravinder Reddy[1]
[1]University of Pennsylvania, Philadelphia, Pennsylvania, USA; [2]Pennsylvania Hospital, Philadelphia, Pennsylvania, USA

Ten asymptomatic subjects between 40-60 years of age were imaged on a 1.5T Siemens clinical MR scanner using the spine array coil. Average $T_{1\rho}$ was measured from maps generated from a series of spin-locked MR images. $T_{1\rho}$ values were measured in region of interest in the center of the nucleus pulposus and the degenerative grade of each lumbar disc was assessed from conventional T_2-weighted images according to the Pfirmann classification system. $T_{1\rho}$ relaxation correlated significantly with disc degeneration ($r=-0.47$, $p<0.01$) and the values were consistent with a previous cadaveric study, in which correlation between $T_{1\rho}$ and proteoglycan content was demonstrated. This suggests a potential utility of $T_{1\rho}$ MRI as a non-invasive assessment of early disc degeneration *in vivo*.

1720. Quantitative Assessment of Clinical Stage of Aplastic Anemia by Using Dual Phase Chemichal Shift Sequence

Eito Kozawa[1], Waka Mizukoshi[1], Atsuko Heshiki[1]
[1]Saitama Medical School, Moroyama-chou, Saitama, Japan

Thirty-two aplastic anemia patients were included in this study with 1.5 T MR imaging units on TE=4.6 msec for in-phase and 2.3 msec for opposed-phase on dual phase chemical shift sequence. We compared the signal intensity ratios (SIRs) of mild type, moderate type and severe type of aplastic anemia patients in 32 patients. The mean SIRs of the three groups were significantly different according to the Tukey-Kramer test ($P < 0.05$). In-phase and opposed-phase dual phase chemical shift MR imaging help in predicting clinical stage of aplastic anemia.

1721. Diffusion Tensor Imaging of the Forearm's Nerves

Dan Stein[1], Arnon Neufeld[2], Moshe Graif[2], Yaniv Assaf[1, 2]
[1]Tel Aviv University, Tel Aviv, Israel; [2]Tel Aviv Sourasky Medical Center, Tel Aviv, Israel

In this study we have shown that successful imaging of the forearm's nerves can be achieved using DTI with the help of a sleeve filled with an inert liquid to abduct the air away from the forearm, thus reducing possible susceptibility induced artifacts. From the DWIs, FA, ADC, $D_{parallel}$, $D_{perpendicular}$ maps have been calculated and their values extracted and compared, proximally and within the carpal tunnel (CT). We found that at the CT FA values are elevated while the ADC, $D_{parallel}$ and $D_{perpendicular}$ values are significantly reduced. The presented work has potential applications in PNS diseases studies such as CT syndrome.

1722. Diffusion Weighted Magnetic Resonance Spectroscopy of Peripheral Nerve at 18.8T

Jacob Ellegood[1], Ryan T. McKay[1], Chris C. Hanstock[1], Christian Beaulieu[1]
[1]University of Alberta, Edmonton, Alberta, Canada

Diffusion anisotropy of water in neural tissue has been examined quite extensively, but compartment specific interpretation of diffusion characteristics is rather complex given that tissue water includes contributions from exchanging intra- and extracellular water. However, intracellular space can be probed selectively by measuring the diffusion characteristics of intracellular metabolites with diffusion weighted magnetic resonance spectroscopy (DW-MRS). The purpose of this study was to measure mean diffusivity and fractional anisotropy of different metabolites (N-acetyl aspartate, creatine and phosphocreatine, choline, glutamate, and taurine) in excised myelinated peripheral nerve of the frog at 18.8T.

1723. Tendon Imaging Using 3D Ultrashort TE Scanning

Jürgen Rahmer[1], Peter Börnert[1], Clemens Bos[2], Jan Groen[2], Giel Mens[2]
[1]Philips Research Laboratories, Hamburg, Germany; [2]Philips Medical Systems, Best, Netherlands

Ultrashort echo-time imaging (UTE) is a technique to image otherwise invisible short-T2 components in tendons, ligaments, etc.. 3D radial free-induction-decay (FID) sampling schemes can be used for volumetric UTE imaging with isotropic resolution. 3D image data allow the extraction of non-planar slices for the visualization of complex anatomies, e.g., the course of tendons in a joint. Conspicuity of tendon tissue can be improved by creating images that contain short-T2 components only, e.g., by forming a subtraction image between the short-TE FID and a later echo. This contribution demonstrates the potential of non-planar slice extraction from 3D UTE subtraction image data for tendon visualization in joints.

1724. Diffusion MRI of Denervated Skeletal Muscle for Early Diagnosis of Peripheral Nerve Injury

Eiko Yamabe[1], Toshiyasu Nakamura[1], Koichi Oshio[1], Yoshito Kikuchi[2], Hiroyasu Ikegami[1], Yoshiaki Toyama[1]
[1]School of Medicine, Keio University, Tokyo, Japan; [2]Saitama Municipal Hospital, Saitama, Japan

T2-weighted MR image of denervated muscle shows high signal intensity because of the increase of extracellular fluid (ECF). However, it takes certain amount of time before this change becomes visible. To resolve this problem, we detected the motion of ECF by measuring both T2 and apparent diffusion coefficient (ADC) using peripheral nerve injury model of rats. While T2 value increased gradually, ADC increased right after injury and decreased 5 days after injury. Four weeks after injury, ADC returned to normal, but T2 stayed at high value. Diffusion MRI can be a useful tool for early diagnosis of peripheral nerve injury.

1725. Determination of Anisotropic Velocity Profiles in Muscle Using Wave-Guide Constrained Magnetic Resonance Elastography

Anthony Joseph Romano[1], Philip B. Abraham[1], Stacie I. Ringleb[2], Phillip J. Rossman[2], Joseph A. Bucaro[1], Richard L. Ehman[2]
[1]Naval Research Laboratory, Washington, District of Columbia, USA; [2]Mayo Clinic, Rochester, Minnesota, USA

In this paper, we implement a previously introduced measurement and analysis approach labeled Wave-Guide Constrained Magnetic Resonance Elastography, which was developed for analyzing waves in guided structures such as muscle, white matter tracts, and neuronal fiber pathways, and which does not assume any a priori anisotropic model. We analyze the waves propagating along particular muscle fiber pathways utilizing space-wavenumber analysis and determine the zero-order anisotropic wave-guide velocities as functions of position. The approach will be demonstrated using a 3-D MRE *in vivo* measurement of a human calf muscle excited acoustically at 90 Hz.

1726. Fanctional Imaging of Muscle Contraction Caused by Electric Stimulation

Yasuharu Watanabe[1], Keisaku Kimura[2], Masahiro Umeda[2], Ichio Aoki[2], Masahiro Higuchi[2], Chuzo Tanaka[2], Shoji Naruse[3]

[1]Meiji School of Oriental Medicine, Suita, Osaka, Japan; [2]Meiji University of Oriental Medicine, Nantan, Kyoto, Japan; [3]Radiology, Kyoto, Kyoto, Japan

The purpose of this study is to visualize muscle contraction during electric stimulation using dynamic DWI. Seven healthy volunteers underwent MRI of the lower extremities with single shot diffusion EPIs and phase contrast gradient echo, respectively. In the results, the DWI signal intensity in the stimulated muscles was decreased by the electric stimulation. The speed of muscle shortening was estimated from the phase contrast images. However, muscle deformation was not enough to explain the signal decrease in DWI. We suggest that the signal reduction in DWI is caused by incoherent water movement in the tissue, caused by the intramuscular structure.

1727. Skeletal Muscle Degeneration and Regeneration Following Femoral Artery Ligation in the Mouse, as Monitored Using Diffusion Tensor Imaging

Anneriet M. Heemskerk[1], Glenda S. van Bochove[1], Maarten R. Drost[2], Gustav J. Strijkers[1], Klaas Nicolay[1]

[1]Eindhoven University of Technology, Eindhoven, Netherlands; [2]Maastricht University, Maastricht, Netherlands

The aim of this study was to evaluate quantitative diffusion MRI for monitoring tissue regeneration following femoral artery ligation in mice. The apparent diffusion coefficient (ADC) was increased and decreased after ligation at 3 and 10 days, respectively, whereas T2 was increased. Regional differences between the ADC and T2 response were observed which corresponded with histological findings of swollen cells and inflammation, respectively. Therefore, the data strongly suggest that the combination of DTI and T2 MRI enables the differentiation of the degenerative and regenerative phases in muscle regeneration.

1728. Dynamic Changes in DTI Eigenvalues and Eigenvectors Following Ischemia-Induced Skeletal Muscle Damage

Anneriet M. Heemskerk[1], Gustav J. Strijkers[1], Glenda S. van Bochove[1], Maarten R. Drost[2], Klaas Nicolay[1]

[1]Eindhoven University of Technology, Eindhoven, Netherlands; [2]Maastricht University, Maastricht, Netherlands

DTI-based characterization of skeletal muscle injury was performed which included detailed analysis of all the eigenvalues and eigenvectors. In normal situations the direction of the principal eigenvector is along the muscle fibers. However, it was demonstrated that upon injury the principal eigenvector may change its orientation to perpendicular to the fiber direction.

1729. Diffusion Tensor MRI for the *In Vivo* Determination of Skeletal Muscle Architecture in Two Ankle Angles

Anneriet M. Heemskerk[1], Gustav J. Strijkers[1], Maarten R. Drost[2], Klaas Nicolay[1]

[1]Eindhoven University of Technology, Eindhoven, Netherlands; [2]Maastricht University, Maastricht, Netherlands

The aim of this study was to detect changes in skeletal muscle architecture using DTI-based fiber tracking. To that end the architecture of the mouse tibialis anterior muscle was determined in two ankle angles. Significant changes in two important architectural parameters, i.e. pennation angle and physiological cross-sectional area, were observed, in accordance with expectations. We conclude that fiber tracking enables reproducible and reliable determination of muscle architecture. The DTI tools developed enable longitudinal studies on wild-type and transgenic mice to assess possible alterations in muscle architecture.

1730. Quantitative Characterization of Mouse Calf Muscle Degeneration After Left Sciatic Nerve Axotomy with Magnetic Resonance Imaging

Jiangyang Zhang[1], Gang Zhang[1], Susumu Mori[1, 2], Kazim A. Sheikh[1]

[1]Johns Hopkins University School of Medicine, Baltimore, Maryland, USA; [2]Kennedy Krieger Institute, Baltimore, Maryland, USA

Research on mouse models of human neuromuscular diseases requires imaging tools for characterization of changes in mouse muscle morphology. In this study, the progression of mouse calf muscle atrophy after left sciatic nerve axotomy was examined using *in vivo* 3D high resolution MRI followed by *ex vivo* 3D MRI. T2 changes in affected muscles were detected. Changes in individual muscle morphology were characterized based on segmentation and computational techniques. We show that the amount of atrophy in different muscles after complete denervation is not uniform.

1731. Effect of Skeletal Muscle T1 Changes on the Determination of Perfusion by Arterial Spin Labelling Combined to NMR Imaging

Céline Baligand[1], Didier Bertoldi[1], Claire Wary[1], Pierre G. Carlier[1]

[1]Institut de Myologie, Paris, France

Using simulations, we calculated the error introduced by possible changes in skeletal muscle T1 on the quantitation of perfusion by arterial spin labeling *in vivo*, we measured the T1 changes during reactive hyperemia in the mouse leg and corrected the ASL perfusion curves for these changes.

1732. Radiologic Evaluation of Hip Measurements: MR Versus X-Ray Correlation

Sarah Ann Shock[1], Andy I. Abeles[2], Mark E. Schweitzer[1], Robert Meislin[1], James Babb[1], Charbel Isaak[1]
[1]NYU, New York, New York, USA; [2]University of Missouri, Columbus, Missouri, USA

Evaluation of hip dysplasia has traditionally been performed using standardized measurements devoloped for use with plain film radiography. The accuracy in appyling these measurements to MR images is unknown. This study suggests that the center edge angle often assessed on pain films can be similarily applied to MR images.

1733. The Study of Ulnar Variance with High-Resolution MRI: Correlation with Triangular Fibrocartialge Complex and Cartilage of Ulnar Side of the Wrist

Hiroshi Yoshioka[1], Toshiokazu Tanaka[2], Teruko Ueno[3], John A. Carrino[1], Carl S. Winalski[1], Philipp Lang[1], Barbara N. Weissman[1]
[1]Brigham and Women's Hospital, Boston, Massachusetts, USA; [2]Mayo Clinic, Rochester, Minnesota, USA; [3]Iwate Medical School, Morioka, Iwate, Japan

The relationship between ulnar variance and TFCC or cartilage of the lunate and the ulnar head was examined in 93 subjects with high-resolution MRI using a 47-mm microscopy surface coil. Ulnar variance measured on MRI showed a strong correlation with TFCC thickness and TFCC angle, while there was no correlation between ulnar variance and cartilage thickness of lunate and ulnar head. High-resolution MRI with a microscopy coil is useful to evaluate the pathology of the ulnar side structures of the wrist associated with ulnar variance.

1734. The Value of MR Imaging Using Microscopy Coil in Evaluation of Finger Masses: Correlation with Pathologic and Surgical Findings

Jung-Ah Choi[1], In Sook Lee[2], Joo Han Oh[1], Heung Sik Kang[1]
[1]Seoul National University Bundang Hospital, Seongnam, Gyeongi-do, Republic of Korea; [2]Pusan National University College of Medicine, Pusan, Republic of Korea

The use of MRI with microscopy coil in evaluation of finger masses is investigated and determined to be useful in preoperative evaluation of finger masses.

1735. Joint Arthrography with MRI Image Overlay: Porcine Trials

Gregory Scott Fischer[1], Anton Deguet[1], Csaba Csoma[1], Russell H. Taylor[1], Laura Fayad[1], S James Zinreich[1], Gabor Fichtinger[1]
[1]Johns Hopkins, Baltimore, Maryland, USA

MR arthrography generally consists of two consecutive sessions: 1) an interventional session where a needle is driven to the joint space and contrast is injected under fluoroscopic or CT guidance and 2) a diagnostic MRI imaging session to visualize the distribution of contrast and evaluate the condition of the joint. We eliminate the separate radiologically guided needle insertion by performing those tasks on conventional high-field closed MRI scanners using a 2D augmented reality image overlay device to help guide needle placement procedures. Twelve trials have been performed on porcine cadaver shoulders in a 1.5T scanner with 100% of needles reaching the joint space on the first insertion attempt.

1736. Feasibility of MR Guided Direct Arthrography

Suzanne Wakeley[1], Martin J. Graves[1], Philip Bearcroft[1], Richard T. Black[1], Elzare van Rooyen[1], David John Lomas[1]
[1]University of Cambridge & Addenbrooke's Hospital, Cambridge, UK

Direct MR arthrography is increasingly used for diagnosing intra articular joint pathology but requires X-ray fluoroscopy for contrast medium introduction and therefore adjacent radiology facilities. This work develops a method for MR guided direct arthrography using in room control and display of the MR system combined with multi-sequence interactive MR fluoroscopy and demonstrates the feasibility in phantom and human joints.

1737. High SNR, Microscopic Imaging of Skin Lesions

Stefan Maderwald[1], Susanne C. Ladd[1], Mark E. Ladd[1], Frank Stock[1], Thomas Paul[1], Anja Liffers[2], Jörg Barkhausen[1], Thilo Gambichler[2], Harald H. Quick[1]
[1]University Hospital Essen, Essen, Germany; [2]Ruhr-University Bochum, Bochum, Germany

A surface RF receive coil dedicated for high-resolution *in vivo* MRI of human skin was designed to open up new perspectives for noninvasive imaging and characterization of human skin diseases. The coil provides high SNR, which allows performing high-resolution imaging within short examination times. *In vivo* measurements were successfully performed and evaluated in ten healthy volunteers and six patients with skin tumors, resulting in images with excellent quality. The imaging concept, combining a high-SNR RF coil and dedicated high-resolution imaging protocols, provides detailed anatomic display of normal human skin as well as skin lesions such as basaliomas and melanomas.

1738. Abnormal Post-Ischemic Reperfusion Patterns in the Skeletal Muscle of Serotonin Deficient Mice Identified by Arterial Spin Labeling Coupled to SSFSE Imaging

Didier Bertoldi[1], Yves Fromes[2], Cécile Fligny[3], Francine Cote[3], Guilan Vodjdani[3], Pierre G. Carlier[1]
[1]Institut de Myologie, Paris, France; [2]Institut de myologie, Paris, France; [3]UMR 7091, Paris, France

Post-ischemic hyperemia patterns were determined in leg skeletal muscles of mice using pulsed ASL combined to SSFSE imaging. In contrast to wild-type animals, serotonin deficient mice, obtained by knock-out of tryptophan-hydroxylase 1 gene, were unable to maintain prolonged post-ischemic vasodilatation. These results suggest that serotonin might play a role in the control of post-ischemic vasodilatation in the skeletal muscle.

1739. Application of 1H and 31P Single Point Imaging (SPI) of Teeth Using Silent Gradients

Marco L.H. Gruwel[1], Peter Latta[1], Marta Tanasiewicz[2], Vyacheslav Volotovskyy[1], Milos Sramek[3], Boguslaw Tomanek[1]
[1]NRC-CNRC, Winnipeg, MB, Canada; [2]Silesia Medical Academy, Katowice, Poland; [3]OAW Visualisierung, Vienna, Austria

Using 1and 31P Magnetic Resonance Imaging (MRI), microimages of teeth wereobtained with a silent Single Point Imaging (SPI) technique. Utilizing sine-shaped gradient ramps significantly reduced the sound pressure level of the experiment. 1H NMR showed distinct resonances from dentin and enamelwith a large difference in spin-spin and spin-lattice relaxation times. 3Dreconstruction of the data allowed for complete visualization of the object.

1740. 3D Visualisation of the Tooth Caries - Potential New Area for Biomedical Application of MRI

Wladyslaw Piotr Weglarz[1], Marta M. Tanasiewicz[2], Tomasz W. Kupka[2], Marco LH Gruwel[3], Cezary Przeorek[4], Andrzej Jasinski[1], Boguslaw Tomanek[3]
[1]Institute of Nuclear Physics, Krakow, Poland; [2]Medical University of Silesia, Bytom, Poland; [3]NRC Institute of Biodiagnostics, Winnipeg, Manitoba, Canada; [4]Comprehensive Cancer Centre, Gliwice, Poland

Spin-echo based MR imaging methods allow for high resolution visualization of the moisture entering into heavily decayed tooth, which are paths for microorganisms causing further damage of the tissue. SE method which gives the highest quality images is relatively slow, and typically require more than 1h time for data collection. With FSE method reasonable quality image is possible to obtain in less than 10 minutes time, which in principle can be considered as applicable *in vivo*. With these methods it is not possible to see any details in mineralized tooth's tissue, especially gradual decrease in tissue density in early stages of the caries development, as it can be seen from CT image. With this respect, the SPI method which allow for visualization of the mineralized tissue is more promising. Its limitations in obtaining high resolution images are long data collection and substantial rf deposition which has to be seriously considered in case of *in vivo* imaging. The potential solution is to compromise resolution. The silent version of the method used in this work overcome another typical disadvantage of SPI, i.e. high level of acoustic noise.

1741. NMR Study of Gallstones from Benign and Malignant Gallbladders

Madhulika Srivastava[1], [2], G. A. Nagana Gowda[2], Ajay Sharma[3], Ashish Gupta[2], V. K. Kapoor[3], C. L. Khetrapal[2]
[1]Department of Surgery, Lucknow, Uttar Pradesh, India; [2]Centre of Biomedical Magnetic Resonance, Lucknow, Uttar Pradesh, India; [3]Sanjay Gandhi Postgraduate Institute of Medical Sciences, Lucknow, Uttar Pradesh, India

Gallstones from chronic cholecystitis (CC) (n=23; benign), xanthogranulomatous cholecystitis (XGC) (n=11; benign), and gallbladder cancer (GBC) (n=11; malignant) were studied using 1H NMR to explore aetio-pathophysiology of gallbladder cancer. Significantly less cholesterol and high calcium were observed in GBC compared to CC ($p<0.0001$; $p<0.002$, respectively) or XGC ($p<0.0001$; $p<0.03$, respectively). Magnesium was high in GBC compared to CC ($p<0.002$). Striking differences in the gallstone composition of the malignant and benign patients that can be obtained rapidly from single pulse NMR methods may provide new insights into the aetio-pathophysiology of gallbladder cancer.

Cancer Models: Detection, Diagnoses, and Staging

Room 4E Tuesday 13:30 - 15:30

1742. Functional Colonoscopy Using Dark Lumen DCE-MRI

Christopher Chad Quarles[1], James Oliver McIntyre[1], David Lee Gorden[1], Martin Lepage, [1,2], Thomas Edison Yankeelov[1], Ronald R. Price[1], Lynn M. Matrisian[1], John Christopher Gore[1]
[1]Vanderbilt University, Nashville, Tennessee, USA; [2]University Sherbrooke, Sherbrooke, QC, Canada

Dark lumen-based colonoscopy has demonstrated reasonable success in detecting colon polyps. The purpose of this study is to develop a new approach to eliminate the colon lumen signal intensity while improving polyp detectability in Min mice using oil as a back-filling agent. The largest dimension of the smallest polyp detected was 1 mm. We also demonstrate the potential of dynamic contrast enhanced MRI to characterize the polyp microenvironment.

1743. Tumor-Antigen Targeted Imaging of Pancreatic Adenocarcinoma

Zdravka Medarova[1], Wellington Pham[1], Young Kim[1], Guangping Dai[1], Anna Moore[1]
[1]Massachusetts General Hospital, Charlestown, Massachusetts, USA

Previously, we have described a dual-modality targeted contrast agent (CLIO-EPPT) for tumor imaging based on specificity for the uMUC-1 tumor antigen. Important questions relevant to targeted imaging studies deal with the possibility of extracting molecular information about tumor biology. With our new studies, we established differential accumulation of CLIO-EPPT in orthotopic pancreatic tumors as compared to a scrambled-control nanoparticle (CLIO-SCR). We also demonstrated that chemotherapy did not lead to impaired probe uptake, which was in agreement with the lack of uMUC-1 downregulation. This investigation describes a molecular imaging approach, which is an early step towards *in vivo* molecular tumor profiling.

1744. A Dendrimer Based Contrast Agent for MR Imaging of Her-2/neu Receptors by a Three-Step Pretargeting Approach

Wenlian Zhu[1], Baasil Okollie[1], Zaver M. Bhujwalla[1], Dmitri Artemov[1]
[1]Johns Hopkins University, Baltimore, Maryland, USA

Herceptin, an FDA approved humanized MAb for the treatments of Her-2/neu positive breast cancer, is also used to selectively deliver anticancer or image agents to Her-2/neu overexpressing tumor cells. Pretargeting approaches that separate the delivery of antibody and anticancer or imaging agents may further reduce toxicity by avoiding the long half-life of the antibody while an avidin/streptavidin-biotin system is used to link the antibody and agents. We have prepared a PAMAM dendrimer generation 4 based DTPA-Gd conjugate for MRI studies. MR enhancement by a three-step pretargeting approach of Her-2/neu positive BT-474 breast tumors in vitro and *in vivo* are shown.

1745. Characterization of Rat Glioma Models by Magnetic Resonance Angiography

Sabrina Doblas[1], Yasvir Tesiram[1], Debra Saunders[1], Quentin Pye[1], Preeti Kshirsagar[1], Rheal A. Towner[1]
[1]Oklahoma Medical Research Foundation, Oklahoma City, Oklahoma, USA

Malignant gliomas, which are the most common primary brain tumors, still lead to poor prognosis because of the difficulty of an early and accurate diagnosis. One of the problems is that the presence of new blood vessels, which is an absolute requirement for tumor growth and spread, must be well documented. Indeed, it has been shown that a dramatically increased angiogenesis is characteristic of high-grade gliomas. In this point of view, magnetic resonance angiography (MRA) can be used as a non-invasive tool to assess angiogenic behavior of gliomas and perhaps provide better diagnosis. We conclude from our study that specific angiogenic patterns of different glioma models (C6, F98 and 9L/LacZ) can be revealed by MRA, which could be a useful method to differentiate gliomas in human diagnosis.

1746. Dynamic Contrast Magnetic Resonance Imaging Detects Premalignant High-Grade Dysplasia in Epithelial Carcinogenesis

Joel Richard Garbow[1], John Engelbach[1], Krista Olson[1], Jeffrey Arbeit[1]
[1]Washington University, St. Louis, Missouri, USA

The ability to study and biologically characterize high-risk pre-malignant epithelial lesions of internal organs will be a tremendous boon to therapy and prevention of invasive malignancies. Here we used dynamic contrast enhanced magnetic resonance imaging (DCE-MRI) to determine differential microvascular biology associated with neoplastic progression in a unique transgenic mouse model of multistage cervical carcinogenesis. Vascular permeability (KPS), measured at the cervical transformation zone using DCE-MRI, is approximately 50% greater in transgenic animals displaying high-grade squamous epithelial dysplasia compared with non-transgenic animals. Sub-epithelial microvascular area, measured from MECA32 immunoperoxidase stained tissue sections, was similarly elevated in the transgenic animals.

1747. Early Detection of Prostate Neoplasm Using Pixel-By-Pixel R1 Mapping Following Gd(ABE-DTTA) Administration in TRAMP Mice

Pal Kiss[1], Ada Elgavish[1], Isam-Eldin A. Eltoum[1], Pal Suranyi[1], Huadong Zeng[1], Tamas Simor[1], Balazs Ruzsics[1], Gabriel A. Elgavish[1]
[1]University of Alabama at Birmingham, Birmingham, Alabama, USA

Detection of prostate cancer in the early, prostate intraepithelial neoplasia (PIN) phase would be important for clinical decision making. In our study, ceMRI was carried out following Gd(ABE-DTTA) administration in a TRAMP mouse model. Pixel-by-pixel R1 mapping was used to differentiate prostate areas with different pathology grades. We found correlation between the areas with significantly different R1 enhancement and areas with different PIN grades as determined by the histological analysis. R1 was found more enhanced in normal areas and areas with low grade mouse PIN (mPIN) versus lower enhancement in areas with high grade mPIN and early adenocarcinoma.

1748. Improved Prostate Cancer Detection Using DCE-MRI and Probability Maps

Xinrui Huang[1], Qiang Wang[2], Yufeng Xu[3], Xiaoying Wang[3], Shanglian Bao[1]

[1]The Key Lab of Medical Physics and Engineering,Peking University, Beijing, People's Republic of China; [2]The Medical School of Peking University, Beijing, People's Republic of China; [3]The First Hospital of Peking University, Beijing, People's Republic of China

Dynamic contrast-enhanced magnetic resonance imaging (DCE-MRI) has been used for the assessment of prostate diseases by examining the kinetic properties of MR time-intensity curve (TIC) variations. The feature parameters to describe the enhancement of TIC are usually evaluated and referenced separately. We combined these parameters with logistic regression to determine the statistical probability model on whether a prostate region is cancerous or not and improved detection of prostate cancer by computing the prostate cancer probability maps.

1749. Tumor Growth with Anisotropic Diffusion

Ashok Kumar[1], Alma Gregory Sorensen[1]

[1]Martinos Center for Biomedical Imaging, Charlestown, Massachusetts, USA

Growth of brain tumors such as gliomas may be modulated by anisotropic brain structures. A computational and mathematical method to simulate the growth of tumor fronts using a Hamilton-Jacobi equation for moving fronts derived from a reaction-diffusion model and Level-Set methods is proposed. Tumor fronts are evolved computationally from the tumor outlines (obtained from contrast enhanced T1 images) using DTI diffusion tensor data. Evolution of tumors driven by full diffusion tensor creates more complex shapes and tends to follow the white-matter fibers much more than a simple isotropic evolution based on trace ADC.

1750. Longitudinal MR Studies of Human Mammary Carcinoma Cell Brain Metastasis in Nude Mice at 7 Tesla

Rui Simoes[1], [2], Antonio Martinez[3], Sebastián Cerdán[4], Angels Sierra[3], Carles Arús[1]

[1]Universitat Autònoma de Barcelona, Barcelona, Spain; [2]Universidade de Coimbra, Coimbra, Portugal; [3]Institut de Recerca Oncològica, Barcelona, Spain; [4]Instituto de Investigaciones Biomédicas Alberto Sols UAM-CSIC, Madrid, Spain

Brain metastasis were induced in BALB/c nude mice by intracarotid injection of MDA-MB-435 human mammary carcinoma cells and its progression characterized *in vivo* by using different MR approaches: T2, CE-T1, diffusion imaging and single voxel spectroscopy at 35 and 136 ms echo time. Brain Metastasis developed in 5 out of 7 animals studied with an heterogeneous kinetics. MRS pattern changes indicated replacement of normal brain parenchyma by aggressive tumour cells while automated pattern recognition analysis showed the potential of this approach as a non-invasive tool for tumour staging and grading in animal models.

1751. High Field MR Imaging of Pre-Invasive Pancreatic Carcinoma in a Transgenic Mouse Model

Palamadai Nilakantan Venkatasubramanian[1], Paul Grippo[2], Richard Knop[3], Alice Wyrwicz[1]

[1]ENH Research Institute, Evanston, Illinois, USA; [2]Northwestern University School of Medicine, Chicago, Illinois, USA; [3]Evanston Northwestern Healthcare, Evanston, Illinois, USA

The EL-Kras transgenic mouse develops premalignant lesions of pancreatic cancer, known as PanINs and is therefore a model of early pancreatic cancer progression. We have imaged pancreas from EL-Kras and normal mice *ex vivo* at high field strength. Our results show that PanINs in EL-Kras mouse pancreas could be differentiated from normal pancreas based only on classical endogenous contrast without the use of external contrast agents.

1752. Characterization and Early Detection of Liver Metastasis by fMRI

Yifat Edrei[1], Eitan Gross[1], Eli Pikarsky[1], Eithan Galun[1], Rinat Abramovitch[1]

[1]Hadassah Hebrew University Medical Center, Jerusalem, Israel

Liver metastases are the major cause of death from colorectal carcinoma. Using fMRI, liver arterial/portal perfusion is detected by CO_2-reactivity, while vessel density by the response to O_2. Currently, we implemented this method in liver metastasis model. In healthy livers, the response to CO_2 was negative and to O_2 positive. In tumors, the magnitude of the response was significantly reduced. These results suggest a higher arterial/portal ratio and decrease in vascularity in metastasis. Using our inhalation approach, we detected areas with SI change 2-4 days earlier than in T_2W-images. This method provides a tool for earlier diagnosis of liver tumors.

1753. Semi-Automated Lymph Node Staging Using LN-MRI

Gozde Unal[1], Greg Slabaugh[1], Bernd Wachmann[1], Thomas Fuchs[1], Tong Fang[1], Robert Krieg[2], Ravi Seethamraju[2], Mukesh Harisinghani[3], Ralph Weissleder[3]

[1]Siemens Corporate Research, Princeton, New Jersey, USA; [2]Siemens Medical Solutions, Erlangen, Germany; [3]Massachusetts General Hospital, Boston, Massachusetts, USA

The current state of lymph node staging in MR images is a laborious and time consuming task due to the large number of data to be validated. A semi-automated approach can increase the efficiency and reduce the amount of time for this task. We present a method which combines advanced segmentation and classification methods to facilitate this goal.

1754. Multiparametric Imaging of Tumor Boundaries Using Linear Discriminant Analysis

Marina Benito-Vicente[1], Pilar López-Larrubia[1], Laura Barrios[2], Patricia Sanchez-García[1], Sebastián Cerdán[1], María Luisa García-Martín[1]

[1]Instituto de Investigaciones Biomédicas "Alberto Sols" CSIC/UAM, Madrid, Spain; [2]CSIC, Madrid, Spain

We provide a new method for tumor boundary evaluation based on the combination of T2, ADC and % MT (Magnetization Transfer) maps rather than on the use of the individual parameter maps. Rats bearing C6 gliomas were subjected to T2, ADC and % MT imaging providing the corresponding maps. Regions containing proliferative tumor, edema and contralateral healthy brain were selected and analyzed individually pixel by pixel, or combined using linear discriminant analysis (LDA). LDA improved the classifications of individual parameters allowing the identification of tumor tissue in 98.9 %, edema in 93.5% and healthy brain in 91.9% of the cases.

1755. Comparison of Spectral Spatial PRESS with TE Averaged PRESS in Breast Choline Detection

Fei Sun[1], Lu Hong[2], Guang Cao[3]

[1]GE Healthcare China, Beijing, People's Republic of China; [2]Tianjin Cancer Hospital, Tianjin, People's Republic of China; [3]GE Healthcare China, Hong Kong, People's Republic of China

Dual band Spectral Spatial PRESS (SS-PRESS) was compared with TE averaged PRESS (J-PRESS) in 72 breast lesions and SS-PRESS demonstrates advantages in prescan successfulness and better SNR than J-PRESS. While the sensitivity and specificity of SS-PRESS was also tested in a 153-breast lesion group. If limited the lesion type to 1.5cm and upper, the sensitivity of SS-PRESS reached 76.7% and specificity is 85.4%. SS-PRESS scan can also be automatically reconstructed by host scanner and exhibit clinical convenience.

1756. Fatty Acid Speciation by NMR Spectroscopy and Potential Methods for Liver Cancer Diagnaosis

Yasvir A. Tesiram[1], Debra Saunders[1], Jeff Griffitts[1], Rheal A. Towner[1]

[1]Oklahoma Medical Research Foundation, Oklahoma City, Oklahoma, USA

We show that using a modified HSQC pulse sequence, at least one peak from the projection of the indirect dimension (13C) can be unambiguously assigned to a fatty acid compound. Incorporating such selectivity into CSI will yield an accurate method for liver cancer diagnosis.

1757. 1H-MR Spectroscopy of the Prostate at 3.0 T with a Phase-Array Surface Coil

Frank Traeber[1], Nuschin Morakkabati-Spitz[1], Ursula Jaeger[1], Mike P. Wattjes[1], Patrick Bastian[1], Alexander Schmitz[1], Jürgen Gieseke[2], Okan Guer[1], Wolfgang Block[1], Renate Bloemer[1], Hans H. Schild[1]

[1]University of Bonn, Bonn, Germany; [2]Philips Medical Systems, Best, Netherlands

Purpose of our study was to optimize acquisition parameters of single-voxel and of spectroscopic imaging sequences for 1H-MRS of the prostate at 3.0 T, and to test the feasibility of highfield MRS without use of endorectal coils in patients suspicious for prostate cancer. Almost in-phase detection of the strongly coupled citrate spins revealing a quadruplet structure at 3.0 T was achieved using TE 132 ms. The summed signals from choline, polyamines, and creatine were related to the citrate intensity, and this metabolic ratio discriminated cancer from benign hyperplasia with 67% sensitivity and 86% specificity in 26 biopsy proven cases.

1758. Line Scan Echo Planar Spectroscopic Imaging of the Prostate at 3T: Feasibility Study

Yasushi Kaji[1], Kagayaki Kuroda[2], Ryo Sugihara[1], Kazuro Sugimura[1]

[1]Kobe Univ. Graduate School of Medicine, Kobe, Hyogo, Japan; [2]Institute of Biomedical Research and Innovation, Kobe, Hyogo, Japan

A line scan echo planar spectroscopic imaging (LSEPSI) sequence is an attractive method which can rapidly give us the metabolites information. The lack of any phase encoding and the gsnapshoth sampling of individual columns both help minimize motion ghosting artifacts. In this study, we generated 1D CSI acquisitions of the prostate tissue columns and assessed the characteristics of obtained data at 3T. Citrate resonance of the prostate could be identified *in vivo*. In addition, the spatial resolution was good to separate the tissue border.

1759. Differentiation of Low from High Grade Oligodendrogliomas by 1H Magnetic Resonance Spectroscopy Imaging and Perfusion Weighted Imaging

Sanjeev Chawla[1], Sumei Wang[1], John H. Woo[1], Jiongjiong Wang[1], Donald M. O' Rourke[1], Kevin Judy[1], Michael S. Grady[1], Ranald L. Wolf[1], Elias R. Melhem[1], Harish Poptani[1]

[1]University of Pennsylvania, Philadelphia, Pennsylvania, USA

The study was performed to ascertain whether combined use of CASL and 1H-MRSI can differentiate low from high-grade oligodendrogliomas. 1H-MRSI and CASL imaging was performed on eleven patients. Average CBF from solid parts of the tumor were normalized to contralateral white matter and assigned as CBFT/W. Absolute concentrations of metabolites from these regions were normalized to contralateral white matter. Although CBF T/W could not differentiate between high-grade and low-grade oligodendrogliomas, 1H-MRSI exhibited high ChoT/W and Lip/Lac T/W in high grade-III tumors than grade-II oligodendrogliomas suggesting a complementary role of the two MR techniques.

1760. Dynamic Contrast-Enhanced MR and Proton MR Spectroscopic Imaging in Localizing Prostate Cancer

Jurgen J. Futterer[1], Tom W.J. Scheenen[1], Stijn W.T.P.J. Heijmink[1], Christina A. Hulsbergen-van de Kaa[1], J. Alfred Witjes[1], Arend Heerschap[1], Jelle O. Barentsz[1]
[1]UMCN, Nijmegen, Gld, Netherlands

The performance of localizing prostate cancer (PCa) throughout the whole prostate of PCa patients with T2-weighted MR imaging, dynamic contrast-enhanced MR imaging (DCE-MRI) and quantitative three-dimensional proton MR spectroscopic imaging (MRSI) was prospectively determined using whole mount section histopathology as the reference standard. Two readers evaluated 34 PCa patients and calculated the localization performance, ROI based (14 in every prostate) receiver operating characteristics (ROC) and kappa statistics, concluding that the localization performance in PCa patients of T2 weighted MR imaging improves significantly by using either DCE-MRI or MRSI.

1761. Imaging Findings of Castleman Disease of the Abdomen and Pelvis

Liangping Zhou[1], Weijun Peng[1], Peihua Wang[1], Bei Zhang[2], Yubao Guan[3], Kangrong Zhou[4]
[1]Cancer Hosipital of Fudan University, Shanghai, People's Republic of China; [2]Shanghai Ruijin Hosipital, Shanghai, People's Republic of China; [3]1stHospital of Guangzhou College, Guangzhou, People's Republic of China; [4]Zhongshan Hosipital of Fudan University, Shanghai, People's Republic of China

10 patients with pathologically proved Castleman disease in the abdomen and pelvis were examed with CT & MRI.The lesions were divided into those with localized (n=9) and disseminated (n=1). The pathologic subtypes of all 9 cases of localized disease were hyaline vascular type.The most suggestive CT & MRI features of localized & hyaline vascular type of Castleman disease include a single larger mass or a single dominant mass with small satellite nodules, enhanced sharply with the attenuation similar to large arteries and areas of central lower radial attenuation with in the larger tumor after intravenous injection of contrast media.The pathologic subtypes of 1 cases of disseminated disease were plasma cell type which manifested as several well-defined nodules lied in the retroperitoneal zone that enhanced sharply with the attenuation similar to large arteries after intravenous injection of contrast media.

Cancer Models: Predicting and Monitoring Therapy Response with MRI

Room 4E Tuesday 13:30 - 15:30

1762. Characterization of the Tumor Micro-Environment After Administration of Glucocorticoids to Understand Their Radiosensitization Effect

Nathalie Crokart[1], Bénédicte F. Jordan[1], Christine Baudelet[1], Gregory O. Cron[1], Julie Hotton[1], Kim Radermacher[1], Vincent Gregoire[1], Nelson Beghein[1], Philippe Martinive[1], Olivier Feron[1], Bernard Gallez[1]
[1]Université Catholique de Louvain, Brussels, B, Belgium

We hypothesized that glucocorticoids may enhance tumor radiosensitivity by increasing tumor oxygenation via inhibition of mitochondrial respiration. EPR oximetry studies indicate an early increase in tumor oxygenation after administration of hydrocortisone, dexamethasone and prednisolone. At the time of maximal reoxygenation, the blood flow (monitored with DCE-MRI) was decreased, and oxygen consumption by tumor cells (measured using X-Band EPR) was decreased. We observed a longer regrowth delay when irradiation was combined with hydrocortisone compared with radiation alone. This effect is not due to a direct radiosensitization effect of hydrocortisone on tumor cells as evaluated by survival clonogenic assay.

1763. Botulinum Toxin Potentiates Cancer Radiotherapy and Chemotherapy

Réginald Ansiaux[1], Christine Baudelet[1], Greg O.Cron[1], Jérôme Segers[1], Chantal Dessy[1], Philippe Martinive[1], Julie De Wever[1], Julien Verrax[1], Valérie Wauthier[1], Nelson Beghein[1], Vincent Grégoire[1], Pedro Buc Calderon[1], Olivier Feron[1], Bernard Gallez[1]
[1]Catholic University of Louvain, Woluwe, Brussels, Belgium

To increase the efficacy of anti-cancer treatments, efforts must be made to find new strategies for transiently opening the tumor vascular bed in order to alleviate tumor hypoxia and improve the delivery of chemotherapeutic agents. We hypothesized that Botulinum Neurotoxin type A (BoNT-A) could lead to inhibition of the neurogenic contractions of tumor vessels and therefore improve tumor perfusion and oxygenation. *In vivo* EPR and DCE-MRI have been performed to assess changes in tumor oxygenation and perfusion status after BoNT-A administration. This characterization of the tumor micro-environment has been used to guide treatment schedule with radiation therapy and chemotherapy.

1764. Botulinum Toxin Increases Tumor Uptake of Gemcitabine Chemotherapy as Measured with Fluorine Spectroscopy

Greg O. Cron[1], Nelson Beghein[1], Réginald Ansiaux[1], Bernard Gallez[1]
[1]Catholic University of Louvain, Brussels, Belgium

Fluorine-19 MR spectroscopy (FMRS) may be used to study non-invasively the kinetics of fluorinated chemotherapy agents in tumor. The purpose of this FMRS work was to investigate how Botulinum neurotoxin type A affects the uptake and elimination of the chemotherapy drug gemcitabine in mouse tumors. The results show that the initial uptake of gemcitabine in treated tumors was 40% higher than in controls ($p<0.001$). No statistically significant difference in elimination time constant was observed. The total quantity of gemcitabine to which the tumor is exposed should therefore be ~40% higher in treated tumors compared to controls.

1765. Blood Flow Increase in 9L Brain Tumors in Response toRadiation Therapy and Chemotherapy as Detected by Arterial Spin Labeling MRI

Amandeep Salhotra[1], Phillip Zhe Sun[1, 2], Peter C.M. van Zijl[1, 2], Zaver Bhujwalla[1], Bachchu Lal[2], John Laterra[1, 2], Jinyuan Zhou[1, 2]

[1]Johns Hopkins University, Baltimore, Maryland, USA; [2]KKI, Baltimore, Maryland, USA

The response to tumor therapies was assessed in a rat model of 9L gliosarcoma through changes in the MRI relaxation times, apparent diffusion coefficients, and blood flow, in which blood flow was quantified by a non-invasive arterial spin label technique. The preliminary results show that the sensitivity of these MRI measures in response of therapy depends on applied therapeutic method and tumor age. There is a persistent substantial increase in blood flow in the region of treated tumors for both radiotherapy and chemotherapy.

1766. Carbogen Breathing Differentially Enhances Blood Plasma Volume and 5-Fluorouracil Uptake in Two Murine Colon Tumor Models with Distinct Vascular Structures

Hanneke van Laarhoven[1], Giulio Gambarota[1], Jasper Lok[1], Martin Lammens[1], Yvonne Kamm[1], Theo Wagener[1], Cornelis Punt[1], Albert van der Kogel[1], Arend Heerschap[1]

[1]University Medical Centre Nijmegen, Nijmegen, Gld., Netherlands

Using USPIO enhanced MRI, 31P MRS, and 19F MRS we measured *in vivo* the effect of carbogen breathing on tumor blood plasma volume, pH and energy status, as well as the effect on 5-fluorouracil (FU) uptake and metabolism in C38 and C26a colon tumors that differ in their vascular structure. Carbogen breathing decreased extracellular pH, increased tumor blood plasma volume and increased FU uptake in both tumorlines, but most significantly in the C38 tumor. Systemic toxicity of FU was also enhanced.

1767. Application of Multiple-Quantum-Filtered 23Na MRI to Monitor Chemotherapeutic Response in RIF-1 Tumors

Andriy Babsky[1], Hong Zhang[1], Shahryar K. Hekmatyar[1], Gary Hutchins[1], Navin Bansal[1]

[1]Indiana University, Indianapolis, Indiana, USA

The effects of 5-fluorouracil on radiation-induced fibrosarcoma (RIF-1) tumors were monitored by *in vivo* single-quantum (SQ) and triple-quantum-filtered (TQF) ^{23}Na MRI, ^{1}H MRI, and PET to evaluate changes in total tissue and intracellular Na^+ content, water apparent diffusion coefficient (ADC), and FDG uptake, respectively. *In vivo* MRI measurements showed correlated increases in SQ ^{23}Na signal intensity (SI) and water ADC after therapy, reflecting an increase in extracellular space. TQF ^{23}Na SI and FDG uptake was lower in treated tumors compared with controls, suggesting decreased glycolysis and/or a decreased cell density in treated tumors.

1768. Evolution of the Tumor Oxygenation and Perfusion at the Early Stage of the Treatment with SU5416, an Inhibitor of Flk-1 Tyrosine Kinase

Réginald Ansiaux[1], Christine Baudelet[1], Greg O.Cron[1], Philippe Martinive[1], Julie De Wever[1], Vincent Grégoire[1], Olivier Feron[1], Bernard Gallez[1]

[1]Catholic University of Louvain, Woluwe, Brussels, Belgium

The transient normalization of the tumor vasculature at the early stage of an anti-angiogenic treatment has been described for several antiangiogenic agents. Our purpose was to assess the validity of this paradigm in the case of an inhibitor of Flk-1 tyrosine kinase, SU5416. EPR oximetry study indicates an early reoxygenation of the tumor. Surprisingly, however, this reoxygenation was not correlated to an increase in perfusion (as shown by DCE-MRI), but more likely due to an inhibition of oxygen consumption by the tumor cells. Consistently, we found that SU5416 potentiates the response to radiotherapy, but not to chemotherapy.

1769. Comprehensive Magnetic Resonance Monitoring of Tumoricidal Effect of a Vascular Targeting Agent in a Rodent Liver Metastatic Model

Yicheng Ni[1], Xihe Sun[1, 2], Feng Chen[1, 3], Frederik De Keyzer[1], Vincent Vandecaveye[1], Willy Landuyt[1], Paul Van Hecke[1], Hide Bosmans[1], Guy Marchal[1]

[1]University Hospital, Catholic University of Leuven, Leuven, B-3000, Belgium; [2]Affiliated Hospital, Weifang Medical University, Weifang, Shandong, People's Republic of China; [3]Zhong Da Hospital, Southeast University, Nanjing, Jiangsu, People's Republic of China

We sought to noninvasively monitor the therapeutic effects of a vascular targeting agent Combretastatin A-4-phosphate (CA4-P) in rats (n = 15) with liver implantation of rhabdomyosarcomas (R1) by using a 1.5 Tesla clinical MR scanner. We applied comprehensive MR techniques including T2-, contrast enhancing T1-, diffusion-, and dynamic susceptibility perfusion-weighted MRI with regional blood volume and flow maps as well as 1H-MRS in correlation with microangiographic and histological findings. With vascular shutdown and angiogenesis being vividly documented, R1 tumors grew significantly slower in CA4-P treated rats than in saline controls. Noninvasive longitudinal therapeutic follow-up in rodent liver tumors proved feasible.

1770. Early Response Measurements of NGR-TNF Efficacy Using MR and Immunohistochemical Methods

Hanneke van Laarhoven[1], Giulio Gambarota[1], Cornelis Punt[1], Jasper Lok[1], Ilja Verhagen[1], Angelo Corti[2], Salvatore Toma[3], Corrado Gallo Stampino[3], Albert van der Kogel[1], Arend Heerschap[1]

[1]University Medical Centre Nijmegen, Nijmegen, Netherlands; [2]San Raffaele H Scientific Institute, Milan, Italy; [3]MolMed S.p.A, Milan, Italy

Targeted delivery to the tumor of picogram doses of TNF-á can be achieved by coupling TNF-á with CNGRC (NGR-TNF), a peptide that targets tumor neovasculature. We assessed NGR-TNF efficacy at an early stage in lymphoma bearing mice. MRI measurements with blood pool contrast agent showed an increased leakage of contrast agent from the vasculature in NGR-TNF treated tumors compared with controls, suggesting NGR-TNF-induced vascular permeability. Immunohistochemical analysis showed a decrease in tumor hypoxia and an increase in labeling index of the S-phase marker bromodeoxyuridine, possibly due to an increase in tumor blood flow after NGR-TNF treatment.

1771. TOOKAD Photodynamic Therapy of Orthotopic PC3-MM2 Prostate Tumors in Nude Rats : Investigation Using BOLD-MRI, Diffusion-Weighted-MRI and Dynamic-Contrast Enhanced MRI

Dominique Blanc[1], Henri Ficheux[1], Nathalie Just[2], Nicolas Guilbaud[2]

[1]NEGMA-LERADS, Magny-les-Hameaux, France; [2]Oncodesign Biotechnology, Dijon, France

Photodynamic therapy (PDT) of cancers is a physico-chemical method for the local treatment of cancers and some other vascular diseases. PDT represents a unique therapeutic means of treating patients that cannot undergo other classical therapies either for operatory contraindications or inefficacy of radiotherapy and chemotherapy. In this study, Tookad PDT was investigated with both invasive and non-invasive techniques to determine the best conditions for appropriate PDT therapy of xenografted human prostate tumors. MRI techniques allowed early determination of tumor response to treatment , informations that may be useful for further clinical investigations of prostate cancer response to Tookad PDT treatment.

1772. MRI Assessment of a Treatment for Non-Small Cell Lung Cancer in a Mouse Model

Ruqayyah M. Al-Hashem[1], Hongbin Ji[2], Mitchell S. Albert[1], Kwok-Kin Wong[2], Yanping Sun[1]

[1]Brigham & Women's Hospital, Boston, Massachusetts, USA; [2]Dana Farber Cancer Institute, Boston, Massachusetts, USA

Epidermal growth factor receptor (EGFRvIII) mutations results in non-small cell lung cancer (NSCLC). In this study we evaluated the efficacy of Traceva on EGFRvIII induced lung tumors in a NSCLC mouse model. A total of 8 NSCLC mice were evaluated, 4 mice with tumor greater than 100mL were treated with Traceva. The NSCLC responded to Traceva dramatically with an average result of 64% reduction in tumor volume within the first 7 days and 90% reduction within 14 days of daily oral treatment. The decrease in tumor volume for these subjects followed an exponential decrease with a regression value of 0.9979.

1773. Ranpirnase-Induced Changes in Blood Flow, Lactate, and ATP Levels in A549 Human NSCLC Measured by Noninvasive Near Infra-Red Spectroscopy and Magnetic Resonance Spectroscopy

Sergey Magnitsky[1], Ulas Sunar[1], Matthew Milkevitch[1], Arjun G. Yodh[1], Intae Lee[1]

[1]University of Pennsylvania, Philadelphia, PA 19104-6069, USA

Cytotoxic RNase, rinpirnase (ONCONASE¢ç: ONC) caused apoptosis in A549 NSCLC cells, along with significant inhibition in tumor growth. Tumor 1H and 31P MRS was used to monitor the lactate and ATP levels on A549 tumor cells after treatment with ONC. Tumor perfusion was noninvasively measured by a Near Infrared Spectroscopy method. We observed ONC-induced increases in tumor perfusion during the first 120 minutes. In contrast, ~20% decrease of lactate level was observed using non-localized MR spectroscopy, caused by the removal of tumor acidic metabolites. In conclusion, ONC may be a new and promising drug for the treatment NSCLC.

1774. A ^{1}H MRS Study of Tumour Overexpression of Dimethylarginine Dimethylaminohydrolase (DDAH) and Response to Taxotere

Basetti Madhu[1], Saira Ansari[1], John R. Griffiths[1], Guy St.J. Whitley[1], Simon P. Robinson[1]

[1]St. George's, University of London, London, England, UK

Overexpression of dimethylarginine dimethylaminohydrolase (DDAH), which metabolises endogenous inhibitors of nitric oxide synthase, indirectly increases nitric oxide (NO). NO has both pro- and anti-apoptotic effects. ^{1}H MRS was used to assess control and DDAH overexpressing tumours prior to and 24 hours after treatment with taxotere. Following treatment, the choline concentration of control tumours significantly increased, but it did not change in tumours overexpressing DDAH. The data are consistent with DDAH overexpression conferring pro-apoptotic activity following taxotere treatment.

1775. Real-Time Imaging of Emerging Resistance During Cancer Therapy

Kuei C. Lee[1], Daniel E. Hall[1], Benjamin A. Hoff[1], Bradford A. Moffat[1], Surabhi Sharma[1], Thomas L. Chenevert[1], Charles R. Meyer[1], Wilbur R. Leopold[2], Timothy D. Johnson[1], Alnawaz Rehemtulla[1], Brian D. Ross[1]

[1]University of Michigan Medical School, Ann Arbor, Michigan, USA; [2]Molecular Imaging Research Preclinical Services, Ann Arbor, Michigan, USA

9L orthotopic tumors were established and treated with two different therapeutic regimens of BCNU. Using diffusion MRI, we were able to demonstrate the sensitivity of this technique to quantitatively measure tumor response and also the emergence of drug resistance due to therapy. This study highlights the ability of diffusion MRI to provide real-time assessment of therapy-induced response for allowing early opportunities to optimize therapeutic protocols.

1776. The ADC Value in Esophageal Caners on Diffusion-Weighted MR Images for Predicting Effect of Chemoradiotherapy

Takashi Koyama[1], Shigeaki Umeoka[1], Tsuneo Saga[1], Ken Tamai[1], Go Watanabe[1], Masahiro Hiraoka[1], Kaori Togashi[1]
[1]Kyoto University, School of Medicine, Kyoto, Japan

The purpose of this study is to investigate whether the ADC values of esophageal cancer can predict the response to chemoradiotherapy., Esophageal cancers treated with chemoradiotherapy were classified as either good response or poor response according to whether the wall thickness of the tumor on CT after chemoradiotherapy decreased in less than half of that before chemoradiotherapy or not. The ADC value of tumor on DWI was compared between good response and poor response group. Esophageal cancer with lower ADC titer showed good response to therapy, but the response to therapy varied among the cancers with higher ADC values.

1777. *In Vivo* MR Diffusion Investigation of Murine Tumors with Bacteria Infiltration

Kaung-Ti Yung[1], Xiangjin Song[1], Gabrielle Ramus[1], Vitaly Chibisov[1], Qiuhong He[1]
[1]University of Pittsburgh Medical Center, Pittsburgh, Pennsylvania, USA

Bacterial-based cancer treatment has shown great potential in attacking poorly vascularized tumor regions, especially when combined with conventional chemotherapeutic drugs. We report an *in vivo* MRI diffusion study of Murine LL/2 tumors injected with genetically altered E. Coli DH5á (Met) or JM109 (Hb) strains. The calculated diffusion maps show distinctive features not apparent in their MRI images with a mean ADC ~ 0.56 x 10-3 mm2/s. In correlation with histochemical staining results, the T2-weighted image of the E. Coli DH5á-carrying tumor showed homogeneous yet fragmental tissue, but the tumor that eradicated the injected E. Coli JM109 strain presented more structural heterogeneity. These results demonstrate that MRI may be an important tool to detect tumor tissue remodeling by different types of bacterial interactions.

Clinical MRS in Cancer

Room 4E Tuesday 13:30 - 15:30

1778. Characterization of High Grade Gliomas Using TE-Averaged PRESS at 3 T

Yan Li[1], Radhika Srinivasan[1], Susan M. Chang[1], Sarah J. Nelson[1]
[1]University of California, San Francisco, California, USA

The purpose of this study was to use single voxel acquisition, TE-averaged PRESS, to acquire the T2 relaxation times of Cho, Cr and NAA and to obtain quantitative metabolite concentrations in tumors using an 8-channel phased array coil at 3 T. TE-averaged PRESS spectra were acquired from eight healthy volunteers and seven glioma patients in NAWM or tumor lesions. The T2 relaxation times of Cho and NAA in tumors were significantly different from those in normal regions. The difference in NAA concentration after T2 relaxation correction was statistically significant between normal and lesions. In addition, Glu showed statistically significantly higher concentration in high grade gliomas.

1779. Quantitative SENSE Spectroscopy of Gliomas at 3T

Esin Ozturk-Isik[1, 2], Albert P. Chen[1, 2], Jason C. Crane[1], Duan Xu[1], Eric T. Han[3], Daniel B. Vigneron[1, 2], Soonmee Cha[1], Susan M. Chang[1], Sarah J. Nelson[1, 2]
[1]University of California, San Francisco, California, USA; [2]UCSF/UCB Joint Graduate Group in Bioengineering, San Francisco, California, USA; [3]GE Healthcare Global Applied Science Laboratory, Menlo Park, California, USA

SENSE MRSI has been implemented for imaging gliomas at high field, and was quantitatively analyzed in comparison to spectra acquired with elliptical k-space sampling. SENSE spectra reduced the spectral scan time from 37:42 min (R=1) to 9:28 min (R=4) for a 16x16x8 array, and resulted in better spatial resolution than the elliptical k-space sampling acquired with comparable scan time. Our results indicated that both SENSE and elliptical k-space spectra resulted in similar spectral patterns over the PRESS box, and were able to distinguish spectra of tumor from normal tissue.

1780. Fast Nosologic Imaging of the Brain

Maarten De Vos[1], Teresa Laudadio[1], Arjan W. Simonetti[1], Sabine Van Huffel[1], Arend Heerschap[2]
[1]K.U.Leuven, Leuven, Belgium; [2]U.M.C.Nijmegen, Nijmegen, Netherlands

A fast, accurate and robust method is developed for nosologic imaging of the brain. To incorporate both spatial information and prior knowledge, the method is based on canonical correlation analysis (CCA). We apply CCA two times: once to detect the tumour type and once to show the heterogeneity of the tissue. We also show how the result on MRSI spectra can be improved by using MRSI and MRI information together. The final result gives a reliable segmentation and classification of the segments.

1781. Enhanced Detection of Glutamine (Gln) and Glutamate (Glu) with 1H MRS Using Single Voxel STEAM: Their Potential to Stage Brain Tumors

Matthew R. Amans[1], Quan Jiang[2], Yang Xuan[1], Shireen Hm-Meeran[1], Lucia J. Zamorano[1], Murali Guthikonda[1], Geoffrey Barger[1], Vivek Sehgal[1], Jiani Hu[1]

[1]Wayne State University, Detroit, Michigan, USA; [2]Henry Ford Hospital, Detroit, Michigan, USA

Glutamine (Gln) and glutamate (Glu) levels are both directly and indirectly (via reactive oxygen species signaling) involved in tumor proliferation and apoptosis, and thus could provide useful information for tumor diagnosis and treatment. Preliminary results demonstrate a consistent and remarkable increase in both Gln concentration (using water as a reference) and Gln/Cr ratio. The results also suggest Gln/Glu could be an early indicator of malignant transformation compared to "traditional" 1H MRS markers such as NAA, Cho, and Cr.

1782. Brain Tumour Diagnosis and Prognosis by *In Vivo* 1H MRS and *Ex Vivo* Metabolomic and Genomic Data. A Prospective Study as Part of ETUMOUR (FP6-2002-LSH503094)

Daniel Monleon[1], Carmen Martinez-Bisbal[1], Beatriz Martinez-Granados[1], Vicent Esteve[1], Eva Piñero-Sagredo[1], Ruben Ferrer-Luna[1], Manuel Mata[2], Jose Piquer[3], Luis Marti-Bonmati[4], Bernardo Celda[1]

[1]Universitat de Valencia, Burjassot, Valencia, Spain; [2]University of Valencia, Valencia, Spain; [3]Hospital de la Ribera, Alzira, Valencia, Spain; [4]Clinica Quiron, Valencia, Spain

There is a great need to improve our understanding of brain tumour biology to improve diagnosis and to develop new treatments. The purpose of this communication is to check the complementarity between *in vivo* 1H MRS and *ex vivo* metabolomic and transcriptomic data for a better diagnosis and prognosis of brain tumour, using the multi-center protocols provided in the LSH-FP6 european project eTUMOUR. Our results demonstrate the viability of a extensive characterization of brain tumour biopsies by spectroscopic and genomic tools. In addition, comparative analysis of *in vivo* 1H-MRS and HRMAS data have been useful for a better identification of *in vivo* spectra and, therefore, for an improved brain tumour classification. This analysis provided brain tumour classifiers for *in vivo* and *ex vivo* MR data. Particular attention has been focused in the metabolomic and phenotypic differences between glioblastomas with different survival time, short as primary and longer as secondary glioblastoma.

1783. *In Vivo* MRS Metabolic Profiles of Human Brain Metastases from Different Primary Cancers

Torill Eidhammer Sjøbakk[1], Roar Johansen[1], Tone Frost Bathen[1], Ursula Sonnewald[1], Kjell Arne Kvistad[2], Steinar Lundgren, [12], Ingrid Susanne Gribbestad[1]

[1]Norwegian University of Science and Technology, Trondheim, Norway; [2]St.Olavs University Hospital Trondheim, Trondheim, Norway

In vivo single volume 1H MR spectra (3T) were obtained from brain metastases in patients with primary breast cancer, lung cancer, colon cancer and malignant melanoma. The MR spectra are dominated of signals from lipids and choline compounds. The spectra were analyzed by principal component analysis, and a trend of clustering dependent on origin of brain metastasis was observed. The metabolic profile of the metastases thus contains information related to its origin. The tumour biology, including MRS determined metabolic profiles, might be valuable clinical information when planning the treatment of brain metastases, and also when deciding to terminate further therapies.

1784. Sequential MRSI and DWI Study for Early Assessment of Response of Breast Cancer to Neo-Adjuvant Chemotherapy: A Pilot Study

K A. Danishad[1], V Seenu[1], S Roell[2], M Vorbuchner[2], N R. Jagannathan[1]

[1]All India Institute of Medical Sciences, New Delhi, Delhi, India; [2]Siemens Medical Solutions, Erlangen, Germany

MRSI and DW-MR imaging were carried out in breast cancer patients prior to neo-adjuvant chemotherapy and after first and third cycle of NACT. After I NACT, significant decrease in choline SNR and an increase in ADC were observed in responders. Choline SNR decreased marginally or increased in non-responders. After III NACT, reduction/absence of choline was observed and ADC further increased in responders. Inhibition of tumor proliferation by chemotherapy caused reduction in choline SNR, while reduction in increases the ADC. The study demonstrates that both MRSI and can be to evaluate the early response of breast cancer

1785. Simultaneous Detection of Choline and Other Metabolites Using SEE-SelMQC for Spectroscopic Imaging of Human Breast Cancer

Qiuhong He[1], Xiaohong Joe Zhou[2]

[1]Univerisity of Pittsburgh, Pittsburgh, Pennsylvania, USA; [2]University of Illinois Medical Center, Chicago, Illinois, USA

A Spin Echo Enhanced Selective Multiple Quantum Coherence transfer (SEE-SelMQC) technique has been implemented on a GE 3T clinical scanner and successfully demonstrated for multiple metabolite detection. The method is capable of simultaneous choline and lactate/PUFAs detection in extracranial human tissues containing high concentration of fat. The excellent lipid and water suppression afforded by SEE-SelMQC is used to remove the baseline artifacts often observed in breast MRS detection of choline. Three-dimensional multiple metabolite imaging is possible in combination with spatial-spectral Sel-MQC methods and fast imaging k-space mapping to localize breast lesions *in vivo*.

1786. MR-Determined Metabolic Phenotype of Breast Cancer Predicts Lymphatic Spread, Grade and Hormone Status

Tone Frost Bathen[1], Line Rørstad Jensen[1], Beathe Sitter[1], Hans Fjøsne[2], Jostein Halgunset[1], David E. Axelson[3], Ingrid Susanne Gribbestad[1], Steinar Lundgren, [12]

[1]NTNU, Trondheim, Norway; [2]St. Olavs University Hospital, Trondheim, Norway; [3]MRI_Consulting, Kingston, Ontario, Canada

MR spectroscopy describes the biochemical properties of breast cancer. We analysed tumour tissue from patients diagnosed with invasive ductal carcinoma grade I, II, and III by HR MAS MRS. Multivariate models relating spectral data to tumour grade, lymphatic spread and hormonal status were designed by application of various multivariate methods. Validation of training results and testing on blind samples gave optimistic results. The tumour biology of the individual patients' disease is becoming an important factor to consider when choosing treatment for breast cancer, and MR determined metabolic phenotype may have a future role as a supplement for clinical decision making.

1787. High-Resolution Magic Angle Spinning (HRMAS) 1H MRS Detects Biomarkers in Pancreatic Cancer

Haihui Cao[1, 2], Gregory Y. Lauwers[2], Carlos Fernandez-del Castillo[2], Andrew L. Warshaw[2], A. Aria Tzika[1, 2]

[1]Massachusetts General Hospital and Shriners Institute, Harvard Medical School, Boston, Massachusetts, USA; [2]Massachusetts General Hospital, Harvard Medical School, Boston, Massachusetts, USA

We report that high-resolution Magic Angle Spinning (HRMAS) 1H MRS has detected lipid accumulation in pancreatic cancer biopsies. Our findings are consistent with the hypothesis that HRMAS 1H NMR permits the identification of novel pancreatic tumor biomarkers, which can allow early diagnosis and could greatly improve prognosis.

1788. Potential of 3D ^{1}H MRSI Localization of Prostate Cancer to Direct TRUS Guided Biopsy in Patients with PSA 4 – 10 Ng/mL

Virendra Kumar[1], N R. Jagannathan[1], Rajeev Kumar[1], S C. Das[1], Lokesh Jindal[1], Sanjay Thulkar[1], S Dutta Gupta[1], S N. Dwivedi[1], A K. Hemal[1], N P. Gupta[1]

[1]All India Institute of Medical Sciences, New Delhi, Delhi, India

In the present study, we evaluated the usefulness of MRSI for the detection of prostate cancer foci in men with raised PSA (4-20 ng/mL) and the feasibility of directing TRUS guided biopsies at the lesions found on MRSI. MR investigations were carried out on 25 men at 1.5 Tesla (Sonata, Siemens) using endorectal coil. MRSI was used to provide z and x-coordinate of the suspicious voxel for TRUS guided biopsy. 15/25 patients showed areas of malignancy in MRSI while 5 (33%) were positive on TRUS guided biopsy. None of the patients who had a negative MRSI were positive for cancer.

1789. 1D High Resolution Magic Angle Spinning Total Correlation Spectroscopy of Prostate Cancer Tissues

Mark Gunnard Swanson[1], Andrew S. Zektzer[1], Kayvan R. Keshari[1], Laura Tabatabai[1], Thomas Butler[1], John Kurhanewicz[1]

[1]UCSF, San Francisco, California, USA

An *ex vivo* 1D high resolution magic angle spinning (HR-MAS) total correlation spectroscopy (TOCSY) sequence was developed to detect the choline containing metabolites (PC and GPC), the ethanolamine containing metabolites (Eth, PE, and GPE), and lactate and alanine. Higher ratios of PC/GPC and significantly higher ratios of PE/Eth, GPE/Eth, and Lac/Ala were observed in prostate cancer versus healthy glandular prostate tissues. The sequence developed in this study allows the detection of PC, GPC, PE, and GPE, without the need to perform 31P spectroscopy, and could be translated to *in vivo* MRS studies of prostate cancer patients.

1790. Potential of ^{1}H MR Spectroscopic Imaging to Predict Negative Biopsy in Men with PSA < 10 Ng/mL

Virendra Kumar[1], Rajeev Kumar[1], Lokesh Jindal[1], Rishi Nayyar[1], Sanjay Thulkar[1], S Dutta Gupta[1], S N. Dwivedi[1], A K. Hemal[1], N P. Gupta[1], N R. Jagannathan[1]

[1]All India Institute of Medical Sciences, New Delhi, Delhi, India

Cancer can be detected in only 30% men with serum prostate specific antigen < 10 ng/mL. There are no markers to identify patients who are unlikely to have cancer and can thus avoid a biopsy. Magnetic resonance spectroscopic imaging (MRSI) identifies areas of abnormal metabolism that may harbor cancer. We prospectively evaluated the use of MRSI to identify patients who are unlikely to have a cancer detected on their biopsy. None of the patient who had no evidence of malignancy in MRSI was found to have cancer on the sextant TRUS guided biopsy. These patients may not harbor clinically relevant cancer prostate and MRSI may have potential to avoid biopsy.

1791. 3D ^{1}H MRSI Based TRUS Guided Biopsies in Men with Suspected Prostate Cancer

Virendra Kumar[1], N R. Jagannathan[1], Rajeev Kumar[1], Lokesh Jindal[1], S C. Das[1], Rishi Nayyar[1], Sanjay Thulkar[1], S Dutta Gupta[1], S N. Dwivedi[1], A K. Hemal[1], N P. Gupta[1]
[1]All India Institute of Medical Sciences, New Delhi, Delhi, India;

The positive biopsy rate of ultrasound guided sextant biopsy is low especially in patients with PSA < 10 ng/mL. The present study was carried out to evaluate the sensitivity and specificity of 3D ^{1}H MRSI directed TRUS guided biopsies in a large cohort of patients categorized on the basis of PSA level (0-10 ng/mL, 10-20 ng/mL, > 20 ng/mL). TRUS guided biopsy was performed by using MRSI derived x- and z-coordinate of the suspicious voxel. The overall sensitivity and specificity of MRSI directed TRUS guided biopsies was 98% and 40% respectively, with PPV=43%, NPV=97 %. The pick up rate of prostate cancer increased with MRSI focused biopsy.

1792. Single Voxel and Chemical Shift Imaging (CSI) of Soft Tissue Sarcomas

Virendra Kumar[1], Madhabanda Kar[1], K A. Danishad[1], S V.S Deo[1], N K. Shukla[1], U Sharma[1], S Dattagupta[1], S Dey[1], S Tulkar[1], N R. Jagannathan[1]
[1]All India Institute of Medical Sciences, New Delhi, Delhi, India

Multi voxel and single voxel spectroscopy were performed on patients with soft tissue tumor to distinguish between benign and malignant lesions and to detect the recurrence/residual tumor based on choline delectability criteria. In eighteen histopathologically proven malignant lesions choline resonance was observed while in four benign lesions including low grade liposarcoma, choline could not be detected. Our study proved that MR Spectroscopy can be used as a reliable tool in differentiating benign and malignant lesions with 100% sensitivity and 100% specificity

Clinical Applications in Cancer

Room 4E Tuesday 13:30 - 15:30

1793. Multi-Contrast Whole-Body 2D Axial MR Imaging During Continuous Table Movement for Tumor Staging

Katja Brauck[1], Michael Zenge[1], Frank Stock[1], Ladd Mark[1], Florian Vogt[1], Joerg Barkhausen[1]
[1]University Hospital Essen, Essen, NRW, Germany

Whole-body MRI has become well established for the evaluation of metastases in patients with malignant diseases. We compared the feasibility and accuracy of a 2D T2 and T1-w real-time whole-body imaging protocol during continuous table movement with PET/CT as the standard of reference in 13 patients. All lesions as seen by the PET/CT with a diameter greater than 6 mm could be visualized by real-time MRI. Contrast-enhanced sequences were the most accurate for tumor detection. Real-time whole-body imaging is a promising method for tumor staging, providing an extended FOV and fewer motion artifacts than breath-held approaches

1794. 3D MR Sialography as a Tool to Visualize and Investigate Radiation-Induced Changes to the Salivary Glands and Ducts in Patients

Eleftheria Astreinidou[1], C.P.J Raaijmakers[1], J. Roesink[1], C Terhaard[1], L. W. Bartels[1]
[1]University Medical Center, Utrecht, Netherlands

A 3D MR sialography protocol was developed and evaluated in 11 healthy volunteers and applied, for the first time, in 9 patients receiving radiotherapy (RT) for head-and-neck tumors pre-RT and post-RT at 6-weeks, 6-months and 1-year. The whole trajectory of the salivary ducts was visible pre-RT but only partly 6-weeks post-RT for those glands receiving dose >20Gy. Recovery was observed at 6-months or 1-year post-RT for doses when the dose was 25-45 Gy, but not when dose > 45 Gy. This is a novel approach in investigating radiation-induced xerostomia as the saliva itself is imaged.

1795. Three-Dimensional Proton MR Spectroscopic Imaging of Human Breast Lesions

Michael A. Jacobs[1, 2], Mari Smith[3], Nagi Khouri[1], David A. Bluemke[1], Peter B. Barker[3]
[1]Johns Hopkins School of Medicine, Baltimore, Maryland, USA; [2]Sidney Kimmel Dept of Oncology, Baltimore, Maryland, USA; [3]Kennedy Krieger Institute, Baltimore, Maryland, USA

We have implemented and investigated the diagnostic value of 3D-MRSI in patients with breast lesions who were scheduled for biopsy. Unilateral, 3D-MRSI with nearly whole breast coverage is feasible in a single session combined with conventional, bilateral breast MRI.

1796. Evaluation of CADstream™ for Serial Automated Breast Tumor Volume Measurements in Patients Undergoing Neoadjuvant Chemotherapy for Breast Cancer

Bonnie N. Joe[1], Alexander Urioste[2], Kiarash Vahidi[1], Jessica Gibbs[1], Evelyn Proctor[1], Zakar Siraj[1], Ying Lu[1], Nola Hylton[1]

[1]University of California, San Francisco, San Francisco, California, USA; [2]University of California, San Diego, San Diego, California, USA

MRI breast tumor volume has recently been shown to be predictive of length of recurrence free survival (LRFS) in breast cancer patients undergoing neoadjuvant chemotherapy. This study evaluates a software package (CADstreamTM, Confirma, Inc.) for automated measurement of serial breast MRI tumor volumes in response to treatment and compares results to established in-house software. CADstreamTM produced similar results to those reported previously using in-house software (correlation coefficients ranged from 0.71 to 0.95, $p<0.0003$ for all visits). The reproducibility of results using commercially-available software supports the robustness of volumetric measurements of tumor response as a surrogate endpoint for survival outcomes.

1797. Characterisation of Breast Tumors with a Model-Independent Analysis of Bolus-Tracking MRI

Smitha Makkat[1], Steven Sourbron[1], Vally Dewilde[1], Filip De Ridder[1], Rob Luypaert[1], Tadeusz Stadnik[1], Johan De Mey[1]

[1]Vrije Universiteit Brussel, Brussels, Belgium

Previously we demonstrated the feasibility of quantifying perfusion parameters in human breast tumors using a model-independent deconvolution analysis of DCE-MRI. In this study we applied a refinement of the protocol to a larger cohort of patients and investigated the value of the measured parameters in tumor characterization. Our results suggest that malignant and benign breast tumors may be classified correctly with the proposed measurement and post-processing protocol, in terms of their perfusion values. However, additional parameters such as those obtained from modeling may be needed to achieve full characterization.

1798. Comparison of Whole Body MRI and Whole Body PET-CT for Staging of Advanced Bronchial Carcinoma – Initial Results

Christian Plathow[1], Susanne Eschmann[1], Philipp Aschoff[1], Vanessa Heinrich[1], Jürgen Schaefer[1], Claus Claussen[1], Thomas Hehr[1], Christina Pfannenberg[1] , Heinz-Peter Schlemmer[1]

[1]Eberhard-Karls University, Tuebingen, Baden-Wuerttemberg, Germany

Whole body MRI using a dedicated sequence protocol for oncologic staging is able to correctly classify T-stage very accurately in patients with advanced bronchial carcinoma. Especially STIR and T1w VIBE 3D post CM sequences seem to be suitable for correct T-staging. Whole body PET-CT seems to have advantages in correct N-staging.

1799. Usefulness of Diffusion-Weighted MR Image in Detecting Pancreas Cancer: Comparative Analyses with T1, T2-Weighed MR Images

Noriaki Muraoka[1], Hirohiko Kimura[1], Hidemasa Uematsu[1], Yasuhiro Fujiwara[1], Isao Yamaguchi[1], Harumi Itoh[1]

[1]University of Fukui, Fukui, Japan

We hypothesized that DWI could be useful to depict the pancreatic cancer, which was not identified by conventional image technique such as T1-WI or T2-WI. Ten subjects with pancreatic cancer were included in this study. We compared the image contrast between tumor and normal pancreatic parenchyma divided by the muscle (C/M ratio) in each image sequence. The mean C/M ratio of the DWI was significantly greater than those of the T2-WI and T1-WI. The mean C/M ratio between T2-WI and T1-WI was not statistically significant. These results support the hypothesis that DWI may be useful to depict the pancreatic cancer.

1800. High-B-Value Diffusion-Weighted MR Imaging of Gastric Cancer: By Segmented Breath-Hold Technique

Xiao Peng Zhang[1], Lei Tang[2], Ying Shi Sun[1], Fei Sun[3]

[1]Beijing Cancer Hospital & Peking University School of Oncology, Beijing, People's Republic of China; [2]Beijing Cancer Hospital, School of Oncology, Peking University, Beijing, People's Republic of China; [3]MR Modality, GE Healthcare, China, Beijing, People's Republic of China

Three diffusion-weighted EPI sequences with different number of acquisitions were performed in 16 patients with gastric cancer. The sequences were segmented into 2-3 breath-holds using a function ¡ pause¡± key if the scan time exceeded patients' duration. The b values were 0, 1000s/mm2, and the MPG pulses were placed in 3 directions. There was no statistical difference in ADC measurement between single breath-hold sequence and segmented breath-hold sequences. Multi-acquisition with segmented breath-hold technique reduced EPI- and ASSET-related artifacts and achieved higher CNR. All 16 cases obtained acceptable images with segmented breath-hold technique combined with multi-acquisition method.

1801. Abdominal Imaging with Extended Field of View in Rectal Cancer Using a Continuously Moving Table: A Feasibility Study

Gregor Sommer[1], Ute Ariane Ludwig[1], Hans-Peter Fautz[1], Oliver Schäfer[1]
[1]University Hospital Freiburg, Freiburg, Germany

Two MRI sequences with continuous table motion were implemented in a standard pelvic imaging protocol for rectal cancer follow up and tested on ten patients: The sequences were a contrast enhanced T1 weighted GRE with fat suppression and a STIR-fat suppressed T2 weighted TSE, covering the whole abdomen in down to one minute with only one breath-hold required. Quality and diagnostic scope of the images were evaluated in an individual case analysis and give promising initial experience about the applicability and usefulness of fast moving table imaging methods as a tool for extending the diagnostic coverage of standard MRI examinations.

1802. Multi-Parametric MR Imaging of Prostate Cancer at 3T

Albert P. Chen[1, 2], Joonmi Oh[1], Eric T. Han[3], Duan Xu[1, 2], John Kurhanewicz[1, 2], Daniel B. Vigneron[1, 2]
[1]UCSF, San Francisco, California, USA; [2]UCSF/UCB, San Francisco, California, USA; [3]GE Healthcare, Menlo Park, California, USA

MR imaging and MR spectroscopic imaging utilizing endorectal coil have become important clinical tools for prostate cancer management. However, the addition of other type of MR techniques such as diffusion imaging and T2-mapping to provide quantative and functional information may improve the sensitivity and specificity of MR to characterize prostate cancer. Challenges have prevented these techniques from being clinically feasible. In this study, we developed a novel 1-hour clinical protocol combining 3T MRI, MLEV-PRESS, DTI-EPI and magnetization prepared/spiral readout T2 mapping to monitor anatomic, metabolic, and relaxivity changes in prostate cancer.

1803. Metabolic Profiling of Preinvasive and Invasive Cervical Cancer Using 1H and 31P Magic Angle Spinning MRS

Sonali S. De Silva[1], Geoffrey S. Payne[1], Patrick Soutter[2], Nandita M. Desouza[1]
[1]Institute of Cancer Research, Sutton, Surrey, UK; [2]Hammersmith Hospital, London, UK

The metabolic profiles of preinvasive and invasive cervical cancer have been evaluated on *ex vivo* tissue samples using 1H and 31P magic angle spinning (MAS)-MRS. 1H spectra were acquired from all samples but samples larger than 20 mg were required to obtain quantiable 31P MAS spectra. In common with many other cancers we have found high levels of PE compared with PC, and that both PC and PE increase from pre-invasive to full cancer.

1804. Deformable Registration of Abdominal Mion-Enhanced MR Images for Presurgical and Radiotherapy Planning of Lymph Nodes

Fred S. Azar[1], Christophe Chefdhotel[1], Ravi T. Seethamraju[2], Mukesh G. Harisinghani[3]
[1]Siemens Corporate Research, Princeton, New Jersey, USA; [2]Siemens Medical Solutions, Boston, Massachusetts, USA; [3]Massachusetts General Hospital, Boston, Massachusetts, USA

In order to determine the extent of metastasis in lymph nodes, pre- and post-MION enhanced MR images of the abdomen are co-registered. This initial patient study tests the performance of a rigid and a non-rigid registration algorithm on abdominal MR data and shows that accurate registration may enable significant improvement in detection rate of lymph node metastasis. In addition nodal information from pre-contrast images may be used to accurately identify nodal boundaries on post-contrast images. Registration of anatomical images with MRAs or CTs, will pave the way for precise surgical planning or radiotherapy.

1805. MR Imaging of Bone Tumors - A Pictorial Review

Guenther K. Schneider[1], Peter M. Fries[1], Alexander Massmann[1], Dieter Kohn[2], Klaus Remberger[1], Roland M. Seidel[3], Roland M. Seidel[3]
[1]UniversityHospital of Saarland, Homburg, Saar, Germany; [2]Saarland University Hospital, Homburg, Saar, Germany; [3]Saarland UniversityHospital, Homburg, Saar, Germany

To present MRI features of both benign and malignant tumors as well as tumor-like lesion. To demonstrate important findings for staging and therapy planning

Nanoparticle Contrast Agents - Methods and Applications

Room 4E Tuesday 13:30 - 15:30

1806. SPIO Positive Contrast In-Vivo by the Use of Diagonal-SPRITE

Andrea Protti[1], *Po-Wah So*[1], *Amy Herlihy*[1], *Jimmy Bell*[1]
[1]Hammersmith Hospital, Imperial College London, London, UK

Superparamagnetic iron oxide particles (SPIOs) have been extensively used in molecular imaging by MRI for the imaging of cells and gene expression. However, being iron based, imaging of such particles causes attenuation of the signal intensity due to severe shortening of T2*. In order to detect the short T2* SPIOs a novel UTE technique, Diagonal-SPRITE was used. Diagonal-SPRITE determined the T2* of phantoms containing either a SPIO-containing solution or saline. In-vivo Diagonal-SPRITE MRI was also performed and positive contrast of SPIOs was achieved by the subtraction of an image at ultra-short and short Tp.

1807. Diffusion is a Major Determinant of Contrast in SSFP-Based Single Cell MRI: A Theoretical and Experimental Study

Trevor Wade[1], *Chris Heyn*[1, 2], *Dave Rutt*[1], *Paula Foster*[1], *Brian Rutt*[1]
[1]Robarts Research Institute, London, Ontario, Canada; [2]University of Toronto, Toronto, Ontario, Canada

In cellular imaging, the static dephasing model of the FIESTAsequence consistently underestimates the signal loss. A new model,based on the theory developed by Kaiser for signal loss in a SSFP sequence due to diffusion, has been modified for theFIESTA sequence to estimate the signal from each subvoxel in animaging voxel. This new model, which includes both dephasing anddiffusion effects, has proved very effective at predicting thesignal from voxels containing iron loaded cells.

1808. Phase Susceptibility-Weighted Imaging of SPIO Nanoparticles

Melanie S. Kotys[1], *Steve H. Fung*[1], *Jianwu Xie*[1], *King CP Li*[1]
[1]National Institutes of Health, Bethesda, Maryland, USA

Molecular imaging of superparamagnetic iron oxide nanoparticles (SPIONs) is an effective method for cell tracking using magnetic resonance imaging (MRI). A new phase-based (δΦ) technique for susceptibility-weighted imaging (SWI) of SPIONs is presented and compared to magnitude-based SWI methods for sensitivity and relation to iron concentration and signal-to-noise ratio (SNR). R_2* appeared non-linear to iron concentration, while δΦappears appeared linear. The SNR for the δΦmethod increased from 3.2 to 80 times that of the R_2* method as concentration increased. Phase-based SWI of SPIONs appears to be linear to concentration of iron and has higher SNR than magnitude-based SWI methods.

1809. Non-Monoexponential Signal Decay Due to Single SPIO Loaded Cells

Joerg Pintaske[1], *Bernd Mueller-Bierl*[1], *Fritz Schick*[1]
[1]University Hospital Tuebingen, Tuebingen, BW, Germany

While the actual field close to superparamagnetic iron oxide (SPIO) loaded cells will certainly be very different from that of a magnetic dipole, far from the cell where field inhomogeneities are most effective the field distribution will closely resemble that of a magnetic dipole. Using a numerical approach we treat SPIO loaded cells as magnetic dipoles in a homogeneous magnetic field and compute the 3D frequency distribution and MR signal decay. The numerical results and experimental findings show non-monoexponential signal decay due to single SPIO loaded cells.

1810. LDL Nanoparticles as Magnetic Resonance Imaging Contrast Agents

Ian Ronald Corbin[1], *Hui Li*[1], *Juan Chen*[1], *Jerry David Glickson*[1], *Gang Zheng*[1]
[1]University of Pennsylvania, Philadelphia, Pennsylvania, USA

Low-density lipoproteins (LDL) are a naturally occurring endogenous nanoplatform in mammals. Lipophilic Gd-DTPA chelates have been incorporated into LDL to produce novel LDL receptor-targeted MRI contrast agents. In vitro studies demonstrated that Gd-labeled LDL retained the physical and functional properties of the native LDL particle. *In vivo* studies show that 24 hrs following iv injection of Gd-labeled LDL into nude mice with HepG2 tumor xenografts that significant contrast enhancement was evident within the tumor. Thus, Gd-labeled LDL demonstrates potential utility as a receptor targeted MRI contrast agent for *in vivo* tumor detection.

1811. Numerical Simulation of Magnetic Field Distortions Caused by Cells Loaded with SPIO Nanoparticles

Joerg Pintaske[1], *Bernd Mueller-Bierl*[1], *Fritz Schick*[1]
[1]University Hospital Tuebingen, Tuebingen, BW, Germany

Superparamagnetic iron oxide (SPIO) nanoparticles have been used to label cells in order to image cell migration with MRI by exploiting the high sensitivity of MRI techniques to the SPIO induced field distortions. In dependence on the specific cell labeling technique the SPIO particles are distributed completely different on the cellular level. We used a numerical approach and studied the magnetic field distortion caused by SPIO labeled cells in dependence on the distribution of SPIO nanoparticles on the cellular level. We show numerically that the magnetic field is sensitive to its shape and intracellular distribution of magnetic dipoles (SPIO particles) only in close proximity to the cell. Outside this region, the magnetic field cannot be distinguished from the magnetic field created by a spherical particle with the same total magnetic moment.

1812. Detection of Blood Volume Changes in the Rat Kidney Using an Intravascular USPIO Contrast Agent

Pippa Storey[1, 2], Lin Ji[1], Lu-Ping Li[1], Pottumarthi Vara Prasad[1, 2]
[1]Evanston Northwestern Healthcare, Evanston, Illinois, USA; [2]Northwestern University Feinberg School of Medicine, Chicago, Illinois, USA

Endothelial function is important in maintaining organ homeostasis, and can be assessed by monitoring vascular responses to mechanical and pharmacological maneuvers. In this study we investigated the potential of MRI in combination with an intravascular USPIO contrast agent ferumoxytol to monitor changes in blood volume noninvasively. Systemic vasodilation was induced in rats by intravenous infusion of adenosine, and the resulting R2 changes in the kidney were monitored using a CPMG sequence. Following injection of ferumoxytol (8mg Fe/kg) the R2 responses to adenosine infusion (500µg/kg/min) in the renal cortex, outer medulla and inner medulla were 8.3±1.7s^{-1}, 15.8±3.7s^{-1} and 13.8±1.4s^{-1} respectively (mean±SEM).

1813. MRI of Mouse Experimental Colitis Using Ultrasmall Superparamagnetic Iron Oxide Particles

Anna E. Larsson[1], Silvia Melgar[1], Erika Rehnström[1], Lennart ET Svensson[1], Erik Michaelsson[1], Paul D. Hockings[1], Lars E. Olsson[1]
[1]AstraZeneca, Mölndal, Sweden

The aim of the present study was to investigate ultrasmall superparamagnetic iron particles (USPIO) as a possible inflammation biomarker by using MRI in an experimental mouse inflammatory bowel disease model. A dose of 1000 or 500 mmol/kg Sinerem, and a T2* sensitive sequence at 4.7 T were used. MRI and histological results demonstrate that USPIOs accumulate in macrophages in the serosa in the proximal part of the colon wall in DSS exposed mice injected with the high dose of USPIOs. In conclusion, USPIOs seem to be a promising inflammatory biomarker in experimental mouse colitis.

1814. Comparison of T2 and T2* for Quantification of Cellular Iron-Uptake at 3.0 T

Hannes Dahnke[1], Rebecca Kuhlpeter[2], Lars Matuszewski[2], Walter L. Heindel[2], Tobias Schaeffter[1], Christoph Bremer[2]
[1]Philips Research Laboratories, Hamburg, Germany; [2]University Hospital Muenster, Muenster, Germany

MRI relaxometry imaging is used for the quantification of super paramagnetic iron oxide (SPIO) contrast agent concentrations. The R2 (=1/T2) and R2* relaxation rates are exploited to obtain information about the concentration. Moreover, the question, whether the contrast agent is incorporated into cells or dissolved in liquid is addressed by measuring the difference R2'=R2*-R2. If the SPIOs are compartmentalized in cells, the R2* relaxation rate is higher than R2; in case the SPIOs are dissolved in liquid the relaxation rates R2 and R2* are similar. We show that SPIO-labeled Human-lung-carcinoma-cells can be distinguished form free SPIO in phantom and *in vivo* studies via the different relaxation properties of R2 and R2*.

1815. Improving Contrast of Iron Oxide Based Cell Labeling with Manganese-Enhanced MRI

Ichio Aoki[1, 2], Yuko Kawai[1], Jun-ichiro Jo[3], Yasuhiko Tabata[3], Masahiro Umeda[1], Toshihiro Higuchi[1], Afonso C. Silva[2], Chuzo Tanaka[1]
[1]Meiji University of Oriental Medicine, Kyoto, Japan; [2]NINDS, NIH, Bethesda, Maryland, USA; [3]Kyoto University, Kyoto, Japan

Negative contrast-agent is useful for organs which have homogeneous positive background such as liver and brain. However, it is difficult to distinguish in areas of inherently low background signal, such as abdomen and cavities. The purpose of this study is to use manganese-enhanced MRI to improve SNR and contrast in tissues prior to administration of iron-oxide-labeled agents or cells. Mn^{2+} can shorten the T_1 and yield better SNR for detecting negative contrast-agents such as iron-oxide particles. This information will be also useful for identifying and masking the signal voids due to local magnetic inhomogeneity or low signal areas.

1816. Sensitivity of Off-Resonance Susceptibility Separation with Superparamagnetic Iron Oxide

Catherine Diane Gard[1], Anthony Z. Faranesh[2], Garry Gold[2], Tom Grist[1], Scott B. Reeder[1]
[1]University of Wisconsin-Madison, Madison, Wisconsin, USA; [2]Stanford University, Stanford, California, USA

Superparamagnetic iron oxide (SPIO) particles have shown promise for labeling and tracking of cells. Using a positive contrast off-resonance separation method, we imaged a phantom with increasing concentrations of SPIO particles. This method acquires images at slightly different echo times to facilitate separation of spins in locally heterogeneous magnetic fields created by SPIO particles. Using a spherical magnetic perturbation model, on- and off-resonance signals were separated and used to measure the sensitivity of this method with free SPIO particles. This method demonstrated a linear increase in signal separation with increasing SPIO concentrations, and was sensitive to concentrations above 54 ig/mL.

1817. Positive Contrast Visualization of SPIO Labelled Cells by Diagonal-SPRITE

Po-Wah So[1], Andrea Protti[1], Tammy Kalber[1], Amy Heavner Herlihy[1], Jimmy David Bell[1]
[1]Hammersmith Hospital, Imperial College London, London, UK

Superparamagnetic iron oxide particles (SPIOs) have been used to label a range of cells. Whilst gradient-echo based pulse sequences are commonly employed, signal voids arising from susceptibility agents such as SPIOs cannot be distinguished from bulk susceptibility differences. The origin of the signal voids may be discerned by the application of Diagonal-SPRITE, a UTE method, which can also be employed to achieve positive contrast. In this study, Diagonal-SPRITE MR methods were used to provide positive contrast of SPIO labelled cells in vitro and *in vivo* by subtraction of Diagonal-SPRITE images obtained at different phase encoding times.

1818. Small Hypovascular Hepatocellular Nodules: Association with Signal Intensity at SPIO-Enhanced MR Imaging in Cirrhotic Livers

Minoru Hayashida[1], Katsuyoshi Ito[1], Ayame Shimizu[1], Masahiro Tanabe[1], Naofumi Matsunaga[1]
[1]Yamaguchi University School of Medicine, Ube, Yamaguchi, Japan

The purpose of this study was to evaluate signal-intensity patterns of small hypovascular hepatocellular lesions at SPIO-enhanced MR imaging. This study included 67 hypovascular hepatocellular lesions in 47 patients. Most hypovascular hepatocellular lesions seen at multiphasic contrast-enhanced dynamic CT in cirrhosis showed iso- (34/67: 51%) or low-signal intensity (21/67: 31%) at SPIO-enhanced MR imaging, indicating that these lesions tended to possess an almost identical or higher number of Kupffer cells in nodules than surrounding liver tissues. This fact may suggest close association between intranodular blood supply and SPIO uptake (numbers and functions of Kupffer cells) of hepatocellular lesions.

1819. Relaxometry of New Nanoparticles at 3 Tesla: Effect of Core Size and Coating on R1, R2, R2*

Michael Gerhard Kaul[1], Nadja Bigall[2], Oliver T. Bruns[1], Harald Ittrich[1], Marija S. Nikolic[2], Wolfgang J. Parak[3], Hannes Dahnke[4], Horst Weller[2], Gerhard Adam[1]
[1]University Medical Center Hamburg-Eppendorf, Hamburg, Germany; [2]University of Hamburg, Hamburg, Germany; [3] Ludwig-Maximilians University, München, Germany; [4]Philips Research Laboratories, Hamburg, Germany

Molecular imaging is one of the major interests in modern diagnostic medicine. New contrast agents with shaped functionality and strong relaxivities are desired. In this study new nanoparticles with different core sizes and coatings were examined and tested. The applied sequences together with the analyzing tools have shown to be an effective package to determine in-vitro relaxivities of new nanoparticles on a clinical 3T scanner. The influence of the core size and the coating on the relaxivities has been shown.

1820. New Synthesis Method of Ultrasmall Iron Oxide Nanoparticles Using Polyvinylpyrrolidone

Ji-ae Park[1], Yongmin Chang, [1], Bo-Hyung Park[1], Seung-Tae Woo[1], Hui-Jin Song[1], Joo-Hyun Kim[1]
[1]Kyungpook National University, Daegu, Jung-gu, Republic of Korea

In this study, we introduced the new synthesis method of PCL coated iron oxide nanoparticles with use of polyvinylpyrrolidone(PVP). The major advantages of our method on the process of polycaprolactone and polyvinylpyrrolidone coated iron oxide nanoparticle(PCL-PVP-NP) is that it is not going through the polymerization of biocompatible polymer. So it can be more easy and inexpensive than existing method. Moreover it has carboxylic groups on the surface of the PCL-PVP-NP. The carboxylic groups are advantageous in that they can be conjugated to other functional group or other proteins. By its ability to make a conjugation with molecular markers such as antibody or small peptide, PCL-PVP-NP becomes a good model system for molecular imaging.

1821. Distinguishing of Magnetically Labeled Cells from Hemorrhage Using Positive Contrast MRI

Eun-Ju Kim[1], Dae Hong Kim[2], Eun-Sook Lee[1], Ho-Taek Song[1], Jin-Suck Suh[1]
[1]Yonsei University, Seoul, Republic of Korea; [2]Korea Basic Science Institute, Daejeon, Republic of Korea

The labeled cells with superparamagnetic iron oxide (SPIO) can be traced using *in vivo* MRI. But the labeled cell and hemorrhage could not be clearly distinguished in conventional T2* weighted MRI. By using the positive contrast MRI method, we present the possibility that SPIO-labeled cells were distinguishable from hemorrhage *in vitro* and *in vivo*.

1822. MR Apoptosis Imaging and Evidence of Apoptotic Nanoprobe Passing Across the Blood Brain Barrier

Donghoon Lee[1], Jonathan Gunn[1], Conroy Sun[1], Omid Veiseh[1], Stacey Hansen[2], Miqin Zhang[1], Jim Olson[2], Richard Ellenbogen[1], Raymond Sze[3]
[1]University of Washington, Seattle, Washington, USA; [2]Fred Hutchinson Cancer Research Center, Seattle, Washington, USA; [3]Children's Hospital and Regional Medical Center, Seattle, Washington, USA

Iron oxide based nanoparticles have been synthesized with PEG (polyethylene glycol) coated and annexin V conjugated in order to achieve target imaging on apoptotic brain tumor, medulloblastoma (D283). Successful particle uptake by apoptotic cells was observed to acquire linear relationship between the degree of apoptosis and iron concentration. The particles (np-PEG-annexin V) injected through tail vein were taken by normal mouse brain for several hours then cleared out approximately 12 hours after the administration. This indicates a strong evidence that the small size of the nanoprobe synthesized for the apoptotic imaging allowed the passage across the blood brain barrier.

1823. Off Resonance Spectroscopic Imaging of Iron Oxide Nanoparticles at Dilute Concentrations and High Field Strengths

Christian Thomas Farrar[1], Guangping Dai[1], Bruce R. Rosen[1], David E. Sosnovik[1]
[1]Massachusetts General Hospital, Charlestown, Massachusetts, USA

Off Resonance Spectroscopic Imaging (ORSI) may provide a powerful new technique for bright contrast imaging of susceptibility based contrast agents. Prior studies with ORSI have been done at 1.5 Tesla and with high concentrations of the contrast agent. The aim of this study was thus to evaluate ORSI at high field strengths and dilute concentrations of iron oxide. Our results suggest that ORSI may be able to (1) selectively image different MION concentrations, (2) selectively suppress susceptibility based artifacts such as air bubbles, and (3) detect MION concentrations as low as 8 ug Fe/ml in fluid solution.

1824. Epidermal Growth Factor Receptor (EGFR) Targeted MRI Using a Probe of SPIO Nanocrystal and ScFv EGFR Conjugate

Hui Mao[1], Lily Yang[1], Xianghong Peng[1], Y Andrew Wang[2], Xiaoxia Wang[1], Zehong Cao[1], Gregory Adams[3], Qing An Yuan[3]

[1]Emory University School of Medicine, Atlanta, Georgia, USA; [2]Ocean NanoTech, LLC, Fayetteville, Arkasas, USA; [3]Fox Chase Cancer Center, Philadelphia, Pennsylvania, USA

We report our investigation of a novel MRI probe consisting of superparamagnetic iron oxide (SPIO) nanocrystals conjugated with the protein (ScFv EGFR, a single chain antibody), developed for MR imaging of EGFR over-expressed in tumors. This EGFR targeted SPIO nanocrystal-ScFv EGFR conjugate exhibits strong T1 and T2 shortening effects. Its strong specificity in binding to EGFR over expressed breast cancer cells was demonstrated by T2 MRI in cell culture. *In vivo* mouse MRI showed T2 contrast enhancement in the liver/spleen and delayed T1 enhancement in the kidney, indicating that this protein-SPIO complex is stable in physiological conditions.

1825. Fast Positive Contrast Imaging Using a Spin-Echo Spiral Sequence

Weitian Chen[1], Wen-Tung Wang[1], Walter J. Rogers[1], Craig H. Meyer[1]

[1]University of Virginia, Charlottesville, Virginia, USA

The presence of super-paramagnetic iron-oxide particles can be visualized either as a negative contrast or a positive contrast. Positive contrast imaging is reported to have improved specificity in iron detection. We developed a rapid slice-selective spin-echo spiral sequence for positive contrast imaging. We achieved positive contrast imaging *in vivo* by using this sequence. The developed technique is less sensitive to respiratory motion than 2DFT positive contrast imaging sequences.

1826. Investigation of USPIO-Induced Field Inhomogeneities in a Rat Stroke Model

Ana-Maria Oros-Peusquens[1], Marco Irkens[1], Michael Schroeter[2], Andreas Saleh[2], Sebastian Jander[2], Nadim Jon Shah[1]

[1]Research Centre Juelich, Juelich, Germany; [2]Heinrich-Heine University Duesseldorf, Duesseldorf, Germany

We investigate the field inhomogeneities generated by ultrasmall superparamagnetic iron oxide particles (USPIO) accumulation in the rat brain following stroke. Two stroke models are used, one induced by photothrombosis (PT), the other by main cerebral arterial occlusion (MCAO). The inflamation produced by stroke is followed by aninflux of macrophages at the site of the lesion. The time scale of this process depends on the stroke pathophysiology. Macrophages can be visualised in MRI by their strong uptake of USPIO from the vasculature. The effect of USPIO accumulation on the local R2* relaxation properties isinvestigated using a gradient echo sequence with multiple echoes. Strong non-exponential decay of the FID is observed frequently. Correspondingly, the Fourier transform of the FID shows lineshapes with forms significantly deviating from a Lorentzian shape. These lineshapes, intensities and widths aremonitored and mapped in several exemplars, at 2 as well as 7 days following induced stroke. A novel visualisation method sensitive to field inhomogeneity is proposed.

1827. Magnetic Resonance Imaging of Viral Particle Biodistribution *In Vivo*

Juhana Hakumäki[1, 2], Jani Räty[1], Timo Liimatainen[1], Thomas Wirth[3], Tuulia Huhtala[1], Teemu Ihalainen[4], Maija Vihinen-Ranta[4], Ale Närvänen[1], Seppo Ylä-Herttuala[1]

[1]University of Kuopio, Kuopio, Finland; [2]Kuopio University Hospital, Kuopio, Finland; [3]Ark Therapeutics Ltd., Kuopio, Finland; [4]University of Jyväskylä, Jyväskylä, Finland

We have studied the possibility of visualizing viral vector particle biodistribution *in vivo* by MRI. An avidin-displaying baculoviral vector (Baavi) was conjugated with biotinylated USPIO particles. The results show that viral particle homing into choroid plexus cells in rat brain can be visualized by MRI and that the labeling does not affect the transfection or homing capabilities of the avidin-coated baculoviral vector. Our study provides the first evidence that viral vector imaging can be performed by MRI using USPIO-labeled, avidin-displaying baculoviruses *in vivo*. Thus, the utility of MRI is expanded also to the very initial steps of therapeutic gene delivery.

1828. Temperature Dependence of T1 Relaxation Time of New Long-Circulating Thermosensitive Liposomes with Encapsulated Gadodiamide

Tungte Wang[1], Martin Hossann[1], Herbert M. Reinl[1], Michael Peller[1], Nicole Teichert[1], Maximilian Reiser[1], Rolf D. Issels[1], Lars H. Lindner[1]

[1]University Hospital Grosshadern, Ludwig-Maximilians-University, Munich, Bavaria, Germany

Recently, a novel formulation of long-circulating thermosensitive liposomes with encapsulated gadodiamide for MR thermometry has been developed. It showed the potential to both release the cytostatic drug and monitor the temperature during the tumor treatment using the combined chemotherapy and hyperthermia. In this work, T1 of these liposomes was measured, while heated from 30 C up to 50 C and subsequently cooled down. The results revealed that the gadodiamide/drug was released due to the phase transition at about 41 C, consistent with the therapeutic temperature for the combined therapy. Moreover, the temperature during the treatment could be derived from the measured T1.

1829. The Modified Fe_3O_4-NH_3^+ with RGD-4C Ligand for Cancer Cell Targeting MR Contrast Agent

Chia-Hao Su[1], Ping-Ching Wu[2], Jun-Cheng Weng[1], Dar-Bin Shieh[3], Chen-Sheng Yeh[2], Jyh-Horng Chen[1]

[1]National Taiwan University, Taipei, Taiwan; [2]National Cheng Kung University, Tainan, Taiwan; [3]National Cheng Kung University, Taipei, Taiwan

A comprehensive totally aqueous phase synthesis of NTA-Ni modified superparamagnetic Fe_3O_4 nanoparticles was presented and the particles diameter is 6.2 ± 1.1 nm. The Fe_3O_4-NTA-Ni particles may act as a modular designed unit rendering molecular orientation control, which was demonstrated in the receptor mediated targeting for cancer cells expressing specific integrins using RGD-4C-6-His fusion peptide as the ligand to self-assemble on the nanoparticle through surface immobilized Ni-NTA. In MR imaging study, we found that the Fe_3O_4-NTA-Ni-RGD-4C-6-His particles exhibited an efficient tumor targeting and contrast enhancement. Furthermore, the results of Pearls?iron stain on the tumor cells also provided the Fe_3O_4-NTA-Ni-RGD-4C-6-His particles as the tumor-targeting probe.

1830. Targeted Contrast Using Gadolinium Labeled G5 Dendrimers

Scott D. Swanson[1], Jolanta F. Kukowska-Latallo[1], Anil K. Patri, [12], James R. Baker, Jr. [1]

[1]University of Michigan, Ann Arbor, Michigan, USA; [2]National Cancer Institute, Frederick, Maryland, USA

A target-specific MRI contrast agent for tumor cells expressing high affinity folate receptor has been synthesized and evaluated. The contrast agent was synthesized using generation five (G5) of polyamidoamine (PAMAM) folate-dendrimer and the bifunctional DOTA chelator that forms stable complexes with Gadolinium (Gd). We report selective uptake in tumor of the G5 dendrimer in NOD scid mice using human KB tumor cells over-expressing folate receptor (FAR+).

1831. Hot Spot Imaging of Microcapsules: An Initial Assessment of Detection with Fluorine and Magnetization Transfer Imaging

Brad P. Barnett[1], Assaf A. Gilad[1], Jesus Ruiz-Cabello[1], Mike T. McMahon[1, 2], Dara L. Kraitchman[1], Aravind Arepally[1], Peter C. van Zijl[1, 2], Jeff W M Bulte[1]

[1]Johns Hopkins University School of Medicine, Baltimore, Maryland, USA; [2]Kennedy Krieger Institute, Baltimore, Maryland, USA

The hallmark of microencapsulation technology is its ability to create a permeability barrier between graft tissue and host immune system. Immuno-isolation of cells encapsulated in alginate-PLL-alginate capsules has proven effective in treating a number of human diseases in small-scale clinical trials. For further advancement in the clinic, a means of imaging microcapsules post-transplantation in order to assess biodistribution and functionality is needed. To this end, we present two techniques to image microcapsules. The first utilizes fluorine imaging to detect capsules loaded with a PFPE agent. The second utilizes magnetization transfer imaging to detect the PLL inherent in APA microcapsules.

1832. Annexin A5 Conjugated Quantum Dots with a Paramagnetic Lipidic Coating for the Multimodal Detection of Apoptotic Cells

Geralda A.F. van Tilborg[1], Willem J.M. Mulder[1], Patrick T.K. Chin[1], Chris P.M. Reutelingsperger[2], Gustav J. Strijkers[1], Klaas Nicolay[1]

[1]Eindhoven University of Technology, Eindhoven, Netherlands; [2]Maastricht University, Maastricht, Netherlands

Apoptosis, or programmed cell death, plays an important role in the etiology of a variety of diseases, including cancer. Visualization of apoptosis would allow both early detection of therapy efficiency and evaluation of disease progression. To that aim we developed a novel annexinA5-conjugated bimodal nanoparticle that is composed of a quantum dot with a paramagnetic lipid coating, which can be used both for *in vivo* optical imaging and MRI. Both fluorescence microscopy and MRI demonstrated a high specificity of the annexinA5-contrast agents for apoptotic cells, which confirms its potential for the detection of apoptosis with both imaging modalities *in vivo*.

1833. Compartmental Assessment of Gadofluorine Contrast Agent Deposition in Atherosclerotic Plaque of WHHL Rabbits and Its Correlation to Lipid Content

Stephen Clark Lenhard[1], Karpagam Aravindham[1], Alan Olzinski[1], Bernd Misselwitz[2], Hanns Joachim Weinmann[2], Beat Jucker[1]

[1]GlaxoSmithKline, King of Prussia, Pennsylvania, USA; [2]Schering AG, Berlin, Germany, Germany

This study was undertaken to more definitively assess the accumulation of Gadofluorine within specific regions of atherosclerotic plaque and to quantitatively examine the correlation between contrast agent uptake and cholesterol content in the lesions.

1834. [19]F MR Techniques Augment Quantitative Molecular Imaging with Paramagnetic Perfluorocarbon Nanoparticles at 1.5T

Shelton D. Caruthers[1, 2], Anne M. Neubauer[1, 3], Frank D. Hockett[1], Rolf Lamerichs[4], Patrick M. Winter[1], Michael J. Scott[1], Patrick J. Gaffney[5], Samuel A. Wickline[1], Gregory M. Lanza[1]

[1]Washington University School of Medicine, St. Louis, Missouri, USA; [2]Philips Medical Systems, Andover, Massachusetts, USA; [3]Washington University, St. Louis, Missouri, USA; [4]Philips Research Labs, Eindhoven, Netherlands; [5]St. Thomas' Hospital, London, UK

Relative to proton-based MR molecular imaging, fluorine MRI/MRS offer additional possibilities in quantifying agents and discerning multiple tracers. Herein, we demonstrate [19]F quantification techniques as compared to T1 measurements using fibrin-targeted paramagnetic perfluorocarbon nanoparticles in clot phantoms. Two fibrin-targeted nanoparticle emulsions were prepared using perfluoro-15-crown-5-ether (CE) or perfluorooctylbromide and applied to clots in varying mixtures. Only the CE particles incorporated gadolinium. With proton imaging, signal intensity and T1 values behaved as expected with CE concentration. Signal intensity on both [19]F imaging and spectroscopy correlated well with nanoparticle concentration. Additionally, the different perfluorocarbons were imaged and quantified independently.

1835. The Optimization of Liposomal Formulations for Molecular MR Imaging

Gustav Jacob Strijkers[1], Willem J. Mulder[1], Ewelina Kluza[1], Klaas Nicolay[1]

[1]Eindhoven University of Technology, Eindhoven, -, Netherlands

The present study was aimed to optimize the relaxivity properties of liposomal molecular MRI contrast agents. Measurements of the molar relaxivities r1 and r2 were done as a function of the content of Gd-DTPA-containing lipid and temperature at 0.47 and 1.41 T. The study demonstrates that liposomes with a high payload of Gd-DTPA-lipid are attractive candidates for the MRI-based detection of sparse molecular targets. The liposomes containing 25 mol% Gd-lipid are most suitable, because they exhibit the highest relaxivity per mM liposomes with acceptable r2/r1 ratio.

1836. A Novel Approach of Quantifying Susceptibilities in Small Objects: Quantitative Diagnosis in MRI

Ching-Yi Hsieh[1], Yu-Chung Norman Cheng[1], Jaladhar Neelavalli[1], Qiang Liu[1], E. Mark Haacke[1]

[1]Wayne State University, Detroit, Michigan, USA

We have studied the simulation and experiment of a small air tube in a gel phantom. The susceptibility difference between the gel and air creates a phase variation in the gel. Based on analyzing MR signals within two specific concentric circles on each complex image, the susceptibilities obtained from different complex images can be accurate within 10%. This complex sum method is promising to be used in quantifying local susceptibilities of small objects. Efforts in this research will lead to the quantification of small amount of iron *in vivo* in future.

New or SMART Contrast Agents

Room 4E Tuesday 13:30 - 15:30

1837. CNS Imaging with a High Relaxivity Contrast Agent: What is the Benefit Over a Standard Gadolinium Agent?

Kenneth R. Maravilla[1], Joseph A. Maldjian[2], Ilona M. Schmalfuss[3], Matthew J. Kuhn[4], Nicoletta Anzalone[5], Marco Essig[6], Lars Gustafsson[7]

[1]University of Washington, Seattle, Washington, USA; [2]Wake Forest University, Winston-Salem, North Carolina, USA; [3]University of Florida, Gainesville, Florida, USA; [4]Southern Illinois School of Medicine, Springfield, Illinois, USA; [5]Hospital San Raffaele, Milan, Italy; [6]German Cancer Research Institute, Heidelberg, Germany; [7]Sahlgrenska University Hospital, Gothenburg, Sweden

Gadobenate dimeglumine (GBD) is a Gd contrast agent with higher relaxivity in blood compared with other approved Gd agents. To explore the clinical utility of increased R1, 151 patients with brain or spine disease underwent two MRI examinations, one with GBD and the other with gadopentetate dimeglumine (GPD). Three blinded neuroradiologists read all cases. Lesion-to-brain CNR was significantly greater after GBD than after GPD ($p<0.0001$), with 3 readers noting increases in enhancement over GPD of 22%, 25%, and 26%, respectively. Readers preferred GBD over GPD for lesion border delineation, definition of disease extent, visualization of lesion morphology, lesion enhancement, and global diagnostic preference ($p<0.0001$ for all). This study confirms the improved enhancement provided by gadobenate dimeglumine for CNS imaging.

1838. Development of Gadolinium Based Contrast Agents to Detect Tumor Apoptosis *In Vivo* Using MRI

Anant Krishnan[1], Andre Neves[1], Mikko Kettunen[1], De-en Hu[1], Maaike de Backer[1], Kevin Michael Brindle[1]

[1]University of Cambridge, Cambridge, UK

The C2A domain of Synaptotagmin I (C2A) shows high affinity binding to phosphatidylserine on apoptotic cells. We are developing Gd3+-based contrast agents (CA), based on conjugation of C2A. GST-tagged C2A directly conjugated to a Gd-DTPA complex produced a CA with a T1-relaxivity of 60 mM-1s-1 (9.4T). Experiments in vitro, showed an increase in signal intensity in T1-weighted images with increasing amounts of C2A-GST-Gd. Experiments *in vivo* showed a decrease in tumor T1 over 24 hours in treated animals injected with C2A-GST-Gd, compared with controls. These data suggest that Gd3+-based contrast agents may detect apoptosis in vitro and *in vivo*.

1839. MRI Detection of Rapamycin and AP-Cav Therapeutic Rescue from Endothelial Over Expression of Akt in Transgenic Mice

Keren Ziv[1], Thuy L. Phung[2], Ori Brenner[1], Kenneth Walsh[3], Laura E. Benjamin[4], Michal Neeman[1]
[1]Weizmann Institute of Science, Rehovot, Israel; [2]Beth Israel Deaconess Medical Center and Harvard Medical School, Boston, Massachusetts, USA; [3]Boston University, Boston, Massachusetts, USA; [4]Beth Israel Deaconess Medical Center and Harvard Medical School, Boston, Massachusetts, USA

Akt, a serine/threonine protein kinase is chronically activated in VEGF stimulated endothelial cells, and induces angiogenesis via its downstream effectors, mTOR and eNOS. MRI was applied here for studying the effect of pharmacological inhibition of mTOR and eNOS on myrAkt-activated vasodilation and elevation of blood volume, in a transgenic mouse model with endothelial inducible expression of dominant active Akt (myrAkt). Rapamycin (mTOR inhibitor) reduced blood volume to a normal level, while AP-Cav (eNOS inhibitor) yielded a smaller un-significant effect. Thus, suppressing the signaling of Akt via mTOR can reverse the angiogenic phenotype of tumor blood vessels induced by VEGF.

1840. Cellular MRI Contrast Via Co-Expression of Transferrin Receptor and Ferritin

Abby E. Deans[1], Youssef Zaim Wadghiri[1], Lisa M. Bernas[2], Xin Yu[1], Brian K. Rutt[2], Daniel H. Turnbull[1]
[1]New York University School of Medicine, New York, USA; [2]University of Western Ontario, London, Ontario, Canada

Cellular MRI contrast is demonstrated in an in vitro system via co-expression of the TfR and FTH genes in a transfected mouse neural stem cell line. Our results demonstrate that transfected cells have increased iron accumulation with no detectable cell toxicity. The differential accumulation of iron results in a significant increase in transverse relaxivities R2 and R2* at 1.5T and 7T, with increased effect at higher field strength. Increased R2* effect is also observed following transplantation into mouse forebrain by T2*-weighted brain imaging and R2* relaxometry at 7T.

1841. The Efficacy of Signal Intensity Change Map Images Obtained Using First Pass Dynamic Fercarbotran-Enhanced MR Imaging for Assessment of Focal Hepatic Lesion Vascularity

Seishi Kumano[1], Keiichi Kikuchi[1], Takaharu Tsuda[1], Hitoshi Miki[1], Teruhito Mochizuki[1]
[1]Ehime University, Toon, Ehime, Japan

First pass dynamic ferucarbotran-enhanced MRI also can be evaluated the vascularity of hepatic focal lesion by using single shot GER EPI sequence. The purpose of this study was to evaluate the efficacy of the signal intensity map images for the detection of hypervascular hepatocellular carcinomas. Continuous 25 phase images were obtained to include the entire liver. Signal intensity change was calculated as exponential fraction (SI=A-kt) with pixel by pixel basis. Signal intensity map images using first pass dynamic Fercarbotran-enhanced MRI can be helpful in determining the vascularity, especially in lesions larger than 2cm.

1842. Non-Invasive Visualization on Drug Delivery of Polymer Drug Conjugates

Furong Ye[1], Tianyi Ke[1], Eun-Kee Jeong[1], Xuli Wang[1], Zheng-Rong Lu[1]
[1]University of Utah, Salt Lake City, Utah, USA

Polymers have become effective carriers in drug delivery due to advantages such as enhanced tumor accumulation. However the *in vivo* delivery mechanism of polymer drug conjugates is not clear based on current biopsy-based method. We intend to explore non-invasive monitoring of *in vivo* drug delivery with contrast-enhanced MRI and quantitative T1 mapping. MRI data clearly revealed the sized effect of the conjugates on their pharmacokinetics; and quantitative T1 mapping is effective to visualize the dynamic accumulation of the conjugates in the solid tumor tissue. It's promising for future study of non-invasive monitoring in drug delivery with polymeric drug conjugates.

1843. Controlled Internalization and Recycling of Her-2/neu by Cross-Linking with an Avidin/streptavidin-Biotin System for MR Enhancement

Wenlian Zhu[1], Baasil Okollie[1], Zaver M. Bhujwalla[1], Dmitri Artemov[1]
[1]Johns Hopkins University, Baltimore, Maryland, USA

Avidin/streptavidin-biotin system is frequently used in pretargeting approaches to link antibody and targeting agent together due to the rapid reaction between avidin/streptavidin and biotin with high affinity. In the ideal pretargeting setting, cell membrane bound biotinylated antibody is tagged by avidin, which subsequently binds to a biotinylated functional agent. However, avidin is a tetramer that can bind to four biotinylated antibody molecules, which results in extensive cross-linking of the antibody before binding it to the funtional agents. We show here the internalization and recycling of Her-2/neu receptors induced by the above cross-linking and its application in MR signal enhancement.

1844. Development of Avidin-Based Positive Contrast Agents to Detect Tumor Apoptosis Using MRI

Andre A. Neves[1], Anant Krishnan[1], Mikko Kettunen[1], De Hu[1], Maaike De-Backer[1], Kevin Brindle[1]
[1]University of Cambridge, Cambridge, England, UK

We have been developing targeted MRI contrast agents (CAs) that can be used to detect tumor cell apoptosis *in vivo*, a prognostic indicator for the outcome of therapy. These CAs are based on the C2A domain of synaptotagmin I and avidin conjugated to gadolinium chelates, having the potential for signal amplification and improved sensitivity. Relatively large increases in T1 relaxation were observed in vitro (up to 2.5-fold) and *in vivo* (up to 1.6-fold) when the complexes bound to apoptotic cells. Ongoing tests *in vivo* will allow the selection of an avidin-based positive CA with adequate sensitivity, specificity and pharmacokinetic properties.

1845. MRI of C6 Glioma Cells Taged with an Opioid Functionalized DTPA-Gd Contrast Agent

Timo Dansauer[1, 2], Ekkehard Küstermann[1, 2], Dieter Leibfritz[1, 2]
[1]University of Bremen, Bremen, Germany; [2]Center of Advanced Imaging (CAI), Bremen, Germany

A paramagnetic contrast agent Bis-normorphine-Gd-DTPA complex is presented, which interacts with opioid receptors of C6 rat glioma cells. Furthermore the synthesis, kinetical stability in media DMEM, T1 and T2 relaxation times respectively are described.

1846. Contrast Agent for Blood Pool Imaging and Targeted Contrast Delivery Using RHA and Gd-DTPA

Jim M. Wild[1], John Woodrow[2], Bernd Misselwitz[3], Richard Johnson[2]
[1]University of Sheffield, Sheffield, Yorkshire, UK; [2]Upperton Ltd, Nottingham, UK; [3]Schering, AG, Berlin, Germany

Significant quantities of Gd-DTPA were attached to the recombinant human albumin (rHA) molecule in the laboratory. The agent has a higher molar R1 and R2 in water (R1 = 7.2 s-1mM-1, R2 = 18.4 s-1 mM-1) than Gd-DTPA (R1 3.5 s-1 mM-1, R2 = 5.5 s-1 mM-1). In-vivo comparisons with Gd-DTPA and a polymeric Gd blood-pool agent, were made in rats and the clearance kinetics were examined. With free sites on the Gd loaded rHA molecule, there are possibilities for binding the agent to antibodies. This was demonstrated and thus the potential applications for targeted molecular imaging are highlighted.

1847. Design and Synthesis of a Novel Gadolinium-Based MR Contrast Gd(DOBAPATA) for MR Imaging of Calcium

Anil K. Mishra[1], Josef Pfeuffer[2]
[1]INMAS, Delhi, India; [2]Siemens Medical Solutions, Erlangen, Germany

A novel MR contrast agent was developed to report on changes in calcium ion concentration. Gd(DOBAPATA) is a hybrid MR contrast agent, which binds gadolinium and calcium selectively. The calcium binding chelating agent was derived from an amino acid and conjugated to the gadolinium binding agent DOTA. EDTA type of chelating agents are known to have high affinity towards calcium and can function as reporters of calcium ions. Bis-amino-phenylalanine tetraacetate was linked with DOTA via amide to function as an extracellular MR contrast agent for imaging calcium ions to report on neuronal activity. Here, we present first in-vitro MR relaxation studies.

1848. Selective MRI and MRS of PEGylated Compounds

Scott D. Swanson[1]
[1]The University of Michigan, Ann Arbor, Michigan, USA

To reduce clearance time, delay breakdown time, and increase clinical efficacy, small molecule pharmaceutical agents are sometimes attached to polyethylene glycol (PEG). We report that PEGylated pharmaceuticals can be selectively detected using MRI or MRS with an increased sensitivity of up to three orders of magnitude. High molecular weight, flexible polyethylene chains, and superposition of many ethylene resonances combine to create a condition favorable for MRI and NMR detection. In this example we have selectively created an image Pegaptanib Sodium with only 32 nmoles of compound.

1849. First *In Vivo* Characterization of a Low Molecular Weight Gd-Metallostar – a Contrast Agent with High Relaxivity

Claudia Weidensteiner[1], Joao Bruno Livramento[2], Philipp Schmidt[1], Rainer Kneuer[1], Peter Roland Allegrini[1], Lothar Helm[2], Éva Tóth[2, 3], André E. Merbach[2]
[1]Novartis Institutes for BioMedical Research, Basel, Switzerland; [2]École Polytechnique Fédérale de Lausanne, Lausanne, Switzerland; [3]Centre de Biophysique Moléculaire CNRS, Orleans, France

In this study, the first *in vivo* characterization of a new contrast agent - a Gd-metallostar $[Fe\{Gd_2L(H_2O)_4\}_3]^{-4}$ (3.7 kDa) - was performed in mice with dynamic contrast enhanced MRI (4.7 T). Its *in vivo* relaxivity and pharmacokinetics were compared to GdDOTA (0.56 kDa). The pharmacokinetics of the metallostar was similar to GdDOTA whereas its relaxivity was much higher. The results confimed that the *in vivo* relaxivity of the metallostar was very close to the value of 13.5 $s^{-1}mM^{-1}$ Gd as measured in saline (compared to 3.3 $s^{-1}mM^{-1}$ Gd for GdDOTA).

1850. Novel Bioresorbable Magnetic Contrast Agent Nanoceramics

Igor Kuriashkin[1], Louise Lee[1], Ryan Haggerty[1], Waltraud Kriven[1]
[1]University of Illinois at Urbana-Champaign, Urbana, Illinois, USA

Nanoceramic particles, such as layered double hydroxides (LDHs), have possible applications as drug delivery carriers. Bimolecules and chemotherapeutic can be intercalated into LDHs, displacing the interlayer anions. A new ceramic contrast reagent for MRI, $(Gd^{3+}\text{-DTPA})^{2-}$intercalated LDHs, have been developed and verified by fluorescent confocal microscopy, EPR and MRI.

1851. Novel Myristoylated Polyarginine Peptides for Molecular Neuroimaging: Initial *In Vivo* Studies

Rob J.A. Nabuurs[1], Mark A. Van Buchem[1], Guangping Dai[1], Anna Moore[1], Wellington Pham[1]
[1]Massachusetts General Hospital, Charlestown, Massachusetts, USA

Recently we have demonstrated that a fluorescently labeled myristoylated polyarginine peptide, MPAP, could cross the blood-brain barrier and be detected by *in vivo* optical imaging. This study assessed whether a gadolinium-modified delivery module, MPA11P, could cross the BBB and could be detected by MRI. *In vivo* MRI was performed using a T1 inversion recovery sequence on nude mice before and after intraperitoneal administration of MPA11P. T1 histograms of manually segmented brain regions showed a peak shift towards a lower T1 time 24 h after injection. Our study suggests that MPA11P-Gd could be detected in the brain by *in vivo* MRI.

1852. Design and Synthesis of Novel Myristoylated Polyarginine Peptides for *In Vivo* Molecular Neuroimaging

Wellington Pham[1], Rob J.A. Nabuurs[1], Mark A. Van Buchem[1], Anna Moore[1]
[1]Massachusetts General Hospital, Charlestown, Massachusetts, USA

Clinical application of potentially useful imaging agents for the detection of neurodegenerative diseases is hampered by the limited access of probes to the BBB. Here we developed Gd-associated fatty acylated polyargine (MPAP-Gd) as a probe to cross the BBB for molecular neuroimaging using MRI. The peptide backbone was synthesized by solid phase chemistry, while a fatty acid group was incorporated using Schotten-Baumann reaction. DOTA was conjugated to the peptide selectively to a lysine side chain on solid support followed by association with gadolinium to afford the final product. Assessment of the probes *in vivo* using MRI is currently underway.

1853. Paramagnetic Metal Probes Used for the Development of High-Relaxivity Protein Targeted Contrast Agents

Stephan G. Zech[1], Hariett B. Eldredge[1], Mark P. Lowe[2], Peter Caravan[1]
[1]EPIX Pharmaceuticals, Inc., Cambridge, Massachusetts, USA; [2]University of Leicester, Leicester, UK

The relaxivity of the gadolinium blood pool contrast agent MS-325 is found to be significantly higher when bound to human serum albumin (HSA) as compared to albumins from rabbit, rat or mouse. Various biophysical methods (NMR, relaxometry, luminescence) are employed with MS-325 surrogates where lanthanide ions Eu, Yb, or Dy have replaced the Gd. Exploiting the unique properties of the other lanthanides, molecular parameters influencing relaxivity are independently determined. While the molecular tumbling time and water hydration number do not change, water exchange is significantly slower when MS-325 is bound to rabbit albumin compared to HSA, resulting in decreased relaxivity.

1854. Comparison of Gd-Bz-TTDA, Gd-EOB-DTPA and Gd-BOPTA in Dynamic MR Imaging of the Liver with Rat Models

Twei-Shiun Jaw[1], Gin-Chung Liu[1], Yun-Ming Wang[1], Shih-Hsien Chen[1], Jui-Shung Hsu[1], Feng-O Shen[1]
[1]Kaohsiung Medical University, Kaohsiung, Taiwan, Taiwan

To evaluate the competitive potential of a new lipophilic paramagnetic complex, Gd-Bz-TTDA with the commercially available MR hepatobiliary contrast agents Gd-BOPTA and Gd-EOB-DTPA, dynamic MR imaging studies for normal and hepatocellular carcinoma (HCC) rats models were performed using a 1.5- T scanner. The results revealed that the enhancement of liver in normal rats injected with 0.1 mmol/kg Gd-Bz-TTDA was significantly more intense and persistent than those injected with the same dose of Gd-EOB-DTPA or Gd-BOPTA after 5 minutes. All agents showed similar enhancement pattern of the implanted HCCs. The liver-lesion contrast to noise ratios were higher in the rats injected with Gd-Bz-TTDA after 30 minutes. The results indicated that Gd-Bz-TTDA can be competitive to the commercially available hepatobiliary agents, Gd-EOB-DTPA or Gd-BOPTA by its more intense and prolonged liver enhancement, which providing better liver-lesion discrimination.

1855. Transcription MRI Contrast Probe Enables the Detection of Different Cerebral Messenger RNA Levels

Shuning Huang[1], Christina H. Liu[2], Guangping Dai[3], Bruce R. Rosen[1], Philip K. Liu[3]
[1]MIT/MGH, Cambridge, Massachusetts, USA; [2]Martinos Center for Biomedical Imaging, MGH, Cambridge, Massachusetts, USA; [3]Martinos Center for Biomedical Imaging, MGH, Charlestown, Massachusetts, USA

Visualization of gene transcription *in vivo* is very important for genotyping, phenotyping, and accessing alterations in gene transcription during normal development or disease processes. Here we report an MR imaging probe that allows us to detect and visualize diferent mRNA transcript levels from two genes in live animals. This molecular imaging probe will enable us to study molecular processes at mRNA level in healthy and diseased animal models.

1856. Ferritin as a Tissue Specific MRI Reporter of Inducible Gene Expression in Transgenic Mice

Keren Ziv[1], Batya Cohen[1], Vyacheslav Kalchenko[1], Alon Harmelin[1], Michal Neeman[1]
[1]Weizmann Institute of Science, Rehovot, Israel

Ferritin, the iron storage protein was suggested as a reporter gene for MRI. We report here generation of novel Tet:EGFP-HAferritin transgenic mice as a platform for tissue/promoter specific tetracycline-inducible expression of HAferritin and EGFP. Double transgenic offspring generated by crossing with mice expressing tetracycline transactivator in the liver were used for analysis of MR visibility and physiological impact of liver selective overexpression of h-ferritin. Expression of ferritin resulted in reduced R2, which was consistent with histologicaly detected intracellular vacuoles in liver hepatocytes. These findings demonstrate the feasibility of MRI detection of inducible tissue specific ferritin overexpression in transgenic mice.

1857. Transcription MRI Detects Altered Cerebral Gene Expression in Live Stroke Animals

Christina H. Liu[1], Shuning Huang, [12], Bruce R. Rosen[1], Philip K. Liu[1]
[1]Massachusetts General Hospital, Charlestown, Massachusetts, USA; [2]Massachusetts Institute of Technology, Cambridge, Massachusetts, USA

We report here an MR imaging probe that allows us to detect and visualize the elevation of mRNA transcript resulting from acute responses to cerebral ischemia simulating cardiac arrest in live animal. This contrast probe will enable us to study molecular processes at the transcription level in normal developmental and disease models using live animals.

1858. Redox-Sensitive Contrast Agents for MRI Based on Reversible Binding of Thiols to Serum Albumin

Natarajan Raghunand[1], Bhumasamudram Jagadish[1], Theodore P. Trouard[1], Robert J. Gillies[1], Eugene A. Mash[1]
[1]University of Arizona, Tucson, Arizona, USA

DOTA-based thiol complexes of gadolinium were synthesized. It was hypothesized that these complexes would form reversible covalent linkages with human serum albumin (HSA) which contains a reactive thiol at cysteine-34. The binding constants of both complexes to HSA, and their longitudinal water-proton relaxivities, were measured in the absence and presence of homocysteine, a competing thiol. Their *in vivo* pharmacokinetics were followed by DCE-MRI, and could be altered by a chase of homocysteine but not saline. Such spontaneous, redox-sensitive and reversible binding of gadolinium complexes to circulating albumin can be exploited for imaging tissue redox and the blood-pool by MRI.

1859. A Bio-Activated Paramagnetic Gd(III) Complex [Gd(DO3A-FPG)] for MRI

Yun-Ming Wang[1], Yu-Ton Chang[1], Yu-Zheng Su[1], Jui-Sheng Hsu[1], Gin-Chung Liu[1]
[1]Kaohsiung Medical University, Kaohsiung, Taiwan

A novel bio-activated MRI contrast agent containing galactopyranose residue, [Gd(DO3A-FPG)], was designed and synthesized successfully. Relaxation time (T1) decreasing (59 %) of enzymatic cleavage of [Gd(DO3A-FPG)] in BSA indicates that the BSA or β-gal binds to Gd(III) chelate after the galactopyranose residue removed. MR image significant enhancement was observed for [Gd(DO3A-FPG)] solution in the presence of β-gal and BSA. [Gd(DO3A-FPG)] possesses enzymatic cleavage, longer rotational correlation time, higher relaxation rate and higher MR image enhancement in the presence of β-gal that might result in a novel type of contrast agent for visualization of gene expression by MRI

1860. Investigations Into the Relaxivity and Complexation Behaviour of GdDOTA-4AmP, a PH Responsive MRI Contrast Agent

A. Dean Sherry[1], [2], Mark Woods[3], Paul Jurek[3], Ferenc Kalaman[1], Md Meser Ali[1]
[1]University of Texas at Dallas, Richardson, Texas, USA; [2]UT Southwestern Medical Center, Dallas, Texas, USA; [3]Macrocyclics, Dallas, Texas, USA

The pH responsive behaviour of GdDOTA-4AmP is of intense interest as an MR contrast agent since its pH response is ideal for use *in vivo*. This poster discusses recent results into how the structure of this complex affects the relaxivity oH response of the complex.

1861. A Smart PARACEST MRI Contrast Agent for Nitric Oxide Detection

Guanshu Liu[1], Marty D. Pagel[2]
[1]Case Western Reserve University, Cleveland, Ohio, USA; [2]Biomedical Engineering, Cleveland, Ohio, USA

We have developed a “smart” PARACEST MR agent that changes its PARACEST effect only after chemical modification by Nitric Oxide. The amine and amide of Yb-DOTA-ortho-Aminoanilide show a PARACEST effect, but reaction with Nitric Oxide converts these functional groups to a hydrazine that doesn’t demonstrate a PARACEST effect. This PARACEST MR agent can also be used to measure pH. This example constitutes a fundamentally new technology platform for “smart” MR agents.

1862. A “smart” PARACEST Agent for Detection of Transglutaminase Activity

Rachel Rosenblum[1], Mark Pagel[1]
[1]Case Western Reserve University, Cleveland, Ohio, USA

We have developed a “smart” PARACEST MR agent that is detectable only after chemical modification by a specific enzyme. Yb-DO3A-pentylamine shows no PARACEST effect, but Transglutaminase catalyzes the reaction of this agent with glutamine to form an amide, which shows a PARACEST effect. This example constitutes a fundamentally new technology platform for “smart” MR agents.

1863. A Transcatheter MR-Guided Fiber Optical Confocal Microscopy System

Sascha Krueger[1], Daniel Herzka[2], Charlotte Cavé[3], King Li[4], Steffen Weiss[1]
[1]Philips Research, Hamburg, Germany; [2]Philips Research, Briarcliff Manor, New York, USA; [3]Mauna Kea Technologies, Paris, France; [4]National Institutes of Health, Bethesda, Maryland, USA

To combine the excellent diagnostic imaging and real-time guidance capabilities of an MR system with the high resolution, sensitivity and selectivity of optical microscopic imaging for studying processes at the molecular level, a confocal fiber-based microscopy system was integrated into an MR-localizable catheter (active tracking). MR imaging and tracking and optical imaging are thus automatically co-registered and can be used complementary. The system facilitates spatially directed optical probing of vascular tissue. Real-time MR images, catheter position updates and optical microscopic images were obtained in a vessel phantom containing stained and unstained gels and chicken meat labeled with FITC-Lectin as targets.

Cell Labeling and Tracking: Methods and Applications

Room 4E Tuesday 13:30 - 15:30

1864. Optimization of a Cell Labeling Strategy for Magnetic Resonance Imaging

Gunter Wolf[1], Klaus Strobel[2], Susanne Gruener[1], Arne Koch[1], Volker Hietschold[3], Nasreddin Abolmaali[1]
[1]TU Dresden, Dresden, Germany; [2]FZ Rossendorf, Dresden, Germany; [3]University Hospital, Dresden, Dresden, Germany

MRI allows the non-invasive tracking of single cells or small groups of cells *in vivo*. Therefore, cells need to be labeled with a suitable contrast agent (CA). In the present study we optimized a cell labeling strategy with MRI. By means of T1-weighted MRI and T1 relaxation time measurements, we systematically investigated the labeling of human non-small cell lung cancer (NSCLC) cells with Gd- and Mn-based CA using five different transfection agents (TAs). Our main goal was to find a combination of CA and TA, which gave the best constrast in MRI. As a result two preferable TAs for labeling NSCLC with Mn or Gd were found. The labeling strategy presented here may be easily transferred to other cells, e.g. any kind of stem cells.

1865. *In Vivo* MR Imaging of the Sequential Recruitment of Macrophages to the Soft Tissue Infection

Jin Seong Lee[1], Hee Jung Kang[2], Heun-Don Jung[3], Keun Ho Lim[3], Sang Tae Kim[3], Tae-Hwan Lim[1]
[1]University of Ulsan College of Medicine, Asan Medical Center, Seoul, Republic of Korea; [2]Hallym University College of Medicine, Seoul, Republic of Korea; [3]University of Ulsan College of Medicine, Seoul, Republic of Korea

Experimental soft-tissue infection in 6 male C3H/HeN mice was induced in the left lower leg. The iron oxide-labeled macrophage was administered through the tail vein 48 hours after inoculation of the bacteria. On sequential MR images after administration of macrophage labeled with iron oxide, the band-shaped lower SI zone was noted in the abscess wall. The relative SI of the abscess wall progressively decreased until 24 hours after the injection of iron oxide-labeled macrophages. In this study we demonstrated that the sequential recruitment of intravenously administered iron oxide-labeled macrophage can be monitored with 4.7T MR imaging.

1866. Cellular Imaging of Rat Aortic Endothelial Cell Monolayer Using a 3T Whole Body Scanner

Frank Seifert[1], Isabela Schmitt-Knosalla[2], Martina Seifert[2]
[1]Physikalisch-Technische Bundesanstalt, Berlin, Germany; [2]Charité Universitätsmedizin Berlin, Berlin, Germany

The aim of this study is to develop methods for an MR based monitoring of the monolayer of endothelial cells seeded onto the luminal side of a vascular graft to get more information about their fate under *in vivo* conditions. Isolated rat aortic endothelial cells were labelled with small iron oxide particles (VSOP). Seeded vascular grafts were transplanted in a rat interposition model into the region of the abdominal aorta. All measurements with aortic grafts in vitro and *in vivo* were performed on a 3T whole body scanner.

1867. Developing Magnetocapsules for Immunoprotection and MR Tracking of Pancreatic Islets Using Clinically Approved Materials

Brad P. Barnett[1], Piotr Walczak[1], Wesley Gilson[1], Assaf A. Gilad[1], Jesus Ruiz-Cabello[1], Carolyn Lauzon[1], Dara L. Kraitchman[1], Matthias Stuber[1], Aravind Arepally[1], Jeff WM Bulte[1]
[1]Johns Hopkins University School of Medicine, Baltimore, Maryland, USA

Due to the significant long-term risk associated with immunosuppressive therapy, only patients with brittle type I diabetes mellitus have been selected as suitable candidates for islet transplantation. A means to immunoisolate islets, allowing engraftment free of chronic immunosuppressive therapy is needed. A plausible alternative, microencapsulation, involves surrounding individual islets with a thin shell that is impermeable to the host's immune system but is permeable to metabolites. If microcapsules could be visualized after implantation, their functionality and biodistribution could be evaluated more effectively. To this end, we have developed alginate-based microcapsule that incorporate Feridex®? in order to create the MR-trackable magnetocapsule.

1868. Antibody Mediated Cell Labeling of Peripheral T Cells with Micron Sized Iron Oxide Particles (MPIOs) Allows Single Cell Detection by MRI

Erik M. Shapiro[1, 2], Laura N. Medford-Davis[2], Cynthia E. Dunbar[3], Alan P. Koretsky[2]
[1]New York University School of Medicine, New York, New York, USA; [2]National Institute of Neurological Disorders and Stroke, National Institutes of Health, Bethesda, Maryland, USA; [3]National Heart, Lung and Blood Institute, Bethesda, Maryland, USA

Labeling cells with iron oxide is a useful tool for MRI based molecular and cellular imaging. Here we demonstrate that peripheral T cells can be labeled with streptavidin coated micron sized iron oxide particles, MPIOs, achieving iron concentrations as high as 50 pg iron per cell. Labeling is facilitated by use of a biotinylated CD5 antibody, which is specific for peripheral T cells. Such labeling allows the detection of single lymphocytes by MRI using conditions well suited for *in vivo* animal work.

1869. Optimization of Dendritic Cell Labeling for MR Tracking After Vaccination in Cancer Patients

Pauline Verdijk[1], Tom W.J. Scheenen[1], Andor A. Veltien[1], Jeff W.M. Bulte[2], Piotr Walczak[2], W. Joost Lesterhuis[1], I. Jolanda M. de Vries[1], Cornelis J.A. Punt[1], Arend Heerschap[1], Carl G. Figdor[1]

[1]Radboud University Nijmegen Medical Center, Nijmegen, Netherlands; [2]Johns Hopkins University School of Medicine, Baltimore, Maryland, USA

Dendritic cell (DC) cancer vaccines are currently being administered as a novel form of cell therapy to boost the immune system in cancer patients. We have demonstrated that MR imaging of DCs labeled with superparamagnetic iron oxide (SPIO) is feasible after intranodal injection in melanoma patients and allows evaluation of the delivery and tracking of the vaccine. In this study we assessed the maximal SPIO content that did not affect the function of DCs and the lowest density of DCs that could be detected by gradient echo MRI with this SPIO level on a 3T clinical MR system.

1870. Chemical Biotinylation of Cells for Molecular Imaging and Cell Tracking

Po-Wah So[1], Tammy Kalber[1], Amy Heavner Herlihy[1], Jimmy David Bell[1]

[1]Hammersmith Hospital, Imperial College London, London, UK

A number of methods have been proposed to label cell for cell tracking *in vivo*. Previously, chemical biotinylation of cells has been used for the isolation and study of cell surface proteins. This relatively fast and simple method can however be readily modified as a rapid and relatively cheap method for the generic labelling of cells for MRI techniques. In this study, the feasibility of imaging chemically biotinylated cells in vitro and *in vivo* by MRI is demonstrated.

1871. In Vitro Evaluation of Cellular Engraftment Parameters of 3 Transfection Methods to Label Mouse Embryonic Stem Cells Using Ferumoxides

Yoriyasu Suzuki[1], Charles Henry Cunningham[1], Micha Drukker[1], Phillip Chung Ming Yang[1]

[1]Stanford University, Stanford, California, USA

In vitro comparison of the engraftment parameters of magnetically labeled mESC with 3 transfection methods using ferumoxides was conducted. Critical biological determinants of cellular engraftment including longitudinal viability, differentiation capacity of mESC into cardiomyocyte of mouse embryonic stem cells (mESC) were compared among transfection techniques. Magnetic labeling of mESC using transfection methods is safe and effective. Although cellular viability and proliferative capability did not show any difference among the 3 methods, the differentiation capability of mESC transfected by Elp was most attenuated and iron uptake by PS was most efficient.

1872. Compatibility of Iron Nanoparticle-Based MRI Cell Tracking and ^{31}P MRS Bioenergetic Measurements

Zhuoli Zhang[1], Kenneth W. Fishbein[1], Chiara Dell'Agnola[1], Steven J. Sollott[1], Kenneth R. Boheler[1], Magdalena Juhaszova[1], Edward G. Lakatta[1], Richard G. Spencer[1]

[1]National Institutes of Health, Baltimore, Maryland, USA

Labeling of cells with superparamagnetic iron oxide particles permits cell tracking by 1H MRI while 31P MRS allows non-invasive evaluation of cellular bioenergetics. We evaluated the compatibility of these two techniques by obtaining 31P NMR spectra of iron-labeled and unlabeled, immobilized HeLa and myoblast cells in vitro. Broadened but usable 31P spectra were obtained, although distortions to metabolite peak area ratios often occurred with cell labeling, particularly for HeLa cells. We conclude that the distortion of peak widths and areas by iron oxide labeling is probably influenced by the inhomogeneous loading of particles among labeled cells.

1873. *In Situ* and *In Vivo* Magnetic Resonance Imaging of Iron Labelled Dendritic Cells in the Mouse

Andreas Hess[1], Dirk Baumjohann[2], Manfred B. Lutz[2], Kay Brune[3], Lubos Budinsky[1]

[1]Institute of Pharmacology, FAU, Erlangen-Nürnberg, Germany; [2]University Medical Center, Dep. Dermatology, Erlangen-Nürnberg, Germany; [3]Doerenkamp Professorship for Innovations in Animal and Consumer Protection, FAU, Erlangen-Nürnberg, Germany

The aim of this study was to visualize DC cells non-invasively by MRIin a mouse model. First, we established and verified an efficientlabelling method for DC's by clinically approved agents: smallparticles of iron oxide (SPIO) and protamine sulfate. Labelled DC'swere injected into one food pad and thesame amount of unlabelled into the other. The cells migrate into thedraining lymph node via lymph vessels. Using a 4.7 T scanner and a dedicated mouseresonator weimaged these popliteal lymph nodes of the DC injected and control sideusing a T2 weighted MSME sequence both *in vivo* and in-situ.

1874. MRI Tracking of Migration of Bone Marrow Cells to the Sites of Injured Arteries

Bensheng Qiu[1], Fabao Gao[1], Sourav Kar[1], Jiangyang Zhang[1], Piotr Walczak[1], Malika Larabi[1], Rong Xue[1], Emma Frost[1], Zhiping Qian[1], Jeff WM Bulte[1], Xiaoming Yang[1]

[1]Johns Hopkins Univ School of Medicine, Baltimore, Maryland, USA

We attempted to develop a new method of using MRI to track the migration of bone marrow (BM) cells to the injured arteries. Feridex-labeled LacZ-BM cells were transplanted into recipient nude mice with cuff-induced injury in the femoral arteries. Both *in vivo* MRI and *ex vivo* 3D MRI showed large hypointense regions at the sites of injured arteries, which were histologically correlated with Feridex- and LacZ-positive cells in the harvested arterial tissues. This study provides the first evidence to support the potential use of MRI to track the migration of magnetically labeled BM cells to the injured arteries.

1875. Temporal Monitoring of an SPIO Labeled, Optically Traceable Tumor Mouse Model

Daniel A. Herzka[1], Jade Quijano[2], Terence Wong[2], Wei Liu[1], Jianwu Xie[2], King C. Li[2]
[1]Philips Research North America, Bethesda, Maryland, USA; [2]National Institutes of Health Clinical Center, Bethesda, Maryland, USA

In this work, we present a dual-labeled mouse tumor model that allows monitoring of cells over time. A cell line of human melanoma cancer cells that constitutively expresses enhanced green fluorescent (EGFP) protein was incubated with superparamagnetic iron oxide (SPIO) particles. The cells were optically traceable using multispectral optical imaging, providing a true measure of viability as only live and functioning cells produce EGFP. Furthermore, the cells were detectable by MR imaging techniques sensitive to susceptibility-based contrast. Tumors were observed using the two complementary imaging modalities over 4 weeks and histology was correlated with imaging results at different time points.

1876. The Efficacy of SPIO-Enhanced MRI in Evaluating Inflammatory Pseudotumors: Imaging and Histopathological Correlation

Yasutaka Kawamura[1], Makoto Ishida[1], Akio Yamaguchi[1], Harumi Itoh[1]
[1]University of Fukui Hospital, Fukui, Japan

Inflammatory pseudotumors in the liver are usually shown as a focal mass on conventional CT and MRI and are difficult to differentiate from neoplasms such as metastases and hepatocellular carcinomas. Interpreting the uptake of SPIO in the lesion due to the phagocytosis of macrophages is really useful in making correct diagnosis using SPIO-enhanced MRI. Applying additional diffusion weighted images after SPIO administration could be useful in detecting small liver tumors and in avoiding false-positive results due to small liver vessels.

1877. *In Vivo* Tracking of Endothelial Progenitor Cells in a Mouse Model of Choroidal Neovascularization

Sergio Li Calzi[1], Kyung-Hee Chang[1], Kyle Padgett[1], Aqeela Afzal[1], Lynn C. Shaw[1], Maria B. Grant[1], John R. Forder[1]
[1]University of Florida, Gainesville, Florida, USA

Endothelial progenitor cells (EPCs) are responsible for neovascularization and are critical components in vascular repair. Neovascularization is altered in many diseases, including diabetes, heart disease and cancer. The ability to noninvasively track these cells is important. EPCs from donor animals were loaded with magnetic iron oxide nanoparticles (MION). No alterations were observed in cell viability, apoptosis, and chemotaxis following loading with MION. Detection of single labeled cells was confirmed by serial dilution into agar followed by MRI (17.6 T). In vitreal injection of EPCs into C57/Bl6J mice following laser-induced choroidal neovascularization resulted in areas of increased density in the retina.

1878. Long Term MR Signal Characteristics of Ferucarbotran-Labeled Mesenchymal Stem Cells: Discrimination of Intra- And Extracellular Iron Oxides Before and After Cell Lysis

Tobias Daniel Henning[1], Jan S. Bauer[1], Thomas Frenzel[2], Elizabeth J. Sutton[1], Yanjun Fu[1], Heike E. Daldrup-Link[1]
[1]UCSF, San Francisco, California, USA; [2]Schering AG, Berlin, Germany

Stem cell-based tissue replacement therapies require the assessment of engraftment and viability of transplanted cells. Iron oxide labeling and subsequent MR imaging provides an efficient method of *in vivo* tracking with high sensitivity and high spatial resolution. This study demonstrates the long term signal effects of iron oxide labeled human mesenchymal stem cells on T1, T2 and T2*-sequences. The differentiation of intracellular versus extracellular contrast agent was made, corresponding to viable and dead cells respectively.

1879. Single Cell MRI with FIESTA: Quantitative Benefits of 3T Vs 1.5T

Soha Ramadan[1], Chris Heyn[1], Brian K. Rutt[1], Paula Foster[1]
[1]Robarts Research Institute, London, Ontario, Canada

In this study we investigate the use of higher magnetic field strength to allow for high resolution FIESTA image data acquisition in reasonable scan times, and the impact of this strategy on contrast generated by iron labeled cells. Mice were injected with MPIO-labeled, brain-seeking metastatic breast cancer cells and imaged at 1.5 and 3T with 3DFIESTA. The contrast generated by iron labeled cells was the same in 1.5 and 3T images matched for SNR and spatial resolution and was greater in higher resolution 3T images. A greater than linear increase in SNR resulted from 1.5T to 3T.

1880. MR Microscopy of Multipotent Astrocytic Stem Cells Labeled with Multimodal Qdots Applied to a Neonatal Murine Model of Hypoxic Ischemic Encephalopathy

Samuel Colles Grant[1, 2], Tong Zheng[3, 4], Gregory P. Marshall II[3, 4], Heesun Yang[3], Debamitra Dutta[3], Heather Cornnell[3], Swadeshmukul Santra[5], Paul H. Holloway[3], Brij M. Moudgil[3], Edward W. Scott[3, 4], Eric D. Laywell[3, 4], Glenn A. Walter[3], Arthur Scott Edison, [23], Dennis A. Steindler[3, 4], Michael D. Weiss[3]
[1]Florida State University, Tallahassee, Florida, USA; [2]National High Magnetic Field Laboratory, Tallahassee, Florida, USA; [3]University of Florida, Gainesville, Florida, USA; [4]McKnight Brain Institute, Gainesville, Florida, USA; [5]University of Central Florida, Orlando, Florida, USA

Hypoxic Ischemic Encephalopathy (HIE) is a major cause of neuronal injury in neonates. A potential treatment may be neural stem cell implantation. MR microscopy can fully evaluate this treatment because it can interrogate stem cell proliferation and the recovery of infarction. In this study, unilateral HIE has been instituted in a neonatal murine model, and multipotent asctrocytic stem cells (MASC) labeled with a unique contrast agent providing MR and optical enhancement have been injected into the effected cortex. MR images acquired in and *ex vivo* display MASC integration along white matter tracts as well as bilateral proliferation in the ventricles.

1881. Imaging of Islet Transplantation in a Pre-Clinical Animal Model Using an FDA-Approved Contrast Agent: *In Vitro* Studies

Natalia Evgenov[1], John Pratt[1], Zdravka Medarova[1], Pamela Pantazopoulos[1], Susan Bonner-Weir[2], Anna Moore[1]
[1]Massachusetts General Hospital, Charlestown, Massachusetts, USA; [2]Joslin Diabetes Center, Boston, Massachusetts, USA

Pancreatic islet transplantation is a powerful clinical tool to treat Type 1 diabetes patients. In order to monitor transplantation efficiency and graft survival, reliable non-invasive imaging methods are critically needed. We used an FDA-approved commercially available contrast agent FERIDEX, to label human pancreatic islets for *in vivo* detection after islet transplantation. Our results showed that labeling was not cytotoxic to human islets and did not affect their insulin secretion. Furthermore, our phantom studies indicated that human islets could be labeled with FERIDEX, in amounts sufficient for their detection by MR imaging.

1882. MR Characterization of Isolated Human Pancreatic Islets

Suraj Serai[1], Lara Leoni[2], Muhammed Haque[2], Jose Oberholzer[1], Richard Magin[1], Brian Roman[2]
[1]University of Illinois at Chicago, Chicago, Illinois, USA; [2]University of Chicago, Chicago, Illinois, USA

To investigate the potential role of Manganese enhancement to measure glucose activated islets, we examined isolated human pancreatic islets. When present during glucose stimulation, extra-cellular Mn can enter ß-cells through voltage-gated calcium channels and its accumulation alters T1 and T2 relaxation times. Preferential enhancement of signal intensity can be obtained by selectively altering these relaxation parameters. Therefore before the study of any contrast agent effects, T1 and T2 of control islets were measured and maps created to establish baseline values. These data were then used to establish parameters for MR image acquisition of activated versus non-activated islets.

1883. Comparison of Labeling Strategies for Stem Cells with Gd-Chelates

Tessa Geelen[1], Uwe Himmelreich[1], Carles Justicia[1], Cordula Strecker[1], Mathias Hoehn[1]
[1]Max-Planck-Institute for Neurological Research, Cologne, Germany

Gd-chelates are suitable for the visualization of deposits of stem cells *in vivo*. The route of internalization of Gd-chelates influences the efficiency of the labeling and the detectability of cells. Electroporation was most efficient for the three cell lines used in the study. Saturation of R1 relaxivity was observed for cells that took up Gd-chelates by endocytosis.

1884. Positive Contrast Imaging of Iron-Oxide Labeled Human Embryonic Stem (HES) Cell and Fibroblast Using SWEET

Young Beom Kim[1], Hyen Suk Kim[2], Dae Kee Kwon[2], Seung-Schik Yoo[3], Byeong Chun Lee[2], Sung Keun Kang[2], Woo Suk Hwang[2], HyunWook Park[1]
[1]Korea Advanced Institute of Science and Technology, Yuseong-Gu, Daejeon, Republic of Korea; [2]Seoul National University, Gwanak-Gu, Seoul, Republic of Korea; [3]Harvard Medical School, Boston, Massachusetts, USA

The MRI detection of superparamagnetic iron-oxide particles (SPIO)- labeled cells is important in cell-replacement therapies. Cells loaded with SPIOs cause signal reduction (negative contrast) associated with dephasing due to the magnetic field inhomogeneity near the cell. Negative contrast agents have drawback of being confused with the signal void caused by other sources such as tissue inhomogeneity or partial volume effects. We provide simple means of detecting SPIO by using susceptibility weighted echo-time encoding technique (SWEET) whereby the subtraction of two sets of image volume acquired at slightly-shifted echo time resulted in enhancement of signal at the cell position.

1885. Tuftsin-Gd-DOTA Conjugates as Potential MRI Reagents for Macrophage Imaging

Jianghua Feng[1], Marco Meloni[1], Stuart Allan[1], Johanna Narvainen[1], Stephen Faulkner[1], Risto Kauppinen[2]
[1]University of Manchester, Manchester, UK; [2]University of Birmingham, Birmingham, UK

Macrophages contain tuftsin receptor that functions to internalize tuftsin for cell activation. Tuftsin was used as a lead molecule to tag the bioactive peptide with FITC or DOTA. Both Tb and Gd petide conjugates were obtained using DOTA-tuftsin. FITC-tuftsin was internalized by mouse macrophages as revealed by confocal microscopy. Time-gated fluorometry showed dose-dependency of fluorescence signal from macrophages incubated with Tb-tuftsin. Finally, T1-weighted MRI signal was strongly enhanced in macrophage preparations exposed to Gd-tuftsin. These results indicate that tagged tuftsin-conjugates retain biological function at the tuftsin receptor and may be used to detect macrophage cells by fluorescence imaging or MRI.

1886. A Responsive MRI Contrast Agent to Monitor Functional Cell Status: A Feasibility Study Using Dendritic Cells

Uwe Himmelreich[1], Carles Justicia[1], Silvio Aime[2], Thomas Hieronymus[3], Martin Zenke[3], Mathias Hoehn[1]
[1]Max-Planck-Institute for Neurological Research, Cologne, Germany; [2]University of Torino, Torino, Italy; [3]RWTH Aachen, Aachen, Germany

An insoluble Gd-DTPA-chelate was developed and tested for conditional activation by intracellular lipases in dendritic cells. The concept of an insoluble, responsive T1-contrast agent has the advantage of zero relaxivity in the inactive state. The contrast agent was also feasible for detection of implanted cells in rats *in vivo*.

1887. Intracellular MR Contrast Agents Based on Cationic Cell Penetrating Peptides: A Comparative Study

Joern Engelmann[1], Wu Su[1], Deepti Jha[1], Ritu Mishra[1], Josef Pfeuffer[1, 2], Kamil Ugurbil[1, 3]

[1]Max Planck Institute for Biological Cybernetics, Tuebingen, Baden-Wuerttemberg, Germany; [2]Siemens Medical Solutions, Erlangen, Bayern, Germany; [3]Center for Magnetic Resonance Research, Minneapolis, Minnesota, USA

For the development of intracellular Magnetic Resonance contrast agents (CAs) it is a prerequisite that they cross the plasma membrane. Cell penetrating peptides (CPPs) are known to transport cargo molecules attached to it into cells. We synthesized intracellular CAs containing known CPPs or modified peptides. Gd-diethylenetriaminepenta-acetic acid (Gd-DTPA) was coupled to CPPs for MR visualization and fluorescence imaging agent fluorescein isothiocyanate (FITC) for tracking the agent inside cells by optical imaging. Compared on the basis of these measurements, modifications in CPPs enhanced the intracellular delivery ability of our CAs providing a tool for stable labeling of cells for MR imaging.

1888. A Novel Dual-Modality MRI/PET Probe

Björn Gustafsson[1], Angelique Y. Louie[1]

[1]University of California, Davis, Davis, California, USA

A novel combined MRI/PET probe, targeted to atherosclerotic plaques, is reported. The probe is based on a maleylated bovine serum albumin with a conjugated 1,4,7,10-tetraazacyclododecane-1,4,7,10-tetraacetic acid ligand system, that can tether both paramagnetic Gd^{3+} and a positron emitter, *e.g.* $^{64}Cu^{2+}$. Experiments in cultured cells demonstrate specific scavenger receptor A-mediated uptake of the probe by macrophages, present in early stages of atherosclerotic plaques, and show measurable contrast in MR image. Biodistribution studies in rat models show rapid clearance from the blood stream as well as clearance of the contrast agent by kidney and liver, which decreases to low levels by 24h.

1889. Identification of the Neural Stem Cells in the Human Brain by Magnetic Resonance Spectroscopy

Louis Manganas[1], Sherry Zhang[1], Petar Djuric[1], Mark Wagshul[1], Mirjana Maletic-Savatic[1]

[1]Stony Brook University, Stony Brook, New York, USA

The main objective of this study is to develop non-invasive imaging methodology for identification, quantitation, and tracking of neural stem cells (NSC) in the human brain, from early development to elderly age. Currently available reagents as well as reagents under development, including gadolinium-labeled contrast agents and SPIO-based derivatives, are not used as common MRI agents in neonates and infants due to their potential side effects. This is why 1H-MRS is emerging as methodology of choice, particularly for imaging infants and young children. Herein, we describe our results on identification of NSC in the human brain, using their unique spectroscopic signature.

1890. Does Endocytosis of Perfluorocarbon Nanoparticles by Progenitor/Stem Cells Alter 19F Relaxation at 11.7T?

Divya Venkataramani[1], Junjie Chen[1], Anne Morawski Neubauer[1], Kathy Crowder[1], Jason Brant[1], Gregory M. Lanza[1], Samuel A. Wickline[1]

[1]Washington University, St. Louis, Missouri, USA

We have reported previously that a unique MRI signal source, fluorine, which is abundant in liquid perfluorocarbon nanoparticles (PFC NP), can be used to provide simultaneous readouts of the 19F and 1H signals at 1.5T and 4.7T when gadolinium chelates are incorporated into the lipid membrane of the PFC NP. To evaluate the proposed use of PFC NP as unique labeling agents for stem cells, we characterized 19F T1/T2 relaxation before and after stem cell labeling, and elucidated the consequences of incorporating different molecules into the lipid layer of PFC NP in phantoms and labeled progenitor/stem cells at 11.7T.

1891. Dual Modality Monitoring of Intracerebral Stem Cell Delivery and Distribution Following Reperfused Ischemia

Piotr Walczak[1], Jian Zhang[1], Assaf A. Gilad[1], Dorota A. Kedziorek[1], Jesus Ruiz-Cabello[1], Randell G. Young[2], Mark F. Pittenger[2], Peter C.M van Zijl, [13], Judy Huang[1], Jeff W. Bulte[1]

[1]Johns Hopkins University, Baltimore, Maryland, USA; [2]Osiris Therapeutics, Inc., Baltimore, Maryland, USA; [3]Kennedy Krieger Institute, Baltimore, Maryland, USA

In animal models of stroke, it has been shown that a modest functional improvement can be achieved through stem cell transplantation. Further advancement depends greatly upon achieving a robust and targeted cell engraftment of the ischemic lesion. Intraarterial cell delivery appears ideally suited, however it may lead to further microvascular occlusion by cellular grafts and needs to be carefully pursued. We propose dual modality monitoring of cell delivery and distribution using Laser Doppler flowmetry and cellular MR imaging in order to improve the efficacy and safety of targeted stem cell therapy in cerebral ischemia.

1892. Superparamagnetic Iron Oxide Labelling for *In Vivo* Follow-Up of HRPE Cell Implants in Non-Human Primate

Joseph Flores[1], Alex L. MacKay[2], John R. O'Kusky[3], Piotr Kozlowski[2], Joseph A. Frank[4], Doris J. Doudet[1]

[1]Pacific Parkinson's Research Centre, Vancouver, BC, Canada; [2]High Field MRI Centre at UBC, Vancouver, BC, Canada; [3]University of British Columbia, Vancouver, BC, Canada; [4]National Institutes of Health, Bethesda, Maryland, USA

Intrastriatal implantation of human retinal pigment epithelial (hRPE) cells has been shown to produce long-term motor improvement in Parkinson's Disease patients and animal models of PD. We present the results of a preliminary study to assess the safety and efficacy of SPIO labelling of hRPE cells for non invasive imaging using MRI. There was no effect of labelling on viability and doubling time of the hRPE cells. The cells implanted in the brain of a monkey were visible *in vivo* on MRI images acquired 7 weeks post-implantation. Post mortem histochemistry confirmed the presence of labelled cells at the implant site.

1893. Difference in Migration Pattern of Mouse and Canine Stem Cells Detected by *In Vivo* MRI

Sergey Magnitsky[1], Raquel M. Walton[2], John H. Wolfe[1, 2], Harish Poptani[3]

[1]The University of Pennsylvania, Philadelphia, Pennsylvania, USA; [2]Children's Hospital of Philadelphia, Philadelphia, Pennsylvania, USA; [3]The University of Pennsylvania,, Philadelphia, Pennsylvania, USA

Murine C17.2 neural stem cells, murine primary neuronal stem cells (NSC?s) and canine neuronal progenitor cells (NPC?s) were labeled with iron oxide particles, transplanted into neonatal brains and monitored by *in vivo* and *ex vivo* MRI. Transplanted C17.2 NSC?s migrated throughout the brain while mouse (NSC?s) and canine (NPCs) cells exhibited much less mobility and most cells concentrated within the lateral ventricles. *In vivo* detection of migration pattern of different NCS in mouse brain indicates differences in engraftment potency of these cell lines and may facilitate stem cell based therapies of neuronal diseases.

1894. *In Vivo* MRI Long Term Follow Up of the Iron Labelled HRPE Cells Implanted in Rat Brain

Piotr Kozlowski[1], Joseph Flores[2], Andrew C. Yung[1], Alex L. MacKay[1], Doris J. Doudet[2]

[1]High Field MRI Centre at UBC, Vancouver, BC, Canada; [2]Pacific Parkinson's Research Centre, Vancouver, BC, Canada

Human Retinal Pigment Epithelial (hRPE) cells attached to gelatine micro-carriers were labelled with iron using Ferumoxide-Protamine Sulfate preparation and implanted in the striatum of a rat brain. T2-weighted images acquired at 3 and 8 weeks post implantation confirmed the presence of iron labelled cells in their original location at both time points. This pilot study shows that the *in vivo* long term MR imaging of the SPIO-labelled hRPE-GM cells is possible. This technique may prove to be a viable method to follow up the hRPE cells for studying the efficacy of the implantation based treatment of Parkinson's Disease.

1895. Endogenous Stem Cell Tracking by MRI After Local Injection of Contrast Agent

Carles Justicia[1], Uwe Himmelreich[1], Pedro Ramos-Cabrer[1], Christiane Sprenger[1], Mathias Hoehn[1]

[1]Max Planck Institute for Neurological Research, Cologne, Germany

There is a continuous production of newly endogenous progenitor cells in the brain during the adult life, restricted to the subventricular zone and the subgranular zone of the hippocampus. An important increase in cell proliferation has been described in these regions after stroke and neurodegenerative diseases. In this work we demonstrate that it is feasible to label endogenous progenitor cells with iron nanoparticles injected intraparenchymally near the subventricular zone, and to follow their natural migration towards the olfactory bulb. We suggest that it is possible to monitor progenitor cell migration also under pathological conditions.

1896. IRON Imaging of Magnetoelectroporated Mesenchymal Stem Cells in a Rabbit Hindlimb Ischemia Model

Dorota Anna Kedziorek[1], Wesley Gilson[1], Danielle Crawford[1], Matthias Stuber[1], Jeff W. Bulte[1], Lawrence Hofmann[1], Dara L. Kraitchman[1]

[1]Johns Hopkins University, Baltimore, Maryland, USA

The goal of the current study was to implement two new methods: magnetoelectroporation and IRON water suppression imaging for the delivery and tracking of mesenchymal stem cells in a rabbit model of hindlimb ischemia.. The MSCs therapy is an option for a treatment for patients with intermittent claudication (IC) or chronic limb ischemia due to infrainguinal peripheral arterial disease PAD. Prior to transplantation into rabbit thigh muscle, the bone-marrow derived MSCs were labeled with iron, using magnetoelectroporation procedure. To track these cells *in vivo*, we have used the IRON method and we have compared it with traditional FSE images.

Phase Contrast and Flow Dynamics

Room 4E Tuesday 13:30 - 15:30

1897. Volumetric Cine Phase-Contrast MRI of the Great Vessels with PC VIPR: Initial Experience

Oliver Wieben[1], Kevin M. Johnson[1], Frank R. Korosec[1], Charles A. Mistretta[1]
[1]University of Wisconsin, Madison, Wisconsin, USA

This study presents initial results for imaging of the great vessels with PC VIPR, a radial trajectory for ECG-gated 3D flow encoding of a large spherical volume with isotropic spatial resolution to provide information on both vessel geometry and quantitative flow of the great vessels. An improved view ordering scheme for retrospective ECG gating and the use of a temporal filter were implemented for improved cine imaging.

1898. Variable Density Excitation Pulses in One-Shot Fourier Velocity Encoding for Valve Flow Imaging

Daeho Lee[1], Julie Camille DiCarlo[1], Adam Bruce Kerr[1], Juan Manuel Santos[1], John Mark Pauly[1]
[1]Stanford University, Stanford, California, USA

Measurement of peak valve flow is important in diagnosing aortic and mitral stenosis. Since it doesn't suffer from partial volume effects, one-shot Fourier velocity encoding (FVE) has been shown to be an effective way of acquiring a velocity distribution in real-time. Reducing readout time by traversing k-space with variable sampling density is advantageous in its higher temporal resolution, insensitivity to off-resonance and field inhomogeneity. Similarly, we can adopt variable density in excitation k-space. In valve flow imaging, a variable density approach improves the contrast of the velocity spectrum by achieving a narrow cylinder with suppressed and incoherent sidelobes in a shorter time.

1899. High Temporal Resolution Phase Contrast MRI Using SSFP

Vinay Manjunath Pai[1], Abram Voorhees[1], Elizabeth Hecht[1], Leon Axel[1], Vivian Lee[1]
[1]New York University, New York, New York, USA

Phase contrast MRI (PCMRI) provides flow information similar to 2D echocardiography without the restrictions of acoustic windows. High temporal resolution PCMRI may prove to be very useful for evaluating valvular dynamics, and for studying flow patterns in the cardiac chambers. A new approach utilizing dual echoes and parallel imaging is presented for obtaining high temporal resolution flow information in a breathhold examination. The results obtained in flow phantoms and humans compare well with flow results obtained using conventional FLASH-based phase-contrast sequences.

1900. Phase Contrast Imaging Using Sensitivity Encoding and Automatic Coil Sensitivity Estimation: A Feasibility Study

Per Thunberg[1]
[1]Dept. of Biomedical Engineering, Örebro University Hospital, Örebro, Sweden

The purpose of this work was to study the feasibility of phase contrast imaging combined with sensitivity encoding, where coil sensitivities are estimated during the actual measurement. The coil sensitivity estimation is performed by acquiring additional autocalibration signals (ACS-lines). A simulated phase contrast imaging measurement was performed using authentic complex valued coil sensitivities and a synthetic object. The data set was reduced corresponding to different reduction factors. Various numbers of ACS-lines were used for coil sensitivity estimation. The results show that it is feasible to obtain accurate velocity and flow measurements. The number of ACS-lines is decisive for the accuracy.

1901. Transtenotic Pressure Gradient Measurements Using Phase Contrast Vastly Undersampled Projection Imaging (PC-VIPR) in a Canine Model

Kevin Michael Johnson[1], Aquiilla Turk[1], Pat Turski[1], Kari Pulfer[1], David Niemann[1], Chuck Mistretta[1]
[1]University of Wisconsin-Madison, Madison, Wisconsin, USA

We have previously reported on a novel MR based imaging sequence, PC-VIPR which can acquire velocity encoded images at speeds up to 50 times that of standard Cartesian imaging by means of angular undersampling. Recently we have been able to utilize this sequence to calculate pressure changes across areas of stenosis from the image data. In this study, we evaluate the ability of PC-VIPR to ascertain transstenotic pressure gradients across carotid stenoses in a canine model. In the evaluation of 20 carotid stenoses PC VIPR measurements were well correlated with invasive catheter based measurements(R=0.75), when the degree of stenosis is less than 70%.

1902. Self-Navigated Phase Contrast MR

Joshua F. P. van Amerom[1], Jim M. Li, Jeffrey A. Stainsby[2], Labonny Biswas[1], Naeem Merchant, Christopher K. Macgowan[1], Marshall S. Sussman
[1]Hospital for Sick Children and University of Toronto, Toronto, Ontario, Canada; [2]GE Healthcare Canada, Toronto, Ontario, Canada

Measurement of flow in pulmonary blood vessels requires some form of correction for respiratory motion. Self-navigated phase contrast MR is a modification of the conventional retrospectively cardiac-gated phase contrast MR sequence. This technique uses the image data itself to determine anatomic position. Data that is poorly correlated with an initial template is discarded and reacquired in real time. In vitro flow phantom tests show that the technique is an improvement over conventional multi-averaged phase contrast in terms of image quality and flow measurement.

1903. Improved Temporal Resolution in Phase-Contrast MRI with Non-Interleaved Velocity Encodings

Craig Alan Hamilton[1], Robert A. Kraft[1], Ersin Bayram[1], William Gregory Hundley[2]
[1]Va Tech/Wake Forest School of Biomedical Engineering and Sciences, Winston Salem, North Carolina, USA; [2]Wake Forest Univ. Health Sciences, Winston Salem, North Carolina, USA

High temporal resolution is required in phase contrast flow measurements in the coronary arteries. We present a new technique which uses non-interleaved velocity encodings followed by spatial registration to double the temporal resolution of coronary flow measurements.

1904. Effect of Background Velocity Error on Measured Time of End-Systole in Patients with Aortic Regurgitation by Phase Contrast MRI

Steven G. Lloyd[1], Himanshu Gupta[1]
[1]University of Alabama at Birmingham, Birmingham, Alabama, USA

Velocity mapping by phase contrast MRI is often used to measure the regurgitant volume in aortic regurgitation, which may be used to grade the severity. This requires calculating the time integral of the diastolic flow velocity. The limits of integration (i.e., systolic and diastolic durations) must therefore be accurately known. Background phase offsets result in small deviations in the measured velocities. We examined the effect of such shifts on the systolic duration. Analysis shows that small offsets of the order of 2 cm/s do not significantly affect the accuracy of systolic and diastolic duration measurements and may be neglected.

1905. Adaptive Navigator Gated Time-Resolved 3D MR Velocity Mapping at 3T: Assessment of Normal and Pathological Vascular Anatomy and Blood Flow

Michael Markl[1], Alex Frydrychowicz[1], Benrd Jung[1], Maxim Zaitsev[1], Jürgen Hennig[1]
[1]University Hospital Freiburg, Freiburg, Germany

An image acquisition and data processing strategy is presented for the assessment of vascular geometry and 3D blood flow based on optimized respiration control, imaging at 3T and advanced 3D visualization. Phase Contrast-MR Angiography data, morphological information and spatially co-registered vascular hemodynamics are derived from the same data set for computer aided 3D visualization of global and local blood flow patterns. Results from volunteer and patient studies illustrate the potential of time-resolved 3D MR velocity mapping for the simultaneous assessment of 3D vascular anatomy and identification of normal and pathological 3D blood flow characteristics in the thoracic aorta.

1906. Rapid Cardiovascular Flow Quantitation Using Slice-Selective Spiral Fourier Velocity Encoding

Joao Luiz Carvalho[1], Krishna S. Nayak[1]
[1]University of Southern California, Los Angeles, California, USA

Flow quantitation is important for the evaluation of many cardiovascular conditions. We propose the use of Fourier Velocity Encoding (FVE) with slice selection and low spatial resolution spiral readouts. Balancing time and velocity resolutions, and fully sampling k_x,k_y in one readout, we were able to acquire aortic valve flow time-velocity histograms with 52 ms temporal resolution and 12.5 cm/s velocity resolution in a single 8-second breath-hold. For measuring carotid flow, higher spatial resolution was obtained with longer acquisition time. This method was tested on flow phantoms and normal volunteers, and the results compared well with Doppler ultrasound.

1907. Validation of Phase Contrast Measurements with Combined Parallel Imaging and Partial Fourier Acquisition

Stefanie Pertschy[1], Rolf Döker[1], Ralph Noeske[2], Dagmar Hartung[1], Michael Galanski[1], Joachim Lotz[1]
[1]Medical School Hannover, Hannover, Germany; [2]GE HealthCare Technologies, Berlin, Germany

Phase contrast measurements with combined partial Fourier acquisition and parallel imaging technique were done at 1.5 Tesla. Cardiac output was measured in normal volunteers and patients with and without partial fourier acquisition and parallel imaging. Precision, accuracy and signal to noise ratios were also measured in vitro. A tendency to overestimate flow volumes by 5% was seen while time of acquisition was reduced by a mean of 64%.

1908. Phase Contrast MRI Velocimetry of a Stereolithographic Total Cavopulmonary Connection at 1.5 T and 3 T

Hiroumi D. Kitajima[1], Kartik Sivaram Sundareswaran[1], Thomas Zdzislaw Teisseyre[1], Oskar Skrinjar[1], John N. Oshinski[2], Ajit Prithiviraj Yoganathan[1]
[1]Georgia Institute of Technology, Atlanta, Georgia, USA; [2]Emory University, Atlanta, Georgia, USA

MRI at 3 T has yet to be applied to in vitro phase contrast velocimetry in complex anatomies. A stereolithographic model is manufactured to reproduce the patient-specific anatomy of a total cavopulmonary connection as imaged by *in vivo* MRI. The anatomic replica is placed in an experimental flow loop, where high-resolution flow data are acquired at 1.5 T and 3 T. Resultant 3-D 3-component flow fields are compared. The extracted hemodynamic data provide keen insight to fluid structures in the complex anatomy and highlight differences of in vitro phase contrast MRI at 1.5 T and 3 T.

1909. Multi-Centre *In Vivo* Evaluation of MR Phase Contrast Flow Measurements

Susan Maguire[1], Martin John Graves[2], Karin Markenroth[3], Nasreddin D. Abolmaali[4]
[1]Mater Private Hospital, Dublin, Ireland; [2]University of Cambridge Hospitals NHS Foundation Trust, Cambridge, UK; [3]Lund University Hospital, Lund, Sweden; [4]Medical Faculty Carl Gustav Carus, Dresden, Germany

We report on a multi-centre, multi-vendor *in vivo* evaluation of cine phase contrast (CPC) flow mapping. We measured the Qp/Qs ratio in a cohort of 53 normal volunteers using non-segmented CPC sequences. Local and central site data analysis was performed, including inter and intra observer reproducibility. Each subject was also scanned three times to assess measurement repeatability. For the central site analysis the Qp/Qs ratio was 1.13±0.08. Intra subject repeatability was 0.09. There were no significant differences between local and central site analysis or between intra and inter observer measurements. Qp/Qs can be measured with acceptable accuracy for clinical applications.

1910. Comparison of Regurgitation and Variation of In-Plane Flow Speed in Branch Pulmonary Arteries After Repair of Tetralogy of Fallot : A Phase-Contrast MR Imaging Study

Sheng-Chun Niu[1, 2], Cheng-Wen Ko[1, 2], Ming-Ting Wu[2, 3], Yi-Luan Huang[2, 3], Yi-Ru Lin[2, 4], Shang-Yueh Tsai[2, 4]
[1]National Sun Yat-sen University, Kaohsiung, Taiwan; [2]Kaohsiung Veterans General Hospital, Kaohsiung, Taiwan; [3]National Yang Ming University, Taipei, Taiwan; [4]National Taiwan University, Taipei, Taiwan

Pulmonary regurgitation has been regarded as an important feature for long-term clinical outcome after repair of Tetralogy of Fallot. The interest of applying phase-contrast cine magnetic resonance (PCMR) as an accurate method for evaluating flow velocity, volume and pattern has also been increasing. In this study, our preliminary result demonstrated the regurgitant fraction is a useful hemodynamic indicator in branch pulmonary arteries after repair of Tetralogy of Fallot, while coefficient of variation of in-plane velocity may reflect the severity of turbulent flow which deserves further investigation for its clinical implication.

1911. 4D Phase Contrast Imaging for the Assessment of Morphology and Haemodynamics in Peripheral Arteries: Feasibility Results from a 3T MR System

Alex P. Frydrychowicz[1], Jan Winterer[1], Jürgen Hennig[1], Mathias FJ Langer[1], Michael Markl[1]
[1]University Hospital Freiburg, Freiburg, Baden-Württemberg, Germany

In this feasibility study we applied time-resolved 3D and 3-directional phase contrast MRI at 3T to iliac and femoral arteries in order to utilize the simultaneously available functional (three-directional blood flow velocities over the entire cardiac cycle) and anatomical information (3D magnitude images) for integration of haemodynamic features into 3D morphological imaging. Advanced data processing permits 3D visualization of the measured haemodynamic information. All results were compared to vascular US. Data from volunteers and a patient with PAOD is displayed for demonstration of the potential of this technique for the evaluation of global and local blood flow characteristics and pathologically altered vascular hemodynamics

1912. Predicting SFA Stenosis Severity with Cine PC Flow Measurements During Suprasystolic Thigh Compression

Honglei Zhang[1], Kiyarash Mohajer[1], Bernard Ho[1], Martin R. Prince[1]
[1]Weill Medical College of Cornell University, New York, New York, USA

Fourteen patients with suspected peripheral vascular disease underwent routine bolus chase peripheral MRA and 2D cine phase contrast flow measurements proximal and distal to SFA disease pre, during and post suprasystolic (200 mm Hg) thigh compression for 3 minutes. During compression, the decrease of flow volume at the lower level was greater in severe stenoses and occlusions. The peak delay was significantly prolonged for severe stenoses. After thigh compression, hyperemia was found in 19 arterial segments. 2D cine PC flow measurement at higher flow rates is helpful to determine if a borderline stenosis is flow limiting.

1913. Superficial Femoral Artery Occlusive Disease Severity Correlates with MR Cine Phase Contrast Flow Measurements

Honglei Zhang[1], Kiyarash Mohajer[1], Daniel Gurell[1], Hale Ersoy[1], Bernard Ho[1], K Craig Kent[1], Martin R. Prince[1, 2]
[1]Weill Medical College of Cornell University, New York, New York, USA; [2]Columbia College of Physicians and Surgeons, New York, USA

Routine bolus chase peripheral MRA was performed on 48 patients followed by 2D cine PC flow measurements for each leg obtained above and below the SFA lesion. Flow pattern, flow volume and velocity data were also obtained from 9 healthy volunteers. The severity of SFA disease was graded as normal, no significant lesion (< 50%), moderate-to-severe stenosis (¡Ý 50%) or occlusion and correlated with flow data. Two variables showed statistically significant positive correlation with the severity of arterial disease, including existence of peak delay ($r = 0.65$, $p < 0.001$) and peak velocity ratio ($r = 0.31$, $p < 0.001$).

1914. A Noninvasive Technique to Evaluate Intracranial Compliance and Pressure Using MR Flow Quantification and Inverse Circuit Analysis

Kagayaki Kuroda[1, 2], Takaomi Kanno[1], Kosuke Maruhashi[1], Yoichi Tanabe[1], Koichi Oshio[3], Masatoshi Honda[4], Isao Muro[4], Mitsunori Matsumae[5]

[1]Graduate School of Engineering, Tokai University, Hiratsuka, Kanagawa, Japan; [2]Institute of Biomedical Research and Innovation, Kobe, Hyogo, Japan; [3]School of Medicine, Keio University, Shinanomachi, Tokyo, Japan; [4]Tokai University Hospital, Isehara, Kanagawa, Japan; [5]School of Medicine, Tokai University, Isehara, Kanagawa, Japan

A noninvasive technique to evaluate intracranical pressure (ICP) and compliance (ICC) based on MR flow measurements and an inverse analysis of inductively coupled electrical circuits, modeling blood and cerebrospinal fluid (CSF) flows in the brain, was devised. Numerical simulations followed by experiments using a brain-circulation-mimicking phantom confirmed that the proposed technique yielded relative indices of ICP and ICC. Studies using 26 healthy volunteers (22-63 years old) and 10 patient volunteers (27-69 years old) revealed that healthy and patient groups could be mapped for significantly different regions using the two-dimensional space formed by the indices.

1915. A New Method for the Determination of Aortic Pulse Wave Velocity

Jamie Harle[1], Martin John Graves[1], Ian B. Wilkinson[1], Simon Howarth[1], Jonathan H. Gillard[1]

[1]University of Cambridge Hospitals NHS Foundation Trust, Cambridge, UK

We have developed a new method for the determination of aortic pulse wave velocity (PWV) using 2D cine phase contrast MRI. The method uses a threshold of the calculated sum flow instead of the conventional threshold of percentage peak velocity for the determination of the time delay. Results are presented from an ongoing clinical trial assessing the determination of aortic PWV within a young and old population group. The new method shows a statistically significant increase in PWV amongst the older population group at the proximal and distal aortic regions which is not seen using the conventional method.

1916. Assessment of the Wall Shear Stress (WSS) of the Abdominal Aortic Aneurysm Using Time-Resolved Three-Dimensional Phase-Contrast MRI (4D-Flow) and a New WSS Mapping Application (Flova)

Yasuo Takehara[1], Haruo Isoda[1], Shuhei Yamashita[1], Hiroyasu Takeda[1], Yasuhide Ohkura[2], Takashi Kosugi[2], Masaya Hirano[3], Marcus T. Alley[4], Michael Markl[5], Norbert Pelc[4], Harumi Sakahara[1]

[1]Hamamatsu University School of Medicine, Hamamatsu, Shizuoka, Japan; [2]Renaissance of Technology Corporation, Hamamatsu, Shizuoka, Japan; [3]GE Yokogawa Medical Systems, Hino, Tokyo, Japan; [4]Stanford University School of Medicine, Stanford, California, USA; [5]University Hospital Freiburg, Freiburg, Barden-Wuerttemberg, Germany

To assess if time-resolved three-dimensional phase-contrast MRI (4D-Flow) data postprocessed by a new application gFlovah can provide 4-dimensional WSS mapping of the abdominal aortic wall affected by aneurysm, 3 consecutive patients with infrarenal abdominal aortic aneurysm (AAA) were examined. WSS of the AAA was significantly lower (less than 0.2 Pa) than that of non-aneurysmal wall near the aneurysm (over 1.5 Pa) in all patients. Combined use of the 4D-Flow and Flova enabled WSS mapping of AAA. The lower WSS in AAA may be reflecting that the aneurismal wall is continuously affected by the growing risk of aneurysmal growth and rupture.

1917. Hemodynamics in the Aorta and Coronary Arteries: a Study with MRI and CFD

John N. Oshinski[1], Suo Jin[2], Don P. Giddens[2]

[1]Emory University, Atlanta, Georgia, USA; [2]Georgia Tech, Atlanta, Georgia, USA

This study determined patient-specific WSS in the proximal coronary arteries by modeling flow in the aorta and coronary arteries. A combination of magnetic resonance imaging (MRI) and computation fluid dynamics (CFD) was used to study the flow fields in 4 subjects. The study showed significant skewing of the velocity profiles in the proximal coronary arteries caused by the presence of a transient vortex at the ostia. Results presented here are consistient with the observation that atherosclerotic plaques preferentially form in areas of low or oscillatory WSS.

1918. Visualization of Hemodynamics at the Carotid Bifurcation with MR Imaging: Cine Vector Representation of Blood Flow Using PC MRA

Takashi Ishimori[1], Reiko Seo[2], Satoru Nakano[3], Toshiaki Kusuhara[1], Motoomi Ohkawa[1], Yuichi Yamashita[4], Satoshi Sugiura[4]

[1]Faculty of Medicine,Kagawa University, Kita, Kagawa, Japan; [2]Kagawa Rosai Hospital, Marugame, Kagawa, Japan; [3]Kurihara Central Hospital, Kurihara, Miyagi, Japan; [4]Toshiba Medical Systems, Otawara, Tochigi, Japan

The feasibility of vector representation of blood flow at the carotid bifurcation based on PC MRA was examined. The visualization of hemodynamics was compared with two different PC techniques, the average blood flow method acquired without ECG gating and the cine method with ECG gating. Cine method enables observation of the changes in pressure flow against vessel wall, which provides detail information of the turbulent flow in carotid artery. The examination of various level of stenosis using this method is considered to be useful in the analysis of how vortex flow and blood stagnation participate in the formation of stenosis.

1919. Comparing Steady and Pulsatile LDV and PC-MRA Flow Measurements in an Anatomically Accurate Cerebral Artery Aneurysm Model

Dorothea Ilse Hollnagel[1], Paul E. Summers[2], Spyros S. Kollias[3], Dimos Poulikakos[1]
[1]ETH Zurich, Zurich, Switzerland; [2]University of Oxford, Oxford, UK; [3]University Hospital, Zurich, Switzerland

Blood flow measurements in cerebral aneurysms are gaining in importance in clinic and research. To verify the accuracy of the non-invasive phase-contrast MRA we surveyed an original geometry cerebral aneurysm model by Laser-Doppler-Velocimetry (LDV) and PC-MRA. Methods: We performed measurements in a Dantec 2D-LDV and 3T-Phillips Gyroscan on a silicone model from a patient's DSA. Constant and realistic flow curves were applied.Results: Both, steady and pulsatile results of LDV and PC-MRA show strong similarities.Conclusion: High accuracy PC-MRA can be used to acquire original patient data even in small arteries and aneurysms for clinic and further research.

1920. The Impact of Vessel Motion and Flow Variability on MR-Based Wall Shear Rate Measurement in the Carotid Artery

Sheng-ping Wu[1], Osama Al-Kwifi[2], Joshua van Amerom[1], Graham A. Wright[2], Christopher K. Macgowan[1]
[1]The Hospital for Sick Children, Toronto, ON, Canada; [2]Sunnybrook and Women's College Health Science Centre, Toronto, ON, Canada

This work investigated the effect of beat-to-beat changes in vessel position and pulsatile blood flow on MR-based measurements of wall shear rates in the carotid artery. The ECG gated phase contrast magnetic resonance images were simulated in MATLAB assuming the spatial resolution of 0.25 mm&, the inner diameter of 7 mm and circular vessel with 108.3 ± 3.8 cm/s peak velocities. The motion and pulsation data from the *in vivo* measurements were integrated to the simulated k-spaces. Consequently, these factors were found to change the calculated WSR slightly (approximately 2%). This indicated that the ECG gated MR PC measurement can be an accurate method for WSR calculation in the carotid artery.

1921. Application of Fourier-Based Phase Unwrapping Algorithm for MR-Venography

Hassan Bagher-Ebadian[1], Quan Jiang[1], James R. Ewing[1, 2]
[1]Henry Ford Health System, Detroit, Michigan, USA; [2]Oakland University, Rochester, Michigan, USA

This study presents an algorithm for unwrapping experimental MRI phase maps in the presence of noise. The algorithm employs Laplacian operators in the Fourier space of the phase map, accomplishing in a single-step deterministic procedure a fast and practical solution for phase unwrapping problems in MR-venography and other MRI applications. In enhancing the vein structures in generated venograms, the algorithm shows a superior performance for images with high phase gradients and noise. The method can also be used to produce maps of static magnetic field inhomogeneity, thus guiding shimming of the MR magnetic field.

1922. Free Breathing MR Flow Measurments in Infants and Young Children with Ventricular Septal Defects: Physiological Aspects and Comparison to Invasive Oximetry

Nasreddin D. Abolmaali[1], Anoosh Esmaeili[2], Jan Schmitt[3], Matthias Heller[4], Mirko Schiemann[4], Arne Koch[1], Thomas J. Vogl[4]
[1]Technical University Dresden, Dresden, Germany; [2]JW Goethe University, Dresden, Germany; [3]Winterberg, Saarbruecken, Germany; [4]JW Goethe University, Frankfurt, Germany

Determination of Qp/Qs using MRvenc in infants and children suffering from VSDs is quick, safe and reliable compared with invasive oximetry. MRvenc under free breathing conditions generates more physiological data as compared with breath holding. Even in small children with high respiratory frequencies motion artefacts were not detectable.

1923. Variable-Density Spiral Imaging for Real-Time Color Flow Cardiac MRI at 3T

Chia-Ying Liu[1], Krishna Nayak[2]
[1]Uinversity of Southern California, Los Angeles, California, USA; [2]University of Southern Calofornia, Los Angeles, California, USA

Real-time imaging provides the ability to monitor dynamic processes and interactively selects scanning planes. The development of color flow mapping in ultrasound has proven to be effective at visualizing regurgitant jets and abnormal flow. It is desirable to have such capability in an MR exam. In this work we develop variable-density spiral k-space acquisitions for phase contrast cardiac flow imaging at 3T. A real-time platform was used for reconstruction of both velocity and density maps and color image display. The performance of uniform and variable density spirals were compared qualitatively and quantitatively for real-time cardiac flow assessment.

1924. CSF Flow in the Aqueduct and Skull Base as a Function of Heart Rate

Mario Forjaz Secca[1, 2], Júlia Duarte[2, 3], José Luis Ferreira[1], Augusto Goulão[2, 3], Pedro Vilela[3]
[1]Univ. Nova de Lisboa, Caparica, Portugal; [2]Ressonância Magnética de Caselas, Lisboa, Portugal; [3]H. Garcia D'Orta, Almada, Portugal

Most studies that quantify CSF flow do it at the level of the Aqueduct measuring two different quantities: Stroke Volume and Flow Rate. Both these quantities vary with Heart Rate. To further understand the dynamics of CSF flow we obtained measurements of Stroke Volume and Flow Rate at the level of the Aqueduct and at the level of the skull base as a function of heart rate within the same person. In both locations we observed a bigger decrease in the SV than in the FR but for each quantity the variations for the Aqueduct and skull base were similar.

1925. Implementation, Validation, and Application of Cine PCMRI for Quantifying Blood Flow in Small Animal Models of Cardiovascular Disease

Joan M. Greve[1], Mary T. Draney[1], Andrea S. Les[1], Nathan Wilson[1], Norbert J. Pelc[1], Charles A. Taylor[1]
[1]Stanford University, Stanford, California, USA

Manipulation of the murine genome to examine the contribution of genes to physiology and pathology has made understanding how to scale from mouse to human increasingly important. Phase contrast MRI (PCMRI) has been used clinically but rarely applied to small animal models. This work describes implementation, validation, and application of through-plane PCMRI to measure blood velocities in the aorta of rats and mice. Prospective gating had no effect on measurements and flow from a pulsatile phantom was accurately measured. Linear baseline corrections best rectified remaining static phase errors *in vivo*. Acquisition took 16 minutes per animal and was reproducible.

1926. Hemodynamics in the Mouse Aorta - A Combined MRI US and CFD Study

Akiva Feintuch[1], Yuqing q. Zhou[1], Jonathan Bishop[1], Lorinda Davidson[1], C. Ross Ethier[2], R. Mark Henkelman[1, 2]
[1]Hospital for Sick Children, Toronto, Ontario, Canada; [2]University of Toronto, Toronto, Ontario, Canada

Atherosclerosis, like many other diseases, has been a target for mouse modeling. Although there exist physiological differences between mice and humans the atherosclerotic patterns observed in the mouse closely resemble those in humans. Due to the well known relation between atherosclerotic patterns and local hemodynamics, it is of interest to compare mouse and human aortic hemodynamics. Computational fluid dynamics (CFD) simulations which can predict distribution and magnitudes of wall shear stress along the aorta require knowledge of boundary conditions in terms of input velocities and flow splits from the aorta to the carotid arteries. In this study both phase contrast MRI and Doppler ultrasound (US) are used to measure the velocity and flow in the aorta and carotids of anesthetized mice during the cardiac cycle. Data from both modalities was used for input and validation of numerical simulations

1927. Tracking Micron Sized Particles as a Means to Validate Bacterial Motion in Flowing Tubes

Hari Prashanth Ramnath[1], Yimin Shen[1], Yu Chung Norman Cheng[1], Chung- Chu Chen[1], Joseph Smolinski[1], Ewart Mark Haacke[1], Gregory William Auner[1]
[1]Wayne State University, Detroit, Michigan, USA

Water containing as low as 100 bacteria per liter is considered to be contaminated and it is necessary to identify the presence of Escherichia coli (E. coli) bacteria before they are being consumed. The main motivation of the research is to improve the sensitivity and the specificity of the Ecoli biosensor. In order to achieve this we have used Magnetic resonance imaging in conjunction with commercial CFD software to track the path taken by bacteria along the flow channel. This priori knowledge will help us in positioning the sensor arrays in the channel at the position of vantage, thereby improving its detecting capabilities.

MRA

Room 4E Tuesday 13:30 - 15:30

1928. Selective Visualization of Blood Flow Using SSFP Non-Contrast MRA with Time-Spatial Labeling Inversion Plus

Yuichi Yamashita[1], Takao Yamamoto[1], Mie Suzuki[1], Ayako Ninomiya[1], Ikuo Aoki[1], Masao Yui[2]
[1]Toshiba Medical Systems Corporation, Bunkyo-ku, Tokyo, Japan; [2]Toshiba Medical Systems Corporation, Nasu, Tochigi, Japan

In acquisition using True SSFP combined with Time-SLIP, blood vessels can be selectively visualized without the use of contrast medium. In addition, hemodynamics can be observed by acquiring images with various BBTI settings. In order to observe hemodynamics, however, several scans should be performed, and as a result, the total scanning time becomes longer and imaging parameter setting becomes more complicated. The findings of the present study suggest that the Continuation Sampling method permits hemodynamics to be observed in a single scan with no need to change settings.

1929. Fresh Blood Imaging (FBI) of Peripheral Arteries: Comparison with 16-Detector Row CT Angiography

Katsumi Nakamura[1], Kiyomi Kuroki[1], Akiyoshi Yamamoto[1], Akihiro Hiramine[1], Mitsue Miyazaki[2], Yuka Matsufuji[3]
[1]Tobata Kyoritsu Hospital, Kitakyushu, Fukuoka, Japan; [2]Toshiba America Medical Systems, Rolling Meadows, Illinois, USA; [3]Toshiba Medical Systems Co., Fukuoka, Japan

Fresh blood imaging (FBI) is a novel non-contrast enhanced three-dimensional MR angiography technique. In this study, we compared FBI with CT angiography in the evaluation of peripheral arterial disease. Sensitivity, Specificity, and accuracy of FBI with regard to detection of 50% or greater luminal reduction were 97%, 98`%, and 97%, respectively. FBI is an accurate and noninvasive alternative to CT angiography for the assessment of aortoiliac and lower extremity arteries in patients with peripheral arterial diseases.

1930. Scoutless Abdominal Angiography at 3 Tesla with Two-Dimensional Acceleration

Andres Carrillo[1], Ajit Shankaranarayanan[2], David Gurr[3], Theodore Steger[3], Wei Li[4, 5], Eugene Dunkle[4], Robert Edelman[4, 5]

[1]GE Healthcare, Evanston, Illinois, USA; [2]GE Healthcare, Menlo Park, California, USA; [3]GE Healthcare, Waukesha, Wisconsin, USA; [4]Evanston Northwestern Healthcare, Evanston, Illinois, USA; [5]Northwestern University, Chicago, Illinois, USA

Recently, a new method using non-selective RF excitation was proposed for the scoutless acquisition of peripheral arteries. This method decreases the overall imaging time by using a non-selective RF pulses, but it does not take advantage of the speed benefits that could be obtained by the use of parallel imaging. By combining the benefits of both techniques a reduction in the acquisition time of abdominal angiography in the order of 30% can be achieved without significant reduction in image quality.

1931. Reduced Acquisition Window with Parallel Technique Improves Non Contrast 3D HASTE MRA Imaging

Jian Xu[1], Niels Oesingmann[1], Alto Stemmer[2], Kellyanne McGorty[3], Elizabeth Hecht[3], Ruth P. Lim[3], Qun Chen[3], Bernd Stoeckel[1], Vivian S. Lee[3]

[1]Siemens Medical Solutions USA Inc., New York, New York, USA; [2]Siemens Medical Solutions, Erlangen, Germany; [3]New York University School of Medicine, New York, New York, USA

Reduced acquisition window with parallel technique improves non contrast 3D HASTE MRA imaging

1932. Flow Preparation Pulse for Abdominal Non-Contrast-Enhanced MRA

Mitsuharu Miyoshi[1], Tetsuji Tsukamoto[1]

[1]GE Yokogawa Medical Systems, Hino, Tokyo, Japan

Steady State Free Precession yields high blood signal image in short scanning time and it enables Non-Contrast-Enhanced MR Angiography in abdomen. However, SSFP produces bright signal not only in artery but also in vein or stationary fluids. We propose new Flow Preparation (Flow Prep) pulse to distinguish artery from vein and stationary fluids. This technique was developed based on bipolar velocity encoding used in Phase Contrast Angiography. Phantom examination showed that signal intensity of the Flow Prep matched with theoretical values. The Flow Prep enhanced the contrast of artery in volunteer scans.

1933. Feasibility of Quantitative Analysis of Non-Contrast-Enhanced MRDSA Using ECG-Gated Two-Dimensional Half-Fourier FSE for the Assessment of Peripheral Vascular Diseases

Katsumi Nakamura[1], Akiyoshi Yamamoto[1], Kiyomi Kuroki[1], Akihiro Hiramine[1], Mitsue Miyazaki[2], Yuka Matsufuji[3]

[1]Tobata Kyoritsu Hospital, Kitakyushu, Fukuoka, Japan; [2]Toshiba America Medical Systems, Rolling Meadows, Illinois, USA; [3]Toshiba Medical Systems Co., Fukuoka, Japan

A 2D non-contrast-enhanced MR digital subtraction angiography (MRDSA) technique using ECG-gated 2D half-Fourier FSE is reported, which employs a flow void phenomenon of pulsatile flow and provides DSA-like images. In this study, we assess quantitative analysis of non-contrast enhanced MRDSA on peripheral arterial diseases. According to the grade of stenosis, starting time of arterial signal decrease was significantly delayed, which was thought the decreased arterial pressure distal to the stenosis. Combination of nonenhanced 3D images obtained using flow-spoiled FBI and non-contrast-enhanced MRDSA allows not only studying morphology of the vessels but flow dynamic information in patients with arterial diseases.

1934. Phase-Adjusted Fresh Blood Imaging (PA-FBI) as a Non-Contrast Peripheral MRA Technique

Mitsue Miyazaki[1, 2], Hitoshi Kanazawa[2], Nobuyasu Ichinose[2], Yoshio Machida[2], Yoshimori Kassai[2], Takashi Okigawa[3], Youhei Nomitsu[3], Hirofumi Wada[3], Joji Urata[3]

[1]Toshiba America Medical Systems, Rolling Meadows, Illinois, USA; [2]Toshiba Medical Systems Corp., Otawara, Tochigi, Japan; [3]Saiseikai Kumamoto Hospital, Kumamoto, Japan

Flow effects in non-contrast enhanced flow-spoiled fresh-blood imaging (FS-FBI) were investigated in terms of signal coherence. In order to gain arterial signal intensity, an ideal condition is to have a large signal difference between diastole and systole. However, to obtain dark blood in systole, a stronger read-out (RO) spoiler pulse was applied and N/2 artifacts appeared in a result. A new method is proposed to maximize the signal difference in diastole and systole, using two coherent pathways in phase changes as a simple model. Application of RF phase offset permits significant improvement in arterial depiction with less N/2 artifacts.

1935. Non-Contrast MR Angiography of the Heart and Great Vessels Using SSFP with Non-Selective Excitation

Vibhas S. Deshpande[1], Mayil S. Krishnam[2], Stefan G. Ruehm[2], John Paul Finn[2], Gerhard A. Laub[1]

[1]Siemens Medical Solutions, Los Angeles, California, USA; [2]University of California, Los Angeles, California, USA

The purpose of this study was to evaluate feasibility of acquiring non-contrast MR Angiography (MRA) images in the chest using a steady-state free precession sequence (SSFP) to evaluate cardiac morphology, and the aortic, pulmonary, and coronary vasculature. Non-selective RF excitation was implemented to reduce TR and sensitivity to field inhomogeneity. SSFP data were compared with contrast-enhanced MR angiography (CEMRA). Results show that SNR and image quality between SSFP and CEMRA are equivalent. Cardiac morphology and coronary vessels are better depicted on SSFP due to ECG-gating. In conclusion, SSFP with non-selective excitation is a promising approach for non-contrast MR angiography.

1936. Non- Contrast- Enhanced 3D SSFP Versus Contrast-Enhanced MR Angiography for Imaging of Heart and Great Arteries in the Chest: Initial Experience

Mayil S. Krishnam[1], Vibhas S. Deshpande[2], Kambiz Nael[1], Gerhard A. Laub[2], John P. Finn[1], Stefan G. Ruehm[1]
[1]UCLA, Los Angeles, California, USA; [2]Siemens Medical Solutions, Los Angeles, California, USA

We have evaluated the feasibility, reliability and clinical application of non contrast free breathing, 3D SSFP technique in the anatomical assessment of the heart, coronaries and thoracic great arteries and compared the results with CEMRA at 1.5T. Two investigators evaluated the SSFP and CEMRA for visibility, image quality, artifact of the heart and extra cardiac great vessels and coronary arteries. Stenoses and aneurysm of the great arteries were evaluated and compared between sequences. 3D SSFP technique is promising for the morphological evaluation of the heart, coronary arteries and extracardiac great vessels.

1937. Technologic Optimization of Noncontrast Magnetic Resonance Pulmonary Angiography

Gopi Sirineni[1], Aaron Darius Cann[1], Puneet Sharma[1], Krishna Pottala[1], Khalil Salman[1], John Oshinski[1], Diego Martin[1]
[1]Emory University, Atlanta, Georgia, USA

We are investigating the use of fast bright-blood noncontrast MR imaging in evaluation of the pulmonary arteries.

1938. Three Dimensional SSFP of Carotid Artery Disease with Diastolic Triggering

Anna Elizabeth Helen Zavodni[1], Derek J. Emery[1], Ashfaq Shuaib[1], Alan Wilman[1]
[1]University of Alberta, Edmonton, Alberta, Canada

A magnetization-prepared, triggered three-dimensional steady-state free precession technique was evaluated for imaging carotid artery disease in patients under investigation after transient ischemic attacks and stroke. The technique was compared to 3DTOF, and continuous 3DSSFP. Correlation was made with doppler ultrasound. The results suggest that triggering the 3D SSFP acquisition to diastole can result in good depiction of slight stenosis (<50%), but often fails in the presence of more significant stenosis.

1939. Comparison Between Variable Rate K-Space Sampling and Sequential K-Space Acquisition with BSSFP and CMT

Randall B. Stafford[1, 2], Mohammad Sabati[1, 2], M Louis Lauzon[1, 2], Houman Mahallati[1, 2], Richard Frayne[1, 2]
[1]University of Calgary, Calgary, Alberta, Canada; [2]Foothills Medical Centre, Calgary Health Region, Calgary, Alberta, Canada

The purpose of this research was to determine whether a variable rate k-space sampling method or a sequential k-space acquisition provides better overall image quality for continuously-moving table (CMT) large field-of-view (FOV) imaging with balanced steady-state free precession (bSSFP). bSSFP CMT large FOV images were collected at the same table velocity using both the variable rate and sequential sampling methods with approximately equal k-space coverage. After qualitative and quantitative comparison between the images, we conclude that sequential k-space sampling is as effective as variable rate k-space sampling during bSSFP CMT large FOV imaging.

1940. Flow Independent Angiography at 3.0T with Dual-Acquisition Balanced SSFP and Multi-Echo IDEAL

Brian A. Hargreaves[1], Scott B. Reeder[2], Huanzhou Yu[3], Ann Shimakawa[3], Jean H. Brittain[4]
[1]Stanford University, Stanford, California, USA; [2]University of Wisconsin, Madison, Wisconsin, USA; [3]GE Healthcare, Menlo Park, California, USA; [4]GE Healthcare, Madison, Wisconsin, USA

Balanced SSFP imaging provides 3D imaging with excellent angiographic contrast, particularly at 3.0T. Two major challenges to this application are fat/water separation and the well known dark signal bands due to field and susceptibility variations. We present a dual-acquisition balanced SSFP technique that combines RF phase cycling with multi-echo IDEAL fat/water separation to simultaneously address both of these challenges with reasonable scan times. Using longer repetition times improves arterial-venous separation, SNR efficiency and spatial resolution while reducing the RF absorption limitations. Flow independent angiograms of the lower leg can be obtained in several minutes without a contrast agent.

1941. Impact of Fat Saturation in Slice-Selective Inversion-Prepared 3D SSFP Renal MRA

Jan Weidner[1], Marcus Katoh[1], Arno Buecker[1], Rolf W. Gunther[1], Elmar Spuentrup[1]
[1]RWTH Aachen University Hospital, Aachen, Germany

The impact of additional fat saturation (SPIR,spectral presaturation inversion recovery) on vessel visualization was investigated in a slice-selective inversion-prepared 3D steady-state free-precession (SSFP) renal MR angiography (MRA) sequence. In 10 patients with suspected renovascular disease, a navigator-gated cardiac-triggered slice-selective inversion-prepared 3D SSFP sequence was performed with and without fat suppression. SNR, CNR and vessel sharpness were analyzed. Results were compared with contrast-enhanced MRA (CE-MRA) as the reference method. Using additional fat saturation, a significantly higher SNR and CNR can be achieved. Vessel sharpness was comparable for both sequences. Hence, fat saturation should be routinely used using this approach.

1942. MOTSA TOF-MRA Using Multi-Oblique-Stacks Acquisition (MOSA)

Sai Kam Hui[1], Jian Yang[1], Shing Chung Cheung[1], Ed XueKui Wu[1]
[1]The University of Hong Kong, Pokfulam, Hong Kong, People's Republic of China

One of the intrinsic advantages of current TOF MRA techniques is their insensitivity to in-plane blood flow or turbulent flow, causing hypointense signal or discontinuity in blood vessels in MRA images. To overcome this problem, a multi-oblique-stacks acquisition (MOSA) technique is proposed to improve the visualization of in-plane blood flows in MRA. The results showed that TOF-MRA obtained from MOSA was improved as compared to that of conventional MOTSA for the same amount of scan time.

1943. Effects of High Field on Magnetization Prepared Angiography

Anthony G. Tessier[1], Alan H. Wilman[1]
[1]University of Alberta, Edmonton, Alberta, Canada

The effects of high-field on a magnetization prepared 3D MRA technique are investigated with numerical simulation and in normal volunteers at 4.7T. Results show that with the higher SNR and longer T1 relaxation times, the technique produces high quality MR angiograms of the intracranial arteries, despite the inherent B1 inhomogeneity due to the RF standing wave effect. The inversion recovery MRA sequence completely suppresses the background while providing sufficient blood in-flow time to achieve high blood-to-background contrast.

1944. Automatic Extraction and Matching of Neonatal Cerebral Vasculature from MRA-TOF Images

Hui Xue[1, 2], Christina Malamateniou[1], Joanna Allsop[1], Latha Srinivasan[1], Daniel Rueckert[2], Jo V. Hajnal[1]
[1]Hammersmith Hospital, Imperial College London, London, UK; [2]Visual Information Processing, London, UK

An automated method to extract and match neonatal cerebral vasculature from MRA-Time of Flight (MRA-TOF) images is presented. Vessel extraction is first performed to find vessel centerlines from 3D MRA-TOF images and the extracted segments are connected iteratively to compose a vessel tree. To study vasculature development from serial MRA examinations of neonates, account must be taken of rapid brain growth, accompanied by extensive vascular development, which changes vessel geometry so that voxel-by-voxel comparison is unreliable. Accordingly a vessel matching algorithm is developed to determine topological correspondence between different branches. The methods were tested on 4 infants each scanned twice.

1945. 3D TOF MRA of the Intracranial Arteries: Effects of Increasing Magnetic Field to 4.7T

Amir Eissa[1], Alan Wilman[1]
[1]University of Alberta, Edmonton, AB, Canada

Utilizing 4.7T magnets in 3D TOF MRA has the expected benefits of higher SNR and more background signal suppression. It also has concerns with respect to RF focusing. The study was done on 15 healthy volunteers with flow compensated 3D TOF MRA sequence. Theoritical considerations were also addressed.

1946. Dynamic Spin Labeling Thick-Slab Angiography: Off-Resonance Correction of Spiral Acquisitions by Vessel-Selective B_0-Fieldmapping

Carsten Warmuth[1], Bernd Hamm[1], Matthias Taupitz[1]
[1]Charité Medical School, Berlin, Germany

Arterial spin labeling in combination with a Look-Locker multiple readout strategy enables acquisition of dynamic angiograms with high temporal resolution. Use of non-cartesian spiral k-space sampling is attractive in terms of SNR, but image quality suffers from off-resonance blurring. We present a method for deblurring spin labeling angiograms by using vessel-selective B_0-fieldmaps, which is especially suitable for 2D thick slab projection acquisitions.

1947. Intracranial Aneurysms at 3.0T: Time-Of-Flight vs. Contrast Enhanced MRA Vs CTA

Kambiz Nael[1], Pablo Villablanca[1], Whitney Pope[1], Ali Nael[1], Gerhard Laub[2], John Paul Finn[1]
[1]David Geffen School of Medicine at UCLA, Los Angeles, California, USA; [2]Siemens, Los Angeles, California, USA

High spatial resolution 3.0T MR angiography including both time-of-flight (TOF) and contrast-enhanced MRA was performed for visualization and characterization of intracranial aneurysms in patients with suspected intracranial aneurysm, and the result was compared to multi-slice CTA.

1948. Segmentation of Venous Vessels Using Multi-Scale Vessel Enhancement Filtering in Susceptibility Weighted Imaging

Andreas Deistung[1], Marek Kocinski[2], Piotr Szczypinski[2], Andrzej Materka[2], Jürgen R. Reichenbach[1]
[1]Friedrich-Schiller-University Jena, Jena, Thuringia, Germany; [2]Technical University Lodz, Lodz, Poland

We introduce a method for extraction of cerebral veins using susceptibility weighted imaging (SWI) data with a multi-scale vessel-enhancement algorithm. This line-enhancement algorithm was applied in 2D projection and 3D SWI data. The algorithm emphasizes veins and the boundary of the brain. Subsequent masking, thresholding and skeletonization removed the boundary, suppressed noise and improved the visibility of vessel connections. It was possible to extract venous vessels out of SWI data down to a diameter of 100 µm, which can be used for high detailed vessel tracking and for the determination of brain regions with malformed venous vessel architecture.

1949. CNR-Based Variable Resolution Reconstruction for Black Blood MRA

Prashanthi Vemuri[1], Eugene G. Kholmovski[1], Dennis L. Parker[1]
[1]University of Utah, Salt Lake City, Utah, USA

In present day MR, faster imaging strategies facilitate imaging with higher spatial resolution. But since noise in MR data is uniformly distributed throughout k-space, an increase in the amount of k-space sampled for increasing the spatial resolution results in the addition of more noise to the image. This abstract derives a theoretical dependence of the CNR of vessels in black-blood MRA on the fraction of k-space used for reconstruction. Based on this analysis, we present a variable resolution reconstruction technique which utilizes the local CNR value to improve the visibility of the vascular structures in black blood MRA.

1950. Regional Cerebral Volume Flow Using Quantitative Magnetic Resonance Angiography

Meide Zhao[1, 2], Sepideh Amin-Hanjani[2], Sean Ruland[2], Anthony P. Curcio[1], Ostergren Lauren[1], Fady T. Charbel[2]
[1]VasSol, Inc., Chicago, Illinois, USA; [2]University of Illinois at Chicago, Chicago, Illinois, USA

An algorithm was developed to determine the volume flows to specific brain areas, i.e., regional cerebral volume flow, and to determine the distribution of cerebral volume flows within different regions of the brain circulation in healthy volunteers. The study population consisted of eighty-three healthy volunteers. All subjects underwent quantitative Magnetic Resonance Angiography (QMRA) study with a standard NOVA head-and-neck protocol (VasSol, Inc., Chicago). Twelve regions in the brain circulation were identified in a partition tree and the volume flow for each region was determined based on the QMRA study results.

1951. High Resolution 2D and 3D Magnetic Resonance Imaging of Murine Carotid Arteries *In Vivo*

Christoph Jacoby[1], Alma Zernecke[2], Ulrich Flögel[1], Yang Chul Böhring[1], Andreas Beck[1], Volker Aurich[1], Christian Weber[2], Jürgen Schrader[1]
[1]Heinrich-Heine-Universität, Düsseldorf, Germany; [2]Rheinisch-Westfälisch Technische Hochschule Aachen, Aachen, Germany

This study was aimed at developing protocols for repetitive monitoring of vascular lesion development in murine carotid arteries *in vivo*. Using atherosclerotic mouse models, 2D and 3D high resolution MR measurements were performed at different time points before and after experimental injury in order to detect different courses of vascular remodeling depending on the degree of injury. MRI measurements were highly correlated to morphometric data obtained 4 weeks after injury. Additionally, high reproducibility as well as low intra- and interobserver variabilities were determined by repetitive measurements and analyses, respectively.

1952. Gadolinium-Enhanced MR Angiography in the Evaluation of Carotid Artery Stenosis: Comparison with Digital Subtraction Angiography in 238 Patients

Nicoletta Anzalone[1], Guiseppe Scialfa[2], Roberto Iezzi[3], Siegfried A. Thurnher[4], Richard Coulden[5], Gianpaolo Pirovano[6]
[1]Hospital San Raffaele, Milan, Italy; [2]Hospital Niguarda ca Grande, Milan, Italy; [3]Hospital SS Annunziata, Chieti, Italy; [4]University of Vienna, Vienna, Austria; [5]Papworth Hospital, Cambridge, UK; [6]Bracco Diagnostics Inc., Princeton, New Jersey, USA

238 patients with suspected carotid artery disease underwent MRA and DSA examinations within 2 weeks. 2D-TOF MRA was performed before and 3D spoiled gradient-echo MRA after the administration of 0.1 mmol/kg gadobenate dimeglumine. According to 4 experienced reviewers (3 MRA, 1 DSA), more segments were technically adequate on CE-MRA than 2D-TOF MRA. Contrast use significantly decreased the technical failure rate for all 3 readers ($p<0.001$). Sensitivity for detecting significant (¡Ý 60%) stenoses ranged from 56.6% to 76.3% and from 57.9% to 86.3% for 2D TOF MRA and CE-MRA, respectively. Specificity increased from 81-83% to 89.5-93.6% and accuracy from 78.3-82.2% to 87.8-89.7 for CE-MRA as compared to 2D TOF MRA.

1953. Intra-Individual Cross-Over Blinded Dose Comparison of Single Versus Double Dose of Gd-DTPA in Contrast-Enhanced Magnetic Resonance Angiography of the Carotid Arteries

Johannes T. Heverhagen[1], Claudia Jourdan[1], Michael V. Knopp[1]
[1]The Ohio State University, Columbus, Ohio, USA

This study was an intra-individual comparison of single-dose and double-dose Gd-DTPA enhanced MRA in the carotid arterial territory with blinded evaluations by two independent radiologists. Carotid MRAs were carried out in eleven healthy volunteers at 1.5 Tesla with a three-dimensional fast spoiled gradient echo sequence. Contrast agent was injected with a power injector keeping the injection time constant for both dosages. Both readers found at least 97% of vascular segments evaluable. Median overall image quality and diagnostic confidence were rated excellent. Our results suggest that a single dosage of approximately 0.1 mmol/kg bw Gd-DTPA may be the preferable dosage in the carotid arteries.

1954. A CE-MRI Study Asssing the Uptake of Gd-DTPA and the Stability of Atheromatous Tissue Within the Carotid Arteries

Aleksandra Radjenovic[1], Michael J. Gough[2], Cedric Abbott[2], Laura A. Rhodes[1], Demos Dellagrammaticas[2], Yvonne Chapman[2], John P. Ridgway[1], Steven Frederick Tanner[1]

[1]University of Leeds, Leeds, UK; [2]Leeds General Infirmary, Leeds, UK

Inflammation is thought to be a factor associated with plaque instability. Contrast enhanced MRI (CE-MRI) has the potential to detect inflammation and may therefore be capable of identifying patients at risk of thromboembolic complications arising from plaque disruption. This study has compared CE-MRI measurements of atheromatous plaques with histological assessment of plaque stability. The results show relatively high levels of enhancement within the unstable carotid plaque indicating that the CE-MRI technique may be of use in non-invasive patient studies assessing plaque stability.

1955. Free-Breathing 2D Time-Of-Flight Pulmonary MRA at 3T

Jian Yang[1], Sa Kam Hui[1], Ed Xuekui Wu[1]

[1]The University of Hong Kong, Hong Kong SAR, People's Republic of China

This study aims to optimize and evaluate a free-breathing 2D TOF PMRA protocol at 3T. The protocol was based on a T1-weighted turbo field echo sequence with static tissue suppression using magnetization transfer plus selective inverse recovery, spectral fat saturation, cardiac gating, respiratory navigator gating, and parallel imaging. Satisfactory pulmonary MRAs were demonstrated in volunteer subjects (N=12). The proposed protocol is clinically relevant for patients who are unable to provide long breath-holds during MRI scans.

1956. Intra-Individual Comparison of 0.5 & 1.0M Contrast Agents in the Evaluation of Chronic Thrombo-Embolic Pulmonary Hypertension

Neil Woodhouse[1], Jim M. Wild[2], Edwin J R van Beek[3], Charlie Elliot[4], Martyn N J Paley[1], Paul D. Griffiths[1], David G. Kiely[4]

[1]University of Sheffield, Sheffield, South Yorkshire, UK; [2]University of Sheffield, Sheffield, South Yourkshire, UK; [3]University of Iowa, Iowa City, Iowa, USA; [4]Sheffield Teaching Hospitals NHS Trust, Sheffield, South Yorkshire, UK

We compared 0.5M Gd-DTPA (Magnevist) and 1.0M Gd-BT-D3OA (Gadovist) in both high-resolution and dynamic time resolved MRA in chronic thromboembolic pulmonary hypertension (CTEPH). Patients were scanned twice within 48 hours receiving the same contrast dose for each examination. There was greater separation of pulmonary and systemic peaks in the Gd-BT-DO3A examinations compared to Gd-DTPA. Parametric comparison between the time-resolved examinations revealed better delineation of the pulmonary arterial and venous circulations using Gd-BT-DO3A. The more compact bolus-profile of Gd-BT-DO3A compared to that of Gd-DTPA results in less contamination of the arterial phase image by cardiac motion and pulmonary-venous and systemic vasculature.

1957. Contrast Detection and Timing for MR Angiography with Self-Navigated DC Signal Detection

Scott Brian Reeder[1], Ethan K. Brodsky[1], Anja C. Brau[2], Walter F. Block[1], Jean H. Brittain[3]

[1]University of Wisconsin, Madison, Wisconsin, USA; [2]GE Healthcare, Menlo Park, California, USA; [3]GE Healthcare, Madison, Wisconsin, USA

In this work, we describe a self-navigated method for the detection of contrast uptake for rapid MR angiographic applications. Using a 3D projection reconstruction angiographic imaging method (VIPR), samples from the center of k-space are collected just prior to the readout gradient in order to measure the DC component of image spatial frequencies. Acquiring this information every TR provides a rapid method for tracking the bolus of contrast as it enters the patient. This method can be generalized to Cartesian image acquisitions and shows promise for improving the timing and detection of contrast boluses.

1958. Reduction of Bolus Profile Artifacts in High Resolution Contrast-Enhanced MR Angiography Using CENTRA and SENSE

Gregory J. Wilson[1], Jeffrey H. Maki[2, 3]

[1]Philips Medical Systems, Cleveland, Ohio, USA; [2]University of Washington, Seattle, Washington, USA; [3]Puget Sound VA HCS, Seattle, Washington, USA

Randomly segmented central k-space ordering (CENTRA) has been proposed as a method to reduce ringing artifacts in high resolution 3D CE-MRA. CENTRA acquires the central portion of ky-kz space in random order, then acquires the periphery in elliptical centric order. This study uses a computer simulation to evaluate CENTRA encoding for reduction of ringing artifacts in high resolution 3D CE-MRA. Results showed CENTRA effectively reduced arterial ringing in clinically relevant simulations. The tradeoffs appeared to be increased mottled noise and increased likelihood of venous enhancement, thus limiting the duration of the central window to 4-6 sec in practice.

1959. Different Injection Duration Combining with Modality of K Space Sampling: Initial Experience with a 3 T Scanner

Kai Lin[1, 2], Zhao-Qi Zhang[2], Biao Lu[2], Wei Sun[3]

[1]Beijing Institute of Heart Lung and Blood vessel diseases, Beijing, People's Republic of China; [2]Beijing Anzhen Hospital, Beijing, People's Republic of China; [3]GE Healthcare, Beijing, People's Republic of China

Does injection duration of contrast medium affects image quality? Do various k space sampling modalities have different sensitivities to the effection? 80 patients were randomly divided into four groups and underwent imaging with different 3D contrast-enhanced MRA scanning and injection protocol combinations. We found that short injection duration of contrast medium leads to more heterogeneous signal intensity. Centric view ordering seems to be more sensitive to short injection duration than elliptic centric view ordering of k space sampling.

1960. Peripheral MR Angiography with Gadobenate Dimeglumine: Results of a Large-Scale Multi-Institutional Experience

Siegfried A. Thurnher[1], Claus Claussen[2], Gunther Schneider[3], Claudio Ballarati[4], Georg Bongartz[5], Stefan Schoenberg[6], John R. Parker[7], Gianpaolo Pirovano[7]

[1]University of Vienna, Vienna, Austria; [2]Eberhardt Karls University, Tuebingen, Germany; [3]Homburg University Hospital, Homburg/Saar, Germany; [4]Hospital Valduce, Como, Italy; [5]University Hospital, Basel, Switzerland; [6]Ludwig Maximilians University, Munich, Germany; [7]Bracco Diagnostics Inc., Princeton, New York, USA

Patients with peripheral arterial disease (n=272) underwent DSA and MRA (2D-TOF sequence followed by 3D-SPGRE sequence after 0.1 mmol/kg gadobenate dimeglumine) within a 30 day period. Both exams covered from the aortic bifurcation to the trifurcation, and DSA results were used as the gold standard. According to the three blinded reviewers the technical failure rate of TOF-MRA was 6.2%-18%. This rate was significant lower ($p < 0.001$) on the CE-MRA exam (2.5%-3.4%), a rate approaching that of DSA (1.4%). Sensitivity for detection of significant disease (¡Ý50%) ranged from 33.2% to 62.8% and from 54% to 80.9% for TOF-MRA and CE-MRA, respectively. When comparing CE-MRA to TOF-MRA, significant increases ($p < 0.001$) in specificity (74.3-88.9% to 89.7-95.3%) and accuracy (68-77.3% to 85-87.5%) were noted. Significantly better reproducibility ($p < 0.00001$) was also demonstrated for CE-MRA vs TOF-MRA (82% agreement, k-value: 0.66 vs 65.2% agreement; k-value: 0.47).

1961. Combining Body and Surface Coils in High Resolution

David G. Kruger[1], Ananth Madhuranthakam[1], Houchun Hu[1], Stephen Reiderer[1], James Glockner[1], Jason Polzin[2]

[1]Mayo Clinic, Rochester, Minnesota, USA; [2]GE Medical Systems, Milwaukee, Wisconsin, USA

Contrast-enhanced continuously moving table angiography has been shown to be effective in maintaining the position of the scanner sweet spot with the dynamic flow of the contrast bolus in peripheral angiography. In this work we incorporate the use of a four-element surface coil along with the body coil in one continuous acquisition. The body coil is used for signal reception from the heart to the popliteal arteries, at which point the surface array is activated to image the popliteal trifurcation region with increased spatial resolution and SNR. Scans are completed in approximately 60 seconds.

1962. Contrast-Enhanced MRI of Occlusive Arterial Disease

Kevan James Thompson Anderson[1], General Leung[1], Nigel R. Munce[1], Beiping Qiang[2], Erin L. MacMillan[3], Michael V. Truong[3], John J. Graham[3], Alan R. Moody[3], Alexander J. Dick[3], Bradley H. Strauss[2], Graham A. Wright[1, 3]

[1]University of Toronto, Toronto, Ontario, Canada; [2]St. Michael's Hospital, Toronto, Ontario, Canada; [3]Sunnybrook and Women's College Health Sciences Centre, Toronto, Ontario, Canada

In this study we investigate the behavior of two different MRI contrast agents (Omniscan and Clariscan) for characterizing occlusive arterial disease attributes such as inflammation and neovascularization in an animal model of total femoral artery blockage. The relative distribution volume of each contrast agent was measured in occlusive lesions of varying age. Consistent with the literature, the results suggest that endoluminal neovascularization increases over the initial 10 weeks and is followed by a progressive collapse of these neovessels. An increase in permeability and associated interstitial space is also experienced over the initial 3-5 weeks and subsides over time.

1963. High-Resolution 3-D Imaging of Chronic Total Occlusions in Peripheral Vessels Using a T-1 Weighted Turbo Spin Echo Sequence with Inner Volume Imaging

Smita Sampath[1], Amish N. Raval[2], Robert J. Lederman[3], Elliot R. McVeigh[1]

[1]Laboratory of Cardiac Energetics, Division of Intramural Research, NHLBI, NIH, DHHS, Bethesda, Maryland, USA; [2]University of Wisconsin, Madison, Wisconsin, USA; [3]Cardiovascular branch, Division of Intramural Research, NHLBI, NIH, DHHS, Bethesda, Maryland, USA

Peripheral arteries are challenging to maneuver during X-ray guided recanalizations due to the absence of a lumen to hold contrast agents and the tortuous nature of the vessels. In this abstract, we investigate the use of a T1-weighted high-resolution 3-D Turbo Spin Echo MRI pulse sequence in combination with inner volume imaging to image and characterize occluded arteries within a reasonable clinical acquisition time of around 5-10 minutes with adequate signal-to-noise ratios at 1.5T with a view toward practical percutaneous X-ray revascularization.

1964. Whole-Body MR Detects Unsuspected Concomitant Vascular Disease in CHD Patients

Susanne C. Ladd[1], Thomas Paul[1], Thomas Schlosser[1], Sophia L. Goericke[1], Isabel Wanke[1], Elke R. Gizewski[1], Michael Forsting[1]
[1]University Hospital Essen, Essen, Germany

A whole-body MR protocol (head, whole-body MR angiography, heart) is applied to coronary heart disease patients, which requires an in room time of 40 minutes. MR results are compared to patients' history. The rate of previously unknown ilio-femoro-popliteal stenoses, myocardial and cerebrovascular infarctions was 60.7%, 14.8% and 68.8%, resp. Prospective studies have to show if whole-body MR can serve as a screening tool for vascular pathologies in these high-risk patients.

1965. Concomitant Atherosclerotic Changes in Whole-Body MR-Angiography and Coronary Calcium Deposit in Patients with Catheter-Staged Coronary Artery Disease (CAD)

Katja Brauck[1], Frank Breuckmann[1], Joerg Barkhausen[1], Susanne Ladd[1]
[1]University Hospital Essen, Essen, NRW, Germany

Patients with coronary artery disease show a high prevalence for concomitant atherosclerotic disease of peripheral vessels. We evaluated the correlations between arterial pathologies as found in whole-body MR angiography and coronary calcium deposit. The results show that whole body MR angiography and coronary calcium deposit (EBT) correlate well, and both depend on the degree of coronary artery disease as defined by catheter angiography. An atherosclerosis index as defined in this study shows to be a promising parameter for the prediction of coronary calcium deposit.

1966. Comprehensive Imaging with Whole Body MRI at 1.5 and 3.0 Tesla in Patients with Longstanding Diabetes

Sabine Weckbach[1], Harald Kramer[1], Denise Friedrich[1], Klaus G. Parhofer[1], Maximilian F. Reiser[1], Christian Glaser[1]
[1]Ludwig-Maximilians-University Munich - Grosshadern, Munich, Germany

The purpose of this study was to implement a high-resolution protocol on a 3 T whole body scanner and evaluate the protocol in asymptomatic patients suffering from diabetes for more than ten years. 45 asymptomatic patients with type 1- or 2-diabetes lasting for more than ten years were examined on a 1.5 T or 3.0 T whole body MR system. Correlation to a group of 200 healthy adults of the same age range who received a whole body MRI for cardiovascular screening was performed. Compared to a healthy control group pathologies such as vascular stenoses, myocardial infactions and chronic-ischemic lesions of the brain were substantially more often found in the diabetes group than in the healthy control group. Due to the integration of several technical advances, whole body MRI with PAT, especially at 3T, is a highly promising method for comprehensive disease specific imaging since typical pathologies in diabetics can be identified with high spatial resolution and patients can potentially be treated earlier.

1967. Flow-Independent Angiography of the Hand with 3D Balanced SSFP Imaging

Tolga Cukur[1], Julie C. DiCarlo[1], Neal K. Bangerter[1], Brian A. Hargreaves[1], Dwight G. Nishimura[1]
[1]Stanford University, Stanford, California, USA

Balanced steady-state free-precession imaging is an excellent candidate for flow-independent angiography when combined with magnetization preparation. However, high signal from fat and off-resonance caused by air-tissue interfaces can degrade vessel visualization. Phase-sensitive fat-water separation is fast and efficient, but fails in the presence of susceptibility variations at air-tissue interfaces. In this work, we use a susceptibility-matching material covering the hand in order to reduce susceptibility variations, and dramatically improve image quality. Optional inversion-recovery and T2-prep pulses further improve contrast between arterial blood and synovial fluid or muscle respectively. High-resolution angiograms with great small-vessel depiction can be acquired within a few minutes.

1968. Signal Characteristic of a 1-Molar Contrast Agent at 1.5 and 3T and Improvements with a Variable TE GRE Sequence

Aurélien Fabian Stalder[1], Michael Markl[1], Jürgen Hennig[1]
[1]University Hospital, Freiburg, Germany

To enhance Gadolinium based CE-MRA, the influence of a 1-molar contrast agent (Gadobutrol/Gd-Bt) has been explored and possible improvements are suggested. Relaxation times and relaxivities were measured for several Gd-Bt concentrations in water at 20 C for 1.5T and 3T. Gd-Bt concentration influence on signal intensity could be effectively simulated and compared to measurements. Although shortened T2* were measured, no significant T2* effect on signal intensity in water was observed. Based on these findings, variable echo time approaches were explored in order to enhance SNR. An adaptive bandwidth approach was implemented and results indicating increased SNR at high concentrations are presented.

1969. Diagnostic Accuracy of Contrast-Enhanced MR Angiography with Various Doses of Gadobenate Dimeglumineu

Gunter Schneider[1], Riccardo Manfredi[2], Luigi Grazioli[3], Siegfried A. Thurner[4], John R. Parker[5], Gianpaolo Pirovano[6]

[1]Homburg University Hospital, Homburg/Saar, Germany; [2]Polyclinic "A. Gemelli" University Hospital, Rome, Italy; [3]University of Brescia, Brescia, Italy; [4]University of Vienna, Vienna, Austria; [5]Bracco Diagnostics Inc., Princeton, New York, USA; [6]Bracco Diagnostics Inc., Princeton, New Jersey, USA

A parallel-group blinded read was conducted to evaluate 4 doses of gadobenate dimeglumine for CE-MRA in terms of the accuracy (sensitivity and specificity) for detecting significant steno occlusive disease in renal, pelvic and carotid arteries. Eighty-four patients with suspected disease of the renal, pelvic or carotid arteries underwent CE-MRA (3D-SPGE sequences at 1.5 T) and DSA. CE-MRA was performed using dose of 0.025, 0.05, 0.1 or 0.2 mmol/kg (21, 25, 17 and 21 patients, respectively). Assessment of MRA and DSA images was performed on a segmental basis by 4 independent experienced radiologists. Overall accuracy was for CE-MRA was high, especially at the 0.1 mmol/kg dose level (95.2-97.3%, $p<0.01$ for 0.1 dose vs other doses).

1970. High Resolution Imaging and Artery-Vein Separation of Contrast-Enhanced MR Angiography in the Lower Extremity Using Vasovist Blood Pool Agent

Maisie S. Wang[1], David Robert Haynor[1, 2], Gregory J. Wilson[3], Romhild M. Hoogeveen[4], Michael G. Hartmann[5], Jeffrey Harold Maki[1, 2]

[1]University of Washington, Seattle, Washington, USA; [2]Puget Sound VAHCS, Seattle, Washington, USA; [3]Philips Medical, Bothell, Washington, USA; [4]Philips Medical, Best, Netherlands, USA; [5]Epix Pharmaceuticals, Cambridge, Massachusetts, USA

Blood pool agents have higher relaxivity and prolonged intravascular half-life compared to Gd contrast agents. Longer scan times can be used for high resolution imaging in the equilibrium phase to improve visualization of the vasculature. We optimized MR parameters (flip angle, TE, TR, bandwidth) to obtain high resolution and contrast-to-noise images of the lower extremity using the Vasovist blood pool agent. Computational tools were developed to perform artery-vein separation on healthy and patient data. We provide imaging guidelines for equilibrium-phase CE-MRA using blood pool agents that may be useful when these agents become clinically available.

1971. Vast Reduction in Reconstruction Time of 3D Time Resolved Inhomogeneity-Corrected Spiral MRA Using Parallel Computing on a 32 Node Cluster

Bryan Kressler[1, 2], Pascal Spincemaille[2], Martin R. Prince[2], Yi Wang, [12]

[1]Cornell University, Ithaca, New York, USA; [2]Weill Medical College of Cornell University, New York, New York, USA

An inhomogeneity corrected spiral reconstruction is implemented and parallelized to run on a cluster of commercially available PC based computers. The parallelized implementation drastically reduces reconstruction time from hours to minutes, rendering time resolved 3D spiral MRA practical for routine clinical use.

1972. Feasibility Study of a Double Self-Gating Technique for Free-Breathing Time-Resolved 3D Imaging

Peng Lai[1], Andrew C. Larson[1], Sonia nielles-vallespin[2], Debiao Li[1]

[1]Northwestern University, Chicago, Illinois, USA; [2]Siemens Medical Solutions, Erlangen, Germany

This work aimed to investigate the feasibility of a double self-gating (DSG, respiratory self-gating + cardiac self-gating) technique for applications requiring free-breathing time-resolved 3D imaging. A new 2-projection method capable of accurate heart displacement measurement is also proposed. Both respiratory and cardiac gating signal were derived from direct measurement of the heart. Our preliminary results showed the potential of using this DSG scheme for suppressing both respiratory and cardiac motion artefacts.

1973. Motion Tracking by Constrained Reconstruction of Orthogonal Projections

Yuexi Huang[1, 2],Graham Wright[1, 2]

[1]University of Toronto, Toronto, ON, Canada; [2]Sunnybrook & Women's College Health Sciences Centre, Toronto, ON, Canada

The AUCTION algorithm (Assignment and Update with CorrelaTION) was developed to reconstruct 3D data sets from orthogonal projections for time-resolved MR angiography. Correlations with a 3D spatial constraint are used to solve the ambiguity problems of the reconstruction. In the presence of motion, however, the data set forming the spatial constraint will be blurred. The mis-registration of the 3D spatial constraint to a particular pair of orthogonal projections may introduce ambiguities in the AUCTION reconstruction. In this work, the motion correction method for the AUCTION algorithm is investigated. The effectiveness of motion tracking by this technique is demonstrated in phantom studies.

1974. Extracting Quantitative Parameters from a Mathematical Model Fitted to Renal Artery Blood Flow Data Obtained by Magnetic Resonance Angiography

Martin Larsson[1], Anders Persson[1], Per Eriksson[2], Örjan Smedby[1]

[1]Linköping University, Linköping, Sweden; [2]Linköping University Hospital, Linköping, Sweden

To investigate the feasibility of quantitative parameter extraction, 8 patients and 5 controls were examined with cine phase-contrast MR velocity measurements and blood flow data were extracted. A mathematical model with parameters describing the temporal course of the curve was fitted to the aorta and renal artery blood flow data. Acceptable curve fitting ($R^2>0.80$) was obtained in 36 of 39 curves. The results suggest that it is technically feasible to fit a mathematical model to renal blood flow data and from it extract quantitative parameters potentially useful for diagnosis of renal artery stenosis.

1975. MRI Scanning by Remote Control

John Paul Finn[1], Roya Saleh[1], Stefan Thesen[2], Stefan G. Ruehm[3], Margaret Lee[1], John Grinstead[4], John Child[4], Gerhard Laub[5]

[1]David Geffen School of Medicine at UCLA, Los Angeles, California, USA; [2]Siemens Medical Solutions, Erlangen, Germany; [3]David Geffen School of Medicine at UCLA, Los Angeles, California, USA; [4]Seimens Medical Solutions, Los Angeles, California, USA; [5]Siemens Medical Solutions, Los Angeles, California, USA

Remote control (RC) MRI scanning was implemented at our institution to address the very real problem of coordinating complex cardiovascular studies with limited available physicians and technologists. Because of our geographically distributed scanner base, and the unpredictable nature of in-patient requests for scans, we often have complex studies scheduled in close temporal proximity, but in widely separate physical locations. Our results indicate that MRI scanning by remote control is entirely feasible and, within the context described, can produce results at least as good as can local control.

Spectroscopy

Room 4E Tuesday 13:30 - 15:30

1976. Longitudinal Measurements of Myocardial Creatine Content in Normal and Creatine Transporter Over-Expressing Mouse Hearts Using Single Voxel ^{1}H-MRS *In Vivo*

Darci Phillips[1], Michiel ten Hove[1], Julie Wallis[1], Stefan Neubauer[1], Jurgen E. Schneider[1]

[1]University of Oxford, Oxford, Oxon, UK

In this study we used single voxel ^{1}H-MRS to longitudinally measure the myocardial creatine content in normal and creatine transporter over-expressing mice at six weeks, four and eight months, respectively, and to reference it to the unsuppressed water signal. Using HLPC, we previously showed that creatine transporter over-expressing mice have elevated but variable creatine levels. Now we demonstrate that cardiac ^{1}H-MRS can be used *in vivo* to non-invasively quantify the myocardial creatine content, to stratify normal and genetically modified mouse hearts according to their metabolite levels, and to follow them longitudinally.

1977. Cardioprotective Effects of a PPAR-Delta Selective Agonist (GW610742X) in a Rodent Model of Congestive Heart Failure

Tom Chih-Chuang Hu[1, 2], Kristeen Maniscalco[2], Alan R. Olzinski[2], Carolyn Williams[2], Stephen C. Lenhard[2], Thomas R. Schaeffer[2], Amy Grill[2], Chris P. Doe[2], Robert N. Willette[2], Beat M. Jucker[2]

[1]Medical College of Georgia, Augusta, Georgia, USA; [2]GlaxoSmithKline, King of Prussia, Pennsylvania, USA

PPAR-δ nuclear receptor is a transcriptional regulator for nutrient metabolism and energy homeostasis and cardiac specific knockout of PPAR-δ results in cardiac lipotoxicity, hypertrophy, and failure. In this study, we examined the potential therapeutic benefit of a specific PPAR-δ agonist (GW610742X) on cardiac LV and RV functional parameters, energetics and substrate metabolism in a rodent model of congestive heart failure. GW610742X treatment resulted in a reduction in RV hypertrophy, pulmonary congestion, and a normalization of substrate metabolism in a rodent model of congestive heart failure.

1978. *In Vivo* 2D Mapping of Cardiac High Energy Phosphates in the Mouse

Ulrich Flögel[1], Christoph Jacoby[1], Axel Gödecke[1], Jürgen Schrader[1]

[1]Universitätsklinikum Düsseldorf, Heinrich-Heine-Universität, Düsseldorf, NRW, Germany

This study was aimed at developing a protocol for an integrated energetic and functional characterization of transgenic mouse models with cardiomyopathies. Using acquisition-weighted 2D ^{31}P CSI at a field strength of 9.4 T, we were able to acquire spectra from the left ventricle of good quality within a reasonable acquisition time of about 75 min. The obtained data were validated against perchloric acid extracts of the same hearts. Analysis of a transgenic mouse line which has been shown to develop signs of heart failure revealed that cardiac dysfunction was accompanied by an impaired energy homeostasis over the entire left ventricle.

1979. Metabolic Imaging of Healthy and Infarcted Myocardium Using ^{31}P Chemical Shift Imaging with Spatial Saturation Pulses

Oliver Geier[1], Meinrad Beer[2], Jan Ruff[3], Wolfram Machann[2], Dietbert Hahn[2], Matthias Spindler[2], Herbert Köstler[2]

[1]Rikshospitalet University Hospital, Oslo, Norway; [2]Universität Würzburg, Würzburg, Germany; [3]Siemens AG Med, Erlangen, Germany

The contamination from tissue adjacent to the myocardium is one of the major restriction for 31P-MR-spectroscopy of the human myocardium. Aim of this work was to present a new 3D CSI-technique which suppresses the unwanted contribution from adjacent organs by means of spatial saturation pulses. The method was applied both to healthy volunteers and first patients with myocardial infarctions.

1980. Efficient Quantitative 23Na Concentrations of Fast and Slow T2 Components in the Human Heart Using UTE-CSI and the Blood Pool as a Reference

Matthew D. Robson[1], Damian J. Tyler[1], Joseph B. Selvanayagam[1], Jane M. Francis[1], Stefan Neubauer[1]
[1]Oxford University, Oxford, UK

Sodium concentrations in the human heart increase during ischemia due to failure of the Na-K pump. Here we have used the Ultra-short TE CSI sequence run with a short repetition time to measure both the short T2 and long T2 components of the sodium signal in humans. We have quantitated these measurements using the myocardial blood pool as a reference and corrected for the receive profile of the RF coil. Myocardial tissue shows a long T2 component of 43.6+/-1.9mM/l (T2* of 18.4+/-1.6ms), and a short T2 component of 10.5+/-2.4mM/l (T2* of 1.21+/-0.41ms) across the whole heart.

1981. The Intra- Versus Extracellular Myocardial Tissue Sodium Contents in the Time Course of Infarct Healing

Hanns Hillenbrand[1], Reza Kharrazian[1], Sebastian Hagelauer[1], Kai Hu[1], Frank Wiesmann[1], Elsbeth Fekete[1], Lisa Bauer[1], Georg Ertl[1], Peter Jakob[1], Wolfgang Bauer[1]
[1]Würzburg University, Würzburg, Germany

Intra- and extracellular tissue sodium contents were measured in myocardial infarction (isolated rat hearts, n=49) in the time course of infarct healing using a chemical shift MR imaging sequence. Significant reduction of intracellular tissue sodium content and significant increase of extracellular tissue sodium content were found in necrosis, in granulation tissue and in scar tissue.

1982. ^{1}H NMR Diffusion Spectroscopy of Oxymyoglobin in Perfused Rat Heart

Ping-Chang Lin[1], Ulrike Kreutzer[1], Thomas Jue[1]
[1]University of California, Davis, Davis, California, USA

Even the role as oxygen storage has been well established, another character of myoglobin, facilated oxygen diffusion, still lacks a reliable value for the intracellular diffusivity of myoglobin to determine if it is physiological significance. A modified pulsed-gradient stimulated echo (PG-STE) sequence was used to measure the signal attenuation of oxymyoglobin in a perfused rat heart during K+ arrest. Our current experimental results represent the diffusion coefficient of myoglobin in the cell is just slightly slower than in solution, which indicates the *in vivo* myoglobin-facilated oxygen diffusion cannot be ignored.

MRS of Cells, Body Fluids, and Others

Room 4E Tuesday 13:30 - 15:30

1983. Insulin Release and Energetic Changes in INS-1 Cell Bioreactors in Response to Glucose Challenge

Robert Woodbury Wiseman[1], Brian Andrew Bieber[1], Lawrence Karl Olson[1], Kenneth A. Krohn[2]
[1]Michigan State University, East Lansing, Michigan, USA; [2]University of Washington, Seattle, Washington, USA

The functional coupling between mitochondria and insulin release was examined in a beta cell model using phosphorus NMR spectroscopy of small cell bioreactors. Results show that a first order change in cytosolic ADP is highly correlated with insulin release and that ATP remained unchanged. This suggests that ADP homeostasis is a controlled variable and offers insight into the role of both adenylates and of mitochondrial energetics in insulin secretion in this cell line.

1984. Across Species Metabonomics: Identification of Common Spectral Changes in Mouse and Hamster Urine, Caused by Parasite Infection

Radka Stoyanova[1], Shuyan Du[2], Yulan Wang[3], Qi Zhao[2], Elaine Holmes[3], Juerg Utzinger[4], Paul Sajda[2], Truman R. Brown[2]
[1]Fox Chase Cancer Center, Philadelphia, Pennsylvania, USA; [2]Columbia University, New York, New York, USA; [3]Imperial College, London, UK; [4]Swiss Tropical Institute, Basel, Switzerland

A metabonomic investigation of the spectral patterns in urine from mice and hamsters infected with parasites is presented. The approach combines 1H NMR spectroscopy with the application of Pattern Recognition technique. Besides the spectral pattern, differentiating the two species, a common spectral pattern across the two species associated with the presence of the disease is also identified. This pattern is related to the depletion of hippurate. Identification of such common biomarkers across species is instrumental for opening an entire sphere of investigations, where drug efficacy in experimental animals can be directly related to treatment outcome and toxicity in humans.

1985. Software Tool for Comprehensive Assessment and Interpretation of Metabolomic Data

Qi Zhao[1], Radka Stoyanova[2], Shuyan Du[1], Paul Sajda[1], Truman R. Brown[1]
[1]Columbia University, New York, New York, USA; [2]Fox Chase Cancer Center, Philadelphia, Pennsylvania, USA

The quantity and complexity of spectroscopic data obtained from metabolomic studies has made data interpretation very difficult. The challenges stem not only from the need to apply data processing procedures to large sets of spectra and connect them with auxiliary information about the samples, but also the necessity to invoke pattern recognition methods to ensure optimal information retrieval. Most existing software deals only with a few aspects of this process and in general acts on a single spectrum. Here we present a software tool, High Resolution Spectroscopy (HiRes), to address all these challenges and provide comprehensive analysis of metabolomic datasets.

1986. High-Resolution ^{1}H NMR Spectroscopy Reveals Differences in CSF Metabolic Profiles for MS Patients with Inflammatory vs. Non-Inflammatory Plaques

Norbert W. Lutz[1], Angele Viola[1], Irina Malikova[1], Sylviane Confort-Gouny[1], Jean-Philippe Ranjeva[1], Jean Pelletier[1], Patrick J. Cozzone[1]
[1]School of Medicine, Marseille, France

Conflicting results have been reported with respect to lactate concentrations in CSF of MS patients vs. nomal levels. We used ^{1}H NMR spectroscopy to compare CSF metabolic profiles of MS patients with or without inflammatory plaques, to test the hypothesis that increased lactate levels in MS patients may be associated with inflammatory plaques. We found that molar concentrations of lactate were indeed moderately increased for locally inflammatory vs. non-inflammatory MS. We also found slightly increased (or decreased) levels of an unassigned compound (or of phenylalanine) for inflammatory-plaque MS, in analogy to results obtained for MS vs. normal CSF.

1987. A Magnetic Resonance Spectroscopy Technique for Evaluating Lung Preservation Strategies

Tian-Teng He[1], Matthias Peltz[1], Robert Y. Chao[1], Michael Erik Jessen[1], Dan Marshall Meyer[1]
[1]University of Texas Southwestern Medical Center at Dallas, Dallas, Texas, USA

The optimal lung preservation conditions for lung transplantation remain controversial. We evaluated the effect of preservation temperature and percent alveolar oxygen on rat lung metabolism by carbon-13 decoupled proton magnetic resonance spectroscopy of lung extracts. Oxygen content and preservation temperature influenced pulmonary metabolism and energetics, particularly after long-term storage. This method offers promise as a rapid and inexpensive technique for testing multiple preservation conditions.

1988. A Metabolomics Study of Necorosis in Sarcoma Using 1H HR-MAS NMR Spectroscopy

Jin-Hong Chen[1], Rachael B. O'Connor[1], Penelope DeCarolis[1], Yuhsin V. Wu[1], Rula C. Geha[1], Samuel Singer[1]
[1]Memorial Sloan-Kettering Cancer Center, New York, New York, USA

Necrosis, the major cell death mechanism in tumors, is an important prognostic factor for cancer metastasis and recurrence. New methods for the quantitative analysis of necrosis are needed. A metabolomics study of necrosis in sarcomas from 17 patients was carried out using 1H hr-MAS NMR spectroscopy, supervised Support Vector Machine (SVM) learning, conventional pathologic analysis and Oil-Red-O staining. Compared to viable tumors, the necrotic tumors were characterized by a 1.5-fold increase in the observed lipid signals and a more than 90% loss of small metabolites and protein amide proton signals. SVM learning confirmed these observations and accurately discriminates necrotic from viable tumors. The substantial loss in the protein amide proton signals in necrotic tissue provides an explanation for the increased water relaxation times detected in necrotic compared to viable tissue.

1989. Evaluation of Human Prostate Tissue Metabolites with HRMAS 1HNMR After Three-Year Storage at -80ºC

Kate Weymouth Jordan[1], Leo Ling Cheng[1]
[1]Massachusetts General Hospital/Harvard Medical School, Boston, Massachusetts, USA

The assumption that tissue sample storage in the –80ºC condition prevents metabolite degradation/alteration has never been tested. In this study 15 human prostate tissues, removed from five prosatectomy patients, that had been stored at –80ºC for 32 months were analyzed with high resolution magic angle spinning (HRMAS) MR spectroscopy, and compared to the original measurements of the same specimens from 2002 when snap frozen for less than 24 hours. Results from this study clearly demonstrate that long-term storage at –80ºC has negligible effects on metabolite concentrations, furthermore, contributions to metabolic profiles are more dramatically altered by innate tissue heterogeneities.

1990. Magnetic Resonance Microscopy of a Glioma Spheriod in a Collagen I Matrix

Shuning Huang[1], David Vader[2], David A. Weitz[2], Gangping Dai, Bruce R. Rosen[1], Thomas S. Deisboeck[1, 2]
[1]MIT/MGH, Cambridge, Massachusetts, USA; [2]Harvard University, Cambridge, Massachusetts, USA

Glioblastoma multiform (GBM) is a highly invasive primary brain tumor with high incidence. It has been an active research area to understand how this tumor cell invades its microenvironment. We have previously employed Glioma multicellular tumor spheroid (MTS) model to investigate the dynamic expansion of tumor cells in a collagen I matrix using light and fluoresce microscopy. However, studies that can utilize the current clinical relevant tools are more desirable. Here we show that it is feasible to use Magnetic Resonant Microscopy (MRM) to study the tumor cell invasion using the same model system.

1991. Diagnosis of Escherichia Coli Induced Urinary Tract Infection by NMR

Ashish Gupta[1, 2], Mayank Dwivedi[3], G. A. Nagana Gowda[1], Abbas Ali Mehdi[2], Raja Roy[4], Amita Jain[5], Mahendra Bhandari[6], C. L. Khetrapal[1]

[1]Centre of Biomedical Magnetic Resonance, Lucknow, Uttar Pradesh, India; [2]King George's Medical University, Lucknow, Uttar Pradesh, India; [3]Sanjay Gandhi Postgraduate Institute of Medical Sciences, Lucknow, Uttar Pradesh, India; [4]Central Drug Research Institute, Lucknow, Uttar Pradesh, India; [5]Department of Microbiology, Lucknow, Uttar Pradesh, India; [6]King George's Medical University, Lucknow, Uttar Pradesh, India

1H NMR spectroscopic method is suggested and applied for the diagnosis of Escherichia coli (E. coli) in the urinary tract infection (UTI). Specific property of E. coli of metabolizing lactose to lactate in urine is exploited. Other common bacteria, such as Pseudomonas aeruginosa, Klebsiella pneumoniae, Enterobacter aerogenes, Acinetobacter baumanii, Proteus mirabilis, Citrobacter frundii do not produce lactate. The method was applied to E. coli (n=96) infected urine samples and the results showed very high sensitivity with reference to conventional method. Diagnosis of E. coli bacteria causing UTI infection in a single step both qualitatively and quantitatively may have useful implications.

1992. In-Vitro NMR Studies of Echovirus 11 Infection in RD Human Cells

Syed Naved Akhtar[1], Rishi Kumar Singh[2], Y Jadegoud[1], G. A. Nagana Gowda[1], T N. Dhole[2], Archana Ayyagari[2], Mahendra Bhandari[3], C. L. Khetrapal[1]

[1]Centre of Biomedical Magnetic Resonance, Lucknow, Uttar Pradesh, India; [2]Sanjay Gandhi Postgraduate Institute of Medical Sciences, Lucknow, Uttar Pradesh, India; [3]King George's Medical University, Lucknow, Uttar Pradesh, India

The effects of Echovirus 11 infection on RD human cell lines (derived from rhabdomyosarcoma) were studied using 1H NMR spectroscopy and optical microscopy. Both uninfected and infected cells, consumed glucose and produced lactate and acetate as extracellular metabolites. In infected whole cells, glycerophosphocholine and uridinediphosphoglucose were observed in addition to the metabolites observed in uninfected cells. Intracellular metabolites of infected cells showed glutamine, glycerophosphocholine and glycine which were not observed in uninfected cells. The uninfected and infected cells did not show any difference in their lipid components. Unlike optical microscopy, NMR spectroscopy identified early stages of infection through metabolic changes.

1993. Quantitative Evaluation of 31P MRS of Tissue Samples Using Magic Angle Spinning

Geoffrey S. Payne[1], Helen Troy[2], John R. Griffiths[2], Martin O. Leach[1], Yuen-Li Chung[2]

[1]Institute of Cancer Research and Royal Marsden NHS Trust, Sutton, Surrey, UK; [2]St Georges Hospital Medical School, London, UK

High-resolution 31P MAS has been compared with high-resolution MRS of extracts of the same tissue samples. MAS produces spectra of superior signal-to-noise ratio, with concentration estimates in good agreement with those of tissue extracts, but leaving tissue intact for histological analysis. Concentration estimates using reference compound acquired in a separate measurement are more reliable than adding compound to tissue within the rotor. The method is well suited to the study of tumour biopsies where only small tissue samples are available and where histological verification is required, for example before and after treatment with new targeted agents that affect phospholipid metabolism

1994. Determination of ^{13}C Labeling Rates in Fatty Acyl Groups from [1,6-$^{13}C_2$]Glucose in Human Glioma Cells

Anthony Mancuso[1], Ralph J. DeBerardinis, [1,2], Craig B. Thompson[1]

[1]University of Pennsylvania, Philadelphia, Pennsylvania, USA; [2]The Children's Hospital of Philadelphia, Philadelphia, Pennsylvania, USA

To match their high growth rates, tumor cells often have elevated levels of enzymes involved in *de novo* fatty acid synthesis, which are essential for phospholipid formation. Inhibition of these enzymes has been proposed as a therapeutic strategy and pilot studies in model systems have yielded optimistic results. To determine if fatty-acyl synthesis can be non-invasively monitored with ^{13}C NMR, we examined human glioma cells during proliferation in medium containing [1,6-$^{13}C_2$]glucose. The results demonstrated that 4 distinct fatty acyl resonances could be observed in real time. In future studies, fatty-acyl labeling rates from other sustrates such as glutamine will be determined.

1995. Detection of Liposomal Uptake to Ovarian Cancer Cells Using ^1H MR Spectroscopy

Yah-el Har-el[1], Kristine Glunde[1], George Sgouros[1]

[1]Johns Hopkins University School of Medicine, Baltimore, Maryland, USA

Elevated phosphocholine (PC) and total choline-containing compounds (tCho) in tumor cells can be detected by ^1H magnetic resonance spectroscopy (MRS). Liposomes consisting of egg phosphatidylcholine and immunolabeled with Herceptin were used to deliver radionuclides to SKOV3 ovarian cancer cells, which contain up-regulated levels of the protein Her2/*neu*. We hypothesize that the presence of these liposomes will be detectable using ^1H MRS in SKOV3 cells following incorporation of these immunoliposomes by these cells. To test this hypothesis, empty immunoliposomes were bound to SKOV3 cells and ^1H MRS was used to detect elevated levels of PC reflected by an increased PC/GPC ratio.

1996. VEGF Overexpression Combined with Hypoxia is Associated with Increased Invasion and Changed Cellular Metabolism in a Human Prostate Cancer Cell Line

Ellen Ackerstaff[1], Dmitri Artemov[1], Flonné Wildes[1], Venu Raman[1], Zaver M. Bhujwalla[1]
[1]Johns Hopkins University School of Medicine, Baltimore, Maryland, USA

High expression of vascular endothelial growth factor (VEGF), high tumoral total choline (tCho) levels and hypoxia have been linked to increased metastasis. We investigated the effects of VEGF overexpression and hypoxia on invasion and metabolism of the prostate cancer cell line, PC-3, co-cultured with human umbilical vein endothelial cells under oxygenation and hypoxia, using our Metabolic Boyden Chamber. VEGF overexpression increased invasion of hypoxic cancer cells and decreased levels of intracellular mobile lipids. Hypoxia tended to increase tCho levels in the cancer cells. Our results may in part explain the increased occurrence of metastasis observed in patients with cancers secreting high levels of VEGF and the associated metabolic changes.

1997. Evaluation of In-Vitro NMR Spectroscopy in Detecting Metastasis in Axillary Nodes in Breast Cancer in a Clinical Setting

N R. Jagannathan[1], Uma Sharma[1], M N. Pavan Kumar[1], V Seenu[1]
[1]All India Institute of Medical Sciences, New Delhi, Delhi, India

In vitro NMR spectroscopy investigation of axillary lymph nodes (n=88) from thirty breast cancer patients revealed the metabolic changes underlying metastases. The concentrations of GPC-PC, choline, lactate, alanine and UDPG and the intensity ratio of GPC-PC/Threonine (Thr) were elevated significantly in metastatic nodes. Using GPC-PC/Thr ratio as a marker MRS detected the metastases with a sensitivity, specificity and accuracy of 80%, 91% and 88%, respectively while nine patients who received neoadjuvant chemotherapy (NACT) the accuracy of MRS in detecting metastases was 75% compared to 96% in those who did not (n = 21) NACT.

1998. 1H-MRS and Metabolomics for Diagnostic Activity Assessment of Hydatid Cysts of the Parasite *Echinococcus Granulosus*

William E. Hull[1], Waldemar Hosch[2], Thomas Junghanss[2], Guenther W. Kauffmann[2]
[1]German Cancer Research Center (DKFZ), Heidelberg, Germany; [2]University Clinic, Heidelberg, Germany

Our pilot study examined 16 samples of cyst fluid obtained from 13 patients bearing hydatid cysts of the parasite Echinococcus granulosus (canine band worm). 1H-MRS at 600 MHz allowed several amino acids, lactate, acetate, formate, succinate, citrate, malate, fumarate, glucose, myo-inositol, betaine, and choline metabolites to be identified and quantified as metabolite/valine ratios. Cysts classified as active or fertile (n = 10) exhibited high ratios for succinate, acetate and malate, as well as detectable fumarate. In inactive, sterile cysts (n = 5), these ratios decreased dramatically ($p < 0.002$), suggesting a high diagnostic potential for these parameters.

1999. The Hepatoprotective Effect of N-Acetylcysteine in Acetaminophen Intoxication is Due to Early Glutathione Replenishment Via Stimulation of Anaplerotic Mechanisms

Tom Chan[1], Valerie-Ann Raymond[1], Marc Bilodeau[1], Dieter Leibfritz[2], Claudia Zwingmann[1, 2]
[1]Hospital Saint-Luc, Montreal, Quebec, Canada; [2]University of Bremen, Bremen, Germany

Acetaminophen (AAP) is converted by the cytochrome P450 pathway to a toxic intermediate, N-acetyl-p-benzoquinone-imine (NAPQI), which is usually completely detoxified through combination with glutathione (GSH). N-acetylcysteine (NAC) is believed to act by regenerating glutathione (GSH) stores. We wanted to identify the effect of NAC on metabolic pathways in mouse liver. After AAP treatment, a rapid depletion of GSH stores parallels a considerable inhibition of anaplerotic flux. Krebs cycle metabolism of acetate, however, was unchanged after AAP treatment, but stimulated by NAC. These data suggest that anaplerotic fluxes play a key role for GSH resplenishment after AAP intoxication.

2000. 13C and 31P NMR Spectroscopy in Perfused Mouse Liver: A Robust Functional Assay for the Assessment of Glucagon Receptor Antagonists

Corin O'Dell Miller[1], Haiying Liu[1], Joseph Leslie Duffy[1], Emma R. Parmee[1], Bei Betty Zhang[1]
[1]Merck, Rahway, New Jersey, USA

A 13C and 31P NMR spectroscopic approach was employed in perfused mouse livers metabolizing 13C-labelled substrates to develop a novel *ex vivo* assay for the assessment of small molecule glucagon receptor antagonists. Three novel thiophene-derived glucagon receptor antagonists were profiled using this approach. The relative inhibitions of glucagon induced glycogenolysis demonstrated by each compound were consistent with their in vitro activities and were also reliable indicators of their intrinsic activities in the liver. That this information could be gained without the need to optimize dosing and pharmacokinetic parameters demonstrates the value of this technique.

Microscopy

Room 4E Tuesday 13:30 - 15:30

2001. 21 Tesla Micro-MRI of Rat Skin

Rakesh Sharma[1], Bruce R. Locke[1]
[1]Florida State University, Tallahasee, Florida, USA

A rapid ultra high resolution *ex vivo* MRI imaging method was evaluated to visualize rat skin structure. The main objectives were: 1.qualitative assessment of viable epidermis, hair, oil and fat-rich skin features by multi-contrast approach; 2.achievement of spatial resolution up to 15 microns; 3. comparison of skin histology with MRI skin features obtained by 21 Tesla magnetic resonance imaging (MRI) imager.

2002. A Modified Golgi Impregnation Method for *InVitro* MR Microscopy

Xiaowei Zhang[1], Russell E. Jacobs[1]
[1]California Institute of Technology, Pasadena, California, USA

The Golgi Black Reaction stains a small eclectic, random, population of neuron. Pretreatment with the powerful oxidant potassium dichromate hardens the tissue, subsequent 'development' with silver nitrate results in black deposits delineating neural cells. Contrast in MRI arises from physio-chemical heterogeniety modulating concentration and relaxation characteristics of water in tissue. Pretreatment with K2(Cr2O7) with or without ProHance yields neuroanatomical contrast that is dramatically improved compared to conventional fixation. Seven distinct layers in the hippocampus of treated mouse brains are easily identified. Enhanced or different contrast leads to better definition of anatomical features and should facilitate identification of abnormalities.

2003. Multiple Mouse Cardiac Imaging

Jonathan Bishop[1], Akiva Feintuch[1], Nicholas Bock[1], Brian Nieman[1], Jun Dazai[1], Lori Davidson[1], R. Mark Henkelman[1, 2]
[1]Hospital for Sick Children, Toronto, ON, Canada; [2]University of Toronto, Toronto, ON, Canada

Multiple mouse MR imaging has recently been introduced for high-throughput imaging of large numbers of mice. The feasibility of this technique for cardiac imaging was studied and retrospective gating was found to provide comparable image quality to prospective gating for three-dimensional imaging in mice. In this abstract, retrospectively gated cardiac images obtained from three mice in parallel are presented.

2004. Magnetic Resonance Imaging Using Standard CMOS RF Coil

Edzer Lienson Wu[1], Tao Wang[1], Jyh-Horng Chen[1], Shey-Shi Lu[1]
[1]National Taiwan University, Taipei, Taiwan

High-resolution cross-section magnetic resonant image of a Plantago asiatica was taken with a 990micron, 45-turn square rectangular spiral surface radiofrequency coil in a 3 Tesla Bruker Biospin MRI machine. This coil is produced by standard CMOS microfabrication technique on silicon substrate, with a 5um line width and spacing. The coil is designed to observe biological subjects at the microscopic scale. Though the resulting image quality did not meet the theoretical predictions, it still demonstrates the imaging feasibility of standard CMOS microfabricated coils. Further optimization and improvements of the coil and sample loading mechanism are required.

2005. Magnetic Resonance Microscopy of a Mouse Model of Attention-Deficit-Hyperactivity Disorder: Role of D4 Dopamine Receptors

Yu Ma[1], Patrick R. Hof[2], Samuel Colles Grant[3], Stephen J. Blackband[4], Hai-Dee Lee[1], Rubinstein Marcelo[5], Helene Benveniste[1]
[1]Brookhaven National Laboratory, Upton, New York, USA; [2]Mount Sinai School of Medicine, New York, USA; [3]Florida State University, Tallahassee, Florida, USA; [4]University of Florida, Gainesville, Florida, USA; [5]University of Buenos Aires, Buenos Aires, Argentina

Studies have shown a wide variety of genetic polymorphisms in attention-deficit-hyperactivity Disorder (ADHD). Genetically engineered mice models are therefore important in studying ADHD. Here we use MR microscopy to characterize brain morphometry in a recently developed mouse model of ADHD that involves neonatal disruption of central dopaminergic pathaways in CF-1 mice as well as in mice deficient of the dopamine-4 receptor.

2006. High-Field Parallel NMR-Microscopy in Small Animals

Sascha Köhler[1], Peter Ullmann[2], Sven Junge[1], Markus Wick[1], Franek Hennel[1], Felix Breuer[3], Peter M. Jakob[3], Wolfgang Ruhm[1]
[1]Bruker BioSpin MRI GmbH, Ettlingen, Germany; [2]Medical Physics, University Hospital Freiburg, Germany; [3]University of Würzburg, Würzburg, Germany

This study demonstrates that MRI in small animals at high fields can greatly benefit from using Parallel Imaging (PI) and that this technique has the potential to gain a similar importance in such applications as in routine clinical MRI. For 3D time-of-flight angiography of the rat and mouse brain it is shown that a PI acceleration factor of two yields almost the same image quality as the corresponding non-accelerated experiment. Using PI in DTI experiments allows to acquire significantly more diffusion directions in the same acquisition time which results in a considerably improved image quality of the derived anisotropy maps. The value of this additionally acquired information about diffusion anisotropy is demonstrated by a DTI study on a formalin-fixed rat brain.

2007. Distinctions Between Islet and Acinar Cells in Mammalian Pancreatic Tissue Using High Field MR Microscopy

Samuel Colles Grant[1, 2], Nicholas Edward Simpson[3], Sally Ann Litherland[3], Stephen John Blackband, [23], Ioannis Constantinidis[3]

[1]Florida State University, Tallahassee, Florida, USA; [2]National High Magnetic Field Laboratory, Tallahassee, Florida, USA; [3]University of Florida, Gainesville, Florida, USA

Through the application of high magnetic fields and radio frequency microcoils, MR microimages of isolated mammalian islets, acinar cells and multicellular insulinoma aggregates were acquired at isotropic resolutions down to 9.4 µm. Several MR contrast mechanisms (T2, T2* and diffusion) were applied to determine the MR characteristics of these samples. High resolution MR images demonstrate that isolated islets possess a unique structural heterogeneity that has previously not been reported. This heterogeneity distinguishes islets from surrounding acinar tissue, a novel distinction for MR imaging. Optical deconvolution confocal microscopy supports these MR observations of intra-islet structural heterogeneity.

2008. *In Vivo* 4D Magnetic Resonance Microscopy of Neurulation and Somitogenesis in Amphibian Embryos

Julian Michael Tyszka[1], Yun Kee[1], Russell E. Jacobs[1], Marianne Bronner-Fraser[1], Scott E. Fraser[1]

[1]California Institute of Technology, Pasadena, California, USA

Magnetic resonance microscopy offers a unique window on deep tissue movements in optically opaque embryos. The aim of this project is to develop MR microscopy for single and multiple embryo, high throughput studies with sufficient spatiotemporal resolution to explore key developmental processes during neurulation and somitogenesis in established amphibian embryonic models.

2009. Imaging Optimization for *In-Vivo* Human Micro Imaging at 7T

Hiroyuki Kabasawa[1, 2], Akira Nabetani[1, 2], Hitoshi Matsuzawa[2], Tsutomu Nakada[2]

[1]GE Yokogawa Medical Systems, Hino-shi, Tokyo, Japan; [2]University of Niigata, Niigata-shi, Niigata, Japan

Ultra high field MRI for human study became available and its application research is under way. High spatial resolution imaging is one of the promised targets for ultra high field MR because of its high SNR. However, imaging technique for human brain micro imaging *in vivo* has not been optimized yet. In this study, human study safety on RF power deposition was evaluated and practical limitation was determined. Imaging protocol optimization follows to acquire 50um spatial resolution at 7T within reasonable time.

2010. High Throughput Microimaging of the Mouse Brain

R. Mark Henkelman[1], Jun Dazai[1], Nir Lifshitz[1], Brian J. Nieman[1], Shoshana Tsatskis[1], Jason Lerch[1], Jonathan Bishop[1], Shoan Kale[1], John G. Sled[1], X. Josette Chen[1]

[1]Hospital for Sick Children, Toronto, Ontario, Canada

We present a new method for high resolution anatomical phenotyping of the mouse brain combined with parallel imaging that enables three brains to be imaged at the same time. The method allows for 32 micron isotropic images of a mouse brain to be produced every four hours.

2011. Passive Staining: A Novel Procedure for 3D MR Histology - Description and Application to the Characterization of Cerebral Anomalies in Doublecortin Knockout Mice

Marc Dhenain[1, 2], Fiona Francis[3], Caroline Kappeler[3], Yoann Saillour[3], Christine Walczak[2], Andreas Volk[2]

[1]CEA-CNRS URA 2210, Orsay, France; [2]Curie Institute, Orsay, France; [3]Cochin Institute, Paris, France

The passive staining protocol consists of soaking a brain in a mixture of gadoteric acid (Dotarem®) and formalin. This procedure strongly reduces the relaxation times in brain samples and improves the contrast between white matter, subcortical structures and the cortex on 3D images recorded by MRI microscopy. Its application to the brain of doublecortin knockout mouse, a model of type-1 lissencephaly, revealed corpus callosum agenesis associated with modification of the hippocampal shape, as well as cingulate cortex hyper-extension and ectopic fiber bundles. This protocol can thus be useful to screen brain anomalies in transgenic mice without performing time-consuming histological studies.

2012. Automated Registration of Histology Sections with *Ex-Vivo* MRM Volumes

Alize E.H. Scheenstra[1], Jouke Dijkstra[1], Rob C.G. van de Ven[1], Louise van der Weerd[1], Johan H.C. Reiber[1]

[1]LUMC, Leiden, Netherlands

This paper presents the semi-automated registration of a single HE-stained histology sections with *ex vivo* Magnetic Resonance Microscopy (MRM) images of the mouse brain. The proposed method preprocesses both the MRM volume and the histology section in such a way that regular 2D-3D registration can be applied to the data.Preliminary results show that for 7 of the 8 histology sections created from 3 mouse brains the corresponding slice in the MRM volume can be found.

2013. NMR Microscopy of Dental Biofilm Metabolism

Paul D. Majors[1], *Jeffrey S. McLean*[1], *Robert A. Wind*[1]
[1]Pacific Northwest National Laboratory, Richland, Washington, USA

We demonstrate the feasibility of using NMR microscopy to measure microbial physiology for dental biofilm samples in a model oral environment. This offers the opportunity for the detailed study of the pathological processes associated with dental caries and resulting tooth decay. Synthetic tooth enamel and glass biofilm support materials are shown to be compatible for MRI, MRS and MRSI measurements. The growth medium must be chosen carefully to support biofilm growth and activity, and provide NMR spectral resolution. Metabolic studies of biofilms may prove useful for understanding normal and pathological function in dental and other biofilms.

2014. Staining Methods for Magnetic Resonance Microscopy of the Rat Embryo

Alexandra Petiet[1], *Laurence W. Hedlund*[1], *G. Allan Johnson*[1]
[1]Duke University Medical Center, Durham, North Carolina, USA

Magnetic resonance histology (MRH) has become a valuable tool in assessing the developing rat embryo. This study describes a staining and fixation method to enhance the SNR. Rat fetuses were immersion-fixed for up to 24 h in Bouin's with ProHance at varied concentrations. The results showed that T1 was reduced, yielding a 5-fold SNR increase. T2 was also reduced with increasing concentration and immersion time, which decreased the SNR. An optimization of those variables has allowed the acquisition of 20-micron 3D images in 3 h, making MRH a routine tool for evaluating embryonic development.

2015. To Cool or Not to Cool: The Question for Skin Microscopy Receive Coils

Julie Camille DiCarlo[1], *Greig C. Scott*[1], *Steven M. Conolly*[2], *Bob S. Hu*[3], *Dwight George Nishimura*[1]
[1]Stanford University, Stanford, California, USA; [2]University of California, Berkeley, Berkeley, California, USA; [3]Palo Alto Medical Foundation, Palo Alto, California, USA

Peripheral vascular disease (PVD) often presents with non-healing skin lesions, and wound-healing concerns make biopsy unfeasible. MRI provides skin contrast and sensitivity depth, but requires SNR improvement to keep imaging times reasonable. We examine the tradeoff of decreased copper resistance at 77 K and cryostat-induced B_1 losses to determine the optimal coil configuration for skin microscopy. Images from a 4x4x1 cm^3 slab of 78x78 μm^2 resolution acquired in ~2 minutes in the skin of a normal subject and diabetic patient with PVD are presented. Results indicate great promise for ischemic skin imaging.

2016. Spatial-Spectral Holographic Interpretation of High Field MR Imaging : Analysis, Implications and Experiments at 7T

Andrew Jeremy M. Kiruluta[1, 2]
[1]MGH, Boston, Massachusetts, USA; [2]Harvard University, Cambridge, Massachusetts, USA

The 3D NMR imaging equation can expressed as a spatial-spectral holographic formulation similar to that in quantum optics. This interpretation arises naturally in NMR from the inhomogeneous linewidth broadening due to either a set of linear orthogonal gradients fields or from chemical anisotropy. We can thus think of NMR k-space as a spatial-spectral holographic grating. The spatial holographic component arises from dielectric effects at high field strength (>4T) when the excitation wavelength is less than or commensurate with the size of the imaging sample. In this work, holographic properties of storage, time-reversal, recognition and triple correlations are experimentally demonstrated.

2017. MR Microscopy of Chemically Fixed Human Embryos with a Large Image Matrix

Yosuke Otake[1], *Shinya Handa*[1], *Katsumi Kose*[1], *Kouhei Shiota*[2], *Shigeto Yamada*[2]
[1]University of Tsukuba, Tsukuba, Ibaraki, Japan; [2]Kyoto University, Kyoto, Japan

3D MR microscopic images of chemically fixed human embryos were acquired with a large matrix size (256×256×512) using a 9.4 T superconducting magnet and a parallel receiver system. The developmental process of human embryos, such as vascular structures in the liver, was clearly visualized through T1 or T2* image contrasts.

2018. A Novel Autocorrelation Method for Measuring the Thickness Anisotropy Tensor of Trabecular Bone

Branimir Vasilic[1], *Felix W. Wehrli*[1]
[1]University of Pennsylvania Medical Center, Philadelphia, Pennsylvania, USA

The full width at half maximum of the autocorrelation function of cancellous bone images provides a good estimate of trabecular thickness. The thickness anisotropy tensor can be calculated from k-space data acquired in MRI. Through numerical experiments on micro-CT data we show that by anisotropic sampling one can substantially improve the resolution with which the principal values of the anisotropy tensor are measured without significantly sacrificing accuracy or sensitivity.

2019. Bi-Exponential Characterization of T2 Relaxation Decay in an Engineered Osteogenic Tissue Model

Huihui Xu[1], Shadi F. Othman[1], Liu hong[1], Richard L. Magin[1]
[1]University of Illinois at Chicago, Chicago, Illinois, USA

In this *in vitro* MR study of tissue engineered bone, the T2 relaxation (at 500 MHz) of developing osteogenic implants was measured over a 4-week period. Both mono-exponential and bi-exponential fits to the T2 relaxation time were investigated. The data show that for the early time points investigated, both a fast and a slow component to the spin-spin relaxation was present, suggesting increasing tissue heterogeneity with bone morphogenesis.

2020. Comparison of Contrast-To-Noise Ratio for *In Vivo* Mouse Brain Imaging at 3T and 7T Under Nearly Identical Scanner Configurations

Mark William DiFrancesco[1], Weihong Yuan[1], Ronald Pratt[1], Scott Dunn[1], Bernard J. Dardzinski[1], Scott K. Holland[1]
[1]Cincinnati Children's Hospital Medical Center, Cincinnati, Ohio, USA

T1 and T2 weighted *in vivo* images of mouse brain were compared for signal-to-noise and contrast-to-noise at 3T and 7T with nearly all other protocol parameters remaining identical. The two Bruker scanners employed in this study were fitted with the same gradient sets and drive electronics and operated with the same software. Identical single-turn-solenoid RF coils were constructed for both field strengths. System details such as RF coil Q and receiver noise figure were measured to allow a consistent comparison of noise. Images optimized for contrast-to-noise were obtained based on relaxometry performed on each mouse. Under these unique circumstances, the influence of field strength on brain image quality was isolated.

2021. High Resolution 3D Brain MR-Elastography

Michael A. Green[1], Ralph Sinkus[2], Lynne E. Bilston[1, 3]
[1]Prince of Wales Medical Research Institute, Sydney, New South Wales, Australia; [2]ESPCI, Paris, France; [3]UNSW, Sydney, NSW, Australia

High resolution *in vivo* measurement of the viscoelastic properties of the brain has been achieved via 3D steady-state MR-Elastography at 3T. Several parameters within the MR sequencing and the mathematical reconstruction have been optimised to produce mechanical waves which are efficiently coupled into the skull allowing maximum amplitude in the centre of the brain whilst maintaining good signal to noise. Quantified results agree well with rheological measurements made on bovine and porcine brain tissue in the literature and they also show very good correlation with anatomical structures such as grey matter, white matter and ventricles.

Transmitters and Receivers

Room 4E Tuesday 13:30 - 15:30

2022. Designing a Transmitter and Receiver for Use in Strong Magnetic Fields

David Ian Hoult[1], Glen Kolansky[1], Dennis Kripiakevitch[1]
[1]National Research Council Canada, Winnipeg, Manitoba, Canada

The advantages of a transmitter and receiver operating close to the MR magnet are outlined, and the importance for the Cartesian feedback method of phased-array transmission emphasised. Attention is drawn to the ubiquitous conventional use of ferrites that precludes high magnetic field operation, and the use of new, balanced, radio-frequency integrated circuits, together with toroidal inductors, is advocated for eliminating ferrites. Examples of new designs include a 20 MHz I-Q modulator with 60 dB rejection of carrier and unwanted sideband, a quadrature splitter with ±0.5o phase accuracy between 300 and 500 MHz and a 150 W ferrite-free RF amplifier.

2023. Shading Reduction at 3.0T Using an Elliptical Drive

Daniel Weyers[1], Graeme McKinnon[1], Ricardo Becerra[1], Susan Mathew[1], Michael Edwards[1]
[1]GE Healthcare, Waukesha, Wisconsin, USA

Dielectric related artifacts are commonly present at 3.0T in patients having an elliptical crosssectional area. This pheneomenon is prevalent in small patients, usually female, with a flat or concave abdomen. The energy propogation through one axis of the body cooresponds to less phase shift, less signal cancellation, and better homogeneity. Using a new transmit chain, an elliptical drive can be used as an alternative to dielectric pads to overcome shading in the trunk and improve B1 homogeneity over a diverse patient population.

2024. Using a Mode Concept to Reduce Hardware Needs for Multichannel Transmit Array

Markus Vester[1], Jürgen Nistler[1], Ralph Oppelt[2], Wolfgang Renz[1]
[1]Siemens Medical Solutions, Erlangen, Germany; [2]Siemens CT, Erlangen, Germany

A concept for a multichannel transmit array is presented which uses spatial Fourier modes instead of single antenna elements. Obvious advantages are reduced hardware needs, intrinsic matching of the antenna to the RF amplifiers and decoulping of the modes. The concept can be used for B1-shim and TX-Sense.

2025. Characterization of Receiver Demodulation for Correcting Off-Axis MR Imaging Degradation

Youngkyoo Jung[1], Yogesh Jashnani[1], Richard Kijowski[1], Walter F. Block[1]
[1]University of Wisconsin-Madison, Madison, Wisconsin, USA

Improper alignment of the gradient coil and the real-time frequency demodulation reference signal, necessary in off-axis imaging, may be one source of the inconsistency of non-Cartesian imaging. As the system delay parameter varies with imaging bandwidth and between scanners, many non-Cartesian imaging methods require trial and error tuning for off-axis imaging. We present an automatic per-patient-based method to precisely measure the timing error in the frequency demodulation reference signal in less than 0.5 s. Off-axis image quality is significantly improved when compensation for demodulation phase errors due to the delay is applied to radial and spiral reconstructions.

2026. A Low Input Impedance MRI Preamplifier Using a Purely Capacitive Feedback Network

Ralph Oppelt[1], Markus Vester[1]
[1]Siemens AG, Erlangen, Germany

A novel MRI preamplifier is presented which achieves a low input impedance without a bulky high-Q input inductor while maintaining a high equivalent noise input resistance. This allows a significant reduction in size and makes the preamp highly suitable for multi channel loop arrays. The low input impedance which is essential for channel decoupling is achieved over a very large bandwidth so that tuning is strongly simplified.

2027. Direct MRI Detection at 3T Using an FPGA-Controlled High-Speed Digital Receiver

Andrzej Jesmanowicz[1], James S. Hyde[1]
[1]Medical College of Wisconsin, Milwaukee, Wisconsin, USA

A new digital receiver with two A/D converters sampling at 100 MHz was implemented for off-line real-time image acquisition. One of the converters directly digitized the RF signal and the other digitized the internal reference waveform. The dynamic range of the A/D converter can be increased to 20 bits at a final output bandwidth 12.2 kHz. All processing, including filtering, mixing, and FT, were done by computer. For an N-channel acquisition system, one needs only N+1 A/D converters.

2028. An RF Small Signal Unit Optimized for a 7T Multinuclear MR System

Jan Bollenbeck[1], Ralph Oppelt[2], Horst Kroeckel[1], Philipp Hoecht[1], Wilfried Schnell[1]
[1]Siemens AG Medical Solutions, Erlangen, Germany; [2]Siemens AG Corporate Technology, Erlangen, Germany

The trend to increasing magnetic field strengths increases the demands on the Radio Frequency Small Signal Unit (RFSU) of the MR system. In this paper we focus on the impact of the increased frequency and dynamic range on the specific electrical requirements. The architecture of an RFSU used in a commercially available Siemens 7T System is presented and the implemented design features used to fulfill the tight specifications are described.

2029. A Solution for the Dynamic Range Problem by Means of a Parallel Image Acquisition

Yosuke Otake[1], Katsumi Kose[1], Tomoyuki Haishi[2]
[1]University of Tsukuba, Tsukuba, Ibaraki, Japan; [2]MRTechnology Inc., Tsukuba, Ibaraki, Japan

The dynamic range problem was solved using a parallel image acquisition. By adding a 33-37dB extra gain channel, the dynamic range of the receiving system was extended to 75-81dB. As a result, clear 3D large matrix spin-echo and gradient-echo images were successfully obtained.

2030. 16-Channel Interface Boxes for Adaptable MRI Array Systems

Nicola De Zanche[1], Jurek A. Massner[1], Christoph Leussler[2], Klaas Paul Pruessmann[1]
[1]University and ETH Zurich, Zurich, Switzerland; [2]Philips Research Laboratories, Hamburg, Germany

Receiver arrays that are adaptable to diverse measurement situations are extremely valuable in the research environment. We have constructed interface boxes that allow up to 16 independent coil elements to be connected and arranged as needed. Our modular approach reuses designs and hardware in order to focus on the problems specific to the particular measurement. The standard interface box accepts coils of various shapes and sizes which are constructed as separate units and can be used in any combination without electrical adjustments because the elements are preamplifier-decoupled.

2031. Noise Figure and Dynamic Range Optimization in Optical Links for MRI Applications

Jing Yuan[1], Peng Qu[1], Juan Wei[1], Gary X. Shen[1]
[1]The University of Hong Kong, Hong Kong, People's Republic of China

MRI applications impose critical requirements in noise figure and dynamic range for optical links used for coil interconnect. To reduce the intrinsic high noise figure of optical links, a low-noise preamp must be used. But it also brings the side effect of dynamic range reduction. Compromise must be made between noise figure and dynamic range to optimize the optical link to meet the critical requirement in MRI. Dynamic range of the current optical link is still a challenge for high field imaging above 3T and needs to be further improved..

MR Safety, Bioeffects, and Acoustic Noise

Room 4E Tuesday 13:30 - 15:30

2032. Modal Analysis of a Single-Layered Gradient Coil Insert for a 4T MRI

Chris Mechefske[1], Wang Fenglin[1], Carl Gazdzinski[2], Brian Rutt[2]
[1]Queen's University, Kingston, Ontario, Canada; [2]Robarts Research Institute, London, Ontario, Canada

Ongoing developments of magnetic resonance imaging technology have lead to high acoustic noise in and around MRI scanners. Many important factors, including the structural dynamic properties, contribute to the vibro-acoustic problem. A non thin-walled dynamic model with the geometric ratio of 8.25 was developed based on modified Love's governing equations. Experimental modal testing on the gradient coil insert was conducted. Remote laser measurements of the gradient coil during scanning in a 4T MRI were carried out. The measured results not only validate the analytical model, but also disclose the real dynamic behavior of the gradient coil during scanning.

2033. Construction and Validation of a Probe for Electric Field Measurements in Gradient Coils

Rebecca Emily Feldman[1], Timothy J. Scholl[1], Blaine Alexander Chronik[1]
[1]University of Western Ontario, London, Ontario, Canada

A probe was developed to measure the total electric field induced by a gradient coil. The probe was used to measure the electric field over the X-Y plane of an empty head gradient coil. The electric field measured was an order of magnitude higher than the simulated electric field due to the changing magnetic field alone. However, when the mouth of the coil was shielded, the measured electric field approached the simulated field. The larger measured electric field is hypothesized to be due to the coils scalar potential.

2034. Magnetic Resonance Imaging in Patients with Neurostimulation Systems

Vicente Martinez Sanjuan[1], Vicente Hervas Briz[2], Juan Carlos Valia, German Cerda Olmedo, Carolina Quiroz, Juan Carlos Quiles Teodoro[3], Federico Mata Escolano[4], Elsa Alonso, Adela Batista, Luis Garcia Ferrer, Julian Celma Marin
[1]Ersa- Hospital General Universitario Valencia, Valencia, Spain; [2]Hospital General Univeristario Valencia, Valencia, Spain; [3]Eresa-Hospital General Universitario Valencia, Valencia, Spain; [4]Eresa-Hospital General Universitario De Valencia, Valencia, Spain

The present study investigates the safety of patients with a spinal cord NSS subjected to MRI. Such NSS are used not only to treat chronic pain but also to manage primary tremor, tremor in Parkinson's disease and epilepsies that are refractory to medical treatment or prove highly disabling.With our imaging protocol, MRI in patients with NSS at spinal cord level produced few and non-serious complications, without patient injury or changes in the system. Patient-reported satisfaction was moreover maximum in all cases.We therefore consider that patient safety is guaranteed when our study recommendations are followed.

2035. Differences in RF-Induced Heating Per Unit of SAR of a Deep Brain Stimulation Implant Across Two MR Systems

Jean Adelaide Tkach[1], Kenneth B. Baker[2], Ali R. Rezai[2]
[1]University Hospitals of Cleveland, Cleveland, Ohio, USA; [2]Cleveland Clinic Foundation, Cleveland, Ohio, USA

The specific absoprtion rate (SAR) is often used as the metric for applied RF power in safety recommendations for performing MRI procedures in patients with elongated, conductive implants. However, no universally standardized method of determining SAR has been adopted by the MR manufacturers. Using a phantom model, we demonstrated substantial diferences in the heating profile of an fully implanted neurostimlation system between two different 1.5T MR scanners using a t/r head coil configuration, the configuration that complies with the FDA approved labeling for MRI safety guidelines associated with implant system evaluated.

2036. RF-Heating Effects on Coated Wires and Pacemaker Leads at 1.5T and 3.0T

Roger Luechinger[1], Volkert A. Zeijlemaker[2], Firat Duru[3], Peter Boesiger[1]
[1]Institute for Biomedical Engineering University and ETH, Zurich, Switzerland; [2]Bakken Research Center, Maastricht, Netherlands; [3]University Hospital, Zurich, Switzerland

Heating effect of the RF-field are in general expected to be higher in higher field strength. By evaluating heating effects at the tip of wires and pacemaker leads it could be found, that due to resonance effects higher heating effect could be seen at 1.5T compared with 3.0T.

2037. Reducing and Monitoring Resonant Heating in MR Guidewires

Ross Venook[1], William Overall[1], Scott Smith[2], John Pauly[1], Greig Scott[1]
[1]Stanford University, Stanford, California, USA; [2]Boston Scientific, Minneapolis, Minnesota, USA

In this work, we studied the feasibility of lossy capacitive top-loading for reduction of RF guidewire heating. We monitored interactions with temperature measurements and optically-coupled MR-compatible RF current transducers. Preliminary results indicate that lossy dielectric loading proximally can reduce resonant heating distally in a guidewire under MRI. In future it may be possible to combine these loading and current-monitoring techniques to detect and prevent unsafe RF interactions during interventional MRI procedures.

2038. Effect of Transmit Array Phase Relationship on Local Specific Absorption Rate (SAR)

Leonardo M. Angelone[1, 2], Nikos Makris[2], Christos Vasios[2], Lawrence Wald[2], Giorgio Bonmassar[2]
[1]Tufts University, Medford, Massachusetts, USA; [2]Massachusetts General Hospital, Charlestown, Massachusetts, USA

This study measured the effect of a transmit array phase relationship on local Specific Absorption Rate (SAR) to determine if B1 shimming could yield significantly different "worse case" local SAR levels compared to standard phase relationships. Two different phase configurations for transmit coils were tested using FDTD simulations with a high-resolution head model. We show that the phase relationship can vary the local SAR distribution, greatly affecting also the SAR values for specific tissues, such as CSF, nose, and nerve.

2039. Simultaneous B_{1+} Homogenisation and SAR Hotspot Suppression by a Phased Array MR Transmit Coil

C. A.T. van den Berg[1], B. van den Bergen[1], H. Kroeze[1], L. W. Bartels[1], J. J.W. Lagendijk[1]
[1]University Medical Centre, Utrecht, Netherlands

In this study it is demonstrated that in 3 Tesla whole-body MR imaging, quadrature performance is severely deteriorated. FDTD simulations with four different patient models demonstrated severe B1+ non-uniformity and elevated SAR deposition, especially for obese patients. These effects can be explained by the dielectric interaction of an elliptical geometry with a circularly polarized RF field. A phased array transmit coil is able to correct for this effect and suppress B1+ non-uniformity and SAR hotspots. This technique would allow higher flip angles and/or higher RF duty cycles at 3T while gaining in flip angle uniformity.

2040. The Effect of Body Size and Shape on RF Safety and B1 Field Homogeneity at 3T

B. van den Bergen[1], C. A.T. van den Berg[1], H. Kroeze[1], L. W. Bartels[1], J. J.W. Lagendijk[1]
[1]University Medical Centre, Utrecht, Netherlands

We present a study about the effect of body size and shape on B1 field homogeneity and the creation of SAR and temperature hotspots at 3T. The typical results that we show are based on FDTD calculations with various anatomies and show a significant influence on B1 field homogeneity, SAR deposition and local temperature rise. This study helps us to understand the effect of body geometry on RF field inhomogeneity and RF safety during MRI scanning.

2041. Safety Considerations Concerning SAR During RF Amplifier Malfunctions in Parallel Transmission

Ingmar Graesslin[1], Konstantinos Falaggis[1], Peter Vernickel[2], Peter Röschmann[1], Christoph Leussler[1], Zhiyong Zhai[3], Michael Morich[3], Ulrich Katscher[1]
[1]Philips Research Laboratories, Hamburg, Germany; [2]TuTech Innovation, Hamburg, Germany; [3]Philips Medical Systems, Cleveland, Ohio, USA

Parallel RF transmission has gained increased interest in MR imaging research. This study investigates the consequences of a malfunction in one of the transmit channels on the resulting SAR. Based on FDTD simulations the local SAR was derived for a decoupled eight-channel body coil loaded with an anatomically detailed body model. The results of the simulation indicate that the failure of a single RF transmit channel can lead to increased local SAR in a given region. To prevent safety hazards, a malfunction control of the RF transmit channels is required in a multi-element transmit MR system.

2042. Minimizing Power of RF Pulse by Genetic Algorithm

Yong Pang[1], Chun Sheng Wang[1], Gary X. Shen[1]
[1]University of Hong Kong, Hong Kong, Hong Kong SAR, People's Republic of China

In excitation phase of MRI, there is only a very small portion of the RF pulse energy used for rotating the net magnetization, most of them are deposited into the imaging object as heat. So, reducing the RF pulse power can effectively decrease the heat deposited. In this work, genetic algorithm is introduced to minimize the power of RF pulse in the pulse design procedure, while keeping the excited profile almost unchanged. Simulation result showed that the power of RF pulse can be reduced by about 17% using GA minimization, while the excitation profile homogeneity almost has no change.

2043. Measuring Local RF Heating in MRI: Simulating Perfusion in a Perfusionless Phantom

Imran Akca[1], Tonguc Onur Tasci[1], Onur Ferhanoglu[1], Didem Bacanli[2], Christopher Yeung[3], Ergin Atalar[1, 4]
[1]Bilkent University, Ankara, Turkey; [2]Baskent University, Ankara, Turkey; [3]National Heart, Lung & Blood Institute, Bethesda, Maryland, USA; [4]Johns Hopkins University School of Medicine, Baltimore, Maryland, USA

In this study, predicting *in vivo* temperature increase by using a gel phantom experiment is presented. The theory behind this estimation comes from our earlier Green's function averaging technique, but fortunately by using this estimation method we do not need to do extensive computer simulations. The steady state temperature increase of *in vivo* can be predicted from phantom measurements therefore difficulty of making *in vivo* experiments can be avoided; moreover this method can be used for setting safety limits in MRI by carefully considering the amount of prediction error that can exist due to mismatch of phantom properties.

2044. Calculated Local and Average SAR in Comparison with Regulatory Limits

Christopher M. Collins[1], Weihua Mao[1], Wanzhan Liu[2], Michael B. Smith[1]
[1]Penn State College of Medicine, Hershey, Pennsylvania, USA; [2]University of Minnesota, Minneapolis, Minnesota, USA

Here we discuss some recent experiences in attempting to compare SAR calculated in the human head and body to regulatory limits. Importantly, even in volume coils at commonly-used frequencies, calculated maximum SAR in any one gram of tissue will exceed FDA limits long before whole-head or whole-body SAR averages. This raises questions about either the interpretation of local SAR calculations in light of the limits, or about interpretation of the limits in light of common practice and new local SAR calculations. Finally, use of numerical calculations for comparison to regulatory limits on local temperature show fairly poor spatial correlation between SAR and temperature, indicating a need for more meaningful regulatory limits.

2045. Evaluating Radio Frequency Heating of Vascular Stents at 3 Tesla Using a Gel Phantom

Nikolaus M. Szeverenyi[1], John J. Wasenko[1], David H. Feiglin[1]
[1]SUNY Upstate Medical University, Syracuse, New York, USA

Many patients with vascular stents could not be scanned at 3T due to safety concerns. No specific safety data was available from vendors, safety websites, or literature. We initiated an *ex vivo* testing program, examining 20-60 mm long stents. Radiofrequency heating tests followed ASTM F2182-02a guidelines. Temperature increased by 2.5 deg at the ends of some stents during an aggressive 15 minute scan. The measurements were converted to SAR values, which correlated to stent length. SAR gains of 4 were observed in long stents. The tested devices were approved as safe for 3T and lower field MRI scans.

2046. Vibro-Acoustic Analysis of Acoustic Liners for MRI Scanners

Chris Mechefske[1], Wie Shao[1], Brian Rutt[2]
[1]Queen's University, Kingston, Ontario, Canada; [2]Robarts Research Institute, London, Ontario, Canada

Vibro-acoustic analysis was conducted to predict the acoustic performance of a MRI liner with different thicknesses based on the coupling of a finite element (FE) structural model and a boundary element (BE) acoustical model. Known forces were applied to the structural FE model of the gradient coil to generate a velocity distribution for the acoustical BE model. The sound field inside the liner bore was predicted. The results show that increasing the liner thickness will attenuate more noise. However, the cost of this attenuation will be a much heavier liner and potentially reduced inner radius of the MRI bore. This study also shows that FEM and BEM are powerful simulation tools for vibro-acoustic analyses.

2047. Reduction of the Acoustic Noise of a Siemens 7 Tesla Scanner

Joerg Stadler[1], Peter Dietz[2], Frank Baumgart[1], Andre Brechmann[1]
[1]Leibniz Inst. f. Neurobiology, Magdeburg, Germany; [2]Simenes AG Medical Soulutions, Erlangen, Germany

The acoustic noise generated by the switching of magnetic gradients of MR-scanners becomes an important safety issue especially at ultra-high field (7 Tesla) as these scanners can produce noise levels above 130-140 dB. We reduced the noise of a 7 Tesla scanner in a two-step procedure: By passive sound insulation, we first reduced the scanner-noise to a level comparable to a conventional 3 Tesla scanner. Second, we implemented a FLASH sequence with long gradient rise time for functional imaging which further reduced the scanner noise to < 50 dB SPL at the subjects ear.

2048. Method for Reducing Gradient Acoustic Noise for an MR Sequence

Labros S. Petropoulos[1], [2], Paul Margosian[1], David Lampman[1], Victor Taracila[2], Robert W. Brown[2]
[1]Hitachi Medical Systems America, Twinsburg, Ohio, USA; [2]Case Western Reserve University, Cleveland, Ohio, USA

An alternative methodology for reducing acoustic noise generated by the gradient structure is proposed. Instead of altering the mechanical and/or electrical structure of the gradient, we utilize the freedom in the choice of specific sequence parameters subject to patient comfort and image quality. The selection of these parameters is made such that intrinsic frequencies of the desired sequence do not coincide with gradient's excitation modes. Using a 1.5T MR system, for example, we reduce the sequences' peak acoustic noise level by 7 dB by simply modifying the TR times, with a scan time penalty of less than 0.8 sec.

2049. Simulation Study of Active Noise Control in a 4T MRI Scanner

Mingfeng Li[1], Teik C. Lim[1], Jing-Huei Lee[1]
[1]University of Cincinnati, Cincinnati, Ohio, USA

A variety of methods have been proposed to reduce acoustic noise emission during MRI scans, but few investigators are pursuing active acoustic noise control due to its complexity. In this study, we are investigating various ANC control system including feed-forward only and feed-back only as well as a hybrid ANC system that incorporates both feed-forward and feed-back controls for the feasibility of reducing MRI noise. In this preliminary report, the simulation results show that the hybrid system performs better than the feed-forward or feed-back controller alone.

2050. Static B_0 Field Monitoring at 3 T and 7 T: An MRI Dosemeter

Ian D. Cavin[1], Jasbinder Chauhan[1], Robert Chettle[1], Ian Taylor[1], Mohamed Henini[1], Paul M. Glover[1], Penny A. Gowland[1], Richard W. Bowtell[1]
[1]University of Nottingham, Nottingham, UK

The study demonstrates, for the first time, the feasibility of monitoring occupational exposure of MR workers to ultra high static magnetic fields using a portable dosemeter. The 3 axis hall probe logging device provides valuable data on the magnitude and the duration of the B_0 exposure and is capable of logging data for upto 8 hours. Routine activities carried out during a typical day can now be quantified and recorded to aid epidemiological investigations. Two MR workers carrying out typical daily tasks revealed integrated field exposure values of 128.7 and 135.5 Tesla seconds at 3 Tesla.

2051. A Static Magnetic Field of an MR Scanner Modulates Brain Activity

Toru Yamamoto[1], Atsuhito Toyomaki[2]
[1]Hokkaido University School of Medicine, Sapporo, Hokkaido, Japan; [2]Hokkaido University Graduate School of Medicine, Sapporo, Hokkaido, Japan

To investigate whether brainwaves are changed by the static magnetic field of a 1.5-T MR scanner, we monitored brainwaves inside and outside the MR scanner in different two days before and after demagnetization of the MR magnet. With our new method to remove the confounding influence of ballistocardiogram, we found that the frontal midline *f*Æ-wave significantly increased during an odd ball task only in the static magnetic field. In contrast, with or without the static magnetic field, no significant difference was observed for all brainwaves during rest condition. Our results suggest that the static magnetic field modulates brain activity.

2052. Thresholds for Perceiving a Metallic Taste at Large Magnetic Field

Ian D. Cavin[1], Paul M. Glover[1], Richard W. Bowtell[1], Penny A. Gowland[1]
[1]University of Nottingham, Nottingham, UK

An experiment is described which attempts to quantify the threshold of perception for metallic taste caused by movements in a large static magnetic field. Subjects were positioned in a field strength of 0.5 T and a gradient of 1 T/m and required to rotate their head horizontally or vertically at frequencies up to 1 Hz. Their experiences were recorded together with a measurement of actual rate-of-change of magnetic field. Fifty percent of subjects reported a metallic taste for horizontal plane movements at a dB/dt of 2.3±0.3 T/s at 0.66 Hz.

2053. Mechanisms for Vertigo Experienced by Subjects in a High Field Environment: Hypotheses and Experiments

Paul M. Glover[1], Penny A. Gowland[1], Richard W. Bowtell[1], Ian Cavin[1]
[1]Sir Peter Mansfield Magnetic Resonance Centre, University of Nottingham, Nottingham, NG7 2RD, UK

There are three possible mechanisms for induction of vertigo related to exposure due to magnetic fields. These are Magnetohydrodynamic effects (MHD); Susceptibility of maculae; and Galvanic vestibular stimulation (GVS) of hair cells due to induced circulating currents. The theoretical basis for each mechanism is examined from both a physics and physiological point of view. A series of experiments are reported and calculations presented which preclude MHD and advance the possibility that the susceptibility of the otolithic organs are the dominant mechanism at high fields. Induced currents are not ruled out completely but there is currently no direct experimental evidence for this mechanism using a controlled experimental dB/dt.

2054. Improving Patient Monitoring During Magnetic Resonance Imaging: Real-Time Restoration and Analysis of the Electrocardiogram

Roger Abächerli[1, 2], Remo Leber[2], Sven Hornaff[2], Cédric Pasquier[1], Freddy Odille[1], Pierre-André Vuissoz[1], Michel Kraemer[3], Jean-Jacques Schmid[2], Jacques Felblinger[1]
[1]IADI INSERM (ERI 13), Nancy, Lorraine, France; [2]Schiller AG, Baar, Zug, Switzerland; [3]Schiller Médical, Wissembourg, Alsace, France

The ECG used for patient monitoring during MRI unfortunately suffers from severe artefacts. We applied filters based on the Linear and Time-Invariant system for the offline and online suppression of the remaining superimposed artefacts during worst case scenarios. We studied and analysed the suppression performances of these algorithms. We Wiener filtering (reference annotations) and the LMS filter (online suppression) to measure real-time analysis performance of the ECG acquired during MRI. An significant improvement of the arrhythmia module performance was found enabling reliable patient monitoring and MRI synchronization.

2055. Intracranial EEG in a High-Field MRI Environment: Safety Evaluation

Shannon M. Boucousis[1], Paolo Federico[1], Bradley Gordon Goodyear[1]
[1]University of Calgary, Calgary, AB, Canada

Safety testing of intracranial electrodes has not yet been performed at high field strengths. A phantom model was constructed for in vitro measurements of electrode movement, temperature, and induced voltage in the static MR environment and during MR imaging protocols. The electrodes showed no measurable movement/torque in the MR environment. Temperature change along the electrodes and surrounding tissue was <1 C over a one-hour scanning period. Induced voltage levels ranged from 100 mV to 3500 mV at a frequency of 127 MHz. These preliminary results indicate that intracranial EEG should be safe in a 3 Tesla environment.

2056. Discrepancy Between Peripheral Nerve Chronaxie Times as Measured Using Electric and Magnetic Stimuli

Bryan James Recoskie[1], Tim James Scholl[1], Christopher M. Collins[2], Blaine Alexander Chronik[1]
[1]University of Western Ontario, London, Ontario, Canada; [2]The Pennsylvania State University College of Medicine, Hershey, Pennsylvania, USA

Peripheral nerve stimulation (PNS) results from induced electric fields during MRI.It is expected that electric field exposure thresholds would be consistent with changing magnetic field exposure thresholds. This assumption has motivated the use of electric field exposure criteria to guide magnetic field exposure criteria in MRI. This study tests this hypothesis by comparing chronaxie times for electric and magnetic strength-duration curves for twenty healthy individuals. The average chronaxie times for the electric and magnetic field conditions were significantly different. This suggests that it is not appropriate to use electric field exposure criteria to guide PNS safety standards in MRI.

2057. MRI Based Measurement of Magnetic Field Distribution Generated by Transcranial Magnetic Stimulation Coils

Sangwoo Lee[1], *Luis Hernandez-Garcia*[1], *William Grissom*[1]
[1]University of Michigan, Ann Arbor, Michigan, USA

Transcranial magnetic stimulation (TMS) suffers from poor spatial localization and specificity, and recent research has focused on improving these characteristics via stimulation coil design. The design of a stimulation coil necessitates models of the electromagnetic fields induced by the coil and experimental validation of such models. In this work, we propose an MRI-based method to measure the TMS probe's magnetic field distribution in the head, and present phantom data to demonstrate the measurement

2058. Thermoelastic Pressure Waves Induced Inside the Human Head by RF Pulses from High Pass Birdcage Coils

Zhangwei Wang[1], *James C. Lin*[2]
[1]Penn State College of Medicine,, Hershey, Pennsylvania, USA; [2]University of Illinois-Chicago, Chicago, Illinois, USA

This paper investigates the thermoelastic pressure waves generated by RF pulses absorbed by human head inside MRI coils. The RF induced pressure waves in a human head (without shoulder and neck) loading high-pass birdcage coils of 64 MHz (1.5T), 300 MHz (7.0T) and 400 MHz (9.4T) were computed using the FDTD method. The effect of different pulse width was also investigated. Results for the peak pressure, SAR and pressure distribution are obtained - indicating that the induced thermoelastic pressure waves are functions of RF frequency, power absorption and pulse width.

Neonatal Brain

Room 4E Wednesday 14:00 - 16:00

2059. Lateral Ventricular Size in Extremely Premature Infants: 3D MRI Confirms 2D Ultrasound Measurements

Johan Bengtsson[1], Sandra Horsch[1], Hugo Lagercrantz[1], Zoltán Nagy[1], Anders Nordell[1], Ulrika Ådén[1], Bo Nordell[1], Mats Blennow[1]

[1]Karolinska University Hospital, Stockholm, Sweden

Cerebral ventriculomegaly at term equivalent age is an important predictor of adverse outcome of preterm infants. In this study we used 3D MRI as a "gold standard" for lateral ventricle volume measurement in order to study the value of 10 different, commonly used 2D ultrasound measurements. 34 extremely preterm infants were scanned with MRI and ultrasound at term age. Of the 10 sonographic ventricular measurements, 6 showed good correlations to MRI volumes. The best correlation was found to the measurements of the frontal horns (frontal horn product= short axis*long axis of the frontal horn, r2=0.947).

2060. Diffusion Tensor Imaging of the Developing Visual Cortex and Visual White Matter Pathways in Premature Newborns

Robert Thomas Held[1], Pratik Mukherjee[2], Srivathsa Veeraraghavan[2], A James Barkovich[2], Daniel B. Vigneron, [12]

[1]UCSF/UCB, San Francisco, California, USA; [2]University of California, San Francisco, California, USA

MR- DTI is a powerful method for the analysis of white and gray matter formation in pre-term infants. In this study, an MR compatible incubator and specialized neonate head coil was used to acquire 41 MR-DTI scans from 29 premature newborns with normal neurodevelopmental outcome at one year. Fractional anisotropy (FA) of the gray matter of the primary visual cortex decreased and white matter of the optic radiations increased with age, respectively. Diffusivity orthogonal to the length of the optic radiations decreased with age. The diffusivity changes did not differ significantly between the hemispheres or genders.

2061. Defining Normal and Abnormal DTI Parameters in Premature Newborns

Srivathsa C. Veeraraghavan[1], Steven P. Miller[1], Pratik Mukherjee[1], Natalie N. Charlton[1], Duan Xu[1], Anthony James Barkovich[1], Daniel B. Vigneron[1]

[1]University of California, San Francisco, California, USA

MR diffusion tensor imaging (DTI) is a powerful technique for assessing tissue microstructure. In this study, 44 DTI-MR exams from 31 premature newborns with normal 1-year neurodevelopmental outcome were used to establish normative DTI values and to investigate quantitative differences in DTI for 20 preterm infants with abnormal outcome. The normative data was used to define anatomic and maturational changes. Subjects with abnormal neurodevelopmental outcome demonstrated spatial heterogenitiy in abnormal DTI values. In 19/20 cases Dav exceeded 2 standard deviations from normal in ≥1 region, however, the specific regions varied between individuals.

2062. High Resolution Diffusion Tensor Imaging of the Corpus Callosum in the Preterm Brain at 3 Tesla

Mustafa Anjari[1], Latha Srinivasan[1], David J. Larkman[1], Joanna M. Allsop[1], Julie Fitzpatrick[1], Frances M. Cowan[1], Joseph V. Hajnal[1], Mary A. Rutherford[1], A David Edwards[1], Serena J. Counsell[1]

[1]Hammersmith Hospital, Imperial College London, London, UK

Structural abnormalities affecting the corpus callosum in infants who were born preterm have previously been reported. We aimed to investigate callosal microstructure using diffusion tensor imaging in order to test the hypothesis that radial diffusivity was elevated in this structure in preterm infants. Diffusion tensor imaging was obtained from 15 preterm infants at term equivalent age and 5 healthy term born control infants. We found that radial diffusivity was significantly elevated in the posterior portion of the body of the corpus callosum. This suggests that microstructural abnormalities, in addition to the previously reported macrostructural abnormalities, are prevalent in preterm infants.

2063. Impact of Preterm Birth on Hippocampal Structure Utilizing Volumetric MRI Techniques

Deanne Kim Thompson[1], Stephen J. Wood, Gary F. Egan[1], Lex W. Doyle[2], Simon K. Warfield[3], Gregory A. Lodygensky[4], Peter J. Anderson[5], Terrie E. Inder[4]

[1]Howard Florey Institute, University of Melbourne, Melbourne, VIC, Australia; [2]Royal Women's Hospital, University of Melbourne, Melbourne, VIC, Australia; [3]Brigham and Women's Hospital, Harvard Medical School, Boston, Massachusetts, USA; [4]St. Louis Childrens Hospital, Washington University in St Louis, St Louis, Missouri, USA; [5]Murdoch Childrens Research Instititue, Melbourne, VIC, Australia

Preterm infants are at risk for adverse neurodevelopmental outcomes. The hippocampus appears vulnerable in this population and may contribute to cognitive, learning and memory deficits. Preterm and term infants underwent volumetric MRI evaluation of the hippocampus by manual segmentation on combined coronal t2w and pdw images obtained at term equivalent. At two years of age, cognitive and motor development was assessed with Bayley Scales of Infant Development (BSID-II). Preterm infants had striking bilateral reductions in hippocampal volume associated with white matter injury. Adverse cognitive functioning at two years of age was related to reductions in hippocampal volume. Interventions are required to improve hippocampal development and long-term cognitive performance.

2064. Volumetric and Diffusion Analysis of the Neonatal Brain

Jonathan Paul Dyke[1], Linda A. Heier[1], Aziz M. Ulug[1], Jeffrey M. Perlman[1], Maricor Castillo[1]
[1]Weill Cornell Medical College, NY, USA

Volumetric and diffusion analysis was performed on 16 premature infants and 9 term infants imaged at 40 weeks gestational age. Prematureinfants showed a decrease in whole brain volume and an increase in the whole brain apparent diffusion coefficient compared with terminfants imaged at the same time. Additional analysis of various cerebralstructures as well as GM/WM segmentation may contribute tounderstanding the source of developmental deficits in prematureinfants seen later in life.

2065. Easy and Effective Acoustic Noise Protection in Neonatal MRI

Marcus Lundh[1], Anders Nordell[1], Johan Bengtsson[1], Zoltan Nagy[1], Sandra Horsch[1], Ulrika Adén[1], Bo Nordell[1]
[1]Karolinska University Hospital, Stockholm, Sweden

High levels of acoustic noise in neonatal MRI can lead to anxiety, motion artifacts, and incomplete examinations due to newborns waking up. Hearing protection is often complicated to apply properly on neonates and there is often an uncertainty if the hearing protection is having the intended effect. Acoustic noise levels during our neonatal MRI studies range from 80-112dB (A-weighted). We have developed a new simple, safe and reliable method for substantial reduction of the acoustic noise (6-24dB). An acoustic hood of dampening materials is placed inside the MR tunnel attenuating the noise and providing a safer environment for the infant.

2066. Determining the Most Consistent Method for MRI Hippocampal Volumetry in Infants at Term

Deanne Kim Thompson[1], Stephen J. Wood, Terrie E. Inder[2], Simon K. Warfield[3], Lex W. Doyle[4], Gary F. Egan[1]
[1]Howard Florey Institute, University of Melbourne, Melbourne, VIC, Australia; [2]St Louis Children's Hospital, Washington University in St Louis, St Louis, Missouri, USA; [3]Brigham and Women's Hospital, Harvard Medical School, Boston, Massachusetts, USA; [4]Royal Women's Hospital, University of Melbourne, Melbourne, VIC, Australia

The hippocampus appears vulnerable in preterm infants who have been found to be susceptible to later learning and memory deficits. This study compares five MRI post-processing techniques to determine the most reliable method for hippocampal segmentation in the newborn brain. In addition, hemispheric asymmetry, known to exist in the adult brain, is examined in term and preterm infants, including sick preterm infants who received postnatal steroids. The most reliable technique for obtaining hippocampal volume was tracing on combined raw coronal t2w and pdw images. There was significant hemispheric asymmetry within all infant hippocampal volumes, except for the preterm infants who had received high dose steroids. This is the first study to systematically analyze the most reliable method for hippocampal volume and hemispheric asymmetry in the newborn brain.

2067. Quantitative DTI Assessment of Periventricular White Matter Changes in Neonatal Meningitis

Richa Trivedi[1], Amit Gupta[2], G K. Malik[2], Rakesh Kumar Gupta[1], Khader M. Hasan[3], Kashi Nath Prasad[1], Ponnada A. Narayana[3]
[1]Sanjay Gandhi Post Graduate Institute of Medical Sciences, Lucknow, Uttar Pradesh, India; [2]King George's Medical University, Lucknow, Uttar Pradesh, India; [3]University of Texas Medical School at Houston, Houston, Texas, USA

Diffusion tensor imaging (DTI) holds significant promise for examining white matter microstructure and fiber integrity. Mean fractional anisotropy (FA) and mean diffusivity (MD) values were acquired in the frontal, parietal, occipital, and temporal periventricular white matter in neonatal meningitis (n=12) grouped as normal (n=5) and abnormal (n=7) on the basis of conventional magnetic resonance imaging (MRI), and compared with healthy controls (n=5). Observed decreased FA values in normal as well as abnormal appearing periventricular white matter in patients was consistent with the expected pathological changes in white matter.

2068. Water Mapping of the Whole Brains of Infants Using an FSE Sequence at 3.0 T

Zhengchao Dong[1, 2], Feng Liu[1, 2], Alayar Kangarlu[1, 2], Bradley Peterson[1], Bradley Peterson[1, 2]
[1]Columbia University, New York, New York, USA; [2]New York State Psychiatric Institute, New York, New York, USA

Water content is an important variable in brain development because it is closely related to the progress of myelination in the central nervous system of humans.A number of methods and applications for measuring water content in the brain with MRI have been reported in the last decade. Several have been quantitative techniques; however, to our best knowledge, they have all been performed in adults or children only, not in infants. Here we present a preliminary study of mapping water content quantitatively in the brains of healthy infants using multi-slice images acquired with a fast spin echo (FSE) pulse sequence.

2069. Brain-Water ADC and 31P MRS Imaging Metabolite Ratios and Intracellular PH in a Piglet Model of Transient Hypoxia-Ischemia

Alan Bainbridge[1], Osuke Iwata[2], Enrico De Vita[1], Daniel A. West[2], John S. Thornton[3], Satchi Iwata[2], Nichola J. Robertson[2], Ernest B. Cady[1]
[1]University College London Hospitals NHS Foundation Trust, London, UK; [2]University College London, London, UK; [3]National Hospital for Neurology and Neurosurgery, London, UK

An earlier study demonstrated a good correlation between ADC and cerebral energetics (measured using surface coil 31P MRS) averaged over a large brain volume. Finer spatial discrimination of 31P data can be achieved using MRS imaging. Our aims were to compare metabolite ratios obtained using 31P MRS imaging with spatially and temporally correlated brain-water ADC following transient HI. There were significant correlations between 31P metabolite ratios and ADC in both the subcortex and the deep grey matter. We have demonstrated the utility of ADC as a surrogate measure of cerebral energetics with higher spatial resolution than previously achieved.

MRS/MRI of Neuropsychiatric Disease

Room 4E Wednesday 14:00 - 16:00

2070. Region and Gender Specific Neurochemical Alterations and Sleep Deprivation in Major Depressive Episodes

Harald Murck[1], Mirjam I. Schubert[1], Dagmar Schmid[1], Petra Schuessler[1], Axel Steiger[1], Dorothee P. Auer[1]
[1]Max Planck Institute of Psychiatry, Munich, Bavaria, Germany

Efficacy of total sleep deprivation (TSD) to treat patients with major depressive episodes (MDE) varies with the clinical phenotype and biological markers such as activity of the stress hormone axis. In this study we aimed to noninvasively investigate neurochemical alterations that may be associated with therapeutic sleep deprivation. 15 patients with MDE underwent serial proton MRS in the frontal and parietal cortex on two consecutive mornings before and immediately after the first night of TSD. A gender specific increase in prefrontal Glx was noted as well as reduced prefrontal Glx/Cr ratios at baseline in responding vs. non responding patients.

2071. Lower GPC Compounds in the Hippocamps and Higher GPE in the Putamen/thalamus Region in Depressed Patients Detected by 3D ^{31}P RINEPT MRSI

Nominated for an ISMRM Poster Award

Gabriele Ende[1], Tim Wokrina[1], Sigi Walter[1], Helga Welzel[1], Christine Kief[1], Traute Demirakca[1], Marco Ulrich[1], Alexander Sartorius[1], Fritz A. Henn[1]
[1]Central Institute of Mental Health, Mannheim, Germany

We conducted a 3D ^{31}P RINEPT MRSI study in patients with major depression (MDD) compared to healthy controls. Our previous ^{1}H MRSI findings of reduced hippocampal choline-containing compounds (Cho) in MDD let us to the hypothesis that glycerophosphocholine (GPC) measured via ^{31}P RINEPT would be decreased in the hippocampal region. We further observed an increase of Cho in the putamen. In concordance with these previous results of changes in the ^{1}H MRS Cho signals in MDD patients we observed a decreased GPC ratio in the hippocampal region and an increased glycerophosphoethanolamine (GPE) ratio in the putamen/thalamus region in MDD patients.

2072. Frontal and Occipital Lobe GABA Changes in Depression, Measured with 1H-MRS

Nominated for an ISMRM Poster Award

C. John Evans[1], Marzena Wylezinska[1], Zubin Bhagwagar[1], Peter Jezzard[1], Akeem Sule[1], Sudhakar Selvaraj[1], Paul Matthews[1], Philip Cowen[1]
[1]University of Oxford, Oxford, Oxfordshire, UK

Previous studies have measured GABA reductions in the human occipital lobe in subjects with mood disorders. However, these changes have not been observed in the frontal lobes of recovered depressed subjects, suggesting either regional variations in GABAergic function, or differences between the subject groups. This study measured GABA levels in recovered depressed and control subjects using 1H-MRS (MEGA-PRESS), in both frontal and occipital lobes. Reduced GABA levels were found in the recovered depressed subjects, with similar decreases detected in the frontal and occipital lobes.

2073. Proton Spectroscopy Study of Adolescent Depression

Vilma Gabby[1], David Hess[1], James S. Babb[1], Oded Gonen[2]
[1]New York University, School of Medicine, New York, New York, USA; [2]New York University, New York, USA

Adolescent Major Depressive Disorder (MDD) represents a major public health concern. There has been scarce of research in this age group. This study examines neurochemistry in adolescent MDD focusing on the striatum and cingulate cortex. Addressing prior inconsistent findings, we use high resolution, 3D multivoxel 1H-MRS, ‹1cm3 voxels to quantify metabolite concentrations. Seven depressed adolescents and seven comparisons were enrolled. Significant higher striatal choline concentrations were observed in the MDD group (p=0.012). Findings are consistent with increased membrane breakdown and suggest that impaired cellular resilience may play a role early in the course of the illness.

2074. MRI Morphometry of the Brain in a Longitudinal Study of Depression

Jamila Ahdidan[1], Lars Kroloekke Hviid[1], Kim Mouridsen[2], Barbara Ravnkilde[1], Anders Bertil Rodell[3], Raben Rosenberg[1], Poul Videbech[1]
[1]University Psychiatric Hospital in Aarhus, Risskov, Denmark; [2]CFIN, Aarhus, Denmark; [3]General Hospital of Aarhus, Aarhus, Denmark

A five year longitudinal study of depression has been performed in order to examine structural morphometric differences of the whole brain, between patients and controls over time. We propose using morphometric methods, such as deformation based morphometry (DBM), to automatically identify structural shape changes of the whole brain associated with depression. These methods can detect changes with a high resolution and accuracy without a priori hypothesis. We present a pilot study performed on five patients and seven controls. Preliminary results have shown a significant change over time between the two groups in the hippocampus and the cerebellum.

2075. Treatment of Adolescent Bipolar Depression with Lithium: Effects on Brain MyoInositol Levels Measured by Proton MR Spectroscopy

Kim M. Cecil[1], Melissa P. DelBello[2], Nick C. Patel[3], Caleb M. Adler[2], Stephen M. Strakowski[2]

[1]Cincinnati Children's Hospital Medical Center, Cincinnati, Ohio, USA; [2]University of Cincinnati College of Medicine, Cincinnati, Ohio, USA; [3]University of Cincinnati College of Pharmacology, Cincinnati, Ohio, USA

This study used proton MRS to identify the effects of lithium on myo-inositol (mI) concentrations in adolescent bipolar depression. Twenty-eight adolescents with bipolar disorder, current episode depressed, received lithium, adjusted to achieve serum levels of 1.0-1.2 mEq/L. Medial, left and right lateral prefrontal mI concentrations were measured at baseline, day 7, and day 42 using short echo (TE 35 ms) MRS acquired at 1.5T. A significant change over time was observed for mI concentrations in the medial prefrontal cortex and right lateral prefrontal white matter. Specifically, day 42 concentrations were significantly higher than those on day 7 in both regions.

2076. Comparison of 1D and 2D MR Spectroscopy in Bipolar Depression

Shida Banakar[1, 2], June Watzl[1], Nader Binesh[2], Mark Frye[2], Albert M. Thomas[2]

[1]LABIOMED at Harbor-UCLA, Torrance, California, USA; [2]UCLA School of Medicine, Los Angeles, California, USA;

Twenty three bipolar depressed patients and twelve healthy controls have been investigated using serial scans of PRESS-localized one-dimensional (1D) MRS and two dimensional (2D) L-COSY sequences. The total acquisition times were 13 minutes for 1D MRS using head transmit/receive and 24 minutes for 2D L-COSY using body "transmit" and 3" surface "receive". LC-Model processed 1D MRS data yielded absolute and relative levels of major metabolites and showed increased Glx levels in bipolar depression. 2D MRS findings were in agreement with 1D MRS and in addition relative levels of metabolites such aspartate and other metabolites at lower concentrations with less coefficient of variance.

2077. Hippocampal Neurochemical Findings in Medication-Free, Euthymic Bipolar Disorder: 1H MRSI Study

Wen-Jang Chu[1], Stephen M. Strakowski[1], Hoby P. Hetherington[2], Xin Wang[1], Cal M. Adler[1], Mellissa P. DelBello[1], John N. Adams[1], Neil P. Mills[1], Yun Gao[1], Kelly B. Javis[1], Jing-Huei Lee[1]

[1]Univ. of Cincinnati, Cincinnati, Ohio, USA; [2]Albert Einstein College of Medicine, Bronx, New York, USA

Bipolar disorder (BD) is a common psychiatric illness, the specific neurobiochemical basis of bipolar disorder still not completely understood. The advance of MRS technique has resulted in a lot of studies reporting abnormalities of neurochemistry in BD brains. Previously reported 1H MRSI studies of the hippocampal metabolites changes in BD are few and contradictory. The present work investigated the hippocampal metabolism in medication-free, euthymic bipolar patients using 2D 1H MRSI at 4 Tesla.

2078. Global Gray/White Matter Ratio and Gray Matter Volume Reflect Abnormal Aging Neurodevelopment in Treatment Naive Schizophrenics

Su Lui[1], Luo Ouyang[2], Wei Deng[1], Tao Li[1], Hong Yang[1], Hehan Tang[1], Lijun Jiang[1], Xiaoqi Huang[1], Bin Song[1], Xiangping Zhou[1], Sumner Maclean[1, 3], Vanessa Sluming[4], Qiyong Gong[1, 4]

[1]West China Hospital of Sichuan University, Chengdu, Sichuan, People's Republic of China; [2]University of Electronic Science and Technology of China, Chengdu, Sichuan, People's Republic of China; [3]Universitatsklinikum, Goettingen, Germany; [4]University of Liverpool, Liverpool, UK

The voxel-based analysis was applied to investigate the association of gray/white matter (G/W) ratio and gray matter volume (GMV) with age in patients with first-episode, antipsychotic-naive schizophrenia. 20 schizophrenia patients and 21 normal controls were recruited, and high-resolution T1-weighted images were acquired using a 3.0T MR system. Our results revealed a disassociation of both global G/W ratio and GMV in frontal and temporal lobes with age in patients with schizophrenia, and this represents an abnormal neurodevelopment associated with these regions which may, in part, explain the impaired cognitive performance in the patients

2079. Cortical Disorganization in Brodmann Areas 9, 46 and 32 in Schizophrenia: Evidence from Brodmann-Based MRI Morphometry

Vaibhav A. Diwadkar[1, 2], Jeffrey J. Nutche[2], Rhonda El-Sheikh[1], Serguei Fedorov[1], Debra M. Montrose[2], Matcheri S. Keshavan[1, 2]

[1]Wayne State University School of Medicine, Detroit, Michigan, USA; [2]University of Pittsburgh School of Medicine, Pittsburgh, Pennsylvania, USA

We present preliminary evidence of a methodology to assess cortical integrity in schizophrenia in Brodmann regions estimated from MRI images. The locations of Brodmann regions 9 & 46 (prefrontal cortex) and 32 (anterior cingulate) were estimated using a Brodmann-Talairach atlas. These regional definitions were used to extract gray and white matter volume from normalized and volume-modulated MRI images of young first-episode schizophrenia and healthy control subjects. Compared to controls, patients showed reductions in the ratio of gray to white volume. The results provide support for this approach of assessing cortical organization in schizophrenia by estimating Brodmann regions *in vivo*.

2080. Working Memory Dysfunction with fMRI Task and Gray Matter Difference in Schizophrenia Patients Using Voxel Based Morphometry

Rahyeong Juh[1, 2], Min Ying Su[1], Chang Uk Lee[2], Tae Suk Suh[2], Orhan Nalcioglu[1]
[1]University of California, Irvine, California, USA; [2]Catholic University of Korea, Seoul, Republic of Korea

The prefrontal cortex (PFC) and parietal cortex are important in performing working memory (WM) tasks. In this study we performed fMRI studies to compare the activation regions between the schizophrenic patients and controls using the 2-back WM task paradigm. In addition, the gray matter (GM) loss between these two groups was compared using the voxel based morphometry (VBM) analysis. The brain regions showing differences in fMRI and VBM studies were compared to investigate the consequence of structural atrophy on functional activation.

2081. 2D and 3D RINEPT {^{1}H}-^{31}P-MRSI in the Human Brain and Its Possible Application to Schizophrenia

Tim Wokrina[1], Marco Ulrich[1], Gabriele Ende[1]
[1]Central Institute of Mental Health, Mannheim, Germany

An altered metabolism of membrane phospholipids has been hypothesized in schizophrenia and various ^{31}P MRS studies have been undertaken to explore possible changes in the phosphomonoesters (PME) and phosphodiesters (PDE) signals. Here a 2D slice selective and a 3D ^{31}P MRSI sequence using RINEPT editing are compared with respect to time demand, spatial resolution and applicability to psychiatric patients. The PME and PDE resonances can be well resolved into phosphoethanolamine, phosphocholine, glycerophosphoethanolamine and glycerophosphocholine resonances. Both sequences have showed to be useful in clinical routine for the study of a possibly altered membrane phospholipid metabolism in schizophrenia even at the low field strength of 1.5 T.

2082. High Energy Phosphate Abnormalities Normalize After Antipsychotic Treatment in Schizophrenia: A Longitudinal 31P MRS Study of Basal Ganglia

Jayakumar Peruvumba Narayan[1], B N. Gangadhar[1], G Venkatasubramanian[1], M S. Keshavan[2]
[1]National Institute of Mental Health & Neurosciences, Bangalore, Karnataka, India; [2]Western Psychiatric Institute and Clinic, Pittsburgh, Pennsylvania, USA

It has been hypothesized that neuroleptics might induce decreased energy demanding processes. Earlier, we have reported increased high-energy phosphate metabolism, consistent with disturbed fronto-striatal activity in antipsychotic-naïve schizophrenia. We followed up these patients for one year reassessed them using Magnetic Resonance Spectroscopy for the effect of antipsychotic treatment on the abnormalities of high-energy phosphate metabolism of basal ganglia. Patients had significantly lower mean PCr/ATP ratio than healthy controls at baseline but not during the follow-up. The observations support the hypothesis that neuroleptics might invoke reduced energy demanding processes.

2083. Assessing the Effect of Comorbidity in Attention-Deficit/Hyperactivity Disorder (ADHD) Using *In Vivo* ^{31}P Spectroscopy

Jeffrey A. Stanley[1], Matcheri S. Keshavan[1], Heidi Kipp[2], Erika Greisenegger[2], Kanagasabai Panchalingam[3], Jay W. Pettegrew[3], Oscar G. Bukstein[3]
[1]Wayne State University School of Medicine, Detroit, Michigan, USA; [2]Western Psychiatric Institute and Clinic, Pittsburgh, Pennsylvania, USA; [3]University of Pittsburgh School of Medicine, Pittsburgh, Pennsylvania, USA

Attention-deficit/hyperactivity disorder (ADHD) is one of the most prevalent neurodevelopmental behavioral disorders. A preliminary *in vivo* phosphorus (^{31}P) spectroscopy study has shown deficits in membrane phospholipid (MPL) precursor levels in the basal ganglia (BG) and prefrontal (PF) regions of children with ADHD compared to healthy control subjects. The purpose of this study is to assess the effect of comorbid oppositional defiant disorder (ODD) and/or conduct disorder (CD) on MPL deficits. Results show greater MPL deficits in ADHD subjects with greater severity in behavioral symptomatology.

2084. Elevated Brain Lactate Response During Visual Stimulation in Panic Disorder

Richard J. Maddock[1], Michael H. Buonocore[1], Linda E. Copeland[1], Anne L. Richards[1], Shawn P. Lavoie[1]
[1]University of California Davis, Sacramento, California, USA

Patients with panic disorder (PD) have elevated brain lactate responses to alkalosis. This has been interpreted as evidence of cerebral hypoxia due to excessive vasoconstriction in PD. However, brain lactate can increase during neural activation under fully aerobic conditions. We tested the hypoxia model of panic disorder by measuring visual cortex lactate responses during visual stimulation in PD patients and normals with proton MRS. Optimal slice-selective gradient order was crucial for obtaining artifact-free spectra. PD patients had significantly greater increases in visual cortex lactate during visual stimulation than normal volunteers. This finding is evidence against the hypoxia model of PD.

2085. Positive Correlation of Glycerophosphocholine with Alcohol Consumption in Frontal White Matter of Light Social Drinkers Revealed by 3D ^{31}P MRSI Using RINEPT Editing

Tim Wokrina[1], Traute Demirakca[1], Matthias Ruf[1], Marco Ulrich[1], Sigrid Walter[1], Helga Welzel[1], Gabriele Ende[1]
[1]Central Institute of Mental Health, Mannheim, Germany

Several studies have previously shown that the ^{1}H MRS signal of choline containing compounds (Cho) is altered in alcohol dependent patients. Also, a positive correlation of alcohol consumption with Cho in frontal white matter (WM) and in the anterior cingulate gyrus of light social drinkers has been reported. To further analyze the impact of alcohol consumption on the brain we investigated 13 healthy light socal drinkers with phosphorous 3D MRSI using RINEPT editing. We found a positive correlation of alcohol consumption with frontal WM glycerophosphocholine/totalP. The results suggest that already small amounts of alcohol lead to adaptive mechanisms to alcohol consumption in the brain.

2086. Brain Volume Measurements Correlate with Impulsivity and Aggression

Renee Ochs[1, 2], Ying Wu[1, 2], Carly Demopoulos[1, 2], Rachel Scheidegger[1, 2], Robert R. Edelman[1, 2], Ann B. Ragin[1, 2]
[1]Northwestern University, Chicago, Illinois, USA; [2]Evanston Northwestern Healthcare, Evanston, Illinois, USA

Brain morphology has not been extensively studied in relation to the personality traits of impulsivity and aggression. This investigation examined brain volume measurements determined by automatic segmentation in relation to ratings of these traits from psychometric instruments. Subjects were scanned with a GE 1.5T MR system and T2 images were processed using SIENAX. The brain parenchyma value was significantly different between groups and correlated with aggression measures. White matter volume correlated with impulsivity and aggression measures. This study suggests white matter involvement in impulsivity and aggression. Factors influencing overall brain volume may be relevant in understanding aggression.

2087. fMRI-Guided Spectroscopy for Evaluation of Speech-Related Brain Areas in Neuropsychiatry

Peter Vermathen[1], Claudia Ehrlich[2], Daniela Hubl[2], Andrea Federspiel[2], Thomas Dierks[2], Chris Boesch[1], Roland Kreis[1]
[1]University Berne, Berne, Switzerland; [2]University Hospital of Clinical Psychiatry, Berne, Switzerland

The study of metabolic causes for auditory hallucinations requires that the main cortical areas of speech processing are investigated by MRS in a single examination. However, 1) spectral quality for these areas is insufficient if they are co-recorded by MRSI without local optimization, 2) speech relevant regions cannot be defined from morphological MRI. An experimental protocol of below one hour was therefore devised including fMRI for localization of Broca's and Wernicke's areas, 3D-MRI for structural evaluation, single-voxel MRS for the challenging regions of frontal Broca's area, and single-slice MRSI for centrally located temporal Wernicke's area as well as auditory regions.

Advanced Imaging in Brain Tumors

Room 4E Wednesday 14:00 - 16:00

2088. Plasticity Changes as Reorganization of Pre-Motor Cortex in Lower Limb Amputees: A VBM Study

Juan Ignacio Romero-Romo[1, 2], Corica Rodgers[3], Juan José Ortiz[2], Leopoldo Gonzalez[2], Angel Romero[2], Fernando Alejandro Barrios[2]
[1]SESEQ, Querétaro, QRO, Mexico; [2]Universidad Nacional Autónoma de México, Querétaro, QRO, Mexico; [3]University of California, Irvine, California, USA

Voxel Based Morphometry (VBM) studies are an unbiased statistical selection of anatomical differences that can localize cerebral structures that differ between populations. These kind of studies provided *in vivo* evidence, of the plastic changes that took place as reorganization in pre-motor cortex of lower limb amputees. The use of VBM helped localize differences in brain structures in particular in pre-motor cortex (BA6) between right lower limb amputees and control subjects.

2089. Structural Abnormalities in Posterior Fossa Brain Tumor Survivors: A Voxel-Based Morphometry Study Based on Free-Form Deformation

Yong Zhang[1, 2], Ping Zou[1], Raymond K. Mulhern[1], Robert J. Butler[3], Robert J. Ogg[1]
[1]St. Jude Children's Research Hospital, Memphis, Tennessee, USA; [2]University of Tennessee Health Science Center, Memphis, Tennessee, USA; [3]Oregon Health and Science University, Portland, Oregon, USA

We used voxel-based morphomotry (VBM) to compare brain structure between survivors of posterior fossa brain tumor (PFBT) and controls to test the hypothesis that focal morphological abnormalities in PFBT patients account for altered brain activation patterns during a continuous performance test (CPT). Free-Form Deformation improved the spatial normalization accuracy for the PFBT patients with surgical voids and enlarged ventricles. Morphological differences were detected, but not located where altered activation occurred, contrary to our hypothesis. Morphological differences in the thalamus and white matter of the internal capsule and corpus callosum may have affected CPT activation indirectly.

2090. Quantitative Analysis of Gd Enhancement Histogram Tails Predicts Transformation in Low Grade Gliomas

Paul S. Tofts[1], Chris E. Benton[1], Rimona S. Weil[1], Daniel J. Tozer[1], Daniel Altmann[1], H Rolf Jager[1], Adam D. Waldman[1, 2], Jeremy H. Rees[1]
[1]UCL, London, UK; [2]Charing Cross Hospital, London, UK

Histograms of percent signal enhancement in low grade gliomas, after injection of double dose Gd, were calculated. Optimising the predictive ability of these histograms, the best feature is the right-hand tail, minus the left-hand tail, all multiplied by the tumour volume. This is the corrected volume of enhancing tissue. In 21 subjects (8 non-transformers, 13 transformers), all but one could be correctly classified using a threshold of 3.0ml. Kaplan-Meier survival curves for the time-to-transformation, based on a 4ml threshold for the uncorrected enhancing volume at the baseline examination, differed substantially ($p < 0.04$ at 5 years).

2091. Using RCBV and CBF to Distinguish Radiation Necrosis from Tumor Recurrence in Malignant Gliomas

Rebecca Ann Lund[1], Scott D. Rand[1], H G. Krouwer[1], Chris J. Schultz[1], Kathleen M. Schmainda[1]
[1]Medical College of Wisconsin, Milwaukee, Wisconsin, USA

Distinguishing radiation necrosis from tumor recurrence is a key aspect of post-radiation follow-up in patients with malignant gliomas. An area of enhancement on MR could represent necrosis of surrounding tissue or tumor recurrence. The aim of the study was to determine if relative cerebral blood volume (rCBV) and cerebral blood flow (CBF) imaging could distinguish between viable tumor and radiation necrosis. The SE rCBV showed a significant difference between normalized rCBV values for low-grade gliomas and radiation necrosis. Both GE and SE CBF showed a significant difference between normalized CBF values for low-grade gliomas and radiation necrosis.

2092. fMRI in Patients with Brain Tumors: Descriptive Serial Cases of Cognitive Function in Pre and Post Surgical Conditions

Erika Aguilar[1], Maria De Iturbe[1], Karla Becerril[1], Priscila Rojas[1], Ana Luisa Sosa[1], Sergio Gomez LLata[1], Ulises Garcia[1], Perla Salgado[1], Jorge Paz[1], Fernando Barrios[2], Erick Pasaye[1]
[1]Instituto Nacional de Neurología y Neurocirugía "MVS", Mexico, DF, Mexico; [2]Instituto de Neurobiología, Juriquilla, Queretaro, Mexico

fMRI is used in planning surgical interventions in patients with brain tumors in order to achieve a maximal tumor resection with minimal disruption. We measured the physical ability, cognitive function and fMRI activation of five patients with brain tumors in different regions in pre and post-surgical conditions. Physical and cognitive abilities were conserved or improved after surgery in most cases, and pre and post surgical fMRI studies showed activation in different localizations of the same eloquent areas involved in the task. fMRI can serve as a guidance to preserve not only the patient´s physical ability, but also his/her cognitive functioning.

2093. Assessing Changes in Tumor Vascular Function Using DCE-MRI: A Tale of Two Analysis Algorithms

Srikanth Mahankali[1], Qing Yuan[1], Alfred WK Yung[1], Edward Franklin Jackson[1]
[1]The University of Texas MD Anderson Cancer Center, Houston, Texas, USA

Two threshold-based, whole tumor ROI analysis algorithms based on ipsilateral, pre-contrast baseline signal intensity, and contralateral, pre-contrast mode-based signal intensity, are used to analyze serial DCE-MRI data following the oral administration of a receptor tyrosine kinase inhibitor in six patients with Glioblastoma Multiforme. The basis for this comparison is that user-defined, whole tumor ROIs are unable to evaluate tumor heterogeneity in malignant lesions and thus may be insensitive to drug action. Data demonstrate varied response outcomes encountered with the different techniques and highlight the need to develop standardized approaches to measurement particularly essential in this era of multi-center trials.

Multiple Sclerosis: Grey and White Matter Lesions

Room 4E Wednesday 14:00 - 16:00

2094. Detection of Subpial Cortical Demyelinating Lesions in Multiple Sclerosis *In Vivo*

Jacqueline Tien Hsiang Chen[1], D. Louis Collins[1], Harold L. Atkins[2], Mark S. Freedman[2], Douglas L. Arnold[1]
[1]Montreal Neurological Institute/McGill University, Montreal, QC, Canada; [2]The Ottawa Hospital-General Campus, Ottawa, ON, Canada

Subpial demyelinating lesions in multiple sclerosis are generally undetectable by conventional MRI *in vivo*, despite the high prevalence of extensive cortical lesional pathology on post-mortem examinations. We used T1-weighted MRI to define the boundary between cerebrospinal-fluid and cortex, and magnetization transfer ratio images to define a boundary between sparsely myelinated and normally myelinated cortex. This allowed the detection of abnormal regions of subpial demyelination extending into the deeper layers of the cortex with a pattern and prevalence consistent with cortical subpial demyelinating lesions.

2095. Abnormalities of Deep Gray Matter Perfusion in Multiple Sclerosis: Dynamic Susceptibility Contrast Perfusion MRI at 3.0 T

Matilde Inglese[1], Sun-Jung Park[1], Glyn Johnson[1], James S. Babb[1], Hina Jaggi[1], Joseph Herbert[1], Robert I. Grossman[1]
[1]New York University, New York, New York, USA

Patients with primary progressive multiple sclerosis (PP-MS) show a relative lower rate of new T2 lesions formation and lower amount of inflammatory lesions compared to patients with relapsing remitting MS (RR-MS). Recent studies have shown decreased perfusion in both lesions and NAWM of RR-MS patients. However, perfusion in PP-MS has yet to be explored. Using dynamic susceptibility contrast (DSC) enhanced T2*-weighted MRI for measuring tissue perfusion, we observed significantly lower cerebral blood flow (CBF) and volume (CBV) in deep gray matter in MS patients as compared with normal controls and in PP-MS patients as compared with RR-MS patients.

2096. Imaging Cadavers - 'cold Brain' MRI Effects and Noninvasive Diffusion Thermometry of the CSF

Paul S. Tofts[1], Daniel J. Tozer[1], David G. MacManus[1], Klaus Schmierer[1], Nick C. Fox[1]
[1]University College London, London, UK

In cadaveric brain imaging, the low temperature gives a variety of interesting ‘cold brain’ effects (also present to some effect in post-mortem tissue). In conventional FLAIR and Spin Echo images the cold CSF is bright because of its reduced T1. The diffusivity of CSF is reduced by a factor of three at 1degC; ADC values of CSF provide a potential non-invasive thermometer to show brain temperature. In one cadaver, the ADC of CSF was 1.1 10-9 m2 s-1, implying a temperature of 1degC. An improved inversion time TI can be found for FLAIR, depending on the brain temperature

2097. *In Vivo* Visualization of Multiple Sclerosis Cortical Lesions by High Resolution MRI at 3T

Francesca Bagnato[1], Lalith Talagala[2], Vasiliki Ikonomidou[2], Alessandro Calabrese[2], Fernanda Tovar-Moll[2], Annie W. Chiu[2], Marco Riva[2], Mary Ehrmantraut[2], Joan M. Ohayon[2], Henry F. McFarland[2]
[1]NIB, Bethesda, Maryland, USA; [2]NINDS / NIH, Bethesda, Maryland, USA

In this study, high resolution spoiled gradient recalled fast inversion recovery images (IR-FSPGR) were obtained in 23 MS patients and 20 healthy volunteers (HV) at 3T using an 8-channel receiver coil array. Initial analyses of 8 patients revealed neocortical lesions (NL) in 7 patients while none in HV. Most NL crossed cortical boundaries or were present exclusively within juxta-cortical areas. Up to 70% of NL were found in frontal lobes. We demonstrate that a high-resolution T1-weighted 3T MRI using multi-channel receiver arrays is effective for NL identification in MS.

2098. Imaging Cortical Lesions at Standard and High Field-Strength (1.5T and 4.7T): Post-Mortem MRI and Histopathology

Jeroen J. G. Geurts[1], Erwin Blezer[2], Hugo Vrenken[1], Annette van der Toorn[2], Chris H. Polman[1], Jonas A. Castelijns[1], Petra J. W. Pouwels[1], Lars Bö[1], Frederik Barkhof[1]
[1]VU University Medical Center, Amsterdam, Noord-Holland, Netherlands; [2]University of Utrecht, Utrecht, Netherlands

Gray matter abnormalities have been linked to physical, including neuropsychological, deficits in Multiple Sclerosis (MS). Cortical lesions are highly prevalent in (progressive) MS, but unfortunately, they are rarely depicted by standard MR imaging (MRI) techniques. In this study, the sensitivity of standard field-strength (1.5T) post mortem MRI for cortical lesions was compared to the sensitivity of high field-strength MRI (4.7T). Type I lesions (mixed gray matter-white matter lesions) were relatively easily visualized (up to 100%) by both field-strengths, while purely intracortical lesions (types II-IV) were rarely detected, even when using high-field MRI.

2099. A Voxel-Based Morphometric Analysis of Clinically Isolated Syndrome Patients

Mason Shieh[1], Daniel Pelletier[1], Kathleen Garrison[1], Darin Okuda[1], Roland G. Henry[1]
[1]University of California at San Francisco, San Francisco, California, USA

Voxel-based morphometry (VBM) is an unbiased method of comparing local concentrations and volumes of brain tissue across images of the brain. VBM analysis has been slow to be applied to multiple sclerosis patients due to lesions that could provoke distortions during spatial normalization and the validity of lesion masking techniques to correct for this problem has not been explored. CIS patients have relatively few lesions and therefore are the best candidates for investigating this technique. Lesions were masked in 32 CIS patients using a modified version of the method outlined in Brett *et al*. and statistically compared to 61 control subjects using SPM. CIS patients showed significant volume decreases in the thalamic regions, while similar results were obtained with much lower significance without lesion masking.

2100. Texture Response of Deep Gray Matter in Patients with Multiple Sclerosis Treated with Minocycline

Yunyan Zhang[1], Luanne M. Metz[1], Hongmei Zhu[2], Voon Wee Yong[1], J Ross Mitchell[1]
[1]University of Calgary, Calgary, Alberta, Canada; [2]York University, Toronto, Ontario, Canada

Deep gray matter (GM) texture change in patients with multiple sclerosis (MS) after minocycline treatment was quantified using the recently developed polar Stockwell transform (PST) analysis on 3T T2-weighted MRI. The texture tended to change from coarseness to finesse 24 months on drug. Such changes were higher in active than in inactive patients. The texture improvement was the largest in the head of the caudate nucleus. This study suggests that the PST may be a new tool to monitor deep GM pathology. Future studies seek to verify these results and to correlate MR texture with clinical indicators of MS.

2101. Quantitative T1 Measurements Suggest Sex-Dependent Gray Matter Involvement in MS

Jeffrey M. Njus[1], Leif E. Vigeland[1], Xin Li[1, 2], Charles S. Springer[1, 2], Maria Taylor[3], Frank W. Telang[2], Patricia K. Coyle[3], William D. Rooney[1, 2]

[1]Oregon Health and Science University, Portland, Oregon, USA; [2]Brookhaven National Laboratory, Upton, New York, USA; [3]Stony Brook University, Stony Brook, New York, USA

Brain 1H2O T1 maps were collected from 16 healthy controls and 17 MS subjects at 4 T. Normal appearing white and gray matter ROIs were selected and T1 values were compared between control and MS groups, and also between sexes. T1 values were increased by 6% in MS NAWM, with men and women showing similar increases. T1 values were also increased in MS NAGM, but only for the women. These findings suggest possible regional differences in MS disease expression between the sexes.

2102. MRI Evidence for a Strong Relationship Between Total Cerebral White-Matter Lesion Load and Clinical Disability in Patients with Multiple Sclerosis

Zografos Caramanos[1], Sridar Narayanan[1], Simon James Francis[1], André Luiz Mendes Matos[1], Maria Carmela Tartaglia[1], Yves Lapierre[1], Douglas Lorne Arnold[1]

[1]Montreal Neurological Institute, McGill University, Montreal, Quebec, Canada

We examined the cross-sectional relationship between clinical disability and total cerebral white-matter lesion load (LL) in a large sample of patients with multiple sclerosis. We found that LLs (particularly T1-LLs) are strongly related to clinical disability when patients that span a wide range of clinical disability are examined. Our results also suggested that – in combination with their mean cervical-cord cross-sectional area, disease duration, and sex – such patients' T1-LLs can account for a large degree of the variance in their clinical disability.

2103. Extensive T2* Heterogeneity in White Matter Studied by High Resolution MRI at 7T

Tie-Qiang Li[1], Alan Koretsky[1], Peter van Gelderen[1], Hellmut Merkle[1], Lalith Talagala[1], Jeff Duyn[1]

[1]NIH, Bethesda, Maryland, USA

High resolution T2*mapping in the human brain were performed at 7T. Surprisingly there was significant heterogeneity in white matter contrast that was not attributed to large veins. This contrast followed major white matter fiber bundles and should enable sensitive detection of changes in white matters. Advantages of the GRE sequence used include the unique contrast mechanisms sensitive to tissue microscopic susceptibility, fidelity against physiological motion artifacts, and relative insensitivity to B1 inhomogeniety

2104. Quantitative Multi-Slice Mapping of the Myelin Water Fraction Using Multi-Compartment Analysis of T2* Relaxation at 3T

Yiping P. Du[1], Renxin Chu[1], Mark S. Brown[1], Bette K. Kleinschmidt-DeMasters[1], Jack H. Simon[1]

[1]University of Colorado Health Sciences Center, Denver, Colorado, USA

Demyelination of white matter in the central nervous system is considered the primary pathology of multiple sclerosis (MS). We present the preliminary results of mapping the myelin water fraction (MWF) using a fast multi-slice imaging technique. A multi-slice echo-planar spectroscopy imaging sequence was used to record the T2* relaxation in each voxel with a scan time less than 10 minutes. Multi-exponential analysis using a 3-pool model was used for quantitative mapping of MWF. The MWF maps, with a matrix size of 256x256, clearly depict the MS lesions in post mortem human brains.

2105. Normal-Appearing White Matter Changes Vary with Distance to Lesions in Multiple Sclerosis

Hugo Vrenken[1], Jeroen J.G. Geurts[1], Dirk L. Knol[1], Chris H. Polman[1], Jonas A. Castelijns[1], Petra J.W. Pouwels[1], Frederik Barkhof[1]

[1]VU University Medical Center, Amsterdam, Netherlands

Goal: To investigate the relation of normal-appearing white matter (NAWM) changes in Multiple Sclerosis (MS) with the lesions visible on conventional MR.Methods: We measured whole-brain, B_1-corrected T_1 relaxation time and magnetization transfer ratio (MTR) maps in MS patients and healthy controls. Histograms of T_1 and MTR were analyzed for NAWM pixel subsets progressively further from the MR visible lesions.Results: While MTR histogram abnormalities were confined to the first two pixel layers around lesions, T_1 histogram abnormalities were more widespread. NAWM distant from lesions had T_1 histograms significantly different from control white matter, while MTR histograms were normal.

2106. The Early MS Pathology in the Corpus Callosum by Atrophy, Magnetization Transfer and Diffusion Tensor Measures at 3T in Patients with a Clinically Isolated Syndrome and a Positive MRI

Jack H. Simon[1], Mark Brown[1], David E. Miller[1], Jeffrey Bennett[1], John Corboy[1], Deb Singel[1]

[1]University of Colorado Health Sciences Center, Denver, Colorado, USA

Baseline characterization of corpus callosum from the earliest disease, after a clinically isolated syndrome in patients with a positive MRI reveals no or minimal change outside focal lesions in the normal appearing white matter (NAWM) by diffusion tensor(fractional anisotropy and apparent diffusion coefficient) and magnetization transfer at 3T. As disease progresses, increased abnormality is detected in the NAWM. As a sizeable fraction of these callosa contain fibers that are at risk for injury as they connect to distant (non-callosal) focal MS lesions, this pathology is likely too dilute to measure within the non-selective tissue class called NAWM.

2107. Registration and Subtraction of 2D-T2SE Images in a Routine Multicentre Multiple Sclerosis (MS) Trial Setting

Bastiaan Moraal[1], Dominik S. Meier[2], Hugo Vrenken[1], Peter A. Poppe[1], Ronald A. van Schijndel[1], Petra Jan Willem Pouwels[1], Charles R G Guttmann[2], Frederik Barkhof[1]

[1]VU Medical Center, Amsterdam, Netherlands; [2]Brigham and Women's Hospital, Harvard Medical School, Boston, Massachusetts, USA

MRI indices are used as a secondary outcome measure in phase III clinical multiple sclerosis (MS) trails. Serial analysis to detect and quantitate disease activity is difficult, inaccurate and time consuming due to repositioning errors and a background of unaltered non-active lesions. Registration and subsequent subtraction circumvent these difficulties. Using data from a multicentre clinical trial, we evaluated the changes in MS lesions on registered and subtracted images, as well as on the original baseline and follow-up images. On the subtracted images, 77% more active lesions (positive activity) were detected. Interobserver agreement has not yet been analysed but is expected to be better for subtracted images.

2108. Semi-Automated Method for Quantifying and Localizing White Matter Hyperintensities on MR Images

Minjie Wu[1], Caterina Rosano[1], Meryl Butters[1], Ellen Whyte[1], Ryan Crooks[1], Carolyn Cidis Meltzer[1], Charles F. Reynolds III[1], Howard Jay Aizenstein[1]

[1]University of Pittsburgh, Pittsburgh, Pennsylvania, USA

White matter hyperintensities (WMH), commonly found on T2 and FLAIR brain MR images in the elderly, are associated with a number of neuropsychiatric disorders. In the current study we implemented and validated a semi-automated method for quantifying and localizing WMHs. We adapted a fuzzy connected algorithm to automate the segmentation of WMHs and used a demons-based image registration to automate the anatomic localization of WMHs. The volumes of automated WMHs were significantly correlated to the accepted gold standard (manual ratings, p=0.0003; correlation coefficient 0.907). As predicted, the WMHs in late-life depression (LLD) clustered in the prefrontal cortex and subcortical regions.

2109. Identification of Abnormal White Matter in Multiple Sclerosis

Kishore Venkata Mogatadakala[1], Sushmita Datta[1], Aziz Hatim Poonawalla[1], Khader M. Hasan[1], Jerry S. Wolinsky[1], Ponnada A. Narayana[1]

[1]University of Texas Medical School at Houston, Houston, Texas, USA

The presence of so called "normal appearing white matter (NAWM)" which appears normal on conventional magnetic resonance imaging (MRI), but is abnormal, is well recognized in Multiple Sclerosis (MS). It is thought that NAWM represents tissue at risk. However, currently, there are few noninvasive techniques for identification of the NAWM. We present a technique that is based on a combination of multi-parametric segmentation of MRI and fractional anisotropy (FA) derived from the diffusion tensor imaging (DTI) in identifying the NAWM.

2110. Is a Two-Pool MT Model Valid in Tissues with Multicomponent T2?

Sharon Portnoy[1], Greg Jan Stanisz[2]

[1]University of Toronto, Toronto, ON, Canada; [2]Sunnybrook & Womens' CHSC, Toronto, ON, Canada

Quantitative MT analysis is usually performed using the Two-Pool Model of MT exchange. However, this model does not account for the multiple liquid T2 components that occur in tissues. Thus, the physical interpretation of liquid pool T2 estimates extracted from Two-Pool Model fits to MT data has remained uncertain. By comparing MT and T2 decay data in white matter, this study demonstrates that T2 measured from MT experiments is equal to the inverse of a tissue's mean transverse relaxation rate. This finding suggests that on the time scale of typical MT experiments, the multiple liquid T2 components are indistinguishable, validating the use of a Two-Pool Model description for steady state MT data.

2111. Corpus Callosum Partitioning Schemes and Their Effect on Callosal Morphometry

Charlotte Ryberg[1], Mikkel Bille Stegmann[2], Karl Sjöstrand[2], Egill Rostrup[3], Franz Fazekas[4], Frederik Barkhof[5], Gunhild Waldemar[1]

[1]Memory Disorders Research Unit, Copenhagen, Denmark; [2]Informatics and Mathematical Modelling, Kongens Lyngby, Denmark; [3]Danish Reseach center for Magnetic Resonance, Copenhagen, Denmark; [4]Medical University, Graz, Austria; [5]VU Medical Center, Amsterdam, Netherlands

Corpus Callosum (CC) is the main fiber tract connecting the two brain hemispheres. The lack of evident landmarks that delimit anatomical and functionally distinct callosal regions has spawned several geometric partitioning schemes to subdivide the CC into regions. The aim of this work was to investigate the statistical impact of six common partitioning schemes for regional analysis of CC in 569 elderly subjects. Irrespective of the method used, CC atrophy was associated with impaired global cognitive and motor function. However, the pattern of associations between CC areas and clinical and functional data depends on the partitioning scheme used.

2112. *In-Vivo* 3D Multi-Component T2-Relaxation Measurements for Quantitative Myelin Imaging at 3T

Burkhard Mädler[1, 2], Alex L. MacKay[2]
[1]UBC Hospital, Vancouver, BC, Canada; [2]University of British Columbia, Vancouver, BC, Canada

We developed a novel 3D multi-echo CPMG imaging sequence that provides an accurate and reliable way to carry out multi-component T2 measurements over most of the brain volume in a clinical acceptable time. RF deposition for multi-spin echo sequences is a concern, especially at higher field strength. We have shown that, by replacing composite hard-pulses with less SAR sensitive slab selective pulses, high quality multi-echo decay curves can still be obtained when a body coil with uniform B1 homogeneity over the brain volume is used. Geometric mean T2 measures as well as myelin water fraction values were in good agreement with previously published data at 3T.

2113. Pattern of Hemodynamic Impairment in Multiple Sclerosis: Dynamic Susceptibility Contrast Perfusion MRI at 3 T

Sumita Adhya[1], Glyn Johnson[1], Joseph Herbert[1], James S. Babb[1], Hina Jaggi[1], Robert I. Grossman[1], Matilde Inglese[1]
[1]New York University, New York, New York, USA

Dynamic susceptibility contrast (DSC) perfusion MR is able to characterize cerebral hemodynamics in patients with stroke and brain tumors. Although it has long been known that inflammation associated with vascular occlusion and fibrin deposition occurs prior to demyelination, it has only recently been suggested to contribute to disease progression in Multiple sclerosis (MS). Using DSC perfusion MRI, we detect lower level of cerebral blood flow (CBF) and volume (CBV) in the NAWM of patients with primary progressive (PP) and relapsing-remitting (RR-MS). CBF and CBV correlated with the expanded disability status scale (EDSS) score.

2114. Diffusion Modeling Using Bayesian Probability Theory Applied to Imaging of Multiple Sclerosis

Joshua S. Shimony[1], Adrian A. Epstein[1], Christopher D. Kroenke[1], Jeffrey J. Neil[1], Anne H. Cross[1], Yvette I. Sheline[1], Abraham Z. Snyder[1], G Larry Bretthorst[1]
[1]Washington University Medical School, St. Louis, Missouri, USA

The diffusion tensor model has proven extremely valuable for modeling the diffusion properties of water in the brain. The model incorporates a monoexponential function for the diffusion attenuation curve. Since the introduction of this model studies from several research groups have shown that this function does not fit the data well at high gradient values. As a result many researchers have applied a biexponential function to the data. We explore a simple alternative model using Bayesian probability theory that provides a unique contrast mechanism and apply it to normal subjects and patients with multiple sclerosis.

2115. Minocycline Impedes the Evolution of Gd-Enhancing Lesions Into Black Holes in Patients with Multiple Sclerosis

Yunyan Zhang[1], Luanne M. Metz[1], Voon Wee Yong[1], J Ross Mitchell[1]
[1]University of Calgary, Calgary, Alberta, Canada

The impact of minocycline on the evolution of Gd-enhancing lesions into 'black holes' was assessed in 10 multiple sclerosis (MS) patients over 3 years. None of the 'new' Gd-enhancing lesions (3/12) in this sample became black holes. 4/9 'old' Gd-enhancing T1-hypointense lesions never developed black holes. Importantly, two 'old' Gd-enhancing lesions showing hypointense T1 changed to normal appearing white matter on months 6 and 36 respectively after the commencement of treatment. This study indicates that minocycline may be beneficial in preventing the accumulation of severe tissue damage in MS.

2116. Application of Single-Slab 3D-FLAIR, 3D-DIR and 3D-T2, Compared to 2D Dual-Echo T2, in Multiple Sclerosis Patients

Bastiaan Moraal[1], Petra Jan Willem Pouwels[1], Hugo Vrenken[1], Charles R G Guttmann[2], Dominik S. Meier[2], Ronald A. van Schijndel[1], Jeroen J G Geurts[1], Frederik Barkhof[1]
[1]VU Medical Center, Amsterdam, Netherlands; [2]Brigham and Women's Hospital, Harvard Medical School, Boston, Massachusetts, USA

In multiple sclerosis (MS) trials a reliable comparison obtained at different time points is often difficult. Registration (and subtraction) might circumvent these difficulties but the relatively think slices of the 2D-T2SE induces blurring. These techniques might benefit from single-slab 3D images that allow the acquisition of thinner slices. A cross-sectional analysis was performed in which the number of lesions in different regions of the brain was determined. The single-slab 3D images showed an improved detection of intracortical and mixed WM-GM lesions (DIR) and deep WM lesions (FLAIR). Future studies have to demonstrate the distinct advantages of the single-slab 3D datasets using registration and subtraction.

fMRI in Animals

Room 4E Wednesday 14:00 - 16:00

2117. Quantifying the BOLD Contribution in CBV-Weighted fMRI at 9.4T

Hanbing Lu[1], Leah Gitajn[1], William Rea[1], Yihong Yang[1], Elliot A. Stein[1]
[1]National Institute on Drug Abuse, Baltimore, Maryland, USA

In fMRI employing iron oxide contrast agent, there are two competing factors that contribute to the fMRI signal: one is the BOLD effect, and the other is the superparamagnetic effect of iron oxide. At high field, the BOLD contamination can be a significant component in CBV-weighted fMRI. This work is intended to determine 1) the optimal iron dose in CBV-weighted fMRI and 2) BOLD contribution in CBV-weighted fMRI signal. We further quantified the intra- and extra-vascular BOLD effect in spin echo fMRI at 9.4T.

2118. Dynamic fMRI Acquisition of BOLD, RCBV, CBF, and Hypercapnic Reactivity for RCMRO2 Calculation During Rat Forelimb Stimulation

Young Ro Kim[1], George Dai[1], Emiri Tejima[2], Joseph B. Mandeville[1], Bruce R. Rosen[1]
[1]Athinoula Martinos Center for Biomedical Imaging/ Massachusetts General Hospital, Charlestown, Massachusetts, USA; [2]Neuroprotection Research laboratory/ Massachusetts General Hospital, Charlestown, Massachusetts, USA

Accurate dynamic measurements of rCMRO2 are useful for understanding various pathological conditions and assessing the integrity of neuronal responses. We calculated the rCMRO2 changes of rat somatosensory cortex during the electrical forelimb stimulation based on the dynamic acquisition of BOLD, functional changes of CBV, CBF, and responses to the exposure of CO2 (5%). Apparent ipsistimulus CBV responses (e.g., left SS response to left forelimb stimulus) were not accompanied by concomitant increase of rCMRO2. We demonstrated that the unbiased acquisition of local hemodynamic parameters is necessary for accurately understanding details of fMRI activities during the rat forelimb stimulation.

2119. MRI Evidence of Resting State Connectivity in Rodent Brain

Kathleen Anne Williams[1, 2], Scott J. Peltier, [12], Stephen M. LaConte, [12], Shella Dawn Keilholz[1, 2]
[1]Georgia Institute of Technology, Atlanta, Georgia, USA; [2]Emory University, Atlanta, Georgia, USA

This work looks for evidence of resting state connectivity in the rat brain similar to that which has previously been observed in humans. Six rats were imaged on a Bruker 11.7 T scanner using a single-shot gradient-echo EPI sequence to acquire T2*-weighted MR images. Power spectra obtained from SI show structure in low frequencies that is not present in spectra from the sagittal sinus or outside the brain, suggesting that resting state fluctuations are present in rats. Correlation maps created using a seed in SI demonstrate increased correlation in the cortex compared to subcortical structures.

2120. fMRI of the Rat's Whisker-To-Barrel Pathway

Ian Mark Devonshire[1], Jason Berwick[1], Paul G. Overton[1], John E. Mayhew[1], Nikos G. Papadakis[1]
[1]University of Sheffield, Sheffield, UK

fMRI of the anaesthetised rat was performed using a small, open-access volume coil and multi-slice asymmetric spin-echo EPI, in response to electrical stimulation of the rat's whiskers. Robust microvascular BOLD and CBV responses were observed in the two extreme stations of the whisker to barrel pathway (cortex and brainstem); the thalamic nuclei were detected inconsistently, possibly due to their small spatial extent. This method will enable future investigations into the relationship between neural and haemodynamic responses in different regions of the brain, information that is essential in order to provide a more accurate understanding and interpretation of fMRI data.

2121. Imaging Dynamic Neural Network in Rat Brains Using BOLD fMRI

Tsukasa Nagaoka[1, 2], Naoyuki Miyasaka, [23], Richard P. Kennan[2], Seiji Ogawa[2, 4], Timothy Q. Duong[1]
[1]Emory University, Atlanta, Georgia, USA; [2]Albert Einstein College of Medicine, Bronx, New York, USA; [3]Tokyo Medical and Dental University, Bunkyo, Tokyo, Japan; [4]Ogawa Laboratories for Brain Function Research, Shinjuku, Tokyo, Japan

This study extended the rat somatosensory stimulation model for dynamic imaging of neural network of the entire brain. We reported robust activations in the contra-lateral somatosensory cortex, bilateral striatum, bilateral thalamus and bilateral reticular formation, not previously possible. The BOLD fMRI signal changes (in the contralateral hemisphere) were 9.8%, 1.4%, 3.2% and 1.4%, respectively. The ability to detect activations in sub-cortical nuclei and higher brain functions beyond the commonly reported primary somatosensory cortices could have many important applications, include the opportunity to study neural network of the entire brain and fMRI evaluation in stroke where injury often covers subcortical regions.

2122. Stimulus Frequency Dependence of the Relationship Between BOLD Signal and Somatosensory Evoked Potential in Rat Cortex

Ikuhiro Kida[1], Mamoru Tamura[1], Toru Yamamoto[1]
[1]Hokkaido University, Sapporo, Hokkaido, Japan

Since the BOLD signals correlate with hemodynamic changes such as deoxygenated hemoglobin and CBF, the stimulus frequency dependence should match both for BOLD signal, deoxygenated hemoglobin and/or CBF. However, an fMRI study using the gradient-echo BOLD signal reports a conflicting result with CBF measurement and optical imaging for the stimulus-frequency dependence in rat forepaw stimulation model. We investigated whether the BOLD signal correlates with hemodynamic changes and neuronal events for the various stimulus frequencies. Result that the spin-echo BOLD signal peaked at 3-5Hz stimulus frequency paralleled with the changes in hemodynamics and the integrated somatosensory evoked potential amplitude.

2123. Subcortical Forepaw Stimulation fMRI Activations in Awake Rats

Qiang Shen[1], Nanna Sulai[1], Timothy Q. Duong[1]
[1]Emory Unviersity, Atlanta, Georgia, USA

fMRI studies in awake and behaving animals could offer many unique advantages. We demonstrated herein that BOLD and CBF fMRI responses under awake conditions are reasonably robust by using three well-established forepaw electrical stimulation model. Larger BOLD percent changes were observed under awake conditions compared to the anesthetized conditions. Most importantly, activations were observed in additional brain structures (predominantly in the subcortical regions and higher order functions) that were not detected in the anesthetized preparations. This study demonstrated the ability to do fMRI under awake conditions, which will have important value in many applications.

2124. Distinct Characteristics of Brain Activity in Cat V1 and LGN in Response to Flicking and Grating Visual Stimuli: A fMRI Study at 9.4T

Nominated for an ISMRM Poster Award

Xiao-Hong Zhu[1], Nanyin Zhang[1], Yi Zhang[1], Wei Chen[1]
[1]CMRR, Department of Radiology, University of Minnesota Medical School, Minneapolis, Minnesota, USA

We have demonstrated the feasibility of high-resolution fMRI at high field for reliably mapping the thalamocortical activation in the cat visual sensory system, a well-established animal model for vision science. In this study, we applied the same fMRI technique to investigate the dependence of neuronal activity in the lateral geniculate nucleus (LGN) and visual cortex (V1) on the type of visual stimulus by using flicking and grating stimuli. Our results demonstrate that both stimuli cause strong BOLD changes in LGN. However, the grating stimulus produces much stronger BOLD changes in V1 than the flicking stimulus indicating the distinct neural characteristics between different brain structures along the visual pathway in response to different stimuli.

2125. Study of Correlation Between Brain Activity and ATP Metabolic Rates by Means of ^{31}P Magnetization Transfer and Electroencephalograph Measurement

Fei Du[1], Yi Zhang[1], Michael Friedman[1], Nanyin Zhang[1], Xiao-Hong Zhu[1], Kamil Ugurbil[1], Wei Chen[1]
[1]Center for Magnetic Resonance Research, University of Minnesota, Minneapolis, Minnesota, USA

Numerous brain studies during the past decades have supported a coupling among brain acitivity and cerebral blood flow (CBF) as well as the cerebral metabolic rates of glucose and oxygen (CMRglc, CMRO2). Adenosine-5'-triphosphate (ATP) is the basic energy currency which provides major energy resource to be directly used in the live organs. In the mammal brain, ATP is mainly generated from the oxidative phosphorylation of glucose and/or phosphocreatine catalyzed by creatine kinase (CK). In this study, the cerebral metabolic rates of ATP syntheses (CMRATP) and brain activity were measured by *in vivo* 31P magnetization transfer approach and EEG respectively at various physiology conditions in the rat brain. The results show that (i) the CMRATP values catalyzed by ATPase and CK reactions are tightly correlated to brain activity; (ii) the relative change of CMRATP is larger for ATPase reaction than CK reaction; and (iii) the *in vivo* measurement of CMRATP should provide an important tool for studying the brain function and bioenergetics.

2126. Functional Magnetic Resonance Imaging of the Rat Spinal Cord After Peripheral Nerve Injury

Katarzyna Majcher[1], Boguslaw Tomanek[2, 3], Andrzej Jasinski[1, 4], Tadeusz Foniok[2], Dave Kirk[3], Dave Rushforth[2], Ursula I. Tuor[2, 3], Grzegorz Hess[5]
[1]Institute of Nuclear Physics, PAS, Krakow, Poland; [2]Institute for Biodiagnostics (West), NRC, Calgary, Alberta, Canada; [3]Experimental Imaging Centre, University of Calgary, Calgary, Alberta, Canada; [4]Pedagogical University, Krakow, Poland; [5]Institute of Pharmacology, PAS, Jagiellonian University, Krakow, Poland

The neuronal activity within the rat spinal cord following a graded reduction of sensory input from the hindpaw was investigated using fMRI. The experiment allowed correlation of the neuronal activation with the increasing nerve injury using spinal cord fMRI. Fast spin echo images were acquired through spinal cord at 9.4T. A consistent decrease in activation volume within the spinal cord was observed following nerve section with a correspondence between increasing injury. The results indicate that spinal cord fMRI provide important information concerning the functional effects of loss of sensory inputs to the spinal cord after peripheral nerve injury.

2127. Functional Imaging of Cat Spinal Cord by CBV-Weighted fMRI

Fuqiang Zhao[1], Changfeng Tai[1], Jicheng Wang[1], Ping Wang[1], James R. Roppolo[1], William C. de Groat[1], Seong-Gi Kim[1]

[1]University of Pittsburgh, Pittsburgh, Pennsylvania, USA

fMRI has been widely used to study brain functions. Although the volume of published literatures in brain functional MR imaging has grown dramatically over the past decade, the number of published studies of functional MR imaging of the spinal cord is limited, suggesting that significant technical challenges are associated with detecting the blood oxygenation level¨Cdependent (BOLD) effect in the spinal cord. In this study the spinal cord fMRI was performed in cat at 9.4T with the high sensitivity of CBV-weighted fMRI. Robust CBV responses within the gray matter of spinal cord were observed during the electrical stimulation of sciatic nerve. Spinal cord functional MR imaging is of great value in both basic research and clinical applications.

2128. Comparison of Neural Activity in the Rat Spinal Cord Using fMRI and Field Potentials During Noxious Electrical Stimulation of the Hind Paw

Jane Lawrence[1, 2], Phillip F. Gardiner[1], Kalan R. Gardiner[1], Patrick W. Stroman, [13], Kris L. Malisza, [12]

[1]University of Manitoba, Winnipeg, Manitoba, Canada; [2]National Research Council Institute for Biodiagnostics, Winnipeg, Manitoba, Canada; [3]Queens University, Kingston, Ontario, Canada

fMRI of the lumbar spinal cord was performed on nine halothane anesthetized rats during electrical stimulation of the hind paw. Electrophysiology was performed in the same animals to identify areas of neuronal activity. Local field potentials were measured extracellularly in the same region of the cord. Both techniques identified the greatest amount of activity around the T13 vertebra. Negative local field potentials were identified from 150 µm to a depth of 1350 µm from the dorsal surface. Comparison of the two techniques verifies that spinal fMRI detects areas of neural activity in the spinal cord.

2129. Neural Basis of Unconditional Fear: Perfusion and Functional Imaging in Aging Rat Bed Nucleus of the Stria Terminalis

Wei Chen[1], Young Kim[2], Karl F. Schmidt[1], Feng Luo[1], Mathew Brevard[1], Jean King[1]

[1]University of Massachusetts Medical School, Worcester,,Massachusetts, USA; [2]MGH/MIT/HMS, Charlestown, Massachusetts, USA

The novel perfusion and fMRI techniques were used to explore the neural basis of unconditional fear in aging rats. The study demonstrates Bed Nucleus of the Stria Terminalis (BNST) is highly involved in mediating behavioral responses to unconditioned stress. The differentia of CBF in aging individuals was observed to contribute to the difference of BOLD signal between the young and old ones in the BNST. This study is very useful for understanding the neuronal, emotional and cognitive components of fear which underlies anxiety disorders. Meanwhile, the study demonstrates that it is feasible to address neural basis of unconditional fear using perfusion and fMRI techniques. In addition aging effects on neurovascular coupling is also possible with these techniques.

2130. Imaging Fear Stress Responses in Monkeys

Josie A. Harder[1, 2], Timothy S. Garelick[1], Wei Chen[1], Jean A. King[1]

[1]UMass Medical School, Worcester, Massachusetts, USA; [2]University of Bradford, Bradford, UK

There are fundamental similarities in responses to threat across mammalian species. These fearful responses to unlearned stimuli (such as predator odor) are relevant to unlearned fear states in humans, including phobias and other psychiatric conditions. In humans, it is known that fearfulness increases with aging. Functional MRI of conscious marmoset monkeys reveals that the amygdala (associated with emotional states including fear) and frontal cortices (which modulate the amygdala) show significantly increased positive BOLD in response to predator scent exposure. Furthermore, we have shown that in aged marmosets this “fear” response is significantly greater than in adolescents.

2131. Functional (BOLD) MRI in Zebra Finch to Investigate the Capacity of Specific Brain Regions to Segregate Meaningful Auditory Signals from a Noisy Background

Tiny Boumans[1], Clémentine Vignal[2, 3], Alain Smolders[1], Marleen Verhoye[1], Johan Van Audekerke[1], Nicolas Mathevon[3], Annemie Van der Linden[1]

[1]University of Antwerp, Antwerp, Belgium; [2]Université Jean Monnet, Saint-Etienne, France; [3]Université Paris XI, Orsay & LBA, Université Jean Monnet, Saint-Etienne, France

Recently, functional BOLD MRI was introduced in a well-documented animal model for vocal learning, the songbird. The present study shows that fMRI can be used for neurocognitive research in songbirds by demonstrating auditory induced activation representing discriminatory properties of auditory regions of the telencephalon in zebra finch brain. The obtained fMRI results match with previously obtained IEG results of a study with the same experimental setup.

2132. Functional MRI of the Songbird Zebra Finch at 3 Tesla

Henning U. Voss[1], Kristen Maul[2], Douglas Ballon[1], Ofer T. Tchernichovski[2], Santosh A. Helekar[3]

[1]Cornell University, New York, New York, USA; [2]CUNY, New York, New York, USA; [3]University of Houston, Houston, Texas, USA

Birdsong in songbirds has emerged as a useful model of human speech in terms of its perception, acquisition and production. We studied the feasibility of functional BOLD MRI in the songbird zebra finch on a 3 Tesla whole body MRI scanner and found significant BOLD signal intensity changes for different kinds of stimuli across different brain regions. By quantifying the activation intensity, it was possible to discriminate between tutored song and other song stimulations. Our results provide insights into how to optimize fMRI in songbirds at 3T.

2133. Quantitative MRI of Cerebral Blood Flow in the Non-Human Primate

Paul A. Greenberg[1], *Joanna E. Perthen*[1], *Anna L. Quijada*[1], *David J. Dubowitz*[1]
[1]University of California San Diego, La Jolla, California, USA

Macaque monkeys are routinely used as a model for studying human neurophysiology. To use macaques to address neurovascular coupling, we need to define cerebral blood flow, blood volume and oxygen metabolism changes in the macaque brain following neuronal activation. In this study we optimized arterial spin labeling for macaque hemodynamics. We quantified resting CBF (44 ml/100mg/min) and CBF change to a CO2 stimulus (38%). We also optimized VASO to measure CBV changes (-2%). These data provide the first quantitative measures of CBF in macaques, and form a basis for further studies of the neurovasuclar relationship in primates.

2134. High Spatial Resolution fMRI Mapping of Digit Topography and the Funneling Illusion in SI Cortex of the Anesthetized Squirrel Monkey

Gregory Harrison Turner[1], *Li Min Chen*[1], *Robert M. Friedman*[1], *John C. Gore*[1], *Anna W. Roe*[1], *Malcolm J. Avison*[1]
[1]Vanderbilt University, Nashville, Tennessee, USA

Intrinsic optical imaging can be used to map cortical activations with high spatial and temporal resolution but is limited by the accessibility of the area of interest and the need for surgery to expose the cortex. With the static field strengths now available for fMRI in both animals and humans, the prospect of non-invasive functional imaging studies of cortical and subcortical areas with high spatial resolution is now at hand. To test the ability of high field fMRI to achieve high spatial resolution, we examined whether fMRI could map the neural correlates of the tactile funneling illusion in SI.

2135. Perfusion-Based fMRI in the Monkey Brain at 7T: Investigations of CASL Parameters

Anne Catherin Zappe[1], *Hellmut Merkle*[2], *Josef Pfeuffer*[1, 3], *Nikos k. Logothetis*[1]
[1]Max Planck Institute, Tuebingen, Germany; [2]NIH/NINDS, Bethesda, Maryland, USA; [3]Siemens Medical Solutions, Erlangen, Germany

Perfusion-based imaging in the monkey primary visual cortex was performed at 7T applying continuous arterial spin labeling (CASL). Increased perfusion sensitivity and SNR at high magnetic field (due to larger T1) was further optimized using a custom-made three-coil setup with a separate neck labeling coil. We investigated the labeling parameters to obtain relative functional cerebral blood flow (fCBF) changes in the anaesthetized monkey. We report excellent functional activation of striate cortex at high resolution of 0.75x0.9mm2 in-plane. Interestingly, the optimal parameter set for obtaining highest signal changes of regional CBF (rCBF) are different from the reported values for imaging gray matter CBF.

2136. Discordant Responses to Cocaine in CBF and CBV: Implications for PhMRI CMRO2 Assessment

Feng Luo[1], *Karl F. Schmidt*[1], *Craig F. Ferris*[1], *Timothy Q. Duong*[2]
[1]UMass, Worcester, Massachusetts, USA; [2]Emory University, Atalanta, Georgia, USA

Two potential confounding effects of extending fMRI CMRO2 calculation to pharmacological studies were investigated by simultaneous direct measurements of CBF and CBV in the same experimental animal. While CBF showed a monophasic increase after cocaine infusion, CBV demonstrated a biphasic response with an initial decrease in CBV followed by prolonged CBV increase. A clear CBF-CBV discordant response to cocaine administration was found during the initial period. CBF-CBV recoupled during the steady state, however, with a significant lower á value in cortical and subcortical regions. Those two effects confound phMRI CMRO2 method on evaluating cerebral oxygen metabolism following cocaine administration.

2137. Characterizing Alcohol-Induced Changes in Forebrain Activity in Awake Rats Using PhMRI and Assessing Brain Tissue Alcohol Pharmacokinetics Using Proton MR Spectroscopy

Feng Luo[1], *Zhixin Li*[1], *Steven Treistman*[1], *Craig F. Ferris*[1]
[1]University of Massachusetts, Worcester, Massachusetts, USA

This study aimed to identify alcohol related neurocircuitry in fully conscious rats using contrast enhanced fMRI-CBV method. In addition, brain tissue alcohol kinetics was monitored by proton MRS. Dopaminergic mesolimbic system activation was detected under alcohol challenge. A significant shorter CBV response was found following a single dose of alcohol administration, albeit sustained brain tissue alcohol concentration. Acute tolerance may play a role in this discrepancy finding. This study also illustrated the advantageous to combine phMRI and MRS techniques to provide compensatory information which is vital important for us to understand the complex neural adaptation processes following acute alcohol administration.

2138. A Multimodality Investigation of Cerebral Haemodynamics and Autoregulation in PhMRI

Alessandro Gozzi[1], *Laura Ceolin*[1], *Adam Schwarz*[1], *Torsten Reese*[1], *Simone Bertani*[1], *Angelo Bifone*[1]
[1]Centre of Excellence for Drug Discovery, Psychiatry, GlaxoSmithKline, Verona, Italy

Pharmacological MRI methods are used to assess central effects of acute drug challenge, but many psychoactive drugs also induce peripheral blood pressure (BP) changes, potentially introducing confounds. We examined BP along with cerebral blood volume (CBV), measured by MRI, and laser-Doppler flow (LDF) changes induced by norepinephrine, a non-brain penetrant vasopressor not expected to elicit changes in neuronal activity. Blood flow autoregulation was preserved over a wide BP range (80-140 mmHg); CBV changes were also non-significant within this range. Above the upper BP threshold, measurable changes in both CBV and LDF were observed, particularly localised in cortical structures.

2139. Mapping Neural Activities of Area Postrema and Nucleus Tractus Solitarius in Awake Rats Using Pharmacological MRI: Relevance as a Potential Biomarker for Detecting Drug-Induced Emesis

Chih-Liang Chin[1], Gerard B. Fox[1], Vincent P. Hradil[1], Mark A. Osinski[1], Steve P. McGaraughty[1], Pamela D. Skoubis[1], Bryan F. Cox[1], Yanping Luo[1]

[1]Abbott Laboratories, Abbott Park, Illinois, USA

Drug-induced emesis, a major concern in patient care and drug discovery, can be triggered by neural activation at brainstem regions, including area postrema (AP) and nucleus tractus solitarius (NTS). Using CBV-based phMRI in awake rats, we imaged neural activities in AP/NTS following the administration of known emetic agents (apomorphine and ABT-594) as a potential biomarker in a species that is routinely used for efficacy studies but does not show emesis. Observed dose-related activities in AP/NTS agree with behavioral measures obtained using a ferret model at relevant plasma levels, indicating phMRI in rats has potential as a biomarker for emesis liability.

2140. Application of Functional Magnetic Resonance Imaging to the Study of 5-HT2C Neurotransmission in Rat Brain

Jennifer Ann Stark[1], Karen E. Davies[1], Shane McKie[1], Steve R. Williams[1], Simon M. Luckman[1]

[1]University of Manchester, Manchester, UK

We are investigating animal fMRI as a tool in discovering new appetite pathways to help develop anti-obesity agents. Here we investigated whether high field fMRI could detect receptor modulation by specific serotonin (5-HT1B and 5-HT2C) receptor antagonists, after stimulation by the anorexigenic mixed 5-HT receptor agonist m-chlorophenylpiperazine (mCPP) in the rat. Animals received either vehicle or mCPP, and a pre-treatment of receptor antagonist or its vehicle. Data were analysed in SPM2 by 1-way ANOVA followed by F tests. The results showed distinct cancellation of mCPP-induced activity by the 2C receptor antagonist. However the 1B antagonist had little effect.

2141. L-Tetrahydropalmatine Induces a Negative BOLD Signal in the Nucleus Accumbens and Orbitofrontal Cortex in Heroin-Dependent Rats

Zheng Yang[1], Guofan Xu[2], Kathleen Q. Yin[2], Gaohong Wu[2], Shi-Jiang Li[2]

[1]Institute of Basic Medical Science, Beijing, People's Republic of China; [2]Medical College of Wisconsin, Milwaukee, Wisconsin, USA

The functional MRI method has demonstrated that cocaine-cue induced positive BOLD signal changes in regions of the anterior medial orbitofrontal cortex (OFC) and the subcollosal cortex correlated with craving ratings in human cocaine users. If this positive BOLD signal could serve as a biomarker for drug craving, a medication that can specifically induce a negative BOLD signal in these regions could have the potential to extinguish the drug craving. A present fMRI study demonstrated that a Chinese herb extract, L-Tetrahydropalmatine (L-THP), significantly induced a negative BOLD signal in these regions in heroin-dependent rats, suggesting that L-THP would have such a therapeutic potential for anticraving.

2142. An fMRI Study of Naturalistic Stimulation of the Rat's Whiskers

Ian Mark Devonshire[1], Paul G. Overton[1], John E. Mayhew[1], Nikos G. Papadakis[1]

[1]University of Sheffield, Sheffield, UK

An MRI-compatible paradigm for naturalistic stimulation of the rat's whiskers was developed using air-puffs. It was applied in a CBV (MION) fMRI study of the anaesthetised rat using an open access volume coil and multi-slice spin-echo EPI. Robust CBV responses were elicited in the cortex and brainstem. Activation in thalamic nuclei was observed inconsistently, due to their small spatial extent. As air-puff stimuli are known to better mimic sensory interactions that occur in behavioural conditions, they are well suited to investigations into the mechanisms of sensory transduction and response modulation. Consequently, fMRI techniques can now be applied to such investigations.

2143. Functional MRI of Hypothalamic Responses to Circulating Glucose and Fatty Acids

Jong-Hee Hwang[1], Tony K T Lam[1], Wei Sun[1], Tsukasa Nagaoka[1], Naoyuki Miyasaka[1], Kan Takahashi[1], Luciano Rossetti[1]

[1]Albert Einstein College of Medicine, Bronx, New York, USA

Hypothalamic sensing of circulating nutrients (e.g. glucose) has recently been implicated in regulation of glucose homeostasis. However, previous reports on hypothalamic activation induced by glucose intake have not addressed the relative contribution of hypothalamic glucose sensing and plasma insulin during hyperglycemia. The purpose of this fMRI study was to examine hypothalamic activation, isolated from changes in insulin levels, compared to the effect of fatty acids sensing, specifically by measuring R2* changes in rats. Glucose infusion resulted in localized R2* increase (T2* decrease) in the medial hypothalamic area. However, no significant localized activation was detected during systemic lipid infusion.

2144. The Role of Cortico-Cortical Connections in Intercortical Plasticity Following Peripheral Nerve Injury

Galit Pelled[1], Kai-Hsiang Chuang[1], Stephen Dodd[1], Alan P. Koretsky[1]
[1]National Institute of Health, Bethesda, Maryland, USA

Peripheral nerve injury has been demonstrated previously to cause remarkable brain organization in the somatosensory area in humans and animal models. The sciatic and saphanous nerve deafferentiation model was applied in rats, in order to investigate the contribution of the cortico-cortical connections to brain reorganization. Using fMRI, we observed that following the injury, the deprived somatosensory cortical region of the hindpaw representation was occupied by the ipsi-lateral, healthy, hindpaw. Furthermore, cortical lesioning of the healthy somatosensory area abolished the bilateral activation of the somatosensory cortex, suggesting, that the reorganization of the deprived cortical region was mediated through the inter-hemispheric connections.

2145. Mapping Neuropharmacological-Evoked BOLD Signals in Rat Brain Under Isoflurane Anesthesia: A Feasibility Study

Xiaodong Guo[1], Ping Wang[1], Mike Robbins[1], Jian-Ming Zhu[1]
[1]Wake Forest University School of Medicine, Winston-Salem, North Carolina, USA

á-chloralose has been used for anesthetic in most fMRI studies on rats, because it preserves neuronal-hemodynamic coupling and have the largest functional response comparing to other anesthetics. But the need of mechanical ventilation and difficulty to maintain animal in a stable physiological conditions over long duration when applying á-chloralose to rats make isoflurane an interesting substitute. Using multishot SE-EPI on isoflurane anesthetized rats, reliable amphetamine evoked BOLD contrast change was detected in rat brain.

Coronary MRA

Room 4E Wednesday 14:00 - 16:00

2146. Preliminary Study of Coronary MRA at 3T: Using 3D Gradient Echo Sequence in a Delayed Post-Contrast Phase

Wei Sun[1], Guang Cao[2], Yi He[3], Zhaoqi Zhang[3]
[1]GE Healthcare China, Beijing, People's Republic of China; [2]GE Healthcare China, Hong Kong, People's Republic of China; [3]Beijing Anzhen Hospital, Beijing, People's Republic of China

The performance of SSFP technique is unsatisfactory at 3T although it is widely used in coronary imaging at 1.5T. It has been reported that the T2 prepared gradient echo sequence at 3T can offer better coronary image quality with less artifacts whereas CNR is inferior than using SSFP. The aim of this study is to investigate the feasibility of using gradient echo sequence to imaging coronaries in a delayed post contrast phase at 3T and also to develop a more efficient target localization strategy. The preliminary experiment on 3 human subjects showed that the CNR can be doubled with the residue contrast after 18¡À3min delay after initial injection for the first pass perfusion.

2147. Coronary Blood Flow Measurement at 3.0T Using Navigator-Echo Gated Phase Velocity Mapping

Kevin R. Johnson[1], Puneet Sharma, John N. Oshinski[1]
[1]Georgia Tech/Emory University, Atlanta, Georgia, USA

Coronary artery blood flow measurements by phase-contrast MRI have been limited by heart motion and the minute size of the coronary arteries. In this study, a navigator-echo gated cine phase velocity mapping technique is described to obtain velocity and flow waveforms of the coronary arteries at 3T. Six right coronary arteries and six left anterior descending coronary arteries were studied with measurable cross-sections in 182/192 (94.8%) total phases.

2148. 3D Coronary Vessel Wall Imaging at 3 Tesla Using DIR with an Obliquely Oriented Re-Inversion Slab

Andrew Nicholas Priest[1], Paul Martin Bansmann[1], Alexander Stork[1], Michael G. Kaul[1], Gerhard Adam[1]
[1]University Hospital Hamburg-Eppendorf, Hamburg, Germany

Coronary vessel-wall imaging can be used to detect atherosclerosis and could thus have important clinical applications. To improve the SNR of this technique, we have implemented 3D coronary vessel-wall imaging at 3 Tesla. A particular problem of this method is that, for black-blood preparation, a 'local re-inversion' pulse must be used to avoid inflow of left ventricular blood, but at 3T the previously used cylindrical prepulse is less robust, and flip angle inhomogeneities reduce the effectiveness of re-inversion. We therefore use an obliquely oriented re-inversion slab, implemented using adiabatic pulses, and have demonstrated the feasibility of this method *in vivo*.

2149. Feasibility of 350 Micron Resolution Coronary MR Angiography at 3T

Ahmed M. Gharib[1], Daniel A. Herzka[2], Vincent B. Ho[3], Robert G. Weiss[4], Roderic Pettigrew[1], Matthias Stuber[4]
[1]NIH, Bethesda, Maryland, USA; [2]Clinical Sites Research Program, Bethesda, Maryland, USA; [3]Uniformed Services University of the Health Sciences, Bethesda, Maryland, USA; [4]Johns Hopkins University, Baltimore, Maryland, USA

Coronary magnetic resonance angiography (MRA) is emerging as a valuable non invasive tool for the evaluation of coronary artery disease (CAD). However, to achieve maximum accuracy in detection of CAD, contemporary MRI methods may benefit from a higher spatial resolution to approach that of the current gold standard x-ray coronary angiography (0.15mm). To date the commonly used in-plane spatial resolution at 1.5T and using gradient echo sequences is ~0.7×1×3mm^3. This study demonstrates the feasibility of acquiring coronary MRA with a voxel size of 0.34×0.35×1.5mm^3 on a commercial 3T scanner.

2150. Automated Identification of Minimal Myocardial Motion for Improved Image Quality in Coronary MRA at 3T

Ali Oguz Ustun[1], Robert George Weiss[1], Milind Desai[2], Matthias Stuber[1]
[1]Johns Hopkins University, Baltimore, Maryland, USA; [2]Cleveland Clinic Heart Center, Cleveland, Ohio, USA

FREEZE, an automated software tool for the identification of the period of minimal myocardial motion is developed and tested. Quantitative analysis demonstrated that vessel length, vessel sharpness, SNR and CNR were significantly improved (all $P<0.05$) when imaging was performed at the software prescribed trigger delay. Consistent with these objective findings, image quality by consensus reading also improved significantly when using the automated prescription of the period of minimal myocardial motion. FREEZE not only improves image quality in coronary MRA but also minimizes operator dependence while 'ease-of-use' is improved.

2151. Development and Evaluation of 3T Whole-Heart Coronary MR Angiography Technique

Ahmed M. Gharib[1], Vincent B. Ho[2], Daniel A. Herzka[3], Julia Locklin[1], Matthias Stuber[4], Roderic Pettigrew[1]
[1]NIH, Bethesda, Maryland, USA; [2]Uniformed Services University of the Health Sciences, Bethesda, Maryland, USA; [3]Clinical Sites Research Program, Bethesda, Maryland, USA; [4]Johns Hopkins University, Baltimore, Maryland, USA

Free-breathing, whole-heart 3-dimension (3D) coronary MR angiogram (CMRA) utilizing Navigator gating at 1.5T has been shown to be a valuable technique for coronary evaluation. Improvements in signal by imaging at 3T field strength provide opportunities for further CMRA optimization. With the further implementation of parallel imaging at 3T, scan times can be shortened or higher spatial resolution may be achieved without perceivable deterioration of image quality. This study: 1. demonstrates the feasibly of performing whole heart, free breath, 3D FFE acquisitions at 3T; and 2. evaluates four different acquisition schemes for optimal coronary artery illustration

2152. High-Resolution Coronary Artery MRA at 3 Tesla with Slow Infusion of an Extravascular High Relaxivity Contrast Agent MultiHance

Xiaoming Bi[1], James Carr[1], Debiao Li[1]
[1]Northwestern University, Chicago, Illinois, USA

Conventional Gadolinium based extracellular contrast agents have been extensively used in coronary MRA. The spatial resolution is limited by confining data acquisition within the first-pass of contrast agent. In this study, we investigated the feasibility of acquiring high-resolution coronary artery images at 3 Tesla with slow infusion of an extravascular, high relaxivity agent MultiHance. The signal enhancing characteristics were also compared to that of a conventional agent. With an average imaging time of 5.46 „b 0.66 minutes, the CNR is improved by 65.6% with infusion of MultiHance. High resolution coronary MRA with slow infusion of MultiHance is feasible at 3T.

2153. Flow-Related Problems in Whole Heart Cine Coronary MR Angiography

Kay Nehrke[1], Peter Börnert[1], Christian Stehning[1]
[1]Philips Research Laboratories, Hamburg, Germany

It was the aim of the present study to investigate the performance of a standard high-resolution b-SSFP sequence in whole heart cine CMRA. For this purpose 3D cardiac cine imaging was performed on healthy adults using a 1.5T whole body scanner. SNR and contrast were quantitatively compared for full and partial spatial coverage of the heart. In all volunteers a considerable decrease of the relative blood signal from the intraventricular cavity was found with increasing spatial coverage of the heart. This effect may be associated with increased "in-plane" flow due to the prolonged transit time of the spins.

2154. Respiratory Self-Gated 4D Coronary MRA with UNFOLD

Lan Ge[1], Peng Lai[1], Andrew Larson[1], Jaeseok Park[1], Xiaoming Bi[1], Debiao Li[1]
[1]Northwestern University, Chicago, Illinois, USA

Because of the need for high temporal and spatial resolution, the major challenge for 4D coronary MRA is to increase imaging speed. Temporal filtering of modulated undersampling artifacts may permit additional complimentary acceleration possibilities for 4D coronary MRA. In this work, we investigated the feasibility of using temporal filtering (UNFOLD) to permit accelerated undersampled data acquisition for 4D coronary MRA. Full k-space datasets of six healthy volunteers were obtained and then undersampled in the phase-encoding direction (factor of 2) to simulate a shorter scan time. The acquisition time was reduced by half while maintaining the image quality. The UNFOLD temporal filtering strategy is feasible to increase data acquisition speed during free-breathing 4D coronary MRA.

2155. Comparison of Inversion Recovery Steady-State Free Precession and Fast Low Angle Shot Sequences for 3D Magnetic Resonance Coronary Angiography

Kai-Uwe Waltering[1], Holger Eggebrecht[1], Kai Nassenstein[1], Thomas Schlosser[1], Peter Hunold[1], Joerg Barkhausen[1]
[1]University Hospital, Essen, NRW, Germany

For the diagnosis of coronary artery disease, invasive coronary artery angiography must still be considered the standard of reference. But recently, breath-hold MR coronary angiography (MRCA) has become feasible using different sequences which have not been compared so far. Following injection of extracellular contrast-agents, signal-to-noise- and contrast-to-noise-ratios rapidly decrease due to the short plasma-half-life-time. Therefore, intravascular compounds with constant blood and myocardial T1-times over several minutes are preferable for the comparison of different breath-hold sequences for MRCA. Our results show an overall improved image quality for IR-SSFP compared to FLASH sequences. Therefore, we recommend SSFP techniques for contrast-enhanced MRCA.

2156. Three-Dimensional Time-Resolved Whole-Heart Coronary Angiography Using a 3D Cones Trajectory

Paul T. Gurney[1], Brian A. Hargreaves[1], Dwight G. Nishimura[1]
[1]Stanford University, Stanford, California, USA

Whole heart, time resolved 3D imaging for coronary angiography is performed using a robust 3D Cones SSFP sequence with excellent spatial (1.1 mm isotropic) and temporal (60 ms) resolution acquired in reasonable scan times.

2157. Adapting Trigger Delays to Heart Rate for Coronary MR Angiography

Garry Liu[1], Graham Arnold Wright[1]
[1]University of Toronto, Toronto, Ontario, Canada

Heart rate variations can reduce both the effectiveness and efficiency of cardiac gating for coronary angiography. Our work explores how heart rate variations can affect cardiac imaging windows and justifies the use of heart rate adaptive trigger delays in a correction scheme. Specifically, the ideal trigger delay is nonlinearly related to the preceding pacing cycle length (RR interval on the ECG) and can be charactized per individual during a prescan exam. With this approach, we anticipate that imaging windows can be extended by approximately 10-20% for a 20bpm increase in heart rate depending on the region of interest.

2158. Motion Measurement Using Echoes During SSFP Dummy Cycles for Whole-Heart MR Coronary Artery

Masao Yui[1], Yoshimori Kassai[1], Shigehide Kuhara[1]
[1]Toshiba Medical Systems Corporation, Otawara, Tochigi, Japan

A new 2D navigator projection method is proposed using echoes data from the dummy cycles of balanced SSFP to estimate cardiac motion for whole heart MR coronary angiography. The echo data are reconstructed, and then a 2D projection of the imaging slab is obtained from every cardiac cycle until all of actual imaging data is acquired. Translation in the SI and AP directions can be estimated around several regions of the heart from the 2D projection images. The translation was compared with the SI translation of the diaphragm position using conventional 1D navigator.

2159. Compensating for Beat-To-Beat Variation in Coronary Motion Improves Image Quality in Coronary MR

Maneesh Dewan[1], Gregory D. Hager[1], Steven M. Shea[2], Christine H. Lorenz[3]
[1]Johns Hopkins University, Baltimore, Maryland, USA; [2]Siemens Medical Solutions, Baltimore, Maryland, USA; [3]Siemens Corporate Research, Baltimore, Maryland, USA

The purpose of this work was to investigate effect of compensating for variations in coronary motion on a beat to beat basis as opposed to assuming respiratory-coronary motion correspondence or acquiring patient specific motion prescans. Initial results demonstrate that direct tracking of coronary motion is feasible, and future work will include integrating the method for online tracking and prediction.

2160. An Automatic Off-Resonance Correction Method for Multi-Slice Imaging

Weitian Chen[1], Craig H. Meyer[1]
[1]University of Virginia, Charlottesville, Virginia, USA

Spiral off-resonance correction using field maps prolongs the scan time and can be unreliable when the maps themselves are corrupted by strong field inhomogeneity. Automatic off-resonance correction methods do not have these problems. However, automatic methods are prone to estimation error, especially at structure interfaces or regions with low signal. When applying automatic methods to multi-slice imaging, the field map can have large discontinuities in the slice direction due to estimation error. Using the continuity of the underlying field, we developed an automatic off-resonance correction method for multi-slice imaging with improved robustness compared to existing automatic methods.

2161. Magnetic Resonance Coronary Angiography Using an Intravascular Contrast Agent: T1 Time Course of Normal Myocardium and Blood

Kai-Uwe Waltering[1], Holger Eggebrecht[1], Kai Nassenstein[1], Thomas Schlosser[1], Peter Hunold[1], Joerg Barkhausen[1]
[1]University Hospital, Essen, NRW, Germany

Recently, breath-hold MR coronary angiography (MRCA) has become feasible, and blood-pool MR contrast-agents (i.e. Gadomer) have been introduced to improve image quality and diagnostic accuracy. The correct setting of the inversion-time TI is a prerequisite for diagnostic image quality in 3D-inversion-recovery-gradient-echo-MRCA. Our data show that a single-injection of Gadomer results in short T1 times of blood and within 15min after injection, whereas myocardial T1-times changes significantly. Therefore TI has to be individually adjusted to optimize the image quality. We conclude that high quality MRCA can be acquired within the first 15min after injection of a single dose of Gadomer.

2162. Breath Hold Magnetic Resonance Coronary Angiography with MS 325: Initial Experiences

Kai Nassenstein[1], Kai Uwe Waltering[1], Frank Breuckmann[1], Thomas Schlosser[1], Peter Hunold[1], Joerg Barkhausen[1]
[1]University Hospital Essen, Essen, Germany, Germany

Our study aimed to evaluate the intravascular contrast agent Gadofosveset (MS-325) for breath hold magnetic resonance coronary artery imaging. T1-values of the myocardium and the ventricular cavity (LVC) were measured at different time points after injection and repetitive 3D IR-FLASH sans covering the mayor coronary were performed. The T1 time of the LVC remained unchanged, whereas the T1 time of the myocardium slightly increased within the first 30 minutes after injection. Although, the contrast to noise ratio of the coronaries and the myocardium slightly decreased, MRCA showed good image quality within 30 minutes after injection.

2163. Optimal Selection of the Subject-Specific Data Acquisition Window for Coronary MRA

Xiaoming Bi[1], Yiu-cho Chung[2], Sven Zuehlsdorff[2], Debiao Li[1]
[1]Northwestern University, Chicago, Illinois, USA; [2]Siemens Medical Solutions, Chicago, Illinois, USA

The selection of trigger delay time (TD) for coronary MRA requires substantial user interactions and experience. We propose to use a motion curve calculated from biplane cine scans to identify the subject-specific time window. The method provides an objective way to identify the TD with minimal user dependency. The results from healthy volunteers showed that the optimal timing for coronary MRA could be predicted by the motion curve. The need for visual assessment of images is eliminated. Implementation of online processing software for the cines will allow automatic generation of the motion curve and determination of optimal TD.

2164. Coronary MR Angiography at 3T During Diastole and Systole

Ahmed M. Gharib[1], Daniel A. Herzka[2], Ali Ustun[3], Milind Desai[4], Julia Locklin[1], Roderic Pettigrew[1], Matthias Stuber[3]
[1]NIH, Bethesda, Maryland, USA; [2]Clinical Sites Research Program, Bethesda, Maryland, USA; [3]Johns Hopkins University, Baltimore, Maryland, USA; [4]Cleveland Clinic Foundation, Cleveland, Ohio, USA

Traditional coronary magnetic resonance angiography (MRA) is performed during the quiescent mid-diastolic period of the cardiac cycle. There is another quiescent period at end systole that has been not exploited for coronary MRA imaging. This study demonstrates the feasibility of imaging during this systolic period without a detrimental effect on image quality. This is made possible by using parallel imaging in the form of sensitivity encoding (SENSE) at 3T to abbreviate the systolic image data acquisition window.

Vessel Wall Imaging

Room 4E Wednesday 14:00 - 16:00

2165. Delayed Enhancement MR Coronary Vessel Wall Imaging in Patients with Suspected Coronary Artery Disease

Tareq Ibrahim[1], David Maintz[2], Josef Dirschinger[1], Silvia Schachoff[1], Albert Schomig, [13], Warren J. Manning[4], Markus Schwaiger[1], René Michael Botnar[1]
[1]Technical University Munich, Munich, Germany; [2]University Münster, Münster, Germany; [3]German Heart Center, Munich, Germany; [4]Beth Israel Deaconess Medical Center, Boston, Massachusetts, USA

Atherosclerosis is a systemic inflammatory disease that affects large and medium sized vessels including the coronary arteries. plaque itself. Native MR coronary vessel wall imaging has been show to allow assessment of coronary wall thickness but requires high spatial resolution and accurate motion correction. Contrast enhanced MRI may be an alternative as the imaging task is reduced to the detection of the presence or absence of contrast uptake. Thus, delayed enhancement coronary vessel wall imaging has been investigated in patients with suspected CAD and correlated with x-ray angiography.

2166. T2 and ADC Values of Coronary Atherosclerotic Plaques Under Fresh and Preserved Conditions

Binjian Sun[1], Don P. Giddens[1], Robert Long Jr.[2], Robert Taylor[2], Diana Weiss[2], Giji Joseph[2], David Vega[2], John N. Oshinski[1]

[1]Georgia Institute of Technology, Atlanta, Georgia, USA; [2]Emory University, Atlanta, Georgia, USA

Quantitative T2 and ADC values are valuable in characterizing atherosclerotic plaque components and in optimizing pulse sequences of multi-contrast MRI. In the present study, we evaluated the T2 and ADC values in typical coronary artery plaque constituents both before and after formalin preservation. The MR scans were conducted on freshly-excised coronary arteries under simulated *in vivo* conditions by using a custom designed tissue culture chamber. Preserved scans were conducted on the same vessels after preserving them in formalin. T2 and ADC distributions of each plaque constituents were measured using the pixels that corresponding to the specific tissue type based on histological sections. The measured T2 values for all plaque constituents showed significant changes between fresh and preserved vessels.

2167. Characterization of Coronary Atherosclerotic Plaque Using Multi-Contrast MRI Acquired Under Simulated In-Vivo Conditions

Binjian Sun[1, 2], Don P. Giddens[1], Robert Long Jr.[2], Robert Taylor[2, 3], Diana Weiss[2], Giji Joseph[2], David Vega[2], John N. Oshinski[1, 2]

[1]Georgia Institute of Technology, Atlanta, Georgia, USA; [2]Emory University, Atlanta, Georgia, USA; [3]Atlanta VA Medical Center, Atlanta, Georgia, USA

Purpose:To compare coronary atherosclerotic plaque characterization using multi-contrast MRI on 1) freshly-excised vessels under simulated *in vivo* conditions, and 2) preserved vessels.Materials and Methods: T1, T2, proton density and diffusion-weighted MR images were acquired on thirteen freshly-excised human coronary arteries from explanted hearts. Vessels were imaged in an MR-compatible tissue culture chamber using a 4.7 Tesla small bore MR scanner. Eight vessels were then preserved in buffered formalin and rescanned following the same imaging protocol. A three-dimensional spatially penalized fuzzy c-means (3D-SPFCM) technique was applied to classify different plaque constituents. The classification results from vessels under ¡ fresh¡± and ¡ preserved¡± conditions were compared with corresponding histological sections.Results: For most plaque constituents, the plaque characterization results show no significant difference between fresh and preserved scans, and little difference between scans and the histological reference standard. In the case of thrombus, apparent signal changes were identified between fresh and preserved images. Overall, MR scans conducted under preserved conditions provided 1.8%-17.5% greater SNR than those conducted under fresh stage.Conclusion: Preservation of coronary vessels did not significantly change the results of plaque constituent characterization using multi-contrast MRI. MR scan techniques and classification methods developed on *ex vivo* coronary specimens can be applied to *in vivo* imaging.

2168. Time Efficient Carotid Artery Imaging Using TSE with Reduced Field of View and Interleaved Double Inversion at 3 Tesla

Seong-Eun Kim[1], Eun-Kee Jeong[1], Eugene G. Kholmovski[1], Dennis L. Parker[1]

[1]University of Utah, Salt Lake City, Utah, USA

Black blood imaging on a 3 Tesla system may provide improved information for evaluation of size and morphology of carotid artery plaque. In comparison with conventional DIR imaging techniques, our interleaved DIR rFOV-TSE technique can improve acquisition efficiency and reduce the total time required for imaging the carotid artery by a factor of 6. These techniques are important at 3T where the high SNR is sufficient to allow implementation of such time reduction techniques.

2169. Multi-Contrast Black-Blood MRI of Carotid Arteries: Comparison Between 1.5 and 3 Tesla Magnetic Field Strengths

Vasily L. Yarnykh[1], Masahiro Terashima[2], Cecil E. Hayes[1], Ann Shimakawa[3], Norihide Takaya[1], Patricia K. Nguyen[2], Jean H. Brittain[3], Michael V. McConnell[2], Chun Yuan[1]

[1]University of Washington, Seattle, Washington, USA; [2]Stanford University, Stanford, California, USA; [3]GE Healthcare, Menlo Park, California, USA

Black-blood imaging of carotid arteries with three contrast weightings (T1, T2, and proton density) has been compared between 1.5 and 3 Tesla magnetic fields. MRI at 3 T significantly improves signal-to-noise ratio and black-blood contrast in high-resolution imaging of the carotid artery wall and atherosclerotic plaque. Advantages of 3 T scanners can be used for an up to two-fold reduction of scan time or a 1.5-fold increase of spatial resolution without scan time and SNR penalties. Quantitative morphological measurements are compatible between 1.5 T and 3 T scanners suggesting that both field strengths can be interchangeably used in progression and treatment studies.

2170. *In Vivo* Automated Quantification of Fibrous Tissue Content in Atherosclerosis Plaque MRI with T2-Mapping and Contrast Enhanced (TMCE) Technique

Jinnan Wang[1], Vasily Yarnykh[1], Chun Yuan[1], Tobias Saam[1], Thomas Hatsukami[2], Marina Ferguson[1], Tong Zhu[1]

[1]University of Washington, Seattle, Washington, USA; [2]VA Puget Sound Health Care System, Seattle, Washington, USA;

In vivo identification and quantification of fibrous tissue content in atherosclerosis plaque has always been envisaged as either controversial or complicate. In this study, an automatic technique based on T2 Mapping and Contrast Enhanced (TMCE) MRI is developed. Results show that this technique is highly sensitive and reliable, which will greatly expedite the computer-assisted analysis in plaque MRI.

2171. Reproducibility and SNR Optimization of Quantitative T2 Atherosclerotic Plaque Imaging with a Dual-Echo Technique

Jinnan Wang[1], Vasily Yarnykh[1], Thomas Hatsukami[2], Chun Yuan[1]
[1]University of Washington, Seattle, Washington, USA; [2]VA Puget Sound Health Care System, Seattle, Washington, USA

T2 mapping of atherosclerosis plaque allows accurate tissue component characterization. In this study, dual-echo fast spin echo sequence is optimized for the purpose of highly reproducible T2-mapping. Both phantom and *in vivo* study show that this optimization approach will greatly promote the reproducibility of T2 mapping technique and the tissue characterization reliability of MRI.

2172. The Forgotten Side: *In–Vivo* Assessment of Inflammatory Atheroma Burden on the Contralateral Side to Symptomatic Carotid Stenosis Using High Resolution USPIO-Enhanced MR Imaging

Tjun Tang[1, 2], Simon Peter Satterly Howarth[1, 2], Ilse Joubert[1], Andrew P. Brown[3], Martin John Graves[1], Peter J. Kirkpatrick[2], Michael E. Gaunt[2], Jonathan H. Gillard[1]
[1]University of Cambridge, Cambridge, Cambridgeshire, UK; [2]Addenbrooke's NHS Trust, Cambridge, Cambridgeshire, UK; [3]Glaxosmithkline, Greenford, Surrey, UK

It is well known that vulnerable atheromatous plaque has a thin, fibrous cap and large lipid core with associated inflammation which can be detected on USPIO-enhanced MR imaging. Studies using USPIO to assess macrophage burden in symptomatic carotid disease have not yet analyzed the contralateral asymptomatic side.20 symptomatic patients underwent multi-sequence imaging at 1.5 Tesla pre and 36 hours post USPIO infusion. Images were manually segmented into quadrants and signal change in each quadrant was calculated following USPIO. Contra-laterally there were 153 quadrants (54%) with a signal drop post USPIO when compared with 201 quadrants (73%) on the symptomatic side. This suggests that investigation of the contralateral side in patients with symptomatic carotid stenosis can demonstrate inflammation in over 50% of plaques, despite a mean stenosis of only 46%. Patients with symptomatic carotid disease having had an endarterectomy should have their contralateral carotid artery followed up.

2173. High-Resolution Carotid MRA and Plaque MRI at 3T: Initial Clinical Experience and Validation of Semi-Automated Plaque Characterization

Kevin DeMarco[1], David Zhu[1], Collen Hammond[1], Grant Henderson[1], William Kerwin[2], William Ross[3], Vasily Yarnykh[2], Chun Yuan[2]
[1]Michigan State University, East Lansing, Michigan, USA; [2]University of Washington, Seattle, Washington, USA; [3]Pathway MRI, Inc, Seattle, Washington, USA

High resolution carotid contrast-enhanced MRA and *in vivo* carotid plaque MRI at 3T has been performed in 24 patients to date. Multi-contrast carotid plaque images could be interpreted in vast majority of patients making it reasonable for clinical use. Plaque characterization at 3T by semi-automated program (Pathway MRI, Inc) has been compared with manual segmentation and validation by comparison with histological evaluation of endarterectomy specimens is on-going. High resolution MRA/MRI helped confirm the degree of stenosis and demonstrated a remarkable amount of complex plaque morphology that was not expected on duplex ultrasound. This has changed patient management in some cases.

2174. An MRI Technique for the Study of the Prevalence of Atherosclerosis

Hunter Reeve Underhill[1], John Robin Crouse[2], Vasily Yarnykh[1], Robert Kraft[2], Tobias Saam[1], Norihide Takaya[1], Baocheng Chu[1], Clement Yang[1], James Greg Terry[2], Chun Yuan[1]
[1]University of Washington, Seattle, Washington, USA; [2]Wake Forest University School of Medicine, Winston-Salem, North Carolina, USA

We present an MRI technique that provides sufficient coverage of both carotid arteries to enable the study of bilateral plaque burden. We applied this technique to a population of patients without a previous history of carotid disease. The additional coverage afforded by this technique enabled us to find a strong correlation between the presence of atherosclerotic changes in one artery and increased wall thickness in the contralateral artery.

2175. MRI Can Detect Intraplaque Hemorrhage in Ex-Vivo Coronary Arteries

General Leung[1], Nigel Munce[1], Richard Bitar[1], Jagdish Butany[2], Graham A. Wright[1], Alan R. Moody[1]
[1]Sunnybrook and Women's College Health Sciences Centre, Toronto, Ontario, Canada; [2]Toronto General Hospital, Toronto, Ontario

Intraplaque hemorrhage (IPH) has been seen as a critical factor in the destabilization and rupture of a vulnerable arterial plaque. 4 coronary arteries and 2 vein grafts were obtained from patients who died of acute myocardial infarction. MR imaging of these *ex vivo* specimens revealed two foci of IPH which were detected with histopathology. Initial results suggest that MRI can be used to aid in post mortem identification of culprit atherosclerotic lesions.

2176. Carotid Atherosclerotic Score--A New Method to Identify High Risk Carotid Plaques Based on Multi-Contrast MRI: Validation and Preliminary Results from Patients

Jianming Cai[1], Tobias Saam[2], Marina S. Ferguson[2], Chun Yuan[2]
[1]Chinese PLA General Hospital, Beijing, People's Republic of China; [2]University of Washington, Seattle, Washington, USA

Pathologically, the risk of atherosclerotic plaque is related to plaque components, especially the status of the fibrous cap which separates vessel lumen from plaque bulk. Our goals are 1) to design a MRI-based Carotid Atherosclerosis Scoring (CAS) system to assign scores based on the topography of plaque components and the status of the fibrous cap, 2) to validate these scores by comparing MRI to histology, and 3) to summarize these quantitative entries into a risk score that can be used clinically for risk assessment. This new CAS system is highly correlated to histologic findings. Higher scores were significantly associated with the presence of recent ipsilateral TIA, stroke or amaurosis fugax.

2177. Distribution of Intraplaque Hemorrhage in Carotid Complicated Plaques Defined by High-Resolution Magnetic Resonance Direct Thrombus Imaging (HiresMRDTI)

Richard Bitar[1], Alan R. Moody[2], Sean Symons[1], General Leung[2], Jagdish Butany[1], Susan Crisp[2], Alexander Kiss[3], D James Sahlas[2], David Gladstone[2], Robert Maggisano[2]
[1]University of Toronto, Toronto, Ontario, Canada; [2]Sunnybrook and Women's College HSC, Toronto, Ontario, Canada; [3]Institutes for Clinical Evaluative Sciences, Toronto, Ontario, Canada

hiresMRDTI detects both deep and superficial intraplaque hemorrhage (IPH). The predilection of IPH for the deeper segments suggests that the majority of IPH in complicated carotid plaques does not arise from the luminal surface and is likely due to adventitial vasa vasorum rupture/leakage.

2178. High Resolution Diffusion Weighted Imaging of Human Carotid Artery Using 2D Ss-RFOV-DWEPI at 3 Tesla

Seong-Eun Kim[1], Eun-Kee Jeong[1], Eugene G. Kholmovski[1], Dennis L. Parker[1]
[1]University of Utah, Salt Lake City, Utah, USA

It has been reported that DWI of excised human specimens can enhance the contrast between thrombus and vessel wall. To attain high resolution DWI of the human carotid, we have developed a 2D single shot reduced FOV preparation in conjunction with an abbreviated EPI readout using a pair of slice selective refocusing RF pulses with the selection gradient in the phase-encoding direction. Because of the single shot acquisition, each image is free from phase errors caused by the diffusion gradients. The results obtained indicate that DWI may be of substantial value as a new contrast for carotid plaque imaging.

2179. Time-Efficient Multislice Black-Blood Imaging with Reduced Field-Of-View Using Quadruple Inversion-Recovery Sequence

Vasily L. Yarnykh[1], Chun Yuan[1]
[1]University of Washington, Seattle, Washington, USA

A new method has been developed for time-efficient black-blood imaging. The method combines two strategies for a reduction of scan time: multislice acquisition and outer volume suppression to reduce the number of phase encodings. These goals are achieved by using a new MSFQIR (multislice Small-FOV Quadruple Inversion-Recovery) black-blood preparative sequence, which consists of two double-inversion pulse pairs applied in orthogonal planes with appropriate combination of inversion delays. The MSFQIR method demonstrated an improvement in time efficiency and a reduction of motion and flow artifacts in black-blood imaging of the aorta.

2180. Non Invasive MRI Vessel Wall Evaluation in Asymtomatic Patients: Comparison of Three MRI Based Parameters in Aorta and Common Carotid Arteries

Karen B. Weinshelbaum[1], Venkatesh Mani[1], Hiroaki Taniguchi[1], Silvia H. Aguiar[1], John E. Postley[2], Robert J. van der Geest[3], Ellen Bondar[1], Daniel D. Samber[1], J H. Reiber[3], Zahi A. Fayad[1]
[1]Mount Sinai School of Medicine, New York, New York, USA; [2]Columbia University, New York, New York, USA; [3]Leiden University Medical Center, Leiden, Netherlands

Different quantitative parameters have been used for non-invasive MRI evaluation of arterial vessel walls to monitor sub-clinical disease, but their reliability in large analyses has yet to be determined. In this study, we compare variation in measurement of three parameters in a large data set. Three parameters, average wall area, average wall thickness and average ratio of wall area/ total vessel area, atherosclerotic disease index (ADI) were calculated. Analysis showed that the ADI had the lowest coefficient of variation in the data for both aorta and carotid arteries. ADI can be used as a reliable parameter for evaluating vessel walls.

2181. Evaluation of Thrombus Organization as a New Parameter for Follow-Up After Endovascular Abdominal Aortic Aneurysm Repair

S. A. Cornelissen[1], M. J. Van der Laan[2], K. L. Vincken[1], C. J. Bakker[1], H. J. Verhagen[1], W. P. Mali[1], F. L. Moll[1], L. W. Bartels[1]

[1]University Medical Center, Utrecht, Netherlands; [2]Hilversum General Hospital, Hilversum, Netherlands

We developed a method to evaluate thrombus organization as a new parameter in the follow-up of patients afterendovascular repair of abdominal aortic aneurysms. Intra-aneurysmal voxels were classified into three categories by using multispectral MRI-data.. In half of the patients a substantial amount of intra-aneurysmal voxels were hyperintense on the T2w-images. We expect that the size and time course of these hyperintensities provide a new parameter in the follow-up of these patients, using the presented methods we were able to reproducibly measure these volumes.

2182. Vessel Wall Imaging in Peripheral Vascular Disease

Timothy J. Carroll[1], [2], Dongxiang Xu[3], Nondas Leoloudas[2], Jin Tan[2], James Carr[2], Debiao Li[2], John Koktzglou[2], Chun Yuan[3], Mary McDermott[2]

[1]Biomedical Engineering, Chicago, Illinois, USA; [2]Northwestern University, Chicago, Illinois, USA; [3]University of Washington, Seattle, Washington, USA

We have performed vessel wall imaging in a series of patients with known vascular disease. Our analysis has shown that plaque burden measured with MRI correlates with other clinical indicators of the severity of vascular disease.

2183. Rapid and Reproducible Measurement of Atherosclerotic Plaque Volume in Peripheral Arterial Disease by MRI

David C. Isbell[1], Craig H. Meyer[1], Walter J. Rogers[1], Frederick H. Epstein[1], Joseph M. DiMaria[1], Nancy L. Harthun[1], Hongkun Wang[1], Christopher M. Kramer[1]

[1]University of Virginia Health System, Charlottesville, Virginia, USA

A high resolution, noninvasive approach to quantifying atherosclerotic plaque in the periphery could have significant clinical and research utility. Fourteen patients with peripheral arterial disease were studied in a 1.5T scanner. Atherosclerotic plaque volume was measured and interobserver, intraobserver, and test-retest variability determined. Sixteen peripheral vessels were studied with total image acquisition time of 12.8 minutes per vessel. Mean volume was 6.76 ± 3.36cm3. For intra-observer R=0.997; inter-observer R = 0.993; test-retest reproducibility R= 0.996. Thus, high resolution measurement of plaque volume in the superficial femoral artery in peripheral arterial disease is feasible, rapid, and reproducible.

2184. Black-Blood Imaging Using a Spin-Echo Spiral Sequence with Flow-Spoiling Gradients

Wen-Tung Wang[1], Peng Hu[1], Craig H. Meyer[1]

[1]University of Virginia, Charlottesville, Virginia, USA

In this work, we investigated the feasibility of black-blood imaging of peripheral arteries using a spin-echo spiral sequence with flow-spoiling gradients. Instead of the upstream spin inversion or saturation, the black blood is caused by the dephasing effect from the moments of the flow-spoiling gradients in the imaging region. The results show that black-blood imaging of peripheral arteries using a spin-echo spiral sequence with flow-spoiling gradients is feasible. Using gradients with a large first moment dephase the flow signal at the cost of a longer echo time.

2185. Multislice Spiral Superficial Femoral Artery Wall Imaging

Christopher Thomas Sica[1], Chris M. Kramer[1], Craig H. Meyer[1]

[1]University of Virginia, Charlottesville, Virginia, USA

A multislice dark blood vessel wall imaging sequence with spiral readouts was developed. Adouble inversion block was used to null the blood signal, with either one or five 3 mm thickslices acquired per DIR block. The SNR and flow suppression were good at a resolution of 0.39 mm, The efficiency of spirals allow for more slices to be nulled following a giveninversion block, and the short TE leads to a high signal from the vessel wall.

2186. The Effect of Slice Thickness on Assessment of Atherosclerosis Geometry Measures

Ruta Gelombickaite[1], Rem van Tyen[2], Gregory Wong[1], Joseph Rapp[1], David Saloner, [12]

[1]VA Medical Center, San Francisco, California, USA; [2]University of California San Francisco, San Francisco, California, USA

This study was performed to assess the impact of reduced resolution, such as is attainable in clinically-relevant studies, on the assessment of plaque geometry. Measurements of plaque volume were made with standard *in vivo* imaging method on six excised carotid endarterectomy specimens. This was compared with measurements made using ultra-high resolution imaging. Measurement of plaque volume and maximal wall area made with 2mm thick slices was found to be in good agreement with that made with the 0.2mm slices. This indicates that studies with 2mm thick slices are sufficient for monitoring changes in plaque bulk over time.

2187. Diffusion Based Model of Contrast Agent Kinetics for Dynamic Contrast-Enhanced MRI

William Sean Kerwin[1], Vasily Yarnykh[1], Chun Yuan[1]
[1]University of Washington, Seattle, Washington, USA

A novel mechanism of contrast agent kinetics in dynamic contrast-enhanced MRI is explored. Contrast agent uptake is assumed to occur by diffusion from a high concentration pool into a poorly perfused substrate adjacent to the pool. Observation of depth of penetration versus time yields an effective diffusion coefficient describing the uptake. *In vivo* experiments show that this model is consistent with contrast agent uptake at the luminal surface of carotid atherosclerotic plaques

2188. High-Resolution MRI with a New Cardiac and Respiratory Gating System for Contrast-Enhanced MRI of the Carotids in the ApoE-/- Mouse

Hasan Alsaid[1], Maher Sabbah[2], Zakaria Bendahmane[1], Odette Fokapu[2], Philippe Robert[3], Claire Corot[3], André Briguet[1], Emmanuelle Canet-Soulas[1]
[1]Laboratoire de RMN Méthodologie et Instrumentation en Biophysique, UCB-CNRS UMR 5012, Villeurbanne, France; [2]UMR 6600, Biomécanique et Génie Biomédical, UTC, Compiègne, France; [3]Guerbet, B.P. 50400, Roissy CdG cedex, France

We propose to evaluate contrast enhancement of carotid wall in ApoE-/- mice using efficient cardiorespiratory gating. Real-time cardiorespiratory gating was implemented using Simulink(MathWorks, Inc). ECG gated images were acquired in the stable expiratory phase. High relaxivity contrast agent Vistarem was injected. Pre and post-contrast T1 (89µm) SE were acquired at 2T MRI in ApoE-/- and C57BL/6 mice at carotid origin. Signal enhancement was measured by Creatools software. This study demonstrates the efficiency of the real time cardiorespiratory gating. Signal of the carotid wall in ApoE-/- increased post-contrast and reaches its maximum 30 to 40min post-contrast and decreased after 60min.

2189. Characterization of Plaque Components in Gadofluorine M-Enhanced Rabbit Atherosclerosis: Toward Quantification of Plaque Progression with Biomechanics

Jie Zheng[1], Dalin Tang[2], Bernd Misselwitz[3], Issam El Naqa[1], Joseph O. Deasy[4], Dana Abendschein[4]
[1]Washington University School of Medicine, St. Louis, Missouri, USA; [2]Worcester Polytechnic Institute, Worcester, Massachusetts, USA; [3]Schering AG, Berlin, Germany; [4]Washinfton University School of Medicine, St. Louis, Missouri, USA

The aim of this study is to evaluate the signal behaviors of multi-contrast atherosclerotic plaque images with Gadofluorine M enhancement in a double-injury rabbit plaque model. In addition, plaque progression was observed with two consecutive MRI scans. Morphology changes in different plaque components were addressed. For one animal, biomechanical stress and strain maps were obtained, in which shear stress and strain increased significantly, whereas the areas of foam cells increased and lumen remained unchanged.

2190. Magnetic Resonance Imaging of Rabbit Atherosclerotic Lesions with MS-325

Marc Lobbes[1], Robbert-Jan Miserus[1], Andrea Wiethoff[2], Alfons Kessels[3], Mat Daemen[1], Jos van Engelshoven[1], Sylvia Heeneman[1], Tim Leiner[1], Eline Kooi[1]
[1]Cardiovascular Research Institute Maastricht, Maastricht, Limburg, Netherlands; [2]Epix Pharmaceuticals Inc., Cambridge, Massachusetts, USA; [3]Clinical Epidemiology and MTA, Maastricht, Limburg, Netherlands

Previous research suggested uptake of MS-325 in the atherosclerotic vessel wall. We hypothesized that MS-325 can be used to detect atherosclerotic lesions in rabbit abdominal aortas. Four groups of 3-4 NZW rabbits each were formed: atherosclerotic and normal rabbits receiving MS-325 or Gd-DTPA. T1w MR images were acquired (1.5T). Post-MS-325 signal enhancement was significantly larger in atherosclerotic aortas than in controls. Post-Gd-DTPA signal enhancement was comparable between atherosclerotic aortas and controls. Thus, preliminary results show specific enhancement of atherosclerotic lesions after administration of MS-325, whereas Gd-DTPA enhanced MRI is not able to distinguish between diseased and non-diseased rabbit vessel walls.

2191. In-Vivo MRSI Detection of Lipid in Carotid Atherosclerotic Plaque

Kai Wolfgang Eberhardt[1], Susan Yeon[2], Dana Cecil Peters[2], Michael Schär[3], [4], Peter Boesiger[1], Sebastian Kozerke[1]
[1]University and ETH Zürich, Zurich, Switzerland; [2]Harvard Medical School, Boston, Massachusetts, USA; [3]Philips Medical Systems, Cleveland, Ohio, USA; [4]Johns Hopkins University, Baltimore, Maryland, USA

Proton MRSI exams with high spatial resolution were performed on five healthy volunteers and three patients with carotid atherosclerosis. Data were acquired using a periodic pulse sequence with balanced gradients and weak excitation according to the Linear Response Equilibrium approach presented recently. The exams enabled the first direct *in vivo* detection of cholesterol and fatty acids in the arterial wall.

2192. Atherosclerotic Plaque Characterization Using NMR Spectroscopy

Said Rahnamaye Rabbani[1], Erasmo Simão da Silva[1], Antonio Carlos Bloise[1], Mauro M. Hanaoka[2], Tito José Bonagamba[3]

[1]São Paulo University, São Paulo, Brazil; [2]São Paulo University, São Paulo, São Paulo, Brazil; [3]São Paulo University, São Carlos, São Paulo, Brazil

Cardiovascular and cerebrovascular diseases, currently the first and third cause of death in developed countries, will soon be a major burden to public health worldwide and therefore there is a great effort to study vascular diseases using different techniques. The aim of the present study is to investigate the feasibility and the efficiency of MRS in detection of different stages of human atherosclerotic plaques. We show that the 13C and 1H High-Resolution spectra reflect the disease severity as the consequence of lipid alterations and consequently the NMR spectra changes.

Body MR: Liver, Contrast Techniques

Room 4E Wednesday 14:00 - 16:00

2193. Evaluation of the Upper Abdomen on Dynamic Enhanced Coronal Liver Acceleration with Volume Acquisition Imaging: Comparison with MDCT

Motoyuki Katayama[1], Takayuki Masui[1], Kimihiko Sato[1], Masahiro Sugiyama[1], Hidekazu Seo[1], Atsushi Nozaki[2], Masaya Hirano[2]

[1]Seirei Hamamatsu General Hospital, Hamamatsu, Shizuoka, Japan; [2]General Electtric Yokogawa Medical Systems, Hino, Tokyo, Japan

Liver Acceleration with Volume Acquisition (LAVA) belongs to 3D SPGR acquisition, which has some advantages, such as high spatial resolution and high signal-to-noise ratio, Coronal LAVA imaging could cover upper abdomen. We compared coronal LAVA imaging with 16 detector-row CT imaging about hepato-biliary disease. The delineation of the cholangio-pancreatico lesions, hepatic lesions and the portal veins showed higher on LAVA imaging than on MDCT imaging. On the other hand, the delineation of the arteries showed higher on MDCT imaging than on LAVA imaging.

2194. Time-Resolved Three-Dimensional Contrast-Enhanced Dynamic MR Imaging of the Whole Liver with a Parallel Imaging Technique

Katsuyoshi Ito[1], Takeshi Fujita[1], Ayame Shimizu[1], Minoru Hayashida[1], Masahiro Tanabe[1], Naofumi Matsunaga[1]

[1]Yamaguchi University School of Medicine, Ube, Yamaguchi, Japan

The purpose of this study was to evaluate the clinical feasibility of time-resolved three-dimensional contrast-enhanced dynamic MR imaging of the whole liver with parallel imaging technique during a single breath-hold, and to assess the utility of continuous imaging from early-arterial through late-arterial phase for evaluating hypervascular HCCs. The study included 82 patients with 51 HCCs. This technique allows the capture of the distinct arterial and portal phases, obviating the use of timing bolus or contrast detection methods, and has a potential to evaluate transitional hemodynamics of hypervascular HCCs during the early-arterial through early-portal phase due to excellent temporal resolution.

2195. Clinical Evaluation of an Ultra High Spatio-Temporal Resolution Time Resolved Dynamic Contrast Enhanced Imaging Technique in Hepato-Biliary Oncosurgical Imaging

Rammohan Vadapalli[1], Manojkumar Saranathan[2], Ramesh Venkatesan[3], Mohan deseilva[4], Aloka Pathirana[4]

[1]Asiri Surgical Hospital, Colombo, Sri Lanka; [2]Indian Institute of Science, Bangalore, Karnataka, India; [3]Wipro GE Medical Systems, Bangalore, Karnataka, India; [4]University of Jayawardhenpura, Colombo, Sri Lanka

MRCP is a critical component of hepatobiliary imaging. However, it is insufficient by itself. A robust, fast multiphase dynamic contrast enhanced sequence is needed to detect and characterize lesions and metastases. We investigated the use of a novel fat suppressed DCEMRI time resolved sequence with ultra high spatio-temporal resolution in hepatobiliary and pancreatic imaging practice, as a useful adjunct to MRCP. Excellent visualization of the arterial and late phases was observed as well as complete correlation with histopathological data.

2196. Comparison of a Recently Developed 3D SPGR Breath-Hold Examination for Abdominal MR Imaging and 2D Fast SPGR Breath-Hold Equivalent for Image Characteristics

Kimihiko Sato[1], Takayuki Masui[1], Motoyuki Katayama[1], Masahiro Sugiyama[1], Hidekazu Seo[1], Atshushi Nozaki[2], Masaya Hirano[2]

[1]Seirei Hamamatsu General Hospital, Hamamatsu, Shizuoka, Japan; [2]GE Yokogawa Medical Systems, Hino, Tokyo, Japan

A recently developed MR imaging sequence denominated liver acquisition with volume acceleration (LAVA) is a 3D SPGR sequence, which enables entire liver imaging within 20 seconds of breath-hold times. We applied the 3D LAVA images to pancreaticobiliary diseases and compared them with the 2D fast SPGR (FSPGR) images. The 3D LAVA images have higher SIRs than the 2D FSPGR images, and the 3D LAVA images can demonstrate pancreas lesion comparable to the 2D FSPGR images. Postcontrast 3D LAVA images can reduce intravascular artifacts. The use of thin-section MR imaging with the 3D LAVA sequences may replace the 2D FSPGR sequences.

2197. Detection and Characterization of Hepatocellular Carcinomas£ºComparison of Gadolinium-Enhanced 3D MR Imaging and Digital Subtraction Angiography in the Same Patient

Huiyi Ye[1], Maoqiang Wang[1], Jing Zhang[1], Youquan Cai[1], Lin Ma[1], Fengyong Liu[1]
[1]PLA General Hospital, Beijing, People's Republic of China

Purpose: To compare the efficiency of gadolinium-enhanced 3D MR imaging and digital subtraction angiography (DSA) for detection and characterization of HCCs. Methods: Unenhanced, gadolinium-enhanced 3D MR imaging and DSA were obtained in 73 patients. RESULTS: The gadolinium-enhanced 3D MR image set and DSA detected 139 (5 lesions ¡Ü1.0cm) and 171 HCCs (37 lesions ¡Ü1.0cm) respectively, and diagnosed correctly 128 HCCs and 133 HCCs respectively. CONCLUSION: The gadolinium-enhanced 3D MR image set is superior to DSA for characterization of HCCs and DSA is superior to the gadolinium-enhanced 3D MR image set for Detection of HCCs (¡Ü1.0cm).

2198. Biliary Enhancement of Gd-BOPTA (MultiHance®) and Gd-EOB-DTPA (Primovist®) - A Study in Healthy Volunteers

Nils Dahlström[1], [2], Torkel B. Brismar[3], Anders Persson[1], Nils Albiin[3], Örjan Smedby[1]
[1]Linköping University Hospital, Linköping, Sweden; [2]Hudiksvall Hospital, Hudiksvall, Sweden; [3]Karolinska University Hospital Huddinge, Stockholm, Sweden

Contrast media that give intraluminal enhancement in the biliary system can provide functional information. In this study the dynamics of bile duct enhancement relative to that of liver parenchyma for Gd-BOPTA (Multihance®) and Gd-EOB-DTPA (Primovist®) was investigated. Ten healthy subjects were repeatedly examined after administration of each agent for five hours. The earlier onset of biliary enhancement and the longer duration of high image contrast between bile and liver with Gd-EOB-DTPA compared to Gd-BOPTA may facilitate the hepatobiliary examination at MRI. Near its biliary enhancement peak, Gd-BOPTA may however provide higher image contrast than Gd-EOB-DTPA within a short time window.

2199. Hepatocellular Adenoma and the Surrounding Liver: A Spectrum of Characteristic Findings at State-Of-The-Art MR Imaging, with Histopathological Correlation

Indra Celine van den Bos[1], Shahid M. Hussain[1], Pieter E. Zondervan[1], Piotr A. Wielopolski[1], Jan N M IJzermans[1], Rob A. de Man[1]
[1]Erasmus Medical Center, Rotterdam, Netherlands

Hepatocellular adenoma (HA) has an increased risk of hemorrhage and malignant transformation in large (>5 cm) lesions. Differentiation with focal nodular hyperplasia (FNH) is important, since HA are sensitive to hormonal levels and may grow during use of oral anticonception, or pregnancy, with risk of potentially life-threatening bleeding. To evaluate image characteristics of liver and lesions, a retrospective analysis was performed with histopathological correlation. It is shown that liver parenchyma in case of HA has often changed in morphology, signal intensity and histopathology. Also, most lesions show either partial or marked fatty infiltration, which may facilitate differentiation with FNH.

2200. MRI Estimation of Donor Liver Graft Steatosis Prior to Orthotopic Liver Transplantation: Feasibility and Evaluation of Possible RF Heating Effects

Kieren Grant Hollingsworth[1], Susan Maguire[2], Martin John Graves[1], David J. Lomas[1]
[1]University of Cambridge, Cambridge, Cambridgeshire, UK; [2]Addenbrookes Hospital, Cambridge, Cambridgeshire, UK

Steatosis of donor liver grafts adversely affects the outcome of human orthotopic liver transplantation and is currently assessed subjectively by the transplanting surgeon. As a preliminary to using an established rapid MRI method for quantifying donor liver graft steatosis this work used a porcine liver "phantom" to assess the feasibility of examining an undisturbed sterile packaged cooled liver graft and any expected or observed heating effects of the MR protocol employed. The protocol allowed rapid quantification of liver fat fraction and no expected or observed increase in 'graft' temperature was demonstrated, making it suitable for use with human liver grafts.

2201. Liver Vessel Enhancement of Gd-BOPTA and Gd-EOB-DTPA

Torkel B. Brismar[1], Nils Dahlström[2], [3], Örjan Smedby[2], Anders Persson[2], Nils Albiin[1]
[1]CLINTEC, Stockholm, Sweden; [2]CMIV, Linköping, Sweden; [3]Department of Radiology, Hudiksvall Hospital, Sweden

The contrast enhancement dynamics in the liver vessels of Gd-BOPTA (MultiHance®) and Gd-EOB-DTPA (Primovist®) was studied in ten healthy subjects. The signal intensity of the common hepatic artery, the middle liver vein, a segmental branch of the right portal vein and the liver parenchyma was obtained native, during arterial and portal venous phases and thereafter at 10 and 130 min after intravenous contrast medium injection. The image contrast between liver and vessels was greater when using MultiHance® compared to Primovist®. MultiHance®is better in clarifying the vascularity whereas Primovist® more clearly displays the liver specific contrast enhancement.

2202. Triple Arterial and Portal Venous Phase Dynamic MRI of Liver: To Differentiate Malignant and Hypervascular Benign Focal Lesions by Enhancement Curve and Parameters

Ying Li[1], Xiao-peng Zhang[1], Lei Tang[1], Kun Cao[1]
[1]Beijing Cancer Hospital, Peking University School of Oncology, Beijing, People's Republic of China

The purpose is to investigate the efficacy of enhancement curve and parameters obtained from triple arterial and portal venous phase dynamic MRI of liver to differentiate malignant and hypervascular benign focal lesions. 35 HCCs and 16 hepatic hypervascular benign lesions were included. The analysis of phase-intensity curve and enhancement parameters showed that there are different MR dynamic enhancement patterns in HCCs and hypervascular benign focal lesions .The positive enhancement integral and maximum slope of increase of hepatic hypervascular benign focal lesions are higher than those of malignant ones, indicating different perfusion characteristics based on different pathologic architectures, which is helpful to differentiate these lesions.

2203. Focal Liver Lesion Detection and Characterization: Comparison of SSEPI Diffusion-Weighted Imaging with T2-Weighted Imaging; Early Experience

Tejas Parikh[1], Stephen Drew[1], Samson Wong[1], Vivian S. Lee[1], Elizabeth M. Hecht[1], Ruth Lim[1], Bachir Taouli[1]
[1]NYU Medical Center, New York, New York, USA

SSEPI diffusion-weighted imaging sequence was implemented in 21 patients with liver lesions, and compared with T2-weighted imaging by 2 independent observers in terms of lesion detection and characterization. A significantly larger number of lesions were detected with DWI when compared with T2 weighted-imaging (overall sensitivity for observer 1/2 was 87.7/81.5% vs. 71.7-69.5%, respectively). In addition, DWI achieved slightly better characterization of malignant lesions. Our early experience shows the potential role of SSEPI sequences implemented in routine liver protocols.

2204. Liver Function Test Using SVD-Based Deconvolutional Analysis in Gd-EOB-DTPA-Enhanced MRI

Anders Nordell[1], Henrik Nilsson[2], Roberto Vargas[1], Eduard Jonas[2], Lennart Blomqvist[1]
[1]Karolinska University Hospital, Stockholm, Sweden; [2]Karolinska Institute, Danderyd Hospital, Stockholm, Sweden

Calculating hepatic extraction applying deconvolutional analysis (DA), will remove the effect of contrast recirculation. Using DA, one thus estimates a hepatic extraction/time curve as if a single bolus contrast passage was used. DA was performed using singular value decomposition (SVD), which is a more robust method than Fourier based DA. In this pilot study we describe dynamic Gd-EOB-DTPA MRI as a segmental liver function test, where we compare traditional contrast enhancement parameters such as time to peak and relative peak value with the hepatic extraction fraction (HEF).

2205. Characterization of Neuro-Endocrine Tumors Using MRI: Longitudinal Study in an Athymic Nude Mouse Model

Loredana Baboi[1, 2], Laurent Milot[1, 3], Frank Pilleul, [13], Jean-Yves Scoazec[4], Olivier Beuf[1]
[1]Université Claude Bernard LYON1, CPE, Villeurbanne, France; [2]Creatis- UMR5515 CNRS - U630 INSERM, Lyon, France; [3]Hôpital Edouard Herriot, Lyon, France; [4]Faculté de Médecine Laennec, Lyon, France

As the main cause of treatment failure in humans, liver metastasis is an important target for therapeutic intervention. Experimental model of endocrine tumors with liver dissemination is available for evaluation of new medical therapeutics such as antiangiogenic therapy. The aim of this longitudinal study was to evaluate the performance of the detection and characterization of the liver metastases using high field MRI. The fraction of lesion over the total liver volume was quantified. Characterization of cystic or non-cystic type of lesions was achieved using various TE.

2206. Automatic Analysis of Hepatic DCE-MRI Data

Daniel Monleon[1], David Moratal-Pérez[2], Luis Marti-Bonmati[3], Ignacio Blanquer[2], Vicente Hernández[2], Jose Carbonell[2], Bernardo Celda[1]
[1]Universitat de Valencia, Burjassot, Valencia, Spain; [2]Universidad Politécnica de Valencia, Valencia, Spain; [3]Hospital Universitario Dr. Peset, Valencia, Spain

The blood supply to the liver is derived jointly from the hepatic arteries and the portal venous system. The influence of breathing, the large number of pharmacokinetic parameters and the fast variations in contrast concentration in the first moments after product injection reduce the efficiency of traditional approaches. In this communication, we present a tool for easy and automatic analysis of liver DCE-MRI data. Liver DCE-MRI data were measured, co-registered and analyzed for 25 patients. Concentration/time curves obtained by non-linear sampling allowed the capture of contrast concentration peaks, improving the accuracy of parametric images and the correlation of the data to the pharmacokinetic models. We developed computer software for the analysis of concentration/time curves and correlation between the data and different pharmacokinetic models. Parametric images of TTP, rBV and several pharmacokinetic constants were also created. The software developed allowed the automatic semi-empirical or pharmacokinetic analysis of liver DCE-MRI data. This software may also help in the diagnosis of liver diffuse diseases.

2207. Clinical Evaluation of Elliptical Centric Fat Suppressed Time Resolved Imaging in Liver Tumor Characterization

Manojkumar Saranathan[1], Ramesh Venkatesan[2], Venkat Ramanan[2], Ananta Padmanabha[3], Rammohan Vadapalli[3]
[1]Indian Institute of Science, Bangalore, Karnataka, India; [2]GE Healthcare, Bangalore, Karnataka, India; [3]Asiri Surgical Hospital, Colombo, Sri Lanka

Clinical evaluation of a fat suppressed elliptic centric TRICKS (FSTRICKS) pulse sequence for high spatio-temporal resolution dynamic imaging and characterization of liver tumors was the primary purpose of this study. A secondary objective was to assess its potential in providing a pre-surgical planning roadmap in the clinical management of hepatic tumors and lesions. FSTRICKS' role in adequately characterizing and differentiating malignant and benign liver tumors such as HCC (singular tumor or multi-centric nodules with cirrhotic livers), metastatic lesions, focal nodular hyperplasia (FNH), hemangiomas and cystic lesions were studied on 30 patients and MRI results were correlated with clinical histopathology

2208. Clinical Feasibility of Single Breath-Hold Multiphase Dynamic MR Imaging of Liver Using THRIVE-CENTRA-Keyhole Sequence

Myeong-Jin Kim[1], Wha Sun Kim[1], Donald G. Mitchell[2], Jan de Becker[3], Gabriele Beck[3], Masayuki Kanematsu[4], Eun Ju Kim[5], Ki Whang Kim[1]
[1]Yonsei University, Severance Hospital, Seoul, Republic of Korea; [2]Thomas Jefferson University Hospital, Philadelphia, Pennsylvania, USA; [3]Philips Medical Systems, Best, Netherlands; [4]Gifu University, Gifu, Japan; [5]Philips Medical Systems Korea, Seoul, Republic of Korea

THRIVE-CENTRA-Keyhole imaging, a newly developed 3D GRE sequence, provides multiartieral dynamic MR imaging of liver and have a potential for evaluation of hemodynamics of focal liver.

2209. Detection and Characterization of Hepatic Metastases with Superparamagnetic Iron Oxide Enhanced Diffusion Weighted MR Imaging

Nagaaki Marugami[1], Shinji Hirohashi[1], Satoru Kitano[1], Kimihiko Kichikawa[1]
[1]Nara Medical University, Kashihara, Nara, Japan

The purpose of this study is to determine the usefulness of SPIO enhanced diffusion weighted imaging (DWI:b=500) for detection and characterization of the hepatic metastasis.Specificity and Az value of post-contrast DWI was significantly superior to pre-contrast DWI. Detection and characterization of hepatic metastases were improved with SPIO enhanced diffusion weighted MR images.

2210. Inferior Vena Cava Encirclement by Caudate Lobe Hypertrophy: Evaluation by MRI and CT and Its Impact on Caval Preservation During Orthotopic Liver Transplantation

Rashi I. Mehta[1], Donald G. Mitchell[1], Liise Kayler[1], Laurence Parker[1]
[1]Thomas Jefferson University Hospital, Philadelphia, Pennsylvania, USA

Preservation of the recipient IVC is preferred over IVC resection during liver transplantation at most centers due to reduced fluid resuscitation requirements, maintenance of core body temperature, and improved hemodynamic stability. Complete encirclement of the IVC by hepatic parenchyma may cause difficulty in preserving an intact IVC, a problem often encountered intraoperatively, and of particular relevance in the case of a living liver donor, in which case the IVC must be preserved. Routine preoperative assessment of this phenomenon using MRI or CT may be helpful in identifying patients in whom IVC preservation will be difficult, and help plan operative technique

2211. Phase Velocity Imaging of Portal Pressure Gradients for Evaluating Liver Cirrhosis

Yuenan Wang[1], Hyeonjin Kim[1], Alexander Pinus[1], Maolin Qiu[1], R. Todd Constable[1]
[1]Yale University, New Haven, Connecticut, USA

Liver cirrhosis can be characterized by portal hypertension. The current gold standard for diagnosis is biopsy but this is limited by its invasive nature. A new MR model of the portal pressure gradient is presented that provides reproducible non-invasive diagnosis of liver cirrhosis. The method is tested in CCl4 induced cirrhotic and normal rats. This approach revealed statistically significant differences in portal pressure gradient along the portal vein between cirrhotic and normal control rats, suggesting that the portal pressure gradient method is potentially useful in the diagnosis of liver cirrhosis.

2212. Focal Nodular Enhancement on 3D MRI of Cystic Renal Lesions Predicts Malignancy

Ivan Pedrosa[1], Martin P. Smith[1], Gregory S. Adey[1], Martin G. Sanda[1], William D. DeWolf[1], Neil M. Rofsky[1]
[1]Beth Israel Deaconess Medical Center, Boston, Massachusetts, USA

We examined the positive predictive value (PPV) for malignancy of focal nodular enhancement in renal cystic lesions on 3D MRI. A surgical database was reviewed for patients at our institution having pre-operative 3D renal MRI and radical or partial nephrectomy during 52 months. Of 286 nephrectomies, 159 (56%) patients had pre-operative MRI studies. Of these, 21/159 (13%) lesions displayed focal nodular enhancement within a cystic lesion, 14 (67%) of which measured ¡Ü 10mm. Twenty (95%) of 21 lesions were renal cell carcinoma. The demonstration of solid enhancing nodular components provides excellent PPV (95%) for diagnosing neoplastic cystic renal lesions.

Body: GI-GU

Room 4E Wednesday 14:00 - 16:00

2213. Specific Pathogen-Free Transgenic Mice Carrier for Molecular MR Imaging

Cory Robert Wyatt[1], Donna J. Cross[1, 2], Mark Mathis[1], Cecil Hayes[1], Jennifer A. Flexman[1], Kenneth R. Maravilla[1], Satoshi Minoshima[1]

[1]University of Washington, Seattle, Washington, USA; [2]University of Michigan, Ann Arbor, Michigan, USA

Since transgenic mice often have compromised immune systems, they are stored in barrier specific pathogen-free (SPF) facilities that have the highest level of pathogen protection available. If a transgenic mouse is removed from the barrier SPF facility, it cannot be returned, putting the animal at risk during future housing. This dilemma is particularly acute for longitudinal imaging studies, where the same subject is used for repeated imaging sessions. In this study, we developed a device that will maintain a SPF environment while allowing for the longitudinal MR scanning of transgenic mice.

2214. *In Vivo* Sodium Imaging of Mouse Kidney at 9.4 Tesla: A Feasibility Study

Haiying Liu[1], Martin G. Kohler[1], XL Shen[1], Maria L. Garcia[1], Donald S. Williams[2], Richard J. Hargreaves[2]

[1]Merck Research Labs, Rahway, New Jersey, USA; [2]Merck Research Labs, West Point, Pennsylvania, USA

High resolution *in vivo* sodium images of mouse kidney were obtained using a 9.4T NMR scanner in 20min. Both spatial resolution and SNR of the sodium images were sufficient for resolving the sodium concentration gradient at organ level and its change after a 15mpk flurosemide injection in mouse kidney. The result of the study suggests that such a non-invasive imaging based assessment can be used to gain insights regarding to renal function and mechanism of diuretics.

2215. Functional Consequences of Aquaporin-1 Deficiency: Renal MRI in a Pre-Clinical Model

Natarajan Raghunand[1], Theodore P. Trouard[1], Heddwen Brooks[1]

[1]University of Arizona, Tucson, Arizona, USA

The aquaporin-1 (AQP1) water channel is widely expressed in fluid-transporting epithelia and endothelia, particularly in the kidneys. We have employed Dynamic Contrast-enhanced MRI and Blood Oxygen-Level Dependent MRI to study altered renal function in AQP1-knockout (AQP1ko) mice. Decreased filtration function in the AQP1ko mice, possibly indicating compensatory tubuloglomerular feedback regulation, was observed. Decreased filtrate pH and decreased medullary T2* were also observed. A decreased T2* suggests increased medullary workload in AQP1ko mice, while decreased filtrate pH is indicative of altered proton pump activity. Quantitative comparisons between control and AQP1ko mice, and physiological explanations for the differences, will be provided.

2216. MRI-Histopathology Correlation of N-Phenylanthranylic Acid Induced Nephropathy in Rats

Yi-Xiang Wang[1], Graham Betton[1], Eike Floettmann[1], Carsten Leiss[1]

[1]Astra Zeneca, Macclesfield, Cheshire, UK

Eight rats were dosed with N-phenylanthranylic acid (NPAA) 700mg/kg/day for 14 days and four rats were treated with vehicle. After euthanasia, the left kidneys were harvested and placed within a vial containing 10% formalin, and scanned at 9.4T. Histology showed all NPAA treated animals developed various nephropathy changes. With nephropathy kidneys, MRI revealed an increase in kidney size, a loss in the conspicuity of the normal corticomedullary junction, and fine radial bands pointing to the renal papilla with alternating high and low signal. These results suggest that MRI could provide sensitive imaging markers for NPAA induced kidney damages.

2217. Synchronization Strategies in T2-Weighted MR Imaging for Detection of Mouse Liver Metastasis

Loredana Baboi[1], [2], Laurent Milot[1], [3], Frank Pilleul, [13], Carole Lartizien[2], [4], Olivier Beuf[4]

[1]Université Claude Bernard LYON1, CPE, Villeurbanne, France; [2]Creatis - UMR5515 CNRS - U630 INSERM, Lyon, France; [3]Hôpital Edouard Herriot, Lyon, France; [4]CERMEP- Plate-forme ANIMAGE, Bron, France

To detect liver metastasis in clinical practice, respiratory-triggered T2-weighted MR images is the sequence of choice. With conventional acquisition strategies used on small animal MR systems, the slice number is limited and the time between each slice is decreased, favoring the cross talking. Additionally, the T2 contrast is not freely controlled. The proposed strategy enables true T2-weighted imaging with minimal movement artifacts and minimal inter-slice crosstalk, regardless of the respiratory period and the number of slices.

2218. Visualization of Seminiferous Tubules by High Resolution MR Imaging in Rat Testes: The Usefulness in the Evaluation of Spermatogenic Activities

Masayuki Yamaguchi[1], [2], Fukiyuki Mitsumori[1], Nobuhiro Takaya[1], Hidehiro Watanabe[1], Manabu Minami[2]

[1]National Institute for Environmental Studies, Tsukuba, Ibaraki, Japan; [2]University of Tsukuba, Tsukuba, Ibaraki, Japan

To determine whether high resolution MRI aids in evaluating the status of spermatogenesis *in vivo*, MR findings in the rat testes with normal spermatogenesis and with artificially impaired spermatogenesis were compared. T_2 weighted images successfully demonstrated both normal and damaged seminiferous tubules, and depicted the reduction in their outer diameter in the latter, reflecting the decreased number of germ cells in the seminiferous epithelium and the decreased amount of seminiferous tubular fluid. High resolution MRI is promising for the evaluation of the status of spermatogenesis *in vivo* via detecting the changes in appearances of the seminiferous tubules.

2219. Evaluation of Autoimmune Pancreatitis with MR Imaging: A Comparative Study with Helical CT

Zhenghan Yang[1], Weifeng Zhao[1], Min Chen[1], Ye Tan[1], Xiaohua Ye[1], Min Zhang[1], Cheng Zhou[1]
[1]Beijing Hospital, Beijing, People's Republic of China

The aim of this study is to investigate the MR imaging characteristics in patients with autoimmune pancreatitis (AIP), and to evaluate the role of MR imaging in the diagnosis of this entity in comparison with helical CT. MR imaging and dynamic helical CT were performed in 6 patients with AIP. The imaging features of AIP were reviewed and compared between MR imaging and helical CT. Our results indicate that MR imaging is superior to CT in demonstrating characteristic imaging features of AIP, particularly in showing capsulelike rim and diffuse irregular stricture of the pancreatic duct.

2220. Quantification of the Stimulation Effect on the Exocrine Pancreas of Two Doses of Secretin Using MRCP

Maria Antonietta Bali[1], Thierry Metens[1], Marianna Arvanitakis[1], Jacques Devière[1], Celso Matos[1]
[1]Erasme Hospital, Brussels, Belgium

The aim of this study was to evaluate the stimulating effect of two doses of secretin on pancreatic exocrine secretions using MRCP. This study has been realized in ten healthy volunteers. MRCP was repeated two times in each volunteer for each dose (1 and 0.3 CU/Kg). Pancreatic flow output and total excreted volume were derived from a linear regression between MR calculated volumes and time. In all examinations, pancreatic exocrine fluid volume increased linearly with time. Mean pancreatic flow output and total excreted volume were significant lower at the dose of 0.3 CU. Pancreatic exocrine function reacts proportionally to the degree of stimulation.

2221. Role of Secretin Enhanced MRCP in Post Partial Pancreatectomy Patients

Munazza Anis[1], Koenraad J. Mortele[2], Servet Tatli[2], Alisa Suzuki[2], Sukru Mehmet Erturk[2], Peter A. Banks[2], Stuart G. Silverman[2]
[1]Brigham and Women's Hospital,, Boston, Massachusetts, USA; [2]Brigham and Women's Hospital, Boston, Massachusetts, USA

We assess the role of secretin MRCP in patients with partial pancreatectomy and enteric anastomosis where the role of ERCP is limited due to altered anatomy. 2 readers measure different parameters affecting the pancreatic duct, enteric anastomsis and amount of jejunal fluid in pre- and post-secretin MRCPs done in the last 6 months at our institution. A statistical significance was not seen in the visualization of the pancreatic duct, however, improvement in pancreaticojejunal anastomosis visualization was evident.

2222. Free-Breathing and High B-Value Diffusion-Weighted MR Images of Solid Pancreatic Tumors and Tumor-Like Lesions

Mayumi Takeuchi[1], Kenji Matsuzaki[1], Hitoshi Kubo[1], Masafumi Harada[1], Hiromu Nishitani[1]
[1]Univ. of Tokushima, Tokushima, Japan

We evaluated benign and malignant solid pancreatic tumors and tumor-like lesions by free-breathing and high b-value DWI, and corresponding isotropic ADC maps to differentiate benign lesions from malignancies. Nine ductal adenocarcinomas showed very high signal intensity on DWI (ADC=1.44+/-0.37). One treated ductal adenocarcinoma, three mass-forming chronic pancreatitis (0.97+/-0.21), and two benign islet cell tumors (1.55+/-0.05) showed slight high to iso signal intensity. Two autoimmune pancreatitis showed relatively homogeneous slight high signal intensity (1.05+/-0.07). DWI may be useful in primary tumor and metastatic lesion detection of pancreatic ductal adenocarcinoma, and in differentiation from benign tumor-like pathologies.

2223. Pancreatic Duct Visualisation: Secretin MRCP Compared with 2D and 3D MRCP Techniques, Initial Results

Suzanne L. Wakely[1, 2], Evis Sala[1, 2], Lucy Bushby[1, 2], Richard T. Black[2], Martin J. Graves[1], Ruth Beavon[2], David J. Lomas[1, 2]
[1]University of Cambridge, Cambridge, UK; [2]Addenbrookes Hospital, Cambridge, UK

Secretin MRCP (sMRCP) is reported to improve visualisation of the pancreatic duct, its side branches and variant anatomy, although this has cost and side-effect implications. This study compared the diagnostic performance of a) conventional 2D projection MRCP, b) adaptive averaging of real-time MRCP and c) 3D respiratory triggered FSE, with 2D projection sMRCP. Six patients were evaluated prospectively. Qualitative visual analysis was performed by two experienced observers, blinded to acquisition details. The results demonstrate the 3D technique matched or exceeded the performance of the sMRCP technique in all cases and suggest that the use of secretin may be avoided.

2224. Quantification of Renal Volume and Length in Normal Subjects by Magnetic Resonance Imaging

Benjamin Cheong[1], Raja Muthupillai[1, 2], Scott Flamm[1, 3]

[1]St. Luke's Episcopal Hospital, Houston, Texas, USA; [2]Philips Medical Systems, Cleveland, Ohio, USA; [3]Baylor College of Medicine, Houston, Texas, USA

In routine clinical practice, kidney length and kidney volume are measured by ultrasonography (US) using a formula that approximates the bean shaped kidney to an ellipsoid. The purpose of this study is to evaluate the accuracy of such an approximation. In an *ex vivo* model of a porcine kidney, the ellipsoid formula underestimated the kidney volume by 21%, whereas the magnetic resonance imaging (MRI) method to compute volume using disc summation was within 5% of the volume obtained by the water displacement method. In 20 patients with no intrinsic kidney disease, using the ellipsoid formula to compute the volume resulted in an underestimation of 17-20% compared to the volume estimated from MRI data using the disc summation method. The mean kidney length and volumes estimated using MRI in 130 patients with no intrinsic kidney disease are greater than the hitherto reported reference values obtained using US.

2225. Sodium MRI of the Human Kidney

Yael Rosen[1], Nimrod Maril[1], H Glenn Reynolds[2], Alexander Ivanishev[1], Robert E. Lenkinski[1]

[1]Beth Israel Deaconess Medical Center, Boston, Massachusetts, USA; [2]GE Healthcare, Milwaukee, Wisconsin, USA

The corticomedullary sodium concentration gradient may serve to characterize physiological and pathological processes in the kidneys. We demonstrated the capability of 23Na-MRI to map the sodium distribution in the human kidney at 3mm resolution, in a 24-minute scan. Normal volunteers were scanned at 3T using a home-built quadrature surface-coil and a modified 3D-GRE. The images revealed the multi-medullae structure of the human kidney and enabled the measurement of the sodium gradient. This gradient increased significantly after water deprivation. These results suggest that sodium MRI can serve as a valuable non-invasive method for functional imaging of the human kidney.

Body: GI

Room 4E Wednesday 14:00 - 16:00

2226. Clinical Significance of Diffusion Weighted Image in Staging Esophageal Cancer

Aine Sakurada[1], Taro Takahara[1], Tomohiro Yamashita[1], Seiji Nasu[1], Tomohiko Horie[1], Marc Van Cauteren[2], Yutaka Imai[1]

[1]Tokai Univ. School of Medicine, Isehara, Kanagawa, Japan; [2]Philips Medical Systems, Shinagawa, Tokyo, Japan

The purpose is to investigate the detestability of esophageal cancer and lymph node metastases with diffusion weighted image, in comparison with surgical results. For depiction of primary tumor, the sensitivity was 54.2%, 50.0% and 71.4% for reader A, B and C, respectively. Lymph node group-based sensitivity was 51.5%, 36.4%, 30.3% and specificity was 91.1%, 93.4%, 95.9% for reader A, B and C, respectively. Detectability of esophageal cancer and its metastases in lymph nodes were comparative to those of FDG-PET scan in literature. There were no significant differences in ADC value obtained using this method between metastatic and non- metastatic node groups.

2227. *Ex Vivo* MR Diffusion Anisotropy Measurement for the Evaluation of Gastric Tissue Fiber Directions Using 3D Turbo STEAM Sequence

Roger Nana[1], Nader Metwalli[1], Lei Zhou[1], Keith Aaron Heberlein[1], Choong-Ki Eun[2], Xiaoping P. Hu[1], Chi-Woong Mun[1, 3]

[1]Emory University/Georgia Institute of Technology, Atlanta, Georgia, USA; [2]Inje University, Busan, South, Republic of Korea; [3]Inje University, Gimhae, South, Republic of Korea

The aim of this study is to assess the feasibility of *ex vivo* Diffusion Tensor Magnetic Resonance Imaging (DT-MRI) as a diagnosis tool for gastric cancer. Human gastric tissues resected from patients and fixed in 10% formalin solution were used as specimens. High-resolution 3D diffusion weighted Turbo STEAM is implemented on Trio 3.0-T MRI (Siemens, Germany) system with a hand made small specimen coil (I.D. *f*Ö = 74 mm, quadrature-birdcage type, Tx/Rx mode). The sagittal view of a b zero image, diffusion weighted, apparent diffusion coefficient (ADC) map, and fractional anisotropy (FA) color map of a cross sectional normal gastric tissue are generated. The muscle layer can be discriminated from other mucosal and submucusal layers of the gastric tissues in all images. The FA map provides more detail information on the muscle fiber directionalities. The study shows the possibilities of the 3D Turbo STEAM diffusion tensor imaging and can be used as a diagnostic method of gastric cancer disease.

2228. Diffusion-Weighted MR Imaging of Gastric Cancer: Preliminary Studies

Xiao Peng Zhang[1], Lei Tang[1], Ying Shi Sun[1], Jie Li[1]

[1]Beijing Cancer Hospital & Peking University School of Oncology, Beijing, People's Republic of China

Diffusion-weighted MR imaging were performed in 26 patients with advanced gastric cancer, of which 24 cases obtained acceptable images. Four b values (0, 300, 600 and 1000s/mm2) were employed to generate DW images. There was statistical difference of ADCs with different b value sequences. The larger the b values, the lower the ADCs. The SNR of tumors reduced as b values went higher. High-b-value images have better contrast and produce more accurate ADCs, and low-b-value images can be an alternate when the SNR is too low to identify tumor signals.

2229. Dynamic 3D Gastric Imaging Using *k-T* BLAST and Image Processing of the 4D MRI Data of the Human Stomach

Stefan Zwick[1], Andreas Steingoetter[1], Sebastian Kozerke[1], Werner Schwizer[2], Peter Boesiger[1]
[1]ETH and University Zurich, Zurich, Switzerland; [2]University Hospital Zurich, Zurich, Switzerland

The recently developed accelerated acquisition method for dynamic MRI (k-t BLAST) was evaluated for dynamic 3D gastric MRI. An automated segmentation algorithm was implemented to process the 4D datasets. k-t BLAST reconstruction was simulated using 2D reference datasets to determine optimal acceleration factors and training profiles for *in vivo* studies. Accelerated dynamic 3D gastric MRI was performed in volunteers. Based on this data, the developed segmentation tool was evaluated. Simulations were confirmed by *in vivo* studies. The automatic segmentation allowed over 90% contour detection with a volume detection error < 5%. This work presents the first method analyzing gastric function in 3D.

2230. Effect of Fat Emulsion Acid Stability on Gastric Emptying, CCK Release and Satiety: An EPI Study

Luca Marciani[1], Martin Wickham[2], Gulzar Singh[1], Debbie Bush[1], Barbara Pick[1], Jeff Wright[1], Annette Fillery-Travis[3], Richard Faulks[2], Charles Marsden[1], Robin C. Spiller[1], Penny A. Gowland[1]
[1]University of Nottingham, Nottingham, England, UK; [2]Institute of Food Research, Norwich, England, UK; [3]Centre for Research and Dissemination, Norwich, England, UK

Consumption of pre-processed foods high in fat, often added as a fat emulsion, is steadily increasing in the developed countries. Based on our previous work on fat emulsions, this study aimed to investigate whether it would be possible to manipulate intragastric distribution and hence gastric emptying, cholecystokinin levels and satiety feelings in healthy volunteers by simply modifying the intragastric acid stability of the fat emulsions fed to them. We show here that, when compared with an equicaloric acid-unstable emulsion, acid-stable emulsion slowed gastric emptying by about 2.5 fold, increased the levels of circulating CCK and increased the sense of satiety.

2231. Behaviour of Calcium Gelled Alginate Beads in Simulated Gastrointestinal Conditions

Peter Jonathan Wright[1], P Rayment[2], C Hoad[1], I Dalhiwala[2], T Weaver[2], L Marciani[3], R Spiller[3], M Butler[2], P Gowland[1]
[1]University of Nottingham, Nottingham, Nottinghamshire, UK; [2]Unilever R&D, Sharnbrook, Bedfordshire, UK; [3]University Hospital, Nottingham, Nottinghamshire, UK

Alginates are extremely versatile biopolymers with a wide range of applications in the food industry. This study aims to investigate behaviour of gelled alginate beads in physiologically simulated GI conditions. Alginate beads were made by dropping 1.5% alginate solution into 0.37% calcium chloride solution. Beads were placed in simulated gastric and intestinal solutions for 2 and 3 hours consecutively. T2 of the beads was measured and rapidly decreased in gastric conditions with beads shrinking in size. T2 increased in intestinal conditions with beads increasing in size. MRI profiling shows similar T2 pattern occurs within beads with outer ‘shell’ remaining stable.

2232. Crohn’s Disease of Small Bowel:MR Enteroclysis,dynamic Contrast Enhancement,and Cross-Sectional Imaging

Liu Yu Bao[1]
[1]Guangdong Provincial People's Hospital, Guang Zhou, Guangdong, People’s Republic of China

The purpose of this study was to evaluate Crohn’s disease of small bowel using MR enteroclysis,dynamic contrast enhancement,and cross-sectional imaging. The abnormalities of Crohn’s disease and its complications can be identified by MR enteroclysis, dynamic contrast enhancement.Complications of Crohn’s disease can be shown better when MR enteroclysis is performed.

2233. MRI of Colon Wall Thickness - A Biomarker in Experimental Mouse Inflammatory Disease?

Anna E. Larsson[1], Silvia Melgar[1], Erika Rehnström[1], Lennart ET Svensson[1], Erik Michaelsson[1], Paul D. Hockings[1], Lars E. Olsson[1]
[1]AstraZeneca, Mölndal, Sweden

A large body of studies show that MRI is valuable in monitoring patients with inflammatory bowel disease. The present study aimed at investigating if colon wall thickness, measured *in vivo* with MRI, can reflect inflammation in chemically induced mouse colitis. Our results demonstrate that colon wall thickness correlated positively with inflammation scores assessed *ex vivo*, and to serum haptoglobin levels, a systemic inflammatory marker. Hence, colon wall thickness may be a useful biomarker in evaluation of putative drugs. However, future studies are needed to examine if colon wall thickness may serve as a biomarker that can respond to pharmacological treatment.

2234. How to Select B Value of Diffusion-Weighted MR Imaging for Detecting Primary Rectal Cancer

Xiao Peng Zhang[1], Ying Shi Sun[1], Lei Tang[1], Jie LI[1], Kun Cao[1]
[1]Beijing Cancer Hospital, School of Oncology, Peking University, Beijing, People's Republic of China

The aim of this study is to investigate how to select the reasonable b values of DWI for displaying rectal cancer.Materials and Methods Thirty-two patients with rectal cancer with single-shot EPI diffusion-weighted sequences (b=300, 500, 800, 1000 and 1300 s/ mm2) at 1.5T MR scanner (GE Healthcare) with an 8-channel body phase-array coil. The mean ADC values and Signal-to-noise ratio (SNR) of tumors, Contrast-to-noise ratio (CNR) of tumors and normal rectal wall, Signal intensity ratio (SIR) of bladder were calculated and compared. .Results The CNR of tumors and normal rectal wall decreases following the ascending of b values, and the CNR in the DWI of rectal cancer with b=300, 500, 1000 s/ mm2 was significantly higher than that in DWI with b=1300 s/ mm2 and T2 weighted imaging (F£½42.492£p£¼0. 001). The SIR of bladder and background noise in DWI (b=300, 500, 800, 1000 and 1300 s/ mm2) were lower than that in T2 weighted imaging£¨F£½144.786£p£¼0. 05£©. When b values reached 800 s/ mm2 the SIR declined to 2.437¡À 0.844. The mean ADC values of tumor were decreases following the ascending of b values. Discussion and Conclusion The results indicate b 1000 s/ mm2 is reasonable to DWI of rectal cancer. Both the effect of blood perfusion and T2 shine through can not markedly influence the diffusion-weighted imaging of rectal cancer .

2235. Dual Modality Virtual Colonoscopy Workstation: Design, Implementation, and Evaluation

Dongqing Chen[1]
[1]Viatronix Inc., Stony Brook, New York, USA

A commercialized CT virtual colonoscopy system (V3D Colon, Viatronix Inc.) was enhanced to support dark-lumen MR colonography procedure. A volume rendering technique was developed to display 3D endoluminal view for polyp detection using MR images. The new technique allows rendering accurate 3D depth for spatial-intensity-inhomogenety images. The user graphics interface and workflow remained the same as before. That greatly saves training time when old user start using new modality. The new system was evaluated on 12 MR cases. For the good and moderate imaging quality cases, the results are promising

2236. An Inversion Recovery Phase-Contrast EPI Scan for Rapid Simultaneous Encoding of Velocity and T_1 Data for the Single Kidney Glumerular Filtration Rate

Mahmoud Abdulhamid Abdulhusain[1], Michael H. Buonocore[2]
[1]University of California, Davis, California, USA; [2]University of California Davis, Sacramento, California, USA

Current techniques do not allow simultaneous acquisition of velocity and T1 data in a rapid breath-hold scan for renal imaging. This study offers an approach that solves this and reveals a trend that relates T1 to velocity. An inversion recovery EPI scan was modified to enable phase-contrast velocity encoding. Results from a phantom experiment reveal that T1 and velocity data can be acquired simultaneously, and that velocity is only reliable in the plateau periods of the signal curves. These findings show promise for the use of the technique in clinical settings.

2237. Functional Magnetic Resonance Gadolinium Enhanced Imaging of the Kidney: Detection of a Physiological Change in Renal GFR in Response to an Amino Acid Challenge Test

Diego R. Martin[1], Khalil Salman[1], Richard A. Jones[2], J Damien Grattan-Smith[2], Marijn Brumner
[1]Emory University School of Medicine, Atlanta, Georgia, USA; [2]Children's Healthcare of Atlanta and Emory University, Atlanta, Georgia, USA

There is clinical need for improved methods of measuring renal function. This study shows that a dynamic gadolinium enhanced MR imaging technique of the kidney can measure renal functional response to a physiological change induced by an amino acid challenge test. This study helps to demonstrate the capability of this technique to reproducibly measure altered renal function.

2238. Rationale and Validation of a 3-Compartment Kinetic Model for Determining Glomerular Filtration on Gadolinium Enhanced MR Imaging of the Kidney

John Votaw[1], Puneet Sharma[1], Khalil Salman[1], Richard Jones[2], Diego Martin[1]
[1]Emory University, Atlanta, Georgia, USA; [2]Children's healthcare of Atlanta, Atlanta, Georgia, USA

This study develops a 3-compartment kinetic model to describe Gd distribution in the renal artery and kidney, applys the model requirements to an optimized MR imaging technique, and implements the theoretical model to extract measures of renal blood flow and GFR. The 3 compartments represent blood, extracellular space, and glomerular filtration. The model was tested on idividuals receiving a steady infusion of Gd for 60-90 secs, and acquiring dynamic data very rapidly (0.9s/image). Both flow and GFR were quantified, and found to be in the range predicted by standard techniques. This procedure is capable of being implemented in the clinic for flow and GFR quatification in a very short study time.

2239. Comparison of Two Methods to Determine Single Kidney GFR from MR Renography: A Multicompartmental Model and Patlak-Rutland Analysis

Louisa Bokacheva[1], Ambrose Huang[1], Henry Rusinek[1], Manmeen Kaur[1], Qun Chen[1], Elissa Kramer[1], Edward Leonard[2], Vivian S. Lee[1]
[1]New York University School of Medicine, New York, USA; [2]Columbia University, New York, USA

Dynamic contrast-enhanced perfusion images of the kidneys acquired at 1.5 T in 9 patients were investigated for non-invasive evaluation of renal function. Glomerular filtration rates (GFR) were determined by two methods, a multicompartmental model and Patlak-Rutland method, and compared with the results of the reference nuclear medicine measurements. The GFRs derived from multicompartmental model were found to be in better agreement (R^2=0.92) with the reference GFR values from radionuclide studies than the results of Patlak Rutland method (R^2=0.7). It has also been demonstrated that the multicompartmental model analysis is better suited for low dose perfusion studies.

2240. Comparison of a Rutland-Patlak Plot and a Compartmental Analysis for the Assessment of Single-Kidney Glomerular Filtration Rate

David L. Buckley[1], Ala'a E. Shurrab[2], Philip A. Kalra[2]
[1]University of Manchester, Manchester, Greater Manchester, UK; [2]Hope Hospital, Salford, Greater Manchester, UK

The purpose of this study was to compare two approaches for the measurement of single-kidney glomerular filtration rate (SK-GFR) using dynamic contrast-enhanced MRI. Data from 39 separate MR renography studies were analysed using a Rutland-Patlak technique and a compartmental model. Estimates using both methods correlated well with radioisotope assessed SK-GFR - the Rutland-Patlak approach provided a near one-to-one correspondence while the compartmental method overestimated SK-GFR. However, the compartmental model fits to the experimental data were significantly better than those with Rutland-Patlak. Further work, including image registration, is needed to address these issues.

2241. Effect of Diabetes on the Renal Medullary Oxygenation in Rats: An Early Time Course Study

Elisabete Santos[1], Lu-Ping Li[1], Lin Ji[1], Pottumarthi V. Prasad[1]
[1]Evanston Northwestern Healthcare, Evanston, Illinois, USA

Diabetes aggravates renal medullary hypoxia possibly through enhanced regional oxygen consumption. To examine how early such enhanced medullary hypoxia begins, kidneys of control and streptozotoxin induced diabetic rats were investigated by direct regional pO2 and blood flow measurements using invasive fiber optic probes and non-invasive BOLD MRI. Six Wistar Furth rats in each group of control, 2-, 5-, 14- and 28 days after induction of diabetes were tested. Hypoxia was found in renal medulla as early as 2 days following induction of diabetes. Our findings also suggest that the change in renal oxygenation is determined predominantly by increased oxygen consumption.

2242. Magnetic Resonance Imaging Measurement of Renal Blood Flow Determined on First Pass Gadolinium-Chelate Perfusion

Khalil N. Salman[1], Puneet Sharma[1], Richard Jones[2], John Votaw[1], Diego Martin[1]
[1]Emory University, Atlanta, Georgia, USA; [2]Children's Healthcare of Atlanta, Atlanta, Georgia, USA

This study focuses on measuring renal blood flow from first-pass Gd-chelate perfusion imaging. The motivation is that both renal blood flow and glomerular filtration rate can be determined in one study session. The analysis assumed no contrast agent had reached the renal vein, making the window of perfusion analysis about 7 secs. By measuring the concentration of Gd in the kindey and artery over time, flow can be determined via a two-compartment kinetic model. Results show high correlation between this model and first-pass renal perfusion data. The method was validated against traditional phase contrast imaging.

2243. Dynamic Measurement of Renal Perfusion Using CASL: A Tool to Evaluate the Effects of Antihypertensive Agents in Spontaneously Hypertensive Rats

Denise Welsh[1], Alexandre Coimbra[1], Paul J. McCracken[1], Jacquelynn Cook[1], Richard Hargreaves[1], Magdalena Alonso-Galicia[1], Donald S. Williams[1]
[1]Merck & Co.,Inc, West Point, Pennsylvania, USA

This study uses arterial spin labeling (ASL) to monitor changes in renal perfusion following administration of an antihypertensive agent. For validation of this technique, renal perfusion was measured during infusion of ACh or ATII. Test groups were dosed with the ACE inhibitor Enalapril or saline. Infusion of ACh increased renal perfusion, while ATII decreased renal perfusion, demonstrating the ability to dynamically track renal perfusion in near real time. Enalapril produced a significant and sustained increase in renal cortical perfusion compared to saline controls. ASL perfusion MRI provides a non-invasive means of measuring renal perfusion in response to pharmacologic interventions.

2244. An Iterative Convolution Approach for the Non-Invasive Assessment of Cortical Perfusion in Renal Transplant Using DSC MRI

Ryan C. Lipscomb[1], Elizabeth A. Sadowski[1], Arjang Djamali[2], Bryan N. Becker[2], Thomas M. Grist[1], Sean B. Fain[1]
[1]University of Wisconsin, Madison, Wisconsin, USA; [2]University of Wisconsin, Fitchburg, Wisconsin, USA

An iterative convolution approach for estimation of the tissue impulse response function, H(t), is applied to the renal transplant population. We compared renal perfusion calculated using the proposed iterative technique to conventional gamma-variate fitting and show improved physiological accuracy and decreased variability in renal blood flow estimates. The iterative convolution results differentiated between normal transplants and those undergoing acute rejection.

2245. Conversion of the MR Signal Intensity to Gd-DTPA Concentration in Contrast-Enhanced MR Renography

Louisa Bokacheva[1], Keyma Prince[1], Henry Rusinek[1], Niels Oesingmann[2], Qun Chen[1], Manmeen Kaur[1], Ambrose Huang[1], Vivian S. Lee[1]
[1]NYU School of Medicine, New York, USA; [2]Siemens Medical Solutions USA, Inc., New York, USA

A method for calculating Gd-DTPA concentration from the MR signal intensity (SI) has been implemented for dynamic contrast-enhanced 3D renography. The method is based upon the phantom and *in vivo* measurements and differs from frequently used method of relative signal change to calculate Gd-DTPA concentration. The proposed method enables one to account for nonlinearity between SI and higher concentrations of gadolinium.

2246. Diffusion-Weighted MR Imaging of the Prostate: A Primary Study

Guo Xuemei[1], Wang Xiaoying[1], Li Feiyu[1], Jiang Xuexiang[1]
[1]First Hospital, PeKing University, Beijing, People's Republic of China

To evaluate whether diffusion weighted imaging (DWI) can be used to differentiate prostate adenocarcinoma (PCa) from normal prostate peripheral zone (PZ) and prostatitis, ADC values were measured in 13 BPH, 10 prostatitis and 15 PCa patients with different b value of 300, 500 and 800sec/mm2. The mean ADC value of PCa was significantly smaller than that of normal PZ and the prostatitis£but the difference between the prostatitis and the normal PZ had no statistical significance. The result of the study implied that ADC value measured from DWI can be used to differentiate prostatitis and PCa.

2247. Primary Study of Apparent Diffusion Coefficient in the Diagnosis of Prostate Cancer Recurrence After Endocrinotherapy

Feiyu Li[1], Xiaoying Wang[1], Yufeng Xu[1], Jiangxi Xiao[1], Xuexiang Jiang[1]
[1]Peking University First Hospital, Beijing, People's Republic of China

Early and accurate diagnosis of prostate cancer (Pca) recurrence is very important. Some modalities have been used in the diagnosis of Pca recurrence such as PET, MRS and PWI. We also though that DWI and ADC should play their roles in this field. The purpose of this study is to investigate the difference of ADC values between recurrent and non-recurrent Pca after endocrinotherapy. Twenty-eight Pca patients with or without cancer recurrence were recruited and the ADC values of recurrent and non-recurrent regions were measured. Statistically significant difference could be detected between them.

2248. ADC of Prostate Tissue *In Vivo* at 3T

Roger Bourne[1], Peter Stanwell[1], Saadallah Ramadan[1], Phillip Katelaris[1], Carolyn Mountford[1]
[1]Institute for Magnetic Resonance Research, Sydney, NSW, Australia

Apparent diffusion coefficient (ADC) measured by MR *in vivo* reflects physical properties of tissue that correlate with the microscopic architectural structure seen at histopathology. Measurements of ADC on 33 patients by diffusion-weighted EPI at 3T with a single element endorectal surface coil demonstrate more significant differences between benign peripheral zone tissue and adenocarcinoma than previously reported from 1.5T studies. Measurement of ADC of prostate tissue at 3T provides significant diagnostic information to improve the sensitivity and specificity of prostate cancer detection and staging by MR.

2249. The Effect of Different B-Values on the Apparent Diffusion Coefficient in Prostate Cancerous and Non-Cancerous Regions

Feiyu Li[1], Xiaoying Wang[1], Yufeng Xu[1], Jiangxi Xiao[1], Xuexiang Jiang[1]
[1]Peking University First Hospital, Beijing, People's Republic of China

It was reported that ADC would help determination of non-cancerous and cancerous tissues. But it's not enough to distinguish benign from malignant tissues with ADC alone because of the overlapped ADC values. Can the increase of b-value bring the increase of ADC difference between non-cancerous and cancerous tissues? The purpose of our study is to investigate the changes of ADC with different b-values in cancerous and non-cancerous regions, and to determine if b-values have effect on ADC difference between the two tissues. According to the result, it seemed that ADC difference were not changed significantly using different b-values (range 300-800s/mm2).

2250. Effect of Diffusion Weighted Imaging for Detection of Prostate Cancer-Comparison Between Tissue Types-

Tamami Namiki[1], Yoshihisa Namiki[1], Ken Koyama[1], Hiroshi Tanaka[2], Junta Harada[1], Kunihiko Fukuda[2], Mituhiro Ohmura[1], Kouichi Kishimoto[1]
[1]Jikei Kashiwa Hospital, Kashiwa, Chiba, Japan; [2]Jikei University School of Medicine, Nishi-Shinbashi, Tokyo, Japan

Diffusion weighted imagingiDWij of cancer tissue have higher intensity than surrounding prostate tissues. But there is some false negative in this method. We performed ROC analysis of different tissue types. ROC analysis were performed for each of the following combinations 1)benign and well differentiated cancer 2) benign and moderately differentiated cancer 3)benign and poorly differentiated cancer. The areas under the ROC curve for each combinations were 1)0.51 2) 0.69 3) 0.84. These results showed that poorly differentiated cancer is most easy to detect cancer in prostate DWi, and well differentiated cancer is sometimes false negative.

2251. Influence of Local Environment and Differentiation on Experimental Prostate Cancers on Tumor Metabolism and Vascularisation

Christian M. Zechmann[1], Eva C. Woenne[1], Gunnar Brix[2], Nicole Radzwill[3], Martin Ilg[3], Peter Bachert[1], Peter Peschke[1], Stefan Kirsch[1], Hans-Ulrich Kauczor[1], Stefan Delorme[1], Fabian Kiessling[1]

[1]DKFZ, Heidelberg, Germany; [2]Federal Office for Radiation Protection, Neuherberg, Germany; [3]Bruker Biospin, Ettlingen, Germany

Purpose of this study was to investigate the influence of tumor implantation site (intraprostatic/subcutaneous) on growth, vascularisation, metabolism, and histologic phenotype of three different experimental malignant prostate tumors in rats using DCE-MRI and ^{1}H-MRS.Differentiated tumors grew significantly slower in the orthotopic environment while anaplastic carcinomas did not show distinct differences. Significant differences in tumor perfusion were observed between orthotopic and subcutaneous low malignant carcinomas (Dunning-H) and the other sublines. All tumors showed elevated choline-creatine-ratio and signals of free fatty acids increased from benign to anaplastic tumors. Histologically orthotopic Dunning-H tumors showed a higher degree of apoptosis and mature vessels.

2252. Design of an Anatomically and Physiologically Realistic Prostate Phantom

Rolf F. Schulte[1], Mika W. Vogel[1], Timo Schirmer[2], Harry Schilling[3], Adriane Groeger[1], Patrick Gross[1]

[1]GE Global Research, Munich, Germany; [2]Applied Science Laboratory, Hallbergmoos, Germany; [3]Schleifring und Apparatebau GmbH, Fuerstenfeldbruck, Germany

The prostate is emerging as the first clinical diagnostic application of MRS. However, prostate MRS is difficult and requires highly trained specialists. Trainings on healthy volunteers are severely limited due to the commonly used endo-rectal coils. In this work, a dedicated phantom is presented which closely resembles anatomical and physiological characteristics of the prostate, including the surrounding fat layer, rectum and body. Initial MRI and MRS measurements show the usefulness of this phantom as a training and testing device.

Body MRI: Abdominal MRS

Room 4E Wednesday 14:00 - 16:00

2253. Dynamic Metabolic Changes in Liver and Muscle Tissue Under Glucose Administration Detected by ^{31}P MRS

Tim Wokrina[1], Marco Ulrich[1], Maria Gilles[1], Daniel Kopf[1], Gabriele Ende[1]

[1]Central Institute of Mental Health, Mannheim, Germany

Consequences from the metabolic syndrome and type-2 diabetes like weight gain and dyslipidemia are often assigned to insuline resistance. The goal of this study was to show that phosphorous MRS is capable of measuring dynamic changes in metabolite concentrations under glucose administration and to determine which tissue types are mainly involved in the glucose oxidation. Under glucose administration, we found a significant increase of Pi/γ-ATP and PME/γ-ATP metabolite ratios in liver tissue and an increase of the ratio Pi/PCr in calf muscle tissue. The energy cost of glycogen storage buildup in the calf muscle tissue might be brought up by the use of PCr.

2254. Measurement of T1 and T2 in MR Spectroscopic Evaluation of Fatty Liver

Michael Simca Middleton[1], Jeff Schwimmer[1], Mark Bydder[1], Graeme Bydder[1], Claude Sirlin[1]

[1]UCSD, San Diego, California, USA

Accurate MR Spectroscopic (MRS) liver fat quantification requires correction for relaxation effects. Average literature-based relaxation values may be used, but given patient variability, direct measurement may be preferable. Alternatively, sequences may be used that avoid these dependencies. We compared different MRS methods to measure T1 and T2 of liver fat and water. We measured T2 consistently and reliably with breath-hold spectroscopy at multiple values of TE. However, T1 could not be measured reliably using variable TR or variable flip-angle techniques. This suggests that fat fraction may best be determined with sequences that avoid T1 dependence, using patient-specific measured T2 correction.

2255. Fat Storage in the Liver During Feast or Famine

Vincent j. van Ginneken[1], Suzanne R. Kiihne[2], Lisanne Ham[1], Elwin Verhey[3], Rob E. Poelmann[1], Louise van der Weerd[1]

[1]Leiden University Medical Centre, Leiden, Netherlands; [2]Leiden University, Leiden, Netherlands; [3]TNO pharmaceuticals, Zeist, Netherlands

Obesity is becoming a huge problem because food is mostly available on demand. Because the dynamics of lipid accumulation in the liver of a mammal is largely unknown, we qualified and quantified the process of triglyceride (TG) accumulation in a mouse model after 24 hours of starvation and 40 days of a fatty diet using 1H-MRS and mass spectrometry.

2256. Hepatic ATP Synthesis Rates in Healthy Humans

Albrecht I. Schmid[1], Martin Krssak[1], Julia M. Szendroedi[1], Ewald Moser[1], Michael Roden[2]
[1]Medical University of Vienna, Vienna, Austria; [2]Hanusch Hospital, Vienna, Austria

Hepatic ATP synthesis was quiantified using ^{31}P MR-spectroscopy and the saturation-transfer experiment. The quality of the localisation (1D-ISIS) was specific and gave sufficient SNR. This is, to our knowledge, the first published quantification of ATP-synthesis in the human liver. Values and precision of data from the present study are in excellent agreement with data from isolated perfused rat livers *(Thoma et al. 1987)*.

2257. Cardiac / Respiratory Double Triggering for ^{1}H MR Spectroscopy of the Liver

Roland Kreis[1], Peter Vermathen[1], Michael Ith[1], Kim-Ann Lê[2], Luc Tappy[2], Chris Boesch[1]
[1]University Berne, Berne, Switzerland; [2]University of Lausanne, Lausanne, Switzerland

Since intrahepatocellular lipid [IHCL] content is related to insulin sensitivity, studies of the metabolic syndrome often rely on a reliable and non-invasive determination by MR methods. IHCL content was measured with a cardiac/respiratory double triggering sequence that is based on the respiratory amplitude modulation of the ECG signal. Reproducibility was investigated for IHCL and TMA. The method proved sensitive and reliable enough to show a correlation between IHCL content and hepatic, as well as whole body, insulin sensitivity even in a small number of healthy non-obese subjects.

2258. ^{31}P Magnetic Resonance Spectroscopic Imaging of Liver Repopulation by Transplanted Hepatocytes

Charles Landis[1], Kosho Yamanouchia[1], Alan Koretsky[2], Hoby Hetherington[1], Chandan Guha[1]
[1]Albert Einstein College of Medicine, Bronx, New York, USA; [2]National Institute of Neurological Disorders and Stroke, Bethesda, Maryland, USA

Hepatocyte transplantation (HT) is being explored as a therapeutic alternative to whole organ transplantation. However, engraftment, survival, proliferation and immune rejection of transplanted hepatocytes are difficult to monitor because of the invasive nature of liver biopsy procedures and spatial heterogeneity of repopulation of the liver by transplanted cells. Ectopic expression of creatine kinase (CK) in liver enables ^{31}P MRS measurements of phosphocreatine (PCr), a metabolite not normally produced in liver. Using donor hepatocytes isolated from transgenic mice that express CK in liver, ^{31}P MRSI was used to evaluate the survival and proliferation of transplanted hepatocytes. A strong, statistically significant, correlation of *in vivo* ^{31}P MRSI PCr signal and *ex vivo* determined liver CK expression was observed in mice receiving HT.

2259. Non-Invasive Analysis of Gallbladder Bile Composition in Cynomolgus Monkeys Using *In Vivo* 1H-MRS

Basil Künnecke[1], Markus von Kienlin[1]
[1]F. Hoffmann-La Roche Ltd, Basel, CH-4070, Switzerland

Bile is an essential compartment in lipid and cholesterol metabolism which serves the purpose of solubilising hydrophobic metabolites for excretion and dietary uptake. Biliary malfunction is implicated in numerous common diseases such as obesity. Hence, repetitive assessment of bile would be highly desirable. Here, we demonstrate in a cynomolgus monkey model that *in vivo* 1H-MRS provides high-resolution spectra which allow bile composition to be non-invasively and repetitively assessed in situ. Quantification reveals glycine and taurine conjugates of cholate, chenodeoxycholate and deoxycholate as the major biliary constituents. A cross-sectional and longitudinal study provides insight into the variability of bile composition.

2260. *In Vivo* 1H Liver Spectroscopy with Free Breathing 2D PACE

Jian Xu[1], Jan Ruff[2], Alto Stemmer[2], Mark A. Brown[1], Stephan Roell[2], Uwe Boettcher[2], Marianne Vorbuchner[2], Nouha Salibi[1], Bernd Stoeckel[1], Bachir Taouli[3], Vivian S. Lee[3]
[1]Siemens Medical Solutions USA Inc., Malvern, Pennsylvania, USA; [2]Siemens Medical Solutions, Erlangen, Germany; [3]New York University School of Medicine, New York, New York, USA

In vivo 1H Liver Spectroscopy with Free Breathing 2D PACE.

2261. The Usefulness of In Vitro Proton MR Spectroscopy for Characterizing and Differentiating Abdominal Body Fluids

Sang Soo Shin[1], Gwang Woo Jeong[1], Hyung Joong Kim[1], Heoung Keun Kang[1]
[1]Chonnam National University Medical School, Chonnam National University Hospital, Gwangju, Republic of Korea

Computed tomography(CT) is presently the premier imaging modality for evaluating patients with ascites because of its excellent spatial resolution and ability of enhancing small differences in tissue density, giving an accurate determination of the location and extent of fluid collections. However, its ability to characterize the nature of different types of fluid such as abscess, bile, serosanguinous ascites, malignant ascites, chyle is limited. We assessed the in vitro MRS at 1.5 Tesla to obtain some valuable information on discrimination and characterization of various abdominal fluids.

Body MRI: Techniques, Qualitative Measurements, Misc.

Room 4E Wednesday 14:00 - 16:00

2262. MRI Susceptibility Measurement of Hepatic Iron Concentration: Demonstration of Feasibility

Zili Chu[1, 2], Brigitta U. Mueller, [12], Donald H. Mahoney, [12], Kenneth L. McClain[1], Saul J. Karpen, [12], Raja Muthupillai[1, 3], Taylor Chung, [12], Rajesh Krishnamurthy, [12], Zhiyue J. Wang, [12]

[1]Baylor College of Medicine, Houston, Texas, USA; [2]Texas Children's Hospital, Houston, Texas, USA; [3]Philips Medical Systems, Cleveland, Ohio, USA

An accurate measurement of hepatic iron concentration has significant value for managing iron-chelation therapy. A non-invasive MRI liver susceptometry measurement technique that had been developed and validated previously was used to study a group of patients with liver iron concentration up to 19.0 Fe mg /g dry tissue. With a decrease of the echo time of the T2 preparation pulse and an increase of the navigator beam area, the susceptibility measurement can be carried out for heavily iron-overloaded patients. The liver magnetic susceptibility measured by MRI was linearly correlated with biopsy determined liver iron concentration.

2263. Characterizing MRI Parameters of Iron Loaded Rat Liver

Yu Pei Ma[1], Jeffrey J. Luci[1], John P. Wikswo[1], Mark D. Does[1]

[1]Vanderbilt University, Nashville, Tennessee, USA

Accurate non-invasive assessment of liver iron is essential for treatment of iron overload patients. We used an animal model to study how the NMR relaxation parameters change with liver iron contents *in vivo*. Using 4.7T scanner, both the longitudinal and transverse relaxation rate, R1 and R2, increase linearly with iron content, while R2* increases more rapidly when the iron concentration is higher than 0.8 mg Fe/g w. wt.. Comparing with R2, R1 is less sensitive, however, its correlation coefficient with iron content is higher. The magnetic susceptibility of iron overload liver, measured using a SQUID susceptomer, is also presented.

2264. On the Necessity of Flip Angle Correction for Fast T1mapping Using DESPOT 1

Reto Treier[1], Andreas Steingoetter[1], Michael Fried[2], Werner Schwizer[2], Peter Boesiger[2]

[1]University and ETH Zurich, Zurich, Switzerland; [2]University Hospital Zurich, Zurich, Switzerland

This study demonstrates the effect of B1 inhomogeneity on fast T1determination using DESPOT1. We present a method combining this approach with a fast B1 mapping technique allowing accurate T1 quantification in the human abdomen, especially the stomach. Spectroscopic reference data and in vitro and *in vivo* T1maps were acquired at 1.5T and 3.0T. Uncorrected data show a clear underestimation of the nominal T1 values. Applying the combined method, computed T1 values are in close agreement with the reference. The proposed optimized DESPOT1 technique offers new possibilities for fast T1mapping in non-static tissues as is the case for the abdominal region.

2265. Assessment of Colorectal Hepatic Metastases by Quantitative T2 Relaxation Time: a Method for Evaluating Tumour Response to Treatment?

Luigi Funicelli[1], David Collins[2], Baris Kanber[2], Erica Scurr[3], Martin O. Leach[2], Janet E. Husband[3], Dow-Mu Koh[2, 3]

[1]Instituto Europeo Di Oncologia, Milan, Italy; [2]Institute of Cancer Research, Sutton, Surrey, UK; [3]Royal Marsden Hospital, Sutton, Surrey, UK

Quantitative T2 relaxation time has been shown to be more accurate than visual assessment for the characterisation of focal liver lesions. Malignant lesions such as metastases show shorter T2 relaxation times (<130 ms) compared to benign lesions. Dynamic contrast enhanced MR imaging and diffusion-weighted MR imaging are increasingly employed to provide surrogate markers of response for hepatic malignancies. However, the value of quantitative T2 measurements in evaluating the response of liver metastases to treatment has not been previously established. Such measurement may also be potentially useful for assessing the effects of conventional and novel therapeutics.

2266. T2-Weighted MR Imaging with FIESTA Versus Fast Spin-Echo: Comparative Efficacy in Clinical Hepatic Imaging

Alvin C. Silva[1], Sean D. Beaty[1], Amy K. Hara[1], Maitray D. Patel[1], Patrick T. Liu[1]

[1]Mayo Clinic Arizona, Scottsdale, Arizona, USA

Purpose: To assess diagnostic accuracy of FIESTA as complementary sequence to moderately T2-weighted FSE in characterization of focal liver lesions, as compared with conventional heavily T2-weighted FSE.Materials and Methods: Independent, retrospective review of 40 benign/malignant lesions by three radiologists. Qualitative and quantitative evaluation performed, including ROC analysis and lesion CNR.Results: No significant statistical difference in lesion characterization between FIESTA and heavily T2-weighted FSE, as per ROC diagnostic accuracy, with substantial-excellent interobserver agreement. Significant difference in calculated CNR between benign & malignant lesions with FIESTA. Conclusion: FIESTA may replace heavily T2-weighted FSE as complementary sequence for hepatic lesion characterization.

2267. Evaluation of a Balanced 3D Turbo Field Echo Sequence Versus Radial Stack and Thin Slice Single Shot Turbo Spin Echo for Detecting Small Choledochus Calculi and Depicting Choledochus in the Papillary Region

Margaret Melhus[1], Tom Hirschberg[1], Stein Westad Ødegård[1], Tryggve Holck Storås[1]
[1]Ullevål University Hospital, Oslo, Norway

Traditional SSTSE thick and thin slab imaging were compared with 3D B-TFE for accuracy of detection of calculi in choledochus and depiction of the choledochus in the papillary area. 33 patients referred for MRCP were included. Precence or absence of calculi were confirmed by ERCP, peroperative cholangiography or clinical followup.Area (AUC) under empirical Receiver Operating Characteristics (ROC) Curve was used as a measure of accuracy in calculi detection.No statistically significant differences were found in detection accuracy between techniques. The B-TFE images were found to give a better visual depiction of the choledochus in the papillary region.

2268. Rapid EPI-Based MR Elastography of the Liver

Meng Yin[1], Roger C. Grimm[1], Armando Manduca[1], Richard L. Ehman[1]
[1]Mayo Clinic College of Medicine, Rochester, Minnesota, USA

MR Elastography (MRE) is a modified phase-contrast MRI technique for quantitatively assessing the mechanical properties of soft tissues by visualizing the propagating shear waves in soft tissues. A potential application of MRE is to detect and quantitatively assess hepatic fibrosis in patients with chronic liver disease. The spin-echo EPI-MRE sequence is an ultra-fast image acquisition method with equivalent accuracy and improved sensitivity for shear wave imaging. It may play an important role in the 7-D (4-D spatial and temperal resolution, 3-D motion directions) MRE development, with potential to allow the entire acquisition to be accomplished in less than one minute.

2269. One-Breath-Hold Acquisition of the Whole Abdomen in One Minute Using Continuously Moving Table MRI

Gregor Sommer[1], Ute Ariane Ludwig[1], Oliver Schäfer[1], Hans-Peter Fautz[1]
[1]University Hospital Freiburg, Freiburg, Germany

An acquisition method is presented which provides full volume coverage of the entire abdomen in a total measurement time of 70 seconds with only one breath-hold required. The method uses GRE-based transverse 2D-volume acquisition with continuous table motion combined with parallel imaging techniques. The upper 18 cm of the abdomen are recorded during a 20 seconds breath-hold phase which provides an image quality that is comparable to standard multiple-breath-hold approaches with stationary table. An acquisition regime for minimized FOV-usage increases the data homogeneity along the z-direction and makes the technique suitable for being used on short bore magnets.

2270. Do We Need Suspended Breathing with Real-Time Axial Continuously Moving Table MR Imaging?

Amrei Zielonka[1], Sonja Kinner[1], Michael O. Zenge[1], Mark E. Ladd[1], Susanne C. Ladd[1]
[1]University Hospital Essen, Essen, Germany

For three different 2D axial SSFP moving table sequences, we compared quality and potential distortion in the z-direction of breathhold versus non breathhold acquisitions reformatted into sagittal and coronal planes in 5 healthy volunteers. Distances between anatomic structures were comparable. No qualitative distortion is seen without breathhold; only motion artifacts generated by the heart are present, which do not influence the depiction of other structures including the hilar vessels. Further studies have to show if this technique can replace conventional imaging in patients who can not hold their breath; and whether this technique allows reliable, fast whole-body examinations.

2271. Two Approaches to Water/Fat Selective Whole-Body Continuously Moving Table 3D Imaging

Peter Börnert[1], Bernd Aldefeld[1], Jochen Keupp[1], Holger Eggers[1]
[1]Philips Research Laboratories, Hamburg, Germany

Whole-body 3D water/fat selective screening could be of interest in future clinical practice. High fat levels have been linked to a number of obesity-related illnesses, and fat visualization has been shown to be useful for the detection of tumor metastases in the abdominal region. In this study, the feasibility of whole-body continuously moving table water/fat selective imaging was investigated using two different approaches (magnetization prepared and three-point Dixon). It was found that the three-point Dixon fat imaging approach performs best, delivering high quality images.

2272. MR Imaging of Testicular Torsion: Features of Testicular Hemorrhagic Necrosis and Clinical Outcomes

Yuji Watanabe[1], Masako Nagayama[1], Akira Okumura[1], Yoshiki Amoh[1], Kazushige Oda[1], Takayoshi Ishimori[1], Takashi Kiyono[1], Kazuaki Nakada[1], Hideki Mitsui[1], Noriyoshi Morimoto[1], Takashi Tabuchi[1], Masayuki Kumashiro[1], Shinsuke Komaki[1], Takashi Sugioka[1], Osamu Ito[1], Keisuke Ohtsuki[1], Yoshihiro Dodo[1]
[1]Kurashiki Central Hospital, Kurashiki, Okayama, Japan

It has been difficult to differentiate testicular torsion from other scrotal disorders. When patients with acute scrotal symptoms are diagnosed to have testicular torsion, a choice of emergency surgery, orchiectomy or orchiopexy, is required. MR imaging can be useful in the evaluation of patients with testicular torsion. The overall accuracies in the detection of testicular necrosis was 93% for the T2-weighted imagings, 73% for dynamic contrast-enhanced subtraction MR imaging and 73% for intraoperative findings. The preoperative and follow-up MR imaging can help to accurately diagnose testicular torsion and to demonstrate testicular necrosis as well.

Abdominal MR Imaging at 3T

Room 4E Wednesday 14:00 - 16:00

2273. Rapid 3D T1-Mapping in the Abdominal Region at 3.0 T

Aart J. Nederveen[1], Cristina Lavini[1], Karin Horsthuis[1], Gerard J. den Heeten[1], Jaap Stoker[1]
[1]AMC, Amsterdam, Netherlands

In MRI quantitative measures are not frequently used. Quantitative T1-measurement in the abdominal region is however of clinical importance for quantification of contrast agent concentration in suspected lesions. In this study T1-measurements in 8 slices were performed with the classical Look-Locker (LL) sequence using a 3D Turbo Field Echo sequence. The entire volume was acquired within one breathhold, both before and after contrast agent administration. This technique allows for quantitative assessment of contrast agent concentration, thus permitting permeability imaging in areas that suffer from important motion problems.

2274. The Effect of Dielectric Pad on MR Images of the Upper Abdomen at 3T

Masako Kataoka[1], Hiroyoshi Isoda[1], Yoji Maetani[1], Yuji Nakamoto[1], Takashi Koyama[1], Shigeaki Umeoka[1], Ken Tamai[1], Aki Kido[1], Tsuneo Saga[1], Nobuko Morisawa[1], Kaori Togashi[1]
[1]Kyoto University Graduate School of Medicine, Kyoto, Japan

This study aimed to demonstrate the effect of dielectric pad on MR images of the upper abdomen at 3T regarding the improvement of B1 inhomogeneity. 10 healthy volunteer were scanned at 3T scanner using HASTE, T1-FLASH, Fat sat T1 FLASH, and diffusion weighted images. Images obtained with different dielectric pad made of ultrasound gel, water and without pad were compared regarding signal uniformity. The use of pads improved the B1-inhomogeneity in images on HASTE, and DWI, while no significant differences were observed on T1-FLASH images. There were no significant differences between the two different dielectric pads on all sequences.

2275. Single Breath-Hold T1 Measurements Using Segmented Inversion Recovery Prepared TrueFISP Sequence at 3 T

Louisa Bokacheva[1], Ambrose Huang[1], Jing An[1], Niels Oesingmann[2], Henry Rusinek[1], Qun Chen[1], Vivian S. Lee[1]
[1]New York University School of Medicine, New York, USA; [2]Siemens Medical Solutions, Erlangen, Germany

Estimates of T1 relaxation times within a breath-hold are particularly desirable for various applications, including dynamic contrast-enhanced perfusion imaging. Segmented inversion recovery prepared TrueFISP (sIR-TrueFISP) sequence was used to create abdominal T1 maps in the abdomen within one 20 s breath-hold. Abdominal scans with 10 degree sIR-TrueFISP sequence were acquired on 3 T Magnetom TIM Trio system. T1-maps of the axial slices were constructing by fitting the images pixel by pixel. Resulting T1 values for abdominal tissues are in agreement with the conventional inversion recovery method and published results.

2276. *In Vivo* Magnetization Transfer of Liver at 3T

Melanie S. Kotys[1], Ahmed M. Gharib[1]
[1]National Institutes of Health, Bethesda, Maryland, USA

Magnetization transfer (MT) imaging of liver has been shown to be of clinical diagnostic value but can be hindered by breathing artifacts. Further, *in vivo* liver MTR values have not been fully characterized at 3T. A breath-hold segmented MT strategy was used to acquire MT ratio (MTR) maps of the liver with decreased imaging time and no breathing artifacts. The average normal liver MTR value from five volunteers was 18.5% ± 2.8%. This value may more accurately reflect the MTR values for human liver at 3T using a sequence that acquires high-quality, quantitative MTR maps of the liver.

2277. Multiarterial Phase Dynamic MR Imaging of the Whole Liver Using LAVA at 3T

Hua Wang[1], Xiao-Ying Wang[1]
[1]Peking University First Hospital, Beijing, People's Republic of China

The purpose of this study was to explore the efficacy of multiarterial phase dynamic MR imaging of the whole liver using LAVA (Liver Acceleration Volume Acquisition) at 3T to depict small early enhanced hepatic lesions as well as hepatic arterial system. Nine patients with small early enhanced hepatic lesions were included in the study. Multiarterial phase (four phases) imaging of the whole liver during a single breath-hold was performed. Diagnostic quality images were obtained. Early enhanced hepatic lesions and main branches of portal veins were depicted as well as hepatic arterial system on the MIP images of subtraction. The contrast-enhancement dynamic process of small early enhanced hepatic lesions and their relationships with the hepatic vascular systems can be well depicted with increased spatial and temporal resolution.

2278. Imaging of the Liver at 3.0T. : Optimization of Breath-Hold, Volumetric Fat-Suppressed Fast Spin-Echo and Diffusion-Weighted Black-Blood Echo-Planar Imaging

Indra Celine van den Bos[1], Shahid M. Hussain[1], Piotr A. Wielopolski[1]
[1]Erasmus Medical Center, Rotterdam, Netherlands

The advantages of abdominal imaging at 3.0T are yet to be devised. Potential benefits include higher spatial resolution and possibility of thin slice imaging, although fat-suppressed T2-weighted imaging is limited by several factors, which include high specific-absorption-rate (SAR) and artifacts related to increased SNR, paramagnetic effects and field distorsion.To evaluate and optimize T2-weighted imaging at 3.0T, a pilot study was performed on eight volunteers to obtain optimal scanning parameters. Fat-suppressed FSE and diffusion-weighted echo-planar imaging show potential for thin slice imaging with multi-planar reformatting capabilities, improved fat-suppression and suppression of the blood signal with improved detection of focal liver lesions.

2279. MR Imaging of the Liver on Multi-Channel MR Systems at 1.5 and 3Tesla - Initial Experiences

Christoph J. Zech[1], Alexandra Panteleon[1], Karin A. Herrmann[1], Maximilian F. Reiser[1], Stefan O. Schoenberg[1]
[1]Munich University Hospitals - Grosshadern, Munich, Germany

MR imaging at 3Tesla (T) systems offers new perspectives; however, there are a number of challenges for abdominal MRI at higher field strength. The aim of this study was to compare the image quality and lesion delineation in MR examinations of the liver at 1.5 and 3T. The presented results show that MR examinations of the liver are feasible with high quality at 1.5T as well as 3T. Specific artifacts were seen more frequently at 3T, but did not result in a decreased image quality and lesion delineation in comparison to 1.5T.

2280. Comparison of 1.5T and 3T MRI for R2* Measurement of Iron Burden in Transfusion-Dependent Anemias

Pippa Storey[1, 2], Christine Lynn Carqueville[3], Alexis A. Thompson, [23], John C. Wood[4], Cynthia K. Rigsby, [23]
[1]Evanston Northwestern Healthcare, Evanston, Illinois, USA; [2]Northwestern University Feinberg School of Medicine, Chicago, Illinois, USA; [3]Children's Memorial Hospital, Chicago, Illinois, USA; [4]Children's Hospital of Los Angeles, Los Angeles, California, USA

R2* measurements provide a non-invasive way to monitor iron burden in patients with transfusion-dependent anemias such as thalassemia major. The relationship between hepatic iron concentration and R2* has been established at 1.5T but not at 3T. In this study, liver and cardiac R2* values were measured at 1.5T and 3T in 20 control subjects and 6 patients. Normative values were $39.2\pm9.0s^{-1}$ (1.5T) and $69.1\pm21.9s^{-1}$ (3T) in the liver, and $23.4\pm2.2s^{-1}$ (1.5T) and $30.0\pm3.7s^{-1}$ (3T) in the heart. Over patients and controls, the relationship between 3T and 1.5T R2* values was linear, with a slope of 1.93±0.08 (liver) and 1.90±0.19 (heart).

2281. 1.5T vs. 3T Body MRI: Qualitative and Quantitative Comparison of T2 Weighted Images for Liver Lesion Detection

Janio Szklaruk[1], Pryia R. Bhosale[1], Aparna Balachandran[1], Chaan S. Ng[1], Eric P. Tamm[1], Jingfei Ma[1]
[1]MD Anderson, Houston, Texas, USA

Our goal is to compare liver lesion detection with T2 weighted images at 3T MRI and at 1.5T. A total of 56 solid liver lesions were detected at 1.5T and 3T. Three radiologist scored lesion detectability on a 0 to 2 scale: 0=definitely absent; 1 = probably present; and 2=definitely present. The contrast to noise ratio (CNR) of lesion to liver was calculated and compared at 3T and 1.5T. There was no statistical difference in lesion detection at the two different field strengths ($p = 0.15$). There was no statistical significant difference in CNR at the two different field strengths($p = 0.07$).

2282. 3D Multi-Phase Contrast-Enhanced MR Imaging of Cirrhosis: 3.0 T Versus 1.5 T

M Louis Lauzon[1, 2], Magnus Breitling[2], Richard Frayne[1, 2], Houman Mahallati[1, 2]
[1]University of Calgary, Calgary, Alberta, Canada; [2]Foothills Medical Centre, Calgary Health Region, Calgary, Alberta, Canada

Multi-phase 3D breath-hold T1-weighted contrast-enhanced MR acquisitions are critical in diagnosing hepatic lesions. MR imaging at 3.0 Tesla has many potential advantages compared to 1.5 Tesla. Here, we quantitatively compare 3.0 T versus 1.5 T (via signal-to-noise (SNR) and contrast-to-noise (CNR) ratios) pre-contrast and contrast-enhanced scans at the arterial, portal venous and equilibrium phases for cirrhotic livers. The pre-contrast tissues had marginally significant increases in SNR (but not CNR) at 3.0 Tesla compared to 1.5 Tesla ($p \leq 0.05$), whereas the contrast-enhanced comparisons showed a "trend" towards increased SNR/CNR, albeit not statistically significant ($p > 0.1$).

2283. MRC at 3 Tesla with SPACE

Clare M. Haystead[1], Elmar M. Merkle[1], Brian M. Dale[2]
[1]Duke University Medical Center, Durham, North Carolina, USA; [2]Siemens Medical Solutions, Cary, North Carolina, USA

MR cholangiography was performed at 3.0T using a novel pulse sequence called SPACE to improve image quality and temporal resolution. Datasets were acquired in 29 human subjects and compared to a standard respiratory triggered 3D TSE T2w sequence. Utilization of the SPACE pulse sequence resulted in elimination of N/2 ghosting artifacts and decrease in background signal. Despite the statistically lower signal-to-noise ratio, image quality (evaluated by two independent readers) proved to be statistically superior on SPACE imaging. Additionally, SPACE imaging also offered statistically better temporal resolution. Dielectric artifacts on the other hand were slightly more pronounced on the SPACE sequence.

2284. RF Power Optimization for 3D-MRCP Allows Breath Hold Acquistion at 3T

Neville D. Gai[1], Reed F. Busse[2], Daniel J. Schaefer[1]
[1]GE Healthcare, Waukesha, Wisconsin, USA; [2]GE Healthcare, Menlo Park, Wisconsin, USA

Three-dimensional fast-recovery fast spin echo (3D-FR-FSE) has been demonstrated in previous studies to enable high-resolution thin-slice MR Cholangiopancreatography (MRCP) with higher SNR and greater anatomic detail than comparable 2D single-shot fast spin echo (SSFSE) acquisitions. While at 1.5T, the TR may be short enough to acquire a 3D dataset in a breath hold when coupled with parallel imaging, regulatory limits on SAR (specific absorption rate, a measure of patient RF heating) make this more challenging at 3T. We have developed a "SAR-burst" scan that more effectively takes advantages of the higher short-term (10-second-average) limit on SAR level while ensuring that the lower long-term (6-minute-average) limit is met as well. Additionally, the refocusing flip angle is automatically adjusted based on prescription parameters and patient weight to fully utilize available RF power while maintaining high SNR. These optimizations allow 3D-MRCP data to be acquired during a single breath hold at 3T with better coverage and resolution than non-burst mode scans.

2285. Optimization of MR Cholangiopancreatography at 3T: Comparison of 2D Thick Slab Acquisitions to 3D Strategies

Eric Niendorf[1], Martin P. Smith[1], Neil M. Rofsky[1], Ivan Pedrosa[1]
[1]Beth Israel Deaconess Medical Center, Boston, Massachusetts, USA

3T MRI and parallel imaging techniques make quality 3D sequences for magnetic resonance cholangiopancreatography (MRCP) clinically feasible. In this study, 20 patients underwent MRCP that included standard 2D thick-slab SSFSE images and 3D breath hold (BH) and 3D respiratory gated non-breath hold (RG-NBH) FRFSE sequences on a 3T GE system. Image sets were evaluated for visualization of different levels of bile ducts, pancreatic ducts, SNR, and "overall" impression. 3D RG-NBH was significantly better than 2D thick-slab SSFSE for depicting most bile ducts, SNR, and "overall" impression. 3D RG-NBH significantly outperformed 3D BH in all categories.

2286. Detection and Its Clinical Significance of Thoracic Duct Using MRCP Sequence at 3.0 Tesla

De-xin Yu[1], Chuan-fu Li[2], Qian Wang[1], Xiao-ming Zhang[1], Jian-jun Xiu[1]
[1]Qilu Hospital of Shandon University, Jinan City, Shandong Province, People's Republic of China; [2]Qilu Hospital of Shandon University,, Jinan City, Shandong Province, People's Republic of China

Our aim is to detect the dimensions of the thoracic duct with MRCP protocol and to probe the potential morphological changes caused by some disorders. Three MRCP were performed in a total of 139 patients, and the thoracic duct was shown in 69.78%.Most configuration of the cisterna chyli was tubular or saccular. The mean longitudinal, anteroposterior and transverse diameters of the cisterna chyli were 26.04¡À10.45 mm, 5.08¡À2.08 mm, and 5.02¡À2.13 mm respectively. The anteroposterior and transverse diameters of the thoracic duct were 3.08¡À0.44 mm and 3.58¡À0.13 mm in control group. The portal hypertension may influence the dimension of thoracic duct.

2287. Detectability and Measurement of Cisterna Chyli with Heavily T2-Weighted Technique at 3.0 Tesla

De-xin Yu[1], Chuan-fu Li[1], Qian Wang[1], Xiao-ming Zhang[1], Jian-jun Xiu[1]
[1]Qilu Hospital of Shandon University, Jinan City, Shandong Province, People's Republic of China

Our aim is to detect the configuration, dimensions of the cisterna chyli on heavily T2-weighted images and to probe the relationship of its dimensions between in disorders and a control group. Three-dimensional MRCP in 142 patients were performed, AND 29 cases were excluded. The mean longitudinal, anteroposterior and transverse diameters were measured in four groups including the control, portal hypertension, choledochus obstruction, and malignant tumour were compared. The most common configuration was tubular or saccular. The mean longitudinal, anteroposterior and transverse diameters were 26.34¡À10.40mm, 5.20¡À2.18mm, and 5.25¡À2.16mm. The disorders may influence the number of the lymphatic ducts at thoracic duct.

2288. SR-TurboFLASH Measurements of Renal Perfusion: Comparison Between 1.5 and 3T with and Without Parallel Imaging

Henrik Jakob Michaely[1], Harald Kramer[1], Klaus-Peter Lodemann[2], Niels Oesingmann[3], Maximilian F. Reiser[1], Stefan O. Schoenberg[1]
[1]University of Munich, Munich, Bavaria, Germany; [2]Bracco-Altana Pharma, Konstanz, Baden-Wuerttemberg, Germany; [3]Siemens Medical Solutions, New York, USA

An intraindividual comparison of renal perfusion studies in healthy volunteers at 1.5T with parallel imaging (PI), 1.5T without PI and 3.0T with PI is presented. Perfusion was measured using a SR-TurboFLASH sequence after the bolus administration of 7ml of Gd-BOPTA. SNR, image quality and the semiquantitative perfusion parameters were determined.The perfusion parameters mean transit time and time to peak were independent of the technique used. Perfusion imaging at 3.0T was found to yield the highest SNR and the best image quality compared to the sequnences at 1.5T with or without contrast agent.

2289. Evaluation of the Reproducibility of Intrarenal R2* Maps at 3.0T

Yufeng Xu[1], Xiaoying Wang[1], Xuexiang Jiang[1]
[1]Peking University First Hospital, Beijing, People's Republic of China

MRI maps of R2* have been shown to provide a new method for monitoring intrarenal oxygenation noninvasively. In this study we tested the reproducibility of BOLD-MRI R2* mapping at 3.0T in 8 healthy volunteers. The mean R2* values were 15.51¡À1.19Hz in cortex and 34.96¡À1.51Hz in medulla. The coefficients of variance between two examinations were 5.8% in cortex and 4.1% in medulla. Bland-Altaman's analyse showed that there was a good agreement between both renal R2* values. In conclusion, R2* values could be measured in a reproducible way in the renal medulla and cortex at 3.0T.

2290. Dynamic Contrast-Enhanced MRI Study of Male Pelvic Perfusion at 3T: Comparison in Cardiac and Non-Cardiac Patients

Ping Hou[1], Elise JB De[2], Larry A. Kramer[1], Ouida Lenaine Westney[1]
[1]University of Texas, Houston, Texas, USA; [2]Albany Medical College, Albany, New York, USA

Lower urinary tract symptoms and erectile dysfunction may relate to pelvic ischemia which can be demonstrated by dynamic contrast-enhanced (DCE) MRI perfusion values. This primary study has shown that patients with known coronary artery disease (CAD) will differ from those without (controls) with respect to (1) pelvic perfusion in prostate, corpus cavernosal and spongiosal tissues, and (2) pelvic symptoms (erectile dysfunction and lower urinary tract symptoms). Greater enhancement was observed in the control than the CAD for all three tissues with very significant difference.

Fat Quantitation

Room 4E Wednesday 14:00 - 16:00

2291. Fat/Water ^{1}H MRI to Investigate Effects of Leptin in Ob/ob Mice

Judy Rose James[1], JeAnne L. Hertel[2], Andriy M. Babsky[3], Shahrya K. Hekmatyar[3], Charles V. Jackson[2], Navin Bansal[3]
[1]Purdue University, West Lafayette, Indiana, USA; [2]Eli Lilly Research Laboratories, Indianapolis, Indiana, USA; [3]Indiana University School of Medicine, Indianapolis, Indiana, USA

The effects of exogenous leptin on visceral and subcutaneous fat volume in the abdominal region and fat-to-water ratio in the liver of leptin-deficient obese mice were investigated by ^{1}H MRI. Chemical shift selected fat and water ^{1}H MRI of control and leptin treated mice were obtained one day prior to treatment and after seven days of treatment (0.3 mg/kg/day). Among all the parameters measured, hepatic fat-to-water ratio decreased most dramatically with treatment, whereas subcutaneous fat volume in the abdominal region did not change significantly. Noninvasive fat and water MRI may prove very useful for evaluating new drugs for the treatment of obesity and other metabolic disorders.

2292. The Effect of Nutritional Counselling on Hepatic, Muscle and Adipose Tissue Fat Content and Distribution in Non-Alcoholic Fatty Liver Disease

Elizabeth Louise Thomas[1], Audrey E. Brynes[1], Gavin Hamilton[1], Nayna Patel[1], Adam Spong[1], Robert D. Goldin[2], Gary Frost[1], Jimmy D. Bell[1], Simon D. Taylor-Robinson[1]
[1]Hammersmith Hospital, Imperial College, London, UK; [2]College London, St Mary's Hospital, London, UK

The aim of this study was to assess the effectiveness of UK clinical practice, 'lifestyle modification', in reducing in hepatic fat. Whole body MRI and ^{1}H MRS were obtained, before and after 6 months nutritional counselling. A 4% weight loss, was accompanied by significant reductions in most adipose tissue (AT) depots. IMCL was significantly reduced in the tibialis. Decreases in IHCL and sol-IMCL were not significant. Significant correlations were found between decreased hepatic fat and reductions in intra-abdominal and abdominal subcutaneous AT. Improvements in serum AST and ALT were associated with reductions in intra-abdominal AT, but not changes in IHCL.

2293. Automatic Segmenation of Adipose Tissue Distribution in Childhood Obesity

Akila Rajagopal[1], Kendall O'Brien[1], Vincent Schmithorst[1], Maninder Kalra[1], Bernard J. Dardzinski[1], [2]
[1]Cincinnati Children's Hospital Medical Center, Cincinnati, Ohio, USA; [2]University of Cincinnati College of Medicine, Cincinnati, Ohio, USA

About 15 % of children and adolescents ages 6 to 19 are obese; a 200% increase over the past two decades. The amount of visceral fat is associated with other co-morbidities e.g., cardiac disease, diabetes, and sleep apnea. MR imaging can quantify the amount of subcutaneous and intra-abdominal fat noninvasively. Forty two obese children referred for sleep apnea had MR imaging of the abdomen. Automatic and manual segmentation of the adipose tissue distribution was performed. The two techniques agreed to within 5%. The automatic technique was at least 20 times faster than the method with user intervention.

2294. Insulin Resistance, Not Obesity Determines Fatty Liver in Obese Children

Daniel Weghuber[1], Michael Roden[2], Carlo Franz[1], Marek Chmelik[1], Sherin Torabia[1], Martin Bischof[1], Stephan Gruber[1], Werner Waldhaeusl[1], Anton Klingler[3], Kurt Widhalm[1]
[1]Vienna Medical University, Vienna, Austria; [2]Hanusch Hospital, Vienna, Austria; [3]Assign Data Management and Biostatistics, Innsbruck, Austria

Pediatricians face an uprise in the prevalence of childhood obesity and comorbidities, including insulin resistance, and NAFLD. The underlying mechanisms related to the changes in insulin sensitivity (IS) are poorly understood. The present study examined the association of liver fat deposition with IS in obese children. Intrahepatocellular lipids (HCL) of 26 obese children were assessed by MRS: 1H SVS. Insulin sensitivity was estimated by the WBISI. Obese insulin resistant children had significantly higher HCL than their insulin sensitive counterparts. HCL correlated negatively with WBISI after adjustment for BMI. Therefore, insulin resistance, not obesity determines fatty liver in obese children.

2295. MRI Quantification of Liver Fat in an Obese Population

Theresa Tuthill[1], David Raunig[2], Anne Hickman[2], Barry Peterson[2], Brad Wyman[2]
[1]VirtualScopics, Groton, Connecticut, USA; [2]Pfizer, Groton, Connecticut, USA

To further understanding of hepatic steatosis in liver disease and drug toxicity, a non-invasive technique for measuring fat fraction was investigated. Using the modified Dixon technique, twenty-one obese subjects were imaged with a 1.5T GE MRI scanner. Regions of interest were selected to compute fat fraction which ranged from 3 to 18%. Statistical analysis of ROIs showed the technique to be stable. The lack of correlation between liver fat content and BMI or ALT levels shows that liver fat accumulation cannot be simply explained by body weight or circulating liver enzymes in obese subjects.

2296. Quantifying MR Properties of the Cirrhotic Liver Using Explanted Specimens

Brian E. Chapman[1], J. Wallis Marsh[1], Mitchell E. Tublin[1]
[1]University of Pittsburgh, Pittsburgh, Pennsylvania, USA

We present preliminary quantification of the MR properties of cirrhotic livers using explanted livers. Explanted livers were obtained from the OR and imaged prior to routine pathology processing. T1 and T2* values were quantified using spiral based GRE sequences. T2 was quantified using FSE techniques. Fat was measured using in-phase and out-of-phase GRE images. Good separation between HCC and surrounding cirrhotic tissue using T1 and Fat measures were obtained. T2 showed limited separation between HCC nodules and the cirrhotic tissue. T2* measures were not used due to blurring and distortion in the spiral images when long TE values were used.

2297. MRI Estimation of Donor Graft Steatosis Prior to Orthotopic Liver Transplantation: Initial Results with Early Serum Outcome Measures, Surgical and Histological Correlation

Kieren Grant Hollingsworth[1], Jane Smith[1], Neville V. Jamieson[1], Chris J E Watson[1], Michael E. Allison[2], Graeme J. Alexander[1], David J. Lomas[1]
[1]University of Cambridge, Cambridge, Cambridgeshire, UK; [2]Addenbrookes Hospital, Cambridge, Cambridgeshire, UK

Donor graft steatosis adversely affects the outcome of human orthotopic liver transplantation and currently is subjectively assessed visually by the transplanting surgeons. 6 liver grafts were assessed "*ex vivo*" for steatosis by MRI, histology and surgical opinion. Total bilirubin, ALT and prothombin time were measured for 14 days post-transplantation. Of the 3 patients with the highest peak total bilirubin, ALT and prothombin time, 2 had above median steatosis (as measured by MRI). Although there were correlations between the MRI fat measurement and the histological assessment, there was no correlation between the surgical and MRI assessments.

2298. Fat Quantification by Modeling the Variation in Signal Amplitude with TE

Mark Bydder[1], Michael S. Middleton[1], Peter D. Gatehouse[2], Alyssa D. Chavez[1], Claude B. Sirlin[1]
[1]University of California, San Diego, California, USA; [2]Royal Brompton Hospital, London, UK

An important clinical use of Dixon techniques is to quantify fat deposition in organs such as liver. Because the amount of fat deposition relates to the severity and progression of disease, a reliable method to quantify fat would be a valuable tool for diagnosis and follow up of patients. The purpose of this study is to develop reliable methods to quantify fat.

2299. An MR Imaging Method for Quantifying Fat Fraction

John David Biglands[1], Dan Wilson[1]
[1]Leeds Teaching Hospitals NHS Trust, Leeds, West Yorkshire, UK

There are two limitations with the Dixon method of quantifying fat fraction. The ambiguity over whether fat or water is the dominant species, and T1-weighting errors. We propose a method to resolve these limitations by using images taken over a range of TR values and using a least squares fitting method to obtain values for the fat fraction and the T1s. The method has been successfully modelled in a computer simulation incororating random noise into the MR signal.

2300. Effect of Flip Angle on Fat Quantification by Dixon Techniques

Mark Bydder[1], Michael S. Middleton[1], Alyssa D. Chavez[1], Claude B. Sirlin[1]
[1]University of California, San Diego, California, USA

An important clinical use of Dixon techniques is to quantify fat deposition in organs such as liver. Because the amount of fat deposition relates to the severity and progression of disease, a reliable method to quantify fat would be a valuable tool for diagnosis and follow up of patients. The purpose of this abstract is to develop a reliable MRI method to quantify fat.

2301. Quantification of Liver Fat Content Using Selective Saturation at 3.0 T

Xiaohong Joe Zhou[1], Grace Guzman[1], Jennifer E. Layden-Almer[1], Katherine Schwartz[1], Theodore Mazzone[1], Thomas J. Layden[1], Scott J. Cotler[1]

[1]University of Illinois Medical Center, Chicago, Illinois, USA

We describe an MR technique for quantitatively measuring the liver fat content in patients with non-alcoholic fatty liver disease (NAFLD). The technique relies on chemically selective saturation, and requires a calibration scan of a liver phantom with known fat contents. Our results from ten patients indicate that the liver fat content revealed by MR correlates well with optical image analysis. The results also show that pathologists' assessment appears to overestimate fat content and this tendency is accentuated with higher degrees of liver fat. These findings suggest that the proposed technique is potentially useful for evaluating the presence of NAFLD.

2302. A Comphrehensive Fat Composition Measurements in Mice *In Vivo* with High Field MR Systems

Haiying Liu[1], James Mu[1], Corey Miller[1], Bei B. Zhang[1], Donald S. Williams[2], Richard J. Hargreaves[2]

[1]Merck Research Labs, Rahway, New Jersey, USA; [2]Merck Research Labs, West Point, Pennsylvania, USA

An MR based assay has been implemented to provide a comprehensive characterization of body fat composition. A valuable set of body composition parameters have been obtained from both lean and ob/ob mice (N=4/group). These readouts, total fat volume, visceral volume, liver fat content, IMCL, etc. are not easily accessible from a living animal with other conventional measurement techniques. A more complete characterization of the body fat changes in progression of obesity and response to various therapeutic agents is now possible in the same animal.

2303. MRI Adipose Tissue Volume Measures: Comparison of SPGR and Fast Two Point Dixon Methods at 3T

Ann L. Scherzinger[1], Yiping Du[1], Elizabeth Stamm[1], Robert Eckel[1], Jingfei Ma[2]

[1]University of Colorado School of Medicine, Denver, Colorado, USA; [2]University of Texas M. D. Anderson Cancer Center, Houston, Texas, USA

Traditional T1 weighted imaging is compared with a rapid Two Point Dixon (2PD) technique for quantitation of abdominal adipose tissue volumes at 3T. The 2PD technique is shown to give larger but more reproducible adipose tissue volumes. Correlation of measured volumes is strong for the subcutaneous fat compartment but not for the visceral fat compartment.

2304. Automated Fat Quantification Applied to Abdominal MR Images

Qi Peng[1], Roderick W. McColl[2], Paul T. Weatherall[2]

[1]UT Health Science Center at San Antonio, San Antonio, Texas, USA; [2]UT Southwestern Medical Center, Dallas, Texas, USA

A novel fast fat-only imaging method based on a 3D balanced steady-state free precession sequence has been proposed recently. An automated fat quantification method is introduced here for the rapid post-processing of the generated high contrast images. The method is based on a simple fat distribution model which takes both full-volume fat voxels and partial-volume into consideration. The final fat volume can be quantified after a simple automated curve fitting step. The method was tested in a phantom study and the results show that the proposed method can offer rapid and very accurate fat quantification.

2305. Fast Whole-Body 3D Water/Fat Scoring

Peter Börnert[1], Bernd Aldefeld[1], Holger Eggers[1], Jochen Keupp[1]

[1]Philips Research Laboratories, Hamburg, Germany

The amount and distribution of body fat is linked to a number of obesity-related illnesses. Clear knowledge about these conditions may help to improve diagnosis and to define potential risks for individual patients. Whole-body 3D head-to-toe water/fat MR imaging was performed at moderate spatial resolution in a total scan time of 2 minutes using continuously moving table imaging and employing a three-point Dixon technique. Using image-processing algorithms, useful diagnostic information can be derived. Such a short scan could be added to each standard examination in an efficient and patient-convenient way.

Gynecological and Fetal MR Imaging

Room 4E Wednesday 14:00 - 16:00

2306. Advanced Cervix Cancer: Can Simple DCE-MRI Derived Parameters Predict Treatment Response?

Kieren Grant Hollingsworth[1], Evis Sala[1], Mark Anthony Zahra[1, 2], James Brenton[1, 2], Robin Crawford[3], Mark Arrends[1], Li Tee Tan[2], David J. Lomas[1]

[1]University of Cambridge, Cambridge, Cambridgeshire, UK; [2]Addenbrookes Hospital, Cambridge, Cambridgeshire, UK; [3]University of Cambridge, Cambridge, Cambridgeshire, UK

Treatment response in advanced cancer of the cervix is relatively unpredictable. This pilot study evaluates the possible predictive value of simple DCE-MRI derived parameters such as the relative signal intensity (rSI) and slope of contrast medium uptake following rapid bolus injection of gadolinium-DTPA. Six patients were studied prior to and during treatment with chemo-radiotherapy. The initial DCE-MRI parameters (rSI, slope, Ktrans) were not correlated with initial tumour size but did significantly correlate with subsequent percentage volumetric tumour regression suggesting they may have a useful role in predicting treatment response in cancer of the cervix.

2307. Evaluation of Cervical Carcinoma of the Uterus with High B Diffusion-Weighted Imaging: A Comparison with Normal Uterine Cervix

Zhenghan Yang[1], Weifeng Zhao[1], Fei Sun[2], Min Chen[1], Lei Jiang[1], Min Zhang[1], Xiaohua Ye[1], Ye Tan[1], Cheng Zhou[1]

[1]Beijing Hospital, Beijing, People's Republic of China; [2]GE Medical System, China, Beijing, People's Republic of China

The purpose of this study is to investigate the usefulness of DWI in evaluating cervical carcinoma of the uterus. Conventional MR imaging and DWI with high b value were performed in 15 patients with cervical carcinoma and 11 volunteers, and the ADC values were measured. The mean ADC value of the cervical carcinomas was significantly higher than that of normal uterus cervix. On high b value DWI, malignant tissue showed significantly high signal than normal tissues. Our preliminary study indicates high b value DWI and ADC measurement has the potential ability to differentiate cervical carcinoma lesion from normal tissues.

2308. MR Profiles of Cervial Cancer Biopsies Correlate to Apoptosis and Cellular Density

Beathe Sitter[1], Heidi Lyng[2], Tone Frost Bathen[1], Line Rørstad Jensen[1], Gunnar B. Kristensen[2], Ingrid Susan Gribbestad[1]

[1]Norwegian University of Science and Technology, Trondheim, Norway; [2]Health Enterprise Rikshospitalet - Radiumhospitalet, Oslo, Norway

We have compared MR characteristics of biopsies from cervical cancer patients to apoptosis and cellular density. Tumor samples from 20 patients were excised before and after treatment and analyzed using MAS and histopathology. Lipid-CH_2/CH_3 ratio showed weak correlations (Pearson) to cellular density (r^2:-0.33, p: 0.032) and total apoptotic frequency (r^2: 0.30, p: 0.045). Ratios of cholines to lipid-CH_3 showed significant correlations to cellular density (r^2: 0.50, p: 0.001). The apoptotic frequency in such samples is representative for carcinomas and MAS studies can provide valuable information when exploring the potential of *in vivo* MRS as a non-invasive method to monitor apoptosis.

2309. Assessment of the Treatment Response of Uterine Cancer Using Double-Echo Dynamic Perfusion-Weighted MRI

Nobuyuki Kosaka[1], Hidemasa Uematsu[1], Hirohiko Kimura[1], Yoshiyuki Ishimori[2], Tetuji Kurokawa[1], Tsuyoshi Matsuda[3], Harumi Itoh[1]

[1]University of Fukui, Fukui, Japan; [2]Ibaraki Prefectural University of Health Sciences, Ibaraki, Japan; [3]GE-Yokogawa Medical Systems, Ltd., Tokyo, Japan

We hypothesized that perfusion-weighted MRI (PWI) could be used to assess the treatment response of uterine cancer. PWI was performed on 6 patients before and after chemotherapy. The relative tumor blood volume (rBV) was calculated in accordance with a first-pass compartment model. After chemotherapy, rBVs significantly decreased in all cases ($p<0.05$). The reduction rate of rBV and reduction rate of tumor size showed significant correlation ($p<0.05$). Our results suggest that the reduction rate of rBV can be used as a quantitative index for evaluating the effectiveness of therapy in uterine cancer.

2310. Can DCE-MRI Predict the Nature of Ovarian Tumors ?A Correlation Between DCE-MRI and Angiogenesis Biomarkers

Isabelle Thomassin-Naggara[1, 2], Marc Bazot[2], Emile Darai[3], Patrice Callard[4], Claude Marsault[2], Charles-André Cuenod[1, 5]

[1]Laboratoire de recherche en imagerie de la faculté Necker, paris, france, France; [2]Service de radiologie de l'Hopital Tenon, paris, france, France; [3]Service de gynécologie et obstétrique de l'Hopital Tenon, paris, france, France; [4]Service d'anatomopathologie de l'Hopital Tenon, paris, France, France; [5]Service de radiologie de l'Hopital Européen Georges Pompidou, paris, France, France

Purpose: To determine whether dynamic magnetic resonance imaging (DCE-MR) enhancement parameters are associated with angiogenesis markers in order to determine nature of epithelial ovarian tumors.Materials and methods: Forty one patients with epithelial ovarian tumors underwent DCE-MR following by surgical excision and CD 34, anti-alpha smooth actin and VEGFR-2 staining in all lesions (12 benign, 13 borderline and 16 malignant tumours).Results: The myometrium smooth muscle has a typical enhancement curve with a much steeper rise and higher peak than skeletal muscles. There was a significant higher amplitude and faster enhancement of malignant compared to borderline and benign tumors.Benign tumors have a weaker slope of enhancement than borderline and borderline than malignant which have an intensive slope of enhancement.The enhancement amplitude was correlated with total capillary surface, and the slope of raising with weak pericyte coverage index and high VEGFR-2 expression. There was no correlation with the microvessel density.

2311. Magnetic Resonance Imaging Characterization of Uterine Leiomyomata of African American Women Demonstrate an Overall Greater Number of Smaller Uterine Leiomyomata

Alisa Suzuki[1], Fiona M. Fennessy[2], Kelly H. Zou[1], Clare Tempany[1]

[1]Brigham and Women's Hospital, Boston, Massachusetts, USA; [2]Dana Faber Cancer Institution, Boston, Massachusetts, USA

Uterine leiomyomata represent the most common gynecologic tumors. African American women (AA women) are more likely to have leiomyomata. This study is to examine imaging characteristics of leiomyomata in AA women, and compare them to those of their Caucasian counterparts. Study included 31 AA women (422 leiomyomata) and 42 non-AA women (185 leiomyomata). AA women have a greater number of leiomyomata (13.6 SD } 2.8) per person in comparison to Caucasian women (4.4 SD } 5.9) ($p=0.001$). Submucosal and intramural leiomyomata of AA women are significantly smaller in size ($p<0.001$). These findings may help guide clinicians in determining treatment options.

2312. Use of MRI to Quantify Intra-Vaginal Gel Distribution in Human Subjects: Preliminary Analysis of the Candidate Gel Formulation for the Cyanovirin-N Trial

Mark Rosen[1], Amy Hummel[1], Kelly Timbers[1], David Shera[1], Scott Pretorius[1], Frank Malinoski[2], Kurt Barnhart[1]

[1]University of Pennsylvania, Philadelphia, Pennsylvania, USA; [2]Biosyn, Inc., Huntingdon Valley, Pennsylvania, USA

Six female subjects were studied with MRI for quantification of intra-vaginal distribution and spread of candidate gel formulations for the upcoming clinical trial of intra-vaginal cyanovirin-N for prevention of HIV transmission. Gadolinium chelate was added to four different candidate gel formulation (without microbicide). These were then inserted intravaginally into female volunteers for evaluation of intra-vaginal spread of gel and total vaginal surface coverage. Effects of gel formulation, time between insertion and imaging, and simulated intercourse were studied.

2313. Development of a Murine Isogenic Graft Model of Endometriosis: Monitoring by Dynamic Contrast-Enhanced MRI

Inna V. Linnik[1], Steve R. Williams[1], Alex De Giorgio-Miller[2], Philip S. Murphy[2], David L. Buckley[1]

[1]University of Manchester, Manchester, UK; [2]Pfizer, Sandwich, UK

The purpose of our study was to develop non-invasive method of studying endometriosis in a pre-clinical model. We used dynamic contrast-enhanced MRI (DCE-MRI) in a mouse isogenic graft model of endometriosis. Each animal was imaged on days 3, 7 and 10 after tissue implantation. Estimates of baseline T1, Ktrans, ve (interstitial volume) and kep (exchange rate) were obtained for each lesion and time point. No consistent change was observed in any parameter over the time frame studied.

2314. Application of Magnetic Resonance Direct Thrombus Imaging for the Detection and Monitoring of Pelvic Endometriosis

Ranu Taneja[1], General Leung[1], Susan Crisp[1], Richard Bitar[1, 2], David Howe[3], Philip Murphy[3], Alan R. Moody[1, 2]

[1]Sunnybrook and Women's College Health Sciences Centre, Toronto, Ontario, Canada; [2]University of Toronto, Toronto, Ontario, Canada; [3]Pfizer Inc., Sandwich, Kent, UK

Magnetic Resonance Direct Thrombus Imaging (MRDTI) uses a 3D highly T1-weighted fat-suppressed acquisition to visualise methaemoglobin–rich thrombi whilst suppressing surrounding sources of high signal. We applied the same core MRDTI approach to the female pelvis to locate blood products within endometriotic lesions. Application of the MRDTI sequence increased detection of small endometriotic foci. Superimposition onto T2WI improved anatomical localization and differentiation of endometriotic foci from other cystic lesions in the pelvis. This technique may provide a reliable and non-invasive means of diagnosing, quantitating and following up endometriosis.

2315. Reduced Field of View Imaging for Fetal fMRI (F-fMRI)

Laura J. Pisani[1], Roland Bammer[1], Gary H. Glover[1]
[1]Stanford University, Stanford, California, USA

We present a reduced FOV (rFOV) sequence designed for fetal fMRI. Two-dimensional selective outer volume suppression allows rFOV imaging without aliasing of signal from the maternal abdomen. Imaging performance is compared with a conventional full FOV gradient echo sequence. fMRI studies were performed with a) an auditory stimulus and b) oxygen modulation. The rFOV sequence allows tradeoffs between shortening the readout trajectory and lowering gradient slew rates for quieter scanning and increased SNR. Preliminary negatively correlated activation measurements (cc < -.2) from oxygen modulation are reported.

2316. Fetal MRI in Early Second Trimester Pregnancy

Marie Raiend[1], Hashem Amini[1], Håkan Ahlström[1], Ove Axelsson[1], Johan Wikström[1]
[1]Uppsala University, Uppsala, Sweden

MRI was performed of 56 fetuses where routine ultrasound scanning had shown suspected malformations. 3 mm T2 weighted Single Shot TSE sequences were acquired in the axial, coronal, and sagittal planes as well as 8 mm T1-weighted axial images. The main ultrasound findings were verified in 51/56 cases. Additional relevant findings were found in 17/56 cases. Of these were 6/7 cases with CNS lesions, 5/8 cases with oligohydramnios, and all three cases with diaphragmatic hernia. Fetal MRI is feasible in early second trimester, and of special value in cases with suspected CNS lesions, diaphragmatic hernias and oligohydramnios.

2317. Assessment of Liver and Brain Volumes at Post-Mortem Fetal MRI – Comparison to Organ Weights at Conventional Autopsy

Ferdia A. Gallagher[1, 2], Andrew C. Breeze[2], Justin J. Cross[2], Gerald A. Hackett[2], Christoph C. Lees[2], Ilse Joubert[2], Patricia A. K. Set[2], Flora A. Jessop[2], Anita L. Whitehead[2], David J. Lomas[1, 2]
[1]University of Cambridge, Cambridge, UK; [2]Addenbrooke's Hospital, Cambridge, UK

Post-mortem MRI offers a non-invasive alternative to conventional perinatal autopsy when parents decline consent. Many stillborn fetuses appear normally formed, but intrauterine growth restriction may be implicated. Signs of IUGR at autopsy include an abnormally elevated brain weight/liver weight ratio. We sought to determine whether comparable information could be obtained at post-mortem MRI by estimating brain and liver volumes (using ANALYSE software) and comparing these to the actual organ weights measured at autopsy. We observed a high correlation between organ weights and volume estimates and believe that this technique may provide important information when autopsy consent is withheld.

2318. Improving Image Quality in Fetal MRI Using Autocalibrating Reconstruction for Cartesian (ARC) Sampling

Roland Bammer[1], Erika Rubesova[1], Allan White[1], Stefan T. Skare[1], Philip Beatty[1], Anja Brau[2]
[1]Stanford University, Stanford, California, USA; [2]GE Healthcare, Menlo Park, California, USA

While T2-weighted fetal MRI is readily achieved with single-shot FSE, appropriate T1-weighted images are still difficult to obtain. In particular, the image quality is often frustrated by respiratory motion of the mother or fetal movements. A robust new parallel imaging method, Autocalibrating Reconstruction for Cartesian Sampling (ARC), was investigated for its potential strengths and weaknesses in rapid T1w fetal MRI. We could demonstrate that T1w ARC FGRE and LAVA can significantly improve the robustness and reliability of T1w fetal MRI within a single breath-hold of reasonable duration for pregnant women.

2319. Placental Perfusion and Permeability Assessment by Dual Echo DCE-MRI in Mice Using High Concentration of Gadolinium

Fabienne Taillieu[1], Laurent,J Salomon[1], Nathalie Siauve[1], Olivier Clément[1], Daniel Balvay[1], Catherine Vayssettes[1], Yves Ville[2], Charles A Cuenod[1]
[1]Université Paris V Descartes, Faculté Necker, Paris, France, France; [2]Centre Intercommunal de Poissy, Poissy, France, France

This study using dual echo DCE MRI in mice with high concentration of Gd gives a non invasive access to placental microvascular parameters including the perfusion and permeability of the placental barrier. It shows promises to elucidate intrauterine growth restriction pathogenesis as well as to help in the management of compromised pregnancies.

2320. Post-Partum Relaxation Parameter Mapping of Human Placentas at 1.5T : Differences Between Pre-Eclamptic and Healthy Pregnancies

Chardonnay Julia Vance[1, 2], Bruce N. Ames[1], Gary H. Glover[2]
[1]UC Berkeley, Berkeley, California, USA; [2]Stanford University, Stanford, California, USA

Relaxation parameters of seven post partum human placentas were mapped at 1.5T: two from healthy pregnancies, three from mild pre-eclampsia (PE), and two from severe PE. T2 times were not linked to PE. T1 times were more than two-fold higher in placentas from two severe PE versus normal pregnancies (averaging 1693 ms vs 764 ms, respectively). The S.D. of T1 was also higher with PE (280 ms PE vs 70 ms non-PE). Including the mild cases of PE, T1s do appear to correlate with the severity of PE in this small, unmatched data set.

2321. Analysis of Ovarian Vascular Function in PKB[alpha]/Akt1- Deficient Mice Using Biotin-BSA-GdDTPA Enhanced 3D-MRI

Vicki Plaks[1], Elina Berkovitz[1], Brian A. Hemmings[2], Nava Dekel[1], Michal Neeman[1]
[1]Weizmann Institute of Science, Rehovot, Israel; [2]Friedrich Miescher Institute for Biomedical Research, Basel, Switzerland

Angiogenesis plays a vital role in sustaining reproductive processes. PKB/Akt is known to act as a mediator of angiogenesis via the VEGF receptor/PI3K/PKB signaling cascade. This study focuses on the role of PKBá in ovarian function and its implications on embryo implantation and overall fertility utilizing macromolecular contrast enhanced MRI to study ovarian vascular function in PKBá knockout (KO) mice. MRI data analysis revealed reduced vessel density in KO ovaries as compared to WT. This observation along with the absence of spontaneous pregnancies in this model and the apparent reduced fertility after embryo transfer imply that ovarian function is perturbed.

Manganese Enhanced MRI: Multiple Applications

Room 4E Wednesday 14:00 - 16:00

2322. The Use of MEMRI to Assess *In Vivo* Axonal Transport Rates in the Murine Central Nervous System (CNS)

Karen Brown Smith[1], Mitchel E. Deshazer[1], Robia G. Pautler[1]
[1]Baylor College of Medicine, Houston, Texas, USA

Manganese enhanced MRI (MEMRI) has been developed for *in vivo* neuronal tract tracing as well as a marker for neuronal activation. Here we extend the use of MEMRI in the murine olfactory system as a means to detect *in vivo* axonal transport rates. We verified microtubule based axonal transport with responses to temperature changes and pharmacological agents.

2323. Semi-Automatic 3D Segmentation and CNR Measurement of Mn2+ Enhanced Optical Nerve in Adult Rats

Øystein Olsen[1, 2], Vassili Kovalev[3], Maria Petrou[4], Marthe Thuen[2], Pål Erik Goa[2], Christian Brekken[2], Olav Haraldseth[2]
[1]Sør-Trøndelag University College, Trondheim, Norway; [2]Norwegian University of Science and Technology, Trondheim, Norway; [3]University of Surrey, Guildford, UK; [4]Imperial College, London, UK

The purpose of this project was to develop an objective method of calculating Contrast-to-Noise Ratio (CNR) profiles from 3D MRI data of the Mn2+ enhanced optic nerve, based on minimal user intervention. We present a robust and objective a method for calculating the CNR profile of the Mn2+ enhanced optical nerve based on objective image post processing with few user interactions. The method traces the nerve centre, segments the nerve from the eye and calculate the CNR profile with a user defined spatial resolution. Even though the method is dedicated for a specific application it is of general interest.

2324. Detection of Blood-Brain Barrier Disruption in Rat Brain After Osmotic Shock Using Manganese-Enhanced Magnetic Resonance Imaging (MEMRI)

David Bennett[1], Nils Henninger[2, 3], Marc Fisher[2, 4], Chris Sotak[1, 2]
[1]Worcester Polytechnic Institute, Worcester, Massachusetts, USA; [2]University of Massachusetts Medical School, Worcester, Massachusetts, USA; [3]University of Massachusetts Memorial Healtcare, Worcester, Massachusetts, USA; [4]University of Massachusetts Memorial Healthcare, Worcester, Massachusetts, USA

Infusion of manganese two minutes after osmotic disruption of the blood-brain barrier (BBB) resulted in areas of signal enhancement closely correlated with areas of Evans Blue histological staining. For MEMRI experiments using applied neuronal stimulus to generate T1-contrast, this infusion protocol may obscure intended results. This infusion protocol may, however, be a useful alternative for imaging experimental BBB disruption.

2325. MEMRI Reveals Functional Changes in Basal Ganglia Output Nucleus in Parkinson's Disease

Revital Shtarkshall[1], Hagai Bergman[2], Gadi Goelman[1]
[1]Hadassah Hebrew University, Jerusalem, Israel; [2]Hadassah Medical School, Hebrew University, Jerusalem, Israel

Manganese enhanced-MRI was used to follow dynamic connectivity changes in a 6-OHDA Parkinson disease rat model. Using principal component analysis we followed manganese transfer from the CPu to relay nuclei. Two common principal components (PCs) were found in our data; one resembles delayed and sustained manganese accumulation, the other fast increase followed by fast decrease. Both PCs represent the substantia nigra (SN) for control and 6-OHDA groups. However, the volume of the first PC is significantly lower in 6-OHDA rats with no change in the other PC. Volume reduction suggests a reduction in spatial localized connectivity between CPu and SN.

2326. Novel Application of MEMRI Detects Sensory Deficits from Olfactory System Injury in Newborn Rabbit After Antenatal Hypoxia-Ischemia

Alexander Drobyshevsky[1], Alan M. Robinson[2], Matthew Derrick[1], Alice M. Wyrwicz[1], Xinhai Ji[1], Ila Englof[1], Sidhartha Tan[1]

[1]Evanston Northwestern Healthcare, Evanston, Illinois, USA; [2]Northwestern University,, Chicago, Illinois, USA;

Smell deficits elicited by the motor response are observed in our cerebral palsy model of antenatal hypoxia-ischemia in rabbits. Manganese Enhanced MRI was applied to quantitatively asses the difference in manganese uptake and transport by olfactory epithelium neurons between control and post-hypoxic rabbit kits and whether this difference is augmented by specific odors. Amyl acetate exposure resulted in increased augmentation of the signal in control group. There was a significant decrease in manganese uptake in olfactory epithelium and olfactory bulbs in P1 kits following fetal hypoxia.

2327. Quantitative Assessments of Mouse Optic Nerve Projections to the Brain *In Vivo*

Miriam Scadeng[1], James D. Lindsey[1], Jonathan Crowston[1], David J. Dubowitz[1]

[1]University of California San Diego, La Jolla, California, USA

The ability to directly assess axonal integrity throughout the visual system *in vivo* would allow repeated evaluations within the same subject, and a more accurate determination of the rate of disease progression or recovery. We use an intracameral injection of manganese ions (Mn) to track visual cortical projections in the mouse. Mn is seen as increased T1 signal intensity ipsilaterally in vitreous humor and optic nerve, and contralaterally in lateral geniculate nucleus, superior colliculus and visual cortical areas V1 and V2L. This data demonstrate the ability to assess axonal integrity in the visual system across 2 synaptic junctions.

2328. Mapping Cellular Architectonics of Rat Hippocampus Using Manganese-Enhanced and Diffusion Spectrum Imaging

Jun-Cheng Weng[1], Jyh-Horng Chen[1], Pai-Feng Yang[1], Li-Wei Kuo[1], Van Jay Wedeen[2], Wen-Yih Isaac Tseng[3]

[1]National Taiwan University, Taipei, Taiwan; [2]Harvard Medical School, Charlestown, Massachusetts, USA; [3]National Taiwan University College of Medicine, Taipei, Taiwan

Manganese-enhanced magnetic resonance imaging (meMRI) and diffusion spectrum imaging (DSI) both have the potential to probe the neuroarchitecture based on the different biological mechanisms. However, application of these two methods simultaneously and non-destructively in rat hippocampus has never been demonstrated yet. Therefore, the purpose of this paper is to realize the neuroarchitecture of rat hippocampus using meMRI and DSI in 3T MRI. We combined meMRI with DSI anisotropy (DA) to indicate the consistency of the two tools. The results indicate that neuronal architecture of rat hippocampus can be visualized and has high consistency in a systemic administration of Mn^{2+} and water molecular diffusion.

2329. Effects of the Dietary Fatty Acids on Manganese-Enhanced Magnetic Resonance Imaging (MEMRI)

Yu-Ting Kuo[1], [2], Po-Wah So[1], Amy H. Herlihy[1], Jimmy D. Bell[1]

[1]Hammersmith Hospital, Imperial College London, London, UK; [2]Faculty of Medicine, School of Medicine, Kaohsiung Medical University, Kaohsiung, Taiwan

Dietary supplementation of the omega-3 fatty acids have been shown to have beneficial effects on the cardiovascular system in human and animal, but the effect on the brain is not conclusive. MEMRI has been successfully used to study brain structures and activity, but the effect of the long-term dietary intervention on MEMRI is still unknown. In this study, we have performed MEMRI to evaluate the effects of dietary fatty acids on the murine brain. The results suggest MEMRI is able to detect the effects of dietary fatty acids on the brain, with dietary low fish oil supplement showing neuroprotective effect.

2330. Timelapse Mn++ Enhanced MRI in the Living Brain

Elaine L. Bearer[1], Xaiowei Zhang[2], Tim Hiltner[2], J. Michael Tyszka[2], Russell E. Jacobs[2]

[1]Brown Univ, Providence, Rhode Island, USA; [2]California Institute of Technology, Pasadena, California, USA

Neuronal transport has never been directly imaged in the living brain. Transport delivers molecules to distant sites and is useful for tracing neuronal pathways by histology. MEMRI allows investigation of transport parameters and tract tracing *in vivo*. We injected Mn++ into (1) the vitreous of the eye and (2) the optic chiasm and monitored its effect on neuronal activity by VEP. Mn++ transport was imaged over time (every 6min for 2hr) by T1-weighted MR and sighted versus blind mice compared. Mn++ transiently inhibits VEP, rates suggest transport along different intracellular pathways that differ for anterograde and retrograde directions.

2331. Manganese-Enhanced MRI of Rat Brain Function Under Forepaw Electric Stimulation: Comparison Between Accumulative Pain-Evoked Activity and Activity-Induced Manganese-Dependent Contrast

Jun-Cheng Weng[1], Jyh-Horng Chen[1], Chia-Hao Su[1], Wen-Yih Isaac Tseng[2]

[1]National Taiwan University, Taipei, Taiwan; [2]National Taiwan University College of Medicine, Taipei, Taiwan

Neuroimaging methods have been proposed to provide noninvasive approaches for neuroscience research. Functional MRI (fMRI) based on blood oxygenation level-dependent (BOLD) in brain research remains challenging, such as spatial resolution, motion suppression, complex paradigm and drug administration. Therefore, an alternative MRI approach is provided by manganese-enhanced MRI (meMRI), which has the potential to image neural activity by using manganese ion as a MR-detectable contrast agent. The purpose of this paper is to use the direct and effective meMRI in 3T MRI to map accumulative pain-evoked activity (APA) and activity-induced manganese-dependent contrast (AIM) of electric stimulation of rat forepaw. In order to detect diluted concentration of Mn^{2+} in rat brain and to highlight the active area, contour plot of meT1WI and R1 map were implemented. Our results indicated a clear relationship between Mn^{2+} enhancement and pain-evoked activity.

2332. Manganese-Enhanced MRI of Appetite Centres in Ob/ob Mice

Nachiket Abhay Nadkarni[1], Yu-Ting Kuo[1, 2], Amy H. Herlihy[1], Jimmy David Bell[1]
[1]Hammersmith Hospital, Imperial College London, London, UK; [2]Kaoshing Medical University, Kaoshing, Taiwan

Manganese-Enhanced MRI (MEMRI) is a functional neuroimaging tool that could be useful in the investigation of appetite regulation. The leptin deficient (*ob/ob*) mouse is an important model of obesity, and the efficacy of MEMRI needed to be determined in this system. This study provides evidence that *in vivo* MEMRI confirms some previous *in vitro* c-Fos results in the *ob/ob* mouse, for example demonstrating an absence of fasting state regulation of neuronal activity in appetite centres. However, there are discrepancies with c-Fos as to the chronic, long-term effect of leptin deficiency on neuronal activity.

2333. Central Neural Activity in Rats with Tinnitus Evaluated with MEMRI

Carol A. Bauer[1], Luisa Ciobanu[2], Boris Odintsov[2], Thomas J. Brozoski[1]
[1]Southern Illinois University, Springfield, Illinois, USA; [2]University of Illinois, Urbana-Champaign, Illinois, USA

Tinnitus is the perception of sound in the absence of external auditory stimulation. Current evidence implicates inappropriate neural activity in the CNS in this process. The application of imaging techniques has shown that functional changes at more than one brain level are likely responsible for the development and persistence of tinnitus. We used the technique of manganese-enhanced MRI to assess neural activity in the central auditory pathway of rats with psychophysical evidence of tinnitus after acoustic trauma. Using this technique, the long-term effects of trauma are evident as increased neural activity in auditory midbrain over a year after the exposure.

2334. Mapping Cocaine-Induced Brain Activation Using Manganese-Enhanced MRI

Hanbing Lu[1], Zheng-Xiong Xi[1], Leah Gitajn[1], William Rea[1], Clara Scholl[1], Yihong Yang[1], Elliot A. Stein[1]
[1]National Institute on Drug Abuse, Baltimore, Maryland, USA

Cocaine is a potent psychostimulant that produces euphoria, enhanced alertness as well as increases in heart rate and blood pressure. The effects of cocaine on the cardiovascular and cerebral vascular systems raise questions whether and to what extent these vascular effects could potentially confound fMRI data that are based on the hemodynamic response after cocaine administration. Manganese-Enhanced MRI (MEMRI) is an alternative neuroimaging approach that is independent of hemodynamic response. In the present study, we applied this technique to map rat brain activation induced by acute cocaine administration.

2335. Manganese-Enhanced MRI of the Spinal Cord for *In Vivo* Assessment of Damage and Functional Improvement Following Spinal Cord Injury in Mice Treated with 95CDL Antibodies

Bram Stieltjes[1], Stefan Klussmann[1], Michael Bock[1], Ana Martin-Villalba[1], Marco Essig[1]
[1]DKFZ, Heidelberg, Baden Württemberg, Germany

Recent experiments have shown functional recovery after spinal cord injury (SCI) using CD95L antibody treatment. We describe how quantitative MEMRI of the spinal cord (SC) can be used to evaluate the efficacy of novel drugs directed against SCI. We studied the differences of manganese uptake in the SC before and after treatment in SCI mice treated with CD95L antibody. We correlated clinical evaluation of SCI mice with follow up SC MEMRI. MEMRI-derived parameters correlate strongly with the clinical status Thus, MEMRI of the SCI can be used as an objective measure of improved function after treatment for SCI.

2336. Anorexigenic Gut Hormone Oxyntomodulin Modulates Manganese-Enhanced MRI Signal in the Mouse Hypothalamus

Nominated for an ISMRM Poster Award

Owais Bashir Chaudhri[1], Yu-Ting Kuo[2], James R. C. Parkinson[1], Amy H. Herlihy[1], Jimmy D. Bell[2], Sarah A. Stanley[1], Mohammad A. Ghatei[1], Stephen R. Bloom[1]
[1]Imperial College London, Hammersmith Hospital, London, UK; [2]MRC Clinical Sciences Centre, Imperial College London, Hammersmith Hospital, London, UK

Obesity is a major cause of death. The need for new therapies for obesity has led to interest in the mechanisms of energy balance. Gut hormones are important physiological regulators of appetite. Here we use mangenese-enhamned MRI techniques to investigate the site, degree and timing of the effects of the anorexigenic gut hormone oxyntomodulin on MRI signal in the mouse hypothalamus. Oxyntomodulin modulates manganese-enhanced MRI signal in specific areas of the hypothalamus in mice.

2337. *In Vivo* Blood-Brain Barrier Permeability Assessment with Mn-Enhanced MRI (MEMRI)

Sarah Heloko Shahmoradian[1], Yingying Sun[1], Robia G. Pautler[1]
[1]Baylor College of Medicine, Houston, Texas, USA

HexB-/- mice display many phenotypic similarities to humans afflicted with Sandhoff's disease. In this study, manganese-enhanced MRI (MEMRI) was used for the first time to measure blood-brain barrier (BBB) integrity the hexB-/- mice. 5 young hexB-/- mice and 5 old hexB-/- mice as well as age-matched controls were imaged *in vivo* post intraperitoneal administration of MnCl2 to assess the leakiness of the BBB.

2338. Imaging Motor Function *In Vivo* Using Manganese-Enhanced MRI

Xiping Liu[1], Balaraman Kalyanaraman[1], Shi-Jiang Li[1]
[1]Medical College of Wisconsin, Milwaukee, Wisconsin, USA

It is hard to evaluate animal motor function with traditional fMRI. Manganese-enhanced MRI (MEMRI) can reveal event-related neuronal activation during post-event period. After MnCl2 administration, mice were let run on a motor controled mouse treadmill at different time points and for different durations, which truned out to be different motor cortex activations. Therefore MEMRI may be a quantitative method to assess motor function.

Artifacts and Correction: Non-Motion

Room 4E Wednesday 14:00 - 16:00

2339. Restoration of EPI Susceptibility Distortion at 3T: Comparison of Fluid-Dynamic Image Registration with Phase-Encoding Gradient Reversion

Davide I. Imperati[1], Marc Tittgemeyer[1, 2], Andreas Schäfer[1], Harald E. Möller[1, 3]
[1]Max Planck Institute for Human Cognitive and Brain Sciences, Leipzig, Germany; [2]Max Planck Institute for Neurological Research, Cologne, Germany; [3]University Hospital Münster, Münster, Germany

We propose a cross evaluation of restoration methods for EPI images. Two strategies were tested to un-distort the images: image registration of the distorted image with an undistorted (reference) image of similar contrast, and co-registration of two distorted images acquired with inverted phase-encoding. Testing included phantom experiments and *in vivo* imaging of human brain. Results were compared to undistorted reference images to the known phantom structure. Fluid-dynamic image registration appeared to be better than reversed-gradient methods, because it accounts for large displacements and is able to correct for distortions in slice-select gradient direction, too.

2340. Improvement of Gradient-Reversal EPI Undistortion Method Using Local Pixel Adjustment

Xiaoxu Liu[1], Jianhui Zhong[1]
[1]University of Rochester, Rochester, New York, USA

Echo planar imaging (EPI) suffers severe geometry and intensity distortions because of its inherently long acquisition window in the phase encoding direction. Gradient-reversal undistortion method can successfully correct both the geometry and intensity distortions induced by field inhomogeneity. The essence of this method is to find the corresponding points in forward and reverse phase-encoding gradient images. We propose an improved algorithm with local pixel adjustment to find corresponding points in EPI images. It is an effective and fast improvement of the original algorithm.

2341. Multi-Stational Whole-Body MR Imaging with Geometric and Intensity Distortion Correction

Yo Taniguchi[1], Hisako Nagao[2], Takayuki Abe[2], Tetsuhiko Takahashi[2], Hisaaki Ochi[1]
[1]Central Research Laboratory, Hitachi, Ltd., Kokubunji, Tokyo, Japan; [2]R&D Center, Hitachi Medical Corporation, Kashiwa, Chiba, Japan

We have developed a method for obtaining whole body images by smoothly joining multi-stational (MS) images. Both geometric and intensity distortions are corrected using image intensity values with our method, not hardware distortion information. The optical flow method is used to build image warp maps from which the geometric distortions are successfully corrected. More than 300 sets of MS images of human bodies, obtained by various pulse sequences, were tested to evaluate the proposed method, and as a result we were able to obtain good results from all of the images.

2342. Concurrent Geometric Distortion Correction in Mapping Slice-To-Volume (MSV) Motion Correction of fMRI Time Series

Desmond Teck Beng Yeo[1, 2], Jeffrey A. Fessler[1, 2], Boklye Kim[2]
[1]University of Michigan, Ann Arbor, Michigan, USA; [2]University of Michigan Medical School, Ann Arbor, Michigan, USA

The accuracy of measuring voxel intensity changes between stimulus and rest images in fMRI echo-planar imaging (EPI) data, from which brain activation maps are computed, is severely degraded in the presence of head motion. In addition, EPI is sensitive to susceptibility-induced geometric distortions. Head motion causes image shifts as well as field-map changes which result in local changes in geometric distortion. Conventionally, geometric distortion correction is performed, with a static field-map, independently of image registration. This does not account for field-map changes with head motion. This work evaluates the improved motion correction capability of MSV with concurrent iterative field-corrected reconstruction using only an initial field-map. The results from simulated motion EPI data show improved accuracy in image registration and field-corrected reconstruction for the correction of image artifacts complicated by the motion induced field effects.

2343. A Modified Reversed Gradient Method Using the Displacement Map Concept for Geometric Distortion Correction in EPI

Hing-Chiu Chang[1], Teng-Yi Huang[2], Tzu-Chao Chuang[1], Hsiao-Wen Chung[1, 3], Cheng-Yu Chen[3]
[1]National Taiwan University, Taipei, Taiwan; [2]National Taiwan University of Science and Technology, Taipei, Taiwan; [3]Tri-Service General Hospital, Taipei, Taiwan

Reversed gradient method (RG) relies on using gradient with reversed polarity that produces distortion in opposite direction, from which the information on the difference in spatial displacements is then used to correct for distortion. However, RG is problematic in regions with low signals. We proposed a modified RG using the concept of displacement map to solve this problem. Our modified scheme uses 2D surface fitting to smooth the displacement map, it hence has advantages of less computing time with eddy current correction capability. The corrected EPI images show good preservation of quality even near the skull base.

2344. EPI Undistortion Using an Echo Spacing Fitting Method

Xiaoxu Liu[1], Jianhui Zhong[1]
[1]University of Rochester, Rochester, New York, USA

Echo planar imaging (EPI) suffers severe geometry and intensity distortions because of its inherently long acquisition window in the phase encoding direction. In this work, we propose an Echo Spacing Fitting (ESF) EPI undistortion method using two images collected with different echo spacing times and phase gradient directions. It is shown that the previously proposed phase-reversal undistortion method is a special case of the ESF method. This algorithm performs well in correcting distorted EPI image due to field inhomogeneity. More accurate correction can be achieved if 3 or more images with different echo spacing times are acquired.

2345. Can Blessing Influence fMRI Results?

Johan Olsrud[1], Anders Nilsson[2], Peter Mannfolk[2], Anthony Brian Waites[1]
[1]Lund University Hospital, Lund, Sweden; [2]Lund University, Lund, Sweden

In BOLD fMRI activation/blood flow is detected through small induced changes of the local magnetic field. Other factors that influence the magnetic field, such as motion, can easily affect the results. In this study we investigate the influence on GRE-EPI signal when an external object (hand) is extended into the tunnel. It is shown that temporally well correlated signal changes are iduced with a magnitude quite comparable to those normally found in activated areas during an fMRI study

2346. Correct Ghosting and Distortion Artifacts in EPI by Phase Labeling for Additional Coordinate Encoding (PLACE)

Qing-San Xiang[1], Frank Q. Ye[2]
[1]University of British Columbia, Vancouver, BC, Canada; [2]National Institute of Mental Health, NIH, Bethesda, Maryland, USA

A simple method is introduced for both N/2 ghost and distortion correction in EPI. Two images are acquired by otherwise identical sequences differing only by an additional gradient lobe along phase encoding direction, creating a relative phase ramp across the field-of-view. The undistorted original y-coordinate of each voxel is encoded as additional phase information that is used to achieve both N/2 ghost and distortion correction. The technique has been demonstrated successfully in phantom and animal studies. The images can also be used as reference scans to allow both deghosting and undistortion of every image in a time series.

2347. A New Approach Predicting Optimal Imaging Gradient Orientation for EPI

Michael V. Mengershausen[1], Jochen Rick[1], Oliver Speck[1]
[1]University Hospital Freiburg, Freiburg, Germany

Echo planar imaging (EPI) is commonly used for functional magnetic resonance imaging (fMRI). Its sensitivity to susceptibility gradients enables the measurement of the blood oxygen level dependent effect (BOLD). But this sensitivity also implies geometric distortions and signal loss due to field inhomogeneities not related to BOLD. In this work the signal loss, which is dependent on the orientation of the spatial encoding gradients, is predicted in order to prospectively select the optimal parameter setting for the acquisition. The signal loss is calculated by numerical prediction of signal loss, and is based on measured three dimensional B_0 maps.

2348. Image Reconstruction Using Dynamic EPI Phase Correction

R. Scott Hinks[1], Fred J. Frigo[1], Bryan J. Mock[1], Xiaoli Zhao[1], Ryan Sangill[1, 2], Bruce D. Collick[1]
[1]GE Healthcare, Waukesha, Wisconsin, USA; [2]CFIN, Aarhus University Hospital, Aarhus, Denmark

Echo Planar Imaging (EPI) is used for Diffusion Weighted Imaging (DWI), Diffusion Tensor Imaging (DTI) and functional Magnetic Resonance Imaging (fMRI). Inherent in the data collection scheme are phase errors that lead to image artifacts when left un-corrected. Reference scans are often used to estimate phase errors before a scan. For lengthy EPI scans, however, initial phase characteristics may change causing image quality to deteriorate over time. A new technique is proposed to reduce variability in image fidelity during the course of long EPI scans by adjusting phase correction parameters during the scan.

2349. A Fast and Robust Minimum Entropy Based Non-Interactive Nyquist Ghost Correction Algorithm

Stefan Skare[1], David B. Clayton[1], Rexford Newbould[1], Michael Moseley[1], Roland Bammer[1]
[1]Stanford University, Palo Alto, California, USA

Nyquist ghosts in EPI are normally measured by a reference scan in clinical practice. This may take over a minute for a multi-shot, multi-slice and multi-coil EPI scan. Using the EPI rawdata itself, without reference scans or user intervention, it is possible to iteratively search for the minimum entropy of the reconstructed magnitude image by altering the two first order phase correction parameters. The entropy metric is however not a smooth objective function, and may fail if ghosts are high. Here we present a sub-second safe way to find the solution of correcting the ghosts using the minimum entropy.

2350. Real-Time Oblique Echo-Planar Imaging: Ghosting Artifact Reduction in Arbitrary Scan Orientations

Yoon Chul Kim[1], Jon-Fredrik Nielsen[1], Krishna S. Nayak[1]
[1]University of Southern California, Los Angeles, California, USA

In EPI, ghosting artifacts due to gradient timing errors can be corrected if the scan plane is on axis. Oblique scan planes pose additional considerations and conventional methods solve them by measuring gradient delays. We present a new ghosting reduction method of not requiring gradient delay information. It adopts a double-alternating EPI readout, where traversal in k-space alternates every phase-encode and every frame. Sensitivity encoding (SENSE) is used to recover full FOV images. Sensitivity maps are estimated on-the-fly similar to TSENSE, and they are ghost free. Cardiac results indicate that this method makes real-time EPI robust against scan orientation changes.

2351. An Efficient Method to Correct Signal Drop-Out in EPI

Helen Marshall[1], David J. Larkman[1], Jo V. Hajnal[1]
[1]Hammersmith Hospital, Imperial College London, London, UK

Echo planar imaging suffers from signal loss when B0 varies in the through-slice direction. This can be corrected by the z-shim method at the expense of multiple image acquisitions with different correction gradients applied. A method that requires only two z-shim images and an efficient calibration procedure is described and tested. At 3T with a 3mm slice thickness full signal restoration (to within 2% of the correct value) was achieved in 95% of all brain pixels when parameter values were determined for each slice and 94% when a single calibration for the whole brain was used.

2352. Comparison of the B0 Field and Shimming in Human Brains at 3T and 7T

Kathryn Hammond[1], Janine Lupo[1], Doug Kelley[2], Sarah Nelson[1]
[1]University of California, San Francisco, California, USA; [2]Global Applied Science Laboratory, GE Healthcare, San Francisco, California, USA

This study introduces ROMP, “Reconstruction of Multichannel Phase”, a phase-sensitive reconstruction method which can be used to map the B0 field prior to shimming. ROMP mapping is used to demonstrate the increased inhomogeneity of the B0 field at 7T as compared to 3T. An analysis of shimming the field with linear and second order shims shows the need for higher-order shimming at high field strengths or for volumes placed over the sinuses.

2353. Correction Accuracy in B1 Measurement for High Field Image Intensity Correction

Hiroyuki Kabasawa[1], C. Celil Guclu[2], Zhu Li[2]
[1]GE Yokogawa Medical Systems, Hino-shi, Tokyo, Japan; [2]GE Healthcare-Technologies, Waukesha, Wisconsin, USA

To correct for image non-uniformity caused by dielectric effect, *in vivo* B1 mapping-based image correction methods were recently presented. The B1 field or flip angle (FA) field map may be perturbed due to various reasons including susceptibility artifact, tissue relaxation parameters, etc.. To reduce the sensitivity to these measurement errors, a simulation analysis was performed to characterize noise variation in the B1 map. Then a novel B1 field estimation and filtering method was proposed based on the simulation results. The proposed method effectively suppressed artifact caused by B1 measurement inaccuracy.

2354. Improvement in B1-Inhomogeneity Artifacts at 3 Tesla Using Dielectric Cushion

Kendra Marshae Franklin[1], Elmar M. Merkle[1], Brian M. Dale[2]
[1]Duke University Medical Center, Durham, North Carolina, USA; [2]Siemens Medical Solutions, Cary, North Carolina, USA

Our study evaluated the quantitative and qualitative impact of a radiofrequency cushion on 3T abdominal MRI. Twenty healthy volunteers were imaged, with and without the cushion, using multiplanar T2-weighted HASTE and true-FISP sequences, with and without parallel imaging. Quantitative analysis demonstrated a statistically significant reduction in hepatic SNR on coronal T2-weighted HASTE images with the cushion. Qualitative analysis showed a significant decrease of dielectric artifacts on coronal T2-weighted HASTE images. Findings did not correlate with the volunteers’ body mass index. In addition, the radiofrequency cushion did not have any substantial quantitative or qualitative impact on true-FISP images.

2355. A Simple B_1 Correction Method for High Resolution Neuroimaging

Peter van Gelderen[1], Alan P. Koretsky[1], Jacco A. de Zwart[1], Jeff H. Duyn[1]
[1]National Institutes of Health, Bethesda, Maryland, USA

The sensitivity gain available through high field in combination with multi-channel detectors allows a dramatic improvement in resolution for MRI of human brain. However, image intensity variations that result from non-uniformity of transmit and receive B1 fields compromise their interpretability. In this work, we present a simple method that allows for correction of these intensity variations by using a reference scan. The results are demonstrated for high-resolution T1-weighted imaging using a 24-channel detector array at 7 T.

2356. A Composite Spin-Lock Pulse for $\delta B_0 + B_1$ Insensitive $T_{1\rho}$ Measurement

Huairen Zeng[1], Gochberg Daniel[1], Christophe Gatenby[1], Yansong Zhao[1], Malcolm Avison[1], John C. Gore[1]
[1]Vanderbilt University, Nashville, Tennessee, USA

Significant artifacts arise in T1r-weighted imaging from B1 and B0 inhomogeneities. While composite spin-locking preparatory pulses that can correct the artifacts from B1 inhomogeneities have been described, they do not correct artifacts arising from B0 inhomogeneities. These B0 artifacts severely limit the accuracy of T1r relaxation time measurements, especially at lower spin-locking field in high B0 field systems. A new composite spin-locking pulse, which is self-compensating for both B1 and B0 inhomogeneities was proposed. Experimentally obtained T1r weighted images and numerical simulations confirmed that the new pulse greatly reduces the artifacts from B0 inhomogeneities.

2357. g-Factor Guided Denoising for SENSE Reconstructed MR Images with Edge Restoration

Sathya Vijayakumar[1], Feng Huang[1], James H. Akao[1], George Randy Duensing[1]
[1]Invivo Corporation, Gainesville, Florida, USA

Owing to the geometry factor (g-factor), there is a great amount of non-uniformity in the distribution of noise in SENSE reconstructed images. Edges and noise are both high frequency information, low pass filters for denoising cannot distinguish between edges and noise. In this work, we apply a g-factor guided total variation filtering technique to denoise the images and add back the removed information (which includes both noise and edge information) weighted by g-factor to strike a balance between the smoothing and the edge preservation.

2358. Image Support Reduction Technique for Self-Calibrated Partially Parallel Imaging

Feng Huang[1]
[1]Invivo Corporation, Gainesville, Florida, USA

In this work, a simple image support reduction technique is introduced for Partially Parallel Imaging (PPI) techniques. This technique can dramatically reduce the artifacts of images reconstructed by self-calibrated PPI techniques, such as GRAPPA or mSENSE , by applying a filter before and after the PPI. Since the kernels of the PPI algorithms need not be changed, this technique can be easily adopted.

2359. The Impact of Oblique Slicing and Shim Inclusions on Dynamically Shimmed Global Homogeneity

Kevin Matthew Koch[1], Scott McIntyre[1], Terry W. Nixon[1], Douglas L. Rothman[1], Robin A. de Graaf[1]
[1]Yale University, New Haven, Connecticut, USA

Dynamic shim updating (DSU) is a method used to improve global homogeneity through updating of locally optimized shim settings during a multi-volume acquisition. Given the established dependencies of static shimming on higher order shim inclusions and oblique slicing angle, we investigated the impact of these parameters on DSU-utilized global homogeneity. Oblique DSU is complicated by non-obvious shim degeneracies in oblique imaging planes. A method was thus developed to obliquely apply DSU using functional degeneracy analysis. Simulated shimming of measured data was then performed with this method as a function of single-oblique slicing angle and shim inclusion.

2360. Improved Sampling Density Correction for PROPELLER MRI

Christine Marie Kunesh[1], James Pipe[1]
[1]St. Joseph's Hospital, Pheonix, Arizona, USA

Non-uniform collection of data for PROPELLER MRI poses the need for a sampling density correction algorithm. The previous method consisted of a double convolution method that left artifacts in the final image, most commonly seen as a ringing effect. This new algorithm makes use of the regular geometries associated with PROPELLER scans and results in more accurate sampling density correction and lessening of associated artifacts.

2361. Stress Monitoring in Nitinol by Gradient Echo Magnetic Resonance Imaging

Johannes Martinus Peeters[1], Ernst E.H. Van Faassen[2], Chris J.G. Bakker[1]
[1]University Medical Center Utrecht, Utrecht, Netherlands; [2]Utrecht University, Utrecht, Netherlands

The functional properties of Nitinol implants, like self-expansion of stents and filters, are determined by microcrystalline transition, which depends on the thermal-mechanical behavior of the material. As magnetic properties change at crystal structure transitions, magnetization measurements may be used to characterize the thermal-mechanical state. Therefore, a study was performed to investigate the potential of MRI to monitor stress-induced crystal structure transitions. Magnetization changes during elongation of a Nitinol wire were quantified by gradient echo susceptibility artifact analysis and related to measurements with a tensile tester. Results indicate that magnetization measurements can provide direct feedback of stresses in the specimen.

2362. Assessment of Image-Based Registration of Diffusion-Weighted Images Acquired at High *b*-Value

Susana Muñoz Maniega[1], *Mark Elliot Bastin*[1], *Paul Anthony Armitage*[1]
[1]University of Edinburgh, Edinburgh, Scotland, UK

One disadvantage of high *b*-value diffusion MRI techniques is the reduction in signal-to-noise ratio (SNR) of the diffusion-weighted (DW) images due to the large signal attenuation at high *b*-value. This is thought to cause problems when DW images need to be corrected for eddy-current induced distortions and bulk patient motion using image-based registration techniques. Here we demonstrate that one multimodal registration algorithm, FLIRT (www.fmrib.ox.ac.uk), can register DW images with SNR as low as 1.5 within error tolerance. The possibility of using registration techniques at such low SNR facilitates the quantitative pixel-by-pixel analysis in diffusion imaging techniques using very high *b*-values.

2363. Rapid Measurement of Subtle Sub-One-Percent Changes in Transmitter Output and Receive Gain to Monitor Scanner Stability

Jonathan Samuel Jackson[1], *Dan Tozer*[1], *Paul S. Tofts*[1]
[1]Institute of Neurology, London, UK

MR scanner signal instability introduces errors in the quantitative measurement of MR parameters. Here we show new ways of monitoring very small fllip angle and receive changes (<1%) that are rapid and precise using an EPI variant of the Double Angle Method (DAM) and a Noise Image. The method, when combined with temperature measurements of the scanner hardware components will assist in identifying and addressing sources of signal drift in MRI

2364. Leadless Cardiac Gating During Brain Imaging Using a Blood Flow Navigator

Andre Jan Willem van der Kouwe[1], *Thomas Benner*[1]
[1]Massachusetts General Hospital, Charlestown, Massachusetts, USA

The ECG signal is normally obtained in the MR scanner using a pulse oximeter probe or ECG electrodes. We demonstrate that a reliable signal that correlates with blood flow in the neck can be obtained using an embedded blood flow navigator (BFN) inserted in the imaging sequence. We demonstrate the use of the BFN in a 3D FLASH scan of a human head. The BFN yields a blood flow measurement every 150 ms and does not require any external apparatus. This signal may be used for cardiac gating, on-line correction and post-processing of the image.

2365. A Virtual MRI Scanner for Simulating Arbitrary Pulse Sequences on High-Resolution Virtual Phantoms

Jeremy Magland[1], *Branamir Vasilic*[1], *Felix W. Wehrli*[1]
[1]University of Pennsylvania Medical Center, Philadelphia, Pennsylvania, USA

An efficient MRI simulator is described for use with user-specified pulse sequences and high-resolution 3D virtual phantoms. The simulator models T1, T2, and T2* relaxation as well as arbitrary spectral composition. Phenomena predicted by the Bloch equation are accurately represented. For example, artifacts caused by chemical shift, approach to steady-state, off-resonance, or an imperfect B1 field, as well as the effects of finite sampling (e.g. Gibbs ringing), stimulated echo artifacts and partial volume are all handled automatically. The simulator solves the Bloch equation in k-space by storing in memory thousands of coherence pathways which evolve during the sequence. The program is coupled with software for importing arbitrary pulse sequences, so the virtual scanner can be used to compare and optimize novel sequences. Since the computation time depends only on the pulse sequence duration and complexity and not the size of the virtual phantom (besides loading into memory) the scanner can be used to perform realistic MR simulations on very high resolution virtual phantoms, such as segmented micro-CT data sets.

2366. Removal of Sideband Modulations in 1H MRS Without Solvent Suppression

Mahir Sinan Ozdemir[1], *Yves De Deene*[2], *Yves De Asseler*[1], *Ignace Lemahieu*[1]
[1]Ghent University, Ghent, Belgium; [2]Ghent University Hospital, Ghent, Belgium

The majority of *in vivo* proton spectra utilize solvent suppression so as to reduce the dynamic range for the detection of signals originating from low-concentrated metabolites. We previously showed that it is possible to perform absolute quantification of proton spectra without water suppression in a single measurement. Nonetheless, the quality of the unsuppressed water spectra is deteriorated by the water sidebands caused by time varying modulation of the main magnetic field due to mechanical vibrations of the gradient coils. In this work, we proposed a method to remove the gradient-induced sideband modulations and verified the method in a phantom study.

2367. Sub-Second 3D Image Reconstruction with Gradwarp Correction in Moving Table MRI

Roger C. Grimm[1], *Dave G. Kruger*[1], *Jason A. Polzin*[2], *Steve J. Riederer*[1]
[1]Mayo Clinic, Rochester, Minnesota, USA; [2]General Electric Healthcare, Milwaukee, Wisconsin, USA

Large FOV MR imaging using continuous table motion is susceptible to artifacts arising from the nonlinearities of image gradients. Images contain spatially dependent blurring in addition to spatial distortion. Ideally, a 3D Fourier transform and gradwarp correction is required for each acquisition. Despite the seeming intense computational requirements, image reconstruction can be accomplished in 2.3s with an off-the-shelf PC. In a realtime implementation with a 5ms TR, a group-wise recon could be performed every eight TRs. Using an eight-node blade system, total reconstruction times drop to 420ms or a group-wise recon could potential be done for every TR.

2368. Chemical Shift Artifact Correction by Image Processing in Spin-Echo Imaging

Francois De Guio[1], Boubakeur Belaroussi[1], Olivier Beuf[2], Hugues Benoit-Cattin[1]
[1]CREATIS, UMR CNRS #5515, U 630 Inserm, Université Claude Bernard Lyon 1, INSA Lyon, Bât. B. Pascal, 69621 Villeurbanne, France; [2]UMR CNRS 5012, Université Claude Bernard Lyon 1, CPE Lyon, France

Chemical shift artifacts occur in Spin-Echo MR images and are responsible for spatial misregistration. Numerous different techniques have been proposed but they always constrain the acquisition process. We present an image processing method to correct these artifacts. It is based on a pre-scan image of the fat and enables the correction of any Spin-Echo scheme sequence. Algorithm has been tested on several simulated images and on real images with good results.

2369. Efficient Deblurring by Iterative Reconstruction for Spiral-In-Out Imaging

Hua Guo[1, 2], Quan Zhu[1], Todd B. Harshbarger[2], Allen W. Song[1, 2]
[1]Duke University, Durham, North Carolina, USA; [2]Brain Imaging and Analysis Center at Duke University, Durham, North Carolina, USA

By using iterative reconstruction and the field map from the sequential spiral-in and out images, the blurring in spiral imaging can be corrected effectively. The combination of spiral in and out improves the image quality around the susceptibility affected region. This technique can be used for fMRI when the regions of interest suffer from susceptibility induced artifacts.

2370. A Novel Method of Flip Angle Mapping and Calibration

Daniel Joseph Schaefer[1], Ceylan Celil Guclu[1]
[1]GE Healthcare, Milwaukee, Wisconsin, USA

The Double-Angle Method is often used to obtain flip angle maps for the purpose of either calibration or intensity correction. In the case of *in vivo* calibration, the number of images per TR maybe limited by SAR leading to scan time increase. In this work, we present a method for mapping the flip-angle using arbitrary sets of flip angles (theta-alpha theta, where alpha<2) rather than a theta-2theta pair.

2371. Compatibility of Inner Volume Selection and VSS Edge Saturation with SENSE

Ken-Pin Hwang[1]
[1]General Electric Healthcare Technologies, Houston, Texas, USA

The use of quality outer volume suppression techniques capitalizes on the speed benefits of parallel imaging in small FOV applications. This study examines the effectiveness of inner volume selection and FOV edge saturation by very spatially selective (VSS) pulses in a 3D FSE sequence, and observes their effect on artifacts produced by SENSE when aliased signal is present in the FOV. The combination of these techniques acheives near perfect suppression with minimal increase in scan time and is fully compatible with SENSE acquisitions.

2372. Exact Correction of Sharply Varying Off-Resonance Effects in Spiral MRI Using Spatially Varying Deconvolution

Mahender K. Makhijani[1], Krishna S. Nayak[1]
[1]University of Southern California, Los Angeles, California, USA

MRI with non-Cartesian acquisition schemes suffer from blurring artifacts due to off-resonance. Conventional algorithms for off-resonance correction are approximate in nature and assume that the off-resonance map is varying smoothly across the object. This assumption is violated in the case of susceptibility related off-resonance which is sharply varying near certain tissue interfaces. We present a new method for fast and accurate off-resonance correction using spatial domain deconvolution that does not assume smoothness of the field map. Phantom and *in vivo* results are presented.

2373. Susceptibility Artifact Correction in GE Images

Boubakeur Belaroussi[1], Hugues Benoit-Cattin[1], Christophe Odet[1]
[1]CREATIS Laboratory - CNRS UMR 5515 - INSERM U 630, Villeurbanne, France

In Gradient Echo (GE) images, susceptibility artifact induces both intravoxel dephasing and pixel shifting leading to intensity and geometric distortions that may disturb image analysis. In this work, we propose an original image-processing based correction method in GE MR Images when a field map of the imaged object is known. Susceptibility artifact impact is modeled by means of pixel shifting map and intensity distortion map. An original image processing scheme based on MRI simulation is used to build the intensity distortion map to take into account intravoxel dephasing. The proposed method has been successfully tested in real images.

2374. Analysis and Suppression of Off-Slice Excitation in SSFP Imaging

Wenmiao Lu[1], Brian A. Hargreaves[1]
[1]Stanford University, Stanford, California, USA

Balanced steady-state free precession (SSFP) is a fast imaging sequence offering good tissue contrast and high signal-to-noise efficiency. However, it is susceptible to off-resonance effects. In this work we analyze one type of artifact often encountered in SSFP imaging – undesired steady-state excitation outside the selected slice. In practice such undesired excitation often leads to spurious imaging of objects outside the selected slice or through-slice aliasing. To suppress this off-slice excitation, we proposed two filter design approaches to product RF pulse with high stopband suppression. Our designs were verified with simulation and experiments.

2375. Use of the Fresnel Transform to Detect and Correct Field Drift Artefacts in MR Images

Jamu Krishna Alford[1], Blaine Alexander Chronik[1]
[1]University of Western Ontario, London, Ontario, Canada

In MR, main field drift during image acquisition causes phase error that in turn produces image artefact. Drift can come from many different sources, but is often associated with heating of resistive elements in the scanner. When the magnetic drift is different in each line of k-space distortions in the phase-encoded direction appear. Averaging images in order to remove this phase error only further degrades the image quality. A new technique is detailed that can identify and remove the unwanted error. This abstract introduces the mathematical transform and shows example images before and after correction.

2376. Reducing Eddy Currents Artifacts for Self-Navigated Reconstruction in B-SSPF by Super-Segmented Acquisition

Sergio Andres Uribe[1, 2], Michael S. Hansen[2], Redha Boubertakh, [23], Vivek Muthurangu[3], Reza S. Razavi[3], Pablo Irarrazaval[1], Derek L. G. Hill[2]
[1]Pontificia Universidad Catolica de Chile, Santiago, Chile; [2]University College London, London, UK; [3]King's College London, London, UK

A common approach for self-navigated sequences in 3D cardiac imaging is to repeatedly acquire the center profile of k-space. This introduces large jumps in k-space, which produce eddy current artifacts in the images. In this work we developed a novel k-space ordering strategy which involves acquiring the center profile of k-space frequently while avoiding large jumps between each acquisition profile. The results show a marked reduction of eddy current artifacts in the images. Furthermore, this method is an alternative to the standard segmented acquisition, which also suffers from eddy current artifacts.

2377. Correction of Eddy-Current Induced Phase Error in Diffusion-Weighted Imaging

Jie Huang[1], David C. Zhu[1]
[1]Michigan State University, East Lansing, Michigan, USA

The theoretical basis for measuring the spatial derivative of diffusivity of water diffusion in tissues has been established based on a newly derived theoretical relationship between the diffusion gradient and the image signal acquired with a diffusion-weighted spin-echo pulse sequence. The diffusion gradient is linearly related with the phase change of the signal with and without diffusion-encoding gradients (DEG). Measuring the diffusion gradient provides a means of delineating the interface between two tissues with different diffusion magnitudes. However, the eddy currect induced by DEG could cause a large phase error in diffusion-weighted phase images. In this paper, we present a method for measuring the eddy current and correcting the phase error introduced on diffusion-weighted phase images.

2378. A Simple Approach to Measure and Correct for B0 and Linear Eddy Currents

Aiming Lu[1], Bruce L. Daniel[1], Kim B. Pauly[1]
[1]Stanford University, Stanford, California, USA

Eddy currents cause artifacts in MR images or distort slice profile during spectral-spatial excitation, and thus often need to be corrected. However, B0 eddy currents and linear eddy currents affect acquisition differently, and characterization of both terms separately may be require special experiment setup and thus time-consuming. In this work, we present a simple approach to extract the B0 and linear eddy current terms simultaneously. Our phantom studies with a multiple-echo projection reconstruction (PR) sequence demonstrate significantly improved image quality with the correction of both terms when the measurements are used to correct the reconstruction.

2379. Robust Radial Imaging with Predetermined Isotropic Gradient Delay Correction

Peter Speier[1], Florian Trautwein[1]
[1]Siemens AG MED, Erlangen, Germany

Timing Delays δt between gradients and receiver events were characterized for a variety of measurement parameters and systems. The dependency of δt on the physical gradient axis of the readout were found to be negligibly small. The isotropic average values could well be approximated with a linear equation that was parameterized with the receiver dwell time and the coefficients being dependent on system type only. This isotropic linear model was used to adjust the RO pre- and dephaser in radial imaging sequences. Cardiac imaging on volunteers proved that this correction provides robust clinical image quality for radially acquired images.

2380. Correction of Slice Profile Distortion from Metallic Devices

Kim Butts Pauly[1], Garry E. Gold[1]
[1]Stanford University, Stanford, California, USA

Metallic devices remain a source of image artifacts in MRI. In-plane shifts can be eliminated with view angle titlting, and the resulting images reveal the underlying slice profile distortions. These arise from both potato chipping of the slice and intensity modulations from variations in slice thickness. The purpose of this work was to use a thin slice VAT sequence with two averages, the second offset from the spin echo by 60 microseconds, to obtain a field map. This is then used to correct for slice profile distortions.

2381. Improved Slice Excitation for Ultra-Short TE Imaging with B0 and Linear Eddy Current Correction

Aiming Lu[1], Bruce L. Daniel[1], Kim B. Pauly[1]
[1]Stanford University, Stanford, California, USA

MR imaging with ultra short echo times (UTEs are of wide interest to visualize tissues with short T2 or T2*. A self-refocused half RF excitation is usually employed to achieve ultra-short TEs. However, this technique is sensitive to eddy currents induced by the selective gradient, which can result in undesirable slice profile and therefore complicate the interpretation of the images. Here we present an effective method to compensate for both B0 eddy currents and linear eddy currents, and our results demonstrate significantly improvement in slice selectivity.

2382. Stimulated Echo Induced Misestimate on Diffusion Tensor Indices and Its Remedies

Tzu-Chao Chuang[1], Shang-Yueh Tsai[1], Yi-Ru Lin[1], Teng-Yi Huang[2], Tzu-Cheng Chao[1], Cheng-Wen Ko[3], Ming-Ting Wu[4], Hsiao-Wen Chung[1]
[1]National Taiwan University, Taipei, Taiwan, Taiwan; [2]National Taiwan University of Science and Technology, Taipei, Taiwan, Taiwan; [3]National Sun Yat-Sen University, Kaohsiung, Taiwan, Taiwan; [4]Kaohsiung Veteran General Hospital, Kaohsiung, Taiwan, Taiwan

The dual spin-echo technique with twice-refocused gradient provides diffusion tensor images (DTI) immune to eddy-current effects. The resulting estimates of the apparent diffusion coefficient (ADC) and fractional anisotropy (FA), however, were found to be inconsistent with values obtained from conventional DTI. In this work we showed that the measurement errors could originate from the formation of stimulated echo superimposed on the second spin echo, but only in b = 0 images rather than the diffusion-weighted images, leading to over-estimation of ADC and under-estimation of FA. Remedies include appropriate design of crusher gradients or an intentional shift of the echo time.

2383. Fast Dixon Fat/Water Separation with Cartesian Total Sampling Time Sequence

Candice Anne Bookwalter[1], Jeffrey L. Sunshine[2], Jeffrey L. Duerk, [12]
[1]Case Western Reserve University, Cleveland, Ohio, USA; [2]University Hospitals of Cleveland and Case Western Reserve University School of Medicine, Cleveland, Ohio, USA

Continuously sampled sequences (a.k.a., total sampling time (TST) acquisitions) sample data during the entire read gradient application including the traditional flat top, ramps, dephase and rephase lobes in order to capture one full and two partial echoes. The three echoes acquired by a Cartesian TST sequence may be used for fat/water separation. In this study, a simple time spacing of 2.2 ms between the start of the dephase lobe and the true echo allowed Dixon fat/water separation. Phantom and *in vivo* images showed the same contrast between fat and water in the TST data compared to traditional two-acquisition Dixon method.

2384. Fat Suppression and Off-Resonance Corrections for Single and Multi-Echo PC VIPR

Kevin Michael Johnson[1], Oliver Wieben[1], Patrick Turski[1], Darren Lum[1], Wally Block[1]
[1]University of Wisconsin-Madison, Madison, Wisconsin, USA

Radial k-space trajectories have been shown to allow for significant accelerations in image acquisition; however, objects that are off resonance are blurred. In the case of phase contrast (PC) VIPR, the shortening of the readout length, is limited by SNR and data acquisition efficiency. We propose methods to measure 3D field maps without increasing scan time, which may also suppress motion artifacts from fat. Using this field map, we show substantial improvements in image quality in areas where off-resonance blurring has previously been reported.

2385. Signal Drop-Out Reduction in Gradient Echo Imaging with a Hyperbolic Secant Excitation Pulse - An Evaluation Using an Anthropomorphic Head Phantom

Karin Shmueli[1], David Lee Thomas[1], Roger John Ordidge[1]
[1]University College London, London, UK

The Hyperbolic Secant (HS) excitation pulse produces a through-slice quadratic phase variation, partly cancelling the through-slice susceptibility-induced phase gradient that causes signal drop-out. The HS-90 pulse parameters can be altered to vary the quadratic phase coefficient, thereby allowing selection of a pulse for optimal recovery of signal drop-out in specific regions. Different HS-90 pulses were used to excite GE-EPI images of an anthropomorphic head phantom with realistic susceptibility artifacts. Every HS-90 pulse resulted in recovery of dropped-out signal, at the expense of overall signal intensity. The pulse with a 1.22 rad/mm^2 coefficient gave a good compromise between drop-out recovery and signal reduction.

2386. Elimination of Artefacts in Fast Spin Echo Imaging Caused by T2 Decay During the Echo Train by Combining Novel K-Space Ordering ('Feathering') and Parallel Imaging

David William Carmichael[1], David L. Thomas, Roger J. Ordidge
[1]Insititute of Neurology, University College London, London, UK

In multi-echo imaging sequences like the fast spin echo (FSE), the point spread function (PSF) in the phase encoding direction is significantly degraded. This is due to discontinuities in adjacent k-space data obtained at different echo times caused by T2 decay. To improve the PSF, data are acquired alternately at different echo times (called 'feathering') in the regions of discontinuity. Using GRAPPA with feathered array coil data it is possible to reconstruct data over the region of the discontinuity from both echo times. This is used to dramatically improve the PSF, eliminating artefacts in both simulations and FSE images.

2387. Real-Time Electrocardiogram Artifact Correction Using a Finite Impulse Response Filter Signal Processing Method and Computer System

Freddy Odille[1], Cédric Pasquier[1, 2], Roger Abaecherli[1, 2], Pierre-André Vuissoz[1], Gary P. Zientara[3], Jacques Felblinger[1]

[1]Université Henri Poincaré; INSERM ERI 13, Nancy, France; [2]Schiller Médical SAS, Wissembourg, France; [3]Brigham and Women's Hospital and Harvard Medical School, Boston, Massachusetts, USA

During MRI examinations, artifacts on electrophysiological waveforms (ECG, EEG, EMG…) are still a problem for patient monitoring and triggering of acquisitions. A Finite Impulse Response filter method is applied to MR gradient switching induced artifact prediction from gradient waveforms. The predicted artifacts are subtracted from the corrupted ECG in real-time. Validation of the method is presented along with real-time implementation using a specially designed computer and electronics system. Real-time operation was demonstrated at 1 kHz with a delay of only 1 ms introduced by the correction, enabling further real-time processing such as QRS detection and automatic monitoring algorithms.

2388. A Multi-Frequency Amplitude Modulator for Encoding Electrical Signals in MR Images

Christian G. Hanson[1], Lars G. Hanson[1]

[1]Copenhagen University Hospital Hvidovre, Hvidovre, Denmark

Using rudimentary hardware, it has previously been demonstrated that electrophysiological signals can be modulated and encoded in a way similar to the "mag stripe" technique used for representation of sound tracks in movies: The signals are encoded in the oversampled region of the field-of-view discarded by the image reconstruction. Non-MR signals can thereby be recorded by the scanner without affecting the images. A much improved flexible modular 8-channel modulator was constructed for the purpose. Filters, gains, trigger timings and frequencies are controlled via an optical PC-link. The equipment provides easy high-quality recording of non-MR signals.

2389. Strategies for Avoiding Image Artefacts When Scanner is Used for Recording of Non-MR Signals

Lars G. Hanson[1], Arnold Skimminge[1], Christian G. Hanson[1]

[1]Copenhagen University Hospital Hvidovre, Hvidovre, Denmark

Surplus sampling capacity of MR scanners can be used to record non-MR signals as has been demonstrated previously. If the non-MR signals are encoded in the oversampled frequency range of the scanner, i.e. outside the field of view, such signals are invisible in the images but can be extracted from the imaging raw data, a technique resembling "mag stripe" encoding of soundtracks in movies. Even though the non-MR-signals are encoded at frequencies corresponding to positions outside the field of view, there may be ringing artefacts appearing in the MR images. Two strategies for eliminating such artefacts are presented.

Data Processing: Miscellaneous

Room 4E Wednesday 14:00 - 16:00

2390. The DICOM Standard: Is Twelve Bits Enough?

Ken Earl Sakaie[1], Mark J. Lowe[1]

[1]The Cleveland Clinic Foundation, Cleveland, Ohio, USA

The DICOM image storage standard allocates 12 bits per pixel to represent image intensities, even though current hardware typically allows at least 16 bits of resolution. Quantitative imaging requiring large dynamic range may suffer errors due to the 12-bit limit. Simulations and measurements indicate that typical fMRI and DTI experiments can suffer appreciable errors due to the bit-resolution limit associated with the DICOM standard.

2391. A Realistic fMRI Time Series Simulation with Individual Slice Motion, Geometric Distortion and Spin Saturation Effect

Boklye Kim[1], Roshni Bhagalia[2], Desmond T. B. Yeo[3]

[1]University of Michigan Medical School, Ann Arbor, Michigan, USA; [2]University of Michigan, Ann Arbor, Michigan, USA; [3]University of Michigan, ann Arbor, Michigan, USA

Validation of fMRI motion correction and analyses by statistical inference have been the focus of many publications and invoked interests in developing accurate phantom data. Although it has been an area of focus for many investigators, none of the mathemetical phantoms simulating motion artifacts, to this date, do not include accurate account of head motion. Most data sets share a common theme that assumes no inter-slice motion during the time series acquisition. For fMRI time series data acquired using multi-slice EPI, and most likely single shot sequences, each slice is subject to a different set of motion parameters in the presence of subject's head motion. Following the previous work on a synthetic time series constructed with known motion parameters affecting each slice, this work includes geometric distortion exerted on each slice computed with varying field inhomogeneity and spin saturation effect as a result of out of plane head motion.

2392. Displaying Parametric Data from DCE-MRI Investigations of Breast Cancer: How to Present Complex Data

Marco Borri[1, 2], Michael Khazen[1], Martin O. Leach[1]
[1]Institute of Cancer Research and The Royal Marsden NHS Foundation Trust, Sutton, UK; [2]University of Turin, Torino, Italy

Assessment of lesion's uptake kinetics using DCE-MRI involves evaluation of relative extent of enhancement due to contrast agent during the initial phase of about 2 min following the administration, along with analysis of the shape of kinetic uptake curve, which can aid in distinguishing between benign and malignant lesions. An increasing need to combine dynamic functional data with morphology leads to a need to evaluate the merits of different approaches. In this work we compare five different methods of creating colour-encoded kinetics maps where saturation of the colours is modulated by the extent of contrast enhancement during the initial phase.

2393. Fast Volume Visualization Using Pre-Computed Volume Radiance Transfer

Xuejun Hao[1], Dongrong Xu[1, 2], Bradley S. Peterson[1, 2]
[1]Columbia University, New York, USA; [2]New York State Psychiatric Institute, New York, USA

Visualization of 3D medical datasets is an effective way for us to understand the structure and functional relationships in the data, such as human brain and body. Indirect (surface-based) and direct volume (volume-based) display have their relative advantages as well as disadvantages. Indirect volume rendering is fast, whereas direct volume rendering can generate high quality images with subsurface details. Here we propose a novel volume visualization algorithm which combines the advantages of direct- and indirect-volume rendering. Our method can interactively render high-quality images with subsurface details without using expensive special-purpose graphics hardware. We achieve interactivity by pre-computing the volume radiance transfer and storing it with points on a desired isosurface.

2394. Fully Automatic Liver Scan Planning - Slice and Navigator Positioning from Stacked 2D Localizer Scans

Matthias Fenchel[1, 2], Stefan Thesen[1], Andreas Schilling[2]
[1]Siemens Medical Solutions, Erlangen, Germany; [2]Eberhard-Karls-University, Tuebingen, Germany

We present a method for fast and fully automatic positioning of slices and navigators for MR liver examinations. First, a statistical model of the liver is generated from a data pool of scanned livers of probands. Once this model has been generated, we are able to register it to a set of localizer slices from the scanner, maximizing a chosen correlation metric between model and localizers. From the final parameters of the registration process, we easily obtain the geometric information needed to position the slices and the navigator ROI for an examination.

2395. Denoising of Complex MRI Data by Wavelet-Domain Filtering: Application to High B-Value Diffusion Weighted Imaging

Ronnie Wirestam[1], Adnan Bibic[1], Jimmy Lätt[1], Sara Brockstedt[1], Freddy Ståhlberg[1]
[1]Lund University, Lund, Sweden

Magnitude MR images show a Rician noise distribution and a non-zero minimum signal, often referred to as the rectified noise floor. Quantification is severely hampered in low-SNR measurements, for example, high b-value diffusion MRI. To reduce this problem, real and imaginary MRI data in the image domain were filtered, before construction of the magnitude image. The noise-reduction filtering (or denoising) was accomplished by Wiener-like filtering in the wavelet domain. The advantage of denoising the complex MRI data in the image domain, compared with filtering the complex k-space data, is that image artefacts caused by filtering-induced phase errors are avoided.

2396. Enhanced MRI Resolution for Clinical Applications

Mathijs Visser[1, 2], Arianne Van Muiswinkel[1], Calina Ciuhu[3], Gerard de Haan, [23]
[1]Philips Medical Systems, Best, NB, Netherlands; [2]Eindhoven University of Technology, Eindhoven, NB, Netherlands; [3]Philips Research The Netherlands, Eindhoven, NB, Netherlands

Magnetic resonance (MR) scanners are used in hospitals to image human body tissues for diagnosis purposes. A compromise between the acquisition time and resolution of the MRI images must always be made. Many Fourier based techniques, like parallel imaging and partial k-space acquisitions are commonly used. Another solution is offered by image processing methods for resolution enhancement. In this paper we discuss a popular video imaging enhancement technique, based on structure controlled Wiener Filters (SCWF), which we have applied to MRI images. We compare it with some known resolution enhancement techniques in the area of image processing.

2397. A Robust Field-Map Estimation Method Using Dual-Echo GRE with Bipolar Readout Gradient Structure

Desmond Teck Beng Yeo[1], [2], Thomas L. Chenevert[2], Jeffrey A. Fessler[1], [2], Boklye Kim[2]
[1]University of Michigan, Ann Arbor, Michigan, USA; [2]University of Michigan Medical School, Ann Arbor, Michigan, USA

Field-maps are generally required to correct for field-inhomogeneity artifacts like geometric distortion in EPI images and blurring in spiral acquisitions. The standard static field-map estimation method using two separate acquisitions with different echo times is prone to motion errors due to the relatively long period of time between the two acquisitions. A simple phase error correction technique to estimate a field-map from a dual-echo GRE sequence is presented. A dual-echo sequence offers a more efficient and accurate way of generating a magnetic field-map compared to two separate single-echo acquisitions since the data are collected from a consistent subject position, therefore minimizing motion artifacts, without the additional scan time. A pulse sequence that is typically used to acquire fat-water in-phase and out-of-phase gradient echo images simultaneously is used without any modification. The dual echo fast gradient echo (DEFGRE) sequence utilizes two back-to-back continuous readout gradients, which turn out to be in opposite direction. Residual phase error from the non-symmetric readout pulses applied with the opposite polarity is modeled as an affine phase term in the readout direction. Results from phantom and human subject data show that the linearly varying correction term stays constant over time and, hence, can be applied to different data acquired over time. The DC correction term may change with time and is estimated empirically for different scans. The technique can be applied to other MRI scanners for the field-map acquisitions without having to modify the existing dual-echo sequence.

2398. A New Single Acquisition, Two-Image Difference Method for Determining MR Image SNR

Michael C. Steckner[1]
[1]Hitachi Medical Systems America, Twinsburg, Ohio, USA

Various methods are available to compute SNR. These methods differ in how noise is measured and are a balance between robustness and acquisition duration. A new single acquisition method is demonstrated that has the desirable attributes of both single image, and two-image techniques. The single acquisition is acquired with two times larger read direction field of view and matrix size. The resultant k-space data is undersampled into the even and odd data points. The resultant magnitude reconstructed images, with normal matrix size and image FOV, are effectively created simultaneously in time, eliminating any system drift artifacts in the noise measurement.

2399. Object Orientation Independence of Susceptibility Weighted Imaging by Using a Sigmoid-Type Phase Window

Francisco Manuel Martinez Santiesteban[1], Scott D. Swanson[1], Douglas C. Noll[1], David J. Anderson[1]
[1]University of Michigan, Ann Arbor, Michigan, USA

Susceptibility Weighted Imaging (SWI) uses the phase information of MRI, to enhance the contrast of small magnetic susceptibility differences not easily observed in the magnitude images. After filtering, the phase is mapped to values from 0 to 1 by either using positive, negative or triangular windows. Unfortunately, a single-side window is sensitive to the orientation, with respect to the main magnetic field, of the object that produces the phase difference, and the triangular window tends to overestimate the size of the object. In this work, we propose the use of a sigmoid-type window to enhance the contrast of SWI independently of the orientation of the object, as long as it produces a phase change with respect to the surrounding tissue.

2400. T_2*-Based Fat-Water Separation

Carsten Warmuth[1], Bernd Hamm[1], Matthias Taupitz[1]
[1]Charité Medical School, Berlin, Germany

Separation of fat and water signals is usually based on the chemical shift difference. These phase sensitive techniques require the calculation of B_0 fieldmaps and involve phase unwrapping procedures. Here we present an alternative amplitude based method, which does not require computation of a fieldmap. It is based on the biexponential T_2* decay unique to fat protons.

2401. An Efficient and Effective Algorithm for Two-Point Fat-Water Separation

Maria A. Schmidt[1], Karlene M. Fraser[1]
[1]St. George's Hospital, London, UK

A two-point region-growing phase correction algorithm was recently proposed for fat-water separation, based on detecting large phase shifts at the boundary between water-dominant and fat-dominant regions. This work investigates the performance of the phase correction method in the presence of noise and magnetic field inhomogeneity, and proposes two fundamental modifications to the algorithm: (i) to start the region-growing process with images of lower resolution, and (ii) to apply low-pass filters to the final phase-corrected map prior to calculating separate water and fat images. The resulting method is accurate, faster and less sensitive to noise.

Rapid Imaging

Room 4E Wednesday 14:00 - 16:00

2402. K-SpaceTrajectory Measurement with Signal Shifting

Marine Beaumont[1, 2], Christoph Segebarth[1, 2], Laurent Lamalle, [23], Emmanuel Luc Barbier[1, 2]
[1]U 594, Grenoble, F-38043, France; [2]Univ Grenoble 1, Grenoble, F-38043, France; [3]IFR 1, Grenoble, F-38043, France

Different approaches for measuring k-space trajectory have been described in the literature. Self-encoding gradient techniques are time consuming due to the high number of phase encoding steps needed. The approach with off-center slice selections is faster but has apparently not been used to measuring high k-space values, when phase dispersion may lead to signal destruction, and to errors in the trajectories at the k-space periphery. To overcome this difficulty without significantly increasing the acquisition time, we propose an approach whereby a dephasing gradient is applied, prior to the gradient to be calibrated, to shift in time the signal maximum.

2403. Fast Whole Brain T1 Mapping at 3 Tesla

Femke de Smit[1], Hans Hoogduin[1]
[1]University Medical Center Groningen, University of Groningen, Groningen, Netherlands

T1 values are presented for 3T that were measured using a fast inversion recovery method. The method allows whole brain coverage in 2m20s at an isotropic resolution of $2x2x2mm^3$.

2404. Fast Spin Echo for T_2 Quantification at 3T

Feng Liu[1, 2], Bradley Peterson[1, 2], Yunsuo Duan[1, 2], Alayar Kangarlu[1, 2]
[1]Columbia University, New York, New York, USA; [2]New York State Psychiatric Institute, New York, New York, USA

It is known that relaxation measurements require long acquisition time. This is primarily the reason why relaxation quantifications have not been widely used in clinical settings. In this work, T2 Relaxation times were measured in both phantoms and infant brains with acceptable accuracy, using a clinically available fast spin echo (FSE) sequence of high echo train length (ETL=32) with parallel imaging capability. A modified fitting equation was tested to account for the differences between SE and FSE in T2 estimation. T2 maps of infant brains were obtained using this high ETL FSE.

2405. Application of Geometry Distortion Corrected SEPI Sequence

Yingbiao Xu[1, 2], Mark Haacke[1, 2]
[1]Wayne State University, Detroit, Michigan, USA; [2]The MRI Institute for Biomedical Research, Detroit, Michigan, USA

Geometric Distortion Corrected Segmented EPI (GDC-SEPI) utilizes a center out k-space trajectory and a phase map to smooth the phase discontinuities between segments. GDC-SEPI speeds up the acquisition while minimizing the distortion, fat shift, blurring and ghosting associated with SEPI. GDC-SEPI turns arterial signal bright compared with dark signal normally seen in a SEPI, which is important in Susceptibility Weighted Imaging (SWI) to keep the arteries bright so that they do not interfere with the hemorrhagic or venous signal being dark. GDC-SEPI is a good sequence to run in clinical environment for SWI to speed up acquisition.

2406. Accelerated Exponential Fitting for Rapid Relaxation Time Mapping

Holger Eggers[1], Peter Boesiger[2]
[1]Philips Research, Hamburg, Germany; [2]University and ETH Zurich, Zurich, Switzerland

The quantification of relaxation times is commonly based on the fitting of an exponential function to a time series of signal intensities. Solving a non-linear regression problem for this purpose provides accurate estimates, but is rather time-consuming in form of the popular Levenberg-Marquardt method. It is proposed to perform a search for a real root of a polynomial in a small interval instead. This approach is shown to permit a substantial acceleration of the quantification compared to the Levenberg-Marquardt method, while achieving the same accuracy.

2407. Reducing T_2 Blurring in Fast Spin Echo Sequences Using the Point Spread Function

Huairen Zeng[1], Xiawei Ou[1], Yansong Zhao[1], Gochberg Daniel[1], Brian Welch[1, 2], John C. Gore[1]
[1]Vanderbilt University, Nashville, Tennessee, USA; [2]Philips medical system, cleveland, Ohio, USA

Fast (or Turbo) spin echo (FSE, TSE) pulse sequences are widely used in clinical imaging but they suffer from blurring when high spatial frequencies are attenuated by T2-effects. This blurring is especially pronounced at high field when T2 is shorter. We have developed a method to reduce blurring effects using an appropriate point spread function (PSF) measured by a modified TSE sequence but without deconvolution. The method restores image sharpness at reasonable additional scan times.

2408. Improvements in Cerebrospinal Fluid Flow Measurements with Phase Contrast Balanced Steady State Free Precession

Erin Jane McCormack[1], Michael R. Egnor[1], Mark E. Wagshul[1]
[1]Stony Brook University, Stony Brook, New York, USA

To overcome limitations in obtaining accurate quantitative information with phase contrast gradient echo sequences (PC-GRE) for cerebrospinal fluid (CSF), a new technique is presented, phase contrast balanced steady state free precession, which improves accuracy of CSF measurements in multiple regions of the brain. CSF images acquired with PC-GRE suffer from very low SNR, due to the requirement of short repetition times (TR) for adequate temporal resolution, and the elaxation rate of CSF. CSF is often turbulent, causing phase dispersion and further signal loss. PC-bSSFP can overcome these limitations due to its high SNR and robustness against signal loss from turbulence.

2409. Chemical Exchange in Fully-Balanced Steady-State Free Precession

Sean CL Deoni[1]
[1]Institute of Psychiatry, King's College, London, England, UK

Multi-component T1 and T2 relaxation arising from exchanging water pools with different physical environments has been observed in several biological tissues. In this we investigate the effect of chemical exchange on the fully-balanced steady-state free precession (SSFP) imaging signal by solving for the steady-state signal of the Bloch-McConnell expressions. We show that at low TR (5ms), the effect of exchange is negligible on the signal from each exchanging species and, therefore, the SSFP signal can be expressed as a linear summation of each species. This result suggests the future possibility of using SSFP to observe and measure multi-component relaxation *in vivo*.

2410. Graphical Derivation of the Steady-State Magnetization in Balanced SSFP MRI

Zungho Zun[1], Krishna S. Nayak[1]
[1]University of Southern California, Los Angeles, California, USA

Balanced steady-state free precession (SSFP) exhibits different steady-state signal depending on flip angle and resonance-offset, producing a well-known ¡ banding artifact¡±. The steady-state magnetization can be derived from matrix calculations based on excitation, relaxation, and off-resonance precession that should cancel one another in the steady state. Matrix derivations are accurate, but do not provide an intuition behind the signal variation and the banding artifact. In this work, a new graphical derivation of the SSFP signal is presented. For given T1 and T2, the steady-state signal is uniquely determined by a new parameter, the effective flip angle, which is a function of flip angle and off-resonance precession within TR, and along with T2/T1, uniquely determines steady-state magnetization.

2411. Binomial Pulse Suppression to Reduce Ghosting Artifacts in Transient-State BSSFP Imaging

Yin-Cheng Kasuga Huang[1], Teng-Yi Huang[2], Tzu-Chao Chuang[1], Hsiao-Wen Chung[1, 3], Cheng-Yu Chen[3]
[1]National Taiwan University, Taipei City, Taiwan; [2]National Taiwan University of Science and Technology, Taipei City, Taiwan; [3]Tri-Service General Hospital and National Defense Medical Center, Taipei City, Taiwan

Magnetization-prepared transient-state balanced steady-state free precession (TS-bSSFP) images require a good stabilization method to reduce image artifacts due to initial signal oscillations at various off-resonance conditions. However, it is not possible to inhibit signal oscillations near ±180 SSFP angles without an inevitable reduction of contrast we have prepared using just a train of a few RF. We present a method using a binomial composite RF pulse with spoilers to reduce ghosting of this kind, in front of some stabilization method, e.g. Kaiser-Bessel window. Such *binomial scheme* seemed to be effective in our preliminary results of phantom studies.

2412. Oscillating Steady States

Klaus Scheffler[1], Stefan Maderwald[2], Mark Ladd[2], Oliver Bieri[1]
[1]Radiology, Basel, Switzerland, Switzerland; [2]Radiology, Essen, Germany, Germany

The signal formation and properties of steady state free precession (SSFP) in combination with alternating RF pulse phases or alternating spin precession is analyzed. Simulations and experiments demonstrate that the amplitudes of SSFP echo paths are significantly influenced by application of alternating phases either via the exciting RF pulse or via some external mechanism producing alternating spin precession. This behavior can be described using a simple perturbation theory applied to the frequency response profile of balanced SSFP combined with a final signal integration over one balanced SSFP band. The high sensitivity of SSFP echo amplitudes to alternating RF pulse phases or precession is exemplarily used to detect and visualize propagating transverse acoustic shear waves.

2413. Modified T_2-TIDE Sequence: A Preliminary Result

Yin-Cheng Kasuga Huang[1], Teng-Yi Huang[2], Hsiao-Wen Chung[1, 3], Cheng-Yu Chen[3]
[1]National Taiwan University, Taipei City, Taiwan; [2]National Taiwan University of Science And Technology, Taipei City, Taiwan; [3]Tri-Service General Hospital and National Defense Medical Center, Taipei City, Taiwan

Transition into driven equilibrium (TIDE) has less banding artifacts than half-angle-half-TR (HAHT) TrueFISP, and is not as blurred as in HASTE with also less SAR. For variable pure T_2-weighted contrast, T_2-TrueFISP is done by driven equilibrium (DE) HAHT preparation, while T_2-TIDE is TIDE with more 180¢X refocusing RF. We modified the T_2-TIDE sequence presented by Paul *et al*. in *ISMRM* 2005 and obtained images somewhat different from theirs. We also compared T_2-TrueFISP of comparable TE in DE preparation and conventional steady-state TrueFISP (SS-TrueFISP / SS-bSSFP). In conclusion, T_2-TIDE is a better choice than T_2-TrueFISP for fast T_2WI in clinical setting.

2414. Frequency Off-Resonance Effects on Parametric SSFP Imaging

Zhiqiang LI[1], Maria I. Altbach[1]
[1]University of Arizona, Tucson, Arizona, USA

Steady-state free precession (SSFP) techniques are sensitive to the frequency offset caused by field inhomogeneity. In this study we demonstrated the influence of off-resonance effects on the estimation of MRI-dependent tissue parameters obtained from SSFP techniques. If the field inhomogeneity caused by tissue susceptibility can not be neglected, errors in the parameter estimation can be reduced by measuring data at various frequency offsets in order to find the optimal estimate.

2415. Steady State BURST: Signal Amplitudes and the Influence of Gradient and RF Spoiling

Christian Boller[1], Klaus Scheffler[1]
[1]University of Basel, Basel, Switzerland

The signal behavior of a gradient echo BURST sequence is studied under steady-state conditions in simulation and experiment. The separation of echo pathways between excitations is shown to require proper gradient spoiling. Further, the use of phase cycling between sub-pulses in a BURST is shown to be beneficial even in the stead state, both with and without RF spoiling.

2416. Efficient Implementation of Hardware Optimized Gradients for Rapid Imaging Sequences

J. Andrew Derbyshire[1], Elliot R. McVeigh[1]
[1]NHLBI, National Institutes of Health, Bethesda, Maryland, USA

Hardware optimized gradient pulses minimize TRs by optimizing gradientshapes so that at least one of the physical gradient axes operates atthe specified limits during dead-times. We demonstrate a method thatreduces the number of waveform shapes required to be designed from~1000 to 12 (i.e. two per encoding gradient pulse per axis) forscanners that can play a linear combination of two pulse shapessimultaneously on each gradient axis. The method provides a simplerimplementation for optimized pulse sequences providing increased SNRefficiency in rapid, interactive imaging and improved frame rates ininterventional real-time imaging.

2417. Real-Time MRI of Upper Airway Collapse During Inspiratory Loading

Ian Michael Colrain[1, 2], Krishna S. Nayak[3], Jon F. Nielsen[3]
[1]SRI International, Menlo Park, California, USA; [2]University of Melbourne, Melbourne, Victoria, Australia; [3]University of Southern California, Los Angeles, California, USA

Real-time single- and multi-slice upper airway (UA) imaging was performed using an echo-planar gradient echo pulse sequence, achieving 1.56 mm spatial resolution over a 20 cm FOV with a 5 mm slice thickness every 160 ms. Susceptibility resulted in moderate warping artifacts, which were mitigated by shortening the readout duration. Application of a 5 cm H2O load to an awake male subject diagnosed with primary snoring resulted in significant narrowing in UA 2D cross sectional area, primarily in the lateral (R/L) direction. We achieved real-time visualization of UA collapse in response to a known increase in inspiratory load.

2418. Real-Time Tagging of Muscle Dynamics in a 70cm Bore 1.5T Scanner

Elliot McVeigh[1], Mike Guttman[1], Cengizhan Ozturk[1], Silvia Salinas Blemker[2]
[1]NHLBI, National Institutes of Health, DHHS, Bethesda, Maryland, USA; [2]Stanford University, Stanford, California, USA

The purpose of this work was to test the ability of a “wide bore” (70cm diameter), 1.5T MR system to perform real-time tagging of skeletal muscle dynamics We present results from real-time tagging images of the thigh musculature during a full flexion-extension of the knee (motion not previously possible at 1.5T). A real-time SSFP sequence was programmed on a Siemens Espree scanner to yield approximately10 frames/sec, with interactive tagging available via a mouse-click. The tags were visible for approximately 800-1000ms in the real-time images (~10 frames); this was sufficient to visualize the strain in skeletal muscle groups during motion.

2419. Real-Time Quantification of Brain Motion Using Gradient-Echo Phase

William Ryan Overall[1], John M. Pauly[1]
[1]Stanford University, Stanford, California, USA

A new technique for measuring very small displacements is applied to real-time imaging of pulsatile brain motion. Nonlinear encoding provides high velocity-SNR over a broad range of velocities. We demonstrate that this technique can measure motion well below 1 mm/sec without the need for long bipolar encoding gradients. We have generated motion maps with true frame rates above 2 frames per second. The technique may be applicable to prospective motion correction in diffusion imaging.

2420. k-T SPARSE: High Frame Rate Dynamic MRI Exploiting Spatio-Temporal Sparsity

Michael Lustig[1], *Juan Manuel Santos*[1], *David L. Donoho*[1], *John Mark Pauly*[1]
[1]Stanford University, Stanford, California, USA

A method for high frame-rate dynamic imaging exploiting the spatio-temporal sparsity of dynamic MRI sequence of images(scene) is proposed. The k-t space is randomly sampled by random ordering of the phase encodes in time. The dynamic scene is reconstruct by minimizing the L_1 norm of a transformed dynamic scene subject to data fidelity constraints. The proposed method does not require a known structure nor a training set, only that the dynamic scene has a sparse representation. A 7-fold frame-rate acceleration is demonstrated in simulated data and *in vivo* non-gated Cartesian balanced-SSFP cardiac MRI

2421. Whole-Body MR Imaging with Continuously Moving Table and Multiplanar Reformations: Toward Parameter Optimization for SSFP Imaging in Patient Examinations

Sonja Kinner[1], *Amrei Zielonka*[1], *Michael O. Zenge*[1], *Susanne C. Ladd*[1], *Mark E. Ladd*[1]
[1]University Hospital Essen, Essen, Germany

We optimized parameters for whole-body imaging with continuously moving table using a 2D axial SSFP sequence. Our aim was to develop a fast but accurate examination for patients which allows imaging the thorax and abdomen in a single breath hold. After identifying the optimal parameters (sharpness, image quality) in phantoms, they were applied and assessed in volunteers (depiction of small anatomic structures). Slice thicknesses of 6mm with table velocities of 20-22 showed the best results, allowing a 30s breath hold during imaging thorax and abdomen.

2422. Evaluation of the SNR in the Echo-Shifted Pulse Sequence

Alexander B. Pinus[1], *Hyeonjin Kim*[1]
[1]Yale University School of Medicine, New Haven, Connecticut, USA

Following recent interest in the echo-shifted (ES) pulse sequences, this study is concerned with the evaluation of the SNR of the ES signal. In particular, the SNR is evaluated as a function of number of TR periods the echo is shifted, N, and the flip angle. It was found that the SNR decreases as a hyperbolic function of N. The Ernst angle also decreases as a function of N.

2423. MR Imaging of Intermolecular Double-Quantum-Filtered Zero-Quantum Coherence

Zhong Chen[1, 2], *Bingwen Zheng*[1], *Xiaoqin Zhu*[1], *Tianliang Gu*[2], *Jianhui Zhong*[2]
[1]Xiamen University, Xiamen, Fujian, People's Republic of China; [2]University of Rochester, Rochester, New York, USA

A new three-pulse sequence was designed to choose signals from intermolecular ZQCs and avoid contamination from other coherences, using intermolecular double-quantum filtering. Efficient phase-cycling and fast spin echo acquisition with optimal flip angles were proposed to obtain pure iZQC images quickly, to overcome the imperfect RF pulses, and to reduce the effect of the longitudinal magnetization during the evolution period. The method may provide an attractive alternative for iZQC with the CRAZED sequence.

2424. Single-Shot 3D Gradient and Stimulated Echo Imaging

Jürgen Finsterbusch[1, 2], *Wolfgang Weber-Fahr*[1, 2], *Martin A. Koch*[1, 2]
[1]University Medical Center Eppendorf, Hamburg, Germany; [2]University Medical Centers Hamburg-Kiel-Lübeck, Hamburg-Kiel-Lübeck, Germany

An extension of 2D gradient and stimulated echo (GRASTE) imaging ispresented that is capable of acquiring a 3D volume within a singlesub-second acquisition. Within a readout echo train consisting of astimulated and several gradient echoes, all echoes share the same 2Dphase encoding but are differently phase-encoded in 3D direction,Thereby all required 3D phase-encoding steps were covered within areadout interval, i.e. the number of echoes was equal to the number ofacquired sections in the slab. Applications to healthy volunteers at3T are presented and demonstrate the feasibility of single-shot 3DGRASTE.

2425. Sensitivity Encoded Proton Echo Planar Spectroscopic Imaging (SENSE-PEPSI) on Human Brain Using a Large-N Coil Array

Shang-Yueh Tsai[1, 2], *Stefan Posse*[3, 4], *Lawrence L. Wald*[5], *Cheng-Wen Ko*[6], *Hsiao-Wen Chung*[2], *Fa-Hsuan Lin*[1]
[1]Athinoula A. Martinos Center for Biomedical Imaging, Massachusetts General Hospital, Chalestown, Massachusetts, USA; [2]Department of Electrical Engineering, National Taiwan University, Taipei, Taiwan; [3]MIND Institute, 801 University Blvd SE, Suite 200, Albuquerque, New Mexico, USA; [4]University of New Mexico, Albuquerque, New Mexico, USA; [5]Athinoula A. Martinos Center for Biomedical Imaging, Massachusetts General Hospital,, Chalestown, Massachusetts, USA; [6]National Sun Yat-sen University, Kaohsiung, Taiwan

Parallel MRI techniques have been demonstrated to be capable of accelerating data acquisition by using spatial information from RF array coils to substitute for a portion of the data that would normally be acquired using sequentially-applied magnetic field gradients. This is particularly advantageous for spectroscopic imaging (SI) to reduce the long encoding times associated with phase encoding. Proton Echo Planar Spectroscopic Imaging (PEPSI) provides much faster acceleration with a scan time of a minute for a 32x32 spatial matrix. Here, we report initial *in vivo* results using a combination of parallel MRI and PEPSI to further accelerate the SI data acquisition.

2426. Fast Low-Angle Dual Spin-Echo (FLADE): A New Pulse Sequence for Micro-Imaging of Trabecular Bone

Jeremy Magland[1], *Branamir Vasilic*[1], *Felix W. Wehrli*[1]
[1]University of Pennsylvania Medical Center, Philadelphia, Pennsylvania, USA

A new pulse sequence for high-resolution imaging of trabecular bone (TB) at distal extremities is described. Spin echo approaches such as 3D FLASE (Fast Large-Angle Spin-Echo) have proven useful for micro-imaging of TB, as they are less sensitive to artifacts from local susceptibility induced gradients in the vicinity of trabeculae. However, the short repetition time (TR) needed to achieve sufficient resolution within a clinically feasible scan time can cause problems. In FLADE (Fast Low-Angle Dual Spin-Echo), the single spin-echo of FLASE is replaced by a double spin-echo, and the TR is significantly lengthened. The longer TR not only reduces artifacts, but can also be used to improve the detection of patient motion.

2427. Inversion-Optimized, Multi-Slice, Parallel TOSSI (T-One Insensitive Steady State Imaging)

Jamal J. Derakhshan[1], *Martin Blaimer*[2], *Peter Schmitt*[3], *Jeffrey L. Sunshine*[2], *Jeffrey L. Duerk,* [12], *Mark A. Griswold*[2]
[1]Case Western Reserve University, Cleveland, Ohio, USA; [2]University Hospitals of Cleveland/Case Western Reserve University, Cleveland, Ohio, USA; [3]Siemens Medical Solutions, Erlangen, Germany

TOSSI (T-One insensitive Steady State Imaging) can be used to generate pure T2 contrast in steady state free precession imaging. We extend the TOSSI framework to fast multi-slice imaging with optimal T2 contrast by adjusting the inversion pulse timing dynamically, using slice-selective adiabatic RF pulses and by using parallel imaging to obtain higher resolution images at a fixed echo time. We demonstrate that TOSSI can be used to obtain T2W images of the brain in a moving subject, unlike T2W TSE which is severely degraded by motion artifacts. Comparison with other rapid acquisition images, HASTE and SE-EPI, are also presented.

2428. FastDiagonal-SPRITE: A New Method for Diagonal-SPRITE Images

Andrea Protti[1], *Amy Herlihy*[1], *Jean Tessier*[2], *Jimmy Bell*[1]
[1]Hammersmith Hospital, Imperial College London, London, UK; [2]AstraZeneca, Macclesfield, UK

In the study of ultra-short TE (UTE) for biological components an improvement in Diagonal-SPRITE is presented. The technique named FastDiagonal-SPRITE reduces acquisition time compare to Diagonal-SPRITE by reducing the k-space data points collected without decreasing in resolution and S/N. For this reasons the technique is an improvement for *in vivo* MR imaging. New artefacts are studied by point spread function (PSF) and methods to reduce them are presented.

2429. Efficient Phase-Encoding for 3D Turbo-Spin-Echo Imaging with Very Long Echo Trains

John P. Mugler III[1], *Marion I. Menzel*[2], *Wilhelm Horger*[2], *Berthold Kiefer*[2]
[1]University of Virginia, Charlottesville, Virginia, USA; [2]Siemens Medical Solutions, Erlangen, Germany

The conventional phase-encoding method used with turbo/fast spin-echo (TSE) imaging is very inefficient for 3D imaging with a large number of echoes, such as can be achieved by using variable-flip-angle refocusing RF pulses. We developed a phase-encoding scheme that makes efficient use of very long echo trains by accelerating the acquisition along both the in-plane and through-plane phase-encoding directions. This method takes full advantage of the reduction in imaging time offered by such long echo trains and, combined with parallel imaging strategies, yields imaging times that are clinically practical for single-slab 3D-TSE imaging of large volumes.

2430. Flow Sensitivity of CPMG Sequences with Variable Flip Refocusing and Implications for CSF Signal Uniformity in 3D-FSE Imaging

Reed F. Busse[1]
[1]GE Healthcare, Madison, Wisconsin, USA

3D-FRFSE with variable flip refocusing is a means to acquire large volumetric datasets with T2-weighting in a relatively short time. CSF, however, may appear dark in regions of high flow. Here it is demonstrated that motion causes differing amounts of phase to accrue in different spin and stimulated echo pathways, resulting in signal loss when signal pathways do not add constructively. As refocusing flip angles decrease and/or net gradient area between refocusing RF pulses increases, the sensitivity to flow increases. *In vivo* imaging experiments demonstrate that uniformly bright CSF may be attained if minimum flip and net gradient area are limited.

2431. Rapid High-Resolution T_1 Mapping by Variable Flip Angles: Accurate and Precise Measurements in the Presence of RF Field Inhomogeneity

Hai-Ling Margaret Cheng[1, 2], *Graham A. Wright*[1, 3]
[1]The University of Toronto, Toronto, Ontario, Canada; [2]The Hospital for Sick Children, Toronto, Ontario, Canada; [3]Sunnybrook & Women's College Health Sciences Centre, Toronto, Ontario, Canada

The variable flip angle (VFA) approach enables rapid 3D T_1-mapping with superior *precision* compared to conventional methods. To ensure *accuracy*, the influences of B_1 inhomogeneity and noise-bias must be considered in addition to the choice of flip angles. We present an accurate and precise approach that accounts for these influences. A simple, parameter-independent T_1 correction scheme is derived theoretically for B_1-induced error. We identify a noise threshold and show that three properly chosen angles best maintain accuracy and precision across a large T_1 range. Improved T_1 measurements through the proposed approach are demonstrated in simulations, phantoms, and human brain scans.

2432. Time Efficient Flip Angle Measurement at 7T

Duan Xu[1, 2], Charles H. Cunningham[3], Douglas AC Kelley[4], Krishna S. Nayak[5], Albert P. Chen[1], John M. Pauly[3], Daniel B. Vigneron[1, 2]

[1]UCSF, San Francisco, California, USA; [2]UCSF/UC Berkeley, San Francisco, California, USA; [3]Stanford University, Stanford, California, USA; [4]GE Healthcare Technologies, San Francisco, California, USA; [5]University of Southern California, Los Angeles, California, USA

With the non-significant risk classification of 7T, high field MR imaging is poised to advance clinical radiology. Unlike 1.5T and 3T, 7T systems do not have a body coil, so excitations are performed by smaller volume or surface coils, yielding highly variable excitation. In this abstract, we utilized a fast double angle B1 mapping sequence to obtain the flip angle. *In vivo* B1 maps demonstrated as large as 3-fold differences in some regions in effective flip angle experienced by tissue in slice and across slices. They also highlight the differences between excitation offered by coils with different designs.

2433. Sweep Imaging with Fourier Transform (SWIFT)

Djaudat Idiyatullin[1], Curt Corum[1], Jang-Yeon Park[1], Michael Garwood[1]

[1]University of Minnesota Medical School, Minneapolis, Minnesota, USA

A new fast and quiet method for MRI based on acquisition of time domain signal during "adiabatic" sweep excitation is reported. The described approach represents a branch of NMR which by coincidence was not previously developed. The proposed imaging method has reduced motion artifacts because it does not require gradient inversion or the delays associated with forming an echo. The method applies virtually simultaneous excitation and signal acquisition giving significant benefits for studying objects having fast spin-spin relaxation rates. Additionally, gradients do not have to be pulsed and can be run in a small stepwise continuous manner, greatly reducing acoustic noise.

2434. Maintaining the CPMG Conditions with Slice Accelerated Parallel Imaging in 2D Fast Spin Echo

Kevin F. King[1]

[1]GE Healthcare, Waukesha, Wisconsin, USA

Parallel imaging in the slice encoding direction is used with 3D pulse sequences to allow high acceleration while maintaining reasonable geometry factors via 2D acceleration. For T2-weighted imaging, 3D acquisition has relatively long scan time and consequently 2D pulse sequences are frequently favored. Slice direction acceleration can also be used with 2D pulse sequences such as Fast Spin Echo. With Fast Spin Echo, the CPMG conditions must be maintained by aligning the center of the cosine modulation with the time in the RF pulse where the transverse magnetization is effectively created (isodelay point), otherwise ghosting artifacts result.

2435. Phase-Compensated Spin-Echo Sequence Using Hyperbolic Secant Pulses for Both Excitation and Refocusing

Jang-Yeon Park[1], Michael Garwood[1]

[1]Center for Magnetic Resonance Research and Department of Radiology, University of Minnesota, Minneapolis, Minnesota, USA

Frequency-modulated (FM) pulses are frequently used for refocusing to overcome problems due to RF inhomogeneity and to achieve broad bandwidth. An even number of FM pulses have previously been used in spin-echo sequences to cancel the non-linear phase of the transverse magnetization produced by individual pulses. FM pulses have also been applied for both excitation and refocusing, whereby each pulse compensates the phase of the other. Here, the phase profiles are analytically described when hyperbolic secant (HS) pulses are used for excitation and refocusing, and the exact condition for achieving phase compensation is derived for spin-echo imaging using HS pulses.

2436. True T1 Weighted MR Imaging by a Non Selective and Selective RF Sandwich Pulse Scheme: TOBAC T One Beta Alpha Contrast

Michael Deimling[1], Alto Stemmer[1]

[1]Siemens Medical Solutions, Erlangen, Germany

In the present work a new approach to T1 weighted imaging with a simple sandwich RF pulse is examined. Plain, fast gradient echo imaging performed with high flip angles and short TR <<T1 leads to suboptimal T1 contrast in the 2D mode; and in the case of 3D acquisition to a strong contrast variation in slice partition direction. In the steady state the effective slice profile can be much broader than the nominal slice thickness. The suggested sandwich pulse creates a nearly optimal slice excitation resulting in a true T1 contrast and an accurate slice definition.

2437. Single-Shot STEAM MRI with Cross-Sectional RF Excitations

Jürgen Finsterbusch[1, 2], Martin A. Koch[1, 2]

[1]University Medical Center Eppendorf, Hamburg, Germany; [2]University Medical Centers Hamburg-Kiel-Lübeck, Hamburg-Kiel-Lübeck, Germany

The main reason for the inherent lower SNR of single-shot STEAM is the low flip angle in the readout interval that is required to avoid image blurring and depends on the ratio of the resolution and FOV in phase-encoding direction. This is in particular a problem if only a small FOV is of interest but a larger one must be acquired to avoid aliasing as for instance in spine imaging. For these applications, cross-sectional RF excitations can be used to reduce the FOV without aliasing and enhance the SNR due to the larger flip angle that can be used.

2438. Parallel Zoom EVI: Effects of Short TR on Image Quality

Cécile Rabrait[1], Cyril Poupon[1], Patrick Le Roux[2], Alejandro Ribès[1], Denis Le Bihan[1], Franck Lethimmonier[1]
[1]Commissariat à l'Energie Atomique, Orsay, France, France; [2]GE Health Care, Buc, France, France

A new method to perform single shot 3D imaging is introduced. It combines a zoomed Echo Volumar Imaging sequence with 2D parallel acquisition and SENSE reconstruction with a reduction factor of 4. Two artefacts were identified, which result from the high acquisition rates reached. First, an aliasing artefact in the middle of the phase direction has been identified and suppressed. It was created by imperfect outer volume suppression and SENSE reconstruction. Second, the profile along the partition direction has been greatly improved by setting the excitation flip angle to the Ernst angle. Finally, brain volumes acquired at 1.5T are presented.

2439. Broad Oversampling with TIme Efficiency (BOWTIE) for Increased SNR

Candice Anne Bookwalter[1], Kestutis J. Barkauskas[1], Mark A. Griswold[2], Jeffrey L. Sunshine[2], Jeffrey L. Duerk[2]
[1]Case Western Reserve University, Cleveland, Ohio, USA; [2]University Hospitals of Cleveland and Case Western Reserve University School of Medicine, Cleveland, Ohio, USA

The radial continuous sampling sequences (aka Total Sampling Time (TST) acquisitions) are more time efficient than their Cartesian counterparts, however radial sequences exhibit characteristic artifacts. This study proposes a TST sequence where the phase encoding and dephase/rephase lobes are overlapped in order to create a hybrid radial/Cartesian trajectory bowtie. This TST sequence, named Broad Over-sampling With TIme Efficiency (BOWTIE), samples during the traditionally unsampled radial traversal to and from the edge of k-space before and after Cartesian readout. In this study, a BOWTIE sequence was developed for imaging both phantoms and human volunteers for the purpose of SNR gain.

2440. Deriving Oxygen-Sensitive Contrast in Tissue from MRI: A Comparison Between T2*-Weighted, T2-Prepared and SSFP Methods with an Ischemia Leg Cuff Model at 1.5T

Jain Mangalathu Arumana[1], Rohan Dharmakumar[1], Nicole Campbell[1], Debiao Li[1]
[1]Northwestern University, Chicago, Illinois, USA

Current methods for deriving oxygen-sensitive contrast (OC) in tissue are limited by sensitivity, poor SNR, and imaging time. Recently, SSFP imaging has been proposed for detecting oxygen-related changes in tissue. This work, based on previous theoretical studies, (1) investigates the SSFP dependence of OC on TR and flip angle ($f\tilde{N}$) and (2) compares the OC derived from SSFP against T2-prepared and T2*-weighted methods with a leg cuff model. Results show that OC with SSFP is strongly dependent on TR and $f\tilde{N}f$nand that with appropriate choice of these parameters, it is possible to increase OC beyond conventional methods.

2441. Determination of the Variability of fMRI Responses Using Deconvolution Analysis

Bharat Biswal[1], Nitin Chawla[2]
[1]University of Medicine & Dentistry, Newark, New Jersey, USA; [2]University of Medicine & Dentistry of New Jersey (UMDNJ), Newark, New Jersey, USA

A large number of statistical tests (including t-test, cross-correlation, F-test, deconvolution, etc.) are currently used in functional Magnetic Resonance Imaging (fMRI) to localize and quantify task-induced signal changes. It is currently assumed that fMRI time-points are stationary i.e., signal characteristics do not change over time. In this study, time-varying signal characteristics of fMRI signal response were investigated using Impulse response function. Substantial variation in the activation map was obtained for bilateral finger tapping paradigm. The proposed method can be extended to study variation between different experiments, and can also be used to detect habituations, or learning effects.

2442. Rapid Fat Suppressed Imaging: Application to the Cartilage and the Breast

Qi Peng[1], Roderick W. McColl[2], Paul T. Weatherall[2]
[1]UT Health Science Center at San Antonio, San Antonio, Texas, USA; [2]UT Southwestern Medical Center, Dallas, Texas, USA

A pulse sequence implementation of a novel rapid fat suppression strategy is proposed to achieve rapid and effective fat suppression. The pulse sequence performs fat presaturation with short binomial RF pulse train, in combination with sustained short (1-1) spatial-spectral water-selective excitations in a segmented gradient echo shot. The effectiveness of fat suppression of the sequence is tested both on the knee and breast, and the significance this method for further imaging speed improvement is briefly discussed.

2443. Fast Separation of Water, Acetone, Fat and Silicone with a Multiecho Balanced SSFP Sequence

Jochen Leupold[1], Oliver Wieben,[12], Sven Mansson[3], Klaus Scheffler[4], J Stefan Petersson[5], Jürgen Hennig[1]
[1]University Hospital Freiburg, Freiburg, Germany; [2]Madison Clinical Science Center, Madison, Wisconsin, USA; [3]Malmo University Hospital, Malmo, Sweden; [4]University of Basel, University Hospital, Basel, Switzerland; [5]Amersham Health R&D, Malmo, Sweden

Fast chemical shift imaging of water, fat, acetone and silicone is demonstrated on 1H phantoms with a multiecho balanced SSFP sequence and IDEAL spectral reconstruction. The separation of water, fat and silicone is demonstrated *in vivo* as well. The method is particularly promising for spectroscopic (hyperpolarized) 13C imaging.

2444. Rapid 3D-SPGR Imaging of the Liver with Multi-Echo IDEAL

Scott B. Reeder[1], Anthony T. Vu[2], Brian A. Hargreaves[3], Ann Shimakawa[4], Oliver Wieben[1], Charles A. McKenzie[5], Jason A. Polzin[2], Jean H. Brittain[6]

[1]University of Wisconsin, Madison, Wisconsin, USA; [2]GE Healthcare, Waukesha, Wisconsin, USA; [3]Stanford University, Stanford, California, USA; [4]GE Healthcare, Menlo Park, California, USA; [5]Beth Israel Deaconess Medical Center, Boston, Massachusetts, USA; [6]GE Healthcare, Madison, Wisconsin, USA

Dynamic contrast enhanced imaging of the liver requires robust fat-suppression and complete volumetric liver coverage within a reasonable breath-hold interval. In this work we described the combination of IDEAL, a chemical-shift based water-fat separation method, with a multi-echo 3D-SPGR acquisition for rapid volumetric imaging of the liver within a breath-hold. The use of multiple echoes greatly improves the SNR efficiency of this approach, with an effective signal averaging of three in a single TR. Imaging of the entire liver with robust water-fat separation was possible in breath-hold times less than 20seconds.

2445. Intrinsic Fat Saturation of TIDE with Variable Flip Angles Due to Modified Stop Bands

Dominik Paul[1], Maxim Zaitsev[1], Jürgen Hennig[1]

[1]University Hospital, Freiburg, Germany

Many applications of balanced SSFP require suppression of fat signals. Due to modified stop bands in TIDE imaging an intrinsic fat saturation method is presented called FS-TIDE. The TIDE signal-evolution in the transition from TSE-like behavior to TrueFISP was simulated in investigated. The resulting signal notch for off-resonant spins is then used for fat suppression. FS-TIDE is applied to phantoms and healthy volunteers on a 1.5T system. Resulting images were compared to standard TrueFISP with and without fat suppression. It is demonstrated that FS-TIDE provides a method for homogenous fat suppression in abdominal imaging while maintaining SSFP-like image contrast.

2446. Single Quadrature Echo Water-Fat Separation with Robust Phase Correction

Huanzhou Yu[1], Scott B. Reeder[2], Charles A. McKenzie[3], Ann Shimakawa[1], Anja C.S. Brau[1], Norbert J. Pelc[4], Jean H. Brittain[5]

[1]GE Healthcare, Menlo Park, California, USA; [2]University of Wisconsin, Madison, Wisconsin, USA; [3]Beth Israel-Deaconess Medical Center and Harvard Medical School, Boston, Massachusetts, USA; [4]Stanford University, Stanford, California, USA; [5]GE Healthcare, Madison, Wisconsin, USA

Three-point IDEAL (Iterative Decomposition of water and fat with Echo Asymmetry and Least-squares estimation) water-fat decomposition method offers robust separation, however, triples the scan time. To accelerate IDEAL, a reduced sampling scheme is proposed. The new approach acquires one full-resolution echo with water and fat quadrature encoded (separated by $\pm\pi/2$). Two additional echoes are acquired in low-resolution. Robust water-fat separation is achieved with correction for the phase map calculated from the low-resolution images. The scan time is close to a single acquisition. Uniform water-fat separation was obtained in breathheld abdominal imaging and breast imaging, demonstrating its value in time-sensitive applications.

Parallel Imaging

Room 4E Wednesday 14:00 - 16:00

2447. SENSE and GRAPPA Reconstruction of Multi-Shot Multi-Echo EPI Data

David B. Clayton[1], Stefan Skare[1], Rexford Newbould[1], Roland Bammer[1]

[1]Stanford University, Stanford, California, USA

We present both GRAPPA and SENSE reconstructions of multi-shot, multi-echo perfusion-weighted EPI with an effective reduction factor of 4. Although both require no user input and are generally robust to the choice of acquisition parameters, we show that a critical step for SENSE reconstruction is the method and parameters used for generating coil sensitivity maps. While GRAPPA reconstruction could be treated nearly as a black-box and demonstrates extremely robust and reliable performance in all cases treated here, the SENSE reconstruction required some refinement of the details involved in transforming the data from all shots into optimum sensitivity maps.

2448. Rapid Large Field-Of-View Microscopy Using Parallel Imaging

Mary Preston McDougall[1], Steven M. Wright[1], Ian Steele-Russell[2], Naresh Yallapragada[1], Murat Russell[2]

[1]Texas A&M University, College Station, Texas, USA; [2]Texas A&M Health Science Center, College Station, Texas, USA

Microcoils are used to increase the SNR in high-resolution microscopy imaging, with the intrinsic disadvantage that they cover a limited field-of-view. This paper presents a large-scale (FOV) microscopy system comprised of a 64-channel array of microcoils (enabling a large FOV in the phase-encode direction) and a 64-channel broadband receiver (enabling a large FOV in the frequency-encode direction). Conventional surface coil and array images with the same field-of-view and resolution were compared. Despite an imaging time of only nine seconds for the array image as compared to 2.13 minutes for the conventional image, a factor of three higher SNR was achieved.

2449. Single Breath-Hold Whole-Heart MRA Using Variable Density Spirals and Localized Coil Demodulation

Juan Manuel Santos[1], Bob S. Hu[2], Jin H. Lee[1], John M. Pauly[1]
[1]Stanford University, Stanford, California, USA; [2]Palo Alto Medical Foundation, Palo Alto, California, USA

We have previously presented a single breath-hold whole-heart aquisition method that takes advantage of the localized sensitivity of a surface coil. We extend the method to increase the FOV by using an 8 channel cardiac coil and localized demodulation (PILS) without increasing the acquisition time.

2450. Evaluation of Sensitivity Encoded Diffusion Tensor Imaging at 4T

Xiaoping Zhu[1], Geon-Ho Jahng[1], Yu Zhang[1], Jim X. Ji[2], Ashish Raj[1], Hemanth T[1], Mathew Jacob[3], Zhi-Pei Liang[3], Machael W. Weiner[1], Norbert Schuff[1]
[1]VAMCSF/UCSF, San Francisco, California, USA; [2]Texas A&M University, College Station, Texas, USA; [3]University of Illinois at Urbana-Champaign, Urbana, Illinois, USA

We developed an approach to assess quality of sensitivity encoding (SENSE) diffusion tensor imaging (DTI) within the context of fractional anisotropy (FA) evaluation in healthy aging of corpus callosum. DTI were acquired using an eight-channel coil at 4T MRI. With high acceleration factor, SENSE significantly amplified noise, induced bias, and altered biologically distinction features, such as age correlation of FA in genu. Consistent with the changes of the first order statistics described by the linear mixed model, image texture entropy increased globally. In conclusion, SENSE reconstruction can bias DTI results, which need to be considered in clinical applications.

2451. Susceptibility-Weighted Imaging at 3T and 7T Using Multi-Channel Phased Array Coils and SENSE

Janine M. Lupo[1], Douglas Kelley[2], Duan Xu[1], Daniel B. Vigneron[1], Sarah J. Nelson[1]
[1]University of California, San Francisco, California, USA; [2]Global Applied Science Lab, GE Healthcare, San Francisco, California, USA

Susceptibility-weighted imaging is an emergent technique for high resolution, distortion-free imaging of brain vasculature. With the availability of high field MR systems with multi-channel coil capabilities, parallel imaging acquisitions and SENSE reconstruction can be employed to reduce the acquisition time as long as the decrease in SNR does not significantly affect the contrast between vessels and brain parenchyma. This study assesses the feasibility of SWI at 3T and 7T with SENSE. The sensitivity of detecting small vessels is improved at higher field strengths and the implementation of SENSE was not found to significantly reduce the detection of small vessels.

2452. Parallel Imaging of Trabecular Bone Micro-Architecture Using Autocalibrating Technique at 3 T

Suchandrima Banerjee[1, 2], Eric T. Han[3], Anja CS Brau[3], Sharmila Majumdar[1, 4]
[1]University of California San Francisco, San Francisco, California, USA; [2]UC Berkeley, Berkeley, California, USA; [3]GE Healthcare, Menlo Park, California, USA; [4]University of California Berkeley, Berkeley, California, USA

This study implemented autocalibrating partially parallel imaging (PPI) with a GRAPPA based robust reconstruction applied it to invivo MRI of trabecular bone micro-architecture at 3 Tesla in conjunction with a multiple acquisition steady state free precession (SSFP) sequence. Improving signal-to-noise ratio efficiency of multiple SSFP by PPI was demonstrated. Intensity distribution and spatial correlation in the parallel images were characterized and quantitative analysis of bone structural parameters was obtained. Visualization of bone micro-structures was preserved even in images having high reduction factor (R=3) but for their quantification , new image analysis independent of background signal may be required.

2453. Highly Accelerated IDEAL for Volumetric Abdominal Imaging with Fat-Water Separation in a Single Breath-Hold

Ajit Shankaranarayanan[1], Daniel Sodickson[2], Randy Giaquinto[3], Aaron Grant[2], Andres Carrillo[4], David Gurr[5], Ananth Madhuranthakam[6], Huanzhou Yu[1], Ann Shimakawa[1], Sanjay Joshi[5], Charles Dumoulin[3], Scott Reeder[7], Theodore Steger[5], Anja Brau[1], Norman Farrar[2], Neil Rofsky[2], Susan LaRuche[2], Jean Brittain[8], Charlie McKenzie[2]
[1]GE Healthcare, Menlo Park, California, USA; [2]Beth Israel Deaconess Medical Center, Boston, Massachusetts, USA; [3]GE Global Research, Niskayuna, New York, USA; [4]GE Healthcare, Evanston, Illinois, USA; [5]GE Healthcare, Milwaukee, Wisconsin, USA; [6]GE Healthcare, Boston, Massachusetts, USA; [7]Radiology, Madison, Wisconsin, USA; [8]GE Healthcare, Madison, Wisconsin, USA

Initial study of combining a robust fat-water separation technique like IDEAL with high acceleration factors enabled by 32 channel system for breath-held contrast enhanced abdominal imaging is shown here. Net acceleration of 6.3 was achieved in the these experiments. Moreover, the high SNR demonstrated in images from volunteers suggests that even higher acceleration factors may be possible, enabling higher spatial resolution or larger coverage.

2454. Motion-Free Carotid Artery Imaging with a Reduced-FOV Parallel HASTE Sequence

Ling Zhang[1], Eugene G. Kholmovski[2], Junyu Guo[1], Dennis L. Parker[2]
[1]Univerisity of Utah, Salt Lake City, Utah, USA; [2]Utah Center for Advanced Imaging Research, Salt Lake City, Utah, USA

HASTE is a fast sequence which acquires half k-space data in one shot. It is a valid candidate for carotid artery imaging since most physiological motions can be considered frozen during such a short scan time. However, its long echo train length must be reduced to image vessel wall which has a short T2. Reduced phase FOV combined with parallel imaging can greatly shorten the echo train length, reducing T2 decay related blurring to an acceptable level. Multiple averages can be acquired to enhance SNR. The combination of KIPA and Homodyne reconstruction gave acceptable single-shot images.

2455. Autocalibrating Parallel Imaging at 7T-High Resolution, Quantitative and Phase-Sensitive Applications

Suchandrima Banerjee[1, 2], Julio Carballido-Gamio[1], Janine Lupo[1, 2], Jan S. Bauer[1], Duan Xu[1], Doug A. Kelley[3], Daniel B. Vigneron[1, 2], Sarah J. Nelson[1], Sharmila Majumdar[1]

[1]University of California San Francisco, San Francisco, California, USA; [2]University of California Berkeley, Berkeley, California, USA; [3]GE HealthCare, San Francisco, California, USA

The synergy between high field strength and parallel imaging has been discussed in the literature. This study implements an autocalibrating acquisition and GRAPPA based reconstruction to look at three different applications –high resolution imaging of trabecular bone micro-architecture and cartilage and susceptibility weighted imaging of brain vasculature. Our initial studies investigated reduction factors (R) upto 4 and image quality was preserved in all applications till R=4.The study supports the idea that there is an upward shift in maximum speedup factor at higher field.With the availability of appropriate coil hardware imaging at even higher acceleration should be possible.

2456. MR Angiography of the Carotid Circulation Using Two-Dimensional Parallel Imaging on a 32 Channel 3.0T System

Michael Christian Fenchel[1, 2], Kambiz Nael[2], J. Paul Finn[2], Stefan Ruehm[2], Stephan Miller[1], Gerhard Laub[3]

[1]Eberhard-Karls-University Tuebingen, Tuebingen, BW, Germany; [2]David Geffen School of Medicine, University of California Los Angeles, Los Angeles, California, USA; [3]Siemens Medical Solutions, Los Angeles, California, USA

The feasibility of combined in-plane and through-plane parallel-acquisition for isotropic 3D contrast enhanced MR angiography (MRA) of the carotid and vertebro-basilar circulation should be assessed. Six volunteers and five patients with suspected cerebro-vascular disease were examined on a 3.0T MR-scanner. Contrast-enhanced 3D CE-MRA was acquired with parallel-acquisition (GRAPPA) in both phase- and slice encoding-directions. Scoring of image quality on a 4-point-scale [range 0-3] yielded 2.5±1.0 and 2.1±1.0 for extra-cranial and intra-cranial vessel segments in volunteers and 2.8±0.6 and 2.0±1.2 in patients, respectively. This study shows that contrast-enhanced MRA, applying parallel-imaging in both phase- and slice-encoding direction, is feasible at 3.0T.

2457. 3D Time Resolved MRA: Comparison of TREAT (Time –resolved Echo-Shared Angiographic Technique) of the Intracerebral Circulation at 1.5 and 3 Tesla

Jean Yves Gauvrit[1, 2], Meng Law[1], P. Sunenshine[1], Q. Chen[1], R. Carson[1], J. Xu[3]

[1]New York University Medical Center, New York, New York, USA; [2]Hopital R Salengro, Lille, France; [3]Siemens Medical Solutions,, Erlangen, Germany

To compare image quality, SNR, temporal/spatial resolution using Time Resolved MRA of the intracranial vessels at 1.5T with a higher spatial resolution at 3.0T.

2458. A Practical Stopping Criterion for Iterative Non-Cartesian SENSE Reconstruction

Peng Qu[1], Kai Zhong[2], Bida Zhang[2, 3], Jianmin Wang[3], Gary X. Shen[1]

[1]The University of Hong Kong, Hong Kong, People's Republic of China; [2]The Graduate School and Institute of Biophysics,The Chinese Academy of Sciences, Beijing, People's Republic of China; [3]Siemens Mindit Magnetic Resonance Ltd., Shenzhen, Guangdong, People's Republic of China

In non-Cartesian SENSE reconstruction based on conjugate gradient (CG) iteration method, the iteration very often exhibits a ¡ semi-convergence¡± behavior which can be characterized as initial convergence towards the exact solution and later divergence. This phenomenon makes a suitable stopping criterion very critical for automatic implementation of this reconstruction strategy. In this study a practical stopping rule for iterative SENSE reconstruction is proposed. By monitoring the residual norm along the iteration, this stopping criterion can automatically stop the process where artifact and SNR are well compromised and good overall image quality are achieved.

2459. Fast Toeplitz Based Iterative SENSE Reconstruction

Valur Olafsson[1], Sangwoo Lee[1], Jeffrey A. Fessler[1], Douglas C. Noll[1]

[1]The University of Michigan, Ann Arbor, Michigan, USA

Reconstruction of images from sensitivity encoded imaging (SENSE) is computationally demanding when non-Cartesian k-space sampling is used in the data acquisition. Most of the reconstruction time is accounted for by the multiple matrix-vector multiplication required in conjugate gradient (CG) iterations. We present a new fast iterative reconstruction method for SENSE providing off-resonance correction with high accuracy. Simulations show that the proposed method is significantly faster than NUFFT based method with substantial correction for field map.

2460. The Use of Coil Sensitivity Variations in the Read-Direction for Improved Parallel Imaging

Felix Breuer[1], Martin Blaimer[2], Nicole Seiberlich[1], Mark Griswold[2], Peter Jakob[1]

[1]University of Würzburg, Würzburg, Germany; [2]University Hospitals of Cleveland, Cleveland, Ohio, USA

In conventional Cartesian parallel MRI sensitivity variations provided by the receiver array can only be exploited in the phase encoding direction in which undersampling is performed. Potential sensitivity variations in the read-out direction are unused. In this work we show that sensitivity variations in the read direction can additionally be exploited by employing rapidly oscillating phase encoding gradients during the actual read-out process. This strategy allows one to exploit sensitivity variations in one additional dimension resulting in improved parallel image reconstruction quality for both 2D and 3D imaging.

2461. A Reconstruction Algorithm of MR Images Acquired on a Radial K-Space Trajectory for Parallel Imaging

Sungdae Yun[1], YeJi Han[1], HyunWook Park[1]
[1]Korea Advance Institute of Science and Technology, Daejeon, Republic of Korea

A reconstruction method was presented by Pruessmann *et al*. for Sensitivity Encoding (SENSE) with arbitrary k-space trajectory. This method requires gridding step which converts the coordinates from arbitrary grid to Cartesian grid. Therefore, it suffers from the gridding interpolation error in the reconstructed image. In this study, we proposed a reconstruction algorithm for parallel imaging with radial k-space trajectory. The presented method does not require gridding step and can reconstruct the images using only magnitude informationof the projection data which is obtained after the Fourier transform along the radial direction.

2462. Efficient Computation of Autocalibrating Parallel Imaging Reconstructions

Anja C.S. Brau[1], Philip J. Beatty[1, 2], Stefan Skare[2], Roland Bammer[2]
[1]GE Healthcare, Menlo Park, California, USA; [2]Stanford University, Stanford, California, USA

The accuracy of autocalibrating parallel imaging reconstructions such as GRAPPA has recently been shown to improve through the use of a 2D convolution kernel; however, the extension to a 2D kernel significantly increases computation time. We demonstrate that autocalibrating reconstruction methods can be separated into two processing steps and that each step can be independently optimized in terms of computational efficiency. The most computationally efficient means of obtaining the accuracy of a 2D k-space kernel is to find the kernel weights in k-space and then apply the weights in either image space or hybrid space, depending on the specific application.

2463. Pseudo-Cartesian GRAPPA Reconstruction of Undersampled Non-Cartesian Data

Nicole Seiberlich[1], Robin M. Heidemann[2], Felix A. Breuer[1], Martin Blaimer[1], Mark A. Griswold[3], Peter M. Jakob[1]
[1]University of Würzburg, Würzburg, Bavaria, Germany; [2]Siemens Medical Solutions, Erlangen, Bavaria, Germany; [3]University Hospitals of Cleveland, Cleveland, Ohio, USA

The GRAPPA reconstruction of undersampled non-Cartesian data involves two steps: reconstruction of the missing data points, and resampling of the non-Cartesian data onto a Cartesian grid. In all previous work, the reconstruction was performed first, followed by regridding of the then complete k-space data. In this abstract, we propose first regridding of the undersampled data, and then performing a Cartesian GRAPPA reconstruction to arrive at a fully-sampled k-space. This method is advantageous because it allows one to reconstruct arbitrary sampled data with the standard Cartesian GRAPPA procedure, without the need for specialized non-Cartesian GRAPPA reconstruction techniques.

2464. K-Space Inherited Parallel Acquisition (KIPA)

Junyu Guo[1], Eugene G. Kholmovski[1], Ling Zhang[1], Eun-Kee Jeong[1], Dennis L. Parker[1]
[1]University of Utah, Salt Lake City, Utah, USA

The GRAPPA method gives good quality results for low reduction factors but it is less applicable for high reduction factors due to residual aliasing artifacts and substantial noise amplification in the reconstructed images. A novel method for dynamic parallel imaging called K-space Inherited Parallel Acquisition (KIPA) has been developed to overcome the limitations of GRAPPA for dynamic imaging.

2465. Kriging and GRAPPA: A New Perspective on Parallel Imaging Reconstruction

Keith Aaron Heberlein[1], Xiaoping Hu[1]
[1]Emory/GA Tech, Atlanta, Georgia, USA

Parallel MRI is widely used as a method for reduced acquisition. GRAPPA is a reconstruction method that recovers missing samples in the k-space directly using a weighted average estimation model. In the field of geostatistics, a common method for spatial estimation is termed “kriging”. This paper describes the application of kriging to the parallel imaging reconstruction problem. Furthermore, we show that GRAPPA is identical to kriging when considering Cartesian sampling.

2466. Application of TurboSENSE for Non-Cartesian Trajectories

Calvin Lew[1], Frandics Chan[1], Dan Spielman[1], Chunlei Liu[1], Roland Bammer[1]
[1]Stanford University, Stanford, California, USA

TurboSENSE is a method for magnitude-only reconstruction using phase contraints. It offers a better-conditioned solution than SENSE, especially noticeable at high reduction factors. Here, turboSENSE has been extended to non-Cartesian trajectories, where the reconstruction problem is solved similar to iterative methods for SENSE reconstruction. TurboSENSE is specifically demonstrated on variable density spiral trajectories.

2467. Understanding the GRAPPA Paradox

Philip James Beatty[1, 2], Anja C. Brau[1]
[1]GE Healthcare, Menlo Park, California, USA; [2]Stanford University, Stanford, California, USA

Autocalibrating parallel imaging methods such as GRAPPA use low-frequency convolution kernels to calculate the weights needed to unfold the aliased images. Yet GRAPPA has been shown to accurately reconstruct images even if the image contains high-frequency components, such as when the reconstructed FOV is smaller than the object. In this work we examine the GRAPPA paradox: how can low-frequency convolution kernels accurately reconstruct images encoded with high-frequency coil sensitivities? To answer this question, we compare the unfold images generated by GRAPPA and self-calibrating SENSE reconstructions and show that, although functionally the same, they represent fundamentally different approaches to solving the reconstruction problem.

2468. A Theoretical Analysis of Errors in GRAPPA

Feng Huang[1], George Randy Duensing[1]
[1]Invivo Corporation, Gainesville, Florida, USA

GRAPPA has been widely used as a prominent partially parallel imaging (PPI) technique. To understand GRAPPA better and hence further improve its performance, the error sources of GRAPPA are analyzed in this work. The relationship of the performance of GRAPPA to coil geometry, the choice of auto-calibrated signal (ACS) lines, blocks for reconstruction are all discussed based on the analysis of error sources. The discussion can be used to guide the design of coil and reconstruction algorithm. Linear coil distribution was used as an example to confirm some claims.

2469. The Geometry Factor as a Cramér-Rao Bound for Magnitude and Phase

Angel Ramon Pineda[1], Calvin D. Lew[1], Roland Bammer[1]
[1]Stanford University, Stanford, California, USA

The geometry factor in SENSE imaging provides a measure of the noise amplification of the unaliasing process. It gives the ratio of the noise of the reconstructed complex image obtained from the full acquisition over that of the accelerated acquisition. We recast SENSE in terms of the magnitude and phase. Assuming a sensitivity matrix with no errors, we compute the Cramér-Rao bound (CRB) to show numerically that the geometry factor is a normalized CRB for both magnitude and phase. Hence, the minimum variance of the magnitude and phase of the reconstructed images are minimized when the geometry factor is minimized.

2470. Iterative Solution of Transmit SENSE Using a Conjugate Gradient Method

Ingmar Graesslin[1], Ulrich Katscher[1], Ferdinand Schweser[1], Markus Niemann[1], Peter Börnert[1]
[1]Philips Research Laboratories, Hamburg, Germany

Due to the analogy between the design of spatially selective RF pulses and MR imaging, it is possible to adapt the methodology of parallel imaging for parallel trans-mission. Thus, in analogy to parallel imaging, the RF pulse calculation can be performed via direct matrix inversion or via iterative methods. This paper discusses the iterative approach in some detail and compares the two approaches for different scenarios. It turns out, that the matrix approach typically requires longer computation times than the iterative approach. On the other hand, in most scenarios, the resulting excitation accuracy is lower for the iterative approach.

2471. B_1 Homogenisation Using a Multichannel Transmit Array

Jürgen Nistler[1], Rainer Kurth[2], Markus Vester[1], Dirk Diehl[3], Wolfgang Renz[1], Thorsten Speckner[1], Thorsten Feiweier[1]
[1]Siemens Medical Solutions, Erlangen, Germany; [2]University Erlangen, Erlangen, Germany; [3]Siemens CT, Erlangen, Germany

The extending use of high field mri in clinical application needs methods to eleminate shading in image brightness. A possible solution is B1 homogenisation using multichannel transmit arrays. We show results of B1 shim in the liver.

2472. SENSE Accelerated Multiple Excitation Imaging at Ultra High Field

Arthur William Magill[1], Alexa Jones[1], Paul Glover[1]
[1]Nottingham University, Nottingham, UK

At high frequencies (>128MHz) the RF wavelength approaches the dimensions of the human head, leading to a significant B_1 phase variation across the sample. This causes destructive or constructive interference, giving highly inhomogeneous B_1 fields. By employing multiple independent elements excited sequentially using a BURST like imaging sequence, we are able to separate signals due to different transmit elements within the same slice without interference. However, there is a time penalty associated with the sequential excitation. In this work we demonstrate the use of SENSE to accelerate image readout, restoring the speed to near that of a single excitation readout.

2473. Wave-Propagation Based Estimation of Coil Sensitivities

Richard Winkelmann[1], Peter Börnert[2], Olaf Dössel[1]
[1]University of Karlsruhe, Karlsruhe, Germany; [2]Philips Research Laboratories, Hamburg, Germany

Parallel imaging performance is continuously rising, achieving high acceleration factors. SENSE, as a major parallel imaging method, however requires accurate coil sensitivity maps to create high quality images. Standard low-resolution reference scan approaches can fail, which may result in an image artifact in the reconstructed image. This abstract presents an approach to estimate the coil sensitivities, taking the basic coil geometry and a wave propagation model into account. First *in vivo* studies on different anatomies are very promising.

2474. Optimization of Regularization Parameter for GRAPPA Reconstruction

Peng Qu[1], Jing Yuan[1], Bing Wu[1], Gary X. Shen[1]
[1]The University of Hong Kong, Hong Kong, People's Republic of China

The effectiveness of regularization to improve SNR in parallel imaging techniques has been reported in previous works, but how to optimize the regularization parameter remains a problem. In this study, three regularization parameter choice strategies are compared in GRAPPA reconstruction: the L-curve method, the fixed singular value (SV) threshold method, and a novel discrepancy principle approach. *In vivo* experiment results show that the discrepancy-based parameter choice strategy significantly outperforms the others. It can automatically choose nearly optimal parameters for the reconstructions so as to achieve good compromise between SNR and artifacts.

2475. SNR-Adaptive K-Space Filtering for Autocalibrated Parallel Image Reconstruction

Junyu Guo[1], Eugene G. Kholmovski[1], Ling Zhang[1], Dennis L. Parker[1]
[1]University of Utah, Salt Lake City, Utah, USA

All of the autocalibrating methods in k-space like GRAPPA, GARSE calculate the reconstruction coefficients in the fully sampled central k-space and apply them to recover the missing k-space lines in the outside region of k-space. Noise amplification is caused when the coefficients from the high SNR region are applied to the very low SNR region. In this study, an SNR adaptive filter has been extracted from the SNR in k-space and applied to the reconstructed k-space lines to reduce the noise amplification for imaging with high reduction factors.

2476. An Iterative Method for Fast Regularized Parallel MRI Reconstruction

W Scott Hoge[1], Misha E. Kilmer[2], Steven J. Haker[1], Dana H. Brooks[3], Walid E. Kyriakos[1]
[1]Brigham and Women's Hospital, Boston, Massachusetts, USA; [2]Tufts Univ., Medford, Massachusetts, USA; [3]Northeastern Univ., Boston, Massachusetts, USA

Parallel MR imaging is an effective approach to reduce MR image acquisition time. Non-uniform subsampling allows more flexible data acquisition, and increases the potential for high quality images at high acceleration factors. Due to large problem size, iterative methods are often employed to solve the reconstruction problem. Non-uniform subsampling often requires a regularized solution due to poor conditioning, and one challenge is to choose a good regularization parameter. Typically, this requires multiple expensive system solves. Here, we present an efficient LSQR-Hybrid algorithm which provides fast reconstruction while addressing the need for rapid regularization parameter selection.

2477. Bayesian Parallel Imaging with Edge-Preserving Priors

Ashish Raj[1], Gurmeet Singh[2], Ramin Zabih[2]
[1]UCSF, San Francisco, California, USA; [2]Cornell University, Ithaca, New York, USA

Existing parallel imaging methods are limited by a fundamental tradeoff, where suppressing background noise introduces aliasing artifacts. Bayesian methods offer a promising alternative; however, previous methods with spatial priors assume that intensities vary smoothly over the entire image, and therefore blur edges. We introduce an edge-preserving prior which instead assumes that intensities are piecewise smooth, and show how to efficiently compute its Bayesian estimate. This is formulated as an optimization problem, which requires minimizing a large non-convex objective function. Traditional continuous minimization methods cannot be applied. However, it is closely related to some problems in computer vision for which discrete optimization methods have been developed in the last few years. We extend these algorithms, which are based on graph cuts, to address our problem. An empirical analysis indicates a significant improvement in overall quality compared to conventional SENSE methods.

Contrast Mechanisms and MTC

Room 4E Wednesday 14:00 - 16:00

2478. A New Approach to Bright Spot MRI: Visualizing Local Dipolar Fields with the CRAZED Sequence

Cornelius Faber[1, 2], Carolin Heil[1], Benjamin Zahneisen[1], David Balla[1], Richard Bowtell[2]
[1]University of Würzburg, Würzburg, Germany; [2]University of Nottingham, Nottingham, UK

In molecular MRI it is often desirable to obtain positive contrast from iron based contrast agents. Here, we demonstrate how the CRAZED experiment with magnetic field gradient modulation along the magic angle can be used to obtain images with positive contrast from local dipolar fields such as created by SPIOs. Images with high contrast and excellent background suppression can be acquired in 3 minutes scan time.

2479. Effect of Distant Dipolar Field and T_2 on Magnetization in CRAZED-Multiecho Pulse Sequence

Chung Ki Wong[1], Edmund Kwok[1], Jianhui Zhong[1]
[1]University of Rochester, Rochester, New York, USA

It has been recently demonstrated that the finite duration of refocusing pulses in the multiecho acquisition of intermolecular double quantum coherence signal leads to significant signal attenuation. Here we explain such phenomenon by evaluating the effect of distant dipolar field and transverse relaxation T_2 on the magnetization in a CRAZED-multiecho pulse sequence. The result demonstrates the signal rises primarily during the free evolution time in the acquisition period, and the siganl attenuation is proportional to the pulse duration. In addition, for a large range of T_2, maximal SNR is obtained when the pulse duration is half of the pulse separation.

2480. Linear Combination Filtering in White Matter with Steady-State Free Precession (SSFP) Sequences

Logi Vidarsson[1], Kelvin O. Lim[2], Bryon Mueller[2], John Pauly[1]
[1]Stanford University, Stanford, California, USA; [2]University of Minnesota, Minneapolis, Minnesota, USA

Myelin-water has a dramatically shorter T_2 than other braintissues ($T_2 \approx 10$ to 20 ms). Prior myelin imaging methods,acquire a multi-echo dataset and then apply estimation methods toestimate the amount of short T_2 signal. Theacquisition of this multi-echo dataset requires long scan times. Inthis work we use a multiple-flip angle steady state free precession(SSFP) 3D sequence for acquisition. This enables us to generatea 3D 25 slice short T_2 image with a 2 x 2 x 4 mm resolution usingonly 6 min and 50 s of scantime.

2481. PARACEST Detection In-Vivo Using WALTZ-16

Elena Vinogradov[1], Huamei He[2], Angelo Lubag[3], Valerie Humblet[1], James A. Balschi[2], Allan Dean Sherry[3, 4], John Vincent Frangioni[1], Robert E. Lenkinski[1]
[1]Beth Israel Deaconess Medical Center, Boston, Massachusetts, USA; [2]Brigham and Woman's Hospital, Boston, Massachusetts, USA; [3]University of Texas Southwestern Medical Center, Dallas, Texas, USA; [4]University of Texas at Dallas, Dallas, Texas, USA

Chemical Exchange Saturation Transfer (CEST) imaging detects exchange mediated saturation transfer between bound and bulk protons. Exogenous paramagnetic lanthanide complexes (PARACEST) exhibit slow exchange kinetics and large chemical shifts for the lanthanide-bound water molecule. This study used low power (B1 ~200Hz) WALTZ-16 pulses at the bulk water resonance frequency to detect the image contrast effects due to the PARACEST (Tm-DOTA4AmC) agent *in vivo*. Contrast changes due to the PARACEST in the kidneys of mice were observed. At 40 mM PARACEST bolus contrast effect of up to 70% were measured. Studies are underway to quantify the low-detection limit for PARACEST *in vivo*.

2482. MRI Detection of Glycogen (GlycoCEST)

Craig K. Jones[1, 2], Jimin Ren[3], Craig Malloy[3], A Dean Sherry[3], Peter C. M. van Zijl[1, 2]
[1]Kennedy Krieger Institute, Baltimore, Maryland, USA; [2]Johns Hopkins University School of Medicine, Baltimore, Maryland, USA; [3]University of Texas Southwestern Medical Center, Dallas, Texas, USA

We show that glycogen can be detected through the water signal using selective radiofrequency saturation of the hydroxyl protons. This saturation is rapidly transferred to the water protons via chemical exchange, leading to their cumulative saturation and enhanced glycogen detection sensitivity via the so-called chemical exchange saturation transfer (CEST) mechanism. The effect was demonstrated on mouse livers by monitoring the glycogen signal decrease after exposure to glucagon. Comparison of proton-decoupled 13C NMR and CEST MRI was consistent with the glycogen origin of the CEST effect in MRI, which we call GlycoCEST.

2483. Separating Signals from Intra- And Extracellular Water Compartments in Rat Skeletal Muscle *In Vivo* Using MEMRI

John Georg Seland[1], Karl Helmer[2], Govind Nair[2], David Gordon Bennett[2], Christopher Howard Sotak[2, 3]
[1]Norwegian University of Science and Technology, Trondheim, Norway; [2]Worcester Polytechnic Institute, Worcester, Massachusetts, USA; [3]University of Massachusetts Medical School,, Worcester, Massachusetts, USA

Tissue inter-compartmental equilibrium water exchange can significantly affect the quantitative analysis of various *in vivo* MR parameters. In this study, manganese-enhanced MRI (MEMRI) has been investigated as a method for separating and identifying the MR signals from intra- and extracellular water compartment in rat skeletal muscle *in vivo*. In the presence of extracellular manganese (Mn2+) we identified two T1 components in skeletal muscle, which we assign to IC and EC water compartments. The present study indicates that differentiated MR imaging of IC vs EC water may be possible using MEMRI.

2484. Adiabatic Modulation of the Longitudinal and Transverse Relaxations, T1ρ and T2ρ, of Gd-Fullerenol Contrast Agent: Application for the Cellular Imaging.ρ

Shalom Michaeli[1], Dennis J. Sorce[1], Stasia Anderson[2], Elbert Hu[2], Joseph Lin[1], Kamil Ugurbil[1], Michael Garwood[1], Joseph Frank[2]
[1]CMRR, University of Minnesota, Minneapolis, Minnesota, USA; [2]National Institutes of Health, Bethesda, Maryland, USA

Rotating frame relaxation rate constants R1ρ and R2ρ measured using a windowless train of adiabatic full-passage (AFP) pulses placed prior to an excitation pulse are functions of the shapes, lengths, and peak RF power of the AFP pulses. These dependencies lead to the possibility to alternate relaxation contrast and to assess fundamental parameters of the sample. We demonstrate here that adiabatic T1ρ and T 2ρ measurements provide a method to follow relaxation mechanisms of HeLa cells labeling in culture with C(82) Gd-Fullerenol. Theory of paramagnetic relaxations during adiabatic rotation is applied for the data analysis.

2485. Efficiency of Paramagnetic Relaxation Enhancement in Off-Resonance Rotating Frame

Huiming Zhang[1, 2], Yang Xie[1]
[1]ENH Research Institute, Evanston, Illinois, USA; [2]Feinberg Medical School, Northwestern University, Chicago, Illinois, USA

A complete formalism for the relaxivity of Gd-based contrast agents in off-resonance rotating frame at high magnetic field is described. The theoretical simulation and experimental validation were carried out for macromolecule conjugated Gd-DTPA. We found that very high relaxation enhancement efficiency can be achieved in the off-resonance rotating by altering the dynamics of the Gd-DTPA unit at high field.

2486. iDQC MR Imaging with Contrast of Off-Resonance Rotating-Frame Spin-Lattice Relaxation

Bingwen Zheng[1], Zhong Chen[1, 2], Scott D. Kennedy[2], Jianhui Zhong[2]
[1]Xiamen University, Xiamen, Fujian, People's Republic of China; [2]University of Rochester, Rochester, New York, USA

A long-duration, low-power, and off-resonance spin-locking pulse was incorporated into the CRAZED sequence in order to measure the intermolecular double-quantum longitudinal relaxation time in the tilted rotating frame. This modified CRAZED sequence was appended to a fast spin-echo imaging sequence to form images with contrast of the intermolecular double-quantum longitudinal relaxation time in the tilted rotating frame. The results show that both the tilt angle and the effective spin-locking frequency can be used as controllable parameters to manipulate image contrast. The off-resonance spin-locking technique reduces the absorption of rf energy which may be harmful to the patients in clinical applications.

2487. Off-Resonance Spin Echos for Probing the Cellular Microenvironment

Charles H. Cunningham[1], Steven M. Conolly, [1,2], Ian Y. Chen[1], Yoriyasu Suzuki[1], Phillip C. Yang[1], Michael V. McConnell[1], Sanjiv S. Gambhir[1], John M. Pauly[1]
[1]Stanford University, Stanford, California, USA; [2]UC Berkeley, Berkeley, California, USA

A new pulse sequence consisting of spectral-spatial excitation/refocusing pulses and an optional oscillating readout gradient was developed for obtaining positive contrast when imaging regions of concentrated superparamagnetic iron oxide (SPIO). It was demonstrated that the resulting signal can carry information such as the local phase distribution surrounding the cells, which could be used for iron quantification. Also, a proof-of-principle experiment showed that information about a complementary contrast agent such as Gd-DTPA can be measured in the positive contrast signal. This interaction can be measured at a high rate because localization is provided entirely by the RF pulses.

2488. Modeling MRI Contrast Enhancement with Exogenous T_2 Agents

Parker Henry Mills[1, 2], Eric T. Ahrens[1, 2]
[1]Carnegie Mellon University, Pittsburgh, Pennsylvania, USA; [2]Pittsburgh NMR Center for Biomedical Research, Pittsburgh, Pennsylvania, USA

Superparamagnetic contrast agents are a widely studied for emerging cellular-molecular applications. Rational development of new generations of agents requires a computational scheme for predicting contrast enhancement *in vivo*. A general theoretical model is presented to evaluate the minimal concentration of a T2 contrast agent providing satisfactory MRI contrast. The model requires only a few key parameters that are readily evaluated. The model is applicable to a wide range of T2 agents and delivery scenarios. We apply the model to Feridex, a commercial agent, and ferritin, an iron storage protein that can be used as a novel intracellular contrast agent.

2489. Dependency of Oxygen Extraction Calculations from a Static Dephasing Model on Capillary-Radius and Volume Fraction

André Bongers[1], Heiko Schroeder[2], Lothar Rudi Schad[2]
[1]mediri GmbH, Heidelberg, Germany; [2]German Cancer Research Center, Heidelberg, Germany

Recent approaches try to map oxygen extraction fraction (OEF) *in vivo* by measuring average susceptibility difference maps from signal decay measurements with gradient-echo/spin-echo-sequences. These methods utilize a static spin dephasing model to calculate blood volume fraction (l), reversible relaxation rate (R'2) and OEF. An important prerequisite for the applicability of this technique for OEF mapping is that the calculated susceptibility values are independent of capillary radius and volume fraction of the inclusions. In this work, a phantom study was performed to test the dependency of the measured susceptibility differences on l and capillary diameter.

2490. Correction on FID NMR Signal Induced by Mesoscopic Magnetic Field Inhomogeneities at High Volume Fraction

Xiang He[1], Alexander L. Sukstanskii[1]
[1]Washington University School of Medicine, St. Louis, Missouri, USA

At high volume fraction, the FID NMR signal at static dephasing regime deviates from the signal behavior predicated by Yablonskiy and Haacke. When the possibility of overlapping between magnetized objects can not be ignored, the distribution function is not uniform and independent anymore. Using an approach analogy to mean field approximation, the hard sphere model predicates a slightly higher probability for the object residing close to the medium position. The correction of FID NMR singal at the short time and long time scale indicates that underestimation of volume fraction can occur if the correction term is ignored.

2491. 3D-Maps of T1 and Magnetization Transfer (MT) Related Saturation from MT-FLASH Images

Gunther Helms[1], Henning Dathe[2], Steffi Dreha-Kulaczewski[1, 2], Kai Kallenberg[1, 2], Peter Dechent[1]
[1]Göttingen University, Faculty of Medicine, Göttingen, Germany; [2]Göttingen University, Göttingen, Germany

Quantitative magnetization transfer (MT) measurements in brain are commonly performed using FLASH with interleaved MT-saturation. By modeling MT by free evolution of the binary spin bath for short TR and small flip-angles, an MT-related saturation term is identified in the signal equation. Thus, maps of T1, PD-signal, and percentage MT-saturation can be calculated from an MT and two reference 3D-scans (1.25 mm resolution; acquired in 13 min on a 3 Tesla MR-system). The MT-saturation is proportional to the macromolecular fraction and increases with TR. The MT-saturation shows a high contrast between white matter and cortex and multiple sclerosis lesions.

2492. Quantitative Magnetization Transfer Bound Pool Mapping at 3T

Rexford Newbould[1], Chunlei Liu[1], Stefan Ropele[2], Roland Bammer[1]
[1]Stanford University, Stanford, California, USA; [2]Medical University Graz, Graz, Austria

Quantitative magnetization transfer (MT) imaging has been limited at higher fields as most sequences are quite SAR-intensive, and can be hampered by long T1's. Here, a stimulated echo quantitative bound pool fraction (BPF) mapping sequence is presented which has extremely low SAR, and produces high resolution BPF images. The small signal attributable to the MT effect has been magnified by the use of higher field strength, 3.0T. One drawback to the current implementation is sensitivity to Δ B1, which is worse at higher fields, but may be alleviated through alternate RF pulses. Even so, exceptional BPF images with excellent gray/white contrast may be produced.

2493. Optimisation of Quantitative Magnetisation Transfer (QMT) Sequence Acquisition Parameters

Rebecca Sara Samson[1], Mark R. Symms[1], Mara Cercignani[1], Daniel J. Tozer[1], Paul S. Tofts[1]
[1]Institute of Neurology, London, UK

We optimise quantitative Magnetisation Transfer (qMT) acquisition to minimise uncertainty of parameter estimates, using the Cramer-Rao Minimum Variance Bound (CRMVB). Acquisition was optimised theoretically to estimate f/R_A (1-f), a measure of the fraction of protons that are bound to macromolecules, or T_{2B}, their T_2 value, or both (with remaining parameters fixed). For estimation of both parameters, a 39% reduction in the standard deviation (SD) of T_{2B} estimates and a 17% reduction in the f/R_A (1-f) SD were observed experimentally compared to an existing acquisition scheme, verifying theoretical calculations and numerical simulations. Alternatively, qMT acquisition time could be reduced using this approach.

2494. Quantitative Magnetization Transfer and Relaxation in Tissues at 3T

Greg Jan Stanisz[1], Ewa Odrobina, Joseph Pun, Simon J. Graham, Michael J. Bronskill, R Mark Henkelman
[1]Sunnybrook & Womens' CHSC, Toronto, ON, Canada

T1, T2 and magnetization transfer (MT) measurements were performed in vitro at 3 T and 37oC on a variety of tissues: mouse liver, muscle and heart; rat spinal cord and kidney; bovine optic nerve, cartilage, white and gray matter; and human blood. The MR parameters were compared to those at 1.5 T. As expected, the T2 relaxation time constants and quantitative MT parameters (MT exchange rate, R, macromolecular pool fraction, M0B and macromolecular T2 relaxation time, T2B) at 3 T were similar to those at 1.5 T. The T1 relaxation time values however, for all measured tissues increased significantly with field strength. Consequently, the phenomenological MT parameter, magnetization transfer ratio, MTR was lower by approximately 2 to 10%. Collectively, these results provide a useful reference for optimization of pulse sequence parameters for MRI at 3 T.

2495. Systematic Comparison of Magnetization Transfer Contrast in Human Subjects at 3.0, 1.5, and 0.2 Tesla

Petros Martirosian[1], Andreas Boss[1], Michael Deimling[2], Berthold Kiefer[2], Fritz Schick[1]
[1]Section on Experimental Radiology, University of Tübingen, Tübingen, Germany; [2]Department of Magnetic Resonance, Siemens Medical Solutions, Erlangen, Germany

The goal of this study is to evaluate Magnetization Transfer Contrast (MTC) effects for a wide range of tissues (white and gray matter, liver, kidney, spleen, muscle, and articular cartilage) in human subjects at field strengths of 0.2, 1.5, and 3.0 Tesla. MTC MR imaging studies of the head, knee, and abdomen of three healthy volunteers were performed using a new multiple Magnetization Transfer Contrast (mMTC) module. This mMTC pulse module is a modification of a Gaussian shaped MT saturation pulse applied in a proton-density weighted RF-spoiled gradient echo sequence. The sequence allows for both a flexible MT pulse design and performance of consecutive measurements with variable flip angle or variable off-resonance frequency, while keeping other MT pulse parameters constant. Magnetization Transfer Ratio (MTR) maps were calculated on a pixel-by-pixel basis. The results indicate that MTR values are larger at higher magnetic field strengths. The increased MT effect might partly compensate the SAR (Specific Absorption Rate) related problems in MTC applications at higher field strengths.

2496. Magnetization Transfer Effects in Single Slice Spoiled Gradient Echo Imaging

Xiawei Ou[1], John C. Gore[1], Daniel Frank Gochberg[1]
[1]Vanderbilt University, Nashville, Tennessee, USA

We investigated magnetization transfer (MT) effects on the steady state MR signal for a sample subjected to a series of identical on resonance rf pulses, such as would be experienced while imaging a single slice using a spoiled gradient echo sequence. The MT coupling terms for a two-pool system were added to the Bloch Equations, and we derived the resulting steady state signal equation and compared this result to the conventional signal equation without MT effects. We found that the steady state signal is increased by a small amount because of MT. Consequences of this MT effect include 1) inaccuracies in T1 values determined via steady state gradient echo methods and 2) the ability to quantify the MT parameters by fitting the gradient echo steady state signal to the signal equation appropriately modified to include MT effects.

2497. 3T Magnetization Transfer Imaging Reveals Correlation with Cerebral Iron Concentration *In Vivo*

Seth Aaron Smith[1, 2], Jeff W.M Bulte[2], Peter C.M. van Zijl[1, 2]
[1]Kennedy Krieger Institute, Baltimore, Maryland, USA; [2]Johns Hopkins University, Baltimore, Maryland, USA

We present a high field MTR comparison of different gray matter structures in the human brain revealing an outstanding correlation with age-adjusted iron concentration *in vivo* (r = 0.90). Similar studies in ferritin doped agarose phantoms showed an even stronger correlation (r = 0.98) of the MTR with [Fe]. The widening of the water peak with increased iron concentration increases the direct saturation leading to elevated MTR in iron rich regions. This finding is likely to be acutely powerful for the quantification of cerebral changes in iron storage diseases such as Alzheimer's, Parkinson's diseases and many others.

2498. XTC MRI Parameter Optimization: Theoretical Considerations

Kai Ruppert[1, 2], Jaime F. Mata[2], James R. Brookeman[2], Klaus D. Hagspiel[2], John Paul Mugler III[2]
[1]Advanced MRI Technologies, Sebastopol, California, USA; [2]University of Virginia, Charlottesville, Virginia, USA

A typical Xenon polarization Transfer Contrast (XTC) MRI experiment consists of 2 imaging segments separated by a contrast preparation segment. In this work we performed a theoretical analysis of how the available non-equilibrium magnetization of hyperpolarized Xe-129 should be expended to obtain maximum sensitivity to regional variations in the gas-phase depolarization. We found that an individual optimization of the flip angles for the two imaging segments and of the number of contrast-generating RF inversion pairs can improve the error in the resulting depolarization maps by about 200% compared to previously-published results.

Relaxometry

Room 4E Wednesday 14:00 - 16:00

2499. Improved T1 Estimation with Spoiled Gradient Recalled Echo (SPGR) Images Using a Modified Variable Flip Angle Method

Cheng Yang[1], Gerald L. Wolf[2], Gregory S. Karczmar[1], Walter M. Stadler[1]
[1]University of Chicago, Chicago, Illinois, USA; [2]Perceptive, Waltham, Massachusetts, USA

Using multiple sample phantom data acquired with 3D spoiled gradient recalled echo (SPGR) pulse sequence at several flip angles, we demonstrate model failure of the traditional variable flip angle method for T1 estimation. Using a modified variable flip angle method, we show that the effective flip angles are different from the prescribed flip angles. We find the modified method is able to significantly increase the goodness of the fit and the accuracy of T1 estimation. The effect of spatially inhomogeneous flip angles can also be easily corrected with the modified method.

2500. Rapid Data Acquisition for T1 Mapping, Using Multishot EPI and Automated TR Variation at 3T

Xin Liu[1], Yi Feng[1], Tianyi Ke[1], Zheng-Rong Lu[1], Kevin S. Li[1], Glen Morrell[1], Eun-Kee Jeong[1]
[1]University of Utah, Salt Lake City, Utah, USA

MR imaging is a powerful tool to probe the dynamic distribution of contrast agent in drug development. T? mapping is considered as the most reliable imaging method which closely reflects the concentration of the contrast agent in tissue. There have been various acquisition techniques to acquire the MR images for T1 mapping. In this report, a rapid MR imaging technique is described and preliminary results are presented, which used multishot segmented EPI and automated TR variation. The equilibrium signal intensity, which reflects the equilibrium magnetization Mzo(r), was calculated using precontrast data, and used as an additional data to calculate the dynamic T1*(r) at each time point.

2501. Enhancement of *In Vivo* T1 Contrast and Image Quality at Ultrahigh Magnetic Fields (4.7-17.6T) Utilizing Fasting Imaging Techniques

Kyle Robert Padgett[1], Stephen J. Blackband[2, 3], Samuel C. Grant,[3, 4]
[1]University of Miami, Miami, Florida, USA; [2]University of Florida, Gainesville, Florida, USA; [3]National High Magnetic Field Laboratory, Tallahassee, Florida, USA; [4]Florida State University, Tallahassee, Florida, USA

Because of its pervasive use in anatomical imaging, the degradation of T1 contrast at high fields due to longer tissue T1s is particularly vexing. Previous work has demonstrated that sufficient T1 contrast may be obtained at ultrahigh magnetic fields using optimized magnetization preparation. However, the duration required for T1 enhancement substantially increases the acquisition time. These *in vivo* rodent and biologically representative T1 phantom results demonstrate that fast imaging methods can be employed to improve image quality without significantly sacrificing T1 contrast and that fast SE T1 imaging provides significant susceptibility correction while maintaining T1 contrast.

2502. Spin-Lattice Relaxation and Diffusion of Hyperpolarized ^{3}He in Phantoms

Gernot Laicher[1], Ben Anger[1], Brian T. Saam[1]
[1]University of Utah, Salt Lake City, Utah, USA

Spin-lattice relaxation and diffusion of hyperpolarized Helium-3 is measured in a foam phantom as a function of compression and in other phantoms with well-defined surface-to-volume ratios. The spin-lattice relaxivity in the foam phantom is shown to be proportional to the surface-to-volume ratio. Surface-to-volume ratios and tortuosities are extracted from various phantoms.

2503. Quantification and Mapping of T_1 Relaxation Time in the Tongue

Iordanis Evangelou Evangelou[1], Gloria Chi-Fishman[1]
[1]National Institutes of Health, Bethesda, Maryland, USA

T1 measurements of lingual tissue were made in six healthy volunteers in 3.0T and four excised calf tongues for methodology optimization and comparison in 1.5T and 3.0T. *In vivo* human lingual T1 values (1306.76±218.41) are considerably greater than those of the fresh (809.5±228.59) and formalin-preserved (373.91±59.27) calf tongues. Human T1 values also have regional specificity (posterior significantly lower than anterior and mid tongue regions, $p < 0.05$). Our parametric maps, generated from nearly perfect curve-fitting, clearly illustrate lingual anatomy. Further parsing into constituent tissue types will permit detailed quantitative characterization and studies of tissue changes due to disease, aging, and exercise.

2504. Effect of Chemical Exchange on T1 Values Calculated Using DESPOT1

Sean CL Deoni[1], Brian K. Rutt[2], Derek K. Jones[1]
[1]Institute of Psychiatry, King's College, London, England, UK; [2]Robarts Research Institute, London, Canada

In this work we investigate the effect of chemical exchange, such as between the intra and extracellular compartments in human brain white and grey matter, on T1 measurements made using the DESPOT1 (Driven Equilibrium Single Pulse Observation of T1) T1 mapping method. We show that, as can be anticipated, derived measurements have a strong dependence upon acquisition parameters, such as TR and flip angle. In comparison with inversion-recovery measurements, we demonstrate an increased sensitivity to fast T1 components of the DESPOT1 approach, suggesting its utility in imaging applications focused on these components.

2505. Effect of Multi-Component T1 and T2 Relaxation on Derived Single-Component DESPOT2 T2 Values

Sean CL Deoni[1]
[1]Institute of Psychiatry, King's College, London, England, UK

Here we investigate the effect of multiple-component T1 and T2 relaxation on single-component T2 values derived using the rapid DESPOT2 (Driven Equilibrium Single Pulse Observation of T2) T2 mapping method. Further, we compare these values with those calculated using convention the spin-echo approach. An increased sensitivity of DESPOT2 to fast T2 components is demonstrated, even when these components have small volume fractions. This sensitivity may make DESPOT2 advantageous in imaging applications interested in fast T2 components, such as investigations of myelin in multiple sclerosis or during brain maturation.

2506. Measuring T_2 Using a T_2 Prepared Balanced Turbo Field Echo Sequence

Caroline L. Hoad[1], Eleanor F. Cox[1], Penelope A. Gowland[1]
[1]University of Nottingham, Nottingham, UK

T_2 relaxation times were measured using a balanced turbo field echo (bTFE) sequence, prepared with a spin echo, in a 4 quadrant phantom and abdomen of a single healthy volunteer. Various bTFE sequence parameters were varied and T_2 measured by fitting the data to simulations of the magnetisation at the centre of k-space following the applied r.f. pulses. All T_2 phantom data was in good agreement with expected values, although the results were slightly lower than expected values. Repeated measurements in the liver and spleen of a single volunteer produced T_2 data similar to a previous study using HASTE imaging.

2507. Comparison of Global T2 Values and Globus Pallidal T1-Weighted Signal Changes in Sub-Clinical Hepatic Encephalopathy

Albert Michael Thomas[1], Rajesh Kumar[2], Bhagyashree Sawale[2], Amir Huda[3], Steven Han[2]
[1]University of California Los Angeles (UCLA) School of Medicine, Los Angeles, California, USA; [2]UCLA School of Medicine, Los Angeles, California, USA; [3]California State University at Fresno, Fresno, California, USA

T2 values and T1 signal changes in globus pallidus (GP) were calculated in seven patients with sub-clinical hepatic encephalopathy (HE) and 12 controls; whole brain of HE patients were also assessed using T2 relaxometry. Proton density and T2-weighted, and T1-weighted images were collected using a 1.5T MRI scanner. We observed 22.8% increase of T1-weighted signal intensities in the GP region of HE patients, however, T2 values showed a declining trend. Other regions showed increased T2 relaxation values in patients compared to control subjects. Signal increase in GP regions of HE patients and changes in hemispheric T2 values are the major outcome.

2508. T_2 Measurements in the Human Brain at 4.7T Using an Adiabatic Multi-Echo Sequence - Correlation Between T_2 and the Tissue Iron Content

Fumiyuki Mitsumori[1], Hidehiro Watanabe[1], Nobuhiro Takaya[1], Michael Garwood[2]
[1]Natl. Inst. Environ. Studies, Tsukuba, Ibaraki, Japan; [2]CMRR, Univ. Minnesota, Minneapolis, Minnesota, USA

We implemented multiple pairs of adiabatic refocusing pulses in a spin echo sequence to obtain an artifact-free T_2 decay in the multi-echo measurements at high field. The new sequence was applied to obtain T_2 values in the human brain at 4.7T. T_2 values determined in 5 different grey matter regions (ranging from 38 to 64ms) showed strong correlation with published levels of iron in those regions. T_2 values also dispersed from 53 to 64ms in white matters. This result suggested that the T_2 value in the human brain is predominantly affected by the iron distribution rather than its tissue types.

2509. Investigation of Susceptibility-Induced MR Signal Dephasing in Phantom Measurements and Model Simulations for Oxygen Extraction Mapping

André Bongers[1, 2], Heiko Schroeder[2], Lothar Rudi Schad[2]
[1]Mediri GmbH, Heidelberg, Germany; [2]German Cancer Research Center, Heidelberg, Germany

In view of methods currently discussed to map Oxygen-extraction in tissue, this work performed a phantom study to investigate the validity of signal-decay models used to calculate susceptibility differences from spin-echo/gradient-echo measurements. The signal-decay around a spin-echo was measured for capillary inclusions of different radii and compared to model simulations for two distinct dephasing models: One for static spin-dephasing and one with incorporation of diffusion effects. Our measurements show that a substantial diffusion effect has to be taken into account especially for small radii. This indicates that Oxygen-extraction results obtained from the static dephasing approximation might include substantial diffusion errors.

2510. Optimization of Voxel Based Relaxometry Parameters for the Detection of Focal T2 Changes

Gaby S. Pell[1], Heath Pardoe[1], Regula S. Briellmann[1], David F. Abbott[1], Graeme D. Jackson[1]
[1]Brain Research Institute, Melbourne, Victoria, Australia

The voxel-based approach has become a popular method for the analysis of various MR parameters between subject groups. The extension of the method to T2 analysis is termed voxel-based relaxometry (VBR). There are a considerable number of parameter choices to be made when setting up the analysis which may influence the outcome of the analysis. These include the choice of smoothing kernel and the warping procedure through which the images are registered to a standard space. This report examines the sensitivity of the analysis to these parameter choices in a study of a group of patients in which a focal area of T2 increase is expected.

2511. Effect of Spatial Distribution of Magnetic Dipoles on Lamor Frequency Distribution and MRI Signal Decay - A Numerical Approach Under Static Dephasing Conditions

Joerg Pintaske[1], Bernd Mueller-Bierl[1], Fritz Schick[1]
[1]University Hospital Tuebingen, Tuebingen, BW, Germany

Cells loaded with superparamagnetic iron oxide (SPIO) cause relatively strong magnetic field distortions, implying that field superposition effects of neighboring cells have to accounted for. We treat SPIO loaded cells as magnetic dipoles in a homogeneous magnetic field and compute the static 3D frequency distribution and related signal decay for various spatial dipole distributions. We demonstrate that non-monoexponential signal decay can result directly from magnetic field inhomogeneities. Our results provide deeper understanding of how the spatial distribution of SPIO loaded cells affects the MR signal formation and have to be considered for the *in vivo* quantification of SPIO-loaded cells.

2512. Measurement of T2 of an ROI of Arbitrary Shape Using Spatially Selective Excitation

Qin Qin[1], Mark D. Does[2], Robin A. de Graaf,[13], John C. Gore[2]
[1]Yale University, New Haven, Connecticut, USA; [2]Vanderbilt University, Nashville, Tennessee, USA; [3]Yale Medical School, New Haven, Connecticut, USA

A novel protocol of making quantitative T2 measurement using interleaved spatially selective excitation pulses is proposed. This new technique acquires signals from the entire ROI as a single voxel by encoding in the excitation phase rather than after acquisition, resulting in the SNR proportional to the ROI area. The obtained SNR per unit measuring time is potentially significantly higher than the conventional imaging methods. Phantom experiments are conducted to demonstrate the feasibility.

2513. Measurement of Short and Ultra-Short T_2 Components Using Progressive Binomial RF Saturation

Stefan Ropele[1], Christian Enzinger[1], Thomas Seifert[1], Franz Fazekas[1]
[1]Medical University Graz, Graz, Austria

A MR method for measuring T2 relaxation times in tissues is proposed. The method is based on a T2 selective saturation followed by a conventional sequence. Saturation is accomplished by a single binomial RF pulse with constant flip angle. The T2 selectivity is controlled by the pulse duration. A full T2 spectrum can be obtained by performing a series of measurements with varying RF pulse duration. The method was used to acquire T2 spectra in pig liver on a conventional 1.5 T system in vitro. We observed a short T2 component around 17ms and an ultra-short T2 component around 1ms.

2514. Selection of T2 Components from Segmented K-Space Multiecho Data: Improving Efficiency of T2 Relaxometry for Myelin Quantification

Alexey A. Samsonov[1], Andrew L. Alexander[1], Aaron S. Field[1]
[1]University of Wisconsin, Madison, Wisconsin, USA

Analysis of multiexponential T2 relaxation decay of the MR signal from a voxel may provide important information about water compartmentation within the voxel. Usually, collection of such data is time consuming. We propose a new method to significantly improve efficiency of data collection for T2 spectrum analysis in which only a part of the CPMG echo train is used for T2 decay sampling, while the rest of the echoes are utilized for k-space segmentation. The drawback of the method is SNR loss relative to images reconstructed from a full set of echoes. The method was demonstrated with simulated data.

2515. A Dynamic R2*-And-Field-Map-Corrected Imaging for Single Shot Rosette Trajectories

Sangwoo Lee[1], Jeffrey A. Fessler[1], Douglas C. Noll[1]
[1]University of Michigan, Ann Arbor, Michigan, USA

Reconstruction of single shot gradient echo rosette images is challenging in 3T. We present a robust reconstruction method that can reconstruct R2*-and-field-map corrected (and R2* weighted) images from low accuracy field maps. Beyond the robust dynamic field map correction, the proposed method produces a more accurate field map from the phase of reconstructed images. A human experiment results are presented.

2516. Dependence of R_2^* on Oxygenation and Contrast Agent Concentration in Human Blood at 3T

Nicholas Paul Blockley[1], Susan T. Francis[1], Penny A. Gowland[1]
[1]University of Nottingham, Nottingham, UK

The dependence of the transverse relaxation rate, R_2^*, of blood on oxygenation and contrast agent concentration ([CA]) has been measured at 3T. A linear fit to a plot of R_2^* versus deoxyhaemoglobin content yielded $R_2^*=122.0(1-Y)+7.0$, although a quadratic function provided a better fit. The relaxivity of CA was found to be $(-2.74\pm1.23)\times10^{-4}$ s^{-1} M^{-1} (Y~0.4) for concentrations up to 1mM (i.e. R_2^* was observed to decrease with increasing [CA]). Additional experiments at higher oxygenation and at higher [CA] showed that the quoted relaxivity reversed at a certain [CA]. An explanation for this result is suggested.

2517. Tri-Exponential T2 Quantification *In Vivo*

Jinesh J. Jain[1], Wilburn E. Reddick[1]
[1]St. Jude Children's Research Hospital, Memphis, Tennessee, USA

We propose a tri-exponential model, parametric fitting of the T2 relaxation curve, restricting the range for T2 in each compartment - Myelin [20 50] ms, White / Gray [50 120] ms, CSF [120 500] ms, and estimating the probability of the existence of each compartment on a pixel-by-pixel basis. The three T2 components were forced to lie within each compartment with the magnitude parameters allowed to take any non-negative value including zero, to account for missing components. Results from the processing of six healthy normal adults are presented.

2518. MRI Phantoms with Independently-Controllable Biexponential-T2 Decays

Robert Adam Horch[1], Mark D. Does[1]
[1]Vanderbilt University, Nashville, Tennessee, USA

In this work, chemical formulations are presented for biexponential-T2 MRI phantoms at different field strengths. These phantoms are based on aqueous solutions of urea, in which the water relaxation pool can be controlled by inner-sphere contrast agents while the urea relaxation pool remains virtually unaffected. Outer-sphere contrast agents, which affect both water and urea relaxation pools, can then be used concomitantly to enable a wide, continuous range of phantom T2 combinations. Unlike previous biexponential phantoms, the phantoms presented here have negligible constraints on pool size ratios and shelf-life.

2519. Correlation of MR Relaxation Parameters with Tissue Macromolecular Composition

Jeffrey James Luci[1], Tuhin Kumar Sinha[1], Sheerin Khatib Shahidi[1], Dale Shannen Cornett[1], Richard M. Caprioli[1], Benoit M. Dawant[1], John C. Gore[1]
[1]Vanderbilt University, Nashville, Tennessee, USA

Quantitative values of tissue NMR parameters, such as relaxation rates, are directly related to biomolecular composition, and variations of these account for much of the useful contrast available from MRI. We present here a new method to spatially correlate MR relaxation parameters with a myelin map generated from a matrix assisted laser desorption/ionization mass spectrometer (MALDI-MS) run in imaging mode at near MR resolution. Good spatial correlation of the known apparent T_1 and T_2 of white matter with myelin content is demonstrated.

2520. Cross-Site Reproducibility of Myelin Water Estimates

Charmaine Lian Li Chia[1], Thorarin Albert Bjarnason[2], Alex L. MacKay, [23], Gilbert Bruce Pike[1]
[1]Montreal Neurological Institute, Montreal, Quebec, Canada; [2]University of British Columbia, Vancouver, British Columbia, Canada; [3]University of British Columbia Hospital, Vancouver, British Columbia, Canada

The feasibility of myelin water fraction (MWF) measurements in multi-centre studies requires an assessment of cross-site stability in T2 distributions. We acquired T2 relaxation data in a healthy subject using two protocols at two sites and compared the T2 distributions and MWFs in six white and grey matter ROIs. MWFs estimated from data acquired with the same protocol but different sites were in reasonable agreement. However, alternate protocols and MWF estimation methods produced large variations in the estimated MWF. Consistent acquisition protocols and analysis methods are essential in multi-center MWF studies as is a rigorous assessment of cross-site variability.

2521. Free-Breathing, Dark-Blood GESFIDE Pulse Sequence for the Measurement of R2*, R2 and R2' of Myocardium

Ruitian Song[1], *Hee Kwon Song*[1]
[1]University of Pennsylvania Medical Center, Philadelphia, Pennsylvania, USA

An accurate measurement of transverse relaxation parameters is of growing importance in the non-invasive determination of iron concentration in subjects with iron-overloading diseases. In this work, a free-breathing, dark blood GESFIDE (gradient-echo sampling of free induction decay and echo) pulse sequence was developed and implemented for the measurement of R2, R2*, and R2' in the heart. Enhancements to the sequence include a short TE crossed-pair navigator and a navigator-restore inversion pulse to maintain strong respiratory gating signal from the liver. The improved sequence enables robust measurement of transverse relaxation rates of the myocardium in a single free-breathing scan.

2522. Prediction of Iron-Induced MRI Relaxation by Monte Carlo Modeling

Nilesh Ghugre[1], *John C. Wood*[1]
[1]Childrens Hospital Los Angeles, Keck School of Medicine, University of Southern California, Los Angeles, California, USA

MRI is becoming increasingly important in non-invasive quantification of iron-loaded tissue but the underlying biophysics remains poorly characterized. There is indication that unlike the case of free ferritin, susceptibility-based diffusional losses dominate over the contribution of contact mechanisms *in vivo* as a result of ferritin aggregation and sequestration. To examine the potential role of iron fluctuations at the lysosomal scale(~0.4 μm radius), we employed a Monte Carlo model to simulate the effect of particle size and aggregation on iron-induced MRI signal relaxation and compared this with human liver tissue relaxometry; our model predictions suggest that mesoscopic relaxation dominates microscopic effects.

2523. Inversion Recovery in the Presence of Radiation Damping - Implications for Evaluating Contrast Agents

Thomas Roger Eykyn[1], *Wing Chau Tung*[1], *Geoffrey S. Payne*[1], *Martin O. Leach*[1]
[1]Institute of Cancer Research, Royal Marsden NHS Foundation Trust, Sutton, Surrey, UK

Relaxation measurements performed at high magnetic field may be adversely affected by the influence of radiation damping in concentrated samples such as 1H in water. We consider how the measured value of T1 is affected by this phenomenon for a gadolinium-doped water sample and for an un-doped water sample. A method employing pulsed field gradients is proposed for suppressing this effect and the method is validated for measuring the relaxivity of the commercial contrast agent GdDTPA.

Spectroscopic Data Analysis and Quantitation

Room 4E Wednesday 14:00 - 16:00

2524. Decomposition Characteristics of Brain Tissue Investigated at Two Different Temperatures by Means of ^{1}H-MRS

Eva Scheurer[1], *Roland Kreis*[1], *Michael Thali*[1], *Chris Boesch*[1], *Michael Ith*[1]
[1]University & Inselspital Berne, Berne, Switzerland

Decomposition of brain tissue at 20ºC and at 4ºC was investigated by single voxel 1H-MRS in a sheep model over a period of 18 and 85 days, respectively. The results revealed that several metabolites show similar decomposition characteristics at both temperatures, however on a different time scale. Reproducible and unequivocal time courses of individual metabolite concentration allow for an estimation of the postmortem interval at both temperatures.

2525. Spectral Resolution Versus SNR and Acquisition Duration: An Adversarial Balancing Act

Roman Fleysher[1], *Lazar Fleysher*[1], *Songtao Liu*[1], *Oded Gonen*[1]
[1]NYU School of Medicine, New York, New York, USA

Enhancment of the spectral resolution (via longer signal acquisitionduration) versus signal-to-noise-ratio (SNR) trade-off have beendiscussed in the literature. While several approaches are discussed,none culminates in a recipe for an optimal trade-off. In this study, weuse the contrast-to-noise (CNR) metric to rigorously formulate thetrade-off. We demonstrate the benefits of reducing the readout durationto approximately 1.5 x T2*. Shortening data acquisition is the onlyin-situ spectral resolution enhancing filter capable of speeding up theexperiment without severe spectral distortions and/or sensitivity (SNR)losses. It also yields higher CNR than the well-known T2*-matchedfilter.

2526. Automated Separation of Low Quality and Artifact Spectra by Pattern Recognition in the Processing of MR Spectral Images

Bjoern H. Menze[1], *B. Michael Kelm*[1], *Fred A. Hamprecht*[1]
[1]University of Heidelberg, Heidelberg, Germany

We propose a methodology, which automates the decision of a human operator about the quality and interpretability of an MR spectrum. It separates both spectra of low signal-to-noise ratio and spectra corrupted by artifacts. The method is applicable in conjunction with a following quantification or a pattern recognition. The primary application will be in the automated processing of high resolution MR spectral images.

2527. Could We Accurately Measure *In Vivo* Diffusion Coefficients of Brain Metabolites Using Single-Voxel MR Spectroscopy?

Tiejun Zhao[1], Lei Zhou[1], Xiaoping Hu[1]
[1]Emory University/Georgia Tech, Atlanta, Georgia, USA

In vivo diffusion coefficients of water and NAA were determined with localized spectroscopy measurements and were shown to depend on the voxel size. With voxel size less than 10 ml, the measured diffusion coefficients of water in phantom, water *in vivo*, and NAA *in vivo* were 2.04 ¡Ñ 10^{-3} mm^2/s, 0.85 ¡Ñ 10^{-3} mm^2/s and 0.17 ¡Ñ 10^{-3} mm^2/s, respectively, in agreement with earlier reported values using similar voxel size. However, with voxel size as big as 24 ml, the measured *in vivo* diffusion coefficients of water and NAA were 1.5 ~ 3.0 times those of small voxels

2528. Automatic Repositioning of CSI Grids in ^{1}H MRS: Impact on Reproducibility of Metabolite Concentration Measurements

Ileana Hancu[1], Dan Blezek[1], Katherine Turk[2], Gilberto Gonzalez[2], Eva-Maria Ratai[2]
[1]GE Global Research Center, Niskayuna, New York, USA; [2]MGH, Boston, Massachusetts, USA

Longitudinal 1H chemical shift imaging (CSI) exams to study the effects of disease or treatment are becoming increasingly common. One of the sources of variability in such exams arises from imperfect re-localization of the CSI grid in the follow-up exams. A novel approach, based on a priori image registration and acquisition of follow-up CSI grids with identical coverage and orientation as in the baseline exam, is presented here. Streamlined workflow, reduced variability of metabolite concentration measurements, and increased voxel overlaps are noted when this automatic repositioning procedure is compared to the visual CSI grid repositioning approach.

2529. CFIT: A Novel Circle-Fitting Approach to Spectral Analysis

Refaat ElSayed Gabr[1], Ronald Ouwerkerk[1], Paul A. Bottomley[1]
[1]Johns Hopkins University, Baltimore, Maryland, USA

Spectral analysis of *in vivo* spectra is problematic due to low signal-to-noise ratio, overlapping peaks and intense baseline artefacts. We present a new frequency-domain technique for MRS analysis, CFIT, wherein the circular trajectories that result when spectral peaks are projected onto the complex plane, are fitted with active circles. This eliminates the need for phasing spectra. The baseline is dealt with using active contours (snakes). CFIT exhibited the lowest failure rate compared to standard time- and frequency-domain methods applied to 98 real human chest and heart 31P MRS data sets. Its accuracy was comparable to our best current method.

2530. Study of Pilocarpine Model of Epileptic Rats at 7 Tesla by Magnetic Resonance Spectroscopy

Cristina Cudalbu[1], Sophie Cavassila[1], Alexandra Montavont[2], Philippe Ryvlin[2], André Briguet[1], Danielle Graveron-Demilly[1]
[1]Université Claude Bernard Lyon1, ESCPE, Villeurbanne, France; [2]CERMEP and ANIMAGE, Lyon, France

The brain of the pilocarpine rat is a well-studied model of temporal lobe epilepsy that reproduces most of the clinical and neuropathologic features of human temporal lobe epilepsy. The purpose of our study was to analyze by MRS the hippocampus region, 24 hours after the onset of Status Epilepticus. Short echo-time *in vivo* signals of brains of epileptic and healthy rats were acquired at 7Tesla and quantitated using QUEST. We detected a significant increase of the lactate concentration in the hippocampus of epileptic rat brains. Our concentration estimates obtained from the healthy rats are in good agreement with the published values.

2531. Towards Accurate Quantification of Metabolites and Macromolecules in HR-MAS Spectra of Brain Tumor Biopsies Using LCModel

Kirstie S. Opstad[1], Tiernan Byrnes[1], Alison Loosemore[1], B A. Bell[1], John R. Griffiths[1], Franklyn A. Howe[1]
[1]St. George's, University of London, London, UK

HR-MAS ^{1}H MRS of whole biopsies provides detailed biochemical profiles that can be related to the lower resolution spectra obtained *in vivo*. Nevertheless there is still significant overlap of many resonance peaks and contributions from broad macromolecule resonances that impede accurate quantification. We have determined a first set of metabolite and macromolecule resonances needed for an LCModel quantification of brain tumor biopsies. Our data suggests that when fitting resonances of coupled spins systems in high-resolution spectra interactions between metabolites and the macromolecular environment of the biopsy cause small peak shifts not found in solution spectra, which must be accounted for.

2532. Quantitative Proton MRSI of the Human Cervical Spine at 3.0 Tesla

David Bonekamp[1], Richard A. E. Edden[1, 2], Peter B. Barker[1, 2]
[1]Johns Hopkins University School of Medicine, Baltimore, Maryland, USA; [2]Kennedy Krieger Institute, Baltimore, Maryland, USA

1D-MRSI of the human cervical spine and medulla oblongata was performed at 3T using a 2 channel flexible surface coil array. The spine water signal was used as an internal intensity reference for metabolite concentration quantification. An optimized protocol was used to minimize the chemical shift artifact associated with slice selection. Ratios were determined: NAA/Cho=2.32±1.15, NAA/Cr=2.81±1.36 and Cho/Cr=1.26±0.42. Quantification of spectra yielded concentrations: NAA=10.20±7.30, Cr=6.37±4.99 and Cho=1.90±1.30 mmol/kg wet weight. The measured metabolite concentrations are similar to those previously reported in brain in the literature, but are somewhat lower than those reported in the previous SV study of the cervical spine.

2533. Estimated Metabolite Concentrations in the Rat Brain with Quest:A Comparison Between In Vitro and Simulated Basis Sets

Cristina Cudalbu[1], Sophie Cavassila[1], Olivier Beuf[1], Herald Rabeson[1], Dirk van Ormondt[2], Danielle Graveron-Demilly[1]

[1]Université Claude Bernard Lyon1, ESCPE, Villeurbanne, France; [2]Delft University of Technology, Delft, Netherlands

Quantitation of short echo-time MRS signals is usually based on a metabolite basis set. The latter can be obtained either by quantum mechanically simulating the metabolite signals, or by measuring signals of metabolite solutions. The purposes of the present study are: 1) to compare the influence of the basis set on the quantitation results; 2) to estimate the metabolite concentrations in the central region of the rat brain. *In vivo* signals of rat brains were acquired at 7Tesla and quantitated with QUEST. The concentration estimates using the two basis sets are not significantly different and in good agreement with the published values.

2534. Assessment of HR-MAS NMR Prostate Biopsy Tissue Spectra with Principal Component Analysis and Metabolite Quantification

Paul Allen DiCamillo[1], Mark Gunnard Swanson[1], John Kurhanewicz[1], Sarah Jane Nelson[1]

[1]University of California, San Francisco, California, USA

Spectroscopic analysis of tissue samples from transrectal prostate punch biopsies provide a particular challenge due to the inherent tissue heterogeneity, contamination by blood and lipids, and small sample size. Automated and objective approaches to analyze this spectroscopic data and assess patient prognosis are desirable. The application of principal component analysis to high field (11.74T) high resolution magic angle spinning (HR-MAS) prostate biopsy tissue spectra is described and compared to LCModel quantification. The non-destructive nature of HR-MAS allows histological evaluation of the same tissue specimens. These techniques are used to survey prostate biopsy tissue and report on the characteristics of these tissues at high field.

2535. ProFit: Two-Dimensional Prior-Knowledge Fitting of *J*-Resolved Spectra

Rolf F. Schulte[1], Peter Boesiger[1]

[1]University and ETH Zurich, Zurich, Switzerland

A two-dimensional fitting procedure is introduced, capable of extracting the full amount of information from 2D *J*-resolved magnetic resonance spectroscopy data. The fitting procedure uses a linear combination of 2D model spectra. *In-vitro* and *in vivo* experiments on a whole-body 3T MR scanner show the detectability of a wide range of metabolites in the human brain, namely total creatine, N-acetyl aspartate, choline-containing compounds, glutamate, *myo*-inositol, glutathione, *scyllo*-inositol, γ-aminobutyric acid, alanine and ascorbic acid.

2536. Vitamin C Concentration Measured in the Human Brain *In Vivo* Using LCModel Analysis of Fully Resolved 1H Edited Spectroscopy at 7 Tesla

Melissa Jo Terpstra[1]

[1]University of MN, Minneapolis, Minnesota, USA

Since Vitamin C (ascorbate) is an important brain antioxidant, *in vivo* detection could be used to study its role in protection against oxidative stress. In order to increase the sensitivity and specificity of ascorbate detection relative to that initially reported at 4 T, editing was implemented 7 T. The ascorbate concentration measured at 7 T from a 3-fold smaller region of interest, 1.3 ± 0.2 µmol/g (mean ± SD, n=8) with a smaller average CRLB (7 %) was in excellent agreement with that previously measured at 4 T, 1.3 ± 0.3 µmol/g (mean ± SD, n=4), average CRLB 9 %.

2537. Postprocessing of Spectroscopic Imaging Data with Incomplete K-Space Sampling Using a Maximum Entropy Method

Wolfgang Dreher[1, 2], Dieter Leibfritz[1, 2]

[1]University of Bremen, Bremen, Germany; [2]Center of Advanced Imaging (CAI), Bremen, Germany

Measurements with a reduced range of k_Ω -values are beneficial for fast spectroscopic imaging (SI) such as spectroscopic RARE or SSFP based SI because the minimum total measurement time can be shortened or the SNR can be increased. Therefore, a maximum entropy method (MEM) was used for processing incomplete SI data. MEM was employed for spectrum reconstruction or time domain data extrapolation. After tests on simulated data, MEM was applied to spectroscopic RARE data measured *in vivo* on rat brain at 4.7T. The results show that MEM is an efficient and robust tool to process incomplete SI data.

2538. Water as an Internal Reference for Spectroscopic Imaging: Errors Due to Inacurrate Water Relaxation Times

Charles Gasparovic[1, 2], Deidre J. Devier[1, 3]

[1]University of New Mexico School of Medicine, Albuquerque, New Mexico, USA; [2]MIND Institute, Albuquerque, New Mexico, USA; [3]University of New Mexico, Albuquerque, New Mexico, USA

A strategy for using tissue water as a concentration standard in 1H magnetic resonance spectroscopic imaging studies on the brain is presented and the potential errors that may arise due to inaccurate estimates of the various water relaxation times are examined. The sensitivity of the method to such errors is shown to be small at short echo times.

2539. Quantification of Human Brain Metabolites with Different RF Coils

Harald E. Möller[1, 2], Timm Wetzel[1], Marc Tittgemeyer[1]
[1]Max Planck Institute for Human Cognitive and Brain Sciences, Leipzig, Germany; [2]University Hospital Münster, Münster, Germany

Twelve volunteers were investigated repetitively by PRESS using two different RF coils. Upon LCModel analysis, the SNR doubled, and Cramer-Rao lower bounds of major peaks improved with an 8-channel array instead of a birdcage coil. Indications of an overestimation of glutamate/glutamine and myo-inositol were obtained for the birdcage coil. The separation of N-acetylaspartate and N-acetylaspartylglutamate was improved for the array-coil. Intersubject variation was of the order of 6% for total NAA. A standard phased-array headcoil yields improved precision or permits major reductions of the total scan time. Pooling of data recorded with different RF coils is not advocated.

2540. Predicting SNR Gains from Constructive Averaging of Proton Spectra: Theory and Practice

Refaat ElSayed Gabr[1], Michael Schär[1,2], Shashank Sathyanarayana[1], Robert G. Weiss[1], Paul A. Bottomley[1]
[1]Johns Hopkins University, Baltimore, Maryland, USA; [2]Philips Medical Systems, Cleveland,, Ohio, USA

Physiological motion causes dephasing which can undermine the signal-to-noise ratio (SNR) advantage of averaging 1H STEAM and PRESS acquisitions to measure weak metabolites including creatine and choline in the torso. Constructive averaging, wherein each acquisition is individually phased prior to averaging, can reverse SNR loss, but the benefits are highly variable. Here an analytical theory is presented which correctly predicts the SNR advantage of constructive averaging based on measures of the phase variation. The theory is validated with *in vivo* 1H spectra from the human heart and leg, demonstrating useful SNR gains of up to 7-fold.

2541. Blind Spectra Decomposition of MRSI of the Brain with Tumor by Sparse Component Analysis

Chunqi Chang[1], Xiangling Mao[2], Yeung Sam Hung[1], Jian Yang[1], Peter C. W. Fung[1], Dikoma C. Shungu[2], Ed X. Wu[1]
[1]The University of Hong Kong, Hong Kong, People's Republic of China; [2]Weill Medical College of Cornell University, New York, New York, USA

Magnetic Resonance Spectroscopy Imaging (MRSI) is suitable for analyzing brain tumor metabolites *in vivo*. Several tissue types may exist in the tumor lesion area, and thus the measured MR spectra are a linear superposition of the constituent spectra of each of the different tissues. In this abstract we describe a novel approach, based on sparse component analysis, to recover the constituent spectra from the measured mixtures. The method is applied to experimental MRSI data of a brain with tumor lesion, and promising result is obtained. Compared to the existing BSD and cNMF approaches, this method is relatively simple and very fast.

2542. Continuous Saturation Correction in the Presence of Changing Metabolite Concentrations

Nominated for an ISMRM Poster Award

Damian J. Tyler[1], Mark A. Cole[1], Carolyn Carr[1], Daniel J. Stuckey[1], Kieran Clarke[1]
[1]University of Oxford, Oxford, UK

Accurate quantitation of ^{31}P metabolites requires rapid acquisition of many averages. Correction for saturation is then needed. However, correction can be prone to errors if the 'effective' T_1 changes during the course of an experiment, as in an ischaemia-reperfusion experiment. In this work we have implemented a continuous saturation correction scheme based on the 'dual-angle' method. We have demonstrated the feasibility of the technique throughout an ischaemia-reperfusion experiment, even in the presence of an ~75% increase in the 'effective' T_1 of one of the metabolites. The experiments were performed in the same time as a normal spectroscopic experiment.

MRS Sensitivity Enhancement Techniques for 13C and Other Nuclei through Hyperpolarization

Room 4E Wednesday 14:00 - 16:00

2543. Usage of Paramagnetic Contrast Agents to Enhance ^{13}C Signal Detection *In Vitro*

Ruud B. van Heeswijk[1], João M.N Duarte[1], Sabrina Laus[1], Rolf Gruetter[1]
[1]EPFL, Lausanne, Switzerland

A feasibility study of the use of paramagnetic contrast agents to shorten acquisition times in 13C spectroscopy.

2544. Field Inhomogeneity May Substantially Affect Hyperpolarised 129Xe Rat Head Spectra

Jeff Kershaw[1, 2], Kazuhiro Nakamura[1, 2], Atsushi Wakai[1, 2], Yasushi Kondoh[2], Iwao Kanno[2]
[1]Akita Industry Promotion Foundation, Akita, Japan; [2]Akita Research Institute of Brain and Blood Vessels, Akita, Japan

Recent results have uncovered inconsistencies in hyperpolarized 129Xe rat head spectra that seem to correspond to changes in the shimming. To investigate the homogeneity of the field in rat head and as a first step towards studying the possible effects inhomogeneity may have on the 129Xe dissolved phase spectrum, we have implemented a field-mapping algorithm. The results indicate that even with a supposedly well-shimmed state, there is a substantial variation in the field that may cause or contribute to anomalies in rat head spectra.

2545. *In Vivo* Carbon-13 Spectroscopy of Rhesus Monkey Brain at 4.7T: Detecting Rapid Exchange Between α-Ketoglutarate and Glutamate Using Magnetization Transfer

Shizhe Steve Li[1], Jehoo Yang[1], Zhengguang Chen[1], John Bacher[1], Robert B. Innis[1], Jun Shen[1]
[1]National Institutes of Health, Bethesda, Maryland, USA

Aspartate aminotransferase is an enzyme catalyzing the transfer of amino group between aspartate and glutamate. Recently, the *in vivo* carbon-13 magnetization transfer (CMT)effect due to this reaction has been found in the rat brain at 11.7 Tesla by saturating the carbonyl carbon of α-ketoglutarate or oxaloacetate. In this study, the *in vivo* CMT effect caused by aspartate aminotransferase-catalyzed rapid exchange between α-ketoglutarate and glutamate was further validated in rhesus monkey brain at 4.7 Tesla. In particular, the CMT effect was observed for the first time in the carboxylic carbon region by saturating the carboxylic carbon of α- ketoglutarate (C-1).

2546. Fast Metabolic Imaging of Systems with Sparse Spectra: Application for Hyperpolarized ^{13}C Imaging

Dirk Mayer[1], Yakir S. Levin[1], Gary H. Glover[1], Ralph E. Hurd[2], Daniel M. Spielman[1]
[1]Stanford University, Stanford, California, USA; [2]GE Healthcare, ASL-West, Menlo Park, California, USA

A fast spiral chemical shift imaging sequence has been developed for application in hyperpolarized ^{13}C imaging. The sequence exploits sparse spectra and prior knowledge of resonance frequencies to reduce the measurement time by undersampling the data in the spectral domain. Multiple data sets having only frequency components within a certain bandwidth are reconstructed "in-focus" while others are severely blurred ("spectral tomosynthesis"). The sequence was tested at 3 T on a phantom containing approximately 1.5-M solutions of alanine, lactate, and pyruvate-pyruvate hydrate C1-C2 ester at thermal equilibrium polarization, all enriched to 99% ^{13}C in the C1 carbonyl positions.

2547. Least Squares Reconstruction for Sparse Spectra: Application to Hyperpolarized ^{13}C Imaging

Yakir S. Levin[1, 2], Dirk Mayer[1], Yi-Fen Yen[3], Ralph Hurd[3], Daniel M. Spielman[1, 2]
[1]Stanford University School of Medicine, Stanford, California, USA; [2]Stanford University School of Engineering, Stanford, California, USA; [3]GEHealthcare, Menlo Park, California, USA

Hyperpolarization of 13C allows for imaging of an injected compound and its downstream products. A single-interleaf spiral CSI pulse sequence that allows for aliasing of peaks from the broad but sparse 13C spectrum is explored here. A k-space based least-squares algorithm using a priori knowledge of peak characteristics for reconstruction of metabolic images is proposed. Using simulation and phantom measurements, the technique compares favorably to conventional 3-D spectroscopic reconstruction and allows optimization of acquisition parameters such as spectral width and number of echoes. The work implies that very rapid (<100 ms) spectroscopic imaging of hyperpolarized 13C can be performed.

2548. ^3He T_1 in Mouse Lung Estimated from Washout Curve Analysis Under Spontaneous Respiration. Use of SF_6 Gas at Thermal Equilibrium to Evaluate Respiratory Term

Hirohiko Imai[1], Michiko Narazaki[1], Hiroyuki Inoshita[1], Astuomi Kimura[1], Hideaki Fujiwara[1]
[1]Osaka University, Suita, Osaka, Japan

We estimated ^3He T_1 in mouse lung under spontaneous respiration by a novel method, in which SF_6 gas at thermal equilibrium was utilized in combination with the hyperpolarized ^3He gas in the quantitative washout curve analysis. The estimated ^3He T_1 value was moderate compared with the value calculated from literature data measured during breath-hold. Thus, ^3He T_1 is shown to be readily estimated in noninvasive manner.

2549. Hyperpolarizing (1H and 13C) Naturally Occurring Amino Acids to Explore Their Function Via MRI

Joachim Bargon[1], Hanjo Heinrich[1], Ute Bommerich[2], Rahim R. Rizi[3]
[1]University of Bonn, Bonn, Germany; [2]University of Magdeburg, Magdeburg, Germany; [3]University of Pennsylvania Medical Center, Philadelphia, Pennsylvania, USA

L-Phenylalanine (PHE) is hydroxylated in the human body to L-tyrosine (TYR) by phenylalanine hydroxylase (PAH). Therefore, both PHE and TYR can be components of artificial nutrition and are approved for infusions or injections. TYR is eventually converted into L-DOPA and decarboxylated to L-dopamine (DA). A shortage of DA causes Parkinson's Disease. We have generated 1H- and 13C-hyperpolarized PHE and other hyperpolarized amino acids from appropriate precursors via Parahydrogen Induced Polarization (PHIP) both in their true (L) and false (R) chiral form. This allows studying the different chiral isomers individually, serving as magnetically labeled molecular probe in combination with PHIP-enhanced MRI.

2550. Method for Continuous Measurement of Nuclear Para State Enrichment in Hydrogen Gas with Applications to Hyperpolarized Heteronuclear Contrast Agents

Vahid Vahdat[1], Stephen Kadlecek[1], Sheeva Rajaei[1], JiangSheng Yu[1], Kiarash Emami[1], John MacDuffie Woodburn[1], Masaru Ishii[2], Frank Hammond[1], Rahim R. Rizi[1]
[1]University of Pennsylvania, Philadelphia, Pennsylvania, USA; [2]Johns Hopkins University, Baltimore, Maryland, USA

We present a method for quantifying the enrichment of the nuclear para statein a sample of hydrogen based on a measurement of the speed of sound in thegas. This approach makes use of a pair of spherical, resonant cavitiesfilled with normal hydrogen and the sample to be tested, and driven by piezotransducers. Production and quantification of parahydrogen is critical inseveral industries, but its application in the MR community stems from itsuse in the production of novel, hyperpolarized contrast agents for MRIangiography, perfusion measurements, and MRI/MRS examination of in vitro and*in vivo* molecular transformations. The apparatus described provides acontinuous measurement of the reagent quality during production andimmediately before use.

2551. Direct Generation of 1H- And 13C-Hyperpolarized Molecules for MRI from Parahydrogen Via Reversibly Functioning Catalysts

Joachim Bargon[1, 2], Rahim R. Rizi[2]
[1]University of Bonn, Bonn, Germany; [2]University of Pennsylvania Medical Center, Philadelphia, Pennsylvania, USA

Parahydrogen-Induced Polarization (PHIP) yields strong nuclear spin polarization[1] of protons and heteronuclei including 13C. Because of the relatively long T1 relaxation times of quarternary carbons especially, 13C-hyperpolarized molecules appear intrinsically more attractive as contrast reagents for MRI than their 1H-hyperpolarized counterparts. We have demonstrated a technique for reversibly hydrogenating potential contrast agents to generate a hyperpolarized version of a target molecule without synthesizing an unsaturated precursor as was previously required. This development should speed the creation and testing of hyperpolarized agents for bloodflow and molecular imaging.

2552. Early Experience with Simple Methods for Parahydrogen-Induced Hyperpolarization

Aaron K. Grant[1], Elena Vinogradov[1], Daniel K. Sodickson[1, 2], James A. Balschi[3], Robert E. Lenkinski[1]
[1]Beth Israel Deaconess Medical Center, Boston, Massachusetts, USA; [2]Harvard Medical School, Boston, Massachusetts, USA; [3]Brigham and Women's Hospital, Boston, Massachusetts, USA

Liquid-phase hyperpolarized contrast media can be imaged with high sensitivity and virtually no endogenous background signals, and promise to enhance many applications of MRI. We describe a simple and inexpensive technique for assessing the feasibility of candidate substrate compounds for use with parahydrogen induced polarization. The method is illustrated using proton and natural abundance carbon-13 NMR spectra of a sample compound.

2553. A Compact Counter-Flow Xenon Polarizer for Clinical Applications

Jan H. Distelbrink[1], Steven Ketel[2], Jeff E. Ketel[1], Korac MacArthur[2], Craig S. Pelissier[1], Hongguo Zhu[3], F W. Hersman, [1,2]
[1]Xemed LLC, Durham, New Hampshire, USA; [2]UNH, Durham, New Hampshire, USA; [3]Canberra, Meriden, Connecticut, USA

A compact xenon polarizer is in its final stages of development. High polarization and production rate are available with unattended operation. Details and performance characteristics will be presented on the meeting, including the latest polarization figures

2554. Improvements in Spectral Resolution in *In Vivo*-Hyperpolarized 13C-CSI on Pigs Using Spectroscopic GRASE

Jürgen Klaus Hennig[1], Sven Mansson[2], Jochen Leupold[1], Oliver Wieben[3], J Stefan Petersson[4]
[1]University Hospital, Freiburg, Germany; [2]University Hospital, Lund, Sweden; [3]University Wisconsin, Madison, Wisconsin, USA; [4]GE Healthcare, Malmö, Sweden

Hyperpolarized 13C shows *in vivo* relaxation rates in the range of 30-60 s. This allows to observe rapid metabolic turnover after injection of suitable substrates like 13C-pyruvate. In order to maximize spatial and spectral resolution a spectroscopic GRASE-sequence with 13 echoes within each refocusing period was used for data acquisition. The spectral resolution is in the same order as the peak separation, therefore direct Fourier Transformation leads to severe spectral degradation by partial volume effects. These can be remedied by sinc-interpolation leading to significant improvements of spectral amplitude, resolution and peak definition. Equivalence between superresolution reconstruction, frequency sweep reconstruction and sinc-interpolation is discussed.

MR Elastography

Room 4E Wednesday 14:00 - 16:00

2555. Progress in Phased-Array Mechanical Drivers for Magnetic Resonance Elastography

Yogesh K. Mariappan[1], Kevin J. Glaser[2], Richard L. Ehman[2]
[1]Mayo Clinic College of Medicine, Rochester, Minnesota, USA; [2]Mayo Clinic College of Medicine, Rochester, Minnesota, USA

Dynamic MR Elastography measures the stiffness of tissues by imaging propagating shear waves. Typical low frequency (50–200 Hz) shear waves induced in the sample (via transverse or longitudinal drivers) have limitations like high attenuation, shallow wave penetration or low resolution. We investigated a high frequency mode conversion technique wherein high frequency longitudinal waves are induced and stiff regions are detected by imaging the shear waves that are present only in these regions, the waves are highly attenuated in the soft regions. The short wavelength of these high frequency waves will allow for more accurate stiffness measurements of stiff regions.

2556. Three-Dimensional Visualization of Ultrasonically Induced Shear Waves for Elasticity Imaging

Derek D. Steele[1], Kevin J. Haworth[1], Oliver D. Kripfgans[1], Scott D. Swanson[1]
[1]The University of Michigan, Ann Arbor, Michigan, USA

Transient shear wave (TSW) elasticity imaging has shown considerable promise for understanding tissue mechanics and its relationship to disease. Compared to other elasticity imaging methods, TSW imaging may allow one to use a very simple wave-speed based reconstruction. To date, all TSW elasticity imaging has employed one- or two-dimensional (2D) reconstructions. However, three-dimensional (3D) TSW methods may offer more accuracy than 2D methods, as has been shown for static elasticity imaging. Here, we present a 3D visualization of ultrasonically induced shear displacements in a tissue-like phantom which may be used for 3D elasticity reconstruction.

2557. Group-Velocity Inversion in MR Elastography on Skeletal Muscles

Sebastian Papazoglou[1], Jens Rump[1], Dieter Klatt[1], Uwe Hamhaber[2], Jürgen Braun[2], Ingolf Sack[1]
[1]Institute of Radiology, Berlin, Germany; [2]Institute of Medical Informatics, Berlin, Germany

MR elastography (MRE) enables to monitor the full vector-field of a harmonic displacement so that anisotropic elastic parameters of the investigated tissue are accessible. Here, a strategy is introduced for deducing two independent shear moduli from 2D wave images in MRE based on the group velocity of bulk shear waves. The approach utilizes fast SSFP-MRE and automatic detection of direction-dependent wave velocities. The new method is demonstrated on the biceps of 5 healthy volunteers revealing that the shear modulus parallel to the muscle fibers is about 5 times larger than perpendicular to them.

2558. MR Elastography Sequence Comparison: Standard PC MRE vs. Balanced Alternating Steady-State Elastography

Stefan Maderwald[1], Frank Stock[1], Oliver Kraff[1], Armin de Greiff[1], Oliver Bieri[2], Klaus Scheffler[2], Mark E. Ladd[1]
[1]University Hospital Essen, Essen, Germany; [2]University of Basel, Basel, Switzerland

Many pathologies in soft tissues cause a change in the mechanical properties, and magnetic resonance elastography (MRE) offers a non-invasive diagnostic method to visualise these changes. A novel technique for visualization of propagating transverse acoustic shear waves, BASEL (balanced alternating steady-state elastography) is compared to a standard gradient echo MRE phase-contrast (PC) sequence. Tissue-like agarose gel phantoms and *in vivo* experiments were used for the comparison. Typical 2D wave images were produced with both sequence types and the LFE reconstruction technique provided similar average shear modulus results for both datasets. Among other benefits is the reduced acquisition time of BASEL.

2559. High Frequency Mode Conversion Technique for Stiff Lesion Detection in Magnetic Resonance Elastography

Yogesh K. Mariappan[1], Phillip J. Rossman[2], Armando Manduca[2], Anthony Romano[3], Richard L. Ehman[2]
[1]Mayo Clinic college of Medicine, Rochester, Minnesota, USA; [2]Mayo clinic college of medicine, Rochester, Minnesota, USA; [3]Naval Research Laboratory, Washington, District of Columbia, USA

Dynamic MR Elastography measures the stiffness of tissues by imaging propagating shear waves. Typical low frequency (50–200 Hz) shear waves induced in the sample (via transverse or longitudinal drivers) have limitations like high attenuation, shallow wave penetration or low resolution. We investigated a high frequency mode conversion technique wherein high frequency longitudinal waves are induced and stiff regions are detected by imaging the shear waves that are present only in these regions, the waves are highly attenuated in the soft regions. The short wavelength of these high frequency waves will allow for more accurate stiffness measurements of stiff regions.

2560. A Novel Fractal Model to Explain the Rheology of Liver Tissue Using MR-Elastography

Benjamin Robert[1], Ralph Sinkus[1], Jeremy Bercoff[2], Mickael Tanter[1], Mathias Fink[1]
[1]Laboratoire Ondes et Acoustique, Paris, France; [2]SuperSonic Imagine, Aix-en-Provence, France

Steady-state mono-chromatic MR-Elastography is used to measure the complex shear modulus G*(w)=Gd(w)+iGl(w) of *ex vivo* bovine liver tissue within the frequency interval 40-100Hz. The frequency dependence of the shear wave speed can be explained by the classical Voigt model. However, the model fails to describe the frequency dependence of real and imaginary part separately. In order to account for the observed power-law behavior of Gd(w)~Gl(w)~w^0.75 and the constant ratio Gl(w)/Gd(w)=tan(0.15*pi/2) we propose a rheological model which consists of two fractal networks. The frequency powers of the individual networks resemble what has been established for the cytoplasm (~w^0.75) and the cytoskeleton (~w^0.15).

Parallel Transmission Technology

Room 4E Wednesday 14:00 - 16:00

2561. Self-Calibrated Transmit SENSE

Adam Bruce Kerr[1], Charles H. Cunningham[1], John Mark Pauly[1], Randy O. Giaquinto[2], Ronald D. Watkins[2], Yudong Zhu[2]

[1]Stanford University, Stanford, California, USA; [2]GE Global Research Center, Niskayuna, New York, USA

Transmit SENSE provides the capability to significantly accelerate multidimensional selective excitations and reduce RF power absorption. The design of the multicoil transmit RF pulses dependhowever on knowing the transmit sensitivity profiles of the coil array. Previous demonstrations have relied on being able to use a coil with a uniform transmit sensitivity as a reference. In contrast, we present a self-calibrating method that does not impose such restrictions, and is demonstrated to work robustly in the presence of significant dynamic range. The method is validated by demonstrating a large-tip transmit SENSE excitation on an eight-channel system.

2562. Application of RF Current Sources in Transmit SENSE

Hyokwon Nam[1], William Grissom[2], Douglas C. Noll[2], Steven M. Wright[1]

[1]Texas A&M University, College Station, Texas, USA; [2]University of Michigan, Ann Arbor, Michigan, USA

Knowledge of coil pattern is a key requirement in order to implement Transmit SENSE. However coupling between transmit array elements makes it complicated. RF current sources avoid effect of coupling thus each coil pattern can be obtained very easily. Transmit SENSE experiments using RF current sources were performed and results demonstrate that the current source can be used to drive elements in a Transmit SENSE array.

2563. Comparison of a Current Source and a Voltage Source in Transmit SENSE

Hyokwon Nam[1], Steven M. Wright[1]

[1]Texas A&M University, College Station, Texas, USA

: A resonant coil fed by a standard voltage amplifier has been used for RF transmission in MR imaging. However coupling effect in array elements makes it difficult to implement parallel transmission with multiple coils. A novel approach to avoid effect of coupling between transmit array elements is to use RF current sources driving non-resonant structures. This study presents an analysis of a RF current source driving a non-resonant coil and a conventional voltage amplifier driving a resonant coil and shows the advantages of the current source in parallel transmission.

2564. Potential Advantage of High Modes of Birdcage for Parallel Imaging

Chunsheng Wang[1], Peng Qu[1], Bing Wu[1], Gary X. Shen[1]

[1]The University of Hong Kong, Hong Kong, People's Republic of China

The potential advantage of using high modes of a 12-rung birdcage coil for parallel imaging has been investigated. When 11 modes are incorporated, the acceleration factor can be up to 5 with average g-factor within 2. For certain number of channels, the optimized combination of corresponding modes can be obtained.

2565. Transmit Coil Array for Very High Field Head Imaging

Yu Li[1], Charles Saylor[1], George R. Duensing[1]

[1]Invivo Diagnostic Imaging, Gainesville, Florida, USA

In transmit coil array design for very high field imaging, the most challenging issue is the decoupling. This study proposes a new decoupling technique based on the use of CRC mode generated by a concentric double loop coil. It is shown that the coil coupling can be well suppressed when eight surface coils are used for transmission in head imaging at 7T field. With the aid of a power splitter, head images can be acquired using an eight-channel transmit surface coil array on a SIEMENS 7T whole-body scanner.

2566. A Degenerate Bandpass Birdcage as Antenna for a 3T Wholebody Transmit Array

Jürgen Nistler[1], Rainer Kurth[2], Razvan Lazar[1], Markus Vester[1], Wolfgang Renz[1]

[1]Siemens Medical Solutions, Erlangen, Germany; [2]University Erlangen-Nuernberg, Erlangen, Germany

On most MR systems birdcage resonators are used as wholebody transmit antenna. This becomes more difficult for higher frequencies (dimensions near to wavelength). We investigated a 3T degenerate bandpass birdcage, which can be used as a multichannel transmit antenna.

2567. Improved Homogeneity of the Transmit Field Due to Simultaneous Transmission with Phased Arrays and Volume Coils

Nikolai I. Avdievich[1, 2], Hoby H. Hetherington[1, 2]
[1]Albert Einstein College of Medicine, Bronx, New York, USA; [2]Gruss MRRC, Bronx, New York, USA

Due to RF field/ tissue interactions at high-field, 4-8T, the transmit field from head-sized volume coils shows a distinctive pattern of inhomogeneity, with enhanced sensitivity in the center of the brain. Conversely, surface coil phased arrays provide increased peripheral sensitivity. In theory, simultaneous transmission from these two devices could provide a very homogeneous transmission field. To avoid interactions between the two coils, a counter rotating current (CRC) surface coil consisting of two parallel rings carrying opposite currents was used. Using this system enables substantial improvements in the homogeneity of the transmit B1 profile as compared to the volume coil alone.

2568. Obtaining Localized Excitation in Human Abdominal Organs at 7 Tesla

Tamer S. Ibrahim[1], Roney Abraham
[1]The University of Oklahoma, Norman, Oklahoma, USA

In this work, utilizing three-dimensional full wave simulations, we optimize the drive ports of a 32-port volume coil in order to obtain localized excite field distribution within the volume of the human heart. With driving the coil with the optimized excitation, we show the excite field distribution inside the heart and inside a sizeable exterior rectangular volume, and demonstrate that excellent 3-D localization can be achieved in the heart. We conclude that the proposed excitation mechanism shows much potential in allowing MRI systems to selectively image abdominal organs at ultra high field strengths.

2569. An Optimized Four-Channel Microstrip Loop Array at 7T

Bing Wu[1], Xiaoliang Zhang[2], Gary X. Shen[1]
[1]The University of Hong Kong, Hong Kong, People's Republic of China; [2]University of Minnesota, Minneapolis, Minnesota, USA

The microstrip transmission-line (MTL) transmit/receive loop array has been recently developed for MR applications at ultrahigh fields (>4T). In this study, the geometry of transmission-line array, including the substrate thickness and gap between coil elements was investigated by simulation and the capacitive decoupling method was analyzed. Finally an optimized four-channel microstrip loop array was built for 7T.

Parallel Receive Coil Technology

Room 4E Wednesday 14:00 - 16:00

2570. Evaluation of Cost Functions in the Design of RF Coils Optimized for SENSE Imaging

L Tugan Muftuler[1], Gang Chen[1], Orhan Nalcioglu[1]
[1]University of California, Irvine, California, USA

We have previously reported a new approach to MRI RF coil array design that is optimized for SENSE imaging. In this approach the inverse problem is solved to find the current paths that will form the coil, which will maximize the SNR in SENSE imaging (hence minimize the g-factor) within a target volume. In this study, the effect of weights on components of the cost functions used in the least squares approximation were investigated.

2571. Adjustable Simultaneous Inductive Decoupling of Large Arrays

Naresh Yallapragada[1], Mary Preston McDougall[1], Steven M. Wright[1]
[1]Texas A&M University, College Station, Texas, USA

In this abstract we present a novel approach to simultaneously inductively decouple large coil arrays of identical parallel elements. The method utilizes a "flux blocking pad" to control the amount of mutual inductance between coils. The method was successfully tested and implemented in decoupling two elements and was then extended to a 7-element array. Decoupling measurements greater than 20dB have been demonstrated between neighboring elements. The method is simple and elegant and can easily be extended to accommodate large numbers of array elements.

2572. 3D RF Coil Modeling Method and Its Application in Optimized SENSE Coil Design

Gang Chen[1], Lutfi Tugan Muftuler[1], Orhan Nalcioglu[1]
[1]University of California, Irvine, Irvine, California, USA

A new RF coil modeling method was investigated to achieve the more flexible and reasonable constrain to the SENSE coil array optimization problem. In this new method the RF coil is confined in a 3D volume near the object rather than a 2D cylinder surface as in the conventional approach. Simulation results showed that the optimized coil array with the new modeling method has significant improvements on the average SENSE SNR, SENSE SNR uniformity and average and maximum g-factor compared with that of the optimized RF coil array modeled on a 2D cylinder surface.

2573. Head RF Coil Design with Surface Current Density Optimization for SENSE Imaging

L Tugan Muftuler[1], Gang Chen[1], Orhan Nalcioglu[1]
[1]University of California, Irvine, California, USA

We have designed and implemented an MRI RF coil that is optimized for SENSE imaging. Our approach solves the inverse problem where the B1 field is calculated to maximize SNR (hence minimize g-factor) within a target volume. We have implemented this with two different approaches. The first one models the coil with positions of vertices of coil conductor segments. In the second approach, which is described here, a finite element mesh is defined on a coil frame and the surface current density is calculated to generate the desired B1 field within the VOI.

2574. RF Coil Array Optimized for 2D SENSE Imaging

Gang Chen[1], Lutfi Tugan Muftuler[1], Orhan Nalcioglu[1]
[1]University of California, Irvine, Irvine, California, USA

An optimized RF coil array was designed and built for 2D SENSE encoding in 3D Fourier MRI with a modified "target field" method. In this method, the RF coils were modeled by the locations of the metal strip vertices that make up the RF coil. The coil array was designed to achieve maximized average SNR in 80% of the inner volume. Experiments showed enhanced SNR and uniformity in 2D SENSE encoding compared with standard coil designs. A different design that was optimized to achieve more uniform SNR and higher SNR in the center 60% of the volume was also presented.

2575. A 16 Channel Head Coil

Jovan Jevtic[1], Velibor Pikelja[1], Randy Duensing[2]
[1]Invivo Corporation, Pewaukee, Wisconsin, USA; [2]Invivo Corporation, Gainesville, Florida, USA

A new head coil with 16 channels has been designed to improve the SNR in the center of the brain and provide general parallel imaging capability.

2576. Improved A-P Parallel MRI of the Spine Using a Twisted Array

Scott B. King[1], Sathya Vijayakumar[2], Feng Huang[2], Charles Saylor[2], G Randy Duensing[2]
[1]National Research Council of Canada, Winnipeg, Manitoba, Canada; [2]InVivo Corporation, Gainesville, Florida, USA

Spine MRI tends to be done with A-P phase encoding, without the speed-up benefit of parallel MRI, because traditional spine arrays do not have adequate g-factor performance for A-P phase encoding. Here a Twisted Array is shown to improve g-factor not only for parallel MRI in the S-I direction (g<1.3), but now also for A-P parallel MRI, while minimizing the number of Rx-channels used. It may now be feasible to perform R=2 speed-up in the A-P direction for spine MRI.

2577. A Comparison of Methods for Reducing the Number of Channels for SENSE

Dan Kenrick Spence[1], Steven M. Wright[1]
[1]Texas A&M University, College Station, Texas, USA

When combining a large array of coils so that it can be used on a system with a small number of receiver channels, two possible methods that might be used are to combine the array so that each channel is optimized to give the optimal SNR at a different point in the image, or to combine the array so that each channel is optimized to yield the optimal SNR over different regions of the image. These two methods are compared for SENSE imaging when a sixty-four element linear array is reduced to eight or sixteen channels.

2578. A 32 Channel Cardiac Array Optimized for Parallel Imaging

Titus Lanz[1], Peter Kellman[2], Mathias Nittka[3], Andreas Greiser[3], Mark Griswold[4]
[1]Rapid Biomedical GmbH, Rimpar, Germany; [2]NIH, Bethesda, Maryland, USA; [3]Siemens Medical Solutions, Erlangen, Germany; [4]Case Western University, Cleveland, Ohio, USA

In this abstract we present a 32 channel cardiac array which is optimized for parallel imaging of the human heart. The coil array consists of 32 equivalent single coil elements which are distributed equally in an flexible anterior half and a rigid posterior half. *In vivo* 2D TSENSE experiments were performed up to accelerations of 6 and 3D TSENSE up to 8. At 8x, the mean g-factor was 2.2 with 90% of the voxels having a g less than 3.0. These high reduction factors have the potential to allow real-time 2D imaging, or short breathhold 3D imaging.

2579. Single Breath-Hold 3D Cine Imaging of the Thorax Using a New 32 Element Cardiac Coil

Michael Schacht Hansen[1, 2], Marc Kouwenhoven[3], Vivek Muthurangu[2], Derek L. G. Hill[1], Reza Razavi[2]
[1]University College of London, London, UK; [2]King's College London, London, UK; [3]Philips Medical Systems, Best, Netherlands

Three-dimensional whole heart cine imaging is a convenient method for assessing cardiac structure and function. In order to acquire such data in a single breath-hold hold, high acceleration factors are needed. However, this is contingent on the provision of coils with a large number of elements. In this work we show 3D cine images acquired using a new 32-element cardiac coil. Extensive volume coverage is demonstrated for multiple acquisition orientations, which all have adequate image quality.

2580. A Novel 16-Element Coil for SENSE Brain/neurovascular Imaging

Cecilia Possanzini[1], Ulrike Dydak[2], Sebastian Kozerke[2], Marijn Kruiskamp[1], Roger Luechinger[2], Marcel Warntjes[3], Mark van Uden[1], Mika Ylihautala[4], Peter Boesiger[2], Fredy Visser[1]

[1]Philips Medical Systems, Best, Netherlands; [2]ETH and University Zürich, Zürich, Switzerland; [3]CMIV Linköpings universitet, Linköping, Sweden; [4]Philips Medical Systems, Vantaa, Finland

In this paper, we describe the design of a novel 16-element coil for brain and neurovascular applications at 3T capable of SENSE in all directions. We demonstrate that in SENSE imaging, as well as in SENSE spectroscopic imaging, the high SNR and SENSE performances of this coil enables applications which otherwise would be impossible due to the long scanning time.

2581. A 34 Element 3T Brain Coil Array for Multi Dimensional Accelerated Imaging

Scott A. Lindsay[1], Kevin F. King[1], John E. Lorbiecki[1], Ed Benjamin Boskamp[1]

[1]GE Healthcare, Waukesha, Wisconsin, USA

A 34 element Brain dome resonator was developed for multi dimensional accelerated imaging at 3T. The g factor plots show values close to 1 for accelerations up to 4 in both AP and RL directions and accelerations of up to 2 in the SI direction. Images show that total accelerations of 9 are acceptable even for slice widths down to 1.5mm. The coil allows accelerated imaging of multi oblique planes with accelerations in all 3 directions.

2582. Experimental Comparison of Signal-To-Noise Between 16 and 8 Element Receive-Only Brain Gapped Array Coils and Birdcage Head Coil at 3 Tesla

Jerzy Bodurka[1], Jeff Duyn[2], Lalith Talagala[2], Peter Bandettini[1]

[1]NIMH, NIH, Bethesda, Maryland, USA; [2]NINDS, NIH, Bethesda, Maryland, USA

MRI receiver and reception system quality directly influences MRI sensitivity. It has been established that birdcage-type volume RF coil sensitivity less than that of an array of surface coils. Previously, the SNR and noise amplification factor (g-factor) performance of a home-built 16-element gapped receive-only brain array coil have been evaluated at 3 Tesla with a custom built high bandwidth digital MRI receiver. However, the 16-element array SNR performance was compared to other arrays with different number of elements by software combination of individual channels. Here, we present an experimental comparison of SNR between images acquired with separate 16 and 8 element receive-only gapped arrays and the standard birdcage head coil using a commercially available MRI scanner. Compared with a birdcage coil, the 16 element close fitting array provides a 2.7-fold SNR increase over the whole brain, 5.7 –fold increase in the brain periphery and 1.8 fold increase in the brain center. Compared with an 8-element array, the 16-element array was found to provide SNR gains of 10%, 13% and 18%, respectively, in the whole brain, central brain and in periphery.

2583. A Four-Channel Transceive Phased-Array Helmet Coil for 3 T

Wolfgang Driesel[1], Timm Wetzel[1], Toralf Mildner[1], Christopher J. Wiggins[2], Harald E. Möller[3]

[1]Max Planck Institute for Human Cognitive and Brain Sciences, Leipzig, Saxony, Germany; [2]A.A. Martinos Center for Biomedical Imaging, Massachusetts General Hospital, Charlestown, Massachusetts, USA; [3]University Hospital Münster, Münster, NRW, Germany

We describe a novel four-channel transceiver array helmet coil based on strip-line technology for all MRI and MRS applications of the human brain at 3 T. Due to the symmetry of the assembly, a high degree of circularly polarized RF is obtained within the entire brain in the transmit mode. Investigations of the RF distribution indicated a birdcage-like B1 profile in axial slices and a moderate gradient along the z-axis. The design may be exploited for parallel imaging on scanners where no body coil is available.

2584. SENSE-Optimization of a Transceive Surface Coil Array for MRI at 4T

Robert G. Pinkerton[1, 2], Graeme C. McKinnon[3], Ravi S. Menon[1, 2]

[1]Robarts Research Institute, London, Ontario, Canada; [2]University of Western Ontario, London, Ontario, Canada; [3]GE Healthcare, Waukesha, Wisconsin, USA

In the current study, we use a finite difference time domain method to simulate the electromagnetic radio frequency fields of a transceive surface coil array for parallel imaging optimization (specifically, cartesian SENSE). The SENSE optimized surface coil array gap size and acceleration factor is shown to be a function of the ratio of physiological-to-intrinsic noise sources. This ratio is experimentally verified to be approximately 1.3 resulting in an optimum gap size and SENSE acceleration factor of 0.25 and 2 (respectively) to be the optimum design of an 8 element transceive surface coil array for functional MRI at 4 T.

2585. Multipurpose 4+4 Channel Array Setup for Parallel Imaging in 3D

Daniel Gareis[1], Volker Christian Behr[1], Felix Breuer[1], Mark Griswold[2], Peter Jakob[1]

[1]University of Würzburg, Würzburg, Germany; [2]Case Western Reserve University and University Hospitals, Cleveland, Ohio, USA

Aim of this work was to develop a pair of 4-channel proton coil-arrays operating at 1.5T for multipurpose applications feasible for different small regions of the human body.A positioning system with rotary hinges was built, ensuring the fixed parallel orientation of the two coil planes.Encoding in one dimension using PPA acceleration factors of R=2-4 resulted in high-quality imagesFor 3D imaging and data reduction in two phase encoding directions factors R=6-8 are expected to provide reasonable image quality. Applications for the 4+4 channel system are high resolution imaging of wrist, knee, elbow, pediatric heart, ankle, ear or carotids.

2586. A Clover Leaf Coil Array for Neonatal Cardiac Imaging at 3T

David Herlihy[1], David J. Larkman[1], Julie Fitzpatrick[1], Adrienne Foran[1], David A. Edwards[1], Jo V. Hajnal[1]
[1]Hammersmith Hospital, Imperial College London, London, UK

Cardiac MRI of neonates presents a number of special challenges including imaging at high resolution and with a small field of view because of the small size of the neonatal heart. These factors suggest that use of higher field scanners may be beneficial, since they allow improved signal strength and the usual problems associated with torso imaging are likely to be reduced by the small size of the subject. We have therefore designed and tested a dedicated neonatal cardiac coil of clover leaf design for use at 3T

2587. Bilateral Surface Coil for Lower Extremity Imaging at 3T

Ryan Brown[1], Yi Wang[2], Ray F. Lee[3], Joel D. Morrisett[4]
[1]Weill Medical College of Cornell University, New York, NY, USA; [2]Weill Medical College of Cornell University, New York, New York, USA; [3]New York University, New York, New York, USA; [4]Baylor University, Houston, Texas, USA

For lower extremity applications, it is advantageous to acquire data using a dedicated coil. We introduce an eight-channel array for imaging at 3T. The array consists of four surface coils wrapped azimuthally around each leg. It is tailored to the geometry of the lower extremity and offers improved sensitivity compared to standard coils as well as simultaneous imaging of both legs to reduce scan time. Three volunteers were imaged to examine the superficial femoral arteries. The study demonstrated that surface coils can be utilized for bilateral lower extremity imaging.

2588. A Transceive Surface Coil Array for MRI of the Human Prostate at 4 T

Robert G. Pinkerton[1, 2], James P. Near[1, 2], Enzo A. Barberi[3], Ravi S. Menon[1, 2], Robert Bartha, [1,2]
[1]University of Western Ontario, London, Ontario, Canada; [2]Imaging Research Labs, Robarts Research Institute, London, Ontario, Canada; [3]XLRImaging, London, Ontario, Canada

A novel torso transceive surface coil array for prostate magnetic resonance imaging and spectroscopy at 4T is presented. It is shown that a conformal transceive surface coil array that uses 50Ω transmitter amplifiers and receiver preamplifiers is capable of whole volume torso imaging while maintaining the high signal-to-noise ratio (SNR) inherent to surface coil designs. Through implementation of field focusing techniques, a 2-fold increase in SNR and improved homogeneity is shown in the prostate compared to a conventional circularly polarized driving scheme. This novel transceive surface coil array for volume imaging of the human torso at 4T is experimentally demonstrated.

2589. 4 Channel Rat Head Arrays for 7 T and 11.7 T

Titus Lanz[1], Thomas Steinberger[1], Stephen Dodd[2], Fernando F. Paiva[2], Afonso C. Silva[2], Alan P. Koretsky[2]
[1]Rapid Biomedical GmbH, Rimpar, Germany; [2]National Institutes of Health, Bethesda, Maryland, USA

In this work we present a 4 channel coil array design for the rat head which is implemented at two field strengths, at 7 T and 11.7 T. It shows good performance with good isolation of neighbouring channels through the use of capacitive decoupling. Preamplifier decoupling for nonadjacent coil elements was shown to be sufficient. Coil elements are well isolated in the MR images and parallel imaging shows very good properties.

2590. Inductive Decoupling of RF Coil Arrays: A Study at 7T

George Carlos do Nascimento[1], Fernando F. Paiva[1], Afonso Costa Silva[1]
[1]National Institutes of Health, Bethesda, Maryland, USA

The elimination of inductive coupling is a very important step for the use of RF coils arrays in parallel imaging. In the present work, a 4-channel RF coil array for the rat head was designed and built at 7T to use inductive decoupling of the different channels. It shows good performance with excellent isolation of all channels and immunity to standing waves or other parasitic signals, and utilizes high input impedance preamplifiers, which are easier to build and less sensitive to mutual inductance coupling between the RF coils.

2591. A Volume Head Array with 8 Transmit / Receive Channels for 7 T

Alexander Weisser[1], Titus Lanz[1]
[1]RAPID Biomedical GmbH, Rimpar, Germany

An 8 channel volume array for the human head was developed. The 8 coil elements are used for circular polarized transmission as well as for signal reception. The array includes preamplifiers, transmit-receive switches, phase shifters and power splitters. The array elements are arranged in a slightly elliptical manner for adaptation to an average human head shape. This enables roughly uniform loading conditions for each element. For the elements a rectangular loop design was chosen with the loop areas facing the sample to minimize excitation of dielectric resonances compared to other designs (e.g. TEM).

2592. Optimization of 24-Channel Receive-Only Coil Array for Brain Imaging at 7.0 Tesla by the Genetic Algorithm

Shumin Wang[1], Patrick J. Ledden[2], Jeff H. Duyn[1]
[1]LFMI, NINDS, National Institutes of Health, Bethesda, Maryland, USA; [2]Nova Medical, Inc., Wilmington, Massachusetts, USA

An optimization procedure based on the Genetic Algorithm and full-wave electromagnetic simulations is proposed for RF coil array design in SENSE imaging. With the appropriate definition of the cost function, this procedure is applied to a 24-channel head coil array design for brain imaging at 7.0 Tesla. Results show that the optimized design requires overlap for each row of coils and gaps between different rows. The higher the SENSE rate is, the wider the inter-row gap size is required.

RF Coils for Spectroscopy and Animal Studies

Room 4E Wednesday 14:00 - 16:00

2593. 3T Prostate Coils for 1H and 31P MR Spectroscopic Imaging

Konstantinos George Karpodinis[1], Lucas Carvajal[1], Albert Pofu Chen[1], Bert Jimenez[1], Niles Bruce[1], James Tropp[2], John Kurhanewicz[1], Daniel B. Vigneron[1]
[1]University of California, San Francisco, San Francisco, California, USA; [2]General Electric Medical Systems, Fremont, California, USA

High field 3T clinical MR scanners offer the potential of greatly improving prostate MR imaging and spectroscopic imaging but are limited by the lack of FDA-approved endorectal coils. Also, prototype air-filled endorectal coils demonstrate substantial magnetic susceptibility artifacts at 3T. In addition, the higher SNR at 3T offers the potential of human 31P MRSI which could greatly improve the metabolic assessment of prostate cancer. In this study, new endorectal coils were designed and constructed for prostate MRI and both 1H and 31P MRSI to provide high sensitivity with minimal susceptibility artifacts.

2594. An Endorectal Dual Frequency 13C-1H Receive Only Probe for Operation at 3.0 Tesla

James Tropp[1], Paul Calderon[1], Lucas Carvajal[2], Kostas Karpodinis[2], Albert Chen[2], Dan Vigneron[2], Ralph Hurd[1], J-H. Ardenkjaer-Larsen[3]
[1]GE Healthcare Technologies, Fremont, California, USA; [2]University of California San Francisco, San Francisco, California, USA; [3]GE Healthcare Technologies, Niskayuna, New York, USA

We present circuit designs, and results of bench test, plus preliminary images and spectra (from phantoms) for an endorectal dual tuned 13C-1H receive only probe for operation at 3.0 T.

2595. 4T Actively-Detunable Double-Tuned 1H/31P TEM Head Volume Coil and Four-Channel 31P Phased Array for Human Brain Spectroscopy

Nikolai I. Avdievich[1, 2], Hoby H. Hetherington[1, 2]
[1]Albert Einstein College of Medicine, Bronx, New York, USA; [2]Gruss MRRC, Bronx, New York, USA

Typically 31P spectroscopic studies are limited by SNR considerations. Although phased arrays can improve the SNR; to date 31P phased arrays for high-field systems have not been combined with 31P volume transmit coils. Additionally, to provide anatomical reference for the 31P studies, without removal of the coil or patient from the magnet, double-tuning (31P/ 1H) of the volume coil is required. An actively detunable 31P/1H TEM volume transmit/ four-channel 31P phased array was developed for 4T MRSI of the human brain. The coil can be used either in volume-transmit/array-receive mode or in TEM transmit/receive mode with the array detuned.

2596. A Double-Resonant $^{19}F/^{1}H$ Transmit/Receive Solenoid Coil for MRI

Peter Caesar Mazurkewitz[1], Christoph Leussler[1], Jochen Keupp[1], Tobias Schaeffter[1]
[1]Philips Research Laboratories, Hamburg, Germany

^{19}F MR imaging has a high potential for the detection and direct quantification of fluorine-labeled tracers and drugs in the field of molecular imaging. The combination with ^{1}H imaging provides associated anatomical information. So far, this application has been typically supported by separate ^{19}F and ^{1}H RF-coils. We propose a new $^{19}F/^{1}H$ double resonant solenoid transmit/receive coil for 3T, which exhibits practically the same sensitivity profile for the two frequencies. Coil properties are demonstrated in MR-scans of fluorine and water containing phantom.

2597. Developing an RF Coil for MRI and MRS of Human Breast Tissue

Denis Rubin[1], Qiuhong He[1]
[1]University of Pittsburgh, Pittsburgh, Pennsylvania, USA

A simple and efficient RF coil was developed for high-field MRI/MRSI studies of breast cancer. The coil, used as a transceiver, produced highly homogeneous magnetic field that extended beyond the coil and showed no obvious dielectric artifacts at 3T. It was successfully used to obtain imaging and spectroscopy data of human breast tissue.

2598. A Dual Tuned RF Coil for 3T MRI

Y Duan[1], B. S. Peterson[1], F. Liu[1], T. R. Brown[1], Roney Abraham[2], Tamer S. Ibrahim[2], Alayar Kangarlu[1]
[1]Columbia University, New York, New York, USA; [2]University of Oklahoma, Norman, Oklahoma, USA

Proliferation of high field scanners has made MRS of non-hydrogen elements more appealing. The need for access to deep brain regions justifies development of tools to help better understand the existing dual tune coils and provide guidance for their improvement. In this study, FDTD is used to characterize a dual tuned 31P/1H coil. Improvement in performance of the coil is demonstrated as a result of application of this technique in identification of the pure modes, interaction of the two segments of the coil, and its effect on detection of 31P in deep regions of a phantom.

2599. Implantable Multiple-Frequency Inductively-Coupled Coil System for *In Vivo* MR Imaging and Spectroscopy of Bioartificial Pancreas at 11.1 T

Nelly A. Volland[1], Christopher A. Taylor[1], Thomas H. Mareci[1], Ioannis Constantinidis[1]
[1]University of Florida, Gainesville, Florida, USA

Introduction: Development of an implantable multiple-frequency inductively-coupled coil system for non-invasive *in vivo* monitoring of a bioartificial pancreas is discussed. Methods: System (internal coil inductively coupled to external coil) was developed for imaging and spectroscopy at 11.1T. Further optimizations were pursued to make the system receive-only. Results: System has a match of -12.8dB at 190.5MHz and -16.0dB at 470.7MHz. Receive-only system also gave more uniform image of sample compared to transmit/receive system. Conclusions: The multiple-frequency implantable inductively coupled coil system was successfully constructed to resonate at both frequencies. The receive-only system shows further improvement over the transmit/receive system.

2600. Multi-Element Coil for Animal Imaging at 3T

Gilles Beaudoin[1]
[1]CHUM, hôpital Notre-Dame, Montreal, QC, Canada

We describe a 7 channel receive-only coil for 3T imaging of medium sized cat spine. We have observed an SNR gain of 2.5 to 3 at the level of the spine when compared to a CP knee coil, which is the best available coil for this size of animal.

2601. Multiple Animal TEM RF Coil with Cylindrical Cavity Configuration

Hye Young Heo[1], Soo Yeol Lee[1], Kyung Nam Kim[1], Min Hyoung Cho[1], Ik Hyun Kim[1], Tae Suk Park[1]
[1]Kyung Hee University, Yongin, Kyungki, Republic of Korea

We propose a novel multiple animal RF coil to reduce the scan time in rat brain imaging studies. We developed a single-channel transverse electromagnetic (TEM) RF coil consisting of four cylindrical cavities without the noticeable degradation of SNR and homogeneity. The multiple animal RF coil is capable of simultaneous 8 rats imaging in 3.0 Tesla MRI system. As compared with the single animal RF coil, the developed multiple animal RF coil showed only 6~7% lower SNR when they were loaded with CuSO4 phantoms. With the multiple animal RF coil, we have obtained rat brain images successfully and presented the experimental results.

2602. A Coil System for Multiple-Mouse Imaging at 9.4 T

Peter Gerhard[1], Jeremy W. Wellen[2]
[1]RAPID Biomedical, Rimpar, Germany; [2]GlaxoSmithKline, King of Prussia, Pennsylvania, USA

A challenging constraint in pre-clinical MR screening applications is the inherently low throughput with MRI. We report on a quadruple coil system for simultaneous imaging of four mice at 9.4T to increase animal throughput. The individual coils are quadrature driven birdcage resonators for transmission and detection. Design, workbench and MR data are demonstrated. Isolation and SNR allow parallel imaging with acceleration factors of up to 4. B1 homogeneity across the coils is sufficient for whole-body mouse imaging applications.

2603. *In-Vivo* Mice Imaging Using HTS Volume Coil

Yum Wing Wong[1], Geng Li[1], Edward S. Yang[1]
[1]The University of Hong Kong, Pokfulam, Hong Kong, People's Republic of China

Receiver coils using High-Temperature Superconducting (HTS) materials are able to achieve higher quality factor (Q-factor) over conventional copper coils, thus higher signal-to-noise ratio (SNR) or shorter imaging time. Substantial SNR improvements were introduced by surface coils made of expensive HTS thin film. A 5-inch HTS coil using silver-alloy sheathed Bi-2223 tape was first developed, where lower cost, easier fabrication and more flexible coil configuration can be achieved. In our work, an HTS volume coil for *in vivo* mice imaging in low-field MRI system is first demonstrated.

2604. *In-Vivo* Multiple Mouse MRI Using Parallel Receive-Only Coils on a 3.0 T Clinical Scanner for Molecular Imaging Research

Marcelino Bernardo[1, 2], Hisataka Kobayashi[2], Gregory Metzger[3, 4], Yoshinori Koyama[2], Charlene Shaw[1, 2] David Thomasson[5], Peter Choyke[2]

[1]SAIC-Frederick, Frederick, Maryland, USA; [2]National Cancer Institute, Bethesda, Maryland, USA; [3]Philips Medical Systems, Bethesda, Maryland, USA; [4]University of Minnesota, Minneapolis, Minnesota, USA; [5]National Institute of Health, Bethesda, Maryland, USA

Parallel receive-only coils with modified Alderman-Grant resonator elements for multiple mouse MRI of two and four mice were constructed for plug-in use on a clinical 3.0 T scanner. It incorporates a multiple animal support system for gas anesthesia, heat, physiologic monitor, and contrast injector designed without using conducting wires to avoid RF interference and heating. Incomplete isolation between the unshielded coil elements requires SENSE or a reduction in NSA to maintain the same scan time as in the single mouse. The performance of the coil and support system was measured on phantoms and demonstrated in a simultaneous *in vivo* dynamic MRA of two mice during IV injection of two types of Gd-dendrimer agents.

2605. Design of Multiple-Imaging-Region Gradient Coil for Parallel Mouse Imaging

Joshua Thomas de Bever[1], Blaine A. Chronik[1]

[1]University of Western Ontario, London, Ontario, Canada

Imaging of mice using MRI is critical to studies investigating human diseases such as cancer, multiple sclerosis, and stroke. Currently it takes multiple hours to image a single mouse, and several hundred mice may be required to complete a large experiment. This represents a huge time and financial burden for researchers and granting agencies supporting mouse imaging. To address this, we have designed gradient coils capable of imaging three mice in parallel. We show that multi-imaging-region (MIR) coils provide significant performance increases over standard gradient designs by comparing simulated inductance, imaging region size, and gradient efficiency against standard single-region gradients.

General RF Coil Technology

Room 4E Wednesday 14:00 - 16:00

2606. Implementation of STR Body Coil for High Field MRI

Sung-Taek Chung[1], In-Ki Hong[1], Kyoung-Nam Kim[2], Yeun-Chul Ryu[3], Jeong-Han Yi[4]

[1]Korea Polytecnic University, Sihung-si, Kyoungi-Do, Republic of Korea; [2]Neuroscience Research Institute, Gachon Medical School, Incheon, Incheon-si, Republic of Korea; [3]Korea University, Ahnam, Seoul, Republic of Korea; [4]Konkuk University, Chunju, ChungBuk, Republic of Korea

The aim of this study is to design an optimized 3.0T whole-body coil (Tx/Rx) to produce a high sensitivity and quality images and confirm the safety of the coil by SAR calculation.

2607. Optimization of Resonance Mode Stability in RF Coil Design for Very High Field MRI

Charles Saylor[1], Yu Li[1]

[1]Invivo Diagnostic Imaging, Gainesville, Florida, USA

At very high field MRI, substantial B1 field inhomogeneity exists in RF excitation. The causes of this field inhomogeneity can be categorized into three groups: 1) dielectric resonances within the sample; 2) cylindrical waveguide modes because of the size of the RF resonator, and 3) resonance modes generated by the RF coil. In this study, we took into account these factors and used the resonance mode stability to evaluate the B1 field in a volume coil. Based on this method, a 7T volume coil was optimized and both B1 field homogeneity and power efficiency were improved.

2608. Performance Comparison with 15cm Long and 23cm Long Birdcage Coil on 7T

Akira Nabetani[1, 2], Graeme McKinnon[3], Tsutomu Nakada[2]

[1]GE Yokogawa Medical Systems, Ltd., Hino, Tokyo, Japan; [2]University of Niigata, Niigata, Japan; [3]GE Healthcare, Waukesha, Wisconsin, USA

Head loading, rather than coil geometry, dominates the B1 homogeneity at 7T. Hence, at 7T, coil geometry should be optimized with respect to SNR, or excitation power, etc. under head loading conditions. Two self-shielded 7T head-sized birdcage coils, 15cm and 23cm long, were built and compared with respect to Q value, SNR, B1 uniformity, and excitation power. The experimental measurements were also compared with the results of FDTD simulations. Under head loading conditions the 15cm coil performed better with respect to Q, SNR and power requirements, and had enough B1 coverage and similar uniformity to 23cm coil for brain study.

2609. 4T Split TEM Volume Head and Knee Coils for Improved Sensitivity and Patient Comfort

Nikolai I. Avdievich[1, 2], Ken Bradshaw[3], Jing-Huei Lee[4], Hoby H. Hetherington[1, 2]
[1]Albert Einstein College of Medicine, Bronx, New York, USA; [2]Gruss MRRC, Bronx, New York, USA; [3]MRI Instruments Inc., Minneapolis, Minnesota, USA; [4]University of Cincinnati, Cincinnati, Ohio, USA

Due to the presence of end ring currents, split unshielded birdcage coils require an electrical connection between two halves of the coil. For shielded high-field RF coils not only the coil itself but also the shield must be split and reliably connected electrically. Using TEM volume coils can solve this problem due to inductive coupling between elements. We have developed and tested 4 T split TEM volume coils for the head and knee. Splitting the shield does not degrade the coil performance but improves patient comfort and accessibility. For the leg, it also enhances sensitivity by reducing the coil size.

2610. Shoulder Shield for 7.0T T/R Brain Coil

Gordon DeMeester[1], Zhiyong Zhai[1], Michael Morich[1], Christoph Leussler[2], Kai Michael Lüdeke[2]
[1]Philips Medical Systems, Cleveland, Ohio, USA; [2]Philips Research Laboratories, Hamburg, Germany

When using a shielded birdcage 7T T/R brain coil for brain imaging, some unwanted signals and loading comes from the shoulders outside the coil. This can be attributed to the increased coupling and power loss to the shoulders at 298MHz. To reduce the shoulder effect and increase SNR, a shoulder shield, which can be treated as the extension of the RF shield in the radial direction, is introduced. A shoulder shield with optimal openness and position can increase coil efficiency without increasing head SAR.

2611. Design of Multi-Elements Transverse Field RF Surface Coils

Tomas Mazza[1], Maria Alfonsetti[1], Marcello Alecci[1]
[1]Università di L'Aquila, L'Aquila, Italy

We present a multi-elements transverse field figure-of-eight coil (FO8) RF surface coil design, composed by a number of parallel linear current elements positioned in the central region of the coil, that can be useful to select a well defined region of interest (ROI), and to improve the signal-to-noise ratio and the RF field homogeneity in the selected ROI. We demonstrate theoretically and experimentally that this design allows to obtain a ROI of higher sensitivity. Moreover, we show that the size and shape of the ROI can be adjusted by an appropriate selection of the number and spacing of the elements.

2612. Slotted Surface Coil for Magnetic Resonance Imaging at 4T

Sergio Solis[1, 2], Ruiliang Wang[2], Dardo Tomasi[2], Alfredo Odon Rodriguez[1]
[1]UAM Iztapalapa, Mexico, DF, Mexico; [2]Brookhaven National Laboratory, Upton, New York, USA

A slotted surface coil, inspired on the cavity magnetron was developed for magnetic resonance imaging (MRI) at 4T. Imaging tests using a saline phantom demonstrated that the slotted surface coil has deeper RF-sensitivity than the single-loop RF-coil. High quality images of two rats were acquired simultaneously using standard spin-echo pulse sequences, demonstrating that the slotted surface coil can be a good tool for rat images at 4T.

2613. Optimized Litz Coil Design for Prepolarized Extremity MRI

Thomas Grafendorfer[1, 2], Steven M. Conolly[1, 2], Nathaniel I. Matter[2], John Pauly[2], Greig Scott[2]
[1]UC Berkeley, Berkeley, California, USA; [2]Stanford University, Stanford, California, USA

There are a number of applications for low field MRI, including hyperpolarized gas MRI, hyperpolarized 13C or PHIP, and prepolarized MRI. Unlike conventional MRI, there is no SNR advantage to increased field strength above the so-called body noise dominance threshold. It is critical to choose the most sensitive RF coil for low field MRI. It is well known that litz wire is more sensitive than solid copper up to 1 MHz. Here we found that litz wire provides significant (40%-100%) improvement in SNR over solid copper up to 10 MHz.

2614. Using MR Thermometry to Monitor the Frozen Effect in High-Temperature Superconducting RF Coil System

Li-Wei Kuo[1], Ching Yao[2], Kun-Lin Tsai[1], Hong-Chang Yang[1], Jyh-Horng Chen[1]
[1]National Taiwan University, Taipei, Taiwan; [2]National Health Research Institute, Miaoli, Taiwan

High-temperature superconducting RF coil (HTSC) has been proposed to have the capacity of improving the signal-to-noise ratio because of its non-resistive property. However, the thermal insulation of the liquid nitrogen dewar is usually a limitation to perform *in vivo* experiments. In this work, MR thermometry using water proton resonance frequency method was used to monitor the frozen effect and the capacity of the MR thermometry in HTSC experiment was evaluated by the correlation with the absolute temperature measurement. The PRF thermal coefficient was derived as 0.1181 rad/?C and the monitoring architecture can be implemented in the future to improve the quality and safety in HTSC experiments.

2615. A New Method of Fabricating HTS Tape Coil

Yum Wing Wong[1], Edward S. Yang[1]
[1]The University of Hong Kong, Pokfulam, Hong Kong

High-Temperature Superconducting (HTS) materials can introduce substantial improvement in signal-to-noise ratio (SNR) of MR images. HTS tape coil using Bi-2223 tape was developed, which allows easier fabrication, frequency adjustment and lower cost than expensive thin films. Imaging using small-size HTS tape coil is expected to yield higher SNR improvement, but its fabrication is limited by relatively large recoil force experienced. In our work, a new method of fabricating HTS tape coil is demonstrated, which can effectively enhance the protection for HTS tape coil in particular for those of small size. Potential applications include mice imaging in high field MRI system.

2616. On the SNR Gain for Copper and Superconductor Cryogenic Coils

Lian Xue[1], *Leiming Xie*[1], *Maged Kamel*[1], *Jarek Wosik*[1]
[1]University of Houston and Texas Center for Superconductivity, Houston, Texas, USA

We report on simulation of SNR Gain behavior of cryogenic coils as a function of frequency and coil size in arrays, as well as on an accurate technique for experimental verification of SNR Gains based on Q measurements performed on Cu cooled and high temperature superconductor (HTS) coils. The obtained results identify the advantages of using HTS coils over Cu cooled coils and specify the maximum size ranges for sufficient SNR Gain at different frequencies. New designs for HTS coils of various sizes include frequency tuning based on a dielectric layer introduced between HTS layers.

2617. A Direct Modulated Optical Link for MR Coil Array Interconnect

Jing Yuan[1], *Juan Wei*[1], *Peng Qu*[1], *Gary X. Shen*[1]
[1]The University of Hong Kong, Hong Kong, People's Republic of China

A direct modulated optical link for MR coil array interconnect has been developed. The link uses a diode laser to modulate RF signals directly, and needs only one fiber for each channel. It has a power gain of ¨C18dB, noise figure of 29dB and dynamic range of 110dBHz. The noise figure can be reduced to below 1dB by a low noise preamp. Compared with an external modulated optical link, a direct modulated link has simpler link structure, lower cost and more compact size, so it is more advantageous for large coil array interconnect.

2618. Surface Coils with Integrated Differential Amplifiers

Jolinda Smith[1], *Cliff Dax*[1], *Ray L. Nunnally*[1]
[1]University of Oregon, Eugene, Oregon, USA

We have integrated low-noise amplifiers into receive-only surface coils. Because the amplifiers operate in a differential mode, the surface coils may be left untuned. This minimizes coupling between adjacent coils when used as elements of an array.

2619. Microstrip TEM Coil Optimization at 7T

Can Akgun[1], *Lance DelaBarre*[1], *Pierre-Francois van de Moortele*[1], *Carl J. Snyder*[1], *Kamil Ugurbil*[1], *John Thomas Vaughan*[1]
[1]University of Minnesota, Minneapolis, Minnesota, USA

Efficient high-frequency RF coils are needed to realize the gains of ultra-high field MR imaging. Transverse electromagnetic (TEM) resonators which use microstrip elements have provided a solution. To further advance this technology the design parameters of these coils have been investigated with the aim of generating more efficient coils. Specifically substrate thickness, signal line width, and sidewall depth were varied on microstrip designs to achieve desired B1 fields at 7T. Simulations of eight channel TEM coils incorporating these optimized microstrip elements were then used to analyze B1 field for strength and decoupling potentials of different coil configurations.

2620. Optimizing the SNR Performance of the Tunable Strip Detector

Ananda Kumar[1], *Paul Arthur Bottomley*[1]
[1]Johns Hopkins University, Baltimore, Maryland, USA

The intrinsic signal-to-noise ratio (ISNR) performance of a MRI strip detector with lumped tuning capacitors was numerically optimized over a practical range of design parameters. The most important factors determining ISNR performance were found to be strip length, dielectric substrate, and substrate thickness. ISNR analyses showed that optimized strip detectors can yield comparable performance to that of loops optimized for the same depth. A range of strip detectors were fabricated with various design parameters to validate the numerical analyses. The results were in excellent agreement, showing that numerical optimization proves is an effective approach optimizing MRI detector design.

2621. Comparison of the Coax Element and Stripline Element TEM Head Coils at Ultra-High Field

Tamer S. Ibrahim[1], *Roney Abraham*[1], *Lin Tang*[1], *John Thomas Vaughan*[2]
[1]University of Oklahoma, Norman, Oklahoma, USA; [2]University of Minnesota, Minneapolis, Minnesota, USA

In this work, we compare of the performance of two popular RF coils used in high field MRI head applications, namely, the coax element TEM coil and the stripline element TEM coil. The comparison is performed using the finite difference time domain method. We load the coils with an accurate human head model, and tune and operate the coils at the proper frequency for proton imaging at 7 Tesla. We then compare the performance of the two coils by analyzing the B1+ and B1- fields, as well as the MR signals generated by both coils.

2622. A Van Vaals Resonator with a Novel Quadrature Drive Circuit

Matthew George Erickson[1], *Krishna N. Kurpad*[1], *Thomas M. Grist*[1]
[1]University of Wisconsin Madison, Madison, Wisconsin, USA

This work describes a quadrature van Vaals resonator. Circular polarization is achieved by a novel drive circuit which uses current baluns in conjunction with hybrid combiners or a simple phasing harness. The coil incorporates provision for independent control of power and phase in each conjugate pair of conductors, and retains all of the advantages of the original van Vaals design. The device is suitable for use in clinical magnets.

2623. Evaluation of Ferroelectric Resonators as RF Coils for Magnetic Resonance Spectroscopy

Ilia Geifman[1], Iryna Sergeevna Golovina[2]
[1]Oakton Community College, Glenview, Illinois, USA; [2]Institute of Semiconductors Physics, Kiev, Ukraine

The most important problems of any kind of magnetic resonance methods (NMR, EPR or MRI) are their sensitivity or imaging quality. Major new advances in sensitivity and quality of image can be provided by the development of new types of RF coils, especially ferroelectric resonators (FRs), which are the subclass of dielectric resonators. Potassium tantalite (KTaO3) as the best material for microwave/RF resonators for magnetic resonance spectroscopy is proposed. FRs made of KTaO3 are successfully tested in NMR and EPR experiments providing 10- and 100-fold enhancement in their sensitivity, respectively. For those applications, the advantage of the designed FRs made of single-crystal potassium tantalate is that it exhibits no background signals. Another advantage of this material is that in the RF range it has very small frequency dependence of the dielectric constant. We developed FRs without discrete network elements to substitute commonly used birdcage resonators in NMR and MRI. This study demonstrated the advantages of RF resonators made of KTaO3 in comparison with ceramic resonators made of titanium dioxide and/or aluminium oxide.

2624. RF Breakdown in Vacuum Layers for MRI Noise Reduction

Wolfgang Renz[1], Helmut Stark[2], Jürgen Nistler[1], Martin Rausch[1]
[1]Siemens Medical Solutions, Erlangen, Germany; [2]Stark Contrast MRI Coils Research, Erlangen, Germany

Vacuum layers can be used very effectively to reduce noise in mri systems. The integration of rf coils into the vacuum is limited by a decrease in breakdown voltage. We investigated a setup with an rf shield inside the vacuum and the rf coil outside the vacuum. In this setup it was possible to operate the rf coil with a B1 field strength of 50µT without arcing in the vacuum area.

RF Applications: Miscellaneous

Room 4E Wednesday 14:00 - 16:00

2625. Saturated Double-Angle Method for Rapid B1 Mapping

Charles H. Cunningham[1], John M. Pauly[1], Krishna S. Nayak[2]
[1]Stanford University, Stanford, California, USA; [2]University of Southern California, Los Angeles, California, USA

For MRI at high field it is essential to consider the homogeneity of the active B1 field, particularly if surface coils are used for RF transmission. A new method is presented for rapid B1+ magnitude mapping. It combines a double angle method with a B1-insensitive magnetization-reset sequence such that the choice of TR is independent of T1. A multi-slice spiral acquisition gives volumetric coverage in a few seconds. By comparing maps made with different TRs and observing no difference except variations in SNR, it can be concluded that the proposed sequence achieved the desired removal of T1 effects.

2626. Rapid Mapping of the RF Field

Glen Morrell[1]
[1]University of Utah, Salt Lake City, Utah, USA

A rapid method of 3D B1 mapping is presented which uses a combination of RF pulses played about orthogonal axes to create transverse magnetization with phase varying almost linearly with B1 strength over a wide range of flip angles. Previously described limitations of this technique caused by off-resonance from B0 inhomogeneity and chemical shift are overcome by making the RF excitation as rapid as possible. This phase-sensitive method has favorable SNR characteristics and may be useful for B1 mapping for B1 inhomogeneity compensation with multidimensional pulses, coil profile measurement for parallel excitation, and coil sensitivity mapping for improved parallel imaging.

2627. Measuring Coil Sensitivities of Transmit and Receive Arrays with Demonstration of RF Shimming

Nominated for an ISMRM Poster Award

Martina F. Callaghan[1], Jose L. Ulloa[2], David J. Larkman[1], Pablo Irarrazaval[2], Joseph V. Hajnal[1]
[1]Hammersmith Hospital, Imperial College London, London, UK; [2]Pontif Universidad Catolica de Chile, Santiago, Chile

Operating with arrays of coils for both transmit and receive requires determination of spatially varying coil sensitivities in both modes. Using a duel spin echo - stimulated echo sequence the transmit fields of individual coils can be directly measured and receive coil sensitivities can also be obtained. Total time to determine transmit and all receive profiles is < 1min/transmit coil. The method has been tested at 3T with transmit-receive coils and separate transmit and receive array coils using phantoms and *in vivo*. Measured transmit fields have then been corrected using RF shimming taking into account off-resonance effects and eddy currents.

2628. Transmit Array Spatial Encoding (TRASE): A New Data Acquisition Method in MRI

Scott B. King[1], Donghui Yin[1], Sheryl Thingvold[1], Jonathan C. Sharp[1], Boguslaw Tomanek[1]
[1]National Research Council of Canada, Winnipeg, Manitoba, Canada

We propose a new method of spatial encoding using a transmit-array system, called TRansmit Array Spatial Encoding (TRASE), that provides a new way of sampling k-space without the need for phase encode gradients. MRI simulations of a standard GE pulse sequence and an equivalent GE-TRASE pulse sequence show nearly identical k-space data and MR image for both methods. TRASE may provide faster data acquisition, reduce acoustic noise, enable shorter TE thus higher SNR, eliminate dB/dt in phase direction and reduce eddy current and motion artifacts. The TRASE method offers many possibilities for novel k-space trajectories.

2629. Estimating *In Vivo* Spatial Resolution of Magnetic Resonance Images Using Radiofrequency Tagging Pulses

Wen-Tung Wang[1], *Craig H. Meyer*[1]
[1]University of Virginia, Charlottesville, Virginia, USA

This work investigates the feasibility of using the width of tags generated from RF pulses to estimate the true spatial resolution of *in vivo* MR images. The results show that, for visualization and quantification of the spatial resolution, a good estimation can be obtained when the width of the modulation function is narrower than the spatial resolution to be measured. As a rule of thumb, using tags whose modulation width is one half of the best possible spatial resolution can provide both an accurate quantitative and a quick visual estimation of the true spatial resolution.

2630. Spectrally Sensitive Imaging Using Balanced Steady State Free Precession

Roland Bammer[1], *Michael Markl*[2]
[1]Stanford University, Stanford, California, USA; [2]University of Freiburg, Freiburg, Germany, Germany

Conventional b-SSFP in the presence of field inhomogeneities is often confounded by “banding artifact”. Here, the contribution of relaxation times, excitation B1 field, and off-resonant spins to these artifacts in b-SSFP has been characterized. A new variant of b-SSFP has been introduced to map the underlying spectral distribution of spins within a frequency range given by 1/TR. The b-SSFP banding can be characterized as a result of a circular convolution between the underlying spectrum and a filter function determined by relaxation times and B1.

Brain: Miscellaneous MRS

Room 4E Thursday 13:30 - 15:30

2631. ^{1}H MR Spectroscopic Assessment of Age-Related Changes in Young and Middle-Aged Women

Sarah Andrea Dunham[1], Kathleen L. Fuchs[1], Dattesh D. Shanbhag[1], Virginia I. Simnad[1], Jack Knight-Scott[1]
[1]University of Virginia, Charlottesville, Virginia, USA

In this study, we examined the age-related neurochemical and relaxometric differences between healthy young and healthy middle-aged women. 10 ms TE ^{1}H MRS data were collected from healthy women: 7 middle-aged and 5 young participants. Choline (Cho, p=0.028) and myo-Inositol (mI, p=0.041) concentrations were significantly elevated in the middle-aged women relative to the young women, with a mean increase of 24% for Cho and 17% for mI. Additional support for these aging effects is provided by a consistent trend of decreasing relaxometry parameters with increasing age; such as decreasing tissue water T_1, T_2, and local tissue fraction. The combination of water relaxometry and metabolite concentrations gives a detailed description of the tissue changes that accompany normal age-related cerebral atrophic and neurometabolic changes.

2632. Application of Proton MRSI to Assess Metabolic Status of the Brain in Post Traumatic Brain Injury Depression

Mahaveer Degaonkar[1], Vani Rao[1], Jennifer Spiro[1], Alena Horska[1], Peter Barker[1]
[1]Johns Hopkins School of Medicine, Baltimore, Maryland, USA

We hypothesized that TBI depressed subjects would have decreased NAA/Cho and/or NAA/Cr ratios in the frontal gray matter and basal ganglia as these regions have been implicated in structural imaging studies of the pathogenesis of post-TBI depression. Significant reduction of NAA in frontal and subcortical gray matter regions indicates diffuse axonal injury or metabolic depression. The results indicate that the reduction in NAA in post-TBI depression is mostly due to neuronal injury from TBI. We conclude that frontal cortical region and subcortical regions are more prone to TBI injury and neuronal injury due to functional changes may lead to TBI depression.

2633. Hierarchical Linear Modeling of Longitudinal Magnetic Resonance Spectroscopic Imaging

Ping-Hong Yeh[1], John Kornak[2], Hemanth Thayyullathil[1], Dieter Meyererhoff,[1,2]
[1]Northern California Institute for Research and Education, San Francisco, California, USA; [2]University of California, San Francisco, San Francisco, California, USA

A comprehensive analysis of biomedical longitudinal data demands accommodation of between-subjects and within-subject variation, unbalanced designs and missing data. The longitudinal spectroscopic imaging data even complicate the problem by its large sources of variability. The goal of this study is to apply linear mixed models in the assessment of the change of 2 metabolites during short-term recovery from alcohol dependence and compare the results using different random effect model

2634. A Novel Single-Voxel ^{1}H-MRS Sequence for Single-Shot Detection of Brain Glycine

Andrew Paul Prescot[1], Blaise deB Frederick[1], Marc J. Kaufman[1], Perry F. Renshaw[1]
[1]McLean Hospital, Belmont, Massachusetts, USA

Glycine (Gly) serves as an essential coagonist for the glutamatergic N-methyl D-aspartate (NMDA) receptor subtype. NMDA receptor hypofunction is implicated in brain disorders including schizophrenia, and several therapeutic agents targeting glycinergic neurotransmission are currently under development. We recently developed a ^{1}H-MRS echo time (TE)-averaging method capable of monitoring cerebral Gly levels. TE-averaging requires the sampling of multiple TEs thus giving rise to long measurement times. Accordingly, we developed a novel single-shot method capable of suppressing mI whilst retaining the Gly resonance. This method is demonstrated in phantom studies and preliminary *in vivo* data are presented.

2635. Estimation of Myo-Inositol and Macromolecule Contents in Normal-Appearing White and Gray Matter in MS Using 3D-HMRSI at 3T

Hélène Ratiney[1], Darin Okuda[1], Danielle Graveron-Demilly[2], Sarah J. Nelson[1], Steve Hauser[1], Daniel Pelletier[1]
[1]University of California, San Francisco, California, USA; [2]Laboratoire de RMN, CNRS, UMR 5012, Université LYON I-CPE, Lyon, France

The myo-inositol (mI) band at ~3.6 ppm was investigated at 3T using 3D HMRSI, at echo time (TE) of 40ms in 168 patients with multiple sclerosis (MS) and 27 healthy volunteers. The quantification of this frequency region is challenging because of severe background contamination coming from broad macromolecules and surrounding metabolite peaks (the complex Glutamate-Glutamine, taurine, glycine, alanine, glucose). In this present study, we accounted for this background while estimating mI concentration using the quantitation algorithm QUEST. Macromolecule contents in normal-appearing white matter (NAWM) are estimated to evaluate disease-related changes compared to healthy volunteers.

2636. Characterization of the Downfield Part of the Human Cerebral ^{1}H MR Spectrum at 3 T

Roland Kreis[1], Chris Boesch[1], Peter Vermathen[1]
[1]University Berne, Berne, Switzerland

The downfield region of the human cerebral ^{1}H-MR spectrum is still poorly characterized. Peak positions for NAA (N-H), phenylalanine, homo-carnosine, and histidine are established and macromolecules have been identified at 1.5T. There is potential for observation of further peaks – particularly amides - at higher fields. In this study, the TE- and TR-dependence of the downfield region is characterized at 3T. All peaks were found to be better resolved at this field strength; particularly those tentatively assigned to ATP are much better discerned from background. An unassigned peak at 7.3ppm shows anomalous TE-behavior when comparing spectra from 1.5 and 3T.

2637. Fast and High Resolution MRSI Without Aliasing Using Online SFAS and Multiple Regions of Support

Yun Gao[1], Stephen M. Strakowski[1], Stanley J. Reeves[2], Hoby P. Hetherington[3], Wenjang Chu[1], Jing-Huei Lee[1]
[1]University of Cincinnati College of Medicine, Cincinnati, Ohio, USA; [2]Auburn University, Auburn, Alabama, USA; [3]Albert Einstein College of Medicine, Bronx, New York, USA

The acquisition of a complete 2D MRSI data set is very time consuming, which is often unacceptable for clinical studies. Various approaches have been proposed for reducing the scanning time. In some situations, when not interested in signal from the entire object, one may consider using the reducing FOV approach. However, this method often suffers from aliasing. Alternatively, one can use the sequential forward array selection (SFAS) method for reducing the scanning time. In this work, we demonstrate that online SFAS not only provides high resolution MRSI with less data acquisition time, but also eliminates the aliasing unsaturated signal.

2638. Age-Related Changes in Brain Metabolites in Antiretroviral Medication-Stable HIV Patients

Kenneth Yue[1], Linda Chang[1], Daniel Alicata[1], Christine Cloak[1], Kathryn Taketa[1], Thomas Ernst[1]
[1]University of Hawaii, Honolulu, Hawaii, USA

The interactive effect of aging and HIV on brain metabolites in antiretroviral medication-stable HIV subjects is unknown. We studied age-related metabolite changes in three groups: seronegative controls and seropositive subjects with and without cognitive deficits. Localized proton MRS was employed to measure metabolites in four brain regions. Significant age-related increases in frontal gray matter N-acetylaspartate and choline, and status x age interactions, were observed in both controls and HIV neuroasymptomatic subjects. HIV dementia subjects showed lesser age-related increase in N-acetylaspartate in the frontal lobe. These findings demonstrate additive and interactive effects of aging and HIV infection on brain metabolites.

2639. Proton MR Spectroscopic Imaging in Neurofibromatosis Type-1: Relationship to Neuropsychological Testing

Mona A. Mohamed[1], Jessica R. Abel[2], Sheryl L. Rimrodt[2], Laurie E. Cutting[2], Peter B. Barker[1, 2]
[1]Johns Hopkins University, Baltimore, Maryland, USA; [2]Kennedy Krieger Institute, Baltimore, Maryland, USA

13 children with neurofibromatosis type-1 (NF1) and 17 healthy, age-matched control subjects were examined with neuropsychological testing and proton MR spectroscopic imaging (MRSI). NF1 patients showed significantly lower NAA/Cr and NAA/Cho ratios in the thalamus ($p = 0.017$ and 0.04 respectively) and in the parietal white matter ($p = 0.04$ and 0.039 respectively) as compared to the controls. Also, there were multiple, significant correlations for NAA/Cr and NAA/Cho ratios with neuropsychological test scores. These data suggest that the thalami are a central site of involvement in NF1, and that widespread metabolic abnormality is a factor associated with cognitive impairment in NF1.

2640. Effects of Smoking on Brain Metabolite Concentrations

Diana Marie Lindquist[1], Reid Landes[1], Kirstin Gatchalian[1], Richard Yi[1], Warren Bickel[1]
[1]University of Arkansas for Medical Sciences, Little Rock, Arkansas, USA

Several MRS studies of substance abusers have indicated that use of drugs, such as cocaine, methamphetamine, or alcohol, is associated with changes in brain metabolism. However, there are no MRS studies examining the independent effects of smoking, another addictive behavior, on brain metabolites. Therefore, single voxel spectroscopy was used to measure brain metabolite concentrations in thalamus, frontal and parietal cortex, and hippocampus of smokers and non-smokers. Choline was reduced in the frontal cortex of smokers and creatine tended to be increased in frontal and parietal cortex. Smoking status should be considered when analyzing MRS data sets.

2641. MRS Monitoring of the Effects of Mobile Phone Use on the Brain

Abdesslem Khiat[1], Guy Breton[1], Yvan Boulanger[1]
[1]Hôpital Saint-Luc du CHUM, Montreal, Quebec, Canada

Proton magnetic resonance spectroscopy (1H MRS) was used to evaluate changes in cerebral metabolites for 21 extensive users (average use = 5.5 ± 2.2 years at 2.4 ± 1.1 hours/day) of a mobile phone and 15 nonusers. Data were recorded in both the exposed right temporal area and the contralateral left temporal area as well as in the pontobulbar area. No statistically significant changes could be measured for the NAA/Cr, Cho/Cr and mI/Cr ratios between mobile phone users and nonusers subjects and between the exposed and contralateral temporal areas.

2642. Combined DWI and 1H-MRS Study of the Brain of Cirrhotic Patients

Caterina Tonon[1], Raffaele Lodi[1], Claudia Testa[1], Emil Malucelli[1], David Neil Manners[1], Bruno Barbiroli[1]
[1]Policlinico S.Orsola-Malpighi, Università di Bologna, Bologna, Italy, Italy

Previous studies have shown that water ADC is significantly increased in different brain regions of cirrhotic patients being higher in patients with higher venous ammonium. We investigated the relationship between changes in brain ADC and the content of glutamine (Gln) in cirrhotic patients studied by combined 1H-MRS and DWI. Both brain ADC values and Gln/Cr were increased in cirrhotic patients and ADC values correlated positively with Gln/Cr. These findings show that in cirrhotics increased brain cell water content is secondary to brain glutamine accumulation that has been associated to glial swelling in experimental models of hepatic encephalopathy

Brain MRI: The Next Frontier

Room 4E Thursday 13:30 - 15:30

2643. Fast T1 Mapping of the Brain at 7T with RF Calibration Using Three Point DESPOT1 Method

Tie-Qiang Li[1], Sean C. L. Deoni[2]
[1]NIH, Bethesda, Maryland, USA; [2]King's College London, London, England, UK

Rapid T1-maping with high resolution better than 1mm3 voxel size has great potential for clinical applications. The DESPOT1 (driven equilibrium single pulse observation of T1) approach allow accurate whole brain T1 mapping within the clinical timeframe. However, the accuracy of this method is quite sensitive to B1 inhomogeneity encountered at 7T. In this study, a modified approach based on 3 points DESPOT1 measurements is introduced, which allow rapid and high resolution T1 measurements with B1 correction in the Brain.

2644. Ultrahigh Field T2 in Human Brain: Regional Differences and Changes with Age

Petra Schmalbrock[1], Peter Wassennaar[1], Johannes T. Heverhagen[1], Truong-Kha Truong[1], Donald W. Chakeres[1], Michael R. Thompson[2], John Duraj[2], Michael V. Knopp[1]
[1]The Ohio State University, Columbus, Ohio, USA; [2]Philips, Cleveland, Ohio, USA

Brain iron is known to change with aging and in neurodegenerative disease, and this may be indicative of disturbances in iron homeostasis and/or oxidative stress. Thus non-invasive assessment of brain iron is of significant interest. Consequently, measurement of brain iron has been attempted at 1.5T and 3T, however, with mixed results. It is expected that ultrahigh field MRI is significantly more sensitive to susceptibility effects from iron. In this work, T2 was measured at 7T and 8T for different brain regions and ages with the purpose to evaluate ultrahigh field transverse relaxation mechanisms and their dependence on parenchymal iron.

2645. Improving Image Contrast in Conventional Dual Spin Echo at 3.0T with Short TE and Flip Angle Optimization

Chen Lin[1], Mathew A. Bernstein[1], Krzysztof R. Gorny[1], John T. Wald[1], Robert J. Witte[1]
[1]Mayo Clinic College of Medicine, Rochester, Minnesota, USA

At many institutions, dual-echo conventional spin echo has been replaced by FSE and FLAIR in routine brain imaging. However, some groups still regard conventional spin echo as a valuable pulse sequence for use in clinical practice. At 3.0T, peripheral triggering is useful for suppressing flow artifacts on the T2-weighted images. Consequently, TR depends on the heart rate, and is often longer than optimal value, yielding unwanted hyper-intensity of CSF in PD-weighted images. This work explores methods to reduce CSF intensity in conventional dual spin echo at 3.0T, and thus improve the conspicuity of lesions.

2646. A New Technique for Phase Susceptibility-Weighted Imaging of Iron in the Brain

Melanie S. Kotys[1], David M. Thomasson[1], Nicholas Patronas[1]
[1]National Institutes of Health, Bethesda, Maryland, USA

Magnetic resonance (MR) imaging may be an effective method to detect the distribution of iron in the brain using the high sensitivity of the MR phase to the susceptibility effects of iron. A new technique for susceptibility-weighted imaging (SWI) of iron using phase-based ($\delta\Phi$) SWI is presented. R_2* and $\delta\Phi$ SWI mapping were performed on human brain images.$\delta\Phi$calculations used multiple TEs, pairwise subtraction, and lowpass filtering to reveal phase shifts induced by iron-containing brain structures while minimizing susceptibility effects from other sources. This technique shows greater sensitivity and a higher, more stable contrast-to-noise ratio than basic R_2* mapping.

2647. Automatic Detection and Classification of Hypointensity in MR Images of the Brain

Radu Serban Jasinschi[1], Ahmet Ekin[1], Adriaan Cornelius van Es[2], Jeroen van der Grond[2], Mark Augustinus van Buchem[2], Arianne van Muiswinkel[3]
[1]Philips Research, Eindhoven, Netherlands; [2]Leiden University Medical Center, Leiden, Netherlands; [3]Philips Medical Systems, Best, Netherlands

A method for automated detection and classification of hypointense regions on T2-weighted MR images of the Basal Ganglia (BG) is presented. The detection includes the segmentation of the BG and the use of a normalized feature to detect hypointense regions. We validated our approach by comparing the automated results with a radiologist's assessment of patient data, and found good agreement between these results.

2648. Time-Resolved Contrast Enhanced Neuro-Angiography Using HighlY Constrained Back PRojection (HYPR) with a Hybrid Radial/Cartesian Acquisition (PR-TRICKS)

Yijing Wu[1], Patrick Turski[1], Yan Wu[1], Frank R. Korosec[1], Oliver Wieben[1], Jiang Du[2], Charies A. Mistretta[1]
[1]University of Wisconsin, Madison, Wisconsin, USA; [2]University of California, San Diego, San Diego, California, USA

We recently applied a new reconstruction method called HighlY constrained back PRojection (HYPR) on the hybrid radial/Cartesian acquisition PR-TRICKS and achieved both high spatial and temporal resolution in the time-resolved contrast enhanced neuro-angiography.

2649. New Developments in Dynamic Time-Resolved Magnetic Resonance (MR)- Angiography (TREAT) and High Resolution MR-Imaging of Cerebral Arterio-Venous Malformations (CAVM) Using Parallel Imaging at 3T

Karin Anna Herrmann[1], Ulrike Fasol[1], Olaf Dietrich[1], Berndt Wowra[2], Alexander Muacevic[2], Maximilian F. Reiser[1], Stefan Oswald Schoenberg[1]
[1]Ludwig-Maximilians-University Hospitals Munich-Grosshadern, Munich, Bavaria, Germany; [2]European Cyberknife Center Munich, Munich, Bavaria, Germany

New developments in the treatment of cerebral arterio-venous malformations (cAVM) with non-invasive robotic radiosurgery enforce the demand for high-resolution 3D-imaging and dynamic angiographic techniques comprised in one examination. For precise planning of stereotactic treatment, the reliable identification of the central nidus of arterio-venous shunting as the target is crucial for successful treatment. With parallel imaging techniques and 3T technology high spatial and temporal resolution are achieved. For morphologic information, 3D-imaging with isotropic voxel size is available. Dynamic MRA with time-resolved echo-shared acquisition techniques(TREAT)provides high temporal resolution of 1/700ms permitting the delineation of the central nidus within the cAVM in the early arterial phase. Due to the 3D-properties and isotropic voxel sizes of both the morphologic sequences and dynamic TREAT, 3D-postprocessing with multiplanar reformations and image fusion is possible and can successfully be used as a basis for precise planning of stereotactic treatment.

2650. Quantitative Aspects of Measuring Contrast Reagent Extravasation in the Healthy Human Brain

Xin Li[1], William Rooney[1], Charles Springer[1]
[1]Oregon Health & Science University, Portland, Oregon, USA

A sufficiently high magnetic field (>4T) allows detection of extravasation of the common Gd(III) contrast reagents (CRs) in the normal human brain. [This is not caused by the greater field strength.] We use simulations to investigate aspects of Dynamic-Contrast-Enhanced (DCE) MRI experimental design that allow precise and accurate measurement of this.

Dementia MRI/MRS

Room 4E Thursday 13:30 - 15:30

2651. *In Vivo* Detection of Cerebral Glutathione in Aging and Alzheimer's Disease Using Selective Multiple Quantum Chemical Shift Imaging of GSH

In-Young Choi[1, 2], John J. Sidtis[2, 3], Nunzio Pomara[2, 3], Sang-Pil Lee[1, 2]
[1]University of Kansas Medical Center, Kansas City, Kansas, USA; [2]The Nathan Kline Institute, Orangeburg, New York, USA; [3]New York University, New York, New York, USA

GSH is a major antioxidant and implicated in aging and many neurodegenerative diseases. However, reliable *in vivo* measurement of cerebral GSH has been quite challenging. Recently, we have developed a multiple quantum chemical shift imaging technique and demonstrated GSH mapping in the human brain *in vivo*. In various disorders including neurodegeneration, GSH level decreases in pre-symptomatic stages of diseases, indicating GSH loss may be an important contributor to the pathologic processes. Therefore, we investigated the effect of aging and Alzheimer's disease on GSH content. Cerebral GSH was significantly reduced in aging and further decreased in Alzheimer's disease.

2652. Validation Testing of the MRI Calibration Phantom for the Alzheimer's Disease Neuroimaging Initiative Study

Jeff L. Gunter[1], Matt A. Bernstein[1], Bret J. Borowski[1], Joel P. Felmlee[1], Daniel James Blezek[2], Richard P. Mallozzi[2], Joshua R. Levy[3], Norbert Schuff[4], Clifford R. Jack, Jr.[1]
[1]Mayo Clinic and Foundation, Rochester, Minnesota, USA; [2]GE Global Research, Niskayuna, New York, USA; [3]The Phantom Laboratory, Salem, New York, USA; [4]UC San Francisco, San Francisco, California, USA

As part of the Alzheimer's Disease Neuroimaging Initiative a phantom is scanned with each subject. The ability to measure over time, sensitivity to pulse sequence selection and the ability to retrospectively correct intentionally introduced gradient mis-calibrations on volunteer scans are assessed.

2653. Cortical Thickness Analysis in Mild Cognitive Impairment and Alzheimer's Disease

Won-Jin Moon[1], Jong Min Lee[2], Eun Chul Chung[1]

[1]Kangbuk Samsung Hospital, Sungkyunkwan University School of Medicine, Seoul, Republic of Korea; [2]Hanyang University, Seoul, Republic of Korea

With recent advances in neuroimaging technology, it is now possible to study cortical thickness based on cortical surfaces *in vivo*. Cortical thickness in MRI is a direct index across the entire cerebral cortex to analyze the cortical mass.

2654. Regional Measurement of Hippocampal Atrophy in Alzheimer's Disease Using Optimized Manual ROI Segmentation and Voxel Based Morphometry

Rahyeong Juh[1, 2], Min Ying Su[1], Chang Uk Lee[2], Tae Suk Suh[2], Orhan Nalcioglu[1]

[1]University of California, Irvine, California, USA; [2]Catholic University of Korea, Seoul, Republic of Korea

Voxel based morphometry (VBM) has been increasingly applied to investigate differences in brain morphology between a group of patients and control subjects. VBM permits comparison of gray GM volume at voxel-level from the entire brain, thus is an efficient method for assessing regional differences. However, despite its high efficiency, whether VBM can accurately depict atrophy of irregularly-shaped subcortical structures, such as hippocampus, is questionable. The purpose of this study was to assess the regional GM volume loss measured by VBM in AD compared to controls, and to measure hippocampal volume using manually delineated volumetry and compare the results to VBM.

2655. Evidence for Elevated Brain Iron Concentration in Patients With

Anita Ramani[1], Kamila U. Szulc[1], Jens H. Jensen[1], Hanzhang Lu[1], Caixia Hu[1], Steven H. Ferris[1], Joseph A. Helpern[1]

[1]New York University School of Medicine, New York, New York, USA

The purpose of this study was to detect differences in brain iron concentration in patients with Alzheimer disease, subjects with mild cognitive impairment and age-matched controls using magnetic field correlation (MFC) imaging, a novel quantitative MRI method for estimating brain iron. The MFC is a sensitive measure of the regional distribution of iron in the brain, and can be measured using an asymmetric spin echo sequence. We have previously provided feasibility of this method *in vivo*. In this abstract, we have measured regional brain MFC values using parametric MFC maps and histogram analysis.

2656. Iron Deposition in the Putamen

Bharani Krishnamurthy[1], Ewart Mark Haacke[1, 2], Muhammed Ayaz[2], Sheri Harder[3], Daniel Kido[4], Wolff Kirsch[4]

[1]Wayne State University, Detroit, Michigan, USA; [2]The MRI Institute for Biomedical Research, Detroit, Michigan, USA; [3]University of Saskatchewan, Saskatoon, Saskatchewan, Canada; [4]Loma Linda University, Loma Linda, California, USA

Iron deposition in the basal ganglia is part of the normal aging process. It is also known that elevated iron content in the basal ganglia is often an indicator of disease. Goal in this paper is to understand the normal variations in iron with an elderly population so that we can differentiate normal from abnormal iron content. Current approaches for extracting iron content use either R2, R'2 or R*2. In this work, we use the high pass filtered phase images from an SWI (susceptibility weighted imaging) scan. These have been shown to correlate well with iron content in brain tissues

2657. Using SWI as a Means to Better Visualize the Caudate Nucleus in Huntington's Disease

Mark E. Haacke[1], Lakshman Gollapalli[1], Diana H. Rosas[2], Ken Kwong[2]

[1]Wayne State University, Detroit, Michigan, USA; [2]Massachusetts Institute of Technology, Boston, Massachusetts, USA

Research has demonstrated that longitudinal change in caudate nucleus (CN) volume could be observed over a period of time in subjects with Huntington's disease (HD). We use susceptibility weighted imaging (SWI) to study iron changes in the CN and correlate these changes with CN volume. SWI exploits the magnetic susceptibility differences between tissues caused by varying amounts of iron.

2658. Magnetic Resonance Diffusion and Spectroscopy Abnormalities in Different Forms of Creutzfeldt-Jakob Disease

Danielle Ibarrola[1], Marc Hermier[2], Alain Vighetto[2], Pierre Krolak-Salmon[2], Jean-Claude Froment[2], Dominique Sappey-Marinier[1, 3]

[1]IFR19, CERMEP - Imagerie du vivant, Bron, France; [2]Hôpital Neurologique, Bron, France; [3]CREATIS CNRS UMR5515 & INSERM U630 - Université Claude Bernard, Lyon, France

Variant Creutzfeldt-Jakob disease (vCJD) is a rare but important cause of dementia and death in young patients. The purpose of this study is to evaluate a new treatment based on the intra cerebro-ventricular infusion of Pentosan polysulfate (PSP) by following the patients with biological (research of protein 14-3-3 and tau protein in CSF), electrophysiological, clinical and MRI examinations. We report the preliminary MRI findings with DWI and localized short echo MRS obtained from six patients with different CJD forms (1 variant, 1 sporadic, 2 genetic and 2 iatrogen) at the first point of the protocol (before treatment).

2659. Quantitative Magnetic Resonance and Histological Analysis of Primary Motor Neuronal Loss in Amyotrophic Lateral Sclerosis

Mark David Meadowcroft[1], James R. Connor[2], Zachary Simmons[1], Don C. Bigler[1], Jian-Li Wang[1], Michael B. Smith[1], Qing X. Yang[2]

[1]Pennsylvania State University - College of Medicine, Hershey, Pennsylvania, USA; [2]Pennsylvania State University - College of Medicine, Hershey, Pennsylvania, USA

To evaluate and quantify MRI T1 and T2 image and parameter mapping differentials found in the primary motor cortex of amyotrophic lateral sclerosis (ALS) cadaver brains. Four cadaver brains of patients diagnosed with ALS were embedded and scanned with T1 and T2 quantitative parameter mapping protocols. All four cadaver brains exhibited the same lack of gray and white matter contrast within the primary motor cortex. T1 and T2 parameter mapping and region of interest analysis show significance in relaxation values. Magnetic resonance T1 and T2 parameter mapping allows for accurate quantification of contrast differentials in the motor cortex of ALS tissue. This contrast differential is significantly different from other brain regions of interest and was evaluated and verified with histological staining.

Brain: Magnetization Transfer

Room 4E Thursday 13:30 - 15:30

2660. WIMP: Self-Navigating Magnetization Transfer Pool Mapping with Stimulated Echoes

Rexford Newbould[1], Chunlei Liu[1], Stefan Ropele[2], Roland Bammer[1]

[1]Stanford University, Stanford, California, USA; [2]Medical University Graz, Graz, Austria

A new quantitative magnetization transfer (MT) scheme has been proposed which needs neither complex multi-parametric models nor wide-band MT RF pulses. This sequence is used with both un-navigated and navigated spiral acquisitions. Random phase accumulation from diffusion-like preparatory gradients, combined with the need for two separate acquisitions, sensitizes the results to even miniscule compliant patient motions, and has previously precluded the use of a multi-shot acquisition. Motion and phase correction via the variable-density navigated spiral technique allows much higher resolution multi-shot acquisitions, and greatly improves the resultant bound pool fraction (BPF) images.

2661. A Measurement of the Magnetization Exchange Between the Different Water Compartments in Optic Nerve

Hadassah Shinar[1], Uzi Eliav[1], Gil Navon[1]

[1]Tel Aviv University, Tel Aviv, Israel

^{2}H double quantum filtered (DQF) spectrum of bovine optic nerve is composed of a central transition and 3 pairs of quadrupolar split satellites with quadrupolar splittings of the order of 1400, 550 and 300 Hz. In DQF magnetization exchange experiments, where we selectively excite the broad satellites, we have detected a decay of the magnetization of these signals and a concomitant buildup of the central transition with a time constant of about 15ms. To the best of our knowledge, this is the first time that water exchange is detected between the different compartments of nerves.

2662. Describing Magnetization Transfer Parameters in White Matter Using a Four-Pool Model

Thorarin Albert Bjarnason[1], Alex L. MacKay[2]

[1]University of Calgary, Calgary, AB, Canada; [2]University of British Columbia, Vancouver, BC, Canada

In the literature, the NMR behaviour of white matter has been modeled using either two or four proton pools. In this study, the magnetization transfer (MT) two-pool model parameters were derived from the results of a recent four-pool model investigation of white matter in bovine brain. The two-pool MT parameters derived from the four-pool model were in good agreement with previously published two-pool model results. Since the two-pool model ignores the known existence of two water reservoirs in white matter, we believe that future work on modeling MT results should involve at least four pools.

2663. Correlation of Magnetization Transfer Ratio with Cognitive Impairment in HIV

Ying Wu[1], Pippa Storey[1], Andres Carrillo[2], Leon G. Epstein[3], Bruce Cohen[3], Robert R. Edelman[1], Ann Ragin[3]

[1]Evanston Northwestern Healthcare, Feinberg School of Medicine, Northwestern University, Evanston, Illinois, USA; [2]GE Medical Healthcare, Evanston, Illinois, USA; [3]Feinberg School of Medicine, Northwestern University, Chicago, Illinois, USA

Region-of-interest and global histogram magnetization transfer ratio (MTR) measurements were assessed in 11 HIV and 12 control subjects. Reduced MTR was found in HIV patients for whole brain and for all regions studied. Relationships were evaluated between the MTR measurements and attention, memory, constructional, motor, executive functions and overall dementia severity. Significant correlations between MTR and dementia severity were indicated for whole brain and nearly all white and gray matter regions. Whole brain and localized MTR measurements were also correlated with specific cognitive deficits. White matter alterations were more prominently implicated in specific cognitive deficits.

2664. Regional MRI Measures and Disability in Multiple Sclerosis

Robert Zivadinov[1], Ralph HB Benedict[1], Bhooma Srinivasaraghavan[1], Dominic Carone[1], Viritha Yella[1], Nadir Abdelrahman[1], Michael G. Dwyer[1]
[1]Buffalo Neuroimaging Analysis Center, Buffalo, New York, USA

The use of regional brain metrics (both conventional and non-conventional) may allow for increased sensitivity and specificity in explaining clinical disability in patients with MS. To investigate this possibility, we processed MRI scans from 108 MS patients using a semi-automated brain region extraction algorithm (SABRE), from which we obtained maps identifying 5 distinct regions. We then used image co-registration to examine a variety of other MRI metrics on a region-by-region basis. We found that temporal, frontal, and central regions we the best predictors of disability when examining atrophy, T2-LV, and T1-LV respectively.

2665. Intercentre Differences in Multicentre Brain MTR Histogram Studies Can Almost Be Eliminated by Using Body Coil Transmission

Paul S. Tofts[1], Stefan CA Steens[2], Mara Cercignani[1], Daniel J. Tozer[1], Wouter M. Teeuwisse[2], Matthijs JP van Osch[2], Faiza Admiraal-Behloul[2], Gareth J. Barker[3], Mark A. van Buchem[2]
[1]University College London, London, UK; [2]LUMC, Leiden, Netherlands; [3]KCL, London, UK

Six major factors must be understood and controlled in brain MTR histogram generation: 1) Transmitter coil 2) Imager stability and setup procedure 3) MT pulse shape 4) MT pulse sequence 5) Image registration and segmentation 6) Histogram generation. The major uncontrolled intercentre factor has been B1 nonuniformity. By using body-coil transmission this difference was almost eliminated in a two-centre comparison of whole-brain histograms using different manufacturers, and five different normal controls at each centre. Centre mean peak location values differed by only 1.3 percent units. Peak height values did not differ (p=0.32). Body-coil transmission is very desirable for multicentre work.

2666. Fast Magnetization Transfer Imaging, a Comparative Study

Wouter Teeuwisse[1], Matthias van Osch[1], Hans Olofsen[1], Bart Emmer[1], Jeroen van der Grond[1]
[1]Leiden University Medical Center, Leiden, Netherlands

Magnetic transfer imaging (MTI) usually requires long acquisition times. We applied six fast MTI scans with parallel imaging and segmented EPI in nine healthy volunteers. Magnetic transfer ratio (MTR) histogram peak height, peak location and histogram mean value were evaluated. A one-way ANOVA followed by Bonferroni post hoc tests showed no significant differences in histogram peak height, peak location or mean MTR between conventional MTI and fast MTI scans. Moreover, no changes in standard deviation were observed. Our findings show that fast MTI can be applied in a routine clinical setting with acquisition times less than one minute.

2667. Diffusion Tensor and Magnetization Transfer Imaging of the Brain at 3T in Patients with Cirrhosis

Vijay Paul Bob Grover[1], Serena J. Counsell[1], Nayna Patel[1], Joanna M. Allsop[1], Elizabeth J. Bradford[2], Brian K. Saxby[2], Joseph V. Hajnal[1], Simon David Taylor-Robinson[1]
[1]Hammersmith Hospital, Imperial College London, London, UK; [2]Cognitive Drug Research, Goring-on-Thames, UK

Controversy remains regarding the pathogenesis, diagnosis, treatment and monitoring of hepatic encephalopathy; a common complication of cirrhosis. We investigated the cerebral microstructure with diffusion tensor imaging and magnetization transfer imaging of a cohort of patients with cirrhosis. All female patients had minimal hepatic encephalopathy. The magnetization transfer ratio was significantly lower in the frontal white matter. Apparent diffusion coefficients were significantly higher in the anterior corona radiata and genu, body and splenium of the corpus callosum of these female patients. These findings may be compatible with either an increase in brain water or microstructural damage to the white matter tracts.

2668. Longitudinal MTR Changes in Mild to Severe Alzheimer's Disease

Stefan Ropele[1], Faton Gorani[1], Christian Enzinger[1], Birgit Pendl[1], Alexandra Seewann[1], Reinhold Schmidt[1], Franz Fazekas[1]
[1]Medical University Graz, Graz, Austria

Recent magnetization transfer ratio (MTR) studies in Alzheimer's disease suggest that the MTR is sensitive to pathology related tissue damage. We now have performed a longitudinal MTR study in 28 Alzheimer patients to investigate the evolution of whole brain MTR parameters and deep grey matter MTR and their association with cognition. While deep grey matter did not shown any significant changes, all whole brain histogram parameters documented disease progression even on a time scale of 6 months. No significant correlations between specific cognitive tests and histogram parameters were found. However, the MTR metrics at baseline were predictive of subsequent changes in cognitive performance.

2669. Magnetization Transfer Imaging in Distinguishing Early and Adult Onset Schizophrenia in Drug-Naive First-Episode Patients

Xiaoqi Huang[1], Yuqing Wang[2], Su Lui[1], Wei Deng[1], Luo Ouyang[2], Hehan Tang[1], Tao Li[1], Bin Song[1], Xiangping Zhou[1], Sumner Maclean[3], Vanessa Sluming[4], Qiyong Gong[1]

[1]West China Hospital of Sichuan University, Chengdu, Sichuan, People's Republic of China; [2]University of Electronic Science and Technology of China, Chengdu, Sichuan, People's Republic of China; [3]Universitatsklinikum, Goettingen, Germany; [4]University of Liverpool, Liverpool, UK

Early-onset schizophrenia (EOS) is thought to be a unique subtype of schizophrenia compared with its adult-onset schizophrenia (AOS) counterpart. We applied whole brain voxel-wised analysis of magnetization transfer ratio (MTR) to explore the difference of the cerebral tissue in first-episode drug-naive patients with EOS versus AOS. The result showed that there were significant differences of MTR in cerebral regions of EOS which distinguished itself from AOS in MT imaging.

2670. Correlative Analysis of Anisotropy Diffusion Coefficient and Magnetization Transfer Ratio with Serum Antibody Brain Binding and Antiphospholipid Antibodies in Multiple Sclerosis

Mehdi Adineh[1, 2], Michael Kent[1, 2], Ninad Mantri[1], Navin Kausthubh[1], Cemil Kirbas[1], Sehul Shah[1], Kenneth Pugar[1]

[1]The Wallace Kettering Neuroscience Institute, Kettering, Ohio, USA; [2]Wright State University, Dayton, Ohio, USA

We investigated relationships between DTI, MTR, brain-binding serum IgM, and serum antiphospholipid antibody levels in MS and control subjects and to determine if correlations between these parameters exist, and of what significance they may be. Significant correlations between ADC and MTR values were present in subjects without concomitant brain-binding serum antibodies and absent in subjects with concomitant brain-binding serum antibodies. The correlation was dependant on the presence of serum IgM antibodies capable of binding brain tissue. Multiparametric MTR, DTI, immune biomarker studies may be useful tools in differentiating and characterizing disease subtypes, and require further investigation.

Stroke

Room 4E Thursday 13:30 - 15:30

2671. Moyamoya Disease: Visualization of Dilated Medullary Vessels by Flow-Compensated Gadolinium-Enhanced MRI

Eri Kitamura[1, 2], Mitsunori Kanagaki[2], Yukio Miki[2], Akira Yamamoto[2], Yasutaka Fushimi[2], Tsutomu Okada[2], Nobuyuki Mori[2], Ken-ichiro Kikuta[2], Susumu Miyamoto[2], Nobuo Hashimoto[2], Kazuro Sugimura[1], Kaori Togashi[2]

[1]Kobe University Graduate School of Medicine, Kobe, Japan; [2]Kyoto University Graduate School of Medicine, Kyoto, Japan

To our knowledge, dilated medullary vessels in moyamoya disease have not been investigated in detail nor completely understood. Flow-compensation is a way to rephrase the MR signal of moving spins and is useful to visualize small vessels on gadolinium-enhanced MR images. In this study, we investigated frequency of visualization of dilated medullary vessels in moyamoya disease and the effect of flow-compensation technique on the visualization of dilated vessels. The results suggest that dilated medullary vessels are frequently observed on gadolinium-enhanced MRI, which are better visualized with use of flow-compensation technique.

2672. The Feasibility of a Spin-Echo EPI Based Perfusion MRI in Moyamoya Disease on a 3.0T MR System

In-Chan Song[1], Jung-Eun Cheon[1], In-One Kim[1], Kee-Hyun Chang[1], Dong-Gyu Na[1]

[1]Seoul National University Hospital, Seoul, Republic of Korea

We evaluated the feasibility of a spin echo (SE) EPI technique for MR perfusion imaging of moyamoya disease (MMD) on 3.0T MR system. Most MR perfusion techniques used a gradient echo EPI sequence due to a high sensitivity and broader coverage. A SE EPI, however, known to be sensitive to capillary vessels, but less to susceptibility, would be more useful in MMD with collaterals. Our preliminary results suggest a SE EPI sequence on 3.0 T MR provide high SNRs enough for the good quality perfusion map images and the hemodynamic information on MMD in accordance with the results of angiography.

2673. Cerebral Blood Flow Velocity and White Matter Changes in Type 2 Diabetes Mellitus

David Last[1], David C. Alsop[1], Amir M. Abduljalil[2], Kun Hu[1], Jerry Cavallerano[3], Lukas Lepicovsky[1], Christopher Robles[1], Lewis A. Lipsitz[1, 4], Vera Novak[1]

[1]Beth Israel Deaconess Medical Center, Harvard Medical School, Boston, Massachusetts, USA; [2]College of Medicine and Public Health, Ohio State University, Columbus, Ohio, USA; [3]Joslin Diabetes Center, Boston, Massachusetts, USA; [4]Hebrew Seniorlife Center, Boston, Massachusetts, USA

Diabetes mellitus (DM) increases the risk for cerebrovascular disease, through the effects on cerebral microvasculature and blood flow regulation. This study addresses the effects of type 2 DM on cerebrovascular responses to CO_2 challenges and the relationship between white matter changes (WMC) on MRI and cerebral blood flow velocity (BFV) using transcranial Doppler ultrasound in elderly people. BFV was reduced with type 2 DM. Low BFVs were significantly associated with WMC. These investigations may disclose early indicators of cerebrovascular disease.

2674. Cerebral Developmental Venous Anomalies Associated with Loco-Regional Parenchymal Abnormalities

Francesca B. Pizzini[1], Diego San Millán Ruíz[2], Enrico Piovan[1], Alberto Beltramello[1], Daniel Rüfenacht[3]
[1]University Hospital Verona, Verona, Italy, Italy; [2]Geneva University Hospital, Geneva, Switzerland, Switzerland; [3]Geneva University Hospital, Geneve, Switzerland, Switzerland

We report 102 cerebral developmental venous anomalies (DVA) with a high proportion of parenchymal abnormalities found within the drainage territory of the DVA (focal cortical or subcortical atrophy or signal anomalies on MRI). These parenchymal abnormalities are found within the drainage territory of a DVA (30%) which suggests a pathogenic correlation to the DVA . We postulate a possible physiopathological mechanisms to explain that: DVA represents a zone of venous confluence, and may demonstrate thickened walls on histological examination. The combination of these two factors combined could predispose a DVA to develop venous hypertension and subsequent loco-regional parenchymal alterations.

2675. *In Vivo* Human Middle Cerebral Artery Wall Imaging Using High Resolution Magnetic Resonance Imaging

Isabelle Klein[1], Philippa Lavallée[1], Pierre-Jean Touboul[1], Elisabeth Schouman-Claeys[1], Pierre Amarenco[1]
[1]Medical Hospital and University of Bichat, Paris, France

Patients with symptomatic middle cerebral artery (MCA) stenosis are at high risk of recurrent stroke. Only indirect imaging of intracranial atherosclerosis is currently available. Black blood and multicontrast images using high spatial resolution were acquired at the level of MCA stenosis and of normal MCA segments, as documented by angiographic indirect methods. Data imaging and analysis showed a significant, focal, arterial wall thickening underlying each MCA stenosis. The mean wall (plaque) area was 6.99 mm2 (range 4.42 mm2 to 12.06 mm2). HR-MRI provides a non-invasive method to study, *in vivo*, the burden and pathogenesis of intracranial atherosclerosis.

2676. The Relationship Between the Carotid Atherosclerotic Plaque and Cerebral Perfusion-Weighted Imaging: Preliminary Results

Xin Lou[1], Ning Yu An[1], Jian Min Cai[1], Lin Ma[1], Xue Mei Li[1], Wei Sun[2]
[1]PLA General Hospital, Beijing, People's Republic of China; [2]GE Healthcare, Beijing, People's Republic of China

Atherosclerotic disease of the carotid artery is responsible for 20%~30% of all strokes, infarcts or hypoperfusion can occur in the arteries territories as well as cortical or/and internal watershed (WS). Two distinct hypotheses, namely low-flow and micro-embolism, are equally supported by neuropathological studies and remain controversial. We compared the cerebral perfusion-weighted imaging (PWI) of stable with unstable carotid atherosclerotic plaque groups in determining the association of plaque type with hemodynamic change of 30 patients with unilateral severe ICA stenosis. The mean transit time (MTT) ratios of the cortical WS were prolonged significantly in unstable group compared to the stable group. Our preliminary results reveal that the cortical WS infarction maybe due to the microemboli arising from unstable carotid plaque.

2677. The Composition of Acute MCA Thrombus is Heterogeneous: A Comparison of MR Susceptibility Image and CTA

Mingwang Zhu[1], Masahiko Hiroki[1], Hakan Ay[1], Aneesh B. Singhal[1], Nina M. Menezes[1], Chloe Joan Lopez[1], Christopher Melinosky[1], A Gregory Sorensen[1]
[1]Massachusetts General Hospital, Charlestown, Massachusetts, USA

MCA susceptibility sign demonstrates paramagnetic deoxyhemoglobin in red thrombus in acute stroke. A segment of filling defect on CTA reveals the site and size of MCA occlusion. In this study, a complex thrombus containing diamagnetic material was diagnosed if CTA occlusion is >20% larger than susceptibility sign, others were considered as a red thrombus. In 31 CTA identified MCA occlusions, red thrombi were found in 61% while 39% had complex thrombi. Susceptibility sign may underestimate the MCA occlusion. The composition of acute MCA thrombus is heterogeneous in term of magnetization property.

2678. 3 T Vs 1.5 T MR Diffusion and Perfusion Imaging in Hyper-Acute Ischemic Stroke

Robert Karl Kosior[1, 2], Michael D. Hill[1, 3], Jayme Cameron Kosior[1, 2], Richard Frayne[1, 2]
[1]University of Calgary, Calgary, Alberta, Canada; [2]Foothills Medical Centre, Calgary Health Region, Calgary, Alberta, Canada; [3]Foothills Medical Centre, Calgary, Alberta, Canada

This study compares diffusion and perfusion images of patients with hyper-acute ischemic stroke from both 1.5T and 3T MR scanning systems. The images were registered for direct side-by-side comparison and pairing of quantitative measures. Qualitatively, the 3T images exhibited higher SNR and had better resolution. Though not statistically significant, ADC contrast appeared to be greater at 3T, with scan order also having an effect. Overall, the results show that the 3T scanner produces diffusion and perfusion images that are at least as good or better than 1.5T for hyper-acute stroke assessment.

2679. Artifact Simulating Subarachnoid and Intraventricular Hemorrhage on Single Shot Fast Spin Echo Flair Images: A Trap for the Unwary

Alessandro Cianfoni[1], Maria GM Martin[1], Jiang Du[1], John R. Hesselink[1], Steven G. Imbesi[1], William G. Bradley[1], Graeme M. Bydder[1]

[1]University of California, San Diego, San Diego, California, USA

Single-shot-fast-spin-echo fluid attenuated inversion recovery (SS-FSE-FLAIR) images frequently show high signal artifacts in regions not associated with high CSF flow when confused patients are examined. Experiments on volunteers showed that these were due to head motion between the initial inversion pulse and the subsequent 900 pulse. Similar patterns were seen in patients. The artifacts represent a trap since single-shot sequences are frequently used in uncooperative patients who are at risk of intracranial hemorrhage and they simulate this condition on otherwise non-artifacted images. They could be controlled by increasing the width of the initial inversion pulse or using a non-selective pulse.

2680. A New Approach Using the Distribution of Transit Times (DTT) to Determine Improved Absolute CBF Values in Patients with Ischemic Stroke

Marina Salluzzi[1], Richard Frayne[2, 3], Michael R. Smith[1, 3]

[1]Electrical and Computer Engineering, University of Calgary, Calgary, Alberta, Canada; [2]Seaman Family MR Research Centre, Foothills Medical Centre, Calgary, Alberta, Canada; [3]Radiology, University of Calgary, Calgary, Alberta, Canada

A positive patient outcome after ischemic stroke depends on an accurate diagnosis. Absolute cerebral blood flow (CBF) values are often obtained using a scaling factor determined via MR-PET cross-calibration. We propose a new approach using the distribution of transit times (DTT) to estimate CBF values. Simulation studies indicate that is it more appropriate to use a single cross-calibration factor with DTT-based CBF estimates than with CBF values from conventional deconvolution algorithms. The DTT-based approaches lead, therefore, to better (less systematically biased) characterization of the perfusion level in brain tissue.

2681. Pediatric and Adult Global Hypoxic-Ischemic Injury Evaluated by Diffusion-Weighted Imaging and MR Spectroscopy

Karen Angela Tong[1], Anna Dengel[1], Carrie Carr[1], Udo Oyoyo[1], Stephen Ashwal[1], Sarah Uffindell[1], Barbara Ann Holshouser[1]

[1]Loma Linda University Medical Center, Loma Linda, California, USA

Global hypoxic-ischemic injury is a devastating process that results in severe neurological impairment, if not death. There are many etiologies including near-drowning, cardiovascular collapse, respiratory arrest, strangulation, suffocation, and carbon monoxide poisoning. All age groups can be affected, from young children to the elderly. We evaluated non-neonatal patients who suffered hypoxic injury. Apparent diffusion coefficient (ADC) values of specific brain regions were analyzed and compared to MR spectroscopy data and patient outcomes. Significant differences were observed between ADC values of patients and control subjects. The greatest degree of diffusion restriction and lactate levels occurred in patients that died.

2682. Altered BOLD Hemodynamic Response in Patients with Ischemic Stroke

Kaundinya Gopinath[1], Anna Moore[2], Kyung Peck[3], Bruce Crosson[4, 5], Richard Briggs[1]

[1]UT Southwestern, Dallas, Texas, USA; [2]Emory University, Atlanta, Georgia, USA; [3]Memorial Sloan Kettering Cancer Center, New York, New York, USA; [4]University of Florida, Gainesville, Florida, USA; [5]VA Medical Center, Gainesville, Florida, USA

Ischemic stroke is associated with impairment of cerebral hemodynamics, which leads to alterations in cerebral blood flow, blood volume, oxygen metabolism and vasoreactivity, all quantities that influence the BOLD hemodynamic response (HDR). In this study, differences between the HDRs in the infarcted and the intact hemisphere auditory cortex of patients with ischemic stroke were examined, and characteristics of the HDR of normal controls and stroke patients were compared. Stroke hemisphere auditory cortex exhibited significantly wider HDRs and similar amplitude and times-to-peak compared to the intact hemisphere. Normal controls exhibited no inter-hemispheric differences in BOLD HDR.

2683. Visualization of Collateral Supply by Two-Coil Continuous Arterial Spin Labeling

Harald E. Möller[1, 2], Toralf Mildner[1], Christoph Preul[1], Claus Zimmer[3]

[1]Max Planck Institute for Human Cognitive and Brain Sciences, Leipzig, Germany; [2]University Hospital Münster, Münster, Germany; [3]University Hospital Leipzig, Leipzig, Germany

Two patients were investigated by continuous arterial spin labeling with separate coils for labeling and imaging to evaluate the potential for perfusion territory mapping. Labeling was restricted to either the left- or right-sided carotid. No differences between both hemispheres were observed in patient 1 with asymptomatic carotid stenosis. Similarly, signal changes were predominantly observed in the labeled hemisphere in patient 2, who subsequently underwent embolization coil occlusion of the left internal carotid artery. After the intervention, perfusion contrast was created symmetrically in both hemispheres upon labeling the right side, verifying sufficient collateral supply in agreement with balloon occlusion testing.

Methods in Arterial Spin Labeling

Room 4E Thursday 13:30 - 15:30

2684. Toward Quantitative Whole Brain Pulsed Arterial Spin Labeling: Estimation of Transit Time with Cardiac Gating at 3T

Wen-Ming Luh[1], Jerzy Bodurka[1], Peter A. Bandettini[1]
[1]National Institutes of Health, Bethesda, Maryland, USA

To perform pulsed arterial spin labeling experiments of the whole brain, consideration for the tagging and timing is different from prior knowledge when tagging in the brain consist of smaller size of vessels. Due to pulsatility and fast blood velocity in the carotids and vertebrobasilar arteries, cardiac gating is required when tagging below the brain and the QUIPSS-based saturation is no longer effective. In the study, these effects are demonstrated and the transit time from tagging below the brain is estimated with pulsed ASL on a voxel-wise basis.

2685. Dynamic Relationship Between Arterial Transit Time and Perfusion and Its Implications for Fast ASL Quantification

Gregory R. Lee[1], Luis Hernandez-Garcia[1], Vikas Gulani[1], Douglas Noll[1]
[1]University of Michigan, Ann Arbor, Michigan, USA

Previous work in quantifying the perfusion changes during functional experiments using turbo-CASL has assumed a linear relationship between percentage perfusion increase and percentage transit time decrease. The validity of this assumption was explored by measuring CBF and transit time for four different conditions: rest, two levels of motor activation, and rest while breathing 100% oxygen. The relationship of percentage transit time change to percentage flow change was observed to be highly linear (r2>0.9) over the range of perfusions studied. The slope of the relationship was found to be between –0.11 and –0.15 for the subjects scanned.

2686. Mapping of Arterial Transit Time Using Dual-Coil CASL with Sinusoidally Modulated Labeling Function

Toralf Mildner[1], Karsten Müller[1], Stefan Hetzer[1], Robert Trampel[2], Wolfgang Driesel[1], Harald E. Möller[1, 3]
[1]Max Planck Institute for Human Cognitive and Brain Sciences, Leipzig, Saxony, Germany; [2]NYU School of Medicine, New York, New York, USA; [3]University Hospital Münster, Münster, NRW, Germany

A new method for arterial transit time mapping in the human brain using dual-coil CASL is demonstrated. Perfusion contrast is created using a circular double-loop coil (6-cm diameter each loop), which was placed over both common carotid arteries. The method is characterized by short TR's in the range of 500 - 750 ms and a frequency-swept continuous labeling RF for the creation of a quasi-sinusoidally modulated labeling function at the neck. The evaluation of the experiments was performed using spectral methods which provide a measure of coherence and phase shift at this frequency. This information is used to compute maps of the arterial transit time. Robust maps of the arterial transit time with arbitrary slice orientation were obtained in about 4 minutes.

2687. Estimation of Blood Magnetization for Quantification of Arterial Spin Labeling Signal

Kim Cornelia Carolina van de Ven[1, 2], Esben Thade Petersen[1, 3], Xavier Golay[1, 4]
[1]National Neuroscience Institute, Singapore, Singapore; [2]Eindhoven University of Technology, Eindhoven, Netherlands; [3]Nanyang Technological University, Singapore, Singapore; [4]A*star, Singapore, Singapore

A new method is proposed to get an estimate of the average blood magnetization in a user-independent way, using the QUASAR–ASL sequence. T1t and M0t are calculated from measured signals with a Look-Locker based method. Monte Carlo simulations are provided in order to test the robustness of the method. The results of the Monte Carlo simulations show that it is possible to get back to T1t and M0t and measurements on volunteers also give reliable results for the T1t values in the brain. This method is believed to be better compared to the traditional ROI based methods.

2688. Combined Blood:Brain Partition Coefficient and Perfusion Assessment Using QUASAR

Esben Thade Petersen[1], Kim Cornelia Carolina van de Ven[1, 2], Ivan Zimine[1], Xavier Golay, [13]
[1]National Neuroscience Institute, Singapore, Singapore; [2]Eindhoven University of Technology, Eindhoven, Netherlands; [3]ASTAR, Singapore, Singapore

In this study, we used the QUASAR ASL sequence for simultaneous estimation of the blood-brain partition coefficient λ, blood equilibrium magnetization M_{0b} and CBF. For absolute quantification of CBF, a correct estimate of the blood equilibrium magnetization M_{0b} is essential, because it acts as a direct scaling factor on the perfusion. The Look-Locker readout of the QUASAR sequence is preceded by a saturation pulse. This allows fitting of T_1 and M_{0t} and consequently provides an estimate of λ. The method was applied to acquired data and showed better GM/WM CBF ratios. The complete user independence assures reproducible CBF estimates.

2689. The Effect of Fat Saturation on Arterial Spin Labeling

Yufen Chen[1], Todd B. Parrish[1]
[1]Northwestern University, Chicago, Illinois, USA

Multi-channel receive-only coils can improve signal-to-noise ratio (SNR) for arterial spin labeling (ASL) studies because the inversion is no longer limited by the extent of the coil. However, we have observed a global decrease in SNR when pulsed-ASL images were acquired with fat saturation using a receive-only coil. This study demonstrates that both static and temporal SNR of non-fat-saturated PASL images are over 50% higher than those of fat-saturated images. We also present water-excitation as an alternative to fat-saturation.

2690. Sub-Minute Arterial Spin Labelling at 3.0T

Elizabeth A. Moore[1], Frank G. C. Hoogenraad[2], Xavier Golay[3, 4], Ebsen Thade Petersen[3], Maarten Versluis[2], J M. den Harder[2], Ad Moerland[2]
[1]Philips Medical Systems UK, Reigate, UK; [2]Philips Medical Systems, Best, Netherlands; [3]National Neuroscience Institute, Singapore, Singapore; [4]Singapore Bioimaging Consortium, Singapore, Singapore

Arterial spin labelling is generally a low-SNR and time-consuming technique, making it difficult to apply in a clinical setting. Recently a new technique, PULSAR, has been proposed for 3.0T. PULSAR has an efficient pre-saturation technique and EPI-STAR labelling scheme, which are relatively insensitive to B_1 inhomogeneity. High SNR quantitative images can be obtained realitively quickly. The increased SNR can be traded for reduced scan time, to allow qualitative perfusion images to be acquired in less than one minute. The sequence is a promising alternative to Gd-bolus techniques for the clinical evaluation of conditions such as stroke and dementia.

2691. In-Vivo Measurement of Arterial Cerebral Blood Volume Using LL-EPI-FAIR and LL-EPI-STAR

Matthew Jon Brookes[1], Peter G. Morris[1], Penny A. Gowland[1], Susan T. Francis[1]
[1]University of Nottingham, Nottingham, UK

The *in vivo* measurement of arterial cerebral blood volume (aCBV) can provideimportant information about brain physiology. Recently, we have shown thatLook-Locher-Echo Planar Imaging (LL-EPI) can be combined with Flow sensitiveAlternating Inversion Recovery (FAIR) in order to quantify accurately andnon-invasively resting state aCBV. Here, we extend our previous measurementsby comparison of LL-EPI-FAIR with LL-EPI-STAR (Signal Targeting byAlternating Radiofrequency flow encoding with LL-EPI sampling). We show thatthe two sequences yield equivalent measures of resting stateaCBV, and further that the LL_EPI_STAR sequence provides additional flowdirectional information.

2692. Activation Induced Changes in Arterial Cerebral Blood Volume (ACBV) Measured Using LL-EPI-STAR

Matthew Jon Brookes[1], Peter G. Morris[1], Penny A. Gowland[1], Susan T. Francis[1]
[1]University of Nottingham, Nottingham, UK

The *in vivo* measurement of activation-induced change in arterial cerebralblood volume (aCBV) provides important information to understand themechanisms of the BOLD response. Here, we introduce a non-invasive ASLtechnique based on the combination of STAR and LL-EPI sampling to quantify aCBV changes. Results show spatial patterns of both aCBV, and BOLD changes. The technique allows characterization of arterial inflow curves withhigh temporal resolution, representing a major advantage over more traditional ASL methods when used to measure aCBV. Our results show that a significant increasein aCBV is observed on brain activation during a simple motor task.

2693. Reducing Contamination in PASL Using BASSI RF Pulses

Jan M. Warnking[1], G. Bruce Pike[1]
[1]Montreal Neurological Institute, McGill University, Montreal, Québec, Canada

BASSI pulses were parameterized to obtain low RF energy PASL label pulses with minimal contamination of static spins outside the label region as well as highly selective PICORE/QUIPSS II saturation pulses allowing for small label gaps. Contamination effects in a QUIPSS II PASL implementation based on these optimized BASSI pulses are assessed in an *in vivo* study. Residual contamination in the QUIPSS II/BASSI sequence is shown to be reduced by a factor of three, compared to a conventional PASL implementation.

2694. Pseudo Random Amplitude Modulation: A High Efficiency Method to Measure Flow and Perfusion

Truman R. Brown[1], Nina C. Shapley[1], Haiying Tang[2]
[1]Columbia University, New York, New York, USA; [2]Merck Research Laboratories, Rahway, New Jersey, USA

By modulating the inflowing spins with a pseudo random sequence we demonstrate that the entire transit time distribution can be measured in a single unified acquisition.

2695. Sensitivity and Detectability of Regional Differences in CASL Perfusion Between Subject Groups

Ruth L. O'Gorman[1, 2], Steven C. Williams[2], David C. Alsop[3], Fernando O. Zelaya[2]
[1]King's College Hospital, London, UK; [2]Institute of Psychiatry, London, UK; [3]Beth Israel Deaconess Medical Center, Boston, Massachusetts, USA

Despite a growing number of investigations of cerebral perfusion in various subject groups using ASL, the sensitivity and detectability of differences in absolute perfusion between groups have not been systematically assessed. In this study, the detectability of regional differences in ASL perfusion was investigated by implanting computer-generated perfusion increases into resting-state CASL perfusion images for one of two age-matched groups of healthy volunteers. The limits of detection for the implanted perfusion changes varied widely across brain regions, from 10 ml/min/100ml for clusters in the putamen to 30 ml/min/100ml for clusters in frontal white matter.

2696. Quantitative Cerebral Vascular Response Maps: Determination with Pulsed Arterial Spin Labelling

Ulrike Noeth[1, 2], Futoshi Kotajima[3], Ralf Deichmann[2], Robert Turner[2], Douglas R. Corfield[3, 4]
[1]GSF Forschungszentrum fuer Umwelt und Gesundheit, Neuherberg, Germany; [2]Institute of Neurology, UCL, London, UK; [3]National Heart & Lung Institute, Imperial College, London, UK; [4]Keele University, Keele, UK

Hypoxia is a pathological factor associated with respiratory diseases (e.g. sleep apnea). As the brain is particularly vulnerable to effects of hypoxia, the aim of this study was to acquire quantitative perfusion maps of grey matter under isocapnic and hypoxic conditions from which cerebral vascular response (CVR) maps can be calculated. These CVR maps show the local variability of the cerebral vascular response to hypoxia and might help to identify areas which are most prone to damage under hypoxic insults.

2697. AV Shunt Visualization with Arterial Spin Labeled Perfusion MR Imaging

Ronald L. Wolf[1], Jiongjiong Wang[1], John A. Detre[1], Eric L. Zager[1], Robert W. Hurst[1]
[1]University of Pennsylvania Medical Center, Philadelphia, Pennsylvania, USA

Noninvasive imaging methods remain suboptimal for evaluating arteriovenous malformations (AVMs). Our purpose was to investigate the utility of arterial spin labeled (ASL) perfusion imaging for visualizing and possibly quantitating AV shunting in the presence of AVM. Five subjects with AVM were studied with continuous ASL perfusion MRI and reviewed for presence or absence of AV shunt. A semiquantitative estimate of shunt extent was generated using a threshold strategy. We found that ASL perfusion MR techniques could demonstrate AV shunting, providing a potential complementary method for AVM evaluation by detecting the presence and perhaps also quantifying extent of AV shunting.

2698. Regional Effects of Type 2 Diabetes Mellitus on Cerebral Blood Flow and Brain Anatomy Using MRI and Continuous Arterial Spin Labeling MRI at 3 Tesla

David Last[1], David C. Alsop[1], Amir M. Abduljalil[2], Robert P. Marquis[1], Christopher Robles[1], Vera Novak[1]
[1]Beth Israel Deaconess Medical Center, Harvard Medical School, Boston, Massachusetts, USA; [2]College of Medicine and Public Health, Ohio State University, Columbus, Ohio, USA

The regional effects of diabetes (DM) on cerebral vasoregulation and on brain anatomy were studied on 26 controls and 26 subjects with DM. IR-FGE and FLAIR images were acquired to assess the volumes of CSF, gray and white matter and white matter changes (WMC). Using Continuous Arterial Spin Labeling, perfusion maps were acquired over four 5-minute breathing exercises: baseline, CO_2 rebreathing, hyperventilation and a second baseline. Eight regions were defined on each image allowing the computation of the spatial distribution of all parameters. Cerebrovascular reserve was reduced in DM compared to healthy subjects. Brain atrophy affected more DM patients. No difference was observed for WMC. These data suggest that atrophy might affect reserve. The effects of WMC on reserve remain unclear.

2699. Assessment of Hypertension on Cerebral Blood Flow and Dementia Using CASL MRI

Weiying Dai[1], Owen T. Carmichael, [1,2], Oscar L. Lopez[1], James T. Becker[1], Lewis H. Kuller[1], H. Michael Gach, [13]
[1]University of Pittsburgh, Pittsburgh, Pennsylvania, USA; [2]Carnegie Mellon University, Pittsburgh, Pennsylvania, USA; [3]Nevada Cancer Institute, Las Vegas, Nevada, USA

Earlier studies indicated that hypertension (HTN) may be a risk factor for dementia. Regional cerebral blood flow (rCBF) was measured in 20 normal controls, 19 mild cognitive impaired, and 22 early Alzheimer's disease subjects using continuous arterial spin labeled perfusion MRI. Normal subjects with HTN had decreased rCBF in the putamen, globus pallidus and head of the caudate nucleus, left hippocampus and anterior cingulate gurus, with extension to the subcallosal area. Cognitively impaired subjects had decreased rCBF in the putamen and posterior thalamic regions. The effect of HTN on rCBF appears to decrease after the onset of the cognitive decline.

2700. Close Correlation of ASL MRI and Ultrasound Derived Intracranial Blood Flow Velocities

Martin Griebe[1], Kristina Szabo[1], Matthias Günther[1], Rolf Rüdiger Kern[1], Fabrizio Sallustio[1], Michael G. Hennerici[1], Achim Gass[1, 2]

[1]Universitätsklinikum Mannheim, Mannheim, Germany; [2]Universitätsspital Basel, Basel, Switzerland

We compared Arterial Spin Labelling (ASL) based dynamic angiography information blood flow velocity measurements in normal controls and patients with internal carotid artery (ICA) stenoses to transcranial Doppler (TCD). 18 middle cerebral arteries (MCAs) of 9 normal controls and 6 MCAs of 3 patients with unilateral ACI stenosis were examined. For the DynAngio sequence, 36 phases of inflow with a temporal resolution of 36ms and an in-plane resolution of 0.52mm were acquired on a clinical 1.5T scanner. Blood flow velocity was calculated from the covered distance of the vessel signal and the difference of the inflow time between the phases. These were compared to the mean blood flow velocities as detected by TCD. In all subjects, the DynAngio technique showed the inflow of the labelled blood bolus with good quality. TCD measures and DynAngio calculated MCA velocities correlated closely for both controls and ICA patients ($r=0.89$, $p<0.0001$). The DynAngio technique is useful in assessing MCA haemodynamics, providing additional functional information like blood flow velocity.

DWI/DTI : Clinical Applications

Room 4E Thursday 13:30 - 15:30

2701. Functional Connectivity Correlations in the Cortical-Thalamic Network of Patients with Schizophrenia Using fMRI and DTI

David Matthew Carpenter[1], Gustavo Pantol[1], Joeseph I. Friedman[1], Cheuk Y. Tang[1]

[1]Mount Sinai School of Medicine, New York, New York, USA

Hypotheses of functional disconnectivity (lack of communication) between different brain regions attempt to explain several psychiatric disorders. In the case of schizophrenia, it has been proposed that the cortical-thalamic pathways are disrupted. This disconnect can be due to a damage to the connecting pathways (white matter tracts) or due to an imbalance of neurochemistry. In the past these two mechanisms of disconnected communication have been investigated 'indirectly' using synchronous analysis of functional brain imaging data (e.g. PET & fMRI) or directly by looking at the integrity of white matter tracts using Diffusion Tensor Imaging (DTI) [1,2]. Here we sought to investigate the nature of this disconnect by simultaneously looking at the relationship between two schizophrenia abnormalities: 1) the synchronous activation signal in two functionally connected areas in the brain; with 2) the integrity of the interconnecting white matter fibers.

2702. Quantitative Analyses of Dentate Nuclei and Cerebellar Peduncles Based on DTI in Langerhans Cell Histiocytosis

Weihong Zhang[1, 2], Jiangyang Zhang[1, 2], Hao Huang[1, 2], Peter C.M. van Zijl[1, 2], Robert J. Arceci[1], Susumu Mori[1, 2]

[1]Johns Hopkins University, School of Medicine, Baltimore, Maryland, USA; [2]Kennedy Krieger Institute, Baltimore, Maryland, USA

Langerhans cell histiocytosis (LCH) is a rare disorder characterized by the clonal proliferation of immature Langerhans cells. Imaging of this disorder is inadequate in predicting progression of neurologic deterioration. We applied DTI to 4 patients with LCH and compared the white matter anatomy with 6 age-matched controls. Substantial volume loss was found in the dentate nuclei (DN) and the superior cerebellar peduncle (SCP) in all patients. The DN was difficult to define on conventional MRI, but clearly delineated on average DWI and color-coded orientation maps. The DN volume measurement by DTI may provide a useful tool for patients with LCH.

2703. A Preliminary Result of Principal Diffusion Direction Comparison in Attention-Deficit/Hyperactivity Disorder

Tzu-Cheng Chao[1], Hsiao-Wen Chung[1], Pin-Chen Yang[2], Ming-Ting Wu[3, 4]

[1]National Taiwan University, Taipei, Taiwan; [2]Kaohsiung Medical University, Kaohsiung, Taiwan; [3]Kaohsiung Veterans General Hospital, Kaohsiung, Taiwan; [4]National Yang Ming University, Taipei, Taiwan

Diffusion tensor imaging (DTI) is a sensitive imaging technique to investigate white matter integrity and orientation. In this work, we performed group comparisons of principal direction of the white matter, derived from DTI, on subjects with and without attention-deficit/ hyperactivity disorder (ADHD). The preliminary results showed three regions in the frontal lobe and the striatal area with significant fiber orientational difference with p value less than 0.001. The findings of this work may provide insights in the relationship between white matter fiber orientation and cognition and behavior in humans.

2704. A Diffusion-Tensor MRI Study of Brain and Cervical Cord in Benign Multiple Sclerosis Patients

Beatrice Benedetti[1], Paola Valsasina[1], Elda Judica[1], Vittorio Martinelli[1], Angelo Ghezzi[2], Annalisa Pulizzi[1], Giancarlo Comi[1], Massimo Filippi[1]

[1]Hospital San Raffaele, Milan, Italy, Italy; [2]Ospedale di Gallarate, Gallarate, Italy, Italy

In this study, we performed histogram analysis of brain and spinal cord MD and FA from 40 benign MS (BMS) patients, to achieve a better definition of the nature of disability in MS and to define the nature of tissue damage in benign versus secondary-progressive (SP) MS.We found significant differences in the extent of brain GM damage between BMS and SPMS, whereas brain WM and cervical cord metrics do not differ between these two groups. This suggests that cortical functional reorganization may limit the consequences of tissue injury in BMS, possibly related to the sparing of the GM compartment.

2705. Diffusion Weighted Imaging Study of Patients with Essential Tremor

R Lodi[1], G Rizzo[1], D Manners[1], C Tonon[1], C Scaglione[1], P Martinelli[1], B Barbiroli[1]
[1]Università di Bologna, Bologna, Italy, Italy

The pathophysiology of essential tremor (ET), the commonest movement disorder in adults, is still unknown. PET, fMRI and 1H-MRS studies have shown metabolic abnormalities in the cerebellum and other functionally-related brain structures in ET. Diffusion-weighted imaging (DWI) was used to look for evidence of neurodegeneration in the cerebellum and other brain areas in ET patients. ADC values were similar in all brain area in patients and controls. Our findings do not support a neurodegenerative processes in ET and suggest that the reduction in the neuronal marker NAA found in the cerebellum is secondary to functional neuronal changes rather loss.

2706. Differentiating Perihemorrhagic Infarct from Susceptibility Artifact on DWI Images

Scott K. Nagle[1], David B. Clayton[1], Maarten G. Lansberg[1], Gregory W. Albers[1], Roland Bammer[1]
[1]Stanford University, Stanford, California, USA

On DWI imaging of parenchymal brain hemorrhage, a high-intensity rim often surrounds the hemorrhage. Differentiating whether this is due to infarction or susceptibility artifact can be difficult. A simple method, based upon the anisotropy of the susceptibility artifact, can help differentiate between these etiologies. In a clinical series of 55 stroke patients, four of which had parenchymal hemorrhage with hyperintense rim, the use of two DWI sequences with swapped phase- and frequency-encoded directions clearly demonstrated that this was due to artifact rather than infarct. A single DWI sequence was insufficient to make this differentiation with confidence.

2707. Diffusion Tensor Imaging in Differentiation of PLS Patients and Healthy Controls

Liang Xuan[1], Peter A. Hardy[1], David K. Powell[1], Anders Andersen[1], Don M. Gash[1], Charles Smith[1]
[1]University of Kentucky, Lexington, Kentucky, USA

Primary lateral Sclerosis (PLS) is a rare neurologic disease characterized by progressive weakness in voluntary muscle. PLS is associated with upper motor neuron and corticospinal tract degeneration. Early diagnosis of PLS is difficult because its symptoms are similar to several other neurologic diseases. Quantitative diffusion tensor imaging could provide a useful evaluation of white matter changes associated with motor neuron degeneration and hence help to establish the diagnosis of PLS. In this study, fractional anisotropy and apparent diffusion coefficient within the posterior limb of the internal capsule and the centrum semiovale are compared between normal controls and PLS patients.

2708. Mapping Radiation Dose Distribution on the Fractional Anisotropy Map: Applications in the Assessment of Treatment-Induced White Matter Injury

Deqiang Qiu[1], Lucullus Leung[1], Dora Kwong[1], Godfrey Chan[1], Guang Cao[2], Pek-Lan Khong[1]
[1]The University of Hong Kong, Hong Kong, People's Republic of China; [2]GE Medical, Asia, Hong Kong, People's Republic of China

We describe a method to map whole brain radiation dose distribution calculated from radiotherapy planning onto diffusion tensor MR fractional anisotropy (FA) images to study voxel-by-voxel, dose-effect relationships and regional differences to radiation in medulloblastoma survivors. The method was validated on two normal control subjects and applied to two medulloblastoma survivors who had sequential MR scans over a one year period. Dose dependant FA reduction was found in both patients and regional susceptibility of brain regions was also observed. We conclude that the method described is useful in the study of radiation induced brain injury.

2709. Variability in ADC and FA Measurements in Acute Ischemic Stroke

Mirthula Govindaraj[1], Ashley D. Harris, [1,2], Richard Frayne[2]
[1]Foothills Medical Centre, Calgary Health Region, Calgary, Alberta, Canada; [2]University of Calgary, Calgary, Alberta, Canada

ADC and FA are used to examine acute ischemic stroke. Here we calculate the minimum detectable difference in white matter (WM) and grey matter (GM) and examine variability for region-of-interest analysis in ADC and FA. The minimum detectable difference for ADC was 0.16×10^{-3} mm^2s^{-1} and 0.21×10^{-3} mm^2s^{-1} in WM and GM, respectively. For FA, the minimum detectable differences were 0.19 and 0.10 in WM and GM, respectively. There was no variability difference between drawing elliptical or free-hand regions of interest. The reliability was substantial within observers; however, there was much lower reliability between observers.

2710. *In Vivo* Brain 1H-MRS and DWI, and Post-Mortem Study of Patients with Mitochondrial Neurogastrointestinal Encephalomyopathy (MNGIE)

Caterina Tonon[1], David Neil Manners[1], Piero Parchi[2], Roberto De Giorgio[1], Carlo Casali[3], Maria Lucia Valentino[2, 4], Michio Hirano[5], Giuseppe Plazzi[2], Marzio Bellan, Valerio Carelli, Bruno Barbiroli[1], Raffaele Lodi[1]
[1]Policlinico S'Orsola-Malpighi, Università di Bologna, Bologna, Italy, Italy; [2]Università di Bologna, Bologna, Italy, Italy; [3]Università "La Sapienza", IRCCS Mondino-SanRaffaele Pisana, Roma, Italy, Italy; [4]Columbia University, New York City, New York, USA; [5]Columbia University, New York City, New York, USA

Mitochondrial neurogastrointestinal encephalomyopathy (MNGIE) is an autosomal recessive multisystem disorder caused by mutations in the thymidine phosphorilase (TP) gene. The pathophysiology of the typical WM hyperintensities detectable on conventional MRI is unclear. In three patients with molecular diagnosis of MNGIE we found an increase of WM ADC associated with a global reduction in 1H-MRS metabolites. 1H-MRS disclosed reduced levels of WM Cho suggesting that myelin pathology does not occur and that both ADC and 1HMRS changes may be secondary to an increase in WM water content in the absence of significant pathological changes as demonstrated in one of cases presented.

2711. Investigation of the Effects of Concurrent Chronic Cigarette Smoking in Alcoholics– a Preliminary Diffusion Tensor Imaging Study

Stefan Gazdzinski[1], Timothy C. Durazzo[1], Ping-Hong Yeh[1, 2], Geon-Ho Jahng[2], Pratik Mukherjee[2], Dieter J. Meyerhoff[1,2]

[1]NCIRE, San Francisco, California, USA; [2]UCSF, San Francisco, California, USA

Our previous research suggested independent detrimental effects of chronic cigarette smoking on gray matter (GM) volumes in major lobes, neuronal and cell membrane viability in frontal lobes, as well as perfusion of frontal and parietal GM. Here, we used DTI to assess the effects of concurrent alcohol dependence and chronic cigarette smoking on white matter microstructure.

2712. Whole Brain FA Histogram Analysis for Improved Detection of DAI

Shashwath Ashok Meda[1], Koushik Athreya Govindarajan[1], Malek Makki[1], Robin Hanks[2], Jay Meythaler[2], Scott Mills[2], Zahid Latif[1], William Coplin[3], Ewart Mark Haacke[1], Randall Reed Benson[2, 4]

[1]Wayne State University, Detroit, Michigan, USA; [2]Wayne State University School of Medicine, Detroit, Michigan, USA; [3]Detroit Receiving Hospital, Detroit, Michigan, USA; [4]Detroit Medical Center, Detroit, Michigan, USA

Introduction: Each year it is estimated that nearly 2 million Americans sustain a Traumatic Brain Injury (TBI). A majority of this population is associated with Diffuse Axonal Injury (DAI) as a result of either primary or secondary effects of trauma. The gravity of the situation is further exacerbated by the fact that DAI is more clinically and diagnostically challenging than focal injuries. Until now, CT has not been very conclusive and effective in detecting DAI. However, relatively newer MR imaging modalities such as DTI have been shown to be useful in detecting DAI. Thus, our aim in this proposed method is to use whole brain FA (Fractional Anisotropy) histogram measures, targeting white matter anisotropy changes due to TBI to obtain an imaging predictor variable that may serve towards better prognosis and diagnosis of TBI patients.Materials and Methods: Twelve patients with closed head injury, varying from moderate to severe and thirteen adult volunteers with no history of any kind of brain injury were imaged with standard MRI sequences and DTI as a part of a multi-imaging protocol on a Siemens sonata 1.5 T scanner. Conclusion: Thus, significant differences could be detected between the two groups based on whole brain histogram derived measures. Further probable sites of DAI have been identified using thresholding analysis. The diffusion profiles investigated at the major sites of injury have also proved to be statistically different.

2713. Quantitative Evaluation of the White Matter Tracts of the Limbic System Segmented by Diffusion Tensor Tractography: Feasibility Study of the Patients with Schizophrenia

Haruyasu Yamada[1], Shigeki Aoki[1], Hidenori Yamasue[1], Kiyoto Kasai[1], Osamu Abe[1], Mariko Yoshida[2], Yoshitaka Masutani[1], Harushi Mori[1], Tomohiko Masumoto[1], Naoto Hayashi[1], Toshiyuki Okubo[1], Kuni Ohtomo[1]

[1]Graduate School of Medicine, University of Tokyo, Tokyo, Japan; [2]School of Medicine, Kanazawa University, Kanazawa, Ishikawa, Japan

We newly combined diffusion tensor tractography (DTT) and FA analysis for evaluation of the white matter tracts; we used DTT to segment certain white matter tracts and quantitatively analyzed the degree of deterioration of the fibers by measuring FA using semi-automated ROI method. The purpose of this study is to evaluate the clinical feasibility and efficacy of this method in the patients with schizophrenia comparing between the patients and volunteers. The mean FA values of semi-automatically placed ROIs of the patients with schizophrenia were significantly lower than that of controls in the anterior cingulum, fornix, and uncinate fasciculus.

2714. Atrophy and Diffusion Tensor MRI Metrics of Brain Fiber Bundles. Application to Primary Progressive Multiple Sclerosis Patients

Elisabetta Pagani[1], Beatrice Benedetti[1], Elda Judica[1], Marco Rovaris[1], Giancarlo Comi[1], Massimo Filippi[1]

[1]Scientific Institute and University Ospedale San Raffaele, Milan, Italy

In this study, we wished to investigate the pathological status of the pyramidal tract (PYT) and the corpus callosum (CC) in primary progressive (PP) multiple sclerosis (MS) patients. To this aim, an index of atrophy and DT derived metrics were obtained within the PYT and the CC. We studied 47 PPMS and 16 healthy volunteers. A positive correlation was found between the lesion load and the MD in the PYT and CC; this correlation was only weak with the index of atrophy. Compared to patients without clinical disability progression, those who progressed had significantly higher atrophy ($p=0.009$) of the CC.

2715. DTI of the Optic Nerve

Ashok Kumar[1], Andre J.W. Van-Der-Kouwe[1], Alma Gregory Sorensen[1], Paul Caruso[2]

[1]Martinos Center for Biomedical Imaging, Charlestown, Massachusetts, USA; [2]Massachusetts Eye & Ear Infirmary, Boston, Massachusetts, USA

High resolution diffusion tensor MR imaging of the optic nerve is challenging due to the low SNR and distortions. We have obtained high resolution DTI based data and associated maps of fractional anisotropy (FA) and trace ADC of the optic nerve in a human subject at voxel sizes of 1mm x 1mm x 3mm. High resolution DTI of the optic nerve may be useful in the imaging evaluation of optical neuropathies.

The Normal Brain: DWI/DTI Analysis

Room 4E Thursday 13:30 - 15:30

2716. A Refined DTI Study Shows Increased Sensitivity on an MTBI Study: Results Highly Correlated with Proteomic Findings

Tong Zhu[1], Jeffrey J. Bazarian[1], Jianhui Zhong[1]
[1]University of Rochester, Rochester, New York, USA

Recent DTI studies on mTBI show the possibility to detect localized diffusive changes accompanying with axonal injuries in acute mTBI, with either ROI-based or voxel-base morphometry (VBM) methods. Both methods have pros and cons. In this study, we investigated a refined mTBI-DTI analysis method combining both the methods, utilizing ROI analysis on predefined mTBI vulnerable regions in the normalized space and exploring other regions with VBM. Quantitative comparison between the ROI-drawing routine in normalized space and commonly used ROI routine in native space were performed, and the DTI results were well correlated with a blood biomarker proteomic analysis.

2717. Age-Related Changes Analyzed Using Whole-Brain Tissue Histogram: A DTI Study of Two Different B Values

Elin Lundström[1], Per Julin[2], Lars-Olof Wahlund[3], Leif Svensson[1], Kelvin Lim[4], Eva-Lena Engman[1], Lars Bäckman[3], Laura Fratiglioni[3], Anders Frank[1]
[1]Karolinska University Hospital Huddinge, Stockholm, Sweden; [2]Astra Zeneca, Södertälje, Sweden; [3]Karolinska Institutet, Stockholm, Sweden; [4]University of Minnesota, Minneapolis, Minnesota, USA

Mean Diffusivity (MD) and Fractional Anisotropy (FA) obtained from DTI measurements are two quantitative parameters characterizing brain diffusion. In this study, 307 subjects, spanning the ages of 62-99 years were analyzed in terms of MD and FA data. Correlation with these parameters was found with increasing age. These data may allow differentiation in changes in the parameters due to clinical diagnosis to be isolated from normal aging. Further, pronounced differences between MD and FA histograms obtained using different b values agree with theories of diffusion as being multiexponentially dependent.

2718. Myelination and Axonal Integrity of Spinal Cord Sensory and Motor Pathways Revealed by Diffusion Tensor MRI

Craig K. Jones[1, 2], Seth A. Smith[1, 2], John W. McDonald[1], Jonathan A. Farrell[1, 2], Peter Calabresi[3], Susumu Mori[1, 2], Peter C.M. van Zijl[1, 2]
[1]Kennedy Krieger Institute, Baltimore, Maryland, USA; [2]Johns Hopkins University School of Medicine, Baltimore, Maryland, USA; [3]Johns Hopkins Medical Institutes, Baltimore, Maryland, USA

Diffusion tensor images were acquired on the cervical spinal cord from C2 to C6 in four volunteers. Fiber tracking was done in the left and right lateral and dorsal columns and tract-specific fractional anisotropy, apparent diffusion coefficient (ADC) and magnetization transfer (MT) contrast were quantified per slice. The measures had left-right symmetry for both pathways. There was a small statistical difference in ADC between the lateral and dorsal columns.

2719. Fractional Anisotropy as a Tool for Characterization of White Matter Fiber Tract Integrity in the Aging Rhesus Monkey Brain

Alexandre Coimbra[1], Marie A. Holahan[1], Yevgen Tymofyeyev[1], Richard Hargreaves[1], Jacquelynn J. Cook[1], Donald S. Williams[1]
[1]Merck Research Laboratories, West Point, Pennsylvania, USA

We explored the possibility of using DTI as a longitudinal tool for probing fiber integrity in the rhesus monkey by evaluating reproducibility of fractional anisotropy (FA) measurement in the corpus callosum (CC) in a group of four young adult monkeys. Second, as part of a continuing effort to evaluate the potential of quantitative MRI to characterize aging in the primate brain, we made FA measurements in the CC of 47 monkeys aged 3-30 years.

2720. Diffusion Tensor MR Imaging: Analysis of Anisotropy Metrics in the Aging Brain

Yi-Jui Liu[1], Chun-Jung Juan[2, 3], Cheng-Hsien Hsu[1], Ming-Chung Chou[2], Teng-Yi Huang[4], Hsiao-Wen Chung[2], Cheng-Yu Chen[3]
[1]Feng-Chia University, Taichung, Taiwan; [2]National Taiwan University, Taipei, Taiwan; [3]Tri-Service General Hospital and National Defense Medical Center, Taipei, Taiwan; [4]National Taiwan University of Science and Technology, Taipei, Taiwan

Diffusion tensor imaging technique has been widely applied in the investigation of cerebral anisotropy in healthy subjects, aging brain and cerebral pathology using apparent diffusion coefficient (ADC) and fractional anisotropy (FA). The purpose of this study is to elucidate the geographic difference of the diffusion anisotropy of the cerebral gray and white matter using a three-phase (3P) plotting method and a bivariate distance measurement (d3p) in the aging brain. Our results show significant age-related decline in FA, Cl and Cp parameters and significant age-related increase in ADC and Cs in both white matter and gray matter of the aging brain.

2721. Mapping Dynamic Water Diffusion Process Inside Human Brain Based on Numerical Solution of the Diffusion Equation

Wang Zhan[1], *Li Jiang*[2], *Yihong Yang*[1]
[1]National Institute on Drug Abuse, NIH, Baltimore, Maryland, USA; [2]George Washington University, Washington, District of Columbia, USA

Water diffusion is a dynamic process existing in biological tissue. A number of diffusion MRI techniques have been developed to reveal structural information on the tissue based on water diffusion, but no technique is currently available to estimate the dynamic diffusion process of water in the whole brain. We present here a method to map the 3-D dynamic diffusion process based on a numerical solution of the diffusion equation for the entire brain, incorporating the diffusion tensor information obtained by a diffusion tensor imaging (DTI).

2722. Correlations Between Diffusion Tensor Indices and Intravoxel Tissue Volume Fractions in Human Brain

Wang Zhan[1], *Hong Gu*[1], *Elliot A. Stein*[1], *Yihong Yang*[1]
[1]National Institute on Drug Abuse, NIH, Baltimore, Maryland, USA

The intravoxel tissue volume fractions of white matter (WM), gray matter (GM) and cerebral-spinal fluid (CSF) are measured in the human brain by an inversion-recovery (IR) procedure. The voxel-wise fraction anisotropy (FA) and mean diffusivity (MD) are obtained by a diffusion tensor imaging (DTI) technique. Strong correlations are detected between the diffusion tensor indices and the intravoxel tissues fractions. Regression analysis was performed to establish the statistical relationships. The FA and MD maps can be decomposed according to the WM and GM fractions, respectively, and this decomposition provides tissue-specific DTI maps of the brain.

2723. Validation of Diffusion Tensor Imaging

D. Reamer[1], *Fick T. Shush*[1], *F.H. Fool and Hardy*[1]
[1]Institute of Dreams and Imaginings of Trendy Science, Buggtussle, California, USA

We illustrate the problem with examples of established DTI techniques and new processing algorithms, producing generally arbitrary results. We then propose a new correlative technique, TDI, that provides a more practical approach to defining a suitable processing algorithm revealing 3D fiber structure, using more reliable manual rather than automated techniques. Realizing that validation still remains a stumbling block even with this approach, we also propose a revolutionary new technique, Nauti-DTI. Ultimately, our results do nothing to validate DTI itself, but we hope to show that although complex development of new DTI procedures is painful, ultimately this kind of research is a pleasure

Resolving Multiple Fibers and Novel Approaches to DWI Analysis

Room 4E Thursday 13:30 - 15:30

2724. The Effects of Intra-Voxel Fiber Architecture on the Diffusion Tensor Parameters

Ryan Fobel[1], *Greg J. Stanisz*[2]
[1]University of Toronto, Toronto, ON, Canada; [2]Sunnybrook & Womens' CHSC, Toronto, ON, Canada

This study uses numerical simulations to model the effects that various axonal fiber architecture have on the measurable diffusion tensor parameters. As expected, small SNR is a major contributor to measured differences in the DTI eigen values, $\lambda 2$ and $\lambda 3$. However, for DTI data with sufficiently high SNR, differences between $\lambda 2$ and $\lambda 3$ indicate non-uniform fiber architecture within the voxel. In this case, the assumption of axially symmetric diffusion is no longer valid and results in under/overestimation of the minor eigenvalues. A reduced fractional anisotropy, FA and increased axial asymmetry in non-uniform fiber architecture demonstrates the inability of the diffusion tensor methodology to resolve differences in intra-voxel fiber structures. Any hope of differentiating between fiber architectures on a sub-voxel level will require both an increase in measured gradient orientations and a framework beyond the diffusion tensor methodology.

2725. Dependence of the DTI Signal on the Presence of Fiber Crossing

Nicolas Kunz[1], *Rolf Gruetter*[1]
[1]Ecole Polytechnique Fédérale de Lausanne (EPFL), Lausanne, Switzerland

Diffusion tensor (DT) imaging is a powerful tool to delineate fiber directionality. For “pure” fiber orientation, the DT model, which is characterized by six degrees of freedom, is used to characterize diffusion directionality. When two or more divergent fibers are present, the degrees of freedom are increased, but it is unclear if diffusion measurements have the necessary degrees of freedom to resolve the presence of multiple fibers. The aim of the present study was to examine if, based on the DT description, multiple fiber orientations present in a voxel will permit the measurement of more than 6 degrees of freedom.

2726. Linear Persistent Angular Structure MRI and Non-Linear Spherical Deconvolution for Diffusion MRI

Kiran Kumar Seunarine[1], Daniel C. Alexander[1]
[1]University College London, London, UK

This abstract shows that Persistent Angular Structure (PAS) MRI is a special case of Spherical Deconvolution (SD). This observation allows us to a) construct a linear implementation of PAS-MRI and b) exploit the optimal non-linear representation of PAS-MRI for SD. We show experiments comparing both the linear and non-linear implementations of PAS-MRI and SD using several synthetic datasets that simulate crossing fibre populations. Furthermore, we optimize the linear implementations of these methods to minimize the bias of the reconstructed fibre directions.

2727. Application of Independent Component Analysis for Resolving Multiple Fibre Orientations in DT-MRI Data

Laurence Vigon[1], Nikos Papadakis[1]
[1]The University of Sheffield, Sheffield, UK

The use of standard diffusion tensor (DT) models in the brain is based on the fundamental assumption that the diffusion of water molecules is governed by a Gaussian probability density function. However, in cases where the fibers cross within a voxel, this assumption does not hold and the fiber orientation will be estimated erroneously. In this study, a new method for resolving multiple intravoxel fiber orientations is proposed based on Independent Component Analysis. The method was successfully applied in simulated two-fibre DW signals. Its robustness with respect to varying fiber separation angles as well as number of gradient orientations was also demonstrated.

2728. Resolve Fiber Orientation Ambiguity Using HARD Imaging

Xin Hong[1], Adam W. Anderson[1], Zhaohua Ding[1]
[1]Vanderbilt University, Nashville, Tennessee, USA

Conventional Diffusion Tensor Imaging (DTI) cannot distinguish between fiber crossing, joining, kissing or bending in a voxel. Here we show that this ambiguity can be resolved with High Angular Resolution Diffusion (HARD) measurements and a simple model of partial volume averaging Fiber ORientation Estimated using Continuous Axially Symmetric Tensors (FORECAST). It is demonstrated both by numerical simulation and *in vivo* measurements. The technique may be useful for fiber tracking, and fiber bundles segmentation.

2729. Quantitative Analysis of Q-Space MRI Data: Theoretical and Experimental Validation

L Guy Raguin[1], Diego Hernando[1], Dimitris Karampinos[1], Luisa Ciobanu[1], Brad P. Sutton[1], Zhi-Pei Liang[1], John G. Georgiadis[1]
[1]University of Illnois at Urbana-Champaign, Urbana, Illinois, USA

Standard diffusion-weighted MRI (DWMRI) involves the acquisition of images with q vectors on a sphere in q-space (single q value). One prevailing medical application is the study of brain white matter, for which several methods are available to extract quantitative information about the relative anisotropy of the parenchyma and the orientation of the myelinated fibers. We are proposing a quantitative analysis of q-space MRI data (QUAQ) by exploiting the physics of diffusion in fiber networks to extract the relevant parameters and resolve fiber-crossings. Experimental results on a capillary phantom show that fiber crossings can be resolved using a lesser amount of data than existing methods would require.

2730. Bootstrap Tractography Using Multimodal Fiber Orientation Data from High Angular Resolution Diffusion Imaging

Jeffrey I. Berman[1], Pratik Mukherjee[1], Christopher P. Hess[1], Eric T. Han[2], SungWon Chung[1], Roland G. Henry[1]
[1]University of California San Francisco, San Francisco, California, USA; [2]GE Healthcare Global Applied Science Laboratory, Menlo Park, California, USA

Bootstrap analysis, a model independent method of characterizing uncertainty, was applied to fiber tracking using the multimodal intravoxel fiber orientation information from q-ball reconstruction of high angular resolution diffusion imaging (HARDI). Whole-brain HARDI was acquired with 55 gradient directions at b=3000 s/mm2 and repeated 3 times for bootstrap resampling. Bootstrap HARDI fiber tracks, launched from the corpus callosum, traversed regions of crossing fibers to reveal connectivity matching the known anatomy of these commissural pathways. In comparison, diffusion tensor imaging (DTI) fiber tractography using a deterministic streamline method was only able to delineate the superior projection of these commissural fibers.

2731. Regularized Diffusion Tensor MRI for High Angular Resolution ODF Estimation and Fibre Tractography

Jennifer S.W. Campbell[1, 2], Peter Savadjiev[2], G. Bruce Pike[1], Kaleem Siddiqi[2]
[1]Montreal Neurological Institute, Montreal, Quebec, Canada; [2]McGill Centre for Intelligent Machines, Montreal, Quebec, Canada

We describe a regularization algorithm that can be used to infermulti-peaked orientation distribution functions (ODFs) from diffusiontensor reconstructions. These ODFs are compared to those obtainedfrom a direct high angular resolution diffusion (HARD) reconstructionscheme, q-ball reconstruction. The performance of the regularizeddiffusion tensor ODFs is compared to that of the diffusion tensorreconstruction in a fibre tracking experiment. It is concluded thatthe regularization algorithm can be used to infer high angularresolution fibre structure from a low angular resolution (singlediffusion tensor) ODF reconstruction.

2732. Two Tensor Analysis for White Matter Tractography - Methodological Evaluation

Sharon Peled[1], Carl-Fredrik Westin[1]

[1]Brigham and Women's Hospital and Harvard Medical School, Boston, Massachusetts, USA

Two tensor analysis to resolve crossing tracts in white matter can be performed using standard clinical DTI data when certain geometrical constraints are incorporated. In this work the constrained two-tensor method is critically evaluated using simulations to determine: A) in which cases it is applicable, B) what the associated errors in tract determination are, and C) the optimal data acquisition parameters.

2733. Brain Segmentation Using ATP (Automatic Twice PAM) in Multi Diffusion Indices

Yi-Ping Chao[1], Kuan-Huang Cho[1], Chun-Hung Yeh[2], Sue-Ping Tsao[2], Der-Yow Chen[1], Jyh-Horng Chen[1], Ching-Po Lin[2]

[1]Institute of Electrical Engineering, National Taiwan University, Taipei, Taiwan; [2]National Yang-Ming University, Taipei, Taiwan

Non-invasive diffusion tensor imaging (DTI) has been used widely in brain research and clinical applications recently. Various diffusion indices were developed for recognizing the constituents of brain and the nidus of diseases. In this research, Automatic Twice PAM (ATP) clustering algorithm was employed to segment the brain architectures with features of common diffusion indices with no initial information. The segmentation was found to agree strongly with the anatomy atlas. This efficient and robust method also showed the outstanding ability for aiding morphological study and analysis of brain development.

2734. Time-Series' Analysis of the Diffusion Weighted Signal as a Model-Free Approach to Segmenting Tissue

Sean CL Deoni[1], Derek K. Jones[1]

[1]Institute of Psychiatry, King's College, London, England, UK

In this work we investigate the use of a pseudo time-series analysis approach to characterize and segment diffusion-weighted (DW) MRI data. By treating the diffusion data acquired over a range of encoding gradients as a time-series wave-form we hypothesize that similar tissue (shape and orientation) will share common characteristics in their time-series and therefore be maximally correlated. As proof of principle, we apply this approach to *in vivo* thalamic data to segment the thalamic nuclei and show that this simple approach, free of model assumptions, provides reliable delineation of the DW-MRI data.

2735. Method of Measuring Diffusion Anisotropy and Diffusion Gradient Simultaneously with DTI

Jie Huang[1]

[1]Michigan State University, East Lansing, Michigan, USA

Water diffusion in tissues is generally inhomogeneous and anisotropic due to spatial-location variation (gradient) and spatial-direction variation (anisotropy) of tissue structures. Diffusion anisotropy is measured by DTI. A newly derived theoretical relationship between diffusion gradient and the echo signal in a diffusion-weighted spin-echo pulse sequence establishes the theoretical basis for measuring the diffusion gradient. This paper presents a method of simultaneously measuring diffusion anisotropy and diffusion gradient.

2736. From DTI to CTI: The Role of Anisotropic Conductivity of the White Matter Tissue – an EEG FEM Simulation Study

Daniel Güllmar[1], Jürgen R. Reichenbach[1], Alfred Anwander[2], Carsten H. Wolters[3], Jens Haueisen[1, 4]

[1]Friedrich-Schiller-University, Jena, Germany; [2]Max Planck Institute for Human Cognitive and Brain Sciences, Leipzig, Germany; [3]Westfalian Wilhelms-University Muenster, Münster, Germany; [4]Technical University Ilmenau, Ilmenau, Germany

Pre-testing the use of DTI to extract Conductivity Tensor Information we quantified the influence of anisotropic conductivity on EEG source reconstruction. Employing a finite element method model we performed forward as well as inverse simulations and found a weak dependence of anisotropic conductivity on all measures (RDM, MAG, dipole shift, orientation change and change in magnitude). We observed strong correlation between the error measures and the distance to the anisotropy and discovered that the orientation of the dipoles relative to the anisotropic volume as such plays an important role in predicting the influence of anisotropy on the forward solution.

Fiber Tracking and Visualization

Room 4E Thursday 13:30 - 15:30

2737. Current State of Diffusion Simulation Based Tractography

Sarah Mang[1], Ning Kang[2], Jun Zhang[2], Eric S. Carlson[3], Daniel Gembris[1], Reinhard Männer[1]

[1]University of Mannheim, Mannheim, Germany; [2]University of Kentucky, Lexington, Kentucky, USA; [3]University of Alabama, Tuscaloosa, Alabama, USA

We present a diffusion simulation based tracking (DST) algorithm for the investigation of neuronal connectivity using diffusion tensor magnetic resonance imaging (DTI). This front propagating tracking approach is based on the successive simulation of diffusion, governed by the rank-n diffusion tensors, derived from DTI measurements. The use of backtracking allows the reconstruction of outward branching of the tracts. Synthetic and real data examples are used to illustrate the ability of DST to track neuronal fiber pathways non-invasively. Using the whole tensor data, including magnitude and orientation information, makes the approach more robust in the presence of noise.

2738. Anisotropic Fiber Phantom for DTI Validation on a Clinical Scanner

Ramona Lorenz[1, 2], Björn W. Kreher[1], Jürgen Hennig[1], Matthias E. Bellemann[2], Kamil A. Il'yasov[1]

[1]University Hospital Freiburg, Freiburg, Germany; [2]University of Applied Sciences Jena, Jena, Germany

Verification of tensor measurements and validation of different fiber tracking algorithms with anisotropic diffusion requires a phantom with well known structure and anisotropic properties. In this work, the feasibility of using four different fiber phantoms for calibration measurements on a clinical scanner was investigated and their suitability for application of fiber tracking was tested. Among the tested fibers the dyneema fiber phantom was the most suited to validate diffusion tensor measurements. A fiber crossing phantom of dyneema fibers showed promissing results.

2739. Quantitative Validation of White Matter Fiber Tractography by Use of an Anatomically Realistic Synthetic Diffusion Tensor Phantom

Steven Delputte[1], Els Fieremans[1], Yves Dedeene[2], Yves D'Asseler[1], Rik Achten[2], Ignace Lemahieu[1], Rik Van de Walle[1]

[1]Ghent University, Ghent, Belgium; [2]Ghent University Hospital, Ghent, Belgium

Current clinical use of diffusion tensor fiber tractography is limited due to the lack of a golden standard to validate this technique. By taking into account the environmental architectural information proffered by *in vivo* density regularized fiber tracking, we were able to construct a noise-free synthetic diffusion tensor dataset, originating from a ground-truth fiber distribution that resembles the true white matter anatomy as accurate as possible. The phantom was used to quantitatively study the influence of noise on several tractography algorithms. MRI acquisition artifacts can be incorporated into the phantom as well.

2740. Validation of Multi-Fibre Probabilistic Tractography of Corticothalamic Projections in the Göttingen Minipig Brain

Tim Bjørn Dyrby[1], Lise S L Vejby[1], Geoffery J. M. Parker[2], Daniel C. Alexander[3], Nanna M. Lind[4], Olaf B. Paulson[1], Jacob Jelsing[5]

[1]Copenhagen University Hospital, Hvidovre, Denmark; [2]University of Manchester, Manchester, UK; [3]University College London, London, UK; [4]University of Copenhagen, Copenhagen, Denmark; [5]Bispebjerg University Hospital, Copenhagen, Denmark

Diffusion MRI probabilistic tractography enables *in vivo* tracking of axonal fibres in the brain and will be pivotal in studying brain connectivity in the pathological and healthy human brain. In the present study tractography was compared with real fibre tracts visualized using manganese as an anterogradely transported paramagnetic tracer. We demonstrate that it is possible to trace corticothalamic fibres using a high resolution in situ diffusion weighted dataset optimised for the detection of crossing fibres.

2741. A Comparison of Fiber Tracking by Different Numerical Integration Methods

RKS Rathore[1], Getaneh Bayu[1], RK Gupta[2], Divya KS Rathore[1], Ankur Purwar[1], Richa Trivedi[2], Sona Saksena[2], Manoj Kumar Sarma[1], Anup Singh[1]

[1]Indian Institute of Technology, Kanpur, UP, India; [2]Sanjay Gandhi Post Graduate Institute of Medical Sciences, Lucknow, UP, India

We present the results of fiber tracking using Euler (E), Modified Euler (M) and Runge-Kutta (R) schemes, using nearest neighbor (N) and trilinear (T) interpolations and step sizes h=1, ½, 1/3 and 1/4. The tracking results agree with the anatomy of the corpus callosum. The fiber volume from M is larger than from E and R for h = 1/2. The functional evaluations at each step in the tracking are 1, 2 and 4 for E, M and R, respectively. Till an optimum method is achieved, M using h=1/2 with T is recommended as it generates more fiber data volume.

2742. Automated Assessment of Tract Similarity in Group Diffusion MRI Data

Jonathan D. Clayden[1], Mark E. Bastin[1], Amos J. Storkey[1]
[1]University of Edinburgh, Edinburgh, UK

Automated white matter segmentation is a major aim of diffusion MRI based tractography, but no robust methodology yet exists for segmenting tracts consistently across a group of subjects. Presented here are the first results from a tract similarity algorithm that could be used as a basis for such a methodology. We demonstrate that the similarity score that we have developed indicates better matches for the "same" tract in different subjects, than for different tracts in the same subject. This could improve the reproducibility of group tract segmentation in diffusion MRI studies.

2743. Tract-Specific Mapping of Diffusion Anisotropy Index

Li-Wei Kuo[1], Van Jay Wedeen[2], Jui-Chang Tsai[3], Ham-Min Tseng[3], Jun-Cheng Weng[1], Su-Chun Huang[4], Timothy G. Reese[2], Jyh-Horng Chen[1], Wen-Yih Isaac Tseng, [3,4]
[1]National Taiwan University, Taipei, Taiwan; [2]Harvard Medical School, Charlestown, Massachusetts, USA; [3]National Taiwan University Hospital, Taipei, Taiwan; [4]National Taiwan University College of Medicine, Taipei, Taiwan

To visualize white matter tracts reconstructed from diffusion MRI, it is customary to use RGB color-coding representation to show the orientation of each track. This representation method, however, is subject to the selection of the reference coordinates, and seems redundant to visualize a 3D object. Tract-specific mapping of diffusion anisotropy (DA) index could reveal the integrity of underlying axonal fibers, and should be effective in localizing pathological changes of individual tracts. In this study, we tested this hypothesis by applying such tract representation method to patients with brain tumors, to see whether the affected tracts were infiltrated by tumors or not. Reduction of DA was found in specific locations of the tracts that passed through the tumor. In contrast, no change in DA was noted in the tracts that were merely displaced by the tumor.

2744. Visualization of Absolute T1 and T2 Along Specific White Matter Tracts

Derek K. Jones[1], Sean CL Deoni[1]
[1]Institute of Psychiatry, London, UK

We have combined rapid high resolution relaxometry with DT-MRI tractography to visualize, for the first time, T1 and T2 along specific anatomical pathways. The method highlights the gray matter termini of white matter pathways (due to presence of a white matter / gray matter gradient), helps to identify partial volume artefacts, and can be used to perform a more complete characterization of specific pathways than previously possible. The data required to perform these measurements was acquired in 30 minutes, making tract-specific T1 and T2 measurements clinically feasible.

2745. Fiber Tract Based Interrogation of White Matter

Jeffrey Thomas Duda[1], Hui Zhang[1], Tony J. Simon[2], James C. Gee[1]
[1]University of Pennsylvania, Philadelphia, Pennsylvania, USA; [2]University of California, Davis, Davis, California, USA

We present a method for interrogating white matter associated with fiber tracts derived from diffusion tensor MRI. By integrating the diffusivity of the underlying tensors along the direction of the identified fiber bundles, we hope to gain additional information regarding the micro architecture of the tissue. A study was performed examining fiber bundles that passed through the midsagittal corpus callosum in pediatric patients diagnosed with chromosome 22Q11.2 deletion syndrome as well as age matched controls.

2746. Interactive Digital Stereotaxic White Matter Atlas in Talairach Coordinates (SWAT)

Hangyi Jiang[1, 2], Jiangyang Zhang[1], Peter C.M. van Zijl[1, 2], Susumu Mori[1, 2]
[1]Johns Hopkins University School of Medicine, Baltimore, Maryland, USA; [2]Kennedy Krieger Institute, Baltimore, Maryland, USA

An electronic atlas of human brain white matter was established and incorporated into the Talairach stereotaxic coordinate system. Our high-resolution DTI template, the trajectories of the prominent white matter tracts and pre-segmented anatomical regions were transformed into Talairach coordinate and integrated with extensive annotations in this atlas. Four different types of data representation, Talairach, absolute or relative millimeter coordinates, and white matter parcellation map (WMPM), are available for the locations in the deep white matter. The atlas assists the users in comprehensively understanding white matter functional structures and reporting the position of relevant structures and regions in normalized coordinates.

2747. High Spatial Resolution Probabilistic DT Fibre Tracking Using Seeding Points from fMRI Statistical Parameter Maps

Goran Vucurevic[1]
[1]University Hospital Mainz, Mainz, Germany

1x1x2 mm spatial resolution (256x256x64) volume DTI data set obtained with 12 gradient directions (+b0; b=1000) was made with 15 separately stored acquisitions (1.7GB data set) using EPI sequence (GRAPPA image acquisition and reconstruction with acceleration gain 2) and 8 channel head coil in 1.5T MR scanner. For determining of fiber tract seedings, SPM activation maps of 2 different tasks (motoric and speech&visual) were corregistered to b0 volume image of the mean DTI data set. High spatial resolution DTI together with probabilistic fibre tracking resolved most of the problems due to fibre crossings in “lower” resolution DTI.

2748. Connectivity-Based Parcellation of the Midsagittal Corpus Callosum in Human Brain Using Diffusion Probability Tractography

Ruiwang Huang[1], Oleg Posnansky[1], Lars Hoemke[1], Katrin Amunts[1], NJ Jon Shah[1]
[1]Research Centre Juelich, Juelich, Germany

The corpus callosum is the main commissure of the human brain. It is well known that cortical regions project to corresponding regions (homotopic projections) or to different regions (heterotopic) in the contralateral hemisphere. The precise topography of these fibres in the human brain, however, is largely unknown. The aim of the present study is to parcellate the midsagittal corpus callosum (MCC) on the basis of its connectivity. Therefore, we used diffusion probability tractographic tracking in order to analyse the connection distributions between the MCC and seven cortical regions, which are known to send projections through the corpus callosum.

2749. On the Thresholding of Probabilistic Fibre Tracking Maps

Hubert Fonteijn[1, 2], David G. Norris[2], Frans Verstraten[1]
[1]Helmholtz Institute, Utrecht, Netherlands; [2]F.C. Donders Institute for Cognitive Neuroimaging, Nijmegen, Netherlands

Fibre tracking has been established in the last decade as a promising technique to reveal anatomical connectivity *in vivo*. Recently, developments have been made too quantify the confidence in a fibre track, based on local probabilistic models of the principal diffusive direction. However, generally the probability of a connection decreases with distance, due to the fact that the uncertainty of the fibre direction locally adds cumulatively to the uncertainty of the global track. We present a new method in which the probability is normalized for the number of voxels it has hit and we demonstrate its feasibility with an example.

2750. fMRI-Guided DTI Fiber Tracking: A Verification Study in the Basal Ganglia

Philipp Staempfli[1, 2], Carolin Reischauer[1], Thomas Jaermann[1], Anton Valavanis[2], Spyridon Kollias[2], Peter Boesiger[1]
[1]University and ETH Zurich, Zurich, Switzerland; [2]University Hospital Zurich, Zurich, Switzerland

In the last few years, a variety of different DTI tracking algorithms has been proposed. However, there exists no standard procedure to validate tracking results. The focus in this study was to combine fMRI with DTI. Therefore, the somatotopical organization of the putamen was derived twice: Firstly, an fMRI based somatotopy was calculated; secondly, tracking algorithms were applied to derive somatotopical maps. It is shown that fMRI-guided DTI fiber tracking provides a promising tool for reconstructing anatomical networks underlying specific functional systems in the human brain and allows a validation of tracking results.

2751. Identification of Parallel Hippocampo-Fusiform and Amygdalo-Fusiform Pathways in Living Humans

Charles D. Smith[1], Eren Gultepe[2], Erbil Akbudak[2], Nicolas Lori[2], Thomas Edward Conturo[2]
[1]University of Kentucky, Lexington, Kentucky, USA; [2]Washington University, St. Louis, Missouri, USA

Diffusion tensor tracking (DTT) has been used to identify a previously unknown pathway interconnecting Brodmann mid-fusiform area 37 with anteromedial temporal cortex (e.g., amygdala). We investigated whether this pathway contains specific anatomical/ functional components. Using heuristic criteria, we identified two distinct superior and inferior components with characteristic trajectories and anatomical terminations in all 12 subjects: the amygdalo-fusiform pathway (superior), and a newly identified hippocampo-fusiform pathway (inferior). The superior component hooks sharply to terminate at the amygdala, and the inferior component curves gently to terminate at the hippocampal head. These parallel pathways have functional significance for lexical/visual processing and memory formation.

2752. Spatial Resolution Dependence of DTI Tractography in Human Occipito-Callosal Region

Mina Kim[1], Itamar Ronen[2], Kamil Ugurbil[1], Dae-Shik Kim[2]
[1]University of Minnesota, Minneapolis, Minnesota, USA; [2]Boston University School of Medicine, Boston, Massachusetts, USA

DTI and fiber tracking have been used to measure the fiber structural connectivity in humans in a non-invasive manner. However, low sensitivity is a principal limitation of these methods, causing a large number of possibly missing fiber tracts. Here we studied how the spatial resolution affects the sensitivity of the fiber tracing by rescaling data to five different resolutions. Our data suggest that the spatial resolution can change the degree of the asymmetric cross-callosal connections. We conclude from our study that the spatial resolution of the acquired data will have to be taken into consideration in interpreting DTI data.

2753. Efficient Visualization of Fiber Tracking Uncertainty Based on Complex Gaussian Noise

Jan Klein[1], Horst K. Hahn[1], Jan Rexilius[1], Peter Erhard[2], Matthias Althaus[1], Dieter Leibfritz[2], Heinz-Otto Peitgen[1]
[1]MeVis - Center for Medical Diagnostic Systems and Visualization GmbH, Bremen, Germany; [2]FB 2 (Chemistry) and Center of Advanced Imaging (CAI), Bremen, Germany

Visualizing the uncertainty of fiber tracking is an important new challenge in the area of DTI. We present a new method that allows for an efficient computation of diffusion weighted images with user-defined noise, which are used to analyze the tracking uncertainty resulting from image noise. In contrast to the bootstrap method, our technique needs only a single data set so that acquisition time and the time for computing the artificial data can be reduced dramatically. Our visualization of the resulting fiber sets as well as our measurements show that bootstrap noise can be simulated appropriately by complex Gaussian noise.

2754. Comparison of Parametric and Nonparametric Probabilistic White Matter Tractography Methods

Mariana Lazar[1], Andrew L. Alexander[1]
[1]University of Wisconsin, Madison, Wisconsin, USA

Probabilistic white matter tractography methods have been proposed to account for the uncertainty in the local fiber direction estimation due to image noise and artifacts. The goal of this study was to compare the performances of one parametric probabilistic tractography method, the random vector perturbation (RAVE) algorithm, against a non-parametric bootstrap tractography (BOOT-TRAC) method. The RAVE algorithm appears to generate fiber distributions similar to the BOOT-TRAC algorithm for trajectories situated in homogeneous white matter regions and might be a viable substitute for BOOT-TRAC in cases when multiple measurements of the diffusion-weighted images are not available or are difficult to obtain.

2755. Pre-Computed Global Illumination of MR and DTI Data

David C. Banks[1, 2], Kevin Beason[1]
[1]Florida State University, Tallahassee, Florida, USA; [2]Harvard Medical School, Boston, Massachusetts, USA

We demonstrate techniques that incorporate pre-computed global illumination (using photon mapping) together with hardware-based rendering to permit viewing of globally-illuminated 3D structures from MR and DTI data at interactive speeds.

2756. Visualization of Diffusion Anisotropy Using Colored Superquadric Glyphs in DT-MRI

Jinyoung Hwang[1], Yeji Han[1], HyunWook Park[1]
[1]Korea Advanced Institute of Science and Technology, Daejeon, Republic of Korea

This research is to visualize the diffusion anisotropy in DT-MRI using glyphing and color coding. We combined superquadric tensor glyphs for glyphing and color sphere for color coding. We acquired *in vivo* human brain dataset using 6 diffusion weighted images and 1 non-diffusion weighted image using 3T MRI scanner. As a result, the results provide more directional information than conventional method which used either glyphing or color coding.

2757. 3D Visualization of the Diffusion Tensor Ellipsoid in Mouse Brain

Chien-Yuan Lin[1, 2], Yi-Hua Hsu[2], Chung-Yi Hong[2], Jyh-Hong Chen[1], Chen Chang[2]
[1]Interdisciplinary MRI/MRS Lab, Department of Electrical Engineering, National Taiwan University, Taipei, Taiwan; [2]Functional and Micro-MRI Center, Institute of Biomedical Sciences, Academia Sinica, Taipei, Taiwan

The goal of the present study is to propose a new 3D visualization method which can simultaneously extract and display diffusion tensor size, shape and orientation. The results demonstrate that the proposed method is a promising technique for the evaluation of morphologic phenotype and can be used as an effective diagnostic tool for white matter diseases.

2758. DTI&FiberTools: A Complete Toolbox for DTI Calculation, Fiber Tracking, and Combined Evaluation

Björn Wolf Kreher[1], Jürgen Hennig[2], Kamil A. Il'yasov[1]
[1]University Hospital Freiburg, Freiburg, Germany; [2]University Hospital Freiburg, Freiburg,, Germany

DTI and fiber tracking is a new and still developing discipline of MR post-processing. So far there is no commercial and easy extendable tool available. Therefore, most groups working on DTI have to develop their own tools in order to process and visualize their DTI datasets. This is very time consuming, needs know how and costs manpower. In addition, the results between studies and different groups are not comparable, since the used algorithms can differ in some details. In this abstract, a MATLAB based toolbox is introduced, containing GUI based tools for the whole working procedure of DTI and fiber tracking studies, containing data processing, visualization, evaluation, and documentation.

2759. Camino: Open-Source Diffusion-MRI Reconstruction and Processing

Philip A. Cook[1], Yu Bai[1], Shahrum Nedjati-Gilani[1], Kiran K. Seunarine[1], Matt G. Hall[1], Geoffrey J. M Parker[2], Daniel C. Alexander[1]
[1]University College London, London, UK; [2]University of Manchester, Manchester, UK

Camino is an open-source, object-oriented software package for processing diffusion MRI data. Camino implements a data processing pipeline, which allows for easy scripting and flexible integration with other software. Camino implements and integrates standard and advanced algorithms for synthesis, reconstruction, statistical analysis and tractography in diffusion-MRI imaging and is freely available to the research community. We explain the pipeline approach to processing diffusion-MRI data and summarize the main features of the Camino toolkit.

BOLD: Reactivity and CBV

Room 4E Thursday 13:30 - 15:30

2760. Comparison of BOLD and CBV-Weighted fMRI Studies Using Multiple-Refocused Spin-Echo

Tao Jin[1], Seong-Gi Kim[1]
[1]University of Pittsburgh, Pittsburgh, Pennsylvania, USA

In fMRI, spin-echo sequences can provide better spatial localization to the brain parenchyma than gradient-echo sequences because the dynamic-averaging effect is more prominent for field inhomogeneities of small scales. In order to investigate the mechanisms of the BOLD and CBV-weighted SE signal change, high resolution multiple-refocused spin-echo (MSE) measurements were conducted at 9.4T, which suppress the dynamic-averaging effect by the additional refocusing pulses. It was suggested that the T2* effect can contribute significantly to the fMRI contrast in a SE-EPI sequence because of the long EPI readout time. This effect was also evaluated and found to be negligible in our results.

2761. Neurovascular Coupling in the Human Visual and Motor Cortices

Peter Anthony Chiarelli[1], Daniel Peter Bulte[1], Daniel Gallichan[1], Peter Jezzard[1]
[1]Oxford University, Oxford, UK

We simultaneously acquired BOLD and CBF data from three distinct brain regions—the visual cortex, the primary motor cortex, and the supplementary motor area—while alternating between epochs of visual stimulation, motor stimulation, and 4 % CO2-breathing. We calculated hypercapnia calibration values (M) of 4.5, 8, and 7.5 for the visual, motor, and supplementary motor areas, respectively, and we find CBF:CMRO2 coupling ratios of ~4:1, ~3:1, and ~2.5:1 in the three regions. Understanding regional heterogeneity of neurovascular coupling is an important step towards both a better understanding of the brain, and of the imaging signals we use to investigate functional anatomy.

2762. Spatiotemporal Characteristics of BOLD, CBV and CBF Responses in the Cat Visual Cortex

Tao Jin[1], Jicheng Wang[1], Fuqiang Zhao[1], Ping Wang[1], Michelle Tasker[1], Seong-Gi Kim[1]
[1]University of Pittsburgh, Pittsburgh, Pennsylvania, USA

For a better understanding of the relationship between the oxygen metabolism and the hemodynamic responses in fMRI, high resolution BOLD, CBV and CBF signal changes were studied at 9.4T using a cat visual stimulation model. The spatial and temporal dynamics of the CBV and CBF responses were found to be very similar, suggesting a tight coupling between the blood volume and flow regulation. Our results also suggested that an elevated deoxyhemoglobin concentration is more likely to be responsible for the BOLD poststimulus undershoot than an elevated venous CBV.

2763. Quantitative Characterization of Vascular Non-Linearities in BOLD fMRI

Jacco A. de Zwart[1], Peter van Gelderen[1], J Martijn Jansma[1], Jeff H. Duyn[1]
[1]National Institutes of Health, Bethesda, Maryland, USA

Studies of the BOLD response to varying neuronal activity have reported some degree of non-linearity, but are not in quantitative agreement. To some extent, this is due to confounding neuronal effects related to closely spaced stimuli. In this work, we used the m-sequence method with gapped sub-second visual stimuli to characterize the impulse response with minimal neuronal contribution. Results obtained from human fMRI at 3.0 T show a small but significant non-linearity in the form of temporal dispersion, consistent with a lingering blood volume (balloon) effect.

2764. Sources of Systematic Bias in Hypercapnia-Based CMR_{O_2} Estimation Using Functional MRI

Peter Anthony Chiarelli[1], Daniel Peter Bulte[1], Stefan Kazimierz Piechnik[1], Peter Jezzard[1]
[1]Oxford University, Oxford, UK

Aerobic metabolism (CMRO2) during neural stimulation may be estimated from BOLD and CBF measurements by the hypercapnia-normalization method. We present a thorough re-examination of systematic bias in this model for CMRO2 estimation [1,2], focusing on an unexamined dependence on the value of the hypercapnia calibration constant (M), and a marked covariation between the calculated CMRO2?CBF coupling ratio and the apparent linearity of coupling. This work argues for a much more careful measurement of M to minimise this potential bias, and provides an enhanced transparency of the model itself to the MR community.

2765. Model of Vascular Reactivity to Investigate the Basis of Grubb's Relationship Between Cerebral Blood Flow and Volume

Stefan K. Piechnik[1], Peter Chiarelli[1], Peter Jezzard[1]
[1]University of Oxford, Oxford, Oxfordshire, UK

The relationship between cerebral blood volume and flow is important in order to understand the mechanisms of functional imaging contrast and enable calculation of cerebral metabolic ratio. We analyse several models of cerebral circulation including a novel multicompartmental model based on a meta-analysis of studies directly measuring vascular reactivity. The shape of the volume-flow relationship depends strongly on the choice of the model and the contribution of autoregulating segments in the volume of interest. Even though the former can be neglected under physiological conditions, the latter may contribute significantly to the focal characteristics of imaging contrast.

2766. Does Mild Hypoxia Modulate the Stimulus-Evoked BOLD Response?

Stephen Daniel Mayhew[1], Richard Rogers[1], Paul Dunckley[1], Kyle T. Pattinson[1], Irene Tracey[1], Richard G. Wise[1]
[1]University of Oxford, John Radcliffe Hospital, Oxford, UK

We investigated modulations of the BOLD response by mild hypoxia for brief visual, auditory and noxious thermal stimuli. These stimuli were combined with alternating 300-second periods of mild hypoxia (16% FiO2) and normoxia (21% FiO2) in 9 healthy human subjects at 3T. We observed a significant decrease in BOLD response in visual and auditory areas during hypoxia ($p<0.05$). No significant hypoxia-induced modulation of BOLD response was detected in a wide network of regions of the brain that respond to painful stimulation. Our observations suggest a regional dependence of the modulatory effect of mild hypoxia on the BOLD response.

2767. The Confounding Effects of O_2 on CO_2-Induced Cerebrovascular Reactivity as Measured with BOLD MRI

Alexandra Mardimae[1, 2], Marat Slessarev[1, 2], Jay Han[1, 2], Eitan Prisman[2], Julien Poublanc[2], Adrian Crawley[2], Lisa Rodrigues[2], Joseph Fisher[1, 2], David Mikulis[2]
[1]University of Toronto, Toronto, Ontario, Canada; [2]University Health Network, Toronto, Ontario, Canada

Rapid cyclic changes in end-tidal partial pressures of CO_2 ($P_{ET}CO_2$) have previously been used to determine cerebrovascular reactivity (CVR) from BOLD MRI. However, the effects of variable end-tidal partial pressures of O_2 ($P_{ET}O_2$) on BOLD signal are unclear. We cycled $P_{ET}O_2$ and $P_{ET}CO_2$ to study the effects of variable $P_{ET}O_2$ on BOLD signal during CO_2-induced CVR. During high CO_2 stimulus, increases in $P_{ET}O_2$ resulted in an additional increase in BOLD signal beyond that due to CO_2 alone. Hence, $P_{ET}O_2$ should be carefully controlled during measurements of CVR with BOLD MRI.

2768. Vascular Space Occupancy Weighted Imaging with Control of Inflow Effect and Higher Signal-To-Noise Ratio

Wen-Chau Wu[1], Susanne Wegener[1], Richard B. Buxton[1], Eric C. Wong[1]
[1]University of California, San Diego, La Jolla, California, USA

This study proposes an alternative vascular space occupancy (VASO) weighted imaging by optimizing the difference of longitudinal magnetization between blood and non-blood tissues, instead of eliminating blood signal as used in current VASO technique. The presented method provides compatible sensitivity and specificity in the detection of neuronal activation with 1.7-fold higher SNR and less sensitivity to inversion efficiency. With a voxel size of 3.4¡Ñ3.4¡Ñ5.0 mm^3, VASO signal change is 0.6%, which approximately corresponds to a 44 % change in cerebral blood volume. Global saturation immediately after image acquisition is necessary to remove inflow effect.

2769. An Investigation of the VASO Contrast Mechanism Reveals a Novel Method for Quantifying Cerebral Blood Flow

Manus Joseph Donahue[1], Hanzhang Lu[2], Craig Kenneth Jones[1], James J. Pekar[1], Peter Christian Marie van Zijl[1]
[1]Johns Hopkins University, Baltimore, Maryland, USA; [2]New York University, New York, New York, USA

Vascular space occupancy (VASO)-dependent fMRI is a novel imaging technique sensitive to microvascular CBV changes. We demonstrate that, at high resolution at 3T, VASO effects become too large to originate from CBV effects alone. We show that an arterial spin labeling contribution exists due to the use of a non-selective inversion pulse and that a large influence from CSF will cause VASO gray matter signal changes to become more negative than previously expected. When all contributions are considered, multi-TR VASO experiments can be designed that allow for extraction of CBF and CBV within a single pulse sequence.

2770. Resting-State Functional Connectivity Measured by VASO and BOLD

Yihong Yang[1], Hong Gu[1], Elliot A. Stein[1]
[1]National Institute on Drug Abuse, NIH, Baltimore, Maryland, USA

Synchronized low-frequency fluctuations in resting-state fMRI signal have been used to study functional connectivity. So far, BOLD contrast has been the dominant technique for resting-state fMRI, although ASL perfusion imaging has been used in a few studies. Since BOLD signal arises from the complex interplay of blood flow, blood volume and oxygen consumption, the relationship between resting-state fMRI signal and each of these physiological parameters is not clear. In this study, we attempted to use a blood-volume based fMRI contrast to examine the dependence of resting-state fMRI signal on a single physiological parameter.

2771. Cerebral Blood Volume: Measurement and Change

Robert Turner[1], David Thomas[1]
[1]University College London, London, England, UK

Techniques for measurement, by MRI and optical means, of cerebral blood volume (CBV) are compared and contrasted. At least three different physical quantities are commonly described by this term. The Monro-Kellie argument relating to CBV changes is reviewed, and a novel mechanism for the observed CBV changes during functional activation is proposed, with experimental predictions.

BOLD: Hemodynamic Responses

Room 4E Thursday 13:30 - 15:30

2772. Hemodynamic Response in Human Central Olfactory System

Jianli Wang[1], Robert Grunfeld[1], Mark D. Meadowcroft[1], Xiaoyu Sun[1], Erin Zimmermann[1], Paul J. Eslinger[1], Lukas Ansel[1], Michael B. Smith[1], Qing X. Yang[1]
[1]Penn State College of Medicine, Hershey, Pennsylvania, USA

The hemodynamic response function to odors was studied on eight normal human subjects with a single odor single strength stimulation fMRI paradigm. The hemodynamic response was modeled with different length of stimulations using SPM2. The hemodynamic response function modeled with shortened length of stimulation yielded stronger activation map at the same confidence level. This is quantitatively demonstrated by the activation volume in the primary olfactory cortex and the entire brain. These analyses indicate a rapid decay of hemodynamic signal responding to the odor after onset of stimulation.

2773. Laminar Analysis of the BOLD Hemodynamic Impulse Response

David Ress[1]
[1]Brown University, Providence, Rhode Island, USA

We used high-resolution (≤1-mm voxels) to measure the BOLD hemodynamic impulse response function (HIRF) in early visual cortex. The measured data were then aligned with a segmented reference volume to permit examination of the data as a function of depth in the gray matter. The shape and timing of the HIRF change with depth. In particular, we find that the "negative dip" is generally evident only in tissue near the pial surface.

2774. An Efficient Method for Obtaining Subject-Specific HRF Estimates in Event-Related fMRI

Hannah Devlin[1], Joseph T. Devlin[1], Mark Woolrich[1], Karla L. Miller[1], Peter Jezzard[1]
[1]University of Oxford, Oxford, Oxon, UK

We propose an efficient method for estimating the hemodynamic response function (HRF) in event-related design. The method uses optimised basis functions to obtain subject-specific HRF estimates from functional data. We demonstrate that applying the empirically derived HRFs to an independent data set significantly increases sensitivity to BOLD activation in three brain areas compared to using a standard (non subject-specific) HRF. Because the HRF is derived from normal functional data, this increase in sensitivity is achieved without requiring additional scan time.

2775. Reduction of Onset Variability of Event-Related BOLD Responses with Diffusion-Weighted Spin-Echo EPI

Ho-Ling Liu[1,2], Wan-Chun Kuan[1,3], Tieh-Chi Chu[3], Yung-Liang Wan[1,2], Yau-Yau Wai[1,2], Jiun-Jie Wang[1,2]
[1]Chang Gung University, Taoyuan, Taiwan; [2]Chang Gung Memorial Hospital, Taoyuan, Taiwan; [3]National Tsing Hua Univ., Hsinchu, Taiwan

This study aimed to evaluate the temporal properties and variability of hemodynamic responses measured by the diffusion-weighted spin-echo (DWSE) BOLD-fMRI and compare with spin-echo (SE) and gradient-echo (GE) results. Six healthy volunteers participated in the study. Brief visual stimulations were applied in repeated single-trials for the DWSE50 (b=50 s/mm2), DWSE200 (b=200 s/mm2), SE and GE experiments. Statistically earlier onset times and remarkably smaller variance at the same CNR level (controlled by averaging different number of trials) were observed with the DWSE than the GE data, with SE performed in between. No significant difference was found between DWSE50 and DWSE200.

2776. Somatosensory fMRI at 1.5, 3 and 7 T: Measuring BOLD Signal Changes

Wietske van der Zwaag[1], Kay Elizabeth Head[1], Andrew Peters[1], Susan Francis[1], Penny Gowland[1], Richard William Bowtell[1], Peter Morris[1]
[1]University of Nottingham, Nottingham, UK

Somatosensory fMRI studies using isotropic 3 mm resolution, were compared across magnetic field strengths (1.5, 3 and 7 T). fMRI datasets were acquired at four echo times per field strength to allow estimation of the change in R2*. The paradigm involved vibrotactile stimulation of the thumb. ROI's in SI were selected and R2* changes in these regions were computed for each field strength. Delta-R2* was found to increase with field strength.

2777. The Effect of Global Cerebral Vasodilation on Focal Activation Hemodynamics

Bojana Stefanovic[1], Jan M. Warnking[2], Karin M. Rylander[3], Bruce Pike[2]
[1]NINDS, NIH, Bethesda, Maryland, USA; [2]MNI, McGill University, Montreal, Quebec, Canada; [3]MNI, McGill University, Montreal, Quebec, Canada

We investigated the effect of pronounced CO2-induced elevation in baseline cerebral blood flow (CBF) on BOLD and CBF responses to functional activation. A strong attenuation of the BOLD response (by ~57% in motor cortex and ~55% in the visual cortex) and a slight decline in the CBF response (by ~14% in MC and 2% in VC) was observed at significantly elevated basal perfusion level. The findings call for independent quantification of resting CBF in BOLD fMRI studies that involve subjects and/or conditions with markedly elevated global perfusion.

2778. Habituation of the BOLD Response in fMRI of the Human Auditory and Visual Cortex

Mark A. Elliott[1], Luke Bloy[1], Justin Hulvershorn[1]
[1]University of Pennsylvania, Philadelphia, Pennsylvania, USA

An event-related fMRI study which activated the primary auditory and visual cortices was examined for trends in habituation of the BOLD hemodynamic response during the course of the experiment. In both functional regions, the average time-to-peak of the BOLD response decreased significantly with increasing stimulus count. Converely, the amplitude of the BOLD response increased during the experiment, though statistical significance was only observed in the visual cortex. Unlike other studies which have shown reduced and delayed responses (habituation) to successive lengthy stimuli, this result reveals that brief event-related stimuli produced a larger and faster response, consistent with a neuro-vascular priming effect.

2779. Modeling the Temporal Dynamics of the Positive and Negative BOLD Response

Yashar Behzadi[1], Thomas Liu[1]
[1]UCSD, La Jolla, California, USA

As compared to the positive BOLD responses, the negative BOLD responses exhibited greater initial delays, faster rise times, increased peak amplitudes, and a less pronounced post-stimulus undershoot. In this work, we examine the dynamics of the positive and negative BOLD responses using an arteriolar compliance model of the cerebral blood flow response (CBF)coupled with a Balloon model of the venous compartment. The model simulations suggest that the observed differences may be a result of the varying contribution of smooth muscle compliance during increases and decreases of neural activity.

2780. Intravascular BOLD Signal Contribution to the fMRI ADC Changes in the IVIM Model Regime

Tao Jin[1], Fuqiang Zhao[1], Ping Wang[1], Seong-Gi Kim[1]
[1]University of Pittsburgh, Pittsburgh, Pennsylvania, USA

At 9.4T, the functional ADC changes were measured for TE=16ms, 28ms, and 60ms using small diffusion weighting (b<200s/mm2). The observed ADC changes were highly dependent on the TE. For TE=28ms and 60ms, the ADC changes were small (<1%) and mainly located at the middle of the visual cortex, and were attributed to an increase in the arterial blood volume and flow. Much larger ADC changes (~2%) on both the middle and the surface of the cortex were observed for TE=16ms. These results indicated that an intravascular BOLD signal change can contribute to the functional ADC contrast, and the contribution can be significant if the IV signal change is large.

2781. Caffeine Reduces the Initial Dip in the Visual BOLD Response

Joy Liau[1], Yashar Behzadi[1], Thomas Liu[1]
[1]UCSD Center for fMRI, La Jolla, California, USA

The initial dip in the BOLD signal reflects early transient increases in deoxyhemoglobin and appears to be a more specific marker of neural activity than the later positive BOLD signal. However, the initial dip is not consistently observed in human fMRI studies, possibly due to confounding factors, such as medication and drug usage. In this study we show that caffeine (200 mg dose) can reduce or eliminate the initial dip in the visual BOLD signal. Caffeine usage may therefore be a major source of variability in the detection of the initial dip in human fMRI studies.

2782. An Analysis of Micro- And Macro-Vasculature Blood Flow Characteristics During Graded Stimulation

Yi-Ching Lynn Ho[1, 2], Esben Thade Petersen[1, 2], Xavier Golay[1, 3]
[1]National Neuroscience Institute, Singapore, Singapore; [2]Nanyang Technological University, Singapore, Singapore; [3]A*STAR, Singapore, Singapore

Using a recently developed arterial spin labeling (ASL) model-free method with and without crusher gradients to obtain information on both macro- and microvascular blood flow, it was observed that with an increase in contrast in visual stimulation, both arterial and microvascular arrival times were significantly shortened while cerebral blood flow and arterial blood volumes were increased. CBF increases were relatively muted compared to the stark changes in flow velocities. These results pose interesting questions and also have implications for CBF quantification.

2783. Functional Asymmetry in Human Visual Cortex as Revealed by fMRI

Zhaohui M. Liu[1, 2], Xiaoping Hu[1]
[1]Emory University, Atlanta, Georgia, USA; [2]WPI & UMass Medical School, Worcester, Massachusetts, USA

Human visual performance is not uniform across visual field. The origin of this inhomogenity is not clear. Phenomena of horizontal vertical asymmetry (HVA), implying better performance on horizontal than vertical meridian, and vertical meridian asymmetry (VMA), implying better performance in lower than upper visual field, have been studied in psychophysical terms. However, there is little fMRI evidence for these two asymmetries. We investigated these two asymmetries using fMRI and found HVA and VMA can be revealed by fMRI across different subjects. The results of this study may help us understand the neuronal base of these asymmetry phenomena.

2784. Hemodynamics and Nonlinearities of BOLD Response to Ultrashort Visual Stimulation (5ms - 1s)

Kamil Uludag[1], Baris Yesilyurt[1], Kamil Ugurbil, [1,2]

[1]Max-Planck-Institute for biological Cybernetics, Tübingen, Germany; [2]Center for Magnetic Resonance Research, Minnesota, Minneapolis, USA

It has generally been suggested that one cannot temporally resolve alterations in neural activity in the range of milliseconds using BOLD signal since hemodynamic response evolves in seconds. However, in this study using ultrashort visual stimulus durations ranging from 5 milliseconds to 1 second we investigated the hemodynamic response and nonlinearity of BOLD response. We were able to show that 1) a BOLD response to stimulus durations as short as 5 ms is detectable in humans; b) BOLD responses to different stimulus durations are highly non-linear and c) non-linearities depend not only to stimulus duration but also on intensity.

2785. Minimization of Post-Stimulus Undershoot in Heavily Diffusion-Weighted Functional Magnetic Resonance Imaging

Takayuki Obata[1], Moyoko Tomiyasu[1], Kenichi Kashikura[2], Yoshiyuki Hirano[1], Hiroi Nonaka[1], Masaya Hirano[3], Hiroo Ikehira[1]

[1]National Institute of Radiological Sciences, Chiba, Japan; [2]Gunma Prefectural College of Health Sciences, Maebashi, Gunma, Japan; [3]GE Yokogawa Medical Systems, ltd., Tokyo, Japan

To reveal relationship between post-stimulus undershoot in diffusion-weighted functional MRI (DWI) and slow return to baseline in ADC transient feature, we analyzed post-stimulus undershoot in heavily DWI (b=1400 s/mm2), and compared it with that in weakly DWI (b=200 s/mm2). The DWI (b=1400 s/mm2) transient feature showed minimization of the post-stimulus undershoot, significantly different from that in DWI (b=200 s/mm2). The same physiological mechanism might cause undershoot minimization in DWI (b=1400 s/mm2) response and a slow return in the ADC transient feature after stimulation.

2786. Study of Post-Stimulus BOLD Undershoots Between Lateral Geniculate Nucleus and Primary Visual Cortex in Cat Brain

Xiao-Hong Zhu[1], Yi Zhang[1], Nanyin Zhang[1], Jaekeun Park[1], Wei Chen[1]

[1]CMRR, Radiology Department, University of Minneasota Medical School, Minneapolis, Minnesota, USA

One well observed phenomenon in the fMRI study of visual stimulation is a prolonged post-stimulus BOLD undershoot in the activated visual cortex (V1) although whether the undershoot is due to the delayed CBV or $CMRO_2$ recovery compared to that of CBF is still under debated. It is interesting to examine if the same phenomena also exists in the sub-cortical lateral geniculate nuclei (LGN), which is the first stage for processing visual information. We have conducted an fMRI study using a cat model and flicking visual stimulation to examine the BOLD undershoots in both LGN and V1. We only observed undershoot in V1 but not in LGN indicating the dissociation of BOLD dynamics between them.

2787. The Contribution of the BOLD Poststimulus Undershoot to Block-Design Subtraction Outcomes in Cognitive fMRI

Jed A. Meltzer[1], Michiro Todd Negishi[1], R. Todd Constable[1]

[1]Yale University, New Haven, Connecticut, USA

A mixed block / event-related fMRI study was used to explore the extent to which transient aspects of the hemodynamic response give rise to activation and deactivation in a block design contrast between two memory tasks, one of which requires the hippocampus but induces hippocampal deactivation. In the hippocampal-dependent condition, enhanced post-stimulus undershoots were observed, in some regions equal to or exceeding the magnitude of the early positive BOLD peak observed in that condition. This work provides evidence that the relative magnitude of the poststimulus undershoot can determine whether a region is considered activated or deactivated at the block-design level.

2788. Differential BOLD Hemodynamics in Young and Elderly: Emphasis on Post-Stimulus Undershoot

Kaundinya Gopinath[1], Christina Wierenga[2], Timothy Conway[3, 4], Bruce Crosson[3, 4], Richard Briggs[1]

[1]UT Southwestern, Dallas, Texas, USA; [2]UC San Diego, San Diego, California, USA; [3]University of Florida, Gainesville, Florida, USA; [4]VA Medical Center, Gainesville, Florida, USA

Differences in the BOLD hemodynamic response, with particular emphasis on the post-stimulus undershoot, were studied between young adults (20 subjects; 20-34 yrs) and elderly (20 subjects; 68-84 yrs) populations, using a semantic picture naming task. Young adults exhibited significantly greater magnitude of the post-stimulus undershoot than elderly adults in a number of areas in the brain. These areas also exhibited correlated differences in the amplitude and width of the positive BOLD response. The elderly showed greater undershoot magnitudes in a few areas, often correlated with a greater positive BOLD HDR amplitude.

2789. A Two-Compartment BOLD Model of an Infusion of Contrast Agent

Nicholas Paul Blockley[1], Susan T. Francis[1], Penny A. Gowland[1]

[1]University of Nottingham, Nottingham, UK

A model for the BOLD response has been developed taking account of arterial and venous compartments and the effect of a contrast agent infusion. This model has been fitted to CBV data obtained from an infusion experiment and the fitted parameters are consistent with those values obtained in previous studies where flow data has been employed in the model. However, the results show discrepancies in the fit of the post-stimulus undershoot, suggesting that both volume and oxygenation change play a role in its form.

2790. Physical Source of fMRI Signal Phase Change: Theory and Simulation

Fuqiang Zhao[1, 2], Ping Wang[2], Tao Jin[2], Xiaoping Hu[1], Seong-Gi Kim[2]
[1]Emory / Georgia Tech University, Atlanta, Georgia, USA; [2]Pittsburgh University, Pittsburgh, Pennsylvania, USA

The phase change of MRI signal was previously observed in both BOLD fMRI and CBV-weighted fMRI at 4.7T and 9.4T. The observed phase changes are not caused by the intravascular (IV) signal since the IV signal is minimal at high magnetic field; they are not caused by the temperature change during the stimulation either since the phase changes of the BOLD and CBV-weighted fMRI are opposite. The fMRI signal phase changes are caused by the volume-averaged magnetization change due to the Lorentz Sphere effect during the stimulation and its demagnetization. Theory of using the ¡®Lorentz Sphere' concept to describe the magnetic field inhomogeneity of the heterogeneous cortex was provided. A simulation based on the real fMRI data was conducted. The simulation results are consistent with the experimental results.

2791. Source of Phase Change in BOLD and CBV-Weighted fMRI

Fuqiang Zhao[1, 2], Ping Wang[2], Tao Jin[2], Tsukasa Nagaoka[3], Noam Harel[3], Xiaoping Hu[1], Seong-Gi Kim[2]
[1]Emory / Georgia Tech University, Atlanta, Georgia, USA; [2]Pittsburgh University, Pittsburgh, Pennsylvania, USA; [3]University of Minnesota, Minneapolis, Minnesota, USA

The phase change of MRI signal was observed in both BOLD fMRI and CBV-weighted fMRI. For BOLD fMRI, the positive phase change is dominated in the large draining vein area and the negative phase change is also detected in the surrounding area. For CBV-weighted fMRI, the negative phase change is dominated in the middle cortex area where the highest CBV change occurred during the brain activation and the positive change is detected in the surrounding area. All these phase changes are caused by the volume-averaged magnetization change due to "Lorentz Sphere'effect and the demagnetization effect. The fMRI phase change can be used as the complementary information for the mechanism studies of fMRI and help to interpret the physiology change associated with the brain activation.

2792. Phase Map Based Investigation of Intravoxel Signal Dephasing in Gradient Echo MRI

Alexander Rauscher[1, 2], Jan Sedlacik[1], Markus Barth[3], Stephan Witoszynskyj[4], Jürgen R. Reichenbach[5]
[1]IDIR, FSU, Jena, Thuringia, Germany; [2]Core Unit MR Methods, Jena, Germany; [3]Radboud University, Nijmegen, Netherlands; [4]Medical University, Vienna, Austria; [5]IDIR, FSU, Jena, Germany

Macroscopic inhomogeneities of the static magnetic field cause anaccelerated T2` decay due to intravoxel spin dephasing. In lowresolution gradient echo images this leads to a poor signal-to-noiseratio in magnetic inhomogeneous regions. We present a method based onunwrapped single-echo, high resolution phase images that allows tosimulate and investigate intravoxel signal dephasing and BOLDsensitivity in a systematic manner. The method can be used todetermine optimum scan parameters (in-plane resolution, echo time,slice thickness, obliqueness of the imaging plane, z-shimming) on anindividual basis.

2793. Contribution of Residual BOLD Susceptibility-Induced Local Field Gradients in Diffusion fMRI

Shin-ichi Urayama[1], Toshihiko Aso[1], Takashi Hanakawa[1], Naohide Fukuyama[1], Denis Le Behan[1, 2]
[1]Kyoto University Graduate School of Medicine, Kyoto, Japan; [2]CEA, Orsay, France

A transient decrease of water diffusion has been reported during activation of visual cortex using a MRI sequence sensitized to diffusion by a monopolar pair of gradient pulses. However, this sequence could be contaminated by BOLD susceptibility-induced background field gradients. Diffusion fMRI acquisitions were made at 3T from a monopolar sequence and from a bipolar sequence immune to background gradients. The signal increase during activation at b=1200 s/mm2 was similar for both the monopolar and bipolar sequences suggesting susceptibility effects in the monopolar sequence were not significant. By contrast, the signal change at b=2400 s/mm2 was significantly lower for the monopolar sequence, suggesting that BOLD induced background gradients were significantly reducing the local b value and the diffusion activation effect.

fMRI: Combining with Other Modalities

Room 4E Thursday 13:30 - 15:30

2794. Regional Homogeneity: Epileptic Patients vs. Healthy Volunteers

Huafu Chen[1, 2], Xia Zhao[2], Dezhong Yao[1], Guangming Lu[3], zhiqiang zhang[3], Jia-Hong Gao[2]
[1]University of Electronic Science and Technology of China, chengdu, sichuan, People's Republic of China; [2]University of Texas Health Science Center at San Antonio, San Antonio, Texas, USA; [3]Nanjing General Hospital of PLA, Nanjing, Jiangsu, People's Republic of China

The Kendall's Coefficient (KCC) correlation method was proposed previously to measure a regional homogeneity (ReHo) of the time series of a given voxel with those of its nearest neighbors in a voxel-wise analysis. Based on a hypothesis that ReHo could be modulated by epileptic neuronal activity, KCC analysis may be utilized to measure the similarity of time series of neuron activation on the resting-state fMRI data sets to distinguish the activity patterns between epileptic patients and healthy subjects.

2795. Simultaneous Recording of ERP and fMRI for Cortical Source Imaging

Chang-Hwan Im[1], Zhongming Liu[1], Nanyin Zhang[1], Wei Chen[1], Bin He[1]
[1]University of Minnesota, Minneapolis, Minnesota, USA

Feasibility of continuously and simultaneously recording visual evoked potentials (VEPs) with fMRI was assessed by quantitatively comparing cortical source images by means of receiver operating characteristic (ROC) curve analysis. The averaged EEG source images coincided well with simultaneously acquired fMRI activations. Strong correlation was found between the cortical source images of VEPs recorded inside and outside the scanner. Application of fMRI prior information strengthened correlation between estimated source images as well as resulted in source estimates with higher spatial resolution. The present results demonstrate that reliable cortical source images can be acquired during simultaneous fMRI scanning and they may be used for multimodal functional source imaging studies.

2796. Simultaneous fMRI and EEG Source Localization with Visual Motion Stimuli

Myung Ho In[1], Soo Yeol Lee[1], Min Hyoung Cho[1], Byung Hee Han[1], Tae-S Kim[1], Jae Yong Han[2]
[1]Kyung Hee University, Yongin, Kyungki, Republic of Korea; [2]Gachon Medical School, Incheon, Republic of Korea

We have acquired fMRI and 32-channel EEG data simultaneously with a 3.0 Tesla MRI system. For the simultaneous data acquisition, we used an interleaved fMRI-EEG scheme with visual motion stimuli. The ballistocardiogram (BCG) artifacts in the EEG data have been removed by the correlative template subtraction technique. The EEG source localizations have been performed with the cortically constrained inverse BEM model. The temporal information from EEG source localization has been used to resolve the temporal behavior of fMRI. We found that the EEG source localization can be used to enhance the temporal performance of fMRI if activated regions are separated far apart.

2797. Biological Parametric Mapping

Ramon Casanova[1], Ryali Srikanth[1], Aaron Baer[1], Paul J. Laurienti[1], Ann M. Peiffer[1], Jonathan H. Burdette[1], Satoru Hayasaka[1], Joseph A. Maldjian[1]
[1]Wake Forest University School of Medicine, Winston-Salem, North Carolina, USA

In this work we describe a novel form of multimodal integrative image analysis that we have called biologic parametric mapping (BPM). BPM probes functional imaging data using biological measures from other imaging methodologies. The BPM toolbox was developed in Matlab and includes multimodal voxel-wise anova, ancova, and correlation. An SPM insertion tool developed with the toolbox feature permits the use of SPM statistical inference and visualization tools. Simulated and real data is presented demonstrating the power of the BPM toolbox.

2798. A Combined NIR and BOLD fMRI Study of Transient Activation and Deactivation

Lin Tang[1], Christopher J. Cannistraci[1], Blake Niederhauser[2], Malcolm J. Avison[1], John C. Gore[1]
[1]Vanderbilt University Institute of Imaging Science, Nashville, Tennessee, USA; [2]Vanderbilt University, Nashville, Tennessee, USA

Synopsis not available.

2799. Automated Real-Time Tracing of Functional MRI Signals from Multiple Cortical Areas

Seung-Schik Yoo[1], Heather M. O'Leary[1], Hae-Jeong Park[2], Jong-Hwan Lee[1], HyunWook Park[3], Lawrence P. Panych[1], Ferenc A. Jolesz[1]
[1]Brigham and Women's Hospital, Harvard Medical School, Boston, Massachusetts, USA; [2]Yonsei University College of Medicine, Seoul, Republic of Korea; [3]KAIST, Daejon, Republic of Korea

We developed a method to measure functional MRI signals from multiple cortical areas simultaneously in real-time. Using 3 Tesla clinical MRI, the brain anatomy was automatically registered, segmented, and labeled with anatomical and Brodmann's area nomenclature. Subsequently, the blood-oxygenation-level-dependent (BOLD) signal activities were measured from the segmented regions-of-interest, and displayed in real-time. The method was implemented and tested on three healthy volunteers during the performance of the hand motor task using even-related design. In order to further examine the utility of monitoring brain activities without the prior knowledge of the timing of the task, one subject was allowed freely engage the task, and associated brain activities were successfully detected on-fly from the motor-related neural substrates.

2800. Fx3MRI: Simultaneous fMRI Scanning in an Open System

Frank Gerardus Cornelis Hoogenraad[1], Elizabeth A. Moore[2], Frits de Graaf[1], Fredy Visser[1], Johan W. de Jong[1], Mark Stoesz[3], Ad L. Moerland[1]
[1]Philips Medical Systems, Best, The Netherlands, Netherlands; [2]Philips Medical Systems, London, UK, UK; [3]Philips Medical Systems, Cleveland, Ohio, USA

In this experiment we show the possibility of simultaneously scanning 3 subjects in an open MRI scanner, during a simple fMRI experiment with a motor paradigm. fMRI analysis is performed on all subjects simultaneously and in real-time. Clear activation is shown in all subjects showing the feasibility of scanning multiple subjects and thus creating possibilities for experiments whereby interaction between subjects is measured by fMRI.

fMRI: Measurement Techniques

Room 4E Thursday 13:30 - 15:30

2801. A New Method to Record 2D- Movement Kinematics During Functional Magnetic Resonance Imaging (fMRI)

Tammar Kushnir[1], Bjoern Hauptmann[2], Ronen Sosnik[3], Oded Smikt[3], Eli Okon[3], Tamar Flash[3], Avi Karni, [14]
[1]The Chaim Sheba Medical Center, Tel Hashomer, Israel; [2]University Berlin, Berlin, Germany; [3]The Weizmann Institute of Science, Rehovot, Israel; [4]Haifa University, Haifa, Israel

We present a relatively simple fMRI compatible, 2D-movement kinematics recording system that allows one to quantitatively analyze the type, speed and accuracy of drawing and writing-like upper limb movements with high temporal and spatial resolution during fMRI studies. The system consists of a plastic pen with fiber optics and a halogen light power source (placed outside the magnet room), a translucent plastic board (workspace), CCD camera and a PC with a video-capture card. Behavioral experiments using a commercially available digitizer tablet have demonstrated the reliability of the kinematics data, while the quality of brain imaging data acquired concurrently was unaffected.

2802. Characterization and Suppression of System Noise Due to Scanner Instability in fMRI Using a SMART PHANTOM BOLD Simulator

Yu Li[1], Qun Zhao[2], Mark Limkeman[1], Tim Conway[2], Keith D. White[2], Keith McGregor[2], Bruce Crosson[2]
[1]Invivo Diagnostic Imaging, Gainesville, Florida, USA; [2]R&D Brain Rehabilitation Research Center, Gainesville, Florida, USA

In BOLD-based fMRI, system noise source due to scanner instability reduces the contrast-to-noise ratio and adversely affects determination of hemodynamic response functions. The present study aims to characterize fMRI noise correlated to scanner instability experimentally, and to remove this noise in HRF deconvolution. A SMART PHANTOM BOLD simulator was used to calibrate the system noise from a Siemens Allegra 3T scanner. Human subjects were scanned in an event-related task paradigm. Based on the calibrations, the subjects' HRF deconvolutions were denoised.

2803. Reduced fMRI Signal Sensitivity in Motor Areas When Cued by MRI-Compatible Apparatuses

Hsin-Mei Chen[1], Wan-Chun Kuan[1], Yau-Yau Wai[1, 2], Yung-Liang Wan[1, 2], Ho-Ling Liu[1, 2]
[1]Chang Gung Univ., Taoyuan, Taiwan; [2]Chang Gung Memorial Hospital, Taoyuan, Taiwan

This study aimed to evaluate the influence to BOLD signal and noise in motor areas while a movement task was cued with different modalities (goggle, headphone and leg-tapping by experimenter). Five healthy volunteers participated in the study. Greater activation extent was found with leg-tapping, comparing to the other conditions (p=0.004 when comparing with the headphone condition). The results agreed with the slightly decreased SNR when goggle or headphone was used. The study suggests that even when MRI-compatible apparatuses were used for fMRI experiments, researches may still need to consider the possible lessening of SNR and sensitivity.

2804. A New Stimulus for Isolating Optokinetic Eye Movement from Smooth Pursuit

Caroline K.L. Schraa-Tam[1], Aad van der Lugt[1], Marion Smits[1], Maarten A. Frens[1], Philippus C.A. van Broekhoven[1], Josef N. van der Geest[1]
[1]ErasmusMC, Rotterdam, ZH, Netherlands

The traditional small-field optokinetic stimulation with an optokinetic drum or a striped tape would elicit regular eye movement pattern without apparent self-motion. However, this kind of stimulation activates both the pursuit and the optokinetic system for eye movement. We hypothesize that the use of limited lifetime dots moving coherently in one direction would only elicit optokinetic eye movement without the involvement of smooth pursuit eye movement. Our study has, therefore, revealed evidence that the use of moving limited lifetime dots as stimulus elicits only optokinetic eye movements without the involvement of smooth pursuit eye movements.

2805. Evaluation of a Two Compartment Gel Phantom for fMRI

Anders Nilsson[1], Anthony Brian Waites[1], Peter Mannfolk[1], Johan Olsrud[1]
[1]Lund University, Lund, Sweden

Several phantoms simulating the BOLD effect have recently been presented and is an effective alternative to simulated data to optimise fMRI methods. In this work a two compartment agarose gel phantom with different T2 is presented and evaluated with respect to reproducibility between multiple scan sessions. The phantom could be manufactured with specific relaxation properties and the signal time course was found to be reproducible. The phantom is proposed as a tool for optimisation of image parameters and regular QA in fMRI applications.

2806. BOLD Phantom Investigations of the Relationship Between Blood Oxygenation, Flow Variation and Intra- And Extra-Vessel Signal Change

Lan Jiang[1], Roderick McColl[1], Ralph P. Mason[1]
[1]UT Southwestern Medical Center, Dallas, Texas, USA

Deoxyhemoglobin (dHbO2) is paramagnetic and can serve as an endogenous contrast agent causing signal loss in echo planar MR images. BOLD technique has been used to evaluate physiological information in the clinic. This aim is to investigate the relationship between blood oxygenation, flow variation and intra-and extra-vessel BOLD signal change via in vitro phantom system. Experiment was performed in 4.7T scanner. Our results showed BOLD signal in vessel is sensitive to both flow and oxygenation variation. Intriguingly, a significant signal decrease was found in extra-vessel regions when oxygenation was increased. It may contribute to observations interpreted as the steal effect.

2807. Improved Design for Absolute Skin Conductance Response Measurement During Motor fMRI

Bradley J. MacIntosh[1, 2], Richard Mraz[1], Vladimir Verpakhovski, Simon J. Graham[1, 2]
[1]Imaging Research, Sunnybrook & Women's CHSC, Toronto, ON, Canada; [2]University of Toronto, Toronto, ON, Canada

Understanding the basis for fluctuations in fMRI time series baseline has become an active area of research. It remains to be seen whether output from the sympathetic nervous system, which regulates attention and arousal, affects the rest conditions in fMRI experiments that involve volitional movements. As a result, we have developed a novel quantitative skin conductance response (SCR) system that can be used as a surrogate measure of sympathetic activity. We describe the implementation of the SCR system and provide evidence to suggest the addition of complimentary behavioural information helps to refine the interpretation of fMRI signals.

2808. Predictive Eye Estimation Regression (PEER) for Simultaneous Eye Tracking and fMRI

Stephen Michael LaConte[1], Scott J. Peltier[1], Keith A. Heberlein[1], Xiaoping P. Hu[1]
[1]Emory University/Georgia Tech, Atlanta, Georgia, USA

In this paper, we introduce PEER (Predictive Eye Estimation Regression) - a simple, image-based approach to eye tracking that can occur simultaneously with fMRI experiments. We believe this to be the first report of eye tracking based on MR images. Multivariate SVM regression was used to model the relationship between acquired EPI images and fixation position. This SVM model can be used to estimate fixation in fMRI runs with matched sequence parameters. Successful eye tracking during extended periods of fixation and eye movement were demonstrated on a TR-by-TR basis. Notably, PEER does not alter fMRI results and can be applied at any fMRI site.

2809. Recording of Ultrafast (600-Hz) EEG Oscillations with Amplitudes in the Nanovolt Range During fMRI- Acquisition Periods

Petra Ritter[1], Frank Freyer[1], Robert Becker[1], Kimitaka Anami[2], Gabriel Curio[1], Arno Villringer[1]
[1]Berlin Neuroimaging Center, Berlin, Germany; [2]National Center Hospital for Mental, Nervous, and Muscular Disorders, Tokyo, Japan

Our data show that the synchronization between EEG and fMRI in combination with a "steppingstone" sequence allows recording of low-amplitude high-frequency EEG oscillations (HFOs) possibly reflecting cortical spiking activity during truly simultaneous fMRI acquisition. Amplitude modulations of the HFOs in the range of 50 nV induced by varying stimulus repetition rates were resolved.

2810. Failure to Detect Magnetic Source Dephasing Corresponding to ERP Generation

Lin Tang[1], James Christopher Gatenby[1], Malcolm J. Avison[1], John C. Gore[1]
[1]Vanderbilt University Institute of Imaging Science, Nashville, Tennessee, USA

Magnetic Source MRI, Auditory Oddball, ERP, P300, N170

2811. Using MR Magnitude Imaging to Determine the Spatial Distribution of the Changes of Magnetic Field Induced by Sub-μA Electric Current

Ruiwang Huang[1], Oleg Posnansky[1], Avdo Celik[1], NJ Jon Shah[1]
[1]Research Centre Juelich, Juelich, Germany

The spatial distribution of the changes of magnetic field generated by the ultraweak electric current has been measured from the phantom using 1.5T MR scanner. The results demonstrated that the changes of magnetic field induced from sub-[mu]A electric current are detectable by using the MR magnitude imaging in the presence of the magnetic susceptibility enhancement.

2812. BOLD Sensitivity in Multiecho Sequences

Penny Anne Gowland[1], Richard William Bowtell[1]
[1]Unversity of Nottingham, Nottingham, UK

This abstract aims to determine the optimal echo times for BOLD sensitivity in a multi-echo sequence and to determine how sensitivity varies between regions of different relaxation rates, taking into account the interaction between imaging bandwidth and echo time. For a single echo acquisition, the bandwidth should be as narrow as possible given the limitation of image distortions, up to a maximum echo time of 1.5 T2*. In a multi-echo sequence if the signals are combined by weighted summation, the optimum echo interval is reduced, and the variation in BOLD sensitivity to the underlying tissue T2* is increased.

2813. On the Effect of Flow and Modest Diffusion Weighting in fMRI

Maarten Versluis[1, 2], Hans Hoogduin[1]
[1]University Medical Center Groningen, University of Groningen, Groningen, Netherlands; [2]Philips Medical Systems, Best, Netherlands

The effect of flow and modest diffusion weighting in fMRI is studied using a newly developed method which allows a cyclic variation of the amount of flow or diffusion weighting over the scanned volumes in a fast multi-echo SENSE EPI sequence. The multi-echo acquisition allows the creation of $T2^*$ and I_0 maps. Results show that in the motor cortex I_0 reduces and $T2^*$ increases upon execution of a motor task. The reduction in I_0 is significantly larger when flow or diffusion weighting is applied while changes in $T2^*$ remain nearly constant. This indicates that the intravascular contribution to the BOLD effect at 3T is negligable.

2814. Determination of Acoustic Noise Characteristics and Development of Silent EPI for Auditory fMRI

Sebastian Schmitter[1], Michael Amann[1], Lothar Rudi Schad[1]
[1]Deutsches Krebsforschungszentrum, Heidelberg, Germany

As the acoustic MR scanner noise often amounts up to 110 dBA, auditory fMRI signals are often deteriorated. In this work, the scanner's acoustic response function is examined and a silent EPI sequence is developed. The timing of the gradient switching is adapted to the response function. This reduces the acoustic noise by more than 50% compared to a conventional EPI sequence with the same imaging parameters.The silent sequence, which is applied in an auditory fMRI experiment, shows significant activation of the primary auditory cortex and the left middle frontal gyrus.

2815. Frequency Stabilization Using Finite Impulse Response Filtering for BOSS fMRI at 3T

Ming-Long Wu[1], Teng-Yi Huang[2], Pei-Hsin Wu[1], Ming-Chung Chou[1, 3], Cheng-Yu Chen[3], Hsiao-Wen Chung[1, 3]
[1]National Taiwan University, Taipei, Taiwan; [2]National Taiwan University of Science and Technology, Taipei, Taiwan; [3]Tri-Service General Hospital, Taipei, Taiwan

Blood Oxygenation Sensitive Steady State (BOSS) fMRI is suitable for detecting small functional changes in blood oxygenation, which however also leads to native sensitivity to field instability during consecutive scans. In this study, we proposed a frequency stabilization scheme based on finite impulse response (FIR) filtering to achieve substantially reduced frequency drifts. As compared with manufacturer-supplied frequency stabilization scheme, FIR filtering further improved detection of functional signals, such that experimental reproducibility of BOSS fMRI was greatly increased. Applications to visual fMRI at sub-millimeter spatial resolution show activations with good registration on the cortex.

2816. Transient State BOSS fMRI for a Further Increase in Sensitivity

Pei-Hsin Wu[1], Ming-Long Wu[1], Teng-Yi Huang[2], Hsiao-Wen Chung[1, 3]
[1]National Taiwan University, Taipei, Taiwan; [2]National Taiwan University of Science and Technology, Taipei, Taiwan; [3]Tri-Service General Hospital, Taipei, Taiwan

Blood Oxygenation Sensitive Steady-state (BOSS) fMRI is a new method for obtaining functional contrast without showing distortions from image warping or signal dropout. In this study, we show that the BOSS functional sensitivity could be further increased by acquiring imaging data in the transient state, as evidenced from both simulations and experimental results. The results suggest that parallel imaging techniques could thus be combined with BOSS to increase transient-state BOSS contrast and speed up acquisition without substantial signal loss. High-resolution BOSS imaging experiments from checkerboard visual stimulations verified the advantages of parallel BOSS imaging.

2817. Parallel Imaging in Functional MRI: Comparison of Spiral SENSE and GRAPPA and of Calibration Update Schemes

YoonChung Kim[1], Douglas C. Noll[1]
[1]University of Michigan, Ann Arbor, Michigan, USA

In this study, we compare the performance of spiral SENSE and spiral GRAPPA in functional data in terms of SNR in time course, error in image domain compared to fully sampled data and number of activated pixels. Our study also focused on finding reasonable approach to updating calibration data such as sensitivity map or GRAPPA weights in case of minimal or significant head motion. The result shows SENSE has less error in image domain when compared with fully sampled data. Using moving average of calibration data seems to work well in both situation where there is minimal or significant motion.

2818. Feasibility of High Resolution 3D fMRI with Whole Brain Coverage

Yanle Hu[1], Gary H. Glover[1]
[1]Stanford University, Stanford, California, USA

In high resolution fMRI studies, higher SNR is always desired. Although using a surface coil can increase the SNR, it will limit the study to a certain area of the brain. The 3D method has increased SNR compared to that of the 2D method. However it suffers from low temporal resolution especially when whole-brain coverage is wanted and multi-shot spirals are used to achieve the high in-plane resolution. This problem can be mitigated by using the UNFOLD technique. In this work, we showed the feasibility of high resolution fMRI studies over the whole brain with a reasonable temporal resolution.

2819. Partial K-Space Acquisition Method for Improved SNR Efficiency and Temporal Resolution in 3D fMRI

Yanle Hu[1], *Gary H. Glover*[1]
[1]Stanford University, Stanford, California, USA

Due to the existence of physiological noise, the SNR efficiency and temporal resolution for 3D fMRI can be improved by using a partial-k method. In the partial-k method, doubling high frequency components result in twice as much noise from those components. However, in sum these contributions are still relatively small compared to those from low frequency components where physiological noise dominates. For the same scan time, the benefit from increased time frames will overcome the SNR decrease by using the partial-k method which will result in a better SNR efficiency and temporal resolution.

2820. Doubling EPI Resolution by Acquiring Two K-Space Lines Per Readout Gradient Reversal Using TRAIL

Andrew Nicholas Priest[1, 2], *Enrico De Vita,*[23], *Roger John Ordidge*[3]
[1]University Hospital Hamburg-Eppendorf, Hamburg, Germany; [2]UCL Hospitals NHS Trust, London, UK; [3]University College London, London, UK

The resolution of single-shot EPI is restricted because of limits on the readout length due to T2* decay and distortion. A new method is presented which doubles the resolution of EPI in the phase-encode direction without increasing the readout length, based on a modification of the recently published 'Two Reduced Acquisitions InterLeaved' (TRAIL) method (Priest *et al*, MRM 2004). Distortion is reduced by a factor of two. The correction of N/4 Nyquist ghosts in the images is also addressed. The new method is complementary to, and could in principle be combined with, existing approaches such as parallel imaging.

2821. Isotropic, High-Resolution fMRI at 7T Using 3D Stack-Of-Segmented EPI

Karla L. Miller[1], *Graham C. Wiggins*[2], *Christopher J. Wiggins*[2]
[1]Oxford University, Oxford, UK; [2]Massachusetts General Hospital, Charlestown, Massachusetts, USA

High-resolution fMRI can reveal a wealth of information about cortical structure. However, conventional 2D approaches have severely limited resolution in the through-plane direction. This work presents a 3D stack-of-segmented EPI sequence for high-resolution fMRI, which is capable of achieving small, isotropic voxels with reasonable volume acquisition times. In combination with an 8-channel receive coil at 7T, we demonstrate robust activation maps with resolution as high as 0.58x0.58x0.58 mm^3 (0.19 mm^3).

2822. Echo Train Shifted Multi-Echo FLASH for Functional MRI of the Human Brain at Ultra-High Spatial Resolution

Dirk Voit[1], *Jens Frahm*[1]
[1]Biomedizinische NMR Forschungs GmbH, Goettingen, Germany

This work describes the development of a novel technique for fMRI of the human brain at 0.135 µl voxel resolution for a whole section. The approach is based on a multi-echo FLASH sequence with unipolar traversals of k-space in the frequency-encoding dimension and echo train shifting to avoid amplitude discontinuities in the phase-encoding dimension. These strategies ensure a smooth point-spread function and eliminate image ghosting artefacts without the need for any post processing. Multi-echo FLASH studies at 300 µm in-plane resolution (no interpolation) and 1.5 mm slice thickness revealed robust activations in primary visual areas in response to binocular stimulation.

2823. Effects of Local Susceptibility Gradients on Spiral K-Space Trajectory and Effective Echo–Time (TEeff)

Sumati Krishnan[1], *Douglas C. Noll*[1]
[1]University of Michigan, Ann Arbor, Michigan, USA

Rapid imaging methods such as echo-planar and spiral imaging often suffer severe distortions due to the presence of background field inhomogeneities. In particular, the gradient of the background field variation produces a local distortion, which leads to a shifting and skewing of the k-space trajectory. In this work we present a theoretical framework that illustrates the effect of background gradients on the echo-time, TE. We present an experimental verification that localised susceptibility gradients result in an effective local echo-time (TE) that can shift the k-space trajectory either away or toward the "true" k-space center, for the forward and reverse spiral acquisitions respectively.

2824. Counterbalancing Mismatched Magnetization Differences in Functional Arterial Spin Labeling

Yi-Ching Lynn Ho[1], *Esben Thade Petersen*[1], *Xavier Golay*[1]
[1]National Neuroscience Institute, Singapore, Singapore

Functional arterial spin labeling (ASL) allows imaging of cerebral blood flow (CBF) changes during neuronal activity, but the large dynamic changes in CBF defy the assumption of steady-state condition. Large fluctuations of estimated CBF values would therefore often result around the transitions between activation and baseline blocks. Functional runs typically have even volumes per block, resulting in regular control-label occurrences. We propose a simple method of counterbalancing the mismatched magnetization differences by acquiring equal numbers of control and labeled scans for each particular phase in the stimulation cycle by using an odd number of acquisitions between stimulation epochs.

2825. Echo Time Dependence of Basal Ganglia Activation at 3T During Motor Task

Stephane Lehericy[1, 2], Kamil Ugurbil[2], Pierre-Francois Van de Moortele[2]
[1]University Pierre et Marie Curie, Paris, IDF, France; [2]University of Minnesota, Minneapolis, Minnesota, USA

It is generally accepted that BOLD response should be higher when the echo time (TE) matches the T2* of the structure. Therefore, adapting the TE of BOLD gradient echo fMRI time series to T2* may improve signal detection in the globus pallidus, where ferromagnetic particles deposit normally with age, leading to reduced T2*. Activation volume did not change significantly at TE = 42 ms (T2* of the putamen) compared to TE = 28 ms (T2* of the globus pallidus) in these two structures. Therefore, there was no gain in decreasing the TE to match the T2* of the globus pallidus.

2826. Magnetic Field Effect of Neuronal Currents on MRI: A Snail Ganglia Study

Tae S. Park[1], Soo Yeol Lee[1], Ji-Ho Park[1], Min Hyoung Cho[1], Byung Hee Han[1], Sang Yeon Lee[1]
[1]Kyung Hee University, Yongin, Kyungki, Republic of Korea

We observed the response of magnetic resonance signal to neuronal activity in the dissected snail ganglia to investigate faster responding components than the BOLD component. To activate the snail ganglia in synchronization with magnetic resonance signal measurement, we applied 30 Hz electrical stimulation with the pulse width of 2 s to the ganglia just before the 90 degree RF pulse. The magnetic resonance signal intensity, measured with the volume selection pulse sequence in a 3.0 T MRI, decreased about 2.97¡¾1.10 % when the ganglia were activated by the electrical stimulation. We think that the signal decrease is partly due to the magnetic field produced by the neuronal current and partly to the Lorentz force exerted on the neurons when they were firing.

2827. Theoretical Modeling of MRI Signal Changes Induced by Neuronal Magnetic Fields

Yiqun Xue[1], Jinhu Xiong[1]
[1]University of Iowa, Iowa City, Iowa, USA

Whether MRI can be used for direct detection of neuronal activity is a matter of debate. We present here an improved current-dipole model to compute neuronal magnetic field (NMF) generated by neural firing and to calculate MRI signal changes resulting from the NMF. Each dendrite was modeled as a modified current-dipole and interactions between diploes were considered. Our results show that NMF can potentially generate a few percent changes in MRI magnitude signals. Phases of MRI signal tend to be destructively added and are insensitive to NMF in the activated region. Our modeling implies that direct MRI detection of neuronal activity is possible

fMRI Noise and Artifact Compensation

Room 4E Thursday 13:30 - 15:30

2828. Improved Sensitivity of Spinal fMRI by Using Physiological Recordings in General Linear Model Analysis

Patrick W. Stroman[1]
[1]Queen's University, Kingston, Ontario, Canada

Errors are inherent in all fMRI results, and require efforts to minimize their occurrence. In spinal fMRI an error in a single pixel can have more of an impact than in the brain because of the smaller spatial extent of the spinal gray matter. The dominant source of errors in spinal fMRI is hypothesized to be the motion of the cord and artefacts from respiration. Therefore all of the sources of errors would be related to cardiac and respiratory motion. A means of reducing the errors was investigated based on inclusion of physiological recordings in the general linear model.

2829. A Bootstrap Method for Removing Aliased Cardiac and Respiratory Effects in Volumetric Resting State Connectivity Data

Mark J. Lowe[1], Ken E. Sakaie[1]
[1]Cleveland Clinic Foundation, Cleveland, Ohio, USA

Resting state connectivity studies have become increasingly present in the functional neuroimaging literature. It is desireable to acquire volumetric data when assessing functional connectivity in the brain. Aliased cardiac and respiratory fluctuations in volumetric BOLD-weighted data can significantly reduce the specificity of the connectivity effect. A method is proposed to use the large vessel MRI signal present in the data as an estimator of these effects in combination with RETROICOR to remove them.

2830. Efficacy of Data-Driven Respiration Compensation Methods in fMRI Data at 1.5T

Shuowen Hu[1], Akshay D. Kothari[1], Thomas M. Talavage[1]
[1]Purdue University, West Lafayette, Indiana, USA

Respiratory noise is a component of interest in fMRI data. This work identifies those circumstances in which respiratory noise compensation techniques are beneficial. A magnitude-only Gaussian band-reject filter and a complex image-space estimation and removal procedure were assessed for improvement (relative to no compensation) in true and false detections of synthetic activations superimposed on human baseline fMRI data. A clear benefit in the specificity of detected activation is obtained using complex image-space filtering algorithms. However, there is no compelling evidence that respiration-induced noise compensation algorithms are effective when the rate of stimulus presentation is not near the rate of respiration.

2831. Functional MRI of the Human Amygdala Avoiding Susceptibility Artefacts

Carmen Morawetz[1], Claudia Lange[2], Petra Holz[1], Jürgen Baudewig[1], Godehard Weniger[2], Eva Irle[2], Peter Dechent[1]
[1]MR-Research in Neurology and Psychiatry, Medical Faculty, Georg-August-University, Göttingen, Germany;
[2]Department of Psychiatry and Psychotherapy, Medical Faculty, Georg-August-University, Göttingen, Germany

fMRI of the human amygdala is of great interest for scientists in the fields of psychiatry and psychology. However, this region is especially vulnerable to susceptibility artefacts. In the present study we tested some suggested simple modifications of a standard gradient-echo EPI-sequence at 3 Tesla with special emphasis on raw image quality and activation of the amygdala in response to emotional face stimuli. We found that a combined reduction of TE from 36ms to 27ms and section thickness from 4mm to 2mm is sufficient to record reliable activation of the amygdala.

2832. Calibration of fMRI by Simulating BOLD Contrast in the Living Human Brain

Qun Zhao[1], Keith D. White[1]
[1]University of Florida, Gainesville, Florida, USA

fMRI has been widely used for studying human brain activities through blood-oxygenation-level-dependent (BOLD) contrast. However, calibration of fMRI is challenging because repeatability is imperfect even using the same paradigm with the same subject. We here describe SmartCoils, a device which reliably simulates BOLD contrast signals electronically. These simulated signals are proposed as a means for calibrating the sensitivity to detect BOLD contrast in the presence of "physiological noise" produced by a living human brain.

2833. Realistic Computer Generated fMRI Phantoms with Motion Correlated Susceptibility Artifacts

Ning Xu[1], Yong Li[1], J Michael Fitzpatrick[1], Benoit M. Dawant[1], Victorial L. Morgan[1], David R. Pickens[1]
[1]Vanderbilt University, Nashville, Tennessee, USA

As an extension of work on computer-generated phantoms, more accurate, realistic phantoms are generated by integrating image distortions and signal loss caused by susceptibility variations. With the addition of real motions and activations determined from actual fMRI studies, these phantoms can be used by the fMRI community to assess post processing algorithms such as motion correction, distortion correction, and signal loss compensation methods with higher fidelity. We perform activation analysis on these phantoms based on a block paradigm design using SPM, and the results demonstrate that susceptibility artifacts affect activation detection and thus represent a critical component of phantom generation.

2834. Complex Activation Suppresses Venous BOLD in GE-EPI fMRI Data

Daniel B. Rowe[1], Andrew S. Nencka[1]
[1]Medical College of Wisconsin, Milwaukee, Wisconsin, USA

The phase portion of complex-valued fMRI time courses is generally discarded. There is useful temporal information in the phase regarding vascular effects that can be used to suppress activation in undesirable voxels. Nearly all fMRI studies derive functional "activation" based on magnitude-only data. Recently a magnitude activation from complex data with constant phase model was introduced (Rowe and Logan, 2004). Recently interest has arisen to suppress large-vessel BOLD signals postacquisition in high-resolution gradient echo EPI fMRI data by a phase regressor model (Menon, 2002) and the aforementioned complex model. However these two image analysis methods have not been examined together.

2835. Test-Retest Reliability of fMRI Using SmartPhantom

Qun Zhao[1, 2], Keith D. White[1, 2], Tim Conway[1, 2], Keith McGregor[1], Bruce Crosson[1, 2]
[1]University of Florida, Gainesville, Florida, USA; [2]VA Medical Center, Gainesville, Florida, USA

Functional MRI is one of the most demanding imaging applications. It uses blood oxygenation level dependent (BOLD) contrast to map task-related human brain activation. Test-retest reliability of such mappings has been studied using different paradigms and analysis strategies. Many factors, such as within- and between-subject sources of variance, can compromise repeatability. SmartPhantom, a device which provides repeatable and reproducible simulated BOLD activations by radio-frequency coils and a remote-controlled computer, eliminates such variances from the reliability test. Multiple sessions of SmartPhantom data were acquired from a 3T scanner, and the reliability was analyzed using mutual information based divergence measurements.

2836. Application of Distortion Correction Procedures to Spin-Echo EPI for fMRI Studies in the Temporal Lobe

Karl Vincent Embleton[1], Matthew A. Lambon Ralph[1], Geoff J. M. Parker[1]
[1]University of Manchester, Manchester, UK

Spin-echo EPI was used as the basis for an fMRI experiment to detect activation in regions of temporal lobe where changes in magnetic susceptibility precluded the use of gradient-echo EPI due to intravoxel dephasing. Additionally, different ways of applying a previously described distortion correction using dual-direction kspace traversal were tested. These included acquiring data with both interleaved opposite direction kspace traversal and data with a single direction traversal and a dual traversal pre-scan. Cluster analysis of group data showed significant activation in temporal lobe and other brain regions from a distortion corrected dataset

2837. Local Dynamic Shimming for Slice-Wise Image Acquisition

Jung-Jiin Hsu[1], Gary H. Glover[1]
[1]Lucas Center for Imaging, Stanford University School of Medicine, Stanford, California, USA

To compensate for field inhomogeneity caused by local structures, we have implemented active, local dynamic shimming in which shim fields are generated by adjustable electric currents and have a smaller scale of spatial variation, comparable to the target region. The shim currents are optimized slice-wise and output in accordance with the slice being scanned. It is found that the dynamic shimming is effective and offers convenience and flexibility in shim coil design. Thepresent study is focused on the brain for fMRI; nevertheless, other areas of problematic geometry may also benefit.

2838. Dynamic Updates of R_2^* and Field Map in fMRI Using a Spiral-In Quick-Spiral-Out K-Space Trajectory

Valur Olafsson[1], Jeffrey A. Fessler[1], Douglas C. Noll[1]
[1]The University of Michigan, Ann Arbor, Michigan, USA

Collecting fMRI data using a fully sampled spiral-in spiral-out has been shown to give increased activation volumes. The spiral-in is more robust to susceptibility related signal dropouts, while the spiral-out increases BOLD-weighting. We propose to collect fMRI data using a fully sampled spiral-in and a spiral-out with 4-fold reduced FOV, but same resolution as the spiral-in. This increases temporal resolution without losing the advantage spiral-in spiral-out acquisition gives. The data was reconstructed using a joint reconstruction of the dynamic changes in R_2^* and field map. Results show a large increase in activation volumes relative to collecting only spiral-in data.

2839. Double-Sampled EPI in fMRI: A Ghost-Free Acquisition Method with Inherent Field Map Correction Capability

Yi-Ru Lin[1, 2], Shang-Yueh Tsai[1], Teng-Yi Huang[3], Ming-Long Wu[1], Cheng-Yu Chen[4], Hsiao-Wen Chung[1, 4], Nan-kuei Chen[2], Kenneth Kwong[5]
[1]National Taiwan University, Taipei, Taiwan; [2]Brigham and Women's Hospital - Harvard Medical School, Boston, Massachusetts, USA; [3]National Taiwan University of Science and Technology, Taipei, Taiwan; [4]Tri-Service General Hospital, Taipei, Taiwan; [5]MGH-HMS-MIT Athinoula A. Martinos Center for Biomedical Imaging, Charlestown, Massachusetts, USA

Double-sampled EPI (DSEPI) is proposed as a means to improve fMRI quality. Compared with conventional EPI, DSEPI removes Nyquist ghost by separating the k-space data traversed in opposite frequency-encoding directions. The increased geometric distortion due to longer acquisition time is corrected using a field map, which can be generated using the difference in TE for the two sets of data. Experiments on visual fMRI showed SNR improvements by a factor slightly larger than the expected increase from signal averaging alone. It is concluded that DSEPI with inherent field map correction capability is an effective approach for fMRI studies.

2840. Quantification of Motion-Related Artifacts in Simulated fMRI Data Using ICA

Ivana Drobnjak[1], Christian F. Beckmann[1], Mark Jenkinson[1]
[1]University of Oxford, Oxford, UK

We have demonstrated that Independent Component Analysis (ICA) on fMRI data can be used to spatially and temporally identify motion-related artefacts. The used data included rigid-body motion effects for in-plane rotations, including the interactions with B0 inhomogeneities. The data was generated using a recently developed fMRI simulator (POSSUM).

2841. Detection and Correction of Motion-Induced Susceptibility Changes in fMRI Time Series of the Alert Monkey

Josef Pfeuffer[1, 2], Thomas Steudel[1], Hellmut Merkle[3], Nikos K. Logothetis[1]
[1]MPI Biol. Cybernetics, Tuebingen, D, Germany; [2]Siemens Medical Solutions, Erlangen, D, Germany; [3]NIH/NINDS, Bethesda, Maryland, USA

Functional MR imaging in the alert, behaving monkey is increasingly used to provide both electrophysiological and MR data in the context of neuroscience research. So far, several labs reported fMRI data from the awake monkey, but none of them studied and optimized systematically the effects of monkey's motion to fMRI time series. Here, were report a significant refinement of acquisition and correction strategies to minimize magnetic susceptibility artifacts induced by respiration, mouth, and body movement. Real-time feedback of sensor signals correlated with MR navigator data was combined with targeted animal training and fMRI correction strategies.

2842. An Improved ICA Filter for Motion and Ballistocardiogram Artefacts in EEG Recorded in the MR Scanner

Richard Andrew J. Masterton[1, 2], David F. Abbott[1], Steve Fleming[1], Graeme D. Jackson[1, 2]
[1]Brain Research Institute, Melbourne, Victoria, Australia; [2]University of Melbourne, Melbourne, Victoria, Australia

EEG recordings in the MR scanner are subject to ballistocardiogram (BCG) and motion artefacts. Independent components analysis (ICA) has been used to filter the BCG artefact using a combination of correlation with the ECG and visual inspection to identify and remove artefact-related components. Here we present an improvement to this method using an independently acquired measure of subject motion to automatically select components for removal. Our method removes the need for visual selection of components and also generalises this method to filter all motion artefacts rather than only BCG artefacts. We demonstrate this method using simulated and real EEG.

2843. Constrained ICA–based Ballistocardiogram and Electrooculogram Artifacts Removal from EEG Signals Acquired Inside MRI

T. Rasheed[1], T.-S. Kim[1], Y.-K. Lee[1], M. H. In[1], W. H. Lee[1], S. Y. Lee[1], S. Y. Lee[1]
[1]Kyung Hee University, Yongin, Gyeonggi, Republic of Korea

Ballistocardiogram (BCG) and Electrooculogram (EOG) artifacts are troublesome in the simultaneous acquisition of EEG and MRI. We propose a new method for removing both artifacts simultaneously from the EEG signals acquired inside MRI using constrained Independent Component Analysis (cICA). With the designed reference functions for the BCG and EOG artifacts, cICA identifies the independent components (ICs) corresponding to the reference functions. Then artifact-removed EEG signals are reconstructed after removing the identified ICs. The performance of the "cICA with reference" technique has been evaluated by examining the artifact ICs and power spectrum of EEG, EOG, and EKG signals. The results show that this new approach is effective and should be useful in simultaneous EEG and fMRI studies.

2844. BOLD Baseline 'activity' of Auditory Cortex During Silence

Iain D. Wilkinson[1], Mike D. Hunter[1], Simon B. Eickhoff[2], Thomas WR Miller[1], Thomas F. Farrow[1], Peter WR Woodruff[1]
[1]University of Sheffield, Sheffield, South Yorkshire, UK; [2]Institut for Medicine (IME), Research Center Juelich, Germany

Auditory hallucinations occur in health and disease implying the existence of neuronal activity in the absence of external stimuli. This work sought to characterise human auditory BOLD signal during silence. Baseline activity was examined in 12 normal subjects using a SPARSE-EPI protocol. Data show that functionally defined auditory cortex is characterised, during silence, by intermittent episodes of significantly increased signal in up to 30% of its volume. Significant contrast was detected in left primary/association auditory cortices and anterior cingulate. The findings support the presence of a vascular response-mechanism that may underpin spontaneous auditory hallucinations.

fMRI Data and Statistical Analysis Method

Room 4E Thursday 13:30 - 15:30

2845. Sparse PCA a New Method for Unsupervised Analyses of fMRI Data

Karl Sjöstrand[1, 2], Torben E. Lund[2], Kristoffer H. Madsen, [1,2], Rasmus Larsen[1]
[1]Technical University of Denmark, Copenhagen, Denmark; [2]Copenhagen University Hospital, Hvidovre, Denmark

Exploratory analysis of functional MRI data aims at revealing known as well as unknown properties in a data-driven manner devoid of hypotheses on the time course of the hemodynamic response. Common approaches include clustering methods, principal component analysis (PCA) and in particular independent component analysis (ICA). ICA assumes that the measured activity patterns consist of linear combinations of a set of statistically independent source signals. We introduce a competing method for fMRI analysis known as sparse principal component analysis (SPCA). We argue that SPCA is less committed than ICA and demonstrate similar results, with better suppression of noise.

2846. Accurate Localization of Functional Brain Activity Using Structure Adaptive Smoothing

Karsten Tabelow[1], Jörg Polzehl[1], Volodia Spokoiny[1], Jonathan P. Dyke[2], Linda A. Heier[2], Henning U. Voss[2]
[1]Weierstrass Institute for Applied Analysis and Stochastics, Berlin, Germany; [2]Weill Medical College of Cornell University, New York, New York, USA

We applied a structurally adaptive smoothing method, Adaptive Weights Smoothing (AWS), to presurgical fMRI data of 26 epilepsy/tumor patients. AWS adapts to different shapes of activation areas by generating a spatial structure corresponding to similarities and differences between time series in neighbored locations. In numerical simulations, AWS has been shown to be superior over Gaussian smoothing with respect to the accurate description of the shape of activation clusters and less false detections. We found that AWS and Gaussian smoothing yield occasionally significantly different results, and we present examples showing different aspects of the superiority of AWS in presurgical planning.

2847. Temporal Clustering Analysis: 3D Versus 2D Approaches in Functional MRI Studies

Xia Zhao[1], Jie Tang[2], Jia-Hong Gao[1]
[1]University of Texas Health Science Center at San Antonio, San Antonio, Texas, USA; [2]Shenzhen Sinorad Medical Electronics Inc., Shenzhen, Guangdong, People's Republic of China

Temporal clustering analysis (TCA) is a promising data-driven technique for fMRI data analysis. All previous TCA studies were performed on single-slice fMRI datasets. In practice, multiple-slice or 3D fMRI data acquisition are employed in clinical application. The effectiveness of TCA on multiple-slice datasets are evaluated in this study. Both 2D (single-slice) and 3D (multiple-slice) approaches of TCA were used and compared on simulated and *in vivo* fMRI data. Our results demonstrate that best performance of TCA can be achieved by using a 3D approach when only those slices having brain activations were included in data analysis.

2848. Multisubject Fuzzy Cluster Analysis of Functional MRI

Hesamoddin Jahanian[1, 2], Seyyed Mohammad Shams[2], Gholam Ali Hossein-Zadeh[2], Hamid Soltanian-Zadeh[1, 2]
[1]Image Analysis Lab. Radiology Dept., Henry Ford Health System, Detroit, Michigan, USA; [2]Control and Intelligent Processing Center of Excellence, University of Tehran, Tehran, Iran

In fMRI multisubject analysis, some methods suppose specific assumptions on the signal and noise structure which may not hold for fMRI data. A novel method, based on fuzzy cluster analysis is introduced to address this issue. In the proposed method a vector is obtained for each voxel using the cross-correlation analysis of its corresponding time-series. Then, a feature space is derived from the obtained vectors. Fuzzy cluster analysis of the proposed feature space generates the activation map. The proposed method is evaluated using an experimental visual task dataset (consisting of 11 subjects). The results show that the proposed method improves the activation detection sensitivity.

2849. Exploring Spatiotemporal Pattern of Human Motor Cortex from fMRI by Self-Clustering Independent Components with Partner Matching

Zhishun Wang[1], Bradley S. Peterson[1]
[1]Columbia University and NYSPI, New York, New York, USA

It has been agreed that the human motor cortex may include three interacted regions, namely primary motor cortex (M1), supplementary motor area (SMA) and premotor area (PMA). However, the spatial patterns of these areas have not been exactly exhibited by reconstructing activation maps of neuronal activities under a cognitive motor task. And the temporal patterns and relationships between the spatial and temporal patterns in these areas remains unclear or elusive. The aim of this study was to investigate the spatio-temporal patterns of neuronal processing in human motor cortex using functional magnetic resonance imaging (fMRI)combined with self-clustering of independent components based on the proposed Partner Matching algorithm.

2850. Multivariate Analysis of Resting State fMRI in Major Depression Using SeedPLS

Richard Cameron Craddock[1], Svetlana Ye Masalovich[2], Scott J. Peltier[3], Xiaoping Hu[3], Helen S. Mayberg[2]
[1]Georgia Institute of Technology, Atlanta, Georgia, USA; [2]Emory University, Atlanta, Georgia, USA; [3]Georgia Institute of Technology/Emory University, Atlanta, Georgia, USA

Analysis of functional connectivity with Cg25 in major depression from resting state fMRI scans using partial least squares. Extends findings in major depression from FDG PET scans.

2851. 2dTCA for Detection of Irregular, Transient fMRI Activation

Victoria L. Morgan[1], Yong Li[1], Bassel Abou-Khalil[1]
[1]Vanderbilt University, Nashville, Tennessee, USA

The Temporal Clustering Algorithm (TCA) has been developed in order to detect irregular, transient fMRI activation signals when the timing of the stimulus is unknown. Unfortunately, these methods can be especially sensitive to signal changes caused by motion and physiological noise. We have recently developed a modified TCA technique, 2dTCA, that can detect more than one different activation timing pattern within one dataset so that motion or noise can be detected separately from BOLD activation. This work demonstrates the increased sensitivity of 2dTCA over TCA in a set of phantoms with varying motion and one and two activation time courses.

2852. Independent Component Analysis in the Presence of Noise in fMRI

Dietmar Cordes[1], Rajesh Nandy[2]
[1]University of Washington, Seattle, Washington, USA; [2]UCLA, Los Angeles, California, USA

A noisy version of Independent Component Analysis (noisy ICA) is applied to simulated and real fMRI data. The noise covariance is explicitly modeled by a simple autoregressive (AR) model of order 1. The unmixing matrix of the data is determined using a variant of the FastICA algorithm based on Gaussian moments. The sources are estimated using the principle of maximum likelihood by modeling the source densities as asymmetric exponential functions. Complications of noisy ICA and degree of improvement in estimating fMRI sources are investigated.

2853. fMRI Data Analysis by Means of Locally Linear Embedding

Peter Mannfolk[1], Anthony Waites[1, 2], Anders Nilsson[1], Johan Olsrud[1]
[1]Lund University Hospital, Lund, Sweden; [2]Brain Research Institute, Melbourne, Australia

We describe a method for analyzing fMRI data using Locally Linear Embedding (LLE). The feasibility of the proposed algorithm is shown using both simulated as well as motor activation data. LLE can also be used together with other dimensionality reduction techniques and a number of extensions to make the method more robust have been suggested.

2854. Nonparametric Mixture Modeling for Mapping of Brain Activation Using Functional MRI Data

Rajesh Ranjan Nandy[1], Dietmar Cordes[2]
[1]University of California, Los Angeles, California, USA; [2]University of Washington, Seattle, Washington, USA

The hypothesis based approach to the analysis of fMRI data depends solely on the null hypothesis of non-activation. There is usually no specific alternate hypothesis primarily due to the difficulty in parametrically estimating the distribution of the observed test statistic under the hypothesis of activation. Previous approaches to this problem made several questionable assumptions. A novel nonparametric method is introduced in this abstract to formulate a mixture model by which the distribution of the test statistic under activation can be estimated. The statistical power of the test can also be accurately estimated using this method.

2855. Correlation Analysis of Functional Magnetic Resonance Imaging Data Using FPGA Hardware

Markus Gipp[1], Daniel Gembris[1], Gerhard Lienhart[1], Andreas Kugel[1], Reinhard Männer[1]
[1]Universität Mannheim, Mannheim, Germany

We are developing a medical explorative tool for the analysis of the functional brain connectivity, that will provide a high resolution correlation analysis for fMRI (functional magnetic resonance imaging) data and visualization of the results. For the calculation, additional hardware based on FPGAs (field programmable gate array) will be used to speed up the computation, where we estimate an acceleration by a factor of at least 10 compared to an optimized (pure) software implementation. This tool will generate high resolution correlation map results, likely in real-time, that can map functional connectivity in more detail.

2856. Distinguishing Robust Brain Activations Using Consistency Maps

Epifanio Bagarinao[1], Kayako Matsuo[2], Toshiharu Nakai[2], Yoshio Tanaka[1]
[1]National Institute of Advanced Industrial Science and Technology, Tsukuba City, Ibaraki, Japan; [2]National Center for Geriatrics and Gerontology, Obu, Aichi, Japan

In incremental analysis, a technique used in real-time fMRI, each image is incorporated into the analysis one after the other generating a series of activation maps for each added image. Here, we utilized this series of activation maps to construct a gconsistency maph. Consistency maps can be used to distinguish robustly active voxels from recently activated ones and to extract voxels activated early in the task, pieces of information not readily available in activation maps. An ROC analysis showed that consistency maps could also be used to efficiently minimize spurious activations that can occur any time during the scan.

2857. Wavelet-Based Statistical Analysis of fMRI Activation Images

Radu Mutihac[1]
[1]University of Bucharest, Bucharest, Romania

Analysis of an fMRI block-based visual stimulation paradigm was comparatively performed by wavelet analysis and statistical parametric mapping (SPM) based on Gaussian Random Field Theory (RFT). The voxels were isotropic and the same general linear model (GLM) was employed in both SPM and the discrete wavelet transform (DWT) approach. Consequently, an equivalent spline degree for which the low-pass part of the wavelet analysis is basically equivalent to SPM can be computed. The results for two biorthogonal transforms, 3D fractional-spline wavelets and 2D+Z fractional quincunx wavelets, are presented.

2858. Statistical Inference for Wavelet-Denoised Statistical Parametric Maps

Ryali Srikanth[1], Ramon Casanova[1], Paul J. Laurienti[1], Ann M. Peiffer[1], Joseph A. Maldjian[1]
[1]Wake Forest University School of Medicine, Winston-Salem, North Carolina, USA

We present a novel method for thresholding wavelet-denoised statistical parametric maps. Current wavelet-denoising methods produce smoothed statistical maps that then require another thresholding step in the spatial domain. The choice of this threshold has thus far been arbitrary. In our proposed framework, a rejection region is fixed for the wavelet-denoised maps, and the achieved false discovery rate (FDR) is estimated. Various techniques were used to assess the FDR control and their performance was evaluated using both simulated and *in vivo* fMRI data. The methods accounting for spatial correlation of SPMs performed better than methods that do not.

2859. Dynamic Monitoring of the Brain Activation Under Visual Stimulation Using fMRI - The Advantage of a Sliding Window Analysis

Toshiharu Nakai[1], Epifanio Bagarinao[2], Kayako Matsuo[1], Yuko Ohgami[3], Chikako Kato[4]
[1]National Center for Geriatrics and Gerontology, Ohbu, Aichi, Japan; [2]AIST, Tsukuba, Ibaragi, Japan; [3]Ochanomizu University Graduate School of Humanitics and Science, Bunkyo-ku, Tokyo, Japan; [4]Toyohashi Sozo College, Toyohashi, Aichi, Japan

The temporal change of the t-statistics in the V1 and V4 under visual stimuli covering different visual fields with or without coloring was estimated using a sliding window analysis based on a general linear model. By applying a correlation analysis to the time series of t-statistics, it was suggested that the activity in the V4 was bilaterally organized, and the altering color stimuli gave stronger stimulation to the V1 than did the BW stimuli. A sliding window analysis will be useful to evaluate the transition of neuronal activation in response to several sequential task conditions and the correlation among them.

2860. Time Course Analysis of T-Values in fMRI of Tool-Use Gestures with and Without Real Tools

Kayako Matsuo[1], Epifanio Tila Bagarinao[2], Yuko Ohgami[3], Toshiharu Nakai[1]
[1]National Center for Geriatrics and Gerontology, Obu, Aichi, Japan; [2]National Institute of Advanced Industrial Science and Technology (AIST), Tsukuba, Ibaraki, Japan; [3]Ochanomizu University, Bunkyo-ku, Tokyo, Japan

It is likely that motor schemes in our brain gradually formed through our everyday action. Then, the motor schemes may be differently modulated between the right- and the left-handed peoples. We examined the difference comparing tool-use gestures with and without real objects using fMRI. An incremental analysis technique, that investigates the time course of the t-value along the fMRI series, was applied to clarify the difference.

2861. The Degree of Bilateral Organization of the Motor Areas Under Unimanual Motor Execution - A Correlation Analysis Approach Using Dynamic Monitoring of T-Statistics

Toshiharu Nakai[1], Epifanio Bagarinao[2], Kayako Matsuo[1], Yuko Ohgami[3], Chikako Kato[4]
[1]National Center for Geriatrics and Gerontology, Ohbu, Aichi, Japan; [2]AIST, Tsukuba, Ibaragi, Japan; [3]Ochanomizu University Graduate School of Humanitics and Science, Bunkyo-ku, Tokyo, Japan; [4]Toyohashi Sozo College, Toyohashi, Aichi, Japan

The degree of bilateral organization of the motor areas under unimanual motor execution was evaluated using dynamic monitoring of t-statistics. Simple or complex finger movements were performed by the right or left fingers sequentially in one session. The t-statistics time series on the right and left sides highly correlated in the SMA, PMA and thalamus, while laterality of response was observed in the M1, cerebellum and SPL in response to switching of the motion side. These results may suggest that there is no distinction between the neuronal basis of unimanual complex movements and that of the bimanual movements.

2862. Functional MRI Incorporating Information on Voxel-Wise Tissue Volume Fractions

Yihong Yang[1], Wang Zhan[1], Hong Gu[1], Elliot A. Stein[1]
[1]National Institute on Drug Abuse, NIH, Baltimore, Maryland, USA

Functional MRI using ultra-fast image acquisition techniques (e.g. EPI) typically has a spatial resolution of 2-4 mm. Partial volume effects are unavoidable in such image voxels, which would affect sensitivity and specificity of fMRI techniques. We present here a method to incorporate information on tissue volume fractions into fMRI, and therefore enhancing its spatial capability in detecting brain activity. BOLD and ASL perfusion activation maps were assessed in terms of statistical power and tissue volume fractions of gray matter, white matter, and CSF in each voxel. Using the information of tissue volume fractions, activation can be constrained primarily in gray matter.

2863. Jackknife Assessment of Individual Subject Effects on a Mixed-Effect Group Level fMRI Analysis

Pradeep Chilakamarri Venkat[1], Tom Johnstone[1], Andy Alexander[1], Terry Oakes[1]
[1]University of Wisconsin-Madison, Madison, Wisconsin, USA

This study used a jackknife statistical analysis to quantify theimpact of intrasubject effect magnitude and variance on the group T-statistic in mixed effects linear model. Data weredrawn from 40 subjects who performed arapid event related task (Go/Nogo). A linear predictor forthe change in T-statistic upon dropping a single subject from theanalysis yielded R-squared = 0.69 when using the subject'sestimated effect magnitude and standard deviation, and R-squared= 0.89 when using their quotient. Even with this large group, individualsubjects caused changes in T-values of as much as 12%

2864. Comparison of the Signal-To-Noise Sensitivity of Different False Discovery Rate Methods

Murali Murugavel[1], John M. Sullivan[1], Karl G. Helmer[1]
[1]Worcester Polytechnic Institute, Worcester, Massachusetts, USA

The FDR (False Discovery Rate) has become a popular method of correcting for multiple comparisons in fMRI data analysis. These methods differ in their assumptions of the underlying correlation structure between fMRI voxels. Significant difference were obtained when comparing the result of five different FDR algorithms on the p-value results of a hand-flex task fMRI study. The algorithms were also applied to a data set that simulated different signal-to-noise levels. It was found that the differences in number of voxels deemed to be active was correlated tothe degree of assumptions made about the data correlation structure.

2865. Modified Weisskoff Test for Assessing fMRI Stability

Hans Hoogduin[1], Peter Koopmans[1], Remco Renken[1]
[1]University Medical Center Groningen, University of Groningen, Groningen, Netherlands

An adapted version of the test proposed by Weisskoff in 1996 is used to determine the amount of spatial correlations between voxels and the amount of high-pass filtering needed to remove global fluctuations in fMRI time series.

2866. Dotslashen: A Bayesian Decision Support System for fMRI Clinical Investigation

Ricardo Z.N. Vêncio[1, 2], Liana Guerra Sanches[1], Anita Taub[1], Carolina Araújo[1], Marcelo Maria Felix[1], Griselda Esther Jara Garrido[1], Carlos Alberto Bragança Pereira[2], Edson Amaro Jr.[1]

[1]Hospital Israelita Albert Einstein, São Paulo, SP, Brazil; [2]BIOINFO-USP Núcleo de Pesquisa em Bioinformática, São Paulo, SP, Brazil

Functional magnetic resonance imaging (fMRI) technique is gaining applicability in brain clinical investigation and one of the main challenges is the determination of what should be a "normal" fMRI exam. We are developing a normative fMRI database based on epidemiological sampling criteria from a population. We developed a Decision Support System to assist clinicians to decide whether a given brain activation, or lack of activation, is expected from a healthy subject or not. Thirty seven normal volunteers subdivided according to gender and age, participated of these study. Each participant performed fMRI tasks involving visual, motor, somatosensory, language and semantic paradigms comprising 16 conditions. The system make interpretable probabilistic statements such as "It is very likely that the majority of subjects have these regions activated" or "It is likely that almost no subject has these regions activated". This is achieved comparing the findings from the individual patient's fMRI exam with the normative database. Validation procedures for our system are now under clinical investigation. The web-availability and the user-friendness are the main features of our system. Future directions include efforts to continuously populate the database and integrate more refined neuropsychological parameters.

Breast

Room 4E Thursday 13:30 - 15:30

2867. Rapid Fat Suppression in MRI of the Breast with Short Binomial Pulses

Glen Morrell[1]

[1]University of Utah, Salt Lake City, Utah, USA

A method of water-only excitation is presented for MRI of the breast which achieves effective fat suppression for gradient recalled echo imaging in minimum time with the use of short binomial pulses. In contrast to conventional binomial frequency-selective pulses, these short pulses are applied without interpulse delay, allowing for very rapid spectrally selective excitation. Results are presented showing effective water excitation and fat suppression in breast MRI at 3.0 Tesla with total excitation time of 160 microseconds.

2868. Simultaneous Acquisition of Fat and Water Volume Images of the Breast with T2-Like Contrast Using Vastly Undersampled Isotropic Projection (VIPR) SSFP

Catherine J. Moran[1], Aiming Liu[2], Youngkyoo Jung[1], Frederick Kelcz[1], Ethan Brodsky[1], Thomas M. Grist[1], Sean B. Fain[1], Walter F. Block[1]

[1]University of Wisconsin, Madison, Wisconsin, USA; [2]Stanford University, Stanford, California, USA

Two-dimensional T2-weighting is used in conventional breast MRI as a means to better identify pathology. We combine a 3D acquisition method with Linear Combination SSFP to simultaneously acquire fat and water volumes of the breast with T2-like contrast in a single scan. Dual half-echo vastly undersampled isotropic projection acquisition (VIPR) provides sub-millimeter isotropic resolution. Fat and water volumes, capable of being reformatted in any orientation are created in less time than conventionally acquired 2D fat suppressed T2-weighted breast images.

2869. Improved DCE-MRI in Bilateral Breast Imaging with Fat Suppressed TRICKS

Neville Dali Gai[1], Manojkumar Saranathan[2], Sandeep Gupta[3], David Thomasson[1], Catherine Chow[1]

[1]National Institutes of Health, Bethesda, Maryland, USA; [2]Indian Institute of Science, Bangalore, Karnataka, India; [3]GE Healthcare, Hanover, Maryland, USA

We have applied a modified fat suppressed TRICKS sequence for breast DCE-MRI pharmacokinetic modeling (PKM) studies. The enhanced TRICKS sequence provides improved spatial and temporal resolution which is key to improved PKM analysis. Several studies of patients at high genetic risk of breast cancer were carried out. Qualitative analysis of breast lesions show improved visibility with the new technique. Kinetic maps show increased activity in enhanced lesions for the new as well as established technique. The new technique shows greater promise for improved differentiation between malignant and benign lesions in the breast.

2870. The Applicability of K-T GRAPPA for Dynamic Contrast Enhanced MRI

Feng Huang[1]

[1]Invivo Corporation, Gainesville, Florida, USA

Recently a k-t space based method k-t GRAPPA was proposed to exploit local temporal and spatial correlations for dynamic cardiac parallel imaging. This method is not limited to imaging parts with quasi-periodic motion and is potentially applicable to dynamic contrast enhanced imaging. In this work, it is shown that k-t GRAPPA is suitable for dynamic contrast enhanced imaging to improve the spatiotemporal resolution. Theoretical analysis and simulated dynamic contrast enhanced breast magnetic resonance imaging (DCE-BMRI) data were applied to confirm the claims.

2871. High Resolution Bilateral Dynamic Contrast Enhancement Breast Imaging

Jin Hyung Lee[1], Charles H. Cunningham[1], Brian A. Hargreaves[1], Logi Vidarsson[1], Dwight G. Nishimura[1], John M. Pauly[1], Bruce L. Daniel[1]

[1]Stanford University, Stanford, California, USA

Challenges in dynamic contrast enhanced (DCE) imaging includes the fast scan time and fat suppression. These problems have been previously addressed by using stack-of-spiral acquisitions with spectral-spatial excitations. However, bilateral breast exams have been difficult with such an approach due to large amounts of off-resonance in the large volume (both breasts). To solve this problem, dual-band spectral-spatial RF pulses that excite two slabs simultaneously, each with independently controlled shims and center frequency has been previously proposed. In this abstract, we present patient study results demonstrating the capability of such bilateral pulses incorporated into variable-density stack-of-spirals trajectories.

2872. "Direct Imaging" Method for Bilateral Breast Imaging Using Micro-Strip Coils

Jian-xiong Wang[1], Elizabeth Ramsay[1], Yangmei Li[1], Donald B. Plewes[1]

[1]Sunnybrook & Women's College Health Science Centre, Toronto, ON, Canada

For clinical breast cancer screening, contrast enhanced dynamic MR imaging should be conducted bilaterally in order to screen both breasts of a patient in a single clinic visit. This work presents a possible "Direct Imaging" method which takes advantage of the excellent isolation properties of micro-strip coils to obtain images of both breasts in the time usually required to scan a single breast.

2873. Contrast Agent Enhanced Breast Imaging with a Combined 3D Dual Echo Dixon and Parallel Imaging Technique

Jingfei Ma[1], Anthony T. Vu[2], Jong Bum Son[1, 3], Yinan Liu[1, 3], Adrian Knowles[2], Jason Polzin[2], Constance Lehman[4]

[1]University of Texas M. D. Anderson Cancer Center, Houston, Texas, USA; [2]GE Healthcare Technologies, Waukesha, Wisconsin, USA; [3]Texas A & M University, College Station, Texas, USA; [4]Seattle Cancer Care Alliance, Seattle, Washington, USA

Fat-suppressed 3D fast gradient echo imaging with contrast agent injection is presently in widespread clinical use. The existing approaches of fat suppression (FS), however, are sensitive to field inhomogeneity and suffer from partial application of FS pulses due to scan time constraints. In this work, we applied a combined 3D dual echo Dixon and parallel imaging (PI) technique to patient breast imaging. We demonstrate that for the same scan parameters, the Dixon technique achieves an equivalent speed, superior SNR, and more uniform and complete FS when compared to the regular 3D technique combined with PI.

2874. Comparisons of Water-To-Fat Ratios in Malignant, Benign Breast Lesions, and Normal Breast Parenchyma: An *In Vivo* Proton MRS Study

Sunitha B. Thakur[1], Lia Bartella[1], Nicole M. Ishill[1], Elizabeth A. Morris[1], Laura Liberman[1], David D. Dershaw[1], Hedvig Hricak[1], Jason A. Koutcher[1], Wei Huang[1]

[1]Memorial Sloan Kettering Cancer Center, New York, New York, USA

Water-to-Fat (W/F) ratios were calculated from proton MRS reference scans without water suppression and compared between malignant (n = 42), benign (n = 31) breast lesions, and normal breast parenchyma (n = 21). No significant difference was found between the benign lesions and normal tissue, while the malignant lesions had significantly ($p < 0.001$) higher W/F ratios compared to the benign/normal group. ROC curve analysis showed that the malignant group could be differentiated from the benign/normal group with high sensitivity and specificity. Addition of W/F ratio information may improve sensitivity of the choline-detection-based MRS method in breast cancer detection

2875. Breast Cancer Diagnosis Using Single-Voxel MRS Measurement of Apparent Diffusion Coefficient of Water

Curtis Andrew Corum[1], Adeka D. McIntosh[1], Angela L. Styczynski[1], Nathaniel J. Powell[1], Janice R. Kruse[1], Patrick J. Bolan[1], Michael Nelson[1], Tim H. Emory[1], Douglas Yee[1], Todd M. Tuttle[1], Lenore I. Everson[1], Michael Garwood[1]

[1]University of Minnesota, Minneapolis, Minnesota, USA

We report initial results with single voxel spectroscopy using diffusion weighting and LASER localization in breast tumors to measure the apparent diffusion coefficient of water. This is a quick, easy to implement method compared to image-based diffusion measurements. The apparent diffusion coefficient was compared to core biopsy pathology in 15 patients. The difference of the means of the benign and malignant groups is significant. The apparent diffusion coefficient was also compared to single voxel measurement of choline-containing compounds. A significant correlation was found, suggesting that single voxel apparent diffusion coefficient measurement may be useful as a marker for chemotherapy response.

2876. Can MRS Improve Our Ability to Distinguish Between Benign and Malignant Lesions?

Richard Kinh Gian Do[1], Linda Moy[1], Nouha Salibi[2], Cecilia L. Mercado[1], Kelly Anne McGorty[1], Mary Kitazono[3], Elizabeth Hecht[1]

[1]New York University, New York, New York, USA; [2]Siemens Medical Solutions, St. Louis, Missouri, USA; [3]Keck School of Medicine of USC, Los Angeles, California, USA

Single voxel spectroscopy was performed in combination with dynamic contrast enhancement breast MRI at 1.5T and 3.0T in 36 lesions. Two interpretations were performed for each lesion, initially based on the morphologic and kinetic features, and afterwards with the addition of the MRS data. While choline was not detectable in all cases of breast cancer, it was found in 4/5 patients whose MRI was initially interpreted as being negative. In all patients without breast cancer, MRS confirmed the low level of clinical suspicion as no choline was detected. The MRS data helped to distinguish benign from malignant breast lesions.

2877. Localized ^{13}C NMR Spectroscopy in the Human Breast *In Vivo*

Isabelle valentine Iltis[1], Patrick J. Bolan[1], Hellmut Merkle[1], Carl J. Snyder[1], Curtis Andrew Corum[1], Kamil Ugurbil[1], Michael Garwood[1], Pierre-Gilles Henry[1]

[1]Center for Magnetic Resonance Research, Minneapolis, Minnesota, USA

^{13}C magnetic resonance spectroscopy is a useful non-invasive tool allowing the assessment of tumor glucose metabolism, and has been used *in vivo* in animal models, and *ex vivo* in normal and cancerous human breast tissue. To our knowledge, it has never been applied to human breast *in vivo*. Using a ^{1}H localization and a polarization transfer sequence at 4T, we obtained for the first time localized ^{13}C spectra of the normal human breast *in vivo*. This approach will provide a new tool for detection and therapeutic monitoring of malignancies in the human breast.

2878. Improved Measurement of Choline-Containing Compounds in Malignant Breast Tumors Using Multiple Long-TEs Averaging MR Spectroscopy

Hyun-Man Baik[1], Min-Ying Su[1], O. Nalcioglu[1]

[1]University of California-Irvine, Irvine, California, USA

In this study we applied the multiple TEs averaging method with frequency-shift correction to quantify Cho concentration in malignant breast lesions. The measured Cho levels were compared to that measured using the standard method with a single TE obtained from the same voxel to demonstrate the feasibility of this technique for improving Cho quantification. After frequency correction a higher Cho peak was found, and the quantitative concentration was also higher compared to the results obtained using the conventional single TE technique. The results suggest that this technique can provide a higher sensitivity for Cho detection in breast tumors.

2879. Change of ADC Value of Breast Cancer in Patients Undergoing Neoadjuvant Chemotherapy: Preliminary Study

Guangwei Jin[1], Ningyu An[1], Youquan Cai[1]

[1]PLA General Hospital, Beijing, People's Republic of China

Many studies have shown that tumor water diffusion is associated with tumor cellularity. To our knowledge whether diffusion MRI can reflect response of breast cancer to neoadjuvant chemotherapy in the tumor cellular level by ADC (apparent diffusion coefficient) value has not been reported. Fifteen women (total of 17 tumors) with biopsy-confirmed breast cancer underwent bilateral breast MRI-DWI examination (GE EXCITE HD1.5T) prior to neoadjuvant chemotherapy (AT regimen) and after the first cycle therapy. Our results revealed ADC values of all tumors, except for 2, increased to different extent after neoadjuvant chemotherapy (P=0.001), although the size of most tumors shrunk only slightly after 1 cycle therapy. DWI can reflect response of breast cancer to neoadjuvant chemotherapy in the tumor cellular level by ADC value.

2880. Breast Cancer Evaluation Using Diffusion Weighted MR-Imaging – Prior to and Following Chemotherapy Can DWI Predict Chemotherapeutic Response?

Paul Weatherall[1], Qi Peng[2], Yao Ding[3], Roderick W. McColl[3], Debu Tripathy[3], Jonathan M. Chia[4], Ralph P. Mason[3]

[1]University of Texas Southwestern Medical Center, Dallas, Texas, USA; [2]University of Texas Health Science Center San Antonio, San Antonio, Texas, USA; [3]UT Southwestern Medical Center, Dallas, Texas, USA; [4]Philips Medical Systems, Dallas, Texas, USA

This pilot study involving MRI and Diffusion Weighted Imaging (DWI) of 12 subjects with breast malignancies prior to and following chemotherapy suggests that DWI may have predictive value. Patients whose tumors had very low Apparent Diffusion Coefficients (ADC)were much more likely to have a positive response to subsequent cytotoxic chemotherapy.

2881. Do Diffusion Changes Occur Prior to Size Changes in Breast Tumours Undergoing Neoadjuvant Chemotherapy?

Martin Darren Pickles[1], Peter Gibbs[1], Martin Lowry[1], Lindsay W. Turnbull[1]

[1]University of Hull, Hull, East Yorkshire, UK

The purpose of this work was to determine if treatment induced tumour ADC changes occur prior to tumour size changes in a cohort of breast cancer patients undergoing neoadjuvant chemotherapy. The results of 12 patients revealed that significant changes in ADC values occurred after the 1st cycle (p=0.001) while changes in tumour size were not significant at this time-point (p=0.834) and only became apparent after the 2nd cycle of treatment (p=0.043). It is believed that the altered ADC values were as a result of increased water mobility following treatment induced cell damage.

2882. The Role of Apparent Spin-Spin Relaxation in Assessing Response to Treatment in Breast Cancer Patients Undergoing Neoadjuvant Chemotherapy

Martin Darren Pickles[1], *Martin Lowry*[1], *Lindsay W. Turnbull*[1]
[1]University of Hull, Hull, East Yorkshire, UK

The primary objective of this work was to evaluate the possible role apparent spin spin relaxation rate (R2*) has in assessing response to treatment in a cohort of breast cancer patients undergoing neoadjuvant chemotherapy. The secondary aim was to compare R2* with tumour volume in assessing response. The results from 33 patients revealed no significant difference in R2* values or volume between response groups prior to or post 1st cycle time-points. However at the 2nd cycle time-point significant differences were noted (R2* p=0.009, volume p=0.002). Whilst tumour volume consistently outperformed R2* in assessing response the differences were small.

2883. Contrast-Enhanced MRI for Assessing the Response of Invasive Breast Cancer to Neoadjuvant Chemotherapy

Alan Howard Stolpen[1], *Jeong Mi Park*[1], *Mark W. Karwal*[1], *Megha Garg*[1]
[1]University of Iowa, Iowa City, Iowa, USA

Neoadjuvant chemotherapy is used to decrease the size of locally advanced breast cancers prior to definitive surgery. This study evaluates the performance of serial contrast-enhanced MRI for assessing the response of twenty invasive breast cancers to neoadjuvant chemotherapy. MRI demonstrated a range of tumor behaviors, from disease progression, to partial response, to lesion fragmentation, to complete response. The findings at MRI predict the amount of residual cancer at mastectomy or lumpectomy, especially when MRI shows complete or near-complete complete tumor response.

2884. Fast Exchange Regime Analysis of the Response to Treatment in Human Breast Cancer

Thomas Yankeelov[1], *Martin Lepage*[2], *A. Bapsi Chakravarthy*[1], *Kenneth J. Niermann*[1], *Cheryl R. Herman*[1], *Kevin McManus*[1], *Mark C. Kelley*[1], *Ingrid Mayer*[1], *Ingrid Meszoely*[1], *John C. Gore*[1]
[1]Vanderbilt University, Nashville, Tennessee, USA; [2]Universite de Sherbrooke, Sherbrooke, QC, Canada

Models have been developed for analysis of dynamic contrast enhanced MRI (DCE-MRI) data that include the effects of transcytolemmal water exchange. It has been hypothesized that these models are more sensitive to tumor physiology. Here we present the first example of a DCE-MRI analysis of the response to treatment in human breast cancer which incorporates the effects of transcytolemmal water exchange.

2885. Volumetric Texture Analysis of DCE-MR Images of the Breast Using Gray-Level Co-Occurrence Matrix Method

Weijie Chen[1], *Maryellen L. Giger*[1]
[1]The University of Chicago, Chicago, Illinois, USA

We extend the conventional 2D texture analysis technique to 3D using gray-level co-occurrence matrix (GLCM) method, and assess the performance of textural features in the task of distinguishing between malignant and benign breast lesions in DCE-MRI. There are two advantages in our technique: First, the counting statistics are improved in 3D analysis. Second, our analyses were performed on segmented 3D lesions, which render feature extraction not affected by normal tissues surrounding the lesions. We found 3D texture analysis based on accurately segmented 3D breast lesions improved diagnostic accuracy as compared to 2D texture analyses based on 2D ROIs.

2886. Textural Analysis Optimisation in MRI of the Breast

Tom Beach[1], *Peter Gibbs*[1], *Martin D. Pickles*[1], *Lindsay Turnbull*[1]
[1]University of Hull, Hull, UK

Textural analysis, and in particular the spatial gray-level dependence matrices method, is becoming increasingly utilised in MRI. However, there is little published data investigating either the optimal degree of gray-level reduction or the most appropriate pixel separation to utilise in co-occurrence matrices, and subsequent textural parameter calculation. This work aims to optimise these parameter choices in the application of textural analysis to breast MRI.

2887. Bootstrap Ensemble Neural Networks in MRI of the Breast

Peter Gibbs[1], *Muthyala Sreenivas*[1], *Andrew Hunter*[2], *Lindsay Turnbull*[1]
[1]University of Hull, Hull, UK; [2]Lincoln University, Lincoln, UK

The application of neural networks in MRI has previously been limited due to the requirement for a large number of cases to ensure model robustness. Development of appropriate quantitative parameters, reflecting a radiological interpretation, has also proved problematic. This work utilises an ensemble technique based on bootstrap resampling to improve the final accuracy. Textural, shape, and pharmacokinetic derived parameters are used as inputs into the network.

2888. Breast MRI Lesion Classification: Comparison Between Human Readers and Backpropagation Neural Network (BNN)

Lina Arbash Meinel[1], Alan Stolpen[2], Kevin Berbaum[2], Laurie Fajardo[2], Joseph M. Reinhardt[3]

[1]Philips Research USA, Chicago, Illinois, USA; [2]University of Iowa Hospitals, Iowa City, Iowa, USA; [3]University of Iowa, Iowa City, Iowa, USA

Five radiologists with different levels of experience manually classified eighty breast MRI lesions both with and without CAD assistance. The performance of the computer classifier and human readers were compared using ROC curves, which showed that human readers significantly improved with assistance ($p < 0.05$), and the human readers' performance was also evaluated using MRMC analysis, which showed that the human reader performance with and without CAD system assistance can be generalized to the population of cases with a statistically significant improvement ($p < 0.05$).These results show significant advantages to using CAD in classifying BMRI lesions.

2889. Artificial Neuronal Network Analysis of Neoadjuvant Chemotherapy Response Using Quantitative Morphological, Texture and Enhancement Kinetic Parameters

Yong Chu[1], Ke Nie[1], Hon J. Yu[1], Jeon-Hor Chen[1], Orhan Nalcioglu[1], Min-Ying Su[1]

[1]University of California, Irvine, California, USA

33 patients who had a baseline and a F/U MRI study after 1-2 cycles AC were included (17 responders and 16 non-responders). An artificial neuronal network analysis based on the baseline morphology/texture/kinetics parameters was performed to find optimized subset for response classification. A quantitative analysis was performed to characterize the morphology and texture features (10 GCLM and 14 Laws'). By adding the enhancement kinetic parameters, the classification accuracy improves from 76% to 85%. We demonstrated that quantitative analysis of morphology and texture in breast cancer is feasible, and artificial neuronal network may be applied to find an optimized subset for diagnosis, or therapy response prediction.

2890. Clinical Evaluation of Combining Dynamic Contrast Enhancement MRI and Diffusion Weighted MR Imaging for Diagnosis of Breast Lesion

Xiaopeng Zhang[1], Jie LI[1], Yinshi Sun[1], Lei Tang[2], Kun Cao[3]

[1]Beijing Cancer Hospital,Peking University School of Oncology, Beijing, People's Republic of China; [2]Beijng Cancer Hospital, Peking University School of Oncology, Beijing, People's Republic of China; [3]Beijing Cancer Hospital, Peking University School of Oncology, Beijing, People's Republic of China

Contrast enhanced MRI is a sensitive method for breast invasive cancer, but its specificity is unsatisfactory. DWI has been proved to be valuable in differential diagnosis of breast lesion. In this study, we investigated the value of combination morphological feature, pattern of time-signal curve of dynamic contrast enhanced MRI and ADC value of diffusion weighed imaging in improving specificity diagnosis of breast lesion. The results indicated that the combination of dynamic contrast enhancement MRI and diffusion weighted MRI is useful to increase specificity, and could provide valuable information for the diagnosis of those lesions suspicious in dynamic contrast enhancement MRI.

2891. Differentiation of Malignant from Bening Breast Lesions by Diffusion-Weighted Imaging with ASSET Technique

Guangwei Jin[1], Ningyu An[1], Yu Cai[1]

[1]PLA General Hospital, Beijing, People's Republic of China

Forty-six female patients with histologically confirmed malignant (37 with 39 lesions) and benign (9 with 12 lesions) lesions in breasts and 14 health volunteers underwent bilateral breast SE-EPI with ASSET technique (B=1000, acquisition time about 40¡«50s). The mean ADC value of malignant lesions (1.02¡À0.34x10-3 mm2/s) was statistically lower than that of the benign lesions (1.54¡À0.55x10-3 mm2/s) and normal breast tissues (1.88¡À0.28x10-3 mm2/s) ($p<0.001$).The sensitivity, specificity and overall accuracy of ADC value for malignant lesions with a threshold of less than 1.47x10-3 mm2/s was 92.3%, 58.3% and 84.3% respectively. Our results revealed DWI with ASSET technique was of sufficient sensitivity to distinguish most malignant tumors from benign lesions with short acquisition time and satisfying image.

2892. MR-Elastography for Breast Lesion Characterization - The Effect of Rheology on Its Diagnostic Impact

Ralph Sinkus[1], Katja Siegmann[2], Tanja Xydeas[2], Jeremy Bercoff[3], Mickael Tanter[1], Benjamin Robert[1], Mathias Fink[1]

[1]Laboratoire Ondes et Acoustique, Paris, France; [2]University Tuebingen, Tuebingen, Germany; [3]SuperSonic Imagine, Aix-en-Provence, France

MR-Elastography is bound to provide at most two viscoelastic parameters when data are taken at one frequency and when isotropy is assumed for the reconstruction. Tissue resembles a complex hierarchical organization, thus the interpretation of the complex shear modulus G*=Gd+iGl in terms of inherent material parameters becomes rather. We present *in vivo* results for elasticity and viscosity from 33 malignant and 18 benign breast lesions reconstructed with different rheological models. Application of the Voigt model yields elasticities which do not allow good classification. When data are interpreted in terms of Maxwell elasticity and fractal springpot model very good classification is achieved.

2893. Assessment of Magnetization Transfer and Tissue Blood Flow Imaging in Human Breasts Tissue by GREAST

Ka-Loh Li[1], Lisa J. Wilmes[1], Jessica Gibbs[1], Eric Han[2], Greg Zaharchuk[1], Christopher P. Hess[1], Bonnie Joe[1], Nola Hylton[1]

[1]University of California, San Francisco, San Francisco, California, USA; [2]GE Healthcare Global Applied Science Laboratory,, Menlo Park, California, USA

Tissue contrast from magnetization transfer (MT) and blood flow in arterial spin tagging (AST) experiments was investigated in volunteers. Fifteen breast cancer patients undergoing neoadjuvant chemotherapy were imaged using the gradient-echo arterial spin tagging (GREAST) sequence to assess the impact of preserved MT on detection and differentiation of breast lesions. Texture analysis was performed on the GREAST difference (Δ M) image for each tumor to assess response to therapy. Mean and median signal intensity, and the inverse difference moment (IDM)--a texture measure, showed significant (P=0.03, 0.02, and 0.005) changes following chemotherapy. Assuming that MT-induced signal is not significantly changed after treatment, GREAST ΔM images provided useful information in depicting changes in local blood flow in breast tumors.

2894. The Value of T2 Imaging in Establishing Benignancy or Malignancy of Enhancing Lesions Detected by Gd-Enhanced Breast MRI

Frederick Kelcz[1], Mai A. Elezaby[1]

[1]University of Wisconsin, Madison, Wisconsin, USA

For a group of patients with enhancing lesions detected during breast MRI, we measured the ratio of signal intensity of lesion to surrounding fat on T2-weighted fat suppressed imaging. There was considerable overlap in half the patients analyzed, but for the other half, T2 signal intensity was helpful. It was found that lesion to fat ratios greater than 8 indicated high likelihood of benignity while ratios less than 3 were associated with malignancy. T2 imaging results can be especially helpful in deciding how to follow patients with indeterminate enhancement and morphology.

2895. Parametric Mapping of Contrast Kinetics from Rapid Radial DCE-MR Breast Images

Lawrence Dougherty[1], Hee Kwon Song[1], Peter J. Moate[1], Linda White Nunes[2], Mark A. Rosen[1], Raymond C. Boston[1]

[1]University of Pennsylvania, Philadelphia, Pennsylvania, USA; [2]Pennsylvania Hospital, Philadelphia, Pennsylvania, USA

From images acquired using an interleaved radial 3D DCE-MR imaging sequence, dynamic enhancement curves of breast lesions were fit to a kinetic model, yielding several kinetic features (maximal enhancement, maximal enhancing slope, time to maximal slope, and washout slope). Based on the kinetic parameters correlated with pathologic results obtained from 68 breast lesions, color maps were defined that predicted benign or malignant disease. In 9 prospective studies, 4 malignant and 5 benign lesions were correctly classified. Kinetic modeling of lesion enhancement using high-temporal resolution DCE- MRI is a useful means of characterizing benign and malignant breast lesions.

2896. Volumetric Mapping of the Longitudinal to Transverse Relaxation Times Ratio (T1/T2) of the Entire Human Breast

Jaroslaw Nicholas Tkacz[1], Yommy Chiu[2], Hernan Jara[2]

[1]Boston University Medical Center, Boston, Massachusetts, USA; [2]Boston University, Boston, Massachusetts, USA

Purpose: To develop a quantitative MRI technique for mapping the longitudinal-to-transverse relaxation times ratio (T1/T2) of the entire human breast. Methods: Images obtained with the mixed-TSE pulse sequence in the coronal plane of the entire breast were post-processed for generating T1 and T2 distributions, which were spatially co-registered. These were used as input for a T1/T2 ratio algorithm. Adipose and glandular tissues were segmented with a Q-MRI based morphologic algorithm. Results: Representative T1, T2 and T1/T2 maps on two research subjects were generated. Conclusion: A quantitative MRI technique has been developed for mapping the longitudinal-to-transverse relaxation times ratio (T1/T2) of the entire human breast.

2897. Breast MR Electrical Impedance Tomography Toward Breast Cancer Imaging

H. Y. Heo[1], Y. Cho[1], B. I. Lee[1], S. H. Oh[1], T.-S. Kim[1], S. Y. Lee[1], E. J. Woo[1]

[1]Kyung Hee University, Yongin, Gyeonggi, Republic of Korea

To survive from breast cancer, early detection is the key. Recently with the increased awareness of breast cancer, novel breast imaging modalities are being actively developed to overcome inherent limitations of X-ray mammography. Although breast MR scans with contrast agents increase the sensitivity of breast cancer screening and diagnosis, low specificity and inability to image calcifications are known to be the major limitations of MR breast imaging. In this study, we introduce a new breast imaging modality that is under development: breast MR Electrical Impedance Tomography (breast MREIT). With breast MREIT, we hope to improve specificity of MRI by providing conductivity images of breast, since cancerous tissues exhibit much higher conductivity than benign. Our preliminary results show that objects that are not differentiable in MR images are clearly distinguished in conductivity images.

2898. Study of Marker Component for Low Susceptibility Tri-Modalities Breast Tumor Localization

Yangmei Li[1], Claire Holloway[1], Jian-Xiong Wang[1], Donald B. Plewes[1]

[1]Sunnybrook and Women's Health Science Centre, University of Toronto, Toronto, Ontario, Canada

We outline in-vitro investigations of the composition of a new breast localization marker which shows positive contrast in T1 weighted MRI, ultrasound (US) and X-ray. The marker is composed of 0.4mm diameter copper microspheres suspended in a Gd-DTPA added gel formulation. Maximum contrast in T1 weighted MRI was found with the addition of 10mmol/l Gd-DTPA. The amount of copper was used to control the US contrast do not reduce the MRI contrast of the marker. The study demonstrates the potential of the marker for use as a breast surgical localizer.

2899. Negative Pressure Fixation Device to Reduce Motion Artifacts on Contrast-Enhanced MR Imaging of the Breast

Asha Balakrishnan[1], Daniel F. Kacher[2], Steven E. Chavoustie[3]
[1]Massachusetts Institute of Technology, Cambridge, Massachusetts, USA; [2]Brigham and Women's Hospital, Boston, Massachusetts, USA; [3]University of Miami, Miami, Florida, USA

The purpose of this study is to investigate the effect on misregistration artifact when fixing the breast with a negative pressure device in contrast enhancement MRI. The device was integrated into the breast coil, and nine women underwent a breast MRI with and without the device in place. Reduction in motion artifact was observed in six of the nine women. In addition, using negative pressure on the breast enabled clearer imaging of the nipple-areolar complex and the ductal system.

2900. 7T High Resolution Breast MRI

Ray F. Lee[1], Linda Moy[1], Ryan Brown[2], KellyAnn McGorty[1], Cornel Stefanescu[1], Yi Wang[2], Naomi Peck[1]
[1]New York University, New York, USA; [2]Conell University, New York, USA

Although at 1.5T, the limited sensitivity and specificity of breast MRI prevent it from replacing mammography for screening among higher-risk young women, the quality of breast MRI at 7T should be significantly improved due to the intrinsically high signal-to-noise ratio. We have constructed a 7T breast coil and scanned ten volunteers. Our findings prove that at 7T, high resolution ($0.3x0.3x0.8mm^3$) *in vivo* breast images can be easily obtained, and milk duct and glandular tissue structure can also be identified.

2901. Coregistration of Contrast Enhanced MRI and Broadband Diffuse Optical Spectroscopy for Characterizing Breast Cancer

Min-Ying Su[1], Hon J. Yu[1], Natasha S. Shah[1], David J-B Hsiang[1], Rita S. Mehta[1], Albert E. Cerussi[1], Bruce J. Tromberg[1], Orhan Nalcioglu[1]
[1]University of California, Irvine, California, USA

The correlation between broadband Diffuse Optical Spectroscopy (DOS) and DCE-MRI in characterizing breast cancers was investigated. Sequential DOS and MRI studies were performed using external fiducial markers for co-registration. The 3D MRI data set was re-sliced to obtain the DOS scan plane. In all cases, DOS showed a significant tissue optical index ([water]x[deoxy-hemoglobin]/[lipid]) contrast corresponding to morphological information of the lesion shown on DCE_MRI. Sharp TOI peaks were recovered for well-circumscribed masses. These results provide qualitative confirmation of the common signal origin and complementary information content that can be achieved by combining optical and MR imaging for breast cancer characterization.

2902. Diffusion Tensor Imaging of the Breast: Preliminary Clinical Findings

Savannah C. Partridge[1], JoAnn M. Lorenzo[1], Sue Peacock[1], Bonnie M. Thursten[2], John S. McCloskey[2], Wendy B. DeMartini[1], Peter R. Eby[1], Eric L. Rosen[1], Constance D. Lehman[1]
[1]University of Washington, Seattle, Washington, USA; [2]Seattle Cancer Care Alliance, Seattle, Washington, USA

Diffusion-weighted imaging (DWI) elucidates tissue microstructure, and studies have recently shown promising results for tumor characterization. DTI extends standard DWI to assess diffusion anisotropy or directionality in addition to mobility. We hypothesized that disruption of the breast ductal network by invading cancer may cause alterations in water diffusion properties in the tissue that will be reflected by DTI parameters. In this study, DTI parameters were measured and compared in human breast tumors, benign lesions, and normal tissue. DTI demonstrated significantly reduced ADC and increased FA in tumors compared to normal tissue, while benign lesions were comparable to normal values.

Perfusion and Permeability in Cancer Models

Room 4E Thursday 13:30 - 15:30

2903. Distribution of Steady State Contrast Agent Concentration and Interstitial Fluid Pressure in Human Xenografts

Yaron Hassid[1], Raanan Margalit[1], Edna Haran Furman[1], Maya Dadiani[1], Hadassa Degani[1]
[1]Weizmann Institute of Science, Rehovot, Israel

Increased interstitial fluid pressure (IFP) in tumors creates a physical resistance to therapy. We developed a non invasive MRI application, which enabled us to estimate IFP distribution in H460 lung cancer and MCF7 breast tumors implanted in nude mice. The method is based on slow i.v infusion of GdDTPA, and measurements of T1 rates before infusion, and at steady state concentration in the blood and the tumor. Analysis of the T1 rates yields steady state "Tissue Contrast Agent Concentration" maps, extracellular contrast agent concentration maps and consequently IFP maps. These maps correlated with independent IFP measurements by the "wick-in-needle" technique.

2904. Parallel Observation of Left Ventricular Arterial Input Function and Brain Perfusion in Rats Using a Multi-Coil System

Stephen Pickup[1], Sanjeev Chawla[1], Dae-Hong Kim[1], Harish Poptani[1]
[1]University of Pennsylvania, Philadelphia, Pennsylvania, USA

A multi-coil apparatus was constructed for parallel observation of brain perfusion and left ventricular arterial input function in rats. The apparatus provides high SNR images for the target tissues and homogenous saturation of the entire blood pool. The device was used to perform dynamic contrast enhanced imaging in four Fisher rats bearing brain tumors. The resulting data were analyzed using both the Tofts and BOLERO models for tissue perfusion, yielding maps of K^{trans}, v_e and τ (BOLERO only). The BOLERO model consistently yielded more accurate fits of the data than the Tofts model.

2905. Early Effects of Combretastatine A-4-P on Rat Bladder Tumor Heterografts Assessed by Combined Carbogen Based fMRI and T2 Mapping

Carole D. Thomas[1], Christine Walczak[1], Julia Kaffy[2], Renée Pontikis[2], Jacqueline Jouanneau[2], Andreas Volk[1]
[1]Institut Curie, Orsay, France; [2]Institut Curie, Paris, France

The purpose of the study was to assess, on rat bladder tumor heterografts, the early effects of combretastatin A-4-P (CA-4-P) on tumor vasculature and necrosis by combination of carbogen based fMRI and T2 mapping. Three regions with different T2 modifications were observed 35 minutes after CA-4-P administration. Two of these regions showed also systematically different behaviours on fMRI upon carbogen breathing. These preliminary results suggest that CA-4-P effects on tumour vasculature can be detected early by both, classical T2 mapping and fMRI upon carbogen breathing, which might be useful for non-invasive follow-up of antivascular therapy

2906. Contrast Agent Distribution Function (CADF), a New Dynamic MRI Parameter from Simultaneous Measurement of Relaxation Rates R_1 and R_2* by a New Saturation-Recovery Multi-Gradient-Echo Snapshot Sequence: Concept and First Application to Colorectal Tumor Xenografts in Mice

Melanie Heilmann[1], Jean-Luc Dimicoli[1], Carole D. Thomas[1], Christine Walczak[1], Andreas Volk[1]
[1]Institut Curie - Research Center, Orsay, France

Dynamic MRI with administration of paramagnetic contrast agents (CA) typically needs computation of CA concentration from relaxation rates and assumed *in vivo* CA relaxivities. We developed a new protocol, providing a so-called CA distribution function (CADF(t)), which reflects evolution of CA induced susceptibility gradients, without requiring estimation of CA concentrations. CADF(t) was obtained from R_1 (t) and R_2*(t), measured simultaneously by means of a new Saturation-Recovery Multi-Gradient-Echo Snapshot sequence. First *in vivo* measurements of CADF in colorectal tumor xenografts of nude mice suggested the relevance of CADF parameters ($CADF_{max}$,k_a,k_b), related to blood volume, perfusion and permeability, for investigation of tumor microvasculature.

2907. Direct Comparison of Macromolecular Contrast Agent Vistarem with Dotarem for Detecting Drug Effects on Tumor Vasculature by DCE MRI

Peter R. Allegrini[1], Claudia Weidensteiner[1], Paul M.J. McSheehy[1]
[1]Novartis Inst. for BioMedical Research, Basel, BS, Switzerland

Small molecular contrast agent (CA) are less than ideal dynamic for contrast enhanced MRI since the rate limiting step of CA extravasation may be either vascular permeability or blood perfusion in the immature blood vessels. The influence of perfusion variations can be reduced by using macromolecular CA. In this study we measured the effect of anti-VEGF treatment on transfer constant K^{trans} of two different tumor models with the small Gd chelate GdDOTA and the macromolecular CA Vistarem in the same animals. The effect of VEGF antagonist on K^{trans} resulted in a higher dynamic range when measured with the macromolecular CA.

2908. Longitudinal Studies of Angiogenesis in Hormone Dependent Shionogi Tumours

Trevor Wade[1], Piotr Kozlowski[2]
[1]University of British Columbia, Vancouver, British Columbia, Canada; [2]Prostate Centre at Vancouver General Hospital, Vancouver, British Columbia, Canada

Vessel size index (VSI) measurements were performed on 17 mice withsubcutaneous Shionogi tumours. The VSI was tracked as the tumoursprogressed from an androgen dependent state to an androgen independentstate, and no tumour size dependence was found in any of the stages. Apaired t-test on the measurements on the 6 mice that progressed toandrogen independence indicated significant changes in VSI between thestages of tumour progression.

2909. DCE-MRI for Evaluation of Response to Gefitinib: Comparison of Two Treatment Regimens in a Breast Cancer Model

Lisa J. Wilmes[1], Ka-Loh Li[1], Sheye Aliu[1], Donghui Wang[1], Byron C. Hann[1], Mark M. Moasser[1], Nola M. Hylton[1]
[1]University of California San Francisco, San Francisco, California, USA

Dynamic contrast enhanced (DCE) MRI was used to study breast tumor response to two dosing regimens of the epidermal growth factor receptor (EGFR) tyrosine kinase inhibitor, gefitinib. Differences in tumor T10, endothelial transfer constant (Kps) and growth response were seen between the two groups at early and late treatment time points. The 2-day pulse group showed a significant transient decrease in tumor T10 and Kps accompanied by reduced volume shortly after the dosing was completed. For all groups, a correlation between tumor Kps and percent change in tumor size was observed.

2910. Monitoring Micro-Vasculature Damage Induced by Radiotherapy on Mouse Breast Carcinomas Using DCE-MRI

Martin Pellerin[1], Luc Tremblay[1], Benoit Paquette[1], Martin Lepage[1]
[1]Université de Sherbrooke, Sherbrooke, QC, Canada

Microscopic changes in the tumor tissue following radiotherapy occur before variations in shape and volume can be observed. In this study DCE-MRI was used to analyze changes in the microvasculature following the irradiation of mouse breast carcinomas. The transcapillary transfer rate shows a degradation of tissue perfusion that precedes the onset of necrosis and eventually, tumor regression. Diffusion from the tumor periphery rather than perfusion is responsible for the accumulation of contrast agent in the necrotic tumor core. This gives rise to artificially high values of v_e

2911. DCE MRI Detected Differential Response to ZD6126 of Metastatic Versus Indolent Human Melanoma

Nominated for an ISMRM Poster Award

Rong Zhou[1], Hui Qiao[1], Lin Z. Li[1], Xin Li[2], Phyllis Wachsberger[3], Charles S. Springer, Jr[2], Mary JC Hendrix[4], Jerry D. Glickson[1]
[1]University of Pennsylvania, Philadelphia, Pennsylvania, USA; [2]Oregon Health & Science University, Portland, Oregon, USA; [3]Thomas Jefferson University, Philadelphia, Pennsylvania, USA; [4]University of Chicago, Chicago, Illinois, USA

It has been previously demonstrated that metastatic melanoma (C6181) forms its own blood vessels through a vasculogenic mimicry mechanism [1]. ZD6126, which targets the microtubular cytoskeleton of endothelial cells, is shown to induce vascular shutdown leading to tumor necrosis [2, 3]. We hypothesized that metastatic melanoma may have a more immature vasculature, which is more sensitive to ZD6126 treatment. We utilized DCE MRI to study the acute response (within 1 hr after treatment) and found that Ktrans of the metastatic melanoma was reduced over 60% ($P<0.05$) in response to ZD6126 injection, whereas Ktrans of the indolent tumor remains unchanged.

2912. Short-Term Treatment with the Triple Angiokinase Inhibitor, BIBF 1120, Affects Vascular Permeability and Perfusion of Human Tumor Xenografts in Nude Mice

Martin Krssak[1], Monika Kriz[1], Frank Hilberg[1]
[1]Boehringer Ingelheim Austria, Vienna, Austria

This study assessed the effects of short-term treatment with an orally available triple angiokinase inhibitor, BIBF 1120, on tumor vasculature in subcutaneous tumor xenograft in mice. As measured by DCE MRI following a boluses of low- and macro- molecular Gd-based contrast agents, three days of BIBF1120 treatment reduces perfusion and permeability as well as the relative blood volume in models of head and neck (FaDu) and colon (HT-29) carcinoma. These changes can be detected prior to changes in tumor growth rate and they were more pronounced in FaDu xenografts, which presented with higher relative blood volume prior the treatment.

2913. MRI of Calu-6 Lung Tumors for the Assessment of the Anti-Vascular Activity of MN-029

Nathalie Just[1], Veronique Rancier[1], Nicolas Guilbaud[1], Philippe Genne[1], Kenneth Locke[2]
[1]Oncodesign Biotechnology, Dijon, France; [2]MediciNova Inc, San Diego, California, USA

In this study, we characterized the changes in perfusion of subcutaneously xenografted Calu-6 human lung tumors following intravenous infusion of rats with a novel vascular disrupting agent (MN-029). We observed that in rats treated with 10 mg/kg MN-029, tumor Ktrans and extravascular-extracellular volume (ve) parameters were significantly smaller one and three hours post-treatment compared to values obtained before treatment and compared to vehicle-treated rats. Immunohistochemical studies performed after injection of fluorochromes confirmed these results.

Cancer Models: Assessment of Vascular Function

Room 4E Thursday 13:30 - 15:30

2914. Nonlinear Correction of Arterial Input Function Measured with Spoiled Gradient Echo Sequences

Nominated for an ISMRM Poster Award

Matthias C. Schabel[1]
[1]University of Utah, Salt Lake City, Utah, USA

Accurate quantification of arterial input function is a critical step in quantitative contrast kinetic modeling for tissue perfusion. We describe and demonstrate a data analysis methodology for SPGR pulse sequences which explicitly incorporates the nonlinear relationship between signal enhancement and contrast concentration. The algorithm only requires pre-contrast T1 measurement, and is insensitive to tissue T2* and receive B1 inhomogeneities. Phantom and *in vivo* measurements are presented demonstrating the accuracy of the method and the importance of nonlinear effects in AIF characterization.

2915. Modelling DCE-MRI Arterial Input Functions in Rats

Deirdre McGrath[1], Tony Lacey[2], Daniel Bradley[2], Chris Taylor[1], Geoff Parker[1]
[1]University of Manchester, Manchester, Lancashire, UK; [2]Astrazeneca, Alderley Park, Macclesfield, Cheshire, UK

DCE-MRI is used in anti-vascular therapies to quantify parameters associated with vascular function. In compartmental modelling it is necessary to identify an appropriate arterial input function (AIF). It was sought to assess the effects of using various AIF models. Using experimentally acquired high temporal resolution data from rats, four different AIF models were fitted to the data and compared with the use of the raw AIF data by calculating the parameters from the extended Kety model. It was observed that varying AIF models impact results highly, and was recommended that a bi-exponential model provides the closest modelling of experimental AIFs.

2916. An Adaptive Bayesian MRF Approach for DCE-MR Imaging

Volker J. Schmid[1], Brandon Whitcher[2], N. Jane Taylor[3], Anwar R. Padahni[3], Guang-Zhong Yang[1]
[1]Imperial College London, London, England, UK; [2]GlaxoSmithKline, Greenford, England, UK; [3]Mount Vernon Hospital, Northwood, England, UK

We use a hierarchical Bayesian approach to estimate PK parameters for DCE-MRI data. Spatial information is incorporated in a versatile model-building framework by an adaptive GMRF prior. The new approach reduces estimation error and smoothes the PK parameters in homogenous regions, but retains sharp features.

2917. Tissue Assessment in Gliomas: Comparison of Tumor Blood Volume, Vascular Permeability by Perfusion-Weighted MR Imaging and Tl-201 SPECT

Hidemasa Uematsu[1], Tatsuro Tsuchida[1], Hirohiko Kimura[1], Nobuyuki Kosaka[1], Harumi Itoh[1]
[1]University of Fukui, Fukui, Japan

Tl-201 uptake levels are useful in assessing the degree of glioma malignancy. However, the direct contributor to Tl-201 uptake has not been documented. We hypothesized that increased tumor blood volume could be responsible for the Tl-201 accumulation. We evaluated 9 patients with GBM to analyze the relationship among Tl-201 uptake, blood volume and vascular permeability (K(trans)) calculated by perfusion-weighted MRI. A significant correlation between Tl-201 uptake and blood volume was demonstrated ($p<0.05$), while no significant difference was observed between Tl-201 uptake and K(trans). These results support the hypothesis that increased tumor blood volume is responsible for the corresponding Tl-201 accumulation.

2918. Determination of Maturity and Functionality of Tumor Vasculature by MRI: Correlation Between BOLD MRI and DCE MRI Using P792 in Experimental Fibrosarcoma Tumors

Christine Baudelet[1], Greg O. Cron[1], Bernard Gallez[1]
[1]Catholic University of Louvain, Brussels, Belgium

Although BOLD MRI and DCE MRI are useful techniques for noninvasive imaging of tumor vasculature, it is unclear how both techniques are related. We measured vessel maturation and function via BOLD imaging during hypercapnia and carbogen breathing, respectively. These results were then compared to DCE MRI perfusion measurements which were performed on the same animals using P792 (Vistarem®, macromolecular Gd agent with rapid clearance). Parameters derived from BOLD MRI correlated weakly or not at all ($r^2<0.15$) with those derived from DCE MRI. Characterizations of tumor microvasculature imaging using BOLD MRI and DCE MRI thus appear to be largely complementary.

2919. The Role of Vessel Maturation and Vessel Functionality in Spontaneous Fluctuations of T2*-Weighted GRE Signal Within Tumors

Christine Baudelet[1], Greg O. Cron[1], Réginald Ansiaux[1], Nathalie Crokart[1], Julie DeWever[1], Olivier Feron[1], Bernard Gallez[1]
[1]Catholic University of Louvain, Brussels, Belgium

Acute tumor hypoxia (~blood flow instabilities) can be investigated using signal fluctuations in dynamic T2*w gradient echo MRI. We compared histological measures of vascular density (CD31), tumor vessel immaturity (alpha-Smooth Muscle Actin immunoreactivity), and vessel functionality (Hoechst 33242) with 4.7T MRI measures of similar characteristics (MRI during air, 5% CO2, and carbogen breathing, respectively). The results show that adequate vessel functionality and advanced vessel maturation are not crucial factors involved in spontaneous T2*w GRE signal fluctuations, since a large fraction of fluctuations were observed to occur in non-perfused and/or immature vessels.

2920. DCEMRI Detects Effects of Tumors on Adjacent Normal Tissue That Reflect Tumor Grade

Xiaobing Fan[1], Milica Medved[1], Jonathan N. River[1], Marta Zamora[1], Gregory S. Karczmar[1]
[1]University of Chicago, Chicago, Illinois, USA

We studied contrast uptake and washout behavior in muscles near tumors to distinguish normal muscle from muscle near tumor, and to separate the metastatic from non-metastatic tumors. The low molecular contrast agent Gd-DTPA and higher molecular contrast agent P792 were used to acquire dynamic contrast enhanced MRI at 1.5T for rodent prostate cancer AT2.1 and AT3.1 tumors. The results demonstrated that the muscles near tumors were significantly different from the normal muscles and in addition metastatic and non-metastatic tumors have different effects on nearby muscle.

2921. Susceptibility MRI of Vascular Function and Therapeutic Response in LS174T Colorectal Carcinomas Grown Orthotopically in Murine Liver

Tammy Louise Kalber[1], Anderson Joseph Ryan[2], John R. Griffiths[1], John C. Waterton[2], Simon P. Robinson[1]
[1]St. George's, University of London, London, UK; [2]AstraZeneca, Alderley Park, Macclesfield, UK

The response of murine orthotopic LS174T liver metastases to either carbogen breathing or the vascular disrupting agent ZD6126 was assessed by intrinsic-susceptibility MRI. Tumour blood volume was determined by susceptibility contrast MRI with Endorem. Carbogen breathing significantly increased tumour R_2*, consistent with a decrease in [deoxyhaemoglobin] and vascular steal by the highly-perfused normal liver host tissue. ZD6126 elicited a negligible change in R_2* 24 hours after treatment, suggesting a high level of baseline necrosis in the LS174T murine model of liver metastasis.

2922. Lineshape and Susceptibility in a Rat Glioma Monitored by Echo Planar Spectroscopic Imaging

Gary V. Martinez[1], Maria Luisa Garcia Martin[1, 2], Gregory S. Karczmar[3], Jeffrey R. Alger[4], Nikhil Rajguru[1], Robert J. Gillies[1]
[1]University of Arizona, Tucson, Arizona, USA; [2]CSIC-UAM, Madrid, Spain; [3]University of Chicago, Chicago, Illinois, USA; [4]UCLA, Los Angeles, California, USA

This work describes EPSI at 4.7 T based on previous implementations of EPSI at lower fields. We implemented EPSI with two spatial dimensions without water- and outer volume suppression. This is the first time that this sequence has been developed for this field strength. We applied this sequence to time-resolved *in vivo* 1H spectroscopy to observe the pharmacokinetics of contrast reagent (CR) in a rat C6 glioma at high spatial resolution. Intensity and linewidths of the water peaks were affected by CR and were used to follow pharmacokinetics. Furthermore, at high resolution, we observed multiple water resonances near the edge of the tumor that may represent distinct multi-compartment environments in anisotropic peritumoral tissue.

2923. MR Perfusion and 1H Spectroscopic Imaging in the Longitudinal Evaluation of Brain Tumor Angiogenesis

Nominated for an ISMRM Poster Award

Narasimha Shastry Akella[1], Steven D. Buchthal[1], Louis Burt Nabors[1], Jan A. den Hollander[1]
[1]University of Alabama at Birmingham, Birmingham, Alabama, USA

Twelve patients with malignant brain tumors were studied using dynamic susceptibility contrast enhanced MRI and MR spectroscopic imaging performed on a clinical 3T MRI scanner. Relative cerebral blood flow and metabolite concentrations were acquired and these correlated with each other, and also with the clinical diagnoses of the patients. Patients demonstrated increases in Choline and Creatine, and a decrease in NAA in the tumor margins, along with significantly higher relative cerebral blood flow values compared to uninvolved brain regions. The longitudinal variations in these parameters are useful in evaluating the role of angiogenesis in tumor progression and disease prognosis.

2924. Quantitative Assessment of Tumor Microstructure in Canine Brain Using High Resolution DTI Microimaging

Jian-Ming Zhu[1], Ping Wang[1], John L. Robertson[2], John H. Rossmeisl, Jr.[2], Michael E.C Robbins[1], Edward G. Shaw[1]
[1]Wake Forest University School of Medicine, Winston-Salem, North Carolina, USA; [2]Virginia-Maryland Regional College of Veterinary Medicine, Blacksburg, Virginia, USA

The purpose of this work was to demonstrate the potential of acquiring high resolution DTI images of fixed canine brains for studying spontaneously-developed brain tumor models. An accurate and yet quantitative imaging method was developed to map white matter microstructure in fixed canine brain with tumors. Using this procedure, extremely high resolution microstructural images were obtained. This leads a very accurate method to study microanantomical changes involving with tissue damage and integrity for animal models.

2925. Hypoxia Increases Endothelial Cell Invasion and Migration

Barjor Gimi[1], Noriko Mori[1], Zaver M. Bhujwalla[1]
[1]The Johns Hopkins University School of Medicine, Baltimore, Maryland, USA

Human umbilical vein endothelial cells (HUVECs) were labeled with iron-oxide nanoparticles to provide T2-contrast in MRI. HUVEC invasion and motility in extracellular matrix (ECM) gel was characterized in the presence and absence of cancer cells, under both normoxia and hypoxia. The results demonstrated that hypoxia is a potent stimulus for endothelial cell invasion and migration in the absence of cancer cells and that neovascularization may occur through autocrine signaling in endothelial cells. The assay can also be used to characterize synergistic effects of two or more factors in the angiogenic cascade, and can help identify key targets for anti-angiogenic treatment.

2926. MR Imaging of Bone Marrow-Derived Mesenchymal Stem Cells Incorporation Into Tumor Vasculature in Prostate Cancer Models

Lyubov Ostrovskaya[1], Yoshinori Kato[1], Piotr Walczak[1], Baasil Okollie[1], Jeff W. Bulte[1], Dmitri Artemov[1]
[1]Johns Hopkins University, Baltimore, Maryland, USA

Bone marrow–derived mesenchymal stem cells (MSCs) play a significant role in tumor vasculogenesis. *In vivo* techniques to detect incorporation of MSCs to the tumor vasculature are important for detailed studies of tumor progression and for development of novel anti-angiogenic therapies. We used MRI to monitor homing of iron-oxide-labeled-MSCs to the tumor neovasculature in two prostate cancer models with different growth rates. A significantly higher initial accumulation of MSCs was detected in highly aggressive MatLyLu model in comparison to slow growing human PC-3 cancer, suggesting that rapidly growing tumors can depend to a greater extent upon the MSC recruitment.

2927. Monitoring of Cellular Uptake of Gadollinium by Dendritic Cells Useful for Tracking the Cell Trafficking in Tumor Using MRI

Raghvendra S. Sengar[1], Patricia Griffin[1], Daniel Steed[1], Tianbing Yang[2], Lorissa Villa[2], William Chambers[2], Erik Craig Wiener[2]

[1]University of Pittsburgh Cancer Institute, Pittburgh, Pennsylvania, USA; [2]University of Pittsburgh Cancer Institute, Pittsburgh, Pennsylvania, USA

Dendritic cells are the most effective antigen presenting cells and have been used in a variety of approaches to immunotherapy. We have developed a highly sensitive method for monitoring the trafficking of dendritic cells into tumors using the magnetic resonance imaging agent ProHance. This contrast agent has been shown to be taken up by the dendritic cells and can be imaged with MRI. ProHance is further evaluated of it's effects on dendritic cell phenotype and lytic activity of NK cell co-cultures.

DCE-MRI in Cancer: Clinical and Analysis

Room 4E Thursday 13:30 - 15:30

2928. DCE-MRI Perinecrotic Imaging Biomarker Signature and Observed Interpatient Heterogeneity

Dee Wu[1], Yi Zheng[1], Susan Edwards[1], Syed Rahmannan[1], William TC Yuh[2], Nina Mayr[2]

[1]University of Oklahoma Health Sciences Center, Oklahoma City, Oklahoma, USA; [2]Ohio State University, Columbus, Ohio, USA

A newly developed imaging biomarker for the estimation of the state of tumor angiogenesis is described. DCE-MRI data is aggregated in regions evaluated from the exterior toward the tumor interior at high resolution in ten cervical cancer patients. This work proposes a two-regime model: linear region (6-8 mm) depth followed by highly necrotic varying core regime at greater depth. While this two-regime model provides a potentially adequate description, slope and intercepts parameters derived by linear regression were highly variable between patients indicating the potential importance of careful scrutiny of these measures on a patient-by-patient basis and the need for improved individualized healthcare.

2929. Incorporation of Explicit Arterial Input Function for DCE-MRI Quantification: Use in Human Trial of Sorafenib in Renal Cell Carcinoma

Mark Rosen[1], Keith Flaherty[1], Dan Heitjan[1], Brian Schwartz[2], Peter O'Dwyer[1]

[1]University of Pennsylvania, Philadelphia, Pennsylvania, USA; [2]Bayer Pharmaceutical Corp, West Haven, Connecticut, USA

We demonstrate the effects of incorporating a measured arterial input function (AIF) in DCE-MRI quantification, using the results of a recently completed human trial of DCE-MRI to monitor early response of renal cell carcinoma to Sorafenib. Use of a measured, rather than assumed, AIF leads to dramatic alterations in the resulting tumor Ktrans values before therapy. Change in tumor Ktrans following treatment is significantly associated with clinical outcome (time to tumor progression) only when the measured AIFs are utilized.

2930. Pixel-Based Quantitative Analysis of Dynamic Contrast-Enhanced MRI of Lung Tumors

Yu-Jen Chen[1], Woei-Chyn Chu[1], Wen-Yih Isaac Tseng[2]

[1]Institute of Biomedical Engineering, National Yang-Ming University, Taipei, Taiwan; [2]Center for Optoelectronic Biomedicine, National Taiwan University College of Medicine, Taipei, Taiwan

Dynamic contrast-enhanced magnetic resonance image (DCE-MRI) has been known for its efficacy in characterization and treatment monitoring of tumors. Using a pharmacokinetic model, DCE-MRI provides parameters indicating permeability of tumor microvessels which has been shown to be closely related to angiogenesis. Due to heterogeneity of tumor perfusion, a pixel-based quantitative method to analyze tumor perfusion is desirable. To accomplish this, we tried to develop an automatic motion-detection method to co-register the tumors in motion, and tested the pixel-based DCE-MRI technique in lung tumors.

2931. Dynamic Contrast Enhanced MRI as a Priori Predictor of Response in Head and Neck Squamous Cell Carcinoma: Initial Analysis

Amita Shukla-Dave[1], H. Stambuk[1], Y. Wang[1], S. Karimi[1], Y. B. Su[1], D. G. Pfister[1], N. Lee[1], J. A. Koutcher[1]

[1]Memorial Sloan-Kettering Cancer Center, New York, USA

Squamous cell carcinoma of the head and neck (HNSCC) is the fifth most common malignancy in the world and the survival rates have remained relatively unchanged over the past 3 decades. Today with many treatment options available, it is important to have an a priori method to stratify good risk and poor risk categories to improve outcome and quality of life. The present study was designed to assess whether pretreatment DCE-MRI changes can reliably predict response. DCE-MRI was performed in 17 patients prior to chemo-radiation therapy. The initial results suggest that DCE-MRI may prove to be a useful a priori predictor of response in HNSCC patients.

2932. Pharmacokinetic Analysis of DCE-MRI in Invasive Breast Carcinomas: Correlation with Tumour Grade

Aleksandra Radjenovic[1], Barbara J. G. Dall[2], Steven Frederick Tanner[1], Sarah E. Bacon[2], Daina Dambitis[2], John Peter Ridgway[2]

[1]University of Leeds, Leeds, UK; [2]Leeds General Infirmary, Leeds, UK

Analysis of the correlation between quantitative DCE-MRI findings and prognostic factors (such as histological tumour grade) is important for defining the role of this technique in the diagnosis of breast cancer as well as the monitoring of neo-adjuvant therapies. Previous clinical studies where prognostic factors were compared to DCE-MRI reported contradictory results and did not include pharmacokinetic modelling of contrast uptake. In this study, pharmacokinetic analysis of DCE-MRI was performed in patients with histologically confirmed and graded invasive breast carcinomas and a significant correlation between tumour grade and permeability to Gd-DTPA was found.

2933. The Extent and Severity of Vascular Leakage as Evidence of Tumor Aggressiveness in High-Grade Gliomas

Yue Cao[1], Vijaya Nagesh[1], Daniel Hamstra[1], Christina I. Tsien[1], Ross D. Brian[1], Thomas L. Chenevert[1], Larry Junck[1], Theodore S. Lawrence[1]

[1]University of Michigan, Ann Arbor, Michigan, USA

MRI reveals heterogeneous regions within high-grade gliomas, such as a contrast-enhanced rim, a necrotic core, and non-contrast enhanced abnormalities. It is unclear which of these regions best describes tumor aggressiveness. We hypothesized that the vascular leakage volume, which reflects disorganized angiogenesis typical of glioblastoma, would be the best predictor of clinical outcome. Our data suggest that for patients with high-grade glioma, time to progression after radiation therapy is influenced both underlying biological aggressiveness (vascularity) and spread of disease. In contrast, survival depends chiefly on the spread of disease at the time of presentation.

2934. Radiologist Selection of Tumor Regions of Interest for Dynamic Contrast Enhanced MRI Analysis: Effect on Reproducibility and Spread of Modelled and Non-Modelled Parameters

Adrian Tang[1], David Collins[2], James d'Arcy[1], Martin Leach[1], Simon Walker-Samuel[1], Toni Wallace[2], Nandita deSouza[1]

[1]Institute of Cancer Research, Sutton, Surrey, UK; [2]Royal Marsden NHS Foundation Trust, Sutton, Surrey, UK

Radiologist selection can isolate regions within a tumor, which have significantly higher modelled and non-modelled measures of perfusion and permeability with significantly lower variation. However, ROI selection does not improve reproducibility of either modelled or non-modelled DCE-MRI parameters, suggesting that tumor heterogeneity is not the major factor contributing to reproducibility.

2935. What is the Optimal Cohort Size for a Reproducibility Study of Dynamic Contrast-Enhanced MRI?

N Jane Taylor[1], James A. d'Arcy[2], Simon Walker-Samuel[2], David J. Collins[2], Benjamin Knowles[2], J James Stirling[1], Toni Wallace[2], Dow-Mu Koh[2], Adrian Tang[2], Chooi Lee[2], Martin O. Leach[2], Gordon J S Rustin[1], Anwar R. Padhani[1]

[1]Mount Vernon Hospital, Northwood, Middlesex HA6 2RN, UK; [2]Royal Marsden Hospital, Sutton, Surrey SM2 5PT, UK

The measurement of test-retest variability is an integral part of study design of dynamic MRI (DCE-MRI) studies that evaluate the effectiveness of antiangiogenesis and angiolytic drug trials. In this study we investigate the effect of increasing numbers of patients on the reproducibility of DCE-MRI studies in order to define the number of patients needed to adequately define test-retest variability.

2936. Reproducibility of Pharmacokinetic Parameters Using Different Input Functions in a Multi-Center Non-Expert Phase I Oncology Clinical Trial

Vahan Sharoyan[1], David White[2], Radhika Sivaramakrishna[1], Susan Galbraith[3], Ali Guermazi[1], Caroline Reinhold[1], Anwar Padhani[1, 4]

[1]Synarc, Inc., San Francisco, California, USA; [2]Synarc, Inc.,, San Francisco, California, USA; [3]Bristol Myers Squibb Company, Princeton, New Jersey, USA; [4]Paul Strickland Scanner Centre, Mount Vernon Hospital, Northwood, Middlesex, UK

The purpose of this study was to compare the reproducibility of tumor DCE-MRI kinetic parameters in a oncology clinical trial using vascular input functions based on standard (Fritz-Hansen;Weinmann) and individualized (derived from skeletal muscle) plasma clearance coefficients. Overall means, repeatability coefficients and within-patient coefficient-of-variability of transfer constant (Ktrans), extravascular-extracellular space (Ve), rate constant (Kep) , and initial area under the Gd-DTPA concentration-time curve (IAUC) were determined for six patients. Best reproducibility was obtained with Fritz-Hansen coefficients.

2937. Optimal Quantification of DCE-MRI Data Using Reference Tissue Normalisation

Simon Walker-Samuel[1], Benjamin R. Knowles[1], James A. d'Arcy[1], Neil J. Smith[2], Gina Brown[3], Martin O. Leach[1], David J. Collins[1]

[1]Institute of Cancer Research, Sutton, Surrey, UK; [2]Mayday University Hospital, Thornton Heath, Surrey, UK; [3]Royal Marsden and NHS Foundation Trust, Sutton, Surrey, UK

It has been shown that spoiled gradient echo sequences can be designed such that changes in signal intensity are directly proportional to Gd-DTPA concentration in DCE-MRI measurements. This can be usefully exploited in reference tissue-based quantification methodologies. However, the choice of dynamic parameter used in such analysis (signal difference, relative enhancement or enhancement factor) significantly affects the uncertainty in the resultant quantitative parameters. This study aimed to compare the relative uncertainty in each dynamic parameter in order to evaluate which is most appropriate to use in this type of analysis.

Image Reconstruction Methods

Room 4E Thursday 13:30 - 15:30

2938. Noise Reduction in Multiple Echo Data Sets Using Singular Value Decomposition

Mark Bydder[1], Jiang Du[1]

[1]University of California, San Diego, California, USA

Noise Reduction in Multiple Echo Data Sets using Singular Value DecompositionA method is described for de-noising multiple echo data sets using singular value decomposition (SVD). Images are acquired using a multiple gradient or spin echo sequence and the variation of the signal with echo time (TE) in all pixels is subjected to SVD to categorize the components of the signal variation. The least significant components, which tend to characterize noise variation, are suppressed to reduce their contribution. The result of this procedure is a reduction in noise in the individual TE images. A “minimum variance” filter is used to optimally approximate the noise-free images.

2939. Colored Noise and Effective Resolution: Data Considerations for Non-Uniform K-Space Sampling Reconstructions

Rexford Newbould[1], Chunlei Liu[1], Roland Bammer[1]

[1]Stanford University, Stanford, California, USA

Non-Cartesian acquisition schemes, such as PROPELLER and variable density spirals offer a number of distinct advantages over Cartesian methods. These trajectories are designed to repeatedly sample data near the origin of k-space. When sampled data is regridded, regions near the center of k-space have a greater SNR than those at the periphery. The result is colored noise in the final reconstructed image: a loss of SNR near contrast changes, which reduces the effective resolution of the image. The colored noise can be quite distracting when appraising an image. Here we propose a noise recoloring method, which only decreases SNR in frequencies which have artificially increased SNR above that of the acquisition.

2940. Noise Characteristics in POCS (Projection Onto Convex Sets)-Reconstructed MR Images

Mohammad Sabati[1, 2], Haidong Peng[1, 2], Richard Frayne[1, 2]

[1]Foothills Medical Centre, Calgary Health Region, Calgary, Alberta, Canada; [2]University of Calgary, Calgary, Alberta, Canada

Undersampling of the k-space data has been widely used as an effective approach for rapid 2D and 3D MR imaging. Typically, the central zone of k-space is fully sampled but the peripheral zone is partially sampled. The partial Fourier method, for example, reduces the amount of acquired data by asymmetrically truncating the peripheral portions of k-space in either the phase or the frequency encoding directions, or both. Projection-onto-convex-sets (POCS), techniques have been successful in reconstructing such undersampled k-space data. In evaluating the noise properties of the POCS-reconstructed images and comparing them to those obtained in other reconstruction techniques (via SNR and CNR calculations), care is warranted because the iterative non-linear POCS reconstruction method can modify the underlying noise properties of the image. This preliminary study investigates and characterizes the noise in the POCS reconstruction approach.

2941. Improved Conjugate-Gradient Phase Correction Algorithm for Multi-Shot DWI

Jian Zhang[1], Chunlei Liu[1], Michael Moseley[1]

[1]Stanford University, Stanford, California, USA

SNAILS image reconstruction by using CG method is more susceptible to physiological artifacts than SENSE due to worse system condition. We present an improved algorithm (ICG) here by introducing an additional phase correction stage into the original algorithm. By evaluating the performance of both algorithms at various degrees of motion and signal to noise ratio (SNR), we demonstrate that ICG increases both image quality and converging speed significantly. According to the simulation results, the image quality is increased almost independent of SNR, while the improvement in the converging speed is more significant at higher SNR.

2942. Edge-Guided Localized Phase Unwrapping: Application to SWI

Hemanth Thayyullathil[1], Lara Stables[1], Michael W. Weiner[1], Norbert Schuff[1]
[1]DVA Medical Center and University of California San Francisco, San Francisco, California, USA

Accurate measurement of phase is essential in many contexts in MRI, such as in susceptibility-weighted imaging (SWI), flow imaging, and Bo field-maps. In such situations, artificial discontinuities in phase images called 'phase wraps' are not desirable.We have formulated and implemented a computationally efficient phase unwrapping method, which is able to preserve subtle features in the phase images while unwrapping severe phase wraps. Phase values are altered only at regions of wraps, guided by the linked edges present in the wrapped phase image. We have applied the method on both synthetic objects and experimental SWI phase images.

2943. A Method for Automatic Determination of the Global Polarity of Phase Sensitive Inversion Recovery Images

Yinan Liu[1, 2], Jingfei Ma[1]
[1]University of Texas M. D. Anderson Cancer Center, Houston, Texas, USA; [2]Texas A & M University, College Station, Texas, USA

Phase sensitive inversion recovery images reconstructed from a region growing-based algorithm have an intrinsic ambiguity in the global polarity (GP). Determining GP using the previously proposed net magnetization (NM) or “moment of inertia (MI)” is found to be dependent on the imaging parameters such as TI, as well as the field strength. In this work, this dependency was removed with a theoretical calculation of the white matter signal polarity. A hybrid scheme employing both NM and MI was shown capable of automatically determining the correct GP of images collected over a wide range of TI and at both 1.5T and 3.0T.

2944. A Novel Reconstruction Method for Axial 3D Data Acquisition During Continuous Table Movement

Michael O. Zenge[1], Mark E. Ladd[1], Harald H. Quick[1]
[1]University Hospital Essen, Essen, Germany

Slab selective excitation combined with transverse read-out during continuous longitudinal table movement not only facilitates tumor staging and metastasis screening, the unlimited FOV will furthermore ease a variety of routine examinations on state of the art short bore scanners. A novel reconstruction method is presented which features compact implementation, high computational efficiency and is independent of k-space ordering. High-resolution 3D gradient echo data acquisition was performed during continuous table movement. The total acquisition time for a longitudinal FOV of 1800mm with a matrix of 192x119x900 and isotropic resolution was less than 5 minutes. The reconstruction method provided overall exact anatomical images.

2945. High Frame Rate Cardiac Imaging Using Kalman Filtering

Uygar Sümbül[1], Juan M. Santos[1], John M. Pauly[1]
[1]Stanford University, Stanford, California, USA

We develop acquisition and reconstruction methods for real-time cardiac imaging that exploit the redundancy in the temporal direction. We sample less than 60% of a whole frame and try to estimate the missing parts using a Kalman filter. To obtain a corresponding reduction in scan time, and hence a corresponding increase in frame rate, we use a special trajectory to sample a four-interleave spiral image in two excitations. Our reconstruction videos run at twice the frame rate of that of the corresponding conventional real-time imaging method. This method can be combined with other common intra- and inter-frame speed-up techniques.

2946. FE-MRI: Simulation of MRI Using Arbitrary Finite Elements

Paul Simedrea[1, 2], Luca Antiga[3], David A. Steinman[1, 2]
[1]Robarts Research Institute, London, Ontario, Canada; [2]The University of Western Ontario, London, Ontario, Canada; [3]Mario Negri Institute for Pharmacological Research, Bergamo, Italy

MRI simulation of realistic objects is hampered by difficulties in compactly describing curved or irregular object boundaries. In 2001 Truscott and Buonocore showed how the MRI signal equation could be integrated analytically provided the object is discretized into contiguous linear tetrahedral elements; however, they conceded that many such elements would still be required for complex objects. Taking a cue from finite element numerical analysis techniques, here we demonstrate how this limitation can be overcome by numerically integrating the signal equation over finite elements of arbitrary order or shape, thus allowing for much more compact discretizations of complex objects.

2947. Improving the Accuracy of the Chromophore Reconstruction in Diffuse Optical Tomography by Using Structural and Functional-Priors from MRI

Roshanak Shafiiha[1], Mehmet Burcin Unlu[1], Gultekin Gulsen[1], Ozlem Birgul[1], Mark Jason Hamamura[1], Yong Chu[1], Orhan Nalcioglu[1]
[1]University of California, Irvine, Irvine, California, USA

One of the important goals of NIR breast imaging is accurate assessment of the total hemoglobin concentration and oxygen saturation in tissue. The results of this study demonstrate that applying structural and functional-priori from MRI can improve the accuracy of the chromophore reconstruction in optical tomography. We have constructed ethanol-based multi-modality phantoms to investigate the advantage of using functional-priors, specifically water concentration, from MRI to improve the accuracy of the chromophore reconstruction. The ethanol-based phantom provides a new platform for combined MR and optical imaging to assess the effect of water content on the accuracy of other chromophore concentrations.

2948. Improvements in Line Scan Diffusion Weighted Image Reconstruction with a Least Norm Algorithm

Jing Chen[1], *Kim Butts Pauly*[1]
[1]Stanford University, Stanford, California, USA

Line scan diffusion image (LSDI) is inherently blurred in the line scan direction. In addition, intraview motion in the presence of diffusion weighted gradients may cause signal loss in some lines in LSDI. In this work, we use a least norm (LN) algorithm to reconstruct the images to improve the image quality by solving these two problems. High spatial resolution is obtained in the LN image, and the dropped line is recovered with high accuracy.

2949. Density Compensation for TrueFISP Blade Imaging in the Steady State (TrueBLISS)

Kestutis Joseph Barkauskas[1], *Mark A. Griswold*[2], *Jeffrey L. Sunshine*[2], *Jeffrey L. Duerk*[2, 3]
[1]Case Western Reserve University, Cleveland, Ohio, USA; [2]University Hospitals of Cleveland and Case Western Reserve University School of Medicine, Cleveland, Ohio, USA; [3]Case Western Reserve University, Cleveland, Ohio, USA

Rotating blade trajectories, such as RUKSE and PROPELLER have been proposed as improvements for a variety of applications. For these non-Cartesian trajectories, modulation in the gridded K-space can arise at the overlap between blades, which would ideally be addressed by the Density Compensation Function. This work proposes two alternatives to the Jackson method for blade imaging and confirms for TrueFISP Blade Imaging in the Steady State (TrueBLISS) that Amateur Hack is a rapid alternative to the Jackson method, but Iterative Grid / De-Grid yields superior results.

2950. Voronoi Based Sampling Density Correction

Costin Tanase[1], *Fernando Boada*[1]
[1]University of Pittsburgh, Pittsburgh, Pennsylvania, USA

By using algebraic geometry tools, the Voronoi algorithm could be effectivelly implemented as a building block of a general 3D reconstruction tool. The presented work show the versatility of the approach, and hint to the complexity of the true 3D problems when compared to the 2D counterparts. Whenever the hardware limitations are met (limited slew rates, waveform memory) the K-space trajectory could deviate from the theoretical form. The 3D Voronoi decomposition offers a natural framework to address those imprecision. Also, the description of the aliasing patterns could be better understood in the same framework.

2951. Optimized Algorithm for Sampling Density Correction

Kenneth O. Johnson[1], *James Grant Pipe*[1]
[1]St. Joseph's Hospital, Phoenix, Arizona, USA

An optimized method for calculating the weighting coefficients to normalize sampling density is proposed. It breaks up the collection of points to calculate efficiently the localized sampling desity by dividing k-space into an array of compartments. When calculating density only adjacent compartments need to be traversed instead of the entire catalogue of points.

2952. Iterative Deconvolution-Interpolation Gridding

Refaat E. Gabr[1], *Pelin Aksit*[2], *Paul A. Bottomley*[1], *AbouBakr M. Youssef*[3], *Yasser M. Kadah*[3]
[1]Johns Hopkins University, Baltimore, Maryland, USA; [2]GE Healthcare, Waukesha, Wisconsin, USA; [3]Cairo University, Giza, Egypt

We present a simple iterative solution to the problem of image reconstruction from arbitrarily-sampled k-space. The new solution solves a sparse linear system that is equivalent to deconvolution of the k-space with a small kernel. The deconvolution is accurate, and sampling onto a finer grid is not required. Avoiding grid over-sampling preserves storage crucial for 3D trajectories. The new algorithm bypasses the calculation of sampling density compensation functions, and construction of the gridding matrix is simple, fast and requires no regularization. It is thus amenable to situations involving changing k-space trajectories. The algorithm is implemented with *in vivo* spiral MRI.

2953. Fast Iterative Approximate Pseudo-Inverse Image Reconstruction from Data Acquired on Arbitrary K-Space Trajectories

Souheil Inati[1], *Leslie Greengard*[1]
[1]New York University, New York, New York, USA

We present an efficient least squares method for the reconstruction of magnetic resonance images from data sampled non-uniformly in k-space. The procedure only requires knowledge of the sampling locations and can be applied to arbitrary trajectories in 2 or 3 dimensions, including those that are self-intersecting. The method is based on two fast algorithms, the non-uniform fast Fourier transform (NUFFT) and the fast sinc transform, combined with analytic weights, and an iterative procedure.

2954. Data-Sharing PROPELLER Imaging for Increased Temporal Resolution Retaining Spatial Resolution and Image Contrast

Tzu-Chao Chuang[1], Teng-Yi Huang[2], Fu-Nien Wang[1], Yi-Ru Lin[1], Hsiao-Wen Chung[1], Kenneth K. Kwong[3]

[1]National Taiwan University, Taipei, Taiwan, Taiwan; [2]National Taiwan University of Science and Technology, Taipei, Taiwan, Taiwan; [3]MGH-HMS-MIT Athinoula A. Martinos Center for Biomedical Imaging, Charlestown, Massachusetts, USA

The PROPELLER technique was restricted to static imaging due to its multi-shot nature. By introducing the concept of ¡§keyhole¡¨, images that were reconstructed by the data-sharing PROPELLER technique have the temporal resolution of the blades and the spatial resolution of the conventional PROPELLER images. In this work, simulation on dynamic contrast-enhanced perfusion imaging and *in vivo* T2 estimation experiments were used to demonstrate the effectiveness of the proposed method. Results show that dynamic images showing behavior highly consistent with full-k-space images could be obtained without prominent artifacts.

2955. Image De-Blurring of PROPELLER EPI Using a K-Space Weighting Scheme

Tzu-Chao Chuang[1], Teng-Yi Huang[2], Fu-Nien Wang[1], Fa-Hsuan Lin[3], Cheng-Wen Ko[4], Cheng-Yu Chen[5], Hsiao-Wen Chung[1, 5], Kenneth K. Kwong[3]

[1]National Taiwan University, Taipei, Taiwan, Taiwan; [2]National Taiwan University of Science and Technology, Taipei, Taiwan, Taiwan; [3]MGH-HMS-MIT Athinoula A. Martinos Center for Biomedical Imaging, Charlestown, Massachusetts, USA; [4]National Sun Yat-Sen University, Kaohsiung, Taiwan, Taiwan; [5]Tri-Service General Hospital, Taipei, Taiwan, Taiwan

PROPELLER-EPI is a multi-shot technique that could potentially achieve high-resolution diffusion tensor imaging by combining data acquired from rotating blades in the k-space. One crucial step in PROPELLER-EPI image reconstruction is the windowing used for weighing different blades of data. In this work we showed that by lowering the time constants for the exponential window, data obtained far from the echo center, i.e., those inherently exhibiting stronger susceptibility-induced off-resonance distortions, were de-emphasized, thereby reducing the blurring effects. Such resolution benefits were however gained with trade-off in signal-to-noise ratio due to effectively less signal averages.

2956. An Enhanced Phase Correction Algorithm for PROPELLER DW MRI

Ajit Devaraj[1], Ryan G. Robison[1], James Grant Pipe[1]

[1]St. Joseph's Hospital, Phoenix, Arizona, USA

Good PROPELLER reconstruction is closely related to accurate alignment of the blades with the k-space origin. Superfluous phase can distort this alignment, limiting the reconstruction quality. The existing technique for linear phase correction is sub-optimal - it may result in discarding large data strips from the blade edges. Here we present an improved technique - in lieu of elimination, the artifact is accurately quantified and retained. This information is then used in the reconstruction process to inherently compensate for the artifact. We demonstrate the effectiveness of this approach to track linear phase distortion and the possible improvement in reconstruction.

2957. Efficient Multiple Acquisitions by SPEED with Shared Spatial Information

Zheng Chang[1], Qing-San Xiang[1]

[1]University of British Columbia, Vancouver, British Colmbia, Canada

The fast MRI method of Skipped Phase Encoding and Edge Deghosting (SPEED) is effective to accelerate a single image acquisition, but is not yet applied to multiple acquisitions. Multiple acquisitions such as those in multi-point Dixon are spatially registered. They contain highly similar and redundant spatial information. The redundancy can be reduced by SPEED leading to a higher acceleration factor than that achievable in a single image acquisition. For double-acquisitions, if the 1st acquisition is undersampled by 3/5, the 2nd acquisition can then be undersampled by only 2/5, resulting in a total scan time of nearly a single full acquisition.

2958. Average and Time-Resolved Dual Velocity Encoded Phase Contrast Vastly Undersampled Isotropic Projection Imaging

Kevin Michael Johnson[1], Oliver Wieben[1], Patrick Turski[1], Chuck Mistretta[1]

[1]University of Wisconsin-Madison, Madison, Wisconsin, USA

The velocity to noise ratio (VNR) of phase contrast data is linearly proportional to the magnitude of the first moment of the bipolar applied. In general, the bipolar induced phase can only be resolved to ±ð; however, additional information or assumptions can extend that range. We propose time-resolved and time averaged dual velocity encoded (VENC) techniques, with minimal increases in scan time or artifact. Dual VENC sequences are shown to have higher SNR and VNR, as compared to single VENC sequences; as well as improved vessel characterization.

2959. Super-Resolution in Single-Coil Multiple Image Reconstruction Technique

Satoshi Ito[1], Hiroki Fukaya[1], Na Liu[1], Yoshifumi Yamada[1], Kunio Tanaka[2]

[1]Utsunomiya University, Utsunomiya, Tochigi, Japan; [2]Asahikawa Medical College, Asahikawa, Hokkaido, Japan

This paper presents the resolution improvement method for the partially high-resolution image in multiple image reconstruction technique. The signal obtained in the phase-scrambling Fourier imaging technique can be transformed to the description of Fresnel transform equation. Therefore, an image can be reconstructed by inverse Fresnel transform as well as by standard inverse Fourier transform. By combining these two reconstructed images, we can obtain an image that has a higher resolution than standard imaging technique in the center of image. To improve the resolution, super-resolution technique was applied, and it was shown that resolution was fairly improved by a small number of iterations.

2960. Sparse K-Space Sampling Strategies and Projection-Onto-Convex Sets Image Reconstruction for Improved Fast 3D Imaging

Haidong Peng[1, 2], *Mohammad Sabati*[1, 2], *M Louis Lauzon*[1, 2], *Richard Frayne*[1, 2]
[1]University of Calgary, Calgary, Alberta, Canada; [2]Seaman Family MR Research Centre, Foothills Medical Centre, Calgary Health Region, Calgary, Alberta, Canada

One of the three-dimensional (3D) fast MR approaches is to completely sample the central region of the phase-encoding plane while sparsely sample its peripheral region, resulting in the formation of sparsely sampled k-space. For a given scan time, there exists a number of sampling strategies with different distribution patterns of acquired data (k-space). In this research it is shown that it is possible to choose a specific sparsely sampling strategy (k-space), from which POCS image reconstruction will generate the best image to depict high-resolution structures (e.g., small blood vessels). The resulting image quality was assessed by direct image visualization and local performance error.

2961. Autoregressive Moving Average (ARMA) Method for the Reconstruction of MR Images from Sparsely Sampled 3D K-Space

Haidong Peng[1, 2], *Michael Richard Smith*[1], *Richard Frayne*[1, 2]
[1]University of Calgary, Calgary, Alberta, Canada; [2]Seaman Family MR Research Centre, Foothills Medical Centre, Calgary Health Region, Calgary, Alberta, Canada

In order to achieve real-time 3D MR imaging one approach is to collect sparsely sampled k-space datasets. Moving-table contrast-enhanced MR angiography is one such example. Here, we compare different reconstruction of sparsely sampled data by zero filling (ZF) and by TERA. The quality of the reconstructed images was assessed by visual inspection, as well as by both global and local performance errors (PE). It is shown that the proposed CP-TERA results in better image quality than ZF and rTERA from sparsely sampled k-space dataset and that the PE (both global and local) values in CP-TERA image were less than in ZF and rTERA images.

2962. Adaptive-Kernel Reconstruction of Variable-Density Trajectories

Edward Walsh[1], *David Ress*[1]
[1]Brown University, Providence, Rhode Island, USA

An adaptive kernel gridding method is presented for use with non-uniform density spiral and rosette k-space trajectories. Simulations were performed for one-shot acquisitions of 20ms or less duration. Results demonstrate maintenance of the point spread function compared to uniform density spiral acquisitions of the same spatial resolution and field of view. Gradient parameters used in the simulation were compatible with current high-performance body gradient sets.

2963. Scan Time Reduction in Spectroscopic Imaging Using HYPR

John Oliver Perry[1], *Oliver Wieben*[1], *Charles Mistretta*[1], *Scott Reeder*[1], *Yijing Wu*[1], *Yan Wu*[1]
[1]University of Wisconsin - Madison, Madison, Wisconsin, USA

The application of spectroscopic imaging techniques such as CSI are limited in clinical practice mainly for the extensive acquisition times. Here we propose the use of a HighlY constrained backPRojection reconstruction (HYPR), a novel reconstruction technique for spectroscopic imaging with a radial trajectory to significantly reduce scan times. Simulations are presented that demonstrate good results for the obtained spectra and metabolite images, with a speedup factor of 17 over a fully sampled Cartesian acquisition.

2964. Improved Spectroscopic Imaging Using Echo-Planar Scans and Sparse Reconstruction

Mathews Jacob[1], *Bradley P. Sutton*[1], *Justin Haldar*[1], *Zhi Pei Liang*[1]
[1]UIUC, Urbana, Illinois, USA

We find that the model based spectroscopic imaging framework, originally derived for reduced encoding, is more appropriate for fast-scan techniques; these schemes can provide larger k-space coverage in the same scan time as the reduced phase encoding case. This enables us to redesign the model-based framework to these schemes, thus simultaneously achieving high spatial resolution, signal to noise ratio, and low artifacts. We then present a data-adaptive basis selection procedure to rectify some of the problems associated with the current model based techniques. To achieve this goal, we propose to specify the basis functions using linear constraints. We start with a rigid image model, formulated in this framework. We then relax some of its constraints based on the MRSI data. This enables us to make the model flexible, without losing its robustness.

2965. Improved Random Sampling Reconstruction for In-Vivo Data Using Discrete Cosine Transform

Ivan Lillo[1], *Johannes Plett*[1], *Marcelo Guarini*[1], *Roberto Mir*[1], *Pablo Irarrazaval*[1]
[1]Pontificia Universidad Catolica de Chile, Santiago, Chile

When a signal or image has a sparse or compressible representation in some domain, it is possible to obtain few random samples and reconstruct the image by minimizing the L_1 norm of the coefficients in the sparse domain, maintaining fidelity of the acquired samples. In phantoms it is possible to get exact reconstruction. For *in vivo* images, our hypothesis is that a windowed 2D-DCT of the image, similar to JPEG, yields an excellent concentration of information, allowing a good combination of localization versus frequency. We propose an MRI reconstruction based on the DCT, using adaptive and non uniform *k*-space subsampling.

2966. Off-Resonance Correction for 3D Imaging Using a Stack of Spirals Trajectory

Weitian Chen[1], Craig H. Meyer[1]
[1]University of Virginia, Charlottesville, Virginia, USA

A stack of spirals trajectory is one of the commonly used non-Cartesian 3D trajectories, and it can increase the scan efficiency by an order of magnitude compared to standard 3D methods. The main factor limiting the reliability of spiral imaging is image blurring caused by off-resonance effects. We propose a method for performing 3D off-resonance correction for a stack of spirals trajectory by performing 2D off-resonance correction slice by slice in 3D. This method simplifies the calculations and increases the ffectiveness of the image deblurring.

2967. A Hybrid Homodyne Algorithm for Reconstructing Partially Acquired Two-Point Dixon Data

Dustin K. Ragan[1], Jingfei Ma[1]
[1]University of Texas M. D. Anderson Cancer Center, Houston, Texas, USA

Dixon techniques acquire multiple images at different echo times and use their phase differences to separate water and fat. Although widely used for scan time reduction, homodyne techniques, which assume that the imaged object is real, are generally incompatible with Dixon reconstruction. In this work, we demonstrate that in the special case of a two-point Dixon acquisition, an algorithm for combined homodyne and Dixon reconstruction is feasible. Our experiments show that by using the algorithm, high-resolution fat-suppressed images can be generated from partially acquired k-space data, thus substantially decreasing the total scan time.

2968. Fast Automatic Debluring with a Linear Map

Weitian Chen[1], Craig H. Meyer[1]
[1]University of Virginia, Charlottesville, Virginia, USA

Field inhomogeneity can cause image blurring for non-2DFT acquisitions. We propose a fast automatic off-resonance correction method, which performs linear correction without acquiring extra field map datasets. Our method needs only about two times the computation time of image reconstruction by gridding, and it is likely more robust than pixel-by-pixel based automatic methods. Our method can be a useful technique for fast deblurring when field map based off-resonance correction methods are undesirable or unreliable.

2969. Field Inhomogeneity Correction Based on Gridding Reconstruction

Holger Eggers[1], Tobias Knopp[2], Daniel Potts[3]
[1]Philips Research, Hamburg, Germany; [2]University of Luebeck, Luebeck, Germany; [3]Chemnitz University of Technology, Chemnitz, Germany

A new algorithm for the correction of off-resonance effects is proposed. It is based on the same approximation as standard gridding reconstruction, and it is compatible with direct and iterative approaches. It is shown to achieve a similar accuracy as least squares algorithms, while requiring no time-consuming calculation of interpolation coefficients and offering further advantages in terms of computational complexity. Moreover, it permits balancing the accuracy of the gridding reconstruction and of the field inhomogeneity correction in non-Cartesian imaging. The algorithm is demonstrated in simulations and phantom experiments.

2970. Correction of Gradient Error Distortions in Echo-Planar Imaging

Guoxiang Liu[1]
[1]National Institute of Information and Communications Technology, Kobe, Hyogo, Japan

We propose a simple and general approach to correcting the distortion due to RO field gradient errors (mainly those induced by eddy currents) based on the statistical properties of EPI images. The proposed method can correct the linear eddy-current-induced field gradient error along the RO direction even in high-resolution EPI (such as 128x128-pixel imaging) by online processing. We remove the influence of the PE field gradient from the estimation of the first-order phase error (RO gradient induced) of each RO line, and correct the linear distortion using the estimated RO-gradient-induced phase error.

2971. An Inverse Approach to the Recovery of Signal Losses in EPI Images

Guoxiang Liu[1]
[1]National Institute of Information and Communications Technology, Kobe, Hyogo, Japan

This paper derives and implements a method for recovering MRI signal losses caused by Susceptibility-induced magnetic field gradients (SFGs) in regions with large static field inhomogeneities in EPI. Factor to account for SFGs was added in a traditional EPI equation, which was a simple Fourier transform (FT) for expressing the actual k-space data of an EPI scan. The inverse calculation of this "distorted EPI" equation was used as a kernel to correct reduction in intensity during reconstruction. A step-by-step EPI reconstruction method is proposed to avoid complicated phase unwrapping problems.

2972. T2 Estimation Using a Half Fourier Radial Fast Spin-Echo Method

Ali Bilgin[1], Zhiqiang Li[1], Maria I. Altbach[1]
[1]University of Arizona, Tucson, Arizona, USA

A method based on a bent k-space trajectory and half Fourier reconstruction was developed for obtaining high-resolution T2 maps from a single RAD-FSE k-space data set. With this method the effective Nyquist radius is doubled without increasing imaging time compared to the conventional radial k-space trajectory where a full k-space line is acquired per readout period. This significantly reduces the T2 bias for small objects. The proposed method may lead to accurate diagnosis of pathologies in small lesions.

2973. Reconstruction of SWI for Phased Array Head Coil

Hao Shen[1, 2], Guang Cao[3], Zesheng Tang[2]
[1]GE Healthcare China, Beijing, People's Republic of China; [2]Tsinghua University, Beijing, People's Republic of China; [3]GE Healthcare China, Hong Kong, People's Republic of China

Implement two combination methods Average of Sum (AOS) and Root of Square Sum (RSS) to generate SWI image from a 8-channel phased array head coil. Based on several statistic values, analyse and compare these two kinds of methods.

Artifacts and Correction: Motion

Room 4E Thursday 13:30 - 15:30

2974. Improved Accuracy of Shift Calculations Through Appropriate Filtering of High Resolution Navigators

Robert W. Schaffer[1], Dwight Nishimura[1]
[1]Stanford University, Stanford, California, USA

Navigators are used to detect translation and phase-correct corresponding data frames using cross-correlation. The quality of the corrected image is a function of how accurately the shifts can be calculated. When high precision is attempted (as in high-resolution imaging), the SNR can be quite low. While filtering to maximize the SNR at the peak of the cross-correlation may improve shift calculations, we show that a filter that results in more curvature at the cross-correlation peak is superior. Through appropriate filtering, the accuracy of the measured shift and, thus, the quality of the corrected image can be improved.

2975. ContinuousLy Adaptive Windowing Strategy (CLAWS) for Real Time Reduction of Motion Artefacts

Permi Jhooti[1], David Firmin[2]
[1]Royal Brompton Hospital, London, UK; [2]Imperial College, London, UK

Cardiac imaging is still limited by the impact of respiratory artefacts on image quality. Techniques exist to try to limit the problem but the variable nature of breathing ensures inconsistencies in their performance. ContinuousLy Adaptive Windowing Strategy (CLAWS) is a very robust technique against motion and allows images to be constructed as soon as possible with a further real time reduction of artefacts. The operator may terminate data acquisition earlier in the knowledge that the best image possible at this time will be available. CLAWS is appropriate for any imaging situation in which data acquisition is limited by motion.

2976. Registering Spherical Navigator Echoes Using Spherical Harmonic Expansions to Measure 3D Rotations

Andreu F. Costa[1], Maria Drangova[1, 2]
[1]Robarts Research Institute, London, Ontario, Canada; [2]The University of Western Ontario, London, Ontario, Canada

This study presents an evaluation of accuracy and precision of 3D rotation measurements obtained by calculating the spherical harmonic expansions of spherical navigator (SNAV) echo data. Our analysis employed the SOFT freeware package, where SOFT stands for "SO(3) Fourier transform" and SO(3) denotes the group of proper rotations of R^3 about the origin. Although computationally expensive, it is shown that registering SNAVs with this technique is accurate, precise, and robust.

2977. Self-Navigated Detection of Motion in 3D Abdominal Imaging

Anja C.S. Brau[1], Ajit Shankaranarayanan[1], Jean H. Brittain[2]
[1]GE Healthcare, Menlo Park, California, USA; [2]GE Healthcare, Madison, Wisconsin, USA

A generalized self-navigated motion detection technique was previously demonstrated to derive motion information directly from MR data acquired during 2D imaging. In this work, we extend the concept of self-navigation to a three-dimensional sequence to investigate whether motion-correlated DC signal modulation can be detected in 3D volumes. Initial feasibility results using a 3D Cartesian spoiled gradient echo sequence are presented in volunteer abdominal studies, demonstrating the applicability of self-navigated motion detection to volumetric acquisitions in all scan planes. In addition, the effect of fat suppression inversion pulses on the self-navigated signal is investigated.

2978. Real Time Prospective Motion Correction for High Resolution *In Vivo* MRI Using an Optical Motion Tracking System

Maxim Zaitsev[1], Christian Dold[2], Jürgen Hennig[1], Oliver Speck[1]
[1]University Hospital Freiburg, Freiburg, Germany; [2]Fraunhofer Institute for Computer Graphics, Darmstadt, Germany

Subject motion often causes substantial image quality degradation in high-resolution MRI. The sensitivity of standard 2D and 3D imaging methods to motion may be reduced by use of navigator echoes, which, however, lengthen the measurement and require additional excitation RF pulses disturbing the steady state. In this work the possibility of performing prospective motion correction by interfacing the MR scanner with a fast high-precision stereoscopic motion tracking system is demonstrated. Applicability and limitations of this correction approach for high resolution brain imaging in the presence of strong subject motion are evaluated and discussed.

2979. An Elastic Registration Algorithm Based on Strain Energy Minimization and Its Application to Prostate MR Images

Bao Zhang[1], Rao P. Gullapalli[1]
[1]University of Maryland School of Medicine, Baltimore, Maryland, USA

We propose a novel elastic registration algorithm which is based on the minimization of a physically motivated energy function, namely, the strain energy. Gauss-Seidel method was adopted in its numerical implementation. This algorithm was validated on prostate phantom magnetic resonance images. The registration accuracy was 1.0±0.6 pixels. Further validation was also performed on 6 sets of images obtained on patients undergoing endorectal prostate MRI examination. The normalized cross-correlation coefficient, which was used as a similarity measure between the reference and source/registered images, was significantly improved from 0.62±0.12 to 0.98±0.08 by the registration. These results demonstrated the feasibility of the registration algorithm to prostate images.

2980. In-Plane Bulk Motion Correction in 2D Radial Fast Spin Echo MRI

Sudhir Ramanna[1], Joelle E. Sarlls[1], Rexford D. Newbould[2], Arthur F. Gmitro[1], Theodore P. Trouard[1]
[1]University of Arizona, Tucson, Arizona, USA; [2]Stanford University, Stanford, California, USA

An algorithm for correcting motion artifacts in radial-FSE MRI is presented. The technique makes use of the inherent consistency properties of the moments of projections in radial datasets that have previously been implemented in radial-SE. In radial-FSE, however, each radial line (view) acquired within an echo train has a different T2 weighting, and consistency properties cannot be directly applied. With specific view acquisition ordering and data normalization, consistency properties are used to correct translational and rotational motion in radial-FSE. The method is evaluated in simulated data and in experimental data obtained from volunteers moving during MRI exams.

2981. TSE with Average Specific Phase Encoding Ordering for Motion Artifact Suppression

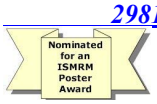

Ling Zhang[1, 2], Eugene G. Kholmovski[2], Junyu Guo[1, 2], Dennis L. Parker[2]
[1]University of Utah, Salt Lake City, Utah, USA; [2]Utah Center for Advanced Imaging Research, Salt Lake City, Utah, USA

A simple method is presented to reduce MR imaging artifact caused by sporadic motion during multi-average acquisition using TSE sequences. The rearrangement of TSE phase encoding (PE) ordering gives each echo train a unique pattern in each average, which makes it possible to detect motion-corrupted echo trains as well as corrupted averages. The corrupted PE views are replaced by corresponding uncorrupted views in the nearest-in-time average. Both phantom and human studies have shown significant suppression of motion artifacts.

2982. Motion Artifact Correction in 3D Multishot EPI-DTI with Real-Time 2D Navigators

Xianfeng Shi[1], Eugene G. Kholmovski[1], Seong-Eun Kim[1], Dennis L. Parker[1], Eun-Kee Jeong[1]
[1]University of Utah, Salt Lake City, Utah, USA

Subject motion during the diffusiongradients can cause motion artifacts in the resultant DW images, and consequently can result in reduced DTI measurement accuracy in multishot DW images. In this report, a motion artifact correction scheme for multi-shot 3D EPI-DTI with one EPI readout per kx-ky or kx-kz plane is described. This technique can be used to reduce artifacts caused by subject motion during diffusion gradients or subject motion between shots or averages and, therefore, to improve the accuracy of DTI measurements.

2983. Optimizing Phase Correction for Multi-Shot DWI with Conjugate Gradient Method and Oversampling

Chunlei Liu[1], Roland Bammer[1], Michael Moseley[1]
[1]Stanford University, Stanford, California, USA

Little is known about optimizing multi-shot DWI for motion correction. With the newly introduced conjugate gradient (CG) phase correction method we can evaluate the phase correction capability of different readout strategies in the presence of k-space undersampling and phase map errors, and thus, empirically optimize the motion correction capability for multi-shot DWI. Through simulation and *in vivo* high-resolution DTI, we demonstrate that trajectories that oversample the center of k-space have more favorable properties for phase correction. CG phase correction combined with oversampling increases tolerance for trajectory and phase map imperfection, thus offers more robustness for motion correction of multi-shot DWI.

2984. Effects of Respiratory Drift on Prospective Motion Correction Factor in Navigator Guided Cardiac Imaging

Maggie M. Fung[1], Sandeep Gupta[1], Wei Sun[2], Ehud Schmidt[3]
[1]GE Healthcare, Hanover, Maryland, USA; [2]GE Healthcare China, Beijing, People's Republic of China; [3]GE Healthcare, Boston, Massachusetts, USA

In prospective motion correction protocols, a patient-specific heart-diaphragm SI correction factor (HDCF) is used to correlate the motion of the diaphragm and the heart for multiple navigator-guided acquisitions. In clinical situations, however, a change in respiratory pattern, over time, is often observed. This study investigates the effects of a drift in end-expiration diaphragm position on the motion correction factor and defines a maximal extend that the end-expiratory level is allowed to change before the scan should be aborted. Results suggest that the correction factor is relatively unchanged for respiratory drifts below 3-4mm and varies greatly for larger drifts.

2985. A Method for Spatial Mapping of Gradient Field Nonlinearity in Magnetic Resonance Imaging

Deming Wang[1], Gary Cowin[1], Katie McMahon[1], David M. Doddrell[1]
[1]The University of Queensland, Brisbane, Qld, Australia

A method for spatially mapping the gradient field nonlinearity within an imaging volume is described. In this method, the gradient coil tensor that provides a full description of the gradient field nonlinearity is derived indirectly from geometric distortion which is measured using a 3D phantom-based technique. The proposed method is demonstrated through the measurement of the gradient field nonlinearity in a Siemens Sonata 1.5 T MRI system. The measured gradient field nonlinearity can be useful for correction of the related errors in, for example, diffusion tensor imaging. The method can be conveniently used to map gradient field nonlinearity in any clinical MRI systems.

2986. Motion Correction for DWI with Segmented EPI: Comparison Between an Iterative Parameter Space Searching Technique and Conventional Navigator Echo Correction

Jeff David Winter[1, 2], Neil Gelman[1, 2], Robert Terry Thompson[1, 2]
[1]Lawson Health Research Institute, London, Ontario, Canada; [2]University of Western Ontario, London, Ontario, Canada

Patient movement in multi-segment diffusion-weighted (DW) imaging generates large inter segment phase differences, which present as ghost artifacts in the final image. An iterative parameter space search was used to determine the optimal phase difference parameters for each segment of multi-segment DW EPI. Eight healthy adult volunteers and five neonatal subjects were scanned at 3.0T with a diffusion weighting of b = 600 s/mm^2. The iterative phase search technique performed significantly better than motion orrection based on the conventional 1D navigator echo technique. ($p < 0.005$ for adults, and $p<0.01$ for neonates)

2987. On the Coregistration of Diffusion Weighted Images

Bennett Allan Landman[1], Jonathan A. D. Farrell, [1,2], Susumu Mori, [1,2], Peter C. M. van Zijl, [1,2], Jerry L. Prince[1], [3]
[1]Johns Hopkins School of Medicine, Baltimore, Maryland, USA; [2]Kennedy Krieger Institute, Baltimore, Maryland, USA; [3]Johns Hopkins University, Baltimore, Maryland, USA

We present a methodology that enables reuse of diffusion weighted data from a single acquisition in subsets. These results closely approximate those independently achievable with optimized schemes of fewer DWDs. First, we show how to derive optimal subsets from an existing master set of DWDs. Second, we perform de novo joint optimization of both master and subsets of particular sizes simultaneously. Our methodology is applicable to any DTI study which computes diffusion tensors from subsets of available data. We demonstrate an efficient means to assess DTI derived contrasts as a function of diffusion encoding scheme and to augment existing schemes.

2988. Improvement in Navigator Echo Displacement Accuracy Using a Pre-Saturation Pulse

Maggie M. Fung[1], Wei Sun[2], Naobuki Takei[3], Sandeep Gupta[1], Thomas K. Foo[4]
[1]GE Healthcare, Hanover, Maryland, USA; [2]GE Healthcare, Bejing, People's Republic of China; [3]GE Healthcare, Hino, Japan; [4]GE Global Research, Niskayuna, New York, USA

In navigator guided cardiac and abdominal imaging, the imaging slab often intersects with the navigator tracker column. As a result, the imaging slab will partially saturate the tracker column and degrade the navigator spatial profile, leading to lower displacement detection accuracy. We proposed a pre-saturation sequence at the end of each image acquisition period to saturate the entire length of the tracker column, thereby allowing uniform recovery of longitudinal magnetization in this region for the next imaging period. Results showed that the proposed technique reduced the partial saturation effects in the navigator spatial profile and increased the displacement detection accuracy.

2989. Evaluation of Conjugate-Gradient Phase Correction Algorithm Under Noisy Conditions

Jian Zhang[1], Chunlei Liu[1], Michael Moseley[1]
[1]Stanford University, Stanford, California, USA

SNAILS image reconstruction algorithm is adapted from SENSE using CG method, by treating the phase correction map of each interleaf as coil sensitivity. However, little is known about the performance of the algorithm under noisy conditions with a worse conditioned encoding matrix. We evaluate the algorithm on simulated SNAILS data with various degrees of motion-induced phase error and a wide range of noise level. It is shown that the iterative CG method corrects phase errors effectively. It does successful reconstructions even at low SNRs.

2990. CASL Perfusion MRI of the Kidney Using Real-Time Tracking, Free Breathing Navigator

H. Michael Gach[1], [2], Thanh Nguyen[3], Yi Wang, [23]
[1]Nevada Cancer Institute, Las Vegas, Nevada, USA; [2]University of Pittsburgh, Pittsburgh, Pennsylvania, USA; [3]Cornell University, Weill Medical College, New York, USA

Continuous arterial spin labeled (CASL) perfusion MRI of the abdomen is very sensitive to physiologic (respiratory) motion between successive control and label acquisitions. Motion compensation techniques like breathholds, respiratory feedback, and navigator are poorly suited for CASL. A real-time tracking, free-breathing navigator-based technique was combined with CASL to measure renal perfusion while minimizing acquisition deadtime and reducing the exertion of the patient. The technique shifts the image slice(s) synchronously with the organ in real-time to minimize control/label subtraction errors. Initial results demonstrate the proof of concept that effectively freezes the position of the organ for at least one image slice.

2991. Self-Navigated 2D SSFP Sequence for Simultaneous Respiratory and Cardiac Motion Detection

Ajit Shankaranarayanan[1], Anja Brau[1], Mike McConnell[2], Jean Brittain[3]
[1]GE Healthcare, Menlo Park, California, USA; [2]Stanford University, Palo Alto, California, USA; [3]GE Healthcare, Madison, Wisconsin, USA

A feasibility study of SelfNavigation approach in the context of 2D SSFP sequence for simultaneous respiratory and cardiac motion detection is shown here. Results comparing the self-navigated data to the respiratory bellow signal and peripheral pulse signal are presented.

2992. Improved Activation Detection in fMRI Studies Using Acquisition and Reconstruction Methods Robust to Susceptibility and Motion Artifacts

Kiran Kumar Pandey[1], Douglas Charles Noll[1]
[1]University of Michigan, Ann Arbor, Michigan, USA

Head motion degrades accuracy and sensitivity of fMRI studies by introducing variability and causing erroneous activation. Motion causes dynamic changes in R2*, amount of signal loss and image distortions from susceptibility. Effectiveness of motion correction algorithms is limited since they do not account for varying susceptibility artifacts during image registration. In fMRI studies, we found that acquisition methods robust to susceptibility induced off-resonance, namely, combined forward and reverse spiral images, significantly improve the quality of activation detection in motion-corrupted data sets. Furthermore, iterative reconstruction with dynamically updated fieldmaps was able to preserve the fidelity of activation maps even in presence of large motion.

2993. Motion Correction for Diffusion-Weighted Segmented EPI: Performance of an Iterative Parameter Space Searching Technique Evaluated with Numerically Simulated Motion Artifacts

Jeff David Winter[1, 2], Neil Gelman[1, 2], Robert Terry Thompson[1, 2]
[1]Lawson Health Research Institute, London, Ontario, Canada; [2]University of Western Ontario, London, Ontario, Canada

The performance of a motion correction technique was assessed by simulating motion artifacts that occur in diffusion-weighted segmented EPI. The simulations involved perturbing the inter-segment phase differences of an artifact free image. The motion correction method evaluated, employs an iterative parameter space search to determine the 0^{th} and 1^{st} order phase corrections for each segment. For images with simulated artifacts having artifact to signal ratios (ASR) of less than 20%, the corrected images displayed very low artifact levels (ASR < 1%). The algorithm accurately determined phase correction values provided that the 1^{st} order phase perturbations were less than certain limits.

2994. Motion Detection and Removal from Registered fMRI Data by Independent Component Analysis Method

Zhilin Wu[1], Yin Xu[1], Guofan Xu[1], Shi-Jiang Li[1]
[1]Medical College of Wisconsin, Milwaukee, Wisconsin, USA

In fMRI studies, head motion costs serious damage to data and motion artifacts still exist even after registration. We applied independent component analysis (ICA) method to find the remaining motion component and to remove it from registered fMRI data. A motion score for each independent component was calculated by cross correlating three translational parameters and three rotational parameters obtained during registration. The component with the largest motion score was the motion component remained in the registered data. A linear combination of the rest independent components and the corresponding coefficients was performed to remove the motion component from fMRI data.

RF Pulse Design

Room 4E Thursday 13:30 - 15:30

2995. A Perfectly Refocused RF Pulse Design Using Zero-Padding

Lei Zhu[1], John Pauly[1]
[1]Stanford University, Stanford, California, USA

In this work, we present an improved algorithm for perfectly refocused RF excitation pulses using zero-padding techniques, based on the conventional SLR algorithm. Three modes of zero-padding are also introduced, and each has its own pros and cons. Simulation results show this method can effectively suppress the residual phase in the excited profile after the beta profile phase precompensation. The choice of the three zero-padding modes and the number of zero-padding samples shows tradeoffs among echo time, phase suppression effectiveness, and RF pulse selectivity.

2996. Application of a Constant Pulse Width VERSE Design to a Silver-Hoult Inversion Recovery Pulse for T1Flair

Neville D. Gai[1], Yuval Zur[2]
[1]GE Healthcare, Waukesha, Wisconsin, USA; [2]G.E. Healthcare, Tirat-Carmel, Haifa, Israel

The RF power deposited at high fields scales roughly as the square of the B0 field. The variable-rate selective excitation (VERSE) technique reduces the SAR deposited by reshaping the RF and slice-select gradient pulses. A desirable feature is to maintain the pulse width of the original pulses constant (mainly for contrast purposes). We have devised and implemented an algorithm based on modeling the scaled waveforms as the Fermi function. The algorithm is applied to a SAR intensive Silver-Hoult inversion recovery pulse used for a T1-weighted fast spin echo inversion recovery sequence. Results show considerable reduction in SAR deposition and/or slice coverage at 3T, especially when used in conjuction with VERSE'd slice excitation and refocusing pulses.

2997. Design of Large-Flip-Angle Half Pulses

John M. Pauly[1]
[1]Stanford University, Stanford, California, USA

Slice selective RF half pulses allow imaging of very short T2 components on conventional scanners. Half pulses designed using a Fourier transform work well at small flip angles, but degrade at 90 degrees. Here we show that high performance 90 degree half pulses can be designed using the Shinnary-Le Roux algorithm to design a slice selective 180 degree pulse, and then using the first half as a slice selective 90 degree half pulse.

2998. Iterative Spectral-Spatial Pulse Design: Toward Full Use of Design Freedom

Chun-yu Yip[1], Sangwoo Lee[1], Jeffrey A. Fessler[1], Douglas C. Noll[1]
[1]University of Michigan, Ann Arbor, Michigan, USA

We propose an iterative spectral-spatial pulse design method that exploits the complex nature of an RF pulse, and the fact that usually only a very selective set of frequency bands are of design interest. For fat suppression, a true null at the fat frequency can be created even with a relatively slow gradient oscillation (at the fat off-resonance frequency). It allows robust fat suppression with fine slice selection, and is potentially beneficial in high fields, in which the fat-water spectral separation is wide.

2999. Contrast Enhancement Using Slice Selective Composite Continuous Rotation Adiabatic Pulses

Ziqi Sun[1], Robert Bartha[1, 2]
[1]Robarts Research Institute, London, Ontario, Canada; [2]University of Western Ontario, London, Ontario, Canada

Slice selective continuous-rotation adiabatic full passage (CRAFP) pulses, a group of AFP pulses with alternating frequency sweep direction, were used to increase the magnitude of nonlinear phase dispersion generated by a customized localization by adiabatic selective refocusing (LASER) sequence. Significantly enhanced contrast was observed in a phantom with two compartments containing different concentrations of nickel(II) doped deionized water in comparison to a conventional spin-echo diffusion weighted (SEDW) sequence and to LASER using non-continuous-rotation AFP (NCRAFP) pulses. The CRAFP pulses were found to be sensitive to magnetic susceptibility with potential applications for contrast enhancement in the presence of paramagnetic agents.

3000. An RF Pulse with Reduced MT Saturation for FSE

James Grant Pipe[1], Nicholas R. Zwart[1], Ryan Grant Robison[1]
[1]St. Joseph's Hospital, Phoenix, Arizona, USA

Fast Spin Echo sequences exhibit SNR loss and contrast changes due to Magnetization Transfer Saturation. Low flip angle refocussing pulses reduce, but do not eliminate this effect, particularly at higher fields. A Low-MT RF pulse was designed in this work, and an example of its performance in a T1 FSE sequence at 3T is given.

3001. Advanced 3D Tailored RF Pulse for Signal Loss Recovery in T2*-Weighted Functional MRI

Chun-yu Yip[1], Jeffrey A. Fessler[1], Douglas C. Noll[1]
[1]University of Michigan, Ann Arbor, Michigan, USA

We present an advanced approach to designing 3D tailored RF pulses for recovering susceptibility-induced signal loss in fMRI. With the new method, effective signal recovery can be accomplished with significantly reduced pulse length and fine slice selectivity. The 3DTRF method is a promising "software" technique that facilitates fMRI of brain regions close to air cavities, with low cost in fMRI temporal resolution.

3002. Multi-Stage Simulated Annealing Optimization of Self-Refocused Radio Frequency Pulses with Short T2

Bashar Issa[1]
[1]UAE University, Al-Ain, Abu-Dhabi, United Arab Emirates

We investigate the design of self-refocused pulses using simulated annealing global optimization techniques with constraints specifying the amplitude of all magnetization components. The magnetization response is calculated by numerically solving the Bloch equations by including T2 terms. The profile of B1 is varied until an error function attains its minimum. The search for minimum is forcefully reset from beginning with smaller search step size. It is hoped that the initial coarse search avoids local minima while the repeated finer search locates the global minimum. We design a self-refocused RF pulse for exciting a rectangular slice with short T2 conditions by restricting T2 to be equal to the pulse length (Trf). The optimized B1 profiles using multi-stage optimization produces transverse magnetization response gain with reduced energy deposition.

3003. Spectral-Spatial Long-T_2 Suppression Pulses for Multislice UTE Imaging

Peder E Z Larson[1], *John M. Pauly*[1], *Dwight G. Nishimura*[1]
[1]Stanford University, Stanford, California, USA

Long-T_2 suppression pulses create excellent contrast for short-T_2 species imaged with ultra-short echo time (UTE) imaging. Previous pulses have been spatially non-selective, making them unsuitable for interleaved multislice acquisitions. This is because the pulse is applied once per TR, causing T_1 recovery to compromise the suppression in later slices. We have designed spectral-spatial long-T_2 suppression pulses for multislice UTE imaging that perform as well as previous pulses and can be applied for every slice, eliminating the problems associated with T_1 recovery.

3004. Double Half RF Pulse for Reduced Sensitivity to Linear Eddy Currents in Ultrashort T2 Imaging

Sonal Josan[1], *Aiming Lu*[1], *John Pauly*[1], *Bruce Daniel*[1], *Kim Butts*[1]
[1]Stanford University, Stanford, California, USA

Half RF pulses used in ultrashort T2 imaging are very sensitive to eddy currents. This work investigates a double half RF pulse in which each excitation is a full pulse split in time, so that long T2s are excited by a full sinc pulse while short T2s are excited by a half pulse. The resulting improved slice selectivity of the long T2s reduces out of slice contribution to the signal, which helps in short T2 quantitation. The short T2 behavior is similar to the normal half pulse. Results from phantom and *in vivo* measurements are presented.

3005. Highly Selective Excitation Method for Short TE Localized ^{1}H MRS of the Frontal Lobe at 3 Tesla

Helene Bataille[1], *Julien Valette*[1], *Philippe Hantraye*[2], *Vincent Lebon*[1]
[1]CEA-SHFJ, Orsay, France; [2]URA CEA-CNRS 2210, Orsay, France

A highly selective excitation method was designed in order to limit extra-voxel contamination on short TE ^{1}H spectra of the frontal lobe at 3 Tesla. The method relies on the combination of two Shinnar-LeRoux (SLR) pulses: a 1.5ms 90 SLR pulse preceded by optimized saturation SLR pulses. As a result, a very sharp selection was obtained, characterized by negligible transition bandwidth and outer-ripples. The SLR excitation method proved efficient for short echo time STEAM spectroscopy of the human frontal lobe: artifact-free spectra were obtained in the 3.5-4.5ppm range, in contrast to spectra localized with sinc3 pulses.

3006. Multi-Band Adiabatic Pulses

Ronald Ouwerkerk[1], *Richard A. Edden*[2]
[1]Johns Hopkins University, SOM, Baltimore, Maryland, USA; [2]Kennedy Krieger Institute, Baltimore, Maryland, USA

Adiabatic inversion pulses are introduced, in which multiple inversion bands are created by summing two or more frequency-shifted adiabatic pulses. Asymmetric hyperpulses or hyperbolic secant pulses were added to create a dual-band inversion pulse with very sharp pass-bands between the inversion bands. The pulses were tested in simulation experiments, and in MR phantom experiments. The pulses had enough B1 insensitivity to be useful in surface coil experiments. Possible applications for this type of pulse are simultaneous suppression of fat and water in 1H-MRS, outer volume signal inversion, or suppression in localized MRS.

3007. Design of Slice Multiplexed Pulses for Simultaneous Multislice Imaging

Kuan J. Lee[1], *Martyn N. Paley*[1], *Paul D. Griffiths*[1], *Jim M. Wild*[1]
[1]University of Sheffield, Sheffield, South Yorkshire, UK

A slice-multiplexed rf pulse that imparts a different linear phase profile to each slice can be used to acquire multiple slices simultaneously and quickly. During read-out, slices are unaliased by using extra slice select gradient lobes, which rephase and dephase individual slices one at a time. Here we describe the improved design of multiplex pulses for 3 or more slices using the Shinnar-LeRoux formalism, and show preliminary *in vivo* results.

3008. Design of Cosine-Modulated Very Selective Suppression Pulses for 3D MRSI at 3T

Joseph Anthony Osorio[1], Duan Xu[1], Charles H. Cunningham[2], Albert Chen[1], Adam B. Kerr[2], John M. Pauly[2], Daniel B. Vigneron[1], Sarah J. Nelson[1]

[1]University of California, San Francisco, California, USA; [2]Stanford University, Stanford, California, USA

At 3T there are inherent advantages for MR spectroscopic imaging (MRSI) of brain tissue, including improved spectral resolution and increased sensitivity. An important aspect of localization in PRESS MRSI is saturating unwanted tissues from the surrounding region of interest, which can contaminate the spectra. This project presents the design of a cosine-modulated very-selective suppression (VSS) pulse that was optimized for high field strengths in order to obtain improved saturation with smaller number of pulses. This study demonstrated the feasiblity of generating improved outer volume suppression pulses for maximum lipid suppression and improved water suppression in phantoms and human subjects.

3009. Single-Sided Quadratic Phase Outer Volume Suppression Pulses

Nikola Stikov[1], Charles Cunningham[1], Michael Lustig[1], John Pauly[1]

[1]Stanford University, Stanford, California, USA

Quadratic phase outer volume suppression (OVS) pulses have high selectivity and low peak RF value. Following the weighted least squares algorithm proposed by LeRoux *et al*., we design single-sided quadratic phase OVS pulses, which maintain the high selectivity at one side of the passband, while treating the opposite side of the passband as a 'don't care' region. By sacrificing symmetry in the pulse to produce quadratic phase in the 'don't care' region, single-sided OVS pulses offer a 10-20% lower peak RF power compared to their double-sided counterparts.

3010. Reduced Field-Of-View RF Pulse Designs with Fat-Suppression

Kyunghyun Sung[1], Krishna S. Nayak[1]

[1]University of Southern California, Los Angeles, California, USA

Increase in acquisition speed can be achieved by exciting only the region of interest (ROI) when the ROI is smaller than the field-of-view. A new 2D spatially selective RF design method to limit the excited FOV with fat-suppression is presented. Minimum-phase filter design is used to reduce the excitation pulse duration while the selectivity of the phase-encoding profile remains the same. The sub-lobe spacing is used to control off-resonance behavior and suppress fat.

3011. 2D and 3D Parallel RF Pulse Design for Inhomogeneity Correction and Volume Localization

Kawin Setsompop[1], Lawrence Wald[2], Borjan Gagoski[1], Vijayanand Alagappan[2], Christina Triantafyllou[2], Franz Hebrank[3], Ulrich Fontius[4], Franz Schmitt[4], Elfar Adalsteinsson[5]

[1]MIT, Cambridge, Massachusetts, USA; [2]A.A. Martinos Center for Biomedical Imaging, Charlestown, Massachusetts, USA; [3]Siemens Medical Solutions, Charlestown, Massachusetts, USA; [4]Siemens Medical Solutions, Erlangen, Germany; [5]Massachusetts Institute of Technology, Cambridge, Massachusetts, USA

Three different designs of 2D and 3D spatially tailored RF waveforms are demonstrated and their performance evaluated in single-channel phantom imaging and in simulation of 8-channel array incorporating experimental B1 field profiles. The result suggested that accelerated multidimensional RF pulses can excite useful B1 profiles in clinically relevant excitation time.

3012. Trajectory Optimization for Variable-Density Spiral Two-Dimensional Excitation

Yakir S. Levin[1, 2], Laura J. Pisani[1], Daniel M. Spielman[1, 2], John M. Pauly[2]

[1]Stanford University School of Medicine, Stanford, California, USA; [2]Stanford University School of Engineering, Stanford, California, USA

This work proposes a simple method to optimize the excitation k-space trajectory for variable density (VD) spiral excitation. Spiral trajectories are approximated as concentric circles, and the Hankel transform is used to compute the resulting slice profile. The circle approximation is validated by comparison to slice profiles resulting from actual spiral trajectories. Using a polynomial to describe placement of the circles (and therefore density), a 1 cm inversion pulse is designed to minimize the height of peak sidelobes. Peak sidelobe height is reduced by 80% compared to uniform density excitation.

3013. Matched Phase Dualband Spatial-Spectral 90º-180º Pulse Pair for MRSI at 3T

Priti Balchandani[1], John Pauly[1], Daniel Spielman[1]

[1]Stanford University, Stanford, California, USA

A pulse sequence has been designed for use at 3T that utilizes a dualband spatial-spectral matched phase 90º-180º pulse pair to excite a thin slice. The sequence enables shorter echo times while still having a spectrally selective profile that suppresses lipids and partially suppresses water. In addition, the pulse pair is designed so that the final echo has completely flat phase. Results of phantom studies show successful suppression of all resonances outside the metabolite passband.

3014. Parallel RF Excitation Design and Testing with an 8 Channel Array at 3T

Kawin Setsompop[1], Lawrence Wald[2], Borjan Gagoski[1], Vijayanand Alagappan[2], Franz Hebrank[3], Ulrich Fontius[4], Franz Schmitt[4], Elfar Adalsteinsson[5]

[1]MIT, Cambridge, Massachusetts, USA; [2]A.A. Martinos Center for Biomedical Imaging, Charlestown, Massachusetts, USA; [3]Siemens Medical Solutions, Charlestown, Massachusetts, USA; [4]Siemens Medical Solutions, Erlangen, Germany; [5]Massachusetts Institute of Technology, Cambridge, Massachusetts, USA

Low flip angle two-dimensional RF excitation pulses for parallel transmission were designed and tested on an 8-channel array constructed for a 3T Siemens Tim Trio scanner modified to handle 8 simultaneous independent RF transmit channels.

3015. A Spatial Domain Method for the Design of RF Pulses in Multi-Coil Parallel Excitation

William Allyn Grissom[1], Chun-Yu Yip[1], Zhenghui Zhang[2], V. Andrew Stenger[3], Jeffrey A. Fessler[1], Douglas C. Noll[1]

[1]University of Michigan, Ann Arbor, Michigan, USA; [2]University of Pittsburgh, Pittsburgh, Pennsylvania, USA; [3]University of Hawaii, Manoa, Hawaii, USA

Current methods for RF pulse design in parallel excitation are based on the small-tip-angle approximation, which allows pulses to be designed using the excitation k-space formalism. In this work we investigated the performance of parallel excitation at large tip angles, using one such design method that is formulated in the spatial-domain. Pulses were scaled to produce tip angles up to 90 degrees, and excitation error was evaluated. We demonstrate that increased error at large tip angles can be attributed mainly to large RF magnitude in accelerated excitation, and can be mitigated using Tikhonov regularization in the design process.

3016. Calculation of B1 Pulses for RF Shimming at Arbitrary Flip Angle Using Multiple Transmitters

Jose L. Ulloa[1], Martina Callaghan[2], Marcelo Guarini[1], Joseph V. Hajnal[2], Pablo Irarrazaval[1]

[1]Pontificia Universidad Catolica de Chile, Santiago, Chile; [2]Hammersmith Hospital, Imperial College London, London, UK

MRI at high field suffers from B1 inhomogeneity. Design in the Small-Tip-Angle (STA) regime allows B_1 pulses that compensate for this. The excessive duration of such pulses has limited their use, but Parallel transmission can shorten excitation times. However, for higher flip angles the STA and existing parallel transmission formalism fail. In this work we extend the model of parallel transmission beyond the STA, by solving the Bloch equation for an array of spatially varying transmitters acting simultaneously. The method was tested by simulating B_1 inhomogeneity correction for 90° excitation with 2 coils to achieve a predicted homogeneous excitation

3017. Generalized Parameter Relations for the Shinnar-Le Roux Pulse Design Algorithm

Kuan J. Lee[1]

[1]University of Sheffield, Sheffield, South Yorkshire, UK

The parameters relating magnetization and polynomial ripples in Shinnar-LeRoux pulse design were first derived by Pauly *et al* (1991) for five classes of pulses. However, these expressions do not cover the entire range of flip angles, e.g. neither the small-tip-angle or 90 relations for excitation pulses are exactly right for a flip angle of 70 . Here, parameter relations have been derived that are more general. Use of the new relations are shown to give simulated slice profiles that have the desired ripple amplitudes for a wider range of flip angles.

Pulse Sequence: Other

Room 4E Thursday 13:30 - 15:30

3018. Whole-Body 3D Continuously Moving Table Imaging Using Radial and Spiral Sampling

Peter Börnert[1], Bernd Aldefeld[1], Jochen Keupp[1]

[1]Philips Research Laboratories, Hamburg, Germany

Whole-body 3D continuously moving table imaging is a current topic of interest for future clinical practice in e.g. angiography and cancer screening. Two new types of sampling schemes, the stack-of-stars and the stack-of-spirals schemes, have been studied in this work to explore their potential with respect to scan efficiency and image quality.

3019. Radial Flow-Gated Phase Contrast Imaging in Carotid Artery

Hsu-Hsia Peng[1], Teng-Yi Huang[2], Wen-Yih Isaac Tseng[1], Hsiao-Wen Chung[1]

[1]National Taiwan University, Taipei, Taiwan, Taiwan; [2]National Taiwan University of Science and Technology, Taipei, Taiwan, Taiwan

Flow measurements by phase-contrast imaging generally requires an ECG signal to synchronize the acquisition of imaging data with pulsatile arterial flow. Recently, self-gated and flow-gated methods via radial scanning are reported for acquiring phase-contrast images on major cardiac vessels without usage of ECG. For carotid arteries with much weaker flow than larger vessels, flow gating without ECG becomes rather challenging. In this study, we accomplished such an aim by employing a correlation method on complex difference images acquired with radial scanning. Quantitative comparison with conventional ECG-gated imaging showed that the proposed method is highly feasible.

3020. Spectroscopic and Imaging Observations of Intermolecular Single-Quantum Coherence

Shuhui Cai[1], Zhong Chen[1, 2], Xiaoqin Zhu[1], Bingwen Zheng[1], Jianhui Zhong[2]
[1]Xiamen University, Xiamen, Fujian, People's Republic of China; [2]University of Rochester, Rochester, New York, USA

A new pulse sequence with three radio-frequency pulses was designed to detect NMR signals originating from pure intermolecular single-quantum coherence (iSQC) in samples with a single resonance peak. The analytical expressions were derived from the modified Torrey's equations with dipolar fields. The spectroscopic and imaging observations and simulated results support the theoretical predictions. The new sequence is insensitive to the imperfection of RF flip angles.

3021. Experimental Validation of a T2r Transverse Relaxation Model Using LASER and CPMG Acquisitions

Simona Nikolova[1], Robert Bartha[1], Chris Bowen[2]
[1]Robarts Research Institute, London, On, Canada; [2]Institute for Biodiagnostics (Atlantic), Halifax, Nova Scotia, Canada

The LASER pulse sequence is sensitive to diffusion of spins through regions with different microscopic susceptibility. The purpose of this study was to investigate the contribution of microscopic susceptibility to LASER signal intensity, and compare it to a conventional CPMG pulse sequence. ORGASOL, polyamide powders were used to generate different magnetic susceptibility in three phantoms. Transverse relaxation rates R2 were measured in each phantom as a function of the spin echo refocusing time (2tcp) within LASER and CPMG pulse sequences. Differences between LASER and CPMG R2 were found in the low tcp range, demonstrating increased sensitivity to microscopic susceptibility in LASER.

3022. Implementation of a Three-Dimensional Double Inversion-Recovery Sequence at 3 Tesla

S.J.P. Jonathan Pierpoint Meara[1], Mark Roger Symms[2], Philip A. Boulby[2], Gareth John Barker[1]
[1]Institute of Psychiatry, London, UK; [2]Institute of Neurology, London, UK

A three-dimensional (3D) double inversion-recovery (DIR) sequence with optimised interleaved inversion has been developed to image selectively the grey matter at a magnetic field strength of 3 tesla. An optimum repetition time was derived theoretically, but it was found that other imaging parameters must be determined empirically due to magnetisation transfer effects. Typical images show that the 3D DIR sequence is successful in imaging the grey matter of the whole brain, while suppressing the signal from white matter and cerebrospinal fluid, in an acceptable scanning time. This sequence has application to diseases that affect the grey matter of the brain.

3023. Single Point Imaging with Minimized Phase Encoding Interval

Peter Latta[1], Marco Gruwel[1], Boguslaw Tomanek[1]
[1]NRC, Winnipeg, Manitoba, Canada

We propose a modification of the Single Point Imaging (SPI), based on the minimization of the phase encoding interval for further signal to noise ratio (SNR) optimization. The results of calculations were confirmed experimentally using 11.7T MRI system. This method is particularly beneficial when the maximum gradient amplitude is limited and the resulting SNR suffers from the T2-related signal attenuation.

3024. Non-CPMG Multi-Echo Spin Echo Imaging with Short Echo Times

Markus Klarhöfer[1], Jochen Hirsch[2], Achim Gass[2], Klaus Scheffler[1]
[1]University of Basel, Basel, Switzerland; [2]University Hospital Basel, Basel, Switzerland

Purpose of the present work was the development of a multi-echo spin echo imaging sequence allowing the investigation of tissue compartments with T2 values of the order of 10ms. To achieve echo times of 2ms and below, a 3D sequence using non-selective hard pulses for excitation and refocusing was implemented. A short repetition time of 160ms and parallel imaging allowed the acquisition of 8 echo images with a spatial resolution of 1.3x2.6x5mm3 in about 11minutes. In preliminary experiments on healthy volunteers bi-exponential signal behaviour was found for short echo times in white matter.

3025. A Fast Spin Echo Triple Echo Dixon (FTED) Technique for Efficient T2-Weighted Water and Fat Imaging

Jingfei Ma[1], Jong Bum Son[1, 2]
[1]University of Texas M. D. Anderson Cancer Center, Houston, Texas, USA; [2]Texas A & M University, College Station, Texas, USA

Previously-published fast spin echo (FSE)–based Dixon techniques for water and fat separation all require multiple scans and often a substantial increase in the echo spacing (esp). In this work, we developed a novel fast spin echo triple echo Dixon (fTED) technique which acquires three raw images in a single scan with readout gradients of alternating polarity and practically no increase in esp. We demonstrate that these three raw images can be used to generate separate water-only and fat-only images and thus allow for high-quality fat-separated T2-weighted imaging of an entire abdomen in only two breadth holds.

3026. Single Slab-Selective 3D CPMG Multi-Echo Sequence with Short Inter-Echo Spacing for Short-Component T2 Quantitation

Dimitris Mitsouras[1], Robert Mulkern[2], Frank J. Rybicki[1]
[1]Brigham And Womens Hospital and Harvard Medical School, Boston, Massachusetts, USA; [2]Childrens Hospital, Boston, Massachusetts, USA

A 3D single-slab Carr-Purcell-Meiboom-Gill pulse sequence was developed for the detection of short T2 components. This application requires both high SNR, typically requiring averaging of the order of 25 mins for single-slice mapping, as well as short inter-echo spacing. This scan time can be used more efficiently for spatial localization in 3D, although high quality slab-selective pulses are necessary. To accommodate these while avoiding elongating the inter echo spacing which would conflict with the detection of fast relaxing components, a dual echo spacing approach was used. Accurate T2 maps over large volumes were thus obtained in typical for the application scan times.

3027. In-Vivo Diagonal-SPRITE Imaging at 9.4T

Andrea Protti[1], Amy Herlihy[1], Jean Tessier[2], Jimmy Bell[1]
[1]Hammersmith Hospital, Imperial College London, London, UK, [2]AstraZeneca, Macclesfield, UK

Recently methods for imaging at ultra short TE's (UTE) have been investigated and show it is possible to detect *in vivo* some of these "MR invisible" components. We are investigating the use of single point imaging (SPI) techniques for *in vivo* UTE imaging at high magnetic fields and have developed a novel version of SPRITE in order to image preclinical disease models. The method, called Diagonal-SPRITE. In-vivo UTE MR images of murine models of brain, lungs and liver are presented.

3028. Comparison of Long-T_2 Suppression Techniques for 3D Ultrashort Echo-Time Imaging

Ulrike Blume[1], Jürgen Rahmer[2], Peter Börnert[2], Dietrich Holz[1]
[1]University of Applied Science Koblenz, Remagen, Germany; [2]Philips Research Laboratories, Hamburg, Germany

Ultrashort echo-time (UTE) imaging can be used to visualize short-T_2 species. To selectively show only the short-T_2 signal components, different approaches have been proposed using appropriate magnetization preparation or multi-echo techniques subtracting the long T_2 signal components. In this work, 3D UTE imaging is performed with focus on musculoskeletal applications, to compare a magnetization preparation approach with the "dual echo" approach for long-T_2 suppression. While magnetization preparation directly yields the desired image contrast, the "dual echo" technique is more time-efficient and seems to be more robust against off-resonance effects.

3029. Anisotropic 3D Radial Sampling for Ultrashort TE Imaging

Jürgen Rahmer[1], Peter Börnert[1]
[1]Philips Research Laboratories, Hamburg, Germany

3D radial free-induction-decay sampling schemes are used in ultrashort TE imaging. These techniques sample a spherical k space volume with isotropic angular resolution, leading to rather long scan durations and large amounts of acquired data. For prolate objects, the number of radial projections can be reduced by angular undersampling in one direction, with only negligible loss in image quality. For this anisotropic sampling pattern, the 3D radial point-spread function is calculated, and phantom as well as *in vivo* scans are presented. Depending on object shape, reductions in scan duration of 25 % or more are possible.

3030. Optimized Short-T_2 SNR and Resolution Using Ultrashort TE Imaging with T_2-Adapted Sampling

Jürgen Rahmer[1], Peter Börnert[1]
[1]Philips Research Laboratories, Hamburg, Germany

Ultrashort echo-time imaging (UTE) employs 2D or 3D radial free-induction-decay sequences to minimize TE. With echo times in the order of 100 µs and below, these techniques enable the detection of species with T2 in the submillisecond range. However, choosing the optimal sampling window duration TAQ for imaging short-T2 components is not trivial. A short TAQ reduces the overall signal-to-noise ratio (SNR), whereas a long TAQ reduces resolution and SNR of short-T2 components due to relaxation effects. To find an optimal TAQ, the point-spread function was calculated for short-T2 signal components acquired using the UTE technique. 3D UTE phantom measurements are presented to verify these simulations.

3031. Acquisition-Weighted Stack of Spirals for High-Resolution Sodium MRI

Yongxian Qian[1], Fernando Boada[1]
[1]University of Pittsburgh, Pittsburgh, Pennsylvania, USA

A novel data acquisition strategy for high resolution sodium MRI, acquisition-weighted stack of spirals (AWSOS), is here demonstrated to be feasible. In the AWSOS method, fast evolving spiral trajectory significantly reduces the fast sodium T2 decay, while the variable data acquisition delay compensates for the T2 decay during slice encoding. Our results from the numerical simulations and phantom studies showed that the AWSOS method is capable of achieving high in-plane resolution (up to 1mm) while keeping the data acquisition time relatively short.

3032. Pulse Sequence Programming in a Dynamic Visual Environment

Jeremy Magland[1], *Felix W. Wehrli*[1]
[1]University of Pennsylvania Medical Center, Philadelphia, Pennsylvania, USA

SequenceTree is a visual NMR pulse sequence programming environment which seeks to provide flexibility within a user-friendly environment. The software is independent of any commercial scanner, but can be interfaced to a variety of scanners, provided that the appropriate conversion tools are created (such a tool has been created for Siemens scanners, and progress has been made interfacing to Bruker). The programmer manipulates sequence objects using mouse clicks and menus, and the software provides a visual display of the sequence at all stages of development. The modular design of SequenceTree allows visual copying and pasting of pulse sequence blocks, and advanced users may create custom objects for use within any sequence. Several dozen pulse sequences have been programmed with SequenceTree by students and researchers in the authors' laboratory.

3033. Fast, Accurate and Precise B_1 Mapping *In Vivo* Using the 180 Null Signal

Nicholas G. Dowell[1], *Paul S. Tofts*[1]
[1]University College London, London, UK

RF field B_1 nonuniformity is the largest cause of error in the quantitative measurement of clinically-relevant parameters in MR images and spectra. Knowledge of the spatial dependence of B_1 will improve the accuracy and precision of such parameters. Here, we present a technique that uses the 180 signal null to construct a B_1 map of the entire brain in less than 4 minutes, independent of T_1, T_2 and PD. The experiment utilizes an existing MR sequence supplied by the scanner manufacturers. Owing to the short scan-time it is envisaged that it may be integrated into existing quantitative MR techniques.

3034. Electrical Conductivity Estimation from Diffusion Tensor and T2: A Silk Yarn Phantom Study

Suk Hoon Oh[1], *Soo Yeol Lee*[1], *Min Hyoung Cho*[1], *Tae-S Kim*[1], *Ik Hyun Kim*[1]
[1]Kyung Hee University, Yongin, Kyungki, Republic of Korea

Conductivity mapping of a human brain is important to enhance accuracy of EEG or MEG source localization in brain function studies. In this study, we have experimentally shown cross-property relation among electrical conductivity, diffusion, and T2, using a silk yarn phantom which mimics neuronal tissues. It has been observed that the electrical conductivity, diffusion, and T2 are strongly correlated among them and all the three physical constants are strongly dependent on the compartmental structure of biological tissues. We think that electrical conductivity of biological tissues can be estimated from their diffusion and T2 values measured with MRI.

3035. Experimental Verification of Electric Properties Tomography (EPT)

Ulrich Katscher[1], *Marius Hanft*[2], *Peter Vernickel*[3], *Christian Findeklee*[1]
[1]Philips Research Laboratories, Hamburg, Germany; [2]University of Applied Sciences, Hamburg, Germany; [3]TuTech Innovation GmbH, Hamburg, Germany

The electric conductivity and permittivity of tissue can be helpful to predict of the local SAR distribution during MR measurements or can potentially be used as an additional diagnostic parameter. This study presents the new approach "Electric Properties Tomography" (EPT), which derives the patient's electric properties from the spatial sensitivity distributions of the applied RF coils. Initial experiments on a standard MR system underline the principle feasibility of EPT. In contrast to previous conductivity / permittivity measurements, EPT does not apply external electrodes or currents and circumvents the solution of an inverse problem, potentially leading to improved spatial resolution.

3036. Defibrillation Electrode Position Study Using Current Density Imaging

Tim P. DeMonte[1], *Dawn B. Jorgenson*[2], *Dinghui Wang*[1], *Angela W. Ma*[1], *Michael L. G. Joy*[1]
[1]University of Toronto, Toronto, ON, Canada; [2]Philips Medical Systems, Seattle, Washington, USA

The MRI technique current density imaging was used to measure current density vectors in a pig. Current was applied through defibrillation electrodes placed in both the apex-anterior (AA) and apex-posterior (AP) positions. The animal was in a state of ventricular fibrillation (VF) during the first acquisition and subsequent acquisitions were made post-mortem (PM). Sufficient data was acquired in a single experimental procedure to compare VF-AA, VF-AP, PM-AA and PM-AP. Comparative analysis was performed for current flow direction using vector plots and streamlines. Comparative analysis of current density magnitude was performed using cumulative distribution plots.

3037. Electric Properties Tomography (EPT) Via MRI

Ulrich Katscher[1], *Marius Hanft*[2], *Peter Vernickel*[3], *Christian Findeklee*[1]
[1]Philips Research Laboratories, Hamburg, Germany; [2]University of Applied Sciences, Hamburg, Germany; [3]TuTech Innovation GmbH, Hamburg, Germany

MR is not yet able to image the electric conductivity and permittivity of tissue. Yet, these parameters are typically measured using external electrodes, defining an inverse problem, leading to limited spatial resolution. This study presents a new approach "Electric Properties Tomography" (EPT), which derives the patient's electric properties from the spatial sensitivity distributions of the applied RF coils. A principle proof of EPT might be feasible with no or only minor modifications of a standard MR. EPT is not based on an inverse problem, and thus, might be able to achieve images of higher quality than achievable with previous approaches.

3038. Accelerating MR Elastography by Means of Keyhole Imaging

Armin de Greiff[1], Stefan Maderwald[1], Mark E. Ladd[1]
[1]University Hospital Essen, Essen, NRW, Germany

Keyhole imaging is a powerful acceleration technique in dynamic data acquisitions. Although seemingly predestined for MR Elastography (MRE), where subsequent datasets only differ in a very limited frequency range from an initial acquisition, it has not yet been applied. To analyze mechanical sheer wave propagation, one typically acquires phase maps with varying offsets to capture a complete cycle of tissue motion. This study analyzes the potential of keyhole imaging for these sequentially acquired images. We acquired the first phase offset with full k-space coverage and replaced a varying number of central k-space lines for subsequent phase offsets. An acceleration factor of eight was achievable without losing relevant information.

3039. Influence of the Transducer Near Field in MR Elastography Wave Images

Sebastian Papazoglou[1], Jens Rump[1], Dieter Klatt[1], Uwe Hamhaber[2], Jürgen Braun[2], Ingolf Sack[1]
[1]Institute of Radiology, Berlin, Germany; [2]Institute of Medical Informatics, Berlin, Germany

In MR elastography (MRE) bulk shear waves radiated by a harmonic surface load are used for testing mechanical properties of soft tissue. Here, it is shown by MRE experiments on gelatine that a longitudinally polarized wave exists in vicinity of the source with wavelengths comparable to the shear wave. We attribute this wave partly to the near field of an extended transducer. It is shown that within the audio regime of MRE and at distances up to one shear-wave length from the transducer the near field might yield to an overestimation of the real shear stiffness of the examined tissue.

Spectral Editing and Localization Techniques

Room 4E Thursday 13:30 - 15:30

3040. Intermolecular Double-Quantum-Filtered Zero-Quantum Coherence in Liquid NMR

Xiaoqin Zhu[1], Zhong Chen[1, 2], Shuhui Cai[1], Jianhui Zhong[2]
[1]Xiamen University, Xiamen, Fujian, People's Republic of China; [2]University of Rochester, Rochester, New York, USA

A double-quantum filtered iZQC pulse sequence was proposed to detect iZQC signals from isolated spin-1/2 systems. Compared to the two-pulse CRAZED sequence for iZQC, the new sequence is insensitive to the imperfection of flip angles thus less susceptible to contaminations of other coherence orders. Experimental observations and computer simulations are in good agreement with the theoretical predictions.

3041. Improved Two-Dimensional *J*-Resolved Spectroscopy

Rolf F. Schulte[1], Thomas Lange[1], Johannes Beck[2], Dieter Meier[1], Peter Boesiger[1]
[1]University and ETH Zurich, Zurich, Switzerland; [2]University of Zurich, Zurich, Switzerland

Localised two-dimensional *J*-resolved spectroscopy (*J*PRESS) is optimised for the *in vivo* detection of *J*-coupled metabolites using magnetic resonance spectroscopy at 3 T. The acquisition of echo signals starts as early as possible (i.e., maximum-echo sampling). This sampling scheme increases sensitivity and decreases overlap of peak tails, hence alleviating baseline problems. The qualitative behaviour of eddy currents in *J*PRESS is outlined and a 2D eddy current correction procedure based on the 1D phase deconvolution method is proposed.

3042. Identification and Exclusion of Motion-Corrupted Data in J-Difference Editing Using Interleaved Navigator Scans

Pallab Bhattacharyya[1], Mark Lowe[1], Micheal Phillips[1], Mark Brown[2]
[1]The Cleveland Clinic Foundation, Cleveland, Ohio, USA; [2]Siemens Medical Solutions, Cary, North Carolina, USA

Subject motion is a known problem in MR spectral quality. This problem is even more severe in technique like J-difference editing, since it is based on the difference of two spectra. Using shot by shot acquisition with MEGA-PRESS approach for GABA editing and identifying motion-corrupted data utilizing water-signal based interleaved navigator scans, we have demonstrated a robust methodology for improved spectral quality control in J-difference editing. We have also demonstrated the possibility of recovering a measurement that otherwise would be corrupted by motion artifact.

3043. Investigation of Flip Angle Dependence in Spatially Resolved 2D Correlated MR Spectroscopy

Nader Binesh[1], Shida Banakar[2], Albert M. Thomas[1]
[1]UCLA School of Medicine, Los Angeles, California, USA; [2]LABIOMED at Harbor-UCLA, Torrance, California, USA

Flip-angle dependence of the last 90 degree rf pulse used for slice-selection as well as coherence transfer in localized 2D COSY was investigated using phantom solutions. The experimental results were compared with theoretical simulations. A phantom containing six metabolites at physiological concentrations was investigated to record 2D L-COSY spectra at different flip-angles of the last rf pulse. Two MRI scanners (1.5T and 3T) with respective quadrature extremity coils were used. 2D spectral simulation was carried out using GAMMA library. Our preliminary findings indicate that the maxima of the 2D cross and diagonal peaks occur at 90 and 180 degrees, respectively.

3044. Prostate Spectroscopy at 3 Tesla Using Two-Dimensional S-PRESS

Thomas Lange[1], Andreas H. Trabesinger[2], Rolf F. Schulte[3], Ulrike Dydak[1], Peter Boesiger[1]
[1]ETH Zurich, Zurich, Switzerland; [2]110 Stapleton Hall Road, London N8, UK; [3]GE Global Research, Munich, Germany

A novel two-dimensional method for the detection of strongly coupled metabolites (2D S-PRESS) is introduced and optimised for prostate spectroscopy at 3T. The technique is based on a PRESS sequence with a constant echo time, but variable inter-pulse delays, which are encoded in the indirect dimension. Two-dimensional S-PRESS gives rise to more clearly arranged spectra than JPRESS and facilitates the distinction of weakly and strongly coupled metabolites. The method enables an improved resolution and characterisation of the citrate signal, allowing for an accurate determination of the spectral parameters (coupling constant and chemical shift difference of the coupled protons) *in vivo*.

3045. Improved PRESS Sequence for Lactate Detection in the Human Vitreous Body

Evelyne Balteau[1], Nathalie Jacqueline Collignon[2], Pierre A. Robe[2], Virginie Sterpenich[1], Gabriel Llabrès[1], André Luxen[1], Pierre Maquet[1]
[1]Liège University, Liège, Belgium; [2]University Hospital of Liège, Liège, Belgium

Magnetic resonance spectroscopy is an attractive tool for non-invasive assessment of vitreous lactate levels, but is hampered by several technical problems such as magnetic field inhomogeneities, water suppression and fat contamination. In this study, numerical simulations as well as *in vitro* and *in vivo* experiments were performed in order to implement improved shimming procedure and PRESS sequence with spectral editing capabilities, yielding better field homogeneity, water suppression and localization accuracy. The experiments demonstrate the feasibility of ^{1}H-MRS lactate detection in the human vitreous body of healthy volunteers, with short acquisition time and reliable lactate doublet assignment.

3046. POM: A Simulation Program for NMR Under Inter- And Intramolecular Interactions

Congbo Cai[1], Zhong Chen[1, 2], Shuhui Cai[1], Jianhui Zhong[2]
[1]Xiamen University, Xiamen, Fujian, People's Republic of China; [2]University of Rochester, Rochester, New York, USA

Few convenient and efficient tools exist that can simultaneously simulate both the macroscopic and microscopic effects in NMR. In this work, the product operator matrix (POM) method combining the non-linear Bloch equations with scalar couplings was introduced, and an efficient numerical simulation program POM was reported. The POM program can be used to simulate various liquid NMR and MRI experiments, which is helpful to understand the physical nature and predict experimental results under complex conditions.

3047. Simultaneous Acquisition of Signals of Different Orders of Intermolecular Multiple-Quantum Coherences

Song Chen[1], Xiaoqin Zhu[1], Zhong Chen[1, 2], Shuhui Cai[1], Jianhui Zhong[2]
[1]Xiamen University, Xiamen, Fujian, People's Republic of China; [2]University of Rochester, Rochester, New York, USA

A new pulse sequence with three radio-frequency pulses was designed to simultaneously acquire iMQC signals of five different coherence orders (n = 2, 1, 0, -1, -2) from isolated spin-1/2 systems. Compared to the CRAZED sequence, more than half of the experimental time can be saved. Both experimental observations and simulated results support the theoretical predictions.

3048. A Novel Method Using a Single Selective Editing Pulse for *In Vivo* Glutathione Editing at 3 Tesla

Yan Zhang[1], Stefano Marenco[1], Daniel R. Weinberger[1], Jun Shen[1]
[1]National Institute of Mental Health, Bethesda, Maryland, USA

Glutathione is an important marker of oxidative stress. Here we propose a new method for glutathione editing which uses a single selective editing pulse and corrects the transient Bloch-Siegert phase shift with precalibrated postacquisition phase correction. The phase correction procedure allows clean subtraction of the intense creatine signals at 3.0 and 3.9 ppm, choline signal at 3.2 ppm and NAA signal at 2.0 ppm. Since only a single editing pulse is used, additional B1 inhomogeneity and coherence leakage caused by a second editing pulse are avoided. The new method is applied to glutathione editing in the human brain.

3049. Further Evidence for a Correlation Between Increased Endogenous GABA Concentration and Decreased Glutamate-Glutamine Cycling Flux

Jehoon Yang[1], Jun Shen[1]
[1]NIMH, Bethesda, Maryland, USA

Increased endogenous GABA concentration has been found to cause increased release of the inhibitory neurotransmitter GABA. Evidence exists in the literature that elevated brain GABA concentration also reduces glutamate release. In this study, accompanying an increase in endogenous GABA concentration caused by administration of the antiepileptic drug vigabatrin, a significant reduction was found in ^{13}C-label incorporation into the predominantly neuronal [4-^{13}C]glutamate from the glia-specific substrate [2-^{13}C]acetate, providing further evidence for a negative modulation of glutamatergic activity by increased endogenous GABA concentration.

3050. J-Resolved Proton Echo Planar Spectroscopic Imaging of GABA in the Human Brain

J. Eric Jensen[1, 2], Blaise Frederick[1, 2], Perry Franklin Renshaw[1, 2]
[1]McLean Hospital, Belmont, Massachusetts, USA; [2]Harvard Medical School, Boston, Massachusetts, USA

Two-dimensional, J-resolved magnetic resonance spectroscopy (2D, JMRS) has been combined with proton echo-planar spectroscopic imaging (PEPSI) to drastically reduce the required scan time needed to sample enough k-space and TE-points to adequately resolve and quantify the gamma-amino butyric acid (GABA) resonance sideband at 2.95ppm from neighboring creatine (Cr) at 3.03ppm at 4 Tesla. This combination of techniques allows us to either drastically reduce the scan-time needed to acquire a whole J-resolved PEPSI (JEPSI) dataset at a modest spatial resolution of 16x16, or to vastly increase spatial resolution to 32x32 in a clinically-sound scan time.

3051. Fast MRSI of Human Breast Using Spiral Sel-MQC

He Zhu[1], Dennis Rubin[1], Qiuhong He[1]
[1]University of Pittsburgh, Pittsburgh, Pennsylvania, USA

We present here a novel MRSI approach combining spin editing and spiral data acquisition. Signal excitation was based on Selective Multiple-Quantum Coherence Transfer (Sel-MQC) technique that selectively excited protons in Poly Unsaturated Fatty Acids (PUFA). Fast spatial localization was achieved by 2-shot spiral imaging. One 2D image of PUFAs was acquired in 64 seconds.

3052. Phase Rotation with Asymmetric RF Pulses in Localized Stimulated Echo Spectroscopy (PRAISES) : A 2.5-Ms TE Sequence for Clinical Spectroscopy

Jack Knight-Scott[1], S. Andrea Dunham[1], Dattesh Dayanand Shanbhag[1]
[1]University of Virginia, Charlottesville, Virginia, USA

The development of ^{1}H-MRS as a standard *in vivo* neurochemical measurement technique in high-field MR depends on the availability of reliable and robust very short echo time (VTE) sequences, compatible for routine clinical examinations. Current VTE sequences are limited for human applications because of their dependency on short-duration, high-amplitude TE spoilers gradients as a primary coherence selection technique. In this work, we present *p*hase *r*otation with *a*symmetric RF pulses *i*n localized *s*timulated *e*cho *s*pectroscopy (PRAISES) as a VTE sequence for clinical MR spectroscopy. PRAISES combines the inherent short TE capabilities of asymmetric RF pulses, RF phase rotation paradigms, and STEAM to deliver a 2.5-ms TE sequence on a 1.5-T MRI system. Preliminary testing of the PRAISES technique is shown for a low-field MRI system; however, the technique is completely translatable to high-field systems and thus an ideal VTE sequence for high-field clinical examinations.

3053. Short Echo Spectroscopic Imaging Combined with Lactate Editing in a Single Scan

Gerd Melkus[1], Philipp Moerchel[1], Volker Christian Behr[1], Markus Kotas[1], Peter Michael Jakob[1], Michael Flentje[1]
[1]University of Würzburg, Würzburg, Germany

In this work, we have shown that a spectroscopic imaging method combined with a lactate editing filter can improve the metabolic information of lipid-rich tissues (e.g. necrotic tumors). After conventional chemical shift imaging, a multiple quantum coherence filter selectively prepares lactate and the signal is detected in a second acquisition window. With this sequence, it is possible to separate lactate from lipids in a single shot without losing the information from the complete 1H spectrum. The method was tested and confirmed using a phantom containing several different metabolites as well as a post-mortem mouse brain.

3054. Optimized Detection of Lactate at 3 Tesla Using the PRESS Sequence

Richard Anthony Edward Edden[1, 2], Peter B. Barker[1, 2]
[1]Johns Hopkins University, Baltimore, Maryland, USA; [2]Kennedy Krieger Institute, Baltimore, Maryland, USA

Single-voxel PRESS spectroscopy can be used to detect an inverted lactate signal at echo times of 1/J. The chemical shift artifact causes the slices selected by the two refocusing pulses of the sequence to differ for the two lactate signals. This disturbs the evolution of coupling, decreasing the signal intensity and compromising its inversion. At 3 Tesla, the artifact is sufficient that the lactate doublet has only 40% intensity and is not inverted, using traditional sinc-gauss pulses. Inversion and 70% detection efficiency can be achieved by using high-bandwidth frequency-modulated pulses. Experimental results agreed well with simulations of the lactate doublet.

3055. Proton Spectral Editing for Separation Between Lactate and Threonine in Human Brain *In Vivo*

Changho Choi[1], Nicholas J. Coupland[1], Sanjay Kalra[1], Paramjit P. Bhardwaj[1], Nikolai Malykhin[1], Dan Gheorghiu[1], Peter S. Allen[1]
[1]University of Alberta, Edmonton, Alberta, Canada

Single-voxel proton J-difference editing for discrimination of the 1.31 ppm resonances of lactate (Lac) and threonine (Thr) in human brain *in vivo*, at 3.0 T, is reported. Three types of spectrally-selective 180° RF pulses (~75 ms long) were employed for manipulating the J evolution associated with their coupling partners at 4.10 and 4.25 ppm. The concentrations of Lac and Thr in the human occipital cortex were estimated as 0.50±0.06 and 0.59±0.04 μmol/g (mean±SD, n = 4), respectively, with reference to Cr at 8 μmol/g.

3056. ^{1}H NMR Spectroscopy Using High Performance Gradients at Sub-Millisecond Echo Time

Vladimir Mlynarik[1], Hanne Frenkel[1], Joao Duarte[1], Ivan Tkac[2], Rolf Gruetter[1]

[1]Ecole Polytechnique Federale de Lausanne, Lausanne, Switzerland; [2]University of Minnesota, Minneapolis, Minnesota, USA

An ultra-short echo time STEAM protocol has been designed for a 9.4 T animal scanner. Actively shielded high performance gradients with the rise time of 120 µs and short excitation pulses enabled reduction of the echo time to 800 µs. A STEAM spectrum of a rat pup shows absence of spurious signals. Spectral lines of some less abundant or poorly resolved metabolites were clearly discernible, the broad lines of macromolecules were more intense. The spectrum has features reminiscent of spectra measured by the pulse-and-acquire technique.

3057. Editing Through Multiple Bonds: Threonine Detection

Malgorzata Marjanska[1], Pierre-Gilles Henry[1], Kamil Ugurbil[1], Rolf Gruetter[2]

[1]University of Minnesota, Minneapolis, Minnesota, USA; [2]Ecole Polytechnique de Lausanne, Lausanne, Switzerland

In *in vivo* ^{1}H spectroscopy, the signal at 1.32 ppm is usually assigned to lactate. This resonance position at physiological pH is shared with threonine, which has similar *J*-coupling and whose coupling partner resonates at 4.24 ppm, very close to that of lactate (4.11 ppm). The close proximity of coupling partners of lactate and threonine renders the measurement of threonine with and without editing technically challenging. The aim of this study was to exploit multiple-bond editing and quantify the threonine signal *in vivo*.

3058. A Novel Approach to Spectral Editing of Glutathione at 7 Tesla Using Echo-Time Independent Signal Modulations in PRESS Sequence

Giulio Gambarota[1], Vladimir Mlynarik[1], Tibor Liptaj[2], Rolf Gruetter[1]

[1]Ecole Polytechnique Fédérale de Lausanne (EPFL), Lausanne, Switzerland; [2]Slovak University of Technology, Bratislava, Slovakia

Various MR methods have been developed, in the last decade, to detect resonances of coupled spin systems which lie underneath singlets. Recently, a novel and simple approach to spectral editing has been proposed for the AB spin system of citrate: this approach exploits the signal J-modulations which occur in PRESS at a constant echo time. In the present study, we investigated with density matrix simulations and experimentally the spectral shape of glutathione at 7 Tesla, with the goal of applying this novel method of difference spectroscopy editing to the protons (ABX spin system) of the cysteine moiety of glutathione.

3059. Simultaneous Measurement of Unobstructed Glutamate and Glutamine Signals in TE-Averaged PRESS Spectra at 3T Using an Optimized Filter Function

Shaolin Yang[1], Elliot A. Stein[1], Yihong Yang[1]

[1]National Institute on Drug Abuse, NIH, Baltimore, Maryland, USA

Glutamate (Glu) and Glutamine (Gln) are important neurotransmitters in the central nervous system. Glu signal at 2.35ppm can be detected using TE-averaged PRESS spectroscopy at 3T with suppression of the neighboring Gln signal. Recovery of Gln signal at 2.45ppm from the same data set while removing the nearby Glu signal has been reported recently. In this study we extended the above techniques to simultaneously measure unobstructed Glu and Gln signals from the same multiple-TE data set using an optimized filter function. Spectral simulation, phantom, and *in vivo* experiments showed that the simultaneously measured Glu and Gln signals are comparable to those obtained separately.

3060. Spectrally-Selective Refocusing for Brain Glutamate and Glutamine Measures: Application to Human Prefrontal and Motor Cortices

Changho Choi[1], Nicholas J. Coupland[1], Sanjay Kalra[1], Nikolai Malykhin[1], Paramjit P. Bhardwaj[1], Dan Gheorghiu[1], Peter S. Allen[1]

[1]University of Alberta, Edmonton, Alberta, Canada

A new proton NMR single-voxel filtering strategy for selective measurement of glutamate (Glu) and glutamine (Gln) in human brain is proposed. Spectrally-selective refocusing by long (> 80 ms) 180° RF pulses, at 3.0 T, was explored for discrimination of the Glu and Gln C4-proton multiplets in separate scans. The refocusing frequencies and echo times, optimized both numerically and experimentally, rendered measurements of Glu and Gln with negligible contamination from N-acetylaspartate and glutathione. Preliminary *in vivo* results from human prefrontal and motor cortices are reported.

3061. Response of the AB Spin System to STEAM Coherence Selection: Novel Avenues for Spectral Editing at Very High B_0

Vladimir Mlynarik[1], Giulio Gambarota[1], Rolf Gruetter[1]

[1]Ecole Polytechnique Fédérale de Lausanne (EPFL), Lausanne, Switzerland

In the past few years, the signal dependence on the echo time (TE) and mixing time (TM) in the STEAM sequence has been investigated for a number of coupled spin systems, at field strengths of 1.5 – 3 T. With increasing B_0, the spectra of coupled spin systems become more sensitive to small changes in the timing parameters (TE and TM) of STEAM sequences. The aim of the present study was to evaluate the effects of higher B_0, (> 3 T) on the AB spin system of citrate and to elucidate the novel coherence behaviour unique to these high B0.

3062. Motor Cortex GABA Concentration as Measured by Double-Quantum Filtering

Sanjay Kalra[1], Changho Choi[1], Peter S. Allen[1]
[1]University of Alberta, Edmonton, Alberta, Canada

The GABA concentration in the human motor cortex, measured by proton double-quantum filtering, is presented.

3063. Water and Metabolite-Modulated MR Spectroscopy and Spectroscopic Imaging

Robin A. de Graaf[1], Laura I. Sacolick[1], Douglas L. Rothman[1]
[1]Yale University, New Haven, Connecticut, USA

An improved method for the simultaneous detection of water and metabolites is described that robustly eliminates spectral contamination from gradient-vibration-induced water sidebands. While the upfield region of the MR spectra is indistinguishable from regular water-suppressed MR spectra, the down-field region shows many enhanced resonances from slowly exchanging protons. The technique is also implemented with MRSI where the water resonance is used for automated frequency and B0 correction and phasing of spectra.

3064. Brain Glutamate Proton Transverse Relaxation Time as Measured by Spectrally-Selective Refocusing

Changho Choi[1], Nicholas J. Coupland[1], Sanjay Kalra[1], Nikolai Malykhin[1], Paramjit P. Bhardwaj[1], Dan Gheorghiu[1], Peter S. Allen[1]
[1]University of Alberta, Edmonton, Alberta, Canada

The proton NMR relaxation times T_2 and T_1 of glutamate (Glu) in the human brain *in vivo*, measured by a newly-developed spectrally-selective refocusing method, are reported. The apparent T_2 of Glu was derived from fitting the C4-proton multiplet area values at six echo times, using both experimental data and density-matrix simulation. The T_2 and T_1 of Glu for the composite gray/white matter tissues were estimated, at 3 T, to be 168±11 ms and 1.23±0.08 s (mean±SD, n = 5) for the prefrontal cortex, and 163±14 ms and 1.22±0.05 s (n = 2) for the motor cortex, respectively.

3065. The Effect of Strong Homonuclear Proton Coupling on a PRESS-Localized Ge-HMQC Sequence

Atiyah Yahya[1], Peter S. Allen[1]
[1]University of Alberta, Edmonton, Alberta, Canada

This work demonstrates that when ^{13}C-coupled protons of a metabolite are simultaneously involved in strong coupling with neighboring protons the outcome to a basic gradient-enhanced Heteronuclear Multiple Quantum Coherence (ge-HMQC) sequence differs from the expected outcome, namely, a 50% yield for ^{13}C-coupled protons, and zero signal for ^{12}C-bonded protons. The effects are exacerbated when the sequence is combined with PRESS to enable 3D localization. Glutamate at 3.0 T was used as an illustrative example, and numerical calculations were confirmed on a 99% $^{13}C_3$ enriched glutamate phantom.

3066. Short TE PRESS Proton NMR Spectroscopy Without Water Suppression. Application to the Human Brain at 3 Tesla

Wolfgang Dreher[1, 2], Christian Schuster[1, 2], Dieter Leibfritz[1, 2]
[1]University of Bremen, Bremen, Germany; [2]Center of Advanced Imaging (CAI), Bremen, Germany

A two-step method for proton MRS without water suppression (WS) was implemented on a 3T head scanner, tested on phantoms and applied to healthy volunteers. Water and metabolite signals can be easily separated by adding or subtracting two data sets acquired either without or with chemical shift selective adiabatic inversion of metabolite signals prior to a short TE PRESS sequence (phantoms: TE=13 ms, *in vivo*: TE=17 ms). The method allows an efficient elimination of gradient induced artifacts. Thus, WS is avoided and the water signal can be used as a reference signal for signal corrections and metabolite quantification.

Spectroscopic Imaging Techniques and Applications

Room 4E Thursday 13:30 - 15:30

3067. Measurement of Temperature Distributions in Cryopreservation Solutions Using Echo-Planar Spectroscopic Imaging

Richard Thompson[1], Sarah Johnson[1], Robert Lambert[1], Locksley McGann[1]
[1]University of Alberta, Edmonton, AB, Canada

Development of protocols for cryopreservation of tissues for transplantation requires accurate monitoring of temperature and cryoprotectant concentrations throughout samples (cooling/warming). In this study, spectroscopic MRI is investigated as a noninvasive method for measuring the spatial and temporal distribution of temperatures in cryoprotectant solutions used for cartilage preservation. We examine the relationships between temperature (as low as -80oC), cryoprotectant concentration and the resulting chemical shifts, line widths and visible concentrations or water and cryoprotectant protons (2 mm resolution, 2 minute scanning). The proton chemical shift difference between water and the cryoprotectant dimethyl sulfoxide (DMSO) presents a unique absolute measure of temperature.

3068. Water Suppression in 1H MRSI by Reference Subtraction

Claudia Domenig[1], Yingjian Yu[1], Andrew Maudsley[1]
[1]University of Miami, Miami, Florida, USA

Robust water suppression in volumetric whole-brain 1H MRSI can be difficult to achieve using conventional acquisition-based or post-processing methods. In this study is examined a new approach to water removal by subtraction of an interleaved water reference SI method. Results indicate that some improvement in spectral baselines can be achieved, resulting in improved spectral fitting of resonances close to water. In addition, some reduction of the residual subcutaneous lipid signal can be achieved.

3069. Natural Linewidth Chemical Shift Imaging (NL-CSI)

Adil Bashir[1], Dmitriy A. Yablonskiy[1]
[1]Washington University in St. Louis, St. Louis, Missouri, USA

Fourier reconstructed phase encoded CSI data suffer from well-known cross-voxel contamination effects. SLIM reconstruction was previously proposed to eliminate this phenomenon. In this study we demonstrate that the presence of even small magnetic field inhomogeneities substantially amplifies inter-voxel signal leakage in both Fourier and SLIM reconstruction approaches. We have developed a new reconstruction algorithm (Natural Linewidth CSI (NL-CSI)) that allows complete removal of magnetic field inhomogeneity effects from the CSI-acquired MR signal. The results show voxel spectra which are free of inter-voxel signal contamination and intra-voxel phase dispersion resulting in substantial improvement of signal lineshape and data specificity.

3070. Implementation of a New Composite Pulse for Excitation in Fast Proton Spectroscopic Imaging at 1.5 T

Zenon Starcuk Jr. [1], Zenon Starcuk[1], Jana Starcukova[1], Petr Krupa[2]
[1]Institute of Scientific Instruments, Academy of Sciences of the Czech Republic, Brno, Czech Republic; [2]St. Anna Faculty Hospital, Masaryk University, Brno, Czech Republic

A new chemical shift-selective composite pulse (1(x)-t-3.5(x)-t-3.2(x)-t-4.0(-x)-t-36.7(-x)-t-36.7(x)-t-4.0(x)-t-3.2(-x)-t-4(-x)) has been developed for the excitation in fast proton spectroscopic imaging at 1.5 T and implemented in sequences on a clinical system Siemens Symphony. The pulse provides a wide bandwidth of excited transverse magnetization framed by sufficiently broad null excitation bands, reducing the need for water/lipid presaturation. Pulse adjustment can control the residual water signal for internal referencing. First experimental results obtained with these sequences are presented. They demonstrate the applicability in measurements without water presaturation and the potential for TR reduction.

3071. Factor-2 Acceleration for 3D EPSI at 4T Using Modified Blipped Phase-Encoding

Andreas Ebel[1], [2], Michael W. Weiner[2], [3], Norbert Schuff[2], [3]
[1]Northern California Institute for Research and Education, San Francisco, California, USA; [2]VA Medical Center, San Francisco, California, USA; [3]University of California, San Francisco, California, USA

To reduce acquisition time for echo-planar spectroscopic imaging (EPSI) by a factor of 2, application of blipped phase-encoding (PE) gradients between even and odd lobes of the readout (RO) gradient was suggested to phase-encode even RO echoes in k-space at an interstitial location along k_{PE}. However, the approach is susceptible to phase inconsistencies between even and odd RO echoes due to B_0 inhomogeneities and gradient imbalance. Feasibility of using a blipped PE gradient in between pairs of even/odd RO lobes to prevent phase inconsistencies from interfering with the phase-encoding is demonstrated for 3D EPSI in normal human brain at 4T.

3072. Fourier Component Imaging of Water Resonance in Human Breast: A New Source of MRI Contrast

Milica Medved[1], Gillian M. Newstead[1], Xiaobing Fan[1], Yiping Du[2], Olufunmilayo I. Olopade[1], Marta A. Zamora[1], Gregory Stanislaus Karczmar[1]
[1]The University of Chicago, Chicago, Illinois, USA; [2]The University of Colorado Health Science Center, Denver, Colorado, USA

A new approach to MRI based on imaging the structure of the water resonance and constructing images proportional to individual Fourier components is proposed. Data from 32 patients with mammographically suspicious findings were acquired using echo-planar spectroscopic imaging at 1.5 Tesla. Frequent inhomogeneous broadening of the water resonance was observed reproducibly in small voxels (< 2 mm3). Images with intensity proportional to peak, and off-peak, components of the water resonance in each voxel were often qualitatively different. Such differences likely reflect underlying anatomy or physiology, and were more frequently observed in patients with invasive disease.

3073. Quantitative Metabolite Mapping in Human Brain at 4T Using Short TE ^{1}H LASER-CSI and Tissue Segmentation

Jennifer Andrea McNab[1], [2], Robert Bartha, [1,2]
[1]University of Western Ontario, London, Ontario, Canada; [2]Robarts Research Institute, London, Ontario, Canada

Quantitative maps of N-acetyl-aspartate, creatine, choline, myo-inositol, glutamate and glucose in healthy human brain have been generated from short echo-time ^{1}H LASER-CSI data for the first time. Tissue segmentation using SPM2 and point spread function characterization facilitated absolute quantification in voxels with mixed tissue content. The combination of a multi-voxel acquisition, detection of more than four metabolites, absolute quantitative concentration measurements, in a time frame that is feasible for clinical research studies (47 min.) and at an informative resolution (nominal voxel size of 0.56 cm^3) makes LASER-CSI a viable and attractive option for future ^{1}H NMR spectroscopic investigations.

3074. Local B_0-Shift Correction for 3D EPSI of Human Brain at 1.5 and 4 Tesla

Andreas Ebel[1, 2], Andrew A. Maudsley[3], Michael W. Weiner[2, 4], Norbert Schuff[2, 4]

[1]Northern California Institute for Research and Education, San Francisco, California, USA; [2]VA Medical Center, San Francisco, California, USA; [3]University of Miami, Miami, Florida, USA; [4]University of California, San Francisco, California, USA

Previously, high spatial resolution acquisition 3D EPSI in combination with a water reference EPSI data set was proposed to accomplish local frequency shift correction in 1.5T human brain metabolite maps, minimizing inhomogeneous spectral line-broadening. At higher magnetic field strength, increased field inhomogeneities typically lead to increased line-broadening. Additionally, increased susceptibility makes shimming of the magnetic field over the whole head more difficult. To determine whether local frequency shift correction still helps limit line-broadening in human brain 3D EPSI at higher magnetic fields, the combination of high spatial resolution acquisition and local frequency shift correction is compared between 1.5T and 4T.

3075. Sensitivity Encoded Three Dimensional Echo Planar Spectroscopic Imaging (3D-EPSI) of Human Brain at 4T

Xiaoping Zhu[1], Andreas Ebel[2], Jim X. Ji[3], Michael W. Weiner[1], Norbert Schuff[1]

[1]VAMCSF/UCSF, San Francisco, California, USA; [2]Northern Institute for Research & Education, San Francisco, California, USA; [3]Texas A&M University, College Station, Texas, USA

We introduce a method of incorporating sensitivity encoding (SENSE) to 3D echo planar spectroscopic imaging (EPSI). Metabolite and interleaved water reference 3D-EPSI, covering the whole brain, were acquired at 4T and reconstructed using SENSE. Frequency shifts of metabolite resonances due to local B0 inhomogeneities in the brain were corrected based on the water resonance line. k-space extrapolation was carried out to reduce lipid contamination. Typical proton spectra from gray matter areas and images of brain metabolites, including NAA, Cr and Cho, are presented, demonstrating the feasibility. Decreases of SNR and spectral resolution in the under-sampled 3D-SENSE-EPSI were investigated and discussed.

3076. Experimental Demonstration of Rosette Spectroscopic Imaging (RSI)

Claudiu Schirda[1, 2], Fernando Boada[2]

[1]University of Pittsburgh, Pittsburgh, Pennsylvania, USA; [2]UPMC, Pittsburgh, Pennsylvania, USA

Low concentrations and long T1's of the physiological Phosphorous 31 metabolites impose severe constraints on the spatial resolution and signal-to-noise ratio (SNR) of the images that can be obtained using conventional spatial encoding schemes.We demonstrate that Rosette Spectroscopic Imaging (RSI) can be used to obtain images of comparable SNR to conventional acquisition schemes but with significantly lower total acquisition time.

3077. Constrained Spectroscopic Imaging with Hard and Soft Anatomical Boundary Constraints

Justin Pritam Haldar[1], Mathews Jacob[1], Andreas Ebel[2, 3], Xiaoping Zhu[3], Norbert Schuff[3], Diego Hernando[1], Bradley Sutton[1], Zhi-Pei Liang[1]

[1]Beckman Institute, University of Illinois at Urbana-Champaign, Urbana, Illinois, USA; [2]Northern California Institute for Research and Education, San Francisco, California, USA; [3]VA Medical Center and Department of Radiology, University of California, San Francisco, California, USA

This paper addresses an outstanding problem in MRSI, i.e., the inversion of noisy, limited Fourier data with anatomical constraints. The proposed method incorporates exact boundary constraints into the basis functions of a spatial-spectral model, and uncertain boundary constraints into a regularizing penalty function. The final reconstruction is obtained by solving a convex optimization problem. By providing an effective way to integrate anatomical images with spectroscopic images, the proposed method can yield higher-resolution metabolite maps than conventional methods.

3078. Unpaired Adiabatic Refocusing Pulses for Volume Selection in Spectroscopic Imaging

Laura Sacolick[1], Douglas L. Rothman[1], Robin A. de Graaf[1]

[1]Yale University, New Haven, Connecticut, USA

Conventional volume selection by adiabatic pulses in spectroscopic imaging is done with pairs of identical pulses. This refocuses the non-linear phase shift introduced by AFP pulses which would otherwise cause intravoxel signal loss. Here we show that sequentially applying single AFP pulses at 45¢ª angles will give good phase refocusing with little signal loss for spectroscopic imaging. Conventional AFP pulses were replaced by FOCI pulses to decrease chemical shift displacement without increasing peak RF power. This new sequence provides good volume selection with half the power and echo time as for a paired AFP sequence.

3079. Sensitivity Encoded Proton Echo Planar Spectroscopic Imaging (PEPSI) in Human Brain at 7 Tesla

Stefan Posse[1, 2], Ricardo Otazo[3, 4], Shang-Yueh Tsai[5], Lawrence Wald[5], Fa-Hsuan Lin[5]

[1]The University of New Mexico, Albuquerque, New Mexico, USA; [2]University of New Mexico School of Medicine, Albuquerque, New Mexico, USA; [3]The MIND Institute, Albuquerque, New Mexico, USA; [4]University of New Mexico, Albuquerque, New mexico, USA; [5]Massachusetts General Hospital, Charlestown, Massachusetts, USA

The increase of the signal-to-noise ratio and the increase in spatial information of the RF coil sensitivity profiles with field strength promise considerable gains in the performance of SENSE accelerated high-speed spectroscopic imaging at 7 T. In this study we demonstrate feasibility of up to 4-fold acceleration of Proton-Echo-Planar-Spectroscopic-Imaging (PEPSI) with one-dimensional SENSE parallel imaging at 7T in phantoms and 2-fold acceleration in human brain using an 8-channel coil array.

3080. Radiofrequency Variations in Spectroscopic Imaging at High Field: Differences in Coupled and Uncoupled Spin Systems

Jeff Snyder[1], Richard B. Thompson[1], Jim M. Wild[2], Alan H. Wilman[1]
[1]University of Alberta, Edmonton, Alberta, Canada; [2]University of Sheffield, Sheffield, Yorkshire, UK

This study investigates the effect of radiofrequency variations due to superposition of standing waves on coupled spin systems both theoretically and experimentally. Experiments performed include simulations, single voxel spectroscopy and spectroscopic imaging on healthy volunteers. Results show a decrease in signal intensity for coupled and uncoupled spin systems when voxels are placed further from the center of the brain. Coupled spin systems glutamate and glutamine experience larger intensity changes than single resonances.

3081. Reduced Echo Time Dualband Spatial-Spectral Pulse Sequence for Brain MRSI at 3T

Priti Balchandani[1], Daniel Spielman[1]
[1]Stanford University, Stanford, California, USA

1H MRSI is a useful technique for measuring metabolite levels in the brain. In this study, the use of a PRESS sequence with only one dualband spatial-spectral (SPSP) linear phase 90º pulse and two standard spatial 180º pulses is proposed for brain MRSI. This sequence provides spectral selectivity while allowing significantly lower echo times than existing SPSP PRESS sequences for the brain. At 3T, shorter echo times result in higher metabolite SNRs. *In vivo* data shows that the linear phase dualband SPSP 90º pulse successfully suppresses fat when compared to the standard GE PRESS sequence at the same echo time.

3082. Metabolic Mapping of the Brain by Volumetric MR Spectroscopic Imaging

Andrew A. Maudsley[1], Ammar Darkazanli[2], Jeffry R. Alger[3], Larry O. Hall[4], Norbert Schuff[5], Colin Studholme[5], Yingjian Yu[1], Andy Frew[3], Dmitry Goldgof[4], Yuhua Gu[4], Raj Pagare[3], Francois Rousseau[5], K. Sivasankaran[1], Brian J. Soher[6], Patrice Weber[5], Karl Young[5]
[1]University of Miami, Miami, Florida, USA; [2]Universiy of Miami, Miami, Florida, USA; [3]UCLA, Los Angeles, California, USA; [4]University of South Florida, Tampa, Florida, USA; [5]UCSF, San Francisco, California, USA; [6]Duke University, Durham, North Carolina, USA

Analysis of MR spectroscopic data from the brain optimally requires comparisons with normal metabolite distributions, which are known to vary by tissue type, region, and demographic factors such as age. For MR Spectroscopic Imaging (MRSI) it is particularly beneficial if this information is available from the whole brain, facilitating statistical tests to detect both local and widespread metabolic changes. To this aim, an integrated set of processing tools has been developed (MIDAS) that provide fully-automated MRSI and MRI data, formation of a brain metabolite database, and comparisons between subject and database metabolite values.

3083. Regional Estimation of T1 Metabolite Relaxation Using 2D MRSI and a Bootstrap Approach at 1.5 T

Helene Ratiney[1], Susan M. Noworolski[1], Michael Sdika[1], Roland G. Henry[1], Radhika Srinivasan[1], Daniel Pelletier[1]
[1]University of California, San Francisco, California, USA

In clinical spectroscopic studies, the use of short repetition times (TR) enables one to meet time constraints but also requires knowledge of accurate metabolite longitudinal relaxation time values (T1) to correct for the resulting strongly T1-weighted signals. We propose a new method to estimate the metabolite T1, at 1.5T, using MR spectroscopic imaging (MRSI) data. The very low signal to noise ratio problem is tackled by using an approach combining Principal Component Analysis (PCA) denoising, bootstrap-like data averaging, and quantitation results quality assessment. A gray matter (GM) versus white matter (WM) contribution to the T1 estimation is also investigated.

3084. Quantitative 3D Spiral 1H MRSI of the Brain with an 8 Channel Phased-Array Coil

Meng Gu[1], Dong-Hyun Kim[2], Daniel Spielman[1]
[1]Stanford University, Stanford, California, USA; [2]University of California at San Francisco, San Francisco, California, USA

In brain 1H magnetic resonance spectroscopic imaging, to obtain high-quality metabolite spectra, it is important to suppress both water and lipids. However, having a residual water signal can be valuable for phasing and quantification. For 3D MRSI, it is essential to use fast imaging methods to reduce scan time while maintaining good SNR. In addition, it is desirable to have robust and efficient quantification. To achieve these goals, we implemented a 3D MRSI sequence at 1.5T with dualband spectral-spatial excitation, spiral k-space readout, 8-channel phased-array acquisition, voxel-by-voxel phasing and automated quantification using LCModel.

3085. Proton MRS of Bilateral Substantia Nigra in the Human Brain at 4 Tesla with Hadamard Encoding

Gulin Oz[1], Ivan Tkac[1], Jodi Lowary[1], Paul Tuite[1], Rolf Gruetter[1]
[1]University of Minnesota, Minneapolis, Minnesota, USA

Substantia nigra (SN) is the primary affected brain region in Parkinson's disease. ^{1}H MR spectra were acquired at 4 tesla simultaneously from two voxels (2.2 ml VOI) encompassing the right and left SN of ten healthy volunteers using Hadamard encoding, excluding central CSF spaces. The neurochemical profile including GABA, glutamate and glutathione was quantified using LCModel in individual subjects. Significantly higher GABA and lower glutamate concentrations relative to reported cortical values were measured, in good agreement with single voxel spectroscopy of the unilateral SN and neurochemistry literature. No right-left asymmetry was observed.

3086. Automatic Outer Volume Suppression (OVS) Slice Placement for Proton-Echo-Planar-Spectroscopic-Imaging (PEPSI)

Ting Li[1], Manel Martinez-Ramon[1], Greg Heileman[2], Stefan Posse[3]
[1]MIND Institute, Albuquerque, New Mexico, USA; [2]University of New Mexico, Albuquerque, New Mexico, USA; [3]MIND Imaging Center, Albuquerque, New Mexico, USA

It is demonstrated that high-speed spectroscopic imaging using the PEPSI method, sensitivity encoded by an 8-channel surface RF coil array, can be 4-fold accelerated without significant loss in spectral quality by using GRAPPA parallel imaging. This approach enables PEPSI acquisitions to be performed in less than 3 minutes for 3D spatial encoding and in just a few seconds for 2D spatial encoding. It is shown that the quality of the reconstruction can be improved by adjusting the SNR of the GRAPPA calibration reference to the SNR of the PEPSI-data.

MR Spectroscopy: x Nuclei and Other

Room 4E Thursday 13:30 - 15:30

3087. A New Complex of Diperoxovanadate with 2-(2′-Pyridyl)-Imidazole: Synthesis, Structure, Interaction and Bioactivity

Yanglin Pan[1], Jianghua Yan[1], Shuyu Yang[2], Xuejun Li[2], Shuhui Cai[1], Zhong Chen[1]
[1]Xiamen University, Xiamen, Fujian, People's Republic of China; [2]Xiamen First Hospital, Xiamen, Fujian, People's Republic of China

A new diperoxovanadate complex NH_4 [$OV(O_2)_2${2-(2′-pyridyl)-imidazole}]·$4H_2O$ was synthesized. Its solution structure was characterized by multinuclear (^1H, ^{13}C, ^{14}N, and ^{51}V) as well as multi-dimensional (DOSY and C-H COSY) NMR techniques in the interaction system of NH_4VO_3/H_2O_2/2-(2′-pyridyl)-imidazole at room temperature. It affected the proliferation of tumor cell and normal one in a different manner. In addition, it inhibited the specific activity of ALP (alkaline phosphatase) in gastric cancer cell MGC-803.

3088. *In Vivo* Large Flip Angle ^{31}P MRS in the Human Brain at 3T

RoseAnn M. Blenman[1], John D. Port[1], Joel P. Felmlee[1]
[1]Mayo Clinic College of Medicine, Rochester, Minnesota, USA

As *in vivo* ^{31}P MRS is implemented at higher field strengths, quantitative techniques must meet the challenges of measuring metabolites with lengthening T_1 relaxation times in clinically feasible scan times. Our approach was to develop a short TR, short TE, large flip angle (LFA) technique at 3T that maximizes the SNR of long T_1 ^{31}P metabolites. The specific components PCr, PE, and PC are respectively maximized with flip angles of 140°, 130° and 120° with respective mean signal gain of 1.71 ± 0.20 (mean ± std), 1.76 ± 0.42 and 1.39 ± 0.26. *In vivo* data show that the LFA technique is successfully employed to maximize SNR.

3089. Comparison of Cardiac Phosphorous Spectroscopy at 1.5T and 3T

Damian J. Tyler[1], Lucy E. Hudsmith[1], Stefan Neubauer[1], Kieran Clarke[1], Matthew D. Robson[1]
[1]University of Oxford, Oxford, UK

Normal healthy volunteers (n=10; 5m, 5f) were scanned at both 1.5T and 3T using an acquisition weighted chemical shift imaging sequence (AW-CSI). A voxel of interest was selected anatomically, and spectral peaks were quantified using jMRUI to determine the signal to noise ratio (SNR). There was a significant increase in SNR (~100%) at 3T compared with 1.5T which could be used to increase the spatial or temporal resolution of ^{31}P cardiac spectra.

3090. Characterisation of Muscle Type Lipid Relaxation Parameters for Quantification of Intramyocellular Lipids Evolution in Zucker Rats

Rachida Fissoune[1], Denis Grenier[2], Emmanuelle Canet Soulas[2], André Briguet[1]
[1]Laboratoire de RMN CNRS UMR 5012, Lyon, France; [2]Laboratoire de RMN CNRS UMR 5012, Lyon, France

1H-MRS is being increasingly used for investigations of human and animal muscle physiology. It is currently the only technique that enables non-invasive monitoring of IMCL levels *in vivo*The knowledge of apparent relaxation times of IMCL and EMCL in muscle tissue is required for optimization of sequence parameters and for quantification. Up to now, all reported IMCL quantifications in rats were performed using creatine as reference. However, in some applications creatine concentration could be influenced by age and animal model. In present study, the relaxation parameters of the two pools of lipids in zucker rats at 7 teslas are determined. Quantification of lipids independently to creatine is proposed.

3091. Changes in Specific Metabolic Pathways Are Essential Steps in the Early Apoptotic Process in the Liver

Sven Gottschalk[1, 2], Tom Chan[1], Valerie-Ann Raymond[1], Marc Bilodeau[1], Dieter Leibfritz[2], Claudia Zwingmann[1, 2]
[1]Hospital Saint-Luc, Montreal, Quebec, Canada; [2]University of Bremen, Bremen, Germany

To clarify whether changes in glucose metabolism occur prior to the already known events in the apoptotic process, and whether these can be prevented by the immunosuppressant Cyclosporine A (CsA), we used multinuclear NMR spectroscopy and molecular studies to characterize metabolic pathways in mice liver during anti-Fas-induced apoptosis. An upregulation of specific metabolic pathways of glucose was the earliest indicator of the effect of Fas on the liver. CsA prevented apoptosis and energy failure at late stages, while the reversal of Fas-induced metabolic upregulation at early stages preceded the protective effect of EGF on programmed cell death. These phenomena provide useful hints for the understanding of early mechanisms controlling apoptotic cell death.

3092. High Resolution Magic Angle Spinning MR Spectroscopy Reveals Biomarkers of Insulin Resistance in Burn Trauma

Haihui Cao[1, 2], Loukas G. Astrakas[1], Qunhao Zhang[2], Hongyue Yu[1], Michael N. Mindrinos[3], Ronald G. Tompkins[2], Laurence G. Rahme[2], A. Aria Tzika[1, 2]
[1]Massachusetts General Hospital and Shriners Institute, Harvard Medical School, Boston, Massachusetts, USA; [2]Massachusetts General Hospital, Harvard Medical School, Boston, Massachusetts, USA; [3]Stanford University, Palo Alto, California, USA

NMR visible intramyocellular lipids (IMCLs) have been associated with insulin resistance. We report that Magic Angle Spinning (MAS) 1H NMR Spectroscopy has detected, with high resolution, differences in IMCLs from control and burned mice. The IMCLs of the latter was linked to insulin resistance. We suggest that increased levels of NMR visible IMCLs in burn trauma is a biomarker for insulin resistance. This has led us to the concept that suppression of IMCLs may represent a candidate strategy for a partial relief of insulin resistance and muscle wasting (or cachexia) resulting from burn trauma.

3093. OVS-Localized ^{31}P NMR Spectroscopy in the Primate Brain

Julien Valette[1], Martine Guillermier[2], Philippe Hantraye,[1,2], Vincent Lebon[1]
[1]CEA-SHFJ, Orsay, France; [2]URA CEA-CNRS 2210, Orsay, France

In this work ^{31}P NMR spectroscopy is performed in the monkey brain using a surface coil at 3T. Optimized localization is achieved in an 8mL cubic voxel at zero echo time by Outer Volume Suppression, with no signal loss caused by metabolites fast T_2 relaxation, and negligible contamination from muscle. This localization technique proves to be sensitive enough for combination with inversion-recovery and saturation transfer and subsequent measurement of ATP synthesis rate in the primate brain at 3T.

3094. ^{19}F High Senseitivity Imaging for *In Vivo* Drug Dynamics in Mice at 7T with 5-FU

Yoko Kanazawa[1], Yoshiyuki Hirano[1, 2], Sachiko Koike[1], Michiko Narazaki[1], Eiji Yoshitome[1], Koichi Ando[3], Masafumi Fujiita[2], Minoru Onozuka[4], Hiroo Ikehira[1]
[1]Institute of Radiological Sciences, Chiba, Japan; [2]Gifu University, Gifu, Japan; [3]Institute of Radiological Sciences, Chiba, Japan; [4]Kanagawa Dental College, Yokosuka, Japan

High sensitivity ^{19}F imaging in small animals is demonstrated using fast sequences such as FSE and FISP at 7T. Dynamical study of 5-FU was successful by FSE with chemical shift selective pulses for simultaneous imaging of several resonance lines by interleave. Clear image of anabolites Fnuc was shown at the position of tumors by FSE. The advantage and disadvantage of FISP is discussed. The method will also find an extended use for molecular imaging.

3095. *In Vivo* ^{31}P–{^{1}H} Echo–Planar Spectroscopic Imaging of the Human Brain

Marco Ulrich[1], Tim Wokrina[1], Peter Bachert[2], Gabriele Ende[1]
[1]Central Institute of Mental Health, Mannheim, Germany; [2]German Cancer Research Center, Heidelberg, Germany

Echo-Planar Spectroscopic Imaging (EPSI) is one of the fastest *in vivo* spectroscopic imaging (SI) techniques. Although this method was implemented for various ^{1}H-MRS applications, EPSI of phosphorous-containing metabolites in the human brain has, to our knowledge, never been considered so far. Here we present the development of eight NOE enhanced ^{31}P-{^{1}H} EPSI sequences with short TE, which permit 2-D SI of the human brain providing good quality high resolution ^{31}P-spectra with different spectral widths. These results convincingly show that ^{31}P-EPSI as a very fast and robust data acquisition method to allow for functional MRS studies.

3096. DRESS Strategy for Improving Cardiac P-31 MRS at 3T: Coil & OVS

Hee-Won Kim[1], David M. Peterson[1]
[1]University of Florida, Gainesville, Florida, USA

In order to optimally utilize DRESS sequence for cardiac P-31 MRS, that is sensitive but tends to be contaminated from outside, an home-made oblong shape quadrature surface coil and a tailored outer volume suppression pulse by SLR algorithm were applied. This stragegy showed reduced contamination from adjacent tissues and enhanced sensitivity. This effect from optimal combination of coil/OVS may be exploited in the routine cardiac P-31 MRS application where high signal-to-noise ratio and precise localization capability are required.

3097. Effect of Patient Orientation on Cardiac ^{31}P-MRS

James Lee Schroeder[1], Damian J. Tyler[1], Yaso Emmanuel[1], Matthew D. Robson[2], Michaela Scheuermann-Freestone[1], Stefan Neubauer[2], Kieran Clarke[1]
[1]University of Oxford, Oxford, Oxfordshire, UK; [2]University of Oxford, Headington, Oxfordshire, UK

Normal healthy volunteers (n=10; 5m, 5f) were scanned in both the prone and supine position using a 1.5 T clinical MRI scanner. ^{31}P spectra were acquired using ECG-gated chemical shift imaging (CSI) and peaks were quantified using AMARES fitting. No significant differences in SNR, PCr/ATP ratio, voxel to coil distance, or scan duration were found between the scans performed in the prone and supine position. These results show that supine subject positioning gives may give adequate signal for clinical cardiac spectroscopy, although further work is needed to look at possible increase in breathing motion.

3098. *In Vivo* Measurement of T_1 Relaxation Times of ^{31}P Metabolites in Human Brain at 3T

RoseAnn M. Blenman[1], John D. Port[1], Joel P. Felmlee[1]
[1]Mayo Clinic College of Medicine, Rochester, Minnesota, USA

Apparent T_1 estimates are important for signal-to-noise optimization, accurate quantitation of spectral data, and for correction of partially saturated MRS data. T_1 relaxation times of ^{31}P human brain metabolites were measured at 1.5T, 2T and 7T, but values measured at 3T have not yet been published. *In vivo* T_1 times measured at 3T are 3.57 ± 0.65s (mean±std), 4.88 ± 0.54s, 2.2 ± 0.4s, 3.94 ± 1.43s, 3.11 ± 0.7s for PCr, PE, Pi, GPE and GPC respectively, and 0.98 ± 0.11s for α-ATP, β-ATP and γ-ATP. Possible sources of systematic errors are identified and strategies for their reduction discussed.

3099. Measurement of the Longitudinal Relaxation Time (T_1) of Cardiac Phosphorous Metabolites at 3T

Damian J. Tyler[1], Lucy E. Hudsmith[1], Stefan Neubauer[1], Kieran Clarke[1], Matthew D. Robson[1]
[1]University of Oxford, Oxford, UK

^{31}P spectroscopy is a valuable technique for the *in vivo* measurement of high energy metabolites, which allows the assessment of tissue energy metabolism. The ratio of PCr to ATP provides a measure of the energetic state of the heart and is an indicator of cardiac failure. To obtain reliable PCr/ATP ratios we require knowledge of the T_1 values of the individual metabolites, as well as the TR and local flip angle. In this work we have for the first time measured the T_1 values of PCr and γ-ATP using the 'dual angle' method to be 3.8±0.3s (PCr) and 2.4±0.5s (γ-ATP).

3100. Quantified ^{19}F MR Spectroscopy Reveals Heterogeneous Capecitabine Metabolism in Human Liver

Dennis WJ Klomp[1], Hanneke W.M. van Laarhoven[1], Cees Punt[1], Arend Heerschap[1]
[1]Radboud University Nijmegen Medical Center, Nijmegen, Netherlands

The aim of this study was to develop a method for quantified localized detection of fluorinated compounds in human liver. For this purpose sensitivity-optimized localized ^{19}F MRS methods at 3 Tesla were used to detect MR signals from capacitabine, 5'DFUR, 5'DFCR and FBAL after oral intake of capacitabine. As the rf coil is made tuneable to ^{19}F and ^{1}H, the same localization method is applied to obtain ^{1}H MR signals of water as for the ^{19}F metabolites. Absolute concentrations are obtained of capecitabine and its metabolites *in vivo* which revealed a substantial spatial heterogeneity of these metabolites in human liver.

3101. ^{31}P Spectroscopy Using a Silicon-Based Needle Coil

Franklyn A. Howe[1], John R. Griffiths[1], Loreta M. Rodrigues[1], Richard R.A. Syms[2], Munir M. Ahmad[2], Iain R. Young[2]
[1]St George's, University of London, London, UK; [2]Imperial College, London, UK

Silicon-based detector coils could be manufactured very cheaply in bulk, so they seem an attractive possibility for single use applications such as for insertion into tumours and other tissues for real-time spectroscopy during interventional surgery. We describe the design, manufacture and the first *in vivo* trial of a silicon needle coil for ^{31}P spectroscopy at 81MHz.

3102. Gated 31P Chemical Shift Imaging of Phosphocreatine Changes During Single Muscle Contractions

Ronald A. Meyer[1], Jill M. Slade[1], Theodore F. Towse[1], Mark C. DeLano[1]
[1]Michigan State University, East Lansing, Michigan, USA

Phosphocreatine changes in skeletal muscle during 2 s duration ankle dorsiflexion contractions were measured by gating phosphorus 2D chemical shift imaging acquisitions to times before and after contractions performed at 15 s intervals. The results demonstrate that spatially-resolved measurements of both contractile PCr utilization and PCr recovery rate in human leg muscles can be accomplished by gated 2D chemical shift imaging at 3 T.

Non-Proton MRI

Room 4E Thursday 13:30 - 15:30

3103. Initial Experience with Sodium MRI of Phantoms and Human Brain at 9.4 Tesla

Fred Damen[1], Samantha Holdsworth[2], Ian Atkinson[1], Ed Boskamp[3], Theodore Claiborne[1], Arno Nauerth[4], Belinda Li[3], X Joe Zhou[1], Zhi-Pei Liang[5], Keith R. Thulborn[1]

[1]University of Illinois Medical Center, Chicago, Illinois, USA; [2]University of Queensland, Brisbane, Queensland, Australia; [3]GE Healthcare, Wakasha, Wisconsin, USA; [4]Bruker Biospin, Ettlingen, Germany; [5]University of Illinois, Urbana, Illinois, USA

Initial experiences of using a whole body 9.4 Tesla scanner for sodium MR imaging (105.9MHz) based on twisted projection imaging (TPI) of phantoms and human brain indicate that improved SNR from 3T is achieved without approaching significant specific absorption rate (SAR) set by FDA guidelines. Adequate homogeneity was achieved shimming on the sodium signal. Spatial resolution of better than 5 mm can be achieved in less than 5 minutes without signal averaging.

3104. Sodium Relaxometry (Part 2): Towards the Characterization of the Sodium NMR Environment in the Human Brain Using a Novel Relaxomety Technique

Robert W. Stobbe[1], Christian Beaulieu[1]

[1]University of Alberta, Edmonton, Alberta, Canada

A novel sodium relaxometry technique is used to characterize sodium relaxation in the human brain using both one and two compartment models. The one compartment model yields a bulk tissue value for the fast component of transverse relaxation, which is difficult to measure using multi-echo experiments, and an average value for longitudinal relaxation. However, the two compartment model generates a more ideal fit for the measured data. Regression of data from two volunteers (using a gray matter ROI) suggests one compartment has sodium relaxation properties similar to 1-2 percent agar, while the other has a very rapid fast-T2.

3105. 1H and 23Na MRI of Rat Head at 4 Tesla with a Simple Double-Tuned RF Surface Coil

Marcello Alecci[1], Sandro Romanzetti[2], Joachim Kaffanke[2], Avdo Celik[2], Hans Peter Wegener[3], Nadim Jon Shah[2, 4]

[1]Università dell'Aquila, L'Aquila, Italy; [2]Institute of Medicine, Juelich, Germany; [3]Central Electronic Institute, Juelich, Germany; [4]University of Dortmund, Dortmund, Germany

MRI is proving to be a very useful tool for sodium quantification in animal models of stroke, ischemia, and cancer. In this work we present the design and the *in vivo* testing of a simple dual-frequency RF surface coil that permits proton and sodium images of the rat head at 4 Tesla.

3106. Comparison of FLASH and TPI Techniques for Sodium Imaging

Samantha Jane Holdsworth[1], Stephen Edward Rose[1], Katie Louise McMahon[1], Donald Maillet[1], Fred Charles Damen[2], Graham John Galloway[1]

[1]University of Queensland, Brisbane, Queensland, Australia; [2]University of Illinois at Chicago, Chicago, Illinois, USA

The application of sodium imaging to clinical research has been limited by low concentration and short T_2 times *in vivo*. This work assesses the image quality of two sequences previously used for sodium imaging; twisted projection imaging (TPI), implemented with a flexible user-interface, and short-TE FLASH. These techniques were tested on phantom and newborn piglets.

3107. Measurement of Phosphorus Content in Normal and Osteo-Malacic Rabbit Bone by Solid-State 3D Radial Imaging

SeshaSailaja Anumula[1], Jeremy Magland[1], Henry Ong[1], Hualei Zhang[2], HeeKwon Song[1], Suzanne W. Wehrli[3], Felix W. Wehrli[1]

[1]University of Pennsylvania medical centre, Philadelphia, Pennsylvania, USA; [2]University of Pennsylvania, Philadelphia, Pennsylvania, USA; [3]Children's Hospital of Philadelphia, Philadelphia, Pennsylvania, USA

Osteomalacia is characterized by hypomineralization of bone caused by vitamin D deficiency, leading to reduced stiffness and mechanical strength. Currently, there is no non-invasive modality that can measure the true mineralization expressed as mass of mineral per unit volume of bone (degree of bone mineralization, DMB). Here, we hypothesize that DMB can be measured with sufficient precision using 3D radial imaging so that subtle differences in phosphorus content and DMB can be measured between normal and osteo-malacic bone. The results obtained are in agreement with DMB measurements obtained by μ-CT, suggesting that this method might be applicable to studies *in vivo* in laboratory animals and possibly in humans.

3108. Feasibility of ^{13}C-MRI of the Lung Using $^{13}CO_2$ Gas

Wolfgang G. Schreiber[1], Florian Meise[1], Alexander Scholz[2], Ursula Wolf[1]

[1]Mainz University Medical School, Section of Medical Physics, Mainz, Germany; [2]Mainz University Medical School, Mainz, Germany

Recently, sophisticated techniques for visualizing intrapulmonary gas using hyperpolarized ^{3}He or ^{129}Xe, or fluorinated gas compounds have been developed. However, when compared with respiratory gases like N_2, O_2 and CO_2 all of theses MRI contrast gases differ in their physical and physiological properties. Here we demonstrate for the first time the feasibility of MRI using thermally polarized isotopically enriched $^{13}CO_2$ gas in phantoms and rat lungs.

3109. Ultrafast 3D Imaging of Hyperpolarized 13C *In Vivo*

Pratip Bhattacharya[1, 2], K. Harris[2], Alex P. Lin[2], Maria Mansson[2], Valerie A. Norton[1], William H. Perman[3], Daniel P. Weitekamp[1], Brian D. Ross[2]

[1]California Institute of Technology, Pasadena, California, USA; [2]Huntington Medical Research Institutes, Pasadena, California, USA; [3], St. Louis University School of Medicine, St. Louis, Missouri, USA

The goal of this work is to develop a fast 3D method of maximum intensity projection (MIP) imaging using hyperpolarized 13C MR angiography *in vivo*. The PASADENA polarizer was individually optimized for production of two hyperpolarized water soluble molecules. Fast multiple-phase 3D-FIESTA 13C imaging was performed on a GE clinical 1.5T scanner before, during and after injection of the hyperpolarized molecule into the jugular vein of rats. The MIP images thereby obtained demonstrate the extent of signal enhancement in the cardiopulmonary circulation. The sequence was effective for imaging hyperpolarized 13C reagents produced in a custom-built parahydrogen polarizer enhancing SNR 25,000-fold. *In vivo* signal enhancements in PASADENA exceed 2000-fold.

3110. ^{13}C PASADENA Imaging *In Vivo*

Alexander Peter Lin[1, 2], William H. Perman[3], Jochen Leupold[4], Pratip Bhattacharya, [25], Kent Harris[5], Jürgen Henning[4], Brian David Ross[5]

[1]Rudi Schulte Research Institute, Pasadena, California, USA; [2]California Institute of Technology, Pasadena, California, USA; [3]St. Louis University, School of Medicine, St. Louis, Missouri, USA; [4]University Hospital Freiburg, Freiburg, Germany; [5]Huntington Medical Research Institutes, Pasadena, California, USA

Parahydrogen and synthesis allows dramatically enhanced nuclear alignment (PASADENA) can achieve greater than 10,000 times ^{13}C signal enhancement through hyperpolarization. Two ^{13}C PASADENA reagents were infused into a rat simultaneously. Reconstruction of the data demonstrates that 3D spatial, spectral, and temporal information can be obtained using fast multi-echo balanced SSFP ^{13}C imaging *in vivo*.

3111. Orthodeuterium Induced 1H- And 2D-Hyperpolarization for MRI

Joachim Bargon[1], Arndt Limbacher[1], Rahim R. Rizi[2]

[1]University of Bonn, Bonn, Germany; [2]University of Pennsylvania Medical Center, Philadelphia, Pennsylvania, USA

Analagous to hyperpolarization derived from parhydrogen, strongly enhanced signals result from hydrogenations of appropriate substrates with orthodeuterium (o-D2). Although p-H2 is easier to enrich than o-D2, and the relaxation times of the deuterium nuclei (due to their quadrupole moment) are shorter, the T1 of the neighboring 1H nuclei or of other heteronuclei in the partially deuterated hyperpolarized product molecules are considerably longer, which renders this in situ technique attractive to generate 1H-, 13C-, or 15N-hyperpolarized contrast agents for MRI investigations. The enhancement factor for 1H in the hydrogenation with o-D2 of methyl propiolate using the catalyst [Rh(cod)(dppb)]BF4 is > 100.

3112. Transfer of Parahydrogen-Induced Polarization to 19F:

Joachim Bargon[1], Ute Bommerich[2], Lars T. Kuhn[3], Rahim R. Rizi[4]

[1]University of Bonn, Bonn, Germany; [2]University of Magdeburg, Magdeburg, Germany; [3]Oxford University, Oxford, UK; [4]University of Pennsylvania Medical Center, Philadelphia, Pennsylvania, USA

Parahydrogen-Induced Polarization (PHIP) leads to strong signal enhancement in 1H-NMR if unsaturated substrates are hydrogenated with parahydrogen applying an appropriate catalyst. As has been shown before, this polarization can be transferred to heteronuclei such as 13C. For imaging the lung, a 19F-hyperpolarized contrast agent should be available, if possible for inhalation. Normally, this demands aerosols; however, fluorinated gases may also qualify. We have found that hyperpolarization of 19F characteristically depends on the distribution of the 19F and initially para protons in the hydrogenation product, rendering structural isomers suitable for the purpose to a different degree, due to different molecular shapes and associated dipolar couplings. Nonetheless, our preliminary findings suggest that in principle generating 19F-hyperpolarized contrast agents for inhalation to image the lung using 19F MRI is feasible.

3113. ^{17}O Imaging for the Evaluation of Physiological Function in the Tumor Bearing Mice

Michiko Narazaki[1], Yoko Kanazawa[1], Sachiko Koike[1], Koichi Ando[1], Hiroo Ikehira[1]

[1]National Institute of Radiological Sciences, Chiba, Japan

^{17}O-H_2O MRI has been proposed for the blood flow and oxygen consumption rate measurement. To overcome technical difficulty due to the low sensitivity and short T_2 of ^{17}O, highly sensitive $H_2{}^{17}O$ imaging was investigated in tumor bearing mice at 7T. $H_2{}^{17}O$ distribution in non-enriched mice was successfully visualized in 10 min by FISP. An i.v. injection of 5% ^{17}O saline dramatically improved image quality. Regional ^{17}O image intensity was in good agreement with the ^{17}O NMR intensities of excised organs. FISP is useful for $H_2{}^{17}O$ imaging. This method will be applicable to the oxygen consumption mapping in brain and tumor.

ELECTRONIC POSTERS

White Matter Disease

Room 4A Monday 14:00 - 16:00

14:00 *3114*. **A 30 Minute Imaging Protocol at 1.5T Exploring Higher Spatial and Functional Information Around White Matter Lesion and Brain Morphology in a Large Scale Epidemiological Study of the Aging Brain**
Computer 1

Piotr Wielopolski[1], Meike Vernooij[1], Marion Smits[1], Henri Vrooman[1], Monique Breteler[1], Gabriel Krestin[1], Aad van der Lugt[1]
[1]Erasmus MC, Rotterdam, ZH, Netherlands

We describe the choices made for the MR pulse sequences for the study of the brain in a second stage of the large epidemiological study of the aging brain using the newer MR imaging hardware/software available clinically at 1.5T. The have tailored the acquisition to a 30 minute protocol providing high resolution multi-contrast capabilities and functional information.

14:00 *3115*. **Subacute Changes in T2 Signal Evolution: Time-Series Modeling of Degenerative and Restorative Processes in MS**
Computer 2

Dominik S. Meier[1], Charles R. G. Guttmann[1]
[1]Brigham & Women's Hospital, Harvard Medical School, Boston, Massachusetts, USA

A pathophysiologically motivated two-process model was applied to frequent MRI of new multiple sclerosis (MS) lesions to study the intensity dynamics of new lesion formation in terms of inflammation and degeneration versus resorbtion and repair. Duration measurements were obtained from the model on a per-pixel basis and compared to the duration of contrast-enhancing activity. T2-weighted MRI appears sensitive toward non-inflammatory, subacute lesion evolution in MS.

14:30 *3116*. **Synergies of High-Resolution Multi-Channel Lesion Segmentation in Multiple Sclerosis: MPRAGE, 3D FLAIR, 3D T2WI and 3D DIR**
Computer 2

Yang Duan[1, 2], Nicola Moscufo[1], Petra J.W. Pouwels[3], Jeroen J.G. Geurts[3], Bastiaan Moraal[3], Simon Warfield[4], Dominik S. Meier[1], Frederik Barkhof[3], Charles R.G Guttmann[1]
[1]Center for Neurological Imaging, Brigham & Women's Hospital, Harvard Medical School, Boston, Massachusetts, USA; [2]The Second Clinical College & Affiliated Hospital, China Medical University, Shenyang, Liaoning, People's Republic of China; [3]Image Analysis Centre (IAC), Department of Radiology and Departments of Physics & Medical Technology, Amsterdam,, Netherlands; [4]Center for Neurological Imaging, Brigham & Women's Hospital, Harvard Medical School,, Boston, Massachusetts, USA

A sensitivity analysis of multi-contrast high-resolution MRI for the detection of brain pathology in MS is presented. All combinations of four different channels (MPRAGE, FLAIR, T2W and DIR) were evaluated for accuracy, sensitivity and specificity with regard to white and gray matter lesions in MS. Best sensitivity and specificity was achieved by the combined use of all four contrasts. The DIR sequence is attractive as it enhances WM anomalies relative to normal appearing white matter. In combination with the other high-resolution protocols (particularly FLAIR), a boost in the sensitivity of automated GM lesion detection was observed.

14:30 *3117*. **Establishing a Comprehensive Multiple Sclerosis Imaging Protocol at 7.0T**
Computer 1

Christiane K. Kuhl[1], Jürgen Gieseke[2], Frank Hoogenraad[3], John R. Duraj[4], Carsten Meyer[1], Christoph Manka[1], Frank Traeber[1], Michael Thompson[4], Peter Meier[1], Inge Franke[1], Lukas Scheef[1], Hans H. Schild[1]
[1]University of Bonn, Bonn, Germany, Germany; [2]University of Bonn, Bonn, Germanz, Germany; [3]Philips Medical Systems, Best, Netherlands, Netherlands; [4]Philips Medical Systems, Cleveland, Ohio, USA

There is evidence that MR imaging at higher magnetic fields (3.0T) does allow a more sensitive detection of demyelinating plaques in patients with multiple sclerosis. Aim of this pilot ("proof of principle") study was to establish a pulse sequence protocol for MS patients at even higher magnetic fields (7T). A small cohort of 6 volunteers underwent MR imaging at 7.0T in order to establish a 7.0T MRI protocol that is in accordance with NMSS guidelines, and that consists of T2-w TSE images, FLAIR, and T1-w images before and after contrast. Then, so far 2 patients with multiple sclerosis underwent (contrast enhanced) MR imaging at 7.0T with the protocol; results were compared with the respective patients' findings at 3.0T and 1.5T.

15:00 ***3118***. **Multi-Parametric MR Assessment of T1 Black Holes in Multiple Sclerosis: Evidence That Extracellular Water is Increased But Myelin Loss is Not Greater**
Computer 1
Irene Margaret Vavasour[1], David KB Li[1], Cornelia Laule[1], Anthony L. Traboulsee[1], Alex L. MacKay[1]
[1]University of British Columbia, Vancouver, British Columbia, Canada

The purpose of this study was to compare the total water content (WC), myelin water content (MWC), magnetization transfer ratio (MTR), T_1 relaxation time (T_1) and T_2 relaxation time (T_2) between MS lesions that are hypointense and those that are isointense on T_1-weighted images. Increases in water were evident from increased WC, T_1 and T_2 in both isointense and hypointense T_1 lesions, but the MWC was the same for both lesion types. One possible explanation is that demyelination occurs in both the isointense and hypointense lesions but the hypointense lesions are distinguished by greater axonal loss and increased extracellular water.

15:00 ***3119***. **Myelin Water is an Independent Measure of Pathology in Multiple Sclerosis**
Computer 2
Irene Margaret Vavasour[1], David KB Li[1], Cornelia Laule[1], Anthony L. Traboulsee[1], Alex L. MacKay[1]
[1]University of British Columbia, Vancouver, British Columbia, Canada

The goal of this study was to determine correlations between water content (WC), myelin water content (MWC), T_1 relaxation time (T_1), T_2 relaxation time (T_2) and magnetization transfer ratio (MTR) to determine to what extent these MR measurements are independent measures of brain pathology in MS. MTR was found to be highly correlated with T_1 and WC indicating that edema, inflammation and changes in extracellular water can play a strong role in determining lesion MTR. MWC was not strongly correlated with any other MR measurement and therefore is an independent measure of pathology.

15:30 ***3120***. **A Whole-Brain Voxel-Based Morphometric Study of Early-Blind Chinese Adults**
Computer 2
Wenju Pan[1], Chunlan Yang[2], Guangyao Wu[1, 3], Tianzi Jiang[2], Junmo Sun[3], Hao Lei[1]
[1]Wuhan Institute of Physics & Mathematics, Chinese Academic of Science, Wuhan, People's Republic of China; [2]Institute of Automation, Chinese Academy of Sciences, Beijing, People's Republic of China; [3]Wuhan University, Wuhan, People's Republic of China

Previous studies have demonstrated that the cortices of congenital and early blind (EB) show striking functional plasticity. In this study, voxel-based morphometry (VBM) analysis was performed in 8 Chinese EB subjects and 11 controls to investigate the anatomical changes, if any, in the brain of the EB subjects, presumably resulted from development-related and learning-induced plasticity after early sensory deprivation and long-term living in an environment with no visual input. The results show that, relative to the controls, the EB subjects showed decreased white matter volumes in bilateral optic radiation and reduced gray matter volumes in bilateral primary sensorimoter areas.

15:30 ***3121***. **Imaging Myelin *In Vivo*; Comparison of the T_2 Distribution at 1.5T and 3.0T**
Computer 1
Shannon Heather Kolind[1], Burkhard Maedler[2], David K. Li[1], Alex L. MacKay[1]
[1]University of British Columbia, Vancouver, British Columbia, Canada; [2]Philips Medical Systems, Vancouver, British Columbia, Canada

We investigated the effects of magnetic field strength on *in vivo* T_2-measurements obtained using a multi-echo imaging sequence. Myelin water fraction (MWF) maps agreed well at 1.5T and 3.0T. MWFs were strongly correlated between 1.5T and 3.0T but were higher in gray matter (GM) at 3.0T than at 1.5T. At 3.0T, the signal-to-noise ratio increased significantly, but the fit-to-noise ratio decreased, possibly due to B_1 inhomogeneities. On average at 3.0T, the geometric-mean-T_2 of the intra/extracellular peak decreased by 33% in white matter (WM) and 37% in GM, and the intra/extracellular peak widened by 61% in WM and 165% in GM.

Gray Matter Segmentation

Room 4A Monday 14:00 - 16:00

14:00 ***3122***. **Thalamic Gray Matter Volume Reduction in Mild Traumatic Brain Injury**
Computer 4
Vagish Hemmige[1], Yulin Ge[1], Robert Grossman[1], Henry Rusinek[1]
[1]New York University School of Medicine, New York, USA

Recent reports using animal models suggest that TBI is associated with subtle thalamic gray matter (TG) reduction. In 29 patients and 18 age- and gender-matched controls we measured TG using T1-weighted images and a technique that corrects for partial volume effects. In patients TG was significantly lower than in controls, with a trend for TG to be lower in patients who were examined 3.7±4.3 years after injury as compared with measures done 6.2±10.6 days after injury. Reduced volume of thalamic gray matter could become a radiological marker of thalamic involvement and may correlate with the post-concussion syndrome.

14:00 ***3123***. **Voxel Based Morphometry and Manual Volumetric Analysis of the Cingulate Gyrus in Patients with Juvenile Myoclonic Epilepsy and Frontal Lobe Epilepsy Compared to Normal Controls**
Computer 3

Long Vu[1], Barbara Swartz[2], Kevin Head[1], Mark Mandelkern[1], Orhan Nalcioglu[1], Min-Ying Su[1]
[1]University of California, Irvine, Irvine, California, USA; [2]Epilepsy Center, Hoag Hospital, Newport Beach, California, USA

Voxel Based Morphometry (VBM) and Manual Volumetric Analysis (MVA) were performed to analyze the difference in brain morphology between 19 patients with epilepsy (10 JME, 9 FLE), and 9 controls. VBM analysis reveals that FLE subjects had less cingulate volume than the controls and the JME, confirmed by the results obtained by MVA. Both FLE and JME had atrophy in middle temporal gyrus, insula and parahippocampal gyrus. Atrophy in parahippocampal gyrus may be related to memory deficit in epilepsy patients. The results also suggest that it may be possible to differentiate FLE and JME based on the cingulate atrophy.

14:30 ***3124***. **Abnormal Inter-Hemispheric Brain Asymmetry in Adolescents with Disruptive Behavioral Disorder**
Computer 3

James D. Christensen[1, 2], Yang Wang[1], Kristine M. Mosier[1], Andrew J. Kalnin[1], William G. Kronenberger[1], David W. Dunn[1], Vincent P. Mathews[1]
[1]Indiana University School of Medicine, Indianapolis, Indiana, USA; [2]Regenstrief Institute, Indianapolis, Indiana, USA

A new method of brain asymmetry mapping was used to detect regions of brain structural abnormality in the adolescents with disruptive behavioral disorder. Two regions in the inferior temporal lobe and the occipital/parietal region were found to have decreased asymmetry compared to normal control subjects. These regions are located along the pathway of the ventral stream of visual processing, which is involved in object recognition and visual attention. Abnormal neurodevelopmental of this neural circuitry might contribute to the cognitive dysfunction underlying disruptive behavioral.

14:30 ***3125***. **Midbrain Imaging at 1.5 and 4T Using Susceptibility Weighted Imaging: Optimizing the Imaging Parameters**
Computer 4

Ewart Mark Haacke, Ph.D. [1], Elena Svilenova Manova[1], Muhammed Ayaz[2]
[1]Wayne State University, Detroit, Michigan, USA; [2]The MRI Institute for Biomedical Research, Detroit, Michigan, USA

The midbrain area in particular is an important area to examine when investigating neurodegenerative disorders like Alzheimer's diseases. This region is known to have changes in iron content and recently it has been shown that paramagnetic iron resides in the neuropil and is associated with vessels and vessel wall. Imaging this region with a method sensitive to those iron granules would provide not only valuable anatomical information but also give a clue about the way such neurodegenerative disorders are manifested. The goal of this work is to find the best MR sequences at 1.5 and 4T to image the midbrain.

15:00 ***3126***. **Environmental Lead Exposure Alters Brain Volume: Results of a VBM Analysis**
Computer 4

Kim M. Cecil[1], Caleb Adler[2], Kelly Jarvis[2], Ilayaraja Elangovan[1], Kim Dietrich[3], Bruce Lanphear[1]
[1]Cincinnati Children's Hospital Medical Center, Cincinnati, Ohio, USA; [2]University of Cincinnati College of Medicine, Cincinnati, Ohio, USA; [3]University of Cincinnati, Cincinnati, Ohio, USA

VBM analyses of high-resolution MR images offers novel information about the regions altered by childhood lead exposure. Subjects (N=159) exposed to significant levels of lead during childhood demonstrate reductions in total brain volume with regional gray and white matter deficits that correlate with mean childhood blood lead levels. In particular, frontal lobe gray and white matter reductions may explain deficits in cognitive and behavioral outcomes clinically observed in populations with significant lead exposure.

3127. WITHDRAWN

15:30 ***3128***. **Effects of Aging on Hippocampal Subfields and Whole Brain Gray and White Matter Volumes Measured at 4 Tesla**
Computer 3

Susanne G. Mueller[1], Lara Stables[2], Antao Du[1], Diana Truran[1], Nathan Cashdollar[1], Norbert Schuff[1], Michael W. Weiner[1]
[1]VAMC San Francisco, San Francisco, California, USA; [2]VAMC, San Francisco, California, USA

Aging can be associated with memory changes. However, the results of volumetric studies regarding an age-related loss of hippocampal volume are controversial. We measured hippocampal subfields in 53 healthy and cognitively normal controls (age range 18-85 years) on a high resolution T2 weighted sequence acquired on a 4T magnet. CA1 and entorhinal cortex (ERC) volumes but not other subfields were negatively correlated to aging. The volume loss in CA1 and ERC seemed to accelerate after the fifth decade of life. This was in contrast to volume loss in GM, which seemed to start early in life and progressed continuously.

15:30 ***3129***. **Cerebral Atrophy in End-Stage Renal Disease**
Computer 4

Isak Prohovnik[1, 2], Hedok Lee[1], James Post[1, 2], Oana Sandu[1], Mary Sano[1, 2], Erik Langhoff, [1,2]
[1]Mount Sinai School of Medicine, New York, New York, USA; [2]Bronx VAMC, Bronx, New York, USA

Generalized cerebral atrophy has been found in patients with End-Stage Renal Disease by visual examination, but it has never been quantified or rigorously localized. We studied 10 patients and six controls, using the MMS and MPRAGE MRI scans analyzed by SPM99. We confirmed previous reports of sulcal dilatation and ventricular enlargement, found novel sites of focal atrophy in brain stem and caudate nucleus, and report quantitative relations of atrophy with age and cognitive deficits.

Spinal Cord MRI/MRS

Room 4A Monday 14:00 - 16:00

14:00 *3130*. **The Effects of Pro- And Anti-Angiogenic Factors on Spinal Cord Injury**
Computer 5
Laura M. Sundberg[1], Pallavi Ahobila-Vajjula[1], Ponnada A. Narayana[1]
[1]The University of Texas Health Science Center at Houston, Houston, Texas, USA

In vivo, longitudinal MR studies were performed on a cohort of rats receiving treatments to modulate angiogenesis following spinal cord injury (SCI). Assessment of open-field locomotion and MRI scans were performed on days 7, 14, 28, 42, and 56 post-injury. T2-weighted images were evaluated for lesions; regions of interest, which included areas of hypo- and hyperintense contrast, were manually selected and lesion volumes were quantified. Comparison between treatments suggests that administration of VEGF in the early stages of injury reduces necrosis 56 days after SCI, while treatment with á-VEGF is detrimental.

14:00 *3131*. **Advanced Dynamic MR Imaging of the Cervical Spine Using the New NeuroSwing® Positioning System in Healthy Volunteers and Patients**
Computer 6
Katja Pinker Pinker[1], Josef Liebisch[2], Rolf Schindler[3], Erich Salomonowitz[4], Knut Eberhardt[2]
[1]MR Centre of Excellence, Vienna, Austria; [2]Institute of innovative Diagnostics, Bad Kissingen, Germany; [3]Inside Funktionelle Diagnosetechnik GmbH, Schweinfurt, Germany; [4]Department of Radiology, St.Poelten, Austria

The aim of this study was the functional MRI of the cervical spine in volunteers and patients using NeuroSwing®-positioning-system as an integrated concept with a newly developed external energy-operated device and an optimized software. 40 healthy volunteers and 20 patients were enrolled in this study. Dynamic MRI of the cervical spine was performed (1.5T, 3D-HASTE, True FISP, T1/T2w-TSE). Functional range of movement was comparable with physiological measurements. MRI of the cervical spine with NeuroSwing®?-positioning-system allowed reproducible investigations in arbitrary functional positions. Cryptic lesions were detected in volunteers and patients and allowed improved visualization of nerve roots, ligaments and vertebral joints.

14:00 *3132*. **Axial Single-Shot EPI Diffusion Tensor Imaging of the Human Spinal Cord**
Computer 7
Cristina Rossi[1], [2], Andreas Boss[1], Günter Steidle[1], Petros Martirosian[1], Claus D. Claussen[1], Fritz Schick[1]
[1]University of Tübingen, Tübingen, Germany; [2]La Sapienza University, Rome, Italy

An optimized DTI protocol with single-shot EPI readout for the acquisition of axial slices of the human spinal cord is proposed. The quality of the acquired images and the parametrical maps was improved by systematically acting on the imaging parameters in order to join a higher spatial resolution with a good signal-to-noise ratio. The fractional anisotropy (FA) maps show the characteristic butterfly shape of the gray matter with an in plane resolution of 0.9x0.9 mm2. FA of (0.784±0.040) and (0.532±0.031) were found for white matter and gray matter, respectively.

14:30 *3133*. **Cervical Spinal Cord Evaluation with ECG-Gated Line-Scan Diffusion Tensor Imaging and 3D Tractography: Feasibility**
Computer 7
Masaaki Hori[1], Keiichi Ishigame[1], Shigeki Aoki[2], Tustomu Araki[1], Hiroshi Kumagai[1], Satoshi Ikenaga[1], Toru Horikoshi[1], Hiroyuki Kinouchi[1]
[1]Univ. of Yamanashi, Nakakoma, Yamanashi, Japan; [2]Univ. of Tokyo, Bunkyo-ku, Tokyo, Japan

The purpose of this study was to compare line scan diffusion tensor imaging (LSDTI) with and without ECG-gating and to estimate clinical usefulness of LSDTI with ECG-gating in evaluation of cervical spinal cord pathology *in vivo*. Images with ECG-gated technique were all superior to those without ECG – gated with permissible extent of imaging time, approximately two minutes. Measurements of ADC and FA and visualization of 3D tractography of white matter demonstrated pathological abnormalities. Quantitative tensor measurements and 3D white matter fiber tracking of ECG-gated LSDTI were useful to estimate cervical spinal cord pathology *in vivo*.

14:30 *3134*. **Comparative Study of Syringomyelia and Myelomalacia of the Cervical Spinal Cord by Using MR Diffusion Tensor Imaging**
Computer 6
Lin Ma[1], Kuihong Zheng[2], Wei Sun[3], Hong Lu[1], Yan Wang[1]
[1]PLA General Hospital, Beijing, People's Republic of China; [2]Navy General Hospital of PLA, Beijing, People's Republic of China; [3]GE Healthcare China, Beijing, People's Republic of China

DTI was used in the comparative study of syringomyelia and myelomalacia of the cervical spinal cord. ADC value, FA value, and eigenvalues were quantitatively assessed and differences between the two disease entities were found. ADC in syringomyelia was higher than that in myelomalacia, and FA in syringomyelia was lower than that in myelomalacia. No statistical differences were found among ¦Ë1, ¦Ë2, and ¦Ë3 in syringomyelia, but ¦Ë1 was significantly higher than ¦Ë2 and ¦Ë3 in myelomalacia. The different pathological mechanisms of the two diseases can be assessed by using DTI technique.

14:30 ***3135***. **Diffusion Anisotropy Reflects Progression of Spinal Cord Contusion Injury in Mice**
Computer 5
Joong H. Kim[1], Sheng-Kwei Song[1]
[1]Washington University, St. Louis, Missouri, USA

Relative anisotropy (RA) was examined using both *in vivo* and *ex vivo* DTI on normal and contusion injured mouse spinal cords. Ex vivo RA of ventrolateral white matter from normal mice is not statistically different over a SNR range from 40 – 130. At SNR of 50, *in vivo* and *ex vivo* RA measurements were not statistically different. Both *in vivo* and *ex vivo* measured RA reflects the temporal and spatial progression of white matter damage after contusion injury in mice.

15:00 ***3136***. **Mouse Spinal Cord Ventrolateral White Matter Diffusion Anisotropy Indices Do Not Change In Situ Up to 10 Hours Postmortem**
Computer 5
Joong H. Kim[1], Sheng-Kwei Song[1]
[1]Washington University, St. Louis, Missouri, USA

The DTI derived anisotropy indices of ventrolateral white matter from normal mouse spinal cord *in vivo*, in situ at various times postmortem, and postmortem after immersion fixation were determined. The relative anisotropy (RA), and trace normalized axial (D||) and radial (D*f*Î) diffusivities remained unchanged comparing *in vivo*, in situ postmortem, and postmortem formalin fixed states. This finding supports the application of postmortem DTI measurements with immersion fixed autopsy specimens.

15:00 ***3137***. **Diffusion Tensor Imaging of the Human Spinal Cord: Determination of Normal Regional Metrics**
Computer 6
Stephen M. Hesseltine[1], Meng Law[1], Scott Lopez[1], James Babb[1], Glyn Johnson[1]
[1]New York University, New York, New York, USA

Diffusion tensor imaging (DTI) shows promise in the evaluation of white matter integrity, and may be useful in the evaluation of spinal cord function. The purpose of thise study is to determine normal values of fractional anisotropy, mean diffusivity and the three principle eigenvectors in various spinal cord regions, in a population of normal patients. The data obtained in normal patients may prove useful for comparison with pathologic states.

15:00 ***3138***. ***In Vivo* MR Spectroscopy in the Human Cervical Spinal Cord at 1.5 and 3 Tesla**
Computer 7
Otto Rapalino[1], Meng Law[1], Nouha Salibi[2], James S. Babb[1], Stephen M. Hesseltine[1], Oded Gonen[1]
[1]New York University Medical Center, New York, New York, USA; [2]Siemens Medical Solutions USA Inc, Malvern, Pennsylvania, USA

Obtaining spectra from the spinal cord at 3 T is challenging because of cord pulsation, field inhomogeneity and small structure of the cord. We compare metabolite ratios from the cervical spinal cord at 1.5 and 3 Tesla in 20 normal volunteers. Our 1H SVS protocol uses a modified PRESS sequence with small voxel sizes and optional pulse/ECG triggering. Using this modified pulse triggered PRESS sequence, relative metabolite ratios from MRS of the human cervical spinal cord are comparable and reproducible at 1.5T and 3T.

15:30 ***3139***. **Metabolite Changes from MR Spectroscopy in the Cervical Spinal Cord in Patients with Cervical Spondylosis**
Computer 7
Otto Rapalino[1], Meng Law[1], Nouha Salibi[2], James S. Babb[1], Stephen M. Hesseltine[1], Oded Gonen[1]
[1]New York University Medical Center, New York, New York, USA; [2]Siemens Medical Solutions USA Inc, Malvern, Pennsylvania, USA

Neurosurgical triage of patients with cervical spondylosis is highly dependent on demonstrating abnormal cord signal at conventional MR imaging; however, changes in spinal cord function and symptomatology precede findings of abnormal cord signal. We obtained single voxel spectra at 1.5T from 6 normal volunteers and 8 patients with cervical spondylosis, using a modified PRESS sequence. There was a statistically significant decrease in NAA/Cr ratio and elevation in Cho/NAA in symptomatic patients with spondylosis. The study suggests that changes in metabolite ratios can be detected in patients with cervical spondylosis before the typical signal cord changes are seen on T2-weighted images.

15:30 ***3140***. **Motion Robust T2-Weighted Imaging of C-Spine with Propeller with Fast Recovery Modification**
Computer 6
Ajeetkumar Gaddipati[1], Anand Kumar[1], Rob Peters[1], Roshy Francis[1], Emanuel Kanal[2]
[1]GE Healthcare, Waukesha, Wisconsin, USA; [2]University of Pittsburgh, Pittsburgh, Pennsylvania, USA

T2 weighted C-spine imaging is currently performed with Fast Recovery (FR)-FSE to achieve better contrast than FSE in shorter scan time. However this technique is susceptible to patient motion, (swallowing, coughing) leading to rescanning of patients. Propeller pulse sequence proposed by Jim Pipe gives motion robustness, but falls short in terms of contrast between CSF and spine. Our approach of combining Fast recovery technique with Propeller provides both the contrast of FR-FSE and motion robustness of Propeller

15:30 *3141*. **Dynamic Evolution of Diffusion Abnormalities of Experimental Spinal Cord Infarction**
Computer 5
Jin Song Zhang[1], *Yi Huan*[1], *Li Jun Sun*[1]
[1]MRI Room, Xi'an, Shannxi, People's Republic of China

To establish a novel canine spinal cord infarction models by interventional method and study dynamic evolution of diffusion abnormalities of experimental spinal cord infarction, especially in the hyperacute, acute, and sub-acute phases of experimental spinal cord infarction at post-embolization 1h, 2h, 6h, 24h, 80h and 168h mainly from sagital images. The signal changes were estimated from a decision mechanism based on statistical detection theory and confirmed by histopathologic examination.

Human Proton MRS

Room 4A Monday 14:00 - 16:00

14:00 *3142*. **Water Loading: A Perturbation Model of Metabolic Activity in ^{1}H-MRS**
Computer 8

Jack Knight-Scott[1]
[1]University of Virginia, Charlottesville, Virginia, USA

In this study, we examine the utility of water loading as a metabolic perturbation model for comparing the detection sensitivity of three internal referencing techniques: creatine (ratio), water peak (total water), and absolute quantitation (tissue water).

14:00 *3143*. **1H MR Spectroscopic Imaging in Patients with MRI-Negative Extratemporal Focal Epilepsy**
Computer 9
Monika Dezortova[1], *Milan Hajek*[1], *Pavel Krsek*[2], *Filip Jiru*[1], *Antonin Skoch*[1], *Josef Zamecnik*[2], *Petr Marusic*[2], *Martin Kyncl*[2], *Michal Tichy*[2], *Vladimir Komarek*[2]
[1]Institute for Clinical and Experimental Medicine, Prague, Czech Republic; [2]Faculty Hospital Motol, Prague, Czech Republic

The study deals with the hypothesis if 1H MRS (1.5T) could help in localizing the epileptic focus in seven patients with extratemporal focal epilepsy and normal MRI findings. 2D CSI sequence was directed towards the suspected epileptogenic zone localized by seizure semiology, EEG, SPECT and PET. 1H MR spectra were evaluated using the program CULICH.All patients had a lateralized 1H MRS abnormality, 5 of them had a clearly localized pathology. We found a good correlation between the localization of the 1H MRS abnormality and SPECT as well as EEG. In all cases, histopathological analysis revealed an MRI-undetected cortical dysplasia.

14:00 *3144*. **Proton Spectroscopy of the Corpus Callosum in Healthy Controls: Detecting Microstructural Differences Along the Mid-Sagittal Length**
Computer 10
Emma Wignall[1], *Paul D. Griffiths*[1], *Pamela Greenwood*[1], *Iain D. Wilkinson*[1]
[1]University of Sheffield, Sheffield, South Yorkshire, UK

It is known from histological studies that both axonal density and type vary within the corpus collosum. This work sought to determine whether there are differences on localised proton spectroscopy between the anterior and posterior aspects of the normal corpus collosum. A long echo time (135ms) single-voxel PRESS technique acquired spectra from 10 healthy males. Significant differences in NAA/Cho and NAA/Cr were found between the 2 anatomical locations. Proton spectroscopy shows biochemical differences along the body of the corpus collosum.

14:30 *3145*. **Evidence for Detection of Ascorbic Acid in the Human Brain at 3T**
Computer 10
Dominik v. Elverfeldt[1], *Martin Buechert*[1], *Robert Kaufmann*[1], *Michael Huell*[1], *Jürgen Hennig*[1]
[1]University Hospital Freiburg, Freiburg, Germany

Quantification of vitaminC (Asc) is not trivial due to strong overlap with the spectra of other metabolites. This study aims to evaluate the potential detection with standard MRS in the human brain at 3T. Spectra of 37 healthy volunteers and the time dependency after an inter venous application were examined. LCModel was able to detect Asc and revealed a strong correlation to other metabolite concentrations. Furthermore a significant rise in Asc was observed in the time dependent data. Therefore this data provide strong evidence that ascorbic acid can be detected in the human brain at 3T via LCModel.

14:30 *3146*. **3T MRS Observations of Acetone and Beta-Hydroxybutyrate in an Epileptic Patient Under Ketogenic Diet**
Computer 9
Dah-Jyuu Wang[1], *Robert A. Zimmerman*[1]
[1]Children's Hospital of Philadelphia, Philadelphia, Pennsylvania, USA

Proton MRS at 3T enables direct detections of acetone and beta-hydroxybutyrate in an epileptic child under ketogenic diet. Improvements in sensitivity and spectral resolution at higher field make MRS an ideal tool for monitoring cerebral ketone bodies in patients under ketogenic diet treatment.

14:30 ***3147***. **Interleaved Multi-Voxel In-Vivo Spectroscopy on the Human Brain Using Dynamic Shim Updating**
Computer 8
Kevin Matthew Koch[1], Scott McIntyre[1], Terry W. Nixon[1], Douglas L. Rothman[1], Robin A. de Graaf[1]
[1]Yale University, New Haven, Connecticut, USA

Under a static shim setting, multi-voxel *in vivo* spectroscopy requires that voxels be in close vicinity of one another such that a single static shim setting is sufficient for all voxels. Without sufficient homogeneity in all voxels, spectral resolution quickly degrades and water suppression deteriorates. Utilizing a custom-built pre-emphasized dynamic shim updating (DSU) system, we have performed rapid interleaved multi-voxel spectroscopy for voxels in widely different regions of the human brain.

15:00 ***3148***. **Reproducibility of Short TE MRS at 3 Tesla: Comparison of Hippocampal with Cingulate Spectra**
Computer 8
Aristides Andres Capizzano[1], Ricardo Jorge[1], Laura Acion[1], Vincent Magnotta[1]
[1]University of Iowa Hospitals and Clinics, Iowa City, Iowa, USA

We examined inter and intra-subject variability of single voxel 1H-MRS of the hippocampus and cingulate at 3Tesla. Coefficients of variation were similar to those reported at 1.5T for NAA and creatine (6-13%) with improvements for choline and myo-inositol, which might be relevant to mood disorder studies.

15:00 ***3149***. **Interictal Epileptic Activity Correlates with Metabolic Alterations in 1H-MRS**
Computer 9
Thilo Hammen[1], Michael Schwarz[1], Marc Doelken[1], Frank Kerling[2], Tobias Engelhorn[1], Andreas Stadlbauer[3], Christopher Nimsky[1], Oliver Ganslandt[1], Michael Buchfelder[1], Arnd Doerfler[1], Herman Stefan[1]
[1]University of Erlangen, Erlangen, Bavaria, Germany; [2]Epilpesy Centre Erlangen, Erlangen, Bavaria, Germany; [3]Landesklinik St.Pölten, St.Pölten, Lower Austria, Austria

In this study hippocampal metabolite alterations in 1H-MR Spectroscopy (1H-MRS) were correlated to findings of intensive video-EEG monitoring and duration of clinical features in TLE-patients. Seizures were analysed by frequency of interictal epileptiform discharges (IEDs), ictal activity and duration of clinical symptoms. Significant negative correlation was found between tNAA and degree of IEDs. Duration of clinical symptoms and tNAA/Cr ratio were significant inversely rated. Our study supports that 1H-MRS is able to refer severity of TLE in which tNAA reduction correlates with degree of interictal spiking. Duration of clinical symptoms correlated with increased Cr signal probably reflecting increased energy metabolism.

15:00 ***3150***. **Oral Creatine Supplementation Depresses ATP in Healthy Human Brain**
Computer 10
Jullie W. Pan[1], Kan Takahashi[1]
[1]Albert Einstein College of Medicine, Bronx, New York, USA

Oral creatine supplementation is frequently used to improve muscle function and has been increasingly used to improve neurological function. We used high resolution 31P spectroscopic imaging in healthy control volunteers (n=7) to assess the changes in energetics with 7 days of creatine supplementation at 20g/day. Image guided single voxel reconstruction was used to position the selected regions for optimum consistency. PCr/ATP ratios increased significantly in the thalamus and hippocampus while it was not significantly different in neortical regions. Quantification of the data showed that the ratio increase is primarily due to a decline in ATP.

15:30 ***3151***. **Proton MRS at 3 Tesla in Brain of Schizophrenic Patients: Elevated Glutamate and Reduced NAA in Hippocampus**
Computer 10
Florian Schubert[1], Frank Seifert[1], Karolina Leopold[2], Michael Krebs[2], Martin Schaefer[2], Jürgen Gallinat[2]
[1]Physikalisch-Technische Bundesanstalt, Berlin, Germany; [2]Charite Universitaetsmedizin, Berlin, Germany

Continuing interest in the role of glutamate in schizophrenia prompted us to perform proton MRS in the brain of schizophrenic patients (n=18) and controls (n=30), focusing on quantitation of glutamate and NAA. Press spectra were acquired from the left hippocampus (HC), anterior cingulate and posterior cingulate. Only in the HC glutamate concentration was significantly higher and NAA concentration significantly lower in patients than in controls. The results confirm a recently reported glutamate increase in hippocampus which, parallelled by reduced NAA suggests dysfunctional glutamatergic neurotransmission with concomitant disturbed neuronal integrity in a key region for the pathophysiology of schizophrenia.

15:30 ***3152***. **Serial Concentration of N-Acetlyaspartate in Young Healthy Adults**
Computer 9
Daniel Rigotti[1], Matilde Inglese[1], Beatrice Benedetti[2], James Babb[1], Marco Rovaris[2], Robert Grossman[1], Massimo Filippi[2], Oded Gonen[1]
[1]NYU School of Medicine, New York, New York, USA; [2]San Raffaele Hospital, Milan, Italy

Our aim is to quantify the normal temporal variations over typical clinical-trial periods of the global concentration of the neuronal marker N-acetylaspartate (WBNAA) in healthy young adults. WBNAA was obtained in a group of 14 healthy subjects (5M 9F, 29.6±8.6 years old). Temporal variations were determined with a second and third WBNAA measurement 20±6 and 41±3 months after the first, respectively. The distribution of WBNAA levels at all time points were not different with respect to the mean 12.8±1.3mM ($p>0.5$) or between-subject variance ($p>0.3$). Within subject variance was not significantly different either within 28 months or seperated by at least 33 months ($p>0.7$). The WBNAA in this cohort was statistically stable over the time period of most clinical trials, this rendering the metric a good surrogate marker for neurodegeneration.

15:30 ***3153***. **Local Modulation of GABA Concentration in Human Sensorimotor Cortex During Motor Learning**
Computer 8
Marzena Wylezinska[1], Tamas Zsigmond Kincses[1], Peter Jezzard[1], Christopher John Evans[1], Paul M. Matthews[1]
[1]University of Oxford, Oxford, UK

Cortical representation of movement can be altered by motor learning. Changes in GABA concentration may contribute to this plasticity. GABA levels were measured in humans during motor learning within two brain regions: primary sensorimotor cortex contralateral and ipsilateral to the hand used for the learning task. We reproduced the observation that thirty minutes of motor learning reduced GABA within an 8ml VOI contralateral to the hand used for the learning task. We observed no significant changes in the ipsilateral cortex. These results suggest that GABA is one of the elements that contributes to local cortical changes during fast motor learning.

Brain Tumors: fMRI and DTI

Room 4A Monday 14:00 - 16:00

14:00 ***3154***. **Combined Magnetic Resonance Tractography and Functional Magnetic Resonance Imaging in Neurosurgical Planning**
Computer 11
An Weimin[1, 2], Cai Youquan[1], Meng Xianghui[1], Ma Lin[1], Sun Wei[3]
[1]301 Hospital, Beijing, People's Republic of China; [2]The Navy General Hospital, Beijing, People's Republic of China; [3]GE Medical Health China, Beijing, People's Republic of China

Combined magnetic resonance tractography and fMRI in neurosurgical planning was very useful to reduce function deficit, and maybe can forecase the function recovery.

14:00 ***3155***. **Using Quantitative MR Diffusion Tensor Imaging to Predict Post-Surgical Outcome of Brain Tumors: A Feasibility Study**
Computer 12
Fang-Ying Chiu[1], Wan-Yuo Guo[2], Kun-Hsien Chou[3], Ming-Teh Chen[2], Yi-Ping Chao[4], Hsiu-Mei Wu[2], Shih-Ya Lo[5], Donald Ming-Tak Ho[2], Ching-Po Lin[1]
[1]Institute of Neuroscience, National Yang Ming University, Taipei, Taiwan; [2]Taipei Veterans General Hospital, Taipei, Taiwan; [3]Institute of Biomedical Engineering, National Yang Ming University, Taipei, Taiwan; [4]Institute of Electrical-Engineering, National Taiwan University,Taipei, Taiwan, Taipei, Taiwan; [5]Institute of Radiological Science,National Yang-Ming University, Taipei, Taiwan

Peri-lesional signal abnormality (PSA) of different brain tumors presents different diffusivity. Tissue integrity and water content play a role to the difference. Quantitative analysis of the diffusivity may serve as a prognostic indicator of therapeutic outcome.

14:00 ***3156***. **A Novel DCE-MRI Protocol for the Study of Brain Tumours at 3T**
Computer 13
Sha Zhao[1], Geoff J. M. Parker[1], Caleb Roberts[1], Barry Whitnall[1], Alan Jackson[1], David L. Buckley[1], Lloyd J. Gregory[1]
[1]University of Manchester, Manchester, UK

We present an optimised method for high temporal resolution quantitative dynamic contrast-enhanced (DCE)-MRI of the brain at 3 T. We demonstrate accurate T1 measurement and dynamic contrast enhancement in a glioma patient. We also demonstrate that the method is equally applicable at 1.5 T, allowing the possibility of quantitative cross-platform studies.

14:30 ***3157***. **Comparison of Arterial Spin Labeling and Dynamic Susceptibility Contrast Imaging in Glioma**
Computer 13
Barbara Appignani[1], Eric T. Wong[1], David B. Hackney[1], David Charles Alsop[1]
[1]Beth Israel Deaconess Medical Center, Boston, Massachusetts, USA

T2* cerebral blood volume (CBV) and arterial spin labeling (ASL) blood flow MRI were performed in 20 studies of 18 patients with biopsy confirmed glioma. ASL and CBV relative to contralateral gray matter were significantly correlated ($p<0.02$). However, ASL more clearly demonstrated abnormal hemodynamics in the tumors because of greater signal to gray matter ratio and reduced large vessel and susceptibility artifacts.

14:30 ***3158***. **Region-Of-Interest Analysis vs. Non-Region-Of-Interest Histogram Analysis in the Evaluation of Cerebral Gliomas**
Computer 12
Robert J. Young[1], Erica Pollack[1], Hanzhang Lu[1], James Babb[1], Glyn Johnson[1], Meng Law[1]
[1]NYU Medical Center, New York, New York, USA

Dynamic susceptibility contrast perfusion magnetic resonance imaging (DSC MRI) of gliomas is most commonly analyzed using region-of-interest (ROI) measurements. We compare the routine ROI method with ROI and non-ROI histogram methods in the grading of glial neoplasms. Our results show that our routine analysis using rCBVmax was the most useful technique ($r=0.734$, $p<0.0001$), followed by rCBV peritumoral, tumoral and total tumoral histogram analysis. Further refinement of the total tumoral histogram method may allow for automated, non-ROI based analysis of DSC MRI, potentially improving intra-observer, inter-observer and inter-institutional reproducibility.

14:30 ***3159***. **The Characteristics of BOLD Hemodynamic Response Function of the Primary Motor Cortex in Patients with High Grade Brain Tumors**
Computer 11
Kyung Peck[1], Bob Hou[1], Nicole Petrovich[1], Philip Gutin[1], Andrei Holodny[1]
[1]Memorial Sloan-Kettering Cancer Center, New York, USA

Patients with a high grade glioma may develop compensatory changes in local cerebral vasculature with a resultant loss of vascular reactivity. As the result, different patterns of BOLD hemodynamic properties compared to the controls may be expected from the areas in/around malignant tumors. Time-resolved BOLD fMRI to investigate time dependent HDR within primary motor cortex (PMC) in the presence of an adjacent brain tumor, relative to control subjects was applied. We measured the percent signal change, time to peak (TTP), and full width at half maximum (FWHM) of the BOLD hemodynamic response within the bi-hemispheric PMC of both groups.

15:00 ***3160***. **Diffusion Tensor Tractography to Depict the Course of Facial Nerve Displaced by Large Vestibular Schwannomas**
Computer 11
Toshiaki Taoka[1], Masahiko Sakamoto[1], Hiroyuki Nakagawa[1], Hidehiro Hirabayashi[1], Satoru Iwasaki[2], Akio Fukusumi[1], Shinji Hirohashi[1], Toshisuke Sakaki[1], Kimihiko Kichikawa[1]
[1]Nara Medical University, Kashihara, Nara, Japan; [2]Higashiosaka City General Hospital, Higashiosaka, Osaka, Japan

In this study, using diffusion tensor tractography, we could extract the course of facial nerve displaced by large vestibular schwannoma, and the course agreed with surgical findings in most of the cases. On a surgery of vestibular schwannoma, identification of the facial nerve displaced by the tumor is very importanct to avoid facial nerve injury. However, it is difficult to depict the course of the facial nerve using conventional MR technique. Diffusion tensor tractography is considered to be a powerful tool for predicting the course of displaced facial nerve in vestibular schwannoma preoperatively.

15:00 ***3161***. **Histogram Analysis of Relative Cerebral Blood Volume Measurements in Cerebral Gliomas: An Interobserver and Intraobserver Reproducibility Study**
Computer 12
Robert J. Young[1], Erica Pollack[1], Gabriel Pivawer[1], James Babb[1], Glyn Johnson[1], Meng Law[1]
[1]NYU Medical Center, New York, New York, USA

Dynamic susceptibility contrast perfusion MR imaging (DSC MRI) of gliomas is most commonly analyzed using region-of-interest (ROI) measurements. We compare inter- and intra-observer reproducibility for different techniques of measuring relative cerebral blood volume (rCBV) metrics using both ROI and non-ROI techniques. Routine $rCBV_{max}$ ROI is compared with $rCBV_T$ tumoral and $rCBV_P$ peritumoral ROI as well as $rCBV_{TT}$ total tumoral non-ROI. Total tumoral histogram analysis, a non-ROI method, achieved the lowest coefficient of variation and highest between and within reader reproducibility. Further refinement of non-ROI analysis of perfusion MR data may lead to standardized, automated techniques for analyzing perfusion MR data.

15:00 ***3162***. **Toward Full Visualization of the Pyramidal Tract in Brain Tumor Patients: Tractography Based on Directional Diffusion Function**
Computer 13
Takashi Yoshiura[1], Seiji Kumazawa[1], Futoshi Mihara[1], Tomoyuki Noguchi[1], Osamu Togao[1], Hiroshi Honda[1]
[1]Kyushu University, Fukuoka, Japan

Conventional tractography methods are unable to track the fiber tract beyond the areas of fiber crossing and branching. As a result, the pyramidal tract is only partially visualized. Toward full visualization of the pyramidal tract, we have developed a new tractography method. In this study, we applied this method, which is called directional diffusion function (DDF) tractography, to 7 brain tumor patients. The estimated pyramidal tract was consistent with the anatomical knowledge in all patients. Overall, full visualization of the tract was achieved in 6 hemispheres (43%). Results supported the feasibility and improved visualization of DDF tractography.

15:30 ***3163***. **Reproducible Quantitative Analysis of Corpus Callosum Infiltration and Contralateral Involvement Using a Probabilistic Mixture Model: Relevance in Primary Brain Tumors**
Computer 12
Bram Stieltjes[1], Mathias Schlüter Schlüter[2], Bernd Didinger[3], Marc-André Weber[1], Horst K. Hahn[2], Peter Parzer[3], Marco Essig[1]
[1]DKFZ, Heidelberg, Baden Württemberg, Germany; [2]MeVis – Center for Medical Diagnostic Systems and Visualization, Bremen, Germany; [3]Heidelberg University Hospital, Heidelberg, Baden-Württemberg, Germany

Diffusion Tensor Imaging (DTI) is evaluated for better delineation of tumor infiltration by primary brain tumors. First reports show conflicting results mainly due to difficulties in reproducible determination of DTI-derived parameters. We present a novel method for ROI-analysis based on probablistic voxel classification for a user independent analysis of DTI-derived parameters and tested this method in healthy controls and patients with primary brain tumors. We show that this method leads to an excellent reproducibility and that DTI of the Corpus Callosum can help in the evaluation of ambiguous cantralateral lesions.

15:30 *3164*. **Application of Novel Directionally Encoded Colormaps for Isolating Linear Anisotropic Structures in Human Brain Diffusion Tensor Magnetic Resonance Imaging**
Computer 11
Daniel B. Ennis[1], Gordon Kindlmann[2], Monique Mogensen[1], Talia Vertinksy[1], Scott W. Atlas[1], Roland Bammer[1]
[1]Stanford University, Palo Alto, California, USA; [2]Harvard University School of Medicine, Boston, Massachusetts, USA

Novel directionally encoded colormaps that incorporate tensor mode (DECMs) are generated from DTMRI data. Tensor mode is a measure that distinguishes linear from planar anisotropy. DTMRI were acquired in 2 patients with glioblastoma multiforme (GBM). The use of DECMs for investigating the effect of the tumor by distinguishing between tracts which retain high linear anisotropy within the tumor versus those that were reduced to predominantly planar anisotropy appears to be of great advantage. DECMs in patients with GBM demonstrate the ability to more clearly visualize existing fiber tracks and disrupted fiber tracks within tumors.

Keeping Track of Fibers and Tracts

Room 4A Monday 14:00 - 16:00

14:00 *3165*. **Diffusion Tensor Imaging Data with Ultimate Interpolation Will Not Solve the Crossing-Fiber Problem: A Simulation Study**
Computer 14
Koji Sakai[1], Kei Yamada[2], Koji Koyamada[1], Tsunehiko Nishimura[2]
[1]Kyoto University, Kyoto, Japan; [2]Kyoto Prefectural University of Medicine, Kyoto, Japan

Crossing-fiber problem remains as one of the biggest unsolved issue on diffusion tensor imaging (DTI) based tractography. This problem can be characterized by the following two issues; (a) low fractional anisotropy (FA) voxel causing stopping and/or misdirection of tractography results and (b) undefined structural characteristics of fiber bundles (kissing, crossing, branching, or merging) within the voxel. The former issue (a) corresponds directly to the connectivity of tractography. The latter issue (b) is directly related to the intra-voxel fiber orientation and the relative location of fiber bundles within the voxel. The tensor based algorithm has not yet reached a complete solution to this problem (b). The objective of this paper is to assess whether we are able to solve the crossing fiber problem by higher resolution imaging achieved by tri-linear interpolation of neighbor tensor elements.

14:00 *3166*. **Generalized DTI Fiber Tracking in Continuous Tensor Field**
Computer 15
Bin Chen[1], Allen W. Song[1]
[1]Duke University, Durham, North Carolina, USA

MR-DTI provides directional information that can be used to delineate brain white matter connections non-invasively. In this study, we propose a generalized streamline tracking algorithm with high order propagation accuracy and a single termination criterion to reduce the inaccuracy introduced by user-defined and potentially biased termination criteria during tracking. The integration of the tissue property increases the sensibility to the boundaries of white matter and gray matter. The tracking results on phantom and human data demonstrated the improved tracking accuracy and agreement to the brain anatomy, respectively. The proposed technique also has the ability to integrate with the tensor field regulation techniques before tracking, along with the propagation modulation method such as tensor deflection during tracking.

14:30 *3167*. **Statistical DSI Brain Tractography: A Way to Handle the Kiss-Cross Uncertainty**
Computer 15
Patric Hagmann[1, 2], Xavier Gigandet[2], Van Wedeen[3], Reto Meuli[1], Jean-Philippe Thiran[2]
[1]University Hospital, Lausanne, Switzerland; [2]Ecole Polytechnique Fédérale, Lausanne, Switzerland; [3]Harvard Medical School, Charlestown, Massachusetts, USA

Despite the advent of diffusion magnetic resonance imaging and tractography algorithms, the accurate mapping of complex fiber kiss-crossings areas of the brain remains out of reach. In this study, we present a statistical DSI-based tractography algorithm which explores all possible paths in the brain white matter. We also introduce a cortex connectivity graph whose weighted edges correspond to the connection likelihood. The tests performed on the centrum semi-ovale have shown that a simple thresholding applied to the edges of this graph allows us to image the connectivity of any part of the brain to the desired level of complexity.

14:30 *3168*. **Use of Independent Component Analysis to Estimate Multiple Fibers Within a Voxel**
Computer 14
Manbir Singh[1], Jeong-Won Jeong[1]
[1]University of Southern California, Los Angeles, California, USA

Detection of crossing fibers within a voxel is a challenge in streamline tractography, particularly in clinical protocols where a relatively small number of gradient directions (6-25) are used. After verifying that the probability density function of the DTI data within voxels likely to contain a single fiber was nongaussian, an Independent Component Analysis (ICA) was performed to seperate two components (representing two fibers) in voxels identified as likely to contain crossing fibers. Results suggest that ICA can detect new tracts through fiber-crossing regions that are undetectable by conventional single-tensor streamline tractography.

15:00 ***3169***. **Mapping the Number of Fibre Orientations Per Voxel in Diffusion MRI**
Computer 14
Shahrum Nedjati-Gilani[1], Geoff J. M. Parker[2], Daniel C. Alexander[1]
[1]University College London, London, UK; [2]University of Manchester, Manchester, UK

We present a method to produce a map of the number of fibre-orientations in each voxel of a 3D diffusion MRI acquisition. We fit a hierarchy of models of increasing complexity to the particle displacement density, by finding the best fit to the model parameters in each case. The results from this method were compared with those obtained using spherical harmonics. We found the new method provides denser clusters of fibre-crossings, which indicates a more reliable result. The results obtained from this method could be used as a gold standard for simpler, faster methods of mapping the number of fibre-orientations.

15:00 ***3170***. **Evaluation of White Matter Fiber Clustering Methods for Diffusion Tensor Imaging**
Computer 15
Anna Vilanova[1], Bart Moberts[1], Jarke J. van Wijk[1], Jan Buijs[2], F. Roos[2], Carola van Pul[2]
[1]Eindhoven University of Technology, Eindhoven, Netherlands; [2]Máxima Medical Center, Veldhoven, Netherlands

Fiber tracking generates individual fibers from Diffusion TensorImaging data. In literature, we can find several methods forclustering of white matter fibers. However, it is not clear whichmethod produces the best results. Many combinations exist between:fibers similarity measures, clustering techniques and parameterdefinitions. We present a comparison of some clustering methodsusing a quality measure that was calibrated and validated for thistask. From the tested methods, the results show that the mean of the closest pointsdistance gives the best results as similarity measure, and that thehierarchical single link gives best results concerning clusteringand robustness.

15:30 ***3171***. **Advances in Fiber Tracking Quantification**
Computer 15
Philip G. Batchelor[1], Fernando Calamante[1], David Atkinson[1], Donald Tournier[1], Derek L. G. Hill[1], Alan Connelly[1]
[1]University College London, London, UK

Fiber tracking is either used as a purely qualitative anatomical method, for example showing how tracts avoid or go through a tumor. Curvatures and torsion have been proposed as a method to quantify fiber tracts. One drawback of the proposed method is that curvatures and torsions are very sensitive to discretisation noise. Here, we want to: discuss an appropriate smoothing method, and propose new tools to quantify fiber tracts, and compare them with previously proposed ones. This is demonstrated on synthetic and *in vivo* datasets.

15:30 ***3172***. **Higher Order Tensor Analysis and Higher Order SVD for Diffusion Tensor Analysis**
Computer 14
Philip G. Batchelor[1], Fernando Calamante[2], David Atkinson[1], Derek L. G. Hill[1], Donald Tournier[2], Alan Connelly[2]
[1]University College London, London, UK; [2]Brain Research Institute, Melbourne, Australia

The standard Singular Value Decomposition (SVD) is one of the main tools to study classical DT-MRI data, when they are represented as symmetric, positive definite tensors of order 2 (written D_ik). Current research in diffusion MR, however, is towards Higher Angular Resolution Diffusion Images (HARDI) data, that can be modeled in different ways as multi-exponential or as Higher Order Tensor (e.g. Ozarsalan). In this context, a generalization of the SVD to such data would appear highly desirable. It turns out that such generalizations, called Higher Order SVD (HOSVD) although not well known, do exist. One possible reason for their reduced use is that the generalization is not unique, and some properties are lost. Nevertheless, it seems a potentially too important tool to be neglected. Thus, our aim here is to introduce and investigate the usefulness of HOSVDs in HARDI, discuss and describe these decompositions, and describe mathematically the transition from 2nd order tensor to higher data.

Cancer Models: MRI/MRS Assessment

Room 4A Monday 14:00 - 16:00

14:00 ***3173***. **Difference in Early Intratumoral Changes Induced by Single Dose and Fractionated Radiotherapy in Rat Rhabdomyosarcoma Measured with Diffusion- And Perfusion-Weighted Magnetic Resonance Imaging**
Computer 16
Frederik De Keyzer[1], Vincent Vandecaveye[1], Jill Eckelmans[1], Feng Chen[1], Ronald R. Peeters[1], Pascal Hamaekers[1], Yicheng Ni[1], Robert Hermans[1], Sandra Nuyts[1], Willy Landuyt[2], Hilde Bosmans[1]
[1]University Hospitals Leuven, Leuven, Vlaams-Brabant, Belgium; [2]Catholic University of Leuven (KUL), Leuven, Vlaams-Brabant, Belgium

Early intratumoral changes after single-dose or fractionated irradiation were examined using DW- and DCE-MRI in rat rhabdomyosarcoma. Either a single-dose of 8Gy or a fraction of 3Gy daily (5 days) was given. The tumors treated with single-dose irradiation showed perfusion decrease, no diffusion differences and growth delay of 12 days. The fractionated radiotherapy tumors showed stronger perfusion decrease and strong diffusion increase, translated in an 18-day growth delay. DW-MRI and DCE-MRI indicate perfusion decrease in single-dose radiotherapy, but limited necrosis formation and tumor growth delay. Fractionated radiotherapy resulted in similar perfusion decreases, but more intratumoral necrosis and longer growth delay.

14:00 ***3174***. **Comparison of $T_{1\rho}$ and Diffusion Response Following Chemotherapy in Mouse EL4 Tumors at 9.4 T**
Computer 17
Mikko I. Kettunen[1], De-En Hu[1], Kevin M. Brindle[1]
[1]University of Cambridge, Cambridge, UK

Diffusion MRI provides an early marker of therapy-induced cell death in tumors, yet its use may be sometimes limited by motion. $T_{1\rho}$ MRI has recently been suggested as alternative means to detect early tumor response. In the current study we compared $T_{1\rho}$ and diffusion responses following chemotherapy in mouse EL4 lymphomas at 9.4 T. Following treatment, diffusion values increased yet $T_{1\rho}$ did not change. The current results imply that the use of $T_{1\rho}$ as an alternative for diffusion may not be feasible in all tumor models.

14:00 ***3175***. **Evaluation of Salmonella-Based Suicide Gene Transfer in a Rodent Tumor Model Using *In Vivo* 19F MR Spectroscopy**
Computer 18
Tom Dresselaers[1], Jan Theys[2], Ludwig Dubois[2], Willy Landuyt[1], Paul Van Hecke[1], Philippe Lambin[2]
[1]K.U.Leuven, Leuven, Belgium, Belgium; [2]Maastricht Radiation Oncology Lab/GROW, Maastricht, The Netherlands, Netherlands

Salmonella typhimurium recombinant for cytosine deaminase (TAPET-CD) is a non-pathogenic bacterial-mediated vector system that, in combination with systemic delivery of 5-Fluorocytosine (5-FC), can result in anti-tumor effects (1-4). We already demonstrated that engineered Salmonella persist in tumors for extensive time periods without the need for repeated administration. Importantly, we also showed the feasibility of 19F-MR Spectroscopy (19F-MRS) to monitor *in vivo* the intra-tumoral conversion from 5-FC to the cytostatic 5-fluorouracil (5-FU) (5). Here we report on a longitudinal 19F MRS study of this TAPET-CD/5-FC therapy in mice xenografted with the human colorectal carcinoma HCT116. Initial results in this model indicate that the 5-FU formation, as observed with *in vivo* 19F MRS, 10 days after the first 5-FC administration correlates with the response of the tumor to the therapy (based on tumor growth over several weeks).

14:30 ***3176***. **The PPARγ Inhibitor GW9662 Attenuates Phenylbutyrate-Induced Lipid Metabolite Accumulation in DU145 Prostate Cancer Cells**
Computer 18
Matthew Milkevitch[1], Nancy J. Beardsley[1], Edward J. Delikatny[1]
[1]University of Pennsylvania School of Medicine, Philadelphia, Pennsylvania, USA

1H and 31P MRS were used to monitor the effects of the peroxisome proliferator activated receptor γ(PPARγ)antagonist GW9662 on prostate cells treated with the differentiating agent phenylbutyrate. Phenylbutyrate (PB) causes G1 cell cycle arrest and apoptosis in DU145 cells, along with significant increases in total choline and mobile lipid resonances in 1H spectra and glycerophosphocholine in 31P spectra. Pretreatment of DU145 cells with GW9662 (1μM, 1h)completely inhibited PB induced effects on lipid metabolites and reversed the G1 block. These data provide strong evidence that PB-induced differentiation and lipid metabolic changes are mediated by PPARγ.

14:30 ***3177***. **Apparent Diffusion Coefficient Predicts Survival in a Transgenic Model of Glioma**
Computer 17
Patrick McConville[1], Jonathan B. Moody[1], Alicia R. Kreger[1], William L. Elliott[1], Wilbur R. Leopold[1], Brian D. Ross[2], Eric C. Holland[3]
[1]Molecular Imaging Research, Inc., Ann Arbor, Michigan, USA; [2]University of Michigan, Ann Arbor, Michigan, USA; [3]Memorial Sloan-Kettering Cancer Center, New York, New York, USA

MRI was used to measure tumor volume and apparent diffusion coefficient (ADC), and compared with survival in the tv-a transgenic model of glioma. Mice with high grade gliomas were divided into two groups: vehicle control (n=12) and temozolomide treated (qdx5; 100 mg/kg IP; n=13). In the treated group, ADC showed a robust early increase that correlated with later tumor growth inhibition and was predictive of an eventual survival increase, compared with controls.

14:30 ***3178***. **Dose Response of Rat GH3 Prolactinomas to 5,6-Dimethylxanthenone-4-Acetic Acid (DMXAA) Assessed by Dynamic Contrast Enhanced MRI**
Computer 16
Dominick John McIntyre[1], Lesley D. McPhail[1], Christian Ludwig[2], Philip Kestell[3], John Richard Griffiths[1], Lloyd R. Kelland[4], Simon Philip Robinson[1]
[1]St George's, University of London, London, UK; [2]University of Birmingham, Birmingham, UK; [3]University of Auckland, Auckland, New Zealand; [4]Antisoma Research Ltd, London, UK

Tumour vasculature is an attractive therapeutic target. The dose-dependent effects of DMXAA, a vascular disrupting agent which induces selective occlusion of tumour blood vessels and necrosis, were investigated using dynamic contrast-enhanced (DCE) MRI, measurements of 5-hydroxyindoleacetic acid (5-HIAA), which is a plasma biomarker of DMXAA-induced anti-vascular activity, and tumour necrosis. DCE MRI revealed a significant reduction in K^{trans} and IAUGC of rat GH3 prolactinomas 24 hours after treatment with 350mg/kg DMXAA, but there was no evidence of dose response. A significant increase in 5-HIAA, associated with DMXAA-induced increase in vascular permeability, was measured in response to 200 and 350mg/kg DMXAA.

15:00 ***3179***. **Assesing the Response of Pre-Clinical Tumor Models to Anti-Neoplastic Therapies Using Functional Diffusion Mapping (FDM)**
Computer 16

Bradford A. Moffat[1], Daniel E. Hall[1], Benjamin Hoff[1], Thomas L. Chenevert[1], Brian D. Ross[1]
[1]University of Michigan, Ann Arbor, Michigan, USA

The purpose of this study was to develop a new method for quantifying therapeutic induced changes in ADC maps of orthotopic rodent tumors. This is a departure from the traditional quantification of mean tumor ADC that does not adequately describe the heterogeneity of change in ADC that usually results from anti-neoplastic therapies. FDM enables segmentation tumors into regions response and resistance to therapy. The results significantly correlate with chemotherapy dose and animal survival.

15:00 ***3180***. **Assessment of Emerging Chemotherapeutic Tumor Resistance to BCNU**
Computer 17

Victor D. Schepkin[1], Kuei C. Lee[1], Kyle Kuszpit[1], Mukilan Muthuswami[1], Thomas L. Chenevert[1], Alnawaz Rehemtulla[1], Brian D. Ross[1]
[1]University of Michigan Medical School, Ann Arbor, Michigan, USA

Proton Diffusion (ADC mapping) and Sodium MRI were tested together with the goal of developing a biomarker for tumor cell response during cancer therapy. ADC and sodium demonstrate a remarkable correlation between each other during BCNU therapy of 9L rat subcutaneous tumor, representing the same process of tumor cellularity changes. Two administrations of BCNU chemotherapy using two different doses revealed that aggressive treatment leads to a more advanced decrease in tumor sensitivity. In-vivo results were confirmed by in-vitro assay. The study demonstrates that both imaging modalities can reflect the efficacy of tumor therapy and emerging chemotherapy resistance.

15:00 ***3181***. **Choline Phospholipid Metabolism in Human Ovarian Tumor Progression: A MRS Study**
Computer 18

Egidio Iorio[1], Alessandro Ricci[1], Delia Mezzanzanica[2], Francesca Spadaro[1], Carlo Ramoni[1], Rossella Canese[1], Carmela Rozera[1], Massimo Spada[1], Filippo Belardelli[1], Sandra D'Ascenzo[3], Vincenza Dolo[3], Silvana Canevari[2], Franca Podo[1]
[1]Istituto Superiore di Sanità, Roma, Italy; [2]Istituto Nazionale Tumori, Milano, Italy; [3]University of L'Aquila, L'Aquila, Italy

The role of 1H MRS-detectable phosphatidylcholine (PC) metabolites as fingerprints of tumor progression was investigated in human epithelial ovarian cancer cell lines or cells isolated from patient ascitic exudate (EOC) as compared with non-tumoral, normal or immortalized epithelial cells (EONT). Phosphocholine and total-choline metabolites increased ($P < 0.0001$) in the malignant progression of epithelial ovarian cells. These MRS-detectable biochemical alterations were associated with activation of enzymes involved in both biosynthetic and catabolic PC cycle pathways. PC-specific phospholipase C was massively expressed on the plasma membrane on EOC (but not EONT) cells.

15:30 ***3182***. **Magnetic Resonance Spectroscopy: A Non-Invasive Tool for Monitoring Histone Deacetylase Inhibition**
Computer 18

Madhuri Sankaranarayanapillai[1], William PingYiu Tong[1], Ashutosh Pal[1], William G. Bornmann[1], Juri G. Gelovani[1], Sabrina M. Ronen[1]
[1]UT M.D.Anderson Cancer Center, Houston, Texas, USA

Histone deacetylase (HDAC) inhibitors have emerged as a new class of anti-neoplastic agents having potential anti-tumor activities for targeted therapy. Our goal was to develop a non-invasive MRS based method to monitor HDAC inhibition in PC3 cells. We already showed that Boc-Lys-Tfa(OH) is an HDAC substrate. Here, ^{19}F MRS of cells treated with p-fluoro-suberoylanilide hydroxamic acid (FSAHA) detected increased intracellular BLT levels which correlated with HDAC inhibition. ^{31}P MRS of the FSAHA treated cells detected increased phosphocholine levels (PC) which also correlated with HDAC inhibition. This indicates that ^{19}F and ^{31}P MRS are promising modalities to assess HDAC inhibition.

15:30 ***3183***. **Accelerated Evaluation of Tumor Treatment Response by Diffusion MRI**
Computer 17

Jonathan Bryan Moody[1], Patrick James McConville[1], Richard J. Lister[1], Bradford A. Moffat[2], Thomas L. Chenevert[2], Alnawaz Rehemtulla[2], Brian D. Ross[2], William L. Elliott[1], Wilbur R. Leopold[1]
[1]MIR Preclinical Services, Ann Arbor, Michigan, USA; [2]University of Michigan, Ann Arbor, Michigan, USA

Diffusion MRI (dMRI) in oncology has demonstrated great promise as a biomarker for assessment of therapeutic efficacy. However, tumor heterogeneity can hinder consistent quantification of tumor response to therapy. We present here a novel approach to tumor characterization using dMRI which provides *in vivo* estimates of net tumor cell kill. Moreover, we demonstrate that dMRI-net kill is significantly correlated with conventional net kill derived from tumor growth delay, but was obtained more than seven weeks before conventional net kill was available. The use of diffusion MRI in preclinical drug development may significantly accelerate the *in vivo* evaluation of novel therapeutics.

15:30 *3184*. **Statistical Power of Two Quantitative Biomarkers for Analysis of DCE-MRI Studies of Agents Targeting Tumour Vasculature**
Computer 16
Dominick John McIntyre[1], Simon Phili Robinson[1], Philip Worthington[2], John Richard Griffiths[1], John C. Waterton[2]
[1]St George's, University of London, London, UK; [2]AstraZeneca, Alderley Park, Macclesfield, UK

Dynamic-contrast enhanced MRI is useful for assessing the affects of tumour vascular targeting agents. Two quantitative biomarkers have been recommended for clinical trials, both based on measuring the tissue [Gd] time course: integrated area under the [Gd]-time curve (IAUGC) and the pharmacokinetic transfer constant K^{trans}. We have compared the statistical power of the methods in a retrospective analysis of pre-clinical studies of the vascular disrupting agent ZD6126 and the anti-angiogenic signalling inhibitor ZD6474. Neither method is consistently more sensitive at low dose, and we recommend IAUGC for its simplicity and robustness to fit failures.

Image Reconstruction

Room 4A Monday 14:00 - 16:00

14:00 *3185*. **Comparison of Wavelets and a New DCT Algorithm for Sparsely Sampled Reconstruction**
Computer 20
Johannes Plett[1], Ivan Lillo[1], Marcelo Guarini[1], Pablo Irarrazaval[1]
[1]Pontificia Universidad Catolica de Chile, Santiago, Chile

MRI images can be reconstructed reasonably well from just a few randomly chosen k-space samples through a convex L_1 optimization. We present a new alternative for the domain of the optimization function based on the Discrete Cosine Transform (DCT) and compare it to Wavelets. The results indicate better and faster performance for the DCT algorithm reducing reconstruction errors and increasing Peak Signal to Noise Ratio (PSNR).

14:00 *3186*. **Low Latency vs. Non Linear Phase: A Balanced Approach for UNFOLD Filter Design in Quantitative Real-Time MRI**
Computer 19
Gregory Maclair[1], Mario Ries[1], Chrit Moonen[1]
[1]IMF CNRS /University of Bordeaux 2, Bordeaux, France

Real-time control of interventional procedures such as guidance of catheters or ablation therapy require a high temporal resolution, a low processing latency and methods that preserve the temporal characteristics of the data. Although UNFOLD encoded sequences are interesting candidates for these applications, current filter implementations show either a non-linear phase (IIRs) which alters the temporal characteristics or have insufficient latency (FIRs). This study proposes an IIR filter design which satisfies both constraints of low latency and linear phase.

14:30 *3187*. **Real-Time Imaging of Speech Production Using Radial *k-T* SENSE**
Computer 19
Michael Schacht Hansen[1, 2], Vivek Muthurangu[2], Christof Baltes[3], Sebastian Kozerke[3], Jeffrey Tsao[4], Reza Razavi[2], Derek L. G. Hill[1]
[1]University College of London, London, UK; [2]King's College London, London, UK; [3]Swiss Federal Institute of Technology (ETH), Zurich, Switzerland; [4]Novartis Institutes for BioMedical Research, Inc., Cambridge, Massachusetts, USA

In this abstract we present a method for *k-t* SENSE reconstruction of undersampled data acquired on non-Cartesian trajectories in *k-t* space. This is an extension of a previously presented method to include complementary information from multiple receive coils. The method is applied to real-time radial imaging of speech production. The radial trajectory is ideal for this application since it provides integrated training data. In simulations and *in vivo* data, we show that the radial *k-t* SENSE reconstruction is superior to a modified sliding window reconstruction which has full temporal bandwidth for the central part of *k*-space.

14:30 *3188*. **Reduced Ring Artifacts for PROPELLER Using an Analytical Density Compensation Algorithm During Regridding Into Cartesian K-Space**
Computer 20
Shaorong Chang[1], Mike Hartley[1], Ajeet Gaddipati[1], Dawei Gui[1]
[1]GE Healthcare, Milwaukee, Wisconsin, USA

Though the k-space is uniformly sampled for each blade with PROPELLER acquisition, the accumulated k-space regridding from all blades is sampled more densely in the low frequencies than in the high frequencies. We derive an analytical density compensation algorithm for PROPELLER based on its sampling pattern, and demonstrate that this density compensation algorithm significantly reduces ring artifacts in phantom studies. In addition, this method is computationally efficient without involving kernel convolution and iterative refinement.

15:00 ***3189***. **Tensor Field Model for Phased-Array Imaging: Application for Phase Sensitive Inversion Recovery Reconstruction**
Computer 20
Jim X. Ji[1]
[1]Texas A&M University, College Station, Texas, USA

Phase sensitive inversion-recovery (PSIR) has clinical applications ranging from myocardial infarction detection, brain tumor imaging, to fat/fluid suppression. Using phase-array coils, multi-channel IR data can be acquired and combined to improve the SNR (or to reduce scan time). However, conventional sums-of-squares reconstruction is not optimal for PSIR because it loses the phase information. This paper presents a tensor Markov random field model that can be used to reconstruct PSIR images from phased-array data. The new method does not require additional phase reference scans, or consistency correction of individual coil images. In-vivo brain MR experiments show that the method is robust and efficient.

15:00 ***3190***. **Optimal Data Sampling for Noquist Ciné Imaging**
Computer 19
David Moratal[1]*, Marijn E. Brummer*[2]*, William T. Dixon*[3]
[1]Universitat Politècnica de València, Valencia, Spain; [2]Emory University, Atlanta, Georgia, USA; [3]General Electric Global Research, Niskayuna, New York, USA

Optimization of data selection for Noquist rFOV reconstruction using any size of the static and dynamic regions is investigated by exhaustive search in limited-size problems. Conclusions were extrapolated to Noquist acquisitions with realistic image dimensions that achieved optimal SNR for additive white noise. An upper bound of the attainable SNR as a function of the number of phases is also presented.

15:30 ***3191***. **Improved Translation Correction Applied to PROPELLER Using Expansion-Matching Filter**
Computer 19
Shaorong Chang[1]*, Mike Hartley*[1]*, Ajeet Gaddipati*[1]*, Dawei Gui*[1]
[1]GE Healthcare, Milwaukee, Wisconsin, USA

PROPELLER is robust to rigid body motion with the capability of estimating rotation and translation shifts of each blade. This paper presents a translation correction algorithm using expansion-matching (EXM) filter, which estimates the template position more accurately, thus yielding images with sharper edges and less motion-derived ghosting artifacts in both phantom and volunteer studies. The EXM filter was also designed to adapt to the noise level in images, resulting in accurate motion estimation even in noise conditions.

15:30 ***3192***. **Image Reconstruction of Low SNR Images from Large-N Arrays**
Computer 20
Christina Triantafyllou[1]*, Graham C. Wiggins*[1]*, Andreas Potthast*[2]*, Lawrence L. Wald*[1]
[1]A.A. Martinos Center for Biomedical Imaging, Boston, Massachusetts, USA; [2]Siemens Medical Solutions, Erlangen, Germany

In this work, we simulate the SNR penalty for SoS combination in low SNR images using noise maps and coil sensitivity data obtained from 8, 23, and 90channel head arrays by comparing the SoS method to combination based on coil sensitivity maps. Our findings show noise amplification of the SoS method within a low SNR object increases significantly with the number of array elements and the penalty is maximum near the array elements. For cases where coil sensitivity cases are not available, we test a modified version of the SoS which improves performance in low SNR data from large arrays.

Artifacts and Correction: Motion

Room 4A Monday 14:00 - 16:00

14:00 ***3193***. **Trajectory Optimization Criterion for Convolution in K-T Space**
Computer 21
Feng Huang[1]*, Dan Xu*[2]*, George Randy Duensing*[1]
[1]Invivo Corporation, Gainesville, Florida, USA; [2]University of Illinois at Urbana-Champaign, Urbana, Illinois, USA

For partially acquired dynamic magnetic resonance imaging (MRI), the accuracy of the reconstruction is a function of the k-t space trajectory. Tsao *et al*. discussed the trajectory optimization for k-t SENSE In this work, the expectation of the reconstruction error is used as a criterion of trajectory optimization for reconstruction methods based on convolution in k-t space. The intuitive basis for the optimization is that all of the data with which to construct missing data is acquired with as little redundancy as possible. k-t GRAPPA is applied to dynamic cardiac MRI data to confirm the criterion.

14:00 ***3194***. **TRELLIS MRI: A Novel Approach to Motion Correction**
Computer 22
Julian R. Maclaren[1]*, Philip J. Bones*[1]*, Rick P. Millane*[1]*, Richard Watts*[1]
[1]University of Canterbury, Christchurch, Canterbury, New Zealand

A new technique called TRELLIS (Translation & Rotation Estimation using Linear Least-squares & Interleaved Strips) MRI is presented. This can effectively track the position of the object being scanned and correct for motion artifacts. The same acquisition time and SNR as a conventional algorithm that samples twice then averages can be achieved. Simulation results show good performance under realistic noise levels. Clinical testing is in progress. This algorithm may offer significant improvements over current state-of-the-art algorithms such as PROPELLER MRI.

14:00 ***3195***. **Real-Time Motion Detection Algorithms for Spherical Navigator Echoes in Functional MRI**
Computer 23
Narter Ari[1], Robert A. Kraft[2]
[1]GE Healthcare, Waukesha, Wisconsin, USA; [2]Wake Forest University, Winston-Salem, North Carolina, USA

Spherical navigator echoes (SNAV) can be used to track head position throughout the functional MRI. However, current motion detection algorithms for SNAV require significant computation times and hence limit the feasibility of SNAV technique for real-time functional MRI applications. We developed a real-time SNAV technique, optimized to have a motion detection accuracy of 0.3mm and timing performance of 2300ms for a TR of 2500ms. We developed k-space thresholded Least Squares Conjugate Gradient (kt-LSCG) algorithm for translation detection, and multi-scale DownHill Simplex (ms-DHS) algorithm with normalized Least Squares cost function for rotation detection.

14:00 ***3196***. **Prospective Intra-Image Compensation for Non-Periodic Rigid Body Motion Using Active Markers**
Computer 24
Sascha Krueger[1], Tobias Schaeffter[1], Steffen Weiss[1], Kay Nehrke[1], Tom Rozijn[2], Peter Boernert[1]
[1]Philips Research, Hamburg, Germany; [2]Philips Medical Systems, Best, Netherlands

Small extra-corporal micro-coils (active markers) are used to continuously track the motion of a non-periodically rigidly moving part of the body to perform an intra-image prospective motion correction during image acquisition. At least three markers are used to form a rigid geometry attached to the region of interest. The MR control system computes and updates the required scan geometry to follow the object in real-time. The temporal resolution of this technique is limited by 3 x TR (repetition time) plus ~5ms computation time. Experiments were performed on volunteers using protocols for 3D brain imaging and for kinematic studies of joints.

14:30 ***3197***. **A Self-Navigated Spiral in & Out Pulse Sequence Design for Retrospective Motion Correction**
Computer 24
Murat Aksoy[1], Chunlei Liu[1], Mike Moseley[1], Roland Bammer[1]
[1]Stanford University, Stanford, California, USA

A new spiral sequence design is proposed for retrospective correction of in-planar rigid body motion. The sequence uses a spiral-in section at the beginning of each interleaf to acquire a low resolution image to be used for retrospective detection and correction of motion. Due to the undersampling artifacts that appear during motion correction and reconstruction, parallel imaging methods provide significant increase in image quality. The results of *in vivo* studies including no motion and mild motion are presented.

14:30 ***3198***. **Prospective Motion Correction for Improved Image Volume Alignment**
Computer 23
Andrew James Wheaton[1], Deepak Bhat[1], Frank G. Hoogenraad[2], Michael R. Thompson[1]
[1]Philips Medical Systems (Cleveland), Highland Heights, Ohio, USA; [2]Philips Medical Systems (Best), Best, Netherlands

Misalignment of image volume data in a temporal series due to subject motion can corrupt data analysis. Prospective Motion Correction (PMC) continuously measures changes in geometry during a scan and makes adjustments on the scanner on-the-fly to realign subsequent image volume acquisitions without imposing timing restrictions or limiting minimum TR. PMC is demonstrated to accurately correct subject motion thereby preserving volume-to-volume alignment. The improved data alignment results in superior activation map performance with more intense and less diffuse activation regions compared to post-processing alignment using retrospective registration.

14:30 ***3199***. **Prospective Motion Correction Using Principal Axes Computation from Moments of Spatial Projections**
Computer 22
Naveen Bajaj[1], Manojkumar Saranathan[1]
[1]Indian Institute of Science, Bangalore, Karnataka, India

Prospective motion correction is a challenging problem in MRI. Navigator echoes have been successfully demonstrated for in-plane translation, rotation and periodic motion. In this work, a novel, fast technique based on principal axes computation using spatial moments is explored to effect prospective correction of rigid-body motion (rotation and translation). The algorithm has been tested for both 3D imaging on synthetic phantom data as well as self navigated radial 2D imaging on both phantom and MR brain data.

14:30 ***3200***. **A Single Scan Two-Point Ghost Phase Cancellation Method Using Bunched Phase Encoding**
Computer 21
Hisamoto Moriguchi[1], Mark A. Griswold[1], Jeffrey L. Sunshine[1], Jeffrey L. Duerk[1]
[1]University Hospitals of Cleveland / Case Western Reserve University, Cleveland, Ohio, USA

The two-point ghost phase cancellation (2PGPC) method is a method for suppression of ghost artifacts using two sets of images. However, the scan time of this method must be extended since it requires two image sets. Bunched Phase Encoding (BPE) has recently been proposed as a new fast data acquisition method in MRI. In BPE, the total number of TR cycles and hence the scan time can be reduced. In this study, it is shown that the BPE technique enables us to reduce the total data acquisition time of the 2PGPC method to that of a single acquisition.

15:00 ***3201***. **Modeling of Organ's Motion Using External Sensors**
Computer 21
Cédric Pasquier[1, 2], Freddy Odille[1], Roger Abaecherli[1, 3], Pierre-André Vuissoz[1], Jacques Felblinger[1]
[1]Université Henri Poincaré; INSERM ERI 13, NANCY, France; [2]Schiller Médical, Wissembourg, France; [3]Schiller, Baar, Switzerland

Common MRI sequences suffer from motion limitation, particularly respiratory-induced motion. Navigators are one proposed correction method but simultaneous acquisition of navigators and images could be a limitation. External sensor may constitute a more versatile input for motion model. Combination of several external sensors are tested and the best input function proving good correlation between external sensors and organ's motion is found. After calibration it is possible to estimate the motion of an organ at any instant in the sequence. This enables the adaptation of motion prediction to different organs and different physiology.

15:00 ***3202***. **Identification and Correction of the Intra-Scan Motion Artifact Using Parallel Imaging**
Computer 22
Nan-kuei Chen[1], Ying-hui Chou[1, 2], Lawrence P. Panych[1]
[1]Brigham and Women's Hospital, Harvard Medical School, Boston, Massachusetts, USA; [2]Fu Jen Catholic University, Taipei, Taiwan

It has been shown previously that parallel imaging may be used to improve the spatial-temporal-resolution of dynamic scans, or to reduce the effective echo time and geometric distortions in EPI. Here we propose a new application of parallel imaging technique: identification and correction of intra-scan motion artifact. The phase-encoding in conventional 2D and 3D spin-warp imaging is re-ordered in such a way that the parallel imaging technique can be applied to detect and correct the intra-scan motion. Additional low ky lines are acquired so that the coil sensitivity can be estimated in the presence of subject movement.

15:00 ***3203***. **An Optimized DENSE Acquisition Scheme for Brain Displacement Mapping**
Computer 23
Michaela Soellinger[1], Andrea Kaspar Rutz[1], Peter Boesiger[1], Sebastian Kozerke[1]
[1]University and ETH Zurich, Zurich, Switzerland

Studying pulsatile brain motion caused by cerebral blood flow allows insights into alteration of the dynamics in the cranium in certain brain diseases. We propose a modified DENSE (Displacement Encoded Stimulated Echo) acquisition scheme for 2D cine displacement imaging which allows eliminating phase errors from the spoiling gradients and the EPI read-out train. A 3D phase-unwrap-algorithm was incorporated to permit encoding frequencies up to 10 cycles/mm. With the method proposed 2D displacement data could be acquired over the whole brain in all 3 directions with a spatial resolution of 2x2x4 mm3 and temporal resolution of 25 ms.

15:00 ***3204***. **3D EXTRACT (Extrapolation and Correlation) for Rapid Correction of 3D Rotation and Translation**
Computer 24
Wei Lin[1], Hee Kwon Song[1]
[1]University of Pennsylvania Medical Center, Philadelphia, Pennsylvania, USA

Motion artifacts are particularly problematic for 3D imaging due to the increased scan time. Although in-plane motion has been studied extensively, few previous studies have addressed through-plane motion. In this work, a technique for 3-D rigid-body motion correction based on successive data extrapolation and correlation is described. The technique is fast, and the processing time independent of the range of translational motion. Results demonstrate significant improvement in image quality in TOF angiography experiments.

15:30 ***3205***. **A Sparse Matrix Formalism for Non-Rigid Motion Correction**
Computer 24
Philip G. Batchelor[1], David Atkinson[1], Derek L. G. Hill[1], David J. Larkman[2], Jo Hajnal[2], Pablo Irrarazaval[3], Michael S. Hansen, [14]
[1]University College London, London, UK; [2]Hammersmith Hospital, Imperial College, London, UK; [3]Universidad Catolica de Chile, Santiago, Chile; [4]King's College London, London, UK

Here we discuss a method to perform general non-rigid motion correction of multi-shot images, even when the inverse motion is not known (but the motion itself is found with the help of e.g. a navigator). We explicitly construct a sparse system for the unknown image, whose right hand-side is the motion-ghosted image. We make the assumption that motions happen between shots, in a multishot context, where each shot is a set of regularly spaced lines. The influence of sparseness on computation time and accuracy is studied, and we show an example of correction of a simulated ghosted image, where the motion at each shot is a spline deformation.

15:30 ***3206***. **Internal Reference Scans for Artifact Correction in Multi-Shot Segmented EPI Acquisition**
Computer 23
Gaohong Wu[1], Shi-Jiang Li[1]
[1]Medical College of Wisconsin, Milwaukee, Wisconsin, USA

Due to the different T1 recoveries and T2* decays, the navigator echo method is not sufficient to reduce the ghost artifact arising from the amplitude and phase discrepancies between segments for the recently proposed turbo segmented imaging (TSI) method. In this study, a new artifact reduction method, which acquires the reference data at the k-space center, is proposed and implemented with a gradient-echo EPI using the TSI technique (TS-EPI). This TS-EPI sequence can be used to obtain high spatial and temporal resolution images with minimal motion artifacts for BOLD and ASL perfusion fMRI studies.

15:30 ***3207***. **Translation First PROPELLER MRI Correction**
Computer 22

Brian Welch[1]
[1]Vanderbilt University Institute of Imaging Science, Nashville, Tennessee, USA

PROPELLER MRI is a well-known approach for correction of multi-shot axial T2W images corrupted by in-plane rigid body motion. The standard PROPELLER correction algorithm compensates for in-plane rotation before in-plane translation; however, it is possible to correct in-plane translation first using center of mass consistency properties. This allows the use of complex k-space values (instead of magnitude only) in the subsequent rotation correction step. This improves rotation detection accuracy and enables the detection of all alignments over the full 360º range – impossible using only magnitude k-space data.

15:30 ***3208***. **Automatic Region Tracking for Motion Correction in MR Perfusion Imaging of the Kidney**
Computer 21

Baudouin Denis de Senneville[1], *Nicolas Grenier*[1, 2], *Mario Ries*[1], *Pascal Desbarats*[3], *Chrit Moonen*[1]
[1]Laboratoire Imagerie Moléculaire et fonctionnelle, Bordeaux, France; [2]Service de Radiologie - CHU Pellegrin, Bordeaux, France; [3]LaBRI, Bordeaux, France

Contrast-enhanced dynamic MRI acquisitions give access to renal physiological parameters like measurement of blood flow, blood volume and glomerular filtration. Since the rapid bolus passage hampers the use of gated sequences, rapid T1-weighted sequences have to be employed while free-breathing. As a result, the acquired data contain motion artefacts caused by the respiratory cycle, spontaneous movements and drifts which limit the quantitative analysis of the data. This study proposes a 2D region tracking method for retrospective motion correction without sacrificing temporal resolution which addresses the latter point by a preparative learning phase.

Artifacts and Correction

Room 4A Monday 14:00 - 16:00

14:00 ***3209***. **SNR Improvement by Modification of Wiener Filter for the Applications of Acquiring Multiple Similar Data: Application to Diffusion Tensor Imaging**
Computer 25

Tokunori Kimura[1]
[1]Toshiba Medical Systems Corp., Otawara, Tochigi, Japan

When applying Wiener filter to improve noisy image, the smaller the noise effects on signal power Ps, the better performance on the SNR improvement of noisy data. Here we proposed a modified WF (called mean-Ps) of improving SNR of Ps by averaging multiple similar data for specific applications. We assessed the performance of our proposed method for the standard Fourier WF (FT-WF) as well as the WF applied Fresnel transform (FR-WF) on diffusion tensor imaging (DTI). The mean-Ps method resulted in the better improvement of SNR particularly in FR-WF compared with the conventional method of using single data for Ps.

14:30 ***3210***. **Correction for the Echo-Shifting Related Artifacts in T2* Mapping**
Computer 25

Nan-kuei Chen[1], *Koichi Oshio*[1, 2], *Ying-hui Chou*[1, 3], *Lawrence P. Panych*[1]
[1]Brigham and Women's Hospital, Harvard Medical School, Boston, Massachusetts, USA; [2]Keio University, Tokyo, Japan; [3]Fu Jen Catholic University, Taipei, Taiwan

T2* mapping is a commonly performed MRI procedure, and is useful for characterizing tissue properties. However, our analysis and experimental data show that, in the presence of background susceptibility field gradients (e.g. near the air-tissue interface), the echo-shifting effect and TE-shifting effect will make the calculated T2* maps inaccurate. We further demonstrate that accurate T2* mapping can only be achieved after (1) quantifying the echo-shifting effect (in gradient-echo EPI and gradient-echo imaging) with the k-space energy spectrum analysis algorithm, and (2) correcting for the TE-shifting effect in T2* calculation.

15:00 ***3211***. **Consistent Non-Cartesian Off Axis Image Quality: Removing Multiple Sources of Demodulation Phase Errors**
Computer 25

Yogesh Jashnani[1], *Youngkyoo Jung*[1], *Richard Kijowski*[1], *Walter F. Block*[1]
[1]University of Wisconsin-Madison, Madison, Wisconsin, USA

Off axis imaging using non-Cartesian sequences suffers degradation relative to on axis imaging if an accurate demodulation reference signal is not available. Poorly generated reference signals necessitate hand tuning of a system delay parameter. Removing phase errors due to these timing offsets only partially restores image quality. Deviations in k-space sample locations due to eddy currents and gradient anisotropic delays result in demodulation phase errors, which must be compensated to fully restore image quality. Off axis image quality has been significantly improved by correcting for all sources of demodulation phase errors and k-space location errors during image reconstruction.

15:30 *3212*. **Simplified and Higher Degree-Of-Freedom Correction Method of Spatially Inhomogeneous Noise on Parallel MR Images Obtained with Surface Array Coils**
Computer 25

Tokunori Kimura[1], *Yoshio Machida*[1]
[1]Toshiba Medical Systems Corp., Otawara, Tochigi, Japan

We developed and assessed a simplified method of correcting inhomogeneous noise on parallel imaging and standard surface-coil imaging due to inhomogeneous coil sensitivity. After correcting coil-sensitivity, equivalently nonuniform filtering was performed by weighted summation of non-filtered and uniformly filtered image using coil-sensitivity window. Two types of uniform filters, linear-space-invariant and structure-adaptive, for several smoothing strengths were compared. The proposed method could provide images on which noise was homogeneously reduced and blur was minimized particularly by using adaptive type. Proposed method is useful for improving inhomogeneous noise with preserving structure and can provide easy and higher degree-of-freedom implementations on commercial MRI.

Spectroscopic Localization and Imaging

Room 4A Monday 14:00 - 16:00

14:00 *3213*. **Robust Lipid Suppression Using Multiple Frequency-Selective Pulses for Brain Spectroscopic Imaging at 3T**
Computer 26

Meng Gu[1], *Daniel Spielman*[1]
[1]Stanford University, Stanford, California, USA

In spectroscopic imaging, lipid signal contaminates much smaller metabolite signals, making it impossible to quantify the spectra. PRESS technique has been widely used to suppress lipids at the cost of spatial coverage. At 1.5T, inversion recovery is normally used to obtain full brain coverage with 30-40% metabolite signal loss. At 3T, frequency selective inversion recovery has been implemented to suppress lipids without causing signal loss. However, this method can not fully suppress lipids due to different T1s and B1 inhomogeneity. To address these issues, a robust lipid suppression technique has been proposed and implemented for brain spectroscopic imaging at 3T.

14:00 *3214*. **Separation of C-13 Metabolites with Chemical Shift Imaging**
Computer 27

Scott Brian Reeder[1], *Jean H. Brittain*[2], *Tom M. Grist*[1], *Yi-Fen Yen*[3]
[1]University of Wisconsin, Madison, Wisconsin, USA; [2]GE Healthcare, Madison, Wisconsin, USA; [3]GE Healthcare, Menlo Park, California, USA

A new chemical shift imaging approach for separation of C-13 labeled metabolites is described for the separation of C-13 labeled alanine, pyruvate, and lactate. This method requires a priori knowledge of the resonant frequencies of these species, as well as the relative signal from the two pyruvate peaks, one of which is close to alanine. Using a C-13 phantom at 3.0T, the new method demonstrate good qualitative agreement with echo planar spectroscopic imaging (EPSI), while only using 1/16th as much data as EPSI. This approach may be advantageous for hyperpolarized C-13 metabolic applications for reduced scan time compared with EPSI.

14:00 *3215*. **Volumetrically Resolved TE-Averaged Spectroscopic Imaging**
Computer 28

Dong-Hyun Kim[1], *Roland Henry*[1]
[1]University of California, San Francisco, California, USA

TE-averaged spectroscopy has been shown to isolate glutamate from glutamine at 3T. Extensions of this method to 2D spatial coverage have been previously implemented. In this abstract, we further extend the method to volumetric spatial coverage using spiral based readout gradients. The total exam time is within clinically acceptable range of 16:30 minutes. Echo time steps were carefully chosen to densely sample those area where the C4 proton had bigger amplitudes

14:30 *3216*. **Fast 4D Metabolite Mapping of Hyperpolarized 13C Compounds Using Multiple Echo 3D FIESTA**
Computer 27

William H. Perman[1], *Jochen Leupold*[2], *Pratip Bhattacharya*[3, 4], *Alex Lin*[4], *Kent Harris*[4], *Jurgen Hennig*[2], *Brian D. Ross*[4]
[1]St. Louis University School of Medicine, St. Louis, Missouri, USA; [2]University Hospital Freiburg, Freiburg, Germany; [3]California Institute of Technology, Pasadena, California, USA; [4]Huntington Medical Research Institutes, Pasadena, California, USA

The objective of this work was to develop a technique which will allow repeated measurements of spatial (3D imaging) and spectral (1D chemical-shift) distributions of a hyperpolarized 13C substrate in order to determine spatially localized metabolic kinetics (e.g. spatial distribution of tumor metabolism of 13C-pyruvate to 13C-lactate). A standard 3D FIESTA pulse sequence was modified for multi-nuclear and multiple gradient echo imaging (ME-3DFIESTA). We then imaged 13C-acetate and 13C-2-hydroxyethylacrylate (280 Hz chemical shift) and simultaneously hyperpolarized 13C-hydroxyethylpropionate and 13C-cis-fumarate to demonstrate the feasibility of using fast ME-3DFIESTA 4D imaging to provide spatially localized metabolic information on hyperpolarized substrates and products.

14:30 ***3217***. **A Java-Based, Platform-Independent Viewer for Magnetic Resonance Spectroscopic Imaging**
Computer 26
Andrew Frew[1], Raj Pagare[1], Daniel J. Valentino[1], Andrew A. Maudsely[2], Ammar Darkazanli[2], Jeffry R. Alger[1]
[1]University of California, Los Angeles, Los Angeles, California, USA; [2]University of Miami, Miami, Florida, USA

To provide for convenient viewing of spectroscopic imaging data with correlation to anatomical images, a self contained, platform-independent Spectroscopic Imaging Viewer was developed. The JAVA-based Viewer relies on XML metadata files to provide the flexibility needed to accommodate various types of spectroscopic imaging acquisitions, file naming conventions, files system hierarchies and operating systems. Images are displayed in co-registered space to provide easy correlation of spectroscopic imaging data to anatomical features and information from diverse modalities.

15:00 ***3218***. **Reduction of Acquisition Time in Magnetic Resonance Spectroscopic Imaging Using Wavelet Encoding Method**
Computer 26
Hacene Serrai[1], Richard Young[2]
[1]Institute for Biodiagnostics, Winnipeg, Manitoba, Canada; [2]Institute for biodiagnostics, Winnipeg, manitoba, Canada

The developped method is based on a non Fourier technique to reduce acquisition time and cross-voxel contamination in Magnetic Resonance Spectroscopic Imaging technique.The method is based on the discrete Wavelet Transform which allow spatial localization. The latter is used to reduce acquisition time by a sequential excitations of adjacent and/or non-adjacent voxels with no waiting time (TR) in between.

15:00 ***3219***. **A Comparison of 31P Concentration Measurements Using CSI and RARE MRI**
Computer 27
Robert L. Greenman[1], Xiaoen Wang[1], Aristidis Veves[1]
[1]Beth Israel Deaconess Medical Center/Harvard Medical School, Boston, Massachusetts, USA

In diabetes, functional abnormalities of the foot microvasculature impede the delivery of oxygen to the local tissues resulting in impaired metabolism, which can be measured using phosphorus-31 chemical shift imaging (31P-CSI). However, 31P-CSI suffers from poor spatial and temporal resolution. Phosphorus rapid acquisition with relaxation enhancement (31P-RARE) has been shown to provide higher spatial and temporal resolution and has also been used to assess diabetic foot muscle. The aim of this study was to compare the of the 31P concentrations in the foot muscles of diabetic and normal subjects as measured using 31P-CSI and 31P-RARE.

15:30 ***3220***. **Techniques of Highly Resolved *In Vivo* 1H CSI in Mouse Brain Tumors at 7 Tesla**
Computer 27
Claudia Diekmann[1], Rui Simoes[2, 3], Pohmann Rolf[4], Sebastian Cerdan[5], Carles Arus[2]
[1]Bruker Biospin MRI GmbH, Ettlingen, Germany; [2]Universitat Autònoma de Barcelona, Barcelona, Spain; [3]Universitat Universidade de Coimbra, Coimbra, Portugal; [4]F. Hoffmann-La Roche Pharmaceuticals, Basel, Switzerland; [5]"Alberto Sols" (UAM-CSIC), Madrid, Spain

This study established CSI acquisition on a various mouse models with a novel development of integrated shim and gradient coil gradient in combination with a PRESS localization using a CSI method.

15:30 ***3221***. **Functional Spectroscopy: A New Experimental Method in Exploring the Glutamate-Glutamine Cycle in the Human Brain**
Computer 26
Karsten Specht[1], Renate Grüner[1, 2], Roger Barndon[2], Heidi Karin van Wageningen[1], Lars Ersland[2], Kenneth Hugdahl[1]
[1]University of Bergen, Bergen, Norway; [2]Haukeland University Hospital, Bergen, Norway

In this study, single-voxel H1-MR Spectroscopy (TE 35ms) was used in 20 humans in order to explore changes in the concentration of metabolites in the sensory-motor system, when the explored subject was performing a motor task. That spectrum was compared to a spectrum, measured during rest. The results showed significant differences in the concentration of Glutamate, Glucose and Lactate. By contrast, a reference region in the occipital lobe didn't showed any significant changes under the same conditions.

Spectroscopic Quantitation

Room 4A Monday 14:00 - 16:00

14:00 ***3222***. **Direct Validation of *In Vivo* Localized ^{13}C MRS Measurements of [1-^{13}C] Glycogen in Rat Brain**
Computer 29
Hongxia Lei[1, 2], Tianwen Yue[2], Florence Morgenthaler[1], Rolf Gruetter[1, 2]
[1]EPFL, Lausanne, Switzerland; [2]University of Minnesota, Minneapolis, Minnesota, USA

In vivo ^{13}C MRS is to date the only non-invasive method to assess brain glycogen metabolism under physiological condition. The present study validated *in vivo* ^{13}C MRS measurement of brain glycogen over a wide concentration range within 20%, when comparing with biochemical determined ^{13}C labeled glycogen.

14:00 *3223*. **Metabolic Profiling of *post Mortem* Multiple Sclerosis Brain Using High Resolution ^{1}H NMR Spectroscopy**
Computer 30

Klaus DG Schmierer[1], Marc E. Denham[1], Sebastian Brander[1], David H. Miller[1], Tarek A. Yousry[1], Harold G. Parkes[1]
[1]Institute of Neurology, UCL, London, England, UK

MR spectroscopy (MRS) *in vivo* is being used to probe multiple sclerosis (MS). Pathological substrates of metabolite changes in MS brain are poorly understood. We applied high-field (500MHz for ^{1}H) MRS and quantitative histology to post mortem MS brain. Normal appearing white matter (NAWM) and white matter lesions (WML) were sampled from nine fresh MS brain slices. Chloroform-methanol-water extractions were carried out and ^{1}H NMR spectra acquired. Differences in metabolite concentrations were detected between NAWM and WML including a reduction of myo-Inositol in lesions. More cases will be studied to verify this finding.

14:00 *3224*. **Water as an Internal Reference for Spectroscopic Imaging: Methodology, Application, and Comparison to Other Methods**
Computer 31

Charles Gasparovic[1, 2], Tao Song[3], Deidre J. Devier[1, 4], Arvind Caprihan[5], Paul G. Mullins, [1,2], Rex E. Jung[1, 2], Leslie Morrison[1]
[1]University of New Mexico School of Medicine, Albuquerque, New Mexico, USA; [2]The MIND Institute, Albuquerque, New Mexico, USA; [3]University of California San Diego, San Diego, California, USA; [4]University of New Mexico, Albuquerque, New Mexico, USA; [5]New Mexico Resonance, Albuquerque, New Mexico, USA

The unsuppressed 'internal' water signal was introduced as a concentration reference for single-voxel proton magnetic resonance spectroscopy (1H-MRS) of the brain over a decade ago (1). However, to our knowledge, a detailed description of how this method could be applied to spectroscopic imaging (SI) or an examination of its potential sources of error has yet to be reported. Here we describe a method for using water as concentration reference in SI and its application to a study on gray matter (GM) and white matter (WM) metabolite concentrations in healthy adult subjects.

14:00 *3225*. **Optimization of Echo Time for GABA Editing Using MEGA-PRESS**
Computer 32

Tsuyoshi Matsuda, RT[1], Hirohiko Kimura, MD, PhD[2]
[1]GE Yokogawa Medical Systems, Hino, Tokyo, Japan; [2]University of Fukui, Fukui, Japan

MEGA-PRESS method is used for evaluation of GABA by clinical setting. We propose the optimization of echo time to increase NMR signal from GABA based on MEGA-PRESS methods. We show that the signal intensity of the GABA obtained MEGA-PRESS with TE61ms was higher than TE68ms spectrum which TE calculated from J-coupling both *in vivo* and vitro condition. Although the signal gain may be small using TE=61ms instead of TE 68ms in GABA editing acquisition, this is very important especially for the clinical application, since the acquisition time is limited in clinical setting.

14:30 *3226*. **Effects of Cations and PH on Optimized Assessment of Prostatic Citrate at 3 Tesla**
Computer 32

Kagayaki Kuroda[1, 2], Takaki Maeda[3, 4], Robert V. Mulkern[5], Naoyuki Takei[6], Yasushi Kaji[7], Kazuro Sugimura
[1]Graduate School of Engineering, Tokai University, Hiratsuka, Kanagawa, Japan; [2]Institute of Biomedical Research and Innovation, Kobe, Hyogo, Japan; [3]Kobe University School of Medicine, Kobe, Hyogo, Japan; [4]Tenri Hospital, Tenri, Osaka, Japan; [5]Children's Hospital, Harvard Medical School, Boston, Massachusetts, USA; [6]GE Yokogawa Medical Systems, Hino, Tokyo, Japan; [7]Graduate School of Medicine, Kobe University, Kobe, Hyogo, Japan

Effects of cations and pH on assessment of citrate using PRESS at 3 Tesla were examined in a TE range of 25-300 ms. J-modulated signal intensity curves versus TE of 90-mM citrate solutions with divalent cations shifted markedly with cation concentrations in the order of Ca2+ > Zn2+ > Mg2+. No apparent TE shift was observed for solutions with monovalent cations including Na+ and K+, and for pH values of 6.0-9.0, whereas marked amplitude changes observed. Regardless of the notable TE shift due to divalent cations, peak amplitudes of 130-140 ms were observed for citrate signal of the prostate in each healthy volunteer.

14:30 *3227*. **Single Voxel MRS Measurements Are Not Influenced by Swirling Flow in Phantom Solution**
Computer 31

Chen Lin[1], Kejal Kantarci[1], John D. Port[1], Joel P. Felmlee[1], Clifford R. Jack Jr.[1]
[1]Mayo Clinic, Rochester, Minnesota, USA

MR spectrocopy is a useful technique for both diagnosis and research. However, large variations in MRS result are often obsearved because it's sensitive to scanner performace and calibration. For quantitative MRS, it's necessary to confirm the accuracy through QC tests. While a phantom containing physiological metabolite solution is commonly used for MRSQC, the effect of flow in the solution has been a concern. This work demonstrates that such effect on measured metabolite concentrations is below the level of detection of a typical MRS protocol and, therefore, a solution phantom may be used without waiting for the flow to settle.

14:30 ***3228***. **Metabolite Profiles Obtained with QUEST from HRMAS-NMR Signals of Rat Brains**
Computer 30
Hérald Rabeson[1], Florence Fauvelle[2], Hélène Ratiney[1], Cristina Cudalbu[1], Dirk van Ormondt[3], Danielle Graveron-Demilly[1]
[1]Université Claude Bernard, Lyon I - CPE, Villeurbanne, France; [2]CRSSA/BCM, La Tronche, France; [3]Delft University of Technology, Delft, Netherlands

High-resolution magic angle spinning (HRMAS) 1H spectroscopy is playing an increasingly important role for diagnosis. This technique enables setting up metabolite profiles of *ex vivo* pathological and healthy tissue. Automatic quantitation of HRMAS signals will provide reliable reference profiles to monitor diseases and pharmaceutical follow-up. We show that quantitation of HRMAS signals of rat brains acquired *without* suppression of lipids and macromolecules to avoid metabolite signal loss, is possible with the time-domain semi-parametric algorithm QUEST. Disentangling the metabolite from the background signals was achieved by the `Subtract' approach. About twenty metabolites were reliably quantitated.

14:30 ***3229***. **Repeated Measures Performance of Volumetric Whole Brain Echo Planar Spectroscopic Imaging**
Computer 29
Jeffry R. Alger[1], Andrew J. Frew[1], Raj Pagare[1], Ammar Darkazanli[2], Andrew A. Maudsley[2]
[1]University of California, Los Angeles, Los Angeles, California, USA; [2]University of Miami, Miami, Florida, USA

A repeated measures study was performed on young adult human brain to determine the characteristic precision with which 1.5 T volumetric echo planar spectroscopic imaging can practically determine metabolite levels in single spectroscopic imaging voxels. Automated MIDAS spectroscopic imaging software was used for signal processing and voxel selection. The within-subject coefficient of variation (Standard Deviation divided by Mean) ranged from 3 to 33% for water-referenced NAA, cholines and creatines in three typically studied homogeneous brain regions (Thalamus, Frontal White Matter, Posterior Cingulate). The Anterior Cingulate could not be evaluated due to the presence of static field inhomogeneity.

15:00 ***3230***. **Fast Analysis of 1H Magnetic Resonance Spectroscopic Imaging Data: An Artificial Neural Network Based Approach**
Computer 29
Himanshu Vishwas Bhat[1], Balasrinivasa Rao Sajja[2], Sushmita Datta[2], Ponnada A. Narayana[2]
[1]University of Houston, Houston, Texas, USA; [2]University of Texas Medical School at Houston, Houston, Texas, USA

A radial basis function neural network (RBFNN) based method for fast quantification of phased, as opposed to magnitude, MRSI data is presented. Simulations show this method to be robust in the presence of noise and phase distortions. The metabolite area ratios for normal subjects determined using RBFNN very favorably compare with the published values. The computational time on a typical PC was around 15-20 seconds, compared to 30-40 minutes, for line fitting methods. This method could be applied for real time analysis of MRSI data under parallel computing environment.

15:00 ***3231***. **Accuracy of Exchange Rate Measurement Using CUPS, a Novel Method for Kinetic Analysis**
Computer 30
Craig J. Galban[1], Richard G. Spencer[2]
[1]National Institutes of Health, Bethesda, Maryland, USA; [2]National Institutes of Health, Baltimore, Maryland, USA

A new method for measuring chemical exchange rate constants using progressive saturation, CUPS, (chemical exchange measurement using progressive saturation) is analyzed here. CUPS is based on the influence of chemical exchange on observed magnetizations during the one-pulse experiment and also provides T_1 values which are not confounded by chemical exchange. We performed a detailed evaluation of CUPS in the presence of noise and flip angle errors, and compared our results with errors in the transient saturation transfer (TST) technique for analysis of exchanging systems.

15:00 ***3232***. **Measuring Glutamate in the Human Brain by MRS: Reproducibility Using Time Domain Fitting at 3 Tesla**
Computer 31
Karen E. Davies[1], Eugenia Leitao[1], S Singh[1], S Mistry[1], Samantha Jefferson[1], Shaheen Hamdy[1], Stephen Ross Williams[1]
[1]University of Manchester, Manchester, UK

Measurement of glutamate by MRS is difficult because of overlap with other signals, notably glutamine. However, at 3T the spectra of glutamate and glutamine do not completely overlap, and separation of the resonances is feasible. Here we report results from a reproducibility study in which serial glutamate measurements were made in 3 brain areas in 5 normal volunteers in a 3T magnet. Time domain fitting was performed using prior knowledge derived from phantom measurements and simulations. The within-subjects coefficient of variation for glutamate in each brain region was between 9-13%, similar to NAA (7-11%).

15:00 ***3233***. **Hyperpolarization by DNP Is Applicable to ^{13}C Isotopomer Analysis**
Computer 32
Matthew Merritt[1], Damir Blazina[2], Craig Malloy[1]
[1]UTSW Medical Center, Dallas, Texas, USA; [2]Oxford Instruments Molecular Biotools, Ltd., Tubney Woods, UK

A constant challenge facing magnetic resonance is the low sensitivity. The sensitivity is directly related to the relative populations of the spin energy levels probed by the experiment. Hyperpolarization by DNP at liquid helium temperatures followed by rapid dissolution has been shown to increase the polarization by orders of magnitude. To test the applicability of this method to ^{13}C isotopomer analysis, we have carried out feasibility studies on uniformly ^{13}C labeled glutamate and acetate. Initial experiments demonstrate that this method will work for the range of molecules of interest, and will not be confounded by multiple isotopomers.

15:30 ***3234***. **On the Reliability of ^{13}C Metabolic Modeling Using Two-Compartment Neuronal-Glial Models**
Computer 32

Alexander Shestov[1], Kamil Ugurbil[1], Pierre-Gilles Henry[1]
[1]University of Minnesota, Minneapolis, Minnesota, USA

^{13}C NMR spectroscopy in conjunction with infusion of ^{13}C-labeled substrates can be used to measure metabolic fluxes. In the brain, complex two compartment neuronal-glial models allow determination of a number of metabolic fluxes, including the glutamate-glutamine cycle rate Vnt which is thought to reflect glutamatergic neurotransmission. In this work we use Monte-Carlo simulations to investigate the reliability of metabolic modeling using two-compartment models. We show that Vnt may be unreliable under certain experimental conditions and that additional constraints in the model may be needed for precise determination of this flux.

15:30 ***3235***. **Very Short Echo Time STEAM Improves Detection of Glutamate at 3-T**
Computer 31

Dattesh D. Shanbhag[1], Sarah Andrea Dunham[1], Jack Knight-Scott[1]
[1]University of Virginia, Charlottesville, Virginia, USA

In this study, we examined TE modulation of the glutamate (Glu) and glutamine (Gln) spectral patterns for both the STEAM and PRESS localization sequences at 3-T to determine the optimal TE for resolving Glu and Gln. NMR-SCOPE simulations suggest that at 3-T, Glu is best resolved from Gln at very short echo times (< 10 ms), irrespective of the localization technique. Specifically, the Glu C-4 proton multiplet at 2.34 ppm is well resolved from the nearest Gln resonance, the C-2 proton multiplet at 2.44 ppm. However, since STEAM provides greater suppression of the Gln resonances and is capable of shorter echo times than PRESS, we propose that with the current technology, a very short TE STEAM provides an optimal strategy for the detection of Glu *in vivo*.

15:30 ***3236***. **Water as an Internal Reference for Spectroscopic Imaging: Variability Due to Partial Volume Estimates**
Computer 30

Charles Gasparovic[1, 2], Tao Song[3], Deidre J. Devier[1, 4], Jeremy Bockholt[2], Arvind Caprihan[5], Paul G. Mullins, [1,2], Stefan Posse, [26], Rex E. Jung[1, 2], Leslie Morrison[1]
[1]University of New Mexico School of Medicine, Albuquerque, New Mexico, USA; [2]The MIND Institute, Albuquerque, New Mexico, USA; [3]University of California San Diego, San Diego, California, USA; [4]University of New Mexico, Albuquerque, New Mexico, USA; [5]New Mexico Resonance, Albuquerque, New Mexico, USA; [6]University of New Mexico School of Medicine, Albuquerque, New Mexico, USA

A strategy for using tissue water as a concentration standard in 1H magnetic resonance spectroscopic imaging studies on the brain is presented and the potential errors that may arise due to the partial volume effect and tissue classification are examined. In particular, different estimates of the cerebrospinal fluid contribution to spectroscopic voxels, based on different segmentation methods, are shown to lead to a large variability in estimates of metabolite concentrations in gray matter.

15:30 ***3237***. **Error Bounds for Semi-Parametric Estimation in MRS**
Computer 29

Helene Ratiney[1], Enrico Capobianco[2], Ronald de Beer[3], Dirk van Ormondt[3], Danielle Graveron-Demilly[1]
[1]Université Claude Bernard, Lyon I - CPE, Villeurbanne, France; [2]University of Boston, Boston, Massachusetts, USA; [3]Delft University of Technology, Delft, Netherlands

The presence of a non-parametric background in 1H short echo-time signals invalidates the theory of Cramer-Rao lower Bounds (CRBs) on metabolite estimation errors. As a result, the usual CRBs, derived in absence of background, become unattainable. The increase of the metabolite estimation errors depends on the way of handling a non-parametric background. Seeking alternative lower bounds for each of the many *ways* of handling non-parametric backgrounds is impractical. We improve the situation by deriving a simple, general expression of CRBs that encompasses unconstrained estimation of the initial part of the background signal that is above the noise level.

MRS of Cells, Body Fluids, and Others

Room 4A Monday 14:00 - 16:00

14:00 ***3238***. **Is NMR Spectroscopy a Suitable Tool in Clinical Microbiology?**
Computer 33

Heide-Marie Daniel[1], Vincent Robert[2], Tania C. Sorrell[3], Brion Dolenko[4], Ray L. Somorjai[4], Carolyn E. Mountford[3], Uwe Himmelreich[5]
[1]Université catholique de Louvain, Louvain-la-Neuve, Belgium; [2]Centraalbureau voor Schimmelcultures, Utrecht, Netherlands; [3]University of Sydney, Sydney, Australia; [4]National Research Council of Canada, Winnipeg, Manitoba, Canada; [5]Max-Planck-Institute for Neurological Research, Cologne, Germany

A supervised, hierarchical classification method was developed for the identification of pathogenic yeast isolates based on NMR spectra of cell suspensions. The method is extendable for new, emerging pathogens. Identification was rapid and robust to the sub-species level. In addition, a distance-based classification is able to distinguish unusual isolates from those available in a database, providing hereby a method to identify outliers.

14:00 ***3239***. **Rapid and Simultaneous Analysis of All Major Constituents in Human Bile Using 1H NMR Spectroscopy**
Computer 34

Omkar B. Ijare[1], B. S. Somashekar[1], G. A. Nagana Gowda[1], Ajay Sharma[2], V. K. Kapoor[2], C. L. Khetrapal[1]
[1]Centre of Biomedical Magnetic Resonance, Lucknow, Uttar Pradesh, India; [2]Sanjay Gandhi Postgraduate Institute of Medical Sciences, Lucknow, Uttar Pradesh, India

One step analysis of major bile components in intact bile is difficult due to broad and overlapping NMR signals. This problem is overcome by using dimethylsulfoxide which results in resolved NMR signals. Using rigorous 1D and 2D NMR studies at 400 and 700 MHz, distinct markers for cholesterol, bile acids and glycerophospholipids were identified and used for quantitative analyses of major constituents of bile in a single step. Accurate, rapid and simultaneous analyses of major bile components shown here for the first time may have immense implications for pathophysiology, diagnosis and prognosis of biliary and intestinal diseases.

14:30 ***3240***. **Simultaneous ^{1}H MRS Measurement of Temperature and PH with a Lanthanide Complex**
Computer 34

Daniel Coman[1], Hubert Trubel[1, 2], Robert E. Rycyna[3], Michael Caldwell[1], Fahmeed Hyder[1]
[1]Yale University, New Haven, CT 06510, USA; [2]University Witten/Herdecke, Wuppertal, Germany; [3]Bruker BioSpin MRI, Billerica, MA 01821, USA

In vivo measurements of brain temperature and pH distributions are scarce, mainly due to the lack of non-invasive methods. The proton resonances from the shifting reagent $TmDOTP^{5-}$ are strongly dependent on temperature and pH. Previous linear models used two resonances to determine temperature and pH. We propose a new non-linear model which exploits temperature and pH information that is stored in three of the resonances of $TmDOTP^{5-}$. The variable temperature and pH interdependencies provide a redundant framework, not exploited previously, to allow more accurate calibrations for temperature (±0.05 C) and pH (±0.02) in vitro and *in vivo*.

14:30 ***3241***. **Origin of the Mobile Lipids Detected Intensity Changes in C6 Glioma Cells with Proliferation Rate**
Computer 33

Maria Rosa Quintero-Bernabeu[1], Miquel E. Cabañas[1], Carles Arús[1]
[1]Universitat Autònoma de Barcelona, Cerdanyola del Vallès-Barcelona, Spain

NMR-visible mobile lipids (ML) resonances detected in various tumours and cultured cell lines vary in intensity with growth rate. Our purpose has been to improve our understanding of the origin of this ML variation in cultured C6 cells. Results obtained demonstrate that TAG content per cell does not change between log and post-confluent cells, suggesting that changes in ML resonances in C6 cells arise from biophysical causes rather than from biochemical changes in TAG content per cell.

15:00 ***3242***. **Role of In-Vitro Proton NMR Spectroscopy in Inflammatory Bowel Disorders**
Computer 33

Krithika Balasubramanian[1], Sandeep Kumar[1], Uma Sharma[1], Govind Makharia[1], N R. Jagannathan[1]
[1]All India Institute of Medical Sciences, New Delhi, Delhi, India

This study is aimed at identifying the two types of IBD- Ulcerative colitis (UC) and Crohn's disease (CD) and differentiating it from ITB and normal using ^{1}H NMR spectroscopy. 21 metabolites were assigned and the concentrations of 10 metabolites were determined. Significant decrease in lactate (Lac), glutamate+glutamine (Glu+Gln), myo-inositol (mI) and glycerophosphorylcholine (GPC) were observed in UC patients compared to controls. CD patients showed a decrease in Lac and Glu+Gln while those with tuberculosis (TB) showed a decrease in Lac, Glu+Gln and mI compared to controls. TB patients showed a decrease in Lac and Ace compared to UC and a decrease in Lac, Ace and mI compared to CD.

15:30 ***3243***. **Accurate and Simultaneous Analysis of Six Glycine/taurine Conjugated Bile Acids in Human Bile Using 1H NMR Spectroscopy**
Computer 33

G. A. Nagana Gowda[1], Omkar B. Ijare[1], B. S. Somashekar[1], Ajay Sharma[2], V. K. Kapoor[2], C. L. Khetrapal[1]
[1]Centre of Biomedical Magnetic Resonance, Lucknow, Uttar Pradesh, India; [2]Sanjay Gandhi Postgraduate Institute of Medical Sciences, Lucknow, Uttar Pradesh, India

Glycocholicacid, glycodeoxycholicacid, glycochenodeoxycholicacid, taurocholicacid, taurodeoxycholicacid and taurochenodeoxycholicacid are identified for the first time in intact human bile using several 1D and 2D [1H-1H and 1H-13C] experiments at 400, 700 and 800 MHz and a method is proposed for their accurate analyses. 1H and 13C chemical shifts for ten standard bile acids were determined under physiological conditions and used for unambiguous identification of bile acids in the complex mixture of human bile. Simple one step method for accurate analyses of individual bile acids in bile presented herein may have implications in the study of bile acid metabolism associated with biliary diseases.

Microscopy and Non Proton MR

Room 4A Monday 14:00 - 16:00

14:00 Computer 35 ***3244***. **High-Resolution *In Vivo* MR Imaging of Mouse Knee on a Whole-Body 3-Tesla System**

Wingchi Edmund Kwok[1], Steve Proulx[1], Zhigang You[1], Edward M. Schwarz[1], Saara M. Totterman[2]
[1]University of Rochester, Rochester, New York, USA; [2]Virtualscopics Incorporation, Rochester, New York, USA

Despite recent advancement in new therapies for arthritis, there is a lack of longitudinal studies following therapeutic treatment to evaluate the repair response. In this study, we developed a high-resolution MR imaging technique for imaging mouse knee that enables longitudinal studies in mice. We conducted our study on a clinical 3-Tesla system. We designed and built a dedicated RF coil, and developed high resolution pulse sequences to support the high image spatial resolution needed. Imaging tests on normal wild-type mice and transgenic mice with inflammatory arthritis shows that arthritis changes in mouse knee can be clearly visualized by our technique.

14:30 Computer 35 ***3245***. **Articular Cartilage Under Static Load: A Quantitative Polarized Light Microscopic Imaging Study Correlated with Micro-MRI (µMRI) Findings**

Hisham Alhadlaq[1, 2], Yang Xia[2], Niloufar Fozouni[2], Ilco Aksovski[2]
[1]King Saud University, Riyadh, Saudi Arabia; [2]Oakland University, Rochester, Michigan, USA

Changes in the organization of the collagen fiber network in loaded articular cartilage were investigated through microscopic MRI (µMRI) and polarized light microscopy (PLM) imaging. The relative thickness of the superficial zone (SZ) was shown to be dependent of strain from both MR T_2 maps and PLM maps, validating previously reported µMRI findings. No significant correlations were established for the transitional (TZ) and deep zones. The angle map showed a shift of the middle of the transition between the SZ and the TZ away from the cartilage surface, in agreement with the shift of T_2 peak observed in µMRI results.

15:00 Computer 35 ***3246***. **Monitoring Brain Potassium with ^{87}Rb MRI**

Victor E. Yushmanov[1], Alexander Kharlamov[1], Fernando E. Boada[2], Stephen C. Jones[1]
[1]Allegheny-Singer Research Institute, Pittsburgh, Pennsylvania, USA; [2]University of Pittsburgh, Pittsburgh, Pennsylvania, USA

To monitor K^+ by ^{87}Rb MRI *in vivo*, we developed a protocol of dietary RbCl administration, verified that it does not interfere with ischemic brain K^+ dynamics, and performed ^{87}Rb and ^{23}Na MRI in phantoms and animals at 3T using a Twisted Projection Imaging scheme and a PCOS coil. Brain [Rb^+] safely increased up to 25 mEq/l with feeding duration. Rb^+ did not significantly change the characteristic stepwise pattern of [K^+] decrease in ischemic cortex with a sharp drop at 4 h. Preliminary MRI experiments prove the practicability of ^{87}Rb MRI of the rat brain with a PCOS coil.

15:30 Computer 35 ***3247***. **Quantitative Sodium MR Imaging of the Human Brain at 3.0T**

Belinda S.Y. Li[1], Glenn Reynolds[2], Frederick C. Damen[3], Ian Atkinson[3], Theodore C. Claiborne[3], Michael P. Flannery[3], Xiaohong J. Zhou[3], Fernando E. Boada[4], Keith R. Thulborn[3]
[1]GE Healthcare, Chicago, Illinois, USA; [2]GE Healthcare, Boston, Massachusetts, USA; [3]University of Illinois at Chicago, Chicago, Illinois, USA; [4]University of Pittsburgh, Pittsburgh, Pennsylvania, USA

Quantitative tissue sodium concentration (TSC) provides an effective and direct measure of tissue viability. Higher field strengths and an efficient k-space acquisition scheme are particularly desirable for sodium imaging. This paper shows that accurate TSC values can be measured in human brains at the increasingly common clinical field strength of 3.0T, using a Twisted Projection Imaging technique, obtaining clinically-useful resolution (nominal 0.064cc) in <9min. Improved SNR and reduced partial volume effects at 3.0T allows more accurate TSC quantification at 3.0T than at 1.5T.

Body MR: Liver

Room 4A Tuesday 13:30 - 15:30

13:30 *3248*. **Arterial Spin Labeling TrueFISP Pancreas/Liver Perfusion Imaging at 1.5 Tesla**
Computer 1
Maolin Qiu[1], Jinghua Wang[1], Alexander Pinus[1], Hyeonjin Kim[1], R Todd Constable[1]
[1]Yale University School of Medicine, Hew Haven, Connecticut, USA

The change in the signal intensity of perfusion-weighted images induced by arterial spin labeling is very small, which is even lower in the arterial spin labeling (ASL) TrueFISP Perfusion Imaging due to the low flip angle. The number of repetitions necessary to achieve reasonable SNR makes breath-hold scans difficult for patients in clinical application. In the current work, we investigated the potentials and drawbacks of using a respiratory triggered, ASL FISP imaging sequence at such 1.5 Tesla for quantitative mapping of Pancreas/Liver perfusion.

14:00 *3249*. **BOLD MRI Signal Analysis of Activated Human Liver**
Computer 1
Zhaoyang Fan[1], Marshall S. Sussman[2], Jeffrey A. Stainsby[3], Michael D. Noseworthy[1]
[1]McMaster University, Hamilton, Ontario, Canada; [2]University of Toronto, Toronto, Ontario, Canada; [3]General Electric Healthcare, Toronto, Ontario, Canada

BOLD contrast has been demonstrated in liver, following certain challenges, in rats and humans. The effect is exacerbated in the liver between fasted and postprandial states. In the present study, fasted human liver was stimulated through ingestion of a controlled meal resulting in dynamic modulation of T2*-weighted images. In the healthy liver parenchyma, an approximate 70% decline in BOLD signal intensity followed by elevation to a level 20% higher than baseline (i.e. fasted state) was observed. Analysis of hepatic signal vs. time provides a baseline for healthy liver response to a standardized challenge.

14:30 *3250*. **Breath-Hold Perfusion of Hepatic Malignancies Using Dynamic Susceptibility Contrast-Enhanced Echo-Planar Imaging: A Preliminary Study**
Computer 1
Wu Bin[1], Peng Weijun[1]
[1]Cancer Hospital, Shanghai, People's Republic of China

The degree of the signal drop during the first pass (i.e. perfusion phase) is directly proportional to the concentration of contrast agent in the blood. A graph of transient signal drop versus time can be used to compute hemodynamic blood volume map reflecting the microvascularity of the tissue and detecting hemodynamic blood changes after treatment such as transcatheter arterial chemoembolization(TACE) and anti-angiogensis therapy. In this pilot work, we investigate the feasibility of doing this procedure in abdominal regions, and focus on the quantitative analysis of time-intensity curves as well as the enhancement patterns with further assessment of effectiveness after treatment

15:00 *3251*. **Parameters of Vascular Permeability in Hepatocellular Carcinomas: Assessment with Low- And High-Molecular-Weight Agents in the Rat**
Computer 1
Nicolas Michoux[1], Bernard van Beers[1]
[1]St-Luc University Hospital - Université Catholique de Louvain, Brussels, Belgium

DCE-MRI is increasingly used for non-invasive imaging the tumour microcirculation and monitoring the action of antiangiogenic agents. In practice, the vascular parameters potentially usable in clinics, displayed an unequal sensitivity to the contrast agent and pharmacokinetics model that are used. Recently, the volume transfer constant Ktrans was recommended as primary end-point, although it reflects a combined measurement of the blood flow and permeability in tumors. Investigating three agents and three models, we reassess which parameter should be measured. It is concluded that permeability differences are better assessed by measuring the volume of extravascular extracellular space rather than Ktrans.

fMRI: High Resolution and Visual System

Room 4A Tuesday 13:30 - 15:30

13:30 *3252*. **Perfusion-Based fMRI in Human LGN and Visual Cortex Reveals a Regional Difference in the Coupling Between Cerebral Blood Flow and BOLD**
Computer 3
Kun Lu[1], Joanna E. Perthen[1], Rob O. Duncan[1], Linda M. Zangwill[1], Thomas T. Liu[1]
[1]University of California San Diego, La Jolla, California, USA

It has been observed that the percentage change of BOLD signal in lateral geniculate nucleus (LGN) due to activation is typically 2-3 times smaller than that in primary visual cortex (V1). We investigated the origin of this difference using perfusion-based functional MRI. Our results suggest that the BOLD difference in LGN and V1 may reflect a regional dependence of the coupling between cerebral blood flow (CBF) and CMRO2. Additional experiments are required to test this hypothesis.

13:30 ***3253***. **Multi Modal-Functional Studies in Rat Somatosensory Cortex: Heterogeneity Due to Stimuli**
Computer 2
Peter Herman[1, 2], Basavaraju Ganganna Sanganahalli[1], Fahmeed Hyder[1]
[1]Yale University, New Haven, Connecticut, USA; [2]Semmelweis University, Budapest, Hungary

The functional response to sensory stimuli is heterogeneous. Here we investigated the heterogeneity by varying stimulus parameters at a depth of layer 4 in the α-chloralose anesthetized rat. The neurometabolic-neurovascular responses (BOLD, CBF, pO2) and electrical activity (AP, LFP) were measured in during 30 s forepaw stimulation and as a function of stimulation parameters (0.2, 2.0, and 10.0 mA; 1, 3, and 9 Hz). The correlation between the BOLD-CBF, BOLD-AP, BOLD-FP, CBF-AP, and CBF-LFP responding patterns were ~0.16, ~0.2, ~1.0, ~0.08, and ~0.93, respectively. Therefore the AP signals have closer correlation to CBF and BOLD signals than the LFP signals.

14:00 ***3254***. **Multi-Modal Functional Studies in Rat Somatosensory Cortex: Heterogeneity Across Layers**
Computer 2
Peter Herman[1, 2], Basavaraju Ganganna Sanganahalli[1], Fahmeed Hyder[1]
[1]Yale University, New Haven, Connecticut, USA; [2]Semmelweis University, Budapest, Hungary

The functional response to sensory stimuli is heterogeneous. We investigated the heterogeneity across the cortical layers for a given forepaw stimulus in the α-chloralose anesthetized rat. The neurometabolic-neurovascular responses (BOLD, CBF, pO2) and electrical activity (AP, LFP) were measured in rat somatosensory cortex during 30 s forepaw stimulation (3 Hz, 2 mA, 0.3 ms) as a function of cortical depth. The contralateral responses were significantly larger than ipsilateral responses, both in size and amplitude for all modalities across all layers. The BOLD responses decreased across layers, from top to bottom, whereas the dynamics of the different signals were generally correlated.

14:00 ***3255***. **Detecting LGN Activation in Human Using Quantitative Perfusion-Based fMRI: A Feasibility Study**
Computer 3
Kun Lu[1], Joanna E. Perthen[1], Rob O. Duncan[1], Linda M. Zangwill[1], Thomas T. Liu[1]
[1]University of California, San Diego, La Jolla, California, USA

Although blood oxygen level dependent (BOLD) activation in human lateral genicuate nucleus (LGN) has been detected using functional MRI (fMRI), no perfusion activation in LGN has been reported yet. We demonstrate in this study that perfusion-based fMRI using arterial spin labeling (ASL) MRI can detect perfusion activation in LGN. Background suppression and physiological noise correction are needed in order to achieve necessary signal-to-noise ratio (SNR) to reliably discern activation.

14:30 ***3256***. **Real-Time Mapping of the Visual Field Using Random Stimulus Presentation**
Computer 3
B D. Ward[1], J Janik[1], Yousef Mazaheri[2], Ted DeYoe[1]
[1]Medical College of Wisconsin, Milwaukee, Wisconsin, USA; [2]Memorial Sloan Kettering Cancer Center, New York, New York, USA

For clinical fMRI applications, it is desirable that parameter estimates and statistical results be displayed in real-time. An fMRI retinotopy experiment was conducted using a random visual field excitation paradigm. Real-time mapping of the visual field was simulated, post-experiment, using recursive, multi-parameter Kalman filter estimation of the visual field sensitivity profile for each voxel.

14:30 ***3257***. **Lamina-Specific Anatomical MRI of the Rat Retina**
Computer 2
Haiying Cheng[1], Machelle T. Pardue[2], Peter M. Thule[1], Timothy Q. Duong[1]
[1]Emory University, Atlanta, Georgia, USA; [2]Atlanta VA Medical Center, Atlanta, Georgia, USA

We used MRI to visualize three strips corresponding to established anatomical structures in the rat retina. The inner strip nearest to the vitreous, which appeared relatively brighter on T1-weighted images and was enhanced by Gd-DTPA, was assigned to be the ganglion and bipolar cell layer and the embedded retinal vasculature. The middle strip, which appeared darker on T1-weighted images and was not enhanced by Gd-DTPA, was the photoreceptor layer. The outer strip which exhibited similar characteristics as the inner strip was the choroidal vascular layer. The retinal thickness, including the choroid complex, was 307±20 micrometer by MRI and 185±35 micrometer by histology.

15:00 ***3258***. **Laminar Specificity of the SE-fMRI Signal in Monkey Striate Visual Cortex**
Computer 2
Jozien Goense[1], Nikos Logothetis[1]
[1]Max-Planck Institute for Biological Cybernetics, Tuebingen, Germany

To relate fMRI signals to the underlying neural events, it is necessary to achieve a spatial resolution and specificity that permits visualization of the cortical functional units, e.g. cortical columns or laminae. Because the resolution of GE-fMRI is determined by intracortical veins and therefore limited, we used SE-fMRI, which is weighted towards capillaries, to obtain specific BOLD responses. SE-EPI however is also sensitive to the venous fraction, potentially limiting spatial resolution. By decreasing the EPI acquisition window, we obtained highly specific functional activation. Activation was predominantly located in layer IV, while activation around surface vessels varied with acquisition window length.

15:00 ***3259***. **Non-Linear BOLD Responses for Transient Deactivations in V1**
Computer 3
Lin Tang[1], Malcolm J. Avison[1], John C. Gore[1]
[1]Vanderbilt University Institute of Imaging Science, Nashville, Tennessee, USA

Synopsis not available.

fMRI: Resting State, Reproducability, and Quality Assurance

Room 4A Tuesday 13:30 - 15:30

13:30 ***3260***. **Default Mode Functional Connectivity Altered by Sevoflurane Anesthesia**
Computer 5
Scott James Peltier[1], Chantal Kerssens[2], Stephan B. Hamann[3], Peter S. Sebel[2], Michael Byas-Smith[2], Xiaoping Hu[1]
[1]Emory University/Georgia Tech, Atlanta, Georgia, USA; [2]Emory University School of Medicine, Atlanta, Georgia, USA; [3]Emory University, Atlanta, Georgia, USA

This study investigated how sevoflurane anesthesia affects functional connectivity associated with the posterior cingulate (the "default mode" network). Resting-state MR scans were acquired under different levels of anesthesia (0, 2%, 1% sevoflurane). Across all subjects, the number of voxels covarying with the posterior cingulate was significantly decreased going from the awake state to deep anesthesia, and was subsequently increased going from deep to light anesthesia.

13:30 ***3261***. **Functional Connectivity of Auditory and Visual Areas During Rest and Stimulus Presentation**
Computer 6
Karen J. Mullinger[1], Paul Simon Morgan[1], Dorothee P. Auer[1], Richard W. Bowtell[1]
[1]University of Nottingham, Nottingham, UK

The correlation of signal fluctuations in visual and auditory cortices and changes in the pattern of connectivity occurring due to presentation of visual and auditory stimuli are studied here using whole-brain fMRI. Concurrent EEG recording was used to monitor changes in brain state, and to compare of EEG power fluctuation with BOLD signal variation. The results show that there are significantly sized regions of visual and auditory cortex that exhibit correlated signal fluctuations during the resting state, with a reduction in this correlation when stimuli are presented. Measurement of alpha power indicates a change in electrical activity during stimulus presentation.

14:00 ***3262***. **Reproducible Whisker Stimulation for fMRI and Neurophysiological Studies**
Computer 6
Basavaraju Ganganna Sanganahalli[1], Peter Herman[1, 2], Fahmeed Hyder[1]
[1]Yale University, New Haven, Connecticut, USA; [2]Semmelweis University, Budapest, Hungary

We developed a controllable device for reproducible whisker stimulations to be used in both fMRI and neurophysiological studies. Transverse air flow positioned anterior-posterior to whiskers was the most competent design for experiments inside and outside the magnet, because the amplitude of air puffs from the two pumps could be matched (±3%) and the frequency of the oscillating air puffs from the two pumps could be offset in time (0.1 to 20 Hz). Preliminary results from fMRI (11.7T) and neurophysiological studies show that stimulation of all whiskers increased activity in the contralateral barrel field with a maximum response at 8 Hz

14:00 ***3263***. **The Minimum Detectable Change in fMRI Measurements of Brain Activity Across Imaging Sessions**
Computer 5
Erin A. Douglas[1], Bradley Gordon Goodyear[1]
[1]University of Calgary, Calgary, AB, Canada

To use fMRI to track post-stroke recovery and assess treatment, there is a need to obtain precise and reproducible fMRI measurements of brain function from individual stroke patients. Modest reproducibility of fMRI has been demonstrated, with the laterality index (LI, defined as contralateral minus ipsilateral divided by contralatreral plus ipsilateral activation) showing better reproducibility. In this study we determine the minimum detectable change in fMRI measurements of brain activity across imaging sessions. As a result, this will determine the usefulness of fMRI for clinical evaluations of the progression of functional recovery and reorganization following stroke in individual patients.

14:00 ***3264***. **Determining the Latency Between Spontaneous Respiration Fluctuations and BOLD Signal Changes**
Computer 4
Monica A. Smith[1], Peter A. Bandettini[1], Rasmus M. Birn[1]
[1]National Institute of Mental Health, Bethesda, Maryland, USA

The blood oxygenation level dependent (BOLD) fMRI signal is influenced by spontaneous fluctuations in respiration during rest, yet the latency between respiration changes and BOLD changes has not been fully characterized. The goal of this study is to measure the magnitude and latency of BOLD signal changes due to variations in respiration at rest. These are compared to measurements from a hypercapnic stress. Signal changes to variations in respirations were found to be delayed by ~9 seconds relative to measured respiration changes. Amplitudes and latencies of these BOLD changes during rest were spatially correlated with changes from a hypercapnic stress.

14:30 ***3265***. **Software Tools for Batch Processing, Management and Visualization of Functional MRI Data**
Computer 4
Andrew V. Poliakov[1], Eider B. Moore[1], James F. Brinkley[1]
[1]University of Washington, Seattle, Washington, USA

Functional MRI presents - among many others - informatics challenges, such as efficient and error-proof processing and management of large volumes of data, record keeping and complex visualization. Our software tools X-batch and MindSeer were developed to resolve these common issues. X-batch addresses two needs of fMRI analysis: i) automation of statistical image processing; and ii) management of images and metadata. MindSeer is a cross-platform visualization tool for 3D neuroimaging data. The standalone version is hardware accelerated and provides a highly interactive visualization experience, whereas a web-enabled client/server version allows remote visualization of neuroimaging data on any computer with internet access.

14:30 ***3266***. **fMRI Quality Assurance Using Phase Space Reconstruction of SmartPhantom Simulations of BOLD Contrast**
Computer 5

Jae-Min Lee[1], Qun Zhao[1], Jianbo Gao[1], Keith D. White[1]
[1]University of Florida, Gainesville, Florida, USA

Measurement of contrast-to-noise ratio using chaos theory based phase space reconstruction is proposed for fMRI quality assurance (QA). This analysis estimates the standard deviation of noise from the signal itself, rather than from a background window as in traditional Weisskoff signal-to-noise ratio. The effectiveness of this method for fMRI QA is demonstrated with data collected during multiple sessions using the SmartPhantom, a device which simulates BOLD contrast electronically.

14:30 ***3267***. **Quantitative Evaluation of Multi-Channel fMRI at 7 Tesla with High 1–dimensional Reduction Factors**
Computer 6

Steen Moeller[1], Pierre-Francois Van de Moortele[1], Kâmil Ugurbil[1]
[1]University of Minnesota, Minneapolis, Minnesota, USA

Parallel Imaging (SENSE) of the human head with one dimensional reduction (and maximum aliasing) factors of four can be performed at very high fields (7 Tesla) with low g-factors (average and maximal). In this study, consequences of the use of such a large 1-dimensional reduction and maximum aliasing factor in EPI based fMRI studies conducted at 7 Tesla was examined quantitatively.

15:00 ***3268***. **Improving the Resolution of Functional Maps on the Cortical Surface**
Computer 5

Xiaojian Kang[1], E. William Yund[2], Timothy Herron[3], David L. Woods[1]
[1]University of California, Davis, Martinez, California, USA; [2]HCNLAB, Martinez, California, USA; [3]HCNLAB, martinez, California, USA

A new method, anatomical space analysis (ASA), was proposed, whereby low-resolution functional images are co-registered and resampled directly into high-resolution anatomical space with subsequent data processing performed in high-resolution space. Compared with the widely used functional space analysis (FSA) method, one major advantage of ASA is that minor head movements which are generally assumed to reduce spatial resolution can actually increase spatial resolution by providing multiple samples of the relationship between functional and anatomical space. Both simulations and analyses of real fMRI data show that ASA improves the precision, objectivity and reproducibility of functional brain image mapping.

15:00 ***3269***. **Theoretical Results Demonstrate Fundamental Differences in Venous BOLD Reducing fMRI Activation Methods**
Computer 4

Andrew Scott Nencka[1], Daniel B. Rowe[1]
[1]Medical College of Wisconsin, Milwaukee, Wisconsin, USA

Although often discarded from the analysis of the complex-valued fMRI time series, the phase may contain fundamental information about the source of the BOLD signal. Rowe and Logan's complex constant phase and Menon's phase regressor methods both utilize the phase and magnitude time courses to bias against declaring voxels with task related phase changes (TRPCs) caused by draining veins active. These simulations which determine the different methods' powers of finding voxels of different TRPC/CNR combinations active indicate a marked difference between the complex constant phase and phase regressor methods. The complex constant phase method exhibits more optimal behavior.

15:00 ***3270***. **The Downside of Spatial Normalisation in fMRI of Medial Temporal Lobe Structures**
Computer 6

Matthew Liptrot[1], Thomas Ramsøy[1], Torben Lund[1], Karam Sidaros[1], Mark Christensen[1], Finn Nielsen[2, 3], William Baare[1], Terry Jernigan[1, 4]
[1]Copenhagen University Hospital, Hvidovre, Hvidovre, Copenhagen, Denmark; [2]Copenhagen University Hospital, Hvidovre, Copenhagen, Denmark; [3]Technical University of Denmark, Lyngby, Copenhagen, Denmark; [4]UCSD, San Diego, California, USA

The objective was to investigate the degree that functional and anatomical variance of medial temporal lobe structures, specifically the perirhinal cortex, impacted upon group analyses after standard spatial normalisation. The perirhinal cortex has been indicated as the initial location of damage in Alzheimer's disease, and so a paradigm enabling its reliable activation may allow presymptomatic detection of cortical degradation. Such clinical use would require a standardized template, yet standard spatial normalisation techniques are shown here to greatly affect the location of both the activations and anatomical regions. This has significant implication for any group analyses of the medial temporal region.

fMRI: Animal Models

Room 4A Tuesday 13:30 - 15:30

13:30 *3271*. **Mapping Pharmacological-Evoked fMRI Data Using Independent Component Analysis-Derived Pharmacodynamic Modeling**
Computer 7
Ping Wang[1], Jian-Ming Zhu[1]
[1]Wake Forest University School of Medicine, Winston-Salem, North Carolina, USA

Because the exact temporal model of BOLD changes associated with amphetamine action is difficulty to specify, the hypothesis-driven analysis method is not as exact as in other fMRI applications. We present a scheme that adds the ICA time course into the SPM design matrix (as the priori regressor), the results denoted this scheme can improve the SPM performance. Our further work will include establishing more accurate pharmacokinetic model based on ICA, and the combinations with SPM.

13:30 *3272*. **Thermoregulatory Activity of the Preoptic Area in Rats is Identified with BOLD fMRI**
Computer 8
Greetje Vanhoutte[1], Marleen Verhoye[1], Annemie Van der Linden[1]
[1]University of Antwerp, Antwerp, Belgium

We approached the study of thermoregulation in the rat using BOLD fMRI with experimental modification of body temperature (Tr) as an appropriate stimulus. Increasing BOLD signal (9%) in the preoptic area of the hypothalamus was restricted to a time period of increasing Tr (38¢XC„³39¢XC) and reached a plateau which sustained during subsequent Tr decrease (39.1¢XC„³37.9¢XC). These BOLD changes were depicted after performing region specific signal corrections in accordance to the prescence of a dense vascular network. Rising Tr causes an increase in blood temperature, modifying O2 affinity for hemoglobin and hence resulting in more deoxyhemoglobin changing susceptibility contributions.

14:00 *3273*. **Graded fMRI Response in Rat Rectal Distention Model**
Computer 8
Venelin Kounev[1], Christopher Paul Pawela[1], Reza Shaker[1], James S. Hyde[1]
[1]Medical College of Wisconsin, Milwaukee, Wisconsin, USA

Functional disorders are the most common disease diagnosed by Gastroenterologists. The mechanisms behind these diseases are poorly understood but are believed to involve a disturbance in the interaction between the enteric nervous system, central nervous system, and the autonomic nervous system. The goal of this study was to develop a working fMRI protocol for an animal model of these disorders using rectal distention. A graded neurosensory response was observed for varying levels of balloon inflation.

14:00 *3274*. **Pharmacological Modulation of the Serotonergic System in Rat Brain Detected by fMRI**
Computer 7
Mark Preece[1], Andrew Blamire[2], Peter Styles[1], Trevor Sharp[1], Nicola Sibson[1]
[1]University of Oxford, Oxford, UK; [2]University of Newcastle upon Tyne, Newcastle upon Tyne, UK

Few fMRI studies have directly investigated the serotonin (5-HT) neurotransmitter system, which is involved in various processes including CBF regulation, sleep, learning and mood. In this study, BOLD fMRI was use to investigate regional responses in the rat brain following administration of the 5-HT-releasing agent, d-fenfluramine, both in naïve animals and after depletion of brain 5-HT levels. Significant reductions in BOLD signal were found in both cortical and subcortical regions that were mostly abolished by 5-HT depletion. In contrast, a significant increase in the BOLD response was observed in the motor cortex, which was not sensitive to 5-HT depletion.

14:30 *3275*. **The Effect of Cocaine on the Rat Brain Apparent Diffusion Coefficient, Cerebral Blood Volume and Mean Arterial Blood Pressure**
Computer 7
Congwu Du[1], Yu Ma[1], Bernd Forester[1], Mei Yu[1], Helene Benveniste[1, 2]
[1]Brookhaven National Laboratory, Upton, New York, USA; [2]Stony Brook University, Stony Brook, New York, USA

Cocaine can reduce cerebral blood flow as well as perfusion to other body organs. The mechanisms underlying these changes are still not fully understood. We hypothesized that if cocaine induces vasoconstriction and reduces cerebral perfusion the apparent diffusion coefficient (ADC) could decrease if low (ischemic) perfusion thresholds were reached. The present study examined the effects of an acute cocaine challenge on changes in the rat brain ADC in parallel with measurements of cerebral blood volume (CBV) changes using a newly developed optical system.

14:30 *3276*. **Quantitative fMRI Studies in Rats During Non-Chemically Based Hypotension**
Computer 8
Peter Herman[1, 2], Basavaraju Ganganna Sanganahalli[1], Fahmeed Hyder[1], Andras Eke[3]
[1]Yale University, New Haven, Connecticut, USA; [2]Semmelweis University, Budapest, Hungary; [3]Semmelweiss University, Budapest, Hungary

BOLD changes are commonly used for studying functional brain activity. Data on how systemic physiological changes (e.g., arteria blood pressure, ABP) modify the BOLD response are needed. The change of the BOLD response to stimulation in steps of non-invasively induced arterial hypotension was studied. The BOLD response did not change down to ~80 mmHg of ABP. Below this ABP the BOLD response became significantly higher than the control response. Hence ABP can influence the BOLD response. Consequently the BOLD response alone cannot be used to accurately monitor function in experiments when ABP drops below the threshold of CBF autoregulation.

15:00 *3277*. **BOLD Variations and Reduced CBF Increases Upon Hypoxia Are Indicative for the Hippocampal Vulnerability**
Computer 8

Greetje Vanhoutte[1], Marleen Verhoye[1], Annemie Van der Linden[1]
[1]University of Antwerp, Antwerp, Belgium

We studied the effect of hypoxia on the hemodynamic response in the mouse brain. In particular we focused on the outcome of the hippocampus versus the cortex because the hippocampal formation is known to be highly vulnerable to neuronal damage. The aim of this study was to elucidate how regional differences in hemodynamics might account for vulnerability differences. First, bolus tracking outlined perfusion parameters such as cerebral blood flow and cerebral blood volume in normoxic condition. Next, arterial spin labeling was applied during hypoxia to detect cerebral flow changes and this was correlated to changes in BOLD contrast.

15:00 *3278*. **Functional Magnetic Resonance Imaging of BOLD Changes Accompanying Feeding in Rats**
Computer 7

Jaclyn Ivy Wamsteeker[1, 2], Henry S. Koopmans[1], Tadeusz Foniak[2], Dave Kirk[1], Boguslaw Tomanek, [1,2], Ursula I. Tuor[1, 2]
[1]University of Calgary, Calgary, Alberta, Canada; [2]Institute for Biodiagnostics (West), Calgary, Alberta, Canada

Greater understanding of extra-hypothalamic CNS control of hunger and satiety will be valuable in developing strategies to combat obesity. fMRI was used to study altered BOLD MR signal intensity changes that accompany the administration of liquid food to hungry anesthetized rats. Cluster analysis showed that in all animals a large number of the brain voxels in all slices examined had a marked reduction in BOLD signal intensity after food infusion. However, the activation response to electrical forepaw stimulation was enhanced after feeding. Both suggest altered vascular reactivity and/or coupling between cerebral blood flow and glucose/oxygen utilization post-feeding.

fMRI: Language, Pain, Psychiatric Disorders

Room 4A Tuesday 13:30 - 15:30

13:30 *3279*. **New fMRI Approaches for Acupuncture Studies**
Computer 10

Jeng-Ren Duann[1], Jeon-Hor Chen[2, 3], Tsung-Jung Ho[3], Chung-Ming Chen[3], Wu-Chung Shen[3], Tung-Wu Lu[4], Jaung-Geng Lin[3]
[1]University of California San Diego, La Jolla, California, USA; [2]University of California Irvine, Irvine, California, USA; [3]China Medical University and Hospital, Taichung, Taiwan; [4]National Taiwan University, Taipei, Taiwan

We performed an fMRI experimental design consisting of single block to avoidbaseline turnover caused by lasting effect of acupuncture sensation. We demonstrated that a De-Qi sensation could last for more than two minutes in a psychophysical test, which could alter the predefined contrast of a multiple block fMRI experiment setting. An fMRI experiment on acupoint ST42 with single-block design and analyzing the image data using GLM with temporally shifting the reference time course to account for possibly different onsets of brain response in different subjects, when compared with the GLM without temporal shifts, demonstrated additional activities in the thalamus and limbic system.

13:30 *3280*. **Diminished Hemodynamic Responses During Processing of Mood Congruent Emotional Adjectives in Depressed Patients**
Computer 11

Traute Demirakca[1], Cornelia Herbert[1], Johanna Kissler[2], Dirk Wildgruber[3], Tim Wokrina[4], Gabriele Ende[4]
[1]Heidelberg Academy of Sciences, Heidelberg, Germany; [2]University of Konstanz, Konstanz, Germany; [3]University of Tübingen, Tübingen, Germany; [4]Central Institute of Mental Health, Mannheim, Germany

The primary objective of the presented fMRI study was to determine whether passively reading pleasant and unpleasant adjectives leads to mood congruent activation differences in depressed patients. Emotional adjectives compared to neutral words yielded significantly deminished hemodynamic responses within the bilateral inferior frontal cortex and the left superior frontal gyrus in depressed patients. Considering the different emotional aspects (pleasant, unpleasant) only the contrast unpleasant > neutral revealed a significant difference between patients and healthy controls. Patients exhibited a higher BOLD response in the right frontal pole of the temporal lobe. The valence specific differences might indicate different implicit verbal processing in patients.

13:30 *3281*. **Sentence Comprehension of Two Languages : An fMRI Study with Korean-English Bilinguals**
Computer 9

Hyo Woon Yoon[1], Seoungbok Lee[2], Jun-Young Chung[1], HyunWook Park[1]
[1]KAIST, Daejeon, Republic of Korea; [2]Chungbuk National University, Cheongju, Republic of Korea

Concerning the neural mechanism of bilingual sentence comprehension, the issue of whether the processing of L1 and L2 are identical or not, is currently a subject of debate. In the present study, we investigated the neural mechanisms of L1 (Korean) and L2 (English) using functional magnetic resonance imaging techniques.

14:00 ***3282***. **Neural Correlates of Morphological Processes in Hebrew**
Computer 9
Atira Bick[1], Gadi Goelman[2], Ram Frost[1]
[1]Hebrew University, Jerusalem, Israel; [2]Haddasa Hebrew University Hospital, Jerusalem, Israel

Our study provides evidence concerning the existence of morphological related activity in an explicit task design. Using fMRI we identified two locations involved in morphological deposition of visually presented words and showed that this activity does not result from the joint contribution of orthographic and semantic properties. Since our results show activation that is independent of semantic overlap, the possibility that this activations results from semantic factors alone seems unlikely. These results coincide with the behavioral data previously obtained in Hebrew, demonstrating the important role of morphological processing in reading, thereby suggesting that morphological analysis is an independent language process.

14:00 ***3283***. **Auditory Processing of Different Stimuli in Depressed Patients vs. Healthy Subjects as Assessed by fMRI**
Computer 11
Bettina Pfleiderer[1], Martin Christ[1], Carsten Konrad[2], Hermina Hihn[1, 2], Nikolaus Michael[2, 3]
[1]University Hospital Münster, Münster, NRW, Germany; [2]University Hospital, Münster, NRW, Germany; [3]Evangelische Stiftung Tannenhof, Remscheid, NRW, Germany

Assessment of auditory cortical processing by fMRI of patients with depression vs. healthy controls pre and after electroconvulsive therapy (ECT). Responses to positive emotional stimuli (music) were compared with responses to neutral stimuli (sine tones). Patients prior ECT generally revealed a reduced response to music stimuli, which may correlate with the symptom of "non-feeling". When presenting tones, medium depressed patients activated a compensatory network (associative visual network). Severely depressed patients were no longer capable of recruiting a compensatory network, instead presenting hyperactivation mainly of frontal brain areas. Depressives prior to ECT reveal altered auditory processing, which normalizes after successful ECT.

14:00 ***3284***. **fMRI During Spinal Cord Stimulation in Chronic Pain Patients**
Computer 10
Jaroslav Tintera[1], Jiri Kozak[2], Ivan Vrba[3], Jiri Vrana[4], Hubert Polacek[4], Richard Rokyta[4], Ibrahim Ibrahim[1], Andrej Stancak[4]
[1]IKEM, Prague, CZ, Czech Republic; [2]Faculty Hospital Motol, Prague, CZ, Czech Republic; [3]Hospital Na Homolce, Prague, CZ, Czech Republic; [4]Charles University Prague, Prague, CZ, Czech Republic

Electrical spinal cord stimulation (SCS) is used to alleviate intractable neuropathic pain. We performed fMRI study in 8 patients during SCS with the block design comprising 3 conditions: a) SCS, b) heat painful stimulation (HPS) applied to the leg and c) simultaneous HPS and SCS.Significant activation during SCS was found in dorsal medial primary motor cortex (M1, Brodmann area 4) corresponding to foot motor area in all patients. The de-activation was found in the primary somatosensory cortex corresponding to representation of the tight or hip. The SCS-related activation in the foot motor area increased during heat pain stimulation.

14:30 ***3285***. **BOLD Signal Changes in Tonic Pain**
Computer 10
Arthur Peter Wunderlich[1], Gregor Stuber[1], Roland Klug[2], Wolfgang Freund[1]
[1]Diagnostic Radiology, Univ.-Clinic Ulm, Ulm, Baden-Wuerttemberg, Germany; [2]Neurology, Univ.-Clinic Ulm, Ulm, Germany

To study neural correlates of tonic pain perception, we investigated 15 healthy subjects while stimulating them electrically for 52 sec, causing tonic pain. Subjects were advised to supress pain sensation. Activation was repeated six times with 26 sec rest. Data were analysed with SPM99, modeling the activation block as early (first 13 sec) and late phase. In the group analysis, activation shifted from anterior insula in the early phase to posterior insula and primary sensory area in the late phase. The differential contrast early minus late reveals the caudate nucleus, the posterior insula dominates the opposite contrast.

14:30 ***3286***. **Brain Activation During Alternation Learning in Social Anxiety Disorder: An fMRI Study**
Computer 11
Tammar Kushnir[1], Ruth Gross-Isseroff[2], Sofi Marom[2], Abraham Weizman[2], Hagai Hermesh[2], David Manor[1]
[1]The Chaim Sheba Medical Center, Tel Hashomer, Israel; [2]Geha Mental Health Center, Petach Tikva, Israel

Social anxiety disorder (SAD) is a very common psychiatric condition. However, the dysfunctional neural network remains to be elucidated. There are indications that cortical and subcortical regions related to the orbitofrontal cortex (OFC) underlie some of the manifestations of this disorder. This study challenges the OFC by using a learning paradigm, alternation learning, which is specifically subserved by this region in both human and subhuman species. fMRI study during performance of this paradigm by SAD patients, showed frontal activation encompassing the fronotemporal, including the OFC and intraparietal cortex, and demonstrated relationship between symptom severity and the pattern of activation.

14:30 ***3287***. **Age Related Connectivity Changes in fMRI Data from Children Listing to Stories**
Computer 9
Prasanna Rasika Karunanayaka[1], Scott Kerry Holland[1], Vincent Jerome Schmithorst[1], Ana Solodkin[2], Elena Plante[3]
[1]Cincinnati Children's Hospital Medical Center, Cincinnati, Ohio, USA; [2]University of Chicago, Chicago, Illinois, USA; [3]The University of Arizona, Tuscon, Arizona

To investigate age-related changes in brain connectivity associated with language development in children, we performed a large scale fMRI study (313 children) of narrative story comprehension. Structural Equation Modeling (SEM) was combined with the results of a group independent component analysis (ICA) of fMRI data to examine the associated age related changes in brain connectivity. We found age-related changes in brain connectivity corroborating recent hypotheses regarding the functional segregation in Broca's and Wernicke's areas, the right hemispheric dominance in narrative comprehension and the age dependent increase in left hemispheric dominance for language processing.

15:00 *3288*. **Brain Activity Pattern of Dyslexic Readers Approaches the Pattern of Normal Readers Following Training with a Reading Acceleration Paradigm**
Computer 9
David Manor[1, 2], Anna Sterkin[2], Meirav Balas[2], Michael Kowen[2], Zvia Breznitz[2], Avi Karni, [1,2], Tammar Kushnir[1]
[1]The Chaim Sheba Medical Center, Tel Hashomer, Israel; [2]Haifa University, Haifa, Israel

A special training procedure, the acceleration reading training (ART) results in a persistent improvement of reading effectiveness of both normal readers and reading-impaired (dyslexic) readers. We used fMRI to study the long term affect of ART on brain activation of dyslexics. Our results suggest that improved reading following ART is accompanied by altered brain activation pattern in dyslexics that approaches the activation pattern evoked in normal readers. We propose, that ART may have resulted in the establishment of a more effective cortical network for reading in the dyslexic brain, more similar to the one employed by normal readers.

15:00 *3289*. **'More' May Be 'less': Deficient Dichotic Listening Performance in Autism is Associated with Hyperactivation of Bilateral Language Brain Regions**
Computer 11
Jonathan Bentwich[1, 2], Mirjiana Maletic-Savatich[3], Elisabeth Caparelli[2], Airen Anshul, Bernd Foerster[2], Michael Cohen, Kith Pradhan[2], Jim Ma[2], Helene Benveniste[2]
[1]Stony Brook University's Cody Center for Research of Autism, Upton, New York, USA; [2]Brookhaven National Laboratory, Upton, New York, USA; [3]Stony Brook University, Stony Brook, New York, USA

The observation that autistic individuals exhibit a left (rather than right) ear advantage is usually interpreted as indicating their reversed right hemisphere lateralization of language processing. However, preliminary DL fMRI data analysis indicates a greater activation of the left (than right) language regions in the HFA group. Even more surprising is the association between the deficient HFA DL performance and their increased activation of bilateral language areas (relative to normal controls). Along with the HFA's deficient activation of attentional and social-communication regions, these results may suggest that autistic individuals over-activate language areas but fail to process important social-communication information.

15:00 *3290*. **Characterization of Non-Evoked Pain After a Surgical Incision**
Computer 10
Bettina Pfleiderer[1], Anne Meinhardt[1], Christian Wagner[1], Peter K. Zahn[1], Esther Pogatzki-Zahn[1]
[1]University Hospital Münster, Münster, NRW, Germany

Little is known about the functional significance of distinct brain regions after tissue injuries like postoperative pain. The activation of different brain areas after an experimental surgical incision was assessed. A distinct temporal profile of activity within specific brain regions occurred: 0-2 min after incision an increasing activation of the limbic system (BA23/24) was observed. During incision there was an activation of frontal brain regions (BA 6-9). Peak brain activity occurred 4.5-10 min after incision and subsequently neuronal activity decreased. There was a strong correlation 0-10 min after incision between non-evoked pain ratings during incision and ventrolateral thalamus activation

fMRI: Novel Detection Methods, Noise, and Artifact Removal

Room 4A Tuesday 13:30 - 15:30

13:30 *3291*. **Blood Oxygenation (BOX) Level Dependent Functional Brain Imaging Using Steady-State Free Precession**
Computer 12
Jin Hyung Lee[1], Paul Thomas Gurney[1], Rohan Dharmakumar[2], Graham A. Wright[3], Brian A. Hargreaves[1], Ajit Shankaranarayanan[4], Karla L. Miller[5], Dwight G. Nishimura[1], John M. Pauly[1]
[1]Stanford University, Stanford, California, USA; [2]Northwestern University, Chicago, Illinois, USA; [3]University of Toronto, Toronto, Ontario, Canada; [4]GE Healthcare, Menlo Park, California, USA; [5]Oxford University, Oxford, UK

Conventional BOLD imaging suffers from image distortion, signal dropout and low spatial and temporal resolution. The proposed method, which we refer to as BOX (Blood OXygenation), eliminates most of the problems by using SSFP acquisitions. Changes in the concentration of deoxyhemoglobin introduce frequency shifts and T_2 relaxation time changes. Previous methods that incorporated SSFP for fMRI relied on the frequency shift to generate oxygen contrast. Such techniques suffer from the sensitivity to off-resonance. BOX exploits T_2 changes to generate oxygen contrast over a broad range of off-resonance frequencies which results in distortion-free high spatio-temporal resolution 3D coverage.

13:30 *3292*. **Precompensation of Spiral Trajectory for Reduced Temporal Fluctuation Noise in fMRI**
Computer 13
Christine S. Law[1], Gary H. Glover[1]
[1]Stanford University, Stanford, California, USA

Image quality in functional magnetic resonance imaging (fMRI) depends heavily on fidelity of imaging trajectory actually used. Even with careful calibration, actual imaging trajectories will always deviate from their design; images are typically acquired using imperfect trajectories. We developed a linear precompensation technique to minimize deviation between design and measured trajectories. We found that image aliasing artifacts from trajectory imperfection are reduced by precompensation. Fluctuation noise caused by motion can also be reduced using our technique.

13:30 ***3293***. **An ICA Based Method to Process Simultaneous EEG-fMRI in Epilepsy**
Computer 14
Jose P. Marques[1], Francisco Sales[2], Miguel Castelo-Branco[1], Patricia Figueiredo[1]
[1]Universidade de Coimbra, Coimbra, Portugal; [2]Hospital da Universidade de Coimbra, Coimbra, Portugal

A methodology based on independent component analysis (ICA) of the EEG signal recorded simultaneous to an fMRI acquisition is explored in this abstract. Due to the large amplitude of EEG signal during epileptic seizures, ICA has little problem in separating out the component(s) relating to that interictal activity. The relevant components are then used to model the time course of the event related design. This approach, when compared to the more conventional methodology, seems to have increased sensitivity to BOLD changes relating to interictal activity, whilst preserving the most relevant regions of activity found with the conventional methodology.

14:00 ***3294***. **Ballistocardiac Artifact Removal from the EEG Recorded in fMRI and Its Application to the Epileptic Interictal Spikes**
Computer 14
Sung Suk Oh[1], Jun-Young Chung[2], HyoWoon Yoon[2], Joong Koo Kang[3], HyunWook Park[2]
[1]Korea Advanced Institute of Science and Technology(KAIST), Daejeon, Republic of Korea; [2]KAIST, Daejeon, Republic of Korea; [3]University of Ulsan College of Medicine, Ulsan, Republic of Korea

The simultaneous recording of fMRI and EEG provides an efficient signal for the high spatiotemporal brain mapping because each modality provides complementary information. One of remarkable examples of combining these two techniques is an analysis of the epileptic interictal spike. A major difficulty in interpreting EEG signals including the epileptic interictal spike from simultaneous EEG/fMRI data is that severe artifacts are induced in the EEG by the pulsatile motion of the heartbeats. We propose a novel algorithm to remove the ballistocardiac artifact using the characteristics of ballistocardiac artifacts, removing artifacts caused by heartbeats and preserves the epileptic interictal spike perfectly.

14:00 ***3295***. **Effect of Background Suppression and Physiological Noise Removal on the Sensitivity of Arterial Spin Labeling fMRI**
Computer 13
Yashar Behzadi[1], Khaled Restom[1], Joanna Perthen[1], Thomas T. Liu[1]
[1]UCSD, San Diego, California, USA

Perfusion-based functional magnetic resonance imaging (fMRI) with arterial spin labeling (ASL) has the potential to provide a more accurate reflection of neural activity than the more commonly used blood oxygenation level dependent signal. However, ASL techniques tend to be less sensitive due to inherently low signal-to-noise and have been of limited use in cognitive fMRI studies, in which activations tend to be less robust and more variable than primary sensory studies. This study examines the effect of background suppresion and physiological noise correction on the sensitivity of perfusion fMRI both in the visual cortex and the hippocampus.

14:00 ***3296***. **fMRI Activation in Human Visual Cortex Measured with Steady State Free Precession at 3 Tesla**
Computer 12
Kai Zhong[1], Jochen Leupold[1], Jürgen Hennig[1], Oliver Speck[1]
[1]University Hospital Freiburg, Freiburg, Germany

This paper analyzes the SSFP signal and contrast behavior at 3 T in fMRI, using a fully balanced multi-echo SSFP sequence with a wide range of TR/TE values. The fMRI activations obtained at different TR/TE times were evaluated, compared to numerical simulations, and the contrast mechanism is discussed. SSFP shows a behavior similar to gradient echo at moderate TR. Signal decays with TE rather than showing a maximum at TR/2. The contrast can be explained by a BOLD mechanism.

14:30 ***3297***. **BOX fMRI Using Multiple-Acquisition Steady-State Free Precession Imaging for Full-Brain Coverage**
Computer 12
Jin Hyung Lee[1], Paul Thomas Gurney[1], Serge O. Dumoulin[1], Brian A. Wandell[1], Ajit Shankaranarayanan[2], Dwight G. Nishimura[1], John M. Pauly[1]
[1]Stanford University, Stanford, California, USA; [2]GE Healthcare, Menlo Park, California, USA

A new fMRI method, which we refer to as BOX (Blood OXygenation), generates oxygenation level dependent contrast using the T_2 sensitive steady state of SSFP imaging. BOX has large coverage over the off-resonance frequency range because SSFP imaging is sensitive to T_2 changes over a broad range of off-resonance frequencies. However, there are still areas of no signal referred to as banding. Such banding can be easily removed with two acquisitions. By using two acquisitions, distortion-free high spatio-temporal resolution 3D full-brain coverage can be obtained.

14:30 ***3298***. **Detection Versus Physiological Noise Suppression in Event-Related fMRI: Optimisation of an Adaptive Cardio-Respiratory Filter**
Computer 13
Olivier Barret[1], Mario Ries[1], Jacco A. de Zwart[2], Peter van Gelderen[2], Chrit T. W. Moonen[1]
[1]IMF CNRS / University of Bordeaux 2, Bordeaux, France; [2]National Institutes of Health, Bethesda, Maryland, USA

Recently, it has been shown that, adaptive model-free time-domain filtering can significantly reduce physiological noise in fMRI data-sets. However, any passive filtering step before the fMRI analysis reduces also the fMRI signal. Therefore the balance between noise suppression and the loss of fMRI sensitivity has to be carefully considered. This study evaluates the filter-performance and the impact on the fMRI detectability of a model-free time-domain filter for a typical event-related fMRI experiment with help of numerical simulations and experimental data.

14:30 ***3299***. **Simultaneous EEG and ASL Perfusion fMRI During Resting and Mental Calculation: A Preliminary Study**
Computer 14

Hengyi Rao[1], David F. Dinges[1], David Censits[1], Don DuRousseau[2], David Roalf[2], Ze Wang[1], Geoffrey K. Aguirre[1], John A. Detre[1], Jiongjiong Wang[1]
[1]University of Pennsylvania, Philadelphia, Pennsylvania, USA; [2]Human Bionics LLC, Purcellville, Virginia, USA

The present study concurrently recorded EEG and ASL perfusion fMRI during three states of eyes closed (EC), eyes open (EO), and mental calculation (MC). Perfusion fMRI revealed greater visual activation for EO than EC, and greater frontal and parietal activations for MC than EC. EEG spectral analysis revealed greater alpha component in posterior brain for EC than EO, and greater delta and theta components in frontal areas for MC than EC. Both fMRI and EEG results were consistent with existing literatures in each modality, demonstrating the feasibility of simultaneous EEG and ASL perfusion fMRI for multi-model neuroimaging studies.

15:00 ***3300***. **The Utility of Synchronization, PCA and Filtering for Removing MRI Artefacts from Simultaneous EEG Recordings**
Computer 14

Hendrik Mandelkow[1], Pascal Halder[2], Daniel Brandeis[2], Peter Boesiger[1]
[1]University and ETH Zurich, Zurich, ZH, Switzerland; [2]University of Zurich, Zurich, ZH, Switzerland

The removal of MRI gradient artifacts from simultaneous EEG recordings is facilitated most effectively by eliminating drift between the MR scanner time base and the EEG clock. Precisely synchronized EEG-MRI recordings can be achieved by the use of a commercially available phase-locking device. We use simulations as well as EEG-MRI data recorded in a water phantom to assess the effectiveness of synchronized recordings in comparison to and in combination with other artefact reduction methods. Such post-processing methods like sampling time correction (STC) and principal component analysis (PCA) are seen to yield advantages mostly at frequencies above 80Hz but not in the crucial EEG range below 50Hz.

15:00 ***3301***. **A Filtered Subtraction Approach for the Reduction of Physiological Noise in Perfusion Based fMRI**
Computer 13

Khaled Restom[1], Yashar Behzadi[1], Joanna E. Perthen[1], Thomas T. Liu[1]
[1]University of California, San Diego, La Jolla, California, USA

A previous study has shown that an image based retrospective method (RETROICOR) for the reduction of physiological noise could be modified to increase the sensitivity of ASL studies. The previously proposed method divided the tag and control images into two independent time series. Here we introduce an improved method that removes physiological noise from a perfusion time series formed from the filtered subtraction of the tag and control images. The proposed method improves the sensitivity to functional activation by a factor of four as compared to the previous method.

15:00 ***3302***. **Modelling Optic Nerve Axonal Fields for Direct Neuronal Detection MR Studies**
Computer 12

Martyn Paley[1], Li Sze Chow[1], James Wild[1], Kuan Lee[1], Elspeth Whitby[1], Paul Griffiths[1], Greg Cook[1]
[1]University of Sheffield, Sheffield, Yorkshire, UK

The optic nerve carries all visual information from the eye to the brain through 1 million axonal fibres. Simulation of the magnetic field modulation which could feasibly be produced by the optic nerve has been developed to help understand the factors affecting the ability of MR to measure weak axonal fields *in vivo*. The calculated waveforms were applied to a D-A converter to modulate a phantom and images were analysed using the ghost reconstructed alternating current estimation (GRACE) method. 3T GRACE images were also acquired in three volunteers with a strobe stimulus showing preliminary evidence for optic nerve ghosts *in vivo*.

Body GI

Room 4A Tuesday 13:30 - 15:30

13:30 ***3303***. **Diffusion-Weighted MR Imaging of Ulcerative Colitis with the Sensitivity Encoding Technique for Monitoring Inflammatory Activity: Initial Experience**
Computer 15

Hiroki Haradome[1], Akihisa Nakamura[2], Takashi Honda[2], Toshiaki Nitatori[2], Youko Ikei[2], Gen Koyama[2], Shin-ichi Takahashi[2]
[1]Kyorin University School of Medicine, Mitaka, Tokyo, Japan; [2]Kyorin University School of Medicine, Mikata, Tokyo, Japan

The combination of diffusion-weighted imaging (DWI) with parallel imaging has been applicable to inflammatory bowel disease. DWI is also more sensitive to inflammatory status of the tissue, than conventional MR imaging due to its realizing reflect to increasing inflammatory cell density. We evaluate the usefulness of DWI with the sensitivity encoding technique (SENSE-DWI) for detecting and monitoring colonic inflammatory activity in patients with UC in this study. Preliminary results suggest that SENSE-DWI enables to estimate site and degree of active inflammation in UC and may be useful for monitoring UC activity or assessing its therapeutic effectiveness.

13:30 *3304*. **Diffusion Tensor Hepatic MR Imaging with Parallel Imaging Technique for the Evaluation of Focal Hepatic Lesions**
Computer 16

Hiroki Haradome[1], Tomoaki Ichikawa[2], Hironobu Soh[2], Tsutomu Araki[2]
[1]Kyorin University School of Medicine, Mikata, Japan; [2]Yamanashi Medical University School of, Nakakoma, Yamanashi, Japan

Diffusion tensor imaging (DTI) with parallel imaging may conduct more detailed imaging analysis for the diffusion phenomenon in the liver because DTI can provide information regarding not only amount of diffusion (apparent diffusion coefficient: ADC) but also anisotrophic direction of diffusion (fractional anisotrophy: FA). The purpose of this study was to determine whether DTI with parallel imaging was useful for the characterization of focal hepatic lesions. DTI with parallel imaging technique allow raising the precision in diagnosis of differentiating benign from malignant hepatic lesions with the combination of ADC and FA measurements.

13:30 *3305*. **Transverse Relaxation Rates (R2*, R2, and R2') of Iron-Overloaded Livers of Thalassemic Mice at 1.5T and 3T**
Computer 17

Ruitian Song[1], Wei Lin[1], Felix W. Wehrli[1], Quikan Chen[2], Toshio Asakura[2], Hee Kwon Song[1]
[1]University of Pennsylvania Medical Center, Philadelphia, Pennsylvania, USA; [2]Children's Hospital of Philadelphia, Philadelphia, Pennsylvania, USA

Transverse relaxation rates, including R2*, R2 and R2', of thalassemic murine livers have been investigated using the GESFIDE (gradient-echo sam-pling of free induction decay and echo) technique at 1.5 and 3T field strengths. The parameters were all well correlated with murine liver iron content at both 1.5 and 3T (r = 0.72-0.79). Within the range of iron concentrations investigated, there was also a high degree of linear correlation among the three parameters (r = 0.93-0.99). The relaxivities for all three rates were approximately doubled at the higher field strength, in agreement with previ-ous observations.

14:00 *3306*. **Characterization of Focal Hepatic Lesion Containing Fat with Balance SSFP Chemical Shift Imaging Sequence**
Computer 17

Zhenghan Yang[1], Fei Sun[2], Min Chen[1], Cheng Zhou[1]
[1]Beijing Hospital, Beijing, People's Republic of China; [2]GE Medical System, China, Beijing, People's Republic of China

The aim of this study is to investigate the usefulness of balance SSFP chemical shift imaging sequence in characterization of focal hepatic lesion containing fat in comparison with spoiled gradient recalled echo (SPGR) T1-weighted chemical shift imaging sequence. In-phase/opposed-phase SPGR T1WI and in-phase/opposed-phase images balance SSFP were performed in 37 patients with various focal hepatic lesions. Our results indicate that compared with SPGR T1-weighted chemical shift imaging sequence, balance SSFP chemical shift imaging sequence can provide similar or more information in characterization of focal hepatic lesions containing fat.

14:00 *3307*. **Detectability of Small Metastatic Liver Tumors Evaluated with Low-B-Factor Diffusion-Weighted Images with Ferucarbotran**
Computer 16

Tastuyuki Tounan[1], Kiminori Fujimoto[2], Sanae Azuma[1], Noriyuki Ono[1], Sunao Mastushita[1], Naohumi Hayabuchi[2]
[1]Chikugo City Hospital, Chikugo, Fukuoka, Japan; [2]Kurume University School of Medicine, Kurume, Fukuoka, Japan

The aim of this study is to evaluate the detection of small (? 2cm) metastatic liver tumors using low-b-factor diffusion-weighted image with/without super paramagnetic iron oxide particle (ferucarbotran) and to compare the tumor-liver signal contrast-to-noise ratio between long echo time and short echo time.As a result, it was thought that the delectability of small (? 2cm) metastatic liver tumors on low-b-factor DWI was improved by the administration of ferucarbotran. For the detection of metastatic liver tumors (< 1 cm), short TE-DWI with ferucarbotran is superior to conventional long TE-DWI with/without ferucarbotran.

14:00 *3308*. **ADC Measurement of Abdominal Organs and Lesions Using Parallel Imaging Technique**
Computer 15

Takeshi Yoshikawa[1], Hideaki Kawamitsu[1], Donald G. Mitchell[2], Yoshiharu Ohno[1], Kazuhiro Kubo[1], Masahiko Fujii[1], Kazuro Sugimura[1]
[1]Kobe University Graduate School of Medicine, Kobe, Hyogo, Japan; [2]Thomas Jefferson University, Philadelphia, Pennsylvania, USA

ADC measurement was reported to be useful in the abdominal field. However, blurring and susceptibility artifacts diminish the image quality and reliability of the values. Parallel imaging can reduce readout time, improving image quality. Our objective was to assess the reliability and usefulness of parallel imaging for ADC measurement of abdominal organs and lesions. The results of our phantom and clinical studies shows the effect of parallel imaging on calculated values is considered to be minimal. However, problems still remain in measurement at left lobe of the liver and pancreas. Measurement at periphery of the image should be avoided.

14:30 *3309*. **Influence of Respiratory Motion in Body Diffusion Weighted Imaging Under Free Breathing**
Computer 15

Isao Muro[1], Taro Takahara[2], Yutaka Imai[2]
[1]Tokai University Hospital, Isehara, Kanagawa, Japan; [2]School of Medicine,Tokai University, Isehara, Kanagawa, Japan

Our results show a stable motion such as calm respiration is completely different from IVIM, which causes signal loss on DWI.The images provided using this method serves high resolution, high quality and high SNR. Because viewing from the other direction was possible, the multi planner reconstruction (MPR) images of an axial scanning image was significant in a diagnosis.

14:30 ***3310***. **Non-Breath-Hold Diffusion Weighted Imaging for the Body: Signal Characteristics, Artifacts and Lesion Conspicuity**
Computer 16

Mamoru Takahashi[1], Yasuo Takehara[2], Katsutoshi Ichijo[1], Norihiro Tooyama[1], Harumi Sakahara[2], Atsushi Nozaki[3]
[1]Seirei Mikatahara General Hospital, Hamamatsu, Shizuoka, Japan; [2]Hamamatsu University of Medicine, Hamamatsu, Shizuoka, Japan; [3]General Electric Yokogawa Medical System,Ltd, Hino, Tokyo, Japan

The purpose of this study is to assess utility in body diffusion weighted imaging.@111 consecutive patients were examined using a 1.5T MRI scanner and abdominal images using non-breath-hold diffusion weighted SE-EPI were obtained. All malignant and inflammatory lymphadenopathy showed extremely high CNR. The signal of the lesions was higher than surrounding tissue in 88% of the malignant neoplasm, in 58% of the benign neoplasm and in 66% of the inflammatory processes. The sensitivity and specificity for diagnosis of malignant neoplasm were 82% and 58% respectively. Body diffusion weighted imaging may be a useful in terms of highlighting the lesions

14:30 ***3311***. **Quantitation of Hepatic Steatosis in Oncologic Patients Using a Fast Dual-Echo Dixon Technique**
Computer 17

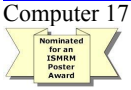

Madelyn P. Vuong[1], Haesun Choi[1], Asif Rashid[1], Lyle D. Broemeling[1], Jean N. Vauthey[1], Jingfei Ma[1]
[1]MD Anderson Cancer Center, Houston, Texas, USA

The purpose of this study is to validate the single breath-hold dual-echo Dixon technique for hepatic fat fraction quantitation with histopathologic correlation. A water/fat phantom study was performed and clinical patients with hepatic metastasis were scanned prior to hepatic resection. Using this technique, fat fractions measured on MR images were highly accurate in the phantom study and highly correlated with histopathological specimens in the clinical patients.

15:00 ***3312***. **Intraportal Venous Flow Distribution: Evaluation with Unenhanced Oblique TrueSSFP MR Angiography Perpendicular to Portal Vein Using a Selective IR Tagging Pulse**
Computer 17

Masahiro Tanabe[1], Katsuyoshi Ito[1], Ayame Shimizu[1], Minoru Hayashida[1], Naofumi Matsunaga[1]
[1]Yamaguchi University School of Medicine, Ube, Yamaguchi, Japan

We evaluated three-dimensional distribution of intraportal blood flow from SMV and SpV by means of unenhanced oblique trueSSFP MR angiography perpendicular to the portal vein using a selective IR tagging pulse. The study included 14 subjects. Whirling flow in the portal vein was observed in 57% (8/14) on the oblique MR images perpendicular to the portal vein while it was not seen on the coronal MR images. This technique has a potential to assess correlation between SpV and SMV inflow to the portal vein, and to evaluate the three-dimensional distribution of intraportal venous flow caused by the whirling flow.

15:00 ***3313***. **Respiratory Triggered Diffusion Weighted MR Imaging of the Liver**
Computer 16

Patrick Asbach[1], Christian Klessen[1], Patrick A. Hein[1], Alto Stemmer[2], Bernd Hamm[1], Matthias Taupitz[1]
[1]Charité Campus Mitte, Berlin, Germany; [2]Siemens AG, Erlangen, Germany

Aim of this study was to implement a respiratory triggered echo-planar-imaging (EPI) based DWI sequence and in a first step to evaluate image quality and contrast parameters of focal liver lesions in comparison to a T2-weighted turbo spin-echo (TSE) sequence. 4 healthy volunteers and 8 consecutive patients with 16 focal liver lesions were prospectively evaluated. Respiratory triggered EPI based DWI is feasible since good image quality and good liver-lesion contrast can be achieved.

15:00 ***3314***. **Selective Visualization of Hypokinetic Small Bowel Loop Using Small Motion Probing Gradient with Low B Value**
Computer 15

Taro Takahara[1], Aine Sakurada[1], Marc Van Cauteren[2], Shuichi Kawada[1], Tamaki Ichikawa[1], Tomohiko Horie[1], Yutaka Imai[1]
[1]Tokai University School of Medicine, Isehara, Kanagawa, Japan; [2]Philips Medical Systems, Shinagawa, Tokyo, Japan

Cine MRI surpasses CT in the diagnosis of strangulated small bowel obstruction because it can evaluate peristaltic function of the obstructed loop. However it is difficult to visualize a strangulated loop selectively because non-strangulated loops also show high intensity on cine MRI. We hypothesize that low b-value images may highlight hypokinetic loops by suppression of the signal from the intestinal lumen in adjoining small bowel loops with normal peristaltic function. The results show that signal intensity of the strangulated loop on low b value (50 sec/mm2) image is much larger than normal loop and therefore the strangulated loop can be visualized selectively.

Body MRI: Hepatobiliary: Novel Techniques

Room 4A Tuesday 13:30 - 15:30

13:30 *3315*. **Comparison of Respiratory-Triggered and Breath-Hold Partial Kz High Special Resolution 3D FSE MRCP Using ASSET for the Evaluation of the Pancreatobiliary System**
Computer 18
Takayuki Masui[1], Motoyuki Katayama[2], Kimihiko Sato[1], Masahiro Sugiyama[1], Hidekazu Seo[1], Atsushi Nozaki[3], Masaya Hirano[3]
[1]Seirei Hamamatsu General Hospital, Hamamatsu, Shizuoka, Japan; [2]Seirei Hamamatsu General Hospital, Hamamatsu, Japan; [3]GE Yokogawa Medical Systems, Hino, Tokyo, Japan

Spatially high resolution MRCP can be obtained using 3D FR FSE in combined use of ASSET and partial Kz using an 8 channel phased array coil. BH 3D FR FSE MRCP with acceptable image quality may be obtained, which may provide competitive information to RT 3D FR FSE MRCP. Compared with BH 3D MRCP, RT 3D MRCP requires longer imaging time however, the information of high spatial resolution MRCP is useful and acquisition time less than five minutes may be acceptable in clinical settings. Thus, when RH 3D MRCP is not diagnostic, BT 3D MRCP may be additionally obtained for the evaluation.

14:00 *3316*. **Evaluation of *k-T* BLAST and *k-T* SENSE for Dynamic 3D Intestinal MRI Using a 32-Channel Phased Array Coil**
Computer 18
Andreas Steingoetter[1], Stefan Zwick[1], Sebastian Kozerke[1], Werner Schwizer[2], Peter Boesiger[1]
[1]ETH and University Zurich, Zurich, Switzerland; [2]University Hospital Zurich, Zurich, Switzerland

The newly developed acceleration methods (k-t BLAST/SENSE) and a 32-channel phased array coil were applied and evaluated for the assessment of intestinal function after established small bowel distension in 2 volunteers. Simulations of k-t methods were performed on 2D reference data. Optimal acceleration parameters were derived for *in vivo* imaging. 3D volumes (12-20 slices of 6mm, FOV=400mm) were dynamically acquired every 590–925ms. Despite temporal blurring at the moving intestinal walls image quality allowed accurate detection of peristaltic frequency. The k-t methods allow dynamic acquisition of large 3D abdominal volumes at demanded temporal resolutions and image quality.

14:30 *3317*. **Dynamic Liver Imaging Using an Image-Based Navigation Approach**
Computer 18
Urs Gamper[1], Martin von Siebenthal[2], Philippe Cattin[2], Sebastian Kozerke[1], Peter Boesiger[1]
[1]University and ETH Zurich, Zurich, Switzerland; [2]Computer Vision Laboratory ETH Zurich, Zurich, Switzerland

Despite recent advances in accelerated data acquisition and the availability of more parallel receiver channels, dynamic 3D imaging of large volumes remains challenging. In this work, an image based navigation approach is presented. In combination with the large coverage and the improved parallel imaging performance of a 32 channel coil, time-resolved 3D images of the complete liver during free breathing could be reconstructed.

15:00 *3318*. **Arterial-Phase Bolus-Track Liver Examination (ABLE): Optimization of Liver Arterial Phase Gadolinium Enhanced MRI Using Centric Re-Ordered 3D Gradient Echo and Bolus Track Real-Time Imaging**
Computer 18
Puneet Sharma[1], Jan De Becker[2], Gabriele M. Beck[2], Harry Friel[3], Bobbie Burrow[1], Diego Martin[1]
[1]Emory University, Atlanta, Georgia, USA; [2]Philips Medical Systems, Best, Netherlands; [3]Philips Medical Systems, Cleveland, Ohio, USA

This study delvelops a new liver perfusion timing technique to enable robust and repeatable arterial phase imaging ("ABLE"). This was facilitated by a new sequence that acquires low frequency k-space segments during the initial portion of the scan (~4sec), before acquiring higher k-space values (CENTRA-Thrive). As a result, the effective timing of image contrast was controlled, rather than empirically timed methods where low k-space is distributed over the entire scan. The sequence was implemented 8 seconds after appearance of Gd in the celiac axis by using bolus-trak. Results showed that CENTRA-Thrive was optimally timed in 95% of cases compared to 67% for tradtional Thrive techniques (non-CENTRA). This method allows consistent arterial phase timing for liver tumor imaging, and allows for potential automation.

Body/GU/Kidney

Room 4A Tuesday 13:30 - 15:30

13:30 *3319*. **Evaluation of Intra-Renal Oxygenation in Mice by BOLD MRI at 3.0T Human Whole Body Scanner**
Computer 19
Lu-Ping Li[1], Lin Ji[1], Scott Lindsay[2], Pottumarthi V. Prasad[1]
[1]ENH, Evanston, Illinois, USA; [2]GE Healthcare, Milwaukee, Wisconsin, USA

BOLD MRI technique has been used in non-invasive evaluation of intra-renal oxygenation levels under normal conditions and during physiological and pharmacological maneuvers at both 1.5T and 3.0T in humans and rats. In this study, we have extended these observations to mouse kidneys. Some disease models are available primarily in mice especially ones that involves genetic mutations. The preliminary data presented here were acquired on human whole body scanner using a custom designed 2 cm loop coil. The BOLD response in mice to the administration of furosemide is similar to that previously seen in human and rat kidneys.

14:00 *3320*. **Evaluation of Intra-Renal Oxygenation During Water Diuresis: A Time Resolved Study Using BOLD MRI**
Computer 19

Santosh Tumkur[1], [2], Anthony Vu[3], Lu-Ping Li[1], Pottumarthi Prasad[1]
[1]Evanston Northwestern Healthcare, Evanston, Illinois, USA; [2]Northwestern University, Evanston, Illinois, USA; [3]GE Healthcare, Milwaukee, Wisconsin, USA

BOLD MRI applied to the kidney has been shown to be useful in the functional evaluation of healthy and diseased states. Preliminary results using a 3-D mGRE sequence at 3.0T and 1.5T to evaluate intra-renal oxygenation changes following administration of furosemide has demonstrated great promise. Following a pharmacological maneuver, the 3-D mGRE sequence permitted the examination of a temporal BOLD response within the renal medulla without sacrificing spatial coverage. In this study, we evaluated the feasibility of using the 3-D mGRE sequence at 3.0T for following temporal responses during water loading. The waterload protocol was performed with and also without cyclooxygenase inhibition by naproxen in order to evaluate the influence of prostaglandins on the observed response.

14:30 *3321*. **Robust Assessment of the Renal Physiological Response Using Breath-Hold Whole Kidney T2 Measurement**
Computer 19

Hui Mao[1], Deigo Martin[1], Xiaoping Hu[1], Chunchun Ni[1], Khalil Salman[1], Bobbie Burrow[2]
[1]Emory University School of Medicine, Atlanta, Georgia, USA; [2]Emory University Hospital, Atlanta, Georgia, USA

Using widely available GRASE method intra-renal functional response to the intravenous infusion of amino acids can be assessed via multi-slice and multi-echo T2 measurement. Nine healthy volunteers participated in the study. T2 measurement was carried out at 1.5T with 8 TEs and 10 axial slices. A 20% amino acid solution was infused. Increased T2 was observed in the renal cortex (9.6%), but not the medulla, after infusion of amino acids, consistent with acute response to the metabolic challenge. The time dependent T2 change can be observed during the infusion, demonstrating the robust detection of renal functional response using this method.

15:00 *3322*. **Diffusion Tensor Imaging of the Kidney with Respiratory Triggering: Optimization of the Parameters to Demonstrate Anisotropic Structure on FA Map**
Computer 19

Masako Kataoka[1], Aki Kido[1], Akira Yamamoto[2], Yuji Nakamoto[1], Takashi Koyama[1], Hiroyoshi Isoda[1], Yoji Maetani[1], Shigeaki Uemoka[1], Ken Tamai[1], Tsuneo Saga[1], Nobuko Morisawa[1], Susumu Mori[2], Kaori Togashi[1]
[1]Kyoto University Graduate School of Medicine, Kyoto, Japan; [2]Johns Hopkins University, Baltimore, Maryland, USA

This study aimed to demonstrate the feasibility of DTI of the kidney with respiration-triggered acquisition or multiple breath-holding and to explore the best imaging parameters for cortex-medulla differentiation on FA(fraction anisotropy) map. DTI of the rt. kidney from healthy volunteer were analyzed (n=6). 6 different sequences with different acquisition technique, slice thickness, number of signal averaging, and b values were compared. DTI of the kidney with respiration-triggered acquisition was feasible with excellent cortex-medulla differentiation. 3-mm thickness, 3 averages, with b = 0, 200 or 400 produce the best images. Images with multiple breath holding resulted in poor quality.

Body/GU

Room 4A Tuesday 13:30 - 15:30

13:30 *3323*. **Prostate Cancer Screening: The Clinical Value of Diffusion-Weighted Imaging and Dynamic MR Imaging**
Computer 20

Akihiro Tanimoto[1], Jun Nakashima[1], Hiroshi Shinmoto[1], Shigeo Okuda[1], Sachio Kuribayashi[1]
[1]Keio University School of Medicine, Tokyo, Japan

Eighty-three patients (44 had prostate cancer) with elevated serum PSA levels were evaluated by T2W, DWI and dynamic MRI at 1.5 T prior to needle biopsy of the prostate. The values from these imaging modalities were compared for the detection of prostate cancer. The ROC analysis indicated that the sensitivity, specificity, and accuracy for the detection of prostate cancer were improved by adding DWI and dynamic MRI. In patients with elevated serum PSA levels, the combination of T2W, DWI, and dynamic MRI may be a valuable tool for detecting prostate cancer and avoiding an unnecessary biopsy without missing prostate cancer.

13:30 *3324*. **Title: Evaluation of Infertility in Women with Dynamic Multi-Phase MR Hysterosalpingography: a Comparison of MR Hysterosalpingography with Conventional Hysterosalpingography**
Computer 21

Jennifer E. Ochsner[1], Elizabeth A. Pritts[1], Mark A. Kliewer[1], Thomas C. Winter[1], Frank Korosec[1], Karl K. Vigen[1], Thomas M. Grist[1], Elizabeth A. Sadowski[1]
[1]University of Wisconsin, Madison, Wisconsin, USA

The purpose of this project is to develop a protocol for dynamic multi-phase MR hysterosalpingography and to compare it to conventional hysterosalpingography in the evaluation of tubal patency and uterine pathology. Ten female subjects with a history of infertility underwent both conventional hysterosalpingography and MR hysterosalpingography. Our data indicates that MR hysterosalpingography is comparable to conventional hysterosalpingography in the evaluation of tubal patency and superior to conventional hysterosalpingography in the evaluation of uterine pathology. Therefore, MR hysterosalpingography has the potential for a single complete pelvic imaging examination in the assessment of female infertility without the risk of ionizing radiation.

13:30 ***3325***. **Menstrual Cycle Related Magnetic Resonance Spectroscopy of Normal Uterus**
Computer 22
Kun Cao[1], Xiaopeng Zhang[1], Lei Tang[1], Yingshi Sun[1]
[1]Beijing Cancer Hospital & Peking University School of Oncology, Beijing, People's Republic of China

To investigate the feature of normal uterus' MRS, and its relationship with menstrual cycle, seven generative healthy female volunteers underwent pelvic MR scan at three different point of their menstrual cycle - premenstrual, post menstrual and ovulatory phase. MRS were acquired and set SNR no less than 2 as the base line of a discernable signal. Choline is the only signal that could be detected in every case, while its peak varies according to different point of a cycle, highest in premenstrual phase. Such change indicates that choline peak is a normal signal of uterus, maybe derived from of endometrium.

13:30 ***3326***. **Sequence Design for Prostate Spectroscopy with an External Transceive Phased Array Coil at 4T**
Computer 23
James P. Near[1, 2], Robert G. Pinkerton[1, 2], Robert Bartha[1, 2]
[1]University of Western Ontario, London, Ontario, Canada; [2]Robarts Research Institute, London, Ontario, Canada

An external transceive surface coil array has been developed as an alternative to the invasive endorectal coils most commonly used for prostate imaging. Such an RF coil cannot be effectively operated with conventional pulse sequences due to the inhomogenous transmit field that is produced. Therefore, a pulse sequence is presented that performs outer volume suppression, water suppression, localization and fat suppression with insensitivity to B1 inhomogeneities. Outer volume suppression is achieved using BISTRO, and localization is performed with LASER, both of which are fully adiabatic. Imaging and spectroscopy are demonstrated in phantoms with this coil and pulse sequence at 4T.

14:00 ***3327***. **MR Imaging and Three-Dimensional H-1 MR Spectroscopic Imaging for Recrudescence of Lower Urinary Tract Symptoms After Transurethral Resection of the Prostate**
Computer 23
Liangping Zhou[1], Weijun Peng[1], Xiaoying Wang[2], Xuexiang Jiang[2]
[1]Cancer Hospital of Shanghai, Shanghai, People's Republic of China; [2]1st Hospital of Beijing University, Beijing, People's Republic of China

14 cases of post-TURP patients with LUTS caused by prostatic disease; including 8 cases of Pca, 5 of BPH, and 1 of transitional cell carcinoma of prostatic urethra confirmed by histopathology of operation or biopsy were evaluated by MRI & three-dimensional H-1 MR spectroscopic imaging (3D 1H MRSI).The length the widened prostatic urethra and the width of the inner outlet of bladder of the LUTS team were statistically shorter than those of the compared team.The average ratios of Cho+Cre/Cit in the regions of cancer (2.21¡Â0.79) were statistically higher than those of the normal prostate tissue.The results of this study demonstrated that MRI possesses the capability to observe the related changes of prostate and the prostatic urethra after TURP. A relatively high accuracy can be achieved by using MRI and 3D 1H MRSI to diagnose the recrudescence of LUTS caused by residual or recurrent disease of prostate after TURP.

14:00 ***3328***. **MR Imaging of the Female Pelvis at 3T:evaluation of Image Heterogeneity Using Different Dielectric Pads**
Computer 22
Masako Kataoka[1], Hiroyoshi Isoda[1], Yoji Maetani[1], Yuji Nakamoto[1], Takashi Koyama[1], Shigeaki Umeoka[1], Ken Tamai[1], Aki Kido[1], Tsuneo Saga[1], Nobuko Morisawa[1], Kaori Togashi[1]
[1]Kyoto University Graduate School of Medicine, Kyoto, Japan

This study aimed to evaluate the improvement of signal inhomogeneity at pelvic MR imaging at 3T using two different dielectric pads on T2WI, T1WI and HASTE. Six healthy females were scanned by 3 T MR scanner and series of imaging was repeated with the use of US gel pad (doped with Gd-DTPA), water-filled solution bag (doped with MnCl2), and without using pad. Variation of signal intensity of fat was used to evaluate homogeneity. Images obtained with both pads (US gel or water) significantly improved signal inhomogeneity and there was no significant difference between these pads regarding the improvement of homogeneity.

14:00 ***3329***. **MR Evaluation of the Female Urethra: Is There a Role for Dynamic Imaging?**
Computer 21
Genevieve L. Bennett[1], Elizabeth M. Hecht[1], Samson Wong[1], Vivian S. Lee[1]
[1]New York University, New York, USA

The purpose of this study is to determine the value of dynamic imaging in the MR evaluation of the female urethra. In 99 patients with urethral symptoms, dynamic imaging with a True Fisp sequence revealed that 33.3% had unsuspected organ prolapse. Among the 12 patients with urethral pathology, such as urethral diverticulum, 50% also demonstrated prolapse. Our data show that the addition of a dynamic sequence to the MR evaluation of patients with urethral symptoms is of added diagnostic value.

14:00 ***3330***. **The Apparent Diffusion Coefficients (ADC) in Normal Prostate and Prostatic Cancer -Compare Single Shot Echo Planner Image (SS-EPI) with Line Scan Diffusion Image (LSDI)-**
Computer 20
Takeshi Yoshizako[1], Akihiko Wada[1], Nobue Uchida[1], Shinji Hara[1], Takafumi Kajitani[1], Kouji Uchida[1], Hajime Kitagaki[1]
[1]Shimane University Faculty of Medicine, Izumo, Shimane, Japan

Diffusion weighted image (DWI) by single shot echo planner image (SS-EPI) on prostatic cancer is sennsitive to motion artifacts. Line scan diffusion image (LSDI) is inherently insensitive to motion artifacts. The purpose of this study was to compare the apparent diffusion coefficients (ADC) of SS-EPI with that of LSDI in normal prostate and prostatic cancer. There was no significant difference between ADC by SS-EPI and by LSDI. Prostatic ca. ADC and normal prostate ADC by LSDI was inherently insensitive to motion artifacts.

14:30 *3331*. **Prostatic Lesion of Low ADC Value: Evaluation by Using Targeted Biopsy**
Computer 20
Yuji Watanabe[1], Masako Nagayama[1], Tohru Araki[2], Akira Okumura[1], Yoshiki Amoh[1], Kazushige Oda[1], Takayoshi Ishimori[1], Takashi Kiyono[1], Kazuaki Nakada[1], Hideki Mitsui[1], Noriyoshi Morimoto[1], Takashi Tabuchi[1], Masayuki Kumashiro[1], Shinsuke Komaki[1], Takashi Sugioka[1], Osamu Ito[1], Keisuke Ohtsuki[1], Yoshihiro Dodo[1]
[1]Kurashiki Central Hospital, Kurashiki, Okayama, Japan; [2]Araki Clinic, Kurashiki, Okayama, Japan

The detectability of prostate cancer by using systematic biopsy has not been very high. In order to determine the detectability of ADC map for prostate cancer, biopsy was performed to target at lesions suspected of cancer by ADC map in this study. Lesions less than 1.3x10-3 mm2/sec of ADC value have been sampled by targeted biopsy and evaluated histologically. Among 68 lesions examined by targeted biopsy, total 35 lesions (52 %) proved to be adenocarcinoma. Low ADC values in combination with targeted biopsy can provide higher detectability of prostate cancer.

14:30 *3332*. **Uterine Contractions Evaluated on Cine MR Imaging in Patients with Uterine Leiomyomas**
Computer 21
Mizuki Nishino[1], [2], Kaori Togashi[3], Asako Nakai[3], Katsumi Hayakawa[2], Shotarou Kanao[2], Kazuhiro Iwasaku[2], Shingo Fujii[3]
[1]Beth Israel Deaconess Medical Center, Boston, MA, USA; [2]Kyoto City Hospital, Kyoto, Japan; [3]Kyoto University, Kyoto, Japan

Submucosal leiomyoma is one of the most recognized causes of infertility. We aim to evaluate uterine peristalsis in patients with uterine leiomyomas using kinematic MR imaging. We performed kinematic HASTE MR imaging of the midsagittal plane of uterus in 26 patients with leiomyoma, and evaluated peristaltic movements at the endometral–myometrial junction and focal myometrial movements adjacent to leiomyomas. Uterine peristaltic movement were partly interrupted by submucosal leiomoymas, but not by myometrial or subserosal leiomyomas. Focal myometrial movements was noted only adjacent to submucosal leiomyomas. These findings are considered to represent dysfunctional contractility, and may be related with pregnancy loss.

14:30 *3333*. **Contrast-Enhanced MR Arteriography to Detect Ovarian Artery Supply to Uterine Fibroids in Patients Scheduled for Uterine Artery Embolization: Comparison with Conventional Angiography During Uterine Artery Embolization for Fibroids**
Computer 22
Naoko Kashitani[1], Susan M. Ascher[1], James B. Spies[1], Pamela A. Flick[1], Reena C. Jha[1]
[1]Georgetown University, Washington, District of Columbia, USA

100 patients with uterine leiomyomata scheduled for UAE were imaged contrast enhanced MR angiography before the procedure. Ovarian artery detection rates between CE MRA and conventional angiography were compared. The sensitivity, specificity, PPV, and NPV of CE MRA for detecting ovarian arteries supply to the uterus and/or fibroid was 71.4%, 89.2%, 66.7% and 97.6%, respectively. Our results suggest a potential role for CE MRA pre-UAE because a negative CE MRA may eliminate the need for routine aortography during UAE.

14:30 *3334*. **MR Imaging and Three-Dimensional H-1 MR Spectroscopic Imaging of Benign Lesion of Prostatic Peripheral Zone: Comparison with Prostate Cancer**
Computer 23
Liangping Zhou[1], Weijun Peng[1], Xiaoying Wang[2], Xuexiang Jiang[2]
[1]Cancer Hospital of Shanghai, Shanghai, People's Republic of China; [2]1st Hospital of Beijing University, Beijing, People's Republic of China

16 cases of benign disease of prostatic peripheral zone all proved pathologically or clinically, MR imaging and 3D 1H MRSI were performed in each case. Most of benign lesion were nodular and well-defined lesion.Prostate cancer presented mainly as patch-like lesion with nodular feeling and ill-defined.The average ratio (0.68¡À0.17) of choline+creatine/citrate (Cho+Cre/Cit) of benign lesion were significantly less than that of prostate cancer.Combined the results of MR imaging and 3D 1H MRSI will play a important role in diagnosing benign lesion of prostatic PZ.

15:00 *3335*. **Serial Change of Non-Cancerous Low Intensity Area in the Peripheral Zone of Prostate on Repeated T2-Weighted MR Imaging**
Computer 23
Shinji Hirohashi[1], Masahiko Sakamoto[1], Nagaaki Marugami[1], Rina Hirohashi[1], Satoru Kitano[1], Toshiaki Taoka[1], Kimihiko Kichikawa[1]
[1]Nara Medical University, Kashihara, Nara, Japan

This study reveals that the distribution of low intensity area in the peripheral zone of prostate may change and even the focal low intensity area mimicking prostatic cancer may appear and disappear on the repeated T2 weighted MR imaging even in the patients without clinically significant prostatic cancer. Radiologists should know the non-cancerous low intensity area in the peripheral zone can vary on the repeated MR examination and sometimes these low intensity areas might mislead the diagnosis.

15:00 *3336*. **Minimally-Invasive Perinatal Autopsy: Post-Mortem MRI with Percutaneous Organ Biopsy**
Computer 22
Patricia Ai Khoon Set[1], Andrew C. Breeze[1], Justin J. Cross[1], Gerald A. Hackett[1], Gerald A. Hackett[1], Christoph C. Lees[1], Ilsa Joubert[1], Flora A. Jessop[1], Anita L. Whitehead[1], David J. Lomas[1]
[1]Addenbrooke's Hospital, Cambridge, UK

The decline in postmortem consent rates worldwide has led to MRI as a proposed alternative to perinatal autopsy, and researchers have examined their comparability. Despite increasing experience post-mortem MRI remains an unproven and investigational technique and there remains a question on its value in clinical practice. This study analyses the feasibility of MRI with percutaneous biopsy as an alternative to conventional autopsy. Thirty fetuses underwent whole-body post-mortem MRI and organ biopsies prior to conventional autopsy. The results support that Minimally-invasive perinatal autopsy is feasible.

15:00 *3337*. **Preoperative Assessment for Pelvic Adhesions: Value of Multi-Phase and Multi-Slice Kinematic FIESTA Imaging**
Computer 21
Motoyuki Katayama[1], Takayuki Masui[1], Kimihiko Sato[1], Masahiro Sugiyama[1], Hidekazu Seo[1], Atsushi Nozaki[2], Masaya Hirano[2]
[1]Seirei Hamamatsu General Hospital, Hamamatsu, Shizuoka, Japan; [2]General Electric Yokogawa Medical Systems, Hino, Tokyo, Japan

Due to improvements of software and hardware, 2D steady-state Free Precession (FIESTA) sequence provides good image quality with high signal-to-noise ratio within a second per slice. We tired to apply fat-sat FIESTA sequence to kinematic FIESTA imaging@for the evaluation of pelvic adhesions. As a result, negative and positive predictive values, sensitivity, specificity, and accuracy for adhesions were 97.7%, 83.8%, 91.2%, 95.6%, and 94.7%, respectively. In conclusion, kinematic FIESTA imaging provided exact information about pelvic adhesions.

15:00 *3338*. **Diffusion Tensor Imaging of the Prostate: Low Anisotropies in Central Gland and Peripheral Zone in Men with Adenocarcinoma**
Computer 20
Joseph R. Roebuck[1], Steven J. Haker[1], Clare M. Tempany[1], Frank J. Rybicki[1], Stephan E. Maier[1], Robert V. Mulkern[1]
[1]Brigham and Women's Hospital, Boston, Massachusetts, USA

High quality diffusion tensor imaging of the prostate as performed with endorectal coil technology, line scan diffusion imaging, and multiple signal averages has revealed much smaller fractional anisotropy (FA) values in the gland than previously reported. The low FA values indicate that obtaining microstructural information from the gland with DTI will be challenging, though some structure is apparent in the primary eigenvector maps.

Lung Imaging: Techniques and Application

Room 4A Tuesday 13:30 - 15:30

13:30 *3339*. **Q-Space Analysis of Lung Morphometry *In Vivo* with Hyperpolarized ^{3}He Spectroscopy**
Computer 24
Dattesh D. Shanbhag[1], G.Wilson Miller[1], Talissa A. Altes[2], Jaime F. Mata[1], Jack Knight-Scott[1]
[1]University of Virginia, Charlottesville, Virginia, USA; [2]Childern's Hospital of Philadelphia, Philadelphia, Pennsylvania, USA

A spectroscopic technique for making morphometric measurements in lungs *in vivo* using a q-space approach for hyperpolarized ^{3}He gas diffusion is presented. Q-space spectroscopic data was collected from healthy volunteers and COPD patients. Two distinct length scales were resolved: in healthy the mean displacements were: 188 µm and 474 µm. In case of COPD, mean displacements were elevated (265 µm and 530 µm). Excellent correlation was found between q-space data and ^{3}HE DWI ADC data. The q-space parameters agreed remarkably well with historical alveolar morphometry data. Detailed lung microstructural information can be obtained using a very low volume of inhaled 3He.

13:30 *3340*. **Quantitative Free-Breathing Oxygen-Enhanced Imaging of the Lung**
Computer 25
Johannes F. T. Arnold[1], Florian Fidler[1], Peter Michael Jakob[1]
[1]University of Würzburg, Würzburg, Bavaria, Germany

Many studies of the human lung have been performed using oxygen as a contrast agent. Two major kinds of approaches were established: A T1-weighted approach and a quantitative approach based on T1-measurement. T1-weighted OE-MRI is favourable in terms of temporal and spatial resolution as well as multislice capability, but on the other hand, because only relative signal changes are detected, various undesired dependencies arise. In contrary, T1-mapping would ease standardization for routine clinical OE lung MRI. Therefore, we propose a hybrid of the T1-weighted and the T1-mapping approach which makes use of the individual advantages of both methods.

14:00 *3341*. **Diffusional Kurtosis Imaging in the Lung Using Hyperpolarized ^{3}He**
Computer 25
Robert Trampel[1], Jens H. Jensen[1], Ray F. Lee[1], Igor Kamenetskiy[1], Georgeann McGuinness[1], Glyn Johnson[1]
[1]New York University School of Medicine, New York, USA

The study of lung structure is of great interest since many pulmonary diseases are associated with abnormalities in the small airways. Conventional diffusion magnetic resonance imaging of hyperpolarized ^{3}He is only capable of monitoring the gas over short time, and hence length, scales because of the short T_2* of the gas. Therefore the method is only sensitive to small structures of the lung (e.g. the alveoli) and is relatively insensitive to changes occurring in larger structures such as the bronchioles and bronchi. We present a method using diffusional kurtosis imaging (DKI) that is particularly sensitive to diffusion over longer distances.

14:00 *3342*. **Feasibility of Using Hyperpolarized He-3 Diffusion Weighted Images to Segment the Airway Tree**
Computer 24
Eric Peterson[1], Sean Fain[1], Rafael O'Halloran[1], James Holmes[1], Robert Pyzalski[1]
[1]University of Wisconsin Madison, Madison, Wisconsin, USA

By acquiring diffusion and non-diffusion weighted hyperpolarized He-3 images of the lung, the airways can easily be separated from the parenchyma by computing the apparent diffusion coefficient (ADC) map. An airway mask can then be generated by performing region growing on the ADC map. By using this strategy, the typical functional information from the He-3 MRI can be combined with the structural information from the airway mask. This could be used in a similar manner to CT based airway segmentation techniques to measure and map out the airways for further analysis.

14:30 *3343*. **Long-Term Reproducibility of Apparent Diffusion Coefficient Using Hyperpolarized 3He MRI in Healthy Volunteers**
Computer 24
Sandra Diaz[1], Per Åkeson[1], Ingrid Casselbrant[1], Eeva Piitulainen[1], Per Wollmer[1], Göran Pettersson[2], Peter Magnusson[2], Barry Peterson[3]
[1]Malmö University Hospital, Malmö, Sweden; [2]GE Healthcare, Malmö, Sweden; [3]Pfizer Inc., Groton, Connecticut, USA

Hyperpolarized He diffusion MRI has been used to estimate the size of the lung alveoli. If a method is possible to use in a clinical setting is dependent of its reproducibility. The aim of the study was to examine the long term reproducibility of 3He ADC MRI in non-smoking healthy volunteers. The average mean ADC value for all subjects was 0.216, 0.217 and 0.218 cm2/sec at baseline, at 6 months and at 12 months respectively (NS). An intra-individual mean ADC variation of 0.97 to 4.1 % was found. The method seems robust enough for the evaluation of emphysema.

14:30 *3344*. **MR Signal Intensity Changes of the Lung Parenchyma; Comparison with Pulmonary Function Test and Quantitative CT Evaluation**
Computer 25
Tae Iwasawa[1], Hiroshi Takahashi[1], Takashi Ogura[1], Yuji Watanuki[1], Akira Asakura[2], Toshiyuki Gotoh[2], Sei-Ichirou Kagei[2], Jun-Ichi Nishimura[1], Tomio Inoue[3]
[1]Kanagawa Cardiovascular & Respiratory Ctr, Yokohama, Kanagawa, Japan; [2]Yokohama National Univ., Yokohama, Kanagawa, Japan; [3]Yokohama City Univ., Yokohama, Kanagawa, Japan

We evaluated relative changes in lung signal intensities (LSI) on 2 sets of 3D-MR images obtained with full inspiration and full expiration in 5 normal volunteers and 12 patients with COPD. Average of relative changes in LSI in the patients was 18.5[plusmn]5.2%, smaller than those in normal volunteers of 46.3[plusmn]1.8 %. In the patients relative change in LSI showed a significant correlation to FEV1.0 (p=0.043). There was no significant correlation between relative change in LSI and RA-950 (the percentage of relative lung area occupied by attenuation values of less than -950 HU on CT images).

15:00 *3345*. **Rapid Lung Volumetry with Ultrafast Dynamic MRI During Forced Vital Capacity (FVC) – Correlation with Spirometry**
Computer 25
Andrew J. Swift[1], Gary H. Mills[2], Neil Woodhouse[1], Stan Fichele[1], Jochen Seidel[2], Edwin JR van Beek[1, 3], Jim M. Wild[1]
[1]University of Sheffield, Sheffield, Yorkshire, UK; [2]Sheffield Teaching Hospitals, Sheffield, Yorkshire, UK; [3]University of Iowa, Iowa, USA

The purpose of this study was to investigate the feasibility of using ultrafast 2D imaging to accurately sample the Forced Vital Capacity (FVC) manouever. The volume exhaled in the first second (FEV1) is the most clinically useful spirometric index, as such temporal resolution of regional volume/time curves is paramount. Using an elliptical model of the axial cross-section of the lungs enabled rapid volume-time curves to be derived from interleaved coronal and saggittal 2D scans. The results show a good correlation with spirometry and represent the first time an FVC manoeuver has been accurately traced with MRI.

15:00 *3346*. **Effect of SNR and Thresholding on the Apparent Diffusion Coefficient in Hyperpolarized He-3 MRI**
Computer 24
Rafael Luis O'Halloran[1], James H. Holmes[1], Tallisa Anne Altes[2], Sean B. Fain[1]
[1]University of Wisconsin, Madison, Wisconsin, USA; [2]University of Virginia, Charlottesville, Virginia, USA

A novel method that applies either automatic or interactive thresholding directly on the SNR of the non-weighted image is presented. With this approach, the mean ADC is largely dependent of image SNR. Also, a theoretical model for the dependence of standard deviation (SD) on SNR is confirmed in a free diffusion phantom. Deviation from purely stochastic SD is demonstrated in the lungs of a smoker with 40 pack years and may provide a means for extracting SNR-independent information about regional variation in lung microstructure.

Thermal Therapy

Room 4A Tuesday 13:30 - 15:30

13:30 *3347*. **Influence of Prostate Perfusion on High-Intensity Focused Ultrasound Cancer Ablation: A First-Pass MRI Study**
Computer 26
Marlene Wiart[1], Laura Curiel[2], Albert Gelet[3], Denis Lyonnet[3], Jean-Yves Chapelon[2], Olivier Rouviere[3]
[1]Creatis UMR CNRS 5515 U630 INSERM, Lyon, France; [2]U556 INSERM, Lyon, France; [3]Edouard Herriot Hospital, Lyon, France

Our aim was to test the hypothesis that perfusion level influences clinical outcome after transrectal high-intensity focused ultrasound (HIFU) ablation of prostate cancer. T1-weighted first-pass MRI was performed in 48 prostate cancer patients. Regional prostatic blood flow (rPBF) was estimated using a new modeling approach that takes contrast agent leakage into account. rPBF values obtained were in good agreement with PET studies. Patients with post-treatment PSA nadir > 0.2 ng/ml (indicative of residual cancer) had a significantly higher rPBF. This *in vivo* study confirms simulation results showing that perfusion level is one of the factors influencing HIFU treatment outcome.

14:00 *3348*. **Simultaneous Monitoring of Temperature and Magnetization Transfer for HIFU Treatment**
Computer 26
Hsu-Hsia Peng[1], Teng-Yi Huang[2], Hsiao-Wen Chung[1], Chih-Ching Wu[1, 3], Wen-Shiang Chen[3, 4], Wen-Yih Isaac Tseng[1]
[1]National Taiwan University, Taipei, Taiwan; [2]National Taiwan University of Science and Technology, Taipei, Taiwan; [3]National Health Research Institutes, Taipei, Taiwan; [4]National Taiwan University Hospital, Taipei, Taiwan

The utilization of MRI for guiding high-intensity focused ultrasound (HIFU) beams can not only greatly increase the localized accuracy during HIFU heating procedures but also can be used to evaluate the HIFU-induced lesions after treatments. Our study investigated the feasibility of estimating temperature changes and magnetization transfer (MT) contrast simultaneously during HIFU heating treatments, using an interleaved dual gradient-echo technique which reflected heating conditions and degree of protein denaturation. Experiments on temperature-varying and HIFU-treated gel phantoms demonstrated that the method exhibited high precision in temperature measurements and expected trends in MT ratio variations.

14:30 *3349*. **Characterization of the Thermal Response of Light Activated Nanoshells in Phantom Using MR Temperature Imaging**
Computer 26
Andrew Miller Elliott[1], Roger Jason Stafford[1], Anil M. Shetty[1], D Patrick O'Neal[2], Chris Bourgoyne[3], John D. Hazle[1]
[1]M.D. Anderson Cancer Center, Houston, Texas, USA; [2]Louisiana Tech. University, Ruston, Louisiana, USA; [3]Nanospectra Biosciences Inc., Houston, Texas, USA

Gold-silica nanoshells are a class of nanoparticle that can be tuned to absorb strongly in the near infrared, making them an attractive agent for delivering targeted thermal therapy. This research uses proton resonance frequency based MR temperature imaging as an aid in evaluating changes in bulk thermal properties and associated spatiotemporal temperature distribution in gel-based phantoms with varying optical properties and nanoshell construction. Physical parameters, such as thermal diffusivity and absorption coefficient are shown to vary predictably with concentration and demonstrably affect the distribution of temperature and rate of heating region and the intensity of resulting temperatures.

15:00 *3350*. **Dynamic Contrast Enhanced Imaging After Canine Prostate Cryoablation**
Computer 26
Erin Liu[1], Donna Bouley[1], Bruce L. Daniel[1], Kim Butts Pauly[1]
[1]Stanford University, Stanford, California, USA

MR-guided cryoablation is a promising minimally invasive therapy for prostate tumors that are solitary and unilateral. The roles of imaging are targetting, monitoring, and post-therapy evaluation. The purpose of this work was to evaluate previously frozen prostate tissue with dynamic and 3D contrast enhanced imaging. Three canine prostates were frozen under MRI guidance. After complete thaw to normal body temperature, dynamic CE and 3D CE images were acquired. The enhancement patterns and timecourses are evaluated and compared to TTC stained sections.

MR Intervention

Room 4A Tuesday 13:30 - 15:30

13:30 *3351*. **Tracking Planar Orientations of Active Interventional Devices for Realtime Image Guided Procedures**
Computer 27
Shashank Sathyanarayana[1], Pelin Aksit[2], Aravind Arepally[3], Parag Karmarkar[3], Meiyappan Solaiyappan[3], Ergin Atalar, [3,4]
[1]Johns Hopkins University, Baltimore, Maryland, USA; [2]GE Healthcare, Milwaukee, Wisconsin, USA; [3]Johns Hopkins Medical Institutes, Baltimore, Maryland, USA; [4]Bilkent University, Bilkent, Ankara, Turkey

We describe a method to track the planar orientation of active interventional devices without using localizing RF microcoils. The method is demonstrated in an *in vivo* mesocaval shunt procedure that required accurate orientation of an active transvascular needle catheter. We determined the plane of the catheter using two projection images, adjusted the scan plane to follow the catheter plane, and displayed its orientation with respect to a previously acquired target plane, thus minimizing navigation time.

13:30 *3352*. **MRI-Guided Transvenous Pancreatic Injections**
Computer 28

Parag Karmarkar[1], Di Qian[1], Ergin Atalar[1, 2], Bradley Barnett[1], Aravind Arepally[1]
[1]Johns Hopkins University, Baltimore, Maryland, USA; [2]Bilkent University, Ankara, Turkey

There is a growing interest in delivering cellular therapeutics e.g. islet cells, stem cells, etc. to the pancreas for treatment of type II diabetes. We demonstrate the feasibility of delivering therapeutic agents to the pancreas in swine (n=3). The pancreas is accessed from the mesenteric venous system, and using custom active MRI catheters and needle system using real-time MRI guidance to deliver agents to the pancreas. This approach has the potential to accurately deliver agents to the pancreas and surrounding anatomy.

14:00 *3353*. **Real-Time Projection Based Technique for Tracking Ferromagnetic Devices**
Computer 28

Eric Aboussouan[1], Ouajdi Felfoul[1], Jean-Baptiste Mathieu[1], Gilles Beaudoin[2], Sylvain Martel[1]
[1]École Polytechnique de Montréal (EPM), Montréal, Québec, Canada; [2]Centre Hospitalier de l'Universite de Montréal (CHUM), Montréal, Québec, Canada

A novel MR-tracking method specifically developed to locate the ferromagnetic core of an untethered microdevice is described. This microdevice aims at being propelled by magnetic gradients generated by a clinical MRI system for endovascular operations. The tracking method relies on the application of RF excitation signals tuned to the equipotential curves generated by the magnetic signature of the object being tracked. A proof of concept is achieved by comparing the MRI positioning data obtained with the proposed technique with those obtained by a camera. The average positioning error is found to be 1.2 mm.

14:00 *3354*. **A Safe and Practical Guide Wire for Use During Passive Tracking in Endovascular Interventional Procedures**
Computer 27

Johannes Martinus Peeters[1], Jan-Henry Seppenwoolde[1], Chris J.G. Bakker[1], Lambertus Wilhelmus Bartels[1]
[1]University Medical Center Utrecht, Utrecht, Netherlands

The lack of an MR-dedicated guide wire has seriously hampered the development of endovascular interventional MRI. We present such a wire designed for tracking with susceptibility-based passive device visualization. This technique is safe and resembles existing clinical procedures. A prototype was developed, consisting of a Nitinol tip segment with stainless steel 410 markers and a plastic base. This prototype was tested in in vitro and *in vivo* animal experiments aimed at catheterization of the renal and hepatic arteries. Depiction of the guide wire was excellent at various tracking speeds. Its mechanical properties were sufficient for use in MR-guided endovascular interventions.

14:30 *3355*. **Positive Contrast Passive Catheter Tracking and Endovascular Device Visualization Using IRON MRI**
Computer 27

Wesley D. Gilson[1], Matthias Stuber[1], Lawrence V. Hofmann[1], Saurabh Shah[1], Parag Karmarkar[1], Jeff W.M. Bulte[1], Dara L. Kraitchman[1]
[1]Johns Hopkins University, Baltimore, Maryland, USA

Many new developments are being made for interventional MRI guidance of endovascular procedures. This study explores IRON MRI for *in vivo* tracking and visualization of MR-compatible endovascular devices. MR angiograms were acquired as roadmap images, and real-time IRON MRI with GRASE image acquisition was performed to guide and place a stainless steel stent in the iliac artery of canines. High resolution IRON MRI clearly visualized the stent with a hyperintense signal. IRON MRI promises to provide a means of performing interventional MRI without the need for passive markers or active coil systems.

14:30 *3356*. **Phased-Array Coil for Image-Guided Treatment of Occlusive Arterial Disease**
Computer 28

Kevan James Thompson Anderson[1], John J. Graham[2], General Leung[1], Nigel R. Munce[1], Alexander J. Dick[2], Graham A. Wright[1, 2]
[1]University of Toronto, Toronto, Ontario, Canada; [2]Sunnybrook and Women's College Health Sciences Centre, Toronto, Ontario, Canada

In this study we propose a novel phased-array intravascular imaging coil consisting of two orthogonal solenoids located at the tip of a catheter. Unlike previous opposed-solenoid designs, the configuration is able to obtain images ahead of the catheter when it is oriented in the same orientation as the static magnetic field. This is of particular interest when guiding a catheter-based device through occlusive lesions during percutaneous treatment. A design is presented and the sensitivity volume of the coils is described through simulation and phantom studies. An *in vivo* application in a porcine femoral artery is also presented.

15:00 *3357*. **Comparison of Intraarterial MRA at 3.0T with X-Ray Digital Subtraction Angiography to Detect Renal Artery Stenosis in Swine**
Computer 28

Thomas K. Rhee[1], Jonathan K. Park[1], Ty A. Cashen[2], Wanyong Shin[2], Brian E. Schirf[1], Andrew C. Larson[1], Pottumarthi V. Prasad[1], Debiao Li[1, 2], Timothy J. Carroll[1, 2], Reed A. Omary[1, 2]
[1]Northwestern University Feinberg School of Medicine, Chicago, Illinois, USA; [2]Northwestern University, Chicago, Illinois, USA

The accuracy of 3D MR angiography(MRA) of renal artery stenosis(RAS) at 1.5T using either intravenous or intraarterial(IA) gadolinium contrast injection is equivalent to digital subtraction angiography(DSA) but MRA still overestimates stenoses. We tested the hypothesis that IA MRA of RAS in swine at 3.0T was as accurate as DSA in the setting of percutaneous transluminal angioplasty(PTA). In 6 pigs, RAS measurements obtained from DSA and MRA pre-PTA($p=0.99$) and post-PTA($p=0.07$) were not statistically significant. Additionally, MRA measurements of RAS correlated closely to DSA measurements of RAS ($r^2=0.92$). Thus, IA MRA of RAS in swine at 3.0T is as accurate as DSA.

15:00 *3358*. **Dual Echo Tip Tracking with Orthogonal Dephaser Gradients**
Computer 27
Sven Müller[1], Wolfhard Semmler[1], Michael Bock[1]
[1]German Cancer Research Center, Heidelberg, Germany

A projection technique for marker coil localization is proposed which utilizes two projections acquired in a double-echo technique. The two echoes differ in the preparation of the projection signal which is optimized to suppress background from lengthy cable structures in one direction. After Fourier transformation, a point-wise multiplication of the projection data is performed to enhance the localized marker coil signal. For optimal signal preparation a maximum signal-to-background-ratio of about 200 was achieved.

Tissue Segmentation and Coregistration

Room 4A Tuesday 13:30 - 15:30

13:30 *3359*. **An Automated Image Registration Methodology Using a Hybrid Genetic Algorithm Strategy**
Computer 29
Wei Huang[1], John M. Sullivan[1]
[1]Worcester Polytechnic Institute, Worcester, Massachusetts, USA

An image registration using optimization of voxel similarities was presented, coupled with a hybrid genetic algorithm. It was shown to be a robust and accurate registration strategy. The registration quality was superior to the conventional alignment techniques. Significantly, the GA was not strongly sensitive to the initial start location nor was it susceptible to local minima/maxima. One of the greatest benefits of the GA is the lack of a required quality start location. The automated centroid mask coupled with the sequential application of GA alignments mimicked manual registration sequences. The GA demonstrated excellent alignments with an accuracy of over 98 percent. The mask strategy was proved to be an efficient method to substantially enhance both speed and alignment accuracy.

14:00 *3360*. **The Effect of the Water-Fat Shift Differences on Automatic Co-Registration of MR Images**
Computer 29
Hans Olofsen[1], Roald van der Landen[1], Wouter M. Teeuwisse[1], Faiza Admiraal-Behloul[1], Mark A. van Buchem[1], Johan H. C. Reiber[1], Matthias J. P. Van Osch[1]
[1]Leiden University Medical Center, Leiden, Netherlands

The goal of this work was to determine the effect of water-fat shift (WFS) differences on the co-registration of MRI scans. The images of two sequences (T2 and FLAIR) with several WFS parameters have been co-registered first manually and then automatically. The results show that automatic co-registration can lead to errors when the images have different WFS settings.

14:30 *3361*. **Robust Method to Measure Tendon Strain**
Computer 29
Jane C. Asmuth[1], Nelly A. Andarawis[1], Nicholas J. Tustison[1], Brian B. Avants[1], Joseph J. Sarver[1], Louis J. Soslowsky[1], James C. Gee[1]
[1]University of Pennsylvania, Philadelphia, Pennsylvania, USA

A non-invasive method to compute the strain field of the supraspinatus tendon under loading is presented. MRI slices of the loaded and unloaded tendon are registered to find a deformation field from which the strain is derived. Tendon MRI images lack contrast and texture and are challenging to register. To guarantee well-behaved results, user-traced splines mark out tendon contours and steer a registration algorithm that models the tendon as a continuum. The strain results from this method are consistent with the strain predicted by finite element model analysis.

15:00 *3362*. **An Automatic Method for Visceral Adipose Tissue Measurement in the Metabolic Syndrome**
Computer 29
Vincent Roullier[1, 2], Christophe Aube[3], Pierre-Henri Ducluzeau[4], Christine Cavaro-Menard[1], Jérôme Lebigot[4], Guillaume Calmon[2]
[1]LISA CNRS-FRE2656, Angers, France; [2]GE Healthcare, Velizy, France; [3]Departement Imagerie, Angers, France; [4]CHU Angers, Angers, France

The metabolic syndrome is pathology in strong increase. The ratio between the surface of intra-abdominal fat and subcutaneous fat appears as a good predictor of this pathology. The measure of this ratio by MRI needs a long and tedious manual segmentation by the experts. We propose a fast and automatic method based on fuzzy algorithms to evaluate this ratio. This method is tested on 10 patients with a metabolic syndrome. Statistical results are studied in comparison with the expert quantification. The potential of this algorithm for a fast and reliable quantification was demonstrated in this study.

Rapid Imaging: Pulse Sequences and Techniques

Room 4A Tuesday 13:30 - 15:30

13:30 *3363*. **Avalanching Amplification of MRI Lesion Contrast by Nonlinear Feedback**
Computer 30
Yung-Ya Lin[1], Susie Yi Huang[1], Massoud Akhtari[1], Gary W. Mathern[1], Dennis J. Chute[1], Harry V. Vinters[1], Sandip Datta[1], Jamie D. Walls[2]
[1]University of California, Los Angeles, Los Angeles, California, USA; [2]Harvard University, Cambridge, Massachusetts, USA

Extracting image contrast from small variations in MRI parameters is vital in distinguishing physiological changes leading to a pathologic state. We present a new approach to enhance MRI contrast based on nonlinear feedback fields induced by the spins themselves. Changes in the distribution of an initially unstable magnetization configuration act back on the spins through the feedback fields to amplify contrast. We demonstrate avalanching amplification of MRI contrast due to small differences in resonance frequency under the distant dipolar field and radiation damping feedback interactions and observe up to 20 times improved contrast in epileptogenic lesions and malignant brain tumors.

13:30 *3364*. **A 3D Golden-Angle Projection Reconstruction Technique for Dynamic Contrast-Enhanced MRI**
Computer 31
Hee Kwon Song[1], Wei Lin[1], Lawrence Dougherty[1], Mitchell D. Schnall[1]
[1]University of Pennsylvania Medical Center, Philadelphia, Pennsylvania, USA

A 3D golden-angle, projection reconstruction technique for dynamic contrast-enhanced MRI is presented. The utilization of the golden angle for incrementing the views permits increased flexibility during reconstruction, compared to previous PR-based dynamic methods. The tradeoffs in the temporal and spatial resolution could be determined retrospectively, providing a high spatial resolution series for lesion architecture, or a high temporal resolution series for dynamic enhancement assessment. Further, with temporally selective data filtering, both high spatial and temporal resolution could be achieved in a single image series. The feasibility of the technique is demonstrated in a 3D dynamic contrast-enhanced exam of the breast.

13:30 *3365*. **Rapid 3D Imaging with an Undersampled Shells K-Space Trajectory**
Computer 32
Yunhong Shu[1], Stephen J. Riederer[1], Matt A. Bernstein[1]
[1]Mayo Clinic College of Medicine, Rochester, Minnesota, USA

The shells trajectory is a 3D non-Cartesian data acquisition method with improved efficiency compared to Cartesian sampling. This work demonstrates that undersampling can be combined with the shells trajectory to further accelerate the acquisition. The undersampling was implemented by removing interleaves from shells with larger radii. The undersampling rate was determined by a Kaiser window with a variable shape parameter â. Different â values were examined, and an acceptable maximum value of 3.2 was found from phantom and volunteer experiments. It is shown that up to two-fold acceleration can be achieved with reasonable image quality and resolution, and minor artifacts.

14:00 *3366*. **An Interleaved Center Frequency Acquisition Method in Transition-Band SSFP fMRI: Increased Spatial Off-Resonance Coverage**
Computer 32
Jongho Lee[1], Juan M. Santos[1], John M. Pauly[1]
[1]Stanford University, Stanford, California, USA

To increase the off-resonance frequency coverage in transition-band SSFP fMRI, different center frequencies are interleaved in one volume acquisition time. A short transition period of linear center frequency change is introduced to decrease the signal oscillation between the different center frequencies. The activation maps match with those of the conventional method (repeated experiments with different center frequencies) while maintaining the same experimental conditions.

14:00 *3367*. **An Extension to UNFOLD to Handle Breathing Motion, and Flexibility in K-T Sampling Schemes**
Computer 31
Bruno Madore[1], W. Scott Hoge[1]
[1]Harvard Medical School, Brigham and Women's Hospital, Boston, Massachusetts, USA

UNFOLD is a fast-imaging method, used in dynamic imaging. It suppresses aliasing artifacts by forcing them to behave in a conspicuous manner through time, so they can be filtered away. But motion, and/or departures from a regular sampling scheme in k-t space, can disturb UNFOLD's temporal strategy, and reduce its ability to suppress artifacts. Our method is an extension to UNFOLD, able to handle these types of disturbances. We show here, in a myocardial-perfusion application, that our extended approach significantly suppresses artifacts, when breathing motion is present. Furthermore, we show that it can handle departures from the usual UNFOLD k-t sampling strategy, which is useful, for example, when designing self-calibrated parallel imaging methods.

14:00 *3368*. **Non CPMG Phase Modulation, the Easy Way**
Computer 30
Patrick LeRoux[1]
[1]GE Healthcare, Buc, IDF, France

The non-CPMG sequence using quadratic phase modulation permits to acquire full signal Fast Spin Echo images, even in the presence of voluntary or unvoluntary phase modulation (an example of application is Diffusion Weighted acquisition in Spine studies). But it needs also a stabilization period whose description has been difficult to implement for the ones not familiar with the theory. We give here an implementation which can be easily reproduced.

14:30 ***3369***. **Absolute B1-Mapping from Repeated Varying Flip Angle RF Excitations**
Computer 30
Alexandru Cernicanu[1], Daniel Kim[2], Tushar Manglik[2], Vinay Pai[2], Leon Axel[2]
[1]University of Pennsylvania, Philadelphia, Pennsylvania, USA; [2]New York University, New York, New York, USA

The inhomogeneity of the RF pulse flip angle needs to be considered in quantitative studies. We propose a method to gauge this variation by calculating the actual B1 seen by each pixel in the field of view. The method relies on the acquisition of 40 measurements at different nominal flip angles and takes into account B0 inhomogeneity effects on the effective flip angle. We imaged a cylindrical phantom and calculated the B1 map and the corresponding effective flip angle map. The B1 calculation method is robust, and it shows important B1 and corresponding flip angle variations (up to 10%).

14:30 ***3370***. **Fat-Water Separation in Dynamic Objects, with a Novel Approach Based on the Dixon and UNFOLD Methods**
Computer 31
Riad S. Ababneh[1], Bruno Madore[2]
[1]Brigham and Women's Hospital, Boston, Massachusetts, USA; [2]Brigham and Women's Hospital, Harvard Medical School, Boston, Massachusetts, USA

We present a novel approach for fat-water separation in dynamic objects. The approach can be seen as a hybrid combination of the Dixon method and of the UNFOLD method. While UNFOLD typically involves changing the sampling function from time frame to time frame to separate aliased and non-aliased signals, our approach changes TE from time frame to time frame instead, to separate fat and water signals. As a result, fat signal is forced to behave in peculiar ways through time, so it can be detected and separated from the (high-temporal resolution) water signal.

14:30 ***3371***. **Fast Structural Brain Imaging Using an MDEFT Sequence with a FLASH-EPI Hybrid Readout**
Computer 32
Ralf Deichmann[1]
[1]Institute of Neurology, London, England, UK

A sequence for the fast acquisition of T1 weighted structural brain images with whole brain coverage and isotropic resolution of 1 mm is presented. The sequence is based on MDEFT with a FLASH-EPI hybrid readout. Several techniques for artefact suppression are implemented, like echo time shifting, asymmetric k-space sampling, and navigator echo acquisition. It is shown experimentally that the hybrid MDEFT sequence with a total duration of 8 min yields the same signal-to-noise and contrast-to-noise ratios as a 12 min MDEFT sequence based on a standard FLASH readout.

15:00 ***3372***. **Validation of an Improved Single Shot Flow Mapping Method**
Computer 32
Jin Zuo[1], Mark Bolding[1], Donald B. Twieg[1]
[1]University of Alabama at Birmingham, Birmingham, Alabama, USA

As a variant of SS-PARSE (Single Shot Parameter Assessment by Retrieval from Signal Encoding), V-SS-PARSE, a single shot imaging method has been developed to realize fast and straightforward flow quantification by solving an inverse problem. Magnitude, velocity, relaxation rate and frequency information can be retrieved without any extra reference image acquisitions, as demonstrated by phantom studies. Retrieved magnitude and velocity maps show results comparable to those obtained by phase contrast methods (correlation of $r > 0.99$), even with the brief single shot 70 ms acquisition.

15:00 ***3373***. **Improved Generalized Series Reconstruction for 3D MRI Using Shaped Data**
Computer 31
Sinha Neelam[1], Manojkumar Saranathan[1]
[1]Indian Institute of Science, Bangalore, Karnataka, India

The work proposes reconstructing partial k-space DCE-MRI using the TRIGR algorithm on a star-shaped (SS) data truncation window. The SS mask contains more energy than the standard rectangular mask (RS), since all points along SS lie close to the ky-kz axes. Two methods of TRIGR extrapolation on SS data were examined and compared to conventional rectangularly truncated (RS) TRIGR data. Analysis on phantom and DCEMRI data sets from patients with cancer reveal SS-TRIGR to be significantly more accurate than RS-TRIGR using just 15% of k-space for small structures.

3374. WITHDRAWN

Rapid Imaging: Applications

Room 4A Tuesday 13:30 - 15:30

13:30 ***3375***. **Temporal Variability of R_2* Estimates in Single-Shot Methods**
Computer 33
Hrishikesh Deshpande[1], Donald B. Twieg[1]
[1]University of Alabama at Birmingham, Birmingham, Alabama, USA

The sensitivity and accuracy of fMRI depend critically on the ability to measure small changes in R2*. To compare the temporal variability of R2* estimates using MEPI and SS-PARSE, phantom studies of repeatability were performed.

14:00 *3376*. **Multiple Echo 3D Hybrid Radial SSFP: Initial Applications in a Single Breath-Hold Cardiac Imaging**
Computer 33
Jing Liu[1], Youngkyoo Jung[1], Karl K. Vigen[1], Walter F. Block[1]
[1]University of Wisconin - Madison, Madison, Wisconsin, USA

3D hybrid radial acquisitions using steady state free precession (SSFP) contrast have already achieved strong results in coronary, cardiac function, and peripheral vasculature imaging. We present methods to sample k-space faster by utilizing the normally unused frequency dephaser, rephaser pulses, and gradient ramps besides the conventional readout. This technique is first applied in a single breath-hold multiple phase cardiac study.

14:30 *3377*. **Dynamic Imaging of Muscles During Speech Using Interleaved Spiral FLASH**
Computer 33
Bradley P. Sutton[1], Jeffrey Tsao[2], Hideo Shinagawa[3], David P. Kuehn[1]
[1]University of Illinois at Urbana-Champaign, Urbana, Illinois, USA; [2]Novartis Institutes for BioMedical Research, Inc.,, Cambridge, Massachusetts, USA; [3]Tokyo Medical and Dental University, Tokyo, Japan

Analysis of function of muscles involved in speech processes requires high spatial and temporal resolutions. We applied a spiral FLASH sequence to imaging the levator veli palatini muscle during natural speech. Image quality was found to be similar to a Cartesian FLASH sequence, but the gradient-induced auditory noise was reduced, allowing improved recording of speech. Adequate temporal resolution was achieved using a sliding window reconstruction to better visualize the muscle motion.

15:00 *3378*. **Spiral MRI on Rat Brain and Rat Heart at 7 Tesla**
Computer 33
Jerome Voiron[1], Laurent Lamalle[2]
[1]Bruker BioSpin MRI GmbH, Ettlingen, Germany; [2]IFR1 - Unité IRM 3T, Centre Hospitalier Universitaire, Grenoble, France

With possibly shorter TEs, shorter gradient application duration and gradient moment nulling, spiral MRI can be an interesting alternative to EPI. Its features are particularly relevant for functional MRI studies as well as for cardiovascular, perfusion and diffusion applications, especially when robustness to B0 inhomogeneity becomes critical. *In vivo* experiments on rat at 7 T using spiral MRI were performed. They demonstrate that this technique could even be better appropriate than EPI at high B0 field. To our knowledge, this is the first described study demonstrating the spiral technique for rat imaging with good spatial resolution at high field.

Data Processing and Pulse Sequences: Other

Room 4A Tuesday 13:30 - 15:30

13:30 *3379*. **Current Density Impedance Imaging in Porcine Heart**
Computer 35
Weijing Ma[1], Dinghui Wang[1], Tim DeMonte[1], Adrian Nachman[1], Dawn Jorgenson[2], Michael Joy[1]
[1]University of Toronto, Toronto, Ontario, Canada; [2]Heartstream operation, Phillips Medical System, Seattle, Washington, USA

Current density impedance imaging (CDII) is a novel technique that can non-invasively image the internal conductivity of an object. In this study, CDII was used to measure the conductivity distribution of the porcine heart. The experimental results showed conductivity variations due to internal heart structures. The CDII-measured conductivity is consistent with direct dielectric measurements, which demonstrates the capability of CDII in imaging biological tissues. Reliable conductivity images will provide invaluable information for bioelectricity research such as the myocardium defibrillation study.

13:30 *3380*. **TrueFISP Blade Imaging in the Steady State (TrueBLISS)**
Computer 34
Kestutis Joseph Barkauskas[1], Claudia M. Hillenbrand[2], Mark A. Griswold[3], Jeffrey L. Sunshine[3], Jeffrey L. Duerk[3]
[1]Case Western Reserve University, Cleveland, Ohio, USA; [2]St. Jude Children's Research Hospital, Memphis, Tennessee, USA; [3]University Hospitals of Cleveland and Case Western Reserve University School of Medicine, Cleveland, Ohio, USA

Blade Imaging strategies have significant oversampling of low spatial frequencies, which allows self-correction of inconsistencies across data segments. Applications for blade imaging exist beyond its conventional use in TSE-based anatomic and diffusion scans of the head. This work proposes Blade Imaging in the Steady State with TrueFISP magnetization preparation (TrueBLISS), which achieves the highest SNR per unit time with T2 consistency across the blades while maintaining the self-correction features of the blade trajectory. TrueBLISS demonstrates expected image contrast and low artifact levels in the abdomen of an asymptomatic volunteer.

14:00 *3381*. **TPI-SENSE for Fast Ultra-Short TE MRI**
Computer 34
Yongxian Qian[1], Andy Stenger[2], Fernando Boada[1]
[1]University of Pittsburgh, Pittsburgh, Pennsylvania, USA; [2]University of Hawaii at Manoa, Honolulu, Hawaii, USA

This study demonstrates the combination of twisted projection imaging (TPI) with sensitivity encoding (SENSE) parallel imaging as a means to further accelerate data acquisition in ultra-short TE MRI. Studies on computer models and phantoms were performed with projection reductions in polar (ring) direction and azimuthal (rotation) direction. Both simulation and phantom images reconstructed from the undersampled data sets illustrated that the TPI sampling scheme, due to its inherent 3D nature, can tolerate larger reduction factors than comparable 2D sampling schemes.

14:00 ***3382***. **Multiple Current Injection Schemes in Magnetic Resonance Electrical Impedance Tomography**
Computer 35
Mark Jason Hamamura[1], Lufti Tugan Muftuler[1], Ozlem Birgul[1], Orhan Nalcioglu[1]
[1]University of California, Irvine, California, USA

In this study, we investigate the effects of using data from different combinations of current density distributions for reconstruction in Magnetic Resonance Electrical Impedance Tomography. The results indicate that selection of the optimum current injection scheme requires balancing overall contrast with spatial resolution in the periphery regions.

14:30 ***3383***. **Electrode Misalignment Correction Algorithms in Magnetic Resonance Electrical Impedance Tomography**
Computer 35
Mark Jason Hamamura[1], Lufti Tugan Muftuler[1], Ozlem Birgul[1], Orhan Nalcioglu[1]
[1]University of California, Irvine, California, USA

Misalignment of electrode locations during reconstruction in Magnetic Resonance Electrical Impedance Tomography (MREIT) can lead to artifacts and diminished contrast in the resulting conductivity image. In this study, we demonstrate the ability of three correction algorithms to improve the reconstruction.

14:30 ***3384***. **Comparision of MR Elastography and Compressive Loading Shear Modulus Estimates for Agar Gel Inclusions**
Computer 34
Timothy C. Dunn[1], Sharmila Majumdar[1, 2]
[1]University of California San Francisco, San Francisco, California, USA; [2]University of California Berkeley, Berkeley, California, USA

The purpose of this study was to compare shear modulus estimates of small agar gel inclusions using dynamic MR Elastography at 3T and quasi-static compressive mechanical testing. MRE at 500 Hz was performed on cylindrical agar gel inclusions (2 cm diameter, 3 cm height) of varying concentration (0.5 to 2.0%) embedded into a homogeneous agar gel background. Compressive mechanical tests were performed on cylindrical samples from the same batch. The slope and intercept of shear modulus versus agar concentration were found to not be significantly different for the two methods.

15:00 ***3385***. **Fast EPI Based 3D MR Elastography of the Brain**
Computer 34
Scott A. Kruse[1], Roger C. Grimm[1], David S. Lake[1], Armando Manduca[1], Richard L. Ehman[1]
[1]Mayo Clinic College of Medicine, Rochester, Minnesota, USA

Magnetic Resonance Elastography (MRE) studies of cognitively impaired patients must be performed in a clinically acceptable amount of time. Previous 3D studies were prohibitively long. The goal of this work was to capture the full 3D wave field using a 2D multi-slice SE-EPI sequence. 24 elastography slices can be acquired in as little as 3 minutes.

15:00 ***3386***. **Dynamic MREIT Using Sub-Milliamp Currents**
Computer 35
Mark Jason Hamamura[1], Lufti Tugan Muftuler[1], Ozlem Birgul[1], Orhan Nalcioglu[1]
[1]University of California, Irvine, California, USA

In this study, we tracked the diffusion of sodium chloride within an agarose gel phantom by measuring its conductivity distribution over a span of 12 hours using the technique of Magnetic Resonance Electrical Impedance Tomography (MREIT). The results demonstrate that MREIT can monitor changes in conductivity over time using sub-milliamp injected currents.

Vascular and Stroke

Room 4A Wednesday 14:00 - 16:00

14:00 *3387*. **Cerebral Blood Flow and Arterial Transit Time Measurements in Patients with Chronic Occlusive Cerebrovascular Disease Using Continuous Arterial Spin Labeling on 3T-MR: Correlative Study with CO2 PET Examination**
Computer 1

Hirohiko Kimura[1], Hiroyuki Kabasawa[2], Tatsuro Tsuchida[1], Yoshiharu Yonekura[1], Harumi Itoh[1]
[1]University of Fukui, Fukui, Japan; [2]GE Medical Systems, Tokyo, Japan

Multi-slice continuous arterial spin labeling (CASL) is a means of non-invasive MR perfusion assessment that provides a quantitative map of cerebral blood flow. However, it has not been investigated whether the hemodynamic changes that accompany cerebrovascular disease affect the utility of CASL in the assessment of CBF. The goal of the current study was to propose a two-compartment model for the quantification of CBF and arterial transit time and to compare CASL-CBF and CO2 PET-CBF in the assessment of regional cerebral blood flow in patients with chronic occlusive cerebrovascular disease.

14:30 *3388*. **Accuracy of MR Angiography and Transcranial Doppler for Cerebral Collateral Flow: A Comparison with IaDSA in 97 Patients with Carotid Occlusion**
Computer 1

Jeroen Hendrikse[1], Willem PThM Mali[1], Jeroen Van der Grond[2]
[1]UMC, Utrecht, Netherlands; [2]UMC, Leiden, Netherlands

The presence of functional collaterals is associated with relatively low stroke risk. Still it remains undetermined whether non-invasive methods can replace iaDSA for cerebral collateral flow measurements. In the present study we show that MRA and TCD collateral flow measurements should be interpreted with caution, for the presence of collateral flow via the anterior circle of Willis MRA and TCD are equally and highly accurate. For the posterior communicating artery, TCD tends to overestimate and MRA tends to underestimate the presence of collateral flow compared to iaDSA. Combined assessment with MRA and TCD did not result in substantial diagnostic gain.

15:00 *3389*. **Preliminary Study of Wall Shear Stress of an Intracranial Aneurysmal Model Based on the Data of Time-Resolved Three-Dimensional Phase-Contrast MRI**
Computer 1

Haruo Isoda[1], Shuhei Yamashita[1], Yasuhide Ohkura[2], Takashi Kosugi[2], Hiroyasu Takeda[1], Yasuo Takehara[1], Shoichi Inagawa[1], Masaya Hirano[3], Marcus T. Alley[4], Michael Markl[5], Norbert J. Pelc[4], Harumi Sakahara[1]
[1]Hamamatsu University School of Medicine, Hamamatsu, Shizuoka, Japan; [2]Renaissance of Technology Corporation, Hamamatsu, Shizuoka, Japan; [3]GE Yokogawa Medical Systems, Hino, Tokyo, Japan; [4]Stanford University School of Medicine, Stanford, California, USA; [5]University Hospital Freiburg, Freiburg, Barden-Wuerttemberg, Germany

We developed a postprocessing software for 4D data sets obtained by 3D cine phase-contrast MRI (4D-Flow) called "Flow visualization and analysis (Flova)". Flova can calculate wall shear stress (WSS) in a few minutes based on the data of both 4D-Flow and MR angiography. We evaluated the accuracy of WSS obtained by Flova using a straight tube with a 16mm diameter and constant flow. We calculated the WSS of a silicon intracranial aneurysmal model three times actual size with constant flow by Flova. The aneurysm model had relatively weaker WSS in the bleb than in the surrounding aneurysmal wall.

15:30 *3390*. **Combining Segmentation and Arterial Spin-Labeling to Evaluate Cerebral Blood Flow Within Vascular Territories in Children with Sickle Cell Disease**
Computer 1

John O. Glass[1], Amir Paydar[1], Gisele Hankins[1], Ping Zou[1], Winfred C. Wang[1], Russell E. Ware[1], Wilburn E. Reddick[1], Robert J. Ogg[1], Kathleen J. Helton[1]
[1]St. Jude Children's Research Hospital, Memphis, Tennessee, USA

Sickle cell disease (SCD) is a devastating hematological disease marked by vaso-occlusive events leading to vasculopathy, brain injury and stroke. Prospective data from 28 patients were analyzed. T1, T2, PD, and FLAIR images were coregistered with ASL images and twelve vascular territories were manually drawn. Automated segmentation differentiated GM and WM for each vascular territory, and quantitative analysis of CBF was performed. CBF was elevated throughout the brain, consistent with previous studies in SCD patients. This study demonstrates that ASL combined with automated image segmentation is useful to investigate brain perfusion in a population known to be at risk for vascular events.

MRI in Animal Models

Room 4A Wednesday 14:00 - 16:00

14:00 *3391*. **Morphological Assessment in a Transgenic Cacna1a Knockin Migraine Mouse Model Using Automatic Segmentation of High-Resolution Whole Brain MR**
Computer 3
Rob C. G. van der Ven[1], Roald van der Landen[1], Louise van der Weerd[1, 2], B Hogers[1], R. R. Frants[1], Rob E. Poelmann[1], Arn M.J.M. van den Maagdenberg[1], Suzane R. Kiihne[2], Johan H.C. Reiber[1], Mark A. van Buchem[1], Faiza Admiraal-Behloul[1]
[1]Leiden University Medical Center, Leiden, Netherlands; [2]Leiden University, Leiden, Netherlands

Migraine is a neurological paroxysmal disorder affecting up to 16% in the general population. Familial hemiplegic migraine type-1 (FHM-1) is an autosomal dominant subtype of migraine with aura caused by mutations in the CACNA1A gene. Recently, we generated a transgenic knockin mouse model of migraine containing a human pathogenic R192Q FHM1 mutation in the mouse Cacna1a gene. The purpose of this work was the phenotypical characterization of brain structures in our migraine mouse model, assessing volume and morphology of the cerebellar white matter and the brain ventricles.

14:00 *3392*. **High-Resolution 3D MRI to Identify Neurodegeneration in a Huntington Disease Mouse Model Brain**
Computer 4
Shoshana Tsatskis[1], Jason P. Lerch[1], Jeffrey Carroll[2], Michael R. Hayden[2], R Mark Henkelman[1]
[1]The Hospital for Sick Children, Toronto, ON, Canada; [2]Centre of Molecular Medicine and Therapeutics, University of British Columbia, Vancouver, BC, Canada

Magnetic resonance imaging was used to detect neuroanatomical differences between eight-month-old fixed Huntington Disease (HD) mouse model brains and their wild-type littermates. A four-channel 7.0-T MR scanner with a 6-cm inner bore diameter gradient set was used to acquire anatomical images of brains within skulls. Significant differences in deformation magnitudes were found in the bilateral striatum, the right cerebral cortex, and isolated regions of the thalamus. These results suggest that HD-related neurodegeneration can be detected earlier than initially believed, and suggest that MR-based measures can provide essential information about neuroanatomical integrity for clinical trials in HD mouse models.

14:00 *3393*. **Multixeponential T2 Relaxation Analysis of Multislice MR Images in a Stroke Model**
Computer 2
Boguslaw Tomanek[1, 2], Adele Nguyen[1], Min Qiao[1], Jeff Dunn[2], Cheryl McCreary[2], Phil Barber[2], Anna Tomanek[2], Tad Foniok[1], Kvieta Burda[3], Ursula Tuor[1]
[1]National Research Council of Canada, Calgary, Alberta, Canada; [2]University of Calgary, Calgary, Alberta, Canada; [3]Jagiellonian University, Krakow, Malopolska, Poland

A multiexponential analysis of T2 relaxation times within brain injured by hypoxia-ischemia was investigated. T2 maps were acquired using a 128-echo multi-slice spin echo sequence using either Gauss or sinc selective 90º and 180º pulses 48 hours after a transient episode of cerebral hypoxia-ischemia. A least squares multiexponential method was used to fit the T2 decay curve. As expected following stroke, there was an increase in T2 in the ischemic region irrespective of MR sequence used. Control parietal cortex was best described by a monoexponential and ischemic cortex by a biexponential T2 when Gauss selective pulses were used. In contrast, with sinc pulses both control and parietal cortex had mono-exponential T2 characteristics. For both Gauss and sinc pulses, in regions that included CSF bi-exponential T2 fits with a long and regular component were optimal. It appears that imperfections of the Gauss selective pulse can contribute to the bi-exponential character of T2 in regions such as stroke.

14:30 *3394*. **The Ratio of T2* and T1 Relaxivities in Experimental Cerebral Tumor and Normal Brain**
Computer 2
James Russell Ewing[1, 2], Hassan Bagher-Ebadian[1], Ramesh Paudyal[1, 2]
[1]Henry Ford Health Systems, Detroit, Michigan, USA; [2]Oakland University, Rochester, MIchigan, USA

Five male Fischer rats with implanted cerebral tumors were studied at 7 Tesla using a Look-Locker inversion-recovery imaging sequence (TOMROP). ?2, the ratio of T2* to T1 relaxivities after injection of the contrast agent (Gadomer), was calculated. In the leaky tumor vascular bed, ?2 was a factor of 5.6 smaller than it was in the contralateral normal side. Thus, in vascular beds permeable to the contrast agent, this observation impacts all attempts to use T2* contrast as a measure of contrast agent concentration in estimating such physiological variables as blood flow, blood volume, and vascular permeability.

14:30 *3395*. **USPIO-Enhanced MRI at 7T in a Mouse Model of Focal Cerebral Ischemia**
Computer 4
Jean-Baptiste Pialat[1, 2], Marlene Wiart[2], Tae-Hee Cho[2], Samir Moucharrafie-Naime[2], Norbert Nighoghossian, [23], Yves Berthezene[1, 2]
[1]Hopital de la Croix-Rousse, Lyon, France; [2]Laboratoire Creatis UMR CNRS 5515, U630 Inserm, Lyon, France; [3]Hopital Neurologique, Lyon, France

The purpose of our study was to evaluate the inflammatory response in a mouse model of focal cerebral ischemia with ultrasmall superparamagnetic iron oxide (USPIO). Two days post-injury, hypointense region was observed in the caudate putamen on the ischemic hemisphere and strongly hypointense region appeared also within the corpus callosum contralateral to the lesion. No signal change was noted in healthy animals with USPIO injection, nor in stroke-induced animals without USPIO injection. Although the mechanisms underlying the hyposignal need further pathological investigations, these abnormalities may account for a global inflammatory process with transcallosal migration of USPIO particles.

14:30 ***3396***. **Functional Imaging of Ketamine in the Rat Brain: A Model for Glutamate Dysfunction in Schizophrenia**
Computer 3

Carmen De Groote[1], *Shane McKie*[1], *Bill Deakin*[1], *Stephen Ross Williams*[1]
[1]University of Manchester, Manchester, UK

Ketamine is a widely used drug to model schizophrenia in humans and rodents. We used pharmacological-challenge fMRI (pMRI) to study the effect of ketamine on blood-oxygen level dependent (BOLD) responses in the rat brain. Gradient-echo images covering the whole brain were acquired at 7T before and for 65 mins after ketamine infusion at two doses (10 and 30 mg/kg), in alpha-chloralose anaesthetized rats. Ketamine produced significant BOLD changes over time in brain regions relevant to schizophrenia. Ketamine pMRI in the rat may be a useful tool in preclinical schizophrenia research.

15:00 ***3397***. **The Effects of Prolonged Dexamethasone Treatment and Single MRI Procedure Under Anesthesia on Hippocampal and Prefrontal Cortex Volume in Rats**
Computer 3

Mirjam I. Schubert[1, 2], *Raffael Kalisch*[1], *Alexandra Wigger*[1], *Rosa Hemauer*[1], *Osborne FX Almeida*[1], *Rainer Landgraf*[1], *Dorothee P. Auer*[1, 2]
[1]Max Planck Institute of Psychiatry, Munich, Bavaria, Germany; [2]University of Nottingham, Nottingham, Nottinghamshire, UK

Hippocampal volume loss in humans and rodents supposedly results from elevated glucocorticoids. To further investigate structural changes in limbic system, i.e. hippocampus, anterior cingulate and retrosplenial cortex, non-adrenalectomized rats with and without long-term dexamethasone treatment were examined by *in vivo* MR-morphometry at 7T. No hippocampal volume loss was found in dexamethasone treated rats. Unexpectedly, the procedure itself led to reduced ACC and RSG both in untreated and dexamethasone treated rats. This study further questions the validity of the assumed dexamethasone-induced MRI detectable HV loss, but suggests extrahippocampal brain plasticity in response to a single stressful event in conjunction with anesthesia.

15:00 ***3398***. **Neurodevelopmental Consequences of Perinatal Hypoxia in C57B/L6 Mice Assessed by *In Vivo* DTI and Behavior**
Computer 4

Halima Chahboune[1], *Laura Ment*[1], *William B. Stewart*[1], *Michael L. Schwartz*[1], *Stephen M. Strittmatter*[1], *Aaron W. McGee*[1], *Douglas L. Rothman*[1], *Fahmeed Hyder*[1]
[1]Yale University, New Haven, Connecticut, USA

In vivo DTI has great potential for assessing neurodevelopmental changes. Here we show alterations in morphology of developing axonal pathways in developing mouse brain when exposed to hypoxia. Chronic sublethal hypoxia (<10%) at the 3rd day (P3) after birth (in C57B/L6 mice) for a week provides an injury model which replicates neuropathologic findings that accompany preterm birth. Normoxic and hypoxic mice were studied with DTI through development (P15 to P45). We report that the normal developmental changes in fiber organization of corpus callosum and cingulate are perturbed by hypoxia. These results are supported by histology as well as behavioral assays

15:00 ***3399***. **Manganese-Enhanced MRI Reveals Laminar Structures in the Rat Retina**
Computer 2

Haiying Cheng[1], *Yongjun Liu*[1], *Timothy Q. Duong*[1]
[1]Emory University, Atlanta, Georgia, USA

Three distinct anatomical “layers” in the rat retina were resolved using manganese (Mn) enhanced MRI. The inner and outer “layers” were significantly more enhanced than the middle “layer” by Mn. Gd-DTPA enhanced T1-weighted images was used to enhance signals from vascular layers located at two opposing boundaries of the retinal thickness. The Mn-enhancement differences between awake + ambient light and anesthesia + dark was substantial, suggesting activity-dependent accumulation of Mn in the retina. Manganese-enhancement MRI thus offers a unique means to investigate structure and function of the retina with laminar specificity, which may be altered in retinal diseases.

15:00 ***3400***. **Quantitative Imaging of Magnetization Transfer in the Myelin Mutant *Shaking* Pup**
Computer 2

Alexey A. Samsonov[1], *Andrew L. Alexander*[1], *Ian D. Duncan*[1], *Aaron S. Field*[1]
[1]University of Wisconsin, Madison, Wisconsin, USA

Quantitative MT imaging (qMTI) allows estimation of several parameters governing MT effects in tissues, and may potentially improve the specificity of MTI. We report first qMTI results in the shaking (sh) pup, one of the “myelin mutant” animal models of dysmyelinating disease in humans. The putative myelin-related parameters, bound pool fraction and cross-relaxation rate, appear markedly decreased in the WM of the sh pup relative to the control. Longitudinal relaxation rate is markedly decreased in the sh pup; this observation contradicts any implications of axonal specificity attributed to T1 relaxation based on the “T1 black holes” of chronic MS lesions.

15:30 ***3401***. **Diffusion Tensor Imaging Detects White Matter and Gray Matter Changes in a Mouse Model for Alzheimer**
Computer 4

Greetje Vanhoutte[1], *Bianca Vanbroeck*[1], *Samir Kumar-Singh*[1], *Christine Van Broeckhoven*[1], *Annemie Van der Linden*[1]
[1]University of Antwerp, Antwerp, Belgium

Using magnetic resonance diffusion tensor imaging (DTI), this study investigates changes in regional fractional anisotropy (FA) in the brain of APP_Au transgenic mouse, a model of intracellular beta-amyloid diffuse plaque deposition associated with Alzheimer's disease. We showed reductions in FA values in comparison with control mice for both white and gray matter: cortex, corpus callosum, hippocampus and cerebellum. Because of its correlation with tissue microstructure and non invasive nature, DTI offers unique insights in the underlying cellular architecture. DTI-based observed abnormalities are becoming a valid tool as a potential biomarker of AD-associated pathology.

15:30 ***3402***. **Decreased ADC in a Mouse Model of a Lysosomal Storage Disease**
Computer 3
Lingyun Hu[1], Yingying Sun[1], Robia G. Pautler[1]
[1]Baylor College of Medicine, Houston, Texas, USA

Mice that lack the hexosamidase b gene (hexb-/-) are a model of the lysosomal storage disease, Sandhoff's disease. In this study, we utilize diffusion-weighted magnetic resonance imaging to evaluate physiological changes in the hexb-/- mouse brain in terms of fluid diffusivity as a consequence of GM2 ganglioside and glycolipid accumulation. The apparent diffusion coefficient (ADC) values in the cortex and striatum of the Hexb -/- mice and control mice at 3-4.5 months old were evaluated and verified with histology.

Diffusion and Perfusion: Pediatric Brain

Room 4A Wednesday 14:00 - 16:00

14:00 ***3403***. **CASL Perfusion MRI in Normal Infant Brain Development**
Computer 7
Ze Wang[1], Maria A. Fernandez-Seara[1], David C. Alsop[2], Wen-Ching Liu[3], April Benasich[3], Jiongjiong Wang[1], John A. Detre[1]
[1]University of Pennsylvania, Philadelphia, Pennsylvania, USA; [2]Harvard University, Boston, Massachusetts, USA; [3]University of Medicine and Dentistry of New Jersey, Rutgers, New Jersey, USA

Continuous arterial spin labeled perfusion MRI was carried out in normally developing 6- and 12-month old infants while asleep without sedation. The resulting cerebral blood flow images showed an increase in frontal CBF between 6 and 12 months of age, consistent with prior observations using FDG-PET. These results demonstrate the feasibility of using perfusion MRI to noninvasively monitor functional brain development.

14:00 ***3404***. **Anisotropy and Diffusivity Changes in Corpus Callosal Subregions in Chronic Pediatric Traumatic Brain Injury**
Computer 5
Larry Allen Kramer[1], Khader M. Hasan[1], Ambika Sankar[1], Mary R. Prasad[1], Jocelyne Bachevalier[2], Jack Fletcher[1], Linda Ewing-Cobbs[1]
[1]UTHSC-Houston, Houston, Texas, USA; [2]Emory, Atlanta, Georgia, USA

Volume, fractional anisotropy (FA) and transverse diffusivity of segmented corpus callosum (CC) was measured in chronic traumatically brain injured children (TBI) and controls utilizing diffusion tensor and conventional imaging techniques. We found that CC volumes were globally reduced compared to controls. FA and transverse diffusivity varied across the specific callosal regions in both groups reflecting histological differences of each region. Transverse diffusivity demonstrated the most significant differences between groups, particularly in the genu, posterior body and isthmus. Transverse diffusivity is an indicator of the integrity of myelin and may provide a more precise and sensitive measure of chronic TBI.

14:00 ***3405***. **Characteristics of Abnormal Diffusivity in Normal-Appearing White Matter Investigated with Diffusion Tensor MRI in Tuberous-Sclerosis Complex**
Computer 6
Malek Makki[1], Diane Chugani[1], Harry Chugani[1]
[1]Children's Hospital of Michigan, Detroit, Michigan, USA

Abstract: Changes in diffusivity and anisotropy revealed in normal appearing white matters (NAWM) brain tissues beyond the origin of tuberous sclerosis complex (TSC) lesions may be important to help localize lesions in MRI negative patients. Six TSC patients and twelve age-matched normal control subjects were studied to evaluate diffusivity and anisotropy in NAWM to investigate whether there are microstructural abnormalities.

14:30 ***3406***. **Functional and Connectivity Asymmetry Observed in the Visual System of an Infant with White Matter Lesions on MRI**
Computer 6
M Alex Dresner[1], Serena J. Counsell[1], Latha Srinivasan[1, 2], Ramsey M. Raafat[1], Frances M. Cowan[2], Joanna M. Allsop[1], Mary A. Rutherford[1, 2], Joseph V. Hajnal[1], A David Edwards[1, 2]
[1]Imperial College London, London, UK; [2]Hammersmith Hospital, London, UK

We present our findings of combined fMRI and probabilistic tractography of the visual system in a 2 year old infant who was born preterm and developed bilateral periventricular leukomalacia and right sided periventricular haemorrhagic infarction. These lesions were evident on serial, conventional MRI. fMRI and DTI obtained at 3 Tesla demonstrated asymmetrical activation in the visual cortex and connectivity distributions in the optic radiations, with diminished activation and connectivity distributions in the hemisphere with the porencephalic cyst.

14:30 Computer 5 ***3407***. **White Matter Volume and Anisotropy in Very Low Birth Weight Preterm Born Children: Association with Cognitive Outcome**

Pek-Lan Khong[1], Deqiang Qiu[1], Ada Yung[1], Grace Poon[1], Connie Leung[2], Se Chua[1], G McAlonan[1], Barbara Lam[1]

[1]The University of Hong Kong, Hong Kong, People's Republic of China; [2]The Duchess of Kent Children's Hospital, Hong Kong, People's Republic of China

We tested the hypothesis that mean white matter (WM) volume and fractional anisotropy (FA) are reduced in children born very low birth weight preterm (n=25, mean age=10.14 years) compared to healthy term born age-matched children (n=13) and that these parameters correlate with Wechsler full scale IQ scores (FSIQ). WM volume and FA were significantly lower in the preterm group compared to controls ($p=0.014$, $p<0.001$ respectively). WM volume was the only independent variable significantly affecting FSIQ after adjusting for gestational age, birth weight and gender ($r2=0.420$, $p=0.011$), suggesting that this parameter is a reliable predictor of cognitive outcome in these children.

14:30 Computer 7 ***3408***. **Perfusion Imaging in a Pediatric Stroke Patient Population Using Pulsed Arterial Spin Labeling-Initial Experience**

Shannon Christine Agner[1], Daniel J. Licht[2], David W. Silvestre[2], Rebecca Ichord[2], Robert Zimmerman[2], John A. Detre[1], Jiongjiong Wang[1]

[1]University of Pennsylvania, Philadelphia, Pennsylvania, USA; [2]Children's Hospital of Philadelphia, Philadelphia, Pennsylvania, USA

Arterial spin labeling (ASL) perfusion is a useful tool in imaging cerebral blood flow (CBF) in adults with cerebrovascular disease. In addition, ASL has been shown to have unique advantages in the pediatric population. In this study, we assess the hemodynamic status in children with acute arterial ischemic stroke (AIS) due to M1 segment MCA stenosis using pulsed ASL (PASL) perfusion imaging. This application demonstrates feasibility and utility of PASL in acute and longitudinal AIS imaging in pediatrics.

15:00 Computer 7 ***3409***. **Anatomic Variations of the Circle of Willis in Neonates: A High Resolution MRA Study at 3 Tesla**

Christina Malamateniou[1], Serena J. Counsell[1], Joanna M. Allsop[1], Julie A. Fitzpatrick[1], Latha Srinivasan[1], Lara Leijser[1], Leigh E. Dyet[1], Frances M. Cowan[1], Joseph V. Hajnal[1], Mary A. Rutherford[1]

[1]Hammersmith Hospital, Imperial College London, London, UK

The Circle of Willis (CoW) is a ring-like arterial structure that serves as potential collateral pathway and is known to display anatomical variations in adults. We used MRA at 3Tesla to identify CoW anatomic variations in the developing brain and to correlate those with known differences in development and disease. We recruited 19 preterm at term and 12 term infants with normal MRI and 10 infants with vascular disease. Differences in the occurrence of the anatomic variations and completeness of the CoW were found between preterm and term infants, those with and without vascular disease and between boys and girls.

15:00 Computer 5 ***3410***. **Discrepant FA Reduction Between the Frontal and Parietal Lobes of Post Irradiation Medulloblastoma Survivors: Preliminary Findings of Regional Susceptibility?**

Deqiang Qiu[1], Lucullus Leung[1], Dora Kwong[1], Godfrey Chan[1], Guang Cao[2], Pek-Lan Khong[1]

[1]The University of Hong Kong, Hong Kong, People's Republic of China [2]GE Medical, Asia, Hong Kong, People's Republic of China

In this study of 16 medulloblastoma survivors and corresponding age-matched control subjects, we tested the hypothesis that fractional anisotropy (FA) in the frontal lobe is more severely reduced than the parietal lobe after whole brain irradiation. Quantitative measurement of regional mean FA was performed using automatically generated masks. We found significant FA reduction in the frontal lobe, but not parietal lobe, in the medulloblastoma survivors compared to controls. Although more severe FA reduction in the frontal lobe was found, this difference did not achieve statistical significance. However, a trend of regional susceptibility of the frontal lobe to radiation was suggested.

15:00 Computer 6 ***3411***. **Maturation of the Corpus Callosum from Birth to Adulthood: Evaluation with Fractional Anisotropy and Diffusion Tensor Tractography**

Kazuyuki Ohgi[1], Akiyoshi Yamashita[1], Takashi Furukawa[1], Hirotaka Seura[1], Katsuhito Gotoh[2], Tomoko Matsubara[2], Syuhei Takemoto[2]

[1]Japanese Red Cross Med CTR, Tokyo, Japan; [2]Toshiba Medical Systems Corp., Otawara, Tochigi, Japan

This study illustrates white matter maturation of corpus callosum (CC) from birth (infancy) to adulthood by using fractional anisotropy (FA) and diffusion tensor tractography (DTT). FA provides useful scalar information in the white matter maturation of CC. DTT can illustrate additional information of developing individual axonal tracts of CC when compared in the same seeding ROI settings and in the same threshold FA values. But special attention should be required for the threshold FA values that can greatly affect delineation of the fibers on DTT.

15:30 *3412*. **Serial Quantitative Diffusion Tensor MRI of the Term Neonates with Hypoxic-Ischemic Encephalopathy (HIE)**
Computer 6

Richa Trivedi[1], G K. Malik[2], Rakesh Kumar Gupta[1], Khader M. Hasan[3], M Hasan[2], Amit Gupta[2], C M. Pandey[1], P A. Narayana[3]
[1]Sanjay Gandhi Post Graduate Institute of Medical Sciences, Lucknow, Uttar Pradesh, India; [2]King George's Medical University, Lucknow, Uttar Pradesh, India; [3]University of Texas Medical School at Houston, Houston, Texas, USA

Serial diffusion tensor imaging (DTI) at two-time points (at birth and at three months) was performed in term neonates with hypoxic-ischemic encephalopathy (HIE) and healthy controls to quantify the white matter abnormalities. On comparing fractional anisotropy (FA) and mean diffusivity (MD) change over time, we observed significant reduction in age related FA increase in periventricular white matter in HIE children where as significant reduction in age related MD decrease in HIE children was observed in deep gray matter region as compared to healthy control. These abnormalities in diffusion tensor imaging (DTI) matrix suggest difference in gray and white matter maturation in neonates with hypoxic-ischemic injury.

15:30 *3413*. **Regional White Matter Anisotropy and General Intelligence in Preterm Born Children: A Voxelwise Analysis**
Computer 5

Pek-Lan Khong[1], Deqiang Qiu[1], Ada Yung[1], Grace Poon[1], Connie Leung[2], Barbara Lam[1]
[1]The University of Hong Kong, Hong Kong, People's Republic of China [2]The Duchess of Kent Children's Hospital, Hong Kong, People's Republic of China

We evaluated 22 (12 male, age range 9.2 yrs- 11.5 yrs, all right handed) very low birth weight preterm born children for regions of significant correlation between white matter fractional anisotropy and Wechsler full-scale IQ scores using voxelwise analysis in SPM2 adjusting for the effects of age and gender (FDR corrected $p<0.05$, cluster size > 30 contiguous voxels). Regions of statistically significant positive correlations were found in bilaterally symmetrical regions in the occipito-temporal, temporo-parietal and frontal lobes. These areas overlap with those found in the normal pediatric population, suggesting that fiber organization/integrity in specific white matter regions underlie general intelligence.

15:30 *3414*. **Arterial Spin Labeling in Children: BOLD and CBF Hemodynamic Response to Visual Stimulation**
Computer 7

Pamela Moses[1], Joanna E. Perthen[1], Catherine Mier[1], Thomas T. Liu[1]
[1]University of California, San Diego, La Jolla, California, USA

To assess potential differences between children and adults in hemodynamic response to brain activation, arterial spin labeling was used for measurement of blood oxygen level dependent (BOLD) and cerebral blood flow (CBF) responses during visual stimulation in 8 year olds, 12 year olds and adults. The peak amplitude of percent signal change for the BOLD signal and CBF was comparable for children and adults. The post-stimulus period, however, showed a lower BOLD signal in adults than children. The deeper undershoot in the adults' BOLD data may reflect a slower return to baseline for cerebral blood volume in the mature brain.

Brain: Diffusion Imaging

Room 4A Wednesday 14:00 - 16:00

14:00 *3415*. **DWI of the Spine with a Non-CPMG Single-Shot Fast Spin-Echo Sequence: Initial Experience**
Computer 9

Ali Yusuf Oner[1], Turgut Tali[1], Azim Celik[2], Fatih Celikyay[1], Patrick Le Roux[3]
[1]Gazi University School of Medicine, Ankara, Turkey; [2]GE Medical Systems, Istanbul, Turkey; [3]GE Medical Systems, Buc, France

There are limited number of researches on spinal DWI, and it has been particularly used for the distinction of acute benign osteoporotic and malignant vertebral compression fractures. The purpose of this study is to prospectively evaluate the improvement in the signal to noise ratio (SNR), with the use of a newly developped non-Carr-Purcell-Meiboom-Gill (non-CPMG) single-shot fast spin-echo (ssFSE) sequence, in the DWI of the spine and its affect on apparent diffusion coefficient (ADC) measurements.

14:00 *3416*. **Cognitive Impairment in Parkinson's Disease: Preliminary DTI Findings**
Computer 8

Michael H. Chappell[1, 2], Tim J. Anderson[2, 3], John C. Dalrymple-Alford[1, 2], Saskia van Stockum[1, 2], Richard Watts[1, 2]
[1]University of Canterbury, Christchurch, Canterbury, New Zealand; [2]Van der Veer Institute for Parkinson's and Brain Research, Christchurch, Canterbury, New Zealand; [3]University of Otago, Christchurch, Canterbury, New Zealand

Cognitive impairment adds a significant burden to Parkinson's disease patients, with many progressing to frank dementia. This diffusion tensor imaging pilot study investigated whether the apparent diffusion coefficient (ADC) and fractional anisotropy (FA) may be suitable markers of this cognitive decline. They were tested for correlation with key neuropsychological measures at each voxel. It was found that ADC was a more sensitive marker than FA, with strong correlations in several regions of the brain, including the periventricular regions, the medial temporal lobe, and the thalamus.

14:30 *3417*. **ROC Analysis Based Visualization of Pathological Brain Regions in Patients with Epilepsy Using Multi-Modal MR Imaging (DWI, T2 and CSI)**
Computer 8

Jacobus F.A. Jansen[1, 2], M. Eline Kooi[1, 2], Albert P. Aldenkamp[1, 3], H. J.Marian Majoie[1, 3], Rianne P. Reijs[1, 3], Marc C.T.F.M de Krom[1], Paul A.M. Hofman[1], Klaas Nicolay[2, 4], Walter H. Backes[1, 2]
[1]University Hospital Maastricht, Maastricht, Netherlands; [2]Eindhoven University of Technology, Eindhoven, Netherlands; [3]Epilepsy Centre Kempenhaeghe, Heeze, Netherlands; [4]University Hospital Maastricht,, Maastricht, Netherlands

The analysis and comparison of data from multiple MRI modalities suffers from the inherent differences between the modalities (e.g. contrast mechanism or spatial resolution). A general method to identify pathological brain regions as detected by inherently different MRI modalities was developed. This method enables a thorough assessment of the local abnormal, potentially pathological, state of a tissue in a patient with a certain cerebral disease. A receiver-operating-characteristic (ROC) curve analysis based visualization of abnormal brain regions was implemented in patients with epilepsy using three MRI modalities, namely diffusion and T2 weighted imaging and spectroscopic imaging.

14:30 *3418*. **Optic Nerve Injury Increases Water Diffusivity**
Computer 9

Junqian G. Xu[1], Avi Z. Snyder[1], Glenn Foster[1], Robert T. Naismith[1], Anne H. Cross[1], Sheng-Kwei Song[1]
[1]Washington University in St. Louis, St. Louis, Missouri, USA

An *in vivo* diffusion tensor imaging study was performed on nine healthy volunteers and three chronic optic neuritis patients at 1.3 mm^3 isotropic resolution. Increased mean water diffusivity associated with decreased diffusion anisotropy was observed in the injured eyes of the patients.

15:00 *3419*. **ADC and Proton Spectroscopy Reflect Cellular Pathology in Patients with Creutzfeldt-Jakob Disease**
Computer 9

David Neil Manners[1], Piero Parchi[1], Raffaele Lodi[1], Caterina Tonon[1], Claudia Testa[1], Sabina Capellari[1], Giulia Pierangeli[1], Pietro Cortelli[1], Pasquale Montagna[1], Bruno Barbiroli[1]
[1]Università di Bologna, Bologna, BO, Italy

Sporadic Creutzfeldt-Jakob disease (sCJD) is the most commonly occurring form of prion diseases, a group of rare, fatal neurodegenerative disorders associated with the accumulation of mis-folded PrP protein. Four patients with sCJD were studied by diffusion-weighted imaging and proton spectroscopy, and results compared with post mortem histology in four brain areas. The presence of gliosis and neuronal loss was found to be associated with a relative reduction in N-acetyl aspartate (NAA) and an increase in apparent diffusion coefficient, while spongiosis was linked to a reduction in ADC but not in NAA.

15:30 *3420*. **Changes of White Matter Integrity and Brain Activation in Diffuse Brain Injuries: Assessed by fMRI and DTI**
Computer 9

Chunchun Ni[1], Hui Mao[1], Felicia Goldstein[1], Tara Ravichandran[1], Randall Scheibel[2]
[1]Emory University School of Medicine, Atlanta, Georgia, USA; [2]Baylor College of Medicine, Houston, Texas, USA

We used a combined fMRI and DTI approach to investigate the white matter damage and related changes of brain activation pattern in patients with diffuse brain injuries. Ten of 12 TBI patients showed reduction of FA in the selected frontal regions compared to those of controls. Some patients further exhibited asymmetrical reduction of FA in the frontal regions. The N-back working memory task led to the greater activation in patients as compared to the healthy controls. 8 patients showed positive correlation between DTI and fMRI results, i.e., increased activation areas and more bilateral presentation in N-back working memory tests.

15:30 *3421*. **Diffusion-Tensor Imaging of Cerebral Glioma at 3 T MRI: Analysis of Fractional Anisotropy and Mean Diffusivity**
Computer 8

Ho Yun Lee[1], Dong Gyu Na[1], In-Chan Song[1], Ji Hoon Kim[1], Kee-Hyun Chang[1]
[1]Department of Radiology, Seoul National University College of Medicine, Seoul, Republic of Korea

Although MD values were significantly different between low-and high-grade gliomas, FA values were not significantly different and not useful for differentiating low-grade from high-grade glioma. In high grade gliomas, FA value of enhancing tumor was significantly lower than non-enhancing tumor or peritumoral T2 bright regions, but FA values were not different between non-enhancing tumor and non-enhancing peritumoral T2 bright region. The higher mean MD value of non-enhancing peritumoral T2 bright regions than that of non-enhancing tumor suggests that decrease of FA value may reflect not only white matter's disruption by tumor infiltration but also expansion of extracellular space due to vasogenic edema. Therefore, distinction between vasogenic edema and tumor infiltration only by FA value is difficult at 3T DTI.

Brain Arterial Spin Labeling Techniques

Room 4A Wednesday 14:00 - 16:00

14:00 *3422*. **CASL Perfusion MRI with Non-Segmented Low Flip Angle 3D EPI**
Computer 12
S. L.. Talagala[1], G. S. Slavin[2], J. Ostuni[1], S. Chesnick[1]
[1]National Institutes of Health, Bethesda, Maryland, USA; [2]GE Healthcare, Milwaukee, Wisconsin, USA

Previous 3D arterial spin labeling (ASL) perfusion studies have used spin-echo trains. Since these sequences can lead to high SAR, we assessed 3D continuous ASL (CASL) using a train of z-phase encoded, low flip angle EPI readouts. A complete 3D data set was acquired following each ASL preparation period. High quality 3D CASL images were obtained using a separate neck labeling coil at 3.5X3.5X4 mm3 resolution in ~5 minutes. 3D and 2D CASL were found to have similar temporal and spatial SNR and perfusion signal. This approach should allow high field, 3D CASL fMRI studies without any sensitivity penalty.

14:00 *3423*. **When Perfusion Meets Diffusion – *In Vivo* Measurement of Water Extraction and Permeability in Human Brain**
Computer 10
Jiongjiong Wang[1], Keith S. St Lawrence[2], Maria Fernandez-Seara[1], John A. Detre[1]
[1]University of Pennsylvania, Philadelphia, Pennsylvania, USA; [2]Lawson Health Research Institute, London, Ontario, Canada

A hybrid MRI technique was introduced by marrying a continuous arterial spin labeling (ASL) method with a twice-refocused spin-echo diffusion sequence. Diffusion weighted ASL signals were acquired with systematically varied b values up to 300 s/mm2, and were modeled based on a biexponential decay model. Water extraction fraction was estimated by differentiating the amount of labeled water in the vascular and tissue compartments, based on their diffusion characteristics. According to the single-pass approximation model, we further estimated the water permeability of human brain based on the derived water extraction fractions.

14:00 *3424*. **Magnetic Resonance Imaging of Cerebral Borderzones**
Computer 11
Jeroen Hendrikse[1], Esben Thade Petersen[2], Peter Jan Van Laar[1], Xavier Golay[2]
[1]UMC, Utrecht, Netherlands; [2]National Neuroscience Institute, Singapore, Singapore

Numerous studies have tried to establish the vulnerability of cerebral borderzone areas to a drop in perfusion pressure. Thusfar no imaging method can depict the exact location of the cerebral borderzone regions. Here we show that it is possible to visualize the borderzone regions between the distal branches of the cerebral arteries with arterial spin labeling MRI based on an increase in arterial blood transit time of 0.43±0.04 s towards these areas. Unexpectedly, a 37±9% reduction in arterial blood volume and 20±7% reduction in cerebral blood flow was observed in the cortical borderzone areas.

14:30 *3425*. **Accurate Measurement the Transit Time and Tag Delivery Time of Pulsed Arterial Spin Labeling: Comparing 8-Channel Phased Array Coil and Quadrature Birdcage Coil**
Computer 11
Wei Sun[1], Guang Cao[2], Xin Lou[3], Youquan Cai[3]
[1]GE Healthcare China, Beijing, People's Republic of China; [2]GE Healthcare China, Hong Kong, People's Republic of China; [3]PLA General Hospital, Beijing, People's Republic of China

The recently developed 8-channel phased array coil gives us an opportunity to improve the SNR of pulsed arterial spin labeling (PASL) not only from the array receivers but also from the wider tagging bands with the whole-body excitation coil. In this study, we accurately measured the transit time and tag delivery time of PASL using both 8-channel phased array coil and quadrature birdcage coil. The results show that the tag delivery time was about 100ms longer for the former. This will certainly help to improve the SNR of PASL. Besides this, the transit time was also obtained and could be used for accurate CBF calculation.

14:30 *3426*. **Automatic Planning for Regional Perfusion Imaging**
Computer 10
Ivan Zimine[1], Esben Thade Petersen[1], Frederic Sardou[1], Xavier Golay[1, 2]
[1]National Neuroscience Institute, Singapore, Singapore; [2]ASTAR, Singapore, Singapore

Regional Perfusion Imaging (RPI) is a method allowing imaging of individual perfusion territories from major feeding arteries that could become a valuable clinical tool for evaluation of patients with cerebro-vascular disorders. Careful planning of the inversion slab is a prerequisite for correct estimation of regional perfusion. So far, manual planning using MR angiography sequences was used for correct positioning of the labeling slabs. However, due to tortuous vascular anatomy, such manual planning is time consuming and very operator dependent. Here, we propose a fast method for automatic planning requiring only minimal user input using processing of TOF images.

14:30 ***3427***. **Whole Brain 3D Velocity Selective Arterial Spin Labeling Using a Background Suppressed Flow Weighted Spiral Fast Spin Echo Acquisition**
Computer 12

Eric C. Wong[1], Wen-Chau Wu[1], Julie Bykowski[1]
[1]University of California, San Diego, La Jolla, California, USA

In velocity selective ASL (VSASL), arterial spins are tagged based on their velocity, rather than their location. This spatially non-selective tagging method allows in principle for the elimination of transit delays in the delivery of tagged blood to the target tissues, and is therefore promising for perfusion imaging in pathology where flow can be slow or circuitous. Because the tag is spatially non-selective, VSASL is particularly amenable to volumetric image acquisition methods. We demonstrate here whole-brain VSASL using a flow-weighted background suppressed 3D stack-of-spiral fast spin echo acquisition.

15:00 ***3428***. **Accurate Perfusion Quantification Using Pulsed Arterial Spin Labeling: Choosing Appropriate Sequence Parameters**
Computer 12

Joanna E. Perthen[1], Khaled Restom[1], Yashar Behzadi[1], Kun Lu[1], Thomas T. Liu[1]
[1]UCSD, San Diego, California, USA

Pulsed ASL techniques can provide quantitative measurements of resting and functional CBF using the QUIPSS II modification. However, accurate quantification of CBF requires that the scan parameters fulfill various conditions. In this study, we show that optimal pulsed ASL scan parameters show a strong dependence on experimental conditions (e.g. tag angle, brain region) and must therefore be tailored to specific study conditions rather than employing a universal approach or adopting literature values. Data from the visual cortex and hippocampus are presented to illustrate the impact of tag angle and brain region and to demonstrate how appropriate parameters can be chosen.

15:00 ***3429***. **Changes in Flow Territories in Patients with Symptomatic Carotid Artery Stenosis Before and After Carotid Desobstruction: A Selective Arterial Spin Labeling MRI Study**
Computer 10

Peter Jan van Laar[1], Jeroen Hendrikse[1], Willem Mali[1], Matthias van Osch[2], Jeroen van der Grond[2]
[1]University Medical Center, Utrecht, Netherlands; [2]Leiden University Medical Center, Leiden, Netherlands

It has been forwarded that in patients with severe internal carotid artery (ICA) stenosis, a decrease in blood flow distal to the stenosis contributes to the clinical symptoms. Compensatory processes include the recruitment of collateral arteries, however their actual contribution remains unknown. We studied the flow territories of the extracranial arteries in 24 patients with severe ICA stenosis and 40 control subjects with selective arterial spin labeling. The reversibility of changes was investigated after carotid endarterectomy or stenting. Our data show that prior to intervention, collateral flow indeed significantly contributes to the ipsilateral hemisphere. After carotid desobstruction flow territories normalize.

15:00 ***3430***. **The Effect of Arterial Blood Velocity Variation Over the Cardiac Cycle on the Temporal SNR of the CASL Perfusion Time Series**
Computer 11

Maria Asuncion Fernandez-Seara[1], Jiongjiong Wang[1], John A. Detre[1]
[1]University of Pennsylvania Medical Center, Philadelphia, Pennsylvania, USA

Continuous arterial spin labeling techniques use flow driven adiabatic inversion of blood water proton spins to image perfusion. Arterial blood velocity changes over the cardiac cycle can have a significant effect on the degree of inversion. In this work, we have performed simulations and experiments to study the effect of two parameters, TR and labeling time, on efficiency variability and as a result on the SNR of CASL perfusion time series. We have demonstrated that temporal SNR can be increased by increasing the duration of the labeling pulse to cover two or more cardiac cycles.

15:30 ***3431***. **Measurement of White Matter Perfusion Using ASL-MRI at 4T**
Computer 11

Geon-Ho Jahng[1], Michael W. Weiner[1], Norbert Schuff[1]
[1]University of California, San Francisco, San Francisco, California, USA

To achieve white matter (WM) perfusion using a pulsed arterial spin labeling (ASL) method, using various post labeling delay times was optimized to measure WM perfusion, The ASL protocol was applied on 7 subjects using EPI and Turbo-Flash (TFL) acquisitions at 4 Tesla. The ratios of gray matter (GM) to WM CBF were consistently higher on TFL (average 1.61) than on EPI (average 1.45). Furthermore, TFL acquisitions achieved more stable CBF measurements than EPI in various brain regions. In conclusion, by optimizing post labeling delay times in conjunction with TFL based acquisitions, WM CBF can be measured at 4T MRI.

15:30 ***3432***. **Comparison of ASL Kinetic Curves Between Subjects and Between Brain Areas**
Computer 10

Daniel Gallichan[1], Peter Jezzard[1]
[1]University of Oxford, Oxford, UK

Resting ASL data were acquired at 10 inversion times in 5 healthy subjects. Hand-drawn anatomically-based ROIs revealed distinct differences in the shape of the kinetic curve across brain regions, corresponding to the differences in structure of their feeding arteries. These regional variations show strong consistency between subjects. The data also indicate that certain regions with particularly long arrival times may not be suitable for quantitative CBF measurement at the commonly used single inversion time of 1.4s.

15:30 *3433*. **Improvements to Control Scan of ASL-Perfusion MRI by Improving Null Pulse for Use with the Repeated Shallow Flip Angle Excitations**
Computer 12

Geon-Ho Jahng[1], Gerald B. Matson[1], Michael W. Weiner[1], Norbert Schuff[1]
[1]University of California, San Francisco, San Francisco, California, USA

The goal of this work is to improve the sensitivity of arterial spin labeling (ASL) perfusion MRI by reducing excitation of inflowing spins during the control pulse. We propose an improved control scheme for pseudo-continuous ASL based on the repeated shallow flip angle excitations using a null pulse. Computer simulations demonstrate immunity of the proposed null pulse over flow velocity of 20-60 cm/sec and off-resonance conditions up to +/- 40 Hz. In conclusion, the new null pulse should improve the control scan of continuous ASL based on repeated shallow flip angle excitations, thus improving sensitivity of ASL perfusion.

Diffusion Applications in Cerebral Ischemia

Room 4A Wednesday 14:00 - 16:00

14:00 *3434*. **Topographical Evaluation of DTI Corticospinal Tractography and Ischemic Stroke Utilizing Spatial Normalization**
Computer 13

Akira Kunimatsu[1], Daisuke Ito[2], Yasuhiro Nakata[2], Natsuko Kunimatsu[2], Shigeki Aoki[2], Osamu Abe[2], Yoshitaka Masutani[2], Hiroyuki Kabasawa[2], Haruyasu Yamada[2], Izumi Anno[1], Manabu Minami[1]
[1]Institute of Clinical Medicine, University of Tsukuba, Tsukuba-shi, Japan; [2]Graduate School of Medicine, University of Tokyo, Tokyo, Japan

We aimed to assess feasibility of employing DTI corticospinal tractography combined with spatial normalization in evaluation of corticospinal tract involvement within capsular or pericapsular infarction in relation to motor functional recovery in stroke patients. Corticospinal tractograms obtained from healthy volunteers were overlaid onto isotropic diffusion-weighted images of patients after spatial normalization. The normalized corticospinal tractogram was engulfed by normalized infarction in all patients and the degree of involvement related presence or absence of motor functional recovery ($p<0.05$).

14:00 *3435*. **Measurement of DTI Metrics in Hemorrhagic Brain Lesions: Its Possible Implication in Imaging Interpretation**
Computer 14

Mohammad Haris[1], Rakesh Kumar Gupta[1], Nuzhat Husain[2], Khadar M. Hasan[3], Lily Pal[1], Ponnada A. Narayana[3]
[1]Sanjay Gandhi PostGraduate Institute of Medical Sciences, Lucknow, Uttar Pradesh, India; [2]King George's Medical University, Lucknow, Uttar Pradesh, India; [3]University of Texas Medical School at Houston, Houston, Texas, USA

MR evolution of cerebral hemorrhage and hemorrhage within brain tumor has been described in literature. In this study, we report high fractional anisotropy (FA) with low mean diffusivity (MD) in early stage and low FA with increase MD in late stage of hemorrhage. However in case of hemorrhagic tumor, all stages of hemorrhage showed high FA with low MD. We have explained these findings on the basis of structural pattern of red blood cells and fibrin mesh as observed on histopathology. We conclude that the presence of hemorrhage in the tumor may simulate the compressed fiber tracts on diffusion tensor imaging.

14:30 *3436*. **Apparent Diffusion Coefficient of Extra- And Intracellular Sodium in Rat Skeletal Muscle: Effects of Prolonged Ischemia**
Computer 14

Andriy Babsky[1], Hong Zhang[1], Shakhryar K. Hekmatyar[1], Navin Bansal[1]
[1]Indiana University, Indianapolis, Indiana, USA

Intra- and extracellular sodium (Na^+_i and Na^+_e, respectively) and water apparent diffusion coefficients (ADCs) were monitored in rat skeletal muscle before and during 4h global ischemia using *in vivo* ^{23}Na and ^1H MRS. $TmDOTP^{5-}$ infusion through the jugular vein was used to separate the Na^+ signals from the two compartments. [Na^+_i] increased by 2.5 times 4 hours after the onset of ischemia. Before ischemia, Na^+ ADCs in both compartments were similar. However, Na^+_e ADC decreased 30-40% 2-4 hours after ischemia, while Na^+_i ADC remained mostly unchanged. Water ADC also remained unchanged after ischemia.

14:30 *3437*. **Correlation of Three-Dimensional Colour-Coded Tractography by Diffusion Tensor Imaging in Acute Ischemic Stroke with 60-Day NIHSS Scores**
Computer 13

lai Can[1], Zhang Shizheng[1]
[1]Sir Run Run Shaw Hospital affiliated zhejiang University, Hangzhou, Zhejiang, People's Republic of China

Background¡ªWe tested the feasibility of a new MRI technique (Three-dimensional color-coded diffusion tensor imaging) that provides visualization of the corticospinal tracts *in vivo* in a group of stroke victims.Summary of Report¡ª27 patients with subcortical infarctions involving the white matter of the supratentorial brain were evaluated. corticospinal tracts (CST) on the lesional side and the precise location and the extent of pyramidal tract damage were successfully depicted in all cases. The position of the CST relative to the infarct was in good agreement with clinical outcomes (NIHSS scores). Conclusions¡ªOur proposed fiber-tracking method was shown to be a clinically feasible technique that correlates well with clinical outcome.

15:00 ***3438***. **Real Time Physiologic Monitoring of Intra Arterial RtPA Therapy in a Canine Model of Acute Embolic Stroke**
Computer 13

Mehdi Rohany[1], Ali Shaibani[1], Wanyong Shin[1], Ty Cashen[1], Kathleen R. Harris[1], Timothy J. Carroll[1]
[1]Northwestern University, Chicago, Illinois, USA

The increasingly important role of Magnetic Resonance (MR) perfusion and diffusion imaging in understanding the pathophysiology of stroke caused increasing attention to combined MR-IR suites as a future management standard in acute stroke. In this study we demonstrate a MR compatible canine model for real time physiologic monitoring of IA rtPA thrombolytic therapy by measuring Apparent Diffusion Coefficient (ADC) values and quantitative cerebral blood flow (qCBF) values in infarcted regions during the IA rtPA injection.

15:00 ***3439***. **Deconvolution of Compartmental Water Diffusion Coefficients in Stroke Using DW-IR MEMRI**
Computer 14

Govind Nair[1, 2], Mohammad Salman Shazeeb, [1,2], James Bouley[3], Karl G. Helmer[1], Mark Fisher[3], Christopher H. Sotak[1, 3]
[1]Worcester Polytechnic Institute, Worcester, Massachusetts, USA; [2]University of Massachusetts Medical School, Worcester, Massachusetts, USA; [3]UMassMemorial Health Care, Worcester, Massachusetts, USA

The mechanism of the decrease in apparent-diffusion coefficient (ADC) of water in the brain during cerebral ischemia is not well understood. We sought to separate and individually measure the relative contributions of intra- and extracellular water ADC changes during ischemia using Mn2+ as an intracellular MRI contrast agent. The ADCs measured showed a significant reduction in both intra- and extracellular ADC during cerebral ischemia.

15:30 ***3440***. **Spiral Rapid Diffusion Tensor Imaging Sequence on a 7T Small Bore Magnet: Application on Traumatic Rat Brain**
Computer 14

Yohan van de Looij[1, 2], Marine Beaumont[1, 2], Olivier Verdonck[1, 2], Christoph Segebarth[1, 2], Jean-François Payen[1, 2], Hana Lahrech[1, 2]
[1]INSERM U594, Grenoble, France; [2]Univ Joseph Fourier, Grenoble, France

Implementation of a very accurate fast Diffusion Tensor Imaging (DTI) sequence on a high field small bore magnet is a challenge since Fractional Anisotropy (FA) mapping requires high precision. The aim of this work was to implement a fast DTI sequence on a 7T small bore magnet with different calibration stages in order to assess the accuracy and precision of Apparent Diffusion Coefficient (ADC) measurements. A Twice-Refocused Spin Echo (TRSE) sequence was implemented. Spiral scanning was preferred to EPI since it offers several advantages for DTI studies. Implemented sequence was applied to *in vivo* traumatic brain injury in rats.

15:30 ***3441***. **Moyamoya Disease: Histogram-Based Quantitative Analysis of Diffusion Tensor Imaging**
Computer 13

Nobuyuki Mori[1], Yukio Miki[1], Yasutaka Fushimi[1], Tsutomu Okada[1], Eri Kitamura, [1,2], Ken-ichiro Kikuta[1], Takashi Hanakawa[1], Shin-ichi Urayama[1], Nobuo Hashimoto[1], Hidenao Fukuyama[1], Kaori Togashi[1]
[1]Kyoto University Graduate School of Medicine, Kyoto, Japan; [2]Kobe University Graduate School of Medicine, Kobe, Japan

Whole brain histogram (WBH) of diffusion tensor imaging (DTI) (WBH-DTI) has been applied for quantitative analysis of various neurological disorders. We analyzed WBHs-DTI of ischemic moyamoya disease (MMD) and of normal control using 3T MRI. MMD with evident infarction (EI) showed significant difference in WBH-DTI, and MMD without EI showed significant difference only in the bin analysis of WBH of fractional anisotropy (FA) (WBH-FA), compared with normal control. WBH-DTI was shown as feasible analytic tool in ischemic MMD, and the WBH-FA might promisingly detect subtle ischemic damage in brain tissue before the advent of EI in conventional imaging.

Diffusion: Clinical Applications

Room 4A Wednesday 14:00 - 16:00

14:00 ***3442***. **The Change of Tissue Microenvironment Elucidated: The Combined FA and Trace Defined a Circle in a Normal Aging Study**
Computer 19

Jiun-Jie Wang[1], Chia-Lung Yang[2], You-Zen Lu[3], Yau-Yau Wai[3], Tzuu-Kang Chy[3]
[1]ChangGung University, TaoYuan, Taiwan; [2]Chang Gung University, TaoYuan, Taiwan; [3]Chang Gung Memorial Hospital, TaoYuan, Taiwan

To integrate the information contained in separated DTI indices, a simple relationship between FA, trace and the amplitude of the diffusion tensor was noticed. It defined a circle in the plane, which explained the age related changes in DTI as a shift of balance in the water diffusion in tissues microstructures. 12 subjects divided into 2 age groups were studies by DTI.

14:00 *3443*. **Probing Tumor Microenvironment Using Diffusion Tensor Spectroscopy and Imaging**
Computer 16
Yousef Mazaheri[1], Cornelia Matei[1], Terence Gade[1], Jason A. Koutcher[1]
[1]Memorial Sloan Kettering Cancer Center, New York, New York, USA

Past studies have established elevated levels of choline (Cho) metabolites as markers of malignancy. However, the mechanisms in the active transport and diffusion of choline across cellular membranes are not fully understood. The goals of this study are to measure the diffusion characteristics of choline in an attempt to understand the characteristics of tumor microenvironment and the transport of metabolites. In particular, we have used diffusion tensor spectroscopy (DTS) and imaging (DTI) to: 1. measure diffusion of Cho and water in a tumor animal model, and 2. compare our finding to pathology maps. We present our preliminary results.

14:00 *3444*. **MR Diffusion Tensor Imaging in the Evaluation of Transplantation of Degradable Scaffold Seeded with Neural Stem Cells to Acutely Injured Canine Spinal Cord**
Computer 17
Guo Xuemei[1], Wang Xiaoying[1], Ni Shilei[1], Jiang Xuexiang[1]
[1]First Hospital, PeKing University, Beijing, People's Republic of China

To observe the effect of transplantation of degradable scaffold seeded with neural stem cells to acutely injured canine spinal cord with DTI. Eighteen canines had spinal cord hemisection. 7 were transplanted with scaffold seeded with neural stem cells, 5 with scaffold only, 5 without transplantation, and 1 without injury. After injury, the ADC values of the injured spinal cord increased and FA values decreased. The ADC and FA values of both side of the spinal cord were significantly different in the control group, but not in the other two groups. So, DTI can provide useful information of spinal cord injury and regeneration in experimental study.

14:00 *3445*. **A Combined VBM and DTI Investigation of Brain Structure and Connectivity in 22q11 Deletion Syndrome**
Computer 18
Chris Chaddock[1], Lucy Lee[2], Jennie Newton[2], Torsten Baldeweg[3], Richard Frackwoiak[2], David Skuse[3]
[1]Institute of Psychiatry, London, UK; [2]Wellcome Department of Imaging Neuroscience, London, UK; [3]Institute of Child Health, London, UK

22q11 deletion syndrome is a genetic syndrome associated with increased rates of schizophrenia. Voxel Based Morphometry and Diffusion Tensor Imaging techniques were used to investigate brain structure. Grey matter density was reduced in the cingulate and bilaterally in the temporal lobes, whilst increases were seen in the insula. White matter density was reduced bilaterally in middle and superior frontal gyri, whereas increases were seen posteriorally to the corpus callosum. DTI data provided evidence of disrupted WM coherence in fronto-temporal areas, although further work is needed to understand how GM and WM loss affects the anatomical location of WM tracts.

14:00 *3446*. **A Correlational Analysis of Cognitive fMRI, DTI, and Clinical Assessment of Multiple Sclerosis**
Computer 15
Raymond Wei-Meng Lau[1], Bradley Gordon Goodyear[1]
[1]University of Calgary, Calgary, AB, Canada

To date, MR imaging studies of Multiple Sclerosis have not investigated the inter-relationship of cognitive fMRI and white matter integrity as measured by DTI, as well as their correlation with current clinical assessments. Understanding these inter-relationships may provide a more complete description of the progression of MS, and could lead to an imaging protocol that, in combination with behavioral assessment, is a comprehensive and accurate clinical evaluation. The objective of this study was to identify correlations between existing clinical measures of MS severity with brain activity measured using fMRI and with ROI-based measurements of fractional anisotropy.

14:30 *3447*. **Assessments of Diffusion Sensitivity in Identifying Brain Lesions in Clinically Isolated Syndrome Subjects**
Computer 15
Yasheng Chen[1], Valerie Jewells[1], Hongyu An[1], Elizabeth Bullitt[1], Weili Lin[1]
[1]The University of North Carolina at Chapel Hill, Chapel Hill, North Carolina, USA

The main thrust of this study was to determine the sensitivity of diffusion weighted imaging in delineating MS lesions in clinically isolated syndrome (CIS) subjects, a cohort of subjects who experience one exacerbation consistent with MS but have not been clinically diagnosed as MS patients. Clinically used T2-weigted images were used as the "gold standard" to define the ground truth of MS lesions.

14:30 *3448*. **Diffusion Weighted Imaging of Ocular Adnexal Lymphomas: Usefulness in Differential Diagnosis and Early Predictor of Response to Therapy**
Computer 18
Letterio Salvatore Politi[1], Andrés J. Ferreri[1], Stefania Bianchi[1], Sandra Pieralli[1], Nicoletta Anzalone[1], Paolo Vezzulli[1], Andrea Falini[1], Giuseppe Scotti[1]
[1]San Raffaele, Milan, Italy

We assess feasibility and optimal MR parameters of Diffusion Weighted Imaging (DWI) of the orbits. We demonstrated clinical usefulness of DWI in the diagnosis of Ocular Adnexal Lymphomas (OAL). OAL show ADC values (610 +/- 54 x 10-6 mm2/sec) significantly lower than other orbital diseases ($p<0.01$) and normal orbital structures ($p<0.002$). Further, changes in ADC could represent an additional helpful tool for monitoring the outcome of OAL and predicting response to therapy, since an increase in ADC value precedes volumetric reduction of the lesion.

14:30 ***3449***. **Radiation Induced Injury of the Lens and Retina in Rat Eyes: Assessment with Diffusion Tensor Imaging**
Computer 17

Lung-fa Kao[1], Xiao Wen Mao[2], Andre Obenaus[2], Sheng-Kwei Song[1]
[1]Washington University, St. Louis, Missouri, USA; [2]Loma Linda University, Loma Linda, California, USA

Radiation injury to eyes is a significant concern for astronauts during the space exploration and to patients undergoing radiation therapy. In the present study, we examined the effect of high Z, high energy (HZE) particles irradiation on the integrity of rat eyes using diffusion tensor imaging. Injuries to the lens and retina of the irradiated rat eyes were detected. Diffusion tensor imaging may be a potential modality to quantify radiation induced injury to the eye.

14:30 ***3450***. **Apparent Diffusion Coefficient Values in Endometrial Cancer: Comparison with the Normal Endometrium and Correlation with Histologic Grades**
Computer 16

Ken Tamai[1], Takashi Koyama[2], Shigeaki Umeoka[1], Tsuneo Saga[1], Shingo Fujii[1], Kaori Togashi[1]
[1]Kyoto University, Kyoto, Japan; [2]Kyoto University Hospital, Kyoto, Japan

This preliminary study was to investigate whether ADC values of the endometrial cancers differ according to the histologic grade of the tumor and whether they differ from those of the normal endometrium. Study population included 19 patients with endometrial cancer and 12 patients with cervical cancer who were pathologically confirmed to have normal endometrium. Our results showed that ADC values of endometrial cancers are significantly lower than those of normal endometrium. ADC values of high-grade tumors showed decreased titer compared with those of lower grade although estimation of histologic grade based on ADC values seems difficult because of considerable overlap.

14:30 ***3451***. **Age Related Cognitive Decline and White Matter Changes Studied by Diffusion MRI**
Computer 19

Efrat Sasson-Sarig[1], Glen M. Doniger[2], Yaniv Assaf[1, 3]
[1]Tel Aviv University, Tel Aviv, Israel; [2]NeuroTrax Corporation, New York, New York, USA; [3]Tel Aviv Sourasky Medical Center, Tel Aviv, Israel

Normal aging is accompanied by pathologies that affect cognitive abilities of the elderly population. Imaging studies found age related white matter (WM) changes in the frontal lobe. WM of young and old subjects was investigated using q-space imaging (QSI) and DTI, correlated with their cognitive performance. The results showed higher q-space displacement and reduced FA in frontal WM, related to age and cognitive performance. It was concluded that structural pathophysiological alternations in WM can be related to age and cognitive performance using DTI and QSI, with a larger effect revealed by QSI.

15:00 ***3452***. **Voxel Based Analysis of ADC, FA and Hemispheric Asymmetry in Normal Aging**
Computer 19

Siamak Ardekani[1], Usha Sinha[1]
[1]UCLA, Los Angeles, California, USA

Age related microstructural changes in brain white matter (WM) could be studied utilizing DTI. We examined alterations in FA and ADC employing voxel and ROI based analysis. A non-linear registration algorithm was used to align subject image volumes to a common template. The results showed significant age related decline in FA in frontal WM, genu and body of corpus callosum, posterior limb of internal capsule and anterior and posterior limbs of external capsule. Regional hemispheric asymmetry in FA and ADC showed decrease in asymmetry with age. The voxel based findings were confirmed by ROI based analysis.

15:00 ***3453***. **Fiber Tractography in Patients with Gliomas: Assessment of the Extent of Tumor Cell Infiltration in Brain Fiber Tracts**
Computer 16

Andreas Stadlbauer[1, 2], Erich Salomonowitz[1], Christopher Nimsky[2], Rolf Buslei[2], Michael Buchfelder[2], Oliver Ganslandt[2]
[1]Landesklinik St. Poelten, St. Poelten, Lower Austria, Austria; [2]University of Erlangen-Nuremberg, Erlangen, Bavaria, Germany

We retrospectively correlated fiber tracking using MR DT imaging with different FA threshold values and histopathological data of 25 patients with gliomas WHO grade II or III. A FA threshold of 0.15 to 0.2 seems to be best suitable to gain realistic fiber tract reconstruction around an infiltrating intrinsic brain tumor. Additionally we demonstrated potentially tumor cell infiltration of intact brain fiber tracts.

15:00 ***3454***. **Abnormal Thalamic Diffusivity in Patients with Tuberous-Sclerosis Complex Revealed with Diffusion Tensor MRI**
Computer 17

Malek Makki[1], Diane Chugani[1], Harry Chugani[1]
[1]Children's Hospital of Michigan, Detroit, Michigan, USA

We performed DT-MRI on six patients with tuberous sclerosis complex and twelve age-matched normal control subjects to evaluate diffusivity and anisotropy in subcortical brain regions that are important in seizure propagation. We evaluated bilaterally the thalamus and the caudate nuclei that appear normal with conventional MRI to investigate whether they have microstructural abnormalities. Patients showed significantly increased diffusivity in the thalamus in both hemispheres when compared to normal controls. The increase in diffusivity was mainly due to a significant increase in direction orthogonal to the axons. Changes in diffusivity and anisotropy revealed in normal appearing brain tissues beyond the origin of TSC lesions may be important to help localize lesions in MRI negative patients.

15:00 ***3455***. **Relationship of Quantiative DTI Abnormalities in the Temporal Lobes and Language Functioning in Autism**
Computer 18

Jill Hunter[1, 2], Elizabeth Wilde[1], Zili Chu, [1, 2], Li Xiaoqi[1]
[1]Baylor College of Medicine, Houston, Texas, USA; [2]Texas Children's Hospital, Houston, Texas, USA

We examined the relationship of diffusion tensor imaging in the left and right temporal lobes in an autistic population compared with matched normal controls and correlated this with neuropsychological measures of language and communication skills in addition to performing volumetric analysis of the temporal lobes in these same subjects. Group differeces were found and will be reported.

15:00 ***3456***. **Relationships Between Brain Water Content and Diffusion Tensor Imaging Parameters (Apparent Diffusion Coefficient, Fractional Anisotropy) in Multiple Sclerosis**
Computer 15

P. E. Sijens[1], R. Irwan[1], J.H. Potze[1], M. Oudkerk[1]
[1]UMCG, Groningen, Netherlands

Fifteen multiple sclerosis patients were examined by diffusion tensor imaging (DTI) to determine fractional anisotropy (FA) and apparent diffusion coefficient (ADC) in a superventricular volume of interest of 8×8×2 cm3 containing gray matter (GM) and white matter (WM) tissue. PRESS 2D-CSI of the same volume was performed without water suppression to map water content. Water content was increased in patients compared with controls, FA decreased and ADC increased. The demonstrated relationship between DTI parameters and water content in multiple sclerosis patients suggests potential for therapy monitoring in normal appearing brain tissue.

15:30 ***3457***. **Benign Multiple Sclerosis: Less Tissue Injury on Diffusion Tensor Imaging**
Computer 15

Yulin Ge[1], Effie Papadaki[1], Meng Law[1], Joseph Herbert[1], Hina Jaggi[1], Robert I. Grossman[1]
[1]New York University School of Medicine, New York City, New York, USA

Multiple sclerosis (MS) is a chronic inflammatory demyelinating disease that is heterogeneous in terms of clinical course. Benign MS is referred to as patients who initially diagnosed with clinically definite MS, but have experienced a benign course for a long time period such as over 10 years without relapse. This study is to characterize the corpus callosum injury in patients with benign MS using diffusion tensor imaging as compared with patients who have a typical relapsing-remitting course of MS. Our results showed less tissue structural damage in patients with benign course.

15:30 ***3458***. **Neurodevelopmental Studies in C57B/L6 Mice Assessed by *In Vivo* DTI**
Computer 18

Halima Chahboune[1], Laura Ment[1], William B. Stewart[1], Douglas L. Rothman[1], Fahmeed Hyder[1]
[1]Yale University, New Haven, Connecticut, USA

In vivo DTI for mouse brain studies is the ultimate goal of neurodevelopmental studies because various mutants or transgenic models are used to mimic several key neurological disorders which manifest through development. Here we assess the feasibility of *in vivo* DTI (at >9.4T) with high angular resolution and quantify the overall growth and maturation of microstructures in normal C57B/L6 mouse brain from P15 to P45. The most noticeable changes in DTI parameters were found in the corpus callosum. However other areas which were subject to maturation in normal brain development were also implicated from our results.

15:30 ***3459***. **Diffusion Tensor MRI in Intermittent Explosive Disorder**
Computer 17

Huiling Peng[1], Konstantinos Arfanakis[1], Daniel A. Fitzgerald[2], K Luan Phan[2], Emil L. Coccaro[2]
[1]Illinois Institute of Technology, Chicago, Illinois, USA; [2]University of Chicago, Chicago, Illinois, USA

Intermittent explosive disorder (IED), which is characterized by episodic, impulsive aggression, is an important social and clinical problem. The purpose of this investigation was to study the diffusion characteristics of the whole brain in patients with IED. Turboprop-DTI was used in this study, in order to produce DTI data that are relatively free of susceptibility-related artifacts in regions such as the frontal and temporal lobes. A significant reduction of FA was detected in the fornix, forceps minor, and posterior cingulate cortex of patients with IED compared to healthy controls.

15:30 ***3460***. **Difference of Apparent Diffusion Coefficient with Diffusion Weighted MR Imaging in Esophageal Cancer with Different Pathological Differentiation**
Computer 16

Ning Wang[1], Xiao Peng Zhang[2], Lei Tang[2], Ying Shi Sun[2], Kun Cao[3]
[1]Peking University School of Oncology & Bejing Cancer Hospital, Beijing, People's Republic of China; [2]Peking University School of Oncology & Bejing Cancer Hospital, Beijing, People's Republic of China; [3]Radiology, Peking University School of Oncology &Bejing Cancer Hospital, Beijing, People's Republic of China

Purpose: Compare the difference of ADC in esophageal cancer with different pathological type, determine the role of ADCs in differentiating the pathological type. Materials and Methods: Thiryt-nine patients were examined with SS-EPI DWI sequences at 1.5T MR scanner, 2NEX and breath-hold techniques were employed. To calculate the ADCs of esophageal cancer obtained with two motion-probing gradients (b=0 and b=500sec/mm2). To compare the difference of ADCs in esophageal cancer with different pathological type grouped by the pathology test after operation or biopsy, Results: There was no statistical difference between two type pathological differentiation (p>0.5).

15:30 ***3461***. **Age-Related Alterations of Cerebral White Matter: Analysis of Normalized Diffusion Tensor Images of Healthy Subjects Grouped in Narrow Age Ranges**
Computer 19

Khin Khin Tha[1], Satoshi Terae[1], Kohsuke Kudo[1], Hiroyuki Soma[1], Toru Yamamoto[2], Yuri Yoshida[1], Ichiro Yabe[1], Hidenao Sasaki[1], Kazuo Miyasaka[1]
[1]Hokkaido University Graduate School of Medicine, Sapporo, Japan; [2]Hokkaido University School of Medicine, Sapporo, Japan

Information about age-related effects on fractional anisotropy (FA) of cerebral white matter of subjects grouped in narrower age ranges is limited. This study evaluated age-related changes of cerebral white matter, using normalized FA images of 132 healthy subjects, aged 22-67 years. Both region-of-interest (ROI)-based and voxel-based morphometry (VBM) analysis were performed. FA of cerebral white matter declined with age. Earliest decline in FA was noted in frontal white matter. Study on normalized FA images of subjects grouped in narrower age ranges provided age- and region-specific alterations of cerebral white matter.

Diffusion: Processing and Analysis

Room 4A Wednesday 14:00 - 16:00

14:00 ***3462***. **Automated 3D Fiber Tracking Based on Two-ROI Approach as a Reliable Tool for the Detection of Corticospinal Tract Degeneration in Amyotrophic Lateral Sclerosis**
Computer 20

In-Chan Song[1], Yoon-Ho Hong[2], Kwang-Woo Lee[1], Kee-Hyun Chang[1], Dong-Gyu Na[1]
[1]Seoul National University Hospital, Seoul, Republic of Korea; [2]Seoul National University Boramae Hospital, Seoul, Republic of Korea

We developed a so-called two-ROI approach in which 3D fiber bundle tracking was performed using two reference ROIs to delineate the corticospinal tract in patients with amyotrophic lateral sclerosis (ALS). Reliability of this approach was analyzed, and the possible changes of diffusion properties were assessed. FA is highly variable along the corticospinal tract in DTI maps, which indicates that possible mismatching in anatomical levels and boundary of ROI can affect the result. Two-ROI approach may reduce such an operator-induced bias in defining a ROI, and can be used as a reliable tool for demonstrating the corticospinal tract degeneration in ALS.

14:30 ***3463***. **Improved Sensitivity in the Temporal Lobe Epilepsy by Measuring the Area and Volume of the Diffusion Anisotropy Tensor**
Computer 20

Jiun-Jie Wang[1], Chia-Lung Yang[1], You-Zen Lu[2], Yau-Yau Wai[2], Tzuu-Kang Chyi[2]
[1]ChangGung University, TaoYuan, Taiwan; [2]Chang Gung Memorial Hospital, TaoYuan, Taiwan

A reduced Fractional Anisotropy and increase trace were often noticed as an indication of the change of the micro-structure in Epilepsy. To improve the CNR and sensitivity of the diffusion anisotropy index on Epilepsy studies, we performed a systematic analysis by comparing the measures of the amplitude, area and volume on the normalized diffusion deviation tensor. The result shows that the measures of area and volume have improved sensitivity and better delineation of the lesion than the corresponding FA. The diffusion anisotropy index is more specific to the detection of seizure compared with trace.

15:00 ***3464***. **Assessing White Matter Abnormalities in HIV Patients Using Diffusion Tensor Imaging Statistics Through Elastic Image Registration**
Computer 20

Hongyu An[1], Yasheng Chen[1], Jeffery Smith[1], Colin Hall[1], Kevin Robertson[1], Kathy Wilber[1], Wendy Robertson[1], Lester Kwock[1], Elizabeth Bullitt[1], Weili Lin[1]
[1]The University of North Carolina at Chapel Hill, Chapel Hill, North Carolina, USA

Diffusion tenor imaging has been demonstrated capable of delineating white matter abnormalities in neurodegenerative diseases. However, it is unclear whether or not DTI will be able to delineate the severity of HIV. We have employed spatially normalized DTI statistics in evaluating the three different clinical stages of HIV patients and results suggest that the statistically detected DTI abnormalities could be a potential biomarker for the severity of HIV disease.

15:30 ***3465***. **Voxel-Based Morphometry Using Diffusion Tensor Imaging to Determine the Brain Regions Affected Following Mild and Severe Traumatic Brain Injury**
Computer 20

Jiachen Zhuo[1], Ritesh Patel[1], Andrew Rosenkrantz[1], Kathirkamanthan Shanmuganathan[1], Xuanxuan Su[2], Rao Gullapalli[1]
[1]University of Maryland Baltimore, Baltimore, Maryland, USA; [2]University of Maryland Dental School, Baltimore, Maryland, USA

DTI has recently shown promises in the evaluation of the TBI patients. In this study, the sensitivity of DTI parameters in differentiating injury conditions was studied along with the regional extent of injury using voxel-based morphometry in comparison with normal controls. Our results suggest that while ADC may be a more sensitive marker for the extent of injury, FA may be more specific in determining the areas that are more severely injured. The pattern of injuries seen here seem to indicate that the more mild injuries start at the periphery of the brain and as the severity of the injury increases the deeper brain structures are involved.

Diffusion: Spine

Room 4A Wednesday 14:00 - 16:00

14:00 ***3466***. **DWI of the Spinal Cord with Limited FOV Single-Shot EPI**
Computer 21
Emine Ulku Saritas[1], Charles H. Cunningham[1], Jin Hyung Lee[1], Dwight G. Nishimura[1]
[1]Stanford University, Stanford, California, USA

Diffusion weighted imaging (DWI) of the spinal cord is important in the diagnoses and better understanding of damage to the long fiber tracts. Single-shot diffusion-weighted echo-planar imaging (ss-DWEPI) provides excellent robustness against motion-induced phase perturbations, but does not provide sufficient quality images. In this work, we achieve higher resolution spin-echo ss-DWEPI images, without the need for a longer readout, by taking advantage of the highly rectangular geometry of the spine. By using a 2D echo-planar RF excitation pulse and a 1800 refocusing pulse, we limit the FOV in the phase-encode direction and suppress the signal from fat simultaneously.

14:30 ***3467***. **Twice Refocused Inner Volume EPI DTI of the Spinal Cord: Initial Findings**
Computer 21
Frederik Bernd Laun[1], Bram Stieltjes[1], Lothar Schad[1]
[1]Deutsches Krebsforschungszentrum, Heidelberg, Baden-Württemberg, Germany

DTI of the spinal cord is hampered by high demands of resolution and several sources of artefacts. Here we present a cardiac gated inner volume technique combined with an EPI read out that may overcome these problems. The obtained image quality is good and repeated evaluation of the FA and ADC within the spinal cord show a high reproducibility. Since we used two 180 slice selective refocusing pulses in phase direction during a twice refocused spin echo diffusion preparation, the proposed method can be used for multislice acquisition increasing time efficacy and spinal cord coverage.

15:00 ***3468***. **Diffusion Study in Human Cervical Spinal Cord *in-Vivo* Using Biexponential Model**
Computer 21
Tomasz Banasik[1, 2], Andrzej Jasinski[1, 3], Marcin Hartel[2], Marek Konopka[2], Piotr Pieniazek[2], Tomasz Skorka[1], Wladyslaw Piotr Weglarz[1]
[1]H. Niewodniczanski Institute of Nuclear Physics PAS, Kraków, Poland; [2]Silesian Diagnostic Imaging Center Helimed, Katowice, Poland; [3]Pedagogical University, Kraków, Poland

Multi b value diffusion study in the human spinal cord was performed *in vivo* on the group of volunteers. The b factor varied up to 7000 s/mm2 in ten steps. Non mono-exponential signal intensity decay was observed and data were fitted to the bi-exponential diffusion model, using a IDL based, in-house written software. Fast and slow components was calculated for GM and WM structures. The maps of diffusion coefficients and fractions were also created.

15:30 ***3469***. **Q-Space Simulations on Mouse Spinal Cord White Matter Tract Histologic Images**
Computer 21
Henry H. Ong[1], Punam K. Saha[1], Eric D. Schwartz[1], Felix W. Wehrli[1]
[1]Department of Radiology, University of Pennsylvania, Philadelphia, Pennsylvania, USA

Q-space imaging allows indirect assessment of porous material microstructure, yielding measures of pore size. The Fourier Transform of the q-space echo attenuation (propagator) is a molecular displacement probability density function. Q-space imaging of biological structures is complicated by the presence of extra-cellular and intra-cellular signal (e.g. water) and molecular exchange between these compartments, the consequences of which are poorly understood. Here, we investigate these effects by performing simulations on histologic images of mouse cervical spinal cord white matter tracts. We found that propagator full-width-half-maximum correlated with axon size over a wide range of extra/intra-cellular T2 and exchange per-meability values.

Artifact Correction in DWI

Room 4A Wednesday 14:00 - 16:00

14:00 ***3470***. **Automatic Correction for Signal Intensity Drift in Diffusion Weighted Images**
Computer 22
Jesper Frandsen[1], Ryan Sangill[1], Leif Østergaard[1], Dora Zeidler[1], Peter Vestergaard-Poulsen[1]
[1]Aarhus University Hospital, Aarhus, Denmark

DTI under full duty cycle may lead signal drift. This signal drift causes overestimation of Apparent Diffusion Coefficient, underestimation of the Fractional Anisotropy, and error in the estimation of the primary diffusion direction used for tractography. Here we present a novel way to correct for the signal drift at no or little extra cost in acquisition time.

14:30 ***3471***. **The Influence of Ghost Correction Accuracy on the Image Quality of GRAPPA Accelerated EPI**
Computer 22
Stefan Skare[1], David B. Clayton[1], Rexford Newbould[1], Mike Moseley[1], Roland Bammer[1]
[1]Stanford University, Palo Alto, California, USA

We are assembled a 192x192 3-shot GRAPPA DW-EPI protocol in the clinics, where the GRAPPA weights are estimated on the T2w image and applied to each shot in the DWI's. Nyquist ghosting between odd/even echoes are normally corrected for by reference scans as a part of prescan. We show here that if this reference scan is not ideal, the GRAPPA weights are altered which produces noise enchancements in the DWI's.

15:00 ***3472***. **Effects of Correction of Susceptibility Distortion on DTI Measures**
Computer 22
Xiaoxu Liu[1], Tong Zhu[1], Jianhui Zhong[1]
[1]University of Rochester, Rochester, New York, USA

Diffusion tensor imaging is becoming very important for studies of neurological disorders such as Alzheimer's disease. DTI data are usually collected with an EPI sequence, which suffers from susceptibility distortion. Consequently, DTI results such as fiber tracking and FA values in specific areas can be mis-interpreted. We undistorted the DWIs collected from a 3T scanner using field maps then compared the DTI results generated from the original and corrected DWIs. Fiber tracking and index maps after correction show more fidelity than original ones. Measurements in corpus callosum show that FA values increase while FA variance reduces significantly after the correction.

15:30 ***3473***. **Reduction of the Effect of Cardiac-Induced Motion for Typical DTI Protocols**
Computer 22
Sofia Chavez[1], Simon Graham[1, 2]
[1]Sunnybrook and Women's College Health Sciences Centre, Toronto, Canada; [2]University of Toronto, Toronto, ON, Canada

Cardiac-induced pulsatile motion can reduce signal intensity in diffusion weighted images. However, it has not been widely reported to affect results when typical diffusion tensor imaging (DTI) protocols are employed. As a result, contradictory advice is being advocated in the literature and in practice, there is no accepted standard in terms of implementing cardiac gating for DTI. A simple mathematical formulation of the effect of signal averaging and confirming experiments resolve the apparent discrepancy and provide an explanation and assessment of the sensitivity of typical DTI protocols to cardiac-induced motion.

Body/MSK - Breast MR

Room 4A Wednesday 14:00 - 16:00

14:00 ***3474***. **Highly Constrained Backprojection: A Method for High Spatial and Temporal Resolution in DCE-MRI of Breast Cancer**
Computer 23
Sean B. Fain[1], Oliver Wieben[1], Yijing Wu[1], Yan Wu[1], Charles A. Mistretta[1], Jean Brittain[2], Frederick Kelcz[1]
[1]University of Wisconsin, Madison, Wisconsin, USA; [2]GE Healthcare, Madison, Wisconsin, USA

This work exploits the sparse nature of contrast-enhanced subtraction data in DCE-MRI to constrain the location of signal changes associated with contrast kinetics in breast tumors. Spatial resolution and signal to noise is preserved by using a composite image made up of a wider temporal aperture of projections, with contrast dynamics determined by a much smaller subset of projections. The technique is well suited to data sets in which the object is relatively static. Results in simulations show accurate contrast kinetics in a complex lesion with as few as 40 projection angles while maintaining high spatial resolution and SNR.

14:30 ***3475***. **Comparison of MRI Features of Infiltrating Lobular Carcinoma with Invasive Ductal Carcinoma Based on ACR BI-RADS MRI Lexicon**
Computer 23
J-H Chen[1, 2], M-Y Su[1], H J. Yu[1], H-M Baik[1], O Nalcioglu[1]
[1]University of California, Irvine, Irvine, CA, USA; [2]China Medical University Hospital, Taichung, Taiwan

This study was to analyze and compare the different morphological appearances and kinetic features between ILC and IDC, using the features defined in ACR BI-RADS MRI lexicon. ILC displayed more diverse morphological appearances than IDC. The non-mass-like enhancement patterns were higher in ILC than IDC (7/29 vs. 1/30). Regarding kinetic features, ILC had a higher possibility showing moderate or slow early enhancement phase than IDC (9/35 versus 1/35). While 91% IDC (32/35) demonstrated the typical malignant kinetic pattern with fast early enhancement and wash-out in the delayed phase, this pattern was only seen in 51% ILC (18/35).

15:00 ***3476***. **Dynamic BOLD Contrast in the Breast Using Heart Saturation**
Computer 23
Rebecca Rakow-Penner[1], Laura Pisani[1], Bruce L. Daniel[1], Gary H. Glover[1]
[1]Stanford University, Stanford, California, USA

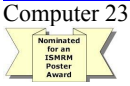

Effectively measuring BOLD contrast in breast tissue has been a challenge due to motion artifacts from the nearby beating heart. This study provides a new method for measuring BOLD contrast by saturating the signal from the heart and stimulating the BOLD response by jittering inhalation of pure oxygen. With the application of this new pulse sequence and method design, BOLD contrast in the breast can be measured more reliably and with greater signal response.

15:30 *3477*. **A Dual-Phase Kinetic Volume Rendering Approach to Present 3D T1-Weighted DCE-MRI Data of the Breast on 2D Images Combining Morphology and Kinetic Characteristics**
Computer 23
Michael Khazen[1], Martin O. Leach[1]
[1]Institute of Cancer Research and The Royal Marsden NHS Foundation Trust, Sutton, Surrey, UK

T1-weighted 3D dynamic contrast-enhanced magnetic resonance imaging (DCE-MRI) of the breast provides an effective clinical tool for the characterization of breast cancer. One of the problems associated with DCE-MRI of the breast is distinguishing lesions from blood vessels that often display contrast agent uptake kinetics similar to many malignant tumours. Although blood vessels have characteristic shape features, these features may be difficult to assess on sectional image. We present a method to address this problem by extracting both morphologic and kinetic information from the data and producing colour-encoded volume rendering of tissue contrast agent kinetics combined with morphology.

Clinical Multimodal and Assessment of Response

Room 4A Wednesday 14:00 - 16:00

14:00 *3478*. **Quantification of Response of Hepatocellular Carcinoma(HCC) to Bevacizumab by Contrast Enhanced MRI**
Computer 25
Emil Cohen[1], Jonathan Schwartz[1], John Mandeli[2], Deborah Lehrer[2]
[1]Mount Sinai School of Medicine, New York, New York, USA; [2]Mount Sinai Medical Center, New York, New York, USA

Quantiative assessment of effects of an anti-angiogenic agent on hepatocellular carcinoma by conrtast enhanced MRI demonstrating good correlation between change in size and degree of change in contrast enhancement.

14:00 *3479*. **Oncological Imaging: Whole-Body MRI for Staging of Patients with Malignant Lymphoma**
Computer 26
Bernd B. Frericks[1], Bernhard Meyer[1], Thomas Albrecht[1], Alexander Huppertz[2], Karl J. Wolf[1], Frank K. Wacker[1]
[1]Charité, Campus Benjamin Franklin, Berlin, Germany; [2]Siemens, Berlin, Germany

Aim of this study was to evaluate the diagnostic accuracy of whole-body MRI for staging of 27 patients with malignant lymphoma. 4 MR sequences were compared to whole-body CT. Regarding lymph node involvement T2w-STIR was superior to CT in the neck and the abdomen and comparable in the thorax. Bone marrow involvement as well as extraosseous extranodal findings were best detected by T2w-STIR. Whole-body MRI is a valuable imaging modality for staging of lymphoma patients with T2w-STIR being the most sensitive sequence reaching results that are superior or at least comparable to CT.

14:00 *3480*. **MRI Compared to CT in Whole-Body Slice Area Measurements**
Computer 24
Joel Kullberg[1], Jan-Erik Angelhed[2], John Brandberg[2, 3], Hans Frimmel[1], Eva Bergelin[2], Lena Strid[2], Håkan Ahlström[1], Lars Johansson[1], Lars Lönn[2, 3]
[1]Uppsala University Hospital, Uppsala, Sweden; [2]The Sahlgrenska Academy at Göteborg University, Göteborg, Sweden; [3]Sahlgrenska University Hospital, Göteborg, Sweden

A high correlation between MRI and CT area determinations has been demonstrated. Total slice area accuracy, distributed over the whole body, of a gradient echo MRI sequence was studied on 10 subjects using CT as reference. 28 axial CT images were acquired and the corresponding MR images were visually selected from a whole-body scan based on congruence in anatomical structures. Automatic area measurements using intensity thresholds were performed for both modalities. The subject-wise summed slice areas gave the linear relationship MRI=0.938·CT+919, R=0.998.

14:30 *3481*. **Whole-Body Pet-MRI - Co-Registration and Image Fusion in Pattients with Cancer**
Computer 24
Roberto Cortes Domingues[1], [2], Michel Pontes Carneiro[3], Luiz Celso Hygino da Cruz[4], Karla Sideira Porto[4], Leonardo Pitanga[4], Rômulo Cortes Domingues[4], Romeu Cortes Domingues[4]
[1]CDPI / Multi-Imagem, Rio de Janeiro, RJ, Brazil; [2]Multimagem Pet, Rio de Janeiro, RJ, Brazil; [3]Multimagem PET, Rio de Janeiro, RJ, Brazil; [4]CDPI, Rio de Janeiro, RJ, Brazil

The purpose of our paper is to evaluate the feasibility of fusion functional positron emission tomography (PET) data with anatomical magnetic resonance (MR) images, using highly-quality whole body MRI imaging.Two years ago, high-quality whole body MRI imaging would take 2 hours, and now with the new designs of transmit-receiver coils, easier movement of the imaging table, and new data-acquisition techniques have allowed rapid imaging of the entire body with highly-quality in 20 to 30 minutes.The preliminary results indicate that the described technique has the potential to emerge as an all-encompassing alternative to conventional multimodality tumor staging strategies.

14:30 *3482*. **Evaluation Early Response of Hepatocellular Carcinoma After Transcatheter Arterial Chemoembolization(TACE) with 1H Magnetic Resonance Spectroscopy *In Vivo***
Computer 26

Wu Bin[1], *Peng Weijuns*[1]
[1]Cancer Hospital, Shanghai, People's Republic of China

Transcatheter arterial chemoembolization (TACE) has significantly improved the survival for patients with inoperable hepatocellular carcinoma(HCC).However, there is no reliable imaging method to detect the early response to such treatment quantitatively. The choline-containing compounds(Cho) in hepatic tumors detected by 1H MRS has known to be linked to malignancy.The purpose of the current study is to find the feasibility of using 1.5T MR scanner clinically in acquiring reliable spectroscopic procedures and to investigate the potential value of 1H MRS in the assessment of the early metabolic processes in large HCC after TACE.

14:30 *3483*. **Neoadjuvant Chemotherapy in Breast Cancer: Prediction of Post-Surgery Disease-Free Survival Using DCE-MRI, Water ADC Mapping and Proton Spectroscopic Imaging**
Computer 25

David John Manton[1], *Anne Hubbard*[2], *Martin Lowry*[1], *Anthony Maraveyas*[1], *Martin D. Pickles*[1], *Daniel J. Tozer*[3], *Lindsay W. Turnbull*[1]
[1]University of Hull, Hull, East Yorkshire, UK; [2]Hull and East Yorkshire Hospitals NHS Trust, Hull, East Yorkshire, UK; [3]Institute of Neurology, London, UK

MRI and unsuppressed proton spectroscopic imaging were carried out at 1.5 T in 16 women before and after neoadjuvant chemotherapy for primary, inoperable breast cancer (six courses). Water ADC was measured, pharmacokinetic parameters were derived from DCE-MRI, and water T2 and water:fat signal ratios were determined spectroscopically. Three of the women developed metastases during clinical follow-up and Kaplan-Meier survival analyses were undertaken. Pharmacokinetic exchange rate, water:fat ratio, water T2 and ADC data all correlated significantly with the length of post-surgery disease-free survival (p=0.049 log-rank tests) suggesting that quantitative MRI and spectroscopic imaging may have prognostic utility in this patient group.

15:00 *3484*. **Tumor Volume Regression During Therapy in Cervical Cancer: Does the Tumor Regress Faster with Combined Radiation/Chemotherapy Than with Radiation Therapy Alone?**
Computer 25

Nina A. Mayr[1], *Jian Zhong Wang*[1], *William TC Yuh*[1], *Joseph F. Montebello*[1], *Vincent A. Magnotta*[2], *Kenneth F. Wegner*[3], *Susan M. Edwards*[3]
[1]The Ohio State University, Columbus, Ohio, USA; [2]University of Iowa, Iowa City, Iowa, USA; [3]University of Oklahoma Health Science Center, Oklahoma City, Oklahoma, USA

There was no difference in the overall volume regression speed for cervical cancer patients with either combined radiation/chemotherapy (CRT) or with radiation therapy (RT) alone. It is the individual regression rate that predicts outcome, regardless of CRT or RT.

15:00 *3485*. **Diffusion-Weighted and Dynamic Contrast-Enhanced Imaging at 3.0 T of Prostate Cancer**
Computer 26

Uulke Age van der Heide[1], *Cecile R.L.P.N. Jeukens*[1], *Peter R. Luijten*[1], *Marco van Vulpen*[1]
[1]UMC-Utrecht, Utrecht, Netherlands

The purpose of this study is to improve the accuracy in localizing and delineating the tumor within the prostate, using a combination of anatomical and functional (diffusion-weighted and contrast-enhanced) imaging at 3.0 T. To this end DCE-MRI and DWI scans were made of 6 patients with biopsy proven prostate cancer. Regions with low ADC and high blood flow were identified. While both features are indicative of the presence of tumor, our data show only partial overlap between the identified volumes, suggesting complementary functional data that can be used in the disease manangement in prostate cancer patients.

15:00 *3486*. **Whole Body MR Imaging vs. FDG-PET: Comparison of Diagnosis Accuracy of M-Stage in Lung Cancer Patients**
Computer 24

Yoshiharu Ohno[1], *Hisanobu Koyama*[1], *Munenobu Nogami*[1], *Hideaki Kawamitsu*[2], *Daisuke Takenaka*[1], *Kazuro Sugimura*[1]
[1]Kobe University Graduate School of Medicine, Kobe, Hyogo, Japan; [2]Kobe University Hospital, Kobe, Hyogo, Japan

Whole-body MRI has the capability for cancer screening and/ or staging similar to FDG-PET. However, no direct comparisons about diagnostic accuracy of M-stage in lung cancer were reported. The purpose of the present study was to prospectively compare diagnostic accuracy of M-stage between whole-body MRI and PET in lung cancer patients. 70 lung cancer patients underwent whole-body MRI and PET, and compared their diagnostic capabilities on per patient basis. There were no significant difference of diagnostic capability between two methods ($p>0.05$). In conclusion, whole-body MRI can accurately diagnose M-stage in lung cancer patients, similar to PET.

15:30 *3487*. **Combined Stereoscopic X-Ray and MR Imaging ("XMR") for the Evaluation of Prostate Brachytherapy Implants with Comparison to Standard CT-Based Dosimetry**
Computer 24

Peter Acher[1, 2], Kawal Rhode[1], Stephen Morris[2], Marc Miquel[1], Kate Mcleish[1], Ronald Beaney[2], Charles Deehan[2], Rick Popert[2], Stephen Keevil[1]
[1]King's College London, London, England, UK; [2]Guy's & St Thomas' NHS Foundation Trust, London, England, UK

Introduction. Combined MRI and stereoscopic X-ray (XMR) may provide an alternative to CT for the dosimetric analysis of permanent prostate brachytherapy (PPB) implants. This study compares dosimetric results from both modalities.Methods. Ten patients underwent both a CT and an XMR study following PPB. Dosimetric analysis was carried out on both and parameters compared.Results. Bland-Altman analysis showed mean D90 values from XMR 1.1% higher than CT with wide limits of agreement (95% confidence interval) of -17.5% to 19.7%.Conclusion. XMR-based results are different to those from CT and are likely due to superior soft-tissue definition and source localisation.

15:30 *3488*. **Combined MRI/MRS Protocol for Specificity Improvement in Breast Cancer Detection**
Computer 26

Luminita Alina Tudorica[1], Paul Fisher[1], Khaldoon Dulaimy[1], Brian O'Hea[1], Terry Button[1], Wei Huang[2]
[1]State University of New York, Stony Brook, New York, USA; [2]Memorial Sloan-Kettering Cancer Center, New York, New York, USA

The goal of this study was to determine if a combined MRI/MRS protocol of dynamic contrast enhanced (DCE) T1-weighted MRI, 1H MRS, and perfusion MRI improves specificity in detection of breast malignancy. 87 patients with positive mammography findings were studied. After DCE MRI showed fast contrast enhancement, single-voxel 1H MRS and perfusion MRI examinations were performed. DCE MRI showed 100% sensitivity and 56% specificity in detection of breast cancer. The specificity improved to 85% with the addition of 1H MRS, and to 100% with the further addition of perfusion MRI.

15:30 *3489*. **Dynamic Contrast-Enhanced MRI as a Predictor of Residual Tumor After Photodynamic Therapy with TOOKAD (WST09) for Locally Recurrent Prostate Carcinoma After Radiation Therapy**
Computer 25

Masoom A. Haider[1], Brian Wilson[2], Sean Davidson[2], Robert Weersink[2], Mark Gertner[2], Andrew Evans[2], Ants Toi[1], John Trachtenberg[3]
[1]University of Toronto, Toronto, Ontario, Canada; [2]Princess Margaret Hospital, Toronto, Ontario, Canada; [3]University Health Network, University of Toronto, Toronto, Ontario, Canada

The purpose of this study was to determine if DCE-MRI could predict the presence or absence of residual prostate cancer in patients after ablative treatment with photodynamic therapy (TOOKAD-PDT) for locally recurrent cancer after radiation therapy. DCE-MRI predicted residual tumor with sensitivity 10/10 (100%), specificity 5/7 (71%), PPV 10/12 (83%), NPV 5/5 (100). DCE-MRI can play an important role in not only delineating treatment response in this population but also help guide therapy and determine whether re-treatment is necessary without the need for repeat biopsy. DCE-MRI is an accurate method for predicting the presence of residual tumor after TOOKAD-PDT.

Analysis and Accuracy of DCE - MRI

Room 4A Wednesday 14:00 - 16:00

14:00 *3490*. **A Joint Bayesian Method for Robust Estimation of PK and AIF Parameters for DCE-MR Imaging**
Computer 28

Matthew Richard Orton[1], Simon Walker-Samuel[1], David J. Collins[1], Martin O. Leach[1]
[1]Institute of Cancer Research, Sutton, Surrey, UK

When applying pharmacokinetic (PK) models to DCE-MRI data it is necessary to provide on estimate of the arterial input function (AIF). We propose a novel Bayesian method that allows the AIF to be directly estimated from the tissues of interest. This leads to accurate estimates of the PK parameters, and allows for the incorporation of prior information that can assist the inference. This approach was tested on data taken from liver metastases. In this example the posterior distribution for the AIF parameters was well localised, and the maps of the Bayesian derived PK parameters agreed well with existing methods.

14:00 *3491*. **Assesing T_1 Accuracy for DCE-MRI Functional Imaging: The Effects of Measurement Sequence and Number of Flip Angles**
Computer 27

Benjamin Richard Knowles[1], Simon Walker-Samuel[1], Martin O. Leach[1], David J. Collins[1]
[1]Institute of Cancer Research, Sutton, UK

Fast imaging sequences are essential for good temporal resolution in DCE-MRI. There are many available for potential use, and all have advantages and disadvantages. Four sequences were evaluated for their effectiveness in DCE-MRI. Attributes examined were T1 calculations, imaging times and SNRs. The sequences examined were IR, SR, and 2D, 3D GRE. The SR and IR sequences gave the best SNR and had the fastest imaging times, whilst the 3D GRE sequence performed adequately and all three produced similar T1 accuracies. 2D GRE gave highly inaccurate T1 values. 3D GRE also has the advantage of providing volume coverage.

14:30 ***3492***. **A Double Bolus Injection Protocol Improves the Precision of K^{trans} in Clinical DCE-MRI Analysis**
Computer 27
Caleb Roberts[1], David L. Buckley[1], Geoff J.M. Parker[1]
[1]University of Manchester, Manchester, Greater Manchester, UK

To achieve high precision in quantitative dynamic contrast-enhanced MRI (DCE-MRI) analysis it is necessary to sample the arterial input function (AIF) and subsequent tissue time course with high temporal definition. Using simulations we explored the effects of mis-sampling both a single and double bolus AIF and resulting tissue uptake curves over a range of temporal resolutions on tracer kinetic analysis. Our study suggests that in DCE-MRI studies where temporal resolution is longer than 9 seconds, a double bolus injection protocol is beneficial in achieving greater precision of kinetic modeling parameters.

14:30 ***3493***. **Standardization of RCBV Values Improves Tumor Contrast**
Computer 28
Todd Robert Jensen[1], [2], Kathleen M. Schmainda[2]
[1]Marquette University, Milwaukee, Wisconsin, USA; [2]Medical College of Wisconsin, Milwaukee, Wisconsin, USA

To allow for better longitundinal and interpatient comparisons, a method to standardize rCBV values has been tested with results showing better separation of white and gray matter rCBV values.

15:00 ***3494***. **DCE-MRI Functional Imaging Using an Endorectal Coil: Limits on Measurement Accuracy**
Computer 28
Benjamin R. Knowles[1], Simon Walker-Samuel[1], Nandita M. deSouza[1], Martin O. Leach[1], David J. Collins[1]
[1]Institute of Cancer Research, Sutton, UK

T1 calculation using a look up table is a fast and accurate method often used in DCE-MRI. Many functions can be used to create a look up table, and five different functions were compared. Look up tables were used to create concentration – time curves from clinical data. A pharmacokinetic model was fit to the curves, and values of Ktrans, ve and kep were compared. We recommend the use of an inverse (y = a + b/x) function for use in gradient echo DCE-MRI, as there is a theoretical basis for using this function, and error propagation is additive.

15:00 ***3495***. **Comparison of a Reference Region Model to Direct AIF Measurement in the Analysis of DCE-MRI Data**
Computer 27
Thomas Yankeelov[1], Greg O. Cron[2], Christina Addison[3], Julia Wallace[4], Ruth Wilkins[5], Bruce Pappas[4], Giles Santyr, [46], John C. Gore[1]
[1]Vanderbilt University, Nashville, Tennessee, USA; [2]Catholic University of Louvain, Louvain, Brussels, Belgium; [3]Ottawa Health Research Institute, Ottawa, Ontario, Canada; [4]Carleton University, Ottawa, Ontario, Canada; [5]Health Canada, Ottawa, Ontario, Canada; [6]Robarts Research Institute, London, Ontario, Canada

We directly compare the output obtained from a reference region model for the analysis of dynamic contrast enhanced MRI data with the output obtained from a direct AIF measurement analysis.

15:30 ***3496***. **Arterial Input Functions from Sub-Second MR and CT Imaging: Quality and Accuracy**
Computer 27
Elizabeth Charles-Edwards[1], Kate Newbold[2], Elly Castellano[2], Adrian Tang[1], James D'Arcy[1]
[1]Royal Marsden NHS Foundation Trust and Institute of Cancer Research, Sutton, Surrey, UK; [2]Royal Marsden NHS Foundation Trust, London, UK

Pharmocokinetic models require arterial input functions (AIFs). AIFs from MR and CT data acquired at a temporal resolution of 0.5 sec from patients with head and neck cancer are compared in terms of quality and accuracy, to each other and to an MR AIF derived from arterial sampling. MR-derived AIFs have similar peak concentrations to that obtained by arterial sampling whereas, though less noisy, the peak concentrations shown in CT-derived AIFs are nearly 3 times higher. This is probably due to increased contrast agent volume, a factor that must be accounted for if CT-derived AIFs are applied to DCE-MRI data.

15:30 ***3497***. **Imaging and Multi-Parametric Analysis of Cancerous Tissue (IMPACT): Prostate Cancer (PCa)**
Computer 28
Yousef Mazaheri[1], Jason A. Koutcher[1], Amita Shukla-Dave[1], Hedvig Hricak[1]
[1]Memorial Sloan Kettering Cancer Center, New York, New York, USA

We introduce a novel approach to combine multiple MR parameters for detection and assessment of prostate cancer (PCa). Our technique combines MR diffusion weighted imaging (DWI) and MR spectroscopic imaging (MRSI) by partitioning tissue populations into three clusters: (2 healthy tissues, 1 tumor). The K-means algorithm and priori information of prostatic and tumor metabolic and ADC values are used to define the three classes. Voxels identified as tumor are further partitioned into high, medium, and low degrees of suspicion.

Contrast Mechanisms

Room 4A Wednesday 14:00 - 16:00

14:00 ***3498***. **Optimal Sampling for Quantitative Magnetization Transfer**
Computer 29
Mara Cercignani[1], Daniel C. Alexander[2]
[1]Institute of Neurology, UCL, London, England, UK; [2]Dept of Computer Science, UCL, London, England, UK

We present a method based on the CramerRao lower bound to optimize the sampling strategies for multi-parametric quantitative MRI techniques. The method is then applied to quantitative magnetization transfer (MT), where a number of parameters is estimated by fitting a non-linear model to the MRI signal obtained with different MT weightings. Simulations and real data show improved precision and accuracy in recovered parameters, suggesting that a reliable quantification of MT parameters from data collected in clinically acceptable scan times is feasible when using an optimal MT point sampling scheme.

14:30 ***3499***. **Fat Suppression Strategies for Off-Resonance (IRON) Imaging of Magnetically-Labeled Stem Cells High in Iron with 0% Fat**
Computer 29
Saurabh S. Shah[1], Wesley D. Gilson[2], Robert G. Weiss[2], Bradley P. Barnett[2], Jeff W M Bulte[2], Dara L. Kraitchman[2], Matthias Stuber[2]
[1]Johns Hopkins University, Baltimore, Maryland, USA; [2]Johns Hopkins University School of Medicine, Baltimore, Maryland, USA

IRON imaging is a method that enables the signal-enhanced visualization of superparamagnetic particles. However, since IRON method intrinsically highlights all off-resonant protons, the presence of fat leads to ambiguous image information. Based on theoretical considerations, we have developed different approaches for fat suppressed IRON imaging. The effectiveness of these fat suppression methods has then been tested in-vitro, and a fat suppressed IRON imaging method with maximized signal-to-noise ratio was identified.

15:00 ***3500***. **Quantification of B_0 and B_1 Effects on the Estimation of MT Parameters at 3.0 T**
Computer 29
Mara Cercignani[1], Mark R. Symms[2], Philip A. Boulby[2], Gareth J. Barker[3]
[1]Institute of Neurology,UCL, London, England, UK; [2]Institute of Neurology, UCL, London, England, UK; [3]Institute of Psychiatry, King's College London, London, England, UK

Quantitative magnetization transfer (MT) imaging relies on fitting a non-linear model to a series of MT-weighted images collected with MT pulses of variable amplitude and offset frequency. Any imperfection in the B_1 field results in a deviation from the nominal pulse amplitude, while any imperfection in the B_0 field results in a deviation from the nominal offset frequency. Here we quantify the error introduced by B_1 and B_0 field inhomogeneities into the MT parameters estimated from data collected at 3.0 T, showing that in some areas of the brain this error can be as large as 50%.

15:30 ***3501***. **Investigation and Modeling of Magnetization Transfer Effects of Conventional and Hyperecho TSE Sequences at 1.5T and 3T**
Computer 29
Matthias Weigel[1], Jürgen Hennig[1]
[1]University Hospital Freiburg, Freiburg, Germany

2D turbo spin echo sequences (TSE) with a large number of slices find widespread applications in clinical routine MRI examinations. One undesirable side effect of this type of acquisition is that adjacent slices lead to an “artificial” magnetization transfer (MT) effect, thus, contrast changes. Low flip angle TSE sequences have become common to limit SAR. In this work, MT effects for different multi-slice TSE sequences with arbitrary flip angles are quantified and compared to a TSE180 at 1.5T and 3T. A modified model derived from “classic” MT experiments is presented that can accurately describe the measured data.

New Contrast Agents

Room 4A Wednesday 14:00 - 16:00

14:00 ***3502***. **New Dendritic Gd-Based Contrast Agents with PEG Cores for Tumor Imaging**
Computer 30
Yanjun Fu[1], Hans-Jurgen Raatschen[1], Michael Wendland[1], Viktor Novikov[1], Hubertus Pietsch[2], Zachary Boyd[1], Mark Knudsen[1], Danute Nitecki[1], David Shames[1], Robert Brasch[1]
[1]University of California San Francisco, San Francisco, CA, USA; [2]Schering AG, Berlin, Germany

Intravascular Gd-based contrast media have prolonged angiographic effect and great potential in MR imaging to quantitate microvascular characteristics. To overcome existing drawbacks of current macromolecular formulations, a series of new Gd-based dendritic contrast agents with polyethyleneglycol cores (PEG, MW 3400 to 12000 Da) and different generations (4 and 5) was originally synthesized. Representative compounds (e.g. Gd-based PEG12000-Gen4 dendrimer) showed great potential as blood pool agents with molecular weights less than 25 kDa, and 2-fold higher relaxivity than Magnevist, and were able to differentiate microvascular permeaility between implanted human breast cancer and normal musculature in athymic rats by DCE-MRI technique.

14:00 ***3503***. **Molecular Magnetic Resonance Imaging of Pulmonary Emboli with Gadofluorine**
Computer 31

Karl Michael Ruhl[1], Marcus Katoh[1], Arno Buecker[1], Bernd Misselwitz[2], Rolf W. Gunther[1], Thoralf Niendorf[1], Elmar Spuentrup[1]
[1]RWTH Aachen University, Aachen, Germany; [2]Schering AG, Berlin, Germany

Systemic application of Gadofluorine allows for selective visualization of fresh pulmonary thromboembolism in a swine model using the IR sequence. Emboli can still be visualized more than 24 hours after injection of contrast media. Although a relative high Gadolinium concentration was found, further investigation are needed to prove a specific binding. Especially the very long half life time have to be taken into account as diffusion into the clot based on high blood pool levels may also support Gd concentration within the clot.

14:30 ***3504***. **Simultaneous Hyperpolarization of Multiple 13C Molecules In Vitro & *In Vivo*: Towards Rapid Metabolite Mapping by MRS & MRI**
Computer 31

Pratip Bhattacharya[1, 2], Valerie A. Norton[1], Alex P. Lin[2], Kent Harris[2], Jochen Leupold[3], William Perman[4], Jürgen Hennig[3], Brian D. Ross[2], Daniel P. Weitekamp[1]
[1]California Institute of Technology, Pasadena, California, USA; [2]Huntington Medical Research Institutes, Pasadena, California, USA; [3]University Hospital, Freiburg, Germany; [4], St. Louis University School of Medicine, St. Louis, Missouri, USA

The goal of this work is to achieve simultaneous hyperpolarization of multiple 13C reagents for fast imaging and spectroscopy of metabolites in vitro and *in vivo*. To facilitate routine hyperpolarization trials by PASADENA, GE Healthcare, Malmo has developed an automated polarizer for the initial steps of synthesis and polarization transfer, presently installed at Huntington Medical Research Institute, Pasadena. The polarizer was individually optimized for the production of two hyperpolarized water soluble molecules. Since the difference in J couplings for both the molecules is small, it is possible to apply polarization transfer sequence optimized for one to the other with negligible (2-3%)loss in polarization. The formation of dual hyperpolarized product was observed in vitro & in vivo by fast 13C CSI and Multiple Echo 3D FIESTA sequences developed on a clinical 1.5T GE scanner. The spatial, spectral and dynamic information of multiple hyperpolarized species can be obtained in real time.

14:30 ***3505***. **Detection of Inhomogeneous B_1 Deposition *via* PARACEST Thermometry**
Computer 30

Shanrong Zhang[1], Raymond W. Sze[1, 2]
[1]University of Washington, Seattle, Washington, USA; [2]Children's Hospital & Regional Medical Center, Seattle, Washington, USA

Recently, a novel MR thermometry has been demonstrated *in vitro* that is based on the application of exogenous PARAmagnetic Chemical Exchange Saturation Transfer (PARACEST) agents. By using this new technique, the inhomogeneous patterns of B_1 deposition have been successfully detected for a phantom with 1 cm diameter that sits on the center of a 2 cm surface coil. Therefore, we believe that such technique may find important application, for example, in detection of "hot spots" in high field MRI diagnoses.

15:00 ***3506***. **Molecular Imaging of Inflammation in Atherosclerosis Plaque Using Functionalized MRI Contrast Agent**
Computer 30

Hasan ALSAID[1], Geneviève De Souza[1], Marie Claude Bourdillon[2], Frédéric Chaubet[3], Abdulrazzaq Sulaiman[4], Charaf Zahir[3], Eric Lancelot[5], Didier Letourneur[3], André Briguet[1], Emmanuelle Canet-Soulas[1]
[1]Laboratoire de RMN UMR CNRS 5012. UCB Lyon1-ESCPE, Villeurbanne, France; [2]EA 3740, Université UCB-Lyon1, Faculté Médecine Laennec, Lyon, France; [3]INSERM U 698, Hôpital X. Bichat, Paris, France; [4]CREATIS, UMR 5515 INSERM U 630, Radiologie, Hôpital Cardiologique, Bron, France; [5]Guerbet, B.P. 50400, Roissy CdG cedex, France

We propose to evaluate arterial wall contrast enhancement with new macromolecular agent functionalized to target atherosclerostic plaques inflammation in ApoE-/- mice. The CMD-A2-Gd-DOTA (P717) was modified into functionalized product (CM8S) to target adhesion molecule P-Selectin. Each product were marked with rhodamine and evaluated in ApoE-/- and C57BL/6 mice at 2Tesla MRI by pre and post-contrast T1 (90µm) SE. Signal enhancement was measured by Creatools software. The MRI data were correlated to histo-pathology, immunohistochemistry and immunofluorescence. Measurements show specific enhancement with CM8S in ApoE-/- where it is co-located with P-selectine as shown by immunohistochemistry and fluorescence but not in control mice.

15:00 ***3507***. **Rapid Toxicity Screening of Novel PASADENA MRI Contrast Agents**
Computer 31

Anna Reisen Freundlich[1, 2], Pratip Bhattacharya,[23], Geza Techy[2], Brenda Ward[2], Marylou Ingram[2], Brian David Ross[2, 3]
[1]Rudi Schulte Reseach Institute, Santa Barbara, California, USA; [2]Huntington Medical Research Institutes, Pasadena, California, USA; [3]California Institute of Technology, Pasadena, California, USA

The 'PASADENA' method of *in vivo* MR-imaging results in >10,000 fold signal increase and sub-second images but employs toxic 13C contrast agents. Compounds used as contrast agents were assessed for cytotoxicity. Dose-response curves were expressed as IC10/50. In vitro toxicity of the hydrogenation-catalyst, "Perfos", was entirely eliminated by passage through a membrane filter. A novel, water-soluble PASADENA reagent, sodium cis-fumarate showed cytotoxicity two orders of magnitude lower than 2-hydroxyethyl acrylate (HEA), precursor to the sole existing PASADENA reagent 2-hydroxyethyl propionate (HEP). 13C cis-fumarate provides a safer, metabolizable contrast agent for *in vivo* hyper-polarized 13C imaging and spectroscopy.

15:30 ***3508***. ***In Vivo* Imaging of Brain Endothelium Activation with a Novel Targeted Iron-Oxide Based Contrast Agent - LacNAc-CLIO**
Computer 31
Sander van Kasteren[1], Daniel Anthony[1], Sandra Campbell[1], Damineh Morsali[1], Ben Davis[1], Nicola Sibson[1]
[1]University of Oxford, Oxford, UK

One of the earliest events in an inflammatory response is the expression of specific adhesion molecules, e.g. selectins, on endothelial cells which enables the migration of leukocytes from the bloodstream into the surrounding tissue. We have previously demonstrated that a novel gadolinium-based contrast agent, Gd-DTPA-B(sLe^X)A, can be used to identify early endothelial activation in a cytokine-induced model of CNS inflammation. We are now developing new agents based on an amine-functionalised cross-linked iron oxide (CLIO) particle, and here demonstrate the application of *N*-acetyllactosamine-CLIO-particles (LacNAc-CLIO), which are a truncated variant of an sLe^X-derivatised CLIO-particle, for the detection of CNS inflammation *in vivo*.

15:30 ***3509***. **In Vitro Tumor Cell Targeting with the Folate Receptor Specific MR Contrast Agent P866**
Computer 30
Olaf Saborowski[1], Jan Stefan Bauer[1], Yanjun Fu[1], Claire Corot[2], Heike Elisabeth Daldrup-Link[1]
[1]University of California San Francisco, San Francisco, California, USA; [2]Guerbet Group, Paris, Roissy CDG, France

The vitamin folic acid has become a useful ligand for targeted cancer imaging and therapies, because it binds to a tumor associated antigen known as the folate receptor (FR). The purpose of this in vitro study was to evaluate the specific uptake of the new FR specific MR contrast agent P866 by varying tumor cell lines. P866 showed a specific uptake in FR positive breast cancer cells. The P866 uptake resulted in a significant T1-effect for all targeted tumor cells, and this effect was significantly higher at 1.5 T compared to 3T.

SMART/Selective Contrast Agents

Room 4A Wednesday 14:00 - 16:00

14:00 ***3510***. **MR Detection of Tumor Cells Labeled with USPIO Using DOPS Liposomes**
Computer 32
Vinod Kaimal[1, 2], Scott K. Holland, [1,2], Vincent J. Schmithorst[2], Xiaoyang Qi[2]
[1]University of Cincinnati, Cincinnati, Ohio, USA; [2]Cincinnati Children's Hospital Medical Center, Cincinnati, Ohio, USA

Human neuroblastoma cells were labeled *in vitro* with dextran coated USPIO nanoparticles delivered using DOPS liposomes. Increased USPIO content in the liposomes was achieved using a chemical linking method. The cells were detected using high resolution T2* weighted gradient echo MRI.

14:30 ***3511***. **Sensitivity and Detection Limits of MRI, CT and SPECT for Holmium-Loaded Microspheres**
Computer 32
Peter Roland Seevinck[1], Jan-Henry Seppenwoolde[1], Tim C. de Wit[1], Johannes Frank Nijsen[1], Freek J. Beekman[1], Alfred D. van het Schip[1], Chris J. Bakker[1]
[1]University Medical Center, Utrecht, Netherlands

The diagnostic potential of Holmium-loaded microspheres (HoMS), a promising therapeutic anticancer agent for internal radiation therapy, was studied using clinical scan protocols on MRI, CT and SPECT. By phantom experiments, the dependence on HoMS concentration of the performance of the modalities was investigated. Despite the low activated fraction of Ho-166, both sensitivity and low contrast detectability were highest for SPECT, followed by MRI and than CT. All three modalities proved to be capable to detect concentrations of HoMS in the therapeutic range. Task specific demands in realistic situations define which combination of imaging modalities is most suitable.

15:00 ***3512***. **RGD Targeted Poly(L-Glutamic Acid)-Cystamine-(Gd-DOTA) Conjugate for Detecting an Angiogenesis Biomarker α *v*β *3* Integrin with MR T1 Mapping**
Computer 32
Tianyi Ke[1], Xuli Wang[1], Eun-Kee Jeong[1], Dennis L. Parker[1], Yi Feng[1], Zheng-Rong Lu[1]
[1]University of Utah, Salt Lake City, Utah, USA

Specific and effective imaging of angiogenesis is critical for more accurate detection of angiogenic diseases and assessment of the effectiveness of antiangiogenic therapies. RGD targeted poly(glutamic acid)-cystamine-(Gd-DOTA) conjugate was prepared for detecting the angiogenesis biomarker ?v?3 integrin with MRI. The binding affinity of the targeted conjugate was evaluated by an in vitro method. The *in vivo* targeting efficacy of the targeted agent was investigated in an animal tumor model with conventional MRI and T1 mapping. The RGD containing conjugate was efficacious for *in vivo* targeting the ?v?3 integrin, which was effectively detected by quantitative MR T1 mapping.

15:30 ***3513***. **Aggregation of an Endogenous MR Reporter Protein to Increase Relaxivity**
Computer 32
Kevin M. Bennett[1], Erik M. Shapiro, [1,2], Alan P. Koretsky[1]
[1]National Institutes of Neurological Disease and Stroke, Bethesda, Maryland, USA; [2]New York University School of Medicine, New York, New York, USA

Ferritin has been proposed as a reporter protein for MRI. However, levels of ferritin expression levels in the brain must be relatively high to achieve practical relaxivity changes. In this work, ferritin aggregation was used to improve transverse relaxivity in vitro using cross-linking of ferritin with a succimidyl ester. The cross-linking was then undone by cleaving the spacer between ferritin cages. Because cross-linking can be achieved *in vivo*, it is proposed as an endogenous molecular reporter strategy that sensitizes the MR signal to R2 changes on the order of seconds or less.

Stem Cells/Cost Effectiveness

Room 4A Wednesday 14:00 - 16:00

14:00 ***3514***. **Magnetic Resonance Fe_3O_4-NH_3^+ Nanoparticles Coated with Anti-Epidermal Growth Factor Receptor Antibody for *In Vitro* Probing on Non-Small Cell Lung Cancer**
Computer 33
Wei-Ting Lin[1], Chia-Hao Su[2], Ang Yuan[3], Jyh-Horng Chen[2]
[1]Interdisciplinary MRI/MRS Lab, Institute of Biomedical Engineering, National Taiwan University, Taipei, Taiwan; [2]Interdisciplinary MRI/MRS Lab, Department of Electrical Engineering, National Taiwan University, Taipei, Taiwan; [3]Department of Internal Medicine, National Taiwan University Hospital, Taipei, Taiwan

Magnetic nanoparticles play a significant role in MR study because of its superparamagnetic characteristic. In the previous study, the aqueous Fe_3O_4-NH_3^+ nanoparticles show excellent negative contrast in MR images for *in vitro* and *in vivo* experiments due to reducing proton relaxation times of T1 and T2, and also been convinced its biocompatibility, hemocompatibility, and low cytotoxicity at *in vitro* tests. Magnetic nanoparticles MR probe has already been a sharp weapon for tumor detection. In this study, we choose non-small cell lung cancer as our probing target. EGFR in NSCLC is overexpression and correlated with a high metastatic rate, poor tumor differentiation, and a high rate of tumor growth.We use Fe_3O_4-NH_3^+ nanoparticles coated with antibodies to target the extracellular domain of epidermal growth factor receptor in non-small cell lung cancer cells and monocyte. *In vitro* experiments, it shows a significant targeting difference between NSCLC and monocyte.

14:30 ***3515***. **Multimodal Imaging Probes for Vascular Endothelial Growth Factor Receptor**
Computer 33
Hye-Won Kang[1], In-Kap Ko[2]
[1]University of Massachusetts Medical School, Worcester, Massachusetts, USA; [2]Dartmouth College, Lebanon, New Hampshire, USA

Detecting molecules expressed on activated macrophage is a challenging task relevant for atherosclerosis imaging. To detect specific MR signal sensitivity at early stage of atherosclerosis, novel imaging probes were developed for potential targeting macrophages in atherosclerotic plaques. We focused on a nanosized carrier of paramagnetic contrast agents, specific immuno-biomarker with potential multi-modality applications. Biocompatible nano-sized micelles were synthesized using a combination of a lipophilic Gd-DTPA, near-infrared fluorochrome and anti-VEGFR antibody. These probes were highly expressed on activated J744A.1 cells with liposaccharide and the expression was detectible by both MRI and optical imaging. Our research suggests that new multi-modal imaging probes could be further applied for visualization of atherosclerotic plaques *in vivo*.

15:00 ***3516***. **Feasibility of Multi-Platform, Multi-Site Clinical Trials of Proton MRS**
Computer 33
Leonard Petrus[1], Dar-Yeong Chen[2], Brian David Ross[3]
[1]Hill Radiology, Pasadena, California, USA; [2]Toshiba America Medical Systems, Irvine, California, USA; [3]Huntington Medical Research Institutes, Pasadena, California, USA

A major impediment to the acceptance and reimbursement of clinical MRS for diagnosis is the absence of clinical and societal efficacy, using the Thornbury and Fryback criteria of Evidence Based Medicine (EBM). Multi-site trials on 100's of patients are essential. A minimum requirement for multi-site MRS trials is comparability of results achieved across the many different MRS platforms available. As part of the effort to standardize MRS procedures we establish that two major vendors (Toshiba: Vantage 1.5T) and GE Healthcare: LX 1.5T) generate statistically indistinguishable MRS results in normal and in common brain pathologies.

15:30 ***3517***. **Dependence of Concentration and Field Strength on MRI Properties of Polyvinyl Alcohol Cryogel**
Computer 33
Kyle James Wilson[1], Tim Orr[1], Neil Gelman[1], Gerald Moran[2], Gord Campbell[3], Robert Terry Thompson[1]
[1]Department of Medical Biophysics, University of Western Ontario, London, Ontario, Canada; [2]McMaster University, Hamilton, Ontario, Canada; [3]Integrated Manufacturing Technologies Institute, NRC, London, Ontario, Canada

It is not always practical or ethical to use human subjects for optimization and testing of MR pulse sequences. Thus, a tissue-mimicking phantom would be useful. Polyvinyl Alcohol Cryogel (PVA-C) has shown promise as a tissue mimicking material. By combining PVA and deionized water, heating for 2 hours and then going through a freeze thaw cycle PVA-C is produced. PVA-C was produced at several concentrations (3-30%) and a range of T1 (700-1860ms) and T2 (70-460ms) values were obtained. Using this data to match T1 and T2 properties of different tissues will allow the development of various realistic phantoms.

Molecular Imaging/Stem Cells

Room 4A Wednesday 14:00 - 16:00

14:00 ***3518***. **Comparison of MR Lymphangiography with a G6 Macromolecular Contrast Agent Obtained at 1.5T and 3.0T Systems**
Computer 34
Yukihiro Hama[1], Marcelino Bernardo[2], Yoshinori Koyama[1], Celeste A. Regino[1], Martin W. Brechbiel[1], Peter L. Choyke[1], Hisataka Kobayashi[1]
[1]NCI/NIH, Bethesda, Maryland, USA; [2]SAIC-Frederick, NCI/NIH, Bethesda, Maryland, USA

Since most of macro-molecular contrast agents show decreased R1 and increased R2 relaxivities in a high magnetic field, T1 contrast induced by macromolecular contrast agents can be compromised on 3T compared with 1.5T. We consecutively performed MR lymphangiograpy in mice with a G6 dendrimer-based nano-sized contrast agent both on 3T and 1.5T to evaluate the effect of high magnetic field on a macromolecular contrast agent. The lymph node-to-fat contrast was compromised with both 3D-fastSPGR and 3D-FIESTA-C on the 3T system compared with the 1.5T system probably because of decreased R1 relaxivity of G6 agent and possible T2 and T2* effects.

14:30 ***3519***. **Ultrastructural Characteristics of Feridex Endocytosis by Human Peripheral Mononuclear Cells and Mesenchymal Stem Cells**
Computer 34
John S. Pratt[1], Anna Moore[1], Alma Gregory Sorensen[1]
[1]Massachusetts General Hospital, Charlestown, Massachusetts, USA

In this study, unique findings regarding the agglomeration state of internalized Feridex were observed in both PBMCs and HMSCs using transmission electron microscopy. In both PBMC monocytes and HMSCs, linear bands of sequestered Feridex nanoparticles were observed at the cell surface. The high concentrations of internalized bands of Feridex ranging from 0.5 - 2 microns suggest that the magnetic properties of Feridex in intracellular compartments are vastly different from ferumoxides suspended in solution.

15:00 ***3520***. **Targeting of Membrane Type1-Matrix Metalloproteinase (MT1-MMP) by Using Ultrasmall Superparamagnetic Iron Oxide (USPIO) Particles to Hepatocellular Carcinoma Cells *In Vivo***
Computer 34
Yongmin Chang[1, 2], Bo-Hyung Park[2], Jae-Chang Jung[3], Young-Mi Lee[3], Ji-ae Park[2], Hui-Jin Song[2], Seung-Tae Woo[2], Joo-Hyun Kim[2]
[1]Kyungpook National University Hospital, Daegu, Jung-gu, Republic of Korea; [2]Kyungpook National University, Daegu, Jung-gu, Republic of Korea; [3]Kyungpook National University, Daegu, Buk-gu, Republic of Korea

Membrane-type 1 matrix metalloproteinase (MT1-MMP) has been implicated in various physiological and pathological processes. Especially, MT1-MMP is highly expressed in different cancers, and overexpression promotes migration, invasion and metastasis of cancer cells in vitro as well as *in vivo*. In this study, we investigate tumor specificity of MT1-MMP at molecular biology level and examine the possibility of MT1-MMP as a tumor marker using conjugation of streptavidinylated USPIO and biotinylated monoclonal antibody (mAb) MT1-MMP in MRI.

15:30 ***3521***. **Comparison of SPIO and USPIO for In Vitro Labelling of Human Monocytes with Respect to MR Detection and Cellular Activation Status**
Computer 34
Raoul David Oude Engberink[1], Susanne M. van der Pol[2], Ed Dopp[2], Helga E. de Vries[2], Erwin L. Blezer[1]
[1]University Medical Center Utrecht, Utrecht, Netherlands; [2]VU Medical Center, Amsterdam, Netherlands

MR imaging of target cells requires an efficient labelling method and the intracellular presence of contrast agents must not interfere with cellular function. To this end we studied in vitro labelling of primary human monocytes with iron oxides comparing SPIO Endorem with USPIO Sinerem. After labeling, cell viability, migratory capacity and cytokine profile were tested. Incubation of monocytes with Endorem (1mg Fe/ml) was optimal with respect to MR signal and unaltered cell viabilty/activity. In contrast, incubation with the smaller sized Sinerem, did not result in significant MR signal. In vitro labelling of primary monocytes with Endorem shows great potential for *in vivo* tracking of monocytes.

RF Coil Decoupling

Room 4A Thursday 13:30 - 15:30

13:30 ***3522***. **LC Decoupling Circuit for Arbitrarily Placed Coils**
Computer 1
Bing Wu[1], Peng Qu[1], Yong Pang[1], Gary X. Shen[1]
[1]The University of Hong Kong, Hong Kong, People's Republic of China

The conventional decoupling technique of coil overlap leads to stringent constrains on how the elements are placed. This fixed overlap may not always be appropriate for parallel spatial encoding. Some alternative decoupling methods are to insert capacitors or LC circuit networks between coils to minimize their mutual coupling. To clearly illustrate the LC decoupling circuit, the technique by inserting decoupling-capacitors (Cd) or decoupling-inductors (Ld) for isolation arbitrarily placed coils was studied. Also we compare the decoupling performance by using Cd and Ld at variable magnetic fields.

13:30 ***3523***. **The Effect of Over/Underlap of Surface Coil Elements on AP Direction Acceleration**
Computer 2
George Randy Duensing[1], Sathya Vijayakumar[1], Scott B. King[2]
[1]Invivo Corporation, Gainesville, Florida, USA; [2]National Research Council of Canada, Winnipeg, Manitoba, Canada

In this work, the effect of the overlap and underlap of surface coil elements on the acceleration in the AP direction was studied. Simulated B-fields and E-fields of loops with different extents of overlap/underlap were processed using the SENSE algorithm to understand the g-factor and SNR performance.

14:00 ***3524***. **An Eight-Channel, Non-Overlapping Phased Array Coil with Capacitive Decoupling for High Resolution MRSI and Parallel DWI of the Brain at 3.0 T**
Computer 2
Cornelius von Morze[1, 2], James Tropp[3], Duan Xu[1, 2], Christopher P. Hess[1], Pratik Mukherjee[1, 2], Kostas Karpodinis[1], Lucas Carvajal[1], Daniel B. Vigneron[1, 2]
[1]UCSF, San Francisco, California, USA; [2]UCSF/UCB Joint Graduate Group in Bioengineering, San Francisco, California, USA; [3]GE Healthcare, Fremont, California, USA

We describe an eight-channel, non-overlapping phased array coil designed for high resolution MRSI and parallel DWI of the brain at 3.0 T. The non-overlapping design is desirable for its high peripheral SNR and reduction in noise in parallel imaging. The combination of a capacitive bridging technique and the standard system preamps eliminate the crosstalk due to the mutual inductance inherent to the design. The expected SNR improvements are validated *in vivo* for the aforementioned applications through imaging studies conducted on five volunteers.

14:00 ***3525***. **Decoupling Method for High Frequency Strip-Line Probes Gives Truly Independent Elements**
Computer 1
Alexa Jones[1], Paul Glover[1], Arthur Magill[1]
[1]University of Nottingham, Nottingham, UK

We are presenting a method for decoupling strip line elements in RF volume coils for high field (7T) Parallel imaging. Previous transceiver coils have relied on the strip line elements containing most of the magnetic field within the strip line by reducing the strip/ground plate separation, or by including a material with high dielectric properties. This solution limits coupling by restricting the B1 penetration. Using experimental and finite element modelling we have shown that strip line elements can be completely decoupled without detuning the elements by placing an inter-element decoupling strip in an optimum position, without restricting RF penetration.

14:30 ***3526***. **Developments in Active Rung Design for Parallel Transmit Coils**
Computer 1
WonJe Lee[1], Krishna N. Kurpad[1], Eddy B. Boskamp[2], Thomas M. Grist[1]
[1]University of Wisconsin at Madison, Madison, Wisconsin, USA; [2]GE Healthcare, Waukesha, Wisconsin, USA

Decoupling between neighboring current elements is essential in the design of parallel transmit arrays. In this work, the effect of various impedance matching schemes on the active rung design was investigated in terms of the correlation between the driven current amplitude and the induced current suppression. Experimental results showed a trade-off between the two parameters in the single ended active rung and suggest a need to explore multiple MOSFET configurations.

14:30 ***3527***. **A Non-Overlapping Phased Array Coil for Parallel Imaging of the Hip at 3.0 T**
Computer 2
Cornelius von Morze[1, 2], Suchandrima Banerjee[1, 2], James Tropp[3], Kostas Karpodinis[1], Lucas Carvajal[1], Daniel B. Vigneron[1, 2], Sharmila Majumdar[1, 2]
[1]UCSF, San Francisco, California, USA; [2]UCSF/UCB Joint Graduate Group in Bioengineering, San Francisco, California, USA; [3]GE Healthcare, Fremont, California, USA

We introduce an eight channel phased array coil for high resolution parallel imaging of the hip, facilitated by the high SNR provided by high field strength (3.0 T) and an optimized FIESTA-c sequence. A non-overlapping design consisting of small receiver loops was selected based on the good parallel imaging performance predicted by numerical parallel reconstruction simulations. Capacitive meshes and system preamplifiers provided the necessary decoupling. We demonstrate the capability for rate-3 acceleration for hip imaging, and predict that accelerations up to 4-5 along a single direction should be possible for this coil.

15:00 *3528*. **Array with Multiple Loops for Vertical Field System**
Computer 2
Bing Wu[1], *Juan Wei*[1], *Gary X. Shen*[1]
[1]The University of Hong Kong, Hong Kong, People's Republic of China

For vertical field MRI applications, the structure of the loop array is quite different from those in a horizontal-magnetic-field system. The conventional decoupling techniques are hard to be extended to vertical MRI system. Therefore, the loops for vertical MRI system are quite difficult to decouple. So far the coil array with up to two loop coils have been investigated on open low-field MRI, the array with more than three loop coils is sparsely reported. In this study, we present a decoupling technique using inductors for vertical-field loop coils. A four-channel array consisted of 3 loops and a saddle coil has been built for human knee at 0.5T vertical MRI system.

15:00 *3529*. **Self-Decoupled Asymmetric Saddle Coil Array for SENSE Imaging**
Computer 1
Pei Hsuon Chan[1]
[1]GE Healthcare, Aurora, Ohio, USA

The quest for lower g-factor and higher reduction factor for a SENSE-optimized coil array often results in a trade-off of lower intrinsic SNR for higher SENSE SNR due to the non-overlap nature of the adjacent coils. In this paper, we present an asymmetric saddle (Asaddle) coil array with each of its Asaddle coils having one wing significantly smaller than the other and being able to decouple from its adjacent Asaddle coils without overlap. The Asaddle coil array not only can preserve the intrinsic SNR as a conventional array but also can provide significantly lower g-factor than the conventional array.

Electromagnetic Analysis and Simulations

Room 4A Thursday 13:30 - 15:30

13:30 *3530*. **A Single-Shot Optimization to Achieve Homogenous 3-D Whole-Body Excitation at 3 Tesla**
Computer 3
Roney Abraham[1], *Tamer S. Ibrahim*[1]
[1]University of Oklahoma, Norman, Oklahoma, USA

In this work, we implement a single optimized phased-array excitation scheme on a 3 Tesla whole-body RF coil to maximize the B1+ (transmit) field uniformity throughout a large abdominal 3-D portion of a human body load. We compare the uniformity of the B1+ field (in the entire 3D abdominal volume encapsulated within the coil structure) resulting from the one unique optimized phased-array excitation to the uniformity resulting from standard quadrature excitation and conclude that the proposed optimized excitation scheme holds much potential in producing highly homogeneous images of large abdominal volumes at 3 Tesla.

13:30 *3531*. **A Comprehensive Look at the Electromagnetics of High Field MRI**
Computer 4
Tamer S. Ibrahim[1], *Chad Mitchell*[2], *Roney Abraham*[1], *Petra Schmalbrock*[3]
[1]University of Oklahoma, Norman, Oklahoma, USA; [2]Uniformed Services University of the Health Sciences, Bethesda, Maryland, USA; [3]Ohio State University, Columbus, Ohio, USA

In this work, numerical and experimental studies of the TEM resonator at ultra high field (UHF) are performed using the finite difference time domain method at 340 MHz and using an 8 Tesla MRI system. An in-depth look at the homogeneity of the excite field as well as the local- and global- polarization of the electromagnetic waves inside the head-coil's cavity is provided for the coil's standard mode of operation when it is empty and loaded. Based on the numerical and experimental results, which are in excellent agreement, an electromagnetic characterization of the meaning of "loading" RF head-coils during UHF experiments is provided.

13:30 *3532*. **Evaluation of Equivalent Circuit Analysis of Double-Tuned RF Coils by Method of Moment**
Computer 5
Xiaomin Zhu[1], *Xiaohua Jiang*[1]
[1]Tsinghua University, Beijing, People's Republic of China

A generalized equivalent circuit model is presented for analysis of both single-tuned and double-tuned radio-frequency (RF) coils for Magnetic Resonance Imaging (MRI) systems. Based on the basic principle of ECM, a generalized equivalent circuit model with $N_1 \times N_2$ meshes is proposed to describe RF coils with complicated configurations in more details, even including the ending modes in the model of birdcage coils. Experimental results show that compared with the numerical analysis by method of moment (MOM), the equivalent circuit method (ECM) appears to be acceptably accurate for the fields not exceeding 3 Tesla.

14:00 *3533*. **Comparison of Three Applied Volume Coils at 7T**
Computer 5
Chunsheng Wang[1], *Jing Yuan*[1], *Peng Qu*[1], *Gary X. Shen*[1]
[1]The University of Hong Kong, Hong Kong, People's Republic of China

The B_1^+field homogeneity, SAR and SNR of shielded birdcage, TEM and microstrip volume coils are compared at 7T in this work by finite difference time domain (FDTD) method. It seems that the birdcage coil has the best unload B_1^+ homogeneity but the TEM has the best loaded B_1^+ homogeneity. On the other hand, the microstrip coil seems better in terms of SAR and average SNR than other two coils at ultra high field MRI.

14:00 ***3534***. **Noise Correlation Matrix for Multiple RF Coils Derived from First Principles of Statistical Physics**
Computer 4
Yi Wang[1], Ryan Brown[1], Pascal Spincemaille[1], Ray Lee[2]
[1]Weill Medical College of Cornell University, New York, New York, USA; [2]New York University, New York, New York, USA

First principles of statistical physics (Boltzmann's distribution and the fluctuation-dissipation theorem) are used to analyze the current fluctuations in a system of linear circuits. Accordingly, the correlation matrices of total noise and of noise at a given frequency are formulated as functions of circuit properties. These noise correlation matrices are connected consistently through the Kramers-Kronig relation. Experiments using a network analyzer and an MR scanner confirmed the predictions from statistical physics.

14:00 ***3535***. **Impact of Coil Diameter and Number of Coil Elements on B1 Destructive Interferences with Stripline Coil Arrays at 7 Tesla**
Computer 3
Pierre-Francois Van de Moortele[1], Can Akgun[1], Carl Snyder[1], Lance DelaBarre[1], Gregor Adriany[1], Tommy Vaughan[1], Kamil Ugurbil[1]
[1]University of Minnesota, Minneapolis, Minnesota, USA

It has been shown that destructive B1+ interferences between complex B1+ vectors result in "bright center, dark periphery" patterns in axial images of the brain with coil arrays at 7T. We investigate, with 1, 8 and 16 stripline coil arrays how B1+ profile is impacted by altering a) distance between coil elements and sample and b) number of coil elements. We demonstrate, at 7 Tesla, that larger diameter coil arrays, and more numerous coil elements result in much smoother patterns of B1 destructive interferences in the periphery of a phantom (even though those destructive interferences still have large amplitude).

14:30 ***3536***. **A Method Based on Infrared Techniques for Experimentally Verifying RF Coil Full-Wave Modeling**
Computer 3
Tamer S. Ibrahim[1]
[1]University of Oklahoma, Norman, Oklahoma, USA

In this work, a method of examining a coil's RF field distribution over any unoccupied region of the coil is presented. This technique is based on the use of infrared sensing. The proposed method was implemented and tested on a high field RF volume coil operating at 340 MHz. Very good agreement was achieved between the infrared measurements and numerical data obtained utilizing the 3D finite difference time domain method. The results demonstrate that the proposed technique is practical, robust, and efficient for making accurate measurements of the electric field distributions in loaded and unloaded MRI RF coils.

14:30 ***3537***. **A Flexible Flow Model for Gradient Coil Design for the Purpose of Clinical MRI**
Computer 4
Viktor Vegh[1], Huawei Zhao[1], David M. Doddrell[1], Graham J. Galloway[1], Ian M. Brereton[1]
[1]University of Queensland, Brisbane, Queensland, Australia

In this work a gradient coil design technique is outlined that uses a numerical wave equation solution methodology along with an optimization technique to obtain the propagating wave fronts through an inhomogeneous porous media, which essentially determines the winding patterns of the different gradient coils in the appropriate coordinate system. It is shown that such an approach is flexible and can be used to design quality gradient coils with large imaging regions. The quality of the gradient coils is measured through a number of key variables, and these are compared to the Siemens Sonata gradient coil set.

14:30 ***3538***. **A Novel Method of Measuring the B1 Field Components of an Unsegmented Linear Coil**
Computer 5
Jan Weis[1], Peter Andris[2], Ivan Frollo[2], Håkan Ahlström[1]
[1]Uppsala University Hospital, Uppsala, Sweden, Sweden; [2]Institute of Measurement Science, Bratislava, Slovakia, Slovakia

Inhomogeneity of the radio frequency field B1 leads to intensity variations in MR images and to spatial dependence of spectral line amplitudes. Our study introduces a simple method of measuring the B1 field components of an unsegmented linear coil. The B1 field distribution is replaced by the static magnetic field caused by DC current flowing through the coil. The technique involves rotating the coil 90-degrees so that measured B1 component is aligned with B0 and measuring the shift of resonance frequency using a spectroscopic imaging sequence. The method is designed for the coils operating up to 20 MHz.

15:00 ***3539***. **Optimization of a Multi-Channel Transmit, Quadrature Receive Birdcage Coil**
Computer 5
Chunsheng Wang[1], Gary X. Shen[1]
[1]The University of Hong Kong, Hong Kong, People's Republic of China

A multi-channel transmit, quadrature receive birdcage coil are optimized by using singular value decomposition (SVD) method. Compared with conventional transceiver quadrature birdcage, this coil has dramatically improved B_1^+ filed homogeneity and relative SNR, with slight penalty of increased average SAR.

15:00 ***3540***. **On Minimization of Net Lorentz Force on Gradient Coil**
Computer 4
Qin Liu[1]
[1]GE Healthcare, Waukesha, Wisconsin, USA

A theoretical study of the net Lorentz force on the gradient coil is presented. Analytical expressions for the Lorentz force on a cylindrical x gradient coil by a cylindrical magnet were derived. Conditions for the minimization of the net Lorentz force were obtained. It was found that the optimization of the magnetic shielding for a shielded gradient coil set would naturally lead to the minimization of the net Lorentz force exerted on it by the magnet.

15:00 *3541*. **Numerical Considerations for Calculating SAR, Power Deposition, and B1 Field in Ultra High Field Whole-Body Full-Wave Simulations**
Computer 3
Roney Abraham[1], Tamer S. Ibrahim[1]
[1]University of Oklahoma, Norman, Oklahoma, USA

For MRI RF volume coil simulations, we analyze the effect of the size of the loaded body model on the calculations of power deposition, specific absorption rate (SAR), and B1+ field distribution. This is accomplished by loading a TEM resonator with five body models that are identical except for the number of cells each contain in the direction orthogonal to the axial plane. We calculate various parameters relevant to the aforementioned issues in the five cases to determine the approximate cutoff size required to achieve accurate results.

A Focus on MR Engineering

Room 4A Thursday 13:30 - 15:30

13:30 *3542*. **Digital Wireless Transmission for MRI**
Computer 6
Juan Wei[1], Bing Wu[1], Jing Yuan[1], Gary X. Shen[1]
[1]The University of Hong Kong, Hong Kong, People's Republic of China

Analog wireless transmission has been reported for MRI application recently to reduce the interference among the array cables. In this work, we have designed and implemented a new transmission system based on digital wireless technique of WLAN IEEE 802.11b. Frequency Division Multiplexing (FDM) method also is proposed to expand possible more array channels for future MR applications.

13:30 *3543*. **RF Coil Interface for Translational Research on Clinical MR Systems**
Computer 7
David Michael Peterson[1], Robert J. Fitzsimmons[1], Jeffrey R. Fitzsimmons[1]
[1]University of Florida, Gainesville, Florida, USA

MR research on animal systems has been well quantified. However, with the mission to move toward translational research, it is imperative to have appropriate coil setups for animals on clinical systems, so that similar experiments can be performed on humans with the same pulse sequences. Therefore, there is a specific need for an RF interface that allows the researcher to effectively design coils that will work with animal and human models. To aid this design an RF interface was built to design, build and verify RF coil geometries.

13:30 *3544*. **Time Constant Sensitivity of Eddy Current Characterizing Pulse Sequence**
Computer 8
Daniel B. Ennis[1], Marcus T. Alley[1], Brian A. Hargreaves[1], Norbert J. Pelc[1]
[1]Stanford University, Palo Alto, California, USA

Bloch simulation was used to demonstrate that a pulse sequence designed to quantify the MR systems reponse to gradient induced eddy currents is sensitive to short time constant eddy currents.

13:30 *3545*. **Registration Technique of Endoscopic Scintillator on MRI Using Optical Position Sensor for Early Detection of Gastrointestinal Stromal Cancer**
Computer 9
Hiroshi Sato[1], Hiroshi Watabe[1], Noboru Teramoto[1], Kazuhiro Koshino[1], Akihide Yamamoto[1], Jun-ichiro Enmi[1], Takao Goto[2], Yuji Iwadate[2], Tetsuji Tsukamoto[2], Hidehiro Iida[1]
[1]National Cardiovascular Center Research Institute, Suita, Osaka, Japan; [2]GE Yokogawa Medical Systems, Hino, Tokyo, Japan

FDG-PET is widely used for clinical screening, but its sensitivity for small cancer is insufficient. Previously reported combined PET-MR approaches have same limitations and require massive developments. We propose a cost-effective registration technique of a high sensitive endoscopic scintillation probe on MR images using optical sensor and infrared reflective marker attached on subjects. Dummy probe with point signal source was intubated into the esophagus of a swine and also into a simulated phantom to evaluate accuracy and repeatability of actual locations for MRI and PET fusion imaging. Maximum S.D. of 4mm indicated proposed approach should be feasible.

14:00 *3546*. **Feasibility and Challenges of Dual-Modality Pinhole SPECT / MRI Systems**
Computer 9
James William Kristian Odegaard[1], Parisa Jamali[1], Hao Peng[1], William Bradfield Handler[1], Timothy J. Scholl[1], Blaine Alexander Chronik[1]
[1]University of Western Ontario, London, Ontario, Canada

The benefits and challenges in creating a system combining pinhole SPECT and MRI are explored. By using a field-cycled MRI system operating at low readout field strength, a number of concerns, such as susceptibility-related field perturbations, are alleviated. Though mutually combative, these two imaging modalities are very useful for a combination of structural and functional imaging. The system we are designing is geared towards dual-modality imaging of small animals.

14:00 ***3547***. **Structural-Acoustic Analysis, Identification and Control of a 4T MRI Scanner**
Computer 8
Mingfeng Li[1], Teik C. Lim[1], Christy K. Holland[1], Suzanne E. Boyce[1], Jing-Huei Lee[1]
[1]University of Cincinnati, Cincinnati, Ohio, USA

A series of experiments were conducted at 4T to identify the major acoustic noise sources and their contributions to sound pressure levels. Quantification of a set of generalized impulse response functions (IRFs) can be applied to synthesize the actual operating response for any given gradient excitations. Temporal and spectral analysis of the data reveals the existence of harmonics, non-harmonics and broadband characteristics, which can be accurately synthesized through the IRFs. These should be useful in guiding the development of a suitable active noise control (ANC) system. The preliminary ANC simulation demonstrates that at least 20 dB noise reductions are achievable.

14:00 ***3548***. **The Accuracy of Transmitter Gain Optimization at 7T**
Computer 7
Douglas A C Kelley[1]
[1]GE Healthcare, San Francisco, California, USA

The determination of optimal transmitter gain at 7T is complicated by standing wave effects in lossy dielectrics, resulting in poor contrast in many studies. This study demonstrates, however, that the errors are small at low flip angles.

14:00 ***3549***. **A Helmet Coil with Reduced Out-Of-Volume Sensitivity for Human Brain Imaging at 7 T**
Computer 6
Wolfgang Driesel[1], Christopher John Wiggins[2], Graham Charles Wiggins[2], Lawrence L. Wald[2], Toralf Mildner[1], Harald E. Möller[1, 3]
[1]Max Planck Institute for Human Cognitive and Brain Sciences, Leipzig, Germany; [2]Massachusetts General Hospital, Charlestown, Massachusetts, USA; [3]University Hospital Münster, Münster, Germany

At high fields (e.g. 7T), RF head coils can have significant sensitivity in the neck and shoulder region, which creates aliasing artefacts when used with a head gradient coil. We present an RF coil design for 7T that achieves good SNR in the brain while minimising signal from the head and neck regions.

14:30 ***3550***. **Comparison of Four Different Birdcage Type Coils**
Computer 6
Wanzhan Liu[1], Christopher M. Collins[2], Michael B. Smith[2]
[1]University of Minnesota, Minneapolis, Minnesota, USA; [2]Penn State College of Medicine, Hershey, Pennsylvania, USA

Four birdcage-type coils are built to experimentally examine the effects of the end-ring/shield configuration on SNR in a head at 125 MHz. The configurations include a) a conventional shield (conventional), b) a shield with annular extensions to closely shield the end-rings (surrounding shield), c) a shield with annular extensions connected to the rungs (solid connection), and d) a shield with strips of copper tape connected to the rungs(thin wire connection). In a human head, the conventional and the surrounding shield configuration result in higher SNR than the solid connection configuration, which has a SNR higher than the thin wire configuration.

14:30 ***3551***. **Parallel Transmit with a Single Exciter and a Multi-Channel Controller**
Computer 7
Mika W. Vogel[1], Dirk Lange[1], Patrick Gross[1], Florian Wiesinger[1], Wolfgang Loew[1], Hartmut Koenig[1], Rolf Schulte[1], Ronald D. Watkins[2]
[1]GE Global Research, Munich, Bayern, Germany; [2]GE Global Research, Niskayuna, New York, USA

The use of multiple RF excitation coils, each connected to an exciter board with microsecond control over the individual waveforms has been proposed as a solution in the context of TransmitSENSE. This requires substantial changes to a clinical MR scanner, and addition of expensive hardware. Here we assess the potential of scalar amplitude and phase control in a simplified setup, using a single RF exciter in combination with a Multi-Channel Controller (MCC) to split and adjust the excitation waveform. The concept was tested using four transmit coils, arranged in a planar configuration to assess performance with very strong B1 variation.

14:30 ***3552***. **Sound Level Measurements in MR Scanners: A Comparative Study**
Computer 8
Krzysztof R. Gorny[1], Diana M. Lanners[1], Matthew A. Bernstein[1]
[1]Mayo Clinic, Rochester, Minnesota, USA

We report results of high precision sound level measurements carried out at our site in clinical GE 1.5T and 3T, short and long bore MR scanners. The measurements were performed for typical “quiet” (i.e., conventional spin echo), and the “loud” FIESTA pulse sequences. We observe an unexpectedly large noise increase on 3T relative to 1.5T short bore scanners. In contrast, small noise level changes were observed in 3 and 1.5T long bore scanners. We speculate that the significant noise increase in 3T short bore scanners may be caused by less efficient vacuum isolation on that system.

14:30 ***3553***. **A Novel Quantitative Method for Measuring the Torque Acting on Cardiovascular Implantable Devices in NMR Scanners**
Computer 9
Rossella Canese[1], Giuseppe D'Avenio[1], Franca Podo[1], Mauro Grigioni[1]
[1]Istituto Superiore di Sanità, Rome, Italy

A new method for the quantitative evaluation of the torque by which a cardiovascular device tends to be aligned along the static magnetic field is here proposed and validated. The method is based on a torsion balance, which enables accurate measurements of small forces. In our experimental set-up the method allowed measurement of torques as small as 10-5 N*m and is therefore applicable to small devices such as stents.

15:00 ***3554***. **Clinical Safety of Magnetic Resonance Imaging on Recently Placed Coronary Artery Stents**
Computer 9
Donna S. Lesniak[1], Brian A. Seeck[1], Joseph A. Craft[1], George S. Chrysant[1], Robert J. Gropler[1], Pamela K. Woodard[1]
[1]Washington University School of Medicine, St. Louis, Missouri, USA

Because of uncertainty regarding safety, some manufacturers of coronary artery stents have recommended waiting a period of 8 weeks after stent placement before magnetic resonance imaging (MRI). Of 211 patients imaged by MRI within 2 weeks after either bare metal or drug eluting stent placement, none had serious adverse cardiac events. Fifteen of the 211 patients were imaged within 24 hrs of stent placement. It appears safe and feasible to perform MRI early after coronary stent placement using a wide variety of stents.

15:00 ***3555***. **MR Imaging of Mouse Heart *In Vivo* at 4.7T Using the Homebuilt RF Probehead and Gradient System**
Computer 8
Sylwia Heinze-Paluchowska[1], Tomasz Skorka[1], Andrzej Jasinski[1, 2], Roman Wiertek[1], Piotr Skora[1], Jacek Kiczek[1], Pawel Borowiec[1]
[1]H. Niewodniczanski Institute of Nuclear Physics PAS, Krakow, Poland; [2]Department of Dielectric and Biophysics, Pedagogical University, Krakow, Poland

In this report, results of Magnetic Resonance Imaging (MRI) of cardiac function in mice *in vivo*, using the homebuilt gradient coils and specialized RF probehead are demonstrated. An unshielded gradient system with inner diameter of 60 mm was designed and constructed for the 4,7T/310 magnet with MARAN DRX console (Resonance Instruments). Dedicated probehead, constructed to fit the gradient system, consists of the RF birdcage coil and the animal handling system. The homebuilt probehead and gradient system enabled us to achieve good quality cardiac MR images of wild-type mice (FVB) and transgenic mice with heart failure (Tgαq*44). Morphological and functional changes can be studied non-invasively applying these hardware components.

15:00 ***3556***. **Slant-Slice Imaging with an Inhomogeneous Field**
Computer 7
Charles L. Epstein[1], Jeremy F. Magland[2]
[1]University of Pennsylvania, Philadelphia, Pennsylvania, USA; [2]Hospital of the University of PA, Philadelphia, Pennsylvania, USA

Slant-slice imaging is an acquisition technique for use with a strongly inhomogeneous background field, which has the SAR and time efficiency of spin-warp imaging. It allows for considerable latitude in the design of specialized MR imaging systems and produces images with high SNR and resolution.

15:00 ***3557***. **Comparison of a TEM Head Coil with an 8 Channel Head Array Coil at 3 Tesla**
Computer 6
Ralf Mekle[1, 2], Rolf Gruetter[1, 2]
[1]Ecole Polytechnique Federale de Lausanne, Lausanne, Switzerland; [2]University of Lausanne, Lausanne, Switzerland

Dedicated hardware, such as transverse electromagnetic (TEM) volume radiofrequency (rf)-coils, have been developed to exploit the inherent advantage of an enhanced signal-to-noise ratio (SNR) at higher fields. Such TEM coils have been successfully utilized at B0¡Ý4T. Since 3T MRI scanners have emerged as valuable clinical and research tools, the goal of this study was to evaluate a TEM head coil in comparison with an 8 channel head array coil on a 3T system. In conclusion, phantom and human head data indicate favorable SNR values for the 8 channel coil at the cost of increased image intensity variations and rf-power deposition.

Dynamic Contrast Enhancement Perfusion: Methodology

Room 4A Thursday 13:30 - 15:30

13:30 ***3558***. **Evaluation and Minimization of the Difference in MR Perfusion Maps Among Softwares**
Computer 10
Kohsuke Kudo[1], Makoto Sasaki[2], Kei Yamada[3], Satoshi Terae[1], Khin Khin Tha[1], Yuri Yoshida[1], Kazuo Miyasaka[1]
[1]Hokkaido University Graduate School of Medicine, Sapporo, Hokkaido, Japan; [2]Iwate Medical University, Morioka, Iwate, Japan; [3]Kyoto Prefectural University of Medicine, Kyoto, Japan

In MR perfusion, different analysis software produces different perfusion maps. The purposes of this study are, (1) to evaluate the difference of perfusion maps analyzed by different softwares, and (2) to assess the methods to minimize those variations.Source data of MR perfusion were postprocessed by 15 different ways by using 8 commercially available softwares. Visual assessment was performed with and without automated color-scale adjustments (ACSA).The appearance of perfusion maps significantly differed between the types of analysis softwares. The differences became smaller with ACSA.The ACSA can be used to minimize the variations of MR perfusion maps.

13:30 ***3559***. **T1-Related Errors on Dynamic Susceptibility Contrast Perfusion MR Measurements**
Computer 11
Matthias J.P. van Osch[1], Evert-jan Vonken[2], Fernando Calamante[3]
[1]Leiden University Medical Center, Leiden, Netherlands; [2]University Medical Center, Utrecht, Netherlands; [3]Brain Research Institute, Melbourne, Australia

Bolus-tracking perfusion MRI monitors changes in the transverse relaxation rate during the first pass of a bolus of contrast agent. Most studies employ a single echo sequence to maximize coverage. However, the underlying assumption of single echo sequences is that T1-effects of the contrast agent are negligible. By means of simulations and *in vivo* measurements we show that T1-effects can lead to serious overestimation of CBF and CBV. A sufficiently low flip angle should therefore be used for single echo sequences.

14:00 ***3560***. **Detection of Dispersion from Bolus-Tracking MRI Improves Cerebral Blood Flow Quantification: A Simulation Study**
Computer 11
Francesca Zanderigo[1], Alessandra Bertoldo[1], Gianluigi Pillonetto[1], Claudio Cobelli[1]
[1]University of Padova, Padova, Italy

Currently, CBF is estimated from the maximum of the dispersed deconvolved curve R'(t) instead from the "true" R(t) at time t=0. This leads to underestimation of CBF. Thus, a deconvolution method able to detect the non dispersed component R(t) is needed. A nonlinear stochastic regularization method (NSR) has been proposed to account for smoothness and non-negativity of R'(t). Here, the NSR ability in discriminating between non dispersed and dispersed components of the effective residue function is shown on simulated data. NSR shows to detect the degree of bias affecting CBF estimates thus improving CBF quantification.

14:00 ***3561***. **Reproducibility of Dynamic Susceptibility Contrast MR with Standard and Block-Circulant Deconvolution Matrix**
Computer 10
Wei-Ting Zhang[1], Caterina Mainero[1], Ona Wu[1], A. Gregory Sorensen[1]
[1]Massachusetts General Hospital, Charlestown, Massachusetts, USA

Repetitive dynamic susceptibility contrast magnetic resonance imaging within hours is both potentially useful and feasible. The primary aim of this study is to determine the test-retest reproducibility of relative cerebral blood volume (rCBV) and flow (rCBF) acquired with the interval of half an hour. The secondary aim is to investigate the effect of different matrixes used for singular-value decomposition (SVD) with a single arterial input function (AIF) (sSVD) or a block-circulant matrix of AIF (oSVD), on the reproducibility of rCBF. Results showed good reproducibility of rCBV. The reproducibility of rCBF from oSVD was better than that from sSVD.

14:30 ***3562***. **Automatic Selection of Arterial Input Function on Dynamic Contrast-Enhanced MRI Images: Comparison of Different Methods**
Computer 10
Denis Peruzzo[1], Alessandra Bertoldo[1], Francesca Zanderigo[1], Claudio Cobelli[1]
[1]University of Padova, Padova, Italy

Cerebral blood flow (CBF), blood volume (CBV), and mean transit time (MTT) can be estimated from DSC-MRI with gadolinium images by deconvolution given the arterial input function, AIF(t), and tissue concentration, C(t). Often AIF is found by manually inspecting tracer concentration maps which is very time consuming and operator dependent. In our study we compare 5 methods of AIF automatic selection, including a novel one. The performance of the methods are tested on a stenosis data set. To analyze the impact of partial volume presence a simulation study was also performed.

14:30 ***3563***. **Improved Deconvolution of Bolus Tracking Data Using Wavelet Thresholding**
Computer 11
Lisa Willats[1], Alan Connelly[2], Fernando Calamante[2]
[1]University College London, London, UK; [2]Brain Research Institute, Melbourne, Victoria, Australia

Combining the techniques of maximum-likelihood expectation-maximisation and wavelet thresholding for the deconvolution of bolus tracking data is shown to be an effective method for accurately characterising the distorted shape of the tissue residue function recovered using a global arterial input function. In particular, when delay and/or dispersion of the bolus occur in the feeding vessels, the proposed methodology enables the resulting distortion to be quantified and distinguished from a true perfusion abnormality. A dispersion index can be defined and used in conjunction with delay and perfusion estimations to improve the interpretation of perfusion data.

15:00 ***3564***. **Estimation of Cerebral Perfusion Parameters Using Bayesian Probability Theory**
Computer 11
Joshua S. Shimony[1], John J. Lee[1], Colin P. Derdeyn[1], William J. Powers[1], Thomas O. Videen[1], Joanne Markham[1], Abraham Z. Snyder[1], G Larry Bretthorst[1]
[1]Washington University Medical School, St. Louis, Missouri, USA

Dynamic susceptibility contrast MR methods have several drawbacks that limit its accuracy. These drawbacks include using a single arterial input function (AIF) for the entire brain and the need to perform a numerical deconvolution on the logarithm of noisy data. We implemented a tissue perfusion model that has several advantages over standard methods, including the estimation of a separate AIF for each pixel and estimation of additional perfusion parameters of clinical interest. The model parameters were estimated using Bayesian probability theory in a group of patients with hemodynamic impairment and compare favorably with PET and standard DSC perfusion estimates.

15:00 ***3565***. **Minimizing Slice Profile Effects in T1W Perfusion Imaging**
Computer 10
Irene K. Mikkelsen[1], Göran Starck[1, 2], Karam Sidaros[3], Maria Widmark[2], Maria Ljungberg[2]
[1]Göteborg University, Göteborg, Sweden; [2]Sahlgrenska University Hospital, Göteborg, Sweden; [3]Hvidovre Hospital, Hvidovre, Denmark

T1 perfusion measurements during bolus passage may be performed using saturation-recovery TurboFLASH with a small flip angle, $_{\alpha}$. The repeated use of $_{\alpha}$ with imperfect slice profile generates imperfect signal profiles. Using the sequence in baseline T1-measurement provides estimates of T1, and also M0 and $_{\alpha}$, which are fixed during the boluspassage. We show that fixating $_{\alpha}$ on the nominal value during parameter estimation may cause severe underestimation of T1 leading to erroneous perfusion estimates. If, however, $_{\alpha}$ is allowed to vary, T1 is accurately estimated. Based on this, a procedure for estimating T1 at realistic noise levels is proposed.

Myocardial Perfusion

Room 4A Thursday 13:30 - 15:30

13:30 *3566*. **In-Flow Effects in Determination of Arterial Input Functions**
Computer 15
Leon Axel[1], Daniel Kim[1]
[1]NYU Medical Center, New York, New York, USA

Studies of dynamic contrast enhancement of tissue in MRI require accurate measurement of the arterial input function, in order to correct for the effects of contrast delivery to the tissue. If images of a large artery or the left ventricle (LV) cavity are included in the image, the blood signal can be used to approximate the arterial signal supplying the tissue. However, motion of the blood through the imaging plane may affect the signal. We sought to investigate the magnitude of this effect in the context of a representative application, studies of myocardial perfusion with first-pass contrast enhancement.

13:30 *3567*. **Quantitative Assessment of Subendocardial Perfusion Abnormality in Hypertrophic Cardiomyopathy: Correlation with Myocardial Scar**
Computer 13
Kakuya Kitagawa[1], Tairo Kurita[1], Masaki Ishida[1], Katsuya Onishi[1], Takeshi Nakano[1], Kan Takeda[1], Hajime Sakuma[1]
[1]Mie University School of Medicine, Tsu, Japan

Transmural distribution of myocardial blood flow was determined in nine patients with HCM by using Patlak plot analysis of stress-rest perfusion MRI. In HCM patients, the endo/epi flow ratio significantly decreased to 0.92 +/- 0.14 during stress compared to resting state (0.99 +/- 0.13, $p<0.001$). In segments exhibiting delayed hyperenhancement, the endo/epi ratio was reduced in comparison with the segments without delayed hyperenhancement both in the resting state and during vasodilator stress, indicating close relationship between scar formation and subendocardial perfusion abnormality in patients with HCM.

13:30 *3568*. **A Dual-Bolus Imaging Method for the Estimation of Myocardial Distribution Volume**
Computer 14
Nathan Pack[1], Edward VR DiBella[1], Christopher J. McGann[1]
[1]University of Utah, Salt Lake City, Utah, USA

Contrast enhanced myocardial perfusion imaging allows for the quantitation of regional blood flow and distribution volume, Vd. The magnitude and spatial distribution of Vd may provide additional information to complement delayed enhancement imaging that can assist clinicians in tracking the progress and impacting the therapeutic strategies of various disease states. Here we present a novel dual-bolus imaging method that may provide a means to more accurately quantitate the late kinetics of tissue enhancement and regional Vd in the myocardium.

13:30 *3569*. **Rotational Long Axis Stress Myocardial Perfusion Imaging**
Computer 12
Yi Wang[1, 2], Saadi A. Siddiqi[1], Sunil T. Mathew[1], Nora Ngai, PhD[1], Olakunle Akinboboye[1, 2], Nathaniel Reichek[1, 2]
[1]St. Francis Hospital, Roslyn, New York, USA; [2]State University of New York, Stony Brook, New York, USA

We evaluated myocardial perfusion using a rotational long axis view in clinical patients initially referred for pharmacokinetic stress testing and nuclear imaging. The results showed a clear distinction in perfusion reserve between normal and abnormal segments determined by SPECT, with mean flow reserve in normal regions twice as large compared to the regions with defects. Thus, we believe that rotational long axis myocardial perfusion imaging is not only technically easy to implement and provides improved apical and basal delineation, but also yields comparable stress perfusion results as conventional short axis imaging.

14:00 *3570*. **Significance of Myocardial Ischemia in Hypertrophic Cardiomyopathy: Relation of Regional Perfusion Abnormalities to Left Ventricular Hypertrophy Assessed by Magnetic Resonance Imaging**
Computer 12
Carsten Rickers[1], Barry Maron[2], Michael Jerosch-Herold[3], Chris Hart[1], Norbert Wilke[4], Andrej Zenovich[2], Prasad Panse[4], Hans Heiner Kramer[1]
[1]University Hospital Kiel, Kiel, Germany; [2]Mpls. Heart Institute and Foundation, Minneapolis, Minnesota, USA; [3]University of Minneapolis, Portland, Oregon, USA; [4]University of Florida, Jacksonville, Florida, USA

We hypothesized magnetic resonance perfusion imaging would allow more precise quantitative assessment of regional blood flow distribution in Hypertrophic Cardiomyopathy (HCM). Using first pass MR perfusion imaging we found that the cardiomyopathic process in HCM is most marked in hypertrophied regions of the LV. MR perfusion abnormalities were most prominent in hypertrophied compared to non-hypertrophied areas. Adverse consequences of HCM (i.e., sudden death and progressive symptoms), often associated with marked LVH may be due, in part, to myocardial ischemia.

14:00 *3571*. **Cardiac BOLD Imaging with Cine 2D-Balanced SSFP**
Computer 14

Rohan Dharmakumar[1], Richard Tang[1], Kathleen Harris[1], Andrew C. Larson[1], Yiucho Chung[2], Graham A. Wright[3], Debiao Li[1]
[1]Northwestern University, Chicago, Illinois, USA; [2]Siemens Medical Solutions, Chicago, Illinois, USA; [3]University of Toronto, Toronto, Ontario, Canada

Poor image quality, long scan times, and inadequate oxygen sensitivity have been the limitation for cardiac BOLD imaging. Based on recent observations of oxygen-sensitive contrast with steady-state methods, this work examines the potential of 2D-balanced SSFP imaging for detecting myocardial oxygen deficits due to coronary stenosis in an animal model. The results show that high quality temporally resolved images showing BOLD contrast may be obtained within the framework of cine imaging. The cine imaging allows for simultaneous detection of wall motion abnormalities and flow/oxygen deficit regions within a single breath hold.

14:00 *3572*. **Myocardial Blood Flow Can Be Quantified in Sub-Gram Regions of Interest in Clinical MR First Pass Perfusion Studies**
Computer 13

Li-yueh Hsu[1], Federico E. Mordini[1], Daniel Mirota[2], Gareth Funka-Lea[2], Andrew E. Arai[1]
[1]National Institutes of Health, Bethesda, Maryland, USA; [2]Siemens Corporation Research, Princeton, New Jersey, USA

The minimal region of interest in first pass MR perfusion for myocardial blood flow quantification was studied in normal subjects. The optimal size spatial filter for homogeneous flow estimation was determined and applied to quantify rest and stress perfusion and to demonstrate perfusion defects in ischemic patients.

14:00 *3573*. **Fast Mapping of Myocardial Blood Flow: A New Algorithm with Intravascular MR First-Pass Imaging**
Computer 15

Thomas Goldstein[1], Haosen Zheng[1], Michael Jerosch-Herold[2], Robert Gropler[1], Jie Zheng[1]
[1]Washington University in St. Louis, St. Louis, Missouri, USA; [2]Oregon Health and Science University, Portland, Oregon, USA

Current first-pass perfusion quantification algorithms are relatively slow and noise-sensitive, making them impractical for clinical applications. The purpose of this study was to develop a method for fast mapping of myocardial perfusioj, aiming to potential clinical use. The algorithm developed is a linear deconvolution alogirthm. The algorithm was compared to the previously validated B-Splines algorithm with both simulations, and *in vivo* analysis on normal dogs. It was found that both algorithms perform similarly in term of accuracy. However, the novel algorithm can perform perfusion mapping in less than 3 seconds, as opposed to several minutes for the B-Spline algorithm.

14:30 *3574*. **High-Resolution Imaging of Myocardial Perfusion**
Computer 15

Dan Xu[1], Yijen Lin Wu[2], T. Kevin Hitchens[2], Chien Ho[2], Zhi-Pei Liang[1]
[1]University of Illinois at Urbana-Champaign, Urbana, Illinois, USA; [2]Pittsburgh NMR Center for Biomedical Research, Carnegie Mellon University, Pittsburgh, Pennsylvania, USA

Dynamic MRI of myocardial perfusion is a useful tool for assessing physiological conditions of the cardiac tissues (e.g., tissue rejection following heart transplantation). However, because of cardiac motion and the limited data acquisition speed of the existing MRI techniques, it has been very difficult to acquire dynamic images in very high spatiotemporal resolution. To address this problem, this paper presents a new generalized-series model-based imaging method. This method decouples the acquisition of the steady-state component of the desired dynamic object function from the transient component, and uses the steady-state component to build the basis functions to constrain the reconstruction of the object function, making it possible to obtain high spatial and temporal resolution simultaneously. The proposed method has been validated using experimental data, which produce excellent results with only 8 dynamic encodings per temporal frame.

14:30 *3575*. **Efficacy of Pattern Recognition of Early Detect and Late Enhancement in Cardiomyopathy**
Computer 13

Yasuyuki Kobayashi[1], Takanori Yasu[2], Keisuke Tanno[2], Osamu Tanaka[2], Yukihisa Ogawa[1], Naohiko Osada[1], Yasuo Nakajima[1], Kenji Yodo[3]
[1]St Marianna University School of Medicine, Kawasaki-shi, Kanagawa, Japan; [2]Omiya Medical Center, Jichi Medical School, Saitama-shi, Saitama, Japan; [3]Toshiba Medical Systems Co., Saitama-shi, Saitama, Japan

Rest and pharmacological stressed perfusion MRI is a very useful tool to assess the intramural microvascular circulation. Furthermore late enhancement is useful to assess the fibrosis, edema, granulation tissue and inflammation of cardiac muscle in cardiomyopathies. Pattern recognition of perfusion MRI and late enhancement is considered to be very useful for diagnosis and follow-up of cardiomyopathy, and predicting the prognosis.

14:30 *3576*. **Myocardial Perfusion Recovery After Percutaneous Coronary Intervention Using First-Pass Contrast-Enhanced MRI**
Computer 14

Mao-Yuan Marine Su[1], Kai-Chien Yang[2], Chao-Chung Wu[2], Woeichyn Chu[1], Wen-Yih Isaac Tseng[3]
[1]Institute of Biomedical Engerening, National Yang-Ming University, Taipei, Taiwan; [2]Department of Internal Medicine, National Taiwan University Hospital, Taipei, Taiwan; [3]Center for Optoelectronic Biomedicine, National Taiwan University College of Medicine, Taipei, Taiwan

Percutaneous coronary intervention (PCI) for patients with chronic stable angina aims at restoration of blood flow in the stenotic coronary arteries. Traditional coronary angiography and nuclear tracer imaging have serious limitations for judging the magnitude and timing of recovered myocardial perfusion after PCI. In this study, we performed first-pass contrast-enhanced myocardial perfusion MRI at 3T MR system to determine the timing and magnitude of perfusion recovery by evaluating the change in myocardial perfusion reserve (MPR) index in a serial follow-up. We found that MPR index in ischemic segments was restored as early as 24 hours after successful PCI. The improvement of myocardial perfusion lasted at least for one week and tended to persist at one month following PCI.

14:30 *3577*. **Accuracy of Assuming Uniform Temporal Sampling in the Analysis of Cardiac Perfusion MRI Datasets**
Computer 12

Edward Victor Rebok DiBella[1], Eugene G. Kholmovski[1]
[1]University of Utah, Salt Lake City, Utah, USA

Myocardial perfusion studies acquire images of multiple slices in each heart beat. It is typically assumed that the bolus tracking images are uniformly sampled in time. This is often not an accurate assumption, due to missed triggers and heart rate changes. This work shows that up to ~20% change in regional perfusion estimates from a two compartment model or the upslope analysis method is possible from assuming uniform temporal sampling. Larger errors were found with an adenosine stress pre-bolus study. Temporal sampling information should be included in the processing of dynamic contrast enhanced cardiac perfusion studies.

15:00 *3578*. **T2* Measurement During First-Pass Contrast Enhanced Cardiac Perfusion Imaging**
Computer 12

Peter Kellman[1], Anthony H. Aletras[1], Li-yueh Hsu[1], Elliot R. McVeigh[1], Andrew E. Arai[1]
[1]NHLBI/NIH, Bethesda, Maryland, USA

First-pass contrast enhanced cardiac perfusion imaging will experience T2* effects at peak concentrations of contrast agent. Reduction in signal intensity of the LV blood due to T2* losses may effect estimates of the arterial input function used for quantitative perfusion measurement. Imaging artifacts may also result from T2* losses as well as off-resonance due to the bolus susceptibility.The purpose of this study was to directly measure T2* and B0-field maps in the LV cavity during first-pass perfusion. For single dose (0.1 mmol/kg), the LV blood pool T2* had mean value 9 ms (N=10) at peak enhancement.

15:00 *3579*. **Myocardial First Pass Persusion Imaging with Integrated Parallel Acquisition (IPAT): A Comparison of TrueFISP and TurboFlash Sequences**
Computer 14

Daniel Theisen[1], Bernd Wintersperger[1], Armin Huber[1], Olaf Dietrich[1], Maximilian F. Reiser[1], Stefan O. Schoenberg[1]
[1]University of Munich, Munich, Bavaria, Germany

In the present study, SR-TrueFISP and TurboFLASH sequences with factor 2 partially parallel acquisition (iPAT) using GRAPPA algorithm for image reconstruction were compared with the established, non-accelerated TurboFLASH technique to assess the value of iPAT in myocardial first-pass perfusion imaging. Sequences were compared by means of artifacts, signal-to-noise ratios (SNR), contrast-to-noise ratios (CNR)and semiquantitative perfusion parameters. Saturation recovery TrueFISP technique provided higher signal-to-noise/contrast-to noise ratios and improved image quality in comparison with the spoiled GRE technique. The most reliable semiquantitative perfusion parameters “maximum upslope” and “peak signal intensity” showed significantly highest values for TrueFISP images. In addition, the combination with parallel acquisition techniques lead to a significant decrease in number of susceptibilty artifacts in comparison with the established TurboFLASH sequence.

15:00 *3580*. **Automated Respiratory Motion Correction Approach for Pixel-Based Analysis of First-Pass MR Myocardial Perfusion Studies**
Computer 13

Henrik Pedersen[1], Kay Nehrke[2], Steffen Ringgaard[1], Won Yong Kim[1]
[1]Aarhus University Hospital, Aarhus, Denmark; [2]Philips Research Laboratories, Hamburg, Germany

A novel and fully automated approach for pixel-by-pixel correction of respiratory motion in first-pass MR myocardial perfusion studies is presented. The proposed method uses additionally acquired navigator echoes to divide the image frames into a number of distinct motion states. This, in combination with knowledge of the signal in neighbouring pixels, can be used to remove the respiratory signal contaminations in each pixel. Preliminary results based on examination if eight patients suggest that this technique reduces respiratory motion to a negligible level. This may significantly facilitate pixel-based analysis of first-pass MR myocardial perfusion studies in a clinical setting.

15:00 ***3581***. **Pixel-Based and Model-Free Quantification of Myocardial Perfusion Using First-Pass Dynamic Contrast-Enhanced MRI**
Computer 15
Hsi-Yu Yu[1], Mao-Yuan Marine Su[1], Su-Chun Huang[1], Bai-Chin Lee[1], Yen-Wen Wu[1], Wen-Yih Issac Tseng[1]
[1]National Taiwan University Hospital, Taipei, Taiwan

A model-free approach was proposed in this study, in which myocardial perfusion can be directly quantified based on the initial rise of the signal-time curves in the left ventricular cavity and myocardium. Our approach lies on an assumption that in the early period of the first-pass perfusion Gd-DTPA only flows into but not flows out from the regional myocardium. Therefore, the signal intensity in the regional myocardium M in this period is determined by the signal intensity change of the left ventricle as AIF, denoting V, delayed time Td related to transport of Gd-DTPA from the left ventricle to myocardium, and perfusion rate £\.

Cardiac Wall Motion: Human

Room 4A Thursday 13:30 - 15:30

13:30 ***3582***. **Improved Spatial Resolution and Reduction of Artifacts in Strain-Maps with Phase-Unwrap HARP**
Computer 19
Andrea Kaspar Rutz[1], Salome Ryf[1], Sebastian Kozerke[1], Peter Boesiger[1]
[1]University and ETH, Zurich, Switzerland

Myocardial strain-maps obtained with HARP are often corrupted by visible artifacts, mainly caused by a low CNR of the tagged images. Improving CNR and/or spatial resolution at the cost of temporal resolution is limited for HARP due to wraps in the HARP-phase. In this work, an improved method for peak-combining HARP-images is introduced, yielding half the number of phase-wraps compared to conventional peak-combination HARP. Furthermore, unwrapping HARP-images allows the analysis of datasets with large motion between consecutive time frames. Thus, high quality strain-maps with increased spatial resolution can be generated.

13:30 ***3583***. **Improved Efficiency in Cine DENSE Using Low Resolution Phase Reference Images**
Computer 16

Xiaodong Zhong[1], Bruce S. Spottiswoode[2], Frederick H. Epstein[1]
[1]University of Virginia, Charlottesville, Virginia, USA; [2]University of Cape Town, Cape Town, Western Cape, South Africa

The purpose of this study was to investigate whether low resolution phase reference images could be acquired to reduce the total scan time without significantly increasing errors in measured myocardial displacement and strain in DENSE MRI. A cine DENSE sequence was modified to acquire phase reference images with different spatial resolutions. Data showed that displacement and strain errors increase as the phase reference image resolution decreases. Using no phase reference data lead to the largest errors in displacement and strain. Replacing the full resolution reference scan with an appropriate low resolution scan decreased acquisition time by 20% with minimal errors.

13:30 ***3584***. **Coil Combination Method for Peak-Combination HARP**
Computer 17
Andrea Kaspar Rutz[1], Salome Ryf[1], Gérard Crelier[1], Sebastian Kozerke[1], Peter Boesiger[1]
[1]University and ETH, Zurich, Switzerland

An efficient algorithm for combining signals from multiple coil elements using peak-combination HARP is presented. Phase contributions originating from the different spatial locations of the coil elements are compensated for without requiring an additional coil calibration scan. Using a 32-element phased array coil, myocardial tracking results of the proposed combination method were in good agreement with the results of the combination method by Roemer. Improved tracking results were achieved compared to the analysis with one coil element and the RMS-combination of all coil elements. HARP-analysis can be clearly improved applying the proposed coil combination method without requiring a reference scan.

13:30 ***3585***. **The Optimisation and Validation of Cardiac Mass and Function at 3 Tesla**
Computer 18
Damian J. Tyler[1], Lucy E. Hudsmith[1], Steffen E. Petersen[1], Jane M. Francis[1], Stefan Neubauer[1], Kieran Clarke[1], Matthew D. Robson[1]
[1]University of Oxford, Oxford, UK

The functional exam is the cornerstone of every cardiac MR protocol. The emergence of clinical 3T scanners provides the exciting possibility to further develop techniques which suffer from low SNR at 1.5 T (eg cardiac spectroscopy) but for 3T to be a useful cardiac tool, it must be robustly capable of performing the functional exam. We have optimised and validated the measurement of cardiac function and mass at 3T by careful comparison with routine protocols at 1.5T. We have demonstrated that although no better than 1.5T, the 3T functional exam can be used for the accurate assessment of cardiac function.

13:30 *3586*. **Real Time Ejection Fraction Monitoring with M-Mode MRI**
Computer 20

Corinna Maier[1, 2], Christine H. Lorenz[3]
[1]Siemens Corporate Research, Princeton, New Jersey, USA; [2]University of Heidelberg, Heidelberg, Germany; [3]Siemens Corporate Research, Baltimore, Maryland, USA

Monitoring the ECG for ischemic changes during dobutamine stress testing or MR-guided interventions is not possible in the MR environment due to the magnetohydrodynamic effect. However, wall motion and global cardiac function can be assessed in real time by MR and interleaved with other types of MR acquisitions. We converted real time MR to an m-mode (motion mode) representation analogous to echocardiography to allow (a) a simple continuous display of cardiac function and (b) simplify real time segmentation and automatic extraction of LV ejection fraction. Preliminary results show that the method may be useful as a monitoring method for CMR.

14:00 *3587*. **Efficiency and Reproducibility of the Right Ventricular Long Axis MR Imaging Plane for the Evaluation of the Right Ventricle**
Computer 20

Joseph Rhett Whitnah[1], Lee M. Mitsumori[1], Jeffrey Harold Maki[1, 2], Kelley Robert Branch[1], Edward A. Gill, [13], Karen Kathleen Stout, [14]
[1]University of Washington, Seattle, Washington, USA; [2]Puget Sound VAHCS, Seattle, Washington, USA; [3]Harborview Medical Center, Seattle, Washington, USA; [4]Children's Hospital & Regional Medical Center, Seattle, Washington, USA

Cardiac MRI is time consuming, requiring multiple scans and significant post-processing time. Right ventriclular (RV) functional analysis using true transaxial planes has been shown to be more reproducible than short axis planes (SAX) in normal individuals, and may require fewer slices and less post-processing time. An oblique right horizontal long axis plane (RHLA) paralleling the inferior wall of the RV optimizes imaging of the RV apex. Functional RV analysis using the RHLA can be completed with fewer slices and in less post-processing time with better reproducibility than the SAX. Surveillance of RV function may be optimized by using these data.

14:00 *3588*. **Imaging 2-D Myocardial Motion and Chamber Blood Flow Simultaneously with EGGS SPAMM & SPAMM (Encoded Gradients for Gauging Speed in Sinusoidal SPAMM and Co-Sinusoidal SPAMM Acquisitions)**
Computer 18

Smita Sampath[1], Elliot R. McVeigh[1]
[1]Laboratory of Cardiac Energetics, Division of Intramural Research, NHLBI, NIH, DHHS, Bethesda, Maryland, USA

It has been shown that myocardial motion quantification using HARP or DENSE in conjunction with CSPAMM techniques reduce artifacts in the strain maps due to the suppression of interference from the recovering dc peak. In this abstract, we present a new method—velocity-encoded CSPAMM — that encodes 2-D blood velocities simultaneously during CSPAMM acquisitions, providing multi-phase measurements of chamber blood flow velocity patterns in addition to myocardial displacements.

14:00 *3589*. **Realtime Imaging of Regional Function of the Heart Using Fast-SENC at 3 Tesla**
Computer 17

Li Pan[1], Ahmed S. Fahmy[2], Robert G. Weiss[1], Amy Spooner[1], Matthias Stuber[1], Nael F. Osman[1]
[1]Johns Hopkins School of Medicine, Baltimore, Maryland, USA; [2]Johns Hopkins University, Baltimore, Maryland, USA

Fast-SENC imaging has been proposed as a technique that can image regional function of the heart in a single heart beat. In this study, the feasibility to use fast-SENC imaging at 3T has been demonstrated. A fast-SENC imaging sequence with interleaved spiral acquisitions has been implemented on a 3T system to measure the regional function of the heart. The images were acquired both in normal subjects, and post-infarction patients with identified dysfunctional region compared with delayed enhancement imaging. Fast-SENC shows its potential to dynamically detect the onset of ischemia during dobutamine stress test, or image the patients with cardiac arrhythmia.

14:00 *3590*. **Left Ventricular Function Assessment in a Single Breath-Hold Using a 2D FIESTA with Steady-State Preparation**
Computer 16

Patrice Hervo[1], Jean Pierre P. Laissy[2], Jean Michel M. Serfaty[2], Ramin Bazeli[2], Sylvie Chillon[2], Elisabeth Schouman-Claeys[2], Glenn Slavin[3]
[1]GE Healthcare Technology, Buc, France; [2]University Hospital of Bichat, Paris, France; [3]GE Healthcare Technology, Baltimore, Maryland, USA

We developed and validated a method to assess in a single breath-hold the left ventricular function, using a 2D FIESTA-SP pulse sequence (gated FIESTA with Steady State preparation) with scan time efficiency to nearly 100%. Image quality and measurements of EF, SV, LVEDV, LVESV, LVMassED and LVMassES were compared with those derived from a series of separate breath-hold single-section conventional FIESTA acquisitions.

14:00 *3591*. **Single Breath Hold 3D Cine Cardiac Imaging Using Spiral SSFP**
Computer 19

Bryan Kressler[1], [2], Pascal Spincemaille[2], Thanh D. Nguyen[2], Martin R. Prince[2], Yi Wang, [1,2]
[1]Cornell University, Ithaca, New York, USA; [2]Weill Medical College of Cornell University, New York, New York, USA

A single breath hold 3D cine imaging sequence is developed to allow visualization of the ventricular volume. The sequence is based on balanced SSFP to provide good blood myocardium contrast without use of an injected contrast agent, and a spiral trajectory to allow fast data acquisition. A sliding window reconstruction is employed to produce images from 16 cardiac phases, allowing visualization of the ventricles throughout the cardiac cycle.

14:30 *3592*. **Cine Viability Cardiac MRI Using Contrast-Enhanced 3D Balanced Steady-State Free Precession Imaging**
Computer 19

Yasuo Amano[1], Tatsuo Kumazaki[1]
[1]Nippon Medical School, Tokyo, Japan

The purpose of this study was to demonstrate the possibility of contrast-enhanced 3D cine balanced steady-state free precession (SSFP) imaging as cine viability cardiac MRI that exhibit the myocardial wall motion and viability in the same imaging sections simultaneously. Patients underwent 2D cine balanced SSFP, pre- and postcontrast 3D cine balanced SSFP, and delayed contrast-enhanced 2D MRI. Contrast-enhanced 3D cine balanced SSFP imaging provided high SNR and CNR of the damaged myocardium, as well as accurate estimations of the ejection fraction and myocardial mass. Contrast-enhanced 3D cine balanced SSFP imaging may be useful for cine viability images of the heart.

14:30 *3593*. **Rapid Assessment of Cardiac Function Using 2D CINE SSFP in Conjunction with K-T BLAST and K-T SENSE**
Computer 16

Thoralf Niendorf[1], Marcus Katoh[1], Harald Peter Kuehl[1], Helena Grawe[1], Jürgen Bunke[2], Marc Kouwenhoven[2], Rolf W. Guenther[1]
[1]University of Aachen, University Hospital, Aachen, Germany; [2]Philips Medical Systems, Best, Netherlands

The feasibility of accelerated 2D CINE SSFP imaging for global LV function assessment is demonstrated. High accelerations are used to support the extended slice coverage. To avoid prohibitive noise amplification due to coil sensitivity encoding, spatio-temporal correlations are exploited using the k-t BLAST and k-t SENSE approach. The accelerated 2D imaging paradigm presented here holds the promise to extend the capabilities of clinical breath-hold CINE imaging from a single slice to multiple slices per breath-hold though myocardial border sharpness remains a challenge as very large accelerations are explored.

14:30 *3594*. **Diffuse and Heterogenous Systolic Dysfunction in Hypertrophic Cardiomyopathy with Myocardial Tagging**
Computer 17

Byoung Wook Choi[1], [2], Susan B. Yeon[1], Warren J. Manning[1], Idith Haber[3], Martin Maron[4]
[1]Beth Israel Deaconess Hospital, Boston, Massachusetts, USA; [2]Yonsei University College of Medicine, Seoul, Republic of Korea; [3]Children's Hospital, Boston, Massachusetts, USA; [4]Tufts-New England Medical Center, Boston, Massachusetts, USA

Hypertrophic cardiomyopathy (HCM) is characterized by myocardial hypertrophy, which may be associated with myocyte disarray and fibrosis. These structural abnormalities may cause ventricular systolic and diastolic dysfunction. However, the relationship between structural and functional abnormalities has not yet been well defined. In a cohort of subjects with HCM, we studied the extent and pattern of left ventricular systolic impairment as assessed by tagged CMR in relation to wall thickness and delayed enhancement. Systolic dysfunction in HCM is regionally heterogeneous and involves hypertrophied as well as nonhypertrophied segments. MPS is positively correlated with EDWT. The epicardial layer shows dysfunction more frequently than mid or endocardial layer. Tagged MRI may be helpful for detection of transmural and nontransmural dysfunction in nonhypertrophied and hypertrophied segments.Delayed enhancement was frequently found in septal junction regions and in segments with marked hypertrophy, which showed more systolic dysfunction.

14:30 *3595*. **Experiment and Simulation-Based Optimization of Blood-Myocardium CNR in Cardiac SSFP Imaging**
Computer 18

Kyunghyun Sung[1], Yoonchul Kim[1], Gerald M. Pohost[1], Krishna S. Nayak[1]
[1]University of Southern California, Los Angeles, California, USA

Cardiac SSFP provides high SNR and excellent blood-myocardium contrast. Prescribed flip-angles are chosen based on simulations that assume on-resonance, achieving the prescribed flip-angles, and ideal slice profiles. We measure SNR and CNR in 3T cardiac SSFP scans using product sequences. SNR and CNR measurements are compared with simulations that include measured off-resonance, measured flip angle variations, and actual slice profiles. The greatest discrepancy between detailed and conventional simulation was the use of actual flip angles. We recommend using a localized pre-scan to calibrate the flip angles in regions of interest so that the prescribed flip angle can be set appropriately.

14:30 *3596*. **Constrictive Pericarditis: Assessement of Diastolic Function by Velocity Encoded Flow Measurements and by Assessement of Septal Motion**
Computer 20

Kerstin Ulrike Bauner[1], Armin Huber[1], Henrik Michaely[1], Stefan O. Schoenberg[1], Maximilian F. Reiser[1]
[1]University of Munich-Grosshadern Hospitals, Munich, Germany

In addition to morphological assessment transmitral and transtricuspid velocity encoded flow measurements and evaluation of septal motion were perfomed to analyze diastolic function in constrictive pericarditis. 23 patients with constrictive pericarditis were examined with MRI. 10 healthy subjects served as controls. The amplitude of E and A wave and the ratio of the amplitudes of the E and A-Wave were calculated. To evaluate septal flattening, septal motion was assessed on short-axis cine MR images and the ratio between the largest and shortest diameter of the left ventricle was calculated to express septal flattening.

15:00 *3597*. **Increasing the SNR and Data Acquisition Efficiency of Displacement-Encoded MRI by the Use of TrueFisp Imaging at 3T and TSENSE Parallel Imaging**
Computer 20

Daniel Kim[1], Vinay M. Pai[1], KellyAnne McGorty[1], Peter Kellman[2]
[1]New York University, New York, USA; [2]National Institutes of Health, Bethesda, Maryland, USA

Displacement-encoded MRI is a promising method for quantifying 2D intramyocardial function with relatively high spatial resolution and without the need for explicit tag detection. However, it yields low signal-to-noise ratio (SNR) due to the 50% signal loss inherent to stimulated echoes and due to the SNR limitation imposed by breath-hold acquisition. The subtraction of sub-sampled phase images recovers a portion of the signal loss and eliminates the need for acquiring phase reference images. The purpose of this study was to improve the SNR by the use of TrueFisp imaging at 3T and data acquisition efficiency by the use of TSENSE.

15:00 *3598*. **Detection of Myocardial Wall Motion Abnormalities Using Real-Time TSENSE**
Computer 18

Orlando P. Simonetti[1], Stephen C. Cook[1], Ghalib Bello[1], Subha V. Raman[1]
[1]The Ohio State University, Columbus, Ohio, USA

The study compares real-time TSENSE SSFP cine imaging with conventional segmented breath-hold SSFP cine. Imaging was performed on 27 subjects referred for clinical CMR for a variety of indications. Real-time imaging without breath-hold or ECG synchronization, and segmented, retrospectively gated, breath-hold SSFP were performed at identical slice positions. Myocardial wall motion was scored for real-time and breath-hold images using a 17-segment model. Scores for all 17 segments showed very good agreement (median $\kappa = 0.75$) between the two techniques. Real-time cine with TSENSE can be used effectively to evaluate regional wall motion.

15:00 *3599*. **32-Channel Real-Time MRI at ~50 Frames Per Sec for Irregular Heart Motion**
Computer 17

Christopher J. Hardy[1], Robert D. Darrow[1], Luca Marinelli[1], Pelin Aksit[2], Thomas K.F. Foo[1], Robert G. Weiss[3], Paul A. Bottomley[3]
[1]GE Global Research, Niskayuna, New York, USA; [2]GE Healthcare, Waukesha, Wisconsin, USA; [3]Johns Hopkins University, Baltimore, Maryland, USA

In patients with irregular heart rhythm, scan acceleration techniques that use prior knowledge can produce suboptimal results. We have developed a 32-channel real-time cardiac MRI system and used it to image the heart at up to 48 effective frames per second during exercise stress testing, without the use of training data sets. This technique may also be useful for assessing beat-to-beat variations in contraction that differ dramatically in normal and stunned myocardium from that in non-viable myocardium after irregular heart beats.

15:00 *3600*. **Cine DENSE MRI of Left Ventricular Dyssynchrony: Development and Initial Clinical Experience**
Computer 16

Rajan A. Patel[1], Xiaodong Zhong[1], Bruce S. Spottiswoode[2], Patrick A. Helm[1], John M. Christopher[1], John D. Ferguson[1], James P. Hummel[1], Christopher M. Kramer[1], Frederick H. Epstein[1]
[1]University of Virginia, Charlottesville, Virginia, USA; [2]University of Cape Town, Cape Town, South Africa

Cardiac resynchronization therapy (CRT) for patients with end stage heart failure improves hemodynamics, symptoms, exercise capacity, quality of life, and mortality. When current criteria are used to select patients for CRT, as many as 30% of patients are non-responders. The present study established the ability of cine DENSE and late gadolinium-enhanced MRI to detect mechanical dyssynchrony and scar, respectively, in heart failure patients. The ability to assess dyssynchrony and viability in a single exam may improve the ability to accurately select patients for CRT.

15:00 *3601*. **Mechanical Asynchrony or Myocardial Shortening as MRI Predictors of Response to Biventricular Pacing. Which is Best?**
Computer 19

J. J. Zwanenburg[1], M. J. Gotte[2], J. T. Marcus[1], J. P. Kuijer[1], C. C. de Cock[1], J. van Dijk[1], O. Kamp[1], M. B. Hofman[1], A. C. van Rossum[1]
[1]VU University Medical Center, Amsterdam, Netherlands; [2]University Medical Center Groningen, Groningen, Netherlands

Background: To select responders to cardiac resynchronization therapy (CRT). Purpose: To investigate whether regional myocardial function should be characterized by mechanical asynchrony, or by instantaneous measures (differences in strain at one time). Methods: Using MRI myocardial tagging, asynchrony of circumferential shortening was measured in 12 heart failure patients. Further, instantaneous measures were: the coefficient of variation in end-systolic strain, the peak shortening reserve, and the septal strain at end systole. CRT was applied, and increase in dP/dtmax defined the response. Results: Only the instantaneous measures (but not asynchrony) predicted the response to CRT ($P < 0.01$).

MSK/Body: Cartilage

Room 4A Thursday 13:30 - 15:30

13:30 *3602*. **In-Situ Observation of T2 and ADC Changes in Cartilage During Collagen Depletion**
Computer 27
Arturo Cárdenas-Blanco[1], Cristián Andrés Tejos[2], Da Xing[1], Laurance D. Hall[1]
[1]Herchel Smith Laboratory, University of Cambridge, Cambridge, UK; [2]Pontificia Universidad Catolica de Chile, Santiago de Chile, Chile

This study reports the in-situ chemical and structural changes suffered by cartilage during enzymatic collagen depletion process, similar to the degradation process produced in osteoarthritic joints. Measuring T2 and the Apparent Diffusion Coefficient, it was found that each structural zone of the cartilage experimented different changes on the enzyme activity and the restriction to free water mobility during the degradation process.

13:30 *3603*. **T1ρ Imaging of Articular Cartilage Using a CPMG Pulse Train for Spin Locking**
Computer 26
Garry E. Gold[1], Eric Han[2], Brian A. Hargreaves[1], Graham A. Wright[3], Jean H. Brittain[2]
[1]Stanford University, Stanford, California, USA; [2]GE Healthcare, Menlo Park, California, USA; [3]University of Toronto, Toronto, Ontario, Canada

T1ρ imaging is a promising method for detecting degenerative changes in articular cartilage. Spin locking for this technique is commonly performed using a continuous radiofrequency pulse. The purpose of our study was to compare spin locking using a CPMG pulse train with a standard continuous radiofrequency pulse in T1ρ imaging of cartilage. These two methods of spin locking produced equivalent relaxation times across a range of frequencies. Increasing spin lock frequency produced increasing T1ρ relaxation times. CPMG T1ρ imaging is a promising method of articular cartilage imaging.

14:00 *3604*. **3D-$T_{1\rho}$-Weighted MRI of the Hip Joint at 3T**
Computer 26
Conrado Furtado de Albuquerque Cavalcanti[1], Renata Vieira, Sait Kubilay, Mark Schweitzer, Ravinder Regatte
[1]Hospital for Joint Diseases - NYU Medical Center, New York, New York, USA

The purpose of the work was to demonstrate the feasibility of measuring 3D-T1*f*â MRI for *in vivo* quantitation of hip cartilage at a 3T clinical scanner. The global average T1£l value of the hip cartilages varied from 38.381 to 42.0049 ms. The average regional T1£l values varied from 34.7239 to 39.4343 ms, and from 42.1434 to 45.0563 ms for anterior and posterior regions, respectively. The preliminary results demonstrate that it is possible to quantify 3D-T1*f*â MRI of hip joint *in vivo* without exceeding the RF power deposition at 3T clinical scanner.

14:00 *3605*. **Towards a Quadrupolar MRI Contrast (QMRIC) for Detecting Early Degenerative Changes in Cartilage Tissue**
Computer 27
Alexej Jerschow[1], Wen Ling[1], Mark E. Schweitzer[1], Ravinder R. Regatte[1]
[1]New York University, New York, New York, USA

The purpose of the work is to demonstrate the feasibility of achieving a quadrupolar MRI contrast mechanism (QMRIC) in 23Na MRI of cartilage tissue. The pulse sequences are based on frequency-swept pulse methods. Quadrupolar couplings are measured in bovine cartilage as a function of proteoglycan depletion. Numerical optimizations are used to achieve a high efficiency in the selection of the signals from ordered sodium environments.

14:30 *3606*. **Diffusion Tensor Imaging of Human Hyaline Articular Cartilage at 1.5T**
Computer 27
Lucianna Filidoro[1], Olaf Dietrich[1], Jürgen Weber[1], Maximilian Reiser[1], Christian Glaser[1]
[1]LMU Munich, Munich, Bavaria, Germany

In view of osteoarthritis, diffusion tensor imaging (DTI) was used to analyze the structure of human hyaline articular cartilage. The experiments were performed on clinical 1.5T MRI systems with a maximum resolution of 468×468µm². Using a self developed software package, maps of diffusion tensor trace, anisotropy, eigenvalues, and eigenvectors were visualized. The general applicability of DTI experiments to articular cartilage structural analysis was strengthened. The findings are in good agreement with current literature about the collagenous fiber architecture of cartilage.

14:30 *3607*. **Linear Combination SSFP at 3T: Improved Spectral Response Using Multiple Echoes**
Computer 26
Yogesh Jashnani[1], Aiming Lu[2], Youngkyoo Jung[1], Richard Kijowski[1], Walter F. Block[1]
[1]University of Wisconsin-Madison, Madison, Wisconsin, USA; [2]Stanford University, Stanford, California, USA

3D isotropic high resolution imaging with high contrast of relevant musculoskeletal joint tissues has been implemented successfully using linear combination SSFP at 1.5T. Using the optimal TR at 3T is difficult due to lack of adequate time for spatial encoding. A multiple echo technique is presented which improves the spectral response by exploiting the different phase progression of fat and water during the TR.

15:00 *3608*. **Rapid 3D Articular Cartilage Imaging with Reduction of Truncation Artifacts**
Computer 26
Rebecca Rakow-Penner[1], Garry Gold[1], Bruce Daniel[1], Jarrett Rosenberg[1], Samuel Mazin[1], John Pauly[1], Gary H. Glover[1]
[1]Stanford University, Stanford, California, USA

Three-dimensional knee imaging is useful for cartilage imaging but scan times can be prohibitively long. This study demonstrates a technique that can shorten scan time by about 40% by partially filling k-space using a linear prediction model, thus reducing truncation artifacts. Two radiologists reviewed images produced by this technique and determined them to be as acceptable as the gold standard images.

15:00 *3609*. **Feasibility of DGEMRIC and T2 Mapping at 1.5T in Detecting Patellar Cartilage Lesions**
Computer 27
Erkki Rauvala[1], Risto O. Ojala[1], Eveliina Lammentausta[2], Ilkka Hannila[1], Osmo Tervonen[1], Jukka S. Jurvelin[2], Ilkka Kiviranta[3], Miika T. Nieminen[1]
[1]Oulu University Hospital, Oulu, Finland; [2]University of Kuopio, Kuopio, Finland; [3]Jyväskylä Central Hospital, Jyväskylä, Finland

This study shows that the detection of cartilage lesions can be improved by combining T2 mapping and dGEMRIC with weighted images typically used in clinical MRI evaluation of cartilage degeneration. Further, combining these MRI methods may provide unique and clinically significant information on the degenerative mechanism behind cartilage changes.

Cardiac Wall Motion: Animal

Room 4A Thursday 13:30 - 15:30

13:30 *3610*. **Effects of Diastolic Properties During Remodeling in Heart Failure**
Computer 22
Peter N. Costandi[1], Lawrence R. Frank[1], Andrew D. McCulloch[1], Jeffrey H. Omens[1]
[1]University of California, San Diego, La Jolla, California, USA

Genetically engineered murine models of heart failure have proven valuable in characterizing remodeling and its ultimate decompensation to failure. Mice lacking a cytoskeletal protein present with a clinical picture of dilated cardiomyopathy and transition to failure as adults. Longitudinal high field cardiac MRI showed improved ejection fraction and stroke volume temporally concurrent with an abrupt phase of chamber dilatation. Hemodynamic analysis showed elevated end-diastolic volume but decreasing pressures. Computational modeling estimated passive properties revealing that global compliance increased as a function of geometric alterations. Diastolic dysfunction may therefore influence the progression of compensatory remodeling and its eventual transition to failure.

13:30 *3611*. **High-Resolution CSPAMM Rat Heart Tagging on a 1.5T Clinical MR System**
Computer 21
Marko K. Ivancevic[1], Jean-Luc Daire[1], Jean-Noel Hyacinthe[1], Gerard Crelier[2], Sebastian Kozerke[2], Karin Montet-Abou[1], Idil Tatar[1], Denis R. Morel[1], Jean-Paul Vallee[1]
[1]Geneva University Hospital, Geneva, Switzerland; [2]University and ETH, Zurich, Switzerland

MRI cardiac tagging allows regional myocardial strain quantification with the possibility of transmural resolution. There is an increasing need to quantify myocardial contraction at a subendocardial scale in small rodents, which have acquired a central role in studying mechanisms of cardiovascular disease in recent years. However, tag imaging of small animals has significant challenges. It has only been performed on high field (>4T) research-dedicated MR systems. Feasibility of MR-tagging at 1.5T on an occlusion-reperfusion model in rat heart with transmural resolution is shown in this study.

14:00 *3612*. **Improved Cardiac Tagging Resolution at 14.1 T Enables Principal Strain Measurements in the LV Wall of a Mouse Model of Regional Dilated Cardiomyopathy**
Computer 21
Janusz H. Hankiewicz[1], E. Douglas Lewandowski[1]
[1]University of Illinois at Chicago, College of Medicine, Chicago, Illinois, USA

Changes in the principle strains (E1 and E2) in the LV wall were examined by combined high resolution DANTE tagging (0.45 mm line spacing and 0.1 mm line thickness) and fast gradient echo imaging at 14.1 T in a transgenic mouse model of pure, dilated cardiomyopathy, in which protein kinase C epsilon is overexpressed. The principle E1 strain is reduced in regions of LV wall thinning associated with the development of LV dilation. The findings demonstrate changes in E1 in the LV of the transgenic mouse model, of progressive ventricular dilatation, predate eventual transitioning to heart failure.

14:00 *3613*. **Altered Myocardial Strain Patterns as a Novel Mechanism for Pacing-Induced Ventricular Remodeling: An MRI Tagging Study**
Computer 22
Jia Zhong[1], Darwin Jeyaraj[1], Chris Flask[1], Lance Wilson[1], David S. Rosenbaum[1], Xin Yu[1]
[1]Case Western Reserve University, Cleveland, Ohio, USA

Pacing induced ventricular electrical remodeling (VER) may lead to heart failure and increased cardiac mortality. To investigate the mechanisms for VER, MRI tagging was performed on 5 mongrel dogs with pacing leads implanted in right atrium and on the surface of anterior and posterior LV wall. Segmented circumferential and radial strains were measured. Similar strains were found between ventricular segments during atrial pacing. However, pacing from LV wall preferentially increased strains in the late-activated segments. The increased strains were associated with prolongation of action potential duration. Our results indicate that altered strain patterns may represent a potential mechanism for VER.

14:30 ***3614***. **Investigation of Cardiac Function in Insulin Resistant Rats Using Triggered Cine MRI**
Computer 22
Gurushankar Govindarajan[1], Lixin Ma[1], Timothy Hoffman[1], Craig Stump[1], Shawna Cooper[1], Zachary Resch[1], James Sowers[1]
[1]University of Missouri-Columbia and Harry S.Truman VA Hospital, Columbia, Missouri, USA

Insulin resistant conditions such as diabetes and the metabolic syndrome are associated with a cardiac dysfunction and remodeling. These maladaptive changes in diabetics are also known as diabetic cardiomyopathy. These changes include cardiac hypertrophy, and diastolic and systolic dysfunction.Cine cardiac MRI can be used to detect and quantify these changes in LV anatomy and function in these insulin resistant Rats. This Non-invasive study to measure the anatomic and physiological changes in heart in insulin resistant rodent models may provide us a powerful tool to study the cardiac functions longitudinally in a controlled setting.

14:30 ***3615***. **Imaging of Myocardial Edema and Function at High Resolution with T2-Meta-DENSE: The Hypokinetic Zone Corresponds to the Area of Edema**
Computer 21
Anthony Homer Aletras[1], Gauri S. Tilak[1], Andrew Ernest Arai[1]
[1]LCE-NHLBI-NIH, Bethesda, Maryland, USA

T2-meta-DENSE is a new method that can acquire T2-weighted images (TE=60 ms) and DENSE displacement maps in end-systolic images. Phase images from the images with TE of 6.5ms yielded strain maps. The images are inherently registered on a pixel-by-pixel basis allowing comparisons of myocardial edema and function following myocardial infarction at high spatial resolution. Black-blood contrast is due to intravoxel dephasing in the blood pool. Six dogs were studied 2 days after transient coronary occlusion. Good correlation (R=0.97) was found between the size of the hypokinetic and the edematous zones.

15:00 ***3616***. **Characterization of 3D Myocardial Wall Motion in the Mouse with MR Tagging**
Computer 21
Jia Zhong[1], Wei Liu[2], Xin Yu[1]
[1]Case Western Reserve University, Cleveland, Ohio, USA; [2]Philips Research North America, Briarcliff Manor, New York, USA

Mouse models are playing an important role in the investigation of human cardiac diseases. The development of rapid, noninvasive methods for characterizing ventricular motion in these animals can provide new opportunities to elucidate molecular mechanisms of myocardial function. We developed a novel 3D strain analysis method combining HARP and homogeneous strain analysis. The present method also allows direct validation of 2D strain calculation. Segmented radial, circumferential, and longitudinal strains were quantified in 2-month-old C57/BL6 mice (n=6). Large peak strains were observed in the anterior-lateral wall. We also found a high correlation in radial and circumferential strains between 3D and 2D quantification.

15:00 ***3617***. **Feasibility of C-SPAMM Rat Heart Tagging After Manganese Injection**
Computer 22
Jean-Noel Hyacinthe[1], Marko Ivancevic[1], Jean-Luc Daire[1], Jean-Paul Vallée[1]
[1]Geneva University Hospital, Geneva, Switzerland

Manganese Enhanced Magnetic Resonance (MEMR) is used to depict the myocardial area at risk in models of coronary occlusion-reperfusion. In such models, MR tagging allows the evaluation of myocardial motion defects during the stunning phase. However, the relaxation effects of manganese may affect tag fading and hence the quality of strain measurement. Imaging 6 rat hearts (CSPAMM at 1.5 T and HARP analysis), we show a contrast to noise ratio increase and no differences in circumferential strain measurements after MnCl2 injection. Thus, MR tagging could be used in combination with MEMR to study the acute phase of coronary artery disease.

MSK/Body: Muscle, Marrow, Arthritis

Room 4A Thursday 13:30 - 15:30

13:30 ***3618***. **Longitudinal Study of Clinical and Quantitative MR Characterization of the Knee in Children with Juvenile Rheumatoid Arthritis**
Computer 31
Dagnachew Walelign Workie[1], Bernard Joseph Dardzinski[2], Brent Graham[2]
[1]UCI Medical Center, Orange, California, USA; [2]Cincinnati Children's Hospital Medical Center, Cincinnati, Ohio, USA

Longitudinal study on 17 subjects with juvenile rheumatoid arthritis (JRA) was performed at three time points: enrollment, 3 months, and 12 months. The longitudinal studies included quantitative DCE-MRI, clinical and laboratory assessments. When compared to the enrollment values, all pharmacokinetic (PK) parameters, clinical and laboratory measures at 3 months and 12 months showed a significant decrease, except for the CHAQ-DI and CRP at 3 months. In most comparisons, the average PK values showed excellent correlation with clinical and laboratory assessments. The decrease of PK parameters might reflect diminution of disease activity and could be used as an objective follow-up of JRA patients.

13:30 ***3619***. **Real-Time Measurements of Knee Muscle Moment Arms During Dynamic Knee Flexion-Extension Motion**
Computer 29

Silvia Salinas Blemker[1], Elliot McVeigh[2]
[1]Stanford University, Stanford, California, USA; [2]National Institutes of Health, Bethesda, Maryland, USA

The goal of this study was to evaluate the feasibility of measuring knee muscle moment arms over a full range of motion using real-time MRI in a 70cm bore Siemens Espree 1.5T scanner. Subjects flexed and extended their knees through a 140-degree range of motion at 8 cycles/minute. The images conveyed the complex path of the rectus femoris muscle, and moment arms estimated from the images compare well with literature values. This method can be applied to characterizing moment arms of other complex muscles under various loading conditions – data that will greatly advance our understanding of *in vivo* muscle function.

13:30 ***3620***. **Quantification of Bone-Water Concentration in a 3T Whole-Body Imager Using Solid-State Imaging**
Computer 30

Aranee Techawiboonwong[1], Hee Kwon Song[1], Maria A. Fernandez-Seara[1], Felix W. Wehrli[1]
[1]University of Pennsylvania Medical Center, Philadelphia, Pennsylvania, USA

The majority of bone water resides in the microscopic pores of the lacuno-canalicular system, leading to extremely short T_2 (~400 μs). Imaging of bone therefore requires solid-state imaging (SSI) techniques. Here we hypothesized that bone water can be quantified and thus potentially pore volume determined *in situ*. As a model for varying pore volume we controlled H_2O content by partial exchange with D_2O. The SSI experiments on animal bone show that high measurement precision can be achieved at 3T and therefore *in vivo* quantification appears feasible.

13:30 ***3621***. **Quantification of Acute Peripheral Muscle Edema in Rats Using MRI**
Computer 28

Shantanu Dhamija[1], Terry Major[1], Serguei Liachenko[1]
[1]Pfizer, Inc., Ann Arbor, Michigan, USA

A clinically translatable MRI method for the detection of edema in the hind legs of spontaneously hypertensive rats is developed. The method is based on the MRI measurement of the proton transverse relaxation in skeletal muscle. The present study validates the MRI T2 measurements as a differentiating marker of peripheral muscle edema after acute infusion of the reference calcium channel blockers with a dose-response approach.

14:00 ***3622***. **In Vitro Demonstration of Shear Strain Distribution of the Human Gastrocnemius-Soleus Aponeurosis During Submaximal Isometric Contraction Using Velocity-Encoded Phase Contrast MRI**
Computer 28

Dongsuk Shin[1], Sinyeob Ahn[1], Haedong Lee[1], John Hodgson[1], Taija Finni[1], Reggie Edgerton[1], Shantanu Sinha[1]
[1]University of California, Los Angeles, California, USA

It has been postulated in muscle physiology literature that aponeurosis structures are made up of thin adjacent layers. We have developed phase contrast MRI based techniques to monitor tissue displacements with sufficiently high resolution. We use it to demonstrate *in vivo* in the human lower leg, that during isometric contraction, (i) the gastrocnemius (GM) moves to a different extent than the soleus on the other side of the aponeurosis, (ii) along the length of the SOL-GM aponeurosis, the displacements of these muscle groups are spatially heterogenous, and (iii) across the aponeurosis, a spatial shear strain distribution is generated.

14:00 ***3623***. **Comparison of Edema Conspicuity in Routine Knee MR Examinations Using IDEAL, STIR, and T2 Fat Suppressed Images at 3.0 T**
Computer 30

Perry Horwich[1], Daniel Sacchetti[1], Charlie McKenzie[1], Mary Hochman[1], Scott Reeder[2], Neil M. Rofsky[1]
[1]Beth Israel Deaconess Medical Center, Boston, Massachusetts, USA; [2]University of Wisconsin Medical School, Madison, Wisconsin, USA

This work examines the conspicuity of edema in soft tissues and bone marrow using short tau inversion recovery (STIR), T2 weighted imaging with chemically selective fat saturation (T2WI-FS), and Iterative Decomposition of water and fat with Echo Asymmetry and Least-squares estimation (IDEAL) imaging at 3.0T. Replacing STIR imaging with T2WI-FS, or water-only IDEAL images, has the potential to decrease scanning time and improve homogeneity of fat suppression. Images were acquired in 10 patients, referred for routine knee MR, and analyzed. IDEAL imaging scored highest for homogeneous fat suppression while STIR scored highest for overall edema conspicuity.

14:00 ***3624***. **Measurement of Skeletal Muscle Injury with Gadomer**
Computer 29

Anthony Z. Faranesh[1], [2], Dara L. Kraitchman[3], Elliot R. McVeigh[2]
[1]Stanford University, Stanford, California, USA; [2]National Institutes of Health, Bethesda, Maryland, USA; [3]The Johns Hopkins University, Baltimore, Maryland, USA

In this study skeletal muscle injury was evaluated using contrast enhanced MRI with the macromolecular contrast agent Gadomer. Quantitative T1 mapping and compartment modeling were used to calculate the peak contrast agent concentrations in ischemic and normal tibialis anterior muscles in a rabbit model. Significant differences were measured in the peak tissue contrast agent concentration between day 14 and day 28 after the induction of ischemia. These methods may have potential to track changes in tissue physiology related to inflammation and necrosis.

14:00 ***3625***. **T1-Weighted Perfusion Studies Using a Hollow Fiber Cartridge Perfusion Phantom: A Preliminary Study to Simulate Clinical Data from the Knees of Children with JRA**
Computer 31

Dagnachew Walelign Workie[1], Bernard Joseph Dardzinski[2], R. Scott Dunn[2]
[1]UCI Medical Center, Orange, California, USA; [2]Cincinnati Children's Hospital Medical Center, Cincinnati, Ohio, USA

Quantitative (DCE-MRI) has been shown to be a useful technique to investigate disease activity in different organ systems. In this study a hollow fiber cartridge (HFC) perfusion phantom that simulates capillary perfusion from DCE-MRI protocols is presented. The phantom was able to mimic signal enhancements from the synovium and physes of knees of children with JRA. Therefore, the HFC perfusion phantom can be used as a tool to investigate the permeability of capillary membranes based on pharmacokinetic modeling and predict the feasibility of quantitative methods to monitor disease activity in JRA.

14:30 ***3626***. **Early Diagnosis of Rheumatoid Arthritis with Microscopic MR Imaging of the Fingers**
Computer 31

Yuji Watanabe[1], Masako Nagayama[1], Akira Okumura[1], Yoshiki Amoh[1], Kazushige Oda[1], Takayoshi Ishimori[1], Takashi Kiyono[1], Kazuaki Nakada[1], Hideki Mitsui[1], Noriyoshi Morimoto[1], Takashi Tabuchi[1], Masayuki Kumashiro[1], Shinsuke Komaki[1], Takashi Sugioka[1], Osamu Ito[1], Keisuke Ohtsuki[1], Yoshihiro Dodo[1]
[1]Kurashiki Central Hospital, Kurashiki, Okayama, Japan

Rheumatoid arthritis (RA) is a chronic systemic disease affecting approximately 0.5-1.0% of the adult population. It is difficult to accurately diagnose the early RA because of a broad spectrum of disease manifestation. Microscopic MR imaging can give detailed information about synovial thickening of metacarpophalangeal and interphalangeal joints of hand fingers. The sensitivity and specificity of MR findings for RA diagnosis included 100% and 23% for diffuse synovial thickening, 37% and 77% for irregular synovial thickening, 30% and 92.3% for irregular nodular synovial thickening with bone erosion as well, respectively. Microscopic MR imaging will allow for early diagnosis of RA.

14:30 ***3627***. **Spin-Labeling Muscle Perfusion Imaging at 3 Tesla**
Computer 29

Andreas Boss[1], Petros Martirosian[1], Claus D. Claussen[1], Fritz Schick[1]
[1]University of Tübingen, Tübingen, Germany

The aim of this study was to demonstrate the feasibility of ASL muscle perfusion imaging using a clinical MR set-up at 3 Tesla. Eight healthy volunteers (mean age 32) participated in this study. A pulsed ASL sequence with FAIR spin preparation and TrueFISP readout strategy was implemented in a 3 Tesla MR scanner. Perfusion-time curves could be recorded with a temporal resolution of 6.4 sec. The perfusion of the musculature reached a maximum approximately 2 minutes after exercise with perfusion values of up to 220 ml/min/100g tissue showing good delineation between active muscles and non-active muscles.

14:30 ***3628***. **Potential of SPIO in the Differential Diagnosis of Bone Metastasis and Inflammation - Animal Experiments**
Computer 30

Natsuko Tsuda[1], Takashi Tsuji[1], Naoki Kato[1], Yuko Fukuda[2], Kumiko Ando[2], Reiichi Ishikura[2], Norio Nakao[2]
[1]Nihon Schering K.K., Osaka, Japan; [2]Hyogo College of Medicine, Nishinomiya, Hyogo, Japan

We investigated the potential of superparamagnetic iron oxide (SPIO) in the differential diagnosis of bone metastasis and inflammation using the animal models. VX2 tumor cells or croton oil were injected into the femora of rabbits. SPIO was intravenously injected at a dose of 8 micro mol Fe/kg. The signal intensity of tumor did not change after a SPIO injection, whereas signal intensity of normal bone marrow and inflammation decreased. Our results showed that SPIO was useful to detect bone marrow tumors. In addition, SPIO may have potential in the differential diagnosis of bone metastasis and inflammation.

14:30 ***3629***. **Flow Heterogeneity Within Muscle of Calf, Forearm, and Foot Using Continuous Arterial Spin Labeling,**
Computer 28

Thomas F. Floyd[1], Jiongjiong Wang[1], Guoqiang Yu[1], Emile R. Mohler, Iii[1], Jeffery Carpenter[1], John Murphy[1], John A. Detre[1]
[1]University of Pennsylvania, Philadelphia, Pennsylvania, USA

Continuous Arterial Spin Labeling is applied at 3 Tesla to the measurement of regional blood flow in muscle of the forearm, foot, and calf. Heterogeneity of flow within various muscle groups is described along with repeatability of the approach and the potential application to physiologic and pathophysiologic study of microvascular flow in muscle.

15:00 ***3630***. **MRI Assessment of Changes in Calf Fluid Level During Medication Challenge**
Computer 28

Chun Zuo[1], Robert Dobbins[2], Derek Nunez[2], Rose Villafuerte[1], Michelle Butman[1], Michael Henry[1], Yiwu He[2], Barbara Orban[2], Andrew Brown[3], John Brown[3], Perry Renshaw[1]
[1]McLean Hospital, Belmont, Massachusetts, USA; [2]GlaxoSmithKline, RTP, North Carolina, USA; [3]GlaxoSmithKline, Greenford, England, UK

We have evaluated the feasibility of using proton and sodium MRI to detect possible fluid retention in eleven young and healthy male subjects during medication challenges of nifedipine and fludrocortisone. Fluid level change was determined by MRI signal changes compared to baseline. Physiological parameters including body weight were also measured for comparison. Sodium MRI was found sensitive for the detection and showed that fludrocortisone caused a +4% increase in calf fluid level versus a weight gain of 1.4% compared to baseline within 2 weeks while nifedipine induced a +2.5% calf fluid accumulation versus a 0.8% weight gain within 3 weeks.

15:00 *3631*. **Ultrafast T2* Mapping of Bone Marrow at 1.5 Tesla and 3.0 Tesla**
Computer 30
Renato Toffanin[1, 2], Marcello Cadioli[3, 4], Giuseppe Scotti[4], Maria Assunta Cova[5]
[1]PROTOS Research Institute, Trieste, Italy; [2]ARCHES, Castellana Grotte, Italy; [3]Philips Medical Systems, Monza, Italy; [4]San Raffaele Scientific Institute, Milano, Italy; [5]University of Trieste, Trieste, Italy

The purpose of this study was to evaluate the feasibility of a multi-shot EPI sequence for the ultrafast T2* mapping of bone marrow. Experiments were performed on the calcaneus of six healthy volunteers at 1.5 Tesla and 3.0 Tesla. A standard gradient-echo sequence with similar acquisition parameters was also used for comparison. T2* parametric maps without and with B0 correction were calculated off-line. The results indicate that ultrafast T2* mapping of bone marrow is feasible at 1.5 Tesla and at3.0 Tesla. Furher studies have to be performed to investigate the full potential of the proposed approach in the clinical investigation of osteoporosis.

15:00 *3632*. **High Resolution MR Imaging of Paraspinal Muscle Injury Following Minimally Invasive and Conventional Open Posterolateral Lumbar Fusion**
Computer 29
Kathryn Jane Stevens[1], Karen Lucy Griffiths[1], Sabine Bammer[1], Stephan E. Maier[2], Todd Alamin[1], Roland Bammer[1]
[1]Stanford Medical Center, Stanford, California, USA; [2]Brigham's and Women's Hospital, Boston, Massachusetts, USA

Post-operative MRI scans were performed on 12 patients, approximately 6 months after either a minimally invasive or open single level posterolateral lumbar spinal fusion (6 minimally invasive, 6 open). Edema and atrophy in the paraspinal muscles were evaluated using conventional MRI sequences, and quantitative differences were calculated using axial dual spin echo sequences and line scan diffusion-weighted imaging. Striking differences in muscle edema were demonstrated between the minimally invasive and open spinal groups. The mean T2 and ADC measurements were significantly lower in the minimally invasive group, suggesting that less muscle damage occurs using a minimally invasive approach.

15:00 *3633*. ***In Vivo* High-Resolution Three-Dimensional Magnetic Resonance Imaging of a Rat Knee Osteoarthritis Model Induced by Meniscal Transection**
Computer 31
Yi-Xiang Wang[1], F R. Westwood[1], S M. Moores[1], A Ball[1], C Heapy[1], R Pickford[1], J J. Tessier[1], J Bowyer[1]
[1]Astra Zeneca, Macclesfield, Cheshire, UK

The study was aimed to evaluate *in vivo* high-resolution 3D MRI in demonstrating the joint structural changes in rat left knee osteoarthritis induced by meniscal tear, with 10 operated and 5 sham-operated animals. MR scan was carried out 44 days after surgery at 4.7T, using a spoiled multi-echo fat-suppressed 3D GRE sequence. In operated rats MRI demonstrated the meniscus tear, cartilage and bone damage at the medial tibial plateau. In five animals single or multiple high signal areas were observed within the epiphysis of tibia, consistent with cyst signal. Patho-anatomical changes seen on MRI were consistent with histopathological data.

Time Resolved MRA: Trick or Treat

Room 4A Thursday 13:30 - 15:30

13:30 *3634*. **Time Resolved Contrast-Enhanced Carotid and Cerebral 3D MR-Angiography with Echo-Sharing and GRAPPA**
Computer 23
Kiriaki Kollia[1], Stefan Maderwald[1], Marc Uwe Schlamann[1], Michael Forsting[1], Isabel Wanke[1]
[1]University Hospital Essen, Essen, Germany

Aim of the study was to improve temporal-resolution of the ce-MRA for the supraaortic and cerebral vessels by evaluating a time-resolved 3D ce-MRA combining parallel acquisition technique and echo-sharing (TREAT). 14 patients (4 with untreated and 4 with treated cranial AVM, 4 with intra- and extracranial vessel stenosis respectively, 2 with intra- and extra-axial tumor respectively) were examined using a new time-resolved ce-MRA technique. The temporal-resolution was sufficient to evaluate nidus delineation, arterial supply, early-draining veins, collateralisation and feeding arterial tumor-branches. Patients with intracranial vessel stenosis or occlusion and with treated AVM might profit from this technique the most.

13:30 *3635*. **Time-Resolved Three-Dimensional Pulmonary MR Angiography Using a Spiral-TRICKS Sequence**
Computer 24
Jiang Du[1], Mark Bydder[1], Richard M. Znamirowski[1], Steve C. Rose[1], Graeme M. Bydder[1]
[1]University of California, San Diego, San Diego, California, USA

Evaluation of the pulmonary circulation is important in the assessment of many disease processes such as pulmonary embolism, hypertension and vascular anomalies. Time-resolved contrast enhanced MR angiography provides the contrast dynamics in pulmonary vasculature, thus very useful for perfusion and angiography study. The short arterial-venous transit time requires fast dynamic imaging sequences. Here we present a hybrid 3D spiral sequence which combines a spiral readout trajectory in-plane and Cartesian slice encoding through-plane in a TRICKS scheme, thereby providing both high spatial resolution and high temporal resolution.

13:30 ***3636***. **Time Resolved Echo-Shared Angiography Techniques (TREAT) with Dedicated Peripheral Angiography Matrix-Coils and High Acceleration Factors at 3T: Initial Experience**
Computer 25

Harald Kramer[1], Volker Matschl[2], Peter Schmitt[2], Henrik J. Michaely[1], Michele Picciolo[1], Maximilian F. Reiser[1], Stefan O. Schoenberg[1]
[1]University Hospital of Munich - Grosshadern Campus, Munich, Germany, Germany; [2]Siemens Medical Solutions, Erlangen, Germany, Germany

One of the last drawbacks of MRA compared to conventional digital subtraction angiography was the absence of dynamic information. The implementation of view-sharing techniques helped to overcome this step. The combination of dedicated angiography coils, parallel imaging and high field strength make it possible to increase temporal resolution to less than 3 seconds per frame at good spatial resolution.

14:00 ***3637***. **Stepping-Table Gadolinium-Enhanced MR Angiography for the Run-Off Study of Lower Extremity Arteries: Two-Injection Techniques Using Combination of TRICKS for the Calf and Two-Step Scanning Technique with Automated Bolus-Detection Algorithm for the Abdomen and Thigh**
Computer 25

Tonsok Kim[1], Takamicchi Murakami[2], Masatoshi Hori[1], Hiromitsu Onishi[1], Kaname Tomoda[1], Hironobu Nakamura[1]
[1]Osaka University Graduate School of Medicine, Suita-city, Osaka, Japan; [2]Osaka University Graduate School of Medicine, Suita-city,, Osaka, Japan

TRICKS is useful for the visualization of the calf arteries without venous overlap. However, incidence of venous overlap on arteries of the thigh is slightly increased with our technique. Improvement of contrast material injection technique is necessary.

14:00 ***3638***. **Time-Resolved MR Angiography for Pulmonary Embolism: Preliminary Results**
Computer 24

Hale Ersoy[1], Samuel Z. Goldhaber[1], Ronald B. Skorstad[1], Joshua L. Rosebrook[1], Tianxi Cai[2], Frank J. Rybicki[1]
[1]Brigham and Women's Hospital, Boston, Massachusetts, USA; [2]Harvard Medical School, Boston, Massachusetts, USA

The 3D pulmonary Gd-MRA has high accuracy in the diagnosis of pulmonary embolism (PE). However, routine implementation has been limited by technical and practical factors such as venous contamination and the need of high spatial resolution to evaluate small arterial segments. In 15 consecutive patients with suspected PE, 3D TRICKS MRA provided high temporal resolution (9 phases, 1 phase / 3.5 sec) pulmonary arterial only imaging. The high spatial resolution of the technique enabled confident diagnosis of PE through the segmental branches. Inter-rater image quality agreement was very good for lobar arteries (kw=0.85) and good for segmental arteries (kw=0.77).

14:00 ***3639***. **Efficacy of Detection of Significant Carotid Artery Stenosis with TREAT Imaging at 1.5T and 3.0T**
Computer 23

Henrik Jakob Michaely[1], Harald Kramer[1], Kerstin Bauner[1], Kambiz Nael[2], Maximilian F. Reiser[1], Stefan O. Schoenberg[1]
[1]University of Munich, Munich, Bavaria, Germany; [2]UCLA, Los Angeles, California, USA

The efficacy of time-resolved echo-shared angiographic technique (TREAT) in the detection of carotid artery stenosis (CAS) is investigated. After 10ml injection of contrast agent TREAT imaging was started. A temporal resolution of 2.3sec/3D-Volume or 1.2sec/3D-Volume was achieved. 40 patients were examined (30/10 1.5T/3.0T). Differences in contrast agent arrival were analyzed on an offline workstation.12/15 patients with CAS > 75% revealed a flow delay while only 3/14 patients with CAS < 75% and no patient without CAS had a delayed flow.The detection of a delayed flow in TREAT is highly indicative of a significant CAS.

14:30 ***3640***. **Diagnosis of Subclavian Steal Syndrome Using a Novel Time-Resolved Magnetic Resonance Angiographic Technique**
Computer 23

Rashmi Virmani[1], Timothy J. Carroll[1], Ty A. Cashen[1], Karin Dill[1], Matthew Walker[1], James C. Carr[1]
[1]Northwestern University Medical School, Chicago, Illinois, USA

The purpose of our study was to diagnose subclavian steal syndrome using a novel time-resolved 3D CE-MRA technique using combination of two complimentary undersampling techniques: TREAT(Time-Resolved Echo sharing Angiographic Technique) with GRAPPA (SENSE based parallel imaging technique). This technique demonstrates the anatomy of cervicothoracic vessels in a fast, noninvasive way and also quantifies clearly the amount and direction of blood flow-through vessels of small caliber and thus provides dynamic information, inherent in DSA exams. This technique can be considered as a valuable substitute for invasive techniques like DSA and may also be used to plan interventions at the same time.

14:30 ***3641***. **Time-Resolved 3D Contrast-Enhanced MRA in Adult Congenital Heart Disease**
Computer 24

Michael Christian Fenchel[1], [2], Roya Saleh[2], Margaret Lee Hsiang-Shung[2], Howard Dinh[2], Kambiz Nael[2], Stefan Ruehm[2], J. Paul Finn[2]
[1]Eberhard-Karls-University Tuebingen, Tuebingen, BW, Germany; [2]David Geffen School of Medicine, University of California Los Angeles, Los Angeles, California, USA

Aim of the study was to investigate whether temporally-resolved 3D contrast-enhanced MRA can unravel complex flow patterns and functional vascular status in patients with surgically treated adult-congenital-heart-disease (ACHD). Thirty-five consecutive patients with ACHD were examined on a 1.5T MR-scanner acquiring coronal time-resolved 3D-MRA and high-spatial-resolution 3D-MRA of the thorax. High image quality was evident in time-resolved and high-spatial-resolution MRA datasets. Time-resolved 3D-MRA can be effective in unraveling complex vascular anatomy in patients with ACHD. It yields clinically relevant information in a substantial number of patients in comparison to conventional MRA, such that both techniques should be regarded as complementary.

14:30 *3642*. **A Comparison of Static and Dynamic 3D Magnetic Resonance Angiography for the Diagnosis of Infrapopliteal Disease in Patients Using TREAT and IPAT**
Computer 25
Lincoln Olivio Diniz[1], Karin Dill[1], James C. Carr[1], Timothy J. Carroll[1], Reed A. Omary[1], Rashmi Virmani[1]
[1]Northwestern University, Chicago, Illinois, USA

We compared high resolution CE-MRA, using a novel time resolved MRA pulse sequence TREAT and iPAT, with conventional static CE-MRA for the assessment of infrapopliteal peripheral vascular disease. Time resolved MRA using TREAT and iPAT produced detailed images of the infrapopliteal arteries with temporal resolution of 5 seconds per frame. Images from time resolved MRA exams included clinically relevant information that can alter diagnosis. Change in diagnosis was due to asymmetric flow, slow flow, and reconstitution of distal runoff vessels on delayed frames, thus identifying a target vessel for surgery, which may result in significant changes in clinical management.

15:00 *3643*. **Time-Resolved Three Dimensional Contrast-Enhanced MR Imaging of the Hand**
Computer 25
Hidekazu Seo[1], Takayuki Masui[1], Motoyuki Katayama[1], Kimihiko Sato[1], Masahiro Sugiyama[1], Atsushi Nozaki[2], Masaya Hirano[2]
[1]Seirei Hamamatsu General Hospital, Hamamatsu, Shizuoka, Japan; [2]General Electtric Yokogawa Medical Systems, Hino, Tokyo, Japan

We evaluated the usefulness of a time-resolved contrast-enhanced three-dimensional MR angiography with the three-dimensional Time-Resolved Imaging of Contrast KineticS (TRICKS) pulse sequence for vessels and the vascularities of the soft tissue anomalies in the hand. As a result, TRICKS MR angiography of the hand can provide the vessel anatomy and the semiquantitative perfusion of soft tissues without consideration of time for triggering imaging after contrast injection.

15:00 *3644*. **Peripheral Angiographic Applications of HYPR TRICKS**
Computer 24
Yan Wu[1], Yijing Wu[1], Frank R. Korosec[1], Oliver Wieben[1], Orhan Unal[1], Jiang Du[2], Dana Peters[3], Charles A. Mistretta[1]
[1]University of Wisconsin Madison, Madison, Wisconsin, USA; [2]University of California San Diego, San Diego, California, USA; [3]Harvard University, Boston, Massachusetts, USA

We applied the HighlY constrained back PRojection (HYPR) algorithm to the PR-TRICKs MRA technique. HYPR is a method that permits great improvements in temporal resolution in radial acquisitions by producing time frames using only a small subset of the total number of projections necessary to satisfy the Nyquist criterion. Streak artifacts that would ordinarily result from constructing images using a dramatically reduced number of projections are ameliorated by constraining the unfiltered back projected data to regions in which vessels are known to exist. In order to determine the location of the vessels, a vessel map is produced using data from multiple time frames. Because the data for each of the time frames is produced from projections that are acquired at slightly different angles, data from multiple time frames can be combined to produce high SNR, low artifact composite images (or vessel maps). Using the HYPR method, the temporal resolution can be improved by more than a factor of 80 as compared to a fully sampled multi-phase data set.

15:00 *3645*. **Non-Contrast Time Resolved Pulmonary MRA with ECG-Triggered 3D HASTE**
Computer 23
Jian Xu[1], Niels Oesingmann[1], Abram Voorhees[2], Alto Stemmer[3], Vivian S. Lee[2], Jing An[2], Bernd Stoeckel[1], Qun Chen[2]
[1]Siemens Medical Solutions USA Inc., New York, New York, USA; [2]New York University School of Medicine, New York, New York, USA; [3]Siemens Medical Solutions, Erlangen, Germany

No contrast MRA with 3D HASTE.

Parallel Imaging

Room 4A Thursday 13:30 - 15:30

13:30 *3646*. **Fast, High Spatial Resolution MRI of the Ankle with Parallel Imaging Using GRAPPA at 3.0T**
Computer 32
Jan Stefan Bauer[1, 2], Suchandrima Banerjee[1], Tobias Daniel Henning[1], Cameron Barr[1], Roland Krug[1], Sharmila Majumdar[1], Thomas Marc Link[1]
[1]University of California, San Francisco, California, USA; [2]Technische Universitaet Muenchen, Muenchen, Germany

Magnetic resonance imaging at 3.0T has shown potential for enhancing musculoskeletal imaging. In most studies the higher SNR obtained at 3.0T compared to 1.5T has been used to improve image quality and spatial resolution. In routine clinical sequences, however, scan time is also a major consideration. This study demonstrates that parallel imaging with GRAPPA reconstruction provides a feasible way to substantially cut down imaging time without loss of image quality.

13:30 ***3647***. **Decoupling in Multi-Channel Bilateral Breast Imaging with Quadrature Coils**
Computer 35
Steen Moeller[1], Prashanthi Vemuri[2], Carl Snyder[1], Lance DelaBarra[1], Patrick J. Bolan[1], Tommy Vaughan[1], Kâmil Ugurbil[1], Michael Garwood[1]
[1]University of Minnesota, Minneapolis, Minnesota, USA; [2]University of Utah, Salt Lake City, Utah, USA

RF coils with quadrature elements have higher sensitivity compared to those with simple loop elements, but the final composite images produced using these coils exhibit non-uniform intensity over the FOV. If two quadrature elements are used for simultaneous acquisition of independent FOVs, as for bilateral breast imaging, the coupling from the quadrature coils exhibits an artificial non-linear spatial variation. This work deals with the decoupling of signal for such bilateral breast imaging studies acquired with quadrature coils.

13:30 ***3648***. **Robust GRAPPA Reconstruction and Its Evaluation with Perceptual Difference Model (PDM)**
Computer 33
Donglai Huo[1], David Wilson[1]
[1]Case Western Reserve University, Cleveland, Ohio, USA

In GRAPPA, a least-squares technique is used to solve the over-determined equations and get the "fitting" coefficients. We developed the Robust GRAPPA whereby robust estimation techniques are used to estimate the coefficients with discounting of k-space data outliers. One implementation, Slow Robust GRAPPA used iteratively re-weighted techniques, and compared to an ad hoc Fast Robust GRAPPA implementation. We evaluated these new algorithms using the Perceptual Difference Model (PDM). We systematically investigated 7500 images with independent variables combinations. We conclude Robust GRAPPA method gives significant improvements as compared to standard GRAPPA. PDM is very helpful in optimizing the MR reconstruction algorithms.

13:30 ***3649***. **Calculation of SNR Degradation Due to Non-Ideal Weighting Coefficients**
Computer 34
Jianmin Wang[1], Bida Zhang, [1,2], Jing Luo[2], Yan Zhuo[2]
[1]Siemens Mindit Magnetic Resonance Ltd., Shen Zhen, Guang Dong, People's Republic of China; [2]Key Laboratory of Cognitive Science, The Graduate School ad Institute of Biophysics, Beijing, People's Republic of China

GRAPPA is known as its high robustness and low residual artifact, but the fitting process may introduce additional uncertainty to the weighting coefficients. We present here a general method to calculate SNR degradation due to non-ideal weighting coefficients and use equivalent weighting coefficients for GRAPPA to analyze its noise behavior. The result shows that although the SNR degradation for GRAPPA is mathematically the reciprocal value of SENSE g-factor, it depends not only on the coil geometry but also on the image contrast. It is also observed that the GRAPPA algorithm has the ability to sacrifice SNR to achieve lowest artifact power and to optimize SNR when artifact power is low.

14:00 ***3650***. **Convolution Kernel Decision Scheme for Reconstruction in K-T/k Space**
Computer 34
Feng Huang[1], George Randy Duensing[1]
[1]Invivo Corporation, Gainesville, Florida, USA

In this work, a novel reconstruction algorithm is introduced. The method is based on allowing the convolution kernel to be selected on the basis of prior acquisitions or from ACS lines within the acquired data. Because of the size of the convolution kernel, temporal resolution of the images reconstructed by k-t GRAPPA may be reduced. To improve the temporal resolution, it is proposed that the choice of the convolution kernel should be guided by the convolution matrix generated with acquired data. Experiments showed that the proposed method could generate better results than k-t GRAPPA with a fixed, small kernel definition.

14:00 ***3651***. **View Ordering in GRAPPA Fast Spin-Echo Methods**
Computer 33
Anantha Raman Krishnan[1], Zhiqiang Li[1], Ali Bilgin[1], Maria I. Altbach[1]
[1]University of Arizona, Tucson, Arizona, USA

It is demonstrated that the location of the auto calibration lines for parallel imaging schemes should be selected carefully, when the k-space lines are acquired with different signal weighting. To illustrate this point, we study the effects of auto-calibrated parallel imaging in fast spin-echo data and propose a view ordering scheme that minimizes the artifacts due to the differences in signal weighting caused by T2 decay.

14:00 ***3652***. **dSENSE: Direct *k*-Space Reconstruction for Non-Cartesian Parallel MR Imaging**
Computer 35
Julien Sénégas[1], Tobias Knopp[2], Holger Eggers[1]
[1]Philips Research, Hamburg, Germany; [2]University Luebeck, Luebeck, Germany

A new, non-iterative algorithm is proposed for the reconstruction of non-Cartesian acquisitions in parallel imaging. It performs the reconstruction in k-space, where each sample is estimated by a linear combination of only a subset of the acquired data. The weights of the linear combination are derived from the coil sensitivities using Fourier transforms and linear algebra. It is shown that the theoretical mean square error of the reconstruction is a useful guideline to locally select the subset of the acquired data for the estimation. The algorithm is demonstrated on simulated and measured radial and spiral acquisitions.

14:00 ***3653***. **Parallel 2D and 3D Spectroscopic Imaging Using GRAPPA**
Computer 32
Felix Breuer[1], Dimitri Ebel[1], Jan Ruff[2], Martin Blaimer[3], Nicole Seiberlich[1], Mark Griswold[3], Peter Jakob[1]
[1]University of Würzburg, Würzburg, Germany; [2]Siemens AG Medical Solutions, Erlangen, Germany; [3]University Hospitals of Cleveland, Cleveland, Ohio, USA

In this work the GRAPPA algorithm has successfully been applied to 2D and 3D spectroscopic parallel imaging. We demonstrate that the flexibility of the GRAPPA approach allows one to derive the reconstruction weights either from a few extra acquired CSI data in the center of the phase encoding k-space or alternatively from a fast fully-encoded low-resolution reference pre-scan. Four-fold accelerated 2D CSI phantom and 3D *in vivo* head experiments are presented with both high spectral and good image quality.

14:30 ***3654***. **Trajectory Optimization in K-T GRAPPA**
Computer 32
Rui Yan[1,2], Feng Huang[2], James Akao[2], Charles Saylor[2], Hu Cheng[3], Randy Duensing[2]
[1]University of Florida, Gainesville, Florida, USA; [2]Invivo Corporation, Gainesville, Florida, USA; [3]Indiana University, Bloomington, Indiana, USA

Dynamic imaging in MRI incorporates temporal correlation between frames. Several reconstruction methods have been proposed to exploit temporal correlation, e.g., UNFOLD, TSENSE, k-t BLAST and k-t SENSE and k-t GRAPPA. The further choice of sampling pattern in k-t space affects SNR, unwrapping artifact, and temporal resolution. Tsao J. *et al*. give the optimal sampling patterns for k-t BLAST and k-t SENSE by qualitatively analyzing the point spread function (PSF) in x-f space. This paper focuses on the optimization strategy applied to k-t GRAPPA and conjectures a quantitative criterion for trajectory optimization.

14:30 ***3655***. **HomoSENSE: A Filter Design Criterion on Variable Density SENSE Reconstruction**
Computer 35
Rui Yan[1,2], Feng Huang[1], James Akao[1], Charles Saylor[1], Hu Cheng[3], Randy Duensing[1]
[1]Invivo Corporation, Gainesville, Florida, USA; [2]University of Florida, Gainesville, Florida, USA; [3]Indiana University, Bloomington, Indiana, USA

Variable density (vd) parallel imaging provides freedom of optimizing k-space trajectory either to increase reconstruction SNR or reduce low frequency aliasing. The reconstructions using variable density such as SPACE RIP, Generalized SMASH, and Generalized SENSE consider this problem globally by solving huge matrix equations, which is time consuming. Parallel processing to different acceleration factor regions, such as Madore's method and later King's method, reduces the reconstruction time but can have either a ringing artifact at edges or bias. This paper discusses a filter design strategy in vdSENSE to reduce bias while still filtering out the ring effect, named as homoSENSE.

14:30 ***3656***. **Prior-Regularized GRAPPA Reconstruction**
Computer 33
Fa-Hsuan Lin[1]
[1]Massachusetts General Hospital, Charlestown, Massachusetts, USA

An auto-calibration scan (ACS) can improve parallel MRI reconstructions, including the popular GRAPPA method. Usually, the ACS is collected at the center of k-space, constituting low-resolution prior information. Previously, we have reported the advantage of prior-informed SENSE reconstruction with reduced noise amplification. Here we propose a prior-regularized GRAPPA reconstruction to further stabilize the reconstructed images at high acceleration rates. We demonstrated prior-informed GRAPPA on a 3T high-resolution anatomical scan. This method can be generalized for optimized k-t space sampling to provide priors with identical spatial resolution.

14:30 ***3657***. **A Fast Approach to Processing Coil Sensitivity Maps Using a Neural Network**
Computer 34
Martin Buehrer[1], Peter Boesiger[1], Sebastian Kozerke[1]
[1]ETH Zuerich, Zuerich, Switzerland

Obtaining information about coil sensitivities is crucial when using sensitivity encoding. Raw sensitivity maps, which can be calculated by dividing single-coil images by the body-coil image, are often impaired by noise, especially in regions with low spin density (e.g. in the lungs). In this work a neural network is used for fast fitting and extrapolation of the raw sensitivity data. Using this approach the computation time for processing the raw sensitivity maps could be reduced by a factor of twelve relative to polynomial fitting approaches.

15:00 ***3658***. **Multi-Tissue Based Coil Sensitivity Estimation for Optimal SNR Reconstruction in Phased Array MRI**
Computer 34
Prashanthi Vemuri[1], Eugene G. Kholmovski[1], Dennis L. Parker[1]
[1]University of Utah, Salt Lake City, Utah, USA

In typical MR studies, the sum-of-squares (SoS) reconstruction algorithm is applied for the combination of phased array MR images. The intensity of the SoS reconstructed image is modulated by a spatially variable function due to the non-uniformity of coil sensitivities and also has sub-optimal SNR and intensity bias. In this work, we have presented an iterative algorithm for the estimation of individual coil sensitivities using a multi-tissue Gaussian model. The estimated coil sensitivities are used for optimal SNR reconstruction which results in images with intensity modulation removed and with reduced intensity bias.

15:00 ***3659***. **Coil Combination and Elimination for Improved Reconstruction Efficiency in Parallel Imaging**
Computer 33
Luca Marinelli[1], *Christopher J. Hardy*[1]
[1]General Electric, Niskayuna, New York, USA

To accommodate the need for higher acceleration factors, coil arrays for parallel imaging applications have, in recent times, roughly doubled the number of channels each year. The resulting data flow can overwhelm reconstruction engines. We introduce and compare a class of algorithms to reduce the number of effective channels through linear combinations and elimination of coils that do not contribute significantly in the region of interest. Eigenvectors of the noise correlation matrix can be used to build a basis of effective sensitivity functions at each point in space. We validate these methods with a 32-channel cardiac array and acceleration R=1,2,4.

15:00 ***3660***. **Joint Image Reconstruction and Sensitivity Estimation in SENSE (JSENSE)**
Computer 35
Leslie Ying[1], *Jinhua Sheng*[1], *Bo Liu*[1]
[1]University of Wisconsin, Milwaukee, Wisconsin, USA

Parallel imaging has emerged as an effective tool to reduce imaging time in various dynamic imaging applications. This paper considers the inaccuracy of coil sensitivity estimation in conventional reconstruction methods such as SENSE, and reformulates the image reconstruction problem as a joint estimation of the coil sensitivities and the desired image, which is solved by an iterative algorithm (JSENSE). Simulation based on an eight-channel configuration demonstrates that the proposed method effectively corrects the sensitivity errors and thereby improves reconstruction especially when large acceleration factors are used.

15:00 ***3661***. **A Spatiotemporal Model-Based Method for Dynamic Imaging Using Phased Array Coils**
Computer 32
Dan Xu[1], *Leslie Ying*[2], *Zhi-Pei Liang*[1]
[1]University of Illinois at Urbana-Champaign, Urbana, Illinois, USA; [2]University of Wisconsin at Milwaukee, Milwaukee, Wisconsin, USA

This paper presents a model-based dynamic imaging method with time-sequential sampling in k-t space using phased array coils. The temporal signal variations of the dynamic object function are absorbed in the temporal basis functions while the spatial signal variations are incorporated in the series coefficients. Parallel data acquisition is used to improve the frame rate, thus reducing potential model fitting error. Simulations based on experimental cardiac data are carried out, which show that the proposed method can reconstruct motion artifacts-free images with very high spatiotemporal resolution.